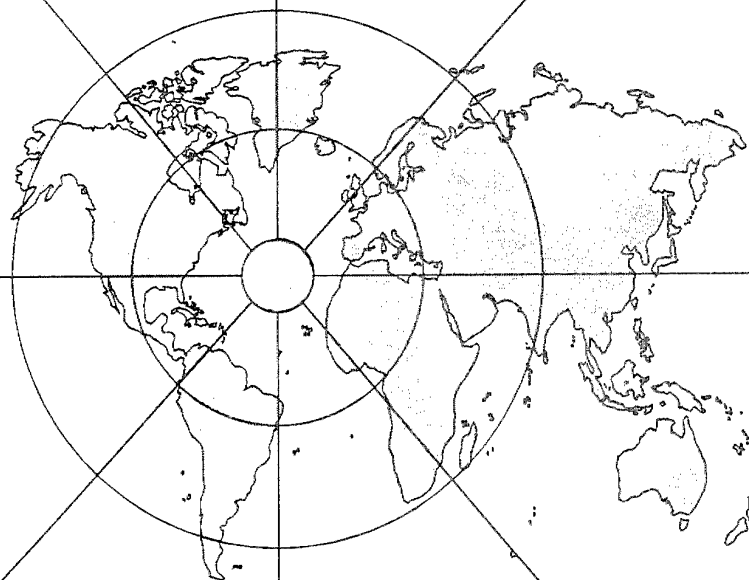


Proceedings of the
Forty-Fifth

IWCS



**INTERNATIONAL
WIRE AND CABLE
SYMPOSIUM**

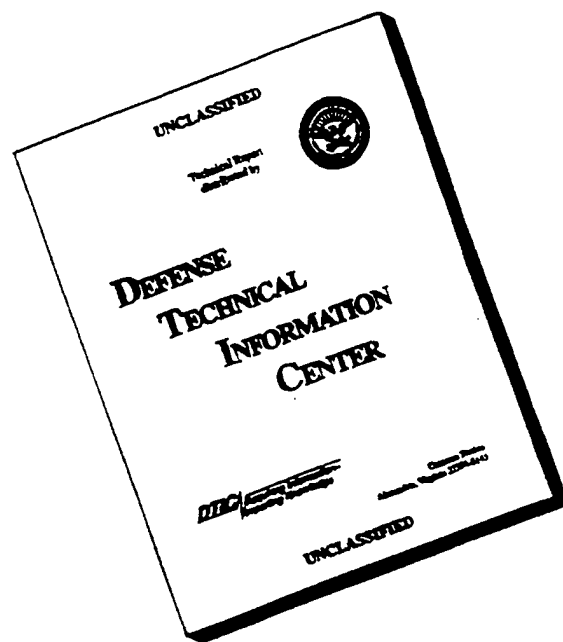
NOVEMBER 18 THRU 21, 1996

Sponsored by
International Wire and Cable Symposium,
Inc. (IWCS)
Eatontown, New Jersey

With Participation by
US Army Communications-Electronics Command
(CECOM)
Fort Monmouth, New Jersey

19970512 049

DISCLAIMER NOTICE



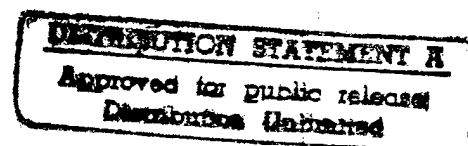
**THIS DOCUMENT IS BEST
QUALITY AVAILABLE. THE
COPY FURNISHED TO DTIC
CONTAINED A SIGNIFICANT
NUMBER OF PAGES WHICH DO
NOT REPRODUCE LEGIBLY.**

PROCEEDINGS OF 45TH INTERNATIONAL WIRE AND CABLE SYMPOSIUM

Sponsored by
International Wire and Cable Symposium, Inc. (IWCS)
Eatontown, New Jersey

With Participation by
US Army Communications-Electronics Command (CECOM)
Fort Monmouth, New Jersey

**RENO HILTON HOTEL
RENO, NEVADA
NOVEMBER 18, 19, 20 AND 21, 1996**



DTIC QUALITY INSPECTED 3

APPROVED FOR PUBLIC RELEASE: DISTRIBUTION UNLIMITED

MISSION

The International Wire and Cable Symposium provides a forum for the exchange of technical information amongst suppliers, manufacturers, and users on technological advancements in materials, processes, and products used for voice, data and video signal transmission systems.

TECHNICAL PAPERS

Tuesday, November 19

9:00 am	SESSION 1	Communications Infrastructure Initiatives: Investing for Global Competitiveness <i>Track 1-- Fiber Optic Cables</i>
1:00 pm	SESSION 2	Submarine Cable and PMD
1:00 pm	SESSION 3	Aerial Cables <i>Track 2 -- Copper Cables</i>
1:00 pm	SESSION 4	Residential Broadband Networks <i>Track 3 -- Materials</i>
1:00 pm	SESSION 5	Insulation, Jacketing & Flame Retardant

Wednesday, November 20

		<i>Track 1 -- Fiber Optic Cables</i>
8:00 am	SESSION 6	Splicing and Enclosure
8:00 am	SESSION 7	Optical Networks <i>Track 2 -- Copper Cables</i>
8:00 am	SESSION 8	Copper Cable Connections <i>Track 3 -- Materials</i>
8:00 am	SESSION 9	Advances in Fiber Coatings <i>Track 1 -- Fiber Optic Cables</i>
2:15 pm	SESSION 10	Fiber Optic Cable Design
2:15 pm	SESSION 11	Testing and Field Evaluation I
2:15 pm	SESSION 12	Emerging Wireless Networks <i>Track 3 -- Materials</i>
2:15 pm	SESSION 13	Fiber Coating Reliability
4:00 pm	SESSION 14	Poster Papers

Thursday, November 21

		<i>Track 1 -- Fiber Optic Cables</i>
8:30 am	SESSION 15A	Fiber Optic Cable Design (Cont)
10:00 am	SESSION 15B	High Fiber Count Cable
8:30 am	SESSION 16	Testing and Field Evaluation II <i>Track 2 -- Copper Cables</i>
8:30 am	SESSION 17	High Performance Twisted Pair Cables <i>Track 3 -- Materials</i>
8:30 am	SESSION 18	Materials in Fiber Optic Cables <i>Track 1 -- Fiber Optic Cables</i>
1:00 pm	SESSION 19	Ribbons, Fiber to the Home and Air Blown Fiber
1:00 pm	SESSION 20	Fiber Optic Connectors/Components
1:00 pm	SESSION 21	Fiber Properties and Reliability <i>Track 2 -- Copper Cables</i>
1:00 pm	SESSION 22	Coaxial Cables

PAPERS

The papers in this volume were printed directly from unedited reproducible copies prepared by the authors. Responsibility for contents rests upon the authors and not the symposium committee or its members. All rights reserved by the International Wire and Cable Symposium, Inc., 174 Main Street, Eatontown, New Jersey 07724.

PROCEEDINGS/PUBLICATIONS INTERNATIONAL WIRE AND CABLE SYMPOSIUM (IWCS)

Proceedings - Bound - Available from IWCS

39th IWCS Proceedings - 1990 - \$20.00

40th IWCS Proceedings - 1991 - \$20.00

Copies of original proceedings not listed above can be reproduced for \$75.00 per copy plus shipping.

44th IWCS Proceedings - 1995 - \$40.00

45th IWCS Proceedings - 1996 - \$50.00

Publications - Bound - Available from IWCS

Index of IWCS Papers (1983-1990); PUB #1001RP-1991 - \$15.00

PIC Insulation Testing Field Experience; PUB #1003RP-1992 - \$25.00

Fiber Optic Cables; PUB #1004RP-1992 - \$25.00

Extra Copies of the 1996 Proceedings can be obtained for: 1 - \$50; 2 - \$100; 3 - \$150; 4 - \$190; 5 - \$230; 6 - \$270; 7 - \$310; 8 - \$350; 9 - \$390; 10 - \$430; 11 and above - \$430 plus \$30 for each additional copy.

Shipping/Handling:

Proceedings

\$ 7.00 per copy USA only

\$15.00 per copy Surface Mail

(overseas - 4 to 6 weeks)

\$35.00 per copy Airmail (Europe)

\$40.00 per copy for (Asia)

Publications

\$ 4.00 per copy USA Only

\$ 7.00 per copy Surface Mail

(overseas - 4 to 6 weeks)

\$15.00 per copy Airmail

(Europe and Asia)

Payment: Make a check or bank draft payable in U.S. Dollars drawn on U.S. Bank only to the INTERNATIONAL WIRE & CABLE SYMPOSIUM, INC. or use your VISA/MC/AMEX by providing number and expiration date and forward request to: International Wire and Cable Symposium, Inc., 174 Main Street, Eatontown, NJ 07724. Telephone inquiries may be directed to Ms. Pat Hudak (908) 389-0990. Prices are subject to change.

Photocopies are available for complete sets of papers for 1964 thru 1995. Information on prices and shipping charges should be requested from the:

US Department of Commerce

National Technical Information Service (NTIS)

Springfield, Virginia 22161

Telephone: (703) 487-4650

Include Title, Year and "AD" Number

13th Annual Wire Cable Symposium (1964)	- AD 787164
15th Annual Wire Cable Symposium (1966)	- AD A006601
16th International Wire Cable Symposium (1967)	- AD 787165
17th International Wire Cable Symposium (1968)	- AD 787166
18th International Wire Cable Symposium (1969)	- AD 787167
19th International Wire Cable Symposium Proceedings 1970	- AD 714985
20th International Wire Cable Symposium Proceedings 1971	- AD 733399
21st International Wire Cable Symposium Proceedings 1972	- AD 752908
22nd International Wire Cable Symposium Proceedings 1973	- AD 772914
23rd International Wire Cable Symposium Proceedings 1974	- AD A003251
24th International Wire Cable Symposium Proceedings 1975	- AD A017787
25th International Wire Cable Symposium Proceedings 1976	- AD A032801
26th International Wire Cable Symposium Proceedings 1977	- AD A047609
27th International Wire Cable Symposium Proceedings 1978	- AD A062322
28th International Wire Cable Symposium Proceedings 1979	- AD A081428
29th International Wire Cable Symposium Proceedings 1980	- AD A096308
30th International Wire Cable Symposium Proceedings 1981	- AD A110859
31st International Wire Cable Symposium Proceedings 1982	- AD A125662
32nd International Wire Cable Symposium Proceedings 1983	- AD A136749
33rd International Wire Cable Symposium Proceedings 1984	- AD A152119
34th International Wire Cable Symposium Proceedings 1985	- AD A164384
35th International Wire Cable Symposium Proceedings 1986	- AD A180828
36th International Wire Cable Symposium Proceedings 1987	- AD A189610
37th International Wire Cable Symposium Proceedings 1988	- AD A200903
38th International Wire Cable Symposium Proceedings 1989	- AD A216023
39th International Wire Cable Symposium Proceedings 1990	- AD A233634
40th International Wire Cable Symposium Proceedings 1991	- AD A244038
41st International Wire Cable Symposium Proceedings 1992	- AD A259235
42nd International Wire Cable Symposium Proceedings 1993	- AD A279242
43rd International Wire Cable Symposium Proceedings 1994	- AD A293473
44th International Wire Cable Symposium Proceedings 1995	- AD A303506
Kwic Index of Technical Papers, International Wire Cable Symposium (1952-1982)	- AD A027588



MESSAGE FROM THE PRESIDENT/DIRECTOR

The International Wire and Cable Symposium (IWCS) Committee and CECOM, Fort Monmouth, NJ extend a welcome to all symposium attendees. The committee is excited over the program scheduled for the symposium and also the return to Reno, Nevada after four successful years on the east coast of the USA. The opening plenary session scheduled for Tuesday, entitled "Communications Infrastructure Initiatives: Investing for Global Competitiveness," with its potential for creating major changes in the telecommunication industry should set the stage for an exciting and interesting conference.

The program includes three days of technical presentations, covering copper/fiber cables and materials; one full day of educational short courses and a day and a half of company exhibits/displays. Mixed in with the technical presentations and displays are special activities, beginning with Monday Night Football sponsored by the AlphaGary Corporation, followed by the contributor's sponsored Tuesday Night Hospitality Hour and the Awards Luncheon on Wednesday. The increasingly popular Poster Session scheduled for Wednesday afternoon also seems to be the gathering place for exciting and enjoyable discussions. In addition, the large number of International attendees and presenters from more than thirty countries each year, help to expand and diversify the technical information available during the symposium.

The committee respectfully bids farewell to several of its faithful and devoted members. Richard Rossi our present chairman, Dr. Felix Kapron, Laurence Jones and Paul Kopera are leaving the committee. I extend to each, the committee's sincere thanks and appreciation for their dedication, cooperation and support.

To insure the continued success of the symposium, the committee solicits the support and participation of all members of the wire and cable industry. Therefore, comments and suggestions are welcomed.

The symposium for years 1997 and 1998 will be at the Marriott Hotel in Philadelphia, Pennsylvania.

A handwritten signature in dark ink, appearing to read "Elmer F. Godwin". The signature is fluid and cursive.

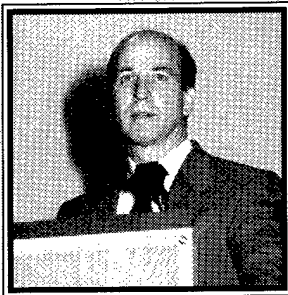
*Elmer F. Godwin
President/Director*

HIGHLIGHTS OF THE 44TH IWCS

International Wire and Cable Symposium

November 13, 14, 15 and 16, 1995
Philadelphia Marriott Hotel, Philadelphia, PA

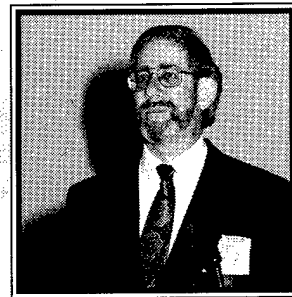
Announcements/Greetings



BRIAN D. GARRETT
IWCS Chairman
CommScope, Inc.
Claremont, NC



BARRY S. SALIS
U.S. Army CECOM
Fort Monmouth, NJ



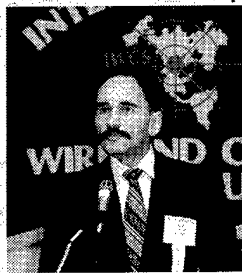
Guest-Speakers - Plenary Session



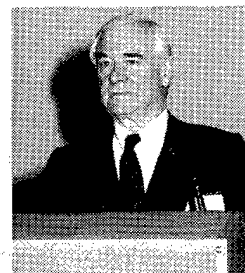
DR. DONALD KECK
Corning
Corning, NY



JOHN HOOD
CommLink Systems, Inc.
Ontario, Canada



DR. FELIX P. KAPRON
Chairman, Plenary Session
Bellcore
Morristown, NJ

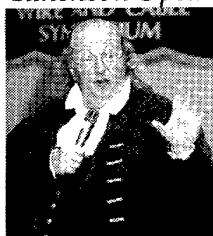


GILLES DUPUY d'ANGEAC
Alcatel Cable Group
Clichy Cedex, France



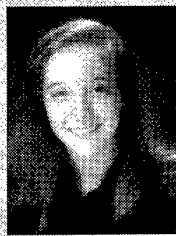
DR. OSTEN MAKITALO
Telia Research
Haninge, Sweden

Luncheon Speaker



RALPH ARCHBOLD
as
Ben Franklin
Philadelphia, PA

Scholarship Recipients



SARA RANSOM
2nd Year
Scholarship Recipient
Massachusetts Institute
of Technology



JASON CHANG
1st Year
Scholarship Recipient
Princeton University

Award Winners



**OUTSTANDING
TECHNICAL PAPER**

TOSHIO KURASHIMA
NTT Laboratories - Ibaraki, Japan
(Also accepting for Kazuo Hogari,
Satoshi Matsubashi, Dr. Tsuneo
Horiguchi, Dr. Yahei Koyamada,
Yutaka Wakui and Hiroshi Hirano)



OUTSTANDING POSTER PAPER

JAN BJORKMAN
Telia AB
Farsta, Sweden
(Also accepting for Dr. Sverker
Forsberg - Swedish University of
Agricultural Sciences,
Uppsala, Sweden)



BEST PRESENTATION

**ANTHONY
RECHICHI**
Accepting for
BARRY J. KEON
Telstra
Clayton, Australia

Several Winners from the Survey Questionnaire



BRIAN D. GARRETT
CommScope, Inc.
Claremont, NC



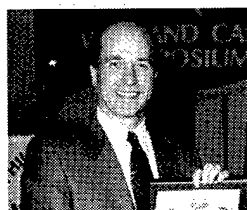
DR. KOICHI INADA
Fujikura Ltd.
Chiba-ken, Japan



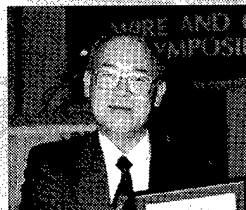
DR. JOYCE P. KILMER
Optotec, N.A.A.
New York, NY



IWC Retirees



BRIAN D. GARRETT
CommScope, Inc.
Claremont, NC

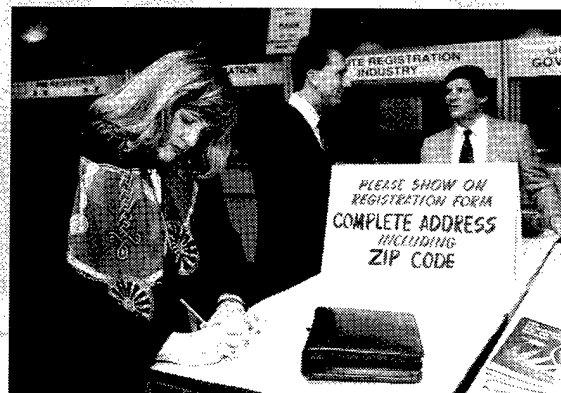
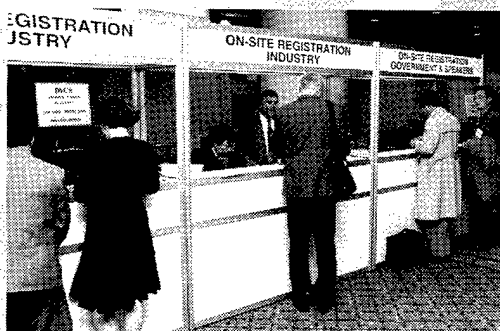
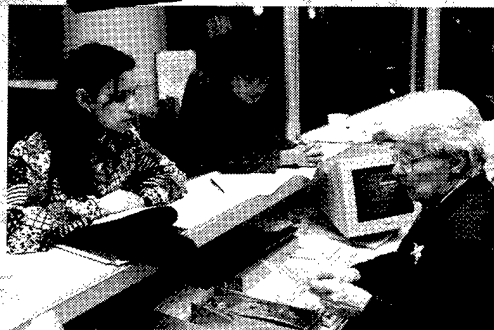
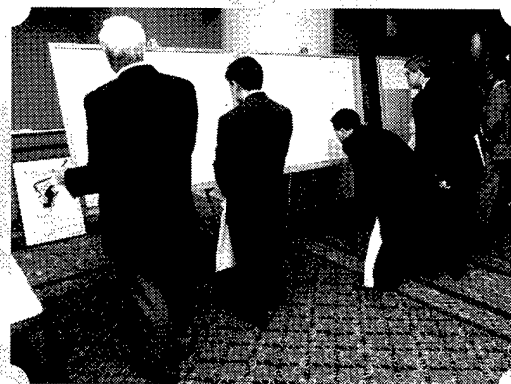
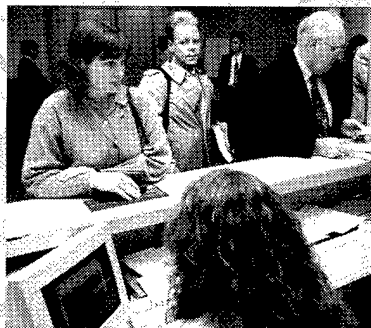
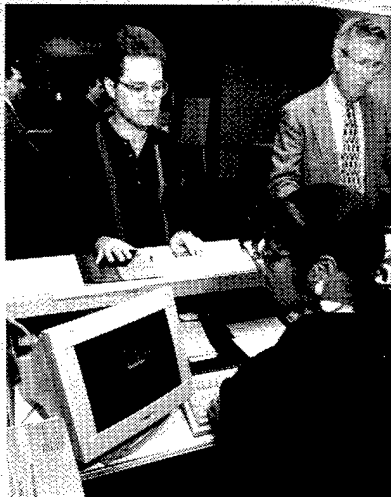


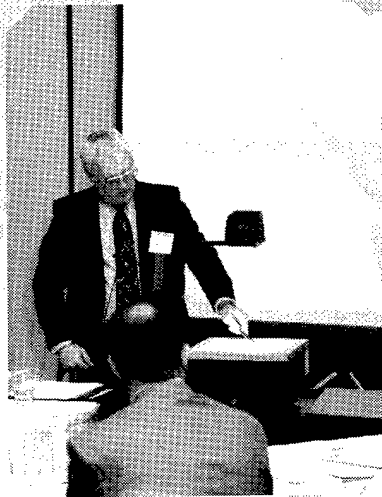
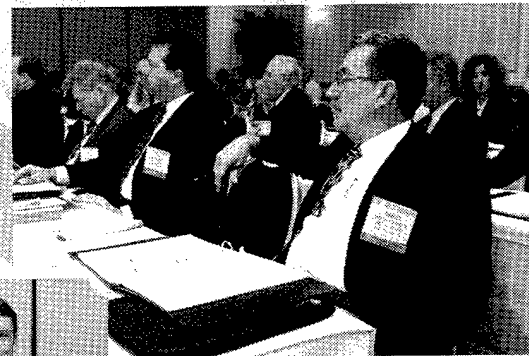
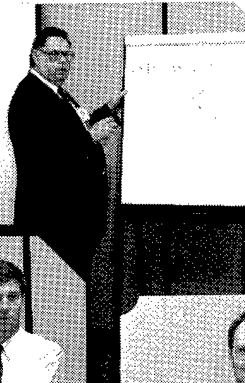
DR. KOICHI INADA
Fujikura Ltd.
Chiba-ken, Japan



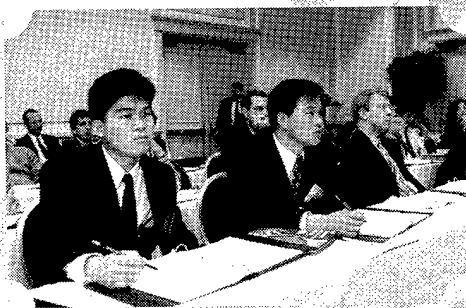
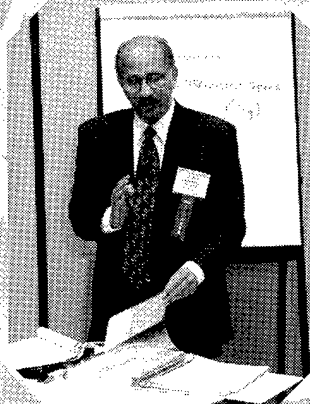
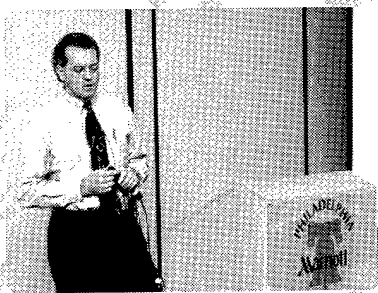
DR. JOYCE P. KILMER
Optotec, N.A.A.
New York, NY

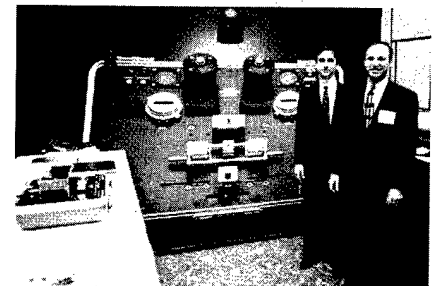
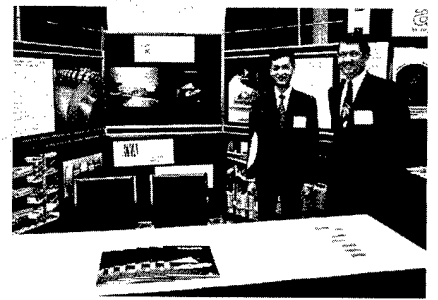
Registration

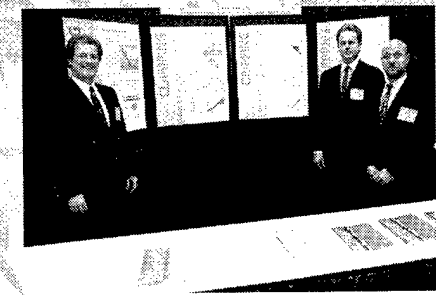
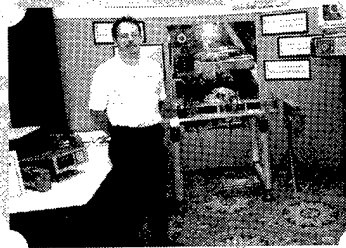
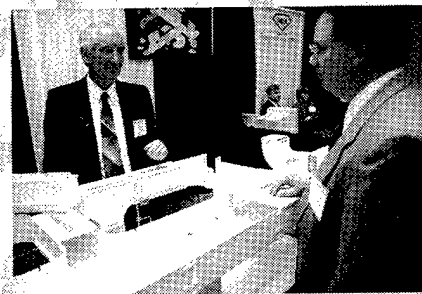
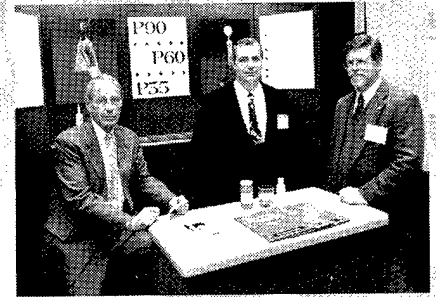
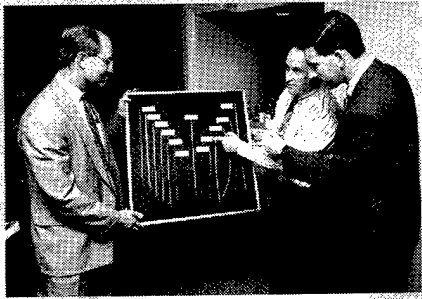


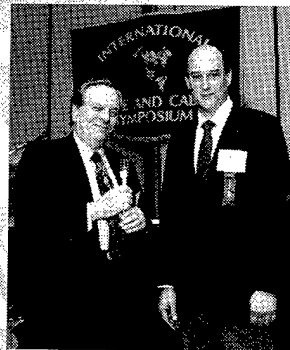
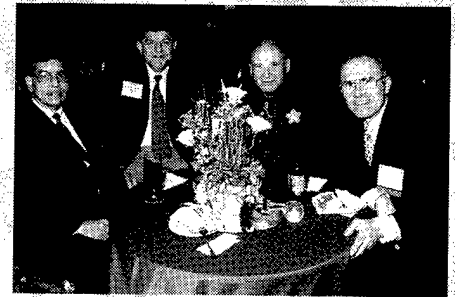
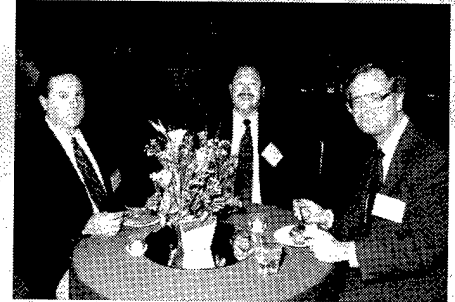
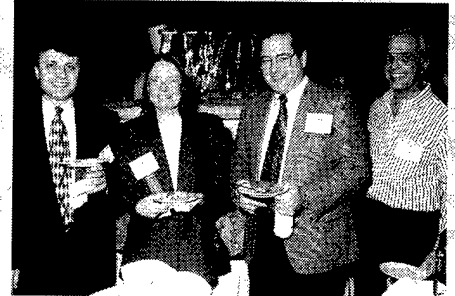
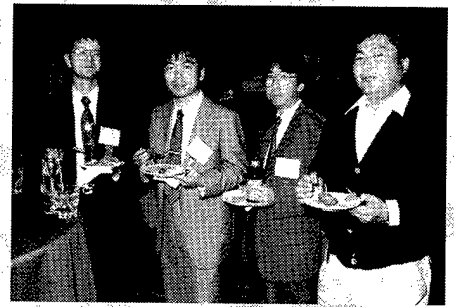
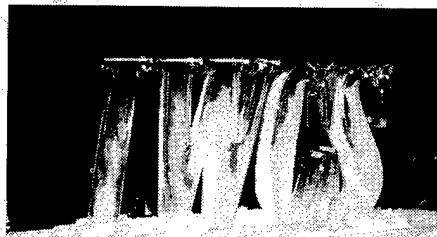
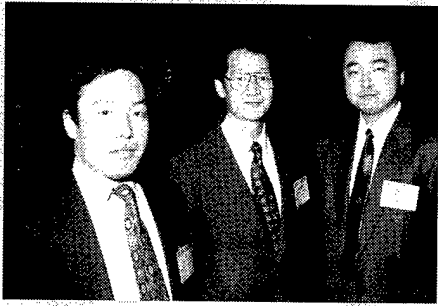


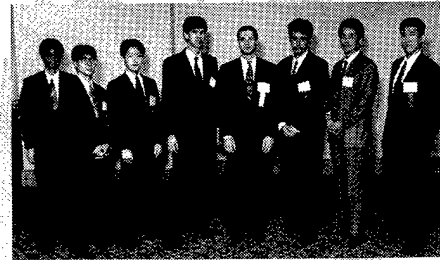
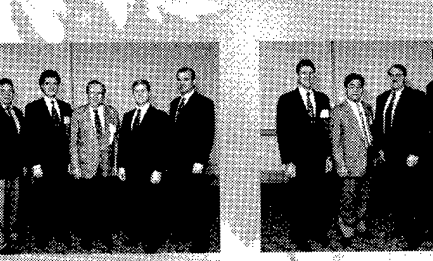
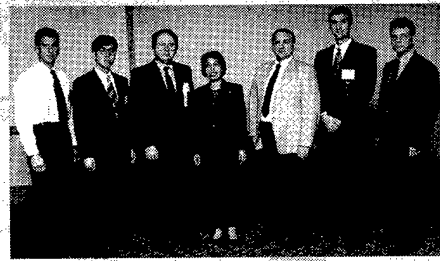
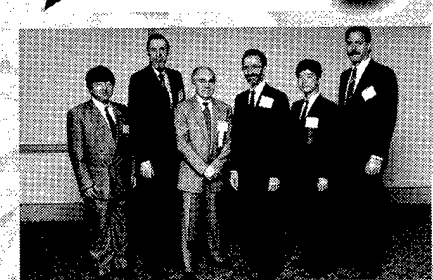
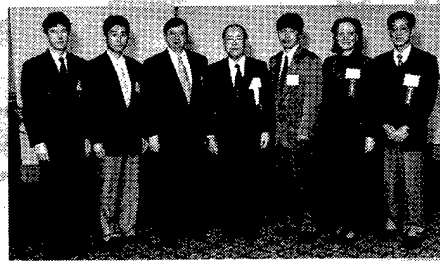
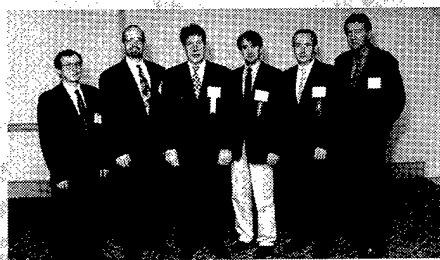
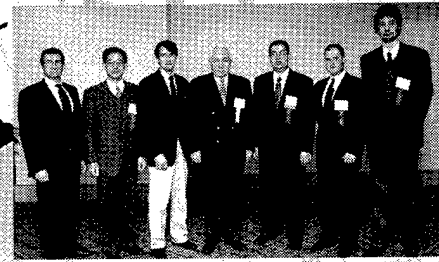
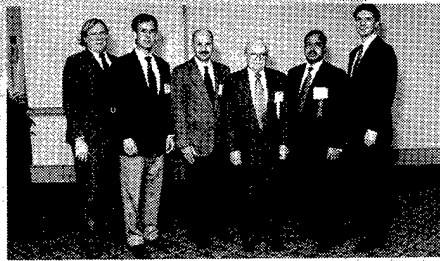
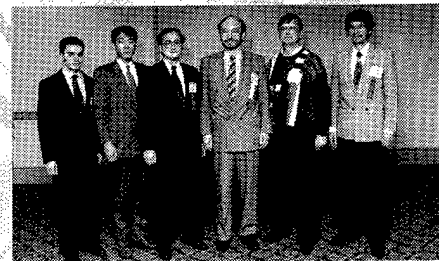
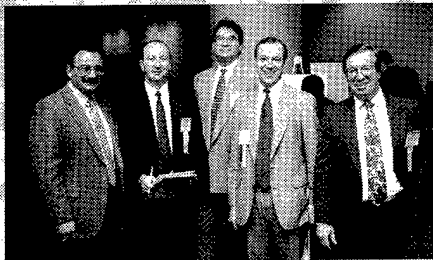
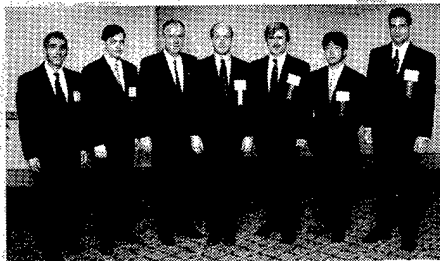
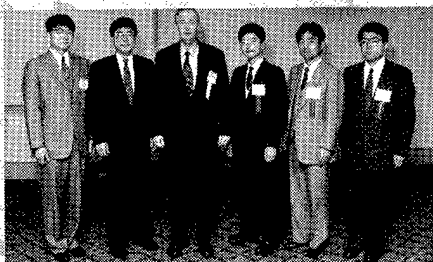
Educational

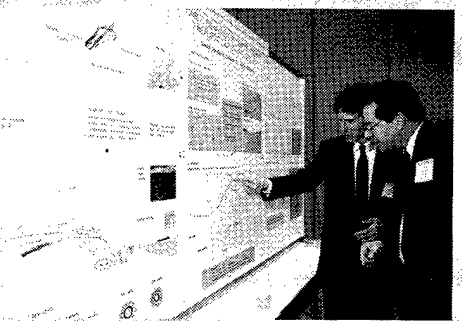
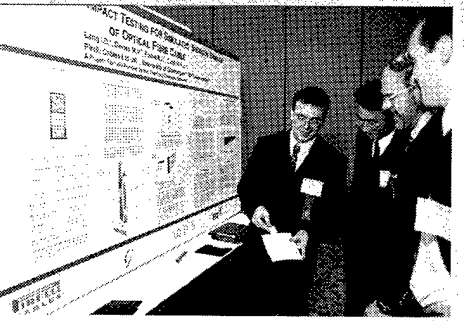
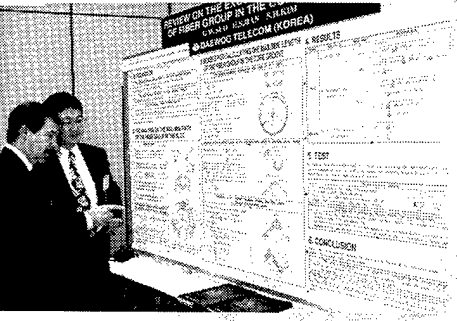
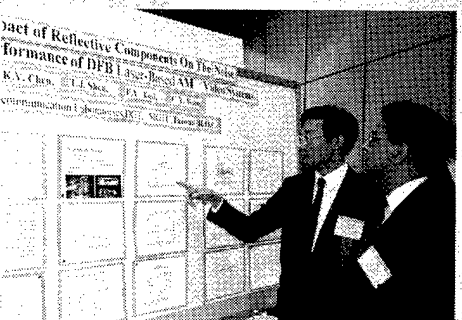
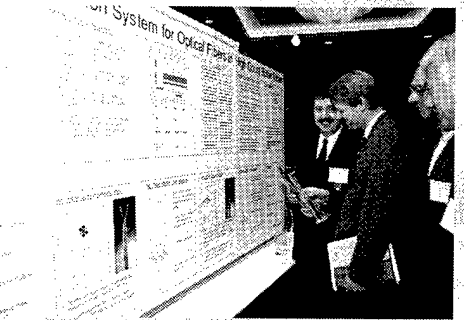
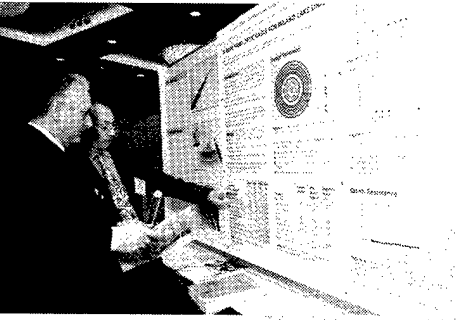
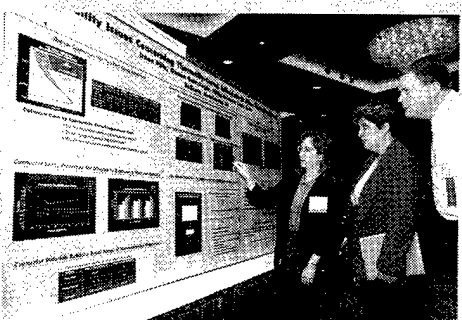
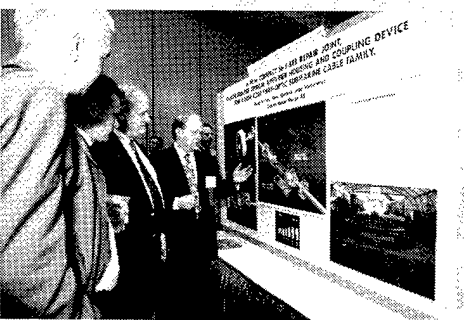
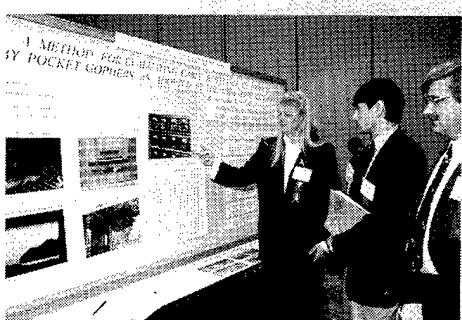
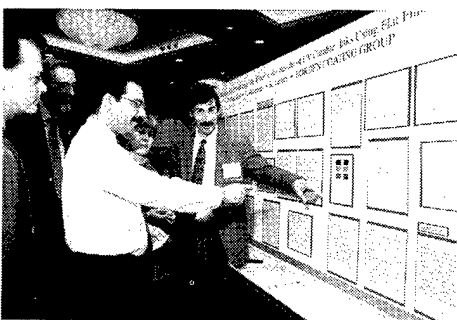
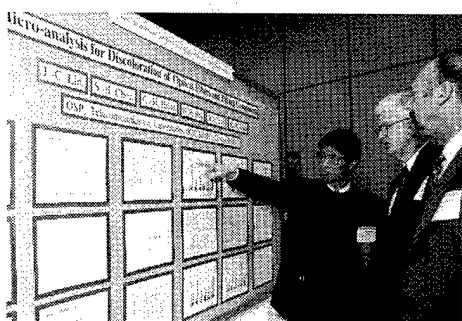
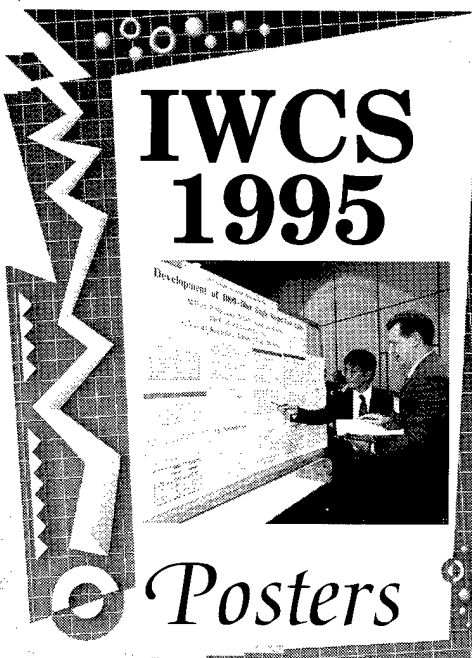
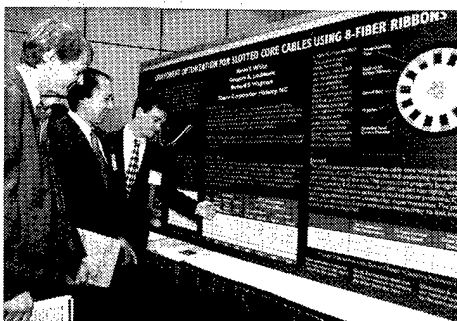
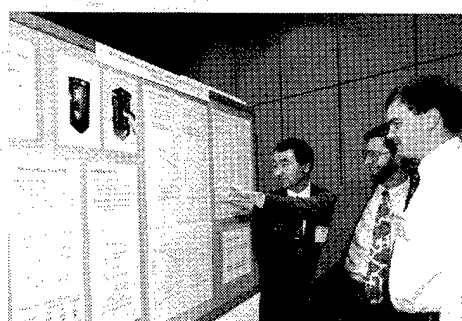
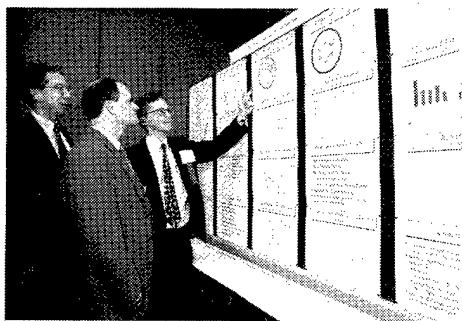












AWARDS

Outstanding Technical Paper

- | | |
|--|------|
| H. Lubars and J. A. Olszewski, General Cable Corp. — "Analysis of Structural Return Loss in CATV Coaxial Cable" | 1968 |
| J. P. McCann, R. Sabia and B. Wargotz, Bell Laboratories — "Characterization of Filler and Insulation in Waterproof Cable" | 1969 |
| D. E. Setzer and A. S. Windeler, Bell Laboratories — "A Low Capacitance Cable for the T2 Digital Transmission Line" | 1970 |
| R. Lyenger, R. McClean and T. McManus, Bell Northern Research — "An Advanced Multi-Unit Coaxial Cable for Toll PCM Systems" | 1971 |
| J. B. Howard, Bell Laboratories — "Stabilization Problems with Low Density Polyethylene Insulations" | 1972 |
| Dr. H. Martin, Kabelmetal — "High Power Radio Frequency Coaxial Cables, Their Design and Rating" | 1973 |
| D. Doty, AMP Inc. — "Mass Wire Insulation Displacing Termination of Flat Cable" | 1974 |
| T. S. Choo, Dow Chemical U.S.A. — "Corrosion Studies on Shielding Materials for Underground Telephone Cables" | 1975 |
| N. J. Cogelia, Bell Telephone Laboratories and G. K. Lavoie and J. F. Glahn, US Department of Interior — "Rodent Biting Pressure and Chemical Action and Their Effects on Wire and Cable Sheath" | 1976 |
| T. K. McManus, Northern Telecom Canada Ltd. and R. Beveridge, Saskatchewan Telecommunications, Canada — "A New Generation of Filled Core Cable" | 1977 |
| F. Suzuki, S. Sato, A. Mori and Y. Suzuki, Sumitomo Electric Industries, Ltd., Japan — "Microcoaxial Cables Insulated with Highly Expanded Polyethylene By Chemical Blowing Method" | 1978 |
| S. Masaki, Y. Yamazaki and T. Ideguchi, Nippon Telegraph and Telephone Public Corporation, Japan — "New Aluminum Sheath Cable Used for Electromagnetic Shielding" | 1979 |
| P. Kish and Y. BeBorgne, Northern Telecom Canada Limited, Montreal, Canada — "General Crosstalk Model for Paired Communication Cables" | 1980 |
| C. J. Arroyo, N. J. Cogelia, Bell Laboratories, and B. J. Darsey, Western Electric — "Thermal Behavior of Experimental Plenum Cable Sheaths Determined in a Radiant Heat Chamber" | 1981 |
| R. H. Whiteley, Raychem Ltd. — "A Comprehensive Small Scale Smoke Test" | 1982 |
| V. A. Fentress, Raychem Corp. and D. V. Nelson, Stanford University — "Fracture Mechanics Evaluation of the Static Fatigue Life of Optical Fibers in Bending" | 1983 |
| M. Fujise and Y. Iwamoto, KDD Research & Development Laboratories, Tokyo, Japan — "Self-Core-Alignment Arc-Fusion Splicer Based on a Simple Local Monitoring Method" | 1984 |
| James A. Krabec and John W. Kincaid, Jr., Belden Technical Research Center — "Advances in the Optimization of Multi-Layer Shield Design" | 1985 |
| Simon D. Dadakarides and Bruce B. Lusignam, Stanford University — "Magnetically Loaded Cables" | 1986 |

Best Presentation

- | | |
|--|--|
| N. Dean, B.I.C.C. — "The Development of Fully Filled Cables for Distribution Network" | |
| J. D. Kirk, Alberta Government Telephones—"Progress and Pitfalls of Rural Buried Cable" | |
| Dr. O. Leuchs, Kable and Metalwerke—"A New Self-Extinguishing Hydrogen Chloride Binding PVC Jacketing Compound for Cables" | |
| S. Nordblad, Telefonaktiebolaget L. M. Ericsson—"Multi-Paired Cable of Nonlayer Design for Low Capacitance Unbalance Telecommunications Network" | |
| N. Kojima, Nippon Telegraph and Telephone—"New Type Paired Cable for High Speed PCM Transmission" | |
| S. Kaufman, Bell Laboratories—"Reclamation of Water-Logged Buried PIC Telephone Cable" | |
| R. J. Oakley, Northern Electric Co., Ltd.—"A Study Into Paired Cable Crosstalk" | |
| G. H. Webster, Bell Laboratories—"Material Savings by Design in Exchange and Trunk Telephone Cable" | |
| J. E. Wimsey, United States Air Force—"The Bare Base Electrical Systems" | |
| Michael DeLucia, Naval Ship Research and Development—"Highly Fire-Retardant Navy Shipboard Cable" | |
| William L. Schmacher, AMP Inc.—"Design Considerations for Single Fiber Connector" | |
| Richard C. Mondello, Bell Labs—"Design and Manufacture of an Experimental Lightguide Cable for Undersea Transmission Systems" | |
| I. Wadehra, IBM Corporation—"Performance of Polyvinyl Chloride Communication Cables in Modified Steiner Tunnel Test" | |
| J. J. Refi, Bell Laboratories—"Mean Power Sum Far-End Crosstalk of PIC Cables as a Function of Average Twist Helix Angle" | |
| G. S. Anderson, Belden Corporation—"Installation of Fiber Optic Cable on 457 Meter Tower" | |
| A. Yoshizawa, The Furukawa Electric Co., Ltd.—"Structure and Characteristics of Cables for Robots" | |
| J. R. Bury, Standard Telecommunication Laboratories, Ltd., Hailow, England—"Development of Flame Retardant, Low Aggressivity Cables" | |
| William E. Dennis, Dow Corning Corporation, Midland, Michigan—"Hydrogen Evolving Tendencies of Cable Fillers and Optical Fiber Coatings" | |
| Stephen Hornung, British Telecom Research Laboratories—"Manufacture and Performance of Fibre Units for Installation by The Viscous Drag of Air" | |
| Dave Fischer, Superior Cable Corp.—"Progress Towards the Development of Lighting Test for Telecommunication Cables" | |
| John C. Chamberlain, Siecor Corp.—"Zero Halogen Fire Retardant Fiber Optic Shipboard Cable" | |

Outstanding Technical Paper

1987

Stephen B. Pierce — Conel Laboratories — "Digital Transmission on Customer Premises Wiring"

1988

Martin C. Light Jr., James A. Moses, Mark A. Sigmon and Christopher A. Story — Siecor Corp. — "Design and Performance of Telecommunication Cable Optimized for Low Fiber Count"

1989

Michel Plasse, Lise Desroches and Paul-Andre Guilbert — Northern Telecom Canada Limited — "High Performance Twisted-Pair Cable for LAN Systems"

1990

Trevor N. Bowmer, Russell J. Miner, Irene M. Plitz, Joseph N. D'Amico and Lal M. Hore — Bellcore — "Thermal Stability Tests for Polyolefin Insulations"

1991

Shigeru Tomita, Michito Matsumoto, Tetsuro Yabuta and Takuya Uenoya — NTT — "Preliminary Research into Ultra High Density and High Count Optical Fiber Cables"

1992

Nathan E. Hardwick III and Kris Kathiresan — AT&T Bell Laboratories and J. G. Hartley — Georgia Institute of Technology — "Analysis of Fiber Optic Cable Design Conditions in Vicinity of Steam Lines — Ruptured and Pristine"

1993

Dr. Yoshinori Namihira and Toshio Kawazawa — KDD R&D Laboratories; and Naoki Norimatsu — KDD Company, Limited — "PMD Reduction of Optical Fiber Cables for Transoceanic Optical Amplifier Submarine Cable Systems"

1994

Toshio Kurashima, Kazuo Hogari, Satoshi Matsuhashi, Dr. Tsuneo Horiguchi, Dr. Yahei Koyamada and Yutaka Wakui — NTT Access Network Systems Laboratories; and Hiroshi Hirano — NTT Technical Assistance & Support Center — "Measurement of Distributed Strain in Frozen Cables and Its Potential for Use in Predicting Cable Failure"

1995

Jean Luc Lang and Jean-Francois Libert — Alcatel Submarine Network; David I. Curtis and Peter Worthington — STC Submarine Systems Ltd. — "Optical Performance of Submarine Cables in Optically Amplified High Bit Rate Systems"

Outstanding Poster Paper

William Wood — Bell Communication Research — "Performance Analysis of Optic Fiber Cleavers"

Dr. R. Raman — Contel Laboratories — "Loss at Dissimilar Fiber Splices"

Werner Bernard and Susan C. Grant — Siecor Corporation — "Fiber Optic Drop Cables in the Subscriber Loop"

Steve Lischynsky, Helmut Lukas, Robin McIntyre and Grant Pacey — Bell-Northern Research Ltd. — "New Technology for a Single Mode Mechanical Splice"

G. Scott Glaesemann — Corning Inc. — "The Effect of Proof Testing on the Minimum Strength of Optical Fiber"

Svend Hopland and Albert Klykken — Norwegian Telecom — "Installation of Submarine Fiberoptic Cables in Rugged Coastal Terrain"

Willem Griffioen — PTT Research — "Mechanical Lifetime of Optical Fibers"

Dr. Sverker Forsberg — Swedish University of Agricultural Sciences; and Jan Björkman — Telia AB — "Release of Lead from Lead-Sheathed Telecom Cables in Soil"

Richard S. Wagman, Gregory A. Lochkovic and Kevin T. White — Siecor Corporation — "Component Optimization for Slotted Core Cables Using 8-Fiber Ribbons"

Best Presentation

Richard Rossi — General Cable Company — "Cable Sheathing Design and Performance Criteria"

Janice B. Haber — AT&T Laboratories — "Single-Mode Media and Apparatus for Fiber to the Home"

Michel de Vecchis — Les Cables de Lyon — "Results on a Large Scale Installation of a Fibre Optic Distribution Network"

Harold W. Friesen — AT&T Bell Laboratories — "An Improved Characteristic Impedance Measurement Technique"

Sue V. Wolfe — STC Submarine Systems — "Structure and High Voltage DC Behaviour of Submarine Cable Mouldings"

Peter Latoszynski — Telecom Australia — "Development of Co-Extruded Polyethylene/Polyamide 12 Insect Resistant Telecommunications Cable"

Timothy S. Dougherty — AT&T Network Cable Systems — "The Temperature of Aerial Plant and Its Effect Upon Foam-Skin Insulation Life" and Wolfgang Wenski — Kabelmetal Electro GmbH — "First Large Scale FITL Installation: Experience From Opal '93"

Barry J. Keon — Telstra — "The Effects of Optical Fiber Coating and Ink Materials on the Corrosion of the Glass Surface"

Dr. Dan L. Philen — AT&T Bell Laboratories — "Optical Fiber for Amplified Undersea Systems"

ELMER F. "ACE" GODWIN SCHOLARSHIP

1994

**Sara Ransom, Massachusetts Institute of Technology,
Freshman -- Materials Science Engineering Major**

**Jurron Bradley, Vanderbilt University, Senior --
Chemical Engineering Major**

1995

**Jason Chang, Princeton University, Freshman --
Chemistry Major**

**Fionna Murray, Virginia Tech, Junior -- Mechanical
Engineering Major**

GOLD SUSTAINING CONTRIBUTORS

A F A Industries
20 Jewell Street
Garfield, NJ 07026

Akzo Nobel Aramid Products
801-F Blacklawn Road
Conyers, GA 30207

Alcatel Cable
30, rue Pierre Bérégovoy
92111 Clichy Cedex
France

AlphaGary Corporation
170 Pioneer Drive
Leominster, MA 01453

Amoco Chemicals
801 Warrenville Road
Lisle, IL 60532

Ausimont USA
10 Leonards Lane
Thorofare, NJ 08086

Cable Systems International
505 N. 51st Avenue
Phoenix, AZ 85043

Camden Wire Co., Inc.
12 Masonic Ave.
Camden, NY 13316

Chase & Sons
19 Highland Ave.
Randolph, MA 02368

Corning Inc.
35 West Market St.
MP-R0-02
Corning, NY 14831

DSM Desotech Inc.
1122 Saint Charles St.
Elgin, IL 60120

DuPont Company
PO Box 27001
Richmond, VA 23261

DuPont Fluoroproducts
Chestnut Run Plaza
Wilmington, DE 19880-0711

Ericsson Cables AB
Kabelvägen 1
824 82 Hudiksvall
Sweden

Essex Group, Inc.
1710 Wall St., PO Box 1750
Ft. Wayne, IN 46801-1750

Facile Holdings, Inc.
185 6th Avenue
Paterson, NJ 07509

Fujikura Ltd.
1-5-1, Kiba, Koto-ku
Tokyo, 135
Japan

The Furukawa Electric Co., Ltd.
6, Yawata-Kaigandori
Ichihara, Chiba, 290, Japan

Fusion UV Systems, Inc.
910 Clopper Road
Gaithersburg, MD 20878

GE Plastics
1 Plastics Avenue
Pittsfield, MA 01201

General Cable Corp.
4 Tesseneer Drive
Highland Heights, KY 41076

The Geon Company
One Geon Center
Avon Lake, OH 44012-0122

Habia Cable
Tierpsvägen 8
815 75 Söderfors
Sweden

Hitachi Cable, Ltd. (Hitaka Works)
5-1-1 Hitaka-Cho
Hitachi-City 319-14
Japan

LaserMike
8001 Technology Blvd.
Dayton, OH 45424

Lucent Technologies
Bell Labs Innovations
2000 Northeast Expressway
Norcross, GA 30071

Neptco Incorporated
30 Hamlet Street
Pawtucket, RI 02861

Nippon Telegraph and Telephone Corp.
1-7-1 Hanabatake
Tsukuba, Ibaraki, 305
Japan

Nokia-Maillefer, Inc.
1856 Corporate Drive, Suite 135
Norcross, GA 30093

GOLD SUSTAINING CONTRIBUTORS

NORDX/CDT

105 Marcel-Laurin Blvd.
Saint-Laurent, Quebec
Canada H4N 2M3

NOVA Chemicals

6711 Mississauga Road, Suite 200
Mississauga, Ontario
Canada L5N 2W3

Olex Cables

207 Sunshine Road
Tottenham, VIC 3012
Australia

Optical Fibres

Second Avenue
Deeside Industrial Park
Deeside, Flintshire
United Kingdom

Owens-Corning

Fiberglas Tower T-12
Toledo, OH 43659

Penreco/Pennzoil Products Co.

4401 Park Ave.
Dickinson, TX 77539

Plasma Optical Fibre B.V.

P.O. Box 1136
5602 BC Eindhoven
The Netherlands

PPG Industries, Inc.

22921 Judith Drive
Plainfield, IL 60544

Quantum Chemical Company

11500 Northlake Drive
Cincinnati, OH 45249

Siecor Corporation (R, D & E)

PO Box 489
Hickory, NC 28603

SpecTran Corporation

50 Hall Road
Sturbridge, MA 01566

The Stewart Group Inc.

259 Steelcase Road W.
Markham, Ontario
Canada L3R 2P6

Sumitomo Electric U.S.A., Inc.

21221 S. Western Ave., #200
Torrance, CA 90501

Teknor Apex Company

505 Central Avenue
Pawtucket, RI 02861

UBE Industries (America), Inc.

666 Fifth Avenue, 14th Floor
New York, NY 10103

Union Carbide Corporation

39 Old Ridgebury Road
Danbury, CT 06817-0001

WaterGuard Cable Products, Inc.

14135 I-10 East Freeway
Houston, TX 77015

Weber & Scher Mfg. Co., Inc.

263 Sussex Avenue
Newark, NJ 07107

Witco Corporation

One American Lane
Greenwich, CT 06831-2559

SILVER SUSTAINING CONTRIBUTORS

ACOME

Paris & Mortain, France

Air Logistics Corporation

Pasadena, CA 91107-3120

BICC Cables Limited

Warrington, Cheshire, United Kingdom

Ciba Additives

Tarrytown, NY 10591

Kabelmetal Electro GmbH

Hannover, Germany

Kromberg & Schubert GmbH u. Co.

Rhede and Wuppertal, Germany

MEHLER Industrietextilien GmbH

Fulda, Germany

Measurement Analysis Corp.

Torrance, CA 90505

Mitsubishi Cable Industries, Ltd.

Chiyoda-ku, Tokyo, 100, Japan

Oswego Wire Inc.

Oswego, NY 13126

Pirelli Cables

Lexington, SC 29072

Showa Electric Wire & Cable Co., Ltd.

Sagamihara, Kanagawa, 229-11, Japan

Siemens AG

München, Germany

Telia AB

S-12386 Farsta, Sweden

T. & T. Marketing, Inc.

Allamuchy, NJ 07820

TABLE OF CONTENTS

TUESDAY MORNING—9:00 AM—12:00 PM (NOON)

Reno Ballroom

Announcements/Greetings

Elmer F. Godwin, President/Director, IWCS, Inc., Eatontown, NJ

Richard Rossi, Chairman, IWCS

Barry S. Salis, Deputy Director, Space and Terrestrial Communications, U.S. Army, CECOM, Fort Monmouth, NJ

PLENARY SESSION 1: COMMUNICATIONS INFRA-STRUCTURE INITIATIVES: INVESTING FOR GLOBAL COMPETITIVENESS

Chairperson: John Sicotte, Corning Inc., Corning, NY

Panelists: Pei Ai Hua, Ministry of Post & Telecommunication, Beijing, China; Luis M. Molleda Susaeta, Telefonica, Madrid, Spain; Carlos Fernando Ximenes Duprat, Telebras, Brasilia, Brazil; Alex B. Best, Cox Communications, Inc., Atlanta, GA

1

TUESDAY AFTERNOON—1:00 PM—5:00 PM

Tahoe Room

TRACK 1—FIBER OPTIC CABLES

SESSION 2: SUBMARINE CABLE AND PMD

Chairperson: Dieter S. Nordmann, Kabelmetal Electro GmbH, Hannover, Germany

New Submarine Cable Design for Long Haul, High Bit Rate Systems—J.-F. Libert, Y. Charles, Alcatel Submarine Networks, Calais Cedex, France

8

Cabling Effects on Fiber PMD—F. Cocchini, A. Chiantore, Fibre Ottiche Sud, Battipaglia, Italy; G. Carones, A. Ginocchio, Pirelli Cavi S.p.A., Milano, Italy

13

Polarisation Mode Dispersion Field Measurements—A Survey of the Swedish National Network—K. Brising, Telia Network Services, Transport Networks, Farsta, Sweden

18

Simulation of System Length Limitations Induced by PMD—D. Gallagher, G. Wildeman, Corning Inc.; W. Jackson, M. Fedoroff, Siecor Corp.

27

Characterization of Optical Groundwire's Cabled Polarization Mode Dispersion Performance as a Function of Axial Strain and Temperature: A Case Study—R. C. Roman, Alcoa Fujikura Ltd., Spartanburg, SC; M. L. Lundergan, S. A. Cooper, Corning Inc., Corning, NY

37

TUESDAY AFTERNOON—1:00 PM—5:00 PM

Crystal Rooms 3/4/5

TRACK 1—FIBER OPTIC CABLES

SESSION 3: AERIAL CABLES

Chairperson: Michel Rousseau, Alcatel Cable, Clichy, France

Optical Phase Conductor for Medium Voltage Overhead Power Lines—R. Böhme, G. Hög, M. Hoffart, U. Jansen, K. Nothofer, Kabel Rheydt AG, Mönchengladbach, Germany

43

High Reliability Optical Ground Wire for Overhead Transmission Systems—R. T. Traut, W. F. Wright, G. N. Fontaine, M. J. Cyr, D. P. Dumont, Simplex Technologies Inc., Newington, NH

50

A Fully Instrumented Installation and Trial of a Novel All-Dielectric Self-Supporting Cable System for Very High Voltage Overhead Power Lines—N. R. Haigh, S. M. Rowland, A. J. Taha, BICC Cables Ltd., Helsby, UK; C. N. Carter, The National Grid Co. plc, Leatherhead, UK

60

Development and Characterisation of a New Dielectric Cored OPGW—A. Stringer, K. A. Ahmed, G. Gitlits, J. S. Jasik, Olex Cables, Melbourne, Australia; D. M. Burgess, R. C. Kemp, Commonwealth Scientific and Industrial Research Organisation, Australia; S. A. Wade, G. W. Baxter, S. F. Collins, Victoria University, Melbourne, Australia

68

Development of Small Size and High Performance Central Stainless Tube Optical Ground Wire Using Colored Thread Binders for Identification of Fiber Bundles—T. Yokokawa, K. Yonezawa, Y. Suetsugu, K. Nagatomi, S. Tanaka, Sumitomo Electric Industries, Ltd., Yokohama and Osaka, Japan

77

Optimized Design and Characteristics Analysis for High-Count and Downsized OPGW—S. C. Park, J. C. Jo, Y. I. Lee, H. J. Kang, Thihan Electric Wire Co., Ltd., Kyungki-Do, Korea

85

TUESDAY AFTERNOON—1:00 PM—5:00 PM

Carson Rooms 1/2

TRACK 2—COPPER CABLES

SESSION 4: RESIDENTIAL BROADBAND NETWORKS

Chairperson: Dr. Marek Kapuscinski, NORDX/CD, Quebec, Canada

Coaxial Cable with Integrated Ribbon-Slots in the Jacket and Accessory Part for Broadband Network—E. Esposito, A. Di Francesco, A. Tedeschi, G. Di Censo, Teleco Cavi, Roseto degli Abruzzi (TE), Italy

92

Optical Fiber and Copper Cables and Passive Components for FTTB/FTTC Network—E. Cressan, O. Bouffant, G. Le Traon, O. Daguiillon, R. Petit, J. Moalic, France Telecom, CNET/LAB, Lannion, France

100

Modular Components for Hybrid Fibre Coax Networks in Different Climatic Zones—H. Schürmann, J. Seidenberg, P. E. Zamzow, Kabel Rheydt AG, Mönchengladbach, Germany

108

Corrosion Control for Grounding Electrodes at Telecommunication Sites—M. Parente, MP Technologies, Hendersonville, NC; G. Schick, Bellcore, Morristown, NJ

115

Tomorrow's Residential Gateway to Broadband Services—S. Godo, Nortel Technologies, Ottawa, Ontario, Canada

122

Cabling for High Speed LANs—C. T. Di Minico, Digital Equipment Corp., Littleton, MA

129

TUESDAY AFTERNOON—1:00 PM—5:00 PM

Carson Rooms 3/4

TRACK 3—MATERIALS

SESSION 5: INSULATION, JACKETING & FLAME RETARDANT

Chairperson: James R. Leech, Union Carbide Corporation, Somerset, NJ

Lifetime Predictions of Flame Retardant Polymers by Thermogravimetric Analysis—S. Rampalli, Andrew Corp., Orland Park, IL

139

Evaluation of the Enhanced Thermo-Oxidative Aging Performance of an Improved Telephone Wire Insulation Compound—G. D. Brown, J. M. Cogen, M. J. Keogh, Union Carbide Corp., Somerset, NJ

167

Advanced LLDPE Compounds in Cable Jacketing—C. J. Kmiec, J. R. Leech, Union Carbide Corp., Somerset, NJ

177

Leakage Current Smoke Corrosivity Testing—Comparison of Cable and Material Data—J. T. Chapin, Lucent Technologies, Bell Laboratories, Norcross, GA; L. M. Caudill, DuPont, Wilmington, DE; P. Gandhi, R. Backstrom, Underwriters Laboratories, Northbrook, IL

184

Reduced Smoke Flame Retarded W&C Formulations—R. L. Markezich, Occidental Chemical Corp., Grand Island, NY

194

TUESDAY EVENING**Hilton Pavilion****Hospitality Hour—6:30 PM–8:00 PM****Suppliers Forum—6:30 PM–8:30 PM****Admission by badges issued to all registrants****WEDNESDAY MORNING—8:00 AM–11:45 AM****Tahoe Room****TRACK 1—FIBER OPTIC CABLES****SESSION 6: SPLICING AND ENCLOSURE****Chairperson:** Nils Artlöve, Telia AB, Farsta, Sweden

CATV Components in Underground Technology—*F. Grajewski, W. Stieb, Alcatel Kabelmetal, Stadthagen, Germany; P. Zamzow, J. Seidenberg, Kabel Rheydt AG, Mönchengladbach, Germany* 201

Cleaving Tool for Optical Fibers Ribbon—*M. Boitel, H. Aoustin, J.-M. Cailleaux, T. Mahe, A. Pecot, France Telecom, CNET, Lannion, France* 207

Fusion Mass-Splices for Optical Fibers Using Micro Mass Axis Alignment Device—*M. Kubota, K. Yoshida, M. Mikawa, NTT Access Network Systems Labs., Ibaraki, Japan; T. Morimitsu, Institute of Systems & Information Technologies, Fukuoka, Japan* 214

Advances in Mass Fusion Splice Loss Increase Optical Fiber Cable Installation Productivity—*S. C. Mettler, N. W. Sollenberger, K. W. Jackson, Bell Laboratories, Lucent Technologies, Norcross, GA* 221

Structural Mechanics Aspects of Fractures of Optical Fibers in Connectors—*W. W. King, B. G. LeFevre, D. L. Stephenson, Lucent Technologies/Bell Laboratories, Norcross, GA* 228

WEDNESDAY MORNING—8:00 AM–11:45 AM**Crystal Rooms 3/4/5****TRACK 1—FIBER OPTIC CABLES****SESSION 7: OPTICAL NETWORKS****Chairperson:** Richard Rossi, General Cable Company, Edison, NJ

Development of Digital Line Multiplexing Optical Transmission Equipment—*T. Yoshimura, S. Dogi, K. Hayashi, Kansai Telecommunication Technology Co., Ltd., Osaka, Japan; T. Kasetani, K. Sekiya, K. Shimoohsako, Furukawa Electric Co., Ltd., Kanagawa, Japan* 236

2.5 Gbit/s Repeaterless Fiber Optic Link: Optimization and Testing of a Remotely Pumped Erbium-Doped Fiber Amplifier Realized with Commercial Optical Components—*F. Pozzi, D. Moro, M. Maglio, SIRT S.p.A., Cassina de' Pecchi (MI), Italy* 246

Fully Engineered 4-WDM 10 Gbps Optical Transmission System—*K. Susai, T. Kasetani, H. Nakamura, A. Fujisaki, Furukawa Electric Co., Ltd., Tokyo, Japan* 253

Management for Deployment of Optical Access Network—*T. Ito, M. Nakagawa, D. Tomizu, M. Ninomiya, NTT Access Network Systems Labs., Ibaraki-ken, Japan* 260

WEDNESDAY MORNING—8:00 AM–11:45 AM**Carson Rooms 1/2****TRACK 2—COPPER CABLES****SESSION 8: COPPER CABLE CONNECTIONS****Chairperson:** Leo Chatter, DCM Industries, Inc., Union City, CA**Moderator:** John Siemon, The Siemon Company, Watertown, CT

Coaxial Connector Retention: An Optimization Study—*W. Eng, Jr., Pacific Bell, San Ramon, CA* 266

Shield Efficiency Test Method for Balanced Shielded Twisted-Pair Cable & Connecting Hardware—*V. A. Rybinski, The Siemen Co., Watertown, CT* 277

Balance Measurements of UTP Connecting Hardware—*B. Lord, D. Tardif, P. Kish, J.-H. Walling, Nordx/CDT, Lachine, Québec, Canada* 287

Testing Patch Cords with Terminated Plugs Using Time Domain Measurements—*H. Koeman, Fluke Corp., Everett, WA* 295

WEDNESDAY MORNING—8:00 AM–11:45 AM**Carson Rooms 3/4****TRACK 3—MATERIALS****SESSION 9: ADVANCES IN FIBER COATINGS****Chairperson:** Xavier Mann, AT&T Fitel, Carrollton, GA

Evaluation of Protective Polymer Coatings for Optical Fiber Applications—*P. L. Tabaddor, C. J. Aloisio, H. C. Chandan, R. C. Moore, N. W. Sollenberger, C. R. Taylor, J. M. Turnipseed, Lucent Technologies Inc., Bell Laboratories, Norcross, GA* 302

Highly Reliable and Long-Life UV Curable Resin Coating System Optimized for Optical Fiber Applications—*Y. Kato, K. Asano, K. Ohsono, K. Yamada, H. Shimane, S. Hinoshita, Hitachi Cable, Ltd., Ibaraki-ken, Japan* 312

Reliability of the Adhesion of the Glass-Primary Coating Interface on Optical Fibers—*A. Murata, K. Ohashi, S. Araki, Fujikura Ltd., Chiba, Japan* 322

Manufacturing and Characterization of Colored, Fatigue Resistant Optical Fiber—*G. F. Orzel, J. F. Bourhis, Alcatel Fibres Optiques, Conflans Ste. Honorine, France; B. J. Overton, C. McNutt, A. Lopez, Alcatel Telecommunications Cable, Claremont, NC; S. Vanpouille, J. Y. Barraud, Alcatel Alsthom Recherche, Marcoussis, France* 328

WEDNESDAY—11:45 AM–2:15 PM**Hilton Pavilion****AWARDS LUNCHEON****Admission by badges to all registrants****WEDNESDAY AFTERNOON—2:15 PM–5:00 PM****Tahoe Room****TRACK 1—FIBER OPTIC CABLES****SESSION 10: FIBER OPTIC CABLE DESIGN****Chairperson:** Manuel R. Santana, Lucent Technologies, Bell Laboratories, Norcross, GA

Down Sized Fiber Optic Duct Cable—*S. Niiyama, A. Nishimura, R. Oka, S. Takagi, Sumitomo Electric Industries, Ltd., Yokohama, Japan* 333

Optical Fiber Ribbon Cable Designs for a Wide Range of Applications as the Availability of FTTH is Realized—*F. Legros, Y. Roussel, D. Brault, JY Guerin, ACOME R&D Dept., Mortain, France; JP Louboutin, D. Boscher, CNET Laboratory, France Telecom, Lannion, France* 340

Significant Improvement of Loose Tube Cable Spliceability Based on New Cable Dry Design—*P. Gaillard, O. Tatat, Alcatel Cable OFCCC, Bezons, France; C. McNutt, J. Holder, Alcatel Telecommunications Cable, Claremont, NC; A. Bouvard, Alcatel Cable France, Calais, France* 353

New Generation Craft-Friendly Cable for Outside Environments—*C. E. Clyburn III, C. L. Tedder, Siecor Corp., Hickory, NC* 359

Development of a Riser Rated Indoor/Outdoor Loose Tube Fiber Optic Cable—*S. M. Chastain, J. W. Thornton, AT&T Fitel, Carrollton, GA* 369

A 1-mm^φ Miniature Optical Fiber Cord Adaptable for Mu-Type Connectors—*M. Sato, S. Iwano*, NTT Opto-electronics Labs., Ibaraki-ken, Japan; *M. Tachikura, N. Tomita*, NTT Access Network Systems Labs., Ibaraki-ken, Japan ... 374

WEDNESDAY AFTERNOON—2:15 PM–5:00 PM

Crystal Rooms 3/4/5

TRACK 1—FIBER OPTIC CABLES

SESSION 11: TESTING AND FIELD EVALUATION I

Chairperson: Inge B. Kovacs, Consultant for Polycheck Limited, Hackettstown, NJ

Characterizing Field Handleability of Optical Fiber Through the Measurement of Strength After Mechanical Stripping—*A. Dwivedi, J. L. Smith*, Corning Inc., Corning, NY 381

Useful Technique for Measurement of Return Losses of Multiple Optical Devices—*J.-Y. Ha, B.-C. Lee, Y.-T. Lee, K.-H. Han*, Korea Telecom, Taejeon, Korea 391

Remodeled Automatic Fiber Testing System for FTTH Trials—*Y. Yoshii, K. Tomita, K. Omoto, N. Nakao, M. Kuroiwa*, NTT Technology and Development Support Center, Chiba, Japan 396

Wide Range Optical Low Coherence Reflectometer for High Resolution Fault Detection and Component Characterization—*M. Bottanelli*, SIRT I S.p.A., Cassina de'Pecchi (MI), Italy 402

Newly Developed Administration System for Remotely Controlling Optical Network Monitoring Equipments at Multiple Locations—*H. Maki, T. Zakoh, Y. Hata, Y. Takenami, T. Matsuda, T. Taguchi*, Sumitomo Electric Industries, Ltd., Kanagawa, Japan 407

Fiber-Strain Measurement Using Brillouin Optical-Fiber Time-Domain Analysis—*C. J. Sandwith, R. I. Odom*, University of Washington, Seattle, WA; *W. D. McCormick*, Lucent Technologies Inc., Greensboro, NC; *J. A. Thornton*, U.S. Navy, Crystal City, VA; *D. R. Wise*, TRW, Fairfax, VA. 415

WEDNESDAY AFTERNOON—2:15 PM–5:00 PM

Carson Rooms 1/2

TRACK 2—FIBER OPTIC CABLES

SESSION 12: EMERGING WIRELESS NETWORKS

Chairperson: Dr. Howard Wichansky, U.S. Army Communications—Electronics Command (CECOM), Fort Monmouth, NJ

Overview of PCS Standards: The Recipe for Acronym Soup—*C. H. Halevi*, Bellcore, Red Bank, NJ 428

PCS for Tactical Users—*R. Barton, W. Sepper, W. Wahl*, Lockheed Martin Western Development Labs., San Jose, CA; *P. Hugo*, U.S. Army Communications Electronics Command, Ft. Monmouth, NJ 438

Code Division Multiple Access (CDMA) Systems for Wireless Applications—*R. Olsen*, QUALCOMM Inc., San Diego, CA 449

WEDNESDAY AFTERNOON—2:15 PM–5:00 PM

Carson Rooms 3/4

TRACK 3—MATERIALS

SESSION 13: FIBER COATING RELIABILITY

Chairperson: Dr. Stephen Hornung, British Telecom Laboratories, Ipswich, United Kingdom

Reliability of Optical Fibers in Steam and Petrochemical Environments—*D. R. Biswas, C. R. Kurkjian, O. S. Gebizlioglu*, Bellcore, Morristown, NJ 456

Structural Changes in Polyacrylate Coatings Exposed to Degrading Environments—*P.-A. Höglström, S. Karlsson, U. W. Gedde*, Royal Institute of Technology, Stockholm, Sweden .. 464

Thermal Stability of Coated Optical Fiber—*A. Suzuki, M. Ban, T. Hattori, N. Akasaka, Y. Matsuda*, Sumitomo Electric Industries, Ltd., Yokohama, Japan 471

Effects of Ink on the Performance of Color Coded Fibers—*E. M. Vogel, J. D. Mann, I. M. Plitz, T. N. Bowmer, R. A. Frantz, C. J. Wiecezorek*, Bellcore, Morristown, NJ; *B. J. Keon*, Telstra, Melbourne, Australia; *P. R. Foy*, Rutgers University, FOMRP, Piscataway, NJ 479

WEDNESDAY AFTERNOON—4:00 PM–6:30 PM

Reno Ballroom

SESSION 14: POSTER PAPERS

Chairpersons: Dr. Reiner J. Gerdes, TransTel Group Inc., Atlanta, GA and Dieter S. Nordmann, Kabelmetal Electro GmbH, Hannover, Germany

A New, Extremely Versatile, Access Network Cabling Concept for Migration to Optical Fiber—*W. Griffioen, H. Nijstad*, KPN Research, Leidschendam, The Netherlands; *A. T. M. Grooten, A. van Wingerden*, NKF Kabel BV, Delft, The Netherlands; *G. Brown*, Mainetti (UK) Ltd., Jedburgh, Scotland; *D. F. Hawkins*, Eden Ltd., Uxbridge, United Kingdom; *G. Plumettaz*, Plumettaz SA, Bex, Switzerland.... 485

Tapered Slot Test. A High-Speed Bending Test Method for Measurement of B-Value of Fibers—*T. Svensson*, Telia Research AB, Haninge, Sweden; *A. Hjorth*, Royal Institute of Technology, Stockholm, Sweden 490

Development of Electro-fiber Optic Cable Containing Metal Tube Armored Fiber for Deep Sea Tow—*H. Ishisaki, S. Imamura*, Ocean Cable Co., Ltd., Tokyo, Japan; *H. Momma*, Japan Marine Science and Technology Center, Kanagawa-ken, Japan 495

144 Fiber All Dielectric Aerial Cable for Railway Applications—*R. Böhme, G. Hög, M. Hoffart, K. Nothofer, S. Richter*, Kabel Rheydt AG, Mönchengladbach, Germany 500

Development of Downsized Slotted Rod Optical Fiber Cables—*F. Hosoi, M. Hara, E. Konda*, Furukawa Electric Co., Ltd., Chiba, Japan 506

New Designs for CATV Fiber Monitoring Systems Combined with Automatic Fiber Transfer and Branching Fiber Surveillance Functions—*K.-H. Lai, C.-C. Lee, K.-Y. Chen, C.-S. Wang, C.-P. Chen*, Chunghwa Telecom Co., Ltd., Taiwan, R.O.C. 511

Design Considerations of Stimulation Brillouin Scattering and Dispersion on 1550nm AM 80 Channel CATV System—*C.-C. Lee, K.-H. Lai, K. Chen, K.-Y. Chen, C.-S. Wang, F.-Y. Tsai*, Chunghwa Telecom Co., Ltd., Taiwan, R.O.C. 515

Innovative Insulation Solution for Zero Halogen Fire Retardant Communication and Power Cables—*D. Sawyer, L. P. Artingstall, J. Preston, S. Dell, S. Cochard*, Lindsay & Williams Ltd., Manchester, England 520

Development of Repeaterless Optical Fiber Submarine Cable System for Extensive Application—*T. Nishida, M. Kiuchi, O. Nagatomi, H. Yoshioka*, Ocean Cable Co., Ltd., Kita-Kyushu, Japan 527

Weatherability of Polyethylene Black Compound—*Y. Kamei, S. Taoka*, UBE Industries, Ltd., Chiba, Japan 532

Study on Ultraviolet Degradation Characteristics of Optical Fiber Ribbons—*K. Shiraishi, H. Nakamura, M. Ito, T. Shiono*, Showa Electric Wire & Cable Co., Ltd., Kanagawa, Japan 537

True Thermal Characteristics of Optical Ground Wires During Fault Current Events Established Using Optical Fibre Distributed Temperature Sensing—*I. G. Knight*, BICC Cables Ltd., Helsby, U.K. 542

Ageing of Fibres and Ribbon in Water and Filling Compound—*J. Björkman*, Telia Network Services, Farsta, Sweden; *T. Svensson*, Telia Research AB, Haninge, Sweden 547

Temperature and Speed Effects on Hand Stripping of 12-Fiber Ribbons— <i>C.-K. Chien, H. R. Cole, J. R. Toler</i> , Corning, Inc., Corning, NY	554
Investigation of Pullout Force for Coating Adhesion in Optical Fiber— <i>C.-K. Chien</i> , Corning Inc., Corning, NY	558
Color Measurement of Optical Fiber: A Comparison of Visual, Micro, and Macro Methods— <i>S.-H. Chou, J.-C. Lin, C.-M. Hsiao, H.-P. Hsu, Y.-c. Lin, K.-Y. Chen</i> , OSP, Telecommunication Labs., Taiwan, R.O.C.	561
Analysis of the Economics of On-line Colored Ribbon Manufacturing— <i>B. Arvidsson</i> , Ericsson Cables, Hudiksvall, Sweden; <i>J. K. Tanskanen</i> , Nokia-Maillefer, Vantaa, Finland	566
Effect of Dynamic Visco-Elastic Properties and Compatibility of Jelly Compounds on Optical Fiber Cable Performance— <i>A. Murata, K. Oohashi, S. Araki</i> , Fujikura Ltd., Chiba, Japan	570
Using Triboelectric Technology to Apply Powders While Reducing Factory Contamination— <i>F. T. Hughes</i> , Nordson Corp., Duluth, GA	575
Fusion Splicing Robot for Optical Fiber Ribbons— <i>H. Yusa, T. Watanabe, K. Watanabe, K. Osaka</i> , Sumitomo Electric Industries, Ltd., Yokohama, Japan	580
Characteristics of the Reusable Ribbon Splice on the Polluted Water Immersion Test— <i>Y. T. Lee, J. Y. Ha, K. H. Han</i> , Korea Telecom, Taejeon, Korea	585
Design of Spring Clamp for Optical Aerial Cable— <i>M.-G. Kim, S.-K. Oh, B.-C. Lee, Y.-T. Lee, S.-D. Baek, K.-H. Han</i> , Korea Telecom, Daejeon, Korea	590
New Concepts in Optical Spliceability Versus Optical Design— <i>J. P. Bonicel, J. Personne</i> , Alcatel Cable, Bezons, France; <i>G. Le Noane</i> , France Telecom-CNET, Lannion, France; <i>B. Joly, A. Vincent</i> , Alcatel Cable Interface, Bezons, France; <i>C. Vergez</i> , Alcatel Contracting, Clichy, France	595
Optoclip II Multiway—Multiway Connector for Singlemode Access Networks— <i>H. Aoustin, M. Boitel, D. Morellec, A. Pecot</i> , France Telecom, Lannion, France; <i>V. Stappers, J.-J. Maillard</i> , Cie Deutsch, Rueil Malmaison, France	599
Failure Analysis of Field Service Optical Fiber Splice Protector— <i>T.-C. Chang, J.-M. Hsiao, W.-J. Chen, H.-P. Hsu, Y.-c. Lin</i> , OSP, Telecommunication Labs., Taiwan, R.O.C.	604
Effective Force Transfer Mechanism in a Novel Cable Pulling Machine— <i>R.-S. Kuo, M.-S. Lu, C.-H. Chen, L.-J. Huang, S.-T. Chang, S.-W. Lai</i> , OSP, Telecommunication Labs., Taiwan, R.O.C.	610
1650-nm Monitoring Technique for Optical Fiber Cable Line Degradation— <i>S.-W. Wang, F.-Y. Tsai, S.-C. Chen, W.-Y. Guo</i> , OSP, Telecommunication Labs., Taiwan, R.O.C.	614
Development of the Portable Terminal for the Information Free Access System Employing FM-SCM Transmission Method— <i>H. Omura, H. Nakayama, H. Nasu</i> , Furukawa Electric Co., Ltd., Kanagawa, Japan; <i>K. Tezuka</i> , Tokyo Electric Power Co., Kanagawa, Japan	618

THURSDAY MORNING—8:30 AM—12:00 PM (NOON)

Crystal Rooms 3/4/5

TRACK 1—FIBER OPTIC CABLES

SESSION 15A: FIBER OPTIC CABLE DESIGN (CONTD.) <i>Chairperson:</i> Dr. Peter R. Bark, Siecor Corporation, Hickory, NC	
Design and Performance of a High-Capacity, Compact, Modular Ribbon Cable Comprising 24 Fiber Ribbons— <i>K. W. Jackson, R. J. Brown, M. D. Kinard, K. M. Kroupa, M. R. Santana, P. M. Thomas</i> , Lucent Technologies Inc., Norcross, GA	623

A Method to Evaluate Ribbon Behavior in Slotted Core Cables— <i>E. Opel</i> , Siemens AG, Neustadt bei Coburg, Germany	631
--	-----

THURSDAY MORNING—8:30 AM—12:00 PM (NOON)

Crystal Rooms 3/4/5

TRACK 1—FIBER OPTIC CABLES

SESSION 15B: HIGH FIBER COUNT CABLE <i>Chairperson:</i> Dr. Peter R. Bark, Siecor Corporation, Hickory, NC	
Development of 3000-Fiber Cable Using 16-Fiber Ribbons— <i>H. Iwata, M. Nozawa, N. Kashima</i> , NTT Access Network Systems Labs., Ibaraki, Japan; <i>T. Tanifuji</i> , Telephone Organization of Thailand, Patumtani, Thailand ..	638
Design and Performance of a 3200-Fiber Hybrid Scr/U-Groove Cable Using 16-Fiber Ribbons— <i>F. M. Sears, P. R. Bark, M. A. Clarke, H. G. Cooke, C. K. Eoll, L. E. Herman, W. S. Jackman, R. O. Livingston, S. S. Sodhi, R. S. Wagman</i> , Siecor Corp., Hickory, NC	645
Development of 3000-Fiber Cables with 8- and 16-Fiber Ribbons— <i>N. Okada, T. Omori, K. Watanabe, K. Kobayashi, M. Miyamoto</i> , Fujikura, Ltd., Chiba, Japan	657
Development of 3000-Fiber Multislotted Core Cable— <i>M. Hara, M. Saito, E. Konda, K. Nagai, M. Oku</i> , Furukawa Electric Co., Ltd., Chiba, Japan	665

THURSDAY MORNING—8:30 AM—12:00 PM (NOON)

Crystal Rooms 1/2

TRACK 1—FIBER OPTIC CABLES

SESSION 16: TESTING & FIELD EVALUATION II <i>Chairperson:</i> Dr. Reiner J. Gerdes, Transtel Group Incorporated, Norcross, GA	
Design of the Novel Supervising Network Using the Information Free Access System— <i>H. Nasu, H. Nakayama, H. Omura</i> , Furukawa Electric Co., Ltd., Kanagawa, Japan; <i>K. Tezuka</i> , Tokyo Electric Power Co., Kanagawa, Japan	669
Investigation of Single-Mode Fiber Loss Properties by OTDR Measurements— <i>P. L. Guenot, P. Nouchi, O. Mercereau</i> , Alcatel Fibres Optiques, Marcoussis, France; <i>B. Poumellec</i> , Université Paris Sud, Orsay, France	679
Time-Varying Optical Fiber Strain Measurement by Using Brillouin Ring Amplifying System— <i>M. Kamikata, M. Miyamoto</i> , Fujikura Ltd., Chiba, Japan; <i>O. Ogawa</i> , Tokyo Electric Power Co., Kanagawa, Japan	689
Fundamental Theoretical Analysis of Optic Fiber Payout from Fiber Optic Data Link Bobbin— <i>A. Akiyama, H. Kubo</i> , Japan Defense Agency, Tachikawa, Japan; <i>M. Shibata</i> , Kawasaki Heavy Industries Ltd., Gifu, Japan; <i>S. Araki</i> , Fujikura Ltd., Chiba, Japan	695
Development of a 50 Hz High Current System and a Unique Impulse Current Generator and Their Application in Testing the Fault Current Rating and Impulse Performance of an OPGW— <i>D. M. Burgess, R. C. Kemp</i> , CSIRO Division of Applied Physics, Lindfield, Australia; <i>A. Stringer</i> , Olex Cables, Tottenham, Australia	704
Study and Analyses of Rodent Attacks in Optical Fiber Cables— <i>P. J. P. Curado, C. Pitombo, D. dos Santos Rosa</i> , Telebrás, Campinas, Brazil; <i>A. C. Pereira Netto, J. E. Filho, M. E. Latini</i> , EMBRATEL, Rio de Janeiro, Brazil	711
Minimizing Lightning Damage in Regions of High Earth Resistivity— <i>D. Vokey</i> , Norscan Instruments Ltd., Manitoba, Canada; <i>G. Gallagher, K. Young</i> , Newtel Communications Inc., Newfoundland, Canada	718

THURSDAY MORNING—8:30 AM—12:00 PM (NOON)

Carson Rooms 1/2

TRACK 2—COPPER CABLES

SESSION 17: HIGH PERFORMANCE TWISTED PAIR CABLES

Chairperson: Hans A. Mayer, Olex Cables (Division of Pacific Dunlop Ltd.), Melbourne, Australia

Moderator: Masood Shariff, Lucent Technologies, Middletown, NJ

Development of Flame Retardant Halogen-Free Clean UTP Cables Applied up to ATM Data Speed—A. Nakayama, K. Watanabe, S. Ishi, S. Hinoshita, Hitachi Cable, Ltd., Ibaraki, Japan 726

Coating Flow Simulation of 24 AWG Wire with FEP Fluoropolymer—P. B. Kuyt, Daikin America Inc., Orangeburg, NY 736

An Accurate, Noncontact Length and Speed Measurement Technique for the Wire and Cable Industry—M. W. Nielsen, B. Osmondson, TSI Inc., St. Paul, MN 743

Crosstalk Measurements as a Means to Characterize the Balance of Data Grade Wires—J.-H. Walling, M. Bélanger, NORDX/CDT, Lachine, Quebec, Canada; V. LeNir, V.P.S. Enterprise, Montreal, Quebec, Canada 751

The Inter-Standard Gap—F. J. Mlinarsky, Scope Communications, Inc., Northboro, MA 762

Networks of the Future: Gigabit Ethernet and Other News From IEEE 802.3—G. O. Thompson, Bay Networks, Inc., Santa Clara, CA 773

THURSDAY MORNING—8:30 AM—12:00 PM (NOON)

Carson Rooms 3/4

TRACK 3—MATERIALS

SESSION 18: MATERIALS IN FIBER OPTIC CABLES

Chairperson: John R. Sicotte, Corning Incorporated, Corning, NY

Reliability of Dry Waterblocking Materials—A. G. Bringuier, C. E. Clyburn III, Siecor Corp., Hickory, NC 779

Effect of Additives and Atmosphere on Hydrogen Outgassing of Organic Materials—J.-F. Libert, F. Ruelle, Alcatel Submarine Networks, Calais Cedex, France 788

Investigation of the Lateral Strength of Buffer Tubes—Z. Gao, W. Pfandl, W. Stöcklein, Siemens AG, Neustadt, Germany 793

Effect of Color Concentrate on Reliability of Poly(Butylene Terephthalate)—P. E. Neveux, Jr., Sumitomo Electric Lightwave Corp., Research Triangle Park, NC 800

Reliability of Spliced GRP Strength Elements—P. E. Neveux, Jr., S.-R. Stokes, Sumitomo Electric Lightwave Corp., Research Triangle Park, NC; J. S. Radley, G. V. Payne, Neptco, Inc., Granite Falls, NC 809

Ballistic Protection of Aerial Cables—A New Economical Solution with a Special Impact Modified Polyamide—M. Hochuli, EMS-Chemie AG, Domat/Ems, Switzerland 817

THURSDAY AFTERNOON—1:00 PM—5:00 PM

Crystal Rooms 3/4/5

TRACK 1—FIBER OPTIC CABLES

SESSION 19: RIBBONS, FIBER TO THE HOME AND AIR BLOWN FIBER

Chairperson: Hirotooshi Hondo, Furukawa Electric Company, Ltd., Kanagawa, Japan

Development and Design Approval of Two Fibre, Singlemode Enhanced Performance Fibre Unit (EPFU)—P. Morris, Optical Fibres, Flintshire, U.K. 821

A Novel Method for the Installation of Lightweight Optical Fibre Units into Tubing—J. P. Wells, A. Cadden, Optical Fibres, Flintshire, Wales, U.K.; G. Brown, P. J. Clayton, Mainetti (UK) Ltd., Roxburghshire, Scotland, U.K. 828

Evaluation of the ABF-Multiplex Installation Technique and Its Application in Customer Access Optical Fiber Network—Y. Matsumoto, T. Kubo, M. Ohta, K. Sanjo, K. Tokumaru, Kansai Electric Power Co., Inc., Osaka, Japan and Sumitomo Electric Industries, Ltd., Osaka, Japan 835

Study of Optical Fiber Ribbon Structural Dimensions—T. Kawano, M. Ito, T. Murase, H. Nakamura, T. Shiono, M. Saegusa, Showa Electric Wire & Cable Co., Ltd., Miyagi-Ken, Japan 845

Development of Optical Fiber Ribbon Materials with Novel Surface Character—T. Hirai, J. Yoshizawa, M. Sugimoto, Z. Komiya, T. Ukachi, Japan Synthetic Rubber Co., Ltd., Ibaraki, Japan 851

THURSDAY AFTERNOON—1:00 PM—5:00 PM

Crystal Rooms 1/2

TRACK 1—FIBER OPTIC CABLES

SESSION 20: FIBER OPTIC CONNECTORS/COMPONENTS

Chairperson: Dieter S. Nordmann, Kabelmetal Electro GmbH, Hannover, Germany

Fiber Gratings: Temperature and Mechanical Sensitivity of Narrow Band Transmission Filters Using Diffraction Packaging Solutions—S. Pitassi, F. Pozzi, A. Marcone, V. Spano, SIRT S.p.A. Cables and Optical Technologies, Milan, Italy 860

Study of the High-Speed Connection for Pre-Connectorized Optical Fiber Cables—Y. Tamekuni, K. Sunaga, T. Ueda, M. Honjo, T. Yamanishi, Sumitomo Electric Industries, Ltd., Yokohama, Japan 869

Development of a Stacked Connection Method for High Density Pre-Connectorized 3000 Fiber Cable—T. Nozawa, Y. Tamaki, H. Yokosuka, Fujikura Ltd., Chiba, Japan 875

Connector-Transfer Type Compact and Low Insertion Loss Optical Switch for Multi-Fiber Ribbons—T. Sato, M. Okuda, S. Ohmizu, T. Shigematsu, Furukawa Electric Co., Ltd., Chiba, Japan 882

High-Reliability Dispersion Compensator Using Negative Slope DCF—R. Sugizaki, Y. Akasaka, S. Arai, K. Furukawa, Y. Suzuki, T. Kamiya, H. Hondo, Furukawa Electric Co., Ltd., Chiba, Japan 888

2x400 SMF Optical Switch Using Axial Alignment with Counterpart Fibers in a V Groove—S. Naraoka, S. Yamaguchi, K. Kamiko, Furukawa Electric Co., Ltd., Chiba, Japan 894

2x800 Direct Fiber Transfer Opto-Mechanical Switch—H. Furukawa, Y. Nomura, H. Yokosuka, Fujikura Co., Ltd., Chiba, Japan 900

THURSDAY AFTERNOON—1:00 PM–5:00 PM

Carson Rooms 1/2

TRACK 1—FIBER OPTIC CABLES

SESSION 21: FIBER PROPERTIES AND RELIABILITY

Chairperson: Dr. Raymond E. Jaeger, SpecTran Corporation, Sturbridge, MA

- High Speed Axial Strength Setup for Measurement of the <> Value—A. Gouronnec, N. Evanno, France Telecom, Lannion, France 906
- Effect of Draw Conditions on Zero-Stress Aging Strength of Silica Based Optical Fiber—P. R. Stupak, M. Supczak, V. A. Cusanello, D. Mazzaresse, D. Roland, M. Smith, SpecTran Communication Fiber Technologies, Inc., Sturbridge, MA 914
- Simple Optical Fibre Reliability Model for Cable Designers—F. Donaghy, Alcatel TCC, Liverpool, N.S.W., Australia 922
- Effect of Water Quality and Quantity on Strength Degradation of Fused Silica Fiber in Water Tests—J. V. Overgaard, P. Haslöv, H. Knuuttila, A. Mazzotti, P. Regio, T. Svensson, T. Volotinen, S. Dodd, Tele Denmark, Denmark; DRAKA-NKT, Denmark; Nokia Cables, Finland; FOS, Italy; CSELT, Italy; Telia Research, Sweden; Ericsson Cables, Sweden; Optical Fibers, U.K. 928
- Novel Index Profile for Improved Large Effective Area Fiber—P. Nouchi, Alcatel Fibres Optiques, Marcoussis, France; P. Sansonetti, C. Le Sergent, Alcatel Alsthom Recherche, Marcoussis, France..... 939

THURSDAY AFTERNOON—1:00 PM–5:00 PM

Carson Rooms 3/4

TRACK 2—COPPER CABLES

SESSION 22: COAXIAL CABLE

Chairperson: Fred Narayan, Phelps Dodge, Coral Gables, FL

- Thermal Aging Effects on Coaxial Cable's Transmission and Its Life Expectancy—L. M. Hore, V. J. Ferraro, O. G. Chavez, J. D'Amico, Bellcore, Morristown, NJ 946
- Improving the Shielding Effectiveness of Coaxial Cables—A. R. Panicali, Telebras R&D Center, Campinas, S. Paulo, Brazil 955
- Optimization of Leaky Feeders for Broadband Wireless Communication Systems—K. Schulze-Buxloh, M. Davies, RFS Kabelmetal, Hannover, Germany..... 959
- Study on Highly Expanded Insulation Material for Coaxial Cables by Non-Fluorocarbon Foaming Technique—T. Higashikubo, T. Zushi, H. Kuzushita, K. Suga, T. Yamamoto, M. Wada, Mitsubishi Cable Industries, Ltd., Amagasaki, Japan..... 968
- Measuring RF Emissions from a Moving Coaxial Drop Cable—J. N. D'Amico, Bellcore, Morristown, NJ; G. F. Appgar, Bellcore, Red Bank, NJ..... 977

OPENING SPEAKERS



RICHARD ROSSI
Chairman, IWCS
Vice President, Sales
General Cable Company
Edison, New Jersey

Richard Rossi has been a member of the Wire and Cable Industry for over 30 years. He has been with General Cable Corp. for all of this time, most of them in an Engineering capacity, culminating in his appointment as Vice President, Engineering in 1991. More recently, he has been appointed Vice President, Sales, Communications Products.

Mr. Rossi has been involved with the International Wire and Cable Symposium since co-authoring and presenting his first paper in 1973. Since then, he has co-authored and presented a number of additional papers and was voted "Best Presentation" at the 1987 IWCS. He has been a committee member of IWCS since 1991.



BARRY S. SALIS
Deputy Director, Space and Terrestrial
Communications
U.S. Army Communications-Electronics Command
Fort Monmouth, New Jersey

Mr. Barry S. Salis has attained the position as Deputy Director of the Space and Terrestrial Communications Directorate after holding increasing positions of responsibility during his 24 year Government career.

Providing policy and guidance for the directorate he ensures the resources are allocated for attainment of the multifaceted communications mission of the directorate. He serves on various levels of command level TQM panels, international and joint panels.

Previously he was Chief, Information Security Division, Space and Terrestrial Communications Directorate, USACECOM responsible for all Army RDT&E in the security area which includes: COMSEC, TEMPEST, COMPUSEC, Key Management, Certification and Accreditation, and Network Security. Support to many PEO and PM Offices, various Directorates, and other non-traditional customers is provided routinely by the entire division. The division also supports evaluation and integration of commercial video products with computer and communications systems to meet the Army's Digitization of the Battlefield thrust.

While serving in the Army Signal Corps for three years from Oct 1971 to Oct 1974 he worked as an engineer in the COMSEC Division, COMM/ADP Lab, USAECOM at Ft. Monmouth, NJ. Continuing in the same organization as a civilian engineer he worked as Project Leader for the Secure Wire Access Terminal, a VINSON COMSEC ancillary equipment, working it from the development through the production phases. He also was Project Leader for the PARKHILL COMSEC equipment as well as numerous other INFOSEC developments as part of the overall Army tactical system architecture. Assigned to lead an internal task force, he was involved in the initial concepts for usage of modeling and simulation to evaluate combined arms doctrinal changes which today are being implemented.

In 1985 he became Chief of the COMSEC Development Branch, responsible for the embedded COMSEC programs, Key Management, system support to PM Offices to include the Special Operations Forces Office, and system integration and testing.

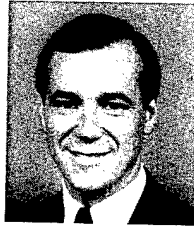
Mr. Salis obtained his BSEE degree from Drexel University, Philadelphia, PA in 1971 and his MSEE from Fairleigh Dickinson University, Teaneck, NJ in 1978. He is married to Jan Freeman Salis. They have two children, Rachel and Howard.

Mr. Salis is a member of and on the board of Directors for the Association of the United States Army (AUSA) and the Armed Forces Communications and Electronics Association (AFCEA).

PLENARY SESSION

Communications Infrastructure Initiatives: Investing for Global Competitiveness

CHAIRMAN



John R. Sicotte
Corning Incorporated
Corning, New York

John Sicotte is the manager for Corning's North American Sales and Applications Engineering Departments. His responsibilities include commercial sales and technical and engineering support of optical fiber customers.

John joined Corning in 1978 as an engineer in the Manufacturing and Engineering Division. He joined the Telecommunications Products Division in 1982 as a market analyst. He was named a senior applications engineer in 1983, and a senior sales engineer in 1985. He became sales and marketing manager for the industrial and government market in 1990. In

1991, he became the manager for North American Applications Engineering. Sales duties were added to his position in 1993.

John holds a master's of business administration from Syracuse University, and a bachelor's degree in civil and environmental engineering from the University of Rhode Island, Kingston.

He is a member of the Society of Photo-Optical Instrumentation Engineers and a member of the Board of Trustees of the International Wire and Cable Symposium.

PANELISTS

Luis Molleda, Sub-Director of Transmission & Outside Plant Department of Technology & Technical Normative, Telefonica, Madrid, Spain

Pei Ai Hua, Sr. Engineer & Director of Telecom Trunk Construction Management, Ministry of Post & Telecommunication, Beijing, China

Carlos Fernando Ximenes Duprat, Manager of Engineering, Telebrás, Brasília, Brazil

Alex Best, Senior Vice President of Engineering, Cox Communications Inc., Atlanta, Georgia

TELECOMMUNICATIONS IN CHINA

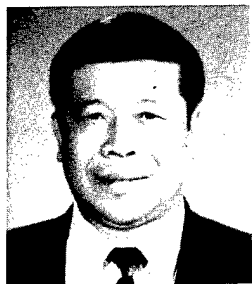
Mr. Pei Ai Hua

Ministry of Post and Telecommunication, Beijing, China

Telecommunications infrastructure construction is a major priority of the People's Republic of China. The State and the Ministry of Post and Telecommunication have undertaken numerous system projects over the last decade. Many prominent telecommunications companies from around the world have been involved in the construction of these systems.

One significant MPT project recently completed was the Beijing - Jiujiang - Guangzhou Telecommunications Backbone Line. This was one of twenty-three First Grade MPT projects of the 9th Five Year Plan of the State. Designed to operate at 2.4 Gbps transmission rates over a route length of greater than 3400 km, this was the first significant MPT system to utilize dispersion shifted fiber technology.

Looking forward, the future of the telecommunications industry in China is very exciting. Aggressive plans for building a state-of-the-art communications network are in place. The projected growth in the China market promises to provide continued challenge and opportunity for the MPT and its suppliers.



Mr. Pei Ai Hua
Sr. Engineer and Director of Telecom Trunk
Construction Management
Ministry of Post and Telecommunication
No. 8 Men Lou Xiang
Jiao Zi Hu Tong
Xuan Wu District
Beijing, China

Mr. Pei has been engaged in teaching, scientific research and technical management in the field of post and telecommunications for almost 30 years.

As a lecturer at several universities in China, he has taught courses on Radio Communications, Electromagnetic Field & Electromagnetic Wave, High Frequency Electric Circuit, Low Frequency Electric Circuit, Pulse and Digital Logic, Microwave Communication and Radio and Electric Waves. Within the Managing Center of Main Lines Communication Construction of the Ministry of Post and Telecommunication, Pei was charged with the First Grade main lines communication construction.

He has been responsible for many key optical fiber communications projects including Shanghai - Nanjing, Shanghai - Fujian, Fuzhou - Guangzhou, Zhengzhou - Xian Chegdu, Xian - Lanzhou - Urumqi, Urumqi - Yilli, Chuangjiang - Wuhan, Shanghai Wuhan, Nanjing - Hangzhou, Jinan - Qinqdao, Beijing - Huhchoate - Yinchuan - Lianzhou, Hangzhou - Fuzhou - Guizhou - Chengdu, Beijing - Zhujiang - Guangzhou and Dalian Shanghai.

Mr. Pei is skilled in microwave communication, radio communication and optical communication. He has been involved in the debugging of microwave main lines, and independently completed the research and manufacture of a phase discriminator and pressing oscillator. He has also been involved in the research and manufacture of a 2 Ghz microbelt and microwave machine and the research and manufacture of a coherent light communication system, the key project in the 8th Five Year Plan of the State. Pei also designed the key parts of a photoelectric prober and 0-2 Ghz low noise, wide belt preamplifier.

Mr. Pei co-authored the book "High Frequency Electronic Circuits", and is an accomplished author of telecommunications articles and papers.

In addition to having studied at the Changchun Telecommunication School, the Beijing Post and Telecommunication University and the China Science and Technology College, Pei is a Master Postgraduate of Photoelectricity Technology from the Electronics Engineering Department at the Changchun Optics and Precision Machinery University.

BROADBAND COMMUNICATIONS INITIATIVES

Alex B. Best

Cox Communications, Inc., Atlanta, Georgia

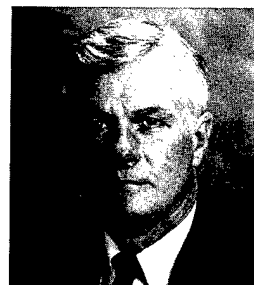
As a result of the rewrite of the Telecommunications Bill in this country, there are a large number of industries positioning themselves as a one-stop shop for providing video, voice, and data services to residential customers. Among this industry group are long distance carriers, local phone companies, and cable operators.

Even larger in number are the types of networks being deployed to provide these services. These include satellite, copper, PCS, hybrid fiber/coax, fiber, MMDS, and LMDS, just to name a few.

Only one of these networks is both present in front of a large number of homes in this country and has the capacity and targetability to provide all three services. This of course is the cable operators' hybrid fiber/coax network.

Cox, along with most other large MSO's in this country have been actively upgrading their networks over the past few years to add fiber, increase capacity, and activate the upstream return path. By the end of 1998, about 75% of Cox's homes passed will be fed from a network that includes fiber down to 1,000 home nodes, has a capacity of 750 Mhz, and is two-way capable.

Beginning in 1996 and early 1997, we will begin deploying technology in the home that allows us to provide wireline telephony (cable phone), high speed data (Internet access), and digital video. We are convinced that our ability to provide a one-stop shop for these three services, plus our capability of transporting these services over a single infrastructure, will lead to our success as being the low-cost provider in all of these businesses for the foreseeable future.



Alex B. Best
Senior Vice President of Engineering
Cox Communications, Inc.
1400 Lake Hearn Drive
Atlanta, Georgia 30310

Alex B. Best, Senior Vice President of Engineering, joined Cox Cable Communications in April 1986 as Vice President of Engineering. He was promoted to his present position in January 1989.

He joined Cox following twenty years with Scientific Atlanta, where he was involved in nearly every aspect of that company's CATV product development and business application. His last position prior to his appointment at Cox was that of Principal Engineer.

He received B.S. and M.S. degrees in electrical engineering from the Georgia Institute of Technology, and completed the Program for Management Development (PMD) at Harvard Business School.

He has been a member of the National Cable Television Association's (NCTA) Engineering Advisory Committee since 1978 and presently serves as its chairman. He has been a member of the Society for Cable Television Engineers (SCTE) since 1975. He is a member of the board of directors of CableLabs, Inc., a research and development group funded by the cable television industry. In addition, he is a member of the board of directors of the Southern Cable Television Association (SCTA).

He was the 1977 recipient of the NCTA's Vanguard Award for Science and Technology and received the SCTA's Polly Dunn award in 1992 for his dedication to the cable industry. In 1994, he was inducted into the SCTE's Hall of Fame.

TELEFONICA INITIATIVES IN GLOBAL COMMUNICATIONS

Luis M. Molleda

Telefónica De España, Madrid, Spain

At the end of the 80's the Argentinean government considers the privatisation of the National Communications Company (ENTEL).

Telefonica de España, taking into account on the one hand the traditional links with the South American countries and on the other hand the large potential of the telecommunications markets of those countries, decides to invest and incorporates itself in the group called Telefónica de Argentina which opts for the control of the communications in the southern zone.

Later, and facing the prospects that the entire region offers, it incorporates itself by means of significant investments in the operations of various different countries, being present today in Argentina, Chile, Perú, Columbia, Venezuela, México and Puerto Rico, and without ruling out any new incorporation that would further reinforce its presence in the region.

This presence fits within a global network project called the "Proyecto Panamericano" which, led by Telefónica de Argentina, CTC de Chile and Telefónica del Perú, could convert the companies of the group into the principal provider of global network services in the region.

In its initial phase the network will offer communications services between the businesses of the region, and in the medium term expand its area of action to all of America, including the United States, along with connection to Europe and the rest of the world.

The connections with the United States are guaranteed because of the incorporation into the group of the Compañía de Larga Distancia (TLD) of Puerto Rico, which by virtue of the new North American Communications Law is authorised to originate all types of telephony traffic in the country.

The connections with the Europe are assured on the one hand because of Telefónica de España a with its vast network of submarine cables, and its more than sixty satellite communications stations. On the other hand this network will have a natural link into the rest of Europe via UNISOURCE, the alliance formed by the operators of Holland, Sweden, Switzerland and Spain, with a participation of 25% each.

Finally, the connection with the rest of the world will be achieved via WORLDPARTNERS, the alliance between UNISOURCE, the North American AT&T and the Asians KDD (Japan) and Singapore Telecom.

By way of summary one can conclude that the activity of Telefónica de España is directed towards the creation of a provider of global network services throughout the world, with powerful resources and costs slightly below those that would exist if each local operator were to establish their international connections in an isolated manner. That is to say, global communications with local investment.



Luis M. Molleda
Subdirector of Technology Department
Telefónica de España
Emilio Vargas 4, 4^a
28.043 Madrid, Spain
Phone : (1) 584.6710
Fax: (1) 584.6972

Born on November 19, 1941. Industrial Engineer from the High Technical School of Bilbao. Joined Telefónica in 1969 and worked successively in Outside Plant Engineering Department, Research and Study Department and now in Technology Department as Subdirector of Transmission and Outside Plant. From 1970 to 1980 was delegate to Telefónica in the CCITT Study Groups V and XV, and from 1970 to 1992 in the Study Group VI, as Vice President of the SG and President of the Working Group on Fiber Optic Plant and Technology. From 1988 to 1994 was member of the European Management Committee of the European Conference on Optical Communications. Presently is the Vice President of the Study Group 6 (Outside Plant) in the new ITU-TS.

BRAZILIAN TELECOMMUNICATIONS SYSTEM

Carlos Fernando Ximenes Duprat

Telebrás, Brasília, Brazil

The objective of this presentation is to show the composition of the Telebrás System in a global view and its Program for the Recovery and Expansion of the Telecommunications and Postal Systems - The "PASTE" which represents an investment program in the sector and a global view of the digitalization of the long distance and local trunking networks by means of optical cables.

TELEBRÁS, through its 28 operating subsidiaries, is the main supplier of public telecommunications in Brazil. In December, 1995, TELEBRÁS represented about 94% of the total public telephone stations and approximately 91% of the national network. Through their subsidiary, Empresa Brasileira de Telecomunicações S/A - EMBRATEL, TELEBRÁS owns and operates all the installations of interstate and international telephone transmission in Brazil. Through the other 27 subsidiaries, TELEBRÁS is the main supplier of the intrastate telephone traffic. The TELEBRÁS system also offers telephone related services such as: data transmission, cellular phones and telegraphic messages, telex, video text, image and sound. Based on their receivables of US\$ 11.4 billion in 1995, TELEBRÁS is the second largest company in Brazil.

TELEBRÁS is controlled by the Brazilian Federal Government which, under the law, is obliged to hold the majority of the TELEBRÁS shares. The TELEBRÁS operations are therefore subject to substantial regulatory controls by the Federal Government. Since 1974 the TELEBRÁS system holds the virtual monopoly of the public telecommunications services exploration in Brazil. In August 1995, the Brazilian Constitution was changed in order to allow the Federal Government to give permission to private companies to supply the telecommunications public services.

The Recovery and Expansion Program of the Telecommunications System and the Postal System - PASTE represents an audacious

investment program, promoted by the government and complemented by the substantial private/human, management and financial resources with the purpose of modifying the Brazilian communications sector into an effective agent for the development of the country, incentivating national productivity and assuring the universal access to the communications services.

The total investment for the PASTE is estimated in US\$ 75 billion, being 50% in the first period of its execution (1995 - 1999) and the balance in the second period (2000 - 2003).

The demand for optical fibers required by the Brazilian Telecommunications System considering both long distances and local networks will be presented.



Carlos Fernando Ximenes Duprat
Engineering Department Manager
TELEBRÁS
SAS Q. 06 - B1. "E" - 4º Andar
70313-900 Brasília, Brazil

Mr. Duprat received his degree in telecommunications engineering in 1976 with post-graduation in operational research. He works at TELEBRÁS System since 1975, with experience in operating companies CETEL and TELERJ, and since 1991 works at TELEBRÁS Holding, initially as manager of Technical Planning Department and at present as manager of the engineering department.

LUNCHEON SPEAKER



DR. JIM KEELAN
Communication Unlimited
Arvada, Colorado

Dr. Keelan has had an interesting life as a former juvenile delinquent, a former football player, and a former Catholic priest. He has attended thirteen universities, holds five undergraduate and graduate degrees, and has taught at universities in the states of Washington, Hawaii, and Colorado.

He is the author of books, audio and video tapes on Laugh Your Way to Health, Having Fun and Being Yourself, B.S. (Beat Stress) and Live Longer, and How to be Married and Still be Yourself. He has appeared on the CBS television program 60 Minutes.

NEW SUBMARINE CABLE DESIGN FOR LONG HAUL, HIGH BIT RATE SYSTEMS

Jean-François LIBERT - Yves CHARLES

ALCATEL SUBMARINE NETWORKS

536 Quai de la Loire - BP 849 - 62225 CALAIS CEDEX - FRANCE

ABSTRACT

Future long haul high bit rate systems incorporating WDM (Wavelength Division Multiplexing) will require more protection of the fibers as well as a greater reliability of the cable.

To meet these requirements, a new cable was designed which particularly protects optical fibers against bending and microbending, and exhibits better performances with regard to abrasion and dielectric strength.

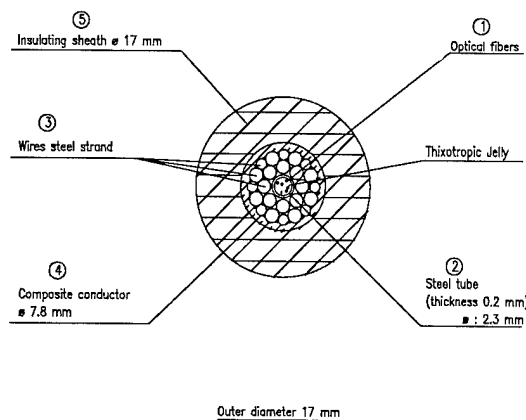
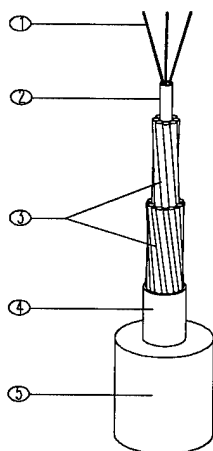
This paper outlines how the OALC4 cable (figure 1), the new Alcatel Submarine Networks cable product ensures the above requirements for amplified systems.

I - BENDING, MICROBENDING

The increase of the requested bit rates for submarine telecommunication cables has resulted in the need for special fibers characterised by large mode field diameters (8.7 μm - 9.0 μm).

Such fibers allow bit rates greater than 10 Gbit but in return are much more sensitive to bending and microbending effects. The OALC4 cable has overcome these effects.

Figure 1 - OALC4 LW cable



The cable structure is based on a steel tube in which are enclosed the fibers. The fiber slack and the filling jelly, which acts as a buffer, prevent any fiber strains during all steps of the cable manufacturing. From the tubing to the insulation process no increase of attenuation is revealed.

Furthermore, the tube also protects the fibers against the strains resulting from a hydrostatic pressure when the cable is laid on the sea bed (the cable is designed to go down to 8000 m depth)

The pressure resistance of a tube is given by the Von Mises equation :

$$P = s \frac{k^2 - 1}{\sqrt{3} k^4}$$

where :

P = External tube pressure

S = Yield strength

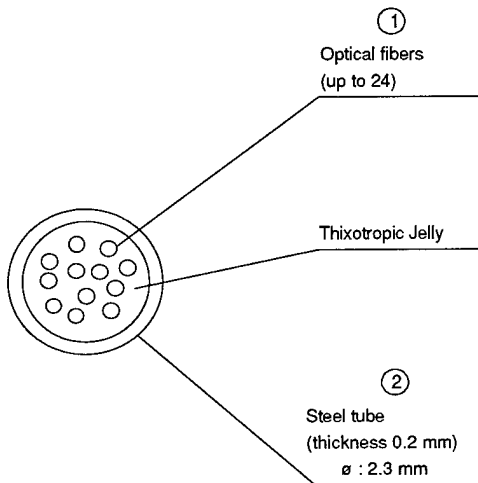
K = Diameter ratio (OD/ID)

Due to the tube characteristics (figure 2), the fiber core of the OALC4 cable, alone, can bear a pressure corresponding to 1 000 bars, with a comfortable safety margin.

Applied to the steel tube the above formula gives a pressure resistance of 1300 bars. (k of the steel tube is 1.21). This corresponds to a water depth of approximately 13 000 meters for a cable designed to go down to 8 000 meters.

Experiments were also carried out to check the quality of the longitudinal tube welding. A cable sample was put inside a pressure vessel under a pressure of 1000 bars and no damage was observed.

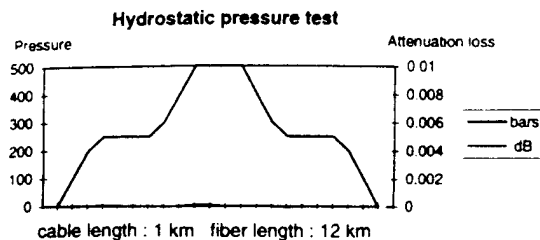
Figure 2 - Fiber structure



In addition to this, the composite conductor design, with its vault structure, increases the efficiency of the pressure resistance of the cable. This additional protection ensures that no effect of bending and microbending will happen when cable is laid on the deep sea bottom.

In order to confirm this, another experiment was performed. A cable sample of 1 000 meters length was put inside a longitudinal pressure tube. The optical attenuation was recorded with regard to the increase of the isostatic pressure (fig 3).

Figure 3 - Optical attenuation / isostatic pressure



As shown in the figure 3, the efficiency of the vault structure to prevent any bending and microbending effect on fiber is clearly revealed.

II - CABLE RELIABILITY

In ten years, the transmission of a single fiber pair has multiplied by more than 35. Therefore the cables which now protect the fibers have to be more and more reliable.

Many improvements have been made to the OALC4 cable as a result of our experience in this field of optical cable :

- Management of hydrogen,
- Dielectric performances,
- Abrasion resistance,
- Handling performances,
- Behaviour in a sea bed environment.

Management of hydrogen

The OALC4 cable design provides a double hydrogen barrier with the composite conductor, where the strength member is surrounded by a formed, welded and reduced copper tape but also with the optical core itself, where, as already discussed, the hermetic steel tube provides a hydrogen barrier very close to the fibers.

This stainless steel tube is welded by a laser beam.

The hydrogen transmission rate through a cylindrical barrier is given by the following expression :

- cylindrical metallic barrier

$$Q = \frac{K * 2 * \Pi * p^{1/2}}{Lnr1 - Lnr2}$$

- cylindrical polymeric barrier

$$Q = \frac{K * 2 * \Pi * p}{Lnr1 - Lnr2}$$

where

- K = permeability constant
- r1 = outside radius of cylinder
- r2 = inside radius of cylinder

The value of K for a polymeric material and for stainless steel are respectively $2.3 \cdot 10^{-8} \text{ cm}^3 / \text{cm} / \text{sec} / \text{atm}$ and $1.3 \cdot 10^{-14} \text{ cm}^3 / \text{cm} / \text{sec} / \text{atm}^{1/2}$.

Hence, the ratio between the permeability constants of polymer and stainless steel tube has an order of magnitude of 10^{+6} .

Therefore, for a given external hydrogen pressure, the shield provided by the OALC4 cable fiber structure is much more efficient compared to a standard polymeric fiber core.

To end this section, it should be stressed that both the steel tube and the copper tape are not overlapped but welded and that the tube shield is very close to the fibers.

Dielectric performances

Nowadays, submarine cable networks involve, longer and longer cable lengths ; 10 000 km links have become a standard. As a consequence, the dielectric strength of the insulant has to be greater and the design life of the whole cable has still to be assured for 25 years.

The polyethylene used in the OALC4 cable is compliant with these stringent requirements. Its selection is the result of several years of studies.

An Alcatel Submarine Networks IWCS paper last year explained in detail the interesting performances of the OALC4 cable insulant.

Abrasion resistance

The above mentioned polyethylene also exhibits a high abrasion resistance, as confirmed by practical experiments.

Because it is a high density polyethylene, it naturally assures a better resistance against abrasion compared to low density polyethylenes. A large range of polyethylenes were submitted to the « taber » test . The test method used conforms with the ASTM 1044 standard.

The polyethylene of the OALC4 cable (table 1) presents very good performances compared to the Low Density polyethylene.

Table 1 : «taber» test

CABLE TYPE	OALC4 POLYETHYLENE ABRASION LOSS (mm ³)	STANDARD POLYETHYLENE ABRASION LOSS (mm ³)
-	70	110

Some additional tests were also carried out to compare the abrasion resistance of this high density polyethylene to some others HD PE. The following ranking can be made (table 2).

Table 2 : Abrasion Resistance

Type of polyethylene	Abrasion resistance
PE HD 1	3*
PE HD 2	2*
PE HD 3	1*

* The smaller the numbering of the ranking, the better the abrasion resistance.

In table 2 the OALC4 polyethylene is identified as PE HD 3.

Handling performances

Laying operation

The OALC4 cable has a high density which is also beneficial for laying operations. Hydrodynamic constant (38 degree knots) allows a laying with a small angle and so that the cable length between the top and the bottom of the water column is greater compared to the current long haul system cable. This provides more time to operators to react in the case of problems.

For instance, in the case of a lay at 6 knots in an 8 km water depth, the ship will benefit 6% more time to analyse and solve the laying problem (bad slack control, high tension, etc...). This extension of 6 % may appear small but can be very effective in adverse situations.

The OALC4 armoured cables provide also a good behaviour during marine operations. The complete range of cable protection is provided from the Single Armoured Light to the Rock Armour cable. All these designs are made with high grade galvanised steel wires. The wires are preformed to the cable diameter during a pre-processing stage. This operation cancels any residual torque on the final cable and prevents any cable problem during sea operations.

Storage capability

The cable storage capability is also very important for long haul systems, since long lengths of cable are involved which require more and more transits and loading operations. Because the capacity on ships cable tanks are not infinite, the OALC4 cable, due to its small outer diameter, contributes to solving the problem of time and cost. This cable with its outer diameter of 17 mm increases by more than 30 % the storage capability compared to current cables. Not only does this present a benefit for cable storage on cablesips but also for cable storage inside the cable depots for spare cables.

Mechanical characteristics

The small size of the cable, which as seen above, provides many advantages but is not a limiting parameter with respect to cable tensile performances. The OALC4 cable strength member is made up of high grade steel wires (2100 Mpa) arranged to form a vault which is a very compact structure. Hence, the cable modulus, which is the water depth for which the cable can sustain its own weight before breaking is 23 km. This elevated figure easily supports a comparison with the current long haul system cables and demonstrates the actual safety margin of a cable.

Regarding armoured cable types, the following table shows that the OALC4 armoured cables have very high tensile strengths. For instance the Ultimate Tensile Strength of each of these cables is higher than the typical figure for current designs.

Table 3 : Armoured cable - Mechanical Performances

Cable Type	Ultimate Tensile Strength
SAL	280 kN
SA	370 kN
DA	560 kN
RA	370 kN

In situ behaviour

Most of the long haul submarine links include deep sea cable. This chapter deals with the specific difficulties which may occur in deep water and the behaviour of the OALC4 cable in one of these cases :

- current cable stability
- suspensions
- strumming

Current cable stability

The current cable stability is the sea bed current from which a cable starts to move.

It can be determined by the value of the S factor expressed by :

$$S = \frac{\mu * (w - t_d)}{t_l}$$

where :

μ = friction coefficient between cable and sea bed

w = cable weight in water

$t_d = \frac{1}{2} C_d \rho D v^2$ (drag force)

$t_l = \frac{1}{2} C_l \rho D v^2$ (lift force)

A cable starts to move on the sea bed when $S = 1$

Following are given the current cable stability for the OALC4 cable and for other standard long haul system cables (table 4).

Due to its small diameter (17 mm) and to its very compact structure, the OALC4 cable is very dense and so it is as stable as current cables.

Table 4 : Current cable stability

CABLE TYPE	CABLE 1	OALC4 CABLE	CABLE 2
Current stability cable (normalised figures)	0.9	1	1.1

Suspensions

In areas where there were difficult laying condition or strong sea bed currents, some cable suspensions may occur. At the contact points of the suspension some contact forces are involved.

The expression of these contact forces is given by :

$$T = \frac{w * l^2}{8 * f}$$

where :

T = contact force

w = cable weight

l^2 = span length

f = sag

This formula shows that for a given span and a given sag the involved contact force is proportional to the weight of the cable.

Since the OALC4 cable is 30 % lighter than a conventional deep sea long haul system cable, the cable strains at the location of the contact points of the eventual suspensions will be reduced at least by the same order of magnitude.

A comparative test was carried out and as presented in the following table (table 5) the good behaviour of the OALC4 cable polyethylene was confirmed.

Table 5 : Number of cycles requested for insulant degradation

CABLE TYPE	OALC4 CABLE	STANDARD CABLE
Number of cycles	65 000	15 000

The OALC4 cable is at least 4 times better than current cables in such a situation.

Strumming effect

Although rare, all cables may strum.

This strumming effect appears when a cable is in suspension and under tension and when the fundamental resonant frequency caused by tranverse current.

This is mathematically described as followed.

$$Fi = \frac{1}{2 * l} * \left(\frac{\pi^2}{me} * \frac{EI}{l^2} + \frac{T}{me} \right)^{1/2}$$

$$Fs = \frac{0.2 * V}{d}$$

Fi = fundamental resonant frequency of the span

Fs = vortex shedding frequency

Ei = cable flexural modulus

me = effective mass of the cable

Nevertheless, any cable type may be submitted to strumming effect. The best way to avoid this phenomenum is to ensure a correct laying operation but, on the cable itself, solutions may be found to reduce the strumming damages. This was done for the OALC4 cable since, in addition to its good abrasion resistance, the cable has got a low flexural modulus. This allows the cable to fit well with wild bottom profiles and goes in the way to reduce cable suspensions and so strumming effects.

CONCLUSION

The OALC4 cable meets the requirements of the new high bit rate submarine systems.

The package design prevents bending and microbending and ensures the integrity of the optical path.

Furthermore, in addition to its good technical aspect, the design also supports high system reliability. The selective choice of a high density polyethylene in conjunction with the optimisation of the design insures a good dielectric behaviour and a good cable resistance against environmental agressions as abrasion, sea bed current, strumming effect.

The design also provides some others benefits such as a large increase of the storage capacity (30 % higher than conventionnal cables), and a high tensile performance (the cable modulus of the cable is 23 km).

Authors

J.F LIBERT

Alcatel Submarine Networks

536 Quai de la Loire

62225 Calais Cedex

Jean-François LIBERT received his engineering degree from «Hautes Etudes Industrielles» of Lille (FRANCE). He joined Alcatel in 1984. He is now Technical Manager for Optical Submarine Cable in Calais.

Y. CHARLES

Alcatel Submarine Networks

536 Quai de la Loire

62225 Calais Cedex

Yves CHARLES was born in 1967. He is graduated from Ecole Universitaire Des Ingénieurs de Lille (E.U.D.I.L). He joined Alcatel in 1993 where he is in charge Cable design and product qualification in Calais (FRANCE).

CABLING EFFECTS ON FIBER PMD

Franco Cocchini*, Antonio Chiantore*, Giovanni Carones^ and Alessandro Ginocchio^

* FOS, Fibre Ottiche Sud, Battipaglia, Italy - ^ Pirelli Cavi S.p.A., Milano, Italy

ABSTRACT

Samples of standard G652 fibers from different manufacturers have been measured for PMD value. The fibers were tested as drawn as well as following various cabling steps for different cable designs. Temperature cycles between -30°C and +60°C have been monitored on finished cables. PMD is confirmed to be a highly randomic phenomenon which can be described and forecast only in a statistical manner. The effect of the stresses induced on the fibers in each cabling step have been clearly demonstrated.

INTRODUCTION

Polarization Mode Dispersion (PMD) has become an important issue in both high quality analog systems and high speed digital systems which utilize single-mode optical fibers, since it can significantly degrade transmission quality.

PMD occurs due to birefringence, i.e. the relative propagation delay between the two polarization states of the fundamental mode, induced on the fiber by the superposition of core ellipticity, asymmetric lateral stresses and twisting. All these events vary randomly along the fiber, thus producing mode coupling, i.e. the exchange of optical energy between modes.

Mode coupling and birefringence have opposite effects on PMD, since increasing mode coupling reduces PMD, while increasing birefringence increases PMD. The final PMD in the network depends both on the intrinsic fiber performance and on the environmental conditions (e.g. colour and ribbon processing as well as cabling, installation and thermal conditions) [1-8].

The performance may depend on the fiber and cable designs. We will present the results of PMD measurements in various cabling steps on three types of cables:

- loose tube cable
- slotted core cable (loose design)
- ribbons in slotted core cable.

Different performances could be obtained with other combinations of fiber and cable designs. Standard fibers (G652) of various manufacturers have been considered in this work.

EXPERIMENTAL PROCEDURES

Various techniques have been proposed to measure PMD. Our experiments were performed basically with two different equipments:

- the EG&G instrument (wavelength scanning method) which utilizes a LED source in the second and third window;
- the GAP Optique instrument (time domain, interferometric) which utilizes a LED source at 1550 nm.

The results of the measurements on the same samples show good agreement between the two instruments [9].

No particular difference can be observed in the measurements in second or in third window (fig.1). Therefore, in the following, all references are to values around 1550 nm.

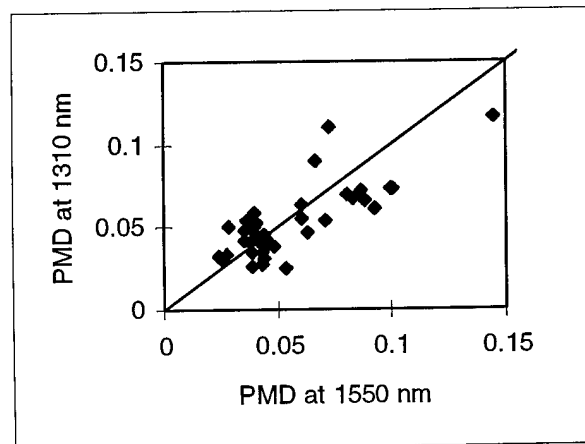


Figure 1. Typical PMD measurements ($\text{ps/km}^{1/2}$) of natural fibers in the range around 1310 nm vs 1550 nm.

The measurements on the fibers were performed on samples wound over a large measurement spool at zero tension ($\varnothing = 300$ mm). The induced PMD due to bending on such a spool is less than $0.01 \text{ ps/km}^{1/2}$ [4]. Therefore, the effect on the intrinsic PMD of the fiber is assumed to be negligible.

Minor effects can be caused by fiber-to-fiber contact due to undesirable coil superposition. However, especially on short samples, this event is rather unlikely. This is supported by the good reproducibility of the measurements after repeated winding operations on the same sample, which is of the same order of the uncertainty of the measurements itself.

The fibers under test have revealed a good homogeneity along the parent blank and the quadrature sum rule [8] is proven to be fully satisfied, i.e.

$$(1) \quad \text{PMD}(L) = \sqrt{\frac{\sum_i \text{PMD}(L_i)^2 L_i}{L}}$$

$$\text{with } L = \sum_i L_i.$$

Therefore, the measurements on both short and long pieces on the measurement spool at zero tension are representative of the intrinsic PMD of the fibers.

On the contrary, measurements on shipping spools, where the fiber is wound at a low constant tension of about 70 g, are not representative of

the intrinsic PMD since a certain level of added birefringence and mode coupling is inevitably introduced (fig.2). The contribution to the birefringence due to the lateral load seems the dominant effect for fiber of low intrinsic PMD, while mode coupling seems more effective on fiber of higher intrinsic PMD.

The measurements on ribbons have been performed on large drums at low constant tension. In this case, due to the flat geometry, undesired coil superpositions are easily checked and avoided. Lateral load effects are assumed to be of the same order to those observed in the measurements of fibers on the shipping spool. As shown in the following, this contribution is negligible with respect to those of the ribbon matrix itself.

The measurements on the cables have been performed on large drums ($\varnothing > 1$ m), and in the case of the ribbon cable, also after installation.

COLOURING EFFECTS

The process of colouring the fibers with inks introduces a certain amount of stress whose effects are similar to those observed in the measurements on the shipping spools. The contribution to the birefringence due to the lateral load affects mainly the fibers with low intrinsic PMD, while mode coupling appears on fibers of higher intrinsic PMD (fig.3).

However, in this case the stresses due to the ink application are larger than those observed in the shipping spool measurements. This is reflected in

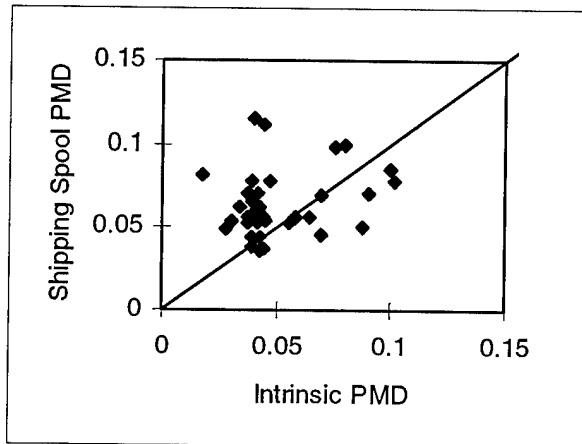


Figure 2. PMD measurements ($\text{ps/km}^{1/2}$) of natural fibers on shipping spool vs measurement spool at zero tension (intrinsic fiber PMD)

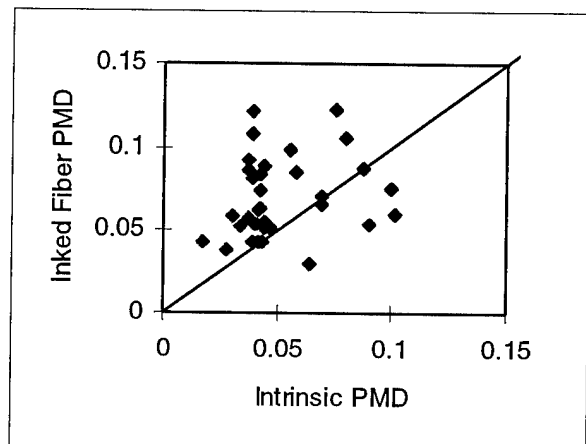


Figure 3. PMD measurements ($\text{ps/km}^{1/2}$) of coloured fibers vs natural fibers, both on measurement spools at zero tension.

the higher average values and standard deviation as reported in fig.4. Due to the viscoelastic nature of the coating and ink materials, relaxation of such stresses could be observed over long time periods.

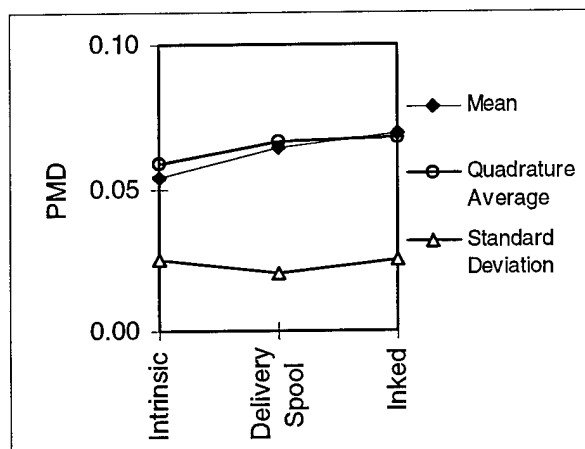


Figure 4. PMD (ps/km^{1/2}) mean value, quadratic average (eq.1) and standard deviation for: natural fibers at zero tension (intrinsic value), natural fibers on delivery spool and coloured fibers at zero tension.

LOOSE DESIGN CABLES

A SZ loose tube cable and a slotted core cable (loose design) have been manufactured with a part of the fibers described so far. The PMD values obtained are reported in fig.5. The results

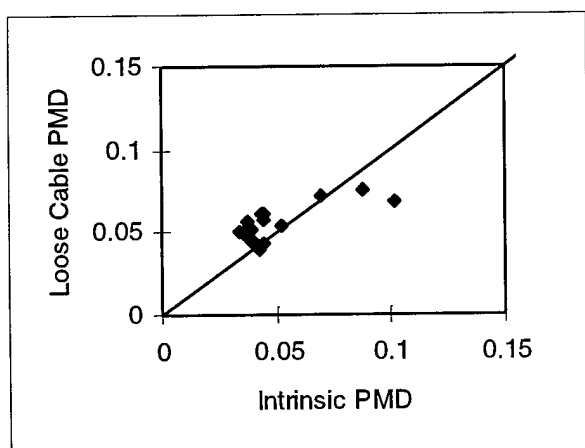


Figure 5. PMD measurements (ps/km^{1/2}) of cabled fibers (loose) vs intrinsic fiber PMD.

are rather consistent with the intrinsic PMD values of the fibers. This is due to the fact that the fibers experience low stresses in loose cables. This is reflected in the almost equal average values observed in the measurements on fibers at zero tension and in cable, as reported in fig.6. A decrease of the standard deviation after cabling is observed, probably due to a residual mode coupling at the higher PMD values. Temperature effects will be presented in a following section of this paper.

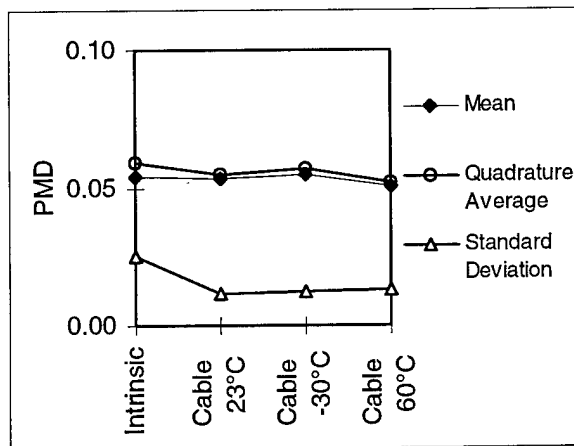


Figure 6. PMD (ps/km^{1/2}) mean value, quadratic average (eq.1) and standard deviation for: natural fibers at zero tension (intrinsic value), loose cabled fibers at 23, -30 and 60 °C.

RIBBON CABLES

A part of the fibers were used to produce ribbons and the relevant ribbon type cable (slotted core design). In this case an increase of PMD is evident due to the stresses induced by the ribbon matrix (fig.7). This effect is partially reduced, but still present, in the measurements on the cabled ribbons (fig.8 and 9). Partial stress relaxation of the viscoelastic matrix can explain this reduction. In fig.9 is also reported the resulting PMD value after cable installation. A further reduction of the averages can be observed.

The effects of the fiber position within the ribbon and in the slot can be seen in table I. A larger PMD can be observed on the fibers positioned at the external sides of the ribbons [10], while no effect can be observed due to the position of the ribbon in the slot. In fact, the variation on the

averages are small and of the same order to those observed in the different slots.

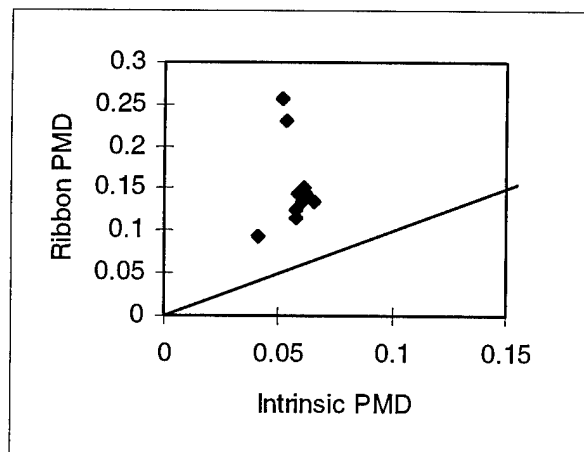


Figure 7. PMD measurements ($\text{ps}/\text{km}^{1/2}$) of ribboned fibers vs intrinsic PMD.

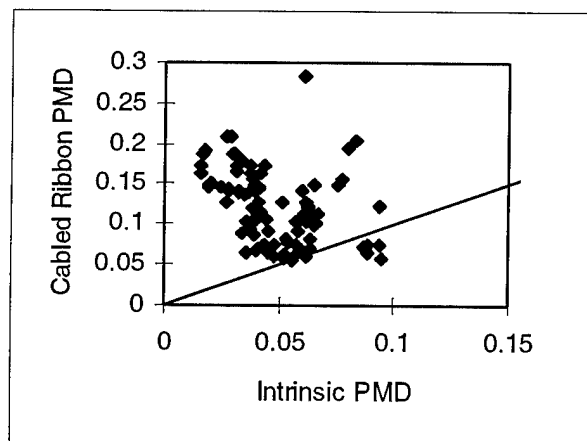


Figure 8. PMD measurements ($\text{ps}/\text{km}^{1/2}$) of cabled ribbon fibers vs intrinsic PMD.

TEMPERATURE EFFECTS

The manufactured cables were also tested in different temperature conditions. In the case of loose cables no temperature effect was observed, as shown in fig. 6 and 10.

Also in the case of ribbon cables only minor temperature effects were observed, as shown in fig. 9 and 11. A slight increase at -30°C and a decrease at $+60^\circ\text{C}$ can be interpreted as due to

the thermal expansion of the coatings and the matrix which bound the fibers.

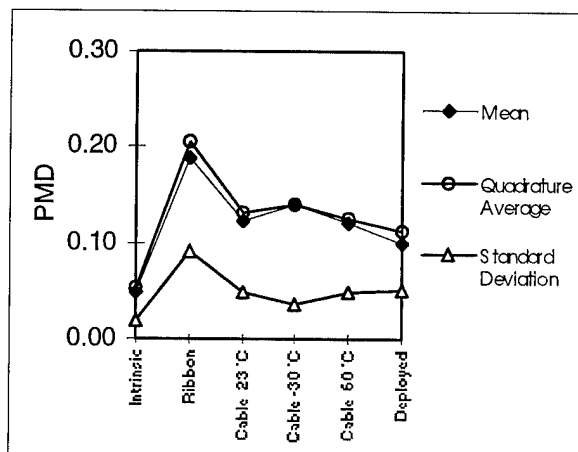


Figure 9. PMD ($\text{ps}/\text{km}^{1/2}$) mean value, quadratic average (eq.1) and standard deviation for: natural fibers at zero tension (intrinsic value), ribboned fibers, cabled ribbon fibers at 23°C , -30°C and 60°C and installed cable.

Fiber Position	Mean	Quadrature Average
External Fibers	0.145	0.150
Internal Fibers	0.098	0.105
Slot 1	0.129	0.134
Slot 2	0.106	0.136
Slot 3	0.126	0.132
Slot 4	0.124	0.124
Slot 5	0.101	0.113
ribbon 1 (inner)	0.128	0.138
ribbon 2	0.103	0.132
ribbon 3	0.114	0.124
ribbon 4	0.127	0.136
ribbon 5 (outer)	0.113	0.122

Table I. PMD ($\text{ps}/\text{km}^{1/2}$) mean value and quadratic average (eq.1) of cabled ribbon fibers as a function of the position of the fiber in the ribbon, the slot and the position within the slot.

CONCLUSIONS

- Loose design cables

On standard G652 fibers neither sensible PMD variations have been observed after the cabling process nor temperature effects on cabled fibers.

- Ribbon in slotted core cable

An increase in the PMD values, due to the ribbonizing process, has been noticed. This increase has been slightly reduced after cabling. The installation process has not caused a sensible variation in the PMD values, while only minor temperature effects, due to the thermal expansion of the ribbon coatings, have been observed.

In any case the measured PMD values of all fibers tested (in different test/cabling conditions) do not represent a limiting factor for the present analog/digital transmission systems for underground/aerial applications.

ACKNOWLEDGEMENTS

The authors acknowledge Sirti and CSELT for the collaboration in the measurements on the installed ribbon cable, M.Artiglia for useful discussions, A.Pannullo and D.Buccella for the help in the measurements.

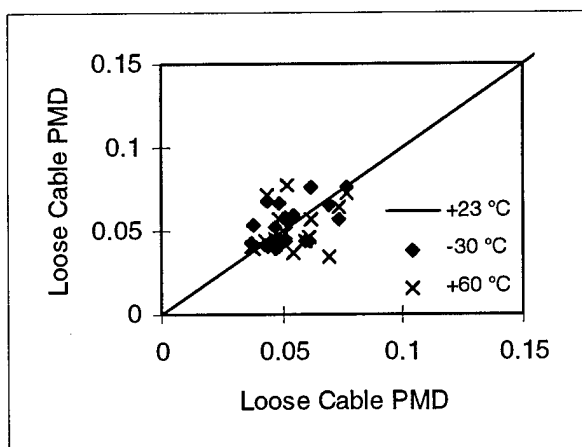


Figure 10. PMD value (ps/km^{1/2}) of loose cabled fibers at three temperatures (23, -30 and 60 °C).

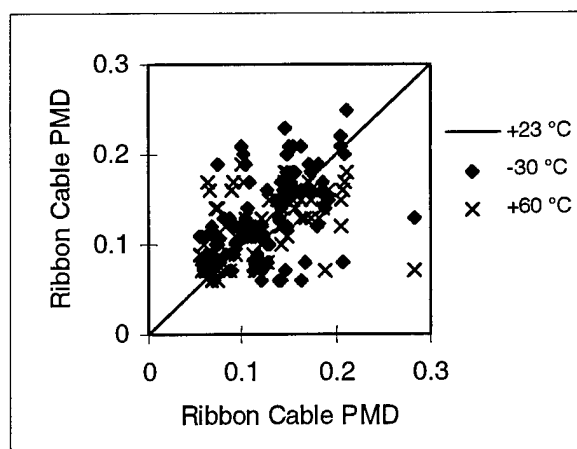


Figure 11. PMD value (ps/km^{1/2}) of cabled ribbon fibers at three temperature (23, -30 and 60 °C).

REFERENCES

- [1] A.F.Judy, W.T.Greene and J.B.Haber, 42nd IWCS, 630 (1993)
- [2] G.Carones, F.Donazzi, R.Gaspari and A.Ginocchio, 42nd IWCS, 639 (1993)
- [3] S.Grindstaff, J.Hill and O.Daneshvar, 42nd IWCS, 647 (1993)
- [4] T.Sekito, Y.Suetsugu, Y.Yamazaki and Y.Saito, 43rd IWCS, 665 (1994)
- [5] D.Boscher, J.C.Bizeul, J.P.Louboutin and C.Mauguen, 44th IWCS, 347 (1995)
- [6] P.Gaillard, M.Carratt, A.Gouronnec and G.Vuillaume, 44th IWCS, 353 (1995)
- [7] A.Gouronnec, R.Goarin, M.Auvray and G.Le Moigne, 44th IWCS, 359 (1995)
- [8] D.Gallagher, M.Ashby and M.Federoff, 44th IWCS, 366 (1995)
- [9] M.Artiglia, A.Chiantore and A.Rossaro, OFMC'95, I.4 (1995)
- [10] A.Galtarossa, G.Giannello, C.G.Someda and M.Schiano, Phot.Tech.Letters 6, 1232 (1994)

POLARISATION MODE DISPERSION FIELD MEASUREMENTS - A SURVEY OF THE SWEDISH NATIONAL NETWORK

Kim Brising

Telia Network Services, Transport Networks, S -123 86 FARSTA, Sweden

ABSTRACT

An investigation of polarisation mode dispersion in Telia's trunk network has been performed to ensure reliability for future upgrading of the network capacity to higher bit rates. A large number of fibre optic cable routes have been measured. The results are presented with a discussion on some observations. It may be said in conclusion that the results point to a highly reliable network with low values of polarisation mode dispersion.

INTRODUCTION

Asymmetries of the fibre core and mechanical influences like tension, pressure and twisting of the fibre give rise to birefringence. The two actually possible polarised light modes in a single-mode fibre will then have a slightly different group delay and thus give rise to polarisation mode dispersion, henceforth abbreviated PMD.

The interest in PMD has grown concurrently with the demand for higher bit rates and longer distances between repeaters; due to the statistical nature of PMD, it could not easily be compensated, like chromatic dispersion.

In order to examine our network, measurements of installed cables have been carried out since last autumn. The measurements were made in different parts of Sweden and represent an average of different cable and fibre types installed since 1985.

MEASUREMENT METHOD

Measurement principle and set-up

The measurement instrument applied uses the interferometric technique^{1,2}. The equipment consists of two units:

- a sender with two LEDs, with the wavelengths 1300 nm and 1550 nm respectively and a polariser.
- a software-controlled receiver.

An outline diagram of the method and the measurement set-up is shown in figure 1.

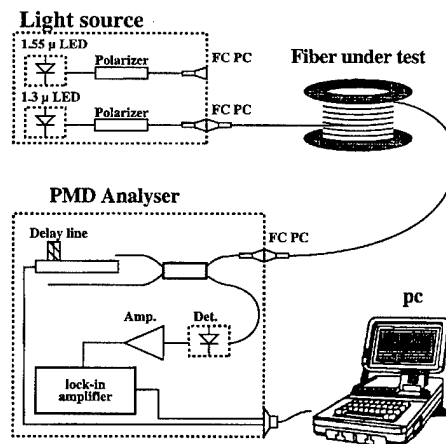


Fig. 1 Measurement principle and set-up

Measurement reliability

During the survey, comparisons were made with other instruments using the same or a different technique (fixed analyser). These comparisons showed a good correlation between the instruments³.

The accuracy of our measurement equipment is specified to be better than ± 0.05 ps in the range from 0.1 to 30 ps.

The accuracy of the measurements is not only related to the measurement instrument or technique. There is also an uncertainty due to the statistical nature of PMD⁴. With high PMD the uncertainty is small but with low PMD the uncertainty has proved as high as 40% in our survey. On the other hand, this uncertainty will not very much affect the distribution of data as presented later in this paper (figure 5), since the uncertainty in absolute figures for low values will be small.

Generally, we have made just one measurement of each fibre, which we think may be justified by the discussion above. However, in the beginning of this survey we made two or more consecutive measurements on each fibre but we seldom found differences above 10% between the consecutive values. Therefore, our approach has been to give priority to measurements on as many routes with different cable types as possible.

CABLE AND FIBRE TYPES

In this section the cable and fibre types used in this survey are presented. The fibre types used in each cable type are summarised in table 1. Cross-sections of the cable types are shown in figures 2 to 4. Henceforth, the cable types are often referred to by their figure numbers.

Slotted core cables with ribbons

For the last seven years, slotted core cables with fibre ribbons have been installed and are today the predominant cable type in Telia's trunk network. Three different suppliers have been engaged, in this paper called A, B and C.

Figure 2 shows the design: The slotted core element has six slots with up to four ribbons packed in each slot. Each ribbon has four single-mode fibres. The fibre types are manufactured according to the OVD or VAD process, dependent on the supplier of the cable. For a short period, cables with MCVD fibres of the matched clad-type were also delivered by one supplier.

The cable core is water-protected by a filling compound and is covered by a polyethylene sheath. The cable is installed in so-called split ducts, ploughed together with the cable into the

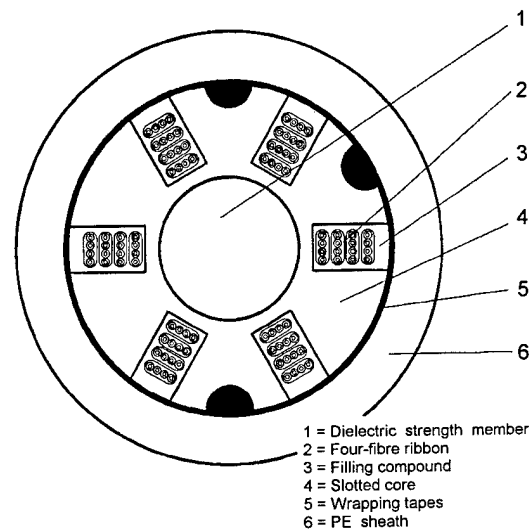


Fig. 2 Slotted core cable with ribbons

ground, or in ducts by means of pulling or blowing technique.

Other slotted core designs

Other slotted core designs used in our network are shown in figures 3a - e. They could briefly be described as follows:

- a) Loose tubes with up to six fibres a tube are used. There is one tube in each slot. OVD fibres were used. This cable type is a precursor of the ribbon cable described in the last sub-section and installed as mentioned above.
- b) Fibres with primary coating (250 μm), directly in the slots. There may be up to four fibres a slot. This cable type was used only for a short period, supplied by only one manufacturer, called D. VAD fibres were used.
- c) Tight secondary coated fibres (900 μm) directly in the slots. Contrary to the other slotted core designs described so far, this design has twelve slots. There is only room for one fibre a slot. This cable type was also used in a steel-armoured version for direct ploughing in the ground. Also, these types were used for a relatively limited period and delivered by one manufacturer (C). VAD fibres were used.
- d) Aerial cable, figure-8 design, with suspension steel wire, slotted core design with six slots, loose tubes with up to four fibres a tube. (Compare the design in figure 3 a). This design is presently used. Suppliers are A and B.

Slotted core designs

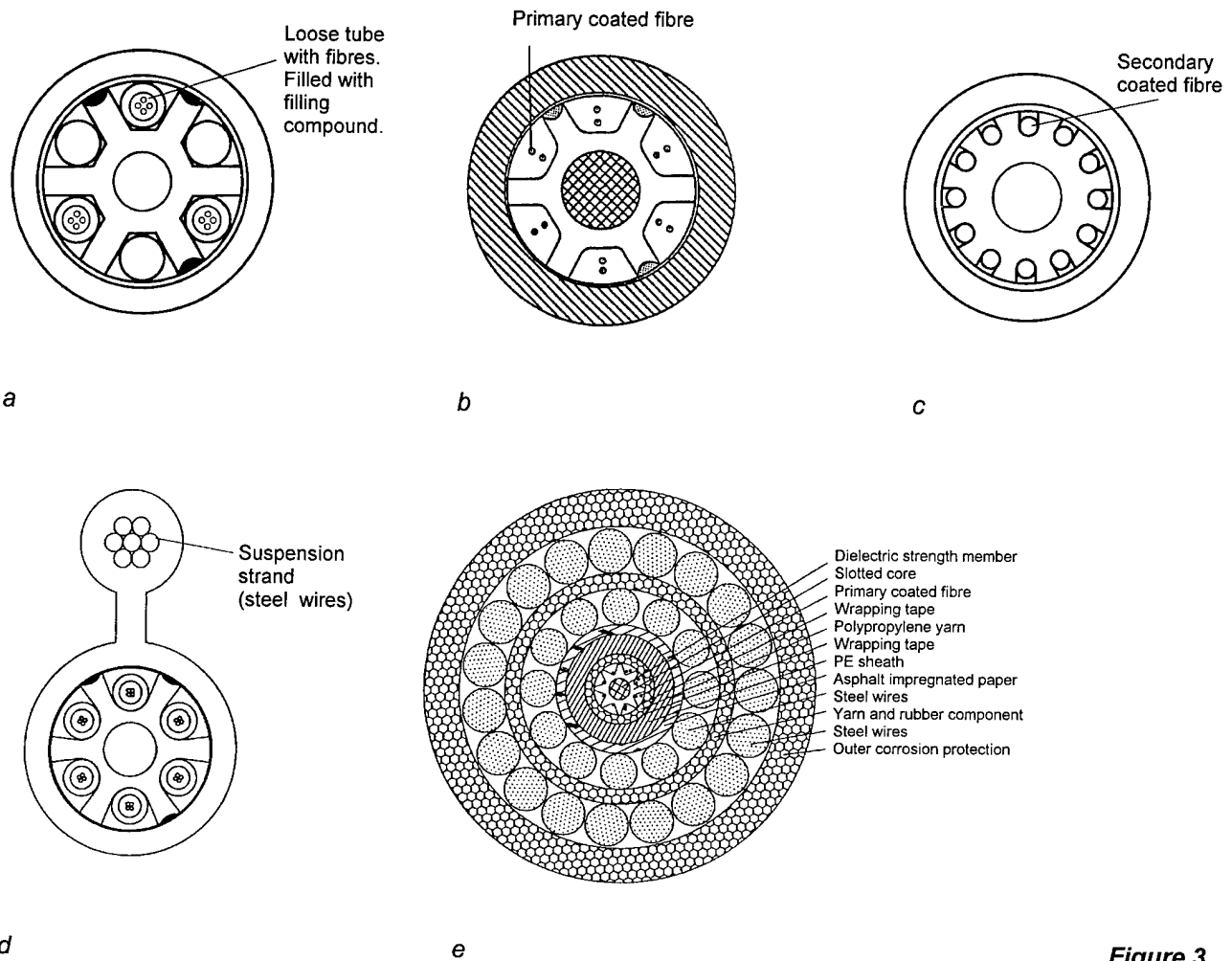


Figure 3

Non-slotted core designs

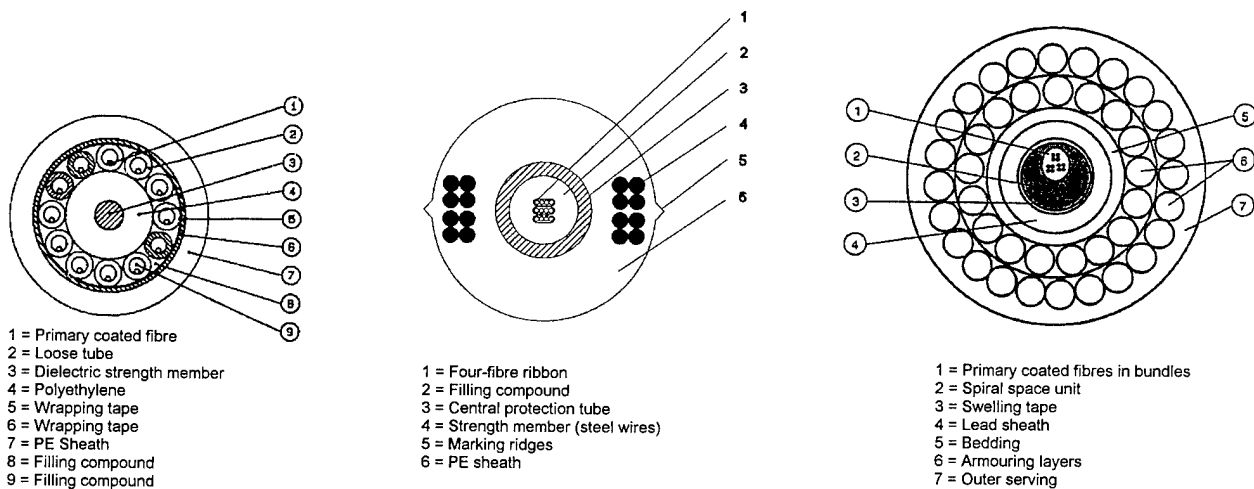


Figure 4

- e) Submarine cable, slotted core design with eight slots with primary carbon-coated OVD fibres directly in the slots. There are two versions of this cable type, one with single and one with double armouring.

Non-slotted core designs

There are also minor parts of our network where cables of the non-slotted core designs are used. The following designs are represented in our survey, shown in figures 4a - c:

- Up to twelve loose tubes with one fibre, each stranded around a dielectric strength member. There is an outer polyethylene sheath or a steel-wire armour between an inner and outer polyethylene sheath. This cable type was a precursor of the ribbon-cable with loose tubes described above (figure 3a).
- Aerial cable of uni-tube design with up to six ribbons. Steel-wires are incorporated in the sheath. This cable type has not yet been introduced in our network. The measurements were made recently in a field trial.
- Submarine cable with fibres in four-fibre bundles covered by yarn in a so called spiral space unit, which is a tube with a helical hollowness. This cable type has double or single-layer armouring.

Cable-type	Supplier	Fibre Type
Slotted core, ribbon, fig. 2	A	OVD, (VAD)
Slotted core, ribbon, fig. 2	B	OVD, (MCVD)
Slotted core, ribbon, fig. 2	C	VAD
Slotted core, fig. 3a	A and B	OVD
Slotted core, fig. 3b	D	VAD
Slotted core, fig. 3c	C	VAD
Slotted core, fig. 3d	A and B	OVD
Slotted core, fig. 3e	E	OVD
Non-slotted core, fig. 4a	A	OVD
Non-slotted core, fig. 4b	B	OVD
Non-slotted core, fig. 4c	F	OVD

Table 1.

The fibre types in parenthesis have been used by the supplier only for shorter periods but are represented in our survey.

OVD = Outside Vapour Deposition

VAD = Vapour Axis Deposition

MCVD = Modified Chemical Vapour Deposition

All the types mentioned are represented in our investigation in approximate proportion as to how common they are in the network.

RESULTS

Almost 500 fibres have been measured in more than 50 cable routes. The route lengths are from 5 to 70 km. The results are encouraging. Of all measured fibres, 99% show a PMD below 0.5 ps/ $\sqrt{\text{km}}$, an internationally suggested limit to ensure reliability in high-speed networks.

The distribution of all measurements is shown in fig. 5. The mean values at the wavelengths 1300 nm and 1550 nm are 0.12 ps/ $\sqrt{\text{km}}$ and 0.11 ps/ $\sqrt{\text{km}}$, respectively. As many as 82 % and 88% of the values at the respective wavelengths fall below 0.2 ps/ $\sqrt{\text{km}}$.

Table 2 below summarises some results pertaining to all cables and cable types. The number of routes and measured fibres is given together with averages of all measured fibres of each cable type. Minimum and maximum values are also given. In general terms, the following may be said:

- Slotted-core cables with ribbon, fig. 2, have the same percentage distribution as the overall distribution. The averages are also the same.

We then relate the other designs to the slotted core cable with ribbon, in consideration of the average values:

- Slotted-core cables with loose tubes, fig. 3a, show somewhat higher values, but the slotted-core aerial cables, fig. 3d, with loose tubes show lower values.
- The slotted core cables with primary or secondary coated fibres, figures 3b and 3c, show lower values, except for the submarine cable, fig 3e, which shows higher values.
- The loose tube design cables, fig. 4a, show considerably higher values.
- The aerial and the submarine cables, figures 4b and 4c, show lower values.

It should be considered that for several cable types the number of measured fibres is small, see table 2. More discussion on the significance of the results will be found in the section *Discussion*.

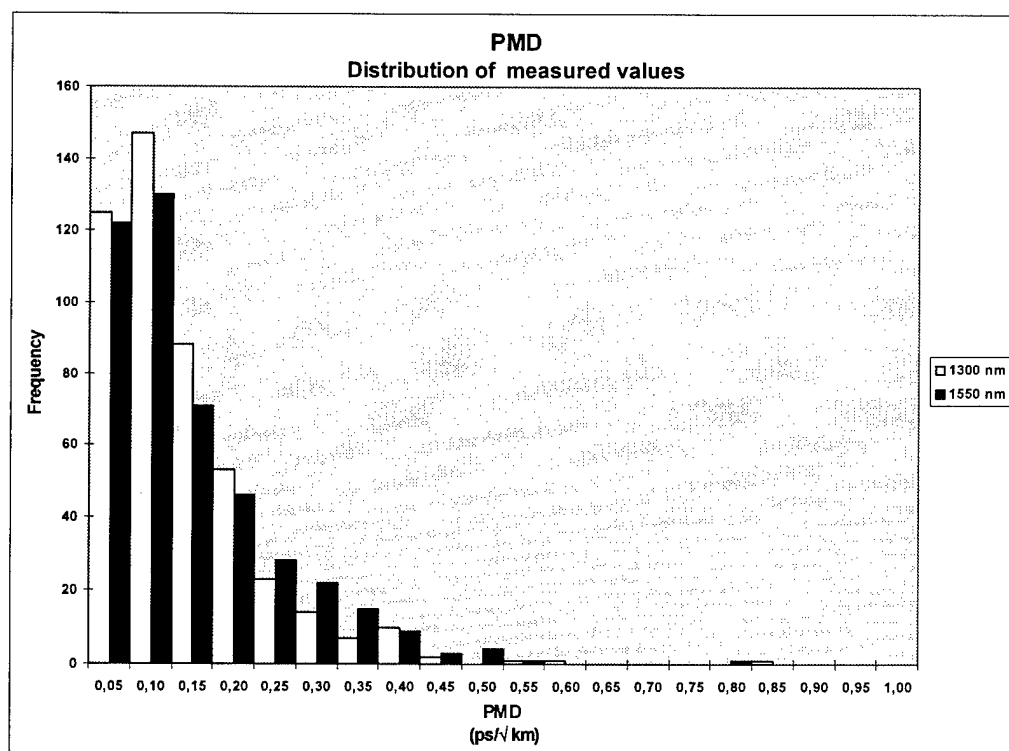


Fig. 5
Distribution of
all measured
PMD values

No of routes	No of fibres	Cable type	PMD (ps/√km)					
			1300 nm			1550 nm		
			Min	Max	Mean	Min	Max	Mean
54	472	All types	0.013	0.833	0.122	0.014	0.809	0.112
32	354	Slotted core, fig. 2	0.014	0.517	0.120	0.014	0.572	0.111
5	36	Slotted core, fig. 3a	0.024	0.482	0.165	0.025	0.436	0.137
2	12	Slotted core, fig. 3b	0.021	0.198	0.073	0.026	0.096	0.059
4	10	Slotted core, fig. 3c	0.013	0.155	0.057	0.017	0.112	0.043
3	12	Slotted core, fig. 3d	0.031	0.244	0.094	0.029	0.205	0.081
1	12	Slotted core, fig. 3e	-	-	-	0.024	0.368	0.162
3	10	Non-slotted core, fig. 4a	0.135	0.833	0.276	0.105	0.809	0.244
1	6	Non-slotted core, fig. 4b	0.061	0.149	0.092	0.040	0.130	0.090
1	8	Non-slotted core, fig. 4c	0.028	0.245	0.084	0.037	0.195	0.073

Table 2 A summary of minimum, maximum and mean-values of PMD of different cable types

OBSERVATIONS

Differences in PMD due to the position of the fibres in a ribbon

For the slotted core cables with ribbon, fig. 2, some interesting observations were made: On several routes a noticeable difference could be seen between PMD values depending on the

position of the fibre in the ribbon. On these routes, PMD values of the two outermost fibres of a ribbon were generally lower, while the two innermost fibres showed considerably higher values. This "pattern" is seen mainly in cables from two of our suppliers, namely A and B. In cables from our third supplier, C, this phenomenon has only been observed on the occasional route.

The results from one cable route showing the pattern described are indicated in figure 6. Here the average over all innermost fibres measured is 0.32 ps/√km at 1550 nm, and somewhat higher at 1300 nm. The corresponding average over the outermost fibres is 0.044 ps/√km. This remarkable difference is not typical. The higher values are more often between twice and four times as high as the lower values.

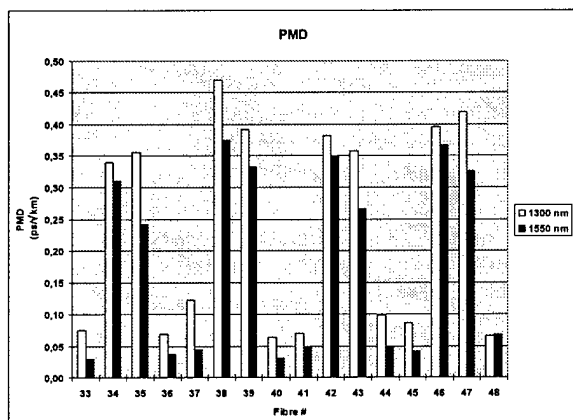


Fig. 6 Measurements representing four 4-fibre ribbons in one slot

Similar observations have been reported earlier by others even if their experience of PMD due to the position in the slot differs from ours⁵.

Differences in PMD due to the position of the ribbon in a slot

The results in figure 6 represent ribbons in one slot where the highest fibre numbers are found in the ribbon closest to the centre of the cable core. No significant difference in values due to the position of the ribbon can be seen in this case which also is true of the most measured cables. However, there are observations of some cables that indicate slightly higher PMD values closer to the centre of the core.

Differences in PMD before and after installation of cables

Together with our suppliers we are carrying on a study of what will happen to PMD after installation. At the time of writing we have only preliminary results. These indicate only relatively small changes in PMD after installation. No trends towards lower or higher values can be seen.

Differences in PMD due to the wavelength

As can be seen from table 2, PMD is somewhat lower at the wavelength 1550 nm than at 1300 nm. By analysing different routes you find that this is not generally true. For some routes the PMD of each measured fibre is generally higher at 1300 nm, but mostly there is no obvious trend as regards the measured fibres in a route; on some fibres the 1300 nm values are higher, on others it is vice versa. However, results obtained from ribbon cables show a slight overrepresentation of higher values at 1550 nm in cables from supplier C in contrast to those from suppliers A and B; see table 3 in the next section.

For all routes the correlation of the PMD at 1300 nm and 1550 nm respectively has been calculated. Most often the correlation is good but there are important exceptions. Ribbon cables from supplier C show poor correlation between the wavelengths, with a negative correlation coefficient in several cases.

DISCUSSION

In this section we will discuss more in detail how we can relate PMD to different cable types, fibre types, suppliers or any other parameter.

Fibre-type

Table 1, in the section *Cable and Fibre Types*, summarises the kinds of fibres used in the respective cable types from different suppliers.

Supplier A, who normally uses OVD fibres, used VAD fibres for a short period. Two routes representing this fibre type were measured. The data show no statistically significant differences in PMD between the fibre types.

Similarly, supplier B who also normally uses OVD fibres, used another fibre type for a short period, namely MCVD fibres. Also here, no statistically significant differences in PMD could be seen between the fibre types.

Generally, no obvious fibre-related PMD can be stated for the other cable types except for the oldest one, of the loose tube design (fig. 4a). The earliest single-mode fibres did not have the tight geometrical tolerances available today. Small geometrical tolerances are of great importance for low PMD values. Therefore, it is likely that the values of the few measured fibres of the loose tube design are significant of all cables from that time.

It should also be noted that different acrylates of fibres and ribbons have been used over the years but no statistical significance of PMD can be noted.

Ribbon

As already discussed, PMD can be dependent on the fibre's position in a ribbon. Most cables with this pattern have OVD fibres but we believe that this is not related primarily to the fibre itself. As mentioned above, supplier A has used VAD fibres for a short period. One of the routes with this fibre type show the position-dependent pattern, the other one does not. Furthermore, all our suppliers show data representing very low PMD on fibres, whatever the fibre type.

From our suppliers we also know that the PMD may increase considerably in the ribbon process. The differences in PMD due to the position of the fibre in a ribbon have been observed already after the ribbon process.

Thus it seems that the ribbon process could have an important impact on the PMD.

Cable types

As stated in the section *Results*, there is a small difference between slotted core cables with ribbon and loose-tube cables (figures 2 and 3a). This may be related to the cable design; the loose-tube design has a considerably shorter pitch than the ribbon design. But one should bear in mind that the amount of data on the loose-tube design is considerably smaller than on the ribbon design.

As already mentioned, the design with loose tubes stranded around a dielectric strength member (fig. 4a) gives considerably high PMD values. Beside the impact of the fibre discussed above, the cable design may also have an influence on PMD; again, a short pitch is used.

The representation of cables of other designs is limited, which makes it difficult to draw any general conclusions about these types. However, most measurements show very low PMD values, which makes us confident in our belief that no extreme PMD values will be found.

With the discussion of ribbon in mind, it should also be mentioned that from our suppliers we know that PMD generally decreases after the cabling process, even if the position-dependent PMD in a ribbon may remain.

Thus we believe that the cable design could generally have an impact on PMD, but this survey does not show how much.

Installation

As already mentioned, the process of installation of the cable seems to affect the PMD only marginally.

Environment

The measurements have been carried out on different seasons at temperatures ranging from a few degrees below zero and with ground frost to typical spring and summer temperatures of up to 20°C. We have not seen any considerable differences in the distribution of PMD measured under these different temperature conditions.

It should also be mentioned that some routes have been measured twice at different times of the year. The differences in the values mostly fall within the uncertainty of the measurement method.

Supplier

A comparison of the ribbon cables from suppliers A, B and C respectively is shown in fig. 7. For each supplier, approximately the same amount of fibres has been measured. Note that the y axis in figure 6 is in per cent. In table 3 the average, minimum and maximum values are summarised.

The distribution between suppliers A and C seems to be very similar despite the fact that the differences in PMD for outer and inner fibres in a ribbon is evident for supplier A but not for C. The reason is that several cables from supplier A with position-dependent PMD show overall low values.

Generally, supplier C has lower values than A (and B) which appears from the average values in table 3.

The generally higher PMD values for supplier B are mainly related to one cable route where many fibres were available. In this cable, the many high values of the innermost fibres have an evident impact on the statistics as can be seen from figure 7.

As the cable design of all the three suppliers is very similar, the most likely explanation of the obviously lowest values for supplier C is the different processing of the cable and the ribbon.

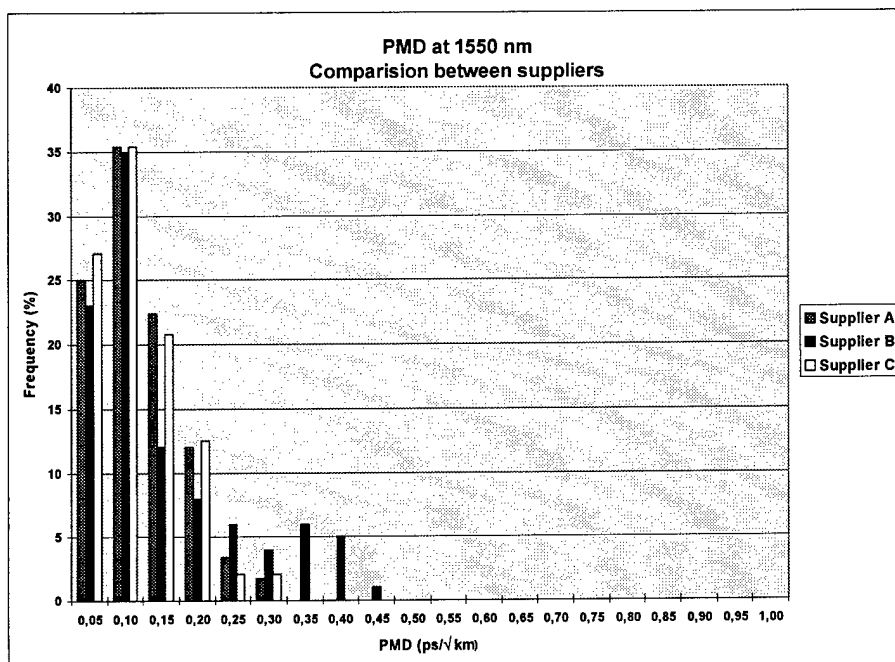


Fig. 7
Distribution of PMD of
slotted core cables with
ribbons. A comparison
between suppliers.

Supplier	No of routes	No of fibres	PMD (ps/√km)					
			1300 nm			1550 nm		
			Min	Max	Mean	Min	Max	Mean
A	11	152	0.014	0.343	0.115	0.017	0.293	0.101
B	8	100	0.015	0.517	0.161	0.024	0.450	0.129
C	11	96	0.017	0.282	0.077	0.014	0.278	0.093

Table 3 A summary of minimum, maximum and mean-values of PMD of slotted core cables with ribbons manufactured by different suppliers.

CONCLUSION

PMD as measured in Telia's trunk network show quite low values. The amount of data is sufficient to state that our network could be upgraded to higher bit rates in the future without limitations considering PMD.

Cables from the late 1980s until now show low PMD values, well below 0.5 ps/√km. Only individual values are slightly higher.

In older cables from the mid 1980's, high PMD values have been observed, but no values above 1 ps/√km have been measured.

The PMD values are more related to the cable design than to the fibre type. Also the ribbon process could have a considerable impact on the

PMD; considerably higher PMD has been observed in the inner fibres than in the outer ones. Further studies will be required to show whether this position-dependence could be an important parameter controlling the ribbon process.

ACKNOWLEDGEMENTS

I would like to thank Stig Karlsson, my colleague during all the measurements, with whom I travelled thousands of kilometers through our country. I would also like to thank Erland Sundberg at Telia Research for valuable viewpoints regarding the content and wording of this contribution. Many thanks also to Lars Sundeman and Jan Björkman for valuable support from the very beginning of this project.

REFERENCES

1. N. Gisin, J.P. Von der Weld and J.P. Pellaux: Polarization Mode Dispersion of Short and Long Single-Mode Fibers, J. of Lightwave Tech, Vol. 9, 821, 1991
2. N. Gisin, Polarization Mode Dispersion: Definitions, Measurements and Statistics, Symposium on Optical Fiber Measurements, Boulder, 1994
3. B. Arvidsson, H. Mickelsson and K. Brising: A practical comparison between two different PMD measurement methods, Symposium on Optical Fiber Measurements, Boulder, 1996
4. N. Gisin, B. Gisin, J.P. Von der Weld and R. Passy: How accurately can one measure a statistical quantity like Polarization Mode Dispersion?, to be published
5. A. Galtarossa and M. Schiano: Polarization Mode Dispersion in High-Density Ribbon Cables, OFMC 1993

AUTHOR

Kim Brising
Telia Network Services
Farsta
Sweden



Kim Brising obtained his MS degree in engineering physics from Chalmers University of Technology in 1981. He has worked several years within the fibre optic cable industry. He joined Telia in 1994, and is now working with fibre-optic cable related subjects and measurement techniques.

SIMULATION OF SYSTEM LENGTH LIMITATIONS INDUCED BY PMD

**D. Gallagher, G. Wildeman
W. Jackman, M. Fedoroff**

**Corning Incorporated
Siecor Corporation**

ABSTRACT

Polarization Mode Dispersion (PMD) is a factor to be considered when designing long-haul, high-data-rate digital systems. This dispersion mechanism varies with time and does not fit easily into traditional system performance prediction procedures. A technique has been developed to predict the range of system performance from a population of PMD values. In this paper the technique is explained and demonstrated using a population of PMD measurements made on production Siecor stranded loose tube cables, containing Corning SMF-LS™ fiber. This technique also can be used to evaluate the sensitivity to variations in system assumptions or budgeting. For purposes of this demonstration of PMD limitations, other sources of system degradation are treated as constants. The model can be expanded to incorporate other length dependent, or incrementally increasing, system limiting factors.

BACKGROUND

The recent development of commercially available fiber amplifiers allow long unregenerated system lengths. This technology, combined with the development of

high-data-rate systems, has converted Polarization Mode Dispersion from a classroom theoretical study into a critical factor in the design of optical fiber systems. PMD has unusual statistical properties which complicate dispersion budgeting. [1,2,3,4,5]

INTRODUCTION

The problem solving approach used in this analysis can be broken down into three primary components. First, system and hardware sensitivity is investigated to estimate a target for total allowable dispersion due to PMD. [6] Because single channel 40 gigabit systems are not yet available commercially, it is necessary to make assumptions about high-data-rate system configurations. Second, a series of assumptions and rules is developed to determine the relationship between individual fiber PMD values and concatenated system performance. And third, Monte Carlo simulation is used to predict the system length limitation based on a population of cabled fiber PMD values and the final system PMD target.

The output of the simulation is the distribution of system lengths at which the PMD target has been

reached using randomly selected fiber PMD values. To understand the relative importance of system parameters, changes are introduced to these parameters and the change in simulation output analyzed. For the sensitivity analysis, only the minimum, median and maximum lengths are reported.

Concatenation Rules and Assumptions

Assumptions must be made concerning the relationship between a set of individual cabled fiber PMD measurement values and the expected performance of the concatenated system over time.

1. ***Variability of Fiber PMD*** It is assumed that each cabled fiber has random variability which can be described by a Maxwellian distribution.[7] Each measurement of PMD is considered to be an estimate of the mean of that Maxwellian distribution. In this simulation, the term "variability factor" is used to represent the ratio of a "worst case" PMD of a fiber to its mean.

2. ***Concatenation*** The simulation uses addition in quadrature to predict the PMD of a concatenated link from the constituent fibers and the fiber amplifier's PMD values. [8]

3. ***Variability of the Concatenated Link*** It is assumed that the PMD of the concatenated link has variability which can be described by a Maxwellian distribution, defined by a

mean equal to the quadrature sum of the component fiber PMD values.

4. ***Variability of the Fiber Amplifier in the System*** It is assumed that the fiber amplifiers in the system have non-random, deterministic PMD.

Monte-Carlo Simulation Description

Monte Carlo simulation is a proven technique for quantifying the probability distribution of outcomes for a distribution of input values. This analysis begins with a baseline set of system parameters and the PMD measurements of a population of cabled fibers. The simulation quantifies the probabilities associated with the concatenated length at which these inputs create limitations due to PMD.

The PMD budget, τ_{MAX} , is calculated by multiplying the bit period (the inverse of the data rate) by the bit fraction (the fraction of the bit period budgeted for PMD). The resulting value represents the worst case PMD excursion allowed with the given system parameters.

Equation 1 calculates τ_{SYS} , the cumulative system PMD, as sequential fibers are added. When this value reaches τ_{MAX} , the system length is appended to the output length distribution, until ten thousand system lengths have been generated.

$$\tau_{\text{sys}} = \left[\sum_{i=1}^n (\tau_{\text{fi}} \times V \times \sqrt{L_c})^2 + \tau_a^2 \times \text{INT} \left(\frac{n \times L_c}{L_A} \right) \right]^{\frac{1}{2}} \quad (1)$$

Where:

- τ_{sys} = cumulative system PMD
- n = current number of concatenated lengths in the span
- τ_{fi} = normalized fiber PMD of the "i" th fiber
- V = variability factor
- L_c = cabled fiber length
- τ_a = amplifier PMD
- L_A = amplifier spacing
- INT = the integer function

The cabled fiber length (L_c), the amplifier PMD (τ_a) and the amplifier spacing (L_A) are treated as constants within each simulation.

Simulation Inputs

The PMD data used to demonstrate the simulation were generated from Jones Matrix measurements [9,10] made on production Siecor stranded loose tube cables containing Corning SMF-LS™ fiber. This Monte Carlo simulation requires PMD measurements from a population of at least one hundred cabled fibers for repeatable output. For the examples presented in this study, measurements from more than five hundred cabled fibers were used.

After evaluating the predicted ranges of the system parameters, and theoretically predicting the system sensitivities to changes in

the parameters, a baseline set of Monte Carlo input values for the demonstration, shown in Table 1, was established. For some of the parameters, such as cable length, bit rate and variability factor, conservative baseline values were selected. For instance, twelve kilometer cabled fiber lengths are not routinely installed, and 40 Gbps system components are not available commercially.

After the baseline model was run, the system was studied for sensitivity. Each parameter under study was iterated through the sensitivity variations listed in Table 1, using the baseline values for the other parameters.

Table 1: Monte Carlo Simulation Inputs

Parameter	Amplifier Spacing (km)	Amplifier PMD (ps)	Cabled Fiber Length (km)	Bit Rate (Gbps)	Bit Fraction (%)	Variability Factor
Baseline	120	0.25	12	40	25	4.2
Sensitivity Variations	80	0.05	4	5	10	3.0
	90	0.10	8	10	15	3.6
	100	0.20	16	20	20	
	110	0.50			30	
		1.00				

RESULTS

Baseline Results. The distribution of PMD limited system lengths shown in Figure 1 was generated using the baseline system parameters described in Table 1. The authors believe that there are other sources of degradation which limit systems to much shorter lengths. The regularly spaced higher frequencies show the incremental length limitations caused by the PMD of the fiber amplifiers. This "comb" effect becomes stronger as the fiber amplifier's PMD increases.

Sensitivity Results. The results can best be understood in relation to the contribution of the varied parameters to τ_{MAX} or τ_{SYS} in the simulations.

Contributors to τ_{MAX} . Bit rate and bit fraction are both direct contributors to τ_{MAX} and would be expected, from the definition of τ_{MAX} and Equation 1, to have a square root relation to the system length. The sensitivity analyses for bit rate (Figure 2) and

bit fraction (Figure 3) show that relationship. The system length is inversely proportional to the square root of the bit rate and directly proportional to the square root of the bit fraction. This response is a direct result of the use of addition in quadrature to predict concatenated PMD.

Fiber Contributions to τ_{SYS} . The summation term in Equation 1 is the fiber contribution to the system PMD. This term is directly proportional to the variability factor within the term. The results for the variability factor sensitivity (Figure 4) show decreasing system length with increased variability factor. For negligible amplifier PMD, the other term in Equation 1 would become zero and the system length would be inversely proportional to the square root of the variability factor. Figure 4 shows the relationship to be slightly less than square root proportional because of the finite amplifier PMD used in the baseline parameter values.

As expected, the sensitivity analysis of cabled fiber length (Figure 5)

shows that median length performance is independent of the cabled fiber length value. The variability in the system length distribution, however, is reduced by decreased cable length; there are more discrete cabled fibers in each system length and the impact of fibers in the extremes of the population is reduced.

Amplifier Contributions to τ_{SYS} . The sensitivity of system length to amplifier PMD (Figure 6) shows little variation until amplifier PMD approaches 1 ps. This non-linear response is predicted by the squared amplifier PMD value in the amplifier term of Equation 1. In that term in Equation 1, the number of amplifiers in the system is inversely proportional to the amplifier spacing. For the moderate amplifier PMD used in the baseline case, the decrease in system PMD with increased amplifier spacing (Figure 7) is visible but small. The system length is more sensitive to a change in amplifier PMD than to a similar change in amplifier spacing.

FINAL COMMENTS

The authors have presented a technique to characterize the probability of PMD induced length limitations in high-data-rate, digital systems. The model includes inputs for the expected PMD variability as well as variable system design parameters.

This technique has been demonstrated using a set of sample parameters and a population of cabled fiber PMD measurements from production Siecor stranded loose tube cables containing Corning SMF-LS™ fiber. These results show that for this fiber population, if PMD were the only limiting factor, system lengths in excess of 1000 kilometers could be achieved. Other factors will cause system length limits to be much shorter than this.

In addition, the sensitivity analysis indicates that cable length, amplifier spacing and amplifier PMD under 1.0 ps have little impact on the overall system length. Other factors having a direct square root relationships are the bit rate, variability factor and bit fraction.

REFERENCES

1. D.A. Nolan and D.Q. Chowdhury, "Mode Coupling Model for the Jones Matrix Eigenanalysis Method," NIST Special Publication 864, 1994.
2. A. Galtarossa, et al., "Polarization Mode Dispersion in Long Single-Mode Fiber Links: A Review," Fiber

and Integrated Optics, Volume 13, pp. 215-229.

3. F. Curti, et al., "Statistical Treatment of the Evolution of the Principal States of Polarization in Single-Mode Fibers," Journal of Lightwave Technology, Vol. 8, No. 8, Aug. 1990.

4. Y. Suetsugu, et al., "Effects of Random Mode Coupling on Polarization Mode Dispersion and Power Penalty in Single-Mode Fiber Systems," *Optical Fiber Technology* 1, pp. 81-86, 1994.

5. F. Curti, et al, "Concatenation of polarization mode dispersion in single-mode fibers," *Electronic Letters* 25,(1989) 290-292.

6. A.F. Mitchell, J.V. Wright et al, "The Future of Optically Amplified Submarine Systems," *Sub-Optique Conference*, 1993.

7. F. Matera and C. G. Someda, "Random Birefringence and Polarization Dispersion in Long Single-Mode Optical Fibers, " *Anisotropic and Nonlinear Optical Waveguides*, Elsevier, 1992.

8. D. Gallagher, et al, "Cable and System PMD Prediction, " *Proceedings of the Forty-Fourth IWCS* (1995), pp. 366-371.

9. D.Q. Chowdhury and D.A. Nolan, "Quantitative Comparison Between the Jones Matrix Eigenanalysis & Wavelength Scan Method for Polarization Mode Dispersion Measurement: A Simulation Study," *NIST Special Publication 864*, 1994.

10. B.L. Heffner, "Accurate, automated measurement of differential group delay dispersion and principle state variation using Jones Matrix Eigenanalysis," *IEEE Photonics Technology Letters*, Vol. 5, No. 7, pp. 814-817

AUTHORS

Dan Gallagher has been with the Telecommunications Products Division of Corning Incorporated since 1986. He currently is the Supervisor of Optical Measurements at the Center for Fiber-Optic Testing. In the past, Gallagher has worked in Product and Process Development in Corning's Wilmington, N.C. manufacturing facility and as a project manager in Product Engineering in Corning, N.Y. He has a Bachelor of Science in Mechanical Engineering from the University of Iowa.

George Wildeman is a marketing manager in Corning's Opto-Electronics Group, responsible for amplifier and components products marketing activities in the telephony market. Wildeman joined Corning's Optical Fiber Business in 1990 and transitioned to Corning's Component Product Business in 1996. Previous to Corning, Wildeman spent five years as a systems engineer providing support for several Navy and NASA satellite communications programs. Wildeman holds a M.S. Electrical Engineering degree from Johns Hopkins University and a B.S. Electrical Engineering degree from Ohio State University.

William S. Jackman received a Bachelor of Science in Engineering Science from Montana State University in 1972. Since he joined Siecor in 1981, he has been heavily involved with measurements and performance modeling. Jackman

has been a Senior Product Evaluation Engineer in Siecor's RD&E facility since 1992.

Mike Fedoroff received his B.Sc. in Mechanical Engineering in 1987 from the University of Saskatchewan and M.Sc. from the same institution

in 1990. Since joining Siecor's Optical Cable plant in Saskatoon, Canada, Fedoroff has primarily been involved in optical cable development and testing. Other activities include a six-month assignment to support International sales in Europe.

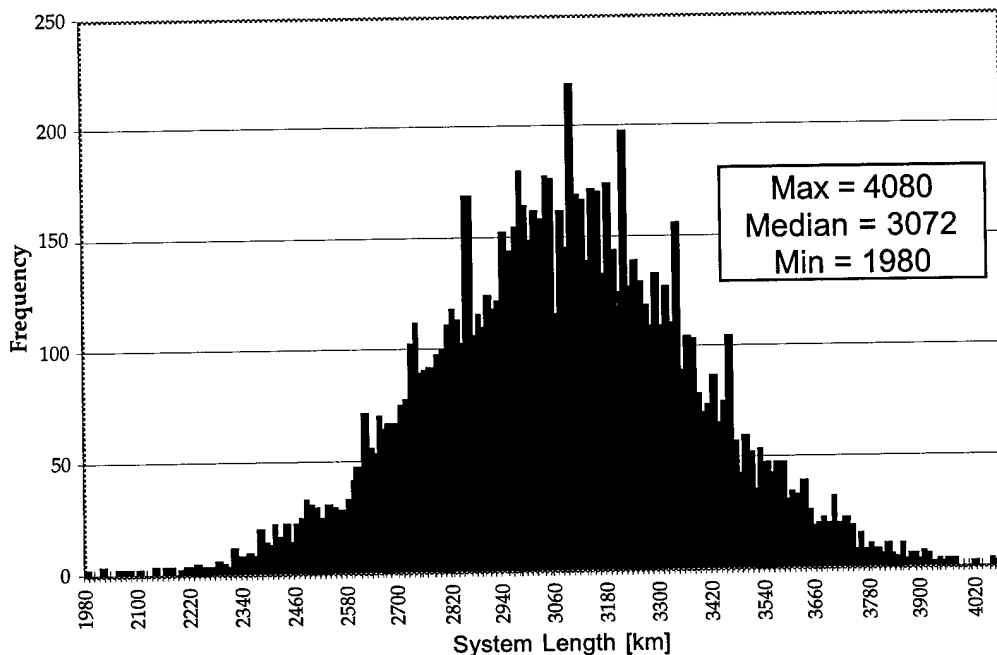


Figure 1: System Length Distribution from Baseline Model Inputs

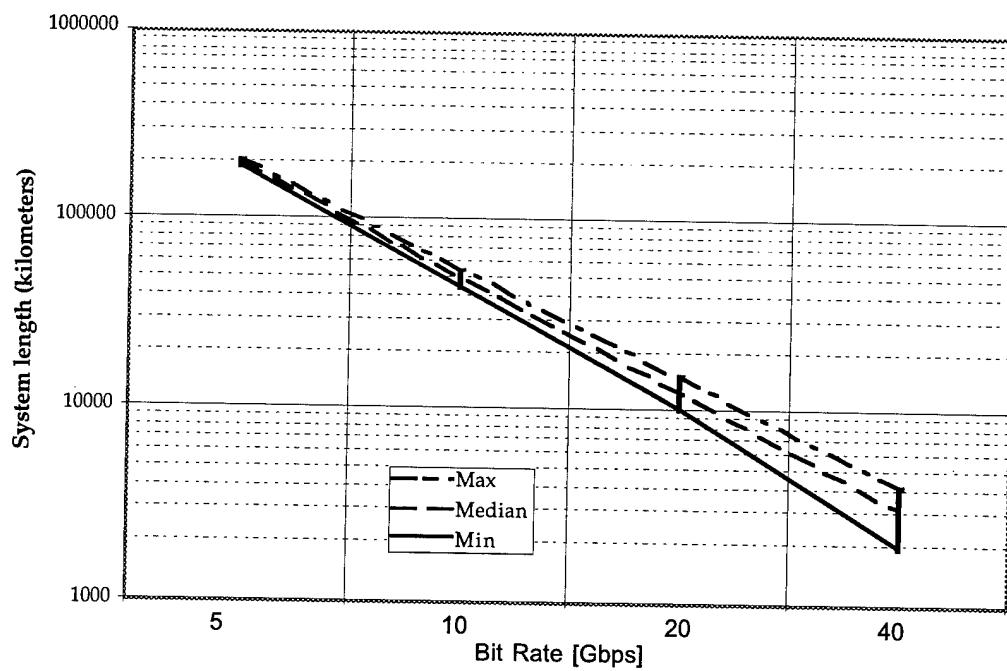


Figure 2: Bit Rate

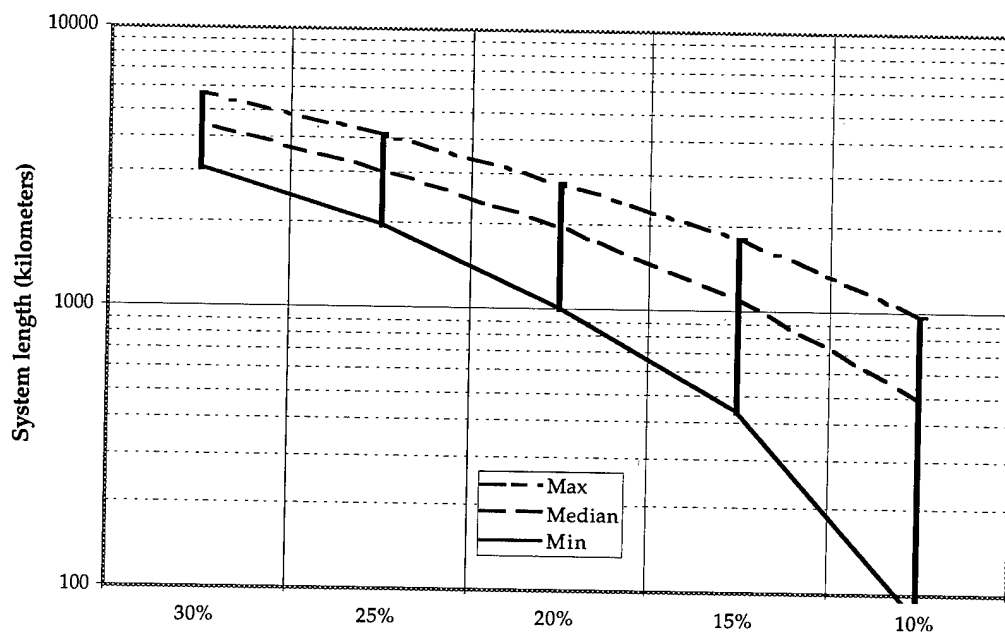


Figure 3: Bit Fraction

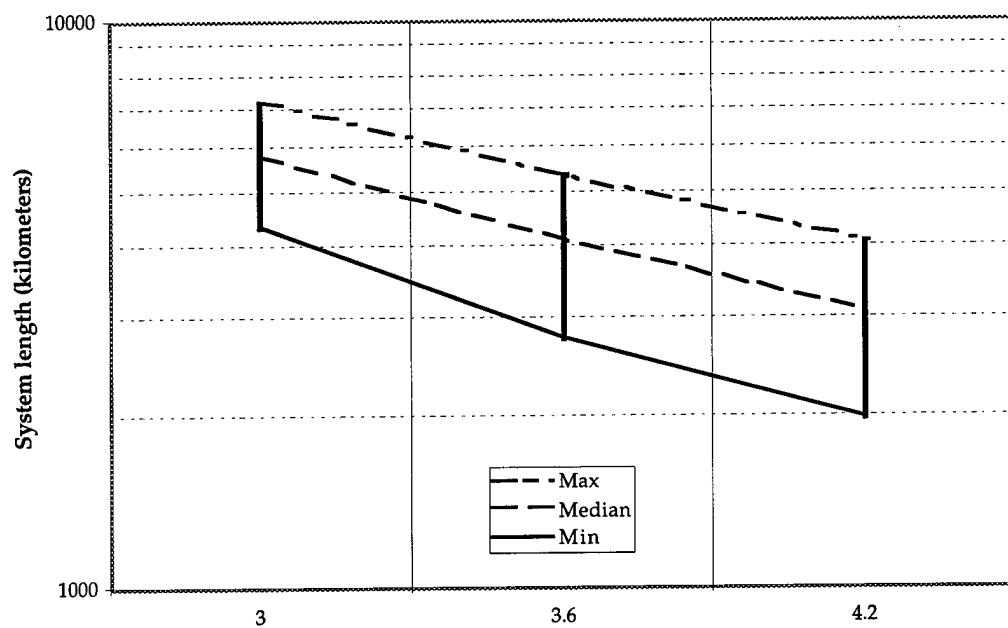


Figure 4: Variability Factor

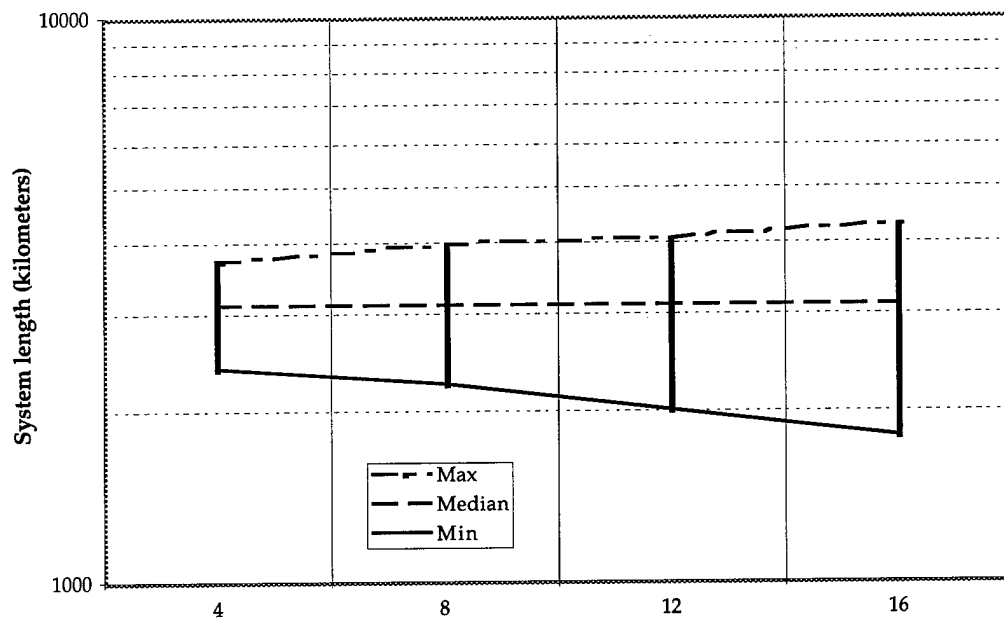


Figure 5: Cabled Fiber Length [km]

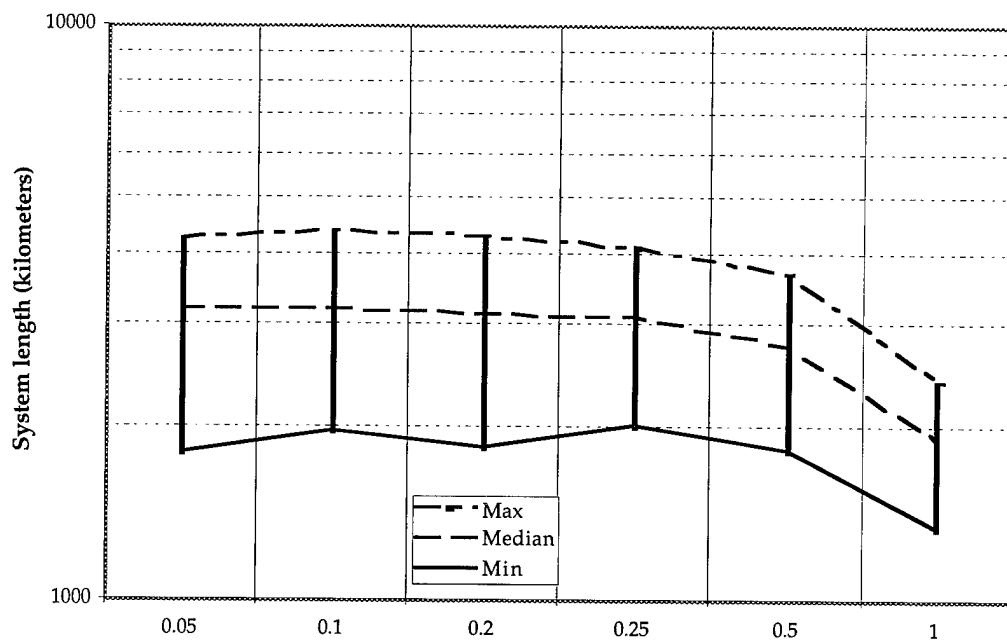


Figure 6: Amplifier PMD [ps]

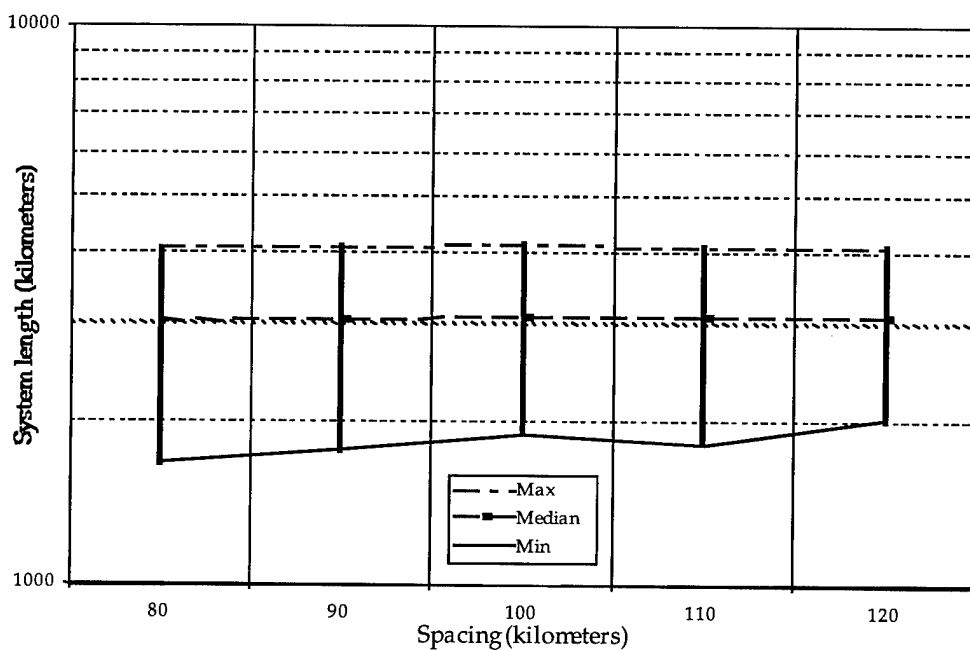


Figure 7: Amplifier Spacing [km]

Characterization of Optical Groundwire's Cabled Polarization Mode Dispersion Performance as a Function of Axial Strain and Temperature: A Case Study

R.C. Roman, Alcoa Fujikura Ltd., Spartanburg, SC 29304
Mark L. Lundergan, Corning Incorporated, Corning, NY 14831
Sheila A. Cooper, Corning Incorporated, Corning, NY 14831

ABSTRACT

Experiments have been conducted to examine polarization mode dispersion (PMD) in two optical groundwire (OPT-GW) cable designs. OPT-GW cables are designed for use by electric utilities and provide both system ground protection and fiber-optic telecommunications capability.

Testing included PMD as a function of manufacturing, tension and temperature. PMD was measured during each step of the OPT-GW manufacturing process. Long-length tension tests were performed on approximately one km lengths of each cable design. The cables were installed and tension testing performed on outdoor structures. In this study, PMD, length and attenuation were measured at discrete axial tensile loads. Additionally, a temperature cycling and thermal aging test was performed on the cables.

Results show the OPT-GW cables are capable of very low fiber PMD using a 245 micrometer acrylate coated non-zero dispersion-shifted (NZ-DSF) fiber design. Measured PMD change during cable manufacture is minimal and measured PMD change at very low temperatures is very slight. Results also show tensioning of the two OPT-GW cable designs, well beyond their intended installation and service stress values, resulted in no increase in fiber PMD.

INTRODUCTION

Very high data rate time division multiplexed (TDM) systems are becoming increasingly practical with the availability of new high speed optical components, electro-optic

components and fiber designs such as NZ-DSF. One of the many system performance parameters in such a high data rate system is PMD. In order to quantify the impact of cabling on fiber PMD performance and to study fiber PMD in its installed and deployed state, the cable and fiber manufacturer studied PMD in two OPT-GW cable designs and in two simulated OPT-GW installations.

It is recognized that PMD increases in proportion to fiber birefringence (1), and that a tight structure, controlled fiber strain cable design such as an OPT-GW cable, may give rise to extrinsic fiber birefringence caused by anisotropic stresses along the cable's length.

To quantify the effect of this external birefringence on fiber PMD, experiments were carried out simulating expected worst-case environmental and mechanical stress conditions. Testing of NZ-DSF fiber in OPT-GW cables included, for the first time, PMD performance as a function of axial strain as measured in an installed state and PMD performance as a function of temperature. Other attributes such as attenuation, length and strain were monitored to further the understanding of this fiber in a tight structure OPT-GW cable.

CABLE DESIGN, APPLICATION and ENVIRONMENT

OPT-GW cable is designed for use by electric utilities and serves the dual purpose of providing both electrical system ground protection and fiber optic communications capability. OPT-GW cables must protect the electrical transmission system from lightning damage and fault current conditions. The

cables are designed for long length aerial spans on "high-tension" towers. Optical fibers are placed inside the cables to provide for data, voice and video communications capability.

The typical cable designs are illustrated in Figure 1. OPT-GW cables are made of three primary components; the optical fiber "units", the aluminum pipe, and stranded aluminum clad steel and aluminum alloy wires. Twelve optical fibers are stranded and encapsulated around a central member in each fiber unit. The fiber units then are cabled or bundled. Two of the test cables contained three 12-fiber units (36 fibers total) and the other two contained four 12-fiber units (48 fibers total). Both cable designs are very common.

The bundled units then are placed in an aluminum pipe using a continuous forming, welding and diameter reducing process. The pipes are different in size to accommodate different fiber counts. The pipe provides hermetic protection from the outside environment. Finally, aluminum-clad steel and aluminum alloy wires are stranded around the pipe. The wires provide the electrical properties of the cable and also provide the required tensile strength.

A typical operating environment for this type of cable is characterized by significant variation in cable temperature and axial strain during its lifetime (2). The cable is installed in the open and can experience extreme temperature, wind and ice loading stresses throughout a given year.

THE EXPERIMENT

To understand the fiber PMD performance of OPT-GW cables, the cables were tested:

- During cable manufacture
- As a function of tension
- As a function of temperature

Each fiber was tested before cabling and at several points during the cabling process. Of the four cables manufactured in this experiment, two were selected for temperature cycle testing and two were used for long length tension testing.

PMD measurements were made using both Wavelength Scanning (Fixed Analyzer) and Jones Matrix Eigenanalysis (JME) techniques, with excellent agreement between the two. All PMD values reported in this paper show the change in quadrature (RMS) average for all fibers in the cables. All attenuation and length measurements were performed with standard, industry accepted equipment and measurement techniques.

Cable Manufacturing Results

In all, 122 NZ-DSF fibers were processed into four cables: two 36-fiber and two 48-fiber cables. Other "control" fibers (n=46) were included in the cables for comparison and are not included in the analysis. PMD changes (Δ) through the manufacturing process were very slight. Table 1 shows the quadrature average results of the manufacturing process (average Δ of all fibers in one cable design) along with the total number of NZ-DSF fibers in all four cables.

Table 1: Average PMD change in manufacturing process

<u>Cable Design</u>	<u>Quadrature Average (Δ)</u>	<u>n</u>
36 Fiber	0.019 ps/(km) ^{1/2}	53
48 Fiber	0.020 ps/(km) ^{1/2}	69

Tension Test and Results

Long-length tension tests were performed on one-kilometer lengths of OPT-GW cable, of each design. The cables were installed on an outdoor test structure located near Toronto, Ontario, Canada. Using standard attachment hardware in a somewhat non-standard installation configuration, the two cables were positioned such that large amounts of controlled axial tension could be applied. Figure 2 is an illustration of the experimental set up. To enable measurements of PMD, attenuation and

length, the cables were installed in a long loop between several test towers so that the cable ends were accessible at the measurement point.

The optical fiber units inside the OPT-GW cables were directly coupled to the cable's metallic structure to enhance cable-to-fiber strain transfer during tensioning. The goal was to achieve cable-to-fiber strain transfer well beyond that which is expected from "normal" installations.

The cables were installed and measured for length, PMD and 1550 nm attenuation at strains from 10% Rated Breaking Strength (RBS) to 70% RBS. OTDR length measurements were compared to expected strain values for each cable design at each tensioning level to validate that the strain coupling method was transferring as expected.

Table 2 shows average calculated strain for the two cable designs and the average measured strain of all fibers within the two cables tested. This data shows that strain was transferred to the fibers inside the cables.

Table 2: Measured versus calculated fiber strain (average of all fibers measured)

<u>% RBS</u>	<u>Calculated Average Strain</u>	<u>Measured Average Strain</u>
10	0.059 %	0.060 %
30	0.178 %	0.160 %
50	0.298 %	0.268 %
70	0.416 %	0.440 %

PMD and 1550 nm attenuation also were measured at the discrete axial tensile load levels between 10% and 70% cable RBS. The change in PMD as a function of axial load is shown in Figure 3. There were no statistically significant increases in the population of PMD values measured throughout the range of applied loads.

Figure 4 shows the 1550 nm attenuation as a function of tension. All attenuation values were under 0.05 dB/km delta and well under the typical 0.30 dB/km cable requirement. Both results indicate that the fibers were insensitive to tension in these OPT-GW cable designs.

Temperature Cycling Results

The temperature cycling and thermal aging tests were performed using a Bellcore GR-20-CORE profile with modified temperature limits. The modified limits come from typical OPT-GW customer requirements. PMD and attenuation were sampled at the high and low temperature points prior to the thermal aging, at the end of the thermal aging period and at high and low temperatures after thermal aging. The temperature profile is shown in Figure 5.

The PMD versus temperature results are shown in Figure 6. The attenuation versus temperature results are shown in Figure 7. The PMD results show little change over the temperature range with the most notable change at -40°C. As can be seen, the temperature cycling results were well within the typical requirements for attenuation change versus temperature as described above.

CONCLUSION

Results show the OPT-GW cable designs using non-zero dispersion-shifted fibers are capable of satisfactory and functional performance with respect to attenuation and PMD even under adverse conditions. The measured fiber PMD change at tensions from 10% to 70% RBS (0.060% to 0.416% strain) was very small.

These results suggest that significant variations in fiber strain resulting from aerial deployment do not have a negative impact on the overall PMD of the fibers. To the authors, this suggests that external birefringence from expected cable stresses were either below the threshold at which resulting PMD increases can be detected, or, such increases were overcome by

another mode coupling mechanism within the cable/fiber structure.

Temperature dependence results also indicate the two OPT-GW cable designs, tested well beyond their intended installation and service temperature values, perform well with respect to PMD and attenuation. Changes in both attenuation and PMD were minimal with the largest observed change in PMD occurring at the -40°C point.

Statistical modeling and Monte Carlo simulations (3) constructed with this data indicate that OPT-GW cable with NZ-DSF fiber, at today's fastest commercial data rates, is capable of being deployed in long repeater-to-repeater segments with no danger of bit error due to PMD.

ACKNOWLEDGMENTS

Corning Incorporated: The authors thank J. Eugene Brarens, Joseph B. Dempsey and Dan Gallagher for their technical advice, direction and experimental expertise.

Alcoa Fujikura Ltd.: The authors thank Bernd D. Zimmermann, M. Kurt Dallas, John R. Sacchetti, J. Harold Campbell, Lynn Southern, Judy Neale and Bob Roach for their technical and analytical inputs.

Ontario Hydro Technologies: The authors also wish to thank Mike Kastellein, Rod Wolfendale and Craig Pon for their technical expertise and assistance with the long length tension test.

REFERENCES

- 1 Y. Suetsugu, et al., "Effect of Random Mode Coupling on Polarization Mode Dispersion and Power Penalty in Single-Mode Fiber Systems," Optical Fiber Technology, vol. 1, PP 81 - 86, 1994
- 2 M. L. Lundergan, et al., "Mechanical and Optical Functionality of Field-Aged Optical Ground Wire Cable," NFOEC Proceedings, 1996

- 3 D. E. Gallagher, et al., "Simulation of System Length Limitations Induced by PMD," IWCS Proceedings, 1996

AUTHORS



R.C. "Bob" Roman received his BA degree from Newberry College, Newberry, South Carolina in 1982. He has been an associate of Alcoa Fujikura Ltd. since 1985 where he has worked as an Associate Engineer in Research and Development and Quality Engineering Manager. Presently he is Quality Assurance Manager for AFL's Telecommunications Division located in upstate South Carolina. Bob is a member of the American Society for Quality Control and is a Certified Quality Engineer. He also is a member of the Institute of Electrical and Electronics Engineers and a member of the Society of Cable Telecommunications Engineers.



Mark L. Lundergan is a Senior Applications Engineer with Corning Incorporated, Telecommunications Products Division, North American Sales and Engineering. He has been employed within Corning's fiber technology business for over sixteen years. Lundergan received dual technical degrees from Corning Community College and a Mechanical Engineering degree from Alfred University, Alfred, New York.



Sheila A. Cooper is a Senior Product Engineer in Corning Incorporated's Telecommunications Products Division. She received her BS in Physics from Michigan Technological University. She joined Corning at the Center for Fiber-Optic Testing in 1988. Her previous experience includes work with mass splicing technologies and other field applications.

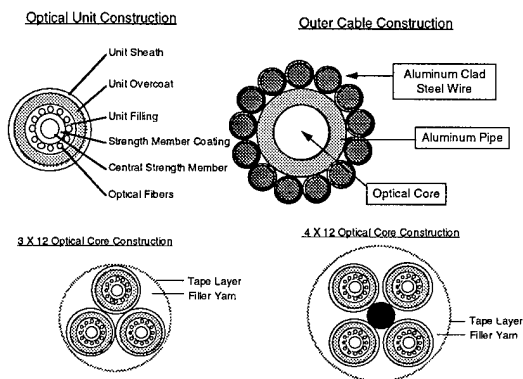


Figure 1 - Optical Groundwire Construction

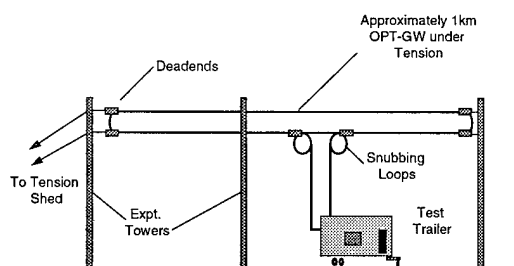


Figure 2 - Long Length Tension Test Configuration

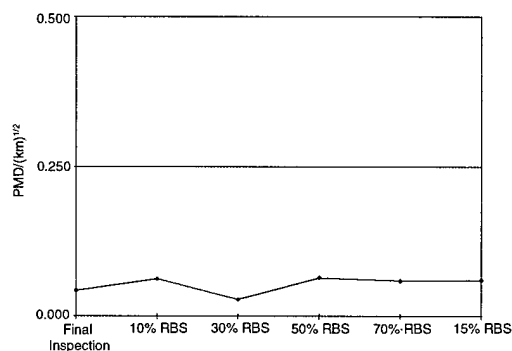


Figure 3 - PMD vs. Axial Load

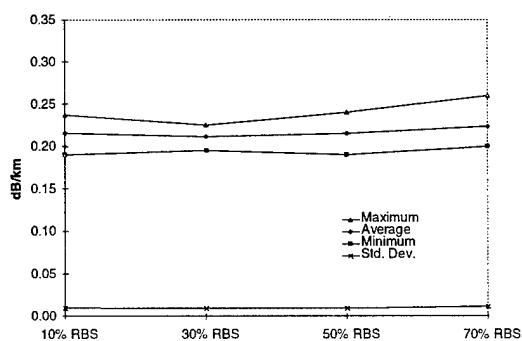


Figure 4 - Attenuation vs. Axial Load

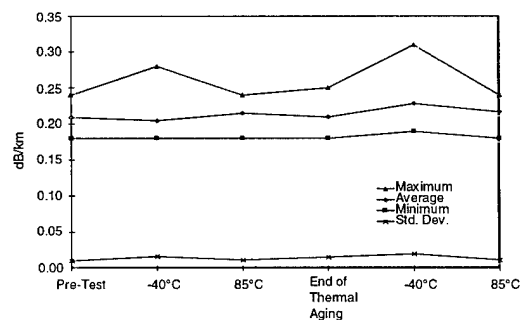


Figure 7 - Attenuation vs. Temperature

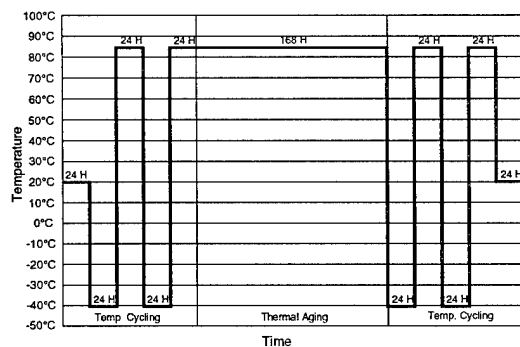


Figure 5 - Temperature Cycling Test Profile

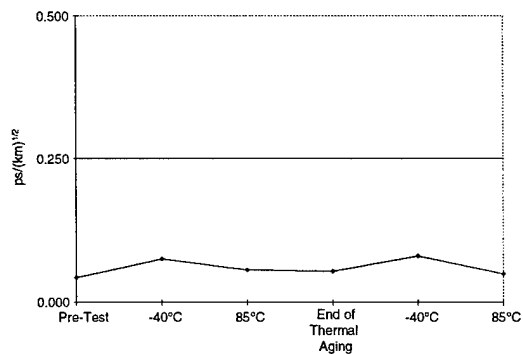


Figure 6 - PMD vs. Temperature

OPTICAL PHASE CONDUCTOR FOR MEDIUM VOLTAGE OVERHEAD POWER LINES

Ralph Böhme, Georg Hög, Michael Hoffart, Ulrich Jansen, Klaus Nothofer

KABEL RHEYDT AG, Mönchengladbach, Germany

ABSTRACT

During the last decade the installation of self-supporting cables in high voltage lines has become more and more important. Well known and often described applications in this field are Optical Ground Wires (OPGW) and All Dielectric Self Supporting Cables (ADSS).^{1,2}

Especially in medium voltage lines which often do not have ground wires, it can be advantageous to implement optical fibers into a phase conductor. This cables will further be called Optical Phase Conductors (OPPC).

The special conditions and requirements for cables, installation and maintenance are described in this paper.

INTRODUCTION

Self-supporting optical cables for use in high voltage lines have been wide spread during the last years. They are basis of independent telecommunication lines of power utilities. The provision of electrical energy in wide areas requires the employment of modern remote data transmission control systems to manage local and temporary variations in energy demand. On the other hand it is of interest for power utilities to build up networks for commercial reasons because of completed or planned deregulations of telecom monopolies. Necessary for such systems are safe connections which allow big transmission rates. Many high voltage lines are nowadays equipped with optical fibers in OPGW and/or ADSS.

In medium voltage lines the situation is a little bit different because most of them do not have an earth wire which can be substituted by OPGW. Additionally the towers of this lines are typically not very high and do not have much space to install ADSS. Another point is often the weak construction which does not allow additional loads. The best way to equip such lines with fibre optics is the use of OPPC. In the past some trials were

made with this technique but it was not fully accepted.³ Since the demand of telecommunication links in overhead lines has rapidly grown the interest for phase conductor applications also increased.

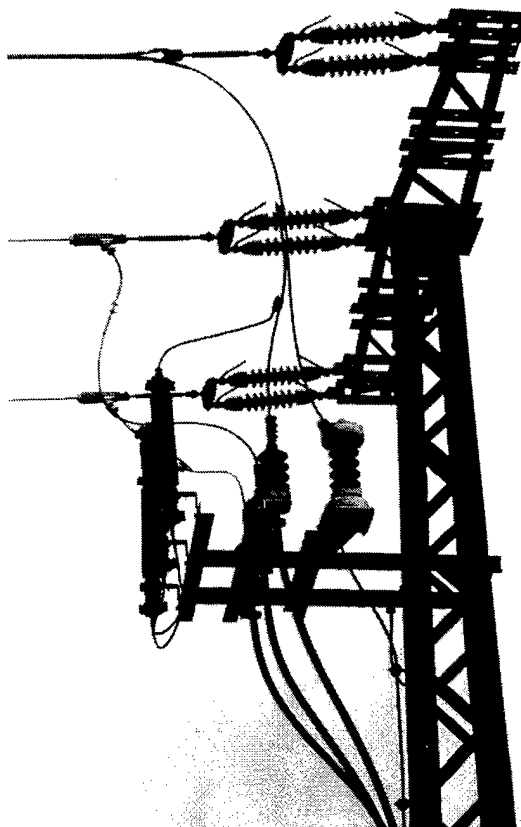


Fig. 1: Termination Tower with Separator

CABLE TECHNIQUE

For optical phase conductor applications it is necessary to have a cable construction which is closest to the conventional one. The resistance of the OPPC should be almost the same as for the phase conductor in order not to cause problems in

the threephase current system. To prevent additional loads on the towers and to ensure sag equality, diameter and mechanical values should also be very similar.

This can excellently be realized by cables with fibres in steel tubes. This construction was often described for use as OPGW.^{1,2} Wellness and reliability has been proven in many installations for several years. The same cable technique is also basis for OPPC applications. Figure 2 shows a comparison of a typical phase conductor⁴ for use in medium voltage lines and the corresponding OPPC.

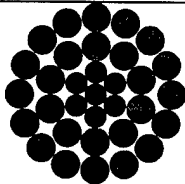
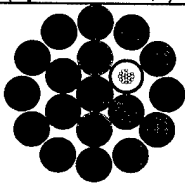
Type	DIN 48204-95/15-Al/St	ASLH-D(S)bb 1x18E9/125 (Ay/Aw 95/12-9,2)
Figure		
Diameter [mm]	13,6	13,9
Weight [kg/km]	383	368
Ultimate Tensile Load [kN]	35,2	42,7
DC-Resistance [Ω /km]	0,306	0,334
Continuous Current [A]	350	332
Coefficient of Thermal Expansion [$10^{-6}/K$]	18,9	20,4
Modulus of Elasticity [N/mm^2]	77	68,6

Fig. 2: Comparison of Standard Conductor with Equivalent OPPW

The construction of OPPC has to be a little different to that of the usual conductor in order to have sufficient space for the steel tube(s). The steel tube has to have minimum dimensions to contain a desired number of fibres with a strain window of at least 0,5%. This is a value which is typically recommended in Germany and many other countries. It ensures that optical fibres are not tensioned in any environmental condition.

Weight, diameter, mechanical and electrical characteristics are very similar so that it is possible to install the cable with sag equality in a wide temperature range. This ensures that the appearance of the line is not changed.

TEMPERATURE LOAD

Performance of the cable

An argument which is often used against OPPC is the permanent loading with high temperatures caused by continuous currents. Such conditions can lead to degradation especially of plastic materials. This is no problem for steel tube cables because the construction does not contain plastic materials.

The optical unit, that means the steel tube with fibres and filling compound is designed to withstand high temperatures for long periods. This was proved several times in temperature tests according to Bellcore standard GR 20. This test includes an ageing period at 85°C for seven days.

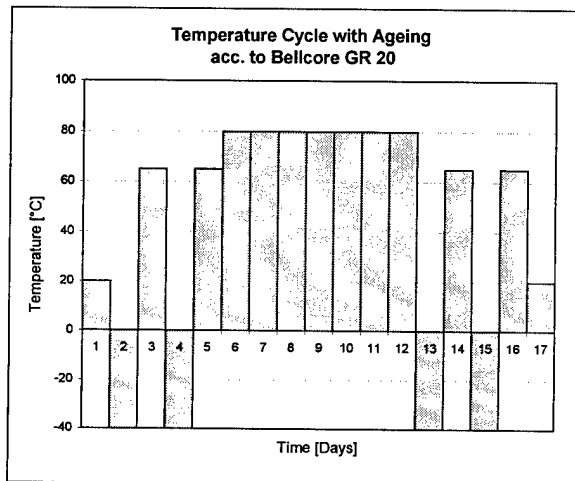


Fig. 3: Temperature Cycling Plan

Above mentioned OPPC was tested in a climatic chamber with the temperatures as shown in Fig. 3. Attenuation was measured with an OTDR at 1240nm and 1550nm. Fig. 4 shows that there is no significant change of attenuation at both wavelengths. The measurement at 1240nm gives an indication whether there is any generation of hydrogen in the cable. Fibres and filling compound are hermetically closed by the steel tube which is a good hydrogen barrier. This ensures that there will be no hydrogen effects over lifetime even at high temperatures.

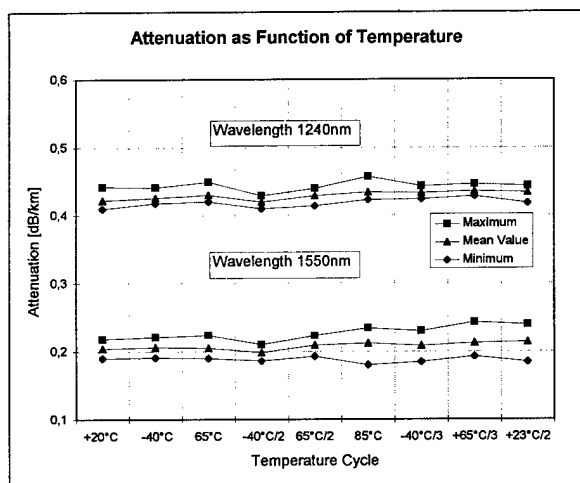


Fig. 4: Attenuation of OPPC as Function of Temperature

In compatibility tests the performance of fibres and filling compound was tested. In the 30 days lasting temperature test the components were continuously heated to 65°C, 85°C and 100°C. Fibres and filling compound showed only slight changes in colour. Fibre strippability and strength remained unchanged. Also the rheological data of the filling compound did not change measurable.

Temperature due to continuous current

There are some calculation methods usual all over the world.^{5,6,7,8} Most of the calculation results of current carrying capacities differ within 10%.⁵ Basis of those calculations is mostly a heat balance equation like from IEC 1597 as follows:

$$P_j + P_{sol} = P_{rad} + P_{conv} \text{ [W]} \quad (1)$$

where

- P_j is the heat generated by Joule effect
- P_{sol} is the solar heat gain by the conductor surface
- P_{rad} is the heat loss by radiation of the conductor
- P_{conv} is the convection heat loss.⁵

Joule effect

Power losses P_j due to Joule effect are given by equation (2)

$$P_j = R_T \cdot I^2 \quad (2)$$

with

- R_T Electrical resistance of the conductor at a temperature T [Ω/m]⁵
- I Conductor Current [A].⁵

From equations 1 and 2 the steady state current carrying capacity can be calculated:

$$I = \sqrt{\frac{P_{rad} + P_{conv} - P_{sol}}{R_T}} \quad (3)$$

Electrical resistance R_T is the temperature and frequency dependent alternate current resistance of the conductor.

Following graphics are based on above mentioned formulas with use of particular calculation methods from various references^{5,6,7,8}.

Radiation

The radiated heat loss P_{rad} is mainly a function of temperature difference between conductor and the environs. Beside this it is dependant from conductor diameter and the condition of the surface. In the calculations for figure 5 it is assumed, that the emissivity coefficient is 0,5, which is the value for an oxidized and slightly soiled aluminium surface.^{6,7}

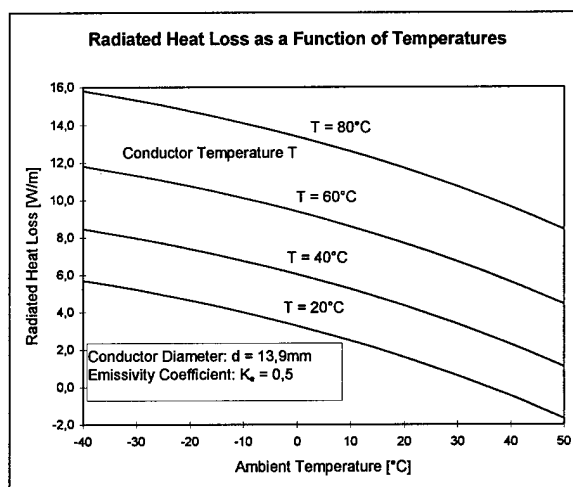


Fig. 5: Radiated Heat Loss

Convection

Convection heat loss mainly depends on the wind speed and the temperature difference between conductor and air. Since some characteristics of the air are also temperature dependant, P_{conv} can not only be described as a function of temperature difference.

In some literature a forced and an unforced convection is distinguished, that means with and without wind. This requires different formulas for this

cases. It is also common to use different calculation methods for laminar and turbulent flow. Fig. 6 is valid for mostly laminar flow.

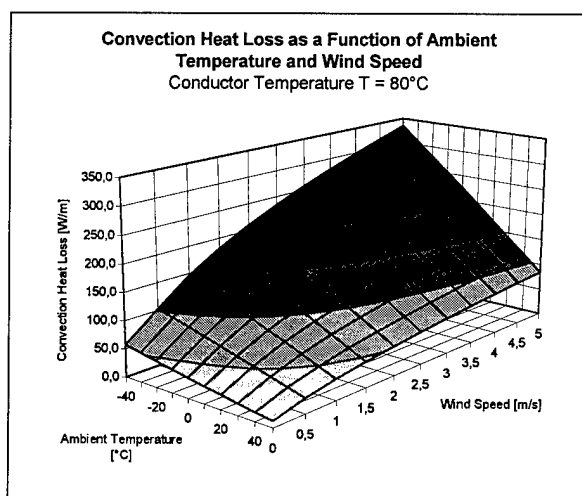


Fig. 6: Convection Heat Loss

Solar Heat Gain

The solar heat gain is a function of intensity of solar radiation, conductor diameter and absorption coefficient. Solar intensity at the border of atmosphere has a value of 1330 W/m^2 in average related to a black body.⁶ Parts of the light are absorbed and reflected. This mainly depends on weather conditions and pollution. Beside this the intensity on earth is a function of ray angle.

Fig.7 shows the heat gain due to solar radiation. The intensity which is given here is meant to be directly at the cable.

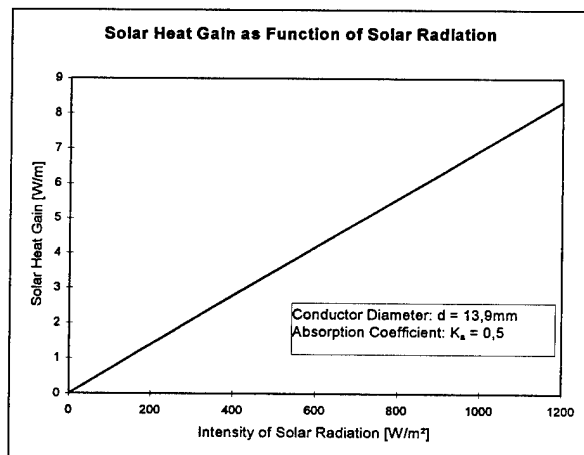


Fig. 7: Solar Heat Gain

For a calculation of the current carrying capacity according to (3) certain limits and preconditions have to be fixed. According to DIN 48204 the maximum conductor temperature shall not exceed 80°C at 35°C ambient temperature and a wind speed of $0,6 \text{ m/s}$. Current frequency is said to be 60 Hz for calculation.⁴

Keeping this current constant for various conditions gives the momentary temperatures of the conductor as shown in Fig. 8. Calculations for this graphic were made with the assumption that the line is permanently operated at maximum load.

The highest temperature of 117°C according to this calculation is reached at 40°C ambient temperature and no wind. A condition with high temperature and no air movement is very rare. Further more phase conductor temperature is a steady state which takes a long time of constant conditions to adjust. Taking this into account it can be assumed that such temperatures are reached very seldom and not for long periods.

For most ambient conditions the conductor temperature is below 60°C .

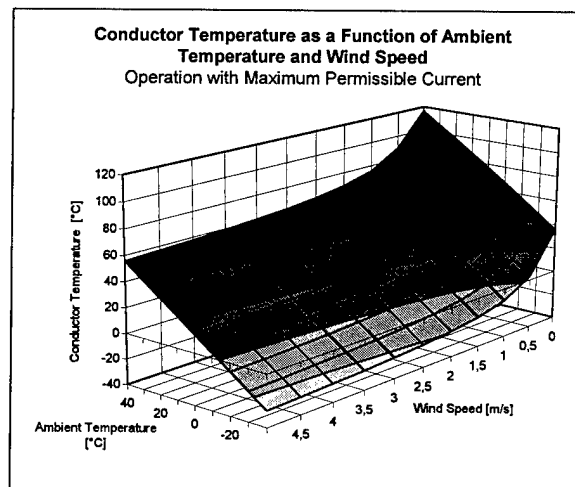


Fig. 8: Conductor Temperature in Operation

INSTALLATION TECHNIQUE

The installation of OPPC in regard to stringing is very similar to that of OPGW. This means in case of steel tube cables that stringing is almost equal to that of usual ropes.

Splice Technique

The technique for splice connections especially at the ends of the line but also in the line has to be different to that of OPGW because of the voltage level.

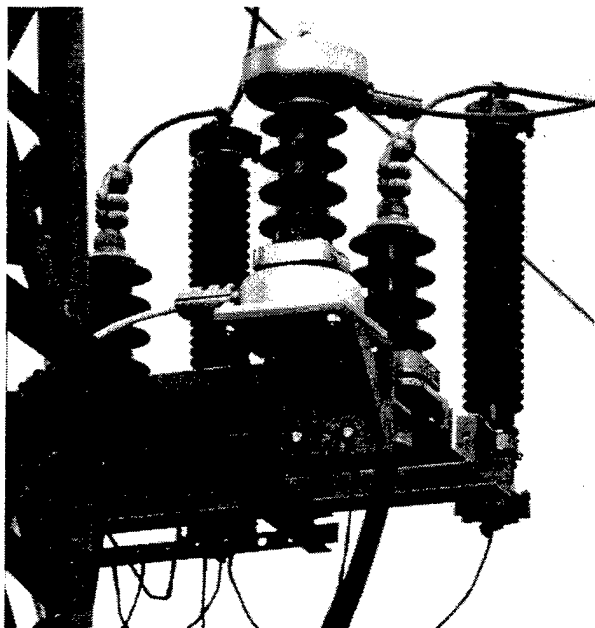


Fig. 9: Separator Installed on a Tower

Separators. In an OPPC electrical current and communication signals are conducted in one cable. Therefore it is necessary to separate them at any point where the communication link is connected with ground level. This happens at both ends of the line, where the optical fibres have to be linked to the terminal devices. (Fig. 9) This can also occur in the line, if a connection to a substation or another line has to be made.

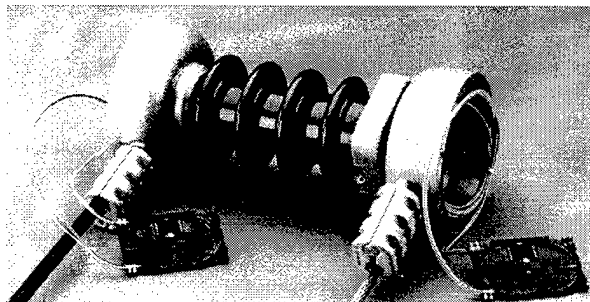


Fig. 10: Separator with Splice Rooms

A separator consists of a porcelain body with two splice rooms at the top and at the bottom. It contains optical fibre bundles which are led through the porcelain body which is foamed with PUR. In the top and bottom part splice cassettes are located for connection of OPPC and approach cable via incorporated fibres.⁹ (Fig. 10)

The unit can either be installed in hanging or standing arrangement.

Joint Closures. For connection of OPPC in the line, joint closures have to be used. They shall have no conducting contact to the tower. This can be realised by placing usual joint boxes on insulators. A more neat solution is to use a box which can be installed without any contact to the tower. This joint box is shown in figures 11 and 12.

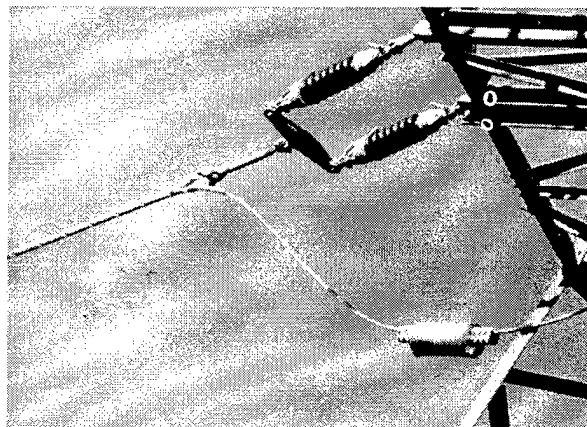


Fig. 11: Joint Closure on Strong Tower

It is connected to the OPPC with parallel groove clamps at strong towers between the insulator strings. This is a part of the line where there are only small longitudinal forces on the cable. So the joint box has mainly the function to house the splices of optical fibres and to conduct the electrical current of the line.

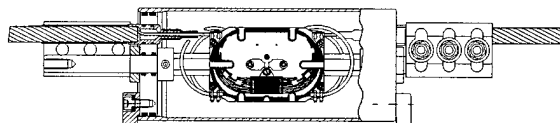


Fig. 12: Drawing of Joint Closure

Cable Fittings

For steel tube cables helically formed fittings are recommendable. They have the advantage of low locally concentrated pressure on the cable and distribute the inlet of the line traction over a longer zone.

At strong poles the fittings consist of a cable guard and a helical dead end.(fig. 1 and 11) It is fixed to the insulator(s) as any other usual clamp. This is a well known solution which has proved its reliability in many OPGW installations all over the world.

At suspension poles armour grip suspensions are used in case of hanging insulators. In this case the installation is also like that of OPGW.

If suspension poles are equipped with standing insulators, as wide spread in medium voltage lines, preformed insulator ties can be used. Such standing insulators can be designed in single or double arrangement which mainly regards to the line forces. If necessary the OPPC can additionally be protected by a cable guard.

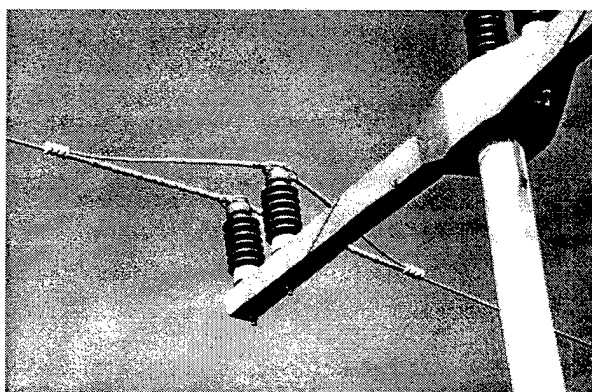


Fig. 13: Suspension Pole with OPPC on Standing Insulators

Conclusion

The installation of OPPC especially in medium voltage lines is a good alternative to other common techniques to equip overhead lines with optical fibres.

The big advantage of this technology is, in case of steel tube cables, that the line gets no additional loads. Reliability is equal to that of OPGW and meet highest demands. Additional costs are only caused by the need of separators at both ends of a line. Compared to the overall system price this extra costs are almost neglectable.

REFERENCES

1. Haag, Hög et al. 'Self Supporting Optical Fibre Aerial Cable Constructions and Related Fibre Parameters for the Transmission at $\lambda=1550\text{nm}$ ', International Wire and Cable Symposium Proceedings 1991, pp. 206-217
2. Haag, Hög et al. 'Optical Ground Wire and All Dielectric Self-Supporting Cable - A Technical Comparison', International Wire and Cable Symposium Proceedings 1994, pp.380-387
3. Haag 'Lichtwellenleiter - Phasenseilluftkabel', Elektrotechnische Zeitschrift etz, Bd. 108 (1987) H. 5, pp. 170 - 176
4. DIN 28204 'Leitungsseile - Aluminium-Stahl-Seile', German standard, April 1984
5. IEC 1597 'Overhead Electrical Conductors - Calculation Methods for Stranded Bare Conductors', First Edition 1995-05
6. A. Webs 'Dauerstrombelastbarkeit von nach DIN 48201 gefertigten Freileitungsseilen aus Kupfer, Aluminium und Aldrey', Elektrizitätswirtschaft Heft 23, December 1963
7. R. Fischer, F. Kießling 'Freileitungen - Planung, Berechnungen, Ausführungen', Springer Verlag Heidelberg, 1989
8. Cigre WG 22.12 'The Thermal Behaviour of Overhead Conductors', Electra No. 144, October 1992, pp. 107 - 125
9. NOKIA KABEL GMBH 'LWL - Verbindungstechnik', Technical Product Description VT-LW-07, 01.95

AUTHORS

Ralph Böhme



Ralph Böhme (42) received his Dipl.-Ing. degree from the Bergische Universität Wuppertal in 1986. He joined KABELRHEYDT in the same year. As a member of the development department for optical fiber cables he is responsible for the development and engineering of all dielectric aerial

al cables (ADSS) cables.

Ulrich Jansen



Ulrich Jansen (32) received his Dipl.-Ing. degree from the Rheinisch-Westfälische Technische Hochschule Aachen in 1990. He joined KABELRHEYDT in the same year. As a member of the development department for optical fibre cables he is responsible for the development of optical

ground wires (OPGW).

Georg Hög



Georg Hög was born in 1950. After studying electronics at the Technische Hochschule Aachen he joined KABELRHEYDT as a development engineer for copper cables in 1977. In 1980 he became responsible for the development of symmetrical telecommunication cables. In 1985 he

became the head of the development department for optical fiber cables. From 1987 to 1988 he was the head of the technical department of BETEFA (special cables for telecommunications). Since 1995 he is responsible for the technical sales department of telecommunication cables.

Klaus Nothofer



Klaus Nothofer was born in 1956. He obtained his Dipl.-Ing. degree from the Fachhochschule Düsseldorf and joined AEG KABEL (now KABELRHEYDT) in 1981 as development engineer for optical fiber cables. From 1984 he was responsible for the optical fiber cable manufacturing technology.

In 1993 he became leader of the Optical Fiber Cable Design Group. He was appointed Manager of Optical Fiber Cable Development and Design in 1994.

Michael Hoffart



Michael Hoffart (39) is General Manager of the Telecommunication Cable Product Group. He received his Dipl.-Ing. degree from the Bergische University, Wuppertal in 1983. He joined KABELRHEYDT on graduation and has been engaged in the fields of optical meas-

urement techniques and telecommunication cables. From 1990 to 1995 he was General Manager of the Optical Fibre and Optical Cable Plant.

Mailing Address:

KABEL RHEYDT AG
Bonnenbroicher Straße 2-14
41048 Mönchengladbach
Germany

HIGH RELIABILITY OPTICAL GROUND WIRE FOR OVERHEAD TRANSMISSION SYSTEMS

R.T. Traut W.F. Wright G.N. Fontaine M.J. Cyr D.P. Dumont

Simplex Technologies Inc., Newington, New Hampshire

ABSTRACT

This paper describes a comprehensive design and development program, which has resulted in the creation of a family of new OPGW designs. These designs provide features that are important to overhead transmission engineers and system planners. The foremost design feature is the long-term reliability of the optical fibers and all components of the new OPGW cables. These cables incorporate well proven robust design elements taken from extensive experience in the design, development and manufacture of deep water transoceanic fiber optic cables. The authors present the OPGW design requirements, design rationale, and a discussion of hardware compatibility. The results from an extensive series of qualification tests are summarized. OPGW installation, application and system requirements are discussed.

I. INTRODUCTION

This paper discusses the design and qualification of two new Optical Ground Wire (OPGW) designs intended to provide a wide range of flexibility in terms of fiber and fault current capacities. Optical transmission reliability is comparable to that of transoceanic submarine fiberoptic cable systems.

Available fiber capacities are 1 to 48 for Design A (Figure 1) and 49 to 144 for Design B (Figure 2).

Fault current capacities are tailored to specific utility requirements by varying the number, size, and conductivity of the outer strand wires.

Both designs incorporate the reliability features and manufacturing techniques used on SL transoceanic fiberoptic telecommunications cables.¹ Due to the cost and down-time (lost revenues) associated with repairing submarine cable systems, their reliability requirements far exceed those economically justifiable for terrestrial systems. The typical availability requirement for a submarine telecommunications cable system is around 99.99%. The typical system reliability budget allocates zero FITs (component failures in 10^9 hours) to fiber and cable. The installed base of SL submarine fiberoptic cables, which currently exceeds 130,000 kilometers, has demonstrated this level of reliability.

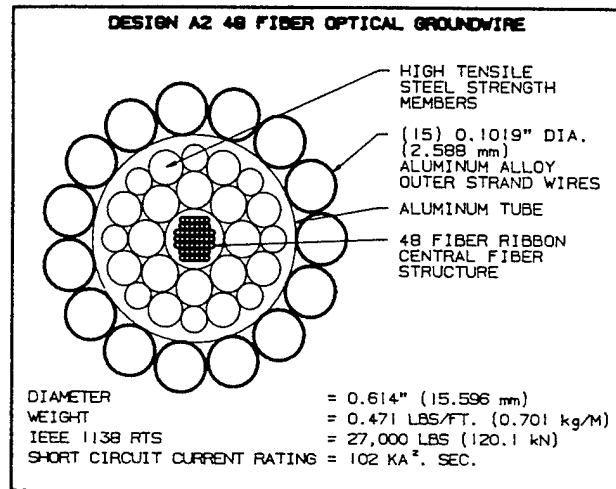


Figure 1 - OPGW Design A2

Some of the key SL cable reliability features that have been incorporated into these new OPGW designs include:

- * High fiber proof test levels to support in-service fiber strain levels
- * Isolation of fibers from microbending and excessive macrobending forces
- * Positive control of fiber strain levels and distribution.
- * High modulus strength member with low residual elongation characteristics
- * Isolation of the optical core from crushing forces
- * Hermetically sealed optical core and strength member
- * Fully waterblocked core and strength member

Other benefits derived from adapting the SL cable's center strength member construction and tight buffered optical core to these new OPGW designs include:

- * High strength to weight ratio
- * Low torque generation
- * Resistance to arc erosion
- * Thermal protection of the optical core
- * Stable optical loss characteristics with changing temperature and tensile loading
- * Efficient cost-effective utilization of materials

In this tight buffer OPGW cable, the Central Fiber Structure is shear coupled to the steel strength members.

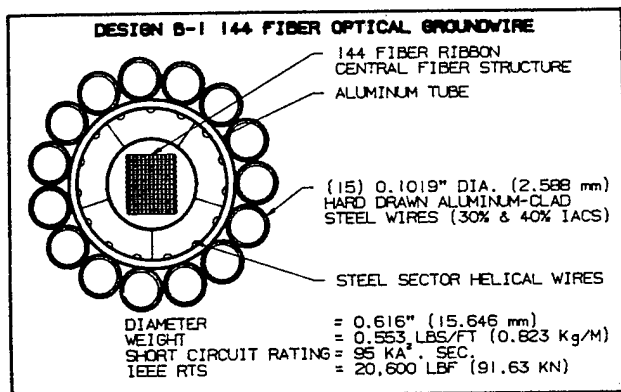


Figure 2 - OPGW Design B1

This design provides a high level of fiber reliability because once the cable's stress-strain characteristics are determined, cabled fiber strain becomes a known and predictable parameter. A conservative fiber reliability assessment can then be made by applying statistically determined values from fracture mechanics theory.

Another superior attribute of this design is the restriction of fiber movement achieved through the encapsulation of the fibers by a benign matrix material. This design eliminates the possibility of fiber crossovers that could occur in a design where fibers have unrestricted movement in a tube or a slot.

II. DESIGN REQUIREMENTS

Reliability of the OPGW cable is the foremost design requirement. For the optical ground wire to perform with high electrical, mechanical and optical reliability over decades of continuous service it must possess certain design characteristics. All design features must work together to provide the three primary system functions required of OPGW. These are: (1) Protection of the optical fibers against lightning damage, over-temperature, hydrogen, radial forces, vibration, non-uniform fiber strain, and excessive axial strain during installation, extreme weather conditions and transient fault currents, and (2) Lightning arc strike capability sufficient to protect all cable components against thermal or mechanical damage during strike severity dictated by the system keraunic zone, and (3) Fault current capacity sufficient to meet or exceed system $\text{KA}^2 \cdot \text{sec.}$ requirements without over-heating, excessive transient sag or compromise of clearances, or damage to any OPGW component, or significant increase in optical attenuation.

Electrical Reliability

The electrical reliability of OPGW is determined by

the provision of the correct cross-sectional area of the metal components, the choice of materials, and the configuration of the components. Since the primary electrical function is the shielding of the power conductor phases, the OPGW must possess an outer stranding material of the right type and of adequate size to prevent any significant lightning arc erosion damage. Significant damage would be any damage which would degrade the future electrical, mechanical or optical reliability of the span. Damage due to lightning arc erosion which is sufficient to part or melt outer wires would be an indication that the OPGW outer strands were underdesigned, or that the lightning magnitude was underestimated for the installation site. The amount of arc erosion damage, for a given OPGW design and lightning stroke waveshape, can be predicted mathematically.^{2,3} In performing arc erosion tests, to accurately produce the effects of the most severe lightning stroke within a given keraunic zone, it is important to test for the long-duration portion of the waveshape. The long-duration portion can produce significant damage on some designs. The short duration portion can be successfully withstood by nearly all designs. A lack of resistance to arc erosion can result in thermal and mechanical damage to underlying components, including the sealed aluminum tube and the optical fibers.

The secondary, but very important, electrical function of OPGW is to have sufficient fault current capacity to prevent transient heating beyond the design temperature. Heating beyond the designed temperature (usually 180°C), could result in long-term degradation of the fiber coating, undesirable increases in optical attenuation, or unacceptable transient sag of the OPGW which could compromise power phase mid-span clearances. Since the OPGW is an inherent part of the electrical ground system, it must be capable of withstanding a high electrical current for a given duration. The industry convention is to express the fault current rating as kiloAmps squared x seconds in order to normalize the rating and avoid confusion regarding the duration. For example, a rating requirement for 24,000 (symmetrical) Amperes for 15 cycles at 60 Hz (0.25 seconds) is equivalent to 144 kiloAmperes squared x seconds. The fault current rating, determined by the system engineer, is generally specific to the system. The selected OPGW design must meet or exceed the fault current rating without exceeding the design temperature.

Mechanical Reliability

The mechanical reliability of OPGW is determined by how well the design is matched to the system environment in which it is installed. The design must

incorporate features which (A) provide sufficient protection to the optical fibers, and (B) prevent damage to the metal components during manufacture, installation and long-term service. The long-term mechanical reliability of the fibers and the metal components are closely related. The stresses within the fibers are influenced directly by the effective modulus of elasticity of the OPGW design, and by the effective axial stiffness (AEC) of the design. In addition, the stresses within the optical fibers can increase significantly over time unless the OPGW design has a low long-term creep characteristic. In addition to providing sufficient steel cross-section within the OPGW design, to produce the desired effective modulus of elasticity and the resulting AEC, the steel configuration is also important in producing a low long-term creep characteristic. In order to provide low creep, the steel strength components should be configured at a low angle of application within the central structure and should be tightly applied without any significant slack. The steel angle of application must be selected to produce good flexibility during manufacture and installation while also providing high crushing stability and impact resistance. In order to hermetically seal the central fiber structure as well as the central steel strength members, the entire central structure should be water-blocked with a non-migrating compound and then enclosed within a continuously axially welded and formed aluminum tube. This tube is primarily to provide sealing against water, but also has important functions as a strong and light-weight binder, a coupling component between the outer strand wires and the central steel wires, and as a contributor to the fault current capacity and the conductance. Depending upon the system requirements, the outer stranding of the OPGW cable should consist of a single or dual layer of wires selected to meet the electrical and mechanical requirements. The material should be either 6201-T81 aluminum alloy⁴ or hard drawn aluminum clad steel⁵ (HDACS) of a selected conductivity, or a combination. In order to minimize cable weight, the lightest wire material that will meet all the electrical and mechanical system requirements should be selected. The outer strand wires are significant contributors to the cable strength and axial stiffness (AEC). After careful analysis of the system span, tension, sag, clearance, elevation changes, short circuit rating, and extreme temperature, wind and ice condition requirements, the OPGW designer can recommend the lightest OPGW design. In all cases, hardware that is compatible with the OPGW design must be selected.

In order to assist in matching or exceeding the sag and clearance maintenance requirements of the system, a low coefficient of linear thermal expansion is

desirable. The lower this value, the less extreme are the sag and tension changes during changing ambient temperatures and during transient short circuit occurrences.

Optical Reliability

Optical reliability of OPGW is, of course, inter-related with electrical reliability and mechanical reliability. The fiber is well-protected when the design requirements, discussed above, are carried out in the OPGW design. With accurately specified system requirements, OPGW designs that positively protect the fibers against any degrading effects are readily available. Designs which securely protect the fibers from excessive axial stress, radial forces, hydrogen, excessive heat and vibration effects prove to be cost effective when they demonstrate the ability to endure over decades of dynamic service. Since fibers are always a significant part of the OPGW cable cost, and account for the majority of the cable cost in higher fiber count designs, it is desirable to ensure that the OPGW design has the inherent design features to provide protection to the fiber under long-term service.

Optical reliability can be divided into two categories. The first, freedom from long-term fracture due to static fatigue, is assured by proof testing of OPGW fibers to a level consistent with well-established experience.^{6,7,8,9} By careful analysis of the cumulative life-time spectrum of tensile stresses occurring on the fibers during manufacture, installation and long-term service, and with conservative design selection, the designer can assure lifetime protection from static fatigue.

Totally coupled "tight buffer" OPGW designs provide the highest degree of strain uniformity and control. Every location on every fiber is permanently under strain control from the moment it is cabled. In addition, encapsulated fibers in these designs are not subject to radial displacement, crossing adjacent fibers (e.g.: microbending), adverse response to aeolian vibration, or axial migration with potential non-uniform axial fiber stresses.

The second category of optical reliability is the requirement for long-term stability of the optical signal attenuation. Cable and system designers expect long-term attenuation stability with no significant increase. In the totally coupled tight buffer designs, this is a result of the permanent positioning of all fibers, thereby eliminating any possibility of the occurrence of the loss increase mechanisms mentioned in the preceding paragraph. Also, with the fibers permanently strain-controlled they are always operating at safe stress levels. It is well known that totally coupled tight buffer designs do not exhibit attenuation increase as a result of the fibers operating constantly at variable safe stress

levels. The new OPGW designs presented in this paper meet the Design Requirements described above as well as the requirements of IEEE-1138-94¹⁰ and system specifications of OPGW users.

Compatibility with Hardware

OPGW must also be fully compatible with system hardware such as dead-ends and suspension hardware. In order to put the OPGW design through the rigorous testing of IEEE-1138-94, and other requirements, the hardware must also be included in the test configuration. In order to qualify hardware for use on an OPGW system, the hardware must also pass qualification specifications¹¹ and any special requirements of the OPGW user.

III. OPGW CABLE DESIGN

Central Fiber Structure

The Central Fiber Structure, located at the center of the cable, is designed to hold a wide range of fiber counts (1 to 144), enables convenient fiber handling, and allows easy fiber identification through the use of fiber optic ribbons.

The Central Fiber Structure is composed of one or more fiber optic ribbons positioned in a symmetrical stack at the center of the structure, which is encapsulated with a urethane acrylate coating material. This coating forms a uniform cylindrical sheath over the fibers which creates a robust fiber handling component. The encapsulant is physically and chemically similar to the optical fiber coatings.

Each fiber in a ribbon is identified via individual color coatings. When multiple ribbons are present, individual ribbon identification can be determined by noting a ribbon's position with respect to the top or the bottom of the stack. This stacked fiber optic ribbon design enables mistake proof identification of each fiber in the structure.

Fiber optic ribbons have achieved widespread acceptance in the fiber optic cable industry. The high fiber packing efficiency that ribbons offer contribute to the design of small diameter, high fiber count cables.¹² To illustrate the high packing efficiency of the tight buffer ribbon construction, consider a 36 fiber loose tube cable core constructed of six, 3 mm dia. loose tubes around a 3 mm central member which has a cross-section area of 64 mm², in comparison to a compact 36 fiber ribbon core constructed with six, 6 fiber ribbons, which has a fitted circle cross-section area of approximately 5 mm². The cross-sectional area of the stacked ribbon package offers a significant space savings compared to the loose tube structure.

The "edge bonded" fiber optic ribbons used in this

construction, consist of multiple fibers (typically an even number up to a maximum of 12), which are placed in contact, side by side, in a common plane. A thin layer of coating material bonds the fibers together and creates an encapsulation over the fibers to form a smooth coating layer. The encapsulation material in an edge bonded ribbon typically adds 1 to 2 thousandths of an inch over the dimensions of the colored fibers.

The Central Fiber Structure (CFS) is engineered to provide performance characteristics that enhance long term fiber reliability and provide desirable fiber handling qualities. Some important features of the CFS include:

1. A tight buffered structure that offers a high degree of fiber protection.
2. The UV-curable acrylate encapsulant is readily mechanically stripped to access the fiber optic ribbons.
3. Fiber optic ribbons that offer easy fiber identification, accessibility and efficient splicing for crafts people.
4. Excellent long term oxidative and hydrolytic stability of the UV-curable encapsulant.

The Central Fiber Structure in this "tight buffer" OPGW cable is shear coupled to the cable's steel strength member package, therefore the fibers experience the same strain as the cable. Since cable loads (and strains) can be predicted, the fiber's strain environment can be predicted. Proper design of the OPGW cable permits fiber strain to be controlled to a conservatively low level and thus ensure fiber reliability. The high packing density of ribbonized fibers in the unit also enhances the cable's light weight and small diameter. This Central Fiber Structure and tight buffer cable design have their origins in an undersea cable design where robust, high reliability performance characteristics are demanded.

Fiber reliability, (i.e.: the conservative prediction of fiber integrity over a specified lifetime), is achieved in the OPGW cable by eliminating critical fiber flaws, and by protecting the fibers from detrimental levels of axial stress, corrosive chemicals, or other environmental factors that would promote subcritical crack growth in the fibers while in service.

To ensure that the optical fibers are capable of achieving their expected reliability rating, each fiber is proof tested to a value that insures the elimination of critical, life shortening flaws. The flaws that remain after proof testing are subcritical and thus fracture mechanics theory allows fiber reliability to be predicted in accordance with statistical models. Additionally, cumulative effects of the cable's in-service environmental factors (installation tension, temperature extremes, wind and ice loading, shunt fault effects, etc.)

are taken into consideration to establish a fiber reliability prediction.

Central Strength Member

The central strength member provides most of the tensile strength for the OPGW. It provides mechanical, thermal, hermetic, and arc-erosion protection for the optical core. It also mechanically couples the optical core to the rest of the ground wire structure, which is essential for control of fiber strain and to prevent pull-in of the central fiber structure at the ends of the ground wire during installation and service life.

Design A utilizes the high tensile steel strength wire package from the SL submarine cable design, which consists of three wire sizes that lock up to form a vaulted structure with high resistance to distortion and crushing. This strength package has been verified to protect the optical core from hydrostatic pressures in excess of 10,000 psi and asymmetric crushing loads in excess of 550 lbf/in.

To accommodate the larger optical core for the 49 to 144 fiber OPGW options, Design B utilizes a solid sector steel tube having cross-sectional area, tensile strength, and outside diameter similar to the strength wire package for Design A.

A welded EC grade aluminum tube is formed around the strength member for both designs. This tube is swaged into the outer interstices of the steel wire package for Design A or slots in the outer surface of the steel sector wires for Design B to ensure load transfer from the aluminum and aluminum clad outer wires to the steel center strength member. This load transfer mechanism has proven to be highly reliable in SL submarine cables under extreme dynamic loading conditions.

Outer Strand Wire Structure

The OPGW designs shown in Fig. 1 and 2 are representative of two families of designs. Other designs within the groups are tailored to meet specific system requirements related to span lengths, sag and tension requirements, fault current rating, lightning severity, or other requirements unique to the system. Generally, these cables use either a single or dual wire layer design in order to meet the system requirements while keeping weight and cost as low as possible. In the case of dual wire layers, the layers are applied in contrahelical lay directions. Such designs are generally either very low in torque generation or torque balanced. A torque balanced design will exhibit virtually no free end torque or rotation during installation.

The outer strand wires are the primary protection of the aluminum tube against lightning arc erosion. In some keraunic zones it is desirable to include more steel

in the outer strand wires to prevent arc erosion damage.

In these new OPGW cables, the outer strand wires supplement an already high modulus center steel structure to control cable strain under tension. While, in most of the new designs, the outer strands share a significant portion of the tensile load, the loss of a few outer strand wires on one of these designs would be less potentially damaging to the cable reliability. Materials of the outer strand layer(s) are either hard-drawn aluminum-clad steel (HDACS), made in accordance with ASTM B-415 or 6201-T81 aluminum alloy made in accordance with ASTM B-398, or a combination. HDACS wires used may be 40%, 30%, 27% or 20% IACS conductivity, depending upon the particular system needs.

Because of the very low creep characteristics of these designs, which is provided primarily by the central steel strength members, these cables can often be lighter in total weight than other OPGW designs with the same fault current ratings.

Due to the enclosure of the central fiber structure within the steel strength members, during transient fault currents or lightning strikes, less heat is generated in the steel than in the aluminum components. Since no aluminum components are adjacent to the optical unit, the fibers see less heat than in most other OPGW designs.

OPGW Hardware

Since OPGW introduction in the early eighties, numerous hardware manufacturers have developed, and now offer as standard fare, hardware specifically designed for use with OPGW cables. Since OPGW cables contain optical fibers internal to the cable, the hardware used must not crush the cable. Hardware containing formed armor wires has become popular for use with OPGW cable, since the formed armor wires provide a uniform compression around the circumference of the cable, thereby minimizing the amount of crushing the cable experiences. The formed armor wires also provide an increased stiffness in the OPGW cable at the hardware location preventing concentrated bending strains. By layering the formed wires, the added stiffness can be gradually reduced, to further reduce the tendency of forming concentrated bending strains.

The two main types of hardware used are dead-ends and suspensions. Dead-end hardware must be capable of supporting both the full weight and the full tension load of the suspended cable at each tower. Suspension hardware, on the other hand, is required to support only the full weight of the cable and a small portion of the tension load, caused by uneven ice loading or variation in elevation.

In addition to providing mechanical support of the OPGW cable, the hardware must also be capable of supporting the current associated with short circuits and lightning strikes. Therefore, the short circuit rating of the hardware should be greater than the short circuit rating of the bare OPGW cable.

Unfortunately, a unified industry standard for the testing and qualification of OPGW hardware has yet to be established. Consequently, IEEE 1138-1994¹⁰, and the ANSI C119.4-1991¹³, has been relied upon for testing procedures and requirements to evaluate OPGW hardware. In addition to these standard test documents, several testing procedures recommended by a manufacturer of OPGW hardware have been incorporated into an internally-developed hardware specification.¹¹

All dead-end and suspension hardware used with OPGW cable must be subjected to the aeolian vibration, galloping and short circuit testing as required by IEEE 1138-1994. The suspension hardware is also subjected to unbalanced load and sustained load at angle tests. In addition to the IEEE-1138 specification, the dead-end hardware must pass the maximum load and sustained load test as outlined in ANSI C119.4-1991. Although not specifically intended for use with OPGW cables, ANSI C119.4-1991 is an industry standard which was developed for use in a similar application.

The unbalanced load is similar to the maximum load test outlined in ANSI C119.4-1991 except that a suspension is used in place of one of the dead-ends. The purpose of the unbalanced load test is to simulate unbalanced loading that may take place in the field as a result of uneven ice loading or variations in elevation. The unbalanced load test is performed at 15% RTS (IEEE rated tensile strength) of the OPGW cable.

The sustained load at angle test is similar to the sustained load test outlined in ANSI C119.4-1991 except that a suspension is placed between the two dead ends and then elevated until a 30° turning angle exists. The tension is raised to 50% RTS of the OPGW cable for 168 hours. The purpose of the sustained load at angle test is to verify that the suspension will not adversely effect the cable at the maximum turning angle.

IV. TEST RESULTS

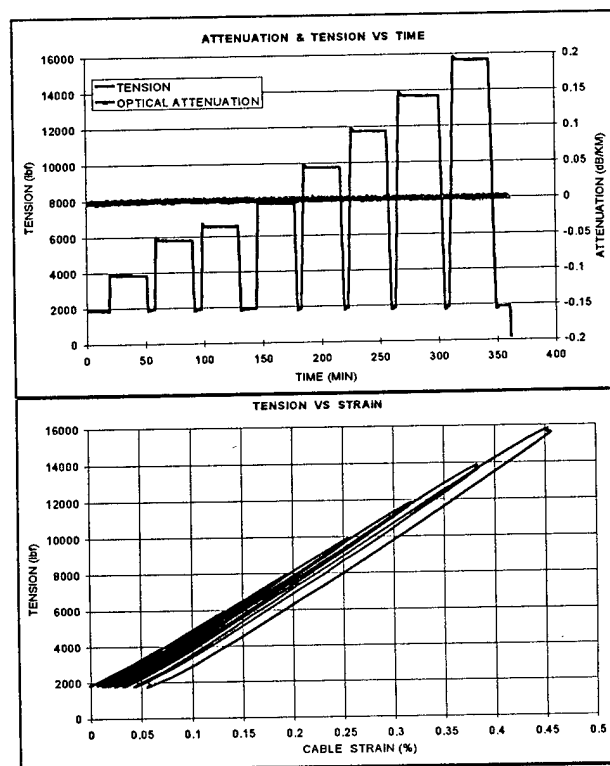
An extensive series of qualification tests have been conducted on both the A2 and B1 OPGW cable designs. The testing was designed to simulate installation conditions as well as the most severe operating conditions. The results are summarized in Table 1.

Table 1 - Qualification Testing of OPGW Designs A2 & B1

TEST	OPGW A2 RESULTS	OPGW B1 RESULTS
Stress-Strain (TTE)	ACCEPT	ACCEPT
24" Sheave Tests	ACCEPT	ACCEPT
Fiber Strain	ACCEPT	ACCEPT
Impact Test	ACCEPT	ACCEPT
Crush Test	550 lbf/in w/o affecting optical atten. 1000 lbf/in w/o permanent change in optical atten.	1000 lbf/in w/o affecting optical atten.
Water Ingress	ACCEPT	ACCEPT
Temperature Cycle Test	ACCEPT	In Progress
Creep Test	In progress	0.02% - 0.03% @ 25% RTS in 10 yrs
Aeolian Vibration	ACCEPT	ACCEPT
Galloping Vibration	ACCEPT	In Progress
Short Circuit Test	ACCEPT (100 KA ² sec rating)	In Progress
Thermal Coefficient	14.83 ppm/°C	
Thermal Coefficient under tensile loads	In Progress	13.3 ppm/°C @ 25% RTS
Breaking Strength Tests	26,455 lbf	25,350 lbf

Tension Characteristics

Stress - Strain tests were performed on one-hundred meter sections of both A and B designs. The objective of the tests was to characterize the cable strain, fiber strain, optical attenuation and torque performance of

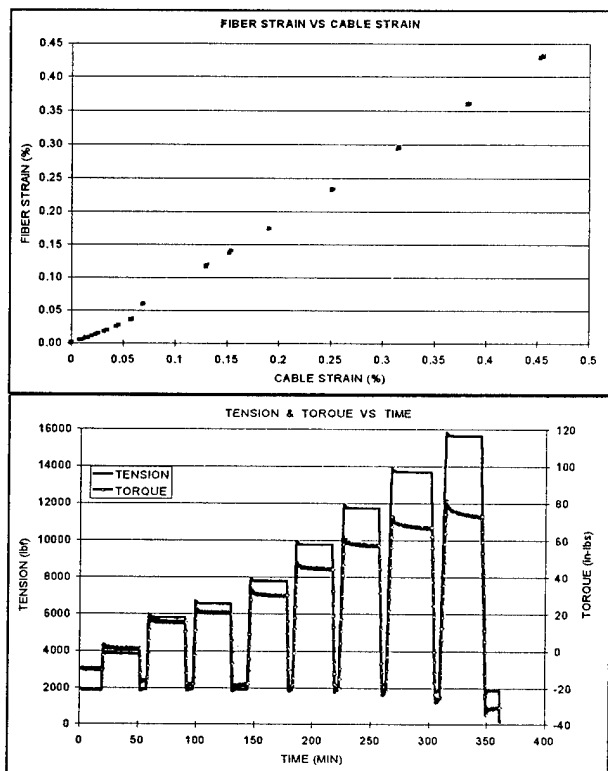


Figures 3 & 4 - A2 Stress-Strain Tests

cable under tensile load conditions. The cables were exposed to the tension loads profiled in Figures 3 and 4. Cables were terminated with formed type dead-end grips with each end prevented from rotating. Tensile loading had no effect on optical attenuation.

The fiber strain was monitored and verified fiber coupling to the cable (Figure 5) and torque vs. tension was measured (Figure 6).

Breaking strength tests were performed using OPGW dead ends. Breaking strength was defined as the tension at which the first wire failed. The results are shown in Table 1.



Figures 5 & 6 - A2 Stress-Strain and A2 Tension vs. Torque

Sheave Tests

Sheave tests were performed on both A2 and B1 cable designs to subject the cable to bending conditions to simulate installation and to characterize the installation effects on optical performance and physical cable integrity. The IEEE 1138-1994 was used as a guideline; however, an entire matrix of tension-sheave bend cycles was generated to provide much more engineering information than would otherwise be possible.

One hundred meter cable samples were prepared and installed into the tensile bed. The cable was threaded through the reverse bend carriage (Figure 7) with two

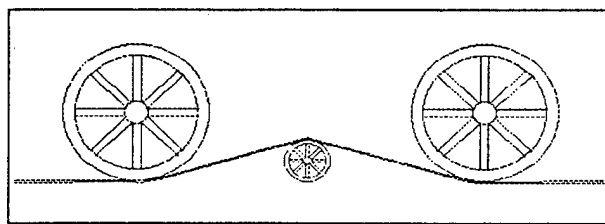


Figure 7 - Reverse Bend Carriage

79" sheaves mounted in the outside positions and a 24" sheave mounted in the middle position with approximately 36° bend over the 24" sheave. The cables were marked into six sections and exposed to the tensions and bends over the 24" sheave outlined in Table 2.

Table 2 - Sheave Test Sequence on 100 Meter Test Lengths

CABLE SECTION	TENSION	BENDS
A	12.5% RTS	30
B	12.5% RTS	50
C	12.5% RTS	70
D	25% RTS	30
E	25% RTS	50
F	25% RTS	70

The results of both the A and B designs show the sheave bends had no affect on optical attenuation (Figures 8 and 9). The results of the cable dissection indicated no damage to or bird-caging of the outer strand wires of either cable. The aluminum tube was not breached and remained in good condition throughout all cable sections. Minor aluminum tube deformations occurred in only the most severely tested cable sections and were well within IEEE 1138-1994 limits.

Temperature Cycling Test

A sample of the OPGW A2 cable was subjected to two thermal cycles between -30°C and +60°C. The change in optical attenuation over the temperature range at 1.5 μ m wavelength was acceptable (Figure 10).

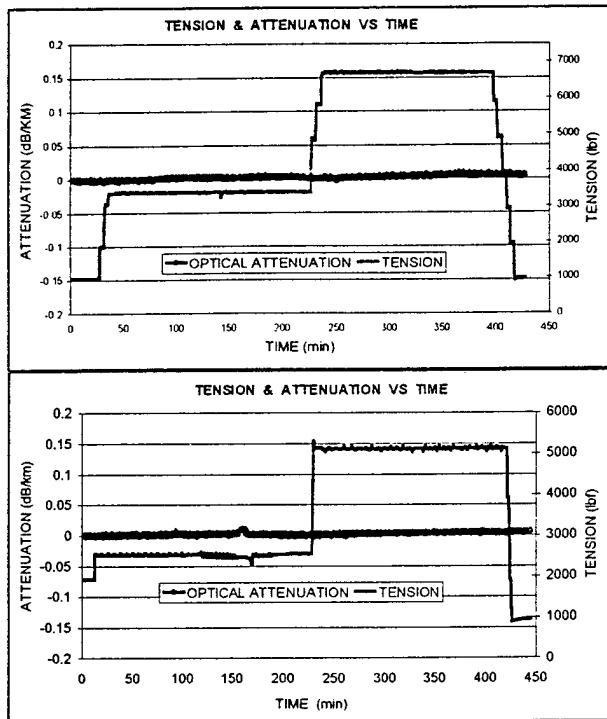
Aeolian Vibration Tests

Aeolian vibration tests were conducted as specified in IEEE 1138-1994 and carried out on OPGW A2 and B1 to simulate fatigue performance under typical aeolian vibration conditions. Both cables performed well mechanically and optically, well within IEEE 1138-1994 requirements.

Galloping Tests

A galloping test was conducted as specified in the

IEEE 1138-1994 and carried out on OPGW A2 to characterize both the mechanical fatigue and optical performance under typical galloping conditions. The cable performed well both mechanically and optically. Galloping testing on OPGW B1 is in progress.



Figures 8 & 9 - Design A2 & B1
IEEE 1138 Sheave Test - Attenuation vs. Time

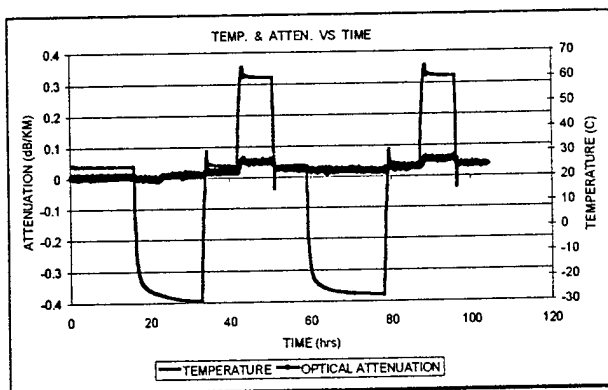


Figure 10 - Design A2 Temperature Cycling
Attenuation vs. Time

Short Circuit Tests

A short circuit test was conducted as specified in IEEE 1138-1994 and carried out on OPGW A2 to assess the physical and optical performance of the cable under fault current conditions. The results revealed no damage to the cable, and the optical attenuation was conforming. Short circuit testing of OPGW B1 is in progress.

Creep Tests

Tests were performed¹⁴ on both designs to determine the long term creep characteristics which are necessary for sag and tension calculations for system design. Results from both designs indicate very low creep characteristics. For example, the B1 test predicts a 10 year creep at 25% RTS in the 0.02% to 0.03% range.

Additional Testing

Many non-standard tests were performed to gather engineering information. A device was designed and built to impose high-cycle, low-magnitude bending at controlled variable strains. A second device was utilized for imposing low-cycle, high-magnitude bending at controlled variable strains. These tests were conducted to verify all predicted bending strain cycle limit values for the aluminum tube.

Tests were performed to yield the thermal coefficient of linear expansion under varying load conditions. For example, the results of the tests indicate a coefficient of 13.3 ppm/°C for OPGW B1 at 25% RTS.

V. OPGW APPLICATION AND INSTALLATION

OPGW cables A2 and B1 may be installed following the standard practices outlined in IEEE 524-1992¹⁵, provided the special conditions for OPGW stated in the standard are followed; specifically the use of sheaves with a diameter that is 40 times the diameter of the OPGW cable. For the A2 and B1 design, this requires the use of 24 inch minimum diameter sheaves.

The cost of installing vibration dampers is minimal when compared to the cost associated with the fibers. Since the fibers represent a major portion of the cost of OPGW cable, especially in the high fiber count versions, the use of dampers is highly recommended to protect the investment in OPGW cables.

Since the A2 and B1 OPGW cables incorporate fiber ribbons, the use of mass fusion splicing technology is recommended. Mass fusion technology has become achievable due to the improvements in fiber quality such as core-cladding eccentricity, fiber diameter tolerances and control of residual cast. The main advantage of mass fusion splicing technology over single fiber fusion splicing technology is the reduction

in splice time. Although mass fusion splicing technology is preferred from a time savings standpoint, single fiber fusion splicing technology can still be used since the fibers are easily separated from the fiber ribbons.

VI SYSTEM REQUIREMENTS

System requirements are usually clearly identified in the OPGW Utility Specification. To provide the most suitable and cost-effective design, it is also important that the cable designer/supplier work closely with the OPGW user system and transmission line engineers. Since sag, lateral loading on structures, hardware selection, creep characteristics, coefficient of thermal expansion, strength, elastic modulus, weight, diameter, etc. are of mutual interest, this cooperation can yield the best result. The proper installation of the cable is extremely important to the long-term performance. Coordination of the OPGW user system requirements with the installation recommendations of the OPGW supplier is vital to successful installation and long-term trouble free service.

VII CONCLUSION

The new OPGW cables meet all the requirements that we have established including the requirements of IEEE 1138-1994. A rigorous qualification testing program has been successfully performed on two new OPGW designs. These prototype cables represent two large families of OPGW designs. The A2 design represents the "A" series of designs for fiber counts up to 48 fibers. The B1 design represents the "B" series of designs for fiber counts up to 144. The design verification and qualification program has demonstrated that these designs meet the electrical, mechanical and optical reliability requirements necessary for the dynamic long-term performance of OPGW.

Design qualification tests have included IEEE-1138 requirements which include sheave, aeolian vibration, galloping, short circuit, creep, cable/fiber strain vs. tension, temperature cycling, water ingress, crush, and impact testing. In addition, special tests to accurately measure the coefficient of linear thermal expansion, under variable tension and temperature, have been completed. All results verify the suitability and reliability of these new OPGW designs.

The results of this extensive program verify the following important features of these OPGW cables:

- * Very low creep characteristics comparable to high steel content ACSR designs
- * Suitable low optical attenuation during all tests
- * Permanent control of the strain levels of all fibers at

all operating conditions, at safe levels for long-term reliability, through use of totally coupled tight buffer designs

- * High strength to weight ratio and high effective modulus of elasticity
- * Low coefficient of thermal expansion
- * Long-term electrical, mechanical and optical reliability

VII REFERENCES

1. A.AdI, T.M.Chien, T.C.Chu, "Design and Testing of the SL Cable", Undersea Lightwave Communications, IEEE Press, 1986, pp. 233-249
2. J.P.BoniceI, O.Tatat, U.Jansen, G.Couvrie, "Lightning Strike Resistance of OPGW", IWCS 1995 Proceedings, pp. 800-805
3. F.Meier, N.Nibbio, F.Gaille, "Effects of Lightning Flashes on Overhead Power Ground Wires With Optical Fibers"
4. ASTM Standard B-398-90, "Standard Specification for Aluminum-Alloy 6201-T81 Wire for Electrical Purposes"
5. ASTM Standard B-415-92, "Standard Specification for Hard-Drawn Aluminum-Clad Steel Wire"
6. S.E.Miller, I.P.Kaminow, "Optical Fiber Telecommunications II", Academic Press Inc., 1988, pp. 146-153
7. S.R. Nagel, "Review of the Depressed Cladding Single-Mode Fiber Design and Performance for the SL Undersea System Application", Undersea Lightwave Communications, IEEE Press, 1986, pp. 157-175
8. S.Sakaguchi, "Drawing of High-Strength Long-Length Optical Fibers for Submarine Cables", Undersea Lightwave Communications, IEEE Press, 1986, pp. 189-203
9. G.S.Glaesemann, "Predicting the Mechanical Reliability of Optical Fibers and Components", IWCS 1995 Short Course Notes
10. IEEE Std. 1138-1994, "IEEE Standard Construction of Composite Fiber Optic Overhead Ground Wire (OPGW) for Use on Electric Utility Power Lines", IEEE Power Engineering Society, 1994
11. "Qualification Requirements for OPGW Hardware", SX Specification No. 446, 1996, Simplex Technologies Inc.
12. K.W.Jackson, M.R.Santana, N.W.Sollenberger, R.J.Brown, K.M.Kroupa, S.H.Webb, "A Modular Ribbon Design for Increased Packing Density of Fiber Optic Cables", IWCS 1993 Proceedings, pp. 20-27
13. ANSI C 119.4-1991, "American National Standard for Electrical Connectors - Connectors for Use

Between Aluminum-to-Aluminum or Aluminum-to-Copper Bare Overhead Conductors", American National Standards Institute

14. "A Method of Stress-Strain Testing of Aluminum Conductor and ACSR and A Test Method for Determining the Long Time Creep of Aluminum Conductors in Overhead Lines", 1971, The Aluminum Association
15. IEEE Std 524-1992, "IEEE Guide to the Installation of Overhead Transmission Line Conductors", IEEE Power Engineering Society, 1992



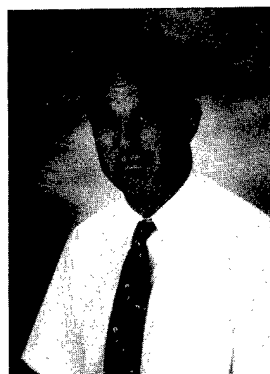
Richard T. Traut
Simplex Technologies Inc.
P.O. Box 0479
Portsmouth, NH 03820

Dick Traut is Manager of Development Engineering with Simplex Technologies Inc. He joined Simplex as a Senior Development Engineer in 1978. His experience includes 29 years in product design and R&D engineering in the power and communications cable industries. He has written numerous technical papers and holds 3 patents. He is a member of IEEE. His education includes a B.S.E.E.T. degree from Roger Williams College (1976) and an M.B.A. from New Hampshire College (1983).



William F. Wright
Simplex Technologies Inc.

Bill Wright is a Senior Engineer in the Development Engineering Group at Simplex Technologies Inc. He received his B.S. in Physics from Saint Mary's University in 1979. His primary responsibilities include development and testing of undersea fiber optic cables, and the evaluation of optical fiber performance.



Gregory N. Fontaine
Simplex Technologies Inc.

Greg Fontaine is the Manager of Product Design and Applications Engineering at Simplex Technologies Inc. He joined Simplex in 1978 and has a B.S.M.E. degree from the U.S. Naval Academy and an M.B.A. degree from New Hampshire College.



Michael J. Cyr
Simplex Technologies Inc.

Mike Cyr is a Senior Development Engineer with Simplex Technologies Inc. He joined Simplex in 1986 as a Process Engineer where he worked on the splicing and coupling of both co-axial and fiber optic cables. In September of 1993, he joined the Development Engineering Group at Simplex and is currently working on the development and coupling of high-fiber count cables. Mike received his B.S. from the University of Maine in 1986.



David P. Dumont
Simplex Technologies Inc.

Dave Dumont is a Development Engineer at Simplex Technologies Inc. He joined Simplex in 1987 and has an A.S.E.T. degree from New Hampshire Technical Institute and is currently completing requirements for a B.S.E.T. degree from the University of New Hampshire.

A FULLY INSTRUMENTED INSTALLATION AND TRIAL OF A NOVEL ALL-DIELECTRIC SELF-SUPPORTING CABLE SYSTEM FOR VERY HIGH VOLTAGE OVERHEAD POWER LINES.

Neil R. Haigh, Simon M. Rowland, Arif J. Taha, and Chris N. Carter*

BICC Cables Ltd, Helsby, UK.

***The National Grid Company plc, Leatherhead, UK.**

ABSTRACT

Dry-band arcing is accepted as being an obstruction to the use of All-Dielectric Self-Supporting (ADSS) fibre optical cables in high voltage environments. The concept of a resistive rod which, when installed on the cable, eliminates any damaging currents from the ADSS cable surface and thereby allows its use on high voltage lines has been developed. This has resulted in the manufacture of resistive rod and accessories, and their installation on a 400 kV line, in an environment which provides severe levels of pollution. Installation was carried out with circuits energised. The surface currents travelling along the resistive rod and ADSS cable system are being monitored continuously. Early results from this trial suggest that ADSS cables may be used in high voltage environments provided they are protected by a resistive rod attachment. The installation procedure demonstrated the ease with which such a protection device can be added to the cable. The paper describes the installation and the first results obtained from the trial. All results have been acceptably consistent with the software model used to develop this product.

INTRODUCTION

The application of fibre optic cables on high voltage overhead lines has been established practice for many years. However, the quantity of cable being installed has increased dramatically over the last 10 years as deregulation of telecommunications

services, and increased commercial pressures in the electricity supply industry have combined to bring the two industries together. New networks which exploit the existing electricity transmission distribution infrastructure are now commonly being implemented in competition with the established public telephone networks^{1,2}.

The first cable which incorporated fibres on HV overhead lines, and which has since become the most popular choice, is optical ground wire (OPGW). A number of alternative cable types have since been developed. None of the generic cable types should be considered inherently better or worse than the others, each having certain advantages in particular situations. In particular, OPGW, the composite earth wire which incorporates optical fibres, is very attractive if a new line is being built or an older one is being refurbished. Spiral wrap cable on earth wires is attractive if rapid deployment is important. Spiral wrap on phase conductors or composite phase wires might be attractive if the system has no earth wire.

When considering which type of cable might be used, a number of important issues arise. Cost of the cables and accessories, cost and speed of installation, the number of fibres available in each cable, the reliability of the cable system and of the installation methods, and the supply chain are all important. The cost of installation is a significant part of the system cost, and is largely dependent on two issues; the speed of deployment and

whether one or more circuit outages are required for installation.

In most cases, all-dielectric, self-supporting (ADSS) optical cable can be installed without having to de-energise electrical circuits; it also has the advantage of being physically separate from the power system. This is particularly useful where renewal or uprating is necessary on a line which has existing optical cable either attached to or within an existing conductor. As an example, it would normally take several weeks to replace, with OPGW, an earthwire which had optical cable wrapped on it. It is unlikely that the telecommunications provider using the wrapped cable could be able to tolerate this duration of loss of service. A self-supporting cable installed before work on the earthwire commenced would overcome the problem. However, at present the application of ADSS cables is limited to lines with system voltages of about 150 kV and below; although there is a range of circumstances which make some lower voltages unsuitable and some higher voltage lines suitable. These issues have been widely discussed in the literature^{3,4,5,6}.

A new product has been developed which overcomes the electrical degradation problems which limit the application of ADSS cables. This system and its installation have been discussed previously^{7,8}. Essentially the system involves installing a typical ADSS cable, which may be carried out without de-energising power circuits. Following this, a controlled degree of conductivity is introduced to the portion of the cable adjacent to the towers. This is achieved by simply clipping a conductive rod onto the cable and pushing the rod towards mid-span. The result of this, schematically shown in Figure 1, is typically 50 m of semiconductive cable at each end of the span. This conductive region controls the field and currents over the whole cable length, as described by Nichols et al⁷. The main difference between this system and that of making the whole of the ADSS cable semiconductive is that the conductive rod can be made with greater accuracy and control, and that during service, any stresses and strains on the cable are decoupled from

the rod. Thus the failures suffered by semiconductive cables can be avoided⁹.

FIELD TRIAL

A number of physical installation trials and one brief electrical trial all suggested that the system would be both effective and simple to implement. A final trial has been designed to demonstrate the long term reliability of the system. To this end a one year, fully-monitored trial of stress control fittings on a standard all-dielectric self supporting cable on a double circuit 400 kV power line has been initiated. The line chosen for the trial is in a coastal location noted for its severe marine pollution, which provides the main threat of dry-band arcing to ADSS cables. The three phase-conductor bundles of each of the two power-line circuits are vertically disposed on either side of the lattice-tower supports, which carry a single, central over-running earth wire.

The ADSS cable is supported from the bottom of the lower cross arm, slightly off the route centre-line. In this position the dry-condition, mid-span space potential on the ADSS cable is approximately 20 kV. Two adjacent spans of cable have been erected, one protected by stress control fittings and one unprotected. The stress control fittings have a resistance per unit length of 400 kOhm/m. The surfaces of these cables have been artificially aged to make them hydrophilic. Had this not been done, the cables would need to have been in the air for a considerable time, perhaps for years, before processes such as UV radiation degradation aged them sufficiently to allow them to suffer from dry-band arcing. Solar powered, intelligent, data logging and telecommunications equipment is mounted on the central tower shared between the protected and unprotected spans of the ADSS cable, together with instruments for gathering meteorological data. The data can be accessed remotely via a cellular telephone network.

A block diagram of the set-up is shown in Figure 2. The parameters measured include: temperature, wind speed and direction, rainfall, relative humidity and the earth

leakage current flowing from both the protected and unprotected cables. Provision has been made to lower the spans at regular intervals to enable the cable surface to be examined for damage. This will not only allow comparison of the two spans, but may also allow detection of imminent failure of the unprotected span before a catastrophic breakage.

THEORETICAL PREDICTIONS

In the position in which the cable is strung the midspan potential of the dry-cable is predicted by the Electran software³ to be 20 kV. The associated software plot is shown in Figure 3.

In a previous paper⁸ an explanation of the structure and use of a novel current calculating software package was given. This has been a necessary development since the resistance of the ADSS rod is now designed not to be uniform along its length. The data is supplied in a tabular format and can be reviewed as a diagrammatic cross-section of the tower. An example of the output information is given in Figure 4. Knowledge of all the information presented there is necessary for successful product design.

BICC software has been used to calculate the current on the cable in the trial installation in a variety of conditions. Of most importance is the current seen on the unprotected cable adjacent to the clamp. If this can reach a few mA then damage due to dry-band arc activity is expected within the year. The important parameters on the protected ADSS cable are the current which may flow through the rod, which might result in the rod heating up, and the current flowing at the rod tip, where dry-band arcing might still occur. From experience of testing and trials it is considered that if this latter current is less than 1 mA then damage will not occur as a result of arcing activity^{5,10}. The heating in the rod can be calculated from the product of the square of the worst case current and the rod resistance per unit length. Assuming a high of 5 mA gives a value of 10 W/m which is readily dissipated, so no significant heating will result.

The software has enabled a product to be designed which is universally applicable to virtually all overhead lines which are mechanically suitable for ADSS installation.

EXPERIMENTAL RESULTS

The live-line installation of the ADSS cable and the rod was carried out without any difficulties. There is no complicated or automated mechanical equipment required to install the rod, and this, together with its light weight, meant that the terrain made no difference to the speed of installation.

Although at the time of writing the trial had been running for only 7 weeks, it can already be seen that the stress control fittings are working in the intended fashion; typical results are shown in Figure 5. In dry conditions, a current of around 1.7 mA flows continuously from the stress control fitting to ground, and no leakage current is drawn from the unprotected cable. In wet conditions, earth leakage currents flow from the unprotected cable; their magnitudes vary according to the levels of marine pollution that govern the specific resistance of the cable, but to date they have not exceeded the 1 mA threshold above which dry-band arcing might be expected to cause damage. In these conditions small increases can also be seen in the corresponding current flowing from the protected span. These are caused by the decrease in the resistance of the wet protected portion of the cable which is in parallel with the stress control rod. Small variations in the rod leakage current are also caused by shifts in the wind speed and direction (not shown here) which change the relative positions of ADSS cable and phase conductors.

DISCUSSION

Software predictions of current are superimposed upon the experimental data in Figure 5. In dry conditions a cable conductivity of 100 MOhm/m predicts the observed current of 0.1 mA. In the same conditions the protected span is predicted to see 1.4 mA somewhat less than the 1.7 mA actually seen. Moisture on the cables increases their conductivity enough to raise the current to 0.3 mA on the unprotected span. This does not change the current

significantly on the span with the rod since the rod is considerably more conductive than the moisture.

Figure 5, shows that, after a dry period, wetting of the cable resulted in the current rising rapidly (point X). The current decreased afterwards, consistent with continued rain washing off the pollutants (salt) which had built up previously under dry conditions. This type of information will verify the model which was used to design the complete system. However further evidence of the performance of the system is necessary for complete verification, since it is only in extreme conditions in which dry-band arcing will damage the cable.

The site chosen for the trial has particularly onerous environmental conditions. Salt spray is commonplace and this followed by mild wetting from dew, for example, is expected to create conditions for damage at some time in the near future. In these circumstances the cable resistance may fall to only a few hundred kOhm/m when currents of several mA will result. It is expected therefore that the unprotected span will fail, although it is difficult to predict when. However, it is hoped that this will be within the coming Winter of 1996/7. The spans under test will be lowered at three monthly intervals to inspect for damage. Only if the protected span remains undamaged whilst the unprotected span fails will the experiment be fully satisfactory. Over the coming period novel data will be generated on the effect of blow-out on current seen on protected and unprotected cables.

CONCLUSIONS

A new cable system has been developed which can be installed on the highest voltage overhead lines, with circuits live, and which is separate from existing phase conductors and earth wires. The experimental results obtained from a full scale trial installation have begun to verify the models used to design the system, although continued effort is required to fully understand the system.

The product will not be necessary on all high-voltage spans, but will allow implementation of ADSS cables on any high-

voltage, long-span route. This provides a cost effective method of installing optical fibres on the highest voltage systems. It is at present the only method of doing so whilst keeping the optical fibres separate from the electrical system.

ACKNOWLEDGEMENTS

The authors would like to thank BICC Cables Ltd. and The National Grid Company plc for permission to publish the material in this paper. The authors would also like to acknowledge the support of their colleagues in carrying out this work.

REFERENCES

- 1/ J R Martin 'Optical Fibre for power utilities' CIGRE 1993 regional meeting, Australia, October 1993, 174-185
- 2/ S C Sharma 'Solutions for Fibre Optic cables installed on overhead Power Transmission lines- a review' IETE Technical review 11 (1994) 215-222
- 3/ C N Carter and M A Waldron 'Mathematical Model of dry band arcing on self-supporting, all dielectric optical cables strung on overhead power lines' IEE Proc C 139 (1992) 185-196
- 4/ A J Peacock and J C Wheeler 'The development of Aerial Fibre Optic Cables for Operation on 400 kV Power Lines' IEE Proc A 139 (1993) 304-313
- 5/ S M Rowland and I V Nichols 'The effects of dry-band arc current on ageing of self-supporting dielectric cables in high fields' IEE Proc.- Sci. Meas. Technol. 143 (1996) 10-14
- 6/ S M Rowland, F Easthope 'Electrical Ageing and Testing of Dielectric, Self-Supporting Cables for Overhead Power Lines' Proc IEE Part A 140 (1993) 351-356
- 7/ I V Nichols, C A Platt, S M Rowland, A J Taha, C N Carter 'A novel system for the installation of all-dielectric self supporting optical cables on high voltage overhead

power lines' 44th Proc International Wire and Cable Symposium (1995) 171 - 177

8/ I V Nichols, C A Platt, A J Taha, C N Carter, S Neve 'The development of a post-fit system for an all-dielectric self-supporting optical cable' 36th Session CIGRE 1996

9/ P G Cristaudo and D L Maskell
'Communications - the new power house for

the Australian electricity supply industry' CIGRE 1993 regional meeting, Australia, October 1993, 149-159

10/ G. Carlton, C.N. Carter, A.J. Peacock, R. Sutehall, 'Monitoring on all-dielectric, self-supporting optical cable for power line use' 41st IWCS Reno, November 1992, 59-63

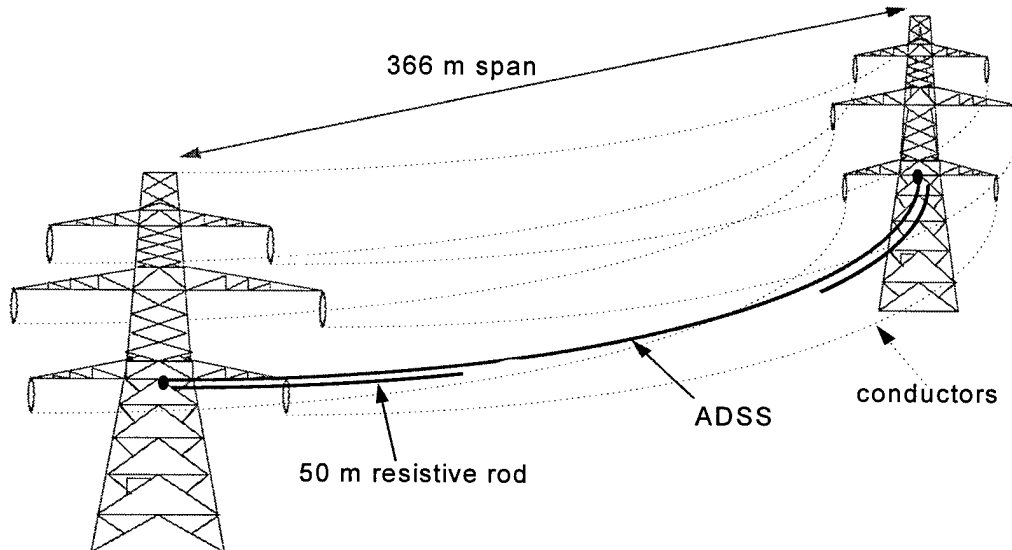


Figure 1 A schematic of installed rod system on a typical span

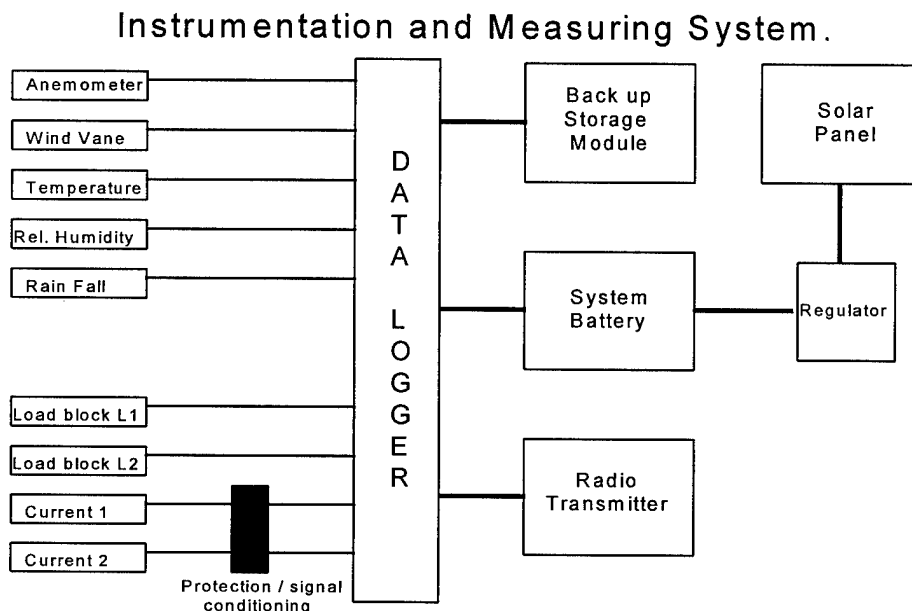


Figure 2 Block diagram of the monitoring equipment

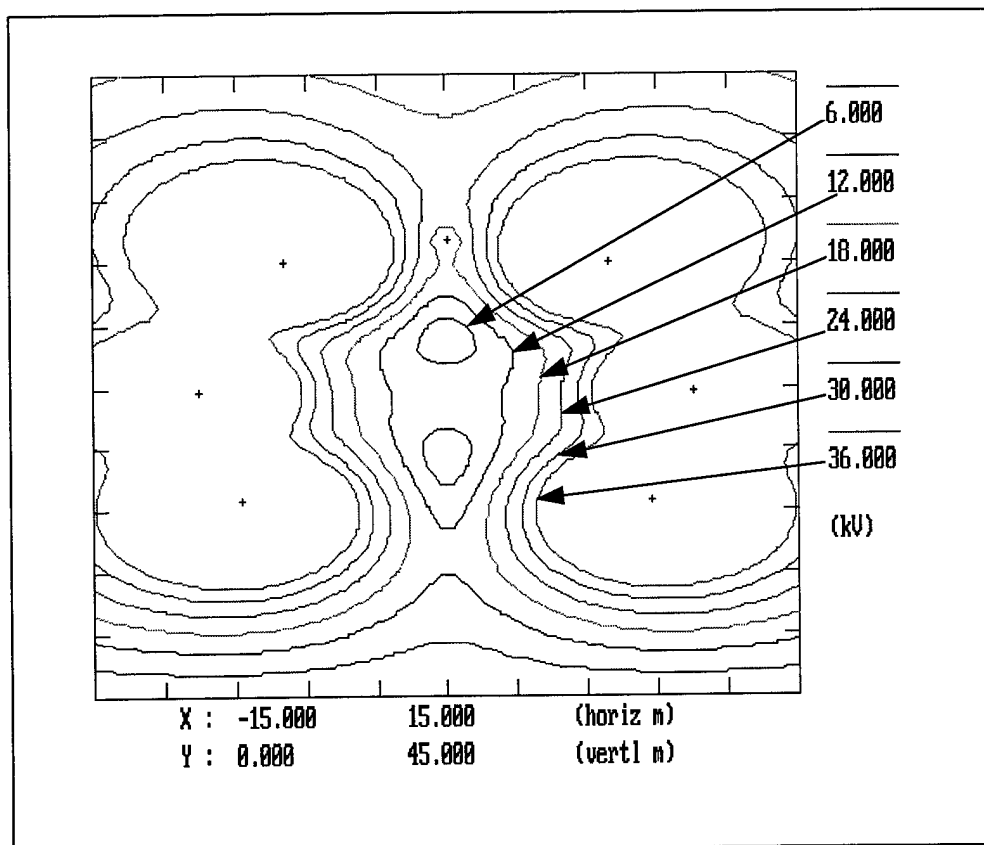
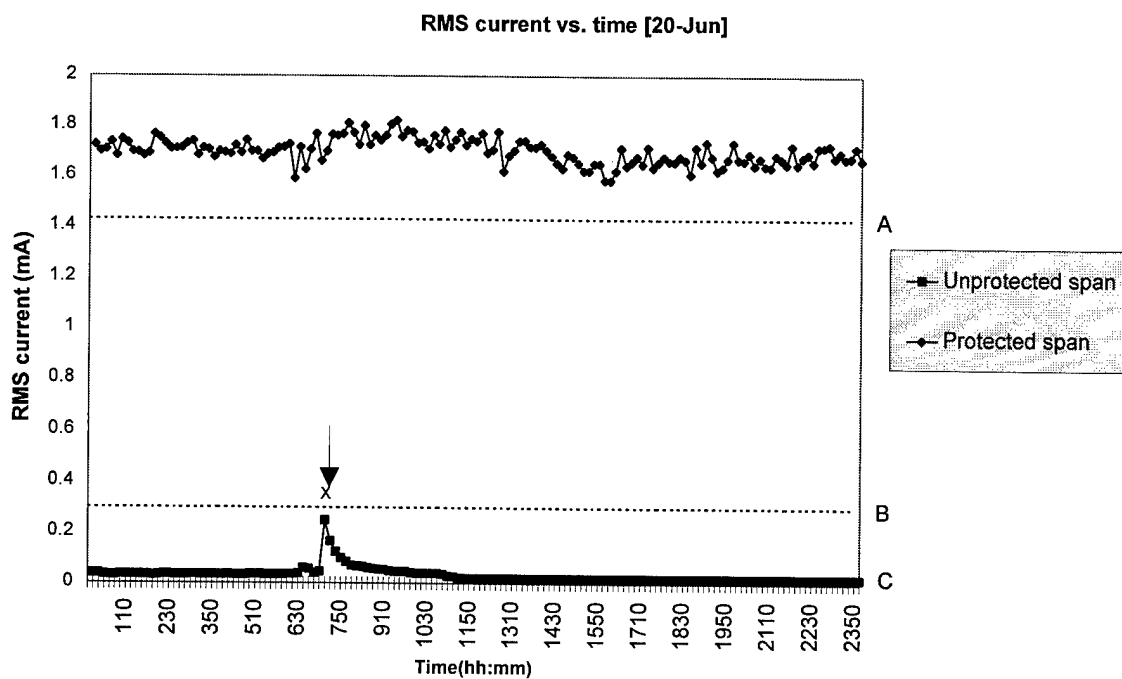


Figure 3 The contours of voltage on a plane perpendicular to the cable at midspan.

Results and Outputs Window			
Print			
Calculation Results			
Index	Description	Dimension	Value
59	Calculation is Invalid if Resistance is below	kOhms/m	51.2981
60	Length over which 63% of Current is collected	m	55.15346
Assuming Current Flow Across Boundary			
Index	Description	Dimension	Value
61	Current flow to support	mA	2.523368
62	Current Flow through Boundary	mA	0.9618734
Assuming Dry Band at Zone Boundary			
Index	Description	Dimension	Value
64	Current flow to support	mA	1.840203
65	Voltage across dry band	kV	14.10887
Assuming Metallic Conductivity for Whole Cable			
Index	Description	Dimension	Value
67	Support Current	mA	4.209162
Assuming No Current Flow			
Index	Description	Dimension	Value
68	Mid span space potential	kV	19.86482
Exit			

Figure.4 An example of the predictions required for system design



A - Predicted current on protected span when wet.
 B - Predicted current on unprotected span when wet.
 C - Predicted current on unprotected span when dry.
 Rainfall occurred at X.

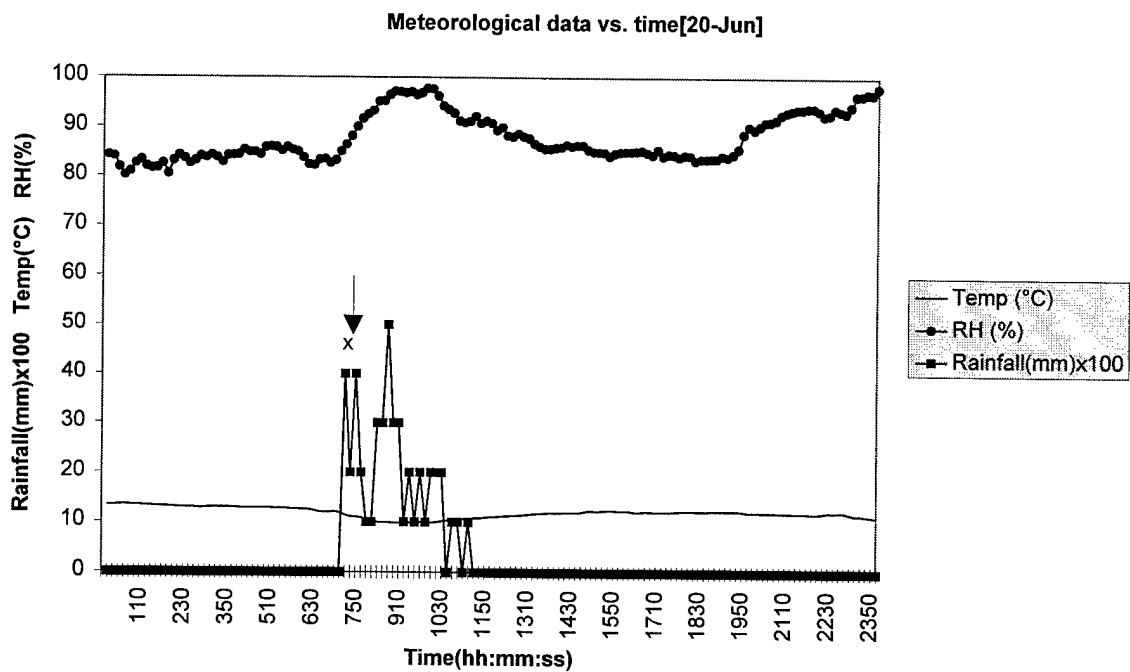
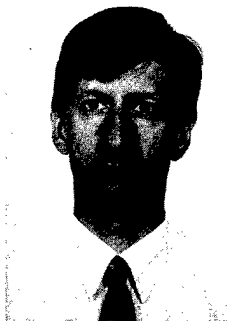


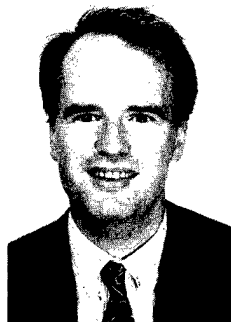
Figure 5 Typical Results From Trial Installation



Simon Rowland

BICC Cables Ltd
Helsby Tech Centre
Helsby
Cheshire WA6 0DJ
United Kingdom

Simon Rowland was born in London, England. He obtained a BSc from the University of East Anglia and a PhD from the University of London. He joined BICC Cables from STC Technology Ltd in 1989 where he worked on power cable insulation materials. He is Programme Manager for Telecoms Research and Development at The Helsby Technology Centre.



Neil Haigh

BICC Cables Ltd
Helsby Tech Centre
Helsby
Cheshire WA6 0DJ
United Kingdom

Neil Haigh was born in Cheshire, England. He graduated with a BSc and PhD from the University of London, specialising in applied optics. He joined BICC in 1988 and is actively involved in the area of optical fibre measurements. He is a Principal Research Engineer and Project manager for the HV ADSS development.



Arif Taha

BICC Cables Ltd
Helsby Tech Centre
Helsby
Cheshire WA6 0DJ
United Kingdom

Arif Taha graduated from Manchester University with a BSc in Materials Science. He has since received an Instrumentation MSc, and a PhD in Electrical Engineering. He has been actively involved in developing optical cable systems for application on long-span, high-voltage power distribution networks for BICC since 1995.



Chris Carter

National Grid Co. Plc
Kelvin Avenue
Leatherhead
Surrey KT22 7ST
United Kingdom

Chris Carter graduated in 1963 from the University of London. He has since worked on magnetohydrodynamic power generation, superconducting magnet design, ac loss measurements in superconductors, failure mechanisms in the joints of power cables and since 1979, the development of optical communications on power lines.

Development and Characterisation of a New Dielectric Cored OPGW

Alan Stringer, Khawaja A. Ahmed, Douglas M. Burgess*, Gabriel Gitlits, Jan S. Jasik,
Ronald C. Kemp*, Scott A. Wade**, Gregory W. Baxter**, Stephen F. Collins**

Olex Cables, Melbourne, Australia

** Victoria University (VU), Melbourne, Australia

* Commonwealth Scientific and Industrial Research Organisation (CSIRO), Australia

ABSTRACT

The application of an Optical Ground Wire (OPGW) to provide an optical fibre communication link on high voltage overhead transmission lines is well established. Recent trends in OPGW design include the production of cables which are small in size, have higher fibre count and low manufacturing costs. Another very important consideration is the reliability of the OPGW. The optical transmission link should operate successfully over the planned life of the power transmission line which is usually in excess of 30 years.

In this paper we present the development and characterisation of a new dielectric cored OPGW. This paper will also present the design, development and results of a complete range of mechanical, electrical, thermal and optical tests to prove the short and long term reliability of this cable. Another focus of the paper will be on a newly developed technique for temperature measurement inside the optical core which is of great importance to establish a sense for the long term reliability of the optical fibres. A test rig was also developed to analyse the electrical characteristics of the cable which simulates the fault currents as well as lightning strikes on OPGW.

1- INTRODUCTION

As we are approaching the information age there is an ever-increasing demand for communication channels with large transmission bandwidth. Optical fibres, due to their numerous advantages are an obvious choice for future communication networks. With the recent privatisation trend in telecommunications and power utilities around the world, there is a growing interest in the increase of transmission capacity in such applications. In the past, power authorities were using these facilities for

their internal communications, monitoring and control. However, with deregulation and privatisation there are great opportunities for the power authorities to have their own full communication systems which will meet internal and commercial needs alike.

OPGW is one of the attractive approaches to put optical fibre on the power transmission line towers.^{1,2} This technique has been widely used in utility networks. OPGW acts as a protective ground wire in high voltage transmission circuits while simultaneously providing optical fibres for communication links. OPGW is a cost effective option when installing new or replacing existing ground wires. Also, in developing countries, where telecom networks are not very well-established, power transmission networks usually get priority over telecom networks. This provides a wide scope for the applications of aerial optical cable.

High voltage power transmission circuits are designed with a long service life in mind, usually in excess of 30 years. Therefore, long term reliability of these cables is of paramount importance. OPGW cables should provide a ground wire function as well as a reliable optical channel over the life of the project. Only rigorous testing of various operating characteristics of OPGW cable can give us this level of confidence.

The exposure of optical fibre to high temperature variations can affect the mechanical and optical properties and also their aging behaviour in the long term. During a fault current or a lightning strike, OPGW temperature can rise in the vicinity of 175 °C or more depending upon a number of factors such as magnitude of the action integral (I^2t), ambient temperature, material type, number of layers and the construction of the optical core. Depending upon the application, fibres with appropriate material and coatings should be used. Knowledge regarding fibre temperature is important for the selection of optical

fibre in order to make a reliable prediction of the expected lifetime of the cable. Therefore information about the temperature of the optical fibres inside the OPGW core is very important.

We have successfully developed and tested a very simple and accurate technique of measuring the temperature inside the optical core of OPGW. This method is based on a special rare-earth doped fibre which is spliced to one of the fibres and can be handled like standard optical fibre. Section 3, discusses this unique temperature monitoring system in detail.

This paper discusses the design of a new and improved version of dielectric-cored OPGW, results of various electrical and mechanical tests performed. In section 2 of this paper, the issues related to the mechanical design of OPGW are discussed. Section 4 presents a computer model to predict the temperature profiles in different layers of the cable as a function of time. Finally, Section 5 presents the results of mechanical and electrical tests performed on this cable.

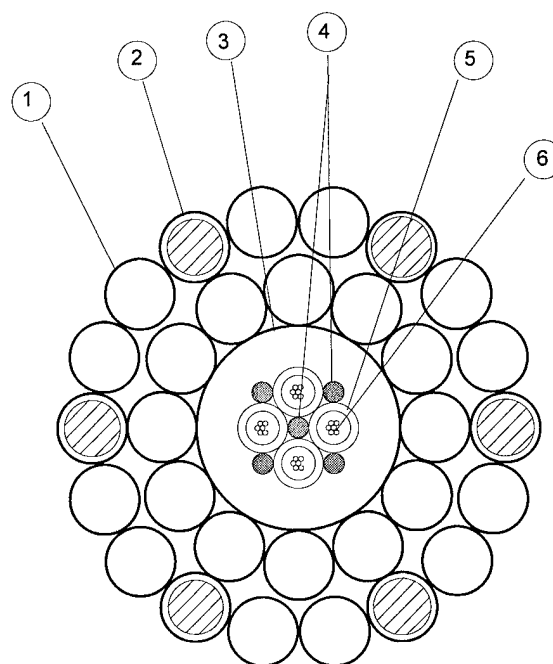
2- CABLE DESIGN

The main purpose of an OPGW, whilst providing an optical communication channel, remains to work as a ground conductor. An ideal OPGW design will, therefore, have electrical characteristics, mechanical strength and properties equivalent to that of a metallic conductor used as a ground wire, whilst having a suitable fibre count and keeping the diameter small. For given electrical and mechanical requirements, a small and light weight OPGW will have better wind/ice loading and consequently, lower forces on towers.

Both the electrical conductors and the optical unit, carrying optical fibres in the OPGW, must be capable of withstanding the stresses presented by the overhead groundwire installation and the environmental conditions. Just like the conventional optical fibre cable, the design has to accommodate all the mechanical factors imposed by the application e.g. tension, wind loading, creep etc.

This design, shown in Fig. 1, is an extension of an existing product developed to emulate the properties of a standard aerial conductor (Grape - 30/7/2.50 mm ACSR/GZ, refer Table 1). A dielectric-cored OPGW cable is a combination of an aerial conductor and dielectric optical fibre cable. In this design, the inward radial heat flow, resulting from lightning strike on or a fault current in the metallic strands, is restricted because of their low radial thermal conductivity of the order of the order of 1% of that in

the solid material.³ The radial heat flow through the strands is thus much less than would occur in a solid material of the same thermo-physical properties.



- | | |
|---|---------------------|
| 1 | Al Alloy Wire |
| 2 | Al Clad Steel Wire |
| 3 | XLPE Sheath |
| 4 | Reinforcing/Fillers |
| 5 | Loose Tubes |
| 6 | Optical Fibres |

Fig 1 Cross-Section of OPGW

In the trial OPGW, the optical unit housed a total of 24 optical fibres which were placed in a group of six in each of the four loose tubes. This assembly was helically stranded and sheathed with Cross-Linked Polyethylene (XLPE) which allows the optical unit to be exposed to higher temperature transients than would otherwise be possible with traditional thermoplastic materials. The XLPE layer provides mechanical strength for the optical unit as well as, very importantly, a thermal buffer to reduce the inward flow of heat to the optical fibres.

The central optical fibre unit is surrounded by a layer of 12/2.75 mm aluminium alloy 1120 wires and an outer layer comprising 12/2.75 mm aluminium alloy 1120 wires and 6/2.75 mm aluminium clad high tensile steel wires. A brief description of the cable's electrical and mechanical properties and its comparison with the GRAPE conductor is given in Table 1.

During manufacture, installation and service, the cable is exposed to radial, tensile and torsional strains. An understanding of the interplay of various forces on different layers and components is very

helpful in determining the cable's behaviour during field applications. The following analysis was performed to gain this understanding of the design limits and establish manufacturing processes.

Description	OPGW	GRAPE
Diameter of optical unit, (mm)	8.1	-
Overall diameter, (mm)	19.1	17.5
Al Type	Alloy 1120	EC grade
No. of Al wires	24	30
Al wire diameter	2.75	2.50
Steel Type	Al-Clad	Galvanized High Tensile
No. of Steel wires	6	7
Steel wire diameter	2.75	2.50
Mass, (kg/km)	688	675
Cross-section area, (mm ²)	178	181
Minimum breaking load, (kN)	81	63.7
Modulus of elasticity, (GPa)	88	90
Calculated DC resistance at 20 °C, (ohm/km)	0.189	0.196
Coefficient of linear Expansion, (°C ⁻¹)	19.2x10 ⁻⁶	18.4x10 ⁻⁶
Sag & Tension @ 40 °C for 300 m span [EDS Conditions stringing tension = 20% of the conductor breaking load at 15 °C]		
Sag, (m)	6.15	6.84
Tension, (kN)	12.8	11.0

Table 1 Comparison of OPGW with GRAPE

The equations presented in literature^{4,5,6} describe mechanical characteristics of a helically stranded single layered cable. Following equations describe the torsional and tensile properties of a multi-layered cable containing helically wrapped elements and loose tubes.

$$M = H_1 \varepsilon_c - H_2 \phi \quad (1)$$

$$T = P_1 \varepsilon_c - P_2 \phi \quad (2)$$

where M is the cable's twisting moment and T is the tensile load carried by the cable,

$$H_1 = \sum_{i=1}^m (Cos^2 \theta_i - \nu_i Sin^2 \theta_i) (n_i E_{si} A_{si} R_i Sin \theta_i)$$

$$H_2 = J_c G_c + \sum_{i=1}^m (n_i J_{si} G_{si} Cos^2 \theta + \pi R_i^2 Sin 2\theta_i n_i E_{si} A_{si} Sin \theta_i)$$

$$P_1 = E_c A_c + \sum_{i=1}^m (Cos^2 \theta_i - \nu_i Sin^2 \theta_i) n_i E_{si} A_{si} Cos \theta_i$$

$$P_2 = \sum_{i=1}^m \pi R_i Sin 2\theta_i n_i E_{si} A_{si} Cos \theta_i$$

n_i is the number of strands in the i th layer, m is the number of layers, E_s is the Young's Modulus of strand material, ϕ is the untwist turns experienced per unit length when the cable is under tensile load, A_s is strand cross section, R is strand's distance from the cable axis and θ is the lay angle. J is the moment of inertia, G is the torsional rigidity,

$\nu = -\frac{\delta R/R}{\varepsilon_c}$ is the radial contraction, $\varepsilon_c = \frac{\partial \ell}{\ell}$, and

subscript "c" refers to the core properties. A right hand lay angle is defined as positive and a left hand lay as negative θ .

The coefficients H_1 , H_2 , P_1 , and P_2 were computed for the experimental OPGW cable using the material properties of various cable components shown in Table 2. Using equations (1) & (2) and assuming $\nu=0.5$, we calculated the tensile modulus (T/ε) of the cable under two conditions;

$$\text{Twist restrained } (T/\varepsilon)_{(\phi=0)} = 57.3 \text{ kN/\%}$$

$$\text{Unrestrained } (T/\varepsilon)_{(M=0)} = 57.01 \text{ kN/\%}$$

The validity of the analysis was confirmed by comparing the results of mechanical tests, with the above theoretical predictions. The ratio T/ε was found experimentally by applying tensile load on the cable whose ends were restrained from rotating. The measured ratio was

$$T/\varepsilon_{(\phi=0)} = 58.35 \text{ kN/\%}$$

which is within 3% of the predicted value.

Component	Young's Modulus, Shear Modulus (GPa)	Cross-sectional Area (mm ²)
Cable Core	E=6.79	51.53
Al	E=68, G=25.50	142.55
ACS	E=162, G=60.81	35.64

Table 2 Material properties of cable components

When the cable is heavily loaded, another important cable parameter is its twisting moment⁵ which can be calculated using above equations. Using (1), and assuming $\varepsilon_c = 1.0\%$, the twisting moment of the cable was calculated to be

$$M_{(\phi=0)} = H_1 \varepsilon_c \cong 1.33 \text{ Nm /kN}$$

which was not very significant for this design and would not have affected the cable behaviour.

3- A NOVEL TEMPERATURE SENSING TECHNIQUE

Under fault current conditions the cable is exposed to sudden electrical/mechanical shocks. To examine the dynamic thermo-physical properties of the cable undergoing fault current conditions, a novel temperature monitoring technique has been developed, in collaboration with Victoria University, to accurately measure the temperature inside the OPGW core.

Previously, thermocouples have been a usual choice for measuring temperature in OPGW during testing. They can be used with relative ease to monitor the temperature at the outer metallic strands. However, the process becomes cumbersome and practically difficult when an attempt is made to use thermocouples to measure the temperature in the optical unit. It is not only extremely difficult to place them in small optical units but there could be mechanical interference along the fibre path leading to anomalous attenuation changes during the tests. Also a great deal of care has to be taken to determine the location of thermocouples in the cable, which have to be close to the termination of cable in order to access them.

The temperature sensor used here is based on a rare-earth doped fibre. The sensor fibre can be easily placed in the cable core with other fibres

making it an attractive and practical technique. This sensing method can measure up to 500°C with an accuracy of approximately 1°C. In this experiment a section of the doped fibre, which was fused into a length of standard fibre, was incorporated into the OPGW using the normal tubing process. This section of doped fibre was then used to monitor the temperature of fibres during fault current testing.

3.1 Basic principle

The fluorescence intensity ratio technique depends on the relative population of two close-lying excited state energy levels of a rare-earth ion. The populations of the two excited state levels are thermally dependent and may be characterised using a Boltzmann distribution. The radiative decay from these levels to a common lower lying level produces two adjacent bands in the fluorescence spectra. Through appropriate filtering the intensity of each band may be measured, and a ratio taken whose value will be a monotonic function of temperature. The advantages of taking such a ratio are that it will be independent of the intensity of the excitation source, require only simple data analysis schemes to interpret and be resilient to fibre bend loss (due to the similar spectral range of each fluorescence). A more detailed discussion of the generic properties of the fluorescence intensity ratio technique is given elsewhere.⁷

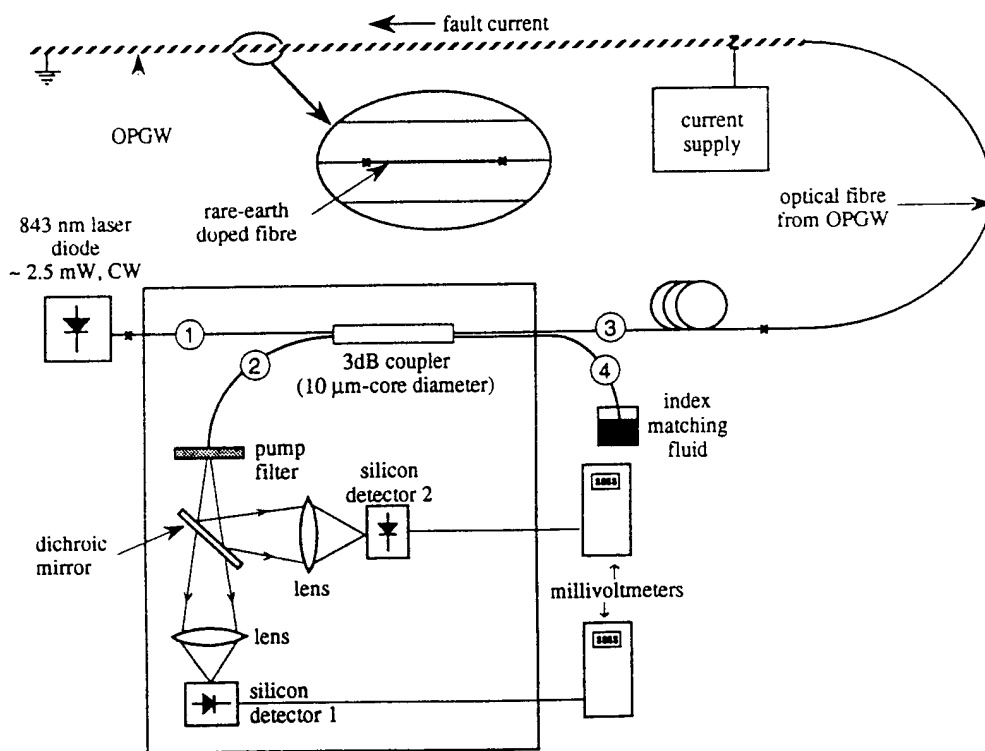


Fig. 2 Experimental Set up using a novel temperature monitoring system based on rear-earth doped fibre

3.2 Experimental details

The thermalising levels utilised in this work were the $^2F_{5/2}^a$ and the $^2F_{5/2}^b$ excited state sub-levels in the rare-earth ion Yb^{3+} . The Yb^{3+} doped silica fibre used was fabricated at the Laboratoire de Physique de la Matière Condensée, Université de Nice, using an MCVD process together with solution doping. It had a doping concentration of approximately 350 ppm and was 95 cm in length. It should be noted that shorter lengths of doped fibre could be employed by simply using a higher dopant concentration.

The experimental arrangement used for these tests is shown in Fig. 2. Approximately 2.5 mW of light from a pigtailed 843 nm laser diode, spliced to port 1 of a 3 dB coupler, was used to pump the rare-earth doped fibre, which was connected via a length of standard optical fibre to port 3 of the coupler. The counter propagating fluorescence, measured at the output of port 2 of the coupler, was separated into the fluorescence originating from the $^2F_{5/2}^a$ level (focused onto detector 1) and that originating from the $^2F_{5/2}^b$ level (focused onto detector 2) using a dichroic mirror. During the tests, the output from each of these detectors was monitored using multimeters. A Schott glass RG850 absorbent filter was used to block the pump light reflected by splices and fibre ends from entering the detectors. The data from the two multimeters were acquired and subsequently analysed by a computer. Test results obtained are presented in section 6.

4- Computer Model for Temperature Prediction

A computer model has also been developed to predict the temperature distribution in various cable layers. In order to obtain the transient temperature distribution within the cable during a fault current event, it is necessary to solve the heat transfer equation within the layered cable structure. Experience shows that a number of simplifying assumptions could be made. The solution procedure is confined to the interior of the cable with radiative and convective boundary conditions being set at the cable surface.

The stranded conductors are assumed to be of a uniform material with an appropriate effective density to take account of the voids and with a radial thermal conductivity very much less than the axial thermal conductivity.⁸ Similar assumptions for optic fibre unit axial symmetry can then be assumed. These assumptions simplify the heat transfer equation to

$$\frac{1}{r} \frac{\partial}{\partial r} \left(rk \frac{\partial T}{\partial r} \right) + q = \rho C_p \frac{\partial T}{\partial t} \quad (3)$$

where T is the temperature, r the radial distance from the cable axis, k is the thermal conductivity, ρ is the density, C_p is the specific heat and t is the time. Heat is generated within the strands by the fault current and is represented by q .

Equation (4) is then solved using the method of finite differences. The cable is divided into a number of radial control volumes, Δr in width, appropriate to the cable dimensions. The temperature, thermal conductivity, density and specific heat are assumed to vary linearly within the control volumes. The boundary conditions at the OPGW surface involve the convective heat transfer coefficients with air, the emissivities of the cable and surroundings and the air temperature. The boundary conditions at the OPGW surface have been established from the heat balance at the surface shown in Eq(5):

$$\kappa \frac{\partial T}{\partial R} = h(T_m - T) + FS_n[(T_m + 273.15)^4 - (T + 273.15)^4] \quad (4)$$

where R is the cable radius, T_m is the temperature of the surrounding medium, T is the surface temperature of OPGW, h is the convective heat transfer coefficient at the cable surface and F is a configuration factor given by:

$$F = \frac{1}{1/E_c + (R/R_t)(1/E_t - 1)} \quad (5)$$

where R_t is the radius of the surrounding region, E_c is the emissivity of the cable surface and E_t the emissivity of the surroundings. Values of the emissivity of the cable and surroundings are assumed initially and later empirically adjusted.

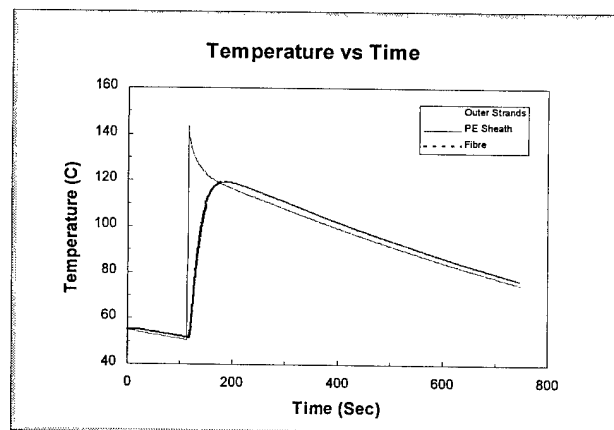


Fig. 3 Computer Model Output - Temperature at various OPGW Layers versus Time

The transient solution of Eq (3) is obtained by using Crank-Nicholson⁸ implicit method to move forward in time. The Crank-Nicholson method has been chosen as being more robust than either pure implicit or pure explicit methods. The temperature at nodal position n and at time-step number i for a time step size of Δt is given by:

$$T(n, i) = T(n, i-1) + \frac{1}{2} \Delta t \left(\frac{\partial T(n, i)}{\partial t} + \frac{\partial T(n, i-1)}{\partial t} \right) \quad (6)$$

The time derivatives of temperature in Eq (4) are obtained by writing Eq (3) in finite difference form resulting in a set of linear equations which then can be solved for the nodal temperatures.

The model gives temperature at the interface of various layers as a function of time. A data file based on the materials characteristics and test conditions was put into the model to simulate the cable under test. The model output is shown in Fig. 3. Initial cable temperature was set to be 55 °C. A simulated fault current of 20 kA is then applied for 0.45 seconds. The temperature of the outer strands then rises to 140 °C. The heat flows inwards and the temperature of the inner units gradually starts to increase after a delay as these units are protected by thermal buffers. It should also be noted that the temperature of the fibre does not reach the peak value achieved by the stranded conductor layers, due to the thermal buffering.

5- TEST RESULTS

5.1 Electrical Tests:

To carry out the electrical tests, a major lightning and fault current testing facility⁹ has been established at the National Measurement Laboratory of the *Commonwealth Scientific and Industrial Research Organisation (CSIRO)*. The facility is capable of testing the cable at fault currents of up to 25 kA over a 60m length and of conducting impulse current tests with peak currents of 150 kA to simulate lightning strikes.

The fault current test was conducted in accordance with IEEE 1138. A 55 metre long OPGW section was suspended between two concrete blocks in a hairpin loop. In order to increase the fibre length under test, four fibres per tube were concatenated to give a total test fibre length of 880 metres. Optical attenuation was monitored by an optical power meter used in a differential mode with a measurement resolution of 0.001 dB. The output of the power meter is also connected to a chart recorder. Load cells were used to measure the

tension. A sag monitoring device was placed in the middle of the span. The surface temperature of the outer metallic strands was measured using thermocouples whereas a special temperature sensing fibre (as described in section 3) was used to monitor the temperature in the optical core of the OPGW.

The cable was exposed to test current pulses with an amplitude of 20 kA rms (50 Hz) for 0.45 seconds. In order to observe the behaviour of OPGW during a fault current, the optical attenuation, temperatures, tension, and sag were recorded and plotted on a personal computer.

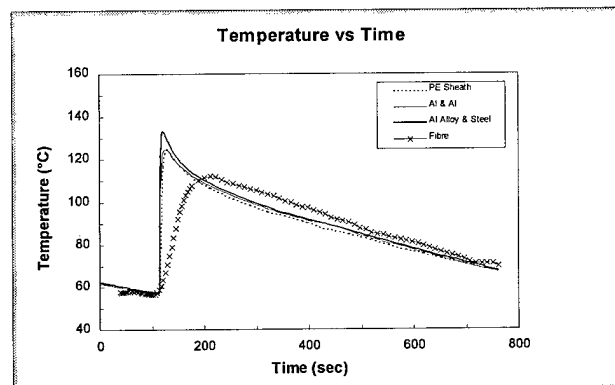


Fig. 4 OPGW Temperatures vs Time

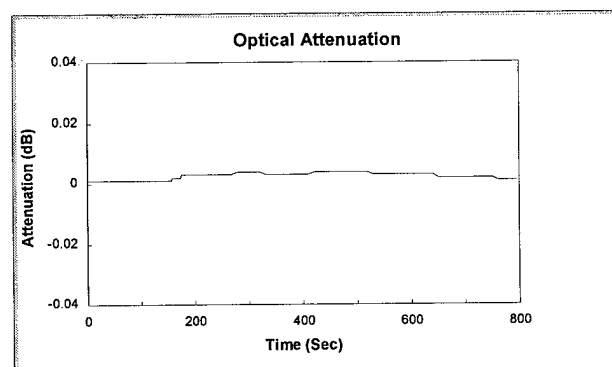


Fig. 5 Optical Attenuation vs Time

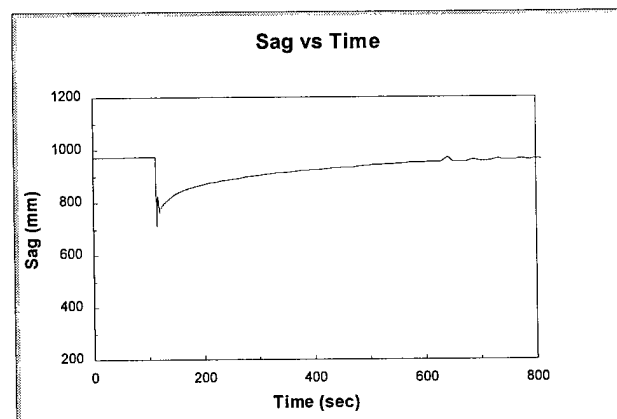


Fig. 6 Sag of OPGW vs Time

In Fig. 4, OPGW temperatures are plotted versus time. With the application of the fault current, the temperature of the metallic strands rises to 140 °C from an initial temperature of 55 °C. The temperature rises with a delay to a peak value of 110 °C, which is in good agreement with the computer model predictions shown in Fig. 3. The variations in optical attenuation, shown in Fig. 5, were insignificant during the test proving the optical transmission reliability of the cable.

Fig. 6 and Fig. 7 show the OPGW sag and tension in the two arms of the hair pin loop, respectively, as a function of time. The cable was, initially, suspended at a tension of 15 kN at a clearance of almost one metre from the ground. With the application of the current pulse, the cable sagged 200 mm from its original position. This corresponds to a sag of 0.55% for a 36 m span.

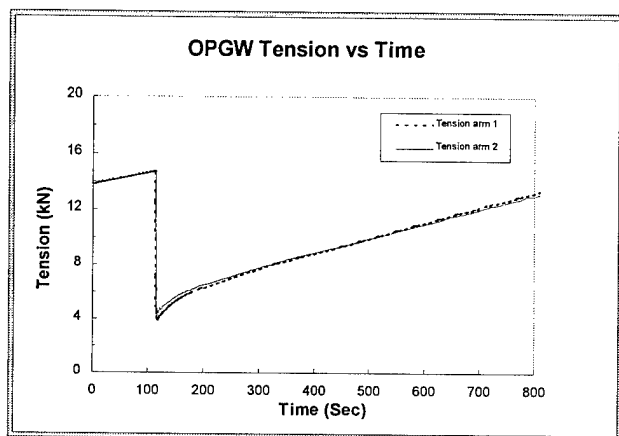


Fig. 7 Tension vs Time

5.2 Mechanical Tests:

The tensile performance of the cable was tested using spiral deadend termination fittings. A 17 m section of cable was used for the test and concatenation of fibers gave a 100 m length under test. There was no change in optical attenuation and fibre strain up to 68 kN. Beyond which the fibre strains at a similar rate as the cable. Fig. 8 shows a plot of cable strain and fibre strain versus cable tension.

6- SUMMARY

A newly developed OPGW cable has been introduced and design concepts have been discussed. The optical fibres are placed at the core and are thermally buffered by a layer of a thermoplastic material with superior thermo-physical properties. Electrical and mechanical tests have also been presented which prove cable reliability.

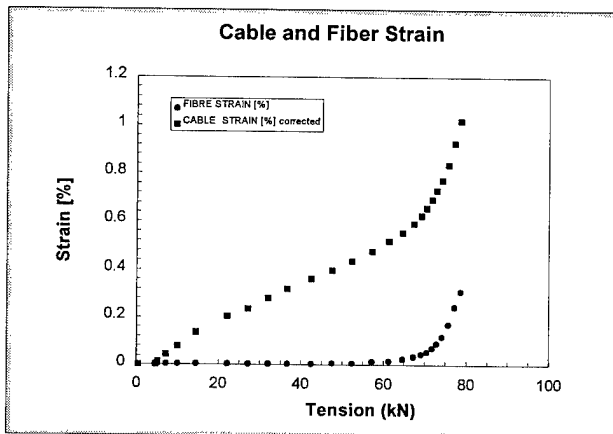


Fig. 8 Plot of cable strain and fibre strain versus tensile load.

We have shown the application of an optical fibre temperature sensor to measure temperature in an environment which was unsuitable for conventional (ie. thermocouple) sensors. This optical temperature sensor meets many of the criteria necessary for successful commercial development¹⁰, by providing reasonable accuracy whilst remaining relatively low in cost.

A computer model has also been discussed which predicts the temperature distribution at various layers of the Cable. Its validity has been proved by a close match of the experimental results and the predicted values.

REFERENCES

- [1] D. Brewer, "Experience of optical fibre cables on overhead lines," CEPSI, 1994, pp. 629-651.
- [2] I.E. Kertscher, "Design and construction of self-supporting aerial fibre optic cables, OPGW fibre optic overhead ground wires and high performance coaxial cables," Wire and Cable Panorama, 1995, pp. 35-44.
- [3] V.T. Morgan, "The radial temperature distribution and effective radial thermal conductivity in bare solid and stranded conductors, IEEE/PES Winter Meeting Atlanta, Georgia, 1990.
- [4] J. Bustamante, "The fatigue strength of steel wire ropes-part1," Wire Industry, 1994, pp. 678-683.
- [5] J.J. Atienza, "Computer programs for the design of steel wire ropes," Wire Industry, 1992, pp. 39-42.
- [6] T.C. Cannan, and M.R. Santana, "Mechanical Characterisation of cables containing helically wrapped reinforcing elements," 24th International Wire and Cable Symposium, 1975, pp. 143-149
- [7] G. W. Baxter, S. A. Wade, S. F. Collins, G. Monnom and E. Maurice, "Rare-earth doped optical fibres for point temperature sensing", Accepted for

presentation at In-Situ Optical Sensors Conf. (SPIE), Denver, 1996.

[8] J. Crank and P. Nicholson, "A practical method for numerical evaluation of solutions of partial differential equations of the heat conduction type," Proc. Camb. Phil. Soc. 43, 1947, pp. 50-67.

[9] D.M. Burgess, R.C. Kemp, and A. Stringer, "Development of a 50 Hz high current system and a unique impulse current generator and their application in testing the fault current rating and impulse performance of an OPGW," Submitted to IWCS, 1996.

[10] K. T. V. Grattan and Z. Y. Zhang, *Fibre Optic Fluorescence Thermometry*, Chapman and Hall, London, 1995.

ACKNOWLEDGMENTS

Scott Wade would like to acknowledge the financial support of the Australian Government through the provision of an Australian Postgraduate Award (APA) scholarship.

Alan Stringer
OLEX Cables,
207 Sunshine Road,
Tottenham, Victoria 3012
Australia

Alan obtained degrees in Electronics and Electrical Engineering at the City University in London where he spent formative part of his career in the cable making industry, researching into the impact of oil contamination in the barrier joints of 400 kV oil-filled cable systems. Subsequently he worked on the development of a Computer integrated manufacturing system and nonconnecting cable measurement systems. After emigrating to Australia in 1986, he joined Olex Cables and investigated the quality issues of

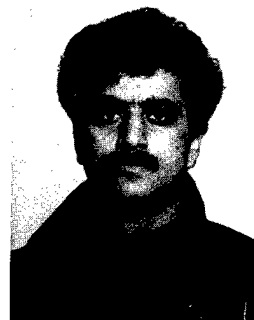


manufacturing ultra-long cables for the submarine optical fibre cable systems. After a brief spell as a systems specialist for communications and special cables, he moved to his current position of Engineering Manager, optical fibre cables, in the Communications Division.

Khawaja Aamer Ahmed
OLEX Cables,
207 Sunshine Road,
Tottenham, Victoria 3012
Australia

Aamer received his B.Sc. (Honours) degree in Electrical and Electronic Engineering from the University of Engineering & Technology Lahore, Pakistan in 1991 and the Master of Engineering Science degree from the University of Melbourne, Australia in April 1994.

From 1991 to 1992, while working for R&D department of Carrier Telephone Industries, Islamabad, Pakistan, he made numerous contributions in the development of a digital radio system. He joined Photonics Research Lab of the University of Melbourne as a member of research staff and he worked on various projects on semiconductor lasers, solitons and high-bit-rate optical transmission systems. In his current role as a development engineer with OLEX Cables, he is involved in the design, development and testing of optical fibre cables.



Douglas Maxwell Burgess
CSIRO Division of
Applied Physics,
National Measurement
Laboratory, Bradfield Road,
Lindfield, NSW 2070, Australia.

Douglas completed a six year traineeship with the federal with the federal department of Civil Aviation, following secondary education. During this time an Electrical Engineering Certificate was obtained. In 1980, he joined the High Voltage Laboratory the National Measurement Laboratory, predominantly being involved with high voltage testing and measurements as well as standards development. An Electronics and Communications certificate was completed in 1982, concentrating on digital systems. Since 1992, he has designed and develop high current systems for testing of OPGW.



Gabriel Gitlits
*OLEX Cables,
 207 Sunshine Road,
 Tottenham, Victoria 3012
 Australia*

Gabriel graduated from the Moscow Telecommunication University in communications engineering. In 1974, he received his PhD degree from All Union Institute of Optical and Physical Measurements, Russia. He has been involved in research, design and development of systems and products for both radio and fibre based networks. Dr. Gitlits has extensive experience in the telecommunications industry. He is the author of numerous books, articles and inventions in fibre optics, signal processing, data transmission and EMC. Since 1995, he has been working in OLEX Cables, specialising in the development and production of OPGW as well as other aerial cables.

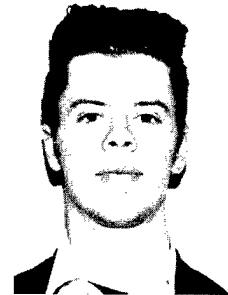


of Birmingham in 1964. He then joined the CSIRO Division of Physics, Australia as a Research Fellow. Since then he has worked on electron spin resonance, temperature measurement and standards, heat transfer and more recently on various heat transfer related problems associated with the cable industry. He is now a senior Principal Research Scientist with the CSIRO division of Applied Physics.

Scott Wade
*Department of Applied Physics,
 Victoria University,
 P. O. Box 14428
 Melbourne, Vic. 8001, Australia*

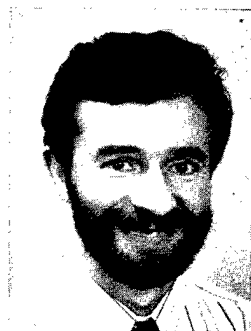
Scott Wade graduated with a B.Sc.(Hons.) degree in 1994 from Victoria University, Australia.

He is currently a PhD. student at Victoria University where his thesis subject is the development of a fibre optic temperature sensor based on fluorescence in rare-earth doped fibre.



Jan S. Jasik
*OLEX Cables,
 207 Sunshine Road,
 Tottenham, Victoria 3012
 Australia*

Jan Jasik graduated from the University of Melbourne with a Bachelor in Industrial & Manufacturing Engineering (Honours) in 1990. After joining OLEX Cables the same year, he has been engaged in the development of Optical fibre cables and manufacturing processes. His major contributions are in the area of optical fibre colour coating, buffer tube extrusion, tube stranding and in development of new ways of cable sheathing. In 1994, he undertook one year long Manufacturing Technology Fellowship program in Japan, where he joined Nippon Light Metal, Kambara Works and worked on the project of Productivity increase of metallic dies for the extrusion of Aluminium products.



Gregory Baxter
*Department of Applied Physics,
 Victoria University,
 P. O. Box 14428
 Melbourne, Vic. 8001, Australia*

Gregory Baxter graduated with a B.Sc.(Hons.) degree in 1982 and received the PhD. degree in 1990 from the University of Melbourne, Australia.

He is with the Optical Technology Research Laboratory within the Department of Applied Physics at Victoria University, Australia. His current research interests include solid-state miniature lasers and the use of rare-earth-doped optical fibre for temperature sensing.



Ronald C. Kemp
*CSIRO Division of Applied
 Physics,
 National Measurement
 Laboratory, Bradfield Road,
 Lindfield, NSW 2070, Australia.*

Ronald Kemp graduated from the University of Bristol with a B.Sc. Honours degree in Physics in 1961 and received a PhD from the University



Stephen Collins
*Department of Applied Physics,
 Victoria University, P. O. Box 14428
 Melbourne, Vic. 8001, Australia*

Stephen Collins graduated with a B.Sc.(Hons.) degree in 1979 and received a PhD. in 1985 from the University of Melbourne, Australia.

He is currently head of the Department of Applied Physics at Victoria University, Australia. His current research interests include fibre optic sensors and optical amplifiers at visible wavelengths.

DEVELOPMENT OF SMALL SIZE AND HIGH PERFORMANCE CENTRAL STAINLESS TUBE OPTICAL GROUND WIRE USING COLORED THREAD BINDERS FOR IDENTIFICATION OF FIBER BUNDLES

T. Yokokawa, K. Yonezawa, Y. Suetsugu, K. Nagatomi, and S. Tanaka

Sumitomo Electric Industries, Ltd.

ABSTRACT

The small size and high performance central stainless (SUS : Steel Use Stainless) tube OPGW was realized by the proper design of fiber excess length (XSL), the precise control of XSL variation and the use of colored thread binders for simple identification and for reducing interaction between fiber bundles and between fiber bundles and the tube. As a result of investigation of heat resistance and various mechanical properties, it was confirmed that the OPGW with the central SUS tube has excellent characteristics in comparison with the conventional OPGW. Moreover, the low PMD has given the prospect of the OPGW for the use in future high bit rate optical transmission systems.

1. INTRODUCTION

Higher fiber count in even smaller cross section has been recently required for Optical Ground Wire (OPGW). An OPGW with a central stainless

steel tube (SUS tube) structure which consists of the SUS tube including optical fibers as a cable core and surrounding stranded wires^{1, 2} has the great potential to realize larger fiber density. One challenge for the central tube structure has been the identification of more than twelve fibers because of the limited available colors. One way for the identification is a special ring-mark coding on inked fibers³. Instead, we have adopted a simple and an easy identification system using colored thread binders, where each binder with different color bundled six or twelve conventional inked fibers. The other challenge has been the stability of fiber excess length (XSL) since large deviation from the nominal XSL might results in degradation of fiber reliability. For the XSL stability we have adopted S-Z reverse lay stranding method, which greatly improved the stability. In this paper, the OPGW with the central SUS tube design is presented, and its high and stable optical performances are discussed.

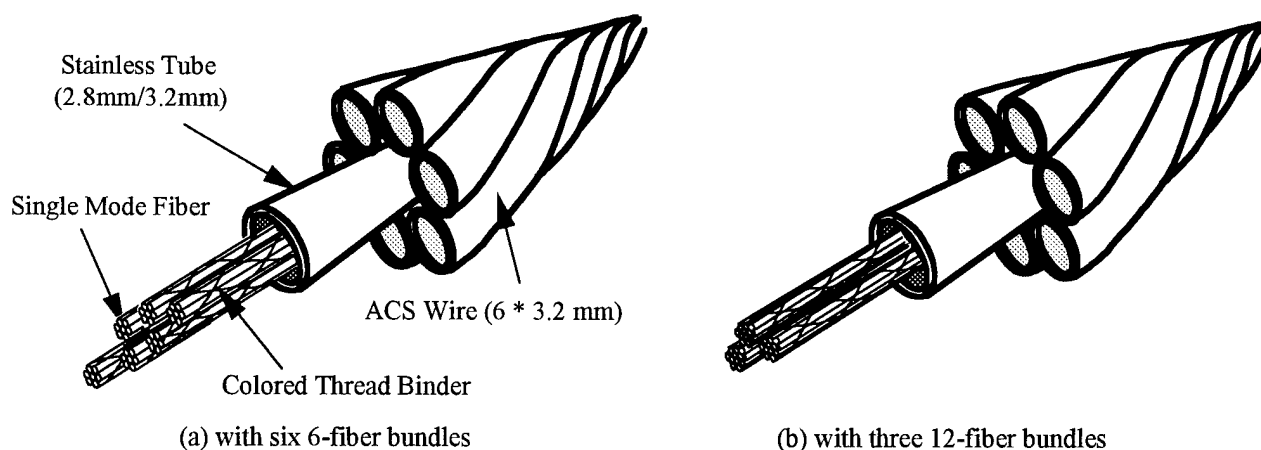


Figure 1 Design of the central SUS tube OPGW using colored thread binders, (a) with six 6-fiber bundles and (b) with three 12-fiber bundles.

2. CABLE CONSTRUCTION

Figure 1 shows the design of OPGW with the central SUS tube. The central tube containing 36 fibers (six 6-fiber bundles or three 12-fiber bundles) has an inner/outer diameter of 2.8/3.2 mm. Single-mode fibers of 0.25 mm coating diameter are used and each bundles is bound by different colored cotton threads. Moreover, 6 aluminum-clad steel wires (ACS wires) whose section diameter is 3.2 mm are stranded around the central SUS tube. In order to reduce interactions between fiber bundles and SUS tube inner wall, the 225 denier cotton thread binders are chosen fuzzy and large in its cross section to act as buffer layers. Further increase in fiber count can be done simply by increasing the number of fiber bundles.

3. STABILITY OF XSL CONTROL

The SUS tube for such a design should have appropriate XSL for the long term reliability of fibers being free from failure probability. Necessary XSL can be determined by the OPGW elongation taking possible kinds of situation, such as installation, temperature change, aerodynamic load, etc. into account. Thus, we have determined the necessary XSL as 0.35%.

In manufacturing line, straight pay-off of fibers (bundles) results in large deviation in XSL from the nominal value. Avoiding this variation occurrence, conventional helical stranding or S-Z stranding can be used, and we adopted the S-Z reverse lay stranding because it needs not to equip a large-scale stranding machine. In tubing process as shown Figure 2, each of six 6-fiber bundles or three 12-fiber bundles is bound with colored cotton threads and stranded

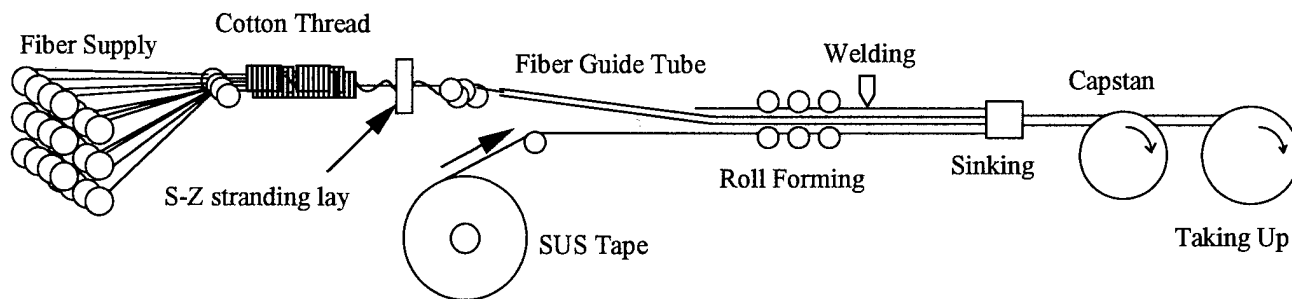


Figure 2 Production of the fiber bundles in a SUS tube

with S-Z reverse lay, while inserting into the SUS tube. Using this tandem manufacturing line, position of each fiber-bundles in the SUS tube at the capstan can be changed and be decreased the XSL variation. From Figure 3(a) and Figure 3(b), it can be seen that the XSL variation among the fiber bundles is significantly improved approximately from 0.17% to 0.04% or even less by the S-Z reverse lay stranding.

4. OPTICAL PERFORMANCE

Various kinds of evaluation test were conducted on the manufactured 24-fiber OPGW and also the manufactured OP unit.

4-1. Attenuation change in a manufacturing process

The measurement result of transmission loss at 1550 nm for the SUS tube OPGW was shown in

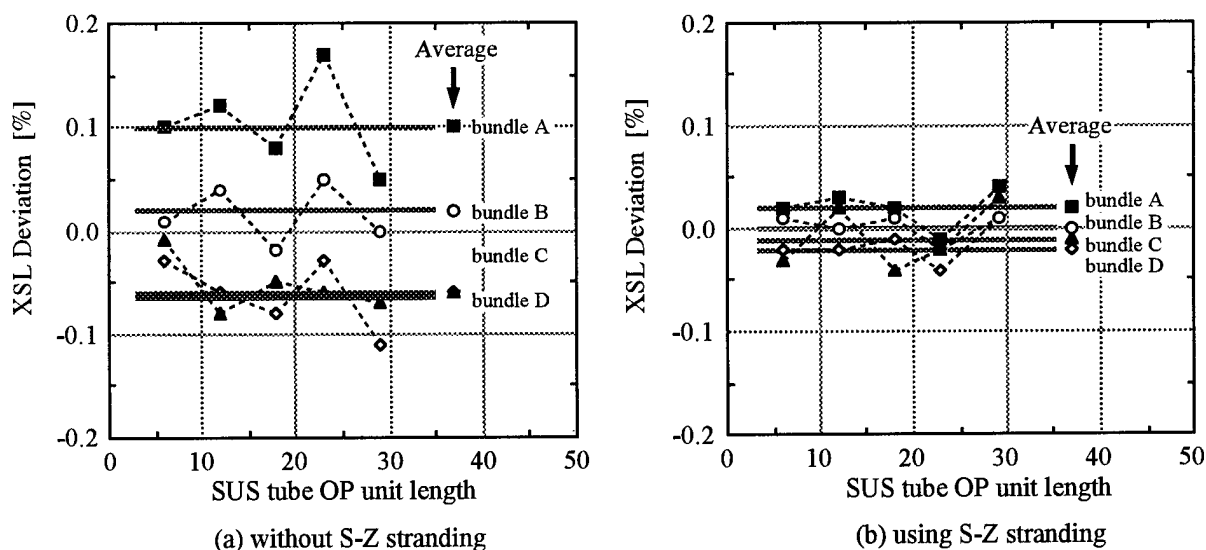


Figure 3 The longitudinal XSL deviation of each bundles

Figure 4. Stable attenuation was confirmed throughout the process with the maximum deviation of 0.02 dB/km. Average loss of the OPGW was 0.197 dB/km.

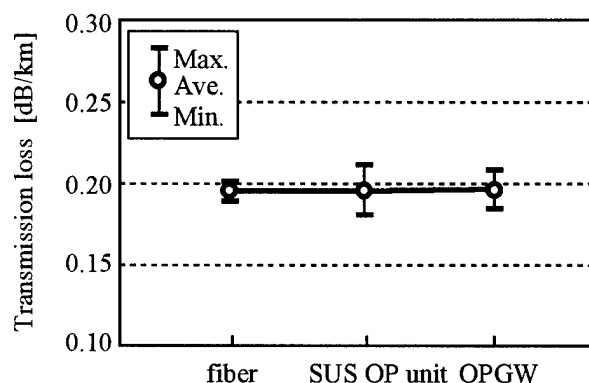


Figure 4 Attenuation change in a manufacturing process

4-2. Polarization-mode dispersion (PMD)

Polarization-mode dispersion (PMD) is one of parameters which determines the properties of optical transmission systems. For the first time, PMD in the OPGW with the central SUS tube was measured by the interferometric method. The low PMD below 0.1 ps/ $\sqrt{\text{km}}$ was obtained and has given the prospect of the OPGW with the central SUS tube for the use in future high bit rate optical transmission systems.

4-3. Temperature dependence

The transmission loss stability with wide range temperature variation was experimentally investigated for this SUS tube OP unit. Transmission loss variation due to change in temperature was continuously monitored at a

wavelength of 1550 nm. The six fibers in a 500 m SUS tube OP unit sample were fusion spliced to form a 3.0 km-long test sample loop. It was subjected to temperature cycling following the temperature profile as shown in Figure 5. After the cycling test it was subjected to heat aging test following the temperature profile as shown in Figure 6.

Figure 5 and 6 also show the transmission loss change at 1550 nm of the SUS tube OP unit for the cyclic and continuous temperature, respectively. The deterioration of the monitoring transmission loss were less than 0.01 dB/km at 1550 nm for each temperature pattern and each of loss increase doesn't remain when it returns to room temperature. From these investigations of temperature dependence, the SUS tube OP unit with colored thread binders

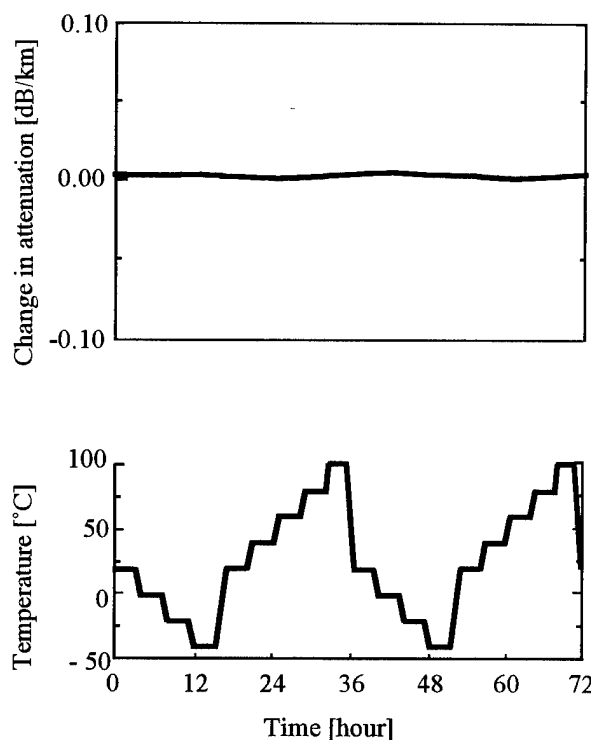


Figure 5 Temperature cycling test

has good stable transmission properties for wide temperature range from -40°C to $+100^{\circ}\text{C}$.

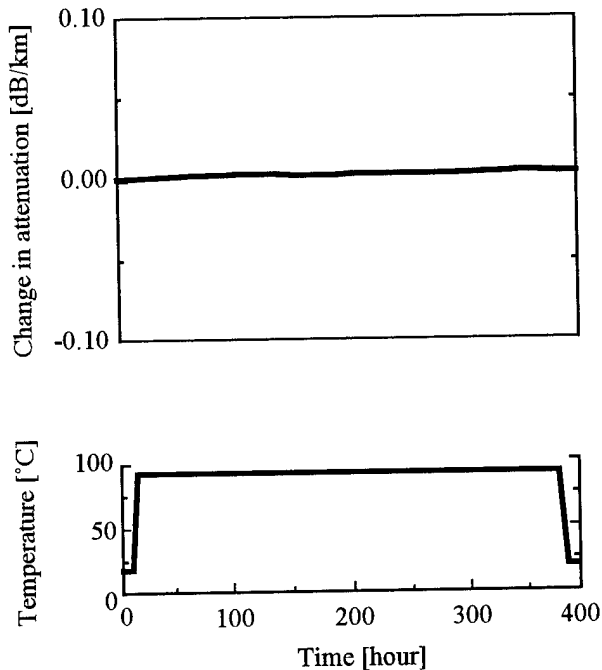


Figure 6 Long term aging (continuous 90°C temperature) test

4-4. Short-circuit test

Short-circuit test is an important test item to evaluate practicability of OPGW, for such test was conducted to simulate accidental fault in power transmission lines.

Figure 7 shows the scheme of the short-circuit experimental set-up. Alternating current of 3.7 kA was applied repeatedly 10 times to a 8m-long SUS tube OPGW for 1.0 second to simulate fault current. Six fibers in one bundle were fusion spliced to form a 48m-long loop transmission line. Temperature of the SUS tube and the transmission loss change at a wavelength 1550 nm were continuously monitored.

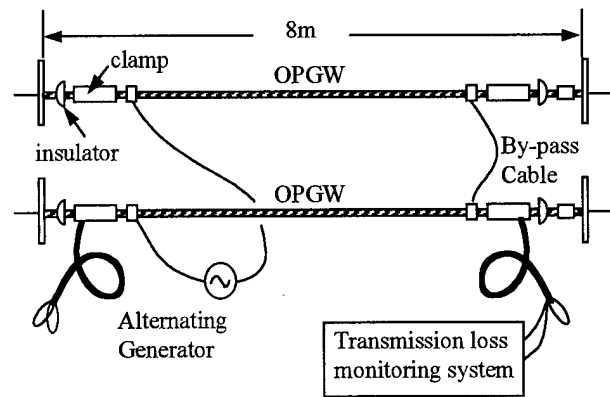


Figure 7 Short circuit experimental set-up

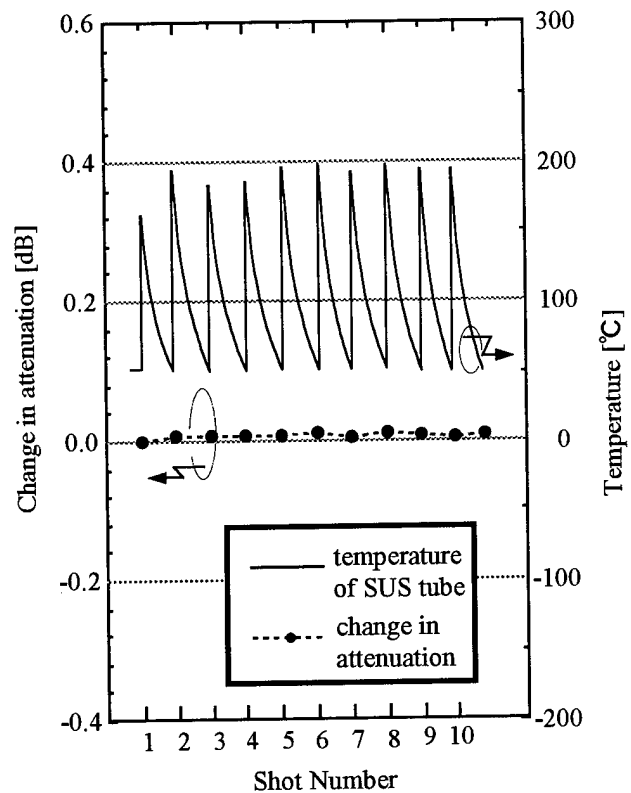


Figure 8 Peak temperature and transmission loss change of the SUS tube OPGW in short circuit test

Temperature of the optical fiber and transmission loss change are shown against applied current in Figure 8. No loss change of the optical fibers was observed under high temperature conditions around 200°C . In addition to the evaluation result of above-

Table 1 Various mechanical tests and results

Test Item	Test Conditions	Test Results
Crushing Force	Plate width : 50 mm Fusion splicing : 6 fibers Crushing force : 800kg	< 0.01 dB
Tensile Load	Sample length : 5 m Fusion splicing : 6 fibers Tensile load : until 80% UTS	< 0.01 dB
Vibration	Sample length : 30 m Fusion splicing : 6 fibers Stringing tension : until 20% UTS Cycle : 86 Hz Amplitude : 32 mm Number of times: 6×10^7 times	< 0.01 dB
Twist	Sample length : 30 m Fusion splicing : 6 fibers Stringing tension : 20% UTS until 1 rotation / 1m	< 0.01 dB
Bend	Bending diameter (D) : 80mm, 120mm, 200mm Fusion splicing : 6 fibers Bending angle : 180 degree	< 0.01 dB
Squeezing	Sample length : 15 m Fusion splicing : 6 fibers Stringing tension : 25% UTS Bending angle : 30 degree Pulley : 450 mm Round-Trip cycle : 20 cycles	< 0.01 dB

mentioned temperature dependence, it was confirmed that the SUS tube OPGW using colored thread binders had excellent heat-resistance.

4-5. Mechanical properties

The results of mechanical tests for the OPGW with the central SUS tube are shown in Table 1. Optical loss was continuously monitored at 1550 nm wavelength during each mechanical tests. In regard to all of test items, stable and excellent results were confirmed with no attenuation increase.

5. CONCLUSION

The small size and high performance central SUS tube OPGW was realized by the proper design of fiber XSL, the precise control of XSL variation and the use of colored thread binders for simple identification and for reducing interaction between fiber bundles and between fiber bundles and the tube. In point of cable design, it is easy to increase the fiber count by increasing the number of fiber bundles. Moreover, the low PMD has given the prospect of the OPGW for the use in future high bit rate optical transmission systems.

REFERENCES

[1] H. Haag, et al., "Optical Ground Wire and All Dielectric Self-Supporting Cable," in Proc. 43rd IWCS, pp. 380-387, (1994).

[2] J. P. Bonicel, et al., "Optical Ground Wire A Worldwide Technical Survey and Comparison," in Proc. 42nd IWCS, pp. 42-47, (1993).

[3] H. Haag, et al., "A New identification System for Optical Fibers in High Count Buffer Tubes," in Proc. 44th IWCS, pp. 546-549, (1995).

Kohichi Yonezawa



Sumitomo Electric
Industries, Ltd.
Electric Conductor
Division

1-1-3, Shimaya, Konohana
-ku, Osaka, 554 Japan

Kohichi Yonezawa was born in 1969 and received his B.E. degree in Electrical Engineering from Nagoya Univ. in 1992.

He joined Sumitomo Electric Industries, Ltd. and has been engaged in design and development of electrical conductor for transmission line. Mr. Yonezawa is a member of Transmission Line Engineering Section in Electric Conductor Division.

Tomoyuki Yokokawa



Sumitomo Electric
Industries, Ltd.
Yokohama Research
Laboratories

1, Taya-cho, Sakae-ku,
Yokohama, 244 Japan

Tomoyuki Yokokawa was born in 1968 and received his B.E. and M.E. degrees in Electrical Engineering from Waseda Univ. in 1994.

He joined Sumitomo Electric Industries, Ltd. and has been engaged in research and development of optical fiber cables. Mr. Yokokawa is a member of the Communication Department in Yokohama Research Laboratories and a member of the Institute of Electronics, Information and Communication Engineers of Japan.

Yoshiyuki Suetsugu



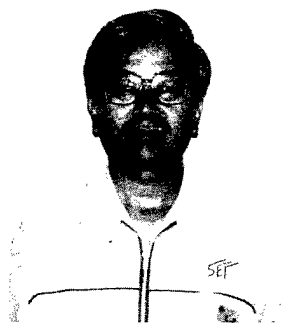
Sumitomo Electric
Industries, Ltd.
Yokohama Research
Laboratories

1, Taya-cho, Sakae-ku,
Yokohama, 244 Japan

Yoshiyuki Suetsugu was born in 1961 in Tokyo. He received B.S. degree in physics and Ph.D. degree in applied physics both from Tsukuba Univ. in 1984 and 1996, respectively.

He joined Sumitomo Electric Industries, Ltd. in 1984 and has been engaged in design and characterization of optical fibers and optical cables at Yokohama Research Laboratories. Dr. Suetsugu is a senior engineer of the Communication Department in Yokohama Research Laboratories and a member of the Institute of Electronics, Information and Communication Engineering of Japan.

Kazuhiko Nagatomi



Sumitomo Electric
Industries, Ltd.
Electric Conductor
Division

1-1-3, Shimaya, Konohana
-ku, Osaka, 554 Japan

Kazuhiko Nagatomi was born in 1946 and received B.E. degree in mechanical engineering from Kyushu University. He joined Sumitomo Electric Industries, Ltd. in 1971 and has been engaged in design and development on overhead transmission line conductors & accessories. Mr. Nagatomi is a member of the Institute of Electrical Engineers of Japan.

Shigeru Tanaka



Sumitomo Electric
Industries, Ltd.
Yokohama Research
Laboratories

1, Taya-cho, Sakae-ku,
Yokohama, 244 Japan

Shigeru Tanaka received his M.E. and Ph.D. degrees from Tokyo Univ. in 1976 and 1989. He joined Sumitomo Electric Industries, Ltd. in 1976, and has been engaged in research and development of optical fiber and cables. Dr. Tanaka is a manager of Communication Department in Yokohama Research Laboratories and a member of the Institute of Electronics, Information and Communication Engineers of Japan.

Optimized Design and Characteristics Analysis for High-count and Downsized OPGW

S.C. PARK, J.C. JO, Y.I. LEE, H.J. KANG

THIHAN ELECTRIC WIRE CO., LTD.
785, KWANYANG-DONG, ANYANG-CITY, KYUNGKI-DO, KOREA

ABSTRACT

To satisfy the recent demands for longer distance and larger capacity communication, it is necessary to make the multicore OPGW which contain the high-count fibers without increasing the outer cable diameter. For the optimized multicore unit design, we analyzed the effect of heat aging, heat shock test and excess length according to different kinds of unit construction. Also we have developed high-count and ribbonized OPGW which use the ribbon. This paper describes the ribbon design and the test result for newly developed OPGW.

1. INTRODUCTION

According to the increase of optical fiber demands and application of OPGW, it is realized that the developed high-count OPGW is essential for telecommunication networks. Generally, the coating material for OPGW is used fluorocarbon polymer resin, polyimide tape and loose tube in those days. But their use reached the uppermost limit for high-count and downsizing. Normally to meet the severe heat resistance, 400 μ m diameter fibers coated by silicone resin are used in conventional OPGW. However UV

coated fiber is used most widely in the world. To construct the vast optical networks, it is important to reduce the cable weight and diameter. Since OPGW is subjected to electrical current such as induction and short circuit, the cable is heated by itself. For this reason, OPGW is required higher heat resistant property than commonly used optical fiber cable. The conventional UV acrylate fiber withstands maximum 120°C. But, assuming that it is applied to induction circuit and lightning the OPGW, the conventional optical units should withstand more than 250°C aging for short term and more than 150°C aging for long term. However the ribbonized OPGW is required 180°C aging for short term and 120°C aging for long term test in low voltage power cable. Hence, heat short test and mechanical test were conducted to evaluate the transmission characteristics of a new ribbonized OPGW.

2. OPGW DESIGN

2.1 Newly Developed Ribbon

In order to make sufficient heat resistant ribbon, we manufactured the UV silicone and fluorocarbon polymer coating type

ribbon unlike conventional ribbon. Besides enduring the ribbon heat resistant, the ribbon matrix material helps to protect the optical fibers from lateral force that can lead to microbending due to the supplied tensile strength. Recently conventional ribbon which coated by UV acrylate resin has been widely used, but newly developed ribbon was made by the developed UV silicone acrylate resin to ensure strong stiffness and lateral force. And then, this thin ribbon was smeared by thermal silicone resin and, jacketed by fluorocarbon polymer resin that has melting point over 300°C against roughness and heat resistance. The newly developed ribbon requires the adhesion of UV acrylate and silicone to ensure heat resistance, and stiffness of its surface to guarantee fiber characteristics when ribbon is inserted into a AL spacer. As a result, Fig. 1 shows the new developed ribbon construction that coated silicone and fluorocarbon polymer by using the conventional ribbon. We design the compact ribbon in order to maintain heat resistance and stiffness.

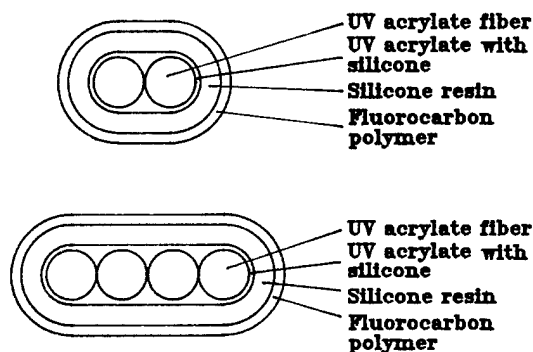


[Fig. 1] Cross-section of a new 2 & 4-ribbon

2.2 Theoretical Analysis of Excess Length

The OPGW is subjected to some tensile force during installation, and is affected by

the stress of environmental conditions. Therefore, to evaluate application of ribbon unit, we observed tensile properties theoretically and practically. It is very important to evaluate the excess length of fibers in the slotted rod for optimized cable design as well as tensile properties. We theoretically consider 6-core unit and new ribbon unit under the effect of excess length for newly developed OPGW. The OPGW is composed of excess length in optical fiber stranding unit and inserting process of AL spacer.

$$E_{\text{total}} = E_{\text{unit}} + E_{\text{inserting}} \dots\dots\dots (1)$$

① Excess length of stranding unit (E unit)

E unit is the excess length of each unit of stranded around FRP rod. Excess length of stranding unit can be calculated by following formula (2).

$$E_{\text{unit}} = \sqrt{\left[\frac{\pi D'}{P} \right]^2 + 1} \dots\dots\dots (2)$$

P : lay length(mm)

D' : the length of center-to-center between the optical fiber over central strength member(mm)

② Excess length of inserting (E inserting)

The difference of excess length in unit between bottom and top of the AL spacer is given by the following formula.

$$E_c = \frac{2\pi^2 (D-h)(h-d)}{P^2 + \pi^2 (D-d)^2} \dots\dots\dots (3)$$

P : Pitch (mm)

D : Diameter of AL spacer(mm)

d : Diameter of unit(mm)

h : Height of groove (mm)

Considering the minimum bending radius,

$$E_{\text{inserting}} = \frac{(h-d)}{4(D-d)\left(1 + \frac{P^2}{\pi^2 (D-d)^2}\right)} + \frac{Ec}{2}$$

Especially, Fig. 2 shows the excess length of ribbon unit into AL spacer.

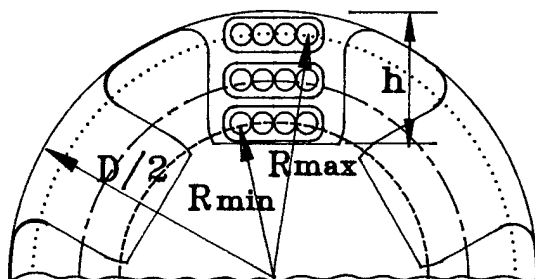


[Fig.2] Analysis of the excess length of ribbon fiber

2.3 Comparison of Each Unit Structure

We have investigated six types of unit with different structure to optimize OPGW design. To compare the six types of unit under same condition, we inserted the manufactured each unit into a same AL spacer. Fig. 3 and Table 1 shows the structure of OPGW and characteristics of OP-unit. Type I and II are ribbon unit as mentioned above.

(a) Type III : Fluorocarbon polymer coating type using silicone fiber

The samples of 400 μ m silicone coating fiber to meet the heat resistant requirement and soft silicone resin was filled in interspaces of these fibers to form a basal unit and extruded by fluorocarbon polymer resin. This type was commonly used an early stage

because silicone has a good property of heat resistant.

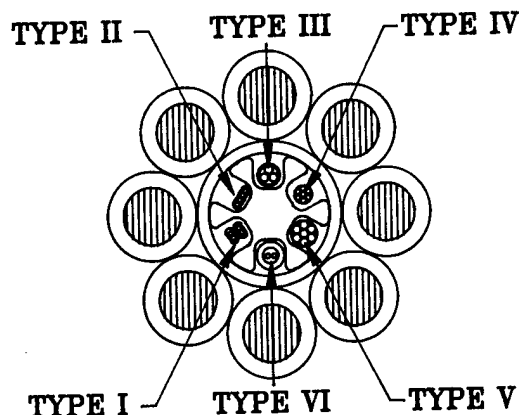


Fig. 3 Cross-section of a six-groove OPGW

[Table 1] Characteristics of OP-unit

Type	Structure	Fiber	Outer coating diameter	Unit diameter	NO. of fiber
I		250 μ m UV acrylate	Silicone & fluorocarbon polymer	0.6 \times 0.9mm	2
II		250 μ m UV acrylate	Silicone & fluorocarbon polymer	0.6 \times 1.4mm	4
III		400 μ m Silicone	Silicone & fluorocarbon polymer	ϕ 1.15mm	3
IV		250 μ m UV acrylate	Polyimide	ϕ 0.8mm	6
V		400 μ m Silicone	Polyimide	ϕ 1.25mm	6
VI		250 μ m UV acrylate	PBT & Silicone	ϕ 1.4mm	2

(b) Type IV : Polyimide tape wrapping type using UV acrylate fiber

To minimize the unit core in comparison with silicone fiber, 250 μ m UV acrylate fibers were stranded around 0.25mm FRP rod, and wrapping by polyimide tape. This unit is one of the smallest structure.

(c) Type V : Polyimide tape wrapping type using silicone fiber

Type V is composed of 0.4mm silicone fibers which have stranded around 0.4mm FRP rod, and was wrapping by thin and heat resistant polyimide tape to improve the heat resistance. This structure makes coating removal easier than fluorocarbon polymer coating to improve fiber splicing efficiency.

(d) Type VI : Loose tube type using UV acrylate fiber

This type was manufactured by PBT in the form of a loose tube type that contain 2-fiber. The structure of Type VI has not impair the OPGW's strain or lateral effect.

as shown in Fig. 4. The change of transmission loss and the deterioration of outer material in 6-core unit of UV acrylate optical fiber and loose tube were increased more than 0.10dB/km at 1.55 μ m wavelength. But, in case of the OPGW with silicone fiber unit and ribbon that coated fluorocarbon polymer, the transmission loss changes were less than 0.05dB/km, also the degree of deterioration is not so severe.

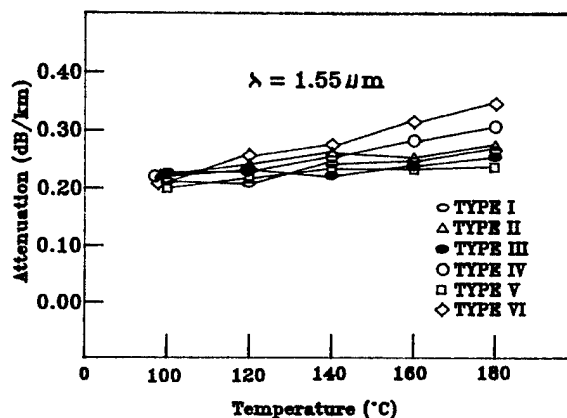


[Fig.4] Attenuation against short term heat aging

3. OPTICAL CHARACTERISTICS

We have evaluated the characteristics with above mentioned 6 types of unit.

3.1 Short term heat aging test

Due to lightning and electromagnetic induction current, the OPGW may be laid in high temperature. Therefore, the specimens, OP unit with a length 300m was looped at both ends, exposed to heat hysteresis in chamber (Peak temperatures were 100°C, 120°C, 140°C, 160°C and 180°C). The changes of transmission loss in 8-cycle were continuously measured at 1.55 μ m wavelength

3.2 Long Term Heat Aging Test

This test method was chosen by the similar reason as the short term aging test and the OPGW is necessary to endure long compatibility. The specimens exposed at 80°C, 100°C, 120°C respectively for 400 hours in chamber and observed transmission loss and the deterioration. The characteristics of attenuation loss in each specimen is shown in Fig. 5 and is less than 0.05dB/km in silicone fiber and new ribbon unit. On the other hand, the unit using UV acrylate fiber and loose tube was changed up to 0.15dB/km at 1.55 μ m wavelength.

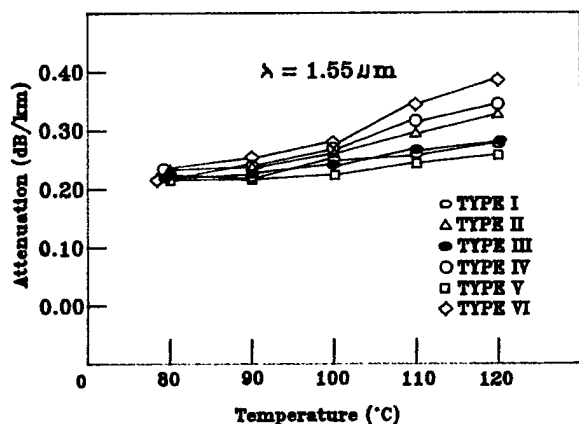


[Fig.5] Attenuation against long term heat aging test

3.3 Tensile Test

The changes in transmission loss and fiber strain caused by application of tensile force were measured. Fig. 6 is shown the characteristics of strain and tensile force with attenuation loss while tensile tests were performed by applying up to 50kN. The variation of attenuation maintained a stable

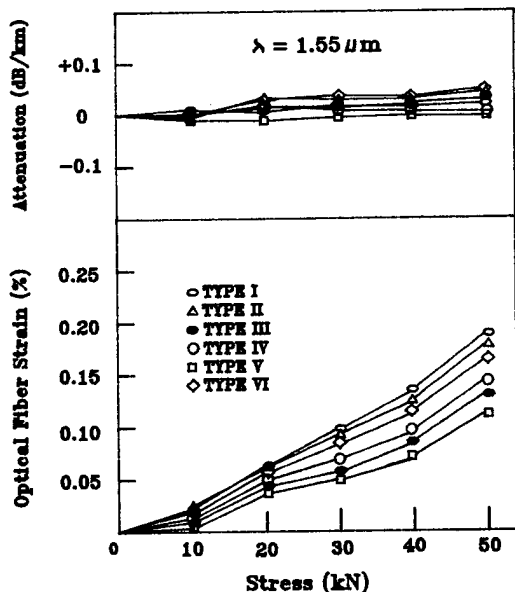


[Fig.6] Characteristics of fiber strain and attenuation according to stress

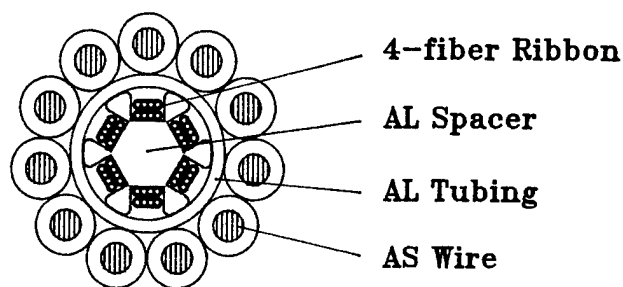
state within 0.05dB/km. Though the ribbon unit have the shortest excess length compare to other kinds of units, the ribbon fiber strain reached 0.18% at stress of 50kN and exhibited good result equivalent to conventional fiber.

4. CONCLUSION

As above mentioned, we have developed newly ribbon type high-count OPGW up to 48-fiber as shown Fig. 7 and the comparison of conventional OPGW and new developed ribbonized OPGW are summarized in Table 2. This ribbon type OPGW can be accommodated to 48-core into downsizing AL spacer compared to conventional 36-core OPGW. In addition, newly developed ROPGW(Ribbonized Optical Ground Wire) is considered as one of the suitable structure for high-count OPGW in low voltage. The practical temperature limit of commercial silicone fiber with PI tape wrapping unit and newly developed ribbon was good characteristics in 180°C for the short term(8-cycle) and 120°C for long term(400 hours) for OPGW application. Besides, UV silicone resin coating ribbon for OPGW has a trustworthy value in mechanical test. Therefore, by investigating OPGW that contained ribbon unit, we have found it possible to expect to allow a fast increase in fiber-packing density as compared with the existing conventional 36-core OPGW and improve fiber splicing efficiency at the same time.

**Table 2 Comparison of conventional OPGW
and newly developed ribbonized OPGW**

Item	Conventinal OPGW	Newly developed ribbonized OPGW
NO. of fiber	36	48
Unit structure	Silicone fiber & PI tape	UV ribbon & fluorocarbon polymer
Unit diameter	8.0mm	7.5mm
OPGW diameter	13.7mm	13.2mm

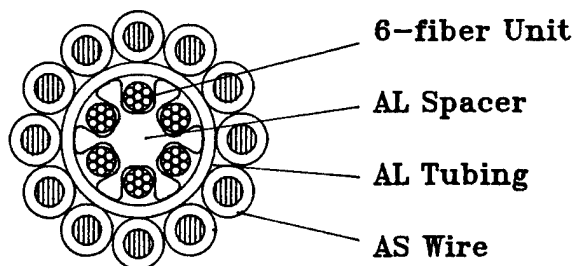


(b) Newly developed 48-core ROPGW

**[Fig.7] Construction of conventional OPGW
and Newly developed OPGW**

REFERENCES

1. K. Nakagaki et al., "Development of High-Performance Composite Fiber-Optic Overhead Ground Wire", Proc. of 35th I.W.C.S., 1986.
2. I. Matsubara, Y. Kitayama, S. Nishiyama, T. Kikuta, "Development of large-capacity composite fiber-optic ground wire", Conference of the Institute of Electric Engineers of Japan, 1065, 1986.
3. H. Satomi, K. Yutaka, H. Kazou, "Multi-hundred-fiber Cable Composed of Optical Fiber Ribbons Inserted Tightly into Slots" Proc. of 35th I.W.C.S., 1986



(a) Conventional 36-core OPGW

BIOGRAPHIES



Sang-cheol, PARK

Taihan Electric Wire
Co., Ltd. Korea

S.C. PARK received his B.A. degree from A-juo University in 1994. He joined Taihan Electric Wire Co., Ltd. and has been engaged in engineering department of optical fiber. Now he is a engineer of Fiber Optics Engineering Department.



Young-ik, LEE

Taihan Electric Wire
Co., Ltd. Korea

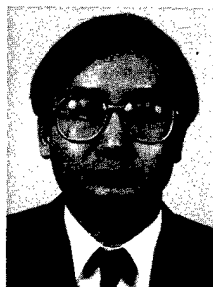
Y.I. LEE received his M.S. degree from Yonsei University in 1981. He joined Taihan Electric Wire Co., Ltd. and has been engaged in engineering department of optical fiber. Now he is a section manager of Fiber Optics Engineering Department.



Jin-cheol, JO

Taihan Electric Wire
Co., Ltd. Korea

J.C. JO received his B.A. degree from Kwangun University in 1992. He joined Taihan Electric Wire Co., Ltd. and has been engaged in engineering department of optical fiber. Now he is a engineer of Fiber Optics Engineering Department.



Hee-jeon, KANG

Taihan Electric Wire
Co., Ltd. Korea

H.J. KANG received his B.A. degree from Hanyang University in 1979. He joined Taihan Electric Wire Co., Ltd. and has been engaged in engineering department of optical fiber. Now he is a general manager of Fiber Optics Engineering Department.

COAXIAL CABLE WITH INTEGRATED RIBBON-SLOTS IN THE JACKET AND ACCESSORY PART FOR BROADBAND NETWORK

E.Esposito,A.Di Francesco,A.Tedeschi,G.Di Censo

Teleco Cavi, Roseto degli Abruzzi (TE),Italy

ABSTRACT

This paper describes the new hybrid cable construction where the ribbons containing the optical fibers,are placed into the slots realized on the coaxial cable external sheath.Such a solution presents the advantages :

- a) of having the optical fibers externally,
- b) not influencing the coaxial element characteristics at high frequency,
- c) using, as framework, aluminium or copper coax cables of standard dimensions and productions already consolidated on world-wide market.

We want to point out that the optical fibers are sufficiently protected and they keep their performance up according to Telecom Italy specifications.

The optical,electric,environmental and mechanical characteristics will be presented.

The accessories don't require any special solution such to increase the installation costs;the standard RF connectors,already consolidated on world-wide market,are used.

As regards the accessories,tests of mechanical and environmental characteristics will be presented.

INTRODUCTION

The Telecommunications industry's growing interest for broadband services ,such as broadcast video and interactive multimedia services,added to traditional telecommunications systems,imposes a series of technical and economic analyses of the possible architectural and system solutions of the access network.

In Italy, a broadband network based on the construction of a flexible network infrastructure,able to evolve gradually in response to changes in the service offered, is in course of development.

The purpose of all operators is the gradual and extensive introduction of optical fiber in the access network.

For such a reason,the HFC broadband network foresees the coax/optical fiber ribbons cable installation at experimental level.

These types of cables will be used in the network terminal area between the fiber node and the subscriber.

CABLE DESIGN AND PERFORMANCE

Cable Construction

The cable construction is based on a standard aluminium coaxial trunk cable that is normally used in HFC broadband network.The cable coaxial component is also used as framework.

On the coaxial cable external sheath, the Ribbon Slotted core (4 R) has been carried out.

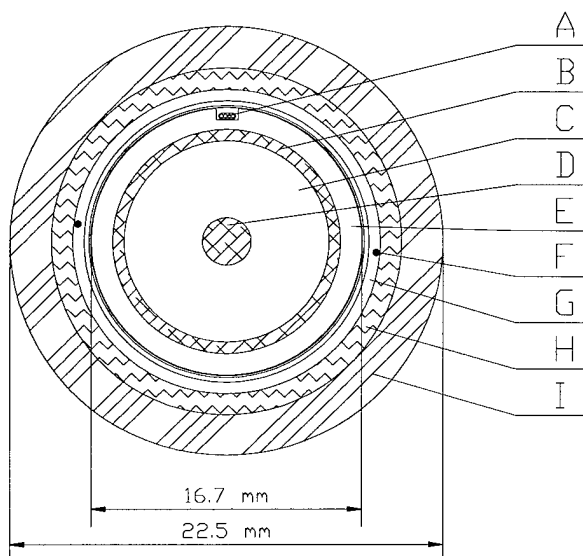
On the slotted core a mechanical protection has been realized ensuring the fiber optical, mechanical and environmental characteristics.

Figure 1 shows a cable cross section design and Figure 2 a sample cable.

Inner conductor . A copper-clad aluminium makes up the inner conductor .It contains 10 % copper by volume,corresponding ,in such a case,to 0.08 mm .The inner conductor diameter is 3.15 mm.

Insulation . The insulation consists of physically foamed polyethylene of about 80 % blowing degree .

Outer Conductor . The outer conductor is made up of welded aluminium tube with a 0.35 mm wall thickness.



- A : 4 optical fiber ribbon
- B : Outer conductor Al
- C : Foamed PE insulation
- D : Inner conductor Al + Cu
- E : Slotted core
- F : Rip Cord
- G : Aramid yarns
- H : Corrugated steel tape
- I : Outer PE sheath

Figure 1 : Cable cross section design

Slotted core . A flooding compound between the outer conductor and the slotted core provides additional protection against corrosion.

The slotted core material consists of a standard medium density polyethylene .

The slot is wound up in closed helicoidal type; four optical fibers ribbon has been put inside it down.

The slot size and the helix lay have been planned so that the fiber optic mechanical stress or the attenuation increase were not introduced .

The Standard Ribbon in according with IEC 794 /1/ has been used.

External protection . In order to meet Telecom Italy specification some protections have been provided.

On the slotted core there are the Rip cord, Aramid yarns, Corrugated steel tape and outer polyethylene sheath.

The main construction characteristics are summarized in Table 1.

TABLE 1 : Main dimensional Cable Characteristic

TEST	M.U.	MAX	MIN	MED
INNER CONDUCTOR	mm	3.16	3.13	3.14
DIELECTRIC DIAMETER	mm	12.99	12.87	12.92
OUTER CONDUCTOR :				
THICKNESS	mm	0.36	0.35	0.355
DIAMETER	mm	13.79	13.62	13.70
SLOTTED CORE: DIAMETER	mm	16.93	16.79	16.85
STEEL TAPE : OVERLAP	mm	9.85	9.74	9.80
OUTER SHEATH : THICKNESS	mm	1.81	1.62	1.71
OUTER DIAMETER	mm	22.78	22.55	22.65

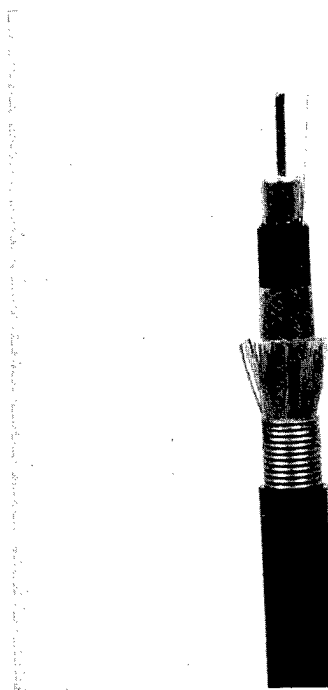


Figure 2: Cable sample

Electrical and Optical Characteristics

Coaxial structure . The cable construction hasn't modified the standard aluminium coaxial cable electrical performance .

Table 2 and Table 3 show low and high frequency measurements after temperature cycling (+ 20 °C , - 30 °C , + 60°C) .The most important parameters,such as : return loss, impedance regularity and characteristic impedance didn't change.

Optical structure . In order to realized Ribbon SMR fibers are used .

Geometrical and trasmissive tests have been carried out.

Table 4 shows the fibers cabled typical performance.

Mechanical and Environmental Characteristics

Several tests have been carried out in order to determine the agreement of the completed cable to mechanical and environmental specifications.

Tensile performance . A 100 m cable was tested by load of 1500 N : no change in fibers attenuation has been found ; the cable and fibers strain was less then 0.25 % .No change in electrical parameters during the test.

Crush Test . The crush test was carried out on a force of 5000 N : The impedance regularity turned out less then 46 dB at 2500 N .No change in fibers attenuation at 5000 N.

Impact . The test was carried out on an anvil diameter of 20 mm : No breaks of fibers or change in attenuation at 5 kg x m .The impedance regularity turned out less then 46 dB at 1kg x m .

Torsion . A 1 m cable sample was tested at a load of 100 N :No change in electrical or optical parameters has been found.

Temperature cycle .Increase of fibers attenuation at temperature cycling and attenuation residue after a complete cycle have been tested.The results, shown in Table 5,meet the reference specifications.

Bending . The test was carried out by 3 cycles on a mandrel of diameter 20 times the cable diameter according to the optical fiber cable specifications and 1 turn on 600 mm diameter according to the coaxial cable specifications

**TABLE 2 - Temperature cycling :
Electrical Characteristics**

TEST	M.U.	T 20°C	T -30°C	T +60°C
Characteristic Impedance	Ohm	75,87	75,35	75,41
Capacitance	nF/km	49,85	49,85	49,81
DC-Resistance inner conductor	Ohm/km	3,48	2,75	3,91
DC-Resistance outer conductor	Ohm/km	1,93	1,54	2,20
DC-Resistance loop	Ohm/km	5,41	4,29	6,11
Velocity ratio (v/c)	%	88	88	88
Return Loss f < 600 Mhz	dB	>32	>32	>32
Return Loss f > 600 Mhz	dB	>30	>30	>30
Impedance Regularity	dB	>46	>46	>46

TABLE 3 - Temperature cycling :Attenuation

Frequency (MHz)	M.U.	T = 20°C	T = -30°C	T =+60°C
5	dB/100m	0.45	0.42	0.49
30	dB/100m	1.09	1.03	1.20
47	dB/100m	1.40	1.26	1.48
100	dB/100m	2.07	1.87	2.18
200	dB/100m	2.95	2.65	3.11
300	dB/100m	3.64	3.27	3.83
450	dB/100m	4.51	4.05	4.74
600	dB/100m	5.25	4.71	5.51
862	dB/100m	6.39	5.72	6.71
960	dB/100m	6.77	6.06	7.11
1000	dB/100m	6.92	6.19	7.26

Typical optical and electrical performance are conforming to the specifications.

Water penetration . A 3 m cable sample was tested for a duration of 24 h : No water penetraton at the opposite end of the cable has been cheeked.

Table 5 describes the results of the tests ,the requirements and the reference specifications.

TABLE 4 - Geometrical and Transmissive Tests on the cabled fibers

TEST	REQUIREMENTS	SPECIFICATION STANDARD	TYPICAL PERFORMANCE
CLADDING DIAMETER	$123 \leq \phi_{CL} \leq 127\text{mm}$	CECC EN 188000 Method 101	$124.8 \leq \phi_{CL} \leq 125.3\text{mm}$
ERROR CONCENTRICITY CORE/CLADDING	Concentricity $\leq 1\text{mm}$	CECC EN 188000 Method 101	Concentricity $\leq 0.3\text{mm}$
ERROR CIRCULARITY CLADDING	Circularity $\leq 2\%$	CECC EN 188000 Method 101	Circularity $\leq 0.53\%$
DISPERSION CROMATIC	$D_{MAX} (1285, 1330\text{nm}) \leq 3.4 \text{ ps / nm x km}$ $D_{Mean} (1285, 1330\text{nm}) \leq 3.0 \text{ ps / nm x km}$ $D_{MAX} (1550\text{nm}) \leq 20 \text{ ps / nm x km}$ $D_{Mean} (1550\text{nm}) \leq 17 \text{ ps / nm x km}$	CECC EN 188000 Method 308	$D_{MAX} (1285, 1330\text{nm}) = 2.85 \text{ ps / nm x km}$ $D_{Mean} (1285, 1330\text{nm}) = 2.78 \text{ ps / nm x km}$ $D_{MAX} (1550\text{nm}) = 16.46 \text{ ps / nm x km}$ $D_{Mean} (1550\text{nm}) = 16.40 \text{ ps / nm x km}$
LAMBA ZERO (λ_0)	$1306 \leq \lambda_0 \leq 1324 \text{ nm}$	CECC EN 188000 Method 310	$1314 \leq \lambda_0 \leq 1315.4 \text{ nm}$
MODE FIELD DIAMETER	$9.1 \leq M \leq 9.7 \text{ mm}$	CECC EN 188000 Method 315	$9.21 \leq M \leq 9.39 \text{ mm}$
PEAK H ₂ O	$\leq 2.1 \text{ dB / km}$	CECC EN 188000 Method 301	$\leq 2.1 \text{ dB / km}$
CUT - BACK	$\lambda = 1310 \text{ nm} :$ $\alpha_{mean} \leq 0.38 \text{ dB / km}$ $\alpha_{max} \leq 0.44 \text{ dB / km}$ $\lambda = 1550 \text{ nm} :$ $\alpha_{mean} \leq 0.22 \text{ dB / km}$ $\alpha_{max} \leq 0.28 \text{ dB / km}$	CECC EN 188000 Method 301	$\lambda = 1310 \text{ nm} :$ $\alpha_{mean} = 0.35 \text{ dB / km}$ $\alpha_{max} = 0.37 \text{ dB / km}$ $\lambda = 1550 \text{ nm} :$ $\alpha_{mean} = 0.22 \text{ dB / km}$ $\alpha_{max} = 0.25 \text{ dB / km}$
CUT - OFF	$1160 \leq \lambda_c \leq 1320 \text{ nm}$	CECC EN 188000 Method 312	$1189 \leq \lambda_c \leq 1209 \text{ nm}$
O.T.D.R.	$\lambda = 1310 \text{ nm} :$ $\alpha_{mean} \leq 0.38 \text{ dB / km}$ $\alpha_{max} \leq 0.44 \text{ dB / km}$ $\lambda = 1550 \text{ nm} :$ $\alpha_{mean} \leq 0.22 \text{ dB / km}$ $\alpha_{max} \leq 0.28 \text{ dB / km}$	CECC EN 188000 Method 303	$\lambda = 1310 \text{ nm} :$ $\alpha_{mean} = 0.35 \text{ dB / km}$ $\alpha_{max} = 0.37 \text{ dB / km}$ $\lambda = 1550 \text{ nm} :$ $\alpha_{mean} = 0.21 \text{ dB / km}$ $\alpha_{max} = 0.24 \text{ dB / km}$

ACCESSORIES

Components already consolidated on world-wide marked, are used for connecting the coaxial and optical part of the cable.

Mechanical and environmental tests on brancher, protective ribbon tube and protective splice cassette has been developed.

Connector Standard RF connector can be used for connecting the cable coaxial part. Figure 3 shows the coaxial cable with connector.

Ribbon Brancher The ribbon brancher, used for separating the optical fiber from the main cable, avoids the mechanical stress on the fibers.

Figure 4 shows the brancher cross section .

Protective ribbon tube . An additional protective ribbon tube must be used for connecting the ribbon to the splice box.

TABLE 5 - Mechanical and Environmental tests on the cable

TEST	CONDITIONS	REQUIREMENTS	SPECIFICATION	TYPICAL OPTICAL PERFORMANCE	TYPICAL ELECTRICAL PERFORMANCE
TENSILE PERFORMANCE	100 m cable Load = 1500 N	<ul style="list-style-type: none"> • Optical: Cable and Fibers Strain : $\leq 0.25\%$ No change in Attenuation • Electrical: No change in Electrical parameters 	IEC 794 - 1 - E1 CECC EN 187000 Method 501 C.T. 1436	Cable Strain : $\leq 0.075\%$ Fiber Strain : $\leq 0.017\%$ No change in Attenuation	No change in : - Characteristic impedance - Capacitance - DC - Resistance - Velocity Ratio - Return Loss - Impedance regularity - Attenuation
CRUSH	Plate/Plate Load = 5000 N	<ul style="list-style-type: none"> • Optical: No change in Attenuation • Electrical: Impedance Regularity Under Study 	IEC 794 - 1 - E3 CECC EN 187000 Method 504 C.T. 1436	No change in Attenuation at 5000 N.	Impedance Regularity : < 46dB x 2500 N
IMPACT	Anvil diameter 20 mm Number of impacts : 1 in 3 different places	<ul style="list-style-type: none"> • Optical: Under Study • Electrical: Impedance Regularity Under Study 	IEC 794 - 1 - E3 CECC EN 187000 Method 504 C.T. 1436	No change in Attenuation or Breaks of fibers at 5 kg x m.	Impedance Regularity : <46dB x 1Kg x m
TORSION	Length of the sample : 1 m Load : 100 N N°3 twist cycles Twist angle: $\pm 90^\circ$ Twist angle $\pm 180^\circ$	<ul style="list-style-type: none"> • Optical: No visible damage No change in Attenuation • Electrical: Impedance Regularity Under Study 	IEC 794 - 1 - E7 CECC EN 187000 Method 508 C.T. 1436	No visible damage. No change in Attenuation for twist angle $\pm 90^\circ\text{C}$ and $\pm 180^\circ\text{C}$	Impedance Regularity : No change.
TEMPERATURE CYCLING	1 Cycle - 30°C + 60°C	<ul style="list-style-type: none"> • Optical: Increase of attenuation at 1550 nm $\leq 0.15\text{ dB/km (max)}$ $\leq 0.05\text{ dB/km (mean)}$ No increase residue of attenuation at 1550 nm after complete cycle. • Electrical: No increase residue of electrical parameters 	IEC 794 - 1 - F1 CECC EN 187000 Method 601 C.T. 1436	At 1550 nm : $\leq 0.08\text{ dB/km (max)}$ $\leq 0.05\text{ dB/km (mean)}$ No increase residue of attenuation	No increase residue of electrical parameters
WATER PENETRATION	Length of the sample: 3 m Test duration : 24 h	No penetration water to the opposite end.	IEC 794 - 1 - F5 CECC EN 187000 Method 605	No penetration water to the opposite end.	
BENDING	3 cycles on 20 times cable diameter.	<ul style="list-style-type: none"> • Optical: No visible damage of the fibers or the cable. 	IEC 794 - 1 - E11 CECC EN 187000 Method 513	No visible damage of the fibers or the cable	
	1 turn on 60 cm diameter.	<ul style="list-style-type: none"> • Electrical: Impedance Regularity: No change. 	C.T. 1436		Impedance Regularity : No change.

The protective tube consists of a tube ,a strenght member and an external sheath.The tube is in Nylon,the strenght member in Aramid yarn and the sheath in LSOH blu color (Figure 5).

Cassette splice box . Standard water tight splice cassette is used for joining the optical fiber ribbon.

Figure 6 illustrates an example of cables and accessories assembled : two hybrid coaxial cables have been connected ,by a splitter, with a trunk cable and the optical part , by splice cassette, with an optical fiber cable.

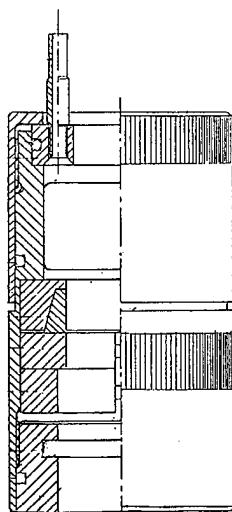


Figure 4 : Brancher Cross section

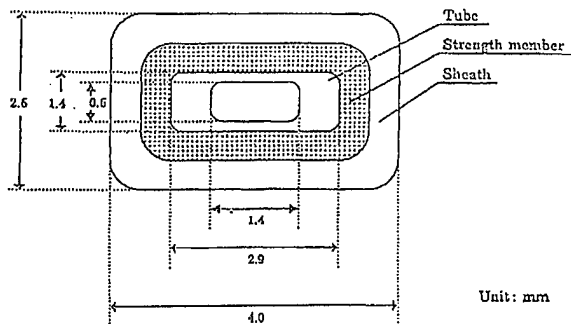


Figure 5 :Protective tube Cross section



Figure 3 : RF assembled Connector

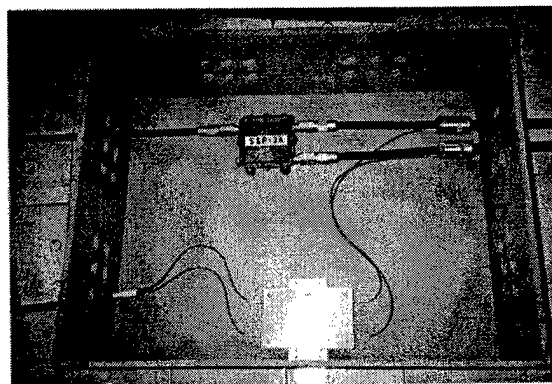


Figure 6 : Cable and accessories assembled

MECHANICAL AND ENVIRONMENTAL TESTS ON ACCESSORIES

Some tests have been developed for verifying that the accessories ability is in accordance with the specifications.

-The temperature cycling has been carried out on Brancher and protection splice cassette .

-The temperature cycling in water on protection splice cassette.

-The tensile performance on ribbon brancher and protective tube,

The torsion on protective tube.

The Tables 6,7,8,9 show that all tests are conforming to the reference specifications.

Table 6 :Temperature cycling on ribbon brancher and protection splice cassette

Test type O.P.M.	T= 23°C rif.			T = -30 °C x24 h		T = +60 °C x 24 h		T= 23°C fin.	
	dB	dB		dB	dB	dB	dB	dB	dB
Splice loss	$\lambda = 1310$	$\lambda = 1550$		$\lambda = 1310$	$\lambda = 1550$	$\lambda = 1310$	$\lambda = 1550$	$\lambda = 1310$	$\lambda = 1550$
Red fiber	0,00	0,00	$\Delta\alpha$ 1	-0,02	0,01	0,01	-0,01	-0,02	-0,03
White fiber (1)	0,00	0,00	$\Delta\alpha$ 2	-0,01	0,00	-0,02	-0,01	-0,02	0,00
White fiber (2)	0,00	0,00	$\Delta\alpha$ 3	-0,03	0,02	-0,02	0,00	0,01	0,01
Violet fiber	0,00	0,00	$\Delta\alpha$ 4	-0,01	-0,01	-0,01	-0,02	0,01	-0,01

TABLE 7 : Temperature cycling in water of the protection splice cassette

Test type O.P.M.	T= 23°C rif.			T = -15 °C x24 h		T = +60 °C x 24 h		T= 23°C fin.	
	dB	dB		dB	dB	dB	dB	dB	dB
Splice loss	$\lambda = 1310$	$\lambda = 1550$		$\lambda = 1310$	$\lambda = 1550$	$\lambda = 1310$	$\lambda = 1550$	$\lambda = 1310$	$\lambda = 1550$
Red fiber	0,00	0,00	$\Delta\alpha$ 1	-0,01	0,00	-0,03	-0,01	-0,02	-0,01
White fiber (1)	0,00	0,00	$\Delta\alpha$ 2	0,01	-0,01	0,00	0,00	0,01	-0,02
White fiber (2)	0,00	0,00	$\Delta\alpha$ 3	-0,01	-0,06	-0,01	-0,07	0,00	-0,05
Violet fiber	0,00	0,00	$\Delta\alpha$ 4	-0,01	-0,03	0,00	-0,06	0,01	-0,06

TABLE 8 :Tests on Ribbon Brancher

TEST	M.U.	Ref.Method	Results	Required
Tensile performance	KN	C.T.1216	1,36	1,00
Torsion		C.T.1216	OK	+/-90° x 3 times

TABLE 9 : Test on Protective ribbon tube

TEST	M.U.	Ref.Method	Results	Required
Tensile performance	KN	C.T.1216	0,256	0,10

CONCLUSIONS

A new hybrid fiber/coax cable for access network has been developed.

The cable has been realized using ,as framework, aluminium coaxial cable of standard dimensions and productions already consolidated

on world wide market.The idea of putting the ribbon outside the cable allows an easy accessibility to optical fibers and having an hybrid fiber/coax cable with an high fibers counter(upper 100 O.F.).The above mentioned idea allows of having an access network more

flexible in order to answer to future services with the subscribers require.

Results obtained show that the fibers are sufficiently protected and their performances agree Telecom Italy specifications.

The Accessories are commonly utilized in the world at low costs and their use don't increase the installation costs. The tests results on accessories show their agreement to the mechanical and environmental access network specifications.

The use of such a cable allows a cost's reduction compared with the saving on civil works during the first cables installation.

REFERENCES

1. "Optical fibre cables" IEC 794
2. "Optical fibres" IEC 793
3. "Optical fibres" CECC EN 188000
4. "Optical fibre cables" CECC EN 187000
5. "Coaxial cables used in cabled distribution networks Part 4 :Sectional specification for distribution and trunk cables" EN 50117-4
6. "Coaxial cables used in cabled distribution networks Part 1 :Generic specification" EN 50117-1



Ernesto Esposito was born in Roseto degli Abruzzi (Italy). He received the Doctorate in Telecommunication Engineering in 1976 from the University of Bologna. From 1978 he is employed in Teleco Cavi where, after an experience in optical and copper cables design, he is now in charge of the

"Research and Development" and "Quality Control Departments".



Andrea Di Francesco was born in Teramo (Italy). He received the Doctorate in Electronic Engineering in 1985 from the University of Ancona.

From 1987 he is employed in Teleco Cavi, where he gained experience in the design and manufacture of optical cables.

At present he is person responsible of the optical cable laboratory .

Arnoult Tedeschi was born in Torin on 19.9.1948. He has worked in Ceat Cavi from 1971 up to 1988 in the copper and optical fiber laboratory. From 1989 he is the person responsible of optical cable production in Teleco Cavi.



Giordano Di Censo was born in Pescara (Italy). He received the Doctorate in Electronic Engineering in 1991 from the University of Ancona. From 1993 he works in Teleco Cavi in the Research and Development Department. He has been

dealing with cable design, and data cables in particular.

OPTICAL FIBER AND COPPER CABLES AND PASSIVE COMPONENTS FOR FTTB / FTTC NETWORK

Authors: E.Cressan - O.Bouffant - G.Le Traon - O.Daguillon - R.Petit - J.Moalic

France Telecom - CNET/LAB - Lannion, FRANCE

ABSTRACT

This paper introduces the FTTB/FTTC architecture from the exchange to the home terminals for new, high-bit-rate applications. Several of the choices that were made for the "Multimedia sur Armor" Field Trial currently being conducted in the town of Lannion in the Brittany region of France, are also described herein. The first portion of the document focusses on Passive Optical Elements. The new generation of fiber optic cables are light and compact. These cables are made of elements such as ribbons and microelements. These structures enable fusion or mechanical mass splicing, which significantly reduces time in the field. In addition, the compact layout of these cable elements inside the different closures makes them more attractive. The second part of this document addresses the copper network: specifically, the public distribution and private home network. This portion also describes the architecture, the transmission and copper cabling systems, and the tests conducted in order to determine the copper configuration for the Field Trial.

INTRODUCTION

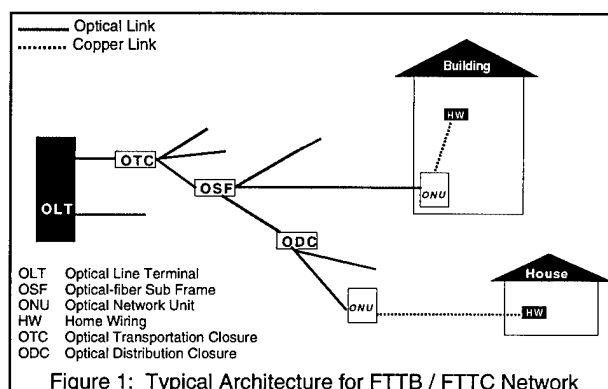
Different architecture solutions are employed by network operators in order to connect residential and small business customers. The most common types of architecture are described in the paper "Fiber-based Access Networks" [1]. This paper focusses on the FTTB / FTTC architecture (see Figure 1) adapted to the "Multimedia sur Armor" Field Trial. The copper transmission system uses ATM Forum 25,6 Mbit/s Interface (NRZI sequence, 4B5B encoded). This choice was made because the concerned chip set was the only one available on the market.

In terms of the actual "Multimedia sur Armor" Field Trial, in the Lannion area, about one hundred

customers are actively involved. Broadband services include:

- Multimedia on PC (Internet access, local services including movie trailers, news, etc.);
- Multimedia on Set Top Box (MOD: movies-on-demand, etc.).

POTS is also included.



The entire passive optical network is a new one, based on the latest in state-of-the-art developments and research. A new generation of light, compact optical cables has been installed. This represents a total of about 1,000 kilometres of fiber with a cable carrying capacity ranging from 4-to-288 fibers.

Due to the chosen system (ATM forum 25,6 Mbit/s Interface), the copper cable network needs newly installed cables for the public distribution and private home networks. For connection and home wiring, 4-pair FTP cables and shielded plugs are used. In the future, the aim is to use the existing copper network with a point multipoint system [2].

OPTICAL PASSIVE ELEMENTS

FTTC/B architecture implies optical deployment up to the connection point (near customers). Table 1

shows the general characteristics of the various elements in the passive optical network that were used for the "Multimedia sur Armor" Field Trial. Certain elements are described in the following paragraphs, including: optical cables, splicing techniques, splice closures, connectors, couplers and optical ends.

Optical Elements	General Characteristics
Frame	2 racks/capacity 512 fibers 1 rack for transportation cables 1 rack for equipment
Couplers	OLT: 4 couplers 1:2 4 couplers 1:8 Splice enclosure: 6 couplers 1:8
Optical Cables	4 to 288 fibers 16 km
Splice Enclosure	14
Optical Fiber Sub Frame	2
Optical Network Unit	32 (up to 4 subscribers)

Table 1: General Characteristics of Passive Optical Elements

Optical Cables

Optical cables constitute the link between the frame, located in the OLT (optical distribution access node), and the ONU (Optical Network Unit). Between these two points, optical cables can be divided into two different categories (see Figure 1):

- the transportation cable: located between the OLT and the OTC (Optical Transportation Closure), and/or between the OSF (Optical fiber Sub-Frame) and the OTC.
- the distribution cable: located between the OSF and the ODC (Optical Distribution Closure), and /or the ODC and the ONU.

Main Characteristics of the Cables.

Cables modularity is either 4 or 8 optical fibers-per-cable element. The 4-fiber modularity is due to the fact that 4 fibers are needed per OLT: one upstream, one downstream, one for FTTH extension and one spare fiber. In order to obtain a higher degree of compactness, the 8-fiber modularity was selected for the transportation cables, which requires more fibers. Based on these modularities, different cable capacities have been elaborated. Table 2 illustrates the length and carrying capacities of the installed cables.

About 25% of excess fiber was included in anticipation of future Field Trials.

Cable Carrying Capacity	Installed Cable Lengths (metre)
4	3 240
8	2 700
16	1 550
24	200
48	2 565
72	1 941
96	1 350
144	858
288	1 522

Table 2: Length of Installed Cables

In order to establish limits to Civil Engineering operations, the cables are limited in diameter and weight. Table 3 shows the target dimensions of the cables used in the ducts.

Maximum Capacities	8	24	72	144	288	512
Modularity	4 or 8 optical fibers					
Diameter (mm)	5	7	11	13	16	21

Table 3: Cable Capacity and Diameter

The Field Trial cables have the following fiber capacities: 288, 144, 96, 72, 48, 24, 16, 8 and 4. Higher capacity cables are used for transportation and the lower capacity cables are used for distribution. When the coupler is set at the OLT, transportation cables have a high fiber capacity. However, when it is set at the OSF, for example, the cable capacity is reduced. The weight per cabled fiber in a transmission network cable (generally loose tubes with a maximum capacity of 60-fibers) can be three-to-six times higher than these new cables. The main characteristics of the cables installed in the ducts are described in Table 4.

Maximum carrying Capacity	8	24	72	144	288	512
Tensile Performance	Tmax=sup(1,5×weigh per unit length, 30 daN)					
Crush (daN/cm)	20		25			
Temperature Cycling	Δα≤0,1 dB/km between -10°C and +60°C at 1550 nm reversible Δα between -30°C and +60°C at 1550 nm					
Cable Bend	10 ×Ø and Δα≤0,1 dB/km at 1550nm					
Kink	5×Ø, no kink and no strength member or sheath damage					

Table 4: Main Characteristics of Duct Cables

The Distribution Network cables are made of different cable elements including: ribbons, microsheatheaths and micromodules. Both microsheatheath and micromodule elements consist of a very thin sheath wrapped around the 4 or 8-fiber bundle. For example, the following three Figures

show the structure of the 96-optical fiber-cable made with 8-fiber ribbons, the 72-optical fiber-cable and the 16-optical fiber-cable. These latter two are composed of microsheaths and micromodules, respectively.

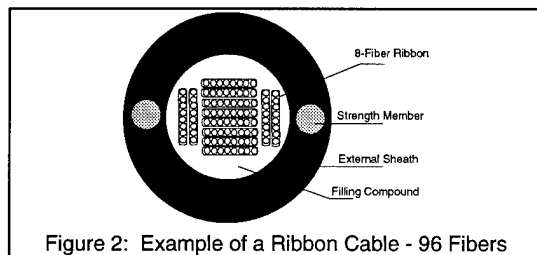


Figure 2: Example of a Ribbon Cable - 96 Fibers

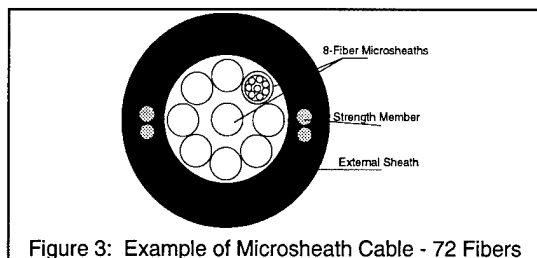


Figure 3: Example of Microsheath Cable - 72 Fibers

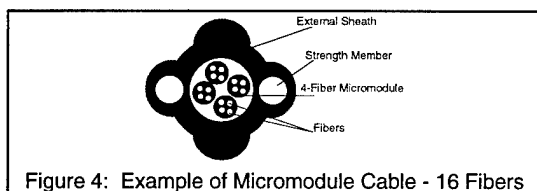


Figure 4: Example of Micromodule Cable - 16 Fibers

Aerial cables were also installed. One such structure is represented in figure 5.

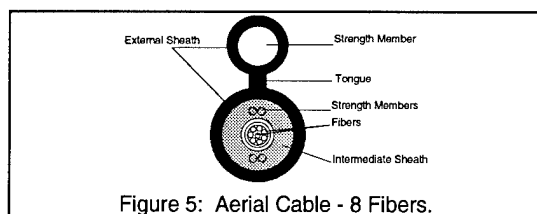


Figure 5: Aerial Cable - 8 Fibers.

Cable Installation. Three different installation methods were used: pulling, blowing and manual installation. The pulling method was used to install high capacity cables directly into buried ducts. Table 5 provides the pulling tension applied to certain cables during installation.

Cable (Number of Fibers)	Maximal Tension Admitted	Installed Length	Tension During Installation
288	550 daN	880 m	264 daN - 195 daN with microballs
144	460 daN	860 m	36 daN
96	75 daN	580 m	12 daN
48	75 daN	680 m	12 daN

Table 5: Pulling Tension Applied During Installation

Due to their limited length and weight, all of the small capacity cables were easily installed, either manually or using the blowing method.

After installation, the optical characteristics were measured and evaluated. No significant changes were recorded.

In conclusion, the new generation optical fiber cable is well adapted to this type of application due to its reduced size and weight, and is, as such, easy to install.

OPTICAL CONNECTIONS AND ENDS.

For Lannion Field Trial, a passive optical network was made in order to provide maximum flexibility for optical fiber switching. A point-to-multipoint network topology was used with two PONs (Passive Optical Networks) employing couplers in either the OLT (Optical Line Terminal), and/or in the ODC (Optical Distribution Closure), or the OSF (Optical Sub Frame). In the present Field Trial, 1:2 and 1:8 couplers were used with "planar wave-guide" technology which enabled a high coupling rate.

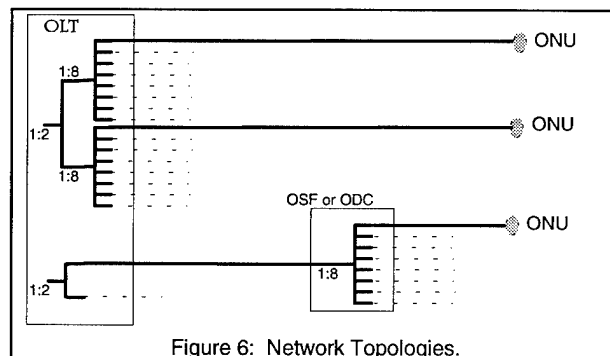


Figure 6: Network Topologies.

When couplers are placed in the OSF or the ODC, they are either spliced directly in the field (in a cabinet or underground enclosure), or pre-packaged in cassettes or trays and then spliced. The latter solution reduces splicing time and ensures good coupler reliability.

Optical Splicing.

Two splicing methods were used: fusion and mechanical splicing. In fusion splicing, the fibers are melted together at their joining point using an electric arc. There is no doubt that this method provides long-term reliability, because it rebuilds the silica guide. In Mechanical splicing, the connection between the fibers is established by physical contact. This technique requires angle-cut fibers and gel possessing the same refractive index as the glass core of the fibers in order to

obtain low IL (Insertion Loss) and high RL (Return Loss) (< -55dB).

The cables selected for the Field Trial (ribbon, microsheath and micromodule) enable the comparison of different splicing techniques (both fusion and mechanical):

- mass splicing for ribbon fibers;
- mass splicing for ribbonized fibers made from microelement; and,
- single-fiber splicing.

Table 6 illustrates the splicing performances obtained when using each of these techniques.

	Splicing Loss Average	Return Loss	Splicing Rates
Mass Ribbon Splicing	0,15 dB	< -55 dB	5 mn for 8 fibers
Mass Ribbonized Splicing	0.20 dB	< -55 dB	10 mn for 8 fibers
Single Splicing	0,10 dB	< -55 dB	5 mn for 1 fiber

Table 6: Optical Splicing Performance.

The latest developments in mass splicing, cable preparation and fiber identification improved the cable productivity. In fact, it took the same time to splice an 8-fiber ribbon as it did a single fiber.

For microsheath or micromodule cables, mass and single splicing were used. With mass splicing, a special tool was used in order to lay out the fibers like a ribbon. This mass, ribbonized splicing technique took approximately twice as long as mass ribbon splicing. This was primarily because the tools were not well-adapted. In fact, for small cable capacity, (less than 24 fibers), single splicing (fusion or mechanical) is a more appropriate method.

Optical Connector.

At the ends (OLT and ONU), push-pull single fiber connectors (with low IL and high RL), based on cone-to-sphere alignment, were used. The fibers do not touch, and the use of an index matching (a thin film inserted into the adapter) provides a low IL. A high RL is obtained by angle polishing in addition to the index matching.

Eight pigtail connectors were spliced with transportation ribbon cables using the ribbonized, or fan-out technique. The fan-out is pre-packaged in the factory, which enables the use of mass ribbon splicing. In the field, this method provides a significant reduction in time.

Optical Passive Ends.

Optical Fiber Frame. The Optical fiber Frame placed in the OLT ensures the switching between the transportation fibers and the equipment fibers. Table 7 shows the general characteristics of the Optical Frame.

Optical Fiber Sub Frame. The OSF (Optical fiber Sub Frame), placed in a building or cabinet, ensures switching between transportation and distribution cables. The OSF function is identical to that of the Optical Fiber Frame, except for its reduced capacity. It enables storage and fiber identification.

Table 8 shows an example of the OSF configuration for the present Field Trial.

Optical Frame	General Characteristics
Maximum Capacity	2 racks of 576 fibers
Rack Dimensions	Rack 19" (42U)
Cable Termination Box number/ rack	8 cable termination boxes(4U) of 72 fibers
Optical Connectors	Single push-pull connector or 8 connectors fan out
Splice	Single or mass
Switching Operation	by single patch cables
Couplers	1:2 and 1:8 in cable termination box (1U)

Table 7: Optical Fiber Frame Characteristics.

Optical Sub Frame	General Characteristics	
Capacity	Transportation 96 OF	Distribution 3 x 48 and 1 x 24 OF
Optical Connectors	Single push-pull connector or 8 connectors Fan Out	
Splice	Single or mass	
Switching Operation	by single patch cables	
Couplers	1:8 in cable termination box (1U)	

Table 8: OSF Characteristics.

Optical Splice Closures.

The OSC (Optical Splice Closures) are equipped with cassettes, or trays, and enable the organization of splices and the storage of spare fibers. The OSC provide storage for the excess fibers and loops which are required for fusion or mechanical splicing. The OSC ensure that the minimum fiber bend radius of 30 mm is respected. The OTC (Optical Transportation Closure) and the ODC (Optical Distribution Closure) protect the ensemble against aggression from the external environment. As such, adherence to strict requirements on sealing, mechanical strength and durability is required. The OTC and the ODC are located in underground chambers, and must be easily opened. Table 9 describes the main differences between the OTC and the ODC.

	Optical Transportation Closure	Optical Distribution Closure
Capacity	512 OF	96 or 48 OF
Organisation	Splice tray	Splice tray or cassette
Cable Capacity	6 maximum	2 to 12 cables
Fiber Storage	No	Yes
Design	Dome closure	Box or dome closure
Easy Re-entry	Yes	Yes
Couplers	No	Yes (1:8)
Splice	Mass	Single and/or Mass

Table 9: Differences between the OTC and the ODC.

The organization of the different elements (ribbon, microsheath and micromodule) inside the splice closures must facilitate mass splicing. As such, the splice closures, originally designed for single splicing, must be modified.

In conclusion, new splicing techniques employed in the present Field Trial significantly improved productivity. In order to obtain the same splicing rate for ribbonized splicing, more appropriate tools are required. In addition, the Field Trial has proven that Passive Optical Components are well-adapted for high capacity cables and for fiber organization.

THE COPPER NETWORK

This portion of the document focusses on the copper network (the public distribution network and

the private home network, called home wiring) used for the "Multimedia sur Armor" Field Trial. The following is a description of the transmission system, the copper cabling system and the tests conducted in order to determine the configuration for the Field Trial (transmission and electromagnetic tests).

The architecture between the ONU (Optical Network Unit) and the terminal plug is a point-to-point configuration with a passive Network Termination (NT).

System and Services

Two types of services are delivered to the customers: POTS and broadband services. The transmission system uses the ATM Forum 25,6 Mbit/s Interface (NRZI sequence, 4B5B encoded) to transport the broadband services over two pairs. The system is symmetric, using one pair per direction. One pair is used to transportation the existing POTS line (retained as a backup facility). The other pair is required for the new POTS line that uses the optical infrastructure.

Cabling System (Figure 7)

From the ONU to the terminal plug, Foiled Twisted Pairs cables (FTP) are used.

Distribution Network. The branching cable is a FTP multiplier cable called "88/98" (France Telecom standard) which has a category

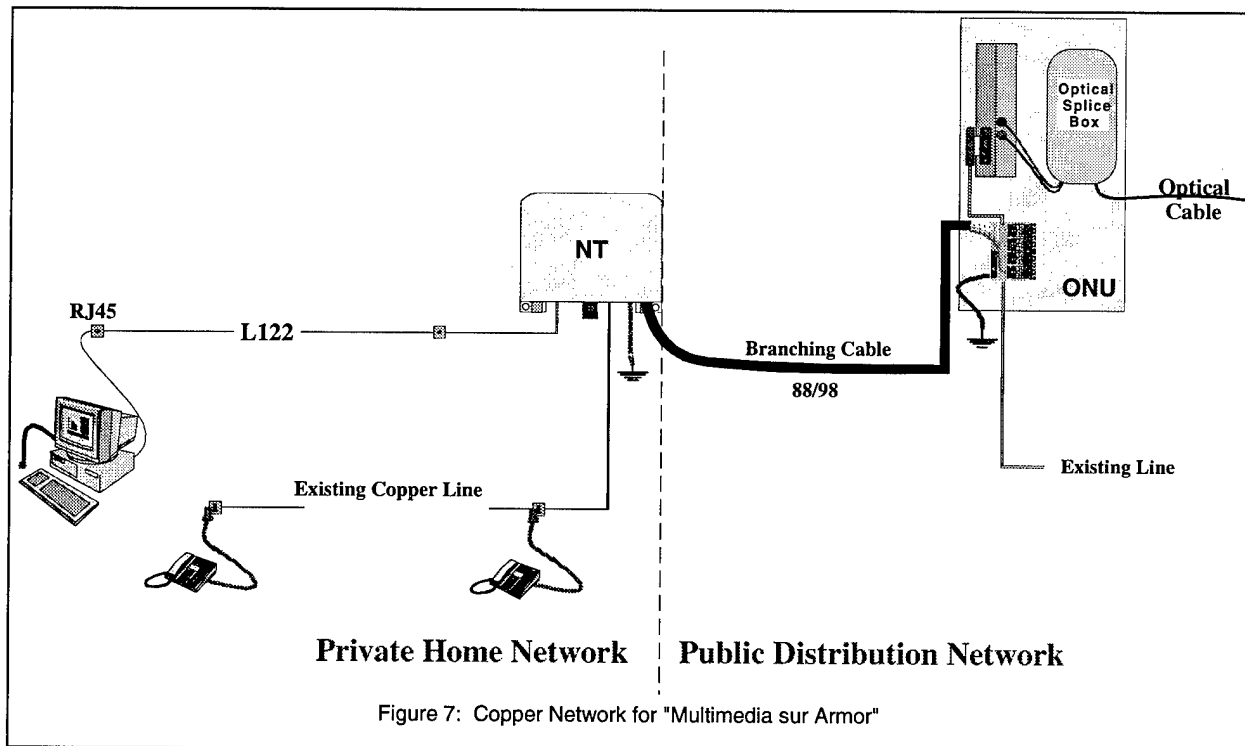


Figure 7: Copper Network for "Multimedia sur Armor"

4 cable performance (ACR, NEXT, etc.). The cable is a quad structure that has a 4-pair capacity (P1/P2 in Q1 and P3/P4 in Q2).

The passive NT is a wall-mounted box located at the entrance to the customer premises.

Home Wiring. The home network is composed of a 4-pair FTP category 4 cable, called "L122" (France Telecom standard) for the broadband services and two plugs. The existing wiring is used for the two POTS.

Measurements

Reach Tests. The reach on different cables was measured with the ATMF 25,6 Mbit/s transmission over two pairs (Figure 8).

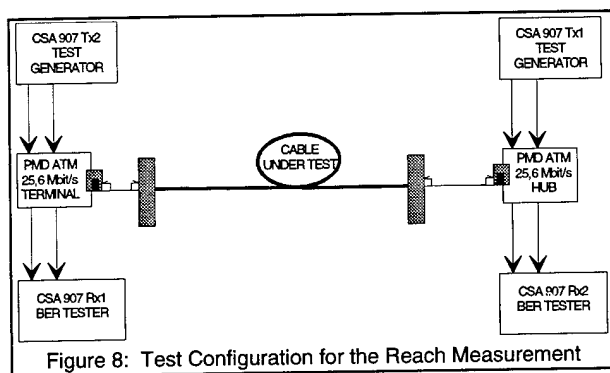


Figure 8: Test Configuration for the Reach Measurement

For the branching cable, the test is conducted for configurations using different pairs. The results are shown in Table 10.

Length (m)	Used Pairs	BER	
300	P1/P2	10^{-4}	$3 \cdot 10^{-5}$
	P1/P3	$7 \cdot 10^{-5}$	$< 10^{-10}$
250	P1/P2	$< 10^{-10}$	$< 10^{-10}$
	P1/P3	$< 10^{-10}$	$< 10^{-10}$

Table 10: Reach on the Branching Cable

The POTS traffic has no influence at these lengths. With 250 m of "88/98" branching cable, transmission is satisfactory ($BER < 10^{-10}$) for each configuration.

The cables under testing for the home wiring are the existing 4-pair cables used in France for customer premises cabling, and the UTP-5 cable (consult Table 11 for the characteristics and reach results for the P1/P4 pairs).

Cable	Type	Cat.	Freq.	Use	Reach (m)
L120	FTP	5	100 MHz	LAN	390
L122	FTP	4	1 MHz	ISDN	250
278	UTP	3	3400 Hz	POTS ISDN	30 to 140
UTP5	UTP	5	100 MHz	LAN	280

Table 11: Reach on Home Wiring

The reach for the "278" UTP-3 cable (30 to 140 metres) depends upon the cable. The "L120" FTP-5 cable has a better reach (390 metres) than either the UTP-5 (280 metres) or the "L122" FTP-4 (250 metres). However, for ease of installation, the choice is narrowed to the "L122" or the UTP-5.

EMC Testing. The aim of this test is to provide information relative to electromagnetic behaviour between the different cabling systems. Two EM Compatibility tests were conducted: immunity and emission.

EM Immunity Testing: the cabling system's electrical fast transient sensibility is determined according to the procedure outlined in the standard IEC 1000-4-4 (previously, the IEC 801-4). The test objective is to couple common mode noise bursts onto telecommunication cables via a capacitive clamp. The generator level is specified at four different levels: 250, 500, 1000 and 2000 V. This corresponds to the four severity levels on I/O signal, data and control lines. The equipment reference configuration for the testing is provided in Figure 9.

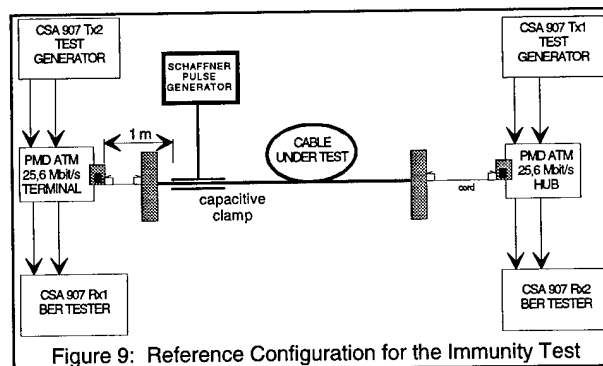


Figure 9: Reference Configuration for the Immunity Test

Table 12 shows the performance of the cabling systems for ATMF 25,6 Mbit/s transmission. It provides the maximum voltage delivered without error, using the Schaffner generator ($BER < 10^{-10}$), on the Field Trial configuration (200 metres of "88/98" cable and 50 metres of diverse home wirings).

Cable	IEC 1000-4-4 Standard			
	Level 1	Level 2	Level 3	Level 4
L122	YES	YES (550 V)	NO	NO
UTP5	NO (< 200 V)	NO	NO	NO

Table 12: Field Trial Cable Performance

At 200 V, the BER for the UTP-5 is $1,5 \cdot 10^{-7}$. For the immunity test, measurements show that "L122" FTP cable outperforms the UTP-5 cable. Level 2 was attained for this configuration with the use of a screen.

EM Radiated Emission Testing: using identical test configurations, the antenna is placed one metre away from the floor and the test cable. The transmission equipment is placed in the Faraday cage. The reception analysis bandwidth is fixed at 30 Hz (no signal with a 100 KHz bandwidth is used in the EN 55022 standard), and the span is set at $32 \text{ MHz} \pm 2,5 \text{ KHz}$.

Table 13 provides the maximum level obtained by the radiated emissions for the Field Trial configuration. Figure 10 illustrates the behaviour of the UTP-5 and the "L122" cables. The PC configuration indicates that the screen is connected to the ground on both sides of the link for the FTP cable (a PC is a Class 1 device). The TV configuration (Class 2 device) implies that the screen is connected to the ground only on the emission side.

Cable	Radiated Emissions max level in dB μ V/m Horizontal Polarisation	Radiated Emissions max Level in dB μ V/m Vertical Polarisation
L122 TV	33	19
L122 PC	10	10
UTP5	43	34

Table 13: Field Trial Cable Performance

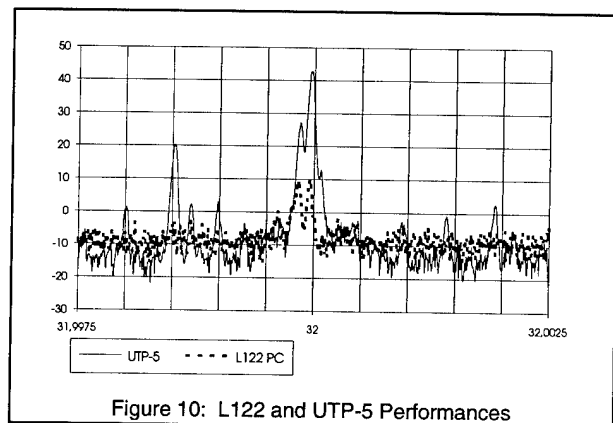


Figure 10: L122 and UTP-5 Performances

Both cables comply with France Telecom standard specifications (level $< 46 \text{ dB}\mu\text{V/m}$). However, for the radiated emissions, measurements prove that the "L122" FTP cable outperforms the UTP-5 cable. The shielded cables present less radiation emissions than the unshielded cables).

Due to the chosen system (ATM forum 25,6 Mbit/s) and the electromagnetic requirements, the configuration retained for the "Multimedia sur Armor" Field Trial is a maximum copper cables length of 250 metres. So, the copper network is constituted with the following maximum lengths: 200 metres for the "88/98" branching cable and 50 metres for the "L122" in the home wiring.

CONCLUSION

Brand new passive optical and/or copper materials were analyzed. The optical infrastructure part is now fully realized. The "Multimedia sur Armor" Field Trial was an effective means for validating the potential of an optical network realized using these compact cables and associated optical elements. At the beginning of 1997, the copper portion of the network will be completed and all services will be available to the hundred customers implicated in the Field Trial.

REFERENCES

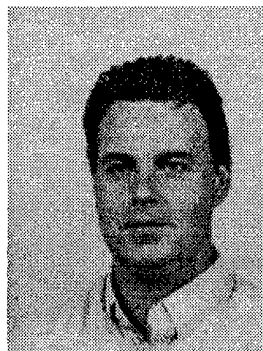
- [1] Fiber based access networks: How far in line with home network cabling - G. du Chaffaut and M.Lissillour - 5th Symposium on premise wiring and lan for smart buildings - May 96.
- [2] Optical Access Networks in France: deployment for business customers and introduction in residential areas for Multimedia services - D.Chapelain France Telecom/CNET - Workshop IEEE, Nuremberg - Sept. 95.

AUTHORS



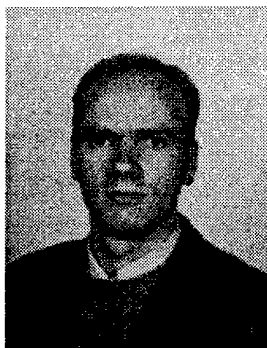
Emmanuelle CRESSAN was born on October 2, 1967. In 1994 she received the title of Docteur of the University of Rennes (Physics and Chemistry of Materials). Working in the Telecom Cables and Connection Equipment Department since 1994, she is in

charge of the optical cables (establishing specifications, performing tests, european standardization, implementation of cables in Field Trials).



Gilles LE TRAON was born on December 17, 1968. He received his engineering degree from the Ecole Nationale d'Ingénieur de Brest (ENIB) in 1992. He joined the National Research Center of France Telecom in 1994. Working in the Telecom Cables and

Connection Equipment Department, he is in charge of optical fibers connections and passive components.



Olivier BOUFFANT was born on January 15, 1968. Graduated from the University of Toulon in Electronics in 1992, he joined the National Research Center of France Telecom in 1994. Working in the Telecom Cables and Connection Equipment Department,

he is in charge of the new high bit rate applications on the Customers Premises Cabling Systems.



Regis PETIT was born on November 12, 1954. He joined the National Research Center of France Telecom on July 1, 1981. Assistant in Research and Development, he is in charged of infrastructure coordination for the "Multimedia sur Armor"

Field Trial.



Olivier DAGUILLON was born on November 23, 1967. In 1995, he received the title of Docteur of the University of Clermont-Ferrand. He joined the National Research Center of France Telecom in 1995 where he is in charge of studies relating to EMC of

the Subscriber's Telecommunication Terminations.



Jean MOALIC was born on March 28, 1944. He joined the National Research Center of France Telecom on December 1967. He was mainly involved in early demonstrators of optical systems, including both digital access systems and analogue CATV systems. He is now in charge of the passive

infrastructure and the head-end of the "Multimédia sur Armor" Field Trial.

MODULAR COMPONENTS FOR HYBRID FIBRE COAX NETWORKS IN DIFFERENT CLIMATIC ZONES

Heinrich Schürmann, Jürgen Seidenberg, Peter E. Zamzow

KABEL RHEYDT AG, Mönchengladbach, Germany

ABSTRACT

New services on hybrid fibre coax (HFC) networks require to adapt the specifications on the infrastructure. First of all the bandwidth has to be upgraded to 750 or 862 MHz. Secondly, services like cablephone request an increased reliability and availability of the network.

Cables and components will be proposed which are adapted to the extended specifications. The properties of coaxial cables under different climatic conditions like the RF attenuation, the current rating for remote feeding and the sag in case of aerial installation are discussed.

INTRODUCTION

By the introduction of fibre optics into CATV networks the number of cascaded coaxial amplifiers has been decreased significantly. Older designs are using fibre nodes serving around 2000 passed homes. Actually 500 passed homes are fed by one optical receiver typically. However, networks operating already purely passively (without any coaxial amplifier separated from the optical receiver) are starting to become popular. Depending on the bandwidth and topology around 50 to 200 passed homes are belonging to one fibre node in this case as shown in Fig. 1.

With the introduction of fibre optics also the bottleneck 'bandwidth' has been overcome. The increased bandwidth capacity of the fibre optic system consequently led to a tendency of realizing increased bandwidth coaxial cable systems, too. Meanwhile the original 300 MHz bandwidth has been upgraded towards 550 MHz, 750 MHz or even 862 MHz. The number of available analogue TV channels has doubled from around 40 to 80 channels. Furthermore hundreds of digital video channels coded in MPEG2, transmitted in 64 QAM format can be distributed.

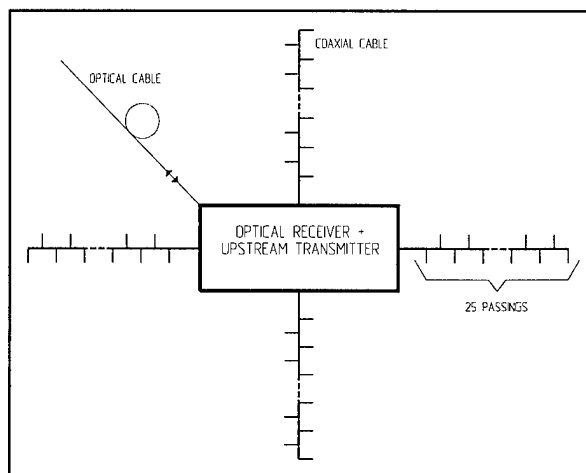


Fig. 1: Topology of modern HFC fibre node cells

Now bidirectional transmission is going to become more and more important. The huge amount of available transmission capacity invites further services to be offered via the HFC network. Cablephone and cabledata are new services requiring a return path capability on the HFC network. Alternatively, with limited performance a return path could be realized on a further network (e.g. telephony network). However, this requires the presence of two networks, the HFC for the downstream and the telephony network for the upstream transmission at the same time.

To handle all new upcoming services in general today's requirements on modern HFC networks are characterized by

- bandwidth up to 750 or 862 MHz
- full return path capability
- remote powering for cablephone equipment

The following sections will focus on the properties of components required to realize this type of HFC networks.

Finally a review of the properties for different climatic regions is given.

ADAPTATION OF THE CABLE INFRASTRUCTURE FOR MODERN HFC NETWORKS

The cable infrastructure for modern HFC networks has to meet the tendency that the bandwidth of the system is increasing towards 750 or 862 MHz and at the same time the number of passings per fibre node is decreasing. It is very attractive in terms of cost¹ and reliability to have no active elements like coaxial amplifiers within the cable infrastructure. Additionally by omitting all active elements the network becomes inherently bidirectional, that means it offers full return path capability. However, the maximum number of passings per fibre node is limited to a number of around 100 assuming 4 coaxial trunk lines to be driven by one optical receiver due to the attenuation of the coaxial cables and couplers at the upper bandwidth limit.

Since the cable infrastructure might remain purely passive at least for the CATV service no remote powering on the trunk lines is required any longer. Only for other services offering a very high availability as telephony services remote powering of interface equipment at the customer premises will still ask for maintaining remote powering on the trunk lines. The power required to power a cablephone interface is typically in the order of 1.5 W maximum per subscriber and 0.5 W in average taking into account the statistics of the service. The total average power for a fibre node containing 500 subscribers (5 subscribers per passing in average) therefore adds up to be around 250 W net, or 300 W including losses on the cable infrastructure. If we assume that 4 trunk cables are used to feed all the node area this power is carried as 75 W per trunk cable. With a remote power supply voltage exceeding 60 V less than 1.5 A of current has to be inserted into the trunk cables.

In comparison to traditional CATV networks with a large number of cascaded coaxial amplifiers where the current might be as high as 15 A modern HFC networks are operated at much lower currents. In case of no cablephone service the remote powering can even be omitted completely.

The new powering demands have a strong impact on the properties of the passive components like the TAP couplers:

network topology	HFC for CATV services	HFC for CATV services	HFC for CATV and cablephone services
# of subscribers per fibre node	2000	100	100
Required Tap Coupler Property			
bandwidth	550 MHz	862 MHz	862 MHz
remote power capability on trunk	15 A	0 A	1.5 A
remote power capability on TAPs	0 A	0 A	0.5 A
return loss	fine	fine	excellent
immunity against electromagnetic radiation	fine	fine	excellent
reliability	fine	fine	excellent
security against vandalism	fine	fine	excellent

Table 1: Properties of TAP couplers for HFC networks

Table 1 shows that in contrast to traditional tap couplers modern HFC networks in one case require no remote powering at all or in the other case require even remote powering via the taps. More attention has to be paid to achieve a good return loss and immunity against electromagnetic interference in order to avoid problems with 64QAM transmission. Furthermore reliability issues like protection against lightning etc. and protection against unauthorized access or vandalism become more important.

Table 2 shows the required properties of cables for HFC networks^{2,4}. Due to the increased bandwidth a tendency towards larger size cables can be observed. This tendency is also true for the drop cables. In order to fulfill the requirements on immunity against electromagnetic radiation and reliability a drop cable with welded outer conductor instead of a aluminium foil-braid-foil construction is proposed. Table 3 gives the characteristical data for the new AK 320 cable and the equivalent RG11 cable.

network topology	HFC for CATV services	HFC for CATV services	HFC for CATV and cablephone services
# of subscribers per fibre node	2000	100	100
Required Trunk Cable Properties			
bandwidth	550 MHz	862 MHz	862 MHz
cable size due to bandwidth	0.42" .. 0.86"	0.54" ... 1.125"	0.54" ... 1.125"
remote power capability on trunk	15 A	0 A	1.5 A
return loss	fine	fine	excellent
immunity against electromagnetic radiation	fine	fine	excellent

Table 2: Properties of trunk cables for HFC networks

Table 3 shows that with almost the same mechanical dimensions improved electrical properties³ are achieved. The simplified production of the outer conductor in the AK 320 compared to the RG11 helps to lower the production costs.

cable type	AK 320	RG 11	
property			
diameter inner conductor	1.74	1.63	mm
diameter insulation	7.2	7.2	mm
diameter outer conductor	7.6	8.1	mm
diameter sheath	9.2	10.2	mm
attenuation at			
200 MHz	5.9	6.4	dB/100m
862 MHz	13.1	14.4	dB/100m
return loss	30	20	dB
DC resistance			
inner conductor	11.2	30.0	Ω/km
outer conductor	6.1	20.0	Ω/km
screening attenuation	> 110	> 80	dB

Table 3: Properties of AK 320 and RG11 drop cables

NEW REMOTE POWERING APPROACH FOR THE CABLEPHONE NETWORK TERMINATION

Additionally the drop cables for cablephone services are also used for the remote powering of the cablephone customer's network termination

unit (NTU) . In order to achieve a flexibility in connecting or disconnecting the subscriber to the cablephone service it is advantageous to power the NTU not via the inner conductor of the coaxial drop cable but by 4 additional small copper wires with a diameter of 0.4 or 0.6 mm (AWG 27 ... 23) inserted into the sheath of the drop cable as shown in Fig. 2.

It is assumed that the ground voltage is applied via the outer conductor whereas the remote voltage is applied via all 4 wires in parallel.

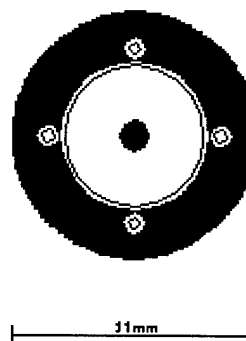


Fig. 2: Coaxial drop cable with integrated remote power wires

Of course, this cable requires a tap coupler offering access to the remote power supply. Fig. 3 shows a picture of a tap coupler which offers the possibility to connect or disconnect the remote power wires of the drop cable.

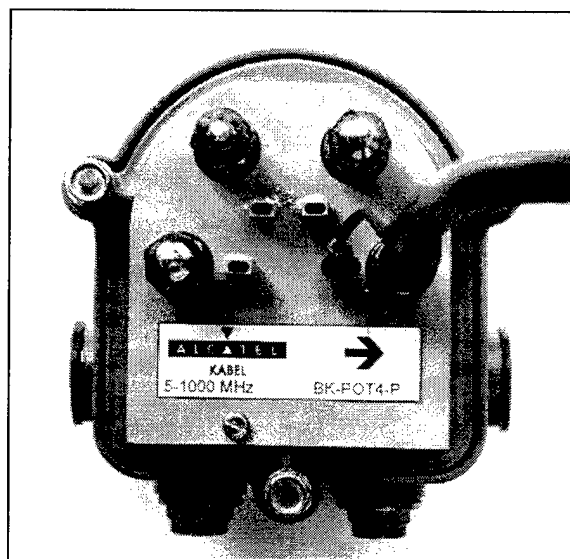


Fig. 3: Tap coupler with remote power connectors

The RF-properties of the separate remote power wire solution are superior compared to the remote powering via the inner conductor of the coaxial cable since the remote power diplexers in the tap coupler and the customer's network termination are omitted giving by the way also a cost improvement.

Table 4 gives a view on the maximum distance for a voltage drop of 3% (=2V) assuming 60 V of remote voltage and 0.5 A of supply current, which is equivalent to 20 subscribers for cablephone connected to one passing.

cable type	AK 320	RG 11
copper wire \varnothing		
0,4 mm (AWG 27)	98 m	74 m
0,6 mm (AWG 23)	185 m	113 m

Table 4: maximum length of drop cable for 3% of voltage drop at 60V/0.5 A

PROPERTIES OF COAXIAL CABLES IN DIFFERENT CLIMATIC ZONES.

In different climatic areas it is important to keep in mind especially the transmission properties of coaxial cables. The sensitivity of the transmission characteristics to other climatic factors like humidity are negligibly small. However, the long term reliability might be depending on this parameter. Fig. 4 shows the global temperature profile with the average minimum and maximum temperatures. In the northern countries the coldest temperatures are observed with an average minimum of -25°C and maximum of $+10^{\circ}\text{C}$. In contrast in the countries close to the equator the hottest temperatures with an average minimum of $+25^{\circ}\text{C}$ and a maximum of $+40^{\circ}\text{C}$ are found. To obtain the absolute minimum and maximum temperatures an additional 15°C of variation of the average values should be assumed. The greatest temperature span of 35°C occurs in the very north and the very south compared to only 15°C in the tropical and subtropical areas.

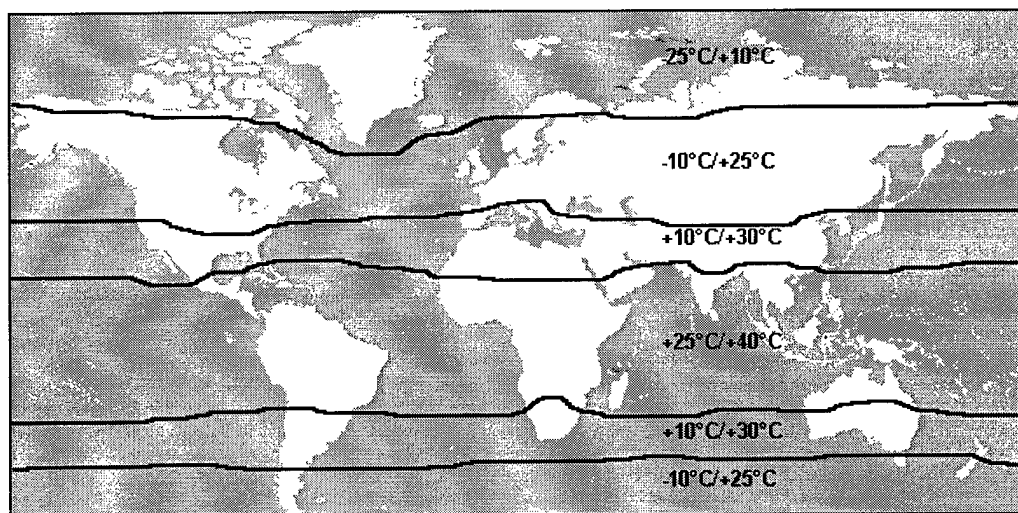


Fig. 4: Global ambient temperature profile with average min. and max. temperatures

The temperature of installed cables depend on several factors:

- the kind of installation (e.g. aerial or buried)
- the ambient temperature
- additional sun radiation

- heat created by dissipated power in the coaxial cable due to resistive loss of the cable in combination with remote supply currents

The last factor has to be beared in mind particularly for small size coaxial cables like the

AK 320, 500 and 540. Therefore in the following diagram only the smaller size coaxial cables are characterized, where all the impacts are worst. Fig. 5 shows the attenuation of the AK320, 500 and 540 coaxial cables in the frequency range 5 to 1000 Mhz for a cable temperature of -20°C and +70°C.

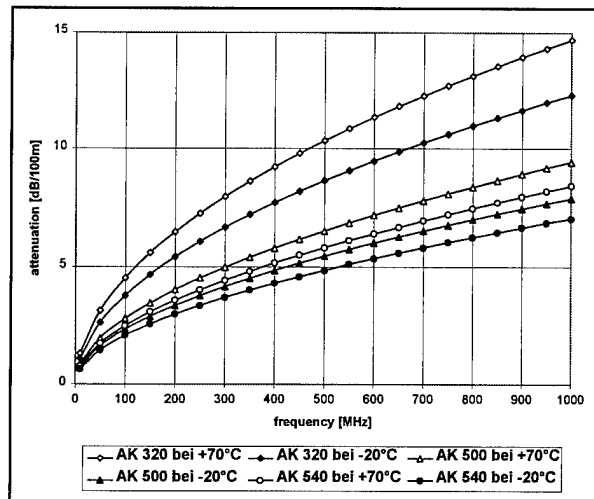


Fig. 5: Attenuation of the AK320, 500 and 540 cables between 5 and 1000 MHz

The variation of the attenuation obviously increases with frequency. This effect is more pronounced for the smaller size cables. Compared to the attenuation at +20°C the variation is -8% and +10% at -20°C and +70°C, respectively. It is important to consider this temperature dependend slope when designing coaxial cable networks for large bandwidths and especially aerial installation.

Impact of heat created by remote supply currents

Remote supply currents might create an additional temperature increase of the cable due to resistive losses of the cable. Since buried cables don't suffer the same ambient temperature variation like aerial cables the effect of course is only important for aerial cables. The maximum cable temperature typically is specified to be 70°C.

Fig. 6 explains the maximum allowed remote current (DC or 50/60 Hz AC) as a function of the ambient temperature and the sun radiation⁵.

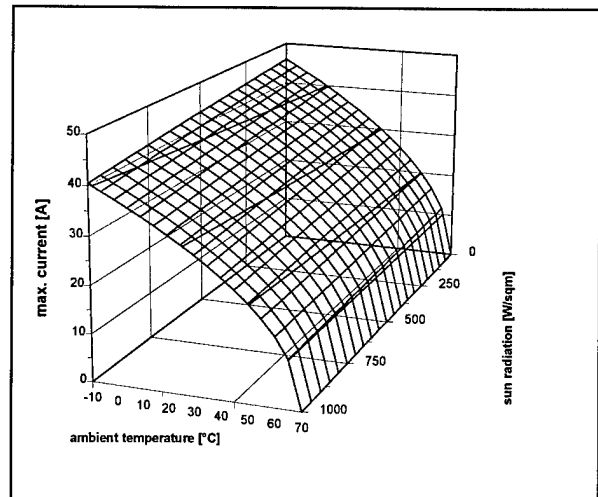


Fig. 6: Maximum remote current of the AK 500 as a function of the ambient temperature and sun radiation

The diagram is a result of a thermal simulation of the cable including natural air convection and sun radiating orthogonal on the cable axis. The results have been proven empirically, too.

Table 5 gives a set of conditions out of this diagram as well as the results for the AK320 and AK 540 cables

	maximum remote current		
cable type	AK 320	AK 500	AK 540
climate zone			
standard (ambient temperature +25°C sun radiation 400 W/m²)	17,0 A	32,9 A	34,2 A
subtropical zone (ambient temperature +35°C sun radiation 600 W/m²)	14,6 A	28,3 A	29,4 A
tropical zone (ambient temperature +45°C sun radiation 800 W/m²)	12,0 A	23,2 A	24,2 A

Table 5: Maximum remote current for different climatic zones and the cable types AK 320, AK 500 and AK 540

It turns out that for the smallest cable, the AK320, assuming aerial application in the tropical zone the maximum remote current is below the standard maximum value of 15A. In contrast to this, for the AK 500 the maximum remote current might exceed 15 A. However, the additional temperature increase due to electrical losses will give a higher RF attenuation than expected from

the ambient temperature and sun radiation only. This has to be recognized when designing networks in tropical regions.

Sag of coaxial cables in case of aerial installation

It is very attractive in terms of installation costs to install aerial cables on poles. The easiest way is to use a cable already combined with a messenger to form a 'figure 8' construction. However, it is important to determine the sag as a function of pole spacing and temperature. Fig. 7 gives the sag at +20°C for the AK 320, AK 500 and AK 540 cables with standard messenger at +20°C as a function of the pole spacing. For pole spacings below 40 m the sag remains below 1 m.

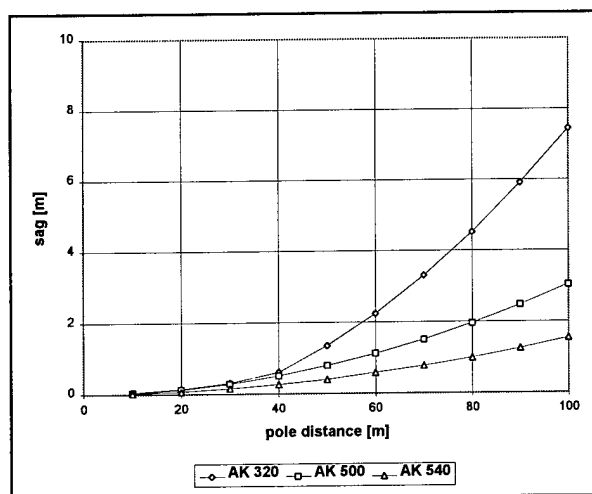


Fig. 7 : Sag as a function of pole spacing for +20°C for AK 320, 500 and 540

Fig. 8 additionally shows the sag variation as a function of the cable temperature compared to +20°C. For pole distances up to 40 m the sag variation is less than 15 cm. Compared to the absolute sag the sag variation stays relatively small for all pole distances.

CONCLUSION

The increasing demands on HFC networks supporting cablephone and cablemodem services have been analyzed. A remote powering

solution for the customer's network termination unit has been proposed.

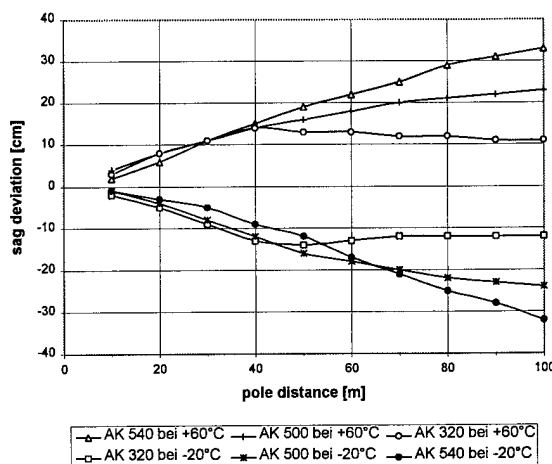


Fig. 8: Sag variation as a function of pole spacing at -20°C and +60°C for the cable types AK 320, 500 and 540

The thermal behaviour for different climatic regions has been discussed. It turns out that a temperature dependent slope of the attenuation has to be considered for networks working with large bandwidth like 750 or 862 MHz.

ACKNOWLEDGEMENTS

The authors gratefully acknowledge the cooperation of Mr. Hartmut Gohdes of RFS Hannover in calculating the thermal loading of RF cables

REFERENCES

- ¹Dale F. Lutz, Cost Analysis of HFC Rebuilds/Upgrades, Proceedings of papers presented at the SCTE Cable-TEC Expo '96, June '96, Nashville, TN
- ²Coaxial cables used in cabled distribution networks Part 4: Sectional specification for distribution and trunk cables, EN 50117-4
- ³Standard Specification for Polyethylene Plastic Molding and Extrusion Materials, ASTM D 1248
- ⁴Coaxial cables used in cabled distribution networks Part 1: Generic specification, EN 50117-1
- ⁵RFS (Hannover) catalogue issue 9.



Heinrich Schürmann (53) is responsible for engineering of CATV cables and components. He reached his Dipl.-Ing.-Degree from the RWTH Aachen, Technical University of Aachen/Germany. In 1971 he joined KABEL RHEYDT first being engaged in the development of symmetrical

and coaxial cables. In 1980 he changed to the optical fibre department and was responsible for data processing. At the beginning of 1996 he joined again the product group CATV.



Jürgen Seidenberg (39) received his Dipl.-Ing.-degree and Ph. D. in telecommunications engineering from the RWTH Aachen, Technical University of Aachen / Germany. He joined KABEL RHEYDT in 1989. Presently he is head of the department of optical transmission

systems for CATV as well as technical manager for CATV cable



Peter E. Zamzow (56) is director of the Telecommunication Division. He finished his post-graduate studies in telecommunications in Munich and Graz as Dipl.-Ing. He joined AEG KABEL (later: KABEL RHEYDT) in 1970. He has been engaged in development and production of telecommunication

cables. In 1980 he became head of the fiber optic division at AEG KABEL and in 1982 he was nominated as a senior engineer. Starting in 1992 he was infrastructure manager of the new Optical Fiber Cable Plant Rheydt. Since July 1994 he is director, manager of the product group CATV, product line telecommunication, sector Germany.

mailing address:

KABEL RHEYDT AG
Department NB
Bonnenbroicher Str. 2-14
D-41238 Moenchengladbach
Germany

+49 2166 27 2991 (phone)
+49 2166 27 2992 (fax)

Corrosion Control for Grounding Electrodes at Telecommunication Sites

Michael Parente

**MP Technologies
P.O. Box 2577, Hendersonville, NC 28793-2577
Phone (704) 891-8970**

George Schick

**Bellcore
445 South Street, Morristown, NJ 07960-6438
Phone: (201) 829-2549 Fax: (201) 829-5886**

Abstract

The grounding electrode system for small telecommunication sites that contain electronic equipment often consists of a buried bare-copper ground ring connected to ground rods. In locations where it discharges dc stray currents, the system may corrode at an unacceptable rate. This paper proposes a grounding electrode system that uses high-silicon-chromium cast-iron anodes in combination with ground rods and an insulated ring. Calculations predict a satisfactory corrosion life, even if significant dc currents are discharged.

Introduction

Telecommunication networks increasingly use small buildings, below-ground vaults, or cabinets to shelter electronic equipment. These electronic sites, typically remote from a town, require a grounding electrode system for electrical protection, and for a connection to earth on telecommunication services that use earth as part of the signaling path.

The grounding electrodes must remain effective over the life of the site, typically planned for 20 years. However, at locations where the electrodes are subject to the

discharge of dc stray currents, corrosion may disable the grounding system much sooner.

This paper examines the dc current distribution in grounding electrodes at a representative electronic site. It determines levels of dc stray currents that cause excessive corrosion loss in the electrodes, and proposes an alternative design that extends the life of the electrode system.

Grounding Electrodes at Telecommunication Sites

The grounding electrode system at an electronic site in the United States of America must comply with provisions of the National Electrical Code (NEC) [1] and must also have sufficiently low earthing resistance to enable certain types of signaling used by the telecommunication network. The grounding system that has evolved to satisfy these needs typically consists of a buried exterior ground ring that is connected to two or more ground rods [2]. The ring often is bare, solid, 2-AWG copper wire, and the rods are copper-clad steel with a 5/8-inch diameter and a length of 8 feet. (Figure 1)

If the ground ring is buried at a depth of at least 2.5 feet, and has a length of at least 20 feet, it satisfies the grounding electrode requirement of the NEC. Similarly, the two ground rods, if spaced at least 6 feet apart, also satisfy the NEC. The combination of the ground ring and rods provides a sufficiently low earthing resistance for signaling on the network.

Corrosion Caused by DC Stray Current

The grounding electrodes of Figure 1 are connected to earthing terminals inside the electronic enclosure from which they are bonded to the neutral conductor of the powerline and also to the shields of the telecommunication cables that enter the site. Either the neutral conductor or the shields may be a source of dc stray current that is discharged from the grounding electrodes into the earth. The resulting corrosion rate of the system depends on the level of dc stray current, its division among the two ground rods and the ring, and the surface area over which current leaves the electrodes.

Division of Current

Division of current between parts of an interconnected grounding-electrode system is inversely proportional to their individual earthing resistance. That is, the current into each ground rod depends on its resistance to earth relative to the resistances of the other rod and the ring, assuming that each is independently connected to earth. The actual earthing resistance of each electrode depends on local variations in earth resistivity near the electrode, and on the contact of each portion of the electrode with the earth. Calculations under idealized, homogeneous conditions are made here to illustrate the principles, but actual values for installed electrodes will differ, depending on local conditions.

In the following example, it is assumed that the ground rods are 5/8 inch in diameter and 8 feet long, and the ground ring is 24 feet on a side, 2.5 feet deep, and 2-AWG bare copper. Earth resistivity is not a factor in determining the division of current under

homogeneous conditions, but for illustrative purposes, it is assumed to be a uniform 1000 meter-ohms.

The earthing resistance of one ground rod is about 400 ohms [3]. The resistance of the 24-foot-square ring is calculated to be 68.5 ohms [3]. Mutual resistance between the electrodes affects the combined earthing resistance if the electrodes are interconnected. For this example, the combined earthing resistance is increased to about 63 ohms from a level of about 51 ohms that would result if they were far apart [3].

If the three electrodes are interconnected and a dc current, I , is injected into the combination, the current divides and exits to earth in inverse relation to the earthing resistance of each electrode. For our example, assuming no mutual coupling, about 0.75 I leaves through the ring, and about 0.125 I leaves each ground rod. See Figure 2.

Earth resistivity affects the earthing resistance of each electrode, but not the division of current among them. For instance, if the earth resistivity were uniformly 100 meter-ohms, the resistance of the ring would be 6.8 ohms, and each rod would be 40 ohms, but the ring would still carry 75 percent of the current.

Corrosion Rate

DC stray currents rarely corrode ground rods uniformly. In uniform earth, most current leaves near the tip of the rod, so corrosion would be greatest there. Commonly, local nonuniformity of the earth, or uneven electrical contact with the earth, cause the corroding current to exit preferentially over small areas of the rod. This example assumes that current exits from 12 inches of the rod. If failure of the ground rod is considered to occur when all material in the 12-inch segment is lost, the level of stray current that causes failure can be estimated. One foot of 5/8-inch steel rod weighs about 1 pound, and steel corrodes at a rate of 20.1 pounds per year per ampere [4]. Therefore, one ampere corrodes 1 foot of steel ground rod in about 18 days. Because the cladding of the ground rod

is thin, and the density of copper is close to that of steel, these calculations apply for practical purposes to copper-clad steel ground rods.

For our example, one rod conducts only 0.125 of the current into the combined 3-electrode system. So, 1 ampere of dc stray current into the system would cause loss of the rod in $18/0.125 = 144$ days (0.41 year). If the rod were to last 20 years, current into the 3-electrode system would have to be less than $0.41/20$, or about 20 mA.

To learn the rate at which the copper grounding ring corrodes, assume that, because the ring has no sharp ends and is buried in a uniform backfill, it corrodes uniformly. The 2-AWG copper ring has a length of 96 feet and weighs 18.2 pounds. Copper corrodes at a rate of 22.8 pounds per year per ampere [4]. Since the ring conducts 0.75 of the total current into the 3-electrode system, 1 ampere into the system causes the entire ring to corrode away in $18.2/(.75)(22.8) = 1.1$ years. If the ring is to endure 20 years, the dc stray current, I , into the system would have to be less than $1.1/20 = 53$ mA.

In this example, the controlling factor is avoiding corrosion of the ground rods, which requires that the total dc stray current into the representative 3-electrode grounding-electrode system be less than about 20 mA.

Since corrosion of the rods is controlling, additional ground rods would extend the life of the system. Using the same calculation technique to provide an estimate of the extended life, the ground ring with four rods would have a threshold of dc stray current of about 26 mA; the ring with six rods would have a 32 mA threshold. In this example, the addition of standard ground rods does not significantly increase the life of the system.

Levels of DC Stray Currents

High levels of dc stray currents can be expected in the vicinity of dc electrified railway systems (e.g., heavy rails, light rails and subways) and impressed-current cathodic protection systems of non-telecommunication

below-ground structures. We measured the stray dc current, picked up in a manhole from a cathodic protection rectifier and transmitted by a cable shield to the grounding system of an electronic site, to be 1.9 amperes. In another case, the dc stray current was not measured, but it corroded 93 inches of a 10-foot, 5/8-inch diameter stainless-steel ground rod in approximately 10 years. This loss of material would be caused by a continuous current of approximately 400 mA over 10 years. DC electrified rail systems may provide considerably larger stray dc currents than cathodic protection rectifiers.

Alternative Grounding-Electrode System

This paper proposes an alternative grounding-electrode system that uses four high-silicon-chromium cast-iron anodes [5] together with an insulated copper ring. Because it is insulated, the ring does not help lower earthing resistance, but the ring configuration is used because it provides a redundant connection of the four anodes to the electronic site as well as a diversion of surge currents from the enclosed equipment. The anodes are similar in shape and function to ground rods, and are intended to provide a low resistance to earth while enduring for the life of the installation even in the face of dc stray currents.

Long-life Ground Rods

High-silicon-chromium cast-iron anodes are composed of about 79% iron, 15% silicon, and 5% chromium [6], and are commercially available as rods 5 feet long and 2 inches in diameter. They typically are used as anodes for impressed-current cathodic protection systems, but they also can function as long-life ground rods.

The calculated earthing resistance of a 5-foot, 2-inch-diameter anode in an earth resistivity of 1000 meter-ohms is about 470 ohms, which is almost as low as the 400 ohms of a standard 8-foot ground rod (5/8-inch diameter). If the anode is installed by boring and backfilling with a slurry of bentonite, the resistance is lower. In field tests, an anode in bentonite had an earthing resistance that was

significantly lower than standard rods in the same location. In 1989 at a telecommunication central office, three 5-foot long, 2-inch-diameter high-silicon-chromium cast-iron anodes were placed in a 98-foot-deep well and surrounded with coke breeze to serve as an auxiliary grounding system. Their original resistance to ground was 11.6 ohms, and this resistance dropped in two years to 10.5 ohms. The system works well, and we do not expect corrosion problems[7].

The corrosion rate reported by a supplier and other sources [8] of high-silicon-chromium cast iron is much lower than that of steel ground rods. The anode is corroded by stray currents at a rate of about 0.94 pound per year per ampere (versus 20.1 pounds per year per ampere for steel) [6]. The bentonite backfill promotes uniform corrosion over the entire surface, so a single 5-foot anode (44 pounds) would require 1.6 amperes to be 75% corroded (assumed end-of-life) in 20 years. If four anodes were placed in a four-electrode system, the combination would withstand more than 6 amperes. These currents are significantly higher than for the foregoing grounding-electrode system.

High-silicon-chromium cast-iron anodes are anodic to copper, so they help protect from local corrosion effects any exposed copper in the wires that interconnect the electrodes. Furthermore, the anodes are resistant to local corrosion effects, even in soils of high chloride content, or in soils containing sulfate-reducing bacteria.

Because they are less than 8 feet in length, the 5-foot anodes do not satisfy requirements of the NEC for rod electrodes. Accordingly, they should not be used as the sole grounding electrodes for ac power service. They may, however, be used as supplements to acceptable grounding electrodes.

Our field experience, indicating 1.9-ampere stray dc current entering the earth through the grounding system of a CEV, is well within the capabilities of the 6-ampere system described in a previous section.

Proposed System

If the electronic site is in a stray-current area, and if excessive stray dc currents enter the earth from the grounding electrodes, an alternative design using high-silicon-chromium cast-iron anodes is proposed. The alternative system shown in Figure 3 includes an external ring configuration to divert surge currents, and has sufficiently low earthing resistance for signaling.

The proposed grounding-electrode system uses four 5-foot, 2-inch-diameter high-silicon-chromium cast-iron anodes, one at each corner of the ring. Two standard copper-clad steel ground rods (8-foot length, 5/8-inch diameter) are included to comply with the NEC.

A significant difference from the standard grounding system is the use of an insulated copper ring instead of the bare ring. The insulation is intended to avoid corrosion of the ring by stray dc currents; it is needed because a bare ring would conduct about half the total current of the proposed grounding-electrode system, and would entirely corrode within 20 years if the current into the system exceeded about 75 mA.

The combined earthing resistance of the six rod electrodes is about 80 ohms in uniform earth that has a resistivity of 1000 meter-ohms. This value of earthing resistance is sufficiently low for signaling on ground-return systems. This alternative grounding-electrode system should withstand any reasonably expected stray dc current over a 20-year system lifetime.

References

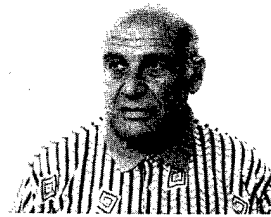
- (1) 1993 National Electrical Code ANSI/NFPA 70-1993
- (2) "Proposal for a Recommendation Covering Bonding Configurations and Earthing at Remote Electronic Sites," Contribution by the United States of America to the ITU-T, Contribution 5-5, January 1994.
- (3) E. D. Sunde, *Earth Conduction Effects in Transmission Systems*, Dover, NY, 1968.
- (4) H. H. Uhlig, *Corrosion and Corrosion Control*, John Wiley, NY 1971.
- (5) M. C. Fontana and N. D. Greene, *Corrosion Engineering*, McGraw-Hill, NY 1967.
- (6) W. T. Bryan, *Use of High-Silicon Chromium Iron Anodes for Deep Ground Beds*, Conference Paper, 26th Annual NACE Conference, Philadelphia, PA, March 1970.
- (7) R. A. Langhage, Private communication.
- (8) *NACE Corrosion Engineers Handbook*, 2nd edition, p. 104, 1991, Editors: R. S. Teller, R. Baboian and C. C. Munger.



Michael Parente chairs the IEEE Working Group for Data, Communications, and Signaling Circuit Surge-Protective Devices.

From 1988 to 1992 he was Special Rapporteur for Grounding to the International Telecommunications Union. He has lectured on the subject of electrical protection and grounding of telecommunications networks in the USA and Europe. His publications and patents cover all aspects of electrical protection of networks, and include many of the systems designs and performance requirements in widespread use by network providers.

Until 1993 he was Director, Electromagnetic Compatibility, at Bell Communications Research, and is now an independent technical consultant. He is a Fellow of the IEEE, and holds an MSEE from Polytechnic University of New York.



George Schick has a Dipl. Eng. degree in Electrochemistry/Electrometallurgy from the University of Grenoble, France, an MS degree in Metallurgy from MIT, and a PhD in Metallurgy and Materials Science from New York University. He worked for Bell Telephone Laboratories, Inc. from 1961 to 1983 in the area of corrosion. In 1984 he joined Bell Communications Research where he is working on corrosion control of the telecommunications plant and on the effects of the environment on optical fibers. Dr Schick was elected Fellow of NACE International and received the Francis L. LaQue Memorial Award from ASTM.

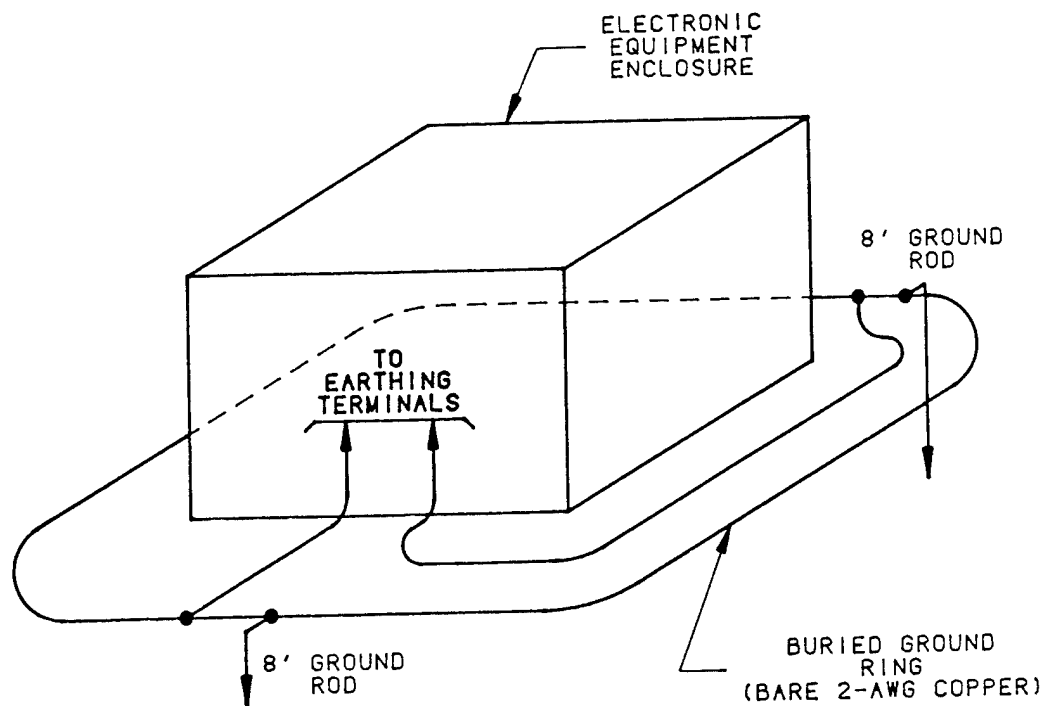


Figure 1. Representative Grounding Electrodes for Electronic Equipment Enclosure

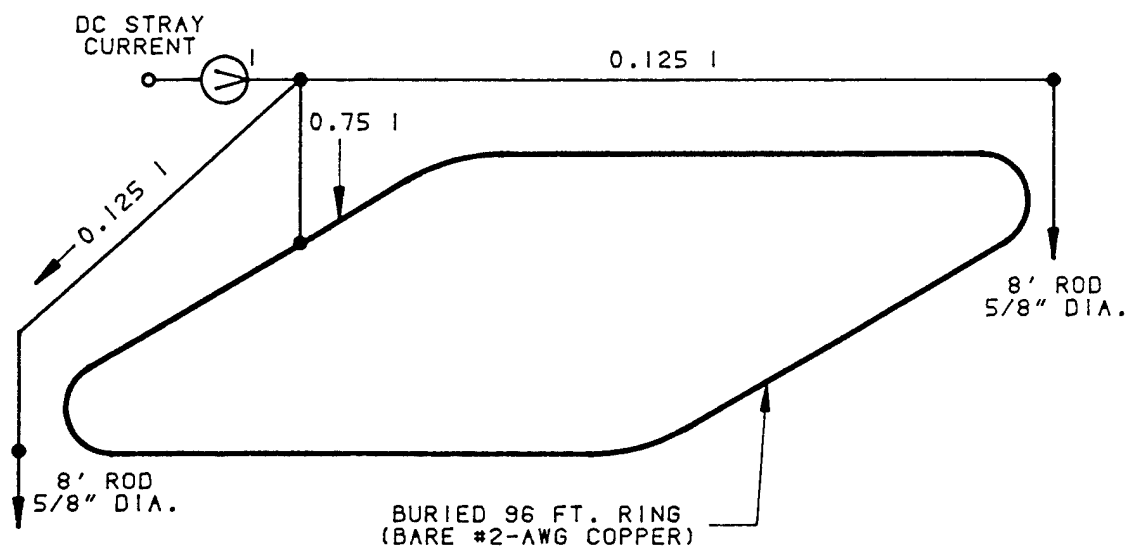


Figure 2. Division of Stray Currents Among Grounding Electrodes

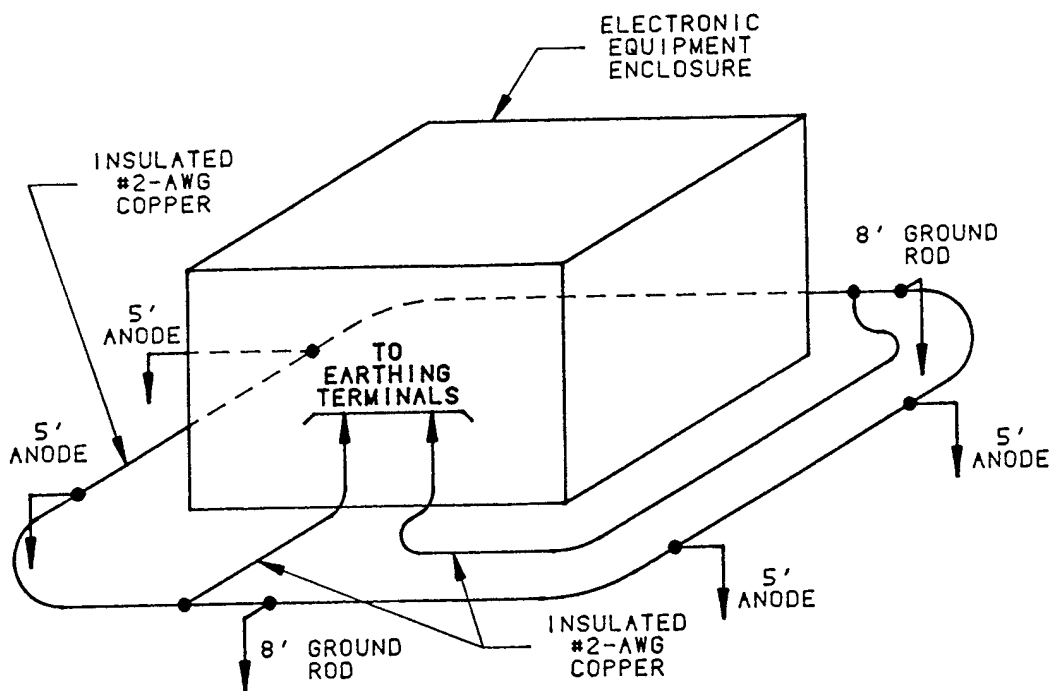


Figure 3. Proposed Grounding Electrode System for Stray-Current Areas

TOMORROW'S RESIDENTIAL GATEWAY TO BROADBAND SERVICES

**Severin Godo
Manager - Transmission System Enhancements**

NORTEL Technologies in Ottawa, Ontario, Canada

ABSTRACT

VARIOUS INDUSTRY SECTORS ARE PARTICIPATING IN ESTABLISHING THE INTERFACE BETWEEN THE RESIDENTIAL USER AND THE BROADBAND NETWORK SERVICES OF THE FUTURE.

THIS PAPER DESCRIBES THE RESIDENTIAL GATEWAY - AN INTELLIGENT ACCESS NETWORK-TO-CONSUMER INTERFACE DEVICE CAPABLE OF PROCESSING AND DIRECTING COMMUNICATION BETWEEN THE DIVERSE SERVICE TERMINALS WITHIN THE RESIDENCE AND ANY NETWORK ACCESS PROVIDER. IT FOCUSES ON THE RESIDENTIAL GATEWAY CONCEPT ITSELF AS BEING DEVELOPED BY TIA TR41.5 AND THE CONCEPT'S RELATIONSHIP WITH THE PREMISES CABLING NETWORKS OF THE RESIDENTIAL BROADBAND FUTURE.

1.0 INTRODUCTION

In North America, the concept of a residential gateway has resulted largely from telecommunication deregulation that has led to competition in the access network and consumer ownership of the premises distribution.

In the past, most in-house networks were either virtually or actually an extension of a network from a local access service provider. Hence, terminals and their protocols had to meet the specifications of the access network.

The current situation, dominated by open standard interfaces for plain old telephone service (POTS) and cable television service, offers the benefits of consistency and low consumer price from using well-defined interfaces for the access networks. However, services offered by an end-service provider are still limited by the capabilities of the local access network. This service provider must use a protocol that can exist with the limits of the local access network (e.g. spare POTS or TV channels).

With terminals becoming increasingly intelligent and with the introduction of interactive, broadband services, the types of terminals that can be connected to the in-house network are becoming increasingly varied. Without some level of coordination (and standardization), the creation of new terminal types (and their corresponding services) will be haphazard which would result in high consumer costs, serious interoperability problems and resulting consumer fears. The complexities before us are illustrated in Figure 1.

A residential gateway, developed as per the architectural concept being formulated in Telecommunications Industry Association subcommittee TR41.5¹, is reflected in this paper. The concept will facilitate low cost user devices and will make it easier for the customer to have simultaneous access to multiple, logically independent communications. In addition, it will permit service providers to provide portable services that will be available whenever the user requires communications.

It is the vision of TR41.5 that the tomorrow's residential gateway will be realized such that the consumer is less aware of the type of network that provides local access service and is less aware of restrictions placed by terminals dedicated to a particular service. In this vision a consumer may place a call using for example a wireless terminal in the home, continuing the connection moving to the car, driving to work and in the office. Throughout the connection, the consumer is unaware of the call being seamlessly transferred or switched among various public and private networks. In this vision, consumer equipment may provide similar features and provide services to other terminals to share these features (e.g. intelligent room thermostat providing information to television or computer for possible interaction). This paper also reflects on the relationship of the residential gateway concept with premises cabling networks of residential broadband future.

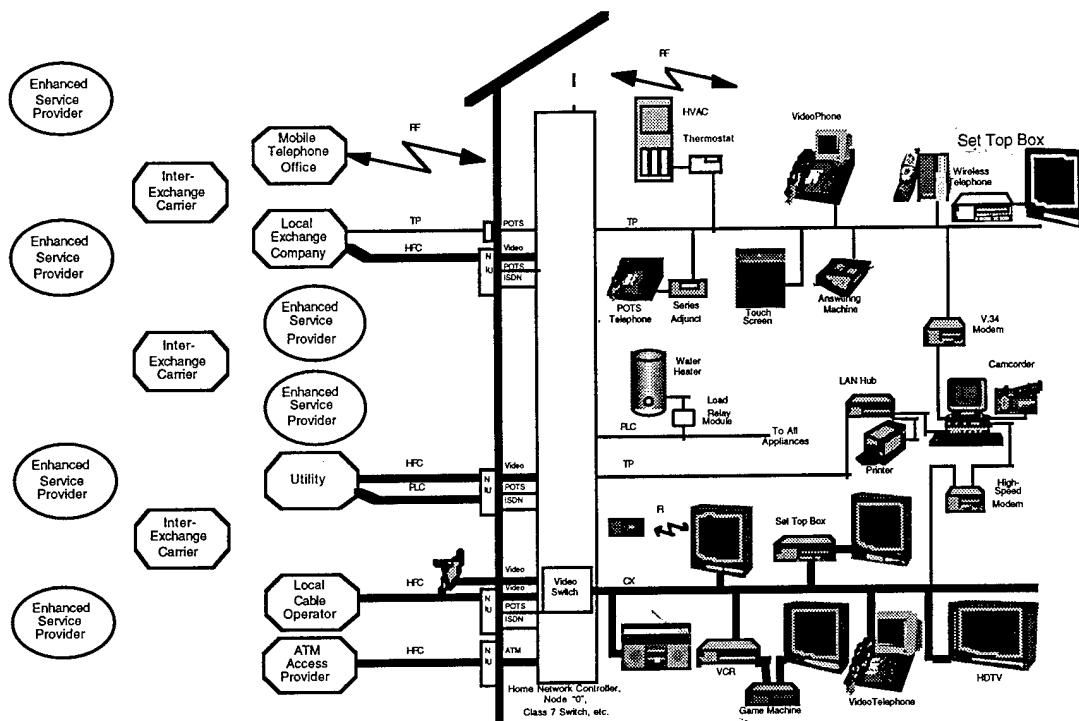


Figure 1. Premises Architectures for Multimedia Services

2.0 A CONCEPTUAL RESIDENTIAL GATEWAY ARCHITECTURE

The conceptual architecture being developed by TIA-TR41.5 is shown in figure 2 and overviews the logical structure of the access and in-house networks. Its arrangement of functional blocks may differ in a physical implementation (e.g. some blocks

may be nulled). The architecture defines groupings and reference points, similar to those found in ISDN Basic-Rate Recommendation ITU-T I.411. Each particular function is not necessarily restricted to a single group. Furthermore, the functions identified for each group are not exhaustive.

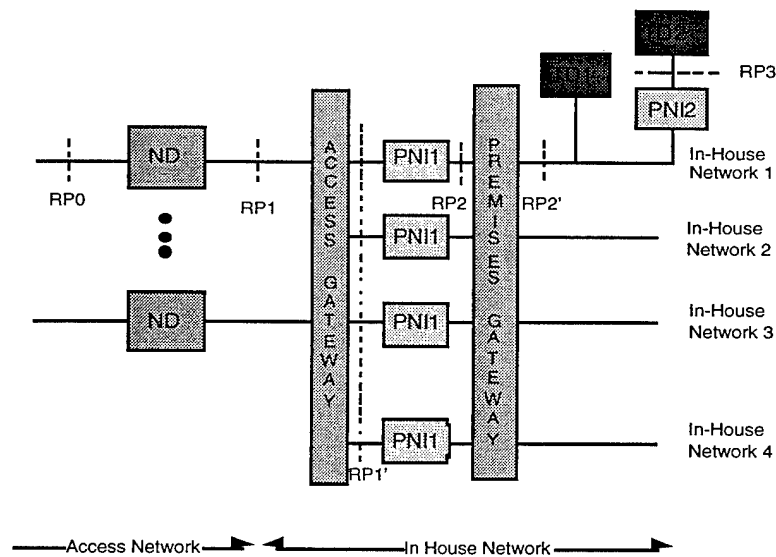


Figure 2. Conceptual Premises Architecture

2.1 Network Device (ND)

The ND provides the proper physical and electrical termination of the network access link, and a legal separation between the access network owned by the public network operator and the in-house network owned by the consumer.

The ND includes broadly layer-1 equivalent functions and could provide multiple open and standard interfaces to other multiple customer equipment. ND functions may include:

- Line transmission termination
- Legal separation from Access Service Providers' networks
- Layer 1 line maintenance and performance monitoring functions
- Timing
- Layer 1 multiplexing
- Interface termination, including multi-drop termination employing layer 1 contention resolution
- Communications access network media change
- Electrical protection of access network in the event of power transfer
- Encryption for privacy and confidentiality
- Powering, grounding and bonding.

The functionality present at Reference Point 1 (RP1) is a perfect subset of the one provided at Reference Point 0 (RP0). The Service Provider for the access network may have functionality at RP0 for network maintenance and provisioning that terminates in the network device, and thus does not appear at RP1. All functionality available to the consumer at RP1 is also present, in some form, at RP0.

2.2 Access Gateway (AG)

The AG maps the functionality from one or more access networks between one or more in-home networks.

An AG device basically provides routing and/or switching and firewall functions between the access interface and the in-home networks that may be carried on multiple media (e.g., twisted pair, power line, wireless or coax). It also requires that mutually acceptable administrative procedures be established between the two networks. To achieve system interoperability AG functions (which broadly belongs to OSI layers 1, 2 and 3) may include:

- Layers 2 and 3 protocol handling/translation and multiplexing
- Routing/Switching
- Protocol translation/adaptation
- Concentration, rate conversion, multiplexing or signal translation
- Firewall
- Maintenance functions (e.g. fault isolation)
- Interface termination, impedance matching, rate conversion and other Layer 1 functions
- Media change in the in-house network

The functionality present at RP1' is identical to the one provided at RP1 within the limitations of the media and protocol mapping. The AG should not intervene with the functionality available from or going to the access network. However, it is recognized that due to limitations of existing protocols that it may not be possible to map all of the functionality from one network to another network, such as from a broadband

access network to a narrowband in-house network. For example, a local area network controller or PBX can provide AG functions at layers 1, 2, and 3. A simple router can provide AG functions at only layers 1 and 2. In a specific access arrangement, the AG group may consist of only physical connections.

2.3 Premises Network Interface 1 (PNI-1)

The PNI-1 generates one or more in-house network(s) for in-house use to provide functionality (common to all PNI-1s) beyond that provided by the access networks.

PNI-1 may provide features on the in-house network that are not available on the access network (e.g. signaling via an out-of-band control channel). Likewise, the PNI-1 may or may not pass through to the in-house network information and signaling that is received from the access network interface. For example, the PNI-1 (e.g. PBX, terminal controller) may act as a 'lightweight' proxy signaling agent for devices in the home that are connected to it. PNI-1 functions may therefore include:

- Layers 2 and 3 protocol handling
- Layers 2 and 3 multiplexing
- Maintenance functions
- Interface termination and other Layer 1 functions
- Media change of the generated in-house network (e.g. coax to twisted pairs)
- Addition of new functionality from corresponding access network

The functionality present at RP2 is a superset of the one provided at RP1'. However, it is also possible for an PNI-1 to not provide certain functionality that is available from the access network (e.g., a simple PBX can provide PNI-1 functions at layers 1, 2, and 3. A simple terminal controller can provide PNI-1 functions at layers 1 and 2 and layer 3 if it involves routing capabilities. A simple time division multiplexer can provide PNI-1 functions at only layer 1. In a specific access arrangement, the PNI-1 group may consist of only physical connections.

2.4 Premises Gateway (PG)

A PG provides a routing between one premises network and another premises network.

Often the networks that the PG is routing between are based on different media (e.g., coax and twisted pair). Their functions, which broadly belongs to OSI layer 1 and higher layers, may include:

- Layers 2 and 3 protocol handling
- Layers 2 and 3 multiplexing
- Routing/Switching
- Protocol translation/adaptation
- Concentration
- Maintenance functions; and
- Interface termination and other Layer 1 functions
- Media change in the in-house network

The functionality present at RP2' is identical to the one provided at RP2 within the limitations of the media and protocol mapping. The PG should not intervene with the functionality available from or going to the PNI-1 or access network. However, due to limitations of existing protocols it is recognized that it may not be possible to map all of the functionality from one network to another network, such as from a broadband to a narrowband network. Also, a local area network controller or PBX can provide PG functions at layers 1, 2, and 3, and a simple router can provide PG functions at only layers 1 and 2. In a specific premises network arrangement, the PG group may consist of only physical connections.

2.5 Terminal Equipment (TE)

The TE grouping is further divided into three classes:

- Terminal Device 1
- Premises Network Interface 2
- Terminal Device 2

Terminal Device 1 (TD1) interfaces directly to an in-house network and provides functionality to the end-user, possibly cooperating with other devices to provide that functionality.

TD-1 includes functions containing interfaces compliant with the protocol stack defined for the RP2' reference point. Its functions, which broadly belongs to OSI layer 1 and higher layers, may include:

- Protocol handling
- Maintenance functions
- Interface functions compliant with the RP2' reference point

Examples of TD1s include facsimile machine or telephone with layer 1 functions on a loop-start POTS line, a simple television on an analog video line, digital telephones, some data terminal equipment, and integrated work stations, or combinations of equipment that provide these functions.

Premises Network Interface 2 (PNI-2) device provides conversion from network dependent signals to network independent signals.

PNI-2 includes functions that allow one or more independent TD devices to be served by the in-house or access network. This allows devices that were built prior to the definition of the in-house or access network to co-exist with the in-house or access network. It also allows devices to be built to a standard PNI-2 interface that are proprietary or independent of the access network technology. Its functions, which belong to OSI layer 1 and higher layers, may include:

- Protocol handling
- Maintenance functions
- Interface functions
- Other equipment or network interface functions
- Connection functions to other equipment
- Interface to proprietary networks.

The functionality present at RP3 is a subset of the one provided at RP2'.

Because PNI-2 adapts the in-house network or access network for use by one or more devices that are not capable of interfacing directly to the in-house or access network, the functionality found at RP3 is typically less than RP2'.

For example, a set-top box can provide PNI-2 functions at layer 1 to a television set, a personal computer, and an audio entertainment system. A simple modem/fax card can provide PNI-2 functions at layers 1 and higher to a personal computer. Terminal adapters between physical interfaces at ISDN reference points R and S, or R and T, are examples of equipment or combinations of equipment that provide PNI-2 functions.

Terminal Device 2 (TD2) terminates a network or interface that does not comply with the in-house network or access network and provides functionality to the end-user, possibly cooperating with other devices to provide that functionality.

TD2 functions may include:

- Protocol handling
- Maintenance functions
- Interface functions
- Connection functions to other terminal device equipment.

TD2 includes TD1 functions, but with an interface other than those supported by the in-house network. A TD2 could be proprietary

equipment or legacy equipment that is incompatible with the in-house network (e.g. a personal computer can provide TD2 functions at layers 1, 2, and 3 and higher but it uses a PNI-2 to access the premises network. A CEBus (Consumer Electronics Bus) compatible thermostat can use layers 1, 2, and 3 on a power-line or on an unshielded twisted pair line to provide TD2 functions to other heating and ventilation equipment).

2.6 Logical Architecture

Although the conceptual reference architecture in Figure 2 illustrates the reference architecture from a physical perspective, the logical or software architecture is equally important. Given the vast array of access options and lower layer standards that will evolve over time, it will be important to develop a software architecture that relieves application developers from having to know and account for differences in the underlying details. The need to develop this architecture is consistent with the evolution towards a "client/server" relationship between the end devices that consumers use to access services and the services themselves. A common set of "middleware" software capabilities will therefore be necessary to enable the abstraction of the underlying communications detail. TIA TR41.5 is also addressing the basic middleware concept consistent with work being done by the Multimedia Communications Forum (MMCF)².

3.0 RELATIONSHIP WITH PREMISES CABLING NETWORKS OF RESIDENTIAL BROADBAND FUTURE

Current in-house networks

The premises environment is likely to consist of several independent networks based on different media types (e.g. non-graded twisted pair for telephony, coaxial cable of varying grades for video, and power lines for electric power, control signaling and low speed data). Power wires are usually star-wired from a breaker panel to one or more rooms where they may be daisy-chained to various appliances. It is often a poor network for communication.

Typical phone lines are run daisy-chained through the house. It is typically two pairs of D-station wire, with only one pair connected, and the second pair available for new services, such as a second line or to power the lighted dial on the phone.

The coax cable is normally a tree and branch form, usually maintained adequately for television viewing, but commonly has defects such as poor shielding, bad connectors, or unterminated extensions.

Migration of in-house networks

People are reluctant to change and usually, they will not want to change their ways unless there is a compelling motivation (e.g. solving a major problem, increased convenience). To get customers to use in-home networks as tools to increase control in their lives, save time, and filter out the good information from the glut, enhancements to the in-home network with gateway, new media and new consumer products must prove itself. The intelligence in the home must be used to seamlessly process information to be more convenient for the customer. At first, only the motivated few early adopters are willing to struggle with a new product concept or new service (e.g. telecommuting, Internet). They may attempt to reuse existing equipment and in-house networks to access emerging desired services, and may or may not achieve satisfactory results. As new lines, terminals, and services are added to achieve desired results, home networks will become increasingly interactive, increasingly use multimedia functionality, become increasingly digital, and will require media capable of handling high bit-rates/bandwidths. Available services will include:

- Phone
- ISDN for computers or digital phones
- Cable TV, Satellite TV
- Cellular phone, paging
- Computer data access by modem
- Various reporting signals over modem for electric metering, HVAC, and security.
- Residential Broadband by twisted pair or coax for video and high speed data services.

Initially, implementation solutions will likely be clustered into a single room in the home (e.g. Category 5 cable to a home office for ISDN or residential broadband services.). Further upgrades may eventually be needed to provide access to desired services throughout the house. Methods by which home networks can usually be enhanced for services beyond the existing wiring include:

- Install appropriate new wires to the end-point where the service is needed.
- Install multiple transmitters and receivers on existing power, or phone lines, or CATV lines, avoiding the frequencies used by the existing analog service.

- Install wireless (RF or IR) transmitters and receivers where needed.

Few consumers are expected to anticipate the value of emerging services and upgrade all in-house networks and equipment simultaneously.

In general, we can estimate that as customers migrate to increased services, in the early days of the transition they will add analog units. There will be few services and the home network will be fairly simple. As demands increase, the network will become more complex, and the emphasis will shift to adding digital units in later years. Today, we can think of the common house as being all analog, even if some analog signals carry digital bits. In the analog-to-digital transition period, both technologies will be working side by side with emphasis shifting to digital networks for new applications. In the long term the emphasis will be heavily digital, although the analog lines, analog TV, phones, and tapes may not disappear entirely.

It is expected that a high-speed digital access network will be realized eventually that will be reliable, easy to use, and will provide fair access to all content providers. Early versions of such networks can be seen in field service trials today (e.g. hybrid-fiber-coax, asymmetric digital subscriber line, local multi-point distribution system, etc.), and network providers are tasked with major challenges to meet all requirements of reliability, ease of use and a fair access for all content providers. Roll-out on a large scale is still awaiting market acceptance, which is expected by the year 2000. The home will then need to be enhanced with a high speed digital network (twisted pair, coax, fiber, power line, wireless or a combination thereof) to accommodate these access technologies. This enhancement will essentially consist of:

- Deployment of a scaleable, modular residential gateway
- Re-use of exiting wiring distribution, to the extent practical
- New terminal devices that will handle a wide variety of services

4.0 INDUSTRY ACTIVITIES

In order to assist in realizing common telecommunications industry goals for equipment and service development that will benefit consumers, equipment manufacturers and service providers alike, TIA TR41.5 is actively examining the premises infrastructure necessary for various communications systems to meet

emerging "information highway" requirements. Their near-term objective is to develop the above conceptual architecture that would permit realizations of premises gateways for connecting existing and new consumer terminals (voice, video and data) of various technologies to various types of access networks. The architecture document is on schedule to be released before year-end 1996. TR41.5 has recently started a second document on a fast-track development schedule that will specify a realization of an evolvable, modular gateway consistent with the architectural concept.

A number of other industry forums and standards groups are looking at developing

gateway arrangements, but their focus is by and large is on interconnecting specific terminal types to applications for specific access solutions. In a broad sense, these include:

- Video (e.g. CATV industry)
- Home Automation (e.g. Utility and Alarm industries)
- Telephony, Data (e.g. Telco, Cellular, Wireless)

Some of the most active forums besides TR41.5 working the lower OSI layer functions, are shown in Table 1:

Table 1: Other External Standards Forums

Forum	Related application areas
ATM Forum, Residential Broadband Group	ATM to the home
ITU-T SG Multimedia	Home distribution and network termination
Digital Audio-Visual Council (DAVIC)	Home distribution and network termination for digital video - i.e., video -on-demand
ATIS T1E1.2	Network termination for wideband access facilities (N. America based)
ETSI NA5 and TM3	Network termination for wideband access facilities (Europe based)
ISO/IEC Joint Tech. Comm.1/SG 25/WG3	Home electronic systems
Video Electronics Standards Assoc. (VESA) ³	Digital in-house networks for multimedia

5.0 CONCLUSIONS

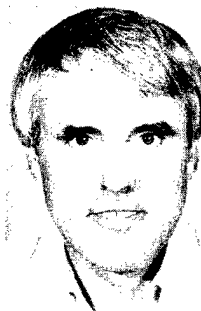
The telecommunications industry is undergoing tremendous changes with the advent of multimedia and 'information highway' and with moving to a dynamically competitive free market environment. This is forcing industry to rethink and redesign the very nature of the products and services they deliver. The resulting changes will influence the architecture of the in-house network significantly and make it necessary to deploy the concept of a residential gateway to coordinate the connections between service providers on the access networks and the terminals delivering the services.

The concept of a residential gateway being developed by TIA TR41.5 includes functionalities that will accommodate all known existing and emerging services from all service provider. This gateway will facilitate low cost user devices, re-use of existing wiring infrastructures (to the extent practical) and make it easier for the customer to have simultaneous access to multiple, logically independent communications.

References:

1. ANSI/TIA SP draft 2.0 - Multimedia Premises Reference Architecture, 1996
2. MMCF/95-009, Reference Architecture Model Specifications, Multimedia Communications Forum (MMCF), 1995
3. VESA Open Set Top - Home network working document, Home network subcommittee, version 2.3, 1995

Biography:



Severin Godo, P. Eng. has over 20 years of telecommunications experience with Nortel Technologies and Bell Canada. As a manager of the Transmission Systems Enhancement group within Nortel, he is involved with development of broadband access technologies and is participating in various Industry standardization committees including TIA TR41 and ISO/IEC JTC1 SC25.

Cabling For High Speed LANs

Christopher T. Di Minico
Digital Equipment Corporation
550 King Street, Littleton, MA 01460
chris.diminico@lkg.mts.dec.com

ABSTRACT

With the dramatic increases in desktop computing power and the need to network between users, a new generation of LAN technologies has evolved. Cabling options identified to meet the demand for the increased data transmission throughput are 100 ohm balanced twisted pair cabling and optical fiber.

The technologies discussed in this paper are, 100BASE-T, (Fast Ethernet), 100VG-AnyLAN (Demand Priority), Fiber Distributed Data Interface (FDDI), and Asynchronous Transfer Mode (ATM). The physical layer cabling requirements of each technology will be discussed with special emphasis on 100 ohm twisted pair cabling. The cabling will be presented with respect to both the transmission performance and the size of the network topologies allowed (i.e., cabling distances). The paper focuses on the installed cabling performance (i.e., connectors terminated to cable within a structured topology).

Additionally, LAN technology transceiver designs will be presented as background for a discussion on cabling performance specifications (specified in MHz) vs LAN technologies specifications (specified in Mb/s).

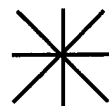
BACKGROUND

Cabling is a key consideration when designing networking products. The broad market penetration and acceptance of 10BASE-T (10 Mb/s Ethernet) was due to its suitability for operation on the 100 ohm twisted pair cabling installed to work area wall outlets for telephony applications. The star wiring topology (Figure 1), where individual cable pairs are distributed radially from a centralized telecommunication closet to each work area, facilitated the deployment of multi-port Ethernet repeaters.

Telecommunication cabling standards (e.g., TIA/EIA-568-A, and ISO/IEC 11801), developing in parallel with the evolving twisted pair technology, specify categories of twisted pair cabling performance (i.e., Category 3, Category 4, and Category 5). 10BASE-T cabling, associated with Category 3, is the most widely installed twisted

pair cable. New technologies, designed to connect to the desktop, test their market penetration based on cabling considerations. The Category 3 cabling option affords the broadest opportunity for market penetration.

Figure 1 Star Topology

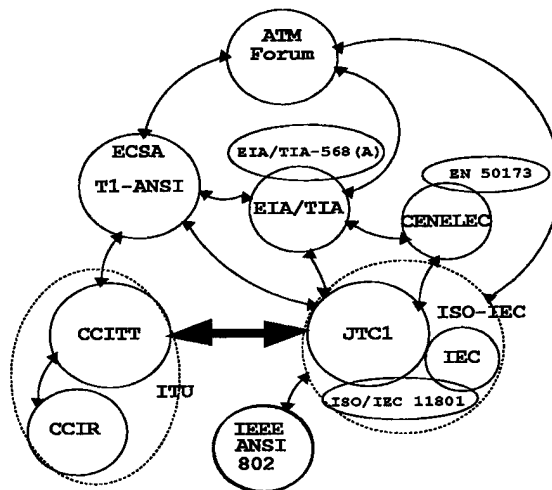


Cabling Standards

Either TIA/EIA-568-A (The Commercial Building Telecommunications Cabling Standard), or ISO/IEC 11801:1995(E), or both, are referenced in the cabling specification of the LAN technologies presented in this abstract.

The scope of these cabling standards includes the cabling topology, performance, components, installation practices and the field tests. The telecommunication standards environment is illustrated in Figure 2.

Figure 2 Telecommunication Standards



EN 50173 - European Standard: Performance requirements of generic cabling schemes
ISO/IEC 11801 - Generic Cabling for Customer Premises
EIA/TIA-568(A) - Commercial Building Telecommunications Cabling Standard

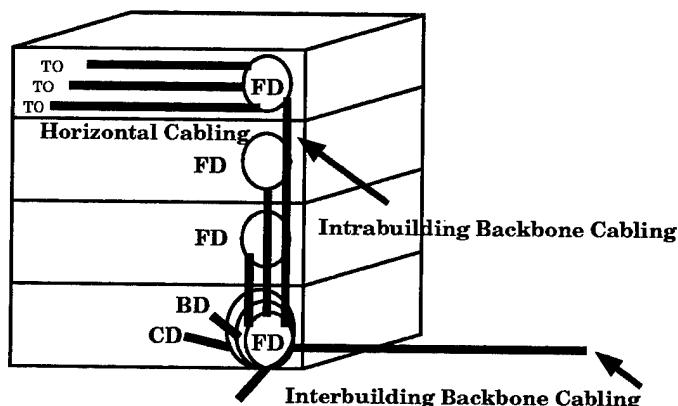
Cabling Topology. TIA/EIA-568-A and ISO/IEC 11801:1995(E) Cabling Standards both share the same basic Cabling System Structure. **Figure 3** illustrates the ISO 11801 Generic Cabling System.

The Cabling System includes cables, patch cords, and connectors for the Horizontal Cabling, Intrabuilding Backbone Cabling, and Interbuilding Backbone Cabling.

The distributors (CD, FD, BD - **Figure 3**) are structures that support termination of building wiring and facilitate inter-connection or cross-connection to equipment using a patch cord.

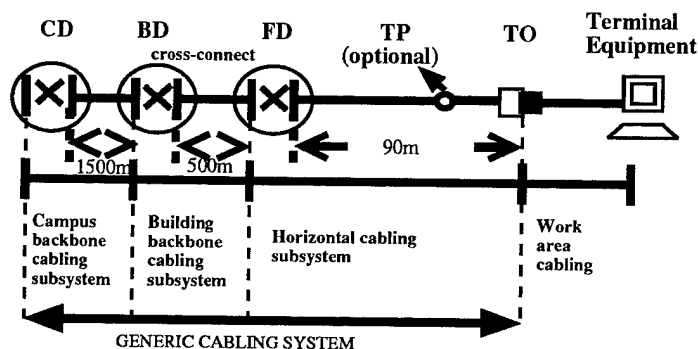
Figure 3 ISO/IEC Generic Cabling System

TO= telecommunication outlet
FD= floor distributor, BD =building distributor
CD= Campus Distributor



Cabling Distance. In **Figure 4** Horizontal Cabling distances were primarily based on the physical plant (i.e., the area of floors in a building). Backbone Cabling distances were based on application specific distance limitations.

Figure 4 ISO 11801 Generic Cabling Distances



Cabling Performance. 100 ohm twisted pair cabling in both TIA-568-A and ISO 11801 is specified in categories of performance:

- Category 3 - specified to 16 MHz
- Category 4 - specified to 20 MHz
- Category 5 - specified to 100 MHz

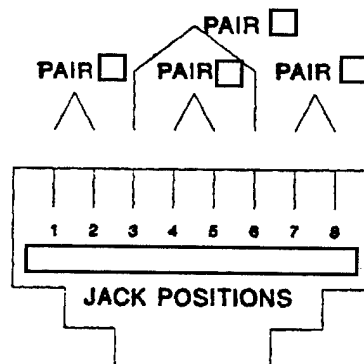
Cable electrical transmission specifications.

- DC Resistance Unbalance
- DC Resistance
- Mutual Capacitance
- Capacitance Unbalance: Pair to Ground
- Characteristic Impedance
- Structural Return Loss (SRL)
- Attenuation
- Near End Crosstalk (NEXT) Loss

Connector electrical transmission specifications.

- DC Resistance
- Return Loss
- Attenuation
- Near End Crosstalk (NEXT) Loss

Figure 5 Telecommunication Outlet (ISO/IEC 603.7) 8-position modular jack (front view) pin/pair assignments



Cabling Horizontal Link Performance. The transmission characteristics of the horizontal cabling (Figure 6) for TIA/EIA568-A (Tables 1 and 2) are component-based while those for ISO/IEC 11801 (Tables 3 and 4) are application-based. Additionally, ISO/IEC11801 specifications are based on the **Link** (i.e., does not include work area cable and equipment cable) while the TIA/EIA568-A specifications are based on the **Channel**. The TIA/EIA568-A Minimum Channel NEXT Loss (Table 1) is derived from the component specifications (e.g., the Channel NEXT loss is the in-phase vector sum of the crosstalk introduced by the components in the channel). The maximum attenuation (Table 2) is equal to the sum of the attenuation of each component in the channel. For the ISO/IEC-11801 Link (Figure 6), the Minimum NEXT and maximum Attenuation (Tables 3 and 4) are based on the applications listed in Annex G. of that standard. The ISO links are classified by performance (Class A through Class D). Class D is associated with Category 5 performance.

Figure 6 Horizontal Cabling Topology

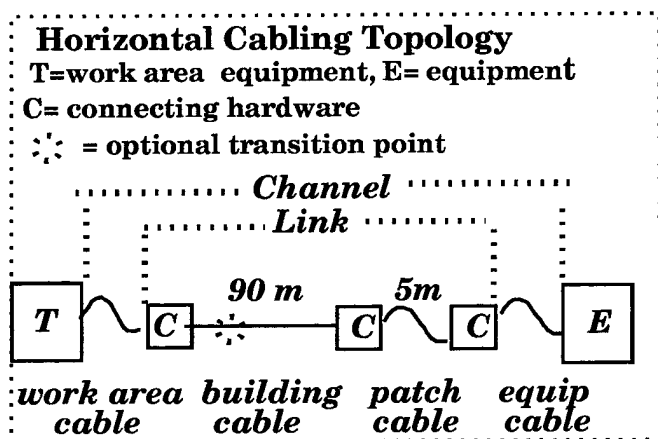


Table 1 TIA/EIA-568-A Minimum Channel NEXT Loss (dB)

Frequency (MHz)	Category 3	Category 5
1	39.1	60.3
4	29.3	50.6
8	24.3	45.6
10	22.7	44.0
16	19.3	40.6
20	N/A	39.0
25	N/A	37.4
31.25	N/A	35.7
62.5	N/A	30.6
100	N/A	27.1

Table 2 TIA/EIA-568-A Maximum Channel Attenuation Values (dB)

Frequency (MHz)	Category 3	Category 5
1	4.2	2.5
4	7.3	4.5
8	10.2	6.3
10	11.5	7.0
16	14.9	9.2
20	N/A	10.3
25	N/A	11.4
31.25	N/A	12.8
62.5	N/A	18.5
100	N/A	24.0

Table 3 ISO 11801 Minimum Link NEXT Loss (dB)

Frequency (MHz)	Class C	Class D
.1	N/A	N/A
1	39	54
4	29	45
10	23	39
16	19	36
20	N/A	35
31.25	N/A	32
62.5	N/A	27
100	N/A	24

Table 4 ISO 11801 Maximum Link Attenuation Values (dB)

Frequency (MHz)	Class C	Class D
.1	N/A	N/A
1	3.7	2.5
4	6.6	4.8
10	10.7	7.5
16	14.0	9.4
20	N/A	10.5
31.25	N/A	13.1
62.5	N/A	18.4
100	N/A	23.2

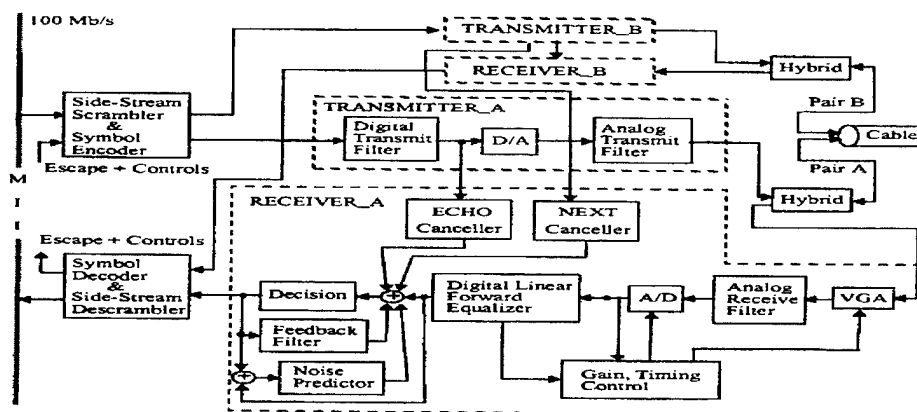


Figure 7. 100BASE-T2 Transceiver

Block diagram of a 100BASE-T2 transceiver

Attenuation To Crosstalk Ratio. The attenuation-to-crosstalk ratio (ACR) is the difference between the crosstalk loss and the attenuation of the link in dB. These values are provided in ISO/IEC 11801 (Table 5). ACR is related to the signal-to-crosstalk ratio (SCR) specified in LAN technologies [often specified more accurately as the crosstalk-to-insertion loss ratio (NIR)]. ACR does not include transceiver variability as do SCR and NIR.

The ISO/IEC 11801 claims that the Class D ACR values were based on the applications referenced in Annex G of that document. For example, an insertion loss to NEXT loss of 30 dB at 16 MHz is specified for TP-PMD (twisted pair FDDI). However, the ACR at 100 MHz (Table 5) is not application related. There are no technologies that specify a 4 dB ACR at 100 MHz. Additionally, with the introduction of networking technologies that implement crosstalk cancellation, cabling choices should not be based on ACR [i.e., making trade-offs between attenuation (cable length) and crosstalk].

Table 5 Minimum ACR Values (dB)

Frequency (MHz)	Class D
1	N/A
4	40
10	35
16	30
20	28
31.25	23
62.5	13
100	4

Field Testing of 100 ohm Cabling Performance

Cabling transmission performance depends on both the component performance and the installation procedures. The TIA/EIA Technical System Bulletin-67 (TSB-67) was developed to address field test tool accuracy and field test parameters (provided below) for post-installation performance measurements of 100 ohm twisted pair cabling.

TIA/EIA - TSB-67 Test Parameters.

Wire Map- to verify cable pair to connector pin termination (Figure 4), and identify connector errors.

Attenuation- the signal loss in a channel or link

Length-the maximum length

NEXT- pair-to-pair signal coupling between adjacent transmitters and receivers.

MHz vs Mb/s

Attenuation and near-end crosstalk loss for cabling are derived from swept frequency measurements. Specifications range from 0.1 MHz to 100 MHz. The attenuation and NEXT values represent the loss of a sinusoidal voltage at the specified frequency and should not be confused with bandwidth limitations, bit rate, or baud (i.e., 622 Mb/s does not necessarily require cabling specified to 622 MHz). Modulation, the additional variations of amplitude, frequency or phase, and signal conditioning are used to transform the desired bit rate into an acceptable signaling rate (baud) based on the design objectives.

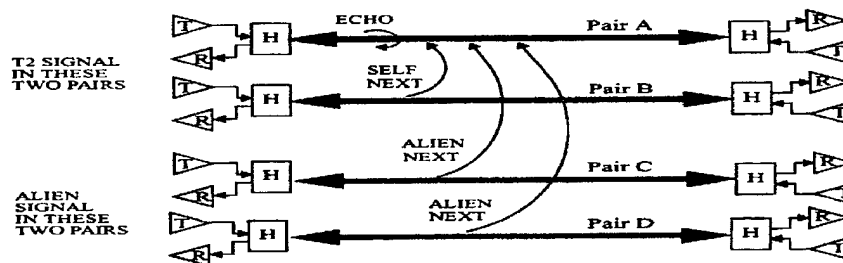


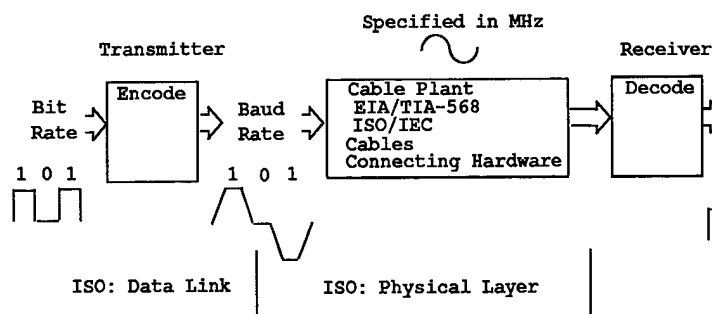
Figure 9. NEXT environment

Example 4-Pair NEXT Scenario

Figure 8 illustrates the signal reference for bit rate and baud. Bit is an abbreviation for binary digit. Bit rate is the number of bits transferred per unit of time expressed in bits per second or in millions of bits per second (Mb/s). Baud is the unit of signaling speed on the physical media, equal to the number of discrete conditions or signal events per second.

Data Transmission. Design objectives dictate the complexity of the modulation technique, signal shaping, and the need for crosstalk cancellation. The most ambitious of the 100BASE-T proposals is 100BASE-T2 (Figure 7) [T2]. This proposal relies on signaling techniques that require digital signal processing (DSP) and mixed-signal silicon technology for operation on two pair of Category 3 cabling (or better). (Class A-ISO/IEC 11801). In addition, 100BASE-T2 objectives are to operate in the NEXT environments illustrated in (Figure 9) [T2] and to meet FCC Class A or B, and CISPR 022 Class A or B.

Figure 8. Signaling Reference



The following discussion will be in reference to the 100BASE-T2 transceiver (Figure 7). The **Equalizer**, placed in the path of the receiver, is a filter used to reduce the effect of intersymbol interference (ISI) which appears as an overlap of adjacent symbols introduced by phase or amplitude distortion in the channel (link). Pulse shaping aids in controlling ISI by rolling off the frequency spectra, minimizing the signal bandwidth. **Encoding** is the translation of a discrete set of sample values into a code. In a binary code, each code state is represented by the presence or absence of a pulse (voltage). The two states of a binary code are customarily denoted as 0 and 1. In a ternary code, there are three distinct code states. MLT-3 code is represented by 1, 0, -1. **Scrambling** spreads the power of a signal over a wider frequency spectra.

Crosstalk Environment

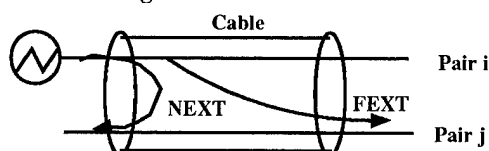
Figure 9 characterizes the cabling infrastructure associated with 10BASE-T including the support of multi-pair bundles used for multiple applications. Based on parallel data transmission and multi-application usage, additional sources of crosstalk, other than self NEXT, must be considered. For example, in a four-pair 100BASE-T2 configuration, three possible multi-application include:

- T2 and voice
- multiple T2
- T2 and 10BASE-T

Alien Crosstalk. represents NEXT or FEXT coupling that cannot be canceled in the same fashion as self NEXT (i.e., crosstalk from alien connections). When associated with two possible alien disturbers, the crosstalk is characterized as Multiple-disturber NEXT (MDNEXT) and Multiple-disturber ELEFEXT (MDELFEEXT) .

FEXT. (far-end crosstalk) represents crosstalk coupling measured at the opposite end of a cable from the transmitter (source).

Figure 10. Far-end Crosstalk



ELFEXT. (equal level far-end crosstalk) represents crosstalk coupling measured at the opposite end of a cable from the transmitter (source). The cable bias is removed by subtracting pair attenuation from FEXT (far- end crosstalk) to get the equal level results.

.Shared and Switched LAN

In a LAN, stations can share a single communication channel using a Media Access Protocol (MAC) or they may attach to a "switch". In a shared LAN, stations connect to a hub, possibly a repeater or concentrator, which forms a broadcast channel for the stations. All stations receive the transmissions from any other station. Station operation is **half duplex**. There may be only one station originating data on the LAN at one time, determined by the MAC protocol.

The same stations described above may be connected to a switch. There may be only one active originator on each switch port at any single instant. The switch copies packets from an input port to the specific output port(s) required while other ports may send or receive a different packet. When connected directly to a switch, a LAN station may operate in **full duplex** mode, therefore access control is not necessary.

Propagation Delay and Delay Skew

In a shared 100BASE-T LAN, round trip delay, which includes the cabling propagation delay, is a key parameter. Additionally, delay skew, the difference in propagation delay between pairs, is critical for implementations employing simultaneous transmitters such as 100BASE-T4 (half-duplex) and 100BASE-T2 (full duplex).

The specification for 100BASE-T4 is provided below as an example.

IEEE Std 802.3u-1995 - type 100BASE-T4:

Section 23.6.2.4.3 - Difference in link delays - The difference in propagation delay, or skew, under all conditions, between the fastest and slowest simplex link seg-

ment in a link segment shall not exceed 50 ns at all frequencies between 2.0 MHz and 12.5 MHz. It is a further functional requirement that, once installed, the skew between all pair combinations due to environmental conditions shall not vary more than +/- 10 ns, within the above requirement.

HIGH SPEED TECHNOLOGY OVERVIEW

In this section, each of the four protocols will be reviewed with a focus on the cabling topology and the 100 ohm twisted pair cabling specification..

FDDI

FDDI is a 100 Mb/s LAN which uses a token ring protocol to schedule station access. FDDI is the type of ring where each station removes its own transmission and operates without a central controlling station. It can support up to 500 stations on a single LAN with a maximum of 100 km of duplex cable.

Cabling Topology. FDDI provides support for Category 5 and 150 ohm STP [TP-PMD], multimode fiber [PMD], as well as single mode fiber [SMF-PMD]. The topology is a dual ring of trees, in which the FDDI dual ring is extended to a tree structure by the use of concentrators. The number of levels in the tree is limited only by the allowable station count and the maximum extent of the network. FDDI protocols provide relatively thorough fault isolation capabilities as well as standardized ways of adding fault tolerance in the dual ring and, in trees, with dual homing [Hutchison][Ocheltree][Willebeek].

Table 5. Twisted Pair FDDI (TP-PMD)

	TP-PMD
Cabling	100 m Link segments ISO/IEC class D performance per TP-PMD
Connecting Hardware (IEC 603-7)	8 position modular jack pin/ pair assignment TX (1, 2)- RX(7,8)
Signaling	4B/5B block code Scrambled MLT-3 100 mb/s (125 M baud)

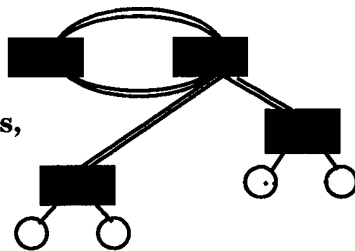
Table 6. Summary of 100BASE-T Cabling

Table 6. 100BASE-T	100BASE-X (copper)	100BASE-T4	100BASE-T2 (Draft)
	100BASE-TX		802.3v/D2 March 5,1996
Horizontal Cabling Topology	100 m Link segments ISO/IEC class D performance per TP-PMD with additions	100 m Link segments ISO/IEC class C performance with additions	100 m Link segments ISO/IEC class C performance with additions
Category 3		4 pair- 3 pair data 1 pair collision detect	2 pair - Bi-directional
Category 4		4 pair- 3 pair data 1 pair collision detect	2 pair - Bi-directional
Category 5	2 pair - 1 pair receive 1 pair transmit	4 pair- 3 pair data 1 pair collision detect	2 pair - Bi-directional
Connecting Hardware (IEC 603-7)	8 position modular jack pin/ pair assignment TX (1, 2)- RX(3 ,6)	8 position modular jack pin -pair assignment TX(1,2) -RX(3,6) BI(4,5)-BI(7,8)	8 position modular jack pin-pair assignment BI_DA(1,2) - BI_DB(3,6)
Network Extent	Two repeater networks of ~200m span	Two repeater networks of ~ 200 m span	Two repeater networks of ~ 200 m span
Signaling	4B/5B block code Scrambled MLT-3 100 mb/s (125 M baud) FDDI PMD	8B6T code data rate per pair 1/3 of 100 Mb/s(33.333.mb/s)	PAM5X5 full duplex 25 Mbaud

Figure 11. FDDI Topology

Topology:

**Dual Ring,
Dual Ring of Trees,
Hierarchical Star**



100BASE-T

100BASE-T, also called Fast Ethernet, is a protocol developed in IEEE 802.3. It is an extension of the Ethernet /802.3 MAC protocol [ISO] for operation at 100 Mb/s.

The operation and architecture of 100BASE-T is nearly identical to that of its 10 Mb/s ancestor. 100BASE-T supports a broadcast channel made up of point-to-point media segments connected via repeaters, similar to the topology of 10BASE-T. Stations attach to the network without requiring the MAC to perform any initialization protocol. This significantly simplifies the implementation.

A key parameter of the CSMA/CD protocol is the slot time, which is the period of time required for a station to be sure that it has not experienced a collision in a properly functioning LAN. Its relationship to the round trip delay is expressed in ISO/IEC 8802-3 as follows:

$$\text{Slot time} = \text{round trip delay} + \text{max jam time}$$

Jam time is the amount of time specified for transmitting a collision enforcement to ensure that a collision is detected by all transmitting stations.

Table 7. Summary of 100BASE-T Network Topology

Table 7. Network Topology	balanced copper	fiber	balanced cable and fiber T4 and FX	balanced cable and fiber TX and FX
DTE-DTE (1) Figure 9. (1)	100 m	412 m	na	na
One Class I repeater Figure 9. (2)	200 m	272 m	231 m (100m balanced cable)	260.8 m (100m balanced cable)
One Class II repeater (2)	200 m	320 m	304 m (100 m balanced cable)	308.8 m (100 m balanced cable)
Two Class II repeaters Figure 9. (3)	205 m	228 m	236.3 m (105 m balanced cable)	216.2 (105 m balanced cable)

Scaling the data rate by a factor of ten while not modifying the MAC's 512 bit slot time requires that the network diameter shrink by a factor of 10. This limits the station to station separation of the network to a maximum of approximately 210 meters.

Cabling Topology. The 100BASE-T topology is significantly different from the 10BASE-T topology. Only one level of the building wiring hierarchy can be supported. Because of timing restrictions, the collision domain can contain no more than two repeaters. The MAC limit of 1024 stations is not changed. The supported media types include Category 3, Category 5, and 150 ohm Shielded Twisted Pair (STP) [100BASE-T]. Support for multimode fiber is also included by incorporating the FDDI PMD [PMD] specification for operation on multimode fiber, but the 2 km distance supported by that PMD is not allowed, due to the timing constraints previously mentioned (Figure 12).

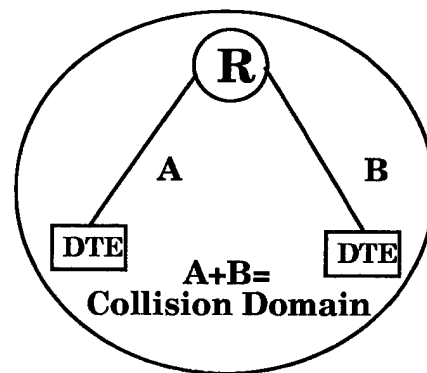
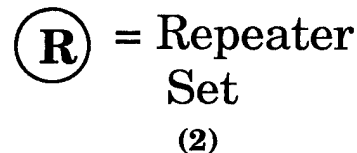
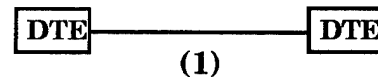
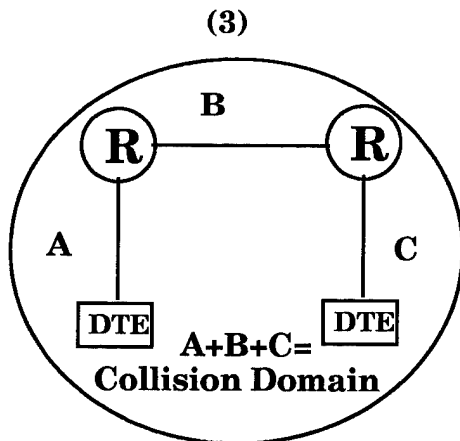


Figure 12. 100BASE-T Network Topology



ATM

Asynchronous Transfer Mode (ATM) is different than the other protocols described. ATM is connection oriented, point-to-point, full duplex and uses a small, fixed packet size called a "cell". It is primarily a format for use by switches and includes no access arbitration protocol.

The PHY (physical) layer of ATM contains a Convergence Sublayer (CS) and a PMD sublayer. The convergence sublayer maps cells into a PMD service. The convergence protocol provides for delineation of the cells in the serial bit stream.

DATA RATE (Mb/s)	SONET DESIGNATION	ITU	OC-N	DS-N	MEDIA
44.736				DS-3	
155.52	STS-3c	STM-1	OC-3c		MMF
155.52	STS-3c				150 ohm STP
100					FDDI-MMF-PMD

Table 8. ATM User-Network Interface Version 3.1

Cabling Topology. ATM at 155 Mb/s will include support for Category 5, 150 ohm STP, multimode fiber [UNI3.1] and singlemode fiber [Bellcore]. The topology is a mesh of switches, which means a switch in the network can be reached from another point using multiple routes involving independent sets of switches. ATM also provides a virtually unlimited end-to-end extent, since no MAC protocol sets the timing constraints for end-to-end extent

Table 8. Twisted Pair ATM 155.52 Mb/s

Cable	Category 5
Horizontal Cabling Topology	100 m Link segments per TIA/EIA -568-A
Connecting Hardware (IEC 603-7)	8 position modular jack pin/ pair assignment ATM Network Equipment receive +:(1), receive -(2) transmit+(7). transmit-(8) ATM User Device receive +:(7), receive -(8) transmit+(1). transmit-(2)
Network Extent	virtually unlimited
Signaling	155.52 Mb/s Line code Non-return to Zero (NRZ)

VG-AnyLAN

VG-AnyLAN, also called 100VG-AnyLAN and Demand Priority, a 100 Mb/s protocol developed in the IEEE 802.12 working group [AnyLAN]. It supports the 802.3 or 802.5 frame formats, but the protocol itself is different from each of those protocols. While a network can operate with each frame format, it is configured to run either 802.3 or 802.5 frame format, not both at the same time.

Cabling Topology. VG-AnyLAN supports Category 3 Category 5 and 150 ohm STP, as well as fiber optic links of 2 km at 1300 nm and 500 m at 800 nm [AnyLAN]. The topology consists of cascaded hubs, as in the 10BASE-T architecture. The supported end-to-end distance restrictions are specified in relationship to repeater types (A through G) [AnyLAN].

Figure 13. VG-AnyLAN Network Topology

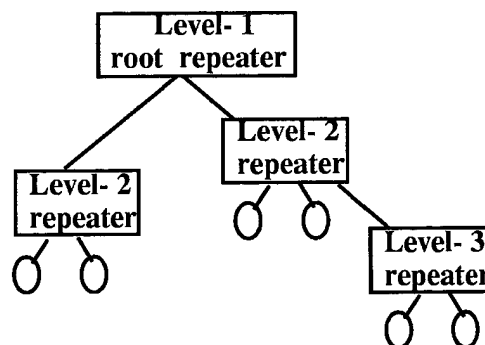


Table 9. Twisted Pair VG-anyLAN (4-UTP)

Cable	4 Pair (4-UTP) Category 3, 4, 5
Horizontal Cabling Topology	100 m Link segments ISO/IEC 11801
Connecting Hardware (IEC 603-7)	8 position modular jack pin/ pair assignment end node and repeater uplink. TP:0(1, 2), TP:2 (4,5) TP:1(3 ,6), TP:3(7,8) repeater downlink TP:0(7, 8), TP:2 (3,6) TP:1(4 ,5), TP:3 (1,2)
Network Extent	100 meter segments lengths between up to 3 levels of cascaded re- peaters
Signaling	NRZ encoded 30 M baud/Pair (120 Mbaud)

SUMMARY

High speed LAN technologies are evolving at a rapid rate. Due to its market penetration, 100 ohm twisted pair horizontal cabling is playing a significant role in that evolution. Presently, the feasibility of Gigabit ethernet on Category 5 cabling is under evaluation by the 802 Higher Speed Task Group (HSSG). The four high speed LAN technologies presented here all have 100 ohm twisted pair cabling options. These were characterized here both in a structured cabling environment and within their respective network topologies.

Author Christopher T. Di Minico, Principal Engineer Digital Equipment Corporation, B.S.E.E Northeastern University

Acknowledgment

Special thanks to William J. Cronin, Jerry D. Hutchison, K.K. Ramakrishnan, and Henry Yang for their contribution to the protocol descriptions [Digital].

References

[100BASE-T] IEEE Std 802.3u-1995 (Supplement to ISO/IEC 8802-3:1993 "MAC Parameters, Physical Layer, Medium Attachment Units and Repeater for 100 Mb/s Operation, Type 100BASE-T

[AnyLAN] IEEE Std 802.12-1995 , " Demand Priority Access Method, Physical Layer and Repeater Specification for 100 Mb/s Operation.

[Bellcore] Bell Communications Research, Synchronous Optical Network (SONET) Transport Systems: Common Generic Criteria, Document Number TA-NWT-000253, Issue 8, Oct., 1993.

[Digital] Digital Equipment Corporation, A Comparison of High Speed LANs, 19th Conference On Local Computer Networks, October 2-5, 1994

[FMAC] ANSI X3.139-1987, Fiber Distributed Data Interface (FDDI) - Token Ring Media Access Control (MAC).

[Hutchison] J. Hutchison, "The Role of Concentrators in FDDI Rings", Proceedings of IEEE 15th Conference on Local Computer Networks, Minneapolis, MN (October 1990), pp. 24 - 40.

[ISO] ISO 8802-3:1989, Information processing systems - Local area networks - Part 3: Carrier sense multiple access with collision detection (CSMA/CD) access method and physical layer specifications.

[Ocheltree] Keneth Ocheltree, "Using Redundancy in FDDI Networks," Proceedings of IEEE 15th Conference on Local Computer Networks, Minneapolis, MN (October 1990), pp. 261 - 267.

[PMD] ANSI X3.166-1990, Fiber Distributed Data Interface (FDDI) - Physical Layer Medium Dependent (PMD).

[SMF-PMD] ANSI X3.184-1993, Fiber Distributed Data Interface (FDDI) - Single Mode Fiber Physical Layer Medium Dependent (SMF-PMD).

[SMT] ANSI X3.229-1994, Fiber Distributed Data Interface (FDDI) - Station Management (SMT).

[TP-PMD] X3T9.5/93-022 " Fiber Distributed Data Interface (FDDI) - Twisted Pair Physical Layer Medium Dependent (TP-PMD) Rev 2.1", 1 March 1994.

[T2] 100BASE-T2 Physical Layer for Fast Ethernet Overview of Operation Version 2.0 March 4, 1996

[UNI] The ATM Forum, "ATM User Network Interface, Version 3.1 (UNI3.1) Specification ", draft of 28 May 1994.

[UNI3] The ATM Forum, "ATM User Network Interface, Version 3.0 Specification ", September 1993.

[Willebeek] M. Willebeek-LeMaire & A. Ruiz, "FDDI Network Availability Analysis", Proceedings of IEEE 16th Conference on Local Computer Networks, Minneapolis, MN (October 1991), pp. 24

LIFETIME PREDICTIONS OF FLAME RETARDANT POLYMERS BY THERMOGRAVIMETRIC ANALYSIS

Sitaram Rampalli

Andrew Corporation
10500 W. 153rd Street, Orland Park, Illinois, USA.

ABSTRACT

This paper discusses systematic studies on the thermal and thermooxidative behavior of various commercial flame retardant polymers suitable for wire and cable applications. Increasing use of these materials on a variety of cables has prompted this study with a view to understand more about the nature of their thermal and oxidative degradation. Thermogravimetric analysis (TGA) is used to follow the weight loss with temperature in these polymers.

Two sets of experiments were performed. In the first study, constant heating rate technique was used to record the weight loss thermograms. From these thermograms, the rate constants and the activation energies were computed. Using this kinetic data, the lifetime of the flame retardant polymers was estimated.

In the second study, dynamic heating rate thermogravimetry experiments were performed by employing the High Resolution TGA. This technique allowed increased resolution of various thermal transitions in these materials. Experiments both under thermal and thermooxidative conditions of degradation were performed. A brief summary of the results obtained by using this technique is presented. The information obtained from these two approaches was found to be highly useful in understanding the nature and the thermal life of the flame retardant polymers.

INTRODUCTION

Flame retardant polymers for wire and cable applications have become more common in the recent years. Depending upon the end use of a given cable construction, these polymers can either be used for outer sheathing (jacketing) or for primary insulation. The surge in the consumption of the flame retardant polymers for wire and cable applications is in response to the wide spread stringent codes and regulations on the fire propagation and smoke toxicity issues that

have taken into effect in various countries around the globe. As a result of these regulations there is the proliferation of several different flame retardant formulations in the market place.

At the present time, wire and cable manufacturers can select the flame retardant materials from two main categories. These are:

- (1) polymers that are inherently flame retardant
- (2) polymers that are compounded with a suitable flame retardant additives.

High performance engineering plastics like polyetherimide (PEI), polyetheretherketone (PEEK), etc., fall under the first group of polymers which are inherently flame retardant. Even though, these materials have excellent performance properties, their high cost, high stiffness, combined with difficulties in processing are the major factors for their limited use in wire and cable applications. Consequently, a vast majority of the materials for use on cables are manufactured by using the second approach. Under this category, common workhorse materials such as polyolefins, vinyls, elastomers etc., are modified by using either a single or a combination of several different flame retardant additives for achieving the required flame retardancy and reduction in smoke toxicity. Once again, these additives can be either halogenated or nonhalogenated compounds. Chlorinated and brominated compounds are the main halogen containing additives, whereas, metallic hydroxides, phosphorous compounds, and other organometallics are the main constituents of typical nonhalogenated flame retardant compounds.

The presence of flame retardant additives in the base polymer(s) has a profound influence on their thermal and thermooxidative stability. Sometimes, cables are installed under severe environmental conditions as for example, cables used in the engine rooms of large ships or in underground tunnels, mines, and in nuclear reactors fall under these types of applications. For

cables using under such adverse conditions, in addition to the flame retardancy, the material should have adequate thermal and thermooxidative stability. Many times it is quite possible that the additives that are used to impart the flame retardancy to the base polymer can also lower the thermal and oxidative stability of the final formulations. It was found that magnesium hydroxide, a common nonhalogenated flame retardant additive exerts a significant degradative action on polyamides via hydrolysis from the water released from the magnesium hydroxide¹. Similarly, certain types of brominated additives in polyesters were found to be capable of modifying the degradation kinetics with reduced activation energies and rapid weight loss². The thermal degradation of ethylene-ethyl acrylate copolymer with some inorganic fillers was also investigated³. It appears that the mechanisms of formation of degradation products from the blends of EEA copolymer with aluminum trihydrate, magnesium hydroxide, and titanium dioxide are altered in the presence of the fillers. Thermal analysis techniques were used to study the mechanism of fire retardancy in polypropylene filled with chlorinated paraffins and also in combination with phosphorous^{4,5}. The effects of polymeric versus monomeric flame retardants on the thermal and flammability characteristics of low density polyethylene by thermogravimetry were also reported in the literature⁶. The influence of particulate fillers on various polymers with special reference to flammability and smoke suppression is summarized in a recent book⁷.

Relatively very little systematic work has been reported in the literature on the kinetics of decomposition of the commercially available flame retardant compounds used in wire and cable applications. Results on the ultraviolet and oxidative thermal aging studies on the flame retardant polymers by high pressure differential scanning calorimetry were reported in my previous paper⁸. The present study deals with the applications of thermogravimetric analysis for the evaluation of kinetics of decomposition of flame retardant polymers. Experiments were conducted both under thermal (inert) and thermooxidative conditions of degradation. Varying heating rate technique is employed to evaluate the kinetics of decomposition and hence the lifetime estimation on these materials. Results on the dynamic heating rate technique using the novel form of thermogravimetry known as "High Resolution TGA" are also included in the present study.

THEORETICAL BACKGROUND

Thermogravimetry provides a rapid method for determining the temperature-decomposition profile of a material. From such a profile, it is possible to determine the degradation kinetics of the material. By using the kinetic data, the lifetime of a given material under specific conditions of temperature can be estimated with reasonable accuracy. Several different techniques were reported in the literature on the kinetics of polymer degradation using the data generated from the thermogravimetry experiments. Most of the methods are based on the following approaches:

1. Constant heating rate TGA
2. Dynamic heating rate TGA
3. Stepwise isothermal TGA
4. Constant reaction rate TGA

Only the first two methods are used in this work to evaluate the kinetic parameters for the thermal and thermooxidative decomposition of flame retardant polymers.

Constant Heating Rate TGA:

This method was first developed by Flynn and Wall⁹. This technique requires three or more weight loss versus temperature experiments on the samples at different heating rates. This approach assumes the basic Arrhenius equation:

$$\frac{d\alpha}{dt} = z \exp\left(-\frac{E_a}{RT}\right) (1-\alpha)^n \quad \dots(1)$$

where:

- α = fraction of decomposition
- t = time (seconds)
- z = pre-exponential factor (1/seconds)
- E_a = activation energy (J/mole)
- R = gas constant (8.314 J/mole K)
- n = reaction order (dimension less)

equation (1) can be rearranged to get equation (2):

$$E_a = \left(-\frac{R}{b}\right) \frac{d \ln \beta}{d(1/T)} \quad \dots(2)$$

where

$$\frac{d \ln \beta}{d(1/T)} \quad \text{is a constant}$$

b= is a constant assuming n=1

β = heating rate ($^{\circ}\text{C}/\text{min}$)

T= temperature of weight loss ($^{\circ}\text{C}$)

Using a point of equivalent weight loss beyond any initial weight loss due to volatile evolution, a plot of $\ln \beta$ vs $1/T$ is constructed. The slope of this straight line plot is used to calculate the activation energy (E_a). The pre- exponential factor (z) is calculated by the interactive method developed by Zsako and Zsako¹⁰.

Toop has postulated a relationship between the activation energy of degradation and the estimated life of insulation compounds¹¹.

$$\ln t_f = \frac{E}{RT_f} + \ln \left[\frac{E}{\beta R} P \left(\frac{E}{RT_c} \right) \right] \quad \dots (3)$$

Where:

t_f = estimated time to failure (min)

E = activation energy (J/mol)

T_f = failure temperature (K)

R = gas constant (8.134 J/mole K)

$P(E/RT)$ = value from a numerical integration table in

reference 11

T_c = temperature for 5% weight loss at β (K)

β = heating rate ($^{\circ}\text{C}/\text{min}$)

To calculate the estimated time to failure (t_f), the value for the temperature (T_c) at the constant conversion point is first selected for a slow heating rate (β). This value, along with the activation energy (E_a) is used to calculate E/RT . This value is then used to select a value for $\log P(E/RT)$ from the numerical integration table given in the paper by Toop. The numerical value for $P(E/RT)$ can be calculated by taking the antilogarithm. By selecting a value for failure (or operation temperature (T_f)) it is possible to calculate the estimated time to failure (t_f) from the equation (3).

It is also possible to estimate the maximum use temperature (T_p) for a given lifetime (t_f) by rearranging the equation (3).

$$T_f = \frac{E/R}{\ln t_f - \ln \left[\frac{E}{\beta R} \cdot P \left(\frac{E}{RT_c} \right) \right]} \quad \dots (4)$$

From equations (3) and (4) plots of estimated lifetime at various temperatures can be constructed. The actual experimental details using this technique are the subject of ASTM standard E1641-94¹². A computer software is now available for generating the data using these equations¹³.

Dynamic Heating Rate TGA:

This technique is the basis for the High Resolution Thermogravimetry¹⁴. In the constant heating rate TGA the information obtained from the experimental data is limited to one step decomposition and first order kinetics. In the case of high resolution TGA approach, it is possible to determine the kinetic parameters such as, energy of activation and reaction order for each step in a multi component or complex material system.

In the dynamic heating rate TGA, both heating rate as well as the rate of weight loss vary continuously during the decomposition. The heating rate is decreased, however, as the rate of weight loss increases. This approach allows very high heating rates to be used in regions where no weight changes are occurring while avoiding transition temperature overshoot. The principal outcome of this technique is enhanced resolution of individual events in the weight loss versus temperature scans.

Decomposition kinetics from variable heating rate experiments can be obtained by using the following equation¹⁵.

$$\ln \left(\frac{H_r}{T^2} \right) = \left(-\frac{E_a}{R} \right) \left(\frac{1}{T} \right) - \ln \left[\frac{zR}{E_a} n(1-\alpha)^{n-1} \right] \quad \dots (5)$$

where:

H_r = heating rate at the peak ($^{\circ}\text{C}/\text{min}$)

T = Temperature at the peak (K)

assuming α is a constant, dH_r / dT is zero at the peak

maximum, and $d(d\alpha / dT)$ is zero.

If the reaction order (n) is one, then the equation (5) simplifies to:

$$\ln\left(\frac{H_r}{T^2}\right)\left(\frac{E_a}{R}\right)\left(\frac{1}{T}\right) - \ln\left[\frac{zR}{E_a}(n)\right] \quad \dots(6)$$

Plotting $\ln(H_r/T^2)$ versus $(1/T)$ permits the determination of activation energies of decomposition. In this method, the calculation of activation energy is

for this study. A generic description of these materials is presented in Table I. All the materials in the present study were assigned alphabetical letters to avoid the trade names.

Equipment:

Thermogravimetric analyzer, Model 2950 equipped with High Resolution option from TA Instruments, New Castle, Delaware, USA., was used to study the kinetics of thermal and thermooxidative degradation of the flame retardant polymers. Figure 1 shows the photograph of the TGA unit used in the present study.

TABLE I
DESCRIPTION OF THE MATERIALS USED IN THE PRESENT STUDY

MATERIAL	GENERIC DESCRIPTION	
	Base Polymer	Nature of the Flame Retardant Additive(s)
A	Blend of Polyethylene copolymer With rubber modifiers	Aluminum Trihydrate
B	Polyethylene copolymer(s)	Magnesium Hydroxide
C	Functionalized Ethylene Propylene Rubber (EPR)	Aluminum Trihydrate
D	Polyurethane	Proprietary char forming additives
E	Elastomeric Polyethylene	Chlorine
F	Low Density Polyethylene	Organic Bromine/Antimony Oxide
G	Polyvinyl Chloride Alloy	Compounds of Lead, Barium, Zinc, and Antimony.
H	Polyvinyl Chloride	Compounds of Lead, Antimony, and Barium.

independent of the reaction order and the reaction mechanism.

EXPERIMENTAL

Materials:

Several commercially available halogenated and nonhalogenated flame retardant polymers were selected

Electronic grade helium (99.9999% pure), and research grade ultra high purity air were used as the purge gases in the thermogravimetric analyzer for thermal and thermooxidative studies respectively.

Constant heating rate TGA experiments were performed at heating rates of 1, 2, 5, 7, and 10° C/min. For dynamic heating rate experiments, the high resolution setup on the TGA was used. The resolutions

were 4, 4.5, 5, 5.5, and 6. The sensitivity setting was maintained at 3 in all the experiments.

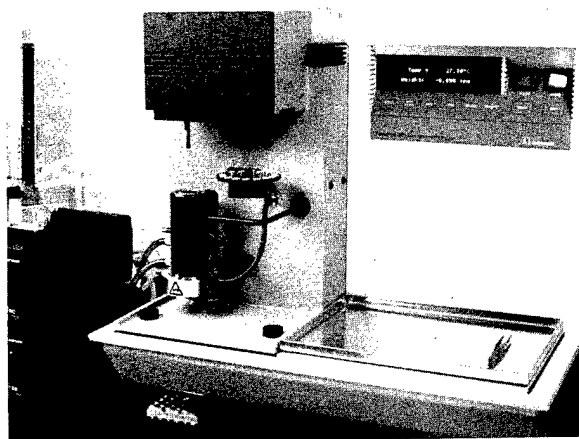


Fig. 1 Thermogravimetric Analyzer

RESULTS AND DISCUSSION

Thermal Degradation Studies:

Pure thermal degradation studies were carried out in an atmosphere of helium. Helium was chosen because of its ultra low levels of oxygen and high thermal conductivity. These studies are highly useful in understanding the influence of thermal energy alone on the polymers in the absence of other chemical reactions which normally occur in the presence of oxygen. Further, information obtained on the materials under pure thermal degradation is of importance in optimizing the processing conditions - such as extrusion and injection molding for these materials. The course of degradation of the polymers under thermal conditions is a function of the structure of the polymer itself as well as the presence of traces of impurities and other additives.

Thermal degradation is characterized by the breaks in the primary bonds in the chemical structure of the polymer. A number of experimental indicators are used to quantify the phenomenon of thermal decomposition of polymers¹⁶. These are:

1. Temperature of initial decomposition ($T_{d,o}$).
2. Temperature of half decomposition ($T_{d,1/2}$).
3. Temperature of the maximum rate of decomposition ($T_{d,max}$).
4. The amount of char residue at the end of pyrolysis.
5. The average energy of activation.

Figures 2, 3, 4, and 5 show the TGA and DTG curves for the materials at 1 and 10°C/min representing the lowest and the highest heating rates used in the present study. Table II shows the values of $T_{d,o}$, $T_{d,1/2}$, $T_{d,max}$, and the amount of char residue for all the materials tested. These values are computed at the heating rate of 1°C/min. It is clear from these figures and the Table II, that material B has the highest initial decomposition temperature (269°C) whereas, the material G has the lowest initial decomposition temperature (84°C). The temperature of half decomposition ($T_{d,1/2}$) is highest for material E and lowest for material G. It is also evident from the DTG curves that for materials A, B, & C the maximum weight loss occurs between 425-430°C, whereas for material D, the corresponding temperature is around 273°C, thus indicating that material D is least stable among all the nonhalogenated materials tested. Similarly materials G & H are the least stable among all the halogenated materials tested.

The percent weight loss per minute at the maximum decomposition temperature is highest for material G, which happens to be formulation based on PVC with a high level of flame retardant filler loading. As it can be seen from the DTG curves that most of these materials exhibited more than one $T_{d,max}$ thus indicating several stages of degradation, although other weight loss events may be associated with volatile additives that are present in the formulation.

Thermooxidative Degradation Studies:

Oxidative degradation studies were performed using ultra pure air as the purge gas in the thermogravimetric analyzer. Thermal degradation presents no practical problems beyond the processing stage, since most of the cables made with these flame retardant compounds are not designed to function at elevated temperatures. On the other hand, in the case of oxidative degradation can happen even at room temperatures and below. The oxidative process is accelerated at elevated temperatures. Oxidation sometimes can occur even in the solid state.

Figures 6, 7, 8, and 9 show the TGA and the corresponding DTG curves for the materials at a heating rate of 1 and 10°C/min under air purge. Once again these two heating rates are the minimum and maximum used in this study. Table III shows $T_{d,o}$, $T_{d,1/2}$, $T_{d,max}$ values and the amount of char residue for all the materials at 1°C/min. As it can be seen from Figures 6 and 7 that the overall general trend in the weight loss for the nonhalogenated materials under thermooxidative conditions is very similar to the one observed under thermal decomposition. The materials

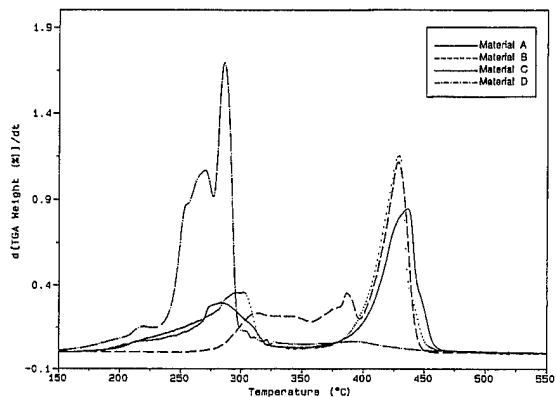
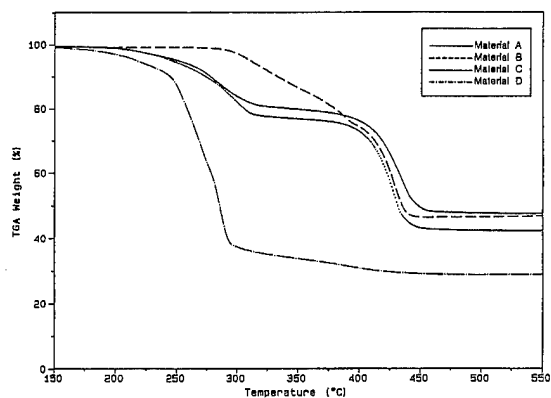


Fig. 2 TG and DTG Curves of Nonhalogenated Polymers in Helium
Heating Rate: 1°C/min

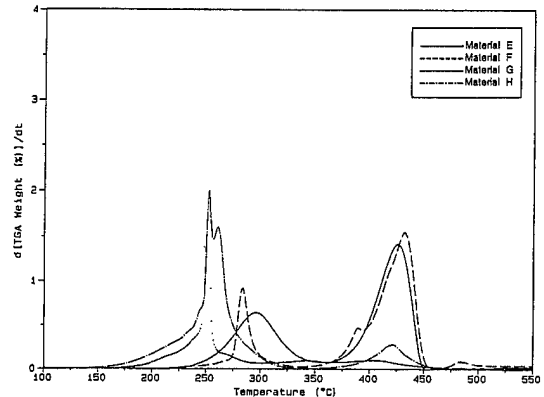
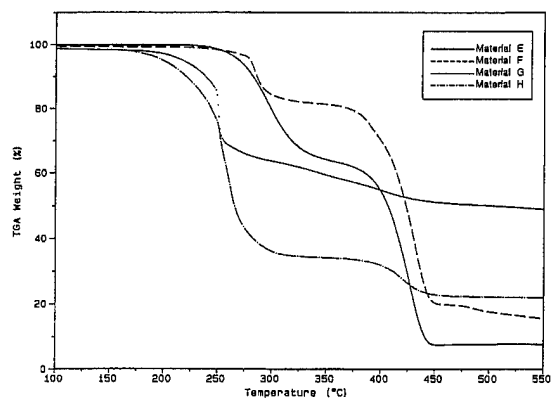


Fig. 4 TG and DTG Curves of Halogenated Polymers in Helium
Heating Rate: 1°C/min

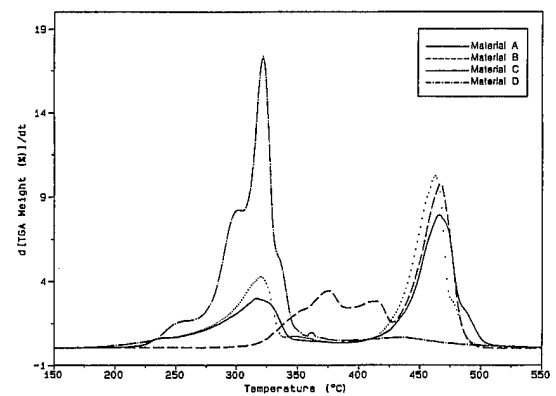
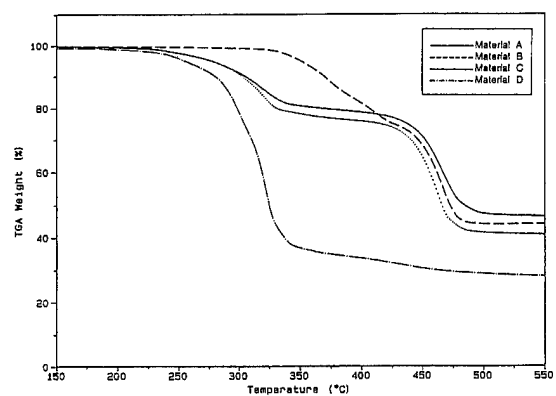


Fig. 3 TG and DTG Curves of Nonhalogenated Polymers in Helium
Heating Rate: 10°C/min

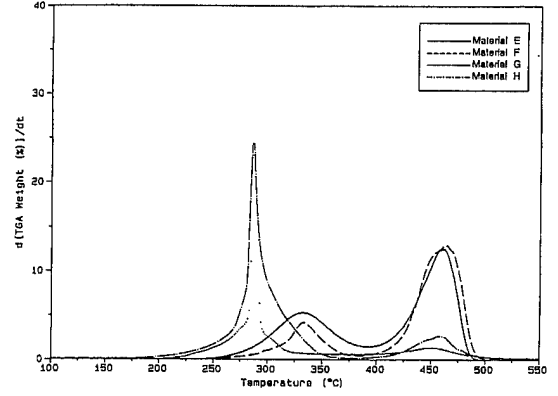
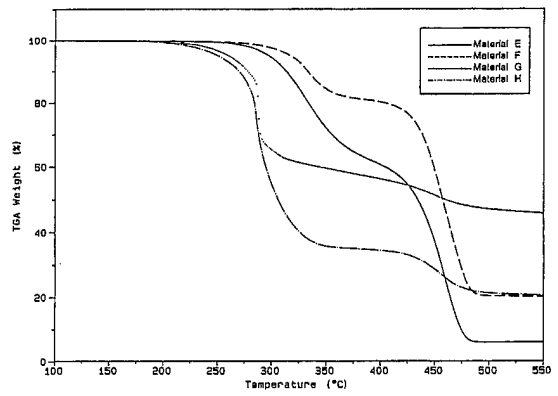


Fig. 5 TG and DTG Curves of Halogenated Polymers in Helium
Heating Rate: 10°C/min

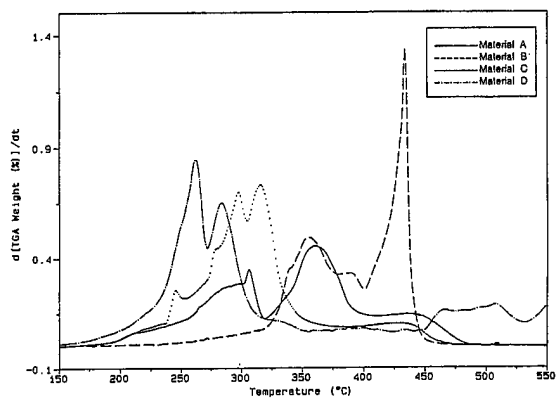
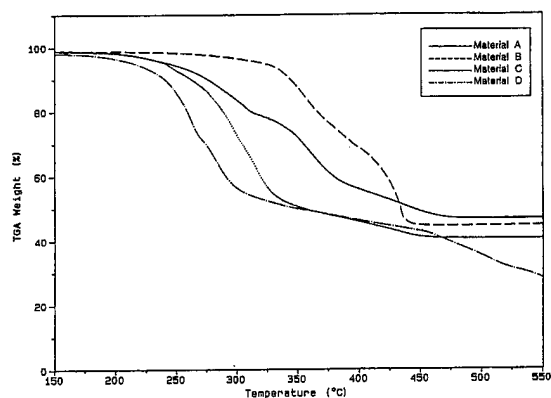


Fig. 6 TG and DTG Curves for Nonhalogenated Polymers in Air
Heating Rate: 1°C/min

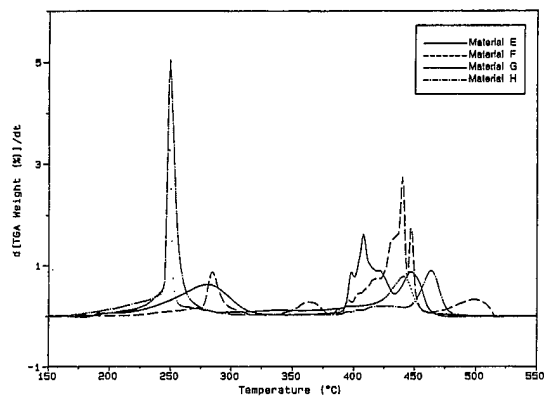
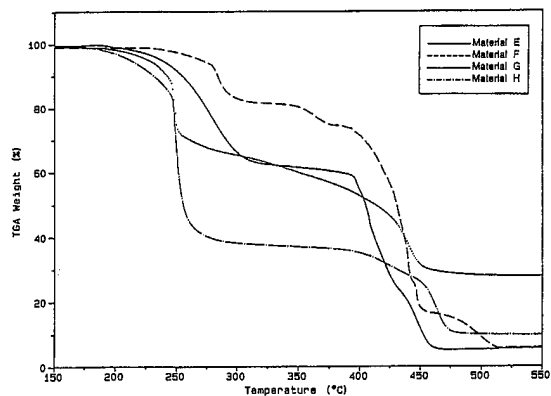


Fig. 8 TG and DTG Curves for Halogenated Polymers in Air
Heating Rate: 1°C/min

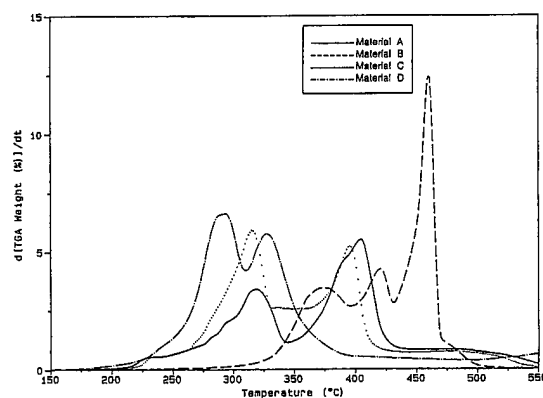
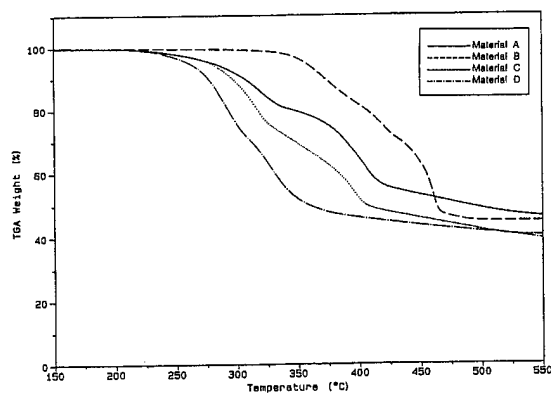


Fig. 7 TG and DTG Curves for Nonhalogenated Polymers in Air
Heating Rate: 10°C/min

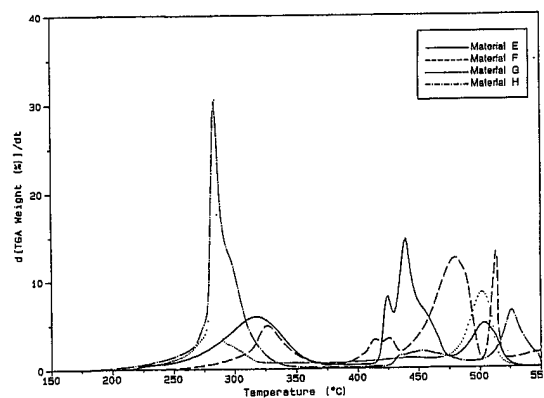
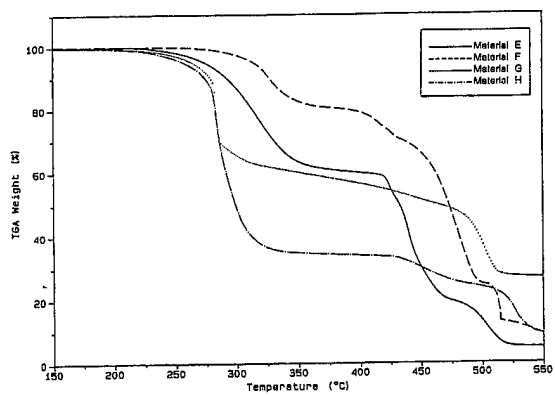


Fig. 9 TG and DTG Curves for Halogenated Polymers in Air
Heating Rate: 10°C/min

TABLE II
THERMAL DEGRADATION OF FLAME RETARDANT POLYMERS IN *HELIUM*
HEATING RATE: 1°C/min

Material	$T_{d,0}$	$T_{d,1/2}$	$T_{d,max}$	Percent Weight Loss per minute @ $T_{d,max}$	Residue
A	197.13	409.89	284 437	0.30 0.85	47.55
B	268.70	403.31	425	1.11	46.72
C	202.45	405.49	429	1.16	42.29
D	170.19	273.20	269 286	1.07 1.71	28.91
E	247.97	416.56	432	1.57	15.34
F	253.21	401.12	296 426	0.65 1.43	7.74
G	84.00	251	251	3.80	48.98
H	144.24	257.85	251	2.30	33.00

$T_{d,0}$ = Temperature of initial decomposition (Temperature at which the weight loss is just measurable)
 $T_{d,1/2}$ = Temperature of half decomposition (Temperature at which the weight loss reaches 50% of its value)
 $T_{d,max}$ = Temperature of the *maximum* rate of decomposition

D and **B** showed the lowest and the highest thermal stability. Compared to thermal decomposition, the oxidative process showed several steps in the weight loss curve. This is more prominent in the case of halogenated polymers, especially above 325°C. The temperature of initial decomposition ($T_{d,0}$) for materials **E** and **F** is less under oxidative conditions, when compared to thermal exposure; this is not unusual. However, for material **G** and **H** the $T_{d,0}$ is much higher under oxidative conditions of degradation than in thermal degradation. This is due to the fact that these two materials contain lead oxide (PbO) as a part of the flame retardant package. Studies have shown that lead oxide can exert an inhibitory effect on auto-oxidation of several polymers¹⁷.

The last column in the Tables II and III is the amount of residue left behind in the pan at the end of the experiment. Since the thermal degradation experiments are conducted in an atmosphere of inert gas (helium) free from oxygen, some of the residue consisted of char

and metal oxide fillers. By subtracting the amount of residue left behind in the pans in the experiments under helium and air, we can obtain the actual char residue formed under thermal conditions of degradation. It has been shown that there was a correlation between char residue and the oxygen index of the polymers¹⁵. In general, higher the char residue, lower is the flammability of the polymer. Among the current materials investigated, the char residue from the halogenated polymers is significantly higher than those of the nonhalogenated materials. Of all the materials tests, material **G** has the highest percentage of char residue. In fact this material has very low flammability and a very high oxygen index number (>50%) and it is intended for plenum cable applications.

Kinetic Analysis of Flame Retardant Polymers:

Thermal Degradation:

One of the standard methods for evaluating the kinetic

TABLE III
THERMOOXIDATIVE DEGRADATION OF FLAME RETARDANT POLYMERS IN AIR
HEATING RATE: 1°C/min

Material	T _{d,0}	T _{d, ½}	T _{d,max}	Percent Weight Loss per minute @ T _{d,max}	Residue
A	134.33	346.28	315 361	0.480 0.372	46.64
B	265.00	382.37	350 435	0.520 0.815	45.06
C	169.28	304.14	297 316	0.708 0.747	40.50
D	101.82	284.09	250 262	0.861 0.680	27.96
E	238.51	428.41	275 440	1.000 3.793	5.83
F	213.72	402.06	397 408	1.054 2.217	5.74
G	194.04	316.5	249 441	4.181 0.800	27.86
H	173.82	252.95	258 470	5.744 1.250	9.79

parameters and hence the life of the cable insulation is done by using the laboratory ovens. The samples are aged at various temperatures and plots of lifetime versus failure the reciprocal of the failure temperature are constructed. The method assumes first order kinetics and uses extrapolation to estimate the long lifetimes encountered at normal use temperature. Even though, this procedure is highly useful in evaluating various materials, it is very time consuming and laborious - especially if the material under test is very stable.

Thermogravimetry is a very rapid, reliable and accurate methodology for the evaluation of kinetic parameters such as, order of the reaction, energy of activation, and hence the polymer lifetimes. Decomposition kinetics of the flame retardant compounds under thermal and thermooxidative conditions was evaluated by using the method described in the section under "theoretical background".

Each material under study is temperature programmed at five different heating rates. The specimen weight loss is recorded as a function of temperature. The temperatures for a constant decomposition level are determined by using the resulting thermal curves. The kinetic activation energy is then determined from a plot of the logarithm of the heating rate versus the reciprocal of the temperature of constant decomposition level. The activation energy thus obtained is used to calculate the estimated lifetime at a given temperature or the maximum operating temperature for given estimated lifetime.

Figure 10 shows a series of thermal curves under thermal conditions of degradation for materials A thru H. These thermal curves depict weight loss up to 20%. The next step in the data evaluation is the selection of percent decomposition. Typically, a value in the initial stages of the decomposition curve is highly desirable, since the mechanism of degradation here is more likely to be that of the actual product failure. A value of 5%

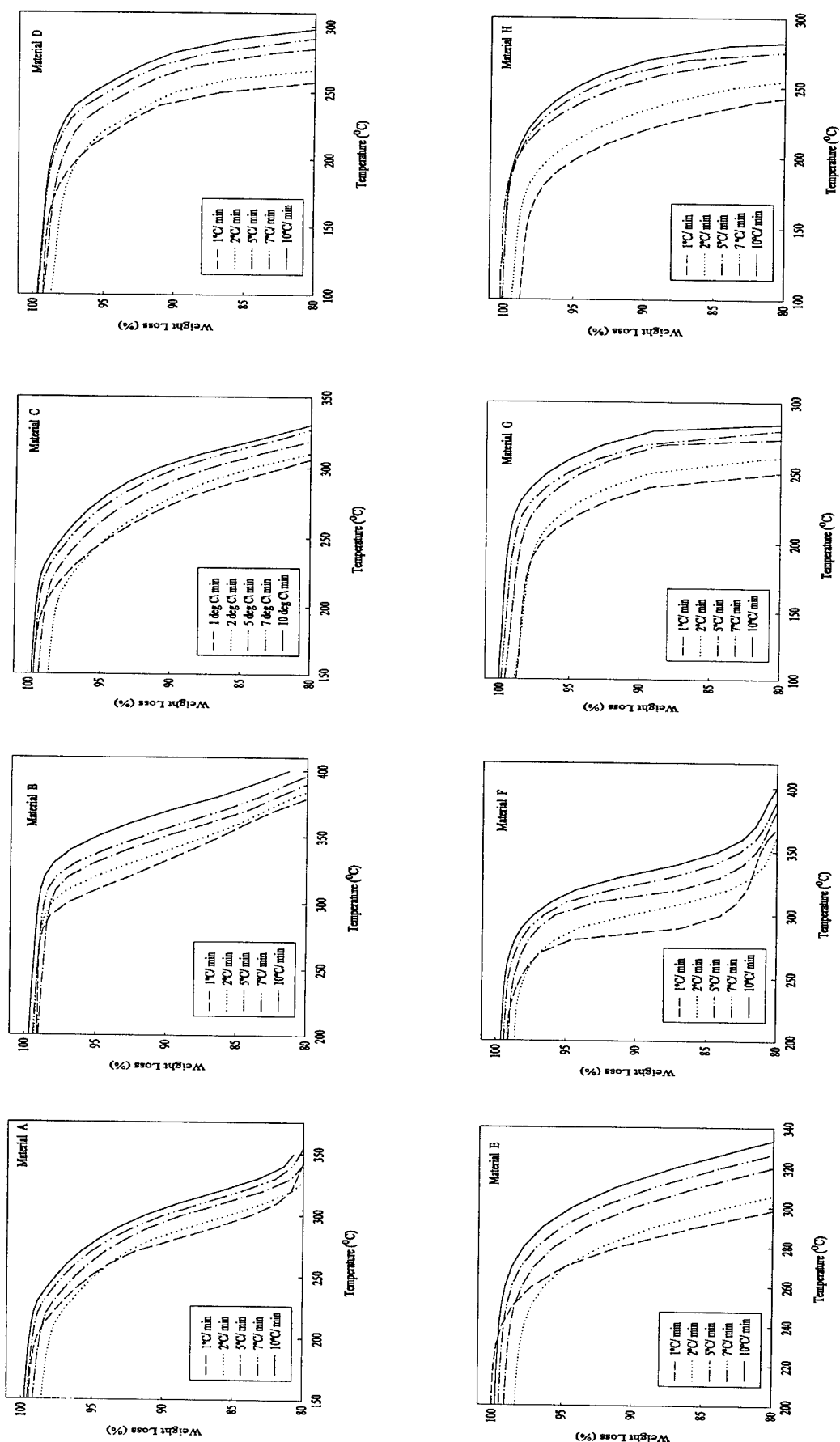


Fig. 10 Thermal Stability of Flame Retardant Polymers in Helium

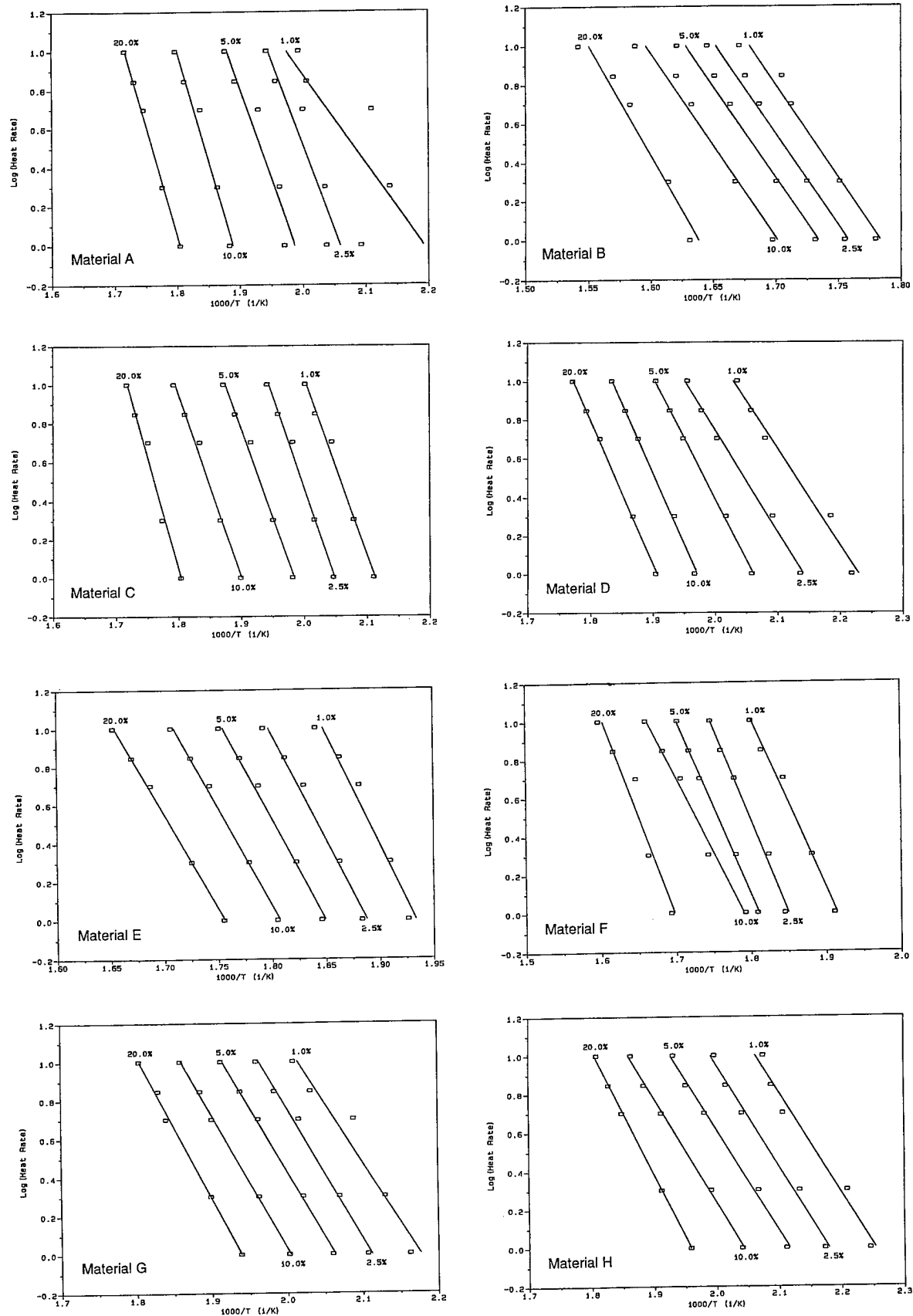


Fig. 11 Log Heating Rate vs Temperature of Flame Retardant Polymers in Helium

decomposition (sometimes known as 'conversion') is the commonly chosen value.

After selecting the appropriate conversion level, the temperature (kelvin) at that conversion level is measured for each thermal curve. A plot of the logarithm of the heating rate versus the corresponding reciprocal temperature at constant conversion is prepared. Figure 11 shows a series of such plots for materials A thru H. Even though, a 5% conversion value was selected for the final computation of the lifetime, conversion levels up to 20% are included in these plots. The slopes of the lines will be constant, if the degradation mechanism is the same at all conversion levels. Only for the material A, the lines at low conversions are different from those at 5% and above conversions. For all other materials (B thru H), the slopes remained fairly constant.

Using the slopes of the lines from Figure 11, the activation energy for thermal decomposition at 5% conversion level was calculated using the equation (2) for each of the materials under study. The activation energy values are shown in Table IV. It can be seen that the activation energy at 5% conversion case is very similar to that of the 1, 2.5, and even up to 10% for all the materials in this study. This represents the failure mechanism is fairly consistent at these conversion levels. This point further proves that the selection of 5% conversion represents a close approximation of the actual product failure.

Estimation of the Lifetime:

The next step in the data analysis is the estimation of the lifetime and/or the maximum use temperature of the materials at a given lifetime. This is done by using the equations (3) and (4) as discussed in the earlier section.

Figures 12 and 13 show the plots of estimated lifetime of the materials as a function of temperature under thermal conditions of aging in helium. From a closer look at these plots it can be concluded that, among nonhalogenated polymers material B, is highly stable; whereas, among the halogenated polymers, materials E, & F are highly stable. Even though, materials G & H have very similar compositions, there are substantial differences in their thermal lifetimes. Thus, for example, it will take 5 years for material G to degrade by 5% at 100°C; whereas it will only take less than an year for material H. It appears that chlorinated and brominated materials as a group are thermally more stable than either polyvinyl chloride or other compounds formulated from PVC.

Thermooxidative Degradation:

Thermooxidative degradation occurs when both temperature and oxygen are acting on the material simultaneously. In this type of degradation, the presence of certain additives such as metallic salts, catalyst residues, as well as the tacticity of the base polymer itself will play a very important role in determining its oxidative stability.

Kinetic analysis under thermooxidative conditions of degradation was performed in the same manner as it was done under thermal degradation. Figure 14 shows a series of thermal curves for all the materials under air atmosphere. From these plots the percent decomposition at various heating rates was calculated. Plots of log of heating rate versus the reciprocal of the temperature are shown in Figure 15. The activation energies at various decomposition levels were calculated and are shown in Table V. It is evident that once again the material B has the highest activation energy at almost all conversions - more specifically at 5% conversion. This clearly demonstrates that the material B is by far the most stable material under thermal as well as thermooxidative conditions of exposure.

Estimation of the Lifetime:

The lifetime of the flame retardant materials as a function of temperature was estimated using the procedures described in the previous section under thermal degradation. Figures 16 and 17 show such plots. As it can be seen from these plots that among all the nonhalogenated flame retardant materials tested, material B, once again showed a very high level of stability under thermooxidative conditions of aging. Materials A, & C are very similar in their overall oxidative stability, thus indicating that their basic chemical composition is virtually identical. Material D has the least amount of oxidative stability. In general all these three materials have similar lifetime under thermooxidative conditions aging when compared to thermal degradation. Among the halogenated flame retardant materials tested, the material F (brominated polyethylene) is highly stable, whereas the material H is least stable.

The magnitude of the effects of thermal and thermooxidative degradation of various flame retardant polymers is reflected in their estimated lifetime. These results are tabulated in Table VI. It is no surprise that the lifetimes under thermal decomposition conditions is significantly higher for most of the materials except for materials G & H. One possible reason for this

TABLE IV

ACTIVATION ENERGIES OF THERMAL DEGRADATION AT VARIOUS CONVERSIONS

Material	Conversion (%)	Activation Energy (kJ/mol)
A	1	111.3
	2.5	140.2
	5	144.6
	10	175.2
	20	192.7
B	1	190.4
	2.5	181.5
	5	179.5
	10	186.2
	20	205.1
C	1	134.1
	2.5	148.8
	5	140.7
	10	151.2
	20	196.8
D	1	97.2
	2.5	101.3
	5	117.4
	10	129.3
	20	128.6
E	1	194.1
	2.5	181.9
	5	175.3
	10	168.5
	20	166.8
F	1	146.7
	2.5	174.0
	5	174.1
	10	131.8
	20	173
G	1	99.7
	2.5	109.0
	5	113.7
	10	122.1
	20	134.2
H	1	102.7
	2.5	103.4
	5	99.5
	10	103.5
	20	125.9

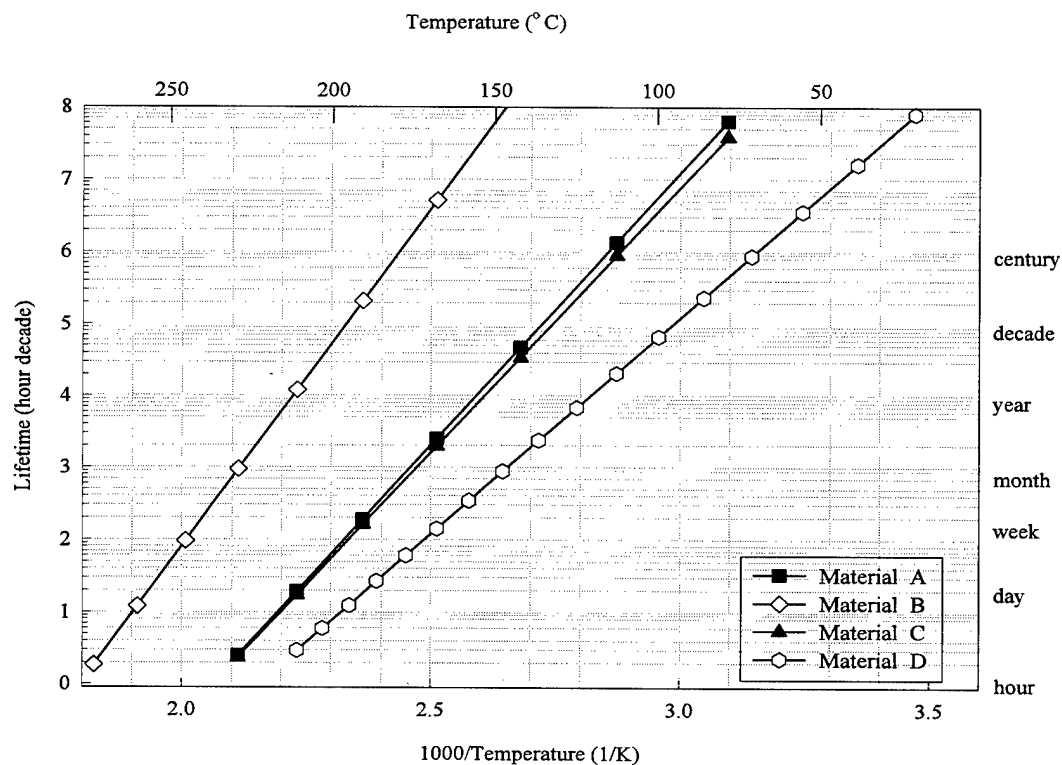


Fig. 12 Plots of Estimated Lifetime as a function of Temperature for Nonhalogenated Polymers in Helium

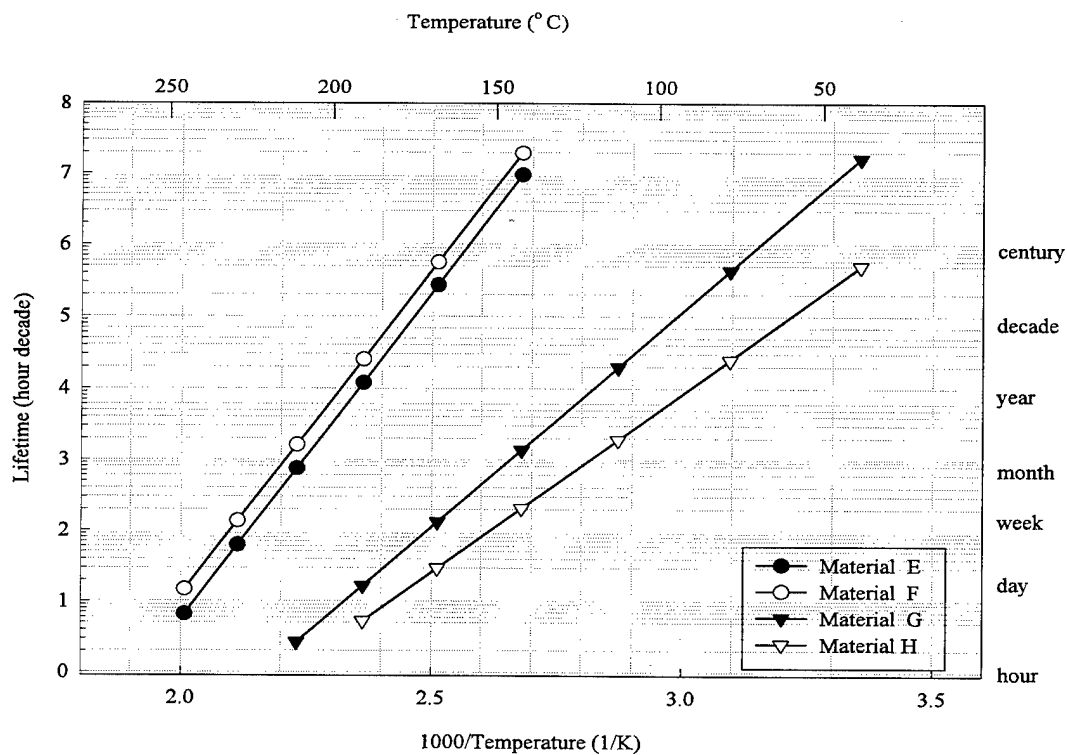


Fig. 13 Plots of Estimated Lifetime as a function of Temperature for Halogenated Polymers in Helium

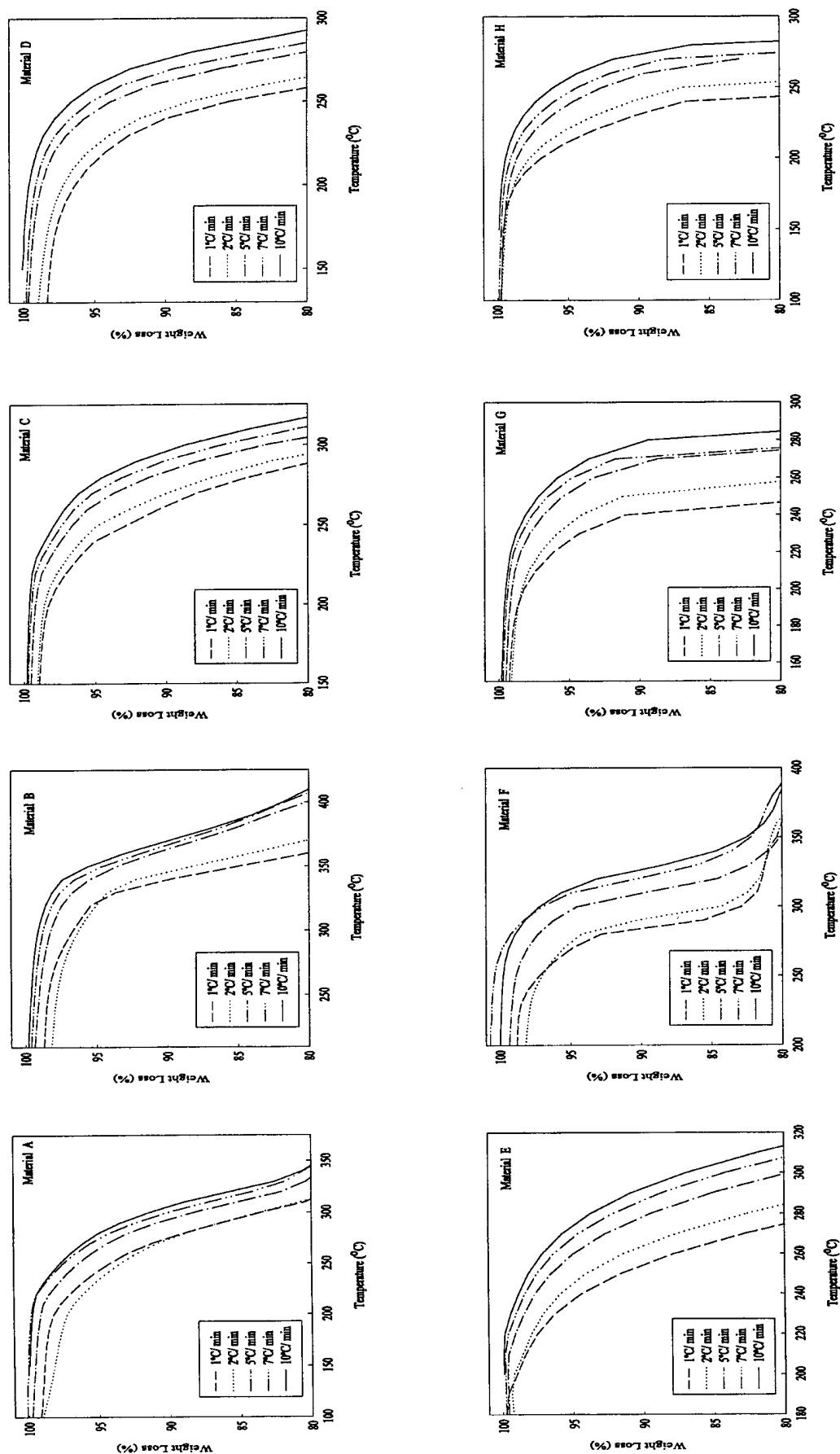


Fig. 14 Thermooxidative Stability of Flame Retardant Polymers in Air

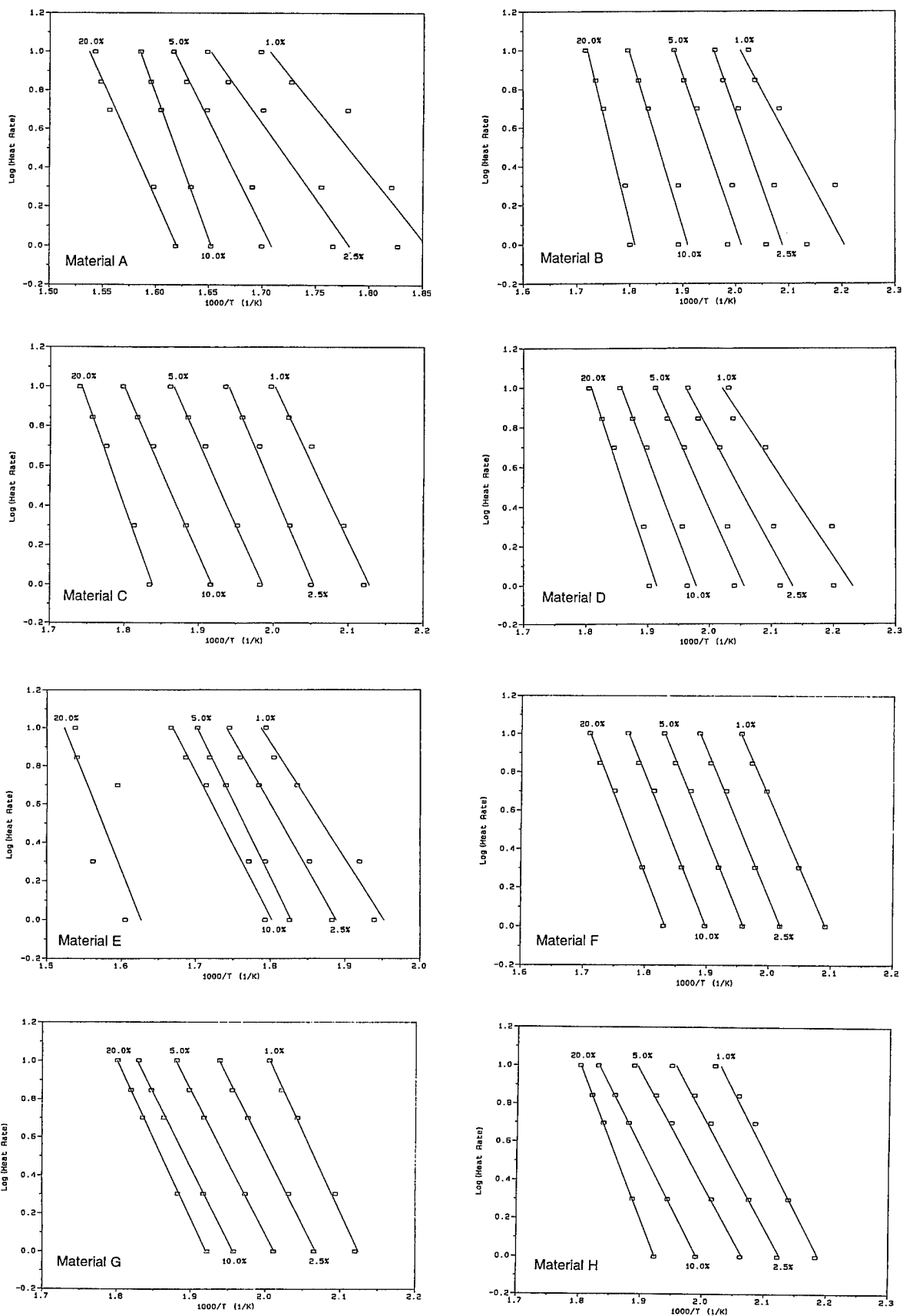


Fig. 15 Log Heating Rate vs Temperature of Flame Retardant Polymers in Air

TABLE V

ACTIVATION ENERGIES OF THERMOOXIDATIVE DEGRADATION AT VARIOUS CONVERSIONS

Material	Conversion (%)	Activation Energy (kJ/mol)
A	1	137.7
	2.5	156.3
	5	149.9
	10	160.4
	20	186.6
B	1	108.8
	2.5	129.1
	5	186.5
	10	254.1
	20	243.0
C	1	132.5
	2.5	132.1
	5	131.8
	10	142.4
	20	169.9
D	1	85.3
	2.5	100.7
	5	111.7
	10	125.0
	20	136.8
E	1	135.5
	2.5	134.7
	5	135.5
	10	138.8
	20	143.8
F	1	124.8
	2.5	134.3
	5	146.6
	10	124.1
	20	290.9
G	1	149.1
	2.5	142.3
	5	142.6
	10	150.2
	20	156.1
H	1	108.7
	2.5	97.9
	5	95.3
	10	110.0
	20	145.6

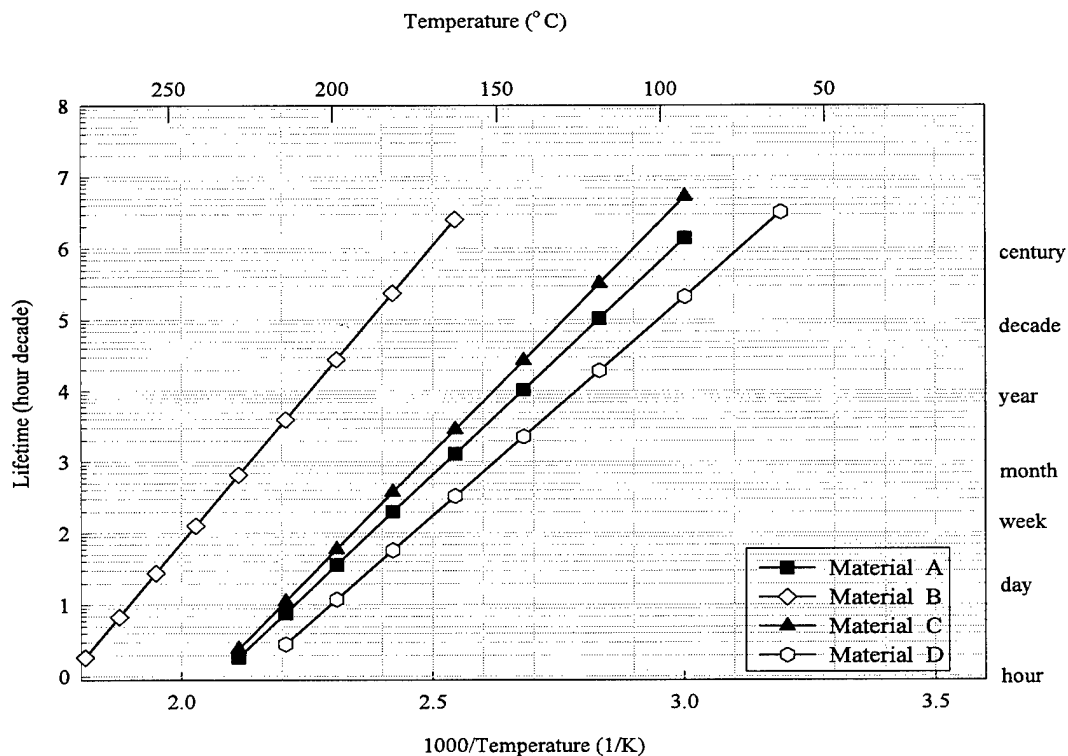


Fig. 16 Plots of Estimated Lifetime as a function of Temperature for Nonhalogenated Polymers in Air

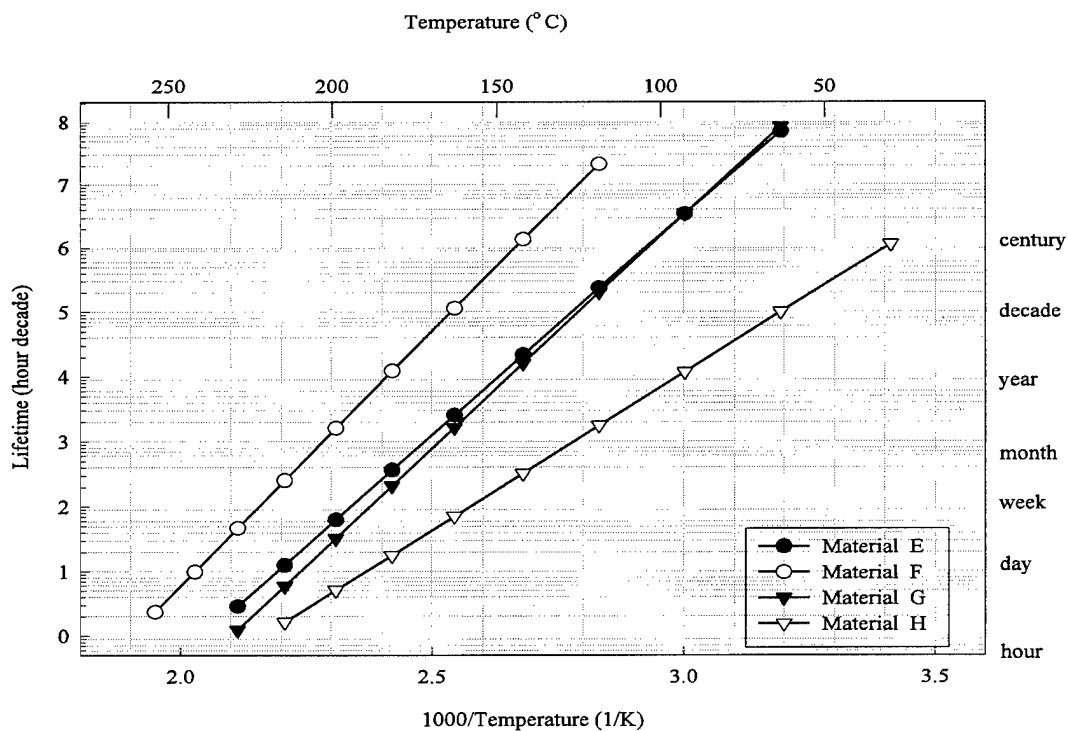


Fig. 17 Plots of Estimated Lifetime as a function of Temperature for Halogenated Polymers in Air

TABLE VI

ESTIMATED LIFETIME OF THE FLAME RETARDANT POLYMERS AT 5% CONVERSION

Material	Temperature, °C	Estimated Life (hrs.)	
		Thermal	Thermooxidative
A	25	5.85E+9	1.41E+10
	50	6.42E+7	1.31E+8
	75	1.35E+6	2.38E+6
	100	47400	74200
B	25	4.07E+14	2.27E+15
	50	1.50E+12	6.75E+12
	75	1.24E+10	4.62E+10
	100	1.94E+8	6.17E+8
C	25	1.71E+10	8.04E+8
	50	1.50E+8	1.32E+7
	75	2.60E+6	3.89E+5
	100	77400	18400
D	25	2,31E+7	1.19E+7
	50	5.94E+5	3.63E+5
	75	25800	18300
	100	1710	1380
E	25	1.42E+13	1.90E+9
	50	5.97E+10	2.77E+7
	75	5.51E+8	7.41E+5
	100	9.53E+6	32200
F	25	2.60E+13	1.48E+11
	50	1.14E+11	1.53E+9
	75	1.08E+9	3.04E+7
	100	1.93E+7	1.02E+6
G	25	1.30E+7	2.23E+9
	50	3.74E+5	2.71E+7
	75	17900	5.98E+5
	100	1290	22000
H	25	8.43E+5	8.86E+5
	50	37700	45200
	75	2640	3540
	100	263	390

increase in the thermooxidative stability as opposed to pure thermal stability might be due to the effective scavenging of the oxygen at the polymer surface by one of the additives (very likely the lead oxide) present in these materials. This in turn retarded the overall oxidative degradation process. This once again confirms the high initial decomposition temperatures ($T_{d,0}$) observed earlier for these two materials. As for material **B** (polyethylene copolymer with magnesium hydroxide filler), the estimated life appears to be very much identical under both thermal and thermooxidative

conditions of aging. This might be due to an effective antioxidant package present in this material.

To evaluate the effects of various fillers and additives on the degradation of the flame retardant polymers, experiments were conducted on the base polymer. For this study, a sample of material **A** was subjected to Soxhlet extraction using boiling xylene. The extraction was carried out for about 8 hrs. After the extraction, the dissolved polymer was precipitated with acetone from the xylene extract. It was then filtered and dried

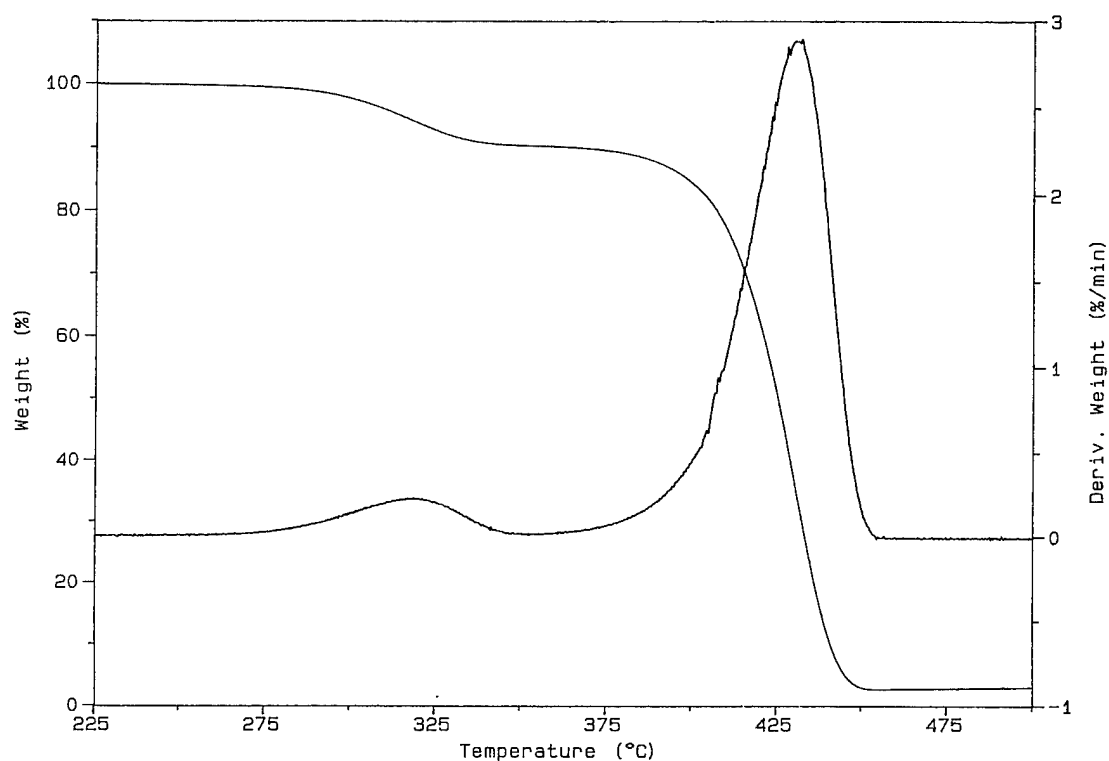


Fig. 18 TG and DTG Curves of Extracted Polymer from Material A

overnight in a vacuum oven. TGA experiments at various heating rates were conducted on the extracted polymer in helium atmosphere.

Figure 18 shows the TG and DTG curves of the extracted polymer from material A. The temperature of the initial decomposition ($T_{d,0}$), and the temperature of half decomposition ($T_{d,1/2}$) were found to be 295°C and 424°C respectively. These temperatures are considerably higher than the corresponding temperatures for the unextracted polymer (refer Table II). The maximum rate of weight losses were: 0.23% and 2.89% per minute at 218 and 432°C respectively. Figure 19 shows an overlay of TG and DTG curves of material A, before and after extraction along with the

weight loss curve for the pure aluminum trihydrate. In the case of ATH most of the weight loss occurs 200 - 265°C due to the elimination of water molecules. The first peak on the DTG curves for the unextracted material is the combined weight loss for ATH and one of the polymers in this material. In the case of extracted material, this small peak is shifted towards higher temperature (around 325°C).

The above observations suggests that the presence of inorganic fillers such as, aluminum trihydrate can significantly reduce the thermal stability of the base polymer. One reason for this might be the hydrolysis of the polymer chain by the water molecules formed during the thermal degradation.

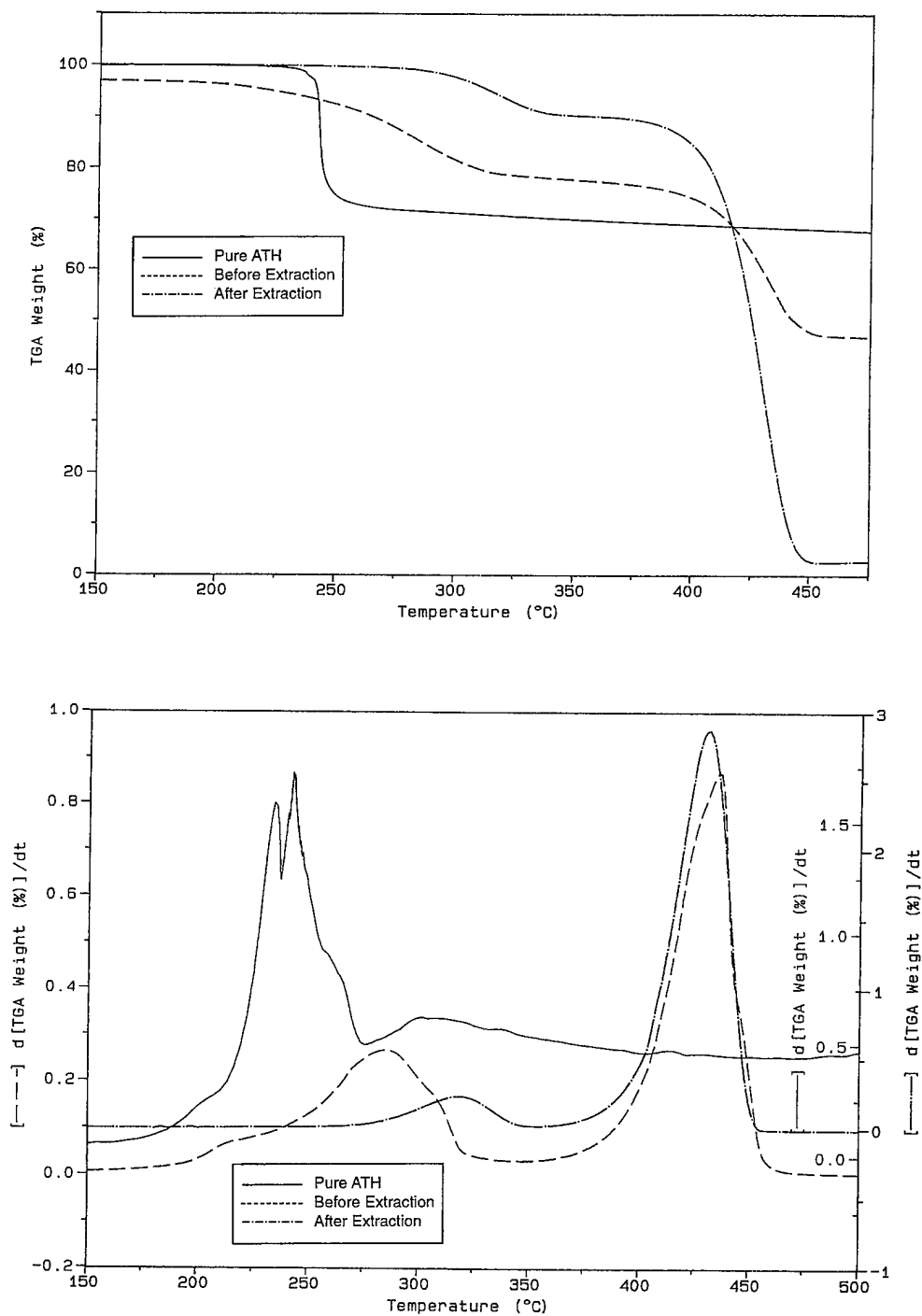


Fig. 19 Overlay of TG and DTG Curves of ATH and Material A

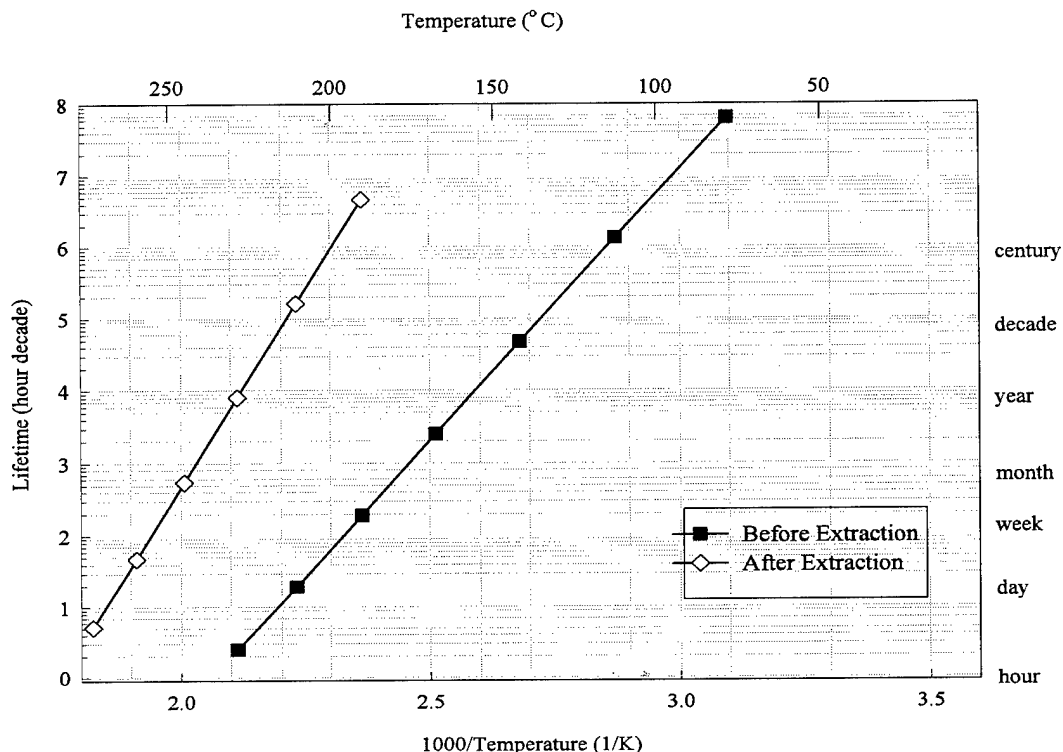


Fig. 20 Lifetime vs Temperature Plots of Material A before and after Solvent Extraction

Kinetic Analysis on the Extracted Polymer:

To understand further, the influence of various fillers and other additives on the thermal life of the base polymer used in the flame retardant formulations, kinetic experiments were carried out on the extracted polymer sample. These experiments were done by subjecting the sample at various heating rates in helium as described in the previous section. From the plots of log heating rate versus temperature, the lifetime was estimated. Figure 20 shows one such plot for material A before and after extraction with xylene. Like in the previous cases, a 5% conversion was selected for estimating the lifetime of the polymer.

It is quite clear from this plot that the base polymer used in the formulation of the material A has far better thermal stability and this has reduced significantly after

compounding with the filler. From the slopes of these plots it can be predicted that the gap between the life expectancy of these two materials widens significantly at lower temperatures. All this proves that there is a trade off between the required flame retardancy and optimum thermal stability in the final formulation. Additives are required to provide adequate flame retardancy to a given polymer composition and at the same time they also lower the thermal stability of the polymer in question. Similar observations were made under thermooxidative conditions of degradation.

DYNAMIC HEATING RATE TGA

Dynamic heating rate thermogravimetry experiments on all the flame retardant polymers were carried out under thermal and thermooxidative conditions. To accomplish this, the TGA module was operated under high resolution mode. Experiments were done using various resolution settings. The outcome of these experiments is summarized in this section.

Dynamic heating rate TGA is a very powerful tool for isolating the subtle thermal transitions, such as weight loss with temperature in a given sample. The heating rate is continuously varied automatically by the instrument in response to the changes in the sample weight. Initially the heating rate was programmed at 30°C/min. This heating rate drops to a much lower value in response to the weight changes in the material.

Figure 21 illustrates a typical thermogram of the material A generated under thermooxidative conditions using the dynamic heating rate experiments. The heating rate dropped to approximately 9°C/min at the first weight loss event. It further dropped to about 2°C/min as the weight loss progressed. Finally, when there is a significant weight loss around 350°C, the heating rate also dropped to a near zero before moving back up. Similar observations were made with other materials in this study.

Figure 22 shows the differential thermograms (DTG) overlays of the dynamic heating rate and constant heating rate thermograms of all the materials under thermal conditions of degradation. Similarly, figure 23 is the corresponding DTG overlays under thermooxidative conditions of degradation. It is fairly obvious that the DTG curves under dynamic

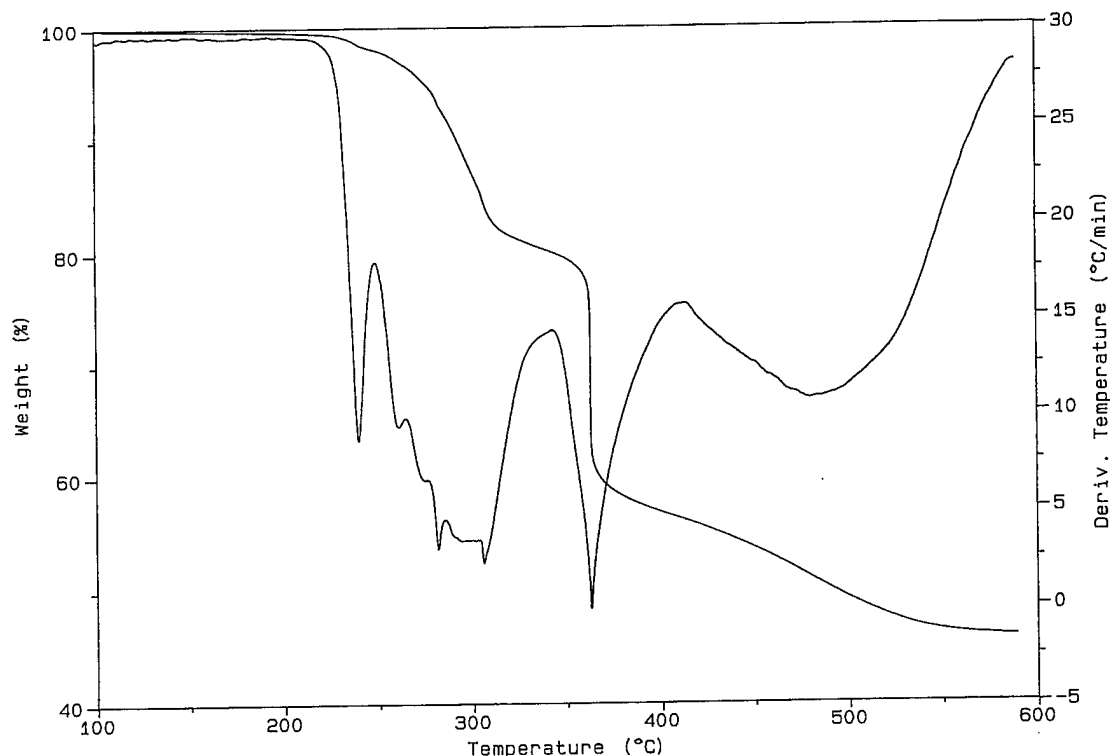


Fig. 21 Weight Loss Profile of Material A under Dynamic Heating Rate TGA in Air

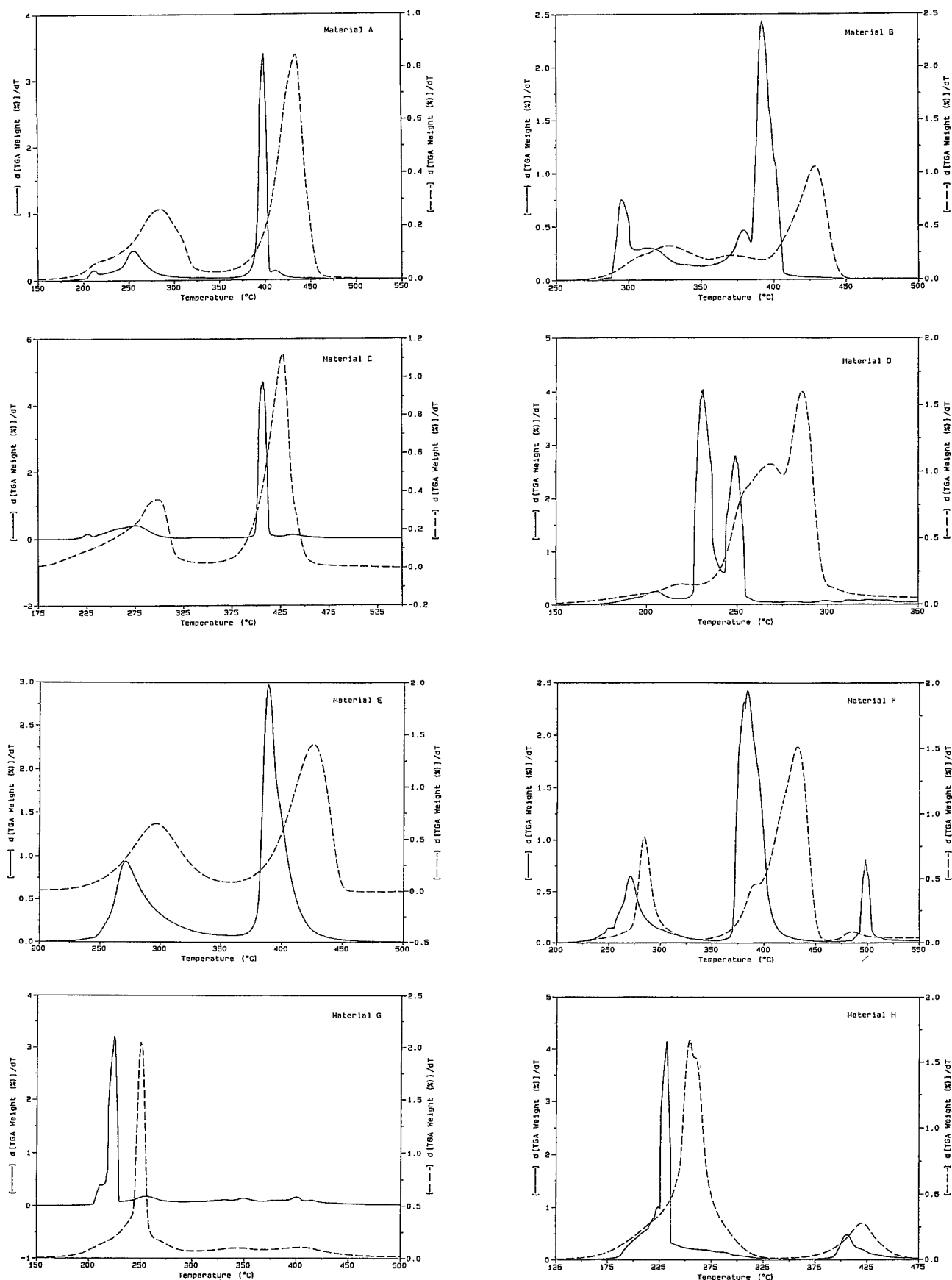


Fig. 22 Dynamic and Constant Heating Rate DTG Curves of Flame Retardant Polymers in Helium
 [———] Dynamic Heating Rate [- - - -] Constant Heating Rate at 1°C/min

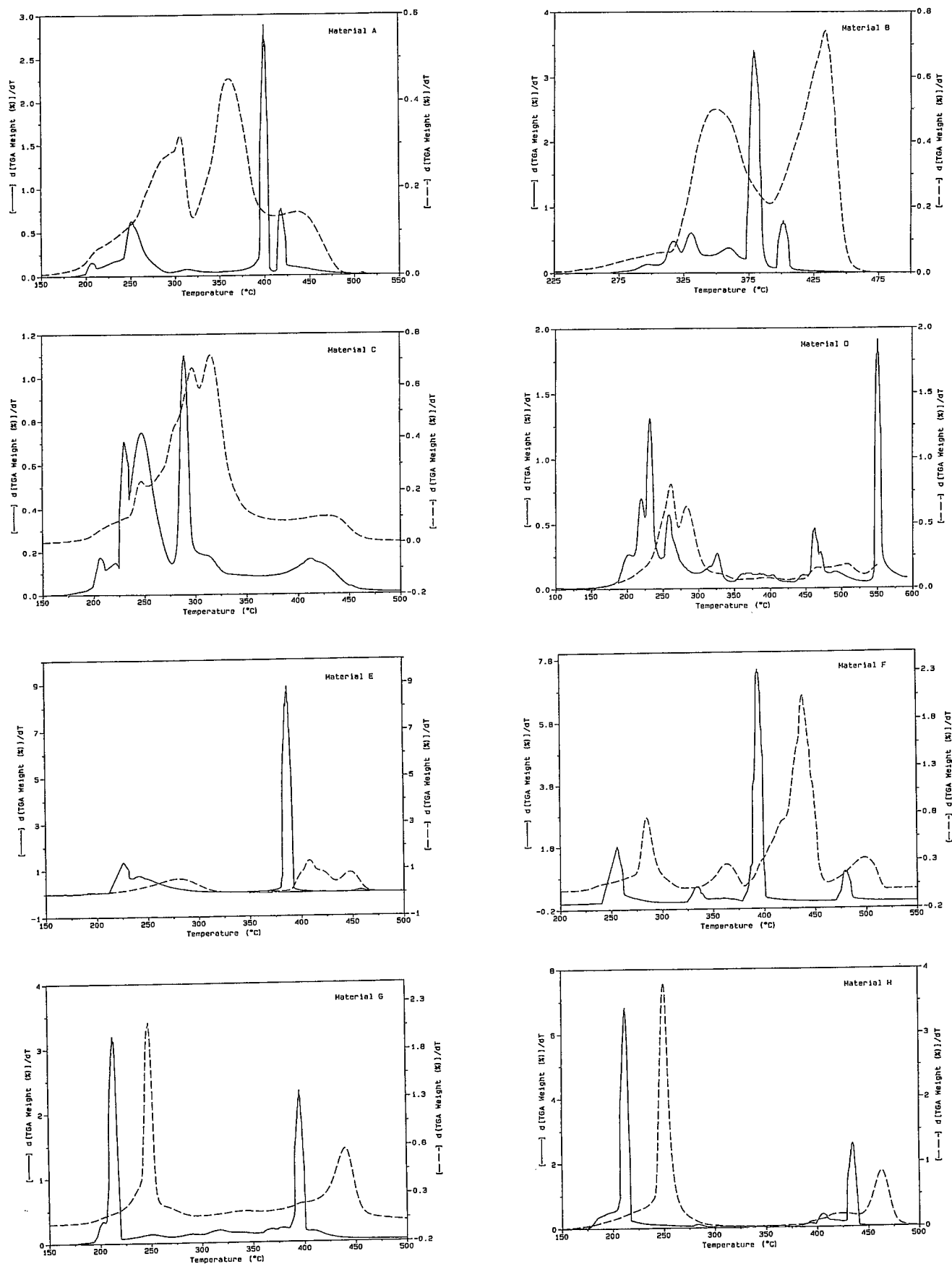


Fig. 23 Dynamic and Constant Heating Rate DTG Curves of Flame Retardant Polymers in Air
 [———] Dynamic Heating Rate [- - - -] Constant Heating Rate at 1°C/min

heating rate mode showed considerable improvement in resolving various weight loss peaks when compared to the standard constant rate heating mode at 1°C/min TGA. For example, in the case of material A, (Fig. 26) there are four distinctly separate weight loss peaks with well defined peak temperatures. Whereas, the DTG curve obtained by constant heating rate TGA showed considerable broadness in the peaks and hence the weight loss event(s) are not very distinct. In some cases, under constant heating rate experiments, certain weight loss peaks are totally absent. This is shown very dramatically in the thermooxidative degradation of material D (Fig. 28). Five separate weight loss peaks were found in the case of dynamic heating rate scan, whereas, the same material when scanned under constant heating rate showed only two clear peaks.

It is possible to perform a detailed kinetic analysis on each of the individual weight loss peaks by using the equation (6). The activation energy associated with each weight loss event will be highly useful in understanding more about the thermal behavior of these flame retardant compounds. Work along these lines is in progress and the results will be communicated at a later date.

Thermal Rating of the Flame Retardant Polymers:

Based on the results obtained, an attempt was made to assign thermal rating to all the materials studied. The temperature index as defined in the ASTM D2307, permits comparison of the temperature/time characteristics of an electrical insulating material. Toop¹¹ first tried to calculate the thermal index using the information on the activation energy. However, it was not very clear the exact point of conversion at which the activation energy must be calculated for evaluating the temperature index. Shrinet et.al¹⁷ have done extensive work on the evaluation of the temperature index of the standard polymers using the thermograms obtained at a heating rate of 1°C/min in TGA experiments. In this work, the temperature index of the flame retardant materials is essentially derived based on the calculations given in the Shirnet's paper.

The method for the determination of the temperature index assumes that the activation energy value for the material must be taken during its initial decomposition stage on the slowest heating rate curve. However, it should be emphasized that taking the values too early in the thermograms of the complex materials such as the flame retardant polymers is not preferable. This is because the weight loss in the material in the initial stages is mainly due to the decomposition of the

volatile additives, rather than the actual base polymer itself. Keeping this in mind the activation energy at 5%

TABLE VII
TEMPERATURE INDICES OF THE FLAME
RETARDANT POLYMERS

Material	Temperature Index (°C)	
	Thermal	Thermooxidative
A	118	117
B	171	186
C	112	103
D	79	73
E	146	104
F	152	130
G	77	102
H	54	57

decomposition level was chosen for calculating the temperature index of these materials.

The results of the thermal index calculations under thermal and thermooxidative conditions of degradation are summarized in Table VII. It is clear from this table that the temperature index is highest for material B and lowest for material H, both under thermal and oxidative conditions.

CONCLUSIONS

An exhaustive and elaborate study to determine the expected life of various commercially available flame retardant polymers for wire and cable applications was undertaken. Since these materials are relatively new—especially the nonhalogenated polymers, information on the thermal and thermooxidative behavior is very much essential in understanding their long term survivability and product failure. In this objective in mind the above work was performed in a systematic manner. Based on the above studies the following conclusions can be drawn:

1. The thermograms of the materials tested showed more complex degradation pattern under oxidative (air) conditions of decomposition, when compared to pure thermal (helium) decomposition. In the case of thermal degradation, the principal mechanism is either depolymerization or random chain scission. In the case of thermooxidative degradation, there are several autocatalytic reactions which are reflected in their thermograms.
2. For materials **G & H**, the temperature of initial decomposition ($T_{d,0}$) is much higher under oxidative conditions of decomposition. This might be due to the presence of lead oxide in their formulation which was known to hinder the auto-oxidation of the polymer.
3. The char residue was higher for the halogenated polymers and it is highest for the material **H**, which is a formulation based on PVC and various other additives. This indicates that material **H** has low flammability and high oxygen index when compared to the other materials. Indeed, this material is intended for plenum applications.
4. Kinetic analysis on the materials using the constant rate thermogravimetry has indicated that materials **B, E, & F** showed highest activation energy at the 5% conversion level in thermal decomposition. In thermooxidative decomposition, only material **B** showed a high activation energy. Material **H**, which is a PVC formulation showed the lowest activation energy.
5. Kinetic analysis on the base polymers (after removing all the additives by solvent extraction) showed considerable thermal stability when compared to the fully formulated polymer. This suggests that even though the additives and other fillers in the system are essential for providing the necessary flame retardancy, at the same time the thermal life of the final formulation decreases. It is therefore essential to select a flame retardant additive package which will not deteriorate the thermal characteristics of the base polymer.
6. Dynamic heating rate experiments showed much more clear cut weight loss events during the degradation of the flame retardant compounds when compared to the constant heating rate experiments. The information so obtained from dynamic heating rate experiments is highly valuable in assessing overall flame retardancy of these materials. Thus it might be possible to pinpoint the exact temperature range within which

a particular component in a given formulation starts decomposing. However, use of hyphenated techniques such as, TGA-IR and GC-MS will greatly enhance the quantification of the individual weight loss events.

7. The temperature index of the materials was evaluated based on the experimental data and it was found that material **B** has the highest number. TGA technique is much faster than conventional oven aging technique for evaluating the thermal indices of polymeric materials.
8. Overall, among all the flame retardant polymers studied, material **B**, which is a polyethylene copolymer compounded with magnesium hydroxide as the flame retardant additive showed the highest level of stability both under thermal thermooxidative conditions of degradation, whereas, material **H**, which is a polyvinyl chloride formulation with metal oxide additives showed the least amount of thermal stability.

REFERENCES

1. P. R. Hornsby, J. Wang, R. Rotheron, G. Jackson, G. Wilkinson, and K. Cossick
Polymer Degradation and Stability, **51**, 235(1996)
2. J. D. Cooney, M. Day, and D. M. Wiles
J. Appl. Polym. Sci., **29**, 911-923 (1984)
3. I. C. McNeill and M. H. Mohammed
Polym. Degradat. Stabil., **48**, 189-195 (1995)
4. G. Camino and S. L. Costa
Polym. Degradat. Stabil., **3**, 423-30 (1981)
5. S. Percec, F. Popescu, and M. Dima
J. Thermal. Anal., **20**, 311-9 (1981)
6. R. Antony, M. Brahmakumar, and C. K. S. Pillai
Polym. Sci., **1**, 407-11 (1994)
7. R. N. Rotheron (Ed.)
Properties of Composites in *Particulate Filled Polymer Composites*
Harlon Longman, pp 207-34, 1995.
8. S. Rampalli
Proc. 42nd Intl. Wire & Cable Symposium, St. Louis, USA., November 15-18, 1993.

9. J. H. Flynn and L. A. Wall
Polym. Lett., **14**, 323 (1966)
10. Zsako and Zsako
J. Therm. Anal., **19**, 33 (1980)
11. D. J. Toop
IEEE Trans. Elec. Insul., **E1-6**, 2 (1971)
12. ASTM Standard **E1641-94**
American Society for Testing and Materials,
Philadelphia, PA.
13. R. L. Blaine
TA Instruments Applications Brief, **TA 84**.
14. TA Instruments Application Brief, **TA -023**
15. D. W. Van Krevelen
Properties of Polymers, 3rd Edition, Elsevier
16. N. S. Allen
Degradation and Stabilisation of Polyolefins,
Applied Science Publishers, London, 1983.
17. V. Shrinet and P. A. Krishna Moorthy
J. Appl. Polym. Sci., **50**, 367-371(1993)

ACKNOWLEDGMENTS

I would like to thank Mr. Phil Kurowski for his dedicated and meticulous laboratory work on thermal analysis. I would also like to extend my sincere appreciation to Andrew Corporation for their encouragement and for granting me the permission to communicate this paper.



Sitaram Rampalli is a Senior Research Chemist in the Research and Development Group, Andrew Corporation, Orland Park, Illinois. He received his Ph. D. Degree in Chemistry from the Indian Institute of Technology, Bombay, India, and a Master's Degree in Polymer Science from the University of Akron, Ohio. Currently he is responsible for the selection, evaluation, and recommendation of various polymeric materials for wire and cable applications. He holds five patents and several publications in scientific and technical journals.

Dr. Rampalli is a Senior Member in the Society of Plastics Engineers, and a member in the American Chemical Society. He is involved in the teaching of the polymer science courses at the Illinois Institute of Technology and DePaul University, both in Chicago. He is also conducting the educational short course on "Polymers in Wire and Cable Industry" at the IWCS.

Dr. Rampalli's research interests are in the area of characterization and analysis of polymeric materials used in electrical and electronic applications, polymer degradation, and structure-property relationships in polymers.

EVALUATION OF THE ENHANCED THERMO-OXIDATIVE AGING PERFORMANCE OF AN IMPROVED TELEPHONE WIRE INSULATION COMPOUND

Geoffrey D. Brown, Jeffrey M. Cogen, Michael J. Keogh

Union Carbide Corporation, Somerset, New Jersey

ABSTRACT

Providing robust stabilization of HDPE foam/skin telephone wire insulation for grease-filled cable applications is a significant technical challenge. The interaction between cable filling compound and insulated singles typically results in a substantial decrease in long-term insulation aging performance. In recent years, insulation stability testing requirements have been revised to specify oven preconditioning of grease filled cables to better model this interaction. Implementation of these more rigorous requirements has resulted in commercial filled telephone cable products with substantially improved oxidative stability. Although prior work included optimization of the traditional insulation stabilization system for improved filled cable performance, substantial investigation of alternative stabilization technologies failed to identify improved candidates. Some industry concern has persisted about long-term product performance in severe climate applications.

A new insulation stabilization technology has now been developed that provides a significant improvement in foam/skin insulation aging performance for grease filled cable, as demonstrated in several accelerated aging tests. This patented system will boost insulation aging performance for hot climate applications and against more rigorous testing requirements.

Results of cable aging studies are used to demonstrate the performance of the new stabilization system. In these studies, filled foam/skin test cables incorporating the new stabilization system were prepared and tested against reference samples containing the traditional antioxidant systems. The cable age

testing evaluations included the Bellcore OIT and 90°C pedestal test methods. OIT trend analysis was also utilized to map performance during cable preconditioning and periodically during the 90°C pedestal testing. Accelerated pedestal testing at 110°C was used to demonstrate the expected improvement in aging time before insulation cracking. Methodology to overcome the well known variability in cable testing was incorporated into these cable aging studies and is reviewed.

The results are discussed in the context of Bellcore TR-NWT-00421, Issue 3, Revision 1 and MAT 1101, which represent International Specifications with stringent performance requirements.

INTRODUCTION

Despite an increasing use of fiber optics in outdoor telephone network cables, the use of copper twisted pair telephone cables remains extensive, especially in local loop applications. The recent emergence of economically viable high frequency digital communication over copper is likely to further contribute to the persistence of some copper in the local loop environment. In addition, the vast infrastructure of installed copper cable will require new cables for repair and incremental expansion. Therefore, it remains essential that any newly-installed copper cable be designed to provide many years of useful service life.

Since the mid-80's, there have been considerable improvements made in the long-term oxidative stability of foam/skin insulation in grease filled cable applications. In 1987, work by L. E. Davis¹ demonstrated the need to

include substantial oven preconditioning of cable samples prior to performing accelerated aging studies on insulation. This cable preconditioning models the commercial use where interim storage and outdoor exposure prior to final installation allows for substantial interaction between the insulation and the surrounding cable filler. Subsequent network installation can include interconnection of cables in outdoor enclosures, typically called pedestals or junction boxes, where the sheathing and cable filler are removed to allow interconnection of the insulated wires. Especially in hot climates, the exposed insulated wires in these pedestal boxes experience a severe thermo-oxidative environment. For example, peak summer temperatures in pedestal boxes located in the Southwestern United States have been measured at greater than 50°C.² In addition, outdoor junction boxes such as Subscriber Loop Carrier cabinets that contain powered circuitry show even higher temperatures, with measurements above 60°C. Given these severe application requirements, there is a good likelihood that premature insulation cracking failures will be observed if the insulation stabilization system is not properly designed.

In 1989³, Bellcore incorporated 70°C cable preconditioning into the testing procedure for copper telephone cables with polyolefin insulation. The revised requirements include two weeks of preconditioning prior to oxidative induction time (OIT) testing and four weeks of preconditioning prior to the long-term 90°C pedestal aging test. The inclusion of cable preconditioning was estimated⁴ to reduce pedestal aging time before cracking at 90°C by 60% relative to 90°C pedestal testing without preconditioning. The change in insulation aging performance can be attributed to a combination of extraction loss⁵ of insulation antioxidant(s) into the cable filler and absorption of cable filler oils⁶ into the insulation material. Because of the problem of extraction loss to the cable filler, antioxidant systems optimized for aircore cable were found⁷ to be inefficient when used in filled cables. For example, the widely used tetrakis [methylene (3,5-di-*tert*-butyl-4-hydroxyhydrocinnamate)]methane (AO-1) primary antioxidant undergoes a high degree of extraction from the insulation into the cable filler, as illustrated in Figure 1. Despite this relative inefficiency, commercial use of AO-1 in this application has continued.

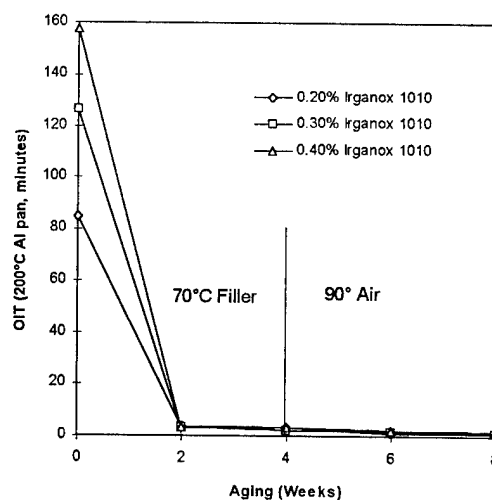


Figure 1: Effect of cable filler exposure on OIT of film samples containing AO-1 antioxidant, demonstrating the large and rapid OIT loss.

In contrast to AO-1, the bifunctional 1,2-bis (3,5-di-*tert*-butyl-4-hydroxyhydrocinnamoyl) hydrazine (MD-1), which serves as a primary antioxidant and a copper deactivator, demonstrated good performance after cable filler exposure as illustrated in Figure 2. In the late 80's and early 90's, commercial product evolved to formulations with increased MD-1 to satisfy the revised Bellcore testing

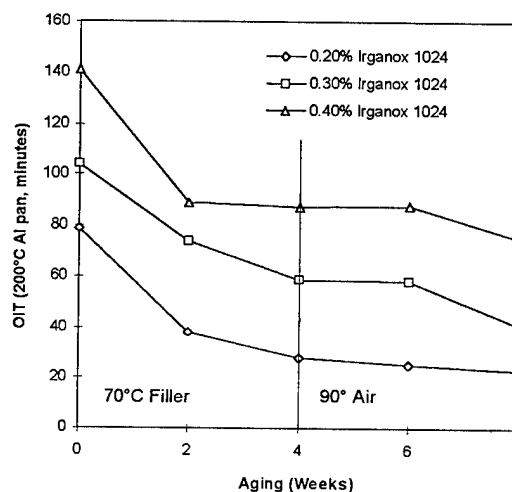


Figure 2: Effect of cable filler exposure on OIT of film samples containing MD-1 stabilizer, demonstrating a much higher level of OIT retention than observed with AO-1.

requirements, with the current Bellcore requirement calling for a combination of AO-1 and MD-1. Research has continued in search of a "next generation" stabilization system for filled copper cable insulation to provide an improvement in aging performance over the AO-1/MD-1 system. Such an improved insulation stabilization system would enhance performance in severe climates and testing conditions and would provide a safety factor to compensate for non-optimal cable system variables.

GENERAL CONSIDERATIONS FOR EVALUATION OF INSULATION PERFORMANCE

Difficulties in accurately measuring insulation aging performance complicate the search for improved insulation materials. Insulation aging performance, especially in grease filled cables, is dependent on several key system variables in addition to selection of the insulation compound. Such variables include the insulation type and thickness, the insulation fabrication process, the copper conductor, the insulation colorants, the pair twisting process, the cable filler composition, and the cable fabrication process. Figure 3 illustrates differences in cable system performance that were observed in a controlled study in which identical insulation compound was supplied to four different cable fabricators. Each prepared 25 pair 26 AWG test cables using ETPR type cable filler, and these cables were then tested in a single laboratory. A substantial range of OIT performance was observed in the insulation from the finished cables, especially after preconditioning, as indicated by the approximate 200% range of OIT data after two weeks of 70°C cable preconditioning. These results clearly demonstrate the complexities involved in benchmarking compound performance in a fabricated article that incorporates a number of other significant system variables.

Aside from the insulation compound itself, the cable filler type and quality is typically the cable system variable having the largest effect on insulation aging performance. There is a broad range of cable filler materials used on a worldwide basis including polyethylene wax/petroleum jelly (PE/PJ), extended thermoplastic rubber (ETPR), and polyisobutylene based systems (also known as

"synthetic"). A wide range of modifiers and additives are incorporated into the many commercially available grades of cable filler materials. This broad array of cable filler materials encompasses significant differences in supplier formulating capabilities, specification and end-use requirements, regional market influences and customer preferences.

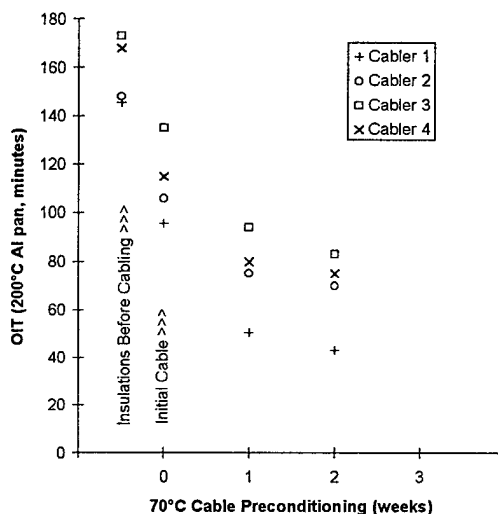


Figure 3: Foam/Skin insulation OIT testing results for test cables incorporating identical HDPE compound, demonstrating wide range of results obtained with cables made by different cablers. Identical samples (same blend) of HDPE solid and cellular compounds were fabricated by four different North American cablers into 25 pair 26 AWG filled foam/skin test cables with ETPR type cable filler. Union Carbide performed oven aging and insulation OIT testing on all of the cable samples.

Cable filler selection criteria include cost, regional raw material supply situations, fabrication processing and end-use handling characteristics, cable drip and water penetration performance, and elevated temperature physical (oil separation) and thermo-oxidative stability. Because of the potential for absorption of cable fillers into the insulation, some cable specifications indicate maximum allowable levels of filler absorption into insulation materials and/or requirements for testing insulation physical properties after grease exposure. However, the influence of cable filler formulation types and constituents on insulation thermo-oxidative stability has been little reported.

Table 1 shows the results of some insulation/cable filler compatibility testing obtained using a relatively small sampling of the commercial cable fillers. In this model, 0.25 mm films of solid insulation material were immersed in vials of the cable filler and placed in 70°C circulating air ovens. Changes in the OIT value of the film were monitored after various immersion periods.

The results of the model study indicate a wide range of effect on OIT among the different cable fillers. Although it is not proper to assume a direct quantitative scale-up of such model study results to actual finished cable, a similar range of performances would be anticipated for cable testing. These results underscore the importance of a carefully controlled system approach to insulation evaluation and illustrate the need for a safety factor in insulation material aging performance to accommodate less than optimal cable filler.

	OIT (200°C Aluminum Pan), minutes			
	Initial Dry Sample	1 Week	2 Week	4 Week
PE/PJ Type 1	114	69	60	65
PE/PJ Type 2	114	62	52	47
PE/PJ Type 3	114	85	66	74
average PE/PJ	114	72	59	62
range PE/PJ	114	62-85	52-66	47-74
PIB/Synthetic Type 1	114	83	69	59
PIB/Synthetic Type 2	114	75	68	52
PIB/Synthetic Type 3	114	100	91	63
PIB/Synthetic Type 4	114	70	65	57
PIB/Synthetic Type 5	114	78	67	45
ave. PIB/Synthetic	114	81	72	55
range PIB/Synthetic	114	70-100	65-91	45-63
ETPR Type 1	114	54	39	32
ETPR Type 2	114	49	39	38
ETPR Type 3	114	49	39	36
ETPR Type 4	114	38	35	37
ETPR Type 5	114	45	41	35
average ETPR	114	47	39	36
range ETPR	114	38-54	35-41	32-38

Table 1: Results of some insulation/cable filler compatibility testing obtained using a relatively small sampling of the various cable filler types. In this model, 0.25 mm films of solid insulation material were immersed in vials of the cable filler and placed in 70°C circulating air ovens. Changes in the OIT value of the film were monitored after various immersion periods.

Another complexity in evaluating product performance is the choice of accelerated aging methodology. An Insulated Cable Engineers Association (ICEA) working group effort⁸ refined the insulation OIT test method as detailed in ASTM D-4565.94.⁹ However, moderate lab to lab testing variation still persists. In addition, two series of ICEA sponsored round robin studies¹⁰ on the 90°C pedestal test showed very large lab to lab testing variations. ICEA efforts to utilize an oven apparatus for foam/skin insulation aging to improve inter-lab repeatability were unsuccessful. However, 90°C pedestal test consistency within a given laboratory has been shown to be reasonably good on a number of occasions. Therefore, side by side OIT and 90°C pedestal testing of experimental insulation material against a commercial reference sample was selected as the method of choice to assess relative performance.

LABORATORY SCREENING STUDIES

Screening for promising new stabilizer systems was achieved using a model test that includes the cable filler interaction as well as thermal aging. Solid films (0.25 mm thick) of the insulation samples were immersed in excess cable filler at 70°C for four weeks. OIT trend performances of different polyethylene antioxidant systems were followed during the four week 70°C filler immersion, using a single supply of cable filler for all formulations. OIT trend testing was continued during subsequent aging of the wiped film samples in a static air apparatus in a 90°C circulating air oven environment. This screening method was used to identify promising antioxidant formulations for further study.

Cellular samples are not used in the film/cable filler immersion screening model. When cellular samples are immersed in excess cable filler, the samples become saturated with cable filler oils completely filling the cells. In contrast, for cellular or foam/skin insulations in filled cables, the cells do not fill and the insulations equilibrate at a much reduced level of oil absorption.

Within cable, geometry constraints and a limited supply of cable filler cause this equilibrium at a much reduced level¹¹ of filler oil absorption. A "test tube" model was used to simulate the cable environment to better model cellular insulations. In this model, a tightly packed bundle of foam or

foam/skin insulated wire is pushed into a test tube filled with preheated cable filler. This simulates the geometry and cable filler exposures experienced in filled cable. As in the film screening study, samples are evaluated at various stages of cable filler exposure, and the samples are oven aged in air following four weeks of cable filler exposure.

"Test tube" model results for the system eventually selected for commercial scale up are illustrated in Figure 4. The control sample was made using a commercial cellular material formulated to meet the current Bellcore TR-NWT-00421, Issue 3, Revision 1 requirements.

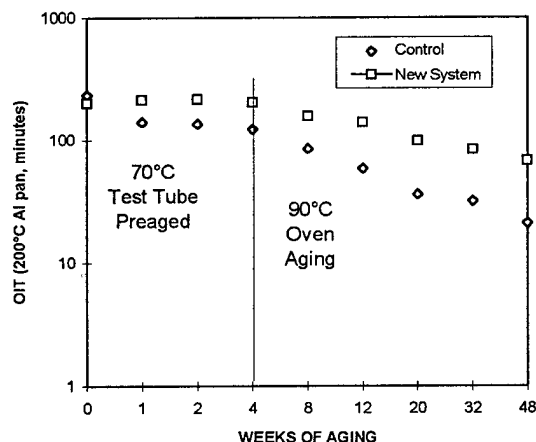


Figure 4: 24 AWG cellular insulation "test tube" model results for the system eventually selected for commercial scale up. The control sample was made using a commercial cellular formulation formulated to meet Bellcore TR-NWT-00421, Issue 3, Revision 1.

CABLE STUDIES

Cable Fabrication

The modeling results confirmed promising insulation aging performance for a number of antioxidant formulations. The next step was to proceed with full scale foam/skin cable evaluations. This evaluation included a reference sample incorporating current commercial insulation materials which was fabricated and tested side by side with the developmental formulations. The following guidelines were utilized to accurately evaluate the developmental compounds:

- 1) Single lots of raw materials were utilized and all compounds were prepared during a single campaign in order to limit compound variables to those under evaluation.

- 2) Foam/skin insulation of the reference and developmental samples were prepared in back to back extrusion trials in order to ensure near equivalence of foam/skin variables such as equipment details, processing conditions and colorants used.

- 3) The insulated wires were pair twisted on a single twisting machine to ensure a similar twinning process.

- 4) The reference and experimental insulated wires were prepared into lengths of 25 pair test cores. A color code tape was included for subsequent sample identification.

- 5) The cores of reference and experimental product were spliced together prior to cable filling/jacketing. The cable filling/jacketing process was performed at steady state conditions following standard production. This provided equal processing conditions and cable filler materials for the reference and experimental samples.

These guidelines ensured that the effect of cable variables other than insulation formulation were held constant, thus allowing a meaningful comparison of the reference cable sample with the developmental cable samples. Subsequent cable testing followed a similar protocol, with side by side testing of the reference and developmental samples.

First Round Accelerated Aging Studies

An initial set of cabling trials was used to select the developmental candidate showing best overall performance. Figure 5 shows the OIT trend during 90°C pedestal aging for the selected candidate versus the reference sample incorporating the current commercial product. Although the test evaluates time to insulation cracking, the OIT trend testing provides substantial early information about the relative performances prior to cracking. As evident in Figure 5, the new system features improved OIT retention during cable preconditioning and also a reduced rate of decline in OIT performance during 90°C pedestal aging.

Both the reference sample and the developmental product easily passed the Bellcore requirement for 260 days of pedestal aging at 90°C without insulation cracking. To confirm these results and perform complete product qualification testing on the selected sample, a second round of cabling studies was conducted.

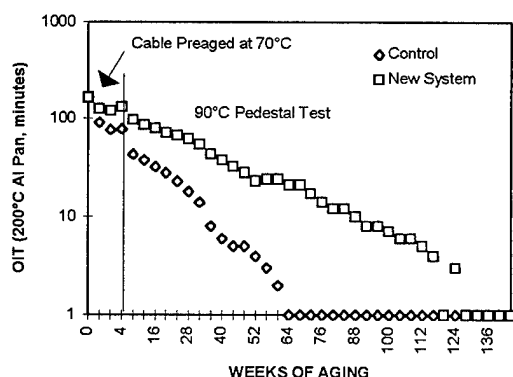


Figure 5: OIT results obtained in the first round 90°C pedestal aging study for the developmental formulation and the commercial reference sample (control).

Second Round Accelerated Aging Studies and Bellcore Technical Audit

This second round of studies followed the same general evaluation guidelines as outlined above, starting with preparation of new compound samples and fabrication of new developmental and commercial reference cable samples.

Figure 6 shows the 90°C pedestal OIT trend results for this second round of cabling trials.

In addition to the in-house testing, a Bellcore technical audit was commissioned to perform the 90°C pedestal testing on lengths of the second round test cables. Spot samples were obtained from the Bellcore pedestals and tested using the same DSC-OIT apparatus and procedure as the in-house testing. These are the "Bellcore" data points shown on Figure 6. There was good consistency between the independent Bellcore 90°C pedestal testing and the pedestal evaluations done in-house. Both studies confirm the original findings that the developmental product provides better OIT retention after cable preconditioning and during 90°C oven aging. As of August 5, 1996 none of the second round cable samples showed any cracking in the 90°C pedestal test, with both samples having "passed" the minimum requirement.

To provide some early insulation cracking data, a pedestal evaluation was performed on the second round samples at an accelerated 110°C condition. This data is shown as Figure 7. Note that the OIT trend testing during the 110°C pedestal testing shows similar characteristics to the 90°C pedestals. As a result of the substantially accelerated aging, cracking in both the reference sample and the developmental sample was obtained, with the developmental cable showing a substantial improvement over the reference cable. A similar performance improvement is anticipated for the 90°C testing.

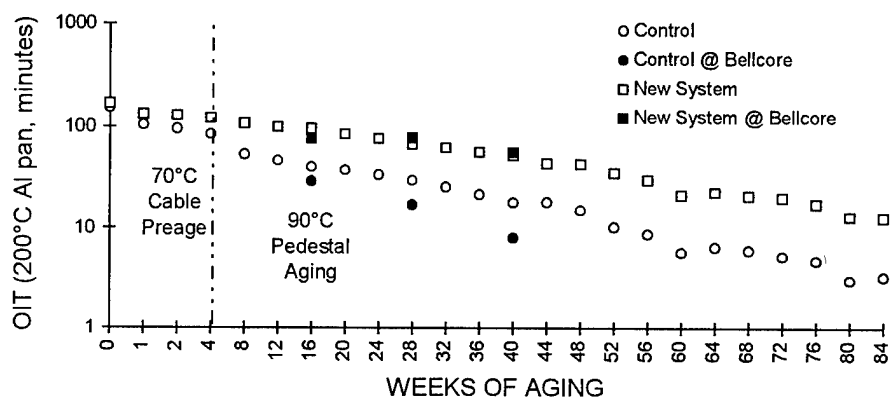


Figure 6: OIT results obtained in the second round 90°C pedestal aging study for the developmental formulation and the commercial reference sample (control). Union Carbide OIT measurements from the Bellcore audit samples are provided for comparison.

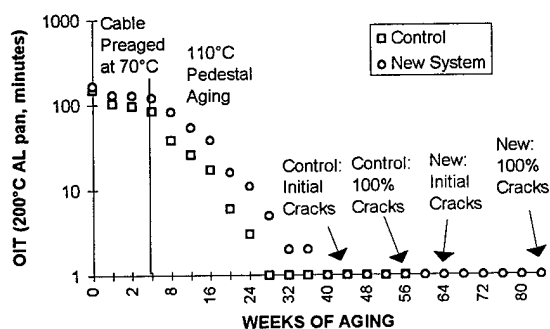


Figure 7: OIT results obtained in the second round 110°C pedestal aging study for the developmental formulation and the commercial reference sample (control).

CABLE TRIAL SUMMARY		DRY WIRE	FILLED CABLE	70°C PREAGE		90°C PED AGING		
				2 WK	4 WK	8 WK	28 WK	40 WK
CABLER #1 (1st Round)	Control	183	166	77	43	38	14	6
	New System	184	163	119	97	85	54	38
CABLER #1 (2nd Round)	Control	197	154	95	84	44	26	18
	New System	191	166	128	120	99	62	44
CABLER #2	Control	186	147	89	82	36	Not Yet Available	
	New System	188	147	117	115	61		
CABLER #3	Control	168	155	90	78	Not Yet Available		
	New System	166	120	111	86			

Table 2: Comparative OIT results (200°C Al pan, minutes) for Union Carbide testing of samples from different cabling trials comparing the new cellular compound to a commercial control sample. All evaluations were performed on 26 AWG foam/skin insulation with 80°C ETPR type cable filler.

Additional Cable Evaluations

Additional foam/skin cable evaluations were initiated at other cable producers. Table 2 provides a comparison of key OIT data from the various foam/skin cable evaluations available to date.

Each of the evaluations confirms the advantages obtained using the new system, with the new formulation providing a significant improvement over the traditional system after preconditioning and pedestal aging.

CABLE TESTING SPECIFICATIONS

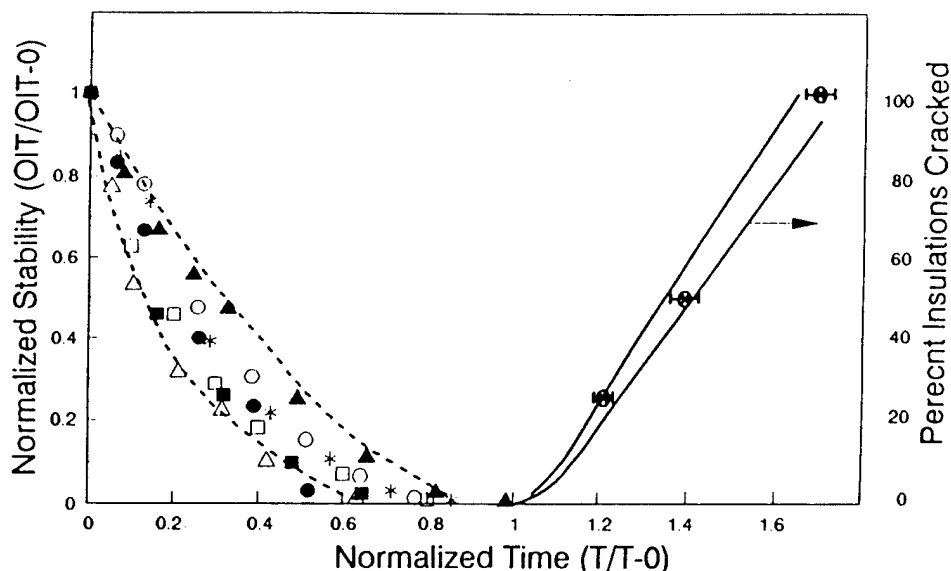
Demanding insulation age testing specifications are becoming more prevalent as industry knowledge about insulation aging performance in grease filled cable becomes more widespread. The Bellcore TR-NWT-000421 and MAT 1101 (seen in Saudi Arabia and the Philippines) are examples of specifications

incorporating rigorous insulation age testing requirements. These include the minimum two week 70°C cable preconditioning needed to incorporate the effects of cable filler/insulation interactions. The cable preconditioning is followed by insulation testing to demonstrate good retention of oxidative stability. The Bellcore specification as refined in 1992¹² incorporates a 260 day/90°C pedestal aging protocol to evaluate for premature insulation cracking. The Bellcore specification also includes more frequent insulation OIT testing, with a 60 minute minimum OIT required following two week cable preconditioning.

MAT 1101 includes a requirement for a retained 20 minute OIT following four weeks of cable preconditioning and 26 weeks of insulation aging in an 80°C oven. This very severe insulation testing requirement includes both the effect of cable filler interactions and the characteristic decline in insulation OIT during oxidative aging. The 26 week OIT pedestal data in Table 2 is indicative that the new product will provide superior performance. A MAT 1101 80°C oven evaluation has been initiated with the new formulation.

The Bellcore TR-NWT-000421 Issue 3 Revision 1 specification also includes a requirement for HPLC testing of AO-1 and MD-1 antioxidants in insulation removed from cable before preconditioning. This compositional fingerprint requirement was based on cables that tested well in the OIT and 90°C pedestal tests following the prescribed two and four week preconditioning. The main advantage of the HPLC procedure was fast testing time compared to the very lengthy pedestal test for periodic QA testing of production cable samples.

Bellcore is now modifying the TR-NWT-000421 specification to accommodate new insulation antioxidant systems providing good 90°C pedestal and OIT performances. A proposed revision¹³ has been distributed for industry comment prior to being finalized. The Issue 3 Revision 2 specification would provide two options for insulation age testing. The Part A option will continue current requirements including HPLC for insulation antioxidant systems incorporating the conventional AO-1/MD-1 system. The Part B option, intended to accommodate the possibility of new and improved formulations, will waive the HPLC



Copyright © 1996 Bellcore. Reprinted with permission.

Figure 8: Bellcore composite data showing OIT trend versus time to insulation cracking. Time is normalized to T-0, time to first cracking for the respective samples. OIT is normalized to OIT-0, which is the OIT value at start of insulation aging.

requirement following demonstration of good performance in initial pedestal evaluation. Both options will continue the pedestal test for initial cable producer qualification and for requalification of substantial changes in the cable product.

The proposed Bellcore revision incorporates an interesting graphical analysis of OIT data from 90°C pedestal tests (Figure 8). T. Bowmer performed this analysis on available data for a number of test cables based on the AO-1/MD-1 antioxidant system. The plot shows insulation OIT versus a normalized time, with T_0 defined as the first pedestal cracking of the respective sample.

This analysis shows that the OIT trend data exhibit an exponential decline within 0.6 to 0.8 time units, leveling out to a small residual value of one minute or less. The sample then exhibits a plateau period ranging from 0.2 to 0.4 time units before exhibiting first pedestal cracking. The analysis indicates a reasonable predictive capability for pedestal cracking based on early OIT trend results. Based on this concept, Bellcore has incorporated a requirement for pedestal testing with OIT trend modeling into the proposed specification update. The new Bellcore requirements call for minimum percent retained OIT values after four and eight weeks of pedestal testing. Comparison of Figures 7 and 8 shows a similar OIT versus cracking characteristic for the new formulation in 110°C

pedestal testing; the 90°C testing is still in progress.

CONCLUSION

A carefully designed cable evaluation program has successfully led to the development and commercial introduction of a new cellular compound providing improved foam/skin insulation aging performance. Methods to accomplish a successful demonstration of the product improvements have been reviewed in detail. A key feature of this program is side by side preparation and testing of a commercial reference sample with the developmental material. The side by side evaluation holds constant the many other cable system variables which can influence insulation aging performance. In this manner, the impact of a designed change can be accurately measured. The program also confirmed that careful side by side pedestal testing within a single laboratory provides good comparative data, supported the utility of OIT trend measurements during age testing as a predictive tool, and demonstrated the value of a minimum two week 70°C cable preconditioning to measure the impact of cable filler interactions on insulation aging performance.

A recommendation to include a side by side evaluation of a commercial reference sample has been incorporated into the new Bellcore TR-NWT-000421 specification. Similar require-

ments are recommended for other worldwide cable testing specifications.

ACKNOWLEDGMENTS

The authors are indebted to several individuals and organizations for their support. Rick King and his colleagues at Ciba-Geigy provided significant assistance to our laboratory development programs. Tim Dogherty, Ed Nelson, and Maureen Chan of AT&T provided excellent support to the initial cable evaluation. Scott Koehler and his colleagues at Cable Systems International skillfully implemented the commercial qualification studies. Trevor Bowmer and Lal Hore from Bellcore provided consultation and support in both the Bellcore Pedestal Testing Audit Study and in preparing the proposed revision to the TR-NWT-000421 specification. Jim Tyler and colleagues at Essex Group, Inc. and Dick Welter and colleagues at Superior TeleTec skillfully implemented cable performance evaluations. And finally, we acknowledge our many colleagues at Union Carbide who supported and helped implement this program.

REFERENCES

- ¹ Davis, L. E., "A Global Test Method for Long Term Stability of Solid and Foam Skin Insulation," Proceedings of the 36th International Wire and Cable Symposium, 1987, pp.475-479.
- ² T. N. Bowmer, R. C. Coker, and R. J. Miner, "Field Temperatures in Outside Plant," Proceedings of the 39th International Wire and Cable Symposium, 1990, pp. 335-342.
- ³ BELLCORE, "Generic Requirements for Metallic Telecommunication Cables," Technical Reference TR-TSY-000421; Issue 2, Revision 1, March 1989.
- ⁴ T. N. Bowmer, R. J. Miner, I. M. Plitz, J. N. D'Amico and L. M. Hore, "Thermal Stability Tests for Polyolefin Insulations," Proceedings of the 39th International Wire and Cable Symposium, 1990, pp. 316-327.
- ⁵ K. D. Dye, V. J. Kuck, F. C. Shilling, M. G. Chan and L. D. Loan, "Analysis of Stabilizer Concentrations in Polyolefin Cable Materials," Proceedings of the 38th International Wire and Cable Symposium, 1989, pp. 98-104.
- ⁶ Eoll, C. K., "The Aging of Filled Cable with Cellular Insulation," Proceedings of the 27th International Wire and Cable Symposium, 1978, pp. 156-170.
- ⁷ Brown, G. D., "Performance of HDPE Insulation Antioxidants in Filled Cable Applications," Proceedings of the 36th International Wire and Cable Symposium, 1987, pp.337-343.
- ⁸ Kuck, V. J., "An Improved Method for Measuring the Stability of Polyolefins," Sixth International Conference on Plastics in Telecommunications, pp. 3/1-3/10, September 1992, London.
- ⁹ American Society of Testing and Materials, "Standard Test Methods for Physical and Environmental Performance Properties of Insulations and Jackets for Telecommunications Wire and Cable," 1994 Annual Book of ASTM Standards, ASTM D-4565-94 Section 17.
- ¹⁰ T. N. Bowmer, R. J. Miner, I. M. Plitz, J. N. D'Amico and L. M. Hore, "Thermal Stability Tests for Polyolefin Insulations," Proceedings of the 39th International Wire and Cable Symposium, 1990, pp. 316-327.
- ¹¹ Foord, S. G., "Compatibility Problems in Filled Cellular Polyolefin Insulated Telephone Cables," Proceedings of the 22nd International Wire and Cable Symposium, 1973, pp.23-29.
- ¹² BELLCORE, "Generic Requirements for Metallic Telecommunication Cables - Thermal Oxidative Stability Requirements for Cables With Polyolefin Insulated Conductors," Technical Reference TR-NWT-000421; Issue 3, Revision 1, December 1992.
- ¹³ BELLCORE, "Generic Requirements for Metallic Telecommunication Cables - Thermal Oxidative Stability Requirements for Cables With Polyolefin Insulated Conductors," Technical Reference TR-NWT-000421; Issue 3, Revision 2, July 1996.

BIOGRAPHY

Geoffrey D. Brown received a MSME degree from Bucknell University in 1977. After graduation, he joined Specialties Polyolefins

Research and Development Department at Union Carbide Corporation. Since 1983, he has worked on the development of insulating and jacketing materials in the Telecommunications and Flame Retardant Wire and Cable Product Groups.

Jeffrey M. Cogen received a B.A. in Chemistry from Cornell University in 1984 and a Ph.D. in Organic Chemistry from the University of California at Berkeley in 1988. Since 1992 he has been a Chemist in the Specialty Polyolefins Division of Union Carbide Corporation where he has conducted research in the area of polymer additives and stabilization.

Michael J. Keogh is a Corporate Fellow in the Specialty Polyolefins Division of Union Carbide Corporation. He received a B.S. in Chemistry from Manhattan College and a Ph.D. in Organic Chemistry from Purdue University. He has been involved in research and product development for wire and cable applications for 22 years. He holds over 60 U.S. patents in this and related areas.

ADVANCED LLDPE COMPOUNDS IN CABLE JACKETING

Chester J. Kmiec and James R. Leech

Union Carbide Corporation
Somerset, New Jersey

ABSTRACT

Telephone cable jacketing was one of the first large uses of High Pressure Low Density Polyethylene (LDPE). Through extensive product development, compounds were made that offered ease of application, durability and long-term cable protection. These products were viewed as major advances over the traditional sheathing materials of the day. The introduction of broad molecular weight Linear Low Density Polyethylene (LLDPE) offered several additional advantages over LDPE for cable jacketing. These included improved low and high temperature performance, toughness, better abrasion resistance, lower moisture vapor transmission and excellent Environmental Stress Crack Resistance(ESCR).

As described in this paper, further advancements by Union Carbide Corporation in catalyst and gas-phase fluidized bed polyethylene process technology, as well as molecular structure control, are encompassed in the next generation of polyethylene products with enhanced end-use properties for Wire and Cable applications. The end-use advantages over the current broad molecular weight LLDPE cable jacket compounds are demonstrated in terms of tensile properties and low temperature performance, while maintaining abrasion resistance and ESCR. These advanced LLDPE resins also offer enhanced extrusion performance over the broad molecular weight LLDPEs currently used in cable jacketing.

INTRODUCTION

LDPE use into telephone cables was pioneered in the 1950s. The black jacketing offered a well balanced blend of properties that provided good performance and value. LDPE materials were developed with good ESCR, low temperature flexibility, moisture resistance and ease of processing, allowing large scale use in jacketing applications.

The development of the low-pressure, gas-phase fluidized bed UNIPOL® polyethylene process (UNIPOL Process is a registered Trademark of Union Carbide Corporation) in the 1970s provided polyethylene with excellent ESCR characteristics, improved low and high temperature performance and better abrasion resistance than LDPEs. LLDPE use has grown considerably over the last two decades, resulting in essentially total displacement of LDPE for telephone jacketing applications in the USA. It also has been widely accepted as the material of choice throughout most of the rest of the world.

UNIPOL process LLDPEs are produced under mild polymerization conditions, typically at pressures less than 2.4 MPa (350 psi) and reaction temperatures of less than 100°C. This low pressure process provides a broad range of LLDPE resins for wire and cable, blown film, cast film, pipe and tubing applications. LLDPE has essentially a linear backbone with only short chain branches, about 2 to 6 carbon atoms in length. In LLDPE, the length and frequency of branching, and, consequently, the density, is predominately controlled by the type and amount of comonomer used in the polymerization.

The majority of the LLDPE resins on the market today have a narrow molecular weight distribution, best suited for film and molding applications. LLDPE resins with broad molecular weight distributions are more suited for wire and cable applications, where the broad molecular weight provides enhanced processing and performance characteristics.

Advancement in low-pressure, gas-phase fluidized bed polyethylene process, catalyst technology (e.g. metallocenes) and product technology continues in the 1990s. The technology improvements allow control of the molecular structure, wherein advanced LLDPE compounds are being produced bringing enhanced properties and value to telecom cable jacketing.

These advanced broad molecular weight LLDPE materials provide the wire and cable industry with jacketing materials having extrudability like that of LDPE, (i.e., better extrudability than even the conventional broad molecular weight LLDPE). These new materials can also offer improved properties over both LDPE and conventional LLDPE jacketing, particularly with respect to tensile strength, elongation, and low temperature brittleness.

ADVANCED LLDPE COMPOUND PROPERTIES

Within the US markets, the use of LDPE materials for telecommunication jacketing has undergone a dramatic reduction in favor of broad molecular weight LLDPE based jacketing products. The advantages of tensile properties, low temperature performance, abrasion resistance and ESCR characteristics of LLDPE materials significantly improved the performance of the telecommunication cable. Advanced LLDPEs have been found to offer further improvements in the performance characteristics of low pressure polyethylene's for telecommunication cable jacketing. TABLE 1 compares various experimental advanced LLDPEs with a conventional LLDPE jacketing material, using a typical black jacketing formulation.

In general, the advanced LLDPE based formulations yielded tensile strength at break 20-70% higher than the LLDPE control and elongation typically 10-40% higher. Tensile at yield in most cases were also significantly improved over the control. These tensile strengths improvements were achieved while maintaining equivalent ESCR performance versus the LLDPE control. The higher Melt Flow Ratio (MFR) values indicate a broader MWD for the new materials, which translates into improvements in extrusion.

TABLE 1
Advanced LLDPE Compounds Property Comparison

<u>Property</u>	<u>ADVANCED LLDPE "A"</u>	<u>ADVANCED LLDPE "B"</u>	<u>LLDPE Control</u>
Density (kg/m ³)	937	937	937
M (dg/min)	0.55	0.64	0.55
Melt Flow Ratio	115	130	80
Tensile @ Break (MPa)	23.7	25	16.5
Tensile @ Yield (MPa)	13.8	14.2	11.3
Elongation (%)	780	930	680

Note: All formulations contain 2.5% carbon black

Comparison of an advanced LLDPE compound to a LLDPE and LDPE control was made in terms of abrasion resistance, low temperature brittleness, electrical and stiffness properties as illustrated in TABLE 2. Abrasion resistance of the new material is comparable to the conventional LLDPE, both of which are significantly better than the LDPE control. Notched low-temperature brittleness testing was carried out using a modified version of ASTM D-746 with a 0.508mm notch. The results show that the advanced LLDPE example yielded a 25% improvement over the LLDPE control and a 300% improvement over the LDPE based jacketing material. The Dielectric Constant and Dissipation Factor of the advanced LLDPEs are comparable to the LLDPE and LDPE controls and relate to the excellent intrinsic dielectric properties of polyethylene.

TABLE 2
Advanced LLDPE Properties

Property	ADVANCED LLDPE "A"	LLDPE Control	LDPE Control
Tabor Abrasion (mg/100 cycles)	16	15	22
LTB $\bar{\epsilon}_{50}$ Notched (°C)	-49	-39	-10
Dielectric Constant @ 1MHz	2.53	2.54	2.48
Dissipation Factor @ 1 MHz	0.000346	0.000329	0.000300

Note: All formulations contain 2.5% carbon black

FIGURE 1 compares the Elastic Modulus (E') versus temperature at a given frequency (1.0 Hz). The advanced LLDPE shows similar performance to the controls at lower temperatures. At the higher temperatures, the new material maintains a higher elastic modulus over the both the LLDPE and LDPE controls, and relates to improved melt strength.

FIGURE 2 illustrates the Coefficient of Thermal Linear Expansion (CTE) for the advanced LLDPE material. The CTE is shifted to the right for the new material, thus indicating less expansion. A material with a lower CTE would be advantageous in a finished cable, especially where temperature cycling is encountered.

EXTRUSION PERFORMANCE

Historically, high molecular weight polyethylenes were required to improve the physical properties. This increase in molecular weight also increased the melt viscosity, resulting in higher extrusion pressure, extrudate temperature and drive power (motor amperage). The development of LLDPE resins allowed for excellent physical properties even at lower molecular weights (i.e., higher melt index). However, even the conventional broad molecular weight LLDPEs used in telecommunication jacketing applications are typically of higher viscosity than the LDPE materials under

FIGURE 1

ELASTIC MODULUS

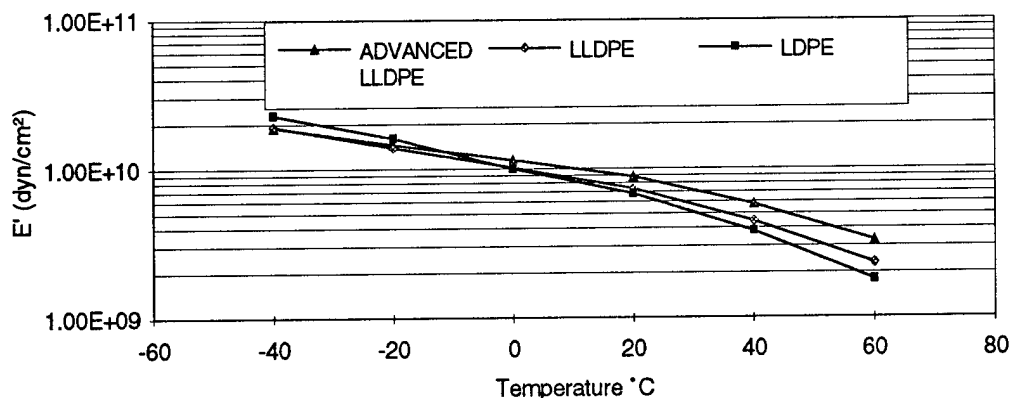
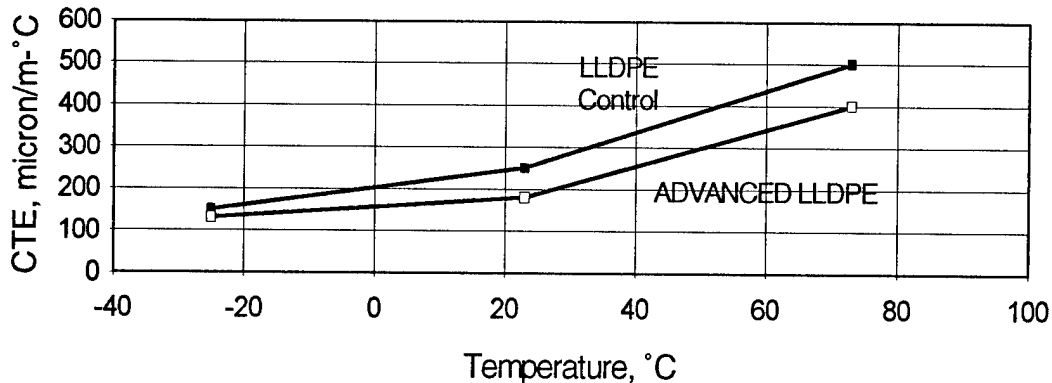


FIGURE 2

Coefficient of Thermal Linear Expansion



the shear conditions experienced in jacket extrusion. The increase in melt viscosity results in a higher melt temperature than achieved with LDPE. The even broader molecular weight advanced LLDPEs were found to narrow this processing gap between conventional LLDPE and LDPE, while improving tensile strength, elongation, and low temperature brittleness properties.

Goettfert rheological characteristics of an advanced LLDPE compound versus the conventional LLDPE and LDPE jacketing compounds is shown in FIGURE 3. The results indicate that advantageous cable jacketing extrusion performance exists versus the conventional LLDPE. The curves also indicate that the advanced LLDPE is similar to the rheological characteristics of a LDPE in the typical jacketing shear extrusion range.

To confirm the expected extrusion performance advantages, advanced LLDPE based formulations were evaluated on a Davis-Standard wire line using 14 AWG copper with a jacketing thickness of 30 mils. TABLE 3 illustrates that a reduction in extrusion pressures

and extruder drive motor power were achieved at a 61m/min. wire line speed with the new material. In general, a head pressure reduction of 14% and 13% lower power were observed during the extrusion trial. No melt fracture was observed under these conditions. Furthermore, when the line speed was nearly doubled (116m/min.) for the advanced LLDPE material versus that of the control, the resulting pressures were similar to the LLDPE control at 61m/min. Again no melt fracture was observed with the advanced LLDPE. The LLDPE control gave pronounced melt fracture at 116 m/min..

The advanced LLDPEs also were found to offer the advantage of reducing extrusion processing temperatures without sacrificing line speed. The lower processing temperatures resulted in a lower melt temperature, which could allow a shorter cooling trough or reduce the amount of heat to the core. TABLE 4 illustrates that the advanced LLDPE "A" material was successfully run at lower temperatures than previously utilized in Table 3. At a melt temperature of 199°C a smooth jacket was obtained with "A" where the LLDPE

FIGURE 3

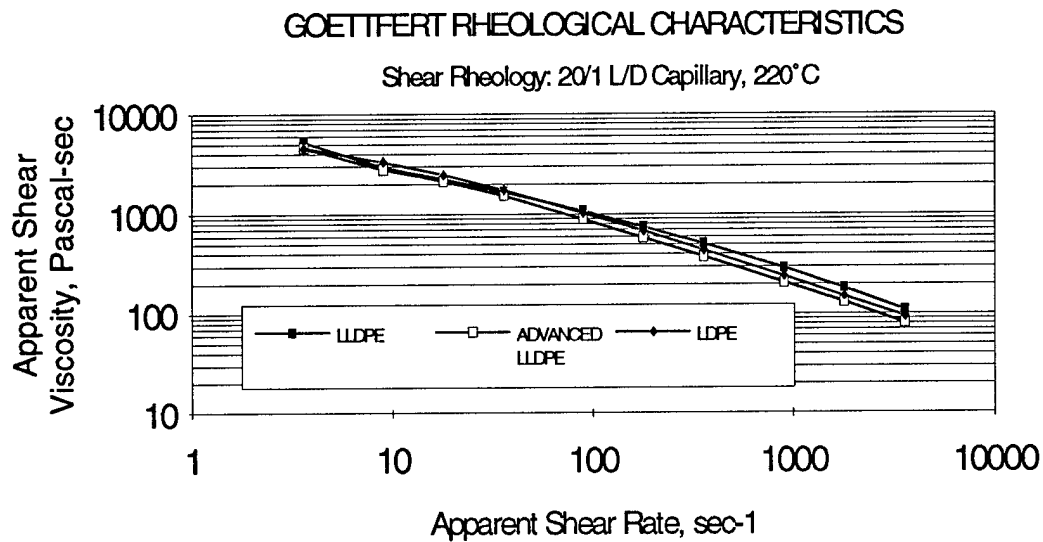


TABLE 3

Advanced LLDPE Extrusion Performance

	<u>ADVANCED LLDPE "A"</u>	<u>LLDPE Control</u>	<u>ADVANCED LLDPE "A"</u>	<u>LLDPE Control</u>
Density (kg/m ³)	937	937	937	937
Melt Index (dg/min.)	0.55	0.55	0.55	0.55
Melt Temperature (°C)	215	208	216	235
Pressures (MPa)				
Breaker Plate	21.7	24.8	25.6	29.7
Head	17.9	20.7	20.7	24.8
Screw rpm	35	37.5	68	63
Screw amps	35	40	47	52
Linespeed (m/min.)	61	61	116	116
Cable surface	smooth	smooth	smooth	melt fracture
Extrusion Rate (kg/hr.)	19.8	20	35.8	35.6

Note: Extrusion temperature profile of 175°C - 215°C used for these extrusion runs .

TABLE 4
Wire Line Speed Comparision

	ADVANCED LLDPE "A"	LLDPE Control	ADVANCED LLDPE "B"	ADVANCED LLDPE "B"
Density (kg/m³)	937	937	937	937
Melt Index (dg/min.)	0.55	0.55	0.64	0.64
Melt Temperature (°C)	199	199	187	209
Screw rpm	35	31	36	67.5
Screw amps	37	40	39	49
Linespeed (m/min.)	61	61	61	116
Cable surface	smooth	melt fracture	smooth	smooth
Extrusion Rate (kg/hr)	19	19	19	35.9

Note: 1) Extrusion temperature profile for advanced LLDPE "A" and LLDPE control set at 188°C.

2) Extrusion temperature profile for advanced LLDPE "B" set at 176°C.

control exhibited rough jacket surface (melt fracture) at this temperature. Further lowering of the melt temperature by 12°C using the advanced LLDPE "B" material, again yielded cable with a smooth surface at a line speed of 61 m/min. The new LLDPE "B" material did not develop melt fracture when the line speed was increased to 116 m/min. However, as expected, the resulting pressure and amperage increased at the higher line rate.

CONCLUSIONS

The advanced LLDPE materials manufactured from the low-pressure, gas-phase, fluidized bed, polyethylene process have shown improvement in processing

performance over the conventional broad molecular weight LLDPE materials used in jacketing. These new LLDPEs minimized equipment limitations through increased processing flexibility from increased line speed or lowering of processing temperatures. The lower processing temperatures can lead to shorter cooling times or less heat history for the cable core. The advanced LLDPEs narrow the processing gap between LLDPE and LDPE, while maintaining the advantageous properties of LLDPE materials. Significant advantages over the conventional LLDPEs were also noted in tensile, elongation and low temperature brittleness properties.

AUTHORS

James R Leech
Union Carbide Corporation
Weston Canal Center
P.O. Box 450
Somerset, New Jersey 08875-0450

Since 1989 Jim has been Technology Manager for Union Carbide's Telecommunication's business. He has had almost 25 years in polymer Research and Development, the last 20 at Union Carbide. He holds an M.S. in Chemistry (University of Pittsburgh) and an M.B.A. in Chemical Marketing (Fairleigh Dickinson University). He has been involved in LLDPE product development since the late 1970s for applications ranging from injection molding to pressure pipe and wire and cable extrusion. He is Vice Chairman for this year's IWCS

Chester J. Kmiec
Union Carbide Corporation
Weston Canal Center
P.O. Box 450
Somerset, New Jersey 08875-0450

Chet is a Development Scientist at Union Carbide Corporation. He has 22 years experience in Polymer Applications Research and Development, the last seven years at Union Carbide. He holds a B.S. in Plastics Technology from Lowell Technological Institute and an M.B.A. from the State University of New York at Buffalo. He has been involved in polymer application development in areas covering flame retardants, peroxide crosslinking and polyethylene product development for applications which include hose, tube and wire and cable extrusion. Current responsibilities include new product development for telecommunications cables.

LEAKAGE CURRENT SMOKE CORROSIVITY TESTING - COMPARISON OF CABLE AND MATERIAL DATA

J. Thomas Chapin

Lucent Technologies, Bell Laboratories, Norcross, GA

Loren M. Caudill

DuPont - Wilmington, DE

Pravin Gandhi, Robert Backstrom

Underwriters Laboratories, Northbrook, IL

ABSTRACT

This paper is the third in a series which presents electrical leakage current measurements on interdigitated test patterns exposed to smoke effluent from plastic materials and telecommunications cables. Six commercial US and European cables were selected for testing. The leakage current behavior of each cable was measured and related to the fire performance rating of the cables. The cable leakage currents data are also compared to material data in order to investigate the effects of co-combustion of all combustible components in the cable. Co-combustion can affect the chemistry and particulates of the smoke effluent which may also affect the leakage current results. This relationship is discussed. Supplemental data are also reported on the cable materials such as heat of combustion, ash content and elemental analysis in order to provide insight into the combustion and leakage current behavior.

INTRODUCTION

This paper is the third in a series on the subject of the reliability of digital electronic equipment when exposed to non-thermal fire damage conditions. In this paper the effects of smoke effluent on printed circuit board test patterns were investigated by measuring the change in leakage current as a function of relative humidity (RH). The smoke effluent was generated by degrading materials in a combustion tube furnace. The materials tested are commonly used in copper and fiber optic telecommunications cables. By measuring the dependence of leakage current on RH, one can gain

insight on how smoke deposits react to moisture and to assess the potential for recovering smoke exposed equipment.¹ The effects of RH on leakage current and the utilization of interdigitated test patterns to study electronic reliability has been widely reported in ongoing dust contamination studies.²⁻⁵ These test patterns have been used by AT&T Bell Laboratories, Bellcore and other laboratories concerned with corrosion and electronic reliability for a number of years.

The first paper in this series reported on the combustion of six reference materials using a tube furnace and a cone calorimeter.⁶ Six material classes were investigated: halogenated and non-halogen flame-retardant polyolefins, standard and smoke suppressed PVC materials and fluoropolymers. The results indicate that both the chemistry of the materials and their combustion conditions affect the smoke effluent and the corresponding leakage currents on the test patterns. Surprisingly, the results did not necessarily correlate with halogen content, as has been widely concluded.⁶ The increase in leakage current is far more complex than halogen content of the degraded material and is more likely related to the chemistry of the smoke effluent, particle size distribution and deposition conditions. It has been demonstrated that graphitic carbon in the smoke arising from petroleum fires in Kuwait adversely affected leakage current on test patterns and electronic equipment.⁷ Also, flame-retardant formulations have become far more complex in recent years with the recognition that numerous additives can be employed in the formulation to retard flame spread, reduce acidic gas emissions, suppress smoke or enhance char formation.

The second investigation in this series expanded the range of materials and compared the results of the leakage currents on test patterns to pH and conductivity measurements made in accordance with the International Electrotechnical Committee (IEC) Standard 754-2, Standard Method for Measuring pH and Conductivity of Materials. This acid gas and conductivity method is frequently cited in European cable specifications. The results indicate that there is correlation between halogen content and measured solution pH and conductivity, as expected. However there is not a correlation between pH, conductivity and leakage currents. High leakage currents were measured on samples with high solution pH values (greater than 4.3) and low conductivity values (less than 10 microSiemens). Certain fluoropolymers and low-smoke PVC materials in the series tested exhibited low pH values and high conductivity also had low leakage currents. The perception that there is a direct relationship between halogen content and smoke corrosivity (electronic reliability) is oversimplified. The information gained from the IEC 754-2 tests may have relevance in predicting generalized corrosion for certain applications, but acid gas alone is not the primary contributor to failure in digital electronic equipment.

The present paper reports on the leakage current behavior of test patterns exposed to smoke arising from burning copper telecommunications cable and compares the results to individual material measurements. This work is distinguished from the earlier work in that the chemistry and particulates formed during combustion are determined by the combustion of all of the combustible components in the cable. As is the case with material formulations, cable constructions have become more complex, utilizing numerous materials for specific end-use requirements, not all related to fire behavior. For this reason, tests that utilize the entire cable product as the test specimen will provide the most meaningful information to the end user who is faced with predicting electronic reliability in fire situations.

INTERNATIONAL STANDARDS FOR FLAME SPREAD AND CORROSIVITY

Flame Spread

Copper and fiber optic cables designed for indoor use must exhibit fire retardant behavior that meets the local fire requirements. In the US, National Electrical Code^(R) defines performance-based tests for residential, general purpose, riser or plenum

applications. In Europe and throughout the rest of the world, there are a variety of IEC and country-specific fire standards that are cited in cable specifications. Many of these methods are being reviewed for relevance and harmonization to international standards. This work is being conducted in code bodies such as, the IEC and CENELEC (European Committee for the Electrotechnical Standardization).

For flame spread, the comparison between US and IEC tests is found in Table 1. No equivalent "plenum" or "riser" tests exist in the IEC fire test methods. UL 1581 and IEC 332-3C are vertical tray tests that are similar, but not equivalent. The same situation applies to UL 1581 VW-1 and the IEC 332-1 tests which are small scale, single cable small burner tests.

Table 1. Fire Test Methods

US Test	US Marking ^a	IEC ^b
UL 910 Plenum	CMP, OFNP	na ^c
UL 1666 Riser	CMR, OFNR	na ^c
UL 1581 Vertical Tray	CM, OFN	IEC 332-3C
UL 1581 VW-1	CMX	IEC 332-1

^a Copper and optical fiber nonmetallic cables.

^b No marking required, rating in cable specifications.

^c No equivalent test

Smoke Corrosivity

The evaluation of the corrosivity of combustion products from polymer insulated copper wires, polymer coated glass fibers, and cable jackets is a topic of vigorous discussion in standards organizations world wide⁷⁻¹².

Several test methods have been standardized to assess the corrosion hazards arising from the evolution of gases generated in a fire involving these products. However, many of these methods may not be suitable for assessing the hazards to telecommunications equipment in particular, since the relevant property related to telecommunication equipment reliability is not measured directly. Thus, it is essential that new test method(s) under consideration be based on appropriate technical data that they are useful in hazard assessment of these equipment.

At present, most smoke corrosivity methods found throughout the world assess smoke corrosivity by measuring changes in pH or conductivity of water extracts, or by measuring metal loss. These methods fail to accurately predict the electronic reliability of digital equipment, since it has been found that failure usually arises from the degradation of insulation resistance rather than direct metal loss. These conclusions are based on experience gained from telecommunications equipment fires. Further, pH and conductivity methods assess only one characteristic of fire effluent - acid gas. A list of country-specific and international smoke corrosivity test is found in Table 2 in Reference 6.

CORROSION-RELATED EQUIPMENT FAILURES

There are damage mechanisms associated with real fires that are of greater consequence than acid gas generation and metal loss. With respect to corrosive components in the smoke, acid gases are important, but ionic contaminants associated with fillers, flame retardants, colorants, processing aids and/or impurities in the polymers, or by-products of the polymerization reactions, can also be important. The most common cause of equipment malfunction following exposure to smoke from cable combustion is not loss in thickness of structural metals or metal circuitry from direct deposition of corrosive gases but rather electrical shorts and arcing that cause cross-talk and malfunctioning components². The low insulation resistance associated with smoke-related contamination leads to metal migration (dendrites), electrolytically corroded conductor lines (quite distinct from the direct corrosion caused by deposition of corrosive smoke on conductors), and other electrochemical degradation processes^{4,5}. The full array of contaminants from the smoke includes the halide gases, of course, but also includes other ionic contaminants, organic gases, and, in some cases graphitic carbon. High humidity exacerbates the effects of ionic contaminants^{4,5}. However, if graphitic carbon is formed in a fire, it has been found to be conductive at all humidity levels. Data reported in a Comizzoli's paper⁴ about the effects of these kinds of contaminants on electrical leakage are shown in Figure 1.

The figure shows that ionic contamination, from several different sources, produces electrical leakage on an AT&T standard interdigitated test pattern that

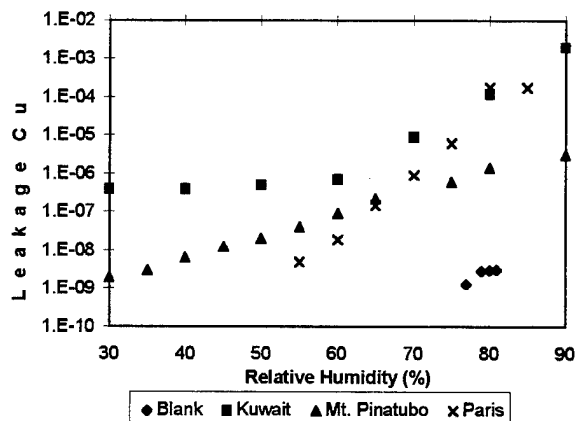


Figure 1 - Influence of Relative Humidity on Leakage Current for Dust Particulate from Various Sources

exhibits a pronounced exponential dependence on humidity. It is this exponential dependence that necessitates tight control of humidity if the functionality of smoke damaged equipment is to be restored. One of the curves in the figure is for soot deposited on equipment exposed to the oil fires following the Gulf War (identified as "Kuwait"), show that graphitic carbon can also cause failures. In this case, even short term restoration of service requires cleaning the equipment.

MATERIALS USED IN TELECOMMUNICATIONS CABLES

Telecommunications cables have become far more complex in the past several years due to increased customer and regulatory requirements, as well as improvements in overall transmission performance. Indoor optical fiber cable designs are now commercially available (exceeding 100 fibers) that meet stringent UL 910 Plenum and UL 1666 Riser test requirements. These cables often contain multiple subunit cables and buffered fiber constructions that may require several thermoplastic materials, strength members and other inorganic or cross-linked materials for specific purposes. Likewise, high performance copper cables have evolved that meet or exceed Category 5 transmission performance in unshielded and shielded constructions.

These advanced cable constructions employ the full range of materials commonly used in

telecommunications industry, such as: polyolefins, plasticized semirigid PVC materials, fluoropolymers, polyamides, polyesters and so on. These materials are either intrinsically flame retardant or additives are employed to provide enhanced smoke or acid gas suppression or flame spread resistance. In fact, UL444 Standard for Copper Telecommunications Cables has 17 separate materials categories that define aging and mechanical test requirements.

In order to describe the materials selected for this investigation, the material samples were broadly divided in three categories, 1) polyolefins (PO), 2) PVC compounds (PVC) and 3) fluoropolymers (FP). The materials and their general properties are described in Table 2.

Table 2. Classes of Materials Used in Telecommunications Cables	
Material Class	Polymer Components/Flame Retardancy
Polyolefins - PO	<ul style="list-style-type: none"> Hydrocarbons: polyethylene, polypropylene Oxygenated copolymers: ethylene with vinyl acetate, ethyl acetate Halogen-free and halogenated formulations Heats of combustion from 5,500 to 20,000 BTU/lb.
PVC materials - PVC	<ul style="list-style-type: none"> Polyvinyl chloride resin and chlorinated rubbers Plasticized, semirigid, smoke suppressed, low acid gas Heats of combustion from 5,500 to 12,000 BTU/lb.
Fluoropolymers - FP	<ul style="list-style-type: none"> Homopolymers, copolymers with various fluorinated monomers and copolymers with fluorine and chlorine-containing monomers Heats of combustion from 2,200 to 7,000 BTU/lb.

TEST PLAN

Based on these data shown in Figure 1, and our experience with smoke damaged electronic equipment, a more appropriate test of smoke corrosivity is to expose interdigitated test patterns to the smoke effluent and measure leakage current as a function of humidity. Measured current/humidity curves are then compared to threshold curves for various damage levels. Of course the threshold levels depend on the geometry of the circuitry on the test substrate. A test pattern in common use that fits the minimum requirements for corrosivity testing is the ASTM IOC B25 pattern¹³, which has also been adopted by Bellcore for some of its electrical leakage test specifications. Alternatively, the AT&T pattern can be used¹⁴, or, optimally, a new pattern can be developed that would enable leakage current and electrical resistance to be measured simultaneously.

Whatever test substrate is used, it should have the test circuit repeated several times so that the precision of the data can be assessed and confidence limits can be specified in comparing different materials and different test positions within the same test.

EXPERIMENTAL

Commercial copper cables were selected for this investigation and tested intact and as separate components. The cables were all of the same construction; 4 pair, 24 awg insulated twisted pairs with a surrounding jacket. This is commonly referred as a UTP (unshielded twisted pair) construction. The jackets varied in thickness, according to the type of jacket material. The identification of each cable and their material constructions are found in Table 3.

Table 3. Identification of Cables and Cable Components					
Cable ID	Fire Rating	Jacket Material ID	Jacket Thickness (in.)	Insulation Material ID	Insulation Thickness (in.)
A	CMP	FP1	0.007	FP1	0.0075
B	CMX	PVC9	0.036	PO1	0.0070
F	CMP	PVC4	0.016	FP1	0.0065
G	CMR	PVC7	0.023	PVC8	0.0075
H	IEC 332-3C	PO7	0.031	PO1	0.0070
K	IEC 332-1	PO8	0.016	PO1	0.0100

The gross heat of combustion (in BTU/lb.) for each cable component is found in Table 4.

Table 4. Gross Heat of Combustion (BTU/lb.) Data for the Cable Components			
Rating	Cable ID	Jacket	Insulation
CMP	A	2246	2246
CMX	B	8440	19436
CMP	F	6827	2219
CMR	G	9248	9600
IEC 332-3 C	H	6082	19436
IEC 332-1	K	6215	19436

The description of each cable material is found in Table 5.

Table 5. Outline of Cable Materials and General Chemistry	
Material ID	General Description
FP1	Fluorinated polymer
PO1	Non-flame-retarded polyolefin
PO7	Nonhalogen, flame-retarded polyolefin
PO8	Nonhalogen, flame-retarded polyolefin
PVC4	Low-smoke PVC
PVC7	Flame-retarded PVC
PVC8	Plasticized PVC
PVC9	Plasticized PVC

The tests were conducted using a combustion tube furnace (modifying the IEC 754-2 test protocol). The test apparatus, samples, corrosion targets and test procedure are described below.

Combustion Tube Furnace

The combustion tube furnace consisted of furnace, silica tube, combustion boat, air supply system and a mixing chamber for the combustion products. The tube furnace had an inside diameter of 60.3 mm and a heating zone of 300 mm. The test temperature was controlled by an electronic temperature controller. The silica tube was 1600 mm long, 47.5 mm inside diameter and had a wall thickness of 2.75 mm. The silica tube was placed in the tube furnace such that it extended 400 mm from the rear end of the furnace. The rear end of the tube was ground and was fitted with a glass adapter connected to an air supply from a dry compressed air cylinder. A porcelain combustion boat, 97 mm in length was used to hold the test sample during the test.

The mixing chamber was made from polymethyl methacrylate (PMMA), with dimensions of 310 x 310 x 340 mm. A stainless steel plate was attached to the inner side of part of the chamber connected to the silica tube. The purpose of the plate was to protect the PMMA surface from flames or hot gases emanating from the silica tube. The top of the mixing chamber was a blowout panel to release excessive pressure. The chamber had a 6.3 mm opening at the bottom of one of the sides to permit exhaust of combustion products to a smoke abatement system. The mixing chamber was placed 385 mm away from the end of the tube furnace, such that 55 mm of the silica tube protruded inside the chamber. A photograph of the test assembly is shown in Figure 2.

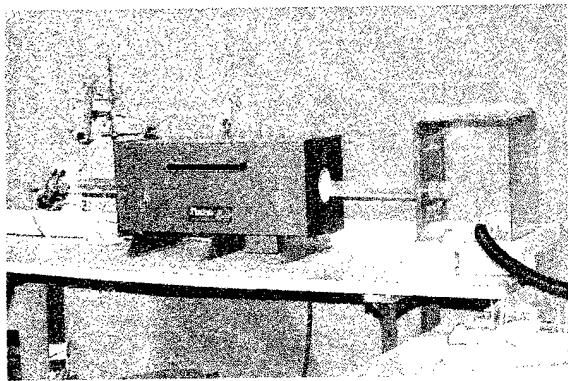


Figure 2 - IEC 754 Tube Furnace with Collection Chamber for Leakage Current Experiments

The leakage current on the target was measured using a Keithley picoammeter/voltage source Model 487. Switching between targets was accomplished with a Keithley Model 7001 switch system. The 30% to 90% controlled RH environments were produced using a General Eastern RH generator Model C-1.

Test Samples

A sample weight of 1000 ± 5 mg, was used for materials and cable samples (copper included). The samples are identified in Tables 4 and 5.

The cable jacket and insulation samples were subjected to heat of combustion analysis and semiquantitative elemental analysis on the ash to identify the types of elements present in the formulations. The gross heat of combustion test was performed in accordance with ASTM D2015.

Corrosion Target

Commercially available leakage current targets, Model PCBS P/N REMOD were supplied by Precision Prototypes, Inc. The comb pattern spacing was 12.5 mils with all copper surfaces solder tinned and mounted on a printed circuit board laminate 0.062 in. thick. A schematic of the circuit is shown in Figure 3. Prior to testing, the target was cleaned in an ultrasonic bath with 75% isopropyl alcohol, followed by rinsing in deionized water for 30 seconds, and drying with compressed nitrogen.

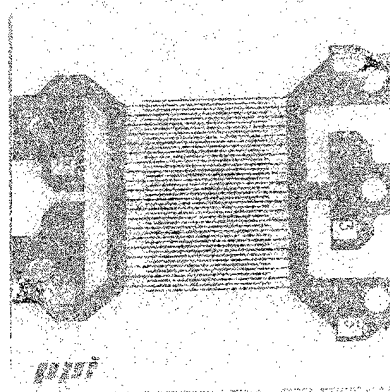


Figure 3 - Comb Pattern Leakage Current Target

Test Procedure - Combustion Tube Furnace

For each test, the following test procedure was used. Test temperatures of 935°C at test position "P1" (300 mm from the entrance of the furnace), and 900°C at position "P2" (600 mm from the entrance of the furnace) were established in the tube furnace. One corrosion target was placed at the bottom and at one of the ends of the mixing chamber. The test samples were weighed to an accuracy of 1 mg, and evenly distributed on the bottom of the combustion boat. The test samples with the combustion boat were also weighed. The combustion boat with the test sample were placed inside the rear end of the tube prior to test initiation. The end was closed with the adapter, and an air flow rate of 5.0 liters per minute was established through the silica tube. The combustion boat was then moved, using a push rod, to the test position "P1". The combustion products were allowed to react with the corrosion target for 1 hour. At the end of one hour, the target was removed and leakage current characteristics were determined. The combustion boat with residue was weighed and the sample weight loss was determined. Two tests were performed for each test sample.

RESULTS

The results obtained from the combustion tube furnace tests are presented herein. The leakage current data collected for the combustion of whole cable are shown in Figures 4, 5 and 6.

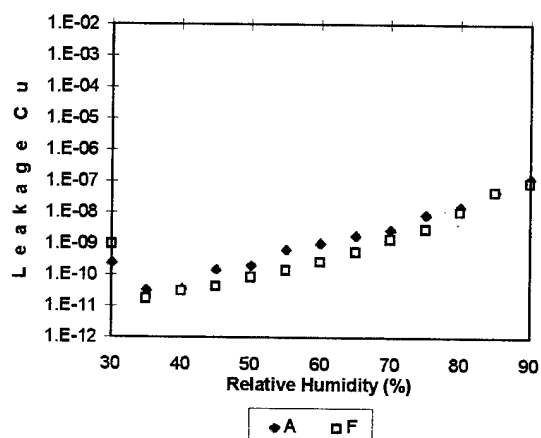


Figure 4 : Leakage Current for CMP Rated Cables

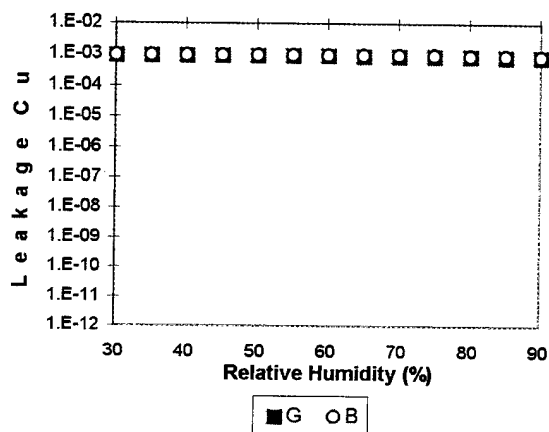


Figure 5 : Leakage Current for CMR/CMX Rated Cables

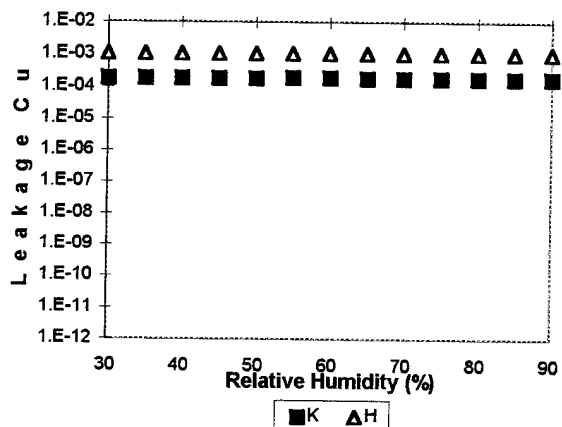


Figure 6 : Leakage Current for 332-1/332-3C Rated Cables

The Leakage current data for the jackets and insulation of all the cables are shown in Figures 7 and 8.

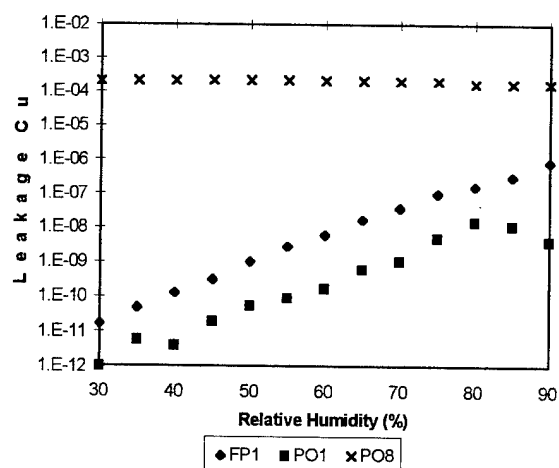


Figure 7 : Leakage Current for FP and PO Class Materials

Material PO7 shorted and exhibited high leakage current behavior similar to Material PO8.

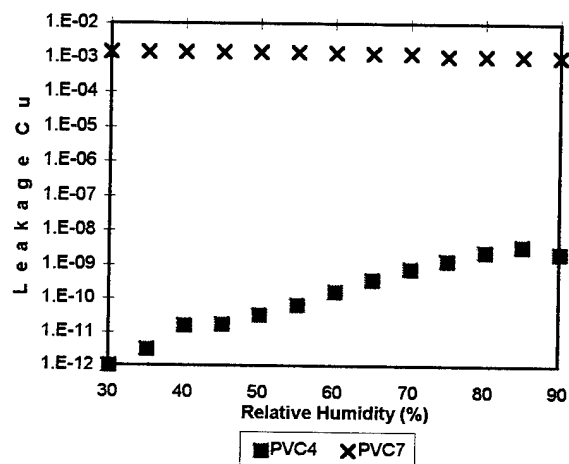


Figure 8 : Leakage Current for PVC Class Materials

Material PVC9 shorted and exhibited high leakage current behavior similar to Material PVC7.

Table 6. Common Elements in Formulation of Cable Jacket and Insulation						
Cable	Jacket	% Ash	Elements	Insulation	% Ash	Elements
A	FP1	<0.1	C, H, F	FP1	<0.1	C, H, F
B	PVC9	9.45	C, H, O, Al, Sb, B, Ca, Pb, Mg, Mo	PO1	<0.1	C, H
F	PVC4	22.47	C, H, O, Cl, Al, B, Ca, Cu., Fe, Pb, Mg, Mo, P, Zn	FP1	<0.1	C, H, F
G	PVC7	7.20	C, H, O, Al, Sb, B, Ca, Pb, Mg, Mo	PVC8	5.52	C, H, O, Al, Sb, Ca, Pb, Mg, Zn
H	PO7	46.53	C, H, O, Al, Ca, Mg	PO1	<0.1	C, H
K	PO8	58.80	C, H, O, Al, Ca	PO1	<0.1	C, H

The list of elements present in the cable jacket and insulation materials is presented in Table 6

DISCUSSION

The leakage current data for the six cables show a dramatic difference between fire performance levels. Based upon existing leakage current data, a semilogarithmic dependence of leakage current on RH is expected. This is observed for the plenum (CMP) rated cables (Cables A and F). These two cables exhibit low leakage current over the entire range of relative humidity. However, the other four cable constructions (Cables B, G, K and H) show exceedingly high leakage currents that are independent of RH. This is expected to be due to the formation of graphitic smoke deposition on the targets consistent with the Kuwait particulate study (see Figure 1).

This data are supported by the leakage current data on individual material samples. For example, FP1, PVC4 and PO1 (Figures 7 and 8) show low leakage currents, while material samples PO7, PO8, PVC6 and PVC9 (Figures 7 and 8) exhibit high leakage currents. Cable A is composed of FP1 as the jacket and insulation material which individually and combined show low leakage currents on the test pattern. The same is true of Cable F which is

composed of PVC4 as the jacket and FP1 as the insulation.

The other four cable constructions which show high leakage currents are: 1) Cable B which is composed of PVC9 and PO1, 2) Cable G which is composed of PVC7 as the jacket and PVC8 as the insulation, 3) Cable H which is composed of PO7 as the jacket and PO1 as the insulation, and 4) Cable K which is composed of PO8 as the jacket and PO1 as the insulation. Cable samples H and K contain PO1 as the insulation which individually exhibits a low leakage current when tested alone. However, when combined with jacket materials that exhibit high leakage currents (PO7 and PO8) the combined effect is a smoke effluent that is more conductive.

The materials of construction used in Cables A and F have been found to also have low smoke generating propensity as measured by UL 910. In general, it is anticipated that the leakage current results will be influenced by the type of smoke generated (particle size distribution, chemistry and morphology) and also by the fire conditions (e.g., ventilation). The relative weight of these factors with respect to leakage current still need to be investigated in future research programs.

Finally, the percent ash content and elemental analysis data if presented in Table 6., provide a

profile of the elements found in the jacket and insulation materials. Note that the ash content varies greatly for the PVC and flame-retardant polyolefin formulations. Metal hydrates of aluminum and magnesium have been added to provide flame retardancy which increases the ash content. Other additives are included in some formulations to suppress smoke and enhance char formation. The high leakage currents can not simply be explained by the presence or absence of these elements. The conductivity of the smoke effluent is more likely influenced by the formation of conductive, graphitic smoke particulates, which at present is not easily predicted.

CONCLUSIONS

The leakage current data for the six cables show a dramatic difference between fire performance levels. The cables that meet UL 910 flame spread and smoke density requirements also show low leakage current behavior in the test patterns. The lower fire performance cables show higher leakage currents under the same test conditions. The data on the cable jacket and insulation materials is also consistent with the cable data, where co-combustion of all cable materials occurs. High leakage currents were measured on "nonhalogen" cables that meet IEC 754-2 criteria for pH and solution conductivity. Materials that meet this requirement are considered "low, or non-corrosive". These new results contradict this conclusion. Also, the data confirm earlier conclusions that there is not a direct correlation between halogen content and smoke corrosivity as it relates to electronic reliability. Further investigation is required to understand the relationship between smoke effluent (gas and particulate compositions) and leakage current behavior.

ACKNOWLEDGEMENTS

The authors wish to thank Ms. Mamatha Ratnam and Mr. Jim Walnock for contributing to data analysis and text development, Mr. Mark Wayne and Mr. Barry Powers for their contributions in obtaining the pH, conductivity and leakage current results, Dr. Doug Sinclair and Mr. Bob Comizzoli for their technical expertise and experimental consultation.

REFERENCES

1. Cider, L. "Cleaning and Reliability of Smoke Contaminated Electronics", *Fire Technology*, Third Quarter 1993, pp. 226-245.
2. Sinclair, J.D., "Corrosion of Electronics", *Journal of Electrochemical Society*, March 1988, pp. 89C-95C.
3. Comizzoli, R.B., Frankenthal, R.P., Milner, P.C. and Sinclair, J.D., "Corrosion of Electronic Materials and Devices", *Science*, Vol 234, 1986, pp. 340-345.
4. Frankenthal, R.P., Siconolfi, D.J. and Sinclair, J.D., "Accelerated Life Testing of Electronic Devices by Atmospheric Particles: Why and How", *V140*, No. 11, November 1993, pp. 3129-3134.
5. Comizzoli, R.B., "Materials Developments in Microelectronic Packaging Conference Proceedings", Montreal, August 1991, ASM International, pp. 311-316.
6. Chapin, J.T., Sinclair, J.D., Comizzoli, R.B., Gandhi, P., Peins, G.A., *IWCS Proceedings 1995*, pp. 432-436.
7. Briggs, P.J., "Smoke Generation-Developments in International Test Methods and Use of Data for Selection of Materials and Products", *Fire Safety Journal*, V20, 1993, pp. 341-351.
8. Comizzoli, R.B., Frankenthal, R.P., Lobnig, R.E. Peins, G.A., Psota-Kelty, L.A., Siconolfi, D.J., and Sinclair, J.D., *Interface Fall 1993*.
9. Fazzari, A.M., Stratta, J. J., and Panzer, L.M., "Plastic Building Products with Reduced Combustion Emissions", *Technical Proceedings 43rd Annual Conference*, Composites Institute, 1988, pp. 8A.1-8A.4.
10. IEC Technical Committee (TC) 89 is responsible for the development of international standards pertaining to smoke corrosivity and safety issues.
11. Bottin, M.F., "Acidity and Corrosivity Measurements of Fire Effluent", *International Wire and Cable Symposium Proceedings*, 1990, pp. 205-213.
12. ASTM D5485 - Fire Test Response Standard For Determining the Corrosive Effect of Combustion Products from Electrical Insulation's or Coverings using the Cone Corrosimeter ASTM, 1916 Race Road, Philadelphia, PA.
13. Electronic Controls Design, Inc., 13626 S. Freeman Road, Mulino, Oregon 97042.
14. Precision Prototype Inc., 255 Midland Ave, Garfield, NJ 07026 Target PTBF P/N



J. Thomas Chapin is a Member of Technical Staff in the Chemistry, Environment and Safety Group at Lucent Technologies, Bell Laboratories in Norcross, Georgia. He is responsible for fire technology research and materials development for copper and fiber optic cables. He joined AT&T Bell Laboratories in 1980 after working at the Upjohn Company for three years. He received his B.S. in Chemistry and Ph.D. in Polymer Science from the Institute of Materials Science at the University of Connecticut. Since 1980 he worked in the areas of outside plant materials failure phenomena, optical fiber coating development and fiber optic cable development. He has been awarded 11 patents and has 15 publications.

REDUCED SMOKE FLAME RETARDED W&C FORMULATIONS

Ronald L. Markezich

Occidental Chemical Corporation, Technology Center, Grand Island, New York

ABSTRACT

Flame retardant wire and cable formulations with greatly reduced smoke have been developed. This has been accomplished using traditional halogenated flame retardants with a unique combination of fillers and inorganic salts. Smoke levels on combustion are greatly reduced and less acid gases are produced.

Using mixtures of a thermally stable chlorinated flame retardant with inorganic salts such as magnesium hydroxide show a synergistic effect in the oxygen index test. the antimony oxide level may be reduced and yet still maintain high oxygen indexes and physical properties. Various polyolefins have been evaluated, PE, EVA, EPDM, and EEA.

The FR-EVA wire and cable formulations using this combination of flame retardants give less smoke when burned in the NBS smoke chamber and produces less acid gases.

The chlorinated flame retardant additives yield much less smoke than the brominated flame retardant additives in a wide variety of wire and cable polymer formulations when tested in the NBS smoke chamber. The combination of chlorinated flame retarded with magnesium oxide can give a NBS smoke number or less than 100 Ds maximum in both the flaming and smoldering modes.

Results of flammability, smoke evaluations, corrosivity, physical and other properties will be compared and discussed for these new formulations versus traditional formulations.

INTRODUCTION

Millions of pounds of polyolefins and polyolefin copolymers containing halogenated additives have been produced over a number of years to meet the high standards of the wire and cable industry. Formulators are now faced with the additional task of how to provide the same critical performance in

combustion properties while providing reduced smoke and corrosivity during combustion.

Progress is continually being made to introduce compositions with reduced smoke generation by methods, such as substituting aluminum trihydrate for halogen additives.⁽¹⁾ Technology has also been developed which allows the continued use of the traditionally accepted halogenated additives and achieve lower smoke.^(2,3,4) While this technology lowers the smoke during combustion, the corrosivity of the gases is probably effected very little.

We have now developed a method my using a combination of a halogened flame retardant and magnesium hydroxide to flame retard wire and cable materials which results can result in lower smoke and also lower corrosivity.

For a preliminary report on this technology see references 4 and 5.

MATERIALS AND PROCEDURES

The additives discussed in this paper and their sources are listed below:

CFR	Dechlorane Plus® (Diel-Alder adduct of hexachloro-cyclopentadiene and 1,5-cyclooctadiene) Occidental Chemical
Mg(OH) ₂	Zerogen®35 Solem Division of JM Huber Corporation
Talc	Mistron ZSC Cyprus Industrial Minerals
Silicon 1	D-4,7051 Dow-Corning Corporation

The ethylene vinyl acetate copolymer (EVA) used in these evaluations was obtained from commercial

sources and contained 9% vinyl acetate and had a melt index of 3.2. The other polyolefins used were also obtained from commercial sources.

The experimental samples were mixed on a two roll mill to obtain homogeneous samples. Compounded samples were sheeted and granulated prior to molding. Molding was accomplished by standard techniques. Samples for smoke evaluation were molded into 6 by 6 inch sheets from which specimens were cut.

Testing

Oxygen Index: The test employed is the ASTM D-2863. The minimum concentration of oxygen, expressed as volume percent in a mixture of oxygen and nitrogen that will just support flaming combustion.

Smoke Generation: Testing was performed in a NBS Smoke chamber according to ASTM E-662. The samples, 3 by 3 inch by 0.085 inch thick were exposed to radiant heat plus propane microburners (flaming combustion). Smoke evolution was continually recorded during the test period. Results are reported as specific optimal density, D_s . The smoke density testing was done VTEC Laboratories

Cone Calorimeter: Testing of materials was conducted by Underwriters Laboratories Inc.®, Northbrook, Illinois, in general accordance with the procedure specified in the proposed ASTM D 0.21.4. The sample size was 6 inch by 1/4 inch thick. The tests were conducted in the horizontal orientation and the radiant flux of the cone heater was set at 50 kW/m. The initial exhaust mass flow was 30 g/s.

Corrosivity: The gases from the cone calorimeter were tested for corrosivity using a corrosion target Model No. 030788-S 0.35-8061 (nominal 45,000 angstrom span) from Rohrback Cosasco. A CK-3 corrosometer from Rohrback Cosasco was employed to measure the corrosion of the probes.

RESULTS

Table 1 gives some typical talc filled FR-W&C formulations using CFR as the flame retardant in combination with magnesium hydroxide. The total flame retardant level is constant at 25% with 5% Sb_2O_3 . Figure 1 shows a graph of the % $Mg(OH)_2$ versus oxygen index. There is a synergistic effect between the chlorinated flame retardant and magnesium hydroxide which gives the highest O.I. with 20% CFR and 5% $Mg(OH)_2$.

The use of alumina trihydrate, instead of magnesium hydroxide, in these talc filled EVA W&C formulations does not show the same synergistic effect as $Mg(OH)_2$ does (shown in Figure 2).

Table 2 shows FR-EVA formulations that have been tested that do not contain talc. The oxygen indexes of these formulations are shown in Figure 3. There is a maximum oxygen index when the mixture contains 5 to 10% $Mg(OH)_2$ with 5% Sb_2O_3 .

Table 3 shows FR-PE and FR-EEA formulations that have been tested. Figure 4 shows the oxygen indexes of the FR-PE formulations. There appears to be little synergistic effect between CFR and $Mg(OH)_2$ in the PE system.

The plot of the oxygen indexes of the FR-EEA is shown in Figure 5. There is a maximum oxygen when the mixture contains about 10% $Mg(OH)_2$ and 15% CFR.

The FR-EPDM formulations that were tested are shown in Table 4 and the oxygen indexes are plotted in Figure 6. There is a large synergistic effect in the talc filled sample while the samples that do not contain talc do not show the same degree of synergy.

Table 5 lists the formulations that were tested in the cone calorimeter, and the corrosion values of Samples 1 to 3 are listed in Table 6. The use of the mixed CFR/ $Mg(OH)_2$ gives a four- to five-fold decrease in corrosion values.

Table 7 gives the results of several non-talc formulation with different levels of silicon compound added. As the silicon level increases the oxygen index increases. There is no effect on tensile elongation, but there is an effect on the NBS smoke values. In the flaming mode formulation #4 gives a D_s of 72 at 4 minutes.

The results of a 20% talc filled formulation is shown in table 8 with different levels of silicon compound added. There is no effect on oxygen index. All of the D_s smoke values in the flaming mode at 4 minutes are less than 80, and the D_m numbers are all 112 to 101 for the materials.

Table 9 gives the results of 20% talc filled formulations using mixed CFR/ $Mg(OH)_2$ system. There is no effect on oxygen index with increasing silicon compound, but the tensile elongation increases.

The NBS smoke values at 4 minutes are less than 50 Ds for 1 the samples.

SUMMARY

Flame retarded wire and cable formulations using a mixture of a chlorinated flame and magnesium hydroxide show a synergistic effect in the oxygen index flammability test and produce less smoke and have lower corrosivity when burned. It is possible to make a material that gives less then 100 Dm in the NBS smoke test.

REFERENCES

1. J. R. Pedersen, et al, "Low-Smoke, Halogen Free Ship-Off Shore/On Shore Cables with Improved Flame Retardance and Fire Resistance," IWCA, Cherry Hill, November, 1983.
2. J. J. Duffy and C. S. Ilardo, "New Reduced Smoke, Flame Retardant Wire and Cable Formulations Containing Halogenated Additives," IWCA, Reno, November, 1984.
3. C. S. Ilardo and R. L. Markezich, "Reduced Smoke Flame Retardant Formulations for High Performance Applications," Wire Association International Conference, Atlanta, May, 1988.
4. C. S. Ilardo, "Flame Retardant Polyolefins Compositions," U.S. Patent 4,567,214 (1986).
5. R. L. Markezich and D. G. Aschbacher, "Reduced Smoke and Less Corrosive Flame Retardant W&C Formulations," Wire Focus '93, Cherry Hill, New Jersey, September, 1993.
6. R. L. Markezich and D. G. Aschbacher, "Reduced Corrosive and Lower Smoke Flame Retardant W&C Formulations," IWCA, St. Louis, November, 1993.



BIOGRAPHY

Ronald L. Markezich is Technical Manager/Flame Retardants at Occidental Chemical Corporation, Technology Center, Grand Island, New York. He holds a B.A. degree in Chemistry from Knox College, Galesburg, Illinois and a Ph.D. in Organic Chemical from University of Wisconsin at Madison. He spent five years at General Electric's Corporate Research & Development Center at Schenectady, NY and two years at General Electric's Plastics Division in Mt. Vernon, Indiana. The last sixteen years have been at Occidental Chemical Corporation. He has eighteen U.S. Patents and over sixty publications.

Table 1
FR-EVA W&C FORMULATIONS

Weight %	1	2	3	4	5
EVA	47.9	47.9	47.9	47.9	47.9
CFR	25	20	15	10	5
Sb ₂ O ₃	5	5	5	5	5
Mg(OH) ₂	0	5	10	15	20
Talc	20	20	20	20	20
Agerite Resin D	1.4	1.4	1.4	1.4	1.4
Luperox 500R	0.7	0.7	0.7	0.7	0.7
Results					
O.I. (%)	28.1	28.75	28.41	27.42	27.25
Tensile % Elongation	350	320	300	190	140

Table 3
FR-PE or FR-EEA W&C FORMULATIONS

	1	2
PE or EEA	47.9	67.9
CFR	25 to 0	25 to 0
Mg(OH) ₂	0 to 25	0 to 25
Talc	20	0
Sb ₂ O ₃	5	5
Agerite Resin D	0.7	0.7
Luperox 500R	1.4	1.4

Table 4
FR-EPDM W&C FORMULATIONS

	1	2
EPDM	40.5	53.5
LDPE	8	13
CFR	18 to 0	20 to 0
Mg(OH) ₂	0 to 18	0 to 20
Talc	20	0
Sb ₂ O ₃	5	5
Agerite Resin D	1	1
Luperox 500 R	1	1
Zinc Oxide	2	2
Paraffin Wax	2	2
Vinyl Silane A-172	0.5	0.5

Table 2
FR-EVA W&C FORMULATION
(No Talc)

Weight 1%	1	2
EVA	67.9	62.9
CFR	30 to 5	30 to 5
Sb ₂ O ₃	0	5
Mg(OH) ₂	0 to 25	0 to 25
Agerite Resin D	1.4	1.4
Luperox 500R	0.7	0.7

Table 5
FORMULATIONS TESTED IN THE CONE
CALORIMETER
(Weight %)

	1	2	3
EVA	47.8	47.8	51.8
CFR	25	15	15
Sb ₂ O ₃	5	5	1
Talc	20	20	20
Mg(OH) ₂	---	10	10
Luperox 500R	1.4	1.4	1.4
Agerite Resin D	0.7	0.7	0.7
Ferric Oxide	0.1	0.1	0.1

Table 6
CORROSION VALUES W&C
FORMULATIONS

	1	2	3
Metal Loss End of 60 Min Exp. (angs)	6577	1733	1673
Metal Loss 24 Hour Exposure (angs)	9840	2077	2235

Table 7
FR-EVA W&C FORMULATIONS
(NO TALC)

Weight %	1	2	3	4
EVA	67.9	66.9	65.9	64.9
CFR	25	25	25	25
Sb ₂ O ₃	5	5	5	5
Agerite Resin D	0.7	0.7	0.7	0.7
Luperox 500R	1.4	1.4	1.4	1.4
Silicon 1	0	1	2	3
Results				
OI	24.75	26.25	27.25	27.25
Tensile % Elongation	444	451	455	444
NBS Smoke				
Flaming	172	108	139	72
Ds 4.0 min	123	74	78	112
Dm (Corr)				
Smolding				
Ds 4.0 min	4	5	15	4
Ds (Corr)	110	97	123	85

Table 8
FR-EVA W&C FORMULATIONS
(20% TALC)

Weight %	1	2	3	4
EVA	47.9	46.9	45.9	44.9
CFR	25	25	25	25
Sb ₂ O ₃	5	5	5	5
Talc	20	20	20	20
Agerite Resin D	0.7	0.7	0.7	0.7
Luperox 500R	1.4	1.4	1.4	1.4
Silicon 1	0	1	2	3
Results				
OI	28.25	28.25	28.75	28.25
Tensile % Elongation	323	334	247	260
NBS Smoke				
Flaming Ds 4.0 min Dm (Corr)	76 110	39 112	56 112	46 101
Smolding Ds 4.0 min Dm (Corr)	3 100	3 116	3 101	4 125

Table 9
FR-EVA W&C FORMULATIONS
(20% TALC MIXED
CFR/MS(OH)₂)

Weight %	1	2	3	4
EVA	47.9	46.9	45.9	44.9
CFR	15	15	15	15
Sb ₂ O ₃	5	5	5	5
Mg(OH) ₂	10	10	10	10
Talc	20	20	20	20
Agerite Resin D	0.7	0.7	0.7	0.7
Luperox 500R	1.4	1.4	1.4	1.4
Silicon 1	0	1	2	3
Results				
OI	29.25	28.25	28.75	28.25
Tensile % Elongation	163	290	340	336
NBS Smoke				
Flaming Ds 4.0 min Dm (Corr)	44 73	47 103	37 77	42 116
Smolding Ds 4.0 min Dm (Corr)	42 54	52 44	2 58	2 67

Figure 1
OXYGEN INDEX OF FR-EVA/
20% TALC/5% Sb₂O₃
25% CFR Minus % Mg(OH)₂

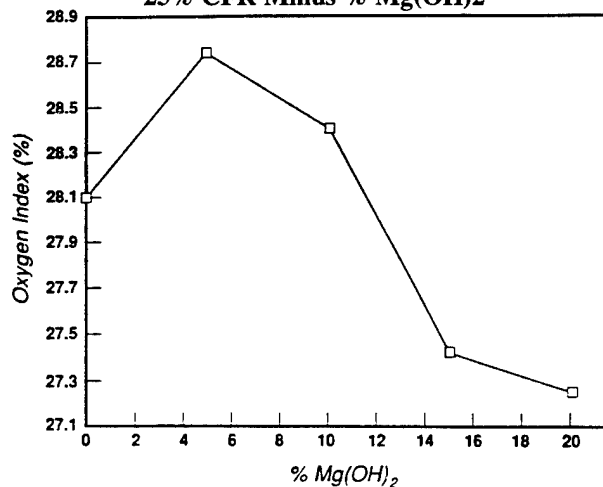


Figure 2
OXYGEN INDEX OF FR-EVA/
20% TALC/5% Sb₂O₃
25% CFR Minus % ATH or Mg(OH)₂

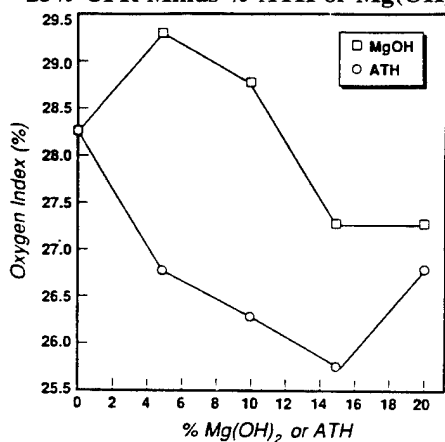


Figure 3
OXYGEN INDEX OF FR-EVA (No Talc)
30% CFR Minus % Mg(OH)₂

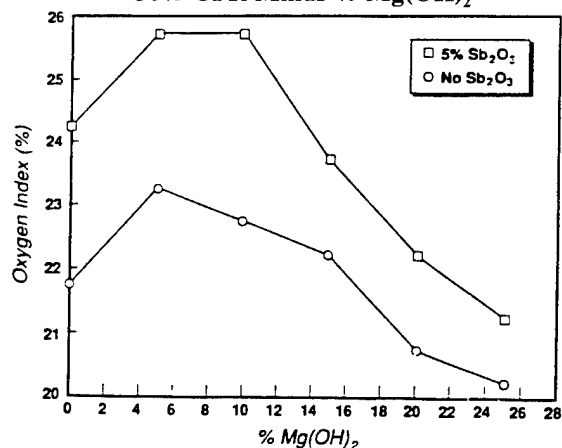


Figure 4
OXYGEN INDEX OF FR-PE
25% CFR Minus % Mg(OH)₂ with 5% Sb₂O₃

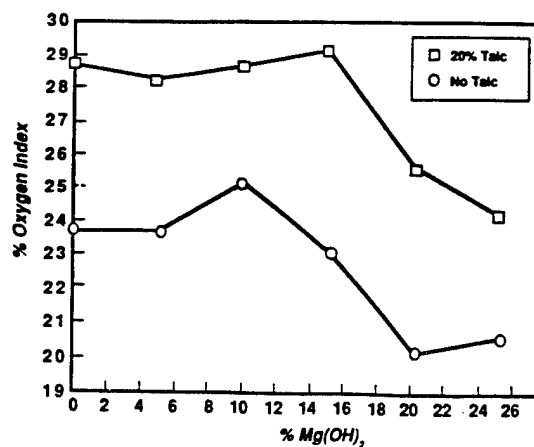


Figure 5
OXYGEN INDEX OF FR-EEA
25% CFR Minus % Mg(OH)₂ with 5% Sb₂O₃

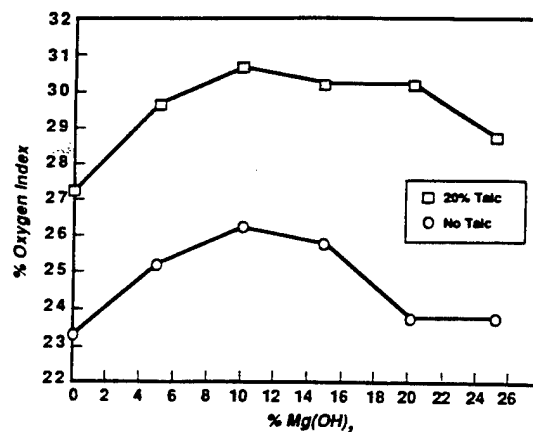
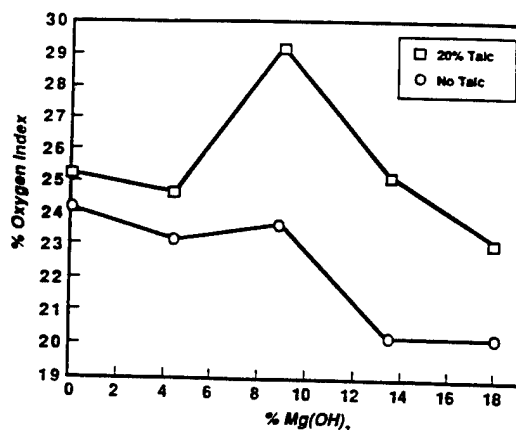


Figure 6
OXYGEN INDEX OF FR-EPDM
18% CFR Minus % Mg(OH)₂ with 5% Sb₂O₃



CATV COMPONENTS IN UNDERGROUND TECHNOLOGY

Franz Grajewski*, Werner Stieb*, Peter Zamzow**, Jürgen Seidenberg**

*ALCATEL KABELMETAL **KABEL RHEYDT AG

ABSTRACT

An entirely new technology to overcome heat generation problems in housings for CATV components is described. The combination of underground installation and a specially-designed diffuser insure that the dissipated power of the electronics is carried off into the ground. This takes place at the low temperature level which is normally found in the ground at a depth of one-half meter. Temperature calculations confirm this to be a very effective technology to solve heat generation problems in connection with CATV components. In addition, optimal protection against adverse mechanical influences and moisture is secured. Easy access to the components is possible at any time.

INTRODUCTION

While traveling through the country one can readily notice unsightly gray boxes of various sizes located at many corners. Insiders identify them readily easily as housings for different kinds of telecommunication equipment. Their number is increasing steadily.

The main reason for this development is the result of ever-increasing new and additional telecommunication services provided to the population. These require new cable networks and new systems technology. There is a clear tendency to the effect that more and more electronic equipment must be installed near the end user. This automatically raises the question where to house all those components.

To install them in buildings so as to provide free access for maintenance is often impossible for legal reasons. Therefore, interconnection cabinets are used more and more for the installation of electronic components. This approach, however, creates some other problems, such as:

- defacing of the landscape, especially in old towns;
- exposure of the equipment to traffic accidents and vandalism. Extended damage to the lines of large customers can entail huge expenses;
- the thermal boundary conditions for electronic components in above-ground housings are subject to extreme oscillations. Temperatures above 80°C are frequently encountered. Temperature control is therefore a major problem.

Two years ago we introduced to the Deutsche Telekom an underground housing system, which was specially designed for HYTAS application. It consists of a two-shell housing whose outer shell is made from concrete as protection against mechanical forces. The inner part is a polymeric box which covers the electronic components and seals them hermetically against dust and moisture.

This system has confirmed the advantages of underground technology over the past two years. However, it is not suitable for the use with CATV components. We therefore designed a new system for this special application.

DESIGN OF THE CATV UNDERGROUND HOUSING

Basic Design Requirements.

An underground housing for CATV components must meet the following minimum requirements:

- fast and easy access to the components without the need to work the ground;
- a single-shell housing, designed to ensure adequate sealing of the internal components, on the one

hand, and protection against external mechanical forces in the cover area, on the other hand;

- a cable entry section consisting of a 60 mm dia. tube;
- an inner housing volume with a back plane area 40 mm x 250 mm, 120 mm deep, designed to contain twelve components;
- sufficient cable slack to allow for the complete removal of the components from the housing;
- with the overall power generated by the components 95 W, the maximum temperature may not exceed 60°C, even under unfavorable weather conditions, such as are found in the tropics.

Housing Design.

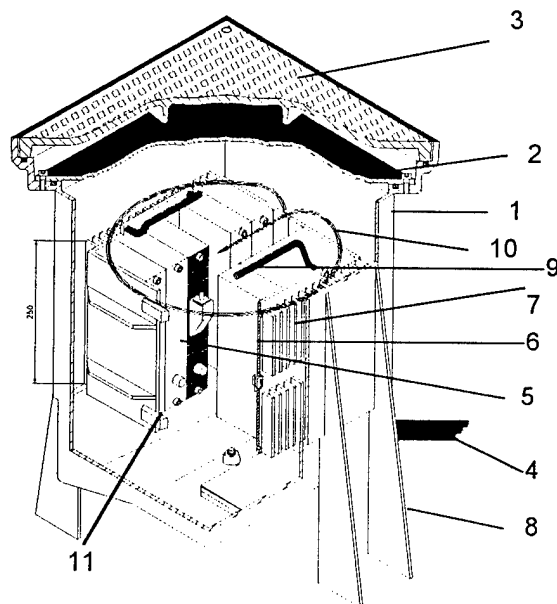


Fig.1 Basic Design Elements of the CATV Underground Housing

In order to meet the described requirements we selected a cast iron housing as shown in Fig. 1.

For the single-shell design polymeric materials are eliminated for economical reasons and also for reasons of heat conduction into the ground. Cast iron is a cheap and strong material with adequate heat conductivity. Therefore, all external parts of the housing body are made from cast iron.

The rectangular body 1 is closed by two cast iron covers. These are required to maintain the separation between mechanical protection, ensured by the outer cover (3), and the hermetic sealing of the inner space, which is assured by cover (2). The cables (4) are led into the box from the bottom and sealed by resin. The CATV components (5) are mounted with their back planes onto a special rack (6).

The rack is made out of aluminum. It has a capacity to carry up to twelve components with a back plane area 40 mm x 250 mm and a depth of 120 mm. To achieve good thermal contact the components are screwed onto the rack. The rack with its cooling fins (7) is in contact with the cast iron wall of the housing, thus ensuring good heat transfer to the outer wall. Handles (9) and the cable slack (10) permit complete removal of the rack from the housing. An opening mechanism makes it possible to unlatch the rack and to provide easy access to all connectors and components.

Opposite the rack which is provided with the cooling fins is the outer housing to which triangular cooling fins (8) are attached. These increase the surface area for heat transfer into the ground.

THERMAL ANALYSIS OF THE INTERNAL TEMPERATURE EVOLUTION

The basic requirement for CATV application is that the temperature of the internal air space must not exceed 60°C at any time. This is important especially if fiber amplifiers are used, because their reliability is drastically reduced at higher temperatures.

Our analysis was done on a theoretical basis for the following reasons:

- state-of-the-art FEM computer programs³ which permit 3-dimensional, time-dependent calculations with a justifiable investment of time and of sufficient accuracy are now available.

- an empirical analysis is too involved because it is nearly impossible to simulate in the laboratory the conditions which exist in the ground.
- one must expect that geometrical modifications will become necessary (number and thickness of fins, wall thicknesses) which can create substantial tooling costs.

Calculation Model and Boundary Conditions

Since this is a symmetrical problem only one-quarter of the housing needs to be used for the calculations.

Fig. 2 shows a section of the rack with the electronic components.

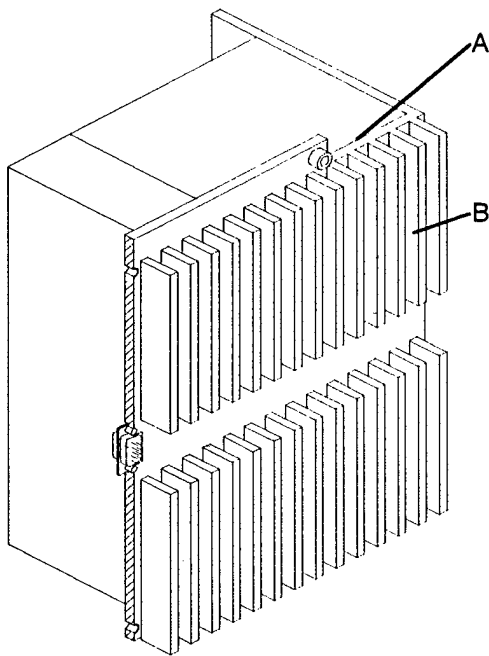


Fig.2 Preliminary Calculations at the Fins of the Rack

To get information about what happens at the fins of the rack, preliminary calculations were done under the following assumptions

- the temperature at the back plane is 60 °C (point A in fig.2);
- the heat transmission coefficient

$\alpha = 4 \text{ W/m}^2 \text{ K}$ at the sides of the fins (point B)

The result confirmed that there is no significant heat transmission into the air. This means, that the heat is conducted completely through the fins into the outer wall.

Accordingly, the following three-dimensional calculations were done with the boundary conditions set as shown in fig. 3.

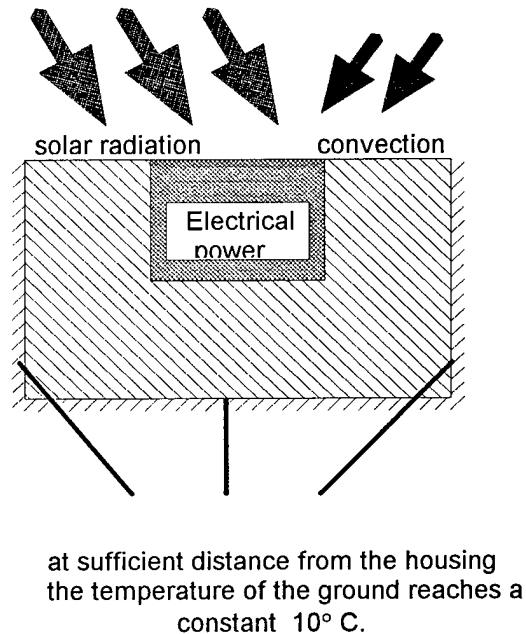


Fig. 3 Boundary Conditions

The convective heat exchange is characterized by $\alpha = 7.7 \text{ W/m}^2 \text{ K}$. The maximum temperature during the day is 30°C and the minimum temperature during the night is 10 °C. The solar radiation is estimated as $1000 \text{ W/m}^2 \text{ K}^{1,2}$.

These boundary conditions are then combined to an effective temperature of the air over the ground and that over the cover of the underground housing. This function is shown in Fig. 4.

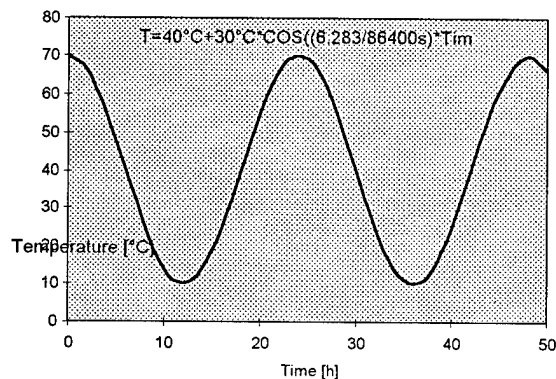


Fig.4 Effective Temperature of the Air Above the Surface

Fig. 5 shows the model of the underground housing for the three-dimensional calculations.

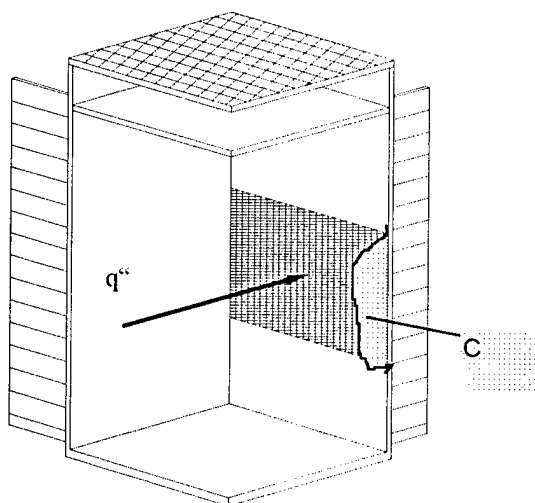


Fig. 5 Model for Three-Dimensional Calculation

A surface power density of $q''=1100 \text{ W/m}^2$ is effective over the hatched area in fig. 5. The fins were changed into a rectangular shape having the same area as the triangular shape in fig. 1

CALCULATION RESULTS

Section C in fig. 5 was detected as the area where the highest temperatures develop. Fig. 6 shows the temperature evolution in this section over two days under the conditions described above.

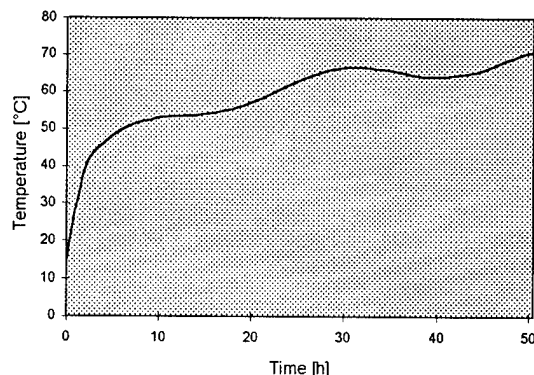


Fig. 6 Temperature Evolution in the Area of Maximum Temperatures

The influence of the day and night rhythms can be clearly seen. Also, one notices that the curve moves asymptotically towards a final mean temperature about 68°C . Around this mean value the temperature will oscillate by $\pm 3^\circ\text{C}$.

Even though the boundary conditions simulate extreme weather conditions, these may occur especially in tropical regions. This means that this system does not fulfill the basic requirement which is to limit the maximum temperature in the system to 60°C

OPTIMIZATION OF THE SYSTEM

In fig. 7 the temperature distribution is shown qualitatively in direction toward the corner of the housing.

The calculation shows that there is a negative temperature gradient in direction of the corner. This means that the heat flow is not only directed through the fins into the ground.

There is also a heat flow into the side walls, which are not in contact with the electronic components

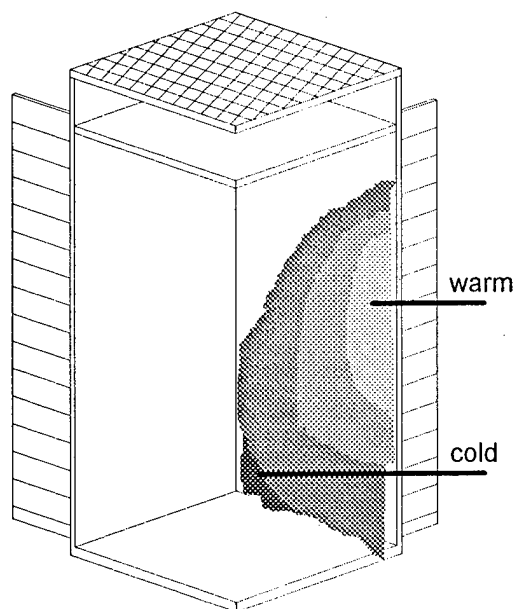


Fig. 7 Temperature Distribution

Two measures of optimization can be derived from these results:

- increase the wall thickness of the housing
- increase the number of fins, especially the arrangement of additional fins at the edges of the housing.

Our first two-dimensional calculations show that this method will be successful. Three-dimensional, time-dependent calculations are currently being conducted to confirm these computational results.

CONCLUSIONS

Even under extreme weather conditions it is possible to control the temperature evolution within an underground housing for CATV components without complicated cooling fans that require maintenance and additional power. A precondition for this is to design the geometry of the housing not only from point of view of handling, but also to optimize it so that the generated heat is safely transmitted into the ground.

It is also shown that today we have strong instrumentation for designing. Three-dimensio-

nal, time-dependent calculations point out the weak points in the design, before the building of prototypes, which then must be tested with costly test series. Usually one needs more than one prototype for the optimization. This expensive procedure can be reduced to a minimum.

ACKNOWLEDGMENTS

The authors wish to thank Mr. Hofheimer of Cable Consultants Corp./Larchmont NY for his valuable assistance in the editing of this paper.

REFERENCES

- /1/ VDI Wärmeatlas
Berechnungsblätter für den
Wärmeübergang
5. erweiterte Auflage
VDI Verlag
- /2/ Klimaanforderungen an
fernmeldetechnische Einrichtungen der
Deutschen Bundespost
Ersatz für FTZ A 01 AN 1 /
Entwurf, Ausgabe Sept. 1977
- /3/ Handbücher zum FEM Programm Mark
Volume A User Information
Copyright 1994



Franz Grajewski
ALCATEL KABELMETAL
31655 Stadthagen
Germany



Werner Stieb
ALCATEL KABELMETAL
31655 Stadthagen
Germany

Dr.-Ing Franz Grajewski (40) studied mechanical engineering at Aachen's Technical University. From 1984 to 1988 he assumed a scientific fellowship at the University's Institute of Polymer Processing. After Graduation he joined ALCATEL KABELMETAL as manager R&D/Heat-Shrink Technology. Since 1991 he is General Manager of the product group Accessories and Heat-Shrink Technology.

Dipl. Ing. Werner Stieb (38) after receiving his electrical engineering degree from the University of Kaiserslautern in 1986 joined ALCATEL KABELMETAL as a development engineer in the field of telecommunication cables. Today he is responsible for product marketing of fiber optic accessories in the product group Accessories and Heat-Shrink Technology.



Jürgen Seidenberg
KABEL RHEDT AG
41048 Mönchengladbach
Germany

Jürgen Seidenberg (39) received his Dipl. -Ing.-degree and Ph. D. in telecommunications engineering from the RWTH Aachen, Technical University of Aachen / Germany. He joined KABEL RHEYDT in 1989. Presently he is head of the department of optical transmission systems for CATV as well as technical manager for CATV cable.



Peter Zamzow
KABEL RHEYDT AG
41048 Mönchengladbach
Germany

Peter E. Zamzow (56) is director of the Telecommunications Division. He finished his postgraduate studies in telecommunications in Munich and Graz as Dipl. -Ing. He joined AEG KABEL (later KABEL RHEYDT) in 1970. He has been engaged in development and production in telecommunication cables. In 1980 he became head of the fibre optic division of AEG KABEL and in 1982 he was nominated as a senior engineer. Starting in 1992 he was infrastructure manager of the new Optical Fibre Plant Rheydt. Since July 1994 he is director, manager of the product group CATV, productline telecommunication, sector Germany.

CLEAVING TOOL FOR OPTICAL FIBERS RIBBON

Michel BOITEL, Hervé AOUSTIN, Jean-Marc CAILLEAUX, Thierry MAHE, Alain PECOT

FRANCE TELECOM - CNET

LANNION, FRANCE

ABSTRACT

The return loss for connections using cleavage and matching materials changes during climatic tests as refractive indexes are temperature dependent.

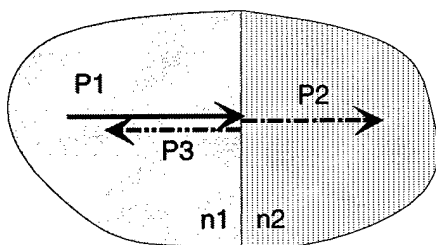
If the cleavage surface is at right angle with the fibre axis, we showed that none of the matching material we could identify can maintain a RL better than 43 dB, between -30 and +80°C. To reach the characteristics required in most telecom specifications (50 or 55 dB), the fibre end must be cleaved with an angle.

The cleaving tools commonly used were originally designed for fusion splicing, then to give a perfectly right angle between the surface and the fibre axis. If the fibre is twisted before the cleavage, there will be an angle of a few degrees, depending on the torsion stress.

We designed a cleaving tool (patented) based on a torsion principle which cleaves the fibers ribbons with a 6° angle, allowing the RL specifications to be respected at every temperature.

INTRODUCTION

When light travels across a boundary between two materials which have different refractive indexes, a part of the light is transmitted, the other is reflected.



The RL is given by the Fresnel law :

$$RL = 10 \log \frac{P_3}{P_1} = 20 \log \frac{n_2 - n_1}{n_2 + n_1}$$

What occurs when light is reflected ?

- degradation of lightwave components
- errors in digital communications and distortion in analog communication systems
- reduction of the transmitted power

Most of Telecom specifications require a Return Loss of at least 50 or 55 dB at each connection.

Fusion splices rebuilt the fibre structure and then guarantee a high Return Loss in every condition.

Physical Contact connectors with Advanced Polishing (APC) can have a high RL when connected. When not mated, the reflection grows up to 15 dB, according to Fresnel law for a straight interface between fibre and air.

Mechanical splices or bare fibre connectors (ref. (8)) are basically constituted of a groove filled with an index matching fluid in which cleaved optical fibers are aligned.

When the fibre is cleaved with a right angle, the refractive index of the fibre core and matching material can be very close, the Return loss is then high (up to 65 or 70 dB in some conditions). Unfortunately, the index of both materials does not change in the same way with the environmental conditions. Therefore, the reflected light does not remain at that very low level during temperature evolution (between -30°C and +80°C in FT specifications for fibre connections).

A classical solution to reduce a return loss due to a refractive index difference is to give an angle to the fibre end, by polishing or

cleavage. It ensures that the reflected light is not guided back into the fibre.



A reliable way of cleaving fibre ribbon with an angle is given in the second part of this article.

MATCHING MATERIALS TESTING

We identified, provided with and tested ten matching materials. The tests include a chemical analysis, a refractive index measurement between 5 and 80°C and a RL measurement between -30 and 80°C.

CHEMICAL ANALYSIS

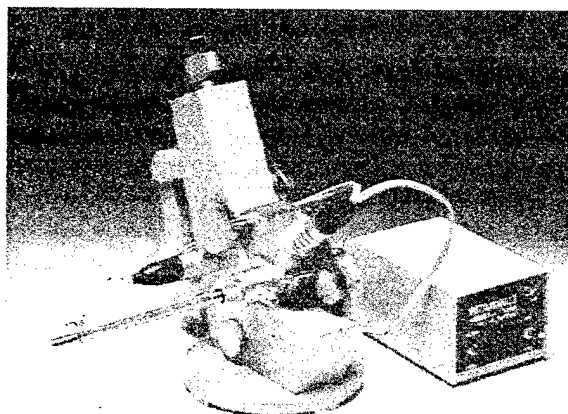
	chemical composition
1	poly-isobutylene
2	polysiloxane containing propyl or butyl radicals
3	polymethyl-phenyl siloxane
4	polymethyl-phenyl siloxane
5	polymethyl siloxane
6	polymethyl siloxane
7	polysiloxane, high rate of phenyl radicals
8	polysiloxane, low rate of phenyl radicals
9	polysiloxane, low rate of phenyl radicals
10	polysiloxane

The matching material n°1 is a poly isobutylene with a low molecular weight.

From 2 to 10, they are all different kinds of silicon greases, with differences due to several radicals, influencing the refractive index or viscosity.

REFRACTIVE INDEX MEASUREMENT

The evolution of the refractive index, at visible wavelengths, between 5 and 80°C was measured with a dipping refractometer, the temperature limitations being due to the apparatus (cooling and heating by liquid water)



Dipping Refractometer

See Figure 1 for results.

As for silica the refractive index does not change much in this temperature range, it clearly implies that those materials will not maintain a low return loss (even if the analysis is not made at the wavelengths commonly used for telecommunications).

TEMPERATURE DEPENDENCE of the RETURN LOSS

To evaluate the influence of the temperature on the return loss we have cleaved fibres with a perfectly right angle and dipped them in the material under testing. The reflectance was measured during temperature variations, in a climatic chamber.

Three measurement methods were experimented :

FIG 1 : Temperature dependance of the matching materials refractive index (visible wavelengths).

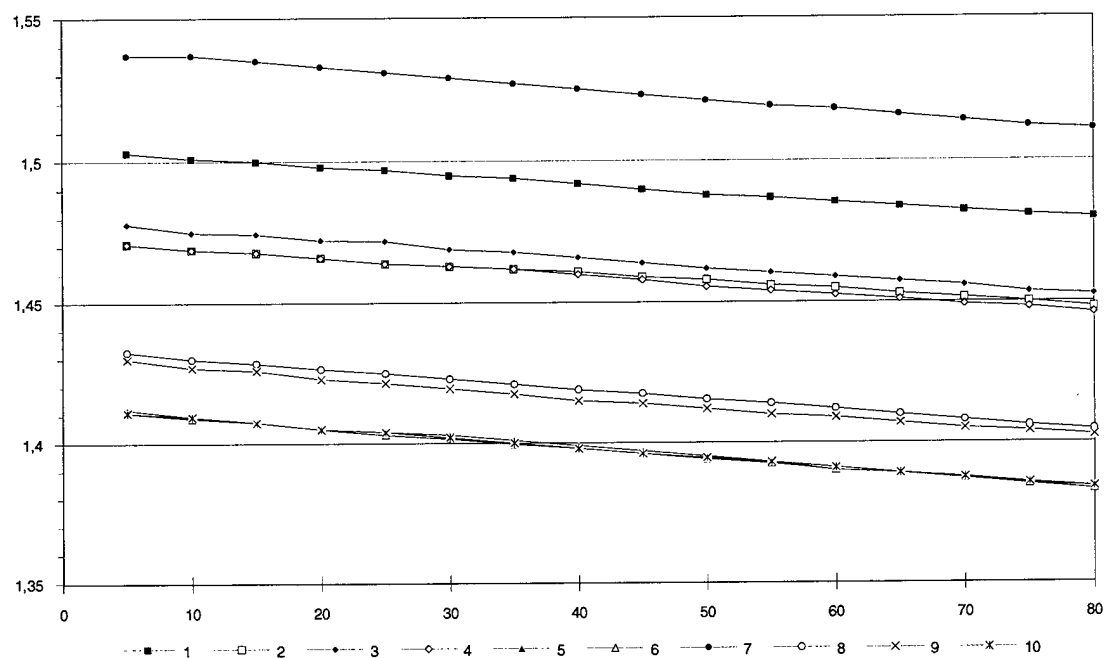
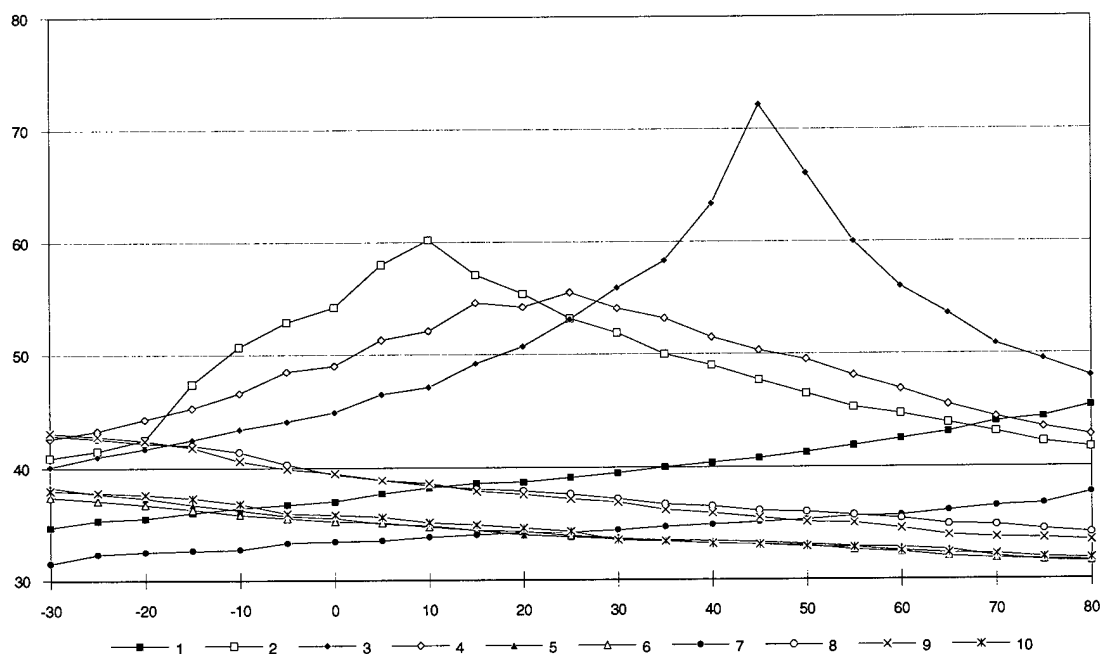
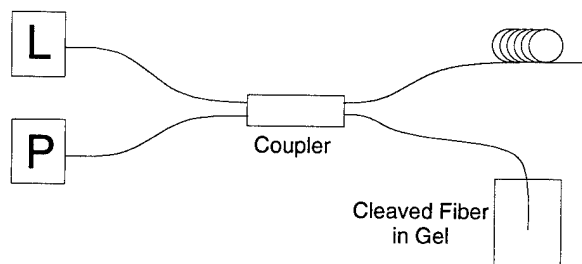


FIG 2 : Temperature dependance of the return Loss (1300nm)

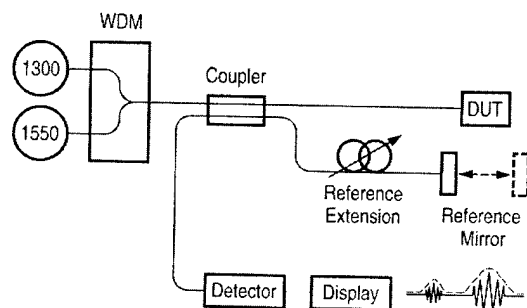


- Power meter and coupler



- Optical Time Domain Reflectometer

- Precision reflectometer, based on a Michelson interferometer using low coherence light sources



At lab temperature, we obtained for $\lambda = 1300 \text{ nm}$:

	coupler	OTDR	interferometer
1	39	39	39
2	61	60	59
3	54	53	53
4		65	67
5	35	35	34
6	35	35	
7	34	33	
8	39	39	38
9	38	39	38
10	35	35	

We considered that the results given by the three methods were very similar. As it was the easiest method, we used the OTDR in the following experiments.

The figure 2 shows our results.

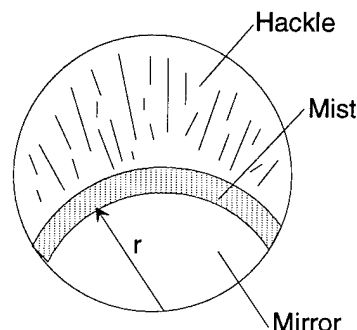
None of the tested matching materials can maintain a return loss better than 43 dB between -30 and $+80^\circ\text{C}$, for a cleaved fibre, the endface making a right angle with the optical axis.

CLEAVING TOOL for fibre ribbons or microsheaths

BASIC CLEAVAGE PRINCIPLES

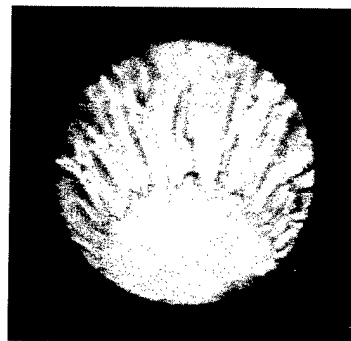
The basic principle of cleavage is to use the propagation of a crack to obtain a flat and regular surface suitable for light transmission.

In a non-crystalline material, there is no cleavage plane, a fracture tends to be propagated in a direction perpendicular to the main stress. A typical fracture is separated in three areas : mirror, mist and hackle.



The cleavage starts when the applied stresses reach a minimum, the mirror surface spreads until the energy is too high to create only two surfaces, then start the two others, mist and hackle.

If a traction T is the only force applied to the fibre, an energetic analysis of the fracture shows that $T\sqrt{r}$ is a constant (in a constant environment).



Fracture obtained with $T=5\text{N}$

To design a cleaving tool using only traction, it is necessary to calibrate a tension force between a minimum to start the fracture and a maximum to have a r larger than the fibre diameter.

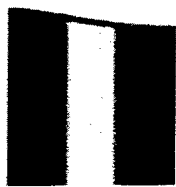
An optimisation of the stress distribution can be obtained if a double bend replaces the traction, in the middle part of the bend, there are only tensile stresses decreasing from the outer to the inner part of the curved fibre. A fracture will start easily in the high stress area, but as the strain decreases, the kinetic energy of the fracture propagation will grow slowly, the apparition of the hackle area is then delayed.

According to the principles roughly described before, most of the existing tools have been designed in order to cleave fibers with a perfectly right angle which is required to realize fusion splices.

If shear stresses are added, the fracture will be deviated, leading to an angled endface.

Those stresses can be obtained by a flexion added to a traction or by an asymmetric double bend.

A more reliable method is to twist the fibre. It is already used for cleaving single fibers, and with our tool, it is also applicable to multifibre (ribbon, microsheath) cleavage.



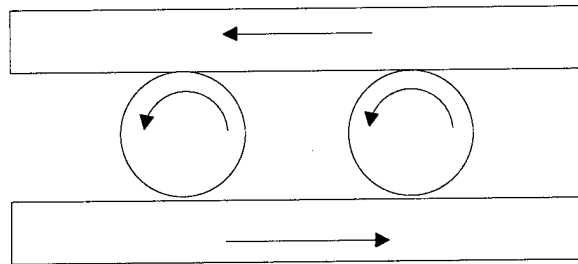
angle-cleaved fibre (torsion)

TOOL DESCRIPTION

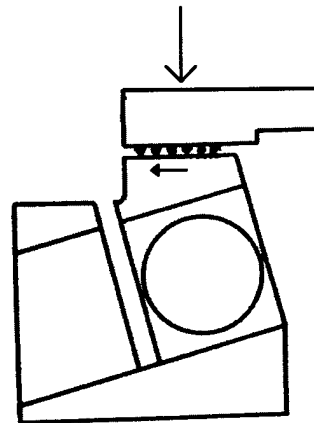
The principle of this tool is patented.

The fibers are clamped at one end. At the other one the clamp is made of two parts, a upper rigid plane and a lower deformable beam. When the clamp is closed, a translation occurs

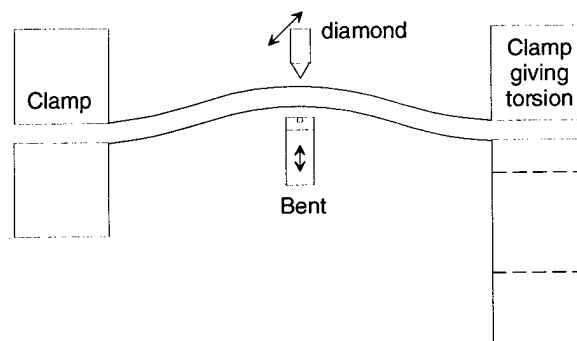
between the two planes, giving the fibre a controlled twist.



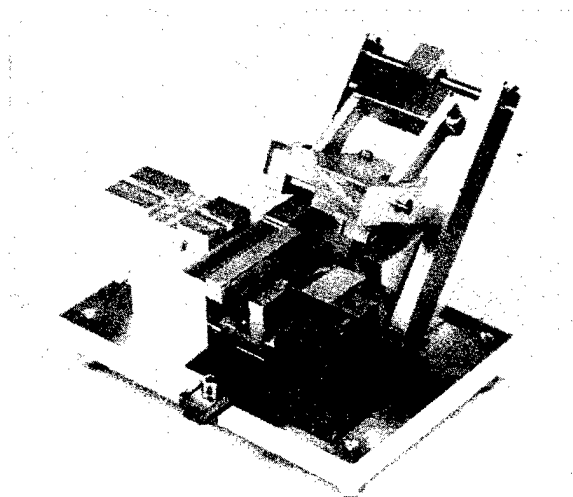
When the upper clamp goes down, the two thin beams around the circular hole in the lower clamp bend, moving the upper plane from the right to the left.



A diamond is used to scratch the fibre, a double bend is applied for the final cleavage.



A prototype have been designed on the basis of those principles :



PERFORMANCES

Most of the previous works were undertaken to design tools which would give no angle at all. To obtain repetitive angles in different climatic conditions is not really easier, an accurate measurement of these angles is then important.

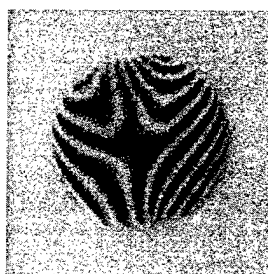
Three methods were used to measure the angle in the core area.

Measurement Methods

Profile projector

The operator turn the fibre until the fibre shows its greatest angle and measures it (in the core area). The quality and repetitiveness of this method depends greatly on the operator ability.

Interferometer



Fibre cleaved using the patented tool
(5° between the fibre and the interferometer axis)

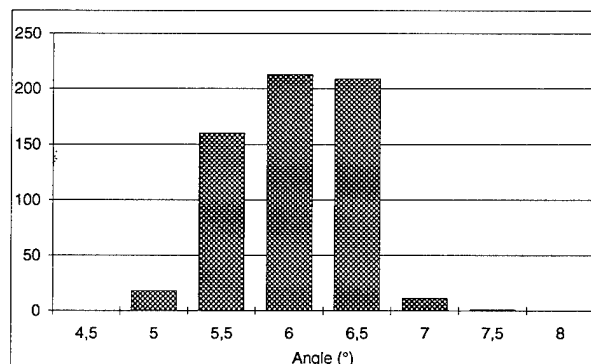
A Michelson interferometer is used to create fringes at the fibre end. A micrometric displacement turns the fibre until the core area is perpendicular to the interferometer objective. The micrometer vernier gives the angle between the plane around the fibre core and the optical axis.

Beam deviation

Light is injected in the fibre, the angle between the refracted beam and the fibre gives almost directly the cleavage angle.

The results obtained by the three methods are quite repetitive and are the same more or less an average of 0.5 °.

RESULTS



The results include fiber cleavages undergone at high (40°C) and low (0°C) temperature, with the prototype (photograph before)

CONCLUSION

We have shown that none of the matching materials that we know can maintain a high return loss in the temperature range specified by France Telecom.

The most reliable method to obtain an angle is to use torsion. We suggest a tool design suitable for fibre ribbons, microsheaths or even single fibers.

ACKNOWLEDGEMENT

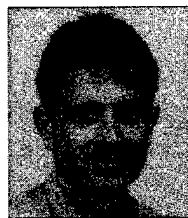
To M. R. Lever and M. J.Y. Moisan for the chemical analysis of the index matching materials.

To M. J.L. Descamps for his help in testing the optical properties of the same materials.

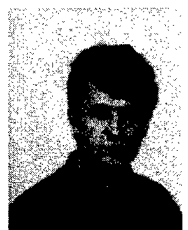
REFERENCES

- (1) A. GRIFFITH "The Phenomena of rupture and Flow in Solids" Phil. Trans. Roy. Soc. Vol. A221 1920.
- (2) JP DOMERGUE et al "Méthode de clivage d'une fibre optique : définition et expérimentation" Revue Technique Thomson CSF, vol 13, n°4, Décembre 81.
- (3) EB SHAND "Experimental Study of Fracture of Glass : I, The Fracture Process" J. Amer. Ceram. Soc, vol 37, 1954 p559
- (4) TA MICHALSKE, BC BUNKER "The Fracturing of Glass"
- (5) E YOFFE, "The Moving Griffith Crack" Phi. Mag. vol. 42, 1951
- (6) JW CRAGGS "On the Propagation of a Crack in an Elastic Brittle Material" J. Mech. Phys. Solids, vol. 8 1960)
- (7) R.J. FERINA "Precision Length Oblique Cleaving of Ribbon Fibers for High-Performances Mechanical Splices" IWCS 1994.
- (8) AOUSTIN, STAPPERS "Optoclip II Multiway, Multiway Connector for Singlemode Access Networks", IWCS 1996.
- (9) BOITEL "Taux de reflexion des raccords de fibres optiques, comportement thermique, facteur influençant" OPTO 90.
- (10) MITSURU KIHARA "Temperature Dependence of Return Loss for Optical Fiber Connectors with Refractive Index-Matching Material" IEEE Photonics Technology Letters, vol 7, No 7, July 1995

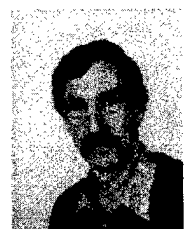
AUTHORS



Michel BOITEL Graduated from the Ecole Nationale Supérieure d'Optique in 1969. He joined the CNET in 1970 and is now engaged in fiber connection R&D.



Hervé AOUSTIN Graduated from the Ecole Nationale Supérieure des Arts et Metiers in 1990. He is engaged in fiber connection R&D since he joined the CNET in 1992.



Jean-Marc CAILLEAUX is a member of the cable and connection department. He is presently engaged in fibre connections and enclosures tests and specifications.

Thierry MAHE is a member of the cable installation and optical fibre connection group in CNET. He is presently engaged in fibre connection R&D.



Alain PECOT graduated from the Institut National des Sciences Appliquées in 1979. He is the manager of the cable installation and optical fibre connection group, in the CNET.

All authors : CNET LAB
2, Avenue P. MARZIN
22 307 LANNION
FRANCE

FUSION MASS-SPLICES FOR OPTICAL FIBERS USING MICRO MASS AXIS ALIGNMENT DEVICE

Manabu Kubota*, Koichi Yoshida*,
Masahiko Mikawa*, Takenori Morimitsu**

*NTT Access Network Systems Laboratories
Tokai, Naka, Ibaraki, 319-11 Japan

**Institute of Systems & Information Technologies /Kyushu
Momotihama 2-1-22 Sawara-ku, Fukuoka, 814 Japan

ABSTRACT

This paper describes a micro mass axis alignment device with piezo elements and its application in a mass fusion splicer. Splicing performance tests are carried out on the manufactured prototype of splicer. The splicer achieves an average splice loss of about 0.02dB for dispersion-shifted four-fiber ribbons.

INTRODUCTION

In the conventional mass fusion splicing process [1] [2], fibers are aligned by using V-grooves. This means that axis alignment depends on the accuracy of the V-grooves. Misalignment must be minimized to reduce the splice loss of fibers. So high precision V-grooves and fibers with low core eccentricity have been fabricated recently. However, the V-groove can become contaminated with dust from the actual installation environment or with coating residue produced when fiber is stripped. Once dust adhered to the V-grooves, it is difficult to remove because of their adhesive power and electrostatic force. The result is that misalignment errors can easily occur and lead to an increase in splice loss. Therefore, a high precision alignment device is required for the low loss splicing of fibers.

A fusion splicer which handles only one fiber can be equipped with a core axis alignment device as shown in Fig.1 [3]. However, it is difficult to use this design for a compact mass axis alignment device, because it must include V-grooves, cantilever springs, micro positioners and

conventional motors, which limits the size. This led to the development of the micro mass axis alignment device which reduces axis miss alignment errors.

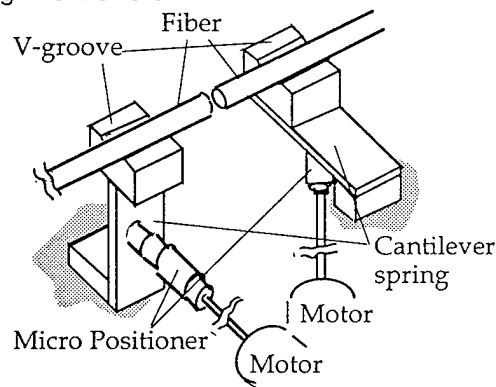


Figure 1. Core Axis Alignment Device for One Fiber

S.Aoshima et.al proposed a compact mass axis alignment device by using piezo elements as shown in Fig.2 and achieved individual movement of optical fibers [4]. However this device had two problems to fabricate practical mass splicer. First, the device consists of so many parts that assembling and adjustment is difficult. Second, axis alignment is adversely affected by dust between the arms, frictional force, and dust between fiber and micro arm as shown in Fig. 3.

This paper presents a new micro mass axis alignment device which works properly in practical fields to overcome these deficiencies. Moreover, we describes the characteristics of fabricated device and the performance of splicer which uses this device.

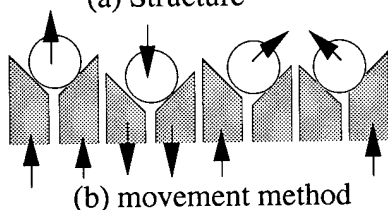
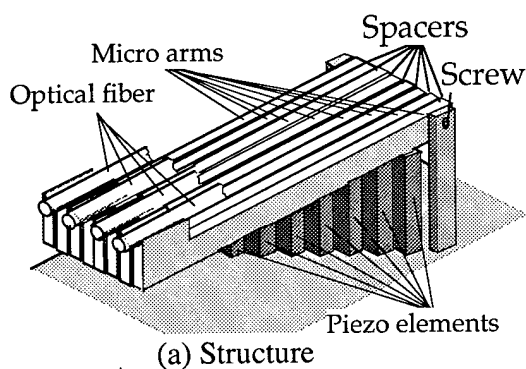


Figure 2. Previous Mass Axis Alignment Device

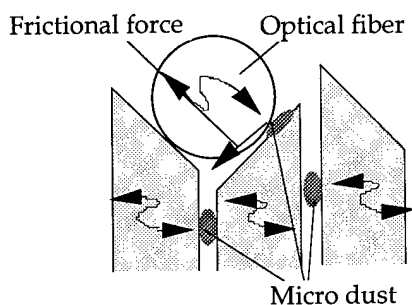


Figure 3. Interference by Micro Dust

MICRO MASS AXIS ALIGNMENT DEVICE

Device Structure

Figure 4 shows the structure of the new micro mass axis alignment device. This device has four micro arms with flexure hinges which can align individual optical fibers. V-grooves which hold the optical fibers are formed at the tips of the micro arms and each micro arm is actuated by a pair of piezo elements. The piezo elements are installed in an inverted V configuration. The four micro arms are fabricated on one monolithic part and no adhesive or bolt is used. This means that there is no need to assemble or adjust the micro arms.

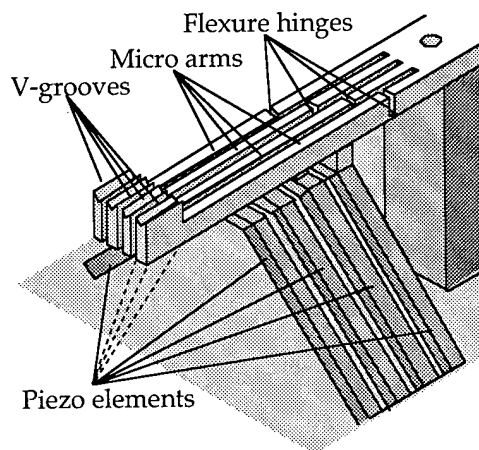


Figure 4. Proposed Mass Axis Alignment Device

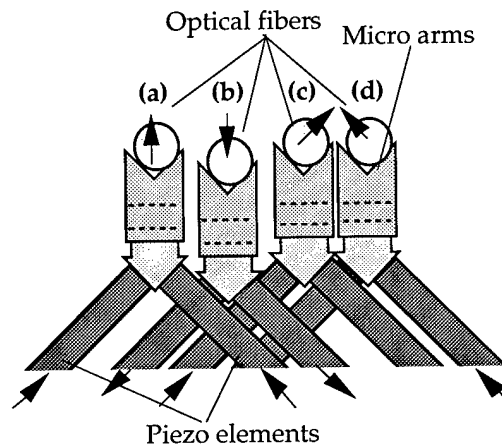


Figure 5. Movement Mechanism

Figure 5 shows the movement mechanism. The optical fiber moves upwards or downwards when both piezo elements are extended or contracted, as shown in Fig. 5 (a) and (b), respectively. It moves upwards to the right or left when only the left or right element is extended, as shown in Fig. 5 (c) and (d), respectively. Thus these micro arms can be moved vertically and horizontally with sub-micron order precision by controlling the voltages applied to the piezo elements. Each optical fiber can be positioned independently on a two dimensional surface by moving the appropriate micro arm. This design provides wide

clearances of each micro arm and this device is free from frictional resistance. This means that the alignment of fibers can not be interfered with micro dust.

This device is manufactured using micro machining technology and so is sufficiently small to be installed in a mass fusion splicer. The device is designed for four-fiber ribbon splicing but the number of micro arms can be changed for use with five or eight fiber ribbons.

Device Characteristics

We fabricated a micro mass axis alignment device and tested its characteristics. First, we performed on axis alignment experiment to confirm that the movement mechanism operated as designed. The movement of fiber was observed on a TV monitor.

Figure 6 shows experimental results for the axis alignment area. The following voltages were applied to the left and right piezo elements at the points shown in the figure.

Point (Left, Right): O (0V, 0V), A (150V, 0V), B (150V, 150V), C (0V, 150V)

The optical fiber can be moved to any position within the area OABC as shown in the figure by controlling the applied voltage to the piezo elements.

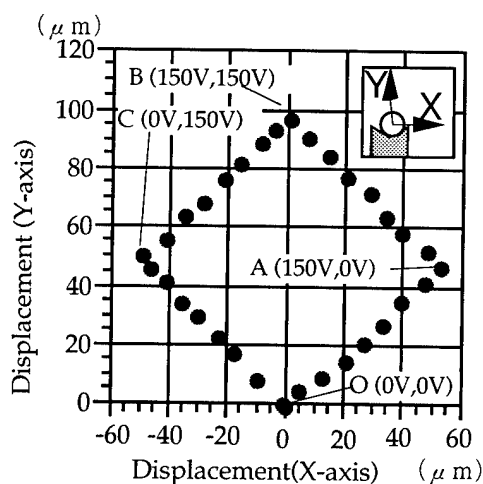


Figure 6. Experimental Results for Axis Alignment Area

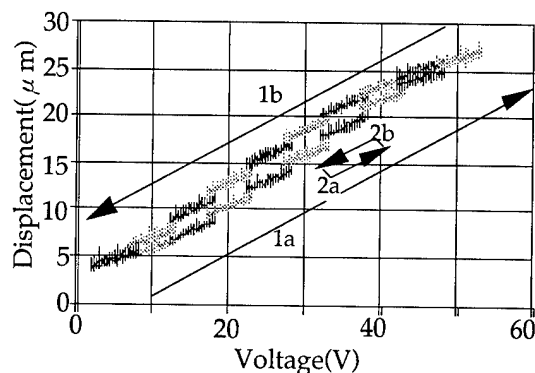


Figure 7. Relation between Voltage and Displacement

Figure 7 shows the relation between the displacement of micro arm and the voltage applied to the piezo elements. Piezo elements has hysteresis characteristic as shown by 1a→1b in the figure. But if the displacement range is small (2a→2b), the hysteresis characteristic is negligible and the slope of the data lines is constant throughout. This means it is possible to control the position of the fiber is by using feedback control^{[5][6]}. The motion of optical fiber is stable during these experiments.

These results confirmed that new alignment device has sufficient characteristics for fiber alignment.

Fusion Mass-Splicer using Micro Mass Axis Alignment Device

Figures 8 and 9 show a photograph of a mass fusion splicer equipped with the micro mass axis alignment device and a close up of the device, respectively. The splicer is 220mm long, 280mm wide and 195mm high. This machine is also equipped with CCD image analysis system comprising two cameras and a mirror and a piezo element controller which employs a micro-processor to control the micro mass axis alignment device. The fiber axis is monitored via two-dimensional observation with the CCD system which has two magnification modes (high and low). The low magnification mode is used to monitor fiber alignment. It corresponds

to the observation system of a conventional splicer. Four fibers can be observed and aligned simultaneously with sub-micron order and this reduces the alignment time. The high magnification mode is used to estimate splice loss. Although only one fiber can be seen at one time in this mode, core deformations and splice failures can be observed clearly.

Thus the newly developed splicer has two special features not provided by the conventional mass fusion splicer. One is the micro mass axis alignment device and the other is the image analysis system which has two magnification modes.



Figure 8. Manufactured Fusion Splicer

Performance of Fusion Mass-Splicer using Micro Mass Axis Alignment Device

We investigated performance of the developed splicer experimentally with dispersion shifted four-fiber ribbon. Once the fiber ribbons are positioned, fibers are aligned automatically as shown in Fig. 10 and the misalignment of each fiber is reduced to below $0.3 \mu\text{m}$.

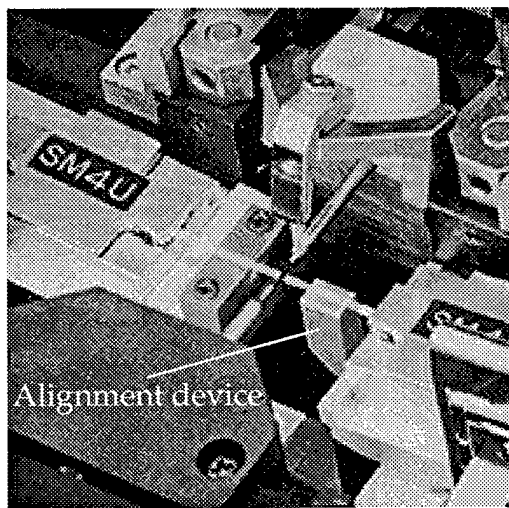
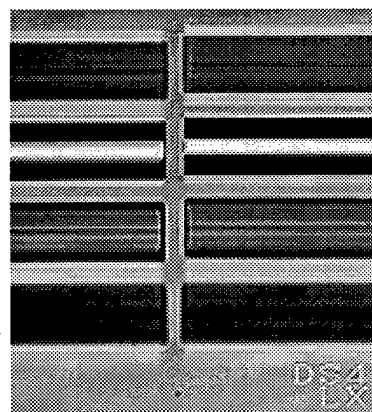
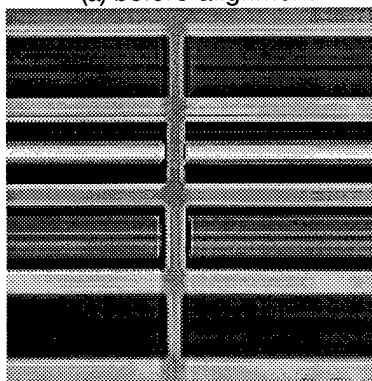


Figure 9. Alignment Device



(a) before alignment



(b) after alignment

Figure 10. Photograph of Alignment Process

A histogram of the time required for alignment is

shown in Fig. 11. The average time required for alignment is about 90 seconds.

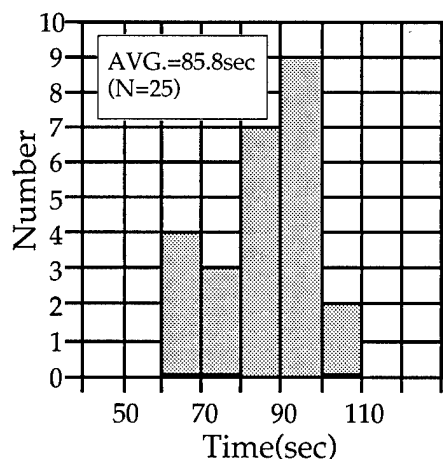


Figure 11. Histogram of Required Time for Alignment

The splice loss histogram was obtained by using the splice machine shown in figure 12. The average loss is 0.02dB.

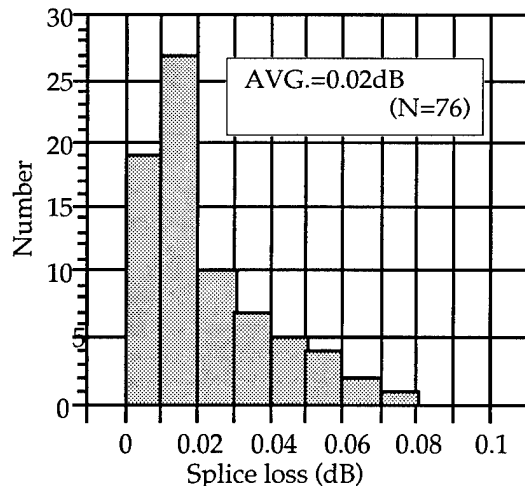
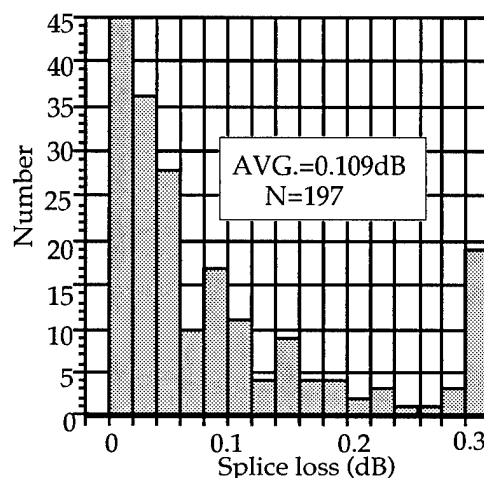


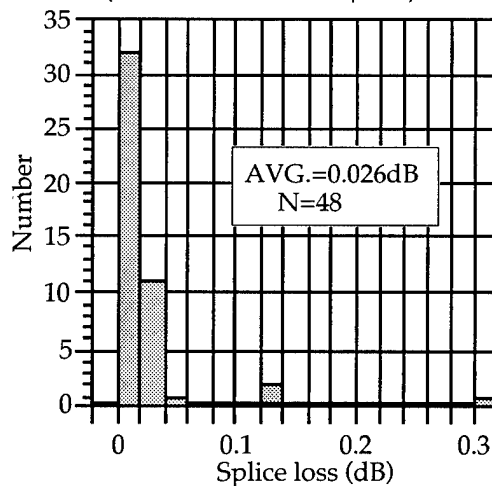
Figure 12. Splice Loss Histogram for Four Ribbon Dispersion Shifted Fiber

To confirm the effectiveness of the micro mass axis alignment device, we undertook another splice experiment with the developed and conventional splicers. The fiber used in this experiment was the same as that used in the previous experiment. The only difference was that, in the first experiment the fiber was wiped

with alcohol to clean it, but not in the second. Before placing the ribbons on the machine the fibers were simply stripped and cleaved without being cleaned, thus leaving residue on the fiber surface. Therefore, the leaving residue is considered to interfere with fiber alignment when the conventional mass fusion splicer was used.



(a) Splice Loss Histogram
(Conventional Fusion Splicer)



(b) Splice Loss Histogram
(Fusion Splicer using Micro Mass Axis Alignment Device)

Figure 13. Splice Loss Histogram for Four Ribbon Dispersion Shifted Fiber (with out cleaning)

Figure13 (a) and (b) show a histograms obtained

using the conventional mass fusion splicer and the developed splicer, respectively. From Figure 12 (a) and (b) , it is noted that the average loss with conventional splicer was about 5 times larger than that with new splicer. The new splicer achieves low loss splicing without cleaning.

DISCUSSION

This section discusses the effectiveness of our micro mass axis alignment device and the newly developed splicer which uses this device. We obtained the following results from fiber splicing experiments.

The micro mass axis alignment device works properly, so the misalignment of optical fiber was greatly suppressed below $0.3 \mu\text{m}$. This indicates that our new micro mass axis alignment device operated as designed and was controlled with accuracy. Required time for alignment can be reduced with software improvement.

The splicer achieved low loss splicing of fibers, which suggests the micro axis alignment device endured the impact of discharge arc and held the optical fibers during arc fusion.

The average loss with the conventional splicer became worse because of misalignment resulting from the residue on the fiber surface. But the new splicer was not affected by the residue. This means that new micro mass axis alignment device works well, and it is therefore expected to function well in a dusty environment. More over, very low loss splice is obtained with this splicer and the need for re-splicing is reduced. This, in turn, reduces the overall cost of fiber installation.

CONCLUSION

A micro mass axis alignment device which uses piezo elements was proposed for low-loss fiber ribbon splicer. We tested the fiber splicing performance of the manufactured splicer. It achieved an average splice loss of about 0.02dB for dispersion-shifted four-fiber ribbons. This

results confirms the effectiveness of our micro mass axis alignment device. This splicer is especially suitable for use when a low splice loss is required such as for long distance or submarine cables.

ACKNOWLEDGEMENT

The authors thanks to K.Ishihara, Y.Koyamada, T.Yabuta and K.Nishimura for their continuous encouragement. The authors also thanks M.Matsumoto, S.Furukawa and I.Sankawa for useful discussions.

REFERENCES

- [1] M.Tachikra and N.Kashima, "Fusion mass splices for optical fibers using high frequency discharge", Journal of Light Wave Technology, Vol.LT-2, No.1, pp.25-31, 1984
- [2] M.Miyauchi, M.Matsumoto, T.Haibara and N.Kawasaki, "Design and Performance of Mass Fusion Splice for Single-Mode Fiber Ribbon", The Transactions of The IEICE, Vol.E72, No. 8, PP. 912-918, 1989
- [3] Y.Kato, S.Seikai, T.Tanifuji, "Arc-fusion splicing of single-mode fiber: an apparatus with an automatic core-axis alignment mechanism and its field trial results", Journal of Lightwave Technology, Vol.LT-2, No.4, pp.442-447, 1984
- [4] S.Aoshima, N.Yoshizawa and T.Yabuta, "Compact Mass Axis Alignment Device with Piezo elements for Optical Fibers", IEEE Photonics Technology Letters, Vol.4, No.5, pp.462-464, 1992
- [5] M.Kubota, K.Yoshida, M.Mikawa and T.Morimitsu, "Plural Micro Arms one Body Formation Type Micro Mass Axis Alignment Device for Optical fibers", Proceedings of the 34th SICE Annual Conference Domestic Session Papers, pp.793-794, 1995
- [6] M.Mikawa, K.Yoshida, M.Kubota, and T.Morimitsu, "Visual Servoing Based on H_∞ Control Theory for Micro Mass Axis Alignment Device", Proceedings of the 35th SICE Annual Conference Domestic Session Papers, pp.75-76, 1996

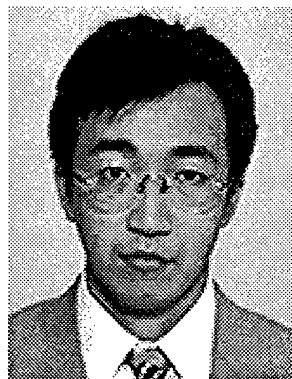


Manabu Kubota

NTT Access
Network Systems
Laboratories

Tokai, Naka, Ibaraki,
319-11 Japan

Manabu Kubota was born in Hokkaido, Japan, on June 13, 1966. He received a B.E. degree in mechanical engineering from the University of Osaka Prefecture in 1991 and a M.E. degree in precision machinery systems from Tokyo Institute of Technology in 1993. He joined the NTT Field Systems R&D Center in 1993, where he has been engaged in the research on micro mechanisms. Mr. Kubota is a member of the Japan Society of Precision Engineering and Robotics Society of Japan

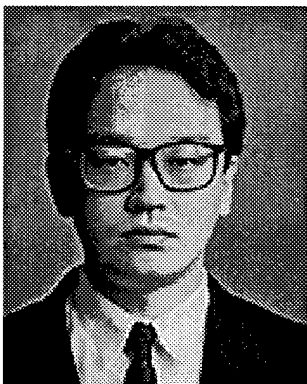


**Masahiko
Mikawa**

NTT Access Network
Systems
Laboratories

Tokai, Naka, Ibaraki,
319-11 Japan

Masahiko Mikawa was born in Kyoto, Japan, on July 9, 1968. He received B.E. and M.E. degrees all in mechanical engineering from Osaka University in 1993 and 1995, respectively. He joined the NTT Access Network Systems Laboratories in 1995, where he has been engaged in the research on visual feedback. Mr. Mikawa is a member of the Society of Instrument and Control Engineers and Robotics Society of Japan.



Koichi Yoshida

NTT Access
Network Systems
Laboratories

Tokai, Naka, Ibaraki,
319-11 Japan

Koichi Yoshida was born in Kumamoto, Japan, on June 21, 1963. He received B.E., M.E. and Dr. Eng degrees all in electrical engineering from Kyushu University in 1987, 1989 and 1995, respectively. He joined the NTT Transmission Systems Laboratories in 1989, where he has been engaged in research on robotics for teleoperation. He is presently a research engineer in NTT Access Network Systems Laboratories. Dr. Yoshida is a member of the Society of Instrument and Control Engineers and Robotics Society of Japan.



**Takenori
Morimitsu**

Institute of
Systems &
Information
Technologies
/Kyushu

Momotihama 2-1-22
Sawara-ku, Fukuoka,
814 Japan

Takenori Morimitsu was born in Fukuoka, Japan, on October 18, 1947. He received B.E. and M.E. degrees in mechanical engineering from Kyushu University in 1970 and 1972, respectively. He joined NTT Electrical Communication Laboratories in 1972, where he has been engaged in research on submarine cable transmission systems and access network systems. He is a member of the American Society of Mechanical Engineers, the Japan Society of Mechanical Engineers, the Institute of Electronics, Information and Communication Engineers, and Robotics Society of Japan.

ADVANCES IN MASS FUSION SPLICE LOSS INCREASE OPTICAL FIBER CABLE INSTALLATION PRODUCTIVITY

Stephen C. Mettler
Neil W. Sollenberger
Ken W. Jackson

Bell Laboratories
Lucent Technologies
Norcross, Georgia

ABSTRACT

Mass splicing of optical fiber ribbons has been used to reduce installation costs since the onset of modern lightwave communications. The continuous improvement, over the last few years of fiber geometry, ribbon quality and alignment accuracy of mass fusion splicing machines has made the loss performance of mass splicing extremely competitive with single-fiber splicing while further improving the process speed and reliability. Mean 12-fiber mass fusion splice losses of 0.03 to 0.04 dB are being achieved with both matched clad and depressed clad fiber ribbons. The use of fiber ribbons reduces cable size which allows longer pull lengths and, therefore, fewer splices. Ribbon cables reduce storage and fiber organization problems at splice points and allow faster restoration times in repair situations. Also, with simple mid-span and fiber end separation methods, individual fibers are accessible for single-fiber splicing when needed. These factors combine to make ribbon cable very attractive.

INTRODUCTION

The cost of cable installation is an important factor in the economics of extending optical fiber further into the loop distribution plant. Larger fiber-count cables are being used for these applications. The cost of these installations can be reduced by using cable of central tube design with the core consisting of varied modular fiber ribbons offering a wide range of fiber counts. The cable uses a variety of ribbons including a maximum ribbon size of 24 fibers. Combining fiber ribbon and the increased efficiency of mass

fusion splicing can greatly reduce the time and cost of cable installation.^{1,2,3} The ribbons provide many combinations of mass splicing arrangements that offer very high productivity and reliability.

In the past, the use of mass splicing incurred a loss penalty over single-fiber fusion splicing. Since then, fiber and cable manufacturers have made significant improvement in fiber core eccentricity and outside diameter control and in factory-made fiber ribbon quality. There has been a simultaneous improvement in the speed and the alignment precision of mass fusion splicing machines. These advances have greatly reduced the splice loss differential between single-fiber and mass fusion splicing while further reducing the splicing time. Some of the evolutionary improvement in mass splicing has been shown.^{4,5} Recent loss data shows that mass fusion splice loss now competes directly with time-consuming single-fiber splicing.

Optical fiber fusion splice loss depends on the degree of alignment of the fiber cores and on the amount of core deformation caused by the fusion process. Single-fiber fusion splicing machines can magnify the fibers and align their cores in three dimensions before splicing. Any fiber core eccentricity present will produce transverse offset when the surface tension of the molten glass pulls the fibers into alignment on their outside diameters (ods) during fusion. This movement also causes core distortion. In mass fusion splicing, individual fiber alignment is not possible and initial alignment is controlled by the positions of the fibers in v-grooves. Core alignment therefore depends on the combination of fiber core eccentricities, fiber od differences,

ribbon geometry and the alignment and cleanliness of the splicing machine v-grooves. The final splice loss, for each fiber pair, depends on the core misalignment and core distortion caused by the surface tension effects and how well the machine maintains fiber alignment during splicing. Surface tension effects can be more important for mass fusion because the longer arc times (15 to 30 seconds for mass fusion vs. 1 to 2 seconds for single-fiber fusion) allow more time for self-centering with respect to the fiber ods. In addition, poor ribbon structure may perturb the position of the fibers in the heating zone, producing higher splice loss. Ideally, the ribbon should have all fibers in contact with the adjacent fibers and in one plane. As fiber and ribbon geometry improve, both core distortion and final misalignment are reduced during the od self-centering effect and splice losses decrease.

MODELING

The statistical distribution of splice loss that can be expected between random fibers can be found using Monte-Carlo techniques.⁶ Fibers are selected at random from the manufactured fiber core eccentricity statistical distribution, which is a Rayleigh probability distribution. The Rayleigh core eccentricity distributions are truncated, both in practice and in the computer simulation, at the maximum allowed eccentricity. The current industry standard tolerance for maximum core eccentricity is 0.8 μm , however, there is no specification on mean eccentricity.

The effects of changing both the mean and the maximum core eccentricities were examined for the case of pure transverse offset caused by core eccentricity. The angular orientations of the two fibers in each splice are also randomly selected from a uniform distribution. This process simulates single-fiber splicing with fiber od-to-od alignment, but does not include core distortion effects. Splice loss due to transverse offset is calculated for each pair of fibers using the single-mode fiber splice loss model.⁷

The summary splice loss statistics in Table 1 show the results of applying different maximum eccentricity tolerances to Rayleigh core eccentricity distributions with different means.

Each row in the table represents a mean core eccentricity and each column is defined by the maximum eccentricity tolerance. The first line in each block in the table contains the mean splice loss, the second line the σ and the third line the maximum of the 10,000 splice losses in that computer run. The maximum theoretically possible splice loss, if both fibers have the maximum core eccentricity, is the same for all the blocks in each column and is shown at the bottom of the column. The results in the table used fibers with mode field diameter (MFD) of $9.3 \pm 0.5 \mu\text{m}$, but remain the same for fibers with MFD of $8.8 \pm 0.5 \mu\text{m}$. The effects of including randomly varying MFD on actual splice loss is very small and made no difference in the statistics shown.

TABLE 1: EFFECT OF CORE ECCENTRICITY ON SINGLE-MODE FIBER SPLICE LOSS

Splice Loss Statistics - Single-mode Fiber at 1.3 μm			
Mean Eccentricity	Maximum Core Eccentricity		
	0.5 μm	0.6 μm	0.8 μm
0.15 μm	0.01	0.01	0.01
	0.01	0.01	0.01
	0.10	0.10	0.11
0.20 μm	0.02	0.02	0.02
	0.02	0.02	0.02
	0.17	0.20	0.21
0.25 μm	0.03	0.03	0.03
	0.03	0.03	0.03
	0.19	0.25	0.33
0.30 μm	0.04	0.04	0.05
	0.03	0.04	0.05
	0.21	0.29	0.44
0.35 μm	0.04	0.05	0.07
	0.04	0.05	0.06
	0.22	0.31	0.46
Maximum Loss	0.23 dB	0.33 dB	0.57 dB

The results shown in this table can be used to establish realistic splicing expectations for both single-fiber and mass fusion splicing:

1. Both the mean and the σ of the splice loss distribution depend primarily on the mean of the core eccentricity distribution. Once the manufactured Rayleigh eccentricity distribution mean drops below $0.35\text{ }\mu\text{m}$, the maximum eccentricity tolerance has very little effect on splice loss mean and σ .
2. The maximum core eccentricity tolerance primarily impacts the maximum splice loss seen for any mean eccentricity. Even with the best mean eccentricity, the application of even the lowest maximum core eccentricity tolerance, $0.5\text{ }\mu\text{m}$, means that there will be some fibers for which the present maximum splice loss tolerances being used in the field, 0.05, 0.10 and even 0.20 dB, may not be possible.
3. The maximum loss seen in the 10,000 splice computer run decreases as mean eccentricity decreases, regardless of the maximum core eccentricity tolerance. The probability of having a splice near the theoretical maximum increases as mean core eccentricity increases.
4. Core eccentricities being achieved by fiber manufacturers are approaching the level that core deformation caused by external perturbing factors, i.e., ribbon geometry, v-groove cleanliness, etc., tends to dominate the splice loss. Core eccentricity is approaching the limits of our ability to measure it.

Figures 1 & 2 are cumulative frequency distributions of splice loss from the different Monte-Carlo runs showing the effect of varying maximum core eccentricity (Fig. 1) and mean eccentricity (Fig. 2). The statistics of the distributions are given in the table, Fig. 1 for the case of $0.25\text{ }\mu\text{m}$ mean eccentricity and Fig. 2 for $0.80\text{ }\mu\text{m}$ maximum eccentricity. The three splice loss distributions in Fig. 1 are very similar except for the extreme tail of the distribution, as seen from the maximum splice losses in Table 1. The core eccentricity maximum tolerance has little effect on overall splice loss when mean eccentricity is this low. Overall splice loss is driven primarily by mean eccentricity as shown in Fig. 2. Regardless of any other factors

affecting splice loss, improving the mean eccentricity by only $0.1\text{ }\mu\text{m}$, from 0.3 to $0.2\text{ }\mu\text{m}$, cuts the mean splice loss in half.

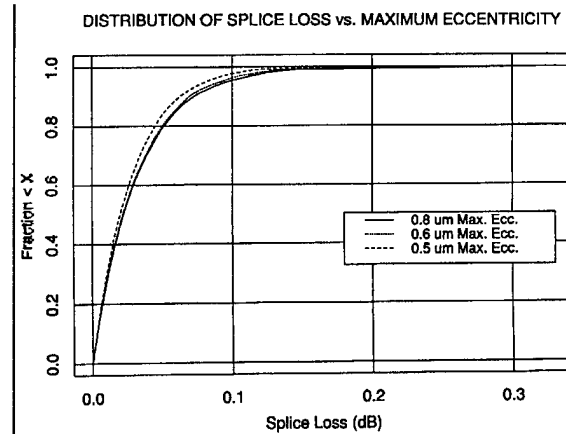


FIGURE 1: Mean Core Eccentricity = $0.25\text{ }\mu\text{m}$

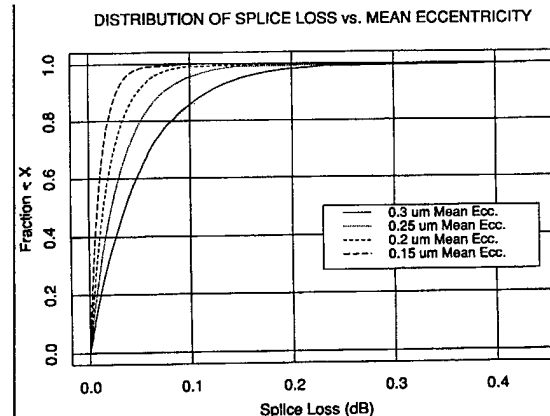


FIGURE 2: Maximum Core Eccentricity = $0.80\text{ }\mu\text{m}$

The total splice loss that can be expected along any optical fiber path (or span) depends on the overall splice loss distribution and the number of splices per path. In any system with more than a few splices per span, one higher-loss splice will not seriously raise the total span loss. Setting a reasonable splice loss target for individual splices can save time and expense because most spans will have enough splices that the mean splice loss will be achieved after four or more splices. As the number of splices per span goes up, averaging reduces the spread of the total path splice loss; the σ goes down and the average loss on the worst path goes down. This behavior can be modeled by grouping the random splice loss distributions generated using core eccentricity. The splice loss distribution for

0.25 μm mean and 0.8 μm maximum eccentricity was used. This splice loss distribution matches the experimental data seen with a fiber core eccentricity distribution with a mean of 0.15 μm . Adding the effect of an additional 0.1 μm mean core eccentricity provides a way to model the additional splice loss caused by core distortion seen in fusion splicing.

The 14,400 random splices in the Monte-Carlo run were grouped two-at-a-time, three-at a-time, four-at-a-time, etc., to simulate the number of splices per span. The statistics of the resultant distributions are shown in the table below. For example, for a span with four splice points, while the mean splice loss remains 0.03 dB, the σ drops to 0.02 dB and the worst individual path had a mean splice loss of 0.12 dB.

TABLE 2: SPLICE LOSS STATISTICS FOR SPANS WITH MULTIPLE SPLICES

Core Eccentricity of 0.25 μm Mean & 0.8 μm Maximum						
Per-Splice:	Number of Splices per Span					
	1	2	3	4	5	6
Mean (dB)	0.03	0.03	0.03	0.03	0.03	0.03
σ (dB)	0.03	0.02	0.02	0.02	0.01	0.01
Worst Case Mean (dB)	0.33	0.21	0.15	0.12	0.12	0.09

The one splice column gives the statistics of the overall 25,000 random splice distribution. This column is the base data for the rest of the table. The statistics are developed by taking the cumulative splice loss for each span, dividing by the number of splices in that span and then taking the statistics of the resultant splice loss distribution. This set of statistics shows how averaging reduces the σ and the maximum average splice loss seen. These results show that the highest cumulative splice loss per span is much less than the worst case which would be the number of splices in the span times the worst single-splice splice loss of 0.33 dB. Obviously, less splices in each span lowers the total span splice loss.

Twelve-fiber mass fusion splicing can also be simulated by grouping the splices twelve-at-a-

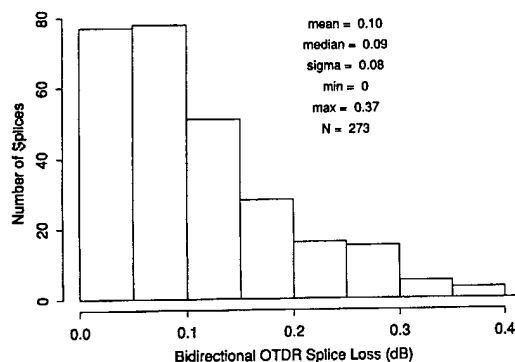
time. This provides a basis for judging when a good twelve-fiber mass fusion splice has been made. This process gave a mean splice loss per fiber of 0.03 dB with a σ of 0.01 dB and a maximum twelve-fiber mean of 0.07 dB per fiber splice for 0.25 μm mean and 0.8 μm maximum core eccentricity. These statistical results are in good agreement with the experimental data. The results can be combined with the experimental results to develop the remake rules for field splicing.

EXPERIMENT

Splicing experiments were performed using current 12-fiber factory-made ribbons and the newest splicing machine. Stripping and cleaving were performed with the tools that came with the machine. Both depressed-clad (DC) and matched-clad (MC) fibers were spliced. The fibers were manufactured using either the modified chemical vapor deposition (MCVD) process or the vapor axial deposition (VAD) process. Fibers were randomly selected from inventory and the 1996 data used fibers with mean core eccentricity of < 0.20 μm . Splice loss was measured using bidirectional OTDR and estimated using the machine Profile Alignment System (PAS). All splicing was random; **no identical fiber splice losses are included in the data.** Current results are compared to data from previous experiments using older fiber ribbons and earlier model splicing machines and to the Monte-Carlo studies.

The measured loss distribution in Figure 3 shows 1993 results with depressed clad fiber ribbon. Several different earlier model splicing machines were used, the differences between machines were statistically insignificant. In a real installation some splices would have been remade improving the results somewhat, however, the losses still would not have been as low as the 1996 data below.

FIGURE 3: DEPRESSED CLAD FIBER - 1993



The measured splice losses for the current fiber ribbons and the new machine are shown in Figures 4, 5 and 6. Figure 4 shows MC to MC, Figure 5 DC to DC and Figure 6 DC to MC splice loss distributions. One splice was remade in both Figures 4 and 5 for high loss (> 0.5 dB) which would probably have been remade in the field. Using a 0.25 dB maximum splice loss standard would have required only one splice remake out of 28 mass splices in the MC experiment and only one out of 14 in the DC case. The splicing machine PAS system correctly caught both instances of high splice loss. The data in the DC to MC experiment demonstrate that mass fusion splicing different types of fibers is just as easy as either single-fiber fusion of different fibers or mass fusion of like fibers.

FIGURE 4: MATCHED CLAD FIBER - 1996

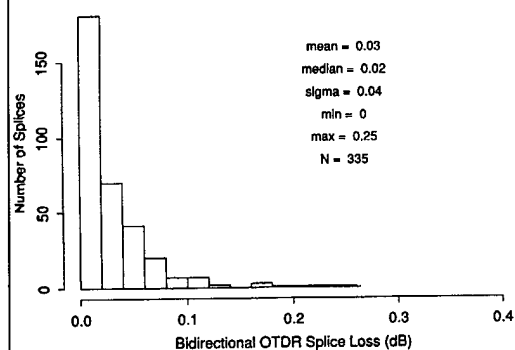


FIGURE 5: DEPRESSED CLAD FIBER - 1996

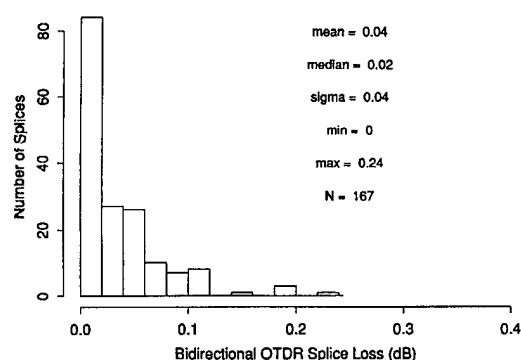
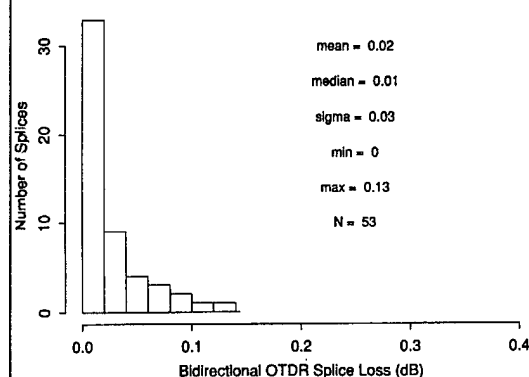


FIGURE 6: DEPRESSED CLAD TO MATCHED CLAD FIBER - 1996



A previous experiment had been performed using the same matched clad ribbons used for the data in Figure 4 using an earlier model splicing machine. The mean splice loss in that case was 0.045 dB with a σ of 0.05 dB. Comparing these results to Figure 4 indicates that improvements in the splicing machine have contributed about 0.01 to 0.02 dB of the improvement seen between the 1993 and 1996 mean splice loss.

These experimental results demonstrate that mass fusion splice losses are approaching both the theoretical minimum predicted by the Monte-Carlo studies, as shown in Table 1 for lower core eccentricity fiber, and single-fiber fusion experimental results.

CONCLUSIONS

Quality improvements in fiber, ribbon and splicing machines have, as predicted,⁸ resulted in lower mass fusion splice loss. As mass fusion splice loss is reduced, the number of remakes

required is reduced, further improving the efficiency of both initial installation and restoration of cut cables. These results show that further productivity improvement can be anticipated as 24-fiber ribbons, currently in production, are spliced either split into 12-fiber subunits or as 24-fiber ribbons in the future.

The continuous improvements in fibers, ribbons and splicing machines that have made the results shown here possible should continue, producing further reductions in splice loss and increasing splicing efficiency. There are limitations on the further improvement in splice loss performance. Core eccentricities below 0.2 μm test the limits of eccentricity measurement capability. Splice losses are approaching the level that they are lower than the noise in even bidirectional OTDR measurements. Many of the splices in these experiments produced negative bidirectional OTDR loss measurements which were assigned a value of zero. OTDR loss measurements depend on the quality of the OTDR, the training and capabilities of the operator and the distance to the splice. Individual splice loss measurements were seen to vary by as much as ± 0.03 dB, however, the 12-fiber mass fusion splice loss average repeatability was ± 0.01 dB.

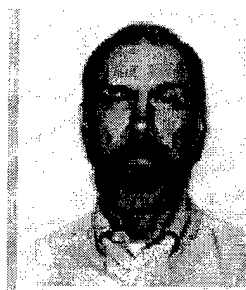
ACRONYMS

1. DC - Depressed Clad
2. MC - Matched Clad
3. MCVD - Modified Chemical Vapor Deposition
4. MFD - Mode Field Diameter
5. od - outside diameter
6. OTDR - Optical Time Domain Reflectometer
7. PAS - Profile Alignment System
8. VAD - Vapor Axial Deposition

REFERENCES

1. Patrick Neville, "Maintaining the network in New York," *Lightwave*, March, 1991.
2. Fred L. Fleming and Kent B. Brown, "A mission for mass-fusion splicing," *Telephony*, September 28, 1992, p. 28.

3. Patrick W. Hart and John F. Thompson, "Multifiber Splicing, a Brief Analysis," Raychem Outside Plant Seminar, September 22, 1993.
4. Mackie, G., Duke, D., Karl, G. & Menard, R., "Evolution of Fusion Splicing Technology and Application Based on Fiber Geometry," NFOEC '95, Boston, MA, June 18-22, 1995, p. 93.
5. Mallya, A., Paz, R., Kiritsy, E. R., Perry, R. E., Cooper, S. A., Young, J. C. & Linchuck, B. A., "Mass Fusion Splicing Attenuation Performance and Its Use in a Consumer Broadband Network," *ibid.*, p. 133.
6. Mettler, S. C., "Monte-Carlo Analysis of the Effect of Mode Field Diameter Mismatch on Single-Mode Fiber Splices," *Proceedings of 8th NFOEC*, April 21-24, 1992, Washington, D.C., p. 647.
7. Marcuse, D. "Loss Analysis of Single-Mode Fiber Splices," *B.S.T.J.*, Vol. 56, May-June, 1977, p. 703.
8. Anthony Pellegrino, Sunil Joshi & Rich Contreras, "Evolution of Single-Mode Optical Fiber Splicing Past, Present and Future," *Proceedings of 8th NFOEC*, April 21-24, 1992, Washington, D.C., p. 621.



Stephen C. Mettler is currently a Distinguished Member of Technical Staff in the Advanced Instruments group at Lucent Technologies/Bell Laboratories in Atlanta, Georgia. He received the B.S. in Engineering from

the U.S. Air Force Academy in 1962 and was an Air Force pilot for eight years. He received M.S. (Physics, 1972) and Ph.D. (Mechanical Engineering, 1976) degrees from Purdue University. He has worked in optical fiber splicing for the last twenty years. He has published over twenty five papers, is co-author of a book and a book chapter on optical fiber splices and connectors and holds three patents

in fiber optics.



Neil W. Sollenberger is a Member of Technical Staff in the Outside Plant Fiber Group at Lucent Technologies/Bell Laboratories in Norcross, Georgia. He is responsible for various aspects in the design and

development of outside plant fiber optic cables. Prior to his current assignment, his responsibilities have included the design and development of both copper and fiber optic closures and terminals, as well as cabinets for loop electronics. Neil Sollenberger joined AT&T Bell Laboratories in 1978. He has a B.S. degree in Agricultural Engineering from University of Georgia, and he has a M.S. degree in Mechanical Engineering from Georgia Institute of Technology.



Kenneth W. Jackson is a Distinguished Member of Technical Staff in the Fiber Optic Cable and Materials Development and Engineering Department at Lucent Technologies/Bell Laboratories, Norcross, Ga. He is

responsible for the design and development of outside plant cables. He joined the Western Electric Company in 1970 having received a B.S.M.E. from Auburn University. He joined AT&T Bell Laboratories in 1981 having received an M.S.M.E. and Ph.D. in Mechanical Engineering from the Georgia Institute of Technology. Since 1981 he has worked in the areas of Optical Fiber Fabrication, Fiber Optic Connector Design and Development, Materials Design and Fiber Optic Cable Design and Development. He has been awarded 7 patents and has 9 publications. He is a Registered Professional Engineer in the state of Georgia.

Structural Mechanics Aspects of Fractures of Optical Fibers in Connectors

Wilton W. King, Bruce G. LeFevre and Daniel L. Stephenson

Lucent Technologies/Bell Laboratories
Norcross, Georgia

ABSTRACT

Fracture of fiber in a connector occurs when induced tensile stress exceeds local strength, usually governed by a stripping-related flaw. Stress analyses based upon elementary models from structural mechanics are presented to explore the significance of misalignment and of differential thermal expansion of ferrule and backbone. Results of finite-element analysis are used to suggest an epoxy-driven mechanism for fractures observed after thermal cycling. Implications for reliability are discussed.

INTRODUCTION

Connectors and splices are potential weak links in fiber-optic systems. At these components, degradation of performance or complete loss of function can occur in a variety of ways. One form of catastrophic failure is fracture of a fiber, and the risk is high because here is found bare fiber whose intrinsic local strength may have been substantially reduced by the process of removing protective coatings. But a weakened fiber will only fracture if additionally there is stress of sufficient magnitude, in particular tensile stress. In this paper, we explore sources of such stresses in single-fiber connectors with structures typical of current products.

As a first step in connectorization, buffer and coating layers are usually stripped off mechanically. The tools used invariably nick or scratch the bare fiber and the resulting flaws are sites for amplification of stresses and initiation of cracks. Studies such as those of Wei et al¹ and Wagner² have demonstrated that tensile strengths of individual samples of stripped fiber can often be significantly less than 700 MPa (100 ksi). It is the interaction of tensile stresses with a flaw that leads to fracture, and so circumstances that place a fiber in longitudinal compression are not dangerous unless that condition can lead to buckling of the fiber. For a fiber in bending, the significance of a flaw will depend upon

whether the flaw is on the tension side or compression side of the bent fiber. Of course, when a fiber is loaded in longitudinal tension, that is the nature of the stress throughout. For the most part, analyses of fiber fractures in connectors have been in the form of postmortem fractography.^{3,4,5} Typically in these works, characteristics of prefracture stress states have been inferred from fracture surfaces, and plausible qualitative explanations have then been advanced about the likely structural mechanics and circumstances leading to the fractures. A notable exception is the work of Kinney⁶ in which were reported extensive finite-element analyses of thermoelastically induced stresses in biconic connectors.

The present work focuses on cylindrical-ferrule connectors for which typically the ferrule is ceramic with a diameter of 2.5 mm. The fiber is bonded into a small-bore axial hole in the ferrule by an epoxy or similar adhesive. Telecommunications connectors of this type include FC, SC and ST. The analysis which follows builds upon and amplifies earlier work of the authors.^{7,8}

CONNECTOR STRUCTURE

A partially sectioned view of a generic structure for attaching a single-fiber jumper cable to a connector is shown in Fig. 1. The alignment ferrule is mounted in a frame, often called a backbone, which in turn is spring-supported within the connector housing. The type shown is usually referred to as a "pull-proof" connector because the cable jacket and strength elements are attached directly to the external housing of the connector. This isolates the ferrule-backbone assembly from mechanical loads on the cable. When two connectors are mated, the ferrule-backbone is forced rearward and the buffered fiber must either be compressed in the cavity behind the backbone or slide back into the cable structure. Such isolation is not produced when the cable is attached directly to the backbone. Then the cable is

free to slide relative to the connector housing when mating occurs and the spring is compressed. Whenever buffered fiber is connectorized, it is this latter configuration that pertains.

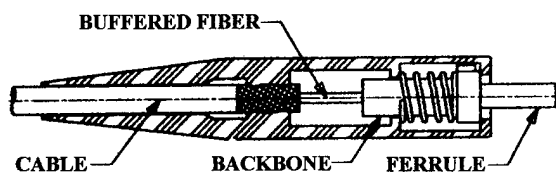


Figure 1 Pull-Proof Connector

Details of fiber attachment can be seen in the section view (Fig. 2) of the backbone and ferrule assembly. Bare fiber is adhesively bonded in the central small hole (or capillary) in the ferrule. An entry funnel at the back of the ferrule facilitates threading the fiber into the ferrule. The length l is the length of bare fiber from the capillary entry to the buffer. Commonly in telecommunications, connectors the design intent is for the buffer to fit up snugly to the end of the ferrule, meaning l is intended to be roughly the depth of the entry funnel, about 1 mm. However other designs⁹ have sometimes intended much longer lengths of unbuffered fiber. The exterior surface of the buffer coating is adhesively bonded to the backbone, and adhesive injected into the ferrule opening prior to fiber insertion is assumed here to no more than fill the funnel.

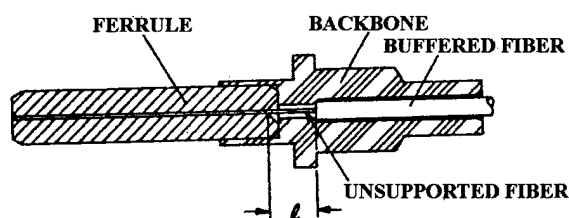


Figure 2 Backbone-Ferrule-Fiber Assembly

Significant differences in mechanical and thermal properties of materials in the ferrule-barrel-fiber-adhesive system play crucial roles in many of the mechanisms for development of stresses. The ferrule is commonly ceramic, and it and the silica fiber are relatively stiff materials having relatively low coefficients of thermal expansion.¹⁰ With higher coefficients of thermal expansion are the adhesive (usually an epoxy) and the metal of which the backbone is usually constructed. The metal typically has stiffness comparable to the silica and the

ceramic, while the epoxy has substantially less stiffness.

STRUCTURAL ANALYSIS

The focus of attention is the region between the end of the buffered fiber and the entry to the capillary hole in the ferrule. It is reasonable to assume that the assembly process leaves the fiber free of axial thrust at the temperature at which the adhesive cures. For some adhesives this might be room temperature and for epoxies upward of 100°C. Because of the low coefficient of thermal expansion of the glass, subsequent cooling would compress the fiber. So, where a heat-cured epoxy is used, a beneficial compressive bias would be expected at room temperature.

In what follows, "back-of-the-envelope" calculations are used to shed light on several obvious potential sources of tensile stress in the bare fiber. These are: thermal mismatch of fiber and backbone; and transverse misalignment of buffered fiber with the ferrule capillary. Finally, a rather subtle epoxy-driven mechanism for fracture in thermal cycling is discussed using results of finite-element analysis.

Representative material properties used for quantitative estimates include coefficients of thermal expansion, α , for epoxy, backbone and glass respectively as $60 \times 10^{-6}/^{\circ}\text{C}$, $20 \times 10^{-6}/^{\circ}\text{C}$ and $0.5 \times 10^{-6}/^{\circ}\text{C}$ (negligible). Elastic moduli, E , have been taken to be 4GPa for epoxy and 70GPa for the glass fiber.

Fiber-Backbone Thermal Mismatch

Assuming the structural stiffness, i.e. product of elastic modulus and cross-sectional area, of the fiber to be much less than that of the backbone, the backbone may be taken to expand or contract freely, "bossing" the fiber. Thus the differential strain generated by a temperature change δT is $(\delta\alpha)(\delta T)$ where $\delta\alpha$ is the difference in coefficients of thermal expansion. Stress induced in the fiber is then $E(\delta\alpha)(\delta T)$ where E is the elastic modulus of the fiber. So a reasonable estimate of tensile stress, σ , induced in the fiber for a 60°C rise in temperature from the stress-free state is

$$\begin{aligned}\sigma &= 70(20 \times 10^{-6})(60) = 84 \times 10^{-3} \text{GPa} \\ &= 84 \text{ MPa (12 ksi)}\end{aligned}$$

This stress would generally be of insufficient magnitude to be of concern.

If the unsupported fiber is so long that compressive stresses generated by cooling cannot be stably sustained, the fiber will buckle, and the associated tensile stresses developed may cause fracture. It is important to recognize that unlike the bending associated with a misalignment, buckling is a form of structural collapse inherently associated with longitudinal compressive thrust.

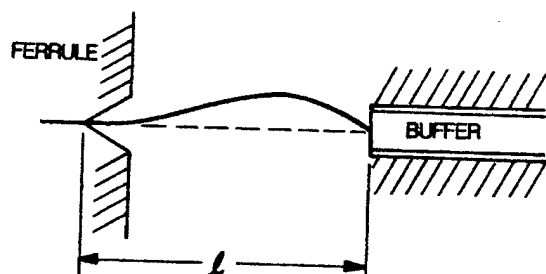


Figure 3 Buckling Mode

Buckling is very sensitive to conditions of support. Where the fiber enters the ferrule it is reasonable to assume a clamped end; where the bare (or coated) fiber enters the buffer a reasonable choice of support is a hinge (see Fig. 3). This leads to a buckling load of

$$P = 2.05 \frac{\pi^2 EI}{l^2} \quad (1)$$

about midway between the reasonable extremes of $\frac{\pi^2 EI}{l^2}$ and $\frac{4\pi^2 EI}{l^2}$ appropriate to a pinned-pinned column and a clamped-clamped column respectively.¹¹ In Eq. (1), $I = \frac{\pi r^4}{4}$ where r is the fiber radius. The critical compressive strain is then approximately $5 \left(\frac{r}{l} \right)^2$, and the critical condition

for buckling, were a backbone to be subjected to a temperature drop δT , becomes

$$(\delta \alpha) (\delta T) = 5 \left(\frac{r}{l} \right)^2 \quad (2)$$

Cooling from an epoxy-cure temperature to room temperature gives a drop of about 100°C, and so with the same backbone properties as before

$$(20 \times 10^{-6})(100) = 5 \left(\frac{r}{l} \right)^2$$

$$\left(\frac{l}{r} \right)^2 = 2500 \quad (3)$$

Thus for a fiber radius of 62.5µm, Eq. (3) gives a critical length of about 3 mm. So, for a longer length, buckling will occur and tensile stresses will be induced by the bending of the fiber. Accurate computation of those stresses is difficult even if one ignores the bound on displacements provided by the backbone wall. Suffice it to say that once the critical compressive thrust has developed, additional backbone shrinkage will produce very rapid development of transverse bending. In practice, exceeding the critical conditions for buckling should be regarded as tantamount to failure.

The conditions of the calculations just carried out correspond to those of a rather dramatic set of failures encountered several years ago. Field connectorization of a set of connectors was improperly done, unsupported fiber too long, and within twenty four hours a significant percentage had apparently suffered fiber fracture. The buckling pattern, or mode, of Fig. 3 yields peak bending at the ferrule opening and also near the midspan. Examples of fractures at these locations are shown in Fig. 4 and Fig. 5.

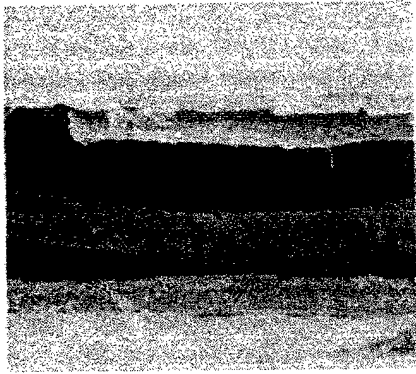
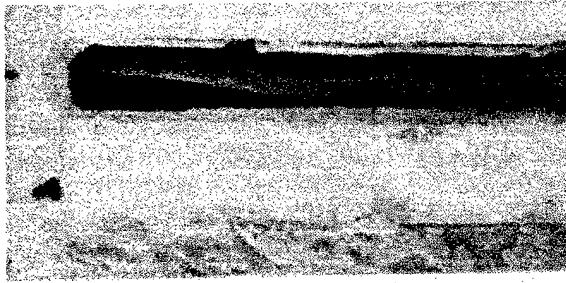


Figure 4 Fiber Buckling: Midspan Fracture
(from Ref. 8)

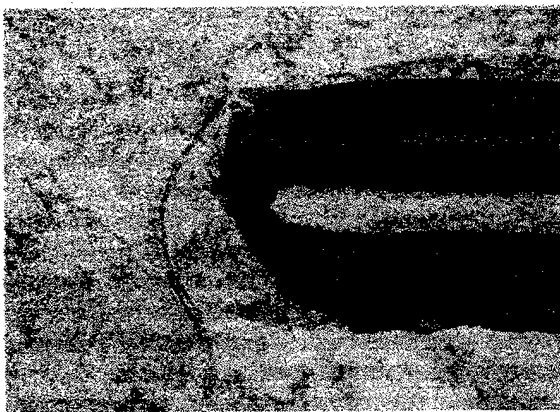
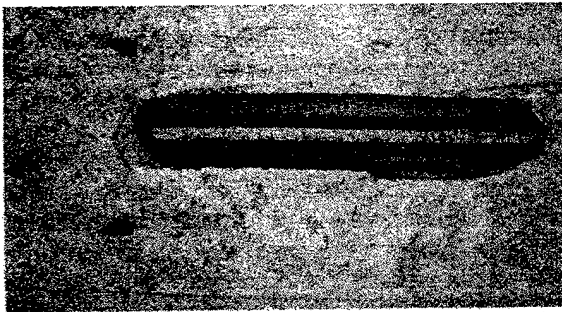


Figure 5 Fiber Buckling: Ferrule-End Fracture
(from Ref.8)

Misalignment

Ends of the unsupported fiber may be offset because of transverse misalignment of the backbone and ferrule bores and because of fiber-coating-buffer concentricity tolerances. The element from structural mechanics that pertains here is a transversely-loaded slender bar (beam)¹¹. For short fiber lengths (approaching 1mm) the theory becomes rather inaccurate since the fiber diameter is typically 0.125mm. The conservative position with regard to bending stresses is to take each end of the fiber to be clamped as shown in Fig. 6. Then, with transverse offset Δ , the maximum bending stress is

$$\sigma = \frac{6Er\Delta}{l^2} \quad (4)$$

and it occurs at the ends of the span.

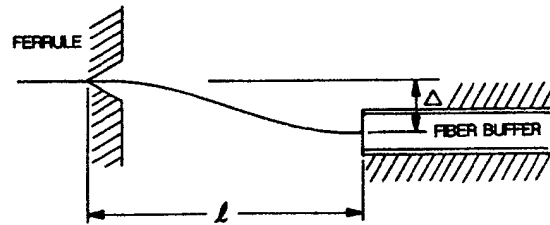


Figure 6 Transverse Misalignment

As an example, with $E = 70$ GPa, $r = 62.5\mu\text{m}$, and $l = 2\text{mm}$, an offset $\Delta = 0.005$ mm produces a maximum bending stress of 330 MPa (48 ksi). This is itself a substantial stress, and four times it would be indicated by (4) for the minimum usual length of 1mm. Even if the support at the buffer is taken to be a hinge, as in Fig. 3, the maximum bending stress is only halved relatively to (4). That is, for a clamped-hinged support system

$$\sigma = \frac{3Er\Delta}{l^2} \quad (5)$$

In spite of the rather large stresses suggested here, the writers have not encountered field or laboratory failures that seem to be clearly attributable to this mechanism. This is probably due to a combination of tight manufacturing tolerances along with the opportunities for adjustment and accommodation provided by the soft inner layers of dual-coated fibers and by buffer-backbone clearances.

Epoxy Role (?) in Thermal Cycling

Over a period of several years the writers have encountered a number of fiber fractures occurring during thermal cycling and with the fractures consistently located at the throat of the ferrule entry funnel. Degradation of optical transmission, indicating progressive failure as occurred in one experiment, is depicted in Fig. 7. The fracture surface, including probable initial surface flaw, is shown in Fig. 8.

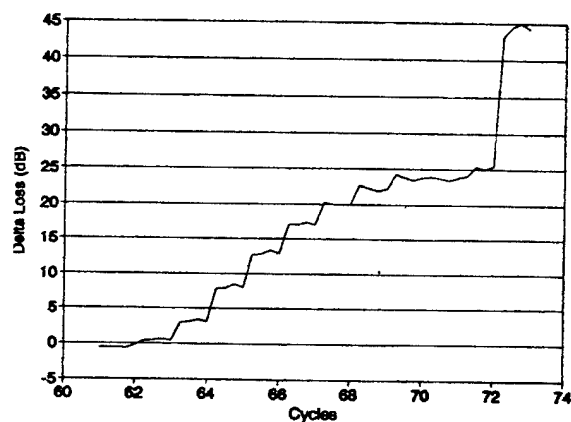


Figure 7 Progressive Failure with Thermal Cycling

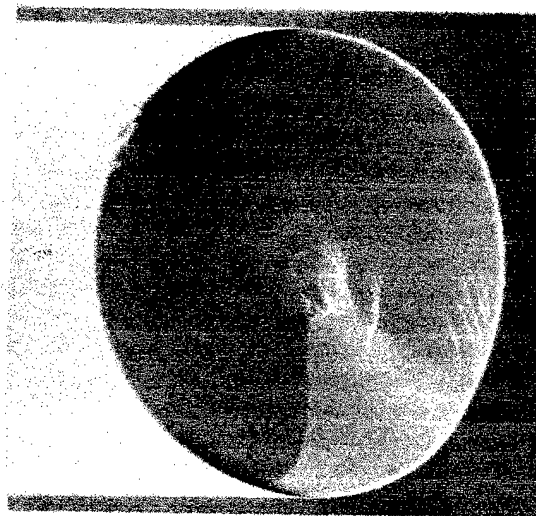
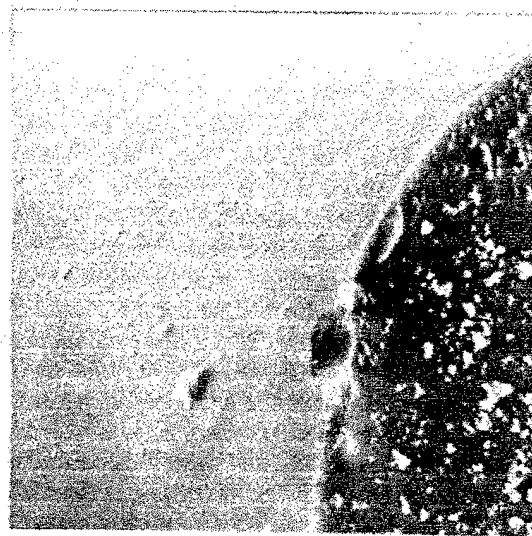


Figure 8 Fracture Surface: Fiber at Funnel Throat

Since the adhesive in this structure was a heat-cured epoxy and the free length of fiber was insufficient for buckling, a source of tension was not readily apparent for thermal cycling between -40°C and 75°C . However, where cooling occurs, the epoxy more or less filling the ferrule entry funnel will try to contract much more rapidly than other components. The epoxy will pull the fiber back toward the funnel throat and also tension will develop at the funnel-epoxy interface. Subsequent heating will simply act to relieve these stresses.

Were the epoxy-funnel bond to break, then cooling would cause the epoxy to "pinch" the fiber and would cause neither tension nor compression at the throat. And this has been verified by finite-element studies. With subsequent heating, the epoxy plug

may "push off" against the funnel wall and generate maximum tension in the fiber precisely at the throat of the funnel. Axial distribution of this tension for a temperature rise of 100° C is given in Fig. 9 along with the finite-element model used.

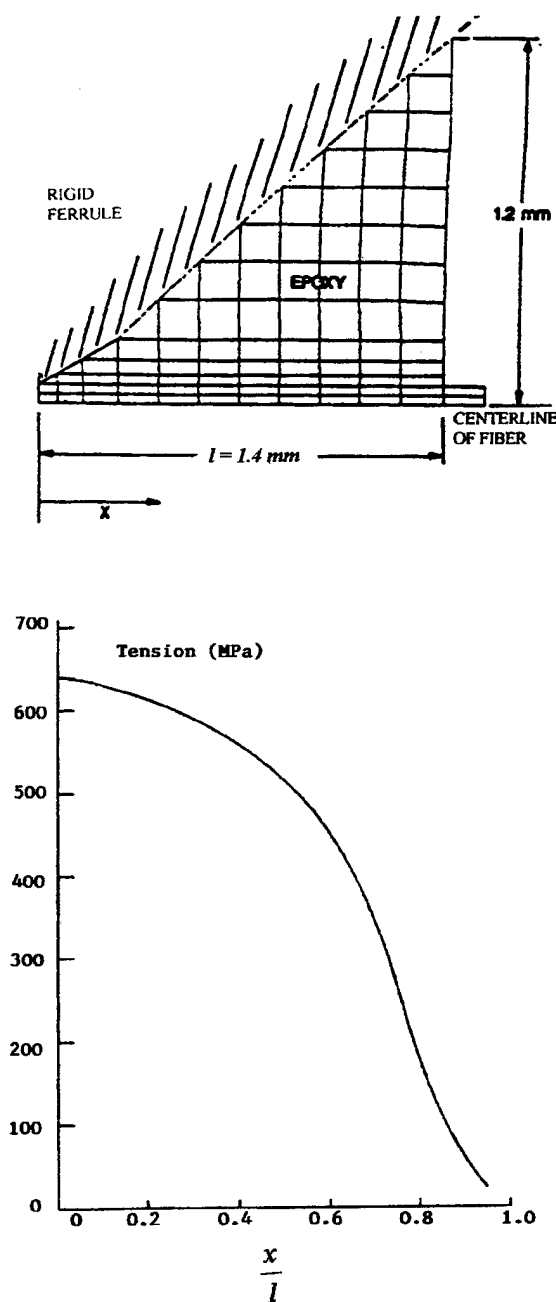


Figure 9 Thermally Induced Fiber Tension in Entry Funnel (from Ref. 8)

Opportunities for Fracture of Buffered Fiber

Buckling in Pull-Proof Connectors. If cable construction is too tight, the buffered fiber in a pull-

proof connector (Fig. 1) will be constrained against sliding back when connectors are mated. Buckling of the buffered fiber can ensue. Even though buffered fiber is of high strength, long term reliability will be at risk if permanent buckling is permitted. Estimates of stresses and elaboration on cable design to avoid this problem may be found in the work of Holman et al.¹²

Sharp Bending at Boots. Buffered fiber exiting a connector boot is vulnerable to fracture by sharp bending even under relatively benign handling conditions if the end of the boot is very stiff. This is particularly true when loose tubing is used to play the role of a buffer, an example being connector termination of individual coated fibers separated at the end of a ribbon structure. The tube may locally collapse in a form of buckling (kinking) carrying the fiber into a severe local bending.

FIBER BREAKS AND CONNECTOR RELIABILITY

The relationship between fiber breaks and connector reliability is best understood within the framework of concepts and terminology under development by industry standards bodies.^{13,14} Reliability is the time dependent failure probability in a particular service environment and is consequently determined by the combination of all failure modes, one of which is fiber breakage. The probability of occurrence of each mode is a function of both design and quality, the latter being a measure of several parameters of the product population including the level and consistency of "defect" occurrence. Reliability and quality are interrelated, but must be separated conceptually to fully understand the role of fiber breaks.

Failure analysis of field and laboratory test samples shows that fiber failures in connectors originate predominantly at regions of surface damage produced during a mechanical stripping operation (to remove the buffer/coating). Dynamic tensile strength data indicates that damage occurs approximately 1% of the time in a typical stripped section of fiber and the consequent reduced strength may fall into the range of stresses produced by the mechanisms presented in this paper. The coincidence of damage and a stress of suitable magnitude, both of which are directly or indirectly related to assembly of the connector, constitutes a defective unit subject to early failure by dynamic overload or static fatigue (under static or cyclic stress). Correctly assembled connectors are not subject to fiber breakage under normal conditions.

The authors are unaware of any documented fiber failures in connectors not showing evidence of significant damage (buckling of long stripped sections is a possible exception) and have been unable to induce static fatigue failures in undamaged stripped fibers, except under extreme conditions of stress, temperature, and humidity.

The frequency of occurrence of defective connectors which are candidates for fiber breakage is a quality issue related to the assembly process and its controls. To assess its impact on reliability, an analysis must address the defect population and account for the following: (a) the defect population is small compared to the main population, and (b) the failure rate should decrease rapidly over time as the defective components are eliminated from the overall population. In principle, the time dependent failure rate can be estimated from life-stress models based on accelerated test data, but this is complicated by the requirement for extremely large sample sizes needed to accurately estimate low failure rates. This kind of information, if available, has not been published. An alternative approach is to rely on field data, but neither is this information available because of non-uniform reporting procedures and proprietary concerns. At present, the best available estimates based on highly accelerated life tests place the cumulative (life-time) failure fraction at less than 0.1%. That limit can be reduced by one of several available screening methods with some trade-off in cost.

CONCLUSION

Using models from structural mechanics, tensile stresses in bare fiber within a ferrule-backbone assembly have been estimated. These stresses are generated either by geometric misalignment or by the consequences of the wide range of coefficients of thermal expansion found in a typical connector structure. Representative numerical results suggest that the calculated stresses are much lower than expected fiber strengths, and so for fracture to take place a substantial flaw must occur or the stress must be persistent and be accompanied by environmental intrusion.

ACKNOWLEDGMENT

The writers are grateful to Brenda Odom for her very skillful manuscript production.

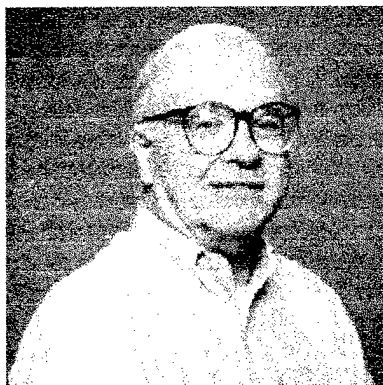
REFERENCES

1. T. Wei, H. H. Yuce, C. H. Hasz and P. L. Key, "Degradation of Fiber Strength During Coating Stripping," Proc. 38th IWCS, 1989, pp. 199-204.
2. W. R. Wagner, "Extrinsic Fiber Damage and its Effect on the Reliability of Optical Fiber Connectors and Splices," Fiber Optic Components and Reliability, Proc. SPIE, Vol. 1580, 1991, pp. 168-185.
3. W. R. Wagner, "Failure Analysis of Fiber Optic Connectors," Advances in Ceramics 22, Fractography of Glasses and Ceramics, Am. Ceramics Soc., 1988, pp. 389-402.
4. H. H. Yuce, J. P. Varachi, Jr. and T. Wei, "Analysis of Optical Interconnection Failures by Analytical Techniques," Proc. 9th NFOEC, 1993, pp. 251-256.
5. T. Wei, B. T. Devlin, H. H. Yuce and J. P. Varachi, Jr., "Failure Mode Analysis of Fiber Components," Proc. 11th NFOEC, 1995, pp. 1081-1085.
6. M. Kinney, "Optical Fiber Stresses within a Biconic Connector," Failure Prevention and Reliability - 1987, ASME DE-19, 1988, pp. 75-79.
7. J. M. Anderson, A. G. Hardee, W. W. King and B. G. LeFevre, "Design Considerations Relating to Thermally Aggravated Fiber Stress in a Connector Cavity," Proc. ASM Int'l. 4th Electronic Materials and Processing Congress, 1991, pp. 225-228.
8. B. G. LeFevre, W. W. King, A. G. Hardee, A. W. Carlisle and K. B. Bradley, "Failure Analysis of Connector-Terminated Optical Fibers: Two Case Studies," J. of Lightwave Tech. Vol. 11, 1993, pp. 537-541.
9. P. Singh, G. T. Gaylon, G. M. Jordhamo and G. W. Peterson, "Fiber Optic Duplex Connector Design Evolution and Analysis," Proc. ASM Int'l. 5th Electronic Materials and Processing Congress, 1992.
10. B. G. LeFevre, "Materials in Fiber Optic Connections," Proc. ASM Int'l 4th Electronic Materials and Processing Congress, 1991, pp. 215-223.

11. E. P. Popov, Engineering Mechanics of Solids, Prentice-Hall, New York, 1990.
12. J. R. Holman, A. C. Jenkins, N. T. Subh and R. Travieso, "Reliability of Optical Fiber Cables for New Connector Systems," Proc. 43rd IWCS, 1994, pp. 795-801.
13. IEC Guideline on Passive Optical Component Reliability, Sections 1-6, IEC/SC86B Working Group 5: Reliability of Fiber Optic Interconnecting Devices and Passive Components, Committee Draft in Ballot, August 15, 1996.
14. TIA Draft Standard (PN 3127), Procedures for Calculating the Reliability of Fiber Optic Connectors, Splices, and Passive Branching Devices, Part 1: General and Guidance. TIA Working Group FO 6.3.8: Reliability of Connectors, Splices, and Passive Branching Devices, part 1: General and Guidance, TIA Working Group FO 6.3.8: Reliability of Connectors, Splices and Passive Branching Devices, Letter ballot in Circulation, May, 1996.

Authors' Mailing Address:

Lucent Technologies/Bell Labs
2000 Northeast Expressway
Norcross, GA 30071



Wilton King is Emeritus Professor at the Georgia Institute of Technology where he served on the faculty for twenty seven years. In 1991 he joined AT&T Bell Laboratories (now Lucent Technologies) in Norcross, Georgia, where he designs and analyzes fiber-optic connector products.



Bruce G. LeFevre is a Member of Technical Staff at Lucent Technologies/Bell Laboratories, Norcross, Georgia. He received his B.S. (Colorado School of Mines) and Ph.D. (University of Florida) in Physical Metallurgy. He joined AT&T Bell Laboratories in 1976 after ten years on the faculty of Georgia Institute of Technology. He has been involved in the study of metals and alloys used in the manufacture of cables and connectors; and is currently working with fiber-optic interconnections, with emphasis on design and reliability.



Dan L. Stephenson is a member of Technical Staff in Fiber Optic Connector Design at Lucent Technologies, Norcross, Georgia. He joined Bell Labs in 1969 as a graduate of Alamance Community College with an Associate in Machine Design.

DEVELOPMENT OF DIGITAL LINE MULTIPLEXING OPTICAL TRANSMISSION EQUIPMENT

Toshimasa Yoshimura*, Shinichirou Dogi*, Katuya Hayashi*,
Tokuhide Kasetani+, Kensaku Sekiya+ and Kazutaka Shimoohsako+

*Kansai Telecommunication Technology Co., Ltd., Osaka, Japan
+The Furukawa Electric Co., Ltd., Kanagawa, Japan

Abstract

KANSAI TELECOMMUNICATION TECHNOLOGY and FURUKAWA ELECTRIC have developed new optical transmission system. By employing the FDM, this system handles different kinds of services such as secondary rate of private line($6\text{Mbps} \times 1$) and ISDN primary rate($1.5\text{Mbps} \times 4$). Small remote terminals developed and operated outdoors, saves installation cost and improves the distribution performance of fibers.

More than ten systems have been in service since October 1995. In this paper, we describe system configurations, merits of this system and parameter of optical transmission path.

Introduction

A demand of I interface services, especially one on metallic cable having a 128k or lower bit rate per second, increase rapidly these days. As the needs of lines which are low speed and small number of multiplexing will increase, after now new services on optical cable, such as N-ISDN network, PHS and Frame relay, will grow near future.

Figure 1 shows a configuration of the conventional system. The system has problems to the following needs.

1. Communication service companies cannot provide services for users apart from large stations 7km or more because of metal transmission limitations
2. Poor investment efficiency due to the system architecture. Under the present circumstances, customers require average of 3 channels, however optical transmission equipment for I interface and ISDN network has a capability to connect hundreds channels to subscribers directly.

Our objectives are described as follows :

1. Effective use of optical cables and service offering for long distance users.
2. Employing the FDM technique, optical signals carries to the small stations nearest customers, then the signals are transmitted through metal cable in order to comply the customers needs for I interface (low bit rate, limited number of lines) at a competitive price.
3. Our equipment meeting ISDN services that have been in service since October 1995, using optional units.

We have developed transmission equipment having solutions for the problems.

Figure 2 shows a configuration of a proposed system.

Merits of the FDM

Table 1 shows comparison between the FDM and the TDM. At a certain configuration, such as ISDN 8 lines transmission, the TDM has an advantage in terms of cost. However, once the configuration is fixed, it is difficult to increase the number of lines in the TDM. Difficulty is provided by deploying new MUX/DEMUX in the TDM system. At the point of flexibility for multiplexed lines, the FDM has an advantage.

Since CODEC and MUX/DEMUX are necessary at the TDM when different kinds of services (i.e.: video signals and private line signals) are handled simultaneously, we have adopted the FDM method.

System configuration

Figure 3 shows system configuration. At a center office, each 8U MUX multiplexes eight U-lines coming from ISDN switches. A 1.5Mbps and 6Mbps QPSK modems modulate ISDN primary rate signals (1.5 Mbps) and the secondary rate of private line signals coming from private line digital switches, respectively. Modulated frequency is 100M to 200MHz. After the frequency multiplexed, these signals are intensity moderated and converted into optical signals.

At remote terminals, received optical signals are

converted to electrical signals again. The QPSK sub-carrier is demodulated in order to obtain its original signals such as ISDN primary rate signals and the secondary rate of private line signals. ISDN primary signals obtained are divided into eight ISDN BRI by 8U-Mux and are transmitted to subscribers using metal lines. On the other hand, DS2Mux divides the secondary rate of private signals into twelve I interfaces (64kbps, 128kbps).Then signals are transmitted to subscribers using metal lines.

We obtained the optical transmission distance of 40km or longer on 1.3 μ m SMF.

Specification of system

Table 2 shows specification of the system. Up to twelve private high speed lines and thirty-three ISDN BRI lines are supported in the system. The system can transmit these different services on two fibers. Assuming the system handles private lines exclusively, as many as 24 lines are supported simultaneously. In the case of ISDN lines only , it handles 64 lines.

We use both FDM and TDM as methods for optical transmission line extension as shown in Figure 3.

Transmission parameters

Table 3 shows specifications for digital modulation and demodulation. We adapted digital modulation method QPSK as because its durability for non-linear noise and efficient use of the band width.

Required minimum CNR (carrier to noise ratio) for a digital demodulator is calculated 25dB in order to meet BER criteria of 10^{-8} . Signal degradation due to thermal noise at receives and a 5dB as a path margin are also considered.

In the optical transmission system, CNR should be maintain 25dB or larger in the entire path. Based on transmission experiments, allowable distortion is 40dBc (1). Distortion is mainly generated at DFB-LD and driver AMP of E/O converter.

In order to meet the specifications for digital modulation and demodulation with a 40 km path, parameters of E/O and O/E are summarized in Table 4. These parameters are calculated from modulation factors and Noise Figure of pre-amplifier at Table 3.

Total CNR (CNR_A) of optical transmission path is given by optical transmitter CNR (CNR_T) and optical receiver CNR (CNR_R) as follows :

$$CNR_A = (CNR_T^{-1} + CNR_R^{-1})^{-1}$$

$$= \left(\left(\frac{m^2}{2} \right) \frac{1}{RIN \cdot B} \right)^{-1}$$

$$+ \left(\frac{\frac{m^2}{2} I_p^2}{2 q I_F B + 2 q I_L B + \frac{4 K T B F}{R_L}} \right)^{-1} \right)^{-1}$$

m : modulation factor

RIN : relative intensity noise

B : band width I_p : optical current

I_L : surface leakage current q : charge

T : temperature K : Boltzmann's constant

R_L : load resistance

F : Noise Figure of pre-amplifier

Figure 4 shows CNR as a function of optical received power. Figure 5 shows CNR and CTB as a function of modulation factor.

It is realized that the influence of RIN on CNR_A around 25 dB is negligible and minimum optical received power is determined by CNR_R . We chose the modulation factor which we can obtain 6dB margin for both CNR and CTB. Modulation factor of 6Mbps is adjusted larger than that of 1.5Mbps in order to obtain the same optical received power. Difference of modulation factors is associated with difference of noise band width at demodulators.

Conclusion

We have developed digital line multiplexing optical transmission equipment, and have obtained performances in the field test. Using the FDM technique in public communication networks, different kind of services (Private line: 6 Mbps and ISDN 4 lines) are successfully transmitted in the same fiber.

Reference

- (1)SEKIYA, et al : 'Experiments on DEQPSK Signal Transmission with CTB', 1993 IECE Spring Conference, B-998



Toshimasa Yoshimura received the B.S. and M.S. degrees from Osaka University, Osaka, Japan in 1977 and 1979, respectively.

In 1979, he joined the Kansai Electric Power Co., Ltd. In 1993, he went on loan to Kansai Telecommunication Technology Co., Ltd.

Since 1996, he is on loan to Osaka Media Port Co., Ltd. Currently, he is working at sales department for a vice-director.



Katuya Hayashi received the B.S. degree from Kyoto Kogei Seni University, Kyoto, Japan in 1988. In 1988, he joined the Kansai Electric Power Co., Ltd. Currently, he is working at Communication System Group, Information & Communications department.



Shinichirou Dogi received the B.S. degree from Meiji University, Tokyo, Japan in 1988.

In 1988, he joined the Kansai Electric Power Co., Ltd. In 1994, he went on loan to Kansai Telecommunication Technology Co., Ltd.

Since 1996, he is working at Communication System Group, Information & Communications department, the Kansai Electric Power Co., Ltd.



Tokuhide Kasetani received the B.S. degrees from Nagoya Institute of Technology, Nagoya, Japan in 1984.

In 1984, he joined the Furukawa Electric Co., Ltd. Currently, he is working at Information and Electronics Laboratory, where he has been engaged in the development on optical transmission systems.



Kensaku Sekiya received the B.S. degree from Chiba University, Chiba, Japan in 1992.

In 1992, he joined the Furukwa Electric Co., Ltd. Currently, he is working at Information and Electronics Laboratory, where he has been engaged in the development on digital modem system.



Kazutaka Shimoozsako received the B.S. degree from Tokyo Denki University, Tokyo, Japan in 1988.

In 1988, he joined the Furukawa Electric Co., Ltd. Currently, he is working at Access network design, Multimedia equipment / System department.

Table 1 Comparison between FDM and TDM

Item	FDM	TDM	Remark
Mixture of services	good	fair, requires an additional MUX/DEMUX	Private line 24 channels + ISDN line 64 channels
Optical transmission distance	good	good	≥ 40 km
MTBF	good	good	dominated by MTBF of the LD module
Cost at a basic configuration	fair 8 modems are necessary.	good A TDM handles ISDN 8 lines.	A configuration based on ISDN 8 lines.
Flexibility for number of lines	good Simply putting an additional modem.	fair The number should be set initially. Otherwise, an upper level of equipment needed.	
Flexibility for increasing subscriber	good No fiber installation required. Optical coupler enable an additional subscriber	fair A additional subscriber place requires fiber installation.	
Analog signals mixture	good Basic setting can transmit video and voice signals.	poor CODEC and MUX/DEMUX are necessary.	
Total evaluation	good	fair	

Table 2 Specification of System

Item		Specification	
		Private line transmission	ISDN line transmission
maximum number of channels		12 channels	32 channels
Kind of line		High speed digital (64kbps,128kbps)	2B+D basic interface
Optical transmission	Multiplexing method	TDM and FDM	
	Multiplex speed at TDM	6.312Mbps	1.544Mbps
	FDM frequency band	100~200Mhz	
	Digital modulation method	QPSK	
	Optical modulation method	Direct intensity modulation	
	Wavelength	1.3 μ m	
	Transmission line	SMF	
	loss bagged	≥ 20 dB	
	Transmission distance	40km (typical)	
Subscriber transmission	Data rate	320kbps	160kbps
	Available channel	B1,B2	B1,B2,D
	Symbol	B8ZS	2B1Q
Transmission quality		$BER \leq 10^{-8}$	

Table 3 Specification for digital modulation and demodulation

Item	Specification	
	Private line transmission	ISDN line transmission
Moduration method	QPSK	
Bit rate	6.312Mbps	1.544Mbps
Symbol rate	3.156Mbps	0.772Mbps
CNR	25dB	
Allowable distortion	≥ 40 dBc	

Table 4 Optical transmission parameters

Item		Specification
Optical transmitter (E/O)	Optical element	DFB-LD
	RIN	-150dB/Hz
	Optical modulation factor	15.8%/ch (private line) 10.8%/ch (ISDN)
	Band width	6.3Mhz (private line) 1.5Mhz (ISDN)
Optical reciever (O/E)	Optical element	PIN-PD
	Quantum efficiency	85%
	Surface leakage current	20nA
	Noise figure	3.5dB
	Load resistance	50 Ω

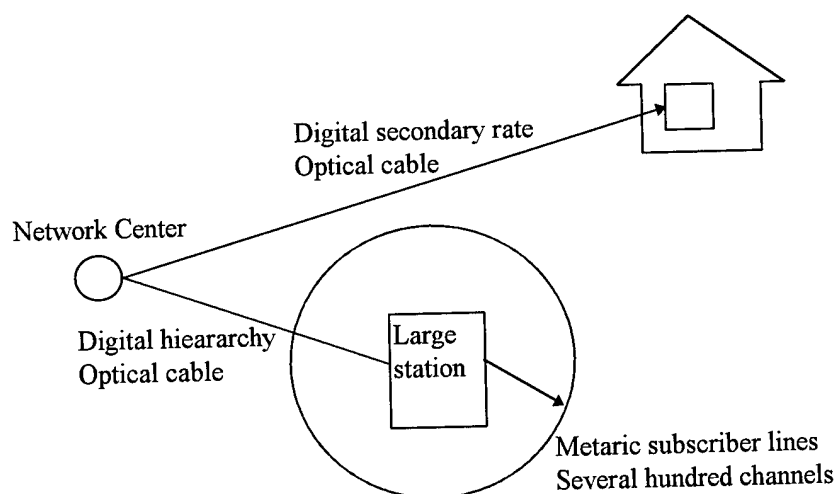


Fig 1 Configuration of the conventional system

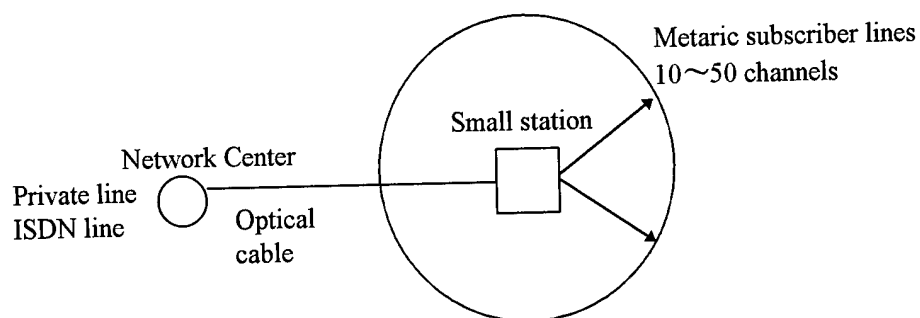


Fig 2 Configuration of a proposed system

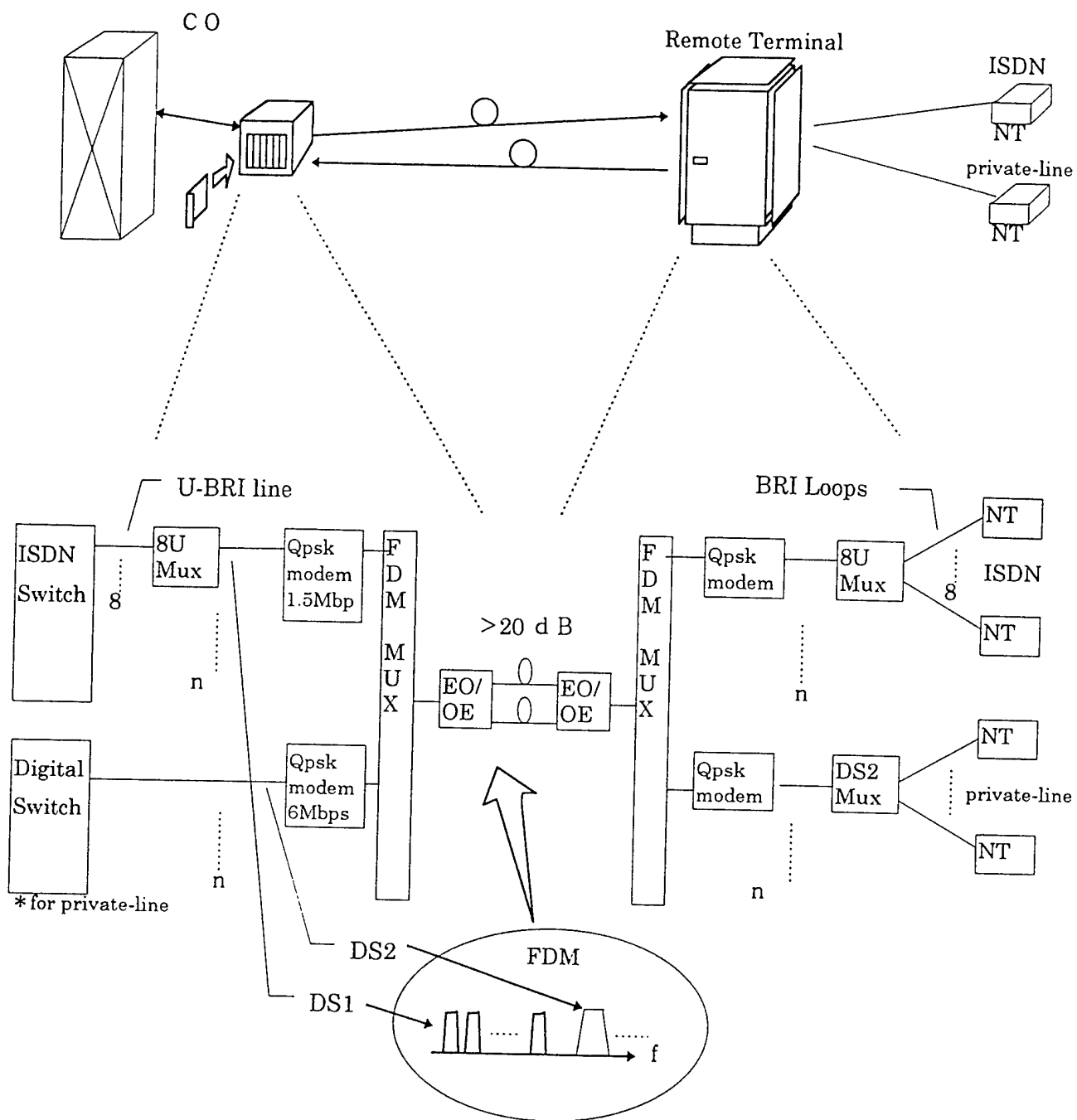


Fig 3 System configuration

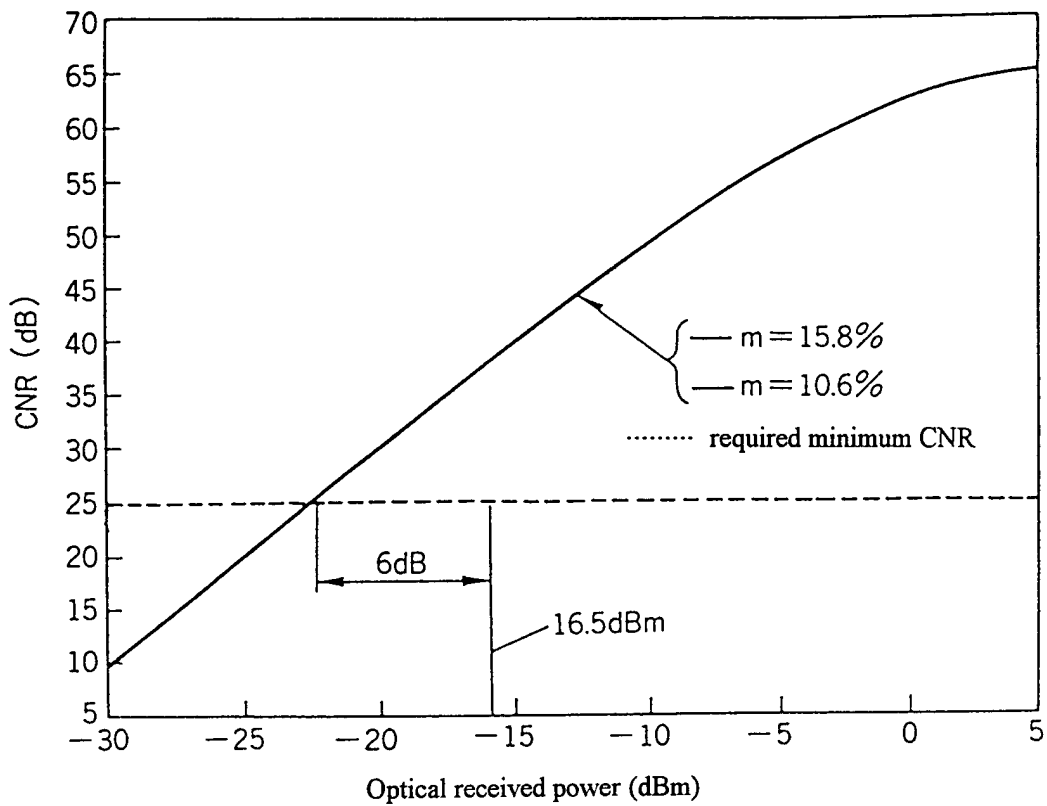


Fig 4 CNR vs optical received power

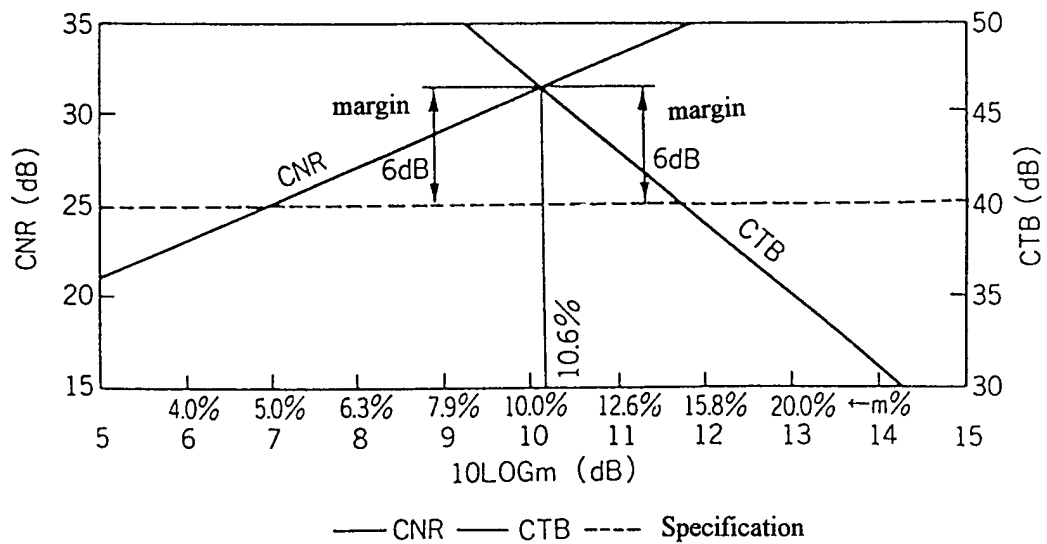


Fig 5 m vs CNR, CTB

2.5 Gbit/s REPEATERLESS FIBER OPTIC LINK: OPTIMIZATION AND TESTING OF A REMOTELY PUMPED ERBIUM-DOPED FIBER AMPLIFIER REALIZED WITH COMMERCIAL OPTICAL COMPONENTS

Francesco POZZI, Daniele MORO, Maurizio MAGLIO
SIRTI S.p.A., Cables and Optical Technologies
Via E.Fermi 2, 20060 Cassina de' Pecchi (MI) ITALY

ABSTRACT

In this paper we report a 2.5Gbit/s repeaterless transmission system over single mode dispersion shifted fiber (SM-DS) with a remotely pumped amplifier realized with commercially available optical components.

1. INTRODUCTION

Long distance repeaterless transmission is one area of digital communication where new research achievements find direct application to commercial systems due to the continuously growing demand of links in the range between 150 and 300 km for terrestrial as well as submarine connections.

The transmission distance can be increased in many ways: firstly by using an optical postamplifier in order to boost the transmitter power, secondly by placing a preamplifier in front of the receiver in order to increase the signal power level over the receiver noise or finally by making use of in line amplifiers along the link.

Another attractive way to further increase the power budget of a repeaterless link is to make use of remotely pumped amplifiers. They basically consist of a piece of Erbium doped fiber placed typically some tens of kilometers away from the transmitter (Remotely Pumped PostAmplifier) or from the receiver (Remotely Pumped PreAmplifier). They are pumped by a high power 1480nm emitting laser placed at the transmitter or at the receiver side respectively. The pump power is injected directly into the same fiber utilized to transmit the signal. As the system does not incorporate any active component along the link or electrical power fed through the fiber optic cable it is much more reliable and need less maintenance expenses than traditional configurations.

Therefore they are preferable in several practical situations such as in submarine cables.

Moreover as any other optically amplified link, the system still remains completely transparent to the information code so any upgrading (increase in the bit-rate or in the number of transmission wavelengths) can be carried out by simply changing the terminal apparatus.

2. OPTICAL AMPLIFIER REALIZATION AND OPTIMIZATION

The principal aim of this stage is to realize a low noise optical preamplifier. The main design parameters available are the pumping configuration and the active fiber length¹. It is well known that forward pumping configuration provides the best noise figure because of the greater population inversion in the first part of the fiber. Moreover for every fiber type, pump power and signal wavelength there is an optimum active fiber length which maximizes the gain. If the fiber is longer than this value its last part is underpumped and causes a reduction of the signal output power. On the other hand if it is shorter some pump power cannot be utilized in order to amplify the signal.

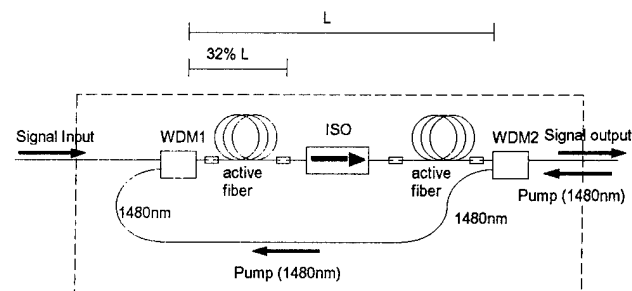


Fig.1 Optical amplifier in forward pumping configuration

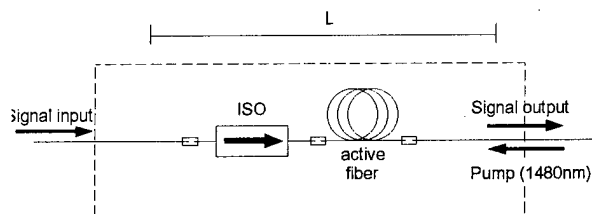


Fig.2 Optical amplifier in backward pumping configuration

In optical amplifiers for remote pumping application the pump power is normally small (a few milliwatts²) and counterpropagating with respect to the signal. So we can propose two possible amplifier arrangements as previously shown in figures 1 and 2.

In the forward pumping configuration (fig.1) the pump power is taken from the line and is injected into the fiber in a copropagating scheme. The right choice of the Wavelength Division Multiplexers (WDM1 and WDM2) with low insertion loss can minimize unwanted pump loss. The use of micro-optic WDM can also provide wide signal bandwidth which is an important feature in multiwavelength systems. The use of a low loss polarization insensitive isolator placed at about 32% of the whole length of the active fiber can further improve the noise and gain performances of the amplifier³ and partially compensate the WDM insertion loss. Input and output isolators can also be included into the device in order to completely isolate it from any unwanted external backreflection.

In the backward pumping configuration (fig.2) the pump is counterpropagating with respect to the signal. The low loss input isolator enables the protection of the device from reflections at the input port but no isolator can be placed at the output unless we make use of two line fibers: one devoted to the signal and the other to the pump.

Having all this in mind, we optimized the amplifier using the cut-back technique. Starting from a fiber of 25 meter long we have progressively reduced its length and measured the amplifier performances in terms of noise and gain. The characterization of the device has been carried out by using the optical measurement method.

In the realization of the amplifier a key factor could be represented by the insertion loss of splices between fibers of different geometrical characteristics. Repetition of the fusion process has revealed to be one possible solution in order to increase the guiding properties of the splice region. We show below the gain and noise figure measured in the 1550nm band versus pump power in the range of greater interest (7.5mW 12.5mW). We have taken into consideration different fiber lengths (23 and 14 meters) and configurations. The signal input power is supposed to be -30dBm

which is of the same order of the expected preamplifier sensitivity.

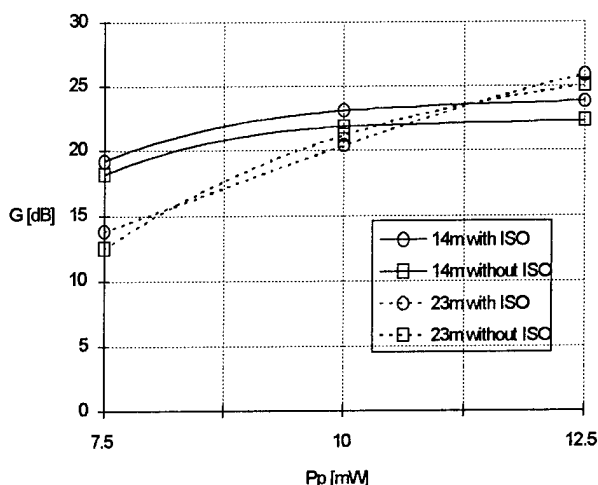


Fig.3a Gain (G) versus pump power (Pp) for L equal to 14m and 23m in forward pumping with and without isolator ($\lambda_{\text{signal}}=1550\text{nm}$, $P_{\text{signal}}=-30\text{dBm}$).

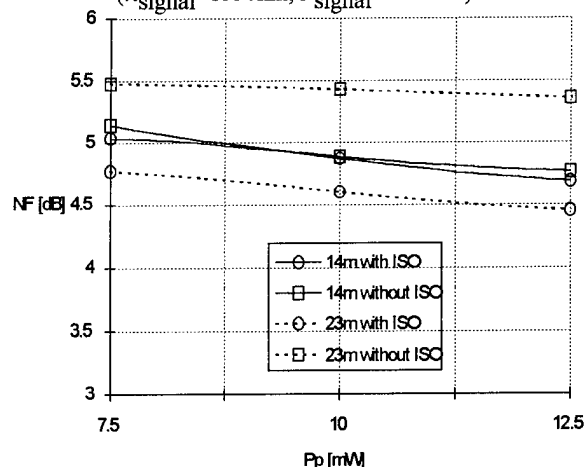


Fig.3b Noise Figure versus pump power for L equal to 14m and 23m in forward pumping with and without isolator ($\lambda_{\text{signal}}=1550\text{nm}$, $P_{\text{signal}}=-30\text{dBm}$).

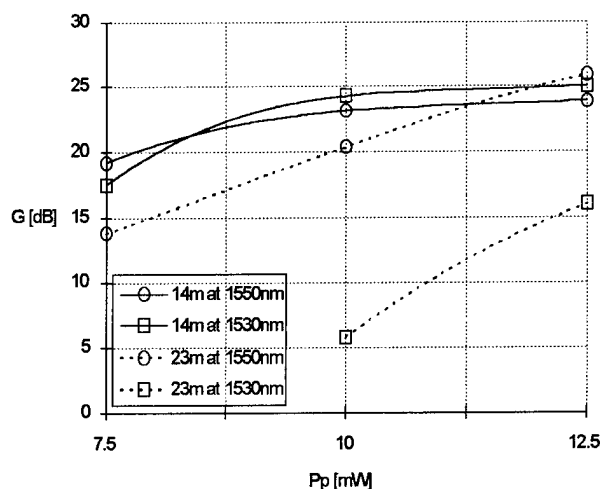


Fig.4a Gain (G) versus pump power (Pp) for L equal to 14m and 23m in forward pumping with $\lambda_{\text{signal}}=1550\text{nm}$ and $\lambda_{\text{signal}}=1530\text{nm}$ ($P_{\text{signal}}=-30\text{dBm}$).

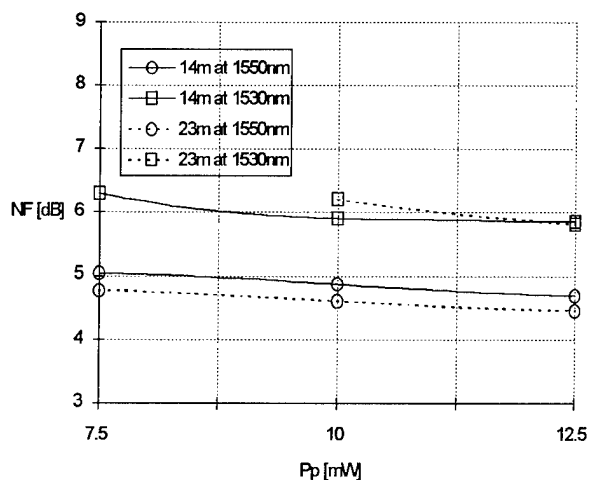


Fig. 4b Noise Figure versus pump power for L equal to 14m and 23m in forward pumping with $\lambda_{\text{signal}}=1550\text{nm}$ and $\lambda_{\text{signal}}=1530\text{nm}$ ($P_{\text{signal}}=-30\text{dBm}$).

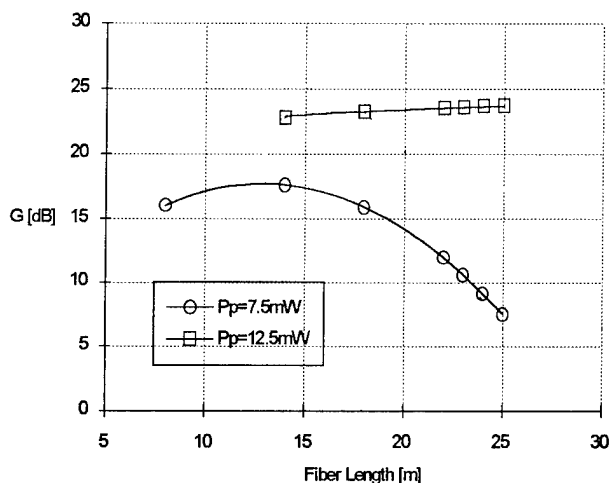


Fig. 5 Gain versus fiber length in forward pumping with pump power of 7.5mW and 12.5mW ($\lambda_{\text{signal}}=1550\text{nm}$ and $P_{\text{signal}}=-30\text{dBm}$).

As expected if the fiber length is decreased the gain is improved till the optimum length. From the graph reported in figure 5 we can deduce that the optimum fiber length is about 14m. The use of an isolator can further improve the device performances particularly for longer active fibers (fig. 3a, 3b). As shown in figure 4a and 4b a reduction in fiber length results in gain equalization. In fact due to the better inversion into the active fiber at low pump powers we have an increase in the gain at 1530nm with respect to 1550nm.

The gain in the backward pumping scheme has shown to be a little bit higher than in the forward one because the pump power in this case is not affected by passive components insertion loss. On the contrary the noise figure is higher because of the worse inversion of the first part of the active fiber.

For this reason it is necessary to verify experimentally which configuration is more suitable for the remote pumping application.

3. REMOTE PUMPING MEASUREMENTS.

The power budget (PB) is a very important parameter introduced in order to characterize communication system performances. It can be defined as the greatest tolerable signal attenuation, normally expressed in dB, which assures a bit error rate (BER) lower than a previously determined value (i.e. 10^{-10}).

Therefore in a conventional optically amplified link, schematically shown in figure 6, the power budget is expressed as follows:

$$PB = (P_{tx} - P_{in}) + (P_{out} - P_{rx})$$

where P_{in} and P_{out} are the input sensitivity and output power of the amplifier respectively.

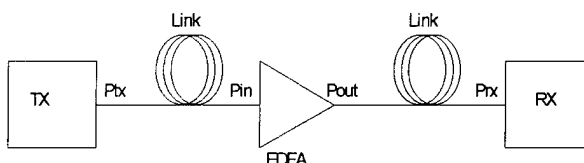


Fig. 6 PB in a conventional optically amplified system.

3.1. Description of the remote pumping test-bed.

We show below the scheme of a repeaterless link with a remotely pumped preamplifier:

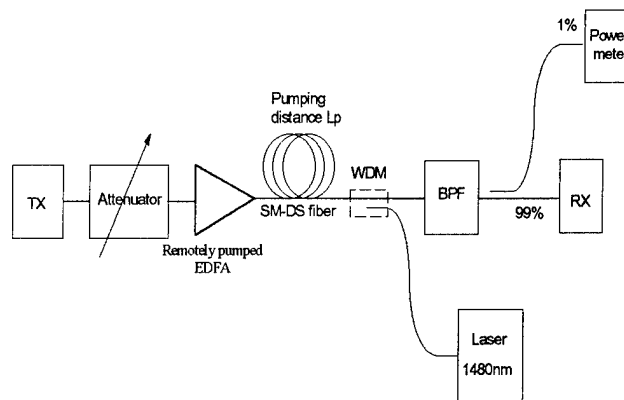


Fig. 7 Set-up for remote pumping measurements.

The transmitter-receiver couple is a SDH analyzer which allows bit error rate evaluation, while the line is a Single Mode Dispersion Shifted fiber (SM-DS) with an attenuation of 0.27dB/km in the 1480nm band and 0.25dB/km at 1550nm.

BPF is an optical filter with -3dB full width half maximum of about 1.3nm. Finally the pump source

is an high power ($>100\text{mW}$) laser diode with emission in the $1.48\mu\text{m}$ band.

The 1% coupler is connected to a Power Meter (PM) or an Optical Spectrum Analyzer (OSA) in order to give real-time measurement of received optical power.

3.2. Experimental characterization of the system with remotely pumped preamplifier.

In this section we report the main results in terms of total power budget for the different amplifier configurations and fiber lengths using the experimental set-up shown in figure 7.

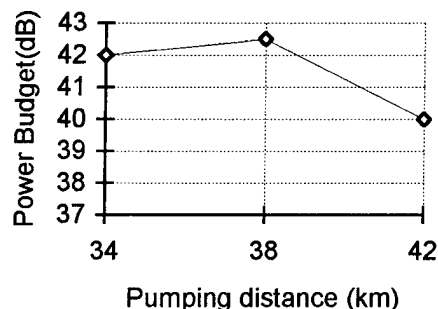


Fig.10 Power budget as a function of the pumping distance with forward pumped amplifier and fiber length equal to 23m.

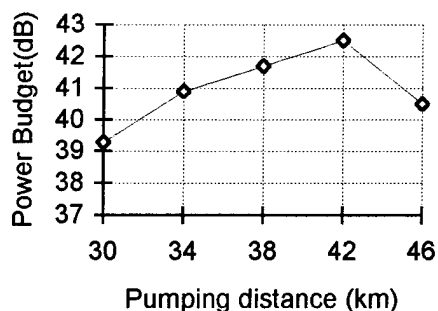


Fig.11 Power budget as a function of the pumping distance with forward pumped amplifier and fiber length equal to 18m.

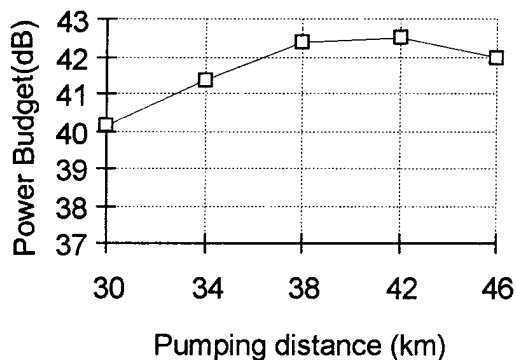


Fig.12 Power budget as a function of the pumping distance with forward pumped amplifier and fiber length equal to 14m.

From these experimental results it is apparent that there is, for any amplifier configuration, an optimum pumping distance which maximizes the power budget. For longer spans the decrease in pump power deteriorates the amplifier performance which results in a decrease in the power budget. On the other hand below the maximum there is no amplifier sensitivity improvement able to compensate the power budget decrease associated with the distance reduction. As shown from figure 10 to 12, optimum distance increases as the active fiber is shortened because less pump power is needed for correct operation.

The use of a booster amplifier with a saturated output power of $+15\text{dBm}$ with the remote preamplifier placed at the optimum distance previously found, has been demonstrated not to reduce the system sensitivity giving a total available power budget of 57dB .

The realized amplifier has also been tested in locally pumped configuration in order to check its noise performance. Pump power higher than 15mW in forward pumping configuration gave a sensitivity of about -34dBm . Sensitivity penalty less than 1dB was observed in remote pumping configuration at optimum pumping distance.

In case of counterpropagating amplifier scheme, the corresponding power budget curve versus pumping distance is illustrated in figure 13.

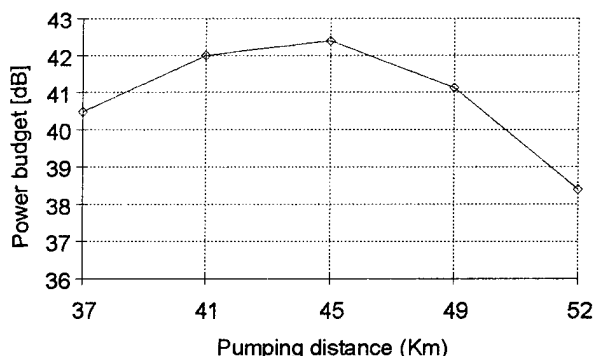


Fig.13 Power budget as a function of the pumping distance with backward pumped amplifier and fiber length equal to 14m.

As expected the optimum distance is further increased but the sensitivity is worse so the best power budget is approximately the same as in the previous case.

As a matter of fact, this last configuration has shown many problems in terms of reliability, probably linked to backreflections from the optical line due to the lack of an isolator at the output of the amplifier. Apparently the only way to make this configuration to work is to use two different fibers: one for the pump and the other for the signal.

3.3. Raman gain measurement

The presence of high pump power in SM-DS fiber is well known to give Raman gain⁴. In remotely preamplified systems it gives a direct contribution to the available power budget. In figure 8 we show the laboratory test-bed used to measure Raman contribution. It is an experimental situation very similar to that of the actual remote pumping configuration:

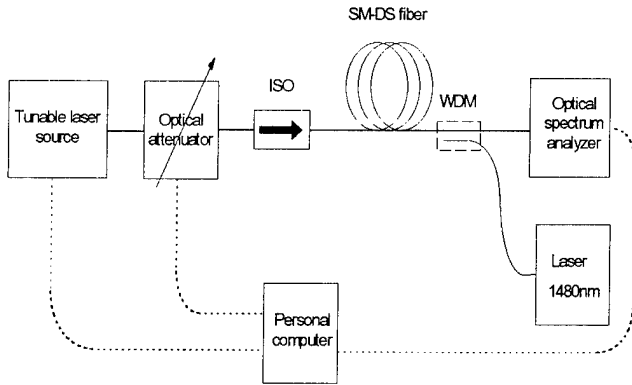


Fig.8 Set-up for raman gain measurements.

The laser diode injects the pump power into the fiber. The attenuator sets the actual input signal power to the line and the optical spectrum analyzer (OSA) is used in order to measure the output power.

We made our experimental tests on a 46km long fiber with different pump power levels as shown in the following figure at 1550nm and 1560nm:

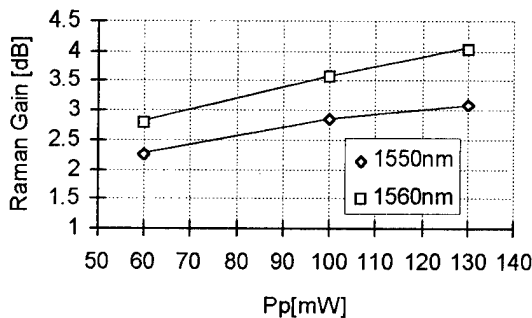


Fig.9 Raman gain as a function of the pump power at 1550nm and 1560nm.

The qualitative behaviour as well as the quantitative results are in good agreement with those commonly reported in literature⁵.

4. SYSTEM PERFORMANCES EVALUATION FROM AMPLIFIER PARAMETERS

In this section we obtain an expression to evaluate system performances as function of the amplifier parameters.

As the system power budget is strictly dependent on the error probability, our first target is to find out an analytical expression for system BER performance in case of different pumping distances.

The amplifier gain and noise figure have been experimentally measured as a function of pump and signal input powers. The result of interpolation in case of 14m active fiber length in forward pumping configuration are reported in figures 14a and 14b.

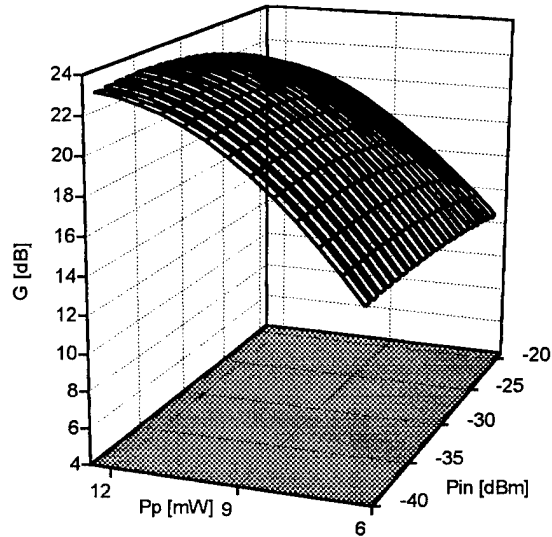


Fig 14a. Optical amplifier gain vs signal input (pin) and pump power (Pp).

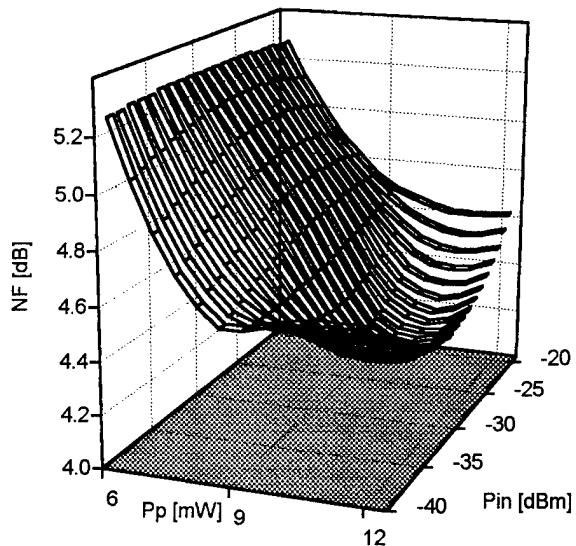


Fig 14b. Optical amplifier noise figure vs signal input (Pin) and pump power (Pp).

From the noise figure definition we can obtain the output signal to noise ratio (SNR):

$$SNR_{out} = SNR_{in} / NF_L$$

Where NF_L is the amplifier noise figure.

In current analysis the noise contribution, due to non linear Raman amplification in fiber link, is neglected. In fact it is known that in a cascade of two amplifiers, the noise is mainly generated in the first one.

The input signal to the amplifier is affected only by shot noise so the noise power spectral density at the photodiode output is⁶:

$$N_e = 2qI_s \langle M^2 \rangle = 2 \frac{\eta q^2}{h\nu} P_{in} \langle M^2 \rangle$$

Where I_s is the mean signal current, η the avalanche photodiode efficiency, P_{in} the mean optical power at the amplifier input, h the Planck constant, ν the optical frequency, q the electronic charge and $\langle M^2 \rangle$ the mean square value of the photodiode gain.

Moreover the average electrical power (P_{em}) generated by the signal input is:

$$P_{em} = \left(\frac{\eta q}{h\nu} P_{in} \langle M \rangle \right)^2$$

Where $\langle M \rangle$ is the mean photodiode gain. Finally the SNR at the receiver output as function of the input power and the amplifier noise figure is given by:

$$SNR_{out} = \frac{\eta P_{in}}{2h\nu B_e \cdot F \cdot NF_L} \quad \text{where}$$

$$F = \langle M^2 \rangle / \langle M \rangle^2 \quad \text{is the APD noise figure}$$

where B_e is the electrical bandwidth of the receiver.

At the photodiode output, the electrical signal has a gaussian distribution and the BER can be easily calculated from the well known formula reported below⁷:

$$BER = Q \left(\frac{m_1 - m_0}{\sigma_1 + \sigma_0} \right)$$

The m_1 term is the optical signal intensity of the '1 bit', m_0 is that of the '0 bit' while σ_1 and σ_0 are their standard deviations, and Q is the Gaussian distribution function. As m_0 is zero and σ_0 is significantly less than σ_1 , the BER can be written only as function of the SNR at the receiver. The following expressions allow us to estimate the system power budget.

$$BER = Q(\sqrt{SNR_{out}}) = Q(\sqrt{P_e/N_e})$$

with P_e received '1 bit' electrical power ($2 \cdot P_{em}$), then

$$BER = Q \left(\sqrt{\frac{\eta P_{in}}{h\nu \cdot B_e \cdot F \cdot NF_L}} \right)$$

with $P_{rx} > -28\text{dBm}$

We calculated the optical pump power at the amplifier for many pumping distances. Afterwards, for different input signal powers, we first evaluated the amplifier noise figure and gain from figure 13, then we estimated the system power budget corresponding to the established BER value (10^{-10}) taking into account that the optical power necessary for the receiver correct operation must be greater than -28dBm .

In the following figure we illustrate the analysis results.

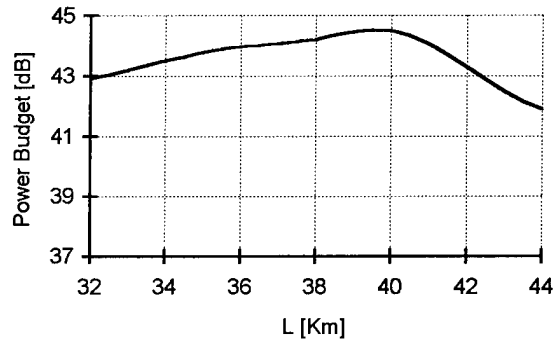


Fig.15 Power budget as function of the fiber link length assuming $\eta=0.7$, $B_e=2\text{GHz}$ and $F=6$.

The qualitative behaviour is in agreement with the experimental curve previously reported (fig.12).

5. CONCLUSIONS

A 2.5Gbit/s repeaterless transmission system over dispersion shifted fiber with remotely pumped preamplifier has been reported.

We experimentally demonstrated that forward pumping configuration with active fiber length of 14 meters is the best choice for our application. In this case in fact the amplifier gives enough gain, low noise and wide bandwidth.

The best sensitivity measured for a BER of 10^{-10} with the amplifier in the optimum configuration (-34dBm) undergoes a maximum penalty of about 1dB when the prototype is placed in the remote pumping set-up and the corresponding maximum available power budget was about 42dB. The Raman contribution to the power budget was estimated to be nearly 3dB.

The use of a booster with a saturated output power of +15dBm gave a total available power budget of 57dB.

References

- [1] E.Desurvire, "Erbium doped fiber amplifiers", J. Wiley & Sons 1994.
- [2] P.B. Hansen et Al. "374 km transmission in a 2,5Gbit/s repeaterless system employing a remotely pumped Erbium-doped fiber amplifier", IEEE Photonics technology Letters, Vol.7, No.5, pg. 588, May 1995.
- [3] S. Yamashita, T. Okoshi, "Performance improvement and optimization of fiber amplifier with midway isolator", IEEE Photonics Technology Letters, Vol. 4, No. 11, November 1992.
- [4] G.P. Agrawal, "Non linear fiber optics", Academic Press, 1989 pg. 218.
- [5] V.L. da Silva, "Comparison of Raman efficiency in optical fibers", OFC '94 Technical Digest, WK 13, pg136.
- [6] N.A. Olsson, "Lightwave system with optical amplifiers", Journal of lightwave technology, Vol. 7, No. 7, July 1989.
- [7] R.M. Gagliardi, S. Karp, "Optical communications", J. Wiley & Sons 1995.

Authors

Francesco Pozzi was born in Gallarate, Italy, in 1968. He received the doctor degree in Electronics Engineering from "Politecnico di Milano" in 1993. In 1995 he joined R&D Dept. of SIRTl where he has been engaged in passive optical components and optical amplifier as a Junior Engineer.

Daniele Moro was born in Castellanza, Italy, in 1971. He received the doctor degree in Telecommunications Engineering from "Politecnico di Milano" in 1995. At the beginnig of 1996 he joined R&D Dept. of SIRTl where he has engaged, as Junior Engineer, in the field of optical component characterization and of broadband network design.

Maurizio Maglio was born in Crema, Italy, in 1961. Since 1985 he has been working as an Engineer in R&D Dept. of SIRTl. After a long experience on passive components, in particular multi-mode and single-mode coupler. Since 1995 he has been engaged in active optical components.

FULLY ENGINEERED 4-WDM 10 Gbps OPTICAL TRANSMISSION SYSTEM

Kyota Susai, Tokuhide Kasetani, Hiroshi Nakamura, Akira Fujisaki

The Furukawa Electric Co., Ltd., Tokyo, Japan

ABSTRACT

The Furukawa Electric has developed a four channel, 2.5 Gbps WDM-OFA transmission system. The system consisting of 6 OFAs in series can transmit signals up to 560 Km. Equipped optical supervisory channel (OSC) provides integrated alarms and performance monitoring, the system is ready to deploy. From BER (Bit error rate) performance measured in a long haul setting (with a 560 Km SMF path and 6 OFAs in between), we evaluate power penalties at a 560 Km transmission setting. Also, influence of optical power into OFA on power penalties is discussed. Based on the SNR (Signal to Noise Ratio) calculation as well as an optical level diagrams, we propose the system configuration.

INTRODUCTION

As a volume of telecommunications is increasing, there has been a growing demand for high speed transmission systems. The WDM (wavelength division multiplexing) -OFA based on the wavelength multiplex technology and optical fiber amplifiers is a key solution in order to comply with a demand at a competitive cost.

The Furukawa Electric has developed a four 2.5 Gbps Dense WDM-OFA transmission system. The system, ready to deploy, attains a transmission rate as high as 10 Gbps and as far as 560 Km.

In this paper, we describe an outline of a prototype system, measured transmission performance along a 560 Km SMF (Single mode fiber) path.

Finally, we propose the system configuration based on the SNR calculation as well as optical level diagrams.

EXPERIMENT

System configuration

The schematic view of system configuration and

specifications are provided in Figure 1 and Table 1, respectively. Assuming a 80 Km as a spacing between the nearest OFAs, our objectives of transmission distance between clock-regenerating is as long as 560 Km with 6 OFAs in between.

Table 1. Specifications (4 channel system)

Optical input	wavelength	1265 to 1360, 1430 to 1580 nm
	power	-3 to -18 dBm
TX mux output	wavelength	1546, 1550, 1554, 1558 nm
	Format	complies with Sonet / SDH standards for 2.4 Gbps
Common Fiber output power		+14 dBm
Common fiber type		non-DSF
Booster or in-line OFA	Noise figure	<5.5 dB
	Output power	+14 dBm
Size		62.5W, 32.5D, 22.4H cm
Power consumption		< 67 W with in-line OFA < 13 W for in-line OFA
Environmental	Temperature	0 to +40 degree centigulate
	Humidity	5 to 95% R.H. non condensing
Alarms	WDM TX	input /output optical power failure power supply failure
	Booster OFA & in-line OFA	input /output optical power failure power supply failure pump laser failure
Remote control		OFA on/off output level of OFA (optional)
Safety for Laser hazard		automatic shutdown

Physical dimensions of the WDC (Wavelength Conversion and Multiplex) shelf is illustrated in figure 2. Each input signal with wavelength of 1310 or 1550 nm, is actively converted into selected wavelengths by the O/E package and the TX package. The prototype has laser carrier wavelengths of any combination of 1546, 1550, 1554 or 1558 nm.

Figure 1. Schematic view of the system architecture

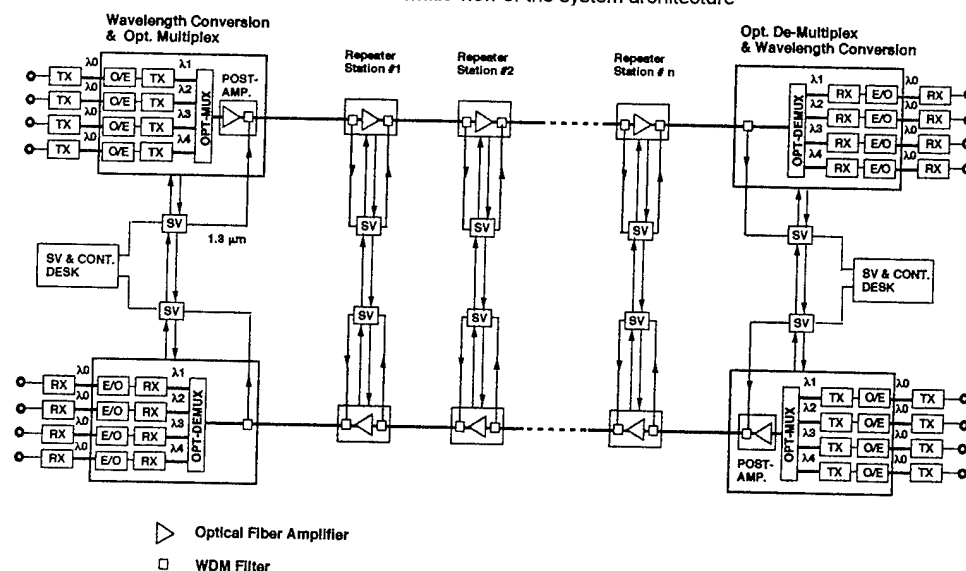
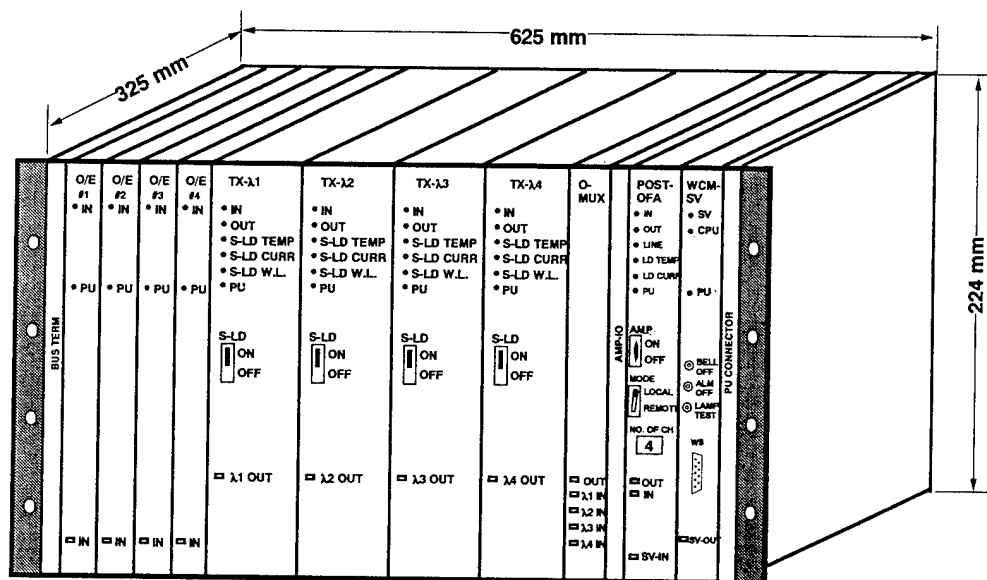


Figure 2. Physical dimensions of WDC (Wavelength Conversion and Multiplex) shelf



Modulation is performed by a LiNbO_3 base externally modulator unit in TX cards. Transmission performance was evaluated using 2^7-1 pseudo-random bit sequence, 2.488232 Gbps, NRZ (non return to zero) pattern signals.

In the OFA cards, NF (Noise figure) less than 5 dB has been achieved by employing a 980 nm and 1480 nm pumping laser at the condition that the OFA input power is -17 to -23 dBm and output power is 7.5 to 8.5 dBm.

A transmission path for this experiment consists of a 560 Km of the SMF (1310 nm zero dispersion fiber). Assuming dispersion of the SMF at 1550 nm is 17 ps/nm/Km, accumulated dispersion after 560 Km transmission is calculated 9520 ps /nm. Because the loss of the fiber is 0.2 dB/Km at 1550 nm, an optical attenuators are placed before each

OFA in order to adjust optical input power into the OFA at a selected level in experiments. By using the AGC circuit, output power of the OFA is adjusted +14 dBm for any input power. At the end of the path, a demultiplex card separates the composite signal into the individual signals at the different wavelengths. Photocopy of the entire system and the OFA card is shown in Photo 1 and 2. Table 2 provides main parameters of the OFA card.

Table 2 Main parameters of the OFA card

Size	3.5W, 32.5D, 22.4H cm
Power consumption	<13 W
Optical input	-16 to -28 dBm
Optical output	+8 +/- 1 dBm
Alarms	Input, Output, LD temp, LD current

Photo 1 Prototype system outlook

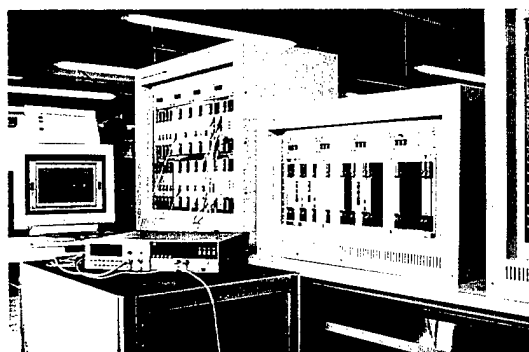
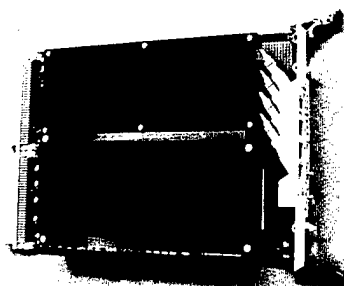


Photo 2 OFA card



Optical supervisory channel (OSC)

A telemetry system provides comprehensive status information on all components of the link. Performance and integrated alarm is remotely monitored from central stations located at each end of the link. Besides the SNR of the signal, almost all items useful for operation is monitored.

Several wavelengths for the optical supervisory channel (OSC) are proposed⁽¹⁾. Table 3 shows comparison among possible wavelengths. The reachable distance are based on the assumption of installed fiber loss (including splices and cable margin) at each wavelength range. There are design tradeoffs associated with each of these possible choices.

Components for the 1510 nm wavelength (e.g. laser diode, filters, etc.) are currently of limited availability. Until these components are mature and readily available, alternative wavelengths of 1480 nm or a wavelength in the 1310 nm band may be used. The selection of the 1480 nm wavelength may preclude the use of remote-pump fiber amplifiers, and may suffer extension ratio penalties arising from amplifier pump leakage. The selection of 1310 nm wavelength may preclude the use of that wavelength for alternative traffic.

In this prototype, we chose 1310 nm as OSC because of wide variety of components availability.

Table 3. Proposed wavelengths for SV (Bit rate = 1.5 Mbps)

Wave-length (nm)	output power (dBm)	loss (dB/Km)	received power (dBm)	reachable distance (Km)	note
1310	3	0.5	-40	80	distance limited
1480	18	0.4	-40	150	poor cost effectiveness
1530		0.3	-40		limited LD availability
1550	3	0.3	-40	130	filter insertion loss

RESULT AND DISCUSSION

OFA gain uniformity

Figure 2 shows an example of optical spectrum after 560 Km transmission. From optical spectrum at each OFA output, gain tilt along the path was summarized in Figure 3(a) and 3(b) for the OFA input of -20 dBm and -28 dBm, respectively. According to our system design, input power of -20 dBm and -28 dBm corresponds to the nominal and the lower limit of input power, respectively.

Figure 2. Optical spectrum after 560 Km transmission (OFA input power: -20 dBm)

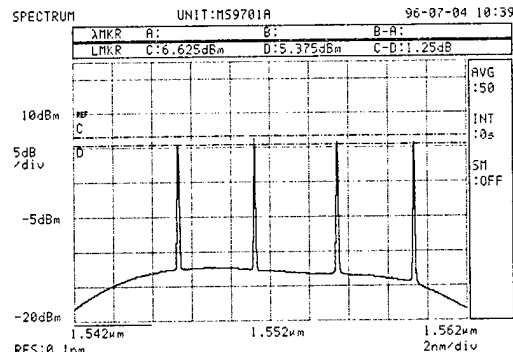


Figure 3 (a) Out put power variation along the 560 Km path (OFA input power: -20 dBm)

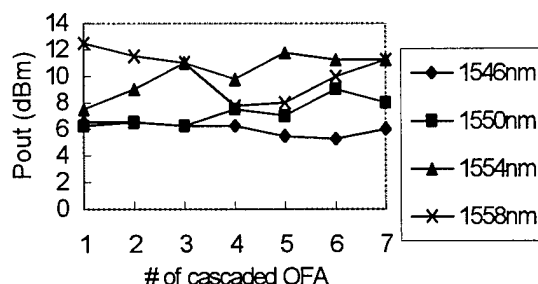
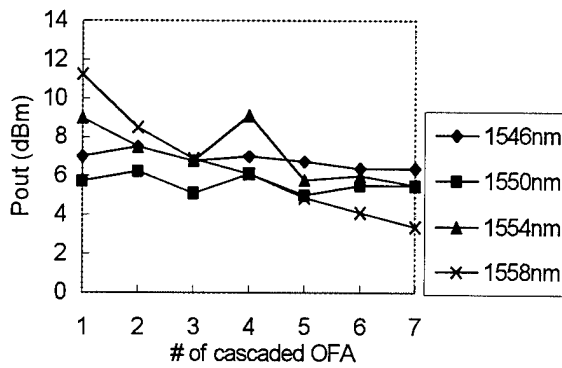


Figure 3 (b) OFA output power variation along the 560 Km path
(OFA input power: -28 dBm)



Based on the gain tilt measurement, it is realized that each optical signal is amplified equally at the OFAs along the path if the input power is -20 dBm. On the other hand, OFA output power of the 1558 nm channel decreases as the signal transmits the path than those of others if the input power is -28 or smaller.

According to the observation, the OFA input power of -16 dBm to -28 dBm would be preferred in order OFAs to amplify every channel uniformly.

BER performance

Figure 4 (a), (b), (c) and (d) show BER performance after 560 Km transmission for each optical channel. BER smaller than 1×10^{-12} is measured in order to verify no BER floor. It is realized that BER decreases as RX received power increases. No BER floor is observed if OFA input power is greater than -28 dBm.

BER measurement at a back to back setting are also provided in figure 4 (a) to (d). Power penalty smaller than 2 dB is achieved when OFA input power is greater than -28 dBm. When OFA input power is -30 dBm or smaller, however, BER performance degrades rapidly, and we observe BER floor.

Figure 4 (a) BER characteristic at 1546 nm channel

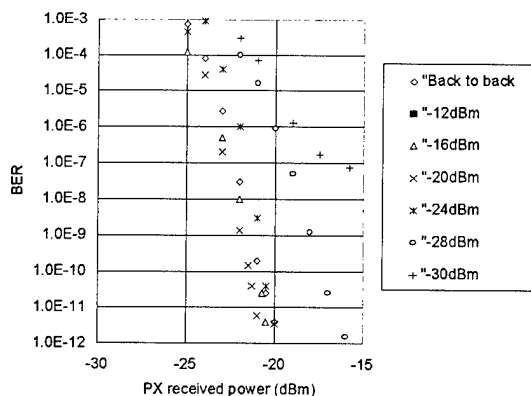


Figure 4 (b) BER performance at 1550 nm channel

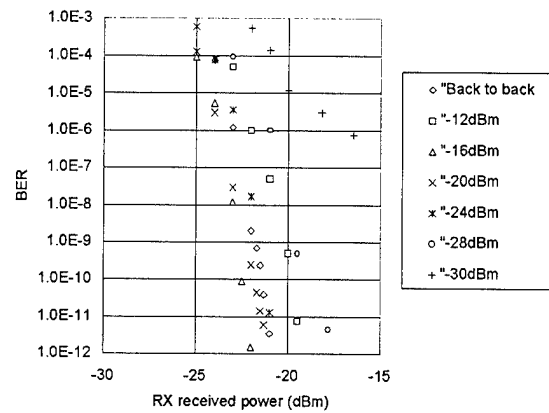


Figure 4 (c) BER performance at 1554 nm channel

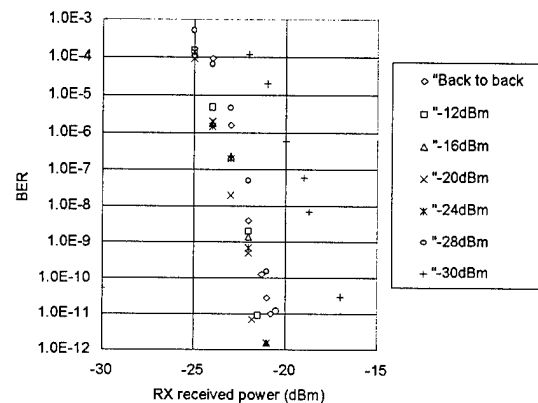
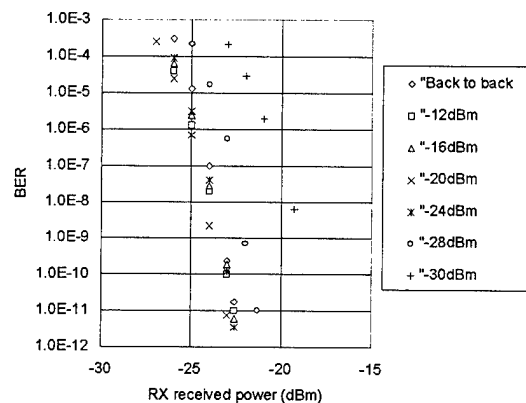


Figure 4 (d) BER performance at 1558 nm channel



Calculated BER characteristics based on SNR

Influence of OFA input power on BER performance is evaluated in terms of the SNR of the signal. Considering noise accumulation of OFAs, the SNR is given by:

$$\text{SNR} = \frac{G^2 \langle N_{in} \rangle^2}{(2kG(G-1)F \langle N_{in} \rangle + k^2(G-1)^2 F^2 \Delta \nu) B}$$

(1)

where,
 G: OFA gain
 $\langle N_{in} \rangle = P_{in} / h \nu$
 P_{in} : OFA input power
 h : plank constant
 ν : frequency of the signal
 K : number of cascaded OFAs (=6)
 F : NF (Noise figure) of each in-line OFA (=4.5 dB)
 $\Delta \nu$: bandwidth of an optical filter (=3.5 nm)
 B : bandwidth of receivers (=2 GHz)

When G is large enough, equation (1) is simplify as follows:

$$SNR = 2\langle N_{in} \rangle^2 / (2kF\langle N_{in} \rangle + k^2 F^2 \Delta \nu) B \quad (2)$$

Based on BER measurement at the back to back setting, we calculated SNR at receivers.

Then total SNR is given by equation.

$$1/SNR \text{ (total)} = 1/SNR(\text{OFA}) + 1/SNR(\text{receiver}) \quad (3)$$

In the model we use to investigate the influence of noise on BER, BER is associated with the SNR. Assuming that noise power and signal power are expressed Gaussian distribution, The BER performance can be calculated from Q factor ($Q=6$ for 10^{-9} BER, for example) ⁽³⁾.

$$BER = 1/(2\pi)^{1/2} \exp(-Q^2/2)/Q \quad (4)$$

$$Q = ((S(1))^{1/2} - (S(0))^{1/2}) / ((N(1))^{1/2} - (N(0))^{1/2}) \quad (5)$$

where $S(1)$, $N(1)$, $S(0)$ and $N(0)$ are the total signal and noise power on the logical ones and logical zeros, respectively.

Figure 5. Comparison between theoretical and measured BER

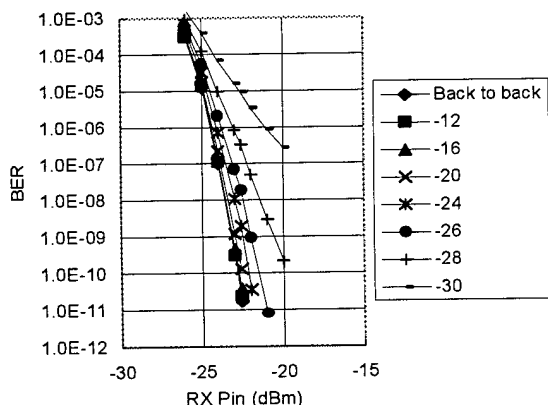


Figure 5 shows estimated BER as a function of optical input power into OFAs. It is clear from these results that calculated BER agrees with observed one. Minimum RX input power achieving

BER of 1×10^{-10} degrades as the number of cascaded OFA increases.

Allowing power penalty smaller than 1 dB, OFA input power higher than -26 dBm requires in order to meet this criteria.

Figure 6 (a) and (b) show examples of observed eye patterns after the 560 Km transmission. It is realized that eye pattern degrade as signal transmits.

Index of eye-opening is large enough when OFA input power is -28 dBm although degradation of the pattern due to dispersion of the SMF observed ⁽²⁾. On the other hand, an eye pattern observed with OFA input power of -30 dBm shows degraded eye-opening.

Figure 6 (a) Observed eye-diagram corresponds to OFA input power of -28 dBm

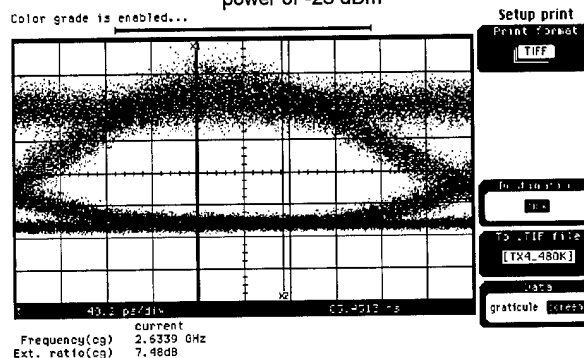
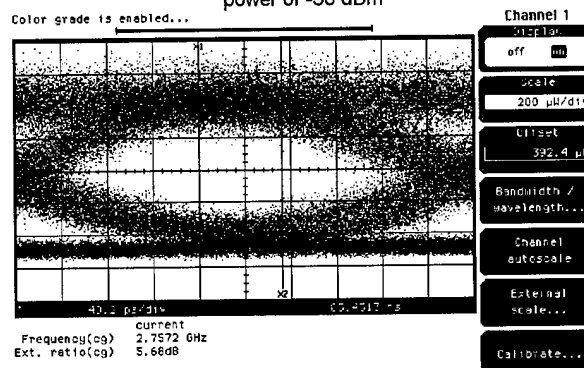


Figure 6 (b) Observed eye-diagram corresponds to OFA input power of -30 dBm



Summary of experiment

To summarize this section, adjusting OFA output power of 8 dBm, OFA input power of -28 dBm or higher can achieve power penalty smaller than 1 dB according to BER evaluation. Span loss between OFAs is allowed up to 36 dB.

System design based on level diagram

According to the BER characteristic investigation, it is realized that maximum attenuation range between OFAs are as large as 36 dB.

Based on the result, we propose a system architecture in terms of an optical level diagram. Assuming 3 dB of system margin, 0.25 dB / Km of fiber loss, 0.5 dB of a splice loss, 1 dB connector loss, total loss of the 80 Km path is 29 dB. Thus, we obtain 7 dB as a path margin.

If there are no connector or splice after 80 Km at each path, maximum span spacing between OFAs becomes as long as 108 Km ($= 80 + (36 - 29) / 0.25$). In this case, five OFAs are required for a 560 Km transmission instead of six OFAs in between.

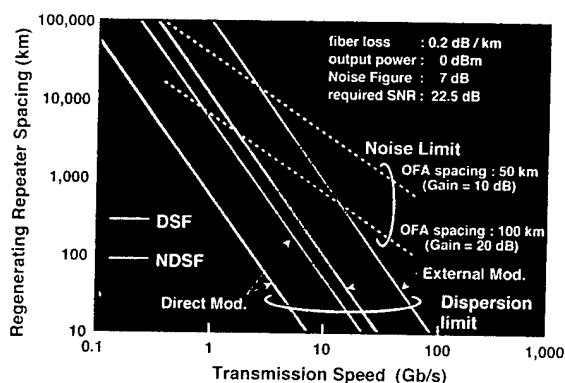
Based on the SNR evaluation, transmission length limit is investigated in the setting of cascaded OFAs.

We assume the followings:

Bit rate: 2.5 Gbps
Fiber loss: 0.25 dB / Km
Connector loss: 1 dB / 20 Km
Splice loss: 0.1 dB / Km
System margin: 3 dB

Figure 7 shows relations among total transmission length, number of OFAs connected in series and spacing of OFA stations. Transmission limit due to fiber dispersion is also shown. From the figure, it is recognized that our system design for the prototype (a 560 Km transmission path, 6 OFAs in series) is in the successfully transmission region. In WDM system, on the other hand, gain tilt among wavelengths should be taken into account.

Fig. 7 Relations among total transmission distance, number of OFA and OFA spacing



CONCLUSION

Four channel, 2.5 Gbps WDM-OFA transmission system has been developed. The system consists of transmitters, WDM filters, receivers and 6 OFAs in series can transmit signals up to 560 Km. Equipped supervisory sub-system, providing integrated alarms and performance monitoring,

the system is ready to deploy. The BER characteristics measured with a long haul setting, we evaluate power penalty at 560 Km transmission setting. Also, influence of optical input power of OFA on power penalty is discussed. Based on SNR (Signal to Noise Ratio) calculation as well as optical level diagram, system design is also discussed.

ACKNOWLEDGMENTS

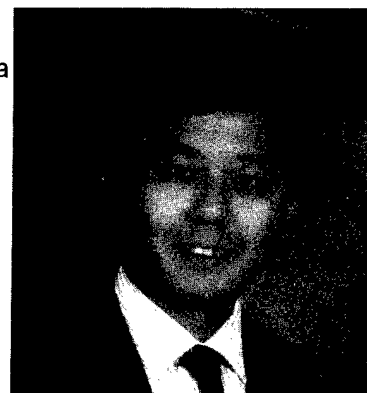
Authors would like to express their thanks to Mr. E. Yoneda for useful discussion and Mr. K. Omae for his continuous encouragement. We also thank Mr. K. Ohtahara, Mr. K. Sekiya and Mr. T. Kosuge for their support.

REFERENCES

- (1) Draft Recommendation G.mcs, Optical Interfaces for Multichannel System with OFA, CCITT
- (2) Iwano et. al., "600 Km Transmission Experiment with 8 channel 2.4 Gb/s Narrow Band-WDM System", IECE Spring Conference, B1129, 1996
- (3) Y. K. Park et. al., "Optical Preamplifier Receivers", Optical Fiber Tech., 1, 59-71 (1994)

AUTHORS

Kyota Susai
5-1-9, Higashi-Yawata
Hiratsuka, Kanagawa
254 Japan



Kyota Susai received the B.S. and M.S. degrees from Tohoku University, Miyagi, Japan in 1987 and 1989, respectively. In 1989, he joined the Furukawa Electric Co., Ltd. Currently, he is working at Information and Electronics Laboratory, where he has been engaged in the development on optical transmission systems.

Tokuhide Kasetani
5-1-9, Higashi-Yawata
Hiratsuka, Kanagawa
254 Japan



from Waseda university Tokyo Japan. He is a
member of IEICE of Japan.

Tokuhide Kasetani received the B.S. degree from
Nagoya Institute of Technology, Aichi, Japan in
1984. In 1984 h joined the Furukawa Electric Co.,
Ltd. Currently he is working at Information and
Electronics Laboratory, where he has been
engaged in the development on optical
transmission systems.

Hiroshi Nakamura
6, Yawata Kaigan-dori
Ichihara, Chiba
290 Japan



Hiroshi Nakamura received the B.E. degree from
Tokyo University, Tokyo, Japan in 1992. In 1992,
he joined the Furukawa Electric Co., Ltd.
Currently,
he is working at Optical Fiber Production
Department, where he has been engaged in the
development of optical fiber measurement
techniques.

Akira Fujisaki
6, Yawata Kaigan-dori
Ichihara, Chiba
290 Japan



Akira Fujisaki joined Furukawa Electric in 1987
after receiving BS degree in electrical engineering

MANAGEMENT FOR DEPLOYMENT OF OPTICAL ACCESS NETWORK

Tamaki ITO, Mamoru NAKAGAWA, Daisuke TOMIZU, and Makoto NINOMIYA

NTT Access Network Systems Laboratories
Tsukuba-shi, Ibaraki-ken, JAPAN

ABSTRACT

A new management method has been established for efficient deployment of an optical access network. This method has been applied partly deploy an optical access network for the first time using real data of one of the NTT's central office areas. The selected central office mainly covers a commercial and industrial region. This paper describes the management procedure and the simulation results.

1.INTRODUCTION

Installation of an optical trunk network for providing multimedia services, is almost finished. It is obvious that the access network must also be upgraded. That is to say, it is essential to install an optical fiber network. NTT plans to deploy optical fiber cables in all private homes by the year 2010, and in major business customers' buildings in the large cities by the year 2000.[1][2]

Such backgrounds it was occasionally discussed how to manage access network. However firm management method has not been established yet. Investigation must be carried out to determine the priority for installation of optical fiber cables in the business area. This will depend on the availability of facilities' and market conditions, and on what kind of services will be used by major users. Thus, facilities must be synthetically evaluated for efficient investment planning. Management of access network facilities which is based on quantitative data, is essential for establishing a future network.

This paper presents a management procedure for efficient planning and establishment of an optical access network using real data.

This management method is supported by a

computer system developed by our project group and is based on an object-oriented software technology. This technology can reduce the development period for making application programs because of its re-usability.[3]

2.MANAGEMENT PROCEDURE

The access network management procedure is shown in Figure 1 as follows:

selecting central office area, setting optical cable distribution area, analyzing fixed distribution area, setting optical cable route, analyzing fixed distribution area(FDA), setting optical cable architecture, ,setting the number of optical cable cores, determining situation of existing underground facilities, determining extent of process and investment (Figure 1).

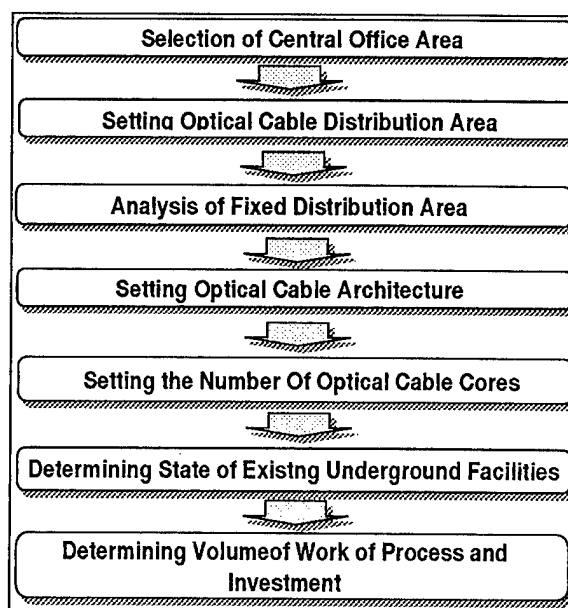


Figure 1 Management flow of optical access network

2.1 Selection of Central Office Area

NTT has about 7000 central offices, divided into six groups (SA, A, B, C, D and E in larger order), depending on the size of the city (Table 1). Central office M selected at this time belongs to group B, which comprises a mainly commercial and industrial region. The priority of optical deployment is not high. Optical fiber has not been installed yet. However a customer has ordered a high-speed digital service that requires optical fiber construction. Thus, office M was selected not only to satisfy this customer's requirement but also in consideration of economical, effective, and efficient future network plan.

Table 1 Central office grouping

Group	Location of Office	Number of Offices
SA	Large Business Area	13
A	GDM *	156
B	City having Prefectural Office	261
C	Middle Class City	197
D	Small City	6525
E	Rural Area	

*Government-Designated Municipalities

2.2 Setting Optical Cable Distribution Area

Optical cable distribution areas are set to make the most effective use of existing underground facilities, and to achieve smooth replacement of metallic cables by optical fiber cables, considering the road plan, geographical features, city development, etc.[4] Distribution areas have already been determined by the staff of the central office M. Four distribution areas (P,Q,R, and S) have been decided. (Figure 2)

2.3 Analysis of Fixed Distribution Area

The Fixed Distribution Area (FDA) is a minimum unit for access network management. Each FDA was ranked based on the monthly charge per line, the business customer ratio, the number of major customers, the number of important lines, the number of wooden poles, the number of fed pairs, the number of total lines, and the number of leased lines. These parameters are combined to evaluate

the overall FDAs. The maximum number of each parameter is equally divided into five stages. Each stage has a value of 5 to 1 in the order of largest to smallest. The higher the evaluation point, the higher the degree of importance. FDAs with totals of more than 25 were set as high priority FDAs. Classification according to the total number of points in each FDA is displayed visually (Figure 3).

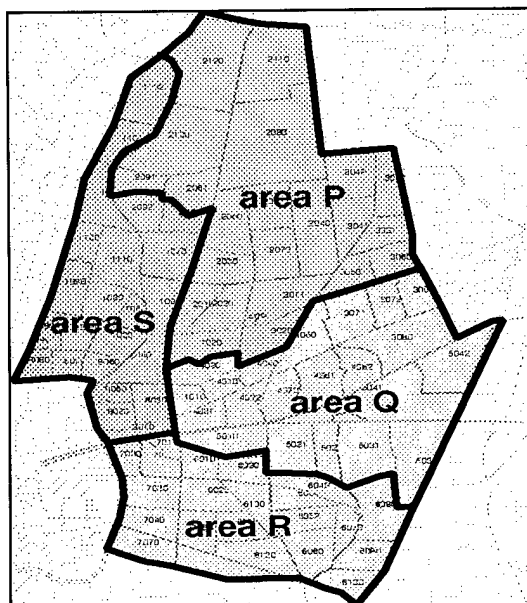


Figure 2 Optical cable distribution area

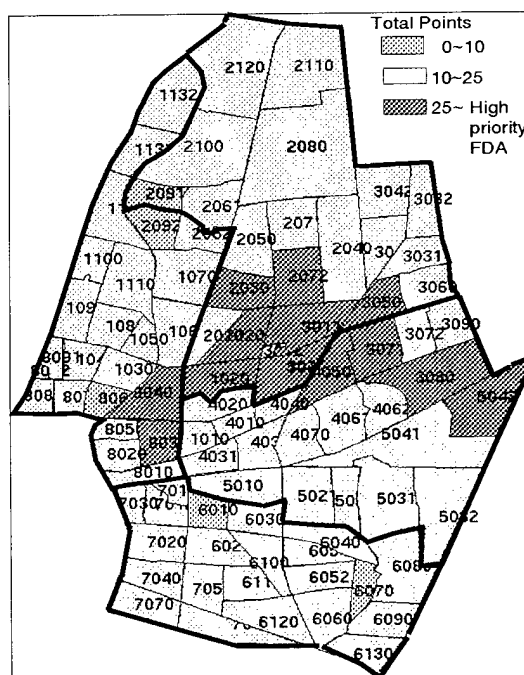


Figure 3 High priority FDAs

2.4 Setting Optical Cable Architecture

Cable route was set to make the most effective use of the existing conduit, considering the future plan, with high priority to the FDA in each optical distribution area as set in 2.2. According to the central office group and zone usage in city planning, three types of network design are decided: loop, combined loop and star, and star (Table 2). As the central office M is in a commercial and industrial area and the central office group is B, combined loop and star was selected. As described, effective use of the existing conduit was also considered.

Optical cable distribution area P was planned for 1995. It has FDA 3042 which needed optical cables for a high-speed digital service. Area Q was planned for 1996 to cancel the lessening capacity of FDA 5031. Areas R and S were planned for 1997 and 2000 for the same reason. Actual routes in area P are shown in figure 4.

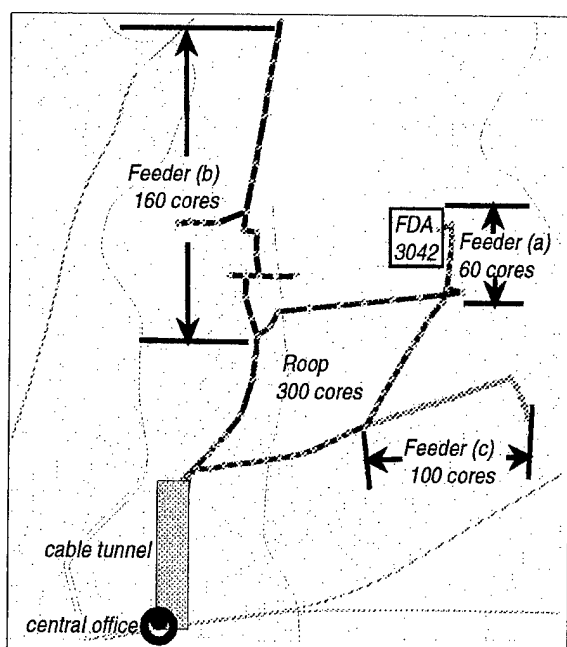


Figure 4 Planned optical cable routes in area P

2.5 Setting The Number of Optical Cable Core

To determining the number of optical cables in the core, the following information was required: the number of lines required in the customer's building or house for each service, information from salesperson about the customer's needs, and the capacity of metallic cable.

From this information the number of cores required for each user building or each FDA was summed

up.

Demands for services through optical cable, for example high speed digital, ISDN1500Kbit/s, video, etc, were investigated in each customer building. The number of cores per system of Remote Terminal(RT), Low-speed Data Subscriber Line Termination(LD-SLT), high speed digital, ISDN1500Kbit/s, multi media, and video need 4,4,2,2,2, and 1 core, respectively (Table 3).

Four additional cores were provided allow for new service demand in each FDA and two more for fault correspondence reserve in each building termination.

Accordingly the necessary core of area P where construction was sped up was calculated. The result was 428 cores. The loop wiring area actually becomes 214 cores of $428/2$. Adding four cores for maintenance and four cores for the express order circuit, the final number became 222. The number of cores in star wiring sections (a), (b), (c) were calculated in the same way. The results were 42, 104, 72. The lead-in building cable requires double of cores that is for fault correspondence reserve and for services. The customer who ordered high-speed digital service requires, 8 cores in his building.

Table 2 Distribution form of optical cables

	residential area	industrial area	commercial area
SA / A			
B / C			
D / E			

■ loop ▨ loop & star □ star

Table 3 Number of cores in each service

services	number of cores
RT, LD-SLT	4/system
High speed digital	2/svstem
ISDN1500bit/s	2/system
Multi Media	2/system
Video(FV-4M)	1/system
For new service demand	4/FDA

2.6 Determining the State of Existing Underground Facilities

The state of the existing conduit route in which the optical cables would be installed was examined. A new conduit must be constructed in case of metallic cable plan, if no or only one conduit is available in each Man hole(MH) section. However, complete optical cable establishment can reduce the number of full-conduit sections in the future. The necessity for civil engineering work is examined to investigate planned conduits in each MH section.

The state of the conduit in area P where construction was actually sped up was examined in accordance with this policy. No section had no free conduits, but three parts of seven section had only one (X, Y, Z). Each part was examined in detail (Figure 5). Part X had two routes. Provisional action by multiple installation of cables in one conduit was adopted for Part Y, because there were enough conduits for the future plan. In part Z, one cable was scheduled to be removed as the cable route was shortly going to change. Therefore, no civil engineering works were assumed in the feeder cable network.

2.7 Determining the Volume of Work and Investment

The length of cable, the number and kind of devices connected with optical cable, and the civil engineering processes are multiplied by the unit price to estimate the total investment.

The actual calculation was done from the central office to FDA 3042 that needed optical cable for high-speed digital service.

For the loop wiring section, 222 cores were necessary(2.5). So 300-core cable was selected. For the star wiring section, 60-core cable was selected, and 16-core cable was selected for the lead-in building. The cable lengths were, 300-core 7.6Km, 60-core 0.5Km, and 16-core 0.5Km. One frame of the Fiber Termination Module (FTM) is connected with optical cable. Civil engineering processes were required for only 20 meters in the lead-in building. These and unit prices were multiplied. Finally, the cost was roughly estimated as ¥103.4 million(\$9.4 million)(Table 4).

Before this optical cable installation, additional metallic cable installation will be needed on the same route in 1997, because the capacities of FDA 3041, 3042, and 3032 are expected to be zero

in 2000. The metallic cable construction cost including civil work in X and Y sections is as about twice of the optical cable.

Table 4 Optical cable construction cost

items	proceed	unit price	investment
300-core cable	7.6Km	\$1.15 million	\$8.8 million
60-core cable	0.5Km	\$0.4 million	\$0.2 million
16-core cable	0.5Km	\$0.006 million	\$0.003 million
civil work	0.02Km	\$10 million	\$0.2 million
FTM	1frame	\$0.2 million	\$0.2 million
Total			\$9.4 million

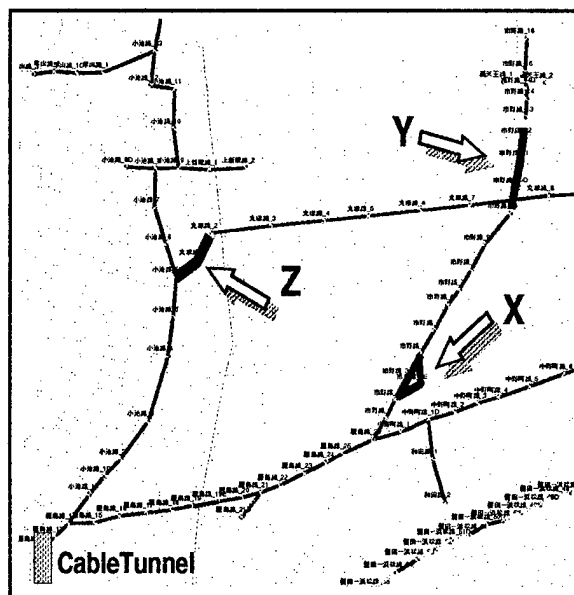


Figure 5 State of established conduits

2.8 Result

Since optical cable construction depends on this management method, we evaluated the central office M from the index, that is, the ratio of the FDA that the optical cable passes through. This ratio is up to 10%. The term from acceptance of customer order to offering services which needs optical cable is shortened in those FDA.

The following effects will be expected:
minimizing civil engineering work by effectively
using current equipment, reduction of maintenance
cost, cancellation of MH section which has no free
conduit.

4. CONCLUSION

In access network planning, two points have to
be taken into consideration. One is the standpoint
of the customer who receives service. The other is
the standpoint of the carrier who maintains
equipment and offers timely services.

It is important to deploy an optical network
efficiently, determining customer's needs and
offering service. It is also important in constructing
facilities to accurately analyze current facilities. We
used real data according to the management
procedure which had been shown at this time. We
can thus obtain a quantitative effect as shown in
the result of 2.8.

This management method is useful not only for
central office M but also for all the central offices, in
flexibly changing the evaluation point of each
parameter.

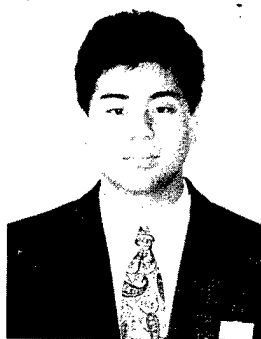
ACKNOWLEDGEMENTS

The authors wish to gratefully acknowledge the
cooperation of engineers at the Shizuoka Branch.
Thanks are also due to Tetsuji Abe, and Toshinao
Kokubun for their stimulating discussions.

REFERENCES

- [1]H.Ishihara "Access Network Upgrading for
Multi-Media Era" Proceeding NTT Technical
Journal Jun.1995 Vol.7 No.6 in Japanese
- [2]Y.Wakui "Environment of Optical Access
Network and Overview of Development
Technology" Proceeding NTT Technical Journal
Apr.1994 Vol.6 No.4 in Japanese
- [3]Y.Kataoka, Y.Kawakami, Y.Kato, Y.Mitsunaga,
"Visual Programming to Access Huge Database of
Subscriber Cable Networks", IEICE Proceedings of
the Fall Conference, D-350, 1993.
- [4]H.Ishihara "Design for Access Network
Facilities" Proceeding Ohm Co., Ltd .in Japanese

AUTHOR'S BIOGRAPHY



Tamaki Ito
NTT Access Network Systems Laboratories
1-7-1 Hanabatake, Tsukuba-shi, Ibaraki, 305
JAPAN

Tamaki Ito received his B.E. degree in agriculture
from Nagoya University in 1989. He joined NTT in
1989. He is engaged in the development of
operation system as a system engineer at NTT
Access Network Systems Laboratories, Japan.



Mamoru Nakagawa
NTT Access Network Systems Laboratories
1-7-1 Hanabatake, Tsukuba-shi, Ibaraki, 305
JAPAN

Mamoru Nakagawa is Senior Engineer Supervisor
at NTT Access Network Systems Laboratories. He
received his B.E. degree in electrical engineering
from Sophia University in 1978. He joined NTT in
1978. He is engaged in the development of
operation system as a system engineer at NTT
Access Network Systems Laboratories, Japan.



Daisuke Tomizu
NTT Access Network Systems Laboratories
1-7-1 Hanabatake, Tsukuba-shi, Ibaraki, 305
JAPAN

Daisuke Tomizu received his B.E. and M.E. degrees in civil engineering from Kyoto University in 1992 and 1994. He joined NTT in 1994. He is engaged in the development of access network management system at NTT Access Network Systems Laboratories, Japan.



Makoto Ninomiya
NTT Access Network Systems Laboratories
1-7-1 Hanabatake, Tsukuba-shi, Ibaraki, 305
JAPAN

Makoto Ninomiya received his B.E. and M.E. degrees in civil engineering from Waseda University in 1991 and 1993. He joined NTT in 1993. He is engaged in the development of access network management system at NTT Access Network Systems Laboratories, Japan.

COAXIAL CONNECTOR RETENTION: AN OPTIMIZATION STUDY

Wing Eng, Jr.

Pacific Bell
San Ramon, CA

ABSTRACT

Coaxial Connector Retention has been an ongoing concern at Pacific Bell for several years. Many of the hardware related DS3(44.736Mb/s) outages in our company can be traced to improperly terminated coaxial connectors. This paper describes the important aspects and process improvements of coaxial connector terminations: coaxial cable designs, cable stripping methods, cable preparation methods, connector crimping methods and connector retention sample testing. Aspects of improper coaxial cable preparation are discussed. Data is provided to show that upgrades in cable products and termination-related products and procedures have markedly improved the retention of central office BNC connectors from a minimum average of 15 pounds to a minimum average of 80 pounds.

1. INTRODUCTION

For several years Pacific Bell has primarily terminated BNC(locking) coaxial connectors on 26 AWG, silver plated, solid copper center conductor coaxial cable. Cable stripping has been achieved using three types of devices; hand tool strip, power tool strip equipped with a manual cut-depth adjustment, and power tool strip equipped with a programmable cut-depth adjustment. The termination preparation and crimping tools used included hooked-end spudgers for flaring of the coaxial cable outer braid, center contact pin crimp tool and outer crimp sleeve crimping tool equipped with crimp die. Retention testing on coaxial connector terminated samples was occasionally performed.

Due to process variations in coaxial cable stripping and coaxial connector termination procedures, tested samples of connectorized cables, at times, produced retention results under 15 pounds. This resulted in a team effort at Pacific Bell to improve the minimum BNC connector retention from 15 pounds to 50 pounds. The team assessed that changes to the coaxial cable and outer crimp sleeve crimping tool and die would offer the best opportunities to realize a major enhancement in coaxial connector retention. Previous upgrades made to BNC connectors used at Pacific Bell convinced the team that any additional changes to the connector itself was unnecessary.

2. PROCESS IMPROVEMENT DETAILS

The tin plated copper braid of the 26 AWG coaxial cable was increased(strengthened) from 39 AWG to 36 AWG braid. Figure 1 depicts the design of the coaxial cable. The center conductor is made of 26 AWG, silver plated, solid copper. The dielectric layer surrounding the center conductor is made of foamed polyethylene. Immediately above the dielectric is a thin layer of aluminum-mylar tape(not shown). The 36 AWG tin plated copper braid lies directly above the tape. Together, the tape and braid comprise the overall shield of the coaxial cable. Lastly, the core of the cable is jacketed with an outer layer of flexible PVC material.

An important concern in the design of the 26 AWG coaxial cable is to retain the same outer diameter over the new 36 AWG tin plated copper braid as over the old 39 AWG tin plated copper braid. On the 26 AWG cable with 36 AWG braid, the overall shield thickness

remains the same by using a thinner aluminum-mylar tape over the dielectric. This is important to insure that no changes to the blade depth cuts of cable strip machines is needed. Also, retaining the same outer diameter over the braid will negate problems of cutting into a larger outer diameter braid.

For illustrative purposes, Figure 2 depicts the three components of a typical BNC connector before termination onto the 36 AWG coaxial cable.

Figure 3 illustrates the flare of the tin plated copper braid. Uniformity in the flaring of the braid is essential for achieving an optimal connector outer sleeve crimp.

The center contact pin crimping tool, illustrated in Figure 4, is used to establish a gold-plated center pin crimp to the center conductor of the 26 AWG coaxial cable.

The most important aspect of the connector termination process is illustrated in Figure 5 which shows the position of the components of the BNC connector immediately before the outer crimp sleeve is crimped onto the 26 AWG coaxial cable. The retention of the BNC connector to coaxial cable is overwhelmingly dependent upon the integrity of the outer crimp sleeve-to-tin plated copper braid crimp.

The outer crimp sleeve tool handle was improved from an uncalibrated, moderately ergonomic, tool, per Figure 6, to a calibrated, very ergonomic, tool crimp handle per Figure 8. Factory calibration of the outer crimp sleeve handle assures that 290 Newtons of closure force, measured approximately 40 mm from the tip end of the handle, is imparted onto the outer crimp sleeve per crimp. Previously, the uncalibrated tool handle crimp force could be altered by adjusting a selector wheel. In the calibrated mode, the calibrated selector wheel value is pre-set in the factory with laser alignment marks etched onto the wheel and tool handle body to ensure against modifications to the calibration set.

The die for the outer crimp sleeve tool handle has two hexagonal cavity closures. The formerly used "standard" die was inserted into the uncalibrated handle with the .178 inch hex "B" cavity closure for connector termination of 26 AWG coaxial cable positioned nearest the tip of the handle as illustrated in Figure 7. The new improved die has repositioned the .178 inch

hex cavity closure for connector termination of the 26 AWG coaxial cable to be closest to the pivot point of the calibrated outer crimp sleeve handle as illustrated in Figure 9. This improved die is called the "Flip-Flop" Die.

3. CABLE TERMINATION PROCEDURES

To insure uniformity of connector termination procedures, uniformity of subsequent retention testing and interpretation of results, all BNC connector terminated coaxial cable samples were prepared by the author.

Both the 39 AWG braid type and 36 AWG braid type of 26 AWG coaxial cables were stripped using a power tool strip equipped with a programmable cut-depth adjustment. This coaxial cable stripping tool was selected for use because it provided repeatable uniform cable strips and was easy to adjust for depth of cuts and length of cuts for the different layers of the coaxial cable. Visual inspection under 10X magnification was used to verify that no cutting(scoring) of the tin plated copper braid was made to coaxial cable samples except in cases when improper cable stripping methods were being studied.

The pace of flaring of the coaxial cable tin plated copper braid was of nominal speed(not rushed) to simulate the work speed of a good installer. The braid was flared in a nominally uniform manner as a hooked-end spudger was consistently employed. No special effort, such as "re-flaring the braid" was used in trying to make the flaring of the braid as uniform as possible.

Finally, crimping of the outer crimp sleeve was performed as repeatably as possible for all connectorized cable samples.

4. PREPARATION OF TEST SAMPLES

Twenty-five BNC connectorized coaxial cable samples were prepared for each of the following seven, sequentially applied, type of terminations:

- 1.) 26 AWG Center Conductor, 39 AWG Braid, Uncalibrated Crimp Handle, Standard Die

- 2.) 26 AWG Center Conductor, 39 AWG Braid, Uncalibrated Crimp Handle, Flip-Flop Die
- 3.) 26 AWG Center Conductor, 39 AWG Braid, Calibrated Crimp Handle, Flip-Flop Die
- 4.) 26 AWG Center Conductor, 36 AWG Braid, Calibrated Crimp Handle, Flip-Flop Die
- 5.) 26 AWG Center Conductor, 36 AWG Braid, Calibrated Crimp Handle, Flip-Flop Die, 0.005 Inch Deep(1 Braid Strand Thick) OverCut of Braid
- 6.) 26 AWG Center Conductor, 36 AWG Braid, Calibrated Crimp Handle, Flip-Flop Die, 0.103 Inch Long(30% Length Reduction) Shortening of Braid
- 7.) Repeat sample preparation of "4.)", above.

For several years at Pacific Bell, BNC coaxial connectors had been terminated onto 26 AWG coaxial cable using technique "1.)", above, resulting in a nominal average of 15 to 20 pounds of connector retention.

5. TEST RESULTS AND DISCUSSION

Sample Set #1

The initial set of twenty-five samples of 26 AWG coaxial cables equipped with 39 AWG tin plated copper braid was terminated with BNC connectors using the uncalibrated outer crimp sleeve tool and standard crimp die. The histogram pull-test results per figure 10 demonstrate the marginal performance of the tested samples. The mean value of connector retention was 16.90 pounds with 3.73 pounds as the value of one standard deviation.

The relatively "flat" distribution of retention values demonstrates the full effect of non-uniform braid flaring(strand clumping) on the crimp process. Moving the outer crimp sleeve over any sections of non-uniformly flared braid prior to crimping has little, if any, combing effect on the braid. The low average retention result and relatively large standard deviation is

due to the small force imparted by the uncalibrated crimp tool and standard die onto the outer crimp sleeve, which contains the relatively thin 39 AWG braid and its sections of non-uniformly flared braid.

Sample Set #2

The second set of twenty-five samples of 26 AWG coaxial cables equipped with 39 AWG tin plated copper braid was terminated with BNC connectors using the uncalibrated outer crimp sleeve tool and "flip-flop" die. The histogram pull-test results per figure 11 show a relatively "normal distribution" with substantial peak around 51 pounds. The mean pull-out value was 51.22 pounds with one standard deviation being 6.18 pounds. This mean retention value was more than three times that of the previous (figure 10) mean standard crimp retention value.

The effects due to non-uniform braid flaring(strand clumping) on the crimp process are apparently overcome by the relative strong force imparted onto the outer crimp sleeve by the uncalibrated crimp tool and the "flip-flop" die.

Sample Set #3

The third set of twenty-five samples of 26 AWG coaxial cable equipped with 39 AWG tin plated copper braid was terminated with BNC connectors using the calibrated outer crimp sleeve tool and "flip-flop" die. The results from the histogram, per figure 12, show a mean retention value of 57.01 pounds with 6.47 pounds as the value of one standard deviation. The "normal distribution" shows a moderately high peak at 59 pounds. Note the "high-end" cut-off of test results around 66 pounds which is supposedly due to braid breakage limitations. The use of the calibrated crimp tool adds about 11% improvement to the connector crimp retention value compared to the result of using an uncalibrated crimp tool.

Sample Set #4

The fourth set of twenty-five samples of 26 AWG coaxial cable equipped with 36 AWG tin plated copper braid was terminated with BNC connectors using the calibrated outer crimp sleeve tool and "flip-flop" die.

The histogram results, per figure 13, show a mean retention value of 84.33 pounds with 4.48 pounds as the value of one standard deviation. The "standard distribution" result shows an obvious peak around 85 pounds and the high end cut-off around 92 pounds is indicative of the upper limits of braid breakage. The use of 36 AWG braid in the coaxial cable adds about 48% improvement to the result of the retention pull test values of the BNC connector compared to the result of using 39 AWG braid coaxial cable.

It should be noted that any "clumpings of braid strand" resulting from non-uniform flaring of the braid tend to be "combed out" when positioning the outer crimp sleeve over the flared braid immediately prior to crimping.

It is anticipated that improving BNC connector retention values to an average of over 80 pounds will result in the substantial reduction of many coaxial connector-related outages experienced at Pacific Bell.

It should be understood that the chances of a six sigma type defect (2 BNC defects per billion terminations) now resides at approximately 57 pounds which is over 3 times the former mean retention value (see figure 10) of 16.90 pounds!

Sample Set #5

The fifth set of twenty-five samples of 26 AWG coaxial cables equipped with 36 AWG tin plated copper braid was terminated with BNC connectors using the calibrated outer crimp sleeve tool and "flip-flop" die. However, an intentional cable stripping defect was introduced; cutting into the braid by 0.005 inches or one strand of braid thickness. Even with the defect, the histogram results, per figure 14, demonstrate a "normal distribution" with a mean retention value of 69.89 pounds and one standard deviation of 3.97 pounds. The peak value of the distribution is around 71 pounds.

The relatively modest impact of cutting into the braid on the connector retention value (reduction of around 17%) can be explained by the substantial force of the outer sleeve crimp modifying retention loss due to cut damage in the cable braid.

Sample Set #6

The sixth set of twenty-five samples of 26 AWG coaxial cables equipped with 36 AWG tin plated copper braid was terminated with BNC connectors using the calibrated outer crimp sleeve tool and "flip-flop" die.

Shortening the normal braid cut length 30% (0.103 inches) was intentionally done to evaluate the impact of this defect upon retention performance.

The histogram results, per figure 15, show a curious "plateau" behavior of peak retention values centered around the mean "peak" value of 52.47 pounds (retention reduction of around 38%). The one standard deviation of 6.61 pounds is illustrative of the wide distribution of peak value data resulting from the inability of the outer crimp sleeve to "comb out" the 36 AWG braid efficiently. In fact, in this situation, only the middle one-third of the crimp sleeve makes contact with the intentionally shortened braid.

In comparing the two types of defects imparted onto the outer braid of the 26 AWG coaxial cable, braid length shortening is substantially more detrimental to connector retention results than is braid overcutting.

Sample Set #7

The seventh set of twenty-five samples of 26 AWG coaxial cables equipped with 36 AWG tin plated copper braid was terminated in the identical manner as "Sample Set #4" in order to establish the repeatability of the crimping force imparted by the calibrated outer sleeve crimp tool equipped with "flip-flop" die. The histogram results show, per figure 16, a mean value for retention of 82.86 pounds and one standard deviation of 3.90 pounds. The calibrated tool handle and "flip-flop" die demonstrated good repeatability of crimping force.

6. CONCLUSIONS

The successful termination of BNC connectors onto central office 26 AWG, silver plated, solid copper center conductor coaxial cables is achievable. The degree of success will largely depend on the use of the calibrated outer crimp sleeve tools and "flip-flop" dies as noted in the following 2 sample test results.

In using 26 AWG coaxial cable equipped with 39 AWG braid, a mean average of 57.01 pounds and one standard deviation of 6.47 pounds for connector retention was achieved.

In using 26 AWG coaxial cable equipped with 36 AWG braid, a minimum mean average of 82.86 pounds and maximum of one standard deviation of 4.48 pounds for connector retention was attained.

In summary, taking 26 AWG coaxial cable equipped with 39 AWG braid and an uncalibrated outer crimp sleeve tool and standard die as product points of reference, the following process improvements will yield the following approximate improvements in BNC connector retention:

<u>Process Improvement</u>	<u>BNC Retention Upgrade</u>
Add "Flip-Flop" Die	200% Increase
Add Calibrated Tool	10% Additional Increase
Add 36 AWG Braid	50% Additional Increase
All 3 Above Mentioned Process Improvements	400% Total Increase (Over Product Point of Reference)

The 26 AWG coaxial cable had its 36 AWG braid "overcut" by 1 strand thickness deep(0.005 inches) to study the impact of braid cuts. The reduction in BNC connector retention was approximately 17%.

The 26 AWG coaxial cable had its 36 AWG braid shorted by 30%(0.103 inches) to study the impact of shortened braid. The reduction in BNC connector retention was approximately 38%.

Although care should be taken to avoid cutting into the braid or shortening the normal-cut strip length of braid during the cable stripping process, use of a calibrated outer crimp sleeve tool, "flip-flop" die and 26 AWG coaxial cable with 36 AWG braid will minimize the effects of such damage and can still produce a very adequate crimp with reasonable connector retention performance.

ACKNOWLEDGMENT

I am grateful to the following persons who have assisted me in the preparation of this paper: Mr. Gerry Dillon, Mr. Hank Hanig, Mr. Pat Hart, Mr. Joe Martinez, Mr. Jim Muite, Mr. Greg Brown, Ms. Debbie Carmain, Mr. Jeff Carmain and Ms. Kim Tran.

REFERENCES

1. J.H. Benjamins, "Double Shielded, Close Tolerance 75 Ohm R.F. Coaxial Cable Specification", Issue 2, 1987, Attachment 2.
2. EIA-364-38A, TP-38A Cable Pull-Out Test Procedure for Electrical Connectors(ANSI/EIA-364-38A-85)
- 3.) J.Elko, et al, Shielding Effectiveness of Coaxial Drop Cables and Simulated Aging by Flexure, IWCS, 1994
4. M.A. Wright, Private Communication



Wing Eng, Jr., joined Pacific Bell in 1981. He has worked in the testing and evaluation of metallic cables for the past 9 years. Mr. Eng received his BA in Astronomy and MS in Physics from UCLA in 1972 and 1974, respectively. He is a member of PMI, Project Management Institute, and may be reached at:

Pacific Bell
2600 Camino Ramon
RM 3S850D
San Ramon, CA 94583

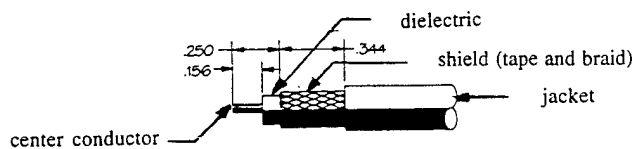


Figure 1. Coaxial Cable Stripping

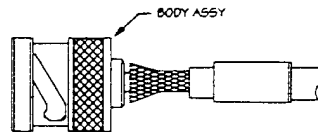


Figure 5. Coaxial Connector Body Assembly

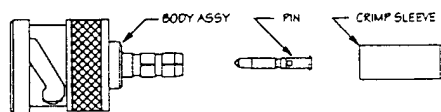


Figure 2. Coaxial Connector Components

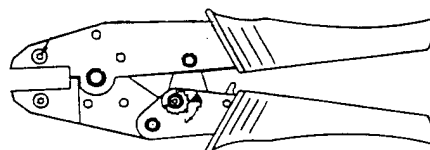


Figure 6. Uncalibrated Crimp Handle

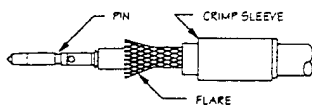


Figure 3. Coaxial Connector Braid Flare

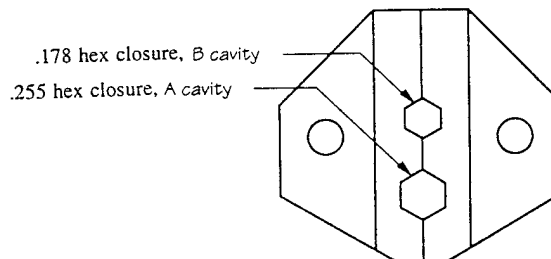


Figure 7. Standard Crimp Die

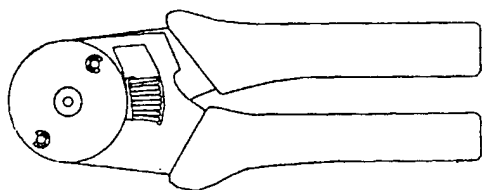


Figure 4. Center Contact Pin Crimp Handle

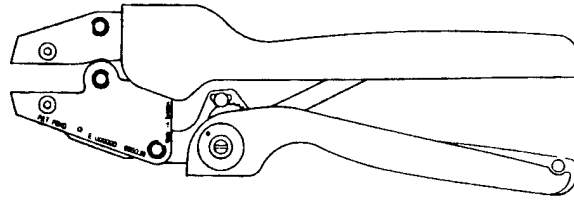


Figure 8. Calibrated Crimp Handle

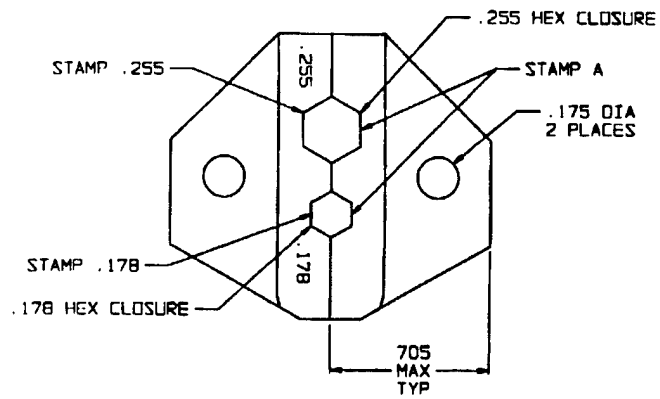


Figure 9. "Flip-Flop" Die

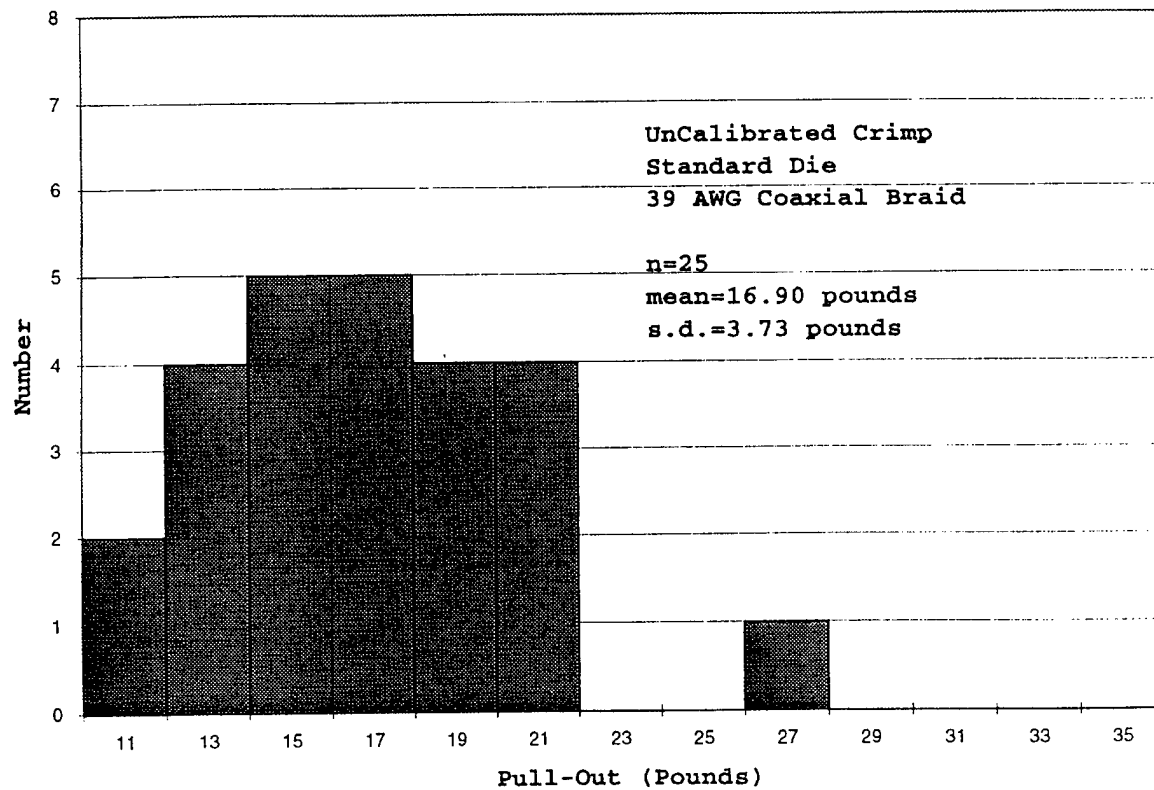


Figure 10. Connector Retention

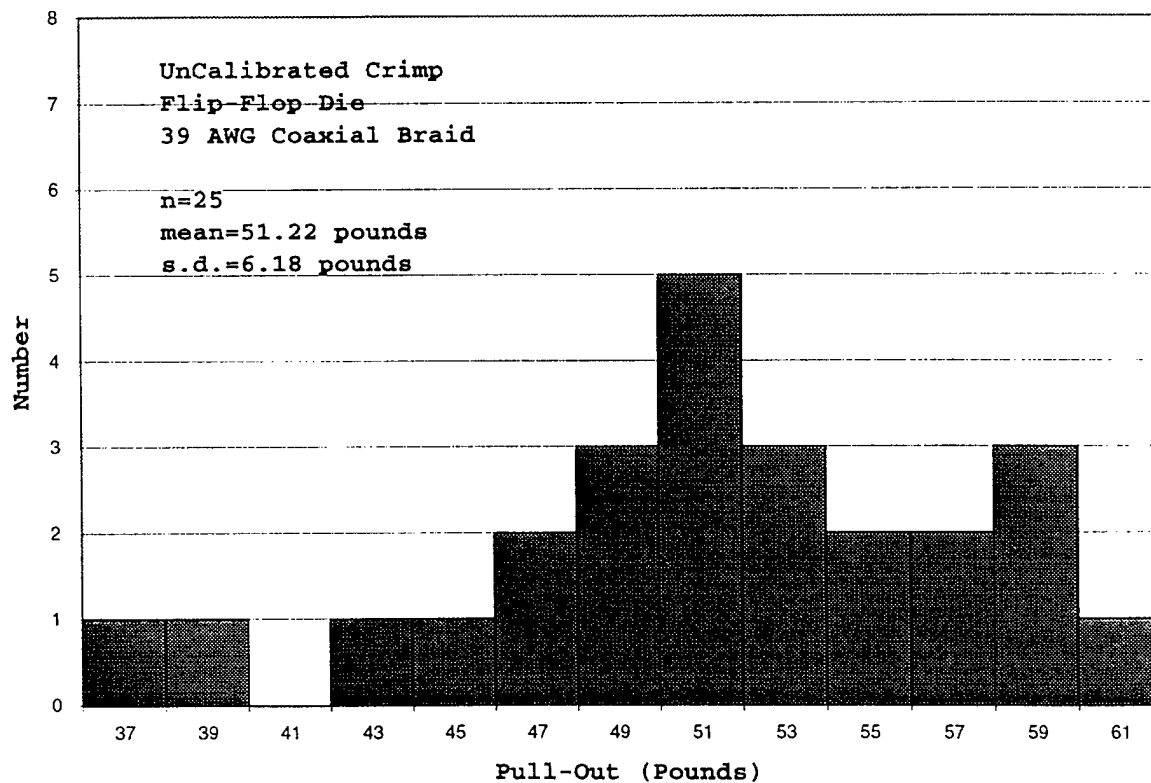


Figure 11. Connector Retention

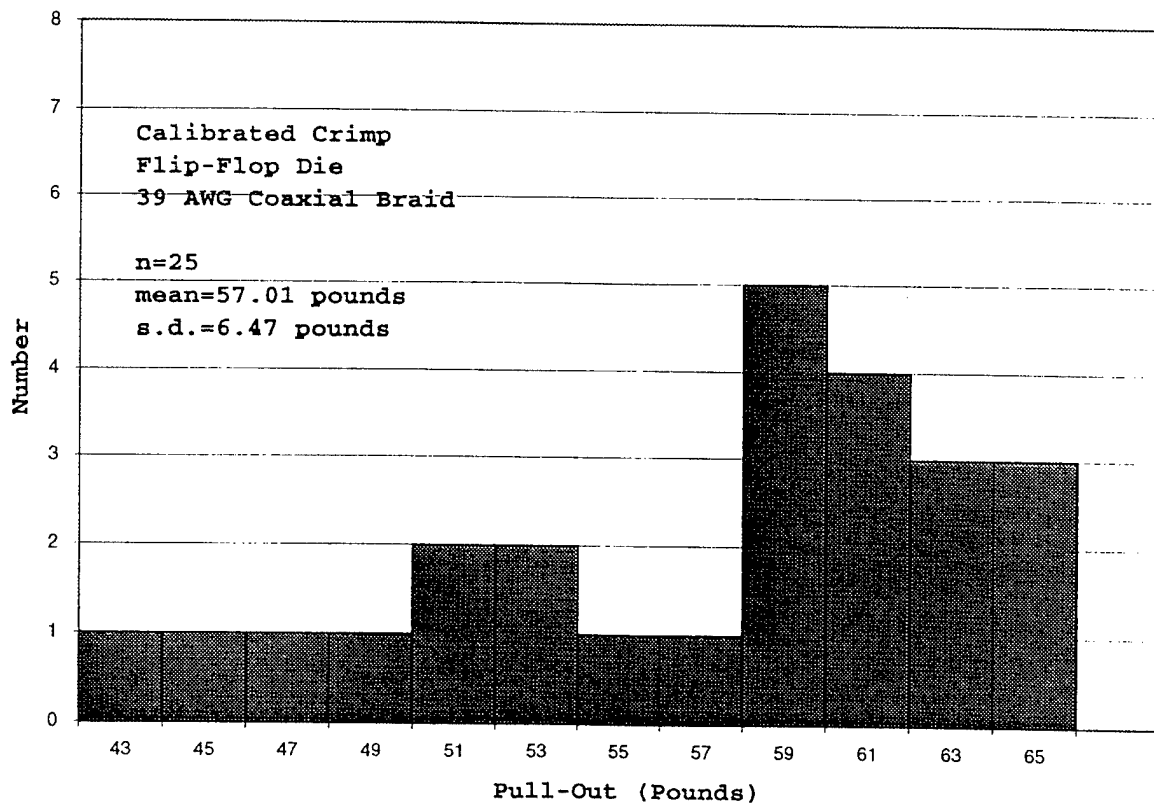


Figure 12. Connector Retention

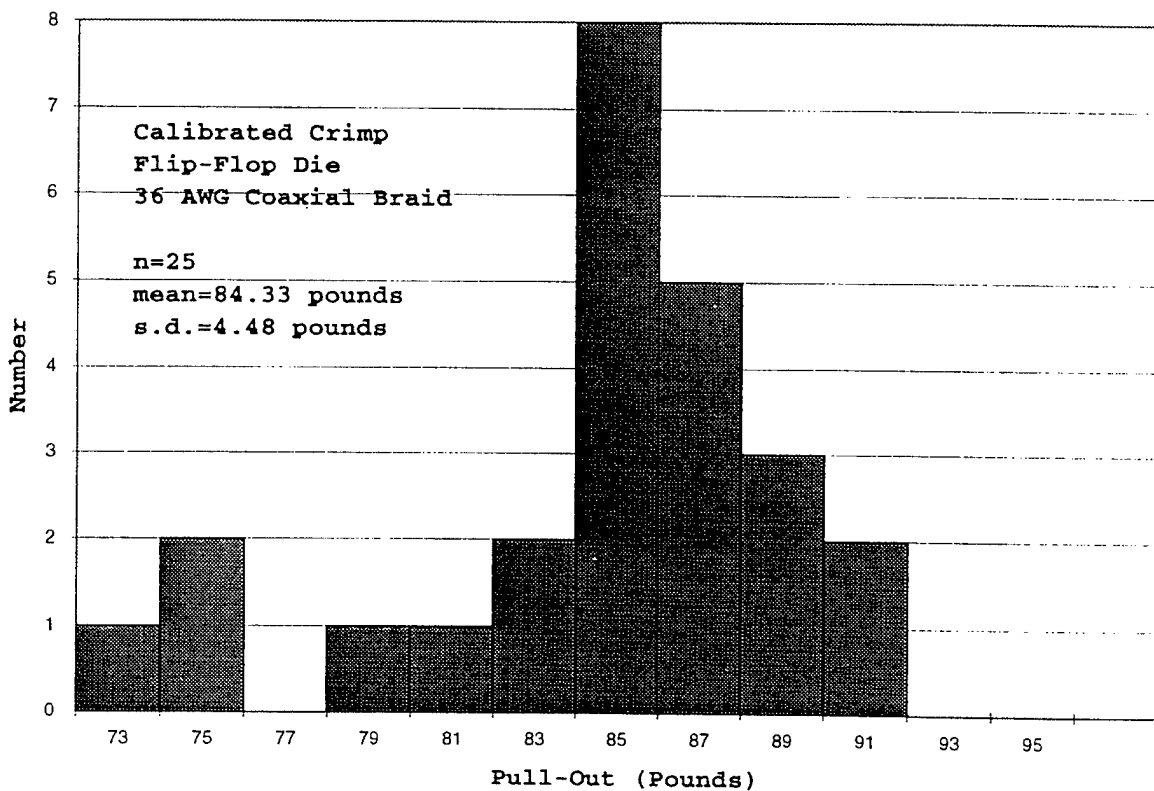


Figure 13. Connector Retention

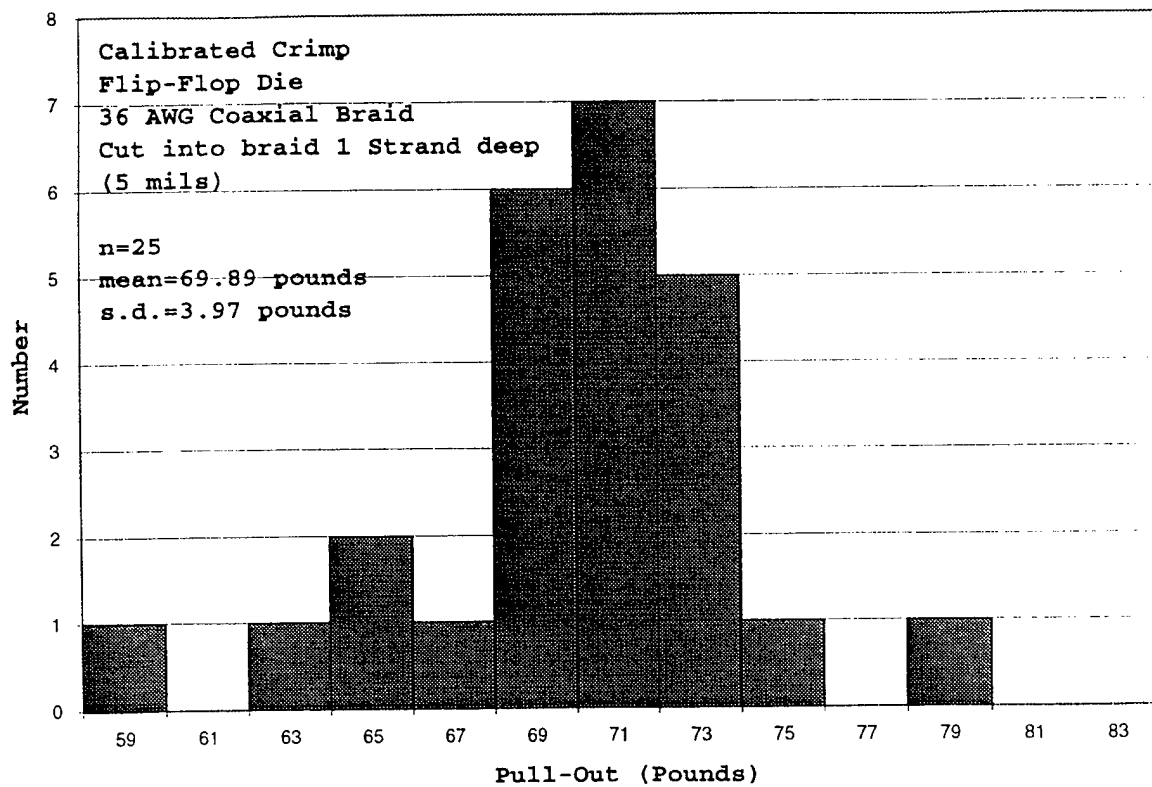


Figure 14. Connector Retention

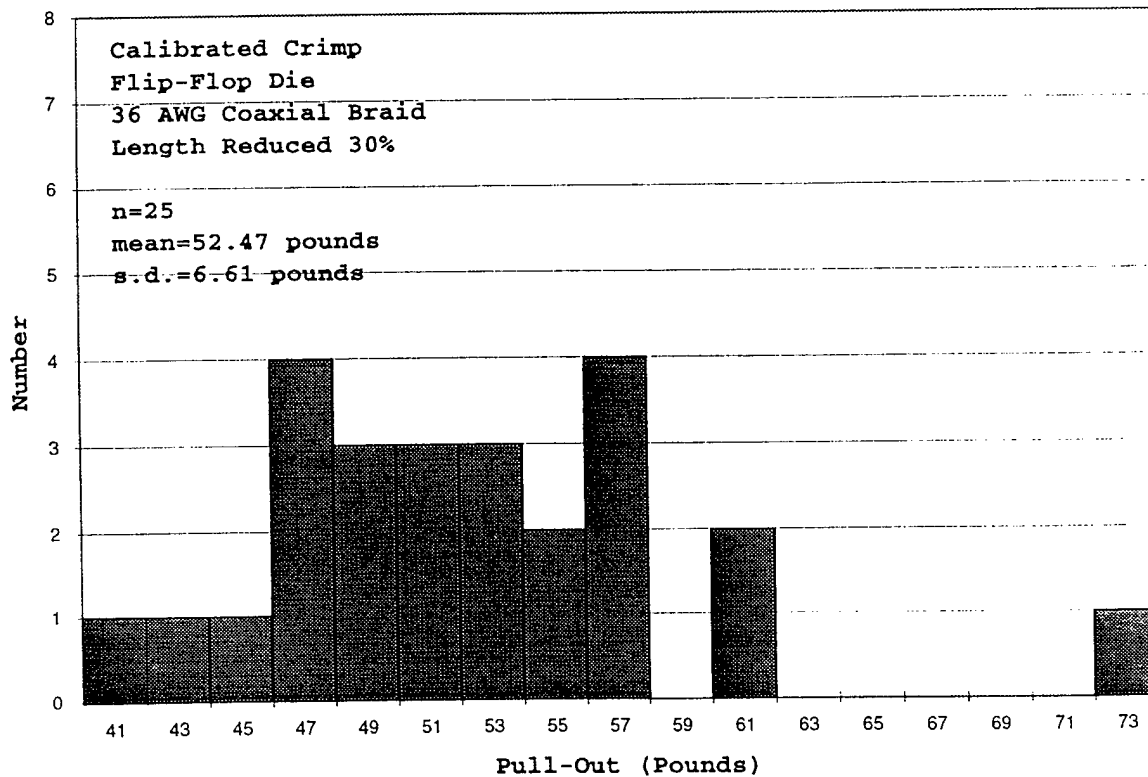


Figure 15. Connector Retention

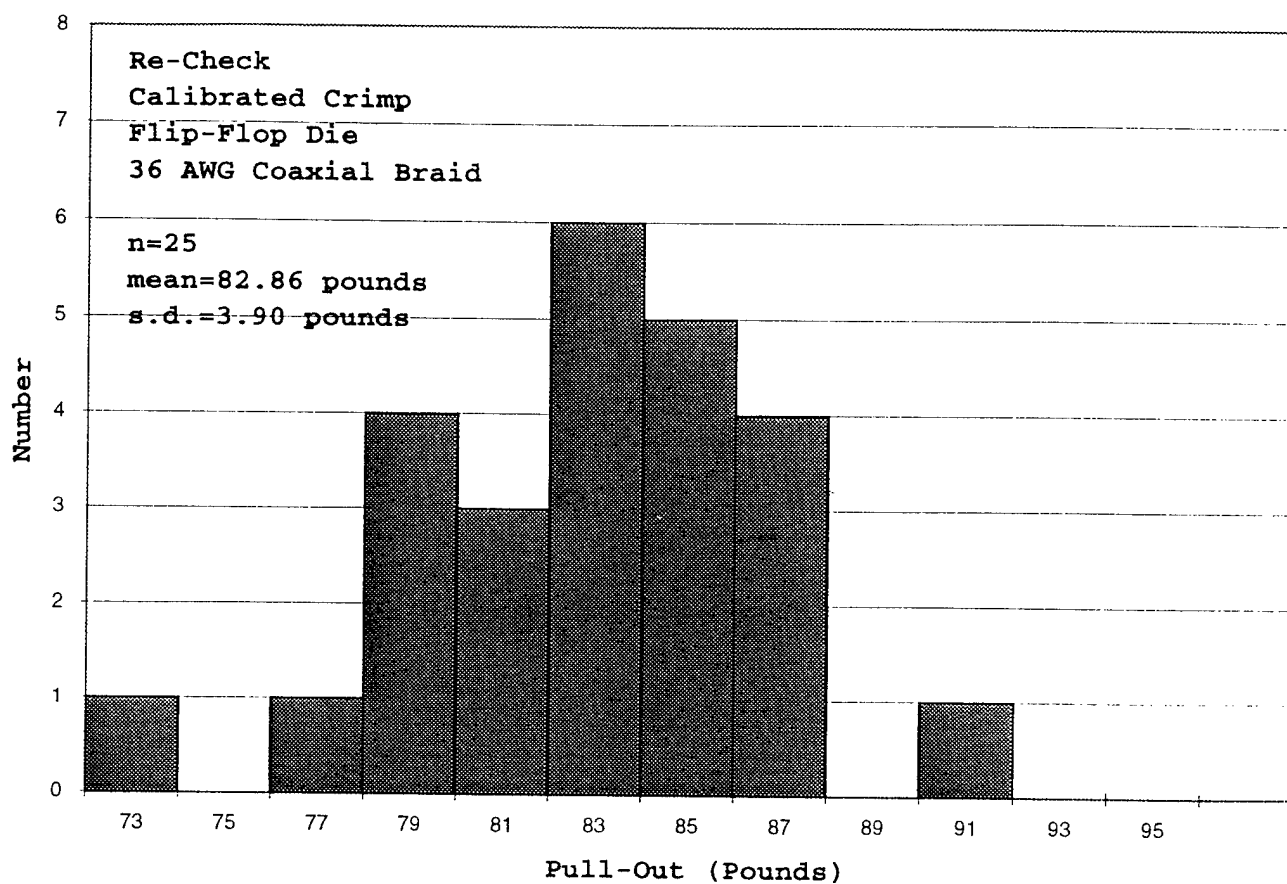


Figure 16. Connector Retention

SHIELD EFFICIENCY TEST METHOD FOR BALANCED SHIELDED TWISTED-PAIR CABLE & CONNECTING HARDWARE

Valerie A. Rybinski

The Siemon Company, Watertown, Connecticut

ABSTRACT

Shield effectiveness directly affects the electromagnetic compatibility (EMC) performance of balanced shielded twisted-pair cable and connecting hardware. Historically, complex and costly measurement procedures suffering from poor repeatability were used to characterize shield effectiveness. These procedures were limited in frequency range and were not suitable for measuring the shield effectiveness of connectors.

Recent refinements of the well known "triaxial" measurement technique have provided a means to quickly and accurately characterize the shield effectiveness of both cables and connecting hardware. This paper focuses on shield effectiveness and the refined transfer impedance test method, with particular emphasis on screened connecting hardware results. It addresses models used in the development of transfer impedance test methodology and describes the test set-up and fixtures used to achieve improved accuracy over an extended frequency range. Much of this information is provided in the context of ongoing research by standards groups whose charter is to fully understand and characterize shield effectiveness for cabling components and links. In the context of this paper, the term screened cable or cabling is intended to describe systems with two or more unshielded pairs (or one or more quads) within an overall foil, braid, or both. The screen itself is sometimes referred to as a shield.

INTRODUCTION

As communications speeds increase, concern grows over noise and its potentially disruptive effects on balanced (twisted-pair) telecommunications cabling. Electromagnetic

compatibility (EMC) describes a cabling system's ability to minimize radiated energy levels (emissions) and resist noise interference from outside sources (immunity). Balanced screened twisted-pair cable and connecting hardware that exhibit low emissions and high immunity may have good balance, shield effectiveness, or both. Shield effectiveness describes the shield termination integrity along the entire telecommunications system and the integrity of the installation's grounding. Because any shield, if not manufactured and/or terminated properly, will behave as an antenna, both radiating and receiving noise, shield effectiveness evaluations become necessary to ensure proper EMC performance.

TRANSFER IMPEDANCE

Traditionally, shield effectiveness has been quantified by measuring shield transfer impedance. Transfer impedance is simply a ratio of the voltage induced upon the shielded transmission line (in volts) versus the magnitude of the interfering noise current (in amperes) measured in ohms (Ω) as shown in Equation (1).

$$Z_t = \frac{V_{ind}}{I_{int}} \quad (1)$$

Lower transfer impedance values correlate to higher shield effectiveness.

Several international standards exist referencing "triaxial" test-set-ups used to measure transfer impedance, (most notably IEC 96-1¹ and IEC 169-1-3²), but their scopes are applicable to coaxial transmission lines only. It has been found that, by modifying the existing coaxial measurement techniques, it is possible to define a repeatable, accurate, and cost-effective method for determining the shield effectiveness

of balanced twisted-pair constructions via laboratory transfer impedance measurements³. Refinements to the measurement technique are characterized by linear and accurate results up to 100 MHz.

THE TRIPLE COAXIAL (TRIAxIAL) METHOD

The transfer impedance measurements described are collected within a radio frequency (RF) shielded copper fixture using the triple coaxial (triaxial) termination method. The transmission tests described also typically require the use of a network analyzer or equivalent, coaxial cables, screened twisted-pair (ScTP) test leads, and impedance matching terminations. The measurement set-up is qualified to a measurement bandwidth of at least 10 kHz to 100 MHz.

The "triaxial" method is aptly named because the terminated fixture is comprised of the following three circuits:

- (1) the cable conductor core (fused at each end),
- (2) the shield under test, and
- (3) the RF shielded copper case.

One of the shortcomings of earlier transfer impedance test methods was that linear measurement resolution was only possible in the frequency range up to 30 MHz. In order to solve this problem, the size of the RF shielded copper case was reduced to about half of that previously recommended. The reduced copper case size accommodates a shorter length device under test, from which linear and accurate measurements can be collected up to 100 MHz. Measurement capability at higher frequencies is under investigation.

The revised RF shielded copper case consists of a 146 mm x 146 mm x 75 mm sealed copper main case attached to a 38 mm x 50 mm x 50 mm secondary case (see figure 1 in Appendix A). The main and secondary cases are fitted with removable lids. Case walls and fitted lids are constructed from 2 mm thick sheet copper. An aperture from the main to secondary case is provided by two fitted 18 mm diameter modular rings. The cases are securely welded and mounted to a 2 mm thick copper ground

plane. The copper case is fitted with $50\Omega \pm 1\%$ metal film feeding and terminating resistors to match the characteristic impedance of the network analyzer and minimize cable to fixture power loss.

In reference 3, Oehler and Stetter show that the equivalent circuit diagram for the shielded copper case and device under test is represented as shown in figure 1 below.

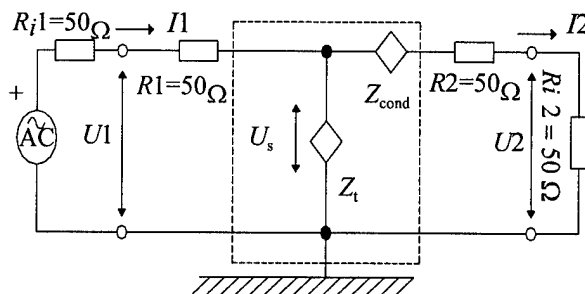


figure 1
Equivalent Circuit Diagram
Copper Case and Device Under Test

where:

- R_1 = feeding resistor = 50Ω
- R_2 = terminating resistor = 50Ω
- U_1 = transmitter voltage (volts)
- U_2 = receiver voltage (volts)
- $R_{i1} = R_{i2}$ = characteristic impedance of the network analyzer = 50Ω

The following equations describe the circuit diagram shown in figure 1:

$$U_1 = I_1 \cdot R_1 \quad (2)$$

$$U_2 = I_2 \cdot R_{i2} \quad (3)$$

$$U_s = I_2 \cdot (R_2 + R_{i2}) \quad (4)$$

$$U_s = Z_i \cdot I_1 \quad (5)$$

The voltage across the cable shield (U_s) is derived using the following assumptions:

$$Z_{cond} \ll R_2, \text{ and} \quad (6)$$

$$I_2 \ll I_1 \quad (7)$$

Assumptions (6) and (7) are only valid for conditions when the impedance of the shield is substantially less than the 50Ω characteristic

impedance of the network analyzer (typically applicable to sample lengths shorter than .3m).

From a substitution operation follows:

$$Z_t = \frac{1}{l_{cable}} \cdot \frac{R_{i1}}{R_{i2}} \cdot (R_2 + R_{i2}) \cdot \frac{U_2}{U_1} \quad (8)$$

Measured shield attenuation, in decibels (dB), is described by the relation:

$$a_s = 20 \cdot \log \left(\frac{U_2}{U_1} \right) \quad (9)$$

By applying the shield attenuation definition and entering the values for R_2 and R_{i2} , the resultant transfer impedance may be expressed as:

$$Z_t = 2 \cdot R_{i1} \cdot \frac{U_2}{U_1} = 100 \cdot 10^{\frac{a_s}{20}} \Omega \quad (10)$$

In the preceding equation, the transfer impedance measurement for cable is normalized to $\Omega/100$ m. The unit length requirement drops out for connecting hardware transfer impedance measurements.

Through the relation in (10), it can be seen that shield transfer impedance is closely related to shield attenuation, a measurement easily collected in a laboratory environment with a network analyzer. Using the model in figure 1, for a theoretically perfect shield construction, one hundred percent of a transmission signal induced on the shorted cable core would follow the shield-to-ground path and the receiver would detect no signal; correlating to one hundred percent signal attenuation and a transfer impedance value of 0Ω . In the real-world, the transfer impedance of the shield would allow some signal power, varying with frequency, to reach the receiver. For both connecting hardware and cables, the shield transfer impedance performance generally remains constant at lower frequencies and starts to degrade in the frequency range of 1 - 10 MHz. The shield attenuation to transfer impedance relationship is inversely proportional; i.e. low measured signal attenuation correlates to high shield transfer impedance which, in turn, correlates to lower shield effectiveness.

Because the transfer impedance derivation includes assumptions which only hold true for short test sample lengths, the applicability of this measurement technique for longer length cable and link measurements is still under investigation. As a preliminary approach to solving this problem, it may become necessary to adjust the values of the feeding and terminating resistors for longer length samples.

TEST SET-UP AND APPARATUS

The following test equipment and components are required to collect transfer impedance data using the triaxial test method:

- (1) Network Analyzer (50 Ω characteristic impedance)
- (2) Coaxial adapters as required to make network analyzer port connections (Author's note: SMA adapters were used, however, other adapters may also be acceptable)
- (3) HF Sealed Copper Case
- (4) 60-40 (Tin-Lead) Rosin Core Solder
- (5) Aluminum Soldering Flux
- (6) Precision $\pm 1\%$ 50 Ω metal film resistors
- (7) ISO/IEC 11801⁴ 4-pair, category 5, stranded and/or solid, screened (single foil, conductive side facing in, with drain wire) cable.
- (8) Embossed tin EMI/RFI foil shielding tape (adhesive backing optional)
- (9) Shielded modular plug connectors

MEASUREMENT PROCEDURE

The measurement procedure for collecting transfer impedance data closely follows the traditional methodology for gathering triaxial measurements with some additional refinements incorporated to allow for twisted-pair cable constructions and high frequency measurement capability.

Products under test may consist of shielded connecting hardware terminated on either end to 75 mm lengths of shielded cable or shielded cable lengths of 300 mm or less (the applicability of longer sample lengths is still under investigation). Connecting hardware intended to be mated with a shielded modular plug is

terminated with a 75 mm length of shielded patch cable on the mated-plug end and a 75 mm length of shielded solid cable on the insulation displacement contact (IDC) end.

The following points highlight the key practices necessary to successfully collect transfer impedance measurements using the refined triaxial measurement technique.

- The twisted-pair conductors, screen, and drain wire (if present) on the near-end of the device under test are soldered and formed into a fused conductor core. A precision $\pm 1\%$ $50\ \Omega$ feeding metal film resistor is soldered to the conductor core. The end of the feeding resistor is soldered to the input coaxial adapter of the main copper case (see figure 2 in Appendix B).
- The screen and drain wire (if present) of the far-end of the device under test is soldered to a 25 mm square or circular segment of embossed EMI/RFI foil tape and secured to the main copper case by a compression fit between the modular and fixed rings.
- The far-end twisted-pair conductors are soldered to form a fused conductor core and passed through the modular ring aperture. A precision $\pm 1\%$ $50\ \Omega$ terminating resistor is soldered between the conductor core and the output coaxial adapter of the secondary copper case. It is critical that the fused conductor core does not come in contact with any portion of the modular rings or aperture opening.
- All shield connections must maintain a 360° solder contact. The use of aluminum soldering flux is highly recommended. Soldered connections may be protected by embossed tin EMI/RFI foil tape (optional).
- The measurement network analyzer is calibrated for attenuation as specified by the manufacturer of the test equipment. Generally, the calibration consists of performing a 'thru' normalization on the network analyzer to compensate for the $50\ \Omega$ coaxial test leads and adapters.
- Shield attenuation measurements are collected and the corresponding transfer impedance is calculated.

TYPICAL DATA

Shield attenuation sweeps collected using the refined triaxial method for a properly terminated cable or connecting hardware sample are characterized by a linear 20 dB/decade slope. Fixturing problems associated with failing to maintain a full 360° shield-to-modular ring contact or other shield continuity problems will result in slope deviations. Serious screening problems attributable to the device under test will also result in attenuation slope deviations. Transfer impedance values are typically plotted on a log-log scale for the purpose of demonstrating measurement linearity.

The solid line curves in figures 2 and 3 depict shield attenuation data and corresponding transfer impedance performance for a typical screened mated plug/jack style connector.

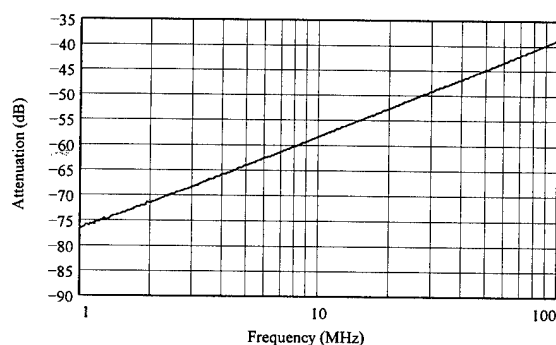


Figure 2
Shield Attenuation Performance for a
Typical Mated Plug/Jack Screened Connector

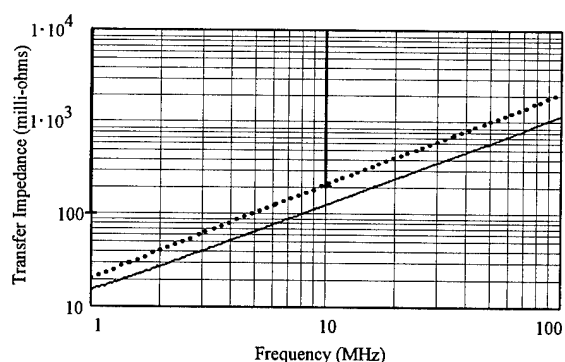


Figure 3
Calculated Transfer Impedance for a
Typical Mated Plug/Jack Screened Connector

Note that the transfer impedance measured for the screened connector is expressed in milli-

ohms. Both attenuation and transfer impedance curves properly depict the 20 dB/decade characteristic slope indicating that the connector is inserted properly into the triaxial fixture.

Generally, the trend of the shield attenuation curve is to flatten out at lower frequencies (< 1 MHz) or when the effects of the test set-up noise floor (readings < -85 dB) begin to dominate the measurement. This effect is readily seen when measuring screened cable.

The curves in figures 4 and 5 depict shield attenuation data and calculated transfer impedance performance for a .15 meter length of ISO/IEC 11801 4-pair, category 5, solid, screened (single foil, conductive side facing in, with drain wire) cable.

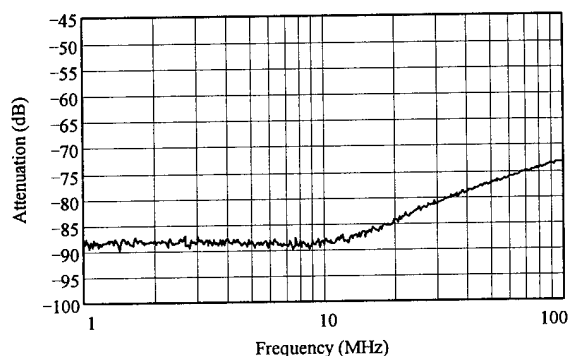


Figure 4
Shield Attenuation Performance for
.15 m of a Typical Screened Solid Cable

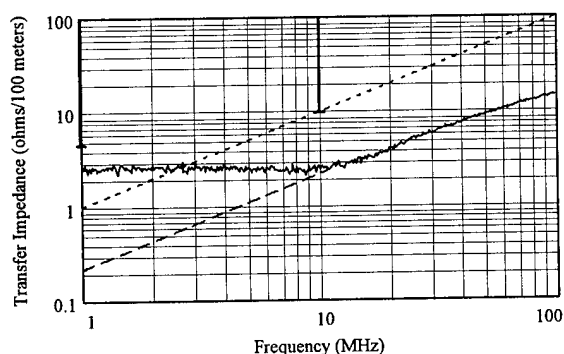


Figure 5
Calculated Transfer Impedance for
.15 m of a Typical Screened Solid Cable

Note that the transfer impedance measured for screened cables is expressed in $\Omega/100$ meters. The attenuation and transfer impedance curves

also depict the proper 20 dB/decade slope, but only in the range of 10 to 100 MHz where the noise floor does not dominate the shield attenuation measurement. A 20 dB/decade dashed extension line drawn in figure 5 is used to approximate the transfer impedance performance of the cable sample in the lower frequency range.

In order to collect cable transfer impedance measurements in the frequency range of 1 to 10 MHz, it would become necessary to collect shield attenuation data for longer length screened cable samples. Theoretically, the shield attenuation performance of cable samples 3 m or longer would be above the fixture noise floor and smoothly correlate to transfer impedance values. Unfortunately, the assumptions used to derive the transfer impedance function from shield attenuation measurements are not valid for cable lengths longer than .3 m. The transfer impedance derivation for longer cable sample lengths is currently under study.

At this time, no other method, including line injection or transverse electromagnetic (TEM) cells, has been successfully refined for accurate and repeatable collection of screened twisted-pair cable transfer impedance data.

For both screened connecting hardware and cables, the frequency range of 1 to 100 MHz was selected for harmonization with the boundaries for category 5 connecting hardware and cable transmission criterion as specified by ANSI/TIA/EIA-568-A⁵, ISO/IEC 11801, and CENELEC 50173⁶.

PERFORMANCE CRITERIA

Currently, the only published standards requirements for 100 Ω screened balanced twisted-pair connecting hardware and cable transfer impedance performance can be found in ISO/IEC 11801 and CENELEC 50173. These standards specify connecting hardware transfer impedance requirements of 100 $m\Omega$ at 1 MHz and 200 $m\Omega$ at 10 MHz (for category 3, 4, and 5 connectors) and cable transfer impedance requirements of 5 $\Omega/100$ m at 1 MHz and 10 $\Omega/100$ m at 10 MHz (for category 3, 4, and 5 cables). The ISO/IEC and CENELEC

requirements can be viewed as limits bars at 1 and 10 MHz on figures 3 and 5.

Qualitative analysis suggests that it may be more appropriate to specify category 3, 4, and 5 transfer impedance performance requirements by applying a slope of 20 to the worst case ISO/IEC and CENELEC limit point for screened connecting hardware and cables. Dotted curves representing the proposed limits can be viewed on figures 3 and 5. These curves are described by the limit equations shown in Table 1 and Table 2 below.

Table 1

Maximum Transfer Impedance Screened Connecting Hardware (mΩ)		
category 3 (1 - 16 MHz)	category 4 (1-20 MHz)	category 5 (1-100 MHz)
$Z_t = 20 \cdot f$	$Z_t = 20 \cdot f$	$Z_t = 20 \cdot f$
where f is the frequency (in MHz)		

Table 2

Maximum Transfer Impedance Screened Cables (Ω/100m)		
category 3 (1 - 16 MHz)	category 4 (1-20 MHz)	category 5 (1-100 MHz)
$Z_t = f$	$Z_t = f$	$Z_t = f$
where f is the frequency (in MHz)		

ACCURACY

The accuracy of the screened balanced twisted-pair transfer impedance measurement is dependent upon two factors:

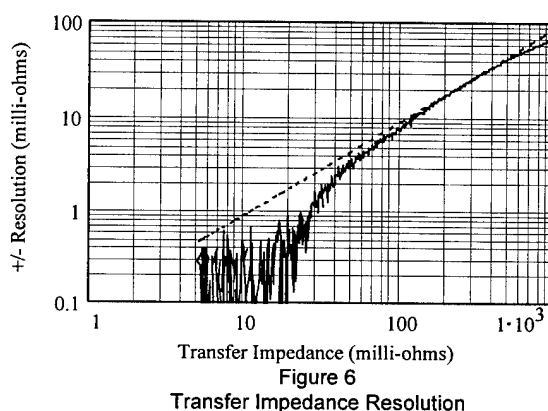
- the accuracy of the network analyzer, and
- fixture measurement repeatability/variability.

The accuracy of the network analyzer is generally considered to be no worse than ± 0.4 dB. This correlates to an equipment measurement error which is dependent upon the magnitude of the measured shield attenuation value. For example, the worst case network

analyzer error applied to -60 dB corresponds to a shield attenuation value of -59.6 dB. The accuracy at -60 dB is equivalent to the difference, in mill-ohms, between the transfer impedance calculated at -59.6 dB and -60 dB or ± 4.7 mΩ (104.7 mΩ - 100 mΩ). Calculated transfer impedance accuracy is better (i.e. $< \pm 4.7$ mΩ) for measured shield attenuation values less than -60 dB and worse (i.e. $> \pm 4.7$ mΩ) for measured shield attenuation values greater than -60 dB.

In addition to equipment error considerations, fixture measurement variances, which are dependent upon the operator's skill in reproducing very similar shield connections for multiple test samples, also contribute to measurement accuracy. It is reasonable to expect a skilled technician to be able to reproduce test results within ± 0.4 dB. Fixture measurement repeatability affects calculated transfer impedance accuracy in much the same way that network analyzer errors do.

The dotted line in Figure 6 shows the combined resolution errors of network analyzer accuracy and fixture repeatability (in milli-ohms) versus the magnitude of measured transfer impedance (in milli-ohms). The chart clearly demonstrates that transfer impedance accuracy is dependent upon the magnitude of measured shield attenuation. Note that the chart resolution begins for a measured transfer impedance of 5.6 mΩ which correlates to an attenuation noise floor of -85 dB.



The solid line in Figure 6 corresponds to the actual worst case error differential measured for five samples of screened cables and connecting hardware. Note that the actual accuracy

performance at high transfer impedance values is much better than predicted.

EFFECTS OF POOR SHIELD TERMINATION PRACTICES

Several experiments were carried out for the purpose of demonstrating the negative effects of improper shield termination practices upon the transfer impedance performance of screened 4-pair 100 Ω connecting hardware. The connecting hardware under test consisted of a mated shielded plug/jack to IDC with shielded cable termination spade enclosed within a metallic 'Faraday cage' style cover. This particular connector, as depicted by the solid line in figure 7, exhibits transfer impedance performance in excess of 75 m Ω below recommended limits at 10 MHz when properly terminated per the manufacturer's instructions. For reference, the recommended transfer impedance limits for connecting hardware are depicted as a dotted line.

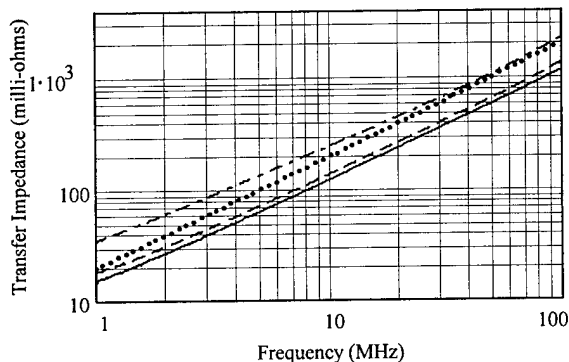


Figure 7
Calculated Transfer Impedance for
Various Shield Termination Scenarios
Limits Depicted as a Dotted Line

The dashed line in Figure 7 depicts the resultant effect of improperly connecting the shielded cable drain wire (the drain wire was left free-floating). This corresponds to a drop in transfer impedance performance of 14 m Ω at 10 MHz. Note that the slope of the transfer impedance curve has begun to deviate from the characteristic 20 dB/decade slope at low frequencies.

The dot-dashed line in Figure 7 depicts the resultant effect when the drain wire is properly grounded, but the cable shield is incorrectly

mated to the termination spade (the non-conductive side of the cable shield was in contact with the spade). This corresponds to a drop in transfer impedance performance of 104 m Ω at 10 MHz; an unacceptable level of shield effectiveness even though a physical shield connection through the drain wire was present! The slope of the transfer impedance curve has significantly departed from the characteristic 20 dB/decade slope.

As these triaxial measurements demonstrate, shield effectiveness can not be guaranteed simply by verifying shield continuity. It is imperative that proper drain wire and cable shield termination practices be followed in order to minimize the risk of potentially disruptive EMC effects.

ONGOING RESEARCH

The Telecommunications Industry Association (TIA) and ISO/IEC technical committees are aggressively pursuing the characterization of shield effectiveness and transfer impedance parameters. It is anticipated that these groups will soon incorporate shield effectiveness performance requirements and a recommended test methodology for measuring transfer impedance into their respective standards on screened cables, connecting hardware, and installed links. Currently, the TIA committee task group researching 100 Ω screened twisted-pair cabling systems (PN-3193) is evaluating the triaxial measurement methodology for incorporation into their Draft Technical Systems Bulletin Specifications for 100 Ω Screened Twisted-Pair Cabling.

CONCLUSIONS

The refined triaxial method is a simple, reliable and repeatable test procedure for characterizing the shield effectiveness of screened cables and connecting hardware via transfer impedance measurements. Higher transfer impedance values correlate to lower shield effectiveness and lower transfer impedance values correlate to higher shield effectiveness. Although past research on the triaxial measurement technique has only been able to demonstrate its capability to perform accurate measurements up to 30 MHz, continued refinements to the set-up and

measurement techniques have demonstrated that this method can be used to provide accurate results at least up to 100 MHz.

As shield effectiveness directly affects the electromagnetic compatibility (EMC) performance of balanced shielded twisted-pair cable and connecting hardware, it is anticipated that the telecommunications industry will embrace the triaxial transfer impedance method as the shield effectiveness test method of choice.

ACKNOWLEDGMENT

Good research demands enormous effort, lots of time, and commitment to the project. The author would like to thank the University of Applied Science, Reutlingen and, especially, Prof. Dr. Albrecht Oehler for his efforts leading to the publishing of this document.

REFERENCES

- [1] IEC 96-1, International Electrotechnical Commission Standard, "Radio Frequency Cables Part 1: General Requirements and Measuring Methods", 1986.
- [2] IEC 169-1-3, International Electrotechnical Commission Standard, "Radio Frequency Connectors Part 1: General Requirements and Measuring Methods, Section Three - Electrical Tests and Measuring Procedures: Screening Effectiveness", 1988.
- [3] University of Applied Science Reutlingen Institute for Electronics (Germany): Thesis Paper, Triaxial Measurement of Shielding Efficiency of Balanced Cabling Components, 1995, by Clause Stetter and Prof. Albrecht Oehler
- [4] ISO/IEC 11801, "Information Technology - Generic Cabling for Customer Premises", 1995.
- [5] ANSI/TIA/EIA-568-A, Telecommunications Industry Association Standard, "Commercial Building Telecommunications Cabling Standard", 1995.
- [6] CENELEC 50173, European Committee for Electrotechnical Standardization, "Performance Requirements of Generic Cabling Schemes", 1995

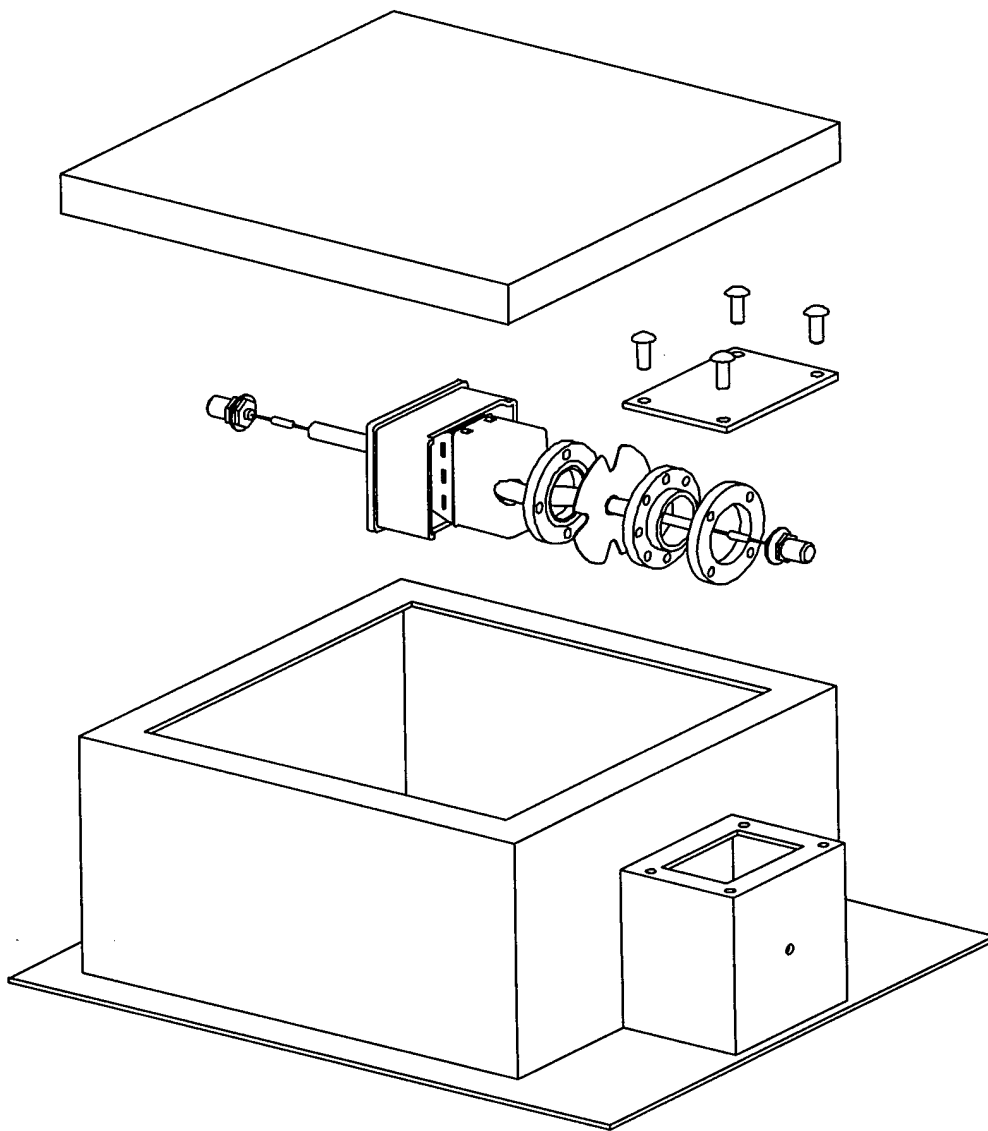
AUTHOR

Valerie A. Rybinski received the B.S.E.E. degree from the University of Connecticut in 1991. Valerie is an electrical engineer at the Siemon Company in Watertown, CT. Her research activity is mainly in the field of shielded and unshielded balanced twisted-pair telecommunications cabling and connecting hardware.



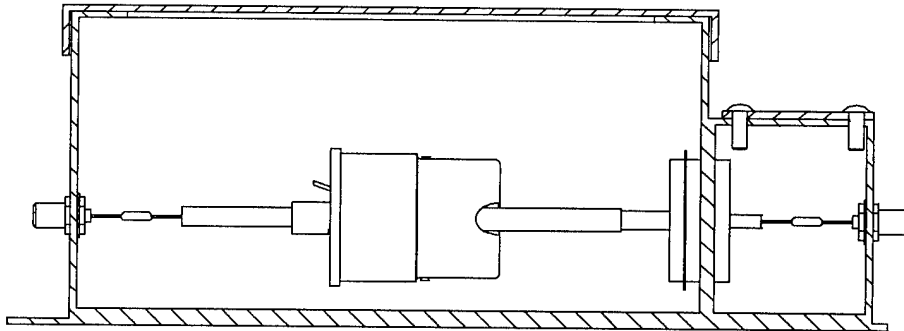
Appendix A

Figure 1: HF Copper Case with Connecting Hardware Test Sample
Exploded View



Appendix B

Figure 2: HF Copper Case with Connecting Hardware Test Sample
Side Termination View



BALANCE MEASUREMENTS OF UTP CONNECTING HARDWARE

Brenda Lord, Dave Tardif, Paul Kish and Jörg-Hein (Jo) Walling

Nordx/CDT
Lachine, Québec, Canada

ABSTRACT

It is known that Electromagnetic compatibility (EMC) performance is affected by the balance of a cabling system. Balance has become an increasingly significant parameter as a result of fast data rate protocols being implemented on local area networks. The various balance parameters for connecting hardware and short links are measured and are shown to be very sensitive to the common mode termination and to the type of balun used. Two types of baluns are compared and results indicate large variations in the transverse conversion loss (TCL) and the longitudinal conversion transfer loss (LCTL) measurements. The common mode impedance looking into the center tap of the test baluns is very different for each type of balun. It is recommended that this parameter be specified in order to ensure consistent balance measurements between labs.

INTRODUCTION

Unshielded twisted pair (UTP) cables have grown in popularity as the media of choice for local area networks and are currently used in over 60% of all desktop interconnections. UTP cabling provides a versatile and economical alternative to traditional coaxial and shielded twisted pair based networks. As transmission rates increase, the application standards committees have developed or are in the process of developing physical layer specifications that support 100 Ohm UTP cables and connecting hardware.

Electromagnetic compatibility (EMC) is one of the critical issues relating to UTP implementations of very high speed LAN equipment such as Twisted Pair Distributed Data Interface (100 Mb/s) and Asynchronous Transfer Mode (155 Mb/s). To this end, the

resulting EMC performance is governed by the design of the equipment as well as the balance characteristics of the UTP channel between the transmitter and the receiver.

This paper describes the mechanism of noise coupling into a UTP channel from external sources. It also relates the magnitude of the induced differential noise component to the longitudinal balance characteristics of a twisted pair circuit, namely the Transverse Conversion Loss (TCL) and the Longitudinal Conversion Transfer Loss (LCTL). Longitudinal balance measurements were performed on various Category 5 connectors and short links. The results show that these measurements are very sensitive to the test configuration, the type of balun used and the common-mode termination. In particular, significant variability in the test results were attributed to the common mode impedance of the test balun (i.e. input impedance looking into the center tap). In order to assure consistency and repeatability between labs, the common mode impedance of the test balun needs to be controlled and specified.

Noise Coupling Mechanism

Three elements are necessary to produce a noise problem. First, there must be a noise source. Second, there must be a receiver circuit that is susceptible to noise. Third, there must be channel for the noise to be coupled from the source to the receiver.

The noise environment consists of primarily two contributors: NEXT from all data signals in the cable (including self NEXT) and externally induced noise from power lines, electric motors, radio and TV broadcast signals, power converters, florescent lights, etc.

Fig. 1 illustrates two mechanisms for noise coupling into the receiver, namely, induced

noise due to external EM field coupling and conducted noise due to external ground loops. Both are equally important.

The induced common-mode coupling voltage (V_e) is a function of the electric field strength (E) and the loop area formed by a conductor of length (l) which is suspended at an average height (h) above the ground plane. The common-mode voltage is the average voltage relative to ground for each conductor of a twisted pair circuit, given by:

$$V_e = (V_{1g} + V_{2g})/2.$$

The differential-mode voltage is the difference in the voltage between conductors of a twisted pair circuit, given by:

$$V_d = (V_{1g} - V_{2g}).$$

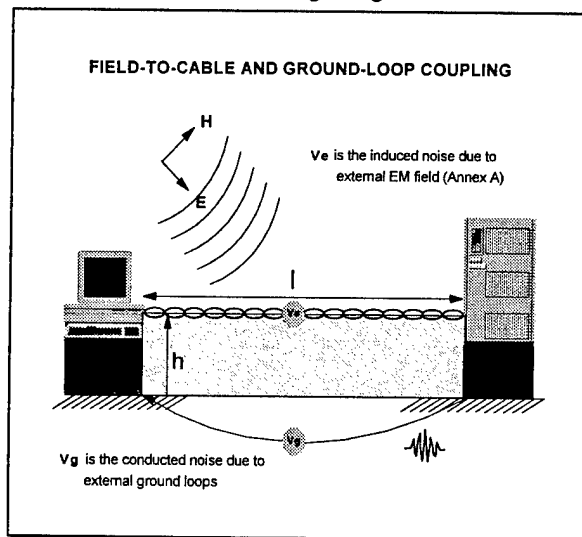


Figure 1. Field-to-Cable and Ground-Loop Coupling

The magnitude of the induced common-mode voltage (V_e) is calculated by using the equation for a circular loop antenna, given by:

$$V_e = 2\pi A E / \lambda$$

This equation is a good approximation for a loop of any shape that satisfies the inequality:

$$2\pi x / \lambda < 1$$

where: x is the distance around the loop,
 λ is the wavelength,
 A is the area of the loop,
 E is the electric field intensity.

The common-mode voltage varies from a minimum value of zero for lengths that are a multiple of λ , to a maximum value for lengths that are multiples of $\lambda/2$. The equation shows that installing the cable close to the ground plane can have a very significant effect in reducing the magnitude of induced common-mode noise coupling. Changing the average height from 1 meter to 0.1 meter reduces the noise coupling by a factor of 10. This is equivalent to reducing the field intensity from 3V/m to 0.3V/m, if the height were constant.

Balance of UTP Cabling

The concept of balance is illustrated in Fig. 2. V_{cm} is the common-mode noise voltage induced in each conductor of a twisted pair. V_g is the conducted noise due to the potential difference of the ground (earth) between the workstation and the hub equipment. For a balanced circuit the noise currents I_n flowing in each conductor of a pair are equal in magnitude and in the same direction, ie.:

$$I_{n1} = I_{n2}$$

Equal currents flowing in each half of the primary winding of a well balanced transformer produce equal and opposite voltages at the secondary winding, resulting in a net cancellation of the noise at the input to the receiver. The common mode rejection of the magnetics can be further improved by adding a common mode choke in series with the transformer. A minimum common-mode rejection ratio (CMR) of 40 dB is desirable for high quality magnetics over the operating frequency range of interest.

Fig 2 also illustrates the effect of isolating the ground connection at one end of the circuit. This has the effect of reducing the noise current flowing through the ground return and can provide a higher noise immunity.

The concept of balanced twisted pairs and the calculation of the induced noise assumes a well balanced cabling link. In practice, cables and connecting hardware exhibit a finite unbalance in capacitance, resistance and inductance, between each conductor and the ground return path. Depending on the degree of unbalance, a part of the common-mode noise signal is converted to a differential-mode noise signal which passes directly to the input of the receiver.

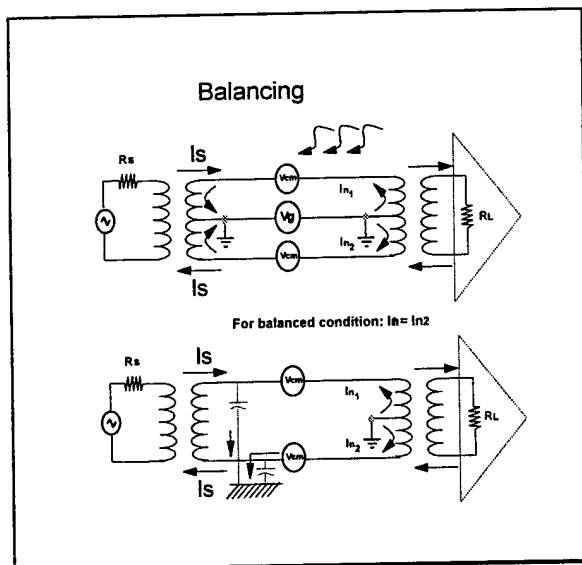


Figure 2. Balancing

The goal is to achieve a balanced circuit in order to control and minimize emissions resulting from the Transverse Conversion Loss (TCL) and differential noise at the receiver resulting from the Longitudinal Conversion Transfer Loss (LCTL).

DEFINITIONS

There are a number of different balance parameters for both a one-port and a two-port network. These are clearly defined in the ITU Recommendation G.117 Transmission Aspects of Unbalance About Earth¹ and Measurements of Unbalance to Ground in Balanced Systems.² The following is a review of the definitions and measuring techniques of the balance parameters that were tested.

To distinguish between a longitudinal and a transverse signal, a longitudinal signal refers to the voltage between an individual conductor and ground, whereas a transverse signal refers to the voltage between two conductors. These two terms are synonymous to a common mode signal and a differential signal respectively. These voltages vary with frequency.

One-port Networks

The following balance parameters are characterized by one-port networks:

Longitudinal Conversion Loss (LCL) is a measure of the ratio of the longitudinal voltage to the transverse voltage for a single twisted pair.

This is measured by transmitting a longitudinal or common mode signal on a terminated pair and measuring the transverse or differential mode signal that is reflected back resulting from the unbalance of the pair for a device under test.

$$LCL = 20 \cdot \log_{10} \left| \frac{V_{CM1}}{V_{DIFF1}} \right| \text{ dB}$$

Transverse Conversion Loss (TCL) is the reverse of the LCL balance parameter whereas the signal being transmitted on a terminated pair is differential and the resultant common mode signal reflected is an indication of the unbalance of the pair for a device under test.

$$TCL = 20 \cdot \log_{10} \left| \frac{V_{DIFF1}}{V_{CM1}} \right| \text{ dB}$$

Two-port Networks:

The following balance parameters are characterized by two-port networks:

Longitudinal Conversion Transfer Loss (LCTL) is the ratio of the common mode signal voltage to the differential signal voltage for a single pair of a device under test. A common mode signal propagates along a pair and the portion of the signal that has been converted into differential is measured on the second port of the network.

$$LCTL = 20 \cdot \log_{10} \left| \frac{V_{CM1}}{V_{DIFF2}} \right| \text{ dB}$$

Transverse Conversion Transfer Loss (TCTL) is the reverse of the LCTL measurement, whereas a differential signal propagates along a pair and the common mode voltage is measured at the receiving port of the network. A ratio of the two voltages is calculated to express the balance parameter.

$$TCTL = 20 \cdot \log_{10} \left| \frac{V_{DIFF1}}{V_{CM2}} \right| \text{ dB}$$

Cross Modal Crosstalk

Considering that cabling systems are not perfectly balanced, the conversion between differential and common mode signals will introduce some additional crosstalk coupling within a multi-pair cabling system. Not only is it important to characterize the differential to differential coupling between pairs, but it is also

important to consider the cross modal crosstalk parameters. Cabling systems that are not well balanced may have significant contributions of cross modal coupling.

Cross modal crosstalk can be defined as the capacitive and inductive coupling between two pairs of a multi-pair cable or, in this case, connecting hardware, such that all the following modes of coupling are studied:

Differential to differential crosstalk is the familiar measurement in which a differential signal is sent on a disturbing pair and measured on a disturbed pair.

Differential to common mode crosstalk implies sending a differential signal on a disturbing pair and measuring the resulting common mode signal coupled onto a disturbed pair.

Common mode to differential crosstalk is the contrary; the signal transmitted on one pair is common mode and the differential mode of the disturbed pair is measured.

Common mode to common mode crosstalk exists when a common mode signal is sent on a disturbing pair and measured on a disturbed pair.

TEST SET UP

Fixture

A test fixture was used to hold eight (8) baluns in an upright perpendicular position. This fixture was securely fixed onto a solid copper ground plane. The distance between the four (4) near end (N.E.) and four (4) far end (F.E.) baluns was eight inches. The four baluns at each end were positioned 90 degrees from each other. The distance between the device under test and the ground plane was two inches.

The fixture initially held eight baluns, referred to as Balun A, that are specified to have a balance of 50 dB throughout the frequency range from 1 - 100 MHz. All tests were repeated with a second set of eight baluns, referred to as Balun B, specified throughout a frequency range of 1 - 350 MHz.

Tests

Tests were performed on two designs of connecting hardware. They were chosen such that Connector 1 uses lead frame technology

and Connector 2 uses printed circuit board technology as a transmission medium. A short link comprising of a Category 5 connector, a seven foot patch cord, and a second Category 5 connector was also studied.

All the above described balance parameters were tested as well as near end and far end cross modal crosstalk parameters. Each parameter was tested in two different configurations as per table 1.

Table 1. Termination Configurations

Test Configuration		1	2
Common Mode Termination	Disturbing Pair		✓
	Disturbed Pair		✓
	Unused Pairs N.E. & F.E.		✓
Differential Mode Termination	Disturbing Pair	✓	✓
	Disturbed Pair	✓	✓
	Unused Pairs N.E. & F.E.	✓	✓

Calibration

Calibration curves for common mode to differential and differential to common mode crosstalk (near end and far end) as well as for all the two port balance parameters were derived using the measured calibration curves for differential to differential and common mode to common mode configurations. The actual calculations can be found in a connected paper.³

RESULTS

Repeatability

Connector 1 was tested, removed from the test fixture, then later retested. A typical result is shown in figure 3.

The curves are exactly the same indicating two things. Firstly, the test set does not introduce additional variations to the results. Secondly, the calculations made for the balance and cross modal parameter calibration curves are correct. Another indication of repeatability is reversing the direction of the signal. That is, swapping the

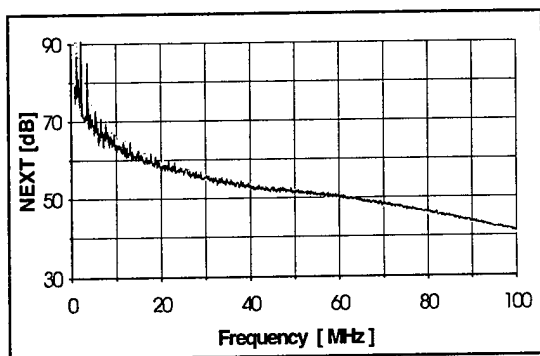


Figure 3: Differential to Common Mode NEXT for Connector 1, Tested and Retested.

transmit and receive ends of the measurement. A typical example of this is shown in figure 4, where the two measurements are superimposed and the expected result is obtained.

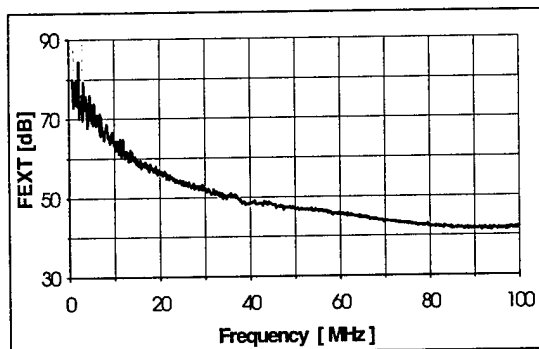


Figure 4. FEXT; Reversing Transmit and Receive.

The Effect of Termination

Figure 5 demonstrates that the differential to differential NEXT results for a short link for tests done with Balun A and then Balun B are similar (excluding the nulls) when using test configuration 2 with common mode termination.

But, figure 6 reveals that this is not true for the same link when using test configuration 1, the differentially terminated configuration. It is clear that short link resonance behavior (i.e. the worst case peak of 29 dB at 87 MHz) is present when using Balun A and not at all present when using Balun B. In fact, there are practically no differences between test set up 1 and 2 (i.e. differentially terminated, and differential and common mode terminated) for most measurements taken with Balun B.

What accounts for the significant difference between measurements using Balun A and

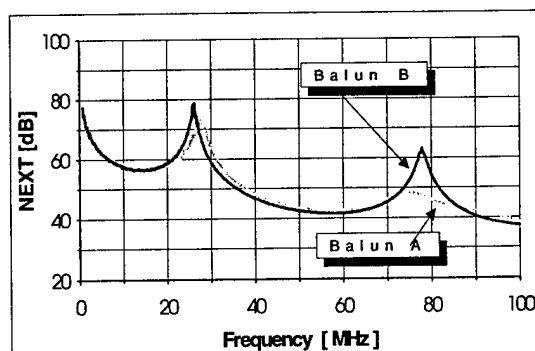


Figure 5. Common Mode and Differentially Terminated Short Link NEXT Measurement for Balun A versus Balun B.

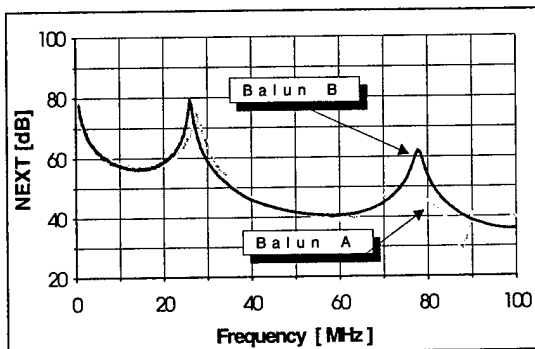


Figure 6. Differentially Terminated Short Link NEXT Measurement for Balun A and Balun B.

Balun B? Are the differences caused by reflections of common mode signals due to common mode mismatch between the baluns and the device under test? If so, is this the reason for the short link resonance phenomena?

In an attempt to understand the cause of these differences, additional tests were performed as follows:

Balance

The balance parameters are not at all similar between Balun A and Balun B. Figure 7 indicates that LCTL results for Connector 1 do not correspond at all when tested with the different baluns. The footprints are completely unlike.

Careful examination of the results show that Balun A exhibits deep nulls at 40 and 70 MHz.

The LCL results for Connector 1 are shown in figure 8. There are less variations in the footprints of the curves although the nulls that appear in the LCTL figure 7 are also present

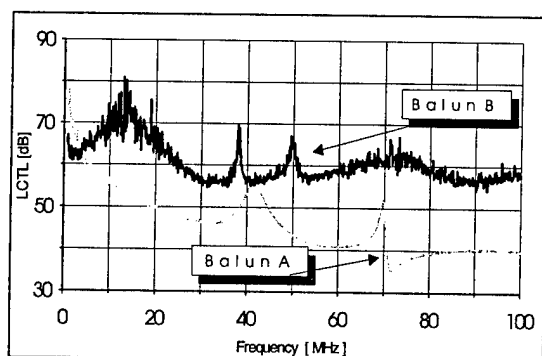


Figure 7. LCTL of Connector 1 measured with Balun A and Balun B

here. These differences are reduced when the unused pairs are common mode terminated as per test configuration 2.

It is also interesting to mention that when using one type of balun, the LCL and LCTL measurement results are completely identical to the TCL and TCTL results respectively. This is an expected finding due to the symmetry of the test circuits for these balance parameters.

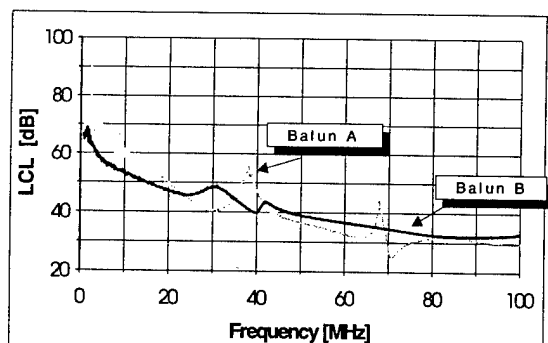


Figure 8. LCL of Connector 1 Measured with Balun A and Balun B.

To eliminate any variables a connector or short link may add to the investigation of the performance of the baluns, the two-port balance networks, i.e. LCTL and TCTL, were measured for 8 inches of unshielded twisted pair. An LCTL result is shown below in figure 9.

Because the test set-up incorporates eight baluns, the LCTL and TCTL curves are different for the different pairs. Each pair represents a different balun combination. This is true for both Balun A and Balun B. The effect of the baluns may add depending on the baluns being used. The deep nulls seen in figure 9 are representative of many measurements taken

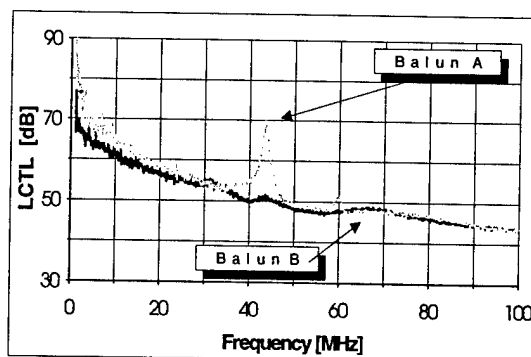


Figure 9. LCTL Measurement for 8" of UTP using Balun A and Balun B

with Balun A. Some results taken with Balun B exhibit similar effects but are usually less pronounced.

According to a paper on Measurements of Unbalance to Ground of Balance Systems⁴, the transformers should have a superior inherent balance to the balance values to be measured. A 12 dB margin may affect the measured value by as much as 2 dB. If a short length (8") of UTP has a balance result of 43 dB when tested with Balun A, the inherent balance of the baluns themselves must be at least 60 dB to not have an effect on the measurement. It will be shown in the following section of this paper that the inherent balance of the baluns does not reflect what is needed for accurate measurements.

DISCUSSION OF RESULTS

Balance of the Balun

The LCL measurements for Balun A and Balun B are shown below in figure 10. Balun B has a significantly better balance in the higher frequencies. The LCL is 58 dB at 100 MHz with a slope of 11 dB per decade. The LCL of Balun A at 100 MHz is 50 dB with a slope of 20 dB per decade. These significant dissimilarities in the inherent balance of the two baluns may account for the differences in the measurements of the balance parameters seen earlier.

Common Mode Impedance

By applying a signal on the common mode port of the balun, terminating the unbalanced primary port in 50 ohms, and measuring an impedance network (LCL = infinity) on the 100 ohm balanced port, it becomes possible to examine the common mode impedance characteristics of each balun.

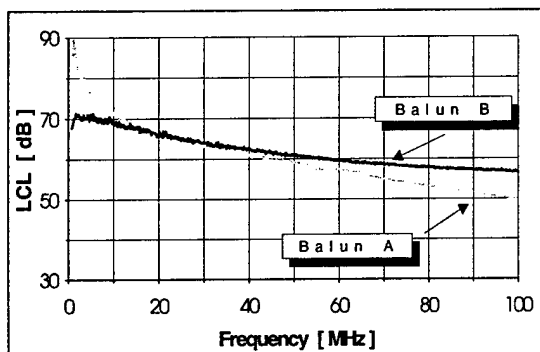


Figure 10. Inherent Balance (LCL) of Balun A versus Balun B

The common mode impedance is represented as reactance versus resistance in figure 11. The common mode impedance of Balun A is significantly different from Balun B.

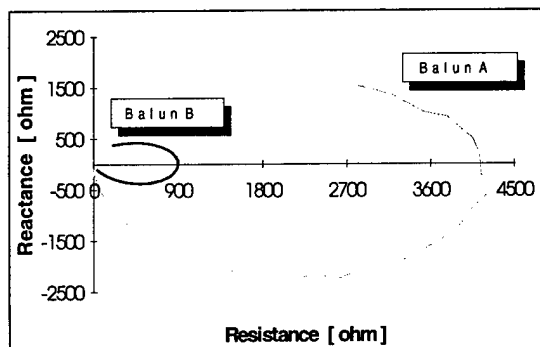


Figure 11. Reactive Component versus Resistive Component of the Common Mode Impedance as seen through the Center Tap of Balun A and Balun B

The resistive component of Balun A is actually negative at 100 MHz (-2 ohms). This is shown clearly in figure 12. It crosses the zero line at 87 MHz. This negative resistance suggests that Balun A amplifies energy at high frequencies.

Balun B, on the other hand, has a higher resistive component which dissipates energy. At 100 MHz, the resistance is 38 ohms.

These values are significant in demonstrating the importance of matching the common mode impedance of the balun with that of the device under test. The common mode impedance of a typical data cable falls in the range of 75 to 100 ohms.

Because Balun A has a higher common mode impedance mismatch, there is more reflected

energy. The reflected energy is present in the measurements as resonance.

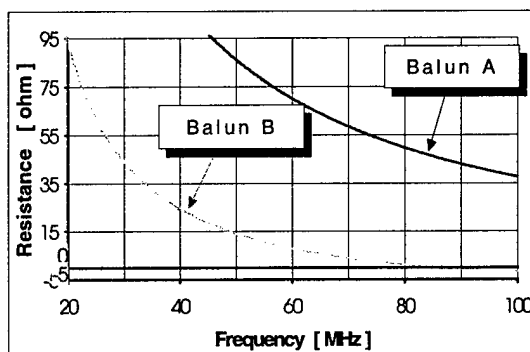


Figure 12. Resistive Component of the Common Mode Impedance as seen through the Center Tap of Balun A and Balun B.

CONCLUSION

Electromagnetic compatibility is an important consideration in the design of high speed LAN equipment. The balance characteristics of a UTP channel, including cable and connecting hardware, plays an important role in reducing electromagnetic emissions as well as reducing the susceptibility to external interference. In this regard, the Transverse Conversion Loss (TCL) is the parameter that governs the electromagnetic emissions emanating from the cabling system. Longitudinal Conversion Transfer Loss (LCTL) is the parameter that governs the level of differential noise that is coupled into the receiver from external sources.

The measurement of TCL and LCTL is very sensitive to the testing configuration, the termination configuration and the characteristics of the baluns that are used for testing. Analysis of the results show large differences in the balance measurements between Balun A and Balun B when testing connecting hardware. These differences are even more apparent in terms of the resonance phenomena when testing short links. Short link measurements using Balun B did not exhibit the worst case resonance peaks that can lead to failures of short links.

The balance of Balun B is about 8 dB better than Balun A at high frequencies. Also, the common-mode impedance looking into the center tap of Balun B has a higher resistive component. It is postulated that the resistive component has a beneficial effect in dissipating and damping out reflected common-mode energy. In fact the

resistive component of Balun A is slightly negative beyond 80 MHz, which is unusual. This would have the effect of adding to the reflected energy and would exacerbate the resonance phenomena.

In order to ensure accurate and repeatable balance measurements it is recommended that the common-mode impedance looking into the center tap of the secondary winding of the test balun needs to be specified over the frequency range of operation which can extend up to 300 MHz.

REFERENCES

- [1] ITU Recommendation: Transmission Aspects of Unbalance About Earth (Definitions and Methods), Fascicle III.1 - Rec. G.117
- [2] North Hills Application Note: Measurements of Unbalance to Ground in Balanced Systems, Sept. 1993
- [3] J.-H. Walling et al : Crosstalk Measurements as a Means to Characterize the Balance of Data Grade Wires, IWCS 1996
- [4] Leo Staschover, North Hills, Measurements of Unbalance to Ground of Balanced Systems, 1991

AUTHORS

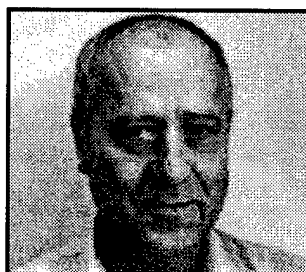


Brenda Lord received her B.E. in Electrical Engineering from Concordia University, Montreal, Canada, in May 1994. She joined Northern Telecom in April 1994 as an engineer in research and development in the connectivity group. Now employed by Nordx/CDT, she works in high frequency testing and component evaluation.



Dave Tardif is studying Electrical Engineering at the University of Sherbrooke, Quebec. He will complete his B.E. degree in 1998. He worked as a Summer Student at the Nordx/CDT Plant in the summer of 1996. His work focused on testing procedures and data acquisition.

Paul Kish received an M.A.Sc. in Electrical Engineering from the University of Waterloo in 1972. He has over 20 years experience with BNR and Northern Telecom in the design and development of telecommunications cables. He is currently Senior Manager, PLM for Broadband Cabling and Standards with Nordx/CDT. Mr. Kish has been an active member of TIA for the last eight years. He serves as the current chairman of TR 41.8.1 working group responsible for the Telecommunications Cabling Standard for Commercial Buildings.



Jorg-Hein Walling finished his studies in Mech. Engng. with a degree in Materials Technology at the Technical University of Berlin. In 1974 he obtained a Doctorate (Dr.-Ing.) at the same University. At the end of 74, he joined Northern Telecom Canada Ltd. Since 1976 he has been senior engineer at the Lachine Cable Plant, working now for Nordx/CDT.

Testing Patch Cords with Terminated Plugs Using Time Domain Measurements

H. Koeman

Fluke Corporation, Everett WA, USA

ABSTRACT

The Near End Crosstalk (NEXT) as a function of distance along the length of a link is obtained in time domain based measurements. Digital signal processing (DSP) techniques may be used to isolate NEXT contributions from segments of the link before performing a FFT operation to obtain a result as a function of frequency. This paper describes its application towards measuring the quality of workmanship of connecting a modular plug to a patch cable. The local NEXT can be measured at each end of the patch cord, thereby providing an excellent indication of quality of the assembly. Time domain based measurements offer the advantage that disturbing effects, present when measuring the patch cord quality using scalar swept frequency techniques, are considerably suppressed.

QUALITY OF WORKMANSHIP OF THE ASSEMBLY

The key quality performance factor of patch cords is Near End Crosstalk (NEXT). The discussion of performance centers therefore around NEXT in this paper. The question is how to define the quality of workmanship of attaching a plug to patch cable and the quality of the components used in the assembly. The cable is disturbed to a certain degree when the jacket is stripped off, and the wires are fitted to slide into the plug. Then a crimping procedure follows, which causes the jacket to be compressed, as well as the connections to the pins of the connector. Not only the connection inside the plug needs to be addressed, also the cable deformation which occurs for a short distance in the patch cable itself. This distance is undetermined, but could be expressed as multiples of the twist rates of the wire pairs in the cable. Practically, this

could be in the order of 10 cm or more. Therefore, the measurement of the quality of a plug/cable interface should include the plug itself plus a short distance of cable.

CURRENT METHODS TO QUALIFY PATCH CORDS

The methods to determine the quality of patch cords considered by standardization organizations all use swept frequency methods. The one method under active consideration by the Telecommunications Industries Association (TIA) in the US is the "de-embedding" method [1]. This method is aimed to determine the quality of the plug-cable-plug assembly by subtracting out the NEXT contributions by the local test jack and the remote terminating jack from an overall link measurement. In order to have a jack design independent result, the de-embedding method uses uncompensated category 3 jack designs. The other method, to be considered a "confidence check", is to measure the patch cord performance in a short link configuration using pre-qualified jacks.

In the de-embedding procedure, the NEXT contributions from local test jack and remote terminating jack must be determined using a reference terminating plug and a reference test plug. The subtraction of the NEXT contribution of the local test jack and remote terminating jacks include both real and imaginary components of signals. Time delay is added in order to subtract the NEXT contribution of the remote terminating jack. The de-embedding procedure contains many steps, each having a measurement uncertainty.

The de-embedded NEXT resulting from a patch cord test is a relatively low number in the range of 24 to 34 dB [2]. The principle of compensation in a jack to achieve category

5 level of performance involves designing an amount of compensation for a nominal plug, centering the compensation between an upper and lower boundary, which may be expected from a compliant plug. These variations can be determined from the uncertainty of the mechanical dimensions as they are specified in [3]. It is obvious that small variations in the uncompensated NEXT cause relatively high variations when a plug is mated with a category 5 jack in a real link.

The challenge of a patch cord standard is to obtain a test station independent measure of the quality of construction, and have this measure of performance to be a good predictor of performance in a link. In some situations there have been good levels of agreement of independent measurements, while in some cases discrepancies remain to be explained. The correlation between the de-embedded NEXT and the NEXT performance in a link is not very good yet: patch cords with a certain de-embedded NEXT value show a 4-6 dB variation in NEXT when the patch cord is measured as a short link [2].

The difficulty of testing a patch cord as a short link is related to effects which disturb the measurement. In each of these cases, reflections from discontinuities play a significant role. First there is the "short link" effect. It is recognized that signal imbalance causes coupling other than differential-to-differential mode and thereby cause excess NEXT components. The common mode signals, particularly if the common mode paths are left unterminated, cause significant resonance effects. For short links excess amounts of 5 dB have been observed. These effects can be shown to be reduced substantially by including full common mode terminations in addition to the differential mode terminations.

Secondly, swept frequency domain tests are affected by reflections from remote terminations, mainly the plug/jack located at the remote end. The specifications for return loss for connecting hardware in [4] and [5] at 100 MHz is 14 dB. This figure represents

a reflection coefficient $\rho = 0.2$. During NEXT the coupled signal splits up in the forward and reverse directions, see figure 1. At a nominal reflection from the remote end, and with little attenuation, a 14 dB error term occurs, which since it is directly correlated with the NEXT signal that arrives directly results in a 1.6 dB error.

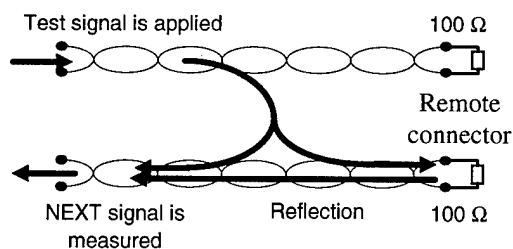


Figure 1: Reflection from remote connector

Therefore, alternate test methods are desirable which are aimed to characterize the quality of terminating a plug to a cable independent of these disturbing effects. Time domain measurement approaches like described in [6] offer an alternate solution.

PROPOSED PATCH CORD ASSEMBLY WORKMANSHIP TEST METHODOLOGY

The proposed patch cord assembly test method is to measure the NEXT associated with the very first portion of a test link. The beginning of the test link consists of a pre-qualified jack with NEXT of $40.5 \text{ dB} \pm 0.5 \text{ dB}$ @ 100 MHz, mating with the plug of the patch cord, see figure 2. The pre-qualification test is performed with a Terminated Open Circuit (TOC) plug measurement of also $40.5 \text{ dB} \pm 0.5 \text{ dB}$ @ 100 MHz [4][5]. It may be desirable to enhance the pre-qualification test by requiring that when using TOC plugs of 40 dB and 42 dB, the mated plug/jack results should be approximately the same.

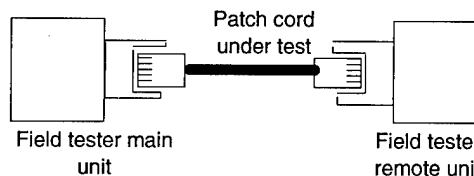


Figure 2: Patch Cord End Test Configuration

Digital signal processing techniques are used to estimate the response of the connection and very beginning of the patch cord. The resulting sensitivity to NEXT at 100 MHz as a function of distance in the current implementation is shown in figure 3.

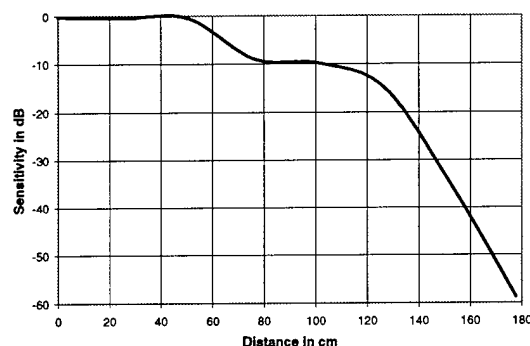


Figure 3: Sensitivity to NEXT @ 100 MHz as a function of distance

It may be noted that NEXT from sources near the local plug are not significantly rejected. As the distance to the local plug increases, the rejection increases quickly. The NEXT from short cable segments of nominally compliant cable, is very small, and therefore the rejection immediately following the plug is not essential. A faster increase in rejection as a function of distance can be accomplished by increasing the resolution of the time domain response. The current sample rate is 500 Ms/s. Any signals that are delayed equivalent to a propagation delay of more than 1 meter are essentially ignored by the measurement. This includes reflections, NEXT from a remote connection, other NEXT from a greater distance than 1 meter, excess NEXT effects from resonating common mode signals, etc.

Practically, the test limit for the plug/jack connection plus the local end of the cable approaches the test limit of the mating connection by itself. Therefore, the dynamic range and the accuracy performance of the tester has to be very good in order to make this measurement in a reliable manner. The test limits are derived from models for plug/jack interfaces and cable. These will be discussed next. The measurement is

repeated from the other end of the patch cord, so that the quality of attachment at both ends is known. Since the workmanship test only uses the ends of the patch cord, the results are independent of its total length. It is possible to add the contributions from each end of the patch cord to obtain a consolidated result for the patch cord as a whole. This is not discussed in this paper.

The principles and implementation of this capability are the subject of patent applications.

MODEL OF PATCH CORD WORKMANSHIP NEXT

The patch cord end includes a plug/jack connection and a short segment of cable. The NEXT model for connecting hardware includes both capacitive unbalance and inductive coupling. It can be shown [7] that the frequency response from both of these components has a 20 dB slope as a function of frequency. We therefore assume that the plug/jack connection NEXT is as defined in [4][5] for category 5 connecting hardware:

$$NEXT_{conn} = 56 - 20 * \log(f / 16) \quad (1)$$

where f is the frequency in MHz.

From the model it might be expected that the phase of the NEXT is approx. 90 degrees relative to the stimulus voltage. In reality, this phase varies quite a bit as a function of frequency as a result of phase delays though the compensation in category 5 jacks [8]. Different category 5 jack designs exhibit different phase responses and some variation may be expected from jack to jack of a specific design. Consequently, the phase is not pre-determined and the NEXT from connector and cable may be considered random.

The NEXT to be expected from a short segment of cable can be estimated by considering a NEXT event, which is attenuated twice by the cable between the NEXT event and the point from where the measurement takes place. The NEXT for a

short cable segment can be obtained using length dependent equations in [9] or [10].

For a short segment of nominally compliant category 5 cable it follows:

$$NEXT_{cable} = 10 * \log(6 * 10^{-9} * f^2 * length) \quad (2)$$

where the *length* is expressed in meters and the frequency *f* in MHz.

The NEXT loss at 100 MHz from a cable segment with length equal to 10 cm, 20 cm, 50 cm and 1 m is shown in table 1.

Table 1: Estimated NEXT loss from a short segment of cable at 100 MHz

Length (cm)	10	20	50	100
NEXT loss @ 100 MHz (dB)	52.2	49.2	45.2	42.2

An important conclusion is that the slope of the NEXT from a short segment of cable, is approximating 20 dB/decade, same as for NEXT expected from connecting hardware. It is therefore expected that the highest accuracy based on this model occurs near the highest frequency where the highest potential for creating random phases between the contribution from NEXT sources along the length of the short cable segment is present [11]. At 100 MHz, given an NVP of 0.67, the wavelength $\lambda = 2$ meters. At $1/8 \lambda$ length, the cable will assume transmission line properties and provide the randomization that is assumed in the short cable model.

MODEL FOR THE WORKMANSHIP TEST

The model for the workmanship test includes the NEXT contribution of the mated reference jack/plug connection plus the short piece of cable. As discussed before, the phase of the NEXT from the plug/jack connection and from the short piece of cable can be assumed to be uncorrelated, certainly near the upper end of the frequency range. If the short piece of cable is really short, the expected NEXT contribution to the overall measured NEXT becomes so small that it is insignificant. If the NEXT from the local end of the cable is significant, it may be

considered to be part of the quality of workmanship attaching the cable to the plug. The NEXT from the cable is reduced slightly by twice the attenuation att_{conn} of the connector.

$$NEXT_{workmanship} = 10 * \log \left(10^{\frac{-NEXT_{conn}}{10}} + 10^{\frac{-NEXT_{cable} + 2 * att_{conn}}{10}} \right) \quad (3)$$

The estimated test limit, using nominal values for connector and cable are shown in figure 4 as a function of cable segment length. Test limits at 100 MHz as a function of cable segment length are shown in table 2.

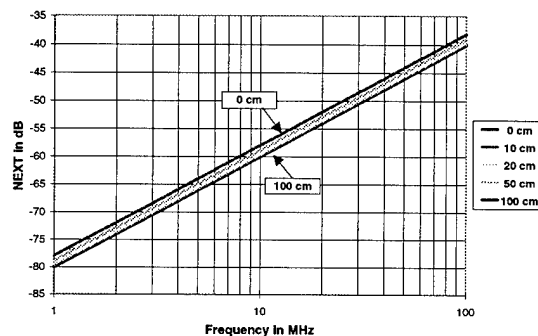


Figure 4: NEXT limits for the workmanship test as a function of frequency

Table 2: NEXT loss for a single connector with a short cable attached

Length cable (cm)	0	10	20	50	100
NEXT loss @ 100 MHz (dB)	40.1	39.8	39.6	39.0	38.1

Note that the NEXT contribution of a good connection is practically always near -40 dB @ 100 MHz, and the NEXT from the cable varies considerably, up to a limit as defined in the ISO/IEC and TIA standards. In addition, the cable NEXT contribution varies a little as a function of the length of the cable portion that is measured. In any of the measurement conditions that are proposed, the NEXT will be dominated by the NEXT from the connection and the workmanship of connecting the patch cable to the plug of that connection.

PRACTICAL RESULTS OF WORKMANSHIP TESTS

The workmanship test is conducted in both directions as for a normal link. When measured in the forward direction, the quality of workmanship at the local end is tested. The test in the reverse direction tests the end of the patch cord that is connected to the remote unit. A typical frequency response for a 2 m long UTP patch cord is shown in figure 5.

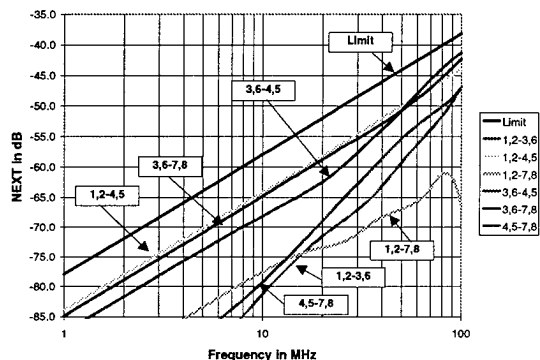


Figure 5: Example of Time Domain Workmanship Measurement, represented in the Frequency Domain

Note that resonance from the NEXT of the remote connector is totally absent. The levels of the test results for the workmanship test are considerably more sensitive than the test limits for a channel or basic link. Disturbing effects have therefore more impact. Nevertheless, the responses that are closest to the limit line tend to exhibit a slope close to 20 dB/decade.

Of particular interest may be the fact that it is relatively easy to obtain passing results on UTP patch cords. However, we have found a large number of failures when ScTP patch cords are tested. This may be an interesting subject of further investigation. It is possible that the crimping procedure and the connection of the shield of the cable to the shield of the cable provides an additional source of capacitive unbalance.

VALIDATION OF TIME DOMAIN WORKMANSHIP TEST METHOD

Frequency swept measurements using network analyzers are widely used to provide a reference for the measurement of NEXT. The following is an imperfect attempt to compare the results of time domain based workmanship tests with those using a network analyzer. For this purpose the following experiment was developed.

A patch cord with a number of intermediate low NEXT connections was constructed. This patch cord consists of:

- A modular (RJ-45) connector with a short piece of cable, terminated at the other end with a low NEXT connector.
- One or more sections of patch cable, with ability to be terminated at one end at the low NEXT connector and at the other end terminating at a low NEXT connector.

A modular (RJ-45) connector, with a short piece of cable, terminated at the other end with ability to connect to the low NEXT connector.

The configuration for a workmanship test using a time domain tester is shown in figure 6.

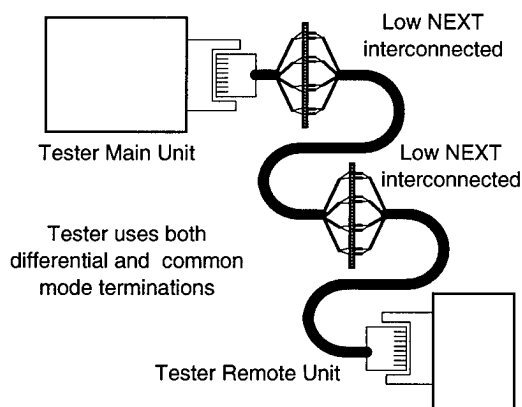


Figure 6: Configuration used for the tester to compare with network analyzer measurement

When the patch cord is measured using a time domain analysis method, sections are connected to form an overall length of approximately 2 meters. The jack at the remote end is the jack of the remote unit associated with the tester and is also pre-qualified for a NEXT of 40.5 ± 0.5 dB @ 100 MHz when terminated with a terminating plug. This remote unit has similar NEXT measurement capability as the main instrument as is the case for normal link testing. The workmanship NEXT can thereby be obtained at both ends of a patch cable. In the particular implementation, approximately 75 cm of cable is included in the workmanship NEXT measurement.

The configuration using the network analyzer is as shown in figure 7. The far end portion of the test cable is removed from the approximate location where the NEXT sensitivity by the tester declines rapidly. A low NEXT connector is present at that location and differential and common mode terminations are applied.

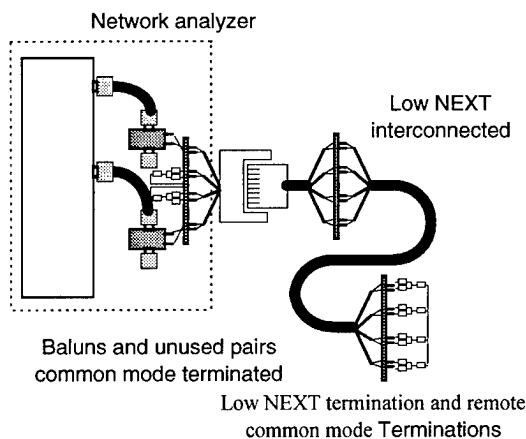


Figure 7: Network analyzer test configuration for comparison with time domain measurement

Additional segments of cable can be added, if necessary, to observe the variations that may be caused by (short) segments of cable at the other end. The baluns at the local end use common mode terminations and the unused pairs have resistive common mode terminations as well. Resistive common mode terminations are used at the remote end.

This measurement arrangement has been chosen to minimize the effects of common mode signals (i.e., the "short link" effect) and reflections from a remote end modular (RJ-45) connector. Reflections from a remote end modular connector can be substantially higher than the reflections from the low NEXT connector with resistive terminations that was used in this experiment.

The results of the time domain test results, converted in the frequency domain using a Fast Fourier Transform are compared directly for the 3,6-4,5 pair combination to the results combination obtained with a network analyzer. A sample comparison is shown in figure 8.

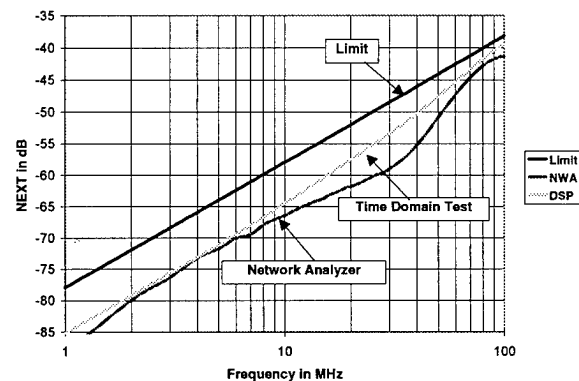


Figure 8: Comparison Time Domain Workmanship Vs Network Analyzer Test

Note that the response of the network analyzer measurement tends to indicate the presence of a reflection from the remote end. Variations were observed with different style jacks used to interface to the test cable. It will remain rather difficult to obtain definite conclusions from the network analyzer comparison tests, due to the noise levels (note the signal levels) and the impact of reflections, which are different in each case. Nevertheless, a reasonable agreement between the results of the two, totally different measurement approaches, is evident, in particular near 100 MHz.

CONCLUSIONS

The time domain based workmanship test for patch cords provides a reliable means to assess the quality of connection of a plug to a patch cable without the reflections and common mode effects that are present when using a swept frequency based test. It is fast and can be used both in the laboratory and in production. There is reasonable agreement with network analyzer tests, particularly near 100 MHz.

REFERENCES

1. Transmission Specifications for Unshielded Twisted Pair Patch Cords. Draft Technical Systems Bulletin, prepared by TIA TR41.8.1 PN-2948 Task Group on UTP connecting hardware.
2. Category 5 De-embedded Modular Cord NEXT Pass/Fail limits. V. Rybinski, Siemon Co., and Sterling Vaden, Superior Modular Products. May 1996. TIA TR41.8.1 PN-2948 Task Group on UTP connecting hardware.
3. International Standard IEC 603-7. Connectors for frequencies below 3 MHz for use with printed boards. Part 7: Detail specification for connectors, 8-way, including fixed and free connectors with common mating features. 1990-04.
4. International Standard ISO/IEC 11801. Information technology - Generic cabling for customer premises. 1995-07-15.
5. TIA/EIA-568-A Commercial Building Telecommunications Cabling Standard. Henricus Koeman. Contribution to TIA TR41.8.1, May 1996.
6. Link Testing in the Time Domain and Performance Advantages over Swept Frequency Measurements. J.S. Bottman and H. Koeman. IWCS Proceedings 1995. Pages 404-411.
7. Modeling of Plug/Jack Connection. Henricus Koeman. Contribution to TIA TR41.8.1, May 1996.
8. Patch Cord Testing as a Short Link. Henricus Koeman. Contribution to TIA TR41.8.1, May 1996.
9. International Standard IEC 1156-1 Multicore and symmetrical pair/quad cables for digital communications. 1994-01.
10. ASTM D-4566: Standard Test Methods for Electrical Performance Properties of Insulations and Jackets for Telecommunications Wire and Cable. 1994.
11. Crosstalk in Outside Plant Cable Systems. G.J. Foschini. The Bell System Technical Journal Vol. 50, No. 7, September, 1971, 2421-2448



Henricus Koeman has a MSEE degree from the Technical University of Delft and a Ph.D. degree from the University of Nymegen (The Netherlands) and is a Principal Engineer with the Fluke Corporation. He is the Fluke representative to the TIA. He is a senior member of the IEEE, a member of the Editorial Review Board of the IEEE Transactions on Instrumentation and Measurements and a licensed professional engineer in the State of Washington. He has been working over 20 years in precision and calibration measurements.

AN EVALUATION OF PROTECTIVE POLYMER COATINGS FOR OPTICAL FIBER APPLICATIONS

P. L. Tabaddor, C. J. Aloisio, H. C. Chandan, R. C. Moore, N. W. Sollenberger, C. R. Taylor and J. M. Turnipseed

Lucent Technologies Inc., Bell Laboratories
2000 NE Expressway, Norcross GA 30071

ABSTRACT

The number and density of optical fibers in cables are increasing as fiber moves closer to the home. Increasingly, fiber is cabled in ribbon form, which places stringent demands on fiber coatings. Fiber manufacturers have responded by enhancing ribbon strippability of the fiber while retaining or improving the coating robustness to long term aging. In this paper, we examine the relationship between the bulk and interfacial properties of four coating systems on commercial fibers and their removability, field performance, fiber reliability and delamination resistance.

INTRODUCTION

In response to increasing customer interest and growth in special end use applications, the optical fiber industry has moved in recent years towards fiber coatings that provide the most consistent performance in both single fiber and ribbon applications. With the progress of optical fiber towards the home, increased exposure of the fiber to harsh environmental and handling conditions has placed stringent demands on the performance capabilities of the coatings. A trend towards high-density, high fiber count cables has led to the development of coatings that facilitate easy ribbon stripping for mass fusion splicing operations, while retaining or improving other performance attributes.

In this paper, we compare the properties of four separate coatings on commercial fibers and consider the influence of bulk and interfacial properties of the primary and secondary coatings on fiber strippability and reliability. We show changes in dynamic fatigue and strength retention under humid aging conditions and estimate product performance in a variety of climatic and installation conditions. We compare

solvent resistance, retention of color along with delamination resistance and correlate the results to the mechanical properties of the coatings. We are currently evaluating the ribbon stripping performance and the results, not included in this paper, will be presented at the symposium.

FIBER COATING PROPERTIES

Completeness of primary coating cure is the key to the mechanical integrity of the fiber. Undercured primary coating can have poor adhesion to the glass, causing decreased fiber strength and delamination resistance. A measure of the cure characteristics of the coatings is therefore the first step in considering the reliability, ribbon stripping and field performance. Besides cure and interfacial adhesion, the bulk properties of the primary and secondary coatings that are defined by the coating chemistry, can affect fiber field performance and ribbon stripping. The ribbon stripping characteristics and delamination resistance are controlled not only by the adhesion between the primary and the glass, but properties of the secondary coating such as elongation, coating geometry and thickness.⁽¹⁾

The fiber pull-out test⁽²⁾ correlates empirically with the degree of cure for a given coating system and is a measure of adhesion between the primary coating and the glass. Here, a tensile force is imposed on a specimen mounted on a rigid tab with a cyanoacrylate adhesive, and the force required to separate the glass fiber from the primary and secondary coatings for a length of 1 centimeter (cm) is measured. This result must be differentiated from single fiber strip force where the protective coating is mechanically removed from the glass fiber along a longitudinal axis and either shreds away or tends to

'accordion' over the gauge length.^(3,4) Typically, properties of the secondary coating such as modulus and maximum elongation determine the strip force. Even when the adhesion levels, as measured by the pull-out test are high, a decrease in the strip force can be engineered by lowering the elongation of the secondary coating without changing the primary coating properties.⁽³⁾ Table 1 summarizes the pull-out and in-situ modulus data obtained for the four commercial coating systems being compared. In each case, three unique fiber samples were tested and the average of the results was recorded.

Table 1. A comparison of the properties of the primary coatings

Fiber	In-situ modulus (psi)	Pull-out (lb.)
A	80.9	2.29 ± 0.14
B	135.4	1.47 ± 0.11
C	180.5	1.75 ± 0.10
D	98.7	1.61 ± 0.11

The *in-situ* modulus, also listed in Table 1, is a diagnostic measure of the low-strain shear modulus of the primary coating. The test procedure is to measure the filar displacement as various loads from 10 to 70 grams are placed at the end of the fiber strand. The modulus can then be obtained from a plot of the load vs. the filar displacement. The *in-situ* modulus is typically proportional to the crosslink density and can be used to measure the cure independent of adhesion.⁽⁶⁾ As shown in Table 1, coatings B, C and D have higher *in-situ* modulus values with considerably lower pull-outs than coating A. While this may initially suggest differences in cure, the disparity is primarily a result of the differences in the chemistry, compositional nature and formulation design of the four coatings.

Fiber strip force measurements (unaged and after aging) were performed on all four coating systems using the method described in EIA-FOTP-178. The corresponding data is summarized in Tables 2 and 3. Not surprisingly, there is no correlation with either of the primary coating properties, *in-situ* modulus or pull-out force, indicating that differences in the physical properties of the corresponding secondary coatings affect strip force.

Table 2. Strip force data for unaged fibers (Sumitomo stripping tool)

Fiber	Unaged Fiber, Strip Force (lb.)		
	0°C	23°C	45°C
A	1.06 ± 0.11	0.75 ± 0.12	0.44 ± 0.10
B	0.92 ± 0.12	0.70 ± 0.11	0.60 ± 0.12
C	1.00 ± 0.11	1.03 ± 0.21	0.92 ± 0.22
D	1.07 ± 0.14	0.96 ± 0.13	1.26 ± 0.31

Table 3. Strip force data for aged fibers (Sumitomo stripping tool)

Fiber	Strip Force Measured at 23°C (lb.)	
	14 days in water at 23°C	30 days at 85°C/85% R.H.
A	0.65 ± 0.11	0.72 ± 0.10
B	0.72 ± 0.11	0.61 ± 0.12
C	1.11 ± 0.23	0.89 ± 0.13
D	1.33 ± 0.22	1.12 ± 0.12

In contrast to fiber C that was relatively unaffected by temperature and fiber D that showed higher values at 45°C, the strip force for the unaged fibers A and B decreased with increasing temperature. For fibers A and B, aged in water and in a high temperature/humidity environment (Table 3), the strip force remained unchanged. For fiber C, the relative change in strip force (unaged-aged) was greater for the fibers aged in the high temperature-humidity environment than the fibers aged in water. Fiber D showed higher strip force with aging in both environments.

FIBER FIELD PERFORMANCE

Accelerated aging measurements have helped in coating design by providing the best possible combination of properties capable of withstanding aggressive humid environments. Changes in the *in-situ* modulus of the primary coatings after exposure to accelerated aging conditions have been used to estimate performance in a variety of climatic conditions.^(7,8,9) High temperature alone can cause oxidative degradation and in combination with humidity (40°C, 75% R.H. simulating extreme Miami conditions), hydrolysis and further breakdown of the network structure can occur. In addition to fiber delamination which causes handling problems, the degradation process can severely alter the color

'accordion' over the gauge length.^(3,4) Typically, properties of the secondary coating such as modulus and maximum elongation determine the strip force. Even when the adhesion levels, as measured by the pull-out test are high, a decrease in the strip force can be engineered by lowering the elongation of the secondary coating without changing the primary coating properties.⁽³⁾ Table 1 summarizes the pull-out and in-situ modulus data obtained for the four commercial coating systems being compared. In each case, three unique fiber samples were tested and the average of the results was recorded.

Table 1. A comparison of the properties of the primary coatings

Fiber	In-situ modulus (psi)	Pull-out (lb.)
A	80.9	2.29 ± 0.1
B	135.4	1.47 ± 0.1
C	180.5	1.75 ± 0.1
D	98.7	1.61 ± 0.1

The *in-situ* modulus, also listed in Table 1, is a diagnostic measure of the low-strain shear modulus of the primary coating. The test procedure is to measure the filar displacement as various loads from 10 to 70 grams are placed at the end of the fiber strand. The modulus can then be obtained from a plot of the load vs. the filar displacement. The *in-situ* modulus is typically proportional to the crosslink density and can be used to measure the cure independent of adhesion.⁽⁶⁾ As shown in Table 1, coatings B, C and D have higher *in-situ* modulus values with considerably lower pull-outs than coating A. While this may initially suggest differences in cure, the disparity is primarily a result of the differences in the chemistry, compositional nature and formulation design of the four coatings.

Fiber strip force measurements (unaged and after aging) were performed on all four coating systems using the method described in EIA-FOTP-178. The corresponding data is summarized in Tables 2 and 3. Not surprisingly, there is no correlation with either of the primary coating properties, *in-situ* modulus or pull-out force, indicating that differences in the physical properties of the corresponding secondary coatings affect strip force.

Table 2. Strip force data for unaged fibers (Sumitomo stripping tool)

Fiber	Unaged Fiber, Strip Force (lb.)		
	0°C	23°C	45°C
A	1.06 ± 0.1	0.75 ± 0.1	0.44 ± 0.1
B	0.92 ± 0.1	0.70 ± 0.1	0.60 ± 0.1
C	1.00 ± 0.1	1.03 ± 0.2	0.92 ± 0.2
D	1.07 ± 0.1	0.96 ± 0.1	1.26 ± 0.3

Table 3. Strip force data for aged fibers (Sumitomo stripping tool)

Fiber	Strip Force Measured at 23°C (lb.)	
	14 days in water at 23°C	30 days at 85°C/85% R.H.
A	0.65 ± 0.1	0.72 ± 0.1
B	0.72 ± 0.1	0.61 ± 0.1
C	1.11 ± 0.2	0.89 ± 0.1
D	1.33 ± 0.2	1.12 ± 0.1

In contrast to fiber C that was relatively unaffected by temperature and fiber D that showed higher values at 45°C, the strip force for the unaged fibers A and B decreased with increasing temperature. For fibers A and B, aged in water and in a high temperature/humidity environment (Table 3), the strip force remained unchanged. For fiber C, the relative change in strip force (unaged-aged) was greater for the fibers aged in the high temperature-humidity environment than the fibers aged in water. Fiber D showed higher strip force with aging in both environments.

FIBER FIELD PERFORMANCE

Accelerated aging measurements have helped in coating design by providing the best possible combination of properties capable of withstanding aggressive humid environments. Changes in the *in-situ* modulus of the primary coatings after exposure to accelerated aging conditions have been used to estimate performance in a variety of climatic conditions.^(7,8,9) High temperature alone can cause oxidative degradation and in combination with humidity (40°C, 75% R.H. simulating extreme Miami conditions), hydrolysis and further breakdown of the network structure can occur. In addition to fiber delamination which causes handling problems, the degradation process can severely alter the color

of the fiber causing uncertainty in future color code identification. The aggressive environments that cause coating degradation and cohesive failure during ribbon stripping, can result in increasing debris on the fiber surface causing alignment problems in mass fusion splicing operations.

To estimate coating field performance, accelerated aging was performed at 125°C, 75°C/85%R.H., 85°C/85%R.H., 95°C/95%R.H. and 120°C/100% R.H. on all four coating systems. For the measurement, 25-50 ft samples were placed in environmental chambers regulated to the desired temperature and humidity for a specified period of time, and physical properties such as color, modulus, pull-out and strip force were monitored periodically. Accelerated aging over a 40 day period at 125°C (simulating 30 years at 40°C) causes oxidative degradation with sometimes rapid color changes.⁽⁷⁾ Figure 1 compares the oxidative stability of the four commercial fibers under evaluation and clearly coatings B, C and D develop color at a faster rate than coating system A.

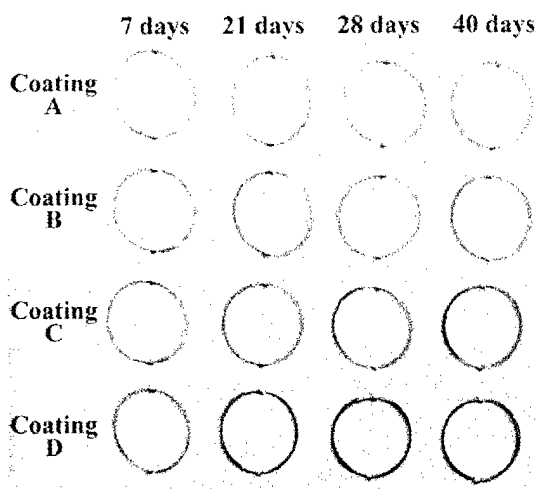


Figure 1. 125°C dry aging program and oxidative stability comparisons

While the 125°C dry aging program provides an estimate of oxidative stability, a more accurate estimate of coating field performance and hydrolytic stability can be made from accelerated aging in high humidity environments.^(8,9) Changes in physical properties, as seen in Figures 2, 3 and 4, also occur in humid environments. Here, variations in *in-situ* modulus, pull-out and strip force after aging at 95°C/95%R.H are depicted.

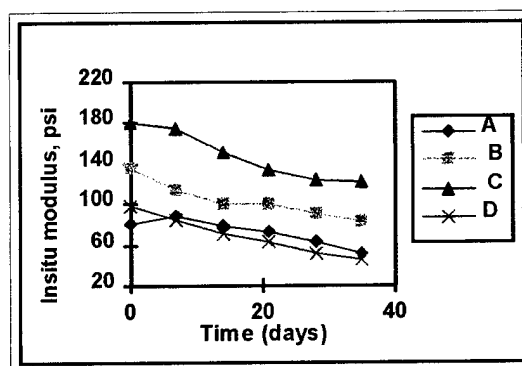


Figure 2. *In-situ* modulus variation with 95°C/95%R.H. aging.

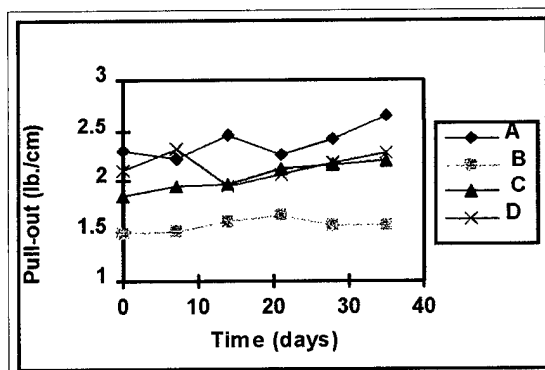


Figure 3. Variation of pull-out force with 95°C/95%R.H. aging

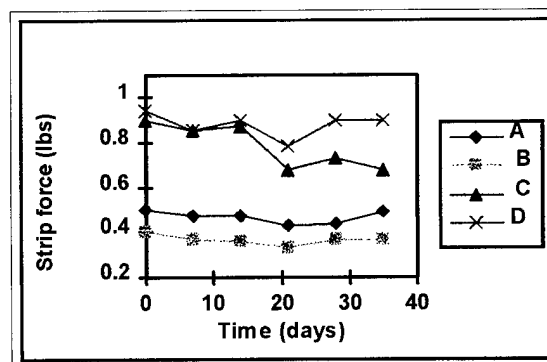


Figure 4. Variation of strip force with 95°C/95%R.H. aging (Microstrip Tool)

While the strip force change for the coatings appears negligible over the aging period, for fibers B, C and D, the degradation process causes increased debris to remain on the glass surface after stripping, requiring more than one alcohol wipe on occasion. Figure 5 compares the residue upon stripping for coating B, both for unaged fiber and fiber aged for 49 days at

95°C/95%R.H. The extent of hydrolytic degradation resulting in increasing cohesive failure is clearly evident.

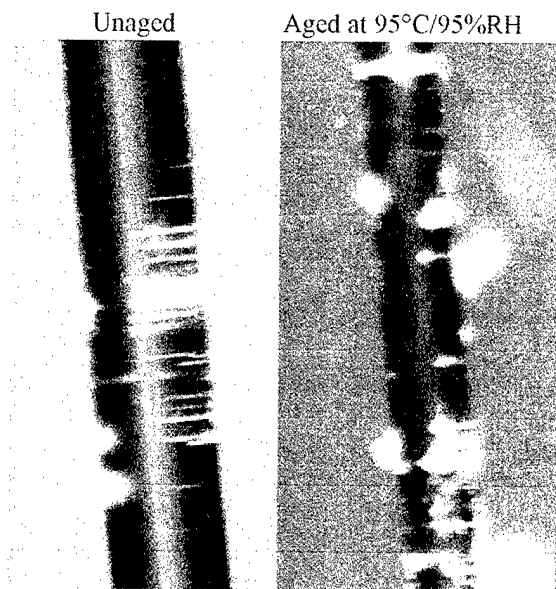


Figure 5. Stripping residues for unaged and aged fibers (49 days)

The decrease in modulus of the primary coating after exposure to moisture is a result of the hydrolysis of the network structure that decreases the crosslink density. Neglecting chain ends, the shear modulus is inversely proportional to the molecular weight between crosslinks M_c as given by

$$G = \rho RT/M_c$$

As the network breaks down, the number of crosslinks decrease and the effective molecular weight between crosslinks increases, consequently decreasing the modulus. It has previously been demonstrated that first order rate equations can be used to describe modulus decay and a rate constant is readily calculated from the slope of $\ln(\text{modulus})$ vs. time plots.^(3,9) For activation energy (E_a) calculations, four sets of accelerated aging conditions were selected and the rate constant k was determined at each temperature. The rate constant k was normalized to 85% R.H., following which, the E_a for the decay process was calculated as the slope of an Arrhenius plot of $\ln(k)$ vs. $1/T$ (Figure 6).

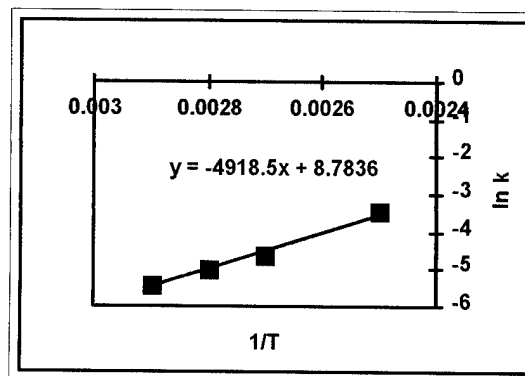


Figure 6. A plot of $\ln k$ vs. $1/T$ for coating system B

The time to reach a prescribed level of degradation (20% of the original modulus in this case) depends not only on the activation energy but the moisture levels as given by

$$t \sim \exp(-E_a/RT)/[H_2O]$$

where $[H_2O]$ is the concentration of water as determined from the relative humidity. Table 4 summarizes the activation energy along with the time for the modulus to degrade to 20% of its original value under simulated Miami conditions of high humidity and temperature (40°C/75% RH). From the data the order of hydrolytic stability of the coatings is determined to be $A > D > B > C$, where the lower activation energy for modulus decay corresponds to lower stability.

Table 4. Activation energy for the hydrolytic decay

Fiber	E_a (calc) kJ/mole	Equivalent days at 40°C/75%RH (simulated Miami conditions)
A	73	5800
B	40.8	914
C	30.8	512
D	52.1	1744

SOLVENT RESISTANCE

With the access of fiber to the home, exposure of the fiber to alcohol and household cleaners is imminent. In the past, solubility parameters as a means of determining the polymer-solvent interaction have been used to estimate the solvent resistance of the optical fiber coatings.⁽³⁾ Coating cure is critical in the extent of solvent penetration, so the design challenge is in tailoring the chemistry and crosslink densities for better chemical and solvent resistance.

The resistance of the coating to a particular chemical or solvent is determined by the physical changes that occur in the coated fiber. Typical effects include swelling of the coating past the edge of the glass and end splitting of the secondary coating with crack propagation either within a certain length or through the fiber specimen. Absolute ethanol (200 proof) was the solvent of choice and coils of coated fiber that were completely immersed in the fluid were periodically examined for swelling and/or splitting. Table 5 summarizes the swelling data obtained for the four commercial fibers under evaluation where the movement of the coatings past the edge of the glass was measured. Clearly, both coatings A and B have better solvent resistance in ethanol than coatings C and D.

Table 5. End swelling measured in absolute ethanol (mm)

Fiber	30min	1 hour	8 hr.	24 hr.
A	0	0	0	0
B	0	0	0	0
C	0	3.3	4	8.8
D	1	2	40	54

FIBER RELIABILITY PARAMETERS

Strength and dynamic fatigue parameters are generally used to characterize fiber reliability. The protective polymer coating can influence the local environment at the primary-glass interface and can consequently affect the fiber strength and fatigue parameters. For the four commercial fibers being examined, both the strength and dynamic fatigue parameters were measured for unaged and aged fibers at 85°C/85% R.H. for 30 days. The data is summarized in Tables 6 and 7, respectively. One fiber was measured for each of the four systems A through D.

Table 6. Effect of aging on strength

Fiber	Median Strength, ⁽¹⁾ ksi	Median Strength, ⁽²⁾ ksi	% Change
A	705	681	-4
B	661	680	3
C	658	735	10
D	690	733	6

⁽¹⁾ Unaged

⁽²⁾ Aged 30 days at 85°C /85% R.H.

For the fibers under investigation, the strength after aging either decreased or showed an apparent increase. While the strength after aging for fiber A was lower, the strength appeared to increase for fibers B, C and D. The apparent increase in strength may be a result of a hydrolytic degradation process generating acidic components at the glass-polymer interface. We believe for fiber A, a slight reduction in strength observed, was due to zero stress aging of the glass.

Table 7. Effect of aging on dynamic fatigue parameter, n

Fiber	Unaged Fiber, n	Aged Fiber, n
A	21	22
B	19	27
C	19	26
D	20	24

In general, with aging, an increase in the dynamic fatigue parameter, n, was observed for all the fibers. Fibers B and C showed a larger increase than fibers A and D. This could also be related to coating stability, however, it must be noted that for aged fibers variations in n are not unusual for different samples of a given fiber.

ADDED LOSS DUE TO WATER IMMERSION

All of the four commercial fibers examined exhibited very little added loss both at 1310 nm and 1550 nm even after 91 days of water immersion. The added loss did not increase monotonically as a function of time as seen in Figures 7 and 8 at 1550 and 1310nm respectively. A typical specification requirement is an added loss of < 0.05 dB/km.

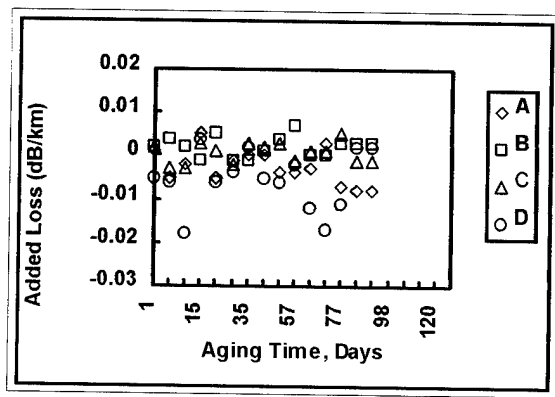


Figure 7. 1550nm added loss due to water immersion at 23°C

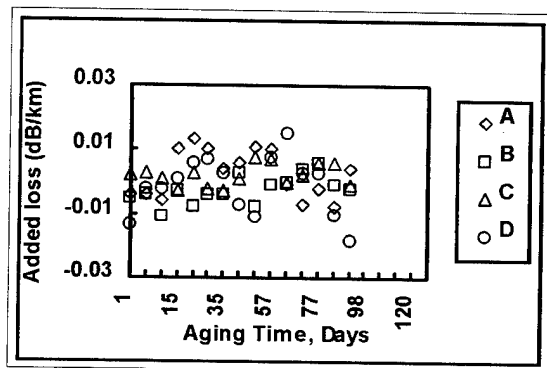


Figure 8. 1310nm added loss due to water immersion at 23°C

DELAMINATION RESISTANCE

It is imperative that the delamination resistance of the coating system be maintained while achieving good stripping performance. For a coated fiber passing over a perturbation, the rate of deformation of the coating is proportional to the longitudinal speed of the fiber. The higher the rate, the higher the modulus of the secondary coating, providing increased protection for the primary and the primary-glass interface. At very low rates the secondary appears to permanently deform. In the intermediate speed region the residual radial tensile stresses, due to processing⁽¹⁰⁾, coupled with the recoil of the secondary coating provide the stresses needed to delaminate the primary-glass interface. The mechanism is analogous to that proposed on a molecular level for a similar observation in the elongation at break for crosslinked rubbers⁽¹¹⁾.

Figure 9 shows the delamination resistance for the four commercial coating systems under evaluation at 0.1, 0.2 and 0.5 m/second. While the coatings appear to perform comparably at the two lower speeds, except for coating C, at 0.5 m/sec coating A clearly exhibits higher delamination resistance.

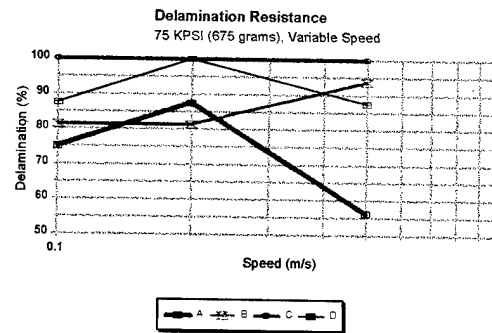


Figure 9. Comparison of delamination resistance for coatings A, B, C and D

In a similar experiment performed using a proof tester, a coated fiber was perturbed using speeds from 0.03 to 15 m/second and proof test levels of 100, 150, and 200 ksi. The data is illustrated in Figure 10 for coating A and similar results were obtained for all four coating systems. While no delaminations are observed above 3 m/second at all of the proof test levels, at speeds down to 0.001 meters/sec, the percent delaminations occurring decreased with increasing observation of secondary deformation.

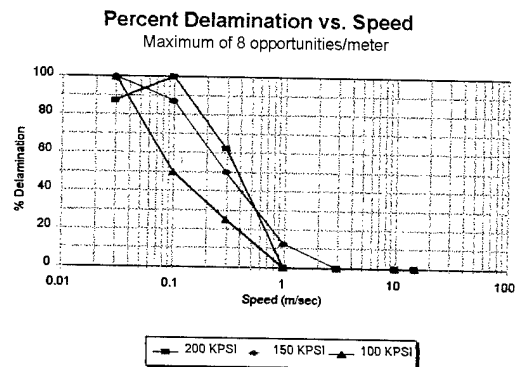


Figure 10. Effect of speed on coating delamination (Coating A)

Figure 11 shows the appearance of a primary-glass interface failure frequently referred to as a delamination. The coated fiber was passed over a 74 mm diameter pulley under 75 ksi tension at 0.2 m/sec. The pulley surface contained five, 280

micron mandrels designed to mechanically perturb the fiber coating. In the index match material, the boundary of the delamination is readily visible. It may be surprising that in all coating systems examined to date, this interface can fail without any visible damage to the secondary outside diameter.

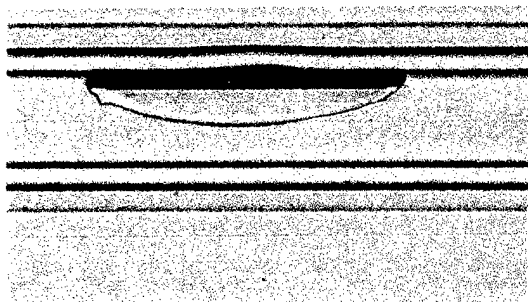


Figure 11. Fiber delamination from imposed mechanical perturbation (Coating B)

SUMMARY AND CONCLUSIONS

Fiber field performance, reliability and delamination resistance was determined for four unique commercial fiber coatings. The overall performance characteristics estimated were correlated to the cure behavior and mechanical properties of the coating systems.

ACKNOWLEDGMENTS

The authors gratefully acknowledge testing support and contributions from Daniel Harper, Donna Reed, Fredrick Korley, Richard Welling, Natasha Celestin, Leo Penn and Robert Towns.

REFERENCES

1. E. H. Urruti, J. R. Toler, G. Kar, C. Chien, J. W. Botehlo, Proceedings of the 41st International Wire and Cable Symposium, p239, 1992.
2. B. J. Overton and C. R. Taylor, Proc. of SPE ANTEC, p392, April 18-21, 1988
3. H. C. Chandan, J. R. Petisce, J. W. Shea, C. R. Taylor, L. L. Blyler, D. Iniss, L. Shepherd, Proceedings of the 41st International Wire and Cable Symposium, p239, 1992.

4. K. W. Jackson, T. L. Parker, J. R. Petisce, N. W. Sollenberger, C. R. Taylor, Proceedings of International Wire and Cable Symposium, p28, 1993.
5. C. R. Taylor, Meeting Digest of OFC, Optical Society of America, Washington D.C, p20, 1985.
6. D. A. Simoff, M. G. Chan, J. T. Chapin, B. J. Overton, Polym. Eng. Sci., vol. 29, p1177, 1989.
7. D. S. Szum, C. P. Chawla, T. E. Bishop, K. P. Murray, J. M. Zimmerman, Proceedings of the 39th International Wire and Cable Symposium, p703, 1990.
8. R. A. Frantz, I. M. Plitz, Proceedings of the 42nd International Wire and Cable Symposium, p850, 1993.
9. G. L. Welch, Proc. Nat'l SAMPE Conf, vol. 2, p649-662, 1970.
10. C. J. Aloisio, W. W. King, R. C. Moore, Proceedings of International Wire and Cable Symposium, p139, 1995.
11. T. L. Smith, J. Polymer Sci. Pt. A 1, p3597 (1960)

BIOGRAPHIES

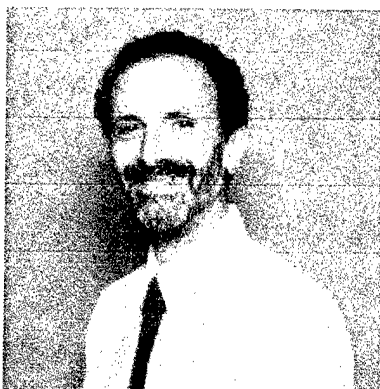


Priya L. Tabaddor

2000 NE Expressway, Norcross, GA 30071

Priya Tabaddor received her Ph.D. in Polymer Chemistry from Virginia Polytechnic Institute and State University in May 1995. Her dissertation focussed on the synthesis and development of high temperature, polyimide nanofoams for thin film dielectric applications. In August 1995, she joined the Materials Technology and Quality Engineering Group at Lucent Technologies. She is currently a

Member of the Technical Staff at Bell Laboratories working on the development of materials for optical fiber applications and related products. She is active in the Fiber Coatings Working Group of the Telecommunications Industries Association.



Charles J. Aloisio

2000 NE Expressway, Norcross, GA 30071

Charles Aloisio began his career with Bell Laboratories in 1952. After two years in the Murray Hill drafting Department and two years in the U.S. Marine Corps, he joined the Chemical Research Department. He worked in the Materials Group with Bell Labs in Indianapolis from 1967 to 1972, while obtaining his MS and Ph.D. from Purdue University. Charles joined the Atlanta Bell labs in January, 1972, as a Member of the Technical staff in the Materials Chemistry Group working on the characterization of polypropylene and polyethylene for cable sheathing and DEPIC insulation. He became the supervisor of the Polymer Characterization Group in 1973 initiating the use of rheology and viscoelastic analysis in a variety of copper and fiber optic applications. Since January, 1992, he has been a Distinguished Member of the Technical Staff in the Material Technology Group, applying rheology and viscoelasticity to fiber optic coating technology.



Harish Chandan

2000 NE Expressway, Norcross, GA 30071

Harish C. Chandan is a Distinguished Member of Technical Staff at Lucent Technologies Inc., Bell Laboratories, Norcross, Georgia which he joined in 1977. He manages the Fiber Qualification Laboratory. His other activities include mechanical reliability of fibers, polymer coatings and glass processing. Dr. Chandan holds a Ph.D. in Ceramic Science from Pennsylvania State University. He is active in the Fiber Reliability Working Group in the Telecommunications Industries Association.



Robert C. Moore

2000 NE Expressway, Norcross, GA 30071

Robert Moore, a Distinguished Member of Technical Staff in the Materials Technology group of Bell Labs in Norcross, Georgia, leads Lucent's fiber coatings processing team. After receiving his Ph.D. in Chemical Engineering in 1986 from the University of California at Berkeley, Dr. Moore joined AT&T's Engineering Research Center in Princeton, NJ, where he developed conductive elastomers. He moved to Norcross in 1990.



Neil W. Sollenberger

2000 NE Expressway, Norcross, GA 30071

Neil W. Sollenberger is a Member of Technical Staff in the Outside Plant Fiber Group at Lucent Technologies/Bell Laboratories in Norcross, Georgia. He is responsible for various aspects in the design and development of outside plant fiber optic cables. Prior to his current assignment, his responsibilities have included the design and development of both copper and fiber optic closures and terminals, as well as cabinets for loop electronics. Neil Sollenberger joined AT&T Bell Laboratories in 1978. He has a B.S. degree in Agricultural Engineering from University of Georgia, and he has a M.S. degree in Mechanical Engineering from Georgia Institute of Technology.

main Fiber Optic Manufacturing site in Atlanta. The group has responsibility for the design and engineering of materials used in fiber optic cable and apparatus products as well as responsibility for the quality of all incoming materials and components. He has previously been Supervisor of the Plastics Engineering and Characterization Group in Atlanta and Supervisor of the Polymer Materials Research, Engineering, and Applications Group at Bell Laboratories in Murray Hill, NJ. Prior to joining Bell Laboratories in 1977, he earned a B.S. in Chemistry from the College of Wooster in Ohio and a Ph.D. in Physical Chemistry from the University of Wisconsin in Madison. His graduate work focused on the physical and viscoelastic properties of polymers. He holds nineteen patents and has authored or co-authored 29 publications.



John Turnipseed

2000 NE Expressway, Norcross, GA 30071

John Turnipseed is a Member of the Technical Staff in the Materials Technology and Quality Engineering Group at Bell Laboratories of Lucent Technologies, where he is engaged in the development and implementation of radiation curable materials intended for use in telecommunications products. He received B.S. and M.S. degrees in Analytical Chemistry from the University of Virginia prior to joining the Western Electric Company in 1972.



Carl Taylor

2000 NE Expressway, Norcross, GA 30071

Carl R. Taylor is currently Bell Laboratories Technical Manager of the Materials Technology and Quality Engineering Group at Lucent Technologies'

HIGHLY RELIABLE AND LONG-LIFE UV CURABLE RESIN COATING SYSTEM OPTIMIZED FOR OPTICAL FIBER APPLICATIONS

Yoshihisa Kato, Kenji Asano, Kazumasa Ohson,
Khodo Yamada, Hideki Shimane, and Shinji Hinoshita

Hitachi Cable, Ltd. 5-1-1, Hitaka-cho,
Hitachi-shi, Ibaraki-ken, 319-14, JAPAN

ABSTRACT

For optical fiber high reliability and long life, we have developed a UV-curable resin coating system that can be used in various terrestrial and submarine applications. Its base composition consists of urethaneacrylate oligomers of the ether type. Optimizing of multi-antioxidants was important in developing this coating system. The best combination of multi-antioxidants was chosen considering the results of heat-resistance evaluation by Dynamic Oxidation Induction Temperature (DOIT), Oxidation Induction Time (OIT) measured with Differential Scanning Colorimeter (DSC), and the relationship between viscoelasticity behavior, softening behavior, change of gel fraction and transmission characteristics. Based on these considerations, we developed primary and secondary coatings that have good environmental resistivity against heat oxidation, metal catalyst degradation, humidity and high temperature and alkaline solutions and then demonstrated their potential for long life.

A prominent achievement is use of the secondary coating resin as the base resin for the color UV ink coating. The coloring system we developed eliminates the possibility of the delamination between the secondary coating and the color UV ink layer. The combination of primary, secondary, and color UV ink layer coatings promises stable duration in jelly application and clear stripping for splicing and connectorization.

1. INTRODUCTION

UV-curable resin has become a common material for optical fiber coating. Optical fiber coating consists of three layers: the primary, the secondary, and the color UV ink layer. For optical fiber coatings, UV-curable urethaneacrylate resin is widely used. Optical fibers are used in various terrestrial and submarine cables. But insufficient research work has been done regarding the life-time of optical fiber coatings.

Recently, on optic/power composite cable, with structure for Composite Fiber Optic Overhead Ground Wire (OPGW), and High-tight unit structure using thermoplastic resin, are seeing increased demand. Such applications require coatings with enhanced heat-resistance. Also, the optical fiber communication networks to link with between states and continents are being expanded. Therefore, high reliability and long-life for long-distance transmission of optical fibers are becoming important. Further, a newly developed coating system must be universally applicable with various kinds of cables for mass-production purposes.

This paper presents various optical fiber characteristics to show the superiority of the newly developed coating system.

2. MATERIAL DESIGN AND FIBER SAMPLE

2.1. Material design

UV-curable urethaneacrylate resin is widely employed in optical fiber coating materials. Among these materials, we selected the ether type because of its resistance against hydrolytic behavior. To enhance the heat-resistance of ether-type acrylate, an optimized combination of multi-antioxidants is used. To study the heating influence for optical fiber coatings, we investigated the relationship between viscoelasticity behavior, softening behavior, change of gel fraction and loss increase characteristics of coating materials and examined those that were the most suitable. Stable coating stripping of optical fiber is an important factor in making high-strength splices for submarine cable applications. The color UV ink layer material used the secondary coating material as a base resin in order to achieve stable stripping of the coat-edge for standard chemical (acid solution) stripping of high-strength submarine cable splices.

Further, for universal applications extending to submarine cable use, we also estimated the lifetimes from the quantity of hydrogen gas evolved from the coating materials.

2.2. Fiber sample

Among the various samples we studied, we show four kinds of representative fiber samples in Table 1. Fiber I is an optical fiber having normal primary and secondary coating materials and color UV ink coating material from the market. Fiber I is not considered especially heat-resistant. Fibers II through IV are samples of varying polyol (ether or ester type) in the oligomer of the primary material and three antioxidants (phenol, amine, or sulfur type), and use the same color UV ink and secondary coating material. In these samples, Fiber II is the fiber that uses the newly developed UV-curable resin coating system. The color UV ink uses the material that has the same composition as the secondary coating material. The antioxidants of the color UV ink and secondary coating material have an antioxidant similar to that used for primary coating material.

3. RESULTS AND DISCUSSION

3.1. Heat resistance of fiber coating materials

Figures 1 and 2 show the results of Dynamic

Table1. Outline of Fiber Samples

Sample type		Optical fiber			
Fiber number		I	II	III	IV
Color material	Color UV Ink A(from the market)	○			
	Color UV Ink B(new color)		○	○	○
Secondary coating material	Secondary A	○			
	Secondary B		○	○	○
Primary coating material	Oligomer A (ether type)		○	○	
	Oligomer B (ester type)				○
	Antioxidant	A (Phenol type)	○	○	○
		B (Amine type)		○	
		C (Sulfur type)		○	
	Others		○	○	○

Notes Fiber II: A fiber using developed coating system.

Color UV ink B: A color UV ink developed for the total coating system

Oxidation Induction Temperature (DOIT) and Oxidation Induction Time (OIT) of each fiber samples measured by DSC (Differential Scanning Colorimeter : PERKIN ELMER 7700). The DOIT was measured under an oxidation atmosphere and at a temperature raising rate of 10°C/min. The OIT was measured under an oxygen atmosphere (after 5 min in a nitrogen atmosphere) at 190°C. In the case of the ether type (polyol in urethaneacrylate oligomer), these results show drastic improvement of the thermal property of the coating materials due to changing the combination of antioxidants. We found that the optimized combination and additive ratio combination of the antioxidants created a synergistic effect on the anti-oxidation performance. On the other hand, in the case of the ester-type acrylate, because its heat-resistance is high compared with that of the ether-type acrylate, oxidation degradation resistance showed good result with a conventional antioxidant. The ester-type acrylate can be used when hydrolysis resistance is not required.

As the next step, we investigated the thermal behavior of coating materials by testing of changes in viscoelasticity, softening temperature, and gel fraction depending on heating.

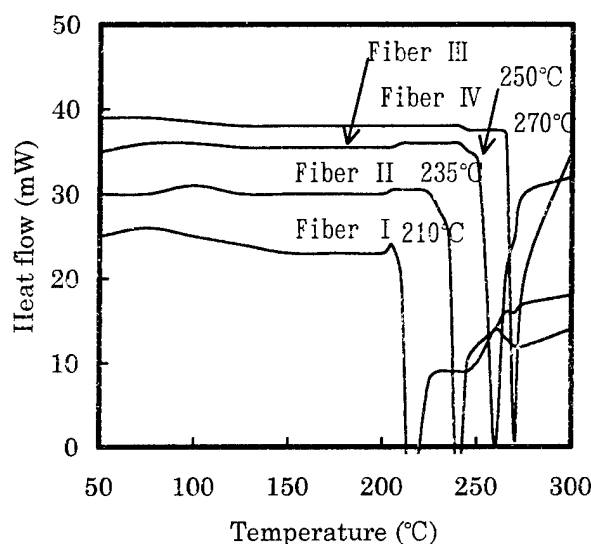


Figure 1. DOIT of Each Fiber Coating

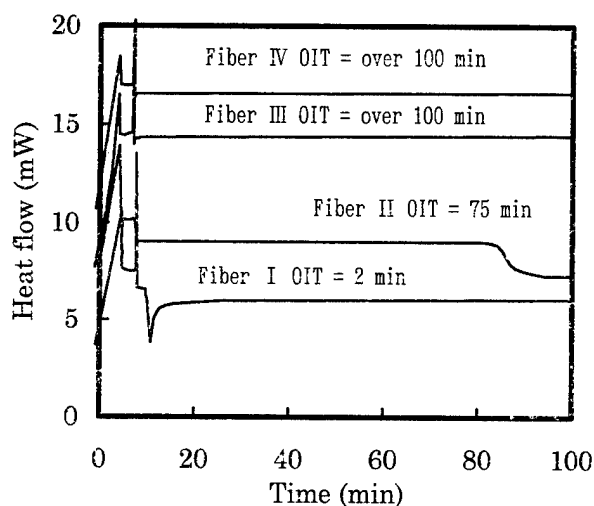


Figure 2. OIT of Each Fiber Coating

Designation	Sheet of material
Fiber I	Primary coating material of Fiber I
Fiber II	ditto Fiber II
Fiber III	ditto Fiber III

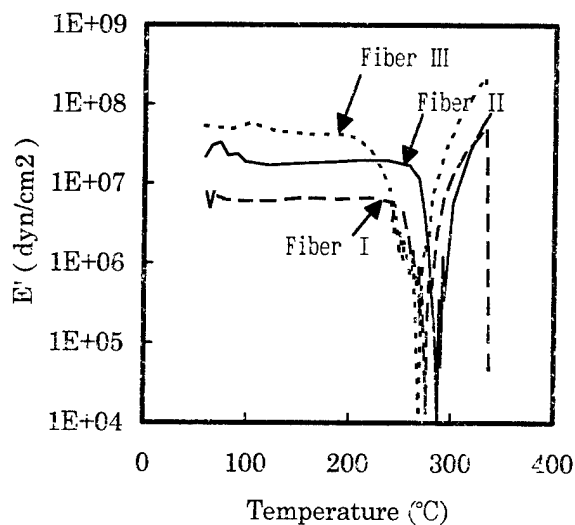


Figure 3. Viscoelasticity Behavior of Each Primary Coating

The results of the measurement of the viscoelasticity behavior of coating are shown in Figure 3. The viscoelasticity of the sheets of primary coating material was measured with viscoelasticity measurement equipment at a temperature range 40 to 350°C. All samples except those designated Fiber

III showed sudden changes in their viscoelasticity at over 220°C. But the sample designated Fiber III changed in viscoelasticity, which started to fall from around 190°C and increased from around 240°C. The difference in the composition of coating materials between Fiber II and Fiber III is the presence of the antioxidant C, which degraded the viscoelasticity drastically. This phenomenon, in which the viscoelasticity falls once and then increases again, can be explained from the change in material, such that molecule chain cutting is initiated first, resulting in softening of material and then a further, strong crosslink reaction occurs, resulting in hardening of material.

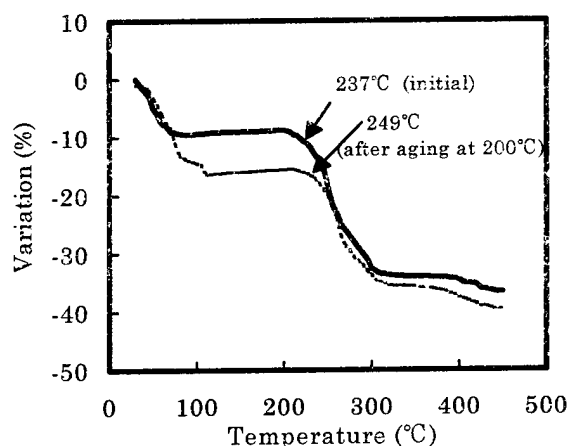


Figure 4. Softening Temperature of Fiber II by TMA

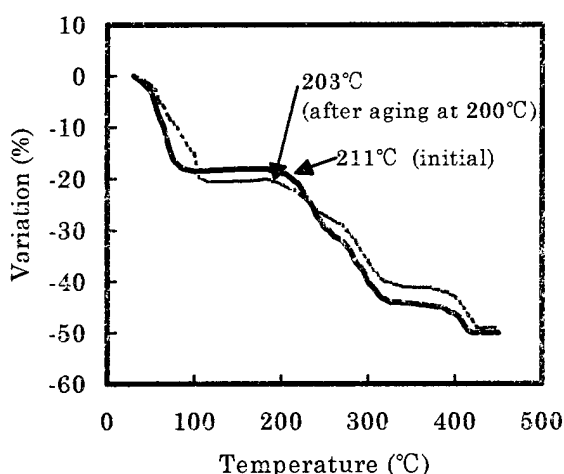


Figure 5. Softening Temperature of Fiber III by TMA

We also confirmed this phenomenon with fiber format by means of cut-through testing while heated. Figures 4 and 5 show the results of the cut-through test which measured the diameter deformation of the fiber, using TMA (Thermo Mechanical Analysis) equipment. The initial (solid line) and aged data (10 min at 200°C, dashed line) of Fibers II and III are shown. Using the antioxidant C (sulfur-type) decreases the viscoelasticity of the primary coating of Fiber III at around 200°C. Consequently, we observed cut-through deformation with the fiber format at around 200°C. A sample of Fiber III (aged at 200°C for 10 min) showed a further decrease in softening temperature from the initial data. While the Fiber II sample showed the opposite reaction.

Further, we confirmed that this influence appears in the change of gel fraction of the coating layer also. Figure 6 shows the change of gel fraction of each fiber sample heated at 200°C. The gel fraction of Fiber III decreased according to the duration of the aging (200°C)

As a result, we found the antioxidant C effective in inhibiting the oxidation degradation of the UV-curable resin. On the other hand, it may change the other properties of the coating which phenomena were observed in viscoelasticity degradation with the

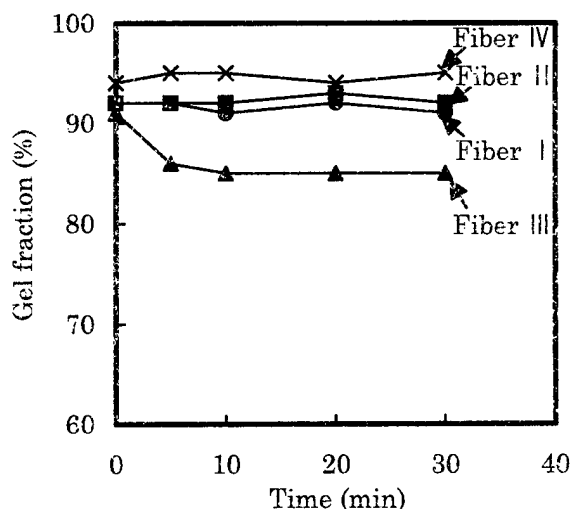
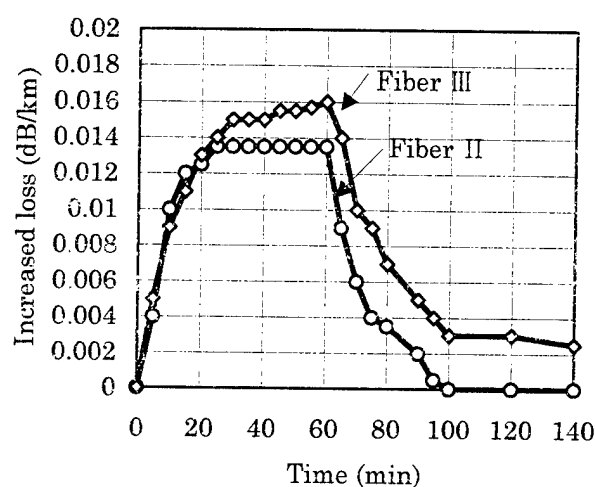


Figure 6. Change of Fiber Gel Fraction by Heating at 200°C

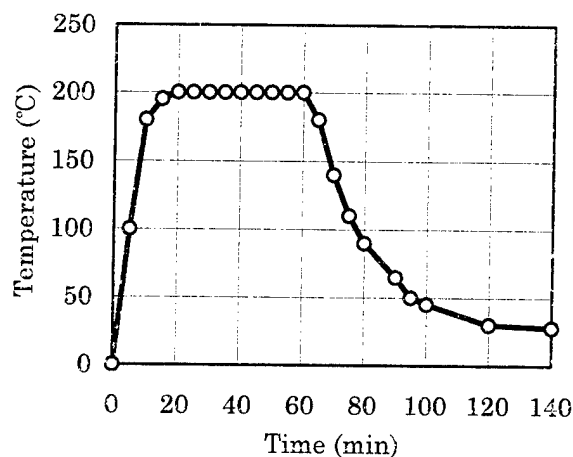
sheet format and cut-through deformation with the fiber format when exposed to high temperature. Such changes could possibly degrade the transmission properties of the optical fiber.

3.2 Effect of attenuation increase due to high temperature

We consider the attenuation increase phenomena for high-tight unit construction, in which the fibers are bound into the thermoplastic compound when making a unit component of the cable. During processing, the fibers are exposed to high temperature through for a short term; their characteristics may be affected.



(a) Attenuation change



(b) Heating temperature condition

Figure 7. Attenuation change due to temperature

Figure 7 shows the transmission attenuation change of Fiber II and III under a high temperature heat-cycle process. The samples were 2 km in length and they were coiled with a diameter of about 300 mm in the thermostatic chamber. The temperature was raised from room temperature up to 200 °C and then cooled down to room temperature again. During the process, the fiber transmission attenuation was measured. We proved that Fiber II, which is designed to prevent the degradation by viscoelasticity, softening temperature and gel fraction, did not show attenuation increase after the heat stress was released. On the other hand, Fiber III did show residual attenuation increase after release of heat stress.

Additionally, We confirmed the Young's modulus of the secondary coating is important in this residual attenuation recovery. Figure 8 shows the relationship between the increase in residual attenuation and the ratio of Young's modulus of the secondary coating of the fiber. This result shows that the increase in residual attenuation varies according to the Young's modulus of the secondary coating and it must be optimized.

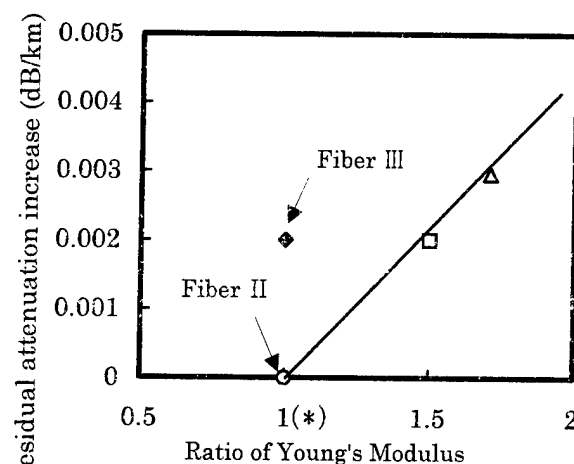


Figure 8. Young's Modulus of Secondary Coating vs. Attenuation Recovery

Note: Ratio 1(*) is referenced with Young's Modulus of secondary coating of Fiber II

3.3. Chemical characteristics

In expanding the usage of optical fibers, the stability and reliability of fiber coatings must be investigated under various environments. Here, we will discuss metal catalyst degradation, hydrolysis resistivity and alkaline resistivity.

To find the extent of metal catalyst degradation, we measured the OIT by DSC at 190°C with a fiber sample and a metal, which contacted with the fiber. Figures 9 and 10 show the OIT chart measurements for Fibers I and II, and typical metals, stainless steel and copper. Table 2 shows the measured OIT values. The oxidation degradation of UV materials depends greatly on the metal contacted. It must be noted that stainless steel promotes oxidation degradation, because the wide use of stainless presents many chances for contact with fibers.

Our newly developed UV-curable resin coating system has excellent performance against such metal catalyst degradation.

Next, we will evaluate the hydrolysis resistivity of Fiber II coatings containing the ether-type polyol compared with Fiber IV coatings containing the ester-type polyol. Figure 11 shows humidity resistance at 85°C, 95% RH, and Figure 12 shows alkaline resisting property at 50°C, 10% NaOH. In those figures, tensile strength retention and elongation retention of each coating are evaluated. Those properties of Fiber IV coatings containing ester-type polyol deteriorate clearly, and this is natural because of its hydrolysis structure.

In contrast, the newly developed UV-curable resin coating system of Fiber II has an ether-type polyol, and it shows excellent environmental resistivity against humidity and alkalinity.

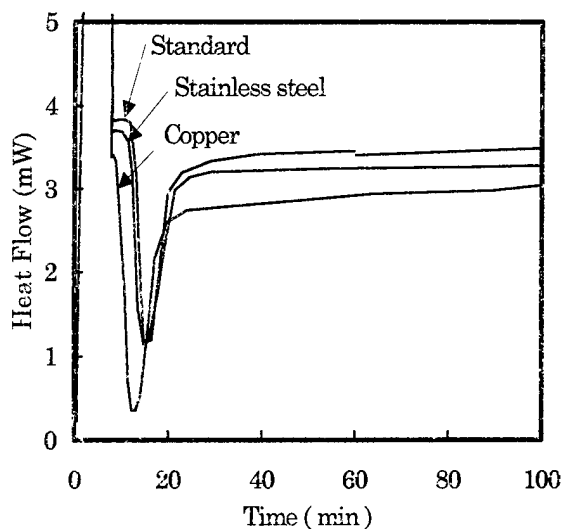


Figure 9. OIT for Fiber I due to Metal Catalyst Degradation

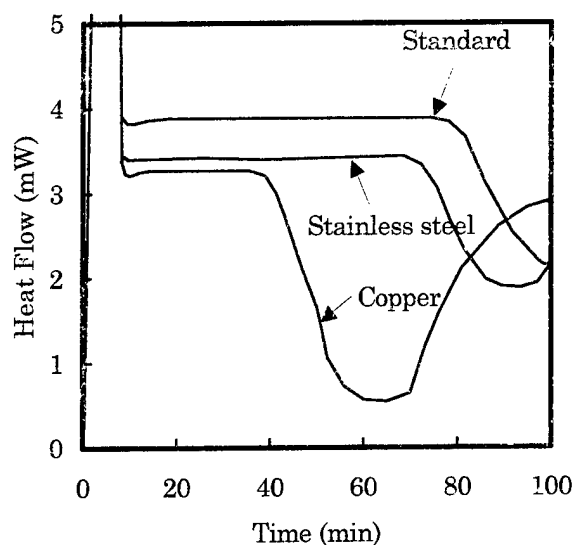


Figure 10. OIT for Fiber II due to Metal Catalyst Degradation

Table 2. OIT of UV Coating Fiber due to Metal Catalyst Degradation

Sample	Standard	Stainless steel	Copper
Fiber I	3	1	Less than 1
Fiber II	75	65	35

Note: Fiber II-A fiber using the developed coating system.

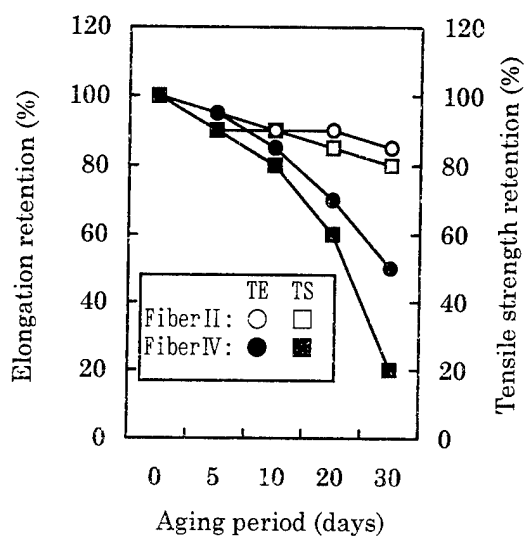


Figure 11. Elongation and Tensile Strength Retention after Aging at 85°C, 95%RH

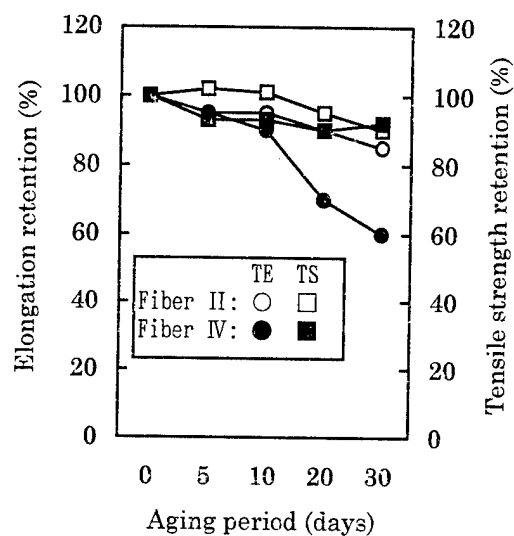
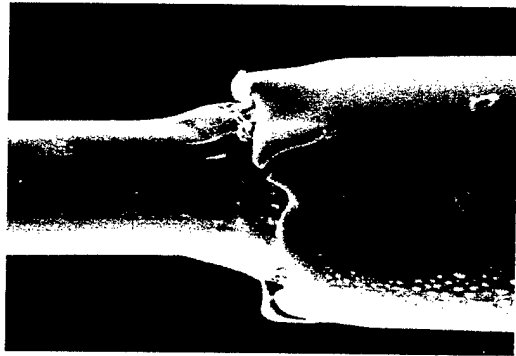
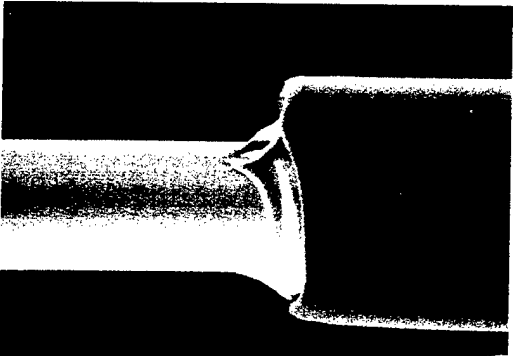


Figure 12. Elongation and Tensile Strength Retention after Aging at 50°C, 10%NaOH

Table 3. Chemical Stripping of UV Coating Fiber

Fiber Sample	Appearance of Fiber after Chemical Stripping	Splice Strength (kgf)
<p>I</p> <p>Combination of primary and color coating from the market (Color UV Ink A)</p>		0.7
<p>II</p> <p>Optimized combination of primary and color coating by New Color (Color UV Ink B)</p>		3.5

3.4. Stripping and splice strength

To achieve high-strength splicing of submarine cable, chemical stripping is indispensable. Table 3 shows the appearance of the chemical stripping and splice strength of Fiber II and Fiber I. Fiber II uses the developed coating system including color UV ink. Fiber I uses the color UV ink coating obtained on the market. If there is any difference in dissolution rate between that of the primary/secondary and that of the color UV ink layer, the coat-edge of each layer will not match. This may bring on bubble troubles in the recoated resin during recoating. Moreover, some materials included in the color UV ink may have a chance to degrade splicing strength when the chemical stripping method is used because there is a possibility of residue, from some material dissolved in the acid solution, sticking on the glass surface.

Consequently, we created an excellent coloring system of high splicing strength with a composition that combines organic pigment and secondary coating resin base.

3.5. Lifetime forecast by heat aging acceleration

The heat-resisting lifetime of Fiber II developed was studied. A clear experimental method has not yet been established for the heat-resisting lifetime of an optical fiber. Various properties (elongation, Young's modulus, viscoelasticity and yellowing of the coatings) may be used for the fitting data with the accelerated aging condition. We selected hydrogen gas evolution because it has the influence of transmission attenuation increase and generated hydrogen due to the oxidation. The hydrogen gas evolution quantitative limit point was assumed to be $1 \mu\text{ l/g}$. By fitting an Arrhenius plot of aging data, we estimated the lifetime of each coating; (primary and secondary). The results are shown in Figure 13. Their activation energies are respectively 22.4 and 26.4 kcal/mol. From the hydrogen gas evolution of primary coating, we estimate the fiber lifetime to be over 25 years at 35°C and over 6500 years at 3°C.

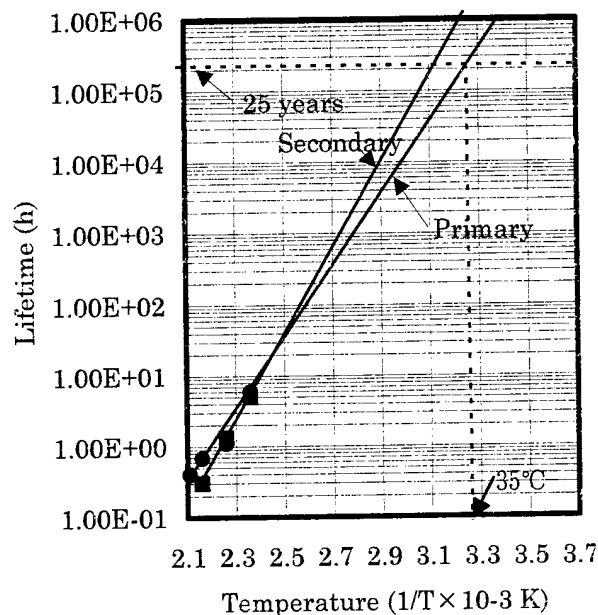


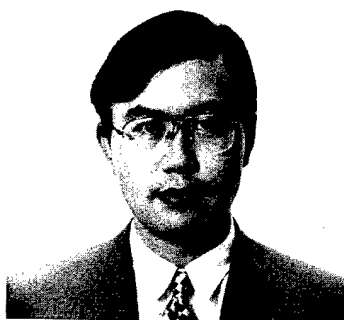
Figure 13. Lifetime estimation of UV curable coatings used by hydrogen gas evolution

4. CONCLUSION

We have created a new concept in fiber coating systems for application in loose or tight unit fiber binding systems for terrestrial and submarine cable use. The base composition of UV-curable resin consists of urethaneacrylate oligomers of ether type. The added technology on the fiber coating system of the terrestrial cable use enables universal application.

The secondary coating UV-curable resin as base resin of color layer ink has promised stable color UV ink coating duration in loose tube application, clear strip separation from the unit binder layer and coat-edge stable stripping in the standard chemical (acid solution) stripping of high-strength splice for submarine cable application.

We have achieved heat-resistive and long-life UV-curable optical fiber coatings by inhibiting thermal oxidation and metal catalyst degradation through application of the synergistic effect of anti-oxidant repellents.



Yoshihisa Kato

Hitachi Cable, Ltd.

5-1-1, Hitaka-cho,
Hitachi-shi, 319-14
Japan

Mr. Kato received his B.E. Degree in Applied Chemistry from Keio University in 1984 and joined Hitachi Cable, Ltd. He has been engaged in research work on ultra-violet curable material used for wire and cables. He is now a researcher in the 2nd Dept., Power System Laboratory.

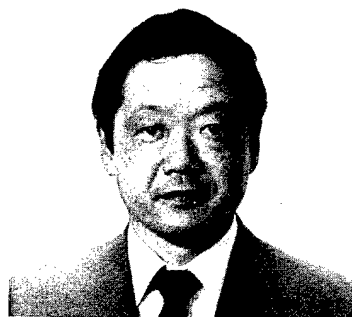


Kazumasa Ohsono

Hitachi Cable, Ltd.

5-1-1, Hitaka-cho,
Hitachi-shi, 319-14
Japan

Mr. Ohsono received his B.E. degree in Mechanical Engineering from the Science University of Tokyo in 1982 and joined Hitachi Cable, Ltd. He has been doing researched in optical fibers. He is now a senior researcher in the 4th Dept., Optoelectronic System Laboratory.

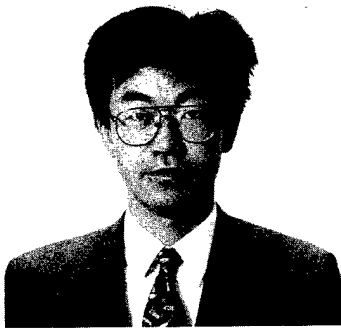


Kenji Asano

Hitachi Cable, Ltd.

5-1-1, Hitaka-cho,
Hitachi-shi, 319-14
Japan

Mr. Asano received his B.S. degree in Polymer Science from Hokkaido University in 1972 and joined Hitachi Cable, Ltd. He currently is engaged in development of new optical fiber coating, wire enamel, and other insulation materials. He is now a chief researcher in the 2nd Dept., Power System Laboratory.



Khodo Yamada

Hitachi Cable, Ltd.

5-1-1, Hitaka-cho,
Hitachi-shi, 319-14
Japan

Mr. Yamada received his M.E. degree in Chemical Engineering from the Science University of Tokyo in 1984 and joined Hitachi Cable, Ltd. He has been engaged in the development and production of optical fiber cable. He is now a senior engineer in the Optical Fiber and Communications Cable Department.



Shinji Hinoshita

Hitachi Cable, Ltd.

5-1-1, Hitaka-cho,
Hitachi-shi, 319-14
Japan

Mr. Hinoshita graduated in Electrical Engineering from Kure National College of Technology in 1970 and joined Hitachi Cable, Ltd. He is currently responsible for the design and development of optical fiber and components of mobile access networks. He is now an executive senior engineer in the Telecommunications Design Department.



Hideki Shimane

Hitachi Cable, Ltd.

5-1-1, Hitaka-cho,
Hitachi-shi, 319-14
Japan

Mr. Shimane received his B.E. degree in Electrical Engineering from Shibaura Institute of Technology in 1993 and joined Hitachi Cable, Ltd. He has been engaged in the design and development of optical fiber cables and telecommunications cables. He is now an engineer in the Telecommunications Design Department.

Reliability of the Adhesion of the Glass-Primary Coating Interface on Optical Fibers

AKIRA MURATA, KEIJI OOHASHI, and SHINJI ARAKI

OPTO-ELECTRONICS LABORATORY, FUJIKURA LTD.
1440, MUTSUZAKI, SAKURA-SHI, CHIBA, 285 JAPAN

ABSTRACT

We studied factors affecting the adhesion force and its stability of glass and the primary coating interface of optical fibers. The adhesion force of the interface is influenced not only by the primary coatings' adhesiveness (T peel force of the coatings), but also by the ratio of the coating thickness and the mechanical properties of the secondary coatings, especially the glass transition temperature. The degree of decrease in the pull-out force of fibers immersed in hot water is affected by the glass-transition temperature and the water content of the primary coatings. Fibers with low-water-content coatings show good stability for interface adhesion. Moreover, the degree of decrease in breakage strength is small in such fibers.

INTRODUCTION

With the rapid growth of optical fiber networks and their application to the subscriber loop, the service environments of optical fibers are becoming increasingly severe. Optical fiber coatings must feature long-term resistance to heat, UV-light, humidity, water, and so on. It has been reported that the adhesion force (expressed as pull-out force and/or strip force) between the glass-coating interface of fibers decreased when the fibers were immersed in water or placed in a humid environment^{1,2)}, and that delamination also occurred^{2,3)}. This decrease in adhesion and the delamination of the interface may cause not only increases in transmission loss^{1,3)}, but also loss of fiber

strength³⁾. The latter phenomenon is known as 'zero-stress aging'. The increased transmission loss and reduction in fiber strength may be caused by irregular lateral pressure and corrosion of the glass surface, respectively. Coating adhesion on the glass-primary coating interface must be stable to ensure fiber property reliability.

In this study, we have investigated the factors that govern the coating adhesion on the glass-coating interface. The content of the adhesive monomer, coating thickness, and mechanical properties of the coatings are noted, and factors affecting the adhesion stability are examined. The time dependence of pull-out force and the fiber strength during water immersion are evaluated, and the effects of water content are discussed.

EXPERIMENTS

We prepared fibers with several types of primary and secondary coatings. The primary coatings varied in terms of peel force and water content. The peel force differs according to the type of adhesive monomer used and the monomer content. The 2.5 % Young's modulus of the coatings were between 0.10 kg/mm² and 0.15 kg/mm². The secondary coatings featured different glass-transition temperatures. The 2.5% Young's modulus of the secondary coatings are approximately 70 kg/mm². Tables 1 and 2 show the typical properties of the coatings. The glass-transition temperatures of the coatings were measured by dynamic mechanical analysis in 1 Hz tensile

Table 1. Typical properties of primary coating

	A	B	C	D	E	F	G	H
T-peel force (g/cm)	55	32	70	24	95	23	8	25
Type of adhesive monomer	b	a	a	a	a	b	c	d
Water content	low	medium	medium	medium	medium	low	medium	high

Table 2. Typical properties of secondary coating

	A	B	C
T _g	low	medium	high
water content	medium	medium	medium

mode. The water content was measured using the Karl Fisher's method at 170°C. The thickness of 0.1 mm or 0.2 mm sheets of coatings cured by 300 mJ/cm² irradiation were used for these analyses.

To evaluate the degree of interface adhesion, we measured the pull-out force between the glass and the primary coatings, as this force most directly represents interface adhesion. The measurement procedure is depicted in Figure 1. The number of samples are 20, and the maximum value of the tests are averaged. We think that strip force is not suitable for the evaluation of interface adhesion, as it is easily affected by Young's modulus and the elongation of the coatings.

Fibers with their edges were enclosed in epoxy resin were immersed in water without stress. After removing the fibers from the water, the fibers are placed in a room controlled

at 25 °C, 50% RH, and then the force was measured. Tensile tests were carried out using 300 mm fibers with a tensile speed of 30 mm/min.

RESULTS AND DISCUSSION

Differences in the pull-out force of fibers coated with various kinds of UV-curable resin

We investigated the original (unaged) pull-out force of fibers. First, we measured the pull-out force of fibers with primary coatings of various peel forces (B,C,D, and E) and one secondary coating (A). The components of B, C, D, and E are nearly the same: only the content of the adhesive monomer is different. The relative pull-out force of the fibers against the T peel force of the coatings are shown in Figure 2. The pull-out force was found to depend on the T peel force. The peel force of primary coatings B, C, D, and E depend on the content of their adhesive monomers, as shown in Figure 3. However, the pull-out force of the fibers using the primary coating containing different kind of adhesive monomer don't fit to

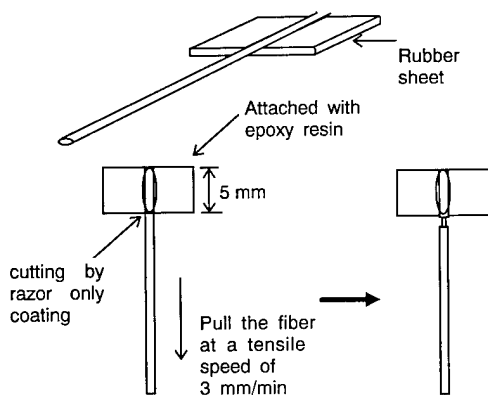


Figure 1. Method of pull-out force measurement

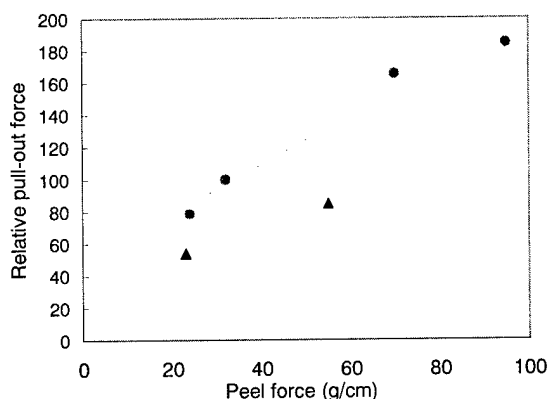


Figure 2. Differences in the pull-out force of fibers with different peel force primary coatings and a secondary coating.

approximation line in figure 2 (depicted as ▲ in the figure). Therefore, pull-out force is proportional to the monomer content, as long as the identical type of adhesive monomer is used. This suggests that the peel force of the coatings is not the only factor, but that other properties (such as the glass transition temperature) affect pull-out force.

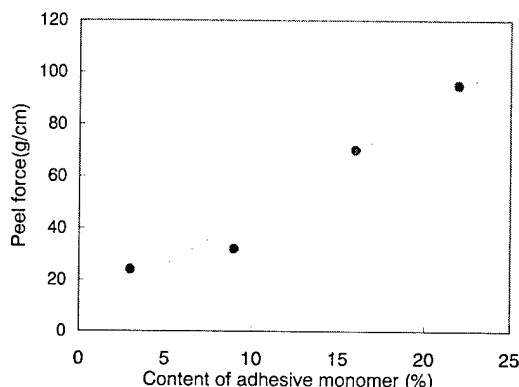


Figure 3. Relationship between the adhesive monomer content and peel force of primary coatings

The relationship between the pull-out force and coating thickness of fibers were measured. The outer diameter and glass diameter were identical in all fibers, while the thickness ratio of primary coating A and secondary coating A were different. The results are shown in Figure 4. The smaller the ratio of the primary coating, the larger the pull-out force of the fibers. This seems to be related to contraction stress in curing. For fibers with an outer coating diameter of 250 μm , a thicker primary coating resulted in a lower pull-out force.

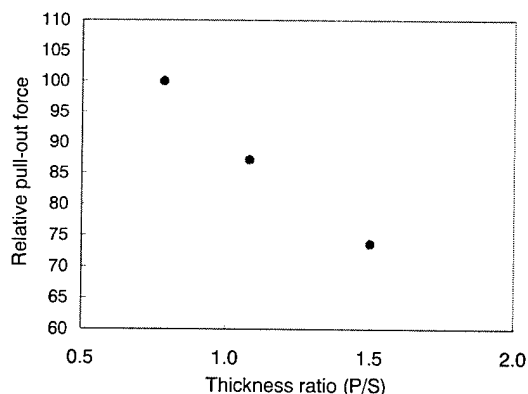


Figure 4. Effect of the coating thickness ratio on the pull-out force of fibers.

The relationship between adhesion stability and the mechanical properties of secondary coatings

As shown in the previous section, the pull-out force of unaged fibers was affected by various factors. The mechanical properties of secondary coatings are one such factor, and such properties have a greater influence on the adhesion stability of the glass-primary interface. We believe that a decrease in pull-out force indicates a decrease in interface adhesion. Therefore, a decrease in the pull-out force may cause partial delamination at the interface. Figure 5 shows changes in the pull-out force of the fibers coated with one primary coating F and three types of secondary coatings A, B, and C, each with a different glass-transition temperature. The fibers were then placed in a room temperature atmosphere. The pull-out forces are expressed relatively in the Figure, and the initial pull-out force of the middle Tg secondary coating is expressed as 100. We used the primary coating with a relatively lower peel force and initial pull-out force. The Initial value was slightly different each other, and the pull-out force of fibers with low-Tg coatings was greater than the other one. The pull-out force of the fiber coated with secondary coatings with a lower Tg temperature did not change over time. On the other hand, the fiber coated with a secondary coating with a higher Tg temperature showed a decrease in the pull-out force over time. The reason for this seems to be the influence of tensile stress on primary coatings from secondary coatings, and it

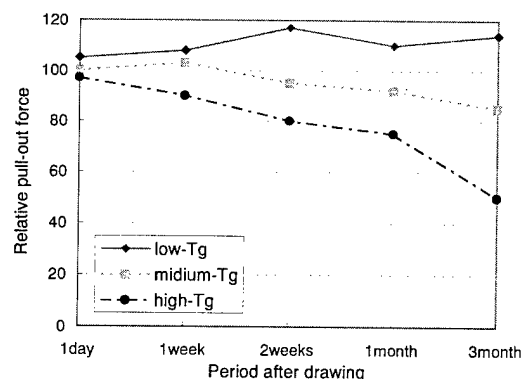


Figure 5. Change of pull-out force of fibers with a primary coating and three secondary coatings at room temperature aging.

depends on the T_g temperature of secondary coatings. When we used the relatively-high-adhesion fibers, the pull-out force of the fibers did not change during room-temperature aging, as shown in Figure 6. However, the decrease in pull-out force may occur in the case of aging in a more harsh atmosphere. This suggests that it is important to choose appropriate primary and secondary coating pairs to maintain adhesion between the glass and the coatings.

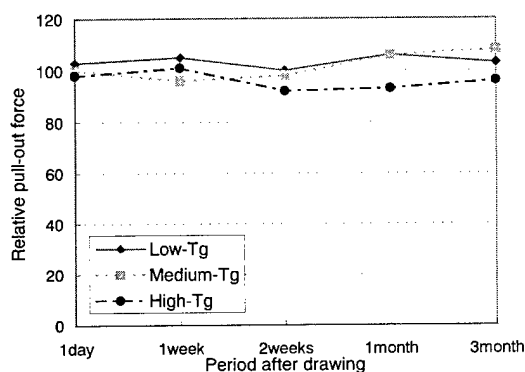


Figure 6. Changes in the pull-out force of fibers with a high adhesive primary coating A and three secondary coatings at room temperature aging.

The relationship between adhesion stability and the water content of primary coatings

The stability of pull-out force and the interface adhesion of the fibers are influenced by the water content of coatings. Therefore, we evaluated the effects of the water content of the primary coatings on the interface adhesion of fibers immersed in water and aged in a humid atmosphere. Figure 7 shows the relative pull-out force of fibers immersed in 60 °C water. The fibers consist of a secondary coating A with a lower T_g temperature, and three types of primary coatings A, C, and H, which differ in water content. After removing the fibers from the hot water, they are left to stand for approximately three hours at room temperature, and then their pull-out force is measured. The results show that the pull-out force of the fiber with a high-water-content primary coating decreases over time. Delamination did not occur in any fibers after

three months of immersion. The swelling of the coating and/or any chemical interaction of water with the interface chemical bond may cause a decrease in pull-out force. Figures 8 and 9 show the changes in the pull-out force of fibers immersed in room-temperature water and aged in a humid (60 °C, 95% RH) atmosphere. The pull-out force of fibers with a high water content decreased slightly, but the extent of the change was smaller than that of the fibers immersed in 60 °C water. It has been found that the 60 °C water immersion test is the most harsh, while aging in a humid environment has a relatively mild affect on the adhesion of the interface. We did not perform the test using high- T_g secondary coatings. In such cases, the pull-out force of the fibers may decrease.

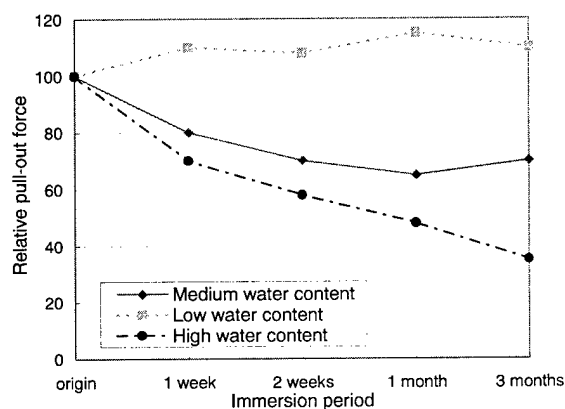


Figure 7. Relative pull-out force of fibers coated with primary coatings with different water content and a secondary coating immersed in 60°C water..

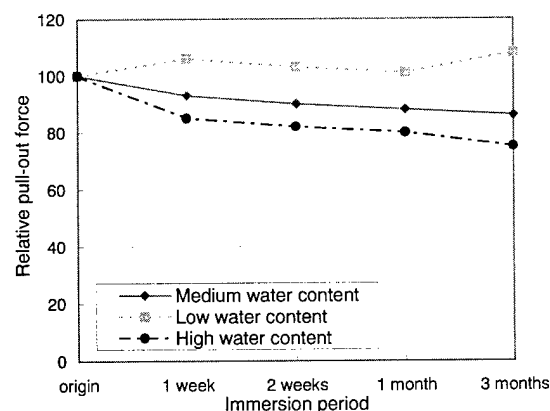


Figure 8. Relative pull-out force of three types of fibers immersed in room temperature water.

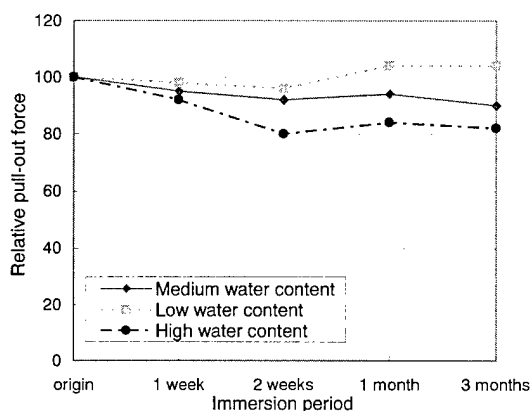


Figure 9. Relative pull-out force of three types of fibers aged in 60°C 95%RH.

Relationship between interface adhesion and the tensile strength of fibers

We investigated the effect of the decrease in pull-out force on the breakage strength of fibers. Figure 10 shows the changes in the of breakage strength of the fiber with the primary coating C with a medium water content and the secondary coating A immersed in water and aged in a humid environment. The strength of the fibers aged in a humid environment did not change, while those immersed in hot water decreased slightly. Figure 11 shows the results for the primary coating A with a low water content and the secondary coating C. The extent of the decrease in strength in hot-water immersion is small. The pull-out force of those types of fiber coatings tend to remain relatively stable. Figure 12 shows a comparison of changes in the strength of fibers with primary coatings with various water contents. It has been found that the adhesion of fibers is also related to fiber strength.

CONCLUSION

The adhesion of glass and the coating interface of fibers is affected by the peel strength of primary coatings and the thickness ratio of the coatings. Fibers coated with primary coatings with a higher peel force show a higher pull-out force when the same kind of adhesive monomer is used. The smaller the

ratio of the primary coating thickness, the larger the pull-out force.

The stability of interface adhesion is affected by the Tg of secondary coatings and the water content of primary coatings. When the low adhesive primary coatings are used, the pull-out force of the fibers with high-Tg secondary coatings decreased over time. The pull-out force of high-water-content primary coatings decreased over time during hot water immersion.

The strength of fibers coated with high-water-content primary coating also decrease over time. Fiber strength has been found to be affected by the degree of adhesion of the interface.

REFERENCES

- 1) A. Ginocchio, A. Portinali, E. Consonni, G. Roba, and F. Nanni, "A New Coating System for Fibers with Enhanced Resistance to Environmental Conditions" 43rd Proc. IWCS, 96 (1994).
- 2) R. A. Frantz, B. J. Keon, E. V. Vogel, T. N. Bowmer, and H. H. Yuce, "The Effects of Optical Fiber Coating and Ink Materials on the Corrosion of the Glass Surface", 43rd Proc. IWCS, 742 (1994)
- 3) F. Cocchini, D. Cuomo, G. Ferri, and A. Pudia, "Influence of Glass-coating Adhesion on the Optical and Mechanical Performances of Fibres in Water", 43rd Proc. IWCS, 66 (1994).

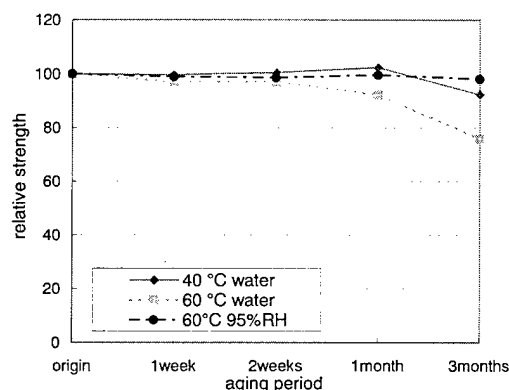


Figure 10. Relative strength of the fibers with the primary coating of medium water content

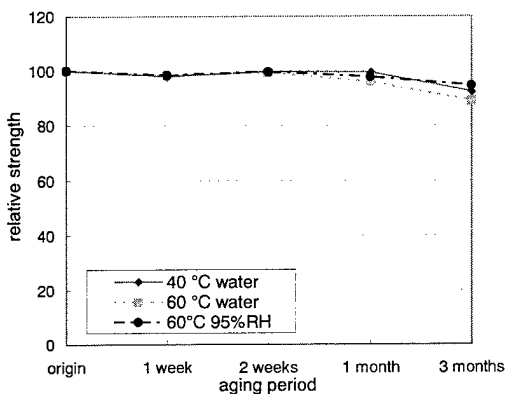


Figure 11. Relative strength of the fibers with the primary coating of low water content

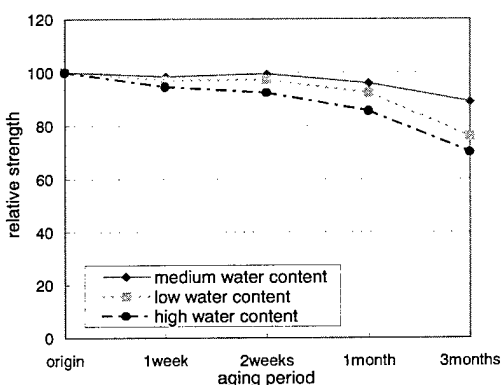


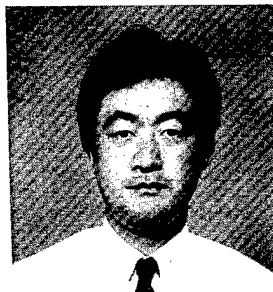
Figure 12. Relative strength of the fibers with three primary coatings immersed in 60 °C water



AKIRA MURATA

Opto-Electronics
Laboratory
Fujikura LTD.
1440, Mutuzaki,
Sakura-shi, Chiba,
285, Japan

Akira Murata was born in 1963. He joined Fujikura LTD. in 1992 after receiving his ph. D. in environmental science from Chiba University. He has been engaged in research and development for optical fibers, and is now an engineer in the Telecommunication Cable Material section and a member of the IEICE of Japan.



KEIJI OOHASHI

Opto-Electronics
Laboratory
Fujikura LTD.

1440, Mutuzaki,
Sakura-shi, Chiba,
285, Japan

Keiji Oohashi was born in 1956. He graduated from the Tokyo Institute of Technology in 1980 with a B.E. degree in chemistry. After eight years of work as an engineer in the field of materials for motor vehicles, he joined Fujikura LTD. in 1988. He has been engaged in research and development for optical fibers and optical fiber coatings. He is now chief of the Telecommunication Cable Material section and a member of the IEICE of Japan.



SHINJI ARAKI

Fujikura LTD.
1440, Mutuzaki,
Sakura-shi, Chiba,
285, Japan

Shinji Araki was born in 1950. He joined Fujikura LTD. in 1974 after graduating from Tokyo Metropolitan University with a B.E. degree in chemistry. He has been engaged in research and development for optical fibers and optical fiber coatings. He is now an assistant general manager in the optical fiber cable manufacturing engineering department and a member of the IEICE of Japan.

MANUFACTURING AND CHARACTERIZATION OF COLORED, FATIGUE RESISTANT OPTICAL FIBER

G.F. Orcel, B.J. Overton⁺, C. Mc Nutt⁺, S. Vanpouille*,
J.F. Bourhis, A. Lopez⁺, J.Y. Barraud*

Alcatel Fibres Optiques, Conflans Ste Honorine, France

⁺ Alcatel Telecommunications Cable, Claremont, North Carolina

* Alcatel Alsthom Recherche, Marcoussis, France

ABSTRACT

Urethane acrylate formulations can be doped with fluorine, by using a fluorinated diol. When the amount of fluorine is optimized, the permeability to water moisture (P) of the coating decreases and the contact angle (θ) increases. The net effect is an increase of the static fatigue parameter « n », which can be predicted from plots of n vs. θ/P .

Fibers with fluorine doped secondary coating can be easily processed through an inking line, using UV curable inks. Such fibers display a very good behavior during aging, showing a very slight decrease of the mechanical properties. The fatigue parameters are not affected by the inking process and values largely in excess of those of regular coatings are obtained: about 29 for aging in water in dynamic fatigue, and near 50 (estimated) for static fatigue.

INTRODUCTION

Optical fibers are used in various applications, which all have different constraints. These applications have usually in common that the fiber must survive in harsh environments in terms of atmosphere and stress. Another aspect is that the fiber must be as small as possible to fit in already existing conduits, easily identifiable, insensitive to microbending and bending, and cost effective.

Alcatel's approach to address these problems is based on the fiber's secondary coating. Most

optical fibers which are available on the market today have a dual polymeric coating, comprised of a primary and a secondary layer of the urethane acrylate family. Alcatel has already introduced a primary coating which takes into account the glass-coating interface and which provides the fiber with improved aging behavior.¹ Alcatel also developed a new secondary coating, formulated with fluorine, which improves the fiber's protection against water aggression.² The first part of this paper presents improvement on the formulation of typical urethane acrylate resins by addition of fluorine for use in optical fiber and ribbon cable applications.

It is essential that this coating be compatible with commercial inks. Although the surface of the fiber is hydrophobic due to the presence of fluorine in the coating formulation, UV inks can be applied very easily. The second part of this paper reviews the latest results on the characterization of colored fiber and especially its resistance to aggressive environments, in terms of atmosphere and stress.

COATING FORMULATION

Most of telecommunication optical fibers produced over the last decade use a dual layer polymeric coating as a protection against the environment. The primary coating, which is in contact with the glass fiber, has a low modulus to protect against microbending optical losses. The secondary coating which is on-top the primary coating has a higher modulus to prevent damages induced by lateral loads. These

polymeric layers must also protect the glass fiber from chemical reaction with the environment and more specifically water moisture. The most popular polymers for long haul application are UV cured urethane acrylates.

These polymers are also used to strengthen flat arrays of fibers in the production of ribbon cables. In this application, the optical fibers are coated with a colored ink. The ribbons must be able to slip one against the other to allow the greatest fiber count in the cable. The most frequent problems encountered in this application is poor slippage between ribbons or too great an adhesion between the ribbon matrix and fiber ink and fluorine doped polymers could then be of great use.

The most common source of degradation of fiber strength is exposure to water moisture. Water molecules diffuse through the coating and react with silica at preferential sites on the glass surface, decreasing the mechanical strength of the optical fiber. This reaction is favored by temperature and stress. The degree of protection offered by the coating can be characterized by a static fatigue test (and the so-called static fatigue parameter « n_s »), where the fiber is exposed under constant stress to water moisture (85 % relative humidity) at 85°C.

Two physical properties can be used to describe the behavior of water with respect to a polymer: the wettability (as measured by the angle of contact θ) and the permeability (P). Attempts have been made to correlate « n_s » to these parameters. For polymers of the urethane acrylate family it was found that the higher the contact angle the higher the static fatigue resistance. Similarly, the lower the permeability, the higher the static fatigue resistance.³ A very good correlation is found when plotting « n_s » as a function of θ/P . A linear relationship (empirical) is obtained as described in figure 1. It can be seen from this curve that for making a coating with a good reliability it is desirable to design a polymer with a high θ/P ratio.

An efficient way of decreasing the water vapor permeability of a polymer is to add fluorine to the formulation. Also, due to the weak interactions between the fluorinated chains, the surface energy of the polymer is lowered, which also decreases the wettability (which corresponds to higher θ).⁴

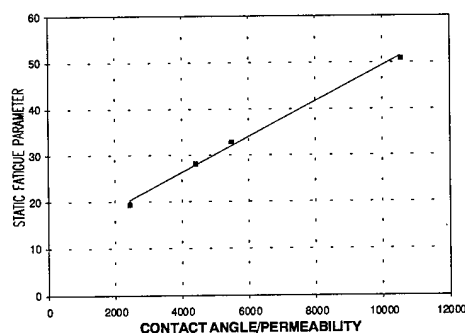


Figure 1: Dependence of the factor n_s on the ratio contact angle/permeability

Urethane acrylate oligomers are the product of a reaction between a diol, a diisocyanate and an hydroxy-alkyl-acrylate. These oligomers are copolymerized with reactive diluents in the presence of photo-initiators under UV light. The crosslinking reaction which takes place is very similar to the one of thermosetting materials, and a high molecular weight solid is obtained.

The characteristics of the diol greatly affect the properties of the final polymer, by modifying the density of urethane bonds and the density of crosslinks. For example, the higher the density of urethane bonds, the higher the T_g ,⁵ and the higher the density of crosslinks, the higher the Young's modulus.⁶ Furthermore, it is easier to incorporate fluorinated chains through the diol. It has already been presented that it is more efficient to fluorinate the side chains than the backbone. The results are summarized in table 1.

The optimized fluorinated secondary coating, in terms of mechanical and thermal properties, when used on top of the conventional primary coating of Alcatel, provides the glass fiber with a significant protection and static fatigue parameters in excess of 50 are obtained.

Optical fibers are not used as such in the field. Most of the time, they are colored with an ink and processed through either a cabling line or a ribboning line. It is important to characterize the influence of post-processing operations on the properties of the fibers. The second part of this paper deals with the determination of the aging characteristics of a colored fiber with a fluorinated urethane acrylate secondary coating.

Table 1: water vapor permeability values of various fluorinated urethane acrylate films

side chain	F	formulation		P
no	no	UA 80%	DR 20%	0.020
yes	no	UA 80%	DR 20%	0.018
yes	no	UA 80%	DR 20%	0.020
yes	yes	UA 80%	DR 20%	0.012
yes	yes	UA 80%	DR 20%	0.011

UA: urethane acrylate

DR: $\text{CH}_2=\text{CHCO}_2(\text{CH}_2)_x\text{O}_2\text{CCH}=\text{CH}_2$

COLORED FIBER

In a precedent paper, we described the aging behavior of fibers colored with thermal and UV curable inks. It was found that although the inking process went very smoothly for both types of ink, the thermal ink peels off after several months of exposure to ambient atmosphere, while the UV curable ink retained its integrity. It was decided to focus for the remainder of this program on UV curable inks. The blue color was chosen because it is usually the most difficult to process.

The fibers were colored with a blue, UV curable ink and introduced into a series of reliability tests. These tests consisted of strength and dynamic fatigue measurements before and after 30 days aging under the conditions of 85°C/85% RH and 85°C water immersion. In addition, the static fatigue stress corrosion factor was determined by the two-point bend method in an environment of 85°C/85% RH.

Dynamic two point bend techniques were used for the strength and fatigue tests in order to focus on the evaluation of the protection afforded by the fluorinated coating. Two point bend methods factor out the contribution of large flaws to the results, a desirable aim since such flaws are external to the performance of the coating in question.

Figure 2 shows the Weibull tensile strength distributions for the fluorinated coating fiber

before and after aging in the 85°C/85% RH environment and immersed in 85°C water. The harsh treatment had a negligible effect on the pristine glass surface, either in terms of strength or distribution. The strength at 50% probability is between 790 and 810 kpsi for the three samples. The fluorination provides an effective barrier.

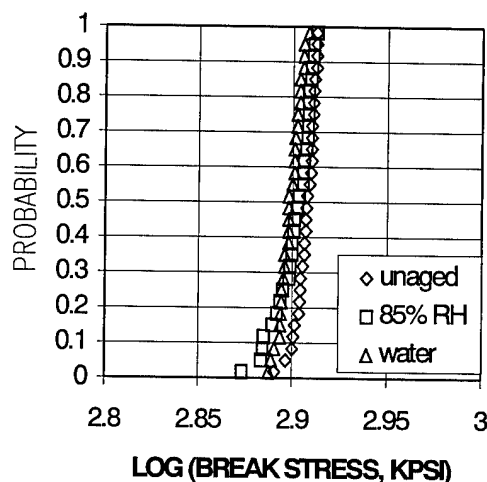


Figure 2: Tensile strength distribution of a blue fiber before and after 30 day aging at 85°C

Figure 3 gives the dynamic fatigue performance of unaged fiber and the fiber after the aging treatments. Thirty samples were broken at each strain rate for all sets of fiber. The stress corrosion factors are given in the legend. In every case the standard error of estimation (SEE) is less than 0.0008, indicating very tightly distributed data.

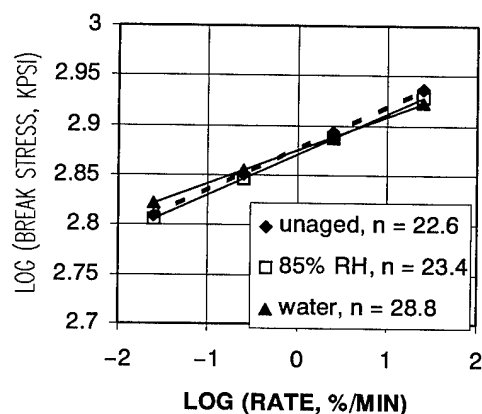


Figure 3: Dynamic fatigue curves of a blue fiber before and after 30 day aging at 85°C

The results indicate that the fiber's susceptibility to stress corrosion actually decreases on aging. Such behavior is usually explained by a blunting of the sharp cracks in the absence of an aggressive chemistry from the coating.⁷ A more aggressive coating would create new flaws or make existing flaws worse to develop.

The extension of these results to the glass in the field, with its distribution of weaker flaws over long length, is legitimate as demonstrated by Griffioen.⁸ The so-called « pristine » glass surface is a surface consisting of a population of chemical bonds that exhibit a distribution of energies to rupture. Consequently, there is a Weibull distribution of break strength even for pristine glass. The n value obtained from fatigue measurements on the pristine glass surface is nearly identical to that obtained from measuring the weak flaws in the fiber.

Figure 4 shows the static fatigue results, where the fiber was tested in two point bending in an environment of 85°C and 85% RH. Three sets of fibers were tested at each stress level. Shown with the data from the fluorinated coating is data taken from the current coating system in use in Alcatel and data from another commercially available fiber. The n -values are given in the legend. The data for the current Alcatel coating and the commercial coating exclude the highest stress point as the fibers broke in less than one hour. The highest stress data is used for the fluorinated secondary samples as the median time to failure was about an hour or more.

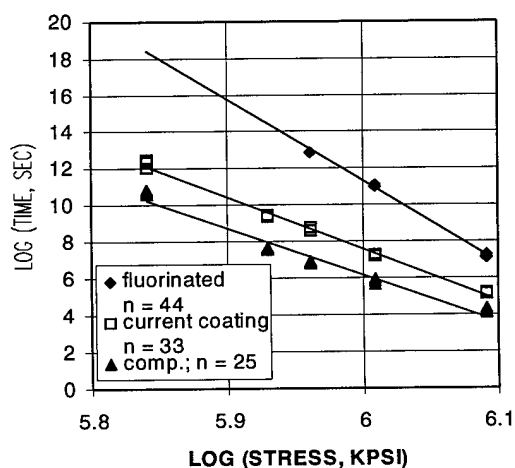


Figure 4: Static fatigue curves for various coatings

The next lower stress level (376 kpsi) is projected to require more than two years to cause failure in the fluorinated secondary coated fiber. This behavior is similar to the one observed for the non-colored fiber. It is thus anticipated that the n value will increase to near 50 when the break for the fourth stress value occurs.

CONCLUSION

Urethane acrylate coatings can be doped with fluorine through the reaction of a fluorinated diol with a diisocyanate. The composition of the polymer can be optimized by decreasing the ratio contact angle/permeability to water moisture. Optical fibers manufactured with a fluorine modified secondary coating show a superior aging behavior and fatigue parameters in excess of 50 are obtained.

The aging properties are maintained after the fiber is colored with a blue, UV curable ink. A dynamic fatigue parameter of 29 obtained on an a fiber aged in water at 85°C for 30 days is reported for the first time for fiber with only UV curable urethane acrylate coating.

ACKNOWLEDGMENTS

The contributions of M Matau (fiber draw), D Benzel and A Bourghelle (inking) are greatly appreciated.

REFERENCES

1. R.J. Overton, C. Lasne, H.M. Michaud, R.G. Sommer, « Designing an Optical Fiber Dual Coating System for Loose Tube and Ribbon Cable Long Line and Local Loop Applications », IWCS, p 701, 1993.
2. G.F. Orcel, J.Y. Boniort, J.Y. Barraud, R.J. Overton, « Hermetic and Polymeric Coating for Military and Commercial Applications », Proceedings of the 44th International Wire and Cable Symposium, 1995, p. 330.
3. B.J. Overton, A.R. Lopez, S.S. Reddy, « Correlating the Material Properties of Fiber Optic Coatings with the Strength and reliability of the Coated Product », *Plastics in Telecommunications VII*, (1995) p.281

4. B. Boutevin, Y. Pietrasanta, in: « Les acrylates et polyacrylates fluorés. Dérivés et applications », (erec edit, 1988)
5. B. Nabeth, I. Corniglion, J.P. Pascault, « Influence of the Composition on the Glass Transition Temperature of Polyurethane and Polyurethane Acrylate Networks », J. Polym; Sci., Polym. Phys. 34, (1996) p.401
6. E. Yildiz, A. Gungor, H. Yildirim, B.M. Baysal, « Synthesis and characterization of UV curable acrylated polyurethane prepolymers, I », Angew. Makromol. Chem., 219, (1994), p.55-66
7. P.C.P. Bouten, D.J. Broer, « Coating Composition and Fiber Lifetime », SPIE vol. 2074, pp. 50-70
8. W. Griffioen, « Discrete Modeling of Crack Growth in Optical Fibers », SPIE, vol. 2290, pp. 56-63

BIOGRAPHIES

Gérard Orcel received his MS and Ph.D. degrees from the University of Florida in the field of Materials Science and Engineering in 1985 and 1987 respectively. He held positions at GelTech and Spectran before joining the R&D group of Alcatel Fibres Optiques in 1992 as Project Manager. Since then, he has been involved in preform design, CVD and draw technology and coating development.

Bob J. Overton is a Senior Principal Scientist in the Fiber Development Group at Alcatel Telecommunications Cable. He received a B.S. in Chemistry from Mercer University and a M.S. in Polymers from the Georgia Institute of Technology. After 14 years with AT&T Bell Laboratories working in fiber optic coatings and cable materials, he joined Alcatel in 1991. At the present time he is responsible for the development of coatings and fiber strength improvement.

Christopher Mc Nutt received his B.S. degree in Chemical Engineering from the University of Tennessee, Knoxville in 1985. He is working as a Project Engineer responsible for materials development at the Alcatel Optical Fiber Cable Competence Center.

Sophie Vanpouille received an engineering degree from Ecole Nationale Supérieure de Chimie de Paris in 1988. She then joined Alcatel Alsthom Recherche to work on polymers for electrooptical modulators. She got a Ph.D. from the Université Pierre et Marie Curie in organic chemistry in 1991. Since then, she has been working on the development of new materials for optical fiber coatings.

Adolphe R. Lopez received a Ph.D. in Material Chemistry from the University of Rennes in 1991. He then worked for one year at Alcatel Alsthom Recherche on coating development. He joined Alcatel Telecommunications Cable in 1992 as Senior Material Scientist in the coating development group.

Jean-Yves Barraud was born in 1941. After a Ph.D. in crystallography he joined Alcatel Alsthom Recherche in 1970, where he held several positions in the field of analytical chemistry and polymer science. He is now Manager of the « Laboratoire Diagnostic Intervention Service », which is devoted to the characterization of materials used by the different Alcatel units in the fields of electrochemistry, energy, and telecommunication. He also leads a group involved in research on polymers for industrial applications.



Christopher Mc Nutt
Alcatel Telecommuni-
cations Cable
Claremont, NC

DOWN SIZED FIBER OPTIC DUCT CABLE

Shinsuke Niiyama, Akira Nishimura, Ryouei Oka, Shigenori Takagi

Sumitomo Electric Industries, Ltd
Engineering Department, Communications Division

1, Taya-cho, sakae-ku Yokohama, Japan

ABSTRACT

A compact fiber-optic cable is effective for low cost and easy handling.

By means of several new cable designs, verified theoretically and experimentally, we developed down sized fiber-optic duct cable.

In this paper, we will introduce the design and test results of our trial cables.

INTRODUCTION

Various counts of fiber-optic duct cables are needed for subscriber network to realize the FTTH.

We planed cable designs of 2 different types, i.e. "high count cable for urban area feeder network" and "low count cable for urban area distribution network and rural area network".

In those cables, ribbon fibers, composed of 250 micro-meter UV-curable acrylate coated single mode optical fiber and polyethylene slot rod, in which ribbon are stranded (ribbon-slot structure), are commonly used by reason of following motivation.

A) 250 μ m fiber is commonly used in conventional cable, so that by using this type of fiber in new cable, multi-fiber splicing to conventional cable becomes possible without peculiar devices.

B) Microbending is caused by fiber coating thickness decrease (Katurasima et.al IWCS 94 Proc PP.37).

C) Ribbon-slot structure is suitable for high density

cable.

D) Slot rod structure, provided herical grooves on its surface, is superior in easy ribbon pick up for mid span access.

E) Water resistance function is provided by a simple design which a water-absorbing tape is tightly wrapped around a slot rod.

We categorize from 400 to 1000-fiber cable as high count cable, also up to 300-fiber cable as low count cable. Compositions of those cables are shown in table-1 and figure-1.

8fiber-ribbon is used in high count region, also 4 fiber-ribbon is used in low count region.

The number of ribbons, stacked into slot grooves, are decided by 2 points of view, namely, cable down sizing and easy ribbon discrimination.

(table-1) Compositions of new compact cable

Category	Low count	High count
Fiber count	20 to 300	400 to 1000
Ribbon	4fiber	8fiber
Cable unit	Single slot rod, provided some herical grooves.	
Number of ribbon per groove	1 to 5	10
Water block material	Water-absorbing tape	

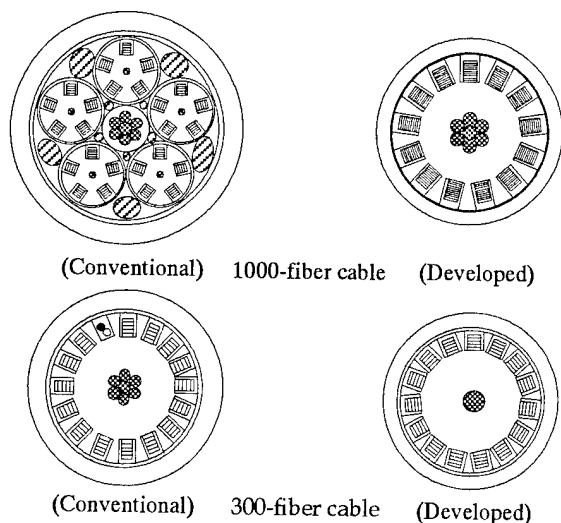
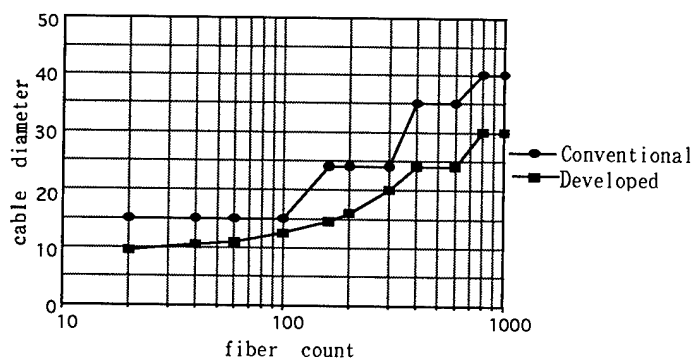


Figure 1. Cable cross section

Figure 2. shows cable diameters of conventional and newly developed. As compared with conventional cables, new cables have 20 to 40 percent smaller diameters.

In the following parts, we will describe our study to realize the down sized cable.



(figure-2) Cable diameter vs. fiber count

CABLE DESIGN

1.THIN COATED RIBBON FIBER

Generally speaking, ribbon coating thickness decrease causes fiber microbend, as well as difficulty increase of coated resin removal.

We made 4 fiber ribbons which had 3 levels of thickness for trial and mounted it into 300-fiber cable to consider ribbon thickness limit.

Thickness were varied from 0.28 to 0.32mm. All size indicate good optical attenuation performance in the temperature limits of -30 to $+70^{\circ}\text{C}$ as shown in figure-3.

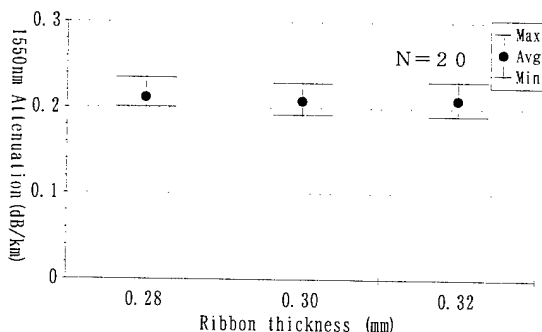
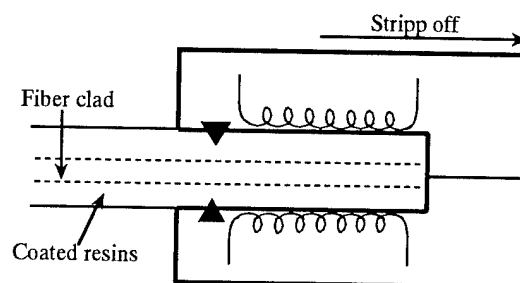


(figure-3) Attenuation of 300 fiber-cable in the temperature limits of -30 to $+70^{\circ}\text{C}$

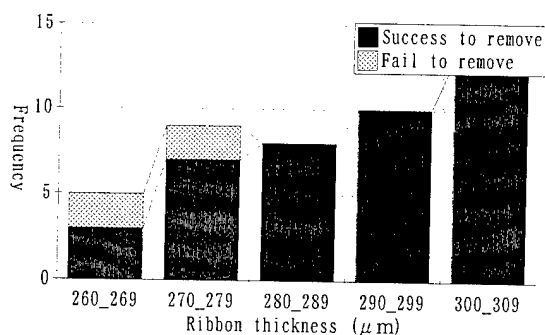
On the other hand, removability is changing for the worse with the thickness decrease.

Figure-4 shows coated resin removal mechanism. At about 30 millimeters from the tip, coated resins are cut, heated and stripped off with the remover. To avoid damaging fiber-glass, width between two edges are set up larger than fiber clad diameter. So with the ribbon thickness getting thinner, cut depth dwindles, finally not enough to strip off.

Figure-5 shows successful removal probability vs. ribbon thickness. The limit of ribbon thickness, required from removability, is $280\text{ }\mu\text{m}$.



(figure-4) Coated resin removal mechanism



(figure-5) Successful removal probability at each size ribbons

2.SLOT ROD DESIGN

Cable diameter changes as slot rod structure.

Figure-6 shows the typical slot rod cross-section.

Rib width must be thick enough against cable crush stress. Groove width and depth must be large enough to mount ribbons. Diameter "D" is fixed by rib width "c", groove width "w" and groove depth "d" according to equation (1) to (2).

$$D^2 = 4(x+d)^2 + w^2 \dots\dots(1)$$

$$\text{Arcsin}\{c/\text{SQRT}(4x^2 + w^2)\} = \pi/n - \text{Arctan}(w/2x) \dots\dots(2)$$

Where "n" is a number of grooves and "x" is a length from center to groove bottom.

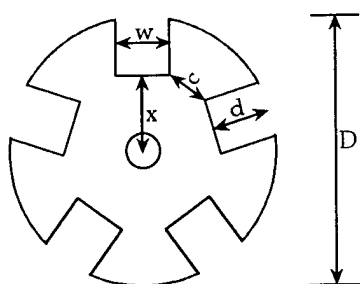


(figure-6) Slot rod cross section

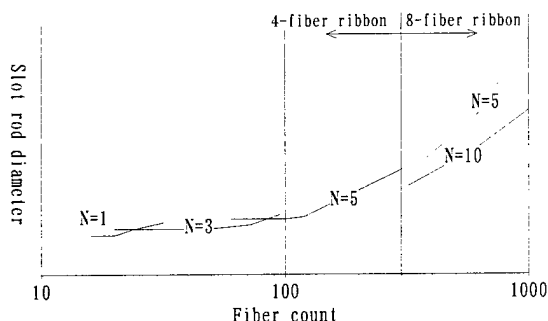


(figure-7) Slot rod diameter vs. fiber count

Calculated slot rod diameters are shown in figure-7. Diameter depends on a number of ribbon "N" which is stacked into each groove. Suitable number for minimizing slot diameter varies with the fiber count.

We used suitable slot rod for every count cable as shown in table-2.

(table-2) Slot rod structure

Fiber count	Ribbon	N	n
20	4-fiber	1	5
40		2	
60		3	
100		5	8
160			
200			
300			15
600	8-fiber	10	8
1000			13

* N is a number of ribbon stack per groove

* n is a number of grooves

3.WRAPPING TAPE

In this cable water-absorbing tape is tightly wrapped around a slot rod for the purpose of groove covering and water resistance.

The tests to evaluating cable water resistance function is shown in figure-8. Water penetration length is in proportion to slot rod groove depth.

About the up to 300-fiber cable, in which slot groove depth is reduced as above mentioned, we used new water-absorbing tape.

Conventional and new water-absorbing tape structures are shown in figure-9.

The amount of water absorbing polymer becomes less than 1/3 times as conventional's. So the cover cloth, which was laminated over the polymer layer of the conventional tape for the purpose of polymer spilling prevention, could be omitted in the new tape.

Thickness of new water absorbing tape is decreased 0.3 to 0.2 millimeter by means of this modification.

Water penetration test results of newly developed cables are shown in table-3. Good performance has been obtained in every size of cables.

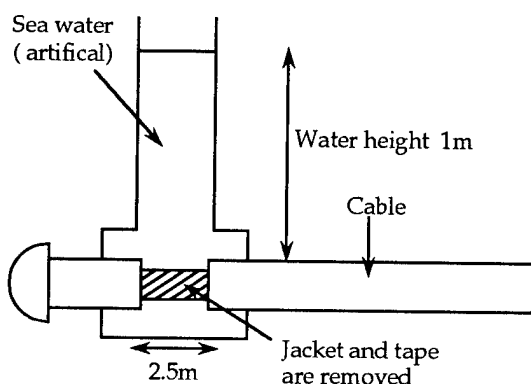


(figure-8) Test procedure for water penetration

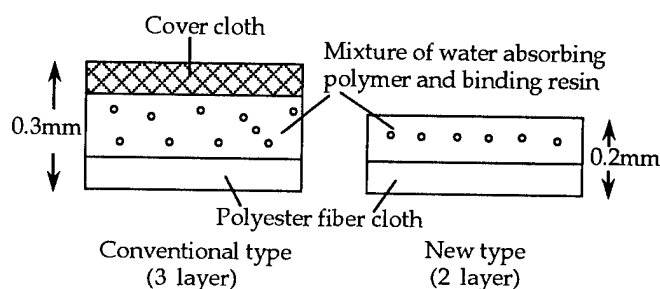


(figure-9) Structure of water-absorbing tape

(table-3) Cable test results of water penetration

Cable size	Used water absorbing tape	Penetration length
Up to 300-fiber	New type	less than 40m
600,1000 fiber	Conventional type	less than 40m

4. OUTER JACKET

So far we have been studying cable fiber design, now outer jacket thickness will be investigated to fix the cable diameter.

For the cable down sizing, it is desirable to make jacket thin. However, duct cable is required tolerance against dynamic force such as rubbing and crushing. We used high strength jacket polyethylene and tested the performance.

Jacket material characteristics of conventional and newly developed cable are shown in table-4.

(Table-4) Jacket material characteristics of conventional and developed cable

	Conventional	Developed
Materials	LDPE	1-LDPE
Density	0.93g/cm ³	0.93g/cm ³
Tension to break	20.8N/mm ²	20.2N/mm ²
Elongation to break	700%	830%
1% Modulus	207N/mm ²	289N/mm ²
Jacket thickness	2.0mm	1.5mm

To evaluate tolerance of our trial cable jacket, we examined squeezing test in extra hard condition as shown in figure-10. Tested cable is passed through 90° bending steel pipe and gone back and forth.

Bending radius is 250 millimeter. Backtension is added and become larger by the friction in the bending pipe. Measured force to pull up the cable was about 3 times as large as backtension.

Test results of conventional and new 100-fiber cable are shown in table-5.

New cable jacket endured more than 50 cycle squeezing under a general tension. Under an extra hard tension, new cable indicates more excellent performance than the conventional cable.

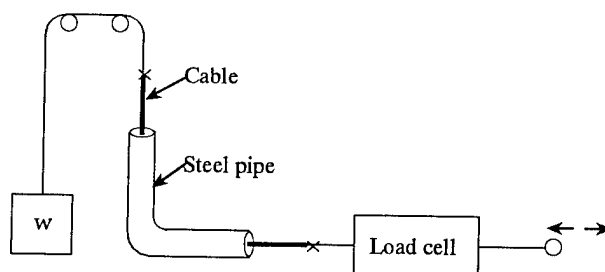


(figure-10) Illustration of cable squeezing test

(Table-5) Cable squeezing test result (n=3)

Backtension	Cycles to jacket break	
	Conventional	Developed
1980N	13~19	22~35
1470N	32~45	41~ more than 50
686N	more than 50	more than 50

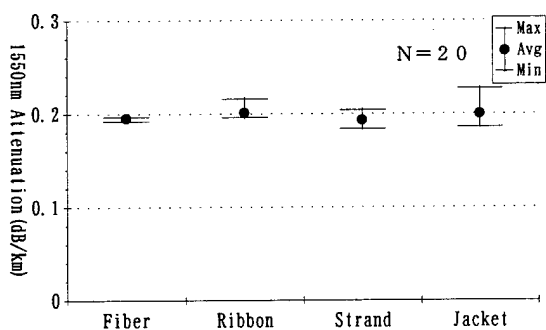
TEST RESULTS OF TRIAL CABLE

We made every size of cables and tested various items simulating the actual environment.

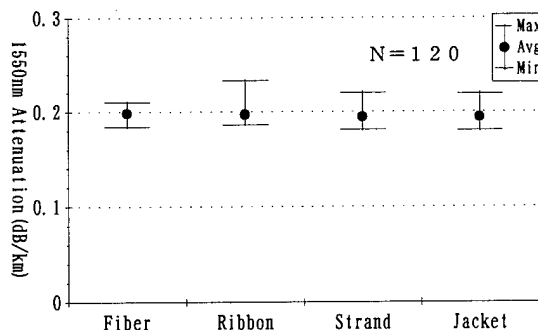
1. TRANSMISSION CHARACTERISTICS

1550nm optical attenuation variation during manufacturing process of representative cable size are shown in figure- 11 to 13. No apparent variations can be seen in any of the processes.

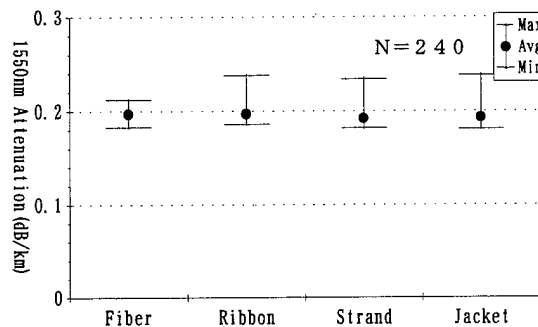
Figure- 14 to 16 show the 1550nm optical attenuation variation under environments of -30°C to $+70^{\circ}\text{C}$, and indicates that stable characteristics equal to those for the conventional cable have been attained.



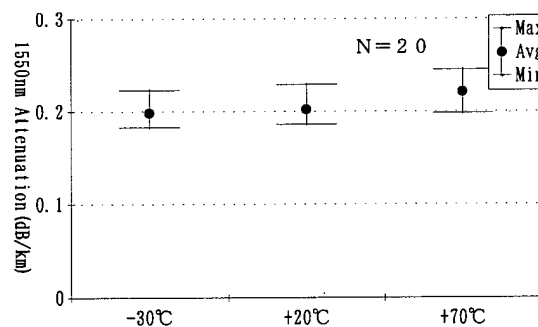
(figure- 11) Attenuation variation during manufacturing process (20-fiber cable)



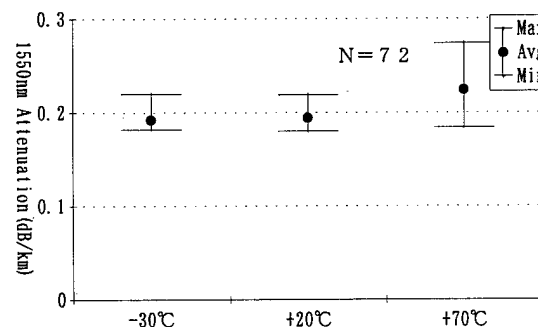
(figure- 12) Attenuation variation during manufacturing process (300-fiber cable)



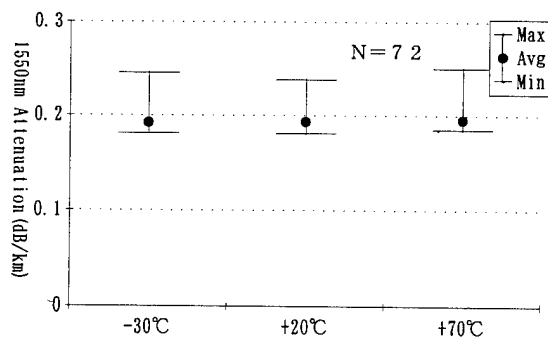
(figure- 13) Attenuation variation during manufacturing process (1000-fiber cable)



(figure- 14) Attenuation (at 1550nm) vs. temperature (20-fiber cable)



(figure- 15) Attenuation (at 1550nm) vs. temperature (300-fiber cable)

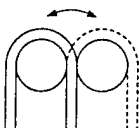
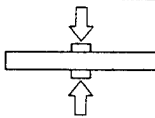
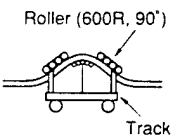
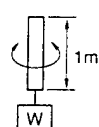
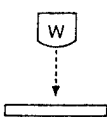


(figure-16) Attenuation (at 1550nm) vs. temperature
(1000-fiber cable)

2.MECHANICAL CHARACTERISTICS

The results of various tests that simulate the external forces applied to the cable damage or an increase of residual attenuation. The results of the tests are shown in Table-6.

(Table-6) Mechanical test result

Test item	Test method	Test condition and result
Bending		Radius; 240mm. Cycle; 10times Angle; 180° Attenuation variation; ≤ 0.1 dB
Bending (low temperature)		Radius; 240mm, Cycle; 10times Angle; 180°, Temperature; -30°C Sheath damage; no damage
Compression		Compression; 1960N, Cycle; 10times Width; 100mm Attenuation variation; ≤ 0.1 dB
Dynamic squeezing	 Roller (600R, 90°) Track	Cable length; 100m, Tensile; 7840N Radius; 600mm, Cycle; 4times Attenuation variation; ≤ 0.1 dB
Torsion	 1m W	Weight; 980N, Angle; 90°, Cycle; 10times Attenuation variation; ≤ 0.1 dB
Impact	 W	Weight; 1kg, Height; 1m, Cycle; 10times Attenuation variation; ≤ 0.1 dB

CONCLUSION

We have developed a series of new fiber-optic duct cable for subscriber network.

In this cable, all components are re-examined and just fitted into the suitable design.

Not a little other types of cable are also needed to realize the "fiber to the home" however, this cable design will be referenced for many other cables, we hope.

Biographical Sketches of the Authors



Shinsuke Niiyama
Sumitomo Electric
Industries, Ltd.
Engineering Department,
Communications division

1, Taya-cho, sakae-ku
Yokohama, Japan

Mr. Niiyama, born in 1969, received his B.S. degree in physics from Osaka University and has joined Sumitomo Electric Industries, Ltd. in 1992. He is now an engineer of optical-fiber and cable design.



Ryouei oka
Sumitomo Electric
Industries, Ltd.
Cable Manufacturing
Department,
Communications division

1, Taya-cho, sakae-ku
Yokohama, Japan

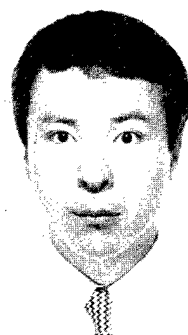
Mr. Oka, born in 1972, received his B.E. degree from Waseda University and has joined Sumitomo Electric Industries, Ltd. in 1995. He is now a process engineer of cable manufacture.



Akira Nishimura
Sumitomo Electric
Industries, Ltd.
Senior Engineer,
Engineering Department,
Communications division

1, Taya-cho, sakae-ku
Yokohama, Japan

Mr. Nishimura, born in 1958, received his M.E. degree from Kyoto University and has joined Sumitomo Electric Industries, Ltd. in 1984.



Shigenori Takagi
Sumitomo Electric
Industries, Ltd.
Cable Manufacturing
Department,
Communications division

1-1-3, Shimaya, konoha-
na-ku, Osaka, Japan

Mr. Takagi, born in 1964, received his B.E. degree in Mechanical Engineering from Tohoku University and joined Sumitomo Electric Industries, Ltd. in 1986. He is now a process engineer of optical fiber and cable manufacture.

OPTICAL FIBER RIBBON CABLE DESIGNS FOR A WIDE RANGE OF APPLICATIONS AS THE AVAILABILITY OF FTTH IS REALIZED

F. Legros, Y. Roussel, D. Brault, JY Guerin; ACOME R&D Department, Mortain France
JP Louboutin, D. Boscher; CNET Laboratory, FRANCE TELECOM, Lannion, France

ABSTRACT

This paper will report on work that has been accomplished to develop new approaches to optical fiber cable designs in preparation for the deployment of the multi-media network.

This work has encompassed the entire range of cables needed in the subscriber network, (from the trunk to the subscriber) in all required applications. Included are cable designs from the very small, 2 fiber cables to high capacity 512 fiber cables, that are consistent in design. This approach along with a new connecting device that has been developed and tested combine to optimize the performance/cost ratio.

Throughout this work, attention has been paid to maintaining simplicity of design and handling.

INTRODUCTION

The deployment of optical fiber in the distribution network has been hampered by various factors:

1. The Cost is Too High (1)

Although costs of necessary components required by the various optical solutions, e. g., HFC, FTTC, FTTH, have been reduced substantially, the overall cost of these systems is still too high for widespread utilization in the network.

Other factors that affect decisions to employ fiber networks relate to merging of services and the costs of various service approaches, the ability of system operators to finance the costs involved, as well as the question of affordability by the end customers.

Copper based solutions are still considered adequate for many systems. FTTC/B or HFC may offer a transitory solution at a lower cost.

2. Properties of Available Optical Fiber Cables are Inadequate.

Beginning in the 1980's, and still continuing, there has been a large deployment of fibers in the long distance networks. For these applications, great care was taken because of the lengths of cable involved, the critical need for reliability, and the belief that the fibers were fragile and subject to installation damage.

These concerns extended to all aspects of manufacturing and installation of the entire system, as well as to the ancillary equipment.

These procedures, although appropriate to the introduction of a new technology with critical performance requirements, has engendered concepts and habits that, while serving to limit risk, may be inappropriate for the widespread application of fiber to the distribution network.

The high costs incurred during the cable laying and splicing operations for these cables (loose tubes or slotted core with single fibers) coupled with the low fiber density the large diameter and substantial weight, remove these designs from consideration for the subscriber loop. Also, when high fiber counts are needed, accessibility of individual fibers is difficult in these "long haul" cables.

Moreover, tensile strength, torsion resistance, bending properties are not adequate for the distribution network basically because physical configurations are generally much more difficult than in the long distance environment. This means that technical compromises must be reconsidered.

3. Early Designs of Cables for the Subscriber Network Lack the Simplicity Necessary for Widespread Deployment.

The first generation of optical cables for the distribution network were complex and required improvement especially in two design areas:

- a. Simplified connections
- b. Flexibility

4. Lack of Standardization

Although International norms for fiber and cables have been established for long distance networks, and are very consistent, the standardization of specifications for most elements of the distribution network still must be established. As an example, inadequate knowledge of the physical properties of fiber, for practical use, e.g., very small bending radii, is a significant limiting factor in the deployment of fiber.

5. Excessive Product Testing

Repeated testing of fibers creates a large additional cost in the finished cable that is not justified by operating experience. Fibers are tested at the original producer, at the fabricator upon receipt, after each step in the manufacturing process, at the finished cable inspection, and upon arrival at the jobsite. This adds a substantial additional cost to the user without adding to the value of the product. More efficient testing equipment is and soon will be available to work with ribbonized cables (OTDR, automatic control of fibers).

6. A Large Investment is Required to Deploy Fiber in the Subscriber Network

System operators are cautious about investing in these projects until the economic benefits vs. the costs are better documented.

To achieve widespread deployment of optical fiber in the distribution system, the performance/cost ratio must be increased. Some approaches have been identified:

1. Technical Breakthroughs are Needed

Possibilities for dramatic cost reduction exist with all components of the network including both active(6) and passive elements. One of the objectives of this work is to consider the passive infrastructure as a whole.

2. Various Approaches to Improved Cable Design and Application

Research has been accomplished in the areas of:

- a. Ultradensification of fibers (13)(14)
- b. Ultradensification utilizing ribbons of optical fibers has been extensively researched (19)(20).
- c. Based on these studies, high fiber count cables have been conceived (21).

On the other hand, low fiber count cables must also be optimized in terms of densification.

- a. Ribbon cable designs have been proposed to meet this goal (23).

Using new installation techniques, mechanical strains may be significantly reduced with cables of more consistent design (24)(25)(26).

Mass splicing is confirmed as a time saving technique.

Additional new concepts, somewhat more radical include ultra thin fibers (22)(29)(30), and bunched multicore fibers (27)(28).

As a result of this study, which approach was selected?

Ribbon cables of various designs incorporate the optimum combination of properties, ease of splicing & identification, and can be designed in an ultra-dense configuration.

To optimize the performance/cost ratio, modular concepts were deployed. This approach resulted in achievement of:

- Ultra densification of fibers.
- Easy handling during installation.
- Flexibility

A comprehensive approach was needed to meet global FTTH requirements:

The solution must allow from low to high fiber counts. Cables must be designed for all applications (duct, direct burial, aerial and within building structures).

The methodology used was a Functional and Value Analysis of:

The global FTTH passive infrastructure
Cable design
The connecting devices

As previously mentioned, this approach has reflected realistic industrial practices to insure conservative costing assumptions.

The result is a global, FTTH oriented solution for the distribution network.

CABLE DESIGN

1. Description of the Basic Concepts

Several technical approaches have been tested to meet the goals as previously described. The

advantages of using optical ribbon cable are well known:

- Mass splicing capability results in a major reduction in connection costs.
- Organization of fibers in ribbon form aids the speed and reliability of fiber management.
- Compact size of ribbon construction vs single fiber makes handling easier.
- The geometry of the coplanar ribbon as a primary module is consistent with a high density secondary module.

Several proposals for solutions have been tested in the context of system value analysis. A sample of functional value analysis of a cable appears in Table I.

The final goal of this method is to finalize a specification. Levels are introduced to be able to select the best techno-economical compromise. Required functions are defined in the distribution network frame, consistent with connecting device functions.

TABLE I

Function	Criterion	Level	Flexibility
Permit optical transmission	Thermal cycling	-30°C, +60°C/ < 0,10 dB/km	1
	Crush resistance	> 40 daN/cm	0
	Tensile strength	> 2 x Weight	1
	Static bending	> 5 x Diameter	1
	Dynamic bending	> 5 x Diameter	1
	Storage temperature	-30°C, +60°C	0
Minimize dimension	Diameter	< 10 mm	0
	Density	> 1 OF/mm ²	1
	Weight	< 60 kg	1
Permit easy accessibility	Time to access		
	To secondary optical modules	< 2 min	1
	To primary optical modules	< 1 min	1
	To optical fibers	< 2 min	1

**Table I: Functional Analysis of Distribution Cable
An Example**

Flexibility has been introduced as a way (i) to reduce costs (ii) and to be able to react in case that solutions proposed do not meet the validation process in field trials.

2. Technical Background

OF ribbon cables in loose tubes are now a basic design concept that consolidates the technical advantages of the ribbon design with ease of manufacture (ability to be introduced in SZ stranded tubes) and with field validation (this design has been successfully laid in a France Telecom experiment named "Tamaris Project"). An example of a 288 fiber cable of this design appears in Figure 1, Loose Tube Design.

However, this generation of cable designs results in too low a fiber density and accordingly are too large in diameter and too heavy.

3. New Concepts

The previous conclusion regarding the loose tube design is a major reason for the work undertaken to introduce new design concepts, the most important of which is encapsulation.

4. Encapsulation

The ribbons are (i) first organized in matrices (ii) and then embedded in a material or a combination of materials, which provide the mechanical and thermal protection that environmental parameters require.

In addition, the mechanical properties of these materials allow easy access to the ribbons. The materials have been selected to obtain a balance of the physical and chemical properties between Young's and the flexibility modulus (the thermal stability of it), the shore hardness, viscosity of the product for ease of processability, and to have the correct optical performance (transmission

characteristics of secondary modules and cables).

A major issue is that ribbons have to have a minimal ability to move within the encapsulation material which is a soft material, and at the same time, they do have to be sufficiently hard to withstand the transverse and lateral forces introduced in the stranding operation.

Another advantage of encapsulation is that watertightness is achieved without the use of jelly fillers thus simplifying or eliminating the costly cleaning operation.

5. Polyfunctional Construction

As much as possible, polyfunctional materials were used in the design of these cables. An example is encapsulation with a thermally stable mechanical protection of the optical primary modules which also provides watertightness whereas loose tube designs require two different materials. Also, the reinforcing elements combine watertightness with good tensile strength.

Finally, this approach provides significant reductions in weight, diameters, and the cost of the cables.

Validation of the reduced cost of connections must be quantified.

6. Validation of New Design Concepts

Combinations of these new designs have been tested to optimize the performance/cost ratio. As an illustration was the patchcord and the unitube design.

Table II displays the global application of developed cables:

TABLE II

Application /Design	Bufferized Ribbon	Slotted core	Patchcord	Unitube
Duct	X	X		X
Direct burial	X			X
Building	X		X	
Aerial				X

Design of Cables

The new generation of cables has been built to optimize the performance/cost ratio. The following drawings illustrate the new designs (Figure II to Figure VII).

- Figure II: Buffered Ribbon Matrices (72 OF)
Figure III: Bufferized Ribbon Matrices (144 OF)
Figure IV: Bufferized Ribbon Matrices (512 OF)
Figure V: Patchcord Design
Figure VI: Slotted Core Design
Figure VII: Unitube Design

This leads to a consistent range of cables as shown in figure VIII.

- Figure VIII: Ultradensification: A Consistent Range of Products.

TEST RESULTS

Thermal cycling, traction, bending, and torsion have been examined.

These tests have been conducted according to International norms (IEC, EN) or recommendations (ITU/T) measurement protocols. When test procedures were not available, specific methods have been carried out, especially the torsion test of the ribbon.

RESULTS ACHIEVED

Synopsis of Basic Performance

Examples of the results achieved are shown in Figures VIII and IX which show the optical transmission properties of the 512 fiber duct cable:

- Figure VIII: Thermal Cycling
Figure IX: Histogram of Attenuation

In Table III we have summarized the principal performance characteristics of a broad range of these new design cables (data is for typical representative cables).

TABLE III Basic Performance of Products

Fiber count (OF)	Application(s)	Weight (kg)	Diameter (mm)	Density (OF/mm ²)	Thermal cycling	Traction (daN)
Bufferized ribbons						
72	Duct/ Direct buried	71	10	0,92	0,02 dB/km	135
128	Building	145	14	0,83	0,08 dB/km	350
512	Duct	360	22	1,35	0,05 dB/km	690
Unitube						
24	Duct/aerial	96	11	0,25	0,05 dB/km	270
48	Duct	70	9	0,75	0,05 dB/km	85
96	Duct	90	10	1,22	0,06 dB/km	90
Slotted core						
4	Duct	15	5	0,20	0,05 dB/km	35
Cable for Patchcord						
4	Building	11	3	0,57	0,03 dB/km	20

FIELD EXPERIMENTS CONDUCTED

1. The Ker-Uhel Project:

In order to proceed with the validation of these new concepts, a decision was made to experiment using the field cables and connecting device. The goals were:

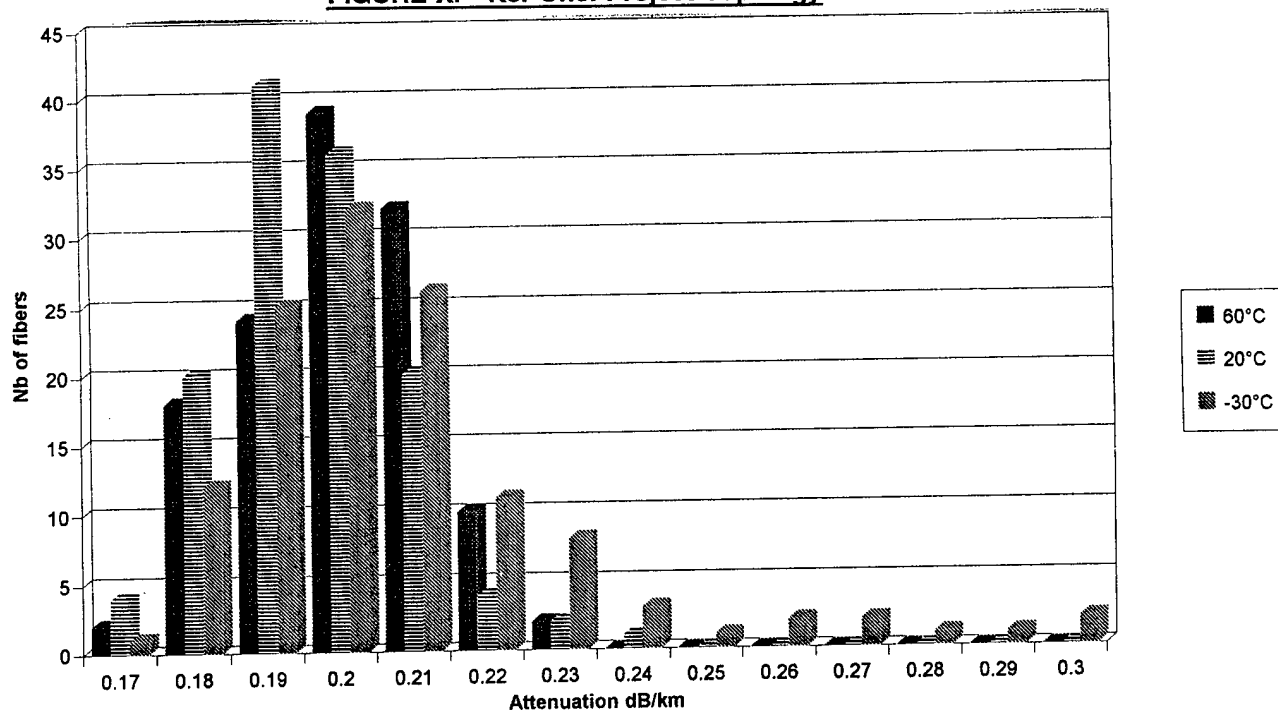
- To check the ability of the design concepts to meet field conditions
- To check that the forecasted advantages (based on theory and laboratory tests):

- a. Enhanced accessibility of optical modules
- b. Advantages of the reduction in weight
- c. Increase in the speed of installation (cable laying, connecting) were achieved.

- To react to unforeseen difficulties in the field installation process.

Detailed description of the topology of this project is shown on Figure XI.

FIGURE XI - Ker-Uhel Project Topology



The choice of cables for this project has been made after taking into account the requirements of the installation and the interest in gaining information from the test. Installation techniques used were both conventional (mechanical pulling) but sometimes pushed to limits or new ones (new France Telecom pushing-blowing techniques (blowing into small diameter tubes) have been tested. Mass connection devices (fusion, mechanical splices and a mass connector) were

selected to offer improved consistency with ribbon cables than the older generation of connectors. Conventional and hybrid (i.e., between ribbons with a different number of fibers). Mass splicing was experimented with in this installation.

The results achieved in the field test of the Ker-Uhel project:

- Ease of installation is globally confirmed
- Reduction in time of the installation compared with conventional designs
- Efficiency of connecting device has been confirmed. The basic criteria are: economy, self efficiency and quality of connection of a new multifiber mechanical splice.
- The results in the field are consistent with laboratory tests and theory.

This leads to a general conclusion: These new designs may now be used to establish a new generation of distribution cables that meet the requirements of field installations at a reduced cost and with improved performance.

CONCLUSION

The consistency of the elements of the passive network infrastructure has been established.

1. Cables

- A new generation of cables based on an ultra dense configuration has been developed
- These compact, light weight, designs enhance accessibility of fibers, modular concepts, (enhanced accessibility of optical modules, e.g., ribbon matrices).
- The ability to produce cables with a wide range of fiber counts using the same design concept has been confirmed.
- This design concept has been proven to be compatible with all installation conditions (duct, direct burial, aerial and within buildings).
- This design concept has been proven to be compatible with all laying techniques including blowing.
- The designs are compatible with new generations of fibers.

2. Connecting Device

- The new connecting device has been field tested for ease of use, simplified organization of fibers and fiber modules, compactness and operational reliability.

3. System Validation

- The entire passive network infrastructure has been confirmed through field trials, integrating with the balance of the network.

ACKNOWLEDGEMENTS

The authors would like to recognize the contributions to this paper from teams of Pouyet and ATI who were involved in the development of closures and splices within this project supported by France Telecom.

BIOGRAPHICAL SKETCHES



D. Brault
(ACOME)

D. Brault has a Chemistry background. He joined ACOME in 1982 and began his activities in working on new polymeric compounds

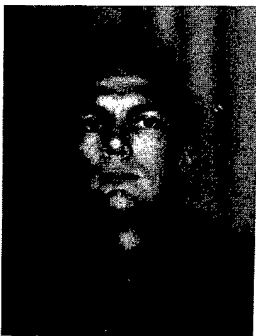
(PVC and zero halogen) within the Study and Research Department. He then moved in 1988 to optical cables activity, being involved in both production team management and new cables project leader. In 1994, he became Optical Cables Studies Manager in the R&D Products Department.



Y. Roussel
(ACOME)

Y. Roussel was born in 1958. He is graduated from Institut Supérieur de Plasturgie d'Alençon. He joined ACOME in 1978. He

worked on materials development and optical cable development. He is now Optical Plant Manager within the R&D Products Department.



JY. Guérin
(ACOME)

JY. Guérin (ACOME) was born in 1962. He received his engineer degree from the Ecole Nationale Supérieure de l'Electronique et

de ses Applications in 1988. He joined ACOME in 1992 where he is in charge of development and projects about passive optical networks within the R&D Products Department.



F. Legros

F. Legros is Senior Manager of the R&D Products Department of ACOME. After having lead Research projects on polymeric materials within

National Centre of the Scientific Research (CNRS) and Study and Research Division of Electricité de France (EDF) he joined ACOME in 1986. He first worked on innovating cables and has been Head of Production and R&D Optical Cables Department. He is now pilot of the R&D program of all new products of ACOME.



D. Boscher

Daniel Boscher, born in 1951, received his engineering degree from the Ecole Nationale Supérieure des Arts et Métiers and joined CNET in 1973.

Working on circular waveguide until 1979, he then joined the optical fibers and cables department. Since 1993 he is manager of the "Fibers, Cables and Measurement" Department.



JP. Louboutin

Jean Pierre Louboutin was born in 1954. Doctor in solid physics, he joined CNET in 1982. He is now Head of Group "Cables in Distribution."

FIGURES

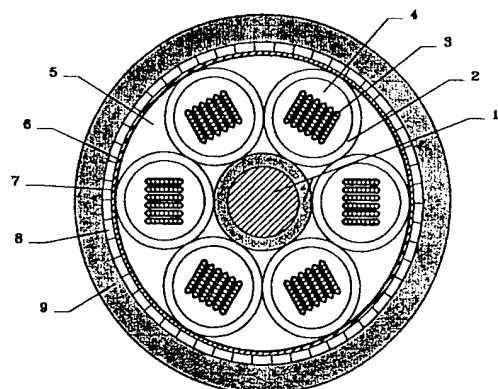


Figure 1. Loose tube design

1. Central strength member
2. Tube material
3. 8 OF ribbon
4. Watertightness compound
5. Watertightness compound
6. Tape
7. Tape
8. Reinforcing element
9. Outer sheath

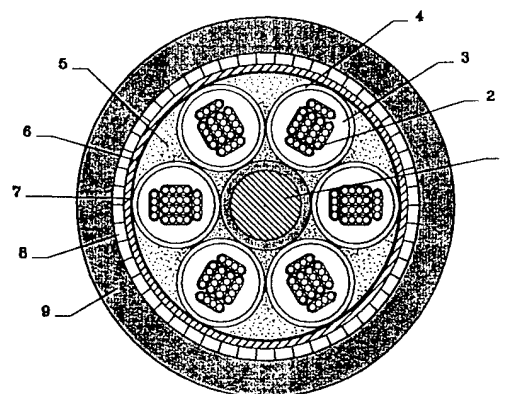


Figure 3. Buffered Ribbon Matrices (144 OF)

1. Central strength member
2. 4 OF ribbon
3. Encapsulation material
4. Encapsulation protective material
5. Watertightness material
6. Tape
7. Tape
8. Reinforcing element
9. Outer sheath

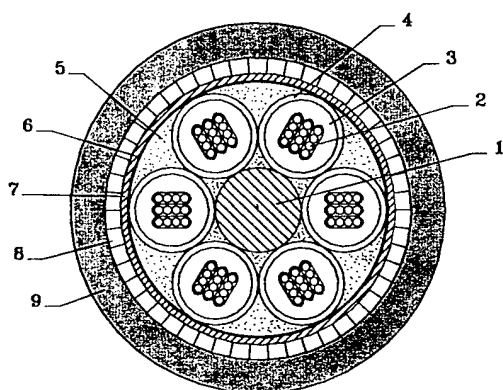


Figure 2. Buffered Ribbon Matrices (72 OF)

1. Central strength member
2. 4 OF ribbon
3. Encapsulation material
4. Encapsulation protective material
5. Watertightness material
6. Tape
7. Tape
8. Reinforcing element
9. Outer sheath

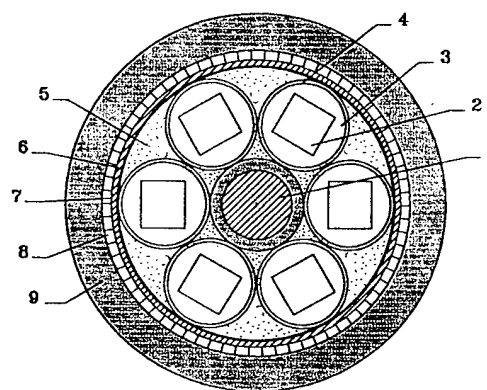


Figure 4. Buffered Ribbon Matrices (512 OF)

1. Central strength member
2. 8 OF ribbon
3. Encapsulation material
4. Encapsulation protective material
5. Watertightness material
6. Tape
7. Tape
8. Reinforcing element
9. Outer sheath

FIGURES

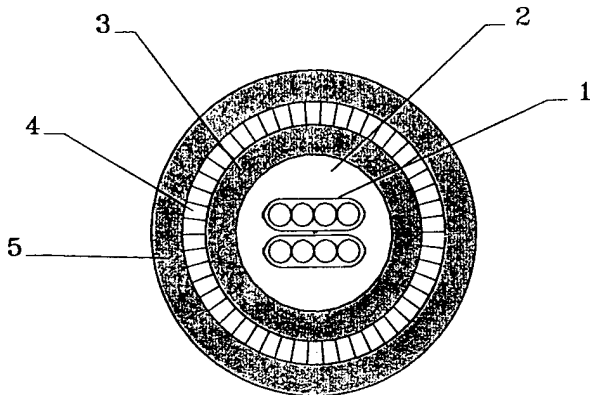


Figure 5. Patch cord design

- 1. 4 OF ribbon
- 2. Encapsulation material
- 3. Polymeric tube
- 4. Reinforcing element
- 5. Outer sheath

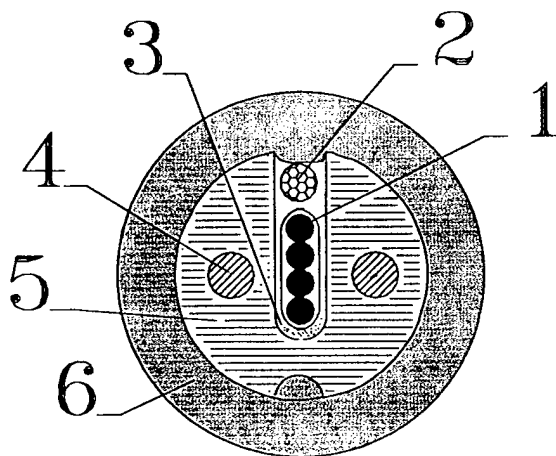


Figure 6. Slotted core design

- 1. 4 OF ribbon
- 2. Filler
- 3. Waterblocking compound
- 4. Strength member
- 5. Plastic core material
- 6. Outer sheath

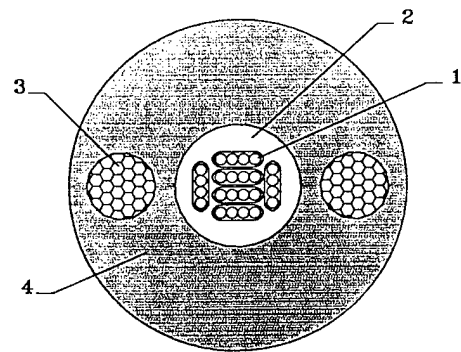


Figure 7. Unitube design

- 1. 4 OF ribbon
- 2. Watertightness product
- 3. Polymeric tube
- 4. Reinforcing element

Figure 8. Ultradensification : a consistent range of products

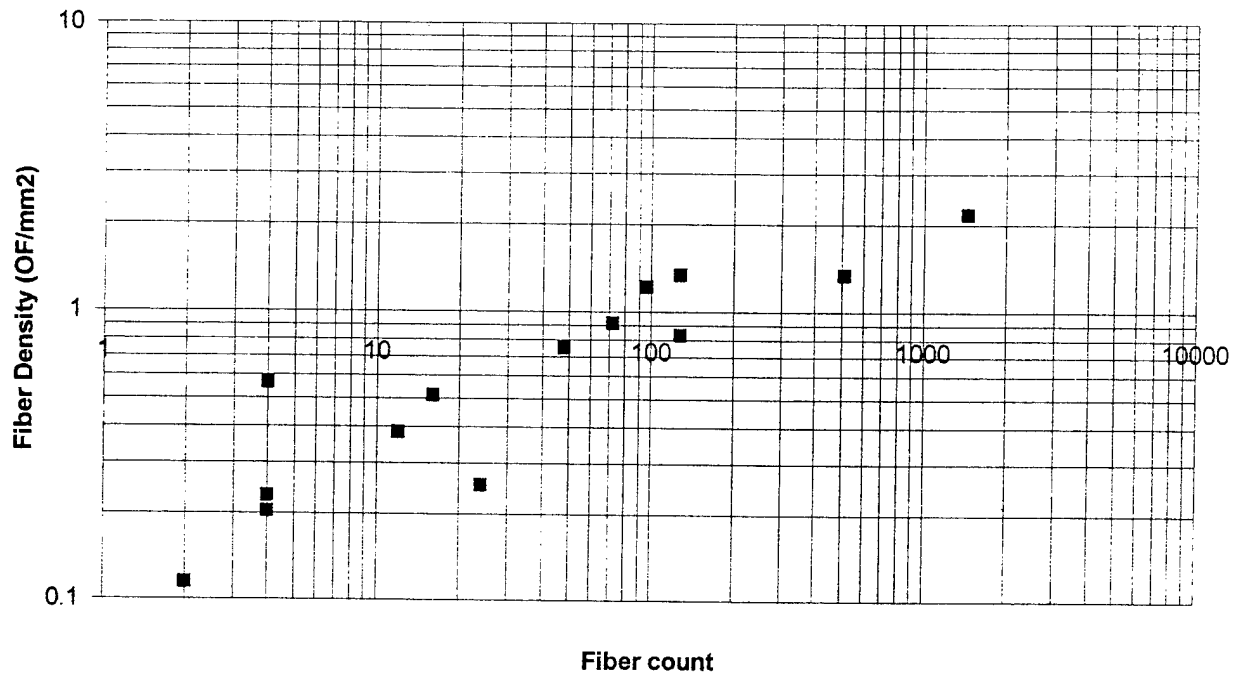


FIGURE IX

Ker-Uhel project topology: a star FTTH network made of ribbon-based cables and hardware

CNET/ACOME/

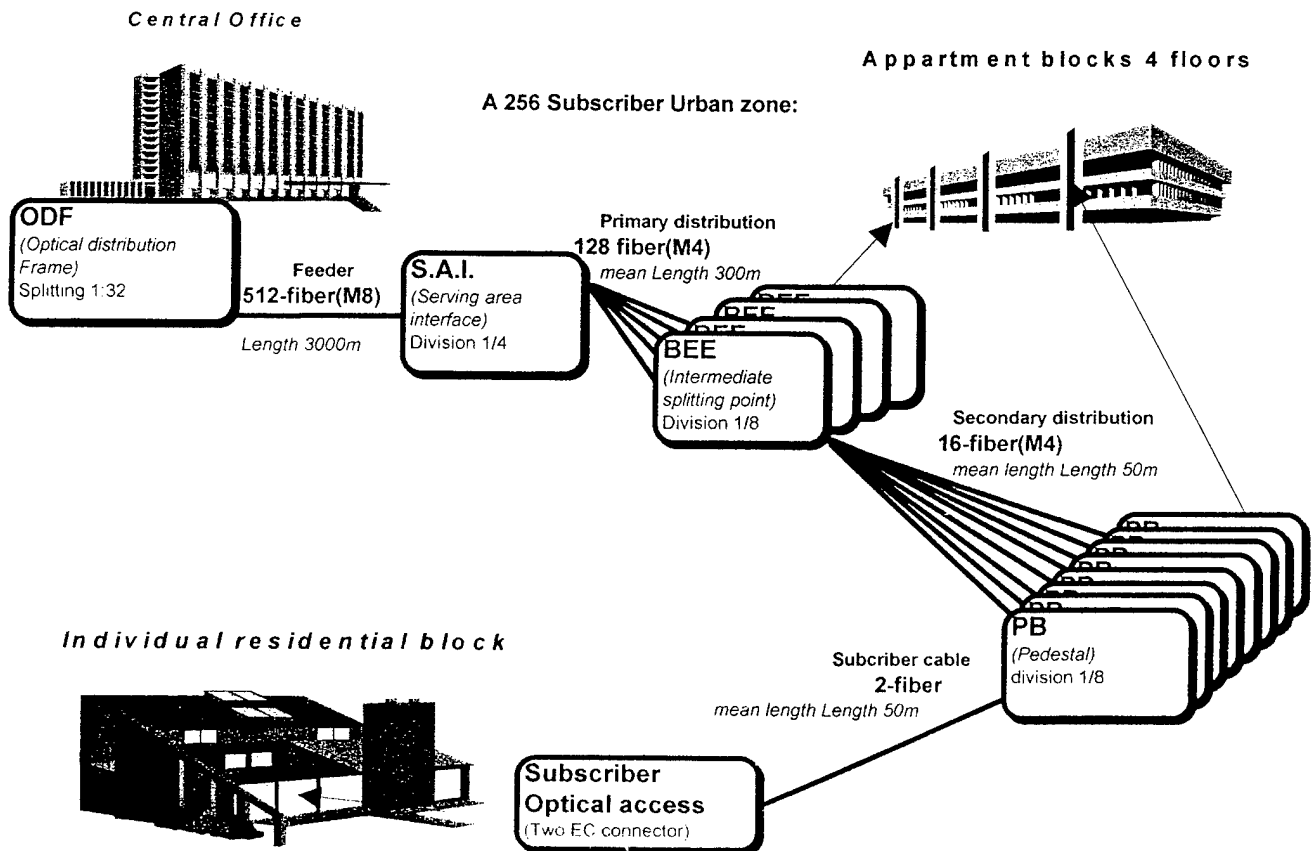
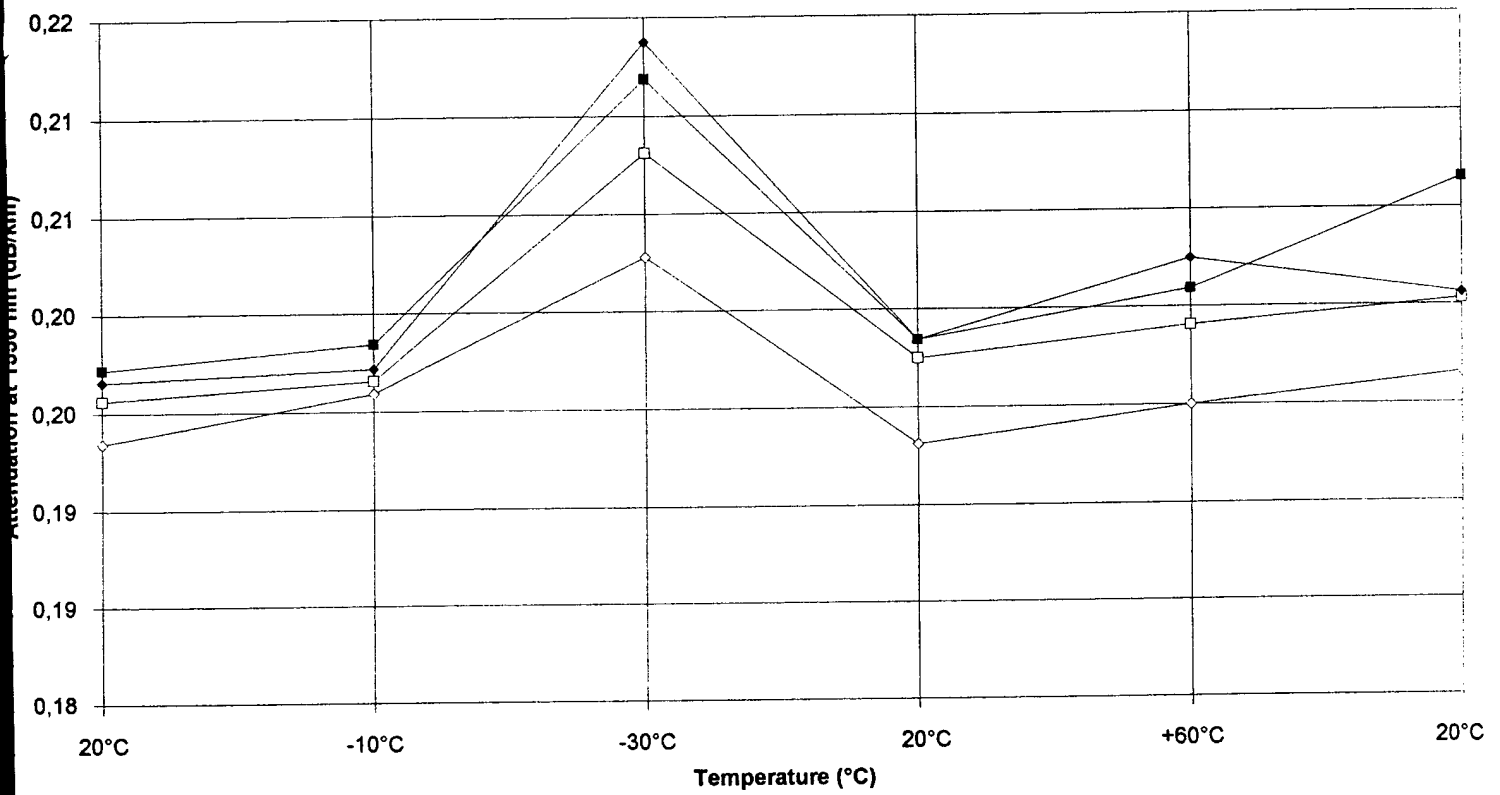


FIGURE X
Thermal cycling (512 OF)



Références.

- (1) Services, Architectures, topologies and economic issues. G.Adams (Nortel) & al. Full Services Access Networks Conference. London. 20.06.96
- (2) Overview of Full Services Optical Access Networks. J.Abiven (France Télécom) & al. Full Services Access Networks Conference. London. 20.06.96
- (3) VDSL Copper Transport System. P.Huish (BT) & al. Full Services Access Networks Conference. London. 20.06.96
- (4) Network Termination and Customer Premises Network. R.Bury (Alcatel) & al. Full Services Access Networks Conference. London. 20.06.96
- (5) FSAN : Operations, Administration and Maintenance. F.Caviglia (CSELT) & al. Full Services Access Networks Conference. London. 20.06.96
- (6) Customer ONU : Cost, Technology and Standardization Issues. R.Baker (Alcatel Optronics) & al. Full Services Access Networks Conference. London. 20.06.96
- (7) D.Boscher, P.Le Goff & F.Legros. Technical & Economical Comparison between Shared & Point to Point FTTH and Analysis of the Cost Evolution as to Determine the Installation of the Fiber.. EFOC'N. Brighton. June 1995.
- (8) Y.Roussel & al. Optical Ribbon Cables : Towards an Innovating Cabling System. EFOC & N'95. Brighton. June 1995.
- (9) M.Tréheux. Technology and Regulation : Some views of the Evolution of Access Networks. EFOC & N'95. Brighton. June 1995.
- (10) Advanced Multiservice Scenarios for Europe. L.A.Ims & al. EFOC & N'95. Brighton. Juin 1995.
- (11) F.Legros, G.Davit. Telecom Network Infrastructure . Telecom Meeting Télécom 95. Genève. 5 October 1995.
- (12) G. Le Noane & al. Vers des réseaux FTTH basés sur de nouveaux composants passifs et actifs et sur de nouvelles techniques d'ingénierie d'installation. Recueil de conférences. OPTO. Paris. March 1996.
- (13) Les câbles à microgaine, une technologie innovante, une réalité industrielle. P.Jamet & al. Recueil de conférences. OPTO. Paris. March 1996.
- (14) Systèmes de câblage optiques à base de rubans : une contribution à la réduction des coûts d'utilisation. F.Legros & al. Recueil de conférences. OPTO. Paris. March 1996.
- (15) Design and Development of a Compact High Fiber Count Ribbon Cable. W.J.McCallum & al. IWCS. pp 8-15. Philadelphie. November 1995.
- (15) J.P.Louboutin & al. Optical Fiber Ribbon Cable Designs for a broad range of Applications as the Availability of FTTH is Realized. IWCS. Reno. 18-21 novembre 1996. (To be published).
- (16). Opening speech. Y.Madec 5th Symposium on Premise Wiring and Lan..Lisbonne-Estori. 7-13 May 1994
- (17) The digital revolution. G.Théry. 5th Symposium on Premise Wiring and Lan. Eilat/Petra. 12-18 May 1996.
- (18) The micro-sheath cable : a novel design of ultralightweight single mode optical cable for low cost subscriber loop. P.Trombert et al. IWCS 1991. pp 24-29
- (19) Preliminary Research into Ultra High Density and High Count Optical Fiber Cables. S.Tomita et al. IWCS 1991
- (20) An Enhanced Ribbon Structure for High Fiber Count Cables in the Loop. K.W.Jackson et al. IWCS 1991
- (21) Design and Development of a Compact High Fiber Count Ribbon Cable. W.G.McCallum et al. IWCS 1995
- (22) Ultra-thin Optical Fiber Ribbon and 108-Fiber Loose Tube Ribbon-Based Cable. X.P.Gao et al. IWCS 1995.
- (23) New Light Weight Small Diameter Fiber Optic Ribbon Cable for the Norwegian Access Network. G.Berthelsen et al. IWCS 1995
- (24) Griffioen. Compendium of laying and installation techniques. Elsevier. 1993
- (25) A New Application of Air Pulled Cable in Microduct for the Local Loop. P.Lesueur et al. IWCS 1995.
- (26) Une nouvelle application du soufflage-tirage en Micro Génie Civil pour le réseau de distribution. A.Pécot et al. Opto 96. March 1996
- (27) Bunched multicore fibers. G.Le Noane et al. IWCS 1994
- (28) Splices and Connectors for Bunched Multicore Monomode Fibers. H.Aoustin et al. IWCS 1995
- (29) Microbending Loss of Thin Coating for Ultra-High-Count Cable. M.Hara et al. IWCS 1992
- (30) Coating Design of Thin Coated Fiber for Ultra-High-Count Optical Fiber Cable. K.Oishi et al. IWCS 1993
- (31) Techno-Economic Study of Optimized Passive Optical Networks. E.Solères. 5th Conference on Optical /Hybrid Access Networks. September 1993
- (32) Telco/Cable Convergence and Local Access Evolution in the United States. J.S.Lively. 5th Conference on Optical /Hybrid Access Networks. September 1993

SIGNIFICANT IMPROVEMENT OF LOOSE TUBE CABLE SPLICEABILITY BASED ON NEW CABLE DRY DESIGN

P. Gaillard¹, C. Mc Nutt², J. Holder², A. Bouvard³, O. Tatat¹

¹ Alcatel Cable OFCCC - Bezons, FRANCE

² Alcatel Telecommunications Cable - Claremont, North Carolina, USA

³ Alcatel Cable France - Calais, FRANCE

Abstract

The aim of this paper is to present a new loose tube cable design combining ABM2 buffer tube material with different experimental solutions to obtain a dry core loose tube cable, without flooding compound between tubes.

The combination of different dry core solutions with ABM2 buffer tubes have been analyzed. The aging and reliability test results are presented and the impact on cable handlability and water tightness are discussed.

With regard to spliceability, the advantages of this new loose tube cable are pointed out compared to standard fully filled loose tube cables.

It is concluded from this study that the loose tube dry core design is a reliable solution, providing a significant improvement over fully filled cables during their end preparations for splicing. Also, the combination of a dry core design and the use of ABM2 tube material demonstrates it is the best solution for a loose tube cable in terms of handling and spliceability.

Introduction

The introduction of optical fiber cables into distribution networks has increased the field technician's comparison between copper pair cables and optical cables for installation and spliceability ease. Therefore, it is particularly essential that optical cables be carefully designed regarding these aspects, such as the simplest possible splicing process is identified, particularly cable end preparation.

This is of significant importance considering the difficulties experienced with optical fiber cable filling and flooding compound removal : it takes time and can cause difficulties in keeping the splicing equipment and tooling clean. It may also impact splice attenuation values if cleaned insufficiently.

In addition to cable cleaning issues, craftsmen also have concerns with buffer tubes flexibility, memory and kink resistance when bending and installing them in splice boxes

and when preparing mid span access without damaging fibers or creating fiber attenuation increase.

During IWCS 95, a paper (1) has been issued, presenting the new ABM2 material in comparison with standard buffer tube materials such as PBT. This evolution of design significantly reduces the tube stiffness and memory, and improves tube handling while maintaining good mechanical properties ; in order to further improve the product the next step is to simplify the cable design by replacing the filling compound with water swellable elements to ensure the longitudinal water tightness between the tubes. These water swellable elements can be more easily and quickly removed, thus providing the opportunity for significant craft labor cost savings by elimination of the time-consuming task of cleaning the buffer tubes before accessing the fibers.

This new cable design (dry core with ABM2 tubes) represents a significant improvement for its implementation on the field, particularly regarding cable ends preparation and handling and storage of loose tube in the splice box.

The dry core design : compared cable structures

Longitudinal watertight structures have been a requirement since the beginning of optical cables development, with solutions based on the filling with an ad-hoc compound of all the interstices and voids of the cable structure. This kind of solution presents, as a main advantage, its physical (voids are filled) and passive aspects ; on an other hand, the following drawbacks can be observed :

- the incorporation of a filling compound into the cable core (compared with a dry solution) leads to a weight increase, which may be penalizing for duct pulling ;
- risks of filling compound dripping into the splice boxes, which can lead to attenuation increases and complicates re-entry for maintenance ;
- possible concerns for the compatibility with other cable components (loose tube material, sheathing material...);

- possible poor adhesion of reinforcement yarns to the outer sheath, which can create troubles when laying the cable using pulling grips or intermediate caterpillars (sheath tearing) ;
- complication of the procedure of cable ends preparation for splicing, as the filling compound has to be wiped out from the tubes and reinforcement members ;
- necessity to use solvents for cleaning tooling and cable elements, which is time consuming and presents potential health concerns ;
- the manufacturing process presents more risks (in terms of scrap rate) compared to a dry process.

In comparison, a dry core solution can be evaluated as follows :

- the cable weight is smaller ;
- the risk of filling compound dripping into the splice boxes is limited to the thixotropic filling compound which is inside the tubes ;
- the swellable materials are generally well compatible with other cable components ;
- the absence of flooding compound ensures a very good adhesion of reinforcement yarns to the outer sheath. This also ensures a good longitudinal water tightness between the yarns and the sheath ;
- the procedure of cable ends preparation for splicing is made easier ;
- the cleaning of the tooling and cable elements is limited ;
- the manufacturing process is less risky.

Different solutions are possible for the design of a dry core structure, either using a water swellable material laid on a cable component (e.g. the core strength member, the binders used to maintain the stranded tubes...), or adding water swellable components (swellable tape, swellable binder, swellable reinforcement yarns...), or using a combination of both.

These solutions have been investigated on various cable designs, such as standard duct dielectric (metallic constructions can be considered similar) cable, either six or six plus twelve positions (fiber counts ranging from 2 to 72 in the first case, and 74 to 216 in the second), or longitudinal, corrugated steel tape armored cable designs with or without an inner protective plastic sheath. The choice of the solution has to be made case by case, considering the estimated free space inside the cable core and compared costs.

The main advantages and drawbacks of these different solutions can be summarized in table 1.

swellable element	advantages	drawbacks
swellable CSM	replaces standard CSM, limited diameter increase	higher cost
swellable binder	replaces standard binder, limited diameter increase	limited swellability may need a short pitch application accumulation of powder on machinery
swellable tape	can present a large swellability, simple to apply, can act as a thermal barrier	higher cost, non negligible diameter increase, requires removal to see ROL
swellable thread	limited diameter increase	may need a short pitch application
swellable reinforcement yarns	replaces standard yarns, limited diameter increase	higher cost
swellable powder applied on one or more cable elements	simplest solution	needs to be realized on line, complicated process

Table 1 : main advantages and drawbacks of swellable elements

Two types of solutions have been selected among these possibilities, and three trial cables have been manufactured in order to compare their effectiveness. A summary of these solutions are compared in table 2.

cable #	core design	watertightness on CSM	watertightness on core & yarns
1	1+6	adhesive (hot-melt)	swellable tape over the core
2	1+6	swellable thread	swellable binders to maintain the core
3	1+6+12	swellable thread	swellable binders to maintain the core

Table 2 : dry cable structures tested

The cables protection consists of dielectric reinforcement yarns (the cable having a water swellable tape over the core being designed with a higher content of aramid yarns) with a high or medium density polyethylene outer sheath (standard dielectric duct designs).

Cable water tightness tests

The cables water tightness has been verified according to the Bellcore GR20 specification (2) (one meter long sample, one meter tap water height), for a duration of 24 hours (aged or unaged samples) at the following stages :

- unaged ;
- after aging 14 days @ 85°C, under dry conditions ;
- after aging 14 days @ 85°C, soaked in water ;
- after aging 14 days @ 85°C, in a 100% RH environment ;
- after aging 14 days of thermal cycles (between -40 and +70°C).

The number of samples per test is 4 ; for cables aged in water and in a humid environment, two of the samples have their ends sealed.

The length of penetration of the water is measured on the cable samples after the 24 hours test, both around the CSM and over the cable core.

In addition to this some other specific tests related to longitudinal water tightness have been realized ; their description and obtained results are given in the next paragraph.

Test results and discussion

The results (average value in cm of water propagation for the four samples and number of leaks) are as shown in tables 3.1 to 3.3 for the three types of cables ; the standard deviations of the test results are low.

aging		leaks	water penetration distance
conditions	time		
initial		0/4	9.8
85°C, dry	14 days	0/4	16.3
85°C, in water	14 days	0/4	8.5
85°C, 95% RH	14 days	0/4	11.3
-40/+70 cycles	14 days	0/4	10.5

Table 3.1 : watertightness results, cable #1

aging		leaks	water penetration distance
conditions	time		
initial		0/4	30
85°C, dry	14 days	0/4	79.3
85°C, in water	14 days	0/4	69.8
85°C, 95% RH	14 days	0/4	88.3
-40/+70 cycles	14 days	0/4	25.3

Table 3.2 : watertightness results, cable #2

aging		leaks	water penetration distance
conditions	time		
initial		0/4	25.2
85°C, dry	14 days	0/4	60.8
85°C, in water	14 days	0/4	39.3
85°C, 95% RH	14 days	0/4	51.8
-40/+70 cycles	14 days	0/4	80

Table 3.3 : watertightness results, cable #3

From these results, it can be noted that :

- all designs listed above passed water penetration requirements ;
- cable design #1 presents some disadvantages in the field, in particular separating the tubes from the CSM due to the use of a hot-melt adhesive, and the additional step of removing the water swellable tape when ROL locations need to be found ;
- cable design #1 has less water penetration due to the presence of hot-melt adhesive ;
- no significant difference has been noted between sealed and non sealed samples during the aging during wet conditions ;
- the water penetration is comparable along the CSM and over the cable core (excepted for cable type #1) ;
- after 14 days @ 85°C in various environmental conditions, all cable designs tested passed the water penetration requirements.

In addition to these comparative aging tests, some additional testing has been conducted ; corresponding description and results are as follows :

- long term penetration test : a cable length type #2 has been submitted to a long term water penetration test ; after 14 days of application of the pressure, the water penetration was measured at approximately 30 cm ;
- long term aging test : a cable length type #1 has been tested for water tightness after a long term aging test of 56 days at 85°C under ambient relative humidity ; the water penetration has been found less than 15 cm after 24 hours of application of the one meter water head pressure ;
- mid span entry test : a cable length type #2 has been tested according to Bellcore GR 20 for thermal test and aging, after being submitted to a mid-span water entry ; no measurable attenuation increase has been detected in the water entry area at low temperatures ;
- chill test : a cable length type #2 has been submitted to a one meter water head pressure for one hour, and then placed in a temperature chamber at -20°C for 1 1/2 hours. The sample was then removed from the chamber and allowed to thaw for approximately 1/2 hour, and was then submitted back to a one meter water head pressure for 1 hour. The length of water penetration was measured at each step of the cycle, which was repeated for a total of 6 times. At the end of the test the water penetration was less than 30 cm.

Cable preparation ability

As already mentioned, the replacement of the filling compound between the tubes in the cable core improves significantly the process for preparing the cable before splicing, either at the cable end or for a mid-span entry.

This is particularly important for the core wrapping removal and for the time spent cleaning tubes ; this point has been emphasized through a comparative evaluation (dry core cable/filled cable) of the time needed for the cable end and mid-span entry. This evaluation has been conducted on a single layer, 72 fiber duct dielectric cable and the obtained results have been extended to a double layer 216 fiber cable (the data are measured on a dry core cable, and extrapolated to a filled core cable on the basis of the comparison made on the 72 fiber cable). It consists of measuring the time which is necessary to prepare a cable end for splicing or to proceed to a mid-span access, for a single tube entry (fibers are made accessible for one tube only) in this latter case. The cable preparation is made using the recommended tooling, and the cable length prepared is 2.5 meters ; the measured time includes the time spent for tools cleaning.

Relevant data are given in table 4, displaying the ratio between the time spent for filled cable and dry cable.

item	OF count	end access	mid-span access
total time	72	1.48	1.72
	216	1.44*	2.17*
access time	72	2.64	1.91
	216	3.33*	2.34*

* : estimated figures

**Table 4 : comparison of dry core/
filled cables entry time**

These results show that the improvement introduced by the dry core structure can be as high as 70% when considering only the access time ; this value is of course less for the total preparation time (the fibers cleaning time reducing the gains on the access time), but still averages 40%.

It has to be added to these results the fact that the limitation of the use of solvents or cleaning agents has a non negligible impact on the tooling durability (e.g. splicing machine) and on the safety and health aspects ; however the impact of these points is not easily quantifiable from a cost point of view.

In addition to this advantage in the cable preparation, the use of the ABM2 material has a significant impact on splice box design and implementation. Regarding this point, the following advantages can be noted :

- currently, the practice of using routing tubes (spiral wrap) and associated labelling is utilized in the routing

of fibers to the splice tray due to the fact that current buffer tube materials do not exhibit adequate kink resistance to withstand the tight bends required in today's small and compact enclosures. ABM2 material is capable of smaller bend diameters, therefore eliminating the practice of using closure routing tubes ; in addition, it is also more pliable, therefore minimizing the potential risk of buffer tube kinking when subjected to multiple splice tray entries. By routing ABM2 buffer tubes directly to the splice tray, tube color identification is readily apparent for future fiber splice applications. Also, by eliminating the need for closure routing tubes, ABM2 saves time and material component costs ;

- cables manufactured with ABM2 buffer tubes are easier to handle and coil, especially in confined areas such as manholes and pedestals ; on the contrary, cables using current buffer tube materials such as PBT and PBT/PC are difficult to handle and manipulate due to their stiffness ;
- due to its enhanced flexibility, ABM2 minimizes the difficulty associated with storing buffer tubes in splice enclosures with limited storage capacity and offers less resistance when storing buffer tubes in splice enclosures. In addition it does not exhibit the tendency to «spring back» like PBT and PBT/PC buffer tubes, which can lead to kinking when the buffer tubes are forced into a tight storage area inside the splice enclosure.

These advantages are mainly related to the limitation of the risks encountered when placing the tubes into the splice closure and are therefore difficult to estimate in terms of time or cost reduction, with the exception of the non-use of the spiral wraps to maintain the tubes.

Miscellaneous tests

In addition to these evaluations, other advantages of the dry core/ABM2 solution can be pointed out :

- such a cable design has successfully passed qualification tests according to the Bellcore GR 20 specification both in 96 and 216 fiber count, as summarized for example for the 216 fiber cable in table 5 ;
- as presented in a previous IWCS paper (1), the ABM2 tubes exhibit a very good behaviour in heat and humidity environments as well as a very good hydrolytic stability, which are important parameters for pedestals and enclosures environment ;
- the yarns adhesion to the outer sheath of a standard dielectric duct cable design has been measured in comparison with the filled design, according to the

test	pass/ fail	performance summary
temperature cycle	pass	max./avg. power change, 0.08/0.00 dB
heat age	pass	max./avg. power change, 0.09/0.01 dB
cable freezing	pass	max./avg. power change, 0.03/0.00 dB
impact resistance	pass	max./avg. power change, 0.00/0.00 dB
compressive strength 500 lbf	pass	max./avg. power change, 0.02/0.00 dB
after load release	pass	max./avg. power change, 0.02/0.00 dB
compressive load 600 lbf	pass	max./avg. power change, 0.08/0.02 dB
after load release	pass	max./avg. power change, 0.02/0.00 dB
cable flex	pass	max./avg. power change, 0.00/0.00 dB
hot & cold bend	pass	max./avg. power change, 0.03/0.00 dB
water penetration, unaged	pass	no drip @ 24 hours
water penetration, aged	pass	no drip @ 1 hours
twist	pass	max./avg. power change, 0.02/0.00 dB
wasp spray	pass	no tube or coating damage
Kellums grip	pass	30 min @ 1000 lbs

Table 5 : 216 fiber cable tests results

ASTM D 4565 test method ; as a result the dry core design (dielectric duct cable) showed an improvement in adhesion compared to a fully filled cable, as the result can reach several tens of daN at 20°C or 60°C, where a filled cable does not exceed 10 daN ;

- the degree of coupling between the CSM and the tubes has been also evaluated, using a tensile machine to measure the strength which is necessary to pull out the CSM from the cable core (coupling force) ; the obtained results show that the use of a dry core/ABM2 design improves the coupling force by an average factor of more than 10, as shown in table 6. The coupling length is defined as the distance required to ensure enough coupling between the CSM and the tubes.

item	coupling force lbs/20 in (N/m)	coupling length ft (m)
ABM2 tube, flooded core	16.9 (147)	10.5 (3.2)
ABM2 tube, dry core	178.2 (1562)	1 (0.3)
improvement ratio dry/filled core	10.5	10.82

Table 6 : coupling length tests results

Conclusion

The association of a loose tube design using ABM2 tube material and a dry core design brings a significant improvement to the tube stiffness, handlability, environmental properties and to the cable preparation for splicing.

In addition, without flooding compound between tubes in the cable core the internal friction coefficients are increased, which leads to a better ability of the cable to withstand installation stresses using pulling grips or intermediate caterpillars, together with a better coupling between the CSM and the tubes which limits the risks of CSM protrusion in the splice boxes due to shrinkage.

Such a design leads to a more reliable solution, with significant labor savings and better acceptance by craftsman.

References

- (1) Adams M., Holder J., McNutt C., Tatat O., Yang M., «Buffer tubes : the next generation», Proceedings of the Forty - Fourth IWCS, 1995, pp. 16 - 21.
- (2) Bellcore, «Generic Requirements for Optical Fiber and Fiber Optic Cable, GR - 20 - CORE», Issue 1, September 1994, Section 6.6.7.

Authors

Pierre Gaillard
Alcatel Cable France, STT/OFCCC
35 rue J. Jaurès BP 20 95871
Bezons cedex, FRANCE

Pierre Gaillard received his engineer degree from the Ecole Catholique des Arts et Métiers (ECAM) in 1980. He joined Alcatel Cable in 1983, where he is now working as a Project Engineer, in the Optical Fiber Cable Competence Center.



Christopher McNutt
Alcatel Telecommunications Cable
Claremont, North Carolina - USA

Christopher McNutt received his B. S. degree in Chemical Engineering from the University of Tennessee, Knoxville in 1985. After working as a Project Engineer responsible for materials development at the Alcatel Optical Fiber Cable Competence Center, he is currently a Material Development Engineer at Alcatel's Claremont facility.



Jim Holder
Alcatel Telecommunications Cable
Claremont, North Carolina - USA

Jim Holder received his B. S. degree in Mechanical Engineering Technology from the University of Dayton in 1983. He worked for 5 years as a Process Engineer at Belden Wire & Cable before joining Alcatel in 1989. At Alcatel, he has worked as a Manufacturing Engineer in both copper and fiber cable plants. He is currently a Senior Cable Development Engineer at Alcatel's Claremont facility.



André Bouvard
Alcatel Cable France
536 quai de la Loire 62225 Calais
Cedex, FRANCE

André Bouvard joined LTT in 1985, where he has been in charge successively of mechanical problems of transmission equipment, splicing and connectorization and definition of industrial processes of the Cable Division. Since the merging of LTT and Alcatel activities he is in charge of the Optical Fiber Cable manufacturing Unit of Calais.



Olivier Tatat
Alcatel Cable France, STT/OFCCC
35 rue J. Jaurès BP 20 95871
Bezons cedex, FRANCE

Olivier Tatat received his engineering degree from the Institut des Sciences de l'Ingénieur de Montpellier (ISIM) in 1982. He joined Les Câbles de Lyon, now Alcatel Cable, in 1985. Now he is working as Project Engineer, in charge of the Materials Group and the development of OPGW in the Alcatel Optical Fiber Cable Competence Center.



A New Generation Craft-Friendly Cable For Outside Environments

Clinton E. Clyburn III, Catharina L. Tedder

Siecor Corporation
Research, Development and Engineering
Hickory, NC

ABSTRACT

This paper presents the development of a new generation stranded loose tube cable employing several advances in components and design. This program was tasked with producing a craft-friendly product appropriate for extensive outdoor proliferation of optical fiber.

The ALTOS™ cable employs new ergonomic polyolefin buffer tubes that display superior performance to conventional polybutylene terephthalate (PBT) tubes in kink, strip, crush and hydrolysis testing. The cable core uses dry waterblocking technology to replace flooding compounds for water penetration protection. This allows for more efficient cable handling and increases friction between core components. A new controlled bond armor is employed for direct buried cables that guards against damage due to rodents and compressive forces and allows simple removal of the outer jacket for mid-span accesses.

All standard industry requirements were met with the ALTOS design. Additional tests to simulate field conditions were conducted to ensure durability. In all mechanical and environmental trials, the new cables performed as well as current commercial loose tube products while offering enhanced handleability.

INTRODUCTION

Initially, stranded loose tube optical fiber cables were used as the trunk or backbone of a telecommunication system. This position would take the cables from a large control area to a centrally-located dispatch location where twisted pair or coaxial cable would then transport the signals. Installation of the optical fiber cable was simple, only two ends of the cable were required for splicing and reentries/mid-span splices were not necessary.

The introduction of broadband services employing optical fiber cables has made cable splicing and termination environments more diverse in terms of hardware and procedures. As fiber proliferates through a network, splicing operations are occurring in more unusual locations. It is common now to find fiber in tight-fitting pedestal, hand-hole and aerial closures. Additional cables in a fixed space means congestion and possible frustration for the craftsman who has to maintain an orderly area.

Adding to the fieldperson's woes in this environment are kinking buffer tubes resulting from being routed too tight for the tube material. Flooding compound throughout the cable requires slow tedious cleaning and soils clothing, tools and the area slated for fiber splicing.

These changing environments are placing increased demands on field personnel and on the products with which they must work. There exists a need for an innovative stranded loose tube optical cable which provides an easier, craft friendly and efficient means of accessing the fibers and installing the cable in these tight environments.

ERGONOMIC BUFFER TUBES

Historically PBT, an engineering thermoplastic, has been the preferred material for commercially available loose tube cables. However, as fiber is moving closer to the home and into the pedestal, space constraints and harsher environments have made it necessary to utilize a more craft-friendly, durable buffer tube material.

Hydrolytic Stability

In long-haul applications, PBT is a suitable selection for buffer tubes. However, with the ever-increasing demand to transmit more information, fiber is being used in new applications where the cable will be

subjected to more diverse environments. Since these environments may include high heat with high humidity and more frequent handling, it is imperative that the buffer tube not be adversely affected by such conditions. The ALTOS buffer tube material is produced from a polypropylene copolymer containing nucleating agents to enhance material properties. This new material, unlike typical PBT, is not susceptible to hydrolysis and has excellent long-term performance¹.

Testing for hydrolytic stability was conducted as per ASTM D348 and D2105. The specification describes the procedure for buffer tube elongation testing after aging for 45 days at 85°C with 85% relative humidity. In this environment, the ALTOS buffer tube retains its unaged elongation value of 760%. Typical buffer tube materials, despite meeting an industry requirement of 10% elongation, suffer significant drops in extension due to these conditions.

It is evident that the new buffer tube is not affected by hydrolysis and will function in hot, humid environments.

Kink Resistance

The pedestal environment with its limited space often requires tight bending radii for buffer tubes. This poses a particular challenge to craft personnel. Even with careful handling, stiff tubes, when subjected to small bending radii, are prone to kinking. Kinking often results in increased attenuation and/or fiber breakage. The ALTOS cable offers an advantage with its flexible, kink-resistant buffer tubes. This material allows the buffer tubes to be easily routed into pedestals and enclosures with little concern that the tube will kink or collapse during handling.

The kink resistance of the 3.0 mm diameter ALTOS buffer tube was measured and compared to a standard 3.0 mm PBT loose tube in a Buffer Tube Loop Test². The Loop test determines the diameter and required force at which a buffer tube will kink.

Samples, 550 mm in length, were cut for testing. A loop with a diameter of 85-90 mm was formed and placed in the grips of a tensile tester. A ring at the cross-over point held the loop in place (Figure 1). The top end of the tube was pulled at 250 mm/min, decreasing the diameter of the loop until kinking occurred.

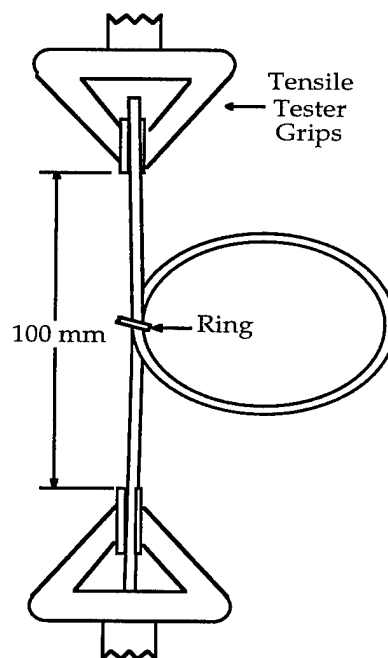


Figure 1: Buffer Tube Loop test

Kinking was determined both by visual observation and by a 10% drop in the force required to pull the buffer tube. The diameter and force at this point were recorded.

The results verify that the ALTOS buffer tube is significantly more flexible than a standard PBT tube. A 3.0 mm diameter PBT tube will kink as it reaches a loop diameter of 40 mm. The ALTOS buffer tube can be subjected to a bend diameter of 8 mm before kinking occurs (Figure 2). Also, it requires more force to induce kinking in the ALTOS tube than in the PBT tube (Figure 3). Note that the practical long-term minimum bend radius for current optical fiber is 25 mm to address stress and fatigue issues. As stronger, more bend-insensitive fiber is developed, this new tube will be able to accommodate tighter limits.

Diameter at Kink

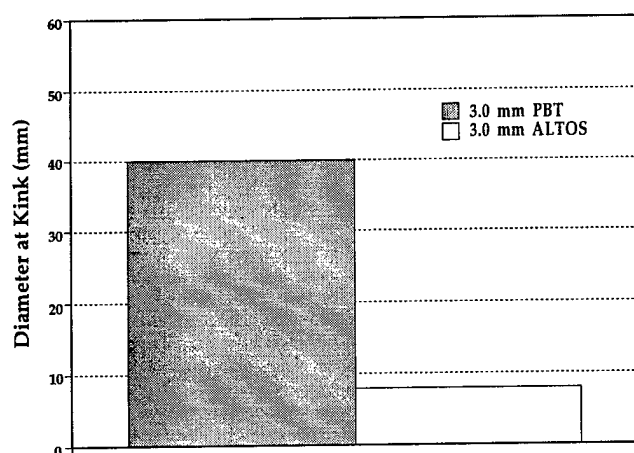


Figure 2: Diameter to kink comparison - ALTOS vs PBT

Kinking Force

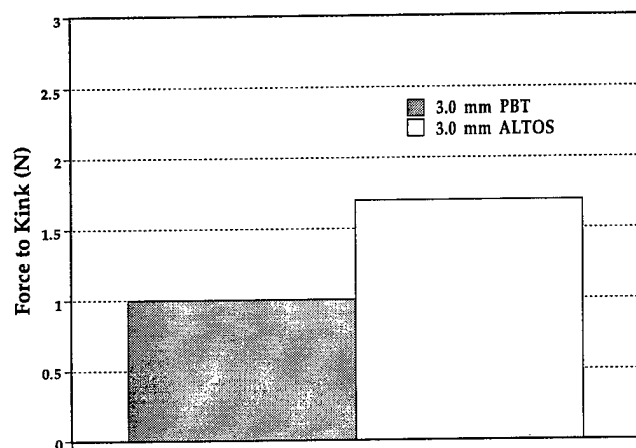


Figure 3: Force to kink comparison - ALTOS vs PBT

Further testing indicates that short term tight bending of the ALTOS buffer tube will not result in attenuation increases as seen with typical PBT tubes. Random samples were assembled of 3.0 mm diameter PBT and ALTOS buffer tubes containing 12 single-mode fibers. Power measurements of 6 fibers per tube were taken on a ten-meter section coil of buffer tube as the loop diameter was decreased. At a 40 mm loop, the onset of kink, the average PBT buffer tube had an attenuation change of 0.49 dB. As the buffer tubes kinked, there was a total loss of signal. No power returned after the PBT tubes were relaxed. Broken fibers were confirmed with post-test dissections. The average ALTOS buffer tube

showed no change at the onset of kink (8 mm) and only an 0.18 dB maximum change after the tubes were completely collapsed. Full power returned as the tubes were relaxed (Figure 4).

Kinking Attenuation

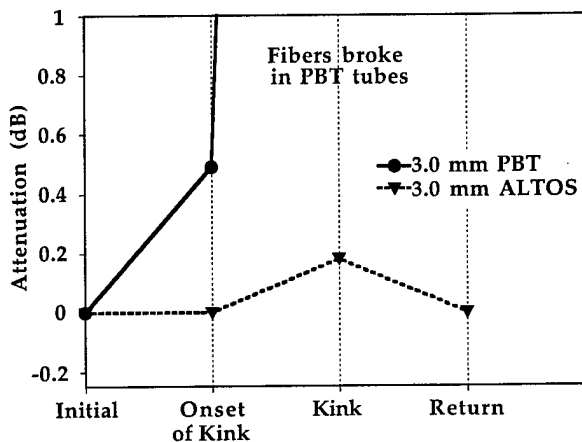


Figure 4: Attenuation of kinked buffer tubes

Fiber Accessibility

As optical fiber is deployed closer to subscribers, more cables are being reentered for fiber splicing. Therefore, it has become increasingly important that the cable components provide easy mid-span access at specified installation temperatures (-30°C to +60°C). In response to this need, the ALTOS buffer tube offers less resistance to entry compared to PBT and polycarbonate PC/PBT tubes, two common commercial buffer tube types.

A test to measure the force required for buffer tube entry was conducted with an Optical Fiber Access Tool (OFAT). The OFAT, a tool commonly used in the field by craftspeople, makes two parallel longitudinal cuts through the buffer tube wall to allow access to the fibers. Testing was conducted in an environmental chamber to provide typical field temperature extremes for installation.

A 250 mm length of tube was secured into the top grip of a tensile tester. New blades were installed and the appropriate blade depth for each buffer tube was adjusted on the OFAT. The tool, attached midway down the tube length, was secured in the bottom grip (Figure 4). Approximately 100 mm of the tube was then pulled through the OFAT at 250 mm/min. The force required to cut through the tube was recorded. The cutting force results were

compared to those of the other two buffer tube types when tested with the same procedure.

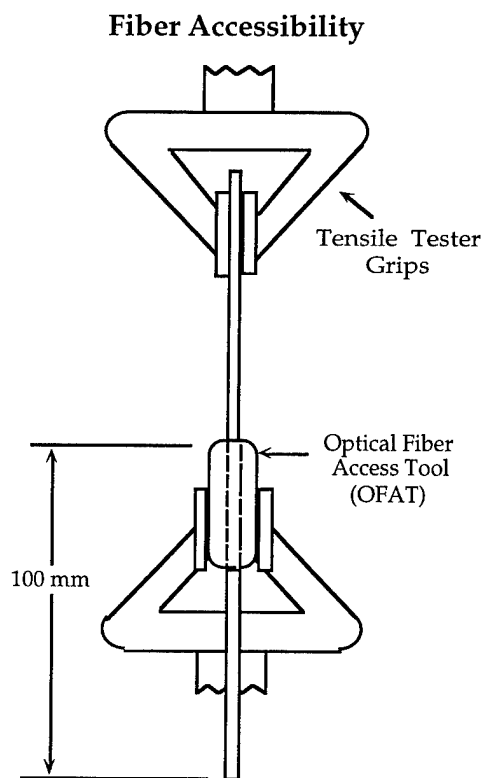


Figure 5: Fiber accessibility testing

The ALTOS tube material offers less resistance to entry than do the other commercially available buffer tubes. At all temperatures, less or comparable force was required to cut through the ALTOS buffer tube wall to gain fiber access (Figure 6). Actual field installations at sub-zero temperatures have verified the findings. At the lowest temperature extreme, the cutting force was approximately the same for all three buffer tube types.

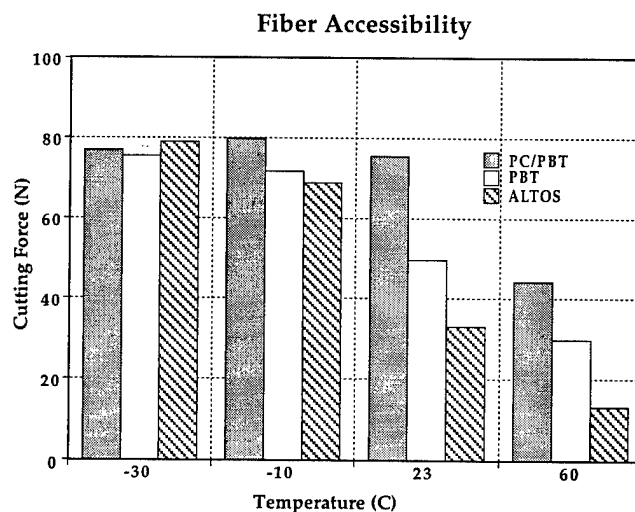


Figure 6: Comparison of forces to enter buffer tubes

Buffer Tube Crush Resistance

During installation, crushing forces are sometimes exerted on cables as they are being routed over mandrels. Although the cable design helps to insulate the buffer tubes from these forces, the buffer tube material must also be resistant to crush. This is especially true at higher installation temperatures where the plastic moduli are lower and cable components are less rigid. The ALTOS cable meets this requirement by providing buffer tubes which are more crush resistant than commercial PBT tubes at the highest typical installation temperature.

Crush resistance of the buffer tubes was determined through Lateral Crush Testing at a temperature of 60°C. Lateral crush testing of buffer tubes measures a material's resistance to diametral loading. This value is indicative of buffer tube performance in cable crush.

Samples of buffer tube, 6.0 mm in length, were cut using Ideal® coaxial cable strippers fit with two parallel blades. The fibers and filling compound were removed prior to testing. A buffer tube test sample was then placed between an upper 2 x 2 cm movable plate and a lower 10 x 10 cm stationary plate to receive a lateral compressive load perpendicular to the longitudinal axis of the tube (Figure 7). The load was applied at a speed of 1.25 mm/min until the buffer tube was 50% of its original diameter. The loads at 5% and 25% tube compressive strain were recorded in N/mm.

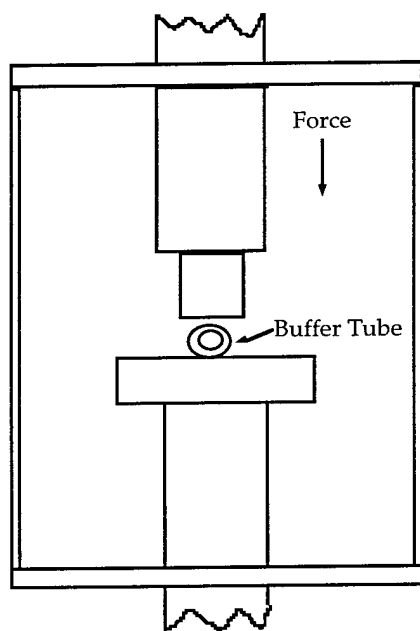


Figure 7: Test setup for buffer tube lateral crush

The ALTOS buffer tube is significantly more resistant to crushing forces at 60°C than a PBT tube, particularly at the onset. At 5% compression, the force required to deform the ALTOS buffer tube is approximately 40% greater than that for PBT (Figure 8).

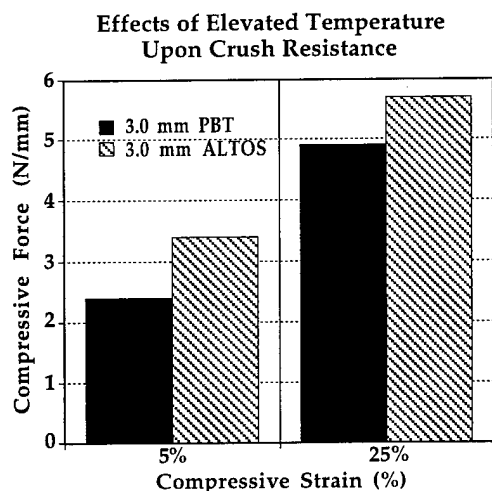


Figure 8: Tube compression force at 60°C

DRY CABLE CORE

The majority of outdoor loose-tube cables installed in the 1990's use flooding compounds through the cable core to prevent axial water migration. In the event the jacket sheath is penetrated, this grease physically stops water from entering the cable and migrating to closure electronics. Though effective, flooding compounds are subject to compatibility problems with other cable components, prone to flow and drip out of cable ends and are very labor-intensive for craft usage. These greases must be thoroughly removed with chemical solvents to ensure a clean environment for fiber splicing.

ALTOS cables employ dry waterblocking technology allowing the absence of flooding compounds in the cable core. These cabling materials contain super absorbent polymers (SAPs) that can hold up to 100x their own weight in water. Their reliability over time and appropriateness for use in outdoor environments has been documented in several studies^{3,4,5,6,7}. The waterblocking scheme is similar to that used in dry core loose tube cables introduced in 1995 (Figure 9). Similar materials were covered in publications from as early as 1988 and have been used in slotted core and single tube designs for many years without incident⁸.

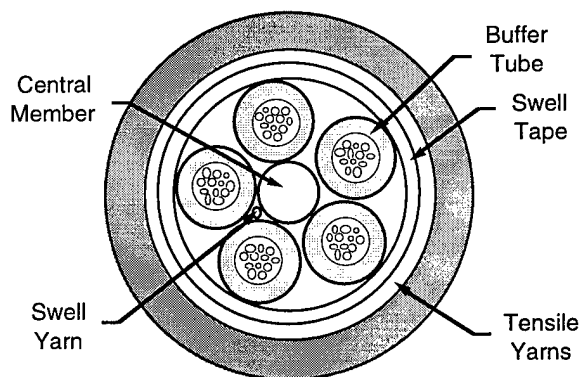


Figure 9: 5 position ALTOS dielectric cable utilizing dry waterblocking technology

Dry loose-tube cable cores provide many advantages to the end user in terms of labor savings and product quality. The waterswell materials are simply cut away to expose clean buffer tubes. Installation tools and the worksite stay clean resulting in higher productivity and worker safety. The dry cable is

lighter than its flooded counterpart meaning longer installation pulls are possible at the same rated tension load.

Standard industry termination procedures call for securing the central member and outer jacket at the cable end. Low temperature optical losses from core pistoning can effectively be avoided with this methodology. Dry core ALTOS cables further inhibit core pistoning when used in conjunction with proper recommended termination procedures.

The absence of grease in the cable core means higher friction coefficients between cable components, which results in better coupling of the strength members. Past studies have shown the coupling forces between buffer tubes and central member in dry core loose tube cables were five times higher than flooded cables⁹.

To determine the magnitude of internal friction difference between flooded and dry ALTOS cables, a test was conducted to observe core pistoning at low temperatures. Three samples of both types of cables in dielectric 5 and 24 tube position sizes were loosely coiled in 50m lengths and placed in a temperature chamber. One end of each coil was clamped to fully couple the cable components. The other end was cut flush and surfaced such that the ends of all cable components were in the same initial axial position.

The coils were then cycled 6 times between -40°C and +70°C. At the end of the last cycle, the cables were cooled to -40°C and held for 72 hours. The distance of central member pistoning out from the cable core was then measured for each sample. The average length for the dry cables was well below that of the flooded versions (Figure 10).

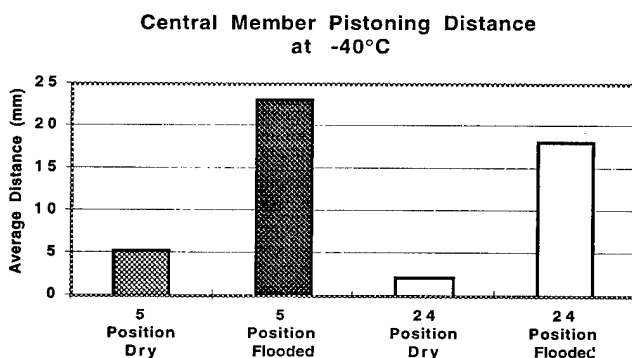


Figure 10: Comparison of Central Member Pistoning in Dry vs Flooded Cables

In loose-tube cables, the central member serves as an anti-buckling agent against cold temperature contraction of the plastics. Ideally, all components would be fully coupled and move as one unit. Unfortunately, end effects mean some degree of independence for the cable plastics. This is further promoted by the lubricity of the flooding greases. Both cable types meet industry requirements when properly terminated and the presence of a dry core does not warrant use violating recommended termination procedures. However the ALTOS dry core provides more friction and higher coupling as seen above.

EASY ACCESS ARMOR

Cables are subject to gnawing and crushing forces by pocket gophers and other rodents desiring to keep their incisors in check^{10,11}. This has necessitated the use of metal armor to protect the cable core. Many armored cable designs commercially available employ an overlapping corrugated metal shield with an unsoldered horizontal seam. If the gopher can get its teeth under this overlap, it is possible to pry open the armor shield and access the buffer tubes.

Most armor tapes employ a laminate coating over the metal which protects the steel from corrosion and bonds the armor to the extruded polyethylene jacket. This makes removal of the outer jacket from the armor extremely difficult during midspan access operations.

The ALTOS armored cable utilizes a proprietary coating treatment on the protective metal tape (Figure 11). This coating allows the horizontal overlap to be sealed, reducing the potential of the rodent from finding an edge to pry open the armor tape. However, this seam can be separated with the twisting force of a craftsman's knife.

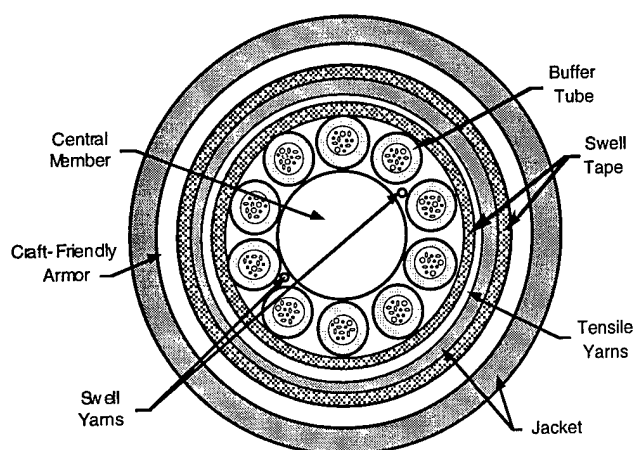


Figure 11: ALTOS 10 position armor cable

The major benefit of this new armor is the controlled bond between the outer jacket and the armor. Field surveys were conducted with armor tapes having several different levels of bond strengths to determine a craft-friendly product. Once a maximum ergonomic level of bond strength was determined from the survey, the ALTOS armor was tailored to consistently separate below that force (Figure 12). The bond does however, meet industry requirements for cable jacket adherence as measured forces are over 30 N/mm when tested in accordance to Section 31 of ASTM D 4565.

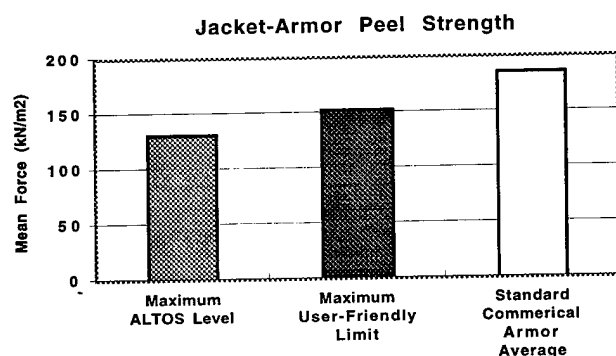


Figure 12: Comparison of Jacket-Armor Peel Strengths from Field Survey

To highlight the value of the removable jacket feature, an efficiency test between standard armor and ALTOS armored cables was conducted with field personnel to expose the cable core in a midspan access operation. Using identical cables (6 buffer tubes) and facilities, 10 cm of outer jacket was removed from the armor in each test and times were recorded. The average time of three craft personnel to remove the standard tightly-bonded jackets was 7:45 minutes. The average time for the ALTOS cables was 1:20

minutes. The standard jacket was consistently ripped in several pieces while the ALTOS jackets peeled off in one piece.

This new armor facilitates midspan entries and allows quick separation of the jacket from the armor to install grounding clips.

CABLE PERFORMANCE: INDUSTRY TESTING REQUIREMENTS

ALTOS cables were produced in dielectric and armored family constructions with a variety of fiber counts between 36 and 288. Dielectric and armored cables were manufactured and tested to different optical, mechanical and environmental industry requirements. Cables contained dispersion-unshifted single-mode fibers. Tests were chosen to subject the cable to rigors beyond what would be found under typical use. Environmental tests for both dielectric and armored ALTOS cables are shown in Table 1. Attenuation results include a 0.05 dB or 0.05 dB/km allowance for measurement repeatability.

Test	Results	Method
Temperature Cycling* (-40° to +70°C, 4 cycles)	Average $\Delta \leq 0.05$ dB/km Maximum $\Delta \leq 0.15$ dB/km	FOTP-3
Cable Aging* (85°C, 168 hours)	Average $\Delta \leq 0.10$ dB/km Maximum $\Delta \leq 0.25$ dB/km	FOTP-3
Cable Freezing*	Average $\Delta \leq 0.05$ dB/km Maximum $\Delta \leq 0.15$ dB/km	FOTP-98
Cable Shrinkage*	90% of fibers ≤ 0.10 dB Δ Remaining 10% ≤ 0.30 dB Δ	GR-20 6.4.4
Water Penetration	No water leakage (1m/1m: 24 hours-unaged, 1 hour-aged 168 hr @ 85°C)	FOTP-82
Lightning Damage	105 kA	FOTP-181
Resistance to Fungus Growth	Grade 0 - 0% growth	ASTM G-21
Filling Compound Flow (80°C)	No compound flow	FOTP-81
Material Compatibility	Buffer tube elongation $\geq 10\%$ (45 days in 85°C water)	ASTM D2105

* Note: Attenuation measurements at 1550 nm

Table 1: Environmental test results of ALTOS cables

Through the rigors of temperature extremes and other environmental punishments, the ALTOS cable met major industry performance requirements.

Armored and dielectric ALTOS cables were extensively tested to various mechanical requirements. The results are shown in Table 2. Attenuation results include a 0.05 dB or 0.05 dB/km allowance for measurement repeatability. Again, all major performance levels were met. Dynamic properties of the cable as observed in impact, cyclic flex and twist were exceptional. Static properties were also reinforced not only by the aforementioned gains from a dry core, but also by new modeling techniques with the ALTOS construction. Integrating cabled material properties versus raw material specifications into cable service simulations allowed the designs to be tailored for specific strengths.

Test	Results*	Method
High Temperature Bend (60°C, 4 turns)	90% of fibers ≤ 0.05 dB Δ Remaining 10% of fibers ≤ 0.15 dB Δ	FOTP-37
Low Temperature Bend (-30°C, 4 turns)	90% of fibers ≤ 0.05 dB Δ Remaining 10% of fibers ≤ 0.15 dB Δ	FOTP-37
Impact (25 cycles)	90% of fibers ≤ 0.05 dB Δ Remaining 10% of fibers ≤ 0.15 dB Δ	FOTP-25
Compression (440 N/cm)	90% of fibers ≤ 0.05 dB Δ Remaining 10% of fibers ≤ 0.15 dB Δ	FOTP-41
Tensile Strength (2700 N)	90% of fibers ≤ 0.05 dB Δ Remaining 10% of fibers ≤ 0.15 dB Δ	FOTP-33
Cable Twist (2m - 2 twists)	90% of fibers ≤ 0.05 dB Δ Remaining 10% of fibers ≤ 0.15 dB Δ	FOTP-85
Cyclic Flex (25 cycles)	90% of fibers ≤ 0.05 dB Δ Remaining 10% of fibers ≤ 0.15 dB Δ	FOTP-104
Cable Jacket Adherence	≥ 14 N/mm force to initiate slippage: jacket/armour	ASTM D4565-S31

* Note: Attenuation measurements at 1550 nm

Table 2: Mechanical test results of ALTOS cables

LONG TERM EXPOSURE TO WATER WITH JACKET BREACH

A possible scenario may be for an outdoor cable with a jacket breach to lie continuously under groundwater for years without detection. The question raised from this situation is whether optical performance of the cable is degraded at temperature extremes as a result of swelled SAP being inside the cable core.

Previous studies have been conducted with slotted core optical fiber cables whose core has been wetted to swell the dry waterblocking materials^{3,12}. Artificial seawater was used as the wetting medium and the cables were subjected to -30°C while monitoring attenuation. No loss increase was noted.

In order to simulate a real field scenario, a section of a 60 dispersion-unshifted single-mode fiber ALTOS dielectric cable was immersed in a tank containing tap water one meter in depth (Figure 13). The jacket of the cable section under the water was breached with a 1x2 cm section removed. The tank was placed in a temperature chamber and cycled 50 times between -40°C and +85°C. Transmitted power was continuously monitored at 1240, 1310, 1550 and 1650nm.

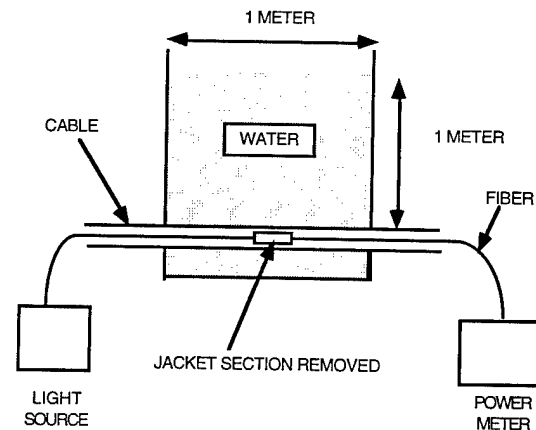


Figure 13: Test setup for submerged breached cable cycling

The results for the maximum attenuation change at 1240 and 1550 nm of 24 monitored fibers are displayed in Figure 14. Each cycling number represents a power measurement at a temperature extreme. No significant change outside of a measurement variability of 0.05 dB was observed. Despite an industry position that hydrogen generation is not an issue with terrestrial cables, note a lack of change at 1240 nm. This reinforces the

idea that swelled waterblocking material does not promote hydrogen. It is thus confirmed that ALTOS cables have stable performance even if water is absorbed in the field without detection.

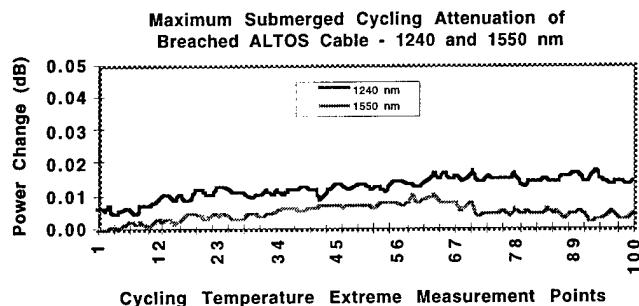


Figure 14: Attenuation change for submerged breached cable cycling test

INSTALLATION TRIALS

A comparison test of installation ease between ALTOS and typical commercial loose tube cables was conducted at Siecor Corporation's Installation Test Facility. Dielectric and armored cables representing a range of fiber counts were installed using air-jetting methods.

A technical duct system route containing several 90° and 180° bends along with multiple elevation changes was selected. A variety of duct diameters and types were used. Comparable cables based on fiber count were tested in tandem to discount temperature effects. All trials utilized duct lubricant.

In all comparisons, the ALTOS cables jetted further than their commercial counterparts. Typical distance increases depended on cable size and duct diameter. Other ALTOS cables permanently placed for long term testing showed no adverse effects on optical performance as a result of installation.

CONCLUSIONS

This paper presents the results of a cable development program designed to expand the benefits of using loose tube cable outdoors. Every facet of the cable design was examined to improve craft efficiency and cable longevity.

ALTOS buffer tubes display superior performance to

typical commercial tubes both in ergonomics and in protection for the fibers. ALTOS tubes are very resistant to kinking, possess improved crush strength and are hydrolytically stable.

The ALTOS cable design is characterized by several improvements over typical loose tube cable offerings. The cable core employs dry waterblocking technology which eliminates the need for flooding greases. Not only does this make the cable craft-friendly for installations, but mechanical properties are improved as the dry core increases coupling between the cable components.

ALTOS armor cables utilize an easily accessible metal shielding that permits craft efficiency in mid-span entries. The outer jacket can be removed from the armor using typical entry techniques with little effort. Stripping trials showed the removal of the ALTOS armor jacket to be faster than standard bonded jackets. The armor tape overlap is sealed to protect against rodents yet can be quickly opened with a standard straight blade cable knife.

The ALTOS cable meets industry requirements for outdoor use. Additional tests were conducted to verify the stalwartness of the design. Cables with breached jackets were temperature cycled while submerged under water. No degradation of optical performance was observed. Cables were air jetted through technical duct systems with distances exceeding that of comparable current loose tube cables.

The ALTOS cable addresses the needs of the end user for the next step in the propagation of fiber optics throughout the telecommunications world. Robustness, reliability and craft-efficiency are delivered in a loose tube package utilizing advances in cabling technology.

ACKNOWLEDGEMENTS

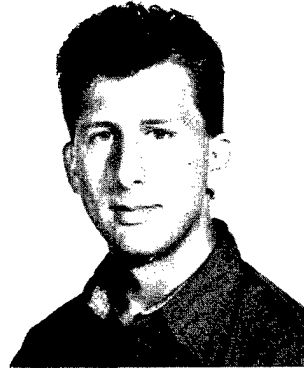
The authors wish to thank everyone involved in the development of the ALTOS cable. Special thanks go out to Larry Barrett, Jason Lail and Eric Caldwell for their hard work in obtaining results for this paper, Don Parris for early work in the program and kudos to Siecor management for the freedom to explore.

REFERENCES

- [1] G. Griswold: "Developing Optimal Processing of Hydrolytically Stabilized PBT for Fiber Optic Cable Core Components", Proceedings of the 42nd International Wire and Cable Symposium, pp. 48 - 55, 1993.
- [2] D. Parris and B. Warner: "Testing of Fiber Optic Cable Core Materials After Accelerated Heat and Humidity Aging", Proceedings of the 39th International Wire and Cable Symposium, pp. 237 - 242, 1990.
- [3] K. Hogari and F. Ashiya: "A Water-Blocking Optical Fiber Cable System Employing Water Absorbent Materials", Proceedings of the American Chemical Society Division of Polymeric Materials - Science and Engineering, Vol. 69, pp. 565 - 568, 1993.
- [4] M. Fukuma, N. Akasaka, S. Suzuki: "Dry Type Water-Blocking Optical Fiber Tape Cable with Slotted Rod", Proceedings of the 36th International Wire and Cable Symposium, pp. 350-356, 1987.
- [5] H. Hiramatsu, N. Ishii and K. Nagai, "Development of Dry-Type Water-Blocking Optical Fiber Cable Using Swelling Material", Proceedings of the 38th International Wire and Cable Symposium, pp. 463-467, 1989.
- [6] A. Bringuier and C. Clyburn III: "Development of a Loose Tube Cable With Non-Flooded Core For Outdoor Plant Environment", Proceedings of the Eleventh Annual National Fiber Optic Engineers Conference, pp. 376 - 386, June 1995.
- [7] C. Clyburn III and A. Bringuier: "A Dry Core Loose Tube Cable for Outside Environments", Proceedings of the 44th International Wire and Cable Symposium, pp. 29 - 36, 1995.
- [8] R. Gravely III and S. Stokes: "An Improved Loose Tube Cable with Dry Water Blocking Elements", Proceedings of the Eleventh Annual National Fiber Optic Engineers Conference, pp. 367 - 375, June 1995.
- [9] P. Patel, M. Reynolds, M. Kinard and A. Panuska: "LXE - A Fiber Optic Cable Sheath Family With Enhanced Fiber Access", Proceedings of the 38th International Wire and Cable Symposium, pp. 72 - 78, 1988.
- [10] G. McCann: "A Method for Evaluating Cable Resistance to Damage by Pocket Gophers as Adopted by the USDA/APHIS/ADC/DWRC", Proceedings of the 44th International Wire and Cable Symposium, pp. 604 - 606, 1995.
- [11] R. Connolly and R. Landstrom: "Gopher Damage to Buried Cable Materials", Materials Research and Standards, MTRSA, Vol. 9, No. 12, pp. 13 -

16, December 1969.

- [12] M. Kawase, "Reliability of Waterproof Optical Fiber Cables", Proceedings of the 42nd International Wire and Cable Symposium, pp. 637 - 644, 1992.



Clinton E. Clyburn III
Siecor Corporation
PO Box 489
Hickory, NC 28603
USA

Clinton E. Clyburn III (Kip) received a B.S. degree in Mechanical Engineering in 1991 and a M.S. in Materials Engineering in 1993 from North Carolina State University. Having earlier service with Raychem Corporation and Alcatel Cable Systems, he joined Siecor Corporation in 1993. He has worked with a variety of design and development projects in cables, materials and testing as well as cable characterization. Kip currently serves as a Product Development Engineer in the Research, Development and Engineering Department.



Catharina L. Tedder
Siecor Corporation
PO Box 489
Hickory, NC 28603
USA

Catharina L. Tedder (Kitty) is currently a Materials Engineer in the Research, Development, and Engineering Department with Siecor Corporation. Since joining Siecor in 1982, she has been active in the development, selection and testing of materials for fiber optic telecommunication cables. She is a graduate from Catawba Valley Community College in Mechanical Engineering Technology.

DEVELOPMENT OF A RISER RATED INDOOR / OUTDOOR LOOSE TUBE FIBER OPTIC CABLE

Scott M. Chastain and James W. Thornton

AT&T Fitel, Carrollton Georgia

ABSTRACT

Fiber optic cables today are being installed in a wide variety of environments. Multiple building networks such as campus environments currently use both outside plant cables and indoor loose tube cables. A new dual purpose cable has been developed for both applications that can reduce terminations and their associated costs.

When designing an indoor/outdoor loose tube cable there are several issues that need to be addressed. First, the jacket of an indoor/outdoor cable must be flame retardant as well as environmentally stable. Also, flooding compounds are often flammable so alternative means of water blocking are necessary. It is also important to consider the flame retardant system and its combustion byproducts.

An indoor/outdoor riser rated cable must be evaluated for both environments. It must undergo riser testing as well as full outside plant cable testing. An indoor/outdoor cable has been designed utilizing a non-halogen polyolefin jacket and dry core technology. The cable satisfies requirements for use in both environments.

Introduction

When designing an indoor/outdoor loose tube fiber optic cable the requirements for both environments must be taken into consideration. The cable should be designed to meet outdoor requirements such as Bellcore GR-20-CORE and RUS-PE90, as well as indoor requirements such as Bellcore GR-409-CORE and applicable NEC codes. Since the outdoor mechanical and environmental requirements are generally more stringent, an indoor/outdoor cable should be tested to meet these standards. Indoor/outdoor cables should perform between -40 °C and +70 °C with no significant attenuation change. The National Electrical Code specifies an indoor riser cable must receive an OFNR rating, and to

receive this rating, the cable must be tested per UL1666. In order to meet UL1666, the maximum flame height shall not reach 12'0" and the maximum temperature rise at twelve feet must not exceed 850 °F(454 °C).

In general, polyethylene jacket compounds are used in the outside plant environment while PVC is traditionally used in riser applications. When choosing a jacket material for an indoor/outdoor cable, the material needs to have the following key characteristics: flame resistance (UL1666), resistance to brittleness at low temperature (-30°C), and UV resistance. Standard polyethylene materials do not perform well during a flame retardant test, while PVC jackets typically do not perform well in the outside plant environment.

Most outside plant cables use petroleum based flooding compounds in the core. These compounds are flammable, so alternative methods of water blocking must be considered. A dry core system using super absorbent polymer (SAP) materials can prevent water migration in loose tube cables. The dry core materials must be reliable and not hinder flame resistance.

Cable Design

Jacket Materials

Two potential jacket materials were considered for the indoor/outdoor cable design: a low smoke poly-vinyl chloride and a non-halogen flame retardant polyolefin.

Poly-vinyl chloride (PVC). Poly-vinyl chloride is widely used and accepted for indoor applications. PVC provides good flame retardance and PVC jacketed cables meet all requirements set forth in the National Electrical Code. However, PVC is a halogen material, and there are growing concerns about the toxicity and corrosivity of its combustion products. PVC can be modified with additives to increase

mechanical, environmental, and thermal performance.

Perhaps the most significant of these enhancements has been the development of a low smoke resin. It is known that the single greatest hazard to personnel and equipment during a fire is smoke.¹ Low smoke PVC can be used to improve the performance of cables for riser spaces, but the material still relies on its halogen content to be effective.

Polyolefins. Polyolefin jacket materials such as polyethylene are accepted industry wide for the outside plant environment. They are economical and offer a good balance of mechanical and thermal properties.

The polyolefins currently being used for outdoor cables are not flame retardant, but flame retardant polyolefin grades have been available for quite some time. The earliest flame retardant polyolefins utilized antimony oxide (a halogen additive) synergist technology, but since the early 1970's non-halogen grades have been commercially available.² These resin blends use metal hydrates to create a non-halogen flame retardant.

Flame Retardant Mechanisms

PVC and non-halogen polyolefins employ different methods to be flame retardant. It is important to consider these differences when developing a flame retardant system for an indoor/outdoor cable.

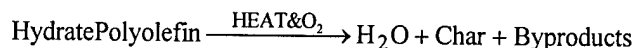
Poly-vinyl chloride. PVC is an effective flame retardant polymer. During combustion, halogenized materials burn out quickly. The sheath materials performance stems from its ability to rapidly lose mass and liberate less heat as flame exposure continues.³ In losing mass, hydrogen chloride gas is generated as follows:



The combustion byproducts may also include CO₂, CO, and H₂O. The char generated is acidic. Additives such as CaCO₃ may be used as a hydrogen chloride acceptor to reduce HCl emissions, but in so doing the flame retardance is reduced. This leads to the fact that the flame

retardance of PVC is directly related to the gaseous HCl.

Halogen Free Polyolefins. Metal hydroxides are commonly incorporated to create a non-halogen polyolefin material. When subjected to elevated temperatures metal hydroxides generate water. The associated reaction is as follows:



The char generated is neutral or slightly basic and other byproducts may include CO₂, CO, and H₂O.

Whereas PVC requires the rapid loss of mass to be effective, non-halogen polyolefins rely on retaining their mass.³ The carbonized char generated and the endothermic dehydration both affect sheath performance. The resins have similar traits to standard polyethylenes while also achieving flame retardant performance equal to or greater than PVC.

Outdoor cables are rated for installation at temperatures as low as -30 °C. In virgin form, most PVC's do not perform as well as polyolefins at low temperatures. In particular, the impact strength of common PVC is greatly reduced at low temperature and this could cause reduced performance in the outside plant environment.

A Flame Retardant System

It is important to understand the mechanisms of PVC and non-halogen polyolefins. In the wire and cable industry many designs utilize flame barrier tapes which work in conjunction with the jacket material to form the sheath system. A change in the jacket requires the reevaluation of the system.

Poly-vinyl chloride jackets historically have used polyimide tapes in the sheath, particularly for large fiber optic cables. Since PVC relies on loss of mass to be effective, it may be susceptible to jacket breaches that would expose the cable core. The polyimide has an extremely high degradation temperature and encapsulates the core to prevent ignition.

Since non-halogen polyolefins work differently, the use of flame barrier tapes such as polyimide films must be explored. Non-halogens partially rely on char, but the endothermic release of water is more important. It is critical that the heat generated in the core be able to transfer energy to the jacket. The dielectric materials used in fiber optic cables are poor conductors and in some instances the use of flame barrier tapes hinder sheath performance by "trapping" heat energy inside the core. A flame retardant sheath system may incorporate a range of jacket materials and/or flame barrier tapes.

PVC or a flame retardant polyolefin can be used to design a flame retardant sheath system, but because it is a non-halogen and offers improved performance at low temperature, a flame retardant polyolefin jacket compound is chosen for the indoor/outdoor application.

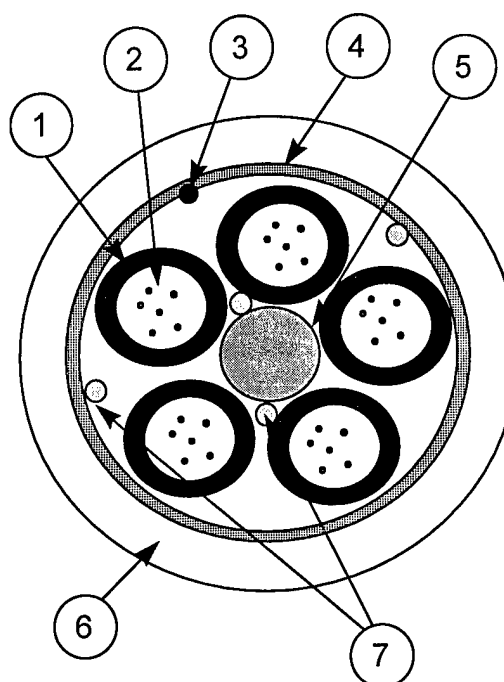
The Core

Outdoor cables commonly use a petroleum based flooding compound to prevent water migration axially down the cable. These compounds are flammable, so alternate water blocking measures must be used.

Non-flooded cable designs are being introduced industry wide. Water swellable tapes and yarns are commonly employed to dry block cables, but the new designs utilize water blocking threads to block the loose tube cable. (See Figure 1) Work has been done to develop this type of water blocking system.⁵ Water blocking elements incorporate polyacrylate superabsorbent powders that swell to many times their original volume when exposed to water. They are applied over the central member and core to water block the cable.

Cable Performance

Cables performed exceptionally well during mechanical and environmental tests with no evidence of mechanical weakness or attenuation increase. The indoor/outdoor cable was tested per GR-20 Issue 1, RUS-PE90, and GR-409 Issue 1.



- | | |
|--------------------|-------------------------------|
| 1 : Buffer Tubes | 5 : Central Strength Rod |
| 2 : Optical Fibers | 6 : Fire retardant Polyolefin |
| 3 : Ripcord | 7 : Super Absorbent Threads |
| 4 : Aramid Yarn | |

Figure 1: Indoor/outdoor Cable

Mechanical Testing

The mechanical testing results of a non-halogen jacketed indoor/outdoor cable are summarized in table 1.

Test Performed	Performance	Test Procedure
Low/High temp	-30 C to +60 C,	FOTP-37
Bend	No Attenuation Change	
Impact	25 impacts, 5 kg mass	FOTP-25
Resistance	No Attenuation Change	
Compressive	220 N/cm, avg.	FOTP-41
Strength	No Attenuation Change	
Cable Twist	10 cycles, L=1.7 m,	FOTP-85
	No Attenuation Change	
	No damage.	
Cyclic Flex	100 cycles, 230 mm,	FOTP-104
	No Attenuation Change	
Cable Tensile	@ 600 lbs, max.	FOTP-33
Test	No Attenuation Change	
Cold Impact	8 N.m, -40°C	RUS PE90
	no damage	

Table 1 - Mechanical Test Results

Cold Impact Testing. To test for low temperature brittleness, samples of both PVC and flame retardant polyolefin jacketed cables were tested for impact resistance at -10 °C, -20 °C, -30 °C, and -40 °C.

The PVC resin used was a commercially available low smoke wire and cable compound. Both types of cable samples were subjected to 4, 6, and 8 N•m impact energies. The flame retardant polyolefin samples showed no damage at any condition for a minimum of twenty impacts. The low smoke PVC jacketed samples showed cracking with as few as two impacts at all conditions tested. One foot samples were also dropped from a height of four feet onto a concrete slab and the PVC jackets cracked at temperatures as high as -20 °C.

Environmental Testing

The environmental results of a non-halogen jacketed indoor/outdoor cable are summarized in table 2.

Test Performed	Performance	Test Procedure
Temp.	Temp -40 +70	FOTP-3
Cycling @ 1550 nm	Requirement: Avg. <0.05 dB Measured: 100% < 0.05 dB	
Cable Aging (7 days, 85°C)	Temp -40 +70 Requirement Avg. <0.10 dB Measured: 100% < 0.05 dB	Bellcore GR-20, Issue 1
Water Penetration	Unaged: 1 meter/24 hrs. Pass Aged: 1 meter/1 hour Pass	FOTP-82
Cable Freeze	-2°C for 24 hrs. No Attenuation Change	FOTP-98

Table 2 - Environmental Test Results

Water Penetration. When water enters the cable, the superabsorbent materials swell and form a gel. During qualification testing all of the cable samples passed unaged and aged water penetration tests per FOTP-82. A one meter static head of water solution was applied to one end of one meter samples for 24 hours. The water solution contained 0.2 grams of sodium fluorescein per liter of tap water.

Sodium fluorescein dye was observed in testing to have an adverse effect on the swell potential of super absorbent polymers, which is consistent with previous results.⁴ Even large dual layer designs can be blocked using sufficient SAP loading. During qualification, all of the water

penetration testing was accomplished with ionic water solutions. After testing, the samples were dissected and the length of water ingress was examined with an ultraviolet light source. In addition, samples were tested during thermal cycling using the method developed by Thornton, et al.⁵ Results are presented in figure 2. This test simulates the long term reliability of loose tube fiber optic cables after a jacket breach.

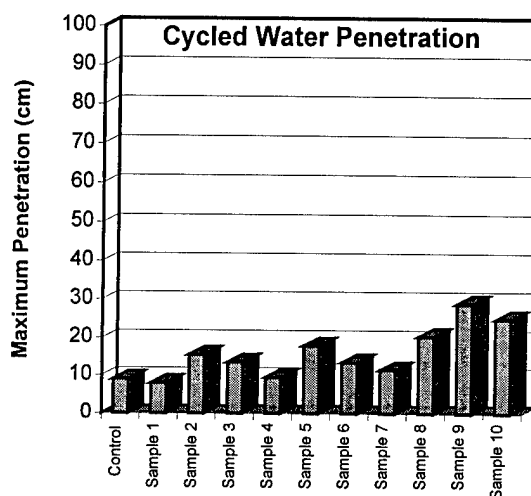


Figure 2: Water Penetration Results

Flame Testing

The potential cable designs were tested for flame resistance per UL1666. Cable designs using both PVC and non-halogen polyolefin jackets were tested. The results are graphically illustrated in figure 3.

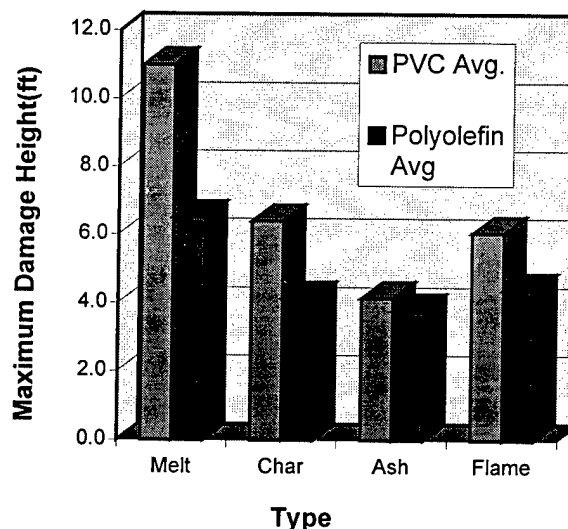


Figure 3: Cable Damage per UL1666

None of the cables tested exceeded the allowable twelve feet for maximum flame height. The maximum temperatures reached during the tests were 459 °F(237 °C) for PVC and 447 °F (230 °C) for polyolefin.

Conclusions

Poly-vinyl chlorides and polyolefins can be used for wire and cable jacketing compounds, and both were considered for use in the indoor/outdoor application. PVC is a good flame retardant and is used for numerous indoor applications, but it is a halogen flame retardant and some low smoke grades do not perform as well as hydrate type flame retardant polyolefins at low temperatures.

The cable that is developed for use in both the outside plant and riser environment utilizes a dry core technology and a non-halogen polyolefin jacket material. This cable was tested for all the industry accepted test requirements such as Bellcore's GR-20 CORE, RUS-PE90, and indoor riser requirements of UL 1666. It met or exceeded all requirements.

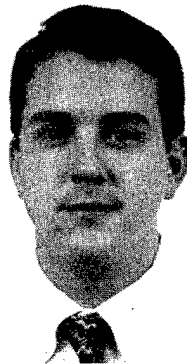
¹ National Fire Protection Association, Board of Directors Report, December 3, 1982.

² Keogh, M.J., et al., "Polyolefin Resin Blends and Additive Technology: Advanced Non-halogen Flame Retardant Compounds", *Proceedings Fire Retardant Chemicals Association*, March 1991.

³ Kanemitsuya, K., "Recent Characteristics of Halogen Free Flame Retardant Materials for Wires and Cables", *Recent Advances in Flame Retardancy of Polymeric Materials*, Volume II, 1991.

⁴ Clyburn III, C. and Bringuier, A., "A Dry Core Loose Tube Cable for Outside Environments", *Proceedings of the International Wire and Cable Symposium*, 1995.

⁵ Thornton, J.W., Chastain, S.M., and Motz, S.D., "Materials, Development, and Field Trials of a Dry Core Cable", *Proceedings of the National Fiber Optics Engineering Conference*, 1996.



Scott M. Chastain
201 Adamson Industrial Blvd.
Carrollton, Georgia 30117

As the materials engineer in the research and development group, Scott Chastain is responsible for the development and qualification of new materials. He received his Bachelor of Materials Engineering from The Georgia Institute of Technology in 1995 and is a member of ASM International.



James W. Thornton
201 Adamson Industrial Blvd.
Carrollton, Georgia 30117

James Thornton holds the position of Design Engineer in the R&D Department at AT&T Fitel Company. He received his Bachelor's degree in Mechanical Engineering in 1995 from the Georgia Institute of Technology. Since joining the company, he has been responsible for the development of Fiber Optic Cable. Mr. Thornton is a member of the American Society of Mechanical Engineers (ASME).

A 1-mm^φ MINIATURE OPTICAL FIBER CORD ADAPTABLE FOR MU-TYPE CONNECTORS

Makoto Sato, Masao Tachikura[†], Nobuo Tomita[†] and Shin'ichi Iwano

NTT Opto-electronics Laboratories and NTT Access Network Systems Laboratories[†]

Tokai-mura, Ibaraki-ken, Japan

ABSTRACT

Since we will have to deal with a large number of fibers in Central Offices in FTTH (Fiber to the Home) systems, the size of the optical fiber cord used for intra-office optical wiring must be reduced to eliminate congestion. This paper describes design concepts for reducing the size of optical fiber cord; increasing volume packing ratio of strength member yarn, utilizing a high-strength yarn, PBO yarn, and utilizing high-strength optical fibers. We also discuss the adaptability of cord to the MU-type connectors in the sense of eliminating fiber buckling in the connector caused by ceramic ferrule movement. The performance of a prototype cord with a 1-mm outer diameter satisfies the usual optical and mechanical requirements.

INTRODUCTION

The size of optical devices used for intra-office optical wiring must be reduced to eliminate congestion, because more than tens of thousands of fibers will terminate at each Central Office in the FTTH system. In particular an optical fiber cord must be developed with a diameter of less than 2 mm, which is currently the smallest available. Recently a high performance 1.6-mm cord (Minicord) was reported for this purpose.¹ This 1.6-mm cord design is based on the conventional designs and contains a 0.9-mm nylon buffered fiber.

We are now designing a high density fiber termination module (FTM) that holds several thousand fiber terminations. Thus we have

assumed a cord reduction factor of four, which means a 1-mm outer diameter cord. Therefore, we must utilize a buffered fiber with a smaller diameter and reduce strength member yarn volume without sacrificing the tensile strength. Furthermore because we plan to adopt the MU-type miniature optical connector² in the FTM, the cord must have a loose structure, that is, the buffered fiber should move within the cord sheath without buckling. The new cord must meet the same mechanical and optical requirements as those for the 2-mm cord with one fourth the cross section. Thus new design concepts had to be formulated.

This paper describes the design concepts to achieve a 1-mm outer diameter optical fiber cord adaptable for MU-type connectors, and we describe the performance of a prototype cord.

REQUIREMENTS

There is no significant alteration in cord usage, and thus the required mechanical and optical properties are the same as those for conventional 2-mm cords. Therefore, the tension should be more than 10 kgf (98 N) at 0.5 % fiber elongation,³ and the optical transmission loss of the cord must be less than 0.28 dB/km at 1.55 μ m. The transmission loss increase must be less than 0.1 dB at 1.55 μ m both in a crush test of 100 kgf (980 N) on 100 mm and in a temperature cycle test between -10 °C and +40 °C.

Since a miniature cord outer sheath is not thick enough to protect the inner buffered fiber, the mechanical performances above must be for the

buffered fiber itself. Therefore, a 0.25-mm UV-coated fiber is not sufficient, and we must adopt a thicker UV-coated fiber. Instead, there may be another approach: adopting a thicker and harder sheath and a 0.25-mm coated fiber. However, the flexural rigidity of a 0.25-mm coated fiber is not high enough to prevent fiber buckling in an MU-type connector. This is of course related to the sliding friction inside the sheath. We discuss the optimum relationship between the flexural rigidity and the sliding friction in the next section.

DESIGN

Loose condition

In MU-type connectors and SC connectors the ceramic ferrule moves back for about 1 mm at most with respect to the body of the connector. Therefore the buffered fiber fixed to the ferrule is pushed into the cord sheath fixed to the connector body. This sliding of the buffered fiber does not always spread throughout the cord. Because the winding of the buffered fiber absorbs the displacement in the cord sheath, the span where the winding occurs is limited near the connector. As shown in Fig. 1, the buffered fiber in the connector body is free. Thus we must design a pushing force that is less than the critical buckling force. Otherwise there will be sharp bend in the buffered fiber that can cause the fiber to break.

Now we consider the model of a winding buffered fiber within the cord sheath. To simplify, we assume a rigid pipe as the cord sheath, and a spiral form of the winding buffered fiber. At a distance of x from the sheath end the element of the buffered fiber of dx in length is pushed from the left with force $P(x)$ and from the right with force $P(x+dx)$. It is also pushed from the wall of the sheath with a friction force $f(x)dx$, where $f(x)$ is the friction force per unit length. In an equilibrium state, these forces are balanced.

$$\frac{dP}{dx} = -f \quad (1)$$

When the fiber is pushed back into the sheath, the friction force f is the maximum statistic friction force f_M . Therefore the pushing force P is

$$P = P_0 - f_M x, \quad (2)$$

where P_0 is the pushing force at the sheath end. The force decreases linearly to the point $\lambda = P_0/f_M$, where the winding of the buffered fiber vanishes.

We can assume the pushing force P as the critical buckling force since the winding amplitude is small within the sheath,

$$P = \frac{\pi^2 EI}{s^2}, \quad (3)$$

where s is the period of winding, EI is the flexural rigidity of the buffered fiber or the product of the effective elastic modulus by the area moment of inertia. As illustrated in Fig. 2 there is a relation between s and the winding compression Δs of

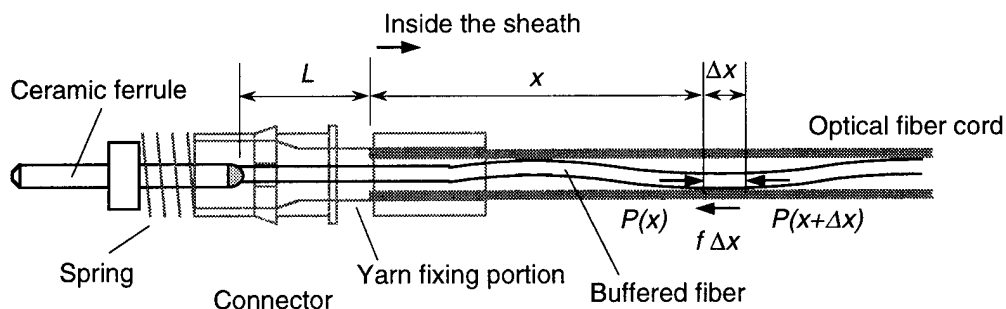


Fig. 1 Cross sectional structure of connector and the winding of buffered fiber in the sheath. Drawing is not accurate and the outer parts of the connector are not illustrated.

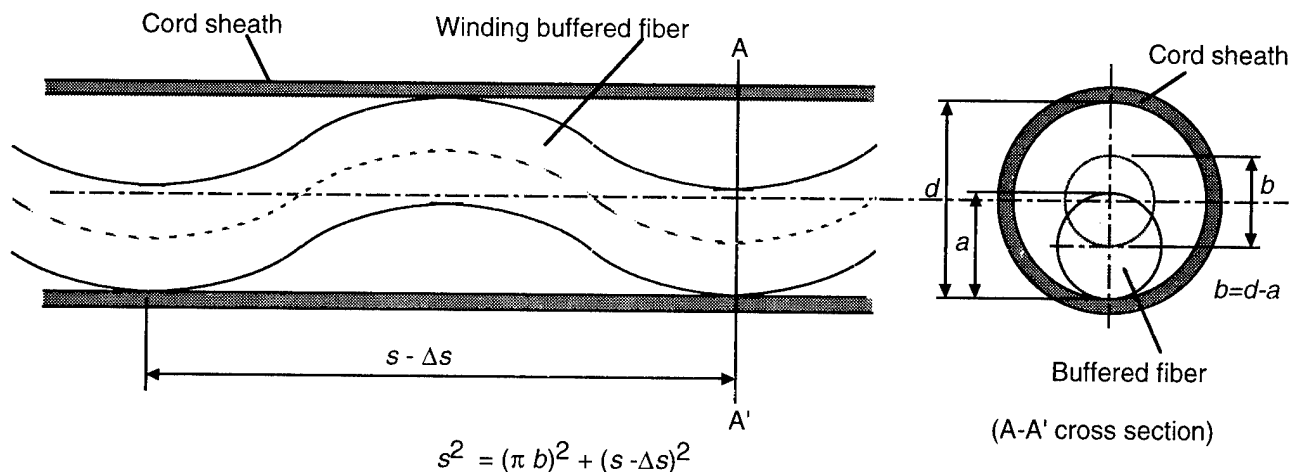


Fig. 2 Buffered fiber coils inside the sheath. Compression of the buffered fiber in length is expressed as $\Delta s/s$. Assuming spiral coils, the observed elastic modulus of the buffered fiber is $2EI/b^2$

thus

$$\frac{f_M}{EI} < \frac{\pi^4 b^2}{4 d_0 L^4}, \quad (10)$$

where L is the free length of the buffered fiber in the connector. Since the values EI and f_M are measurable, then we can judge whether the cord being tested is suitable or not. In the MU-type connector, L is about 5 mm and d_0 is 1 mm at most. Moreover, we can estimate the span of the displacement of the buffered fiber λ with EI and f_M ,

$$\lambda = \frac{2}{b} \sqrt{\frac{d_0 EI}{f_M}}. \quad (11)$$

Because the value of λ should be less than the cord length λ_0 ,

$$\frac{f_M}{EI} > \frac{4 d_0}{\lambda_0^2 b^2}. \quad (12)$$

Since the shortest length of the cord used in the office is 60 cm, we assume λ_0 to have this value.

Consequently, inequalities (10) and (12) are the cord design conditions for f_M and EI values of the buffered fiber.

Miniaturization

Reducing yarn relaxation. Mainly as a result of the fabrication method the aramid yarn in a conventional 2-mm cord is 0.3 % longer than the buffered fiber. Therefore 5500 denier

the buffered fiber, $s^2 = (\pi b)^2 + (s - \Delta s)^2$. Thus the pushing force P is expressed with the ratio of compression as

$$P = E_0 \frac{\Delta s}{s} = \frac{1}{2} E_0 \left(\frac{\pi b}{s} \right)^2, \quad (4)$$

where E_0 is the observed elastic modulus of the winding buffered fiber and b is the difference between the inner diameter of the sheath and the outer diameter of the buffered fiber. Therefore the observed elastic modulus E_0 is

$$E_0 = \frac{2EI}{b^2}. \quad (5)$$

The displacement of the buffered fiber at the distance x is

$$d(x) = \int_x^\lambda \frac{P}{E_0} dx, \quad (6)$$

and thus the sliding length of the fiber at the sheath end is expressed as

$$d_0 = \int_0^{P_0/f_M} \frac{P_0 - f_M x}{E_0} dx. \quad (7)$$

Therefore the pushing force P_0 is expressed as

$$P_0 = \frac{2}{b} \sqrt{d_0 EI f_M}. \quad (8)$$

The pushing force P_0 must be less than the critical buckling force P_c . Therefore,

$$P_0 < P_c = \frac{\pi^2 EI}{L^2}, \quad (9)$$

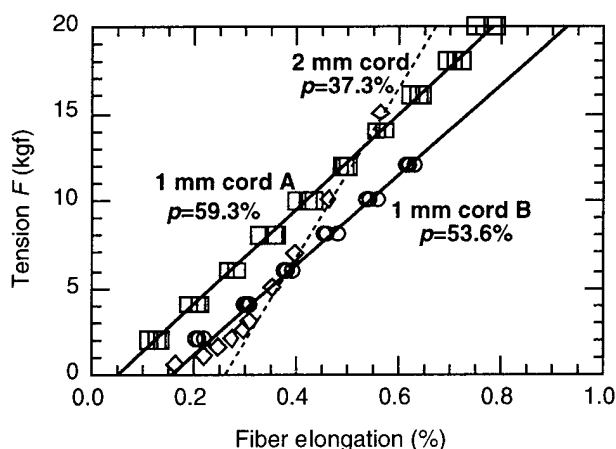


Fig. 3 Elongation-tension curves for loose type cords

aramid yarn as a strength member is required to satisfy the required tensile strength while taking the yarn relaxation of 0.3 % into consideration. It is hard to design 1-mm cord with the same amount of aramid yarn remaining, because the cross sectional area for the yarn is limited. To protect the fiber from crushing force, we decided to use 0.5 mm^φ buffered fiber. Thus we must reduce the amount of yarn. Fortunately, we have found that the yarn relaxation can be reduced by increasing the volume occupancy p of the yarn in the cord sheath. Figure 3 shows the relation between elongation of the fiber and tension in one conventional 2-mm cord and two test samples of 1-mm cord. A cross point on the horizontal axis represents the yarn relaxation. The 2-mm cord uses aramid yarn, while the 1-mm cords use PBO yarn that will be mentioned later. When the occupancy p is increased up to about 60 %, the yarn relaxation is reduced to about 0.1%. This effect enables us to significantly reduce the amount of yarn without sacrificing tensile strength. The tension of the cord F is expressed as

$$F = \frac{\pi p E_y \varepsilon}{4} (d^2 - a^2), \quad (13)$$

where p is the volume occupancy ratio of the yarn, E_y the modulus of elasticity of the yarn, ε the elongation of the yarn, d the inner diameter of the sheath and a the buffered fiber diameter.

Utilizing high strength yarn. Poly(p-phenylen-2,6-benzobisoxazole), PBO, which is a recently developed high strength fiber, has about twice the modulus of elasticity of aramid yarn. According to Eq. (13), the F - d curves for PBO yarn ($E_y=25300$ kgf/mm², and the cross section of unit yarn is 7.12×10^{-5} mm²/denier) are plotted for various ε values in Fig. 4. The occupancy ratio p of the yarn is fixed at 65 %. Empirically the occupancy ratio should be less than 70 % or the movement of the buffered fiber in the sheath will be prevented by the yarn. Assuming that the yarn relaxation is 0.1 %, the solution is found on the F - d curve of $\varepsilon=0.4$ %. To obtain a tension of more than 10 kgf, it is recognized that the inner diameter must be larger than 0.67 mm and the thickness of the sheath must be less than 0.17 mm for the outer diameter to be 1.0 mm.

Increase in optical fiber proof strain. The tensile strength of optical fiber cord should be compared with breakage probability. When high strength optical fiber proof-tested under strain of 0.75 % is used, the allowable maximum elongation equivalent to an ordinary 0.5 % is 0.65 %. Therefore the ε value is assumed to be 0.55 %, and the inner diameter of the sheath is designed to be 0.63 mm (Fig. 4).

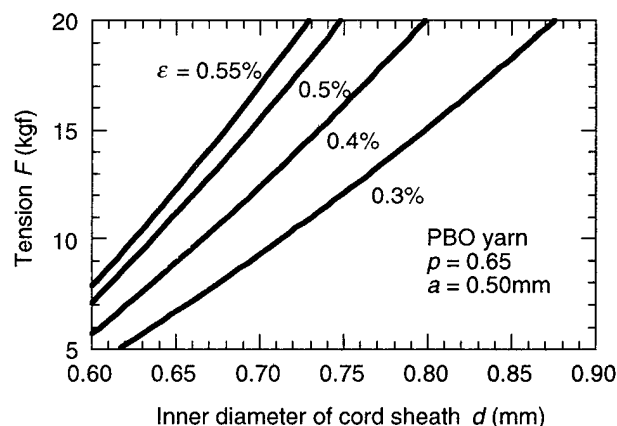


Fig. 4 Relation between tension of the cord and inner diameter of the sheath.

PROTOTYPE PERFORMANCE

We fabricated a prototype cord. The cross sectional structure of the cord is shown in Fig. 5. The 0.5-mm ϕ buffered fiber has a double layer structure with UV curable resins and is packaged with three bundles of PBO yarn in a 0.17 mm thick PVC sheath. The fiber is 0.75 % strain proof-tested. The tension of the cord at 0.65 % elongation was 14.0 kgf. The measured relaxation of the strength member was 0.15 %.

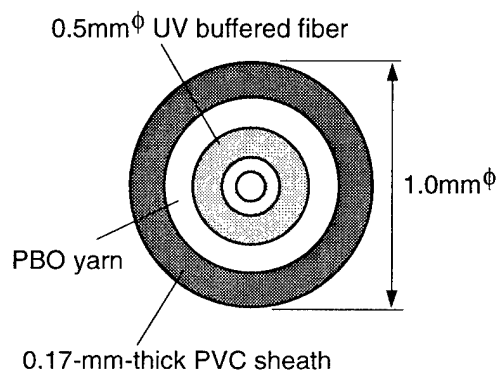


Fig. 5. Cross-sectional structure of a prototype cord

The flexural rigidity of the buffered fiber was 0.57 kgf mm², and the sliding friction force per unit length was 33 gf/cm. With these values the critical buckling force of the buffered fiber in the connector and the pushing force needed for 1-mm sliding are calculated to be 225 gf and 152 gf, respectively (assuming $L=5$ mm). Thus buckling is avoided. The measured pushing force was almost proportional to the sliding length of the buffered fiber into the sheath, and the value at 1.0 mm was 114 gf, which is 25 % smaller than the calculated value. This may be because of the lower estimation in the theory of longitudinal compression of fiber winding. On the other hand, the span of the fiber sliding was estimated as 46 cm, which was short enough.

Table 1. Performance of the prototype cord

<u>Strength member</u>	yarn amount	PBO
	relaxation	0.15%
	packing ratio	65.7%
<u>Buffered fiber</u>	coating	UV resin
	flexural rigidity EI	0.57 kgf mm ²
	sliding friction force	33 gf/cm
	MFD @ 1310nm	9.4 μ m
	λ_c	1.23 μ m
<u>Cord performance</u>	Tension at 0.65% elongation	14.0 kgf
	Temperature cycle test (method IEC 794-1-F1)	<0.05 dB/km
	Crush test (method IEC 794-1-E3)	<0.07 dB
	Transmission loss @ 1550 nm	0.21 dB/km
	@ 1310 nm	0.35 dB/km

The free length of the buffered fiber in the connector may alter according to how the sheath is fixed. According to Eq. (9), when the length L becomes longer than 6 mm, buckling may occur. Buckling is very critical to the free fiber length L . Therefore, in practical cords the flexural rigidity of the buffered fiber should be increase and the sliding friction force should be reduced. For this purpose we must utilize a material for the outer coat of the buffered fiber with a higher elasticity and smoother surface.

The prototype cord satisfied other mechanical and optical requirements (Table 1). The optical transmission loss was 0.21 dB/km at 1550 nm and 0.35 dB/km at 1310 nm. The transmission loss increase was less than 0.07 dB in a crush test and less than 0.05 dB/km in a temperature cycle test.

CONCLUSIONS

We presented design concepts for a miniaturized optical fiber cord. We have clarified the

mechanism of how the buffered fiber slides in the cord sheath, and have expressed the buckling condition of the buffered fiber in an MU-type connector with easily measurable cord parameters, that is, the flexural rigidity of the buffered fiber and the maximum friction force to slide the buffered fiber within the sheath.

We demonstrated that it is possible to design a miniature optical cord with a 1-mm outer diameter by reducing the relaxation of the strength member and using PBO yarn and 0.75 % strain proof-tested fiber, while still satisfying the usual optical and mechanical requirements.

REFERENCES

- 1) D. Mathis, M. Viriyayuthakorn, J. Holman, L. Graham and R. Reagan; Proc. of IWCS, Atlanta, pp.183-188, 1994
- 2) S. Iwano, R. Nagase, K. Kanayama, E. Sugita, K. Yasuda and Y. Ando; IEEE J. Lightwave Technol., Vol. 10, No. 10, pp. 1356-1362, 1992
- 3) C. Tanaka, Y. Katsuyama, Y. Ishida, T. Waki and K. Ishihara; Trans. IECE, Vol. J65-B, No.1, pp.126-133, 1982 (Japanese)



Makoto Sato

NTT Opto-electronics Laboratories
3-9-11 Midori-cho, Musashino-shi, Tokyo, 180
Japan

E-mail: satom@ilab.ntt.jp

Makoto Sato is a Senior Research Engineer in NTT Opto-electronics Laboratories and is engaged in research on optical switches and cables. He joined NTT Electrical Communication Laboratories in 1982, and did his research work on optical fiber splicing and microwave properties of high- T_c superconductors. He received his B. S., M. S. and Ph. D. degrees in Physics from Kyushu University, Fukuoka, Japan. Dr. Sato is a member of IEICE of Japan, the Japan Society of Applied Physics, and the Physical Society of Japan.

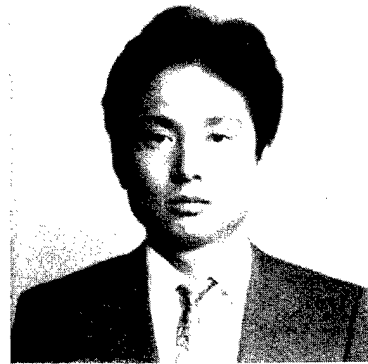


Masao Tachikura

NTT Access Network Systems Laboratories
Tokai-mura, Naka-gun, Ibaraki-ken, 319-11
Japan

Masao Tachikura received B. S. and M. S. degrees in mechanical engineering from Kyoto University in 1974 and 1976, respectively. In 1976, he joined NTT Electrical Communication Laboratories.

Since then, he has been engaged in research and development on optical fiber splicing and connecting techniques, mechanical reliability of optical fibers, and optomechanical switching techniques for optical fibers. Presently he is with the Optical Subscriber Cable Systems Lab. in NTT Access Network Systems Laboratories. Mr. Tachikura is a member of OSA, IEICE of Japan, the Japan Society of Applied Physics, and the Japan Society of Mechanical Engineers.



Shin'ichi Iwano

NTT Opto-electronics Laboratories
Tokai-mura, Naka-gun, Ibaraki-ken, 319-11,
Japan

Shin'ichi Iwano is a Manager, Research Planning Department in NTT Opto-electronics Laboratories. He received his B. S., M. S. and Dr. Eng. degrees in electronics engineering from Kyushu University, Fukuoka, Japan, in 1981, 1983 and 1994, respectively. Since joining NTT Electrical Communication Laboratories in 1983, he has been engaged in research on optical fiber connections and the development of optical fiber connectors. Dr. Iwano is a member of IEEE and IEICE of Japan.



Nobuo Tomita

NTT Access Network Systems Laboratories
Tokai-mura, Naka-gun, Ibaraki-ken, 319-11
Japan

Nobuo Tomita is a Senior Research Engineer and a Supervisor in NTT Access Network Systems Laboratories. He joined NTT in 1974, and was engaged in research on broadband and digital subscriber loops and development of optical fiber cable components. Since 1987, he has been engaged in research and development of operation and maintenance systems for optical trunk and subscriber lines. He is currently engaged in research on high-density optical cable distribution systems inside telephone offices. He received his B. E. and M. E. degrees in electronic engineering from Kumamoto University, Kumamoto, Japan, in 1972 and 1974, respectively, and his Dr. Eng. degree in information engineering from Kyushu University, Fukuoka, Japan, in 1988. Dr. Tomita is a member of IEEE and the Institute of Electronics, Information and Communication Engineers of Japan.

CHARACTERIZING FIELD HANDLEABILITY OF OPTICAL FIBER THROUGH THE MEASUREMENT OF STRENGTH AFTER MECHANICAL STRIPPING

Anurag Dwivedi and Jeffrey L. Smith
Corning Inc., Corning, NY 14831

ABSTRACT

While there are many aspects to fiber handleability such as the ease of processing and testing, this paper relates to the 'field-handleability,' and more specifically to the ability to easily strip the fiber in the field without breakage.

Strength after mechanical stripping (SAMS) of a number of commercially available optical fibers was measured as a function of different strength controlling variables. In addition to SAMS, the peak strip force and strip work were measured to study their correlation with SAMS. The SAMS results for various commercially available fibers are compared with the estimated applied handling stresses in the field. Results are discussed in terms of strength degrading mechanisms, various strength controlling parameters during mechanical stripping, and product functionality.

INTRODUCTION

As fiber deployment moves closer to the home and the number of splices, connectors, couplers, pigtails and other fiber-based components in the field proliferate, understanding and improving the handleability of optical fiber becomes increasingly more important^{1,2}. The attributes that control handleability of a fiber mainly are strength and strippability.

Removal of the polymer coating on silica optical fibers is one of the essential steps in almost every fiber-optic cable installation and repair event. These polymer coatings can be

removed either mechanically or chemically. Although the use of chemicals for stripping is less likely to induce surface damage, this technique is not convenient for field applications. Mechanical stripping is commonly used in the field where stripping tools and mechanical force are used to remove the coatings; this poses risk of damaging the glass surface. It is important to study the strength degradation due to stripping since it may impact the stripping success rate and thus the fiber installation cost. In connectors, couplers, and other fiber optic components, where fiber stripping is the final strength controlling process, the long term mechanical reliability may be impacted due to stripping damage.

Strength of silica optical fibers is dictated by microscopic surface flaws. When a tensile stress is applied on the fiber, these surface flaws act as stress concentrators. This means that the atomic bonds near the crack tip experience a higher tensile stress than applied on the macroscopic sample. Stress concentration is most commonly characterized by the stress intensity factor which, for pure tensile loading, is given by

$$K_I = Y\sigma\sqrt{C} \quad (1)$$

where Y is a crack shape and specimen geometry parameter, σ is the applied stress, and C is the crack depth. When applied stress intensity reaches a critical limit, K_{IC} , the fracture toughness of the material, the sample fails. As evident from equation 1, the failure of a fiber sample is governed by the size of the largest flaw in the uniformly

stressed region of the fiber. If the stress is applied in a humid environment the flaws will grow due to the stress-corrosion (or subcritical crack growth or fatigue), further degrading the strength of the fiber.

The damage to the pristine surface of glass fiber due to stripping, thus, may initiate flaws and consequently degrade the strength of the fiber in accordance with equation 1. Fiber will break if the strength drops below the handling stress applied during or after stripping, cleaving, or splicing.

There are two types of parameters that control the strength of the fiber due to stripping: (a) fiber and coating characteristics such as force required to strip the coating, adhesion of coating to the glass surface, and material characteristics of coating, and (b) stripping tool and process related, such as the surface area in contact with the blades, abrasion due to contamination from dirt or coating debris, hardness of the tool, localized frictional forces generated due to non-symmetric fiber-blade gap configuration, and the practices used by the craftsperson, etc. If a SAMS test is performed in the laboratory the results not only will be impacted by variables exemplified above in types (a) and (b) but also by the test procedure. Since SAMS results are complicated by such a large number of parameters, it is important to perform this testing in a controlled manner to obtain meaningful information.

It is the intent of the present work to characterize the strength degradation due to the damage induced by mechanical stripping of commercial fibers. Tests were conducted in a controlled manner by varying only one strength-controlling parameter that is being studied. Recommendations were formulated for field handling practices and for the analysis of the SAMS data to be used for characterization of handleability and reliability of optical fibers.

BACKGROUND OF STRIPPING PROCESS

Based on the observation of coating debris produced by stripping, one may classify three different coating stripping modes (a) Buckling or crumbling (b) Crumbled-tubes, (c) Tube-off. Typical force vs. distance plots for the crumbling and tube-off modes are shown schematically in figure 1. A 'slip-stick' type force response is demonstrated when coatings crumble. A peak force due to initial coating rupture followed by a monotonically decreasing force (due to interfacial friction) with stripping distance typically characterizes coating tube-off. Most commercial fibers with typical 245 μ m geometry show coating crumbling or buckling as a result of the mechanical stripping process. Fibers with 245 μ m coating dimensions and with extremely low coating/glass interfacial adhesion typically tube off when strip work drops below 20mJ (see figure 10)⁸. Additionally, fiber coatings with very high elastic modulus and/or thicker coating geometry (e.g., 400-900 μ m) are seen to rupture and tube-off during stripping.

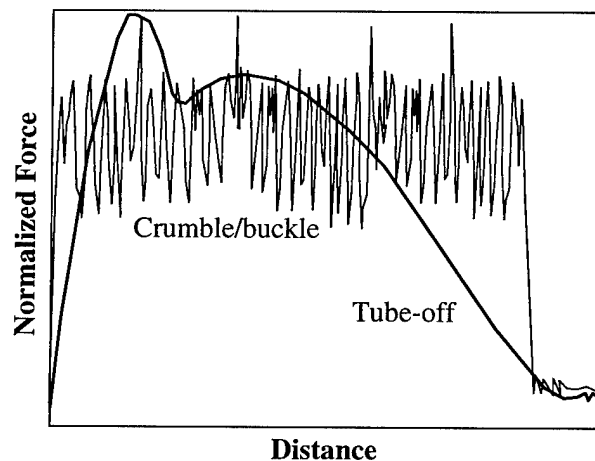


Figure 1: Force vs. distance plot for two coating stripping modes

In a recent study³ it has been shown that most commercial coatings buckle (or crumble) and form an 'accordion' shape during stripping. This buckled mass stores energy during the

stripping process and when that energy exceeds the toughness of the composite coating system, the coating fails. On subsequent stripping, the coating buckles again and fails. This sequence goes on until the entire fiber end is stripped. This process is shown schematically in Figure 2.

Stripping damage to the glass surface is likely to occur during the coating 'bunching and rupturing' events. The spatial extent (1-2 mm for most coatings) of these bunching-rupturing events is such that stripping in any region of the fiber length would simulate the damage imparted by the same tool and technique at the end of the fiber as performed in the field. This argument provides the basis for strength measurement after stripping at the center of a fiber segment (Figure 3) to assess the susceptibility to fiber damage during field stripping. This is, however, true only for the fiber coatings that do not tube-off.

EXPERIMENTAL PROCEDURE

Selection and nomenclature of samples

Samples of various commercially available fibers were tested encompassing a number of glass and coating combinations. For simplicity, and fiber identification, the following nomenclature is used throughout this paper.

T/C-1 : Titania-doped Silica Clad/Coating 1

S/C-1 : Silica Clad/Coating 1

S/C-2 : Silica Clad/Coating 2

S/C-3 : Silica Clad/Coating 3

S/C-4 : Silica Clad/Coating 4 (not a commercial coating)

S/C-5 : Silica Clad/Coating 5

S/C-6 : Silica Clad/Coating 6

To study the effect of coloring ink, both colored and uncolored S/C-1 fibers were tested. Fiber S/C-3 was removed from a newly manufactured cable and was thus color coded. Additionally, SAMS was measured

for the aged S/C-4 removed from a cable that had been deployed in the field for ten years⁴.

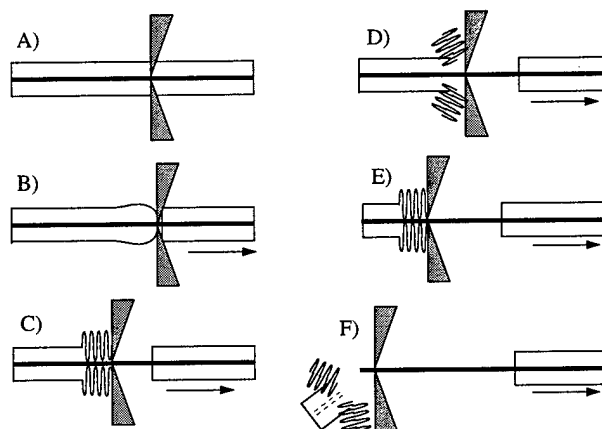


Figure 2: Schematic representation of stripping

Strength after mechanical stripping

SAMS test was performed according to TIA/ITM/XX-(PN3618)⁵ with a few enhancements as described below. A sample set of a minimum of 30 specimens was tested for each fiber. One end of a 2m long fiber was attached to the upper mandrel of an InstronTM strength testing machine. The free end of the fiber was threaded through the guide of a MicrostripTM stripping tool (unless otherwise specified) with 0.006inch (0.152mm) hole diameter blades. The stripping tool was mounted on a specially designed SAMS fixture attached to the InstronTM strength testing machine. A 3cm section of coating was removed from the center of the fiber at a stripping rate of 500 mm/min. The tool was unclamped and the fiber was released from the stripping tool without touching or bending the stripped section. This was accomplished by moving the stripped section up and out of the unclamped stripping tool. The free end then was attached to the lower mandrel of the InstronTM strength testing machine. The fiber then was stretched until breaking at a strain rate of 5%/min which is consistent with TIA/FOTP-28B.⁶

A schematic of the test set-up is shown in Figure 3. It is important to note that in this method the handling of the stripped region is minimized to avoid further degradation of the fiber strength by processes other than the stripping. The SAMS testing was done at laboratory ambient conditions where temperature ranged from 19 to 23°C and relative humidity (RH) ranged from 38% to 48% during the course of testing.

Samples were randomized for SAMS testing to minimize the effect of test/equipment variables on strength. Every break was inspected to ensure that fiber fractured in the stripped section. The breaking stress was recorded for all breaks within the stripped region and results are presented using a Weibull cumulative probability distribution of the failure stress.

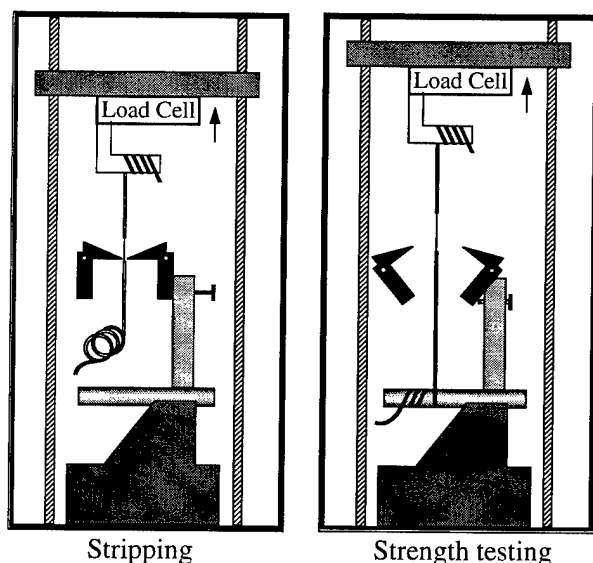


Figure 3: Schematic of SAMS test set-up

Strip Force and Strip Work

Strip force/work measurements were done according to TIA FOTP-178⁷. A sample set of 10 was tested for each fiber. For all fiber samples, 30±3 mm of coating was stripped at a rate of 500±50 mm/min. All fiber stripping was performed using a Microstrip™ tool (unless otherwise specified) with 0.006inch

(0.152mm) diameter blades. The blades were inspected visually and cleaned for any debris and/or build-up from previous use before loading the fiber.

Strip work is the area under the force vs. distance plot resulting from the stripped section of the fiber. All strip force and strip work testing was performed in a controlled environment of 23°C/50%RH.

RESULTS

Test repeatability

To study the effect of blade age on SAMS, testing was performed on a S/C-1 fiber after 0, 100, 200 and 300 strips. Mean SAMS for new blades is measured to be 280±47 (1 std dev) kpsi or 1.93±0.32GPa. SAMS results as a function of blade age are shown in Table 1. Analysis shows that the strength after 200 strips is significantly changed. To eliminate the effect of this test variable, the blades were changed after 200 strips.

Table-1

Blade age (number of strips before SAMS test)	Mean SAMS (assuming normal distribution)	
	kpsi	GPa
0 (New)	280*	1.93*
100	281	1.94
200	325	2.24
300	352	2.43

* Note: 1 std dev for new blades is 47 kpsi (0.32 GPa)

Effect of tool type

SAMS was tested for sample S/C-1 using two different types of tools: Type A, a scissor-action tool, and Type B, a non-scissor-action tool. Results are summarized below in figure 4 for these tools in both 'new' and 'used' conditions. Higher SAMS was observed for 'used' tools. Also, the hole size became enlarged as tools were repeatedly used for

stripping. This prompted us to study the effect of hole size on the SAMS.

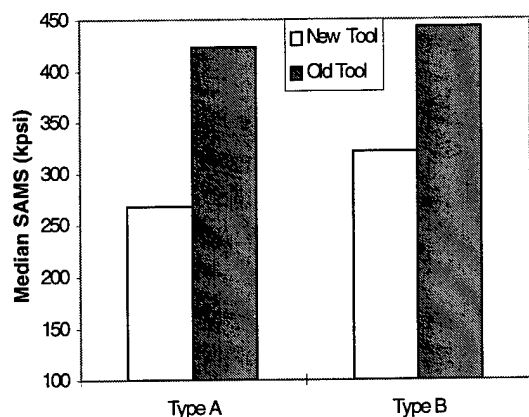


Figure-4: SAMS for different tools

Effect of hole size of the blade

The impact of hole size was studied using tools of Type A, the scissor-action tools. It was noted that commercial tools had a wide distribution of hole sizes. Also, the hole sizes increased significantly as a result of its use for extended period. The hole sizes were determined using an optical microscope. These results are summarized in figure 5. Average starting hole size of a set of selected 'new' Type A tools was 102 μ m. Interestingly, after only 30 strips the average hole size increased to 121 μ m.

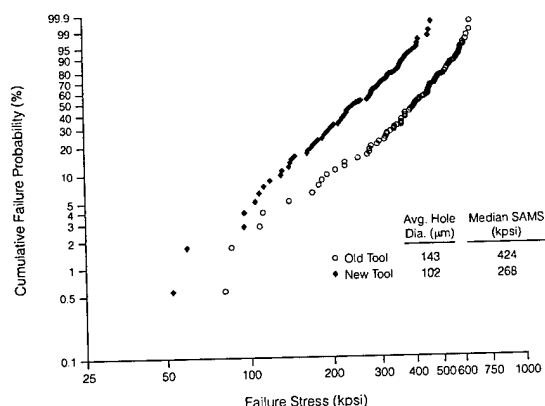


Figure 5: SAMS vs. tool hole size

Similar tools after several months use were found to have an average hole size of 143 μ m.

As evident from this study, hole sizes smaller than the glass diameter (of 125 μ m) can be found; such tools degrade the fiber strength the most. As tools get worn out after use, the hole size increases which results in less fiber damage. Hole sizes slightly bigger than the glass diameter would be optimum since they would impart the least amount of damage during the stripping without leaving a lot of coating residue.

Effect of fiber coating

The effect of fiber-optic coatings on SAMS was studied by testing two fibers made with the same glass composition and manufacturing process but with different coatings. The results are as described in figure 6.

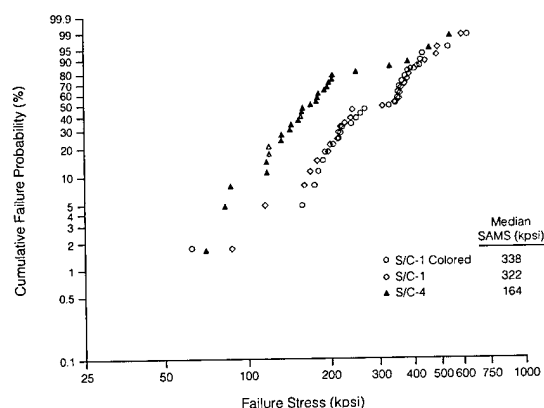


Figure 6: Effect of fiber coatings on SAMS

Effect of fiber coloring

SAMS of S/C-1 fiber was tested with and without coloring. As may be noted from the results shown in figure 6 there is no significant difference between the SAMS of colored fiber and its uncolored counterpart.

Effect of glass surface

Two fibers with the same coating but with different cladding surface compositions were tested. One fiber had pure silica clad whereas the other had titania-doped silica cladding. The results are described in figures 7 and 11.

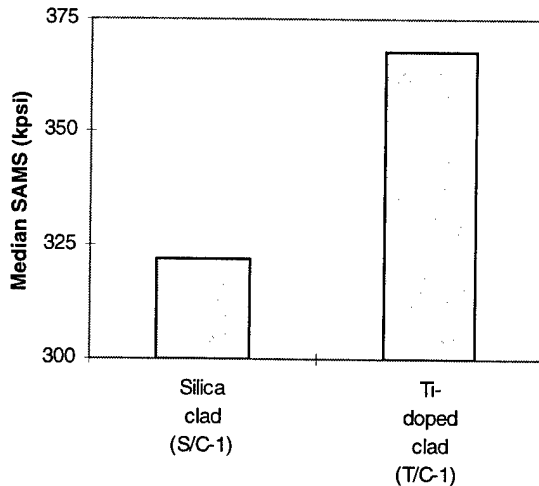


Figure 7: Effect of cladding composition

Effect of aging in the field for 10 years

Fibers S/C-4 were removed from a cable which had been deployed in the field for ten years⁴. SAMS was measured and compared with a recently manufactured fiber with the same glass/coating combination. The results are shown in figure 8.

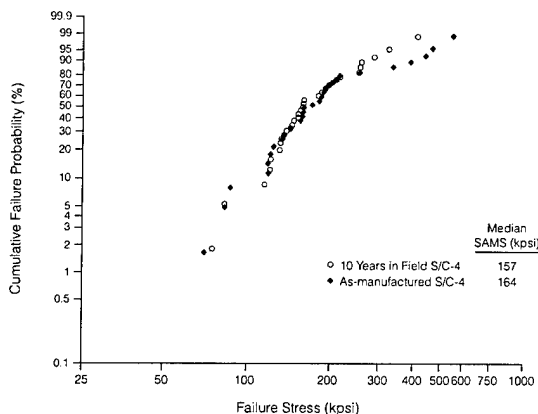


Figure-8: SAMS after 10 years of field aging

Effects of wiping and splicing

Samples S/C-1 were stripped in the center of a 2m fiber segments using the SAMS set-up. The fibers then were carefully broken at the stripped portion. Two individual stripped ends then were wiped using alcohol, cleaved to about 15mm, and fusion spliced together. Spliced strengths then were measured using the same SAMS instrumental set-up and compared to the SAMS for the same fiber. The results are shown in figure 9.

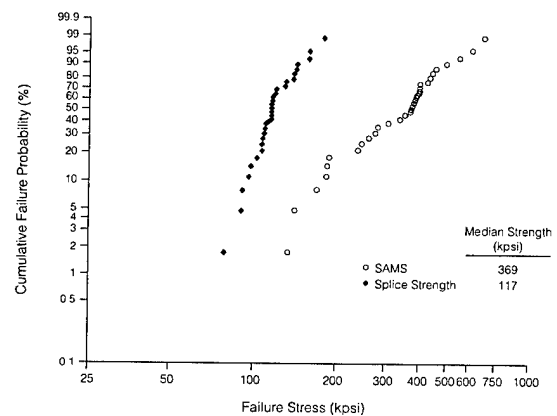


Figure 9: SAMS vs. splice strength

Results show that SAMS is significantly higher than the splice strength. The effects of the individual post-stripping handling steps (wiping, cleaving, and splicing) on the final strength were outside the scope of this paper and remained undetermined. It was observed that none of the breaks occurred at the splice point, however, all breaks occurred within the splice arc region (within 2mm from the joint).

Correlation of SAMS with strip force and strip work

All measured strip force values were well within Bellcore's recommended range of 0.3 - 2.0 lbf (1.35 - 0.90N). The S/C-5 fiber showed the highest strip force (1.16 lbf or

5.20N) and the highest strip work (67.6 mJ) whereas S/C-1 (uncolored) fiber showed the lowest strip force (0.50 lbf or 2.24N) and the lowest strip work (33.5 mJ).

Analysis of the data is presented in figure 10 to demonstrate empirical correlation between SAMS, strip force, and strip work. While the best fit line shows a general trend, the linear correlation between strip force and SAMS, as expressed by equation 2, is rather poor ($r^2=0.422$).

$$\sigma_s = -889.2 S_f + 4701.0 \quad (2)$$

where σ_s is the median SAMS in MPa and S_f is the corresponding peak strip force in N.

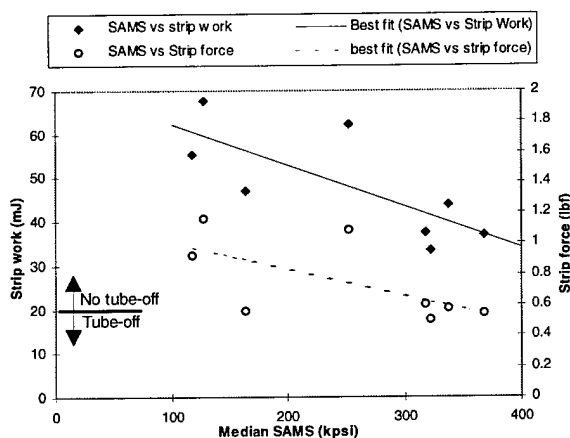


Figure 10: Correlation between SAMS, strip force, and strip work.

Similarly, the linear correlation between SAMS and strip work is expressed by equation 3 and shows a low 'goodness of fit' ($r^2 = 0.570$).

$$\sigma_s = -73.83 S_w + 5261 \quad (3)$$

where σ_s is the median SAMS in MPa and S_w is the corresponding strip work in mJ.

DISCUSSION

Variables Controlling SAMS

The strength after mechanical stripping, SAMS, is considered a functional handleability and reliability parameter.

Unfortunately, the results show poor repeatability due to its sensitivity to a large number of test, tool, and craftsperson parameters. For this reason, this test parameter has been deemed unspecifiable by the TIA⁵. In the present work, extreme care was taken to identify and control the individual strength-controlling parameters, which yielded statistically repeatable SAMS results. This enabled a study of the effects of various parameters on stripping damage.

Based on the results of the present study, the hole size of the tool seems to greatly impact the stripping damage. Hole diameter must be larger than the nominal glass diameter to minimize stripping damage. Also, the results show that several years of field aging in a cable does not affect SAMS.

Other factors impacting SAMS are the characteristics of polymer coating and cladding glass. Coloring ink does not seem to impact SAMS. Results from Figures 7 and 11 confirm the higher abrasion resistance of titania-doped silica clad fibers. It is important to note that there is a poor correlation between strip force and SAMS which indicates that general inference about the susceptibility of commercial fibers to stripping damage is difficult to make based on their relative peak strip force values. However, lower strip force will result in the ease of stripping and improved stripping success rate since it will require smaller force and stress for stripping.

It is worth pointing out that the post-stripping processes such as wiping and splicing, if applicable, have the potential to further degrade the strength. For a majority of applications these are final processes that control the strength of deployed fiber. For silica clad fibers, the impact of such processes (e.g. wiping) seems to be independent of SAMS which would suggest that optimizing fiber parameters for SAMS may not be beneficial for improving long-

term reliability. Rather it is the field practices that would have the greatest impact on the strength and the long term reliability. Higher SAMS, however, is justifiable for maximizing the stripping success rate and for the improved long-term reliability for the applications where fiber stripping is the final strength controlling handling step. Such applications include ultrasonically cleaned stripped fiber-ends used in connectors, couplers, and other fiber optic components.

In summary, the strength-controlling stripping parameters can be classified under four broad categories including (a) craftspeople/field practices (e.g. cleanliness, touching the bare glass, careful handling etc.), (b) tool characteristics (e.g. hole size, tool hardness, and age of the tool, etc.), (c) fiber parameters such as cladding glass, coating, and interfacial characteristics, and (d) the test method (e.g. wiping required or not, stressing rate etc.).

Estimation of handling stresses

Fiber breakage during stripping may impact fiber functionality and installation cost especially in today's environment where the number of fibers being installed and handled is increasing exponentially. A fiber, that is difficult to strip and is susceptible to severe field stripping damage, may break during stripping. The condition for fiber breakage is:

Stripping stress \geq SAMS.

For a tensile stripping process, the highest stripping stress on fiber can be calculated by:

Stripping stress = (Peak strip force)/(Cross sectional area of the glass fiber) (4)

As is shown in figure 10, the highest typical peak strip force of all commercial fibers tested in the present study is about 1 lbf (4.48N). For a 125 micron diameter glass

fiber, this translates into a tensile stripping stress of ~48 kpsi (~331MPa).

As shown in figure 11, the median SAMS for all commercial fibers tested in the present work is significantly greater than the worst case stripping stress of ~48 kpsi (~331 MPa). This suggests a very high stripping success rate (low probability of fiber breakage during stripping) for all commercially available fibers.

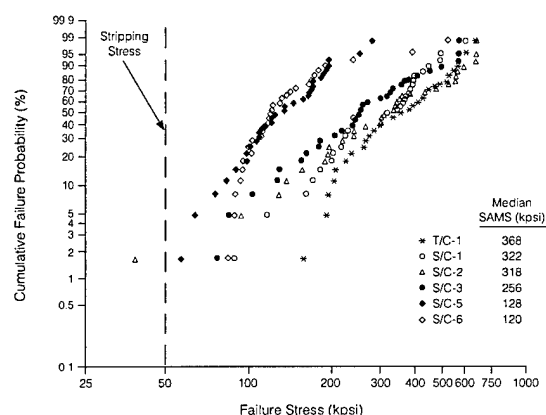


Figure 11: Median SAMS of commercially available fibers.

Field recommendations derived from these results

The authors recommend following field stripping practices based on the results and experience gained from the present study:

- i) Stripping tools/blades must be carefully selected to ensure that the hole size is bigger than the diameter of the glass fiber. Interestingly, the longer the tool is used for stripping, the more strip-friendly it becomes since the hole diameter gradually increases due to wear-out.
- ii) Cleanliness of the tool and the installation environment is extremely important.

Precautions must be taken to avoid unnecessarily touching the bare glass surface with either hands or any other object. Fiber should be completely dry when stripped.

iii) Craftspeople generally bend the fiber during stripping, perhaps because they have the perception that it will clean the coating debris while being stripped. Fiber bending must be avoided during stripping since (a) it may add enormously to stripping stresses and (b) it will increase the blade-glass contact area resulting in more stripping-induced damage. Both, or any, of these effects may reduce the stripping success rate. Thus, stripping should be performed in a tensile mode by keeping the fiber straight and perpendicular to the plane of the tool/blade hole.

iv) Craftspeople must understand that the post-stripping handling of fiber will potentially damage the fiber. Thus these processes, if needed, must be carried out gently and with extreme care. For example, wiping with a soft, clean, and non-abrasive material should be performed only on an as-needed basis, gently, and using minimal pressure to clean the coating debris.

v) For applications where fiber splices may be exposed to severe stress, temperature, and humidity environments, the splices should be proof-tested to ensure minimum strength and long-term reliability. If splicing is not the final strength controlling step, proof testing should be performed after the last strength controlling handling event.

CONCLUSIONS

The following conclusions can be drawn from the results of the present study:

- (1) SAMS can be affected by a large number of variables categorized as:
 - (a) Craftsperson/field practices,
 - (b) Tool characteristics (e.g. hole size), and

- (c) Fiber parameters such as glass, coating, and interfacial characteristics,
- (d) SAMS test method (e.g. wiping required or not, stressing rate).

(2) The strength of stripped portions is sufficient to withstand the stripping stresses for all commercial fibers tested. Commercial fibers are, thus, fully functional for typical installations. Fiber breakage would be seen if stripping/handling stresses are more than the SAMS.

(3) The SAMS for the fibers removed from a 10 year old, field-aged cable remained the same as its as-manufactured counterparts.

(4) SAMS has a very weak linear correlation with the strip force and strip work.

(5) The long-term reliability of stripped portions does not depend on SAMS but is dictated by post-stripping processes such as wiping, cleaving, and splicing. This however is not true for the applications where stripping is the final strength controlling process step.

ACKNOWLEDGMENTS

Authors thank Pat Cruttenden and Jeff Johnson for their support in the areas of strip force testing and splicing respectively, and John Botelho for many helpful discussions.

REFERENCES

- (1) "Mechanical reliability of multi-fiber fusion splices," Yuce et al., IWCS Proceedings, 1992, pp462-466.
- (2) "Optical fiber design for improved mechanical properties," Novack et al., IWCS Proceedings, 1995, pp 162-168.
- (3) "Developments in the Evaluation and Modeling of Mechanical Stripping Behavior of Fiber Optic Coatings," E.H. Urruti, J.W.

Botelho and M.A. Botelho; Proceedings of NFOEC (1995), pp 225-247.

(4) "Mechanical and optical functionality of field-aged optical ground wire cable", Lundergan et al., Proceedings of NFOEC, 1996.

(5) Proposed TIA/EIA/ITM-XX (PN3618), "Characterization of fiber strip damage by dynamic tensile testing."

(6) TIA/EIA/455-28, "Method for measuring dynamic tensile strength of optical fiber."

(7) TIA/EIA/455-178, "Procedure for Measuring Strip Force on Single Fiber."

(8) Private communications with Patrick T. Garvey of Corning Inc.



Anurag Dwivedi is a Senior Engineer in the TPD - International Operations Group of Corning Incorporated. Currently, he is responsible for technical support to optical fiber customers in the Asia Pacific. Anurag joined Corning in 1992 and assumed various responsibilities in the Product Engineering, the Center for Fiber-Optic Testing (CFT), and the International Operations Group of TPD.

Prior to joining Corning, Anurag was employed by Alfred University, as a Post-doctoral Research Associate. Anurag received a M.S. in Ceramic Engineering (1988) and a Ph.D. in Ceramics (1991) from Alfred University, Alfred, NY.



Jeffrey L. Smith is an Opto-mechanical Technician at the Center for Fiber-Optic Testing (CFT), Corning Inc., Corning, NY. Currently, he is responsible for projects related to the mechanical performance of optical fiber products. He joined Corning in 1989 and has been involved with the development, design, implementation, and documentation of new and/or enhanced mechanical test methods and equipment.

Jeff holds an Associate's degree in Electronics Technology, fiber-optic emphasis, from the Pennsylvania College of Technology and is currently pursuing a bachelor's degree in Electrical Engineering.

THE USEFUL TECHNIQUE FOR THE MEASUREMENT OF RETURN LOSSES OF MULTIPLE OPTICAL DEVICES

Joung-Young Ha , Byung-Chul Lee . Young-Tark Lee, and Kwon-Hoon Han

Korea Telecom. Outside Plant Technology Research Laboratory
62-1 Whaam-dong, Yusung-gu, Taejeon, Korea

ABSTRACT

A new measurement method of return loss has been suggested which is useful and allows multiple DUTs (Device Under Tests) to be efficiently tested. The Return loss has been obtained from the optical loss measurement. Compared to the conventional method, the new method showed better characteristics in terms of the test procedures and reproduction.

1. INTRODUCTION

Because of the laser sensitivity to back-reflections, the accurate measurement technique is required for the return loss of optical components (i.e. connectors, optical fiber joints, couplers, WDMs, filters, polarization controllers etc.). Most of environment test of optical components are performed in multiple and/or cascaded configuration.

In this paper, the new measurement method has been suggested which allows the return losses of multiple and/or cascaded DUTs to be measured more efficiently than the conventional method. The test results have been compared between the conventional method and

the new measurement method

2. MEASUREMENT METHODS

2-1. Conventional method

The conventional method^[1] considers a test set-up consisting of an optical coupler, a CW laser source and an optical power detector. With the equipment arranged as in Fig.1.

The reflected power of the reference plug(P_1) and the power reflected by the DUT(P'_1) are measured. The return loss is then calculated according to the following expression.

$$R.L. = -10 \log ((P'_1 - P_1)/P_0) - L_c \quad [\text{dB}]$$

where P_0 is the incident optical power, L_c is the equivalent attenuation between ports 2 and 3 of the coupler.

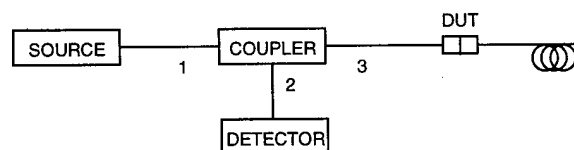


Fig. 1 Conventional Method Set-up

But the conventional method is not appropriate for the test of long-term reliability and multiple DUTs. In order to test multiple DUTs, optical switch is required. The use of optical switch involves the measurements of all the parameters P_0 , P_1 and L_c for every switch port.

Belcore^[2] recommends a transmission measurement method for measuring insertion loss and return loss for multiple DUTs. The measurement system requires a reflector of known reflectance (R_{ref}) and two optical switches. The return loss is obtained according to the following expression.

$$R_{\text{reflectance}} = Pr - K + 10 \log [1 - 10^{-dp/10}] \quad [\text{dB}]$$

where ;

Pr = received power

$$K = Pk - Rk + 10 \log [1 - 10^{-dp/10}]$$

$dp = Pr - Po$

Po = system noise

However, this measurement method not only requires the use of reflector but causes inconvenient when the additional patch cords are added to be cascaded for other tests, such as vibration, tension and thermal cycling test.

2-2. New method

A new measurement method is useful for the various environment tests and allows multiple DUTs to be efficiently tested. The measurement system for multiple DUTs is shown in Fig 2.

The return loss is obtained using the optical loss measurement instead of the optical power measurement.

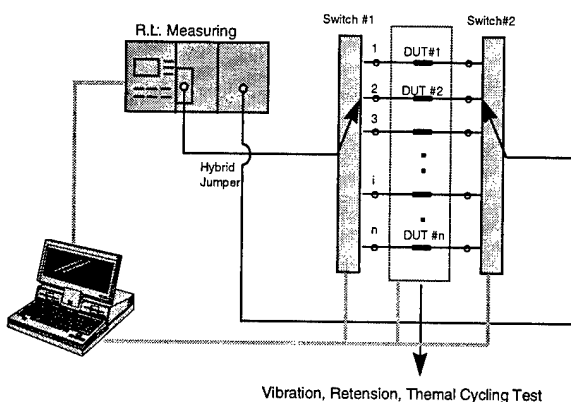


Fig. 2 Measurement System

The return losses are measured at the front and the back of DUT, respectively. The return loss, R.L. of the DUT, can be calculated from the return loss of the back of DUT, $RL2(\text{dB})$, the return loss of the front of DUT, $RL1(\text{dB})$, and the equivalent attenuation up to the front of DUT, $L(\text{dB})$, by the following equation.

$$R.L. = -10 \log (10^{-RL2/10} - 10^{-RL1/10}) - 2L \quad [\text{dB}]$$

where, L is loss from the reference cord to the front of DUT.

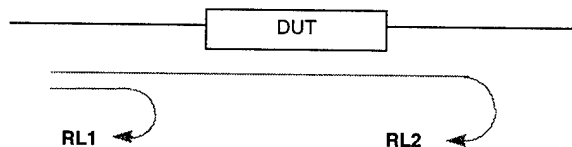


Fig. 3 New Method

3. TEST RESULTS

Fig. 4 shows the experimental set-up for the measurement of return loss. The DUT used

in the test was FC-PC connector. The return losses of the connector were measured at 4 different points with different extension lengths, respectively.

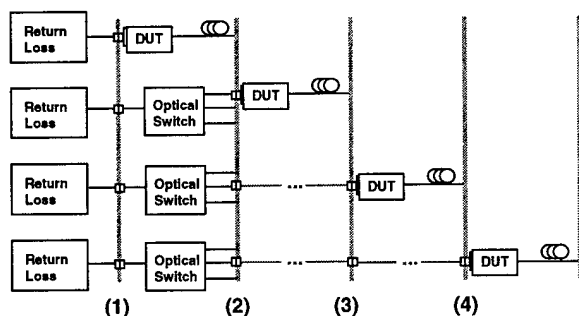


Fig. 4 Experimental set-up for the measurement of return loss

Table 1. Test result

	(1)	(2)	(3)	(4)
RL1[dB]		44.1	38.6	36.5
RL2[dB]		41.8	37.9	36.1
L [dB]		1.05	1.45	1.65
R.L[dB]	43.30	43.55	43.27	43.35

The test result using the new measurement method [Table 1] showed that the return losses were measured to be in good experimental error less than 0.5% for the identical DUT (FC-PC connector).

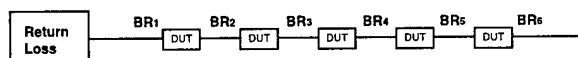


Fig. 5 Experimental set-up for the measurement of cascaded DUTs

The test result indicate that the return losses of the cascaded DUTs in Fig. 5 can be measured as well in the relatively simple way

using the new method.

Fig. 6 shows the test results of the repetitive measurement of the return loss of FC-PC connector using the conventional method and the new method, respectively.

The measurements were made repetitively by reconnecting the connector by 10 times. It was found that the return loss values measured by the conventional method were widely distributed around average value of 44.4dB, while the values by the new method exhibited more consistent values around average of 44.42dB, although the average value of each method was comparable.

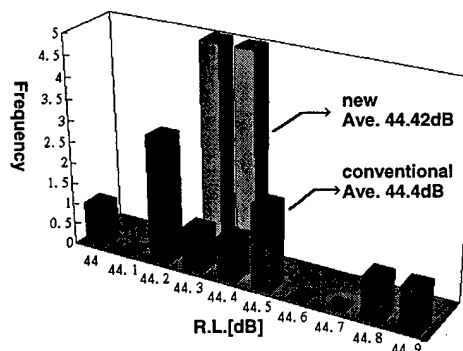


Fig. 6 Test results of repetitive measurement

4. CONCLUSIONS

Return losses of multiple and/or cascaded DUTs were measured using the new measurement method. The new method was relatively simple and easy the measurement of return loss without using reference reflector. When multiple DUTs are measured in cascade, this method allows each DUT's return loss to be measured were efficiently, than the conventional

method.

In addition, the new measurement method was found out to be less affected by the test conditions than the conventional method, giving rise to the more consistent results.

References

1. EIA/TIA STANDARD FOTP-107, "Return Loss for Fiber Optic Components", 1989
2. Bellcore : TA-NWT-001095 "Generic requirement for multi-fiber splicing systems for single-mode optical fibers" Issue 2, 1993. 10

AUTHORS

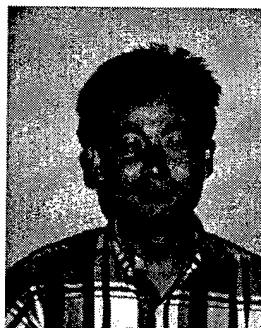


Joung-Young Ha

Korea Telecom.

62-1, Whaam, Yu-sung,
Taejeon, Korea

Joung-Young Ha was born in 1965. In 1989 he received M.S. degree in Electrical Engineering in Kyung-book National University and joined Korea Telecom. He is engaged in the development of mechanical splice .

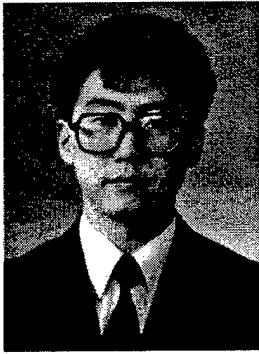


Byung-chul Lee

Korea Telecom.

62-1, Whaam, Yu-sung,
Taejeon, Korea

Byoung-chul Lee was born in 1967. In 1992 he received M.S. degree in physics in Seoul National University and joined Korea Telecom. He is engaged in the design of optical ribbon cable.

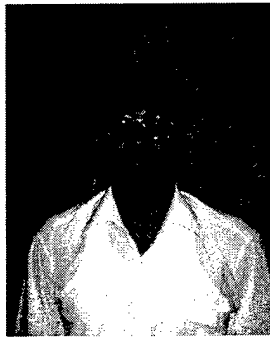


Young-tark Lee

Korea Telecom.

62-1, Whaam, Yu-sung,
Taejeon, Korea

Young-tark Lee was born in 1963. In 1988 he received M.S. degree in Electrical Engineering in Sung Kyun Kwan University and joined Korea Telecom. He is engaged in the design of optical ribbon cable and mechanical splice.



Kwon-hoon Han

Korea Telecom.

62-1, Whaam, Yu-sung,
Taejeon, Korea

Kwon-hoon Han graduated from Seoul National University with B.S. and M.S on Metallurgy and Rutgers University, U.S.A. with Ph.D on Ceramic Engineering. Since he joined Korea Telecom in 1992, he is involved in the development of optical outside plant technologies

Remodeled Automatic Fiber Testing System for FTTH Trials

Yoshiyuki Yoshii*, Kenichi Tomita*, Kiyoshi Omoto*, Naoki Nakao*, Masato Kuroiwa*

*NTT Technology and Development Support Center
1-6 Nakase Mihama-ku Chiba-shi, Chiba 261 Japan

Abstract

This paper describes a new Automatic Optical Fiber Operations Support System (AURORA) that is remodeled and operated to evaluate fibers automatically in accordance with the maintenance management procedures involved in Fiber To The Home (FTTH) trials. The new AURORA has a different wavelength for testing fibers due to Wavelength-Division Multiplexing (WDM) operation for services. Results for operating the new AURORA show excellent performance.

1. Introduction

Optical fibers have wide bandwidths that enable high speed transmission for all kinds of telecommunication networks. It goes without saying that finding and locating faults is important for reliable networks. Operation systems for automatic fiber testing, that are capable of measuring and monitoring fluctuations of optical loss in fiber optic cables by remote operation, are being researched from the viewpoint of effective maintenance⁽¹⁾. Since 1989, NTT has been developing Fiber Transfer and Test Systems (FITASs) and introducing it into long distance networks. The introduction was completed in 1995, and now approximately five hundred FITASs are working and contributing streamline maintenance. On the other side, we have also developed Automatic Optical Fiber Operations Support Systems (AURORAs) and introduced over a hundred systems into both regional trunk and access networks since 1993. Recently, the demand for AURORAs for optical access networks is increasing drastically in conjunction with the deployment of fiber optics in the networks. The AURORA was introduced to maintain the fiber's reliability, especially for business customers. However, since NTT planned Fiber To The Home (FTTH) trials in three towns, it had to be remodeled AURORA to correspond to WDM

operations so that both 1310 nm and 1550 nm were active for residential customers.

2. FTTH Trials

The FTTH trials are conducted at three sites in the suburbs of Tokyo as shown in Figure 1. The systems allow economical presentation of narrow-band communication services to general households by Passive Double Star (PDS) topology using an optical splitter as shown in Figure 2. They can also provide broad-band unilateral video services economically that are suitable for broadcasting-type signal transmission. The trials provide ISDN services as communication services, and also CATV and Video On Demand (VOD) as video services⁽²⁾. The system uses two optical wavelengths, 1310 nm and 1550 nm, over one fiber to take advantage of the optical characteristics of the fiber and to maximize the efficiency of the fiber plant. WDM components have been installed in the central office for the purpose of multiplexing the two wavelengths into a fiber. The trial conditions are summarized in Table 1.

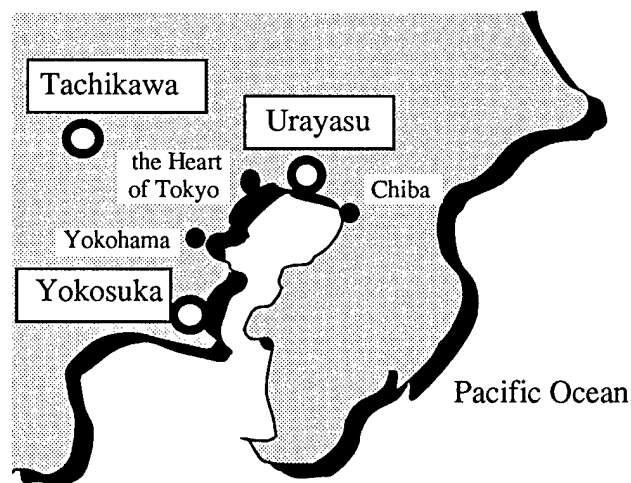


Figure 1 Location of FTTH Trial

3. Remodeling for Trials

Conventional AURORAs have a test wavelength of 1550 nm for fibers that have an active wavelength of 1310 nm. As mentioned above, however, the trial system has two wavelengths, 1310 nm and 1550 nm, for service transmission. Therefore, we had to assign an alternative wavelength for the 1550 nm test wavelength, taking into consideration other optical components and their respective wavelengths.

3.1 System Configuration

The system configuration of AURORA is illustrated in Figure 3. It consists of Measurement Equipment that include an Optical

Time Domain Reflectmeter (OTDR), a light source and an optical power meter, Fiber Switches that can select a fiber to be tested with the least optical loss, Optical Branch Modules that have optical couplers and optical filters for inserting test light into a selected fiber, Termination Cables in which an optical filter is embedded for filtering out test light, a Test Control Module that controls all of the equipment, and Workstations that are used to control AURORA with consoles.

All of the optical splitters of the PDS are installed between Subscriber Line Terminal (SLT) and the Optical Branch Module in the central office to minimize cost⁽³⁾. Thus, the OTDR assembled in AURORA enables fibers to be tested easily without optical splitters which make trace analyzing difficult.

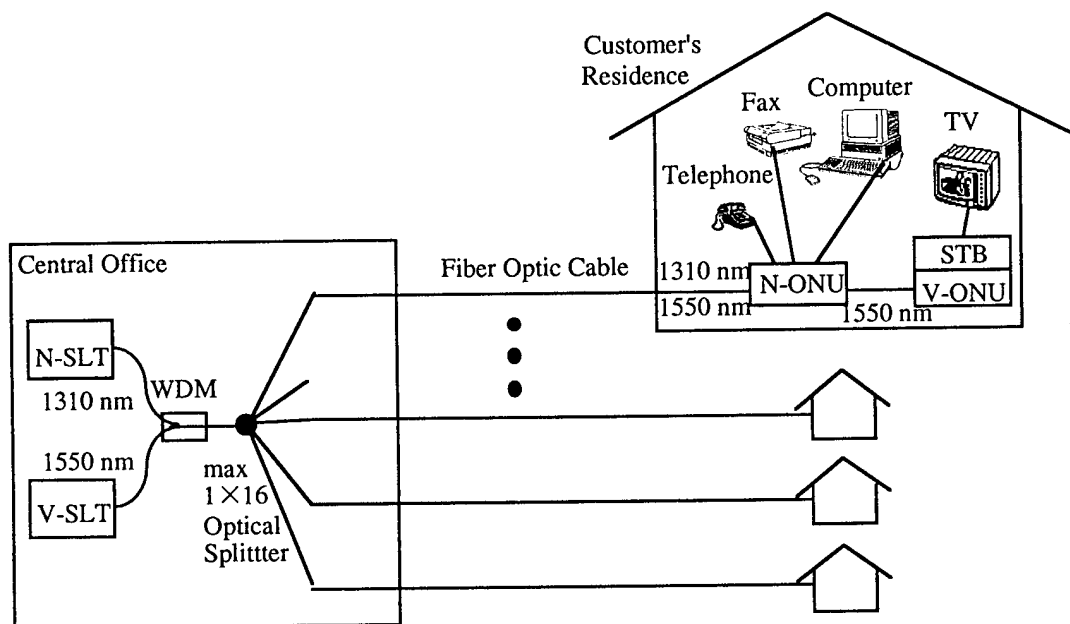


Figure 2 FTTH System

Table 1 Conditions of FTTH Trials

Trial Site	Services	Transmission System	Number of Fiber for a customer	Active Wavelength	Number of Customer	Terminated Fibers in CO	Number of AURORA
Tachikawa	ISDN CATV VOD	N-PDS	1	1310nm and 1550nm	Approximately 300	4,000	1
Yokosuka		ATM-PDS			Approximately 300	1,600	1
Urayasu		ATM-PDS			Approximately 300	6,000	2

3.2 New Test Wavelength

The new test wavelength should meet the following requirements.

- It should be more susceptible than active wavelengths for the purpose of detecting abnormal events easily before the events affect services. This requires a wider wavelength.
- It should be at least 100 nm away from active wavelengths to prevent interference.

We chose 1650 nm as the alternative wavelength based on the above requirements, and also because it had satisfactory results for FITAS in long distance networks⁽⁴⁾.

3.3 Principle

The process in a case of OTDR testing is described below and illustrated in Figure 4. First, an operator sends an order to test a fiber from a remote office. The Test Control Module instructs the Fiber Switch to select the fiber, and the Measurement Equipment to launch the test light. The test light is inserted into the fiber through an optical coupler in the Optical Branch Module and is propagated in the fiber. Back-scattered light caused by the test light is detected as a trace and analyzed to distinguish jointing points and evaluate optical loss. The test light is reflected at an optical filter in the Termination Cable which is tolerant for active wavelengths only. Finally, the results are analyzed and reported to the operator. As compared to conventional AURORA, all optical components, couplers and filters, are modulated to be suitable for new wavelength combinations in addition to 1650 nm LD.

4. Operations

AURORA is a versatile system for not only maintenance but also multipurpose fiber testing. Table 2 tabulates operations of AURORA. The approval test is carried out just after cable installing in order to improve deviant connecting. The pre-service test is carried out just before fibers are dedicated to customers. The preventive test is

carried out automatically once every three months to monitor fiber degradation and once a month to monitor submergence sensors with reference to former OTDR traces. The identification refers to launching a signal light to be detected at the terminal in order to verify that correct fibers are connected in jointing works. AURORA is capable of the above testing by control from remote workstations in accordance with the procedures for service operation. It was definitely indispensable in operating the FTTH networks with minimum personnel resources at the trials.

All Workstations for operating the FTTH system, including AURORA's, were concentrated at the Local Network Operation Center, where several engineers are always stationed, to ensure effective surveillance, analysis and reaction.

They collect a number of equipment alarms and collates them to determine if the alarms originate from a fiber disconnection. In case of fiber disconnection, they operate a Workstation of AURORA, locate the fault and dispatch technicians for quick restoration, minimizing downtime. In fact, AURORA is operated favorably as well as the FTTH networks.

The successful performance of AURORA makes us think that it is very effective for the mass deployment of fibers into access networks.

5. Conclusion

This year, we have a scheme to develop more sophisticated and inexpensive AURORAs for FTTH on the basis of commercial use, not trial use⁽⁵⁾. The described excellent results will surely promote the deployment of AURORA into optical access networks in future.

Acknowledgments

We gratefully acknowledge the invaluable contributions of Mr. Shinichi Sugiura and Mr. Naoyuki Atobe for their stimulation, discussion and encouragement.

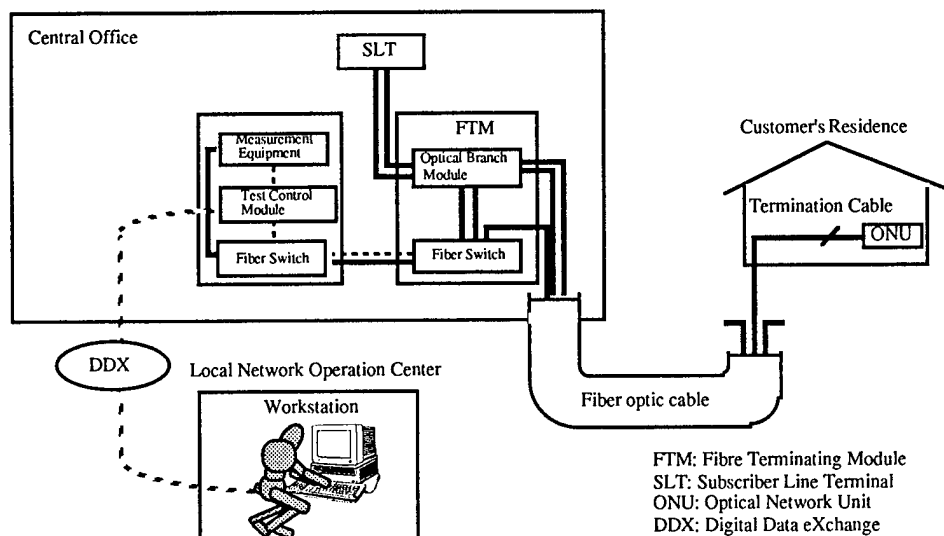


Figure 3 System Configuration

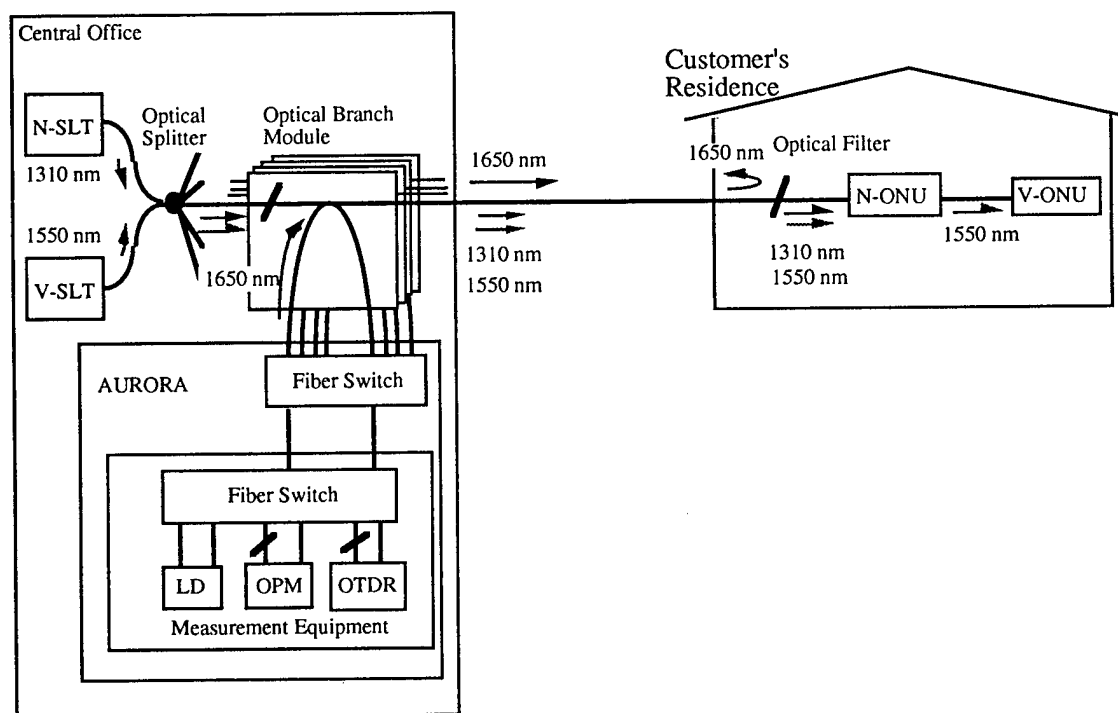


Figure 4 Route of Test Light

Table 2 Operations

	1310 nm	1550 nm	1650 nm
OTDR	Approval Test Pre-service Test	Approval Test Pre-service Test	Preventive Test Fault Location
Optical Power Test	Approval Test Pre-service Test	Approval Test Pre-service Test	
Identification			Fiber Identification at the terminal (Light Source is common to Optical Power Test)

References

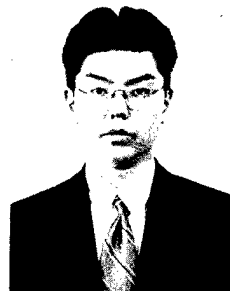
- (1) E. Cottino, D. Deller, S. De Paoli, "1625 nm Monitoring System Design for the Preventive Maintenance of Fiber Optics Plants", 42nd IWCS Proceedings, pp. 799-804, 1993.
- (2) K. Harikae, "Optical Access System Technology to Support Multimedia Service Field Trials", NTT Review, Vol. 7, No. 6, pp. 74-79, November 1995.
- (3) N. Nakao, T. Enomoto, M. Kuroiwa, "Splitter Positions and Testing Wavelength for Optical Fiber Access Networks", 22nd ECOC Proceedings, September 1996 (to be published).
- (4) S. Goto, I. Sankawa, T. Horiguchi, N. Atobe, "Remote Optical-fiber Testing System for Unrepeated Long-span Optical-fiber Trunk Lines", 43rd IWCS Proceedings, pp. 608-613, 1994.
- (5) T. Ebihara, N. Nakao, M. Kuroiwa, "Novel Automatic Remote Fiber Line Testing System and New Fiber Termination Module for Expanding Local Subscriber Loops", 22nd ECOC Proceedings, September 1996 (to be published).



Yoshiyuki Yoshii

Yoshiyuki Yoshii received his Bachelor's degree of Science in solid physics from the Tokyo Institute of Technology in 1990. After joining NTT in 1990, he was engaged in development of operation systems for automatic fiber testing. He is currently a technical staff member of Technology and Development Support Center, Telecommunication Network Laboratory Group, NTT, and is engaged in development of closures for fiber optic cables.

He is a member of the Institute of Electronics, Information and Communication Engineers of Japan.



Kenichi Tomita

Kenichi Tomita graduated from Tomakomai Technical College in 1988.

After joining NTT in 1988, he was engaged in constructing outside telecommunication plants. He is currently a technical staff member of Technology and Development Support Center, Telecommunication Network Laboratory Group, NTT, and is engaged in development of operation systems for automatic fiber testing.



Kiyoshi Omoto

Kiyoshi Omoto received his Bachelor's degree and his Master's degree in civil engineering from Ehime University in 1986 and 1988, respectively.

After joining NTT in 1988, he was engaged in development of fiber optic cables and operation systems for automatic fiber testing. He is currently an Engineer of Technology and Development Support Center, Telecommunication Network Laboratory Group, NTT, and is engaged in development of operation systems for optical access networks.

He is a member of both the Institute of Electronics, Information and Communication Engineers of Japan, and the Operations Research Society of Japan.



Masato Kuroiwa

Masato Kuroiwa received his Bachelor's degree in electrical engineering from Kyushu University in 1981.

After joining NTT in 1981, he was engaged in development of fiber optic cables and operation systems for access networks. He is an Executive Engineer of Technology and Development Support Center, Telecommunication Network Laboratory Group, NTT, and currently responsible for development of operation systems for automatic fiber testing and measurement equipment.

He is a member of the Institute of Electronics, Information and Communication Engineers of Japan.



Naoki Nakao

Naoki Nakao received his Bachelor's degree and his Master's degree in electrical engineering from Okayama University in 1985 and 1987, respectively.

After joining NTT in 1987, he was engaged in development of splicers for copper pairs. He is currently a Senior Engineer of Technology and Development Support Center, Telecommunication Network Laboratory Group, NTT, and responsible for development of operation systems for automatic fiber testing and measurement equipment.

He is a member of both the Institute of Electronics, Information and Communication Engineers of Japan, and the Institute of Electrical and Electronics Engineers, Inc.

WIDE RANGE OPTICAL LOW COHERENCE REFLECTOMETER FOR HIGH RESOLUTION FAULT DETECTION AND COMPONENT CHARACTERIZATION

Mauro Bottanelli

SIRTI S.p.A.
Cassina de' Pecchi (MI), ITALY

ABSTRACT

This paper describes a new transportable and easy to use Optical Low Coherence Reflectometer (OLCR) set-up, that has been designed and developed for field fault detection and optical component characterization. With respect to the typical OLCR features, our reflectometer exhibits a very wide scan range (up to 40 centimeters into fiber) with better than 80 microns spatial resolution and more than 100 dB sensitivity, without using polarization control elements or any kind of signal filtering technique.

INTRODUCTION

Optical communication systems have had a great development in recent years, both in long distance and in distribution networks. The growing interest for higher and higher values of the [bit rate]x[distance] product and for broad band services transmission had required the development of high reliability and high performance optical components.

Commercially available Optical Time Domain Reflectometers (OTDRs) are limited both in resolution and in dynamic range when a centimetric or a sub-centimetric fault location is needed, or when a very low back-reflection component has to be characterized. On the contrary, Optical Low Coherence Reflectometry has been already pointed out in the past as a suitable technique for high resolution fault detection and optical component characterization. Recently, the availability of erbium doped optical amplifiers as light sources

and the growing interest in the development and testing of high technology optical components (couplers, WDMs, filters, attenuators, isolators...) have emphasized OLCR potentiality with respect to traditional measurement method.

This paper describes the design, the development and the first characterization of a new transportable and easy to use OLCR set-up, which has been conceived both for field fault detection and for optical component analysis and quality control applications. The new OLCR set-up has been developed by SIRTI R&D laboratories in cooperation with the Polytechnic of Milan during the last year.

THEORY AND BACKGROUND

Fig. 1 reports the basic scheme of a generic OLCR set-up.

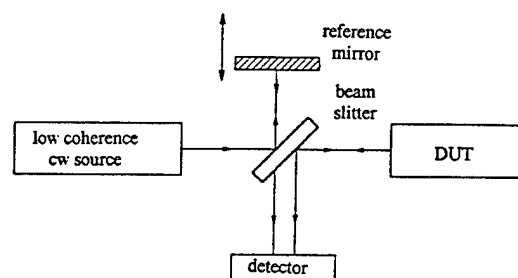


Fig. 1 - Basic scheme of a generic OLCR set-up

The continuous wave low coherence radiation from the light source is parted into a

measurement and a reference beam by means of a beam splitter. After reflections, respectively inside the Device Under Test (DUT) and from the variable length reference path mirror, the beams are combined by the splitter, giving interference patterns on the detector. The set-up therefore reproduces a Michelson interferometer, but, due to the source low coherence time, interference can rise only for very limited difference between the measurement and the reference path, that is: discrimination among different back-scattering points inside the DUT can be obtained with a very high spatial resolution, simply moving the reference mirror by means of a micropositioning stage. The larger the source optical power, the higher the OLCR set-up dynamic range; the narrower the source autocorrelation function, the higher the OLCR set-up resolution. In the past, only Light Emitting Diodes (LEDs) or Super-Luminescent Diodes (SLDs) constituted suitable sources for OLCR set-ups, but better performances can be achieved nowadays by means of the Amplified Spontaneous Emission (ASE) of an erbium doped Optical Fiber Amplifier (OFA). Let us now review the main features of OLCR systems:

- **Spatial resolution:** the shortest spatial distance between two contiguous scattering points that can be distinguished by the system. It can be proved to be:

$$\Delta z = \frac{\lambda^2}{2n\Delta\lambda}$$

where λ and $\Delta\lambda$ are respectively the wavelength and the spectral width of the source, and n is the material refraction index of the DUT.

- **Sensitivity:** the lowest back-scattered signal that can be detected by the system. It can be proved to be:

$$R_{min} = \frac{qB}{\mathcal{I}_{dc}} \quad (\text{shot noise limited case})$$

$$R_{min} = \frac{B}{2\gamma \cdot \delta\nu} \quad (\text{excess noise l. c.})$$

being B the detection band of the optical signal, q the elementary charge, γ the DUT insertion loss, \mathcal{I}_{dc} the photodetector direct current offset and $\delta\nu$ a sort of equivalent source power band width defined by the source power spectrum $G(\nu)$ as:

$$\delta\nu \equiv \frac{\left[\int_0^{+\infty} G(\nu) d\nu \right]^2}{\int_0^{+\infty} G^2(\nu) d\nu}$$

In the first case, the system sensitivity is mainly limited by the photodetector characteristics; in the second, it is limited by the light source intensity fluctuations.

- **Blind space:** the spatial width of some areas inside the DUT where the system can not perform a good measurement, due to the presence of minor lobes in the source autocorrelation function. Those areas are typically adjoining intense light back-scattering centers in the DUT. Their spatial extension can range from 20 mm (multimode LD source) to 5 mm (LED, SLD source) or to 0.5 mm (ASE source) considering the source FW60dB (Full Width at 60 dB from the top of the autocorrelation function).
- **Scan range:** the largest continuous spatial range that can be scanned by the system, typically about 20 centimeters more or less, depending on the system design and purpose.

A NEW OLCR CONFIGURATION

Fig. 2 sketches the main features of our new OLCR configuration. The light source is the amplified spontaneous emission of an erbium doped optical amplifier, having 6 dBm optical output power at 1530 nm, about 8 nm FWHM spectral width, a 1 ps FWHM autocorrelation function width (see figure 3) and a very low polarization degree. Light is launched into a traditional SMR type optical fiber without any particular kind of polarization control, and is

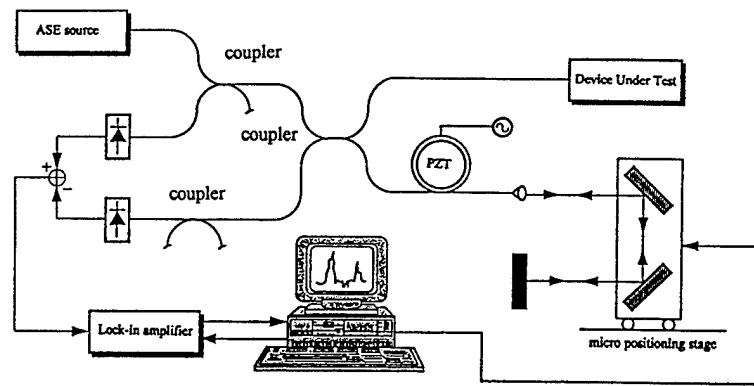


Fig. 2 - Sketch of the new OLCR set-up

parted into measurement and reference beams by means of a 50:50 fusion coupler. A sawtooth ramped piezoelectric cylinder (PZT) as phase modulator (PM) has been inserted on the OLCR reference arm in order to improve the sensitivity by means of a lock-in amplifier detection. A particular micropositioning motorized stage (up to 0.2 micron step resolution) can adapt the reference path to the measurement one, in order to scan up to 40 cm DUT length.

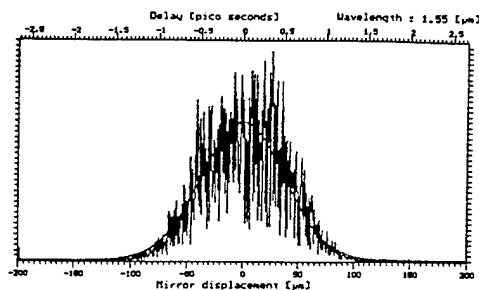


Fig. 3 - ASE source autocorrelation function

Other two 50:50 fusion couplers and two InGaAs PIN detectors have been inserted into the configuration in order to implement the so-called "balanced detection" technique, that is a subtraction between photocurrents deleting the source intensity fluctuation excess noise. In ideal conditions (coupler splitting ratio $k=0.5$, equal detector responsivities, identical detection pigtail paths) the system can be considered shot noise limited only, with even up to a 40 dB sensitivity improvement with respect to the single PIN detection. The opto-mechanical set-up is completely controlled by a personal computer by means of a C language developed program.

A comparison among our new set-up and the most effective traditional OLCR configurations (fig. 4/a, /b and /c) is summarized in the following points 1, 2, 3:

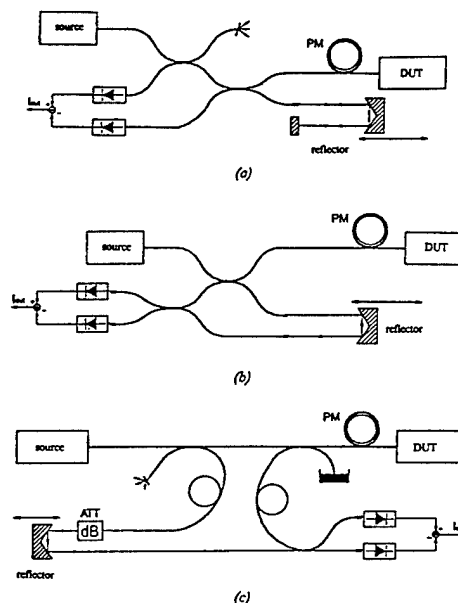


Fig. 4 - Most effective traditional OLCR set-ups

- in the case of a perfectly balanced detection, /b configuration sensitivity can be proved to be theoretically the highest; our configuration and the c/ one have a theoretical sensitivity 3 dB worse than /b. /a configuration can not be considered balanced in any case (it is the worst one). However the real sensitivity also depends on the PZT position: due to macrobending

losses, it can be proved that the PZT placed on the measurement arm can make sensitivity worse, while, as in our configuration, the PZT placed on the reference arm does not influence the sensitivity;

- our and /a configurations have the highest scan range, because they double the moving stage mechanical scan range. Moreover, as far as we know, a 40 cm scan range has never been reported in the literature till now;
- our and /a configurations delete the influence of possible light reflections at the fiber-air interfaces, because in these two configurations unwanted reflected light and the reference light travel along the same physical paths.

NEW OLCR SET-UP CHARACTERIZATION AND FIRST EXPERIMENTAL RESULTS

Table 1 reports our OLCR set-up main features, as measured according to several trial experimental results.

Table 1 - New OLCR set-up mean features

Sensitivity	107 dB
Repeatability	0,86 dB
Reproducibility	0,89 dB
Spatial resolution (FWHM)	75 μ m
Blind space	FW20dB = 260 μ m FW40dB = 550 μ m FW60dB = 1,04 mm
Scan range in the air	60 cm
Scan range in the fiber	40 cm
Measurement mean time (for a 2 cm long DUT)	5 minutes

It is interesting to point out the fact that these such remarkable performances are however still under the maximum configuration theoretical potentialities (the maximum theoretical sensitivity level, for instance, has been calculated to be 142 dB), and that they have been achieved without any kind of particular optical component selection, polarization control systems or hardware end software filtering technique. Those present features can be considered to be sufficient for every practical

measurement purposes, a part from fiber Rayleigh scattering level evaluation, which would require an higher sensitivity and, in general, a very long measurement time.

By means of experimental reports, fig. 5, 6, 7 illustrate the capability of the new OLCR system to be used as fault detector and for component characterization.

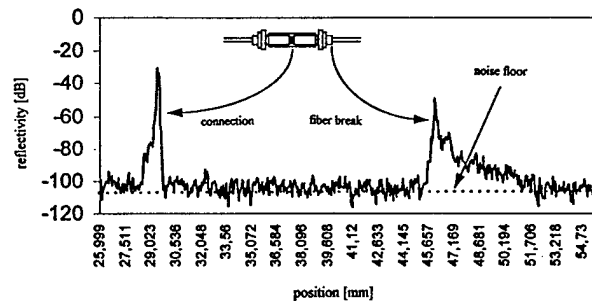


Fig. 5 - Fiber break identification in a connector

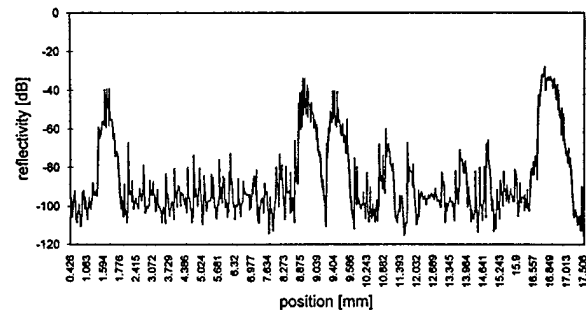


Fig. 6 - 1550 nm optical filter

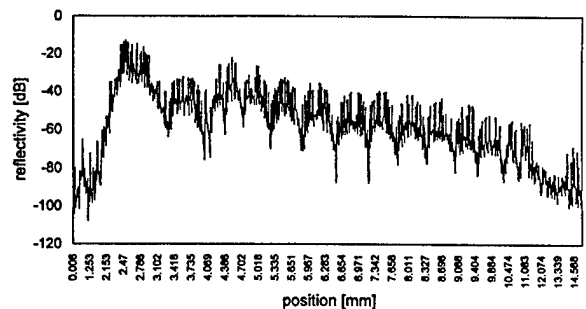


Fig. 7 - All-fiber optical Bragg grating

CONCLUSION

A new OLCR set-up for fault detection and high resolution component characterization has been developed and described. Up to 40 centimeters scan range, better than 80 μm spatial resolution and more than 100 dB dynamic range have been achieved.



Mauro Bottanelli

Cables and Optical
Technologies
R&D Dep. - SIRT I S.p.A.
Via E. Fermi, 2 - 20060
Cassina de' Pecchi (MI)
ITALY

ACKNOWLEDGEMENTS

This work has been developed by the author and by Adolfo Ottonello during a one year stage in SIRT I's laboratories. We would like to thank Mario Martinelli (Polytechnic of Milan) for his invaluable help in theoretical question deepening.

Mauro Bottanelli was born in 1963. He received the Dr. Ing. degree in Nuclear Engineering from Polytechnic of Milan. After a two years activity in the field of industrial automation, he joined SIRT I in 1990 as research engineer in the field of optical fiber and optical component characterization, and of broadband network design. He is a member of the ITU-T 4/15 National Working Group on fibers, cables and optical components.

REFERENCES

- [1] H.H. Gilgen, G. Bodmer, C. Zimmer, "*Optical coherence domain reflectometry as a test method for integrated optics devices*", 2nd Optical Fibre Measurements Conference, Turin, p. 143-146, 1993.
- [2] W.V. Sorin, D.M. Baney, "*Measurement of Rayleigh backscattering at 1.55 μm with 32 μm spatial resolution*", Photonics Technology Letters, vol. 4, p. 374-376, 1992.
- [3] K. Takada, T. Kitagawa, M. Shinizu, M. Horiguchi, "*High-sensitivity low coherence reflectometer using erbium-doped superfluorescent fibre source and erbium-doped power amplifier*", Electronics letters, vol. 29, p. 365-367, 1993.

Newly Developed Administration System for Remotely Controlling Optical Network Monitoring Equipments at Multiple Locations

**Hisao MAKI, Toshiaki ZAKOH, Youichi HATA,
Yoshinori TAKENAMI, Tetsushi MATSUDA, Tetsuya TAGUCHI**

**Sumitomo Electric Industries, Ltd.
1, Taya-cho, Sakae-ku, Yokohama, Kanagawa, Japan**

ABSTRACT

Successfully we have developed remote administration system that has the remote operating functions, not only to monitor optical subscriber lines but also to maintain the network equipments. Applying the network management program, we administrate the network failure by considering each monitoring equipment as the managed object in the network. So, we can recover quickly from the failure in the monitoring system, by means of realizing some functions as follows ; 1) to send the command for tracing the cause of failure, 2) to identify the failure remotely by above management program, 3) to rewrite the control program of each equipment, remotely without replacing the hardware. If the cause of failure is ascertained, this system provides exact and user-friendly operations for an operator in the maintenance center. Certainly, this system will reduce the maintenance cost of optical subscriber lines drastically.

1. Introduction

The optical fiber loops have been introduced in the subscriber network instead of metal cables as in the past. In Japan, NTT has been announced that optical fiber loops will be constructed in the all subscriber lines until 2010.

The technology, that we can monitor the state

of optical fiber line, is established. And the optical fiber monitoring system has already been operated. We can administrate the optical fiber line by monitoring the optical subscriber line with the method of inserting the monitoring light into the communication lines.

While the optical fiber loops have been spread all over the country, it will be necessary to manage this optical fiber monitoring system itself. If the failure occurs in these optical fiber monitoring systems, this maintenance system can find the cause of a failure automatically and identify the part of the failure equipment. These functions of this maintenance system will produce a high efficiency in the optical fiber monitoring system.

We developed the administration system for remotely controlling optical network monitoring equipments at multiple locations all over the country, by combining the technology of testing for optical fiber lines with the technology of network management.

We describe the detail of this development as follows.

2. System Requirements

2.1 Outline of this maintenance system

We show the requirements of administration system for remotely controlling optical network monitoring equipment.

To construct the optical subscriber network, the maintenance of the optical subscriber

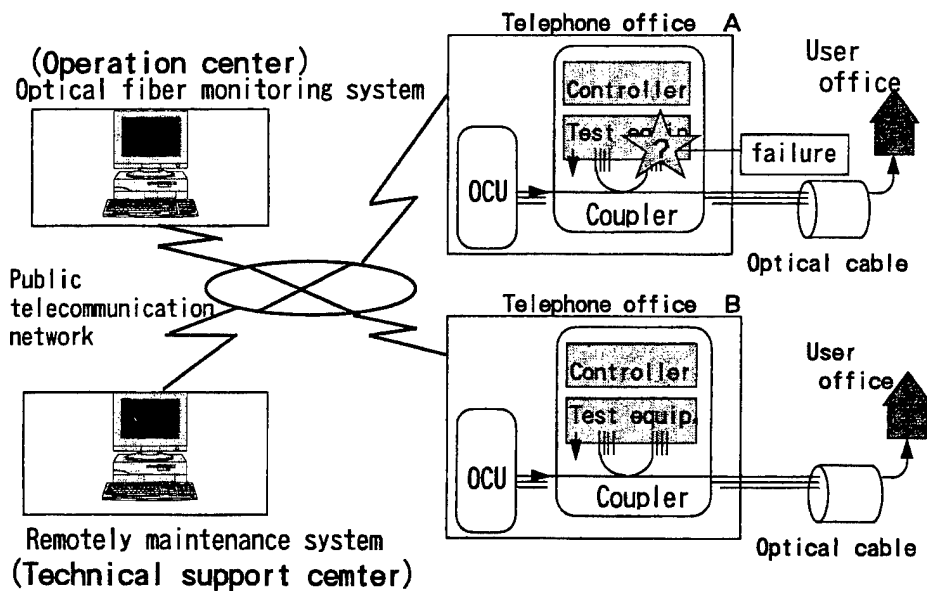


Fig.1 System configuration of maintenance system

network is important matter to keep high reliability of the optical subscriber network and to recover the communication lines from the failure in the network easily.

The function of monitoring the optical subscriber lines realizes a high reliable optical subscriber network.

Automatic optical fiber operation support system (it is called "AURORA"), already used by NTT since 1990 [1], has the main functions as follows ; 1) evaluating the broken points of optical fiber by using OTDR[2], fiber selector and coupler. 2) checking the quality of data and error rate of communication in service.

Further, to investigate the higher reliability, we need the grasp of the information in the monitoring systems at multiple locations and the quick repair of the damaged equipment. Fig.1 shows the relation between the optical fiber monitoring system and this developed network management system.

2.2. Required Functions

We can recover quickly from the failure in the monitoring system, by means of realizing some functions as follows ; 1) to send/receive the command for tracing the cause of failure, 2) to identify the failure remotely by original tracing algorithm, 3) to rewrite the control program of

each equipment in short time, remotely without replacing the hardware.

First of all, the function that we identify the failure state of equipment by using the controlling command is realized by designing the operation program of each equipment. It is important for the program to have the operation about tracing the failure. That is to say, the equipment must send the state of itself in the condition of the failure state.

Secondly, the function that we can make sure of the failure point and support the repair information of estimated cause and its countermeasure is accomplished. After all it becomes complicated for an operator to maintain the monitoring system, in case of wondering that he can't find out an exact cause or an exact countermeasure. If the trouble has happened at each location where the optical fiber monitoring system was introduced, each maintenance center will be in a state of confusion. So it is important for an operator to be supported by the accurate suggestion.

Thirdly, the function that we can automatically change the program of each equipment in the system is useful.

3. System Design

3.1. Basic System Configurations

We define every equipment which constructs the optical fiber monitoring system as MIB (Management Information Base [3]) individually in the network.

If the failure occurs in this network, all information pertaining to the failure is stored in a database. If another network failure occurs, this system automatically retrieves and displays related failure information.

We have developed the algorithm, which can automatically trace the cause of the failure by making a comparison between the detected facts and the records in the past. And we have equipped the mechanism of detecting fact. By using it's mechanism, for example, we can test the optical power in the loop-back of fiber selector or optical branch module, and so we make sure of the optical fiber monitoring system operated normally.

3.2. Integrated Network Management System

We describe the merits of this system.

(1)System architecture

The management system is a large, complex piece of software comprising a man-machine interface, management functions, a management information base (MIB), management protocols and some other functions.

Its architecture, particularly as regards modularity, significantly affects overall system performance. This network management system architecture is a sort of distributed processing environment consisting of independent modules that implement these software functions.

(2)Large-scale network management

In designing this network management system, major emphasis was placed on the management of such interconnected networks and on the communication infrastructure.

(3)Management protocol integration

Equipment management operations are performed via layer protocols and vendor specific management protocols. This network

management system integrates these protocols, allowing the man-machine interface functions and management operations to be executed without regard to any particular protocol.

(4)Flexible management format

As a result of communication load in large networks or decentralization of management departments, it may become necessary to build the management system in a hierarchical manner or install another monitor in a separate location.

This network management system allows the management system to be built in a flexible manner to cope with such situation.

(5)Installation of managed objects

The management information regarding standard protocols, intermediate equipment and vendor specific devices is all provided through extended MIB, which is based on MIB- II . Management system extensibility depends on how easily these managed object definitions can be installed and managed in the system. This network management system offers a tool to automate managed object installation.

(6)Automatic diagnosis in fault management

Fault management is one of the key factors in network management. Automating network fault diagnosis calls for a sophisticated AI system, but a problem lies in the derivation of the diagnostic rules. As the first step in automating network diagnosis, this network management system stores network fault samples in the form of trouble reports to be retrieved later for use in diagnosis. It is also preprogrammed with information on known solutions to common network faults and presents it in the event of a fault.

(7)Man-machine interface

This network management system aims for rapid identification of faulty devices and quick problem determination and solution through its graphical user interface.

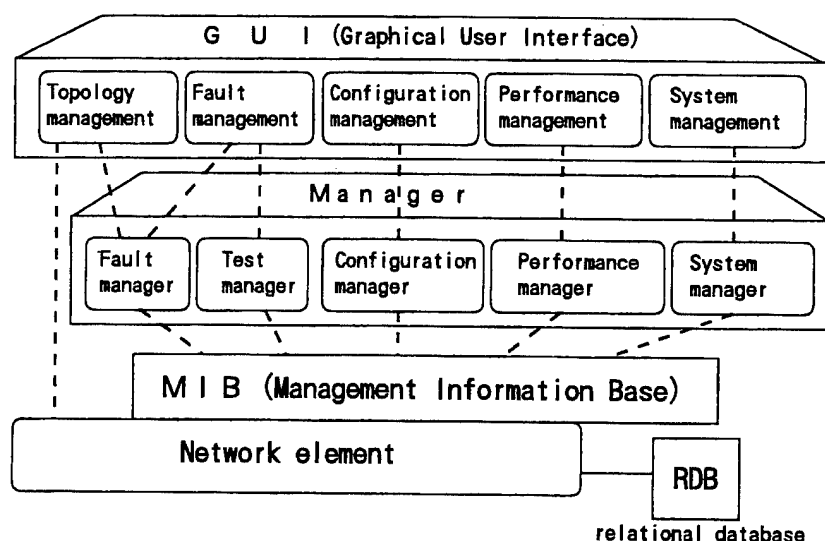


Fig.2 Network management system architecture

3.3. Remote Maintenance Method

We describe the remote maintenance functions. Fig.2 shows this network management system architecture[4].

(1) Configuration management function

1) Automatic configuration definition

The management system requires node and network configuration to be input during initial installation. For a large network, however, inputting information requires considerable time and effort. This network management system offers the user an automatic node discovery capability which reduces the inputting work and facilitates configuration.

2) Physical configuration window

In the network, every equipment in the system is described with physical image.

For the unmanaged equipment, this network management system can make a configuration definition and display it in the topology window. Unmanaged equipment is displayed insensibly, so it can be easily differentiated from managed equipment.

3) Network groups and cluster function

The network configuration display for a large network often does not fit in a single window. To solve this problem, the system displays (as the part of its GUI) the hierarchical relationships between network groups and presents the network configuration of each of these groups.

The system also offers a cluster function which

automatically displays neighboring nodes in a single cluster in the network topology window. The system allows the user to view a network configuration with many nodes in a limited window size.

4) Editing functions in the network configuration window

Node editing functions (such as add, delete, connect and disconnect) are executed in the topology window, which is used for actual network management. Therefore, editing does not interrupt management operations.

(2) Fault management function

1) Fault state

This network management system classifies network faults into hardware, communication protocol, performance and optical state. In the topology window, the fault types are discriminated from one another by color, and acknowledgment by the administrator is indicated by shading. This is especially useful in preventing traces of naturally recovering faults from disappearing from the network topology window.

Fault states are reflected in the network group to which the faulty device belongs to all higher-level network groups. This enables fault detection through network group monitoring alone. If more than one fault occurs at a time, the most serious fault shows up in the network groups.

2) Fault information logging and alarm notification

The system stores fault information in a database as a fault log. It also stores the causes of faults, actions taken and other related information in the form of trouble reports correlated with pertinent faults. When a fault occurs, the system searches the fault log to find and display reports on similar faults that occurred in the past. This network management system can also display preprogrammed solutions to network faults and notify the administrator of fault generation through an alarm relay or over the telephone.

3) Performance management function

This network management system defines the attributes of performance as integral counter values, records a combination of performance attributes at regular intervals, and presents these records as graphs.

(4) System management function

The system management functions in this system offers include file downloading to connecting the products in the network system.

(5) Help function

This network management system provides a hypertext-based on-line help capability that describes window functions and operations. The user can append his/her own help messages to

the help file.

4. Realizing of Each Function

4.1. Network Management Function

(Using configuration management function)

We have realized the remotely maintenance system as a network management system. In this maintenance system, we consider each equipment of optical fiber monitoring system as a network element. We define every equipment which constructs the optical fiber monitoring system as MIB individually in the network.

In this network, every equipment in the optical fiber monitoring system is described with physical image. For unmanaged equipment, this maintenance system can make a configuration definition and display it in the topology window. Unmanaged equipment is displayed insensibly, so it can be easily differentiated from managed equipment. So, we can confirm system construction of optical fiber monitoring system easily. We will reach the detail elements of this system by clicking a upper-layer element on the topology window. Fig.3-a shows the relationship between this maintenance system and the optical fiber testing system.

4.2. Failure Tracing Function

(Using fault management function)

In this maintenance system, we prepared the

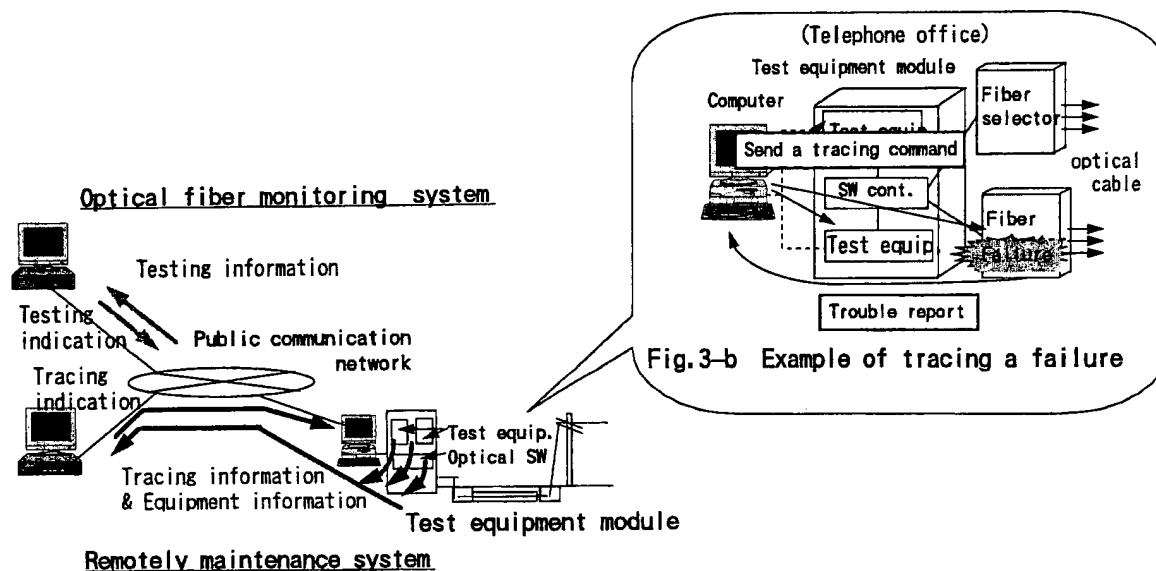


Fig.3-a Relation between monitoring system and maintenance system

command for tracing a failure in the optical fiber monitoring system. Fig.3-b shows the tracing method by using this command. We have developed the algorithm, which can automatically trace the cause of the failure by making a comparison between the detected facts and the records in the past. And we have equipped the mechanism of detecting fact. By using it's mechanism, for example, we can test the optical power in the loop-back of fiber selector or optical branch module, and so we make sure of the optical fiber monitoring system operated normally [see Fig.4].

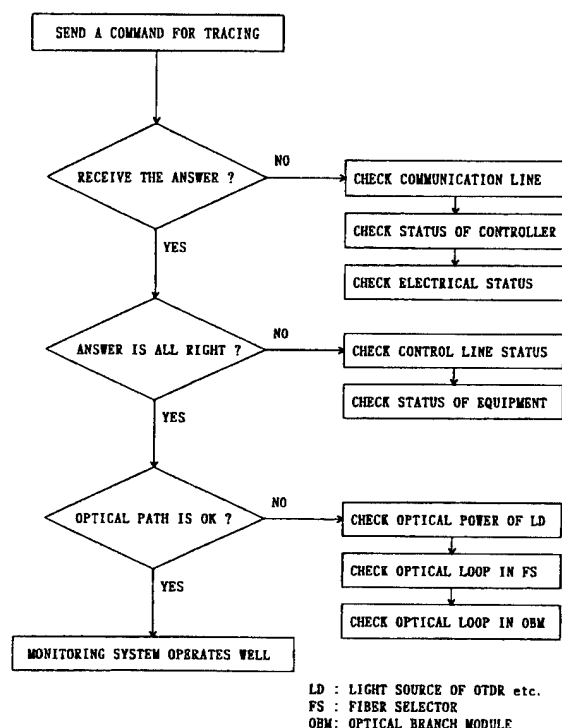


Fig. 4 Algorithm for tracing a cause of the failure

This maintenance system stores failure information in a database as a fault log. It also stores the causes of failure, actions taken and other information in the form of trouble tickets. When a failure occurs in the optical fiber monitoring system, this system searches the fault log to find pertinent failure and display reports on similar failure that occurred in the past.

This network management system can also display preprogrammed solutions to network

faults and notify the administrator through an alarm.

4.3. Program Exchanging Function (Using system management function)

We can recover quickly from the failure in this monitoring system, by means of realizing some functions as mentioned above. After enforcing to send the command for tracing the cause of failure and to identify the failure remotely by above management program, we lastly rewrite the control program of each equipment in less than 30 min., remotely without replacing the hardware.

5. Evaluation of Prototype System

We describe the distinctive points in the Table1.

Table.1 Evaluation of prototype system

Item	Specification
1. the number of managed system	500 ~ 2000 (according to the capacity of HD)
2. the number of fault information	about 400 (originally installed)
3. the time for exchanging program	≤ 30 min. (using public telecommunication)

6. Future Applications

In future ,we will develop expanded system which can administrate whole equipments in the optical network, by extending the definition of MIB to each equipment located from the telephone office to each personal house.

As the architecture of this system is based on the object-oriented network method, we can apply this system easily, not only to expand their function of this system but also to connect this system to another one.

7. Conclusion

We have described an integrated network management system which remotely controls optical network monitoring equipments at multiple locations.

Applying the network management program originally developed, we can administrate the network element, by considering each monitoring equipment as the managed object in the network.

This maintenance system was designed to have the following functions.

- network element management function
- failure tracing function
- program exchanging function

This system has been developed to a level of practical use.

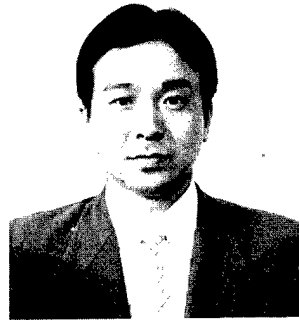
But, it will also be necessary to improve the management functions and the range of solutions about the network faults through this application in the actual network.

References

- [1] N.Tomita, H.Takasugi, H.Suzuki and T.Uenoya
"An automatic maintenance test system for optical subscriber loops", in Proc. EFOC/LAN '91, June 1991, pp.130-134.
- [2] N.Tomita, H.Takasugi, N.Atobe, I.Nakamura, F.Takaesu, S.Takashima
"Design and performance of a novel automatic fiber line testing system with OTDR for optical subscriber loops", IEEE J.Lightwave Technol., vol.12, no.5, pp.717-726, May 1994.
- [3] RFC 1213 : MIB- II (March 1991).
- [4] N.Yoshie, A.Natsume, I.Mizutani, H.Harada, M.Taniguchi, H.Tsuchiya, H.Takahashi,
"Dr_Net integrated network management system", Sumitomo Electric Technical Review, no.36, June 1993.

Biographies

Hisao MAKI



Sumitomo Electric
Industries, Ltd.
1, Taya-cho,
Sakae-ku,
Yokohama, Japan

Hisao Maki was born in 1958. He received his B.E. and M.E. degrees in System Engineering from Kobe University in 1981 and 1983 respectively. He joined Sumitomo Electric Industries, Ltd. the same year and has been engaged in research and development of automatic optical measuring instruments. He is now a senior engineer of Optomechatronics System R&D Dept. Yokohama Research Laboratory. He is a member of the institute of Electronics, Information and Communication Engineering of Japan.

Toshiaki ZAKOH



Sumitomo Electric
Industries, Ltd.
1, Taya-cho,
Sakae-ku,
Yokohama, Japan

Toshiaki Zakoh received B.S. and M.S. degree in Macromolecular Science from Osaka University in 1983 and 1986 respectively. He joined Sumitomo Electric Industries, Ltd. in 1986. He is a senior engineer of Yokohama Research Laboratory. He has worked on coating materials of optical fiber, small-packaged optical transmitter/receiver, operating system of remote fiber testing system. He is a member of Information Processing Society of Japan.



Youichi HATA

Sumitomo Electric
Industries, Ltd.
1, Taya-cho,
Sakae-ku,
Yokohama, Japan

Youichi Hata received B.E. and M.E. degrees in Electronic Engineering from Tokyo Metropolitan University in 1990 and 1992 respectively. He joined Sumitomo Electric Industries, Ltd. the same year and has been engaged in research and development of software design engineering. He is now a research engineer of Optomechatronics System R&D Dept. Yokohama Research Laboratory. He is a member of the Japan Society of Applied Physics.



Tetsushi MATSUDA

Sumitomo Electric
Industries, Ltd.
1-1-3, Shimaya,
Konohana-ku,
Osaka, Japan

Tetsushi Matsuda received B.E. and M.E. in Electronic Engineering from the University of Tokyo in 1985 and 1987 respectively. He joined Sumitomo Electric Industries headquartered in Osaka in 1987. He is a research engineer of Systems and Electronics R&D Center of Sumitomo Electric. He has worked on communication software distributed processing system and software performance tuning tool. He is a member of ACM and Information Processing Society of Japan.



Yoshinori TAKENAMI

Sumitomo Electric
Industries, Ltd.
1-1-3, Shimaya,
Konohana-ku,
Osaka, Japan

Yoshinori Takenami received the B.E. and M.E. degrees in Electrical Engineering in 1988 and 1990 respectively, from Waseda University, Tokyo, Japan. In 1990, he joined Sumitomo Electric Industries, Ltd. He is engaged in the research and development of object oriented distributed systems. At present, he is a research engineer of Systems and Electronics R&D Center of Sumitomo Electric.



Tetsuya TAGUCHI

Sumitomo Electric
Industries, Ltd.
1-1-3, Shimaya,
Konohana-ku,
Osaka, Japan

Tetsuya Taguchi was born in 1955 and received his M.S. degree in Electronic Engineering from Osaka University in 1980. He joined Sumitomo Electric Industries, Ltd. the same year and has been engaged in research and development of video signal technologies and fusion splicing technologies for optical fibers. He is now a chief associate of Systems and Electronics R&D Center of Sumitomo Electric.

FIBER-STRAIN MEASUREMENT USING BRILLOUIN OPTICAL-FIBER TIME-DOMAIN ANALYSIS.

Colin J. Sandwith⁽¹⁾, William D. McCormick⁽²⁾, John A. Thornton⁽³⁾, David R. Wise⁽⁴⁾,
and Robert I. Odom⁽¹⁾

(1) University of Washington, Applied Physics Laboratory, Seattle, Washington

(2) Lucent Technologies Inc., Advanced Technologies Systems, Greensboro, North Carolina

(3) U.S. Navy, Space and Undersea Warfare Command, Crystal City, Virginia

(4) TRW, Systems Intergration Group, Fairfax, Virginia

ABSTRACT

Measurement of fiber strain during cable manufacture and installation has customarily been done either by mechanically measuring the length change in an end-sample or by optically monitoring the overall change in length. The U.S. Navy has undertaken a project to evaluate a new method of incremental strain measurement which uses Brillouin optical-fiber time-domain analysis (BOTDA) to measure the strain at all points along the length of the fiber. The BOTDA system is described, and the results are compared with measurements using the end-sampling technique.

1.0 INTRODUCTION

Brillouin optical-fiber time-domain analysis (BOTDA) is the only known method that can nondestructively measure the relative and absolute strain distribution in long optical fibers and cables. Only one manufacturer is marketing such a system in the United States, and in March 1995 the U.S. Navy undertook an experiment to compare the BOTDA system with the methods of strain measurement used by its current cable suppliers. The test was performed on a 10.4-n.mi. length of single-fiber cable previously deployed for 6 months by the Navy for oceanographic work. The test cable, which was actually two cables joined by a cable-to-cable junction (CCJ), is shown diagrammatically in Fig. 1. The object of the experiment was to compare the BOTDA results with the strain measurements on small samples taken at several locations in the cable. The BOTDA instrument was delivered, demonstrated, and loaned to the project by the manufacturer for several weeks at no cost.

2.0 PRINCIPLES OF BOTDA MEASUREMENT

Figure 2 is a schematic representation of how the BOTDA system uses stimulated Brillouin scattering (SBS) to derive residual fiber strain distribution. Unlike the optical time-domain reflectometer (OTDR), which uses primarily time of flight and attenuation to measure point and other losses but cannot measure strain,¹ BOTDA uses a sophisticated optical technique based on the fact that the Brillouin frequency shift for the optical fiber varies according to the strain induced or existing in the fiber.² Since, to first order of approximation, the Brillouin frequency shift is proportional to the tensile or compressive fiber strain at each point along the length of the fiber, the fiber strain ϵ is proportional to $V_B(\epsilon) = V_B(0)(1 + K\epsilon)$, where $V_B(\epsilon)$ is the strain-dependent Brillouin frequency shift, $V_B(0)$ is the Brillouin frequency shift for zero strain, and K is the coefficient of the Brillouin frequency shift.

The BOTDA sends a very stable continuous wave (cw) signal, called the pump light, at 192,610 GHz into one end of the fiber. Into the other end it sends an accurately controlled set of light pulses, called the probe or pulse light, that are spaced about 10 MHz apart and have a center frequency equal to the cw frequency plus 10 GHz, i.e., 192,620 GHz. By varying the frequency of the pump light, the strain can be determined from $V_B(\epsilon)$. In Fig. 2, the amplitude of the stimulated Brillouin scattering is shown along the vertical (z) axis, fiber length along the diagonal (y) axis, and frequency along the horizontal (x) axis. The set of light pulses is shown as a set of narrow pulses spanning a frequency from 192,610 plus 10.80 GHz (start) to 192,610 plus 11.20 GHz (stop). The frequency span is 400 MHz, which results in 40 pulses spaced 10 MHz apart. The pulse widths can be set from 5 ns to 10 μ s; the shortest pulse provides the best accuracy of location (about 5 to 20 m). The pulse of light whose difference from the cw light is closest to the exact Brillouin frequency shift at each point along the fiber pro-

duces a maximum amplitude SBS that is "reflected" (scattered) back to the source of the pulsed light. The offset between the Brillouin frequency at each maximum SBS and the Brillouin frequency at zero strain determines the strain at each location. By measuring the time of flight of the pulses to and from the scattering points and by determining the frequency of each maximum SBS, it is possible to plot the Brillouin gain distribution (BGD), and from that the fiber strain average distribution (SAD). The output distributions of the SBS from the light pulses close to the Brillouin frequencies are shown as the Lorentzian curves (dashed) in Fig. 2. Negative strain indicates compression, and positive strain indicates tension.

3.0 SYSTEM SETUP AND PARAMETER VALUES

The BOTDA system was set up and operational in less than 1 hour. The time required to make a BOTDA run once the fiber had been connected was about 15 minutes. A typical system setup is shown in Fig. 3. The pump (continuous) laser was set at -3 dBm and the probe (pulsed) laser at -3 dBm. The system is calibrated every 6 to 12 months. The light source was identified as an MQW.DFB.LD (Multiple Quantum Well Distributed Feed Back Laser Diode). The pump and probe lasers are isolated from optical feedback by 60-dB optical isolators. A computer running the UNIX operating system was used for data acquisition and logging.

During the initial demonstration by the manufacturer, the following approximations were mentioned for the relationship between temperature and strain: 1°C is approximately equal to 2.3 MHz (1°C = 1.22 MHz for UV sheathing and 3.689 MHz for nylon sheathing), and 0.01% strain is equivalent to about 525 MHz. A 50-ns pulse could resolve the location of strain to within about 5 m. In a fiber with an index of refraction of $n = 1.5$, a 50-ns pulse is about 10 m long. Hence the resolution is about one-half the pulse width. Pulse length is a tunable parameter. Next-generation production models are expected to come with a 10-ns pulse option.

Measurement of the strain offset from the zero (base) value depends on the accuracy with which $V_B(0)$ is known or set. The sensitivity of the measured strain to the $V_B(0)$ value selected should be fully tested using fibers from various fiber producers and lots. The time constraints and test conditions did not allow such testing to be accomplished during the demonstrations. However, relatively small changes in $V_B(0)$ appear to produce detectable changes in the measured offset from zero strain. A change from 10.952 to 10.938 GHz (14 MHz), for ex-

ample, produced a change of about -0.026% in strain. Quick, off-line experiments indicated that, as would be expected, the zero offset was either not or only slightly sensitive to K , whereas the range of strain was proportional to K .

A K value of 4.78 was used in the demonstration because it reportedly represented the mid value of what had been found in the industry for fibers with an index of refraction between 1.475 and 1.480.

4.0 TEST ON 1-KM LONG UNSTRESSED FIBER

First, a BOTDA test was conducted on a 1-km length of unstressed fiber to calibrate the BOTDA for zero strain in the as-received, loose fiber. This calibration is a critical step, since it sets the zero reference for measured strains in all cables with identical fibers. We compared the fiber strain for the unstressed fiber with that for the BOTDA system's two internal reference fibers (0.5-km dispersion shifted and 0.5-km nondispersion-shifted) and checked the repeatability of the BOTDA measurements by exchanging the input and output ends of the fiber under test.

4.1 Test Setup

To set up the BOTDA system,³ best estimates of $V_B(0)$ and other strain setup values are entered, and a BOTDA run is executed to produce a BGD. The resulting BGD can be used to produce a strain average distribution (SAD) which shows the offset from zero strain produced by the assumed value for $V_B(0)$. The spectrum of the BGD can be analyzed to show how close the assumed value for $V_B(0)$ is to the maximum Brillouin frequency shift. In the BGD display, maximum values for the frequency shift can be determined for specific locations along the fiber. The plotted shape of selected maxima, called the Brillouin gain spectra (BGS), along with the offset from zero strain observed in the SAD, is then used to select a better estimate for $V_B(0)$. The process is iterated until reaching the desired strain value of zero, or in our case 0.001%. Values of 10.952 to 10.940 GHz were tested; 10.938 GHz resulted in a fiber strain of 0.001% and was selected for $V_B(0)$.

4.2 Results

When the BOTDA system was adjusted so that the non-dispersion-shifted internal reference fiber was set to near zero strain, the nominal strain seen in the 1-km-long test fiber was -0.026% (compressive). The repeatability of the SAD on reversing the ends was not good initially

owing to the extremes in localized noise (thought possibly to be due to poor connectors and connector vibration) and the use of a relatively short pulse width of 0.05 μ s. When the noise was eliminated and the pulse width expanded to 0.1 μ s, the repeatability was good. Fusion splices to FCPC (ceramic ferrule screw locking connector series) or equivalent connections are probably required to reduce noise and insertion loss.

The SAD plot for $V_B(0) = 10.938$ GHz is shown in Fig. 4. The dispersion-shifted reference fiber is the short plateau above the horizontal line on the far left. The vertical straight line (cursor) passes through the center of the 1-km loose fiber.

5.0 TESTS ON 10.4-N.MI. POST-SERVICE CABLE

Next, a BOTDA test was conducted on a 10.4-n.mi. (19.29-km) length of post-service cable with a cable-to-cable junction (CCJ) located about mid-length (5.4 n.mi. from one end). The main objective of this test was to determine if the BOTDA system could detect, measure, and locate fiber strain distribution in long lengths of cable and, specifically, in a length of finished submarine cable.

5.1 Cable History and Test Setup

The test cable was recovered after a 6 month deployment by the U.S. Navy as part of an oceanographic project. The cable had been pulled back and forth through sheaves and onto reels under tension many times during deployment and recovery. This tension never exceeded 50% of the maximum rated working tension of the cable. In depot storage the cable was coiled into a tank where it experienced unknown amounts of heat due to a paper and debris fire in the tank. The cable was finally pulled onto a shipping reel and transported across the country to the test site.

The test cable was on a metal reel with both cable ends accessible. The cable ends were stripped back to allow fusion splicing to FCPC optical connectors.

5.2 Results

There is no sure way to predict which of these known actions, if any, produced movements in the buffered fiber. However, translation of the buffered fiber along the cable toward the CCJ during reeling under tension seems in

agreement with both the expected results and the observed fiber strain distribution.

The test showed two noticeable point losses, both more outstanding at a wave length of 1550 nm. The greater loss (0.62 dB avg.) occurred 10.7 km (5.767 n.mi.) from the top end of the reel. The other (0.125 dB avg.) occurred 9.976 km in from the top end. The losses may be due to fiber splices or damage. The loss 9.976 km in from the end labeled "top" is within 27 m of the CCJ location indicated by reeling the cable length through an analog contact cable counter, and within 224 m of the CCJ as roughly measured by the BOTDA.

The first BGD (Fig. 5) indicated an interesting strain distribution in length, frequency-shift, and frequency-shift-amplitude space. Figure 6 shows the strain distribution over an arbitrary distance of 40.218 km. The left side out to about 20 km shows the two reference fibers and the test cable, and the right side is about 20 km of clipped noise. The top end of the cable is at the left, and the bottom end is near the center, just beyond the second circled marker at the high point of about +0.3% strain. As shown near the lower left ordinate, the scale for strain is 0.2% per division (i.e., between the horizontal lines of dots) and the scale for length is 4.03 km per division (i.e., between the vertical lines of dots). A great strain discontinuity (downward spike) is immediately apparent near the center of the cable at the first circled marker, where the CCJ was suspected (and was later proven) to be. Starting about 0.8 km to the left of this spike, the strain continuously decreases, at an increasing rate, from nearly zero to -0.521% (compressive) at the top side of the CCJ. On the bottom (right) side of the CCJ, there is another discontinuity where the strain jumps to about +0.07% (tensile). Intuitively, one suspects that the fiber has been pushed, pumped, or milked toward the CCJ; compressive strain cannot be transferred across the CCJ because, by design, the fiber is held firmly in both ends of the CCJ. The left side of the figure indicates roughly 2-km-long cycles of strain starting at about -0.2%; the cycle reaches a high of about +0.15% about 2 km from the top (left) end of the cable and a low of -0.1% about 2 km from the CCJ spike. Note the 2-km length of tensile strain (+0.05 to +0.10%) starting at the bottom (right) side of the CCJ. There is a 6.5-km length of increasingly compressive fiber strain reaching about -0.15% just prior to a dramatic increase to a tensile strain of +0.3% near or at the bottom (right) end of the cable. The dramatic tensile spike of +0.3% strain on the bottom end was not initially recognized as part of the 10.4-n.mi. cable strain character but was thought to be noise from beyond the end of the cable.

The BOTDA system also has a feature that allows closeup views of localized strain-distribution features and evaluation of localized strain values. A closeup of the greatest compression (the area around the first marker in Fig. 6) is shown in Fig. 7. Use of this closeup feature at selected locations up to but not including marker 2, which was thought to be an end effect, showed fiber strain ranging from +0.145 to -0.521%, a range of 0.666%. Later analysis (mid-May 1995) showed a range of +0.300 to -0.521%, or 0.821%. At the time of the test, no one realized that the strain spike of +0.3% near the bottom end of the reel was real; it was thought at the time to be due to an end effect.

The repeatability of the tests was excellent, (see plots in Fig. 8). When the cable ends were switched, all of the strain distribution features and details were exactly reproduced, as far as could be determined by overlaying plots on a lighted display; however, the value of the strain changed by about +0.01%, the value claimed for the strain resolution of the BOTDA system. Several locations were checked for a change in the relative values of strain when the ends were reversed. The repeatability in strain distribution and local strain was evaluated by comparing closeup displays of several locations of interest. The differences in strain values at these locations were less than $\pm 0.01\%$.

5.3 Discussion

Because the shape and values of the strain distribution were so repeatable when the ends were reversed, the relative value of the strain over the cable length appeared to be reliable.

If we had understood at the time how to use the BOTDA system better, especially the marker 1 and marker 2 features, we could have located the strains and cable features much more accurately (within a few meters) relative to one another. Figure 6 shows the use of the marker feature to show the distance between the maximum compressive strain (marker 1, at the CCJ) and the maximum tensile strain (marker 2, near the bottom), and the range of the strain between the two markers. The distance is 9.188 km and the range of strain is 0.743%, which means the markers were not located exactly at the maximum and minimum strain locations.

The detail of the BOTDA SAD is remarkably good. Clearly if $K = 4.78$ is reasonably correct, then the range of fiber strain exceeds about 0.8%. Perturbation analysis shows that an error of ΔK produces an error in the strain of $\epsilon_{\text{error}} = -(\Delta K/K) \epsilon_{\text{true}}$. Hence a 1% error in K produces an equivalent error in the measured strain range, i.e., 1% of 0.8%.

If $V_B(0)$ is reasonably correct (within 14 MHz of 10.938 GHz), the maximum observed tensile strain is $0.3\% \pm 0.026\%$. Perturbation analysis shows that an error of δ in selecting the Brillouin frequency at zero strain produces an error in the strain of $\epsilon_{\text{error}} = -\delta/[K V_B(0)]$. Here $V_B(0)$ is the nominal value we have chosen.

The observed strain discontinuity of -0.521% about 5.4 n.mi. from the top of the cable (Fig. 6), on the top side of the CCJ, can be explained as compression of the fiber up against the CCJ due to translation during reeling under tension. The CCJ is a reasonable location where such a high strain discontinuity could develop because the buffered fiber is captured at the CCJ.

The test indicated that the BOTDA system could be used for process development, and for checking cables and connections at system integration. It could be used for checking strain distribution during loading or unloading ships, during cable engineering and development testing, and during service conditions where both ends of the cable are available. Such data on fiber-strain distribution could prevent deploying fiber-optic cables that are ready to fail; however, such data are only available by BOTDA.

6.0 COMPARISON OF RESIDUAL FIBER STRAIN MEASURED BY MECHANICAL MEASUREMENT AND BY THE BOTDA SYSTEM

Table 1 compares the residual fiber strains as measured mechanically during production and those measured post-service by the BOTDA. The mechanically measured strain values range from -0.1 to +0.07%, for a total range of 0.17%; the BOTDA strain values range from about +0.292 to -0.521, for a total range of 0.813%. As would be expected after service, the BOTDA results on the 10.4-n.mi. length show a wider range of residual fiber strain.

Table 1. Comparison of production-fiber strains measured mechanically at the power conductor stage and strains measured by the BOTDA system on post-service cable.

Location	Cable Length ID	Cable Length	PROD. FEM	PROD. LEM	POST-SERVICE
			Fiber strain	Fiber Strain	BOTDA Fiber strain
Top	B93D033-2	5.4 n.mi.	-0.060%	-0.096%	-0.521 to +0.150
Bottom	B93D030	5.0 n.mi.	+0.073%	-0.060%	-0.200 to +0.292

FEM = first end manufactured, LEM = last end manufactured.

7.0 COMPARISON OF BOTDA AND MECHANICAL FIBER-STRAIN MEASUREMENTS ON SAMPLES FROM THE POST-SERVICE 10.4-N.MI. TEST CABLE

After the completion of the BOTDA test on the as-received cable reel, the cable was transferred onto a similar reel. The reeling tension was estimated at 90-100 lb. A BOTDA run was then conducted to determine if the strain distribution was affected by the reeled condition or by the CCJ being under turns of the cable. At the same time, the cable's length was determined by running it through an analog contact cable counter. The position of the CCJ was cross checked at that time.

Specimens were then removed at two separate times (samples 1 through 13 during the first reeling and samples 14 through 18 in July 1995). All of the specimens were sent to the original manufacturer for mechanical (destructive) fiber-strain measurements to check the fiber-strain values at three selected locations: at the top of the cable, at the location of the greatest compressive fiber strain (i.e. near the top side of the CCJ), and on the bottom side of the CCJ, as shown in Fig. 9. Months later (in July 1995), after the BOTDA had been returned and after we realized that the 240-m section of high strain near the end of the cable in the original BOTDA plot was not an end effect or an artifact of the testing, samples were taken from this section of cable also.

7.1 Fiber-Strain-Sample Sectioning

The first 100 m from the top of the 10.4-n.mi. sample were removed and discarded; then five strain samples were sequentially crimped, cut, and labeled 1 through 5; 1 was the first sample cut from the top end and 5 was the last sample. Each sample was carefully marked and tagged to indicate the sample number, top end, bottom end, location on the cable, cable ID, and contact person and organization. Reeling then continued until the CCJ was exposed.

BOTDA runs in both directions before and after unreeling to the CCJ showed no detectable change in the shape distribution or approximate values of strain at any of the locations checked.

After being crimped to lock in the fiber strain, five residual fiber strain (RFS) samples (6 through 10) were cut just prior to the top of the CCJ, leaving 30 ft of cable on the top side of the CCJ. A BOTDA run confirmed a strain value of -0.521% at the end of the top length of the cut cable.

Next the CCJ and 30 ft of cable on its bottom side were crimped and cut out. Then three RFS samples (11 through 13) were cut out from the top end of the bottom length of cable.

Later data analysis convinced us that the section of high tensile strain near the bottom end of the 10-n.mi. test cable was not an artifact but actually existed. In July of 1995 we returned to cut five samples (14 through 18) from the high tensile strain area and prepare them for shipment to the manufacturer for mechanical measurement. The BOTDA instrument was not available, because it was on temporary loan only for a few weeks during March and April. The task of relocating the high strain area could have been accomplished in minutes with the BOTDA. As it was, some of the sections had been cut from the bottom end of the cable for other tests, and the exact length of the cable within the high strain had become uncertain. Analysis of BOTDA data indicated that the center of maximum strain was probably about 250 m in from the bottom end of the original cable section. The last BOTDA in the experiment, made on April 7, was used to help locate the high-strain area, but care had not been taken to document the starting point and the reference fibers used, so the BOTDA zero-length reference was unclear. Figure 10 depicts a SAD from this BOTDA showing a short length corresponding to the left end of the lower SAD and right end of the upper SAD in Fig. 8 in which the scale has been expanded to locate the center of the maximum tensile strain. The cursor is placed at the center of the maximum strain, which is at 1.306 km and is +0.300%. However, since the zero reference point for the April 7 BOTDA and the locations of the end of the fiber were uncertain, the location of the high strain in the reeled cable was also uncertain. Hence, samples 14 through 18 were probably cut from one side or the other of the section with the maximum strain.

7.2 Preparation of the Samples for Manufacturer's Measurement of Residual Fiber Strain.

The samples were crimped to prevent fiber movement and were cut into 9.5-ft (2.75-m) lengths for shipment. The actual measurement of residual strain in each sample was performed on a 100-in. (2.54-m) segment from which the jacket and shield had been removed to expose the power conductor. This segment was placed in a fixture specifically designed for strain measurement. The removal of the outer jacket and shield was done in such a way as to not affect the residual strain in the fiber. To measure the residual strain in the fiber, the cable manufacturer carefully removed successive layers of the power conductor and, after each layer was removed, read the precise

change in fiber length directly from a scale with a microscope.

7.3 Results

Table 2 compares the fiber strain distributions measured by the BOTDA system with the strain values measured mechanically for the samples. Samples 6 through 10 are from near the top end of the CCJ, 11 and 12 are from near the bottom end of the CCJ, and 14 through 18 are from the bottom of the cable, where the BOTDA test indicated a 240-m section of high strain. Samples 1 through 5 were not measured because they were of least interest. The conductor on sample 13 was damaged during disassembly and the sample was discarded.

Table 2. Comparison of BOTDA and the manufacturer's test results on the 10.4-n.mi. length of post-service submarine cable.

Sample Cable Length #	BOTDA Fiber Strain %	Manufacturer's Method Fiber Strain %	Technician
6	-0.0520 min. -0.521 max.	-0.488	A
7		-0.436	A
8		-0.30044	B
9		-0.496	A
10		-0.34	B
11	+0.10 avg.	+0.13476	C
12		+0.082	C
14	+0.18 min. +0.292 max.	+0.055	D
15		+0.1007	D
16		+0.091	D
17		+0.126	D
18		+0.18276	E

For samples 6 through 10, the mechanical and BOTDA measurements are in good agreement, with both showing unexpected, extremely high compressive strains. The three mechanical readings by technician A are within 2 to 20% of the values measured by the BOTDA system. The two readings by technician B differ from the BOTDA values by 40% but still show a compressive strain. The agreement between the BOTDA results and these two independent readings is important because it confirms that the BOTDA system can locate and quantify fiber-strain distribution in a long length of cable in a matter of minutes without destroying the cable. The difference of 20 to 60% (depending on which readings are assumed to be correct) between the results of the two laboratory technicians on five probably nearly equal samples and the repeatability of each laboratory technician's own measurements strongly indicate that the mechanical test results are dependent on the technician, and that different technicians may be expected to get results that differ by as much as or more than they differ from the BOTDA readings. Regrettably, with the destructive method there is no permanent record of the data other than the measurements recorded and the cut pieces, which are difficult or impossible to preserve. The BOTDA results are preserved and readily available for detailed analysis and checking.

For samples 11 and 12, the BOTDA and the mechanical results are close, with the mechanical results falling within the range of 0.08 to 0.14 % seen in the BOTDA results. As with samples 6 through 10, the traceability of location in these samples is highly reliable. The BOTDA instrument was available at the time of cutting samples 1 through 13, so that the location of the samples relative to the BOTDA strain results could be verified.

For samples 14 through 18, the results indicate either that the BOTDA system was unable to measure the strain accurately or that the samples were not cut from the center of the length of interest, i.e., the 240-m length where the BOTDA system indicated a strain of +0.292%. Since no BOTDA instrument was available to verify the high strain location in the cable after re-reeling, it is likely that the BOTDA values are correct and that the samples were taken from a length on the edge of the intended location.

8.0 SUMMARY AND CONCLUSIONS

8.1 Summary

A new system based on Brillouin optical-fiber time-domain analysis (BOTDA) has been developed that measures, stores, and allows analysis of data on the strain

distribution in optical fibers. In March 1995, tests were conducted in which the BOTDA system was used to measure the strain distribution in a 10.4-n.mi. length of reeled submarine cable. The distribution was then compared with that measured mechanically in destructive tests of samples from the same cable. The repeatability of the BOTDA results was excellent, and the strain values agreed with those found by mechanical measure. In fact, the BOTDA system located a previously unknown high compressive strain.

Residual strain in the optical fiber of fiber-optic cables induces static fatigue that can cause the fiber to fracture. Prior to the BOTDA system there was no way to measure strain distribution in an intact cable. Using either of the customary methods of strain measurement; ie, mechanically or optically measuring change in length, the fiber-strain distribution, magnitude, and location throughout the entire length of the cable are unknown.

8.2 Conclusions

1. The test results show that the BOTDA system can measure the relative and absolute fiber strain distribution in fiber-optic cable with reasonable resolution. As a testing tool for strain distribution analysis the BOTDA system is unmatched in terms of quickness of data collection and analysis and the amount of data obtainable. The system could be used for manufacturing process development and for checking cables and connections at system integration, as well as during cable design and development and testing. It could also be used to determine the change in fiber strain distribution after handling, field testing, and reeling; such data, in turn, could be used to determine the sensitivity of a cable design to fiber translation and strain buildup. It would be especially valuable during autopsies on post-service or post-test cables, as evidenced by our discovery during the BOTDA test of a fiber-strain condition (high compressive strain on one side of the CCJ and high tensile strain on the bottom end) that was previously unknown.

2. The BOTDA system is the only commercially available instrument for measuring, storing, and analyzing fiber-strain distribution.

3. The BOTDA system can probably measure the location of fiber strain to within 5 to 10 m and the fiber strain distribution along the length of an optical fiber to within $\pm 0.01\%$ of the strain value. The claimed fiber-strain measurement resolution of 0.01% was not proven by our test, but when the fiber ends were reversed, i.e., when the

pulsed and pumped ends were switched, the strain values checked at selected locations were within $\pm 0.01\%$.

4. The time required to run a BOTDA and obtain a SAD on a 20-km-long (and perhaps up to 160-km-long) cable would probably range from several minutes to about half an hour.

5. The tested BOTDA system is relatively expensive. However, the manufacturer is devising means to reduce the cost and is investigating a revolutionary new technique, which requires access to only one end of the fiber or cable and may be less expensive.

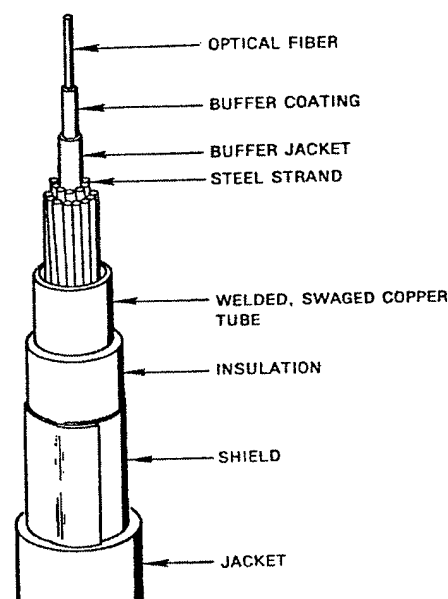


Figure 1. Longitudinal cut-away section of submarine fiber-optic cable.

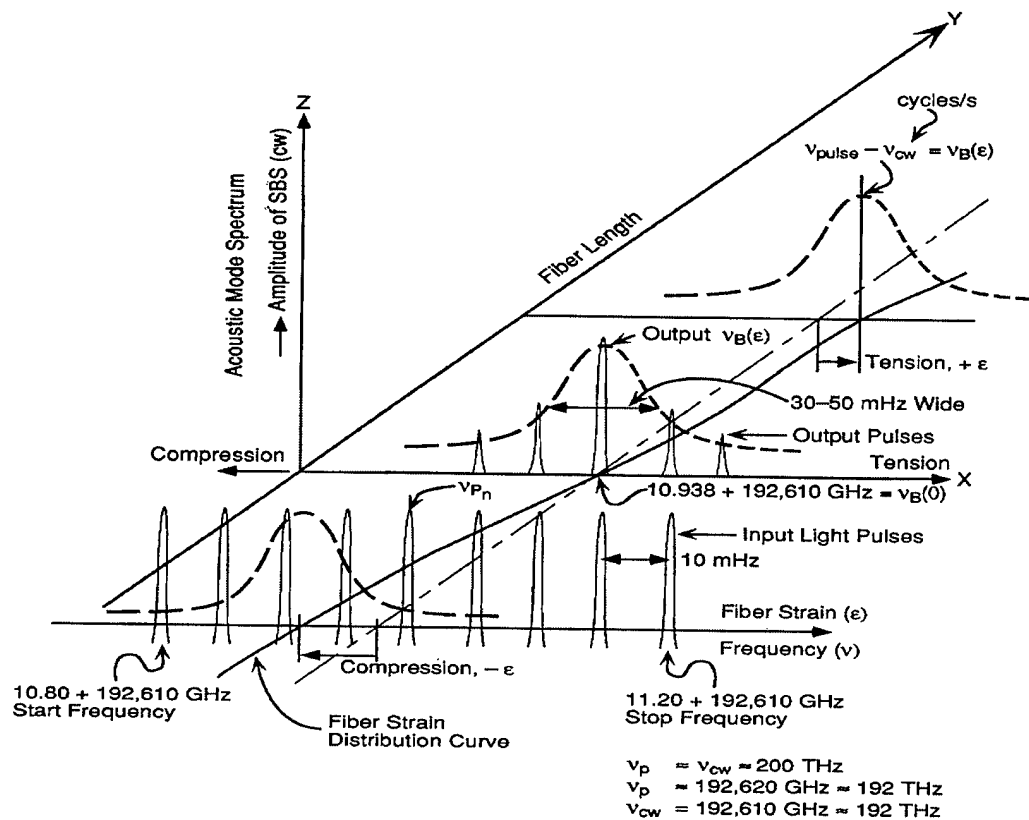


Figure 2. Optical measurement of fiber strain by BOTDA in SBS amplitude, fiber-length, frequency-strain space.

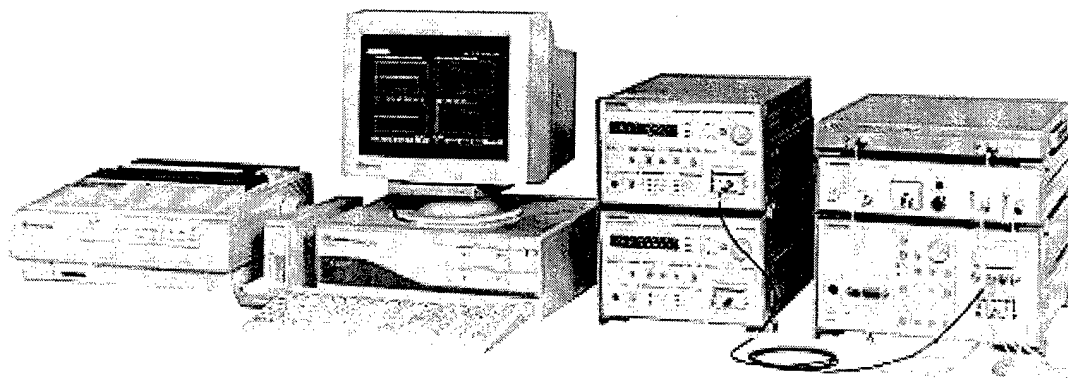


Figure 3. The AQ-8601 BOTDA optical strain measurement system.

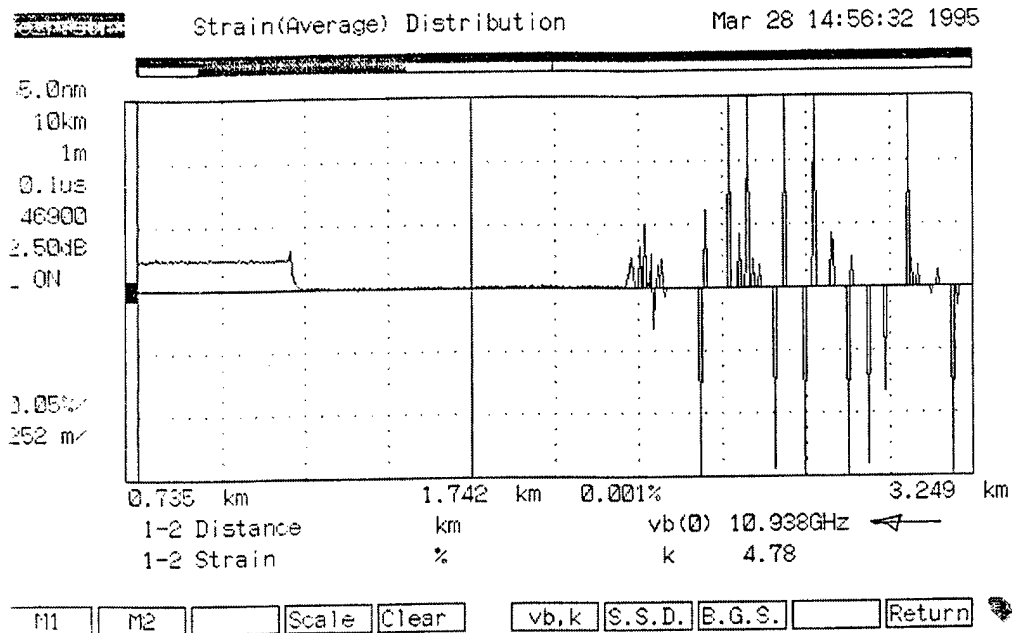


Figure 4. Calibration of fiber strain distribution to zero by using a $V_B(0)$ of 10.938 Ghz.

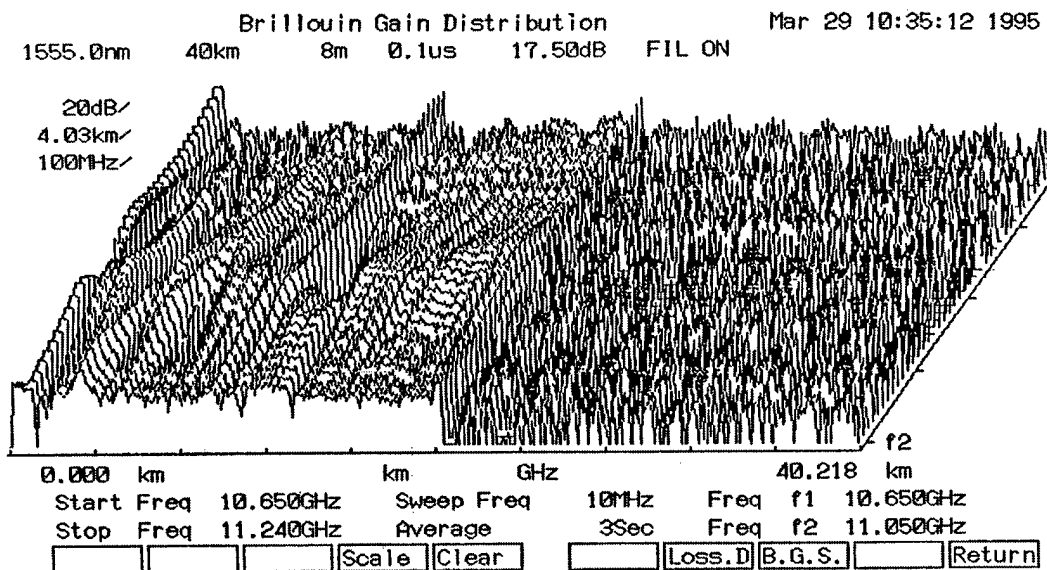


Figure 5. First BDG of 10.4-n.mi. test sample. The top end of the cable is at the far left. The left side of the display is data, and the right side is noise. The hills and valleys reflect the strain distribution.

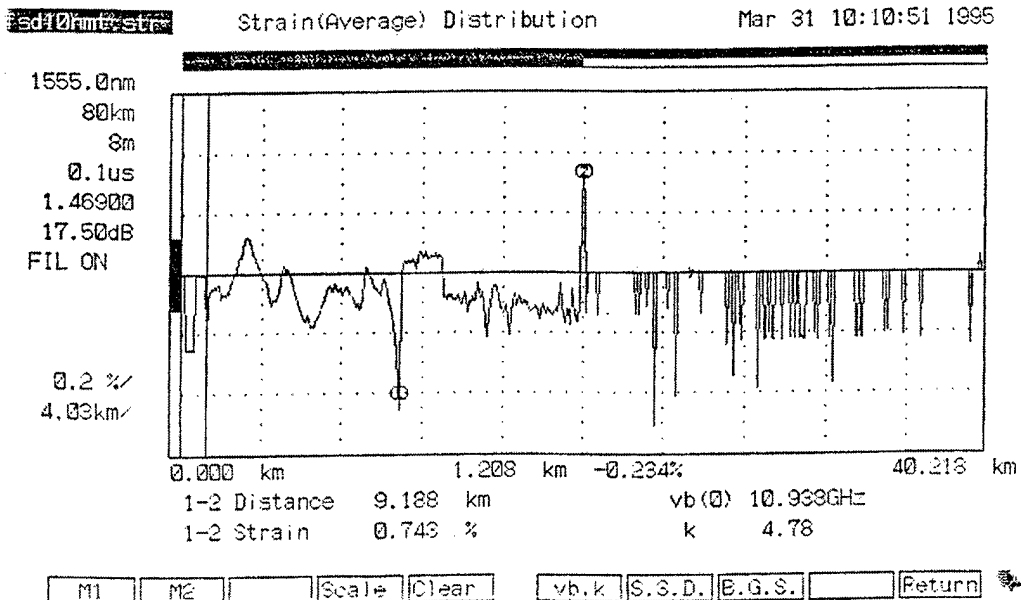


Figure 6. A SAD made from BGD data in Fig. 5. The strain in the two 500-m reference fibers is shown at the left of the vertical cursor line. The dispersion-shifted reference fiber shows a strain of about -0.23, and the nondispersion-shifted fiber shows a strain near zero. The top of the cable is toward the left. The bottom of the cable is near the center of the graph at ≈ 20 km near marker 2. The center of the cable shows the high compressive spike at the location marker 1.

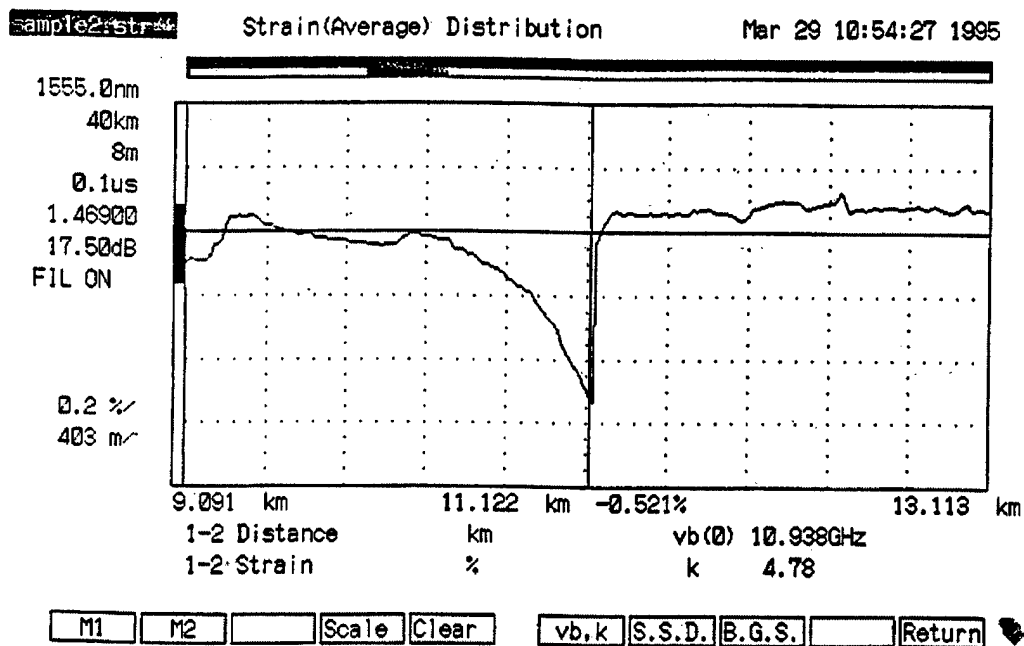


Figure 7. Close-up of strain distribution at marker 1 in Fig. 6 showing a maximum compressive strain of -0.521 % at the cursor location.

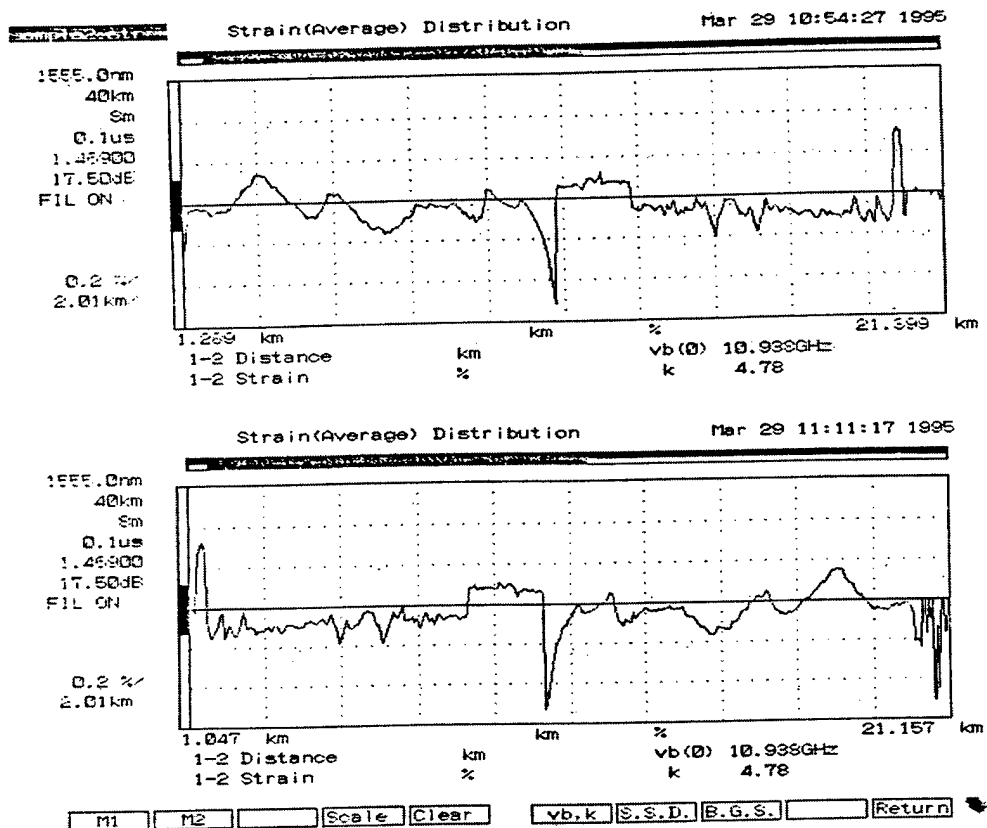


Figure 8. Repeatability of the measurements of the fiber strain when the ends of the 10.4-n.mi. cable going to the BOTDA were switched.

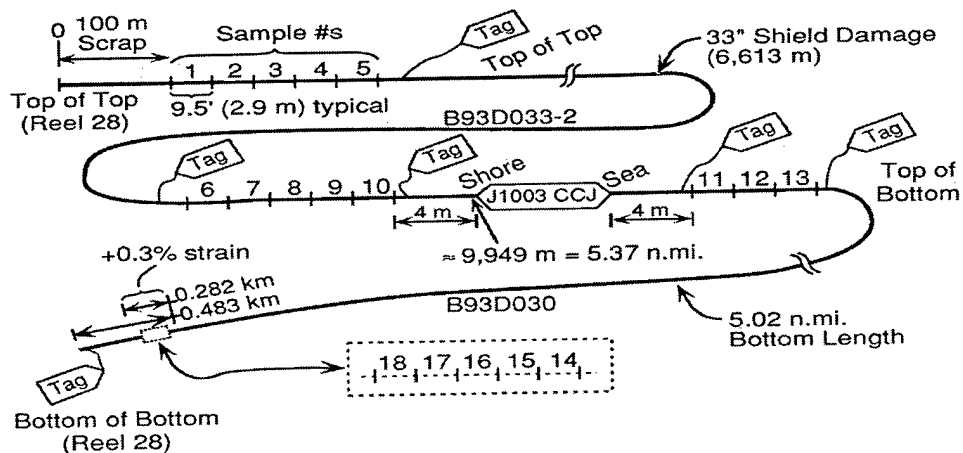


Figure 9. Sketch of cuts made to remove residual fiber strain samples and CCJ from the 10.4-n.mi. cable. Sketch shows sample numbers, CCJ location, shore and sea ends of the cable, tagging, and strain locations.

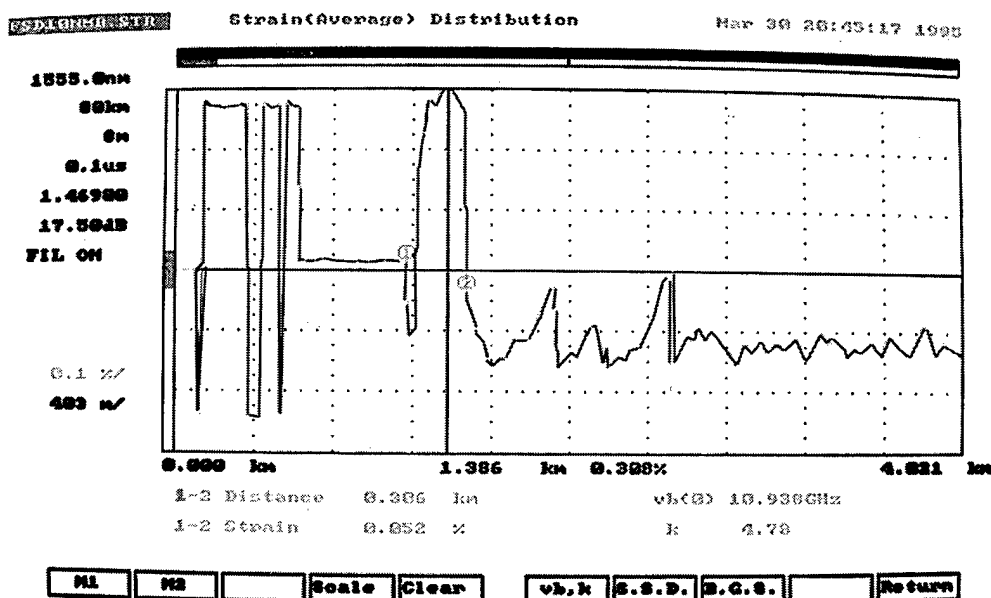


Figure 10. Photographic reproduction of BOTDA screen showing area of high strain near the bottom end of the cable. The character and distribution of the strain can reveal much about the condition of the cable. If previous BOTDAs and the cable history are available, the cause of change may be determined.

lished paper, Applied Physics Laboratory, University of Washington, Seattle, WA, 1995.

9. ACKNOWLEDGMENTS

The authors wish to thank Ted Bookwalter and David Anderson of Alcatel Submarine Networks, Inc., William N. Sparhawk of Simplex Technologies, Inc., and Michael D. Griffin of Ando Corporation for their valuable contributions to the original study.

10. REFERENCES

1. Christian Hentchel, *Fiber Optics Handbook*, Hewlett-Packard GmbH, Boeblingen Instruments Division, Germany, 1989
2. T. Horiguchi, T. Kurashima, and M. Taeda, "Nondestructive measurement of optical-fiber tensile strain distribution based on Brillouin spectroscopy," *Trans. IEICE, J73-B-I*, 144-152, 1990.
3. *AQ-8601 Optical Fiber Strain Measurement System: Abbreviated Instruction Manual*, Ando Electric Co., Ltd., Japan, 1995.
4. Robert I. Odom, "Discussion of optical fiber strain measurement based on Brillouin optical-fiber time-domain analysis," unpub-

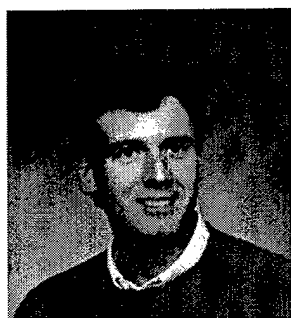
AUTHORS



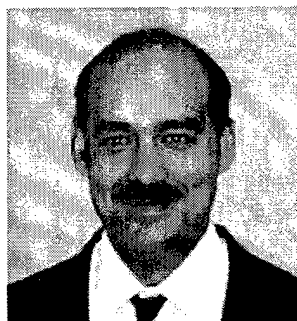
Colin J. Sandwith was born in Friday Harbor, Washington, in 1936. He received a B.S.M.E. in 1961 from the University of Washington and a Ph.D. degree in Material Science in 1967 from Oregon State University. His research centers on failure analysis, marine corrosion, and material science. He is an expert on fiber-optic electro-mechanical cables, connectors, and seals for underwater applications. He is a Principle Mechanical Engineer at the Applied Physics Laboratory, University of Washington, in Seattle, Washington.



William D. McCormick was born in Tacoma, Washington, in 1941. He received a B.S. (1967) in Civil Engineering, a B.S. (1970) in Industrial Engineering from the University of Washington, and an M.S. (1985) in Computer Integrated Manufacturing from Brigham Young University. He is a registered professional engineer in the State of California and is a Member of Technical Staff, Bell Laboratories, Lucent Technologies, Advanced Technology Systems in Greensboro, North Carolina. He currently is designing and building fiber-optic cable systems for military use.



David R. Wise was born in Brownsville, Texas, in 1955. He received a B.S. Degree in Industrial Management in 1983 from Clemson University, Clemson, South Carolina, after serving 6 years in the U.S. Navy Submarine Service. He works for TRW as a Systems Quality Engineer designing and building fiber-optic cable systems for military applications.



John A. Thornton received his B.S. in Ocean Engineering from Florida Atlantic University in 1982 and his M.S. in Civil Engineering from the George Washington University in 1989. Mr. Thornton has worked as an engineer for the United States Navy since 1982. His first 7 years was spent as an ocean engineer designing, installing, and inspecting underwater acoustic training ranges, moorings, and piers. He then worked as the cable development engineer for Fixed Distributed systems, a fixed acoustic system. Mr. Thornton is now the Assistant Program Manager for the Underwater Segment of the Advanced Deployable System, a new acquisition program developing advanced acoustic sensing systems.



Robert I. Odom was born in Seattle, Washington, in 1950. He received a B.S. (1971) in Physics, M.S.E. (1973) in Nuclear Engineering, and Ph.D. (1980) in Geophysics from the University of Washington. In addition to his research in underwater acoustics and theoretical seismology, he has had experience with a number of different laser and fiber-optic systems. He is an expert in acoustic, elastic, and optical wave propagation. He is a Principle Physicist at the Applied Physics Laboratory, University of Washington, in Seattle, Washington.

Overview of PCS Standards: The Recipe for Acronym Soup

Cliff H. Halevi

Bellcore, Red Bank, New Jersey

1. ABSTRACT

For the last four years, standardization of PCS air and network interfaces has been conducted at a feverish pace. Multiple standards committees and a joint standards committee have produced dozens of Interim Standards, Trial Use Standards, Technical Reports and ANSI Standards. The combination of multiple standards bodies, multiple interfaces, multiple standards, and the use of acronyms to refer to all of them, has created a thick acronym soup that is generating an enormous amount of confusion in the industry.

This paper provides a clear, concise understanding of the major U.S. PCS-related standards committees, the standards development process, the multiple air interface standards, PCS terminology, architectures and interfaces, the naming conventions for documents and committees, and will provide an overview of the four main "techno-political" battles being waged in PCS Standards within the U.S.

2. INTRODUCTION

For the last four years, with the FCC auction of PCS-band spectrum looming on the horizon, one of the largest concerted standardization efforts in recent telecommunications history has taken place. Hundreds of telecommunications standards experts, representing thousands of engineers and network planners at their home companies and organizations, have been meeting under the aegis of multiple standards committees. These experts have produced thousands of pages of specifications in dozens of Interim Standards, Trial Use Standards, Technical

Reports and ANSI¹ Standards. These standards define most aspects of PCS systems, from air interface and network interface protocols to service descriptions and network reference models.

The combination of multiple standards bodies, multiple interfaces, multiple standards, and the use of acronyms to refer to all of them, has resulted in a thick acronym soup that makes it difficult for those not directly involved in the process to clearly understand the technologies and interfaces being discussed.

As PCS systems move from the pages of standards documents to the development and deployment of actual systems, a clear understanding of underlying technologies is necessary to decipher competing claims and to facilitate intelligent technology selection decisions.

This paper provides a clear, concise understanding of:

- the definition of PCS
- PCS terminology, architectures and interfaces
- the standards development process, from initial development, to working document, to balloting, comment resolution and final publication
- the naming conventions for documents and committees, including PNs, ISs, dpANS, "J" standards, TR groups, "dot" groups, etc.

¹ American National Standards Institute

- the major PCS-related standards committees, focusing on T1P1, TIA² TR46, JTC and TIA TR45
- the development of air interface standards and the resulting multiple standards that emerged from the JTC
- the four main "techno-political" battles being waged in PCS Standards
 - TDMA vs. CDMA
 - T1 vs. TIA
 - IS-41 vs. DCS 1900
 - Cellular vs. PCS

3. WHAT IS PCS?

3.1 Definition and Characteristics

PCS stands for Personal Communications Services and although the exact boundaries of this definition are a continual source of controversy (e.g., should PCS encompass two-way paging and wireless data over Personal Digital Assistants), the term is commonly used to refer to next-generation wireless telephony systems that are intended to operate at the 2 GHz band being auctioned off by the FCC. PCS systems are intended to differ from today's cellular phone systems in several key respects, namely Cell Size, Power, Quality, Cost and Advanced Features.

1. **Cell Size** - PCS systems are designed to use "microcells" that range from 500 meters to 2 km in radius, which is much smaller than the 5 - 30 km cell radius of today's cellular systems.
2. **Power** - PCS phones are designed to use much less power (as low as 50 mW) compared with today's cellular phones which use 3 W for car phones, and 600 mW for hand-held portables.
3. **Quality** - The use of microcells permits higher frequency reuse and utilization, which allows PCS systems to be designed to provide more bandwidth per user channel. This allows service providers to use voice codecs, if they

choose, that provide voice quality nearly equivalent to wireline telephony.

4. **Cost** - Due to the low power design, the low-cost microcell architecture, and the impending competition between incumbent cellular and new PCS entrants, prices are expected to continually decrease for the foreseeable future, eventually converging with wireline toll pricing. It is even possible, actually quite likely, that in the near future some competitors will offer flat rate pricing to attract and retain users.
5. **Advanced Features** - Perhaps the key differentiator between today's cellular and upcoming PCS systems will be advanced features. Besides the physical characteristics of PCS phones being smaller and lighter, and having much longer battery life due to the low power PCS design, these phones will provide advanced features that derive from PCS's digital technology. These features include:
 - a) **Enhanced Security**, provided by authentication algorithms either built-in to the portable handset, or residing on so-called Smart Cards that plug into the handset
 - b) **Enhanced Privacy**, as a result of digital encryption
 - c) **SMS**, (Short Message Service) in which short text messages can be sent to and from the users handset
 - d) **Integrated Paging**, which allows the phone to use its display to function like a pager
 - e) **Seamless Roaming**, where calls can be received or placed from outside the user's home service area without having to invoke any special commands or dial special access numbers
 - f) **Vertical Services**, integrated or compatible with the services available on today's wireline telephony network
 - g) **Cordless/PCS Integration**, where the PCS handset functions like a cordless phone (i.e. free air time) inside the user's home or office, and uses the PCS network outside

² Telecommunications Industry Association

- h) **Data Interworking**, where the PCS phone can be used as a wireless data terminal to transmit/receive data to/from a laptop or PDA.

3.2 Frequency Band/Channel Allocations

As mentioned previously, the rush to PCS standardization was initiated by the FCC's announced intent to auction off about 120 MHz of spectrum near the 2 GHz band. This spectrum is divided into three 30 MHz blocks (A, B and C) and three 10 MHz blocks (D, E and F). A 20 MHz block is reserved for unlicensed use. The U.S. was then divided into 51 large Major Trading Areas (MTAs) and 493 smaller Basic Trading Areas (BTAs). Two of the 30 MHz blocks are available in each MTA, and the remaining blocks are available in each BTA. Thus, the advent of PCS will result in the addition of six new PCS entrants in any given region to compete with the two incumbent cellular service providers.

Block	Bandwidth	Area	Frequency Range (MHz)
A	30 MHz	MTA	1850-1865 1930-1945
B	30 MHz	MTA	1870-1885 1950-1965
C	30 MHz	BTA	1895-1910 1975-1990
D	10 MHz	BTA	1865-1870 1945-1950
E	10 MHz	BTA	1885-1890 1965-1970
F	10 MHz	BTA	1890-1895 1970-1975
UL	20 MHz	U.S.	1910-1930

Figure 1: FCC PCS Spectrum Allocation

The FCC has divided the auction into phases. They have recently completed the MTA auctions and have so far auctioned off about half of the BTA licenses.

4. PCS ARCHITECTURES, INTERFACES AND TERMINOLOGY

Although the existing PCS Network Reference Models can appear quite formidable and complicated, there are only

a few main interfaces and functional elements that one really needs to know about to have a decent understanding of PCS.

Starting from the user's portable handset, the Air interface in the interface between the handset and the Radio Base Station (BS). Note that in the Bellcore and T1P1 Reference Models, the Radio Base Station functionality is divided into a Radio Port (RP) and Radio Port Control Unit (RPCU) where multiple RPs can subdivide from a single RPCU.

The interface between the Radio Base Station and the (Mobile/PCS) Switch is known as the C-interface in Bellcore and T1P1 terminology, and the A-interface in TR45/TR46 terminology. The A (or C) interface is responsible for carrying signaling for two important kinds of functions: Call Control messages that are carried to the Switch; and Mobility Management messages that are carried (possibly via the Switch) into the network to the Home Location Register and Visiting Location Register (HLR/VLR).

Since the A (or C) interface is between the Radio System and a Switch, it is the interface that is most likely to have two different service provider's networks on either side. This will be even more prevalent as deregulation brings more service providers into the same serving areas. Because of the need to have transparent interoperability between multiple service providers, the development of this interface is one of the most closely watched areas in PCS standards development circles. Many different "flavors" of A-interfaces have been developed, with some being based on SS7³, ISDN⁴, DCS 1900⁵ and even Frame Relay.

Beyond the Switch are the Home Location Register (HLR) and Visiting Location Register (VLR) which contain the PCS

3 Signaling System Number 7

4 Integrated Services Digital Network

5 DCS 1900 is based on Global System Mobile (GSM) which is the European Digital Cellular Standard.

subscribers service profile as well as account, location and routing information.

The primary protocol for communications with these network elements depends on the type of PCS system deployed. The most common intersystem protocol that will be used for North American PCS is IS-41, which is the protocol used to support all North American cellular systems. Some newer PCS systems may use Mobility Management Application Protocol (itself based on IS-41) transported across the A-interface via ISDN Non-Call Associated Signaling or via SS7. PCS 1900 systems that are based on the European GSM digital cellular system use the DCS 1900 Mobile Application Part (MAP) protocol.

5. THE STANDARDS DEVELOPMENT PROCESS

In both TIA and Committee T1, the standards development process begins with an industry need (e.g. an interface or service that needs standardizing), which is articulated in the form of a project request that is brought into an industry standards body.

In TIA, if there is consensus in a subcommittee, a project profile is generated, a project number request form is submitted, and the work is assigned to a Working Group under the Subcommittee. The format of this project number is PN-XXXX.

In Committee T1, the project proposal must be approved by letter ballot before the project can proceed.

At subsequent meetings of the Working Group to which the project is assigned, (this applies to both TIA and T1), participants begin developing a working document by bringing in technical papers, called contributions, that are related to the topic being standardized. These contributions may contain questions, clarifications, tutorials, suggested text for sections of the working document, or alternative text

against contributions brought in by other participants.

These contributions are given unique identifying numbers to aid participants in referring and tracking the input. In TIA, the contribution numbering scheme (e.g. TR46/96.09.26-01) consists of the group name, the year, month, day, followed by a sequential number reset to 1 for each group, each day. In T1, the contribution numbering scheme (e.g. T1P1/96-XXX) contains the name of the subcommittee or Working Group, the year, and a sequential number that is reset to 1 at the beginning of each year.

Regarding the numbering of working documents, TIA uses the "PN" number as the identifier for the working document being developed for that standards project, while T1 gives the working document a number according to the contribution numbering scheme, and appends a revision number following each iteration of the document (e.g. T1P1/96-003R4.)

After the working document has reached the point where it is considered stable, i.e., that it is complete and that there is consensus in the group as to its content, the members of the Working Group conduct a line by line editorial review of the entire document. In TIA, this process is slightly formalized and is known as Verification & Validation (V&V).

Following this review, the members must approve a motion to submit the document for letter ballot, and the document is subsequently mailed out to the committee membership list. The ballot specifies the ballot due date and the type of standards document being balloted.

In TIA, a document can be balloted as an Interim Standard, a Telecommunications System Bulletin (TSB), or a full ANSI Standard. An Interim Standard goes through a slightly streamlined approval process and therefore can not become a full ANSI standard. A TSB is typically used when the document is intended to provide

the industry with clarifications of technical issues, or if it presents changes or enhancements to an existing Interim Standard.

In T1, documents can be balloted as Technical Reports⁶, Trial Use Standards or full ANSI Standards. Technical Reports are used to provide the industry with clarifications of technical issues. Trial Use Standards are analogous to TIA Interim Standards in that the approval process is less rigorous than for full ANSI Standards.

Full ANSI Standards that are developed jointly by TIA and T1 are sometimes referred to as "J" standards, since the numbering format is J-STD-XXX.

Draft standards that are going to be balloted as full ANSI Standards are sometimes referred to by the acronym "dpANS," which stands for draft proposed American National Standard.

As part of the letter ballot process, ballots are returned with industry votes by the specified due date. Respondents can vote Yes, Yes w/Comments, No w/Comments or Abstain. These comments are then reviewed by the group, and every attempt is made to modify the text of the draft standard in order to resolve the comments. Once all comments have been resolved, or an attempt has been made, and given that a sufficient number of Yes votes were received (T1 and TIA have slightly different approval procedures), the draft proposed standard is approved for publication. In the case of ANSI Standards, there is also a behind-the-scenes follow-up process (called BSR-9) where the paper trail of the development and approval process is examined to assure that proper procedures have been followed and that the interests of all industry segments have been given a fair hearing.

⁶ These TRs should not be confused with Bellcore's Technical References, or with TIA's "TR" series Engineering Committees.

6. PCS-RELATED STANDARDS COMMITTEES

6.1 Committee T1

One of the primary standards bodies dealing with PCS issues is T1P1, which is one of the Technical Subcommittees (TSCs) under ANSI-accredited, ATIS⁷-sponsored Committee T1. Although Committee T1 traces its roots to the service provider community, the membership of T1P1 today is mix of service providers (including LEC⁸s, IXC⁹s, cellular and PCS), Manufacturers and General Interest (users, consultants, government, academia).

T1P1 is divided into a number of Working Groups, sometimes referred to as "dot" groups since they are identified as T1P1.1, T1P1.2, etc. Working Groups can be further divided into Subworking Groups. Since 1992, T1P1 has been active in developing PCS-related ANSI Standards and Technical Reports focusing on Services and Architectures, Air Interfaces, Network Interfaces and Network Management. Some of the initial Technical Reports included:

- System and Service Objectives (TR No. 21)
- Privacy & Authentication Objectives (TR No. 22)
- PCS Terminology (TR No. 23)
- Service Capabilities for Low-Power Access to PCS (TR No. 32)
- Network Capabilities, Architectures and Interfaces for PCS (TR No. 34).

More recent work includes: T1.706, *Stage 1 Service Description for PCS*; T1.705, *Stage 2 Service Description for PCS* and the joint development (with TR46) of the PCS air interfaces.

In addition to T1P1, two other T1 TSCs, T1M1 and T1S1, have had a role in the development of PCS standards.

⁷ Alliance for Telecommunications Industry Solutions

⁸ Local Exchange Carriers

⁹ Interexchange Carriers (i.e. Long Distance Carriers)

T1M1 is the T1 TSC responsible for development of OAM&P standards and has issued T1.244, *OAM&P Interface Standards for PCS*, and two PCS-related Technical Reports: *Accounting Management for PCS*, and *Security Management for PCS*.

T1S1 is responsible for the development of network protocols (i.e. CCS SS7, ISDN, AIN, etc.) and has developed T1.651, *Mobility Management Application Protocol for PCS (MMAP)*. The MMAP standard was developed in cooperation with TIA Engineering Committee TR46, for use as a referenced standard in TR46's ISDN-based A-Interface.

6.2 TIA TR46 and TR45

TIA's PCS standardization activity has its roots in the cellular standards work of TIA Engineering Committee TR45. TR45 is the standards body which developed the AMPS analog cellular air interface, the IS-54 TDMA digital air interface for 800 MHz (cellular), the IS-95 CDMA digital air interface for 800 MHz, and IS-41, the intersystem operations protocol which has become the dominant wireless network operations protocol in North America.

In early 1993, in an attempt to create an environment where fledgling PCS technologies could thrive without any constraints imposed from the incumbent cellular interests, TIA formed a separate Engineering Committee, TR46, that was tasked with developing technical standards for the 1800 MHz (i.e. PCS) systems. TR46 set about to develop PCS-related working documents and Interim Standards including:

- PN-3426, Network Reference Models
- IS-104, Service Descriptions for PCS
- IS-651, SS7-based A-Interface
- IS-652, DCS 1900 MAP
- IS-653, ISDN-based A-Interface
- PN-3212, Interworking & Interoperability Between Dissimilar MAPs
- A three volume set of Privacy & Authentication Requirements for PCS

In addition to these standards documents, TR46 also jointly developed (with T1P1) the PCS air interfaces.

TR45 and TR46 are divided into subcommittees (e.g. TR45.2, TR46.1, etc.). Subcommittees are divided into Working Groups, which in turn can be divided into Task Groups. An informal compact notation is used to refer to this organizational hierarchy whereby Task Group 1 of Working Group 2 of Subcommittee TR45.2 is simply referred to as TR45.2.2.1.

Toward the end of 1995, TR45 began lobbying for a change in its scope and charter to allow it to take in the IS-95-based and IS-136-based PCS (1800 MHz) air interfaces, as well as those standards which rely on IS-41. This scope change was eventually approved and is discussed further in Section 8.4.

6.3 JTC

In mid-1992, given the expectation that the FCC PCS Spectrum auction would be held in mid-1995, with subsequent PCS service rolling out in 1996, the standards community was starting to realize that development of a standardized PCS air interface needed to begin as quickly as possible. It was also clear that T1P1 and TR45/TR46 had overlapping interests vis-à-vis PCS and that a turf battle over responsibility for PCS standards would undermine any prospect for rapid air interface development.

In November 1992 a Joint Experts Meeting (JEM) was held to discuss air interface standardization issues. The output of the JEM was a recommendation that T1P1 and TR45/TR46 form a Joint Technical Committee on PCS Air Interfaces. This joint committee became known as the JTC, and immediately set about to develop criteria for development and selection of a PCS Air Interface.

One of the first tasks of the JTC was to attempt to reduce the number of candidate air interface technologies. Although it was recognized at the outset that it may not be possible to select a single air interface that could handle all PCS environments, it was also recognized that a number considerably less than the 16 candidate technologies that

were proposed for consideration would be most beneficial. After several months of trying to foster consolidation, the number of candidate air interface technologies was reduced to the following seven:

- Composite CDMA/TDMA (CC/T)
- IS-95 CDMA upshifted to 1800 MHz
- Personal Access Communications System (PACS)
- IS-136 (IS-54) TDMA upshifted to 1800 MHz
- PCS 1900 (based on European GSM)
- DECT-based
- Wideband CDMA

In mid-1996, the JTC officially disbanded after completing the development, balloting and system testing of six of the seven PCS air interface technologies. (The DECT-based air interface standard was previously transferred to TR41.6 for development.) The PCS air interfaces are briefly described in the next section.

7. AIR INTERFACE STANDARDS

This section describes the PCS air interface standards that came out of the JTC development process:

- **Composite CDMA/TDMA (CC/T)** - This PCS air interface standard is based on the Omnipoint system, which uses a combination of CDMA and TDMA technologies. This standard has been published as T1 Trial Use Standard J-STD-017, and as Interim Standard IS-661 in TIA. Omnipoint has the FCC Pioneer's Preference license for the NY/NJ MTA.
- **IS-95-based CDMA** - This PCS air interface standard is based on a frequency upshifted version of the 800 MHz (1.25 MHz B/W) IS-95 CDMA digital cellular standard. This standard has been published as J-STD-008.

This air interface has been selected for use by a large number of PCS Service providers, including Sprint Spectrum and PCS PrimeCo. A business advantage for this technology is the ability to gain market leverage from 800 MHz cellular IS-95 systems.

- **PACS** - Personal Access Communications Systems (PACS) arose from the consolidation of the Bellcore-originated Wireless Access Communications System (WACS) and Japanese Personal Handyphone System (PHS) proposals.

The system uses an eight-timeslot TDMA air interface for small cell applications with a 2.5 ms frame size and Frequency Division Duplex (FDD) mode for licensed band operation; and a Time Division Duplex (TDD) mode (with either a 2.5 or 5 ms frame size) for the unlicensed band operation.

This standard has been published as J-STD-014 for licensed operation, and includes two Supplements (A and B), for unlicensed operation.

While most of the other PCS air interfaces are based on second-generation cellular digital technology, upshifted to 2 GHz, PACS is a third-generation system that fully embraces the low-power, microcell PCS vision.

Although it is currently only being considered for use by PCS service providers in Alaska (GCI) and Asia, it is also a technology that is ideally suited for Wireless Local Loop, and will likely see increasingly widespread deployment in coming years.

- **IS-136-based TDMA** - This PCS air interface standard is based on a frequency upshifted version of the 800 MHz IS-136 (a.k.a. IS-54) TDMA digital cellular standard. It features a three-timeslot TDMA air interface for large cell applications.

This standard has been published in three sections as J-STD-009, J-STD-010 and J-STD-011. This air interface has been selected for use by AT&T Wireless, among others. A business advantage for this technology is the ability to gain market leverage from 800 MHz cellular IS-136 systems.

- **PCS 1900** - This PCS air interface standard is based on a frequency upshifted version of the GSM European digital cellular standard. It features an

eight-timeslot TDMA air interface for large cell applications.

This standard has been published as J-STD-007. This technology has been selected by Pacific Bell Mobile Services and by BellSouth Mobility DCS.

- **W-CDMA** - This PCS air interface standard is based on a 5 MHz CDMA system. This standard has been published as J-STD-015, and as Interim Standard IS-665 in TIA.
- **DECT** - This PCS air interface standard is based on the European DECT system. It features twelve-timeslot TDMA air interface for small cell applications. Early in the JTC, the DECT work was transferred to TR41.6 for unlicensed applications. The main application for this technology is for wireless PBX.

8. THE "PCS STANDARDS WARS"

Given the enormous financial stakes at risk, it is perhaps understandable that the development of PCS Standards has been marked by a number of highly contentious issues. The tenor of the discussion of these issues has sometimes taken on the characteristics of religious wars. The following subsections provide an overview of the four most bitterly contested issues in PCS Standards development.

8.1 TDMA vs. CDMA

One of the most heated debates in U.S. PCS Standards is the technology and public relations struggle between proponents of IS-95-based CDMA (Code Division Multiple Access) and proponents of IS-136-based TDMA (Time Division Multiple Access). Both of these PCS technologies are derived from the IS-95 and IS-136 second-generation digital cellular standards that are competing to inherit the customer base that is currently being weaned from analog AMPS 800 MHz cellular technology.

While IS-136-based TDMA is a more mature, proven technology, system

limitations and reportedly poor voice codec performance have hampered its popularity. IS-95-based CDMA, on the other hand, claims to increase system capacity by 5 to 20 times, but it is still a relatively new technology so its reliability and actual capacity multiplier still haven't been fully substantiated. With large scale deployment still ahead, the jury is still out on which of the two technologies can establish the biggest nationwide service footprint the soonest.

8.2 IS-41 vs. DCS1900

This debate is similar to the TDMA vs. CDMA battle with the added bonus of protectionist rhetoric. At issue here is that all of the incumbent North American cellular air interfaces, and most of the potential North American PCS air interfaces (IS-95, IS-136, PACS, W-CDMA) use the IS-41 Intersystem Operation Protocol.

The European GSM digital cellular standard has been brought into U.S. Standards bodies, however, and after some "Americanization" has been reborn as PCS 1900. The problem is that PCS 1900 systems use the DCS 1900¹⁰ Mobile Application Part (MAP) for intersystem operations.

On the pro-IS-41 / anti-GSM side, the argument is that the U.S. already has a single network standard (i.e. IS-41); that allowing an incompatible network to be set up would fragment the market and be confusing to consumers; that it would saddle service providers with the unnecessary burden of having to deal with Interworking and Interoperability problems; and that the only ones who would benefit would be the European telecom manufacturers who would gain access to the U.S. telecommunications market.

On the pro-GSM side, the argument is that GSM is not only the single European digital

¹⁰ In the U.S. version of GSM, PCS 1900 refers to the entire radio system, while DCS 1900 refers to the network operations protocols.

standard, but has become a de facto global standard by virtue of the fact that dozens of countries world-wide have deployed, or are planning to deploy, GSM-based systems. Therefore, they argue that U.S. service providers will have to face the Interworking and Interoperability issue anyway unless the U.S. becomes an IS-41 island (albeit a large one) in a GSM world. GSM proponents also point to the fact that GSM technology is tried and tested, and that the service set is mature and quite comprehensive.

Like the CDMA vs. TDMA debate (PCS 1900 is based on TDMA, by the way), the jury is still out on the viability of PCS 1900 systems in the U.S. Even U.S. service providers who are beginning to deploy PCS 1900 systems say that their decision to select PCS 1900 was based on it being the technology that allowed them to get to the market first, not because of any long term commitment to PCS 1900 technology.

8.3 Committee T1 vs. TIA

Standards committees are comprised of people, and as such are not immune from occasional personality conflicts. Like rivalries between neighboring colleges, a sort of rivalry has developed between some of the Technical Subcommittees of Committee T1 and some Engineering Committees of TIA. Some of this is no doubt due to historical factors, given that TIA is a manufacturers trade association, while T1 has traditionally been identified with the wireline carriers.

Differences in procedures, as well as structural differences that contribute to overlapping scopes also contribute to the tension. For example, TIA Engineering Committees are typically organized by technology (e.g. cellular, PCS, Fiber Optics, etc.), while T1 TSCs are typically organized functionally (e.g. signaling, performance, transport, network interfaces, OAM&P, etc.) These differences make it hard to determine which organizations should take the lead and who should follow.

Regardless of the historical origins of the two organizations, any participant who

attends T1 and TIA standards meetings in 1996 would be struck by the observation that, by and large, the membership of the two organizations is becoming largely indistinguishable. Both organizations enjoy the participation of large and small service providers (LECs, IXC's, wireless, cable, satellite) as well as manufacturers. For the vast majority of participants, whose professionalism puts them above the interfactional rivalry, it is hoped that this convergence in membership will lead toward more joint or cooperative standards developments and less unproductive turf battles.

8.4 Cellular vs. PCS (TR45 vs. TR46)

As mentioned previously in this paper, TIA created TR46 to develop PCS standards in an environment free of the constraints that could potentially have been imposed by incumbent cellular interests. At the time, the mantra in PCS circles was "differentiation." That is, PCS was to be presented as a brand new technology that offered users new, advanced features and services, at higher quality and lower cost than current cellular. In other words, cellular was old technology that was doomed to fade away.

Three major things happened that changed this situation. First, the rush to market created a situation where true third-generation wireless technologies were pushed aside in favor of frequency upshifted second-generation digital cellular technologies. Second, the PCS licensees that emerged from the final round of FCC MTA spectrum auctions turned out to be companies with large cellular holdings. Third, cellular technology was rapidly catching up to the specifications of PCS. There was even an attempt to rename cellular as "800 MHz PCS."

Almost overnight, the mantra of "differentiation" was transformed to that of "seamlessness," as licensees sought to ensure that their customers could have access to the same features, quality and services regardless of whether the customer was on a 800 MHz cellular

system or a 1900 MHz PCS system. Further evidence of the convergence of cellular and PCS is the growing use of the term "wireless" to replace both cellular and PCS.

Coinciding with this blurring of PCS and cellular, was the decision by TR45 in late 1995 to change its scope and charter to allow it to reclaim responsibility for IS-95-based and IS-136-based PCS air interfaces, as well as other technologies relating to IS-41. The JTC was wrapping up its air interface development work and was expected to be disbanded within the next few months, so the air interfaces were divided between TR45 and T1P1 for maintenance and enhancements. IS-95 and IS-136 went to TR45, while CC/T, PACS, PCS 1900 and W-CDMA went to T1P1.

The decision to pull IS-41-related PCS standards into TR45 significantly impacted TR46. With most of the standards documents dealing with Service Descriptions and A-interfaces (e.g. IS-651, *SS7-based A-interface*; IS-653, *ISDN-based A-interface*) transferred to TR45, TR46 became a shell, with only PCS 1900 related standards remaining. Since most of TR46's PCS 1900 related work is being done jointly with T1P1, TR46 has essentially become of shadow organization of T1P1.

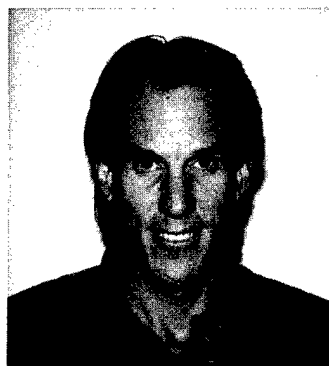
9. CONCLUSION

This paper has attempted to provide a clear, concise understanding of PCS standards development. While it is always a challenge to try to convey an overview of an extremely complex technical topic in just a few pages, it is especially difficult to describe in sufficient detail the nuances of telecommunications standardization, given the interplay of technology and politics. The author hopes, nevertheless, that the reader has gained an understanding of the technologies being standardized, the terminology, processes and procedures involved in standardization, and the recent history and current status of PCS standards.

With the completion of the air interface standards in the JTC, and the completion of the Network Architecture and A-interface standards in T1P1, TR46 and TR45, the main focus of wireless standards activity in 1996 and beyond is expected to concentrate on service descriptions and network issues, such as OAM&P (Operations, Administration, Maintenance & Provisioning), Billing, Emergency Services, Lawfully Authorized Electronic Surveillance, Wireless/Wireline Integration and Wireless Intelligent Networks.

Author

Cliff H. Halevi
Project Director - Standards Management
Bellcore
331 Newman Springs Road, Room 1F-249
Red Bank, NJ 07701
chalevi@notes.cc.bellcore.com



Cliff H. Halevi is currently the Project Director of Bellcore's Standards Management organization, and is Bellcore's voting representative to T1P1 and Committee T1. From October 1993 to September 1995, Cliff was Bellcore's PCS Standards Manager, and has been an active participant in the development of national PCS standards in T1P1, TR46 and the JTC. From January 1994 until March 1996, he was the Secretary of TR46 and of T1P1.3. Bellcore's Standards Management organization provides standards management support, standards development consulting services and standards information products to national and international telecommunications industry clients.

PCS FOR TACTICAL USERS

Mr. Richard Barton, Mr. Werner Sepper and Mr. William Wahl
Lockheed Martin Western Development Laboratories, San Jose, California
Mr. Perry Hugo

U.S. Army Communications Electronics Command, Ft. Monmouth, New Jersey

ABSTRACT

Possible application of Personal Communication System (PCS) technologies to the needs of future, forward tactical users on the battlefield is attractive because of the rapid commercial development of PCS equipment and its relatively low production cost in the marketplace. Looking at cell sizes based on mathematical models of PCS operation, it appears that realistic tactical ranges vary from approximately 3 km to 25 km, depending mainly on the type of surroundings, antenna heights, frequencies used, and system power output. Use of such PCS cells as communication augmentations for military forces requires that they must be low cost and need little or no additional infrastructure. Potential approaches to do this would be to collocate PCS base station components at MSE and TOC sites or to use airborne (or satellite) platforms to provide relays or carry base station components.

INTRODUCTION

As United States military forces invent new tactics for the 21st Century, the concept of shared situational awareness, especially in support of continuous operations, is becoming a focus of both communications and information systems. Whatever its eventual implementation, situational awareness will require both voice and data communications between tactical, strategic and sustaining base information systems.

Links between strategic and sustaining base communities are available through satellite, troposcatter, HF skywave, and other established approaches. Links to forward, tactical battlefields are more difficult because of the frequent need for forward users to hand carry all of their equipment. In addition, future tactical ground force requirements are quite varied and may involve events anywhere in the

world, be at conflict levels from peacetime disaster relief through full armed combat, and need levels of involvement from squads to corps. The only common factor is that reaction time is expected to be very short.

This paper reports some of the results of a study considering the applicability of developing commercial Personal Communication System (PCS) technologies to future forward area battlefield users. It specifically considers Propagation and Deployment of available (or nearly available) PCS components in potential tactical scenarios.

PROPAGATION STUDY

Tactical Cell Sizes

Cell size analysis consists of the evaluation of supportable cell sizes as a function of significant system parameters. Generally, propagation performance or cell size varies according to the actual environment in which it is deployed, frequencies used, base and mobile antenna heights, and type and power of equipment used. User selectable factors, in most cases, include adjustment of base antenna heights and/or effective isotropic radiated power (EIRP), selection of frequencies, and selection of specific site locations based on mission planning predictions of coverage for the actual terrain involved.

Mobile communications adds additional signal degradation factors due to multipath fading, shadowing and path attenuation. Multipath is the receipt of multiple reflected versions of the transmitted signal. Multipath can produce deep fades depending on the instantaneous vector addition of the signal components at the receiver. The rate of change of multipath fade is a function of the relative velocity of the mobile user and the reflecting surfaces affecting the signal. Multipath effects are statistically modeled as a multiplicative

(complex) random variable with Rayleigh amplitude and uniform phase distributions.

Shadowing is the partial or complete attenuation of the direct signal component due to features such as hills, trees, or man-made structures. Shadowing can produce signal strength deviations of all levels. Shadowing loss is typically modeled as a multiplicative (real) random variable with a log-normal distribution.

Path attenuation is the gradual average signal loss variation due to large-scale terrain characteristics and distance. Path losses are a function of path geometry and the propagating environment. Path losses are typically modeled as a function of frequency, antenna height, and range between antennas. These are often user controllable variables.

Additional losses in real environments are due to foliage, shielding of mobile antennas by the human body, and building-vehicular blockages. These should be considered, depending on each application, and are best defined through field experiments with an analysis of actual parametric data.

For the purposes of this study, multipath losses are accounted for in the link budgets by the values selected for the Signal-to-Noise Ratio (SNR) required to close a communication link. Shadowing losses (including blocking due to foliage, bodies, and vehicles) are accounted for by a fixed loss allowance in the link budgets. All the remaining allowable losses can then be attributed to path losses. Thus for various defined environments, path loss models with various frequencies and antenna heights can be used to determine maximum transmission distances that provide a sufficient SNR to close a link. These distances can then be used to show what tactical cell sizes can be expected.

Path Loss Models

A number of path loss models are currently available and were considered for this study. The most widely used are:

1) Free Space Model: Applicable to direct links without terrain effects. Provides a maximum theoretical path distance value for comparison.

2) Longley-Rice Model - Point to point and area modes for prediction of propagation with and without terrain profiles. This model handles both surface and tropospheric refraction. Urban clutter modifications are also available (fit to Okumura's model). The model covers frequency ranges from 40 MHz to 100 GHz, antenna heights of 0.5m to 3000 m and ranges from 1 km to 2000 km. This model tends to under-estimate propagation loss in urban and suburban mobile environments.

3) Okumura Model - Based on measurements made in Tokyo and surrounding suburbs. Correction factors for open areas, suburbs and urban environments are given. This model covers frequencies from 150 MHz to 2.0 GHz, antenna heights for a base station from 30 m to 1000 m and mobile user antennas from 1 m to 10 m, and ranges from 1 km to 100 km. Okumura's urban and suburban corrections over-estimate the losses in the equivalent U.S. areas. The model does not include lower base antenna heights of interest.

4) Hata Model - This model fits equations for Okumura's results over a reduced input parameter range. The model covers frequencies from 150 MHz to 1.5 GHz, base station antenna heights from 30 m to 200 m, mobile antenna heights 1 m to 10 m and ranges from 1 km to 20 km. Hata's equation does not cover the entire range of mobile frequencies (specifically, the 1900 MHz band) and all desired base station antenna heights (specifically 15 m).

5) Walfisch and Bertoni Model - Model is valid for a restricted set of urban cases. The model considers the impact of rooftops and building heights. Coverage for frequencies from 800 MHz to 2.0 GHz, base station antenna heights from 4 m to 50 m, mobile antenna heights from 1 m to 3 m and ranges from 0.02 km to 5 km. The model includes the PCS 1900 MHz band and short-range paths.

6) Lee's point to point loss prediction - Model for the computation of propagation loss on a point to point path within the radio horizon. Ranges are limited to less than 16 km. Model includes path-specific correction for the surrounding environment of the base antenna.

All models attempt to characterize the large-scale average signal losses along the propagation path. These losses are expressed as a function of the distance between the transmitter and the receiver, such that

$$L_p(d) \propto d^n$$

where n is the path loss exponent and $L_p(d)$ is path loss as a function of distance. For direct link conditions (free space), $n = 2$. For urban environments, the value of n can range from 2.7 to 5. A value ranging from 3.5 to 4.0 is typical.

The Hata equations provide a simple area model. The model equations are listed in Table 1. The suburban and urban equations show approximately 15 dB and 20 dB higher losses at 900 MHz than at frequencies below 300 MHz.

The applicability of the model depends on how well the target environment

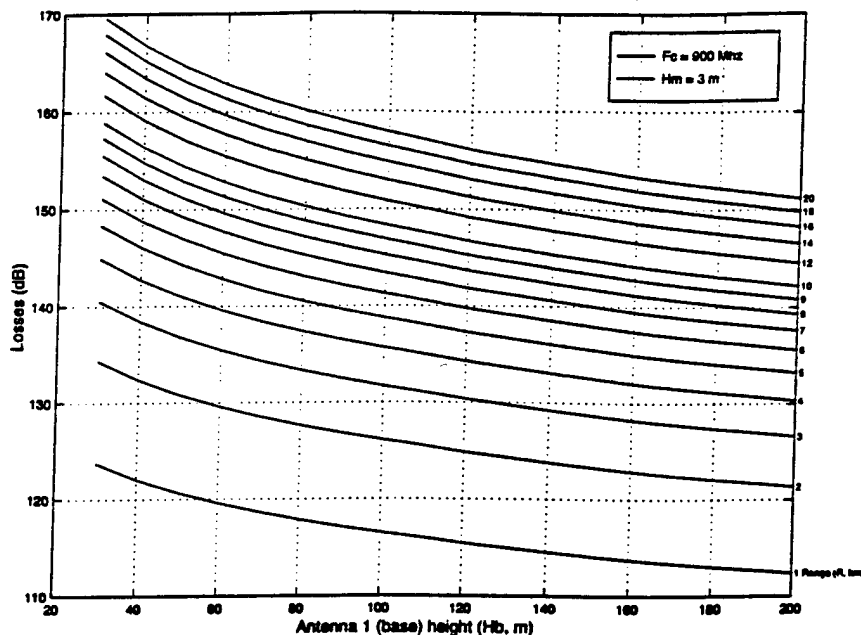
matches the three types of areas defined. Comparisons made between Hata model calculations and measurements in several U.S. urban areas show agreement (A. Mehrotra, Cellular Radio Performance Engineering, Artech House, Boston, MA., 1994). A constant offset in loss versus range is present in some of the tests (4 to 8 dB more loss is predicted by the model). This discrepancy has been attributed to target U.S. cities not matching the Tokyo urban environment. The conclusion is that the Hata loss prediction error cannot be determined accurately without comparison tests for the specific region of interest.

The approach followed in this study for estimating cell size is to reduce the allowable link losses by approximately 6 dB in order to bound the model error. In cases where a close match of the environment exists, this leads to conservative (pessimistic) estimates of the losses. A typical output plot is shown in Figure A.

Table 1. Hata Model Equations

Area	Equations
Urban Area	$L_p = 69.55 + 26.16 \cdot \log_{10}(f_c) - 13.82 \cdot \log_{10}(h_b) - a(h_m)$ $+ (44.9 - 6.55 \cdot \log_{10}(h_b)) \cdot \log_{10}(R) \quad (dB)$ <p>$a(h_m)$ is the correction factor for vehicular station antenna height <u>medium-small city</u> $a(h_m) = (1.1 \cdot \log_{10}(f_c) - 0.7) \cdot h_m - (1.56 \cdot \log_{10}(f_c) - 0.8)$ <u>large city</u> $a(h_m) = 8.29 \cdot (\log_{10}(1.54 \cdot h_m))^2 - 1.1 \quad ; \quad f_c \leq 300 \text{ MHz}$ $= 3.2 \cdot (\log_{10}(11.75 \cdot h_m))^2 - 4.97 \quad ; \quad f_c > 300 \text{ MHz}$</p>
Suburban Area	$L_{ps} = L_p\{\text{Urban Area}\} - 2 \cdot \{\log_{10}(f_c/28)\}^2 - 5.4 \quad (dB)$
Open Area	$L_{po} = L_p\{\text{Urban Area}\} - 4.78 \cdot \{\log_{10}(f_c)\}^2$ $+ 18.33 \cdot \log_{10}(f_c) - 40.94 \quad (dB)$
where f_c is the carrier frequency (MHz) – 150 to 1500 MHz h_b is the effective base antenna height (m) – 30 to 200 m h_m is the vehicular station antenna height (m) – 1 to 10 m R is the distance between the antennas (km) – 1 to 20 km	

Figure A. Output Plot (900 MHz, Urban Area, 3 m Mobile Antenna)



Cell Size in an Interference-Free Environment

Typical link budgets were determined for both Code Division Multiple Access (CDMA) and Advanced Mobile Phone System (AMPS) protocols. The CDMA results are shown in Table 2.

Several assumptions were made about system operation. A total of 26 active users with a 40% voice activity factor was chosen to determine the traffic-loading degradation. The availability of soft handoffs was used to determine the handoff gain at the edge of coverage. A relatively high base antenna

Table 2. Reverse Link Budget Example (CDMA)

CDMA Reverse Link		
Parameters	Budget	Subtotals
Receiver Parameters		
Required Eb/No (dB)	6.0	
Data Rate, 9600 bps (dB)	39.8	
Thermal Noise Temperature, 290 K (dB-K)	24.6	
Boltzmann's Constant (dBm/K-Hz)	-198.6	
Noise Figure (dB)	4.0	
Effective Receiver Sensitivity (dBm)		-124.2
Propagation Loss Allowances		
Foliage Loss (dB)	-3.0	
Body Loss (dB)	-3.0	
Log-Normal Shadowing Loss Margin (dB)	-5.4	
Loss Allowance Subtotal		-11.4
Equipment Loss Allowances		
Receive Cable Loss (dB)	-2.0	
Loss Allowance Subtotal		-2.0
System Gain/Loss Allowances		
CDMA Traffic Loading Effect (dB)	-3.0	
CDMA Soft Handoff Gain (dB)	4.1	
Gain/Loss Allowance Subtotal		1.1
Antenna Gains		
Transmit Antenna Gain (dBi)	.0	
Receive Antenna Gain (dBi)	12.8	
Gain Subtotal		12.8
Transmit Power (dBm)	23.0	
Subtotal		23.0
Allowable Path Loss (dB)		
Subtotal		-147.7
Propagation Model Error Allowance (dB)		6.0
Corrected Allowable Path Loss (dB)		-141.7

gain consistent with a sector antenna is used. The allowable path loss based on these assumptions was computed to be 147.7 dB.

The AMPS calculations used a typical operational SNR of 18 dB. An antenna gain consistent with a high-gain sector antenna is assumed. The transmit power of 10W was selected with the resulting allowable path loss calculated to be 144.3 dB.

Hata analysis results were plotted in terms of constant loss contours to facilitate the determination of the supportable cell sizes based on the allowable path loss obtained from the link budgets. Cases for

open and suburban areas were both considered since they are representative of open battlefield environments. Frequencies of 900 MHz and 1900 MHz were used. The latter were calculated using the Hata model outside its nominal range. The extended model departs by approximately 2.1 dB from the original Hata urban model at 1900 MHz. Since this is within the observed Hata model errors, the original model was used here outside its range to illustrate typical cell size reduction occurring at PCS frequencies. Plots of the resulting calculations are shown in Figures B-1 to B-4.

Table 3 summarizes the supportable cell sizes for typical link budget cases of

Figure B-1. Propagation Loss Contour (Open Area, 900 MHz, 3m Mobile Antenna) **Figure B-2. Propagation Loss Contour (Open Area, 1900 MHz, 3m Mobile Antenna)**

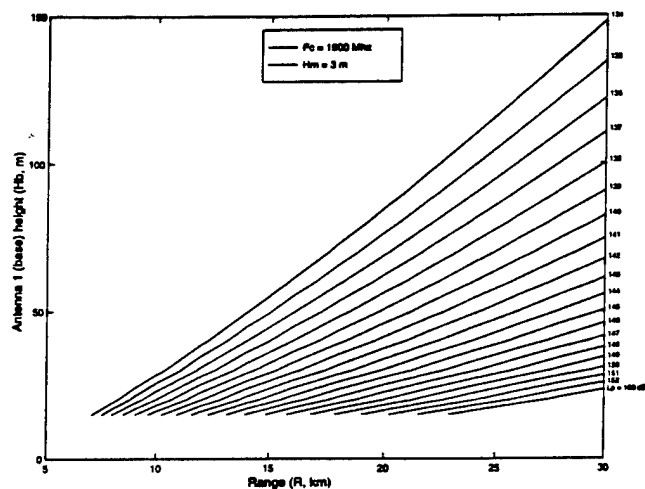
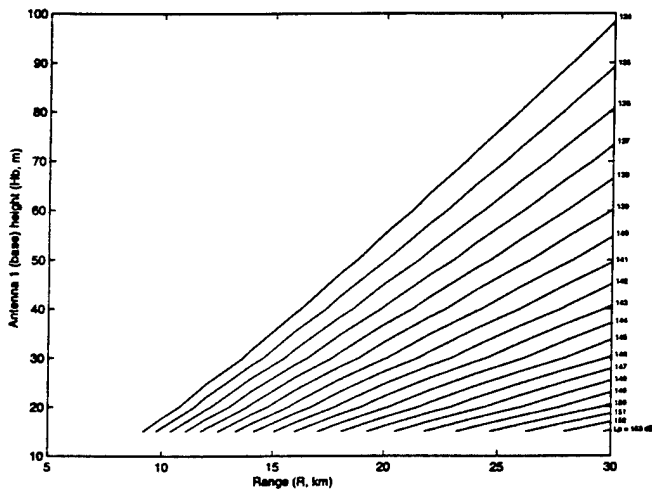
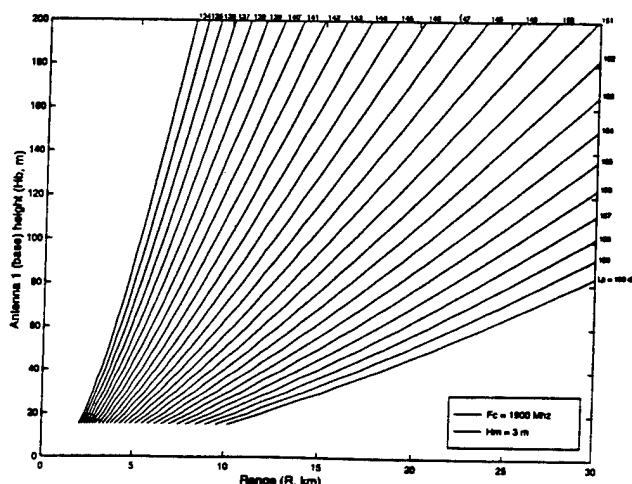
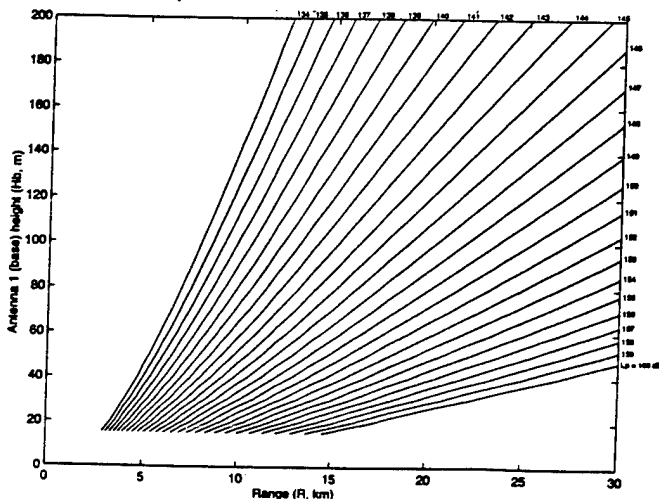


Figure B-3. Propagation Loss Contour (Suburban Area, 900 MHz, 3m Mobile Antenna) **Figure B-4. Propagation Loss Contour (Suburban Area, 1900 MHz, 3m Mobile Antenna)**



approximately 147 dB. it should be noted that the mobile antenna height in all of these examples is 3 m. This is twice as high as a normal walking height. The 3 m elevation is consistent with the antenna (and the user) being on a vehicle.

This analysis shows that cell radii

interference from other users. The effect of co-channel interference is dependent on the ratio of thermal noise to interference power that the system must tolerate at the edge of coverage. Most designs make an allowance for interference degradation over thermal noise. This composite noise (thermal plus

Table 3. Summary Cell Sizes
(147 dB Path Loss, 6 dB Loss Estimation Allowance, 3m Mobile Antenna)

Base Antenna Height (m)	Maximum Cell Radius (km)			
	Open, 900 MHz	Suburban, 900 MHz	Open, 1900 MHz	Suburban, 1900 MHz
15	20.5	6.5	11	3.1
28	30	-	-	-
30	-	9.5	16.3	4.4
50	-	12.9	22.7	5.8
75	-	-	30	-
100	-	20.3	-	8.7
170	-	30	-	-
200	-	-	-	13.8

*Use of Hata Model outside its range.

greater than 7.5 km can be achieved readily with base station mast heights of less than 30 m for cellular frequency bands. These results are consistent with the typical ranges planned for the current military Mobile Subscriber Equipment (MSE) Radio Access Unit (RAU) baseline in open environments with 15m antennas. However, MSE RAU coverages are only marginally satisfied in suburban and urban areas. This reduction in range can be overcome by increasing the transmit EIRP approximately tenfold or by using higher antenna emplacements.

Higher frequency (i.e. 1900 MHz) PCS and wideband PCS equipments are best suited for local area wireless communications coverage in semi-static command post and tactical operation center environments to provide high data rate (i.e. ISDN 144 kbps BRI) wireless services.

Effects of Mutual Interference Environment

Cell sizes are dependent on the composite noise at the receiver. Composite noise includes thermal noise plus

interference) estimate is used to determine the coverage area for a given maximum EIRP and receiver sensitivity. Mutual interference introduces other limitations.

Narrowband frequency division multiple access/time division multiple access (FDMA/TDMA) systems are bandwidth limited. Co-channel interference determines the allowed proximity of neighboring cells using the same frequencies. CDMA systems are interference limited. Co-channel interference limits the maximum number of users per cell.

The use of sectorized antennas reduces the contribution from a portion of the interferers. For FDMA/TDMA, the use of sectorized antennas allows denser frequency utilization. For CDMA, sectorized antennas reduce the interference from a percentage of the users within a cell. This attenuates interferers that are closer to the base at the expense of increasing the antenna gain in the direction of remote interferers in adjacent cells. The CDMA system has the advantage of being able to operate without alignment of antenna sectors. That is, assuming a

uniform location distribution of users within each cell, there is no performance penalty incurred by randomly aligning the sectored antenna setup. This is not the case for FDMA/TDMA, since it requires careful frequency management and antenna alignment to improve the frequency reuse. It should be noted however, that unaligned sectored antennas can be used with FDMA/TDMA to reject external interference from other systems.

FDMA/TDMA systems present a more difficult frequency management problem for a transient tactical infrastructure than does CDMA. CDMA can be deployed as a collection of end-point cells with less coordination of parameters among the bases than FDMA/TDMA. For the latter, proper frequency assignments must be maintained at all times to avoid severe interference. Coordinating the frequency plan of fast-redeploying bases or those providing communications on the move requires a high degree of coordination and control, which may be difficult to maintain under stressed conditions. Consequently, CDMA is easier to use in the tactical mobile environment.

As mobiles are added to the network, interference among mobiles and base

stations for both, a 3/9 reuse pattern for GSM with frequency hopping, a frequency reuse pattern for CDMA of 1 (which means all CDMA frequencies can be reused at all cell sites), 10 MHz of spectrum for both systems with 5 MHz each for forward and reverse links, and a 1000-square kilometer area with loads defined as active traffic channels in a typical urban 50 km/hr multipath environment. The resulting analysis showed initial deployment requirements of 200 base stations for GSM but only 40 base stations for CDMA.

Capacity comparisons of digital cellular air interfaces in a 10 MHz spectrum are provided in the Table 4. CDMA provision of 25 calls/sector/CDMA channel in a fully loaded network includes 35% overhead for soft handoff. In both high and low mobility cases, sector capacity can be greatly increased if neighboring cells are not fully loaded since this provides for automatic dynamic capacity allocation in the network. CDMA, as embodied in IS-95 and IS-665, is recommended over competing TDMA (and GSM) due to its inherent resistance to jamming, interference, detection and improved spectrum efficiency and frequency reuse factors.

**Table 4. Capacity Comparisons of Digital Cellular Air Interfaces
(10 MHz Spectrum with 5 MHz Transmit and 5 MHz Receive)**

Air Interface Parameter	IS-95-A North American Digital	Global System for Mobile (GSM) Communications	IS-54 North American Digital	Advanced Mobile Phone System (AMPS)
Format	Digital	Digital	Digital	Analog
Multiple Access Method	CDMA	TDMA	TDMA	FDMA
Channel Bandwidth	1.25 MHz	0.20 MHz	0.03 MHz	0.03 MHz
Number of Channels	3	25	167	167
Frequency Reuse (3 sector cells)	1/1	3/9	7/21	7/21
Effective Channels	3/1=3	25/9=2.78	167/21=7.95	167/21=7.95
Voice Calls/Channel	25	7.25	3	1
Voice Calls/Sector	75	2.78 x 7.25 = 20.16	7.95 x 3 = 23.85	7.95 x 1 = 7.95

stations determines the required number of base stations. A calculated comparison between GSM and CDMA was made with the following assumptions: three sector base

DEPLOYMENT CONSIDERATIONS

Typical Coverage Patterns

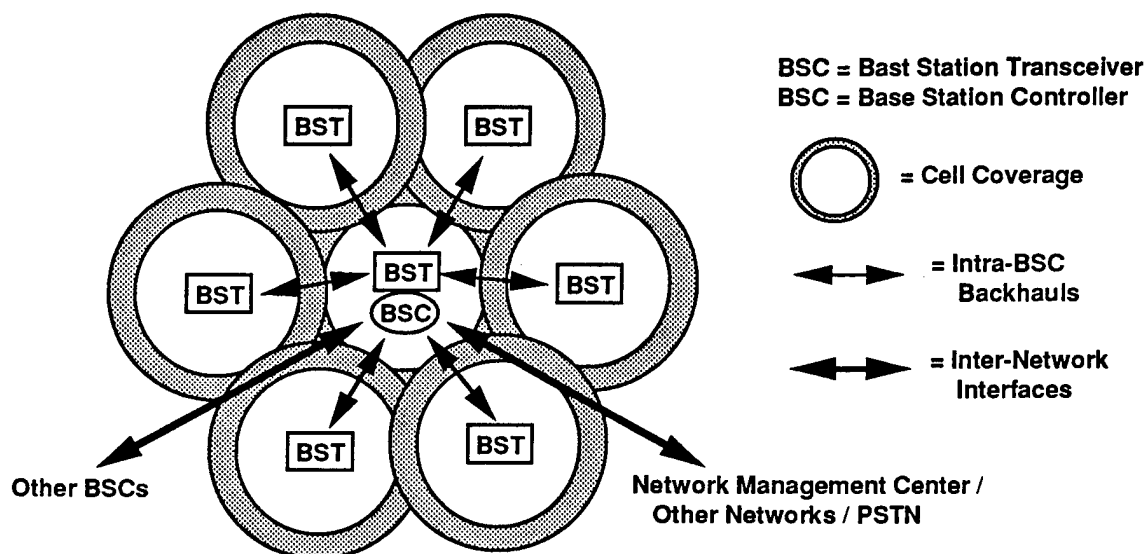
Figure C illustrates a CDMA-type PCS network showing the relationship

between Base Station Transceivers (BST) and Base Station Controller (BSC). The BST provides transceivers, timing reference, backhaul interface, and diagnostics. The BSC provides interconnection between PCS cells, home location register, visitor location register, call control processor, base station manager, network management center interface and interfaces to other networks (PSTN, etc.).

other BSCs are severed. If BSCs regain contact, the connections can be reestablished and the BSCs joined into a single PCS network.

Network management functions for autonomous operation include the ability to manage and coordinate frequency assignments, operation schedules, and other command and control functions. Coordination with adjacent, higher, or lower

Figure C. Typical PCS Network (CDMA Example)



A PCS configuration with a single BSC to one or more BSTs provides point coverage. The BSC operates autonomously from any other PCS cells in the vicinity. Interfaces to other PCS cells as well as to non-PCS networks such as PSTNs, SINCGARS, MSE, etc. are accomplished through gateway interfaces at the BSC. In this way, subscribers in other networks can be reached. However, if PCS subscribers leave the coverage area, their calls cannot be handed over to another PCS cell, even if the other cell is of the same type.

This single-point coverage provides certain advantages in the battlefield. The autonomous operation of such a configuration provides coverage within a unit's area without the need to rely on other or centrally located resources. If other units are adjacent, communication between networks is possible by connection via gateway interfaces at the BSC. But each BSC operates autonomously when connections to

echelons can be accomplished using either the gateway interfaces of the BSC or separate communications channels such as the tactical internet, SINCGARS nets, or satellite communications. The network management function should also include the ability to calculate cell coverage to facilitate the planning for relocation and moving PCS cells.

PCS for Tactical Users

The use of cellular telephone systems, or any new communications system in future tactical scenarios must be accomplished without high acquisition costs, additional personnel, or extensive infrastructure. PCS networks, however require cellular base stations which in turn must be operated and maintained by knowledgeable personnel. Thus, base stations must be collocated with equipment already serviced by technically trained personnel.

Three immediate scenarios for Ground Forces can be postulated. Specific Army application may be insertion into the Area Common User System (ACUS), as specified in the ACUS Modernization Plan and the TRADOC Signal Center Directorate for Combat Development (DCD) Warfighter Information Network (WIN) Concept Paper. Support of Naval and Air Forces are considered in scenarios 2 and 3.

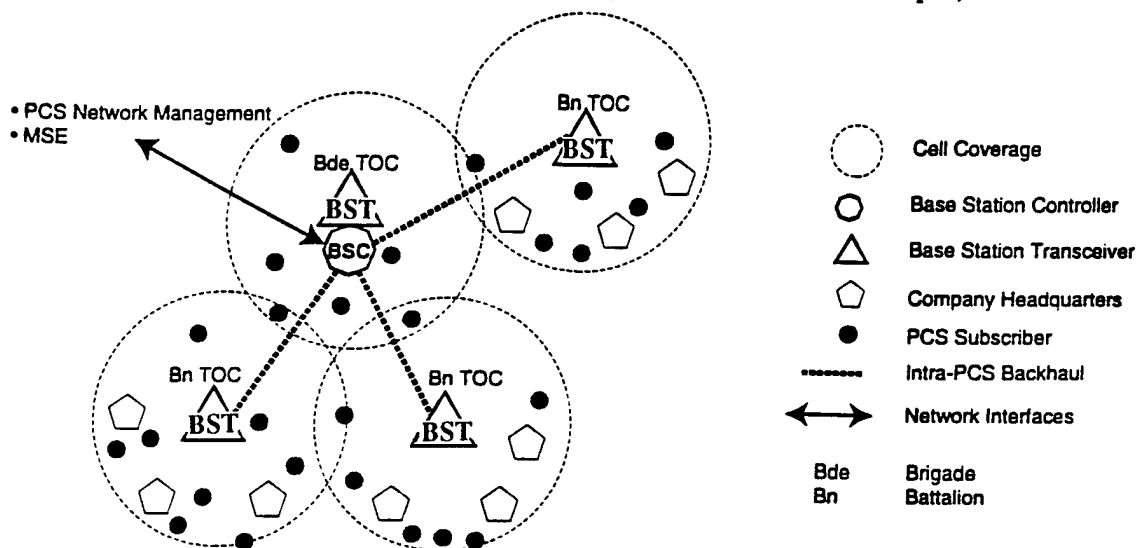
Scenario 1 collocates PCS base stations with MSE and Tactical Operations Centers (TOCs). MSE equipment (switches, network controllers, etc.) is mobile and mounted in shelters for Corps and Division operations while stationary, but with quick setup or move times. MSE includes a separate control system, ISYSCON, to provide system geographic, position, network, frequency and cryptographic variable management. An upgrade of current ISYSCON software tools would be required for cellular and PCS deployment.

Operationally, MSE provides wired telephone, ethernet LAN interfaces and a limited number of mobile telephones. Each

battalions and lower) usually have MSE access only when located within a division rear area or via the mobile phone interfaces. Addition of BSTs to various MSE units and all connected to a single BSC for switching would provide an augmented phone service to all personnel in Division and Corps areas, provide an immediate wireless capability upon unit arrival, and serve local mobile users so long as they remain in range of operational MSE units.

Farther forward, concentrations of suitable vehicles, generators and communications personnel can be found at brigade, battalion, artillery, aviation and other TOCs. Such TOCs are usually configured in HMMWV-mounted Standard Integrated Command Post Shelters (SICPS). Mobile command posts provided by the Command and Control Vehicle (C2V) and Bradley electronic fighting vehicles are also used. Since TOCs are often within line of sight of other TOCs, PCS base stations collocated with TOCs and C2Vs could provide a PCS network down to company level. Figure D shows a typical scenario.

Figure D. Typical PCS Deployment (CDMA Example)



division has four Net Center Switches (NCSs) for redundant area coverage. Large Extension Nodes (LENs) and Small Extension Nodes (SENs) provide user interfaces for headquarters and major support centers. Maneuver units (brigades,

Scenario 2 provides immediate tactical support over a wide area through the use of either satellite or airborne (surrogate satellite) links. Two types of airborne PCS links are suggested. The first is to provide a relay on an airborne platform

(UAV, helicopter, etc.) to function as a link from forward users back to a BST. The Commanders' Tactical Terminal (CTT) system integrated with Guardrail and U-2 aircraft is a current similar example.

A second type of airborne system is putting a BST on an aircraft. This approach provides full communications for all users within the radio "footprint" of the BST. The size of the footprint is determined by the altitude and flight path of the aircraft. Now there would be a standard data link from the airborne BST to a ground-based BSC to provide the required back-haul for switching and netting. Since ground-based BSTs can operate unattended, no functions on the aircraft should be needed beyond possible BST initialization. This approach could provide continuous support to ground force users during fast-moving mobile operations. In addition, it would support separate naval units, especially during littoral operations. It could also provide wide area coverages for air forces without the time and effort to install ground base stations.

Finally, Scenario 3 for immediate, but limited tactical support, would simply use commercial satellite based cellular systems as they become operational between now and the end of this century. This approach is the most limited in both the number of users that could be accommodated and the lack of specific military system capabilities (for example, encryption, call priorities, and resistance to hostile electronic warfare). However, it could support non-hostile operations, such as disaster relief, with immediate linkages back to rear or separated units.

In all these scenarios, consideration should be given to providing microwave or millimeter wave repeaters to provide cellular and PCS cell site range extension and "gap filling." Commercially available cellular and PCS equipment is still highly vulnerable to jamming, interception and deception. Significant military adaptation would be required to "harden" it against network attacks. However, emerging National Security Agency (NSA) Multilevel Information Systems Security Initiative (MISSI) network security components such as FASTLANE/TACLANE in line network encryptors and Fortezza PCMCIA encryp-

tion cards could be applied to enhance information security and reduce vulnerability against deception.

Army, Navy and Air Force future visions are being defined in doctrines such as Task Force XXI, Copernicus-Forward and the Horizon Concept. All of these stress seamless sensor to shooter connectivity. TPCS components might provide such a responsive, flexible, linkage between forward units and their command centers.

CONCLUSIONS

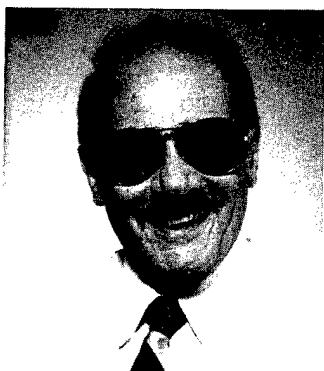
Results of Hata modeling showed that for cellular frequencies, cell radii greater than 7.5 km are feasible with base station antenna heights of less than 30 m. At higher PCS frequencies and in urban areas, cell radii are reduced significantly, but can be increased by either raising the transmit EIRP or by increasing antenna heights.

Use of cellular and PCS communications in the tactical environment requires deployment of base stations, without additional personnel. To do this, base stations for ground forces could be collocated with existing systems having qualified personnel. In Corps and Division areas, MSE units are appropriate candidates. In more forward areas, TOCs and C2Vs provide similar possibilities.

Where it is not appropriate to use ground-based stations in forward areas, relays or PCS base station elements on airborne platforms (or commercial satellite equivalents) might provide immediate, but limited coverage. This is particularly applicable to Naval and Air Force scenarios.

In all cases, PCS could provide an augmentation to current tactical phone systems and act as an immediate, limited wireless capability to provide voice and data support to tactical users. Because PCS developments are supporting a rapidly developing commercial markets, much of their development and production cost will not need to be born by military users. However, because the technology has been developed for commercial users and not the battlefield, PCS components need careful evaluation and some degree of "hardening" to be suitable for most military uses.

AUTHORS



Richard Barton

**Lockheed Martin Western Development
Laboratories, San Jose, California**

Mr. Barton is a Principal Engineer in the System Engineering Directorate of WDL. His experience includes development and design of voice, data and video systems and covers hardware, software, wireline and wireless systems. He holds bachelor and master's degrees from the Univ. of Pennsylvania and is an IEEE senior member, sitting on both its Communications and Computer Societies.



Perry W. Hugo

**U.S. Army Communications-Electronics
Command, Ft. Monmouth, New Jersey**

Currently an electronics engineer with the Space and Terrestrial Communications Directorate, Mr. Hugo's areas cover technical evaluation and tactical implementation of emerging advanced wireless communications for Army Force XXI initiatives. Mr. Hugo is a graduate of the Pennsylvania State University (BS-'83) and a member of the central New Jersey chapter of ADPA.



Werner Sepper

**Lockheed Martin Western Development
Laboratories, San Jose, California**

Mr. Sepper is a Systems Engineering Manager at WDL with responsibilities covering both computer and communications system architecture design and evaluation. Mr. Sepper has been the principal system engineer for the Army All Source Analysis System (ASAS), the Single Source Processor - SIGINT (SSP-S), the C2V Mission Module and several classified programs.



William E. Wahl

**Lockheed Martin Western Development
Laboratories, San Jose, California**

An Advanced Programs Manager at WDL, Mr. Wahl retired from the Army Signal Corps as a Program Manager in 1984. He has since been part of contractor teams for the Army's All Source Analysis System (ASAS), the Air Force's Tactical Reconnaissance System (TRS) and for classified programs. He holds degrees from the Universities of Wisconsin, Kansas and S. California.

CODE DIVISION MULTIPLE ACCESS (CDMA) SYSTEMS FOR WIRELESS APPLICATIONS

Robert Olson

QUALCOMM Incorporated
San Diego, California

ABSTRACT

Code Division Multiple Access (CDMA) air interface standards are published for compatibility between subscriber station and base stations for wideband spread spectrum cellular systems. TIA/EIA/IS-95-A contains the CDMA standard for systems operating in the 800 MHz cellular band while ANSI J-STD-008 defines the CDMA air interface in the 1.8GHz PCS band.

This paper describes system characteristics of a CDMA system designed for simplicity and flexibility. Included is a description of a common network architecture and network planning tools for implementing cellular mobile, PCS and wireless local loop CDMA networks. Also included is a description of a CDMA system base station.

INTRODUCTION

Commercial deployment of cellular mobile phone networks was initiated in the United States in the early 1980's in a 50 MHz spectrum allocation in the 800 MHz band. Since that time, cellular mobile phone services have experienced rapid growth in both the number of subscribers and in the coverage area where services can be obtained. Also, more recently, an additional 120 MHz allocation for Personal Communication Services was allocated in the 1.8-2.0 GHz band as the next generation of cellular services.

Cellular and PCS systems provide telephone services such as voice, data, and facsimile transmission to mobile stations using wireless communications technology.

Calls can be mobile-to-mobile terminated or mobile-to-wireline phone terminated.

Cellular mobile radio systems consist of two major components: the base station and the subscriber stations.

The base station establishes the coverage area in which the mobile stations obtain services, controls the system and the mobiles during call setup, traffic maintenance and teardown, and interfaces to the Public Switched Telephone Network to allow mobile-to-wireline phone calling.

Subscriber stations are mobile radios operated by subscribers and provide access to the base station network when services are desired by the subscriber or when the subscriber receives an incoming call.

CDMA is a digital modulation and multiple access method based on spread spectrum communication. In CDMA, individual channels are separated and distinguished by digital codes. In contrast to other forms of multiple access such as frequency based or time based, the CDMA signals occupy the same spectrum at the same time. The use of CDMA for the air interface in cellular and PCS networks offers improved spectral efficiency, voice quality and communication performance, among other advantages when compared with analog systems and other digital modulation methods for cellular and PCS mobile networks.

The QCMobility system is a CDMA based land mobile network infrastructure product. The equipment is configurable for IS-95-A (800MHz cellular) [1] or ANSI J-STD-008 (1.9 GHz PCS) [2] CDMA air interfaces. The system provides the air interface to the

mobiles using CDMA transceivers located at the cell sites dispersed throughout the coverage area. The system also contains mobile switching center functions supporting subscriber mobility within the home network, and handoff to and roaming within other networks. The system contains digital trunk interfaces to international PSTNs.

The CDMA air interface can simultaneously support high mobility applications such as mobile cellular or PCS phones in vehicles and low mobility applications such as wireless local loop phones and hand held phones used by pedestrians.

CDMA SYSTEM CHARACTERISTICS

CDMA Air Interface

The CDMA air interface between the mobile and the base station is defined in the specifications TIA/EIA/IS-95-A for the cellular band and ANSI J-STD-008 for the PCS band.

A CDMA channel consists of a 1.2288 MHz forward channel and a 1.2288 MHz reverse channel with frequency division duplex operation of the channels. Duplex spacing is 45 MHz in the cellular band and 80 MHz in the PCS band. In both bands, the base to mobile CDMA channel is the higher frequency of the pair. The forward and reverse CDMA channels each contain overhead and traffic channels called CDMA code channels. The code channels perform overhead functions such as synchronization and signaling between the base station and the mobiles and carry the digital voice and data traffic. PCS carries traffic information at up to 9600 bps or 14400 bps. IS-95-A currently specifies cellular traffic at up to 9600 bps. A planned revision of IS-95-A will include 14400 bps traffic service.

A CDMA frequency assignment is a forward channel and reverse channel operating at designated center frequencies, which are separated by the band designated frequency division duplex separation of 45 MHz for the cellular band or 80 MHz for the PCS band.

Frequency Reuse

Frequency reuse is fundamental to modern cellular radio systems. Systems using non spread waveforms require distance between transmitters using the same channel. Analog systems operate with a reuse pattern of $K=7$, which means that the total available spectrum is divided into 7 segments. Modern digital systems using non spread waveforms can achieve a reuse pattern of $K=3$. CDMA with direct sequence spread spectrum signaling allows a reuse factor of $K=1$. This is the most efficient reuse of the spectrum in that all of the spectrum can be used in all sectors of coverage. [3] Frequency reuse in all sectors simplifies frequency planning and allows soft handoff.

Handoff

The CDMA air interface uses a "make before break" method called soft handoff when handing off a call between CDMA cells. With soft handoff, frame selection is done at the Base Station Controller (BSC) on a frame by frame basis. Soft handoff provides a fully transparent call handoff. With soft handoff, the BSC receives multiple copies of each mobile frame that is communicating with more than one Base Station Transceiver Subsystem (BTS). The BSC selects an available frame with no errors based on the cyclic redundancy check attached to the frame. Connection with multiple cells is established before the cell change is made.

When handing off a call between sectors of a cell, the same "make before break" technique is used, but it is termed softer handoff because signal combining is performed in the BTS on a symbol by symbol basis rather than on a frame by frame basis as with soft handoff.

Soft and softer handoff is possible only because CDMA's frequency reuse is $K=1$. Soft and softer handoff improve the performance of CDMA system at the cell boundaries. [4]

Coverage and Capacity

Coverage and capacity requirements in a cellular system determine the number of

BTSs deployed and the geographical placement of them. Each BTS is geographically dispersed from the BSC and requires a link to the BSC and peer level processing capability at the BSC for each channel in the network.

CDMA has attributes which minimize the number of base stations required in either low traffic density or high traffic density cases.

In very low traffic density deployments, the link budget limits the line of sight coverage from the BTS. [5] The processing gain and handoff gain in spread spectrum systems support higher allowable path losses than non spread systems at the same signal levels.

As traffic density requirements increase, the effects of mobile interference limit cell size. The size of cells decreases to accommodate the maximum cell (or sector) capacity of the air interface. The spread spectrum processing gain inherent in CDMA systems makes CDMA less sensitive to interference compared to non spread spectrum systems.

Power Control

CDMA achieves consistent high capacity and quality voice and data service while minimizing average output power. CDMA automatically adjusts cell and mobile power for cell load, cell noise figure, antenna gain, power amplifier output, multipath fading, shadowing, and proximity of the mobiles to the BTS.

CDMA employs both forward link and reverse link power control. Reverse link power is adjusted by both open and closed loop feedback methods which is unique to CDMA based systems.

Power control reduces the transmit power to the minimum required to close the forward and reverse links. Power control reduces the effects of interference to improve capacity of the CDMA channel. Power control adjusts the power levels in the CDMA transmitters on a per sector and a per link basis. The goal of power control is to

manage the interference of users on the same CDMA channel to achieve capacity gains and to deal with near-far considerations for all receivers in the network.

Voice and Data Traffic

IS-95-A CDMA supports voice or data traffic at a base data rate of 9600 bps, including overhead and traffic. ANSI J-STD-008 supports 9600 bps and 14400 bps over-the-air rates. The forward and reverse link channels are used to send voice only, data only, or combined voice and data in the 20 ms frames.

Multipath Performance

CDMA exploits the multipath environment through spread spectrum processing by rake receivers, through time diversity provided by interleaving, through forward error correction on all transmitted bits, through multiple cell/sector diversity provided by soft/softer handoff and through spatial diversity from two receive antennas at the cell.

RAKE receivers track signals and multipath independently and the sum of the signal strengths is used for signal demodulation. Since fades are independent, the result is call clarity with minimal fading even under severe conditions.

High and Low Mobility Services

CDMA offers high and low mobility service with a single air interface. CDMA forward and reverse link power control allows a handset to transmit in microwatts for indoor applications. The same handset may be taken outdoors for high mobility applications.

Distributed Antennas and Leaky Coax

CDMA systems can use distributed antennas and leaky coax to improve system performance in multipath environments found in enclosed areas such as tunnels, parking garages and like structures. The multiple signal reception from the antennas, in conjunction with the use of RAKE receivers, constructively combine the out of sequence signals, resulting in a stronger signal than any of the individual

components. Distributed antennas operate at low transmit levels, typically in the 1 mW range. Maximum coverage area is approximately 2,000 square meters.

Microcells

CDMA Micro cells are RF modules from the BTS which can be physically remoted from the digital, power, and other non-RF parts of the BTS, to provide flexibility of deployment of the BTSs. The modules are connected to the base station using fiber optic cable. The RF performance is identical to full BTS performance and the modules can be remoted to distances of up to 30 Km from the BTS.

Remote Antenna Systems

A CDMA remote antenna system using cable TV infrastructure is planned. The system allows the use of CATV assets in place of PCS base station antennas. The antenna will interconnect with the BTS at the head-end site of the cable network. This allows a CDMA network to be configured without the construction of towers for the PCS antennas.

CDMA SYSTEM IMPLEMENTATION

Network Architecture

An implementation of a CDMA cellular network is shown in figure 1. The network implements either IS-95-A or ANSI J-STD-008, depending primarily on the choice of RF modules in the BTS and the associated antennas. Non RF hardware in the BTS, such as the modems and power conversion equipment, as well as all of the BSC equipment is common to either cellular or PCS bands. Either system supports mobility or local loop services. Application Specific Integrated Circuits implementing key elements of the IS-95-A physical layer are developed for the mobiles and the base station [6].

The Base Station Communication Network provides a path for signaling and traffic packets within the network consisting of BTSs and the BSC. A packet consists of a 20 ms frame containing signaling or traffic information. The network shown uses an

ATM-like variable length packet as the structure of the BCN packets.

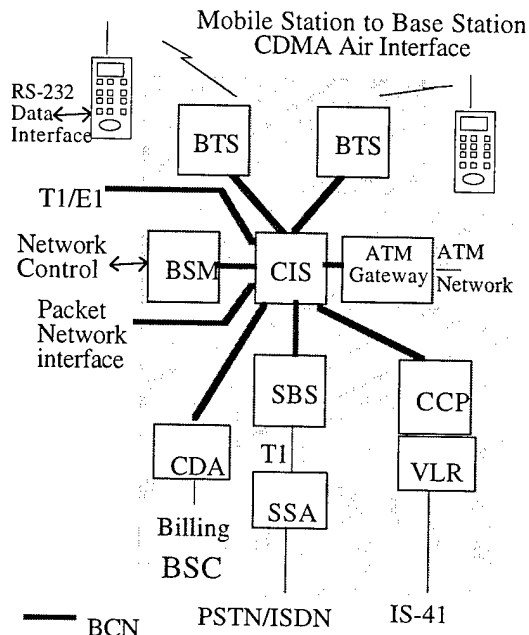


Figure 1. A CDMA Network Architecture

BTS

The BTS provides the basic element of CDMA RF coverage for mobiles. The BTS modulates and demodulates CDMA code channels to communicate with the mobiles. Each BTS provides sufficient channel elements for the overhead, control, traffic maintenance, and handoff up to the BTS capacity. A BTS can be configured with one, two, or three sectors with each sector providing a capacity of 20 simultaneous calls. Typical mobile cellular or PCS BTSs can support up to three sectors per frequency assignment. The number of frequency assignments allowed at each cell site is dependent on the number of 1.25 Hz CDMA channels assigned within the available spectrum. Because the subscribers in wireless local loop systems are static, fewer handoffs need to be accommodated. Thus, a wireless local loop configuration can support up to nine sectors per frequency assignment. Wireless local loop provides capacity of 45 calls per sector. The BTS backhaul interface is T1 unchannelized which uses vocoded voice traffic to efficiently use backhaul capacity.

Base Station Controller

The Base Station Controller (BSC) provides switching and mobility management functions within the network and interfaces with the PSTN.

Base Station Manager

The Base Station Manager (BSM) performs network configuration and overall control. Upon completion of initialization function, the BSM monitors network performance and manages faults.

CDMA Interconnect Subsystem

The CDMA Interconnect Subsystem (CIS) connects the BSC subsystems and the BTSs. The interface format is medium speed serial packets that have framing similar to ATM packets. An ATM gateway can convert the V-ATM packets and ATM cells and interface to an ATM network. CDMA networks will support the ability to handoff calls through the ATM network bypassing the PSTN.

Selector Bank Subsystem

The Selector Bank Subsystem (SBS) processes traffic frames to and from all BTS code channels for traffic to and from the mobiles.

The SBS contains an interworking function to convert PSTN protocols to CDMA protocols. Also included is conversion between the 8 kbps or 13 kbps CDMA vocoder format and the 64 kbps PCM format.

In the reverse direction, the SBS selects the best available CDMA vocoded frame from multiple copies on a frame by frame basis. The SBS converts the CDMA vocoded frame to a PSTN vocoded frame for calls originated or terminated through the PSTN.

For forward traffic, the SBS performs the opposite process, converting PCM frames from the PSTN into CDMA vocoded frames. The SBS sends the frame to the BTS serving the mobile and multicasts the frame to mobiles in handoff regions.

The SBS performs forward and reverse power control to maintain the frame erasure rate established by the BSM.

Call Control Processor / Visitor Location Register

The Call Control Processor (CCP) manages network resources during call setup and teardown. The CCP also contains a database of active mobiles called the Visitor Location Register (VLR). As the VLR processes mobile registrations, it constructs a subscriber database from queries to the Home Location Register which contains subscriber records. The HLR also authenticates registrations. The HLR can be included in the BSC or can be remotely accessed through an IS-41 SS7 link [7].

Supplementary Services Adjunct

The Supplementary Services Adjunct (SSA) provides switching and interface resources to the network. The SSA contains a non-blocking matrix which allows trunk resource such as the SBS, or PSTN trunks to be connected at the 64kbps level. The SSA contains circuits which provide signaling termination between the CDMA network and the PSTN.

Call Detail Access

The Call Detail Access (CDA) collects and distributes call records for billing purposes. User information is provided by the CCP, HLR and SBS. Billing information is available through electronic interfaces or magnetic media.

NETWORK DESIGN

Planning prior to deployment of cellular base stations can be greatly simplified through the use of simulation tools.

QEDesign performs CDMA network planning based on a path loss model and a CDMA network performance model. The software simulation executes on a UNIX workstation and can support multiple network planners simultaneously.

The core databases used by the simulation include terrain, clutter, and demographic databases. Satellite imagery can be used for the terrain and clutter model. The terrain and clutter databases provide information for the CDMA propagation model performed by the simulation. Demographic databases provide a source of predicting traffic density, and thus an estimate of system capacity requirements. Parameters of the databases which effect path loss determination, such as allowances for losses and traffic density, can be edited to allow the user to better control the simulation.

Network planners construct cells by specifying cell RF and antenna parameters to the simulation using a menu driven graphical user interface. When constructed, cells are placed on the imagery map by a cursor or by entering coordinates. When complete, the network simulation contains data for each cell in the network.

The network planner constructs a link budget by entering mobile station and base station RF parameters to the simulation. Path loss adjustments are entered to allow for penetration, cable losses, and shadowing. CDMA parameters including data rate, noise figure and max E_b/N_0 are also entered.

The simulation calculates data sets based on the data bases, the link budget constructed and the CDMA parameters entered. The calculations are performed for each bin in the coverage. Bin size is user entered in arc seconds of latitude and longitude.

The RF model provides a prediction of path loss from each cell site to each bin in the coverage area. The path loss can be displayed in color graphics or numerically by cursor control. The RF model includes the affects of the terrain and clutter models and the link budget established. The RF model indicates areas where coverage can be predicted based on path loss.

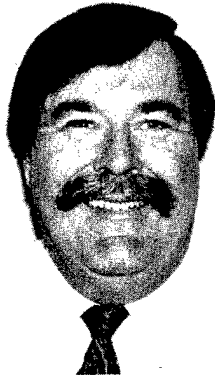
CONCLUSION

Personal Communication Services based on spread spectrum multiple access technology known as Code Division Multiple Access (CDMA) have been developed for cellular band and PCS bands. Applications include cellular land mobile subscribers or wireless local loop subscribers in both bands. The use of microcells and remote antenna systems, including remote antenna systems over cable, are planned to provide flexibility for deployment and coverage extension. Network planning tools are available to analyze network performance including coverage, capacity, handoff, and other parameters.

REFERENCES

- [1] TIA/EIA/IS-95-A "Mobile Station-Base Station Compatibility Standard for Dual-Mode Wideband Spread Spectrum Cellular System", Telecommunication Industry Association, May 1995.
- [2] ANSI J-STD-008, "Personal Station-Base Station Compatibility Requirements for 1.8 to 2.0 GHz Code Division Multiple Access (CDMA) Personal Communications Systems".
- [3] Padovani "Reverse Link Performance of IS-95 Based Cellular Systems", IEEE Personal Communications, Third Quarter 1994.
- [4] Patel, Goni, Miller, Carter, "A Simple Analysis of CDMA Soft Handoff Gain and its Effect on the Cell's Coverage Area", Winlab '95 Symposium.
- [5] Wheatley, Charles, "Trading Coverage for Capacity in Cellular Systems", IEEE MTT-S 1995 International Topical Symposium, pg. 71-77.
- [6] Kerr, Richard, "CDMA Digital Cellular", Applied Microwave and Wireless, Vol 5 Fall Issue 1994, p179-186.
- [7] EIA/TIA IS-41-B, "Cellular Radio - Telecommunications", Intersystem Operations, December 1991.

BIOGRAPHY



Robert Olson received the BSE degree and the MSEE degree from Arizona State University and San Diego State University in 1968 and 1973 respectively. His career includes electronic design and system engineering for multiple access data communication and location tracking networks for twenty years at General Dynamics Electronics Division and at Science Applications International Corporation for two years. He joined QUALCOMM, Incorporated, San Diego, California in January 1996 and is currently involved in CDMA infrastructure applications for cellular and PCS networks.

Robert Olson
5565 Morehouse Drive
San Diego, CA 92121

Reliability of Optical Fibers in Steam and Petrochemical Environments

Dipak R. Biswas, Charles R. Kurkjian and Osman S. Gebizlioglu

Bellcore, Morristown, New Jersey

ABSTRACT

Optical fibers with different coatings were exposed to steam and kerosene environments for 2 h to 33 days. The strength of acrylate coated fibers showed a drop as high as 37% initially then leveled off after 6d steam exposure whereas the drop in strength was less than 10% after 33d in kerosene. In contrast, hermetic carbon coated fibers did not show any change in strength. The strength of fibers was higher than the required proof test level of 100 kpsi and it was also higher than the minimum strength which is required for handleability and successful stripping of fibers for connectorization.

INTRODUCTION

As optical fibers are being deployed rapidly in the outside plant environment, they are likely to be exposed to various harsh environments. These environments may differ significantly depending on the climatic and installation conditions. Exposure to steam and petroleum distillates constitutes one of the harshest environments for these fibers or cables. The underground steam ducts can potentially leak or fail and can react with the optical fiber or cable. The average temperature and pressure of the steam leaking through the pipe can be as high as 400° F (205° C) and 400 psi depending on the size of the steam pipe¹. Other potential exposures to steam may arise from nearby power plants, and cogeneration plants. Petroleum products are

a common contaminant in the underground plant environment in which telecommunication fibers or cables are deployed. These contaminants either from leaks, spills or runoffs can adversely affect the optical fiber or cable. The steam resistant optical cable is designed to handle such harsh environment and the primary function of this cable is to protect the fibers from damage during installation and use. Extensive work has been done on the effect of liquid water and water vapor on the mechanical reliability of optical fibers, substantially less work has been done on the reliability of optical fibers when they are exposed to steam and petroleum distillates.

In this paper, we will address the mechanical reliability, specifically the change in strength of optical fibers with different coatings after being exposed to steam and kerosene environments for nearly 30 days.

MECHANICAL RELIABILITY

The strength, fatigue and strip force were measured on three commercially available standard single mode fibers with different acrylate coatings (Fiber 1, Fiber 2, Fiber 3) and on one carbon/acrylate coated single mode fiber (C). The fibers were placed in a steam chamber under zero stress condition and exposed to steam (130° C and 23 psi) for 2 hr. to 26 days. After aging in steam, the fibers were equilibrated at 70° F and 50% relative humidity for at least 24 hours before measuring the strength, fatigue and the strip force. The surface of glass fibers was analyzed by using atomic force microscopy for any surface degradation. In addition, the coatings were examined by

Dynamic Mechanical Thermal Analyzer (DMTA) for any possible coating degradation and also to measure the coating mechanical properties such as storage modulus E' , loss modulus E'' and the loss tangent ($\tan \delta$). The storage modulus is a measure of stored mechanical energy in tensile or bending deformation, the loss modulus is a measure of loss of mechanical energy in the fiber coating and the loss tangent is the loss modulus divided by the storage modulus. The loss tangent-temperature profile provides information about the glass transition temperature.

The above fibers were also subjected to stress free aging in kerosene at room temperature for 1 to 33 days. The strength and fatigue tests were performed in kerosene at 70° F and 50% relative humidity environments.

STRENGTH AND FATIGUE

STEAM:

The effect of steam aging on the strength of optical fibers is summarized in Table 1 and Figure 1.

Table 1. Effect of Steam Aging on the Strength of Optical Fibers

FIBER	STRENGTH, kpsi					
	Ambient	2h	6h	1d	6d	26d
#1	914.7	902.9 (1.3%)	885.3 (3.2%)	844.8 (7.6%)	652.2 (28.7%)	643.9 (29.6%)
#2	939.4	895.3 (4.7%)	862.2 (8.2%)	735.3 (21.7%)	626.7 (33.3%)	610.1 (35%)
#3	985.6	855.1 (13.2%)	836.9 (15.1%)	735.1 (25.4%)	618.2 (37.3%)	611.2 (38%)
C	548.4	-	-	555.1	551.3	553.1

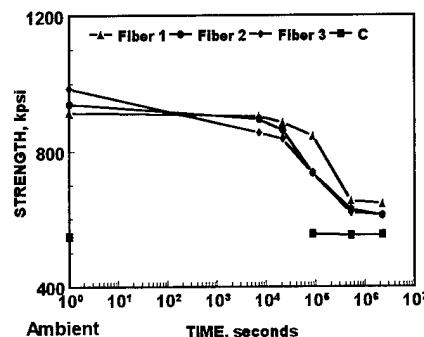


Figure 1. Dependence of strength on aging time in steam.

The results show relatively little change in strength at short times followed by a "knee" and a rapid decrease in strength at longer times. All of the acrylate coated fibers showed relatively similar reductions in strength after steam aging. 1-13% decreases in strength (in parenthesis) were noticed after 2- hour exposure and the highest drop of 38% was observed for fiber #3 when compared with the strength of fibers in ambient condition (70° F and 50% relative humidity). For the acrylate coated fibers 1 - fiber 3), the "knee" (change in slope) occurred after 2 hour exposure to steam after which the strength dropped relatively rapidly and leveled off after 6 days of steam exposure. The reduction in strength is probably caused by the reaction of diffused steam with the glass surface as evidenced from some degree of surface roughness determined from the Atomic Force Microscope photographs (Figure 2). The surface roughening of silica glass is due to the inhomogeneous dissolution of silica in liquid water^{2,3}. This process is thermally activated and its rate is temperature dependent (Arrhenius behavior). The work of Matthewson and Yuce⁴ showed aging behavior for the first time in 85° C / 85% relative humidity similar to that in 85° C in deionized water except the degradation in strength was shifted by an order of magnitude in time.

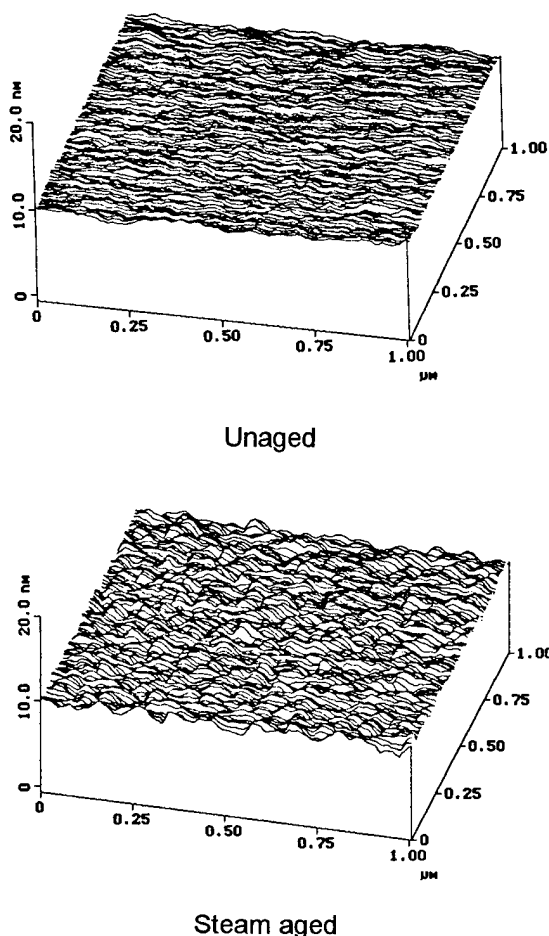


Figure 2. Atomic force microscope photographs of Fiber 3 before and after steam exposure (aging) for 26 days.

From the experimental data on steam aging, one can calculate the time required for any reduction in strength from 130° C exposure to 85° C by shifting the failure time using the following equation:

$$E = R \ln(t_1 / t_2) / (1/T_1 - 1/T_2)$$

where E is the activation energy for the reaction of steam with silica assumed to be 25 kcal/mole, and t_1 and t_2 are the failure times at temperatures T_1 and T_2 . Figure 3 shows the normalized strength vs the aging time at 130° C in steam and shifted to 85° C along with the literature data⁴ for silica fiber aging at 85° C and 85% relative humidity. The 85% humidity data follows a trend

similar to the steam data shifted to 85° C, but it shows an early "knee" and the strength reduction is much sharper and deeper probably due to different coating characteristics. The steam aging behavior of optical fibers with acrylate coatings show a similar trend to the 85 C/85% RH aging of similar optical fibers excepting that in the case of steam, the strength appears to level off within the current experimental time.

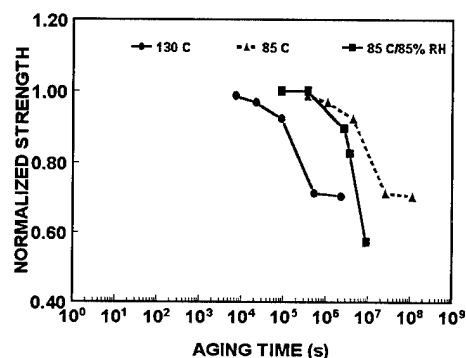


Figure 3. Normalized strength and aging data for Fiber 1 and compared with 85/85% RH data from reference 4 (in filled square).

In the case of the carbon/acrylate coated fibers, there was no change in strength after aging in steam even after 26 days. This indicates that the carbon coating is definitely protecting the fiber from any potential damage due to the diffusion or reaction of steam with the glass surface.

The strength of fibers after 26 day steam exposure was higher than the required proof test level of 100 kpsi and it was also higher than the minimum strength of (~300 kpsi, i.e. 2 GPa) which is required for handleability and successful stripping of fibers for connectorization⁴. All of these fibers were handleable even though there were some changes in the color after the steam exposure. Fiber 3 showed a distinct yellow color after steam aging.

Dynamic fatigue in bending was also evaluated for the above fibers in ambient and after steam aging for 26 days. The results are tabulated in Table 2.

Table 2. Dynamic Fatigue Parameter of Different Fibers

FIBER	Dynamic Fatigue Parameter (n_d)	
	Ambient	Steam Aged
#1	16.6	22.9
#2	19.0	23.2
#3	20.6	25.9
C	78.0	103.0

In general, it has been observed that optical fibers with acrylate coatings after zero stress aging in water or high humidity showed no measurable change in n -values^{5,6}. In case of steam aging, however, the fatigue parameter values show a general increase outside of the experimental error.

KEROSENE:

The effect of aging in kerosene on the 2-point bend strength of optical fibers is shown in Figure 4.

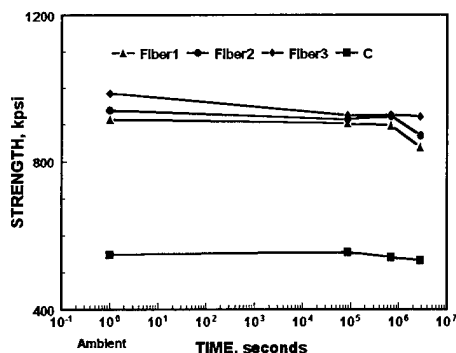


Figure 4. The effect of aging in kerosene on the 2-point bend strength.

The strength reduction after exposing in kerosene was less than 10% after 33 days. The coatings were not discolored and the fibers were easily handleable after aging. The fatigue parameters showed a slight increase after aging in kerosene for 33 days.

STRIP FORCE

The strip force was determined in accordance with the procedure⁷ specified in FOTP-178 with a strip length of 30 mm and a stripping speed of 500 mm/min. The results of unaged vs steam aged fiber samples are shown in Figure 5.

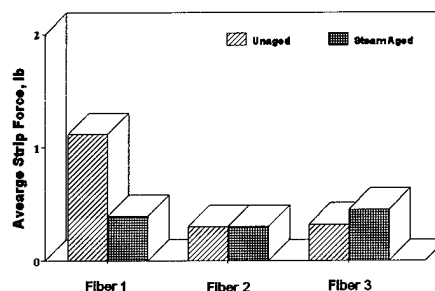
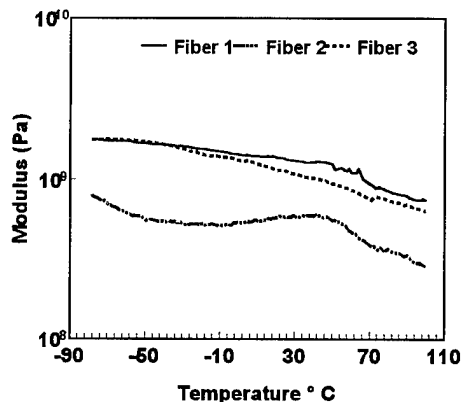


Figure 5. Strip force before and after steam aging.

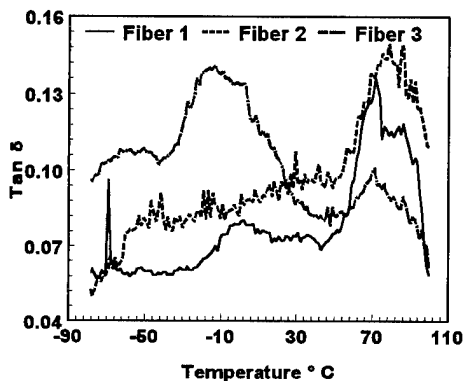
All of the fibers showed a strip force of less than 2 lbs. for both aged and unaged fibers. Only Fiber 1 showed a lowering in strip force after steam aging.

DMTA RESULTS

Fibers 1, 2 and 3 were examined before and after 26-day steam exposure by the in-situ characterization technique using DMTA (Dynamic Mechanical Thermal Analyzer). Figures 6a and 6b show storage modulus - temperature and loss tangent-temperature profiles for these fibers, respectively. While the storage modulus profile of Fiber 2 is placed lower by a factor of 2 compared to those of fibers 1 and 3 over the entire temperature range, the most dramatic difference between these fibers appears in their loss tangent profiles shown in Fig. 6b. In this figure, fibers 1 and 2 show much greater mechanical loss under their secondary coating $\tan \delta$ peaks centered at about 75 °C, while fiber 3 exhibits a $\tan \delta$ profile with a dominant transition centered at about -6 °C.



a)



b)

Figure 6. A comparison of coating mechanical properties for fibers 1, 2, and 3
a) Storage modulus, b) Loss tangent.

Steam exposure for 26 days produces different effects for these three fibers. DMTA profiles of fiber 1 shown in Fig. 7 indicate a general softening over the entire temperature range as evidenced by the lowered E' profile of the steam-exposed fiber. Tan δ profile shifts upward with the appearance of two low-temperature transitions located at about 3 °C and -51

°C. Fiber 1 before steam aging showed a major transition with two peaks located at 71 °C and 86 °C and a minor transition centered at 2 °C. Lowering of E' profile along with growing tan δ profile with multiple low-temperature peaks signifies that this fiber underwent some depolymerization during the steam exposure.

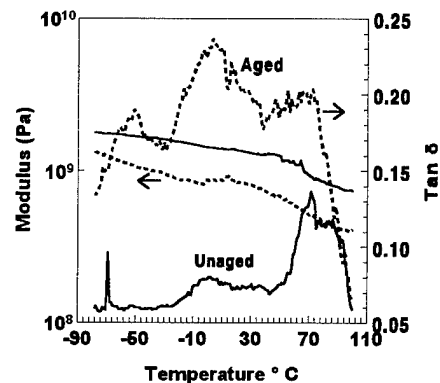


Figure 7. Fiber 1 before and after 26-day steam aging (unaged-solid line, and aged -dashed line).

Fiber 2 showed two major differences in mechanical properties after 26-day steam aging. Its E' profile shifts upward (within a factor of 2) over the entire temperature range shown in Figure 8. Its tan δ profile shows broadening at about the glass transition temperature (T_g) of 70 °C with no appreciable change in its peak value. However, the tan δ profile exhibits three peaks at 0 °C, 18 °C, and -63 °C with greatly increased peak heights. These changes suggest that this fiber might have degraded thermo-oxidatively during steam exposure.

SUMMARY AND CONCLUSIONS

The strength, fatigue and strip force were measured on three commercially available standard single mode fibers with different acrylate coatings (Fiber 1, Fiber 2, Fiber 3) and on one carbon/acrylate coated single mode fiber (C). The strength of the acrylate coated fibers dropped initially then leveled off after 6 day exposure in steam. The drop in strength can be attributed to the reaction between silica glass and the diffused steam. The coatings, in general, underwent degradation after the steam exposure as evidenced by the DMTA analysis. Though Fiber 3 showed a rapid drop in strength initially, the coatings on Fiber 3 did not degrade significantly compared to Fiber 1 and Fiber 2. In case of carbon coated fiber, the steam did not affect the strength indicating a strong resistance to diffusion of steam through the carbon coating to the glass surface. When exposed to kerosene, strength degradation was less than 10 % after 33 day exposure and the fatigue parameter did not change significantly. In the case of both steam and kerosene exposures, the minimum strength measured were significantly above the proof test level of 100 kpsi and minimum safe handling stress of nearly 300 kpsi. With further protection from other steam resistant cable materials, such as hermetic armor and heat resistant jacket⁸, the fiber strength degradation noticed in this work may not be a major concern.

Therefore, with proper cable design and suitable cable materials, optical fibers with acrylate coatings in the cable structure can be exposed to steam and kerosene environments. Hermetic carbon coating on optical fibers can provide even further protection from these environments.

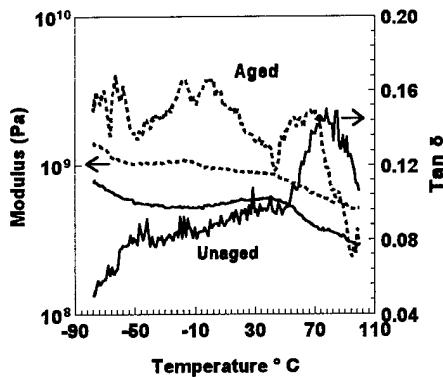


Figure 8. Fiber 2 before and after 26-day steam aging.

Fiber 3 shows minimal change in its E' and $\tan \delta$ profiles after 26-day steam exposure. E' profiles in Fig. 4 suggests that this fiber has undergone no significant change while $\tan \delta$ profiles indicate that the $\tan \delta$ peak temperature (T_g) for the primary coating increased from -14°C to 6°C while the secondary coating T_g (69°C) did not change appreciably. Of these three fibers, Fiber 3 shows no significant change. Even though the initial strength reduction is more pronounced in Fiber 3, it exhibited the highest steam-aging resistance over a 26-day period of aging.

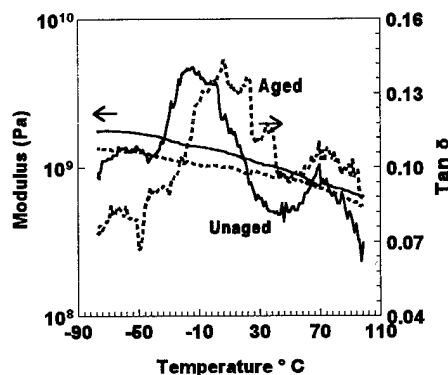


Figure 9. Fiber 3 before and after 26-day steam aging.

ACKNOWLEDGEMENT

The authors would like to acknowledge Irene Plitz, Janet Armstrong and Joel Mann for carrying out the AFM work.

REFERENCES

1. M. Vyas, E. Buckland and P. Neveux, Jr., "Design and Development of Steam Resistant Fiber Optic Cable", Proc of the 40th IWCS, 55 (1991).
2. H.H.Yuce, J.P.Varachi, J.P.Kilmer, C.R.Kurkjian and M.J.Matthewson, "Optical Fiber Corrosion: Coating Contribution to Zero Stress aging," OFC'92, Tech Digest, Postdeadline Paper - PD-21 (1992).
3. D. Innis, Q.Zhong and C.R.Kurkjian, "Chemically Corroded Pristine Silica Fibers: Blunt or Sharp Flaws?," J. Amer. Ceram. Soc., 76, 3173 (1993).
4. M.J.Matthewson and H.H.Yuce, "Kinetics of Degradation during Fatigue and aging of Fused Silica Optical Fiber," SPIE, 2290, 204 (1994).
5. W Griffioen, "Aging of Optical Fibers in Water," Proc. 41st IWCS, 622 (1992).
6. A. Dwivedi, G. Glaesemann and C. Eoll, "Optical Fiber Strength, Fatigue and Handleability after Aging in a Cable," Proc. 43rd IWCS, 728 (1994).
7. Telecommunications Industry Association Arlington, VA., TIA/EIA-455-178A (1996).
8. Bellcore Technical Reference, TR-NWT-001322 (1994).



Dipak R. Biswas received his M.S. and Ph.D. degrees in Materials Science and Engineering from the University of California, Berkeley in 1974 and 1976 respectively. He started working on optical fiber coating development at ITT-EOPD since 1981. After working for Alcatel, SpecTran and Fiberguide, he joined Bellcore in 1994. He is currently working on the reliability of glass fibers with different coatings and plastic optical fibers.



Charles R. Kurkjian received his B.S. degree in Ceramics from Rutgers University in 1952 and his Sc.D. in Ceramics from M.I.T. in 1955. After post-doctoral positions at M.I.T. and the University of Sheffield in England, he spent 35 years at A.T.&T. Bell Labs in Murray Hills, N.J. During this time he did research and development on glass and glass fibers. In September of 1994, he retired from Bell Labs and joined Bellcore in Morristown, N.J. where he continues his work on the strength and reliability of lightguide fibers.



Osman S. Gebizlioglu holds B.S. and M.S. degrees in Chemical engineering from the Middle East Technical University , Ankara, Turkey. After receiving his Ph.D. in the Polymer Materials Program at Princeton University, he was a Monsanto Postdoctoral fellow in the Mechanical Engineering Department of M.I.T. where he investigated the physics of toughening glassy polymers. Since he joined Bellcore in 1987, he has focused his research on polymers used in optical fiber cables and components.

STRUCTURAL CHANGES IN POLYACRYLATE COATINGS EXPOSED TO DEGRADING ENVIRONMENTS

Pär-Anders Högström, Sigbritt Karlsson and Ulf W. Gedde*
Royal Institute of Technology, Department of Polymer Technology,
S-100 44 Stockholm, Sweden

ABSTRACT

The thermo-oxidative and hydrolytic stability of the UV-cured polymer coatings in optical fibers are important to ensure maximum reliability of optical fiber systems. Long-term exposures of UV-cured polyacrylate films were performed in dry and humid air and in water at elevated temperatures. The structural changes of the studied polymers were assessed with infrared spectroscopy, recording the content of double bonds, soxhlet extraction determining the gel content, analyses of extractables with high performance liquid chromatography, measurements of equilibrium swelling in methyl ethyl ketone for the assessment of the crosslink density and dynamic mechanical analysis determining the glass transition temperature and the crosslink density. Migration of uncrosslinked species and post-curing reactions leading to consumption of unreacted vinyl groups occurred initially under all test conditions. Aging under wet or humid conditions led at a later stage to hydrolytic degradation of the polymer network. HPLC showed that aged samples contained no monomeric compounds.

INTRODUCTION

The fragile optical glass fiber is coated on-line directly after the drawing process. The high draw speeds put stringent demands on the coating system. UV-curable urethane acrylates cure at a high rate to give a cross-linked three-dimensional polymer network. The physical properties can be tailored by suitable variation of flexible units between the urethane linkages within the acrylate oligomers. This is utilized in the dual-layer coating system. A soft rubbery primary coating protects the glass fiber and reduces eventual stresses and a hard secondary coating protects the primary coating and fulfills the mechanical and chemical protection of the glass fiber. The polymerization process is very fast and extensive. The conversion of the acrylic double bonds is however not

completed during the UV exposure time. As the oligomers start to crosslink the viscosity increases. If the glass transition temperature, T_g , of the fully cured coating is higher than the cure temperature it will vitrify and attain a glassy state before the reactive groups are converted.¹ An increasing viscosity and a low cure temperature will isolate remaining free radical chain ends within the network. This is a characteristic feature of the outer, high modulus coating when it is prepared as a thin film on a glass plate.² The glass plate acts as a heat sink and decreases the cure temperature. The inner, low modulus coating, with an ultimate T_g below room temperature will not vitrify.³ The extent of cure becomes consequently higher in this case than in the outer layer. There will in all coatings be some low molar mass species remaining, e.g. monomers or photo-initiator. These will with time crosslink or leak out of the network and affect the physical and chemical properties of the coatings.^{4,5} It is thus important to characterize these changes as they can affect the reliability of the optical fiber.

Studies of the thermo-oxidative and hydrolytic stability of acrylate coatings have been reported.⁴⁻⁸ Also a number of test methods have been described to examine physical and chemical properties of the coatings.^{5,9-12} In this work we have performed long-term exposures of UV-cured films to dry and humid air and to water at elevated temperatures to study the kinetics of the degradation. Virgin and aged coatings were characterized with respect to degree of cure, glass transition temperature and crosslink density.

EXPERIMENTAL

Materials

The acrylate resins used were polyether urethane acrylates. Two inner or primary coatings, denoted A and B, and two outer or secondary coatings, denoted C and D were studied.

* To whom correspondence should be addressed.

Film preparation

The coatings were applied on 6x25 cm glassplates using a 100 micrometer Erichsen film applicator. The coatings were cured using a F300 UV-source, Fusion Systems. The UV-radiation was provided with a D-bulb and the films were cured at 0.6 J/cm^2 as measured by a Uvicure radiometer in the UVA-range, 320-390 nm. The films were cured in a box with a nitrogen atmosphere. The box window was made of PMMA having a UV-cutoff at 290 nm. The box was purged with nitrogen for five minutes before curing in order to reduce the concentration of dissolved oxygen in the acrylate resin. The thicknesses of the resulting films were measured with a Mitutoyo microthickness meter.

Aging

The samples were aged for different periods of time ranging from 24 hours to 16 weeks. The aging treatments were performed in moderately circulating dry air at 75, 85 and 95°C, in moderately circulating humid air (85% relative humidity) at 85°C and in deionized water at 85 and 95°C. The temperature were controlled to an accuracy of $\pm 2^\circ\text{C}$. The thicknesses of the 6x25 mm films were 45-55 μm .

Infra-red Spectroscopy

Samples for IR spectroscopy were prepared by cutting the exposed film into small rectangular pieces. The ATR-spectra were recorded with a 1760- FTIR, Perkin-Elmer, using a 10x5x1 mm, 45° KRS-5 crystal. The method was based on the out of plane deformation of the CH_2 -hydrogens in the vinylgroup, $-\text{CH}=\text{CH}_2$, appearing at 810 cm^{-1} . The absorbance of this peak was normalized to a reference peak which was not affected by the degree of crosslinking. The % reacted acrylate unsaturation (% RAU) was determined by comparing the acrylate absorbance of the cured coating to that of the uncured liquid. Data was obtained according to equation (1):

$$\% \text{ RAU} = \left(\frac{R_L - R_F}{R_L} \right) \times 100 \quad (1)$$

where R_L and R_F are relative absorbance values of the 810 cm^{-1} band of the uncured and cured acrylates.

Soxhlet extraction

About 1 g of the cured coating material was placed in an extraction thimble, weighed and extracted for 16

hours with 70 ml diethylether. The thimble was then dried and weighed again. Sample and thimble were conditioned for 6 hours over $\text{Mg}(\text{NO}_3)_2 \times 6\text{H}_2\text{O}$. The gel content (% GC) was obtained as :

$$\% \text{ GC} = \frac{m}{m_0} \times 100 \quad (2)$$

where m_0 and m are the weights of the sample before and after extraction.

Dynamic mechanical analysis

DMTA were performed on a Mark II, Polymer Laboratories. The films were cut into 5x20 mm rectangular strips. Due to the thin film thickness the low modulus inner acrylates could not be tested in the tensile mode. The samples were preconditioned at 60°C for one hour. The specimens were cooled down to 10°C and a temperature scan was run from 10°C to 100°C at a rate of $2^\circ\text{C}/\text{min}$ in dry nitrogen. The elastic modulus (E'), loss modulus (E'') and loss tangent ($\tan \delta$) were obtained at a frequency of 1 Hz.

Swelling

The swelling ratio was measured for the high modulus coatings in methylethylketone (MEK). The samples, 20x20 mm, were dried at 60°C for one hour and then cooled in a desiccator for 10 minutes. The coating pieces were weighed and then submerged in MEK for 24 hours. Solvent was removed from the surface and the sample weight was recorded at 5 second intervals. The evaporation curve, i.e. mass as a function of time, was then adapted to a third degree polynomial to estimate the sample weight directly after removal from the solvent.

HPLC

2.0 mg of the uncured resin was dissolved in 0.10 ml of acetonitrile (ACN) in an autosampler vial. 0.010 ml of the solution was used for the HPLC separation. 2.0 mg pieces of virgin and aged films were immersed in 0.10 ml ACN for 16 hours to extract non-crosslinked material. The elution mixture was ACN/water, 1:1. The flow speed was 1ml/min. Standards were used to identify monomers by retention time.

RESULTS AND DISCUSSION

The residual low molar mass components not bonded to the three-dimensional network have a plasticizing effect on the coating. Aging of the coatings will lead to post-cure and leakage out of low molar mass species. Depending on the aging environment hydrolysis and thermo-oxidative degradation will occur. This affects both physical and chemical properties of the coating. The conversion of acrylic double bonds was estimated with FTIR. Fig.1 shows the % RAU of inner coating A and outer coating C after aging in different environments.

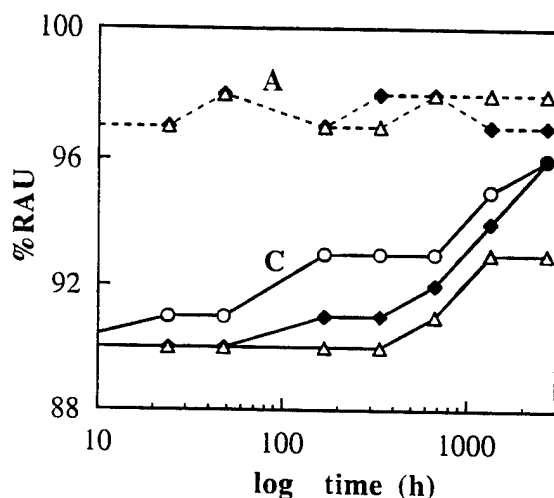


Fig.1 %RAU of inner coating A and outer coating C vs. log aging time. (Δ) 95°C in dry air; (\diamond) 85°C and 85% RH; (O) 95°C in water.

Due to the low glass transition temperature of the inner acrylate coatings they do not vitrify, and cure faster and to higher final degree than the outer coating. The IR-analysis of inner coatings cured in a nitrogen atmosphere show that RAU values are approximately constant at $97 \pm 1\%$ also after prolonged aging. Short aging times in dry and humid heat does not affect the degree of cure of an outer coating. At longer exposure times some low molar mass species crosslink or leak out. In water the RAU value increases already after 2 days, more likely due to extraction out of residual monomer than post-curing. The outer coating materials exhibited initially significantly lower %RAU values than the inner coating materials and also a pronounced increase in %RAU with aging time (Fig.1). There are two obvious reasons for the increase in %RAU: (1) migration of uncrosslinked species to the surrounding medium; (2) post-cure reaction.

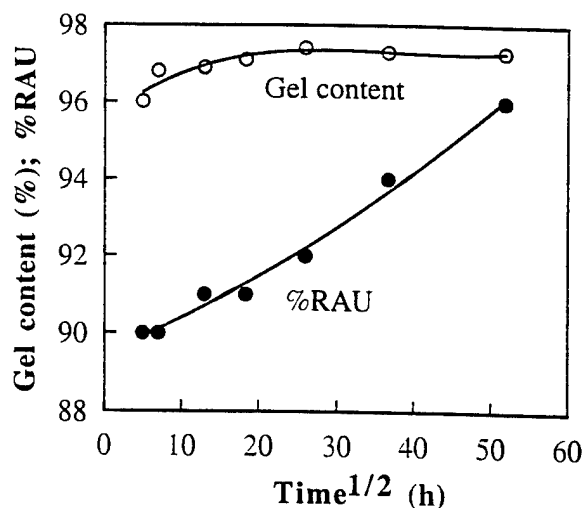


Fig.2 %RAU and gel content of outer coating C (aged at 85°C and 85% RH) plotted as a function of aging time. (\bullet) %RAU; (\circ) %GC.

Fig.2 shows a comparison between %RAU and gel content plotted as a function of aging time. The gel content reached a saturation value after approximately 1000 h of aging whereas %RAU increased monotonously with aging time. These data seem thus to indicate that both mechanisms play some role but due to the significant uncertainty in the IR data it is difficult to assess the relative importance of the two mechanisms on the basis of these data.

Tables 1 and 2 presents the gel content data of both the inner and outer coating materials. The inner coating materials contained more extractables than the outer. It is known from the data presented in Fig.1 that the degree of cure is higher for the inner coating materials. However, the relatively low crosslink density characteristic of the inner coating materials is most probably the main reason for the low gel content of these materials. The gel content became however approximately the same, $98 \pm 1\%$, for both the inner and outer coating materials after extensive aging (16 weeks) at 95°C in dry air (Tables 1 and 2). Migration of uncrosslinked species, migration of small-molecule degradation products and post-curing reaction are possible mechanisms that account for the observed increase in gel content with increasing aging time. Aging under dry conditions caused a continuous increase in gel content during the entire aging period of 16 weeks whereas aging in humid conditions (at 85% RH and in water) caused a decrease in gel content after 1 to 2 weeks of aging (Tables 1 and 2). This is indicative of the occurrence of water-induced (hydrolysis) chain scission of the polymer network.

Table 1A. % gel content of inner coating A

Ageing time	Dry heat			Humid heat 85°C/85%RH	Water	
	75°C	85°C	95°C		85°C	95°C
unaged	91.0	91.0	91.0	91.0	91.0	91.0
1 day	91.0	91.2	91.2	94.6	96.0	96.6
2 days	91.4	92.4	92.3	94.8	96.3	96.8
1 week	94.8	95.0	95.5	96.9	96.5	96.5
2 w	95.7	95.6	96.0	96.8	96.6	96.4
4 w	96.5	96.2	97.2	96.5	96.3	96.3
8 w	96.5	97.1	97.5	96.5	96.2	95.7
16 w	96.8	97.3	97.7	96.3		

Table 1B. % gel content of inner coating B

Ageing time	Dry heat			Humid heat 85°C/85%RH	Water	
	75°C	85°C	95°C		85°C	95°C
unaged	89.0	89.0	89.0	89.0	89.0	89.0
1 day	90.2	90.0	90.2	93.9	95.8	95.8
2 days	90.0	90.0	90.5	95.5	96.6	96.5
1 week	91.5	91.8	92.4	96.7	97.5	97.3
2 w	92.4	94.4	95.0	97.0	97.2	97.0
4 w	94.6	95.7	96.0	96.8	97.0	96.8
8 w	95.2	96.5	96.8	96.5	96.6	96.4
16 w	95.5	96.8	97.2	96.0		

Table 2A. % gel content of outer coating C

Ageing time	Dry heat			Humid heat 85°C/85%RH	Water	
	75°C	85°C	95°C		85°C	95°C
unaged	95.2	95.2	95.2	95.2	95.2	95.2
1 day	95.0	95.3	95.3	96.0	96.6	97.0
2 days	95.5	95.5	95.6	96.8	97.0	96.8
1 week	96.1	96.0	96.2	96.9	97.2	97.0
2 w	97.0	97.2	97.1	97.1	97.4	97.0
4 w	97.2	97.5	97.6	97.4	97.2	96.8
8 w	97.7	97.7	97.9	97.3	97.0	96.7
16 w	97.9	97.9	98.3	97.3		

Table 2B. % gel content of outer coating D

Ageing time	Dry heat			Humid heat 85°C/85%RH	Water	
	75°C	85°C	95°C		85°C	95°C
unaged	95.6	95.6	95.6	95.6	95.6	95.6
1 day	95.6	95.4	95.5	97.5	96.1	96.3
2 days	95.7	95.7	95.8	97.6	96.9	97.0
1 week	96.0	96.1	96.4	97.4	97.2	97.2
2 w	96.8	96.7	97.0	97.4	97.3	97.5
4 w	97.5	97.5	98.0	97.4	97.2	96.9
8 w	97.6	97.7	98.2	97.6	97.0	96.9
16 w	97.9	98.1	98.5	96.8		

which is less obvious in the densely crosslinked network polymers (outer coating materials).

DMTA were used to assess the dynamic mechanical properties of the coatings as they aged. The glass transition temperature, T_g , was defined as the $\tan\delta$ peak value and the equilibrium modulus, E_0 , was obtained from the storage modulus, E' (Fig.3).

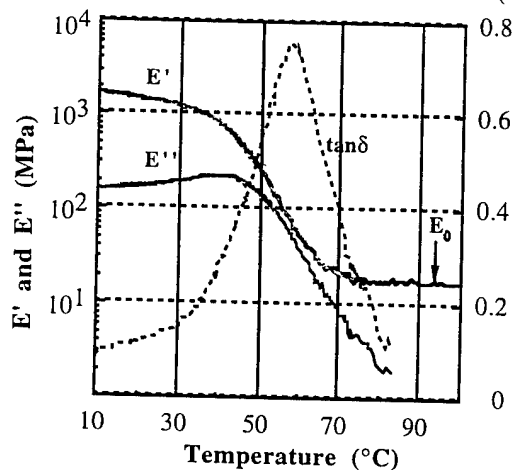


Fig.3 DMTA of outer coating C, aged for 8 weeks at 75°C.

Figure 4 shows that T_g increased with increasing aging time. These data are consistent with the data presented in Figures 1 and 2 and in Tables 1 and 2: the loss of small-molecule species and reduction in concentration of dangling chain ends due to post-curing reaction should lead to a decrease in the relative free volume (at a given temperature) and thus to an increase in T_g . It is interesting to note that the increase in T_g was most pronounced for coatings aged in dry condition. The more moderate increase in T_g for coatings aged in "wet" conditions is most probably caused by the counter acting action from network degradation by hydrolysis.

The equilibrium (rubber) modulus increased moderately with aging time for the coatings aged under dry conditions indicative of a weak increase in the crosslink density, whereas the coatings aged under wet conditions showed a pronounced decrease in E_0 indicative of a progressive hydrolytic network degradation under these conditions (Figure 5).

Swelling measurements were performed to assess the crosslink density. The method was not applicable to the inner coatings. The swelling data for the outer coatings corresponded with the data obtained by DMTA. The degree of swelling decreased weakly with

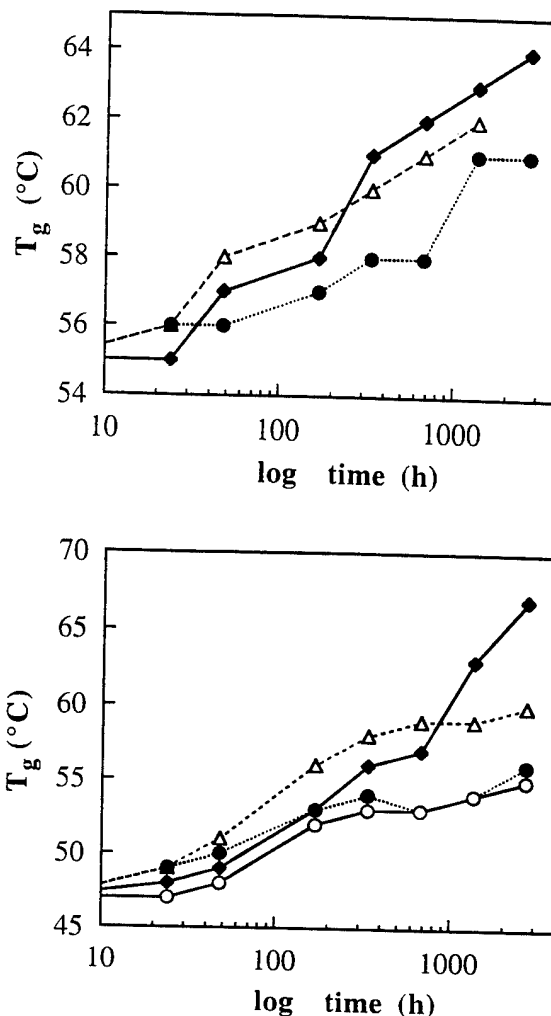


Fig.4. T_g vs. log aging time of coatings C (upper) and D (lower). (o) 75°C in dry air; (♦) 95°C in dry air; (●) 85°C and 85% RH; (Δ) 95°C in water.

aging time for coatings aged under dry conditions characteristic of a moderate increase in crosslink density (post-curing), whereas coatings aged under "wet" conditions showed a progressive increase in degree of swelling indicating the occurrence of hydrolytic degradation's of the network (Figure 6).

High performance liquid chromatography (HPLC) in a few cases combined with mass spectrometry was used to analyze the extractables of the coating materials. Monomers were identified in the uncured resins. Extracts from the aged coatings, contained no monomeric species. The extracted species were thus more complex molecules, non yet being specifically identified.

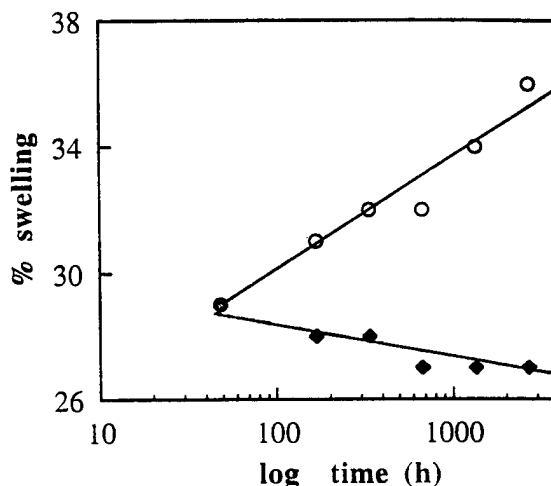
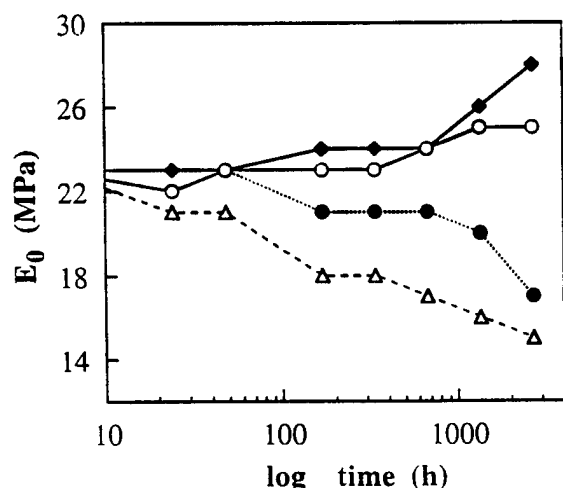
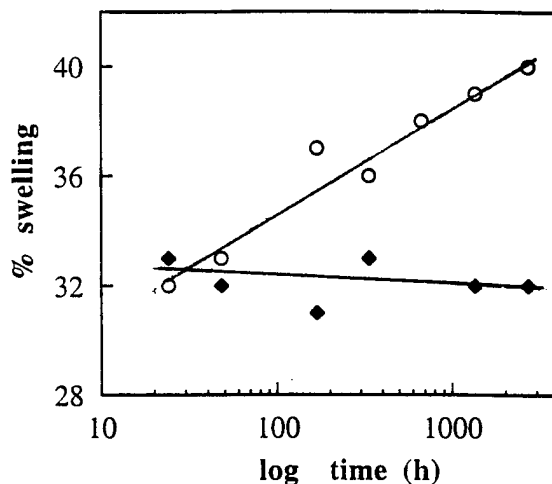
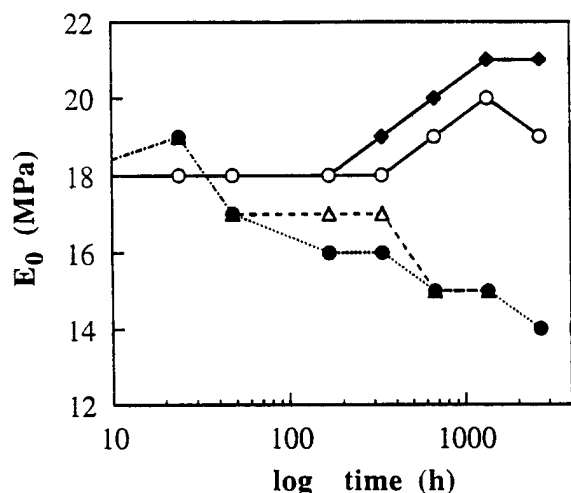


Fig.5. Equilibrium modulus vs. log aging time of coating C (upper) and D (lower). (○) 75°C in dry air; (◆) 95°C in dry air; (●) 85°C and 85% RH; (Δ) 95°C in water.

Fig.6. Swelling ratio vs. log aging time of coating C (upper) and D (lower). (◆) 95°C in dry air; (○) 85°C and 85% RH.

CONCLUSIONS

Polyether urethane acrylates (inner and outer coating materials) were aged under dry and humid/wet (85% RH and in water) conditions at temperatures between 75 and 95°C for 0-16 weeks. Aging under dry conditions caused migration of uncrosslinked species to the surrounding air and post-curing reactions involving unreacted vinyl groups. Network degradation seems insignificant under these conditions. Aging under wet or humid conditions led initially to migration of uncrosslinked species to the surrounding media and to post-curing reactions and at a later stage,

after 1-2 weeks, to hydrolytic degradation of the polymer network. Liquid chromatography showed that the cured resins, aged in different environments, contained no monomeric species.

ACKNOWLEDGMENTS

This study was sponsored by the Swedish Board for Technical and Industrial Development (NUTEK, grant P71-5), Ericsson Cables AB, Hudiksvall and Telia Net AB, Stockholm (Sweden). The authors also wish to acknowledge Karin Nygård-Skalman at Ericsson Cables AB and Jan Björkman at Telia Net AB for valuable discussions.

REFERENCES

1. J.B.Enns and J.K.Gillham, *J.Appl.Polym.Sci.*, **28**, 2831 (1983)
2. D.M.Szum, *Proc.of IWCS*, **43**, 59 (1994)
3. J.B.Enns and J.K.Gillham, *J.Appl.Polym.Sci.*, **28**, 2567 (1983)
4. C.P.Chawla, *Proc.of IWCS*, **43**, 78 (1994)
5. C.P.Chawla and D.M.Szum, *Proc.of IWCS*, 141 (1991)
6. T.Bishop, C.Chawla, D.Szum and E.Poklacki, *Proc. of IWCS*, **41**, 442 (1992)
7. D.A.Simoff, M.G.Chan, J.T.Chapin and B.J.Overton, *Polym.Eng.Sci.*, **29**,1177 (1989)
8. T.E.Bishop and D.M.Szum, *Radtech Europe*, 124 (1991)
9. E.F.L.D'Souza, Technical report/British Tele communications (Jan. 1990)
10. R.A.Frantz, I.M.Plitz and S.R.Schmid, *Proc. of IWCS*, **40**, 134 (1991)
11. H.Takase, Y.Hashiguschi, Y.Takasugi, N.Saito and T.Ukachi, *Proc. of IWCS*, **41**, 279 (1992)
12. J.L.Jostan, R.G.Sommer, M.Hoffart, *Proc. of IWCS*, **41**, 267 (1992)



Pär-Anders Högström received his B.Sc. in Organic Chemistry from the Mid Sweden University in Sundsvall in 1991 and joined Ericsson Cables AB in Hudiksvall, Sweden. He has been working in polymer chemistry in plastics and coatings. He is currently a Ph.D. student in the Department of Polymer Technology, Royal Institute of Technology, Stockholm, Sweden.



Ulf W.Gedde is Professor of Polymer Technology in the Department of Polymer Technology, Royal Institute of Technology, Stockholm, Sweden. Prof. Gedde has published 130 scientific papers, mainly in the field of polymer physics, and one textbook (Polymer Physics, Chapman and Hall, 1995).



Sigbritt Karlsson is Associate Professor of Polymer Technology in the Department of Polymer Technology, Royal Institute of Technology, Stockholm, Sweden. Assoc.Prof. Karlsson has published 100 scientific papers mainly in the field of polymer characterization

THERMAL STABILITY OF COATED OPTICAL FIBER

Atsushi SUZUKI, Megumi BAN, Tomoyuki HATTORI,
Nobuhiro AKASAKA, and Yasuo MATSUDA

SUMITOMO ELECTRIC INDUSTRIES, LTD.
Yokohama, Japan

ABSTRACT

Changes in the chemical structure and mechanical properties of primary optical fiber coating after thermal aging were studied to predict the lifetime of coating. Comparison between the coating aged in air and that in nitrogen using in-situ tests is effective to clarify the degradation process. The degradation process at high temperature proved to be different from that at room temperature range on the coating systems used in this study. When the thermal accelerated aging test is conducted over 150°C, another degradation process leads to the apparent high activation energy in terms of yellowing of the coated fiber and modulus of the primary layer, which brings about an improper overestimation of the lifetime. In this paper, a proper temperature range for the thermal accelerated aging test for lifetime prediction is discussed.

1. INTRODUCTION

While optical fiber networks are widely constructed in the world today, coated optical fibers are exposed to severer environments. The importance of thermal stability of optical fiber has been increasing because of exposure to high temperature environments. Several

studies have been made on the heat resistance of UV curable urethane acrylate for optical fiber coating. These studies proved that mechanical and chemical properties of primary coating is sensitive to heat, and that the most critical performance of coated optical fiber is color change of coating compared with other properties such as transmission loss, strippability and fiber strength^{[1][2][3]}. Yellowing of fiber coating may result in poor color-identification. It is well known that the extent of color change depends on the chemical structure of polyurethane, especially on the portion which is derived from diisocyanate. When the aromatic diisocyanate is used, thermal oxidation of urethane segments generates the chemical origin of coloring^{[3][4]}. For mechanical properties of coating, it is also reported that the degradation of urethane or ether groups leads to the changes in tensile strength^{[5][6]}.

However, most studies have been made on film samples. Only a few attempts have been made on the in-situ evaluation of the fiber coating, especially for the primary coating. It is reported that the crosslinking structure changes by the curing temperature^[7]. Consequently, the degradation process of coating material can also vary in film and fiber coating. Therefore for

accurate lifetime prediction, the properties of coating materials should be measured with in-situ tests.

The purpose of this paper is to evaluate the coating properties using in-situ tests after thermal aging and to estimate the lifetime of the fiber coating.

2. EXPERIMENTAL

2-1. SAMPLE

Test fibers coated with two models of coating systems were prepared to clarify the dependence of the diisocyanate structure to the heat resistance. The primary coating of system A is derived from aromatic diisocyanate, and that of system B is derived from aliphatic diisocyanate. The type of diisocyanate of the secondary coating for both systems is aliphatic. The cure degree of both fiber coatings were evaluated with MEK (methyl ethyl ketone) Extraction Test ^[8]. Measured values of gel fraction for both coating systems are listed in Table 1. Both fiber coatings seem to be cured adequately.

Table 1 Characteristics of test coated fibers

coating system	type of diisocyanate		gel fraction
	primary coating	secondary coating	
A	aromatic	aliphatic	94.1%
B	aliphatic	aliphatic	94.6%

2-2. EVALUATION OF THE SAMPLES

Test fibers were aged in air at 85°C, 100°C, 120°C

and 150°C, and also aged in an inert environment at 120°C in order to investigate the degradation process of the coating systems. Concentration of oxygen in the inert environment was kept below 0.3%. Properties of fiber coatings were evaluated with the following methods after aging.

1. Yellow index (YI)

Test fibers were arranged in parallel as illustrated in Figure 1. Yellow indexes were measured using MINOLTA Color Measurement System CM-3500d with the following parameters:

- Illuminant: D
- Specular Component: Excluded (SCE)
- Area of Measurement: 10mm ϕ
- Background: White Calibration Standard

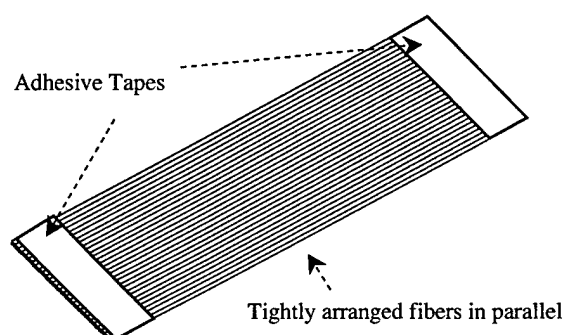


Figure 1 Arrangement of test coated fibers in YI measuring

2. Young's modulus of the primary coating layer

Push In Modulus (PIM) Test ^[8] was applied to evaluate in-situ modulus of the primary coating layer directly. Relative modulus of the primary coating layer is defined with the following equation:

$$\text{Relative modulus (\%)} = \frac{\text{modulus (after aging)}}{\text{modulus (before aging)}} \times 100 \quad (1)$$

3. The chemical structure of the primary coating

IR spectra were measured to evaluate changes in the chemical structure of the primary coating with the Attenuated Total Reflection (ATR) microscopy (model IR-PRAN produced by Spectra-Tech) as illustrated in Figure 2.

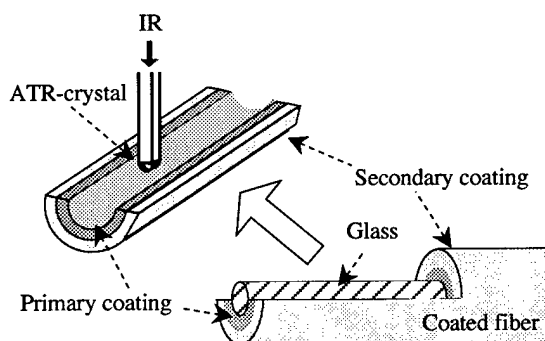


Figure 2 Scheme of ATR-microscope method for the evaluation of the primary coating

Thermal aging causes remarkable changes in IR absorption of the urethane segment at 1533cm^{-1} and the ether segment at 1105cm^{-1} for both coating systems. These changes were analyzed on the basis of absorption at 1511cm^{-1} which scarcely changes before and after aging. Retention of the urethane and ether segments were discussed. Retention of the urethane segment Ru and that of the ether segment Re are given by the equations (2) and (3) respectively:

$$\text{Ru (\%)} = H^{1533}_t / H^{1533}_0 \times 100 \quad (2)$$

where H^{1533}_0 and H^{1533}_t represent IR absorption peak height ratios of the urethane segment to the reference at 1511cm^{-1} before and after aging for time t respectively.

$$\text{Re (\%)} = H^{1105}_t / H^{1105}_0 \times 100 \quad (3)$$

where H^{1105}_0 and H^{1105}_t represent IR absorption peak height ratios of the ether segment to the reference at 1511cm^{-1} before and after aging for time t respectively.

3. RESULT AND DISCUSSION

3-1. YELLOWING

The retention of the urethane segment of primary coatings and YI of coated fibers after aging in air at 120°C for both coating systems are shown in Figure 3. YI increases while retention of the urethane segment decreases as a function of aging time. It is obvious that color change has good correlation with retention of the urethane segment. The coating system B has less color change than the coating system A. On the other hand, little chemical origin of coloring is generated to cause little change in retention of the urethane segment in inert aging at 120°C for both coating systems, as shown in Figure 4. This result suggests that color change is mainly caused by thermal oxidation of the urethane segment and that the coating material derived from aromatic diisocyanate is easily discolored. When the thermal accelerated aging test is conducted, sufficient care should be taken whether thermal decomposition is occurred or not. It was confirmed through inert aging test that thermal decomposition of the urethane segment does not occur below 120°C . Therefore

color change of coated fibers for both coating systems can be predicted by the thermal accelerated aging test below 120°C.

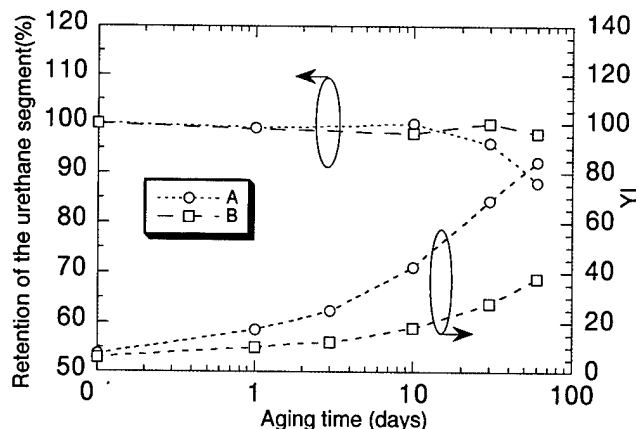


Figure 3 Changes in retention of the urethane segment of the primary coating and YI after aging at 120°C in air

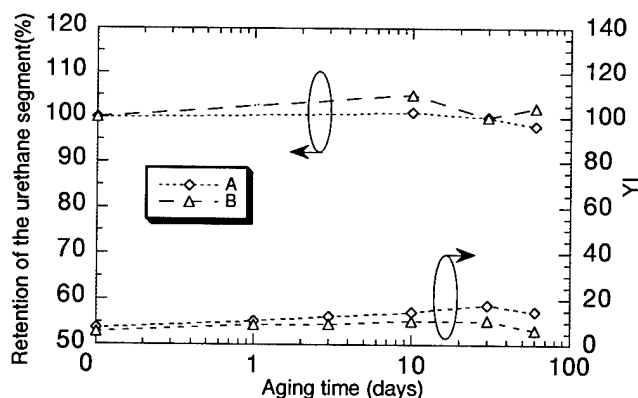


Figure 4 Changes in retention of the urethane segment of the primary coating and YI after inert aging at 120°C

3-2. DEGRADATION OF MECHANICAL PROPERTY

Changes in the modulus of the primary coating layer measured using the PIM test before and after aging are shown in Figure 5. The modulus of the primary coating decreased with increasing aging time in air, however the downward trend of that was not observed in inert

aging. This fact indicates that thermal decomposition does not occur below 120°C for both coating systems. Thus, the lifetime on modulus of the primary coating layer can be predicted through the thermal accelerated aging test below 120 °C.

The slight increase of the relative modulus of the primary coating was observed in inert aging for system A. The curing reaction of unreacted components is supposed to lead to the rise in modulus.

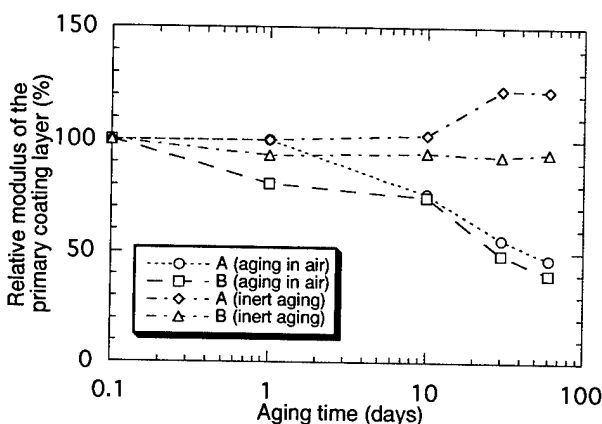


Figure 5 Changes in modulus of the primary coating layer after aging at 120°C

3-3. LIFETIME PREDICTION

It is desirable to obtain the maximum temperature for the thermal accelerated aging test to shorten the aging period practically. The degradation process which is different from that at room temperature range such as thermal decomposition can occur at high temperature range. The proper temperature range for the thermal accelerated aging test was examined.

Figures 6 and 7 show relative modulus and chemical structure respectively after aging at 120 and 150°C in air for coating system A. The relative modulus of the

primary layer aged for 1 day at 150°C is almost the same as that aged for 50 days at 120°C as shown in Figure 6. However, the retention values for the urethane segment and the ether segment after aging at those two temperatures are different from each other as shown in Figure 7. In other words, despite mechanical properties of the primary coating aged for 1 day at 150°C is the same as that aged for 50 days at 120°C, there is the difference between chemical structures of primary coatings. This fact suggests that the degradation process at 150°C is different from that below 120°C and that aging data at 150°C are not proper to use for the lifetime prediction. Thus, the lifetime must be predicted through the thermal accelerated aging test below 120°C for coating systems employed in this study.

The influence of temperature range for the thermal accelerated aging test on the lifetime prediction was also investigated. Two different temperature ranges were examined, namely 85°C-120°C (lower range) and 100°C-150°C (higher range). Lifetime was predicted with respect to the degree of yellowing of coated fibers and the modulus of the primary coating layer using the Arrhenius type assumption.

The degree of yellowing (ΔYI) is defined as the difference in YI between the aged and the original coating with the following equation:

$$\Delta YI = YI (\text{after aging}) - YI (\text{before aging}) \quad (4)$$

The threshold for the degree of yellowing of the fiber coating is assumed to be 30 at which the coating begins to lose transparency. The threshold for the relative modulus of the primary coating layer was taken

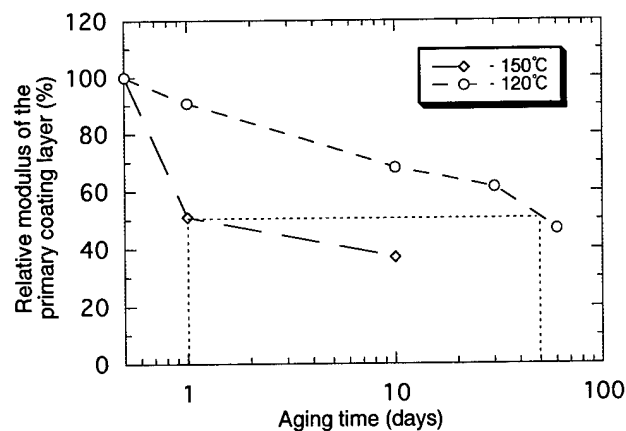


Figure 6 Change in modulus of the primary coating layer of the fiber coated with system A after aging at 120°C and 150°C in air

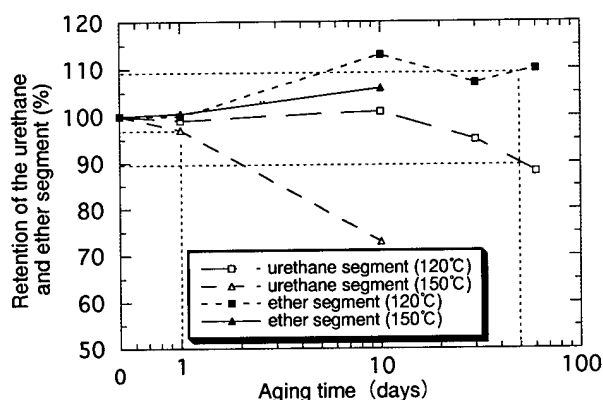


Figure 7 Changes in retention of ether and urethane segments in the primary coating layer of the fiber coated with system A after aging at 120°C and 150°C in air

as 80% for the tentative value. Arrhenius plots on the coating system A and B are shown in Figures 8-10. The Arrhenius plot on the degree of yellowing of the coating system B cannot be shown, because the yellowing of the coating system B is not large enough to estimate the lifetime.

It is found that the apparent higher values of activation energy are obtained if the aging data at 150°C is included as shown in Figures 8-10. Another degradation process at 150°C will make apparent activation energy

higher. Lifetime of fiber coatings under 25°C environment were estimated using these activation energy values. The estimated lifetimes are summarized in Figure 11. It is obvious that the lifetime is overestimated if the aging data at 150°C is included. The proper temperature range has to be verified for the thermal accelerated aging test to predict the lifetime properly.

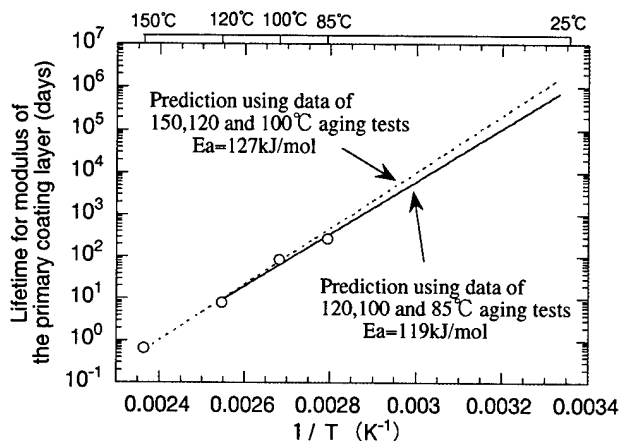


Figure 8 Arrhenius plots on lifetime for modulus of the primary coating layer of the fiber coated with system A

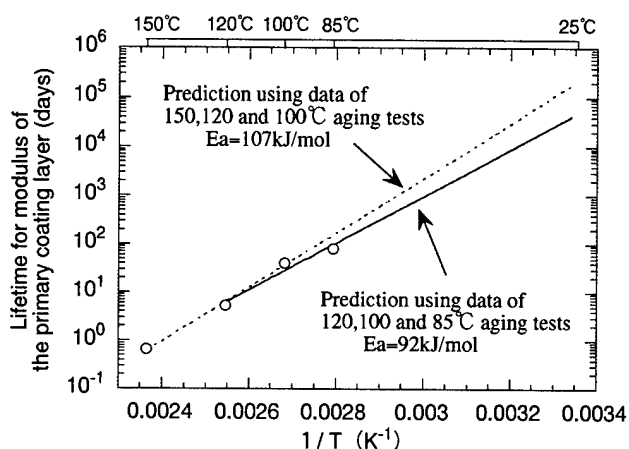


Figure 10 Arrhenius plots on lifetime for modulus of the primary coating layer of the fiber coated with system B

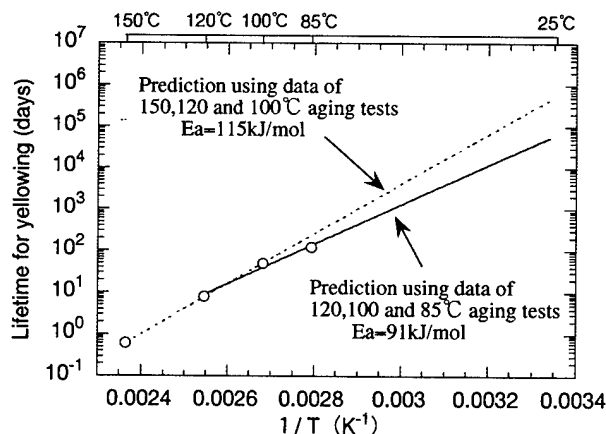


Figure 9 Arrhenius plots on lifetime for yellowing of the fiber coated with system A

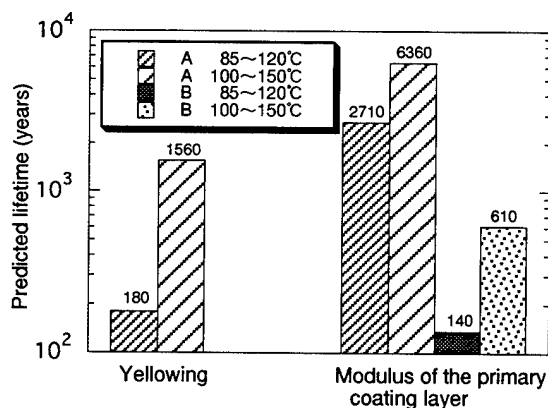


Figure 11 Summary of the predicted lifetime at 25°C

5. SUMMARY

Changes in the chemical structure and modulus of the primary coating layer were studied using in-situ tests after thermal aging. The degradation process at 150°C was different from that at room temperature range. When the thermal accelerated aging test is conducted at too high temperature range, the apparent high activation energy was obtained, and the lifetime of the coating system will be overestimated improperly. The proper temperature range must be applied to predict the lifetime accurately through the thermal accelerated aging test. Chemical analysis using ATR-microscopy and inert aging tests are recommended to determine the proper temperature range for the thermal accelerated aging test. With respect to degradation of the primary coating in the mechanical properties, the predicted lifetime for the coating with the aromatic diisocyanate is much longer than that for the coating with the aliphatic diisocyanate.

REFERENCES

- [1] T.Hattori, N.Akasaka, A.Suzuki, and Y.Matsuda, "Investigation for thermal stability of coated optical fiber", 1995 Spring National Convention Record, The Institute of Electronics, Information and Communication Engineers, B-1025 (1995)
- [2] H.H.Yuce, R.A.Frantz, O.S.Gebzilioglu, I.M.Plitz and T.T.Volotinen, "The mechanical performance of aged dual-coated fibers with varying extents of coating cure" Proc. of 42nd IWCS, 857 (1993)
- [3] A.Murata, K.Kobayashi, K.Oohashi, S.Araki and T.Maruoka, "Heat-resistance behavior and discernibility of color of optical fibers and fiber ribbons", Proc. of 44th IWCS, 151 (1995)
- [4] A.Suzuki, T.Sasaki, T.Hattori, N.Akasaka, and Y.Matsuda, "Investigation for yellowing and mechanical properties of the coated optical fiber", 1996 Spring National Convention Record, The Institute of Electronics, Information and Communication Engineers, B-1051 (1996)
- [5] M.E.Abu-Zeid, E.E.Nofal, F.A.Abdul-Rasoul, M.A.Marafi, G.S.Mahmoud, and A.Ledwith, "Photoacoustic Study of Thermal Degradation of Polyurethane", J.Appl.polym.sci., 28, 2317 (1983)
- [6] G.N.Mathur and J.E.Kresta, "Thermooxidation and stabilization of urethane and urethane-urea block copolymers", Polym.sci.Technol., 26 135 (1984)
- [7] H.Takase, Y.Hashiguchi, Y.Takasugi, N.Saito, and T.Ukachi, "Effect of curing temperature on curing rate and mechanical properties of polyurethane acrylate coatings for optical fiber", Proc. of 43th IWCS, 72 (1994)
- [8] K.Oishi, N.Akasaka, T.Hattori, T.kakuta and Y.Matsuda, "Push-In Modulus Test for primary coating of dual - coated fiber", Proc. of 43rd IWCS, 552 (1994)



Atsushi SUZUKI

*Sumitomo Electric
Industries, Ltd.*

*1, Taya-cho, Sakae-ku,
Yokohama, JAPAN*

Atsushi Suzuki received his M.E. degree in Chemical Engineering from Nagoya University in 1994. He joined Sumitomo Electric Industries, Ltd. in 1994, and has been engaged in research and development of optical fiber and cables. He is a member of the Transmission Media Department in Yokohama Research Laboratories.



Megumi BAN

*Sumitomo Electric
Industries, Ltd.*

*1, Taya-cho, Sakae-ku,
Yokohama, JAPAN*

Megumi Ban received her M.E. degree in Applied Chemistry from Sophia University in 1992. She joined Sumitomo Electric Industries, Ltd. in 1992, and has been engaged in research of polymeric materials. She is a member of the Analytical Characterization Center in Yokohama and a member of the Society of Polymer Science of Japan, the Japan Society for Analytical Chemistry, and the Chemical Society of Japan.



Tomoyuki HATTORI

*Sumitomo Electric
Industries, Ltd.*

*1, Taya-cho, Sakae-ku,
Yokohama, JAPAN*

Tomoyuki Hattori received his M.E. degree in Chemistry from Kyoto University in 1987. He joined

Sumitomo Electric Industries, Ltd. in 1987, and has been engaged in research and development of optical fiber and cables. He is a senior engineer of the Transmission Media Department in Yokohama Research Laboratories and a member of the Institute of Electronics and Communication Engineers of Japan.



Nobuhiro AKASAKA

*Sumitomo Electric
Industries, Ltd.*

*1, Taya-cho, Sakae-ku,
Yokohama, JAPAN*

Nobuhiro Akasaka received his M.E. degree in Chemical Engineering from Tokyo University in 1983. He joined Sumitomo Electric Industries, Ltd. in 1983, and has been engaged in research and development of optical fiber and cables. He is a senior engineer of the Transmission Media Department in Yokohama Research Laboratories, and a member of the Material Life Society of Japan.



Yasuo MATSUDA

*Sumitomo Electric
Industries, Ltd.*

*1, Taya-cho, Sakae-ku,
Yokohama, JAPAN*

Yasuo Matsuda received his M.E. degree in Chemistry from Tokyo University in 1978. He joined Sumitomo Electric Industries, Ltd. in 1978, and has been engaged in research and development of optical fiber and cables. He is a chief research associate of the Transmission Media Department in Yokohama Research Laboratories.

THE EFFECTS OF INK ON THE PERFORMANCE OF COLOR CODED FIBERS

E. M. Vogel, J. D. Mann, I. M. Plitz, T. N. Bowmer, R. A. Frantz, C. J. Wieczorek,
B. J. Keon** and P.R. Foy**

Bellcore, 445 South St., Morristown, NJ 07960, USA

*Telstra, Melbourne, Australia

**Rutgers University, FOMRP, Piscataway, NJ 08855, USA

ABSTRACT

The use of colored inks to code optical fibers raises a number of performance-related issues. For example, problems such as thickness variations along the 3 - 5 micron ink layers can alter the microbending sensitivity of a fiber. Ink layers were found to both improve and exacerbate fiber deterioration. Fiber strength after aging, which is a critical measure for predicting long term mechanical reliability of the fiber, was enhanced by some ink/coating combinations that slowed the penetration of harmful chemicals from the environment. However, we also found ink/coating combinations that accelerated mechanical degradation of the fiber and varied by ink colors - green Vs blue Vs white - showed different aging characteristics. We performed a series of controlled experiments to focus explicitly on the effects of added ink layers. For some ink/coating systems, we have unambiguously traced the root cause of reduced mechanical fiber performance to the added ink layer and its color.

INTRODUCTION

Possible degradations in fiber strength are important as fiber enters the local loop and the potential for increased handling subjects it to loads not previously applied to fibers and cables. Our earlier work has shown that aging optical fibers in water and other environments decreases their strength [1,2]. Our present study is part of an ongoing investigation into the long-term reliability of optical fibers with the emphasis on the coating chemistry and interactions at the glass/coating interface.

Color coding inks applied to optical fibers have usually been perceived solely as a means of identification for the fibers within a fiber optic cable. However, the presence of this color-coding ink layer can affect the fiber's performance and its long-term reliability in a variety of ways. Issues that we and other researchers [1-4] addressed before include:

- color repeatability between suppliers
- repeatability from lot-to-lot
- the stability of each color during aging
- the compatibility of the inks with other materials, notably buffer tube gels or ribbon matrix materials
- the ability to obtain meaningful results with Light Injection/Detection (LID) systems in conjunction with the inked fibers
- any changes in the fiber's sensitivity to microbending-induced losses
- and the potential effects of the ink layer on the aging characteristics, particularly any strength degradation, of the fiber [2].

We have also shown that post-conditioning (drying) can significantly affect the fiber strength and that fibers with different color coding inks exhibit different behavior.

Our data suggested that the color may affect a fiber's long-term mechanical properties. Since the fibers in our previous studies were not from a single preform, batch-to-batch variations may have influenced these aging results. We therefore performed controlled experiments to focus explicitly on the effect of the added ink layer. In this paper, we report on changes in mechanical (strength) and optical (microbending) properties of unaged and aged colored coded fibers.

Work performed while at Bellcore.

EXPERIMENTAL

We applied inks of different colors from a single supplier to a variety of commercially-coated optical fibers. Optical fibers were from standard production runs of two manufacturers, each consisting of a 125 μm diameter silica-based glass fiber coated with a dual layer coating of uv-cured polyurethane acrylate. In each case, we used fiber from a single spool, thus ensuring that the same preform and fiber coating batch were used. We inked successive lengths of each fiber with three different color uv curable inks (Green, Blue, and White). To ensure that the aging behavior of the uninked (natural) coated fiber was uniform along its length, we left uninked sections before, between, and after the inked lengths and measured the performance of these sections as well as the inked fiber both before and after aging.

The commercial fibers were from two suppliers: fiber 1 represents the standard commercial product from supplier 1, while fibers 2a and 2b represent two different vintages of coatings used commercially by supplier 2. All of the inks were applied in the same draw tower under identical processing conditions (speed, temperature, lamp intensity, etc.).

We performed the following tests:

- optical loss and dynamic tensile strength,
- thermal oxidative stability
 - on both unaged fibers and after aging for 14 days in 85 °C DI water
- sensitivity to microbending
 - on both unaged fibers and after aging for 14 days in 85 °C / 85% RH,

All these tests were performed on both unaged fiber and after aging, for uninked (natural) fiber and fiber inked with the three test colors (Green, Blue, and White).

The fiber strength was evaluated by dynamic tensile testing on a screw-driven universal testing machine at a strain rate of 5% per minute, using a gauge length of 0.5 m, in accordance with EIA/TIA-455-28B ("Method for Measuring Dynamic Tensile Strength of Optical Fibers"), in a test environment of 23 °C and 50% RH .

Fiber sensitivity to microbending was measured by a wire mesh test [5]. The fiber samples are arranged in a circle of 0.22 m diameter in a fixed position between rubber plate and wire mesh # 70 and compressed by forces up to about 400 N/m. During compression of the fiber, optical loss was measured at both 1300 nm and 1550 nm nominal wavelengths.

Coating stability was defined by the onset temperature for thermo-oxidation as measured by differential scanning calorimetry (DSC). Changes in coating chemistry of the inked and aged fibers were evaluated with FTIR (Fourier Transform Infrared) spectroscopy.

RESULTS

The optical transmission loss measurements showed no effects from either the inking or the aging processes. However, the tensile strength of the fibers was affected, and in a variety of different ways. These results are shown in Figures 1-3.

Only the uninked version of fiber 1 showed any strength loss after aging, as illustrated in Figure 1. In this instance, the addition of the ink (of whatever color) apparently protected the fiber against the strength degradation typically observed for the natural fiber. In contrast, the results for fiber 2a in Figure 2 showed not only a loss in strength for the aged, uninked sample similar to that for fiber 1, but also an even greater reduction in strength for the inked samples. Finally, the results for fiber 2b, shown in Figure 3, suggest that for this ink/coating combination, the ink is not only providing some additional protection against the environment, but the addition of the ink actually improves the strength of the fiber. Note that all of the inked samples (unaged and aged) have measurably higher strengths than either the unaged or aged uninked (natural) fiber.

The typical responses of the unaged and aged, inked fibers to microbending losses are shown in Figure 4 and 5.

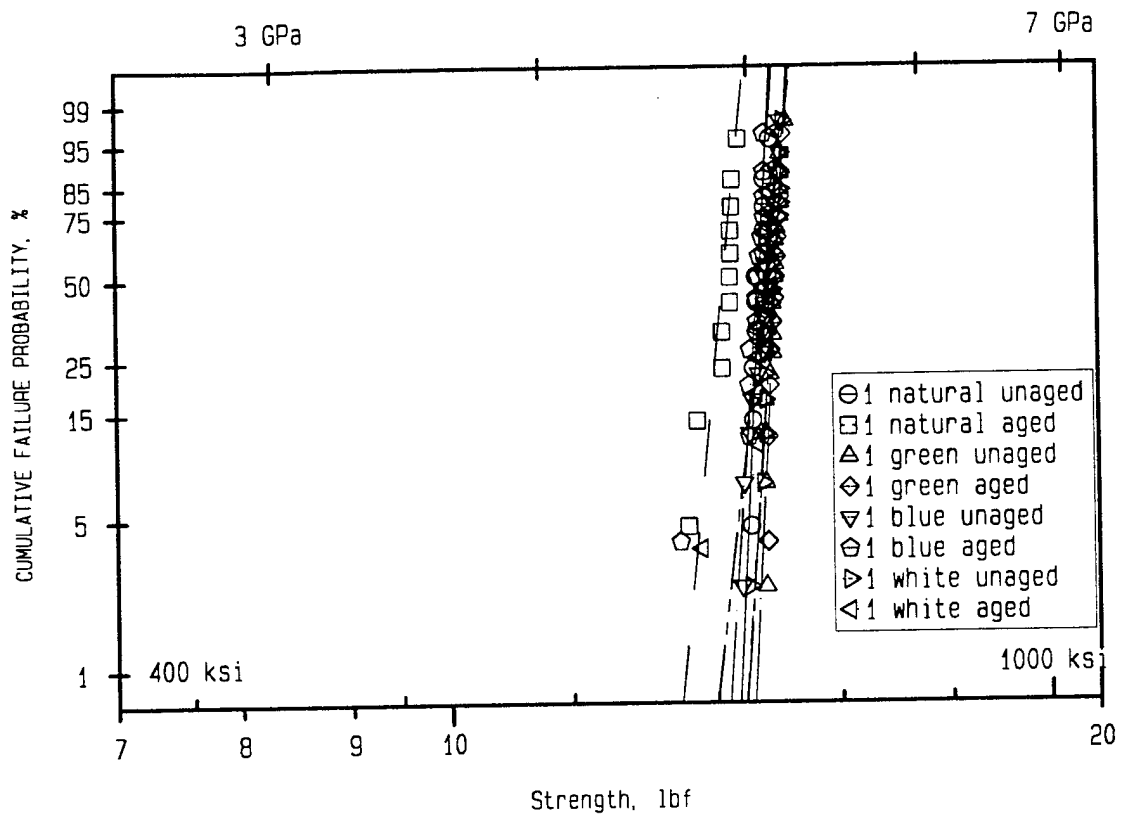


Figure 1: Strength of fiber 1 in natural and inked conditions, unaged and after aging 14 days in 85 °C in DI water.

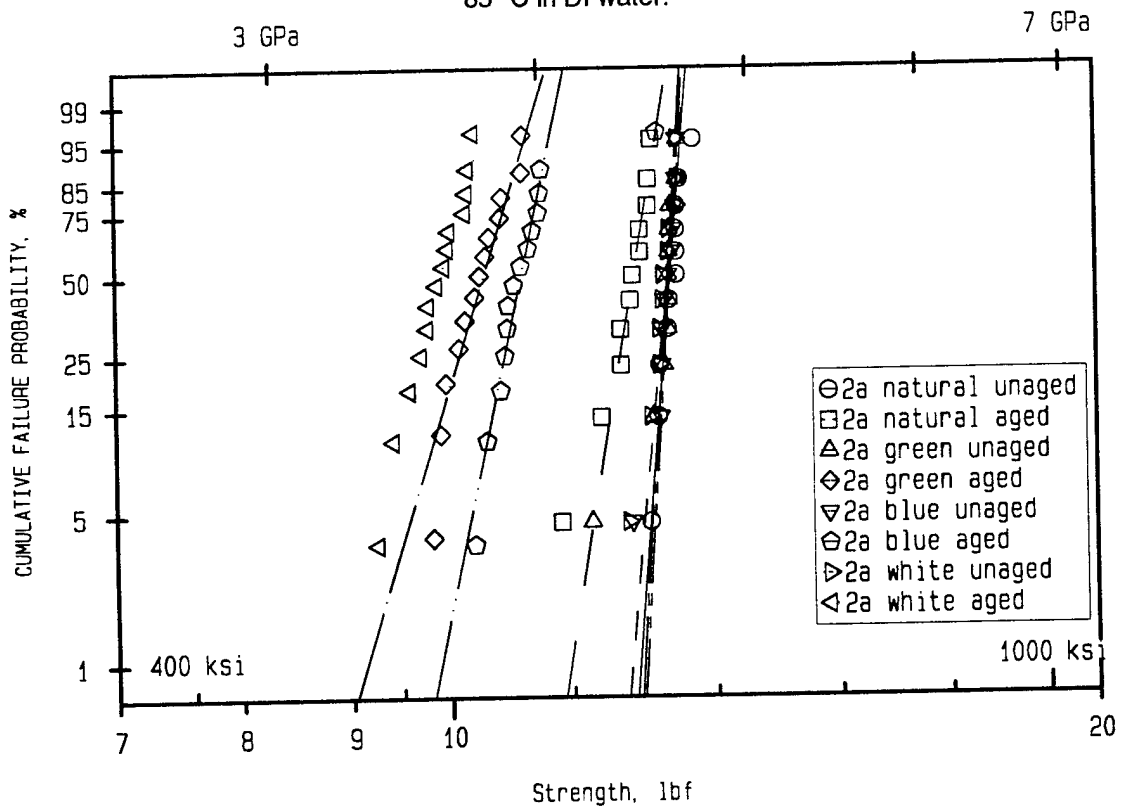


Figure 2: Strength of fiber 2a in natural and inked conditions, unaged and after aging 14 days in 85 °C in DI water.

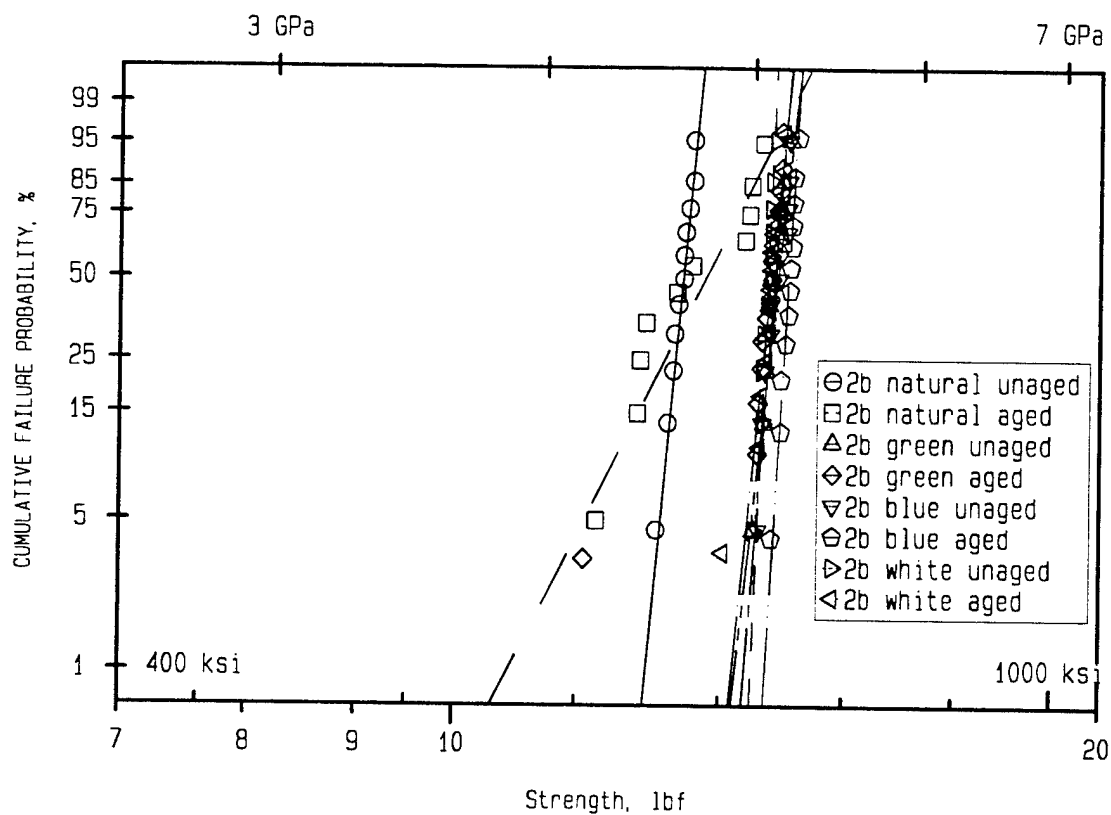


Figure 3. Strength of fiber 2b in natural and inked conditions, unaged and after aging 14 days in 85 °C in DI water.

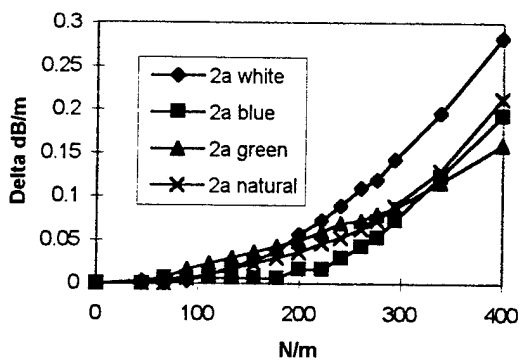


Figure 4. Changes in attenuations of fiber 2a at 1550 nm unaged.

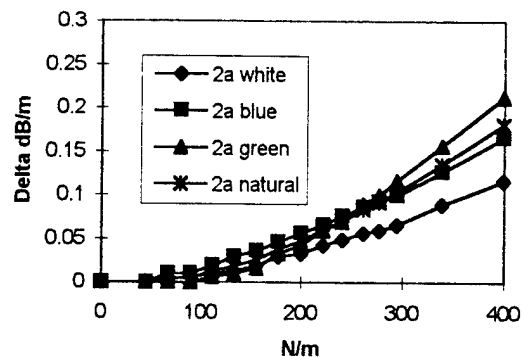


Figure 5. Changes in attenuations of fiber 2a at 1550 nm after aging at 1 month at 85 °C / 85% RH.

Thermal oxidative stability was defined by the temperatures at which oxidation of coating began. The natural (uninked) fiber coating for three different fibers 1, 2a and 2b showed values ranging from 204 to 249 °C and after aging for 2 weeks in 85 °C DI water all fibers showed a reduction in oxygen onset values. In all cases the inking process lowered oxidation resistance, but there was no significant changes in the inked samples after aging. FTIR results showed no obvious changes in the inked fibers after aging. These FTIR studies are continuing to determine if minor chemical changes can be detected and contribute to the fundamental understanding of the degradation mechanism.

DISCUSSION

We have demonstrated unambiguously that some combinations of fiber coatings and inks can detrimentally affect the fiber during aging, reducing the strength by about 20%. However, we have also demonstrated that specific ink and coating combinations can protect against fiber aging. While inks and coatings from a common supplier have most likely—but not definitely—been tested for compatibility by that supplier, the use of inks and coatings from different suppliers may have unexpected and unintended consequences.

Our earlier studies [1,2] showed that fiber strength reductions were 10 % higher for 7 days aging at 85°C in DI water compared with 7 days aging at 85°C in 85% RH conditions. The cable and user industry are actively discussing the relevancy of specific aging conditions to field performance, but this is not the subject of this paper. Therefore, we used the severe aging environment of 85°C in DI water for 14 days to maximize the aging differences between ink/coating combinations.

Changes in the chemistry at the glass/coating interface strongly contribute to the adhesion or delamination process. Our previous work based on gas chromatography/mass spectroscopy [6] suggests that volatile compounds, such as photoinitiators, solvents or stabilizers, are extracted during water aging. Thus, under these aging conditions, water permeates into and through the coatings and reaches the glass surface. Results for fiber 2a in Figure 2 show that the extent of the strength degradation varies with the color of the ink, provides a clear

indication that the ink is actually accelerating the aging effect, probably through differences in the chemical environment at the glass surface. Aging results for ink and coating combination for fiber 2b show that all of the inked samples (unaged and aged) have measurably higher strengths than either the unaged or aged uninked (natural) fiber. This combination appears to enhance the strength by slowing the penetration of water and other chemicals from the environment towards glass/coating interface.

Industry discussions have highlighted the shortcomings of the various microbending tests. During these discussions, the wire mesh test showed relatively good reproducibility in distinguishing poor from acceptable fibers and therefore, we selected the major trends from the wire mesh tests as indicative of the microbending behavior of our fibers. Results of these microbending tests showed no significant performance differences for unaged or aged, inked or natural fibers. The microbending losses were significantly lower at 1300 nm than at 1550 nm. Also there was no evidence of macrobending. The microbend losses of inked fibers was determined previously to be higher than for uninked ones [3]. In addition the magnitude of loss was previously established to depend on the coloring process [3]. Our inking process was the same for all the colors and fibers.

An oxygen onset value is the temperature at which the exothermic oxidation reaction begins as measured by DSC. The lower the onset temperature, the lower is the coating stability. Oxidation resistance is strongly dependent on the coating chemistry or formulation. The initial value for fiber 2a was the smallest and also exhibited the least resistance to oxidation with 10% decrease as compared to the 3 - 5% decrease for the other two coating/ink formulations. Reduced stability can result from intrinsic coating chemistry or extraction of stabilizer additives from the coating formulation by filling compounds or environmental contaminants (e.g., water). The inking process lowered the oxidation resistance in all cases, however after aging, the most significant changes were again observed for fiber 2a.

CONCLUSION

Our results demonstrate that the color of the ink layer is one of the contributing factors that affect

the performance of optical fiber. We have demonstrated unambiguously that combinations of fiber coatings and inks can detrimentally affect the fiber during aging, reducing the strength by as much as 20%. However, we have also demonstrated that certain ink and coating combinations can enhance fiber stability after fiber aging.

The use of inks and coatings from different suppliers may have unexpected, unforeseen, and unintended consequences. As fiber moves deeper into the local loop, there is an increased potential for higher handling stresses and new mechanical loading scenarios for individual fiber and cables. Therefore, it is critical to have an understanding of, and the ability to predict changes in, fiber strength under all likely field conditions, so as to be able to develop requirements and tests to help ensure long term fiber reliability and performance. As a result, we have formulated an additional requirement for strength-testing inked fiber which is incorporated into the Issues List Report for Bellcore's Generic Requirements for optical fiber and cable, GR-20-ILR [7].

We wish to state clearly that our results do not imply that inking deteriorates fiber performance. Inks can offer additional protection against environmental stresses, but the specifics of each ink application (i.e., the ink and coating formulations, ink uniformity, cure, etc.) can strongly modify the extent of this protection, as well as possibly cause counteracting effects.

REFERENCES

1. E. M. Vogel, B. J. Keon, C. R. Kurkjian, R. A. Frantz and H. H. Yuce, "Mechanical Properties of Color Coded Fibers", Proceedings of 1995 National Fiber Optic Engineers Conference, 237 - 247, June 1995, Boston MA.
2. R. A. Frantz, E.M. Vogel and B.J. Keon, "Effects of Color Coding on Optical Fiber Performance and Reliability", Proceedings of the 44th International Wire and Cable Symposium, p.146, 1995.
3. Z. Pasturczyk and C. Saravanos, "Microbend Loss of Colored Optical Fibers Measured over Extended Temperature Range", Proceedings of the 42th International Wire and Cable Symposium, p.527, 1993.
4. J.R. Petisce, M.D. Kinard, S. Siddiqui, and C. Taylor, "Effect of Environmental Aging on Optical Fiber Color Codings," Proceedings of the 42nd International Wire and Cable Symposium, p.552, 1993.
5. P. A. Sutton, J.L.L. Roberts, A. T. Summers and A. Phoenix, "Development of a Non-Destructive Test for Microbending Loss Mechanisms in Cabled Fibre", Proceedings of the 39th International Wire and Cable Symposium, p.450, 1989.
6. R. A. Frantz, B. J. Keon, E. M. Vogel, T. N. Bowmer and H. H. Yuce, "The Effects of Optical Fiber Coating and Ink Materials on Corrosion of the Glass Surface", Proceedings of the 43rd International Wire and Cable Symposium, p.742, 1994.
7. "Generic Requirements for Optical Fiber and Cable Issues List Report", Bellcore, GR-20-ILR, Issue 1A, November 1995.

A NEW, EXTREMELY VERSATILE, ACCESS NETWORK CABLING CONCEPT FOR MIGRATION TO OPTICAL FIBER

W. Griffioenⁱ, H. Nijstadⁱ, A.T.M. Grootenⁱⁱ, A. van Wingerdenⁱⁱ, G. Brownⁱⁱⁱ, D.F. Hawkins^{iv}, G. Plumettaz^v

ⁱKPN Research, Leidschendam, The Netherlands, ⁱⁱNKF Kabel BV, Delft, The Netherlands, ⁱⁱⁱMainetti (UK) Ltd., Jedburgh, Scotland, ^{iv}Eden Ltd., Uxbridge, United Kingdom, ^vPlumettaz SA, Bex, Switzerland

ABSTRACT

A new cabling concept for the telephony copper access network, allowing migration to optical fiber, is presented. Here individual guide tubes run through a telescopic protective tube network with cheap branching connections. This combination turned out to be the key to an upgradeable network at low cost. In this extremely versatile Tube To The Home (TTTH) network small copper cables can be installed or pre-installed, to be removed and replaced by small fiber (or other) cables in the future.

INTRODUCTION

After replacing copper by optical fiber in the trunk network many telecom operators are now fiberizing the Primary Access Network (PAN). The next step, Fiber To The Curb (FTTC) or Fiber To The Home (FTTH), is not an easy one to make because of the very high costs. It is not known which future "killer" application will ever pay for these costs. On the other hand cables lie in the ground for many (more than 20) years. Replacing these cables earlier is not economical. In that case most of the costs must be made again, especially in (but not limited to) countries where the cables are direct-buried and digging is necessary. Besides replacing copper networks by FTTC or FTTH takes a lot of time. Therefore copper access networks laid today ("green field" and renovation) require pro-active alternatives which allow migration to fiber at low cost. And, of course, against little or no extra investments today.

The above requirement seems hard to meet. The copper access network is telescopic: whenever possible, several cables are spliced to cables with more wires. Such a construction is cost-effective: cabling and laying costs can be shared by many customers. However, a telescopic network is not a cheap solution anymore for optical fibers. Splices in optical fibers are more expensive than those in copper and their attenuation is relatively high. Therefore they are avoided as

much as possible. Hence no telescopic structure is preferred, especially not for FTTH. Migration from a telescopic copper to a non-telescopic optical fiber network is difficult. Starting from a non-telescopic copper network is no good solution either, because of costs.

NEW NETWORK CONCEPT

Several alternative copper network concepts for migration to fiber were studied, such as unarmored copper cables in individual tubes and direct-buried hybrid copper/fiber cables. The first mentioned concept is more expensive than the old copper network because the telescopic structure is abandoned. This is also true for the second mentioned concept where individual cables are used because of the fiber. Moreover some excess length of (yet unused) optical fiber must be stored.

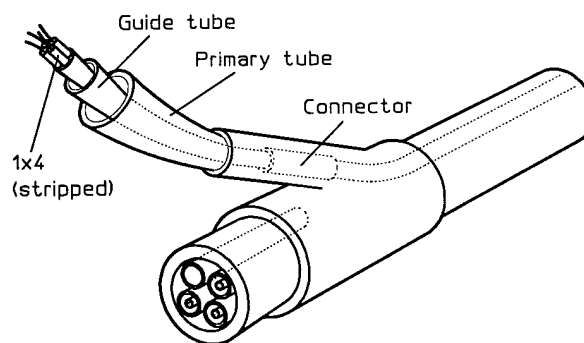


Figure 1 Artist impression of JETNET, in this case with copper quad cables.

By far the cheapest is the new Tube To The Home (TTTH) cabling concept, JETNET[®], presented in this paper (JETNET is a registered trademark of KPN Koninklijke PTT Nederland). Here individual guide tubes run through a telescopic protective tube network. A trunk tube runs through the streets and smaller tubes branch to the subscribers (see Figure 1). Cheap branching

connections are used. Small copper cables can be installed or pre-installed (e.g. using compressed air)¹, to be removed and (individually) replaced by small fiber cables in the future.

In the above concept the guide tubes can be installed in different ways. They can be pre-installed in the protective (trunk) tubes. In that case protective tube and guide tubes can be cut at the same time at branching points and simple Y- or T-connectors can be mounted, after connecting the branching and non-branching guide tubes. Limited space is available for the connectors of the guide tubes. Therefore simple permanent connectors are to be preferred to push/pull-connectors.² The non-branching guide tubes may also remain intact. But then a splittable T-connector is needed. This connector does not need to be pressure-proof. However, it must be "mud-tight" in order to allow (future) renovation.

It is also possible to install the guide tubes after the protective tubing has been laid. This is especially useful when only protective tubes are buried into the ground, to be filled at a later stage. Installing empty protective tubes can be done together with the old copper network, but also when the ground is open for other reasons. For (future) further installation of JETNET digging only at the branch points is then necessary. Filling with guide tubes needs the following procedure. At the branch-points pieces of trunk tube are cut and removed. T-connectors with closed branch-ends are then mounted, with fillers inside to get a smooth channel. Next a bundle of guide tubes is installed, e.g. using compressed air (one operation), filling the entire trunk tube. After shifting the T-connectors there is access to the guide tubes. They can be cut and connected with one or more guide tubes in the branch. Finally the T-connectors are shifted again and mounted.

Another option is also to pre-install the copper cables into the tubing. All JETNET variants cost little or no more than the old copper network. It is not yet clear which variant is most economical.

DESIGN CONSIDERATIONS

The goal is a new copper network with the same electrical and mechanical properties as the old network but with better migration possibilities. The price is aimed to be the same or less. Existing technologies shall be used as much as possible. Optimizing costs is especially important for the copper network (today). For the fiber network (future) this is less critical. Variations in future costs are always small compared to savings in digging costs. A solution is needed which is cheap now and works in the future. Although the network concept must be optimal for fiber in the

"green field" further cost reduction can be obtained later by developing new techniques.

To keep prices low and dimensions small a special miniature copper cable has been developed (see Figure 2a). This cable contains an aluminum shield because of electrical shielding and because of water-tightness. For the optical fiber also a miniature metal (steel) shielded cable has been developed (see Figure 2b).

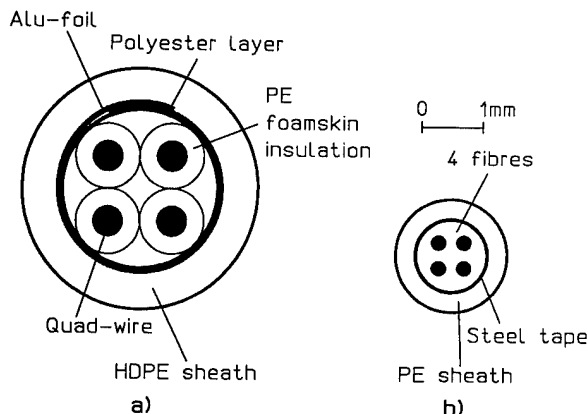


Figure 2 Cross-section of a) copper cable and b) optical cable used in JETNET.

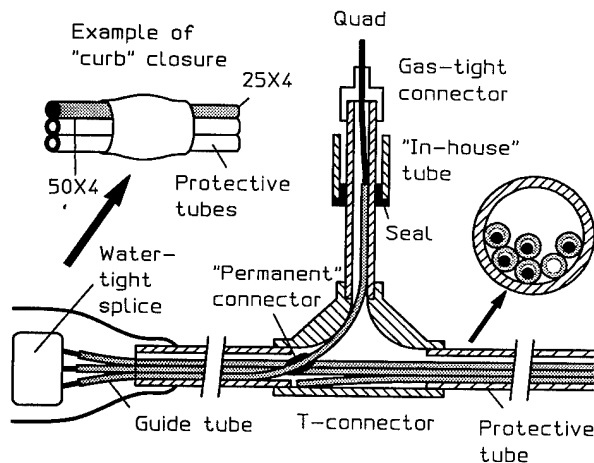


Figure 3 Current concept of JETNET, in this case with copper quad cables.

Examples of techniques for further cost reduction, which can be studied later, are metal-free blown-fibers.³ Not enough is yet known about their behavior in an environment with water. Also metal shields around guide tubes, to keep them dry, can be studied. But, here there is lack of longitudinal water-tightness. Note, however, that no spontaneous fiber fractures have been observed and handleability was still acceptable on blown-fiber trial sites which served for more than 10 years.⁴ Finally a dry-flowing technique is possible for the presented network.

In Figure 3 the currently chosen concept is shown. To each curb 4 protective tubes are connected, with up to 6 guide tubes each. Note that the guide tubes end freely halfway in the branches, to allow longitudinal movement of the guide tubes at "dig-ups".

COMPONENTS

Tubes and connectors

The protective trunk tube is a 37/30 mm high-density poly-ethylene (HDPE) tube. In this tube up to 6 HDPE 7/5.5 mm guide tubes are installed. The guide tubes only partly fill the protective tube (see Figure 3) to protect against mechanical violation. Note that such a construction may protect better than (tight) armored constructions.⁵ The protective branch tubes are HDPE tubes with smaller diameter than for the trunk. The size depends on the results of the impact tests. They are connected to the trunk by a T-connector in which the guide tubes are bent with a minimum radius of 10 cm. The connector is either one piece (pressure-proof) or splittable.

Copper cable

In order to fit into the small guide tubes the quad (twisted-pair) from the old copper network must be stripped. Because a cable with water-barrier was chosen the dimensions of the quad were too large to fit into the guide tubes chosen. Further size reduction has been achieved using foamed PE (see Figure 2a) to allow the metal shield closer to the copper wires with almost no change in the electrical properties. The total diameter over the HDPE jacket is 4.2 mm.

Optical cable

The optical cable has also a water-tight construction, using a laser-welded stainless steel tube (Figure 2b). The diameter over the HDPE jacket (same as for copper quad) is 1.8 mm.

TESTS

Copper cable electrical properties

The electrical behavior of a first prototype of the copper quad, strongly reduced in size, has been measured up to 10 MHz. The characteristic impedance was about ten percent lower than for the old cable. Fine-tuning can be done for the next cable. Attenuation and cross-talk (within the quad) were found to be slightly worse.

Impact tests

A protective trunk tube with 6 guide tubes was tested under a guillotine (specified tip, mass 6 kg, height 0.6 m or more). To detect touching of cable elements copper tubes of 3 mm diameter were used. No deformation could be detected on guide tubes and copper tubes. The protective branch tube with guide tube also passed the impact test. In a non-specified test, the trunk tube was struck heavy blows with a spade, by hand, and posed no problems. Results for the branch tube to be presented at the symposium.

Installing tubes

A bundle of 7 guide tubes was installed into a 750 m long, tortuously laid, protective tube using the assistance of compressed air. First 70 m could be installed by pushing alone. Then, after admitting the compressed air, 380 m (maximum length of the guide tubes) was installed with ease. Installation caused a helical shape of the bundle of tubes (period about 10 m).

Installing cables

Using the assistance of compressed air, the optical cable could easily be installed the required 200 m. The trajectory was very tortuous and a sharp bend (for the T-connector) was applied to the guide tube, 20 m before the end. The minimum bend radius was found to be 10 cm. The copper cable was successfully installed in a 270 m long trajectory. This time the minimum bend radius was 7 cm and also a tube connector was mounted there.

Field trial

A typical Netherlands example of the old copper network is shown in Figure 4a. In the case of optical fiber a division is introduced between Secondary Access Network (SAN), comparable to FTTC, and Tertiary Access Network (TAN), comparable to FTTH. Two curbs C1 and C2 are indicated, serving 2 TAN-areas. The right-most TAN-area is shown in Figure 4b, with JETNET applied. While C2 is a closer curb-location, C1 is used as a worst-case situation (option of shared curb). In fact, for the field trial even extra length has been added (blank portion) to meet the designed maximum test-length of 200 m.

In the field trial all components and handling will be tested and evaluated. Also a dig-up simulation will be performed. Results will be presented at the symposium.

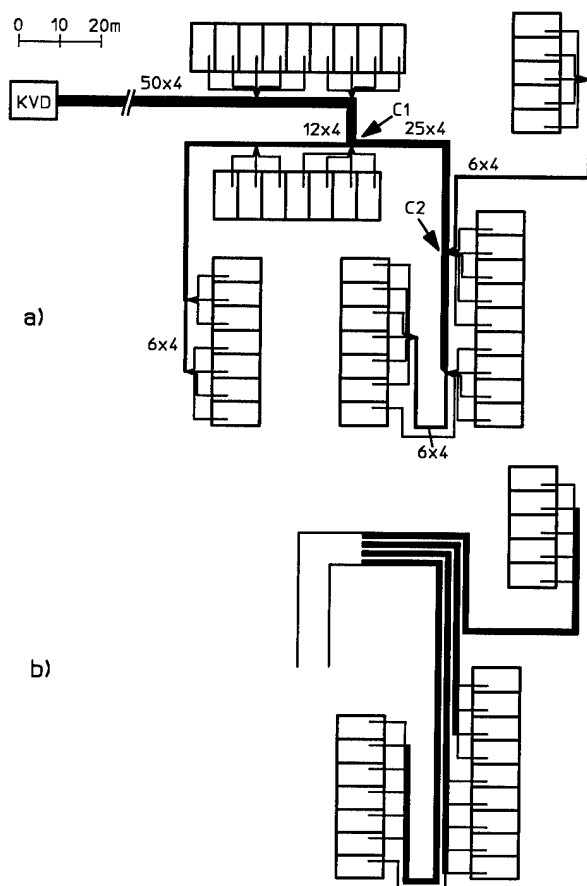


Figure 4 a) Old copper network SAN/ TAN and b) JETNET TAN, also used in the field-trial.

ECONOMICS

The following results from cost calculations refer to the Netherlands situation and are based upon the network shown in Figure 4 (but now with the curb at C2). With the new concept preparing the TAN for migration can be done against only 0-5% extra cabling costs. For this investment more than 90% can be saved in future when upgrading to FTTH takes place, still economical when this takes place beyond the year 2025! This is based on cost spread over the years until FTTH, which is the case for installation in the "green field" and for renovation, not being paid all in the first year. The new concept is also, by far, the cheapest (about half the cabling costs of traditional techniques!) when installing optical fiber in the "green field". Further cost savings come from recovery of the old copper. The network can easily be scaled-up to a redundant one. It is even possible to combine two (e.g. telephony and CATV) networks with "their fingers merged" for the price of slightly more than one. Those networks can still be managed separately, also with respect to migration to fiber.

For the secondary access network (SAN), the part of the network that runs until the curb, it is not necessary to apply the JETNET concept since there is practically no branching in the SAN itself. Just laying empty tubes without branching connections next to the copper network is a sufficient solution for migration.

CONCLUSIONS

The presented network concept has the potential of tremendous cost savings, especially in the TAN (for the SAN just laying empty tubes will suffice). The old copper can be recovered. Migration can be done very fast and can also be done for individual subscribers. Even two separately manageable networks (e.g. telephony and cable television) can be obtained, providing further cost reduction. Upscaling to a redundant network is easy. The concept is future proof, versatile and does not depend on technique. Almost anything is possible, not only copper quad and optical fiber, but also hybrid copper/fiber, coax (in future with high- T_c superconductors?), Tera-chips by pneumatic post?

REFERENCES

1. W. Griffioen, "Installation of optical cables in ducts", Plumettaz, Bex (CH) 1993.
2. European patent EP 0 349 344.
3. M.H. Reeve, S.A. Cassidy, "Installation of optical fibre units using viscous drag of air", *Proc. ECOC* (1983).
4. W. Griffioen, T. Volotinen, P. Wilson, A. Gouronnec, T. Svensson, "Handleability of aged optical fibers", *Proc. 44th IWCS* (1995) 857.
5. K. Nygård Skalman, E. Siönäs, S. Edman, G. Danielsson, "The equipment and cables used in the optical fibre network at Banverket, Sweden", *Proc. Interwire*, Atlanta (USA), November 1992.

BIOGRAPHIES



Willem Griffioen received a MS degree in Physics and Mathematics from Leiden University (Netherlands) in 1980. Worked there until 1984. Joined KPN Research, St. Paulusstraat 4, 2264 XZ Leidschendam, The Netherlands. Responsibilities R&D of Outside-Plant and Installation Techniques.

Worked at Ericsson Cables, Hudiksvall (Sweden) and at Telia Research, Haninge (Sweden) in the scope of exchange/joint projects with KPN Research. Received Ph.D. (Reliability of Optical Fibers) in 1995 from the Technical University of Eindhoven (Netherlands).



Henk Nijstad received a degree in Physics at the University of Twente (Netherlands) in 1993. Completed a 2-year course in Mechatronics with a research project at Oce-Van der Grinten in Venlo (Netherlands). Works from 1995 at the telecom infrastructure department of KPN Research (see previous author for address).



Gerard Plumettaz received a MS degree in mechanical engineering at the Swiss Federal Institute of Technology, Zürich, in 1970 with an emphasis on machine tool techniques. Joined his family business, Plumettaz SA, CH-1880 Bex, Switzerland, in 1971 and became instrumental in product design, development and marketing. Initial task was to design and develop winching concepts for military tank retrieval. Here specialized winching techniques led to the design of underground placement methods. Today, president and chief operating officer of Plumettaz SA continuing to be active in the pursuit of advanced methods in underground placement/technology.



Albert T.M. Grooten holds a MS degree in Materials Engineering of Delft University of Technology (Netherlands). Joined NKF Kabel BV, Schieweg 9, 2627 AN Delft, The Netherlands in 1978. Worked in the R&D department and was International Product Manager for Optical Fiber Cables. After a period as Quality Assurance Manager, introducing the ISO 9001 system, joined the Telecom Sales department of NKF as Marketing Service Manager. Currently holds a position as

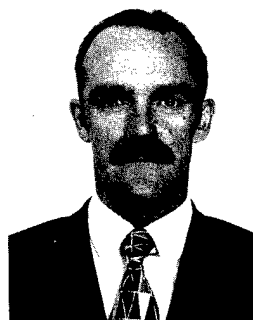
Account Manager for PTT Telecom (Netherlands) and for the Unisource Alliance.



Arie van Wingerden received his B.Sc. degree in Electrical Engineering in 1971. In the same year, joined NKF Kabel BV (see previous author for address) and was involved in various cable development projects and high frequency measuring methods. In 1984 became Engineering Manager of the Project department and responsible for engineering of Outside-Plant and Telecommunication Systems. Current responsibilities are Technology and Quality assurance. Involved in international standardization.



George Brown completed a degree in Economics at Hull University in 1974. Joined Dunlop in production management and gained experience in injection molding rubber components. Moved to Mainetti (UK) Ltd., Oxnam Road, Jedburgh TD8 6NN, Scotland in 1979 as Factory Manager responsible initially for injection molding and then extrusion activities. In 1986 assumed responsibility as General Manager of the Industrial Products Division and then appointed as a Board Member of Mainetti (UK) Ltd. On 1st January 1996 appointed as Chief Executive Mainetti (UK) Ltd. - Industrial Products.



Dave Hawkins received an honors degree in Mechanical Engineering at the University of Aston in Birmingham in 1975. Joined Lucas CAV Ltd. in overseas Department liaising with the South American product plants on all technical matters. Worked with General Motors, the Ford Motor Company and Fiat for some ten years developing the latest generation of fuel line connectors. Set-up Eden Ltd., Unit 11 Chiltern Business Village, Uxbridge, Middlesex UB8 2SN, United Kingdom in 1992 as Managing Director.

TAPERED SLOT TEST. A HIGH-SPEED BENDING TEST METHOD FOR MEASUREMENT OF B-VALUE OF FIBERS

Torbjörn Svensson

Telia Research AB, Haninge, Sweden
torbjorn.k.svensson@telia.se

Anders Hjorth

Royal Institute of Technology, Stockholm, Sweden
anders.hjorth@mailbox.swipnet.se

ABSTRACT

A novel test has been employed for the measurement of the strength of optical fiber at very high stress-rates: the tapered slot test, TST. The properties of the test have been studied from a theoretical view. Design considerations lead to a test instrument for optical fibers which has been applied in some experiments. In this paper are presented the results from testing in TST and two-point bending one carbon coated fiber, and one acrylate coated standard singelmode fiber.

A clean assembly and a remarkable performance are found in this low-budget instrument for high-stress-rate testing. The strength of fiber is readily and accurately measured at stress rates of effectively 11,000 GPa/s. Calculations show that the upper limit for the test is still to be exploited, measurements at stress rates in excess of 100 TPa/s would be practically achievable.

INTRODUCTION

According to the power-law model, stress assisted fatigue of optical fibers can be characterized by two environment-dependent parameters: B, and n. The theory behind this and other approaches is covered by literature, and here is necessary only to know that values of B are useful when lifetime of optical fiber under stress is to be calculated from a known initial strength. An exact value of the initial strength is usually not known, but by assuming that initial strength of fiber locally drops to screen test level, the minimum lifetime of fiber can be estimated, also for very long fibers, cf eq(3) below.

During the last ten years there has been a continual interest in the value(s) of the B-parameter of optical fibers. Vastly disparate values of the B-parameter have been reported, due to different ways of measurement. Most of them are based on mechanical test of fibers at low temperature, in vacuum, or at high stress rate. Testing in ambients environments at high stress-rates is to be favoured mainly because of it's intuitively sound application in regular network environments, to the contrary to low-temperature- or vacuum tests.

The authors' intention with this paper is neither to argue for the application of specific values of the B-parameter, nor to give appropriate values of the n-parameter to be used at the

low fiber stresses typical in network installations^{1,2}, but to present an easy way to do high-stress-rate testing of fiber. Data from this test may be used to evaluate the B-parameter of coated fibers in most environments, and at arbitrary temperatures.

Measuring initial strength of optical fiber by high-speed tensile testing has been expensive and complicated, being accessible only at a few laboratories.^{3,4,5} The proposed test, TST, however implies very small investments. A simple setup based on a ruler and a rotating capstan for pulling the fiber has been used in this study.

In this paper are presented the results from testing in TST and TPB (two-point bending) two standard singel mode fibers, one with regular coating, the other with hermetic coating. From the measurements, and by theoretical considerations are discussed the accuracy of the TST.

THE INSTRUMENT

The TST is an accurate method for testing the bending strength of optical fibers.⁶ A few low-budget parts compose the instrument, no electronics or otherwise sophisticated device is necessary to run the test. Even more remarkable is that the highest stress rates achieved so far by high speed tensile testing are surpassed by the TST. This is owing to the fact that wave propagation and inertia do have negligible effects on the accuracy of TST measurements, at stress rates comparable with other tests based on tensile testing of fiber. Reliable strength data from TST experiments have been produced at a stress rate of 11,000 GPa/s.

A number of experiments have been made with a prototype instrument. The name of the test, tapered slot test, corresponds to the geometry of the instrument. A fiber bend is placed in a shallow slot, covered by a lid during the test. One end of the fiber is gripped, and the other end is pulled with a known speed. The bend moves along the slot and finally breaks, because the taper of the slot implies a gradually decreasing bend diameter on the fiber. See Figure 1.

The significant dimensions of the instrument are the length of the slotted ruler and the width of slot, d. The range of slot

widths used here, $1.30 < d < 3.0$ mm, and a 400 mm slot length are chosen for testing most high-strength optical fibers. In order to avoid static fatigue and break of fibers during mounting, the fiber should be arranged in a large diameter bend, placed outside the top of the slot.

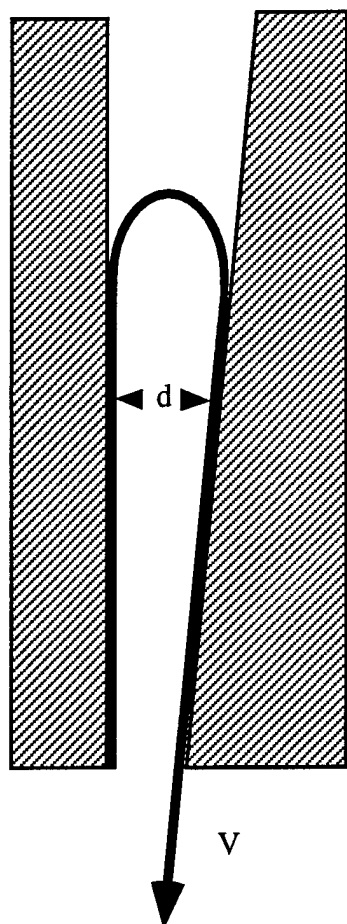


Figure 1. TST, schematic.

The post-failure position of the fracture on the fixed fiber corresponds to the bending diameter at fracture, which is readily transformed to failure stress by algorithms similar to those used in regular TPB tests.

FUNDAMENTALS

Testing of strength intuitively should lead to a useful value of B if made in the same environment as the application of the parameter value. If a B-value in ambient environment and normal humidity is searched for, the test has to be run at very high stress rates. Such conditions may cause severe problems with measurements and the interpretation of data, due to influences from inertia and mechanical waves. The TST pushes forward these problems a considerable step.

In order to evaluate the B-parameter from high-stress-rate data, and to understand the differences between the TPB and TST, a number of useful formulas will be presented.

Stress history

From the "power-law" theory of stress assisted crack propa-

gation in glass can be derived a general expression for the dependence of fracture stress, σ_f , on the time and tensile stress applied, σ , starting from an initial strength, σ_i .

$$\sigma_f^{n-2} = \sigma_i^{n-2} - \frac{1}{B} \int_0^t \sigma^n dt \quad (1)$$

The parameters B and n control the degradation of strength for an arbitrary, positive stress history. It follows by integration of (1) that the strength of fiber in a regular tensile test reads

$$\sigma_f^{n-2} = \sigma_i^{n-2} - \frac{\sigma_f^{n+1}}{B(n+1)\dot{\sigma}} \quad (2)$$

using a constant value of the time-derivative $\dot{\sigma} = d\sigma/dt$. The left-hand term is negligible at low values of $\dot{\sigma}$, and by applying logarithmic derivation of (2) brings the equivalence $n = 1/[d \log \sigma_{fm} / d \log \dot{\sigma}] - 1$, which is used to evaluate the n-parameter from a linear curve fit to median data, σ_{fm} .

Application of B

The major application of B-values is the estimation of fiber lifetime. From the integration of (1) also follows that a static stress, σ_s , will cause fracture of fiber after a time t_s , according to

$$t_s = B \frac{\sigma_i^{n-2}}{\sigma_s^n} \quad (3)$$

Under the assumption that σ_i equals the screen test stress, the lifetime of the weakest part of fiber of any length under static stress is readily calculated from (3). The value of the screen test stress is stated by the manufacturer, and researching the n-value causes few problems. However, knowing the value of B requires a specific measurement.

Calculation of B-value

For regular silica fiber, the strength measured in a tensile test will increase with the applied rate of stress. The values of B and σ_i are inseparable when using data from regular tensile tests. However, due to the fact that there must be an upper limit of tensile stress, a strength asymptote will appear at sufficiently high rates of stress. An accurate evaluation of B should be expected when reaching stress rates such that the following condition is satisfied:

$$\frac{d \log \sigma_f}{d \log \dot{\sigma}} \approx \frac{1}{2(n+1)} \quad (4)$$

Thereby the value of B can be calculated, either by iterative curve fitting to eq (2), or by using the expression

$$B = \frac{\sigma_{f2}^{n+1} - \sigma_{f1}^{n+1} (\dot{\sigma}_2 / \dot{\sigma}_1)}{(n+1) \dot{\sigma}_2 (\sigma_{f1}^{n-2} - \sigma_{f2}^{n-2})} \quad (5)$$

which is derived from eq (2) when applied on two stress rates, $\dot{\sigma}_1$ and $\dot{\sigma}_2$. By inserting the corresponding fracture stresses, σ_{f1} and σ_{f2} , eq (5) follows from the elimination of σ_i .

STRENGTH AND STRESS RATE IN BENDING

Usually, fibers are tested at almost constant rates-of-stress or -strain. An equation as (5) can then be used to evaluate the B-parameter. Commercial instruments for TPB testing usually enable real-time control of the rate during test, but in a TST this is not feasible. Instead, the history of stress and stress rate during loading of the fiber has to be reduced to effective values which can be used in formulas as eq (5).

Strength

The strength is calculated in the same way in TPB and TST. The value of fracture strain reads⁷

$$\epsilon = 1.198 \cdot d_{\text{fib}}/d_{\text{cc}} \quad (6)$$

where ϵ is calculated from the diameter of fiber glass, d_{fib} and center-to-center distance between fiber cores, d_{cc} , which equals the width of the slot (TST) or the plate separation (in TPB), minus the thickness of the coating.

The maximal tensile stress in TPB and TST follows from¹

$$\sigma = E_0[1 + (3 \cdot k/2 - 1/4)/2 \cdot \epsilon] \cdot \epsilon \quad (7)$$

In this study was assumed $E_0 = 70$ GPa and $k = 3$.

Nominal stress rate

A nominal value of the stress derivative in the TST can be defined as the maximum stress divided by the time of loading. By assuming that fracture occurs at the point of symmetry, the nominal stress rate in TST is

$$\frac{d\sigma}{dt} \approx K \frac{V}{d} \sigma_f \quad (8)$$

where V is the pulling speed of fiber and d is the width of the slot according to **Figure 1**. Only dependent on the bending geometry of fiber, K would be $2/\pi \approx 0.637$ for a circular bend. It is known from early works by Matthewson⁷ that the shape of fiber bend in TPB is an approximate ellipse. Recently has been shown by Hjorth that the geometry of fiber in TST is the same as in a TPB, for practical values of the slot angle. Taking into account the longer time of loading an elliptic bend than a circular, the same definition of nominal stress rate would give $K \approx 0.457$.

However it will follow that also this value is about 3 times too high, and the real stress history must be considered by replacing the constant with an n -dependent function $K(n)$.

Effective stress rate

For tensile tests the effective value of stress rate generally is close to the local value at the curve's maximum of stress, mainly because strength degrades more rapidly at higher stresses. In a TST the stress history is strongly non-linear, stress derivative decreases significantly at stress maximum, thus reducing the effective value of $d\sigma/dt$. See **Figure 2**.

The effective value of stress-rate in TST is obtained from the equations (1) and (2), by eliminating terms being equal at the moment of fracture; σ_f and σ_f . What remains is

$$\frac{d\sigma}{dt_{\text{eff}}} = \frac{\sigma_f^{n+1}}{n+1} \int_0^{t_f} \sigma^n dt \quad (9)$$

For practical reasons, a substitution of (9) was searched for. The integral was solved numerically, and from the results an explicit formula has been derived by Hjorth⁸,

$$\frac{d\sigma}{dt} = \frac{\sigma(t_f)^2 V}{E d_{\text{fib}} (n+1)} \cdot \frac{2}{\pi^{1/2}} \frac{\Gamma(\frac{n+3}{4})}{\Gamma(\frac{n+1}{4})} \quad (10)$$

where d_{fib} is the cross sectional diameter of the glass fiber, V is the pulling speed, and E is Young's modulus. A linear elasticity, $\sigma = E\epsilon$ was assumed for simplicity. The function $\Gamma(z)$ may be substituted using Stirling's approximation⁹

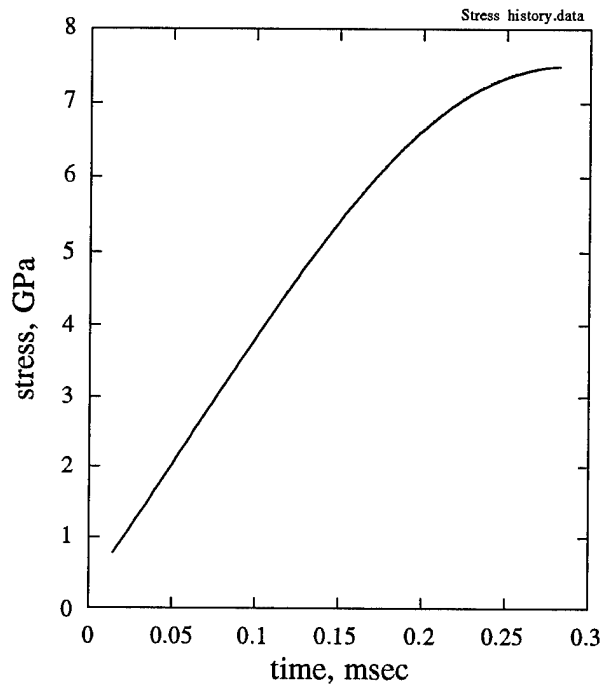
$$\Gamma(z) \approx \sqrt{2\pi} e^{-z} z^{z-1/2} [1 + 1/12z + 1/288z^2 + O(1/z^3)].$$


Figure 2. Example of calculated stress history in TST.

Tabled stress-rate in TST

Equation (8) is applicable on effective stress rates. The value of K is solved by setting the equations (8) and (10) equal;

$$K = \frac{1.198}{n+1} \cdot \frac{2}{\pi^{1/2}} \frac{\Gamma(\frac{n+3}{4})}{\Gamma(\frac{n+1}{4})} \quad (11)$$

Values of K are tabled below, for common values of n .

n	K	$\frac{d\sigma}{dt} \approx K \frac{V}{d} \sigma_f$
18.0	0.151	$V = \text{pulling speed}$ $d = \text{width of slot}$
20.0	0.144	
22.0	0.138	
24.0	0.133	
26.0	0.129	
28.0	0.123	
30.0	0.120	

Table.
K-values for calculation of effective stress rate in TST

DYNAMICS

Theoretical considerations do confirm a negligible influence on measured strength of inertial effects, with the equipment used in combination with the fibers tested. This is true for stress rates including the maximal value employed, 11 TPa/s.

Several plausible errors in TST measurements have been analyzed. Some may be due to trivial factors as parallax of the ruler readings, and the influence of slot tilt due to lid mismatch, other factors may be dynamic gas pressure on fiber bend when covering the slot, and influence on the slot angle on the geometry of bend.⁸ The practical problems have been solved, and remaining errors of major significance are only expected from acceleration along the fiber and vibrations of the bent portion. The reasons for, and type of the errors are:

- 1) transient loading of the pulled end of fiber generates an undetected stress wave which adds to the stress on fiber bend. This causes a too low estimated fracture stress.
- 2) a stationary state of bending waves may establish at a pulling speed equal to the propagation of the wave. Generally, such standing waves will distort the shape of bend, and wrong values of fracture stress will be displayed.
- 3) viewed as a rotation, the motion of the fiber bend obviously will cause tensile stresses which may influence its geometry. However, rotation was shown not to cause any change to the shape of bend, but it adds to the fiber a uniaxial stress. This additional term implies a slightly too high displayed value of fracture stress.

Transient load

The transient stress during acceleration of the fiber may reach considerable strength if the pulling speed is suddenly imposed. The tensile stresses in the transient wave is equal to $\rho C_b V$, thus the fiber may fracture before its bend reaches the slot. Needless to say, this is not the aim of the test. However, owing to the long launching distance, the transient part of tensile wave will decline in due time before the end of test. By reflection and damping a stationary state of tensile stresses in the order of ρV^2 will be reached at the moment of bending failure, but standing waves at the fiber bend may still deform the fiber in an unknown shape.

Standing waves

The mode of vibration of major importance is due to the rotation of a bend along the fiber, according to Figure 3.

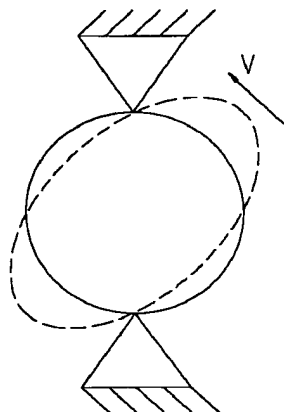


Figure 3. Standing wave

When the velocity of propagation is equal to the pulling speed, the shape of the bend is stationary. This happens at the critical pulling speed

$$V_{cr} = 1.34 C_b \frac{d_{fib}}{d} \quad (12)$$

The longitudinal wave velocity in the fiber, C_b , is in the order of 3,600 m/s in 250 μ m coated fiber. By inserting in eq (12) the value of fiber diameter, $d_{fib} = 125 \mu$ m, and a slot width of $d \approx 2$ mm, the critical velocity for the formation of the first mode is obtained as $V_{cr} = 300$ m/s.

Higher order modes may appear at higher speed. Testing at supercritical velocity should be feasible, either by proper choice of speed and damping, or by smoothing the load onset.

Rotation

Rotation does not cause any change to the shape of bend, since it implies no extra bending moment. On the other hand, rotation adds to the fiber a uniaxial stress equal to $\rho V^2/4$, ρ being the density of fiber. This is usually negligible, since it corresponds to only 7 MPa at 100 m/s.

EXPERIMENTS

Results from comparative tests at ambient temperature, 23°C are shown in Figure 4. Data are from testing in TST and two-point bending two single-mode fibers, called SSM and CC. SSM has a regular acrylate coating, the CC fiber has a hermetic (carbon) coating. The number of specimens tested at each stress rate are: 30 (TST SSM fiber), 25 (TPB of SSM fiber) and 9 (TST of CC fiber).

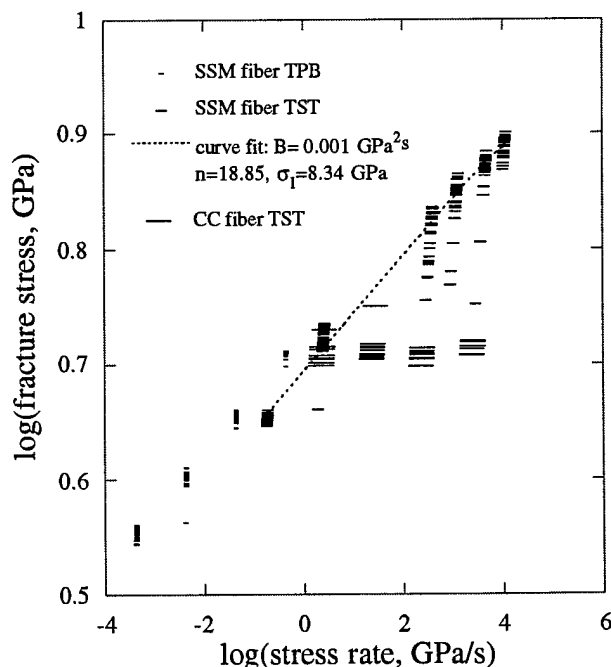


Figure 4. TST data for hermetic fiber (CC), and TPB and TST data for acrylate standard single mode fiber (SSM).

Experimentally, the data from hermetic fiber tested in TST confirm that there is no velocity dependence of the method, for the stress-rates applied here.

A similar n-value of the standard fiber was found in both TPB and TST, but there is a slight mismatch between levels of strength. This was probably caused by different humidity at the two test occasions (50% RH in TPB, 60% in TST). For each occasion the variation was quite small, $\pm 5\%$ RH, and specimens had been tested in a pseudo random order.

Due to the site-dependent humidity, no attempt will be made to evaluate the B-parameter of the standard fiber by including all the data, but on data from the TST only. Unfortunately, the rather linear rate-dependence apparent in Figure 4 gives no clear indication of the initial strength of this fiber. In any case it is illustrative to try a curve fit to eq(2) of data. This gives the parameter values $\sigma_f = 8.34$ GPa, $B = 0.001$ GPa²s, and an n-value of 18.9, when applied on median values of strength and stress rate. The curve fit is shown in Figure 4. Exercises with eq(5) gives a rougher estimate of $B \approx 0.0015$ GPa²s. The calculated values of B are so small that the figures given here should not be too seriously interpreted.

LIMITATIONS

Theoretical considerations have outlined the limits where dynamic effects start to influence the measurement in TST.

In order to retain accuracy at very high speed motion, a value of $\rho V^2/4$ must be added to the ruler-displayed stress because of the fiber bend's rotation. The test should not be made at a pulling speed close to the critical velocity for standing waves according to eq (12). In practice this means a limit of 300 m/s for the TST.

RESULTS

Measurement of the strength of optical fibers has been made by a prototype instrument up to a stress rate of 11 TPa/s. Instruments based on TST method may reach very high stress rates, in excess of 100 TPa/s. Theoretical limitations of the method are described. Additional tensile stresses may appear on the fiber bend under high-speed motion, but their influence on the measurement is negligible up to 100 m/s pulling speed, or stress rates below 60 TPa/s.



Torbjörn Svensson

Torbjörn received his M.Sc and Ph.D. from the Royal Institute of Technology, Stockholm. He joined Telia in 1985. Since then he has been engaged in quality assurance, techniques for testing fibers and cables (holding some patents), and splicing technology. Torbjörn is now at Telia Research, working on reliability of optical transmission systems and components.

Wave propagation and inertia have negligible effects on the accuracy of TST measurements, at stress rates comparable with other tests based on tensile testing of fiber. A brief explanation to this important fact follows from the below features:

- No transient measurement is necessary, since only the post-failure position of fracture is needed. The instrument used is a ruler, which can be calibrated to high accuracy. Fracture stress in TST is calculated afterwards, from the bending geometry of fiber, just as in TPB.
- Deformation is quasistationary at fracture, since vibrations have declined during test launch.
- The size of the bend is almost constant during the stress history of the material. This eliminates vibrations and distortion of the shape of bend.

REFERENCES

1. A. Breuls, "A COST 218 comparison of n-values obtained with different techniques", *Tech Digest OFMC'93*, p 9 (1993)
2. W. Griffioen, "Effects influencing measurement of optical fibre corrosion susceptibility", *Tech Digest OFMC'93*, p 13
3. T. Svensson, "High Strain-Rate Testing of Optical Fibres", *Proc 37th IWCS*, p 217 (1988)
4. T. Svensson, L. Sundeman, and E. Sundberg, "Methods and studies on fibre reliability at Swedish Telecom", *SPIE Vol 1973*, p 180 (1993)
5. A. Gouronnec and N. Evanno, "High Speed Axial Strength .. measurement of the B-value", *These proceedings*
6. SE patent no 503 259
7. M. J. Matthewson, and C. R. Kurkjian, "Strength measurement of optical fibers by bending", *J. Am. Ceram. Soc.*, vol 69, No II (1989)
8. A Hjorth, "Kilrullning. En provmetod för optisk fiber" *M.Sc. thesis*, Royal Inst. of Tech., Stockholm (1996)
9. R. Murray, Spiegel, *Mathematical handbook of formulas and tables*, 28th printing 1992, Mc Graw-Hill Inc.



Anders Hjorth

Anders is under graduate from Royal Institute of Technology, Stockholm. He has a balanced interest in nature, sports and technology, so the attractions of the Stockholm archipelago and the challenges of the Baltic sea tempted him to design and build his proper windsurfing board to be added to his diving equipments. Thus he was well prepared to dive deep into the subject of this paper.

Development of Electro-fiber Optic Cable Containing Metal Tube Armored Fiber for Deep Sea Tow

Hiroshi Ishisaki

Satoshi Imamura

Hiroyasu Momma

Ocean Cable Co.,Ltd
Shibaura Minatoku Tokyo JAPAN

Japan Marine Science and Technology Center
Yokosukashi Kanagawa-ken JAPAN

ABSTRACT

Ocean scientists who study earthquakes or living animals have been demanding electro-optical composite cables which are applicable to the existing winch systems of their research ships, in order to collect real-time information from the deep sea.

We have developed a new Electro-fiber Optic tow cable using metal tube armored fibers (M-PAC) with excellent mechanical characteristics.

In design, we maintained mechanical characteristics of conventional electro-mechanical tow cables. Following factory evaluation test, we conducted a field test at depth of 6000m with connecting an observation system including cameras to the cable end, and obtained very good performance of the Electro-fiber Optic Cable (E-O Cable).

1. INTRODUCTION

As the worldwide trend of ocean scientists in the field of resources, earthquakes, living animals and so on has been toward deep-sea observation year after year, larger systems have been required (Ref.1). On the other hand, many scientists have been demanding development of new tow cables to get more information using the winch system (Fig.1) of an observation ship for economical reasons.

We had used electro-mechanical towed cables (Fig.2) of conventional coaxial type, and complained about their applicable depth of about 4500m, signal amounts and quality. Since 1987, we have started development of an electro-fiber optic tow cable that provides an applicable of 6000m, focusing on excellent

characteristics of newly developed metal tube armored fibers.

Successful development of this cable allows observation of almost all the sea beds in the world.

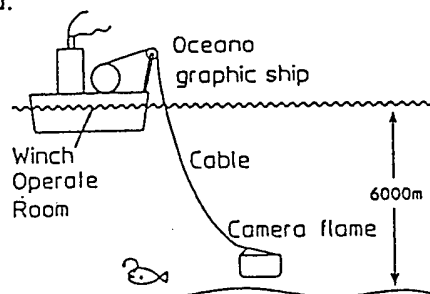


Fig.1 Schematic tow system

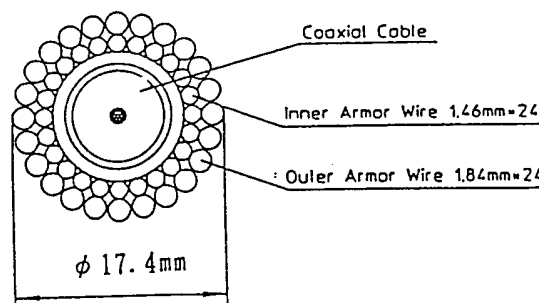


Fig.2 Electro-mechanical cable (Coaxial type)

2. ELECTRO-FIBER OPTIC CABLE

2.1 Requirements

The requirements for tow cables are extremely severe as listed below.

1) To protect fiber reliability from dynamic tension caused wave fluctuations as well as the weight of observation equipment and cable itself of 6000m long.

2) To provide the same outer cable diameter as conventional ones in consideration winch system.

3)To use steel armor so as to withstand wear or impact caused by sea-bed reefs or winching.

2.2 Characteristics of

metal tubed armored fiber

Metal tube armored fiber has extremely attractive characteristics to protect it from external forces such as water pressure,load and humidity.

Table 1 Metal tube characteristics

Material	SUS 304
O.D/W.T *	1.1/0.15 mm
0.2% Modules	536 MPa
Buckling pressure	9.8 kN/mm
Water Tightness	>78 MPa

*O.D:Outer diameter W.T:Wall thickness

2.3 Cable structure and features

The developed cable consists of a stranded insulated conductor with M-PAC,a cushion layer ,a sheath and two armor layers of galvanized steel wires.(Fig.3)

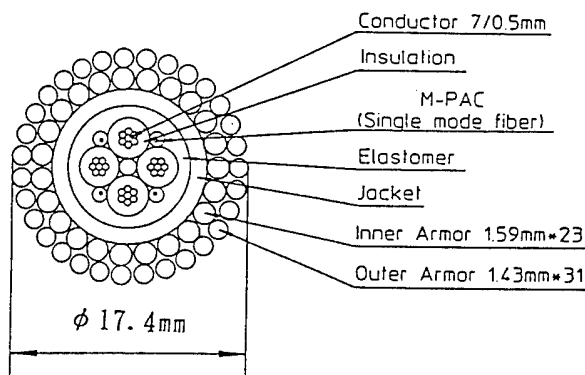


Fig.3 Electro-fiber Optic cable

As well as use of M-PAC, this cable features:

- (1)An elastomer between electro-optical composite and sheath for remarkable improvement of bending strength.
- (2)Armor design that maximizes a ratio of strength to cable weight to minimize the load which is applied to the fiber under outer diameter restrictions.
- (3)2% proof passing fiber with sufficiently stable fatigue and screening characteristics, and without any fiber connection across it.
- (4)Minimization of cable rotation and torque production by loaded armor wires.

Table 2 Difference of E-O and coaxial

	E-O	coaxial
Breaking strength	147kN	163.7kN
Weight in water	0.75kg/m	0.87kg/m
Armor ratio *	1.3	1.9
B.S/W ratio **	22.3	21.6
Bending resistance	> × 10 ***	

*Armor Ratio(A.R) :

$$A.R = \frac{n \cdot d_o \cdot D_o \sin \theta_o}{n \cdot d_i \cdot D_i \sin \theta_i}$$

d:armor wire diameter

n:number of wires per layer

D:pitch diameter of armor layer

θ :lay angle of armor wire

subscripts:0=outer armor, 1=inner armor

**

B.S/W: Breaking strength/Weight in water Ratio

** Compared with no elastomer

2.4 Accelerated test result in factory

Table 3 shows test result.

Table 3 Test result

	condition	result
Tensile test	*42% load of B.S (note1) *span:120m	Fig.5,6,7,8
Flex test (Fig.4)	*tensile=64.7kN *three sheaves (dia 750mm)	*At 2500 times tube and armor wire break(note2)
Dynamic tensile test	*58.8 ± 9.8kN *1cycle =6 sec *8hours	*saturated elongation cable=0.95% fiber=0.65%

note1:42%=64.7kN (cable weight of 6000m+ vehicle+ wave fluctuation)

note2:breaking surface shows fatigue.

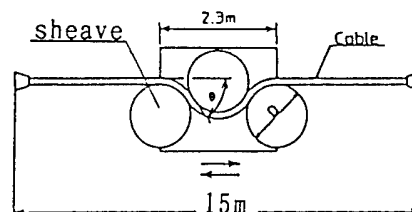


Fig.4 Schematic flex test

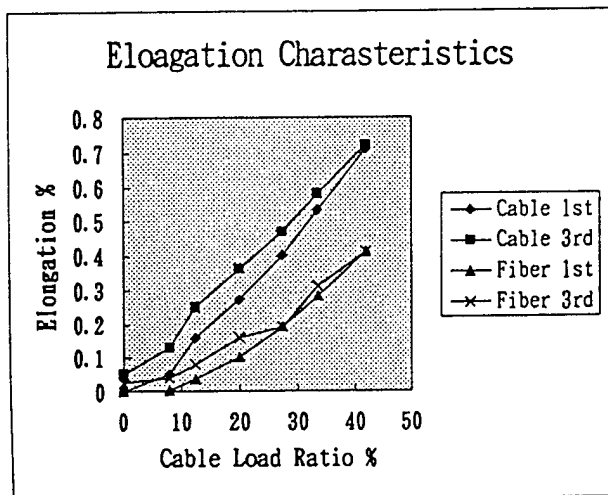


Fig.5 Cable and fiber elongation

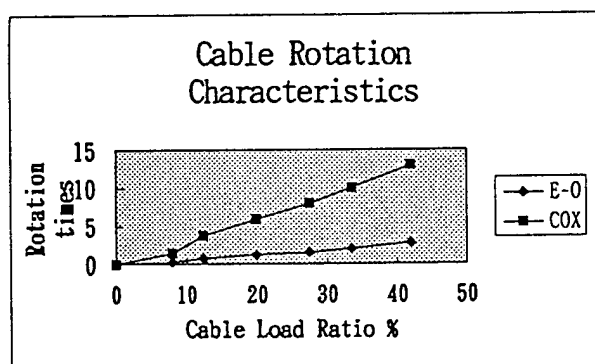


Fig.6 Cable rotation

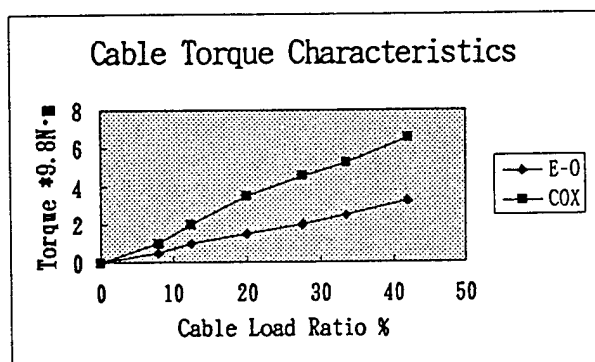


Fig.7 Cable torque

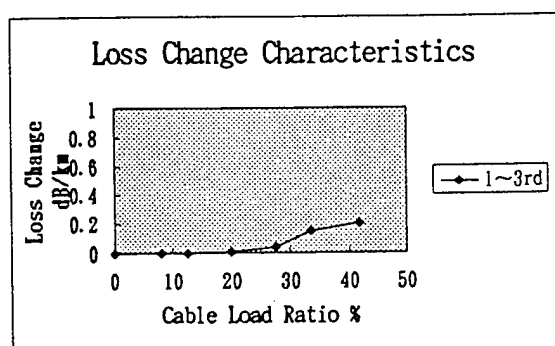


Fig.8 Fiber loss changes

2.5 Fiber reliability (Ref.2)

We calculated the 8 km fiber breaking probability(F) over five years using the factory evolution result and the fiber parameter in 2% proof test, and compared to the result of factory acceleration test. Consequently, we found that use of the fiber within an expected load provided sufficient reliability. (Fig.9)

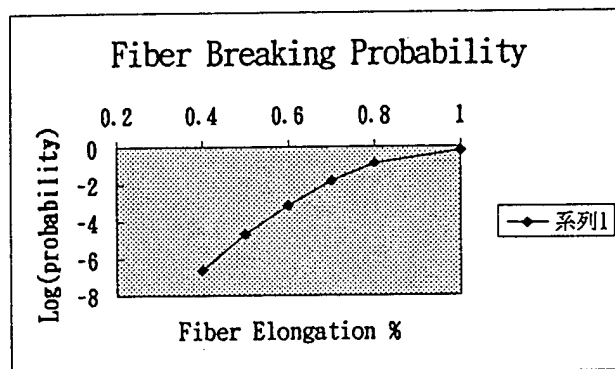


Fig.9 Fiber breaking probability

3. FIELD TEST

3.1 1st step

We winched up a test cable using a traction winch system on the ship, applied a load of 49kN to the cable and passed it through the sheave (O.D 900mm) to and fro.

As a result, we found undulation on the armor wire when we passed the cable through the sheave 7500 times. This was the same as conventional cables. However, we did not find any increasing loss of the fiber.

3.2 2nd step

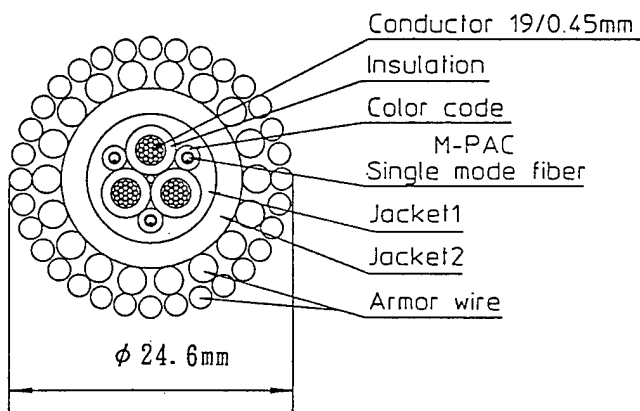
Then we winched up the cable of 8000m long with a special electro-optical connector for an observation equipment, and started testing. During the initial operation, kinks and meandering of cable occurred several times, which resulted residual torque in the cable.

As the cable smoothed out, no kink occurred. Consequently, the cable has continued to provide scientist with clear and wonderful video and data from the sea bed of up to 6607m deep through it. (Ref.3)

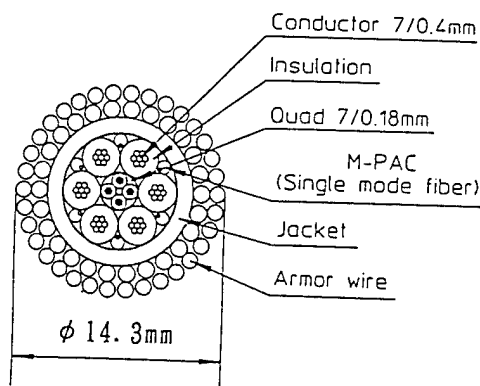
4. CONCLUSION

We have developed a steel armored Electro-fiber Optic cable with metal tube armored fibers and was applied to the water depth of 6000m region. This allows ocean scientist to observe 96% of sea bed in the world ocean using existing winch system.

A similar cables of this kind is shown in Fig10 have been working as well as previous cable, thus providing wonderful results(Ref.4). We have already started manufacturing the stronger cables using carbon coated fiber or high refractive index differential fiber. We expected that the deep sea will be more familiar to ocean scientist in the near future.



TYPE A



TYPE B

Fig 10 Another cable type

Table 4 Another cable list

type	A	B
Cable Dia	24.6mm	14.3mm
Number of M-PAC	3	6
Armor Ratio	1.2	1.25
Weight in water	1.6kg/m	0.5kg/m
Operation depth	6000m	6000m
Cable length	12000m	6100m
B.S	343kN	98kN
Winch system	double	single

5. REFERENCE

- 1)A.Sano etal"Development of the Optical Cable unit in Composite Tether Cable for Deep Sea Unmanned Vehicle System" IWCS 1995,205-210
- 2)Y.MIJAJIMA etal "Study on High-tensile Proof of Optical Fiber" Journal of Light Tech 1983 vol Lt-1 No2 340-346
- 3)MOMMA Hiroyasu,K.Mitsuzawa,T.Hotta,T.Morita and S.Imamura "Laboratory Test and Field Evaluation of Double Armored Electro-optical Cable for the JAMSTEC/Deep Tow" Proc.IEEE/MTS OCEANS'95,vol I,103-108
- 4)H.ISHISAKI etal "Deep Sea Multimonitoring System by Optical Towing Cable"JOURNAL OF The Japan Society for Marine Survey and Technology Sept 1991, 53-59

6. AUTHOR



HIROSHI ISHISAKI

Submarine System DIV
Ocean Cable Co.,Ltd
1-105-2 Hibikimachi
Wakamatuku
Kitakyushu 808,JAPAN

HIROSHI ISHISAKI was born in 1952.He joined Ocean Cable Co.,Ltd after his graduation from Sophia University with B.E in 1976,and and has been engaged in researc and development of fiber,oceanographic cable. He is an engineer of the Submarine System Division,member of the IEICE of JAPAN and JAPAN Society of Applied Physics.



SATOSHI IMAMURA

Ocean Engineering DEP
Ocean Cable Co.,Ltd
1-2-1 Shibaura
Minatoku Tokyo
105,JAPAN

SATOSHI IMAMURA was born in 1957. He joined Ocean Cable Co.,Ltd after his graduation from Ustunomiya University with a B.E in 1979, and has been engaged in engineering department of wire and cable. He is an engineer of Ocean Engineering Department.



HIROYASU MOMMA

Deep Sea Research
Department
Japan Marine Science
and Technology
Center(JAMSTEC)
2-15 Natsushimamachi
Yokosukashi Kanagawa
237,JAPAN

HIROYASU MOMMA was born in 1946 . He joined JAMSTEC in 1972 after he received MSc in Electrical Engineering at Keio University. He is Research Supervisor in Deep Sea Research Department and he is in charge of developing the deep tow system. He is Chief Scientist of the deep tow cruises in JAMSTEC.

144 FIBER ALL DIELECTRIC AERIAL CABLE FOR RAILWAY APPLICATIONS

Ralph Böhme, Georg Hög, Michael Hoffart, Klaus Nothofer, Stefan Richter

KABEL RHEYDT AG, Mönchengladbach, Germany

ABSTRACT

When an optical fiber cable is to be installed along a railway line there is sometimes no possibility to use duct or or buried cables. In these cases the all dielectric self-supporting aerial cable offers a good alternative, because it can be easily installed on existing poles. In case of a tree falling onto the cable, the cable must withstand this event without to be damaged and without any interruption of optical transmission. Because of this a special designed cable with high elasticity is required. Based on experiences with installed cables with up to 24 fibers, a 144 fiber cable was designed for high cable elongation. In combination with a special installation method using suspension rollers full cable operation is ensured for all environmental conditions which occur along a railway line.

BACKGROUND

With the decrease of telecommunication monopolies in many countries the traditional route owners like railway companies and power suppliers aim to participate in this growing market. Especially the long and wide spread railway network can be easily supplemented with optical telecommunication cables. The self-supporting aerial cable is the most important design, if the laying of standard cables in concrete gutters, which run parallel with the track, is not possible or excavations should be avoided. The aerial cables will be installed on the existing poles for the slide wire. For a high reliability the cable must withstand all environmental conditions like temperature, wind and ice load. Due to the fact, that often the tracks are lined with trees, the cable must be in addition protected against tree falling. The cable operation has to be guaranteed even when a tree falls toward the cable and pushes it to the ground. This requires a special cable design and installation technique, which has been approved up to now with cables containing up to 24 fibers.^{1,2,3}

Only between deadend poles helical preformed fittings are used. On all suspension poles the cables is supported by rollers which gives the cable the opportunity of axial movement when required. Because of the axial moveability the sag is pulled out when a tree falls onto the cable. The length that results from pulling out the sag may not be sufficient to provide the extra length which is needed to push the cable to the ground.⁴ Just the high extensibility of the cable ensures that, after removing the tree, the cable rolls back to its original position without having been affected in transmission characteristics. Figure 1 shows schematically a section before and after a tree fell on the cable and, after the tree was removed.

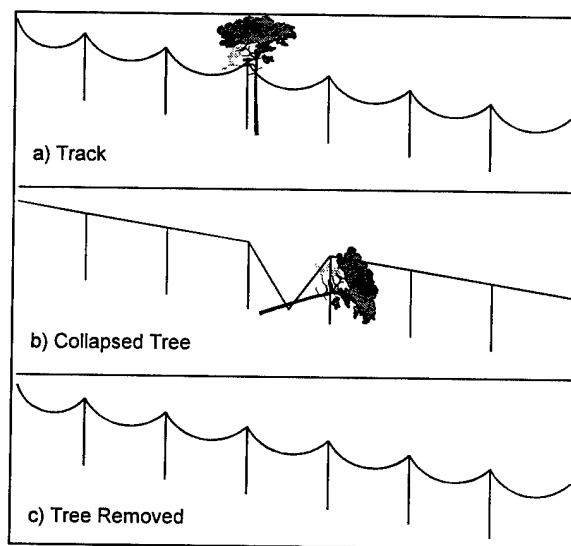


Fig. 1 Collapsing Tree

CABLE DESIGN

Also for higher fiber counts than 24 it was necessary to keep the weight and the dimensions of the cable within tight limits as well as the extremely high elasticity. The cable design must provide a 144 fiber count, not more

than 22mm in diameter and low weight, in order to minimize the additional stress on the poles. Standard suspension rollers which had been in use with the 24 fiber cable should also be used. The special difficulty would be to implement six times the fiber count with sufficient strain margin in a cable with less than the double of the cross section of the 24 fiber cable. To achieve the high elasticity, a thermoplastic central element is chosen instead of the usual FRP rod. A layer of 12 loose tubes, each of which containing 12 colored fibers, is stranded around the central element. In order to achieve the required strain margin without a too small fiber bending radius it was necessary to give the fibers an excess length in the tube of at least 0.1%.

The cable is designed for a maximum operation load of 7.5kN and a corresponding elongation of 1% without any increase of the fiber attenuation. At a tensile force of 10kN the elongation must be greater than 1.2% with a maximum attenuation increase of 0.1dB/km. The cable breaking load must be more than 20kN, which leads to a calculated cable elongation at break of more than 2%. This means that the normally used high modulus aramide yarns could not be used with this cable because the breaking elongation of the high modulus yarns is only 2%, which could cause the cable to break at lower forces than the required 20kN. Therefore low modulus aramide yarns have been used which offer a breaking elongation of more than 3%. For the same reason a thermoplastic central element is used instead of the usual FRP-rod. Although the FRP would not break at the required maximum cable elongation, it was considered that with the suspension roller diameter of only 80mm the additional edge elongation would cause the FRP to break.

The cable is protected by a 2 layer polyethylene sheath with the aramide yarns embedded between inner and outer sheath. To prevent the cable from twisting during installation the aramide yarns are stranded in two layers with opposite pitch. Figure 2 shows the cross-section of the cable.

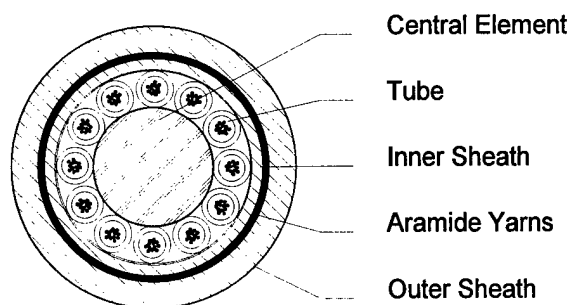


Fig. 2 Cross-Section

With an outer diameter of 21.4 mm the cable has only a weight of 330 kg/km. In consideration of the maximum allowable load to the poles, which are used by the *Deutsche Bahn AG* (German Railway Company), a span-length of 80 m is permissible.⁵

Some characteristics of the cable are summarized in figure 3.

Number of fibers	144 E9/125
Tube diameter	2.8 mm
Wall thickness inner sheath	0.8 mm
Wall thickness outer sheath	2.0 mm
Outer diameter	21.4 mm
Weight	approx. 330 kg/km
Elastic modulus (related to cross section)	3.2 kN/mm ²
Expansion coefficient	16.7 10 ⁻⁶ /K
Max. permissible load	7,5 kN
Breaking load	25 kN
Temperature range	
Transportation/storage	-25°C to +60°C
Installation	-15°C to +50°C
Operation	-40°C to +60°C

Fig. 3 Cable Characteristics

CABLE MANUFACTURING

The buffer tubes each of which containing twelve single mode fibers with an excess length of more than 1 %, are made of polybutyleneterephthalate (PBT) and have an inner and outer diameter of 2.0 and 2.8mm, respectively. One red and twelve yellow tubes are stranded in SZ-technique around the thermoplastic central element. Special attention had to be paid to the stranding. In missing of any rigid strength element the braking forces had to be adjusted very carefully not to have the pitch length longer than the desired value. Even during the sheathing process, the pay-off and take-up forces have to be kept within tight limits, since the thermoplastic central element can bear no compress and tractive forces, but is more or less subject to shrinkage by itself. Every remaining elongation means a reduction of the strain margin. On the other hand, a too low take up force can cause temporary cable contraction which may lead to attenuation increase on the reel.

A sample of the cable is shown in figure 4.

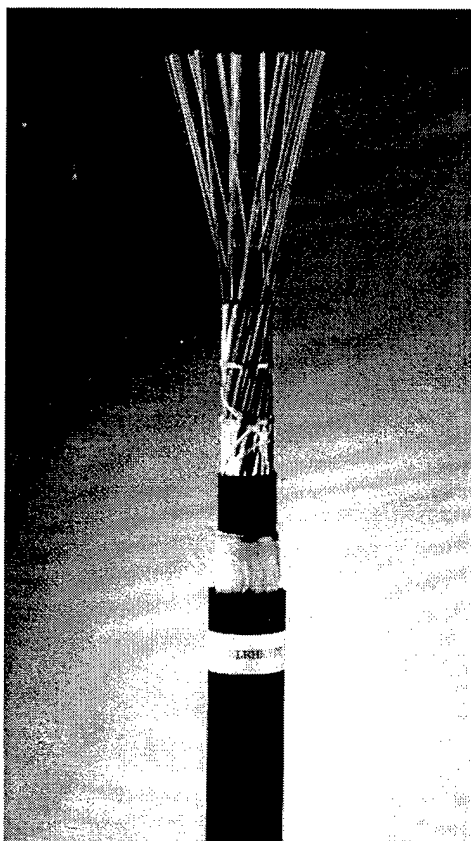


Fig. 4 Stepped Sample

TEST RESULTS

Each production step was followed by measuring the optical attenuation to detect, if the fibers were inadmissible stressed (Figure 5). There was no significant change in the optical attenuation.

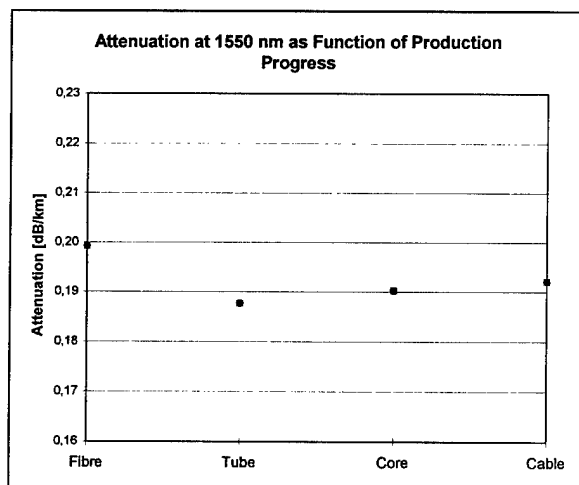


Fig. 5 Attenuation During Manufacturing Process

All designed parameters and required properties were fully met by the completely manufactured cable. The cable was examined in an extensive test program. Especially the elongation characteristics in the tensile test, the behavior at high and low temperatures, the impact strength and the reversed bending strength were of high importance.

Tensile Strength Test

A 130 m cable sample was turned 180° around a deflector roll and stressed up to 15 kN in two cycles. The rotation should simulate the cable installation. The cable ends were fixed with the original helical preformed dead ends which are used later on in the field. The test set up is schematically shown in figure 6.

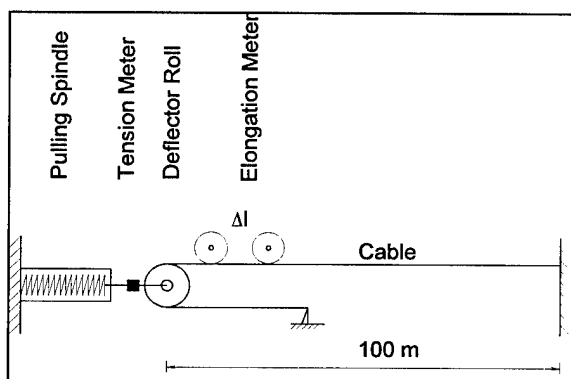


Fig. 6 Tensile Strength Test

The cable elongation (Figure 7), the change in optical attenuation and the fiber elongation (Figure 8) were determined in dependence of the tensile load.

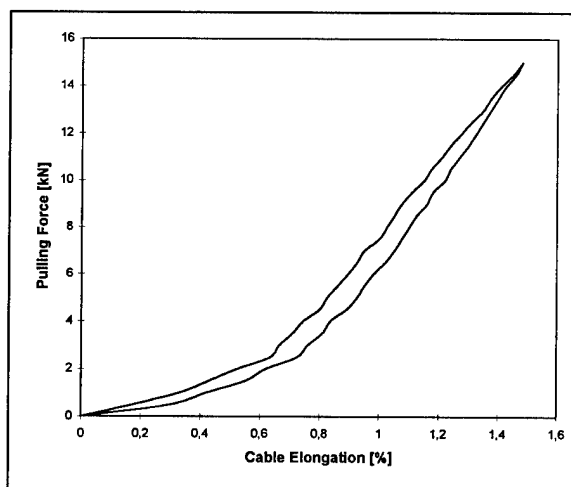


Fig. 7 Stress-Strain Curve

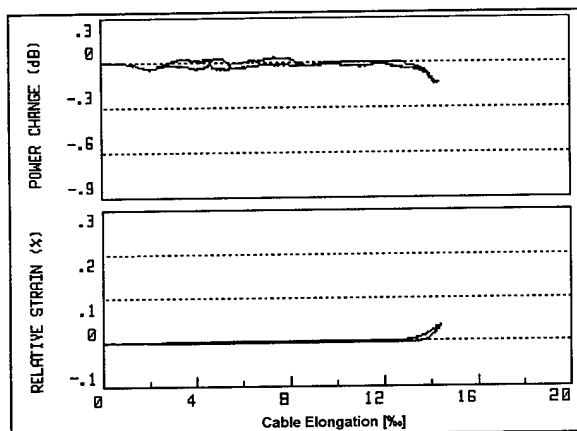


Fig. 8 Attenuation and Fiber Elongation in Dependence of Cable Elongation

It can be seen from the results that the theoretically values for the strain margin are fully met. The fiber elongation starts not until 1,2 % of the cable elongation which shows expressive the excellent manufacturing process. At 12 kN the fiber excess length is exhausted and the optical attenuation increases instantly due to the large stranding angle of the tubes. The breaking load was measured to be 25kN.

Temperature Test

To find out how temperature variations during operation influence the transmission characteristics, the cable was exposed to two temperature cycles with the temperature within the limits of -40°C and $+70^{\circ}\text{C}$ in a climatic chamber. In contrast to underground cables aerial cables are subjected to permanent tensile stress. In order to reproduce the operating conditions as realistic as possible, a part of the cable was wound onto a special designed rack on which the cable was submitted to a defined tensile stress during the temperature test. Figure 9 shows the measuring arrangement.

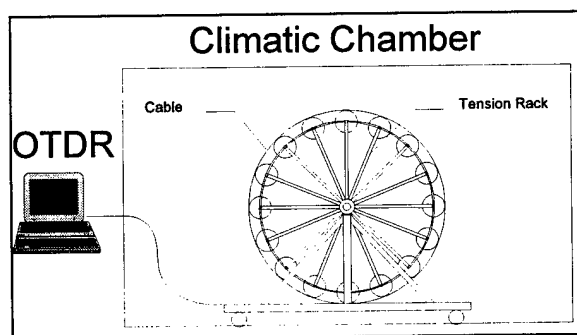


Fig. 9 Temperature Cycle Test

A total cable length of 70 m was wound up in nine parallel layers with a tensile force of 1500N. 2 or 3 fibers of each tube were spliced to 2000m measuring length. At $+20^{\circ}\text{C}$, -25°C , -40°C and $+70^{\circ}\text{C}$ the attenuation was determined with an OTDR.

The results of the temperature cycling test are summarized in figure 10. It can be seen that after finishing the first cycle the attenuation was slightly lower than the initial value. This effect is probably caused by some relaxation of the fibers in the tube, although it can not be excluded that these variations are due to the 29 splices outside of the climatic chamber.

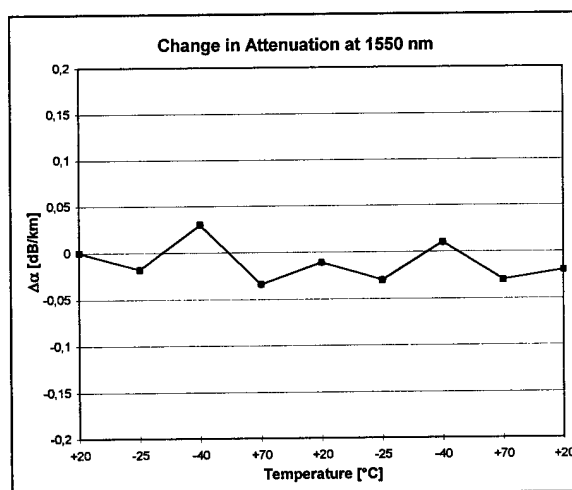


Fig. 10 Change in Attenuation in Dependence of Temperature

Reversed Bending Strength

The cable was bent 50,000 times around a radius of 350 mm with a bending angle of 90° acc. to EN 187000 Method 507. There were no residual changes in optical attenuation. Neither the sheath nor the core were damaged.

Impact Resistance

The impact resistance was checked both at room temperature and at -40°C . The specimen was hit five times with an impact energy of 1 Nm. Neither the sheath nor the fibers were damaged.

CABLE INSTALLATION

The high elasticity of the cable can only be exploit, if the cable is allowed to move axial between the dead ends. This mobility is effected by supporting the cable with rollers, which are easy to attach at the existing poles of the slide wire.⁶

The cable ends are fixed with standard helical preformed dead-ends which are well known also for ADSS on H.V. lines. This installation technique is service-proved with the 24 fiber aerial cables.⁷

Figure 11 shows a roller supported aerial cable along a railway track.

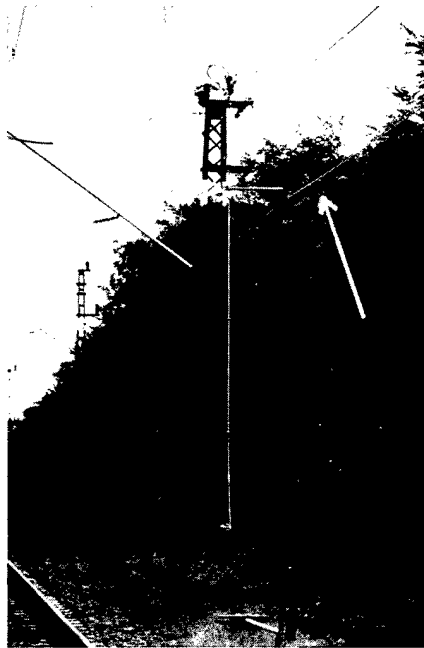


Fig. 11 Railway Track with Roller Supported Aerial Cable

The 144 fiber all dielectric aerial cable can be installed with same technique that was developed for the 24 fiber cable. The standard supporting rollers can be used as the cable diameter matches them.

SUMMARY

An all dielectric and self supporting aerial cable with 144 fibers for installation along the railway tracks was designed and tested. Combined with the special installation technique which uses supporting rollers, the cable offers an extremely high elasticity which allows a collapsing tree to push it to the ground without affecting the transmission characteristics. With its low weight and small diameter the cable has compared to the 24 fiber cables a six times higher transmission capacity. Because of the low weight and the small diameter the additional stress to the existing poles is low and the standard rollers can be used. This 144 fiber aerial cable represents an excellent alternative to underground cables, if the laying in concrete gutters is impossible or excavations should be avoided.

REFERENCES

- ¹ Dr. S. Rauer, Dr. N. Lenge, "LWL-Luftkabel im Rifu-Netz der Deutschen Reichsbahn", Signal + Draht, 85 (1993) 11
- ² A. Bidinger, W. Lynen, R. Ney, "Lichtwellenleiter (LWL)-Luftkabel, Streckenfernmeldekanal an der Bundesbahnstrecke Reutlingen-Tübingen", Signal + Draht, 84 (1992) 3
- ³ B. Diehl, G. Hög, Dr. W. Stremme, "Lichtwellenleiter-Luftkabel mit nichtmetallenen Zugentlastungselementen für den Einsatz entlang von Bahnstrecken", Signal + Draht, 84 (1992) 7/8
- ⁴ R. Ney, "Berechnungen zum Durchhangsverhalten von Luftkabeln", Signal + Draht, 87 (1995) 6
- ⁵ Pflichtenheft für LWL-Luftkabel der DBKom, April 1996
- ⁶ F. Krahn, N. Lenge, G. Weckerle, "Self-Supporting Optical Fibre Aerial Cable With Large Allowable Elongation", Proc. 40th IWCS (1991) 556
- ⁷ A. Bidinger, W. Lynen, R. Ney, "Design And Operation Of An Aerial Fiber-Optic Cable For Railroad Communications", Proc. 40th IWCS (1991) 218

AUTHORS

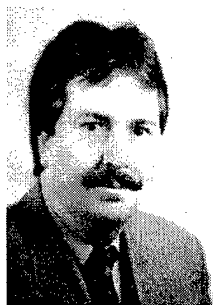
Ralph Böhme



Ralph Böhme (42) received his Dipl.-Ing. degree from the Bergische Universität Wuppertal in 1986. He joined KABELRHEYDT in the same year. As a member of the development department for optical fiber cables he is responsible for the development and engineering of all dielectric aerial

cables (ADSS) cables.

Klaus Nothofer



Klaus Nothofer was born in 1956. He obtained his Dipl.-Ing. degree from the Fachhochschule Düsseldorf and joined AEG KABEL (now KABELRHEYDT) in 1981 as development engineer for optical fiber cables. From 1984 he was responsible for the optical fiber cable manufacturing technology.

In 1993 he became leader of the Optical Fiber Cable Design Group. He was appointed Manager of Optical Fiber Cable Development and Design in 1994.

Georg Hög



Georg Hög was born in 1950. After studying electronics at the Technische Hochschule Aachen he joined KABELRHEYDT as a development engineer for copper cables in 1977. In 1980 he became responsible for the development of symmetrical telecommunication cables. In 1985 he

became the head of the development department for optical fiber cables. From 1987 to 1988 he was the head of the technical department of BETEFA (special cables for telecommunications). Since 1995 he is responsible for the technical sales department of telecommunication cables.

Stefan Richter



Stefan Richter (31) studied material science at the Technische Universität Berlin. He received the degree Dipl.-Ing. in 1994 with a paper about silane crosslinkable polyethylene as low voltage cable insulating material, which was made in cooperation

with the KAISER KABEL GmbH (Berlin). In the same year he joined the BETEFA (special cables for telecommunication) as a production engineer. In 1995 he joined KABELRHEYDT as development engineer for optical fiber cables.

Michael Hoffart



Michael Hoffart (39) is General Manager of the Telecommunication Cable Product Group. He received his Dipl.-Ing. degree from the Bergische University, Wuppertal in 1983. He joined KABELRHEYDT on graduation and has been engaged in the fields of optical meas-

urement techniques and telecommunication cables. From 1990 to 1995 he was General Manager of the Optical Fibre and Optical Cable Plant.

Mailing Address:

KABEL RHEYDT AG
Bonnenbroicher Straße 2-14
41048 Mönchengladbach
Germany

DEVELOPMENT OF DOWNSIZED SLOTTED ROD OPTICAL FIBER CABLES

Fumiki Hosoi, Masami Hara and Eiji Konda

The Furukawa Electric Co.,Ltd. Ichihara, Chiba, Japan

ABSTRACT

We developed downsized slotted rod optical fiber cables. To realize much degree of downsizing, we have reduced the slot height and slot rib width and optimized slot number in a slotted rod. On our design we manufactured downsized cable, and evaluated temperature and mechanical performance of these cables.

INTRODUCTION

Recently optical fiber cable networks are rapidly expanding. In order to construct these network systems successfully, it is important to reduce the total cost of these systems. Therefore it is required to reduce the cost of optical fiber cables.

In conventional optical fiber cables less than 300-count, there are two categories. One is the category of 8~100-count, and the other is the category of 160~300-count. The same slotted rod was used at each category with adjustment of number of fiber ribbons because it was more economical when the cable demand was not large.

Today the cable demand is more and more increasing, we estimated the cable cost could be more economical by designing more downsized slotted rod at every fiber count.

In this paper we describe the concept of the cable downsizing and the characteristics of the downsized cables.

DESIGN CONCEPT FOR DOWNSIZING

The diameter of the slotted rod is determined by various parameters as shown in Fig.1.

For downsizing slotted rod, we took into considerations the three parameters. These were slot height "h", slot number "N", and width of slot rib "b".

Our concept of downsizing is the following.

a) Reduction of "h"

This was carried out by using the thin coated fiber ribbon.

b) Optimization of "N"

Optimum slot number N was calculated at every fiber counts.

c) Reduction of "b"

The slot rib width "b" is reduced by selection of a high modulus material for slotted rod.

These three parameters are explained at the following section in more detail.

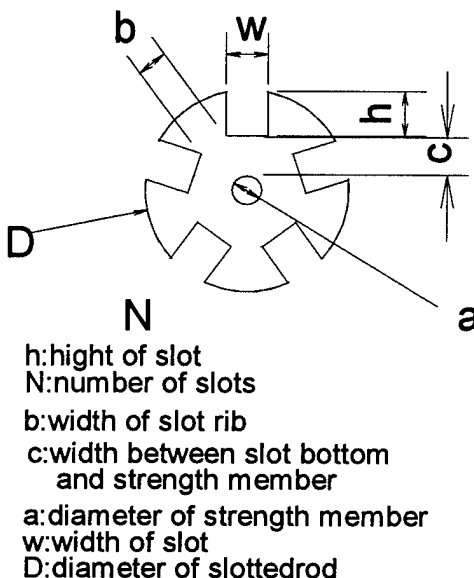


Fig.1 Parameters of slotted rod

THIN COATED 4-FIBER RIBBON

The conventional ribbon had a thickness of 0.4mm. We manufactured ribbons of different thickness and studied their performance.

From the point of view of splicing, we found that ribbon thickness was needed to be more than 0.3mm. The ribbon coating could not be removed clearly by the conventional fiber coating stripper when the thickness was less than 0.3mm.

The 0.3mm ribbon was evaluated to optical and mechanical characteristics as shown in table 1.

This table shows that characteristic of the thin coated ribbon is not different from the conventional one. Then we adopted 0.3mm 4-fiber ribbon. By using the 0.3mm ribbon, the height of slot "h" was reduced by about 25%.

Table.1 Characteristic of 4-fiber ribbons

	Conventional 4-fiber ribbon	Thin coated 4-fiber ribbon
Ribbon thickness(mm)	0.4	0.3
Transmission Loss (dB/km)	Max.0.21 Ave.0.20	Max.0.22 Ave.0.20
Temperature cycling(dB/km) -40~70°C	≤ 0.03	≤ 0.03
Flat plate com- pression(dB) 1000N/100mm	≤ 0.03	≤ 0.03

CONSIDERATION OF SLOT NUMBER "N"

The relation between slot number and slotted rod diameter was calculated for the different slot number and the different fiber counts. Fig.2 shows the results of calculation less than 100 fiber count. From these results, it was found that the diameter of slotted rod took the minimum value when the slot number was five. Therefore we adopted five as the slot number less than 100-fiber count.

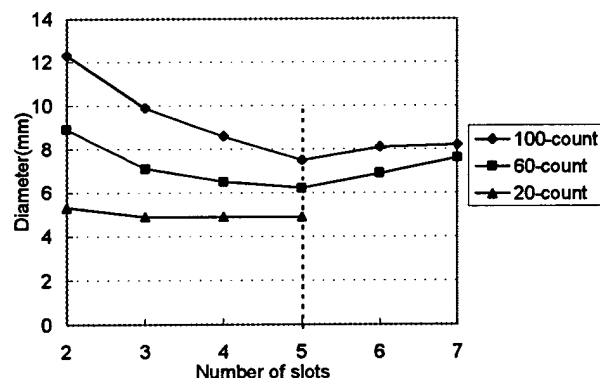


Fig.2 Relation between slot number and slotted rod diameter

In the 160 ~ 300 count cable, large slot height is needed when the slotted rod is minimized. Large slot height results in bad productivity of slotted rod and it connected with higher cable cost.

Therefore in the 160 ~ 300 count cable we adopted the same slot height as the downsized 100-fiber cable, which was out of the question at productivity of the slotted rod. On this slot height we calculated slot number.

REDUCTION OF THE SLOT RIB WIDTH "b"

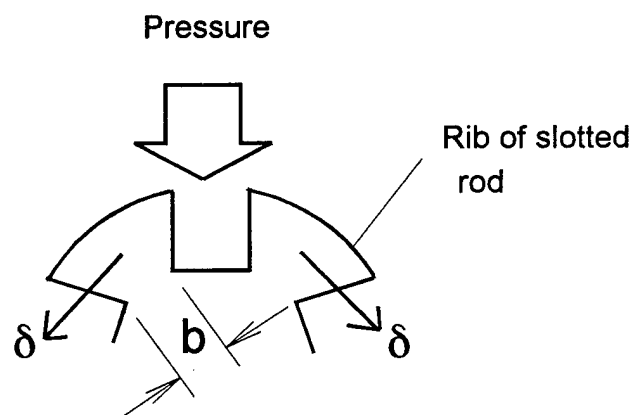
The slot rib width "b" is closely related with the strength of the slotted rod. Behavior of slotted rod under lateral pressure is shown in Fig3. When the slotted rod is under lateral pressure, the rib of slotted rod is bent as shown in Fig3. In order to downsize the slotted rod, the value "b" is must be reduced but the δ , which is the displacement of slot rib as shown in Fig3, become large and it results in deterioration of the cable performance.

The value of δ is depend on not only the slot rib width but also Young's modulus of slotted rod material. Therefore in order to reduce the value of b without deterioration of cable performance, Young's modulus of the slotted rod material must be considered.

To obtain the same strength of slotted rod as the conventional one, we assumed that δ_0 , which was the displacement of downsized slotted rod, was equal to δ_1 , which was the displacement of the conventional slotted rod. Then we calculated the relation between slot rib width of downsized slotted rod "b₁" and Young's modulus of downsized slotted rod "E₁" as shown in Fig.4. Where both "b₁" and "E₁" was normalized "b₀" and "E₀", which were the value of the conventional slotted rod.

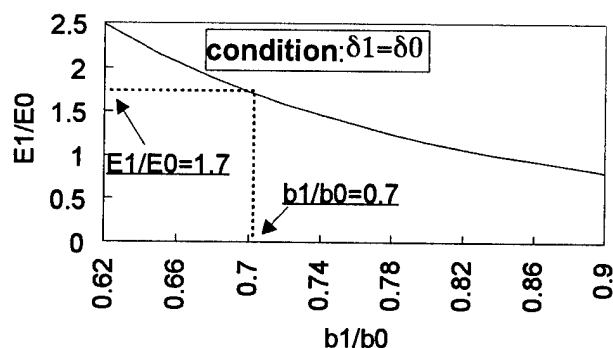
The value b₁/b₀ has a limit, that is 0.7, which is determined by manufacturing technique of slotted rod. E₁/E₀ was 1.7 when the b₁/b₀ took the minimum value 0.7.

According to this result, we selected the most adequate material for the slotted rod.



δ : Displacement of slot rib

Fig.3 Behavior of slotted rod under lateral pressure



$\delta 1$: displacement of rib of downsized slotted rod
 $\delta 0$: displacement of rib of conventional slotted rod
 $E1$: Young's modulus of downsized slotted rod
 $E0$: Young's modulus of conventional slotted rod
 $b1$: width of rib of downsized slotted rod
 $b0$: width of rib of conventional slotted rod

Fig.4 Relation between slot rib width and Young's modulus of slotted rod

STRUCTURE OF DOWNSIZED CABLES

From the above discussion, we have designed and manufactured the downsized cables. Structure of conventional cables and the downsized 20~300 fiber cables are shown in Fig.5 and Fig.6. And comparison of cable diameter between downsized cables and conventional ones are shown in Fig.7.

From these figures it is clear that cable diameter was greatly reduced. Especially in 20-fiber one, diameter is about one half that of conventional one.

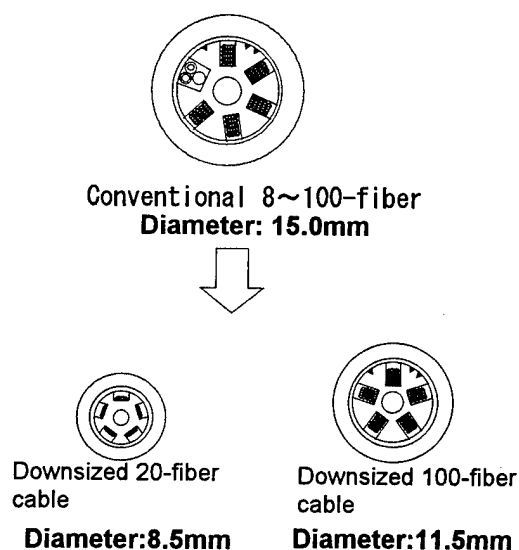


Fig.5 Structure of cables less than 100-fiber count

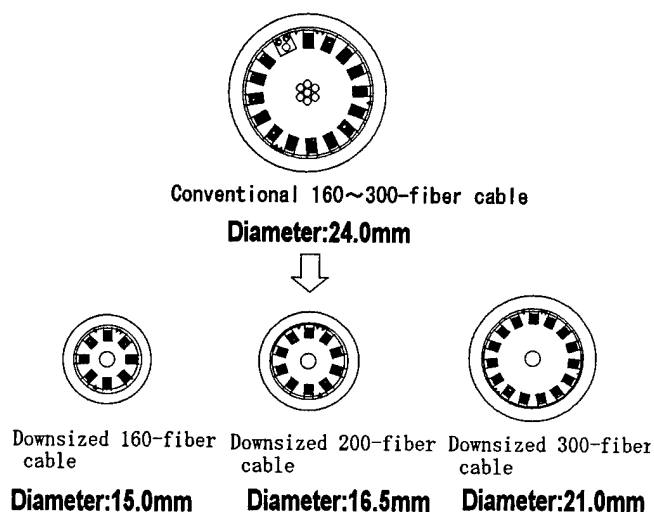


Fig.6 Structure of 160 ~300 fiber cables

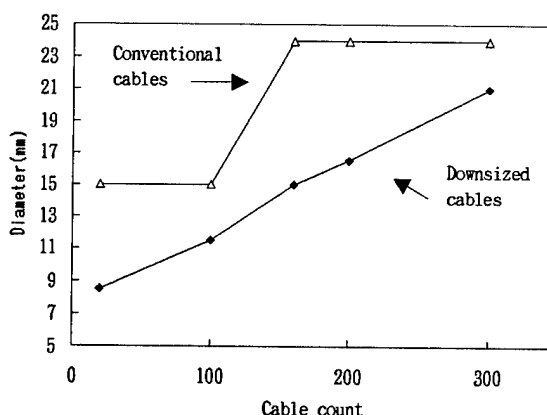


Fig.7 Comparison of cable diameter

CHARACTERISTIC OF CABLES

Transmission loss and attenuation of temperature cycling and mechanical performance were evaluated for downsized cables.

Table.2 shows transmission loss of trial cables at $1.55 \mu\text{m}$. Loss of the trial cables was 0.19 dB/km on the average, 0.18 dB/km at the minimum, and 0.20 dB/km at the maximum. Good result was obtained.

Temperature cycling of the cables at $1.55 \mu\text{m}$ was carried out between -30°C and $+70^\circ\text{C}$. Bend, resistance to lateral pressure, squeeze, torsion, tensile loading, and impact test were carried out to evaluate the mechanical characteristics. Table.3 presents the conditions and the results of these tests. As shown in Table.3, loss increase through these tests is no problem in actual use.

Table.2 Transmission loss ($\lambda = 1.55 \mu m$)

	Downsized 20 and 100-fiber cables	Downsized 160 ~300 fiber cables
Average	0.19 dB/km	0.19 dB/km
Maximum	0.20 dB/km	0.20 dB/km
Minimum	0.18 dB/km	0.18 dB/km

Table.3 Temperature and mechanical characteristic of downsized cables ($\lambda = 1.55 \mu m$)

Item	Condition	Loss change
Temperature cycling	-30°C to +70°C	< 0.03 dB/km
Bend	r=300mm $\pm 180^\circ$ Bending	< 0.01 dB
Lateral pressure	2000N/100mm	< 0.01 dB
Torsion	$\pm 180^\circ$ /2m	< 0.01 dB
Squeeze	Cable 125m Tension 0.2% extending	< 0.02 dB
Impact	Cylinder 1kg 20mm ϕ dropped on cable from 1m height	< 0.03 dB
Tensile	0.3% extending	< 0.02 dB

CONCLUSION

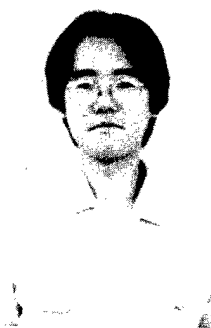
We designed and manufactured the downsized 20 ~300-fiber cables. In order to downsize the cables, we considered reduction of slot height "h" and optimized slot number "N" and selected slotted rod material for reduction of slot rib width "b".

As a result much degree of downsizing was accomplished, such as the diameter in the case of the 20-fiber cable became about one half that of a conventional one.

Mechanical and temperature performances of manufactured downsized cables were evaluated and good results were obtained.

REFERENCE

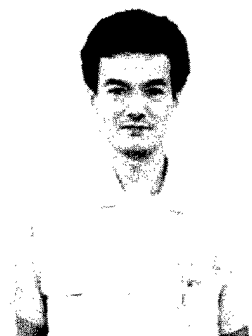
- [1] M.Hara, et al., "development of 1000-fiber Single Slotted Core Cable", 44 th IWCS, 1995



Fumiki HOSOI

The Furukawa Electric Co.,Ltd
6,Yawata Kaigandori,Ichihara, Chiba,290, Japan

Mr. Hosoi received his M.E. degree in Physics engineering from Tokyo University in 1995. He joined The Furukawa Electric Co., Ltd and has been engaged in research and development of optical fiber cable. He is now a research engineer of optical fiber transmission research department, opto-technology laboratory.



Eiji KONDA

The Furukawa Electric Co.,Ltd
6,Yawata Kaigandori, Ichihara, Chiba, 290, Japan

Mr. KONDA joined The Furukawa Electric Co., Ltd. in 1977 and has been engaged in research and development of optical fiber cable. He is now a research engineer of material development and engineering section , research department, opto-technology laboratory.



Masami HARA

The Furukawa Electric Co.,Ltd
6,Yawata Kaigandori, Ichihara, Chiba, 290, Japan

Mr. Hara received his M.E. degree in Physics from Osaka University in 1987. He joined The Furukawa Electric Co., Ltd and has been engaged in research and development of optical fiber cable. He is now a research engineer of optical fiber transmission research department, opto-technology laboratory.

THE NEW DESIGNS FOR CATV FIBER MONITORING SYSTEMS COMBINED WITH AUTOMATIC FIBER TRANSFER AND BRANCHING FIBER SURVEILLANCE FUNCTIONS

Kuo-Hsiang Lai, Chien-Chung Lee, Kuang-Yi Chen, Ching-Shen Wang, Ching-Phon Chen

Telecommunication Laboratories, Chunghwa Telecom Co., Ltd., Taiwan, Republic of China

ABSTRACT

By the new designs, we have successfully combined automatic fiber transfer and branching fiber surveillance functions for CATV Fiber Monitoring Systems in our lab.. This new feature of CATV Fiber Monitoring Systems can satisfy the strong demands of CATV fiber rental customers for distributive transmission and high survivability. The experimental system in our lab. can provide automatic fiber transfer for only 1.5 seconds transfer time. Branching fiber surveillance function is able to monitor up to 32 distributive nodes. The experimental system in our lab. can enhance CATV Fiber Monitoring Systems for high survivability and branching fiber monitoring ability.

INTRODUCTION

Fiber has been wide-spread applied on cable television(CATV) networks recently. The low loss and high capacity characteristics make it play a very important role for trunk transmission. The surveillance problems we suffering on CATV fiber networks convince us that a proper fiber monitoring system is very needed. However, in recent years, Fiber Monitoring Systems (FMS) have been questioned about their advantages in comparison with high cost. Nowadays, FMS can provide fiber fault alarms, automatic detection of fault locations, precautions of long-term fiber degradation and fiber information management. From the view-point of supporting systems, it is not enough for only fiber monitoring. Therefore, we propose FMS combined with fiber transfer function to enhance system survivability. In Optical CATV rental systems, fiber survivability and short down-time are strongly demanded by customers. So, it is suitable for CATV

FMS combined with fiber transfer function. In optical CATV systems, branching distributive architecture has been used a lot. So CATV FMS has to be able to monitor branching fibers.

In this paper, we propose the new design for fiber transfer ability and branching fiber monitoring function. We describe the system architecture and design considerations in system consideration section. We also present our experimental results and system performances in experimental result section.

SYSTEM CONSIDERATIONS

System Design

Optical CATV networks, as shown in Fig.1, can be divided into trunks and passive distributive feeders. Fiber trunk carries AM video signals from the headend to the distributive node over a long distance. By optical splitters or direction couplers, passive distributive feeders send AM video signals to each sub-headend optical node. We propose the approach to combine FMS with automatic fiber transfer and branching fiber monitoring for optical CATV network. The system architecture for this new FMS is shown in Fig.2. This FMS includes automatic fiber transfer subsystem and branching fiber monitoring subsystem. Automatic fiber transfer subsystem, as shown in Fig.3, consists of local fiber selector module (LFSM), remote fiber selector module (RFSM) and transfer control module (TCM). LFSM connects with CATV transmitter, FMS, TCM and fiber routes. RFSM is able to receive optical control signal for fiber selecting. TCM transmits optical control signal to RFSM for selecting fibers and controls LFSM. RFSM connects with CATV receiver and fiber routes. Fiber routes should include at least one spare fiber route. This subsystem can

provide N plus M survivability for the needs of CATV systems. Branching fiber monitoring subsystem consists of branching fiber monitoring module (BFM), fault location module (FLM) and remote terminal module (RTM). Branching fiber routes can be monitored by the fiber surveillance technique for Passive Optical Network (PON). This technique, based on time delay and reflection light detection, has been successfully developed in our lab.. Branching fiber surveillance function is able to monitor up to 32 distributive nodes.

Automatic Fiber Transfer Function

When fiber route occurs faults, TCM receives fault alarm from FMS. TCM will request LFSM and FMS to scan spare fiber first. After confirming spare fiber in a good condition, FMS signals TCM again. Then TCM requests LFSM to connect spare fiber with itself and transmits optical control signals to RFSM for switching trunk line to spare fiber. TCM also controls LFSM to connect CATV transmitter with spare fiber. After FMS completing its checking scanning, the whole fiber transfer is successfully finished. If fiber fault is repaired, we can automatically or manually set TCM to transfer back to the original fiber route. Once we set TCM into automatic re-transfer mode, FMS has to monitor the fault fibers all the time. After the fault is repaired, FMS will signal TCM to execute the re-transfer task. The whole re-transfer process is similar to the transfer process that we have described as above.

In (N+M) fiber selector design, we use 1x2 switches and 1xm switches as the basic components. The main considerable factors are return loss, excess loss and flexibility. The return loss, and excess loss will affect the performance of CATV system. The flexibility will be related to the deployment cost. As shown in Fig.4, there are two kinds of configurations we proposed for (3+1) fiber selector. The architecture in Fig.4b has better return loss and excess loss. However, the architecture in Fig.4a is more flexible. For example, when we want to expand (3+1) fiber selector to (4+1) fiber selector, the architecture in Fig.4a only needs to add one pair of 1x2 switches in S to S cascading. However the architecture in Fig.4b needs to replace all the 1x3 switches.

Branching Fiber Monitoring Function

Branching fiber monitoring module (BFM) uses short optical pulse to probe fiber lines and measure the fiber line loss by reflection signal. Because we add optical identifying unit in remote terminal module (RTM), BFM can measure the losses of all fiber lines at one time. When fiber fault happens, BFM will find out the fault and start fault location module (FLM) to find the fault location. FLM probes the fiber lines by using long optical pulse and decides the exact fault location. These techniques have been successfully developed in our lab..

EXPERIMENTAL RESULTS

For verifying the feasibility of the new design for CATV FMS, we experiment several characteristics of the new design. We set up an experimental CATV optical network, which include a 10km span fiber and four 2km long distributive fiber feeders. We measure the return loss and insertion loss for the experiment network and compare the difference between with the new CATV FMS and without the new CATV FMS. The optical performance result is shown in Table 1. The CATV system with this new FMS has to increase 4.5dB link loss budget and affects return loss only a little.

We measure the effects of the new FMS on AM-VSB NTSC 80 channel system and keep the optical receiving level equal to 0dBm. The results, as shown in Table 2, confirm that it is almost no effects for FMS combined with fiber transfer and branching fiber functions.

We also measure the characteristics of automatic fiber transfer by simulating fiber faults. Its transfer time is less than 1.5 seconds and the repeatability is better than 0.1dB.

Branching fiber monitoring function in our experimental system is able to monitor up to 32 distributive nodes. In four distributive feeders, the monitoring dynamic range of BFM is larger than 21dB. The minimum fault detection loss is able 0.5dB and the fault location time is less than 8 seconds. The monitoring time for branching fiber monitoring function is depend on the program executing speed. In our experiment, it needs extra 0.5 second for one line.

CONCLUSION

We propose the approaches to combine FMS

with automatic fiber transfer and branching fiber surveillance functions for CATV systems. We also have confirmed the performance and effects of this new design. The experimental system which we setup in our lab. can provide automatic fiber transfer for only 1.5 seconds transfer time. Branching fiber surveillance function of our experimental system is able to monitor up to 32 distributive nodes. From the experimental results, the new design for CATV FMS combined with automatic fiber transfer and branching fiber monitoring functions can provide high survivability and the ability of branching fiber surveillance.

REFERENCE

1. Chien-Chung Lee, etc., "New Fiber Monitoring System Without Fiber Selector", IWCS, 1995, pp554-557.
2. Chien-Chung Lee, etc., "Optical Fiber Monitoring Systems for Passive Optical Networks", IWCS, 1994, pp494-498.

ACKNOWLEDGEMENTS

The authors wish to gratefully acknowledge Mr. Feu-Yuan Tsai for his assistance.

Table 1 Optical performance of experimental network

	Network without FMS		Network with FMS	
	1310nm	1550nm	1310nm	1550nm
Return Loss (dB)	-57	-57	-54	-54
Insertion Loss (dB)	-10.8	-9.0	-15.3	-13.5

Table 2 The effects of the new FMS on AM-VSB NTCS 80 channel system

	Network without FMS		Network with FMS	
	1310nm	1550nm	1310nm	1550nm
CNR (dB)	51.1	50.4	51.0	50.0
CSO (dB)	74.9	74.2	72.4	73.2
CTB (dB)	66.7	60.0	65.0	60.1

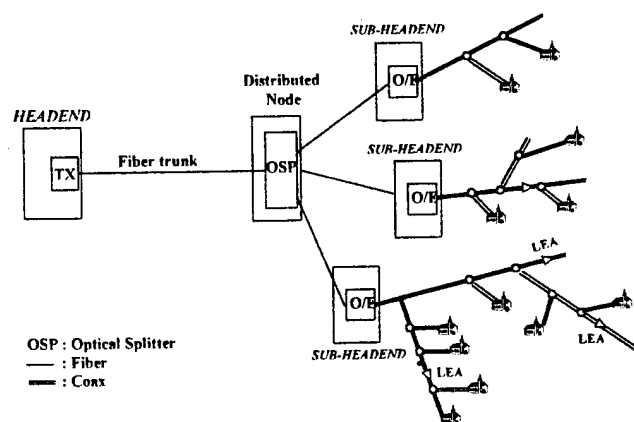


Fig. 1 Optical CATV network architecture

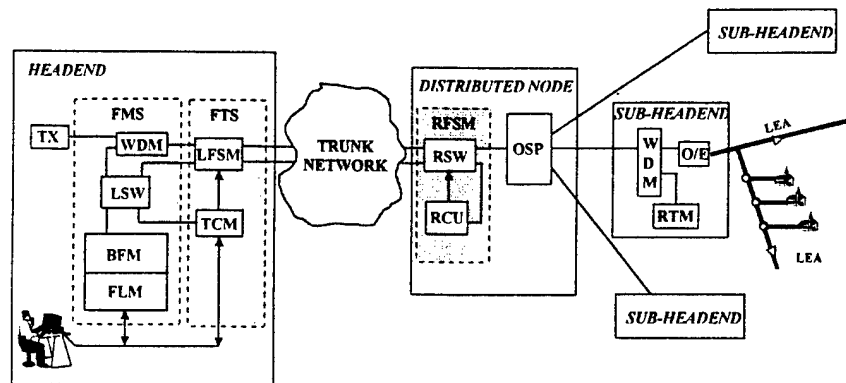


Fig.2 The system architecture for the new CATV Fiber monitoring system

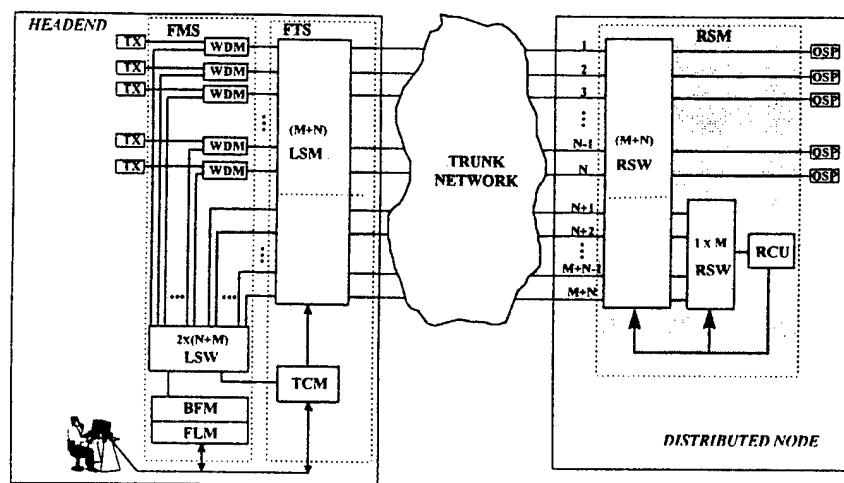


Fig.3 The architecture of automatic fiber transfer system

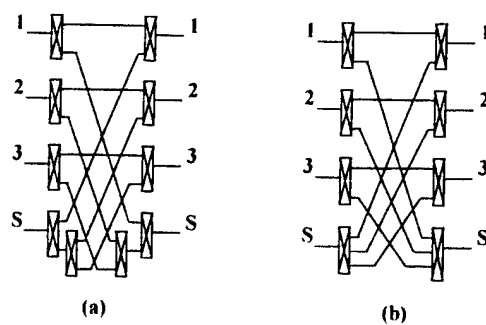


Fig.4 The architecture of (3+1) fiber selector

Design Considerations of Stimulation Brillouin Scattering and Dispersion on 1550nm AM 80 Channel CATV System

Chien-Chung Lee, Kuo-Hsiang Lai, Kelvin Chen, Kuang-Yi Chen,
Ching-shen Wang, Fwu-Yuan Tsai

Telecommunication Laboratories, Chunghwa Telecom Co., Ltd., Taiwan, Republic of China

ABSTRACT

This paper analyzes Stimulation Brillouin Scattering (SBS) and dispersion effects on 1550nm AM 80 channel CATV systems, and compares these theories with our experimental results. SBS effect degrades Carrier-to-Noise Ratio (CNR) and Composite Second Order (CSO) distortion. Fiber dispersion nature causes FM-AM conversion and induces Composite Second Order (CSO) distortion. These two effects are the main limitations for fiber applied on 1550nm AM-VSB CATV systems. We investigate the system parameters related to SBS and dispersion degradation such as optical power level, optical linewidth, SBS gain factor, fiber span and dispersion coefficient. Finally, we summarize all these results for design considerations.

INTRODUCTION

Fiber AM CATV Systems are becoming widespread throughout the cable television industry. To increase system link budgets, higher transmitter powers or lower fiber losses are required. 1550nm AM CATV systems can meet the need for larger link budget, but higher transmitter power and longer fiber link will degrade the system performance caused by fiber nonlinear and dispersion effects. When we use non-shift single-mode fiber as the transmission medium, SBS and dispersion are the main limitations on 1550nm AM CATV systems. Therefore we investigate SBS and dispersion effects on the degradation of 1550nm AM CATV systems. Then we analyze the system parameters related to SBS and dispersion degradation such as optical

power level, optical linewidth, SBS gain factor, fiber span and dispersion coefficient. Finally we summarize all these results and present them as design considerations for 1550nm AM 80 channel CATV system.

BASIC THEORIES

(1) Dispersion-induced distortion

For a modulation signal $m(t)$, the electric field emitted by a laser diode can be described by [1]

$$E(t) = A_0 \sqrt{1 + m(t)} e^{i(\omega_0 t + 2\pi\gamma \int m(\tau) d\tau)} \quad (1)$$

Where m is the intensity modulation, ω_0 is the center optical frequency, and the chirp γ is the ratio of the frequency deviation from the center optical frequency to the normalized intensity modulation. For the 1550nm high power transmitters, the chirp γ approaches zero by using external modulation method. The wave-envelope equation in a lossy, dispersive, and nonlinear medium is [1]

$$\frac{\partial A}{\partial z} + \beta \frac{\partial A}{\partial t} - \frac{i}{2} \beta \frac{\partial^2 A}{\partial t^2} + \alpha A = -ikn_2 |A|^2 A. \quad (2)$$

Where α is the material loss, β and β are the first- and second-order dispersion coefficients in the frequency expansion, $k = 2\pi/\lambda$, and n_2 is the nonlinear refractive index. If we assume a single tone input, $m(t) = m \cos(\Omega t)$, the ratio of the dispersion-induced second-harmonic output intensity to the output carrier intensity can be derived from

equation (1) and (2). [1]

$$2HD|_{DSP} = \frac{1}{4} m \beta \Omega \sqrt{(4\gamma)^2 + (\beta \Omega^3)^2} \quad (3)$$

Likewise, the dispersion-induced third-harmonic distortion normalized to the carrier is [1]

$$3HD|_{DSP} = -\frac{9}{32} (m \beta \Omega^2)^2 (4\gamma^2 + \Omega^2) \quad (4)$$

and

$$\beta = -\frac{\lambda^2}{2\pi c} D \quad (5)$$

Where D is the dispersion coefficient (ps/nm · km). In order to obtain the CSO distortion from the second-order harmonic distortion (2HD), we use the following relationship [2]:

$$CSO_{dB} = 20 \log(\sqrt{N}) + 20 \log(2HD|_{DSP}) \quad (6)$$

Where N is the number of second-order intermodulation products.

For 1550nm, high power transmitters, modulation index m is small and the chirp γ approaches zero. From equation (3) and (4), we can derive that $2HD|_{DSP}$ distortion is larger than $3HD|_{DSP}$ distortion. $2HD|_{DSP}$ can be described by

$$2HD|_{DSP} = \frac{1}{4} m (\beta \Omega)^2 \Omega^4 \quad (7)$$

Therefore CSO distortion is dominated by the modulation frequency Ω . CSO distortion increases when dispersion, fiber length and the modulation frequency increases.

(2) The SBS degradation

Photons will be scattered from index variations induced by sound wave. Owing to the intense injected light, the nonlinear effect will induce sound waves, which then scatter more light. The scattering light provides gain for a backward-propagating Stokes signal. This is the effect that we call SBS. The noise induced by SBS will be greatly increased if the injected laser power exceeds the SBS threshold. So the SBS threshold determines the SBS degradation and the SBS threshold without modulation can be given by [3]

$$P_{thr}^{CW} \approx 42 \frac{A_{eff}}{g_0 L_{eff}} \left(\frac{\Delta \nu_B + \Delta \nu_P}{\Delta \nu_B} \right) \quad (8)$$

Where $\Delta \nu_P$ is the injected laser linewidth, $\Delta \nu_B$

is the spontaneous SBS linewidth (all linewidths are given in terms of HWHM), A_{eff} is the effective core area (μm^2), effective fiber length $L_{eff} = (1 - e^{-\alpha L}) / \alpha$ (km), g_0 is the SBS gain coefficient, L is the fiber length and α is attenuation coefficient. For example, $\Delta \nu_B$ is typically 50MHz for doped silica fibers, $\Delta \nu_P$ is about 10MHz for 1550nm transmitter, A_{eff} is about $80 \mu m^2$ for single-mode non-dispersion-shifted fiber, $\alpha = 0.25 dB/km$, $g_0 = 4 \times 10^{-9} cm/W$, and $L_{eff} \approx 1/\alpha = 17.37 km$ for very long-fiber spans, the SBS threshold is about 5.8mW (7.6dBm). Assuming that the parameters are the same except for $\alpha = 0.4 dB/km$ in 1310nm transmission system, the SBS threshold is about 9.2mW (9.6dBm). The longer fiber length and narrower laser linewidth will decrease the SBS power threshold. In another word, the SBS degradation is more easily induced in these conditions. Because light source is modulated lightly with RF signals in 1550nm AM-VSB transmission system, the SBS threshold for modulated source will increase and the high channels will degrade less than low channels.

EXPERIMENT

The experimental setup is shown schematically in Fig.1. The 1550nm high power transmitter is composed of +5dBm externally modulated transmitter and EDFA. We use Matrix multi-carrier generator to generate NTSC 80-channel carriers. By the spectrum analyzer, the optical power meter and the optical spectrum analyzer, we measure the RF performance in different system parameters. The results are described as follows.

(1) The system parameters measurement

The linewidth of the transmitter without modulation is measured by heterodyne detector. The linewidth is about 6MHz (HWHM). The central wavelength of the transmitter is 1556nm. The experimental fiber has 0.21dB/km attenuation coefficient and 17.2 ps/nm · km dispersion coefficient.

(2) The degradation induced by dispersion

In order to verify the degradation induced by dispersion, we carefully control the launched power

not to exceed the SBS threshold and measure the RF performance in different fiber length. The result is shown in Table 1. The dispersion degradation is not obvious until 60km-fiber transmission. The degradation in high channels is worse than in low channels. To confirm the SBS effect is not induced, we can compare the injected power and the output power, then keep their relationship in the linear regime.

(3) The degradation induced by SBS

We can observe the SBS degradation by high optical power and long fiber-span. However the dispersion degradation will also be induced in long-fiber-span. For identifying the SBS degradation, we subtract the dispersion degradation from low launched power as shown in Table 2. The degradation data include the error from self phase modulation (SPM) but the error is small because of low modulation index. The SBS degradation is increased when launched power is increased. The SNR degradation in low channels is worse than in high channels for SBS. Furthermore, the CSO and CTB degradations in low channels are better than in high channels and the CSO degradation is greater than the CTB degradation.

(4) The degradation induced by dispersion and SBS.

The degradation induced by dispersion and SBS is shown in Table 3. All the degradation data are subtracted by 3m fiber-span, and it means that we only consider the degradation induced by fibers. From Table 3, we know that CNR and CSO are greatly effected by dispersion and SBS. Fig.2 is the number of second-order intermodulation products for each channel in NTSC system.

(5) The tapping effects on the SBS degradation

The experimental setup is shown in Fig.3. Table 4 shows the tapping effects on the SBS degradation. As shown in Table 4, the longer tapping span and the larger tapping value can decrease the SBS degradation.

CONCLUSION

By using Fig.4, we can summarize the fiber effects induced by SBS and dispersion. For certain degradation criterion (for example, CNR=50dB, CSO=61dB and CTB=63dB) and average fiber characteristics (such as dispersion coefficient, attenuation coefficient and SBS gain distribution), we know that the (A) area operating condition in Fig.5 can meet the requirement. The (B) area and (D) area operating conditions are dominated by SBS and

dispersion individually. The (C) area operating condition is both dominated by SBS and dispersion. When we want to implement an AM 80-channel optical CATV System for 1550nm wavelength, we can derive the fiber degradation curve as Fig.5 by experiment or computing. Then we test the performance of this system with non-fiber system, and we measure the optical power and linewidth. Finally, by using the fiber degradation curve and cascading formula, we can predict the system performance from the fiber-span and injected power.

REFERENCE

1. M.R.Phillips, etc., "Nonlinear Distortion Generated by Dispersive Transmission of Chirped Intensity-Modulated Signals", IEEE PHOTONICS TECHNOLOGY LETTERS, VOL.3,NO.5,MAY 1991, pp481-483.
2. B.Clesca, etc., "Second-Order Distortion Improvements or Degradations Brought by Erbium-Doped Fiber Amplifiers in Analog Links Using Directly Modulated Lasers", IEEE PHOTONICS TECHNOLOGY LETTERS, VOL.5, NO.9,SEP. 1993, pp1029-1031.
3. Daniel A. Fishman and Jonathan A. Nagel, "Degradations Due to Stimulated Brillouin Scattering in Multigigabit Intensity-Modulated Fiber-Optic Systems", Journal of Lightwave technology, VOL.11,NO.11,NOV. 1993, pp1721-1728.

TABLE 1 The Degradation Induced by Dispersion (Receiving power=-3dBm)

UNIT: dB	Low Channels			Medium Channels			High Channel		
different fiber-span	CNR	CSO	CTB	CNR	CSO	CTB	CNR	CSO	CTB
3m	50.5	74	60	50.2	73	58.3	50.9	68.8	58
25km	50.3	74.5	58.8	50.2	73.3	58.7	50.8	66.7	58.7
40km	49.9	74.2	61.3	49.5	72.5	58.3	50.5	66	59
60km	50.1	74	60.5	49.8	71	59.3	50.4	60	59

TABLE 2 The Degradation Induced by SBS for 60km fiber-span

UNIT: dB	Low Channels			Medium Channels			High Channel		
different launched power	CNR	CSO	CTB	CNR	CSO	CTB	CNR	CSO	CTB
10.3dBm	-0.5	0.3	0.3	-0.2	-1.4	1.2	0.4	-5.2	1.5
13.3dBm	-0.7	0	0.5	-0.9	-1.4	0.6	0.2	-8.4	0.7
15.6dBm	-11.3	-5.8	-2	-3.5	-10.1	-0.2	-1.2	-12.9	-2.4

* The degradation are referred to 8.3dBm launched power.

TABLE 3 The Degradation Induced by dispersion and SBS for 60km fiber-span

UNIT: dB	Low Channels			Medium Channels			High Channel		
different launched power	CNR	CSO	CTB	CNR	CSO	CTB	CNR	CSO	CTB
8.3dBm	0.1	-0.3	0.2	-0.2	-0.6	-0.2	-0.9	-3.6	-0.5
10.3dBm	-0.4	0	0.5	-0.4	-2	1	-0.5	-8.8	1
13.3dBm	-0.6	-0.3	0.7	-1.1	-2	0.4	-0.7	-12	0.2
15.6dBm	-11.2	-6.1	-1.8	-3.7	-10.7	-0.4	-2.1	-16.5	-2.9

* The degradation are subtracted by non-fiber degradation.

TABLE 4 The Tapping effects on SBS for 60km fiber-span

UNIT: dB	Low Channels			Medium Channels			High Channel		
different tapping	CNR	CSO	CTB	CNR	CSO	CTB	CNR	CSO	CTB
Span: 10km-20km-30km Tapping: a-2dB b-1dB	+7.4	+4.3	+0.3	+5.7	+9.3	-0.3	+3.2	+7.9	-0.6
Span: 25km-10km-25km Tapping: a-2dB b-1dB	+1.9	+3.5	-0.2	+2.1	+2.5	+1.1	+0.9	+2.4	+0.2

* The launched power is 15.5 dBm and the degradation data are referred to non-tapping degradation.

* + means improvement, - means worse.

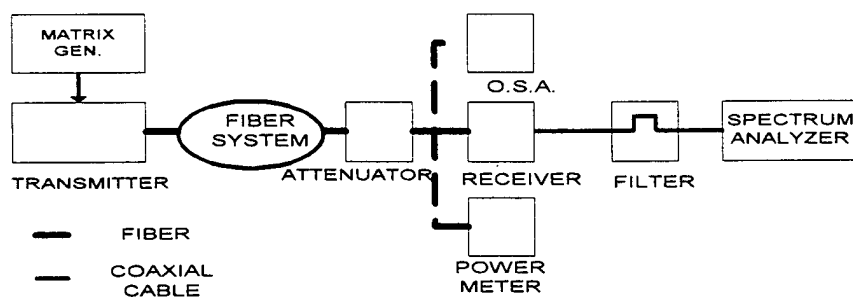


Fig.1 The experimental setup for the degradation measurement of dispersion and SBS

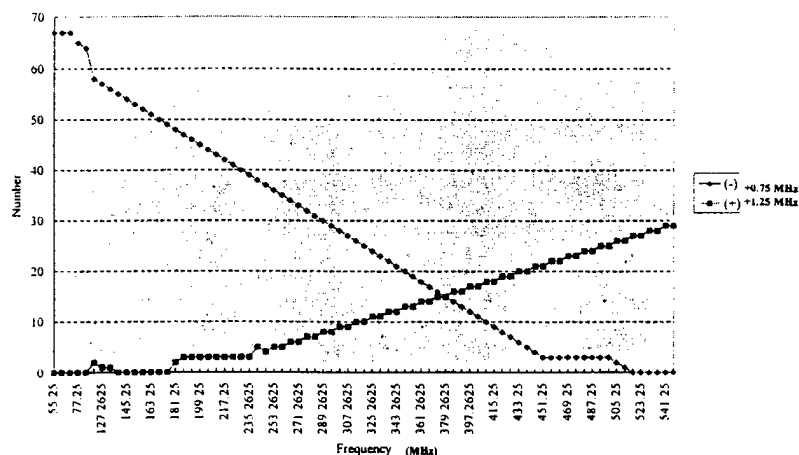


Fig.2 The number of second-order intermodulation products for each channel in NTSC system

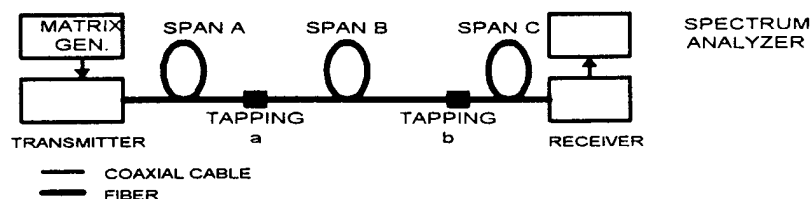


Fig.3 The experimental setup for measuring the tapping effects on the SBS degradation

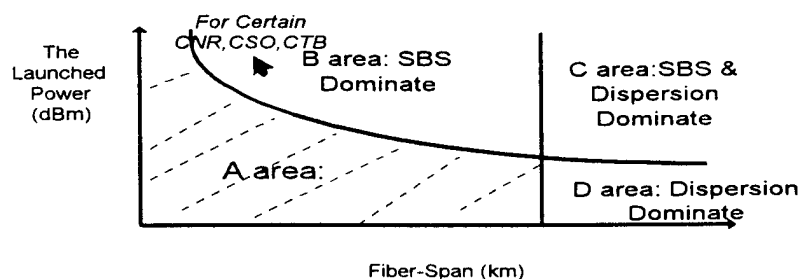


Fig.4 The design considerations for the fiber effects induced by SBS and dispersion

INNOVATIVE INSULATION SOLUTION FOR ZERO HALOGEN FIRE RETARDANT COMMUNICATION AND POWER CABLES

Mr Dudley Sawyer, Mrs Lai Ping Artingstall, Mr Joe Preston,
Mr Steve Dell and Miss Séverine Cochard.

Lindsay & Williams Limited
Manchester
ENGLAND

SUMMARY

There is a commercial requirement for thermoplastic zero halogen fire retardant insulation in ship wiring, low voltage power and communication cable applications. This offered solution allows the similar fire retardancy to be provided to the core of the cable as has already been achieved by zero halogen, low smoke, fire retardant compounds to the outer sheath^{1,2,3}. Excellent speed of processing on standard PVC/LDPE extruders is shown. The compound exhibits high fluid resistance, but still retains all the advantages of being a fully recyclable and high temperature performance thermoplastic. Investment in expensive cross-linking equipment and high inventory are not necessary.

An initial requirement for shipboard wiring cables to IEC 92-351⁴ was targeted for the electrical, mechanical and thermomechanical properties for a successful insulation compound. Added to this, strict criteria for providing totally halogen free, fire retardant and low smoke attributes were essential for the accelerated moves towards safety in shipboard and off-shore installations.

The fire retardancy properties have been measured along with smoke generation and acid gas emissions. These are compared to the performance of typical PVC and LDPE materials.

It is shown that this insulation compound is a viable thermoplastic alternative to both the PVC and LDPE historically used in these applications. A further key attribute of the new compound is its exceptional electrical performance including insulation resistance in water. This widens the potential of the insulation compound to communication applications.

INTRODUCTION

There is a rapidly accelerating move towards inherently safer and environmentally friendly cable designs. The main areas for improvement have been in fire performance (and the combustible products thereof) and environmental issues including recyclability and safe disposal after the cable's working life.

Traditionally PVC and LDPE have been used in the role as primary insulation in low voltage power and telecommunication cables. Although proven reliable insulators they both exhibit limited fire performance that has on occasion allowed cables to continue to burn and worsen the outcome of a building fire.

In the move to design cables sympathetically to the environment, the materials used to insulate copper wires or encapsulate optical fibre elements should be both safe during the manufacturing process and in the service life of the cable or wire. They should also add no further burden when disposed of and more effectively be easily recycled to an additional useful purpose. In particular PVC presents difficulties via its use of heavy metal stabilisers if landfill disposal is intended. Alternatively harmful hydrogen chloride gas can be evolved if incinerated.

Much is known of the extrusion of PVC and LDPE insulation on conventional extrusion equipment. Latterly success in effective extrusion of first generation low smoke and fume compounds on optimized extruder screws has been demonstrated³. The market requires ease of changeover and high line speeds to maintain efficiency and profitability, hence the need for a new generation of low smoke and fume insulation compounds.

For low voltage power and instrumentation cables, especially for shipboard applications, high temperature requirements are known.

Traditionally highly filled thermoplastics, although excellent in fire retardance, when used as primary insulation, have exhibited lesser insulation properties compared to a typical LDPE.

In this paper we describe the development of a new low smoke and fume insulation compound initially targeted for shipboard wiring cables to IEC 92-351⁴. We describe the electrical, mechanical and thermomechanical properties comparing them to typical PVC and LDPE insulations as well as appropriate national standards. The performance of the newly developed insulation compound is also assessed against fire propagation, acid gas, smoke and toxicity.

SAMPLE PREPARATION

Table 1. Sample Identification of insulation compounds.

PVC	Typical PVC compound
LDPE	Typical LDPE
IN 200	First generation zero halogen polyolefinic compound
D93	Latest generation zero halogen polyolefinic compound

Each material was extruded onto 1 mm² solid copper wire at a wall thickness of 0.6 mm nominal. All tests were carried out on these extruded samples unless noted otherwise.

ELECTRICAL PROPERTIES

Zero halogen compounds have long been used for sheathing electrical cables^{1,2,3} and have also found use as a primary insulation in low voltage cables in dry conditions and at an operating temperature up to only 80°C (first generation compounds). The insulating properties of these first generation compounds exhibited values equivalent to those of the best PVC compounds available but falling short of those exhibited by LDPE.

With this new generation insulation compound we now show in table 2 the significant increase in insulation resistance at elevated temperatures.

Table 2. Insulation resistance⁶

For 2 hours at temperature :	PVC	LDPE	IN200	D93
70°C	5×10^{11}	2×10^{15}	7×10^{10}	3×10^{13}
80°C	2×10^{11}	2×10^{15}	6×10^{10}	1×10^{13}
90°C	7×10^{10}	2×10^{15}	6×10^{10}	6×10^{12}
Ohm cm				

Table 3 highlights the improvement in dielectric properties towards the requirements of communication cables where low dielectric constant and loss angle are necessary. Compound D93 has considerably better dielectric properties than PVC.

A prime consideration for cable design is shown in figure 1, the long term insulation resistance comparisons in contact with water at ambient temperatures. Here insulation compound D93 exhibits excellent insulation resistance mirroring the

results of LDPE, well known as a stable insulator in wet conditions.

INSULATION RESISTANCE COMPARISONS AFTER 21 DAYS IN WATER @ 23°C

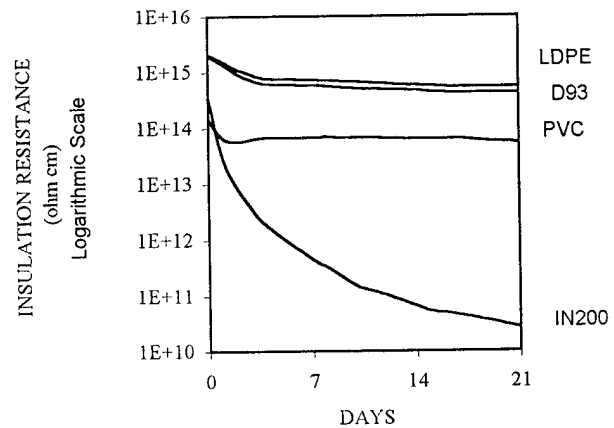


Figure 1. Insulation resistance⁶

PHYSICAL PROPERTIES

Table 4 shows the primary physical properties of the materials. Compound D93 shows higher tensile strength and tear resistance than those shown by the earlier generation zero halogen insulation compounds. These values are comparable to those of PVC and LDPE.

Viscosity is also improved by a factor of 5 as shown by the melt flow rate (MFR) figures. This property is often used as an indicator of ease in processing compounds as can be seen in figure 4. later.

All mechanical, thermomechanical and fluid testing was carried out to IEC 811⁷ unless stated otherwise.

Table 4. Physical properties

Properties	PVC	LDPE	IN200	D93
Tensile strength MPa	15	18	13	17
Elongation %	200	500	185	400
Tear strength N/mm	10	18	5	12
Specific gravity	1.52	0.92	1.53	1.40
MFR (5kg @ 190°C)	9	9	0.2	1
Hardness (Shore D)	40	52	55	73

Table 3. Dielectric measurements⁵

Sample	PVC		LDPE		IN200		D93	
Frequency	ϵ	δ	ϵ	δ	ϵ	δ	ϵ	δ
100 Hz	6.96	0.065	2.26	< 0.001	4.13	0.030	3.03	0.005
1 kHz	6.30	0.082	2.26	< 0.001	4.03	0.018	3.02	0.003
100 kHz	4.27	0.095	2.20	< 0.001	3.72	0.015	2.91	0.003
1 MHz	4.12	0.083	2.26	< 0.001	3.77	0.024	2.94	0.002
ϵ : Dielectric constant, δ : Loss angle								

THERMOMECHANICAL PROPERTIES

Short term thermal ageing results are given in table 5. These demonstrate the excellent performance of compound D93 throughout the full range of ageing temperatures from 80°C to 135°C.

Table 5. Short-term ageing

Properties	PVC	LDPE	IN200	D93
Tensile strength retention (%)				
7 days @ 80°C	102	80	103	102
7 days @ 125°C	brittle	molten	90	115
7 days @ 135°C	brittle	molten	98	85
Elongation retention (%)				
7 days @ 80°C	90	65	85	85
7 days @ 125°C	brittle	molten	50	80
7 days @ 135°C	brittle	molten	40	75
Loss of mass (mg/cm²)				
7 days @ 80°C	0.63	0.05	0.04	0.13
7 days @ 125°C	8.5	molten	0.07	0.10
7 days @ 135°C	11	molten	0.11	0.11
Shrinkage (%)				
7 days @ 80°C	1	1.5	1	1
7 days @ 125°C	12	molten	1	1
7 days @ 135°C	16	molten	5	1

It can be seen at the higher temperatures that problems exist with both LDPE and PVC. LDPE melts and no results are obtainable. PVC shows high loss of mass owing to plasticiser volatility this has lead to embrittlement preventing tensile testing at higher temperatures. IN200, the first generation zero halogen insulation, also shows poor elongation retention at the higher ageing temperatures.

Table 6. Hot pressure

Properties	PVC	LDPE	IN200	D93
Hot pressure %				
at 80°C	15	20	20	0
at 90°C	45	40	50	0
at 100°C	50	65	100	0
at 130°C	100	100	100	5

The results of the hot pressure test are given in table 6. This test is a measurement of the heat deformation properties and a maximum of 50% is invariably specified. It can be seen from the table how compound D93 outperforms the other three materials.

Table 7. Low temperature properties.

Properties	PVC	LDPE	IN200	D93
Cold bend at - 40°C	no cracks	no cracks	no cracks	no cracks
Cold impact at - 40°C	no cracks	no cracks	no cracks	no cracks

Table 7 indicates the low temperature performance in both the cold bend and cold impact tests. These results indicate that compound D93 should be satisfactory at temperatures down to at least - 40°C.

FLUID RESISTANCE

Table 8. Fluid resistance

Properties	PVC	LDPE	IN200	D93
7 days at 23°C in ASTM No 2 oil				
Tensile strength retention (%)	110	80	95	101
Elongation at break retention (%)	90	65	85	90
Volume swell (%)	5	0	2	0
4 hours at 70°C in ASTM No 2 oil				
Tensile strength retention (%)	104	80	85	97
Elongation at break retention (%)	85	65	105	85
Volume swell (%)	1	2	6	1
7 days at 23°C in diesel oil				
Tensile strength retention (%)	105	75	75	103
Elongation at break retention (%)	90	60	95	70
Volume swell (%)	3	6	10	6
4 hours at 70°C in diesel oil				
Tensile strength retention (%)	103	65	20	103
Elongation at break retention (%)	85	65	80	80
Volume swell (%)	13	17	70	7
10 days at 23°C in deionised water				
Tensile strength retention (%)	104	90	85	97
Elongation at break retention (%)	90	65	85	98
Volume swell (%)	0	0	1	0
24 hours at 100°C in deionised water				
Tensile strength retention (%)	101	90	90	96
Elongation at break retention (%)	98	75	90	75
Volume swell (%)	8	2	2	2

It is customary to measure the performance of cable making compounds in ASTM No 2 oil, diesel oil and deionised water at both ambient and elevated temperatures. This data is shown in table 8 and confirms that the performance of compound D93 is comparable to that of PVC and is superior to LDPE and IN200.

FIRE PERFORMANCE

Smoke emission

The ASTM E662⁸ test method was used to assess smoke emission. Figure 2 shows the combined results for the flaming mode tests and figure 3 those for the non flaming mode. Tests in both modes are carried out on 1.5 mm thick plaque samples.

ASTM E662 - Flaming Mode

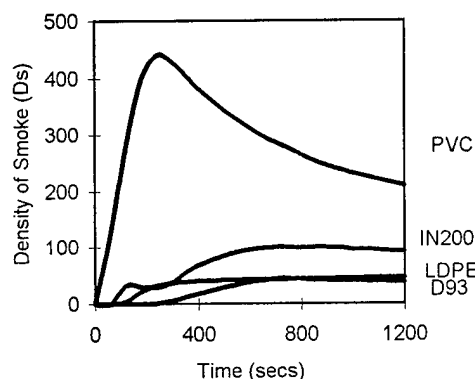


Figure 2. Flaming mode

In the flaming mode compound D93 shows excellent smoke characteristics as does LDPE and is a definite improvement on the IN200 first generation compound. The PVC compound generates smoke at a much faster rate and a far greater quantity than the other materials.

ASTM E662 - Non Flaming Mode

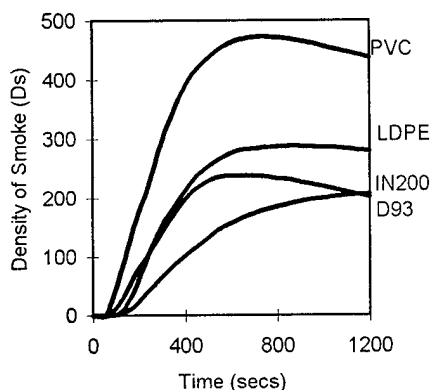


Figure 3. Non flaming mode

The same trend is noted in the non-flaming mode. Here, though, compound D93, demonstrates a clear superiority even over LDPE in that very small volumes of smoke are produced and at a lower rate.

Smoke index

This particular parameter is measured by the method NES 711⁹, a test developed by the British Navy. The index takes account not only of the maximum quantity generated, but also of the rate of evolution of the smoke. This test is also carried out on 1.5 mm plaque samples. Results are given in table 9.

Table 9. Smoke index

	PVC	LDPE	IN200	D93
Smoke index	191	molten	89	28

No result could be recorded for LDPE as the sample melts, falls over the burner and extinguishes the pilot light. However the stark contrast shown between very low index of D93 and the high index of PVC, is an indication that PVC can produce large quantities of smoke very quickly in comparison to the latest generation zero halogen insulation compound D93.

Toxicity

This parameter is evaluated by using method NES 713¹⁰. This test has also been developed by the British Navy. The index is computed by measuring the concentrations of 12 selected gases evolved under fire conditions. D93 is compared to the industry standard in table 10, exhibiting a low index.

Table 10. Toxicity index

	D93	Industry acceptable level
Toxicity	1.4	< 5

Combustion Gases

The most widely used methods of test for the quantities of acid gas evolved during combustion are now grouped in IEC 754¹¹. The results of these tests are given in table 11 and clearly demonstrate the zero halogen, low acid gas nature of compound D93.

Table 11. Combustion gases

Properties	PVC	LDPE	IN200	D93
Acid gas emission %	31	0.5	0	0
pH	2.2	3	6	4.3
Conductivity $\mu\text{S/cm}$	1400	14	14	9

Flame Tests

An essential element in the development of compound D93 was the passing of IEC 332¹² single wire, vertical flame test (LDPE was noted to drip badly). Following this achievement, the oxygen index¹³ was measured to provide data for manufacturing control. Table 12 gives the details.

Table 12. Fire properties

Properties	PVC	LDPE	IN200	D93
IEC 332-1	pass	fail	pass	pass
Oxygen index (%)	22.25	18.5	35	25

PROCESSABILITY

Processing was evaluated in the laboratory using a 25 mm Reifenhäuser extruder fitted with a 3:1 compression ratio screw. Figures 4 and 5 show the outputs and melt temperatures measured as a function of screw speed.

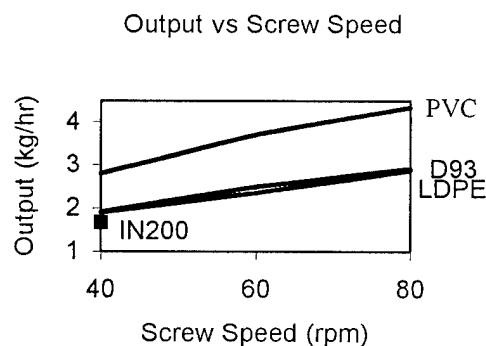


Figure 4. Output

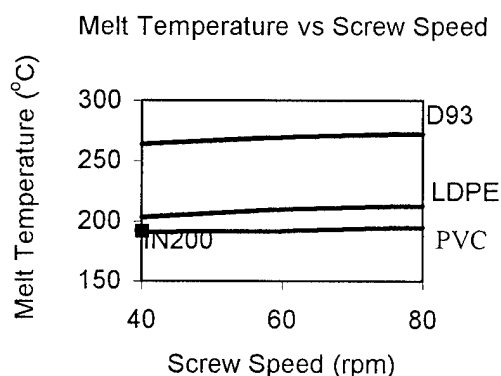


Figure 5. Melt temperature

IN200 could not be run at speeds of above 40 rpm without encountering excessive shear heating problems. However D93 exhibits stable melt temperatures at the high screw speeds commonly required in high speed insulation extrusion.

In the field, compound D93 has been extruded by several major cable companies who have reported line speeds comparable to those used for PVC and LDPE.

DISCUSSION

Table 14 shows two of the national specifications^{4,6} which were used to set the requirements for compound D93 for insulation in electric cables. It can be seen that the performance of the compound D93 exceeds the requirements of IEC 92-351⁴. Further it compares very favourably with BS6746⁶ for PVC insulation.

In all cases the zero halogen low smoke fire retardant properties of D93, allow this novel insulation compound to be used safely in a wide cross section of cable designs.

Table 14. Specifications

Property	IEC 92- 351	TI 1	D93
Tensile strength (MPa)	9 min	12.5 min	17
Elongation (%)	200 min	125 min	400
Ageing 7 days @ 80°C			
Tensile retention (%)	-	+/- 20	- 15
Elongation retention (%)	-	+/- 20	+ 2
Ageing 7 days @ 135°C			
Tensile retention (%)	+/- 30	-	- 15
Elongation retention (%)	+/- 30	-	- 25
Hot pressure @ 80°C (%)	-	50 max	0
Insulation resistance			
@ 23°C (ohm cm)	10 ¹	-	2 x 10 ¹
@ 70°C (ohm cm)	10 ¹² min	10 ¹⁰	3 x 10 ¹²

CONCLUSION

The development of D93, a high temperature thermoplastic insulation compound for both low voltage power cable and communication cables has been described. D93 has been shown to possess excellent electrical and processing characteristics whilst maintaining essential attributes demanded for zero halogen, low smoke, fire retardant cables. D93 has been developed specially with safety and the environment in mind.

REFERENCES

1. H. A. Mayer, et al. : A new generation of non halogenated, flame retardant compounds and cables, IWCS, November 1980
2. Dr J. Taylor, et al. : Recent advances in zero halogen, low smoke, fire retardant compounds, IWCS, November 1987.
3. Dr J. Taylor, et al. : Sheathing power and telecom cables, IWCS, November 1992.
4. IEC 92-351, 1983, Electrical insulations in ships, Part 351 : Insulating materials for shipboard power cables.
5. BS7663 : 1993, Methods of test for determination of permittivity and dissipation factor of electrical insulating material in sheet or tubular form.
6. BS6746 : 1990, Specification for PVC insulation and sheath of electric cable.
7. IEC 811, Insulating and sheathing materials of electric cables - Common test methods.
8. ASTM E 662-83, standard test method for Specific Optical Density of Smoke generated by solid materials.
9. Naval Engineering Standard 711, Determination of the Smoke Index of the products of combustion from small specimens of materials.
10. Naval Engineering Standard 713, Determination of the Toxicity Index of the products of combustion from small specimen of materials.
11. IEC 754, Part 1 (1982) and Part 2 (1991), Test on gases evolved during combustion of electric cables.
12. EC 332-1: 1979, Tests on electric cables under fire conditions. Method of test on a single vertical insulated wire or cable.
13. ISO 4589-1984, Plastics, -Determination of Flammability by Oxygen Index.



Lai Ping Artingstall
Lindsay & Williams Ltd
Ogden Lane Works
Columbine Street
Manchester M11 2LH
England

Lai Ping Artingstall studied "A" levels in both mathematics and chemistry at Central Manchester Colleges prior to joining Lindsay & Williams Ltd in 1990 as a Quality Control Inspector for the Megolon range of compounds. In 1991 she transferred to the development section where she has been instrumental to the development of the latest Megolon range of low smoke, halogen free, fire retardant compounds. Recently qualified to BTec HNC in Polymer Technology she is continuing her studies at Manchester Metropolitan University with a view to attaining BSc (Hons).



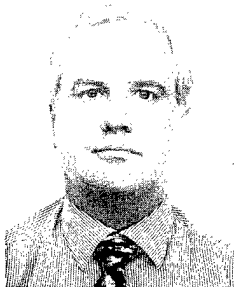
Séverine Cochard
Lindsay & Williams Ltd
Ogden Lane Works
Columbine Street
Manchester M11 2LH
England

Séverine Cochard joined Lindsay & Williams Ltd in 1996 as a Marketing Specialist. She studied at Dunkirk University where she gained a Master's degree in International Trade. She is now preparing a BA in Environmental Studies at the University of Manchester.



Steve Dell
Lindsay & Williams Ltd
Ogden Lane Works
Columbine Street
Manchester M11 2LH
England

Steve Dell joined Lindsay & Williams Ltd from BICC Cables Ltd in 1990. He gained a BSc (Hons) in Mechanical Engineering then finished his formal technical training within the cable industry. He has moved via technical sales role to current position as sales manager cable products for the worldwide promotion of Lindsay & Williams products dedicated to the needs of the cable industry.



Joe Preston
Lindsay & Williams Ltd
Ogden Lane Works
Columbine Street
Manchester M11 2LH
England

Joe Preston joined Lindsay & Williams Ltd in 1970 as a Laboratory Assistant following 2 ½ years experience in the Plastics Industry. He studied chemistry at the North Trafford College of Technology. In 1977 he became responsible for the Quality Control function at Lindsay & Williams. He transferred his efforts in 1982 to Development, working on specialized cable tapes, and in more recent years, the Megolon range of low smoke, halogen free, fire retardant compounds. In 1991 he was appointed Technical Manager of Lindsay & Williams, responsible for all development and quality control functions.



Dudley Sawyer
Lindsay & Williams Ltd
Ogden Lane Works
Columbine Street
Manchester M11 2LH
England

Dudley Sawyer joined Lindsay & Williams Ltd in January 1991 to work on the development of new zero halogen, flame retardant extrusion compounds for the electrical cable industry. He gained BSc (Hons) in Chemistry at the University of Manchester and he has extensive experience of the cable industry having previously spent 21 years with BICC Cables from 1969 - 1990, progressing from Assistant Chemist in the Wire and General Cables Division to Senior Material Technologist.

Development of Repeaterless Optical Fiber Submarine Cable System for Extensive Application

TaKato Nishida, Masahiko Kiuchi, Osamu Nagatomi, Hiroyuki Yoshioka

Ocean Cable Co.,Ltd.
Kita-Kyushu ,JAPAN

ABSTRACT

OCC has developed new compact repeaterless optical fiber submarine cables which contains maximum 24 optical fibers and relevant products. Their excellent performance in practical use through extensive tests and sea trial under severe environments in the sea area of 200m to 5400m in depth.

1. INTRODUCTION

In the trend of global communication network using optical fiber submarine cable technology, the demands for repeaterless optical submarine cable system are increasing to construct cost effective and highly reliable short haul communication system as regional or domestic communication infrastructure which are connected with transoceanic system. In response to such demands, we have developed new compact optical fiber submarine cables for repeaterless system and relevant products.

2. TARGET

Table 1. shows the design target of the repeaterless optical submarine cables and relevant products.

1) Number of fibers

OCC has been supplying 100 fiber core repeaterless optical fiber submarine cable which can be directly linked to a multi-fiber core land cable. Under the analysis of current demands for repeaterless optical submarine cable system, the number was decided as maximum 24 fibers.

2) Water depth

In case of repeaterless optical submarine cable system, it is considered that the cable is generally applied to the water depth up to 3000 m or 4000 m at maximum because of the transmission distance. However the maximum applied water depth should be increased for the expansion of transmission distance due to the remote amplifier technology.

Therefore, the maximum applied water depth was decided as 6000 m.

3) Handling

In order to be handled even by a small cable ship, the small size cables and cable joint boxes were designed to obtain minimum bending radius of 1 meter. The joint box was designed to minimize the jointing time for ship board joints.

4) Reliability

More than 25 years reliability is required for the system.

TABLE 1. DESIGN TARGET

ITEMS	OBJECTIVES
1. Cable 1) Number of fibers 2) Maximum sea depth 3) Handling 4) Design life time	≤ 24 Fibers 6000m To be laid /recovery using existing cable ship laying facility up to 6000m ≥ 25 years
2. Joint box 1) Maximum sea depth 2) Joint construction time 3) Handling 4) Design life time 5) Installation of EDF	6000m 8 Hours To be Laid /recovery using existing cable ship laying facility up to 6000m ≥ 25 years 12 coils

3. DESIGN

3.1 Cable

3.1.1 LW Cable (Cable core)

Figure 1. shows the structure of the lightweight cable (LW cable) which is applied to deep water area. The LW cable is also a cable core of the other cable types described in later.

1) Fiber unit

Maximum 24 fibers are stranded as a single layer around the center wire and embedded in UV-cured resin to form a cylindrical fiber unit. Tight type structure of fiber unit gives high stable performance in cable characteristics.

2) Tension member and Copper tube

High tensile steel wires of 2 sizes are stranded around the fiber unit and the copper tube swagged down tightly on the stranded wires are applied. This composite structure has a high performance against the water pressure and lateral pressure performance. Water blocking compound is filled among tension member and fiber unit to prevent water penetration.

3) Sheath

The sheath consists of high density polyethylene, which has good performance for abrasion, is extruded over the copper tube. The sheath has a role of electrical insulation for Electroding.

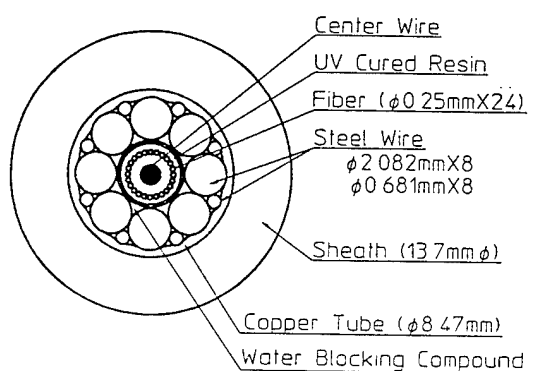


Figure 1 LW Cable

3.1.2 LWS cable

Figure 2 shows the structure of type LWS cable (Light Weight Screened cable). Steel tape is formed longitudinally over the cable core and high density polyethylene sheath is applied. The metal tape protects the cable core from fish bite and/or abrasion encountered in rough sea bed.

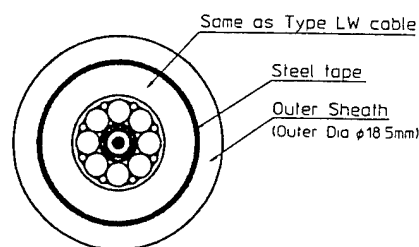


Figure 2. LWS Cable

3.1.3 Armored cable

Two type of armored cable are designed for shallow water area. Structure of the Single Armored cable (SA cable) and Double Armored cable (DA cable) are shown in Figure 3 and Figure 4 respectively.

Table 2 shows the main parameter of each cable.

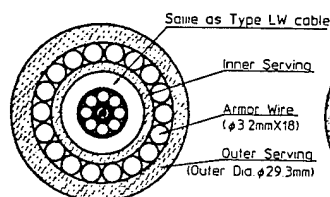


Figure 3. SA Cable

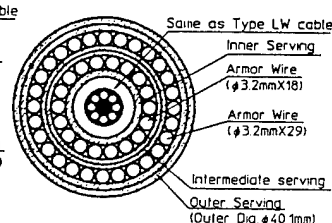


Figure 4. DA Cable

TABLE 2. Cable Parameters

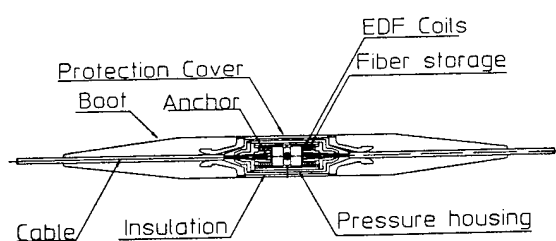
		Unit	LW	LWS	SA	DA
Outer Diameter		mm	13.7	18.5	29.3	40.1
Weight	Air	kN/km	4.66	6.37	18.9	40.5
	Water	kN/km	3.23	3.72	13.2	29.3
CBL		kN	51	51	132	261
NPTS		kN	15	15	30	73
NOTS		kN	38	38	63	127
NTTS		kN	47	47	92	189
DCR (20 °C)		Ω	1.5	←	←	←
IR		Ω /km	1×10 ⁹	←	←	←
Max. Water Depth		m	6,000	5,000	1,500	500

3.2 Joint box

The joint box is used to provide mechanical, electrical and optical connection between cables.

Joint box is applied not only to factory joints but to shipboard joints. Especially, it is important to minimize the jointing time for shipboard joint.

Figure 5 shows the structure of the joint box for armorless cable. Dimension and weight in air are also shown in the figure.



Max.Dia.(mm)	115
Length(mm)	1200
Weight (Kg)	20 (air)

Figure 5. Structure of Joint Box

Key technology to achieve a short jointing time is as follows ;

1) Fiber jointing

The ends of fibers are assembled as ribbon fiber which contains 4 or 8 fibers and splicing of the assembled fibers are carried out. Fiber storage case is designed for assembled fiber splicing technique. As a result, the splicing time can be shortened to approx. 1/3 of the time of single fiber splicing method.

2) Restore of insulation

Pressure housing of joint box are covered with the polyethylene sleeve, and interface between the polyethylene sleeve and cable sheath are restored by the taping technique for shortening the time for assembling.

Polyethylene molding technique can be also applied to the restoration.

In addition the joint box can accommodate the optical amplifier (Er-doped fiber) in the housing with a optical component parts.

4. QUALIFICATION

Qualification on the developed cables and joint box have been carried out in accordance with the test methods described in the relevant recommendation of ITU-T.

Sea trial was conducted to evaluate electrical, mechanical, optical characteristics and handling capability of the cables during laying, holding and recovering in actual sea environment.

1) Qualification on the land

Table 3 lists typical evaluation test items and results.

Figure 6 shows the optical loss change and tension-elongation characteristic in the tensile strength test.

Throughout all tests, the optical loss change satisfied the designed specification.

The cable characteristics are stable, as neither optical loss change nor cable damage is observed even at a load of 4.8 tons close to cable breaking load.

TABLE3. Qualification Test Results

ITEMS	Samples	Test Results
Temperature Stability Target: $\alpha \leq \pm 0.005 \text{ dB/km}$ Condition: $\theta: 0 \sim 35^\circ \text{C}$ Condition: $\theta: -20 \sim 60^\circ \text{C}$	LW LW with JB	$\alpha \leq \pm 0.001 \text{ dB/k}$ $\alpha \leq \pm 0.003 \text{ dB/k}$
Pressure Resistance Target: $\alpha \leq \pm 0.005 \text{ dB/km}$ Condition: $58.5 \text{M} \times 24 \text{hours}$	LW LW with JB	$\alpha \leq \pm 0.001 \text{ dB}$
Tensile Test Target: $\alpha \leq \pm 0.005 \text{ dB/km}$ Condition: $0 \sim \text{NTTS}$	LW,SA,DA	$\alpha \leq \pm 0.001 \text{ dB}$ Refer to Fig.6
Breaking Test Target: $\geq \text{CBL}$	LW SA DA	58KN 147KN 289KN
Mechanical Fatigue Test Target: $\alpha \leq \pm 0.040 \text{ dB}$ Condition: $\text{NTTS} \pm 1 \text{ton} \times 48 \text{hours}$	LW with JB	$\alpha \leq \pm 0.002 \text{ dB}$
Sheave Test Target: $\alpha \leq \pm 0.007 \text{ dB}$ Condition: $\text{NTTS} \pm 1.5 \text{mR} \times 50 \text{cycles}$	LW	$\alpha \leq \pm 0.003 \text{ dB}$
Crush Resistance Target: $\alpha \leq \pm 0.002 \text{ dB}$ Condition: $19.6 \text{KN}/20 \text{cm} \times 1 \text{hours}$	LW	$\alpha \leq \pm 0.000 \text{ dB}$
Impact Resistance Target: $\alpha \leq \pm 0.002 \text{ dB}$ Condition: $20 \text{G}/50 \text{mm}$	LW	$\alpha \leq \pm 0.000 \text{ dB}$
Flexure Resistance Target: $\alpha \leq \pm 0.002 \text{ dB/km}$ Condition: $0.5 \text{mR} \times 50 \text{times}$	LW	$\alpha \leq \pm 0.000 \text{ dB}$
Water Ingress Target: $1000 \text{mv}/2 \text{weeks}$ at 53.6MPa $= 3.3 \text{hours}/100 \text{m}$ at 53.6MPa	LW	14.5hours/100m
Insulation Integrity Target: $\text{IR} \geq 1,000 \text{M} \Omega \cdot \text{km}$	LW,SA,DA	$2 \times 10^4 \text{M} \Omega \cdot \text{km}$
Cable stopper Test Target: $\alpha \leq \pm 0.002 \text{ dB/km}$ Condition: $\text{NTTS} \times 1.5 \text{hours}$	LW,SA,DA	$\alpha \leq \pm 0.001 \text{ dB}$

(α : Loss change)

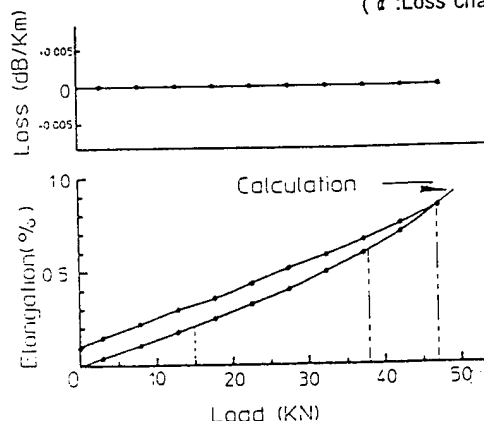


Figure 6. Load-Loss/Elongation Characteristic

2) Results of sea trial

Two kinds of sea trials were carried out to confirm the handling capability of the cables as a final evaluation. The first sea trial was performed to evaluate armored cables including JB in a shallow water area (up to 330 m in depth), and the second sea trial for lightweight cables (including JB) in a deep water area (up to 5400 m in depth).

Figure 8 shows the sea trial diagram and the optical measurement system. The cables for the sea trial contains 12 optical fibers; 6 DSFs and 6 PSCFs, respectively, to evaluate both representative fibers characteristics in the cables.

Because of the severe sea condition, the alteration tension was extreme as shown in figure 9 during laying, holding and recovering in the deep sea area. Sometimes, cable tension increased up to 5 tons (more than NTTs) but cables had very stable characteristics as shown in Table 4. The optical loss change was within ± 0.001 dB/km, and the fiber elongation was within the designed level and reversible against the applied load.

Moreover fine handling performances of cables and joint boxes were confirmed throughout the sea trial.

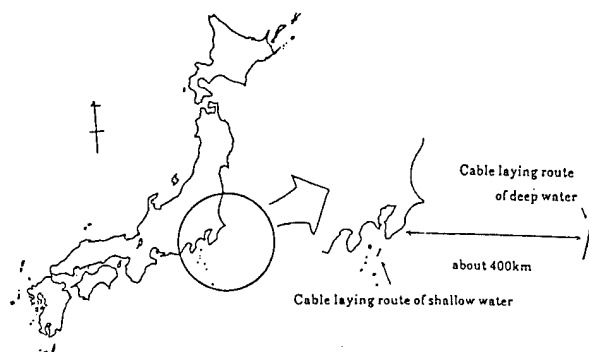


Figure 7. Sea Trial Location

TABLE 6. Results of Sea Trial
(Deep Water)

	Laying	Holding	Recovering
Loss (dB/Km)	PSCF: Max -0.001	Not changed	Max 0.001
	DSF: Max -0.001	Not changed	Max 0.001
Elongation (%)	Max 0.047	Max 0.031	Max 0.047

(UP - DOWN)

	Laying	Holding	Recovering
Loss (dB/Km)	PSCF: Max -0.001	Not changed	Max 0.001
	DSF: Max -0.001	Max 0.001	Max 0.001
Elongation (%)	Max -0.015	Max -0.017	Max 0.031

(UP - DOWN)

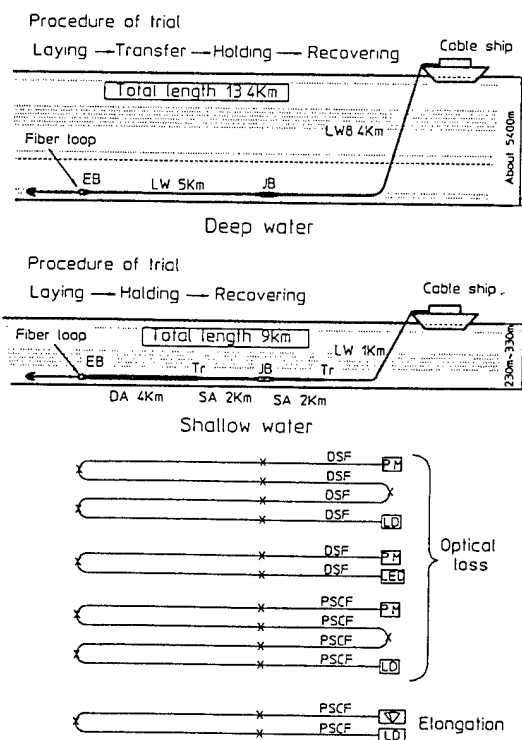


Figure 8. Sea Trial Diagram and Optical Measurement system

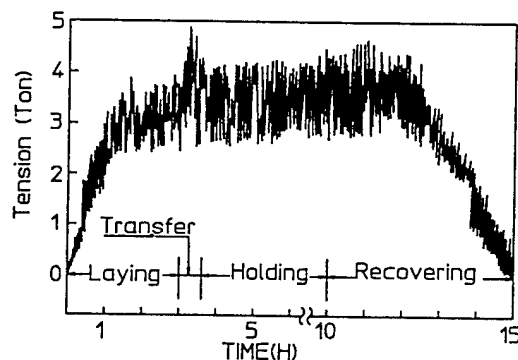


Figure 9. Tension of Deep sea Trial

5. CONCLUSION

OCC has developed new repeaterless optical fiber submarine cables and relevant products to meet the extensive demands to the repeaterless systems. The major characteristics of the cables and relevant products are mentioned below. They will be applied to various repeaterless optical fiber submarine cable systems in future.

- 1) Lightweight, compact cables being capable of accommodating up to 24 optical fibers and providing reliability of more than 25 years.
- 2) The cables can cover sea area up to 6000 m in depth.

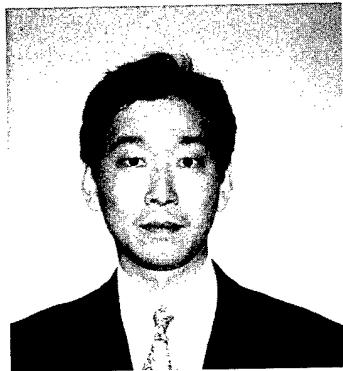
- 3) The cables are highly stable and reliable, in particular optical and tensile characteristics.

6. ACKNOWLEDGEMENT

The authors wish to acknowledge all parties concerned in the development for their assistance and co-operation.

7. REFERENCE

MASAHIKO KIUCHI "Development of small size Optical Fiber Submarine Cable" IWCS '94 234-240



Takato Nishida
Submarine Systems div.
Ocean Cable Co., Ltd.

1-105-2 HIBIKI-MACHI
WAKAMATSU-KU
KITAKYUSHU 808
JAPAN

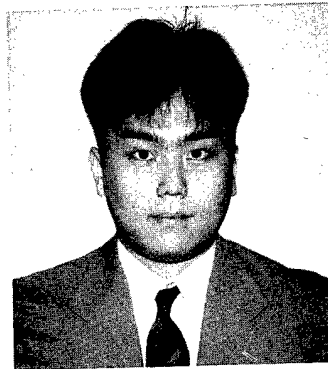
Takato Nishida was born in 1958. He graduated from Musashi Institute of Technology with B.E degree in 1982. He joined Ocean Cable Co., Ltd. and he has been engaged in research and development of optical fiber submarine cable. He is now an assistant manager of submarine systems division.



Masahiko Kiuchi
Submarine Systems div.
Ocean Cable Co., Ltd.

1-105-2 HIBIKI-MACHI
WAKAMATSU-KU
KITAKYUSHU 808
JAPAN

Masahiko Kiuchi was born in 1967. He graduated from Tokai University with B.E degree in 1990. He joined Ocean Cable Co., Ltd and he has been engaged in development of optical fiber submarine cable. He is now an engineer of submarine systems division.



Osamu Nagatomi
Submarine Systems div.
Ocean Cable Co., Ltd.

1-105-2 HIBIKI-MACHI
WAKAMATSU-KU
KITAKYUSHU 808
JAPAN

Osamu Nagatomi was born in 1969. He received B.E degree in 1993 and M.E degree in 1995 from Kyushu University, Fukuoka, Japan. He joined Ocean Cable Co., Ltd. and he has been engaged in research and development of optical fiber submarine cable. He is now an engineer of submarine systems division and a member of SNAJ of Japan.



Hiroyuki Yoshioka
Submarine Systems div.
Ocean Cable Co., Ltd.

1-105-2 HIBIKI-MACHI
WAKAMATSU-KU
KITAKYUSHU 808
JAPAN

Hiroyuki Yoshioka was born in 1954. He graduated from Kyoto Institute of Technology with B.E degree in 1979. He joined Ocean Cable Co., Ltd. and he has been engaged in research and development of optical fiber submarine cable. He is now a section manager of submarine systems division and a member of IEICE and JSME of Japan.

WEATHERABILITY OF POLYETHYLENE BLACK COMPOUND

Yasuhiro Kamei , Shinichi Taoka

UBE Industries, LTD. Ichihara, Chiba, Japan

ABSTRACT

Natural and accelerated weathering tests were conducted for polyethylene specimens with various contents of carbon black. Dependence of crack depth, tensile strength and elongation at break upon exposure time of ultra-violet (UV) light were measured. The results are as follows.

- (1) The crack depth of each specimen became deeper with increase in the exposure time.
- (2) The tensile strength and the elongation at break of each specimen are closely related to the crack depth.
- (3) The degree of damage of a cable can be estimated by the crack depth.

INTRODUCTION

A cable materials using in outdoors must be protected from a damage of a solar light, mainly ultra violet (UV) light. Carbon black is compounded with polyethylene for this purpose. Such polyethylene materials are used for the insulation of a low voltage cable and jacket of a telecommunication cable.

A power cable and telecommunication cable are very important for our current life. If they don't work well, our life becomes very inconvenient suddenly. So the research about the UV performance of these cable materials is very important.

The research about the UV performance of polyethylene began more than 30 years ago, and many reports are represented. Most of the reports, however, investigate the relation between UV performance and mechanical properties.

1). 2). 3). 4). 5)

In this time, we investigated the relation between the UV performance of polyethylene and the

crack depth, and found that the mechanical properties are deeply depends on the crack depth caused by the UV irradiation. We also found that the crack depth depends on the UV irradiation time linearly.

So, by measuring the crack depth, not only the damage level of the materials by the UV irradiation but also the life span of the materials can be estimated.

EXPERIMENTAL

Sample Preparation

Characteristics of polyethylene(PE), carbon black(C.B) and anti-oxidant(A.O) employed as component of carbon black loaded polyethylenes (CBLP) are tabulated in Table 1. Instead of carbon black powder, the master batch composed of carbon black and polyethylene was used because of attaining a good dispersed state of carbon black in CBLP samples. CBLP samples were prepared by melt-blend of the components for 5min at 160°C by means of a Bunbury type mixer with the volume of 2000cc. Compositions of CBLP samples employed in this study are tabulated in Table 2. From these samples, 180mm x 180mm x 1.0mm plaques were molded by compression.

UV Exposure

Accelerated Exposure As an accelerated exposure apparatus, Sunshine Weather-o-Meter(SWOM) equipped with carbon arc lamp in compliance with ASTM G-23 was used. The black panel temperature was 63°C. Water was sprayed for 12min per hour.

Table-1. Characteristics of Components.

material	properties
PE	MFR= 0.1 EVA copolymer (VA content < 3wt%)
C.B	Carbon black : N-110 type Mean diameter : 18milimicron
A.O	Anti-oxidant : phenol type

Table-2. Compositions of Sample.

Sample No.	PE (wt%)	C.B (wt%)	A.O (phr)
A	99.65	0.35	0.2
B	99.30	0.70	0.2
C	98.95	1.05	0.2

Natural exposure Natural weathering was performed in Chiba, Japan where is located at north latitude 35 degrees and east longitude 140 degrees. The samples were faced to the south with the slope of 45 degrees against the horizon

RESULT AND DISCUSSION

Surface of Exposure Sheets

Optical microscope photographs of surfaces and cross sections of various exposure seats are shown in Photo-1. The magnification were x200 for cross section and x40 for surface. From these photographs, the UV irradiation time dependence on the crack occurrence and growing are observed.

Crack growth rate

Fig.1 shows the relation between irradiation time, crack depth and concentration of carbon black. There are time lag (induction time) before occurring the crack in the surface. The induction time becomes longer as the concentration of carbon black increasing. After the occurrence of crack, the crack depth grows in direct proportion to the irradiation time. The growing rate of crack depth becomes slower as the concentration of carbon black increased.

Fig.2 shows the relation between the growing rate of crack depth (slope of the each lines in Fig.1) and the concentration of carbon black. From this figure, the rate of crack depth greatly depends on the concentration of carbon black. A numerical formula of this relation is also shown in this figure. By measuring this crack depth, we can deal the UV performance more quantitatively.

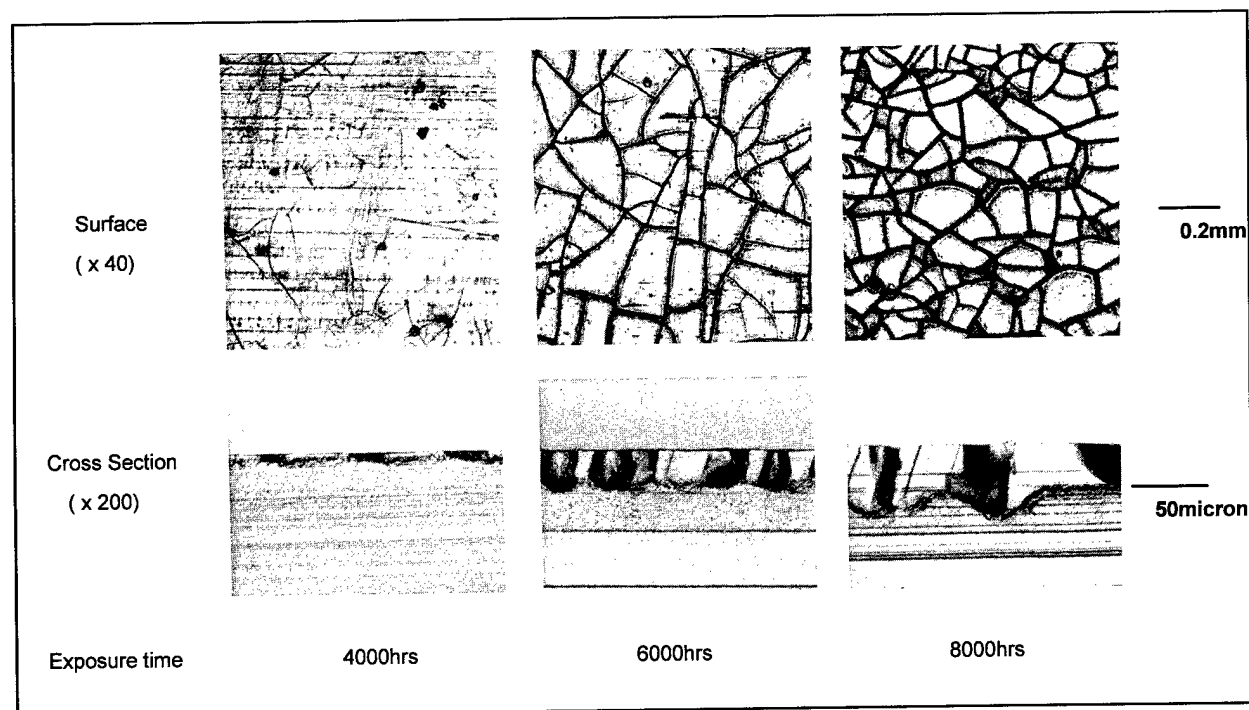


Photo-1 Shape of the Crack that Occurs on an Exposure Sheet (C.B = 0.7%)

Mechanical Properties

Fig.3 and 4 show mechanical properties dependence on crack depth. With increasing the crack depth, mechanical properties decrease. The elongation property is more depends on the crack depth than tensile strength. The crack depth dependence of the tensile strength and elongation are roughly divided in three regions. In the 1st region, the crack depth is below 10 micron, these mechanical properties slightly depend on the crack depth. In the 2nd region, the crack depth is from 10 to 100 micron, the mechanical properties become to depend the crack depth. In the 3rd region, the crack depth is over 100 micron, the mechanical properties fall completely. So the degree of damage of a cable can be estimated by the crack depth.

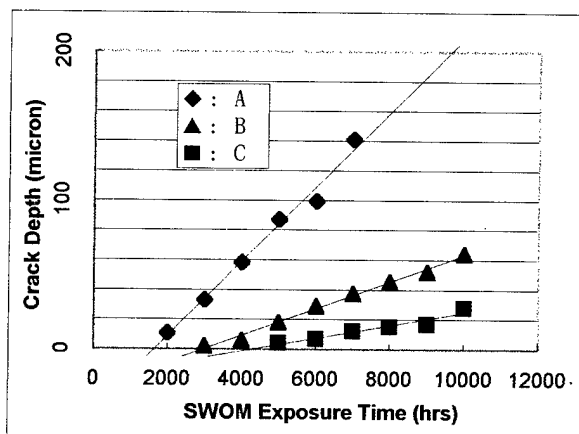


Fig-1. Crack Growth vs. Exposure Time

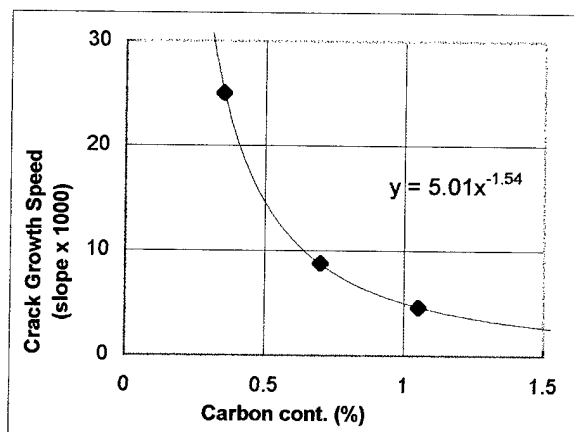


Fig-2. Crack Growth Speed vs. Carbon cont.

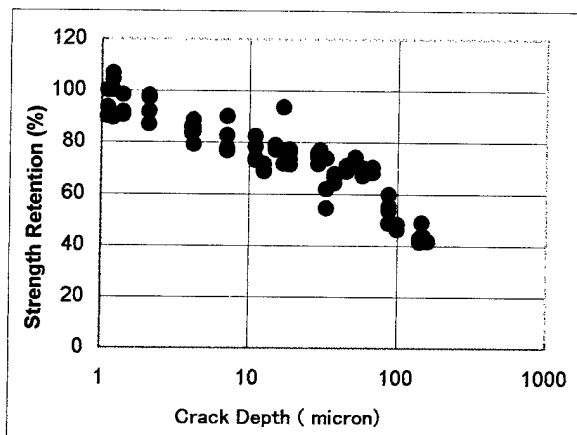


Fig-3. Tensile Strength vs. Crack Depth

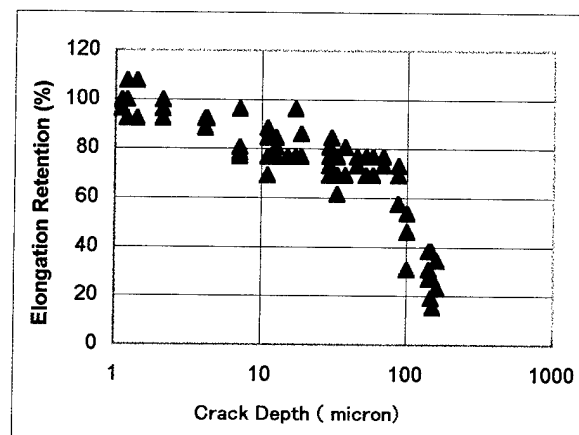


Fig-4. Elongation vs. Crack Depth

From the designing of cable, if the crack depth is below 10 micron it is thought to be safe. So, by checking the crack depth the necessity of exchange of the cable can be judged and we can reduce the extra exchange.

Relationship Between a Natural Exposure

Fig.5 shows the relation between exposure time, crack depth and carbon black concentration. The UV irradiation time to achieve a certain crack depth linearly depends on the concentration of carbon black. From this figure, the concentration of carbon black for the performance of UV irradiation can easily introduce.

Optical microscope photographs of surfaces and cross sections of the seat that was exposed natural weather for 15 years in Japan are shown in Photo-2. The concentration of carbon black is 0.5wt%. The crack depth from the surface reaches 15 microns in these years. To SWOM it approximately corresponds to 3000 hours irradiated sample (calculated from the Fig.5). Therefor, 200 hours of SWOM corresponds about 1year for nature exposure (in Japan).

CONCLUSION

Crack depth dependence of mechanical properties of cable materials are investigated. It was found that crack depth can be used for the measuring of the photo-degradation level.

Crack depth is easy to measure for a small sample. This investigation will helps for a maintenance of cable and design of cable materials.

REFERENCES

- 1) J.B.HOWARD and H.M.GILROY "Natural and Artificial Weathering of Polyethylene Plastics" POLYMER ENGINEERING AND SCIENCE, JULY, 1969, vol. 9, No.4
- 2) F.R.WILLIAMS, et.al, "THE EFFECT OF THE CHEMICAL AND PHYSICAL PROPERTIES OF CARBON BLACK ON ITS PERFORMANCE IN POLYETHYLENE" CABOT CORP. RESERCH AND DEVELOPMENT REPORT.
- 3) "AN ADVANCED CARBON BLACK FOR UV PROTECTION OF CABLE SHEATHING COMPOUND" CABOT CORP. TECHNICAL REPORT S-14A.
- 4) S.H.HAMID. et.al, "WEATHER-INDUCED DEGRADATION OF LLDPE " POLYM.-PLAST. TECHNOL. ENG., 28(5&6), 475-492(1989)
- 5) L.Y.Lee, et. al, "LASER PRINTABLE BLACK CABLE JACKETING COMPOUNDS" 44TH IWCS, 823(1995)

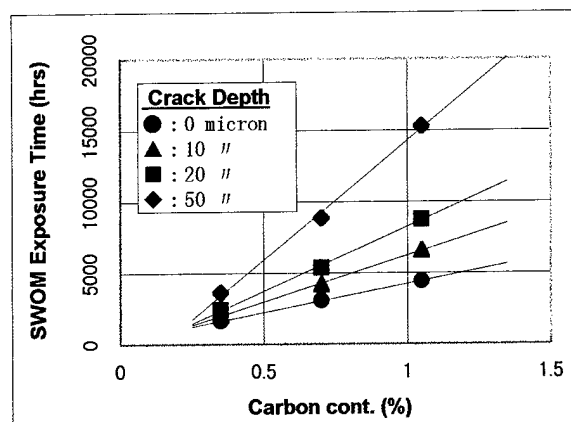


Fig-5. Material Damage.
UV Exposure Time vs. Carbon cont.

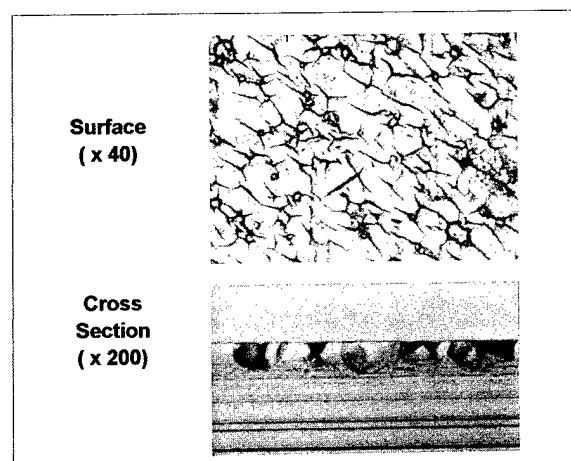


Photo-2. Natural Exposure Sheet
C.B = 0.5wt%, 15years



YASUHIRO KAMEI

UBE Industries, LTD.

8-1, Goi-Minamikaigan, Ichihara, Chiba, 290, Japan

Yasuhiro Kamei received the B.S degree in chemical engineering from Science University of Tokyo in 1985.

He joined The UBE Industries, LTD. In 1985.

He is now an assistant manager of polyethylene team of Research & Technical Dept.



SHINICHI TAOKA

UBE Industries, LTD.

8-1, Goi-Minamikaigan, Ichihara, Chiba, 290, Japan

Shinichi Taoka received the B.S degree in chemical engineering from Kyoto University in 1970.

He joined The UBE Industries, LTD. In 1970.

He is now a manager of polyethylene team of Research & Technical Dept.

STUDY ON ULTRAVIOLET DEGRADATION CHARACTERISTICS OF OPTICAL FIBER RIBBONS

KEIKO SHIRAISHI, HIROSHI NAKAMURA, MITSUO ITO, TAKEO SHIONO

SHOWA ELECTRIC WIRE & CABLE CO., LTD.
4-1-1, MINAMHASHIMOTO SAGAMIHARA KANAGAWA, 229-11, JAPAN

ABSTRACT

It is getting more probable lately that optical fiber cables, which are conventionally installed mainly underground and indoors, are used in a variety of outdoor environment. Degradation characteristics of UV-curable resins for optical fibers and those of optical fibers and fiber ribbons using UV-curable resins under ultraviolet irradiation are therefore studied as a part of reliability study of optical fibers. UV-curable resins used on fiber ribbons are soft, hard and colored resins, and tests are made on these two kinds of UV-curable resins.

INTRODUCTION

Japan is now in the midst of getting into the highly information oriented society represented by digital technologies and computer communication, and the so called Age of Multimedia is about to begin. Demands for optical fiber cables are increasing by leaps and bounds for transmission lines of the new age. In addition, there is a plan in Japan to replace all subscriber lines with optical fiber cables, and demands for optical fiber cables will increase further. It is getting probable, under such circumstances, that optical fiber cables, which are conventionally installed underground and indoors, are used in a variety of outdoor environment.

It is therefore necessary to study reliability of optical fiber cables in outdoor environment, e.g., degradation of optical fiber cable materials and fiber ribbons by ultraviolet irradiation.^{1,2} This study examines degradation behaviors under ultraviolet irradiation of ultraviolet-curable urethane acrylate resins (which are referred to as UV-curable resins) used widely as covering materials of optical fibers and fiber ribbons using such resins.

TEST SAMPLES

Covering Materials (in sheet form)

Table 1 Material characteristics of samples

Sample	A	B	B'
Name	soft resin	hard resin	
Material	urethane acrylate		
Young' s modulus	<0.01	1	1
Elongation	2	1	1
Remarks	·Young' s modulus and elongation are standardized by the values of hard resin B. ·Hard resin B' is hard resin B added with light stabilizer (HALS)		

Table 2 Sheet-forming conditions

	sheet thickness (μm)	irradiation (J/cm^2)
soft and hard resins	200	1.0

UV-curable resins selected for this study are, as listed in Table 1, soft resin A, and hard resin B,³ which are widely used as covering materials of optical fibers. Hard resin B' in the table is hard resin B added with light stabilizer (HALS).

Sheet specimens were prepared under the conditions shown in Table 2 using a metal halide lamp for ultraviolet irradiation for curing.

Fiber Ribbons

The construction of fiber ribbons used in the test is shown in Fig. 1. A single-mode fiber is covered in two layers of a soft and a hard resin in that order, and then coated with a colored resin a few microns thick for identification. Four such colored fibers are then arranged in parallel and covered with a hard resin into a ribbon form.

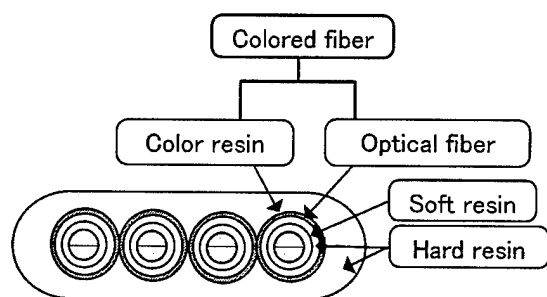


Fig.1 Fiber ribbons structure
(ex. 4 fiber ribbon)

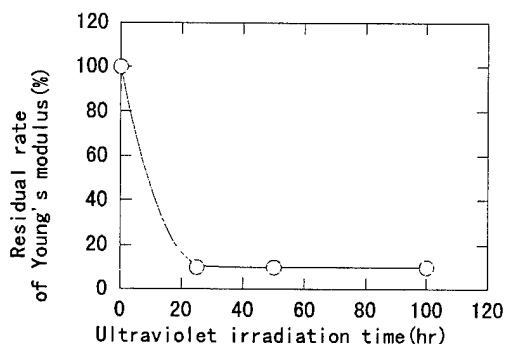
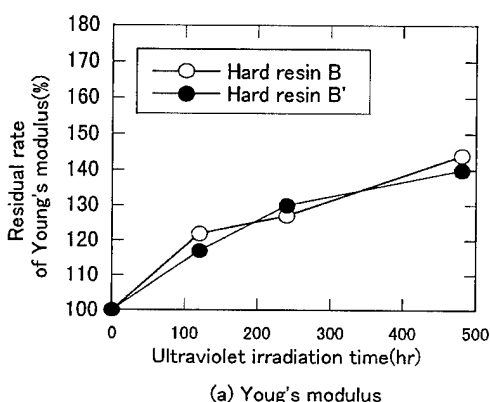
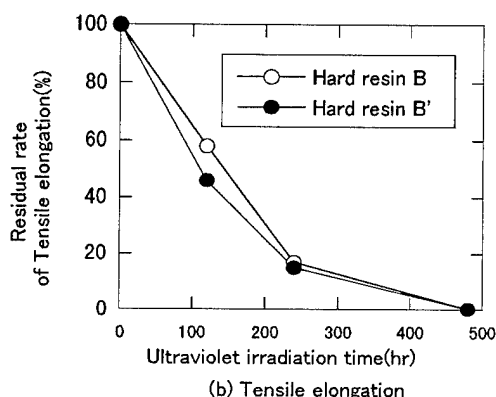


Fig.2 Young's modulus change of soft resin A
(Ultraviolet accelerated degradation test)



(a) Young's modulus



(b) Tensile elongation

Fig.3 Young's modulus and Tensile Elongation Changes
(Ultraviolet accelerated degradation test)

CONDITIONS OF ULTRAVIOLET DETERIORATION TESTS

Accelerated Ultraviolet Deterioration Test

The accelerated ultraviolet deterioration test was carried out, in conformance with JIS K 1415-94, using a sunshine carbon arc as the ultraviolet light source and a black panel of 63°C. Precipitation of 18 minutes every 2 hours was applied.

Outdoor Exposure Test

The outdoor exposure test was carried out, in conformance with JIS K 7219-86, in Sendai, Miyagi, Japan at the height of over 500mm from the installation level. Specimens were directed due south at the elevation of 30° from horizontal plane.

EXPERIMENTS

Sheet Specimens

As for ribbon resins, physical changes were measured by tensile tests giving Young's modulus and elongation. Chemical changes were observed by infrared spectroscopy.

Optical Fiber Specimens of 4 Fiber Ribbons

Optical fibers were subjected to lateral pressure test to measure increase in optical loss at the wavelength of 1.55 μm .

RESULTS

Sheet Specimens

Changes in Young's modulus of the soft resin measured by the accelerated ultraviolet deterioration test are shown in Fig.2, and changes in Young's modulus and elongation of hard resins are shown in Fig.3. Young's modulus of soft resin A decreased rapidly by ultraviolet irradiation, but that of hard resin B increased and its elongation decreased at the same time by ultraviolet irradiation.

Soft resin A, having low Young's modulus, has a

small number of double bonds initially and is low in the cross-link density, and the number of residual double bonds after cross-linking is also low. It is judged therefore that, in the accelerated ultraviolet deterioration test, cutting of main chains of polymer followed by oxidation is occurring mainly, rather than re-cross-linking of residual double bonds, during ultraviolet irradiation.

Hard resin B, having a high initial Young's modulus, on the other hand, has a greater number of double bonds than the soft resin, and thus is high in the cross-link density, and the number of residual double bonds after cross-linking is greater. It is judged therefore that the increase in Young's modulus observed in the accelerated ultraviolet deterioration test comes from re-cross-linking which occurs mainly, rather than cutting of main chains, during ultraviolet irradiation.

As seen in Fig.3, in addition, hard resin B' containing HALS is showing physical changes mostly similar to those of hard resin B, indicating that HALS shows little anti-ultraviolet effect in the hard resin.

An infrared absorption spectrum of hard resin B measured after 480 hours of the accelerated ultraviolet deterioration test is shown in Fig.4. The absorption by carbonyl groups near 1700cm^{-1} is clearly visible even before the ultraviolet irradiation. The absorption width after 480 hours of ultraviolet irradiation is greater indicating the presence of a greater variety of carbonyl groups. Such evidence suggests that cutting of main chains of polymer occurred first by ultraviolet irradiation and then oxidation followed⁴.

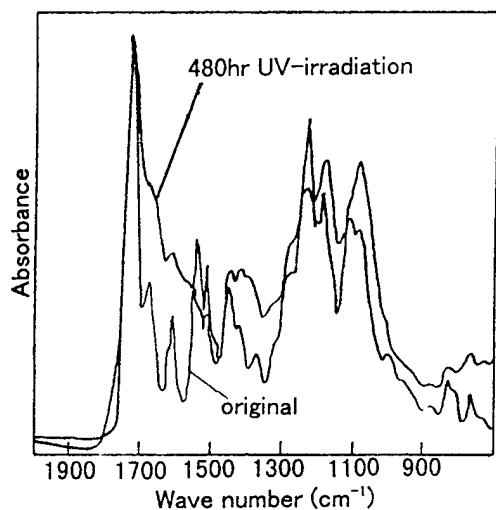


Fig.4 IR of hard resin B

Correlations Between Accelerated Ultraviolet Degradation and Outdoor Exposure

Changes of elongation of hard resin B measured during the outdoor exposure test are shown in Fig.5. As seen in the figure, the elongation decreases as the time of outdoor exposure gets longer. The trend is the same as the case of the accelerated ultraviolet deterioration test.

Correlations between the accelerated ultraviolet deterioration test and the outdoor exposure test were examined as to the time by comparing elongations observed by the respective tests shown in Fig.3 and 5. The result is that 120 hours of accelerated ultraviolet deterioration test roughly corresponds to about 3 months of outdoor exposure test (i.e., the acceleration of the accelerated test is about 20 times of the outdoor exposure test) so far as the elongation of sheet specimens is concerned.

Fiber Ribbons

Ultraviolet degradation Characteristics of fiber ribbons made using soft resin A and hard resin B were evaluated.

Lateral Pressure Characteristics

Lateral pressure characteristics of fiber ribbons were measured at predetermined time points of the accelerated ultraviolet deterioration test. The method and results of the lateral pressure test are shown in Fig.6, and 7, respectively. In the lateral pressure test, the optical loss increment was measured at the wavelength of $1.55\ \mu\text{m}$ while a load (35 kg) was applied to an optical fiber held by sand paper. The loading length was 0.5m.

For the optical fiber subjected to accelerated ultraviolet deterioration, the optical loss increment by lateral pressure was smaller. That is, the lateral pressure characteristic of the optical fiber improved

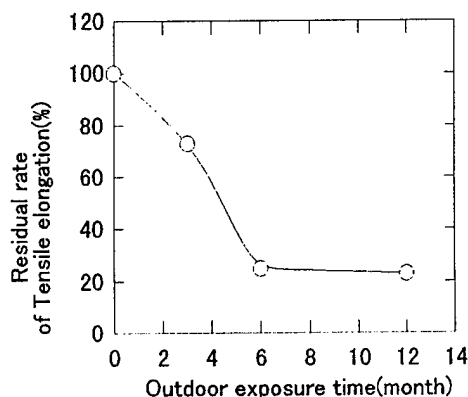


Fig.5 Tensile elongation change of Hard resin B outdoor exposure test

by the accelerated ultraviolet deterioration. It is judged that this improvement comes from Young's modulus of ribbon resin which increases by accelerated ultraviolet deterioration and hence relieves the lateral load to the optical fiber itself.

Optical Fiber Separation

Optical fiber separation refers to a work where the ribbon resin of a 4 fiber ribbon is removed for separation of individual colored fibers. Results of separation of 4 fiber ribbon are shown in Table 3. Optical fiber separation was possible up to 480 hours of accelerated ultraviolet degradation. The hard resin got brittle after 1000 hours of degradation, and it was not possible to separate optical fibers.

Table 3 Separation of 4 fiber ribbons

Ultraviolet irradiation time(hr)	0	240	480	1000
Separation	○	○	○	×

○:GOOD ×:NG

The lateral pressure test was carried out also on colored fibers separated from the fiber ribbon, and results of the test are shown in Fig.7. There was no change in optical loss increment in colored fibers separated after 480 hours of accelerated ultraviolet deterioration. In addition, the appearance and surface of such optical fibers are mostly the same as those of non-irradiated optical fibers. It is judged therefore that colored optical fiber of 4 fiber ribbons show little deterioration even after over 480 hours of accelerated ultraviolet deterioration because of the presence of the ribbon covering.

Bending Characteristics

Bending characteristics of fiber ribbons were evaluated. Relations between the time of ultraviolet irradiation and the bending diameter at which a crack occurred on the surface of 4 fiber ribbon are shown in Fig.8. Cracks occurred at the diameter of about 14 mm for optical fibers subjected to 480 hours of accelerated ultraviolet deterioration, and at about 25 mm for those subjected to 1000 hours of ultraviolet irradiation. As a trend, the bending diameter at which a crack occurs on the surface increases as the time of ultraviolet irradiation gets longer for more deterioration.

CONCLUSIONS

- (a) As for ribbon resins, it has come to be known that Young's modulus of soft resin degrades, but that of hard resin increases during the accelerated ultraviolet deterioration test.

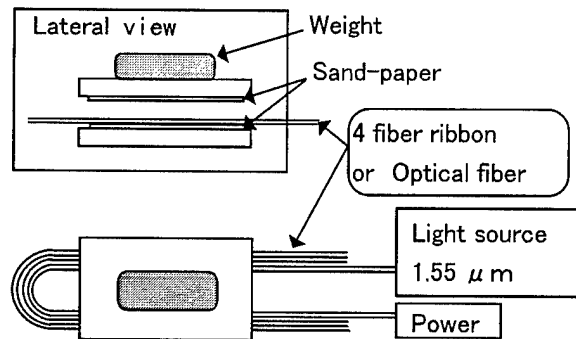


Fig.6 Lateral pressure test method

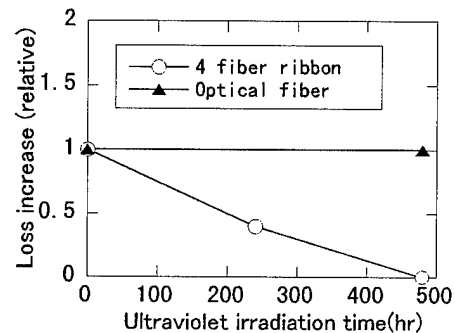


Fig.7 Lateral pressure characteristics

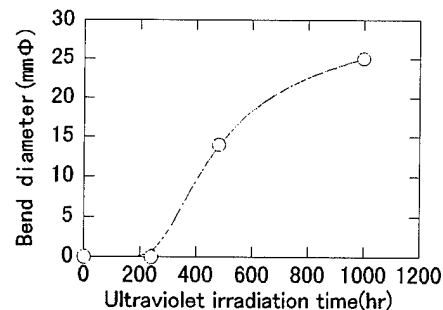


Fig.8 Relative bend diameter of crack occurrence and Ultraviolet irradiation time

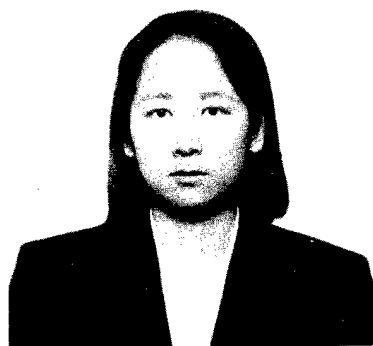
- (b) Effects of the accelerated ultraviolet deterioration test and the outdoor exposure test were compared by measuring elongation characteristics of resins. It turned out, according to the comparison, that 120 hours on the sunshine weather meter was equivalent to about 3 months of outdoor exposure (effecting about 20 times of acceleration)
- (c) As for fiber ribbons, Young's modulus of ribbon resin increased when the ribbon was subjected to accelerated ultraviolet deterioration, and lateral pressure characteristics of optical fibers improved. Cracks occurred more easily on the optical fiber surface in bending test and separation of

optical fibers became more difficult as the elongation of ribbon resin decreased under the accelerated ultraviolet deterioration.

Colored fiber separated from fiber ribbons, in addition, did not show any changes in lateral pressure characteristics up to 480 hours of accelerated ultraviolet degradation. It can be said therefore that fiber ribbons maintain their characteristics for over 480 hours of accelerated ultraviolet degradation.

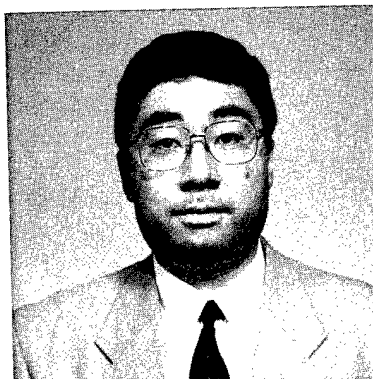
- 1) Shiraishi, et al.:6th Material Life symposium, Material Life Society (1995)
- 2) Shiraishi, et al:B-608 Proceedings of communications society conference of IECE(1995)
- 3) Shiono: Journal of the Japan Society of Polymer Processing ,Vol. 8, NO.5p280-284 (1996)
- 4) B.Ranby et al: "Photodegradation,Photo-oxidation and Photostabilization of Polymer" John Wiley & Sons. (1975)

REFERENCES



Keiko Shiraishi
Showa Electric Wire
& Cable Co., Ltd.
4-1-1,
Minami-hashimoto
Sagamihara
Kanagawa
JAPAN

K.Shiraishi received her B.E. degree from Tokai University in 1993. She joined Showa Electric Wire & Cable Co., Ltd. in 1993. She is an engineer working with the Opto-Electronics R&D of Telecommunication R&D Dept.



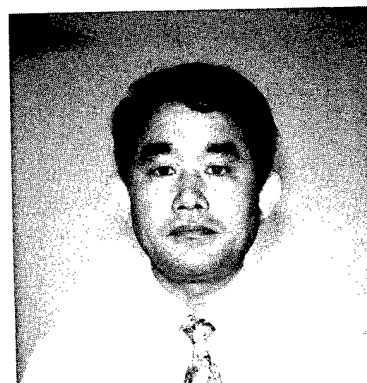
Hiroshi Nakamura
Showa Electric Wire
& Cable Co., Ltd.
1,Nabekura
Funaoka
Shibata-machi
Shibata
Miyagi
JAPAN

H.Nakamura received his B.E. degree from Shizuoka University in 1983. He joined Showa Electric Wire & Cable Co., Ltd. in 1983. He is an engineer working with the Optics & Communications engineering Dept.



Mitsuo Ito
Showa Electric Wire
& Cable Co.,Ltd.,
4-1-1
Minami-hashimoto
Sagamihara
Kanagawa
JAPAN

M.Ito passed from Yokohama Syouko High-school in 1962. He joined Showa Electric Wire & Cable Co., Ltd. in 1962. He is an engineer working with the Opto-Electronics R&D of Telecommunication R&D Dept.



Takeo Shiono
Showa Electric Wire
& Cable Co.,Ltd.,
2-1-1
Odasakae
Kawasaki-ku
Kawasaki
Kanagawa
JAPAN

T.Shiono received his Ph.D. degree in Chemical Engineering from the University of Tokyo in 1979. He joined Showa Electric Wire & Cable Co., Ltd. in 1979. He is the manager of Electric Power R&D Dept.

TRUE THERMAL CHARACTERISTICS OF OPTICAL GROUND WIRES DURING FAULT CURRENT EVENTS ESTABLISHED USING OPTICAL FIBRE DISTRIBUTED TEMPERATURE SENSING

Ian G. Knight

BICC Cables Ltd., Helsby, U.K.

ABSTRACT

Optical ground wires (OPGW) are increasingly being used by power utilities to carry commercial telecommunications traffic. Consequently their reliability is of more concern than it has been at any time since their inception over fifteen years ago.

One of the most severe tests of an OPGW's integrity is its ability to withstand an electrical fault and protect the optical fibres within it. Such events can result in very large temperature rises almost instantaneously.

This paper describes the fault current testing of an OPGW during which distributed optical fibre sensing was used to directly measure the temperatures of the fibres. The impact of the results obtained on OPGW design are discussed.

INTRODUCTION

Optical ground wires (OPGW) were first developed in the late 1970's as a medium for installing fibre optics along high voltage power line routes. The original design concept was to simply place a conventional optical cable core within an aluminium tube and then strand conductor wires around it, to produce a new composite optical cable capable of replacing conventional earthwires. Many variants of OPGW have been developed since these early designs and thousands of kilometres of cable have been successfully installed.

However, despite this successful track record, several fundamental aspects of OPGW performance have remained uncertain over the years, including the temperature to which the optical fibres and various polymeric materials are exposed during electrical fault events. Earthwires are designed such that they do not heat up beyond

a pre-determined maximum temperature, which in the UK is around 180°C, and OPGWs replacing them are expected to exhibit similar mechanical and thermal performance.

Simulated fault current tests are routinely carried out on OPGWs during approval exercises, and traditionally the temperatures which the fibres experience have been considered to be the same as the temperatures measured by thermocouples placed in the metalwork in the outer layer of the cable.

OPGW FAULT CURRENT CHARACTERISTICS

Previous investigations of OPGW fault current performance^{1,2,3} have relied on readings obtained from strategically-placed thermocouples to determine temperatures within the cable structure. This approach is potentially inaccurate, and may lead to misleading results. To gain an accurate understanding of the heat distribution within OPGWs during and after fault events there is a need to be able to measure the radial transfer of heat through the cable, from the metallic strands carrying the short circuit current towards the dielectric core containing the optical fibres. This is important so that the operational environment of the optical fibres can be evaluated and their integrity assured.

Recent technological breakthroughs have produced a distributed fibre optic temperature sensor (DTS) which relies on the temperature sensitive optical scattering phenomena in fibres themselves to measure temperature at every point along the length of the fibre. The most intensively developed of all DTS methods employs the phenomenon of Raman backscatter,⁴ and relies on the temperature dependence of the Raman component of the backscattered light in the fibre.

Combining the analysis of the backscattered

Raman spectrum with conventional optical time domain reflectometry techniques yields a temperature profile along the length of the fibre under test. Pulse length limits the spatial resolution of the DTS system. Pulse repetition rate governs the time needed to obtain a temperature measurement of a given accuracy. Pulse power is also important as this limits the range of the DTS system. There is a trade-off between pulse power, length, wavelength, repetition rates and fibre characteristics that have made the development of an optimum DTS system elusive.

Several trials of distributed temperature sensing systems in power cable temperature sensing applications have been reported in the literature.^{5,6,7,8} The application of DTS systems to OPGW fault event analysis is more unusual and stretches the detection equipment to the limits of its performance. A rapid response time is required (~1 second), whilst needing reasonable spatial resolution because of the short sample lengths used in these tests.

However, the fact that the test samples are short helps because signal levels are not appreciably attenuated due to the fibre length within the sample. Also, the magnitude of the temperature rises experienced, typically > 100°C, means that an accuracy of several degrees in the system is quite adequate to gain a good understanding of the phenomena under investigation.

DESCRIPTION OF TESTING UNDERTAKEN

Cable Design

A strain-free OPGW of the BICC FIBRAL® type (figure 1) was modified for the purposes of these studies. At the centre of this type of design is a core made up of several stranded polymeric loose tubes, each of which houses a number of optical fibres. The lay length of the tubes is chosen to provide a relatively large strain margin (typically ~0.65%) which ensures that the fibres never come under any longitudinal strain under any operational conditions, thus ensuring the maximum possible degree of mechanical protection. The loose tubes are then covered by a layer of thin tapes and a polymeric sheath. This optical core resides in an aluminium alloy tube which affords a high degree of mechanical protection whilst also providing high electrical conductivity. Metallic strands, for further electrical conductivity and mechanical strength, are applied over the tube. The cable is fully filled to prevent longitudinal migration of water.

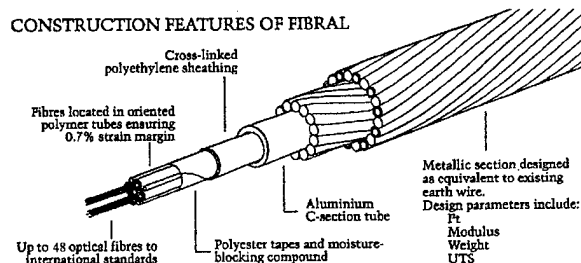


Figure 1. Loose Tube OPGW Design

Several commercial DTS systems are available and the unit chosen for use in this work required the use of 50/125µm fibres which are not normally used in this type of cable. Consequently one such multimode fibre was included in each of the three loose tubes to allow temperature measurement in the optical core.

A small diameter stainless steel tube was included within the single layer of metallic strands surrounding the aluminium alloy tube. This contained a pair of single mode fibres and a pair of multimode fibres, thus allowing simultaneous measurement of optical power and temperature.

The overall diameter of the OPGW was 12.5 mm, and its calculated fault current rating was 57 kA²s. Theoretically this is equivalent to a current of 7.5 kA applied for 1 second being enough to raise the cable's temperature from an initial level of 30 °C to 180 °C.

Experimental Arrangement

A test facility in the UK was identified which possessed equipment capable of allowing up to 40m of conductor to be tested under tension. For the purpose of testing the special OPGW a tension of 500 kg (enough to strain the cable by about 0.1%) was chosen as representative of a typical installation tension. The load on the cable was not adjusted between tests.

All of the sensitive equipment used in the tests was installed a safe distance away from the test area in the observation/control room. A video camera relayed thermocouple readings back to a monitor in the control room. Simultaneously these data were logged to a computer for later examination. The thermocouples were positioned to measure ambient air temperature in the vicinity of the test, and at four places spaced evenly between conductor strands around the circumference of the OPGW.

Optical power measurements (at a wavelength of 1550 nm) were undertaken using fibres within the

optical core of the OPGW during each series of fault current tests. Continuous temperature monitoring during tests was performed by the DTS system using a multimode fibre loop consisting of one of the fibres in the stainless steel tube spliced together with fibres in polymeric loose tubes in the OPGW centre.

A number of short duration currents were applied to the sample. The size, duration, and number of fault currents applied to the samples were variable.

After each fault event the sample was allowed to cool down until its warmest portion approached the ambient temperature. Datalogging continued until the cable almost reached the ambient temperature (typically 10-20 minutes). Visual inspection of the cable was carried out after each event to determine whether any physical damage had occurred.

RESULTS

General

A typical series of DTS temperature vs distance traces collected during an individual test appears in figure 2. Distance along the optical fibre path is represented on the horizontal axis, whilst temperature is on the vertical axis. Each trace shows the temperature profile at a given time (the measurement is made by averaging the transmitted light over a short but finite time, and so does not constitute a truly instantaneous measurement).

The figure shows a rapid rise in temperature over the first half of the optical fibre's path, and a slower rise over the second, right hand half. In this particular case the trace shows temperature of the fibre in the stranded steel tube on the left, and the fibre in the polymeric tube in the cable centre on the right. Thus the metal tube heats up very quickly, whilst there is a lag in the thermal response of the non-metallic core.

Also revealed in the figure is that the temperature in the cable sample is not constant along its length. Hot spots appear at the points near the electrical connections. There is a fibre splice at a distance of 43m, and this is the point where the fibre in the cable core is joined to the fibre in the metal tube. Because of this splicing the points along the fibre optical path at 14m and 71m, and those at 36m and 48m are the same physical points on the cable itself.

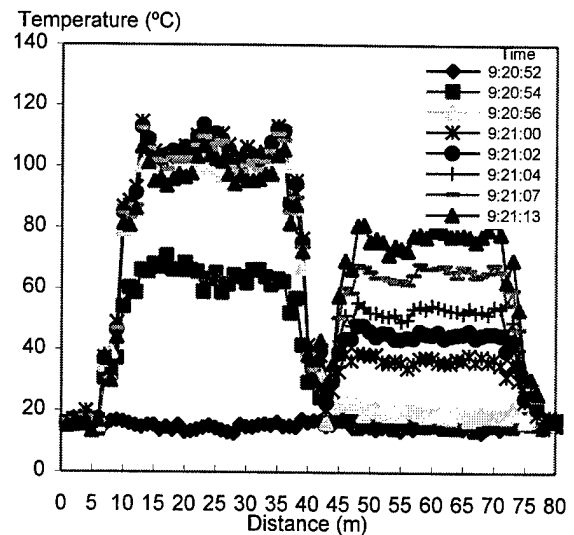


Figure 2. Typical Temperature Profile During Fault Current Test

The large metal mandrel around which the cable is passed in order to allow a tension to be applied to the sample is encountered roughly midway between the electrical connections, at 24m and 60m along the optical path. This gives rise to some curious thermal effects. When a cable was first tested in the morning, or after a long intermission, the mandrel represents a large block of cool material which constitutes a thermal sink, with the result that the cable around it does not reach as high a temperature as other points along the sample. However, after the mandrel has heated up it prevents the cable in contact with it cooling down as fast as the rest of the sample, leading to locally high temperatures during subsequent tests. It also provides some shelter for the cable sample from external environmental effects, such as cooling breezes and precipitation.

The thermocouples applied between and under the OPGW strands were attached at a position about mid-way between one of the electrical connections and the mandrel.

An alternative way of presenting the data obtained is to plot the temperature profile against time for various discrete points along the cable. Figure 3 is an example of such a representation. It shows quite clearly the very rapid heating of the metal tube during after the application of the high current (the current is applied over the course of about 1 second), and also the slower heating up of the optical core.

Two traces are shown for both the metal and

polymeric tubed fibre. One shows the temperature at a point on the large metallic mandrel, and the other is an average of the two points on the cable approximately mid-way between the electrical connections and the mandrel (roughly the same position as the thermocouples).

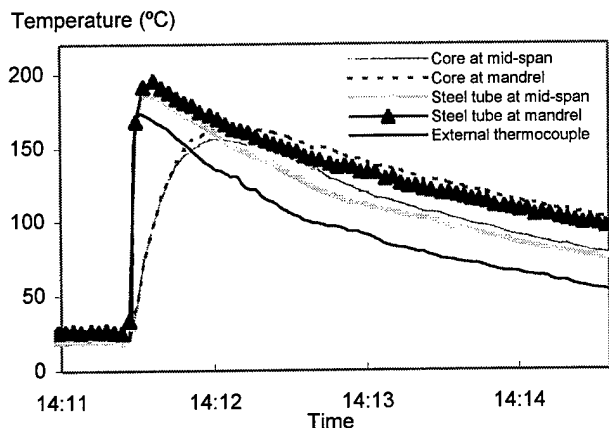


Figure 3. Typical Heating and Cooling Characteristics of an OPGW Under Test

Whilst both of the steel tube traces show a rapid rise and a higher peak temperature than recorded in the polymeric tube, over the course of time the temperatures in the metal and polymeric tubes converge to the same level at the same point on the cable, reflecting a uniform temperature being reached in the cable. It is possible to measure from this data the time delay between the metal tube reaching its peak temperature and the optical core doing so. Typically this delay was in the region of 35 seconds.

Thermocouples consistently recorded lower peak temperatures than those measured by the DTS system. In the phase during and immediately after the application of the fault current this is probably because the majority of the current is conducted along the aluminium alloy tube underneath the wire strands, hence the greatest temperatures are within the cable (although still isolated from the polymeric core). Later, when the temperature distribution has equilibrated across the cable cross-section, the fact that the thermocouples are on the surface means that they will cool more rapidly.

During the testing of the various OPGW samples different levels of fault currents were applied, to a maximum some 40% higher than the calculated maximum rating. No significant attenuation increment was observed during any of these tests, despite temperatures in the core reaching 220°C and those in the stranded steel tube reaching

260°C. No mechanical damage to any of the cable elements was observed as a result of currents up to the design maximum.

Temperature Increase as a Function of I^2t

A large sample of such DTS results was obtained and was used to establish an empirical relationship between the temperature increase experienced by the conductor wires and the magnitude of the action integral (I^2t). Figure 4 illustrates the obtained relationship between the temperature rise experienced by the OPGW and the magnitude of the action integral giving rise to it.

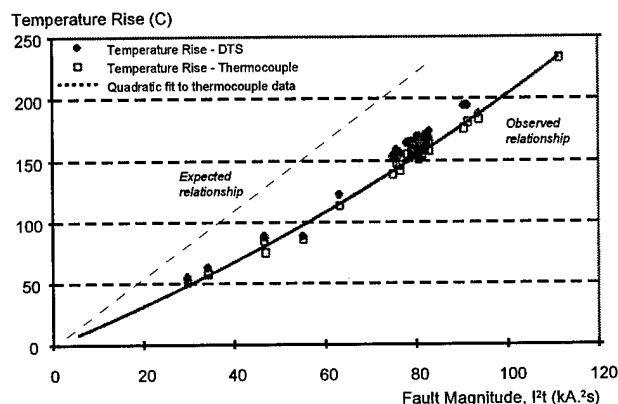


Figure 4. Temperature Rise of OPGW vs I^2t

The temperature rises experienced were significantly less than the theoretical calculations would have suggested. For example, a rise of only about 100°C, instead of the anticipated 150°C, was observed in the metalwork when exposed to the rated fault current for the design. At higher fault currents the relationship was approximately linear.

Temperature Distribution Within the OPGW

The DTS measurements obtained make it possible to directly assess the temperature reached in the optical core of a FIBRAL® type OPGW design during simulated fault events. This relationship is shown in figure 5.

This figure suggests a linear relationship between the temperature increase experienced by the optical core and that affecting the surrounding metalwork. Only 83% of the metalwork's temperature rise is passed on to the core. Thus if the metalwork heated up from 30°C to 180°C then the polymeric core would heat up to only 155°C.

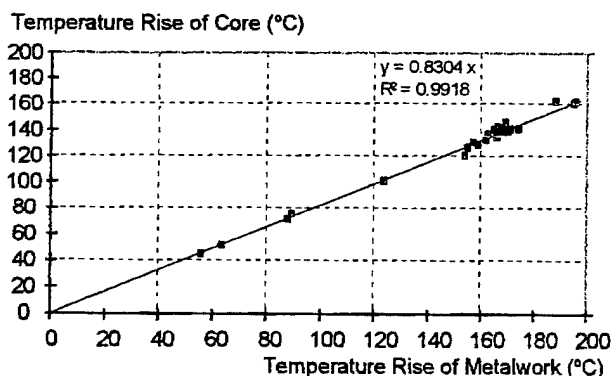


Figure 5. Relationship Between Metalwork and Core Temperature Increases

Not only does the optical core not reach as high a peak temperature as the metalwork, but there is a delay, before it reaches its highest temperature, of about 35 seconds after the fault current flows. Thereafter the core typically has a slightly higher temperature than the surrounding metalwork as heat is gradually lost to the surrounding air.

CONCLUSIONS

For the cable design tested, the temperature rise observed during a fault test was significantly less than anticipated based on the design's calculated fault current rating. The polymeric optical core does not experience as great a temperature increase as the surrounding metalwork. No optical losses were detected during any of the fault events. Together, these facts suggest that the current OPGW design operates within its design criteria, and consequently provides for a high degree of reliability.

A stainless steel tube was successfully incorporated into the OPGW structure and also proved highly resistant to the fault currents applied. However, it is true to say that fibres in such tubes will reach higher temperatures than those contained within the polymeric optical core.

This work also suggests that thermocouples attached to the exterior of a cable sample are prone to lead to anomalous temperature readings.

The DTS system was shown to be a versatile and reliable piece of equipment in this application, allowing temperature traces to be recorded at 1 second intervals.

ACKNOWLEDGEMENTS

The author would like to thank his colleagues in the Telecommunications Cables Systems part of BICC Cables for their assistance in this work, and colleagues at BICC, Erith for the extended loan of their DTS system. The assistance of several staff at the Helsby Technology Centre is also acknowledged.

REFERENCES

- ¹ "Analysis of OPGW Short-Circuit Characteristics", Tanaka, S., et al., Sumitomo Electric Technical Review, p. 147, No. 33, January 1992
- ² "Considerations for Fault Current Testing of Optical Ground Wire", Madge, R.C. et al., IEEE Transactions on Power Delivery, p. 1786, Vol. 7, No. 4, October 1992
- ³ "Performance of Optical Ground Wires During Fault Current Tests", Madge, R., et al., IEEE transactions on Power Delivery, p. 1552, Vol. 4, No. 3, July 1989
- ⁴ Hartog, A., Leach, A., (Nov. 1985), 'Distributed temperature sensing in solid-core fibres'. *Electronics Letters*, Vol. 21, No. 23, 1061-1062
- ⁵ Kent, H., Bucea, G., (Sept. 1992), 'Distributed temperature sensing of high voltage cables - case studies from Sydney, Australia'. *CIGRE paper 21-304*
- ⁶ Harrison, B., Funnell, I., (1991), 'Remote temperature measurement for power cables'. *Proc. 11th International Conference on Electricity Distribution*, paper 3.16
- ⁷ Fitch, A., Basey, W., Nicolls, A.W., (1992), 'Distributed temperature measurement on a power cable using optical fibres incorporated in the construction'. Sixth international conference on dielectric materials, measurements and applications, *IEE Conf. Pub. 363*, 282-5
- ⁸ Angenand, M. et al., (1993), 'Temperature monitoring of XLPE-insulated power cables by means of optical fibres', *Elektrizitätswirtschaft*, 10, 598-602



BIOGRAPHY

Ian G. Knight is head of the cable product design section at BICC Cables' Helsby Technology Centre. He holds a BSc. in Physics with Astrophysics from Birmingham University, and an MSc. in Applied & Modern Optics from Reading University. Since joining BICC Cables in 1990 he has worked in many areas of optical cable design, and in particular in the area of fibre optic cables for overhead power lines.

AGEING OF FIBRES AND RIBBON IN WATER AND FILLING COMPOUND

Jan Björkman
Telia Network Services, Access Networks, Outside Plant
S-123 86 FARSTA Sweden

Torbjörn Svensson
Telia Research AB
S-136 80 HANINGE Sweden

Abstract

The aim of this study on ageing of optical fibres is to find a way of predicting and avoiding possible outages caused by stress-induced failures, and of foreseeing future problems with the handling and identification of fibre. Such problems may arise due to weakening, loss of strippability, discolouring, changes in stress corrosion susceptibility of the fibre, and unknown environmental influences.

Ageing experiments were based on the environments most frequently encountered by fibre: water, jelly, and jelly-coated fibre in water. Ageing temperatures were 23°C and 80°C. Proper cable jellies were supplied by the manufacturers. Aged specimens were tested logarithmically with time, within a one-year sampling period. Three commercial single-mode fibres were tested. Two of these fibres were tested both as single fibres and ribbons.

The tests made here of the aged fibres encompass measurements of fibre strength, stripping force, and complementary observations such as discolouring and delamination of coating. The only drastic changes of post-ageing properties of fibres occurred at a high ageing temperature, 80°C.

In hot water, severe loss of strength of all fibres was observed after sufficient time. In one case the weakening began before one week's ageing, but in the most resistant fibre weakening was delayed by several months.

In cable jelly, all fibres showed a significant increase of strength, and also of their n-values. On the other hand, the n-value was seen to increase also in water.

Finally, an abrupt change of stripping force was observed in one fibre, a total loss of coating adhesion occurred after one year of ageing in water at 80°C.

Background

When the application of optical fibres extends into access networks, this will involve a greater diversity of system components and service environments, as compared to the prevailing transport networks. A growing number of factors which influence the reliability and long-time performance of systems will be encountered: new hardware, harsh and mixed environments, rough handling, tighter specifications, etc.

Although a number of field trials have greatly contributed to the knowledge of factors being crucial for the reliability of fibres and components, new threats may come up. A sure way to trigger potential problems is by scheduled, accelerated testing in the laboratory. The outcome of such testing can be continually studied by various means. Being referred to as well-controlled conditions, the data is of considerable value when extrapolating performance and forecasting failure.

This laboratory study is limited to the most common in-field environment, which is filling compound, water, and combinations hereof. Three types of fibres from cables used by Telia were brought to test. In this paper they are named fibre A, B and C, and ribbon versions of A and C. The fibre coating is polyester urethane acrylate, in all cases.

The test program was scheduled by Telia to run for a 5-year period. This paper presents a summary of the results reported after one year's ageing.

Ageing and testing

Preparation

A loose fibre coil of 200 m length (50 m in the case of ribbon) was put in a cylindrical flat-bottomed glass vessel, a sealed lid being placed on top of the vessel, keeping the ends of fibre outside the vessel. Separate vessels were used for each combination of fibre, ageing temperature, and ageing medium. The ageing media were distilled water and cable gel of appropriate types. Cable jellies were supplied by the manufacturers. The vessels were kept in chambers with a temperature constancy of ± 1 °C. The level of water, when used, was checked periodically and refilled if necessary. Fibre samples were taken after 1, 2, 4, 8, 16, 33, and 52 weeks of ageing, and also on a few more occasions. About 20 m fibre and five m ribbon were taken from the coil on each occasion.

Reconditioning

Before mechanical testing the fibre was reconditioned for a certain period at 23°C, 50% RH, the gel being wiped off the coating. The first samples (1, 2, 4 weeks) were reconditioned only during 2-6 hours. The time for reconditioning was later extended to 7 days (samples 4, 8 weeks, etc) due to the recovery of strength of fibre B on the first days of reconditioning.

Testing

The tests presented here encompass the measurement of fibre strength and n-values, stripping force, and visual observations as discolouring and delamination of the coating.

Bending strength and n-values of fibres and ribbon were measured at 23°C, 50% RH, by two-point bending at four strain rates: 30, 3, 0.3 and 0.03%/min. Samples of 25 fibres or 5 times 4-fibre ribbons were tested at each rate. Regular technique for bending between plates was used. The maximal strain of glass, ϵ was calculated from the diameter of the fibre glass, d_{fb} and the center-to-center distance between fibre cores, d_{cc} by

$$\epsilon = 1.198 \cdot d_{fb} / d_{cc}.$$

The maximal tensile stress in two-point bending follows from

$$\sigma = E_o[1 + (3 \cdot k / 2 - 1/4) / 2 \cdot \epsilon] \cdot \epsilon,$$

In this study it was assumed that $E_o = 70$ GPa and $k = 3$. The value of σ at fracture is the strength, S , from which the n-value of a fibre type is obtained by a linear estimate of the dependence on stress rate, $d\sigma/dt$ of the median strength, \bar{S} of the sample,

$$n = 1 / [d \log \bar{S} / d \log (d\sigma/dt)] - 1$$

The stripping force was measured on reconditioned fibre using the normally applied tools and stripping temperature, which is 90°C for ribbon, and 23°C of single fibre. The tools were periodically checked for wear and damage in a microscope, the knife being replaced a couple of times. The coating was stripped off the fibre along a 30 mm length, at a speed of 60 mm/s. These settings were found most appropriate in order to get a reasonable correspondance with in-field manual stripping. Each strip sample consisted of 10 specimens.

Results

Fibre strength

The two-point bending strength is shown here only at one strain rate, 30%/min, the results at other rates being very similar. Lower-rate curves are just displaced downwards in proportion to the stress-rate dependence of strength. The few diagrams presented, *Figures 1 -- 5*, show median values of strength, and can not give the reader a hint of the scatter between different specimens. Generally the scatter is small, but increases drastically during periods of changes in the average strength because of the inherent characteristics of the test method.

The measurements have shown, that fibre of Type A is the most resistant to water at 80°C. Fibre of Type C showed the quickest degradation of strength, both as single fibre, and in ribbon which is the commonly used form of fibre with this type of coating.

It is interesting to note, that the strength of all fibres and ribbons, A, B, and C was significantly improved by cable jelly at high temperature. The post-ageing strength of fibre was in fact higher than that of unaged fibres.

n-value

The resistance of fibres to stress corrosion in humid atmosphere was measured both before and after ageing. The stress corrosion susceptibility, or the "n-value", was evaluated in the standard climate of 23°C, 50%RH.

In *Figures 6 -- 10* all the curves indicate that high temperature during ageing is beneficial to the post-ageing value of n. In this respect, the advantage of combining gel and hot water is also apparent, especially in fibre B and C. However, the presence of water always leads to a degradation of fibre strength.

It is known that "weak spots" on glass may have significantly higher n-values than are typical for fibres in high-strength condition. In accordance with this, a tendency found here in all fibres aged in hot water, is that higher values of n will develop concurrently with a decreasing value of strength.

In jelly-aged fibre, which still has its original strength there is an improvement in the post-ageing n-value although no weak spots are apparent. During ageing, the gel buffers chemical influences of water. The silane additive apparent in gel may suppress the pH, and aggressors like metal ions may be trapped by other gel constituents. Such effects would prevent corrosion of the fibre during ageing, in this way preserving the fibre strength. The positive influence on n *after* ageing is not understood, however. The n-value is measured after first having wiped off the gel and then reconditioned the aged fibre, so apparently the jelly-improved n-value is caused by permanent effects on the surface of the glass. And the effect has been induced by a coating having properties being altered by ageing. Obviously this is a delicate matter of coating chemistry and reaction kinetics of the glass surface.

The mechanisms behind these observations is an intricate subject which however is beyond the scope of this paper.

Stripping force

Unfortunately, the space allotted does not allow any presentation of all interesting features, e.g the changes of peak in stripping force. In the few diagrams presented here, *Figure 11--15*, the vast amount of data from strip curves has been reduced into simple numbers. One of them is the mean force being averaged along 2 -- 22 mm length of a single strip, the so-called "m.o.s.s". This value has also been averaged, and for each strip sample is presented the "mean of m.o.s.s". See *Figure 11*.

With the exception of what is shown in *Figure 11*, for water in 80°C, the changes in stripping force up to one year of ageing were relatively modest and ageing for reasonably short periods in these environments should not cause any problems with the handling of any of the fibre types. Luckily enough, the degrading fibre strength seems to be accompanied by a diminishing need for stripping force.

However, embrittlement of the coating may cause damage to the glass surface, or bending stresses when handling the fibre. A high level of initial peak force would stress the glass when stripping off the coating. Coating residuals are detrimental for splicing, etc.

Discolouring and delamination

All single fibres were initially transparent, without colouring.

On Type B, a yellow tint is visible after 16 weeks in water at 80°C. As gel-coated, the fibre turns yellow even

earlier, at 4 weeks in water at 80°C, and gets bright yellow after 8 weeks. Ageing during 16 weeks in water at 80°C embrittles the coating, which can be easily peeled off the fibre. Further ageing embrittles the coating so much it is hard to mount in mechanical tests.

Type C behaves in a way similar to that of Type B. The single fibre turns yellowish after 8 weeks in water at 80°C. As gel-coated in water, and in gel only, the fibre turns yellow somewhat earlier. After 16 weeks the coating has a yellow tint (in water), bright yellow (in gel), or intense yellow (gel coated in water). The discolouring is strong after one year in all media at this high temperature.

The strongest discoloration of ribbon occurs when coated by gel in water. After 16 weeks at 80°C it gets a brown tint.

Changes of Type A are quite modest and will not be presented here.

Delamination was observed in fibre ribbons, between the outer protective layer and the coating of each fibre. This may lead to microbend losses and other problems, e.g at freezing. A long term test was therefore run on ribbon in water at 80°C, with simultaneous checks of fibre transmission, during which significant changes in attenuation occurred.

Conclusions

Some fibres resist harsh environments like hot water better than others. Cable jelly is beneficial for fibre strength, but its benefits should not be taken for granted. Factors which may influence the handleability of the fibre, like strength, stripping force, embrittlement and discolouring of coating may vary drastically during the ageing process. Delamination of fibre ribbon may also occur, which increases the risk of microbending losses.

The post-ageing test results obtained indicate some general effects from ageing;

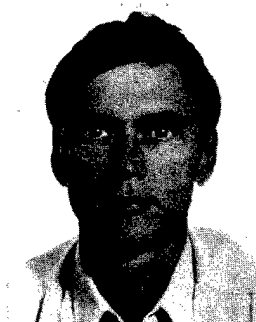
- Ageing at 80°C increases the n-value of fibres.
- The ribbon's outer coating delays/compensates for changes in the strength and stripping force of the fibre.
- An abrupt change of stripping force may occur due to the loss of glass adhesion after ageing in water at 80°C
- Ageing in cable jelly increases the strength and the n-value of fibres.
- Protection of fibre from the aggression of water requires fibre to be completely covered by jelly. Even so, the presence of water will cause degradation of fibre strength.

The authors



Jan Björkman

was born in 1943. With a background in chemical engineering, he joined Telia in 1977, to work mostly with material-related matters, and later with standardization. He is now a senior engineer at Telia Network Services, Access Network, Outside Plant where he is responsible for optical fibres and cables.



Torbjörn Svensson

has a M.Sc. and a Ph.D. from the Royal Institute of Technology, Stockholm. In 1985 he joined Telia where his major engagement was cable and fibre testing techniques, in which field he also holds a number of patents. He is now employed by Telia Research AB, working with the reliability of optical transmission systems and components.

Figures

The diagrams which follow have been so arranged as to make convenient a quick comparison between fibres and ribbon of the same origin. On top of pages are shown the single fibres, on bottom the data from 4-fibre ribbons. Be aware of the mixed order of figure numbers.

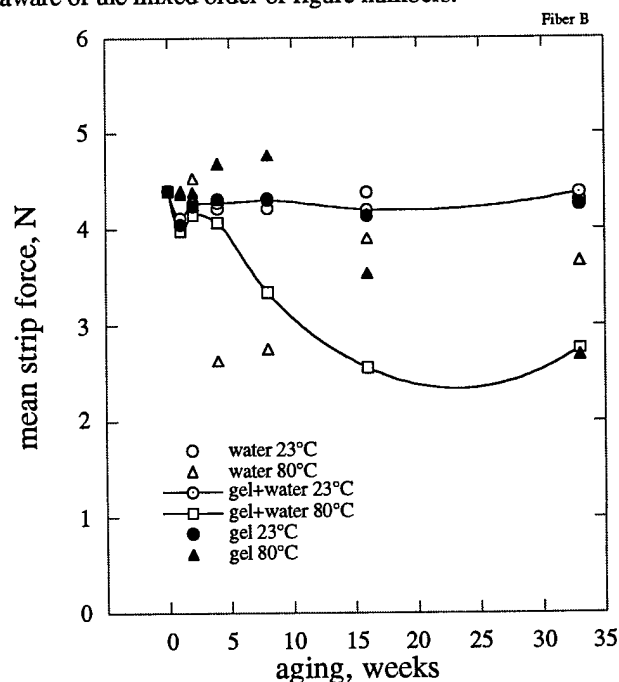


Figure 13. Averaged stripping force of fibre Type B.

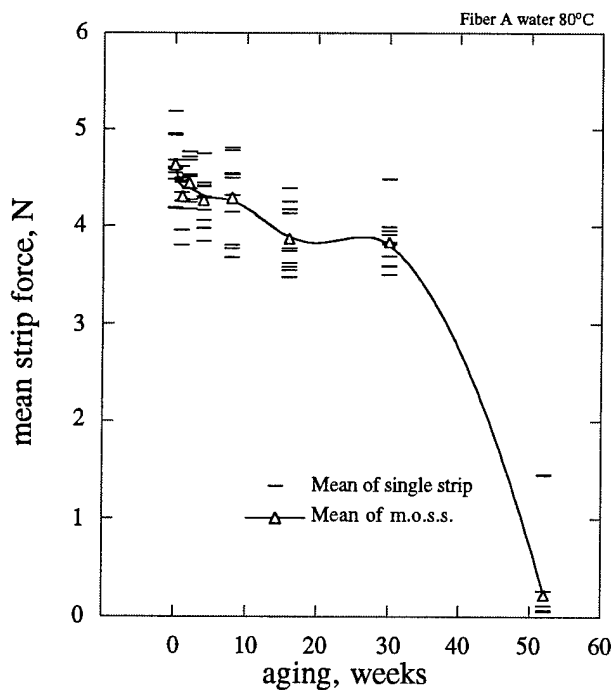


Figure 11. Stripping force of fibre of type A after ageing in water at 80°C. Bars indicate the mean force during a single strip, and the averaged bar values are presented by triangles.

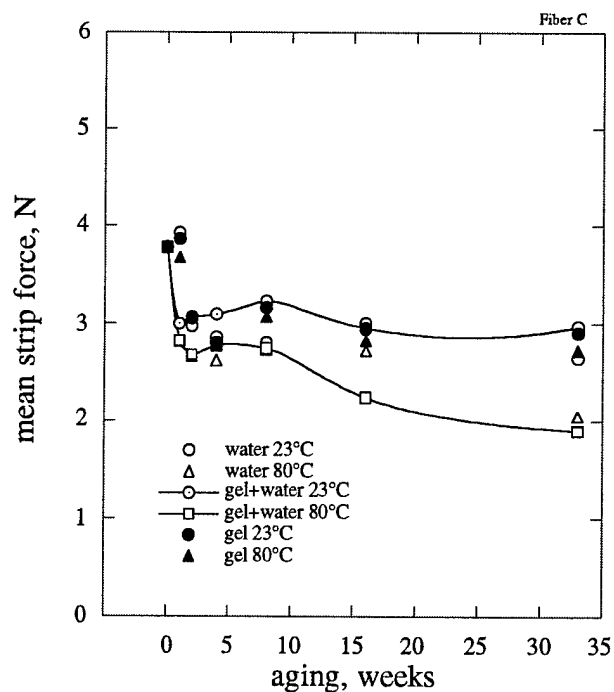


Figure 14. Averaged stripping force of fibre Type C.

Fibre type A and C. Stripping force of single fibre and 4-fibre ribbon

Single fibre Δ

Fibre ribbon ∇

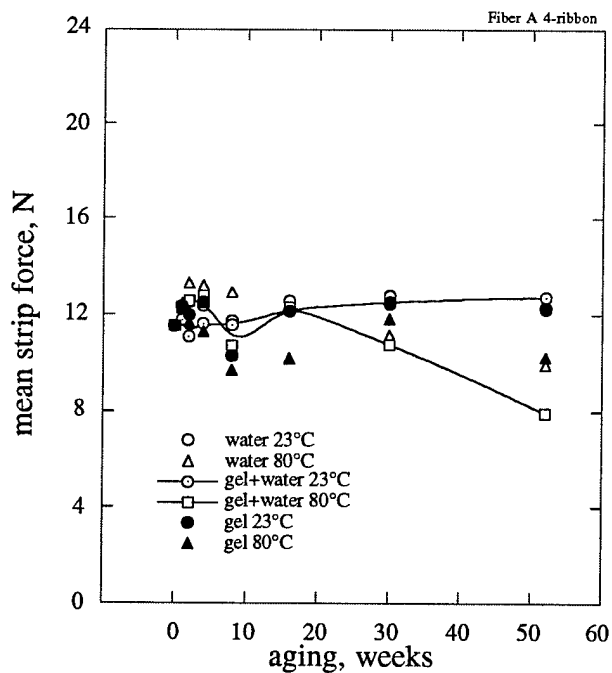


Figure 12. Averaged stripping force of 4-fibre ribbon fibre of Type A.

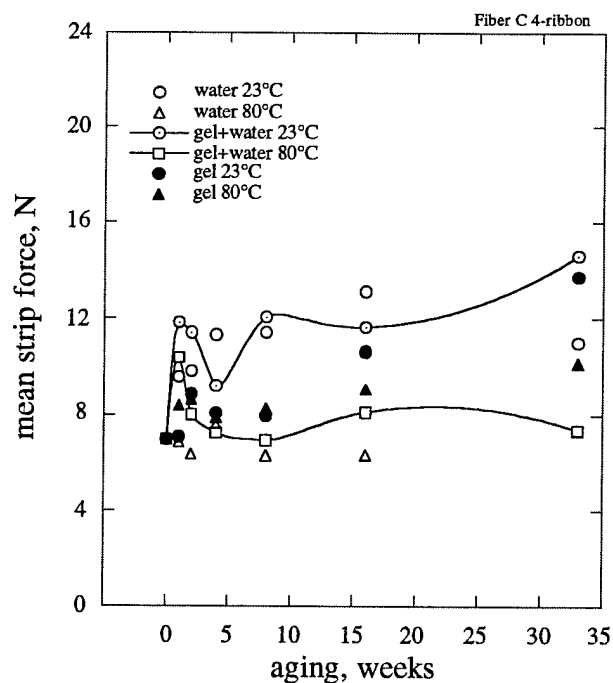


Figure 15. Averaged stripping force of 4-fibre ribbon of Type C.

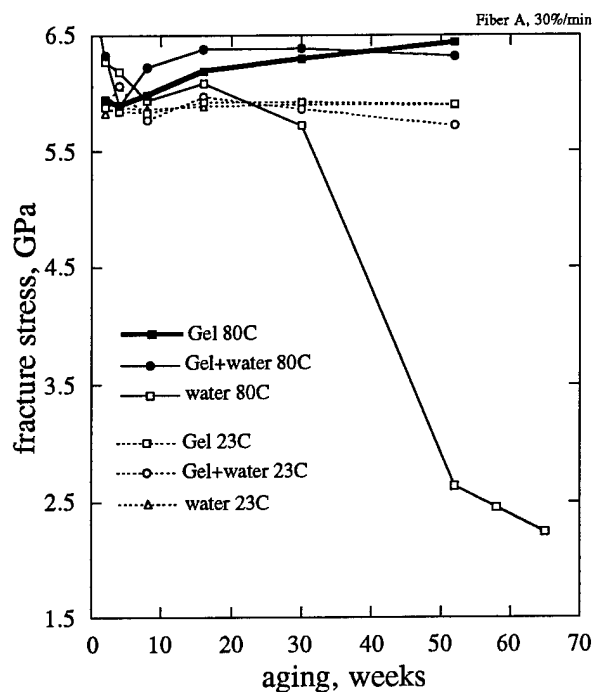


Figure 1. Strength of fibre Type A. Speed 30%/min.

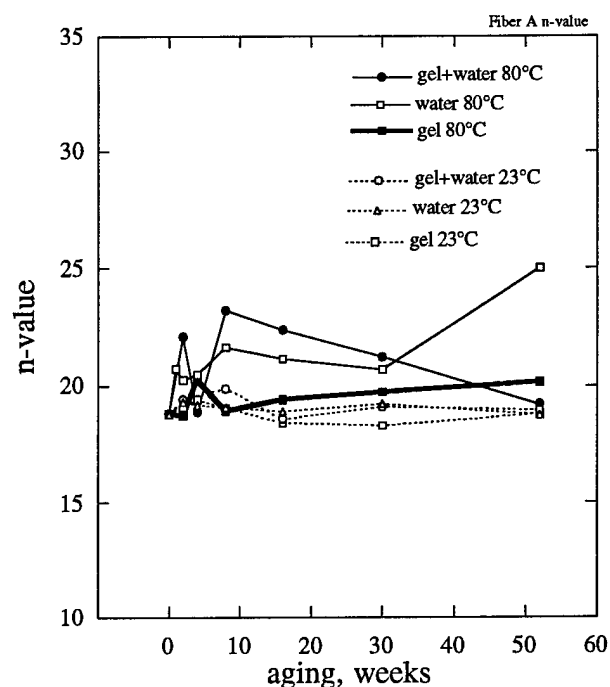


Figure 6. The n-value of fibre Type A.

Fibre A. Strength and n-values after ageing of single fibre and 4-fibre ribbon	Single fibre Δ
	Fibre ribbon ∇

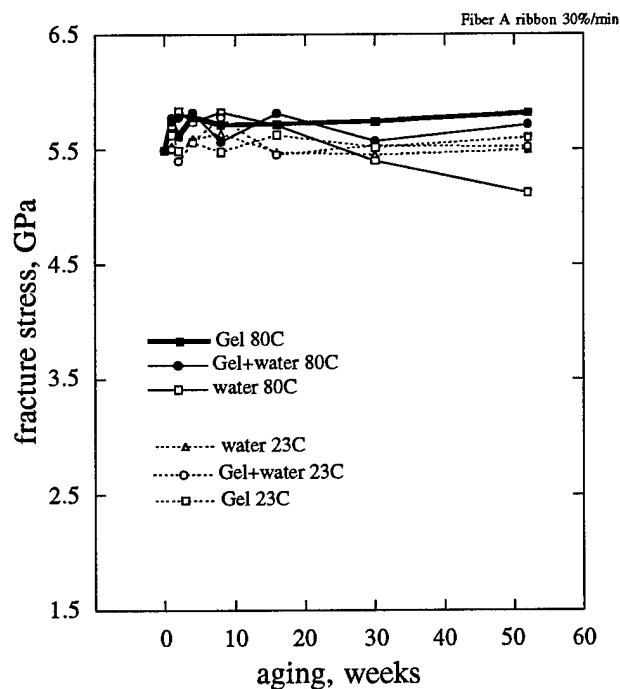


Figure 2. Strength of 4-fibre ribbon Type A.

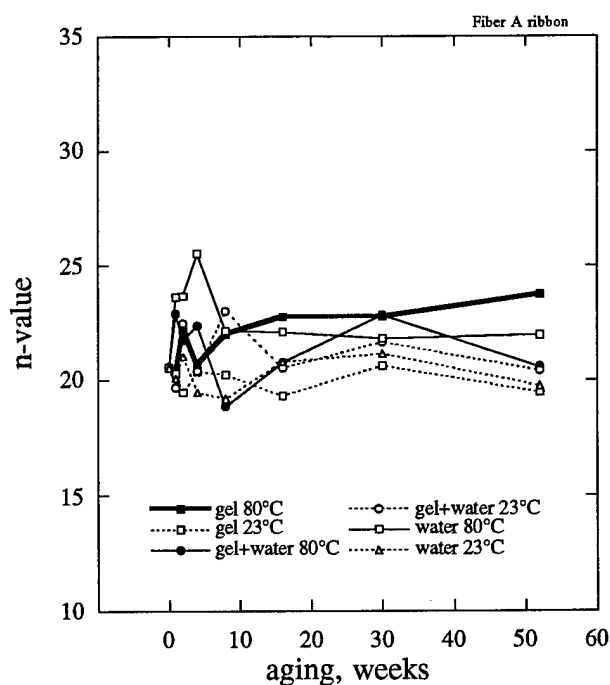


Figure 7. The n-value of 4-fibre ribbon Type A.

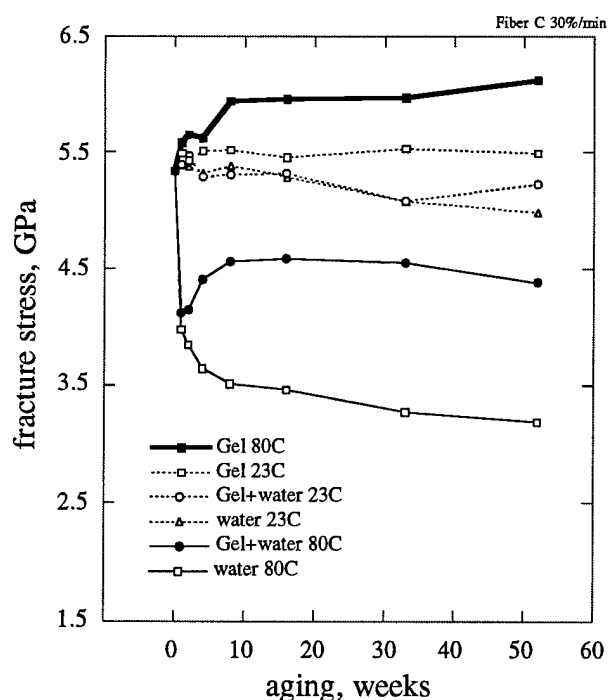


Figure 4. Strength of fibre Type C.

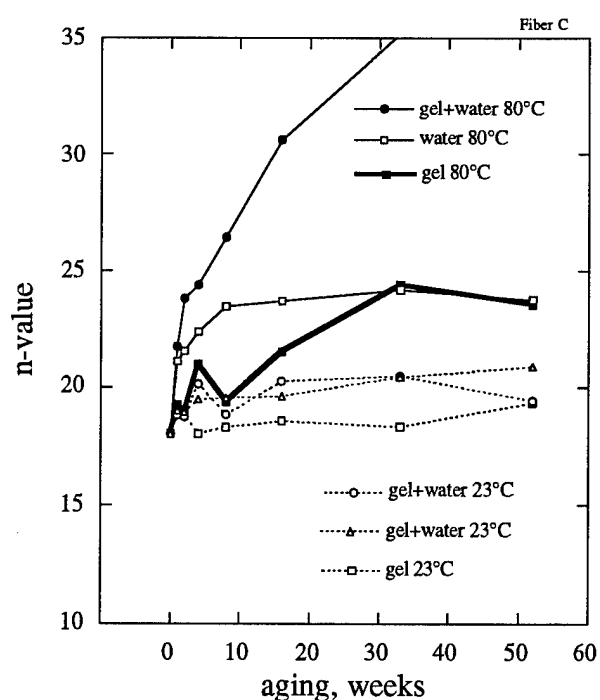


Figure 9. The n-value of fibre Type C.

Fibre C. Strength and n-values after ageing of single fibre and 4-fibre ribbon Single fibre Δ
Fibre ribbon ∇

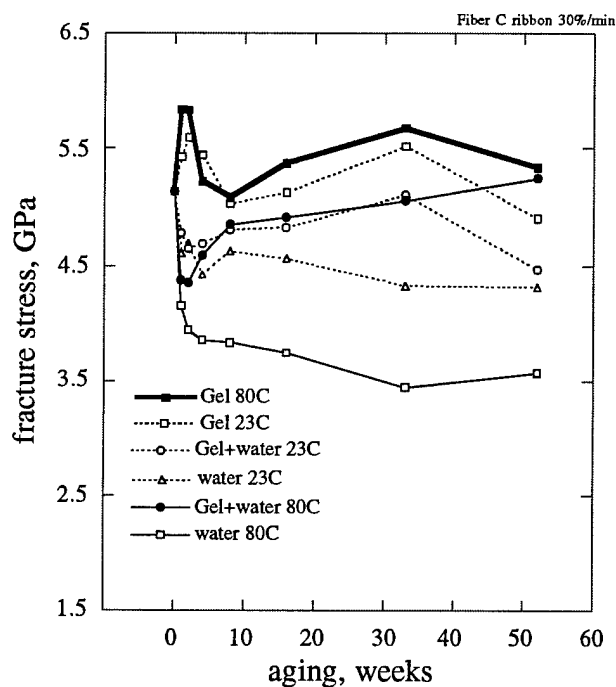


Figure 5. Strength of 4-fibre ribbon of Type C.

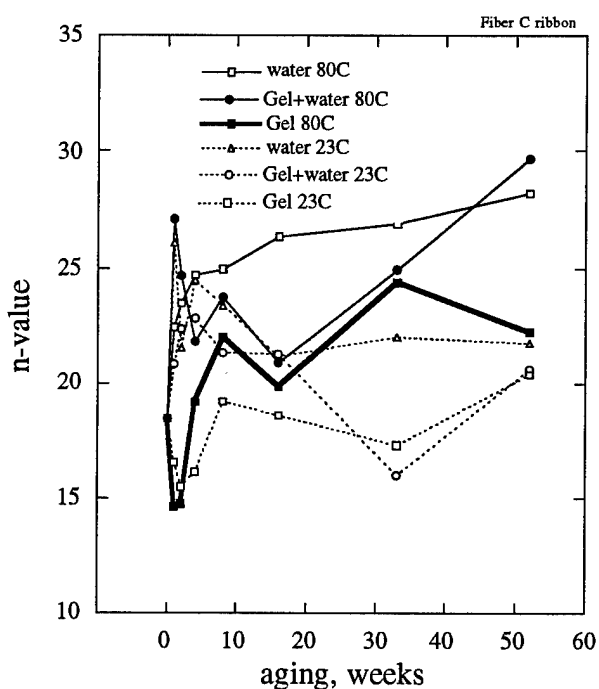


Figure 10. The n-value of 4-fibre ribbon of Type C.

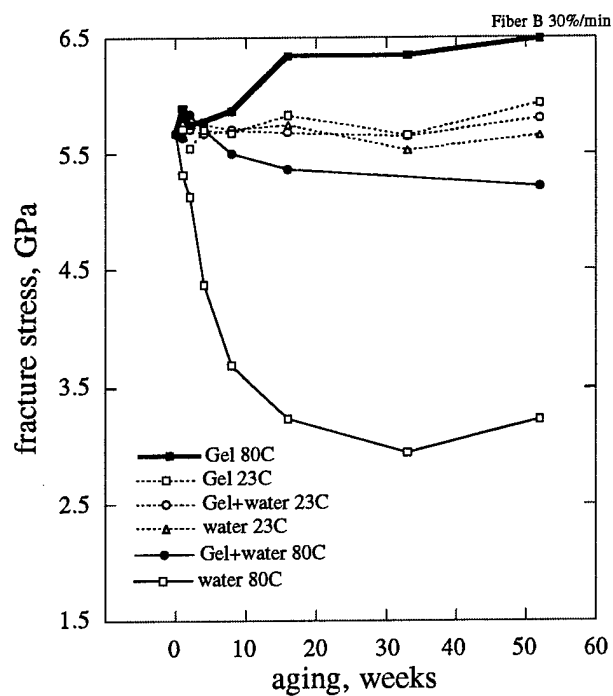


Figure 3. Strength of fibre Type B.

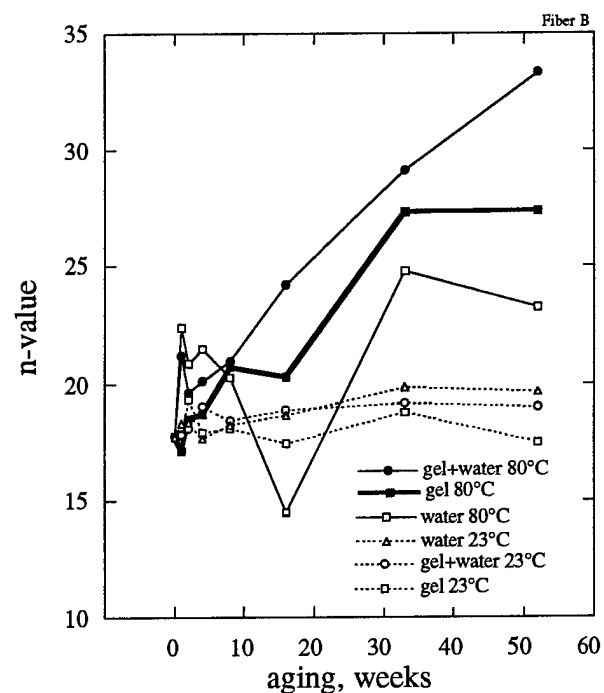


Figure 8. The n-value of fibre Type B.

Fibre B. Strength and n-values after ageing. Only single fibre available

Single fibre Δ

TEMPERATURE AND SPEED EFFECTS ON HAND STRIPPING OF 12-FIBER RIBBONS

Ching-Kee Chien, H. Ralph Cole, and J. Richard Toler
Corning, Inc.
Corning, New York 14831

ABSTRACT

The process of stripping 12-fiber edge-bonded optical fiber ribbons by hand using a thermal stripper has been investigated with the objective of improving the cleanliness of the stripped fibers. While debris remaining on the stripped fibers normally is removed with an alcohol wipe, minimizing the residue improves the chances of obtaining a low-loss fusion splice.

The hand-stripping process was studied by capturing the process on videotape and then analyzing the individual frames to determine the speed of removal of the ribbon matrix and fiber coatings. It was found that the process proceeds at a very uneven speed - the initial part proceeds very slowly, but once the coating bond to glass fails, the speed of the stripper increases quickly.

Temperature was found to have a much bigger effect than strip speed on the stripped ribbon fiber cleanliness. High and low temperatures give more residue than intermediate temperatures.

INTRODUCTION

Optical fiber ribbon cables are being used more frequently because ribbons reduce the time required to splice the fibers, which accounts for a significant portion of the cost of installing cables. When ribbon fibers are spliced in the field, normally they are stripped by hand using a heated stripper to remove the matrix, ink, and fiber coatings. Heated strippers are used because increasing the temperature of the matrix and fiber coatings reduces the force required to remove these coatings to a level below that normally required to break the glass optical

fibers. However, currently available ribbon thermal stripping tools incorporate a temperature adjustment. As a result, a range of temperatures can be found on the heat strip tools which exist in the field. This study was conducted to determine how stripped fiber cleanliness is affected by changes in stripping speed and temperature. Previous papers have covered the control of the stripping process¹ and the roles of the inner and outer primary fiber coatings^{2,3} in the thermal stripping of ribbons.

EXPERIMENTAL METHODS

Strip testing was done with a standard Sumitomo JR-4A heated ribbon stripper. The stripper was either operated by hand or mounted on a Compumotor slide, in which case the speed, distance, and acceleration were controlled by computer. Since previous work on ribbon stripping at Corning has shown no dependence of strip cleanliness on dwell time of the ribbon in the stripper before the stripping process begins, the dwell time in this work was set at 5 seconds for all tests. Stripper temperatures were monitored with a thermocouple placed on the center of the bottom half of the stripper (directly above the heater). The on/off cycle of the Sumitomo stripper was found to produce a temperature range of $\pm 5^\circ\text{C}$. Stated temperatures in this work are given as the middle of this range.

Strip cleanliness was assessed visually under a 2X lens. The rating scale used is shown in Table 1. After the initial inspection, the stripped fibers were wiped with a rubbing alcohol (isopropanol) moistened tissue and the cleaned fibers were re-inspected to determine if all particles were removed.

Table 1

Ribbon Strip Cleanliness Rating Scale

Rating	Appearance
1	Very clean strip - no particles visible under 2X lens
2	≤ 20 particles visible, all removable with one wipe of alcohol-moistened tissue
3	>20 particles visible, all removable with one wipe of alcohol-moistened tissue
4	Many particles visible with no large pieces adhered to the fibers, incomplete removal with one wipe of alcohol-moistened tissue
5	Sections of matrix and fiber coatings remain adhered to the fibers, not cleanable with alcohol-moistened tissue

For all of this work, a 12-fiber edge-bonded ribbon made with standard processes incorporating DSM-Desotech's LTS UV-curable inks, DSM-Desotech's 950-706 UV-curable matrix material, and optical fibers with a developmental fiber coating system were utilized. Ten strips were conducted by hand and the cleanliness rating results were averaged at each condition tested.

RESULTS AND DISCUSSION

Hand Stripping

Investigation of the speeds actually attained during hand stripping of 12-fiber ribbons showed that the speed is extremely uneven. Hand stripping starts at a relatively slow rate. However, after a short period of time (up to one-third of a second), the speed increases rapidly for the remainder of the stripping operation. This is shown in Figure 1 below.

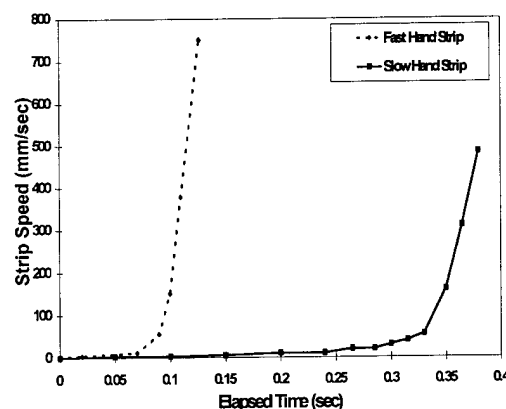


Figure 1 - Hand Strip Speed Vs. Time

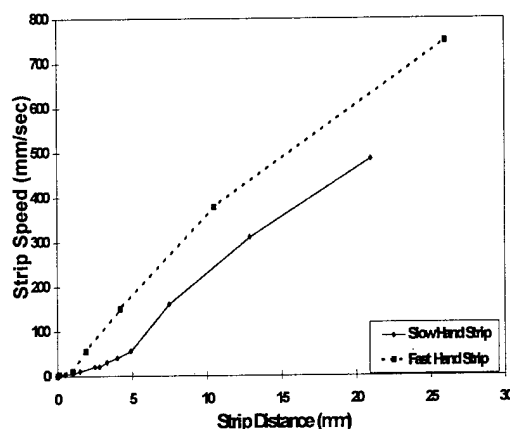


Figure 2 - Hand Strip Speed Vs. Distance

Figure 1 shows that attempting to strip the ribbon slowly by hand just increases the time spent at relatively slow speeds. In both cases, the final strip speed is quite fast and the actual stripping time is practically the same, i.e., less than one second. This is the opposite of the normal perception, in which stripping slowly by hand takes appreciably longer than stripping fast. Figure 2 shows this, in which the two cases are similar in

terms of the speed versus distance traveled by the stripper.

It appears that initially, the coating/ink/matrix material is deformed as force is applied. Once the coating bond to glass is broken, the energy then goes into sliding the tube of coating off the glass fibers. Since sliding the tube of coating from the fibers takes less force than does breaking of the bond to glass, the excess force goes into accelerating the tube removal process. If failure of the coating bond to glass is incomplete, then fragments of the fiber coating remain attached to the glass. These fragments then may be subsequently torn loose by the sliding tube and become particles loosely adhered to the glass fibers when the strip is complete. Such particles are the origin of residue on the stripped fibers. It should be noted that the strip speed vs. time or distance, as shown in Figures 1 and 2, has been observed for two commercial and three developmental fiber coating systems.

Machine Stripping

Ideally, the stripping process conducted by machine should have been carried out at a variety of strip speeds covering the range seen in Figure 1, i.e., very slow up to 750 mm/sec. However, strip speeds in excess of 100 mm/sec were not available for machine stripping during this work. Therefore, ribbon strip cleanliness was evaluated at speeds up to this limit. Stripping of the experimental ribbon at a variety of speeds and temperatures gave the results shown in Figure 3.

As shown in Figure 3, temperatures above 120°C and below 70°C give stripped fibers with more residue than between these two temperatures. Below 70°C, the peak force increases rapidly. This leads to (1) incomplete removal of the matrix/ink/fiber coating tube and (2) one or more broken fibers once the force increases significantly. Above 120°C, the ribbon matrix coating, the ink layer, and the fiber coatings all are converted into powder during the stripping

process. This necessitates more effort in cleaning the stripper between strips in

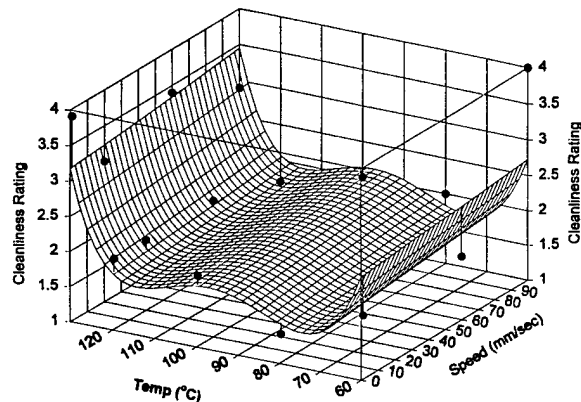


Figure 3 - Ribbon Strip Cleanliness Vs. Temperature and Speed

addition to increasing the residue left on the stripped fibers. The results also show that strip speeds below 100 mm/sec have little to no effect on the strip cleanliness. This pattern of strip cleanliness as a function of temperature shown in Figure 3 also has been observed for many ribbons incorporating a variety of fiber coatings, inks, and matrix materials including commercially available ribbons tested to date. Note that speeds greater than 100 mm/sec were not investigated in this work and might give results leading to different conclusions than those stated here.

SUMMARY

The results of this work lead to the following conclusions:

- (1) The optimum range may differ for other ribbons from that shown here and should be determined for each ribbon type before deciding what temperature range to use.
- (2) Stripper temperature is important in stripping 12-fiber ribbons. Temperatures outside the optimum

range can lead to more residue on stripped fibers and, potentially, to higher loss splices if the residue is not completely cleaned from the fibers.

- (3) The development of ribbon stripping test methods for standards purposes should take stripper temperature into effect since this work shows that temperature can have a large effect.
- (4) Ribbon stripping speeds up to 100 mm/sec do not appear to affect the amount of residue left on the fibers.

ACKNOWLEDGMENTS

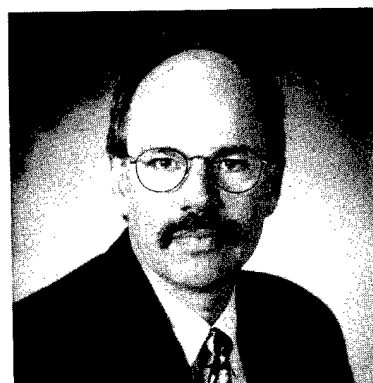
We thank Sandy Coykendall and Clint Hauber for their assistance in coloring fibers and in producing the ribbons tested in this study.

REFERENCES

- ¹ P. K. Kim, N. W. Sollenberger, and K. W. Jackson, Proceedings of the 44th International Wire and Cable Symposium, U. S. Army Communications and Electronics, Fort Monmouth, NJ, 1995, pp. 635-639.
- ² K. W. Jackson, T. L. Parker, J. R. Petisce, N. W. Sollenberger, and C. R. Taylor, Proceedings of the 42nd International Wire and Cable Symposium, U. S. Army Communications and Electronics, Fort Monmouth, NJ, 1993, pp. 28-35.
- ³ R. J. Overton, C. Lasne, H-M. Michaud, and R. G. Sommer, Proceedings of the 42nd International Wire and Cable Symposium, U. S. Army Communications and Electronics, Fort Monmouth, NJ, 1993, pp. 701-707.



Ching-Kee Chien was born in China. He received his B. S. degree in Chemistry in Taiwan and his Ph. D. in Polymer Chemistry from the State University of New York. He joined Corning, Inc. in 1985 where he has worked on coating development for optical fibers.



Ralph Cole is an A&T Associate at Corning, Inc. He received his Associate degree in Electrical Technology from Williamsport Community College and joined Corning, Inc. in 1966. He has worked in a variety of areas including television products, lighting products, and optical fiber coatings.



Dick Toler is Supervisor of Coating Development at Corning, Inc. He received his Ph. D. in Organic Chemistry from the University of Virginia. He joined Corning, Inc. in 1986 and has worked on optical fiber coatings and currently is working on fiber coatings for ribbon applications.

INVESTIGATION OF PULLOUT FORCE FOR COATING ADHESION IN OPTICAL FIBER

Ching-Kee Chien

Corning Incorporated, Corning, New York

ABSTRACT

The pullout force test is used to measure the coating adhesion to glass in optical fiber. The validity of this test is in question. Video study of this test reveals that the coating separates from the glass fiber much earlier than the force reaches to its peak value. The peak force in this test can not represent the coating adhesion. Atomic force microscope (AFM) and electronic spectrum for chemical analysis (ESCA) data suggest a cohesive failure in the inner primary coating, not at the coating-glass interface. Coating shrinkage and the thickness of outer primary coating also play a role to influence the coating separation and peak pullout forces.

INTRODUCTION

An optical fiber is commonly coated with dual layers of acrylate coating to protect it from mechanical handling and field environmental conditions. The inner primary coating is designed to provide optimum adhesion for easy stripping and for maintaining coating integrity under severe environments. One of the challenges is how to measure the coating adhesion to the glass. The pullout force test is widely used to measure the adhesion between fiber and matrix in the composite industry¹. The test is also used to measure the adhesion of coating to glass in an optical fiber among fiber manufacturers². The peak force was designated as the adhesion force. This test is designated as PN-2746 by EIA/TIA. Several papers³ discussed some other factors which can influence the pullout force. They are interfacial pressure, friction coefficient, and work of fracture of the interface. This paper is going to investigate the validity of this test by using video equipment to record the test process.

EXPERIMENTAL

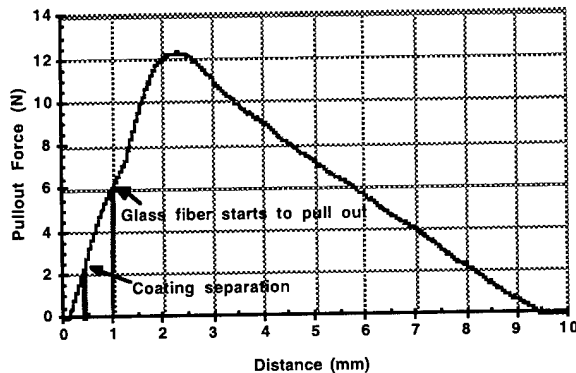
The sample preparation follows the description of the test. The substrate is a 25 mm by 25 mm square microscope slide. The tensile test equipment includes a 10-lb load cell and a Compumotor controlled slide. Two cameras were set up to monitor the fiber movement at the front and the back of the gauged fiber length. The images of the front and the back were superimposed together on a monitor to provide a clear view of coating separation and fiber movement. The test was run at 5 mm/min and the force measurement versus pullout distance was recorded by a computer. As coating separation and fiber movement start, the force measurement was momentarily interrupted to provide a downward spike for marking the events of fiber pull-out.

RESULTS

Video images show the coating starts to separate from the glass shortly after the test begins. The coating separation from the glass fiber was evident from the crack propagation shown at the apparent coating-glass interface. Moments later, the glass fiber starts to pull out from the glued-down coating tube and a bare glass fiber can be seen at the front of the coating tube. The simultaneous movement of the glass fiber at the back end of coating tube was also observed. Both coating separation and glass fiber pull-out were marked electronically in the force measurement. A typical pullout force measurement is shown in Figure 1. It clearly shows that the coating separation from the glass fiber and the pull-out of glass fiber occur much earlier than the force reaches its peak value. In some cases, the glass fiber pulls out of the coating tube about 1 millimeter before the force reaches its peak

value. Therefore, the peak pullout force is definitely not the force to be designated as the coating adhesion to glass. Examined by the atomic force microscope (AFM) and electronic spectrum for chemical analysis (ESCA), the pulled out glass fiber has a thin layer of organic materials remaining on the glass surface.

Figure 1. Pullout force trace vs. distance



These results suggest the coating failed cohesively, not adhesively. In other words, what the test measured is the cohesive strength of the inner primary coating under a tensile load, not the interfacial adhesion force between glass and inner primary coating.

Examination of the same fibers except with a difference in outer primary coating thickness shows a trend in Table 1. The thicker the outer primary coating is, the higher the coating separation and the peak pullout forces are generated. It suggests that part of the peak force is contributed from the cure shrinkage of the outer primary coating. The crimping force from curing the outer primary coating increases the friction and derives a higher coating separation force and peak force.

Table 1. Pullout force of 245 μm OD fiber with different outer primary coating thickness

Outer primary coating thickness (μm)	37.5	32.5	22.5
Coating separation force (N)	4.8	2.9	2.5
Peak pullout force (N)	12.0	9.8	7.2

It is conceivable that the cure shrinkage of an inner primary coating also plays a role. Table 2 shows the pullout force of two fibers. They are exactly the same except with different inner primary coatings. The coating tube can be obtained from a fiber by using the low temperature tubing-off technique⁴. The hole in the coating tube is found to be smaller than the diameter of the glass fiber. The hole shrinkage can be calculated from the difference in the diameter of glass fiber and the hole in coating tube. Among other difference in coating properties, coating A shows a higher shrinkage than that of coating B, which suggest a higher compression force on the glass fiber in coating A and, in result, has a higher pullout force.

Table 2. Pullout force and shrinkage of two fibers with 125 μm diameter of glass fiber

Inner primary coating	A	B
Hole shrinkage (μm)	5.45	0.53
Peak pullout force (N)	23.6	9.1

These results show the peak pullout force can not be designated as the coating adhesion force or the interfacial force between glass and coating. However, the pullout test may be useful for some practical applications, if the failure modes are similar. The pullout force measures the force required to remove a section of coating from glass fiber along the fiber axis under a tensile load. Conceptually, the pullout force can be used as an indicator for strip force of tight buffered fiber and ribbon fiber. Our experience shows the test may be a good approximate indicator for ribbon strip force.

CONCLUSIONS

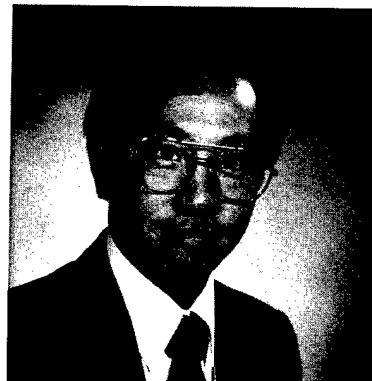
The video recording reveals the coating separation and glass fiber pullout occur much earlier than the peak force. The peak force can not represent the coating adhesion force. Furthermore, the AFM and ESCA results indicate the coating separation is within the inner primary coating, not at the interface. Therefore, the pullout force test is not an adhesion test. Cure shrinkage of coatings and the amount of outer primary coating can influence the pullout force.

ACKNOWLEDGMENT

The author gratefully acknowledge contributions from R.W. Mason.

REFERENCES

1. American Standard Test Method D-1871-84a.
2. Overton B. and Taylor C., Proceedings of SPIE ANTEC, p18-21, 392 (1988); Blyler L.L., Inniss D., and Shepherd L., International Wire & Cable Symposium Proceedings, p239, (1992).
3. Chua P.S. and Piggott M.R., Compos. Sci. Technol., p33-42, p107-119, p185-196 p245-258, vol. 22, (1985); Jiang K.R. and Penn L.S., Comps. Sci. and Technol. vol. 45, p89-103 (1992).
4. Botelho J.W., Optical Fiber Communication, 265, (1994).



Ching-Kee Chien is a Senior Development Scientist at Corning Inc. He received his B.S degree in chemistry in Taiwan and his Ph.D. degree in Polymer Chemistry from the State University of New York. He joined Corning Inc. in 1985 and has worked on coating development for optical fibers.

Color Measurement of Optical Fiber: A Comparison of Visual, Micro, and Macro Methods

S.-H. Chou, J.-C. Lin, C.-M. Hsiao, H.-P. Hsu, Y.-c. Lin, K.-Y. Chen

OSP, Telecommunication Labs, Chunghwa Telecom, Taiwan, R.O.C.

ABSTRACT

Four methods, visual, micro, macro-V, and macro-P, have been used to measure the color of the optical fibers. In this work, the data resulting from four methods are discussed to recognize their correlation and to justify their credibility and practical validity. Visual method provides a personal response but large fluctuation attributed to everyone's different color vision. Micro method supplies extremely low chroma values and sample-specific data. According to the orientation between fiber direction and illumination/receiving geometry, macro-V (perpendicular to each other) and macro-P (coplanar) methods are investigated in this work. Macro-V result has a distorted image due to principle of superposition and reflection law of waves. The conclusion suggests that macro-P method can provide the color data which approach to the personal color imagination and provide credible results.

INTRODUCTION

Color technology is a very complex field; color is a sensation and exists actually in the mind of the viewer only. The stimulus for color is made up of the spectral power distribution curve of a light source, the spectral reflectance curve of an object and the spectral response curve of a detector (an observer).

The principal problem to measure the color of the optical fiber is attributed to the small size of the fiber, 250 μ m in diameter, which is inherent to the optical fiber. For providing a large viewing area near to the size of the standard color chip, usually 20mm by 15mm, the sample of the optical fibers therefore must be laid in an orderly way by hand.⁽¹⁾ The color specification may be performed through the visual measurement or through the use of color measuring instrument.⁽¹⁻³⁾

In visual method, the measurement is executed by comparing with standard color chips. The color data are provided by Munsell notation and the color chips of the Munsell Book of Color as the standards are necessary.⁽³⁾ The standard and the sample must have the same viewing area and are viewed at the same situation. Color is what we see and however is a personal response;

therefore, everyone's color vision is more or less different from anyone else's.

Furthermore, the measurement can be quantitatively performed by using color measuring instruments, spectrophotometer or colorimeter. In instrumental color, due to the small size of the fiber, two methods, micro and macro, were used to measure the color.

Micro method is available to measure an extremely small area, only 4 μ m in diameter, which has been described and discussed previously.⁽²⁾ Because the thickness of the coloring layer for the optical fiber is normally 4 to 5 μ m, a uniform surface however is not easy to obtain. Therefore, the sample location significantly influences the micro results. The data seem more sample-specific due to the measurement area and the uniformity of the coloring layer.

Macro method needs a large viewing area, about 5mm in diameter. Compared with the diameter of the optical fiber, the measurement area by micro method is very small and appears to be flat. On the contrast, the large viewing area is made up of fibers and the pseudo-plane actually includes several curved surfaces. The 0°/45° illumination and receiving geometry was used in macro method. However, due to the fibers placed in good order, different orientations between fiber direction and illumination/receiving may result in different color data. There are two types of the orientations investigated in macro measurement method. One is the fiber direction perpendicular to illumination/receiving plane, called vertical type, or macro-V arrangement, the other is coplanar arrangement, called parallel type, or macro-P arrangement.

Four methods, visual, micro, macro-V and macro-P, are introduced to measure the color of the optical fibers in this work. Three kinds of color notations, (H V/C), (L^* , a^* , b^*) and (L^* , C^* , h), are used to describe the colors. The objective of this work is to discuss the variability of the color data by different measurement methods.

COLOR DESCRIPTION AND MEASUREMENT

Three quantities must be specified to describe color, lightness (V, value), hue (H), and chroma (C). Although

the color notations have been introduced somewhere else,⁽²⁻⁵⁾ it should be noted here again.

A color described by Munsell symbol (H V/C) is used internationally as a basis of color specifications.⁽²⁻⁵⁾ The variables of the Munsell system are presented as a cylindrical polar coordinate system. Munsell Value (V) and Munsell Chroma (C) are expressed by numbers. Munsell Hue (H) is showed by a number and letter combination such as 5R or 10GY where letters represent 10 major hues (Red, Yellow, green, Blue, and Violet, and five intermediates, YR, GY, BG, PB, and RP) and numbers run up to 10, arranged in the same interval on color-ring (called hue circle). Munsell symbol can provide a very clear color sense; the main disadvantage however is the calculation problem.

The CIE system (Commission Internationale de l'Eclairage or International Commission on Illumination) is usually used in connection with instruments for color measurement.⁽²⁻⁵⁾ The 1976 CIE $L^*a^*b^*$ space uses an xyz coordinate system to describe a color, including the lightness coordinate L^* , the red-green coordinate a^* (positive for red, negative for green), and the yellow-blue coordinate b^* (positive for yellow, negative for blue). Comparing with Munsell notation, values of a^* and b^* are used to depict hue and chroma. The main advantage of the $L^*a^*b^*$ notation is the simplicity of the calculation. Furthermore, chroma (C^*) and hue angle (h , in degree) in the CIE system can be calculated by equations (1) and (2), respectively.

$$C^* = ((a^*)^2 + (b^*)^2)^{1/2} \quad (1)$$

$$h = \tan^{-1} (b^* / a^*) \quad (2)$$

Therefore, except (L^* , a^* , b^*), the color data can also be expressed as (L^* , C^* , h). Comparing with Munsell notation, hue is described by an angle in (L^* , C^* , h) data replacing a number and letter combination.

Most modern instruments can be direct-reading in CIE tristimulus values, CIELAB coordinates (L^* , a^* , b^*) and more. The final result of an instrumental color measurement should be a set of numbers describing the nature and magnitude of the sample in color. However, different colorimeters always give different readings for the same colored sample. Therefore, colorimeter readings should never be considered to have any absolute significance and a standard must be provided, such as standard color chips.

EXPERIMENTAL

Six commercially available optical fibers, identified as fibers A, B, C, D, E and F, were used as the samples in this work. Twelve different colors (blue, yellow, green,

red, violet, white, brown, black, aqua, orange, rose and slate) were provided from each supplier. Fibers from A were colored with thermally-cured inks, whereas the others were with UV-cured inks. Generally, the coloring layer cured by exposure to UV light provides a more transparent, thinner and more uniform surface. Four methods, including visual, micro, macro-V and macro-P method, were used to determine the colors of all fiber samples.

For providing a large viewing area, the fibers have to be laid parallel and touching in a holder which is a square hollow with 20mm in each side and about 0.5mm in depth and is made of Teflon plates. Furthermore, the sample containing two layers of fibers orthogonal to each other avoiding background effect is necessary.

Micro measurement equipment has been described previously.⁽²⁾ The measurement diameter was 4 μ m. The 0°/0° illumination and receiving geometry was used. Black background was chosen. The sampling time was 14 sec. The color data were stated as the average of values at ten individual measurement locations to eliminate sample specific problem. Compared with micro method, macro method has some typical different ways as follows. The measurement area was 5 mm in diameter and the sampling time was 2.4 sec due to strong signal. Owing to a large area, the data mean an average of whole area obtained. The 0°/45° illumination and receiving geometry was used. However, there are two different orientations between illumination/receiving geometry and fiber direction investigated, macro-V and macro-P methods.

RESULTS AND DISCUSSION

The colors of seventy-two fiber samples were measured by four measurement methods. Due to a large number of data, only parts of data are represented as examples to be discussed in this paper. If visual method is used, then the colors are presented by Munsell H V/C symbol. If the instrumental methods are used, then the data are originally given by the $L^*a^*b^*$ notation. To discuss color data, transformation of Munsell symbol (H V/C) into (L^* , a^* , b^*) is necessary, and vice versa.

Therefore, to establish the relationship between Munsell notation and $L^*a^*b^*$ notation is inevitable. Firstly, a standard color chip with a given Munsell symbol (H V/C) was measured by a colorimeter to obtain the (L^* , a^* , b^*) data corresponding to this Munsell symbol. Secondly, all (a^* , b^*) points having the same V value should be drawn on an a^*-b^* diagram as calibration reference. Thirdly, the sample color was measured by the same colorimeter, the data (a^* , b^*) then were put on the a^*-b^* diagram having a given L^* value (corresponding to a V value). Finally, depending on the data location related to the points with

the known Munsell symbol, the sample color by Munsell symbol therefore can be obtained.

Blue, yellow and white color data from suppliers A, B, C and E are presented in Table 1. These data measured by all methods are offered by Munsell notation. It clearly shows that the same fiber sample measured by different methods may have significantly different color data, including different hue, different lightness, different chroma, and/or even all. Except this, there are several features displayed in this table.

It should be noted that white is an achromatic color which should have zero chroma value. Actually, as shown in Table 1, the white fibers have somewhat chroma values, about or less than 1 by Munsell chroma value. Furthermore, the data by micro method provide a little low lightness values, probably due to black background effect. By the way, strange hue fluctuation may be attributed to a little colorful color.

Chromatic colors provide some significant meanings. For blue and yellow, although the data measured by different method provides somewhat different hues, the different hues actually change direction slightly comparing with one another. The comparison of the data measured by macro-V with macro-P methods shows that higher lightness values are obtained from macro-V measurements, which are due to different orientations between illumination/receiving and fiber direction. Furthermore, no matter what the supplier is, blue fibers have highest lightness values from micro method, but yellow ones have lowest lightness values. The result from micro method suggests that black background effect becomes more significant for high lightness color, such as white and yellow. Concerning chroma value, the data of micro method have much lower values than those of the other methods, particularly the fibers supplied by B, C and E. The result may be attributed to the low concentration of the pigment and the low opacity of the coloring layer. Furthermore, the inking technology is another factor.

In addition, the yellow fibers supplied from A, C and E have the same data by visual method; different data are obtained by the other methods. There are two possibilities for this issue. Human's eyes are not so sensitive as the colorimeter, or one does not provide enough standard color chips to execute the visual measurement. However, this is one of the disadvantages of visual method.

The color data of green fibers supplied from A and F presented by (H V/C), (L^* , a^* , b^*), and (L^* , C^* , h) are shown in Table 2. The colorimeter is direct-reading in (L^* , a^* , b^*). Using equations (1) and (2) to calculate C^* and h , the color then can be expressed by (L^* , C^* , h).

Furthermore, (H V/C) data also can be obtained by the relationship between Munsell notation and $L^*a^*b^*$ notation. Considering the (L^* , a^* , b^*) data, no matter what the method was used, the green fiber from A has higher values of L^* , a^* , and b^* than those from F. The $L^*a^*b^*$ notation is hard to describe how the hue and the chroma are. (L^* , C^* , h) data can clearly display the chroma values. The comparison of the data of all four methods shows that the data measured by macro-P method provide higher chroma values and are near to those measured by visual method, and ones measured by micro method have extremely low chroma values, specially ones from F. The data presented in Tables 1 and 2 exhibit that different inking technology influences the color data of fibers. The colored fiber cured by exposure to UV light provides an extremely low chroma value due to a more transparent and thinner surface. (L^* , C^* , h) data depict quantitatively the hue difference in degree.

Actually, a^*-b^* diagram and L^* diagram are clear to explain the experimental results. Figures 1, 2 and 3 show the L^* data for 12 colors graphically through L^* diagrams corresponding to suppliers A, D and F, respectively. The points marked the same symbol exhibit that they are measured by the same measurement method. To discuss the data by different methods, the difference below 5 is assumed within experimental error.

For all samples from six suppliers, the L^* values of white and yellow fibers have lowest lightness values measured by micro method comparing with the other methods. On the contrast, the other colors have highest values by micro method and lowest ones by macro-P method. However, white and yellow have much higher lightness value than the other colors. The result concludes that black background effect becomes more significant for high lightness color in micro method. Another feature has to be noted that the data obtained by visual method have large fluctuation and are distributed over a wide range. It implies that everyone's color vision is different from anyone else's. However, although the data by visual method have large fluctuation, the data by macro-P method and visual method are much closed to each other.

Figures 4 to 7 show all (a^* , b^*) data for chromatic colors graphically through the a^*-b^* diagrams that correspond to suppliers A, B, C and E, respectively. The point near to the zero point means that it approaches to an achromatic color. Among the data, no matter what the supplier is, ones obtained by micro method are much near to the zero point shown as achromatic colors. However, with micro method, the chroma values of fibers from A are 23 on average, whereas those from the other suppliers are 13. It shows that the coloring layer cured by UV light supplies low chroma values. Therefore, the inking technology is an important factor to influence the data. Considering the figures, the data by macro-P method and visual method

provide similar and high chroma values, whereas macro-V method provides low chroma values. Furthermore, the higher the chroma values, the more the difference between those obtained by macro method and micro method.

The interesting results are attributed to the essential difference between micro method and macro method, and between macro-P method and macro-V method. Although optical fibers may not provide a wholly uniform surface, small measurement area is supposed to be a uniform surface. On the other hand, the large area by placed the fibers provides a uneven surface, which may affect the signal to the photo detector.

Back to consider the definition of macro-P and macro-V arrangements, by macro-P method, all reflected lights back to the photo detector are still guided at the same direction. Owing to curved surfaces, some positions provide high lightness and the others have low lightness. Therefore, the data by macro-P method should have slightly low lightness value and more accurate chroma and hue values. Macro-V arrangement is the fiber direction perpendicular to illumination/receiving plane. The lights back to the photo detector are reflected from different directions. Due to principle of superposition, construction or destruction, the information from the reflected lights may have a distorted image. Therefore, the result suggests that macro-P method is better than macro-V method attributed to reflection law of waves and principle of superposition.

SUMMARY

Color measurements of optical fibers using visual, macro-P, macro-V, and micro methods have been performed. Different measurement methods however may result in different color data. The result therefore suggests that obtained from the same measurement method, the color data then are comparable. The illumination area and the fiber orientations related to illumination/receiving plane are two important factors to influence the color measurements. It concludes that macro-P method is the best one to measure the color of the optical fiber.

REFERENCES

1. TR-NWT-000020, Bell Communications Research, Technical Reference, Issue 5, 5-8, 1992.
2. J.-C. Lin, S.-H. Chou, C.-M. Hsiao, H.-P. Hsu, Y.-c. Lin and K.-Y. Chen, *Proc. 44th IWCS*, 502, 1995.
3. "Principles of Color Technology", F.W. Billmeyer, Jr. and M. Saltzman, 2nd ed., John Wiley & Sons Co., 1981.

4. R.A. Frantz and I.M. Plitz, *Proc. 42nd IWCS*, 850, 1993.
5. B.J. Keon and R.A. Frantz, *Proc. 43rd IWCS*, 522, 1994.

TABLE 1. Color data (H V/C) of blue, yellow and white fibers from suppliers A, B, C and E by four measurement methods.

	method	A	B	C	E
BL	visual	2.5PB 3/10	10B 3/8	5B 4/8	2.5PB 3/10
	macro-P	3PB 3.0/10.7	10B 3.0/9.0	5.5B 3.9/9.0	2PB 2.9/11.0
	macro-V	5PB 3.9/9.0	2.5PB 4.1/8.5	9B 4.6/7.5	5PB 4.0/8.5
	micro	3PB 5.0/8.0	4.5PB 4.7/2.0	10B 5.0/2.5	5PB 4.5/2.5
YL	visual	2.5Y 8/14	7.5Y 8/12	2.5Y 8/14	2.5Y 8/14
	macro-P	2.5Y 7.8/13.0	6.5Y 8.0/10.0	2.5Y 7.8/12.0	2.5Y 7.7/12.0
	macro-V	2.5Y 8.0/11.0	7Y 8.3/8.5	2.5Y 8.2/10.0	2.5Y 8.2/10.0
	micro	5.5Y 6.9/5.5	9Y 5.9/1.5	6.5Y 6.7/4.0	7.5Y 6.7/3.5
WH	visual	N 9.5	10YR 9/1	0.5Y 9/1	10YR 9/1
	macro-P	7.5Y 8.8/0.3	4Y 8.8/1.1	10YR 8.6/0.7	9YR 8.5/0.8
	macro-V	1GY 9.0/0.4	3Y 9.1/1.0	10YR 9.0/0.6	9YR 8.8/0.6
	micro	4PB 8.4/0.3	2.5Y 7.7/0.2	3.5RP 8.5/0.1	5PB 7.1/0.3

TABLE 2. Color data of green fibers from suppliers A and F by four measurement methods described by (H V/C), (L^* , a^* , b^*) and (L^* , C^* , h).

	green	H V/C	L^* , a^* , b^*	L^* , C^* , h
A	visual	2.5G 5/10	47.50, -51.63, 19.30	47.50, 55.12, 159.5°
	macro-P	2.5G 4.4/8.5	42.21, -44.78, 18.29	42.21, 48.37, 157.8°
	macro-V	2.5G 5.0/6.5	47.66, -35.19, 13.72	47.66, 37.77, 158.7°
	micro	3.5G 6.0/4.5	58.04, -25.90, 9.20	58.04, 27.48, 160.4°
F	visual	5G 4/10	37.87, -51.98, 9.80	37.87, 52.90, 169.3°
	macro-P	7.5G 3.5/9.5	32.74, -46.00, 5.30	32.74, 46.30, 173.4°
	macro-V	8G 4.4/5.0	42.02, -25.34, 2.21	42.02, 25.44, 175.0°
	micro	10G 5.0/2.0	48.17, -11.41, -0.07	48.17, 11.41, 180.4°

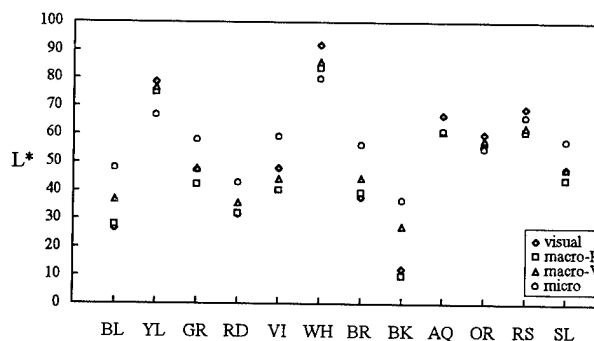


FIGURE 1. L^* diagram for colored fibers from A, the points marked the same symbol measured by the same method.

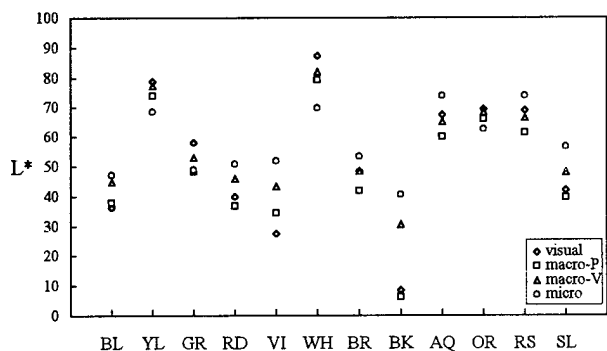


FIGURE 2. L^* diagram for colored fibers from D.

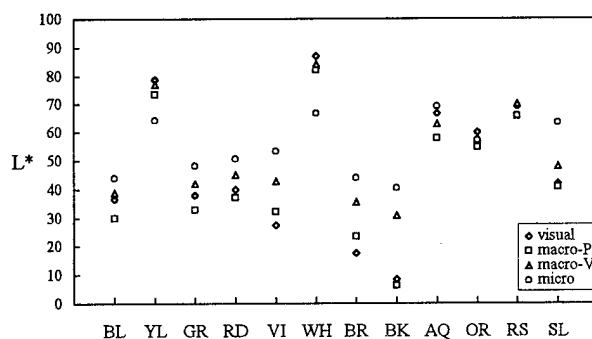


FIGURE 3. L^* diagram for colored fibers from F.

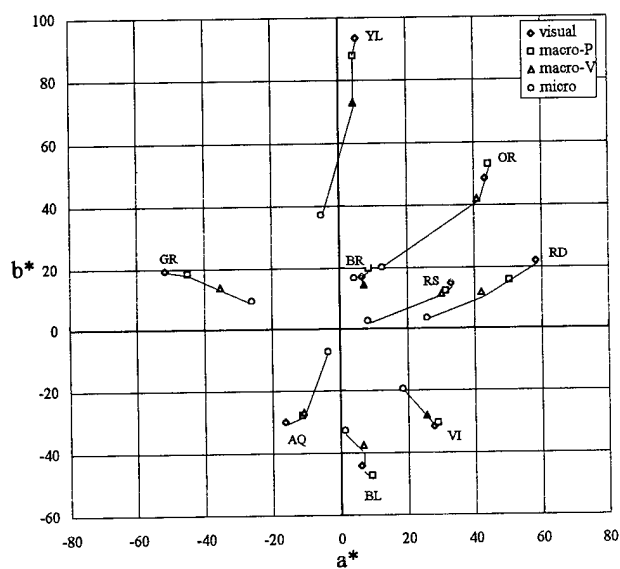


FIGURE 4. Color data of nine colors (without achromatic colors) from A graphically through a^*-b^* diagram, the points marked the same symbol measured by the same method.

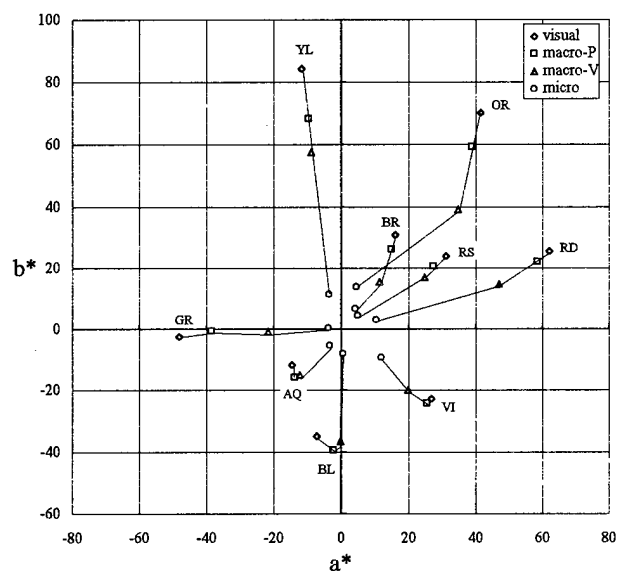


FIGURE 5. Color data of nine colors from B graphically through a^*-b^* diagram.

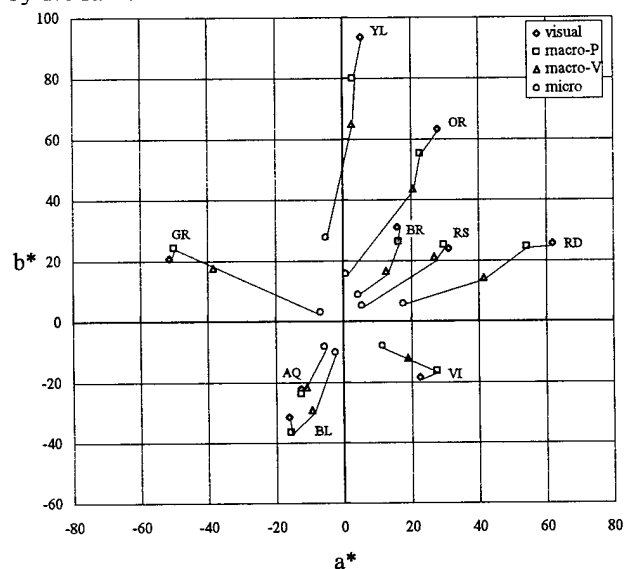


FIGURE 6. Color data of nine colors from C graphically through a^*-b^* diagram.

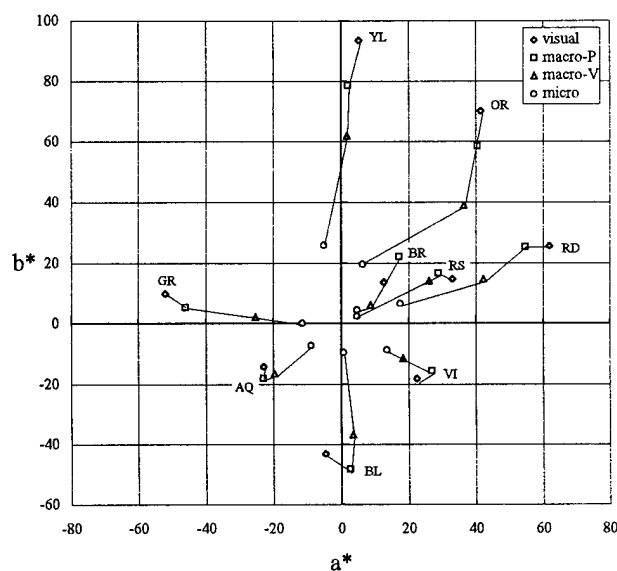


FIGURE 7. Color data of nine colors from E graphically through a^*-b^* diagram.

ANALYSIS OF THE ECONOMICS OF ON-LINE COLORED RIBBON MANUFACTURING

Dr Bertil Arvidsson

Ericsson Cables, Hudiksvall, Sweden

Mr Juha K Tanskanen

Nokia-Maillefer, Vantaa, Finland

ABSTRACT

Ribbon technology is well established in many countries: USA, Japan, Italy and Sweden. Other countries like Malaysia and the Philippines have also introduced ribbons. Several cable manufacturers offer ribbon cables. Since the encapsulated type has the separability requirement, such ribbon cable can also be installed with conventional techniques. It is therefore likely that the ribbon concept has been introduced in more countries than suggested above. This means greater volumes. At the same time, ribbons are finding their way into new applications in the access network and other areas. Also this means greater volumes. Therefore, it is more important than ever to emphasize the benefits of this technology and to utilize it fully in installations.

The focus of this paper is on the ways of optimizing the ribbon process itself and the measuring methods to verify the high quality of the ribbon. The requirements made on ribbons are numerous: attenuation, curl (splicing level) and other

parameters such as polarization mode dispersion (PMD), separability, strippability and high reliability. In view of this it is obvious that the degree of UV-cure is very important for all coating materials in ribbon applications. Especially coloring is critical, since it forms an intermediate material layer, and poor UV-cure immediately results in poor separability.

Today, fiber is colored in a separate line, followed by ribboning. Incorporating coloring with ribboning exposes the fiber to fewer process steps. This reduces processing and increases the reliability of the ribbon product. The standard ribbon process is now mature and the complexity can be broadened through coloring on-line without jeopardizing the final product.

INTRODUCTION

In an earlier work we discussed the on-line method in general, emphasizing long-term environmental tests.¹ Figure 1 shows the on-line concept. The example is a four fiber encapsulated ribbon, where

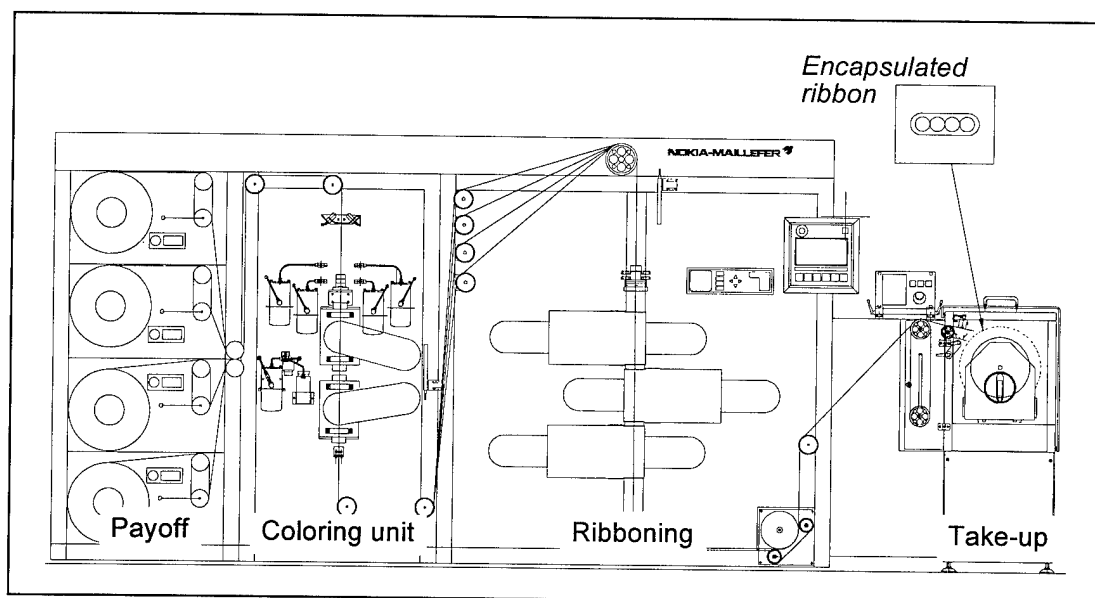


Figure 1 Layout of the on-line ribbon manufacturing process.

each fiber is paid off to the multifiber coloring unit. All fibers are colored simultaneously with one or different colors. The colored fiber is then UV-cured and led to the ribbon die. Also the final ribbon matrix form is UV-cured. Finally the ribbon is wound on a take-up reel.

We have now studied the UV-cure further in respect to the position of the fiber in the lamp during the on-line coloring process. Also the "new" parameter, PMD, is useful when evaluating the process.

NEW REQUIREMENTS

In this project, a new ribbon manufacturing system with on-line coloring was configured (Figure 1). Due to greater volumes and the increased demand for ribbons special attention was paid on economical and productivity factors (line speed, easy material handling and a fast start-up time). Also ramp-up and ramp-down lengths were to be minimized. Another important goal was to maintain good quality - stable coating and coloring conditions and a low tension variation with high processing speed. New maintenance-free technology, such as AC brushless servo motors, offers reliable, accurate and dust-free operation. It was also of interest to study PMD for on-line colored ribbons, since this parameter has recently been specified in many countries.

LINE OPERATION

First the fibers are paid off from double loop payoff units. The tension of each fiber can be measured before ribboning. Optimized tension level is then adjusted during operation either manually or automatically. The fibers are led to the multifiber coloring module where the four fibers are colored simultaneously. The fibers are cured by an efficient UV-lamp system in an oxygen-free environment. The elimination of oxygen expedites the curing process and gives better surface curing for the ribbon.

The fibers are guided to the ribbon coating system. An upper turning wheel balances the fibers that are guided further to the heart of the system, the ribbon coater. The ribbon is made by a compact three-die construction to avoid planarity errors. The nitrogen inert gas system is connected to the coater so that surface curing is not affected through oxygen. Then the ribbon is cured with high power UV-lamps. The ribbon dimensions including the diameter of the colored fibers are measured and displayed in the control cabinet. All parameters can be controlled during the operation on the control panel.

Finally the ribbon is wound in the take-up. Part of this project was to develop a new reel (Figure 2) with conical flanges for outward trapezoidal winding. This way we achieved better stability, easier handling and more ribbon on each reel. Another goal was to handle 50 km ribbon lengths.

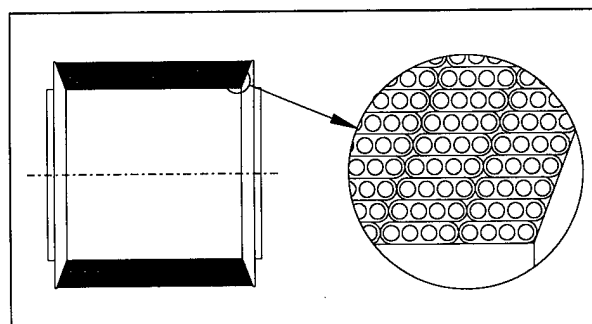


Figure 2 Reel for ribbons.

PROCESS ANALYSIS

We mentioned the importance of proper UV-curing. Wide tests on different UV-systems and curing conditions such as power, UV spectral output, bulb diameter, reflectors and nitrogen flow have been performed. UV-curing applies not only to the fibers before ribboning, but also to the colored fibers and the final product - the ribbon. FTIR-measurements give valuable information when developing the process, especially for establishing the ultimate processing speed limits.¹ Another more direct way is the breakout or separability criterion, i.e. being able to take out the colored fibers without scratching them. In a test run it is therefore useful to run at different speeds and to take samples to find out the rough limits.

Another perceivable parameter is the geometrical shape of the ribbon. Since the fibers are warm after coloring, the conditions in the ribbon die vary from the off-line technique. The stability of separate fibers before ribboning and the ribbon itself is very high. This means a high stability for the whole on-line process.

Finally, we also looked at the influence of fiber dimensions and tension variations on excess length, i.e. the fiber length compared with the ribbon length. The excess length is optimized by automatic control of the tension of each fiber and the coloring conditions.

COLORING ANALYSIS

We have performed and compared FTIR measurements of different laboratories. Because

the equipment, definitions and methods used were different, comparing the results was quite interesting. FTIR results are also relative.^{1,2} We found a good correlation between the results. In this analysis we were particularly interested in UV-curing as a function of the color used, the coloring speed and of the fiber position in the radiance area of the UV-lamp. The latter was of special interest due to on-line coloring. Four fibers were UV-cured simultaneously in the same lamp system. Table 1 shows typical results.

Table 1 UV curing level of fibers at different speeds and positions.

No.	Sample	Process speed [m/min]	Cure level, relative [%]
1	Pos 1	300	98
2	Pos 2	300	97
3	Pos 3	300	97
4	Pos 4	300	98
5	Pos 1	400	96
6	Pos 2	400	96
7	Pos 3	400	96
8	Pos 4	400	96

The fibers were placed side by side (Figure 3). To achieve maximum and equal UV-cure for all fibers they are arranged in a square form around the focusing center.

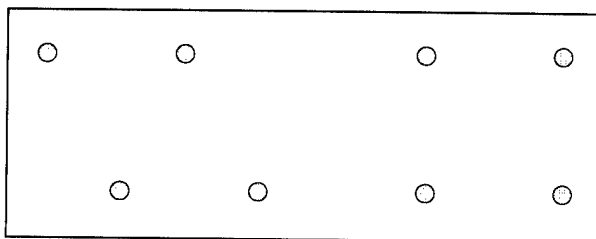


Figure 3 The positions of the four fibers in the coloring die and in the UV-lamp.

The results in Table 1 show that the fiber position in the lamp is under control, but that there is an upper limit for the process speed in order to guarantee the separability requirement for ribbons.

PROCESS EVALUATION

In the early phases of the development work of the encapsulated four fiber ribbon we made several temperature, humidity and water soaking tests as well as geometry with curl, strippability and separability. Now the number of tests is smaller, as we have passed the general development phase involving major changes in the choice of materials. Today it is more interesting to perform a well-selected test program, where some key parameters

have been identified. For the new concept with on-line coloring we focus the tests on ribbon dimensions, water soak, PMD, FTIR, strippability and separability. Strip force is really not needed, because of the subjective method, which has not yet been internationally standardized.

Figure 4 shows the typical results of a water soak test. Earlier we used to let the ribbon soak in the water for very long periods. The requirement in room temperature is no measurable changes after 30 days. For a process evaluation even higher temperatures are sometimes used.

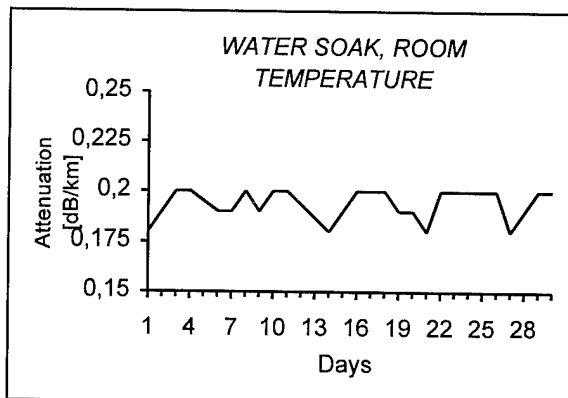


Figure 4 OTDR measurements at 1,550 nm from one end. The graph shows the maximum changes.

Another interesting parameter is PMD.³ By manipulating the ribbon process we can change the PMD pattern in a ribbon. We have used the wavelength scanning technique with Fourier transform from the frequency domain, but acknowledge other techniques as well.^{4,5} In earlier measurements (off-line ribbons) we found slightly higher PMD in the two inner fibers of a four fiber ribbon. PMD has been an interesting tool for the on-line method. We can control the process more precisely by using PMD-measurements. It should be noted that all results (on-line and off-line) are well below the suggested requirement of 0.5 ps/√km.

The FTIR-evaluation indicates that different parameters lead to different curing rates. Changing the reflector and bulb type has little effect on the curing rate (1%). Increasing the speed from 400 to 800 m/min reduced the curing rate by 4-5%. However, doubling the curing power increased the curing rate by 4-5%. This discussion is valid for the cure rate of colored fiber. In principle the same goes for the cure of the matrix material of the ribbon. Increasing the nitrogen flow did not affect the curing level as long as the oxygen level in the curing environment was zero. It affects the cleaning period of the quartz tube of the UV-lamp.

ECONOMY OF THE ON-LINE METHOD

The previous paragraphs clarify the advantage of on-line coloring for ribbon manufacturing. In brief, the most interesting parameters are

- reduced set-up time
- handling
- non-storing of colored fibers
- reduced scrap lengths
- reduced labor
- better stability of the process.

As an example, by using uncolored fibers we were able to reduce the ramp-down scrap length by 30%. Secondly, we expect to save another 50% by optimizing the start-up.

The economics of the whole ribbon production depends on the factory logistics, products and manufacturing programs.

CONCLUSIONS

We focused our work on showing the economy of reducing the number of process steps in ribbon manufacturing by integrating fiber coloring with the new ribbon line. The main advantages are cost savings, simplified logistics and fiber handling. In addition, the quality of coloring and the final product fulfills the same requirements as ribbons colored off-line. At the same time we have increased the productivity of the line.

ACKNOWLEDGMENTS

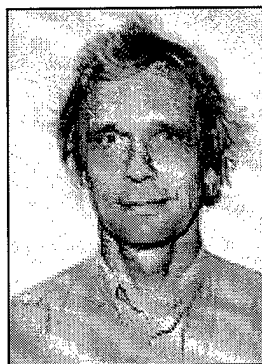
We thank DSM Desotech B.V. for assistance in performing the FTIR cure measurements. We also thank Mr Johan Svanberg and Mr Mats Eriksson at Ericsson Cables and Mr Jari-Pekka Tiesmäki and Mr Mika Nieminen at Nokia-Maillefer for valuable technical discussions.

REFERENCES

¹ B Arvidsson, M Ericsson, J Kohtala, J Tanskanen, "Long-Term Environmental And Process Tests of On-Line Fiber Optic Ribbons", IWCS, Atlanta, 1994.

² J Kohtala, E Peltoluhta, J Tanskanen, "Efficient And High Quality Fiber Identification With UV Curable Inks", Wire Association International, 65th Annual Convention, Conference Proceedings, March 1995.

³ B Arvidsson, H Mickelsson, A Barlow, "A PMD



Dr Bertil Arvidsson,
Ericsson Cables AB,
Telecom Division,
S-824 82 Hudiksvall,
Sweden

Dr Arvidsson, manager of fiber optics at Ericsson Cables AB, Telecom Division, has been involved in optical fibers for several years. One particular area has been ribbon technology. He is active in IEC and CECC with the standardization of optical fibers and cables. Prior to joining Ericsson in 1990, he worked as technical project manager in Sweden, the United States and Switzerland. Before that he was a university lecturer in theoretical physics. He has a Ph.D. in Theoretical Physics from Uppsala, Sweden.



Juha Tanskanen,
Nokia-Maillefer Oy,
P O Box 44,
FIN-01511 Vantaa,
Finland

Juha Tanskanen has a B.Sc. in Mechanical Engineering from Wärtsilä Polytechnic, Finland in 1984 and the M.Sc. in Computer Engineering from Tampere University, Finland in 1991. He joined Nokia-Maillefer as development engineer in 1990 and is currently working as product manager for fiber coloring and ribbon lines.

Study On Fibres In A Cable Factory", OFMC 95, Liege, Belgium, September 25-26, 1995.

⁴ K Brising, "Polarisation Mode Dispersion Field Measurements - A Survey of The Swedish National Optical Network", IWCS, 1996.

⁵ B Arvidsson, H Mickelsson, K Brising, "A Practical Comparison Between Two Different PMD Measurement Methods", Symposium On Optical Fiber Measurements, Boulder, 1996.

Effect of Dynamic Visco-Elastic Properties and Compatibility of Jelly Compounds on Optical Fiber Cable Performance

AKIRA MURATA, KEIJI OOHASHI, SHINJI ARAKI

Opto-Electronics Laboratory, Fujikura Ltd.
1440, Mutuzaki, Sakura-shi, Chiba, 285 Japan

ABSTRACT

We studied the chemical and physical characteristics of jelly compounds, which affect the coating materials of optical fibers, and properties of slotted-core optical fiber cables. We examined the relationship between molecular weight distribution and the swelling of coating materials, in addition to the dynamic visco-elastic properties of the compounds. To attain good performance from slotted-core cables, jelly compounds should be designed to incorporate the following properties:

- 1) Compatibility : Base oil ingredients with low molecular weights should be minimized.
- 2) Mechanical properties : Compounds should have a higher storage modulus in the low applied shear stress region, higher flowing shear stress, and lower dynamic viscosity, based on dynamic visco-elastic analysis.

INTRODUCTION

Jelly compounds are used in loose-tube and slotted-core cables to prevent water contact with optical fibers and fiber ribbons. Jelly compounds are composed of base-oil, fumed-silica, anti-oxidants, and so on. It is essential that the jelly compound does not interact with the optical fibers, especially the UV-curable coatings. Penetration of the oil into the glass-primary coating interface may decrease adhesion and may cause delamination, leading to optical loss increase at low temperatures. Therefore the compatibility of the jelly and the fiber coatings is crucial. Moreover, the dynamic mechanical (visco-elastic) properties of jellies are important in

terms of for drip performance, processability, and optical loss at low temperatures.

Earlier studies have revealed that jelly with low cone penetration values causes increased optical loss at low temperatures¹⁾. Recently, it has been reported that the rheological analysis of jelly compounds is more effective than cone penetration in the evaluation of cable performance²⁾. To minimize optical loss increase at low temperatures, maintaining the visco-elastic properties at room temperature over a wide temperature range is very important³⁾.

In this study, we have investigated that the design of jelly compounds in order to achieve high slotted-core cable performance. First, we investigated the relationship between molecular weight distribution of the jellies and the swelling of UV-curable coatings. We will discuss the effect of swelling on the adhesiveness of glass-primary interfaces. Next, we will show the dynamic visco-elastic properties of the compounds. We observed the storage modulus (G') and flowing shear stress in the region of low applied shear stress, as well as dynamic viscosity in areas of high applied shear stress. We related the visco-elastic properties of the jelly compounds and the results of drip test. Finally we will demonstrate the optical loss properties of slotted-core cables during heat-cycled tests.

EXPERIMENTS

Several compounds with same cone penetration value were used. The molecular distribution of the oil is measured using gel-

permeation chromatography. Mean molecular weights of the jellies are determined by conversion to that of polystyrene. The compatibility of jelly compounds with the UV-curable coatings was measured based on the degree of swelling of the coatings (dimension change). The degree of adhesion was evaluated based on the pull-out force of the fibers at a 3 mm/min testing speed. A rotational rheometer was used to conduct dynamic visco-elastic analysis. Compounds were placed between a plane plate and a cone plate at a 4° angle, and dynamic shear stress was applied at a frequency of 1 Hz. The slotted-core 32-fibers (eight 4-fiber-ribbon in five grooves) cable and poly-ethylene tubing with various inner diameters are utilized in drip tests. Drip testing of cables was carried out based on EIA/TIA-455-81A. In the tube test, tubes filled with jelly compounds are positioned vertically, and the amount of jelly that dripped out was measured. The optical loss of the cables during the +70/-40 °C heat-cycled test were measured by OTDR .

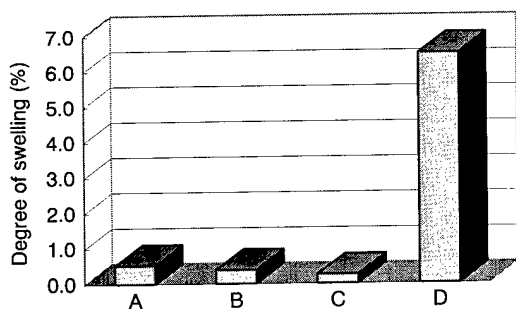


Figure 1-a Degree of swelling of primary coating immersed in four compounds at 25 °C for 1 week

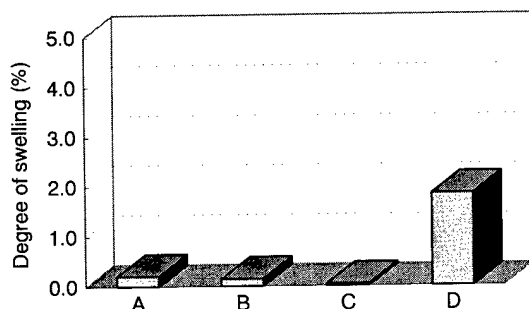


Figure 1-b Degree of swelling of secondary coating immersed in four compounds at 25 °C for 1 week

RESULTS AND DISCUSSION

Relationship between the molecular distribution of the jellies and the swelling of the coatings

We investigated the relationship between molecular distribution and the swelling of UV-curable urethane acrylate resin. Figure 1 shows the degree of swelling of a primary coating (1-a) and a secondary coating (1-b). When UV coatings are immersed in compounds A, B, and C, the coatings do not swell. However, compound D swells not only the primary coatings, but also the secondary coatings. The degree of swelling of the primary coatings much larger than that of the secondary coatings, because of its low cross-linked density. The degree of swelling is affected by the jelly compound, but not by the type of coating.

Figure 2 shows the relationship between the swelling of primary coatings and relative mean molecular weight (M_w : expressed as compound A's $M_w = 100$) and 10 % integrated relative molecular weight in compounds ($M_{w(10)}$). Later factors show good correlation with swelling. It has been found that the degree of swelling is mainly affected by the existence of ingredients with low molecular weight. Even when the mean molecular weights of jellies are relatively large, compounds with sharp molecular weight distributions and those without a low molecular weight do not cause the coatings to swell.

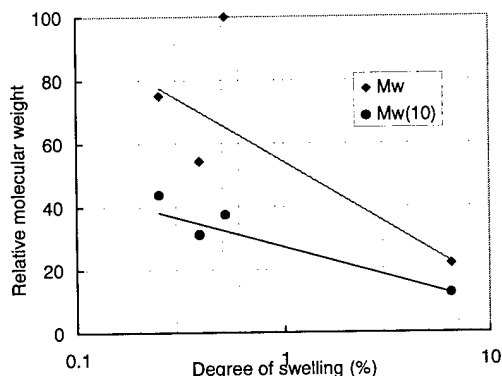


Figure 2 Relationship between the degree of swelling and relative mean molecular weight

Change in the pull-out force of fibers immersed in jelly compounds

Figure 3 shows the pull-out force of 250 μm fibers immersed in jelly compounds A,B, and C at 25 °C and 70 °C. The pull-out force clearly illustrates the adhesion of glass and the primary coating interface. At 25 °C, the pull-out force of fibers only increases slightly over the first two months. At 70 °C, the pull-out force also increases over time. The extents of the increases are nearly the same. This may be the effect by the contraction of the coatings caused by heat. The adhesion of fibers does not change when fibers are immersed in the compounds that do not have a low molecular weight.

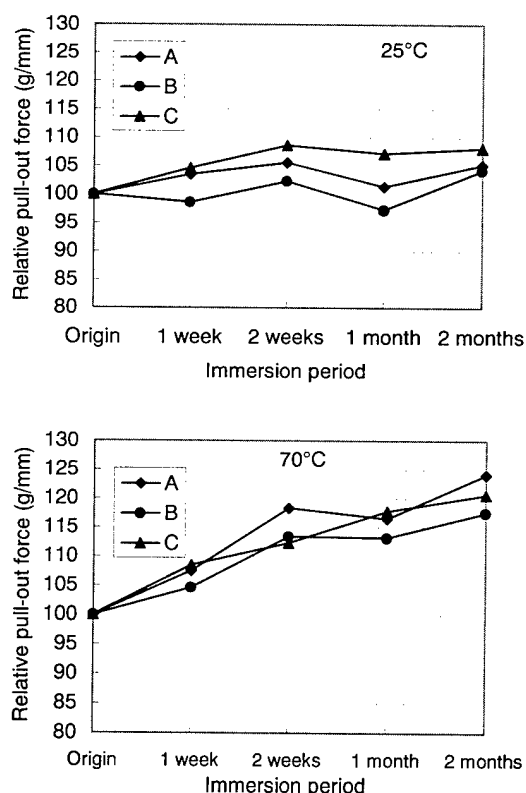


Figure.3 Change in the relative pull-out force of fibers after immersion in jelly compounds at 25°C and 70°C

Dynamic visco-elastic measurement of jelly compounds

We measured the dynamic visco-elastic properties of jelly compounds using a rotational dynamic rheometer. Typical results for compound B at 85 °C is shown in Figure 4. In the region of low shear stress (below 50 Pa), the storage modulus (G') was dominant. In this area, the phase difference indicating that the material is elastic or viscid is low, so the jelly behaves like an elastomer. However, when the shear stress exceeded a certain value, the storage modulus fell suddenly. We defined this value as flowing shear stress. In the region of high shear stress, the loss modulus (G'') is dominant and the phase difference is high, so the jelly behaves like a viscous fluid. G' is correlated with dynamic viscosity, and this value reflects processability, since low-viscosity jellies fill cable grooves and tubes more easily.

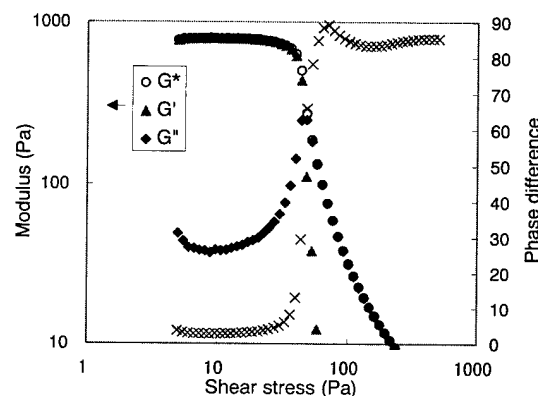


Figure 4 Typical dynamic visco-elastic properties of the jelly compound

Figure 5 shows the temperature dependence of compound B's complex moduli. The moduli at low applied shear stress at various temperatures are nearly the same. However, the flowing shear stress and moduli in the high applied shear stress region decreased as the temperature increased. It is suspected that the jelly drips easily at high temperatures.

Figure 6 shows a comparison of the complex moduli of jelly compounds A, B, C, and E at 85 °C. Even if their cone penetration values of the jellies are nearly the same each other, modulus curves are different.

Differences in the moduli in the low applied shear stress region and flowing shear stress indicate drip performance and processability differ with jelly compounds.

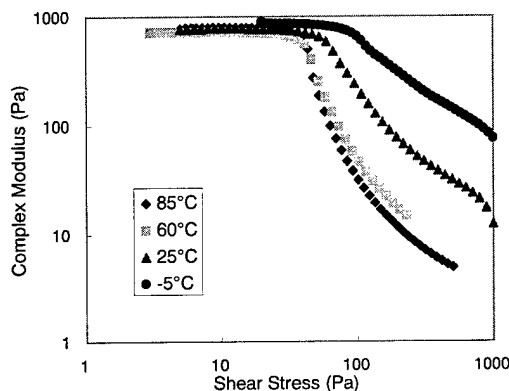


Figure 5. Temperature dependence of the complex modulus of jelly B at 1Hz

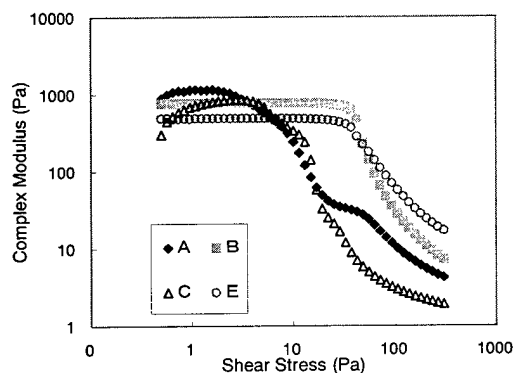


Figure 6. Comparison of the complex modulus of jelly compounds at 85 °C

Drip performance of jellies and the results of optical losses with slotted-core cable

Finally, we confirmed the relationship between visco-elastic properties and drip performance. When we performed the drip test based on EIA/TIA-455-81A using actual slotted-core cable (eight 4fiber-ribbons in five grooves), no dripping occurred at 85 °C. We then performed evaluations using straight PE tubes to clear the relationship between the drip performance and visco-elastic properties. Compounds were loaded into 150 mm length tubes, which were positioned vertically. At

various time intervals, the amount of the jelly that had dripped was measured. Figure 7 shows the relationship between the flowing shear stress and the amount of dripped jelly at 85°C after 24 hours when tubes with an inner diameter of 3 mm were used. The compounds with high flowing shear stress exhibit good drip performance. When tubes with a large diameter were used, the amount of dripping jelly increased. This indicates that jelly drips more readily when tubes or slots with a larger gap are used.

Optical losses of the 32-fiber cable with three

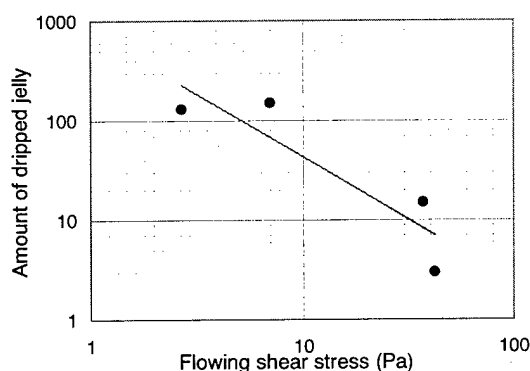


Figure 7 Relationship between the drip performance in PE-tubes and the flowing point in visco-elastic analysis

jelly compounds A, B, and C were tested between -40 °C and 70 °C. Figure 8 shows the average loss of thirty-two fiber during heat-cycled test. No Increase in loss was observed, and this types of jellies were found to show good optical loss performance.

CONCLUSION

To attain good performance from jelly filled slotted-core cables, jelly compounds should be designed to incorporate the following properties: 1) Base oil ingredients with low molecular weight should be minimized. 2) Compounds should have a higher storage modulus in the low shear stress region, higher flowing shear stress, and lower dynamic viscosity, based on dynamic visco-elastic analysis.

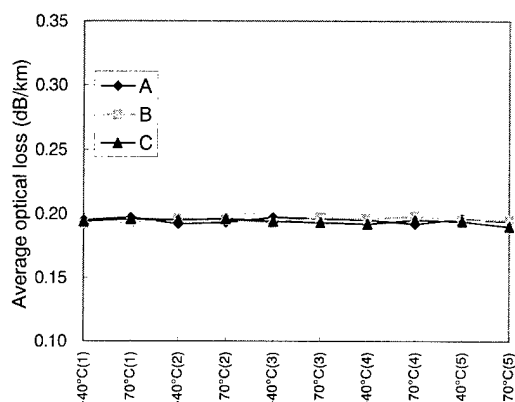
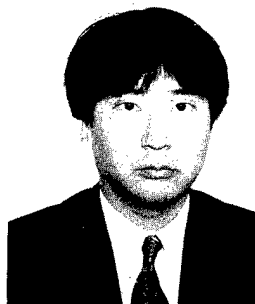


Figure 8 Optical loss at 1.55 μm Change in 32c slotted-core cable during the heat-cycled test.

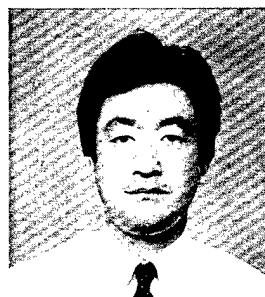
- 1) T. Hattori, N. Akasaka, and M. Fukuma, "Optimal Design of Jelly Compound for Optical Cable", 37th Proc. IWCS, 12 (1988).
- 2) G. Morland, D. Rees, and G. White, "An Evaluation of the Inter-relationship between Rheological Data of Filling Compounds and Fibre Optic Cable Performance" 40th Proc. IWCS, 469 (1991).
- 3) O. S. Gebizlioglu, I. M. Plitz, and M. J. Zammit, "Temperature-dependent Performance of Buffer Tube Gels In Loose Tube Fiber Optic Cables", 44th Proc. IWCS, 457 (1995).



Akira Murata

Opto-Electronics
Laboratory
Fujikura LTD.
1440, Mutuzaki,
Sakura-shi, Chiba,
285, Japan

Akira Murata was born in 1963. He joined Fujikura LTD. in 1992 after receiving his ph. D. in environmental science from Chiba University. He has been engaged in research and development for optical fibers, and is now an engineer in the Telecommunication Cable Material section and a member of the IEICE of Japan.



Keiji Oohashi

Opto-Electronics
Laboratory
Fujikura LTD.

1440, Mutuzaki,
Sakura-shi, Chiba,
285, Japan

Keiji Oohashi was born in 1956. He graduated from the Tokyo Institute of Technology in 1980 with a B.E. degree in chemistry. After eight years of work as an engineer in the field of materials for motor vehicles, he joined Fujikura LTD. in 1988. He has been engaged in research and development for optical fibers and optical fiber coatings. He is now a chief of the Telecommunication Cable Material section and a member of the IEICE of Japan.



Shinji Araki

Fujikura LTD.
1440, Mutuzaki,
Sakura-shi, Chiba,
285, Japan

Shinji Araki was born in 1950. He joined Fujikura LTD. in 1974 after graduating from Tokyo Metropolitan University with a B.E. degree in chemistry. He has been engaged in research and development for optical fibers and optical fiber coatings. He is now an assistant general manager in the optical fiber cable manufacturing engineering department and a member of the IEICE of Japan.

USING TRIBOELECTRIC TECHNOLOGY TO APPLY POWDERS WHILE REDUCING FACTORY CONTAMINATION

Frank T. Hughes

Nordson Corporation, Duluth, Georgia, USA

ABSTRACT

Powders are used at an increasing rate in many of today's wire and cable production lines due to increased performance requirements implemented by both customers and specification agencies. With advances in both powder and machinery technology, powders are now applied in a consistent, repeatable manner. Recently introduced triboelectric technology is a further step in developing equipment to meet the growing requirements of the fiberoptic, power, flexible cord, coaxial and other industries.

This paper will review the different application methods used in the wire and cable industry to apply powder, then discuss some of the application areas where powders are used.

APPLICATION METHODS

Let's start with the most basic equipment and progress to the most sophisticated; triboelectric technology.

Powder Boxes

Because no production equipment was available, users initially developed their own powder boxes. These devices consisted of a metal vibrating box, filled with powder. When the cable passed through the box, some powder would hopefully stick to it. These boxes might also incorporate revolving paddles or pressurized air. Results were normally disappointing with powder covering everything in the plant, except for the cable.

Powder Pump Units

The next units developed for powder dusting applications were units incorporating a pump to draw the powder from a reservoir and spray it onto the cable. Because too much powder was normally placed on the top of the cable, a brush was incorporated to knock off the excess. These units were still inconsistent because no electrostatic charge was present to evenly coat the cable. After a minimum amount of operating time, the powders would clump up and the filters clog, resulting in an inconsistent product and a messy plant environment.

Electrostatic Technology

Electrostatic technology was introduced as an answer to the above problems. The charged powder is drawn to the cable in a very consistent manner, yielding an excellent coating. Using electrostatics has an added benefit of effectively coating the cable's interstices. The charged powder remains on the cable, and does not fall off during following production processes. A filter or collector draws in all remaining powder for reuse, keeping it out of the plant environment and allowing 100% utilization. The main advantages of electrostatic powder application are:

- Consistency and Reproducibility
- Environmental Cleanliness
- Higher Line Speeds
- Reduced Rejects and Returns
- Tighter Amount Control
- Increased Cable Performance

The initial disadvantage of electrostatic type units was their bulky size. Early units could easily take up a 1800 x 1800 x 2500 mm (6x6x8 ft) space. Current technology has greatly reduced this space requirement.

Today three methods of electrostatically charging and dispensing powders are in use:

- Corona Fluid Bed Technology
- Corona Gun Technology
- Triboelectric Charging Technology

Each method has its advantages and limitations.

Corona Fluid Bed Technology

Fluid bed coating technology is the least complex of the three technologies. When corona charging, a power supply generates a charge of 80,000 to 100,000-volts. This charge can be positive or negative, depending on the powder and application requirements.

Dry, pressurized air is blown through a media where it is charged (see figure 1). The charged air then passes through a porous membrane or plate into a reservoir, where it fluidizes and charges the powder. Some of the powder disperses into a cloud of charged particles (because like charged particles repel) through which the cable passes. The powder is attracted to the cable which acts as an effective ground for the electrostatic charge.

When using fluid bed technology, it is very important that the powder fluidizes well. Particle size should average 4 - 50 micron and the powder should not clump easily.

Benefits of this technology include system simplicity and the ability to put on a very light coating when required.

Fluid bed technology limitations include the amount of line space required (760 to 1520 mm or 30 to 60 in.) and their difficulty fluidizing larger micron size powders.

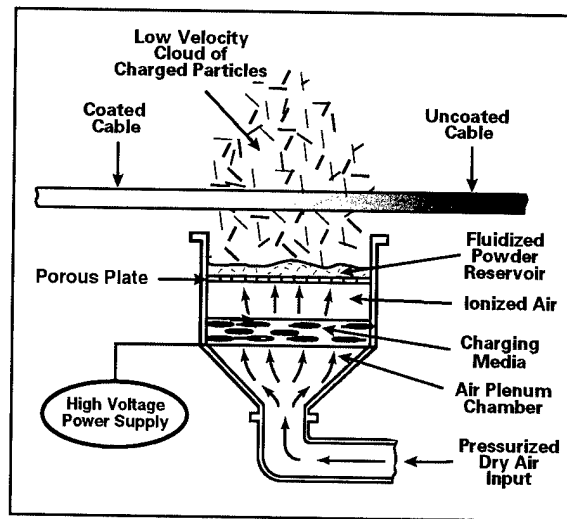


Figure 1 - Corona fluid bed system diagram

Corona Gun Technology

Corona gun technology uses the same 80,000 - 100,000-volt power supply, but utilizes a spray gun instead of charging the air that passes through a fluidized bed.

Dry, pressurized air fluidizes powder in a reservoir so that it can be easily drawn up by a powder pump (see figure 2). The powder pump feeds the air/powder mixture to an electrostatic corona gun which sprays this charged mixture towards the wire or cable traversing through the spray chamber. The charged powder is attracted to the wire and effectively coats the entire circumference. Any extra powder which might escape the unit, and the air which moves the powder through the system is drawn into a collector, where it is filtered and the powder reused.

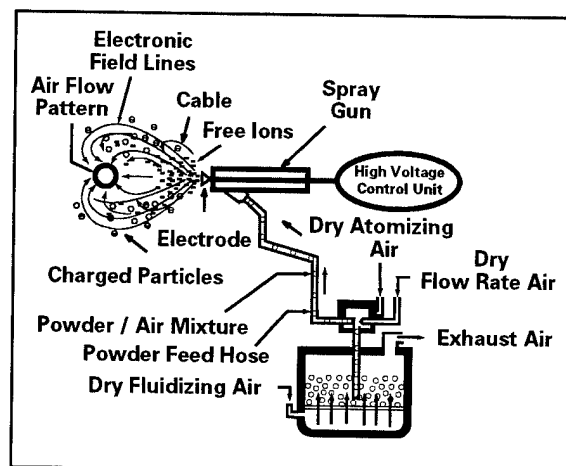


Figure 2 - Corona gun system diagram

Corona gun technology has a number of benefits. The unit utilizes less line space than fluid bed technology. Space requirements are 610 mm (30 in.). Powder particle size can be larger because the powder is sprayed toward the cable instead of needing to form a charged cloud. It is also easier to coat large diameter cables because multiple guns can be utilized and aimed at different portions of the cable diameter.

Technology limitations are the space requirement for the collector, not being able to use powders that impact fuse, and production line speed restrictions.

Triboelectric Charging Technology

The latest innovation in coating wire, cable and other linear substrates is the use of triboelectric technology. Triboelectric technology utilizes the principle of frictional contact or rubbing to create a charge. This same principle is demonstrated in the wintertime when we create a charge by rubbing our shoes on a carpet and getting "zapped" when we touch metal or another person.

Triboelectric equipment has been in use since the 1970s to effectively coat products such as office furniture, yard equipment and recently automobiles. Recently this technology has been introduced to the wire and cable market.

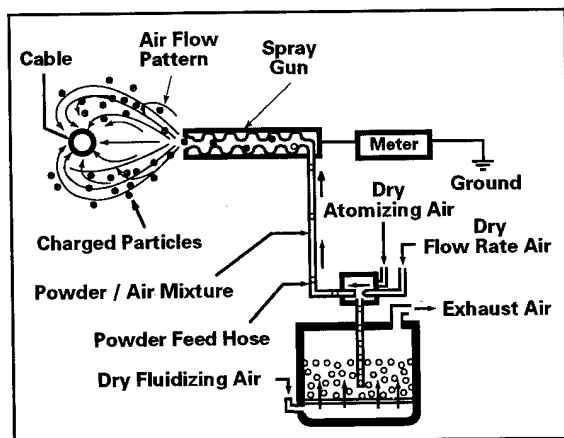


Figure 3 - Triboelectric charging system diagram

As with corona gun technology, dry pressurized air fluidizes powder in a reservoir so that it can be easily drawn up by a powder pump (see figure 3). The powder pump feeds the air/powder mixture into a Tribomatic® gun where it is forced to contact the gun walls. An electrostatic charge is created by this frictional contact. The charged powder is then propelled by the air to the wire or cable, where it forms an effective coating.

The many benefits of triboelectric technology include:

- Because of its very small size, it can fit easily into most fiberoptic, power cable, flexible cord and other lines and is easy to move between production lines.
- The standard coating head is 450 mm (18 in.) long which is cantilevered in design so it can be positioned over drive shafts and other line components.
- The transfer efficiency of the triboelectric system is very high (up to 80%) therefore little unused powder needs to be collected for reuse, eliminating bulky collectors.
- This high transfer efficiency also requires less compressed air, reducing the need for large filters which draw in moist plant air and degrade the powder.
- The closed-loop system utilizes 100% of the powder.
- The coating is more uniform and penetrates even in the smallest interstices. This is because tribo charging doesn't generate a strong electric field between the gun and cable.
- Tribo-charging is more effective on cable that is not highly electrically conductive (e.g. high glass/plastic content) because the system doesn't deposit a large quantity of free ions on the cable as a corona gun might.

- Plant personnel do not come in contact with the powder because the system's automatic powder feed system draws powder right from the suppliers bag, into the system.
- Quantitative data is available for quality control and ISO requirements by measuring the charge acquired by the powder.

However, triboelectric systems are more sensitive to the composition of the surface of the powder particles than other powder application technologies. Therefore, some powders must be modified by the manufacturer to generate an effective charge. Also, highly abrasive powders such as Frit (powdered porcelain enamel) can cause accelerated gun wear.

APPLICABLE POWDERS

Many types of powders are used in the wire and cable industry. Some of the more common are:

- Superabsorbent
- Talc and mica
- Epoxy powders
- Zinc sterates
- Teflon®
- Powdered adhesives
- Paints
- Other polymers

POWDER APPLICATIONS

Let's quickly review some of the more common applications where powder is used in the wire and cable industry.

Fiberoptics

Superabsorbent powders (SAP) are being used at an increasing rate in the fiberoptic industry. SAPs are used to limit the ingress and longitudinal movement of water throughout the cable. The three most common locations for the placement of SAP are (see figure 4): (1) on the outside of the buffer tubes, (2) between the Kevlar® wrap and the corrugated metal tape, and (3) on the outside of the corrugated metal tape.

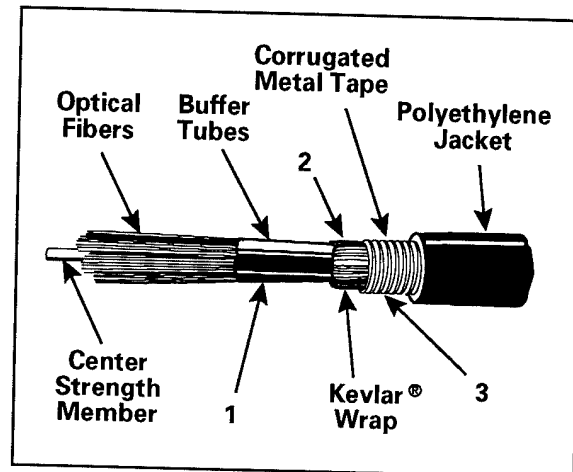


Figure 4 - Typical fiberoptic cable diagram

SAP has also been placed directly on the coated optical fibers and in a number of other locations where loose tube construction is not used.

Power Cables

Superabsorbent powder is also being used by power cable manufacturers. Once again, the goal is to limit water infiltration. The main areas where SAP is placed are (see figure 5): (1) between layers of the central stranded conductor and (2) between and around the concentric neutral conductors. In cables where a metal tape is incorporated, SAP can also be applied to one or both sides of the tape, as required.

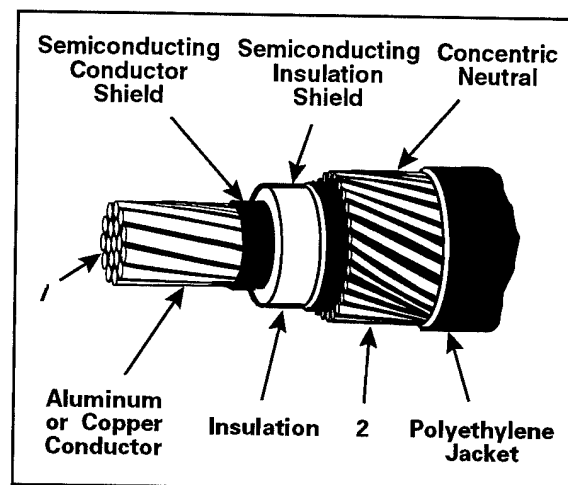


Figure 5 - Typical power cable diagram

Talc and mica powders are also placed on some power cables to aid in stripping and for other various reasons.

Flexible Cords

Talc and mica powders have been used in the flexible cord industry for many years. Many customers phased out its usage because it created a mess. The advancements in electrostatics have once again initiated the use of talc and mica. The major benefits of incorporating the powders are more consistent strippability and better flexibility. Two more common application areas are (see figure 6): (1) around the conductors' insulation and (2) a very light coating on the outer jacket to reduce tackiness.

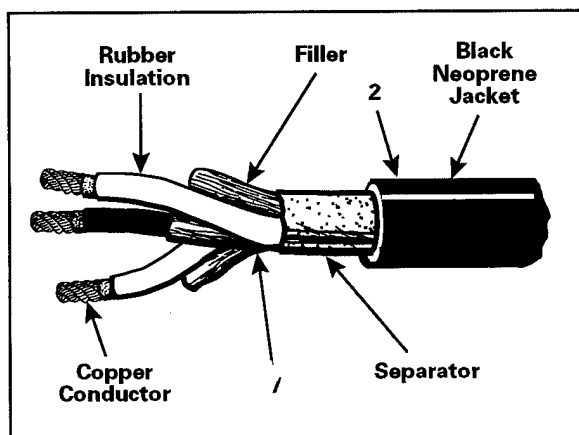


Figure 6 - Typical flexible cord diagram

To get maximum flexibility and strippability, some companies are pursuing the use of Teflon® powder. Other companies find that applying talc using electrostatics assists their penetration of the "fillerless" cable market.

Many other applications use powders to their benefits. These include coaxial cable, transformer wire and the application of protective powders to cable used in bridges, cranes, etc.

CONCLUSION

Electrostatic technology and, specifically, triboelectric systems has benefited many customers attempting to make a better, more profitable product. Its use has also allowed them to introduce new concepts in their wire and cable products.



Frank Hughes
Nordson Corporation
11475 Lakefield Drive,
Duluth, GA 30155
(800) 241-5792

Mr. Hughes resides in Atlanta, Georgia and is Market Manager for Nordson Corporation. He has developed processes used in the wire and cable industry throughout the world. He holds international patents and has given previous papers in the US and Europe.

Fusion Splicing Robot for Optical Fiber Ribbons

Hideaki Yusa, Tsutomu Watanabe, Kazuo Watanabe, Keiji Osaka

Sumitomo Electric Industries, Ltd.
1, Taya-cho, Sakae-ku, Yokohama 244 JAPAN

Abstract

The configuration and performance of the FUSION SPLICING ROBOT (FSR) are presented in this paper which splices optical fiber ribbons automatically. The splice portion is reinforced by using a protection sleeve of heat-shrink tube type. The total process from stripping to reinforcing is done automatically and spliced fiber ribbons can be obtained about 2 min. The average splice loss of 0.04dB, 0.05dB are obtained for single-mode (SM) fiber ribbons and dispersion sifted fiber (DSF) ribbons, respectively. Thereby, splicing productivity is much improved. Compared with conventional technique.

1. Introduction

Recently, high-count high-density optical fiber cables have been introduced to the subscriber networks, which contain as many as 1000 optical fibers. Dramatic improvement of splicing productivity is required to shorten construction period. The FSR has been developed to achieve high splicing productivity. The important feature in the FSR are to reduce the tact time for splicing. The system structure, the splicing procedure, were discussed and proposed.

2. The FSR System

2.1. Configuration

Fig.1 shows the FSR. It consists of a splicing unit and a monitor for viewing the fiber ribbons

and displaying the messages, etc. The specifications of the FSR are shown in Table 1.

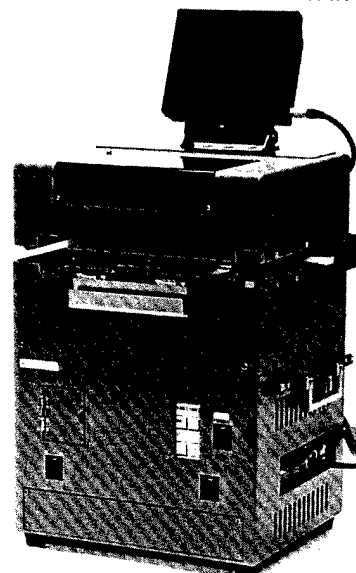


Fig1. Fusion Splicing Robot

Table1. Specifications of FSR

Size	280(W)x230(D)x395(H) mm
Weight	17Kg
Applicable fibers	1)Cladding diameter: 125 μ m 2)Fiber pitch: 250 μ m 3)Profile: SM/DSF 4)Number: 2,4,8 fiber ribbon
Tact time	about 2 minutes

2.2. The splicing procedure

The conventional technology required operator's skills through a few week's training program. On the contrary, the FSR succeeded in splicing, not to rely on one's skills. Therefore, removing tool, the cleaving tool, a gauze and alcohol for wiping the bare fibers are not necessary. Instead, the

residue on fibers is burned off by using short-time discharge.

The FSR has following functions to splice optical fiber ribbons; (a)Removing, (b)Cleaving, (c)Cleaning, (d)Aligning onto the V-groove, (e)Fusion splicing, (f)Splice loss estimation, (g)Testing of proof, (h)Reinforcing. Fig.2 shows the splicing procedure in order to be done by the FSR automatically.

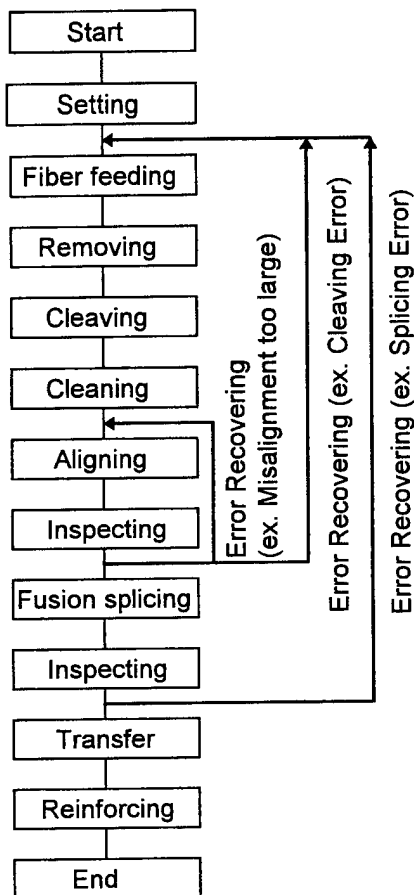


Fig.2 Splicing Procedure

2.3. The Mechanical structure

The FSR is usable in various environments such as in the manholes under the streets, the size and the weight of the robot has been minimized in order to make transportation easy. Each stations (jacket removing /cleaving station, fusion splicing station, reinforcing station) were placed effectively to transfer both sides of fibers by using a pair of manipulators automatically. Fig.3 shows the mechanical structure of FSR.

In this section, each stations for splicing are described.

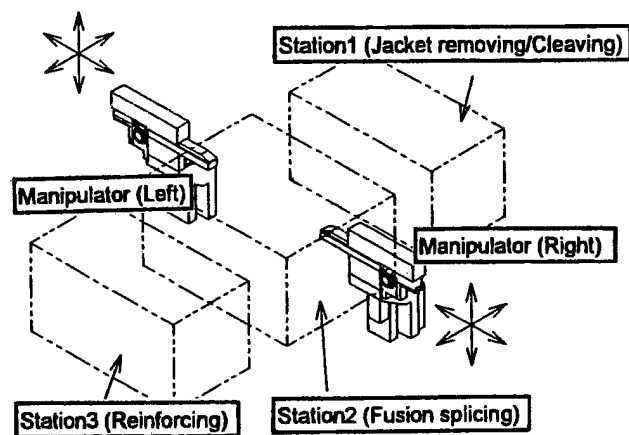


Fig.3 Mechanical structure

(a)Jacket removing/Cleaving station: Fig.4 shows the side view image of the jacket removing /cleaving station. The jacket removing unit is situated at the center of this station and the cleaving units on both sides. After setting the fiber ribbons, these ribbons are fed into the chucking units in each manipulators by the feed rollers, in order to hold the ribbons tightly. The fiber ribbons are carried to the removing unit. The jacket of fiber ribbons are stripped by using a removing unit. Then the fiber ribbons are cleaved altogether by using a cleaving unit.

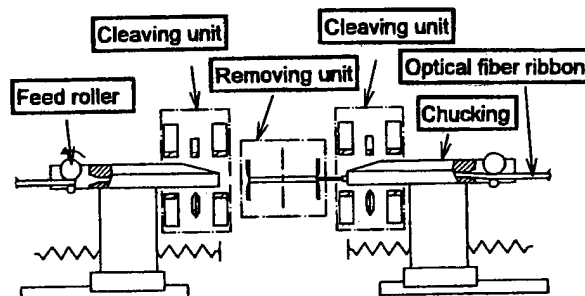


Fig.4 Jacket removing/Cleaving station

(b)Fusion splicing station: Fig.5 shows fusion splicing station which incorporates many functions, cleaning, aligning, inspecting and fusion splicing. The cleaved fiber ribbons are carried to splicing station by a pair of manipulators. At first, the cleaved fiber ribbons are fed forward, passing through the gap of a pair of cleaning electrodes. After the residual coatings on fibers is burned by short-time discharge, the cleaned fibers is placed above the V-grooves. The next step is the aligning on the V-grooves. The sequence about alignment and splicing is

shown in Fig.6. Before and after splicing, the side view of the fibers are monitored by the 2-directional observation system with a mirror and a CCD camera. This system is used both for the positioning of fiber end portions and for the judgment of splicing quality.

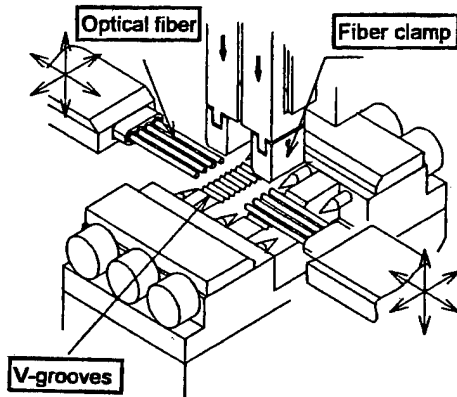


Fig.5 Fusion splicing station

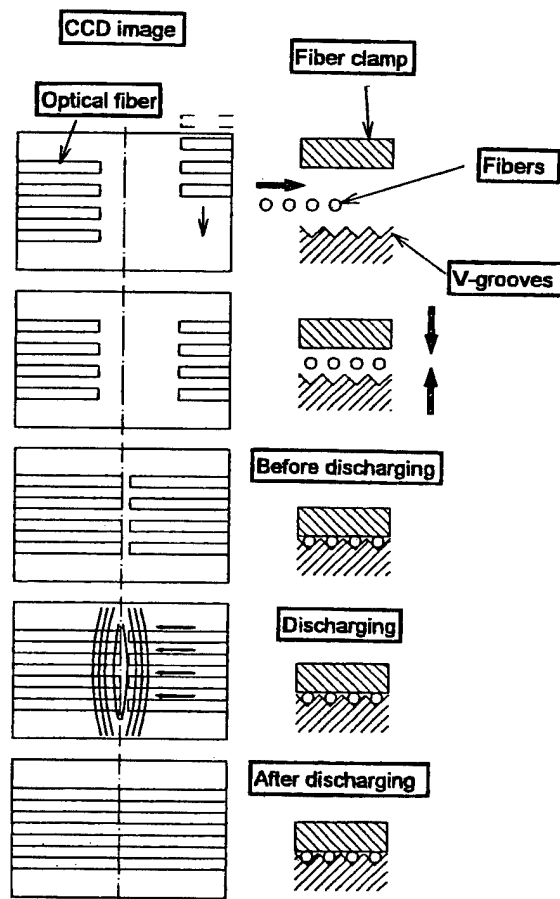


Fig.6 Alignment and splicing sequence

(c)Reinforcing station: Fig.7 shows the reinforcing station. A pair of manipulators makes a synchronized motion and conveys the fiber

ribbons from the splicing station to the reinforcing station.

The automatic reinforcing mechanism using a protection sleeve of heat-shrink tube type is newly developed. The spliced point is reinforced by this sleeve. The splicing procedure for the next fiber ribbons starts during the reinforcing process, so that the tact time is reduced.

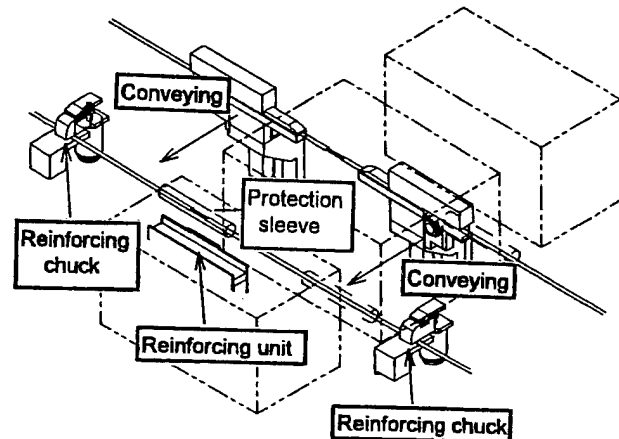


Fig.7 Rein forcing station

2.4. The new alignment concept

The 2-directional observation system for optical fibers is adopted as shown in Fig.8. It enables to measure the misalignment of the fibers' axis accurately, and the estimated loss of the splice points is calculated by using the misalignment, etc. In the previous FSR, the observation system from one direction has been used. But the one-directional observation system is inferior to the 2-directional system in measuring the misalignment accurately. The new and more effective alignment concept was discussed and proposed.

Step1: The basic position for alignment is situated at the position "P-0". A fiber ribbon is conveyed at the decided position "P-1". The microscope is also conveyed at the decided position "M-1". The center of gravity of the fibers' image in the monitor is calculated and conveyed at the position "P-2" on the center line of the microscope.

Step2: The microscope is moved to the position "M-2" at the distance of "2W", where "W" is the distance from the mirror surface to the center of the V-grooves. The center of gravity of the fibers' image, judging from the mirror image, is

calculated again and conveyed at the position "P-3", where P-3 is right above the center of the V-grooves.

Step3: The center of gravity of the fibers is able to be situated above the center of the V-grooves. Then the fibers are lowered until the V-grooves at the distance of "Xd". Finally the fibers are fixed by the fiber clamps.

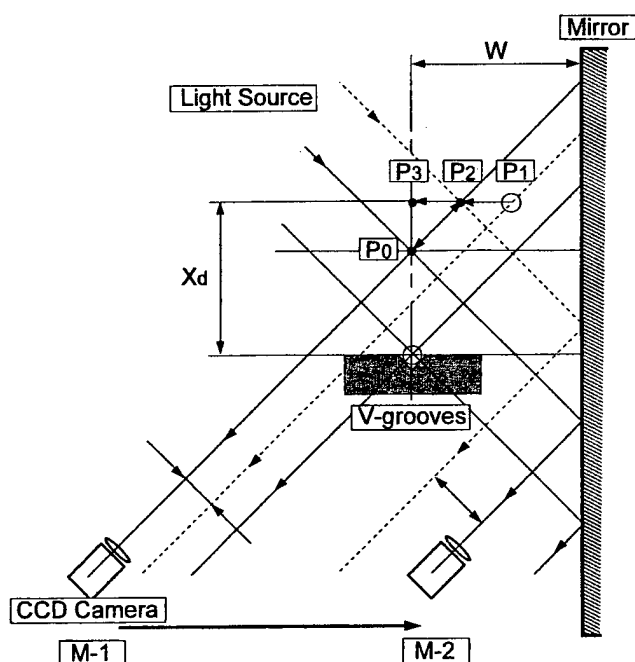


Fig.8 The new alignment system

The experimental results which were obtained in the proposed method above are shown in Fig.9.

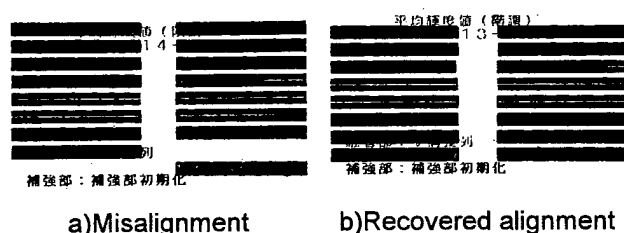


Fig.9 Fiber alignment patterns

There are several patterns of fibers misalignment because the fiber ribbons tend to fan out from the edge of the chucking units. However the CCD-camera can not observe the condition near the chucking units. The optimum conveying distance of optical fibers for aligning to the proper position of V-grooves in each patterns are investigated experimentally. By numerically

evaluating the misalignment, the optical fibers are aligned on the proper V-grooves within three trials.

2.5. Characteristics

The average splice loss of 0.04dB, 0.05dB were obtained for SM2,4,8-fiber ribbons and DSF4-fiber ribbons respectively. The failure strength of spliced portions was as strong as those of spliced using conventional splicers. Concerning with tact time, the spliced portion of optical fiber ribbons could be obtained every 2.2 min. for SM8-fiber ribbons, every 1.8 min. for SM/DSF4, SM2-fiber ribbons in Table2. The splicing productivity will be at least 3 times as high as the conventional mass fusion splicers.

Table2. Splice characteristics

Fiber ribbon	SM8f	SM4f /SM2f	DSF4f
Splice loss (Ave.)	0.05dB	0.04dB	0.04dB
Tact time	2.2 min.	1.8 min.	1.8 min.

3. Conclusions

- (1) The optical fiber ribbons were spliced automatically by using the FSR. The automatically reinforcing mechanism using a protection sleeve of heat-shrink tube type was developed.
- (2) The splicing point showed good characteristics, loss and strength, enough to use the FSR in the field.
- (3) The splicing productivity will be at least 3 times as high as the conventional mass fusion splicers. The FSR succeeded in splicing, not relying on operator's skills.
- (4) The new alignment concept for the FSR was discussed and proposed.

References

- 1) T.Watanabe,et al. "Consideration on the Handling of Flexible, Brittle and Continuous Member in Fusion Splicing Robot for Optical Fiber Ribbons", Proc. of IEEE International.

Conference on Robotics and Automation, pp2413-2419, May 1995.

- 2) T. Haibara, et al. "Single-Mode Multi-fiber Technique for High-Density High-Count Subscriber Cables", IWCS'88, pp576-585.
- 3) M. Matsumoto, et al. "Fully automatic mass-fusion splicer for Singlemode optical fiber ribbons", IWCS'89, pp225-231.

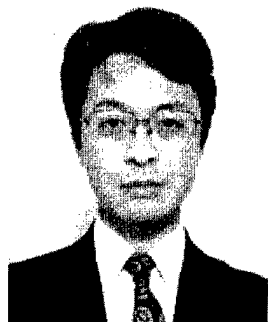


Hideaki Yusa

Sumitomo Electric Industries, LTD.

1, Taya-cho, Sakae-ku
Yokohama, Japan

Hideaki Yusa was Born in 1966 and received his B.S. degree in electronic engineering from Tokyo Metropolitan University in 1990. He joined Sumitomo Electric Industries the same years and has been engaged in research and development of local area network system for data communication technologies and fusion splicing technologies for optical fibers.



Tsutomu Watanabe

Sumitomo Electric Industries, LTD.

1, Taya-cho, Sakae-ku
Yokohama, Japan

Tsutomu Watanabe was Born in 1964 and received his B.S. degree in mechanical engineering from Tokyo University in 1987. He joined Sumitomo Electric Industries the same years and has been engaged in research and development of fusion splicing technologies and



Kazuo Watanabe

Sumitomo Electric Industries, LTD.

1, Taya-cho, Sakae-ku
Yokohama, Japan

Kazuo Watanabe was Born in 1961. He joined Sumitomo Electric Industries in 1980 and has been engaged in research and development of fusion splicing technologies and mechanical switching technologies for optical fibers.



Keiji Osaka

Sumitomo Electric Industries, LTD.

1, Taya-cho, Sakae-ku
Yokohama, Japan

Keiji Osaka was Born in 1955 and received his M.S. degree in precision mechanical engineering from Kyoto University in 1981. He joined Sumitomo Electric Industries the same years and has been engaged in research and development of high NA optical fiber fabrication and fusion splicing technologies for optical fibers. He is now a chief research associate of Optomechatronics System R&D Dept. Yokohama Research Laboratories and a member of Electronics, Information and Communication Engineering of Japan.

CHARACTERISTICS OF THE REUSABLE RIBBON SPLICE ON THE POLLUTED WATER IMMERSION TEST

Y. T. Lee, J. Y. Ha, and K.H. Han

Korea Telecom. Outside Plant Technology Research Laboratory
62-1 Whaam-dong, Yusung-gu, Taejeon, Korea

ABSTRACT

The water immersion test has been performed on the mechanical ribbon splice to investigate the environmental stability of the splice in the outside field. The waters in the different manholes of Korea subscriber areas have been analyzed, and the effects of the polluted water on the performances of the mechanical ribbon splice have been characterized. The ribbon splice showed good results in terms of optical and mechanical performance.

1. INTRODUCTION

Recently the deployment of optical fibers into subscriber network has become a matter of high priority in the telecommunications industry. Korea Telecom has established a base plan - Strategy of FITL (Fiber In The Loop) - to construct an infrastructure of B-ISDN and overcome the problems of copper subscriber networks. Since the FITL needs the large number of cables which also accompanies the increased number of inter-connection points, the reusable ribbon splice which can readily splice fibers have been developed for ribbon (8-fiber) splicing. [1]

Telecommunications outside plant facilities are exposed to adverse environment. One of the adverse field conditions is the polluted water filled in a manhole at many times. The polluted water consists of very different pollutants. These pollutants not only reduce the durability of outside plants facilities but also cause mechanical faults. For instance the polluted water may penetrate into an optical closure due to degraded sealing performance affecting the mechanical splice installed in the optical closure. TA -NWT-001095 of Bellcore first specified the requirements of mechanical splice performance in the adverse field conditions test.[2]

We examined the water in 3 ~ 5 manholes of the regional groups of Korea subscriber area to analyze the main pollutants causing outside plant

facilities to degrade. And the effect of pollutant water on the performance of mechanical splice has been characterized.

2. ANALYSIS OF THE POLLUTED WATER AT MANHOLE

2-1. Selection of manhole

The polluted water of manhole consists of many different pollutants due to the various causes of water penetration. As shown in Table 1, we selected four areas taking into account the incoming water source - coastal area, residential area, industrial area and rural area and each area includes several regional groups (3 ~ 5 manholes per a regional group). We gathered and analyzed the samples extending from May through October. We also investigated the concentrations of the samples and the effects of water contaminants on the outside plant facilities.

2-2. Selection of analysis components

We selected analysis components. By classifying contaminants according to the characteristics of regional groups. First, we measured pH which has an important effect upon outside plant facilities degradation. Measurements were performed directly in the manhole to eliminate pH change which might occur during the sample transportation.

In coastal area, We measured $\text{Cl}^-(\text{Na}^+)$ concentration to find out how much of sea-water flows into manhole. Manholes of residential area may contain harmful materials of living wastes. From this point of view, we analyzed NH_4^+ content because ammonia gas which is produced during anaerobic digestion process of organic materials stands for a degree of contamination in waste water containing lots of organic materials. We expect that the manholes around factory may be filled with incoming industrial waste water including cations such as Fe^{2+} , Cu^{2+} , Zn^{2+} , Pb^{2+} , Ni^{2+} , etc, and anions such as SO_4^{2-} , NO_3^- , etc.

Also we expect that NO_3^- caused by human waste, animals excrement and fertilizer are contained in manhole of rural area.

Table 1 Selected areas of manhole

Areas (number of regional group)	Main factor
Coastal area(4)	Sea-water
Residential area(4)	Living waste water
Industrial area(4)	Factory waste water
Rural area(1)	Agricultural water

2-3. Analysis results

- 1) Temperature : 14 ~ 28 °C
- 2) pH : pH's of water in manhole investigated were about 6 ~ 8 (Table 2). pH in coastal area manhole was 8 ~ 11. This water exhibited basic property . This indicates sea-water has been flowed into coastal manhole since pH of sea-water is around 8.
- 3) The concentration of chloride ion : Table 3 shows Cl^- concentration in each area. Coastal area's manhole showed high Cl^- concentration due to salt. The considerable amount of Cl^- has been also detected in the residential area.
- 4) Nitrogen from ammonia : From the detection of ammonia, we found the water of manhole was contaminated by a lot of organic materials contained in living wastes. As shown in Table 4, residential area exhibited severe contamination due to home waste as indicated by of NH_4^+ concentration as high as about 51.6mg/l .
- 5) Metal ions and SO_4^{2-} : Most of samples had little of metal ion concentration as low as a few $\mu\text{g/l}$.
- 6) Nitrate(NO_3^-) : Generally nitrate was detected in waste or underground water which elapsed for long time with contaminants. As a result of analysis, The higher nitrate concentrations was detected in rural areas than other areas.(Table 4)

Table 2 pH

Areas \ pH	Ave.	Min.	Max.
Coastal	8.04	6.5	11.4
Residential	7.1	5.7	7.9
Industrial	6.65	6.0	7.6
Rural	6.51	6.0	7.5

Table 3 $\text{Cl}^- (\text{Na}^+)$ concentration (mg/l)

Areas	Ave.	Min.	Max.
Coastal	3515(547)	43.3(26)	116,440(5900)
Residential	66.9(49.3)	6.0(1.9)	258.5(175)
Industrial	71.6(66.77)	0.0(2.1)	329(311.2)
Rural	46.8(34.12)	4.6(0.9)	95.4(69.5)

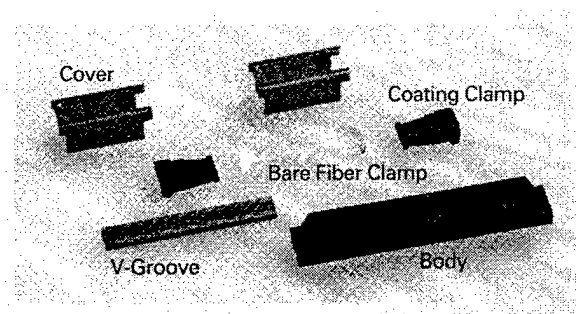
Table 4 $\text{NH}_4^+ (\text{NO}_3^-)$ concentration (mg/l)

Areas	Ave.	Min.	Max.
Coastal	0.48(2.69)	0.02(0.0)	4.3(9.3)
Residential	15(2.25)	0.03(0.0)	51.6
Industrial	4.95(1.8)	0.02(0.0)	20.7
Rural	2.07(3.15)	0.02(0.5)	9.1

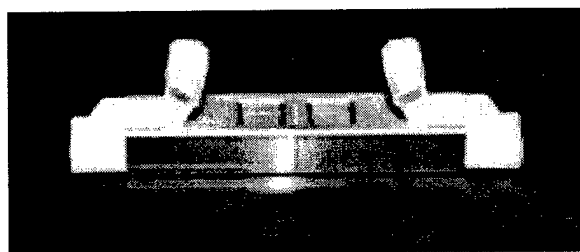
3. ENVIRONMENTAL TEST OF RIBBON SPLICE

3-1. Structural and Optical Performance

The mechanical ribbon splice which has been developed for jointing two SM 8-fiber ribbons consists of body, V-groove, bare fiber clamp, two ribbon coating clamps and two spring covers(Fig1). The size of ribbon splice is 40mm x 6.4mm x 6mm (LxWxH). This splice can be easily assembled, disassembled and cleaned in the factory and fields due to a simple structure as compared to the conventional ribbon splices. The principle of splice is aligning claddings of two 8-fiber ribbons over precise V-groove, and clamping bare fiber and coating by spring cover simultaneously. The clamping method using bare fiber clamp and coating clamp relieve the tensile force and protect the fiber from the environmental effects. We designed bare fiber clamp with seesaw function which ensures splicing at the center of bare fiber clamp and provides low insertion loss by tuning and re-coupling the fibers. In addition, the coating clamp of ribbon splice is designed to rotate by 90 degree so that inserting operation could be achieved while observing the V-groove. Optical performance of the splice showed that mean splice loss was below 0.3 dB and return loss exceeded 40 dB.



(a) Construction



(b) Ribbon Splice

Fig. 1 Photograph of ribbon splice

3-2. Immersion test

The immersion test of the ribbon splice has been performed in the 5 samples which showed the high concentration of pollutant according to the analysis of the flow in water of manhole in Korea. 1) pH=11 considering a basic property in coastal area, 2) pH=2 to test for an acidic property, 3) $\text{Cl}^- = 116,440 \text{ mg/l}$ of maximum to test for a chloride ion, 4) $\text{NH}_4^+ = 51.6 \text{ mg/l}$ of maximum to test for Nitrogen from ammonia and 5) $\text{PO}_4^{3-} = 60 \text{ mg/l}$ of maximum to test for washing detergent. A schematic drawing of the immersion test experiment is shown in Fig. 2.

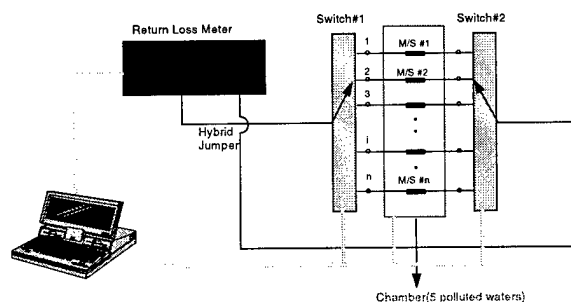
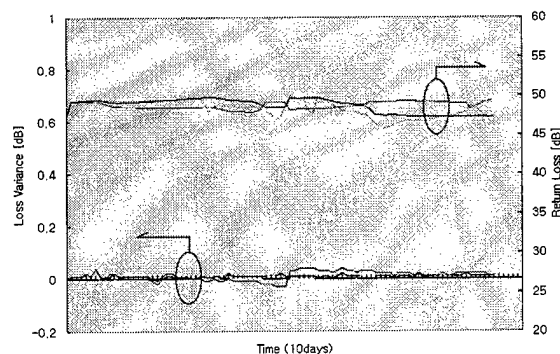


Fig. 2 Experimental set-up for polluted water immersion test

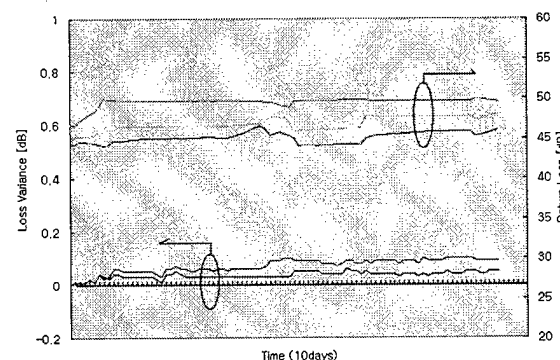
The splices used in this test were spliced below 0.3dB in splice loss and withstood fiber tensile loads of 600g force. The changes in splice loss and return loss have measured on the fibers (2 edge fibers and 1 center fiber) for the respecting mechanical splice which was kept in the polluted water for 10 days at 30 °C taking into account maximum temperature of flow in water into manhole in all seasons.

3-3. The test results

The optical loss changes are shown in Fig. 3. The maximum loss increase of ribbon splice was below 0.1dB and return loss also showed very stable state for all of the tests. After the test, it can also withstand fiber tensile loads in excess of 600g force without significant (0.05 dB) change in loss. The shape of components are showed no deformation or corrosion. These results indicate not only that all parts of the developed ribbon splice could well maintain sealing performance at adverse field conditions, but that the index matching gel exhibits good stability even in the case the pollutant permeates inside the splice.



(a) pH = 11



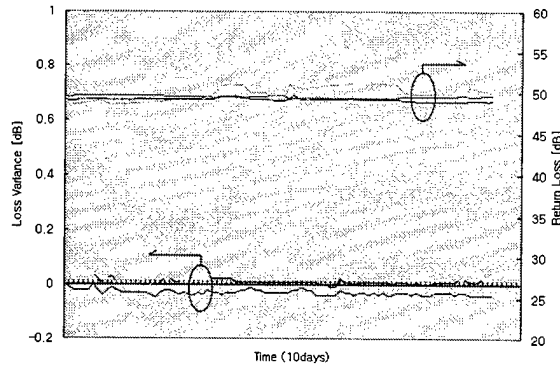
(b) pH = 2

4. CONCLUSION

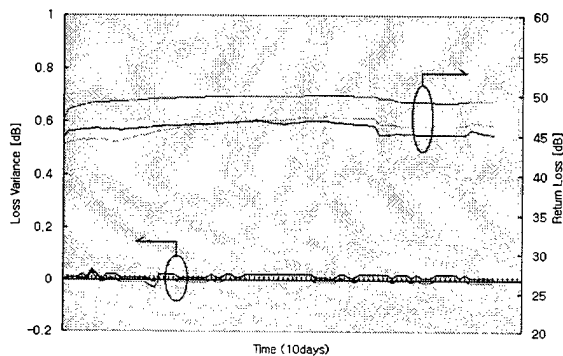
This paper reported the performances of reusable ribbon mechanical splice on the worst pollutant conditions of penetrated water of manhole taking into account the flow in water source - pH =11, pH=2, $\text{Cl}^- = 116,440 \text{ mg/l}$, $\text{NH}_4^+ = 51.6 \text{ mg/l}$, and $\text{PO}_4^{3-} = 60 \text{ mg/l}$, respectively. The ribbon splice showed good results in terms of optical and mechanical performance. These results indicated that the splice can maintain a stable optical signal even in adverse field conditions. This performance requirement of mechanical splice on the adverse field conditions will ensure the ability of the splice to survive in outside environments. In the future, the long term reliability of mechanical splice will be further characterized against adverse environment.

References

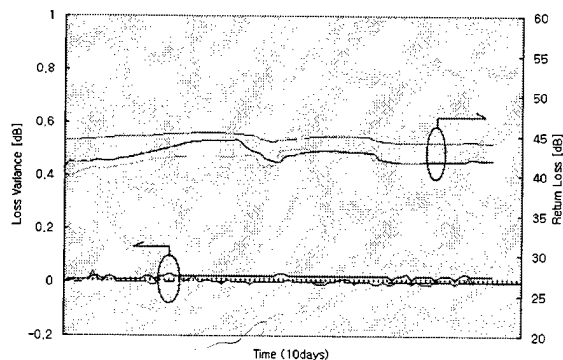
1. Y. T. LEE et al., "The reusable splice for ribbon and single fiber optic cables in optical subscriber loop" proceeding of OECC '96, pp266-267, 1996. 7
2. Bellcore : TA-NWT-001095 "Generic requirement for multi-fiber splicing systems for single-mode optical fibers" Issue 2, 1993. 10
3. C. H. KIM et al., "A study on the counter-measure technology for damage of outside plant product", Annual Report of Korea Telecom, 1993.



(c) $\text{Cl}^- = 116,440 \text{ mg/l}$



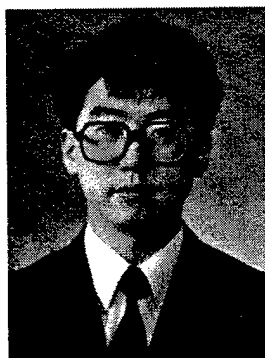
(d) $\text{NH}_4^+ = 51.6 \text{ mg/l}$



(e) $\text{PO}_4^{3-} = 60 \text{ mg/l}$

Fig. 3 Optical performances during immersion test in the polluted water:

AUTHORS



Young-tark Lee

Korea Telecom.

62-1, Whaam, Yu-sung,
Taejeon, Korea

Young-tark Lee was born in 1963. In 1988 he received M.S. degree in Electrical Engineering in Sung Kyun Kwan University and joined Korea Telecom. He is engaged in the design of optical ribbon cable and mechanical splice ..



Kwon-hoon Han

Korea Telecom.

62-1, Whaam, Yu-sung,
Taejeon, Korea

Kwon-hoon Han graduated from Seoul National University with B.S. and M.S on Metallurgy and Rutgers University, U.S.A. with Ph.D on Ceramic Engineering. Since he joined Korea Telecom in 1992, he is involved in the development of optical outside plant technologies



Joung-Young Ha

Korea Telecom.

62-1, Whaam, Yu-sung,
Taejeon, Korea

Joung-young Ha was born in 1965. In 1989 he received M.S. degree in Electrical Engineering in Kyung-book National University and joined Korea Telecom. He is engaged in the development of mechanical splice .

DESIGN OF SPRING CLAMP FOR OPTICAL AERIAL CABLE

Mi-gyoung Kim, Sung-keun Oh, Byoung-chul Lee, Young-tark Lee,
Soon-deok Baek and Kwon-hoon Han

Korea Telecom., Outside Plant Technology Research Laboratory
62-1, Whaam-dong, Yusung-gu, Daejeon, Korea

ABSTRACT

The aerial cable is often suffering from the tension due to suspension in the air which affects the reliability of optical fibers in the cable^[1]. The spring clamp has been developed in an attempt to reduce the tension acting on an aerial cable. The spring clamp which was attached to the ends of the aerial cable could effectively reduce the cable tension, i.e., the cable tension is reduced by 16% for the effective cable weight^[2] 1.2kgf/m.

INTRODUCTION

Since the optical aerial cable between the two poles is exposed to weather, it is continuously suffering from tension. Especially, if an aerial cable is influenced severely by wind, snow and/or temperature, a lot of tension may be induced to an aerial cable. Because the tension of optical aerial cable affects the reliability of fiber^[1], it is necessary to reduce the tension acting upon the optical aerial cable. In general, the shape of aerial cable between two poles can be assumed as a parabolic curve^[2]. The cable tension is related to effective cable weight(cable weight, wind pressure, ice thickness and temperature), span and cable sag^[2], where the cable tension is inversely proportional to the cable sag. Considering this characteristic of cable tension, we have designed the spring clamp(Figure 1) to give an intensional cable sag for reducing the tension of cable which is under the excessive tension.

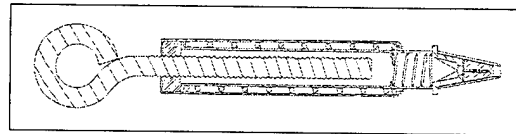


Figure 1. Cross section of spring clamp

THEORY

Figure 2 shows the aerial cable installed between two poles.

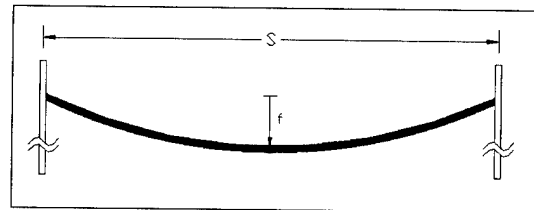


Figure 2. Aerial cable installed

In general, the cable tension T between two poles can be calculated from the following equation^[2].

$$T = \frac{w S^2}{8 f} \quad (1)$$

where

w : Effective cable weight per unit length,
[kgf/m]

S : Spacing of span,[m]

f : Cable sag,[m].

From the above equation(1), we know the cable tension is proportional to effective cable weight and span. On the other hand, it is

inversely proportional to cable sag. Therefore, if the spring clamp whose spring constant is less than that of the aerial cable is attached to the ends of the cable, the sag becomes larger than the case without the spring clamp.

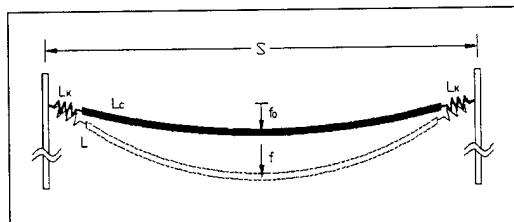


Figure 3. Aerial cable with spring clamp

Figure 3 shows the schematic illustration of the aerial cable installed with the spring clamp. The initial configuration is denoted by the solid line and the deformed one by the dotted line, where, f_0 is the initial sag, f the sag under the environmental conditions, L_c the initial cable length, L_k the initial spring clamp length and L the total length under the environmental conditions. According to the force equilibrium condition, the tension of spring clamp is identical with the cable tension T , then the elongation of the spring clamp can be easily found by the simple relationship between the force and the extension of a linear elastic system expressed by:

$$T = kx \quad (2)$$

where

- k : Spring constant of spring clamp, [kgf/m]
- x : Extension length of clamp, [m].

To reduce the tension of the cable, the spring clamp should be more extendable than the messenger wire of the cable, thus the spring constant of the clamp should satisfy the following condition^[3]:

$$0 < k < \frac{EA}{L_k} \quad (3)$$

where

- E : Young's modulus of messenger wire, [kgf/m²]
- A : Cross section area of messenger wire, [m²].

DESIGN

To reduce the tension of optical aerial cable, spring constant k of spring clamp is the important design factor. Assuming that the initial tension of aerial cable is T_0 and the tension due to several environmental factors is T , the total cable length L (Figure 2) due to several environmental factors can be described as the following equation^[4]:

$$L = 2L_k + L_c + \frac{T - T_0}{EA} L_c + 2 \frac{T - T_0}{k} \quad (4)$$

where

- L_k : Length of spring clamp, [m]
- L_c : Length of cable, [m].

On the other hand, the total initial length between two poles, $2L_k + L_c$ and the total length L due to several environmental factors are as follows, respectively from parabolic curve:

$$2L_k + L_c = S + \frac{8f_0^2}{3S} \quad (5)$$

$$L = S + \frac{8f^2}{3S} \quad (6)$$

where

- f_0 : Initial cable sag, [m]
- f : Cable sag, [m].

Substituting eq.(5) and (6) into eq.(4), the following cubic equation of f is obtained and its solution is well known^[5]:

$$f^3 + f \left[\frac{3w_0 S^3}{64f_0} \left(\frac{3S^2 + 8f_0^2}{3EAS} + \frac{2}{k} \right) - f_0^2 \right] - \frac{3w_0 S^3}{64} \left(\frac{3S^2 + 8f_0^2}{3EAS} + \frac{2}{k} \right) = 0 \quad (7)$$

where

- w_0 : Cable weight per unit length, [kgf/m].

We considered the typical optical aerial cable whose weight is 350gf/m, span length 50m, and initial sag 0.7m. Applying the weather condition of NESC Loading Heavy condition to the above mentioned cable, the cable tension and the extension length of spring clamp Δx have been estimated for the varying spring constants, k (Figure 4).

Using the simulation result in Figure 4, we designed the spring clamp such that its

extension length Δx is 4cm and the spring constant k is 10,000kgf/m. The spring clamp would reduce the tension by 20%(540kgf \rightarrow 444kgf) when the optical aerial cable experiences the NESC Loading Heavy condition.

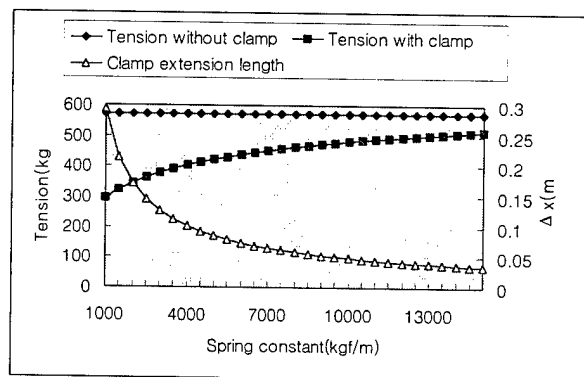


Figure 4. Simulation for clamp design

TESTING

The spring clamp whose spring constant is 10,000kgf/m was manufactured. In case of the cable weight 369g/m, span length 29m, messenger wire 1.6m \times 7 and initial sag 0.5m, the cable tension was measured according to the varying environmental conditions. Because it is not easy to simulate the real environmental conditions, the other factors except the self weight were converted and added to the self weight. Figure 5 shows schematic diagram of testing.

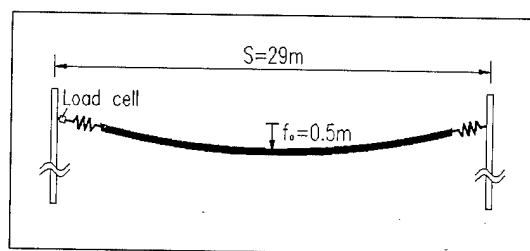


Figure 5. Test method

Figure 6 shows the test results. The experimental values of cable tension were higher than the theoretical values, which results from the experimental error caused by not considering the self weight of load cell.

The test results show that the spring clamp reduce the cable tension by 9% for the effective cable weight of 0.6kgf/m and by 15% for 1.15kgf/m, respectively. It can be seen that the effect of spring clamp is increasing when the environmental conditions are heavier.

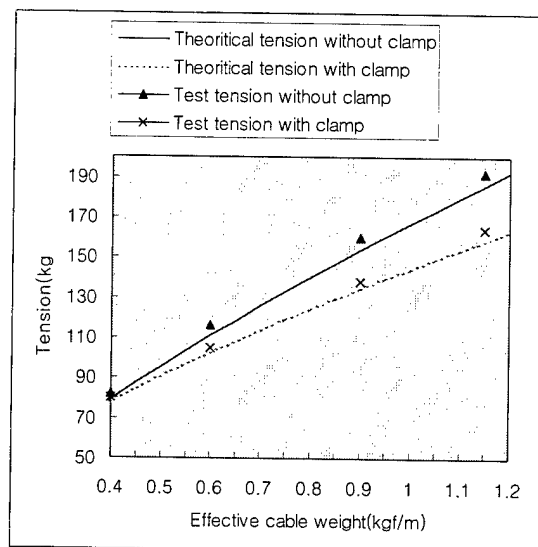


Figure 6. Test results

CONCLUSIONS

To improve the reliability of optical aerial cable, the spring clamp was designed and the range of spring constant was determined to reduce the optical aerial cable tension when it experiences the environmental conditions. Considering the typical optical aerial cable, we designed the spring clamp with spring constant, k of 10000kgf/m and spring clamp extension length, Δx of 4cm. The spring clamp was manufactured and tested. The test results were in good match with the theoretical results. It was also found that the heavier the environmental conditions, the more effective the spring clamp.

REFERENCES

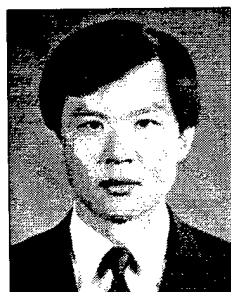
- [1] Shigeo SHIMIZU et al., "Development of optical composite messenger wire", IWCS 1991, pp. 227 - 233.
- [2] P.Stephen Keith et al., "FIGURE-8 FIBER OPTIC CABLE", IWCS 1987, pp. 419 - 425.
- [3] Mi-gyoung Kim et al., "Principle of Spring Clamp", Technical Report TM96-400-042, Korea Telecom., 1996.
- [4] Mi-gyoung Kim et al., "Design of spring clamp", Technical Report TM96-400-006, Korea Telecom., 1996.
- [5] Murray R.Spiegel, "Solutions of algebraic equations", Mathematical Handbook of Formulas and Tables, McGraw-Hill, Inc., 1968, p. 32.

AUTHORS



Mi-gyoung Kim
Korea Telecom.
Outside Plant Technology
Research Laboratory
62-1, Whaam-dong,
Yusung-gu, Daejeon,
Korea
305-348

Mi-gyoung Kim graduated from Korea Advanced Institute of Science and Technology in 1993 with a M.E. Degree on Mechanical Engineering. She then joined Korea Telecom. and is engaged in development and design of fiber optic cables.



Sung-keun Oh
Korea Telecom.
Outside Plant Technology
Research Laboratory
62-1, Whaam-dong,
Yusung-gu, Daejeon,
Korea
305-348

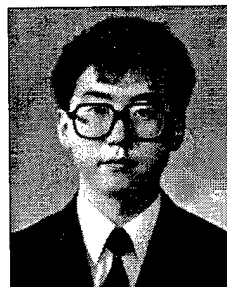
Sung-keun Oh was born in 1961. Since he joined Korea Telecom in 1984, he was engaged in maintenance of optical cable and system, and from 1992 in installation of optical

cable.



Byoung-chul Lee
Korea Telecom.
Outside Plant Technology
Research Laboratory
62-1, Whaam-dong,
Yusung-gu, Daejeon,
Korea
305-348

Byoung-chul Lee was born in 1967. In 1992 he received M.S. degree in physics in Seoul National University and joined in Korea Telecom. He is engaged in the design of optical ribbon cable in the Lab.



Young-tark Lee
Korea Telecom.
Outside Plant Technology
Research Laboratory
62-1, Whaam-dong,
Yusung-gu, Daejeon,
Korea
305-348

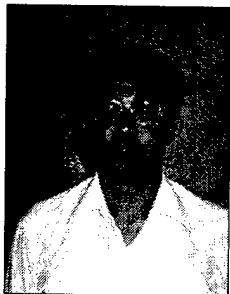
Young-tark Lee was born in 1963. In 1988 he received M.S. degree in Electrical Engineering in Sung Kyun Kwan University and joined in Korea Telecom. He is engaged in the design of optical ribbon cable and mechanical splice in the Lab.



Soon-deok Baek
Korea Telecom.
Outside Plant Technology
Research Laboratory
62-1, Whaam-dong,
Yusung-gu, Daejeon,
Korea
305-348

Soon-deok Baek received B.E. and M.E. from Kyungpook National University, Korea in 1986 and 1988, respectively. He joined Korea Telecom in 1991 and performed the quality assurance work of telecommunication's outside plant facilities including cables and closures for

3 years. He moved to the Outside Plant Research Laboratory in 1994 and is presently engaged in research and development work on optical fiber cables.



Kwon-hoon Han
Korea Telecom.
Outside Plant Technology
Research Laboratory
62-1, Whaam-dong,
Yusung-gu, Daejeon,
Korea
305-348

Kwon-hoon Han graduated from Seoul National University with B.S and M.S on Metallurgy and Rutgers University, U.S.A. with Ph.D on Ceramic Engineering. Since he joined Korea Telecom in 1992, he is involved in the development of optical outside plant technologies.

NEW CONCEPTS IN OPTICAL SPLICEABILITY VERSUS OPTICAL DESIGN

JP. BONICEL (1) - G. LE NOANE (2) - J. PERSONNE (1) - B. JOLY (3) - A. VINCENT (3) - C. VERGEZ (4)

(1) ALCATEL CABLE, Bezons, France ; (2) FRANCE TELECOM-CNET,
Lannion, France (3) : ALCATEL CABLE INTERFACE, Bezons, France ; (4)
ALCATEL CONTRACTING, Clichy, France

1- Abstract

Many papers have already demonstrated that microtube cables have performances well adapted for distribution networks, and therefore turn out to be technically competitive with ribbon cable design.

Moreover, France Telecom is currently launching an experimental network based in a first step on FTTB/FTTC (DORA project), and both above designs will be evaluated on the field.

As it is known that intrinsic technical characteristics are similar in ribbon and microtube design, questions raise about the splicing concern which is an important point for installation.

This paper is intended to give a global idea of the comparative costs when performing splicing operations on the two designs, in comparison with individual splicing process.

2- Description of cables

Cables with 24 OF count («low count»), 144 OF count («medium count»), and 512 OF count («high count») have been compared in terms of spliceability.

Figures 1 to 6 give a cross-section of microtube cables and ribbon cables. Note there is no statement about cable design used for experimenting individual splices. It may be any equivalent fiber count cable of loose design, for example.

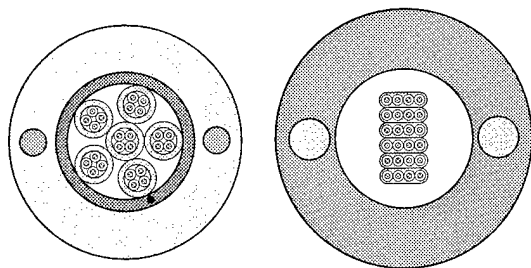


Fig 1&2 - 24 OF microtube and ribbon design

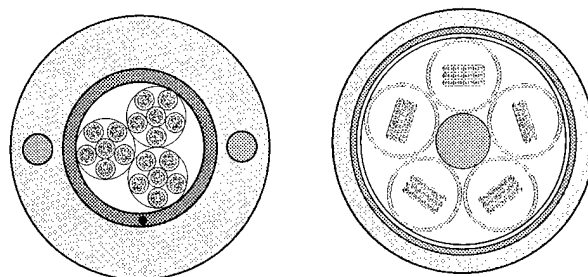


Fig 3&4 - 144 OF microtube and ribbon design

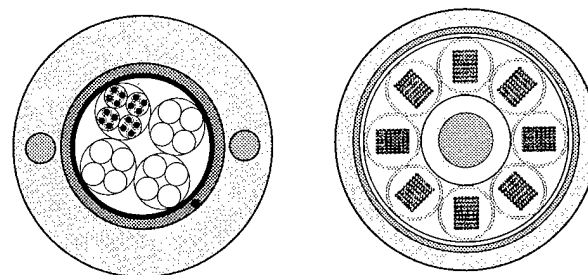


Fig 5&6 - 512 OF microtube and ribbon design

In both microtube and ribbon cables, the OF count per unit is 4 in the 24 OF cable and 8 for the others. This situation corresponds to the DORA project. Furthermore, the influence of modularity is shown for the medium count.

3- Splices closures

Two closures sizes have been used for this experiment :

- a small box that can contain up to 48 single fibre splices, or 96 OF in ribbon fibre splices, or 192 ribbonized fibres issued from a microtube cable design. It has been used for the 24 and 144 OF cable experiment.
- a larger one which is able to contain up to 288 single fibre splices, or 576 OF in ribbon fibre splices, or 1152 OF in ribbonized fibres.

4- Description of single operations for splicing

Table 1 summarizes parameters involved in each operation during splice implementation.

operations	A single splices	B ribbonized fibres splices from microtube cables	C ribbon splices
Preparation of cables - 24 OF count - 144 and 512 OF count	T0 T0	0.9*T0 0.7*T0	0.9*T0 0.7*T0
Ribbonized fibres	not applicable	Tc	not applicable
Splices - fibre preparation . 24 OF . 144 and 512 OF - splices . 24 OF . 144 and 512 OF Total (risk included)	T1 T1 T1 T1 1.15*(T1+T1)	0.5*T1 0.25*T1 0.63*T1 0.38*T1 1.4 *Σ(T)	0.5*T1 0.25*T1 0.63*T1 0.38*T1 1.4 *Σ(T)
Splices protection and installation in the box . 24 OF . 144 and 512 OF Total (risk included)	T2 T2 1.05*(T2)	0.25*T2 0.13*T2 1.2 *Σ(T)	T2 0.5*T2 1.2 *Σ(T)
OTDR measurements . 24 OF . 144 and 512 OF Total (risk included)	T3 T3 1.05 *Σ(T)	T3 T3 1.2 *Σ(T)	T3 T3 1.2 *Σ(T)
Box closing	T4	T4	T4

Table 1 : Description of the operations

For each operation, mass splice duration of microtube cable (case B) and ribbon cable (case C) are related to the correspondent duration Tx spent for individual splices (case A).

The different operations are described and commented hereunder:

4.1- Preparation of cable

This operation consists in cable ends preparation (removing protection), along with the identification of units and fibres.

The corresponding duration is similar for cases B and C, and drops from 10% to 30% compared with A.

4.2- Identifying and ribbonizing fibres

It is a specific task for case B, where it is necessary to take care of fibre identification in order to avoid wrong positioning before ribbonizing operation.

For the realization of the ribbonizing operation various equipment well known and commercially available on the international market can be used.

4.3- Splices

Are included in this item fibre preparation before

splicing (fibre cleaning, coating stripping and cleaving) and all steps related to the splice execution itself : putting fibres or units in the positioning device, performing arc fusion splices, evaluation if splices are correct (loss estimation).

This is the operation for which ribbon or ribbonized unit is quite efficient in terms of cost.

24 OF cable is distinct from the two other fiber count cables because of its lower modularity (4 OF per unit). As a result, the benefit is lower too, but remains significant.

The total duration per operation is affected by a hazard coefficient which is more important in cases B and C due to the fact that if one splice fails, the whole unit must be retreated (splices and measurements).

4.4- Splices protection

Splices are then protected by heat shrinkable sleeves and positioned into cassettes grooves.

Assuming that the increase of attenuation is not greater than 0.1 dB including splice itself and arrangement of units into the box, it is observed that :

- ribbons are less easy to arrange in the box, due to their mechanical polarization and spring effect ;
- correlatively, changes in attenuation may be more important. An important result is that compacity of ribbon units is twice less than microtube bundles. This statement is very significant in a distribution network, where the choice of a small size box is an obvious rule due to the lack of space.

4.5- OTDR measurements

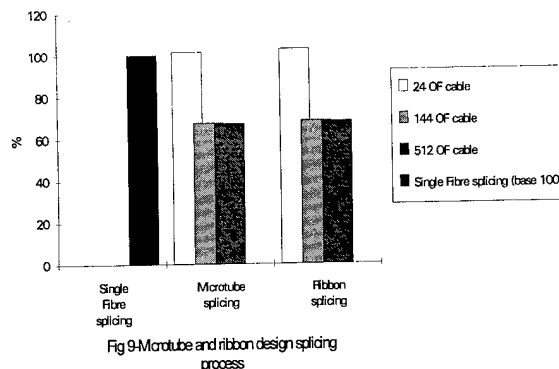
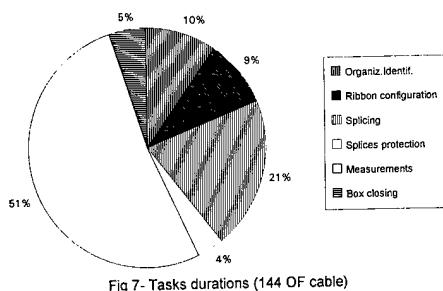
Final OTDR measurements have been performed at 1550 nm in both direction (that means 2 measurements per fibre). In 3 cases, the OTDR intervenes for more than 50% of the total duration for splicing (see pie chart fig. 7).

Comment given in § 4.3, concerning higher hazard coefficient in case B and C, may be reproduced here.

In the other hand, times for cases A, B and C are identical.

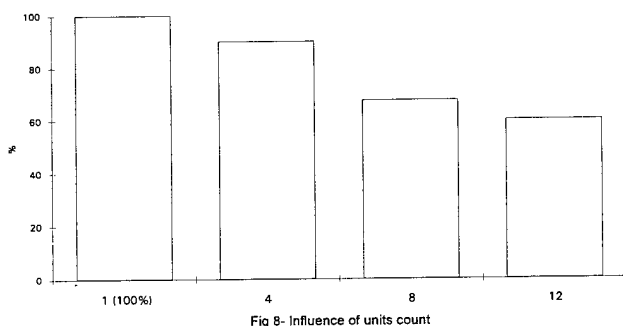
4.6- Box closing

Splicing process ends by closing the box, performing controls and installation in chambers. Times are considered identical, but this could be discussed according to splice closure type which might be different according to cable size.



5- Influence of modularity

The influence of unit OF count is shown in fig. 8.



If network architecture allows, it seems at first sight preferable to adopt high modularity design in microtube cable. However, a specific care must be taken for ribbon cables, substantially for 12 OF ribbons unit installation in boxes.

6- Conclusion

The results are shown in fig 9. For higher cable count, there is no significant time change in splicing ribbonized fibres from microtube cable or ribbon cable.

In both cases, it reduces the cost by more than 30% referring to the single fibre splicing.

One may summarize this conclusion saying that an additional task in microtube cable (said «ribbonizing operation») needs to be made very carefully when identifying and arranging fibres, while the ribbon design, by contrast, is more sensitive in terms of units arrangement in boxes. Respectively, tasks including risk duration are roughly identical.

In low count cable, there is less interest to ribbonize fibres. Moreover, considering a best compacity and handability of microtube units, these one should be preferred in count range below roughly 50 OF cable

References :

- [1] F. Legros, J.L Rochefort, Y. Roussel, D. Brault «Câbles à rubans de fibres optiques», OPTO 92.
- [2] JP. Bonicel, PJ Giraud, M. de Vecchis «Overview of optical fibre ribbon technology», OPTO 92.
- [3] F. Esposito, F. Montalfi, F. Nanni « OF ribbon cable system technology : the Italian experience» IWCS 91.
- [4] KW. Jackson, PD Patel, ML Pearsall, JR Petisce, GA Lochkovic «An enhanced ribbon structure for high fiber count cables in the loop» IWCS, 1989.
- [5] JP Boinet, M. de Vecchis, J. de Vitry «Fibre to the home : no more a trial, an operational reality» ISSLS April 1991, Amsterdam.
- [6] S Hatano, Y. Katsuyama, T Kokubun, K. Hogari : «Multi-Hundred-Fiber cable composed of Optical Fiber Ribbons Inserted Tightly Into Slots», IWCS 1986.
- [7] K.W. Jackson, M.R. Santana, N.W. Sollenberger : «A modular Ribbon design for Increased Packing Density of Fiber Optic Cables», IWCS 1993.
- [8] JP Bonicel, D Keller, G. Kylan, J. Schulte, G. Paternostro, G. Berthelsen, C. Cortines, C. Lasne : «An international Development on Ribbon Technology and Evaluation of Applicability to National Specifications», IWCS 1992.
- [9] P. Trombert, P. Jamet, P. Chéron, G. Le Noane, D. Boscher.» The microsheat cable : a novel design of ultra lightweight single mode optical cable for low cost subscriber loop» IWCS 1991.
- [10] P. Jamet, A. Jarlot - «Manufacturing and field experimentation of microsheat cable for low cost subscriber loop» EFOC/LAN 1992.
- [11] Y. Roussel, F. Legros, D. Brault, JP Louboutin -> Optical ribbon cables : towards an innovating system» EFOC 1995, Brighton.
- [12] T. Sano, T. Watanabe, K. Osaka ->Analysis of mass fusion splice», IWCS 1995.
- [13] D Daems->Evaluation of transient optical losses when handling primary coated, secondary coated and ribbon fiber in the access network».
- [14] P.K. Kim, N.W. Sollenberger, K.W. Jackson-> Capability and control of ribbon stripping as related to ribbon material systems and stripping tools» , IWCS 1995.

Authors

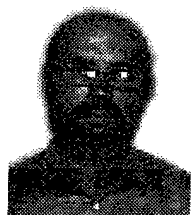
Jean-Pierre BONICEL - ALCATEL CABLE
35 rue Jean-Jaurès 95871 Bezons, FRANCE

Jean-Pierre BONICEL was born in 1952. He received his engineering degree from the Institut des Sciences de l'Ingénieur de Montpellier (ISIM) in 1976. He joined Les Câbles de Lyon, now Alcatel Cable, in 1977 where he was in charge of material and mechanical problems for telecommunication cables. Now, he is head of the telecommunication laboratory, manager for the Alcatel Optical Fibre Cable Competence Center, and Technical Director for the Telecommunications Department.



Georges LE NOANE - FRANCE TELECOM
CNET/LAB/FCI
BP 40 22300 Lannion, FRANCE

Georges LE NOANE, born in 1945, received his engineering degree from the Ecole Nationale des Arts et Métiers and joined CNET in 1974. He began working on optical fibre connector technique, then switches to cables. From 1979 to 1993, he was responsible of optical fibres and cables department. He is now head of division « fibres cables and interconnections ».



Jacques PERSONNE - ALCATEL CABLE
35 rue Jean-Jaurès 95871 Bezons, FRANCE

Jacques PERSONNE, born in 1947, received his engineering degree from the Ecole Spéciale de Mécanique et d'Electricité, Paris, in 1970. He joined LTT in 1971 where he was involved in telecommunication copper cable control and development. He switches in optical cable design in 1981, and joined Les Câbles de Lyon (now Alcatel Cable) in 1986. He is currently in charge of access cable design and responsible of Development Group within Alcatel Optical Fibre Cable Competence Center.



Bertrand JOLY - ALCATEL CABLE INTERFACE
35 rue Jean-Jaurès 95871 Bezons, FRANCE

Bertrand JOLY was born in 1941 in France. He received his graduation from the Aeronautics Engineering school in 1964. As a NASA Fellow, he spent two years at the University of Berkeley, California, where he obtained a Masters and Ph.C. degree in electrical engineering. Since then, he has remained involved in R&D management. B. Joly has been Deputy General manager of Alcatel Cable Interface since 1992, in charge of business development in the field of telecommunications copper and fiber networks. He was appointed head of the Telecommunications Cables Accessory Competence Center of the Alcatel Cable Group in 1991.



Alain VINCENT - ALCATEL CABLE INTERFACE
35 rue Jean-Jaurès 95871 Bezons, FRANCE

Alain VINCENT received his engineering degree from the Conservatoire National des Arts et Métiers, Paris, in 1980. After many activities in the telecommunication equipments field within the Alcatel Cable Group, he joined Alcatel Cable Interface in 1991, where he is in charge of the development of copper and optical fiber telecommunication cables accessories.

Christian VERGEZ - ALCATEL CONTRACTING
30, rue des Chasses 92111 Clichy, FRANCE

Christian VERGEZ was born in Paris in 1952. He received the degree in Electronics Engineering in 1975 from the Ecole Spéciale de Mécanique et d'Electricité, Paris. In 1977, he joined LTT outside plant. He is now at Alcatel Contracting Network Engineering and Installation Department in charge of the design and development of cable accessories.



OPTOCLIP II MULTIWAY

MULTIWAY CONNECTOR for SINGLEMODE ACCESS NETWORKS

Hervé Aoustin, Michel BOITEL
Daniel MORELLEC, Alain PECOT

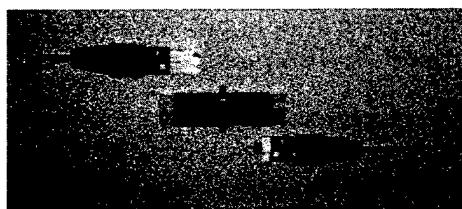
FRANCE TELECOM CNET LAB/FCI/CAI
LANNION, FRANCE

Véronique STAPPERS
Jean-Jacques MAILLARD

Cie DEUTSCH
RUEIL MALMAISON, FRANCE

ABSTRACT

To achieve a distribution network, it is necessary to decrease the cost of each component, this paper describes a new multiway connector, low cost and designed to be installed on the field.



This connector does not include any ferule as others usually do. It is made of two plugs and a receptacle, but the plug does not contain any high precision part : it only maintains and protect the fibers to allow an easy manipulation. The last millimetres of the fibers are protected by a sleeve but remain free. Their ends are cleaved (no polishing). The receptacle includes V-grooves in which the fibers are aligned, the optical continuity between fibre cores is guaranteed by an index matching fluid.

The tool kit which is used is also described in this paper, it includes a ribbon stripping tool which does not need a heavy electrical power supply and an angular cleaving tool allowing a high return loss in any environmental condition.

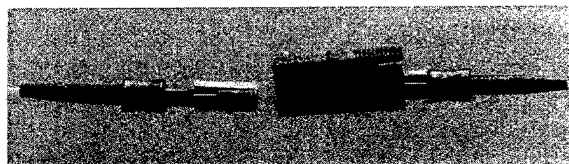
INTRODUCTION

To achieve a large access network, answers have to be found to reduce the price and the volume of passive components. As the cost of optical connection remains far more expensive than those of usual copper

connections, it is necessary to find solutions to decrease their cost in order to allow the construction of a competitive optical fibre network.

The cost limit of most of nowadays connectors is given by the price of the ceramic ferule. In the past, many solutions have been found to make a dematable connection between two fibers without ceramic and even without any ferule. Those light connectors were called "borniers" (translated quite inaccurately by dematable splice), they were first designed for multimodal fibers and allow some tens of connections.

Different kinds were designed but they all basically worked on the same principle : the fibre was stripped, inserted in a plug (by sticking, crimping or both) and cleaved, some millimetres of fibre were free but usually protected by a sleeve or a fork. When connected into the receptacle, the two fibre tips were aligned in a groove (different shapes, different materials) or in some kind of cylinder. Hundreds of thousands of those multimodal connectors have been installed in French video networks (Videocom 1G) since 1985 and are still in use.



first generation of singleway connector

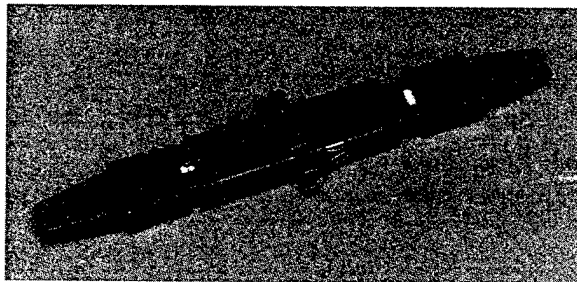
When it was possible, those singleway connectors were improved in order to be able to

connect singlemode fibers, by a new design of the alignment part. An example of this connectors is described in reference (1) and (2). Lately, the plug and receptacle evolved to make a push-pull system, in the dimension of usual connectors (EC, SC), reference (3).

What is required now to allow the deployment of large singlemode access networks is the decrease of the cost and size of optical fibers connections. The solution developed here is the design of a multiway connector, with no ferrule. The dimensions of this 8 fibers connector are those of a classical singleway one.

CONNECTOR PRINCIPLE

The picture shows two plugs and the receptacle, the right-hand plug is half connected.



8-way Push-Pull connector

At the tip of the plug, the fibre last millimetres are free (no ferrule) and, when connected, are precisely aligned into the receptacle, by precision parts.

Description of alignment parts

The two fibers are cleaved, with an angle, to allow a high reflection loss in all thermal conditions, connected or not, as shown in reference (4).

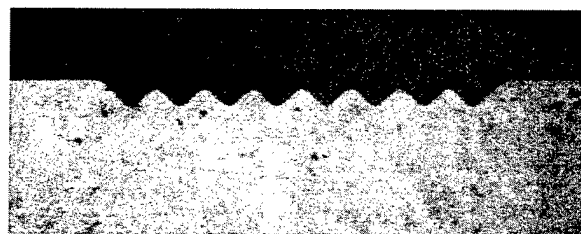
For many years now, the dimension of singlemode fibers diameter and their concentricity are very precise, it is then possible to use the outer surface of the fibre as a reference to align the fibre cores. Numerous

methods can be used, here the fibers are set in precision 90° V-grooves.

Many ways of manufacturing the grooves have been investigated (plastic moulding, ceramics...). Metal stamping trials gave us V-grooves with a good precision and a smooth surface. They can be manufactured at a very low cost, if produced in large scale.

The eight grooves are produced at the same time, the step between them is 250 µm, like fibers in a ribbon.

To obtain a good precision, the stamping needs a soft material, but when inserted in the receptacle, the fibre slips on the V surface and as silica is very hard, soft V would be quickly damaged. The V are therefore stamped in a soft copper alloy and plated with a hard material to reduce abrasion.



Cross Section of the Stamped V-Grooves

The two fibers connected in a groove are in contact (small buckling of the fibre in the plug) but as there is no convex polishing and as the axial force is small, there is not a real physical contact between fibre cores. The two cores are separated by a gap which is filled by a matching fluid set in the V during the receptacle manufacturing. This matching material is a polysiloxane which has a refraction index very close to the fibre core one (at least at laboratory temperature, reference (4)), it decreases Insertion Loss and increases Return loss.

The matching material has a secondary but quite interesting effect : when the fibers enters the alignment part, the gel moves along the fibre, cleaning it from dust or small pollution.

After cleavage, the fibers have different lengths, but are all in contact when connected because of the fibre buckling. During temperature variations this buckling is also

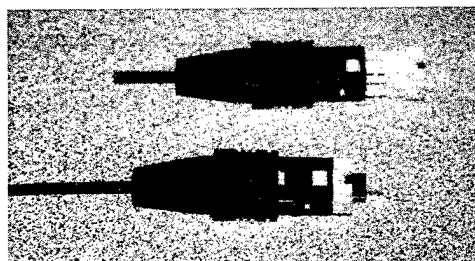
needed to compensate the dilatation of the different parts.

Description of the plug and receptacle

The plug does not contain any high precision part, but it has many significant functions. Its main use is to maintain and protect the fibre during the connection operation.

Most of the parts are plastic moulded, leading to low costs if produced on a large scale.

The striped ribbon, or the microsheath, is stuck in the plug (cyanoacrilate glue) to ensure a high fibre retention. The bare fibers are precisely guided in U grooves in order to position it in front of the precise V-grooves during the connection operation.



Multiway plugs

The Optoclip II multiway has a push pull coupling mechanism, a protection sleeve terminated by a protection cap moves forward or backward during the connection or the disconnection (on the picture : the sleeve is in the plug on the foreground and out, on the fibre in the background). It ensures a full protection of the fibre against dropping or pollution and preserves the operator from laser radiation.

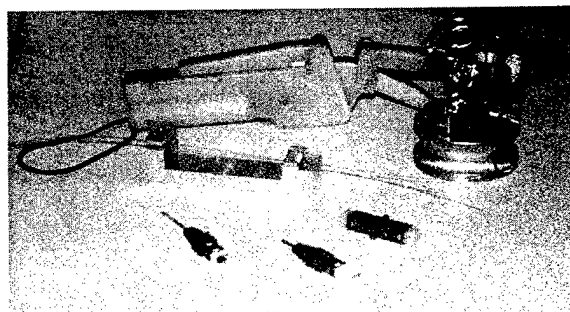
The connector receptacle has a standard size, it can be mounted on SC or EC panels, in usual termination boxes.

TOOL KIT

To connect fibers on-site using the optoclip multiway, the assembling method is :

- setting a plug on the cleaving tool

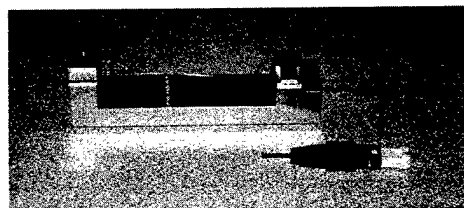
- stripping and cleaning the ribbon or the single fibers
- constituting a ribbon (if single fibers or microsheaths are used)
- inserting of the fibers in the plug
- sticking the fibers
- cleaving them



The procedure is fast, simple and does not need numerous tools.

Ribbon Constitution Tool

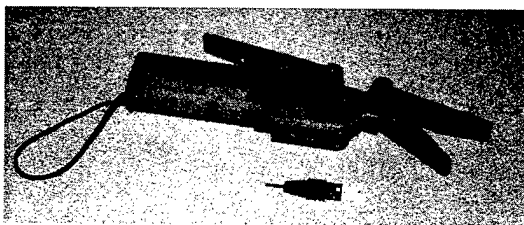
This tool is needed if small capacity or microsheath cables are used. Each single fibre is stripped, inserted in a groove at the end of the tool, with respect to the colour order. The regular ribbon mounting procedure is then used and the tool removed.



The U-grooves which are in the plug aligns quite precisely the fibers, the reconstitution tool is therefore very simple as it does not need to be very precise, its main function is to keep the fibres in good order while the others are stripped and during their insertion in the plug.

Striping Tool

This connector is designed to be mounted on-site. The ribbon stripping tools we know require a heavy electrical power supply (110, 220 V) which is not compatible with our aim. We designed a new tool :



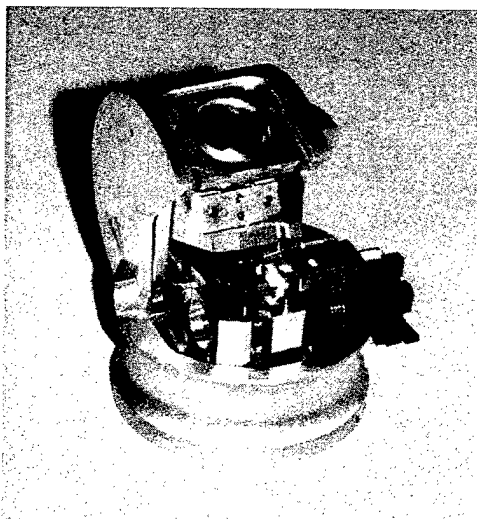
- batteries are in one handle, near a heating electrical resistance. Those batteries allow 100 stripping and can be recharged during the night

- in the same handle is a blade used to cut the outer part of the ribbon

- the other handle hold the ribbon and rotates to give it a tension in order to finally stripe the coating.

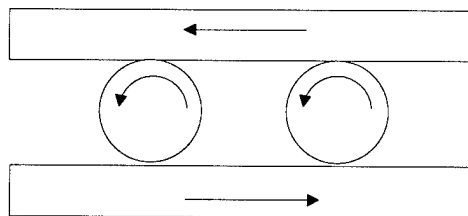
Cleaving Tool

The principle of this tool is patented by France Telecom.



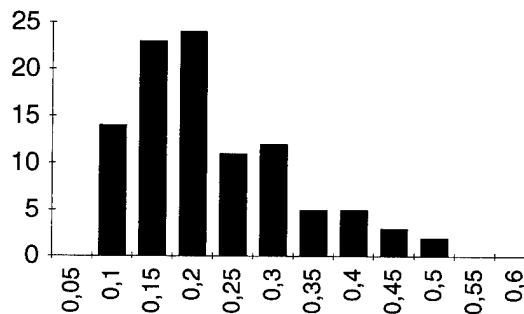
Its principle is widely described in reference (4). It is well known that a double bent of a fibre previously scratched in its middle and clamped at both ends will result in a perfectly straight and flat cleaved surface. If before or during the double bent shear stresses are added, the cleavage will be angular. This shear stress can be created by a change of any of the double bend parameter (motion of the clamped, scratching and bending not in the middle...), in our trials it did not result in reproductive cleaved angle.

Another solution to create this stress is to twist the fibre. It is not as easy for a ribbon as for a single fibre, the solution we have chosen is to clamp the ribbon at one end and to set the other end between two moving planes, which will give the twist.



A more or less classical scratch and a double bend will then cleave the fibre.

PERFORMANCES



This diagram shows the insertion loss measured on a sample of 96 fibre connections.

CONCLUSION

The optoclip II multiway is a solution for a low cost dematable connection, allowing a low insertion loss and a high return loss.

REFERENCES

(1) B. CAPELLE, C. VILLEMMAIN et al. "Borniers optiques monomodes à pertes d'insertion et taux de reflexion très faibles et avec mise en oeuvre très rapide sur site" OPTO 91 Paris.

(2) B. CAPELLE, C. VILLEMMAIN et al. "Singlemode dematable mechanical splice with low insertion and return loss and very fast

termination on the field" OE FIBERS 91, BOSTON.

(3) V. STAPPERS et al. "Low cost fiber optic single mode push pull connector" EFOC&N 94.

(4) BOITEL et al "cleaving tool for fibers ribbon" IWCS 96.

AUTHORS

For CNET :



Hervé Aoustin Graduated from the Ecole Nationale Supérieure des Arts et Metiers in 1990. He is engaged in fibre connection R&D since he joined the CNET in 1992.



Michel BOITEL Graduated from the Ecole Nationale Supérieure d'Optique in 1969. He joined the CNET in 1970 and is now engaged in fibre connection R&D.



Daniel MORELLEC is a member of the cable installation and optical fibre connection group in CNET. He is presently engaged in fibre connection R&D



Alain PECOT graduated from the Institut National des Sciences Appliquées in 1979. He is the manager of the cable installation and optical fibre connection group, in the CNET.

At : CNET LAB/FCI/CAI
3, Avenue Pierre MARZIN
22307 LANNION
FRANCE

For DEUTSCH :

Véronique STAPPERS is European Marketing Manager for Optical Devices for Deutsch.

Jean-Jacques MAILLARD is a member of the Deutsch optical connector design department. He is presently engaged in the Optoclip II Multiway program

At : DEUTSCH
10, rue Lionel TERRAY
92500 RUEIL MALMAISON
FRANCE

FAILURE ANALYSIS OF FIELD SERVICE OPTICAL FIBER SPLICE PROTECTOR

Ting-Chung Chang, Jye-Meei Hsiao, Whei-Jen Chen, Hsi-Pai Hsu, Y.-c. Lin

OSP, Telecommunication Labs, Chunghwa Telecom, TAIWAN, R.O.C.

ABSTRACT

Reliability of fiber splices is a complex issue, because it is affected by labor technique, fusion splice protector method, product design and quality, and the service environment. Postmortem analysis of failure devices is a useful way to improve the optical fiber loop plant reliability. In this paper, we use the microscope analytical techniques of SEM and nondestructive X-ray image to analyze the field failure fusion splice protector samples. In addition, a laboratory simulation of temperature cycling effect on the splices using the same splice protectors was conducted to infer the failure mechanism. From our investigation, the static fatigue resulting from the bending stress that exerted on the weak bare fiber within fusion splice protectors has been identified as the main cause of these failures.

INTRODUCTION

For the goal of fiber to the home, today, more and more fibers have been deployed into the subscriber loop. As the use of fiber spreads throughout the telecommunication plants, short cables of high counts containing numerous fusion splices are becoming more common. When the density of fiber-optic interconnections increases in the loop plant,

the reliability of these devices becomes a issue of importance, because the splices are always the candidates of the weakest link for a subscribe loop fiber system.

An example was reported for a 24-fibers loose-tube-design jelly-filled optical fiber cable. The cable was almost out of service after 1 month of installation, and was found five breaks inside fusion closures. 2 month later, another same type of cable failure occurred in a different route.

All failed samples were identified as breaks at the splices, which were protected by clamp-shell protectors. Further examination is, therefore, initiated to understand the failure mechanism. First, the failure samples were subjected to nondestructive evaluation and conventional analytical techniques of microscopic inspection and SEM examination. Tensile strength measurement was also used to measure the splice strength. Second, A simulating test was established to study that how such clamp-shell protecting splice prepared in the laboratory will perform if under aging tests of temperature cycling, in-service aging, water immersion, bleach immersion, and 70°C oven aging.

EXPERIMENTAL

Nondestructive X-ray image analysis

X-ray images of failure samples were taken by a Nicolet NXR-1400 real time X-ray imaging system.

Simulating laboratory aging tests

Four chain-fiber samples were prepared in the laboratory for simulation tests. Two were constructed from fusing twenty-four individual 10m-fiber to make a total 240m-long chain-fiber with 48 numbers of splices clamped with shell-protectors(but one differs the other by using different clamp tools designated as A and B). The other two chain-fibers were simply a non-spliced fiber but still clamped by 48 clamp-shell protectors. Yet the clamped region was stripped to become bare-fiber. These chain-fibers were then aged inside a 70°C oven and an on-line transmission light was monitored. Other aging tests of temperature cycling, in-service aging, water immersion, bleach immersion (1) were also performed on partial samples.

Tensile strength

Minimum of 25 specimens for each sample were measured in a Universal testing machine using a gage length of 500 mm and a strain rate of 20 mm/min in a laboratory ambient environments of 23°C and relative humidity of 60%.

Coating morphology observation

The fiber samples were cleaned to remove dirt particles which might have collected on aging environments. The fiber samples were stuck on a metal tape and the cleaned fibers are then coated with a gold-palladium coating at a thickness of 40-100 Å. The fiber coating

surface is examined under a scanning electron microscope.

RESULTS AND DISCUSSION

From the nondestructive microfocus X-ray image analysis of field failure fusion splice protector, it showed seven of eight test samples were broken inside the clam-shell fusion splice protector. Figure 1 is the typical pictures of X-ray image of a fractured fiber inside a fusion splice protector of the "clam-shell" type. After removing fiber from the protector and carefully examining the fiber fracture surface using SEM, it shows that most of the fracture surfaces are only comprised the smoothly flat mirror zone as shown by Figure 2. Those mist and hackle zone are not observed. Since the mirror zone was formed during a crack spread. An apparent crack may have been existing after the completion of splicing. Those cracks may have been produced during fiber coating stripping or bare fiber cleaning(2,3,4). When the fused fiber was put into the "clam-shell" protector, it was found that the fiber always somehow bent. Such bending therefor imposed a stress that induced a static fatigue on the fiber. The static fatigue finally lead to a break of fiber at the weakest point where potential cracks have been existing. As a result, relatively poor splicing craftsmanship in the combination of clam-shell induced bending stress may have an immediately effect on the splice, which then will breaks short after the completion of cable installation such as one month or two months after the cable installation.

Results of optical power meter measurement of four laboratory prepared chain-fiber samples aged at 70°C showed that (a) protector tool-A has more effect on the attenuation changes than that of protector tool-B, (b) more pronounced loss was induced for spliced fiber than non-spliced fiber that both are sleeved with protector tool-A while no apparent difference was observed for samples sleeved with protector tool-B between the spliced and non-spliced fibers. As shown on the Figure 3, the splice fibers sleeved by protector tool-A was found having a loss of 3.5 dB of total attenuation while the corresponding non-spliced chain-fiber showing a 2.0 dB of attenuation at 1550nm after 8 weeks aging at 70 °Coven. However, fibers of spliced and non-spliced but sleeved with protector tool-B shows equal loss of 1 dB at 8-weeks of aging. This showed that shell protectors clamped with different brands of tools may have different effects of the induction of attenuation on the fiber splices during thermal aging. This explains why certain types of shell-clamp protectors have higher fatigue failure rates on the splices.

Measurements of the tensile strength of two spliced fibers sleeved with two commercial clam-shell sleeves (designated as protector I, and II) and under environmental aging were shown in Figure 4, 5 and Table 1. It shows that the strength of a spliced fiber clamped with shell protector I and protector II may drop by 83% and 70%, respectively, when comparing to the non-spliced original fiber. Also, the strength of a spliced fiber but without sleeved protectors show a drop of 88% of its non-spliced counterpart and the breaking points were inside the splice-protector region. These indicate that the clam-shell won't help too much to resist the

stress that come to fiber. For Environmental aged protector-sleeved splices, the tensile strength measurements showed that the temperature cycling resulted in 70-80% of drop out of its original fiber-strength and the 45°C water immersion after 30 days gave 75-80% drop. In addition, a significant drop of the tensile strength can also be seen for spliced sleeved optical fiber when aged in a 0.5% bleach solution. All these indicate that the clam-shell protector is not a good environmental protector.

COCLUSION

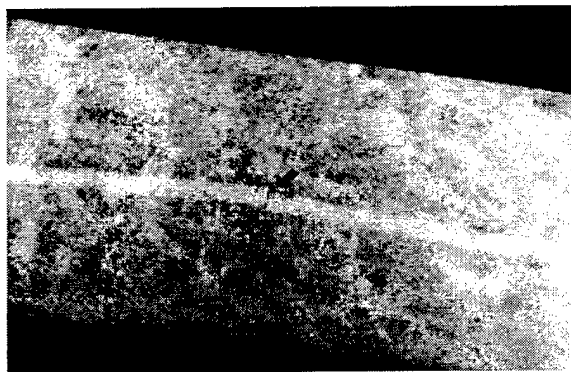
1. From the result of X-ray image analysis and SEM observation in addition to the tensile strength measurement, splice breaks inside clam-shell protector is explained as a fatigue effect result from the protector sleeves.

2. The clam-shell protector may be a convenient installation method but its possibility to induce static fatigue that may lead to splice break and lacking of environmental protecting ability may prompt us to reconsider to use it as a regular deployment method.

REFERENCE

1. Bellcore GR-1380-CORE.
2. T.Wai, H.H. Yuce, C.H. Hase, Proc. 38th IWCS, p199(1989).
3. H.H. Yuce, P.L. Key, T.Wai Proc. 39th IWCS, p400(1990).
4. T.Wai, H.H. Yuce, Proc. 40th IWCS, p199(1989).

Field failure clam-shell protector sample A



Field failure clam-shell protector sample B

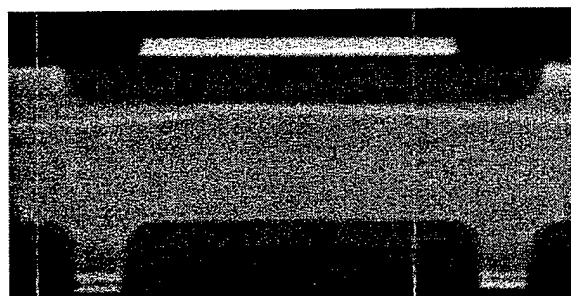


Figure 1 :X-ray image of a fractured fiber inside a fusion splice protector of the clam-shell type

Fracture surface of field failure sample A



Fracture surface of field failure sample B

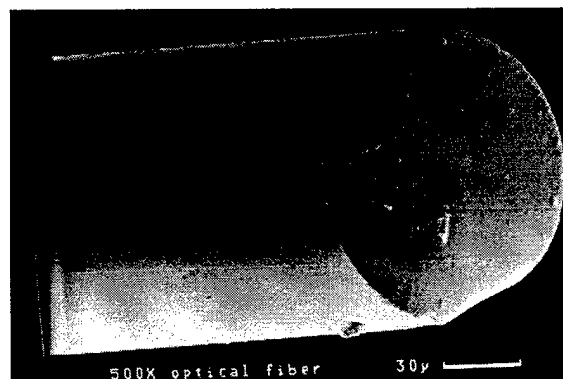


Figure 2 : SEM analysis of fracture surface of fiber removed from protector

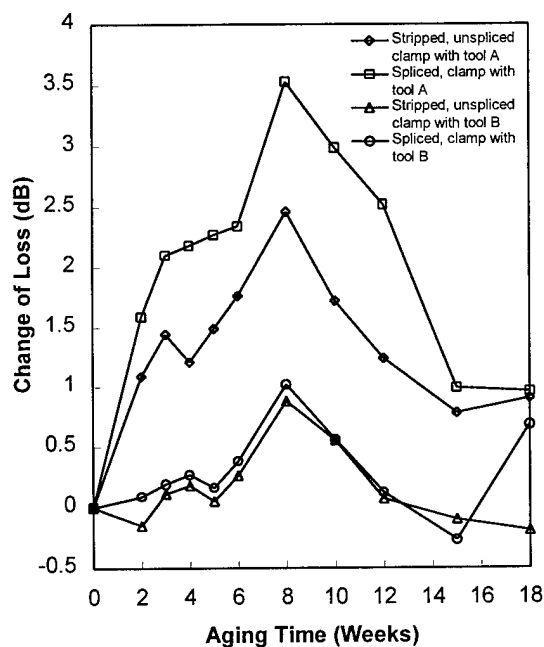


Figure 3 :The optical loss in 1.55 μm of fusion fiber sleeved with clam-shell protector I using tool A and B after aging at 70 $^{\circ}\text{C}$

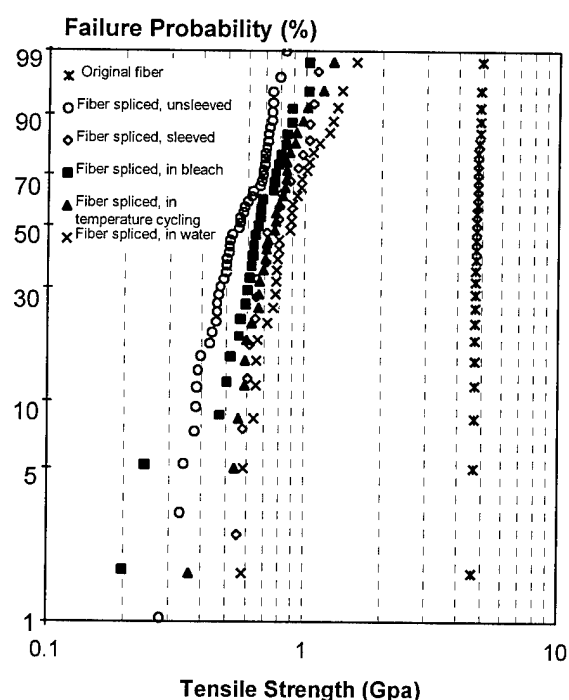


Figure 4 : Effect of aging on the tensile strength of fusion splice fiber protected by clam-shell protector I

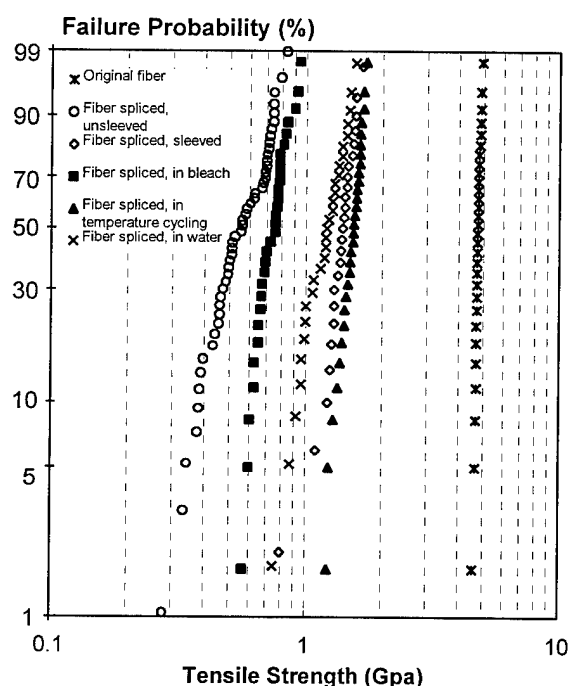


Figure 5: Effect of aging on the tensile strength of fusion splice fiber protected by clam-shell protector II

Table 1: Median tensile strength of spliced sleeved fiber after aging test

Sample	Median tensile strength (kgf)	Probability of fiber break inside the protector
Fiber	5.96	—
fusion fiber (unsleeved)	0.71	—
fusion fiber (protector I)	0.99	19/20
fusion fiber (protector I)-45 °C water immersion	1.11	30/30
fusion fiber (protector I)- 0.5 % bleach immersion	0.83	29/29
fusion fiber (protector I)- temperature cycling	0.96	29/30
fusion fiber (protector II)	1.74	23/25
fusion fiber (protector II)-45 °C water immersion	1.51	28/29
fusion fiber (protector II)- 0.5 % bleach immersion	0.95	30/30
fusion fiber (protector II)- temperature cycling	1.92	27/30

Biographies



Ting-Chung Chang

OSP, T.L.
Chunghwa Telecom
P.O. Box 6-48, Yang Mei
Taoyuan, Taiwan 326,
R.O.C.

Ting-Chung Chang received his M.S. degree in Applied Chemistry in 1984 from Tsing Hua University and then directly joined T.L.. He is now a research scientist and a member of outside plant laboratory in T.L..



Chieh-Mei Hsiao

OSP, T.L.
Chunghwa Telecom
P.O. Box 6-48, Yang Mei
Taoyuan, Taiwan 326,
R.O.C.

Chieh-Mei Hsiao received her M.S. degree in Chemical Engineering from Tsing Hua University. She joined T.L. in 1981 and presently worked as a research scientist and a member of outside plant laboratory in T.L..

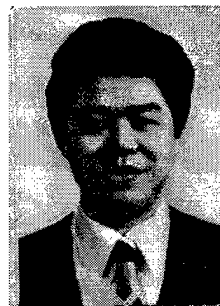


Whei-Jen Chen

OSP, T.L.
Chunghwa Telecom
P.O. Box 6-48, Yang Mei
Taoyuan, Taiwan 326,
R.O.C.

Whei-Jen Chen received her M.S. degree in Applied Chemistry in 1991 from Tsing Hua University and then directly joined T.L.. She is

now a research scientist and a member of outside plant laboratory in T.L..



Hsi-Pai Hsu

OSP, T.L.
Chunghwa Telecom
P.O. Box 6-48, Yang Mei
Taoyuan, Taiwan 326,
R.O.C.

Hsi-Pai Hsu is currently a project manager of the material group of Loop and Outside Plant Laboratory, Telecommunication Labs. . He received his Ph.D. degree in Chemistry in 1983 and has engaged in industrial materials research since then.



Yih-Chyuan Lin

OSP, T.L.
Chunghwa Telecom
P.O. Box 6-48, Yang Mei
Taoyuan, Taiwan 326,
R.O.C.

Yih-Chyuan Lin received his B.S. degree in chemistry in Taiwan and his Ph.D. degree in Photochemistry from Georgetown University. After working as a postdoctoral Fellow in the Institute of Materials Science at the University of Connecticut, he joined Telecommunication Laboratories in 1989 and presently is a project leader of O.S.P. material and construction.

EFFECTIVE FORCE TRANSFER MECHANISM IN A NOVEL CABLE PULLING MACHINE

**R.-S. Kuo, Min-Sung Lu, Chang-Ho Chen,
Lian-Jehn Huang, Shih-Teng Chang, Shih-Wei Lai**

OSP, Telecommunication Labs, Chunghwa Telecom Co. Ltd., Taiwan, ROC

ABSTRACT

Due to the corrosion of the sheath and ingress of water and soil, the friction force between the conduit and the sheath of the cable is large. Therefore, strong force is needed to pull out the scrapped cable. In the conventional method, an eye grip or sleeve is used to hold the outer sheath of the cable to transfer the force. However, the sheath is usually broken and often fails the pull-out task.

For this, a novel system has been developed for the purpose of effective pulling. An iron capsule is used to grip the transmission wire of the cable for effective contact. An aluminum alloy pulley set with a guiding ring assembly is used to transfer the power from the hydraulic power source to the capsule. The pulling engine is capable of adapting to the reaction force such that the pulling power can be adjusted according to the resistance of the cable so as not to break down the cable. The Max. pull-out force of the machine is about 10 tons and the pull-out of the scrapped cable can be made very easily.

INTRODUCTION

In Taiwan, underground telecom cables were installed in the PVC pipe conduits. The construction of an underground outside plant is expensive and time-consuming, therefore, it is of great importance to fully utilize the conduit space. For this, in the case of fault, upgrade or other reasons, the scrapped cables were pulled out to vacate the conduit for another cable installation.

However, the friction force between the conduit and the cable sheath is usually very large such that the removal task often fails with the conventional techniques and equipments. To solve the problem, TL OSP Lab. has developed a novel cable removal machine with hydraulic power winch and epoxy capsules to supply and transfer forces. The maximum pull-out force is about 10 tons. Field trial operations indicate that the machine is capable of extracting scrapped cables for most cases.

CONVENTIONAL METHOD OVERVIEW

A typical Telecom cable is made with metallic conductor wires covered and protected by outer jacket. A common method to pull out cable is to use an eye grip or sleeve to hold the outer sheath of the cable to transfer the pulling forces¹ as shown in Fig.1. Since the sheath is usually made with polymeric material, it was often broken during the pull-out process. With this method, the effective pull force that can be exercised was limited to as low as 2-3 tons. Whereas, the friction force between the conduit and the sheath is often far beyond that range due to:

- a. Ingress of soil and water
- b. Deformation and damage of conduit
- c. Corrosion of cable sheath
- d. Stuck on of the deteriorated lubricant
- e. Other obstacles such as garbage and leaves

Therefore, stronger force is needed to pull out the scrapped cable. And a novel cable holding devices should be developed to transfer the external pulling force directly to the transmission wire core.

EXPERIMENT AND DESIGN OF IRON CAPSULE

The experimental data indicates that the transmission wire is capable of sustaining certain amount of tensile force as listed in Table 1.

Table 1 The Ultimate Tensile Strength of Bare Wire

Diameter of the Wire(mm)	Ultimate Tensile Strength
0.4	3.1 kg
0.5	4.9 kg
0.65	7.8 kg

Since a typical telecom cable contains hundreds to thousands pairs of wires, the accumulated pulling resistance can be very large. For example, the estimated ultimate pulling resistance of a cable with 2400-pairs of 0.4mm diameter wire is approximately:

$$3.1 \text{ kg} \times 2400 \text{ pairs} \times 2 \text{ thread/pair} = 14.8 \text{ tons}$$

To provide such strong force transfer with the mechanical connection between the cable end and the pulling head is difficult. Therefore, chemical connection is chosen.

The iron capsule employed in the connection is shown in Fig. 2. The cable core is plugged into the conic chamber of the hollow iron capsule. Then, a mixture of epoxy adhesives is injected into the chamber. The cable core will integrally associated with the epoxy adhesives after the curing hardening period. The capsule with a pulling cap then forms the cable-epoxy pulling head as shown in Fig. 3. A series of tensile tests on the mixture solid indicate that the ultimate anti-pulling capacity is approximate to 700 kg/cm^2 , about 70% of the tension strength² possessed by the coated wire core. Therefore, the cable-epoxy mixture, confined by the capsule, becomes the force bearer of external pulling force which in turn drags the cable out of the conduit. The connection mentioned can sustain a pulling force larger than 10 tons. The limits is on the tensile strength of the cable; too large a force will elongate and break down the cable in the conduit. The largest pulling force exerted during the cble removal cases coming upon is 9 tons.

CABLE REMOVAL MACHINE WITH HYDRAULIC WINCH

Since the iron capsule was capable of bearing the large pulling force, the next step was the construction of the force generator and transfer media. The final system set up is shown in Fig. 4. The most important elements of the system are the hydraulic power winch and the aluminum alloy pulley reaction frame.

Hydraulic Power Winch

Hydraulic power winch is solidly fixed on the truck deck driven by a hydraulic pump. The pump is powered by a P.T.O.(Pair Transmission Organization) attached to the truck engine. The pulling task is accomplished by using an iron wire drawn from the winch to connect the iron capsule pulling head^{3,4}. The scrapped cable, following the capsule pulling head, is wound on the drum of the hydraulic power winch when it is pulled out from the conduit.

The features of the hydraulic power winch are:

- (1)The maximum pulling forces is 10 tons
- (2)The pulling force is adjustable according to the number of metallic wires and the force sustainable
- (3)The pulling movement is linear and continuous, therefore, the elongation of the cable under tremendous force won't cause problems
- (4)The rotation speed ranges 0-2 rpm. The maximum pulling rate is about 6 meters/min.

Aluminum Alloy Pulley Reaction Frame

The reaction frame is made of 6061T6 high strength aluminum alloy. The total weight is about 67 kg for easy manual transfer and installation. At the upper end, a metallic ladder can be attached for access to the manhole. The purpose of the frame is to transfer the pulling force from the vertical direction above the ground to the horizontal direction inside the manhole. It also functions as the reaction point of the force transfer process².

APPLICATION OF THE CABLE REMOVAL MACHINE

The cable removal machine has offered many benefits to the network plant operation. The re-installation of vacated conduit helps lower down the construction cost and time. The conduit space made available by pulling out scrapped cable is especially precious in highly urbanized areas where road excavation is strictly regulated to prevent traffic jam and impacts on residents. Finally, updating and upgrading of the telecom network are taking place throughout the island and

the cable removal machine, due to its reliable and efficient performance, becomes an indispensable equipment in the network enhancement process.

CONCLUSION

A novel cable removal machine has been developed for effective cable pull-out. By employing iron capsule as force transfer media, the machine maximum pull-out force can be greatly increased to about 10 tons. The important elements of the machine include hydraulic power winch and an aluminum alloy pulley reaction frame. Site trial operations have proven that the machine functions well and the pull-out of the scrapped cable can be made very easily.

REFERENCES

1. "Construction Specification of Underground Cable in Local Outside Plant," CLC-CL1001-1, Spec. of Chunghwa Telecom Co. Ltd., 1983 (in Chinese).
2. Lu, M.-S., et al. : "Review of Underground Cable Removal Techniques," 83-LL-703, Technical Report of Chunghwa Telecom Co. Ltd, 1994 (in Chinese).
3. Chang, C.-F. : "Handy Manual of Standard Mechanical Design Table," Tai-Long Book Co., Inc., Taipei, 1980 (in Chinese).
4. Ong, T.-I. : " Mechanical Design Manual," Kao-Lee Book Co., Inc., Taipei, 1987 (in Chinese).

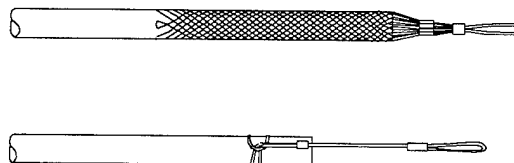


Fig. 1 Conventional Method for Pulling and Installing Cable.
(up) Sleeve (down) Eye Grip.

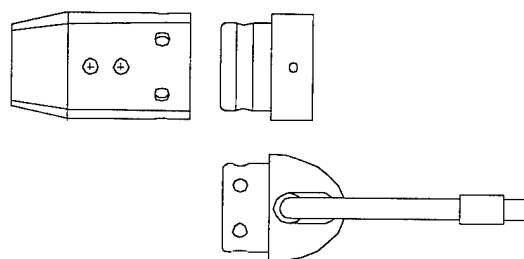


Fig. 2 Cable-Epoxy Capsule and the Fittings.



Fig. 3 Formation Diagram of Cable-Epoxy Capsule Pulling Head

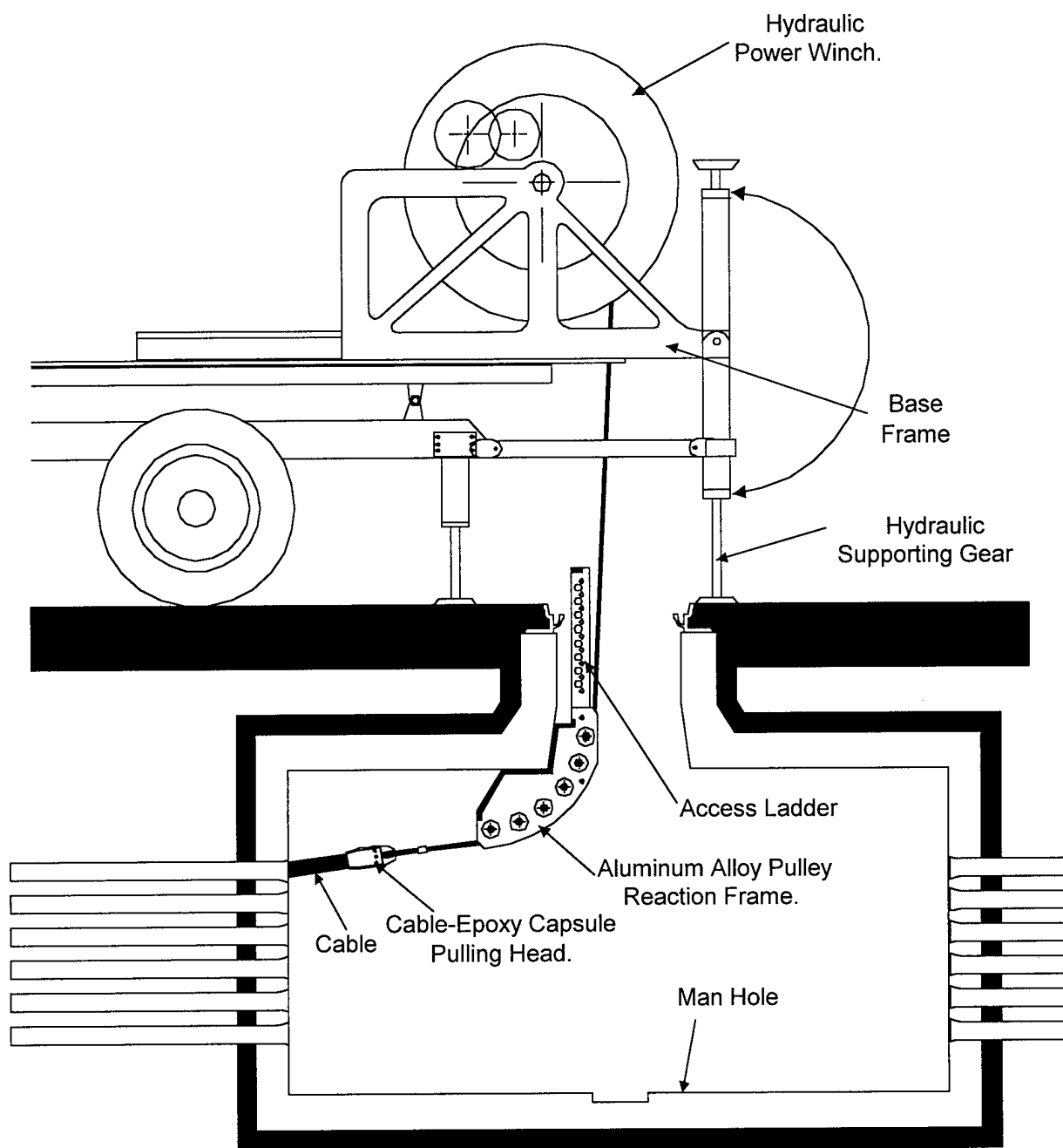


Fig. 4 Schematic Diagram of Cable Removal Machine

1650 nm MONITORING TECHNIQUE FOR OPTICAL FIBER CABLE LINE DEGRADATION

Sheng-Wen Wang, Fwu-Yuan Tsai, Sei-Chun Chen, Wann-Yih Guo

OSP. Telecommunication Labs., Chunghwa Telecom, Taiwan, Republic of China

ABSTRACT

This research applies the high sensitivity to the fiber bending loss of long wavelength (1650 nm) to detect the degradation of fiber optic cable. The suitability of 1650 nm as the monitoring wavelength is studied for the 565Mb/s, and 2.5Gb/s digital signal transmission systems. The required loss threshold value is also determined for a future 1550 nm digital transmission service system while 1650 nm is used as the monitoring wavelength.

INTRODUCTION

To serve the needs of future multi-information services(e.g. image, video signals...) and the dramatic volume increase of telecommunication service brought about by the Asia-Pacific Operation Center, together with the demands for higher quality of telecommunication service, it is vital to accelerate the installation of fiber optic network and the assurance of high quality transmission network. Among the various factors effecting the quality of fiber optic transmission network, the microbending loss[1] introduced when the fiber was formed, or the macrobending loss incurred during the installation of repeater or terminal distributor in the network will degrade quality of the fiber optic transmission. For the fiber optic cable adopted in future fiber optic cable TV network and subscriber loop, plus the fiber optic link that will be applied in ultra-height building, the degradation of fiber relates to the quality of the future telecommunication service.

Traditionally, 1300 nm is used as the transmission wavelength in telecommunication service for fiber network while 1550 nm is used as the monitoring wavelength. There has been a trend to use 1600nm as the monitoring wavelength due to the increasing demands of image and video transmission.

DETECTION OF DEGRADATION IN FIBER CABLE

There are three positions in a fiber cable that can have degradation [2]: (1) fiber in the cable, (2) mechanical

splices closure, (3) terminal distribution box.

Techniques for detection of fiber network will be described in this section.

Microbending loss

Traditionally, microbending loss exists starting from the fabrication of the fiber. It is a distribution loss, difficult to measure when the loss is small. There are researcher using Bernoulli Optical Time Domain Analyzer(BOTDA) to detect cable strain [3]. We can apply the advantage of high sensitive of long wavelength (1650 nm) to the bending loss, with the use of Optical Spectrum Analyzer(OSA) to determine the microbending loss in a fiber cable. Fig.1 is a spectrum of a fiber before cabling. During the cabling process, microbending loss caused by cable jacket and mechanical stress nonuniformity gradually increase. There are obvious changes in the absorption loss in the 1600 ~ 1650 nm wavelength band, as indicated in Fig.2. The accumulated microbending loss in the long wavelength band increases as force is nonuniformly applied during installation, as shown in Fig.3.

Macrobending loss

It is a man-made local bending loss induced by improper fiber installation procedure. It occurs in the mechanical splices closures and terminal distribution box. Because of the higher sensitivity of 1650 nm than 1550 nm to bending, 1650 nm optical time domain reflectometer can be applied in field testing of optical fiber system [4].

LONG WAVELENGTH EFFECTS ON THE PERFORMANCE OF DIGITAL TRANSMISSION SYSTEM

In the previous section we describe the use of 1650 nm wavelength for the detection of fiber cable degradation. The effects of 1650 nm to the performance of digital transmission system will be examined in this section. Uni-direction 100km 1650nm - monitored 565Mb/s - 1550 nm transmission system architecture, as indicated in Fig. 4, was used to measure the eye diagram, bit error rate(BER) and optical receiver power with pseudo-

random NRZ input signal of different bit rate. The isolation capability of a 1650/1550 nm wavelength division multiplexer are all about 12dB, as indicated in Fig. 5 and Fig.6. The directivity is better than 50dB. The contrast ratio of the tunable filter is larger than 30dB.

Fig. 7 is the eye diagram of a 100km uni-direction 1650 nm -monitored 565Mb/s - 1550 nm transmission system. Qualitatively, distinction between 1550 nm signal and 1650nm signal is very clear. Also from the BER measurement, as shown in Fig. 8, there is no power penalty in either 1550 nm transmission signal nor 1650 nm transmission signal for a 100km uni-direction 565Mb/s - 1550nm digital transmission system. In other words, the 1650nm monitoring signal has no deteriorate effect on the performance of the 100km uni-direction 565Mb/s - 1550nm digital transmission system.

The architecture of a 50 km uni-direction 1650 nm - monitored 2.5Gb/s - 1550 nm digital transmission system is shown in Fig. 9. External modulation of the laser diode was used to minimize dispersion of the fiber. Pseudo-random NRZ input signals of different modulation frequency was applied in the same way to measure the eye diagram, bit error rate and optical receiver power of the 1550 nm - 2.5 Gb/s digital transmission system. Fig. 10 or Fig. 11 are the eye diagrams measured before the attenuator for transmission system with wavelength division multiplexer or with tunable filter separately. From a qualitative point of view, it is better to choose a system with tunable filter than a system with wavelength division multiplexer for the reason of low isolation capability in 1650 /1550 nm wavelength division multiplexer (only 12 dB). Therefore we used a tunable filter (contrast ratio > 30dB) in the 50 km 1550 nm - 2.5 Gb/s digital transmission system. From a view of investment in transmission architecture, it is more cost effective to use a 1650 /1550 nm wavelength division multiplexer, with isolation large than 30dB. Fig. 12 is the BER and optical receiver power for a 1550 nm - 2.5 Gb/s digital transmission system. The optical receiver power at BER of 10^{-9} (back to back), receiver power of a 50 km 1550 nm - 2.5Gb/s transmission system and receiver power of a 50 km 1650 nm - monitored 1550 nm - 2.5 Gb/s transmission system are -25.6dBm, -25.6dBm and -25.4dBm respectively. This figure indicates that the effect of adding a 1650 nm monitoring signal into the 1550 nm - 2.5 Gb/s transmission system is almost neglectable, (with power penalty of only 0.2 dB). In the other words, the 1650 nm monitoring signal has no effect on the performance of the 50 km 1550 nm - 2.5 Gb/s digital transmission system.

DETERMINE OF THE THRESHOLD LOSS VALUE

In the preceding section we have proved that the 1650 nm monitoring signal has no effect on the performance of

either 565 Mb/s nor 2.5 Gb/s 1550 nm digital transmission system. Then how do we determine the threshold loss value for fiber cable alarming when using 1650 nm as the monitoring wavelength in a 1550 nm digital transmission system ? We decide that the degradation of fiber cable is due to the local macrobending loss induced by improper installation procedure. Therefore we establish relationship between 1650 nm OTDR and 1550 nm bending loss measurement obtained by power meter for matching index single mode fiber and depressed index single mode fiber. The measurement scheme is shown in Fig.13. Measurement was made for the same bending loss by 1550 nm power meter v. s. 1650 nm OTDR bending loss measurement. Fig. 14 and Fig.15 are 1550 nm v. s. 1650 nm bending loss relation for matching index single mode fiber and depressed index single mode fiber, respectively. Together with BER and optical receiver power graph, threshold loss value for 1650 nm monitoring wavelength used in 1550 nm digital transmission system can be determined. Using 565Mb/s - 1550 nm undersea digital transmission system as an example, the optical receiver power at BER of 10^{-10} is X dBm. The monitoring system needs to alarm before system breakdown. If the alarm is set to go off when the fiber network degrade to a BER of 10^{-8} , the receiver power degrade to Y dBm. The receiver power to be Z dBm when system breakdown occurs with BER of 10^{-6} . When 1550 nm power meter loss changes are (Y - X) dB, (Z-X) dB respectively, reasonable 1650 nm OTDR monitoring loss value and threshold loss value can be determined for different kinds of fibers corresponded to 1650 nm OTDR loss changes.

CONCLUSIONS

This research proposes a technique using long wavelength (1650 nm) for the detection of fiber cable degradation. It has been shown that the long wavelength monitoring signal will not deteriorate quality of the digital transmission system. the required monitoring loss value and threshold loss value for the future long wavelength monitoring system is also suggested.

REFERENCES

- 1.Vivek Arya, Kent A.Murphy, Anbo Wang, and Richard O.Claus,"Microbend Loss in Singlemode Optical Fibers: Theoretical and Experimental Investigation, " Journal of Lightwave Technology, vol.13,no.10,pp.1998-2002,1995.
- 2.Izumi,S.,Yahei,K., Shin-ichi,F., Tsuneo,H.,Nobuo,T., Yutaka,W., "Optical Fiber Line Surveillance System for Preventive Maintenance Based on Strain and Loss Monitoring," IEICE TRANS. COMMUN. , vol. E76-B, no.4 ,pp.402-409,April, 1993.
- 3.Mitsuhiro, T., Tsuneo, H., Toshio, K., Koushi, I., "First Measurement of Strain Distribution Along Field-Installed

Optical fibers Using Brillouin Spectroscopy", Journal of Lightwave Technology, vol.8,no.9,pp.1269-1272, Sept.,1990.

4.Hidetoshi, T., Nobuo, T., Junichi, N., Naoyuki, A., "Design of a 1.65- μ m-Band Optical Time-Domain Reflecto-meter", Journal of Lightwave Technology, vol. 11, no.11, pp. 1743-1747, Nov., 1993.

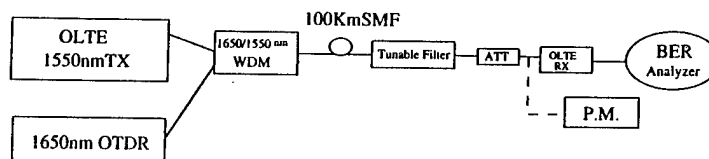


Fig. 4 Uni-direction 1650 nm-monitored 565Mb/s system structure

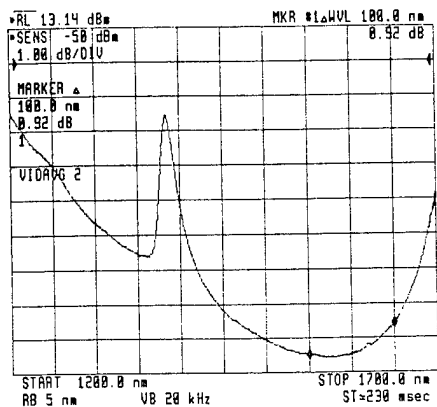


Fig. 1 The spectrum loss of a SMF before cabling

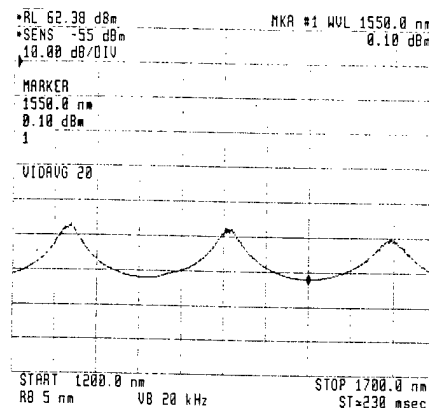


Fig. 5 Output 1550 nm of a 1650/1550 nm WDM

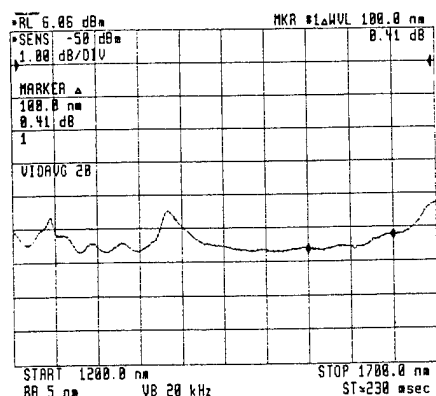


Fig. 2 The spectrum loss of a SMF after cabling

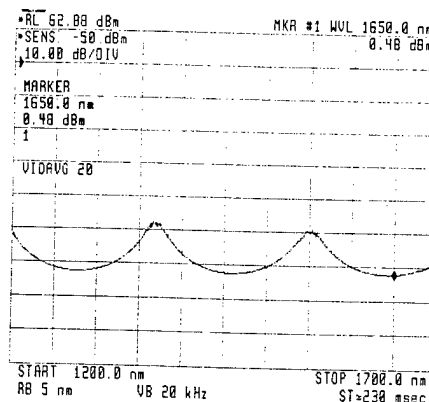


Fig. 6 Output 1650 nm of a 1650/1550 nm WDM

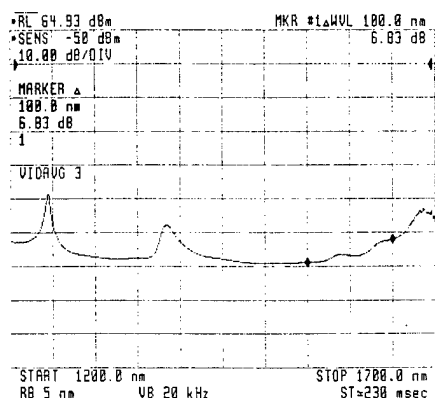


Fig. 3 The spectrum loss of a SMF after installation

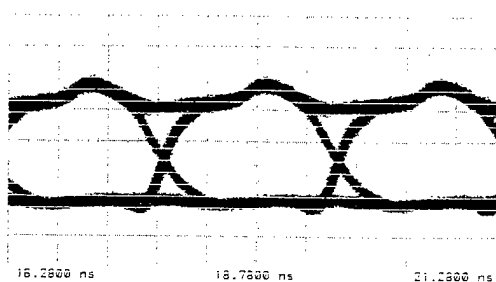


Fig. 7 The eye diagram of a 1650 nm-monitored 565Mb/s system

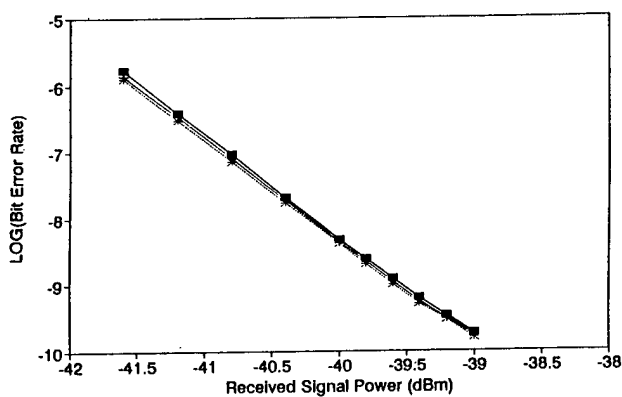


Fig. 8 The BER-Received Power of 1650 nm-monitored 565Mb/s system

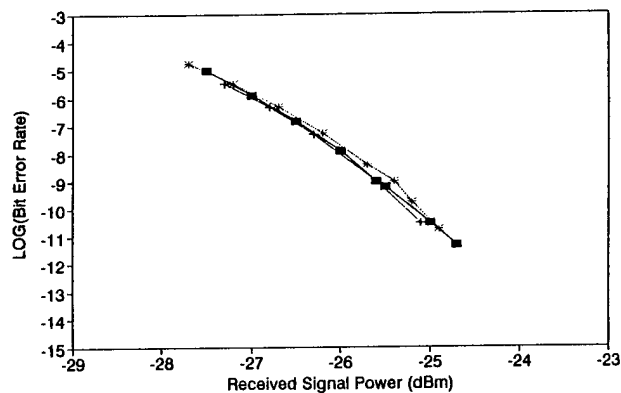


Fig. 12 The BER-Received Power of 1650 nm-monitored 2.5Gb/s system

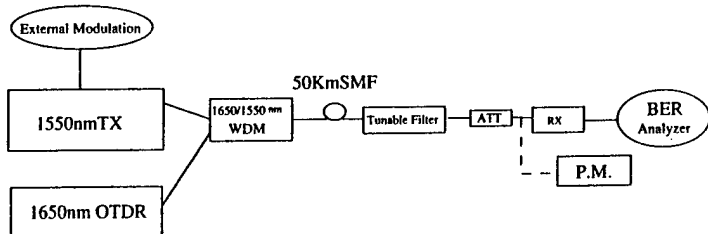


Fig. 9 Uni-direction 1650 nm-monitored 2.5Gb/s system structure

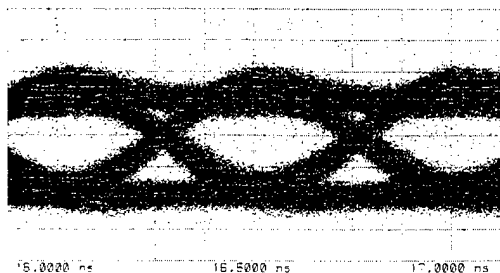


Fig. 10 The eye diagram of a 1650 nm-monitored 2.5Gb/s WDM system

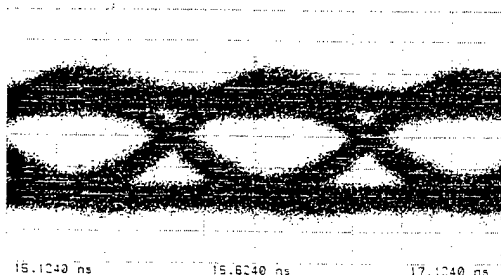


Fig. 11 The eye diagram of a 1650 nm-monitored 2.5Gb/s filter system

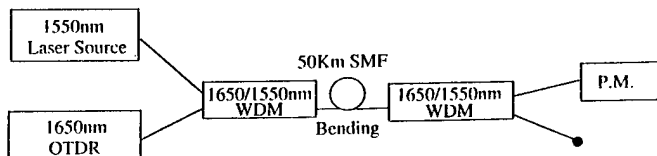


Fig. 13 The threshold loss measurement scheme

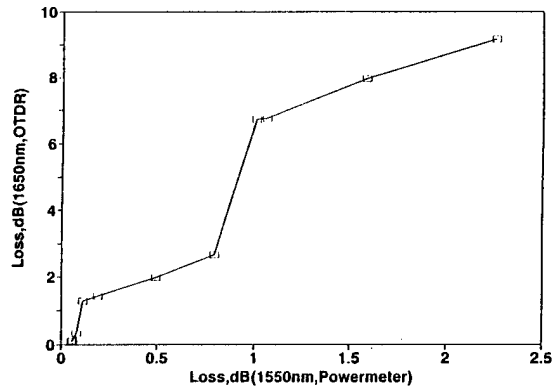


Fig. 14 1550 nm v.s. 1650 nm bending loss for matching index SMF

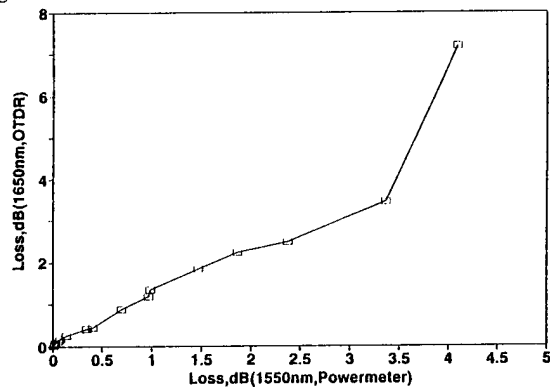


Fig. 15 1550 nm v.s. 1650 nm bending loss for depressed index SMF

Development of the Portable Terminal for The Information Free Access System Employing FM-SCM Transmission Method

Hideyuki OMURA, Haruo NAKAYAMA, Hideyuki NASU
FURUKAWA ELECTRIC CO.,LTD. Information & Electronics Laboratories,
5-1-9, Higashiyawata Hiratsuka, Kanagawa, 254, JAPAN
Telephone:81-463-24-8446 Facsimile:81-463-24-8491

Kenichi TEZUKA
TOKYO ELECTRIC POWER COMPANY Nuclear Power R&D Center,
4-1, Egasaki-cho Tsurumi-ku Yokohama, Kanagawa, 230, JAPAN
Telephone:81-45-585-8938 Facsimile:81-45-585-8943

ABSTRACT

We have developed a highly reliable and cost effective system as the multi-coupler optical communication system which was introduced in [1]. It has already commercialized for some monitoring systems on electrical power cables, railways and express ways. In order to utilize the multi-coupler system, the information free access system have been produced.

In this paper, we present and demonstrate a novel bi-directional free access system including special portable terminals. Finally, we obtained successful results on not only a 20km transmission line but also a 100m atmospheric optical transmission path with 20 optical couplers.

1.INTRODUCTION

Rapidly changing architecture of video transmission or telecommunication system for multi-media service, infrastructure is being consolidated with the optical fiber which take advantage of its low loss and wide band. Such optical fiber transmission lines are very important

to realize video supervising application such as power transmission lines, nuclear power stations, security, construction of roads or railways and so on.

Conventional video supervising systems cannot observe all areas along the transmission line without having blind points, and cannot comply with the requirement of moving an observation point on demand because remote terminals at the observation point must be set up fixedly.

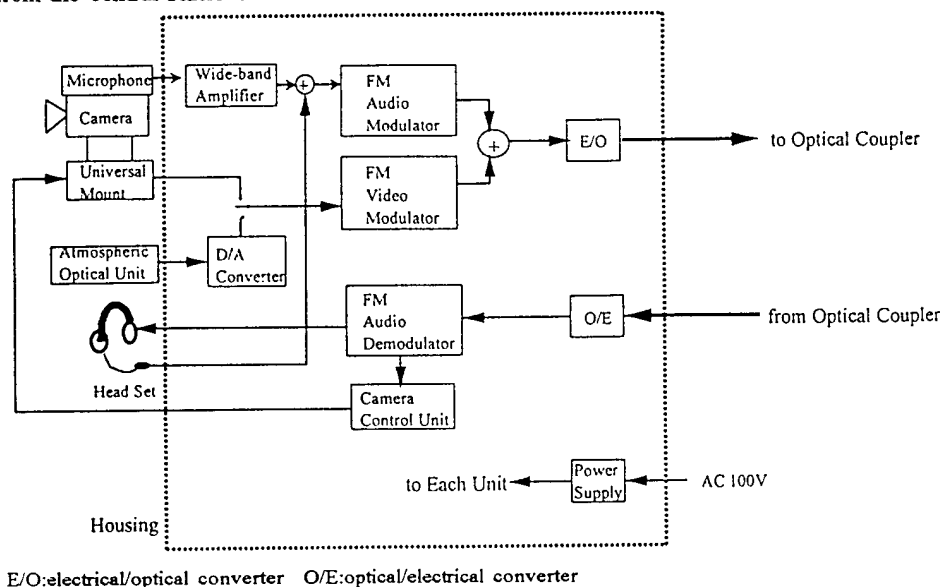
We have developed the information free access system to solve to these problems which conventional systems have. The multi-coupler system(1)(2) employing the FM-SCM video transmission technique(3)(4) has a solution of the problem.

In this paper, we introduce the portable terminal which is indispensable to construct the information free access system. Moreover, we show results of transmission experiments.

2.CONSTITUENT EQUIPMENT OF THE POTABLE TERMINAL

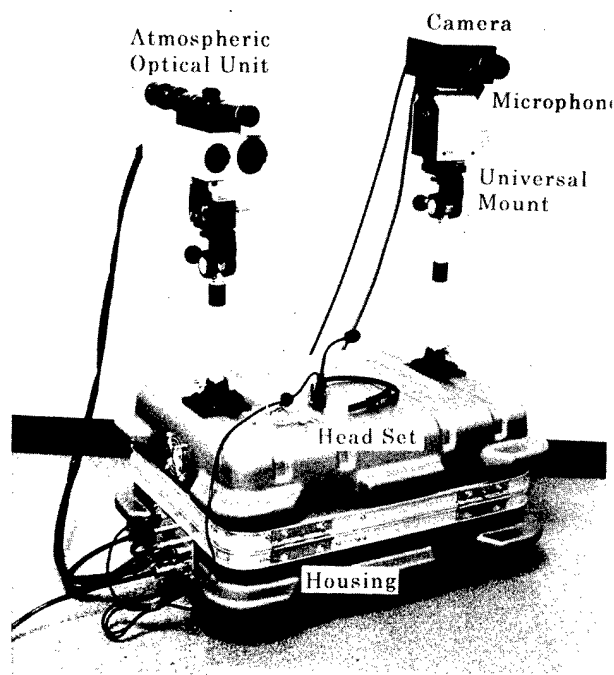
The portable terminal has an interactive transmission

function. This function contributes not only video signals transmission but also telecommunications. Of course, a camera can be controlled by downlink signal from the central station.



E/O:electrical/optical converter O/E:optical/electrical converter

Fig.1 Schematic diagram of the portable terminal



Dimension:516×379×254mm Weight:15.5kg

Photo 1 Novel portable terminal for information free access system

Fig.1 shows a block diagram of the portable terminal.

This terminal consists of an E/O and FM video modulator for video transmission on an uplink, and an

O/E, FM audio modulator and demodulator for communication on a bi-directional link.

Furthermore, a camera, a camera controller unit, a universal mount, an atmospheric optical transmission unit(D/A converter) and an atmospheric optical unit are equipped in the terminal.

When the terminal is set up, a camera, a universal

mount and an atmospheric optical unit are fixed on the housing as shown in Photo 1.

By eliminating some functions according to the requirement, the terminal unit can be made smaller.

In this system, we use the same frequency allocation and the FM modulation format as those used on satellite broadcasting in Japan. Therefore, the tuner which is available on the market can be used for tuning channels in this system.

In our optical atmospheric system, 1480nm laser diodes, which are used for pumping lasers in optical amplifiers, transmit video signals. The output power is 50mW, which is seventeen times as high-power as that of conventional atmospheric optical sources. In this case, optical beam diameter is 2m at an optical receiver site which is 100m distant from the optical source, and received power is 15μW. Furthermore, 670nm laser signals(red color) are transmitted in parallel with main signals as guided signals. Fig.2 shows a schematic diagram of the atmospheric optical unit.

The method we employed can transmit signals longer than the conventional method and make positioning of optical beam patterns very easily.

3.RELIABILITY OF THE INFORMATION FREE ACCESS SYSTEM

Assuming a spare terminal is prepared in reserve, repair time of the portable terminal is negligible. In the case that more than one terminals launch optical signals, the failed portable terminal can be replaced easily without affect performances of other working terminals. In conventional optical repeater systems, however, the failed terminal may preclude the transmission of all signals from other terminals.

The reliability about optical components are generally

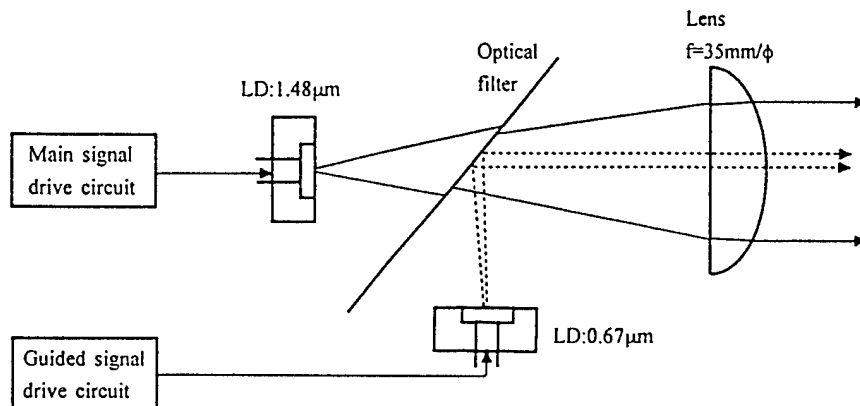


**Fig.2 Schematic diagram of
the atmospheric optical unit**

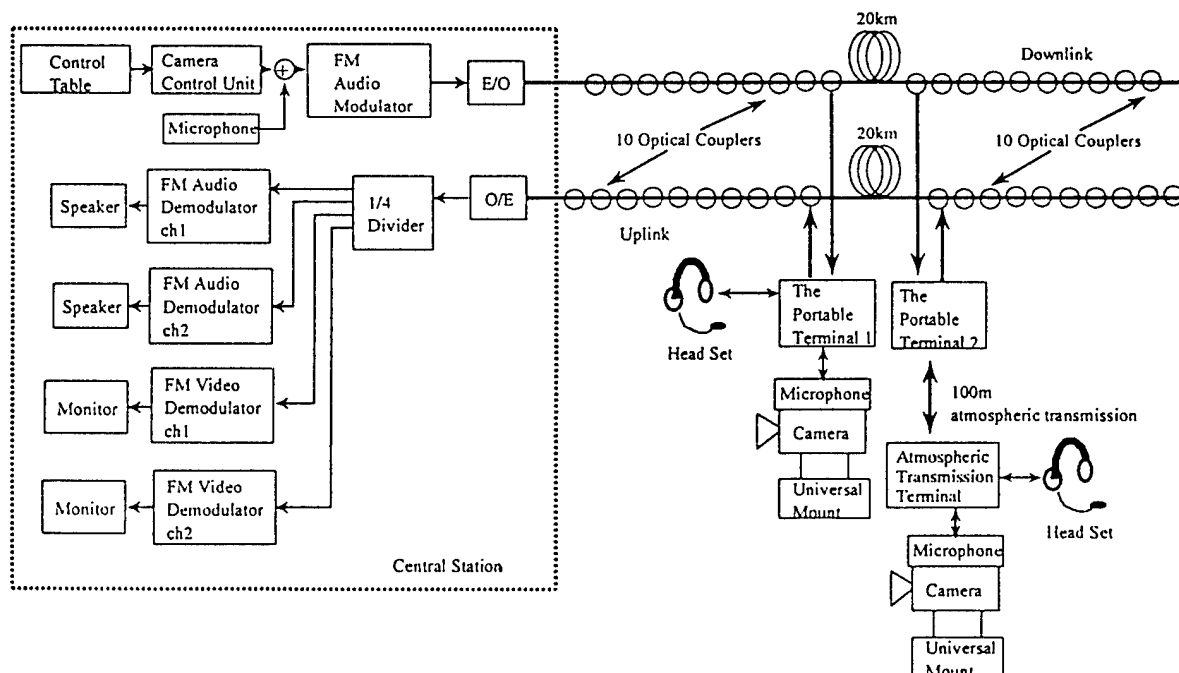


Fig.3 Experimental scheme of 20 couplers free access system

described as follows:

Although the reliability of optical components can not be defined easily. The reliability of optical fiber cables is reported as 1% break probability per 1000km during 20 years while it is loaded with weight of 0.18kgf. Regarding an optical connector using a zirconium oxide sleeve and an optical coupler, the nominal FIT parameters used are smaller than 0.1 and 100 over 20 years, respectively.

Thus, the optical components are much reliable than other electrical parts.

Therefore, our information free access system is suitable for supervising systems in terms of reliability.

4. TRANSMISSION EXPERIMENTS

Transmission experiment was carried out in the setting with 20 couplers and two 20km single-mode fibers as shown in Fig.3.

Two portable terminals were connected to the link, and transmission quality was observed.

The camera launched the NTSC baseband signals to the FM video modulator, and the microphone launched audio baseband signals to the FM audio modulator, which were equipped in the portable terminal 1.

The FM video and audio modulator converted each baseband signal into RF signals and launched them to the E/O, and then optical signals were modulated with RF signals. The modulation depth of video and audio were 55% and 15%, respectively.

In the case of the terminal 2, the atmospheric optical unit received transmitted optical signals, which was modulated with a digital video baseband, from atmospheric transmission terminal. The atmospheric optical unit launched electrical digital video signals to the D/A converter. Since the D/A converter converted digital video signals into analogue video signals, the

same signal transmission sequence was utilized as that in the terminal 1.

As the result, a desirable CNR of 14 dB or over was achieved, and required transmission quality was retained even if the 100m atmospheric transmission was conducted jointly. Furthermore, it was realized that the interactive system was successfully constructed by camera controller unit and based on communication experiments. We succeeded in obtaining desirable CNR of 25dB in the analogue audio transmission.

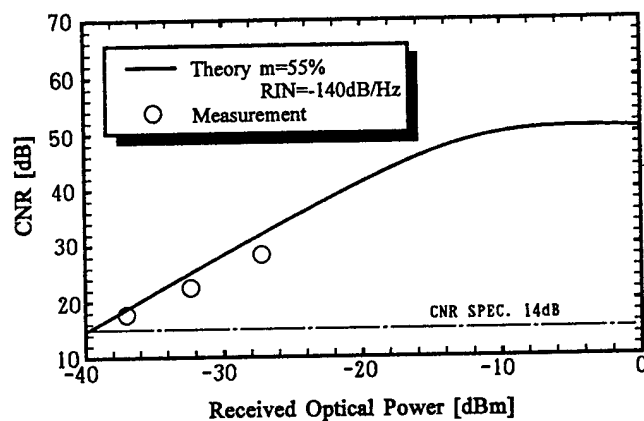


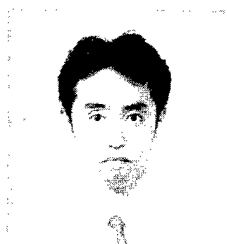
Fig.4 CNR characteristics versus received optical power

5. CONCLUSION

We have developed a portable terminal for the information free access system as a novel supervising system. We demonstrated a video transmission and communication experiments on free access architecture with 20 couplers. Furthermore, 100m atmospheric transmission experiment was carried out with new optical unit equipped a pumping laser of optical amplifier. As the result, it was realized that the interactive and flexible supervising system can be constructed with our portable terminal. Several supervising systems have been deployed using this configuration.

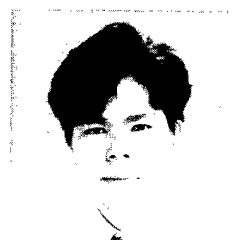
REFERENCE

- (1) OMURA, et al: 'Development of Multi-Coupler Bi-directional Optical Communication System Employing FM-SCM Video Transmission', 44th IWCS, pp380-386, 1995
- (2) MATSUO, et al: 'The Experimental Study of the Influence of Optical Beat Interference on FM-video Transmission System Employing 30ch Multiple Optical Carriers', ECOC'94, We.P.21
- (3) DARCIE.T.E: 'Subcarrier Multiplexing for Multiple-Access Lightwave Network', J.Lightwave Technol.,LT-5,pp1103-1110,1987
- (4) DESEM.C: 'Optical Interference in Lightwave Subcarrier Multiplexing System Employing Multiple Optical Carriers', Electron.Lett.,vol124, pp50-51,1988



Hideyuki Omura
Furukawa Electric Co.Ltd
5-1-9, Higashiyawata
Hiratsuka, Kanagawa, 254,
JAPAN

Hideyuki Omura received the Master Degree in electrical engineering from Tokai University, Kanagawa, Japan in 1987. He joined Furukawa Electric Co., Ltd in 1987 and he has been involved in the development of bi-directional CATV for 4 years. At present he is working in Video transmission system and equipment research section of Information & Electronics Laboratory. Mr. Omura is a member of the institute of Electrical Engineers of Japan.



Hideyuki Nasu
Furukawa Electric Co.Ltd
5-1-9, Higashiyawata
Hiratsuka, Kanagawa, 254,
JAPAN

Hideyuki Nasu received the Master Degree in electrical engineering from Nihon University, Tokyo, Japan in 1995. He joined Furukawa Electric Co., Ltd in 1995. At present he is working in Video transmission system and equipment research section of Information & Electronics Laboratory. Mr. Nasu is a member of IEEE and the institute of Electronics, and Communication Engineers of Japan.



Haruo Nakayama
Furukawa Electric Co.Ltd
5-1-9, Higashiyawata
Hiratsuka, Kanagawa, 254,
JAPAN

Haruo Nakayama received the Master Degree in electronics engineering from Okayama University, Okayama, Japan in 1990. He joined Furukawa Electric Co., Ltd in 1990. At present he is working in Video transmission system and equipment research section of Information & Electronics Laboratory.



Kenichi Tezuka
Tokyo Electric Power Company
4-1,Egasaki-cho Tsurumi-ku
Yokohama, Kanagawa, 230,
JAPAN

Kenich Tezuka received the Master Degree in mechanical engineering from Waseda University, Tokyo, Japan in 1988. He joined Tokyo Electric Power Company in 1988. At present he is working in Nuclear Power R&D Center.

DESIGN AND PERFORMANCE OF A HIGH-CAPACITY, COMPACT, MODULAR RIBBON CABLE COMPRISING 24 FIBER RIBBONS

K. W. Jackson R. J. Brown M.D. Kinard K.M. Kroupa M.R. Santana
P.M. Thomas

Lucent Technologies Inc.
Bell Laboratories
2000 Northeast Expressway
Norcross GA 30071
770-798-3952

ABSTRACT

In this paper we present the design, analysis, and performance characteristics of a new, central tube cable comprising 24 fiber ribbons. The cable can accommodate up to 432 fibers in a sheath OD of less than 19 mm. Other unique features of this high packing density cable design include a simple identification method for ribbon subunits, robustness to excess fiber added loss and enhanced productivity of mass fusion splicing. We also present a simple first order analysis and experimental data that clarify the mechanical performance of high fiber count central tube ribbon cable as related to the geometry of the ribbon and core tube. Lastly, we present environmental and mechanical performance data for critical Bellcore Qualification Tests.

INTRODUCTION

For network providers the competitive environment of telecommunications is becoming time-based. Recent legislative (Telecommunications Act 1996) and technical innovations, coupled with the convergence and bundling of the diverse and traditionally disparate information and entertainment services, have accelerated the deployment of broadband networks. Indeed, compound annual growth rates of more than 20 percent have been

projected for fiber systems and components through the year 2000. These developments have in turn intensified the demand for high fiber count, high fiber density cables. Figure 1 illustrates the growth trend for ribbon cable fiber counts in the U.S.

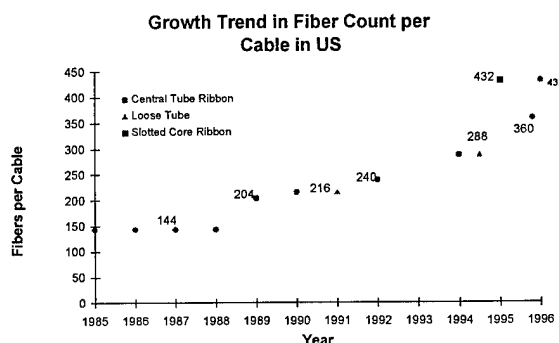


Figure 1 Growth in Cable Fiber Counts in U.S.

A critical success factor for future local and long distance network providers is early presence of a high capacity fiber network that facilitates interactive access to subscribers and content providers. Small size, very high fiber count cables enable network providers to more rapidly establish a high capacity fiber-based network. The 24 fiber ribbon cable described in this paper is specially designed for high fiber count architectures where underground duct space is limited. For example, Cable TV companies often encounter severely limited duct space and thus

need to install the largest amount of fiber possible in their available space. A relevant design and productivity benchmark is the number of fiber miles that can be installed in a 1.25 inch ID inner duct in a given time interval. This in turn is equivalent to the maximum number of ribboned fibers that can be contained within a cable sheath of OD less than about 19mm (0.75 inches).

High fiber density, modular ribbon cables with mass fusion splicing can reduce cable installation time, duct space investment and operating expense associated with network reconfiguration and restoration.. The compact 24 fiber ribbon cable described in this paper can enable network providers to rapidly acquire a high capacity, fiber presence where duct space is severely limited.

BACKGROUND

In the limit, the installation cost per fiber is frequently proportional to the OD of the cable. Significant development work has been conducted on the fundamentals and associated constraints of compact ribbon cable design^{1,2,3,4,5}. The basic approaches have included downsizing the protective coating on the fiber, reducing the thickness of the ribbon and increasing the fiber count per ribbon. Reducing the coating diameter of the fiber can increase the fiber density per ribbon while reducing the matrix thickness can increase the ribbon density in the core cable. Increasing the fiber count per ribbon can also increase the packing density within the cable core. Figure 2 illustrates the various relations for a central tube cable design using¹

$$N_f = \{K_R^2 (D_s - t)^2\} / \{d_f^2 (1 + (h/d_f)^2)\} \quad (1)$$

In Equation (1)

N_f is fiber count

$K_R = d_s/D_c$

d_s is the stack diagonal

D_c is the core id

D_s is the sheath od

$t = (D_s - D_c)/2$

d_f is coated fiber diameter

h is ribbon thickness

Single fiber handling and robustness issues seem to favor maintaining the standard 250 um fiber coating. On the other hand, a thin ribbon design has proven to be appropriate for central core cables where the ribbon stack remains close to the cable's neutral axis when the cable is bent.. Traditionally, in stranded/slotted core cable structures ,where the ribbon stack is located well beyond the neutral axis and is kinematically constrained, thicker ribbons have been used.

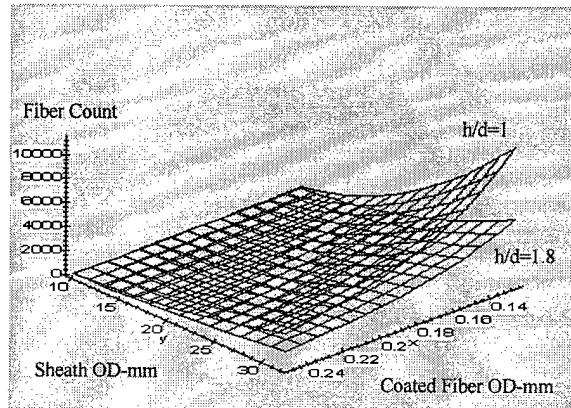


Figure 2: Fiber Count as a Function of Sheath and Fiber Coating Diameter with Normalized Ribbon Thickness as a Parameter

However, recent research indicates that thinner ribbons can also be used in these cables, provided compensating design changes are made in the primary coating of the fiber⁶. Modular ribbons that can be field subdivided into subunits comprising 4, 6, 8 or 12 fibers have been demonstrated and sixteen fiber modular ribbon cables have been commercially deployed. Ribbons comprising a number of pre-identified subunits provide flexibility for routing and rearrangements. In addition, the subunits provide enhanced mechanical robustness over single fibers because the subunits maintain their structural integrity when separated from the main ribbon. Lastly, single fibers or multifiber subunits can be quickly and easily accessed from the ribbon end or midspan.

DESCRIPTION OF CABLE DESIGN

Figure 3a and 3b show the basic characteristics of the 24 fiber ribbon cable for the dielectric and

metallic sheath versions. Figure 3c shows an isometric view of the metallic version.

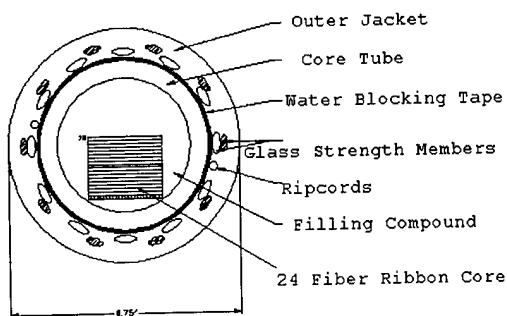


Figure 3a: Dielectric High Fiber Count Cable

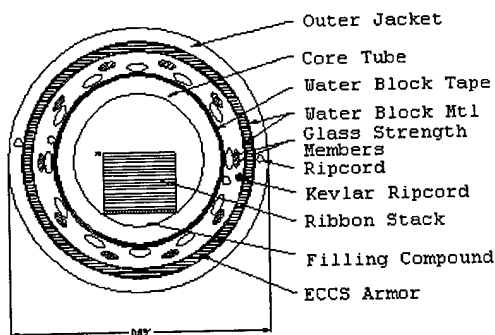


Figure 3b: Metallic High Fiber Count Cable

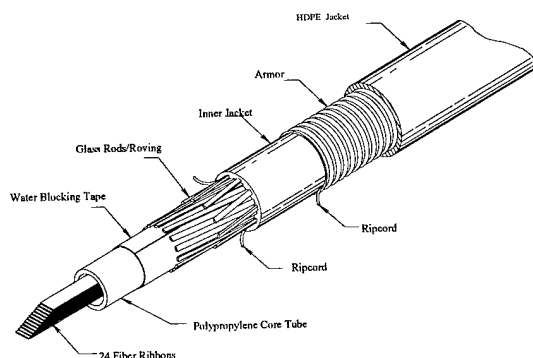


Figure 3c: High Fiber Count Cable

The central tube design was chosen because of its compact and mechanically robust structure. To extend the central tube ribbon cable design to larger sheath diameters and wider ribbons requires special consideration of the radial compression stability of the sheath and the interconversion of torsional and bending energy within the ribbons. These effects are discussed later in this paper.

As shown in Figure 3a, the cable consists of an array of 24 fiber ribbons that are helically placed in the central core tube and surrounded by a water-impermeable, shock-absorbing, jelly-like compound. The ribbon array is given a controlled twist about its own centroidal axis to assure that when the cable is bent, each ribbon is bent only about its principal axis having minimum moment of inertia. Also, because the ribbons within the array are decoupled longitudinally, each ribbon bends independently of the other ribbons in the array. The array itself can move below the neutral bending axis of the cable when the cable is bent so the fibers are inherently protected from tensile strain.

The fibers are well protected against exterior mechanical damage by centrally encasing them within three independently fabricated layers of plastic tubing and a hard, yet flexible, armor that provides enhanced protection against corrosion, lightning and rodents. The dielectric strength members are located outside the core and thus provide a protective "cage" that insulates the fibers from potentially damaging tensile, compressive and shock loads during installation or natural disasters. The central tube cable design protects the fiber much the same way as the sensitive spinal cord is protected in vertebrates. Indeed, the functional elements of the central tube design have several direct biological analogs.

The basic ribbon design is illustrated in Figure 4 for a 24 fiber ribbon comprising Two 12-fiber and three 8-fiber subunits. Within each subunit, the fiber color sequence repeats itself.

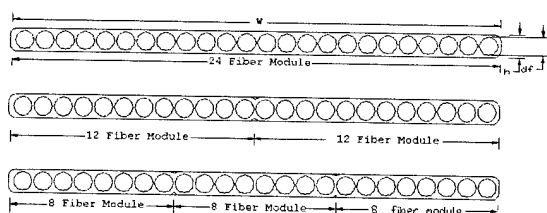


Figure 4: Modular Ribbon Subunit Options

The subunits are easily separated from the main ribbon, are mechanically robust and can be independently mass stripped and fusion spliced. Figure 5 illustrates a binary subunit identification method that is language independent. A subunit is uniquely identified by a sequence of wide and narrow vertical bars. A wide bar represents the number 5 and a narrow bar, the number 1. Thus, in Figure 5, the subunit ID's of 22, 23, 24 equals the corresponding sum of values associated with the wide and narrow vertical bars.

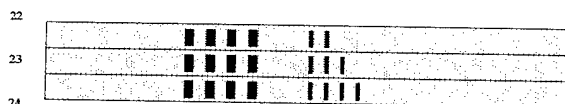


Figure 5: Ribbon Subunit Identification

QUALITATIVE DESCRIPTION OF RIBBON CONFORMATIONS IN A BENT CABLE

Both the design and the manufacture of cables comprising high fiber count ribbons require an understanding of fiber strain as it relates to cable bending. Ideally, one would like to have closed form mathematical relations among key design/process variables including:

- Sheath OD
- Ribbon lay length
- Ribbon Core tube ID
- Width
- Ribbon composite moduli
- Cable bend radius
- Allowable long term stress

Such relations necessarily include geometric assumptions supported by experimental observations.

A well-established design principle for central tube ribbon cables involves imparting a controlled twist to the ribbon stack during cable manufacture to improve bending performance. It is useful to review the physical mechanisms by which the bending performance of a cable can be improved by stack twisting. Observation of the conformations assumed by a twisted stack in a transparent tube under constant curvature indicates that the strain energy of a ribbon composite is alternately stored in bending and torsion. The curvature, $1/R_b$, the bending moment, M_b , and the torsional moment, M_t , are given by

$$1/R_b = M_b/EI \quad (2)$$

$$M_t = K_t \theta \quad (3)$$

where

- E : modulus of ribbon
 I : moment of inertia about bending axis
 K_t : torsional stiffness
 θ : twist angle

Observation of the ribbons under continuous bending indicates that the ribbon bends about its most flexible axis while torsion occurs over a length, L_t in which 180° rotation of the ribbon is obtained.

Figure 6 illustrates a typical configuration of a twisted ribbon as it is bent. As the curvature of the cable is increased, geometrical constraints cause the "effective lay length" of the ribbon stack, $2L_t$ to become shorter to accommodate the ribbon bending only about its most flexible axis. Although the three dimensional conformation of a bent and twisted stack under conditions of positive excess length can become quite complex, the idealized geometry illustrated in Figure 6 illustrates how twisting the ribbon allows it to bend about its most flexible axis when the cable is bent.

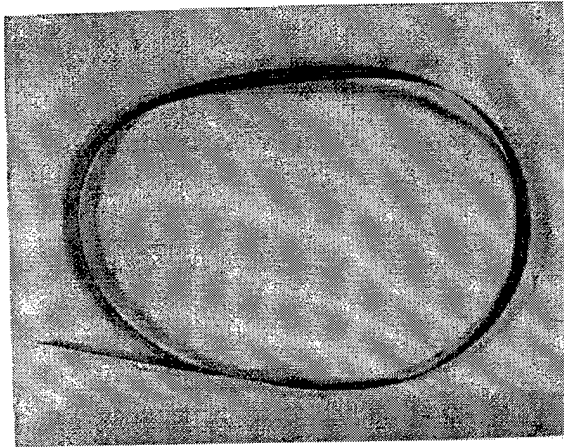


Figure 6: Bending/Torsion Conformations of Ribbon in a Bent Tube.

For field installations, where a cable bend is bounded by straight sections of cable, the ribbons still bend about their most flexible axis and the torsional energy originally present in the bent section can be propagated to the straight sections bounding the bend. Then in the bend, the fiber stress is determined by the bend radius.

COMPRESSION RESISTANCE CENTRAL TUBE

The deflection, Y , of a tube of radius, R , having cross section as illustrated in Figure 7 can be expressed as⁷

$$Y = A_1 P x^3 / b E \quad (4)$$

where

A_1 is a constant
 P is the load
 E is the tube modulus
 $x = R/h$
 R is the mean tube radius
 h is depth of rectangular section
 b is tube length

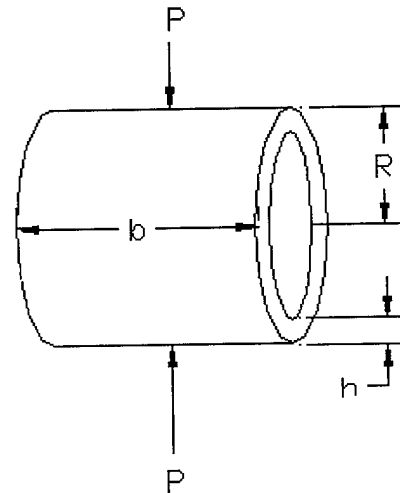


Figure 7 : Geometry for Tube Compression Model

The tube stiffness with respect to compression is given by

$$k = dP/dY = bE/A_1 (h/R)^3 \quad (5)$$

Also, for a tube subjected to uniform external pressure, the critical buckling pressure, P_c , is given by⁸

$$P_c = A_3 E (h/R)^3 \quad (6)$$

Thus, the compression resistance of a tube can be taken as proportional to $E(h/R)^3$. To maintain constant compression resistance as the tube radius increases requires that the product, $hE^{1/3}$, increase in proportion to the increase in R . Figure 8 shows representative results for the Bellcore compression test for the 24 fiber ribbon cable after the requisite design modifications.

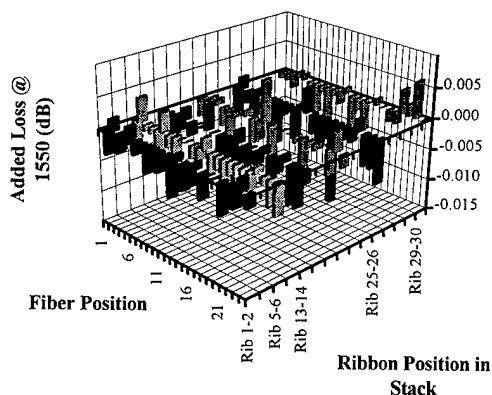


Figure 8: Compression Resistance Performance 225 lbs/in

CABLING AND ENVIRONMENTAL LOSS PERFORMANCE

Figure 9 and Table I show representative loss data for a 360 fiber cable comprising fifteen, 24 fiber ribbons for both matched and depressed clad fibers. The mean and median cable losses are approximately equal and the mean added loss is negligible at both 1310 and 1550 nm. Similar results are obtain at -40C after cable aging for 10 days at 85C.

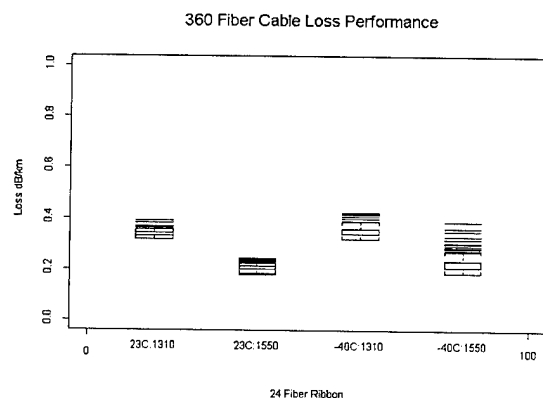


Figure 9: Loss Performance of 360 Fiber Ribbon Cable As Related to Temperature

**TABLE I
360 FIBER CABLE LOSS PERFORMANCE**

TEMPERATURE		CABLE LOSS	
		dB/km	
		1310	1550
25C	MEAN	0.34	0.21
	MEDIAN	0.34	0.21
	STD DEV	0.01	0.01
-40C*	MEAN	0.35	0.23
	MEDIAN	0.35	0.22
	STD DEV	0.018	0.029

* After aging @ 85C for 10 days.

CONCLUSIONS

The results of this investigation demonstrate that the central tube cable design can accomodate up to 432 fibers using 24 fiber modular ribbons. A design methodology for sheath scale-up is presented and verified with excellent performance on industry standard environmental and mechanical tests. The 432 fiber cable can enable telecommunication providers to rapidly establish a high capacity presence even where underground duct space is severely limited.

ACKNOWLEDGEMENTS

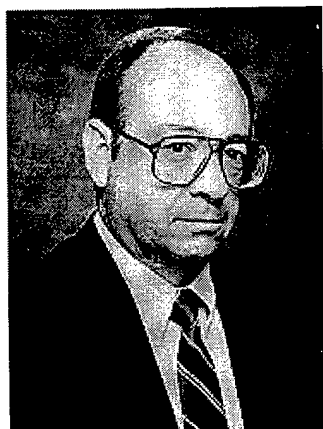
The authors gratefully acknowledge the contributions of W.H. Ficke, N. E. Hardwick, M.Q. Kamino, H. Ly , S.C. Mettler and P.D. Patel.

REFERENCES

1. Jackson, K.W. , M.R. Santana, N.W. Sollenberger, R.J. Brown, K.M. Kroupa, S.H. Webb. " A Modular Ribbon Design for Increased Packing Density of Fiber Optic Cables," 42nd IWCS, (Nov. 1993): 20-26.
2. Tomita, S., M. Matsumoto, T. Yubata, T. Uenoya."Preliminary Research into Ultra High Density and High Count Optical Fiber Cables," 40th IWCS (Nov. 1991): 8-15.

3. McCallum, William J., Martin C. Light, Richard C. Wagman. "Design and Development of a High Fiber Count Ribbon Cable," 44th IWCS. (Nov. 1995): 8-15.
4. Wagman, R.S., P.R. Bark, H.G. Cooke, C. K. Eoll, R.O. Livingston, G. A. Lochkovich, W.W. McAlpine, F.M. Sears, and S.S. Sodhi. "Design Concepts for a 4000-Fiber Cable with Thin Coated Fiber," 43rd IWCS. (Nov. 1994): 12-21.
5. Okada, Naoki., Kohichiro Watanabe, Kazunaga Kobayashi, Matsuhiro Miyamoto. "Ultra-High Density Optical Fiber Cable with Thin Coated Multi Fiber Ribbons for Subscriber Networks," 43rd IWCS (Nov. 1994): 28-34.
6. Kobayashi, K., N. Okada, K. Mitsuhashi, K. Ishida, M. Miyamoto, and S. Araki. "Coating Design of Thin-Coated Ribbons Using 250 um Coated Fibers," 44th IWCS (Nov. 1995): 607-614.
7. Blake, A. . Practical Stress Analysis in Engineering Design, Marcel Dekker, 1990. 310-311.
8. Timonshenko, S.P. and J.G. Gere, Theory of Elastic Stability, McGraw Hill, 1961. c 474-482.

BIOGRAPHY



Kenneth W. Jackson is a Distinguished Member of the Technical Staff in the Fiber Optic Cable and Materials Development and Engineering Department at Lucent Technologies Inc., Bell Laboratories,

Norcross, GA. He is responsible for the design and development of outside plant cables. He joined the Western Electric Co. in 1970 having received a B.S.M.E. from Auburn University. He joined AT&T Bell Laboratories in 1981 having received an M.S.M.E. and Ph.D. in Mechanical

Engineering from the Georgia Institute of Technology. Since 1981 he has worked in the areas of Optical Fiber Fabrication, Fiber Optic Connector Design and Development, Materials' Design and Fiber Optic Cable Design and Development. He has been awarded 8 patents and has 13 publications. He is a Registered Professional Engineer in the state of Georgia.



R. J. Brown is a Member of Technical Staff in the Outside Plant Group of the Fiber Optic Cable Engineering Department at Lucent Technologies Inc., Bell Laboratories, Norcross, GA. After obtaining a BSME

from the University of Maryland in 1969, he began his Western Electric-AT&T-Lucent career in 1970 at the Atlanta Works. While working in Copper Cable Development he received an MSME from Georgia Institute of Technology in 1978 and has been involved in product design, process design, and the manufacture of Fiber Optic cables since 1984. Bob is a Registered Professional Engineer in Georgia and holds three U. S. patents.



Michael D. Kinard is a Senior Development Engineer with Lucent Technologies Inc., Bell Laboratories, Norcross, GA. He holds a BSME from Old Dominion University and an MSME from Georgia Institute of Technology. He

has worked in cable design and development for fifteen years. He holds several patents in the cable design and processing areas.



Kenneth M. Kroupa is a Member of Technical Staff in the Fiber Optic Cable Packaging Department at Lucent Technologies Inc., Bell Laboratories in Norcross GA. He joined the Western Electric Company in 1969 having received a B.S.M.E. from the

University of Illinois. Subsequently, he received an MS in Metallurgy and Materials Science from Lehigh University in 1973 and a MBA from the University of New Hampshire in 1977. Since 1980, he has had production engineering responsibilities in the areas of fiber optic preform manufacturing, final cable inspection, connectorization, and ribbon manufacturing.



Phillip M. Thomas is a Member of Technical Staff in the Fiber Optic Cable Design Group at Lucent Technologies Inc., Bell Laboratories, Norcross., Georgia. He joined AT&T in 1982 after receiving his BMET degree from Southern

Technical Institute. He received his BESM and MSES degrees from the Georgia Institute of Technology. Mr. Thomas is presently involved in the design and development of fiber optic cable for outside plant applications. His past responsibilities included the design and development of fiber optic cable interconnection apparatus, closures, and cable termination hardware.



Manuel R. Santana is the Technical Manager of the Outside Plant Fiber Optic Cable Engineering Group. He is responsible for research, development, design and manufacturing engineering for fiber optic cables used in the

outside plant. He has been involved in research and development in fiber optic cable for 25 years and he has been awarded 12 patents and has 28 publications. In 1991, he was awarded the Hispanic Engineer of the Year for Outstanding Technical Contribution and the Alexander M. Nicolson Trophy (AT&T patent award for commercial value). In 1993, Manuel was appointed AT&T Bell Laboratories Fellow, the highest technical achievement award given by AT&T Bell Laboratories. Manuel joined AT&T Bell Laboratories in 1970 having received his B.S.E.E. from the University of Hartford and his M.S.E.E. from the Georgia Institute of Technology. He is a senior member of the IEEE.

A METHOD TO EVALUATE RIBBON BEHAVIOR IN SLOTTED CORE CABLES

Ernst Opel

SIEMENS AG, D96465 Neustadt bei Coburg, Germany

ABSTRACT

In high fiber count slotted core ribbon (SCR) cables with small clearance in the slots, different optical attenuation values were found at different bending radii. The tests were performed on U-profile test cables (a special slotted core cable) with 16 fiber ribbons varying the temperature from -30 to +70°C. This phenomenon is thought to be caused by the restriction of the free movement of the ribbons in the slots at different cable bend radii.

For a better understanding of the situation a mathematical model was developed and checked with good results. We believe the mathematical model to be a useful instrument to investigate several cable parameters (e.g. pitch length and torsional rigidity or ribbon coefficient of friction) with respect to their effect on ribbon movement under stress.

1. INTRODUCTION

During the development of high fiber count ribbon cables (U-profile cables, SCR cables) attenuation values were found to be dependent on various production and design parameters. In a bending experiment significant attenuation changes were found in the four corner fibers of a ribbon stack. The deformation of the slot cross section can be excluded as a contributing factor because former investigations of bending behavior using finite element analysis (FEA) showed no essential change of the cross section of the slots even under low temperature conditions. It seems obvious that lateral forces from the wall of the slot are the reason for that effect. The herewith associated friction forces do not allow the movement of the ribbon stacks and respectively, the relaxation of the lateral forces. We presume that the ribbon movement is restricted by bending loads and low temperatures.

The movement of the ribbons or ribbon stacks in the slots is caused:

- a) at low temperature by different thermal expansion coefficients of the cable components
- b) at bending load by different local compensation forces.

The movement of the ribbons or ribbon stacks in the slots is restricted:

- a) at low temperature by buckling effects and wall contact (friction).
- b) at bending load by rotation of the ribbon stack and wall contact (friction).

The moveability of ribbon stacks has been investigated in SCR-cables and U-profile cables with helical open slots (nearly rectangular cross section) and no filling compound in the slots. In this report we will describe the influence on moveability of a ribbon stack of different bending loads and temperatures by measuring the pull out force (on a ribbon stack) for a given cable length. Furthermore a mathematical model has been developed to describe the influence of several cable design parameters on the friction forces.

2. CABLE TESTS

2.1 Variation of the bend radii

A U-profile test cable with the following design parameters (Table 1) was used for bending tests:

Table 1. Design parameters of a
U-profile test cable

effective U-profile slot width	= 3.7 mm
effective U-profile slot height	= 3.0 mm
slot wall	≥ 0.5 mm
cable diameter	= 19.0 mm
pitch length	= 400 mm
ribbon stack width	= 3.2 mm
ribbon stack height	= 2.0 mm
cable length	= 900 m
test temperature	= 20°C

Attenuation was measured on a complete cable on reels with diameters of 1.0 m and 1.7 m. Additional measurements were performed on a straight cable. Table 2 shows the average attenuation values of the 4 corner fibers in dB/km.

Table 2. Average values of attenuation changes of 4 corner fibers of a ribbon stack in a U-profile test cable

reel diameter	$\Delta\alpha$ 1550 nm	$\Delta\alpha$ 1310 nm	$\Delta\alpha$ quotient
1.0 m	0.60	0.04	15
1.7 m	0.15	0.04	3.8
straight cable	0.07	0.01	7.0

The quotient $\Delta\alpha(1550 \text{ nm}) / \Delta\alpha(1310 \text{ nm})$ is always greater than two, which is an indication for almost pure macro bending losses. The clearance between the ribbon stack and the slot walls is so small that macrobending occurs at the stressed edge fibers of the ribbon stack. No other fibers showed any significant attenuation changes during the test.

2.2 Variation of the Temperature

Another test cable was made with the following design parameters in Table 3.

Table 3. Design parameters of a SZ-U-profile test cable

cable diameter = 26.2 mm
number of U-Profiles = 10 (SZ- stranded)
pitch length = 500 mm (turning-point 3.1m)
effective U-profile slot width = 3.2 mm
effective U-profile slot height = 3.6 mm
ribbon stack height = 2.20 mm
ribbon stack width = 2.95 mm
16f-ribbons with extra thin fibers
one of the ribbon stacks was protected with cushion layers on the top and bottom of the stack.

A temperature cycle has been done with 500 m of this SZ-U-profile test cable on a reel. Tables 4 and 5 show the average values of the 4 corner fibers in dB/km.(reel diameter = 1.7 m).

Table 4. Average values of attenuation changes of 4 corner fibers of a ribbon stack in a SZ-U-profile test cable without cushion layer

	without cushion layer		
temp.	α 1550 nm	α 1310 nm	$\Delta\alpha$ quotient
- 30°C	1.60	-	-
+ 20°C	0.50	0.46	2.6
+60°C	0.37	-	-

Table 5. Average values of attenuation changes of 4 corner fibers of a ribbon stack in a SZ-U-profile test cable with cushion layer

	with cushion layer		
temp.	α 1550 nm	α 1310 nm	$\Delta\alpha$ quotient
- 30°C	0.25	-	-
+ 20°C	0.25	0.34	1.0
+60°C	0.23	-	-

No fibers other than the corner fibers of the stack showed any significant attenuation changes. The stack without the cushion layer showed macro bending losses at room temperature, while the protected stack showed none. This means that the lateral pressure on the stack is concentrated on the corners of the stack.

3. MEASUREMENT OF THE PULLING FORCES

When pulling a ribbon stack out of a cable of given length, it is necessary to overcome the friction resistance in the cable slot. Therefore the pulling force can be taken as measure of the moveability of a ribbon stack in the cable.

3.1 Experimental set-up

-Preparation of the test cables:
0.7m of the jacket of one cable end was removed from the core.

A ribbon stack was taken out of the slot and drawn through a die. The cable core was removed as well. The ribbon stack was wound around a roll and fixed there. (Fig. 1).

-Measurement device:

A spring balance or a tensile test machine was used for the measurement of the pulling force.

-Test configuration (Fig. 1):

The test cables were put into a temperature chamber while the pulling device was positioned outside. The test cable length (L) was composed with a straight length (Ls) and a bent length (Lb).

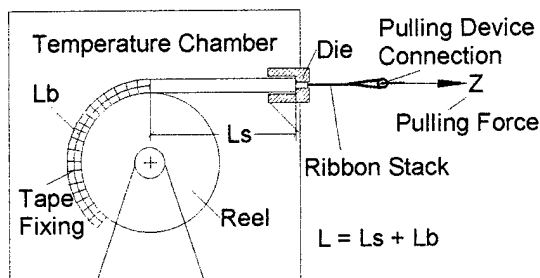


Fig.1. Tensile Test Configuration

3.2 Conditions

The speed of the tensile test and the cable length had to be selected before testing began. Low tensile test pulling speeds tend to result in small pulling force values and high tensile test pulling speeds tend to result in high pulling force values. The effects of temperature and bending can be seen at all speeds. In case of low speed (about 10 mm/min) the pulling force as a function of the pull out length curve gives information about local excess length of the ribbon stack. At high speeds (about 0.5 m/sec) the pulling force provides information about static friction of the whole ribbon stack length. The cable length should be long enough for bending experiments and short enough to be handled in the laboratory. In previous tests we arrived at an optimal test cable length of 7 meters with 0.7 m extra ribbon length on one end.

The bending radii of the cable were checked with following results:

-Small reel-

If a small cable drum diameter (=20 times of cable diameter) is used, the rope friction (reference [6], page A17-18) is the most significant factor and pitch length variations could be neglected for the pulling forces.

-Large (shipping) reel-

By using ship drums

(≥ 40 times of cable diameter)

the bending effects due to temperature cycling could be studied.

If too many turns around a large reel are used, the movement (due to the pulling forces) of the ribbon stack tends to zero.

Some studies were made at 1, 2, 3 & 4 m bent cable lengths on a large (shipping) reel.

3.3 Results

Pulling forces measured by hand with pulling speed ≈ 0.5 m/sec (Tables 6,7 & 8).

Table 6. Pulling forces on a straight 100 F SCR-cable

	pulling force (Z) in N		
temp.	L = 5 m	L = 7 m	L = 10 m
-30°C	16	55	90
+20°C	11	30	36
+70°C	4	14	16

Table 7. Pulling forces on a bent 100 F SCR-cable (reel diameter 600 mm)

	pulling force (Z) / bent length (Lb)			
temp.	Lb = 4 m	Lb = 3 m	Lb = 2 m	Lb = 1 m
-30°C	>750	600	250	150
+20°C	200	140	80	40
+70°C	120	75	60	30

Table 8. Pulling forces on a bent 100 F SCR-cable (Lb = 3 m)

	pulling force (Z) / bending diameter (Db)		
temp.	Db = 0.6 m	Db = 0.8 m	Db = 1.0 m
-30°C	600	200	150
+20°C	140	80	50
+70°C	75	50	25

Table 9. Pulling forces measured with a tensile test machine

cable type	straight cable L=7 m	bent cable Lb=2 m	bent cable Lb=4 m
100 F	7 N	18 N	36 N
24F	3 N	7 N	18 N

pulling speed = 10 mm/min
temperature = 22°C
reel diameter = 40 times cable diameter

4. MODEL OF FRICTION BEHAVIOR

The mathematical model was developed on the basis of the solved "rope friction" problem of mechanical engineering (reference [6]).

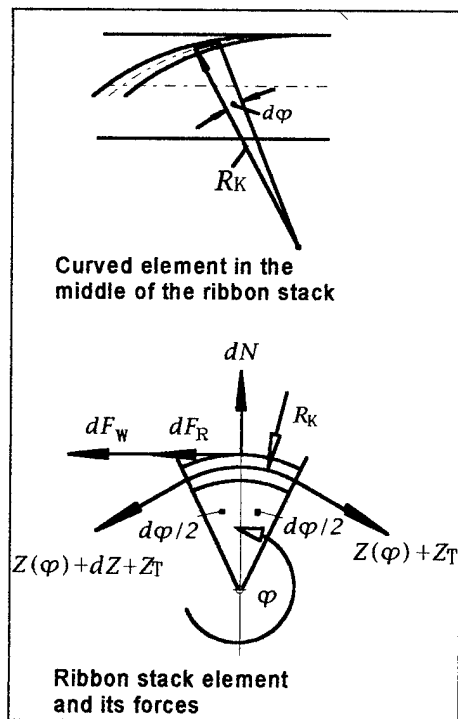


Fig. 2. Forces at a Ribbon Stack Element with the Radius of Curvature (R_k)

Friction law $dF_R = \mu \cdot dN$ (1)

Coefficient of static friction $\mu = \text{constant}$

Specific wall sticking $dF_w = q \cdot R_k \cdot d\varphi$ (2)

Specific friction load q

describes distributed friction

(surface effects, electrostatic attraction, etc.).

In this calculation only the ribbon weight per length unit (m) was considered as $q = \mu \cdot m$

Friction force from ribbon torsion Z_T

Tensile force on the ribbon stack $Z(\varphi)$

at position φ .

Radius of curvature R_k

The equilibrium of the forces results in a differential equation (3) which can be solved by numerical methods.

$$\frac{dZ}{d\varphi} + \mu \cdot (Z(\varphi) + Z_T) + q \cdot R_k = 0 \quad (3)$$

In the case of the unbent cable

$$(R_k = R_{KG} = \text{const.})$$

an elementary solution of eq.(3) can be given.

For a helix the radius of curvature is

$$R_{KG} = R_m \cdot \left[1 + \left(\frac{S}{2 \cdot \pi \cdot R_m} \right)^2 \right] \quad (4)$$

with S = pitch length

and R_m = radius to the middle of the stack

The solution of eq.(3) for a straight cable is

$$Z(\varphi) = Z_0 \cdot e^{-\mu \cdot \varphi} + (Z_T + \frac{q}{\mu} \cdot R_k) \cdot (e^{-\mu \cdot \varphi} - 1) \quad (5)$$

In general the curvature is vectorically composed by the helix and bending curvature.

$$\frac{1}{R_k} \approx \sqrt{\frac{\sin^2 \vartheta(\varphi)}{R_{KG}^2} + \left(\frac{1}{R_{B\alpha}} + \frac{\cos \vartheta(\varphi)}{R_{KG}} \right)^2} \quad (6)$$

$$\text{with } \vartheta(\varphi) = \frac{\varphi \cdot R_{KG} \cdot \cos \alpha}{R_m} + \vartheta_0 \quad (7)$$

The friction force Z_T derives from the torque (M_T)

$$M_T = V \cdot T_r \cdot N_B \quad (8)$$

$$\text{and twist } V = (1 - \eta_e) \cdot \frac{2 \cdot \pi \cdot S}{\pi^2 \cdot D_m^2 + S^2} \quad (9)$$

with T_r = torsional rigidity
 N_B = number of ribbons in a stack
 η_e = degree of relaxation
 S = pitch length
 D_m = helix diameter of the middle of the stack

Friction force from ribbon torsion becomes

$$Z_T = 4 \cdot \mu \cdot P \quad (10)$$

or with $M_T = P B_d$
$$Z_T = \frac{4 \cdot \mu \cdot M_T}{B_d} \quad (11)$$

because of the assumed bearing forces (P) in Fig. 3.

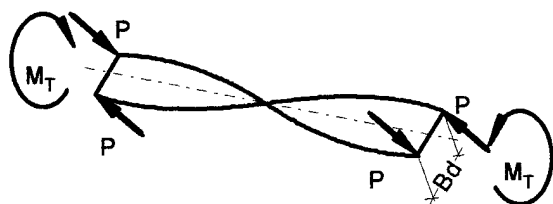


Fig. 3. Twisted Ribbon with Bearing Forces (P)

5. SIMULATION OF PULLING TESTS WITH THE THEORETICAL MODEL

The calculation with the theoretical model had to consider the composite length of the test cables (see situation in Fig. 4). This was completely done in Fig. 5. To avoid the influence of the pulling force loss in the straight part of the cable (L_s), the rectified pulling force (Z_b) at the bent part of the cable (L_b) was taken as representative for the pulling force in Fig. 6,7 & 8.

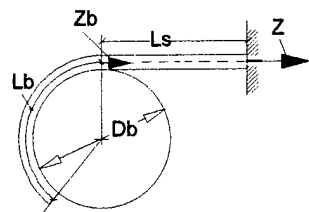


Fig. 4. Composite Cable Length and Rectified Pulling Force (Z_b)

5.1 Limits of the theoretical model

- In the general case equation 3 can't be solved exactly because R_k depends on φ in a complicated way. Therefore a simplified expression equation 6 was used for the numerical evaluations.
- The theoretical model doesn't pay regard to the clearance between stack and slot wall. That means wall contact is assumed along the ribbon stack.
- the coefficient of static friction is assumed to be independent of the speed of the pulling force.

5.2 Comparison of tests and calculations

With a coefficient of static friction of $\mu = 0.388$ and a material temperature of 20°C a good correspondence between calculation and measurement (values from Table 6) was found as shown in Fig. 5.

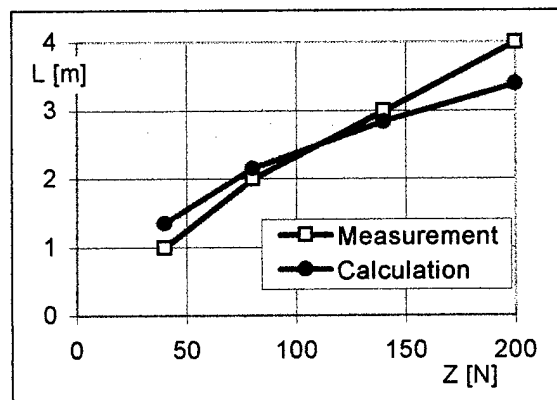


Fig. 5. Comparison of Measured and Calculated Pull out Lengths as Funktion of the Pulling Forces

5.3 Influence of some design parameters according to the theoretical model

Further calculations show the influence of pitch, coefficient of friction and torsional rigidity upon the moveability of the ribbon.

The results are shown in several diagrams.

- In straight cables a long pitch improves the moveability while in bent cables this influence diminishes (Fig.6).
- A massive influence of the coefficient of friction was found under all bending conditions (Fig.7).
- The torsional rigidity of the ribbon stacks produces forces of friction which should not be neglected (Fig.8).

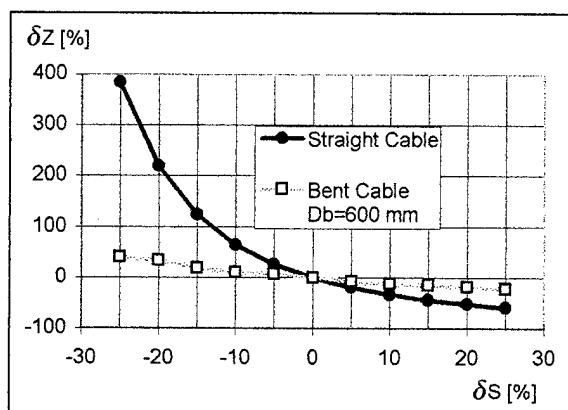


Fig. 6. Relative Friction Force (δZ) as Funktion of Pitch Length Change (δS)

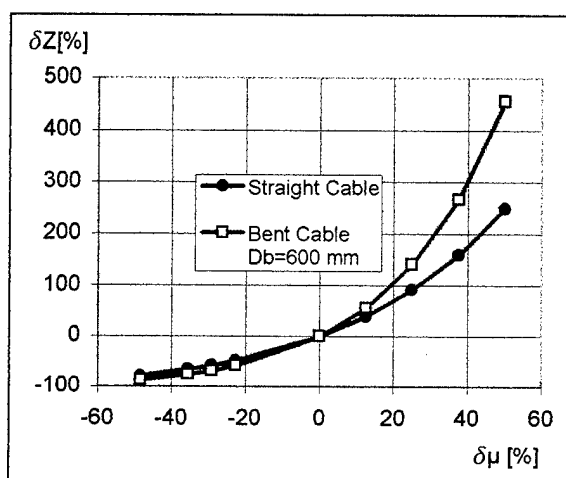


Fig. 7. Relative Friction Force (δZ) as Funktion of Friction Coefficient Change ($\delta \mu$)

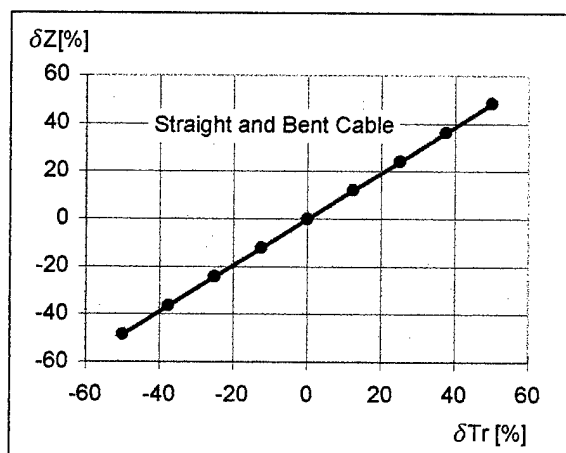


Fig. 8. Relative Friction Force (δZ) as Funktion of Torsional Rigidity Change (δTr)

6. CONCLUSIONS

The simulation of ribbon tensile stresses in cables by a mathematical model may give the cable designers interesting insights in how to optimize the cable design. To avoid attenuation changes, a good moveability of the ribbon stack in the slot would be desirable. In that respect the choice of pitch length seems to be important. Moreover the influence of the coefficient of static friction and the torsional rigidity of the ribbon stacks have to be taken into consideration. We intend to continue our experiments and calculations to find a direct relationship between attenuation changes in bent cables and the friction forces on the ribbon stacks.

7. ACKNOWLEDGMENTS

The author would like to express his thanks to Dietmar Weber and Donald Parris for their support of this paper.

8. REFERENCES

- [1] Tomito, Matsumoto, Nagasawa, Tanifugi (NTT), "Ultra High-Density Optical Fiber Cable with Thin Coated Fibers and Multi-Fiber Connectors", 42st IWCS 1993, pp 5-15
- [2] Patent application DE 4440983 A1, "Formstabile U-Profil"
- [3] Wagman, Bark, Cooke, Eoll, Livingston, Lochkovic, McAlpine, Sears, Sodhi, "Design Concepts for a 4000 Fiber Cable with Thinley Coated Fiber", IWCS 1994, pp. 12-19
- [4] Sears, Cooke, Eoll, Jackman, Lochkovic, McAlpine, Sodhi, Wagman, "Effect of U-groove Torsional Rigidity on Performance of High-Fiber-Count Cable", Optical Fiber Communication Conference Technical Digest, pp. 243-244, 1994
- [5] Kokobun and Katsuyama, "Curing Shrinkage Effects of UV-curable Materials on Fiber Loss Characteristics", IEEE 1990
- [6] W.Beitz and K.-H. Küttner, Dubbel, Handbook of Mechanical Engineering, Springer-Verlag, London, Berlin, New York, 1994, 17th edition, pp. A17-18

9. AUTHOR



Ernst A. Opel

SIEMENS AG ÖN NKE K5
Austr. 101
D-96465 Neustadt bei Coburg
Germany

Ernst Opel is a development engineer in the field of communication cables. He was born in 1959 and received his Dipl.-Ing. (FH) in Feinmechanik from Georg-Simon-Ohm-FH in Nürnberg in 1987. He joined SIEMENS in 1988. Since 1989 he has been engaged in the development of high-density optical fiber cables. In 1994 he joined the cable measurements group where he is responsible for the development of theoretical models.

DEVELOPMENT OF 3000-FIBER CABLE USING 16-FIBER RIBBONS

Hideyuki IWATA, Masaru NOZAWA, Norio KASHIMA, and *Tadatoshi TANIFUJI

NTT Access Network Systems Laboratories
Tokai, Naka, Ibaraki, JAPAN

*Technical Research and Development Department Telephone Organization of Thailand
Muang District, Patumtani, THAILAND

ABSTRACT

In this paper, we describe the design and performance of 3000-fiber cables. They use 16-fiber ribbons which are easily divided into four 4-fiber ribbons or two 8-fiber ribbons. The developed 3000-fiber cables are small in diameter (44 mm and 46 mm) and we have obtained good performance in the field. We also describe a newly developed 16-fiber fusion splice machine and a separator.

These technologies are realized to increase the maximum fiber count in a conduit to 3000 fibers and to reduce cable joining time.

1. INTRODUCTION

High density and small diameter optical fiber cables are required in order to construct "Fiber in the Loop" to support multi media services. We reported 1000-fiber single slotted core cable with a diameter of 30 mm compared with 40mm for multi slotted core cable at the last IWCS⁽¹⁾. The reduced cable outer diameter and weight can be used to increase both the installed length and the maximum fiber count in a conduit for multiple installation from 1000 to 1600. NTT have been using 3600 pair metallic cable in subscriber loops. The installation of optical cable based on single star (SS) architecture will require a fiber count of more than 1600, when metallic cable is replaced with optical fiber cable.

The fiber count of the cable we have developed is close to that of current metallic cable. In this paper, we describe the design and performance of 3000-fiber cable which uses 16-fiber ribbons, and its performance in the field. We also describe a newly developed 16-fiber fusion splicer and separator.

2. HIGH COUNT CABLE DESIGN

Table1 shows NTT's installation condition requirements.

a) Cable outer diameter.

The inner diameter of a conventional conduit is 75 mm, but if the conduit is bent, the maximum diameter for a cable capable of passing through it is less than 73 mm. When the cable is pre-connectorized it requires a pulling head to protect the connectors and this increases the total thickness by 18 mm. In such cases the cable diameter must be less than 55 mm.

b) Cable length.

The mean optical cable installation length in NTT's subscriber loop is 700 m. The maximum cable length is limited by the size of the cable reel currently used in NTT.

The outer diameter of a 700 m long pre-connectorized cable should be less than 50 mm when using the largest NTT reel.

c) Cable weight.

Cable weight is related to installation force. The conventional maximum force should be less than 800 kgf. Therefore the maximum installation length depends on the cable weight.

In some cases, mid span pulling machines for optical fiber cables are used. Their maximum pulling force is 200 kgf. When cables are too heavy, it is impossible to install them between adjoining manholes using this machine.

d) Installation tools.

Current installation tools such as curve guides and duct guides were designed for the current cable diameter. The cable outer diameter should be less than 48 mm for current duct guides when

the pulling force is 800 kgf and less than 50 mm for current curve guides for an 800 kgf pulling force.

e) Workability.

Mid-span access technologies allow the economic construction of efficient feeder and distribution networks for uncertain levels of demand. Therefore high count fiber cable should provide easy workability for mid-span access. It should also be easy to store excess lengths of pre-connectorized cable in a manhole.

f) Fiber ribbon count.

Current NTT cables consist of 4 or 8-fiber ribbons. The fiber ribbon count should be compatible to allow newly installed cables to be joined to existing cables.

Table1 Requirements for 3000-fiber cable

Item	Target value	Note
Cable outer diameter	<73 mm ϕ	
	<55 mm ϕ	Pre-connectorized
Cable length	>700 m	Pre-connectorized
Cable weight	light	200 kgf and 800 kgf pulling force
Installation tools	<48 mm ϕ	duct guide (800 kgf)
	<50 mm ϕ	curve guide (800 kgf)
Workability	easy	mid-span access
		Store excess cable length
Fiber ribbon count	4 or 8	compatible with existing cable

3. CABLE OUTER DIAMETER CALCULATION

The single slotted core cable diameter D_s is given by ⁽²⁾

$$D_s = 2 \left(\sqrt{ \left(\frac{w}{\cos \left(\frac{\pi}{N_s} \right)} + S_w \right)^2 + \left(\frac{S_w}{2} \right)^2 } + B_t + S_t \right) \quad \dots (1)$$

Where W is rib thickness, S_t sheath thickness, B_t is water blocking tape thickness, S_h is slot height, S_w is slot width, and N_s is slot number.

Figure 1 is cross sectional view of a U-groove / single slotted core cable. This cable has U-groove units stranded around a rod with slots. The inner circle radius C_{ur} of the U-groove units is expressed

by

$$C_{ur} = \frac{U_w}{2 \tan \left(\frac{\pi}{N_u} \right)} \quad \dots (2)$$

Where U_w is U-groove unit width and N_u is groove number.

The outer diameter of the central slotted rod D_c is equal to D_s .

When the inner diameter $2C_r$ is close to slotted core outer diameter $D_c + 2B_t$, a high density structure is achieved.

The cable outer diameter D_u is expressed by

$$D_u = 2 \left(\sqrt{ (U_h + C_{ur})^2 + \left(\frac{U_w}{2} \right)^2 } + (2B_t + S_t) \right) \quad \dots (3)$$

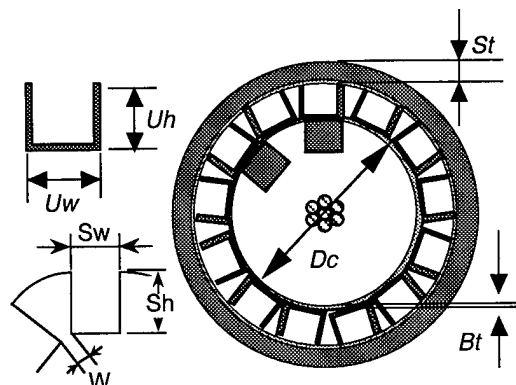


Figure 1 U-groove/single slotted core structure

where U_h is U-groove unit height.

Figure 2 shows the cable diameter for two different cable structures with 8 or 16 fiber ribbons.

The solid line with the filled triangles shows the relationship between fiber count and cable diameter for U-groove/single slotted core cable. For a fiber count of 3000, this cable structure is the most effective in reducing the outer diameter (44 mm).

The dotted line with the filled squares shows the same relationship for multi slotted core cable with 10 stacks of 8-fiber ribbons in each slot. This cable structure is compatible with present manufacturing facilities. For a fiber count of 3000, the diameter of this cable is 55 mm.

The solid line with the filled squares shows the same relationship for multi slotted core cable with 10 stacks of 16-fiber ribbons in each slot. The

solid line with the filled circles shows the same relationship for single slotted core cable with 10 stacks of 16-fiber ribbons. With this cable, a thicker slotted core diameter makes bending difficult.

The diameter of U-groove/single slotted core cable is 25% less than that of multi slotted core cable using 8-fiber ribbons.

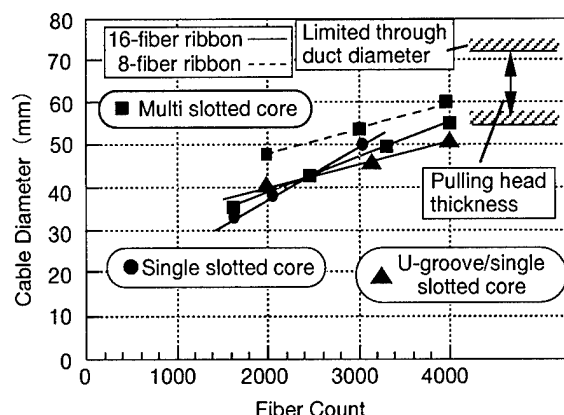


Figure 2 Relationship between Cable structure and diameter

4. 16-FIBER RIBBONS

4.1) Structure

Figure 3 shows a cross sectional view of a 16-fiber ribbon. The ribbon is 0.3 mm thick and 4.3 mm wide. The fiber is 1310 nm single-mode fiber and the outer diameter of the coated fiber is 0.25 mm. The 16-fiber ribbon can be easily divided into four 4-fiber ribbons or two 8-fiber ribbons to make it compatible with existing cables.

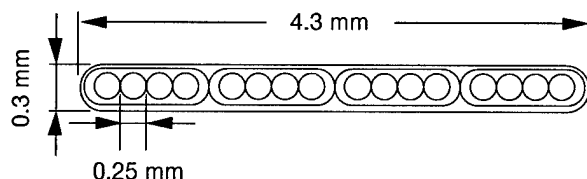


Figure 3 16-fiber ribbon structure

4.2) Performance

Table 2 shows attenuation, mechanical and temperature characteristics for the 16-fiber ribbon. The performance was found to be similar to those of current fiber ribbons.

Table 2 The 16-fiber ribbon performance

Test Item	Note	Result
Attenuation	at 1310 nm (Ave.) 1550 nm	0.35 dB/km 0.20 dB/km
Temperature cycle at 1550 nm	Temperature range: -30 °C ~ +60 °C	< 0.02 dB/km
Lateral force	1 kg/mm	< 0.02 dB
Winding under tension	500 g/340 mm ϕ at 1550 nm	< 0.03 dB/km

4.3) Compatibility with current splicing tools

Table 3 shows the compatibility of 16-fiber ribbon with currently used fusion splicing tools.

a) Newly developed separator.

The optical losses were measured while separating a 16-fiber ribbon into four 4-fiber ribbons or two 8-fiber ribbons using a newly developed separator. Photograph 1 shows this separator. A ribbon can be separated by pushing blades whose width is the same as that of the 4-fiber ribbon. The loss increase was less than 1dB for fibers nearest the point of division. An OE convertor and a sampling oscilloscope were used to measure the high speed change in attenuation. With this measurement system, the time resolution is 50 ms.

b) Stripper, cutter and holder.

A new holder has been developed for 16-fiber ribbon, and other fiber ribbons such as 8 or 4-fiber ribbons can be spliced using existing holders. It is also possible to employ the currently used fiber stripper and cutter.

c) Newly developed 16-fiber fusion splicing machine.

We developed a 0.25 mm pitch 16-fiber fusion splicing machine. This machine can splice 1, 2, 4, 8 and 16 fibers. Its weight and size are similar to those of the currently used 8-fiber splicer. The splice loss was below 0.1dB for 16-fiber splices as shown in Figure 4. The same performance was obtained for 1, 2, 4 and 8-fiber fusion splices. The splicing time of 2.3 minutes is similar to that of the current fusion splicer.

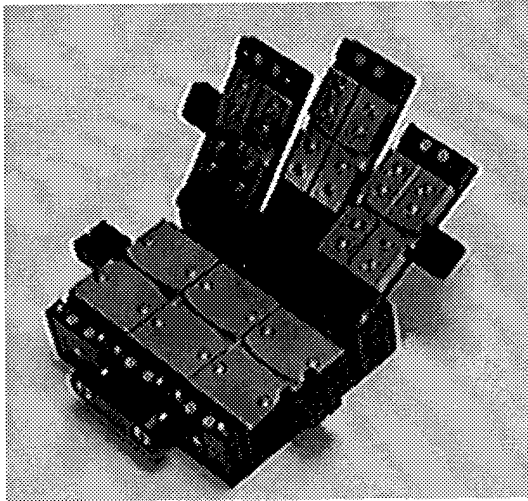
5. 3000-FIBER CABLE

5.1) Structure

One of the 3000-fiber cables we have developed has thirteen U-groove units stranded around a rod with seven slots (Fig. 5(a)).⁽³⁾ Each U-groove and each slot contains ten stacked 16-fiber ribbons. The cable diameter and weight are 44 mm and 1.4 kg/m, respectively.

In the other cable, rods with a helical slot are stranded in two layers (Fig.5(b)). The cable diameter and weight are 46 mm and 1.7 kg/m, respectively.⁽⁴⁾

These diameters are both less than that (55 mm) of the multi-slotted core cable with 8-fiber ribbons (Fig.5 (c)).



Photograph 1 Newly developed separator

Table 3 Compatibility with current fusion splicing tools

Item		Results
Developed Separator	From 16 to 8-fiber	Optical loss change ≤ 1 dB
	From 16 to 4-fiber	
Holder		New 16-fiber holder
Stripper and Cutter		Good
Newly developed 16-fiber fusion splicing machine		Splicing loss ≤ 0.1 dB (1, 2, 4, 8 and 16-fiber) splicing time : 2.3 min

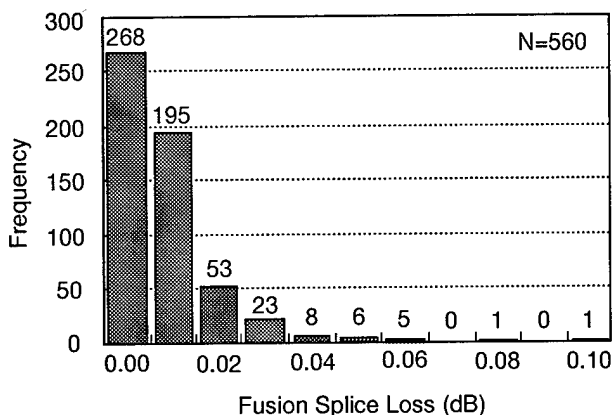
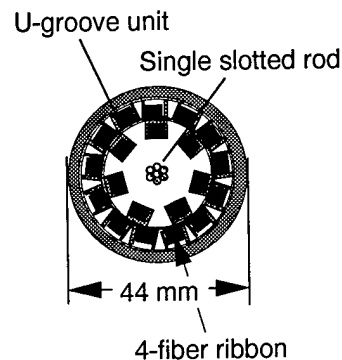
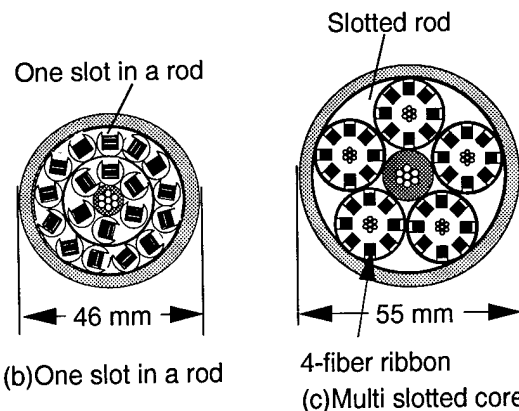


Figure 4 16-fiber fusion splicing loss



(a) U-groove/single slotted core



(b) One slot in a rod

(c) Multi slotted core

Figure 5 Structure of 3000-fiber cables

5.2) Performance

Table 4 shows the attenuation, mechanical and temperature characteristics for the two types of cable. The attenuation performance was similar to that of currently used optical cable. The optical loss changes were measured for temperatures between -30 and +60°C with the cable on a reel 1600 mm in diameter. The optical loss of the bottom corner fibers in a slot increased less than 0.1 dB/km. The mechanical performance in bending, lateral force, tensile and squeezing tests was found to be similar to that of current cable.

Table 4 Trial cable performance (U-Groove/single slotted core)

Test item	Note	Result
Attenuation	at 1310 nm (Ave.) 1550 nm	0.34 dB/km 0.20 dB/km
Temperature cycle at 1550 nm	Temperature range: -30 °C ~ 60 °C	< 0.1 dB/km
Bending	R : 200mm	< 0.03 dB/km
Lateral force	40 N / 5 mm	< 0.02 dB/km
Tension	800 kgf (Strain : 0.2 %)	< 0.02 dB/km
Squeezing	R : 600 mm, 800 kgf	< 0.02 dB/km

5.3) Field test performance

a) Outline.

We evaluated the performance of these cables in the field. Figure 6 shows a schematic view of the underground facilities we used for field tests at our Tsukuba R&D Center. The total conduit length was about 1.0 km. The one slot type cable was connectorized with 8 mechanically transferable (MT) connectors. One connectorized cable 682 m long and another 270 m long were joined at point A. The U groove and single slotted core cable was 1.0 km long. These cables were installed by an optical cable pulling machine with a pulling force of 800 kgf.

b) Cable performance.

OTDR measurements at a wavelength of 1550 nm before and after installation showed no detectable change in optical loss.

c) Joining performance.

The connection loss of a slot in a rod pre-connectorized cable was evaluated in the field. The average connection loss is 0.17 dB both before and after installation.

Figure 7 compares the joining time for 1000-fiber cable using the current method and our new method. The procedure is divided into four stages as follows.

- (1) Removing the pulling head
- (2) Positioning the enclosure
- (3) Joining the cable
- (4) Sealing the enclosure

The joining time is reduced by coupling together two sets of 5 stacked 8-MT plugs and the five excess 8-fiber ribbons are stored by turning them back on themselves in the current enclosure.

The total joining time for 3000 fibers using 375 8-MT connectors is 6 hours. We confirmed that this work can be completed in one day.

d) Installation.

These cables are sufficiently stable with the present installation method.

e) Mid-span access performance.

We have measured the optical loss change at a wavelength of 1550 nm while working on mid-span access. The mid-span access procedure is divided into the following nine stages.

- (1) Removing the cable jacket and water blocking tapes
- (2) Pushing the cable from two sides and taking the fiber ribbons out of the U-grooves or the slots in the outer rods
- (3) Wrapping fiber ribbons in a sheet
- (4) Cutting the U-grooves or outer rods
- (5) Taking the fiber ribbons out of the slots or the inner rods
- (6) Wrapping the fiber ribbons in a sheet
- (7) Cutting the slotted rod or inner rods
- (8) Removing the slotted core or central member core
- (9) Assembling the enclosure parts

The maximum optical loss change for cutting either a U-groove or a rod and removing the slotted core was about 1 dB, but there were no loss changes with the other procedures.

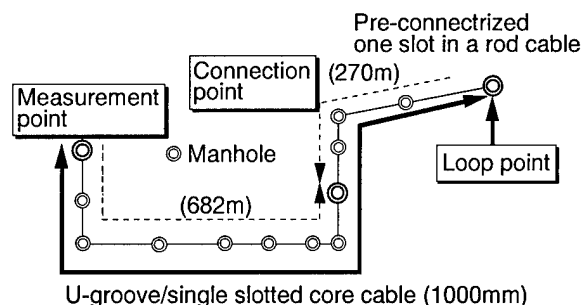


Figure 6 Underground facilities for field test

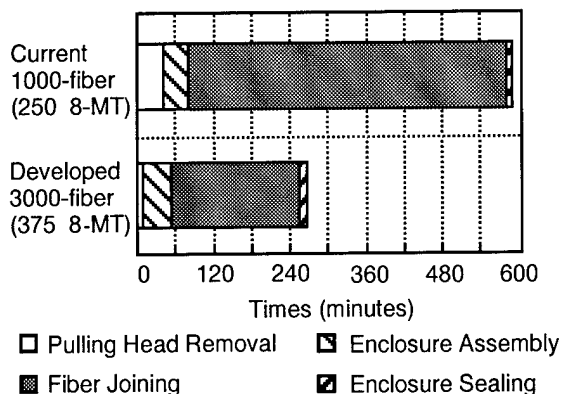


Figure 7 Cable joining time with current and developed method

6. CONCLUSION

Our prototype 3000-fiber cables, with 16-fiber ribbons which can be easily be divided into four 4-fiber or two 8-fiber ribbons, had good characteristics and were sufficiently stable in the field.

We have developed a 16-fiber fusion splicing machine, a holder and a separator.

The 3000-fiber cables are promising with regard to constructing the optical access network. The diameters of these 3000-fiber cables are very small and we have obtained good performance in the field.

ACKNOWLEDGMENTS

The authors are grateful to K.Ishihara, K.Nishimura, T.Yabuta, S.Nagasawa and S.Tomita for their helpful suggestions and comments.

REFERENCES

- [1] H.Iwata, M.Tsutsumi, E.Nakamura, N.Matsumoto, M.Nozaawa, S.Hayami, S.Nagasawa and T.Tanifuji "Pre-connectorized 1000-fiber Single Slotted Core Cable", Proc. of 44th IWCS, pp. 627-634, 1995.
- [2] S. Tomita, M.Matsumoto and T.Tanifuji "High Density Cable Structure for Optical Fiber Ribbons", IEICE TRANS.COMMUN., vol. E76-B, No.4 pp.358-363, 1993.
- [3] F.M.Sears, P.R.Brak, M.A.Clarke, H.G.Cooke, C.K.EoII, W.S.Jackman, R.O.Livingston, W.W.McAlpine, S.S.Sodhi and R.S.Wagman "Design and Performance of a 3200-fiber Hybrid

SCR/U-Groove Cable Using 16-Fiber Ribbons", Proc. of 45th IWCS, 1996.

[4] W.Katsurashima, Y. Kitayama and S.Tanaka "Ultra-High-Count Optical Fiber Cable using Single-Helical-Groove Unit", Proc. of 43rd IWCS, pp. 36-42, 1994.



Hideyuki IWATA

NTT
Access Network
Systems Laboratories
Tokai, Ibaraki,
319-11, JAPAN

Hideyuki Iwata is a research engineer. He was born in 1965 and received B.E. and M.E. degrees in electronic engineering from Yamagata University in 1989 and 1991, respectively.

He joined NTT in 1991. Since 1993 he has been engaged in research on high-density and Aerial optical fiber cable.

Mr. Iwata is a member of IEICE of Japan.



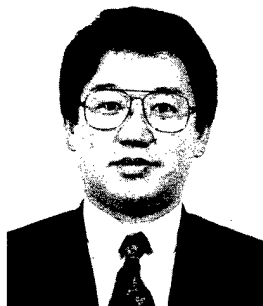
Norio KASHIMA

NTT
Access Network
Systems Laboratories
Tokai, Ibaraki,
319-11, JAPAN

Norio Kashima is a leader of optical fiber cable research group. He was born in 1950 and received B.E. and M.E. degrees from Yokohama National University, Japan, in 1973 and 1975, respectively and a Ph.D. degree from the Tokyo Institute of Technology, Japan, in 1984.

He joined NTT in 1975. He has been engaged in research and development of fiber design, fusion splicing, optical connectors, transmission systems, and access network operation systems, and optical cables.

Dr. Kashima is a member of IEEE and IEICE of Japan.



Masaru NOZAWA

NTT
Access Network
Systems Laboratories
Tokai, Ibaraki,
319-11, JAPAN

Masaru Nozawa is a research engineer. He was born in 1956 and graduated from Aomori Technical High School in 1974.

He joined NTT in 1974. Since 1994 he has been engaged in research on high-density and pre-connectorized optical fiber cable.



Tadatoshi TANIFUJI

TOT
Technical Research
and Development
Department
12-000, THAILAND

Tadatoshi Tanifuji is now a technical adviser of Telephone Organization of Thailand.

He was born in 1949. He received B.E., M.E., and Ph.D. degrees in electronic engineering from Hokkaido University in 1972, 1974, and 1983, respectively.

He joined NTT in 1974. Since 1991 he has been engaged in research on high-density optical fiber cable and jointing technologies.

Dr. Tanifuji is a member of IEEE.

DESIGN AND PERFORMANCE OF A 3200-FIBER HYBRID SCR/U-GROOVE CABLE USING 16-FIBER RIBBONS

Frederick M. Sears, Peter R. Bark, Mary A. Clarke, Harriet G. Cooke,
Christopher K. Eoll, Larry E. Herman, William S. Jackman, Ron O. Livingston,
Shami S. Sodhi and Richard S. Wagman

Siecor Corporation
Hickory, North Carolina

ABSTRACT

An ultra high-density, 3200-fiber, hybrid SCR/U-Groove cable with 16-fiber ribbons containing 250 μm outer diameter (OD) fibers has been successfully designed, manufactured and tested. Processing improvements were made to allow for the manufacture of the large Slotted Core Ribbon (SCR) and U-Groove components required for the 3200-fiber cable structure. This prototype had excellent performance characteristics during all tests. To our knowledge, the cable cross-section packing density of 2.13 fibers/ mm^2 presented here is the highest of any cable design manufactured using standard 250 μm OD fiber.

I. INTRODUCTION

The emerging multimedia access network in Japan requires small diameter, ultra-high fiber count cables in the feeder segment of the optical access network. To meet this requirement, a 4000-fiber, U-Groove cable was previously proposed and developed by NTT¹⁻² (Nippon Telegraph and Telephone). 4000-fiber cable test results have been published for reduced diameter fiber ribbons with 180 and 200 μm OD fibers³⁻⁴. However, issues such as international standardization, compatibility with existing plant and cost postponed the deployment of cables containing fibers with reduced diameters.

Instead, deployment of 1000-fiber, high density slotted-core ribbon (SCR) optical fiber cables has recently proceeded in Japan. These cables use standard OD optical fibers in thin 8-fiber ribbons⁵⁻⁶. However, the need still exists for small diameter, higher fiber count cables with around 3000 fibers for the optical access network.

This need is addressed by the development work reported in this paper.

Table I shows how ultra-high fiber count cables have evolved in Japan. This table summarizes the cable types, fiber counts and cable fiber densities for the optical access network. The multi-rod SCR cable⁷⁻⁸, which was replaced by the single-rod SCR cable, consists of several rods stranded around a central strength member.

In this paper, we present the design, manufacture and testing of an ultra-high density, 3200-fiber, hybrid SCR/U-Groove cable with 16-fiber ribbons containing 250 μm OD fibers. A cross-section of the cable with the maximum complement of fibers is shown in Fig. 1. The inner core of this cable is similar to the core of the 1000-fiber cable, both using slotted rods with stacks of 10 ribbons in each slot. Ribbons in the 3200-fiber cable each contain 16 fibers, instead of 8 fibers as in the 1000-fiber cable. 13 U-Grooves are stranded around a 7-slot rod to construct a hybrid SCR/U-Groove cable. Each U-Groove also contains a stack of ten 16-fiber ribbons. The 16-fiber ribbons are easily separable into four, 4-fiber ribbon subunits.

Various ribbon coating materials were investigated to obtain low ribbon-to-ribbon and ribbon-to-slot/U-Groove friction, and to minimize microbending effects on the ribbon stack corner fibers. Ribbon edge-fiber maximum straight cable strains are calculated for both the inner SCR rod and the outer U-Groove layer. U-Groove strains are also estimated.

Processing improvements were made to allow for the manufacture of the large SCR/U-Groove

components required for the 3200-fiber cable structure. The shapes of the slots and U-Grooves are also important in the design of the 3200-fiber cable. A slot/U-Groove shape was developed which minimizes the cable diameter while providing mechanical integrity.

This paper will address the design and performance of a hybrid SCR/U-Groove cable by focusing on (1) cable design, (2) manufacture of the U-Groove and slotted rod, (3) cable stranding, (4) cable performance, and (5) field installation.

Table I. Evolution of Ultra-High Fiber Count Cables in Japan

	Reduced Diameter Optical Fiber		Standard Optical Fiber		
Cable Fiber Count	4000	4000	1000	1000	3200
Cable Type	U-Groove	U-Groove	Multi-Rod SCR	SCR	SCR/U-Groove
Cable OD (mm)	35	42.5	40	29.4	43.7
Fiber OD (μm)	180	200	250	250	250
Fibers/Ribbon	16	16	8	8	16
Fiber Density (Fibers/ mm^2)	4.16	2.82	0.8	1.47	2.13
References	1,2,3	4	7, 8	5, 6	This paper

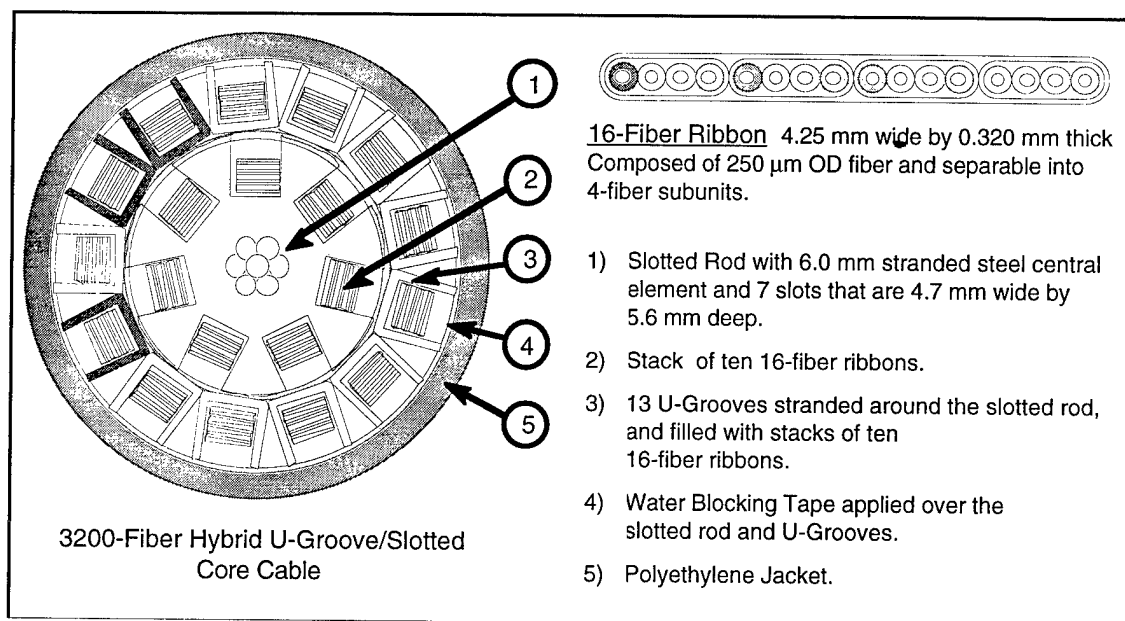


Fig. 1. Cross-Sections of Hybrid 3200-Fiber Cable and 16-Fiber Ribbon

II. CABLE DESIGN

A slotted core design is chosen as the inner core of the 3200-fiber cable since it is slightly more efficient than a U-Groove design in terms of cable diameter. U-Grooves are used as the second layer of the cable because they can be easily applied as a second layer and are removable for access to the inner core.

The 3200-fiber design consists of an inner slotted core with 7 slots and 13 U-Grooves stranded around the slotted core. Each slot/U-Groove accommodates a stack of ten 16-fiber ribbons. Over both the slotted rod and the layer of U-Grooves are water-blocking tapes. The overall polyethylene jacket is 2.5 mm thick.

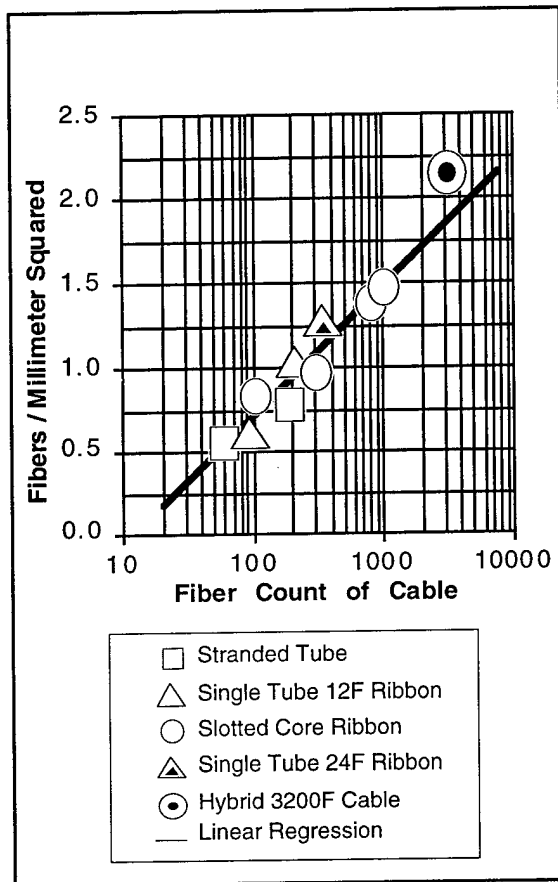


Fig. 2. Comparison of Cable Fiber Density vs. Fiber Count for Various Cables

The nominal cable diameter is 43.7 mm, which gives this hybrid design a fiber packing density of

2.13 fibers/mm² of cable cross-section. The fiber packing density is much higher for this hybrid design than for 3000-fiber count cables made by stranding slotted rods around a central member, where cable diameters can be over 54 mm. Fig. 2 shows a comparison of fiber density versus fiber count for various optical fiber cables using standard 250 μ m OD fiber. Cables compared include stranded tube cables, single tube 12-fiber ribbon cables, slotted core ribbon cables, a single tube 24-fiber ribbon cable and the hybrid 3200-fiber cable. The solid line represents a linear regression fit to the data, excluding the 3200-fiber cable. One can observe that the hybrid 3200-fiber cable has a fiber density above that for the linear regression fit for the remaining cable types.

16-Fiber Ribbons

The 16-fiber ribbons use 250 μ m single-mode fibers, and are separable into 4-fiber ribbon subunits as shown in Fig. 1. They are approximately 0.320 mm thick and 4.25 mm wide. Maximum fiber strains are calculated in the following section for the edge fibers of such a wide ribbon. The materials and their thicknesses are the same as in the 8-fiber ribbon developed for the 1000-fiber slotted core cable⁵. This two-layer ribbon coating was designed to provide good ribbon separation and cable performance. Because the 16-fiber ribbon is separable (by hand or using a separation tool) into 4-fiber subunits, it can be pre-connectorized with either the 4- or 8-fiber standard MT connectors. Once separated, each 4-fiber subunit is mechanically sound and fully surrounded by UV curable material.

16-fiber ribbons are chosen for high fiber count cables since they simplify the stranding operation. 16-fiber ribbons in stacks of ten allow a cable to be designed with a relatively small cable diameter and relatively low fiber strains within the cable. In addition, such stacks allow one to efficiently access fibers in the cable. In contrast, for example, the use of smaller stacks of five 4-fiber ribbons (as used in a 100-fiber SCR cable) would greatly complicate location of a specific fiber amongst 3200.

Straight Cable Fiber Strain

As the number of fibers per ribbon and cable dimensions are increased to obtain a high fiber count cable, fiber strains within the cable become an increasingly important consideration. The lay lengths of the slots and U-Grooves were chosen

to keep maximum strains low while also keeping ribbon twisting low during cable bending. The maximum fiber strains (for the edge fibers in the 16-fiber ribbons) in a straight cable were calculated⁹ to be 0.0498% in the inner slotted rod core and 0.0373% in the outer U-Groove layer.

U-Groove Strain

Another aspect of increasing cable dimensions is the potential for increased bending strains on the U-Grooves. Bending strains encompass the bending due to stranding, the bending due to the shipping reel and the bending due to cable installation.

When the cable is bent, such as when it is on a reel or going around a sheave, the bend radius of the U-Groove is determined by defining a vector equation of the path of the bent helix formed by the U-Groove. This vector equation is written as

$$P = \left[r_C + r_U \cos \left(\frac{2\pi r_C s}{L_U} \right) \right] \cos(s) i + \left[r_C + r_U \cos \left(\frac{2\pi r_C s}{L_U} \right) \right] \sin(s) j + r_U \sin \left(\frac{2\pi r_C s}{L_U} \right) k \quad (1)$$

where

- P = the vector describing the path of the element in a bent cable,
- r_C = bend radius of the cable,
- r_U = radius of element from center of cable,
- $r_C s$ = distance along the axis of the bent cable where s is in radians,
- L_U = lay length of stranded element, and
- i, j, k = unit vectors.

After taking first and second derivatives of Eq. (1) with respect to s , the curvature of the vector at any point along its path can be determined by using the dot products in the following equation¹⁰:

$$\kappa = \frac{\sqrt{(\dot{P} \cdot \dot{P})(\ddot{P} \cdot \ddot{P}) - (\dot{P} \cdot \ddot{P})^2}}{(\dot{P} \cdot \dot{P})^{3/2}} \quad (2)$$

where

- κ = curvature,
- \dot{P} = first derivative of Vector P , and
- \ddot{P} = second derivative of vector P .

The relationship between the curvature and the

bend radius is

$$r_b = \frac{1}{\kappa} \quad (3)$$

where

r_b = bend radius of element.

The strain caused by bending is determined by

$$\epsilon_b = \frac{r_g}{r_b} \quad (4)$$

where

- ϵ_b = the maximum strain due to bending and
- r_g = the distance from the neutral bending axis of the U-Groove to its top.

The maximum bending strain in the U-Groove is estimated using Eqs. (1), (2), (3) and (4). Considering the 3200-fiber hybrid cable design and a cable bend radius of 15 times the cable diameter, the maximum bending strain on the U-Groove is estimated to be 1.1 %. This maximum bending strain is comparable to the component strains seen in lower fiber count cables such as stranded loose tube cables. The measured strain at yield is 5.0% for U-Groove samples which were tested.

III. MANUFACTURE OF U-GROOVE AND SLOTTED ROD

As the size of a ribbon stack increases, the size of the slot or U-Groove containing the stack increases. This makes the slotted rod and the U-Groove more difficult to manufacture. As the size of these components increases, the slotted rod web thicknesses and U-Groove wall thicknesses must be increased to maintain the same crush resistance. Euler's column theory was used to scale the slotted rod and U-Groove thicknesses to maintain the same level of crush resistance⁴. Larger sizes and thicknesses lead to processing challenges for both the U-Groove and the slotted rod.

Both the U-Groove and slotted rod are manufactured by profile extrusion. One difficulty to overcome when component size is increased is the effect of gravity on the extrudate. In each case, the material has a relatively low melt strength. As the material exits from the extruder in a horizontal extrusion set-up, it can deform under its own weight. During the extrusion of either the U-Groove or the slotted rod, provisions are made to control such deformation due to gravity.

There is a special problem to be solved in the case of a slotted rod that is extruded using a stationary die. The issue is nonuniform molten plastic flow as the extrudate leaves the extrusion die, whereby the cross-sectional shape of the extrudate changes relative to the shape of the orifice at the exit face of the die. An indication of the source of the problem may be found in Fig. 3, which shows a comparison of the 3200-fiber SCR rod and the 100-fiber SCR rod circumferential velocities. The circumferential velocities of the extrudate are shown at various radii from the axis of the rod: the larger the diameter of the rod, the larger the velocity gradient generated between the top and the bottom of the slot. The gradient can be ignored for small diameter rods; however, for larger diameters, the extrusion die must be designed to equalize the material flow of the extrudate across the exit face of the die.

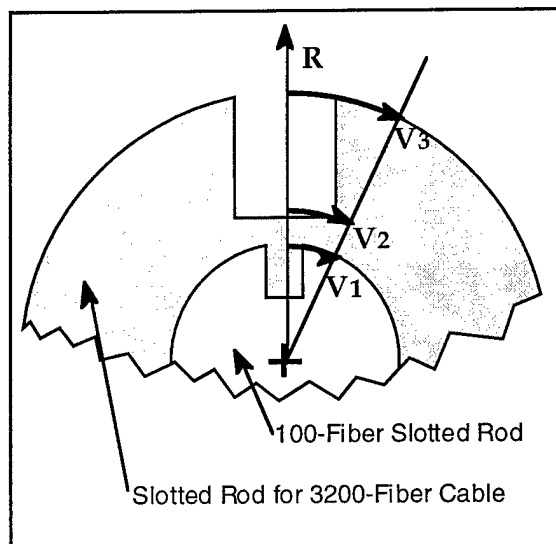


Fig. 3. Comparison of Circumferential Velocities of the Extrudate at Various Radii From the Axis of the Rod

Another processing problem to be overcome for a large U-Groove is the differential cooling across the profile. This problem is solved by compensating with the design of the die so that the stresses are minimized.

IV. CABLE STRANDING

In order to achieve good attenuation performance and to have low fiber strain during bending, the cable stranding process must be precise. Fig. 4 shows the basic layout of the stranding line for the hybrid SCR/U-Groove cable. The stranding method and layout was chosen for simplicity of organization and the ease of ribbon tension control. On the first stranding pass, a reel containing the slotted rod is placed on the rotating payoff and the rod is threaded through the stranding line to the rotating takeup. Seventy 16-fiber ribbons are stranded in the slots, 10 ribbons per slot. Between the ribbon insertion point and the rotating takeup, a layer of water blocking tape and binders are applied. For the prototype cable for which results are being reported here, only one slot was filled.

The reel containing this inner portion of the core is then moved to the rotating payoff and threaded through the stranding line. Thirteen U-Grooves are stranded around the inner core with a handedness opposite to that of the helical slots. A total of 130 ribbons are stranded in the U-Grooves, 10 per U-Groove. An overall layer of swell tape and binders are then applied. Again, for the prototype, 10 sixteen-fiber ribbons were stranded in one of the U-Grooves.

The path of each ribbon and each U-Groove is designed so that bend radii are never less than the appropriate minimum bend radii. Furthermore, the tension on each element, in particular each ribbon, is closely controlled during the stranding process.

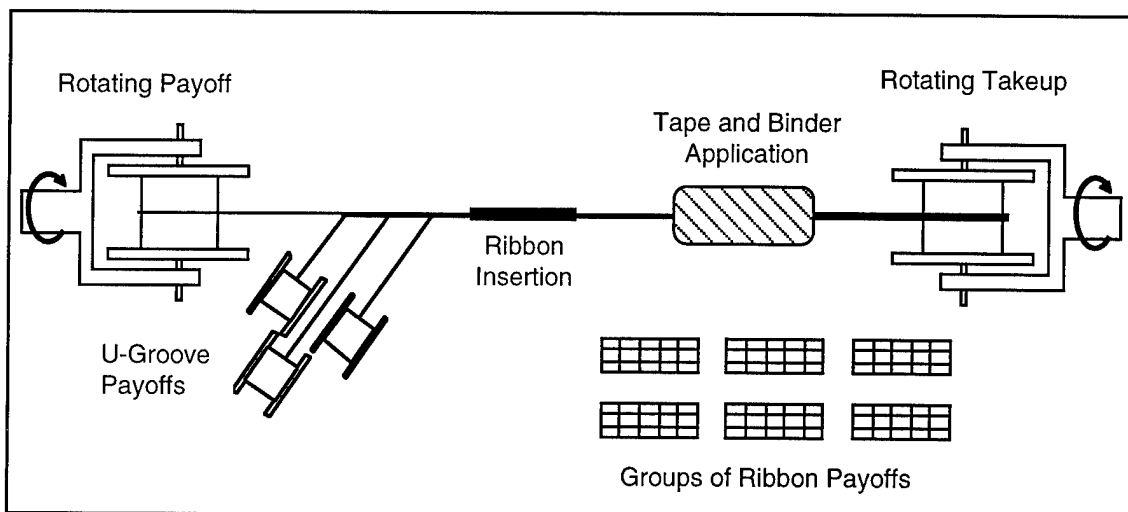


Fig. 4. Stranding Line for the Hybrid 3200-Fiber Cable

V. CABLE PERFORMANCE

Attenuation Measurements

As-Manufactured Attenuation.

Bidirectional OTDR attenuation was measured on all 320 fibers after manufacturing. The mean attenuation at 1550 nm was 0.20 dB/km with a standard deviation of 0.01 dB/km (maximum=0.29 dB/km). At 1310 nm, the mean attenuation was 0.34 dB/km with a standard deviation of 0.01 dB/km (maximum=0.37 dB/km).

Thermal Cycling Attenuation. Of the 160 fibers in each ribbon stack, 40 were measured for attenuation during temperature cycling. Fig. 5 indicates the distribution of those 40 fibers within each stack. With one filled slot and one filled U-groove, 80 measurements were made in total (n=80).

Table II presents a summary of the temperature cycling results for the hybrid 3200-fiber cable. In the row containing the "23°C" data, the mean 1550 nm attenuation after manufacture was 0.23 dB/km with a standard deviation of 0.05 dB/km. The cable had acceptable attenuation performance during thermal cycling, as shown in Table II. The temperature cycling involved two excursions each to -30°C and +60°C. For each temperature, the two sets of results are pooled (n=160). Fig. 6 and Fig. 7 present histograms of the changes in attenuation at 1550 nm for -30°C and +60°C, respectively.

The maximum change in 1550 nm attenuation at -30°C was 0.10 dB/km with a standard deviation of 0.04 dB/km (See Table II). The mean 1550 nm attenuation at -30°C was 0.20 dB/km with a standard deviation of 0.02. The maximum 1550 nm attenuation change at +60°C was 0.11 dB/km with a standard deviation of 0.02 dB/km. The mean 1550 nm attenuation at +60°C was 0.23 dB/km with a standard deviation of 0.04 dB/km.

Mechanical Tests

Attenuation change during mechanical tests was measured at 1550 nm. Measurement accuracy in the bending, elongation and lateral load tests was within ± 0.02 dB. Accuracy for the squeeze test was within ± 0.03 dB.

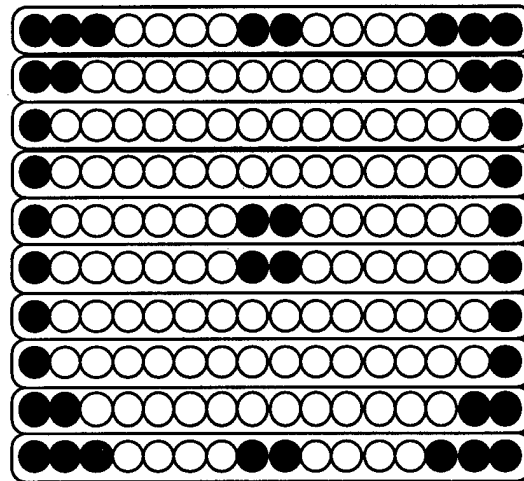
Bending. 200, 300, 400 and 600 mm radius mandrels were used for the bending tests. For the 200 mm mandrel, the maximum attenuation increase observed was 0.03 dB. This occurred in the filled U-groove. For the larger mandrels, no increase larger than the measurement error was observed.

Squeezing. A 0.95 m length of cable was bent somewhat more than 90° around a 600 mm mandrel. The load on the cable was set at 788 kg; this corresponds to 0.20% cable elongation if one uses a tensile modulus of 170 kN/mm² for the 6.0 mm stranded steel central member. No attenuation increase larger than the

measurement error was observed during the squeeze test.

Lateral Load. Lateral loads of 1000 N, 2000 N and 3000 N were applied over a cable length of 100 mm in this test. The load on the cable was maintained for 10 minutes before measurements were taken. No increase in attenuation larger than the measurement error was observed at any of the lateral loads. Furthermore, there was no permanent deformation of the slotted rod or the U-grooves at 3000 N/100 mm.

Elongation. Loads were applied to approximately 19.5 m of cable in this test. The cable was tested at elongations of 0.10%, 0.15%, 0.20% and 0.25%. No increase in attenuation larger than the measurement error was observed for elongations up to 0.25%, corresponding to a load of 984 kg.



Filled circles indicate optical fibers measured

Fig. 5. Stack of Ten, 16-Fiber Ribbons Measured During Temperature Cycling

Table II. Hybrid 3200-Fiber Cable Temperature Cycling Results

1300 nm	Attenuation (dB/km)		Change in Attenuation (dB/km)		Number of Fibers
	Mean	St. Dev.	Mean	St. Dev.	
Initial 23°C	0.34	0.01	---	---	80
-30°C	0.34	0.01	-0.01	0.01	160
+60°C	0.35	0.02	0.01	0.01	160
Final 23°C	0.34	0.01	---	---	80

1550 nm	Attenuation (dB/km)		Change in Attenuation (dB/km)		Number of Fibers
	Mean	St. Dev.	Mean	St. Dev.	
Initial 23°C	0.23	0.05	---	---	80
-30°C	0.20	0.02	-0.02	0.04	160
+60°C	0.23	0.04	0.00	0.02	160
Final 23°C	0.20	0.02	---	---	80

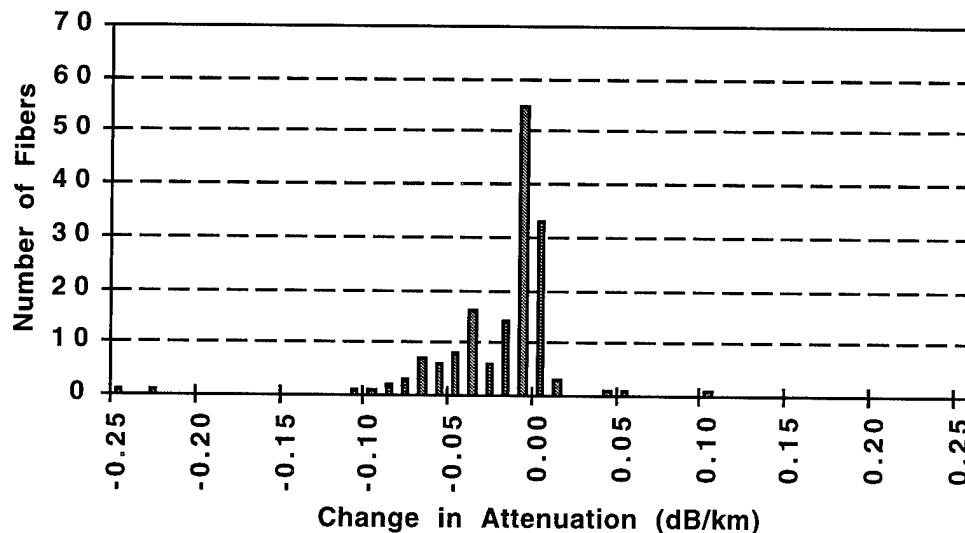


Fig. 6. Attenuation Change at 1550 nm for All -30°C Measurements ($n=160$, mean= -0.02 dB/km, standard deviation= 0.04 dB/km)

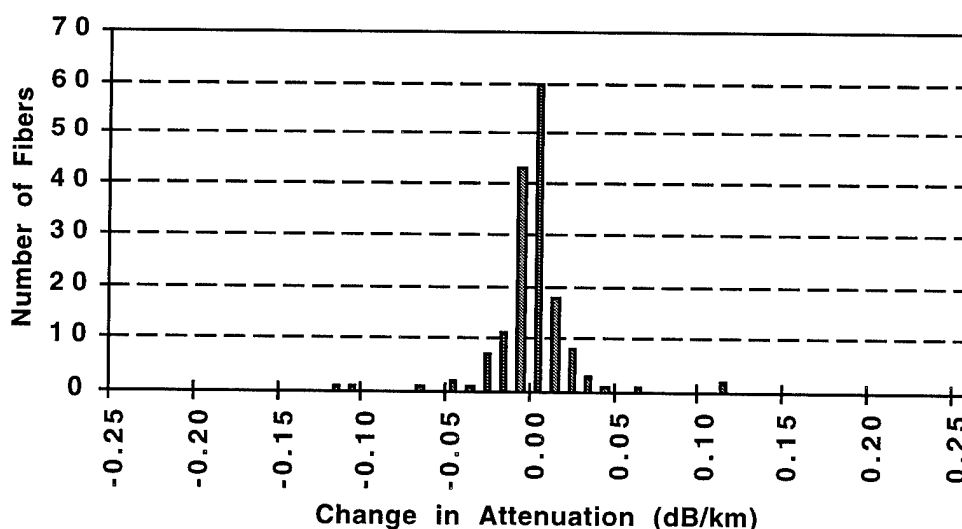


Fig. 7. Attenuation Change at 1550 nm for All $+60^{\circ}\text{C}$ Measurements ($n=160$, mean= 0.00 dB/km, standard deviation= 0.02 dB/km)

VI. FIELD INSTALLATION

A 3200-fiber hybrid SCR/U-Groove cable was manufactured and used for field installation at NTT's Access Network Systems Laboratory. The 1000 meter long prototype cable was installed in a system of ducts at Tsukuba, Japan. Cable attenuation and fiber strain (using a B-OTDA) were

measured before and after installation. Also, mid-span access attenuation measurements and excess cable storage at bending radii down to 350 mm were examined. The 3200-fiber cable met or exceeded the customer's specifications in all tests.

VII. CONCLUSIONS

In summary, we have designed, manufactured and tested a hybrid SCR/U-Groove cable design for up to 3200 optical fibers. The hybrid design has increased fiber density and reduced cable diameter over multi-core SCR cable designs. To our knowledge, the cable cross-section packing density of 2.13 fibers/mm² presented here is the highest of any cable design manufactured using standard 250 µm OD fiber.

Maximum straight cable fiber strains are calculated to be <0.05% for both the inner SCR rod and the outer U-Groove layer. U-Groove bending strains are estimated to be about 1.1%. This is comparable to the component strains seen in lower fiber count cables such as stranded loose tube cables.

The hybrid cable had acceptable attenuation performance during thermal cycling and exhibited excellent performance during mechanical testing. Consequently, the work reported here demonstrates the feasibility of using a hybrid SCR/U-Groove cable for the multimedia optical access network.

REFERENCES

1. S. Tomita, M. Matsumoto, S. Nagasawa and T. Tanifuji, "Ultra High-Density Optical Fiber Cable with Thin Coated Fibers and Multi-Fiber Connectors," *Proceedings of the 42nd International Wire and Cable Symposium*, pp. 5-15, 1993.
2. S. Tomita, "Very-high-fiber-count preconnectorized cable," *Optical Fiber Communications Conference Technical Digest*, paper ThA1, pp. 177-178, 1994.
3. F. Sears et al., "Effect of U-Groove torsional rigidity on performance of high-fiber-count cable," *Optical Fiber Communications Conference Technical Digest*, paper ThA3, pp. 178-180, 1994.
4. R. Wagman et al., "Design Concepts for a 4000-fiber Cable with Thinly Coated Fibers," *Proceedings of the 43rd International Wire and Cable Symposium*, pp. 12-21, 1994.
5. R. Wagman, G. Lochkovic and K. White, "Component Optimization for Slotted Core Cables Using 8-Fiber Ribbons," *Proceedings of the 44th International Wire and Cable Symposium*, pp. 472-478, 1995.
6. H. Iwata et al., "Pre-connectorized 1000-fiber Single Slotted Core Cable," *Proceedings of the 44th International Wire and Cable Symposium*, pp. 627-634, 1995.
7. S. Hatano et al., "Multi-Hundred-Fiber Cable composed of Optical Fiber Ribbons", *Proceedings of the 35th International Wire and Cable Symposium*, pp. 17-23, 1986.
8. T. Uenoya, S. Tomita and F. Ashiya, "Long-term Reliability of 1000-Fiber Water-blocking Cable", *J. Opt. Commun.*, Vol. 12, No. 3, pp. 86-90, 1991.
9. W. McCallum, M. Light and R. Wagman, "Design and Development of a Compact High Fiber Count Ribbon Cable", *Proceedings of the 44th International Wire and Cable Symposium*, pp. 8-15, 1995.
10. E. Kreyzig, Advanced Engineering Mathematics, John Wiley and Sons, p.294, 1962.

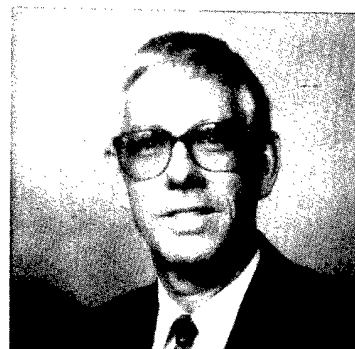


Frederick M. Sears was born in Houston, TX in 1952. He received the S.B. and S.M. degrees from M.I.T. in 1975, in the five year honors program, and a Ph.D. degree from the University of California at Berkeley in 1980, all in mechanical engineering.

In 1980, Dr. Sears joined AT&T Bell Laboratories in Murray Hill, NJ, as a Member of Technical Staff, where he pursued research and development on optical fiber characterization techniques including fiber interferometry, single-polarization fibers, polarization-maintaining fibers and measurements, and optical time-domain reflectometry. In 1984, he transferred to the Atlanta Bell Laboratories location, pursuing optical fiber research and development on modal noise in single-mode lightguide systems, cutoff wavelength, characterization of polarization-maintaining fibers, interconnection of polarization-maintaining fibers, Fabry-Perot fiber interferometry and fiber optic cable design.

Since 1990, Dr. Sears has been at Siecor Corporation in Hickory, NC, where from 1991 to 1995 he managed the Ultra-High Fiber Count Cable development program. He is presently Manager of the Technical Staff in the Research, Development & Engineering Department.

Dr. Sears is a member of the Optical Society of America and Pi Tau Sigma. His volunteer work includes member, board of directors, Plainfield Science Center, 1980-84; member, board of directors, Catawba Science Center, 1993-96; member, OSA Tyndall Award selection committee, 1991; member, Optical Fiber Communications subcommittee on Fibers, Cables and Fiber Components, 1993-97.



Peter R. Bark was born and educated in Germany. In 1963, he received his bachelor of science degree (Diplom-Ingenieur) from the Technical University at Munich. In 1968, he received his doctorate in engineering from the same university. From 1968 to 1971, he was involved in research in molecular beam physics in Munich and in Peymenade, France.

In 1971, he joined Siemens AG in Munich and became involved in the development of telecommunications cable and related hardware. Since 1973, he has been working exclusively in optical fiber technology. In 1978, he joined Siecor Optical Cables, Inc. in the United States as VP of Engineering. In 1980, he became VP and General Manager for Optical Cable Manufacturing and Development. His key task was to build a new factory for fiber optic cables in Hickory, NC, and transfer technology from Siemens in Germany. In 1985, he became VP and Director of Research, Development & Engineering at Siecor Corporation. Dr. Bark is currently the Senior Vice President and Director of Research, Development & Engineering at Siecor Corporation. He has authored and coauthored numerous papers and made a number of key contributions in optical communications.



Mary A. Clarke received her B.S. degree in Materials Engineering from the Virginia Polytechnic Institute and State University in 1991. She worked as a Materials Engineer and then Process Development Engineer in the Research, Development & Engineering Dept. of Siecor Corporation from 1991-1996. Her primary duties included development of slotted rod for high fiber count cables. Currently, she is working towards her doctorate at VPI&SU.



Harriet G. Cooke was born in Carmel, CA in 1966. She received her B.M.E. from Georgia Institute of Technology and her EIT Certificate in 1991. At Georgia Tech, she was involved in NASA sponsored research and design of mechanical arms for lunar applications. From 1991-1996, she worked as a Process Development Engineer in the Research, Development, and Engineering Department at Siecor Corporation, where she worked with profile extrusion and stranding development of Ultra-High Fiber Count cables. She is currently a High Fiber Count Cable Process Engineer at Siecor's Telecommunications Cable Plant. She has been awarded two patents.



Christopher K. Eoll was born in Thunder Bay, Ont., Canada in 1940. He received a B.Sc. in physics and an M.Sc. in theoretical physics from Queen's University in Kingston, Ont., Canada in 1962 and 1964, respectively. In 1967, he was granted a Ph.D. in mathematical physics by the University of Toronto in Toronto, Ont., Canada. Subsequently, he spent two years as a Postdoctoral Fellow at the University of Sussex in Brighton, England and the International Centre for Theoretical Physics in Trieste, Italy.

From 1969 to 1977, he was employed by Canada Wire & Cable Ltd., where his final position was Product Development Manager for the Communication Products Div. He joined Superior Cable Corp. in 1977 as Technical Director. At present, he holds the position of Scientist in the Research, Development & Engineering Dept. of Siecor Corp. He has recently been focusing on various matters relating to optical cables, including aspects of design, materials, processing and light transmission.



Lawrence E. Herman was born in Greensboro N.C. in 1956. He received his B.S. degree in Physics from Lenoir-Rhyne College in 1981. Since 1990 he has been employed at Siecor Corporation where he has worked on

development of ultra-high fiber count cables for the Japanese market. He is currently employed as a Product Development Specialist in the Research, Development and Engineering Department.



William S. Jackman received a Bachelor of Science degree in Engineering Science from Montana State University in 1972. He joined Siecor in 1981 where he has focused on optical measurements and performance modeling. Since 1992 he has been a Senior Product Evaluation Engineer in the Research, Development & Engineering Dept. at Siecor.



Ronnie O. Livingston was born in Loris, South Carolina in 1968. He received his Bachelor of Science Degree in Physics and Applied Mathematics from Presbyterian College in 1990. He has been employed at Siecor since 1992. At Siecor, he has worked with statistical analysis of high fiber count cables, database management and network design. He is currently employed as an Analytical and Systems Engineer in the Research, Development and Engineering Department.



Shami S. Sodhi was born in Amritsar, India in 1964. He received his M.S. in Electrical Engineering from Virginia Polytechnic Institute and State University in 1989. Since 1989 he has been with Siecor Corporation in Hickory, N.C. and is presently Manager of Measurements Systems in the Research, Development and Engineering Department. He has authored and coauthored several papers and is a member of the IEEE.



Richard S. Wagman was born in Dallastown, PA in 1956. He received his B.S. degree in the Engineering Science honors program at Pennsylvania State University in 1978 and his B.S. in Electrical Engineering from Johns Hopkins University in 1984. He joined Siecor in 1985. At Siecor he has worked with cable, materials and test design. He is currently employed in the Research, Development and Engineering Department as a Subject Matter Expert in Cable Design.

All authors can be reached at the following address:

Siecor Corporation - RD
P. O. Box 489
Hickory, NC 28603-0489

Development of 3000-fiber cables with 8- and 16-fiber ribbons

**Naoki Okada, Tatsuya Omori, Kohichiro Watanabe,
Kazunaga Kobayashi, Matsuhiko Miyamoto**

**Fujikura.Ltd., Telecommunication cable section, Opt-electronics laboratory
1440, Mutsuzaki, Sakura-shi, Chiba, Japan**

Abstract

In this paper, the newly designed 3000-fiber cable with ordinary 250 micron fibers are reported. The two types of 3000-fiber cables are proposed. One is the multi slotted-rods type cable with 8-fiber ribbons, and the other is the specially designed H-groove type cable with 16-fiber ribbons. These multi-fiber ribbons are compatible with conventional 4- and 8-fiber ribbons. The 16-fiber ribbon can be divided into two 8-fiber ribbons or into four 4-fiber ribbons as well as the 8-fiber ribbon is divisible into two 4-fiber ribbons. These two types of 3000-fiber cables were designed and manufactured in trials. Their cable characteristics were investigated. As results, it is confirmed that both 3000-fiber cables have good transmission characteristics and mechanical properties.

Introduction

The replacement of metallic cables by optical fiber cables in subscriber loop is promoted as an infrastructure of high speed digital transmission networks. In urban area, the telecommunication cables are installed into underground ducts in Japan. The construction of new ducts are costly. The application of high density, high fiber count cables into available, existed duct is essential for economical construction of new optical networks. Then, ultra high count, high density optical fiber cable is needed. We have attempted to design the new cable which can be accommodated up to

3000-fiber in small cable diameter.

Cable design

In order to achieve the above criteria, following items are considered to design the cable structures.

Firstly, the cable can be accommodate up to 3000-fiber. In Japan, the 3600-pair copper cables are used for the subscriber loops, therefore at least 3000-fiber cable will be needed to replace the copper cables by the optical fiber cables.

Secondly, the cable can be installed into the existed duct whose inside diameter is 75mm. The cable should be designed in small diameter to get easy installation.

Thirdly, the fiber ribbon structure is compatible with conventional 4- and 8-fiber ribbons. Therefore, the 250 micron UV resin coated fibers are used, and the ribbon can be spliced to ordinary 4- and 8-fiber ribbons.

Ribbon structure

The thin coated 8-fiber ribbons have been already developed and used in the actual field.¹ This 8-fiber ribbons are divisible into two 4-fiber ribbons. Moreover, the 16-fiber ribbons with conventional 250 micron coated fibers are investigated to design the high fiber density cable. Considering compatibility with ordinary 4-fiber and 8-fiber ribbon, the 16-fiber ribbons should be divisible into

two 4-fiber ribbons or 8-fiber ribbons. This newly designed 16-fiber ribbon is consisted of four 4-fiber ribbons to get the divisible performance into not only two 8-fiber ribbons but also four 4-fiber ribbons.

The cross sectional view of newly developed 8-fiber ribbon and 16-fiber ribbon are shown in Fig.1. These ribbons have dual coated and encapsulated structures. Therefore, maintaining good transmission characteristics after cabling and good divisibility into 4- or 8-fiber ribbons are achieved.

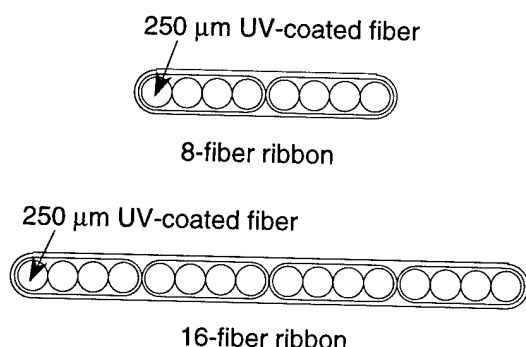


Fig.1 The structures of 8- and 16-fiber ribbon

Cable structure

We have successfully developed the new 1000-fiber cable in small diameter.² This new cable was consisted of the single slotted-rod with the thin coated 8-fiber ribbons, instead of multi slotted-rods structure, as shown in Fig.2.

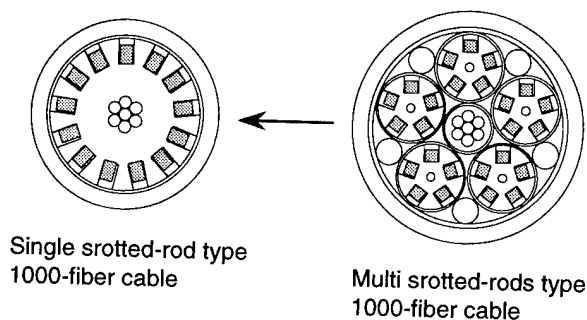


Fig.2 1000-fiber cable structure

In the case of designing 3000-fiber cable, several cable structures may be considered from the view point of the high density fiber packing in a cable.³ In this paper, following three types of cable structures are designed. (1) multi slotted-rods structure with 8-fiber ribbons, (2) multi slotted-rods structure with 16-fiber ribbons, (3) H-groove stranded structure with 16-fiber ribbons are investigated. These structures are shown in Fig.3, and the comparison of the cable diameter and the fiber packing density are listed in Table 1. As results, in the case of multi slotted-rods structure, the cable diameter with 8-fiber ribbons is smaller than that with 16-fiber ribbons. The H-groove stranded structure is smaller than the multi slotted-rods structure. The 16-fiber ribbon structure seems to have too many fibers for the multi slotted-rods structure of the 3000-fiber cable. For using 16-fiber ribbons, the double layer unit-structure based on smaller fiber count in a unit, for example H-groove unit, is applicable.

In order to investigate the optimum 3000-fiber cable structure, theoretical and practical approach were tried.

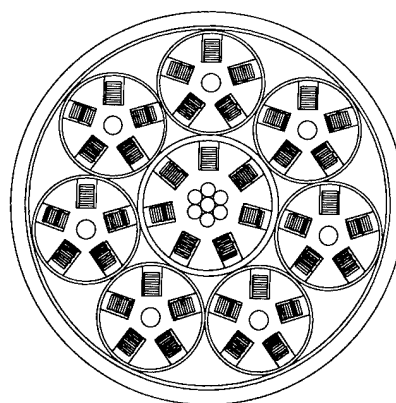


Fig.3 (1) 3360-fiber cable designed by slotted rod units structure with 8-fiber ribbons

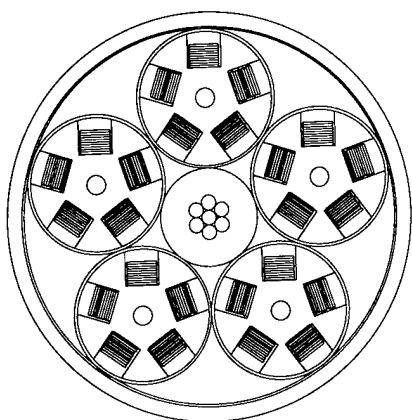


Fig.3 (2) 4000-fiber cable designed by slotted rod units structure with 16-fiber ribbons

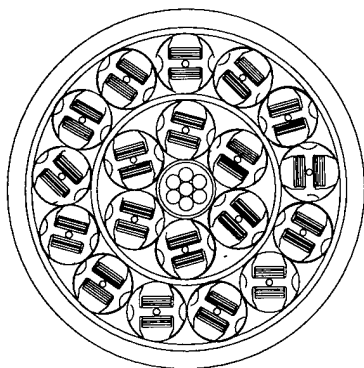


Fig.3 (3) 3040-fiber cable designed by H-groove units structure with 16-fiber ribbons

Table 1 Cable diameter and packing density

Cable structure	Ribbon structure	Cable diameter	Packing density
Multi slotted-rods	8-fiber ribbon	54 mm	1.47 fiber/mm ²
Multi slotted-rods	16-fiber ribbon	55 mm	1.68 fiber/mm ²
H-groove	16-fiber ribbon	49 mm	1.61 fiber/mm ²

Theoretical approach

We reported that the characteristics of the ribbon stranded cables are influenced by the width of the

ribbon and the diameter of the winding drum.⁴ In that paper, the estimated fiber strains which are calculated from the difference between the locus length of the edge fiber and that of the central fiber in the ribbon were proposed to predict the cable performance. As a result, the wide ribbon width may be one of the causes of the cable performance degradation. The slotted-rod with 8-fiber ribbons had been already developed and used in the actual field. Therefore, the multi slotted-rods type 3000-fiber cable with 8-fiber ribbons will be able to be manufactured. However, to manufacture the 3000-fiber cable used the 16-fiber ribbons with the good cable characteristics may be difficult. At first, from the view point of the fiber strain, the details of the cable structure are designed theoretically.

Procedure to calculate the fiber strain

The theoretically estimated fiber strain are calculated by the following procedure. Here, the double helical structures as shown in Fig.4 are investigated. The fiber strain will be most critical at the both edges of the ribbons in the bent cable. Here, these calculation models assume that the ribbons are stranded tightly into the slots.

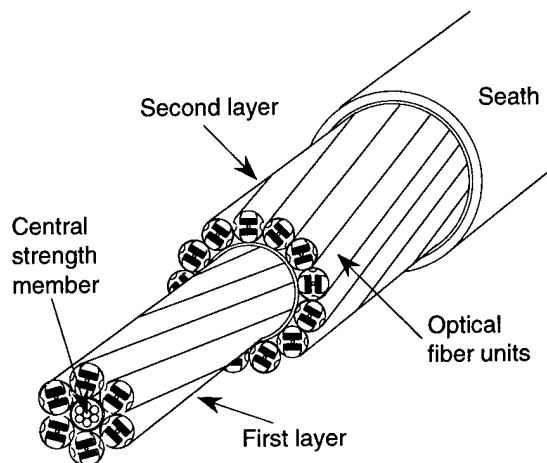


Fig.4 Double helical structure

The parameters to determine the cable structure are shown in Fig.5. And the locus equations of

the edge fiber in the bent cables can be expressed by Eq.1, Eq.2. The estimated fiber strain is defined by Eq.3.

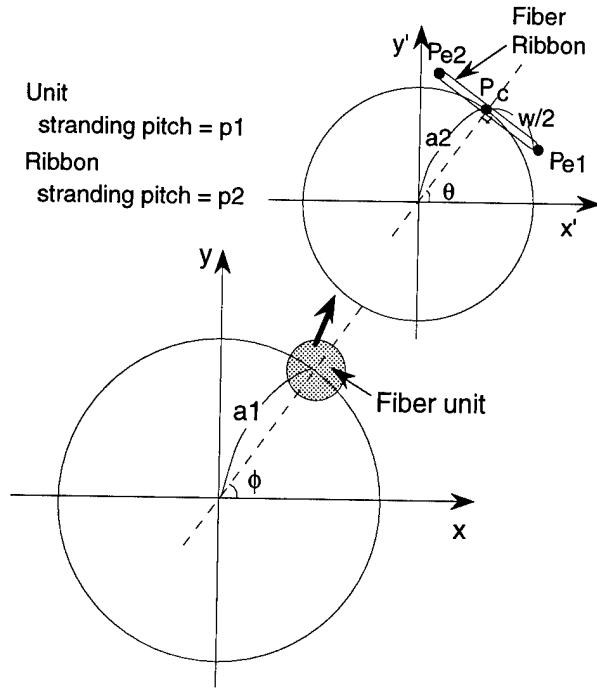


Fig.5 Parameters of double helical stranding

$$\begin{cases} x = a_1 \cos \varphi + \sqrt{a_1^2 + \left(\frac{w}{2}\right)^2} \cos \gamma + s \cos \alpha \\ y = a_1 \sin \varphi + \sqrt{a_1^2 + \left(\frac{w}{2}\right)^2} \sin \gamma + s \sin \alpha \\ z = \left\{ r - a_1 \cos(\alpha - \varphi) - \sqrt{a_1^2 + \left(\frac{w}{2}\right)^2} \cos(\alpha - \varphi) \right\} \sin \xi \end{cases} \quad \text{--- Eq.1}$$

$$\begin{cases} \xi = \frac{\varphi p_1}{2 \pi r} \\ k = \sqrt{a_1^2 + \left(\frac{p_1}{2 \pi}\right)^2} \\ \gamma = \theta \pm \arctan\left(\frac{w}{2 a_2}\right) \\ \varphi = \frac{p_2 \theta}{2 \pi k} \\ s = r - \left\{ r - a_1 \cos(\alpha - \varphi) - \sqrt{a_1^2 + \left(\frac{w}{2}\right)^2} \cos(\alpha - \varphi) \right\} \cos \xi \\ \quad - a_1 \cos(\alpha - \varphi) - \sqrt{a_1^2 + \left(\frac{w}{2}\right)^2} \cos(\alpha - \varphi) \end{cases}$$

$$l = \int_{\frac{2 \pi k \alpha}{p_2}}^{\frac{2 \pi k (\alpha + \eta)}{p_2}} \sqrt{\left(\frac{dx}{d\theta}\right)^2 + \left(\frac{dy}{d\theta}\right)^2 + \left(\frac{dz}{d\theta}\right)^2} d\theta \quad \text{--- Eq.2}$$

$$\varepsilon = \frac{l_{\text{center}} - l_{\text{edge}}}{l_{\text{center}}} \quad \text{--- Eq.3}$$

- w : ribbon width
- a_1 : unit stranding pitch radius
- a_2 : ribbon stranding pitch radius
- p_1 : unit stranding pitch
- p_2 : ribbon stranding pitch
- r : cable bent radius
- φ : unit stranding angle
- θ : ribbon stranding angle
- α : cable bent direction

Especially, in the case of the double helical type, the fiber strain may be determined by the cable bent direction and the stranding position of the fiber and the slotted-rod unit. Therefore, the fiber strain is calculated at the several patterns changing cable bent direction and fiber stranding position.

Results of the calculated fiber strain

The fiber strains are investigated from the view point of the ribbon width, the pitch radius, and the stranding pitch. The results are follows.

Ribbon width. The calculated results are shown in Fig.6. As the ribbon width is wider, the maximum fiber strain becomes larger. The ribbon width dependence is observed obviously.

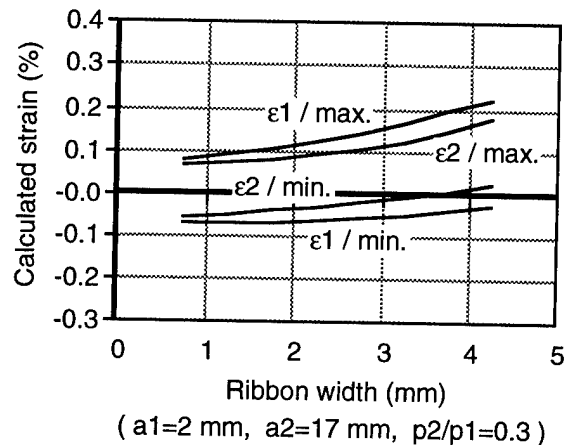


Fig.6 Ribbon width dependence of estimated fiber strain

Ribbon stranding pitch radius. The results are shown in Fig.7. The estimated fiber strain is strongly depended on the ribbon stranding pitch radius. As the ribbon stranding pitch radius is larger, the fiber strain becomes larger. It seems that the ribbon stranding pitch radius is one of the most important parameters to obtain the good cable characteristics.

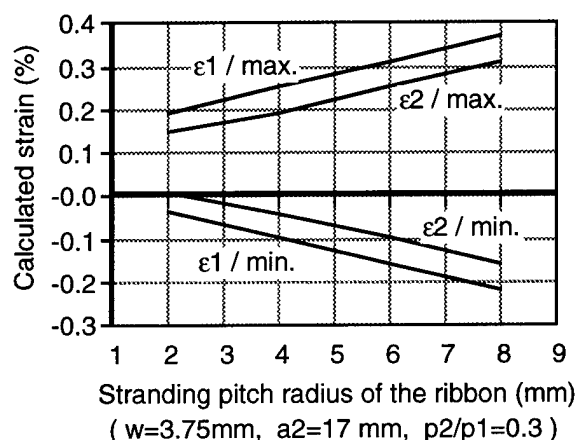


Fig.7 Ribbon stranding pitch radius dependence of estimated fiber strain

Unit stranding pitch radius. The results are shown in Fig.8. The unit stranding pitch radius dependence of the estimated fiber strain seems small.

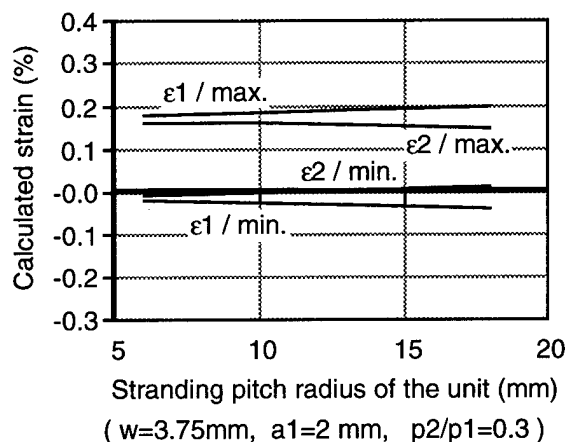


Fig.8 Unit stranding pitch radius dependence of estimated fiber strain

Stranding pitch of the ribbon and the unit.

In order to reduce the fiber strain in the bent cable, the relationship between the stranding pitch of the ribbon and that of the unit are important. The fiber strains are calculated in several stranding pitch of the ribbons and the units, and these results are plotted against the ratio of the stranding pitch of the ribbon and the unit. The results are shown in Fig.8. As a result, the ratio should be designed small at least under 0.5. It means that the unit stranding pitch should be selected over twice of the ribbon stranding pitch. As results of the theoretical approaches, the pitch radius of the ribbon should be designed as small as possible. And the unit stranding pitch should be selected over twice of the ribbon stranding pitch. Moreover, if possible, the narrow ribbon width is better, but the cable diameter may become larger.

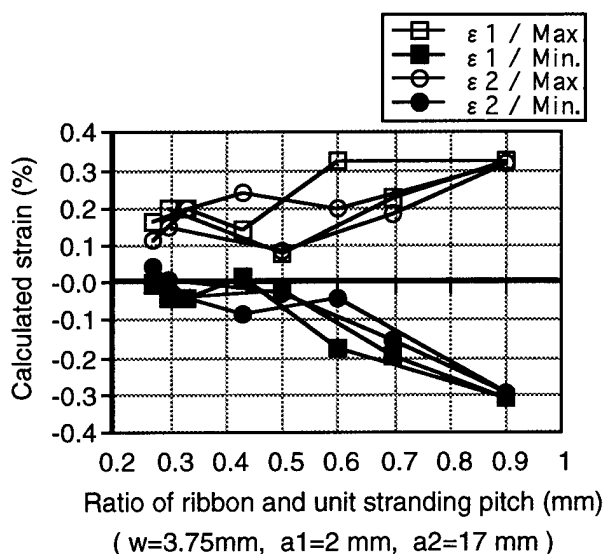


Fig.9 Stranding pitch of ribbon and unit dependence of estimated fiber strain

Cable performance

The two types of the trial 3000-fiber cables were manufactured in laboratory and evaluated the cable characteristics.

One is the multi slotted-rods structure with 8-fiber ribbons. In order to design the cable structure with small diameter, the slotted rod units are stranded around a central slotted rod. The 8-fiber ribbons used in this prototype cable are ordinary structure for the single slotted-rod 1000-fiber cables.

Another is the H-groove units stranded structure with 16-fiber ribbons. This H-groove structure is suitable to design the ribbon stranding pitch radius small. Therefore, as results of theoretical approach, this structure is better than the multi-slotted rods structure.

Cable characteristics

The transmission characteristics, the temperature characteristics, and the mechanical strength were evaluated.

Transmission characteristics. The histogram of the prototype cables wound on the drum are shown in Fig.10. Both the multi slotted-rods cable with 8-fiber ribbons and the H-groove cable with 16-fiber ribbons shows good transmission characteristics.

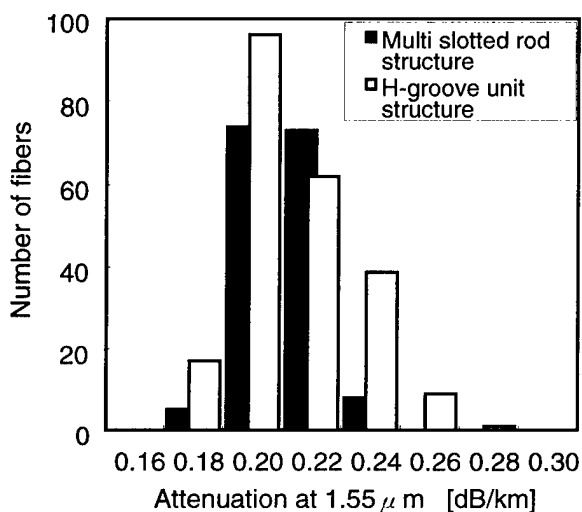


Fig.10 Transmission characteristics of prototype cables

Temperature characteristics. The attenuation of the prototype cables wound on the drum were measured at 1.55 micron. The temperature range is from -30 ~ 70 degree Centigrade. Fig.11 shows the results of the temperature test. The attenuation changes are less than 0.1 dB/km at 1.55 micron on the both cable structures.

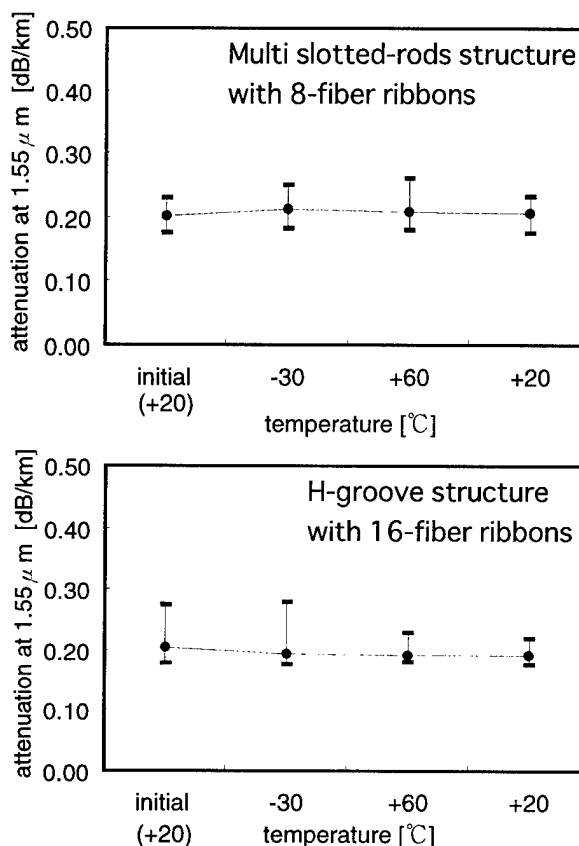


Fig.11 Temperature characteristics of prototype cables

Mechanical strength. The lateral pressure test and high tension pulling test were performed. Especially, in order to install the thick and heavy 3000-fiber cable, the high tension may be demanded. The test conditions and results of the mechanical strength tests are shown in Table 2.

As results of evaluating the basic cable characteristics, both cable structures shows good performance.

Table 2 Mechanical test results

	Test conditions	Cable type	Results
Tensile	9800 N	Multi slotted-rods	Less than 0.02 dB/100m
		H-grooves	Less than 0.02 dB/100m
Lateral pressure	2000 N/100 mm	Multi slotted-rods	No change in loss
		H-grooves	No change in loss

Conclusion

The two types of 3000-fiber cables have designed and manufactured in trial. One is the multi slotted-rods structure with 8-fiber ribbons, the other is the H-groove structure with 16-fiber ribbons. The diameter of these cables are 54mm and 49mm, the H-groove structure with 16-fiber ribbons is smaller than the multi slotted-rods structure with 8-fiber ribbons. Both cables are enough smaller than 75mm which is ordinary under ground ducts in Japan and shows good cable performance. As a results, the technical prospects for the realization of the 3000-fiber cable for the future FTTH networks are obtained.

References

1. H. Iwata, M. Tsutsumi, E. Nakamura, N. Matsumoto, M. Nozawa, S. Hayami, S. Nagasawa, T. Tanifuji, "Pre-connectorized 1000-fiber Single Slotted Core Cable", 44th IWCS, 1995
2. N. Okada, K. Watanabe, K. Kobayashi, A. Sano, M. Miyamoto, "Development of single slotted-rod type 1000-fiber optical fiber cable for subscriber loop", 44th IWCS, 1995
3. H. Iwata, M. Matsumoto, Y. Ishino, S. Tomita, S. Nagasawa, T. Tanifuji, "Field Test Results for

Pre-connectorized Cable with 16-fiber Ribbons", 43th IWCS, 1994

4. N. Okada, K. Watanabe, M. Miyamoto, "Strain Analysis of U-groove Type Cable with Multi Fiber Ribbons", 43th IWCS, 1994

Authors

Naoki Okada

Opto-Electronics
Laboratory
Fujikura Ltd.

1440, Mutsuzaki,
Sakura-shi, Chiba,
285, Japan



Naoki Okada was born in 1964. He joined Fujikura Ltd. after his graduation from Chiba University with a B.E. degree in 1986 and has been engaged in research and development of optical fiber cables. He is now an engineer in the Telecommunication Cable Section and a member of the IEICE of Japan.

Tatsuya Omori

Opto-Electronics
Laboratory
Fujikura Ltd.

1440, Mutsuzaki,
Sakura-shi, Chiba,
285, Japan

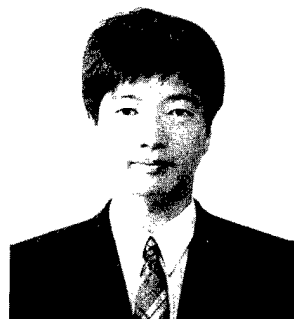


Tatsuya Omori was born in 1967. He received the B.E. degree in electronic engineering from Kogakuin University, Tokyo, Japan, in 1989, and the ME degree in electronic engineering from Chiba University, Chiba Japan, in 1991. He joined Fujikura Ltd. after his graduation from Chiba University with Ph.D. degree in 1994 and has been engaged in research and development of optical fiber cables. Dr. Omori is a member of IEICE of Japan.

Kazunaga Kobayashi

Opto-Electronics
Laboratory
Fujikura Ltd.

1440, Mutsuzaki,
Sakura-shi, Chiba,
285, Japan

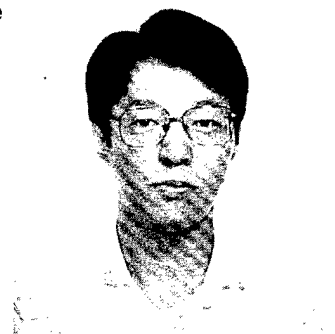


Kazunaga Kobayashi was born in 1961. He joined Fujikura Ltd. after his graduation from Gunma University with a M.E. degree in 1985 and has been engaged in research and development of optical fibers. He is now an engineer in the Telecommunication Cable Material Section and a member of the IEICE of Japan.

Kohichiro Watanabe

Opto-Electronics
Laboratory
Fujikura Ltd.

1440, Mutsuzaki,
Sakura-shi, Chiba,
285, Japan



Kohichiro Watanabe was born in 1959. He received a B.E. degree in electrical engineering from Tohoku University in 1982. Since joining Fujikura, Ltd. in 1988, he has worked on the development of optical fiber cables. He is currently employed in the Telecommunications Cable Section of the Opto-electronics laboratory.

Matsuhiro Miyamoto

Opto-Electronics
Laboratory
Fujikura Ltd.

1440, Mutsuzaki,
Sakura-shi, Chiba,
285, Japan



Matsuhiro Miyamoto was born in 1953. He graduated from Nagoya Institute of Technology with a B.E. degree of electrical engineering. He joined Fujikura Ltd. after his graduation from Tokyo Institute of Technology with a M.S. degree in 1978 and has been engaged in research and development of optical fiber and optical fiber cables. He is now a manager of the optical fiber cable section.

DEVELOPMENT OF 3000-FIBER MULTI SLOTTED CORE CABLE

Masami Hara, Minoru Saito, Eiji Konda, Kiyotoshi Nagai and Masato Oku

The Furukawa Electric Co., Ltd.

Ichihara, Chiba, Japan

ABSTRACT

3000-fiber multi slotted core cable using 8-fiber ribbons composed of 0.25 mm fiber was developed. The cable was designed for a small diameter of 54.5 mm through an optimized number of slotted rods and reduced slotted rod diameter. It was found from a study of the stranding pitch and curvature of slotted rods that a stranding pitch of 1500 mm would produce approximately the same curvature as conventional cable. On the basis of this finding, the cable was fabricated and found satisfactory in both transmission and mechanical characteristics.

INTRODUCTION

For construction of optical fiber networks of future subscriber systems, studies have been carried out to achieve higher density and higher count in optical fiber cables^[1].

The conventional cable having the largest number of fibers is 1000-fiber cable consisting of stacked ten 8-fiber ribbons of 0.3 mm thickness in each slot. An anticipated increase in demand for fiber optics in future would likely create a need for an optical fiber cable having more than 1000 fibers.

A 3000-fiber cable was therefore studied for cable characteristics and the possibility of diameter reduction. The study assumed that the new cable would use 8-fiber ribbons having 0.25 mm fibers as those of conventional cables and would have a slotted rod structure to ensure compatibility with conventional cables. The study is summarized below.

FIBER RIBBONS

One convenient way of increasing both number of fibers and fiber density would be to increase the number of fibers in a ribbon. However, considering the splice with conventional optical fiber cables, it would be better to use the same ribbons as those of conventional cables. Therefore, we studied using the same 8-fiber ribbon as conventional. Figure 1 shows the 8-fiber ribbon. Eight coated optical fibers, 0.25 mm in diameter, were arranged and thickness of ribbon was 0.3 mm.

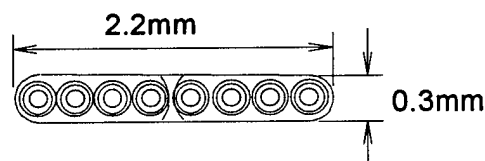


Fig.1 Structure of 8-fiber ribbon

CABLE STRUCTURE

Number of Slotted Rods

For structural compatibility with conventional cables, the structure studied was based on a slotted rod structure consisting of ten ribbons stacked in each slot. The problem in using this slotted rod structure would be to determine the number of slotted rods that would permit the reduction of cable diameter.

Different numbers of slotted rods versus cable diameter were calculated. Figure 2 shows the

results. The calculation assumed that ten 8-fiber ribbons would be stacked in each slot. The calculation results demonstrated that a structure consisting of five slotted rods each having eight slots would minimize the cable diameter.

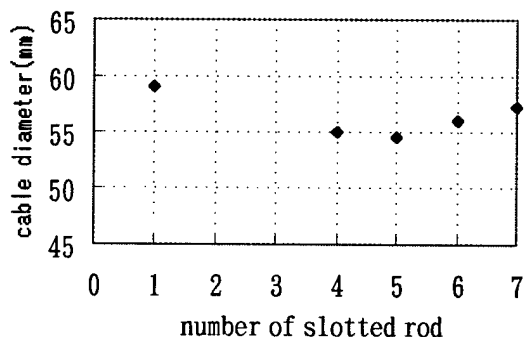


Fig. 2 Relation between number of slotted rods and cable diameter

CROSS SECTION

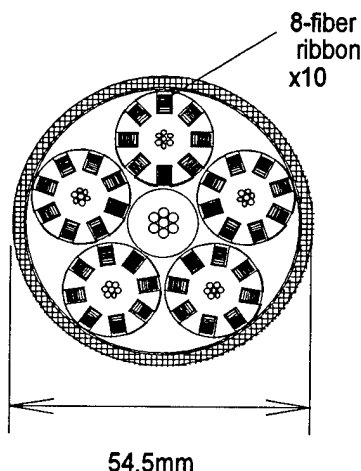


Fig.3 Structure of 3000-fiber cable

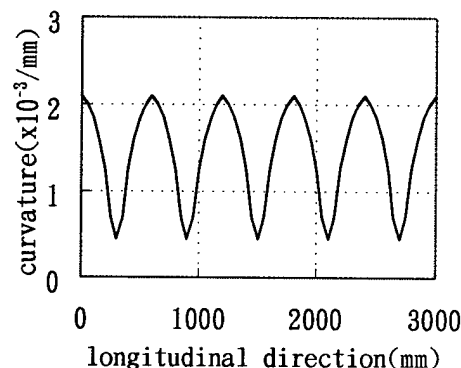
Figure 3 shows the structure of the 3000-fiber cable that will have the smallest diameter. It has a multi slotted core structure with a maximum of 3200 fibers. Each slotted rod consists of eight slots with ten 8-fiber ribbons stacked therein (640 fibers). Five sets of such slotted rods are stranded around the strength member in the center.

The slot dimensions and slotted rod materials were optimized to make the cable diameter of this structure as small as possible. As a result,

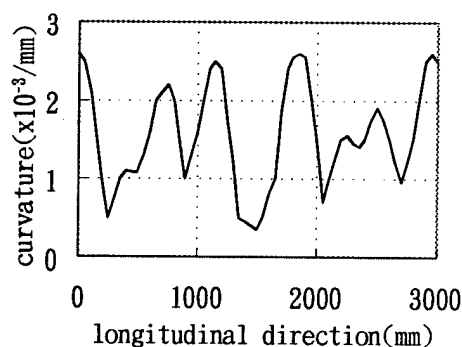
the diameter of the stranded slotted rods, including the wrapping material, was reduced from the conventional diameter of 20 mm to 17.5 mm, and the cable was finished to a diameter of 54.4 mm.

STRAND PITCH

The multi slotted core structure presents the problem of the fiber strain caused by stranding the slotted rods around the strength member in the center. Thus, the fiber curvature radii were calculated for stranding pitches of the slotted rods from 1000 mm to 1500 mm. Figure 4 shows a calculation example of the curvature of the fiber before and after stranding the rods at a 1000 mm pitch, when cables were bent at 800 mm radius. This figure shows the curvature of fiber in the longitudinal direction. It shows that stranding the slotted rod increases the maximum curvature of the fiber.



(a) before stranding



(b) after stranding

Fig. 4 Calculated curvature of the fiber

The maximum curvature after stranding at different stranding pitches were calculated as

shown in figure 5. As the calculation results show, the curvature decreases as stranding pitch increase, and a pitch of 1500 mm produces a curvature approximately equivalent to that of conventional cables.

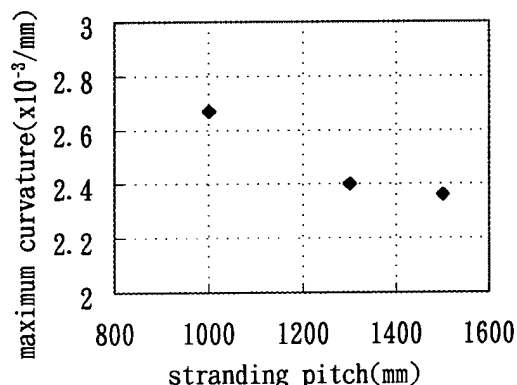


Fig. 5 Relation between stranding pitch and maximum curvature

CABLE CHARACTERISTICS

On the basis of the above findings, a cable was fabricated with the 3000-fiber structure shown in figure 3, and its characteristics were evaluated.

TRANSMISSION CHARACTERISTICS

Figure 6 shows the change in transmission loss in the cabling process. No increase of transmission loss was observed in any of the process. Table 1 shows the transmission loss (1.55 μm) after sheathing. Little increase was observed in the transmission loss of the four-corner fibers. The results were satisfactory.

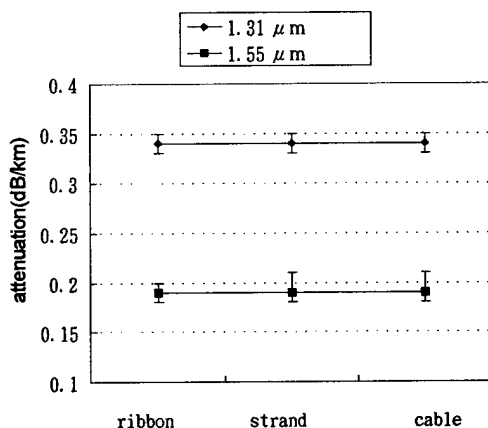


Fig. 6 Change in transmission loss

MECHANICAL CHARACTERISTICS

Table 2 shows the results of various mechanical test. The tensile, bending, lateral pressure, and temperature characteristics were satisfactory without problem.

Table.1 Transmission loss of 3000-fiber cable

	Transmission loss (at 1.55 μm)
Average of edge fibers of bottom and top ribbons	0.20 dB/km
Average of fibers except for above mentioned	0.19 dB/km
Average of all fibers	0.19 dB/km

Table.2 Mechanical characteristic of 3000-fiber cable

Item	Results (at 1.55 μm)
Tensile(1000N)	No loss increase
Bend(R=200mm)	No loss increase
Lateral pressure (3000N/100mm)	No loss increase
Temperature cycling(-30~60°C)	< 0.02dB/km

CONCLUSION

A 3000-fiber cable of multi slotted structure using 8-fiber ribbons, with fiber diameter of 0.25 mm, was fabricated and evaluated. With a diameter of 54.5 mm, the cable demonstrated satisfactory transmission and mechanical characteristics, and it revealed no problems. The study will be continued toward further reduction of slotted rod diameter and, thus, cable diameter.

REFERENCE

- 1) H. Iwata et al., "Field Test Results for Pre-connectorized Cable with 16-fiber Ribbons," 43rd IWCS, 1994



Masami HARA

The Furukawa
Electric Co., Ltd.

6, Yawata Kaigandori,
Ichihara, Chiba,
290, Japan

Mr. Hara received his M.E. degree in Physics from Osaka University in 1987. He joined The Furukawa Electric Co., Ltd. and has been engaged in research and development of optical fiber cable. He is now a research engineer of optical fiber transmission research department, opto-technology laboratory.

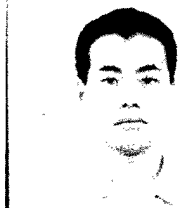


Kiyotoshi NAGAI

The Furukawa
Electric Co., Ltd

2-6-1, Marunouchi,
Chiyoda, Tokyo,
100, Japan

Mr. Nagai received his B.E. degree in electrical engineering from Kyoto University in 1987. He joined The Furukawa Electric Co., Ltd. and has been engaged in production engineering fiber optics & telecommunication division. He is now engaged in design of optical fiber cable at engineering department.



Minoru SAITO

The Furukawa
Electric Co., Ltd.

6, Yawata Kaigandori,
Ichihara, Chiba,
290, Japan

Mr. Saito received his M.E. degree in chemistry from Kyushu University in 1992. He joined The Furukawa Electric Co., Ltd. and has been engaged in research and development of optical fiber cable. He is now a research engineer of optical fiber transmission research department, opto-technology laboratory.



Masato OKU

The Furukawa
Electric Co., Ltd.

20-16, Nobono,
Kameyama, Mie,
519-02, Japan

Mr. Oku received his M.S. degree in Chemistry from Nagoya University in 1991. He joined The Furukawa Electric Co., Ltd. and has been engaged in research and development of optical fiber. He is now a production engineer of optical fiber cable.



Eiji KONDA

The Furukawa
Electric Co., Ltd.

6, Yawata Kaigandori,
Ichihara, Chiba,
290, Japan

Mr. KONDA joined The Furukawa Electric Co., Ltd. in 1977 and has been engaged in research and development of optical fiber cable. He is now a research engineer of material development and engineering section, research department, opto-technology laboratory.

DESIGN OF THE NOVEL SUPERVISING NETWORK USING THE INFORMATION FREE ACCESS SYSTEM

Hideyuki NASU, Haruo NAKAYAMA, Hideyuki OMURA
THE FURUKAWA ELECTRIC Co.,LTD.
Hiratsuka, Kanagawa, JAPAN

Kenichi TEZUKA
TOKYO ELECTRIC POWER COMPANY
Yokohama, Kanagawa, JAPAN

Abstract

Recently, there has been a growing demand for the novel supervising networks in terms of watching road, railroad, bridge and so on, in order to enable operation at a certain point during a certain term. Therefore, we developed the supervising network based on the Information Free Access System which utilize advantages of multi-coupler bi-directional systems consisting of optical passive networks[1]. The novel network consist of two components, which are the Information Free Access System and two types of portable terminals. In this paper, we introduce and demonstrate the architecture and some applications utilizing the network. Furthermore, design of the typical example where the system is applied to traffic construction is also described.

1.Introduction

Observing the constructions and accidents are important to enhance safety, check the present situation under construction and so on. Especially, interactive television function is reasonable means of subjective monitoring on multiple points to support such demand.

In previous work, we had developed the supervising network in order to monitor multiple points simultaneously, by utilizing multi-coupler bi-directional system employing the FM-SCM transmission method. The multi-coupler system have

a great potential to realize highly reliability and cost effectiveness by being consisted of optical passive networks.

The network has been applied to a field of electric power transmission, such as monitoring a power cables, pylons, power stations, transformer substations and so on. In some practical applications, high performance in the field is confirmed.

There has been a growing demand for the novel supervising network whose function differs from that of conventional network in terms of enabling to operation a certain points during a certain term on demand. Monitoring the points of construction and accident of roads, railways and bridges would be possible applications.

In order to meet the needs, we have developed the network utilizing the advantageous features of our previous work. The network consists of the Information Free Access System and two types of potable terminals.

In this paper, we introduce and demonstrate architecture and applications of the network based on the system and the portable terminals. Comparison between the network and conventional ones are also discussed. Moreover, The function of two components equipped in the network are introduced. Design of the typical example for the application evolving to road construction is also described.

2.The conventional supervising network using multi-coupler bi-directional system employing the FM-SCM video transmission

2.1.The configuration of multi-coupler bi-directional system

The configuration of multi-coupler bi-directional system we had developed is shown in Fig.1. In this system, both of optical signal in up ward link and down ward link can be multiplexed and demultiplexed at optical couplers located along an optical link.

In an upward link, optical signals are modulated into sub-carrier having allocated modulation frequency for each terminal. Laser diodes are directly modulated and wavelength spacing to the next optical channels is equal. The optical signals are converted into electrical at a photo-diode in central station by the manner of optical direct detection. Composite electrical signals is separated into the individual signals.

In downward link, the optical signals are modulated into sub-carrier frequencies being allocated for each terminal. By using optical couplers, the optical signals are separated and transmitted to every terminal.

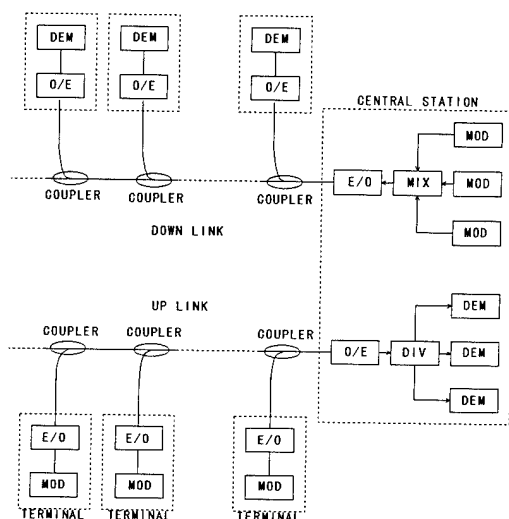


Fig.1 The configuration of multi-coupler bi-directional system.

The system has the following advantages:

(1)High reliability

Comparing with a conventional repeater system (E/O-O/E), number of troubles decreases, because the system is constructed all passive components.

It should be emphasized in this system that any failure of any terminals may not disturb operation of other channels.

(2)Design of system architecture

For all of components being constructed are passive, it is easy to design transmission system architecture. It is not necessary to consider the distortion due to active repeaters.

(3)Cost effectiveness

It has great advantages of cost effectiveness comparing with conventional point to point systems and repeater systems, because fewer components are used in the system.

2.2.The architecture of conventional supervising network

Fig.2 shows architecture of our previous supervising network utilizing multi-coupler bi-directional system employing the FM-SCM video transmission method.

In upward link, sub-carrier frequencies allocated for each terminal are modulated with FM modulator by the video signal from each monitoring camera. The optical signals from each terminal are transmitted to central monitoring equipment. By adjusted to sub-carrier frequency, the video signals can be demodulated by FM demodulator.

In downward link, in order to control zooming and focus of cameras, FM modulated camera control signals are transmitted from the central station to each terminal.

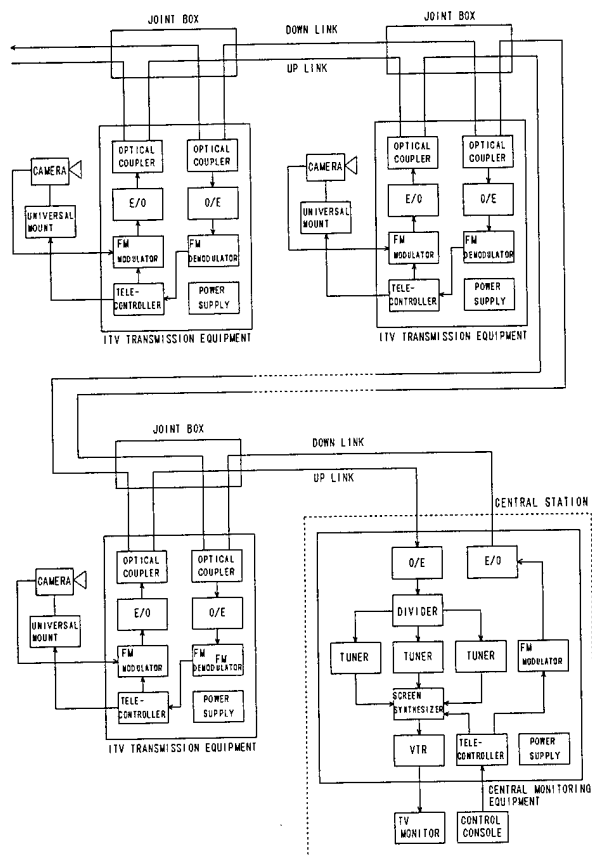


Fig.2 The architecture of the conventional supervising network.

2.3.Application

The conventional supervising networks are mainly applied to the electric power transmission, such as monitoring power cables, pylons, power stations, transformer substations and so on.

Fig.3 shows schematic view in a typical application evolving to observe and operate power cables and pylons in Japan. Camera, transmission equipment and joint box are located in each pylon. The optical signals from each terminal are multiplexed and lead into an optical ground wire (OPGW) by using optical couplers. At the end of a path, OPGW is connected to the equipment located in a transformer substation.

The supervising network have been utilized in the

area where operators cannot reach easily because of the bad weather. Such as heavily snow in winter.

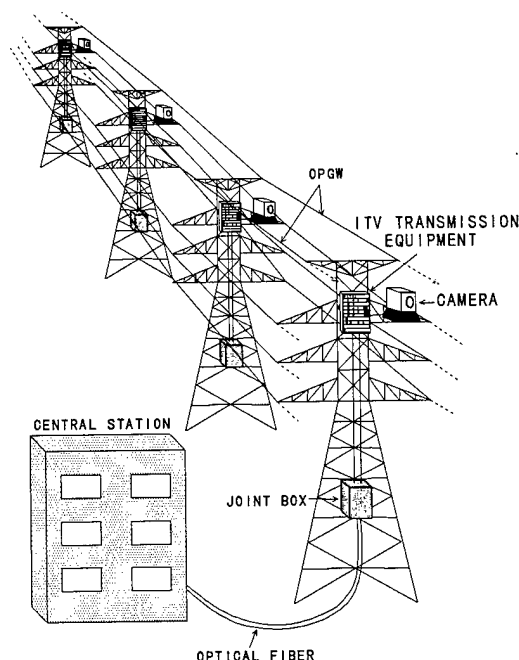


Fig.3 Schematic view of the application of Electric power transmission, as monitoring power cable and pylon.

3.The architecture of the novel supervising network using the Information Free Access System

We found it is difficult for the conventional network described in previous chapter to meet such demand.

Therefore, We developed the novel supervising network using Information Free Access System.

3.1.Information Free Access System

Fig.4 shows the configuration of the Information Free Access System, which is an important component of the network. In this system, series of optical taps are connected at observation points along both fibers.

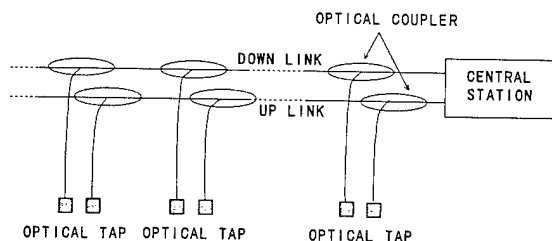


Fig.4 Configuration of Information Free Access System.

3.2. The architecture of the novel supervising network

The architecture of the novel supervising network is shown in Fig.5. The network consists of two components which are the Information Free Access System and the portable terminals. In actual supervising application, the portable terminals are brought to observation points, where optical taps are located, and connected to optical taps. There are two types of portable terminals. Type 1 transmits optical signals into optical tap directly. Type 2 is transmitting the optical signal to the portable converter, which is connected to optical taps, by means of atmospheric transmission method. It is confirmed experimentally that signals can be transmitted in atmosphere up to 100m.

The network provides the function of bi-directional communication. In upward link, video signals are transmitted to central station. On the other hand, in down ward link, signals for camera control are transmitted to each terminal. Bi-directional telecommunications function is also provided. It is convenient for operators at watching points to establish and control the equipment.

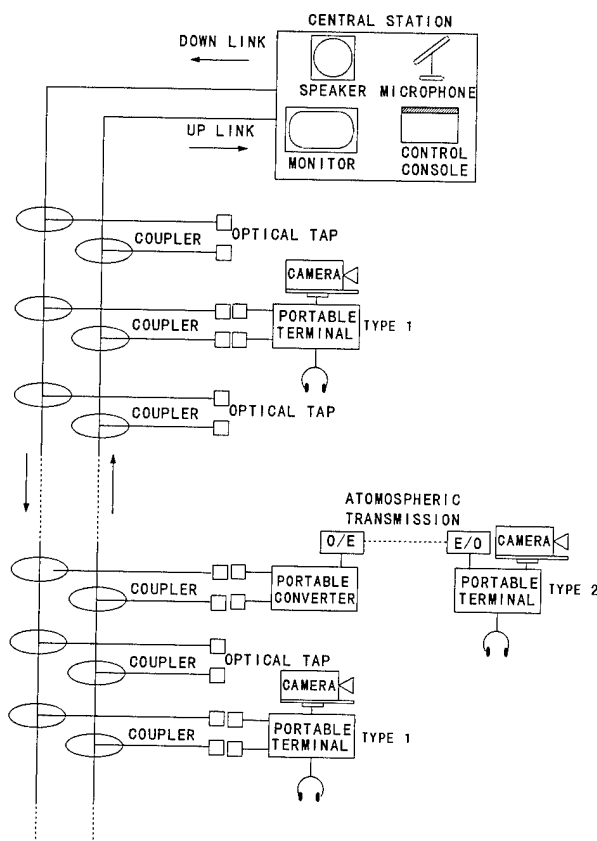


Fig.5 Schematic view of the architecture of the novel supervising network.

3.3. Portable terminals

Portable terminals are indispensable components in the network. We developed two type of portable terminals. The terminals are smaller and lighter for the purpose that only one operator can carry there and establish at watching points. One of portable terminals has atmospheric transmission function in order to achieve the communication where optical fiber can not haul.

3.3.1. Type 1

A photograph and a block diagram of the terminal type 1 are shown in Photo.1 and Fig.6, respectively. It is very easy to carry to other watching points, because it made small and light. The dimensions of the

terminal are 516,379 and 254 mm. The weight of 13.5 kg. Furthermore, camera and cables can be installed into a housing.

In upward links, the video signals from a camera on universal mount and audio signals are transmitted. In downward link, camera control signals. Signals for zooming and focus, and audio signal are received.

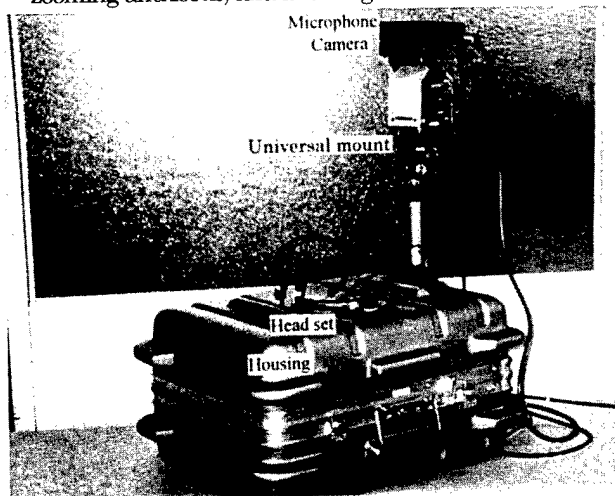


Photo.1 Photograph of portable terminal type 1.

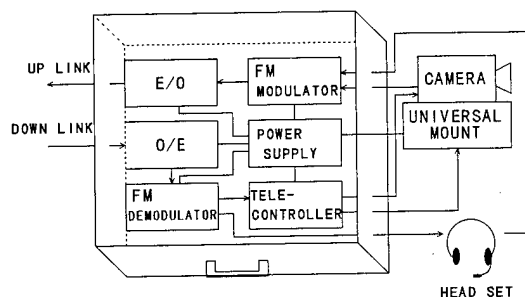


Fig.6 Block diagram of portable terminal type 1.

3.3.2 Type 2

There is the case that some structure or natural product, such as road or river, disturb to haul optical fibers between optical taps and portable terminals. The distance between two components must be separated accordingly. The portable terminal type 2 provides the function of atmospheric transmission in those cases. The weight and dimensions of both

portable terminal type 2 and portable converter are the same as those of type 1.

Photo.2 shows appearance of portable terminal type 2 where atmospheric optical unit is installed on housing.

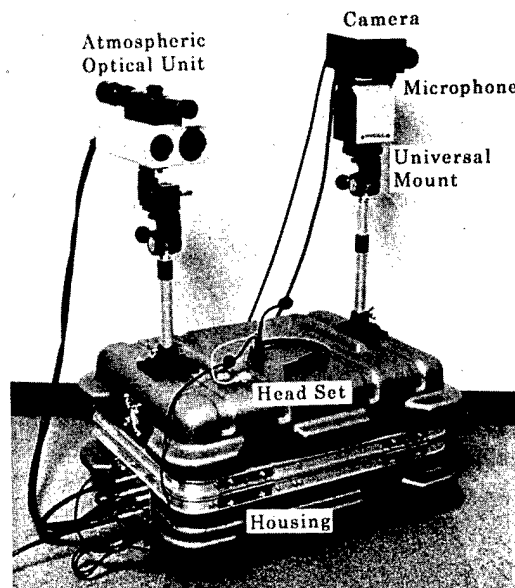


Photo.2 Photograph of portable terminal type 2.

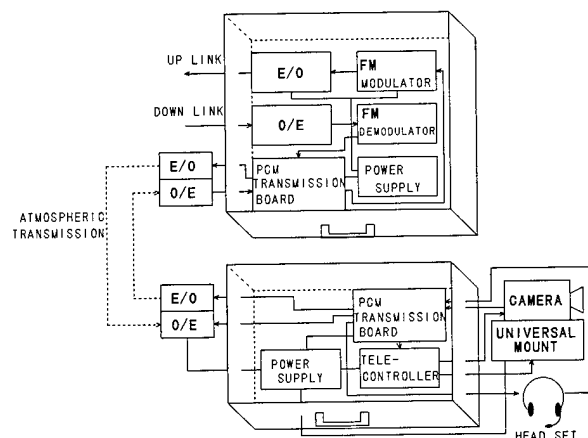


Fig.7 Block diagram of atmospheric transmission using portable terminal type 2 and portable converter.

A block diagram of atmospheric transmission equipment is shown in Fig.7. PCM modulated optical signals are transmitted from one atmospheric optical unit to another. It enables to transmit in atmosphere

as long as 100m so as to meet the specifications of transmission quality and standards of safety laser radiation. In the E/O of the atmospheric optical units, 1.48 μ m laser diode which is widely utilized to pump EDFA (Erbium Doped Fiber Amplifier) is installed. Output power is 50mW.

3.4.Applications

In this chapter, two typical example are described.

3.4.1. Application for traffic construction

In the case of mending a road, the construction points moves as time goes because the construction is conducted in a certain place during certain period. The network is suitable to supervise in such case. Fig.8 shows perspective of the application for mending a road.

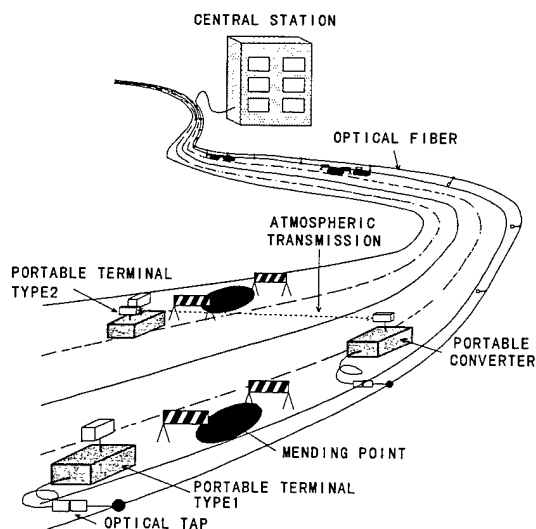


Fig.8 Perspective of the application for mending a road.

In this application, portable terminals are carried to the construction points and connected to the nearest optical taps beside the points. It is impossible in this case to haul optical fibers because traffic lanes and a median strip crossing. Atmospheric transmission can

solve this problem reasonably. It can be also applied to watch the points where traffic accidents has often happened, such as a sharp curve.

3.4.2.Application for railroad crossing

The accident at railroad crossing has been serious problem in Japan. Especially, the suspending crossing gates are often broken by the car passing through after gates are closed. There is a growing demand for watching the points where the accident has often happened. Therefore, the network is suitable for this case. Fig.9 shows perspective of the application on crossing. Optical taps are arranged beside each crossing. For the observation of accidents, portable terminals are established at the problematic crossing. This manner can also be effective for construction of railways.

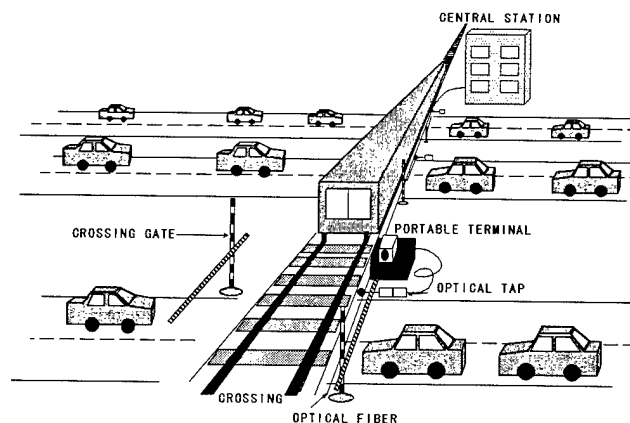


Fig.9 Perspective of the application on crossing of railway.

4.Design of the typical example which is applied to construction of road

In this chapter, the design of the typical example applied to traffic construction is described. Because it desires to reduce the blind points, that optical taps should be located as close as possible.

4.1 Specifications

Specifications for transmission system are shown in Table.1. Assuming as many as 15 portable terminals are in service along a 20km optical link simultaneously.

Table.1 Specifications for transmission system.

Items		Specification
Transmission system		FM-SCM PCM(Atmospheric transmission)
Number of terminals		15
Transmission signals	up link signal	Video(1ch/terminal) Audio(1ch/terminal)
	Down link signal	Audio(1ch/terminal) Camera control (1ch/terminal)
Modulation format	Electrical	FM modulation PCM modulation
	Optical	Direct modulation
Multiplexing		FDM
Frequency band width		Video 1.0~1.3GHz Audio 76~90MHz Camera control 76~90MHz
Light source		DFB laser, FP laser
Optical Output Power	DFB laser	+6 mW
	FP laser	+50mW
Optical wavelength	Up link	1.55 μ m
	Down link	1.31 μ m
	Atmospheric transmission	1.48 μ m
Modulation index	Up link	Video 60%,Audio10%
	Down link	Audio5% Camera control15%
Light receiver		APD
Optical received power		-33dBm
Transmission quality	Video	SNR 41dB CNR 17dB DG 5.5% CSO -22dBc DP 5.5% CTB -32dBc
Length of optical link		20 km
Length of atmospheric transmission		100m

There are two types of light sources. One is the DFB-Laser diode having power 6mW for optical link

transmission. The other is a high power Fabry-Perot laser diode having power 50mW for atmospheric transmission. In upward link, the video signals from terminals are frequency-modulated with FM modulators and the laser diodes are directly modulated. The frequency allocation is same as those used in Satellite Broadcasting in Japan. Sub-carriers are allocated around 1 GHz with channel separation of 38.36 MHz. Desirable CNR is assumed 17dB including 3dB level margin.

4.2 Calculation of CNR

The transmission quality of this network can be described as the characteristics of CNR on upward links.

On multi-coupler bi-directional system employing FM-SCM transmission, CNR is given by the following equation:

$$CNR = \frac{\frac{1}{2} (mMSP_r)^2}{[2e \{ I_{d0} + M^{2X} (I_n + SnP_r) \} + I_t^2 + (MSnP_r)^2 R I_{N_{sys}}] B} \quad (1)$$

Where m is an optical modulation index for each light source, M is the optimized multiplication factor of APD, S is the sensitivity of APD at low bias voltage, X is the excess noise index of APD, I_{d0} is the dark current of APD, I_{dm} is the multiplication current of APD, I_t is thermal noise current of amplifier, P_r is the average received optical power per channel, n is number of channel and B is band width of FM modulation. Numerical parameters are shown in Table.2.

Table.2 Numerical parameters for calculating CNR

m	60 % (1ch/terminal)
S	0.8 A/W
X	0.7
I_{d0}	5.0e-9A
I_{dm}	10.0e-9 A
I_t	30.0e-12 A
B	27.0e6 Hz

On the other hand, when multiplexed optical signals are detected in APD directly, the optical beat interference is observed and it make RIN_{SYS} higher [2]. RIN_{SYS} for n channel is given by the following equation:

$$RIN_{SYS} = \frac{\sum_{i=1}^n (RIN_{LDi} P_{ri}^2) + \sum_{i,j} RIN_{BEATij} (P_{ri} + P_{rj})^2}{\sum_{i=1}^n P_{ri}^2} \quad (2)$$

Where RIN_{LD} is the peculiar value of each laser, RIN_{BEATij} is indicating the effective value for the optical beat interference on two channels which are the nearest wavelength combinations. Measured RIN_{LD} is smaller than -150 dB/Hz for each laser. RIN_{LD} can be negligible, because it is much smaller than RIN_{BEAT} .

In previous work, we experimentally investigated the wavelength spacing of optical channels in order to neglect the beat interference. The wavelength spacing of 0.2 nm over is required, in order to suppress RIN_{BEAT} -130 dB/Hz and smaller.

Under the special condition where P_r and RIN_{BEAT} are the same for every channel and RIN_{LD} is negligible, eq.2 is simplified as:

$$RIN_{SYS} = \frac{4(n-1)}{n^2} RIN_{BEAT} \quad (3)$$

By the way, the multiplication factor of APD is given the following equation:

$$M_{opt} = \left[\frac{2e |I_{d0} + I_t|^2}{eX(I_{dm} + SnP_r)} \right]^{\frac{1}{2-X}} \quad (4)$$

Fig.10 shows calculated characteristic of CNR and received optical power per channel. According to the calculation, P_r should be -33 dBm or over for CNR being 17 dB or over, when 15 points are observed simultaneously. Additionally, P_r should be -32 or over and -35 dBm or over, when 10 and 20 points are observed, respectively.

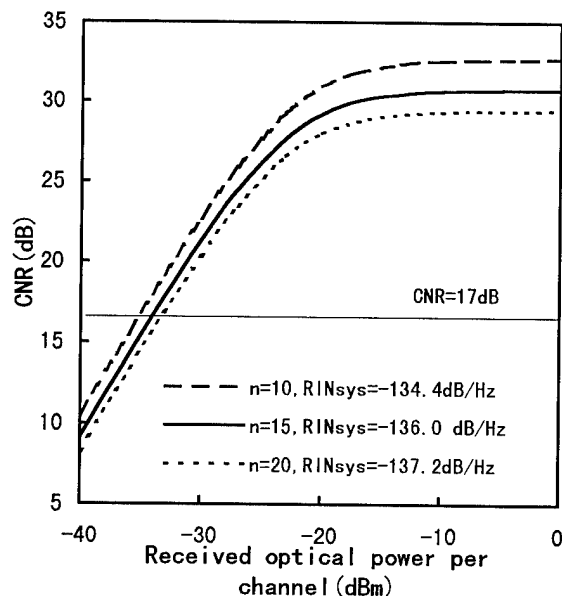


Fig.10 Calculated characteristics of CNR and Received optical power per channel (P_r).

4.3. Estimation of transmission loss

The transmission loss of the network are estimated in Table.3.

Table.3 Estimation of transmission loss.

Items		Loss
Fiber	transmission loss	0.5dB/km
	fusing loss	0.1dB/point
Coupler	transmission loss	$10\log\{n/(n-1)\}$ dB/point
	coupling loss	$10\log(n)$ dB/point
	insertion loss	0.5dB/point

Most suitable optical coupler in the network for supervising is shown in Fig.11. The coupling ratio varies as number of optical taps changes. Additionally, excess loss is neglected.

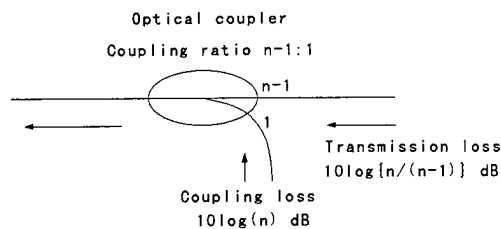


Fig.11 Most suitable optical coupler for the network.

4.4. Investigation of number of optical taps

Total transmission loss is associated with number of optical taps. Fig.12 shows calculated characteristic of total transmission loss from the far end terminal as a function of number of optical taps.

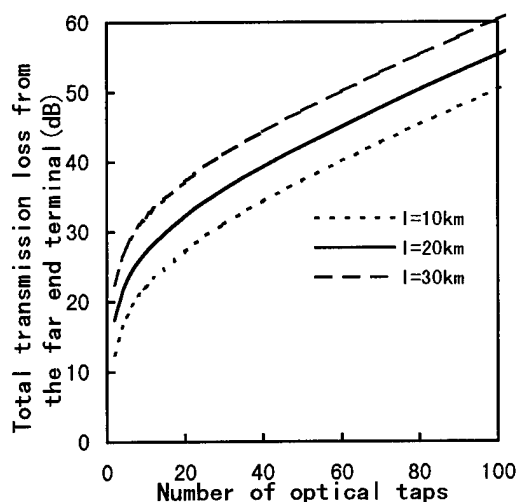


Fig.12 Calculated characteristics of total transmission loss from the far end terminal and number of optical taps.

The calculated results of the lengths of optical link as 10 km and 30 km are also indicated. Total transmission loss from the far end terminal is gradually increased as the number of optical taps and the length of transmission link increased.

To meet transmission quality, optical power from far end terminal should be -33 dBm over.

Fig.13 shows calculated characteristics of received optical power from the far end terminal and number of optical taps. As a result, as many as 45 optical taps can be located along 20 km optical link.

Based on the calculation in the typical example, the optical taps spacing is 450m, and 15 portable terminal can be in service simultaneously.

It is recognized that number of optical taps is varied according to the length of transmission link and number of potable terminals.

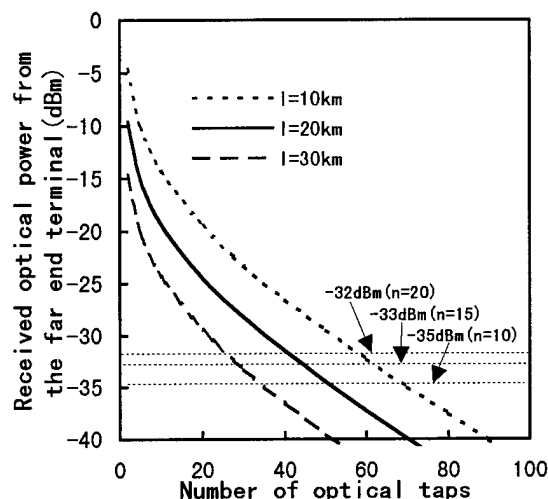


Fig.13 Calculated characteristics of received optical power from far end terminal and number of optical taps.

5. Conclusion

We developed the novel supervising network using the Information Free Access System. By using this network, Several points can be observed during a certain term upon demand simultaneously.

According to a design of the example in traffic construction application, the optical taps can be located with the spacing of 450m along the optical link, and 15 portable terminal are in service simultaneously.

Number of optical taps depends on two factors, which are the length of optical link and number of terminals. Therefore, number of optical taps can varies according to applications.

Reference

- [1]OMURA, et al : 'Development of Multi-Coupler Bi-directional Optical Communication System Employing FM-SCM Video Transmission' 44th IWCS ,pp380-386,1995
- [2]MATSUO, et al : 'The Experimental Study of the Influence of Optical Beat Interference On FM-video Transmission System Employing 30ch Multiple Optical Carriers', ECOC'94, We.P.21



Hideyuki NASU
Furukawa Electric Co.,LTD.
5-1-9, Higashiyawata,
Hiratsuka, Kanagawa, 254,
JAPAN

Hideyuki NASU received the Master Degree in electrical engineering from Nihon University, Tokyo, Japan in 1995. He joined Furukawa Electric Co.,LTD in 1995. He is working in the video transmission system and equipment research section of Information and Electronics Laboratory. He is a member of IEEE.



Haruo NAKAYAMA
Furukawa Electric Co.,LTD.
5-1-9, Higashiyawata,
Hiratsuka, Kanagawa, 254,
JAPAN

Haruo NAKAYAMA received the Master Degree in Electronics Engineering from Okayama university, Okayama, Japan in 1990. He joined Furukawa Electric Co.,LTD in 1990. He is working in Access network design, multimedia equipment and system department. He is a member of the institute of Electronics, Information and Communication Engineers of Japan.



Hideyuki OMURA
Furukawa Electric Co.,LTD.
5-1-9, Higashiyawata,
Hiratsuka, Kanagawa, 254,
JAPAN

Hideyuki OMURA received the Master Degree in electrical engineering from Tokai University, Kanagawa, Japan in 1987. He joined Furukawa Electric Co.,LTD in 1987. Since He has engaged the development of bi-directional CATV system. At present, he is working in the video transmission system and equipment research section of Information and Electronics Laboratory. He is a member of the institute of Electrical Engineers of Japan.



Kenichi TEZUKA
Tokyo Electric Power
Company
4-1, Egasaki-cho Tsurumi-ku
Yokohama, Kanagawa, 230,
JAPAN

Kenichi Tezuka received the Mater Degree in mechanical engineering from Waseda University, Tokyo, Japan in 1988. He joined Tokyo Electric Power Company in 1988. At present, he is working in Nuclear Power R&D Center.

INVESTIGATION OF SINGLE-MODE FIBER LOSS PROPERTIES BY OTDR MEASUREMENTS

P.L. Guenot *, P. Nouchi *, B. Poumellec **, O. Mercereau *

* Alcatel Fibres Optiques, Marcoussis, France

** URA 446 CNRS, Université Paris Sud Orsay, France

ABSTRACT

The dependence of loss properties on different preform elaboration and drawing parameters has been investigated on silica - germanium single mode MCVD fibers. The technique based on bi-directional OTDR measurements between two spliced samples was used to measure relative differences in Rayleigh scattering losses.

At first, this technique has been checked on several index-profiles, then on fibers processed under different non-standard conditions. It was found that none of the studied parameters, except for germanium concentration in the core, influence appreciably Rayleigh scattering level, even though the study of loss spectral dependence versus λ^{-4} leads to assume that Rayleigh losses have strongly grown. Thus our investigation tends to show that induced extra-losses in the I.R. spectra are not consistent with increased Rayleigh losses but rather with other loss mechanisms such as extra-absorption centered toward shorter wavelengths, which spectral dependence is linear versus λ^{-4} in the observed region (1.0 to 1.3 μ m), or λ^{-4} dependent waveguide imperfection losses.

INTRODUCTION

Loss mechanisms of silica-based single mode fibers are considered as relatively well-understood: loss levels are not far from expected low-loss limits for involved profiles and compositions. Loss spectra can be obtained with good accuracy by the well known "cut-back method" but specific accurate measurements of Rayleigh scattering contribution (for example by using integrating spheres or cubes) and absorption component (for example by

microcalorimetry) are not easy to perform on fibers. Rayleigh coefficient is usually estimated using the conventional " $a+b/\lambda^4$ " analysis,¹ that is to say by slope of the infra-red (IR) loss spectra versus λ^{-4} , but precise results cannot be obtained for the following reasons :

a) The conventional $1/\lambda^4$ analysis is based on the assumption that scattering losses prevail over other loss components in the studied portion of the IR loss spectra, these "non-scattering" components being neglected.

b) Mode field diameter, and therefore also Rayleigh coefficient through the portion of light power guided in the core and in the cladding of the fiber, are wavelength-dependent.

c) The Rayleigh scattering coefficient of fiber is wavelength - dependent through the dependence of refractive index of the fiber material on wavelength² (relatively weak).

Walker³ and Heitmann⁴ proposed improved models for analyzing the attenuation components of standard fibers but they rely on many fitting parameters and assumptions. In any case, all these methods do not apply if no clear linear dependence on λ^{-4} appears out of IR loss spectra, or if a "non-Rayleigh" loss phenomenon with wavelength dependence similar to the Rayleigh-scattering one (in the studied range of the IR spectra) exists : for example, waveguide imperfection losses.⁵

Here, we use the bi-directional OTDR (Optical Time Domain Reflectometry) method⁶ at 1.31 μ m and 1.55 μ m to measure Rayleigh scattering loss specific component of GeO₂-SiO₂ single mode MCVD fibers. We first study the relevance of this technique on "standard" fibers. Then our goals are: firstly to clarify the dependence of Rayleigh scattering coefficient on different process parameters such as drawing temperature, vitrification temperature, collapse conditions, and then, to try to conclude on nature of extra-losses induced under different non-standard process

conditions (extra-Rayleigh scattering or not ?) ; secondly to compare the fibers Rayleigh scattering dependence on germanium concentration through the dependence on refractive index, with bulk scattering data.^{7,8,9}

PRINCIPLE OF BIDIRECTIONAL OTDR MEASUREMENTS

Here, we show how the relative difference in Rayleigh scattering coefficient between two fibers can be extracted from spliced-fibers OTDR traces.

It is well known that backscattered power contains information not only about power decay in the fiber but also about local backscattering coefficient $\eta(z)$ depending on the product of scattering loss coefficient $\alpha_s(z)$ and backscatter capture coefficient $B(z)$. It has been shown¹⁰ that the backscattering coefficient fluctuations can be separated from attenuation contribution with a bi-directional OTDR measurement. Let $S(z)$ the backscattered power (dB) when power is injected from the input end of the fiber and $S(L-z)$ (dB) the backscattered power when power is injected from the other end of the fiber (total length L). The difference of $S(z)$ and $S(L-z)$ yields longitudinal distribution of total loss coefficient $\alpha(z)$, while the sum yields longitudinal distribution of backscattering coefficient $\eta(z)$ (or $F(z)$ in units of dB).

When doing bidirectional OTDR measurements on two spliced fibers, summing the two bidirectional traces (power injected from each fiber) yields the relative difference of backscattering coefficient between the two fibers F_s , that is:

$$F_s = 10 \log_{10}(\eta_2(z_0)/\eta_1(z_0)) \quad , \quad (\text{eq.1})$$

where z_0 is the splice location and $\eta_1(z_0)$ and $\eta_2(z_0)$ are the backscattering coefficients of the two fibers 1 and 2 respectively. We show below how the relative difference in Rayleigh scattering coefficient can be extracted from the measurement of F_s .

Backscattering coefficient $\eta(z)$ essentially depends on mode field characteristics and Rayleigh scattering coefficient. Most authors^{11,12,13} have derived simple expression for backscattering coefficient assuming that (a) scattering coefficient $\alpha_s(z)$ does not have any radial dependence, (b) radial mode-field distribution is gaussian (with width W_g), so that :

$$\eta(z) = \frac{\tau v_g}{2} \frac{3\lambda^2}{8\pi^2 n^2} \frac{\alpha_s(z)}{W_g^2(z)} \quad (\text{eq.2})$$

where v_g is the group velocity, τ is the pulse duration and n is the core refractive index. It can be seen from eq. 1 and 2 that the scattering coefficient ratio α_{s2}/α_{s1} can be directly extracted from the measurements of F_s and gaussian width W_{g1} , W_{g2} of each fiber.

This is the method which was used by Fermann et al in 1988.⁶ They proposed comparative measurements of Rayleigh scattering in single mode fibers based on this bi-directional OTDR technique : a low-loss fiber, whose Rayleigh scattering coefficient is supposed to be well known, is used as a reference fiber to which is spliced the fiber under test. As mentioned above, Rayleigh scattering coefficients are supposed to have no radial dependence which is not the case because core and cladding have different doping levels. Also, mode-field distribution is also assumed to be gaussian (eq. 2) and validity of this approximation depends strongly on index profile.

Here, we use a more general formula for $\eta(z)$ relying on the analysis of Hartog.¹⁴ Without any assumption regarding the field radial extension $\psi(R)$ and the radial dependence of scattering loss, Hartog¹⁴ has derived the following expression for backscattering coefficient η :

$$\eta(z) = \frac{\tau v_g}{2} \frac{3\lambda^2}{8\pi n^2} \frac{\tilde{\alpha}_s(z)}{A_{\text{eff}}(z)} \quad (\text{eq.3})$$

where R is the radial coordinate normalized to the core radius a , A_{eff} is the effective area given by

$$A_{\text{eff}} = 2\pi a^2 \left(\int_0^\infty \psi^2(R) R dR \right)^2 / \int_0^\infty \psi^4(R) R dR \quad (\text{eq. 4})$$

and $\tilde{\alpha}_s(z)$ is a field-weighted value given by :

$$\tilde{\alpha}_s(z) = \frac{\int_0^\infty \alpha_s(z, R) \psi^4(z, R) R dR}{\int_0^\infty \psi^4(z, R) R dR} \quad (\text{eq.5})$$

Here, we use eqs. 1 and 4 without any assumption regarding mode-field distribution and radial dependence of Rayleigh scattering. We measure effective areas using VAFF (variable aperture in the far field) data $A_{\text{eff}1}$, $A_{\text{eff}2}$ of each fiber and F_s from the spliced-fibers OTDR traces to extract the ratio $\tilde{\alpha}_{s2}(z)/\tilde{\alpha}_{s1}(z)$.

Table I : Specifications of tested "standard" MCVD fibers.

Sample code	" Standard " MCVD fibers			
	SiO ₂ core	STEP	DSF	TRAP
Index profile	step / SiO ₂ core	step / Ge-doped core	dispersion-shifted fiber	trapeze / Ge-doped core
Δn ($\times 10^{-3}$)	4.9	5.2	12.8	13.9
Process specifications	Standard	Standard	Standard	Standard
Spectral range for "a+b/ λ^4 " fit (μm)	[0.99 ; 1.10] (bi-mode region)	[1.10 ; 1.30]*	[1.15 ; 1.30]*	[1.00 ; 1.30]*
b = Rayleigh coefficient (dB. μm^4 .km ⁻¹)	0.85	0.91	1.14	1.21
a = Intercept (dB/km)	0.00	0.02	0.03	0.00
Fit correlation coefficient	0,9998	0,9999	0,9993	0,9995

* : without taking the [1.22 ; 1.27] μm range into account (OH peak at 1.24 μm)

It is interesting to notice that $\tilde{\alpha}_s(z)$ is slightly different from the intensity-weighted mean value $\bar{\alpha}_s(z)$, which really is the Rayleigh scattering component in fibers. Because of the fourth power of the field in the integral (eq.5), the coefficient $\tilde{\alpha}_s(z)$ we measure gives more weight to the core contribution, compared to $\bar{\alpha}_s(z)$. However, at 1.31 μm , the fibers we study below have a strong mode field confinement, so that $\tilde{\alpha}_s$ and $\bar{\alpha}_s$ are almost equal to the core scattering coefficient α_s (core), within 3% and 12% respectively. At 1.55 μm , the fibers field is less confined so that $\tilde{\alpha}_s$ and $\bar{\alpha}_s$ are within 7% and 16% respectively of the core scattering coefficient.

APPLICATION TO "STANDARD" FIBERS

We first studied the relevance of this technique on a set of MCVD fibers processed under "standard" MCVD and drawing conditions, with different index profiles. These fibers are supposed to be well-known and to have loss level close to theoretical minima values for considered profiles and dopings.

Studied fibers

Four fibers were studied. The first one is a pure silica core fiber (SiO₂ core) with fluorine-doped

depressed cladding, which is used as reference fiber for every measurement. The other ones are germanium-doped core fibers with weakly doped cladding : one step index fiber with core-cladding index difference $\Delta n = 5.10^{-3}$ (STEP), one dispersion shifted fiber with Δn_{core} about 13.10^{-3} (DSF) and one trapezoid index fiber with Δn about 14.10^{-3} (TRAP).

Table I synthesizes specifications of these fiber samples. Reported Δn are measured on preforms. The "a+b/ λ^4 " regression analysis is performed for each fiber in the larger single-mode region of IR loss spectra apparently free from UV, IR, OH absorptions or cut-off contributions, i.e. most of the time between 1.00 and 1.30 μm , without taking the [1.22 ; 1.27] μm range into account, which corresponds to the 1.24 μm OH peak. Figure 1 shows an example of bi-directional OTDR measurement of backscattering coefficient : the standard trapezoid index fiber (TRAP) is spliced to the silica core reference fiber.

OTDR results comparison with λ^{-4} fit values

Figures 2-a and 2-b show results of OTDR measurements of Rayleigh scattering coefficients at 1.31 μm and 1.55 μm respectively (taking effective area differences between reference and studied fiber into account) compared to slope (coefficient "b") of the linear fit of the IR loss spectra versus $1/\lambda^4$. Accuracy of these OTDR results ($\tilde{\alpha}_s$) is estimated at about $\pm 10\%$.

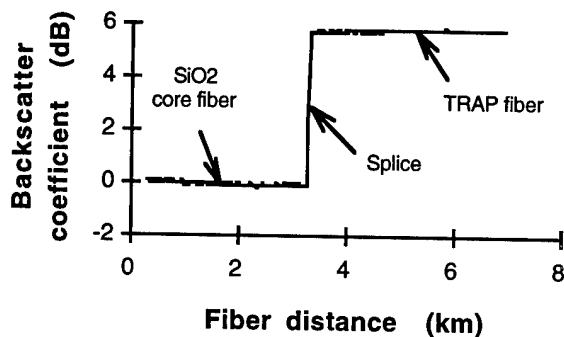


Figure 1 : Example of 1.31 μ m bi-directional OTDR measurement of relative backscattering coefficient.

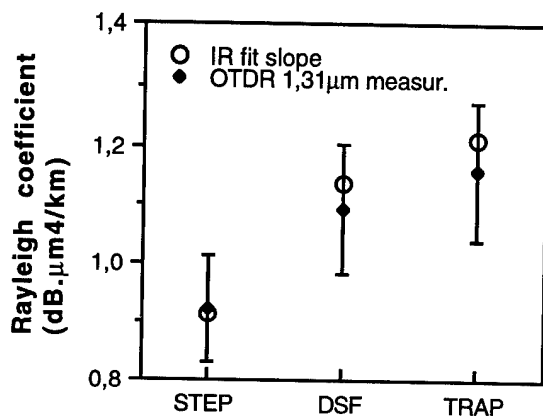


Figure 2-a

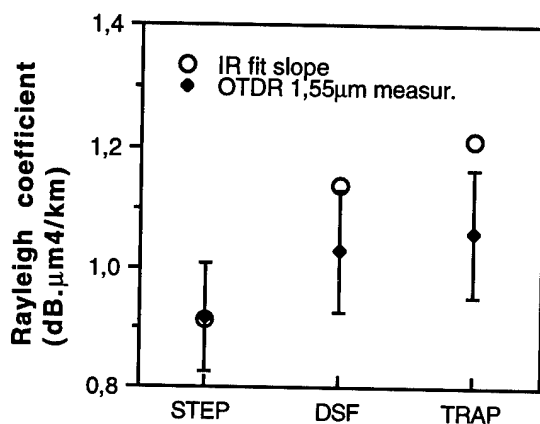


Figure 2-b

Figures 2 : Comparison on standard fibers between Rayleigh coefficients deduced from
(i) $a+b/\lambda^4$ regression slope in the IR loss spectra versus $1/\lambda^4$.
(ii) OTDR measurements at 1.31 μ m and 1.55 μ m, respectively figures 2-a and 2-b.

It is seen that the bi-directional OTDR technique is able to detect Rayleigh scattering coefficient variations, which are revealed on differently doped "standard" fibers by " $a+b/\lambda^4$ " analysis. Agreement between Rayleigh coefficient deduced from IR loss spectra and those deduced from OTDR is much better at 1.31 μ m than at 1.55 μ m. This is because both (a) spectral fit is performed in a wavelength range corresponding to a strong field confinement, and therefore very sensitive to the core contribution and (b) OTDR measurements, as already explained above, gives a large weight to the core contribution. For this reason, the following measurements are only processed at the shortest wavelength, i.e. 1.31 μ m.

RAYLEIGH SCATTERING DEPENDENCE ON FIBER AND PREFORM PROCESS

We then studied a set of trapezoid index fibers similar to previously studied "standard" trapezoid index fiber (Δn about $14 \cdot 10^{-3}$) but processed under different "non-standard" conditions, in order to clarify its loss properties and more specifically Rayleigh scattering dependence on fiber and preform process : although loss levels are clearly above minima values for considered profile and doping, loss spectra of these "non standard" fibers remain almost perfectly linear versus λ^{-4} but with higher slopes, suggesting that nature of induced extra-losses is fully extra-Rayleigh scattering. Here, 1.31 μ m OTDR measurements are used to confirm or to invalidate those dependences.

Studied parameters

Five "non-standard" trapezoid-index fibers has been prepared ; studied parameters are :

- drawing temperature (T_d) : a fiber was drawn under the same speed as the standard fiber (same preform), but under higher drawing temperature (**TRAP H.T_d** fiber) i.e. under lower drawing tension ;

- vitrification temperature (T_v) during CVD phase : a preform was processed with lower vitrification temperature for the core material than standard temperature ; two fibers were drawn from this preform, one under standard drawing conditions (**TRAP L.T_v** fiber) and one under high drawing temperature (**TRAP L.T_v+H.T_d** fiber) ;

- etching before final collapsing pass : a preform was processed without dip suppressing fluorocarbon etching phase before the last

collapsing pass ; the corresponding fiber was drawn under standard drawing conditions (**TRAP w/o e. fiber**) ;

- collapsing atmosphere : a preform was prepared without etching pass and with an inside atmosphere during collapsing passes more reducing than in standard conditions ; it was drawn in standard drawing conditions (**TRAP w/o e. + red fiber**).

OTDR results comparison with λ^{-4} fit values

Table II synthesizes specifications of these fiber samples and results of Rayleigh scattering coefficient calculations deduced from 1.31 μ m OTDR measurements ; the all-purpose reference is as previously our MCVD silica core fiber.

Figure 3 compares OTDR results with slope of the "a+b/ λ^4 " IR regression analysis for all studied trapezoid index fibers : the "standard" one (**TRAP**) and the five "non-standard" ones. Considering the above-studied accuracy of the OTDR method at 1.31 μ m wavelength, it is seen that there is a significant discrepancy between OTDR and λ^{-4} fit values.

OTDR results suggest that Rayleigh scattering coefficients are almost independent of studied process parameters, although IR loss spectra analysis versus λ^{-4} reveal clearly much higher Rayleigh coefficients. For one of the fibers (**TRAP L.Tv+H.Td**), we even measure that Rayleigh scattering loss accounts for only half the slope value of the "a+b/ λ^4 " IR regression analysis.

Nature of induced extra-losses

Let us first consider the example of drawing temperature: it is well-known in germanium doped fibers that linear fit slope of the IR loss spectra versus λ^{-4} increases as drawing temperature increases.⁸ This property is verified here (see figures 3 and 4).

It has been shown that this phenomenon can not be explained by the dependence of mode field confinement on drawing tension.⁸ In our case, cutoff wavelength and refractive index profile have been measured on fibers, revealing that mode field is slightly less confined in trapezoid index fiber drawn at high temperature than in standard one; this could only lead theoretically to lower Rayleigh coefficient, due to lower scattering losses in cladding than in core, and under no circumstances to higher Rayleigh coefficient.

So far, many authors have assumed that this

slope increase is associated to an increased Rayleigh scattering coefficient.^{15,16} Models have been suggested, involving for example dependence of softening temperature or fictive temperature, and therefore Rayleigh coefficient, on drawing temperature;^{15,17} Tsujikawa et al¹⁸ have recently shown significant effects of thermal treatment on Rayleigh scattering in differently doped VAD silica glasses (by direct measurements). Here, OTDR results of Rayleigh loss investigations do not suggest new or complementary useful indications to explain fiber Rayleigh scattering coefficient dependence on drawing temperature, but rather suggest the negation of this dependence phenomenon.

Others CVD and drawing parameters study leads to similar conclusions, as seen in table III.

Consequently, the risen question is as follows : what extra-loss phenomenon which is "invisible" to the OTDR measurements, could lead to almost perfect λ^{-4} linearly dependent loss contribution in the observed IR range ? Three hypothesis are considered :

a) The first hypothesis is an extra Rayleigh scattering localized at the outer part of the OTDR explored region of the fiber (for example at the core-cladding interface or into the cladding) because, as above reported, OTDR measurements give more weight to the core scattering contribution. However, such phenomenon is very unlikely to occur because we do not observe a significant difference in the 1.31 and 1.55 μ m OTDR values, and we do not observe an upward shift of the IR spectral loss curve in the two-mode regime compared to the single-mode regime.¹⁹

b) The second one is waveguide imperfection losses, which not only lead to the well-known wavelength independent loss component but could also lead to linearly λ^{-4} dependent loss contribution, as proposed by Inada et al⁵ ; in this case, the problem amounts to a scattering one, but not Rayleigh type .

c) The third hypothesis is an extra-absorption tail from the visible or more probably UV part of the spectrum. For example, gaussian shape absorption with parameters such as $\lambda_0 = 330$ nm, intensity $I_0 = 10$ dB/km at λ_0 , and half width at half maximum = 1.08eV, leads in the 1.00 μ m to 1.31 μ m range to extra-losses linearly λ^{-4} dependent : $0.02 + 0.21 / \lambda^4$, with correlation coefficient of 0.999997.

Specific scattering and absorption measurements are in progress in order to clarify this question.

Table II : Specifications of tested "non-standard" MCVD fibers and results of Rayleigh coefficient measurements by the bi-directional OTDR technique

" Non - standard " MCVD fibers						
Sample code	TRAP H.T _d	TRAP L.T _v	TRAP L.T _v + H.T _d	TRAP w/o e.	TRAP w/o e + red	DCF H.T _d
Index profile	trapeze / Ge-doped core	trapeze / Ge-doped core	trapeze / Ge-doped core	trapeze / Ge-doped core	trapeze / Ge-doped core	trapeze / Ge-doped core
Δn ($\times 10^{-3}$)	13.9	15.0	15.3	12.7	14.6	34
Process specifications	High drawing temperature	Low vitrification temperature	Low vitrification temperature + high drawing temperature	Without etching phase before collapse	No etching phase + reducing atmosphere during collapse	High drawing temperature
Spectral range for "a+b/ λ^4 " fit (μm)	[1.00 ; 1.30]*	[1.00 ; 1.30]*	[1.00 ; 1.30]*	[1.00 ; 1.31]*	[1.00 ; 1.20]	[1.11 ; 1.31]*
b = Rayleigh coefficient (dB. μm^4 .km ⁻¹)	1.50	1.46	2.39	1.54	1.60	4.12
a = Intercept (dB/km)	0.06	0.05	0.29	0.00	0.46	0.56
Fit correlation coefficient	0.9999	0.9999	0.9993	0.9997	0.9997	0.9997
Rayl. coef. deduced from 1.31 μm OTDR	1.20	1.21	1.27	1.08	1.15	1.80

* : without taking the [1.22 ; 1.27] μm range into account (OH peak at 1.24 μm)

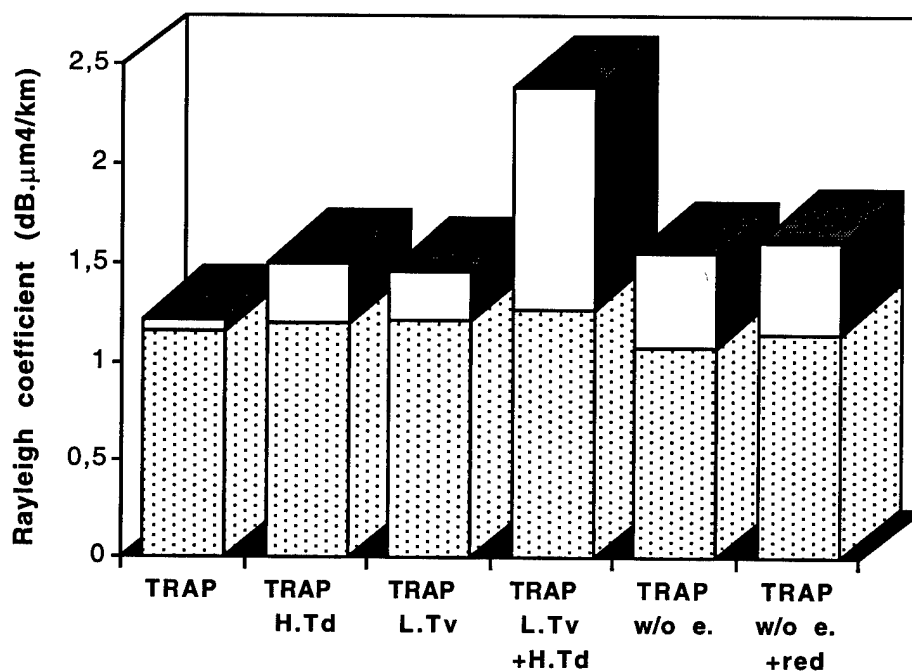


Figure 3 : Rayleigh scattering coefficients comparison on trapezoid index fibers ($\Delta n \approx +14.10^{-3}$)

- (i) Rayleigh coefficients deduced from OTDR measurements at 1.31 μm [dotted part]
- (ii) Rayleigh coefficients deduced from "a+b/ λ^4 " analysis in the IR loss spectra [total amount]

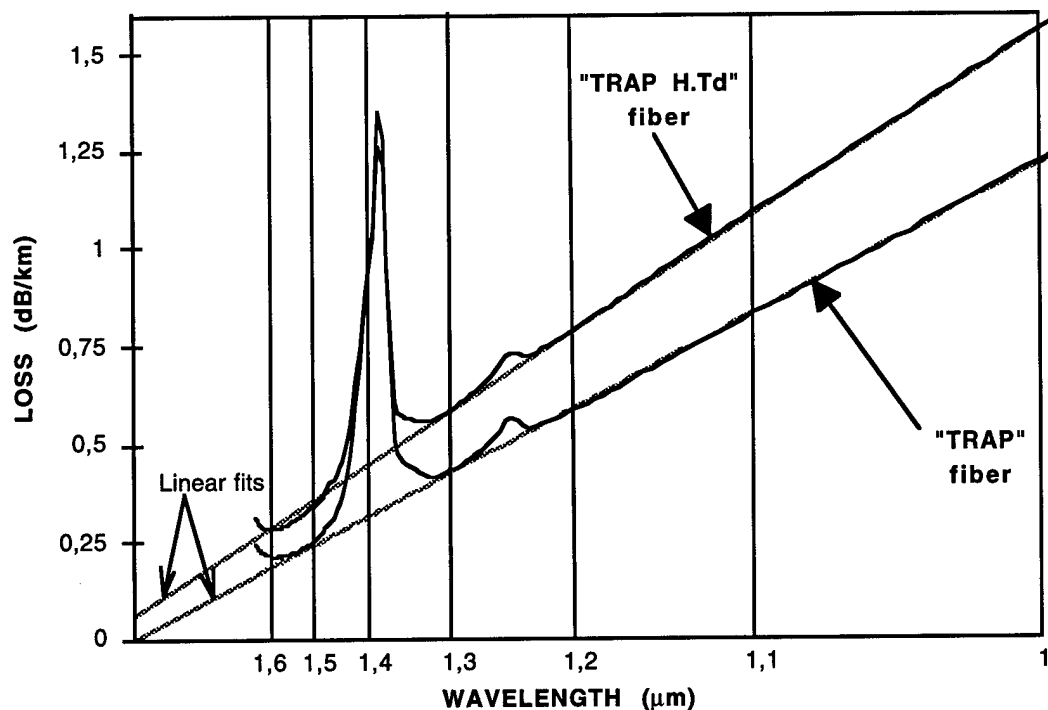


Figure 4: Influence of drawing temperature on loss spectra versus λ^{-4}
 (trapezoid index fibers : $\Delta n \approx +14.10^{-3}$:
 - TRAP fiber : standard drawing conditions
 - TRAP H.Td fiber : high drawing temperature)

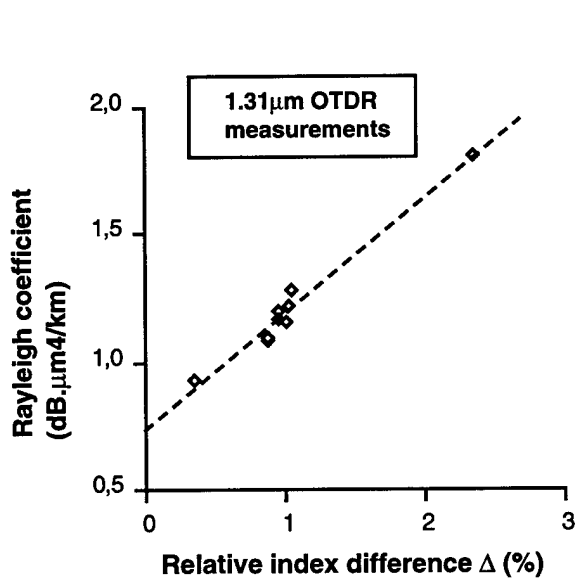


Figure 5 : Relationship between the relative index difference Δ (in percent) of GeO_2 core-doped fibers and Rayleigh scattering coefficient deduced from 1.31 μm bi-directional OTDR measurements (dotted line = linear fit).

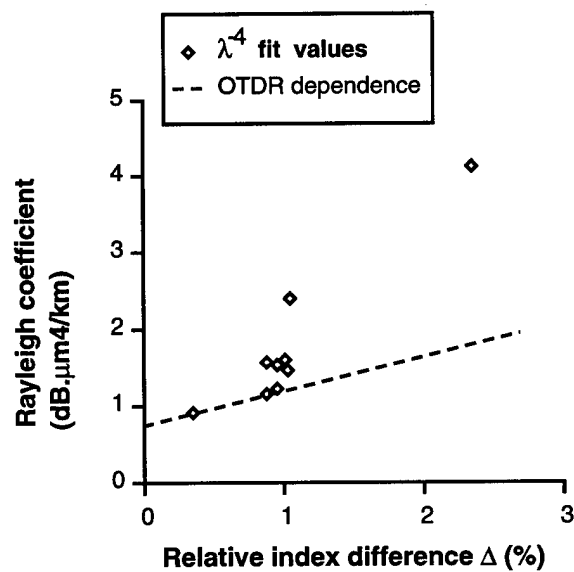


Figure 6 : Comparison on fibers between Rayleigh scattering dependences on core relative index difference, deduced respectively from OTDR (eq. 6) and from linear fit slopes of IR loss spectra versus λ^{-4} .

Table III : summing up of fiber Rayleigh losses dependence on different studied parameters,
investigated by bi-directional OTDR, compared to IR loss spectra versus λ^{-4} analysis.
(Δ is the core-cladding relative index difference)

Studied parameter or phase	Influence on IR total loss level	Influence on IR slope versus λ^{-4} (coef. b of " $a+b/\lambda^4$ " analysis)	Influence on wavelength independent loss component (coef. a)	Influence on Rayleigh coefficient measured according to OTDR
Drawing temperature	strong	strong	strong	none
Vitrification temperature	strong	strong	strong	none
Etching before collapse	strong	strong	weak	none
Collapse atmosphere	strong	strong	very strong	none
Ge concentration in the core	strong	strong not linear	weak for small Δ strong for high Δ	strong $0.73 (1 + 0.61 \Delta)$

RAYLEIGH DEPENDENCE ON REFRACTIVE INDEX

Rayleigh dependence on refractive index has been investigated on a large Δn range, through the study of "standard" fibers (see table I) as well as "non-standard" fibers (see table II) including one trapezoid fiber with highly doped profile (Δn about 34.10^{-3} , DCF H.T_d fiber).

Figure 5 summarizes for all studied fibers the dependence of the Rayleigh scattering coefficient b (dB. $\mu\text{m}^4/\text{km}$) deduced from 1.31 μm OTDR measurements, on the relative index difference Δ . It is found that b increases linearly with the core dopant concentration for our GeO₂ core doped fibers. Parameters of the linear fit are given by :

$$b = 0.73 (1 + 0.61 \Delta) \quad (\text{eq. 6})$$

Figure 6 compares Rayleigh coefficients deduced from loss spectra λ^{-4} analysis to the linear law of eq. 6 deduced from OTDR. It visualizes for our MCVD fibers the discrepancy between results of the two methods, expressed here in term of dependence on refractive index.

This linear Rayleigh coefficient dependence on refractive index measured on fibers by OTDR (eq.6) is close to that measured on GeO₂-doped bulk samples, as well as recently published one for VAD glasses,⁹ $b = b_0 (1 + 0.62 \Delta)$ where b_0 is the Rayleigh scattering coefficient of pure silica glass ($b_0 = 0.8 \text{ dB}.\mu\text{m}^4/\text{km}$)¹⁰, as MCVD glasses.¹⁹ OTDR scattering measurements, as explained in chapter 2, gives a large weight to this

doped part of the fiber, i.e. the core (slightly more than real Rayleigh scattering level of fibers), and a good agreement between OTDR results and bulk data was expected.

Table III sums up all studied parameters and corresponding observed dependences.

CONCLUSION

Bi-directional OTDR measurements have been used to investigate Rayleigh scattering loss properties of GeO₂:SiO₂ MCVD single mode fibers.

"Standard" fibers with different refractive index profiles, known to have loss levels close to minima values, has been measured at 1.31 μm and 1.55 μm , in order to study relevance of this method. It has been found that OTDR measurements of Rayleigh scattering coefficient performed at 1.31 μm wavelength are in good agreement with Rayleigh coefficient deduced from IR loss spectra " $a+b/\lambda^4$ " analysis. OTDR measurements accuracy can be estimated at $\pm 10\%$.

Fibers processed under "non-standard" CVD and drawing conditions have been studied. OTDR measurements reveal that Rayleigh scattering coefficient is relatively insensitive to process parameters such as drawing temperature, vitrification temperature and collapse conditions, although very significant induced extra-losses are linearly λ^{-4} dependent, as if the Rayleigh

scattering losses might have increased. The OTDR study suggests that nature of induced extra-losses is not extra-Rayleigh scattering.

After all, the only parameter which significantly appears to affect Rayleigh scattering of studied fibers is GeO_2 concentration in the core. The investigation of Rayleigh coefficient dependence on core relative index difference (Δ) on a large Δ range leads to almost linear dependence as follows : $0.73 (1 + 0.61 \Delta) \text{ dB} \cdot \mu\text{m}^4/\text{km}$, which is in reasonable agreement with the results obtained by measurements on bulk glass.

ACKNOWLEDGMENTS

The authors would like to thank Dr. J. Auge and Dr. C. Le Sergent for useful discussions and guidance. Thanks are also due to A. Dagorne and R. Meilleur for technical assistance in various phase of the experiments.

REFERENCES

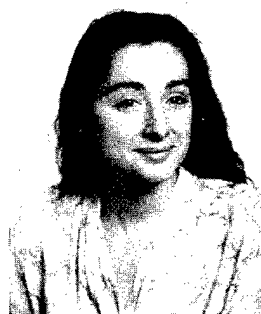
- [1] : K. Inada, *Opt. Commun.* **19**, 1976, p. 437-439
- [2] : H.C. Van de Hulst, *Light scattering by small particles*, Dover publications Inc. New York 1981
- [3] : S. Walker, *J. of Lightwave Tech.* **LT4**, 1986, p. 1125-1131
- [4] : W. Heitmann, *J. of Opt. Commun.* **11**, 1990, p. 122-129
- [5] : K. Inada et al. , in *Proc. 8th Eur. Conf. Optical Commun.* (Cannes, France, 1982, p. 596-600)
- [6] : M.E. Fermann, S.B. Poole, D.N. Payne, F. Martinez, *J. of Lightwave Technology* **6**, 1988, p. 545-551
- [7] : Murata, Hiroshi, "Handbook of optical fibers and cables", *Optical Engineering* **15**, 1988 (ed. M. Dekker)
- [8] : M. Ohashi et al. , *J. of Light. Tech.* **10**, 1992, p. 539-543
- [9] : K. Tsujikawa et al. , *Electronics Letters* **30**, 1994, p. 351-352
- [10] : Di Vita P. et al. , *Electronics Letters* **15**, 1979, p. 467-468.
- [11] : Brinkmeyer E., *J. Opt. Soc. Am.* **70**, 1980, p. 1010-1012.
- [12] : Aoyama K. I. et al. , *IEEE Journal of Quantum Electronics* **17**, 1981, p. 862-868.
- [13] : Nakasawa M., *J. Opt. Soc. Am.* **73**, 1983, p. 1175-1180.
- [14] : Hartog A.H., Gold M.P., *Journal of Lightwave Technology* **2**, 1984, p. 76-82.
- [15] : S. Sudo, H. Itoh, *Optical and Quantum Electronics* **22**, 1990, p. 187-212
- [16] : A.A. Abramov et al, *Electronics Letters* **29**, 1993, p. 1977-1978

- [17] : M.E. Lines, *J. Appl. Phys.* **55**, 1984, p. 4052-4957
- [18] : K. Tsujikawa et al. , *Electronics Letters* **31**, 1995, p. 1940-1941
- [19] : P.L. Guenot et al. , *to be published*



Philippe L. Guenot
Alcatel Fibres Optiques
R&D department
Route de Nozay
91460 Marcoussis
FRANCE

Philippe Guenot, received his engineer degree from CUST of Clermont-Ferrand in 1991. He has been Ph. D. student from Paris XI University in Alcatel Alsthom Recherche laboratories since 1993 and recently joined Alcatel Fibres Optiques as Research Engineer. His current fields of interest are optical and physical properties characterisation in silica-based glasses, and loss mechanisms understanding in optical fibers.



Pascale Nouchi
Alcatel Fibres Optiques
R&D department
Route de Nozay
91460 Marcoussis
FRANCE

Pascale Nouchi received an engineering degree in Physics and Chemistry from ESPCI in Paris, France in 1988. She received her Ph. D. degree in Optical Sciences from the University of Southern California in Los Angeles, in 1992. She then joined the Fiber Optic Department of Alcatel Alsthom Research center. She is now with Alcatel Fibres Optiques.

Bertrand Poumellec
CNRS URA 446
Thermodynamique et Physico-chimie des Matériaux
Université Paris Sud
91405 Orsay Cedex FRANCE

Bertrand Poumellec is graduated from the Ecole Normale Supérieure de Saint-Cloud in 1979. Highest Diploma for teaching (agregation in chemistry in 1979). Doctorate in Geophysics on the olivine silicate in 1980. State doctorate in 1986. He is research leader in the laboratory URA 446 CNRS at the Orsay University (South Paris University). He has dealt with point defects in silica-based materials for 7 years.



Olivier Mercereau
Alcatel Fibres Optiques
R&D department
Route de Nozay
91460 Marcoussis
FRANCE

Olivier Mercereau was born in 1969. He is Bachelor in Physics from Poitiers University. He has been engaged in the Fiber and Photonic Systems Department of Alcatel Alsthom Recherche in 1992. He recently joined Alcatel Fibres Optiques as technician.

A TIME-VARYING OPTICAL FIBER STRAIN MEASUREMENT BY USING BRILLOUIN RING AMPLIFYING SYSTEM

Mitsuru Kamikatanoo**, Osamu Ogawa*, Matsuhiro Miyamoto**

* Tokyo Electric Power Company 4-1, Egasaki-cho, Tsurumi-ku, Yokohama, Kanagawa, 230, Japan

** Fujikura Ltd. 1440 Mutusaki, sakura, chiba, 285, Japan

ABSTRACT

Optical fiber Cables, especially OPGW, sometimes experience large variation in tensile strain which is caused by the resonant vibration, and it is necessary to monitor it for the control of the reliability of optical fiber. Therefore, we developed a new technique to measure time-varying optical fiber strain and strain distribution in a telecommunication cable by using a Brillouin ring amplifying system.

By using this technique, it becomes possible to carry out real time measurement of fiber strain variations at every point of long span fiber cable. This method enables us to obtain Brillouin frequency shifted signal light by simply inputting the pump light into the ring, and to eliminate the need for scanning the frequency of the probe light mentioned in Introduction. Moreover, as the signal light power on the order of mW is obtainable, the averaging process becomes unnecessary, and the strain variation with time of optical fiber can be measured in real time.

1 INTRODUCTION

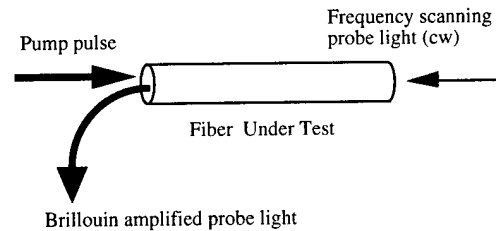
OPGW (Optical fiber composited Ground Wire) is a basic transmission line in power maintenance communication networks. Therefore, diagnosis of the mechanical degradation of the optical fiber incorporated therein and prediction of its service life are important. The OPGW sometimes undergoes a tension variation as large as several ten percent of the constant tension, which is caused by the resonant vibration called "galloping", so diagnosis of this tension variation is also indispensable.

Recently, several methods have been reported which measure fiber strains by utilizing the fact that the amount of frequency shift of Brillouin scattering light depends on the fiber tensile strain.

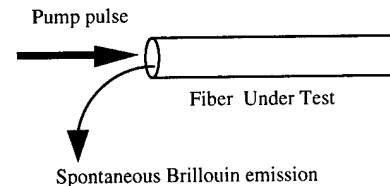
These methods can be classified into two types of methods. One is Pump-Probe Method ("BOTDA": Brillouin Optical fiber Time Domain Analyzer) [1]. According to this method, a pump light and a probe light are launched into the test fiber so as to counterpropagate through the fiber, and the frequency of the probe light is scanned to measure the frequency difference between the two lights which gives the maximum Brillouin gain. The strain distribution in the long span fiber can be known by using a pulsed pump light. However, it is very difficult to measure the vibration phenomenon like OPGW galloping by this method, because of the necessity of fast and accurate frequency scanning of probe light and signal averaging. (See Fig.1a)

The other is B-OTDR (Brillouin-Optical Time Domain Reflectometry) [2]. It can directly measure the very weak spontaneous Brillouin scattering spectrum by using a high sensitive optical heterodyne detector without having to use probe light. But it also needs signal averaging and frequency scanning. (See Fig.1b)

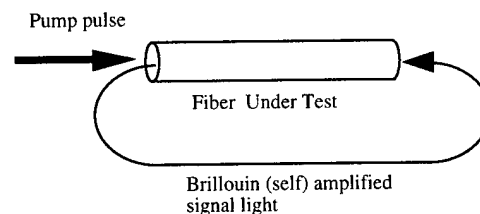
In this paper, therefore, we propose, as a method to solve these problems, a new system of measuring fiber strain distribution using the principle of Brillouin optical fiber ring laser. The proposed system forms a ring optical circuit including the fiber to be measured, optical switches and the EDFA (Erbium-Doped Fiber Amplifier). By controlling the timing to gate the optical switches, we can easily obtain the amplified Brillouin back-scattered signal light at any point of the fiber under measurement. Fig.1c shows the basic concepts of this method.



(a) Pump-Probe Method (BOTDA)



(b) Brillouin-OTDR



(c) Brillouin ring amplifier system
(proposed)

Fig.1 Distributed strain measuring methods

2 CONFIGURATION AND OPERATION

Fig.2 shows the principle and configuration of the proposed system. An optical ring circuit including the test fiber, optical circulator, EDFA, optical switches, optical isolator, and dummy fiber is formed.

The operating process of this system is as follows,

1. The pump light is modulated into periodic pulses by optical switch 1 and launched into the ring through the optical circulator.
2. Brillouin scattering signal light is generated by the pump light everywhere in the test fiber.
3. The signal light propagates through the ring in the direction opposite to that of the pump light.
4. A portion of the signal light separated by a fiber coupler is launched into the measuring system.
5. The timing to open optical switch 2 in the ring is delayed by Δt from that of optical switch 1, so the signal light scattered at a specific position of the fiber can be isolated.
6. The signal light is amplified by EDFA in the ring, which mainly acts to compensate for the loss in the ring circuit.
7. When the gating period of the two optical switches is adjusted to the propagation time T_r , the isolated signal pulse always collides with the pump pulse at the same position where the signal light was first generated, and is Brillouin amplified every round of the ring by the pump pulse, and finally, it reaches a high intensity, showing good phase matching in the steady state.
8. The frequency difference between the pump light and the generated signal light is equal to the Brillouin frequency shift of the fiber at the measuring point, so the fiber strain can be measured.

*It is necessary that the dummy fiber be slightly longer than the test fiber, and that the optical isolator be inserted between those fibers. Defining the time when the first pump light was launched as zero time, and the point where the pump light was launched as the point of origin, the Brillouin back scattering signal light generated by the first pump light beyond the midpoint of the ring circuit requires a longer time than T_r to return to the point of origin. The signal light collides with the next incident pump light with a period of T_r at a different point.

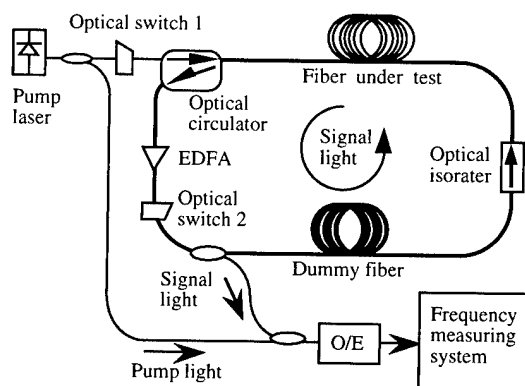


Fig.2 Basic experimental setup

3 THEORY

3.1 Operating conditions

A theoretical description will be given here of the operation of the ring circuit shown in Fig. 2. Fig. 3 shows a simplified model in which the test fiber is regarded as the Brillouin amplifier and the obtained gain as G_B . G_E is the EDFA gain, Γ_{F1} is the fiber transmission loss between the point of incidence of the pump light and the measuring point (Brillouin amplifier), and Γ_{F2} is the fiber transmission loss except Γ_{F1} . Γ_{C1} and Γ_{C2} are the losses by passage through the optical circulator, and Γ_{SW} is the total loss in the optical parts of the ring circuit such as the optical switch and optical coupler. P_{P0} and $P_{P,in}$ are the pump light powers inputted into the ring circuit and the Brillouin amplifier, respectively. The pump light is a pulsed light, but is treated here as being continuous, assuming that the spectrum broadening by pulse modulation is sufficiently small as compared with the Brillouin gain bandwidth (about 50 MHz). Here parameter ξ is defined by Eq. (1).

$$\xi = G_{Bs} G_{Es} \Gamma_{F1} \Gamma_{C1} \Gamma_{SW} \Gamma_{F2} \quad (1)$$

where G_{Bs} and G_{Es} denote the small signal gains at the Brillouin amplifier and the EDFA, respectively. Symbol ξ represents the gain per round of the ring circuit for the small signal light and is a parameter corresponding to the oscillation threshold of the ring laser. That is, when ξ is more than 1, a signal light with strong intensity can be obtained in the steady state. Conversely, when ξ is less than 1, no signal light is produced. Generally, the ring laser oscillates at the ring resonance frequency which gives the maximum gain. With this system, however, the signal light may be regarded as being produced at the frequency, which gives the maximum Brillouin gain, because the overall length of the ring circuit is as long as several ten kilometers and the interval between each point of resonance frequency is very small.

3.2 Transient response

In order to clarify what operation the ring circuit exhibits for a value of ξ , the behavior of the signal light was investigated with input pump light formed into step function. In Fig. 2, the EDFA mainly functions to compensate for the loss and is not essential to the operation of the ring circuit. In this figure, therefore, it was decided to take G_B equal to 1. How the transient response of the signal light power at the output end of the Brillouin amplifier depends on the value of ξ was calculated. The results are given in Fig. 4. The abscissa of the figure is the time standardized by the propagation time for one round of the ring circuit, T_r , and represents the number of rounds of the ring circuit. In this calculation, simultaneous combined equations with several unknowns were solved numerically, taking into account the spectral change of the signal light.

In the region where ξ is more than 1, the signal light power reaches the steady state faster the higher the value of ξ is, and then the signal light power is equal to the saturation power of the Brillouin amplifier. For example, when ξ is equal to 2, the signal light power reaches the steady state in a propagation time for about 30 rounds of the ring circuit (400 μ sec, taking the overall ring length at 80 km). This means that the signal light power responds momentarily to a strain variation of about 0.3 Hz.

On the other hand, when ξ is less than 1, the signal light decays monotonously. In practice, the EDFA is inserted in the ring circuit, so its ASE (Amplified Spontaneous Emission) light is always supplied as an input light to the Brillouin amplifier. Therefore, when ξ is less than 1, the signal light power reaches the steady state at the level of the ASE light.

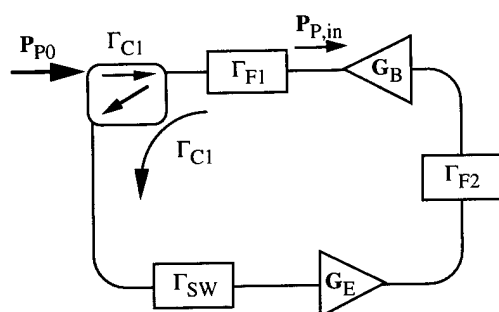


Fig.3 Analytical model of proposed system

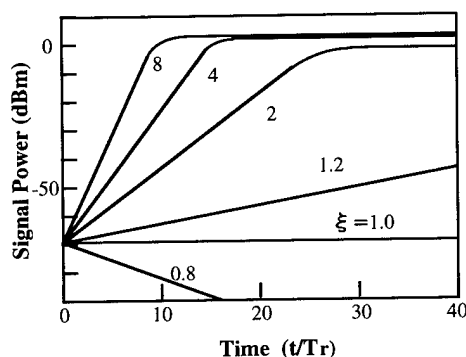


Fig.4 Simulation results of transient responses

4 EXPERIMENTAL

4.1 Experimental setup

A schematic diagram of the experimental setup is shown in Fig. 5. As the pump light source, a Laser Diode (LD) with external cavity whose wavelength is 1555nm and line width is less than 1MHz, is used. AOM1 and AOM2 are Acousto-Optic Modulators and correspond to Optical switches 1 and 2 in Fig.2. As an ordinary AOM causes frequency shift, AOM2 used in Fig.5 is a two-stage AOM to cancel the frequency shift.

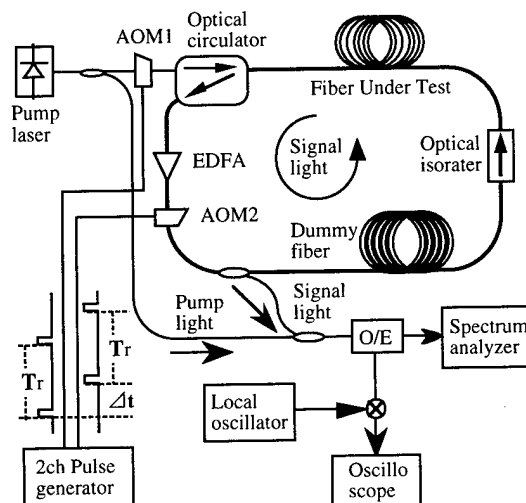


Fig.5 Experimental set up

4.2 Experiment (on Transient Response)

An experiment was made to verify the transient response shown in Fig. 4. The configuration of the measuring system is roughly shown in Fig. 5, but AOM2 was not inserted because it was necessary to detect the signal light, produced in the test fiber (500 m), as a continuous light.

In this system, the pump light was input stepwise, and the variation of the signal light was measured with the spectrum analyzer in the zero span sweep mode. The results are given in Fig. 6. The abscissa is standardized by the propagation time for one round of the ring circuit, T_r , similarly to that in Fig. 4. The ordinate is a linear scale. The signal light power reaches the steady state faster the higher the value of ξ is, which agrees with the tendency shown by the theoretical curve of Fig. 4, and the cycle of fine ripples is equal to T_r . The reason why the two curves of Fig. 6 are different in saturation level is because the EDFA gain was varied to change the value of ξ .

Fig.7 shows the spectrum in the steady state obtained by this amplifier system. It has a very sharp and narrow spectrum on the order of kHz just like a Brillouin fiber ring laser, and its peak frequency has a good agreement with that of the spontaneous Brillouin emission spectrum shown in Fig.8.

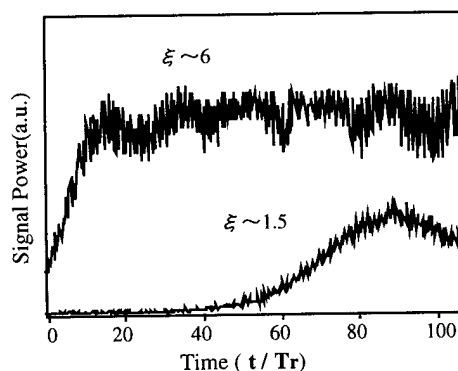


Fig.6 Experimental results of transient responses

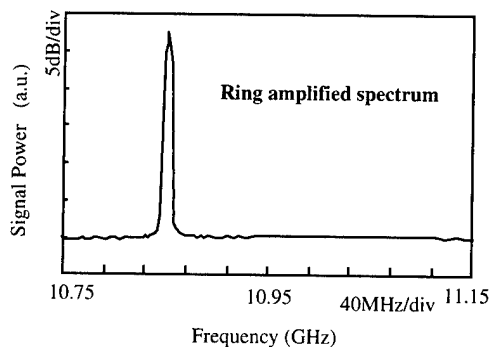


Fig.7 Brillouin spectrum measured by proposal system

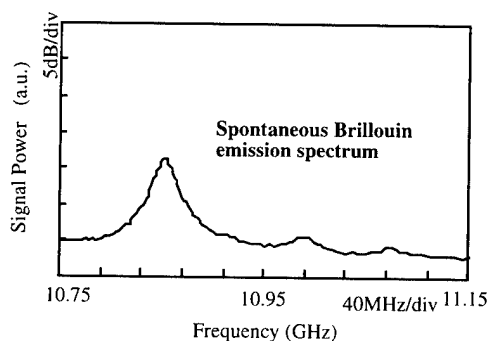


Fig.8 Spontaneous Brillouin emission spectrum

4.3 Measurement of Brillouin frequency shift distribution

Fig.5 shows a schematic diagram of the experimental setup to measure the Brillouin frequency shift at arbitrary positions of the fibers under test. A ring optical circuit is formed, including two types of test fibers and dummy fiber. These fibers are jointed in the following order.

1. Fiber A : 800m, 10.98GHz
2. Fiber B : 500m, 11.31GHz
3. Dummy fiber : 2200m

The pump light power is 50mW, and the gating time for AOMs is 500nsec. The pulse repetition frequency is set at 8.642kHz to match the propagation time of the signal light.

The signal light is mixed with the pump cw light and O/E converted to RF pulse. The RF pulse is still down converted by mixing with the tunable LO (Local Oscillator 10~12GHz) signal, and its pulse waveform is monitored on an oscilloscope.

Experimental results are as follows. Figs.9 and 10 show RF pulse waveforms generated on fibers A and B mixed at several LO frequencies. Fig.11 shows the down converted pulse waveform generated on the boundary of these two fibers. Every pulse is a single pulse picked up from the pulse train. These pulse waveforms are so clear and have low phasing noise. It is assumed that the pulse lights are stimulated Brillouin amplified ones. The Brillouin frequency shift can be known by applying real time FFT to the signal pulse mixed at the fixed LO signal frequency.

It is clear from these results that measurement of Brillouin frequency shift distribution on optical fiber can be achieved with this system.

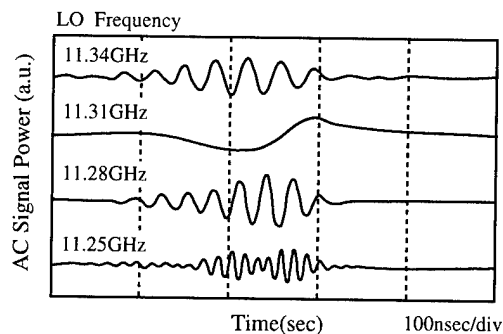


Fig.9 Beat spectra of signal pulse mixed with LO signal (Fiber A $\Delta t=3\text{usec}$)

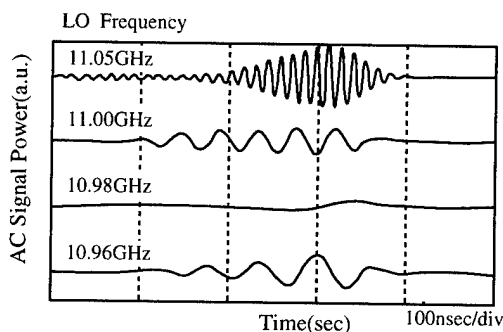


Fig.10 Beat spectra of signal pulse mixed with LO signals (Fiber A $\Delta t=9\text{usec}$)

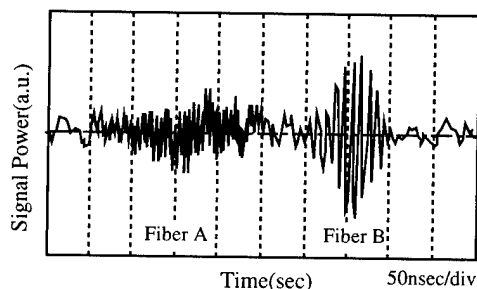


Fig.11 Beat spectrum of signal pulse generated on the boundary between fiber A and fiber B (LO Frequency 11.21GHz $\Delta t=7.87\text{usec}$)

4.4 Experiment for Verification of Operation

The system of Fig. 4 was set up to confirm that measurements can be taken at any position of the long-span fiber. As use of ordinary AOMs results in causing frequency shift, a two-stage arrangement of AOMs was adopted for the optical switch (AOM2) of the ring circuit in order to cancel the frequency shift.

The fibers constituting the ring circuit are jointed in the following order :

1. Test fiber A (not strained): 1,000 m
2. Test fiber B (strained): 200 m
3. Test fiber C (not strained): 1,200 m
4. Dummy fiber: 5,000 m

For fiber B, provision was made to apply strain to it using a pair of pulleys. However, fibers A and B are equal in the amount of Brillouin frequency shift in the unstrained condition. The overall length of the ring circuit including the EDFA is 7.58 km. The pump light launched into the ring circuit is 1 μ sec in pulse width and about 100 mW in peak power. The pulse repetition frequency was set at 26.4 kHz so that it agrees with the light propagation time in the circuit. The Brillouin frequency shift was determined by measuring the beat frequency, caused by the combination of the pump light and signal light signals, by spectrum analyzer.

A sinusoidal tensile strain about 1 Hz in frequency and 0.15% in the variation in amplitude of strain was applied to fiber B, and the beat spectra of the pump light and probe light were measured at 100 msec intervals.

Fig. 12 shows these spectra plotted one over another. As seen in the figure, variations with time of Brillouin frequency shift were measured. The frequencies at which the intensity reaches the maximum level were determined from the waveforms of Fig. 12 and plotted in Fig. 13. The ordinate shows the values converted to strain variation by the proportionality factor of 500 MHz/%. From this, it can be seen that the sinusoidally varying strain was measured accurately for both amplitude and frequency.

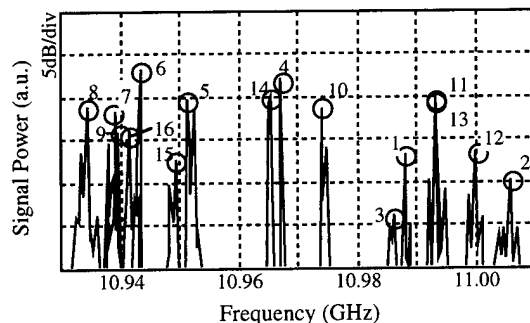


FIG.12 Spectra measured every 100msec

(Added numbers correspond to the sequence of measurement)

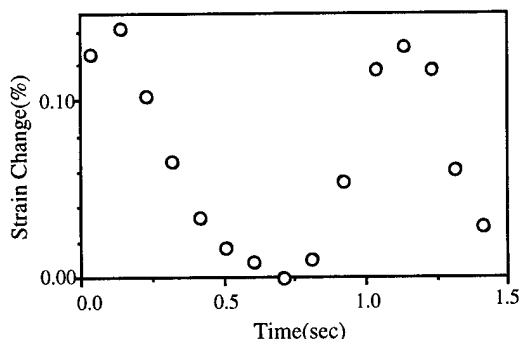


Fig.13 Strain change with the passage of time(fiber B)

CONCLUSION

So far, we have described the new system which makes it possible to measure strain variation or distribution in fibers with a frequency of several hertz such as galloping. At first, a theoretical explanation of the system operation and the results of numerical calculation were given to clarify the operation mechanism. Further, the results of the experiment made to verify the principle of operation were described, and the feasibility of this system was proved.

For the future, we think it necessary to clarify experimentally the range resolution and limits to measurable range and to establish an electric signal processing system to measure the Brillouin frequency shift with higher accuracy.

REFERENCES

- [1] T. Horiguchi et al., "Tensile Strain Dependence of Brillouin Frequency Shift in Silica Optical Fibers", IEEE Photon. Tech. Lett., vol.1, N0.5, pp.107-108 (1989)
- [2] T. Horiguchi et al., "Development of a Distributed Sensing Technique Using Brillouin Scattering", J. Lightwave Technol., vol.13, N0.7, pp.1296-1302 (1995)
- [3] P. Nicati et al., "Frequency Stability of a Brillouin Fiber Ring Laser", J. Lightwave Technol., vol.13, N0.7, pp.1445-1451 (1995)
- [4] O.Ogawa et al. "A New Technique for Measuring a time-varying Optical Fiber Strain", Conference Proceedings of 11th Optical Fiber Sensors, pp.670-673 (1996)



Osamu Ogawa was born in 1964. He received a B.E. degree in communication engineering and a M.E. degree in electronic engineering from Tohoku University in 1986 and 1988, respectively. Then he joined Tokyo Electric Power Company. he has been engaged in researches on optical fiber sensors and optical multiplexing transmission systems. He currently serves as Chief researcher at Computer and Communication R&D Center.

Tokyo Electric Power Company
4-1, Egasaki-cho, Tsurumi-ku,
Yokohama, Kanagawa, 230, Japan



Matsuhiko Miyamoto was born in 1953. He received a B.S. degree from Nagoya Institute of Technology in 1976 and a M.S. degree from Tokyo Institute of Technology in 1978. In 1978 he joined Fujikura Ltd. and has been engaged in research and development of optical fibers and cables. He is a member of the Institute of Electronics, Information, and Communication Engineers of Japan.

Fujikura Ltd.
1440 Mutusaki, sakura, chiba, 285, Japan



Mitsuru Kamikatano was born in 1961. He received a B.E. degree in 1984 and a M.E. degree in 1986 from Tokyo University. In 1991 he joined Fujikura Ltd. and has been engaged in research and development of optical fibers and cables. He is a member of the Institute of Electronics, Information, and Communication Engineers of Japan.

Fujikura Ltd.
1440 Mutusaki, sakura, chiba, 285, Japan

A FUNDAMENTAL THEORETICAL ANALYSIS OF OPTIC FIBER PAYOUT FROM FIBER OPTIC DATA LINK BOBBIN

Akira Akiyama[†], Mitsuru Shibata^{††}, Shinji Araki^{†††}, Hidehiko Kubo[†]

[†] Third Research Center, TRDI, Japan Defense Agency,
1-2-10 Sakae, Tachikawa, 190 Japan

^{††} Aerospace Division, Aerospace Group, Kawasaki Heavy Industries Ltd.
1, Kawasaki, Kagamihara, Gifu, 504 Japan

^{†††} Manufacturing Engineering Department, Sakura Plant, Fujikura Ltd.,
1440, Mutuzaki, Sakura, Chiba, 285 Japan

ABSTRACT

In recent years, FODL(Fiber Optic Data Link) bobbin is used for achieving mobile communication between air vehicles and the ground station. FODL Bobbin is based on developing a long, fine optic fiber wound and unwinding technology on the bobbin under maintaining low transmission loss. The most essential design of FODL bobbin is capable of unwinding reliably in a highly dynamic condition.

In this paper, a fundamental theory of optical fiber payout from FODL bobbin under gravity is deduced for the theoretical analysis of the payout motion of optic fiber from the FODL bobbin. As a result of the computer simulation applying this fundamental theory for unwinding the optic fiber from FODL bobbin under gravity, this fundamental theory covers the basic payout dynamics of the optic fiber on FODL bobbin and in the air simultaneously.

1. Introduction

In recent years, the mobile communication between air vehicles and the ground station using the FODL(Fiber Optic Data Link) bobbin is studied [1, 2]. The FODL bobbin make huge capacity of communication line. This huge capacity of communication line make possible the real time image communication for air vehicles easily.

The construction of the mobile Fiber Optic Data Link requires winding optic fiber on the bobbin precisely and unwinding optic fiber from the bobbin smoothly. The FODL bobbin for the mobile communication is equipped with a long, low transmission

loss, fine optic fiber wound on the bobbin. Currently the wound length of optic fiber on the FODL bobbin reaches scores kilometer.

For the establishment of the smooth unwinding the optic fiber from the FODL bobbin many actual unwinding test at laboratory are carried out. Currently the speed of the smooth unwinding the optic fiber from the FODL bobbin is a few hundred meter per second possibly. For the practical unwinding speed of a few hundred meter per second we make two kind of approach. Firstly we manufacture new FODL bobbins using finer optic fiber and composite materials. Secondaly we analyze the payout motion of optic fiber from the FODL bobbin theoretically.

In general payout motion analysis of fiber, the work of D.G.Padfield in formulating and applying the motion and tention equations of an unwinding yarn is noteworthy [3]. The work of D.G.Padfield is limited to analyze the steady-state payout motion of constant rotating fiber around the symmetrical axis of bobbin. Here the constant rotating fiber around the symmetrical axis of bobbin is located outside the bobbin.

Understanding the dynamic payout motion of optic fiber on the bobbin and in the air is necessary to analyze the unwinding optic fiber from the bobbin. The dynamic payout motion analysis also provide theoretical tool for the design of the FODL bobbin.

In this paper, for the analysis of the dynamic payout motion of optic fiber on the bobbin and in the air simultaneously a fundamental theory of optical fiber payout from FODL bobbin under gravity is formu-

lated [4, 5]. In the formulation of this theory inextensional optic fiber constitutive equation is applied to complete the equations of the motion. This theory also covers the gravity effect for the payout optic fiber motion.

For examining the capability of this theory we make computer simulation. As a result of computer simulation this theory provides the basic dynamic payout motion of optic fiber from the FODL bobbin.

2. Preliminary to the deduction of the equations of motion of optic fiber payout

2.1 Coordinates

Two type of coordinates are set in the space. These coordinates are shown in the Figure 1. One type of coordinates are local Cartesian coordinates. Another type of coordinates are global Cartesian coordinates. Three axes, three base vectors and position vector in the local Cartesian coordinates are described as $(x, y, z), (i, j, k), r$. Three axes, three base vectors and position vector in the global Cartesian coordinates are described as $(X, Y, Z), (I, J, K), R$.

Time is described as t .

2.2 The constitutive equation of optic fiber

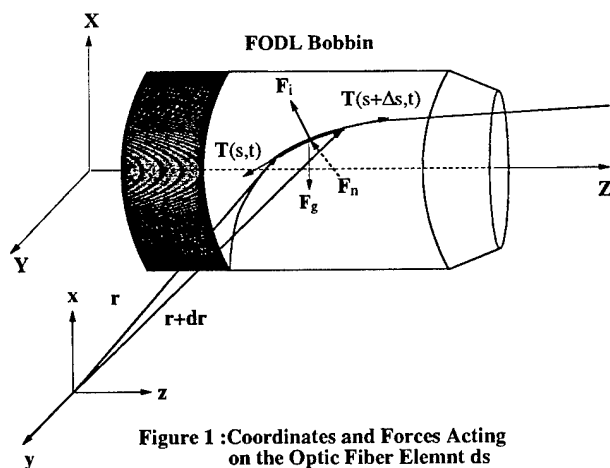


Figure 1 : Coordinates and Forces Acting on the Optic Fiber Element ds

In this analysis optic fiber is supposed as inextensional and perfect flexible string [6, 7].

This supposition originate from small elastic deformation compared with global motion during smooth optic fiber payout motion.

Suppose the length of differentialable optic fiber element ds . The inextensional optic fiber constitutive equation is described with differentialable optic fiber element ds as follows [8].

$$\frac{d(ds)}{dt} = 0 \quad (1)$$

2.3 Forces acting on the optic fiber and relative scope of forces

Forces acting on the optic fiber are tension, inertia, reaction on the bobbin, air drag, friction on the bobbin, gravity, bending moment, torque, etc.

The curvature of moving optic fiber during smooth payout motion is less than the curvature of the FODL bobbin. In this situation optic fiber is considerable as perfect flexible, bending momentless and torqueless.

For understanding of the basic payout dynamics of the optic fiber from FODL bobbin under gravity treated forces are limited to tension T , inertia F_i , reaction on the bobbin F_n , gravity F_g .

$$\begin{aligned} T &= T e_1, F_i = \rho_f \ddot{r}, F_n = F_n t_3, \\ F_g &= \rho_f g g, t_3 = t_{31} i + t_{32} j + t_{33} k, \\ e_1 &= \frac{\partial r}{\partial s} = e_{11} i + e_{12} j + e_{13} k \end{aligned}$$

where

$(\dot{})$: time differential, ρ_f : mass per unit length of optic fiber, t_3 : outer normal vector on the bobbin, g : gravity constant, g : accelerative unit vector of gravity.

3. The deduction of the equations of motion of optic fiber payout

The equations of motion of optic fiber payout is deduced from the balance of forces acting on the differentialable optic fiber element ds in Figure 1. The balance of forces is described by vectors as follows.

$$\frac{T(s+ds, t) - T(s, t)}{ds} + F_g + F_n - F_i = 0 \quad (2)$$

The differential form of the balance of forces at position r is derived from minimizing the differentialable optic fiber element ds with respect to equation (2).

$$\frac{\partial T(s, t)}{\partial s} e_1 + T(s, t) \kappa e_2 + \rho_f g g + F_n t_3 = \rho_f \ddot{r} \quad (3)$$

where

$$e_2 = \kappa^{-1} \frac{\partial e_1}{\partial s}, \kappa^2 = \frac{\partial^2 x}{\partial s^2} + \frac{\partial^2 y}{\partial s^2} + \frac{\partial^2 z}{\partial s^2}$$

The optic fiber is located on the FODL bobbin at initial state. The optic fiber move on the FODL bobbin to the edge of it during payout motion. The velocity of the optic fiber with respect to the outer normal direction on the bobbin is constrained. This

velocity constraint of the optic fiber is written as follows.

$$\dot{\mathbf{r}} \cdot \mathbf{t}_3 = 0 \quad (4)$$

The differentiation of equation(4) with respect to t is

$$\ddot{\mathbf{r}} \cdot \mathbf{t}_3 = 0 \quad (5)$$

F_n in the equation(3) is written by using the inner product of equation(3) and \mathbf{t}_3 and equation(5).

$$F_n = -\frac{\partial T(s, t)}{\partial s} \mathbf{e}_1 \cdot \mathbf{t}_3 - T(s, t) \kappa \mathbf{e}_2 \cdot \mathbf{t}_3 - \rho_f g \mathbf{g} \cdot \mathbf{t}_3 \quad (6)$$

Finally substituting equation(6) for F_n in the equation(3) the equations of motion of optic fiber payout is derived as follows.

$$\frac{\partial T(s, t)}{\partial s} (\mathbf{e}_1 - \mathbf{e}_1 \cdot \mathbf{t}_3 \mathbf{t}_3) + T(s, t) \kappa (\mathbf{e}_2 - \mathbf{e}_2 \cdot \mathbf{t}_3 \mathbf{t}_3) + \rho_f g (\mathbf{g} - \mathbf{g} \cdot \mathbf{t}_3 \mathbf{t}_3) = \rho_f \ddot{\mathbf{r}} \quad (7)$$

4. The procedure for the solution of the equations of motion of optic fiber payout

Continuous optic fiber is dealt with discrete optic fiber string. Minimizing the discretization error by finer discretization the solution of the discrete equations of motion of optic fiber payout give the solution of the equations of motion of optic fiber payout [9].

The procedure for the solution of the equations of motion of optic fiber payout consists of three step. In the first step continuous optic fiber is divided into elements of finite length optic fiber. In the second step for each element the difference equations of motion of optic fiber payout are applied by local Cartesian coordinates. In the last step the difference equations of motion of optic fiber payout for each element are assembled by global Cartesian coordinates and solved by time integration method.

4.1 The equations of motion of optic fiber payout for each element

Variables at each deviation point are shown as variables attached the number of deviation point. Deviation points (s, t) , $(s + ds, t)$ are numbered as (i) , $(i + 1)$. Element $(s, s + ds)$ is numbered as i element. The equations of motion of optic fiber payout in the difference form for each element are written by equation(2), (5) as follows.

$$\frac{T_{(i+1)} \mathbf{e}_{1(i)} - T_{(i)} \mathbf{e}_{1(i-1)}}{ds_{(i)}} + \rho_f g \mathbf{g}_{(i)} + F_{n(i)} \mathbf{t}_{3(i)} = \rho_f \ddot{\mathbf{r}}_{(i)} \quad (8)$$

4.2 The constitutive equation of tention

The constitutive equation of tention rewrites the equations of motion of optic fiber payout having tension to the equations of motion of optic fiber payout not having tension in the form suitable for solving. The constitutive equation of tention is derived by using the optic fiber constitutive equation(1) as follows.

Set $(x_{(i)}, y_{(i)}, z_{(i)})$ as the description point of the motion. the equations of motion of optic fiber payout at the point $(x_{(i)}, y_{(i)}, z_{(i)})$ is described as equation(8). At the same point $(x_{(i)}, y_{(i)}, z_{(i)})$ the equations of motion of optic fiber written by using the optic fiber constitutive equation(1) is as follows.

$$\frac{T_{(i+1)} \mathbf{e}_{1(i)} - T_{(i)} \mathbf{e}_{1(i-1)}}{ds_{(i)}} + \rho_f g \mathbf{g}_{(i)} + F_{n(i)} \mathbf{t}_{3(i)} = \rho_f \ddot{\mathbf{r}}_{(i)} \quad (9)$$

where variables attached (\cdot) mean variables written by using the optic fiber constitutive equation(1).

It is necessary for preserving the length of the optic fiber inextensional in the optic fiber payout motion that forces in the equation(8) are equal to forces in the equation(9) along the optic fiber. That is following.

$$T_{(i+1)} = T_{(i+1)}, T_{(i)} = T_{(i)}, F_{n(i)} = F_{n(i)} \quad (10)$$

$F_{n(i)}$ in the equation(9) is written by using the inner product of equation(9) and \mathbf{t}_3 and equation(5).

$$F_{n(i)} = -\frac{T_{(i+1)} \mathbf{e}_{1(i)} \cdot \mathbf{t}_{3(i)} - T_{(i)} \mathbf{e}_{1(i-1)} \cdot \mathbf{t}_{3(i)}}{ds_{(i)}} - \rho_f g \mathbf{g}_{(i)} \cdot \mathbf{t}_{3(i)} \quad (11)$$

The constitutive equation of $T_{(i+1)}$ in the recurrence form is derived by substituting equation(11) for equation(9) and the inner product of equation(9) and $\mathbf{e}_{1(i)}$.

$$T_{(i+1)} = \ddot{\mathbf{r}}_{(i)} \cdot \mathbf{e}_{1(i)} T A_{(i)} + T_{(i)} T B_{(i)} + T C_{(i)} \quad (12)$$

where

$$T A_{(i)} = \frac{ds_{(i)} \rho_f}{1 - (\mathbf{e}_{1(i)} \cdot \mathbf{t}_{3(i)})^2}$$

$$T B_{(i)} = \frac{\mathbf{e}_{1(i-1)} \cdot \mathbf{e}_{1(i)} - \mathbf{e}_{1(i-1)} \cdot \mathbf{t}_{3(i)} \mathbf{e}_{1(i)} \cdot \mathbf{t}_{3(i)}}{1 - (\mathbf{e}_{1(i)} \cdot \mathbf{t}_{3(i)})^2}$$

$$T C_{(i)} = -\frac{ds_{(i)} \rho_f g (\mathbf{g}_{(i)} \cdot \mathbf{e}_{1(i)} - \mathbf{g}_{(i)} \cdot \mathbf{t}_{3(i)} \mathbf{e}_{1(i)} \cdot \mathbf{t}_{3(i)})}{1 - (\mathbf{e}_{1(i)} \cdot \mathbf{t}_{3(i)})^2}$$

4.3 The difference form equations of motion of optic fiber payout using the recurrence form of tension

Applying equation(10)~(12) to equation(8) the difference form equations of motion of optic fiber payout using the recurrence form of tension is written as follows.

$$ba_{1(i)}\ddot{x}_{(i)} + bb_{1(i)}\ddot{y}_{(i)} + bc_{1(i)}\ddot{z}_{(i)} + \rho_f g b d_{1(i)} + be_{1(i)}\ddot{T}_{(i)} = bf_{1(i)}\ddot{x}_{(i)} \quad (13)$$

$$ba_{2(i)}\ddot{x}_{(i)} + bb_{2(i)}\ddot{y}_{(i)} + bc_{2(i)}\ddot{z}_{(i)} + \rho_f g b d_{2(i)} + be_{2(i)}\ddot{T}_{(i)} = bf_{2(i)}\ddot{y}_{(i)} \quad (14)$$

$$ba_{3(i)}\ddot{x}_{(i)} + bb_{3(i)}\ddot{y}_{(i)} + bc_{3(i)}\ddot{z}_{(i)} + \rho_f g b d_{3(i)} + be_{3(i)}\ddot{T}_{(i)} = bf_{3(i)}\ddot{z}_{(i)} \quad (15)$$

where $ba_{\alpha(i)}, bb_{\alpha(i)}, bc_{\alpha(i)}, bd_{\alpha(i)}, be_{\alpha(i)}, bf_{\alpha(i)}$, $(\alpha = 1, 2, 3)$ are following.

$$\begin{aligned} ba_{\alpha(i)} &= \frac{\rho_f e_{11(i)}(e_{1\alpha(i)} - e_{1(i)} \cdot t_{3(i)} t_{3\alpha(i)})}{1 - (e_{1(i)} \cdot t_{3(i)})^2} \\ bb_{\alpha(i)} &= \frac{\rho_f e_{12(i)}(e_{1\alpha(i)} - e_{1(i)} \cdot t_{3(i)} t_{3\alpha(i)})}{1 - (e_{1(i)} \cdot t_{3(i)})^2} \\ bc_{\alpha(i)} &= \frac{\rho_f e_{13(i)}(e_{1\alpha(i)} - e_{1(i)} \cdot t_{3(i)} t_{3\alpha(i)})}{1 - (e_{1(i)} \cdot t_{3(i)})^2} \\ bd_{\alpha(i)} &= \frac{g_{(i)} \cdot e_{1(i)}(e_{1(i)} \cdot t_{3(i)} t_{3\alpha(i)} - e_{1\alpha(i)})}{1 - (e_{1(i)} \cdot t_{3(i)})^2} \\ &\quad - \frac{g_{(i)} \cdot t_{3(i)} e_{1(i)} \cdot t_{3(i)}(e_{1(i)} \cdot t_{3(i)} t_{3\alpha(i)} - e_{1\alpha(i)})}{1 - (e_{1(i)} \cdot t_{3(i)})^2} \\ &\quad + g_{\alpha(i)} - g_{(i)} \cdot t_{3(i)} t_{3\alpha(i)} \\ be_{\alpha(i)} &= - \frac{e_{1(i-1)} \cdot e_{1(i)}(e_{1(i)} \cdot t_{3(i)} t_{3\alpha(i)} - e_{1\alpha(i)})}{\{1 - (e_{1(i)} \cdot t_{3(i)})^2\} ds_{(i)}} \\ &\quad + \frac{e_{1(i-1)} \cdot t_{3(i)} e_{1(i)} \cdot t_{3(i)}(e_{1(i)} \cdot t_{3(i)} t_{3\alpha(i)} - e_{1\alpha(i)})}{\{1 - (e_{1(i)} \cdot t_{3(i)})^2\} ds_{(i)}} \\ &\quad - \frac{e_{1\alpha(i-1)} - e_{1(i-1)} \cdot t_{3(i)} t_{3\alpha(i)}}{ds_{(i)}} \\ bf_{\alpha(i)} &= \rho_f \end{aligned}$$

4.4 The constitutive equation of $(\ddot{x}_{(i)}, \ddot{y}_{(i)}, \ddot{z}_{(i)})$

The constitutive equation of $(\ddot{x}_{(i)}, \ddot{y}_{(i)}, \ddot{z}_{(i)})$ at i division point as the description point of the motion is derived by the time differentiation of the inextensional optic fiber constitutive equation(1) in the i elemnt.

$$\frac{d^2(ds_{(i)})}{dt^2} = 0 \quad (16)$$

$ds_{(i)}$ in the i elemnt is following.

$$ds_{(i)} = (dx_{(i)}^2 + dy_{(i)}^2 + dz_{(i)}^2)^{\frac{1}{2}} \quad (17)$$

where

$$dx_{(i)} = x_{(i+1)} - x_{(i)}, dy_{(i)} = y_{(i+1)} - y_{(i)},$$

$$dz_{(i)} = z_{(i+1)} - z_{(i)}$$

$(\ddot{x}_{(i)}, \ddot{y}_{(i)}, \ddot{z}_{(i)})$ is rewritten by substitutiing equation(17) for equation(16).

$$\ddot{x}_{(i)} = \ddot{x}_{(i+1)} + X1_{(i)}(\ddot{y}_{(i+1)} - \ddot{y}_{(i)}) + X2_{(i)}(\ddot{z}_{(i+1)} - \ddot{z}_{(i)}) + X3_{(i)} \quad (18)$$

$$\ddot{y}_{(i)} = \ddot{y}_{(i+1)} + Y1_{(i)}(\ddot{z}_{(i+1)} - \ddot{z}_{(i)}) + Y2_{(i)}(\ddot{x}_{(i+1)} - \ddot{x}_{(i)}) + Y3_{(i)} \quad (19)$$

$$\ddot{z}_{(i)} = \ddot{z}_{(i+1)} + Z1_{(i)}(\ddot{x}_{(i+1)} - \ddot{x}_{(i)}) + Z2_{(i)}(\ddot{y}_{(i+1)} - \ddot{y}_{(i)}) + Z3_{(i)} \quad (20)$$

where

$$\begin{aligned} X1_{(i)} &= \text{sgn}(dx_{(i)})dy_{(i)} |dx_{(i)}|^{-1}, \\ X2_{(i)} &= \text{sgn}(dx_{(i)})dz_{(i)} |dx_{(i)}|^{-1}, \\ X3_{(i)} &= \text{sgn}(dx_{(i)})\{(d\dot{y}_{(i)}^2 + d\dot{z}_{(i)}^2) |dx_{(i)}|^{-1} \\ &\quad + (d\dot{y}_{(i)}^2 d\dot{y}_{(i)}^2 + d\dot{z}_{(i)}^2 d\dot{z}_{(i)}^2) |dx_{(i)}|^{-3} \\ &\quad + 2d\dot{y}_{(i)} d\dot{z}_{(i)} d\dot{y}_{(i)} d\dot{z}_{(i)} |dx_{(i)}|^{-3}\}, \\ Y1_{(i)} &= \text{sgn}(dy_{(i)})dz_{(i)} |dy_{(i)}|^{-1}, \\ Y2_{(i)} &= \text{sgn}(dy_{(i)})dx_{(i)} |dy_{(i)}|^{-1}, \\ Y3_{(i)} &= \text{sgn}(dy_{(i)})\{(d\dot{x}_{(i)}^2 + d\dot{z}_{(i)}^2) |dy_{(i)}|^{-1} \\ &\quad + (d\dot{x}_{(i)}^2 d\dot{z}_{(i)}^2 + d\dot{x}_{(i)}^2 d\dot{x}_{(i)}^2) |dy_{(i)}|^{-3} \\ &\quad + 2d\dot{z}_{(i)} d\dot{x}_{(i)} d\dot{z}_{(i)} d\dot{x}_{(i)} |dy_{(i)}|^{-3}\}, \\ Z1_{(i)} &= \text{sgn}(dz_{(i)})dx_{(i)} |dz_{(i)}|^{-1}, \\ Z2_{(i)} &= \text{sgn}(dz_{(i)})dy_{(i)} |dz_{(i)}|^{-1}, \\ Z3_{(i)} &= \text{sgn}(dz_{(i)})\{(d\dot{x}_{(i)}^2 + d\dot{y}_{(i)}^2) |dz_{(i)}|^{-1} \\ &\quad + (d\dot{x}_{(i)}^2 d\dot{x}_{(i)}^2 + d\dot{y}_{(i)}^2 d\dot{y}_{(i)}^2) |dz_{(i)}|^{-3} \\ &\quad + 2d\dot{x}_{(i)} d\dot{y}_{(i)} d\dot{x}_{(i)} d\dot{y}_{(i)} |dz_{(i)}|^{-3}\} \end{aligned}$$

The sign function $\text{sgn}(X)$ takes 1 if X is greater than zero, 0 if X equals zero and -1 if X is less than zero.

At the division point i as the description point of the motion the coordinate components of i division point written by using the inextensional optic fiber constitutive equation(1) and the coordinates is equal

to the coordinate components of i division point written directly by the coordinates as the description of the same physical phenomenon.

$$(\ddot{x}_{(i)}, \ddot{y}_{(i)}, \ddot{z}_{(i)}) = (\ddot{x}_{(i)}, \ddot{y}_{(i)}, \ddot{z}_{(i)}) \quad (21)$$

The constitutive equations of $(\ddot{x}_{(i)}, \ddot{y}_{(i)}, \ddot{z}_{(i)})$ is derived by applying equation(21) to equation(18)~(21).

4.5 The constitutive equations of $(\ddot{x}_{(i)}, \ddot{y}_{(i)}, \ddot{z}_{(i)})$ by the global Cartesian coordinates

The constitutive equation of $(\ddot{x}_{(i)}, \ddot{y}_{(i)}, \ddot{z}_{(i)})$ must satisfy the following equations not to be singular.

$$dx_{(i)} \neq 0, dy_{(i)} \neq 0, dz_{(i)} \neq 0 \quad (22)$$

The coordinate transformation between the local Cartesian coordinates and the global Cartesian coordinates for each element that satisfies equations(22) is set up as follows to use equation(18)~(21) at any point in space.

$$\begin{pmatrix} \ddot{x}_{(i)} \\ \ddot{y}_{(i)} \\ \ddot{z}_{(i)} \end{pmatrix} = \begin{pmatrix} L_{11(i)} & L_{12(i)} & L_{13(i)} \\ L_{21(i)} & L_{22(i)} & L_{23(i)} \\ L_{31(i)} & L_{32(i)} & L_{33(i)} \end{pmatrix} \begin{pmatrix} \ddot{X}_{(i)} \\ \ddot{Y}_{(i)} \\ \ddot{Z}_{(i)} \end{pmatrix} \quad (23)$$

The constitutive equations of $(\ddot{x}_{(i)}, \ddot{y}_{(i)}, \ddot{z}_{(i)})$ by the global Cartesian coordinates are derived from applying equation(23) to the right-hand sides of equation(18)~(21), applying equation(21) to the left-hand sides of equation(18)~(21).

4.6 The difference form equations of motion of optic fiber payout using the recurrence form of tension by the global Cartesian coordinates

The nonsingular difference form equations of motion of optic fiber payout using the recurrence form of tension at any point in space are written as the following equations($\alpha = 1, 2, 3$) by applying equation(18)~(23) to equation(13)~(15).

$$\begin{aligned} & ba_{\alpha(i)} \{ (L_{11(i)} + X1_{(i)}L_{21(i)} + X2_{(i)}L_{31(i)})\ddot{X}_{(i+1)} \\ & + (L_{12(i)} + X1_{(i)}L_{22(i)} + X2_{(i)}L_{32(i)})\ddot{Y}_{(i+1)} \\ & + (L_{13(i)} + X1_{(i)}L_{23(i)} + X2_{(i)}L_{33(i)})\ddot{Z}_{(i+1)} \\ & - (X1_{(i)}L_{21(i)} + X2_{(i)}L_{31(i)})\ddot{X}_{(i)} \\ & - (X1_{(i)}L_{22(i)} + X2_{(i)}L_{32(i)})\ddot{Y}_{(i)} \\ & - (X1_{(i)}L_{23(i)} + X2_{(i)}L_{33(i)})\ddot{Z}_{(i)} + X3_{(i)} \} \\ & + bb_{\alpha(i)} \{ (L_{21(i)} + Y1_{(i)}L_{31(i)} + Y2_{(i)}L_{11(i)})\ddot{X}_{(i)} \\ & + (L_{22(i)} + Y1_{(i)}L_{32(i)} + Y2_{(i)}L_{12(i)})\ddot{Y}_{(i)} \end{aligned}$$

$$\begin{aligned} & + (L_{23(i)} + Y1_{(i)}L_{33(i)} + Y2_{(i)}L_{13(i)})\ddot{Z}_{(i)} \\ & - (Y1_{(i)}L_{31(i)} + Y2_{(i)}L_{11(i)})\ddot{X}_{(i)} \\ & - (Y1_{(i)}L_{32(i)} + Y2_{(i)}L_{12(i)})\ddot{Y}_{(i)} \\ & - (Y1_{(i)}L_{33(i)} + Y2_{(i)}L_{13(i)})\ddot{Z}_{(i)} + Y3_{(i)} \} \\ & + bc_{\alpha(i)} \{ (L_{31(i)} + Z1_{(i)}L_{11(i)} + Z2_{(i)}L_{21(i)})\ddot{X}_{(i)} \\ & + (L_{32(i)} + Z1_{(i)}L_{12(i)} + Z2_{(i)}L_{22(i)})\ddot{Y}_{(i)} \\ & + (L_{33(i)} + Z1_{(i)}L_{13(i)} + Z2_{(i)}L_{23(i)})\ddot{Z}_{(i)} \\ & - (Z1_{(i)}L_{11(i)} + Z2_{(i)}L_{21(i)})\ddot{X}_{(i)} \\ & - (Z1_{(i)}L_{12(i)} + Z2_{(i)}L_{22(i)})\ddot{Y}_{(i)} \\ & - (Z1_{(i)}L_{13(i)} + Z2_{(i)}L_{23(i)})\ddot{Z}_{(i)} + Z3_{(i)} \} \\ & + \rho_f g b d_{\alpha(i)} + b e_{\alpha(i)} \underline{T}_{(i)} \\ & = b f_{\alpha(i)} (L_{\alpha 1(i)} \ddot{X}_{(i)} + L_{\alpha 2(i)} \ddot{Y}_{(i)} + L_{\alpha 3(i)} \ddot{Z}_{(i)}) \quad (24) \end{aligned}$$

4.7 The boundary condition on the surface of the FODL bobbin

4.7.1 The outer normal vector on the surface of the FODL bobbin

Continuous optic fiber is dealt with discrete optic fiber string in the procedure for the solution of the equations of motion of optic fiber payout. In the same procedure the FODL bobbin is dealt with multiangular prism as shown Figure 2.

The outer normal vector on the lateral surface of the multiangular prism is determined uniquely. But the outer normal vector on the side of the multiangular prism does not exist uniquely. Therefore the outer normal vector on the one lateral surface adjacent to the side is assigned to it. This assignment set up the outer normal vector on the lateral surface and on the side of the multiangular prism uniquely.

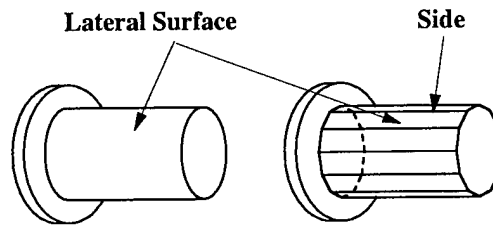


Figure 2 : Circular FODL Bobbin and Regular Multiangular Prism

4.7.2 The boundary condition on the surface of the FODL bobbin

The boundary condition on the surface of the

FODL bobbin is the velocity constraint written by the outer normal on the bobbin as equation(4). The movement of the optic fiber on the bobbin involves the change of the corresponding outer normal direction on the bobbin. The effect of the change of the outer normal direction on the bobbin for the velocity of the optic fiber on the bobbin is derived as follows.

The normal velocity of the division point on the bobbin is constrained by the boundary condition equation(4). Therefore the velocity of the moving division point on the bobbin is transferred as the velocity projected on the new corresponding surface with respect to the direction of the velocity. The magnitude of this new velocity projected on it is derived by using the inextentional optic fiber constitutive equation(1) and the boundary condition equation(4).

Suppose the velocity of the moving division point on the bobbin, the normal vector of the new corresponding surface and the new velocity on it as $\dot{\mathbf{r}}_{(i)}$, \mathbf{t}_3^n and $\dot{\mathbf{r}}_{(i)}^n$ respectively. One has the following equation.

$$\dot{\mathbf{r}}_{(i)}^n = \frac{V_{(i)}(\dot{\mathbf{r}}_{(i)} - \dot{\mathbf{r}}_{(i)} \cdot \mathbf{t}_3^n \mathbf{t}_3^n)}{|\dot{\mathbf{r}}_{(i)} - \dot{\mathbf{r}}_{(i)} \cdot \mathbf{t}_3^n \mathbf{t}_3^n|} \quad (25)$$

The magnitude $V_{(i)}$ of this new velocity is derived from the inextentional optic fiber constitutive equation(1) as follows.

The square of the i element length is written as

$$ds_{(i)}^2 = (\mathbf{r}_{(i+1)} - \mathbf{r}_{(i)}) \cdot (\mathbf{r}_{(i+1)} - \mathbf{r}_{(i)}) \quad (26)$$

Differentiate equation(26) with respect to t and apply equation(1) to equation(26).

$$\dot{\mathbf{r}}_{(i)} \cdot (\mathbf{r}_{(i+1)} - \mathbf{r}_{(i)}) = \dot{\mathbf{r}}_{(i+1)} \cdot (\mathbf{r}_{(i+1)} - \mathbf{r}_{(i)}) \quad (27)$$

Apply the new velocity $\dot{\mathbf{r}}_{(i)}^n$ to the velocity $\dot{\mathbf{r}}_{(i)}$ of equation(27) further. One has The following equation.

$$V_{(i)} = \frac{\dot{\mathbf{r}}_{(i+1)} \cdot (\mathbf{r}_{(i+1)} - \mathbf{r}_{(i)}) |\dot{\mathbf{r}}_{(i)} - \dot{\mathbf{r}}_{(i)} \cdot \mathbf{t}_3^n \mathbf{t}_3^n|}{(\mathbf{r}_{(i+1)} - \mathbf{r}_{(i)}) \cdot (\dot{\mathbf{r}}_{(i)} - \dot{\mathbf{r}}_{(i)} \cdot \mathbf{t}_3^n \mathbf{t}_3^n)} \quad (28)$$

The boundary condition on the surface of the FODL bobbin is rewritten as this new velocity $\dot{\mathbf{r}}_{(i)}^n$ by using equation(25) and equation(28) as follows.

$$\dot{\mathbf{r}}_{(i)}^n = \frac{\dot{\mathbf{r}}_{(i+1)} \cdot (\mathbf{r}_{(i+1)} - \mathbf{r}_{(i)}) (\dot{\mathbf{r}}_{(i)} - \dot{\mathbf{r}}_{(i)} \cdot \mathbf{t}_3^n \mathbf{t}_3^n)}{(\mathbf{r}_{(i+1)} - \mathbf{r}_{(i)}) \cdot (\dot{\mathbf{r}}_{(i)} - \dot{\mathbf{r}}_{(i)} \cdot \mathbf{t}_3^n \mathbf{t}_3^n)} \quad (29)$$

5 Computer simulation

For fundamental theoretical analysis of optic fiber

payout form FODL bobbin a optic fiber payout motion is simulated by computer using the deduced fundamental theory of optical fiber payout form FODL bobbin.

5.1 Conditions for the computer simulation

5.1.1 The discretization of optic fiber and FODL bobbin

For computer simulation the continuous optic fiber is discretized to the discrete optic fiber string. The FODL bobbin is also discretized to the multiangular prism shown in Figure 2.

5.1.2 The initial condition of optic fiber payout

The form specifications of the FODL bobbin and the optic fiber is shown in the Table 1. The initial state of the optic fiber is at rest shown in the Figure 4. Here the optic fiber is wound on the regular 36-multiangular prism. The pulling out point of the optic fiber is on the symmetrical axis of FODL bobbin.

The initial state of the tension is the following.

$$T_{(i)} = 0 \quad (i = 1, 160) \quad (30)$$

Table 1 :Specifications of FODL Bobbin

Item	Details
Form of FODL Bobbin	Inscribed Regular 36-Multiangular Prism
Radius of Inscribed Multiangular Prism	2C (C=26.8mm)
Linear Density	0.08g/m
Length of Element	0.3486C
Winding Pitch	0.25mm/2π
Number of Division Points	160

5.1.3 The condition of optic fiber payout

The wound optic fiber starts to unwind as the pulling out point begins to move on the symmetrical axis of FODL bobbin with $4g$ acceleration. The condition of the pulling out point and the boundary condition of the tension at the opposite end of the pulling out point are as follows.

$$\ddot{Z}_{(160)} = 4g \quad (31)$$

$$T_{(1)} = 0 \quad (32)$$

The division points of the optic fiber on the FODL bobbin move on the lateral surface of the regular 36-multiangular prism during the optic fiber payout.

5.1.4 Time integratin and coordinate transformation

The method of the Runge-Kutta is used for time integration of equations(24) in the computer simulation.

The coordinate transformation between the local Cartesian coordinates and the global Cartesian coordinates for each elemnt is set up at each time integration step as each elemnt has the same angle to each coordinate of the corresponding local coordinates.

5.2 Results of the computer simulation

Results of the computer simulation are shown in Figure 4~7. From these results the optic fiber is unwound as a locus of a trigonometric function. These shapes mean that the circularly wound optic fiber on the bobbin extend to the line. In the Figure 3 a unwound shape of the optic fiber generated by the 4g accelerating fall mass in the experiment is shown. The computed shapes are similar to the experimntal shape. The diffrence between the computed shape and the experiment shape comes from the rotation of the 4g accelerating fall mass in the fall.

These results shows that the fundamental theory is capable of the optic fiber payout dynamics of the FODL bobbin.

6 Conclusion

In this paper,for the analysis of the dynamic payout motion of optic fiber on the bobbin and in the air simultaneously a fundamental theory of optical fiber payout from FODL bobbin under gravity is formulated . The results of the computer simulation shows the fine capability of this theory for the analysis of the dynamic payout motion. This fundamental theory extends to the theory to handle the effect of the stiffness of optic fiber and air drag etc. in the next study.

References

- [1] Cerd Keiser : " Optical Fiber Communications " ,McGraw Hill, Inc(1983).
- [2] Abdul R. Habayeb:" Fiber Optic Guided Weapons" , IEEE LCS THE MAGAZINE OF LIGHTWAVE COMMUNICATION SYSTEMS,Vol.2,No.1,pp.17-28 (February 1991).
- [3] D.G.Padfield: " The Motion and Tention of an Unwinding Thread,Part I" , Proc.Royal Society of London, Series A,pp.382-407 (1958).

- [4] Akira akiyama, Mitsuru Shibata, Shinji Araki : " Fiber Optic Data Link Bobbin For Air Vehicles and Ground Station" , IEICE,3nd Conference of Society of Applied Optic Fiber Technology (1994).
- [5] Akira Akiyama : " A Fundamental Theory of Unwinding Optic Fiber's Motion with Fiber Optic Data Link Bobbin" , IEICE,Vol.J79-B-I No.1,pp.20-27 (January 1996).
- [6] Philip M. Morse,Herman Feshbach : " METHODS OF THEORETICAL PHYSICS" , The McGraw-Hill Book Company (1953)
- [7] Leonard Meirovitch : " ANALYTICAL METHODS IN VIBRATIONS" , The Macmillan Company (1967)
- [8] Shoshichi Kobayashi : " Differential Geometry of Curve and Surface" , Shokabo (1991)
- [9] Klaus-Jürgen Bathe : " Finte Element Procedures in Engineerng Analysis" , McGraw Hill, Inc(1982).

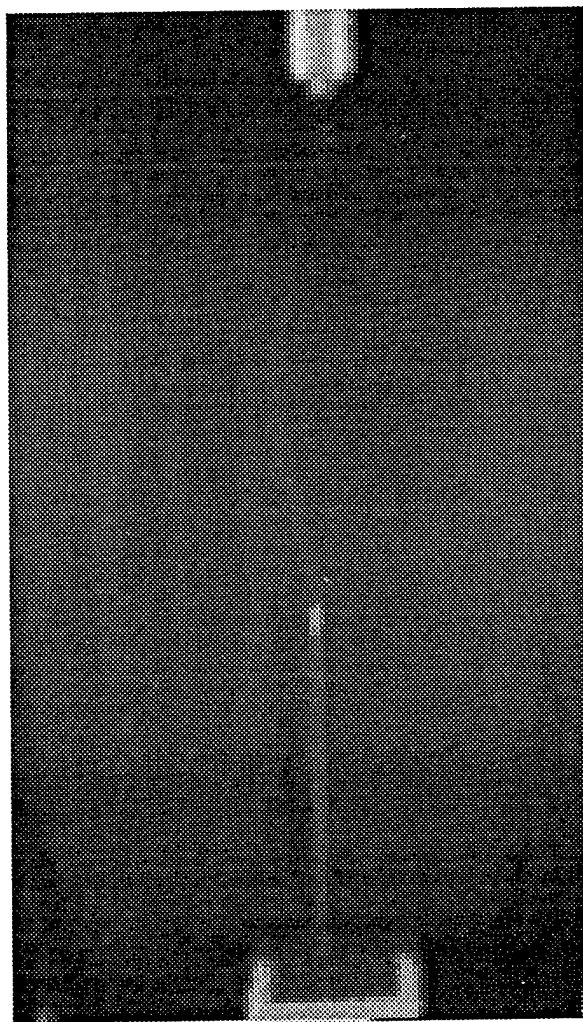


Figure 3 : 4g accelerating fall mass

Figure 4

Figure 5

Figure 6

Figure 7

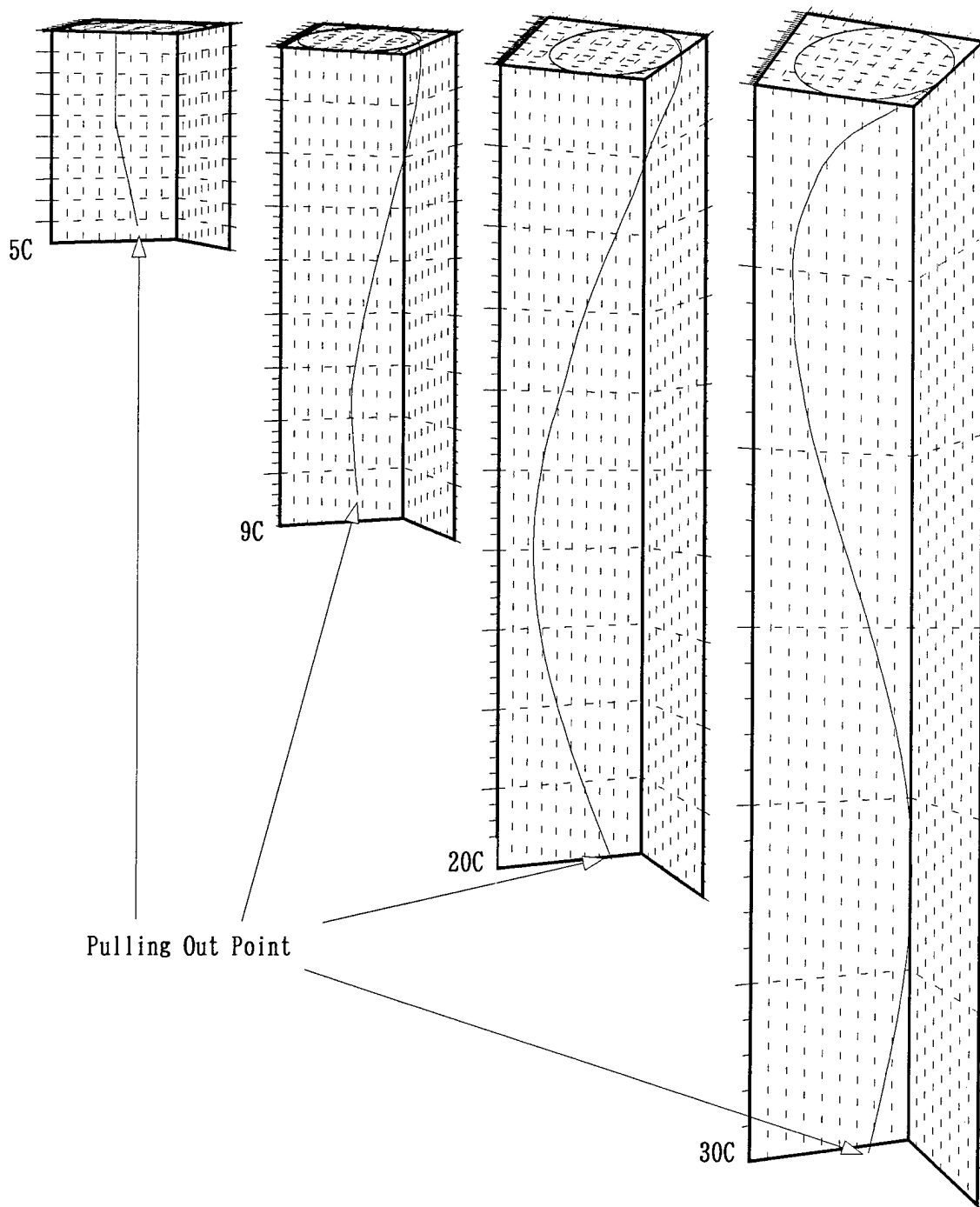
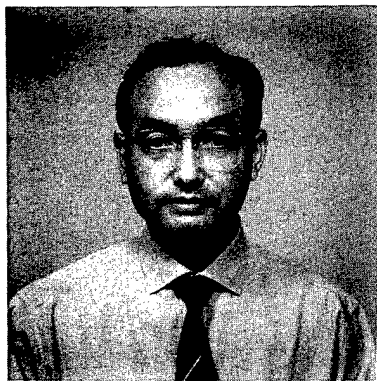


Figure 4-7 : Configurations of Unwinding Optic Fiber



Akira Akiyama
Third Research Center, TRDI,
Japan Defense Agency,
1-2-10 Sakae, Tachikawa, 190 Japan

Mr. Akiyama, who was born in 1952, joined Japan Air Self-Defense Force, JDA after graduating from National Defence Academy in 1975. He has been engaged in research and development of the guided missile after the Ph.D course in AMES,UCSD,USA. He is now a researcher of the 2nd guidance laboratory of the 3rd division,Third Research Center, TRDI,Japan Defense Agency and a member of IEICE of Japan.



Shinji Araki
Manufacturing Engineering Department,
Sakura Plant,
Fujikura Ltd.,
1440, Mutuzaki, Sakura, Chiba, 285 Japan

Mr. Araki, who was born in 1950, joined Fujikura Ltd. after graduating from Tokyo Metropolitan University in 1974 with a B.E. degree. He has been engaged in research and development of optical fibers and optical fiber coatings. He is now assistant general manager,manufacturing engineering department,Sakura plant and a member of IEICE of Japan.



Mitsuru Shibata
Aerospace Division, Aerospace Group,
Kawasaki Heavy Industries Ltd.
1,Kawasaki, Kagamihara, Gifu, 504 Japan

Mr. Shibata, who was born in 1949, joined Kawasaki Heavy Industries Ltd. after graduating from Tomakomai technical collage in 1970. He has been engaged in research and development of the guided missile. He is now assistant manager missile project engineering department,aerospace division,aerospace group and a member of IEICE of Japan.



Hidehiko Kubo
Third Research Center, TRDI,
Japan Defense Agency,
1-2-10 Sakae, Tachikawa, 190 Japan

Mr. Kubo, who was born in 1942, joined Technical Research and Development Institute, Japan Defense Agency after graduating from the Osaka Institute of Technology in 1966 with a B.E. degree. He has been engaged in research and development of the guided missile. He is now chief of the 3rd division,Third Research Center, TRDI,Japan Defense Agency and a member of IEICE of Japan.

DEVELOPMENT OF A 50 Hz HIGH CURRENT SYSTEM AND A UNIQUE IMPULSE CURRENT GENERATOR AND THEIR APPLICATION IN TESTING THE FAULT CURRENT RATING AND IMPULSE PERFORMANCE OF AN OPGW

Douglas M Burgess¹, Ronald C Kemp¹, Alan Stringer²

¹CSIRO Division of Applied Physics, Lindfield, Australia. ²Olex Cables, Tottenham, Australia

ABSTRACT

Optical Ground Wires (OPGW) must continue to provide a secure optical fiber communication link on high voltage aerial transmission lines, both during and after being subjected to fault currents and lightning strikes. The testing of OPGWs prior to installation, under conditions similar to those experienced when in use, is thus of considerable importance to the manufacturers of OPGWs and the supply authorities who use them. As the lightning impulse and heavy current facilities currently available in Australia are unsuitable for testing OPGWs, new facilities have been established at the Australian National Measurement Laboratory (NML) operated by the Commonwealth Scientific and Industrial Research Organisation (CSIRO). The design, development and performance of the new facilities will be discussed.

INTRODUCTION

Although OPGWs were first developed in the 1970's and thousands of kilometres have been installed worldwide, their use in Australia has been quite limited. This situation is expected to change as supply authorities are indicating a growing interest in opportunities for using optic fiber communication networks both for internal communications and monitoring and commercial requirements. This is also likely to be the case in the developing countries to the north of Australia where power transmission networks are being developed. The OPGW establishes an optical fiber communication capability on transmission line pylons while also providing a protective ground wire.

The service life of a HV transmission line may be 40 years and thus a similar requirement holds for OPGWs. Manufacturers and users of OPGWs thus have a critical interest in establishing their reliability and performance¹.

In service, OPGWs are strung on HV pylons with spans of perhaps 0.5 km and when subjected to fault currents will suffer a very rapid extension and sag due to the rapid temperature rise. Requirements for the optic fiber circuit are typically that changes in optical attenuation should be less than 1 dB per kilometre. A fault current test facility for OPGWs thus needs to expose a sufficient length of OPGW to the fault current so that meaningful measurements of optical attenuation and sag can be made. In addition it is also essential to monitor OPGW and fiber temperatures and tension.

The reliability of an OPGW when impacted by lightning strikes is subject to different considerations. A lightning strike may have a peak amplitude of up to 200 kA but occurs only over a very short time frame² although a strike may consist of a number of strokes. The effects of a lightning strike on an OPGW are likely to be felt at the point of impact and may consist of pitting or even breaking³ of the metallic strands in the ground wire. In any event the effects of a lightning strike on an OPGW are not so easily established, or even understood, as in the case of fault currents. There are also physical constraints as the energies involved in lightning strikes cannot be readily simulated in the laboratory. In practice this means that only short lengths of OPGW can be used as test pieces.

APPARATUS

Both high current systems are located inside the High Voltage Laboratory at NML which provides an

experimental environment 45 m long, 21 m wide and 19 m high. Advantages of this location include a stable temperature environment and ready access to a wide range of measuring equipment. Where possible, measurement and control equipment was installed in shielded enclosures to prevent electromagnetic interference (EMI). Particular attention was paid to the routing of cables and positioning of measuring devices, such as voltage transformers, current transformers and a current shunt, so as to minimise interference from nearby high electric and magnetic fields. Other methods used to reduce EMI included isolation through transformers, the use of high signal levels, optical isolation and proper earthing techniques.

50 Hz FAULT CURRENT APPARATUS AND PERFORMANCE

Fault Current Apparatus Two 5 tonne concrete blocks, located 39 m apart on the floor of the laboratory, are used as anchoring points to suspend, under tension, an OPGW in a hairpin loop. In order to minimize circuit inductance and hence maximise supply authority power factor the long parallel sides of the hairpin are placed close together and can be either 0.4 m or 0.8 m apart.

Electrical connections to the OPGW, from the high current transformer, are made at the open end of the hairpin loop near one concrete block. At the closed end of the hairpin loop, a shorting bar is connected between the parallel parts of the OPGW so as to provide a fine current control and to prevent any significant portion of the test current flowing around the closed end of the hairpin which is not under tension. Using this arrangement it is possible to expose up to 65 m of tensioned OPGW to the test current. During testing, mechanical forces are developed between the parallel arms of the hairpin due to opposing magnetic fields. These mechanical forces tend to push the parallel sides of the hairpin apart. To restrain the OPGW, insulating tubes are attached between the arms of the hairpin at about 3 m intervals. A photograph of a suspended OPGW is shown in Fig. 1 and a schematic diagram of the test rig is shown in Fig. 2.

Transformer. An Australian produced 1.1 MVA, 11 kV single phase, dry type, cast resin test

transformer was selected to provide short term high currents for OPGW testing. Advantages of this type of transformer include high winding strength and low voltage drop due to internal impedance which in this case was less than 2 % at full load. In addition, this type of transformer was the most suitable for laboratory installation as no oil retention provisions were required as would be the case in the event of catastrophic failure of an oil filled transformer.

To provide a large output voltage range, four identical secondary windings are incorporated, with each secondary winding provided with a tap allowing either the whole, 1/8 or 7/8 of the winding to be used. Nine separate secondary winding configurations are available, giving from 28 V to 1400 V at no load. Fine output voltage adjustment is achieved by selecting one of 11 taps on the 11 kV primary winding. A photograph of the transformer is shown in Fig. 3.

Control and Protection. For safety and to prevent detrimental effects on the local power grid, it is important to have a reliable and foolproof control and system fault protection scheme. To achieve this, the high current transformer control system is supplied from a dedicated uninterruptible power supply. This ensures voltage stability and surge isolation as well as continuity of control supply, enabling an orderly system shut-down in case of mains failure.

System fault protection is provided by an electronic overcurrent relay, a transformer over-temperature scheme, transformer differential current and switchgear frame leakage schemes. The electronic overcurrent relay enables any of seven different characteristics to be selected to provide the most suitable protection for the test being performed.

To make it possible to conduct symmetrical or asymmetrical high current tests on OPGWs, point-on-wave switching is incorporated in the control scheme. This enables either a maximum or minimum peak current to be obtained on the first half cycle of a high current test.

Electrical Measurements. Electrical quantities are measured using a personal computer (PC) to control an analogue to digital converter which also stores waveforms from a test. The OPGW

test current, transformer output voltage and transformer input voltage and current waveforms are all recorded synchronously. Computer software enables RMS and peak measurements to be made on any part of any trace. An OPGW test current of 20 kA_{rms} has been shown to have a measurement uncertainty of less than $\pm 0.5\%$. Phase angle can also be determined between any two traces enabling a power-factor measurement.

Immediate documentation of test results is possible. Any particular trace or any two traces can be selected to be output to a laser printer.

Operation of 50 Hz System. Once an OPGW has been set up and tensioned, a high current test involves the following sequence of events. Firstly the test transformer is energised by closing an 11 kV vacuum circuit-breaker on the primary side of the transformer. A 'make' switch on the transformer output, in series with the OPGW, is then closed to initiate testing. After the appropriate test period, which is measured with an adjustable protection timing relay, the vacuum circuit-breaker on the transformer primary is opened to complete the test.

A vacuum circuit breaker was selected for use with the high current test system because of its suitability for breaking currents below 2 kA at relatively low power-factor. One disadvantage of using a vacuum circuit breaker is its tendency to current chop and thus produce transient voltage surges that can damage electrical insulation due to uneven voltage distribution. To protect the test transformer from possible insulation damage, high frequency surge diverter networks were installed.

An important component of the high-current system is the 'make' switch which is a modified air circuit breaker. Switching time for this device has to be as consistent as possible to enable accurate point-on-wave switching on the first half cycle of the test current *ie* for symmetrical or asymmetrical test currents. A switching jitter of less than ± 5 degrees has been achieved.

The high current system also has the capability to perform a double fault test. Often faults on transmission lines are of a temporary nature *eg* conductor clashing due to wind. However, system protection will still de-energise the line. To improve supply reliability, many electricity authorities arrange for

circuit breakers to automatically reclose shortly after opening due to a system fault. If a fault is still present on the line after reclosure then the circuit breakers will lock out. OPGWs installed on such a system must therefore be able to withstand the application of two closely spaced high current tests. The 50 Hz high current system described here is designed to be able to perform a second high current test within an estimated 10 seconds of the initial test.

Monitoring of OPGW Behaviour. OPGW temperatures, optical attenuation, tension and sag are all recorded using a data logger/voltmeter controlled by a PC. Quantities such as temperature and optical attenuation can be plotted in real time on the PC monitor to provide a detailed view of OPGW behaviour.

OPGW temperatures are measured using thermocouples both on the surface and, where possible, close to the optic fibers. As a check two thermocouple systems are used. One of these has a digital readout to provide a visual indication of surface OPGW temperatures. Some OPGWs may incorporate a temperature sensitive optic fibre which is preferable to thermocouples.

Optical attenuation is monitored by means of an optical power meter and a differential sensing arrangement so that changes of power level in the light source are corrected for. When operating in differential mode, changes of optical power of 0.001 dB can be monitored. It is important to expose the maximum possible length of optic fiber to the high current and this is done by concatenating the fiber. For a 24 fiber OPGW more than 1 kilometre of fiber can be exposed to the fault current.

The sag and mechanical oscillations of the OPGW are measured using a simple wheel, attached to the OPGW, which travels on a vertical track and rotates a linear variable resistance which is measured by a digital ohmmeter and transferred to the PC. OPGW tension is measured using in-line load cells. Tension adjustment is carried out using in-line turnbuckles.

Performance of the 50 Hz System

The test transformer can deliver up to 100 kA for 1 second. During acceptance testing, a secondary winding temperature rise of only 2° C was recorded

after delivering 65 kA for 1 second. System output limits are mainly determined by a combination of supply voltage drop and duration as well as temperature rise of the supply authority cable from a local substation. So far, testing has required 20 kA to be supplied for 0.45 s through 53 m of the test OPGW. The 19 mm diameter OPGW under test is described elsewhere⁴ and consisted of 2 layers of 2.75 mm diameter strands incorporating 24 aluminium strands and 6 aluminium clad steel strands. The optic fiber unit was centrally located. The 50 Hz system is capable of conducting the same test on 65 m of OPGW which is the maximum length that can be accommodated. Much higher currents can be applied to shorter lengths, for example, an estimated 15 m of the test OPGW can be subjected to a 50 kA test current for 0.5 s.

IMPULSE CURRENT GENERATOR AND PERFORMANCE

As the voltages of a lightning strike cannot readily be simulated in the laboratory, efforts were focused on using short lengths of OPGW as test pieces. In this way peak currents representative of those occurring in lightning strikes can be obtained.

Experiments to date have been carried out using a shorter version of the heavy current test rig in which approximately 8 m of OPGW is suspended horizontally under tension between the two 5 tonne concrete blocks. High voltage porcelain disk insulators are used at each end of the OPGW to insulate it from the blocks. The arrangement is such that optical attenuation in the fibers can be monitored as can fiber temperatures by way of a temperature sensitive optic fiber.

To simulate a lightning strike, an arc is produced on the surface of the OPGW by closing a remotely operated mechanical switch. Closing the switch allows previously charged capacitors to discharge via approximately 1 m of OPGW, the switch, a low inductance wave shaping resistor and a coaxial current measuring shunt. Output voltage from the measuring shunt is fed via a coaxial cable to a differential voltage measuring probe, the output of which is measured with a digital storage oscilloscope. Both the differential probe and the oscilloscope are located in an EMI screened enclosure.

A schematic diagram of the test rig is shown in Fig. 4.

The capacitor bank is rated at 176 kV and can produce up to 300 kA_{pk}. An initial objective of producing a 130 kA_{pk}, 8/20 μ s wave shape has been achieved with a charging voltage of 83 kV. Some surface erosion on the strands of the test OPGW was observed after one discharge but no strands were broken.

The most critical factor controlling the peak current obtainable is the circuit inductance, which translates to the circuit length. Hence special attention was paid to the generator design so as to minimise circuit length. Where possible parallel conductors were used to reduce inductance. A further design consideration was to make the impulse generator demountable so that it can be brought up to a suspended OPGW and assembled around it.

Comparisons of measured peak current with the calculated value obtained from circuit inductance and resistance values has shown that a current measurement error of less than 10 % exists.

In the absence of a recommended standard for lightning resistance of OPGW, it is planned to develop the impulse current generator to achieve a 200 kA peak pulse with a low level DC component following the peak as described in Military Standard MIL-STD-1757A².

CONCLUSIONS

A flexible 50 Hz high current test system for OPGWs has been developed and enables a wide range of test currents and test durations to be achieved. Accurate data relating to the high current and also optical attenuation, temperature, sag and tension can be gathered and recorded. The system has been used to test an OPGW consisting of two layers of strands with currents of 20 kA for 0.45 s.

An impulse current test system for OPGWs has been designed and constructed. In preliminary operation, the system has been able to deliver a 130 kA_{pk}, 8/20 μ s pulse to an OPGW. Damage to the strands consisting of minor surface pitting occurred after one such pulse. It is planned to extend the capabilities of the system to obtain current pulses of 200 kA_{pk}.

REFERENCES

1. "Design, Testing and Validation of Optical Ground Wires and Hardware for use in Hydro-Quebec's 5000 km of Telecommunication Network", E Ghannoun et al CIGRE 22-301, 1996.
2. MIL-STD-1757A: "Lightning Qualification Test Techniques for Aerospace Vehicles and Hardware"
3. "Lightning Strike Resistance of OPGW", J P Bonicel et al IWCS 1995, p800
4. "Development and Characterisation of a New Dielectric Cored OPGW", A Stringer et al IWCS 1996

AUTHORS

Douglas M Burgess
CSIRO Division of
Applied Physics
Bradfield Road
Lindfield 2070
Australia



Douglas Burgess was born in Tamworth, Australia. After completing secondary education he completed an electrical traineeship with the Australian Department of Civil Aviation and also obtained an Electrical Engineering Certificate. In 1980 he joined the CSIRO National Measurement Laboratory and worked in the HV Laboratory on high voltage testing and measurement and standards development. In 1982 he completed an Electronics and Communications Certificate concentrating on digital systems. Since 1992 he has designed and developed high current systems for the testing of OPGWs.

Ronald C Kemp
CSIRO Division of
Applied Physics
Bradfield Road
Lindfield 2070
Australia



Ronald Kemp was born in Dursley, England. He graduated from the University of Bristol with a BSc Honours Degree in Physics in 1961 and received a PhD from the University of Birmingham in 1964. He then joined the CSIRO Division of Physics, Australia as a Research Fellow. Since then he has worked on electron spin resonance, temperature measurement and standards and heat transfer problems associated with the cable industry. He is now a Senior Principal Research Scientist with the CSIRO Division of Applied Physics.

Alan Stringer
Olex Cables
207 Sunshine Road
Tottenham 3012
Australia



Alan Stringer was born in London, England. He graduated from the City University in London with a BSc Honours Degree in Electronics Engineering in 1979 and a PhD in Electronics and Electrical Engineering in 1984. He joined the Central Research Laboratories of BICC where he worked in the Measurement and Instrumentation Division of the Engineering Research Department. He emigrated to Australia in 1986 where he joined Olex Cables, a Division of Pacific Dunlop, as a Senior Development Engineer and is now a Research and Development Manager in the Olex Communications Division.

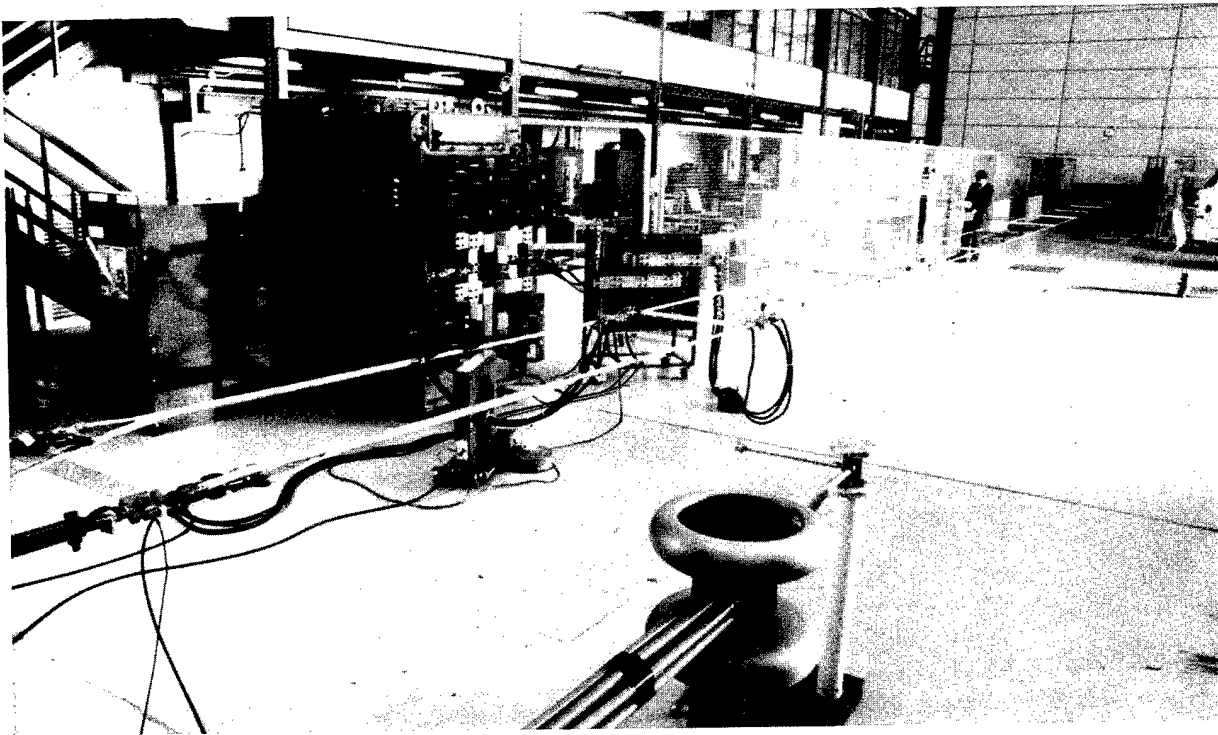


Fig. 1 Suspended OPGW in Short Circuit Test Rig.

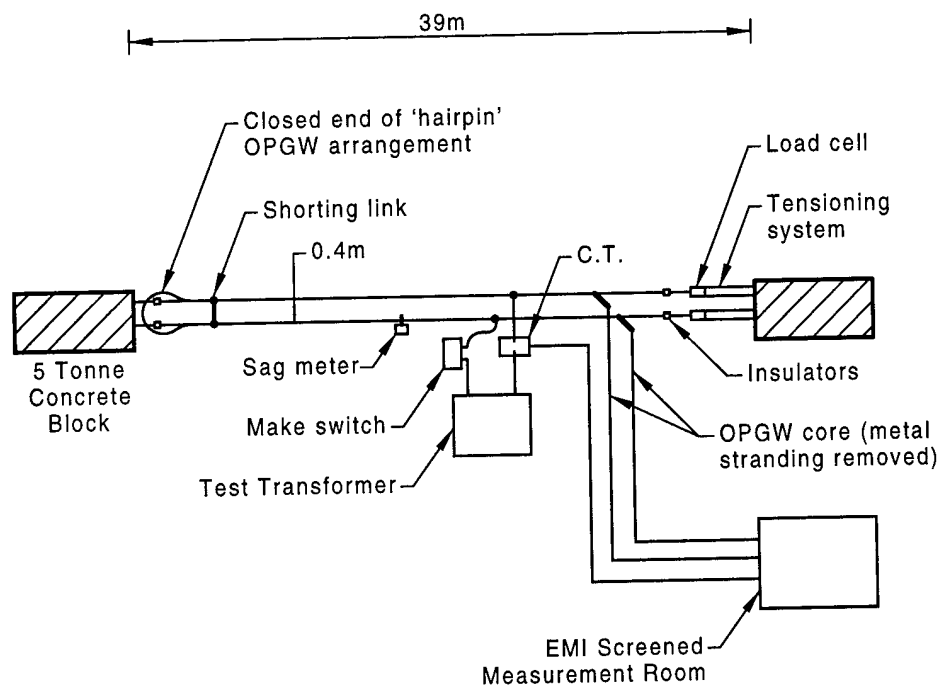


Fig. 2 Schematic Diagram of Short Circuit OPGW Test Rig.

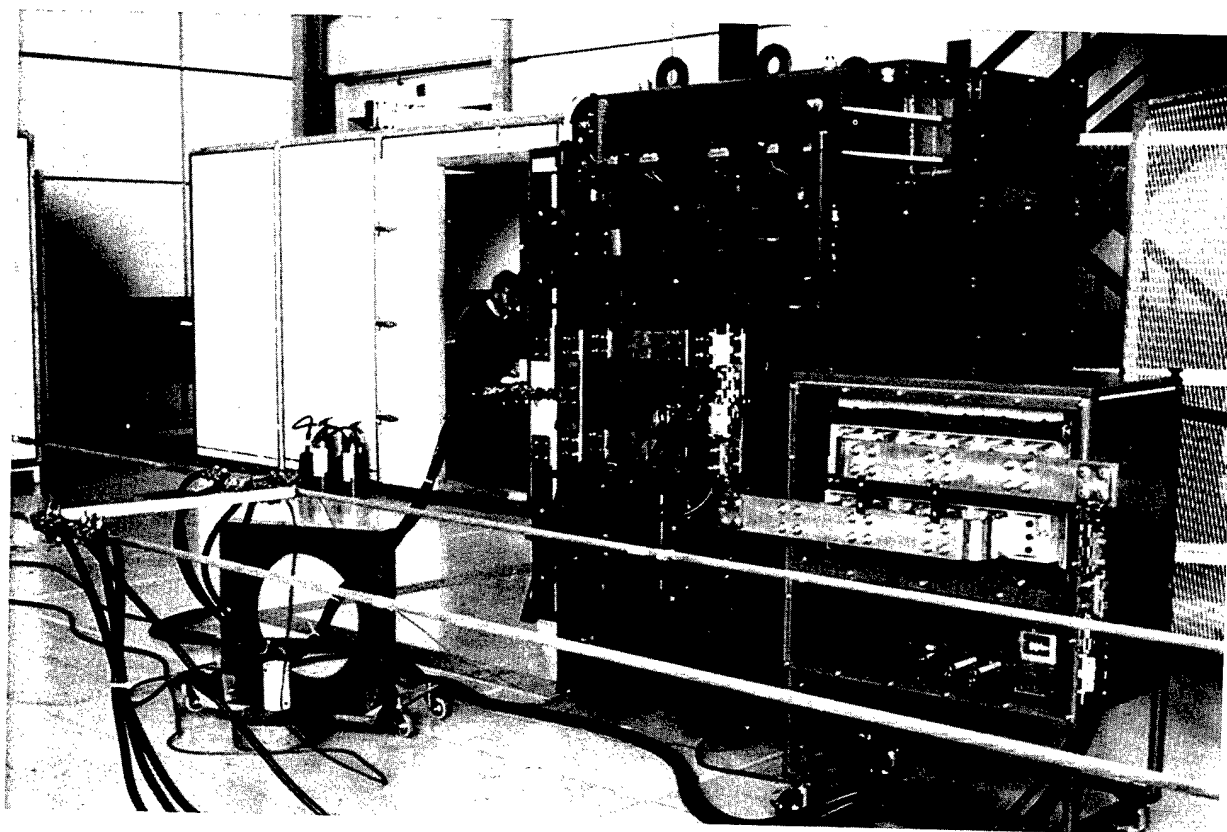


Fig. 3 Heavy Current Transformer.

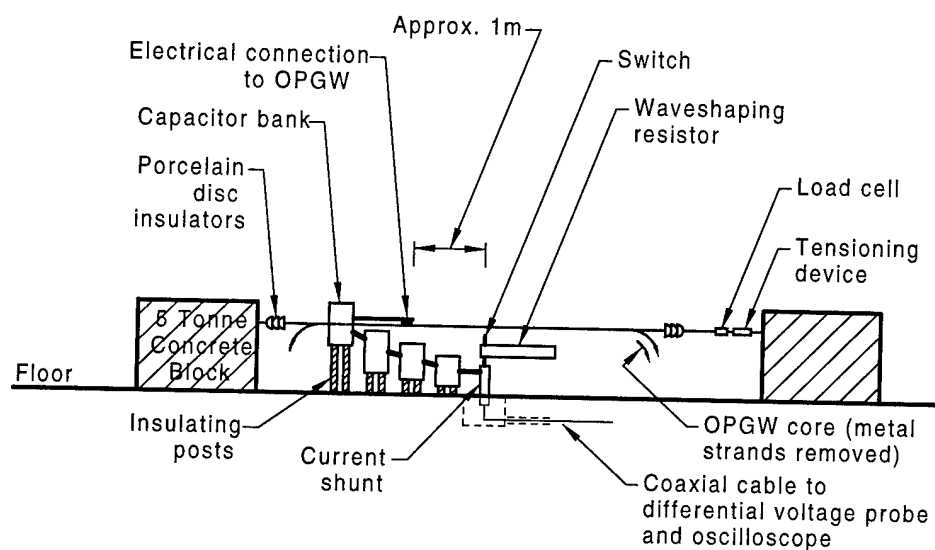


Fig. 4 Schematic Diagram of Impulse Current Test Rig.

STUDY AND ANALYSES OF RODENT ATTACKS IN OPTICAL FIBER CABLES

*Paulo J.P. Curado, *Carlos Pitombo, *Derval dos Santos Rosa
** Antonio C. Pereira Netto, ** João Elias Filho, ** Marcilio E. Latini

*TELEBRÁS - Research and Development Center -Campinas
** EMBRATEL - Optical Systems Division -Rio de Janeiro
Brazil

ABSTRACT

In this work we are going to describe studies conducted to evaluate rodent attack to optical fiber cables for use in buried networks for long distance systems in Brazil.

For facilities an easier installation and electrical protection, these cables must be dielectric; however they are subject to the attack of rodents which are urban and native of the country.

The development of tests to evaluate the resistance of optical cables to rodent attack, and the results of these tests will be presented. These tests were conducted in different models of optical cables specially designed for this purpose.

Therefore, two types of tests have been developed, with and without stimulus to rodent attack, considering that in both cases there is the same degree of aggressiveness.

With these tests, many types of cables were analyzed. Two types tested were considered effective against rodent attacks and acceptable for installation.

INTRODUCTION

The use of buried optical cables in Brazil is relatively recent. At the moment, they are used to interconnect the main Brazilian cities.

Installation of approximately 10,000 km of these cables is under way.

Due to problems with electric protection and maintenance, these cables should be dielectric. These requirements are part of the specifications, which were initially based on international recommendations¹, adapted to conditions in Brazil.

One of the possible problems was the attack of living organisms to optical cables. A previous work² showed the first studies conducted to analyze biological attacks to optical fiber cables and the development of tests to verify their resistance to the attack of fungi and insects were shown.

In the case of rodents, this problem was already detected in the first implantations, with, some cases of interruption of cables which were destroyed by rodents. Although this problem does not interrupt the services, because there are alternative routes, it is necessary to find solutions of cables that are resistant to these attacks.

RODENTS IN BRAZIL

Brazil has a huge territory, a great part of which remains unexplored. The optical cables need to cross these uninhabited areas under completely different conditions.

By mapping the mammals available³ and with the help of institutions dedicated to the study of mammals, several rodents have been detected which can attack optical cables during their working life.

These rodents can be divided into two types: the wild ones and urban ones. Urban rodents are the ones existing in the whole world, which are the house mice, the common rats and big rats. These species live in our cities, and do not have natural enemies. They are extremely aggressive.

Native rodents, which may attack optical cables, may be found all over the country. Those of greater potential are of the gender *Cetnomis* (Tuco-tuco), *Trycomis* (Rabudo or Punaré), among others.

Other rodents can be added to this list, if we consider that the mapping of these species in Brazil is still in development.

A remark to be made on rodents is that the Brazilian legislation does not allow killing native mice, and the use of rodenticides to kill them is forbidden. Therefore, resistant cables are required against rodent attacks.

The use of poison in the cable jacket is not recommended because it does not protect the cable properly, since the animal dies only after destroying the cable. The use of poison during the installation of cables is not only dangerous to operation personnel, but can also contaminate underground water sheets.

INITIAL DEVELOPMENT

The studies were initiated with two basic purposes:

- Evaluation of the cables being installed;
- To establish standard tests to evaluate the rodent attack.

Therefore, 3 types of optical cables designed to be buried were tested together with a cable with a LAP sheath which would serve as a control for comparison. These cables can be seen in Figure 1.

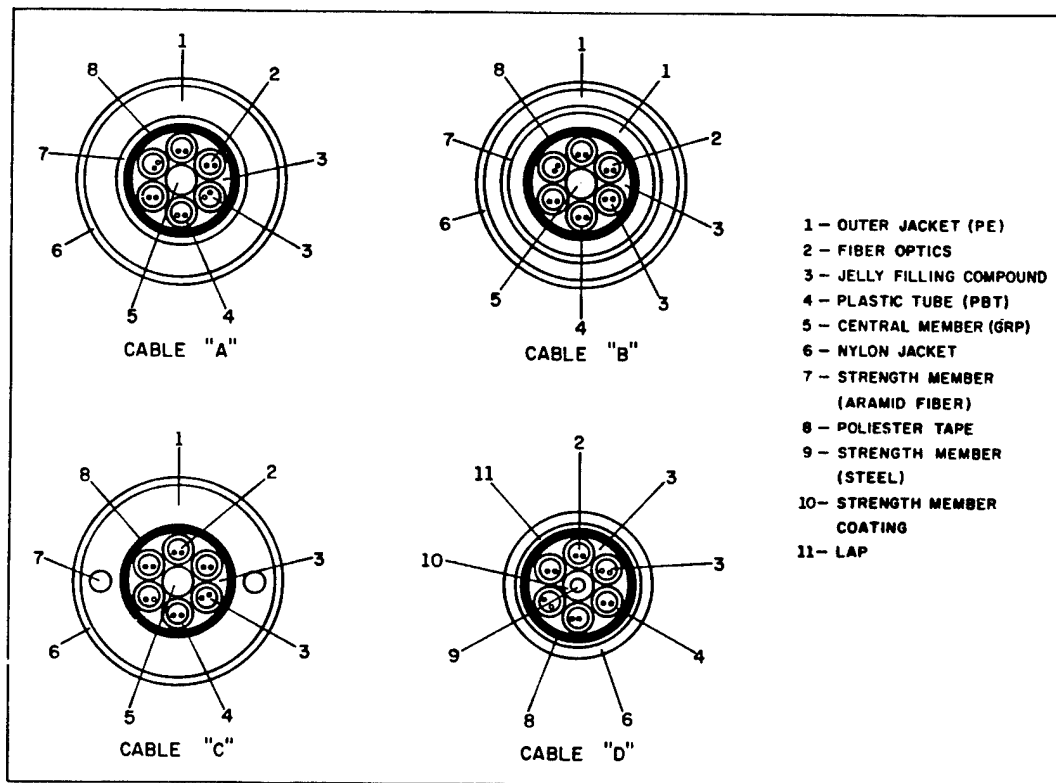


Figure 1 - Optical Cables

In order to analyze these cables, a test was developed using the *Rattus Norvegicus* species, the rat, which was captured in the wild. Laboratory specimens were not used because they do not have the required aggressiveness.

To stimulate the attack, the animals were deprived of water and food. A cage was projected, divided in two halves: one side had the animals' nest and the other had food and water, with a passage between these two compartments.

During the test, a cable was introduced in the passage to prevent the rodent from crossing to the other side to feed. The test lasted three days and the condition of the rodents was controlled daily. In each cage only one rodent was placed.

To analyze the results, according to the depth of the attack to the optical cables, damage indexes were set. These are shown in Table 1.

Table 1 - Damage Index

Index	Damage to the optical cable
0	No damages
1	Damaged jacket
2	Protection against rodents damaged
3	Protection against rodents destroyed
4	Core coating damaged
5	Core coating destroyed
6	Core damaged
7	Cable cut

For each type of cable ten samples were analyzed. The results can be seen in Table 2.

Table 2 - Results of the tests

Index	Quantity of cables			
	A	B	C	D
0	4	5	4	2
1	0	0	0	0
2	0	1	0	0
3	0	0	0	0
4	0	0	3	1
5	1	0	0	1
6	3	2	1	1
7	2	2	2	5
Average	3.7	2.8	3.2	5.0

It can be seen that not all cables had a satisfactory performance, considering that over half of the cables had their optical fibers attacked. Cable D had the worst performance, after cables C, A and B.

Parallel to these tests, one of the types of cables was damaged in the field, which showed the inefficiency of the protections.

Therefore it was concluded that the cables tested were not acceptable when there is need for rodent-resistant cables.

One of the most interesting results found in these tests was that in the cables damaged by rodents the material used as central element remained untouched, which is a good indication that the material can be a barrier against rodent attack. This element is glass-reinforced plastic rod (GRP).

From these results, studies were started to get models of rodent-resistant dielectric cables.

TEST DEVELOPMENT

Although the test was able to evaluate adequately the rodent-resistance of the cables, it has some inconveniences and difficulties. Therefore alternatives were sought to facilitate the conduction of the test.

The rodents chosen, besides being difficult to handle due to their aggressiveness, showed signs of learning, i.e., their individual aggressiveness changed as tests were carried out and it was necessary to get new animals, which is not always easy.

Another difficulty was that, due to the fact that the test was stimulated, i.e., with deprivation of food and water, there should be a break between tests, so the animals can rest.

Taking these factors into account, studies were conducted to develop a test where the stimulus to attack would not be required, besides the rodents' need to wear their teeth.

This way, tests were made with several species of rodents without any stimulus, i.e., the cables were simply left in gages with no partitions. Provisions were taken to protect cable ends.

For each species 4 to 6 cables of the types already shown were tested. The results were

somehow surprising and are shown in Table 3.

Table 3 - Tests with stimulus

Species	Results
<i>Tricomys apereoides</i>	Destroyed cables
<i>Proechimys sp</i>	Did not attack
<i>Bolomys lasiurus</i>	Attack the ends
<i>Akodon cursor</i>	Did not attack
<i>Oxymycterus sp</i>	Attack the ends
<i>Rattus norvegicus</i>	Did not attack

As we can see, the species *Trycomis Apereoides* had the best results to be used in the tests because it damaged the cables at the same level of the stimulated tests conducted with *Rattus norvegicus*. This species can be used to evaluate cables as to their resistance to rodents. Furthermore, it is a very gentle and easy-to-handle species. As the test does not subject the animal to any kind of deprivation, it can be conducted continuously, thus speeding up studies.

The *Rattus norvegicus*, in spite of its high aggressiveness, was not interested in touching the cables.

From the results of the former tests, it was seen that a follow-up on the aggressiveness of the animals is required along the tests to prevent the use of animals that change their behavior due to learning.

Therefore, a system to follow-up on the animals' aggressiveness was established, by following up on relative indexes among animals.

MATERIAL TESTS

From the results in the initial study, we tried to test alternative materials which might be used in optical fiber cables with prospects to protect them from rodent attack.

In the initial course of action, materials were sought which might protect the cables and prevent attack due to the hardness of the material, or due to the discomfort caused to the animal while attacking. Another solution might be a combination of the two.

So, we selected materials commercially available which showed these characteristics. The materials selected were:

- 1 or 2 mm diameter GRP (As indicated in the results of the initial tests).
- Fiberglass filaments.
- 1 or 2 mm diameter rod reinforced with Aramid
- High density polyethylene in 41 mm diameter pipes
- High hardness polyamide
- Fiberglass-reinforced polymers for extrusion (PE or Polyamide).

These materials were tested by using *Rattus norvegicus* in stimulated tests where the materials block the passage of these rodents to reach water and food.

For the tests with rods, test specimens were prepared, where 5 or 6 GRP or Aramid reinforced rod were set parallel on a base and this set blocked the passage of the rodent. The results obtained with this test are shown in Table 4.

Table 4 - Tests Materias

Material	Spl	Damage		
		Total	Partial	No Damage
GRP 1 mm	4	2	1	1
GRP 2 mm	6	0	1	5
Ara. 1 mm	5	4	0	1
Ara. 2 mm	6	1	4	1

The results with GRP rods were very good. The material has good prospects for use in cables.

Polyethylene ducts were tested and did not show a satisfactory performance once they were thoroughly destroyed.

Only one sample of fiberglass-reinforced polyamide, which was not considered viable for the cable manufacturing process because fiberglass damages machines during extrusion. For this material a sample obtained by injection was used. It had a good performance and was not destroyed in the test.

In the case of fiberglass in filaments and high hardness polyamide only test in cables will be possible.

With these results, some models of optical cables were projected so their resistance to rodents could be analyzed.

TESTS WITH CABLES

With the results of the tests in hands, several alternatives for optical cables with protection against rodent attack were proposed. These projects were factory-manufactured and prototypes were built for tests.

In the following Figures 2, 3 and 4 three types of optical cables tested are shown:

- GRP Armor (cable "E")
- Spaced GRP armor (Cable "F")
- Cables protected with fiberglass filaments or fabric and a layer of polyamide in composed protections (Cable "G" and "H").

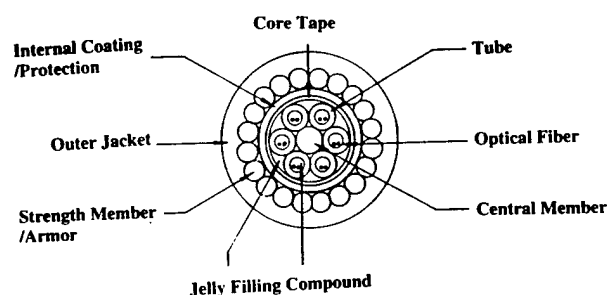


Figure 2 - Cable "E"

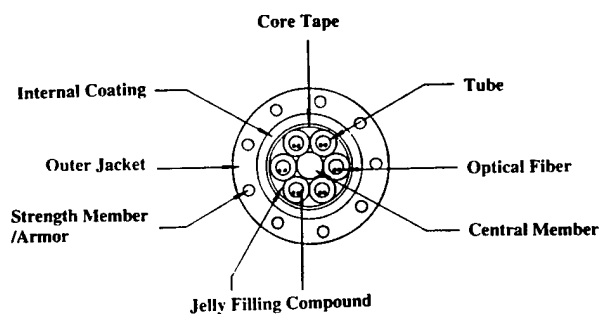


Figure 3 - Cable "F"

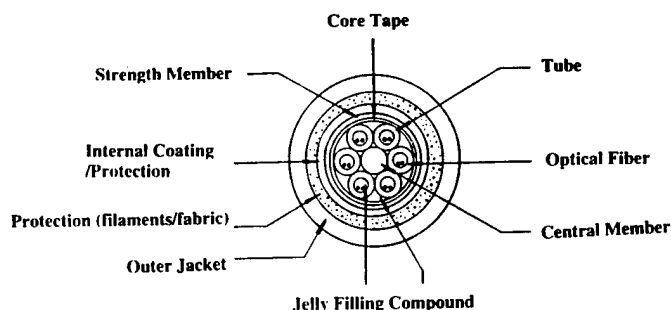


Figure 4 - Cables "G" and "H"

Prototypes of these cables were built and tested. In cable "E" damages above level 1 were not seen and it was necessary to change the animals after this test. For this reason it is possible to show its results against the other cables. Results found for cables "F", "G" and "H" are shown in Table 7.

Table 7 - Test Results

Esp/Cable	F	G	H	Average
1	2	3	4	3
2	2	2	5	3
3	2	4	6	4
4	2	5	4	3.6
5	1	1	1	1
6	0	0	0	0
7	0	1	0	0.3
8	0	0	1	0.3
9	0	0	0	0
10	1	0	0	0
Average	1.0	1.6	2.1	1.5

As we can see, cables F, G and H yielded good results, but the best result was cable E.

With these results it was possible to see that the proposals of cables produced a good result to rodent attack.

The most robust protections, which is the case of cable "E", prevent attack because they are extremely resistant and the animals cannot damage them and sometimes they even get hurt. On the other side, protections such as cables "G" and "H" irritate the animals and prevent them from destroying a

more resistant internal layer. In the cables shown, fiberglass irritates the animals and the internal polyamide layer prevents the nucleus from being damaged.

As to the operational aspect, cables with armor displayed an excessive stiffness, and can hinder the installation process in the case of curves and bends. Cables with double protection are easier to handle, but their protection is not so effective as the protection of the armored cable.

Some alternatives to improve performance of these models are still in the development stage, such as:

- use of fiberglass with a wider diameter, which irritates the animals even more.
- Addition of fiberglass in the coating polymer. This option needs development of the industrial process.

This work continues being developed to improve the solutions already found.

CONCLUSIONS

In this work the considerations and studies conducted to analyze the rodent attack to optical fiber cables were presented.

The results obtained in cables now being used in Brazil were shown. They were considered non-satisfactory to this aspect.

The development of tests was made with and without stimulus for attack. The results of the tests developed verify that the test methodology used was effective in analyzing the cable as to its resistance to rodent attack. It can be used in future developments.

Several materials with characteristics that can protect optical cables from rodent attack were tested and prototypes of cables were built which improved cable resistance. They were considered acceptable for use in buried cable routes.

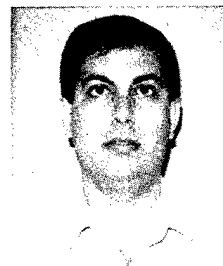
These studies will proceed to improve cable manufacturing process conditions and its handling in implantation.

ACKNOWLEDGMENTS

The authors would like to thank Prof. Ph. D. Rui Cerqueira and Prof. Ms.C. Erika Hingst from UFRJ for their support and conduction of tests, and engineers Ms.C. Atílio E. Regiane and Ms.C. Sebastião Sáhão Jr. for their contribution and suggestions in conducting the works.

REFERENCES

- [1] ITU-T, Outside Plant technology for public Networks, Geneva, 1992.
- [2] Curado, P.; Mendes Filho, M.; Netto, A.C.P.; Elias Filho, J. e Latini, M.E. ; "Optical cable biological attacks analyses", International Wire and Cable Symposium Proceedings, 1995.
- [3] Fonseca, G.A.B. et al; : Lista anotada dos mamíferos no Brasil" [Noted list of mammals in Brazil], conservation International & Biodiversitas foundation, Occasional Paper N. 4, April, 1996.



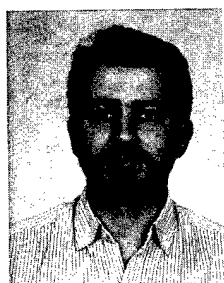
Paulo José Pereira Curado
Telebrás - R&D Center (CPqD)
Campinas, Brazil

Paulo José Pereira Curado was born in 1962. He graduated in Mechanical Engineering from Campinas State University (UNICAMP) in 1985 and in that year he joined Telebrás Research and Development Center in the Outside Plant Department. He has been engaged in research and development of optical fiber cables for trunk lines. Presently he is working with Optical Subscriber Networks in Outside Plant area.



Carlos Pitombo
Telebrás - R&D Center (CPqD)
Campinas, Brazil

Carlos Pitombo was born in 1957. He has been a mechanical engineer since 1980, graduated from Campinas State University (UNICAMP). Since 1989 he has been working at Telebrás Research and Development Center in the Outside Plant Department.



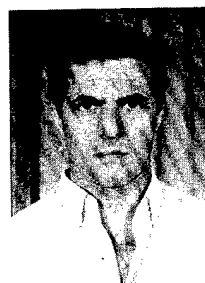
Derval dos Santos Rosa
Telebras - R&D Center (CPqD)
Campinas - SP - Brazil

Derval dos Santos Rosa was born in 1961. He received his B.S. degree and M.S. degree in Chemistry from Campinas State University (UNICAMP) in 1984 and 1991 respectively. In the same University, he received his Ph.D. degree in Materials Science at 1996. Since 1986 he is working at Telebrás Research and Development Center in Outside Plant Department. He was manager of Polymeric Materials Section for 9 years and now is staff member of Materials Technology Division.



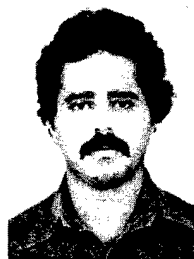
Antonio Costa Pereira Netto
Optical Systems Division Embratel
Rio de Janeiro - RJ - Brazil

Antonio Costa Pereira Netto was born in 1950. He received his B.S. degree and M.S. degree in Telecommunication Engineering from Rio de Janeiro Catholic University (PUC) in 1972 and 1981 respectively. He received his Ph.D. degree from Gama Filho University in 1983. Presently is Optical System Division manager of Embratel.



João Elias Filho
Optical Systems Division - Embratel
Rio de Janeiro - RJ - Brazil

João Elias Filho was born in 1947. He is Telecommunication Technician from National Technical School of Rio de Janeiro. Since 1990 is staff member of Optical System Division of Embratel.



Marcilio Estevão Lattini
Optical Systems Division - Embratel
Rio de Janeiro - RJ - Brazil

Marcilio Estevão Lattini was born in 1954. He received his B.S.C. degree in Telecommunication Engineering from General Roberto Lisboa University in 1982. Since 1992 is staff member of Optical System Division of Embratel.

MINIMIZING LIGHTNING DAMAGE IN REGIONS OF HIGH EARTH RESISTIVITY

David Vokey, Norscan Instruments Ltd.

Gary Gallagher, Keith Young, Newtel Communications Inc.

ABSTRACT

Sections of the Trans-Canada fiber optic cable in the Province of Newfoundland experienced an unusually high incidence of pinholing and "divot" type sheath damage. The cable extends a total distance of 970 km along the Trans Canada highway and is direct buried in split conduit for the entire route. From previous experience^{1,2}, the pinholing was believed to be a result of lightning damage caused by near by ground strikes. However, the "divot" type damage, which is a thumb nail size fractured jacket section, had not been previously reported in the literature.

A study was undertaken to determine the cause of the damage. A theory for the formation of "divot" type faults was developed. Additionally, the research and analysis lead to the conclusion that in conditions of high earth resistance the effects of lightning damage are greatly exaggerated by surface conduction and current dissipation characteristics.

As part of the study, the relationship between ground resistance, grounding, and damage susceptibility was examined. Guidelines for minimizing sheath damage were established. The results of the analysis, recommendations, and subsequent field results are presented.

INTRODUCTION

Newtel Communications Inc. is a full service supplier of local and long distance telephone service as well as providing a complete range of advanced high speed data products such as Frame Relay, ISDN and ATM.

In 1992 construction began on an ambitious undertaking to install a buried fiber optic cable from Cape Ray to St. John's, Newfoundland, a total of 970 km (Figure 1). The cable installation was completed in three phases over a period of three years. The terrain covered during the

installation presented considerable engineering and construction challenges. Large surface and sub-surface rock formations had to be cleared as well hundreds of large boggy areas and rivers had to be crossed. For easy accessibility, the cable was placed close to the provincial highway system and in some locations follows an abandoned railway right of way.

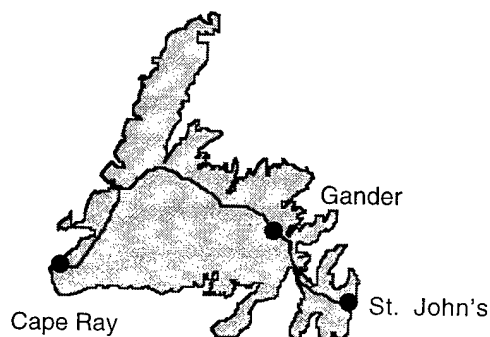


Figure 1: Newfoundland, Canada

A single sheathed cable (Figure 2) was chosen for installation along the entire route. To provide excellent mechanical and moisture protection, the cable is constructed with a PE/steel/PE protective jacket using medium density PE and a 0.15 mm coated and corrugated steel tape armor. The entire route is direct buried at a depth of 1.3 meters and enclosed in a polyethylene split conduit for additional protection against rocks and rodents. Horizontal drilling was utilized to cross major rivers and paved highways. The fiber splice closures along with special test access closures were placed below ground in Optipeds™.

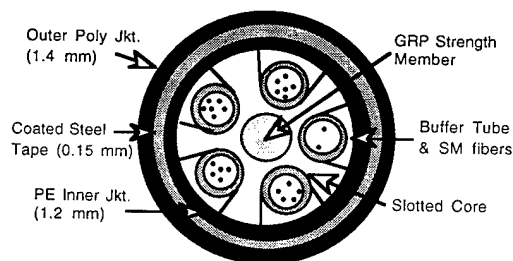


Figure 2: Newfoundland Fiber Optic Cable

The metallic armor is connected to an active monitoring system^{3,4} which continuously measures the dielectric integrity of the outer cable jacket and the condition of the splice closures.

During Phase II construction, sheath damage alarms began to appear in the Phase I sections. Using a combination of long and short range fault locating equipment, the defective areas were identified and repaired. Soon after construction, the newer Phase II began indicating similar types of alarm conditions.

CABLE SHEATH DAMAGE

Initial investigations were focused on the type of damage being unearthed for repair. Two types were identified.

1. Pinholing - A small pin sized hole which penetrates the outer polyethylene jacket. Usually found in clusters over a cable length of 5 to 15 meters. Pinholing is well known and is attributed to electric arcing as a result of a lightning ground strike in the region of a buried cable.

2. Divots - a term used to describe a piece of polyethylene cable covering approximately 0.5 to 1.5 cm in diameter (thumbnail size) (Figures 3&4) which has been separated from the coated steel armor. Up until the time of this study the divot type damage to the outer cable jacket had not been reported in the literature.

Pinholes and divots were appearing in clusters frequently within a 100 meter radius of a repeater site or buried splice location.

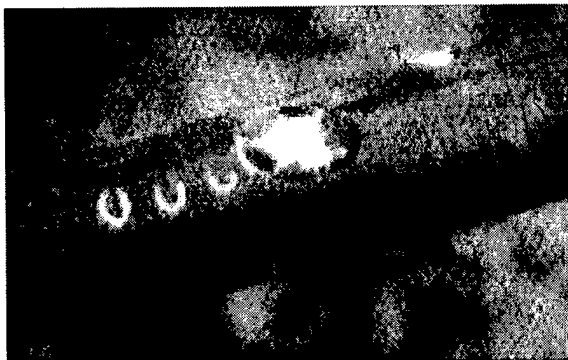


Figure 3: "Divot" type Jacket Damage

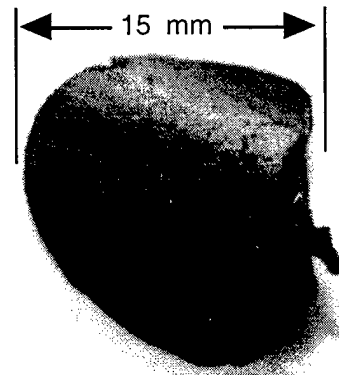


Figure 4: Typical "divot"

FAILURE ANALYSIS

Due to the striking physical similarity and high frequency of the divot class failures it was initially suspected that the cable jacket was defective. In particular, the failure frequently occurred at the meter markings which were stamped into the outer jacket and/or at the steel tape overlap.

Long length cable samples available from the original installation were provided for test and examination. A full battery of electrical and mechanical tests was carried out including :

- Insulation resistance
- 50 kV. dc high voltage in water bath
- 30 kV. ac high voltage in water bath
- Jacket shrinkback
- Tensile and elongation
- Cold impact
- Cold bend

For all tests the cable jacket met or exceeded industry requirements.

Samples of the jacket including both pinhole and divot type damage were collected during repair. A number of divot specimens were examined using;

- DSC analysis
- infrared analysis
- X-ray fluorescence
- microscopic analysis.

The analysis found no deficiencies in the polyethylene material, however, there was evidence of cold fracture of the jacket at the damage site with no significant charring of the polyethylene. This suggested that the fracture was caused by a mechanical force rather than a high energy and high temperature electric arc generated by a lightning stroke.

As the frequency of faults reported began to clearly follow lightning activity in the area, the investigations were directed towards understanding the relationships between lightning, ground resistance, grounding, and cable damage.

THEORY OF DIVOT FORMATION

Ultimately it was the microscopic analysis⁵ that lead to a theory for the formation of the divot type fault. Under careful observation it was noticed that every divot type fault included a pinhole fault. There were many cases of pinhole faults only but in every case of divot type fault there existed a companion pinhole fault. This result is significant as it suggests that a pinhole fault is the precursor to the formation of a much larger divot type fault.

From lab analysis it was determined that the failure mechanism was a cold fracture of the polyethylene jacket. This could be the result only of an outward mechanical force of sufficient magnitude to fracture and to tear away a small piece of the outer jacket.

Referring to Figure 5, a hypothesis for the divot type failure mechanism follows:

1. A near-by lightning ground strike causes a high voltage surge between the surrounding earth and the cable armor which exceeds the dielectric strength of the PE jacket. A small electric discharge occurs which pinholes the cable jacket.

2. Over a period of weeks or months ground water makes its way into the pinhole. At sites where a small void exists at the jacket and armor interface, the water pools near the armor.

3. A second near-by strike easily finds a discharge path at the original pinhole site as the dielectric withstand capability was lost during the first pinholing. If the discharge current is of sufficient magnitude, the resistivity of the pooled water causes heating and instant vaporization of the water. The vapor generates a volume 1700 times larger than the water from which it was formed. The explosive pressure pushes outward and ruptures the cable jacket forming a divot.

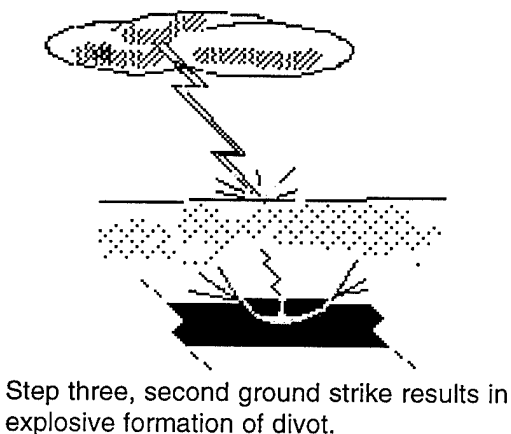
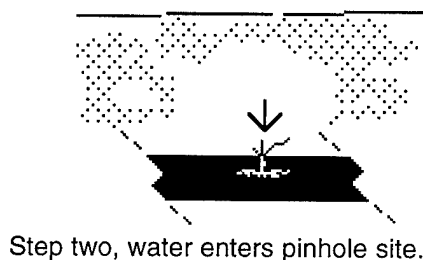
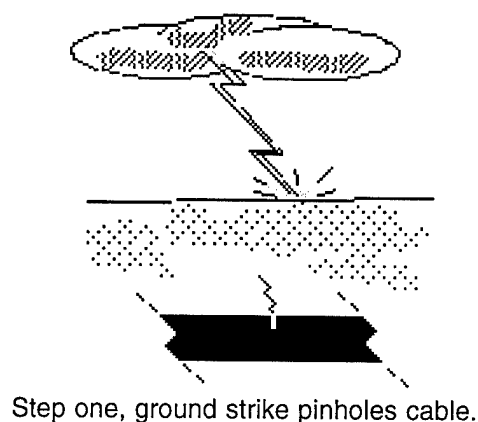


Figure 5: Formation of Divot

LIGHTNING DAMAGE

Isokeraunic maps, which give estimates of the average number of thunderstorm days per year, indicate that the entire island is in a region of relatively low thunderstorm activity with only about five thunderstorm days per year. In spite of this, the incidence of lightning caused cable damage on the cross-island cable appears to be higher than in any other region of Canada.

The local geography and geology were researched in order to understand the nature of

this high susceptibility. The island, affectionately referred to as "the Rock", is part of the Appalachian geological province of North America. The ground at depth ranges from Precambrian rock in the east to a variety of Paleozoic rock in the central and western regions. At a depth of a few meters, the earth resistivity is in the thousands of ohm-meters.

The route parallels the Trans-Canada Highway and traverses several regions of bog and marsh. In many sections, the surface down to a few meters tends to be very wet. Below the immediate bog-like surface, the earth changes abruptly to solid rock formations. This gives rise to a relatively good conducting surface with resistivities on the order of tens of ohm-meters below which is an insulating layer of rock of 1000 ohm-meters or more.

Near-by lightning ground stroke and related cable sheath damage has been studied and reported^{1,6}. Under the assumption of homogeneous soil resistivity, the maximum distance from the center of the stroke to the buried cable which will cause a breakdown in the jacket is estimated to be:

$$r = \frac{I_{ep} \rho}{2\pi V_p} \quad (1)$$

Where:

- r is the distance from the stroke to the cable in meters
- I_{ep} is the peak stroke current in kA
- ρ is the earth resistivity in ohm-meters
- V_p is the dielectric strength of the cable jacket in kV

The surface conditions for a large portion of the cable route in Newfoundland limit the usefulness of equation (1). Using an average peak current of 40 kA, a breakdown voltage of 100 kV and a conductivity of 100 Ω -m, which is high for marshy regions, equation (1) predicts cable breakdown to a maximum of 7 meters from the center of the strike.

Using data from repaired sections, the histogram in Figure 6 plots lightning strike damage. As shown, cable pinholing can occur for distances of 100 meters or more from the center of the strike.

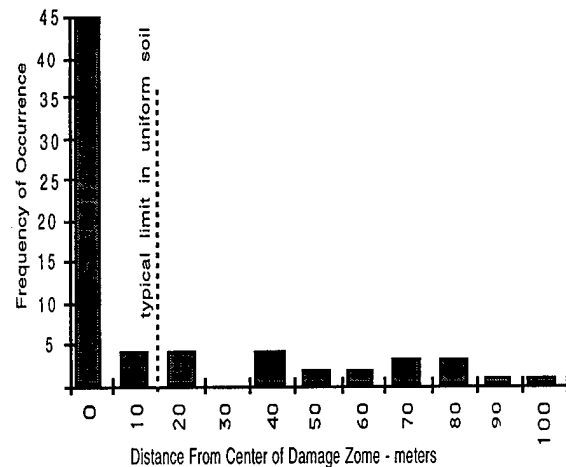


Figure 6: Distribution of faults

Due to the high resistivity and insulating value of the underlying rock a conducting surface volume of finite depth would be a more appropriate model.

Referring to Figure 7, the current density becomes.

$$i(r) = \frac{I}{2\pi r d} \quad \text{A/m}^2 \quad (2)$$

and the electric field intensity is:

$$e(r) = \frac{\rho I}{2\pi r d} \quad \text{V/m} \quad (3)$$

where:

- r is the distance from the stroke to the cable in meters
- I is the stroke current
- ρ is the earth resistivity in ohm-meters
- d is the depth of the conducting surface in meters

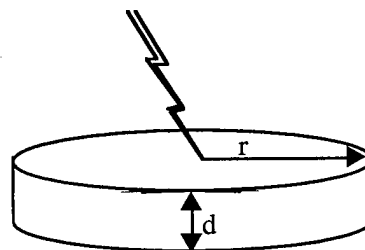


Figure 7: Strike to conducting surface

The voltage at a distance R to a remote ground is given by:

$$V_{ep} = \int_R^{\infty} \frac{\rho I_{ep}}{2\pi r d} dr \quad (4)$$

The integral yields a solution which is reluctant to converge, however due to the longitudinal impedance of the cable armor and high frequency component of the stroke current, a limiting distance of 1000 meters provides a reasonable estimate for the peak voltage for distances up to a few hundred meters.

Solving (4) for finite limits :

$$V_{ep} = \frac{\rho I_{ep}}{2\pi d} \ln r \Big|_R^{1000} \quad (5)$$

A comparison of the two models can be made by evaluating equations (1) and (5) for typical conditions. Assuming a cable sheath breakdown voltage of 100 kV (testing up to 50 kV resulted in no jacket breakdown), a surface resistivity of 20 Ω -m (marsh) for the conducting surface model and a resistivity of 1000 Ω -m (rock) for the semi-sphere model, the radius to which arcing will occur as a function of peak stroke current is plotted in Figure 8.

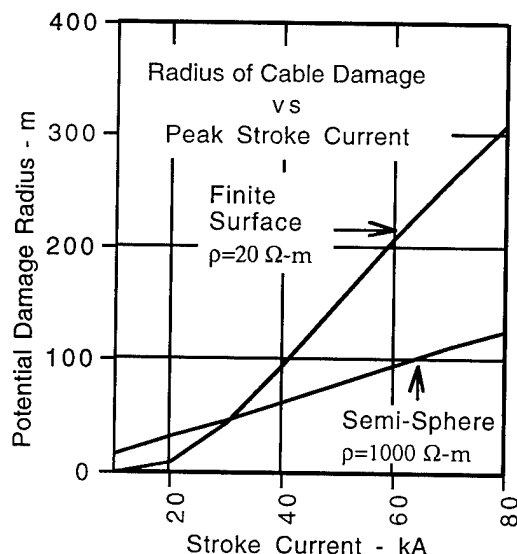


Figure 8: Potential cable damage radius

The conducting surface model, although much lower in resistivity than the semi-sphere model, predicts cable sheath damage to a much larger radius from the center of the strike. This result is consistent with field observations.

GROUNDINGS AND GROUNDING

Grounding protection for the cable armor is done at all repeater sites and splicing points using a combination of gas tube and solid state surge protectors.

In order to remain within system design limits, several repeater sites were placed in remote locations. The power feeds to these locations are typically end-of-line feeds isolated from the main distribution line.

The terms 'zone-of-influence' and 'ground zone' are generally used to describe the area of surrounding earth, approximately 50 meters, which extends from a central grounding point, which at the repeater sites, is the power ground (see Figure 8).

The ground zone, because of proximity, also includes the repeater ground. If the grounding resistances are not sufficiently low, the grounds become electrically coupled.

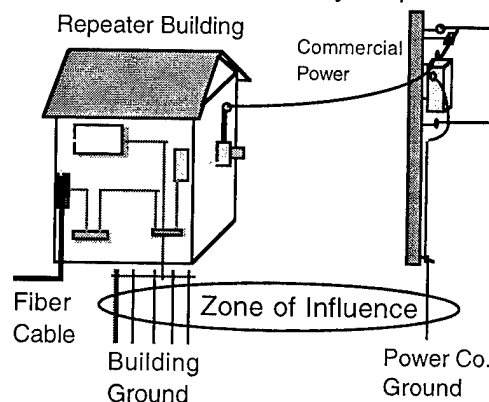


Figure 8: Local grounds at a repeater site

When the grounds are poor at a repeater site, a near-by lightning strike to the power conductors will cause the entire site, including the building grounds, to reach a high voltage relative to a remote ground. During conditions of a ground voltage rise, the cable armor surge protectors operate sending the surge currents out to remote ground over the fiber cable. At

At regular intervals laterals were installed to delta ground grids and experimental chemical ground mats. Careful attention was observed in placing the copper wire to avoid any contact with power guy wires and vertical grounds.

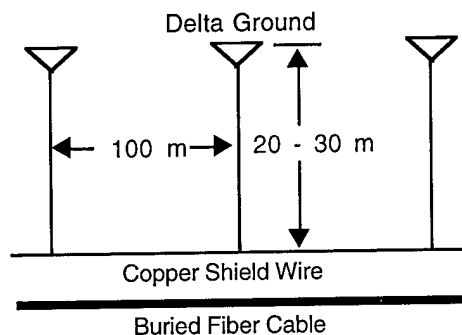


Figure 10: Copper shield wire & grounds

RECENT RESULTS

Recent visits to the sites have shown improving results. The use of exothermic reaction weld connections have greatly improved connection reliability over the 1995-1996 winter. The rate of reported failures continues to drop.

Prompt identification of fiber cable pinholing and 'divots' is made significantly easier with the use of an active monitoring system. To date no single fiber has been found broken or destroyed as a result of a direct or indirect lightning hit.

Based upon damage observed thus far buried fiber cable with unrepaired divots will, over time, start to deteriorate and by exposure and the risk of a high current strike, considerably reduce the expected cable life.

New direct buried fiber cables are now installed using double armored protection. The outer armor is permanently grounded. The inner armor and PE jacket is monitored. Some pinholing of the outer sheath has been reported and in at least one case pinholes have reached the inner armor.

Experimentation with new chemical ground plates is now underway at all repeater sites in special study to observe the long term results of using various chemical mixtures to improve site ground resistance.

CONCLUSIONS

A theory for the formation of "divot" type cable jacket fault has been developed. It is believed that a pinhole fault is the precursor to the formation of a much larger divot type fault. Conditions of high ground moisture and secondary lightning ground strike give rise to divot-type damage.

A surface conducting model has been proposed for estimating lightning damage in regions combining a low resistivity surface over high resistivity rock.

Proper grounding, particularly in regions of high earth resistivity is critical. High resistance grounds at building sites and splice locations, do not offer a path to earth for surge current dissipation. Instead, they provide a connection to earth through which a near-by strike can find an easy path into the cable. Power line grounds should be made as low as possible (25Ω or less) and, where possible, located well away from the building ground.

Monitoring systems are important tools for proactive maintenance. Early warning of cable problems provides the crucial time to identify, locate and repair any damage long before the damage degrades to an outage condition.

Continuous monitoring provides direct feedback as to the effectiveness of new methods and materials in the quest for improved reliability and lower cost of service provision.

several repeater sites with high resistance grounds, the cable has had extensive pinholing for distances up to 1 km .

The same holds true for splice grounds. A high resistance splice ground, rather than provide a path to earth for surge current dissipation, is instead a connection to earth through which a near-by ground strike can find an easy path into the cable. As shown in Figure 9, this is evidenced by lightning damage for dozens of meters on either side of a splice location.

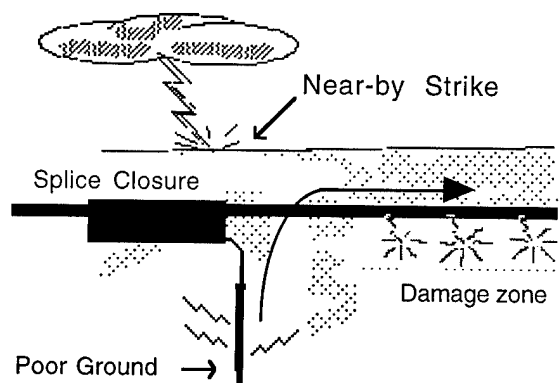


Figure 9: Strike near splice closure

Table 1 lists the ground resistance readings, in ohms, taken in late November 1993 at the ten repeater locations situated approximately 90 km apart.

Table 1: Grounding Resistance Readings

cable Rptr. #	Resistance (ohms)	
	Building	Power
1	104	650
2	88	1200
3	89	230
4	72	540
5	19	370
6	53	1300
7	48	162
8	44	440
9	30	370
10	<u>45</u>	<u>430</u>
Average	59	570

High resistance readings clearly indicate problems with the quality of both the repeater site and power grounding installations.

With unusually high ratio of 9.5:1 for power

ground resistance to a building ground resistance it is expected that a portion of the power line surge currents and voltages developed during a lightning storm, or a switching transient in close proximity of the site would couple from the power ground to the building ground.

RECOMMENDATIONS

Immediate steps were taken to lower site grounding resistance which resulted in an approximately 50% drop in measured readings from the previous readings shown in Table 1.

The following ground improvements were undertaken at each repeater site and resulted in an immediate improvement of pin-holing and divot reports in this area of the cable:

1. Additional standard ground rods.
2. Chemical Rods (Calcium Chloride).
3. Use of ground enhancing materials.
4. Rewiring of all internal building grounds.
5. Replacement of defective protectors.
6. Improved Power bonding.

Due to underlying bedrock, the use of longer rods, which are the industry-accepted standard for reducing earth ground resistance, were not considered. To offset the zone-of-influence condition, low resistance delta grounds were installed at power poles located some distance away outside the immediate zone area.

At the splice locations several deficiencies were discovered:

1. Severely corroded bolts on ground connectors.
2. Missing internal grounding.
3. High ground resistance readings.
4. Loose 'screw type' ground clamps.

After correction, a noticeable drop in pin-holing and divot events was recorded.

The final part of the investigation centered on why some mid-span sections of cable were still reporting problems. Closer observation of these areas revealed that:

1. All cables were placed in open areas.
2. Lack of high objects in the area.
3. No overhead power lines in the area.

A shield conductor was installed in selected test areas(Figure 10). A copper conductor was placed 0.3 m below the surface directly in line with the buried fiber cable for 600 meters.

REFERENCES

1. H. D. Campbell, et.al;"Lightning Pinholes in Cable Sheaths", 27th International Wire and Cable Symposium, Cherry Hill, NJ, 1978
2. S. G. Ungar, "Effects of Lightning Punctures on the Core-Shield Voltage of Buried Cable"
3. D. E. Vokey, "A Means for Monitoring and Protecting Outside Cable Plant Against Moisture", 29th International Wire and Cable Symposium, Cherry Hill, NJ, 1980
4. K. Sontag, "A Fiber Optic Cable Monitoring System", 35th International Wire and Cable Symposium, Reno, NV, 1986
5. R. F. Hamond, Examination Report, ASB-94-114, July, 1994 AECL Research, Whiteshell Laboratories, Pinawa, MB
6. J. A. Olszewski, et.al, "Lightning Considerations in Optical Cables Design", 35th International Wire and Cable Symposium, Reno, NV, 1986

BIOGRAPHY

David Vokey is responsible for research and development at Norscan Instruments Ltd. He graduated from the Manitoba Institute of Technology in 1969 with a Dip. of Tech in Electronic Technology, the University of Manitoba with a Bachelor of Science Degree in Electrical Engineering in 1973 and a Master of Engineering Degree in 1984. Prior to co-founding Norscan Instruments Ltd, he worked for Canada Wire and Cable Ltd. as the Manager of Design and Development and for Siecor Corp. as the Manager of Cable Development with R&D. He is a member of IEEE and an associate member of the Association of Professional Engineers of Manitoba.

Gary Gallagher graduated Cabot Institute St. John's Newfoundland in 1969, he holds a Diploma in Electrical Eng. Technology. He spent 3 years working with a Hydro Utility doing design of overhead and underground distribution systems. For the past 25 years he has worked with Newtel Communications in a variety of technical positions. The last ten years have been spent in doing support for advanced digital switching systems and investigations of better methods to protect equipment from the effects of power and lightning disturbances.

Keith Young has a Bachelor of Engineering in Electrical Engineering from Memorial University of Newfoundland. He has a Diploma o Electrical Engineering Technology from the College of Fisheries in St. John's, Newfoundland. He is a Senior Engineer - Network Access/Electrical Protection with Newtel Communications Inc. He has worked with Bell Northern Research in Nepean, Ontario in the Lightning and Electrical Surge Protection test facilities at Nortel's Corkstown Manufacturing Plant. He is a member of the Association of Professional Engineers and Geoscientists of Newfoundland.

DEVELOPMENT OF FLAME RETARDANT HALOGEN-FREE CLEAN UTP CABLES APPLIED UP TO ATM DATA SPEED

Akinari Nakayama Kiyoshi Watanabe Shinya Ishi Shinji Hinoshita

Hitachi Cable, Ltd., Ibaraki, Japan

ABSTRACT

Recently, UTP cables are required to guarantee low attenuation over a high frequency band so that they can be applied to high-speed data transmission for ATM-LANs. They must also be highly flame retardant and be able to pass fire tests since they are used in buildings. To achieve these requirements, new types of halogen-free flame retardant compounds for the insulation and sheath are investigated. A new flame-retardant polymer compound, which shows superior transmission properties and excellent fire performance, is used in the insulation. In addition, a compound that expands under heat is used in the sheath to raise the flame retardancy of the cables. Consequently, the new UTP cables that use these compounds satisfy the TIA/EIA 568-B Category 5-enhanced covering ATM-LANs, and IEEE.383 VTFT-class flame retardancy standards. These clean UTP cables contribute to the safety of offices and buildings.

INTRODUCTION

Recent premise multiple-pair data-grade wiring technology urgently requires transmitting data at higher speeds for asynchronous transfer mode local area networks (ATM-LANs) as Category 5-enhanced requirements. The lines of unshielded twisted pair (UTP) cables should have adequately

low attenuation over a high-frequency band to cover an ATM transmission system up to STM (synchronous transfer mode)-4 (622 Mbps).

UTP cables should also be flame retardant and pass fire tests since they are used in buildings. Conventional UTP cables consist of polyethylene (PE) insulation that has excellent transmission properties and polyvinyl chloride (PVC) sheaths that are highly flame retardant.

However, PVC, halogenated flame retardant materials, evolve toxic and corrosive gases during combustion. Furthermore the colored smoke evolved from PVC makes taking refuge and fighting the fires difficult¹⁾.

Therefore, the halogen-free clean UTP cables have been developed, which satisfy both the TIA/EIA 568-A Category 5 and Category 5-enhanced electrical tests, and the flame-retardancy standards of vertical tray flame test (VTFT). The results of these developments are described below.

TARGET

The transmission properties of halogen-free clean UTP cables should satisfy Category 5-enhanced, over ATM (622 Mbps) data speed, which we forecast maximum extension to be covered by the symmetrical pair cables. Flame retardancy should pass the VTFT of IEEE.383. Each material used should evolve no halogenated gases with ASTM 1000.001, and smoke evolution should be less than 150 points of smoke density with ASTM E662, NBS smoke density chamber. These targets are summarized in Table 1.

Table 1 Target

Characteristic	Specifications	Requirements
Transmission properties	TIA/EIA 568-A	Category 5 and Cat.5-enhanced
	IEC.11801	Class D and upper grade
Flame retardancy	IEEE.383	Flame propagation ≤ 1.8 m
Toxicity	ASTM 1000.001	HCl ≤ 150 HF ≤ 100
Smoke evolution	ASTM E662	Smoke density ≤ 150

MATERIALS

Conventional halogen-free flame-retardant plastic materials are composed of PE and halogen-free flame retardants such as metal hydroxides (FR-PE). If the FR-PE is applied only to the sheath instead of PVC, good transmission properties and poor FR-PE retardancy result. If, on the other hand, FR-PE is applied to both the insulation and the sheath, good flame retardancy results, but there is much excess loss at the highest frequency band due to the high dielectric constants of metal Hydroxides in the insulation.

To solve this problem, new types of halogen-free flame-retardant compounds for the insulations and the sheaths are investigated.

Insulation

Since single polymers do not have both good transmission properties and high flame retardancy, a polymer alloy material that consists of a low dielectric constant polymer and a flame retardant polymer was considered.

An ethylenic polymer was selected as the low dielectric constant ingredient. For the flame retardant ingredients, an aromatic polymer was selected because of its property to immediately carbonize when heated by fire, which prevents the evolution of flammable gases. A blend of these

polymers, however, lacks certain physical properties such as elongation or flexibility because of the poor dispersion of each ingredient. To improve these physical properties, an ethylenic polymer modified by miscible content of aromatic polymer was investigated.

Consequently, a new flame-retardant polymer material, HFP (Hitachi high-performance clean halogen-free polymer), was developed. The morphology of HFP, observed by transmission electron microscopy, is shown in Figure 1. The ethylenic low dielectric constant polymer makes a mesh-like continuous phase, and the aromatic flame-retardant polymer fills the inside of the mesh-like structure on the submicron order.

The morphology of the blend of the aromatic polymer and PE, the most popular ethylenic polymer, observed by scanning electron microscopy is shown in Figure 2. The aromatic polymer dispersed in PE on a much larger size than that of the HFP.

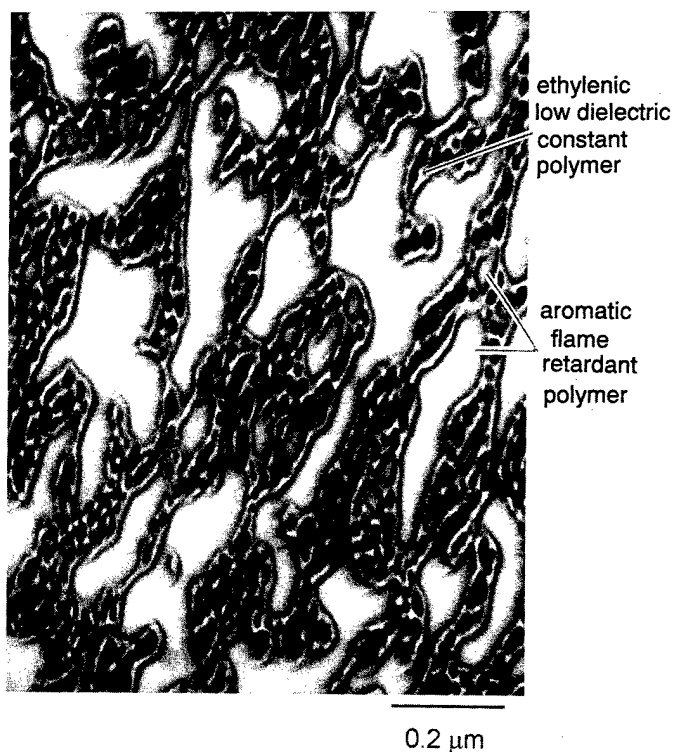
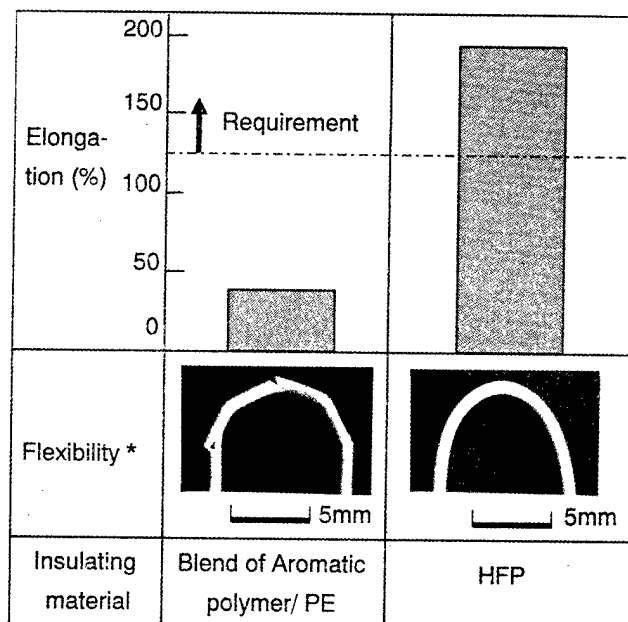
**Figure 1 Morphology of HFP**



Figure 2 Morphology of the blend of aromatic polymer and PE

Figure 3 shows the difference in elongation and flexibility of insulated wire between HFP and the blend of the aromatic polymer / PE. The excellent elongation and flexibility of HFP-insulated wire seem to be caused by its microstructure.

Table 2 shows general properties of the HFP. It has UL-94, V-1 class flame retardancy. The dielectric constant of the HFP has a much smaller value of 2.4, while that of conventional FR-PE has a high value of 3, as shown in Figure 4. HFP has the same order of dielectric loss tangent of 10^{-4} as PE. The dielectric properties of HFP do not change, even at a high frequency band, so the attenuation loss of the UTP cable that uses HFP is expected to be small at high transmission speeds.



* winding diameter : 8mmφ

Figure 3 Comparison of insulating material in elongation and flexibility

Table 2 General properties of HFP for insulation

Characteristic		Require- ment	Perfor- mance
Tensile properties	Tensile strength (MPa)	$8.0 \leq$	45
	Tensile elongation (%)	$125 \leq$	190
Thermal aging (100°C, 48h)	Percent of original of TS	$80 \leq$	103
	Percent of original of TE	$65 \leq$	105
Dielectric properties*	Dielectric constant	—	2.4
	Dielectric loss tangent	—	0.0004
Combustion properties	Oxygen index	—	24
	UL-94	—	V-1

* at 620MHz

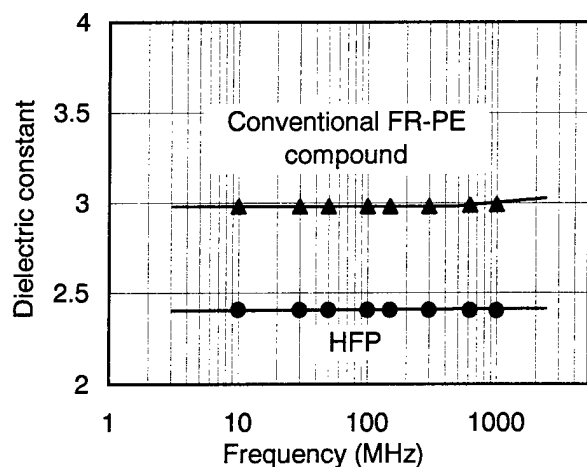


Figure 4 Dielectric constant of HFP and conventional FR-PE

Sheath

Because the UTP cables are unshielded (non metal screen), the heat insulating effect by metal screen, which improves flame retardancy of cables, is not expected. To give the sheath an equivalent effect, creating a bubble layer by heat is thought to be effective. Hence, a new FR-PE that can be expanded by heat is attempted.

The hardening agent contained in this compound, which forms an incombustible layer on the surface of the material during burning, improves the brittleness of cinder of burned sheath. Since the hardening speed is balanced with the thermal degradation speed of polymers, the compound traps the gases inside and changes into a foam in the event of a fire. The conventional FR-PE and newly developed expandable compound after burning are shown in Figure 5. While the former expands 1.5 times, the latter expands approximately 3 times in volume.

If the expandable compound is used in the UTP cable sheaths, the heat insulating effect should prevent fire propagation. The general properties of this expandable FR-PE compound are listed in Table 3.

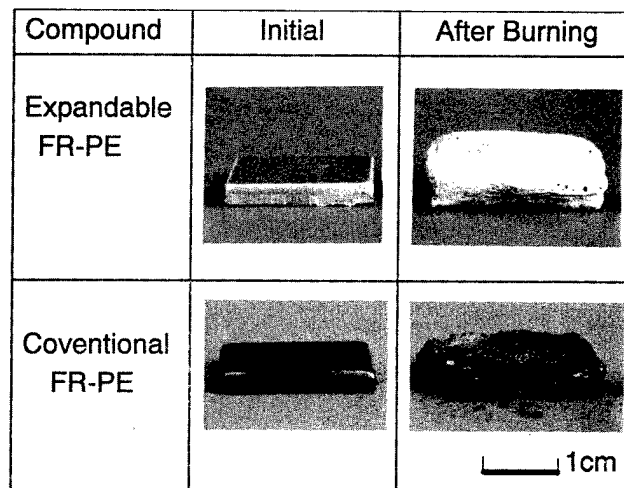


Figure 5 The difference of expansion

Table 3 General properties of expandable flame retardant compound for sheath

Characteristic		Require- ment	Perfor- mance
Tensile properties	Tensile strength (MPa)	$5.0 \leq$	8.8
	Tensile elongation (%)	$300 \leq$	580
Thermal aging (100°C, 48h)	Percent of original of TS	$85 \leq$	100
	Percent of original of TE	$85 \leq$	93
Combustion properties	Oxygen index	—	33
	UL-94	—	V-0

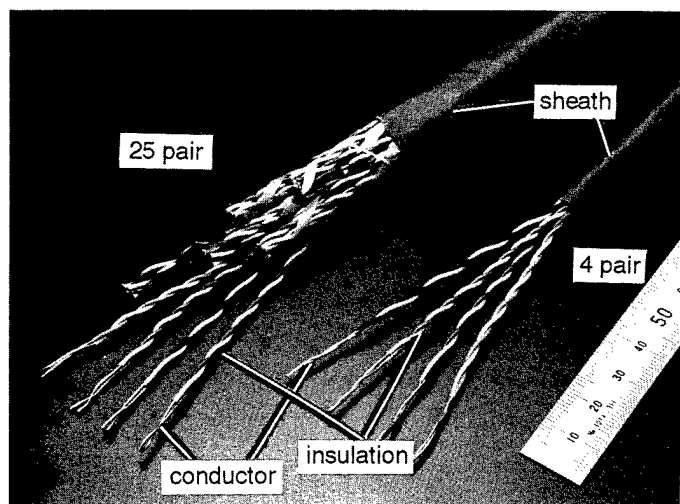


Figure 6 Photograph of 4- and 25-pair UTP cables

CABLE PERFORMANCE

Cable Structures

Both 4-pair and 25-pair UTP cables were manufactured using both HFP and expandable FR-

PE. A photograph of the cables is shown in Figure 6, and the dimensions are shown in Table 4.

Transmission Properties

The transmission properties of the 4- and 25-pair UTP cables are listed in Table 5. Both UTP cables satisfy Category 5 and Category 5-enhanced requirements up to ATM (155 Mbps) data speed. Data is presented up to frequency 500 MHz in order to estimate the performance for the application of ATM (STM-4, 622Mbps NRZ), which requires Peak-Bandwidth of 310 MHz.

Table 4 Dimensions of UTP cables

Item	4 pair	25 pair
Conductor size	24 AWG	
Insulation thickness	0.24 mm	
Diameter (approx.)	5.5 mm	14 mm
Weight (approx.)	35 Kg/Km	180 Kg/Km

Table 5 Transmission properties

Characteristic	Requirement	Performance		Method
		4 pair	25 pair	
Max. mutual capacitance (nF/100m)	5.6	4.8~5.1	4.9~5.3	TIA/EIA 568-A Category 5 and Cat.5-enhanced
Max. capacitance unbalance (pF/100m, pair to ground)	330	< 20	< 50	
Max. characteristic impedance (Ω , 1to100MHz)	100±15	$Z_c(f) = 96.3 + 7.48 / \sqrt{f}$		
Max. attenuation α (dB/100m)	$\alpha = 1.967\sqrt{f} + 0.023 f$	$\alpha = 1.803\sqrt{f} + 0.015 f$ 36 (at 310 MHz) 54 (at 620 MHz)		
Power-sum crosstalk (Worst case)	Under study but ACR is assumed	See Figure 9		IEC.11801

Figure 7 shows the characteristic impedance in the range of 0.01 to 500 MHz. The characteristic impedance of maximum attenuation pair is expressed as follows;

$$Z_c(f) = 96.3 + 7.48 / \sqrt{f} \quad (\Omega) \text{ in } f(\text{MHz}) \quad (1)$$

Attenuation of over 0.01 to 500 MHz for the worst pair among the 25 pairs is shown in Figure 8. The maximum attenuation is expressed as follows;

$$\alpha = 1.803\sqrt{f} + 0.015f \quad (\text{dB}/100\text{m}) \text{ in } f(\text{MHz}) \quad (2)$$

The maximum attenuation at 310 (MHz) and 620 (MHz) are 36 (dB/100m) and 54 (dB/100m) respectively and proved that the developed HFP kept low attenuation up to ATM (622Mbps) data speed by suppressing the attenuation increase due to the dielectric constant and dielectric loss tangent.

The power-sum crosstalk (P.S.XT) for the cases of various pair assignment of the systems is

presented in Figure 9. The XT performance of the developed UTP cables meets the requirements up to ATM (155 Mbps) data speed. There is a possibility that the developed HFP-UTP cable can be used for the ATM (STM-4, 622Mbps NRZ) system when the two-way / two-cable system is used for the purpose of the exemption of the near-end crosstalk (NEXT) requirement ²⁾.

Combustion Properties

The combustion properties are listed in Table 6. The flame propagation of 4- and 25-pair UTP cables in a VTFT of IEEE.383 is respectively 0.4 and 0.75 m, and it is clear that these cables are as flame retardant as UTP cables using PVC sheaths. This is because the new HFP insulation material carbonizes immediately due to the heat of the fire, and prevents the evolution of flammable gases. This highly contributes to improving the flame retardancy of cables. Figure 10 shows the maximum height of flame during a VTFT of 4- and 25-pair UTP cables.

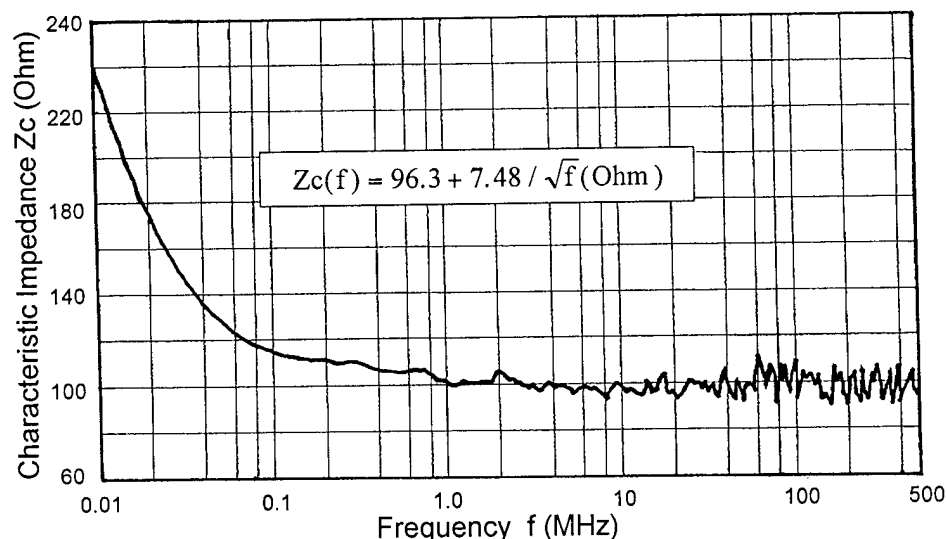


Figure 7 HFP-UTP 25P AWG 24: Characteristic impedance (Z_c)

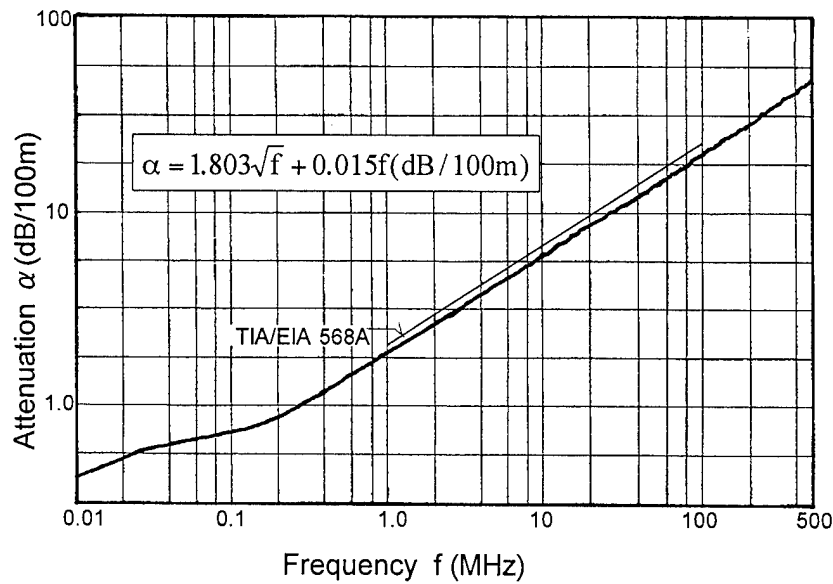
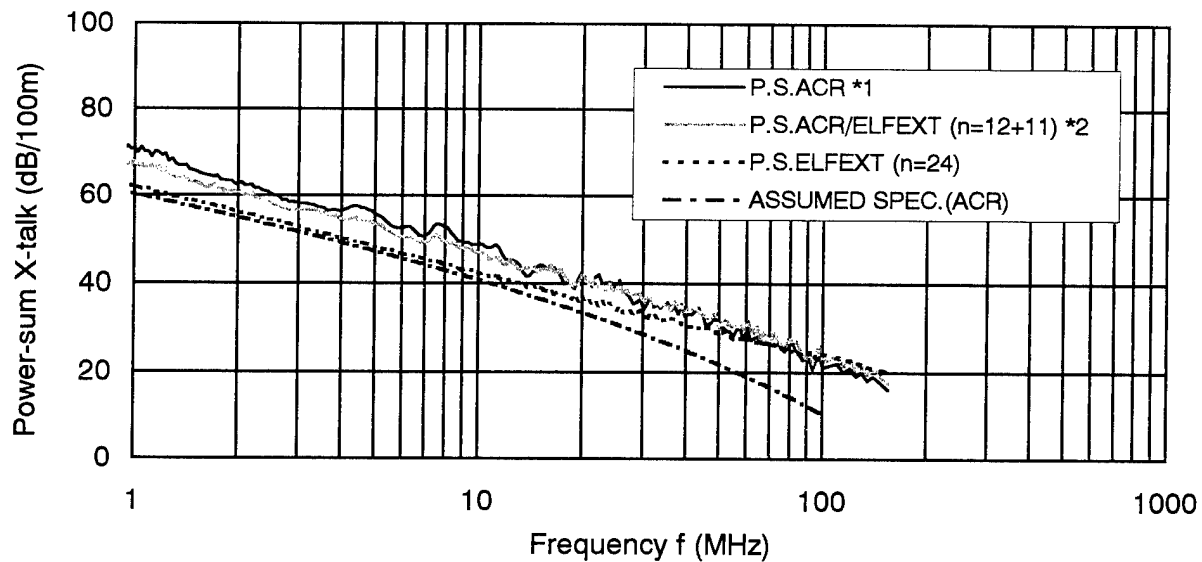


Figure 8 HFP-UTP 25P AWG 24: Maximum attenuation (α)



*1 ACR = NEXT - Attenuation (100m)

*2 ACR/ELFEXT is combination XT for Two-way / One-cable system
ACR's n=12, ELFEXT's n=11, n: Number of disturbing pairs
(12 systems operation is assigned for 24 pairs.)

Figure 9 Performance of P.S. crosstalk vs. frequency

Table 6 Combustion properties

Characteristic	Requirement	Performance		Method
		4 pair	25 pair	
Vertical flame test	Flame propagation $\leq 1.8\text{m}$	0.4	0.75	IEEE.383
Toxicities (sheet test)	HCl ≤ 150 HF ≤ 100	Insulation; 0 Sheath; 0		ASTM 1000.001
Smoke evolution (sheet test)	Smoke density ≤ 150	Insulation; 9 (NF)*, 109 (F)* Sheath; 56 (NF), 86 (F)		ASTM E662 NBS smoke chamber
Corrosivities	pH ≥ 4.0	4.1	4.2	IEC.754-2
	Conductivity $\leq 100\text{mS/cm}$	10	9	

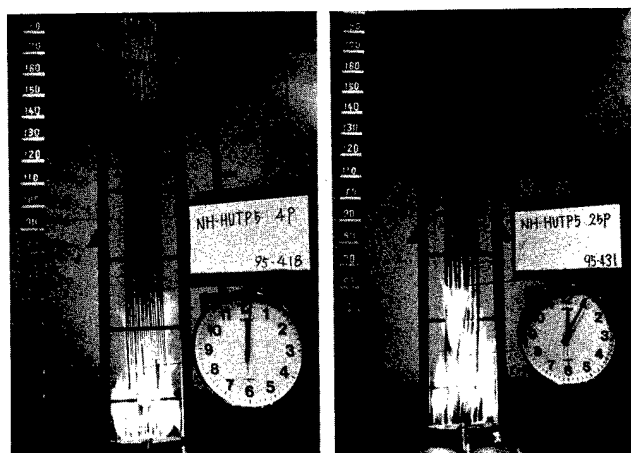
* (NF); Non-flaming method, (F); Flaming method

In accordance with ASTM 1000.001, the toxicity level is low in the event of a fire because no halogenated gases such as HCl and HF are evolved.

The smoke densities of each insulation and sheath compound are measured by NBS smoke density chamber in accordance with ASTM E662. Consequently, the smoke densities of the insulation material and sheath are respectively 9 and 56 in the non-flaming method, and 109 and 86 in the flaming method, although the requirement is less than 150. Therefore, smoke evolution from the whole cable is expected to be small.

The corrosivity is assessed by the pH level and the conductivity of combustion gases based on IEC 754-2. The measured values of pH level and conductivity meet the requirements because no halogenated and sulfuric ingredients are used, which cause evolution of acids.

As mentioned above, since newly developed UTP cables are clean and flame retardant, they will contribute to the security of offices and buildings.



(a) 4-pair UTP

(b) 25-pair UTP

Figure 10 Undergoing VTFT

CONCLUSION

Clean halogen-free flame-retardant UTP cables have been developed. The insulation compound, HFP, developed using polymer alloy techniques, shows excellent transmission properties, fire performance and physical properties. The sheath compound is expandable in the event of a fire and shows superior flame retardancy as compared to conventional FR-PE. The transmission properties of the UTP cables satisfy the TIA/EIA 568-A Category 5 and Category 5-enhanced requirements, and they can be applied to high-speed LAN systems up to ATM data speed. The cables meet the flame retardancy requirements of IEEE.383 VTFT, and have a low level of toxicity, corrosivity and smoke evolution in the event of a fire.



Akinari Nakayama

Hitachi Cable, Ltd.

5-1-1, Hitaka-cho,
Hitachi-shi, Ibaraki,
319-14, Japan

Mr. Nakayama received the M.E. Degree in Organic and Polymeric Materials from Tokyo Institute of Technology in 1994 and joined Hitachi Cable, Ltd. and has been engaged in research and development work for flame-retardant insulating materials. He is now a researcher of the 2nd Department of Power System Laboratory.

REFERENCES

- 1) C.A.Glew, "Halogen vs. Non-halogen Materials for Telecommunications Wire & Cable", International Wire & Cable Symposium Proceeding, P.435-445, 1993
- 2) S. Hinoshita, "Analysis and Improvement of Crosstalk (NEXT & FEXT) for Multi-unit, Backbone UTP Cable applied up to FDDI/ATM Data Speed", International Wire & Cable Symposium Proceeding, P.341-350, 1994

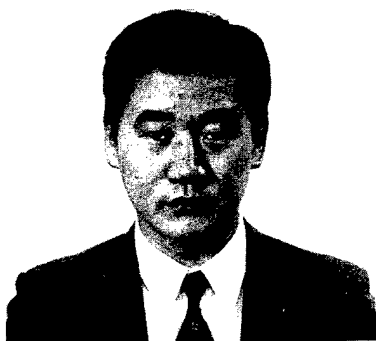


Kiyoshi Watanabe

Hitachi Cable, Ltd.

5-1-1, Hitaka-cho,
Hitachi-shi, Ibaraki,
319-14, Japan

Mr. Watanabe received the M.E. Degree in Organic and Polymeric Materials from Tokyo Institute of Technology in 1979 and joined Hitachi Cable, Ltd. and has been engaged in research and development work for insulating materials of power cables. He is now a senior researcher of the 2nd Department of Power System Laboratory and a member of the Institute of Electrical Engineers of Japan and the Society of Polymer Science, Japan.



Shinya Ishi

Hitachi Cable, Ltd.

5-1-1, Hitaka-cho,
Hitachi-shi, Ibaraki,
319-14, Japan

Mr. Ishi received the B.E. Degree in Electrical Engineering from Shibaura Institute of Technology in 1985 and joined Hitachi Cable, Ltd. and has been engaged in design and development of optical fiber cables and communication cables. He has been involved in design and quality assurance guide for commercial building telecommunication cables.



Shinji Hinoshita

Hitachi Cable, Ltd.

5-1-1, Hitaka-cho,
Hitachi-shi, Ibaraki,
319-14, Japan

Mr. Hinoshita graduated in Electrical Engineering from Kure National College of Technology in 1970 and joined Hitachi Cable, Ltd. and was engaged in research work for broadcasting antenna system and baseband PCM cable. He is currently responsible for design and development of advanced optical fiber and component of mobile access network. He has been an active member of Japan Committee of IEC TC46 / SC46C / WG7 and involved in industry standard for customer premises symmetric cables. He is now a executive senior engineer of the Telecommunication Design Department.

COATING FLOW SIMULATION OF 24 AWG WIRE WITH FEP FLUOROPOLYMER

Pierre B. Kuyt

Daikin America Inc., Orangeburg, New York

ABSTRACT

High speed wire coating with a tubing die is an important industry process. The technology is rather recent, and is not yet fully understood. In this paper, we present a numerical simulation of the flow of a copolymer of tetrafluoroethylene and hexafluoropropylene (FEP) used in a typical wire coating situation. In particular, we wish to predict the location of the attachment point of the polymer on the wire, as well as the stresses and deformations in the melt. The sensitivity of the attachment point with respect to the process parameters and material properties is also investigated.

INTRODUCTION

In the wire and cable industry, the copper wires, such as 24AWG used in twisted pair of local area network cables, are coated with a thin film of fluoropolymer by means of a high speed extrusion process. Actually, the line speed requirements make it impossible to use a pressure coating die, as this would lead to melt fracture¹. In the technology we are considering, the coating occurs outside the die, and results from a vacuum force applied along the inner surface of the melt tube being extruded. The generated melt cone is a critical region of the process where the material is strongly deformed and undergoes high stresses, particularly at the attachment point between the melt and the moving wire. Success and limitations of the process are determined by the stress level. Indeed, too high stress leads to a cone break, bringing the entire extrusion line to a stop.

The purpose of this paper is to show that numerical simulation can be used for predicting relevant information in a process configuration, and to qualitatively assess its feasibility. The difficulty of the numerical simulation originates from the high extrusion speeds and from the dynamic contact point between the wire and the polymer. The location of this contact point is unknown. Such a flow situation has not yet been investigated. The only work remotely connected to this subject was carried out by Sun et al.². They have analyzed the expansion of thick tubes in a sizing die by means of an integral viscoelastic fluid model³; however, the investigated line speeds were very low.

The development of constitutive equations for molten polymer flows and the ever increasing computer performances have opened the door to the simulation of complex industrial processes⁴. In this paper, we use the commercially available computational fluid dynamics package POLYFLOW for simulating the coating process. A differential viscoelastic fluid model will be used for modeling the flow of the fluoropolymer melt. Also a time-dependent simulation will be carried out, in particular, this will allow information to be obtained on

the stability of the coating layer. Viscoelastic models and numerical recipes for calculating flows are widely presented in books^{5,6,7}.

In our present simulations, we compute all variables of interest, i.e. deformation rates, stress components (axial, radial, hoop, shear), velocity distribution and pressure in the melt, as well as the size and shape of the melt cone. We will show that stresses reach a maximum at the tip of the melt cone where the deformations are also the highest. Further along the wire stresses decrease due to the relaxation mechanism. A parametric study is also performed, and this will show how the melt cone is affected by a change of rheological properties and process operating conditions.

PROCESS DESCRIPTION

The process is sketched in Fig. 1. The FEP material exits the tubing die at a flow rate Q . Beyond the die, an internal vacuum F_n is applied and will force the material to enter into contact with the wire moving at line speed V . From the geometric point of view, the annular die is characterized by its inner and outer radii R_i and R_o , while R_c and R_w are the coating and wire radii, respectively. In the process, a melt cone is formed between the die exit and the contact point on the wire, the length of which is denoted by L . Additionally, we may define the Draw Down Ratio (DDR) and the Draw Ratio Balance (DRB) as :

$$DDR = \frac{R_o^2 - R_i^2}{R_c^2 - R_w^2}$$

$$DRB = \frac{R_o/R_c}{R_i/R_w}$$

Each resin is characterized by a range of DDR and DRB where a uniform coating without tear can be obtained. This imposes constraints on the die design, wire size and coating thickness. For example, it was found experimentally, that a DRB significantly less than 1 will most likely result in non circular coating insulation, while a DRB significantly greater than 1 can result in melt tears.

The geometrical data for the tip, die and wire (24AWG) used in this paper are given in Table 1. The melt cone has a typical length L ranging between 0.03 to 0.08 m, and the vacuum force is adjusted accordingly. The line speed V can reach values of 7 m/sec and higher. Finally, in the die head, the fluoropolymer melt has a temperature of 380–390 °C, while the copper wire is often preheated to a temperature of 150°C. Non-isothermal effects, however, will not be considered in this preliminary study.

FLUID PROPERTIES

The material involved in the present flow is a Neoflon™ FEP NP12X fluoropolymer manufactured by Daikin America Inc. Two important properties will be considered in the present analysis: the zero shear viscosity η and the mean relaxation time λ , defined as the inverse of the cross-over frequency between the storage (G') and loss (G'') moduli. These properties have been measured by means of a cone-and-plate rheometer at a temperature of 390°C. The following values have been obtained:

$$\eta = 10^3 \text{ Pa.s,}$$

$$\lambda = 10^{-3} \text{ s}$$

The selection of the fluid model will be based on these rheological properties.

GOVERNING EQUATIONS AND NUMERICAL METHOD

Let \mathbf{D} denote the rate of deformation tensor defined as follows:

$$\mathbf{D} = \frac{1}{2} (\nabla \mathbf{v} + \nabla \mathbf{v}^T)$$

where \mathbf{v} is the velocity field. Let \mathbf{T} denote the extra-stress tensor which can be decomposed as follows:

$$\mathbf{T} = \mathbf{T}_1 + \mathbf{T}_2$$

In this equation, \mathbf{T}_1 is the viscoelastic contribution to the extra-stress while \mathbf{T}_2 is a purely Newtonian component. In the analysis, \mathbf{T}_1 obeys the Phan Thien-Tanner constitutive equation defined as follows⁸:

$$\exp \left[\frac{\alpha \lambda}{\eta_1} \text{tr}(\mathbf{T}_1) \right] \mathbf{T}_1 + \lambda \left[\left(1 - \frac{\zeta}{2}\right) \frac{\nabla}{2} \mathbf{T}_1 + \frac{\zeta}{2} \frac{\Delta}{2} \mathbf{T}_1 \right] = 2\eta_1 \mathbf{D}$$

while \mathbf{T}_2 is given by:

$$\mathbf{T}_2 = 2\eta_2 \mathbf{D}$$

In the above equations, η_1 and η_2 are the partial viscosity factors, and λ is the relaxation time. Also, the symbols ∇ and Δ stand respectively for the upper- and lower-convected time derivative operators. Finally, ζ and ϵ are additional parameters of the Phan Thien-Tanner constitutive equation, which control the shear properties and the extensional viscosity, respectively.

These constitutive relationships are coupled to the momentum and continuity equations respectively given by:

$$-\nabla p + \nabla \cdot (\mathbf{T}_1 + \mathbf{T}_2) = \rho \mathbf{a}$$

$$\nabla \cdot \mathbf{v} = 0$$

where p is the pressure, ρ the density and \mathbf{a} the acceleration vector. In the present case, volume forces (gravity) have been neglected.

The Phan Thien-Tanner fluid model provides realistic predictions for the rheological properties of the melt: it exhibits a shear-thinning behavior, no quadratic first normal stress difference, stress overshoot in shear

start-up and bounded extensional viscosity. Numerical values are required for all five parameters of the model. The zero shear viscosity ($\eta_1 + \eta_2$) and the relaxation time λ will receive the values mentioned above. In the present case, a purely viscous counterpart to the extra-stress is needed in order to overcome instability in shear flow at high shear rate; we have selected $\eta_2/\eta_1 = 1/8$.

Finally, we selected $\zeta = 0.1$ in order to produce a realistic shear-thinning behavior, and $\epsilon = 0.015$ which produces extension thickening followed by extension thinning at high strain rates. Unfortunately, no experimental data is available on the steady-state extensional viscosity, because of technological limitations⁹ in measuring them at strain rates higher than 1 s^{-1} . In Fig. 2, we display the shear and extensional properties, as predicted by the Phan Thien-Tanner fluid model, for various values of the zero shear viscosity and the relaxation time. Shear thinning and extension-thickening are indeed observed.

PROCESS MODELING

We assume the flow process, as sketched in Fig. 1 is axisymmetric. In particular gravity forces will be neglected in the momentum equations. This allows us to select a 2-D axisymmetric geometric model, as displayed in Fig. 3 together with the boundary conditions. In that figure, V_n and V_s are the normal and tangential velocities. We consider only an isothermal flow. Despite the temperature difference between the melt and the wire, this assumption is acceptable, at least in the vicinity of the melt cone, in view of the very high speeds involved in the process.

The location of the dynamic contact point between the melt and the wire (tip of the melt cone) is previously unknown, and actually depends on the process conditions and fluid properties. Here, a time-dependent calculation will be performed, which follows a procedure similar to the start-up of the extrusion line.

Initially, as indicated in Fig. 3, the tube is extruded from the die and a low take-up velocity is applied at the exit of the computational domain together with a vacuum force along the inner free surface of the tube. The line speed is then increased until the nominal value is reached and the contact is established between the melt tube and the moving wire. During the speed increase, the contact point will move backwards to the die exit, and reaches, in some cases, an equilibrium position once the nominal speed has been attained.

For numerical reasons, the contact between melt and wire is governed by means of a slipping law, which relates the tangential force f_s to the relative tangential velocity as follows:

$$f_s = -F_{\text{slip}} \cdot (v_s - V)$$

where F_{slip} is the friction coefficient. Preliminary simulations have shown that, without slipping, deformations are unbounded at the contact. Finally, surface tension effects will also be investigated.

As it can be observed, a lot of independent parameters are involved in the process. Table 2 shows the several cases we will investigate in the next section.

The set of equations presented in the above section with the boundary conditions will be solved by means of the finite element method ⁵. In Fig. 4, we display a typical finite element mesh used for the simulation. It contains 200 finite elements. Calculations have also been performed on refined finite element meshes in the vicinity of the contact point to validate our numerical predictions.

RESULTS AND DISCUSSION

For all the cases mentioned in Table 2, the transient procedure corresponds to a linear increase of the line speed between $t = 0$ and $t = 0.1$ s, followed by a constant value to $t = 1$ s. Unless otherwise specified, results are obtained for a line speed of 4.06 m/s (800 ft/min). Hereafter, we give general comments on the numerical results and on their sensitivity with respect to the several parameters, in accordance with the cases as indicated in Table 2.

Prediction of the melt cone shape and length during start-up

During the start-up procedure, an increasing take-up velocity is applied on the extruded melt. This leads to significant deformations of the extrudate. These deformations are also predicted by the simulations, as shown in Fig. 5. Here, the computational domain is displayed together with the finite element mesh, at different times as the line speed increases. The present situation corresponds to case 4 of Table 2. At time $t = 0$ s, the melt is being extruded, while the take-up velocity is increasing. At time $t = 1$ s, a stable melt cone is obtained. As it will be seen later, stable cones will be obtained for cases 2, 4 and 8, which actually involve low viscous and viscoelastic stresses and high vacuum. For the other cases in Table 2, a stable cone is not reached after 1 s.

Steady state position for the cone length

Stability of the melt cone is a critical factor of the process. For the cases 1 to 9 of Table 2, we display in Fig. 6 the evolution of the cone length L as a function of time. We easily observe that in the absence of vacuum (cases 1 and 3), the cone length L has not reached a steady position after 1 s. Case 2 shows that the vacuum has a stabilizing effect on the contact point, as it can be seen in Fig. 6. Cases 5 to 9 indicate that the cone length increases with viscosity, relaxation time, surface tension and slipping along the wire, while it decreases with vacuum. As it will be shown, a cone length increase is not necessarily accompanied by a stress increase.

Stress predictions

In Fig. 7 we see the stress profiles obtained along the inner surface of the cone, for case 4 at time $t = 1$ s. The die exit is located at the axial distance $Z = 2$ cm. Here we find that the axial stress component is the largest. The peak occurs at the contact point between the melt and the wire, where the stretching is also maximum. Further along the wire, the stresses relax. While a traction state is found in the axial direction, a compression state exists in both radial and circumferential (hoop) directions. In fact, a compression state improves the bonding of the melt on the wire, while a too high traction stress can lead to cone breaks.

Influence of line speed

Fig. 8 shows the effects of the line speed on the cone length, and on the development of axial stress and strain rate at the contact point. This is shown for cases 4 and 7 of Table 2, corresponding to a low and highly viscoelastic material. As expected, we observe that both cone length and axial stress increase with line speed.

Influence of shear viscosity

Cases 4, 5 and 10 involve a melt with increasing shear viscosity. The influence of viscosity on the cone length and on the axial stress and strain rate is shown in Fig. 9. We find that the cone length and the axial stress are very sensitive to the melt viscosity. This can explain why high viscosity grades of FEP are processed at a lower line speed. Furthermore, the effects of temperature on the process can also be easily understood. Indeed, if the temperature drops too rapidly in the cone, leading to a viscosity increase, cone breaks will occur. Note that the shear and extensional viscosities are not two independent material properties, as can be seen in Fig. 2: increasing the shear viscosity also increases the extensional viscosity.

Influence of viscoelasticity

Viscoelastic effects, in particular the extensional viscosity which characterizes the melt response in extension, play a significant role in the coating process. Cases 2, 4, 7 and 11 of Table 2 correspond to FEP melt with increased viscoelastic properties. In Fig. 10, we display the effects of the relaxation time on the cone length and on both axial stress and strain rate. Here we observe that an increase of the relaxation time, hence an increase of the extensional viscosity, leads to an increase of the cone length. This is simultaneously accompanied by an increase of the axial stress and a significant reduction of the axial strain rate.

Influence of vacuum

The influence of the vacuum force is shown in Fig. 11. The curves are obtained on the basis of cases 3, 4 and 8. We observe that the cone length significantly decreases with increasing vacuum. This, accompanied by an important increase of the axial stress, and a moderate increase of the axial strain rate, has also been observed in production trials, where some amount of vacuum is needed for stabilizing the melt cone. Yet, a vacuum excess increases the cone break frequency. Moreover, it is worth mentioning that vacuum increases shear rate at the contact point, which may also affect the cone stability.

Influence of surface tension

Surface tension has been considered in case 9 of Table 2. It is found that it increases the cone length and decreases the axial stress. The effect on the cone length stability is, however, less obvious and needs further investigations.

Influence of slipping along the wire

In Table 2, case 6 corresponds to a situation characterized by a lower friction coefficient for the melt along the wire. This results in a decrease of the axial stress and maximum strain rate. Furthermore, this significantly affects the development of the velocity

profile along the inner surface. This can be observed for case 6 in Fig. 12, where we see that a longer transition length is needed before the melt acquires the wire velocity. Fig. 12 also shows the development of the axial velocity for various process situations, and to some extent, summarizes the previous observations. Finally, Fig. 13 shows profiles of the axial stress for cases 2 to 9 of Table 2. The peaks correspond to the location of the contact points. In particular, we may see that slipping significantly decreases the axial stress, while relaxation time has the opposite effect. The effects of the various parameters on the cone length and axial stress are summarized in Table 3.

CONCLUSIONS

For the first time, the high speed wire coating process in a tubing die was successfully simulated. This was done by means of the simulation software POLYFLOW. In this paper, a time-dependent simulation was performed for an isothermal viscoelastic flow. A differential viscoelastic constitutive equation was used for modeling the fluoropolymer melt. The stresses and deformation rates in the melt cone, as well as the location of the attachment point, were obtained. The influence of the process and material parameters were investigated. In particular, we considered the line speed and vacuum on one hand, and viscosity and relaxation time on the other hand, as well as surface tension and slipping.

Qualitatively the results are in good agreements with the industrial production runs. Typically, the increase of axial stress lowers the line speed for higher viscous and elastic FEP grades. Also, the influence of the line speed and vacuum on cone length and stability were observed. In practice, the melt cone breaks at high vacuum and high speed.

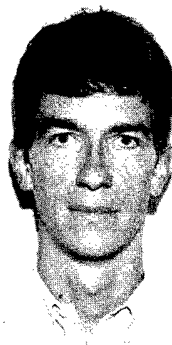
From the quantitative point of view, the actual cone lengths are underestimated in the present simulations. This may originate from some assumptions. In particular, non-isothermal effects and melt slipping on the wire are possible issues. Also a better knowledge of the extensional properties of the material is important. Finally 3-D effects, including gravity, should be considered. All those aspects offer a serious challenge for future numerical studies.

ACKNOWLEDGMENTS

The author would like to thank Dr. B. Debbaut of Polyflow S.A. for his useful discussions and comments.

REFERENCES

- [1] E.E. Rosenbaum, S.G. Hatzikiriakos, "The melt fracture behaviour of Teflon® resins in capillary extrusion", SPE ANTEC, (1995) 1111-1115.
- [2] J. Sun, X.-L. Luo, R.I. Tanner, "The expansion of thick tubes" Theor. and Appl. Rheo. Proc.: XIth Int. Congr. on Rheology, Brussels, (1992).
- [3] B. Bernstein, E.A. Kearsley, L. Zapas, Trans. Soc. Rheol., 7 (1963) 391.
- [4] M.J. Crochet, B. Debbaut, R. Keunings and J.M. Marchal, in *Applications of CAE in Extrusion and Other Continuous Processes*, ed. K.T. O'Brien, Carl Hanser Verlag, München, (1992), Chap. 2.
- [5] M.J. Crochet, R. Davies and K. Walters, *Numerical Simulation of non-Newtonian Flow*, Elsevier, Amsterdam, (1984).
- [6] R.B. Bird, R.C. Armstrong, O. Hassager, *Dynamics of Polymeric Liquids*, Vol. 1: Fluid Mechanics, 2nd edition, Wiley-Interscience, Wiley, New York, (1987).
- [7] Polyflow User's Manual, (1995).
- [8] N. Phan Thien and R.I. Tanner, J. Non-Newt. Fluid Mech., 2 (1977) 353.
- [9] J. Meissner and J. Hostettler, Rheol. Acta, 33 (1994) 1.



Pierre Kuyl
Daikin America Inc.
20 Olympic Drive,
Orangeburg, NY 10962

Pierre Kuyl received both his MS degree in computer sciences and BS degree in mechanical engineering from the university of Louvain-La-Neuve, Belgium. He worked for 3 years at the Computer Aided Engineering center and R&D department of the chemical division of Daikin Industries in Osaka, Japan. He is now responsible for the CAE function of Daikin America in Orangeburg, New York. His area of interest includes rheology, polymer processing and process simulation.

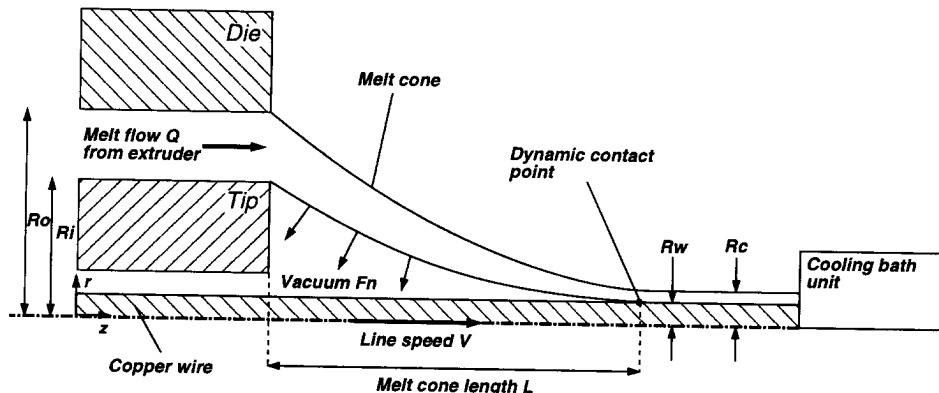


Figure 1. Wire coating process with a tubing die

Table 1. Design Data

DDR	83
DRB	0.99
Radius [cm]	
Ri	0.2362
Ro	0.3962
Rw	0.0255
Rc-Rw	0.0180

Table 2. Material and Process Variables

Case	Rel.Time λ [sec]	Visc. η [Pa.s]	Surf.Tens. σ [N/m]	Vac. F_n [Pa]	F_{slip} [Pa]
1	0.	10^3	0.	0.	10^5
2	0.	10^3	0.	$3 \cdot 10^3$	10^5
3	10^{-3}	10^3	0.	0.	10^5
4	10^{-3}	10^3	0.	$3 \cdot 10^3$	10^5
5	10^{-3}	$5 \cdot 10^3$	0.	$3 \cdot 10^3$	10^5
6	10^{-3}	10^3	0.	$3 \cdot 10^3$	10^3
7	$5 \cdot 10^{-3}$	10^3	0.	$3 \cdot 10^3$	10^5
8	10^{-3}	10^3	0.	$9 \cdot 10^3$	10^5
9	10^{-3}	$5 \cdot 10^3$	$5 \cdot 10^{-2}$	$3 \cdot 10^3$	10^5
10	10^{-3}	10^4	0.	$3 \cdot 10^3$	10^5
11	10^{-2}	10^3	0.	$3 \cdot 10^3$	10^5

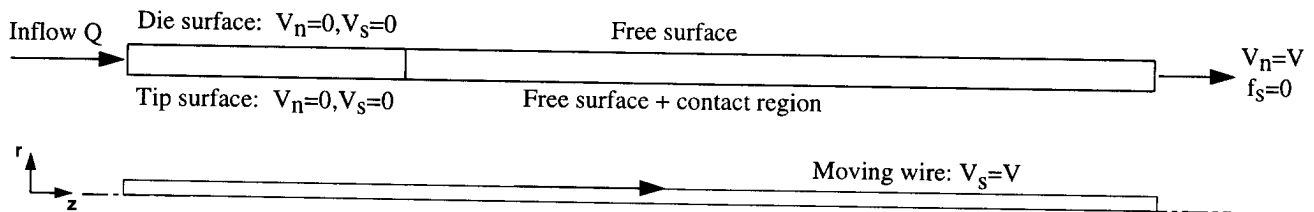


Figure 3. Boundary conditions

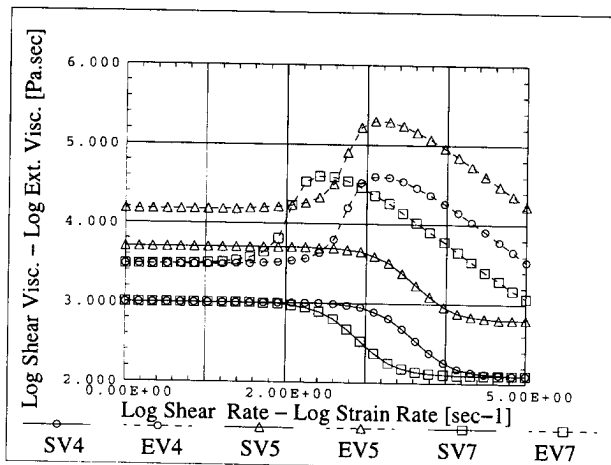


Figure 2. Shear and extensional viscosity for material model of cases 4, 5 and 7.

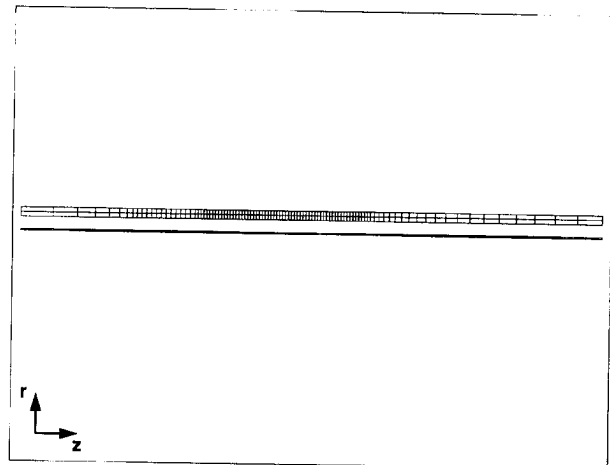


Figure 4. Finite Element Mesh (200 elements)

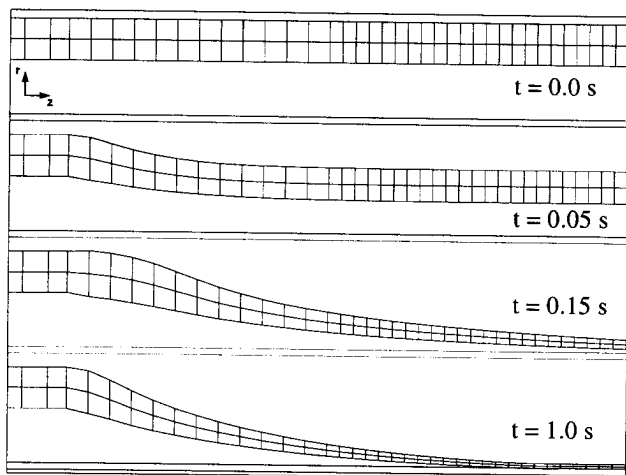


Figure 5. Mesh deformations at different time intervals for case 4.

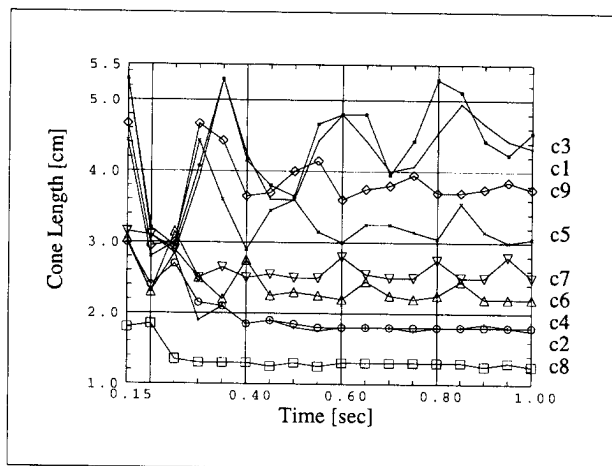


Figure 6. Cone length evolution with time for the different cases of Table 2.

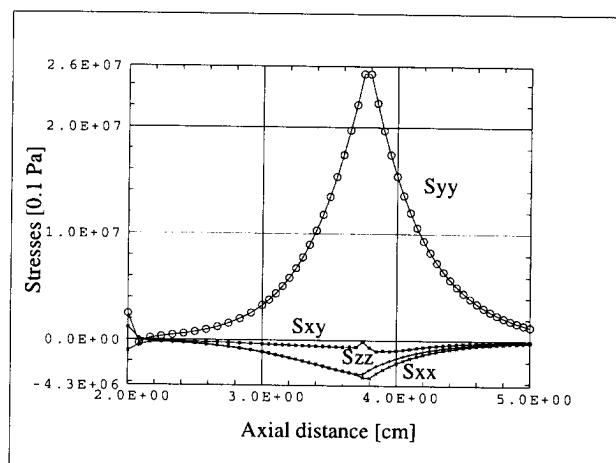


Figure 7. Stress profiles on inside surface at time $t = 1s$ for case 4. Die exit is at $Z = 2cm$.

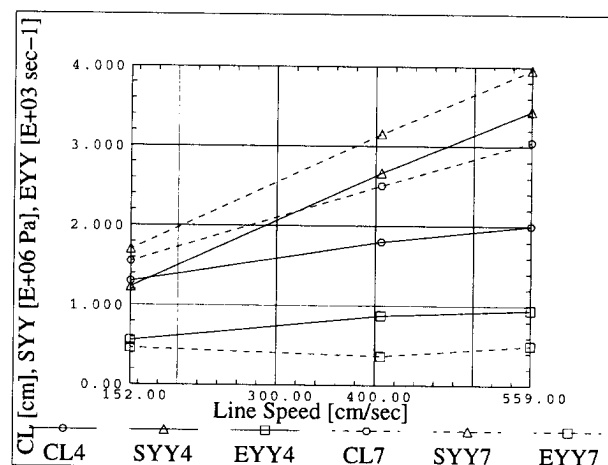


Figure 8. Cone length, axial stress and axial strain rate at contact point for 3 different line speeds.

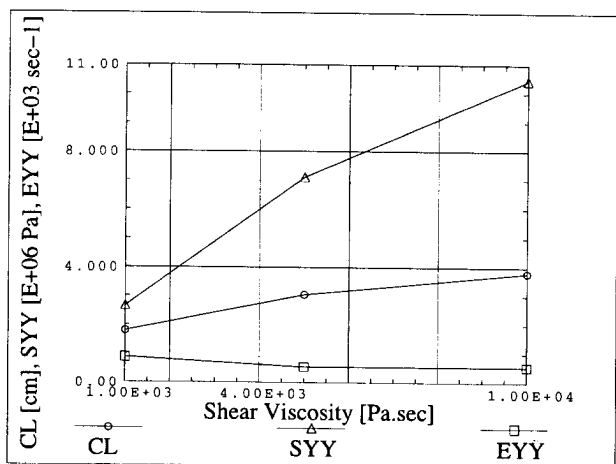


Figure 9. Cone length, axial stress and axial strain rate at contact point for cases 4, 5 and 10.

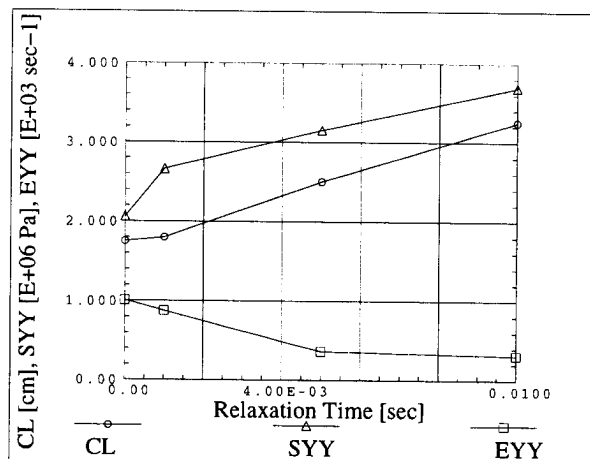


Figure 10. Cone length, axial stress and axial strain rate at contact point for cases 2, 4, 7 and 11.

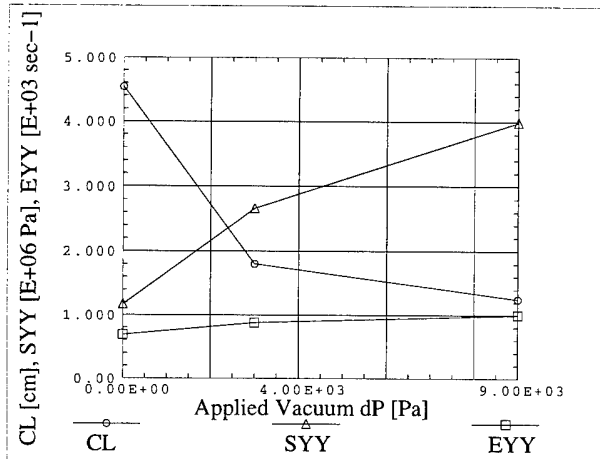


Figure 11. Cone length, axial stress and axial strain rate at contact point for cases 3, 4 and 8.

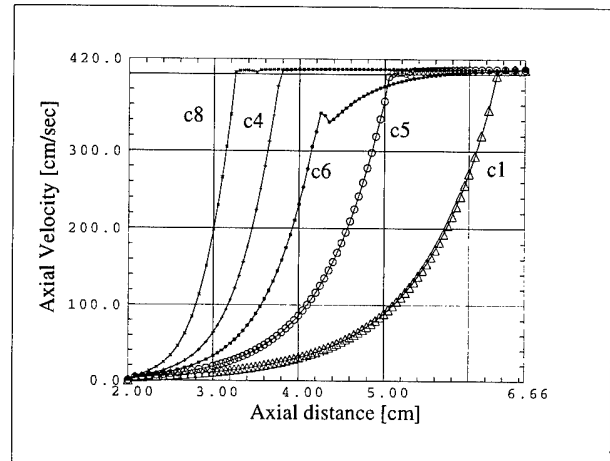


Figure 12. Axial velocity on inside surface for different cases. Die exit is at Z=2cm.

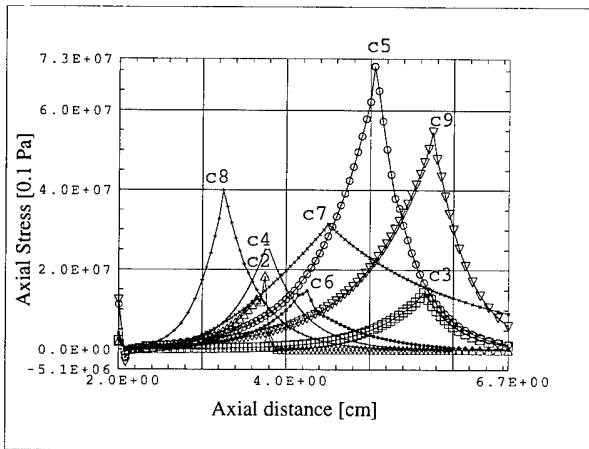


Figure 13. Axial Stress on inside surface at time t=1s for different cases. Die exit is at Z=2cm.

Table 3. Parameters Effects

Parameter increase	Cone length	Axial Stress Sy
Line speed	+	+
Vacuum	-	+
Viscosity	+	+
Relax. time	+	+
Surf. tens.	+	-
Slip on wire	+	-

AN ACCURATE, NONCONTACT LENGTH AND SPEED MEASUREMENT TECHNIQUE FOR THE WIRE AND CABLE INDUSTRY

**Michael W. Nielsen
Brian Osmondson**

TSI Incorporated, St. Paul, Minnesota

Introduction

As global competition continues to intensify, the need to increase productivity and reduce waste is critical to the survival of today's wire and cable manufacturer. One contributing factor to achieving this goal is the ability to measure length and speed with increasing accuracy and precision.

This paper describes a highly accurate, noncontact technology developed by TSI Incorporated to measure both length and speed for the wire and cable industry. Details of the noncontact technology and its advantages for measuring length and speed of wire and cable will be discussed. Test results from a variety of applications and different cables comparing a contact wheel counter system to the TSI LaserSpeed® Model CB100 will also be presented.

Measuring Length and Speed Accurately

The basis of length and speed measurements is to assure with the highest degree of confidence the stated length of the cable or the process speed is indeed accurate. Accurate length and speed measurements are important for many different aspects of the wire and cable industry including:

- To provide the customer with an accurate final length. There are two areas of concern: first, to provide the customer with the indicated length of cable; secondly, to reduce overages and improve profits.
- To provide plant managers and engineers with a proper reference for production capacities, cost analysis, inventory management, and waste reduction.

Common Techniques for Measuring Cable Length and Speed

The most common technique used to measure length and speed is the contact wheel counter system. Length is calculated from the amount of rotation of a contact wheel as measured by an encoder. However, contact wheel counter systems, by their very nature, have several fundamental flaws that make them very prone to measurement errors. These include:

- The amount of slippage or jitter between the wheel and the cable.
- Wear of the contact wheel causing the radius to change.
- Build-up of talcum powder, grease, dirt, or other material between the wheel and cable.

Many different contact tachometer systems have been designed to reduce these measurement errors. They include two-wheel, three-wheel, and four-wheel track systems. However, many of the problems mentioned above still exist to some degree. In general, most tachometer system provide length error of 0.5% or higher; greater than 1.0% error is common.

A New, Noncontact Technique for Accurately Measuring Length and Speed

TSI Incorporated has recently developed a new product, called the LaserSpeed Model CB100, which provides highly accurate and repeatable cable length and speed measurements. Using a long established, noncontact Laser Doppler Velocimetry (LDV) technology, the Model CB100 gauge (Figure 1) eliminates length and speed measurement errors associated with other types of counters. Because of its unique

technology, the Model CB100 can provide length and speed measurement accuracy better than $\pm 0.1\%$, with repeatability better than $\pm 0.05\%$.

CB100 Length and Speed Gauge

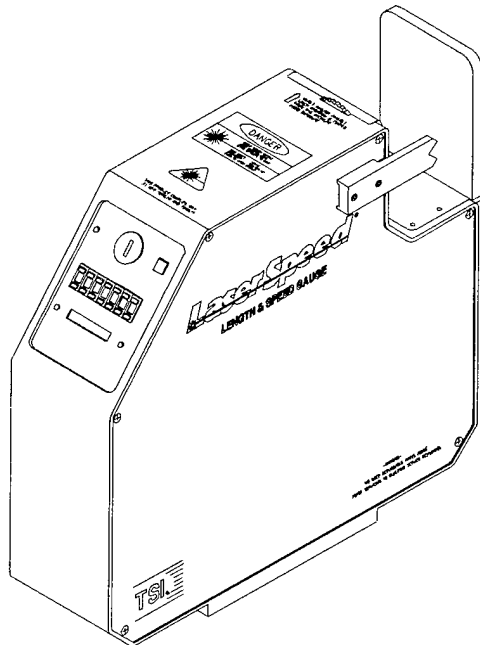


Figure 1

Introduction to Laser Doppler Velocimetry

Laser Doppler Velocimetry is a velocity and length measurement technique based on measuring the Doppler shift in light scattered by a moving surface from two intersecting laser beams. The scattered light is collected and focused onto a receiver, where the light is mixed, or heterodyned. The heterodyned light on the receiver yields two frequencies, the sum and the difference frequency of the Doppler shifted light. The sum product yields a frequency approximately two times that of the original laser beam. This frequency is much higher than the frequency response of the receiver, therefore it is ignored. The difference product is converted by the receiver into an electrical signal whose principle frequency component is directly proportional to the velocity of the material. Each of these concepts will be examined in detail. A schematic of a typical LDV system is shown in Figure 2.

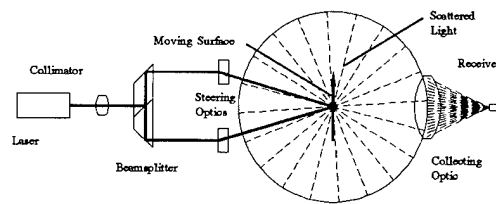


Figure 2

A laser light source is used because it is monochromatic, single frequency, and all the wave fronts are in phase. In other words, the light is coherent. These properties of laser light enable the scattered light from each of the laser beams to mix properly on the receiver.

The beam emitted from the laser is collimated. Collimation controls the divergence (spread) of the light. A collimated laser beam has a constant cross sectional dimension along the length of the beam path. After collimation, the laser beam is split into two, equal intensity beams with an optical beamsplitter. The result is two laser beams with identical optical properties.

The two beams are then crossed, using steering optics, to a fixed location in space. The area where the two beams overlap or cross is called the measurement region (shown in Figure 3).

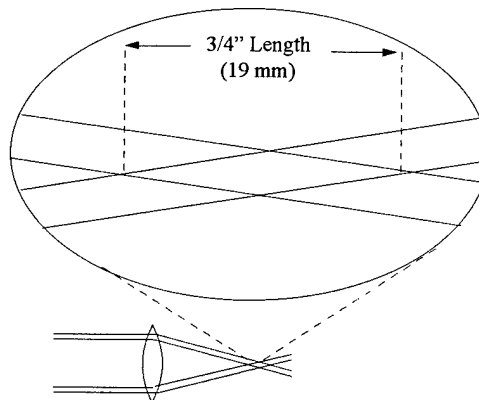


Figure 3

The Model CB100 gauge has a measurement region of approximately 3 mm X 1.5 mm X 19 mm (LWD). This large measurement region is very useful when measuring the length and speed of wires or cables that may not always remain in a fixed position relative to the optical sensor. However, if the wire or cable wanders outside the measurement region no speed or length measurements can be obtained.

The LDV technique measures the velocity component of wire or cable moving perpendicular to the bisector of the angle as shown in Figure 4.

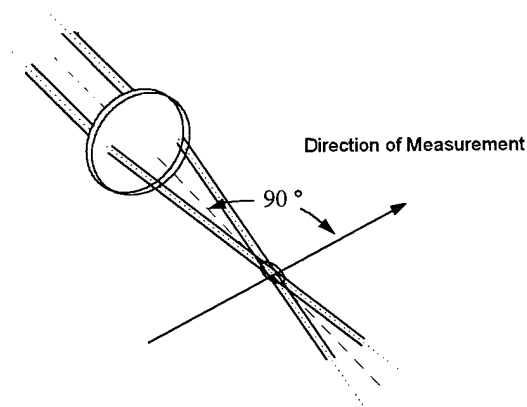


Figure 4

In this figure, the material has a velocity component that is in the same direction as the lower beam and a velocity component that is opposite in direction to the upper beam. The light scattered from the lower beam will be Doppler shifted to a lower frequency (F_1) and the light scattered from the upper beam will be Doppler shifted to a higher frequency (F_2). Mathematically, they are represented below as follows.

$$F_1 = F_{\text{light}} - F_{\text{Doppler}}$$

$$F_2 = F_{\text{light}} + F_{\text{Doppler}}$$

The sum component becomes:

$$F_1 + F_2 = (F_{\text{light}} - F_{\text{Doppler}}) + (F_{\text{light}} + F_{\text{Doppler}})$$

or

$$F_1 + F_2 = 2 F_{\text{light}}$$

Since the frequency of light is around 400 GHz, the sum component ($2 F_{\text{light}}$) will be approximately 800 GHz. This frequency is well above the response of the optical detector, so it can be ignored.

However, by measuring the difference component of the scattered light, one can measure the velocity of the moving material very precisely. The difference component, therefore, becomes:

$$F_1 - F_2 = (F_{\text{light}} - F_{\text{Doppler}}) - (F_{\text{light}} + F_{\text{Doppler}})$$

or

$$F_1 - F_2 = 2 F_{\text{Doppler}}$$

Fortunately, there is also an intuitive model describing LDV. When two laser beams intersect, an alternating pattern of light and no-light fringes are created throughout the measurement region. The light fringes are caused by constructive interference while the no-light fringes correspond to destructive interference of the two laser beams. This concept is shown in Figure 5.

Light is alternately scattered, not scattered, scattered, not scattered, etc., as scattering sites on the wire or cable pass through the interference pattern of the measurement region. This alternating scattered light pattern is converted to electrical energy by the receiver (see figure 5).

The frequency (f) of the electrical signal is proportional to the velocity (v) of the wire or cable. The frequency is multiplied by a length constant, known as the fringe spacing (d), to determine the velocity. The fringe spacing is determined by the crossing angle of the intersecting beams ($2k$) and the wavelength of the laser (λ). Since the crossing angle is fixed and the wavelength is constant, the fringe spacing never changes and is also constant.

In other words,

$$\text{cable speed } (v) = d_f * f$$

where

$$d_f = \lambda / 2 \sin k$$

λ = laser wavelength

k = half angle

f = measured frequency

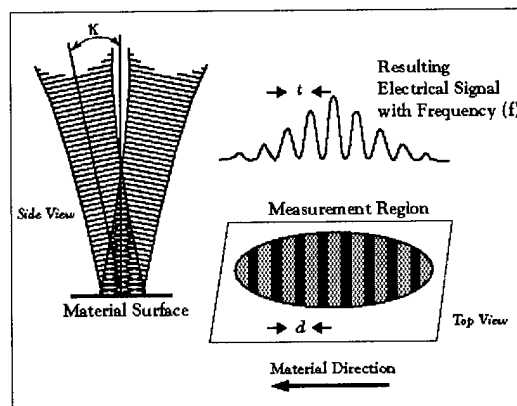


Figure 5

Once the velocity is determined the length (L) of wire or cable passing through the measurement

region can be obtained by integrating the velocity information over the time of interest.

$$L = \int_0^t v dt$$

Laboratory Test Results

To investigate the length measurement capability of the LDV system, a simple but effective test was developed. A belt of a known length (measured using NIST traceable standards) was placed between two wheels. One of the wheels was driven by a motor to rotate the belt. The belt had a small slot which was used as a once per revolution marker. An optical encoder monitored the once per revolution mark. A schematic of the test apparatus is shown in Figure 6.

During the test, the belt length was measured with an LDV system. To reduce measurement error caused by the test apparatus (i.e. the response time of the optical encoder), the length of ten belt revolutions (23.3372 feet) was measured. By increasing the overall measurement length, this effectively reduced the amount of error due to outside influences.

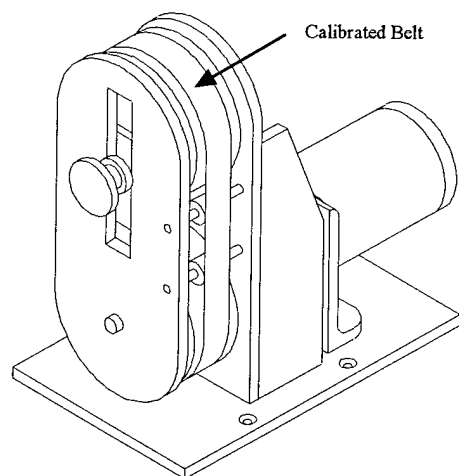


Figure 6

Fifteen hundred individual length measurements were made using the LDV system. The average length, maximum and minimum length, and three standard deviation point are presented in Table 1.

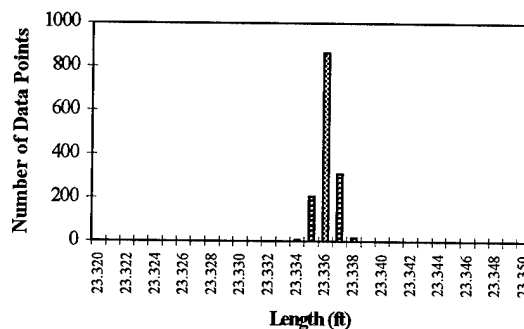
Average	Maximum	Minimum	3 Sigma	% Error
23.336 ft	23.338 ft	23.334 ft	0.00207 ft	0.0089%

Table 1

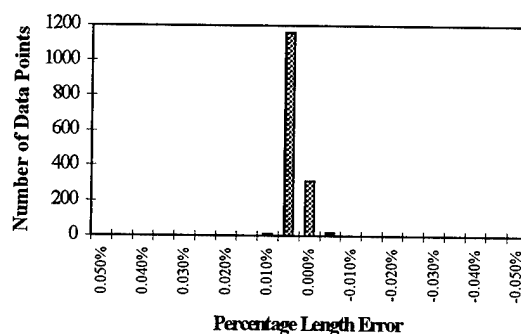
As seen from the data, the CB100 system is capable of measuring length with very high accuracy. The CB100 provided accuracy better than 0.009%.

The 1,500 length measurements are plotted in the following two graphs. These graphs demonstrate the extraordinary accuracy and repeatability of the CB100 system. The data shows the length and percent error measurements grouped in a very tight distribution around the actual belt length.

Length Distribution Chart



Length Distribution Chart



As demonstrated by this data, under ideal conditions, the LDV system can provide incredible length measurement accuracy.

Actual Production Process Measurement Results

It has been reported that noncontact LDV technology is fully capable of providing accurate length and speed measurements for the wire and cable industry. The CB100 gauge has been tested on a variety of wire and cable manufacturing processes. The results overwhelmingly show the benefit of using noncontact measurements over existing contact wheel systems.

Wire Drawing Process

Accurate length measurement of the wire drawing process is critical to reducing scrap. Ideally, the length of wire on the take up reel should be matched so that the next stranding process can be optimized. In the stranding process, if wire splicing is not allowed, the shortest payout reel length will determine the longest stranded cable. There is also industry consensus that suggests there is less down time and greater cost savings if all of the reels run out at the same time, even if the wire can be spliced.

Wire drawing processes produce very fine wire at very high speeds, sometimes over 3000 ft/min. It is extremely difficult, if not impossible to use a contact wheel tachometer system to measure wire length. Instead, many lines use a capstan tachometer to determine the wire length. This technique involves using the capstan radius and number of revolutions to calculate wire length. This methodology is very prone to measurement errors caused by slippage, dirt build-up on the capstan, and movement of the wire up and down the groove of the capstan wheel.

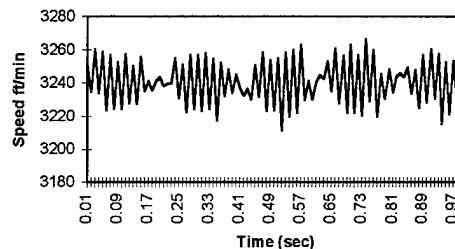
A noncontact system, by its nature, measures the speed and length of the cable directly, not from the capstan wheel. This eliminates all of these problems.

The data below shows the speed of a wire in a drawing process as measured by the CB100 gauge. Notice the speed fluctuations and the periodic pattern over the one second time interval. It is caused by the take up reel rotation. These fluctuations cannot be seen by a capstan tachometer. Therefore, it is impossible for the tachometer to measure

accurate wire lengths. Typically errors associated with capstan tachometers are greater than 1%.

The LDV measurements, on the other hand, closely track the changes in the speed of the wire. Since length is calculated by integrating speed over time, accurate length measurements can be obtained using noncontact LDV technology.

Wire Drawing Machine



High Speed Insulating Line

Just like the wire drawing process, accurate length measurements on high speed primary lines are important to ensure length uniformity on the take up reels, as well as for inventory management purposes. This is critical for matching payout reel lengths for the next process.

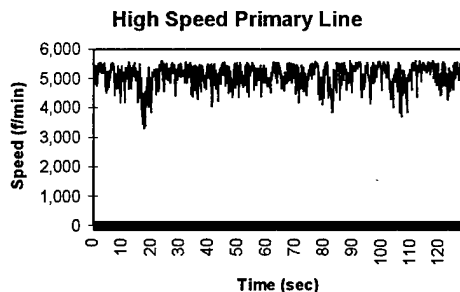
Because the cable speed is very high, most insulating lines use a capstan tachometer to determine the length of the cable. As in the wire drawing process, high speed insulating lines are very prone to measurement errors caused by slippage, dirt build-up on the capstan, and movement of the wire up and down the groove of the capstan wheel.

Noncontact length and speed measurement gauges track the cable speed accurately and precisely. Because the speed and length is measured directly from the cable, problems associated with contact wheel systems can be eliminated.

A CB100 gauge was installed on a high speed primary line which produces 22 gauge wire. The data below shows that the primary line had an average speed of approximately 5,000 ft./min. However, the data clearly shows that the speed is not constant. The variation in speed was caused by the wire moving up and down the

capstan wheel. For a contact wheel tachometer system to accurately measure wire length it must be able to correct for such wire movement changes. This is impossible for capstan tachometers.

Using a noncontact LDV gauge completely eliminates this measurement error. The data clearly shows that the changes in speed can be followed precisely so that accurate length measurements can be obtained.

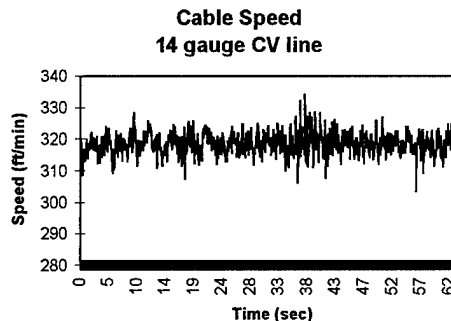


CV or Jacketing Line

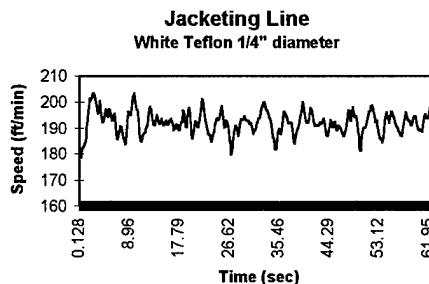
Accurate length and speed measurement is critical for CV and jacketing line applications. Line speed is one of the fundamental control parameters that must be optimized in order to maintain the desired insulation thickness and cable diameter. Most CV and jacketing lines control cable diameter, hence insulation thickness, using a laser diameter gauge and tachometer.

Faster response and more accurate speed measurement could improve cable diameter control and reduce insulating material consumption in the extrusion process. This will ultimately improve finished quality and profits.

The following graph shows CV line speed measurements obtained using LDV. Notice the high frequency fluctuations in speed. These fluctuations are not measurable with a contact wheel tachometer system because the contact wheel has inertia causing the cable to slip.



For CV and jacketing lines, accurate length measurement on the final take up reel is also critical to improving productivity. By closely tracking the speed fluctuations and integrating it over time, take up reel length can be measured very accurately with the CB100. Ultimately, pay out reels can be optimized for the next process (or end customer) which reduces scrap.



Stranding and Cabling Lines

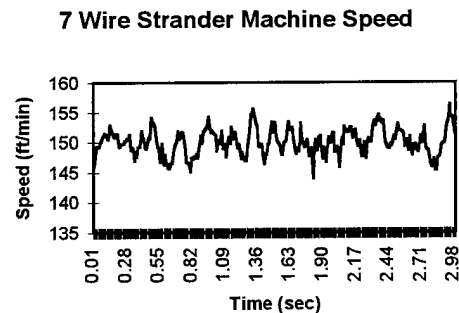
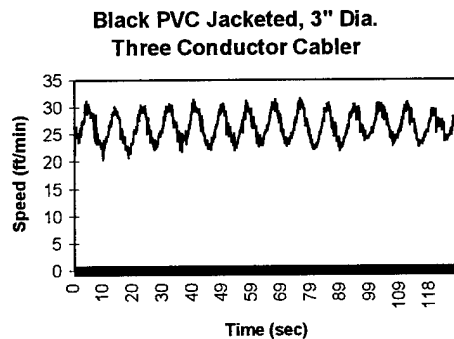
With each step in the cabling process, material cost increases dramatically. Cabling lines are usually very expensive, both in material and handling cost. Any cable overage at this point can adversely affect profitability. Thus, an accurate length measurement guarantees that the customer receives the amount of cable ordered, while minimizing the overage supplied.

There are primarily two problems associated with using contact wheel or belt tachometer systems to measure length on cabling lines. The first problem is the convolutions and rotation of the cable act as a worm gear causing the contact wheel or belt to move faster than the core cable length. The second problem is constant wear on the contact wheel or belt which changes the diameter and thus, the measured length. Such systems often require frequent re-

calibration and maintenance to replace worn parts.

For stranding and cabling lines, a noncontact length measurement gauge has distinct advantages over a contact wheel tachometer. First, the worm gear effect is negated. Second, measurement errors caused by wear are completely eliminated since there is nothing in contact with the cable. In addition, noncontact measurement gauges do not require frequent re-calibration associated with replacing worn wheels or belts. This greatly improves manufacturing uptime capacity.

The following graphs demonstrate the ability of the LDV system to measure cabling and stranding lines. Again, speed is integrated over time to provide an accurate length measurement.



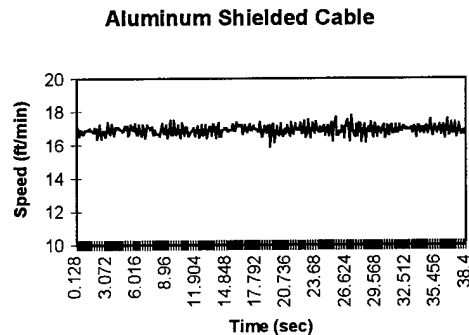
Cable Shielding Line

Another application in which accurate length measurements are very important is the cable shielding line. In this process, a metallic jacket is wrapped around a cable to protect the cable. Material cost in this process is quite high. An accurate length measurement can reduce overage and increase profitability.

Conventional tachometer systems have difficulty measuring on the shielded cable due to the corrugated surface. The tachometer wheels walk up and down the corrugated surface of the cable, increasing the effective cable length. Also, if the cable moves fast enough, the tachometer can bounce creating all kinds of erroneous measurements.

LDV, by its very nature, does not have these problems. The LDV system measures the cable length in a plane perpendicular to the sensor. Therefore, it measures the actual core cable length regardless of cable surface structure or texture.

The following graph demonstrated the ability of the CB100 to measure on an aluminum shielded cable.



Repackaging Line

A repackaging line (Figure 7) is the final step in the cable manufacturing process. This process spools a known amount of cable onto a reel which is then sold to the customer. This is where an accurate length measurement is most critical. If the customer is shipped a short cable, billback charges or lost sales may result. If the customer is shipped extra cable, the manufacturer has given away profits.

Tests were performed on a repackaging line to verify the accuracy of the LDV system. To do this, a stainless steel cable of a known length was used. The cable length was measured with NIST traceable standards. Its length was marked at 1000 feet.

The LDV system was mounted on the repackaging line. The cable was then transferred from a payout reel, through a high

quality tachometer system, past the LDV system, and onto a take up reel. This simple arrangement allowed for several runs of the same cable; therefore, several length tests could be performed.

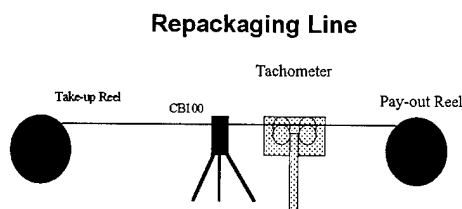


Figure 7

Table 2 shows the actual length of the cable, the length of cable measured by the LDV system, and the length measured by a high quality tachometer system

Actual Cable Length	Tachometer Length Measurement	LDV System Length Measurement	LDV System Error	Tachometer Error
994.041	998	993.779	-0.026%	0.398%
1001.313	1003	1001.057	-0.026%	0.168%
1000.150	1003	999.501	-0.065%	0.285%

Table 2

As shown in Table 2, the LDV system measured the cable length with greater precision than the tachometer. The LDV system measured the cable length with a worst case error of -0.065%. On the other hand, the tachometer system had a worst case error of 0.398%; approximately six times less accurate than the LDV system.

It is important to understand the potential pay back of this higher accuracy. As an example, if this cable manufacturer produced 1,000,000 feet of cable per month, and the cable cost an average of 10 cents a foot, the total revenues per month would be \$100,000. If the LDV system can eliminate overage expense by 0.3%, this would show a cost savings of \$3,000 per month. The LDV system could show pay back in less than five months.

Conclusion

The advantages of a noncontact length and speed measurement system has been proven on all types of wire and cabling manufacturing processes, from bare wire to insulated shielded cable. The LDV system eliminates cable length measurement errors associated with contact wheel or belt tachometer systems which is

caused by slippage, jitter, and wear. In addition, the LDV system can precisely track cable speed changes which makes it ideal for controlling CV or jacketing lines.

Test results performed on a repackaging line show that the LDV system is capable of providing length measurement accuracy better than $\pm 0.1\%$. Comparison between the LDV system and contact tachometer system showed that the LDV system was approximately six times more accurate. As a result, LDV can increase the length measurement accuracy of your process and improve the confidence of stated cable length. Accurate length measurements will reduce shortages to the customer and reduce overages which ultimately improves productivity and quality.

About the Authors

Michael W. Nielsen
TSI Incorporated
PO Box 64394
St. Paul, MN 55164

Mike Nielsen currently holds the position of Senior Applications Engineer in the Process Instruments Division of TSI. Mr. Nielsen's background is in Electrical Engineering. He has held positions in both Manufacturing Engineering and Research and Development. Mike has been involved in design and testing of Laser Doppler Technology for the last fifteen years.

Brian Osmondson
TSI Incorporated
PO Box 64394
St. Paul, MN 55164

Brian Osmondson currently holds the position of Marketing Manager for the Process Instruments Division of TSI. He graduated with a bachelors degree in mechanical engineering from the University of Minnesota in 1986. Brian has been involved with LDV applications for the steel, aluminum, and cable industries during the past four years.

CROSSTALK MEASUREMENTS AS A MEANS TO CHARACTERIZE THE BALANCE OF DATA GRADE WIRES

Jörg-Hein (Jo) Walling *, Martin Bélanger * and Victor LeNir **

* NORDX/CDT, Lachine, Que., Canada

** V.P.S. Enterprise, Montreal, Que., Canada

ABSTRACT

We build a test fixture, to allow measurement of balance, NEXT, FEXT, impedance and attenuation. This test fixture has been designed to also allow the measurement of cross modal crosstalk. We report on measurements which are obtained with this test fixture.

We show that the improvement of the utilization of cross modal crosstalk to assess the balance of a cable, depends also upon the performance of the baluns with respect to their longitudinal balance, though to a lesser degree than the measurement of balance.

The objective of the verification of the validity of our conjecture that balance may be replaced by cross modal crosstalk measurements cannot be unambiguously confirmed.

However, we find cross modal crosstalk to be an helpful, additional indicator to assess the performance of cables with respect to their balance.

We show certain anomalies of the cross modal crosstalk, due to indirect crosstalk coupling over tertiary circuits which yields resonance due to the induced signal reflections in the idle pairs. We show this using different terminations of the idle pairs.

We terminate all unused pairs with respect to their differential mode at the primary port of the baluns. But we also report on tests with additional common mode termination of the unused pairs. The differential to common mode and common to differential mode conversion are measured with the pairs under test terminated not only at the primary port, but also, additionally, at the unused common mode ports of the baluns.

Our findings indicate that balun performance remains a crucial issue and requires improvement and more serious work towards an eventual standardization.

We find this to be true, especially for short links. This issue is covered in a connected paper. [1]

INTRODUCTION

The understanding of balance concepts is gaining renewed importance for the transmission of high bit rate protocols. Electromagnetic Compatibility (EMC) of UTP cables is one of the crucial issues relating to their deployment. Balance characteristics of a UTP channel and its EMC are tightly correlated. Hence, it is mandatory to get a full understanding of the balance performance also of the cables.

Especially today, where the tendency moves towards an increase in the performance for data grade cables, to cope with future demands of new transmission protocols which are under development.

Another area where the balance concepts draw increased attention, is for short link- and plug-connector combination testing. This issue is covered separately in a connected paper. [1]

Therefore, the assessment of the balance performance of wires and cables becomes increasingly important and will have to be addressed.

The present paper is part of a study into crosstalk and balance measurements of cables. We report here only on that part of the study dealing with the results obtained on cables with a length of 100 m.

We reported already on the crosstalk performance of short length data grade wires. [2] Our comparative results of crosstalk using measurements of the complete crosstalk matrices as well as frogging the pairs, i.e. TIP and RING reversal, led us then to the conclusion that the striving for better balun performance is justified. At the same time we reported also on results using baluns with higher longitudinal balance, where these problems seem to be reduced.

Here we report about further developments in this direction. It is known that balance measurements depend to a large extent upon the longitudinal balance performance of the baluns which are used for these tests. For this reason we use the same baluns with improved longitudinal balance, as used

previously [2]. We also use a new type of balun "measuring bridge" having an improvement performance in longitudinal balance at 100 MHz of at least 8 to 10 dB. In the following sections these baluns are designated balun as "A" and balun "B", respectively.

RATIONALE

The utilization of baluns, i.e. of balanced to unbalanced signal transformers is a wide spread, well known and accepted method of testing the cable performances. Baluns are also used to measure the different types of conversion losses. Having both a primary and a common mode port, they can also be used for the measurement of cross modal crosstalks.

We suspect these cross modal crosstalk measurements to be less sensitive to the longitudinal balance performance of the baluns.

It is one our objective to show that the cross modal crosstalk values can be used to describe the cable under test with respect to its suitability for transmission of balanced signals, while coping with the more stringent EMC requirements.

Recently modal decomposition test methods appeared on the market. However, their day to day utilisation is far from being generally accepted. This primarily due to excessive testing times. These are amplified substantially by selecting reasonable frequency point densities per sweep, which increase in turn the resulting calculation times. Though there are potential improvements on the horizon, this drawback has not yet been overcome even under utilization of fast computers. Hence, this area requires further exploration.

Therefore, we use baluns for our test fixture. In an already cited paper [2], we discuss the question whether full matrix measurements of crosstalk shall be made. Alternately we must to consider the performance of the baluns used for the testing of wires and cables and standardize their performance. One of the objectives of this paper is to evaluate cable performances using baluns with different performance, compare the results and derive therefrom the delimitations to standardize on the performance of the baluns used for testing of wires and cables, and their connecting hardware.

We also investigate the sensitivity of differential to differential mode crosstalk, cross modal crosstalk and conversion losses to the ground plane distance.

DESCRIPTION OF CABLES INVESTIGATED

We test extensively two 4-pair cables. The cables are selected for the trials under consideration of basic performance characteristics. One of the cables (cable #1) is characterized having pitches and a

regularity of the twists such as postulated for good balance performance. This cable has, furthermore a large spread of propagation velocities, in order to facilitate the comparison on FEXT and NEXT over the full matrices. Incidentally, this cable has already been used for the tests in [2]. The second cable (cable # 2) has slightly lower twist regularity, yielding a slightly decreased balance performance.

We use these two differing twist regularities, yielding different balances of the cable because they will

- allow a comparison over a wider range of balance values.
- permit a better understanding of the balun performance.
- have substantially different crosstalk performance, both for the regular differential to differential mode crosstalk as well as for the cross modal crosstalk. and for the common to common mode crosstalk.

METHODOLOGY AND MEASUREMENTS

For the measurements we build a test fixture, which allows the automatic measurement of the entire crosstalk matrices, including all the balance measurements from both ends and in the same fan-out. For the termination of the twisted pairs at the far end we use also baluns, which are either terminated at their primary port or additionally at their common mode ports. If we use common mode termination, we also terminate the near end balun, if the port is not connected.

We use for the test set the same baluns used for short link testing, i.e. baluns which have an unbalanced 50 Ohm primary port and a balanced 100 Ohm secondary port with a centre tap for common mode measurements/terminations. The software for this test fixture as well as for the network analyzer has been developed in conjunction with VPS Enterprises.

To assess the impact of adjacent unused pairs, which yield indirect crosstalk coupling over tertiary circuits, we differently terminate the unused pairs. To this extent we use a straight differential mode termination at the primary ports with and without additional common mode termination. Under these conditions we measure four combinations for each crosstalk mode.

In Fig. 1 we have the schematics of the circuit for most of the measurements.[3][4][5][6][7] Both, single and two port measurements can be carried out additionally from both sides of the cable. This is the advantage of far end terminations of the pair or pairs under measurement through baluns.

Definitions and designations of the balance losses, follow the ITU recommendation G.117 [3].

For the cross modal crosstalk we have for $j = k$ balance measurements. Hence for cross modal

crosstalk the diagonal over the pairs of the crosstalk matrix represents a balance mode of the pairs.

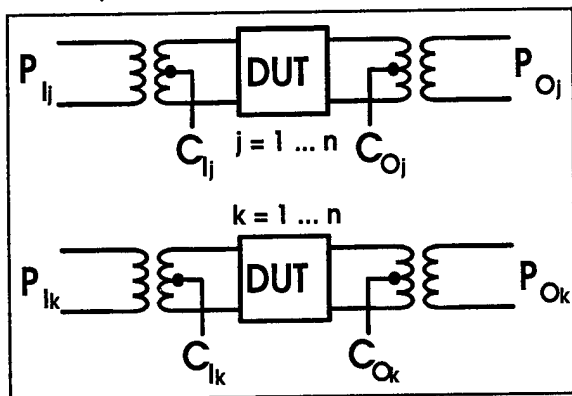


Fig. 1 : Schematics of the test circuit used.

Thus we obtain in case of far end differential to common mode cross crosstalk either OSB or TCTL (the latter with common mode termination at the near end). For common to differential far end crosstalk we obtain under the same conditions with only one degree of freedom the CMR or LCTL values. Here again we use a common mode termination this time at the far end to get LCTL measurements. Identically we obtain for the switch from two to one degree of freedom for the common to differential mode NEXT the LCL and for the differential to common mode crosstalk the TCL values. The schematics for the longitudinal and transverse conversion loss is shown in Fig. 2. [4][8]

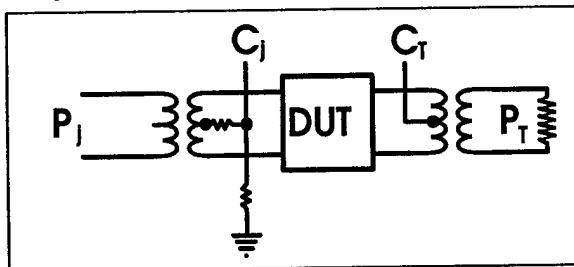


Fig. 2 : Schematics to test the longitudinal and the transverse conversion loss. Indicated is the termination in differential and common mode of the pair under test at the far end.

The calibration for two port balance measurements as well as for differential to common and common to differential crosstalk poses a problem for straight attenuation loss calibration. We assume that the attenuation loss of baluns of the same make are identical. We take then the difference of the averages of the loss between the primary and the common ports, respectively when measured in opposite directions. This yields the average loss of the balun type considered between its primary and common port. To this loss we added the common to common port loss in the direction considered. We have, therefore:

$$P_l C_o = \frac{P_l P_o + P_o P_l}{2} - \frac{C_l C_o + C_o C_l}{2} + C_l C_o$$

$$C_l P_o = \frac{P_l P_o + P_o P_l}{2} - \frac{C_l C_o + C_o C_l}{2} + C_o C_l$$

For the calibration of the single port measurements we use a standard network with an impedance of 100 Ohms, having an LCL=0 dB. The calibration is then checked with standards having LCL=20 dB and an infinite LCL (noise floor determination).

Incidentally, this same calibration procedure can also be used for the previously described two port balance and cross modal crosstalk measurements, under consideration of the through calibration of the common to common ports of the baluns. Hence, some work towards optimizing the calibration procedure remains to be done.

All measurements are carried out over the frequencies of 0.772 to 100 MHz with linear frequency division and 801 frequency points per sweep.

RESULTS

The amount of results obtained for one cable is extremely high and has to be reduced by reasonable filtering. We report only upon some representative results.

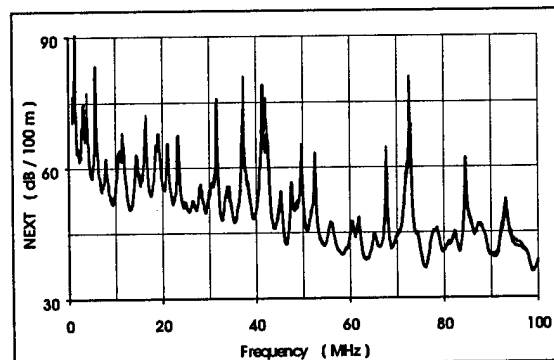


Fig. 3 : Differential to differential mode NEXT of same pair combination measured on different positions of the test set. (Balun "A" and cable # 1)

Before entering into the description of detailed measurements, we report on some sanity checks on our test fixture. After calibration of the test fixture we measure one cable. We then rotate the pairs relative to the positions of the test set and re-measure the same parameters. We then compare the results of the same pairs to each other, measured on different positions. We do this for all possible crosstalk and balance measurements. In Fig. 3 to Fig. 6 are the results for NEXT and FEXT for different modes of crosstalk.

All measurements are carried out keeping the cable under test in a shielded box. This is schematically shown in Fig. 7. However, we report also on some results, obtained without any defined ground plane.

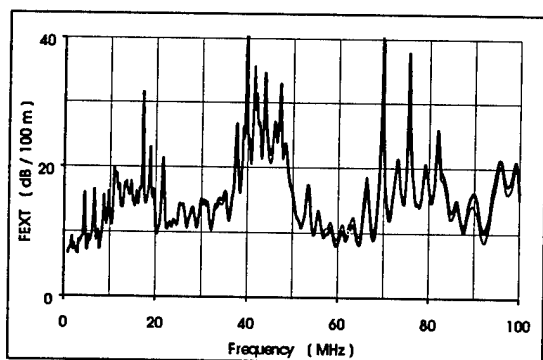


Fig. 4 : Common to common mode FEXT of same pair combination measured on different positions of the test set. (Balun "A" and cable # 1)

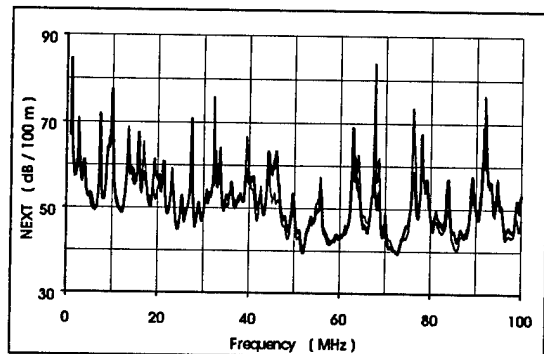


Fig. 5 : Differential to common FEXT of same pair combination measured on different positions of the test set. (Balun "A" and cable # 1)

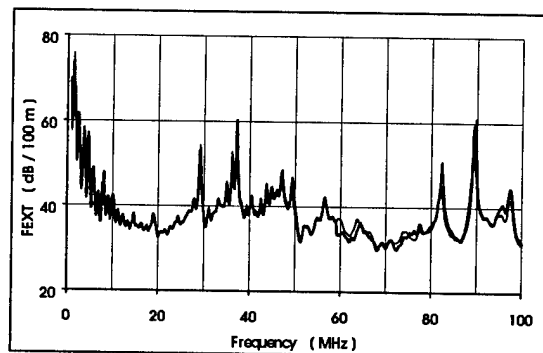


Fig. 6 : Common to differential mode NEXT of same pair combination measured on different positions of the test set. (Balun "A" and cable # 1)

In the Fig. 8 is indicated the differential to common and common to differential mode NEXT for the same pair combination.

In Fig. 9 we have the longitudinal conversion transfer loss (LCTL) for the four pairs of cable #2, both with and without well defined ground plane. In order to show clearly that the ground plane proximity influence increases with improving conversion loss, this graph has been limited to 30 MHz.

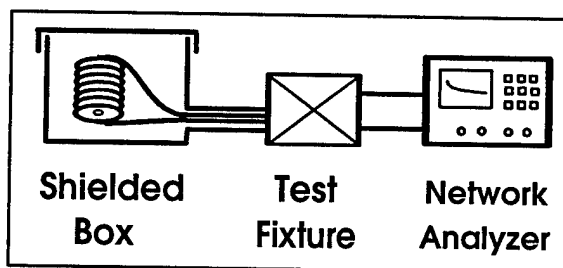


Fig. 7 : Schematics of measurements with well defined ground plane.

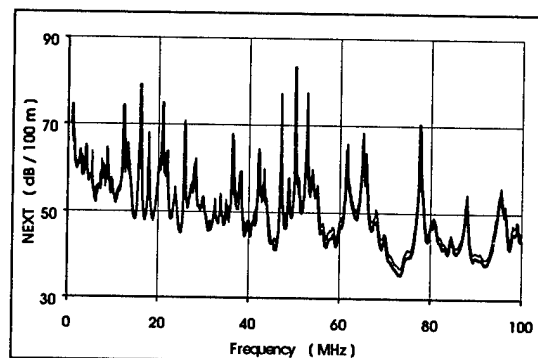


Fig. 8 : Common to differential mode NEXT of pairs 3-4 versus differential to common mode NEXT of pairs 4-3 with no ground plane definition. (cable # 1)

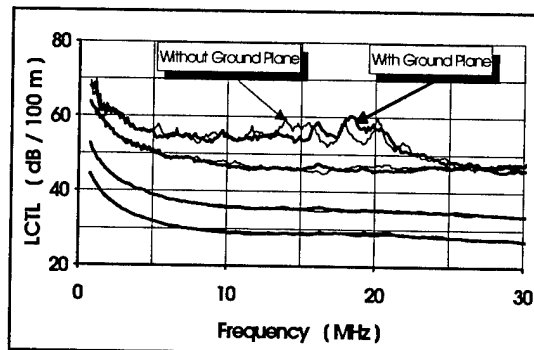


Fig. 9 : Longitudinal conversion transfer loss. All pairs with and without ground plane definition. (cable # 2)

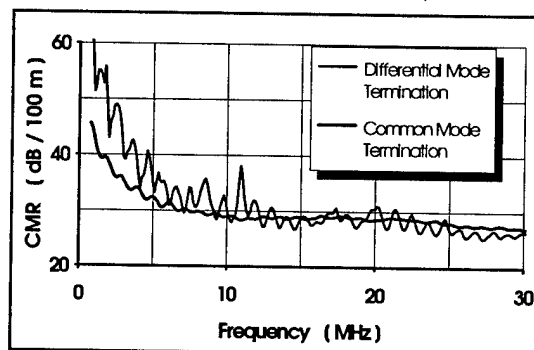


Fig. 10 : Common mode rejection of the same pair, but with differential and common mode termination of the unused pairs. No ground plane definition. (cable # 2)

Fig. 10 finally shows the CMR for the same pair, terminated at the far end at the primary port and terminated also at the common mode port. Again, to better illustrate the reflections in the adjacent pairs and their impact upon the CMR, we limited the frequency in this graph to 30 MHz.

For the two cables, we report some results on tests with different terminations of the unused pairs. We terminate the common mode port of the disturbing and disturbed pairs. Of course, in case of the common to common mode crosstalk we can only compare the differential and additionally a common mode termination of the unused pairs.

Fig. 11 demonstrates the symmetry of the differential to common FEXT matrix using the balun "B".

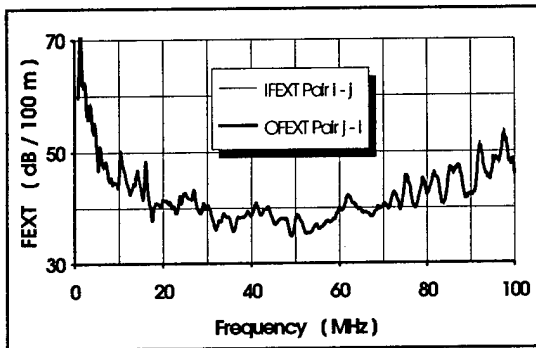


Fig. 11 : Differential to common mode FEXT for the same pair combination measured from the inside and the outside. (cable # 1; baluns B)

Fig. 12 shows the results of differential to differential mode crosstalk with balun "A", and Fig. 13 the same measurements for the identical pair combination with balun "B".

The four traces in each graph are to all practical purposes nearly identical. There are minute differences, not visible on these traces, between differential mode termination and common mode termination of the unused pairs. Hence, we find that the results under partial common mode termination of the pairs under test or of the unused pairs do not notably deviate from those obtained with differential or additional common mode termination on all pairs. Therefore, we will limit our further reporting to those cases where all pairs are terminated in their differential mode with or without an additional common mode termination on all pairs. The differences between both traces is small and is maximum approximately 2 dB.

From the Fig. 12 and Fig. 13 it can be concluded that there are small differences observable, if the differential to differential NEXT is measured with the different baluns. Fig. 14 highlights more clearly the slight differences of differential to differential NEXT if the measurement is taken on the same pair with the different baluns.

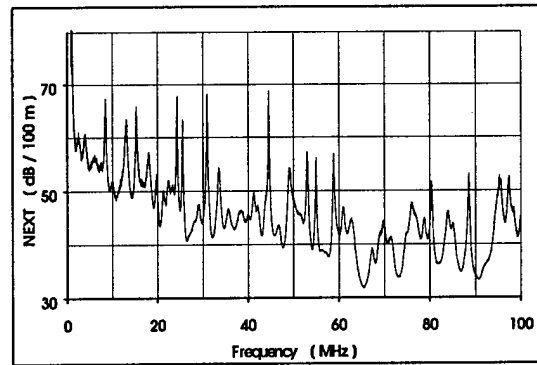


Fig. 12 : Differential to differential NEXT for pairs 2-3 with differential and common mode terminations on disturbing and disturbed pairs as well as on unused pairs. Balun "A", cable #2.

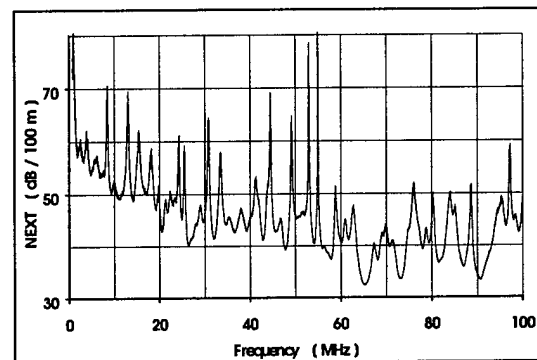


Fig. 13 : Differential to differential NEXT for pairs 2-3 with differential and common mode terminations on disturbing and disturbed pairs as well as on unused pairs. Balun "B", cable #2.

Fig. 14 to Fig. 17 show the comparison for the different baluns while measuring differential to differential, common to common, differential to common and common to differential NEXT, respectively. The differences for differential to differential and common to common mode crosstalk are minor. The differences between the results of the different baluns are higher when measuring the cross modal crosstalk. In each cases, all pairs are additionally terminated in their common mode.

It should be noted, that these measurements were carried out on the pair combination, which includes that pair, for which we report also the balance measurements. In fact, these measurements are carried out on two adjacent pairs, in order to obtain the highest cross modal crosstalk.

The termination mode does not markedly affect the differential to differential and the cross modal crosstalk. It affects, however, substantially the common to common mode crosstalk, and this both for NEXT and FEXT. This is illustrated in Fig. 18 and 19 for the differential to common mode FEXT for both balun types with different terminations.

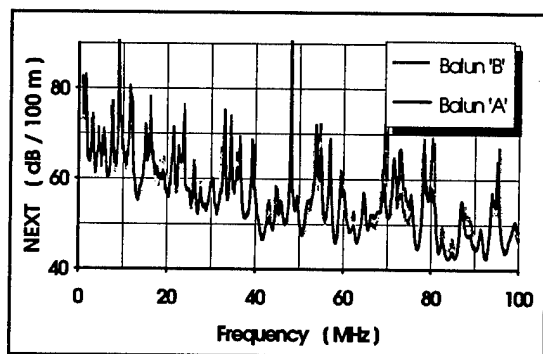


Fig.14 : Differential to differential NEXT measured with the different baluns. Common mode termination of all pairs.

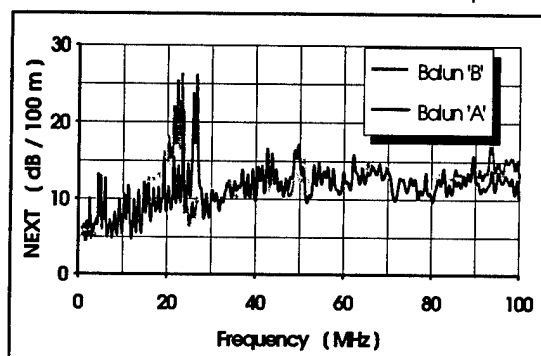


Fig.15 : Common to common NEXT for the same pair combination as in Fig. 14 measured with different baluns.

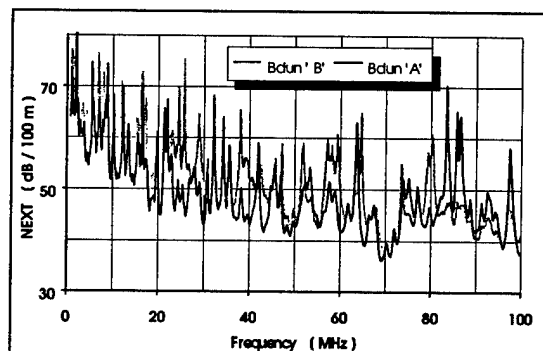


Fig.16 : Differential to common NEXT for the same pair combination as in Fig. 14 measured with different baluns.

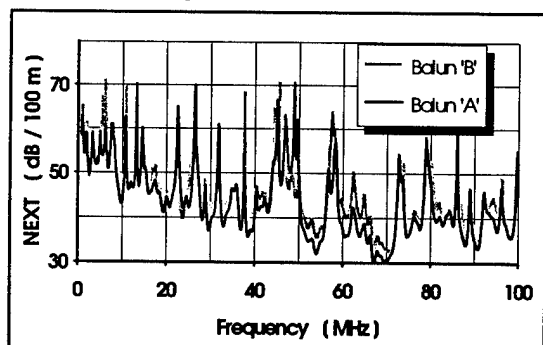


Fig.17 : Common to differential NEXT for the same pair combination as in Fig. 14 measured with the different baluns.

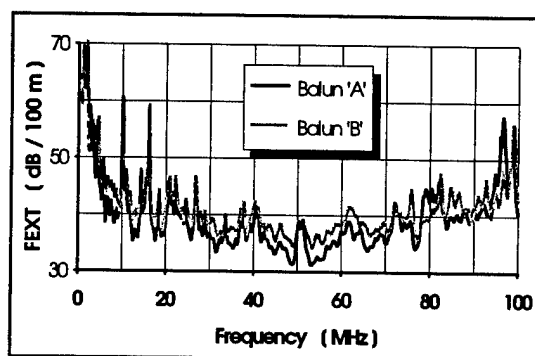


Fig. 18 : Differential to common mode FEXT for different baluns. Unused pairs terminated in differential mode.

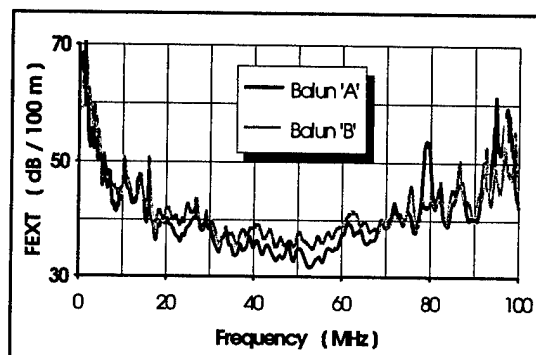


Fig. 19 : Differential to common mode FEXT for different baluns. Unused pairs terminated in common mode.

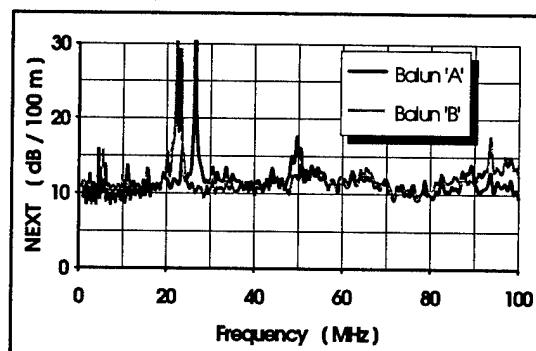


Fig. 20 : Common to common mode NEXT for different baluns. Unused pairs terminated in differential mode.

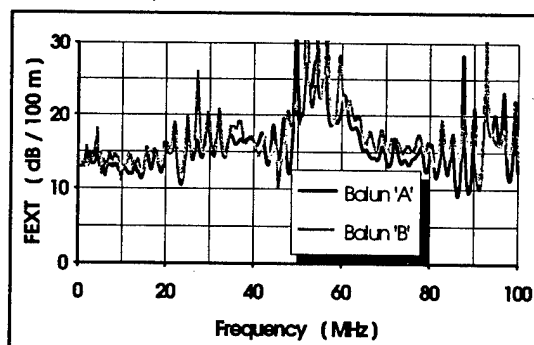


Fig. 21 : Common to common mode FEXT for different baluns. Unused pairs terminated in differential mode.

The Fig. 20 shows for the same pair combination as in Fig. 15 the common to common mode NEXT, however, here the unused pairs are terminated only in differential mode. It is clearly visible that the common to common mode crosstalk is strongly impacted upon by the termination mode of the unused pairs.

The Fig. 21 and Fig. 22 show the same behaviour but for common to common mode FEXT. It is worthwhile to notice that common to common mode crosstalk the trace shows fewer and less pronounced ripples with differential mode termination, than with an additional common mode termination. This is contrary to all other crosstalk modes and is true for both, NEXT and FEXT.

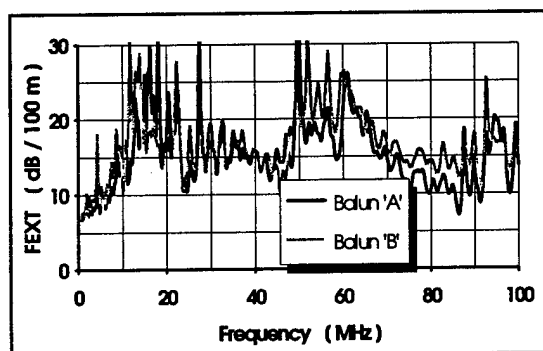


Fig. 22 : Common to common mode FEXT for different baluns. Unused pairs terminated in common mode.

The following reporting on balance measurements refer always to the same pair. As already mentioned, this pair is part of the pair combination for which the cross modal crosstalks are measured.

Fig. 23 and Fig. 24 show thus the longitudinal conversion loss measured with both types of baluns. There is, comparable to cross modal crosstalks a marked difference between the terminations of the unused pairs. The resultant trace is has fewer ripples when the unused pairs are common mode terminated. The same is, incidentally true also for the inverse of LCL, the transfer conversion loss, as may be seen out of the Fig. 25 and Fig. 26.

Fig. 27 and Fig. 28 show the common mode rejection (CMR) and its inverse, the output signal balance OSB. In these cases we indicate only the values with common mode termination of the unused pairs.

Finally Fig. 29 and Fig. 30 indicate the longitudinal conversion transfer loss (LCTL) and the transverse conversion transfer loss (TCTL), also with common mode termination of the unused pairs.

DISCUSSION OF RESULTS

For cable measurements we are able to calibrate the test fixture, which we built, to such an extent that we obtain a very good repeatability of results from position to position. The variability of results is for all

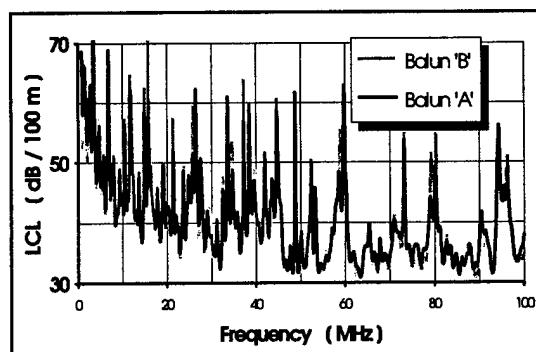


Fig. 23 : LCL for different baluns. Unused pairs terminated in differential mode.

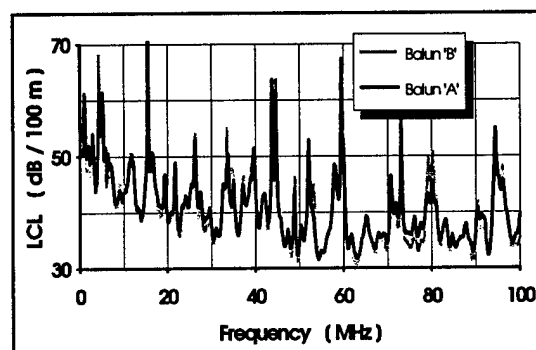


Fig. 24 : LCL for different baluns. Unused pairs terminated in common mode.

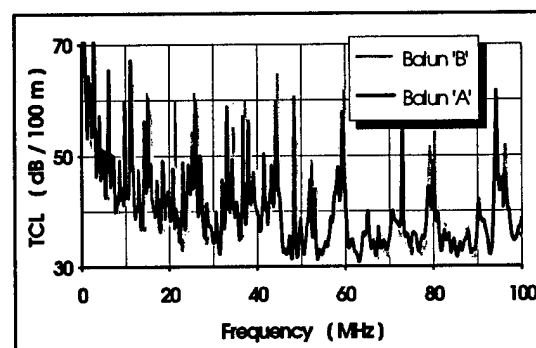


Fig. 25 : TCL for different baluns. Unused pairs terminated in differential mode.

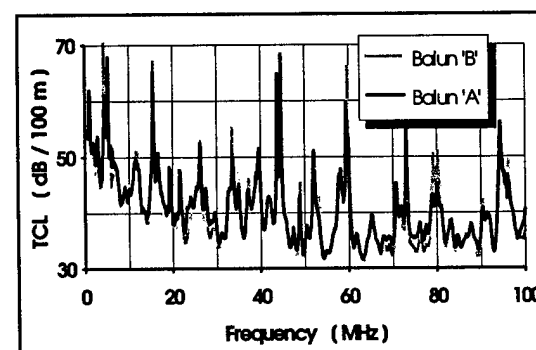


Fig. 26 : TCL for different baluns. Unused pairs terminated in common mode.

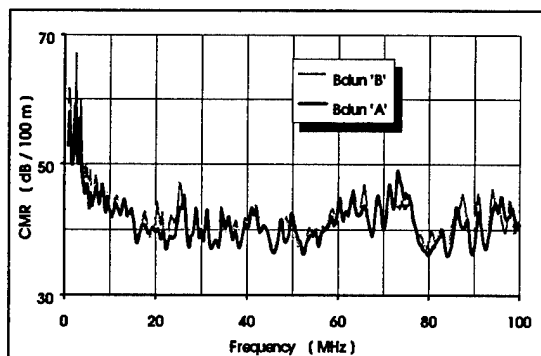


Fig. 27 : CMR for different baluns. Unused pairs terminated in common mode.

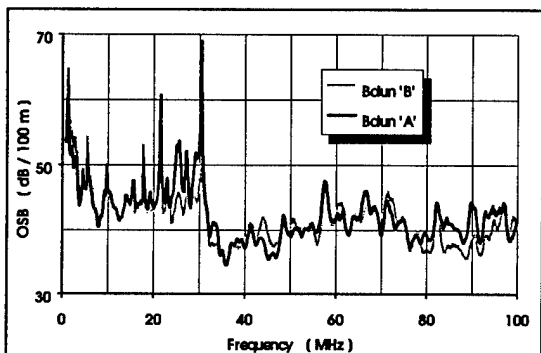


Fig. 28 : OSB for different baluns. Unused pairs terminated in common mode.

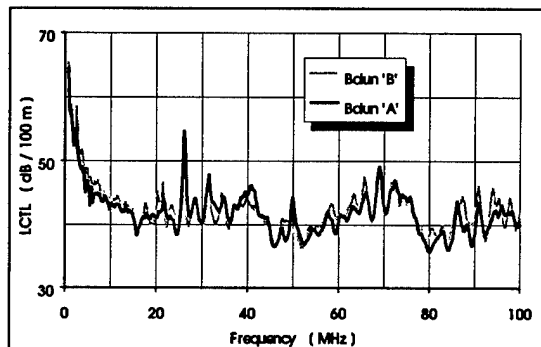


Fig. 29 : LCTL for different baluns. Unused pairs terminated in common mode.

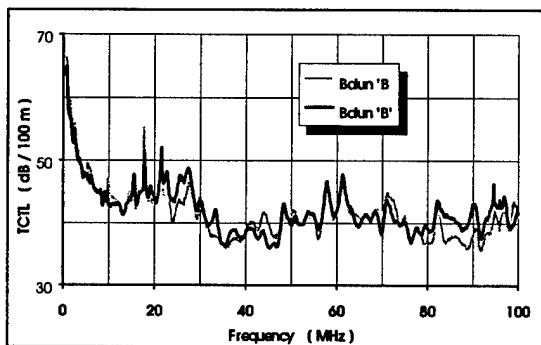


Fig. 30 : TCTL for different baluns. Unused pairs terminated in common mode.

practical purposes zero for differential to differential mode crosstalk. (see Fig. 3) However, we have some minor variations for cross modal crosstalks, which are in the worst case approximately 1.5 dB at the low peaks as may be seen in Fig. 5 and Fig. 6. For common to common mode crosstalk these variations decrease even further. It is worthwhile to note that these variances decrease even more for the balun type "B". One part of these differences may be attributed to our calibration method, where, for simplification purposes, we assume that the baluns are identical in their performance characteristics. This part of the differences is definitely due to the different longitudinal balances of the individual baluns.

The precision of the measurements of our test fixture is furthermore demonstrated by the equality of corresponding differential to common and common to differential mode NEXT measurements on the same pair combination. These have to be theoretically equal if the pairs have a reasonable high longitudinal balance. That this is the case may be seen in Fig. 8.

Generally we find for the balance measurements that the sensitivity to the proximity of the ground plane increases for higher pair balance. Thus pairs having low balances show hardly any sensitivity to the ground plane proximity. This is to be expected, however the degree of this sensitivity decrease is noteworthy. (see Fig. 9)

We observe a substantial impact on the results due to the termination mode of the unused pairs in the cable. The injection of a signal into one of the pairs for balance measurements creates induced voltages in the adjacent pairs by crosstalk coupling. The induced voltages yield a signal reflection in the unused pairs, resulting in oscillatory reflections between the terminations. This yields resonances which in turn impact, due to cross modal crosstalk over tertiary circuits, upon the balance measurements. In fact, if the unused pairs are terminated in differential mode alone then these resonance effects are maximized versus additional terminations in common mode. (see also Fig. 10)

This may be explained due to a high ground plane distance. However, we find this to be generally true for all balance measurements, even with under well defined ground plane conditions. We estimate, therefore, that this is an important feature to be dealt with during an eventual standardization process towards a standard for balance measurements.

We suspected already [2] that the quality of the baluns may impact upon the symmetry of the FEXT matrices. This should hold also for cross modal FEXT measurements, if the propagation constants of the considered pairs are reasonably close to each other. For differential to differential mode FEXT we demonstrated this already in the above mentioned paper. Here we demonstrate this symmetry very

clearly. This is done using baluns with improved balance performance. (see Fig. 11)

For ordinary differential to differential NEXT measurements, we show that the results obtained with different baluns are deviating by approximately 2 dB from each other. We prove furthermore, that the termination mode of the unused pairs has practically no influence at all upon the NEXT measurements. This statement holds also if the pairs under measurement are terminated with respect to common mode. (Fig. 12 and Fig. 13).

We show for cross modal crosstalk that the differences due to the balun may reach values in the order of approximately 3 - 4 dB maximum. (see Fig. 14; Fig. 16 and Fig. 17)

The common to common mode NEXT behaves somewhat peculiar. In fact at lower frequencies the ripple of the result trace is very pronounced for a common mode termination of the unused pairs. (see Fig. 15) Furthermore, in the lower frequency range the average value increases slightly. However, for differential mode termination of the unused, adjacent pairs the ripple is substantially reduced and the level of common to common mode crosstalk is nearly doubled. (see Fig. 20) The last statement holds also for FEXT measurements. (see Fig. 21)

In this context we note that common to common mode FEXT is less affected by a ripple due to reflections in the unused pairs, if they are terminated in differential mode only. (see Fig. 21 versus Fig. 22) The initial lower values of FEXT at lower frequencies are comparable to those obtained for NEXT measurements with additional common mode termination of the unused pairs.

We find that differential to common and common to differential mode FEXT is only affected to a minor degree by the termination mode of the unused pairs. (see Fig. 18 and 19) However, these figures also show clearly some major deviations between the results obtained with different baluns. Generally, we obtain "better results" with the poorer performing baluns. This in itself indicates very clearly that a well defined balun performance is mandatory, if either cross modal crosstalk or balance is to be used as a standardization base.

Our findings let us conclude that cross modal crosstalk measurements may well be used as a means to characterize balance of the cable, though it is clear that we introduce an additional degree of freedom. Here we show only the balance results obtained for one pair of the pair combination in question. The results obtained for the cross modal NEXT for one pair combination are well comparable to the balance (LCL and TCL) measurements obtained for each individual pair combined. (see Fig. 16; Fig. 17 and Fig. 23 to Fig. 26) We expect this to a certain degree, as both measurements are taken

on the same side of the pairs. In fact, as already mentioned, the LCL and TCL measurements are represented by the diagonal of the full cross modal crosstalk matrix under loss of one degree of freedom.

In Fig. 27 to Fig. 28 are indicated the two terminal balance measurements, i.e. balance measurements from the inside to the outside of the cable.

The similarity of the results for CMR and LCTL on one side and of OSB and TCTL should be noted. In fact the similarities are such that for cables only one of these measurements should be carried out, i.e. either CMR and OSB or LCTL and TCTL. The differences between CMR and OSB on one side and LCTL and TCTL on the other side are due to the different unbalances looking into the cable from the inside or from the outside end.

We expect these results to show a certain similarity to far end crosstalk, if the two individual pairs are considered.

However we cannot expect a close similarity to the FEXT measurements directly, as we have to take into account not only IO-FEXT, but also the attenuation. Hence we would need to measure also the corresponding attenuations. In fact, we do not have the values for the attenuations with the common mode port as an input port and the differential port as an output port, and vice versa. However, we would need these values in order to conclude upon the validity of cross modal FEXT as two terminal balance measurements. These points definitely need more work and clarification.

SUMMARY AND CONCLUSION

We build a test fixture with a provision to measure both cross modal crosstalk and all balance modes.

For this test fixture we use two different kinds of baluns, with substantially different performance characteristics. We demonstrate the high degree of performance of our test fixture by carrying out different sanity checks. The results of these checks are very good, thus that we have a high degree of confidence in the validity of our results. We show the degree to which both crosstalk and balance measurements are impacted upon by the balun performance. We find that the cross modal crosstalk is slightly less influenced by the balun performance than balance measurements.

We show that cross modal crosstalk may well be used to characterize the balance of cables though we add one degree of freedom, which generally renders the interpretation of results slightly more complex. However, the cross modal crosstalk and its dependence upon the termination mode of the unused pairs yields a more realistic picture of the real phenomena in a cable with respect to crosstalk and balance.

The balun performance has a prime influence upon the results of the measurements. This is due to unavoidable impedance mismatches. We show this for both baluns in the Fig. 31 and 32. The Fig. 31 indicates the no-load impedance using the reactance-resistance characteristic of both balun types if the primary and the common mode port are left open. Here we show only the results for one balun each.

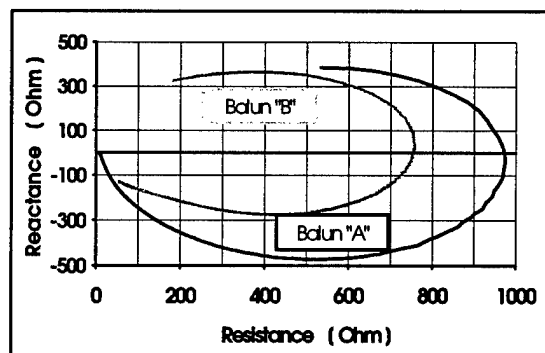


Fig. 31 : Reactance vs Resistance for the different baluns at the secondary or "100 Ohm" port. Primary port is left open.

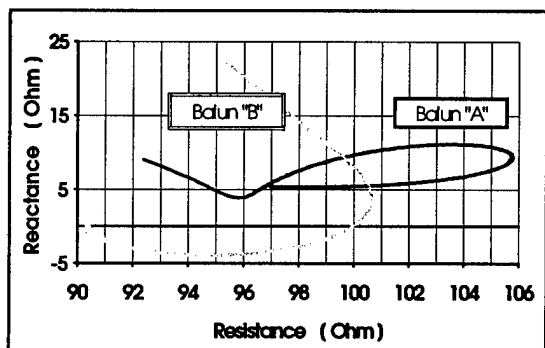


Fig. 32 : Reactance vs Resistance for the different baluns at the secondary or "100 Ohm" port. Primary port terminated in 50

Both no-load impedances are well behaved, though the reactance-resistance locus of balun A is much larger, than for balun B. These loci are practically not altered upon termination of the common mode port. The distortion of the reactance-resistance locus under a 50-Ohm load on the primary port is in both cases substantial. Fig. 32 shows that very clearly for the impedance under a 50 Ohm load. However, the balun B behaves more regular than the balun A. It shows also a lower input resistance variation than balun A. Here the common mode impedance is of lesser importance. However, we show that for short links the common mode impedance is very important. [1]

From our results we may conclude that the performance of the baluns is of prime importance for balance measurements, but of lesser importance for cross modal crosstalk measurements. Though this may be an advantage, it is definitely only gained at the expense of more difficult interpretation of the results.

We cannot, unequivocally, state a preference for cross modal crosstalk over balance measurements, due to the increased difficulty of interpretation. However, if we have the balance measurements, then the cross modal crosstalk measurements are a very valid and helpful complement for the interpretation of the balance results.

As a final summary, we conclude that the balun performance is of prime importance and options to standardize the balun performance should be considered and explored.

REFERENCES

- [1] B. Lord et al : Balance Measurements of UTP Connecting Hardware
45th IWCS 1996
- [2] J.-H. Walling et al : Crosstalk Performance of Short Length Data Grade Wires
44rd IWCS 1994, p.288-297
- [3] NN. : Transmission Aspects of Unbalance about Earth (Definitions and Methods)
ITU - Recommendation G.117, Fascicle III.1 p. 94-107
- [4] L. Staschover : Measurements of Unbalance to Ground of Balanced Systems
Published by: North Hills Electronics, Div. of Porta Systems Corp.
- [5] NN.: ITU-T Recommendation K.10 on Unbalance about Earth of Telecommunication Installations
ITU Rec. K.10 (03/93) p. 1-14
ANSI/IEEE Std. 455-1985, p. 7-22
- [6] M. Graham : Balun Characteristics
Report No. 092-068 Tutankhamon Electronics, May 22, 1992
- [7] L. Staschover : Wideband Signal Transformers
Application Note #WB-1, Oct. 1994, North Hills Electronics, Syosset, NY
- [8] NN. : IEEE Standard Test Procedure for Measuring Longitudinal Balance of Telephone Equipment Operating in the Voice Band

APPENDIX

Abbreviations

We use the following abbreviations :

P	-	Primary or unbalanced differential port of balun
C	-	Unbalanced common port of balun
S	-	Secondary or differential port of balun
j,k,n	-	Indices for pair number
I,O	-	Indices to characterize the inside and outside end of the cable.
T	-	Index to characterize a termination
LCL	-	Longitudinal conversion loss
TCL	-	Transverse conversion loss
CMR	-	Common mode rejection
OSB	-	Output signal balance
LCTL	-	Longitudinal conversion transfer loss
TCTL	-	Transfer conversion transfer loss

Equipment used

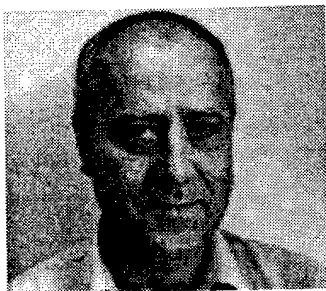
1 Dell Pentium 166 MHz

1 Network Analyzer HP-8751 A
1 S-parameter test set HP-87511A

Software used

Microsoft Visual Basic 3.0
VPS Cabmeas 7.0
Microsoft Access 2.0
Designer 3.0
Microsoft Excel 4.0
Microsoft Word 2.0c
Adobe Premiere LE

Authors



Jörg-Hein (Jo) Walling received his diploma in Mechanical Engineering in 1966 at the Technical University of Berlin. In 1974 he obtained a Doctor's degree (Dr.-Ing.) at the same University. In 1974 he joined Northern Telecom in the Research and Development department. Since 1976 he has been a senior engineer at the NORTEL, now NORDX/CDT, Lachine Cable Plant, responsible for the design of Outside Plant and Data Grade Wires and Cables.



Martin Bélanger received his B.E. in Electrical Engineering from University of Sherbrooke. He joined Technology Cable Group of Northern Telecom Canada Limited, now NORDX/CDT, in 1992. He was initially responsible for cable design and electrical test methods. He is at present responsible for the manufacturing aspects of data grade cables, for quality assurance and for the development of new manufacturing test facilities.



Victor LeNir received a B.Sc in Physics from Manchester University, England in 1960 and a M.Sc. in Computer Science from London University in 1968. He was employed at the Northern Telecom Cable Division in Lachine, Quebec in the Research & Development Group from 1963 to 1991. Since then he is with V.P.S. Enterprises working on the development of specialized, dedicated software packages, especially with regard to data grade wires and cables.

THE INTER-STANDARD GAP

Fanny I. Mlinarsky

Scope Communications, Inc., Northboro, Massachusetts

ABSTRACT

In an ideal world the networking and the cabling standards would be inter-operable. The IEEE, ANSI and The ATM-Forum standards committees developing new networking standards could simply specify a cable plant compliant with TIA-568-A[1] or ISO11801[2].

This kind of cooperative arrangement among the standards organizations could eliminate the redundancy of standardization effort and the duplication of work. But when dealing with the enormous complexity of data communications, can we honestly believe that a jump from 10 to 100 Mb/s will happen flawlessly and quickly, just as the standards dictate? Has any significant advancement in networking technology ever occurred without inter-operability issues?

This paper provides an overview of the emerging 100 Mb/s Local Area Networking (LAN) applications – their physical layer needs and specifications. It examines how well the generic cabling standards such as TIA-568-A[1] and ISO11801[2] address the requirements of the emerging high speed LANs and demonstrates some gaps between the ideal world and the reality today.

How close are we to our goal of standards inter-operability? Can the industry standards ever catch up with the accelerating pace of advancements in the data communications industry? Before we attempt to answer these questions, let's examine the facts.

INTRODUCTION

The Physical Medium Dependent (PMD) layer of a network encompasses the signaling methodology and the physical medium used to transmit digital information. PMD specifications typically define the modulation, the data rate, the maximum acceptable Bit Error Rate (BER)

and the medium. When specifying the medium, or the signaling channel, the networking standards developed by IEEE, ANSI, The ATM Forum and other organizations, typically reference the cabling standards, such as TIA-568-A[1] and ISO11801[2].

Cabling standards are application independent. They form the core of the medium specifications common to all the networking applications but they do not fully address the specific requirements of each network.

So, in addition to referencing a generic cabling standard, the PMD standards typically define unique channel characteristics required to achieve the specified BER performance using the specified modulation scheme. These unique channel requirements, which might include ambient noise, propagation delay, delay skew and other parameters, are often not covered by the generic cabling standards.

The problem is, the cable installer is only required to certify cabling installations to a generic category or class of cabling as defined by TIA-568-A[1] or ISO11801[2] and is not required to verify any network specific channel specifications. And if the installer does nothing more than observe the industry field testing standards, many crucial network-specific channel requirements are not verified because they fall into the inter-standard gap.

This paper examines the implications of incomplete or unspecified PMD channel requirements. Let us begin by reviewing the key cable specifications and their effect on the performance of data communications systems.

PERFORMANCE OF THE PHYSICAL LAYER

A robust physical layer operates at a low BER in the presence of noise, distortion and other hostile conditions in the communications

channel. A low BER means a low rate of re-transmissions of corrupted data and, therefore, a high rate of real data throughput. Data re-transmissions impair throughput efficiency because network bandwidth is unnecessarily consumed while transmitting the same information more than once. Throughput is further impaired when the upper networking layers get involved in detecting and regenerating the corrupted information.

Minimizing the BER of the physical layer is the key to optimizing the rate of data throughput.

SYSTEM ROBUSTNESS

In order to minimize the BER of a communications channel, it is necessary to maximize the data signal's immunity to bit errors in the presence of noise and distortion. The data signal's immunity to bit errors is often gauged by examining its eye pattern.

The Eye Pattern

In qualitative terms, the degree to which a data signal is immune to bit errors is a function of how constricted its eye pattern is. The more constricted the eye pattern the higher the probability of bit errors. The opening in the eye pattern determines the amount of noise that must be added to the signal to cause bit errors.

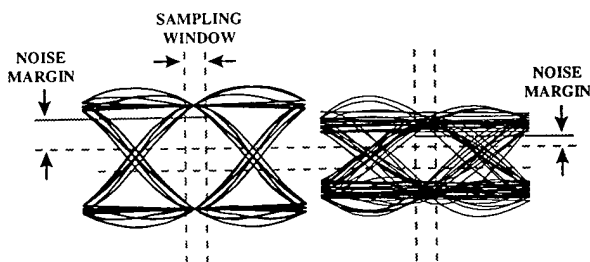


Figure 1

Left -- eye pattern of a good quality signal with a wide noise margin in the sampling window; right -- eye pattern of a poor quality signal with a narrow noise margin

The more constricted the eye pattern, the less noise is required to induce bit errors. The less noise the system can tolerate at a given BER, the less robust the system is.

DISTORTION AND NOISE

Signal distortion contracts the eye pattern opening and thus reduces the transmission system's immunity to noise. Noise, when added

to the data signal, also contracts the eye pattern. Therefore, both noise and distortion, each, contribute to the contraction of the eye pattern. The less distorted the signal, the more noise can be tolerated by the system before bit errors occur. The reverse is also true. The less noise is present in the communications channel, the more distortion can be tolerated.

Distortion

In a twisted pair communications channel, signal distortion is primarily caused by channel attenuation.¹ As the simulation in Figure 2 shows, the high frequency contents of a data signal are attenuated by the channel more than the low frequency contents. The sloping response of channel attenuation distorts the data waveform to such a degree that the eye pattern at the end of a worst case category 5 channel is completely closed. Therefore, before the data can be recovered, it must be equalized to restore the high frequency content of the signal.

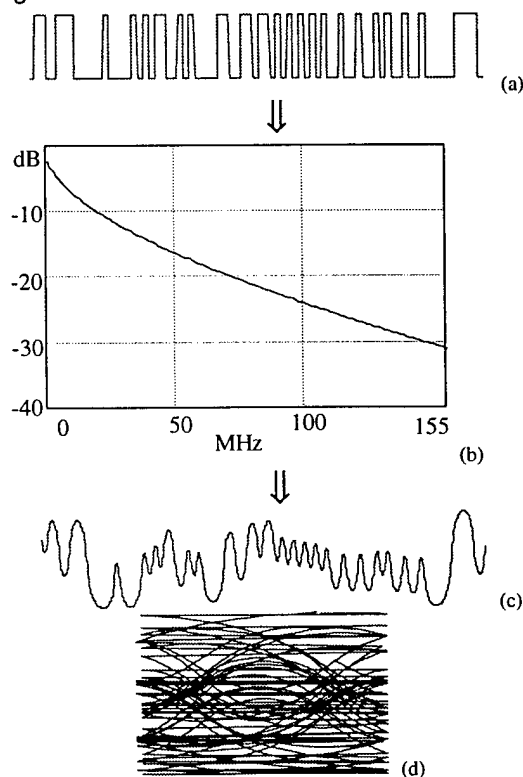


Figure 2

Simulation of a 155 Mb/s NRZ data signal subject to maximum allowable TIA-568-A[1] channel attenuation; (a) ideal, unfiltered 155 Mb/s NRZ data signal; (b) TIA-568-A worst case channel attenuation extended to 155 MHz (Appendix A); (c) simulation of the data signal distortion due to the attenuation; (d) closed eye pattern of the distorted signal

A typical twisted pair receiver includes an equalizer. The receive equalizer has a transfer function designed to cancel the attenuation response, resulting in a signal loss that is uniform over frequency.

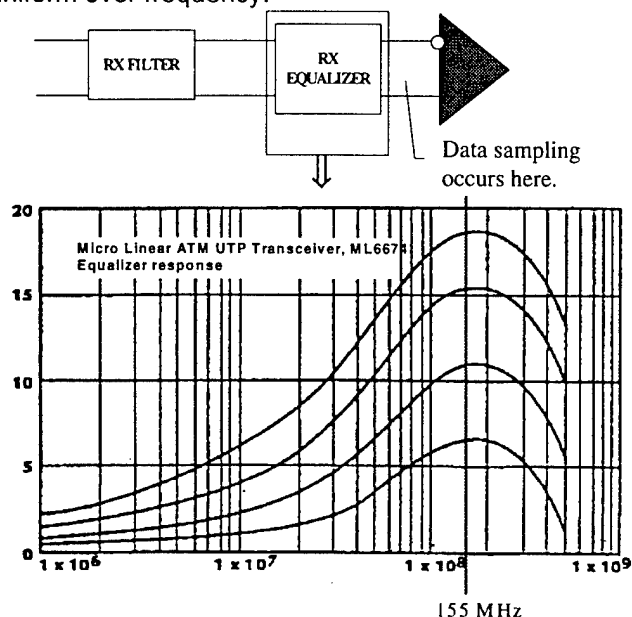


Figure 3

Equalizer curves from the specification of the Micro Linear ATM UTP transceiver, ML667, used in some 155 Mb/s ATM and 100 Base-TX products

The response of the equalizer shown in *Figure 3* slopes upward with frequency, compensating for channel attenuation up to 155 MHz. This is a very common adaptive equalizer that sets the slope of its response based on the measured signal power.

A typical equalizer cancels out the cable attenuation imprecisely and leaves the equalized signal somewhat distorted, as shown below.

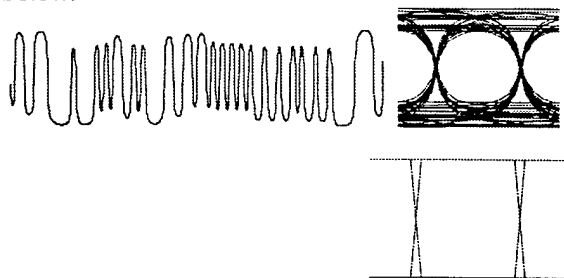


Figure 4

Simulation of a somewhat imperfect (i.e. realistic) equalization of the distorted signal. The eye pattern of the attenuated and subsequently equalized signal (top) is somewhat rounded and more constricted than the transmitted eye pattern (bottom)

Although there are many causes¹ of signal distortion, the distortion in a twisted pair communications channel is primarily due to the imperfect equalization of the channel attenuation response.

Noise

The primary source of noise in a twisted pair channel is the crosstalk between the different pairs in a cable³. Depending on the network topology, the crosstalk coupling onto the received signal could be either at the near end of the cable or at the far end.

A physical layer utilizing two pairs typically transmits on one pair and receives on the other simultaneously. Most of the noise on the receive pair is coupled from the near end transmitter and is known as the near end crosstalk or NEXT. The examples of high speed two pair twisted pair LANs sensitive to NEXT noise are 100 Base-TX[5] and ATM[6,7,8].

Networks such as 100Base-T4[5] and 100VG-AnyLAN[4] transmit on multiple pairs simultaneously. In these multi-pair PMD topologies, the receive signal is subject to far end crosstalk or FEXT. FEXT is the crosstalk coupling from one transmit pair to another as the signal propagates from the transmit end of the cable, the far end with respect to the receiver.

The noise spectrum at a communications receiver is a function of the transmit spectrum and of the cable crosstalk response. In the case of two pair networks, the spectral shape of the noise is a function of the transmit spectrum and of the NEXT response of the cable. In the case of multi-pair topologies, the spectral shape of the noise is a function of the transmit spectrum and of Equal Level FEXT² or ELFEXT [10].

Although noise in a twisted pair communication channel can come from different ambient sources³, it is typically dominated by the crosstalk response of the cable.

Signal To Noise Ratio (SNR)

In a communications channel, the power of the noise is only meaningful when compared to the power of the data signal.

SNR is a measure of the strength of the desired data signal with respect to the interfering noise signal. A low SNR results in bit errors as the

data signal at the station's receiver becomes indistinguishable from noise.

BER is a statistical function of SNR. Feher[9] defines the probability of error function (which is equivalent to BER) for NRZ modulation as

$$BER = P_e = Q(y) = \int_y^{\infty} \frac{1}{\sqrt{2 \cdot \pi}} \cdot e^{-\frac{w^2}{2}} dw \quad (1)$$

where y is the ratio of the peak signal value at the sampling instant to the root-mean-square (rms) voltage of the noise power at the sampling point in the receiver. The noise is assumed to be white Gaussian⁴.

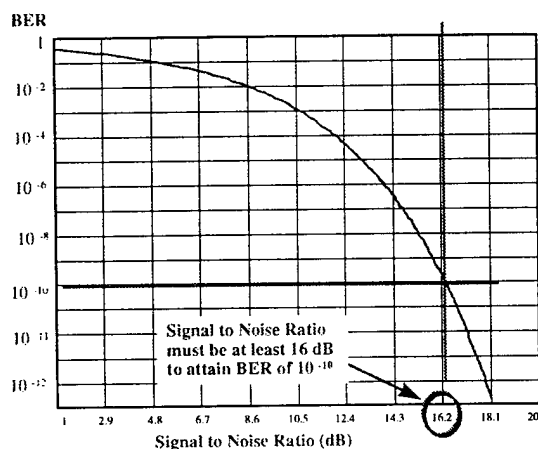


Figure 5

BER vs. SNR function expressed in equation 1 for and NRZ-based communications channel; this function describes the behavior of networks such as 155 Mb/s ATM, which use NRZ modulation

Per Figure 5, for a network such as the NRZ based 155 Mb/s ATM to attain the required BER of 10^{-10} , the SNR would have to be better than 16 dB. The shape of the BER vs. SNR curve is unique for each network topology and signaling scheme but, in all cases, the BER increases with decreasing SNR.

THE INTER-STANDARD GAP BETWEEN THE 155 MB/S ATM STANDARD AND TIA-568-A

The 155 Mb/s twisted pair ATM interface[6] employs two pair full duplex NRZ signaling. At the receiver, the noise spectrum is dominated by the transmit spectrum and by the NEXT response of the cable. The amount of signal distortion is determined by the attenuation response of the cable.

The transmit spectrum of the 155 Mb/s NRZ data signal is shown in Figure 6. The entire first lobe of the spectrum, extending to 155 MHz, is needed for proper data recovery [11].

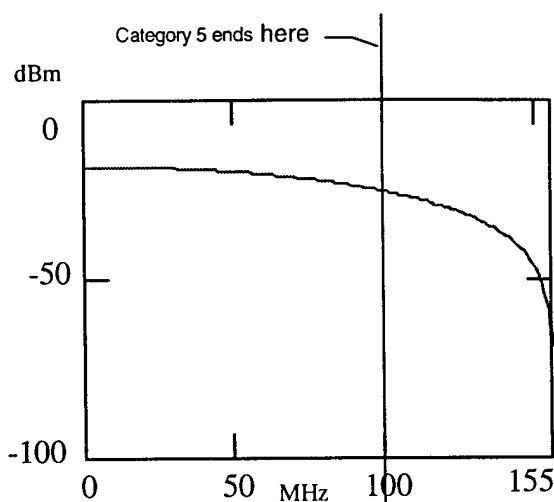


Figure 6

The portion of the 155 Mb/s NRZ signal spectrum needed for proper data recovery

Self NEXT Noise

In specifying the acceptable noise power in the communications channel, the ATM Forum standard AF-PHY-0015.000[6] defines the maximum Self NEXT Channel Noise (Section 5.3.1). The self NEXT noise, composed of the channel near end crosstalk and of ambient noise sources, is not to exceed 20 mV ptp.

To compute the worst case noise power at an ATM receiver, we need to compute the NEXT noise spectrum as a function of channel NEXT and of the useful signal spectrum (Figure 6).

The problem is, TIA-568-A[1] only specifies cabling to 100 MHz and the ATM network uses the category 5 channel beyond this specification.

However, we can easily extend the channel NEXT limit, defined in TSB67[3] beyond 100 MHz (see Appendix A) so as to account for the useful transmit spectrum of the ATM signal.

If the ATM signal is transmitted at the maximum allowable power over a TSB67[3] channel exhibiting the worst case NEXT response (Figure 7), the NEXT noise spectrum at an ATM receiver would be as shown in Figure 8.

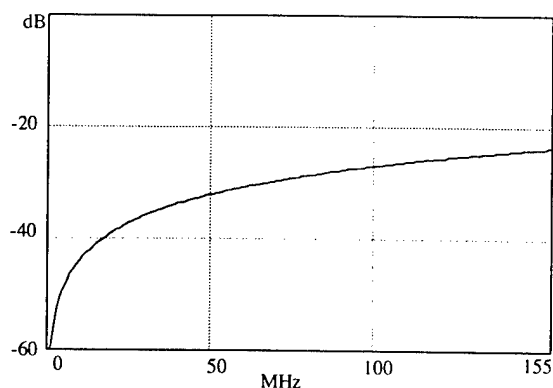


Figure 7

Worst case TSB67[3] channel NEXT response extended to 155 MHz as described in Appendix A

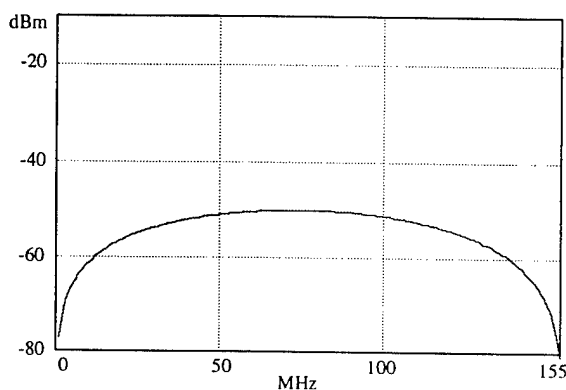


Figure 8

Noise power spectrum at an ATM receiver. This power spectrum is based on the maximum allowable transmit signal of 1060 mV ptp and the worst case TSB67[3] channel NEXT response shown in Figure 7.

Integrating the noise power spectrum results in total noise power of 8.2×10^{-4} mW. Converting total noise power to noise voltage, yields 26 mV ptp. This noise voltage violates the 20 mV limit specified for the Self NEXT Channel Noise (Section 5.3.1).

Based on the Self NEXT noise analysis, the 155 Mb/s ATM physical layer is not likely to achieve the required BER when operating over a worst case category 5 channel.

Signal Distortion

The amount of signal distortion at the end of a worst case TSB67[3] channel is determined primarily by cable attenuation. It is important that attenuation maintain a consistent slope over the entire frequency band of 155 MHz and

meet the extended frequency attenuation limit derived in *Appendix A*. The signal spectrum between 100 and 155 MHz significantly affects the eye pattern opening in the presence of distortion and time domain jitter. This subject is extensively treated in the ATM Forum contribution #96-0444[11].

Discussion

Although the ATM Forum standard[6] states that category 5 satisfies its channel requirements, the above analysis exposes two inconsistencies between the TIA-568-A[1] and the AF-PHY-0015.000[6] standards:

1. The needed signal spectrum extends beyond the category 5 frequency range [11,12].
2. The noise voltage created by the worst case category 5 NEXT response violates the 20 mV ptp limit.

The existing 155 Mb/s twisted pair ATM products compliant with the ATM Forum AF-PHY-0015.000[6] standard use category 5 cabling systems beyond specification. The only reason these products work is that most category 5 installations exhibit substantial margin with respect to the worst case NEXT and attenuation levels and thus deliver the needed performance in the required frequency band of 155 MHz.

However, just because most ATM installations work, does not mean that they are guaranteed to operate at the specified BER and data throughput. The only way to guarantee that a given system will function at the required performance level is to design this system to operate with some degree of performance margin in the worst case environment.

Using components beyond their specification is a poor design practice – it leaves the system vulnerable to products which might create worst case operating conditions and to various installation flaws which might be outside the specified frequency range and thus not detectable by standard field test equipment.

But is The ATM Forum's 155 Mb/s interface the only high speed networking standard exhibiting inconsistencies of definition with the cabling standard upon which it relies for its channel specification?

OTHER EXAMPLES OF INTER-STANDARD GAPS

The gap between The ATM Forum standard[6] and its companion TIA-568-A[1] cabling standard is only one example of a general trend: the cabling standards tend to lag behind the networking standards in addressing the medium dependent specifications required by the new networks.

Often, networking standards introduce their own unique physical layer specifications, not addressed by cabling standards. These specifications include delay skew and ELFEXT. Let us look at a few examples.

Delay Skew

One example of how the cabling standards are often struggling to catch up to the networking standards is the case of the delay skew specification.

Delay skew is the worst case difference in propagation delay among the four pairs in a twisted pair cable.

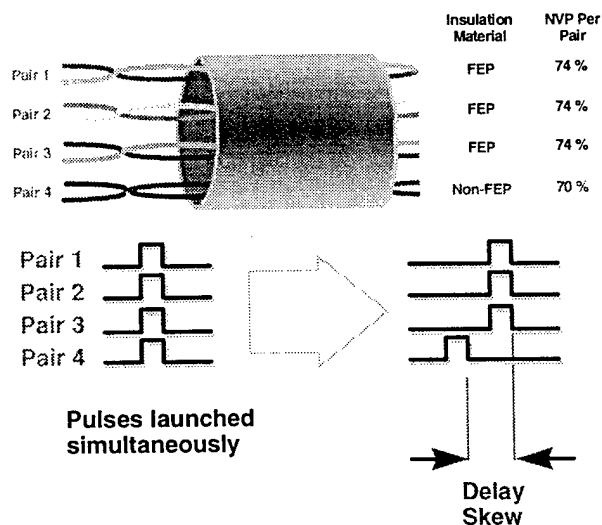


Figure 11

Propagation delay skew among the four pairs in a cable

The LAN standards, such as 100Base-T4[5] and 100VG-AnyLAN[4], which specify transmission over multiple pairs simultaneously, require guaranteed limits on the delay skew among the pairs. The 100VG-AnyLAN[4] standard limits the maximum allowable delay skew to 67 ns

(Section 16.9.1.3) and the 100Base-T4[5] standard limits the maximum delay skew to 50 ns.

Although these multi-pair networking standards have been released since 1995, the delay skew parameter has, until recently, been trapped in the inter-standard gap.

The recent development that has attracted attention to the delay skew issue is the shortage of Fluorinated Ethylene Propylene (FEP) – the material used as insulation in category 5 plenum cables. Because of the FEP shortage, cable manufacturers have introduced cables using a mix of FEP and polyolefin based insulation. As a result of having pairs with different insulation material in the same cable assembly, the delay skew among the pairs has been significantly affected and in some cases has violated the requirements of the multi-pair networks.

The delay skew issue demonstrates the potential perils of using cabling systems beyond explicit specifications. As of this writing (August, 1996), the delay skew specification is being belatedly added to the soon to be released TIA-568-A addendum.

Equal Level Far End Crosstalk (ELFEXT)

ELFEXT is another cabling specification trapped in the inter-standard gap. This parameter is important for proper operation of multi-pair networks since it is the major source of noise for these topologies. As of this writing, TIA-568-A[1] does not specify ELFEXT, while 100VG-AnyLAN[4] places limits on this parameter (Section 23.6.2.3.3).

Although most cabling systems appear to support VG-AnyLAN today, this situation is not guaranteed to last. Currently, the IEEE 802.12 committee is working on the specification for 400 Mb/s 400VG-AnyLAN⁵, which may be more sensitive to the ELFEXT parameter than 100VG-AnyLAN.

Frequency Bandwidth

Channel frequency specifications occupy a prominent place in the inter-standard gap. The committees developing new networking standards are trying to specify cabling requirements so as to assure operation over the widest possible installed base of cabling. For this reason, both category 3 and category 5

networks tend to stretch the specified channel bandwidth limit.

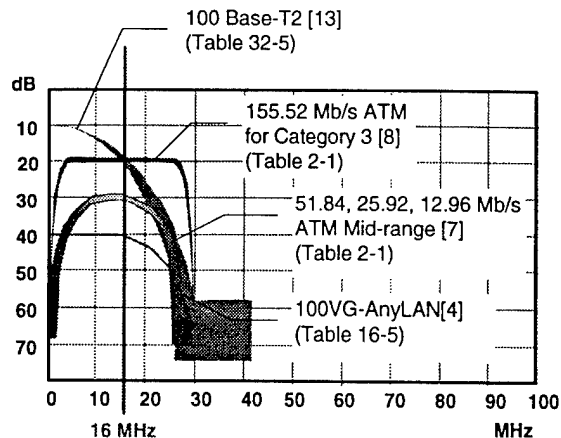


Figure 12

Transmit spectra of several category 3 LANs; these spectra extend beyond the 16 MHz category 3 limits

Figure 12 shows spectra of several high speed networks that specify category 3 cabling. It is easy to see that these networks significantly exceed the 16 MHz frequency limit. Figure 13 shows the spectra of two category 5 LANs, both exceeding the category 5 frequency limit of 100 MHz.

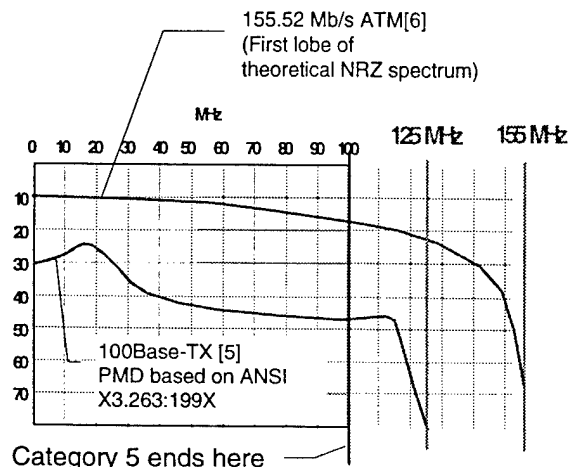


Figure 13

Transmit spectra of category 5 LANs

As already mentioned, the 155 Mb/s NRZ based ATM network has a spectrum extending to 155 MHz. Although it is very easy to show that most ATM products do not filter the first spectral lobe that extends to 155 MHz [11,15], there has been a considerable amount of controversy regarding

the importance of the spectral energy between 100 and 155 MHz.

A recently published Bit Error Rate experiment [12] confirms the dependence of the 155 Mb/s ATM network on channel characteristics above 100 MHz.

This experiment demonstrates that a field installation flaw, such as a bridge tap, which disturbs the channel response beyond 100 MHz (Figure 14) could cause major performance degradation (Table 1) and could substantially deteriorate the BER, causing the link to violate the required BER of 10^{-10} .

Table 1

TEST CONDITION	TIME (min)	# OF ERRORS	BER
no fault	30	6	2.1×10^{-11}
13.8" stub, representing a bridge tap	30	3560	1.2×10^{-8}

Partial summary of BER test results on the same channel with and without an installation flaw – the bridge tap; the bridge tap effected the channel response as shown in Figure 14

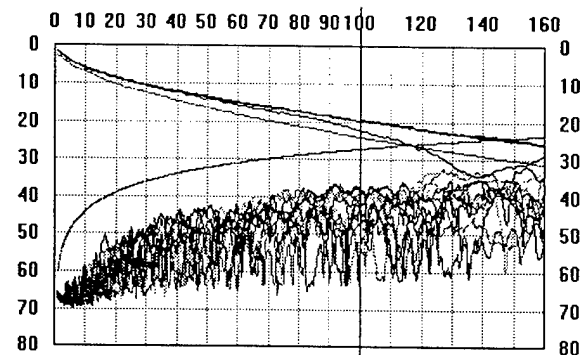


Figure 14

NEXT and attenuation response of a faulty channel with a 13.8" open bridge tap on one of the ATM signal pairs; such a fault is not detectable with a standard 100 MHz field test but significantly effects the performance of the ATM link (Table 1)

This BER experiment reinforces the importance of properly specifying the required channel performance. Since category 5 specification does not extend beyond 100 MHz, most standard field testers would not uncover the installation flaw shown in Figure 14. However, this experiment shows that such a flaw can cause an ATM link to violate the required BER

performance by three orders of magnitude – a very noticeable degradation in data throughput.

SUMMARY

This paper has examined how the specifications of twisted pair cabling affect the noise and distortion environment in a communications channel, thereby affecting the data throughput performance of the channel. We have demonstrated that although the networking standards reference the generic cabling standards for most of their physical layer specifications, the cabling standards tend to lag behind the networking standards in specifying key performance parameters.

Therefore it is not safe to assume that a fully certified category 5 installation will support all the existing and emerging networks. And when field testing twisted pair installations, it may not be sufficient to verify compliance to a cabling standard, such as TIA-568-A[1]. It is important to verify that the network specific requirements are also satisfied.

It is important to remember that the 100 Mb/s networks of tomorrow are considerably more vulnerable to imperfections in the physical layer than are the 10 Mb/s networks of yesterday. And as the LAN industry tries to extract every last bit of performance from category 5 systems, it is important to eliminate the inter-standard gap and to explicitly test the cabling parameters that affect the real rate of data throughput.

FOOTNOTES

¹ Other causes of distortion in a twisted pair channel include imperfections in the Structural Return Loss (SRL) and in the phase response non-linearity of the channel. In a good quality category 5 twisted pair channel, these disturbances typically have far less effect on the quality of the data signal than does the cable attenuation response and, for this reason, are not treated here.

² In qualitative terms, ELFEXT is the far end coupling as seen by the receiver – the attenuated FEXT.

³ Other sources of noise include impulse noise and RF interference. Impulse noise is generally induced by office and building equipment and could be the result of mechanical switching

transients. RF interference is typically generated by TV, radio and other signal transmissions in the air.

⁴ In a twisted pair channel, the noise may not be Gaussian. It is typically dominated by the cable crosstalk and resembles the data signal qualified by the channel crosstalk response.

⁵ As of this writing, it appears that the IEEE 802.12 committee is ready to adapt the 400VG-AnyLAN twisted pair PMD scheme requiring simultaneous transmission on 3 pairs while receiving on the fourth pair. In this case the receive pair might be subject to power sum NEXT from all three transmit pairs.

APPENDIX A

EXTENDING TSB67 NEXT AND ATTENUATION LIMITS BEYOND 100 MHz

TSB67, "Transmission Performance Specifications for Field Testing of Unshielded Twisted-Pair Cabling Systems"[3], defines category 5 field certification limits for Near End Crosstalk (NEXT) and attenuation. The limits are defined for two configurations – Basic Link and Channel.

TSB67 CHANNEL CONFIGURATION

The channel configuration represents a complete link including the patch cables connected to the user device in the work area and to the network equipment in the telecom closet.

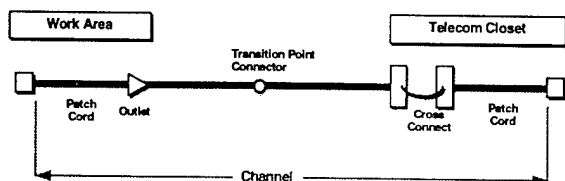


FIGURE A-1

TSB67 channel configuration

TSB67 CHANNEL ATTENUATION

Attenuation is a measure of signal loss. Attenuation response of a category 5 channel is the sum of the attenuation of the cabling and of the connecting hardware comprising the channel.

The attenuation per 100 meters of category 5 horizontal cable is defined in TIA/EIA-568-A[1] Section 10.2.4.6 as follows:

$$AttenCable(f) \leq 1.967 \cdot \sqrt{f} + 0.023 \cdot f + \frac{0.05}{\sqrt{f}} \quad (A-1)$$

The attenuation per 100 meters of category 5 patch cord cable is defined in TIA/EIA-568-A[1] Section 10.5.4.1 as follows:

$$AttenPatch(f) \leq 1.2 \cdot AttenCable(f) \quad (A-2)$$

The attenuation of category 5 connecting hardware is defined in TIA/EIA-568-A [1] Table 10-8 and can be interpolated as a function of frequency by the following equation:

$$AttenConnect(f) \leq 0.1 + 0.003 \cdot f \quad (A-3)$$

The category 5 attenuation certification limit for a channel containing 4 connections, 90 meters of horizontal cable and 10 meters of patch cord cable is defined in TSB67 [3] as the sum of the attenuation limits of the cabling and of the connecting hardware comprising the channel:

$$AttenChannel(f) = 1.02 \cdot AttenCable(f) + 4 \cdot AttenConnect(f) \quad (A-4)$$

The factor of 0.02 is obtained for 10 meters of patch cordage, assuming 20% higher attenuation for the patch cord cable than for the horizontal cable, as $0.2 \cdot 10/100$.

The certification limit for channel attenuation is based on the physical properties of the cabling and of the connecting hardware. These physical properties are expected to behave consistently above the 100 MHz band defined by the category 5 specification.

Because the physical properties of category 5 installations remain consistent over frequency, the maximum allowable attenuation of a 100 meter category 5 channel can be extended beyond 100 MHz, as shown in Figure A-2.

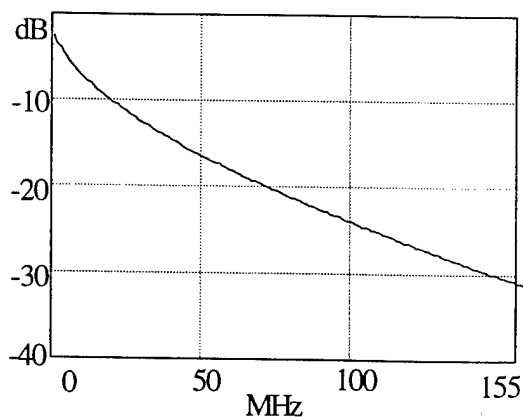


FIGURE A-2

TSB67 channel attenuation limit extended to 155 MHz per Equation A-4

TSB67 CHANNEL NEXT

Near End Crosstalk (NEXT) is a measure of signal coupling from one pair to another. The NEXT response of a category 5 channel is the sum of the NEXT responses of the cabling and of the connecting hardware comprising the channel.

The NEXT of category 5 horizontal cable is defined in TIA/EIA-568-A[1] Section 10.2.4.7 as follows:

$$NEXT_{cable}(f) \geq NEXT(0.772) - 15 \cdot \log\left(\frac{f}{0.772}\right) \quad (A-5)$$

The NEXT at 0.772 MHz is 64 dB for category 5 cable.

The NEXT of category 5 connecting hardware is defined in TIA/EIA-568-A[1] Section 10.4.4.2 as follows:

$$NEXT_{connect}(f) \geq NEXT(16) - 20 \cdot \log\left(\frac{f}{16}\right) \quad (A-6)$$

The NEXT at 16 MHz for a category 5 connector is 56 dB.

The NEXT certification limit of a category 5 channel is the sum of the NEXT limits of the cabling and of the connecting hardware comprising the channel and is computed as follows:

$$NEXT_{connLin}(f) = 10^{\frac{-56 + 20 \log\left(\frac{f}{16}\right)}{20}} \quad (A-7)$$

$$NEXT_{cableLin}(f) = 10^{\frac{-64 + 15 \log\left(\frac{f}{0.772}\right)}{20}} \quad (A-8)$$

$$NEXT_{channel}(f) = 20 \cdot \log(2 \cdot NEXT_{connLin}(f) + NEXT_{cableLin}(f)) \quad (A-9)$$

Equation A-9 defines the NEXT certification limit of a category 5 channel containing 2 near end connections. This equation is based on the physical properties of the cabling and of connecting hardware, which are expected to behave consistently above the 100 MHz band covered by TSB67[3].

Because the physical properties of category 5 installations remain consistent over frequency, the certification limits for NEXT of a category 5 channel can be extended beyond 100 MHz, as shown in the following figure:

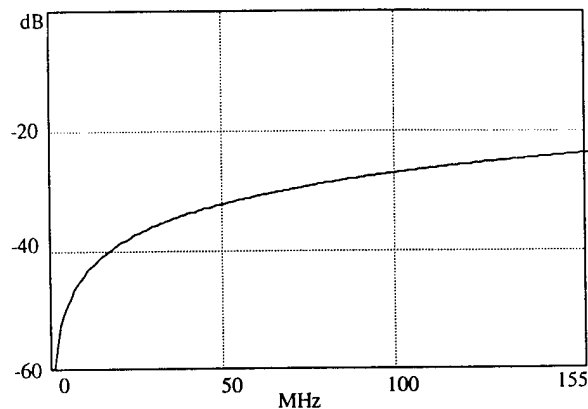


FIGURE A-2

TSB67 channel NEXT limit extended to 155 MHz per Equation A-9

REFERENCES

- [1] ANSI/TIA/EIA-568-A, "Commercial Building Telecommunications Cabling Standard," October 6, 1995.
- [2] ISO/IEC 11801, "Generic Cabling for Customer Premises", 1995.
- [3] TIA/EIA Telecommunications Systems Bulletin, TSB67, "Transmission Performance Specifications for Field Testing of Unshielded Twisted-Pair Cabling Systems", October 1995
- [4] IEEE Std 802.12-1995, "Demand Priority Access Method, Physical Layer and Repeater Specification for 100 Mb/s Operation", November 2, 1995
- [5] IEEE Std 802.3u-1995, "Media Access Control (MAC) Parameters, Physical Layer, Medium Attachment Units, and Repeater for 100 Mb/s Operation, Type 100BASE-T", October 26, 1995
- [6] AF-PHY-0015.000, "ATM Physical Medium Dependent Interface Specification for 155 Mb/s over Twisted Pair Cable", September 1994.
- [7] AF-PHY-0018.000, "Mid-range Physical Layer Specification for Category 3 Unshielded Twisted-Pair", September 1994.
- [8] AF-PHY-0047.000 Letter Ballot, "155.52 Mb/s Physical Layer Specification for Category-3 Unshielded Twisted Pair", November 1995
- [9] Dr. Kamilo Feher, "Wireless Digital Communications", Prentice Hall, 1995
- [10] IEC/TC:SC46C contribution by J.-H. Walling, Dr.-Ing., Nortel (currently NORDX/CDT), "Proposal on the required level of far-end crosstalk of multiple pair data grade cables used for bi-directional traffic", May 1995
- [11] ATM Forum contribution #96-0444, "Physical Layer Requirements for 155 Mb/s Twisted Pair ATM", April 1996
- [12] The ATM Forum contribution #96-0792, "155 Mb/s Bit Error Rate Experiment", June 1996
- [13] IEEE 802.3v/D3.0, "Draft Supplement to IEEE Std 802.3", 100 Base-T2
- [14] ANSI X3.263:199X
- [15] "The ATM Controversy", Scope Communications, Inc., Northboro, MA



Fanny I. Mlinarsky
Scope Communications, Inc.
100 Otis Street
Northboro, Massachusetts 01532

Fanny Mlinarsky has held a number of Engineering and Engineering Management positions at leading communications and test equipment companies including Chipcom, Concord Communications and Teradyne. She has been with Scope Communications since 1993 and is responsible for the development of hand held test tools used by cable installers and network maintenance technicians. Mlinarsky holds a BA in Computer Science and a BS in Electrical Engineering from Columbia University. In her 13 years of experience in the data communications industry, she has actively participated in the development of networking and cabling standards under the auspices of IEEE, ANSI and TIA.

NETWORKS OF THE FUTURE: GIGABIT ETHERNET AND OTHER NEWS FROM IEEE 802.3

Geoffrey O. Thompson

**Chairman IEEE 802.3 / Bay Networks, Inc.
Santa Clara, California**

ABSTRACT

Local Area Network (LAN) speeds are going up to try to keep up with the increased speed and file sizes in personal computers. Geoffrey Thompson, Chairman of IEEE 802.3 will report on recent developments in standardizing Ethernet for operation at a speed of 1 Gigabit/sec. He will also discuss other aspects of 802.3 standards work that impacts cables and cabling.

INTRODUCTION

IEEE 802.3 completed the second speedup of Ethernet since its invention (the first since its standardization) in October of 1995 with the publication of the 100BASE-T Standard (IEEE Std 802.3u - 1995). The success of this effort has resulted in yet another effort to up the speed by factor of ten to 1000 Mb/s. The most popular name for this effort is Gigabit Ethernet although this is not the name that will end up on the standard. The standards effort was officially chartered last spring by the IEEE and is now well underway. There is broad industry participation. There is an industry consortium, the Gigabit Ethernet Alliance, with over 50 members. There are well over a half a dozen well-funded start-ups and the venture capitalists and press are covering our every move.

FIRST A LITTLE HISTORY

Before we start I had better define Ethernet. It is a term that has become very fuzzy over the years. Ethernet is a packet oriented networks communications protocol. In particular it is a single defined packet format (Figure 1a) and the physical systems that have evolved to carry those packets in a LAN environment, especially those standardized in IEEE 802.3.

Ethernet was invented at Xerox Palo Alto Research Center (PARC) in 1973 by Bob Metcalfe, David Boggs and their colleagues. PARC was building a personal computer at that time called the Alto and they wanted to be able to communicate between machines within the PARC campus at greater than modem speeds (1973 modem speeds). It ran at 3 Mb/s over 75Ω Coaxial cable and used Jerrold cable-TV taps. It is now known as "Experimental Ethernet". There were eventually 5-10,000 nodes, mostly Altos and mostly within Xerox. A few were in universities and the Federal Government. The Ethernet patent was filed and a paper was published (Communications of the ACM) in 1976. By then there were at least 500 machines on the net. In 1978-79 Xerox was developing an "Electronic Desktop" product. They were going to tie the machines together with a speeded up version of the Experimental Ethernet (10 Mb/s) called the X-Wire. Metcalfe persuaded Xerox to gather outside partners. Digital Equipment Corporation (DEC) and Intel signed up and the name reverted to Ethernet. The 3 companies published the specification publicly in September 1980 and a number of companies were shipping product within a year. This spec. (Figure 1b) is the base definition of "Ethernet". Initially it was somewhat of a failure. Cabling was too clumsy and expensive. It was too fast for the silicon of the day. That was planned when they wrote the specification but they overdid it a little.

ETHERNET ADAPTS

By now Metcalfe had left Xerox to form a company to (1) bring Ethernet into the larger time and (2) be more flexible and responsive to this particular market than was possible in a big company in another business.

One of the first things this company (3Com) did was to reinvent Ethernet in a new form. The new Ethernet threw out the transceiver cable, used lighter, cheaper more flexible coax, a cable that users could install (RG-58) themselves. They nudged the silicon industry into supplying more and better chips. This new flavor of Ethernet became known as Thin Ethernet, ThinNet or CheaperNet.

By now DEC Intel and Xerox had turned their specification over to the IEEE. The IEEE in turn released it as a formal IEEE standard, IEEE 802.3. The standard named the original thick coax Ethernet 10BASE5 (10 Mb/s Baseband 500 meters) and ThinNet as 10BASE2.

Ethernet now had jumped onto the growth curve of the PC market doing exactly what it was invented to do (remember 1973 and the Alto). We are at about 1983, Ethernet is 10 years old and just really getting started.

ETHERNET ADAPTS AGAIN

If getting facilities involved kept Ethernet from getting a start in the market (thick coax) things were now getting to the point where just the opposite was true. Ethernet wanted to go between departments, facilities didn't like having to run special cable (coax) in the walls and, with deregulation, the phone company had walked away from ownership of all of the installed telephone cabling in buildings. It was too good an opportunity to pass up, even if it was a bandwidth jump from only 3 kHz for voice to 10 MHz. In August of 1987 at least 16 companies showed up to start work on what would become the 10BASE-T version of Ethernet. Pre-standard product started shipping at the same time. Ethernet changed from a bus to a star topology.

ETHERNET TAKES OFF

With the approval of the 10BASE-T addition to the Ethernet/802.3 standard (Figure 2) in 1990 we started getting into big numbers. Millions of nodes per year adding on. Networking gear starts appearing on pegboard hooks in computer stores and the cabling industry puts out a "Generic Premises Cabling" standard, EIA-568 to further support LANs. Cabling architecture is finally as open as the PC architecture is. Success compounds. But with all of this we are into the 90s and Ethernet speed has not changed

in 10 years. In the meantime the size of a floppy disk has gone from 360K to 1.4M, processor speeds are going up significantly every year and so are file sizes.

TIME FOR A SPEED-UP

In the fall of 1992 IEEE 802.3 decided to take a look at raising the speed of Ethernet from 10 Mb/s to 100 Mb/s. Attendance jumped at 802.3 meetings from 20 to 200 so it seemed like the industry was interested. Most of the hard work had already been done. Silicon logic speeds were fast enough that designing chips was no great trick. There was a large body of skill that knew how to both design and use Ethernet. Physical layer standards work had been done at 100 Mb/s by the FDDI group. All we had to do was glue the pieces together and crank out a standard. We did it. The 100BASE-T standard was approved in June of 1995. My estimate is that products including 100BASE-T (Figure 3) represented a market of about \$750 Million in the first 12 months after the standard was approved. This market is dominated by 100BASE-TX which operates on up to 100 meters of Category 5 cable or STP. The market has some other pieces. The most significant of these are switching and full-duplex. There are also fiber flavors and 2 more copper varieties that work over Category 3 cabling, 100BASE-T4 and 100BASE-T2. 100BASE-T2 is worth further comment here as it is the first time that Ethernet has done a standard based on digital signal processing technology. 100BASE-T4 got to 100 Mb/s on Cat 3 by using all 4 pairs and only driving data one direction at a time. 100BASE-T2 uses DSP techniques to do both cross talk cancellation and echo cancellation on only 2 pairs. It can pass data both directions simultaneously.

WHAT NEXT?

100BASE-T is too big a success to just walk away from. Our industry has short product life cycles. The next generation from IEEE 802.3 is called Gigabit Ethernet. (Figure 4)

GIGABIT ETHERNET PROJECT

IEEE 802.3 as a standards body started looking at a next generation project a year ago (Fall 1996). We established that there was enough commercial interest and it was technically feasible. Our parent body formally authorized an IEEE project last Spring (96) (Figure 5) and we are in the

middle of deciding what it will look like. There will be significant refinement of our technical approach between the time this paper is submitted for the proceedings and the date of the talk. In addition to the work being done in the standards group (which meets approximately every 2 months) there is also an industry consortium, The Gigabit Ethernet Alliance (Figure 6), which meets every 2 weeks to try to nudge things along. The Alliance has membership by company and there are over 50 companies involved at this point.

GIGABIT ETHERNET DECISIONS

The major initial market for Gigabit Ethernet is backbone and server room connections rather than desktops, therefore our initial efforts are on fiber and short reach copper. The work is based on keeping the Ethernet MAC pretty much intact and adapting the physical layer from Fiber Channel. (Figure 11) We are speeding it up from 100 MBytes/sec to 1000 Mbits/sec (25%). We will also use the same 8B/10B line encoding that is used by Fiber Channel although we will be able to simplify the code set that they use as Ethernet has simpler requirements. The result: (Figures 12-16)

- ~800 nm, multi-mode fiber
 - 50/125, Up to 500 meters
 - 62.5/125, Up to 200 meters
- 1300 nm, multi-mode fiber
 - 62.5/125, Up to ~800 meters
- 1300 nm, single-mode fiber
 - At least 2 kilometers
- Short reach copper
 - Up to 25 meters using 8B/10B coding and specialty cable assemblies.

We are also investigating a horizontal copper solution that would be suitable for fabrication the next generation of CMOS technology and would operate full-duplex over 100 meters of 4 pair of Category 5 unshielded twisted pair (UTP) cabling. This is a significant challenge both technically and economically. The most promising proposal at this time is based on 4 channels each way. Each 250 Mb/s channel would utilize a 3X3 PAM scheme with pulse shaping, channel equalization and also echo cancellation to support full duplex.

THE RESULT

We expect to have a standard sometime in 1998. You will see pre-standard products significantly sooner than that. We expect that the standard will provide interoperable

products that will provide plug and play upgrades to existing Ethernet networks especially for servers and backbones. We hope that market volumes will be large enough that you will get a 10X speed-up for two to three times the cost of 100 Mb/s.

CONCLUSION

All of this will have a significant impact on cabling. We are trying very hard to tune our work so that it will run on the installed base of fiber and category 5 UTP but we are pushing the limits for low cost (i.e. short wave-length) multi-mode technology. We expect that Gigabit Ethernet will be a significant force in moving the LAN market to single-mode and, hopefully, to dropping prices on 1300 nm transceivers. If there was any doubt in your minds before that 4-pair Cat 5 was the way to go our plans for horizontal copper should settle those doubts. Although we will be pushing the limit on category 5 we are committed to the installed base. This does mean that product and installation quality requirements will not have any slack. Testing and field test equipment requirements will become more sophisticated. We will use up all the capabilities that the specifications have to offer.

ACKNOWLEDGMENTS

I would like to acknowledge my colleagues for the industry broad participation in IEEE 802.3. This open dynamic forum is a key element in the ongoing success of Ethernet. I would also like to thank the Gigabit Ethernet Alliance for their support of the standards process. My thanks as always to Bay Networks for supporting my work and this presentation to you.

REFERENCES

The current standard:

1. ISO/IEC 8802-3 : 1996 (E), ANSI/IEEE Std 802.3, 1996 Edition, CSMA/CD access method and physical layer specifications
2. ANSI/IEEE Std 802.3u - 1995, Supplement for 100 Mb/s Operation (100BASE-T)

Current draft

3. No draft available at manuscript preparation time. Drafts will be posted on:
ftp://stdsbbs.ieee.org/pub/802_main/802.3/gigabit

Other 802.3 documents

4. Not available at manuscript preparation time. Information will be posted on:
ftp://stdsbbs.ieee.org/pub/802_main/802.3/gigabit

AUTHOR

Geoffrey O. Thompson is chairman of IEEE 802.3 and Manager of Standards Development at Bay Networks, Inc. He has been highly active in the development of Ethernet standards since 1983. Before joining Synoptics Communications (now Bay Networks) in 1988, Mr. Thompson spent over 20 years with Xerox Corporation in various research and development positions where he worked on pioneering implementations and products in facsimile, laser printing, computer workstations and local area networking. Mr. Thompson received his BSEE from Purdue University in 1964 and has been issued 3 patents.

Geoffrey O. Thompson
Bay Networks, Inc.
M/S SC01-05
Post Office Box 58185
Santa Clara, CA 95052-8185



Ethernet, the packet format

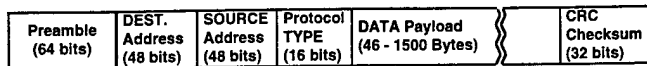


Figure 1a

Ethernet, the physical system (bus) (aka IEEE 802.3 10BASE5)

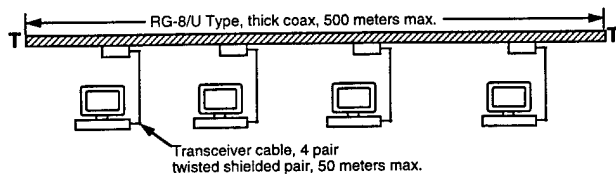


Figure 1b

Ethernet, the physical system (Star Topology)

(aka IEEE 802.3 10BASE-T & 10BASE-F)

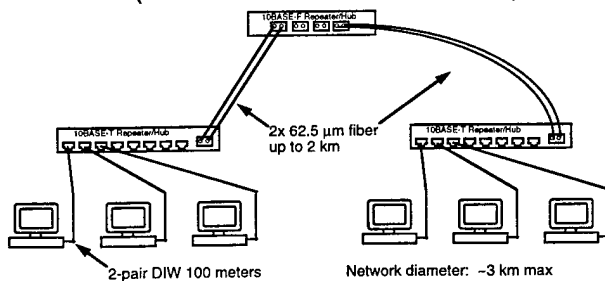


Figure 2

100BASE-TX/FX system (Star Topology)

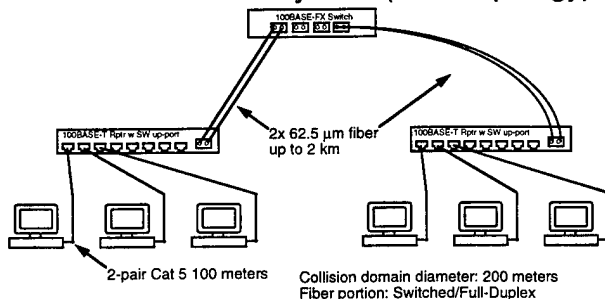


Figure 3

Expected Gigabit Ethernet Topology

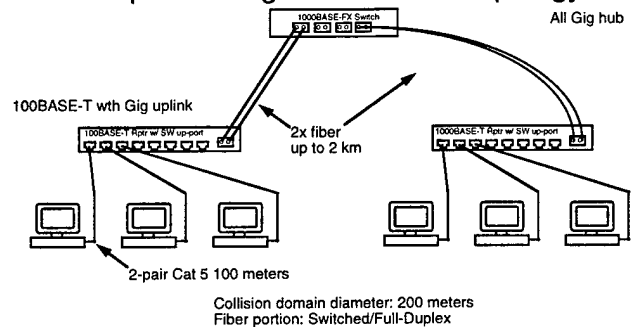


Figure 4

IEEE 802.3z Standardization

- Project Approval 6/96
- Goals
 - Stable Draft Standard 9/97
 - Approved Standard 6/98
 - Variety of Media Options
 - 8B/10B Encoding known, available technology.
 - Advanced Encoding known in infancy.
- No "Holy War" with alternative IEEE groups.

-Figure 5-

Gigabit Ethernet Alliance

- Open industry group
- Goals
 - Interoperability via specifications, testing
 - Standards via IEEE 802.3z
 - Educational via public relations, seminars, tradeshowes
- Over 50 member companies
(2x Fast Ethernet Alliance)

-Figure 6-

Introduction to Gigabit Ethernet

- What is driving the need for "Gigabit" speed?
 - New network applications are changing the bandwidth requirements of existing networks
 - Gigabit Ethernet provides a way to remove network "hot spots" in frame-based Ethernet networks.

-Figure 7-

Migration to Gigabit Ethernet

- Remove Client/Server bottleneck for 100 Mb/s switch networks
- Remove riser bottleneck for 10/100 Mb/s bandwidth to the desktop
- Enable eventual 1000 Mb/s to the desktop

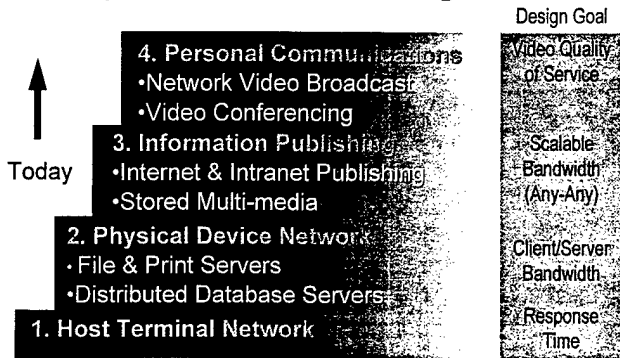
-Figure 8-

Gigabit Ethernet Market Factors

- End-User Acceptance
- Gigabit Ethernet Standards
- Gigabit Ethernet Availability
- Multi-vendor Interoperability

-Figure 9-

Enterprise Network Driving Forces



-Figure 10-

Gigabit Ethernet Overview

- Merger of existing technologies
 - Ethernet MAC
 - Just at 100BASE-T increased speed from 10 Mbps to 100 Mbps, Gigabit Ethernet will increase speed from 100Mbps to 1000Mbps based on the existing IEEE 802.3 MAC.
 - Fiber channel PMD
 - Existing Fiber channel PMD is designed for optical fiber operation at 800Mbps. Gigabit Ethernet designed to increase speed of PMD to support 1000Mbps operation.

-Figure 11-

Gigabit Ethernet Physical Transmission Technology

- Two encoding options:
 - Fiber Channel derived 8B/10B encoding
 - Advanced encoding for UTP horizontal cabling
- Four transmission options
 - 8B/10B Short wavelength (~800nm) CD Laser
 - 8B/10B Long wavelength (1300nm) Laser
 - 8B/10B Custom copper cable, closet jumper
 - Advanced Encoding 4 Pair Cat. 5 UTP

-Figure 12-

Fiber (CD laser) Gigabit Ethernet

- Cable: 2-fiber, 50 micron, 62.5 micron multi-mode
- Connector: MIC, ST or SC (converters available)
- Signaling: 1000Mbps = 1 strand x 1250Mbaud x (80% for 8B10B encoding)
- Data paths: 1 fiber transmit, 1 fiber receive

-Figure 13-

Fiber (1300nm) Gigabit Ethernet

- Cable: 2-fiber, 10 micron single-mode, 62.5 micron multi-mode
- Connector: MIC, ST or SC (converters available)
- Signaling: 1000Mbps = 1 strand x 1250Mbaud x (80% for 8B10B encoding)
- Data paths: 1 fiber transmit, 1 fiber receive



-Figure 14-

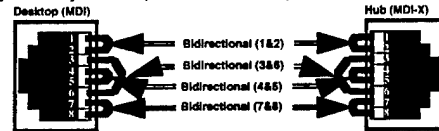
Gigabit Ethernet Physical Transmission Goals

	8B/10B	Advanced Coding
800nm CD Laser	200 Meters (62.5m MM Fiber) 500 Meters (50m MM Fiber)	N/A
1300nm Laser	800 Meters (62.5m MM Fiber) 2 Km (10 m SM Fiber)	N/A
2 Pr Cu XCVR	25 Meters	N/A
4 Pr UTP XCVR	N/A	100 Meters

-Figure 15-

Gigabit Ethernet UTP Cabling

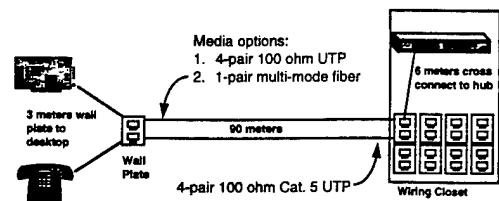
- Signaling: 1000Mbps = 4-pair x 250Mb/s each
- RJ-45 Pinout: same as 10/100BASE-T, except all pairs are bi-directional
- Physical layer is capable of Full Duplex.



-Figure 16-

11801 / 568 Horizontal Cabling

100 meters total



-Figure 17-

Cabling and Topology Summary

- Wire to ISO/IEC 11801 and EIA/TIA-568-A specifications
- Fast Ethernet supports all major cable types
- Fast Ethernet supports large topologies
- Key topology rules:
 - 100m hub to desktop links
 - Bridge/switch between wiring closets
 - Fiber lengths over 100m requires switch

-Figure 18-

Gigabit Ethernet Technology Network Topology

- CSMA/CD Topology
 - Supports 100 Meter radius for CSMA/CD protocol.
- Full Duplex Topology
 - Supports variable distance dependent on media capabilities
 - Supports server, switch and router DTE applications.

-Figure 19-

Gigabit Ethernet - End User Acceptance

- Network management MIBs remain largely the same, familiar tools
- No re-training for MIS and LAN Administrators
- Runs same applications as today's 10BASE-T
- Uses existing cabling infrastructure

Gigabit Ethernet IS Ethernet, Only Faster!

-Figure 20-

Conclusion

- Gigabit Ethernet will play a role in enterprise networks
- Increase server access bandwidth and trunk link speed between switches

-Figure 21-

RELIABILITY OF DRY WATERBLOCKING MATERIALS

Anne G. Bringuier, Clinton E. Clyburn III

Siecor Corporation
Research, Development and Engineering
Hickory, NC

ABSTRACT

This paper presents the performance of different swell materials in various tests that address long-term aging, wet-dry cycling and influence of water temperature. Experiments were designed to resemble conditions experienced in the field. To address the concerns of performance in real field conditions, fluid penetration testing was conducted with polluted manhole waters. Performance of the swell materials was correlated to stranded loose tube cable performance. The dry swellable materials employed proved to be effective when exposed to a variety of environments. This program resulted in the selection of the best performing dry waterblocking materials for stranded loose tube cables in outdoor applications.

INTRODUCTION

As optical fiber cables penetrate further into the worldwide telecommunications infrastructure, the probability for midspan access and cable reentries has increased dramatically. The locations for these operations are not often ergonomic; the craftsman may find himself in an awkward environment with limited space, bad weather and cables containing flooding compounds. These issues result in inefficient cable operations and increase labor costs.

In 1995, some of these issues were addressed with the introduction of a dry core loose tube fiber optic cable for outdoor use^{1,2,3}. Standard loose tube cables use flooding greases for water ingress protection and require tedious cleaning in preparation for splicing and termination. The dry core loose tube cable replaced these flooding compounds with dry water swellable materials.

These materials contain superabsorbent polymers (SAPs) which rapidly swell upon contact with

water and hold many times their initial weight. Although these materials swell in interstitial spaces, the pressure they exert does not change cable performance. In their dry cabled form, they are easily removed with scissors. This improves the efficiency of cable access operations without degrading the cleanliness of the workspace.

Since the introduction of dry water swellable components for the replacement of flooding compound in outdoor cables, reliability of water blocking performance has become a subject of major interest³.

HEAT AGING

Swell materials for cables are most commonly found in the form of tapes or yarns. Heat aging is used as a screening tool to evaluate their performance.

Material Testing

The swell tape selected in this study employed a sodium salt of polyacrylic acid as the active superabsorbent polymer (SAP). The swell yarn selections included:

- Yarn 1: Polyammonium acrylate-coated fiber
- Yarn 2: Crosslinked acrylate copolymer partially neutralized to a sodium salt (i.e. same chemistry as the tape)
- Yarn 3: Olefin/alkyd carboxylate copolymer.

These yarns are comprised of the SAP described above and a polyester fiber and binder, with the SAP portion accounting for 40 to 50% of the total yarn weight.

The conventional laboratory method to measure tape swell height uses a cup and piston assembly where the tape is allowed to swell freely. The procedure for testing yarn absorbency uses a one meter piece of yarn wrapped around a wire basket which is submerged in water for 5 minutes, drained for 1 minute and then weighed.

The water swell tape and yarns were aged at 80° C for 1, 2, 3 and 8 weeks and then allowed to cool for 2 hours in a dessicator at 50% R.H. For the tape samples, swell height was measured in millimeters. For the yarn samples, swellability was measured in grams of absorbed water per gram of yarn (g/g). Each data point presented in Figures 1 through 4 represents the average of five measurements. The average standard deviation was 0.7 mm for the tape swell height , 130% for Yarns 1 and 2 and 300% for Yarn 3 . Aging performance, monitored in distilled and tap water, is represented in the following graphs:

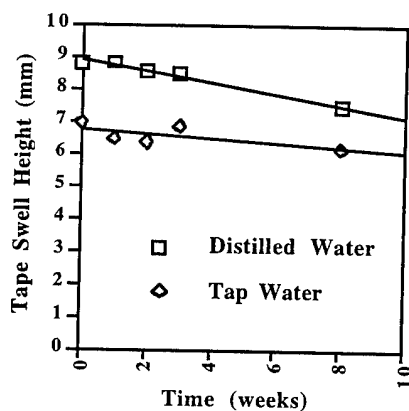


Figure 1: Tape swell height as a function of aging at 80°C

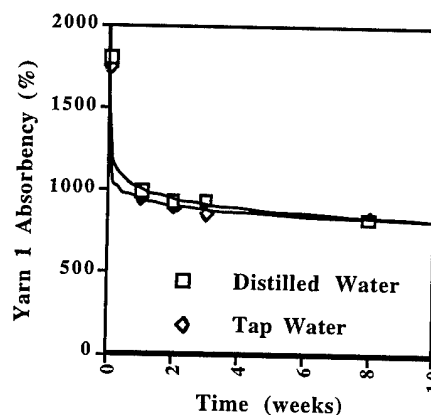


Figure 2: Yarn 1 absorbency as a function of aging at 80°C

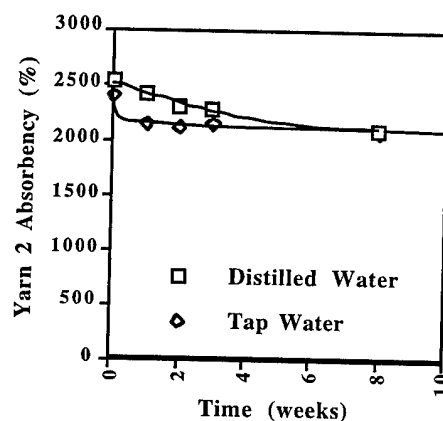


Figure 3: Yarn 2 absorbency as a function of aging at 80°C

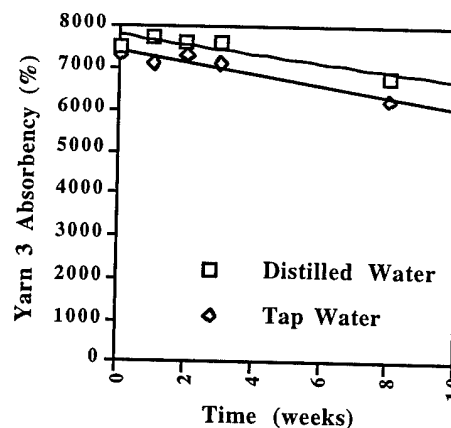


Figure 4: Yarn 3 absorbency as a function of aging at 80°C

From these graphs, the following conclusions were reached:

- The same trends in aging behavior occurred whether distilled or tap water was used.
- At 80°C, no significant degradation of swell performance was observed for the tape in tap water. Tapes stored at 25°C for two years also showed swell heights equivalent to new virgin material.
- For the yarns, initial swell amount and performance after aging depended on their chemistry. Yarn 3 (carboxylate copolymer) exhibited the best initial and final absorbency while Yarn 1 (polyammonium-coated fiber) gave the worst results.
- After 3 weeks at 80°C, the water absorbency for Yarns 1 and 2 plateaued.

In summary, the swell tape and Yarn 2 showed good aging behavior. Yarn 1 exhibited a quick decrease in swell performance after one week, but its swell performance did not degrade further upon subsequent aging. After 8 weeks, Yarn 3 still exhibited decreasing performance. It is important to know that all superabsorbent materials are crosslinked by temperature during their manufacturing process. When held at 80°C, these materials will further crosslink, causing a decrease in swell height and an increase in gel strength, which correlates to a better ability to swell under load. This further crosslinking may explain Yarn 3 behavior in aging.

Additionally, the tape swell rate was monitored because of its direct impact on the cable water penetration performance. A tape which would have a slower rate of swelling may not effectively waterblock the cable. After aging at 80°C for 8 weeks, the swell rates were equivalent to that observed for unaged samples, where 80% of the maximum swell height was reached within the first minute.

Cable Testing

The cables represented in Figure 5 and 6 were used for cable testing. Buffer tubes were 3.0 mm in diameter. This size is one of the largest buffer tubes

commercially available in conventional stranded loose tube cables. This results in spacious interstitial gaps (i.e. the worst cases for water penetration).

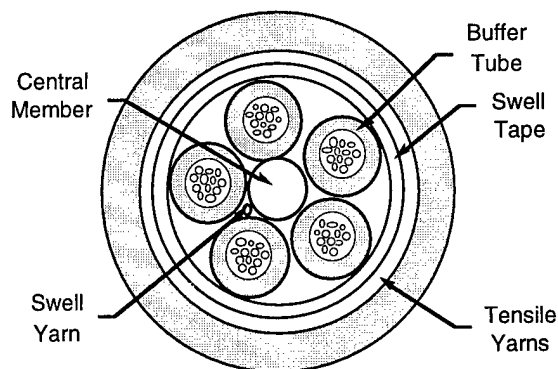


Figure 5: 5 position cable cross-section

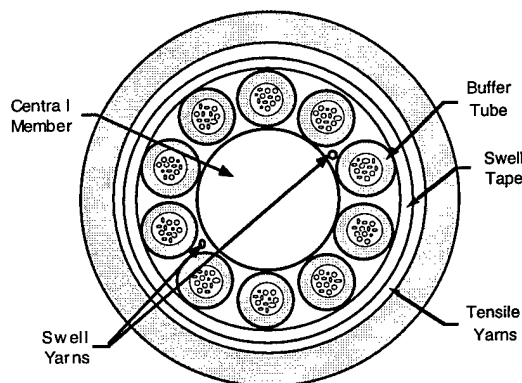


Figure 6: 10 position cable cross-section

The purpose of this testing was to compare the efficiency of the yarns in cables. Yarn 1 was not tested because of its poor aging performance. The measure of performance was a water penetration test in accordance with EIA/TIA-455-82A (FOTP-82). It consists of exposing the cross-section of a one meter section of cable exposed to a one meter head of tap water for 24 hours. After aging in an oven for 1 and 3 weeks at 80°C, cables were tested, then dissected to obtain the water ingress measurements. In Table 1, results were normalized against the

water ingress in the unaged 5 position cable using yarn 2 ($X=1$). Each value represents the average of four measurements. The standard deviation for these comparative results is 0.3. All cables were within the one meter industry requirement.

	Yarn 2	Yarn 3
5 position unaged	1.0	1.4
10 position unaged	1.5	1.5
5 position aged 1 week	1.3	1.5
10 position aged 1 week	1.7	1.7
5 position aged 3 weeks	1.4	1.5
10 position aged 3 weeks	1.7	1.7

Table 1: Water Ingress Data

From Table 1, the following conclusions may be reached:

- Although Yarn 3 has a much higher free swell absorbency than Yarn 2 (Figure 3 and 4), no significant difference could be seen in water penetration performance for the 10 position cable. For the 5 position unaged cable, Yarn 3 actually exhibited slightly worse results than Yarn 2. This may be explained either by a slower rate of swell for Yarn 3 or by a lower gel strength (i.e. little ability to swell under load). It is therefore important to correlate material testing to actual cable performance by dissecting the cable tested.
- Yarns 2 and 3 perform comparably after aging.

Changes in water pressure, water type or gap between buffer tubes will change these results. Note that all water penetration tests performed in this program were conducted with instantaneous exposure to the one meter head. McCallum et al. showed that the ingress distance in dry water swell

cables decreased by a factor of three as the transition time to full pressure increased from zero to ten minutes⁴. This is significant because of the high probability that a breached cable subjected to water pressure would be exposed gradually to a buildup in water level⁵.

SWELLABILITY VERSUS TEMPERATURE

FOTP-82 testing for water penetration uses water at room temperature, typically 23°C. However, in the field the cable may be submerged in ground water which may vary from slightly above 0°C to temperatures close to 40°C. The testing represented in Figures 7 and 8 was conducted to evaluate the effect of water temperature on the tape and Yarn 2 swellability.

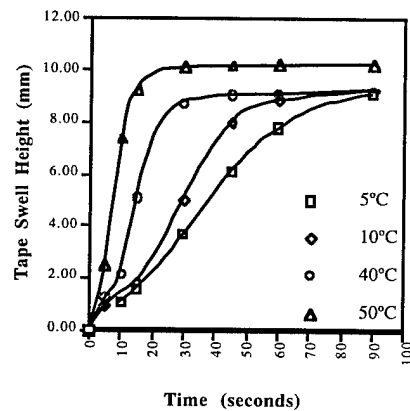


Figure 7: Tape swellability as a function of water temperature

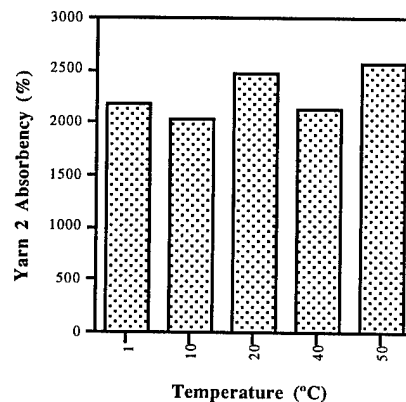


Figure 8: Yarn 2 swellability as a function of water temperature

The SAP used in the tape and Yarn 2 is a sodium salt based polyacrylic copolymer. Each polymer chain is lined with carboxyl groups (COOH) which dissociate in water into negatively charged carboxylate ions (COO⁻). According to the results described in Figure 7, higher temperatures increased the speed of this solvation for the tape. However, even at a cold temperature of 5°C, 80% of the final swell height was reached within the first minute. For both the tape and the yarn, final swell amounts were similar at all temperatures.

SWELLABILITY IN MANHOLE WATERS

Water swell performance depends on the ionic content of the water. When the water contains positive ions, these ions position themselves next to the carboxylate ions, thus limiting the swelling and absorbency capacity of the SAP. In the following study, we investigated the functional impact that this phenomenon would have on the performance of a cable installed underfield conditions. This was achieved by testing cables with water collected from a variety of manhole environments throughout the continental United States. These locations were selected to provide a realistic cross-section of potential installation environments.

Each groundwater was analyzed for ion content by induced coupled plasma using Environmental Protection Agency (EPA) method 200.7. Polyvalent ions are expected to have the greatest effect on water absorbency³. For example, Ca⁺⁺ ions will come in contact with twice as many carboxylate ions compared to a monovalent ion like potassium (K⁺). Groundwaters in Table 2 were collected in metropolitan coastal areas from sites near the shoreline where higher concentrations of salt and other pollutants may be found. These waters were compared to tap waters found in Hickory, North Carolina and in Morristown, New Jersey. Aquamarine™, a commercial sea water replacement and ASTM D1141 substitute ocean water are listed as references. It should be noted that the sea water substitutes are at least two orders of magnitude higher in the concentration of many ions than the field-collected groundwaters.

Ion Type	Na	K	Mg	Ca	Fe	Al
Valence	1	1	2	2	2	3
Hickory, NC Tap Water	9.30	1.10	0.68	2.00	0.17	0.10
Morristown, NJ Tap Water	6.20	0.65	3.00	8.70	0.37	0.89
Philadelphia Manhole	67.50	2.90	0.67	33.6	0.06	0.00
New Orleans Manhole	88.90	8.60	15.90	77.6	0.10	0.00
Stamford, CT Manhole	36.2	5.6	12.6	36.6	2.6	1.3
Winston, NC Manhole	56.5	41.5	2.3	9.6	13.6	16.4
Boston Manhole	108.30	6.80	12.00	8.90	0.29	0.07
Aquamarine Solution	10,300	257	1,306	547	0.00	0.00
ASTM Ocean Water	10,360	261	1,314	418	0.00	0.00

Table 2: Concentration of ions in manhole water (mg/liter concentration)

Initially, the impact of the groundwater ions was examined using the swell materials alone. The swell height for the tape was measured using a "restricted cup". Unlike the conventional method (Figure 8) which measures the swell displacement height with a piston positioned on the tape, this new method⁶ uses a sleeve to restrain the edges of the tape (Figure 9). This situation is more representative of a stranded loose tube construction where the tape is secured and has to fill voids between buffer tubes.

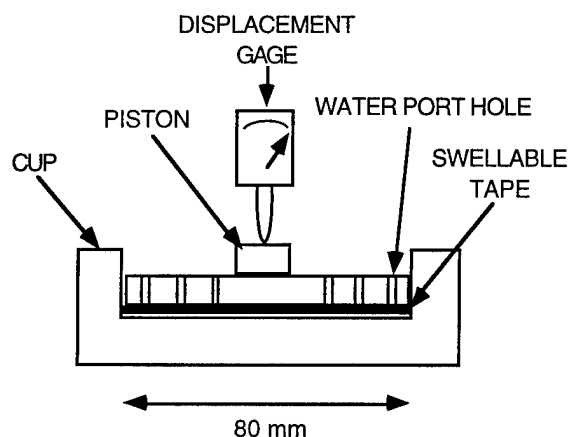


Figure 8: Conventional tape swellability method

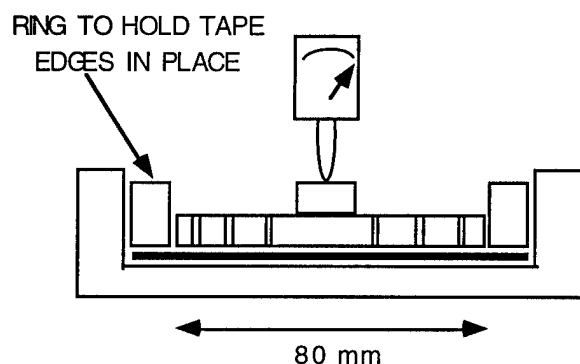


Figure 9: New tape swellability method

Unaged single layer 5 position cables were submitted to 24 hour water penetration tests using the different waters from Table 2. One cable labeled "Hickory aged" was aged for 1 week at 80°C and then tested with local tap water. The dry section was measured in place of the water ingress as such:

$$\text{Dry length(cm)} = 100 - \text{water ingress (cm)}.$$

Using the different manhole waters, all cables tested passed the one meter requirement. Again, values were normalized against the dry length in the unaged 5 position cable. Results from cable testing and material testing using the restricted cup method are displayed in Figure 10.

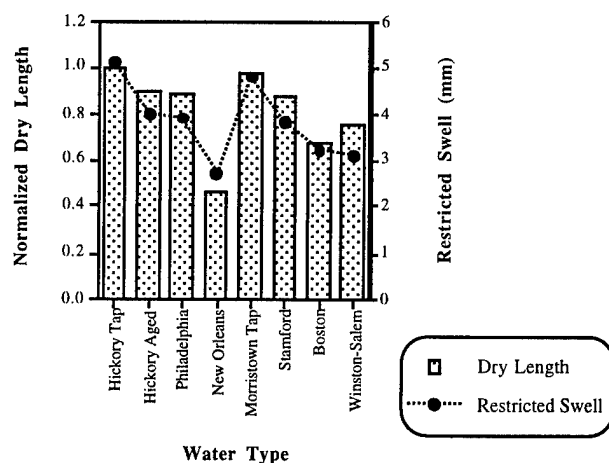


Figure 10: Correlation between restricted cup results and normalized dry length measurements

By analyzing Table 2 and Figure 10, the following conclusions were reached:

- A very good correlation between the swell height in the restricted cup and water penetration results may be observed for the different manhole waters.
- Manhole waters had ion contents greater than tap water. It should be noted that Boston manholes routinely flood from water from the harbor. This provides a functional sample of realistic saltwater contamination of manholes.

Also investigated were a water solution of bleach and a mixture of water and kerosene. A 2% bleach solution was tested to simulate Clorox® being poured into a manhole for cleaning. A 20% kerosene mixture was also tested by agitating the fluid to get mixing both before and during exposure to the cable. The 5 and 10 position single layer cable designs as well as a dual layer 24 position construction exhibited less than one meter ingress when subjected to the standard water penetration test with these solutions.

WET/DRY CYCLING

One concern in the field arises about the effective reactivation of the swellable materials. In other words, if a jacket breach is submerged by water and subsequently dries, would the swellable materials be able to block water penetration again?

Cable Testing

In order to test these conditions, 1 meter sections of cable were first submitted to the standard water penetration test, then placed in an 80°C oven. The sections of cable were tested for the lengths over which the cables dried out. After 5 days at 80°C, only a 10 cm length of the cable had dried while an additional 15 cm was still wet. This observation suggests that complete drying of the cable in the field will probably not occur due to strong hydrogen bonding forces that link the water molecules to the superabsorbent polymer.

However, the test was still pursued. The water penetration testing was conducted on 1 meter cable sections. These samples were allowed to dry for 1 day at 80°C, then retested for 24 hours on a water stand. This constituted one cycle.

After 12 cycles, statistical analysis of the results showed no significant difference between the means of the ingress values.

Material Testing

The conventional swellability method (Figure 8) was used to measure swell height. The tape was allowed to fully swell, then was dried overnight in an 90°C convection oven and subsequently retested. This constituted one cycle. The tape sample remained in the cup while the piston was removed during drying. The result of 12 cycles is presented in Figure 11.

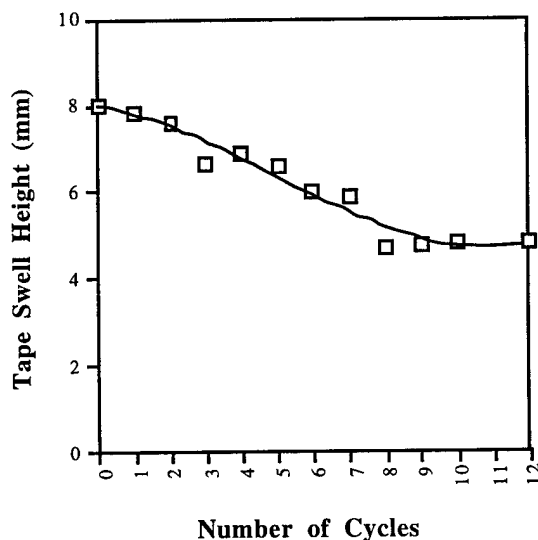


Figure 11: Tape swell height as a function of cycles

Despite a decreasing slope during the first two thirds of the test, a leveling of swell height was observed at the end. Some remarks concerning these results include:

- Some of the swollen gel sticks to the piston and is removed during drying, therefore SAP is lost from one cycle to the other. Around cycle 8, most of the loose gel was depleted.
- Drying at 90°C further crosslink the SAP, thus bringing a decrease in swell height that would not be seen in the field. However, this additional crosslinking increases the ability of the swell material to swell against a load.
- The air circulating in the oven introduces many ions, either present in the oven or outside, for which the SAP has a higher affinity than for water. These ions further decrease the swell height on the next cycle. The SAP manufacturers report a 20% decrease in swellability after 30 cycles when drying is done without forced air.

In summary, a decrease of swell height was measured with the current laboratory procedure. However, the cable performance was not degraded. After 12 wet/dry cycles, no significant change in water ingress was observed.

SEVERE WATER SUBMERSION TESTING

Conditions may exist where a dry core cable with an undetected jacket breach could be subjected to a high water head during a deluge. The condition would most likely be temporary as runoff and drainage would return manhole water levels back to normal levels. However, it is desirable that the waterblocking materials inside the cable be able to control the migration of water during these times when the water level exceeds the standard industry requirement of one meter.

A test was devised to examine severe field conditions where groundwater would rapidly fill a manhole lying at the lowest elevation in an area. In figure 12, a final water height of 6 meters was selected to examine the total flooding of a deep manhole where the damaged cable was lying on the floor. Personnel with field experience have suggested that such a deep manhole would probably fill in 20 minutes or more⁵.

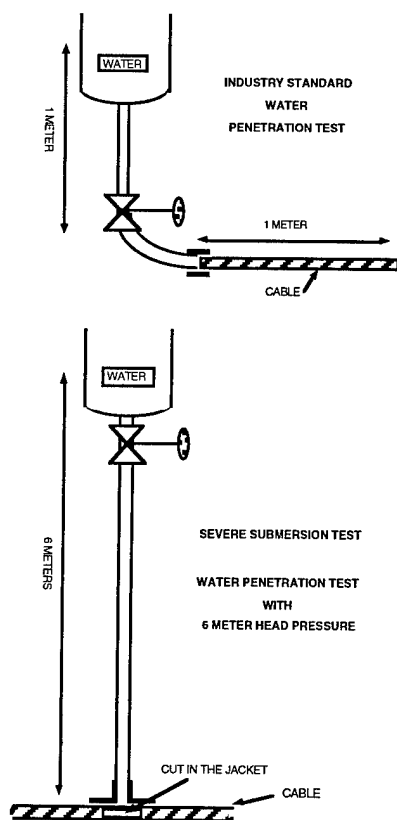


Figure 12: Severe Water Submersion Test Setup

A 1x2 cm section was removed from the cable jacket to simulate a large cut or breach. This section of cable was subjected to flooding using tap water. The fluid head was increased at a constant rate of 30 cm/minute for 20 minutes and then held for 72 hours. Samples were removed afterwards and dissected to measure water ingress.

Tests of 5 and 10 tube position single layer cables showed excellent performance in this severe environment. Average water ingress of the 5 position cables and the 10 position group were slightly below the results found for unaged cables in Table 1. These results were slightly better than the values obtained with the standard one meter test. The reason is due to a gradual buildup of water in the severe environments simulation allowing the waterswell agents to activate. The standard test was employed with an instantaneous application of full water pressure that allows further propagation before the SAP reacts.

CONCLUSIONS

This paper demonstrates methods for evaluating the long-term reliability of dry waterblocking materials and correlation of materials response to cable performance. Swellable yarns and tape were tested in heat aging conditions, wet/dry cycling, and for performance as a function of temperature. In order to address concerns about performance in real field conditions, these materials were evaluated using manhole waters. Though some degradation of swell performance was observed under some of these conditions, the cable's ability to block water ingress within one meter was not compromised. The study resulted in the selection of reliable dry waterblocking materials for long-term cable performance.

ACKNOWLEDGEMENTS

The authors wish to thank everyone involved in the testing performed for this paper. Special thanks go out to Larry Barrett and Wesley Nicholson for their hard work. Merci à Sophie for extensive field testing of swellable materials with various ionic compounds and providing inspiration for further understanding of this technology.

REFERENCES

- [1] A. Bringuier and C. Clyburn III: "Development of a Loose Tube Cable With Non-Flooded Core For Outdoor Plant Environment", Proceedings of the Eleventh Annual National Fiber Optic Engineers Conference, pp. 376 - 386, June 1995.
- [2] R. Gravely III and S. Stokes: "An Improved Loose Tube Cable with Dry Water Blocking Elements", Proceedings of the Eleventh Annual National Fiber Optic Engineers Conference, pp. 367 - 375, June 1995.
- [3] C. Clyburn III and A. Bringuier: "A Dry Core Loose Tube Cable for Outside Environments", Proceedings of the 44th International Wire and Cable Symposium, pp. 29 - 36, 1995.
- [4] W. McCallum, M. Light and R. Wagman, "Design and Deployment of a Compact High Fiber Count Cable with 12-Fiber Ribbons", Proceedings of the 44th International Wire and Cable Symposium, pp. 8 - 15, 1995.
- [5] H. Hartman, Personal Communication.
- [6] Lantor BV-Firet Test Procedure QD1B40R "Restricted Flowing Test".



Anne G. Bringuier
Siecor Corporation
PO Box 489
Hickory, NC 28603
USA

Anne G. Bringuier received an engineering degree in Materials Science and Engineering from the Institut National des Sciences Appliquées (INSA) in Lyon France, an "Advanced Studies Diploma (DEA)" in Macromolecular Science from the University of Lyon in 1985 and a M.S. in Polymer Science and Engineering from Pennsylvania State University in 1987. She worked at Raychem Corporation from 1987 to 1993 in the area of telecommunication closures. In 1993, she joined Siecor where she has been involved with materials selection and design activities for optical fiber cables. Anne is currently a Senior Product Development Engineer in the Research, Development and Engineering Department.



Clinton E. Clyburn III
Siecor Corporation
PO Box 489
Hickory, NC 28603
USA

Clinton E. Clyburn III (Kip) received a B.S. degree in Mechanical Engineering in 1991 and a M.S. in Materials Engineering in 1993 from North Carolina State University. Having earlier service with Raychem Corporation and Alcatel Cable Systems, he joined Siecor Corporation in 1993. He has worked with a variety of design and development projects in cables, materials and testing as well as cable characterization. Kip currently serves as a Product Development Engineer in the Research, Development and Engineering Department.

EFFECT OF ADDITIVES AND ATMOSPHERE ON HYDROGEN OUTGASSING OF ORGANIC MATERIALS

Jean-François LIBERT - Franck RUELLE

ALCATEL SUBMARINE NETWORKS
536 Quai de la Loire - BP 849 - 62225 CALAIS CEDEX - FRANCE

ABSTRACT

Long haul optical submarine systems are designed for a twenty five years lifetime. During this period, low loss stability must be assured. Because, one of the main causes of change in optical fiber attenuation is interaction with hydrogen, it is essential that low hydrogen levels are maintained through the lifetime of the system.

This paper describes the behaviour during ageing of some organic materials used for submarine cable manufacturing. More precisely, the influence of atmosphere and oxidation stabilization has been assessed and mechanisms leading to hydrogen outgassing are proposed. We conclude that hydrogen evolution is linked to some oxydative phenomena and that, as a consequence, organic materials that are sufficiently stabilized against thermal oxidation show a low level of hydrogen outgassing.

1 - INTRODUCTION

Long haul optical submarine systems are becoming longer and longer with point to point spans up to around 10 000 km.

Moreover, bit rates have been continuously increasing for several years and 10 Gbit systems are now being planned for installation in 1997.

As a consequence, failures on such systems are more and more critical and customers ask for more and more reliable systems. Long term behaviour of optical submarine systems must be assessed, and one of the key parameters that has to be taken into account is the natural ageing of the materials used during cable manufacturing.

Indeed, this ageing can have deleterious effects on the optical performances of the cable. One well known effect is the interaction between fibers and hydrogen evolved from materials : significant signal attenuation is caused by chemical reactions that involve - OH formation with doping agents.

Major sources of hydrogen outgassed by materials are polymer degradation, metallic outgassing, as well as natural and galvanic corrosion.

In this paper we describe the work that has been done in order to better understand the phenomena that leads to hydrogen formation during degradation of organic materials.

More precisely, we focussed on the assumed correlation between thermal oxidation and hydrogen outgassing.

Two aspects were investigated :

- effect of stabilization of material against thermal oxidation
- effect of atmosphere surrounding material during ageing

Finally, we postulate a mechanism for hydrogen formation during the polymer degradation.

2 - EXPERIMENTAL

2.1 - Principle

Because hydrogen outgassing is known to be a thermally activated phenomenon, the simplest way to have access to the amount of hydrogen generated by materials is to heat them in sealed cells at higher than service temperatures.

Procedures were adapted to allow the introduction of various gases above the tested material. The hydrogen generated was then measured through a gas chromatograph.

Furthermore, the thermal stabilization of each material was evaluated with an Oxidation Induction Time (OIT) measurement.

Finally, correlations were made between the amount of hydrogen and the thermal stabilization.

2.2 - Procedure

2.2.a - Hydrogen outgassing

For these experiments, a 20 cm³ glass tube (SVL pyrex tube) sealed with a PTFE septum inserted inside a bakelite plug is used.

The filling of the cell with the tested material is performed inside a sealed glove box where a flow of the selected gas is induced.

Of course, sealing of the extraction cell is also performed in the sealed glove box under the same gas flow. This technique has been chosen in order to minimize as much as possible the number of plugs and taps on the cell that can induce critical leaks when small amounts of hydrogen are measured.

The whole is then heated at the required temperature for 18 hours (arbitrary duration). After cooling at room temperature, hydrogen generation is then monitored by withdrawing 500 µl via a gas syringe from the headspace of the sample. The gas is then injected into a gas chromatograph equipped with a thermal conductivity detector. The analyses are performed under the following conditions :

- column :

- * Ø : (1/8)"
- * L : 4,5 m
- * Packed with 60 - 80 meshes silicagel

- carrier gas : Argon N - 60

- flow rate : 10 ml / min

- temperatures :

- * oven : 35° C
- * injection part : 60° C
- * detector : 60° C

2.2.b - Thermal stabilization

This characteristic is indirectly estimated thanks to Oxidation Induction Time measurements. All experiments are performed following the NFT 54-075 french standard.

A Differential Scanning Calorimeter is used. Measurements are made on 15 mg samples at 200° C under 50 cm³ / min oxygen flow rate.

3 - RESULTS

Experiments were performed on two kinds of materials :

- mineral oil based thixotropic jellies (filling compound)
- thermoplastic polyolefinic materials

3.1 - Oxidation Induction Time

3.1.a - Filling compounds

Three kinds of jellies were chosen because they cover a significant range of stabilization against thermal oxydation.

Results are detailed in table 1.

MATERIAL	OIT
Jelly A	7 min
Jelly B	30 min
Jelly C	70 min

Table 1 : OIT on filling compounds

As shown, the jelly C is much more stabilized than jelly A.

3.1.b - Thermoplastic polyolefinic materials

Two kinds of materials were chosen. Results are detailed in table 2.

MATERIAL	OIT
Polyolefin A	20 min
Polyolefin B	90 min

Table 2 : OIT on thermoplastic polyolefinic materials

3.2 - Hydrogen outgassing

A quite significant amount of materials have been chosen because of their significant differences in term of thermal stabilization.

It is now possible to assess the amount of hydrogen following the procedure above mentioned.

3.2.1- Filling compounds

Results are summarized in table 3. Amounts of hydrogen are given in mol / g of material.

100° C			
	N ₂	Air	O ₂
Jelly A	*	4.6 ⁻¹⁰	1.6 10 ⁻⁹
Jelly B	2 10 ⁻¹⁰	7.3 10 ⁻¹⁰	1.4 10 ⁻⁹
Jelly C	*	*	*

120° C			
	N ₂	Air	O ₂
Jelly A	4.5 10 ⁻¹⁰	8.5 10 ⁻¹⁰	3 10 ⁻⁹
Jelly B	9.45 10 ⁻¹⁰	1.3 10 ⁻⁹	3.7 10 ⁻⁹
Jelly C	3.9 10 ⁻¹⁰	3 10 ⁻¹⁰	4.8 10 ⁻¹⁰

135° C			
	N ₂	Air	O ₂
Jelly A	2.65 10 ⁻⁹	3.5 10 ⁻⁹	8.7 10 ⁻⁹
Jelly B	1.85 10 ⁻⁹	5 10 ⁻⁹	6.5 10 ⁻⁹
Jelly C	2 10 ⁻⁹	1.6 10 ⁻⁹	1.55 10 ⁻⁹

140° C			
	Air	O ₂	N ₂
Jelly A	3.65 10 ⁻⁹	3.20 10 ⁻⁹	1.75 10 ⁻⁸
Jelly B	3.3 10 ⁻⁹	7 10 ⁻⁹	1.3 10 ⁻⁸
Jelly C	2.35 10 ⁻⁹	9.5 10 ⁻⁹	3 10 ⁻⁹

Table 3 : Hydrogen outgassing under different ageing conditions

* Under detection limit

Because the observed phenomena are considered thermally activated, they can be described by an Arrhenius law. Arrhenius graphs were then plotted in order to assess the influence of each parameter.

- Influence of atmosphere

Figure 1, 2 and 3 show the behaviour of jelly A, jelly B and jelly C when the atmosphere surrounding them varies.

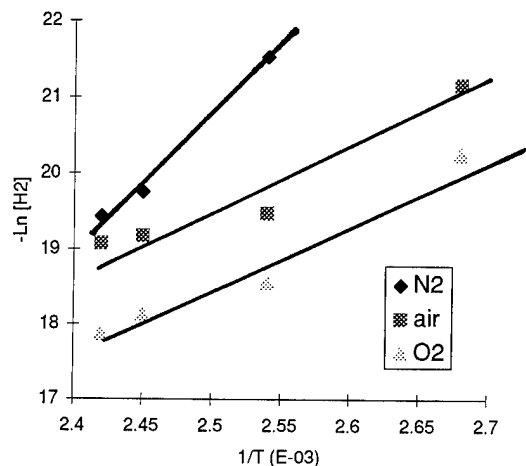


Fig 1: influence of atmosphere on jelly A

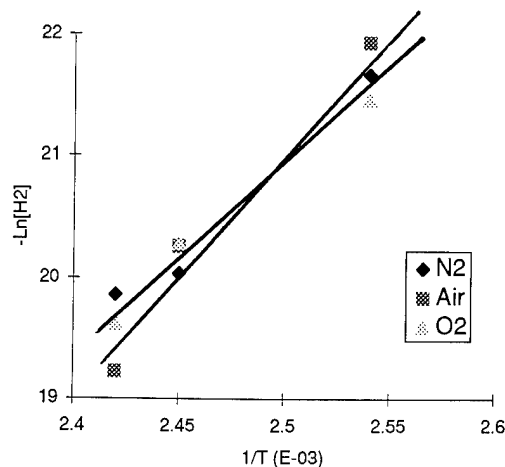


Fig 2: influence of atmosphere on jelly C

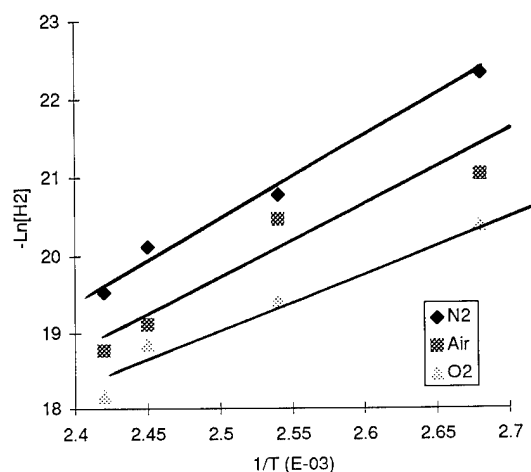


Fig 3: influence of atmosphere on jelly B

When materials were aged under nitrogen, there was no significant difference in term of hydrogen generation.

Activation energy of Arrhenius laws can be derived from these graphs (see table 4).

	E (k Cal / mol) under N ₂	E (k Cal / mol) under O ₂
Jelly A	34	18
Jelly B	21.5	17
Jelly C	30	30

Table 4 : Activation energy under different ageing conditions

Phenomena are much more influenced by atmosphere when Jelly A is considered.

- Influence of stabilization

Figure 4 depicts behaviour of the three filling compounds when aged under the same conditions (18 H under oxygen flow).

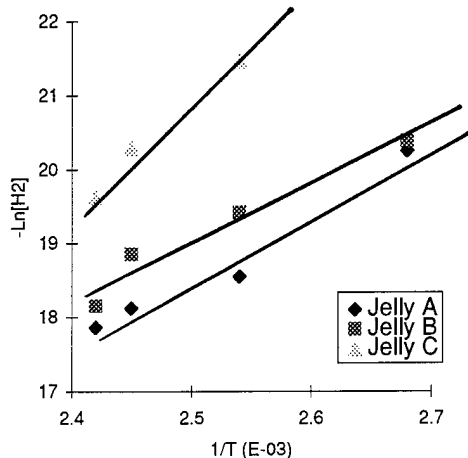


Fig 4: influence of stabilization under oxygen

Again, when materials are aged under nitrogen, there is no significant difference in terms of hydrogen generation.

On the other hand, jelly A exhibits hydrogen evolution that is seven times greater on average, than jelly C.

Moreover, when activation energies are calculated, significant differences can be noticed (see table 5).

	E (k Cal / mol)- under O ₂
Jelly A	18
Jelly B	17
Jelly C	30

Table 5 : Activation energy of filling compounds under O₂

3.2.2 - Thermoplastic polyolefinic materials

Results are summarized in table 6. Amount of hydrogen is given in mol / g of material.

	100° C		
	N ₂	Air	O ₂
Polyolefin A	*	*	4 10 ⁻¹⁰
Polyolefin B	*	*	3.7 10 ⁻¹⁰

* Under detection limit

	120° C		
	N ₂	Air	O ₂
Polyolefin A	3.7 10 ⁻¹⁰	2.95 10 ⁻¹⁰	2.3 10 ⁻⁹
Polyolefin B	4.7 10 ⁻¹⁰	4 10 ⁻¹⁰	6 10 ⁻¹⁰

	140° C		
	N ₂	Air	O ₂
Polyolefin A	1.8 10 ⁻⁹	1.45 10 ⁻⁹	1.4 10 ⁻⁸
Polyolefin B	2 10 ⁻⁹	1.7 10 ⁻⁹	3.9 10 ⁻⁹

Table 6 : Hydrogen outgassing of thermoplastic polyolefins

Hydrogen generation was generally low except for material A aged at 140° C under oxygen : these materials are intrinsically less sensitive to thermal degradation and are also well protected against thermal degradation.

But again, in the hardest conditions (140° C under oxygen), a correlation can be made between stabilisation and hydrogen generation.

4 - DISCUSSION

4.1 - Characterisations after ageing

* color

Most of the materials exhibiting significant hydrogen generation were yellowing : this is a typical manifestation of oxidation.

* infra red

Some infra red analyses were performed in order to try to determine what kind of phenomena occurred during ageing. The only difference that was noticeable between raw material and aged material is located in the 1730 - 1740 cm⁻¹ area.

This area is characteristic of -C = O groups that can be found in aldehydes, ketones and carboxylic acids that are formed during oxidation. On the less stabilized materials, the -C = O absorption peak grows when the said material is aged under oxygen (see figure 5).

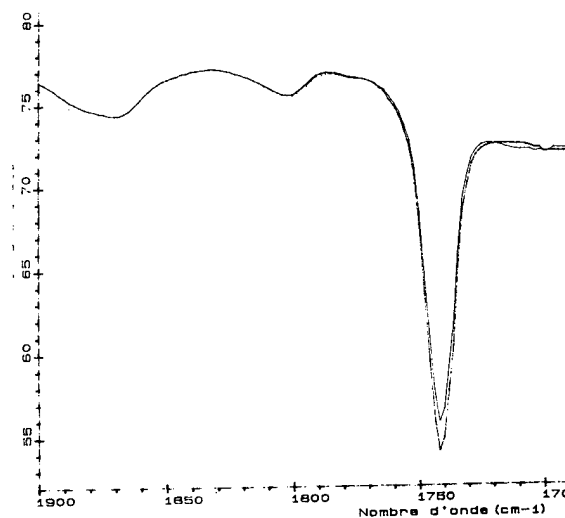
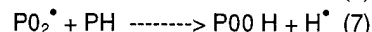
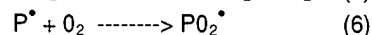
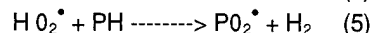
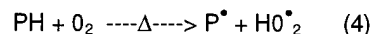
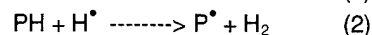
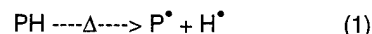


Figure 5 : Infra Red Spectrum

This phenomenon doesn't occur when material is well stabilized nor when the material is aged under neutral atmosphere.

4.2 - Mechanisms

The previous experiments tend to prove that even if hydrogen is formed in a neutral atmosphere, oxygen significantly accelerates this phenomenon. The following mechanism could be proposed to explain degradation leading to hydrogen formation :



All reactions leading to H_2 or H^\bullet formation by abstraction of a hydrogen atom from the polymer (1, 2, 5, 7) depend on both the bond strength of the carbon-hydrogen bond ruptured and of the stability of the radical formed : abstracted hydrogen atoms must be very labile.

Oxygen is essential in formation of alkyl radical P^\bullet and peroxy radical PO_2^\bullet that could then be involved in hydrogen formation.

4.3 - Antioxidants

In the proposed mechanism, formation of free radicals is likely the key parameter for the hydrogen formation.

That's why, if primary antioxidant (also called chain-breaking antioxidant) is introduced in organic materials, formation of free radicals can be inhibited and hydrogen formation reduced.

CONCLUSION

In this study, we assessed the influence of stabilization against thermal oxidation on ageing of organic materials and more precisely on hydrogen formation. Even if the role of oxygen is not clearly defined, it accelerates formation of hydrogen during ageing. In parallel, higher levels of antioxidants in the materials minimize hydrogen outgassing.

As a consequence, the evaluation of hydrogen outgassed in optical submarine cables has to take into account the stabilization and the chemical structure of the materials, their volume but also the amount of air entrapped in the cable during manufacturing.

Authors

J.F LIBERT
Alcatel Submarine Networks
536 Quai de la Loire
62225 Calais Cedex

Jean-François LIBERT received his engineering degree from «Hautes Etudes Industrielles» of Lille (FRANCE). He joined Alcatel in 1984. He is now Technical Manager for Optical Submarine Cable in Calais.

F. RUELE
Alcatel Submarine Networks
536 Quai de la Loire
62225 Calais Cedex

Franck RUELE was born in 1965. He is graduated in chemistry from the «Ecole Nationale Supérieure de Chimie de Clermont-Ferrand». He joined Alcatel in 1991 where he is in charge of cable materials development.

INVESTIGATION OF THE LATERAL STRENGTH OF BUFFER TUBES

Zhan Gao, Walter Pfandl and Waldemar Stöcklein

Siemens AG, Public Telecommunication Networks Division, Neustadt/Germany

ABSTRACT

This paper deals with the experimental measurements and theoretical calculations of the lateral strength of single and dual layer optical fiber buffer tubes. The lateral strength of buffer tubes was determined by using the "crush test" with the equipment proposed by IEC 794-1-E3¹.

One kind of single layer buffer tube and two kinds of dual layer buffer tubes were produced for the tests. The major difference between the two dual layer buffer tubes is that they have different bond strengths between the two layers.

A general relationship between lateral strength and dimensions has been obtained for the single layer buffer tube. For the dual layer buffer tubes, it was shown that the lateral strength depends strongly on the bond between the two layers.

In addition, a linear correlation between the lateral strength and the tensile yield strength has been found for the buffer tubes.

INTRODUCTION

A buffer tube usually consists of a single plastic layer or dual plastic layers as shown in Fig.1. If a new buffer tube is designed, a lot of properties of the buffer tube, for example, cost, tensile strength, flexibility, shrinkage behavior in normal environments and at higher temperatures and higher humidities, physical and chemical aging and the compatibility between the plastic buffer tube material (inner layer of the dual layer buffer tube) and the filling compound should be considered. Because it is not easy to find a polymer which alone meets all the requirements for the buffer tubes, there are only a few polymers which can be used for single layer buffer tubes. Dual layer buffer tubes generally consist of two different polymers which have

different functions. According to the applications, the material combinations of the dual layer buffer tubes will be chosen. Manufacture of dual layer buffer tubes requires higher precision tools, especially, if the thicknesses of the layers are very thin.

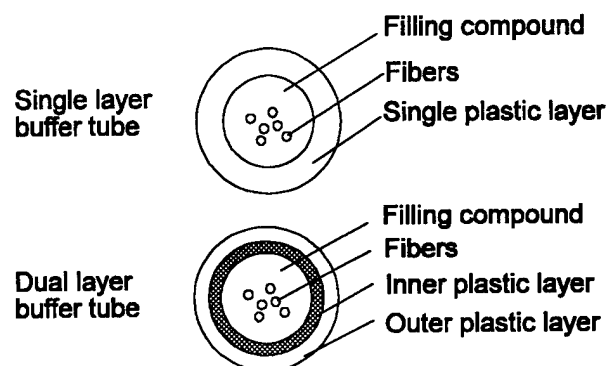


Fig.1: Single and dual layer buffer tubes.

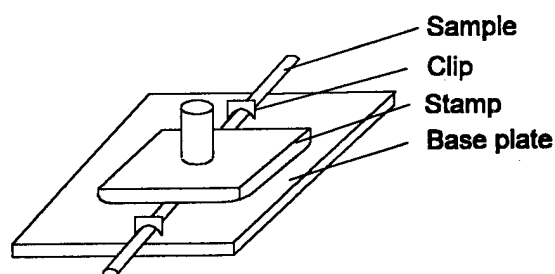


Fig.2: Sketch of the equipment for the crush test.

GENERAL DESCRIPTION OF THE TESTS

Here, the test equipment proposed by IEC 794-1-E3 which is shown in Fig.2 was applied to measure the lateral strength of buffer tubes. A sample with a length of about 30 cm is cut from the buffer tube. The fibers which are included in the buffer tube are removed from the sample.

However, the filling compound remains in the buffer tube, because the filling compound has only a very small influence on the lateral strength. After preparation the sample is put on the base plate of the equipment. Both ends are fixed by clips to prevent the movement and curl of the sample during the test. When the experiment is started, the stamp moves down with a speed of 1 mm/min, while the base plate remains still. The crush length is 10 cm.

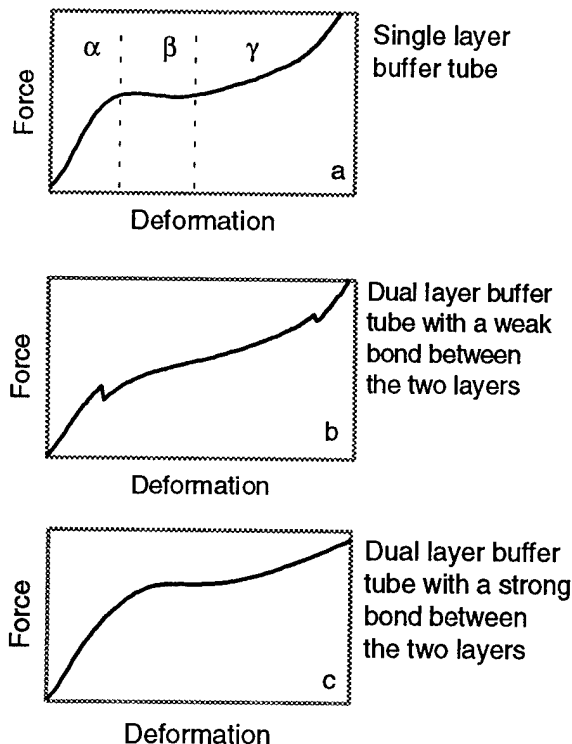


Fig.3: Typical crush test diagrams of three buffer tube types.

Fig.3 shows typical crush test diagrams of three buffer tube types. The x-axis stands for the deflection of the buffer tube in the vertical direction and the y-axis for the lateral force. The experimental curve of a single layer tube is given in Fig.3a and the experimental curves of two different kinds of dual layer tubes are shown in Fig.3b and Fig.3c, respectively. In the case of Fig.3b there is a weak bond between the two layers of the dual layer buffer tube, while in the case of Fig.3c, the bond between the two layers of the dual layer buffer tube is very strong.

Generally, the deformation of the buffer tube during the crush test can be divided into three

regions α , β and γ , which are schematically shown in Fig.3a and in Fig.4. First, when the deformation is small, the force is almost linearly proportional to the deformation. In this region, the deformation of the buffer tube is approximately similar to the small bend of a beam which is supported at the both ends and is pressed by a force at the central point. Most of the deformation in region α is elastic and reversible.

The second region of deformation, β , begins, when the yield point is reached. In this region, the lateral force remains almost constant for a moment as the deformation increases. The deformation in region β is plastic deformation and remains after the lateral force is removed. When the deformation further increases (region γ of Fig.3), the upper half of the buffer tube comes in contact with the lower half of the buffer tube. This results in a strong increase of the lateral force.

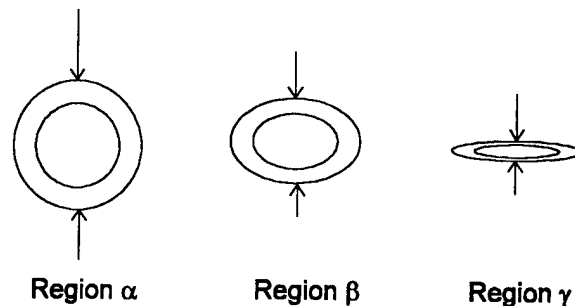


Fig.4: Three regions of deformation of buffer tubes during crush testing.

Some interesting events are shown in Fig.3b for the dual layer buffer tube with a weak bond between the two layers. The curve in this diagram has two discontinuous points, one appears at low deformation and another at high deformation. These discontinuities indicate where the two "weakly" bonded layers separate from one another as a result of the lateral force. Due to the separation of the layers the lateral force falls rapidly. The separation can happen at any deformation, even at a low deformation if the bond between the two layers is weak.

The curve in Fig.3b has a somewhat different form from that in Fig.3a or Fig.3c, especially in the region of deformation around the yield point. The yield point in Fig.3b is not so clear as in the other two diagrams. The lateral force remains at a nearly constant level for a moment when the

yield point is reached in Fig.3a and Fig.3c, while the lateral force in Fig.3b continuously increases with the deformation. This behavior can be explained if we regard the dual layer buffer tube with a weak bond between the two layers as a buffer tube consisting of two separate concentric single layer buffer tubes. Each buffer tube has its own lateral force versus deformation curve. Because of the difference of dimensions of the two buffer tubes, the forms of their lateral strength versus deformation curves are different. The curve in Fig.3b represents the sum of the curves of the two separate single layer tubes and is therefore different from the curve of a single layer tube.

THEORETICAL ANALYSIS AND DEFINITION

The crush test has long been applied in the industry for testing of cylindrical samples. A general solution of the state of the stresses in a cylinder under the crush test is complex²⁻³. For the calculation of the lateral strength of the single layer buffer tubes a simplified equation given by

$$F = C \cdot \frac{(OD - ID)^2}{(OD + ID)} \quad (1)$$

can be applied.

Here F is the lateral strength, C is a constant depending on the material behavior and the test conditions. OD is the outer diameter of the buffer tube and ID is the inner diameter of the buffer tube.

The lateral strength of a single layer buffer tubes can be directly calculated by equation (1) if the constant C is known.

Equation (1) approximately applies for the calculation of the lateral strength of the dual layer buffer tubes as well, when the two layers are strongly bonded together and their mechanical properties are not very different from each other. However, in this case, the constant C is a combined parameter depending on the material behavior of both layers, the ratio of the wall thicknesses of both layers and the test conditions. An approach to find a mathematical description of the constant C for this kind of buffer tube was not done because it is very difficult.

For a dual layer buffer tube with weak bond between the two layers, it is assumed that the buffer tube consists of two separate concentric single layer tubes. The lateral strength of this buffer tube is the sum of the lateral strength of each layer and is given by

$$F = C_1 \frac{(MD - ID)^2}{(MD + ID)} + C_2 \frac{(OD - MD)^2}{(OD + MD)} \quad (2)$$

where F is the composite buffer tube lateral strength, C_1 and C_2 are constants depending on the material behavior of the inner and outer layers, respectively, and the test conditions. ID is the inner diameter of the inner layer and OD is the outer diameter of the outer layer. It is assumed that there is no space between the two layers, therefore the outer diameter of the inner layer is equal to the inner diameter of the outer layer. They are both denoted by MD .

An exact definition of the lateral strength of the buffer tube is difficult and does not yet exist in any international standards. If the lateral force at the yield point is defined as the lateral strength, the evaluated value of the lateral strength may be higher than the real value, because the lateral strength at the yield point is usually the maximum. For dual layer buffer tubes with weak bond between the two layers it is not suitable to define the yield strength as the lateral strength because the yield point for this kind of buffer tube is not clear.

In practice, a cabled buffer tube can be subjected to a high (plastic) deformation. Therefore, the lateral strength of the buffer tube should indicate the capacity to withstand the high (plastic) deformation induced from outside. The plastic deformation energy of a buffer tube in the crush test is given by

$$\begin{aligned} E_p &= \int_0^b F(x) dx - \int_0^a F(x) dx \\ &= \int_a^b F(x) dx \end{aligned} \quad (3)$$

where E_p is the plastic deformation energy of the buffer tube in the crush test, $F(x)$ is the lateral force which is a function of the deformation x , a is the initial point at which the plastic deformation begins and b is the final point of the deformation at which the optical properties of

the fibers in the buffer tube are not yet influenced by the lateral force from outside.

For buffer tubes which were tested here, it was found that plastic deformation of the buffer tubes in the crush test generally begins at the moment when the deformation in the vertical direction reaches about 10 percent of the inner diameter of the buffer tube (10 %-ID). Therefore the initial point, a , in equation (3) is defined as 10 percent of the inner diameter of the buffer tube. The final point of the deformation, b , depends on the free space of the fibers in the buffer tube. According to our experience and the curves shown in Fig.3, we have defined the final point of the deformation, b , as 30 percent of the inner diameter of the buffer tube (30 %-ID).

Dividing the plastic energy E_p by the integration region ($b-a$), we have the average force between the deformation region from point a to point b :

$$F = \frac{E_p}{b-a} \quad (4)$$

We define this force as the lateral strength of the buffer tube. Inserting equation (3) into equation (4), we have

$$F = \frac{\int_a^b F(x) \cdot dx}{b-a} = \bar{F} \quad (5)$$

The average force in the region of the deformation from point a to point b can be automatically calculated and reported by the computer after a crush test has been done.

RESULTS AND DISCUSSIONS

Four commercial polymers were selected to produce buffer tubes for the tests. From one kind of the polymer (P1), single layer buffer tubes with different dimensions were prepared to analyze the relationship between the lateral strength and the dimensions of the single layer buffer tubes. The outer diameter of the single layer buffer tubes was kept constant and the inner diameter was varied. The other production parameters remained constant.

For the dual layer buffer tubes, two kinds of buffer tubes were made. One kind of dual layer buffer tube had the material combination P2

(inner layer) and P1 (outer layer). The bond between the material P2 and the material P1 is weak. Another kind of dual layer buffer tube consisted of the material P3 (inner layer) and the material P4 (outer layer). The bond between the materials P3 and P4 is very strong. The inner and outer diameters of all the dual layer buffer tubes remained constant, only the ratio of the wall thicknesses of the two layers was varied. An overview of the buffer tubes used for the tests is given in Table 1.

Before the crush test, the dimensions of each sample were carefully measured according to IEC-811-1-1⁴ by using an image analysis system. Accurate measurement of the dimensions of the sample is extremely important for proper evaluation of the lateral strength.

Buffer tube	Inner layer	Outer layer	Bond between the two layers
Single layer	P1	-	-
Dual layer	P2	P1	weak
Dual layer	P3	P4	strong

Table 1: Buffer tubes used for the crush tests.

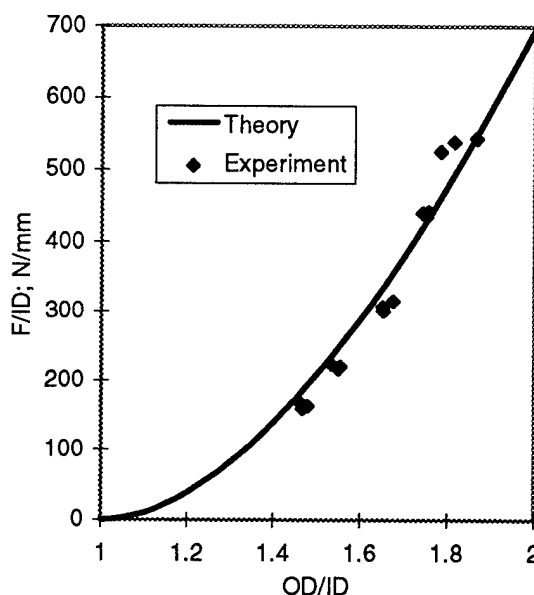


Fig.4: General correlation between the lateral strength and tube dimensions for single layer buffer tubes consisting of the material P1.

The crush testing was carried out at room temperature for all samples and the crush length was 10 cm. The results of the single layer buffer

tubes are shown in Fig.4. In order to achieve a general correlation between the lateral strength and the dimensions for the single layer buffer tube, equation (1) is modified to:

$$F/ID = C \cdot \frac{(OD/ID - 1)^2}{(OD/ID + 1)} \quad (6)$$

This general correlation is presented in Fig.4 where the x-axis stands for the ratio between the outer diameter (OD) and the inner diameter (ID) and the y-axis indicates the ratio between the lateral strength (F) and the inner diameter (ID). The experimentally achieved values are shown by the points. The solid line indicates the theoretical values using equation (6). It is shown that the theoretical calculation has a good agreement with experimental values.

If the dimensions of the single layer buffer tube consisting of the material P1 are known, the lateral strength of this buffer tube can be determined from Fig.4. Likewise, if the lateral strength of the buffer tube is defined, the required dimensions of the buffer tube can be determined from Fig.4.

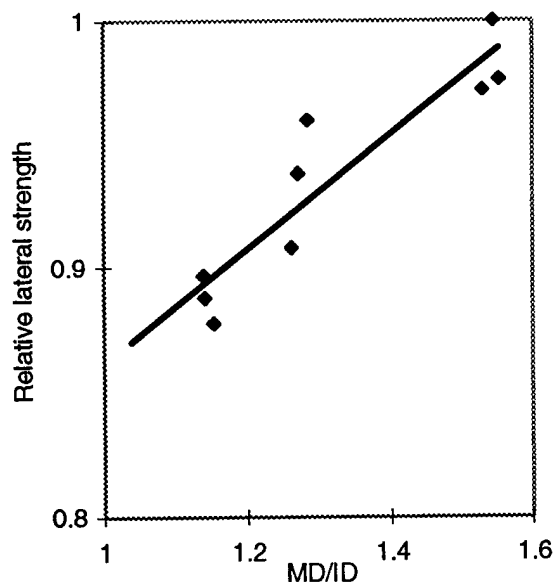


Fig.5: Relative lateral strength of dual layer buffer tubes with a strong bond between the two layers.

The results of the buffer tubes with the material combination P3 (inner layer) and P4 (outer layer) are shown in Fig.5. The x-axis stands for

the ratio between MD and ID and the y-axis indicates the relative lateral strength. The inner and outer diameters of these buffer tubes were constant, only the ratio of the wall thicknesses of the two layers was varied. The bond between the two layers was very strong.

It is shown in Fig.5 that the lateral strength increases with the wall thickness of the inner layer. This is because the Young's modulus of the inner layer is significantly higher than that of the outer layer. The relationship between the lateral strength and the ratio (MD/ID) is approximately linear. This indicates that the lateral strength of the buffer tube in which the two layers are strongly bonded together is nearly proportional to the effective Young's modulus of the buffer tube.

In Fig.6 the results of another kind of dual layer buffer tube consisting of the materials P2 and P1 are shown. In this kind of buffer tube the bond between the two layers is weak.

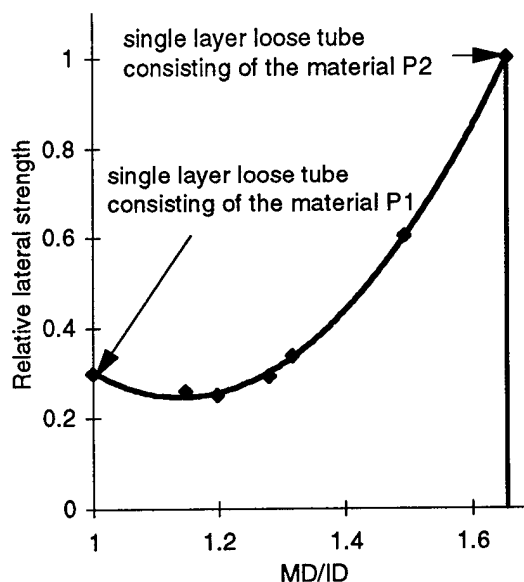


Fig.6: Relative lateral strength of dual layer buffer tubes with a weak bond between the two layers.

The inner and outer diameters of these buffer tubes are constant, only the ratio of the wall thicknesses of the two layers was varied. The Young's modulus of the inner layer is significantly higher than that of the outer layer.

As in Fig.5, the x-axis in this diagram stands for the ratio (MD/ID) and the y-axis for the relative lateral strength. The experimental values are presented by the points. The solid line is achieved by curve fitting the experimental values. It is apparent that the curve in this diagram has a very different form from that in Fig.5. The lateral strength does not simply increase with the wall thickness of the inner layer which has a higher Young's modulus. In the first region of (MD/ID), when the wall thickness of the inner layer, which has a higher Young's modulus, increases, the lateral strength even decreases down to a minimum. Only after this minimum, the lateral strength increases with the wall thickness of the inner layer.

The results in Fig.5 and Fig.6 indicate that the lateral strength of the dual layer buffer tube depends strongly on the bond between the two layers.

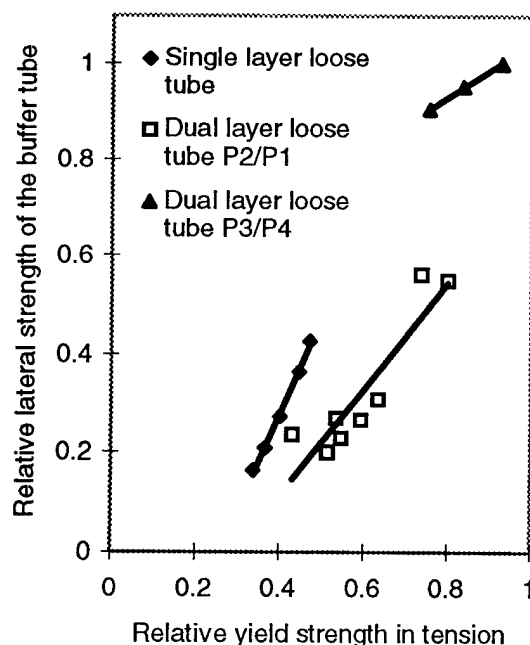


Fig.7: Relationship between the lateral strength of buffer tubes and the yield strength in tension.

In addition, the correlation between the lateral strength and the tensile yield strength of these three kinds of buffer tubes has been analyzed. For each kind of buffer tube a nearly linear correlation (shown in Fig.7) has been obtained. In Fig.7 the x-axis stands for the relative yield strength in tension which was achieved by the

tension tests and the y-axis indicates the relative lateral strength of the buffer tubes.

CONCLUSIONS

The relationship between the lateral strength and the dimensions for single layer buffer tubes is well described by equation (1) or equation (6).

For dual layer buffer tubes in which the two layers are strongly bonded together, a complete mathematical solution of the lateral strength is difficult to achieve. However, the test results indicated that the lateral strength of this kind of buffer tube is nearly proportional to the effective Young's modulus of the buffer tube.

When the bond between the two layers of the dual layer buffer tube is weak, the buffer tube can be regarded as consisting of two separate, concentric, single layer buffer tubes. Such a buffer tube has a lateral strength minimum at a certain ratio of wall thicknesses of the two layers. During crush testing the two layers can be separated. The lateral strength of this kind of buffer tube is generally less than that of a dual layer buffer tube with a strong bond between the two layers.

A linear correlation between the lateral strength and the tensile yield strength is found for each kind of buffer tube tested.

ACKNOWLEDGMENTS

The authors would like to thank the many people who contributed to the design, the preparation of the samples and the tests. They would also like to thank Mr. Don Parris for his help with this paper.

REFERENCES

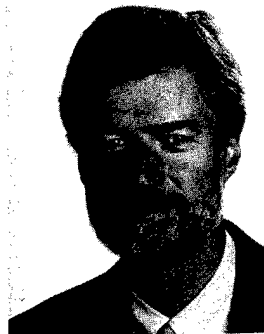
1. International standard, IEC 794-1-E3, 1993.
2. Föppl, A., Vorlesung über technische Mechanik. Volume I. 13. edition, Volume II, 9. edition, 1943 and 1942.
3. Williams, J.G., Stress analysis of polymers, Longman Group Ltd, 1973.
4. International standard, IEC 811-1-1 Part 1, Section 1, Second edition, 1993.



Zhan Gao was born in Shanghai, China in 1963. He received his B.S. and Masters degree in Material Science and Engineering at the University Tongji, Shanghai, in 1985 and 1988, respectively. In 1991, he joined Siemens AG in Neustadt, Germany where his key task was to finish a corporate research project between Siemens AG and the University Erlangen-Nuremberg. Since receiving his Ph.D. from the University Erlangen-Nuremberg in 1994, he has worked in the areas of cable and materials testing and theoretical modeling at the Siemens AG, Telecommunication Cable Research and Development Department.

Mailing address:

Siemens AG, OEN NK E K5
Austrasse 101, 96465 Neustadt, Germany



Waldemar Stöcklein was born in Coburg, Germany, in 1956. He attended the University of Bayreuth, where he studied physics and mathematics. In 1985, he received the Ph.D. degree in physics for basic research in the field of magnetic resonance in "organic metals". From 1986 and 1987, he was an IBM Postdoctoral Research Fellow in the Almaden Research Center in San Jose, CA. In 1988, he joined the Fiber Optic Cable Development Department of Siemens AG in Neustadt/Coburg. He is involved in cable design, fiber characterization and the development of fiber optic test equipment.

Mailing address:

Siemens AG, OEN NK E K5
Austrasse 101, 96465 Neustadt, Germany



Walter Pfandl was born in Fürth, in 1950. He is the head of the Development Group for Optical Fiber and Copper Cables at Siemens AG, in the Public Telecommunication Networks Division. He received his Dipl.-Ing. degree in Material Science from the University of Erlangen-Nuremberg in 1976 and the Ph.D. degree in 1984. In 1985 he led a research group at the Central Development Department of Siemens AG in Erlangen. He has been in his present position since 1993.

Mailing address:

Siemens AG, OEN NK E K
Austrasse 101, 96465 Neustadt, Germany

The Effect of Color Concentrate on the Reliability of Poly(Butylene Terephthalate)

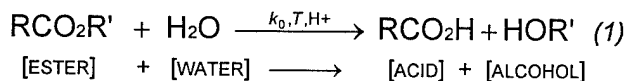
Paul E. Neveux, Jr.
Sumitomo Electric Lightwave Corp.
Research Triangle Park, North Carolina

ABSTRACT

Various poly(butylene terephthalate) color concentrates were evaluated for their effect on the long term reliability of PBT buffer tubes. PBT tubes, made with the color concentrates, were aged at 85°C and 85% RH and tested for tensile properties. Since melt flow had previously been used to successfully determine the degradation rate of natural PBT's, the method was extended to aged PBT color concentrates in order to determine whether or not a correlation existed with tensile property results.

INTRODUCTION

Poly(butylene terephthalate) or PBT is used extensively as a buffer or "loose" tube material in optical fiber cables. Its presence in the local loop/pedestal environment has inspired concerns of reliability since field conditions are expected to have both higher temperatures and moisture levels than buried service environments. Much work has been done to elucidate the major degradation pathway¹ and to insure that PBT optical fiber loose tubes maintain their integrity in the local loop environment.^{2,3,4} It has been shown previously that the mechanism for the degradation of PBT, as with most polyesters, occurs through the hydrolysis of the ester links forming the polymer:



In equation 1 the concentration of water is derived from the temperature and the relative humidity:

$$[\text{H}_2\text{O}] \propto P_{\text{H}_2\text{O}} = \frac{\%RH_T \times P_{\text{H}_2\text{O}(P,T)}}{100} \quad (2)$$

where $P_{\text{H}_2\text{O}}$ is the resulting partial pressure of water at the specified RH and temperature and $P_{\text{H}_2\text{O}(P,T)}$ is the partial pressure of water at pressure P , and temperature, T . The former term is usually taken at 1 atmosphere (or 760 TORR) and can be easily obtained from water vapor pressure tables.⁵

There are two important features to note about equation 1: (a) the hydrolysis process is accelerated by the presence of hydrogen ions, H^+ , and (b) the acid product of the reaction is a source of these hydrogen ions. In essence, the PBT can hydrolyze by an autocatalytic mechanism involving H^+ ions from the carboxylic acid end groups adjacent to the ester linkage.⁶ Reducing the number of carboxylic acid end groups is then a key factor in increasing the lifetime and reliability of PBT tubes. Fortunately, PBT manufacturers have been able to significantly reduce the number of carboxylic acid end groups, thus greatly improving the predicted lifetime of PBT under local loop environments.³

Except for work done with glass fiber reinforced PBT,⁷ none of the work done previously has taken into account the effect that fillers and, more specifically, color concentrates, have on the reliability of PBT. A number of issues arise when considering what effect a color concentrate might have on the longevity of a PBT tube, not the least of which is the concentration of carboxylic acid end groups that might be introduced by the color concentrate. In any case, three basic factors should be considered in a PBT color concentrate: (1) the color or pigment formulation, (2) the grade of PBT resin used as the base for the color concentrate, (3) the conditions under which the concentrate is made, especially the concentration of moisture in the components before extrusion. While the first two factors can and were studied by choice of vendors and concentrates, it was not possible to examine factor 3.

Color formulations are typically made up of two or more component pigments. Formulations will differ from vendor to vendor in their attempt to approach the customers desired product color. The pigments chosen by the formulator may have an effect on the stability of the PBT at the extrusion temperatures required to make the color concentrate. This effect may be due to either a specific chemical pigment-resin interaction or to an inadequately moisture-free pigment. Since it was not possible to determine the color formulation, it was assumed that the pigments did not exhibit any specific chemical degrading interaction.

For the second factor, it is clear that the PBT chosen should be hydrolytically stable since it will essentially be undergoing two extrusion processes: one to manufacture the color concentrate and one to manufacture the tube. However, there are several ways to produce a hydrolytically stable or low carboxylic acid end-group PBT. One way is to increase the molecular weight of the polymer chain, thus decreasing the number of acid end groups in the polymer. Another is to "neutralize" the acid end groups to produce the conjugate base. It is also possible to "cap" the acid end group with a molecule rendering the end group inactive.⁸

In this report, the effect of factors 1 and 2 were examined on the mechanical properties of PBT loose tubes by obtaining (1) standard non-heavy metal PBT color concentrates with the same base resin but different pigment formulations (because they were from two different vendors) and (2) concentrates that had the same color formulation (same vendor, except for black from vendor B, see below) but made from two different hydrolytically stable base resins. In addition to the loose tube mechanical properties, the melt flow rate of the color concentrate as a raw material was determined after aging. Melt flow has been shown previously to be an excellent indicator of the extent of degradation of PBT.³ The correlation between mechanical results of loose tubes and the hydrolysis rate, as obtained *via* melt flow of the color concentrate, was examined.

EXPERIMENTAL

Color Concentrate

The commercial grades of PBT color concentrate pellets obtained for the study were formulated to be

let down with virgin PBT at a ratio of 33 parts PBT to 1 part color concentrate. The concentrates were aged on specially designed stainless steel screen racks at 85°C and 85% RH in environmental ovens. The color concentrate was spread on the racks to allow complete air flow and prevent moisture condensation. After aging the concentrates were dried at room temperature in a desiccator which was continuously purged at 200 ml/min with zero moisture nitrogen for at least 16 hours. The concentrates were measured for melt flow immediately after removing from the desiccator.

Buffer Tubes

The buffer or loose tubes were made by adding color concentrate at a rate of 33 parts PBT to 1 part color concentrate. The same hydrolytically stable PBT resin was used for all tubes using standard operating conditions which includes drying all materials before extrusion. The tubes were filled with a thixotropic gel and contained two optical fibers. The loose tubes were then made into 24" diameter coils, placed onto a perforated stainless steel rack and aged in an environmental chamber at 85°C and 85% RH for up to 60 days. The specimens were removed from the chamber at intermediate intervals to measure the change in the mechanical characteristics with time. The samples were allowed to equilibrate at room temperature for at least 24 hours at $22 \pm 1^\circ\text{C}$ and $50 \pm 5\%$ RH. The samples were then cut to the required test length, the fibers (and consequently, much of the gel) removed, and the ends cleaned with a dry wipe to remove any thixotropic gel.

Mechanical Tests

For the tensile properties, percent elongation and load at yield were examined using an Instron tensiometer with custom designed 50 mm diameter mandrel grips. The gauge length was 200 mm (measured from tube-to-mandrel contact) and the cross-head speed was 10 mm/min (5% strain rate). Three (3) specimens/sample was tested. No attempt was made to prepare the tubes with a machined gauge length section in the tube as mentioned in ASTM D 348.⁹

Melt Flow

Melt Flow was determined using a Tinius-Olsen Model MP987 Melt Flow Plastometer following ASTM D 1238,¹⁰ Procedure B, at a temperature of 250°C and a total load weight of 1000 g, except for black 2B, where the standard 2160 g weight was used.

Because of the fast flow rates of all the PBT color concentrates, except black 2B, a 1000 g weight was used to keep the flow rates below ~60 g/10 minutes and extend the usefulness of the test. Three (3) specimens/sample was tested.

Carbon Black Concentration

Carbon black concentration was determined using the method outlined in ASTM D4218-82,¹¹ except that a Thermogravimetric Analyzer Module attached to a DuPont 9900 Thermal Analysis System was used.

RESULTS & DISCUSSION

Samples Investigated

Shown below in Table 1 are the various types of PBT color concentrate investigated in this study. Three types of base resins were evaluated from Vendor A, while two were investigated from vendor B. Base resins 1 and 2 were hydrolytically stabilized formulations while base resin 3 was not.

Table 1. Color Concentrate Sample Designations

Vendor	Base Resin 1	Base Resin 2	Base Resin 3
Vendor A	1A	2A	3A
Vendor B	1B	2B	(Not tested)

Tensile Testing of Loose Tubes

While there is no universal agreement for the pass/fail criteria of PBT tubes, one prevailing requirement is that the tubes should have a percent elongation at break of $\geq 10\%$ after 45 days of aging at 85°C and a non-condensing humidity of 85% ($[H_2O] = 367$ TORR).¹² However, this requirement requires the tubes to be machined to produce the gauge length. Since machining tubes of these dimensions is very difficult and does not reflect what is actually used in the field, the pass/fail criteria of $\geq 10\%$ percent elongation at *yield* for unmachined tubes after 45 days aging was used. This is conservative since the yield point always occurs before the break.

Figures 1 and 2 show typical percent elongations at yield after 85°C and 85% RH aging of PBT tubes colored with concentrates made with the various base resins from vendor A. The slight increase in

elongation at yield from the control sample is typical and can be observed to occur in as few as 15 days of aging.³ Note that all three base resins, including base resin 3, performed exceptionally well, surpassing the elongation requirements of 45 days by at least 15 days of aging.

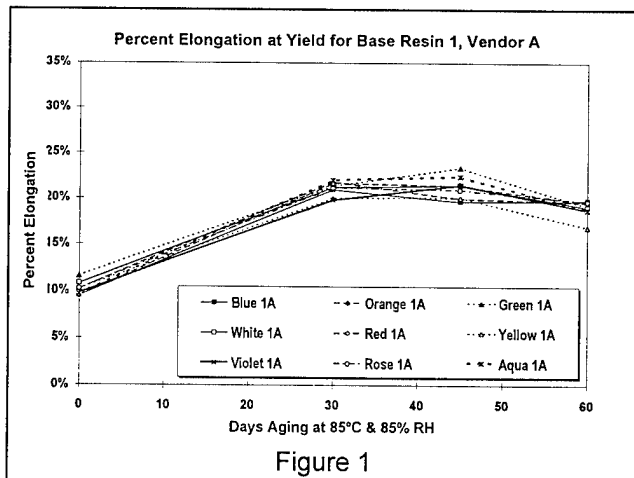


Figure 1

Figure 2 also illustrates the effect of using a hydrolytically stabilized or unstabilized base resin for the color concentrate. No apparent difference can be seen after 60 days of aging at 85°C and 85%RH between the two types of base resins for the colors tested. There are two possibilities for this: (1) the nominal let-down ratio of 33:1 (PBT:CC) was not high enough to significantly impact the results and/or (2) 60 days aging was not long enough to see an effect in the tensile properties. However, as will be seen below, the melt flow testing was able to discern differences between the base resins 1 and 3.

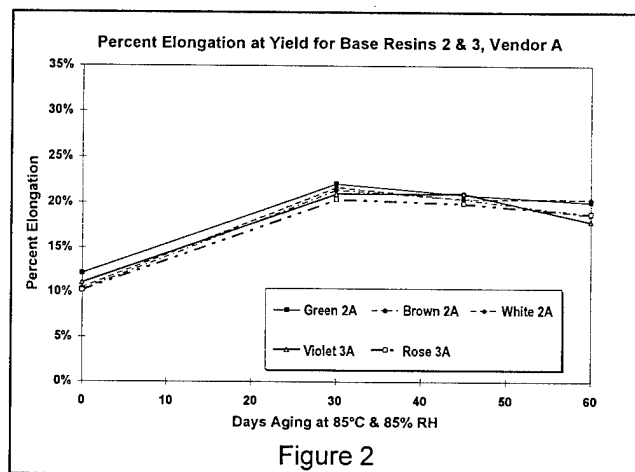


Figure 2

Figures 3 and 4 show the same experiment using concentrates from vendor B. Base resin 1 from vendor B shows similar results to those of vendor A. In contrast, the results of testing color concentrate made from base resin 2 from the vendor B shown in Figure 4 is very different.

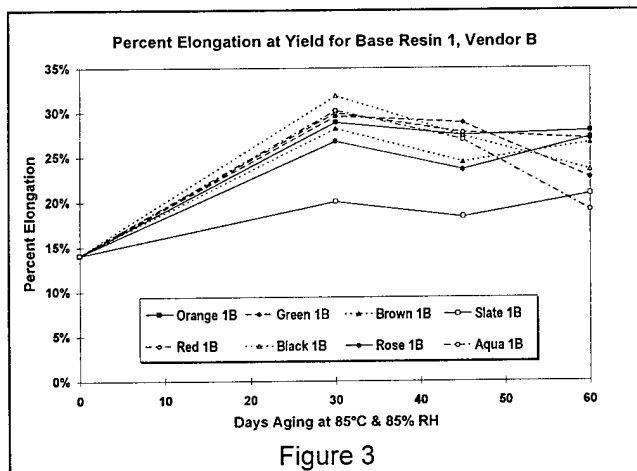


Figure 3

As can be seen, violet and aqua fall below 10% elongation at yield criterion, indicating degradation and potentially poor handling characteristics in the field. Black could not even be tested at 45 days because it was too brittle. Also, it was not possible to test any of the remaining colors at 60 days aging because of excessive brittleness: at some time between approximately 46 and 60 days the samples became too brittle to test.

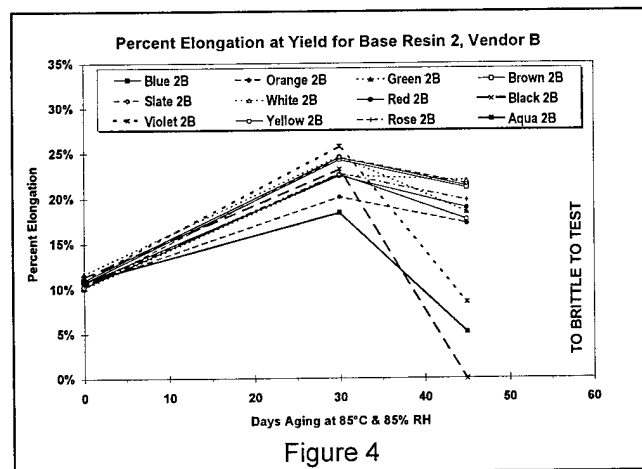


Figure 4

In order to determine the failure mechanism for the black color concentrate, this concentrate was compared with two additional types of black concentrates from vendor B as shown in Table 2.

Note that those concentrates in Table 2 with sample designations 1BH and 2BL were not examined for melt flow characteristics after aging; they were examined only for tensile characteristics.

Table 2. Carbon Black Concentration (Vendor B)

Base Resin 1		Base Resin 2	
Carbon Black Conc.	Sample Designation	Carbon Black Conc.	Sample Designation
12%	Black 1B	14%	Black 2BL
25%	Black 1BH	24%	Black 2B

The elongation at yield results of testing aged tubes made from the concentrates shown in Table 2 is shown in Figure 5. Base resin 1 seems to be unaffected by the concentration but base resin 2 is strongly affected. Note that while all the concentrates made with base resin 2 from vendor B were too brittle to test at 60 days aging (as shown above in Figure 4), the same is not true for the black concentrate made with base resin 2 with the low carbon black level from the same vendor.

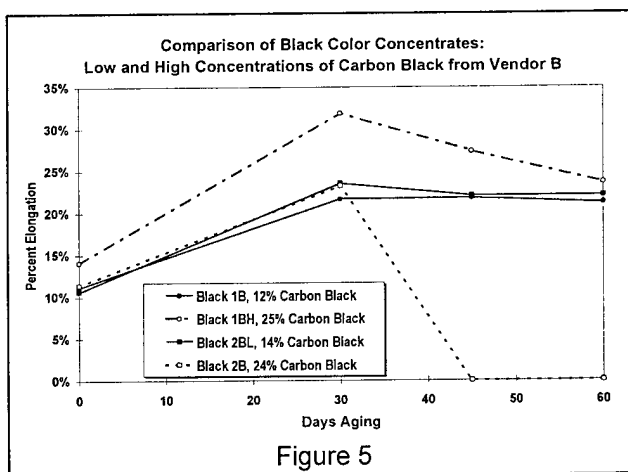


Figure 5

There is no *a priori* reason why the concentration of carbon black should have any effect at all on the reliability of PBT. However, it is well known that carbon black can absorb significant amounts of moisture and the more carbon black is added to make a concentrate, the more moisture can be introduced. It may be that in the case of the black concentrate, excessive moisture was introduced by the carbon black during the manufacturing of the

concentrate causing the eventual premature failure of the PBT tubes.

Melt Flow

The melt flow of PBT has been shown to be directly proportional to the carboxylic acid end group concentration³ which, in turn, is proportional to the molecular weight of the polymer. The method can therefore be used to determine the rate of degradation of PBT such that a plot of the natural log of the normalized melt flow rates versus time yields the rate constant, k , for hydrolysis reaction:

$$\ln(\text{MFR}_t) = kt + \ln(\text{MFR}_0) \quad (3)$$

$$\ln(\text{MFR}_t/\text{MFR}_0) = kt \quad (4)$$

where MFR_t and MFR_0 are the melt flow rates at time, t , and initial time, 0 and k is the reaction rate constant for the specified moisture concentration and temperature. The three base resins examined in this paper were previously examined for their hydrolysis rates and the results, along with the standard error of the slope, are shown below in Figure 6 and Table 3 for comparison. As can be seen the rate of hydrolysis at 85°C and 85% RH is approximately three times greater for the hydrolytically unstabilized PBT compared to the hydrolytically stabilized versions.

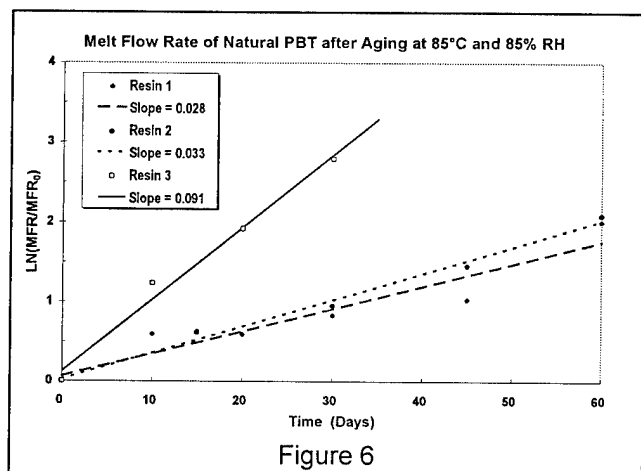


Figure 6

Table 3. Hydrolysis Rates for Natural PBT Resins

Resin 1 Rate	Resin 2 Rate	Resin 3 Rate
0.028 ± 0.005	0.033 ± 0.002	0.091 ± 0.008

In the present case, the method was applied to the PBT color concentrate to see if one could predict the reliability of the PBT by determining the relative rates of degradation of the color concentrates. Because the pigment formulation used to make the concentrate differs from color to color, the melt flow rate for the unaged controls can vary significantly. Therefore, it is not possible to compare the extent of degradation between colors solely on *absolute* melt flow rate at any particular time. Instead, the *normalized* rates, i.e. $\ln(\text{MFR}_t/\text{MFR}_0)$, must be plotted vs. aging time.

It was uncertain at the outset whether or not the pigments would complicate the melt flow results but as can be seen in the figures below, where the plots of $\ln(\text{MFR}/\text{MFR}_0)$ vs. days aging at 85°C and 85% RH are shown, the results are mostly consistent. To confirm that it was possible to see a difference in the hydrolysis rates, concentrates, made with the hydrolytically stabilized (resin 1) and unstabilized (resin 3) base resins with known differences in their hydrolysis rates, were aged. Two colors, rose and violet from vendor A, were examined.

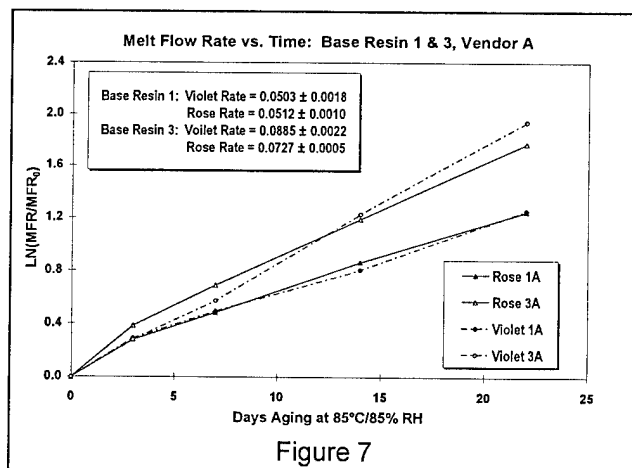


Figure 7

As can be seen in Figure 7 and Table 4, the rates are different but not by the same magnitude as the natural base resins shown in Figure 6 and Table 3. The difference, while attributable to the presence of the pigments, is not completely understood. For three of the concentrates, there appears to be a high initial rate between 0 and 3 days aging, but, after this, the plot is linear. It is not known if it is the pigment causing this phenomenon. Because of the "discontinuity" displayed in the plots, all of the calculated hydrolysis rates shown in the tables do not include the controls (zero days aging).

While there is a significant difference in the melt flow rates between the two base resins of rose and violet, a difference in the tensile properties, as shown above in Figure 1 and 2, is not seen. Further aging of the tubes past 60 days or higher let-down ratios may be necessary to be able to distinguish between these color concentrates.

Table 4. Hydrolysis Rates for Resins 1A & 3A

Color	Resin 1 Rate	Resin 3 Rate
Rose	0.0512 ± 0.0010	0.0727 ± 0.0005
Violet	0.0503 ± 0.0018	0.0885 ± 0.0022

In Figure 8, the rates for all the colors are relatively consistent for base resin 1 from vendor A. Again, there is a large initial increase between 0 and 3 days aging, especially for blue and red. As shown in Table 5, all the hydrolysis rates are less than 0.053 day^{-1} , well below the rates seen with base resin 3.

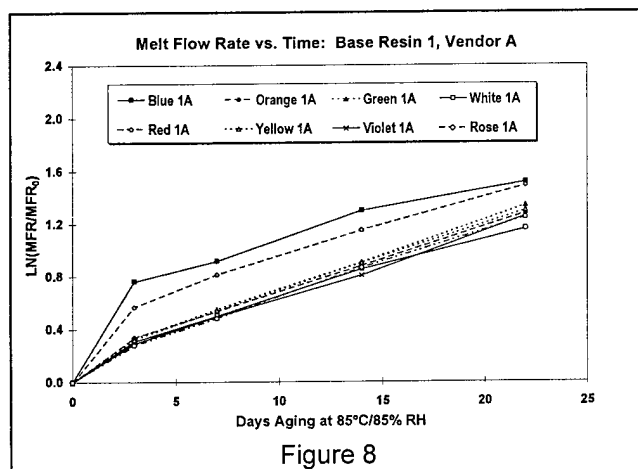
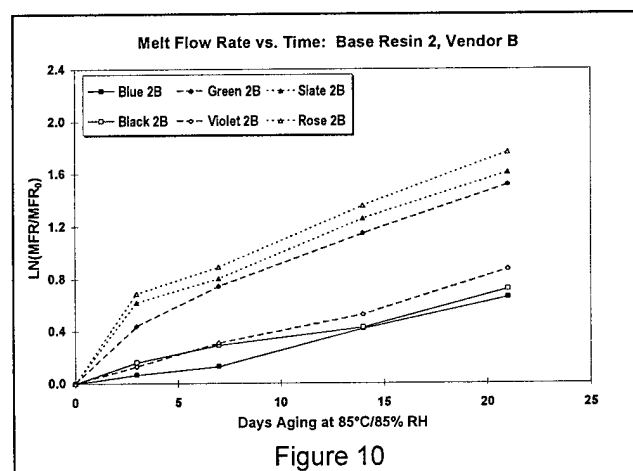
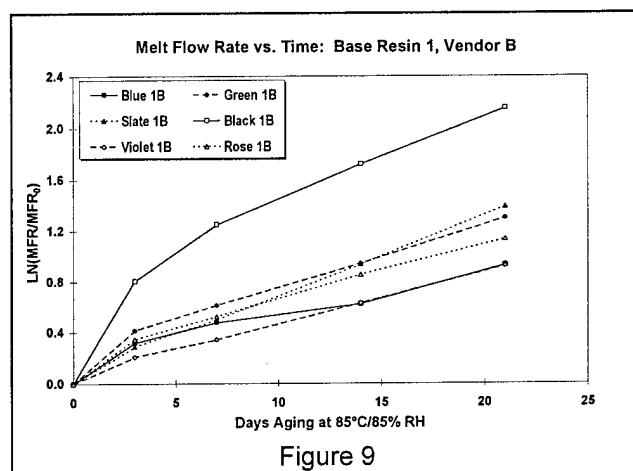


Table 5. Hydrolysis Rates for Resin 1, Vendor A

Color	Rate	Color	Rate
Blue	0.0409 ± 0.0043	Yellow	0.0513 ± 0.0006
Orange	0.0496 ± 0.0002	Violet	0.0503 ± 0.0018
Green	0.0527 ± 0.0005	Rose	0.0512 ± 0.0010
White	0.0451 ± 0.0021	Aqua	0.0491 ± 0.0012
Red	0.0480 ± 0.0025	Average:	0.0487 ± 0.0037

For vendor B, shown in Figures 9 and 10 and Table 6, the results are more varied. With the base as resin 1, the rates for blue, green, violet and rose are less than 0.05 day^{-1} but slate and black are

greater than 0.06 day^{-1} . With base resin 2, three colors, blue, violet, and this time black are less than 0.04 day^{-1} , while the remaining colors, green, slate and rose, are greater than 0.056 day^{-1} . In addition, the initial rates between 0 and 3 days for these latter three colors is much larger than the other colors making them appear segregated. The reason for the increased variability in the melt flow results compared with vendor A is not known.



The results for the black 2B and violet 2B color concentrates were counter-intuitive since the hydrolysis rate was expected to be higher for the concentrate that caused the tube to fail tensile testing at 45 days aging. For violet, the hydrolysis rates for base resins 1 and 2 are virtually the same under the exact same testing conditions. While the reasons are unclear for not seeing differences in violet, some differences can be discerned with black.

Table 6. Rates for Resin 1 & 2, Vendor B

Color	Resin 1 Rate	Resin 2 Rate
Blue	0.0324 ± 0.0034	0.0344 ± 0.0027
Green	0.0491 ± 0.0007	0.0591 ± 0.0030
Slate	0.0618 ± 0.0017	0.0563 ± 0.0024
Black	0.0732 ± 0.0063	0.0301 ± 0.0034†
Violet	0.0400 ± 0.0011	0.0403 ± 0.0028
Rose	0.0442 ± 0.0011	0.0607 ± 0.0017

† 2160 g weight

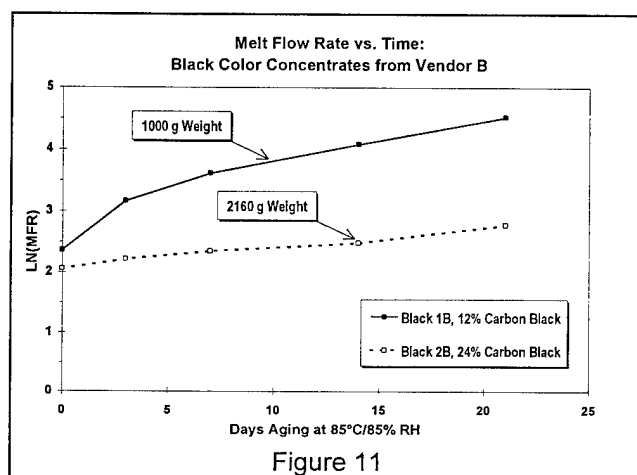


Figure 11

When the black color concentrates are plotted using $\ln(MFR_t)$ instead of $\ln(MFR_t/MFR_0)$, as shown in Figure 11, it is clear that the carbon black concentrate is affecting the rheological properties. So, even if a high rate of degradation was occurring, it would not be detectable due to the masking effects of the high carbon black concentration. Note that because black 2B (resin 2, vendor B) had 24% carbon black, as shown in Table 2, the weight used for the melt flow experiment had to be increased to 2160 g: the 1000 g would not produce any flow with the control sample. The carbon black concentration for black 1B was 11.8%. Despite using more than twice the load to test black 2B, the absolute melt flow at 22 days aging was still only one-third of black 1B.

CONCLUSIONS

Loose tubes made with color concentrates having two different hydrolytically stabilized base resins and obtained from two vendors were aged at 85°C and 85% RH and examined for their tensile properties.

Out of the four concentrates examined, three concentrates produced loose tubes that exceeded by over 15 days the requirement of $\geq 10\%$ elongation at yield after 45 days of aging. This represents a 33% margin over the requirement. However, for one concentrate made with resin 2 from vendor B, the tensile results of loose tubes made with color concentrate clearly indicated a problem with black and to a lesser extent violet and aqua.

To reach these conclusions, over 720 specimens were tested over 60 day periods from 48 colored loose tube samples. Clearly, an alternative method to predict whether or not a particular concentrate would cause a problem, without having to manufacture, age, and test loose tubes, would be advantageous.

Melt flow rheometry¹⁰ is a fast simple test that has been shown to correlate with the decomposition of PBT with high temperature humidity aging.³ Both resins 1 and 2 were shown to be superior to resin 3 in resisting hydrolysis by a factor of three using the melt flow method. If this method could be extended to color concentrates, the failure of color concentrate formulations could be predicted. It has been demonstrated that hydrolysis rates can be obtained from melt flow results but it is clear that the pigments used in the color formulations can affect the rheology of the PBT. For example, when the level of carbon black, as obtained from thermogravimetric analysis (TGA), is approximately 25%, the melt rheology response is completely different than that of a concentrate with approximately 12% carbon black. In this case, it was not possible to rely on the hydrolysis rate as obtained from melt flow analysis. However, for the majority of concentrates, it should be possible to use melt flow analysis to determine hydrolysis rates as long as pigment loading levels for the colors are determined and their effects on the rheology of PBT established.

Where differences were seen in the rate of hydrolysis between color concentrates, the differences were not always seen in the tensile test results, even after 60 days of aging. To clarify the relationship between tensile properties and melt flow rate, the actual time of failure in the tensile testing of the tubes needs to be pinpointed. Tensile properties need to be examined between 45 and 60 days, for those samples that failed between those times, and greater than 60 days, for sample which exhibited no problems up to that time. In this way, the different

colors, base resins, and/or vendors can be distinguished more definitively.

In addition, the effect of the pigment on the rheological properties of PBT needs further investigation. Other test methodologies may be required to fully elucidate this relationship. For example, it may be possible to obtain more information by capillary flow rheometry,¹³ which measures shear stress vs. shear rate, rather than melt flow which measures flow rate with a constant load. Another possible method may be to determine the carboxylic acid end group concentration by titration,¹⁴ however, the pigment(s) present in the concentrate may interfere with obtaining consistent results.

Returning to the three concentrate colors which failed, for black 2B (base resin 2, vendor B) it appears that excess moisture was carried in with the high concentration (24%) carbon black used to make the concentrate leading to premature aging during the manufacture of the concentrate. Further investigation is underway to determine if the same mechanism was responsible for violet 2B and aqua 2B, but moisture in the pigments is still the prime suspect.

For PBT color concentrate vendors, both the pigments and the base resins must be completely dry before manufacturing the concentrate and only the amount of pigment necessary to meet the color requirements be added. The pressures and temperatures used to manufacture color concentrates will definitely cause degradation with moisture present. It may be possible, then, to use melt flow analysis to determine the extent degradation and insure that only quality color concentrates are shipped to the customer.

For cablers, it is clear from this study that the effect of color concentrates on the reliability of PBT be considered prior to use in production. And, while melt flow rates might be used as a screening method to eliminate concentrates with high degradation rates, tensile testing of loose tubes after aging must still be performed to determine the suitability of color concentrates in the final product.

ACKNOWLEDGMENTS

The author would like thank Mr. Gregory Tate for his unending patience and for preparing, aging and testing all of the many samples in this paper. Thanks also go to Messrs. Steve Stokes and Ronald Lindsay for their thoughtful comments and suggestions.

Paul E. Neveux Jr. obtained a B.S. in Chemistry and Biology from Antioch College, Yellow Springs, Ohio. After obtaining a Doctorate in Chemistry at The University of North Carolina at Chapel Hill, he held a post-doctoral fellowship investigating conducting liquid crystal polymers at Duke University, Durham, North Carolina. In 1986, he joined Sumitomo Electric and is currently Sr. Engineer, engaged in materials research and development, and supervisor of the Materials Laboratory. Dr. Neveux is an active member in the Telecommunications Industries Association and the American Chemical Society.

REFERENCES

- ¹ (a) Kelleher, P.G., Wentz, R.P., Falcone, D.R., *Polymer Engineering and Science*, **1982**, 22(4), 260.
(b) Kishore, K., Sankaralingam, S., *Polymer Engineering and Science*, **1984**, 24(13), 1043
- ² Parris, D. R.; *Proceedings of the 38th International Wire & Cable Symposium*, **1989**, 105
- ³ Neveux, P. E., Jr.; Buckland, E. L.; *Proceedings of the 40th International Wire & Cable Symposium*, **1991**, 341.
- ⁴ Gebizlioglu, O.S.; Plitz, I. M.; *Proceedings of the 42nd International Wire & Cable Symposium*, **1993**, 509.
- ⁵ Weast, R.C., ed., *CRC Handbook of Chemistry and Physics*, **1980**, 60th Edition, Section D-196.
- ⁶ GoldSchmidt, H., *Ber.*, **1896**, 29, 2208; Rolfe, A. C.; Hinshelwood, C. N., *Trans. Faraday Soc.*, **1934**, 30, 935.

⁷ Kellerher, P.G., Wentz, R.P., Hellman, M.Y., Gilbert, E.H., *Polymer Engineering and Science*, **1983**, 23(10), 537.

⁸ (a) Rothwell, R. E., Rowan, H. H., Dunbar, J. J., U.S. Patent #4,374,960. (b) Matthies, H.G., *et al.*, Ger. Offen. DE 3,132,371

⁹ ASTM D 348-90, "*Methods of Testing Rigid Tubes Used for Electrical Insulation*," Vol 10.01, American Society for Testing and Materials, 100 Barr Harbor Drive, West Conshohocken, PA 19428.

¹⁰ ASTM D 1238-90b, "*Test Method for Flow Rates of Thermoplastics by Extrusion Plastometer*," Vol 8.01, American Society for Testing and Materials, 100 Barr Harbor Drive, West Conshohocken, PA 19428.

¹¹ ASTM D 4218-82, "*Determination of Carbon Black Content in Polyethylene Compounds by the Muffle-Furnace Technique*," Vol 8.01, American Society for Testing and Materials, 100 Barr Harbor Drive, West Conshohocken, PA 19428.

¹² GR-20-CORE, Issue 1, "Generic Requirements for Optical Fiber and Fiber Optic Cable," BELLCORE, 1994

¹³ Cogswell, F. N., "*Polymer Melt Rheology, A Guide for Industrial Practice*," Goerge Godwin Ltd., London, 1981, pp 15-38.

¹⁴ Kohl, H. A.; *Analytical Chemistry*, **1954**, 26(10), 1614.

Reliability of Spliced GRP Strength Elements

Paul E. Neveux, Jr.,[†] Stephen R. Stokes,[†] J. Scott Radley,[‡] Gregory V. Payne[‡]

[†]Sumitomo Electric Lightwave, Corp.
Research Triangle Park, North Carolina

[‡]Neptco, Incorporated
Granite Falls, North Carolina

ABSTRACT

Commercially available spliced GRP samples were tested for reliability using standard tensile element and cable test methods. To determine the robustness of the splices, twist, cyclic flex and tensile loading and bending were performed. To determine the effect of splices on the cable design parameters, Weibull statistics were applied to the break loads of spliced and unspliced elements, both aged and unaged, to analyze the effect of cable environment aging on tensile strength reliability.

INTRODUCTION

Glass reinforced plastic (GRP) strength elements have served as effective dielectric strength elements in stranded loose tube cables and central tube cables for many years. GRP consists of continuous glass yarns encased in a matrix of thermally or UV-cured epoxy resin. The GRP fills a dual purpose of providing tensile strength and low temperature anti-buckling support to the fiber optic cable. The stock lengths supplied by the various GRP manufacturers do not always match the finished cable length requirements and thus the cable manufacturing process can generate a significant amount of remainder pieces (*i.e.*, < 2 Km) of GRP. Historically, the unusable short pieces were chopped and scrapped for eventual delivery to land-fills.

To address this situation, Neptco, Inc., developed a method of splicing GRP rod to recover the remainder

lengths. This practice allows the cable manufacturer and the GRP manufacturer to better utilize the GRP raw material with a subsequent reduction of scrap and waste. Neptco proof tests every splice to 80% of the rated tensile strength prior to shipping any spliced product. In addition, Neptco annually performs qualification tests of spliced GRP according to Bellcore GR-20-CORE¹

In order to insure that the splices met internal design and customer requirements, test methods and data analysis techniques were developed. Samples of Neptco's commercially available spliced GRP were procured for this analysis. The GRP rod sizes were chosen to represent typical sizes used in stranded loose tube and central tube cables as dielectric tensile and anti-buckling strength elements. The tests and methods were chosen to be representative of typical cable installation and handling practices as well as to measure the mechanical reliability limits of the splices after accelerated environmental aging. The tests, methods and requirements are shown in Table 1.

EXPERIMENTAL

Cyclic Flex and Twist

Four sets of GRP rods with nominal rod diameters of 2.0, 2.7, 3.3, and 4.3 mm were tested. Average sample lengths were 1 meter. Pulling eyes with the appropriate sized collets were used to secure the samples in the test fixtures.

Table 1. GRP Splice Reliability Requirements

Test	Conditions	Requirement
Splice Geometry	GRP diameter	The splice region geometry must meet the same specifications as unspliced GRP.
Cyclic Flex	25 cycles of $\pm 90^\circ$ over a $\leq 55X$ mandrel	No GRP damage
Cyclic Twist	10 cycles of $\pm 360^\circ$ over a 1 meter gauge length	No GRP damage
Tensile and Bending	Simulate installation conditions within a cable by wrapping the spliced GRP around a 560 mm diameter sheave with the splice perpendicular to the bend and applying a tensile load.	The spliced GRP must survive a minimum 1% strain under bending conditions without damage.
Tensile Strength	Unaged	$\geq 80\%$ of rated yield or break strength of unspliced strength element
	Pre-strain on 10" mandrel; Age 7 days in low molecular weight oil at $85^\circ\text{C} \rightarrow 7$ days $85^\circ\text{C}/85\% \text{ RH}$, unstrained	$\geq 80\%$ of rated yield or break strength of unaged strength element

The cyclic flex test was performed per FOTP-104² using the samples described above. All samples were subjected to $\pm 90^\circ$ cyclic flexing. The 4.3 mm and 3.3 mm diameter samples were flexed around a 119 mm diameter mandrel (28X and 36X, respectively) using 14.5 kg and 9.5 kg weights, respectively. The 2.7 mm and 2.0 mm samples were flexed around a 76 mm diameter mandrel (28X and 38X, respectively) using a 9.5 kg weight. Note that the mandrels used to test the GRP rods are significantly smaller than the required 55X making the test much more severe. The test was performed two ways: one with the splice plane parallel to the mandrel bend and another with the splice plane perpendicular to the mandrel bend. Three specimens from each sample were tested for each splice orientation. All samples were initially flexed for 25 cycles at which point they were then visually inspected for damage. If the sample exhibited no damage after 25 cycles, then the samples were subjected to an additional 75 cycles above the required 25 cycles.

The twist test was performed per FOTP-85A³ on the samples described above. All rod samples were initially twisted for $\pm 360^\circ \times 10$ cycles. If no damage was seen the samples were twisted $\pm 720^\circ \times 10$ cycles, then 1 cycle each for $\pm 1080^\circ$, $\pm 1440^\circ$, $\pm 1800^\circ$, $\pm 2160^\circ$, and $\pm 2520^\circ$. Again, these last conditions exceed the performance requirement of the element. Three spliced samples and three unspliced samples of each rod diameter were tested.

Tensile Loading and Bending Test (LT&B)

Testing was performed per FOTP-33⁴ with the changes described below. The samples consisted of 50 meter lengths of GRP rods with the splice in the middle of the length for the spliced samples. Three specimens of each size were tested. A two strand test was performed on all samples. The spliced samples had the splice location centered on the mandrel of the apparatus such that the bend was perpendicular to the splice plane. The percent elongation at each load was measured for each specimen. The load for the 2.0 and 2.7 mm sizes was increased in 50 lbs/strand increments while the 3.3 and 4.3 mm samples were increased at 100 lbs/strand increments. Percent elongation measurements were taken at each load interval until the calculated load at 1% strain was achieved. This load was held for one hour with measurements taken every 10 minutes. After the one hour hold, the load was increased at the same interval until the sample broke.

Tensile Test

For the tensile strength experiments, the 2.0 and 2.7 mm GRP rods were tested. Because specimens frequently slip in the grips outlined in ASTM 3916,⁵ an alternative method was used to prepare the ends of the samples. Two pieces of rod material were cut to the length of the grip and attached to the specimen GRP using polyaramid yarn and epoxy. In this way the ends of the GRP rods could be gripped without crushing or otherwise affecting the integrity of the specimen.

The 2.0 and 2.7 mm GRP rods were stressed and aged per Bellcore GR-20, Issue 1, section 6.1.3.¹ The samples were pre-stressed on a 10 inch diameter mandrel (5X and 3.7X the rod diameters, respectively) before aging. The rods were then aged 7 days in mineral oil followed by 7 days at 85°C and 85% RH in an environmental chamber. The samples were tested on an Instron tensiometer at a strain rate of 1 mm/minute. Five (5) specimens of each size were tested.

RESULTS & DISCUSSION

Table 2 below summarizes the GRP rod sizes examined in the study. Because the Cyclic Flex and Twist tests do not measure a break load to determine the point of failure, the following criteria were used to determine the extent of damage for the test. A GRP break is defined as a clean perpendicular break of the filaments, or a loss of $\geq 20\%$ of the strength element's filaments due to severe fraying, or axial separation of large sections of the filaments in the rod. Severe fraying is defined as filament separation on the outer circumference of the rod resulting in a 5 - 20% reduction in rod diameter.

Table 2 GRP Sizes Examined

Test	2.0 mm	2.7 mm	3.3 mm	4.3 mm
Cyclic Flex	✓	✓	✓	✓
Twist	✓	✓	✓	✓
LT&B	✓	✓	✓	✓
Tensile Test	✓	✓	---	---

Cyclic Flex Test

Table 3 summarizes the cyclic flex conditions used in this report. Because of the way the cyclic flex apparatus was designed, the rods rubbed against the mandrels on each cycle since the mandrels did not rotate or otherwise move with the element. This rubbing caused severe fraying of the glass elements which contacted the mandrel causing a 10 - 20% loss in the diameters of the most of the samples. Despite this unintended damage from the apparatus, the splices greatly exceeded cycle requirements as shown in Tables 4 through 7.

Table 3 Cyclic Flex Test Conditions

Parameter	2.0 mm	2.7 mm	3.3 mm	4.3 mm
Mandrel Diameter	76 mm	76 mm	119 mm	119 mm
Mandrel/Rod	38X	28X	36X	28X
Weight	9.5 kg	9.5 kg	9.5 kg	14.5 kg

For the 2.0 mm GRP, failure was not seen in any of the spliced elements except for one with the splice in a perpendicular orientation that failed on the 30th cycle. For the *unspliced* specimens of the same size, one failed on the 83rd cycle. Neither the 2.7 mm nor the 3.3 mm samples failed after 100 cycles, although there was wear on the surfaces of the rod which contacted the flex apparatus.

Table 4. Cyclic Flex Results for 2.0 mm GRP

Splice Orientation	#	After 25 Cycles	After 100 Cycles	Comment
No Splice	1	pass	---	Break on 83 rd cycle
	2	pass	pass	
	3	pass	pass	
	1	pass	pass	
	2	pass	pass	
	3	pass	pass	
⊥	1	pass	---	Break on 30 th cycle
	2	pass	pass	
	3	pass	pass	

Table 5. Cyclic Flex Results for 2.7 mm GRP

Splice Orientation	#	After 25 Cycles	After 100 Cycles	Comment
No Splice	1	pass	pass	Fraying of rod against apparatus
	2	pass	pass	
	3	pass	pass	
	1	pass	pass	
	2	pass	pass	
	3	pass	pass	
⊥	1	pass	pass	
	2	pass	pass	
	3	pass	pass	

The only specimen which did not meet the pass/fail criteria was one of the *unspliced* 4.3 mm rods. The specimen split axially indicating a shear failure in the matrix. Given that severe fraying was seen in many of the 4.3 mm specimens compared to the other

sizes, it may be that the combination of loading weight (14.5 kg) and mandrel diameter (28X the rod diameter) were too severe. Despite this severity, only one of the 4.3 mm spliced rods failed before the 100th cycle: a parallel oriented spliced specimen broke at the splice on the 39th cycle.

Table 6. Cyclic Flex Results for 3.3 mm GRP

Splice Orientation	#	After 25 Cycles	After 100 Cycles	Comment
No Splice	1	pass	pass	Fraying of rod against apparatus
	2	pass	pass	
	3	pass	pass	
	1	pass	pass	
	2	pass	pass	
	3	pass	pass	
⊥	1	pass	pass	
	2	pass	pass	
	3	pass	pass	

Table 7. Cyclic Flex Results for 4.3 mm GRP

Splice Orientation	#	After 25 Cycles	After 100 Cycles	Comment
None	1	pass	pass	Split axially after 5th cycle
	2	pass	pass	
	3	fail	—	
	1	pass	—	Break on 39th cycle
	2	pass	pass	Fraying of rod against apparatus
	3	pass	pass	
⊥	1	pass	pass	Fraying of rod against apparatus
	2	pass	pass	
	3	pass	pass	

Twist Test

All rod samples were initially twisted for $\pm 360^\circ \times 10$ cycles. No visual damage was seen so the samples were twisted $\pm 720^\circ \times 10$ cycles, then 1 cycle each for $\pm 1080^\circ$, $\pm 1440^\circ$, $\pm 1800^\circ$, $\pm 2160^\circ$, and $\pm 2520^\circ$. As shown in Table 8, there was no apparent visual damage and all samples tested passed the above criteria.

The 2.0 and 2.7 mm samples were further tested to break by continuous rotation in the positive direction. Table 9 below indicates at which point (1 Rotation = $+360^\circ$) the samples failed. As can be seen, no apparent difference was observed between the

spliced and the unspliced 2.7 mm samples. The spliced 2.0 mm samples failed, on average, in 6 fewer rotations than the unspliced specimens.

Table 8. Twist Test Results

GRP Size	Splice	$\pm 360^\circ \times 10$	$\pm 720^\circ \times 10$	$\pm 2520^\circ \times 1$
2.0 mm	No	Pass	Pass	Pass
	Yes	Pass	Pass	Pass
2.7 mm	No	Pass	Pass	Pass
	Yes	Pass	Pass	Pass
3.3 mm	No	Pass	Pass	Pass
	Yes	Pass	Pass	Pass
4.3 mm	No	Pass	Pass	Pass
	Yes	Pass	Pass	Pass

Table 9. Twist to Failure Test Results

GRP Size	Splice	Rotations to Failure
2.7 mm	No	28, 22, 23
	Yes	32, 29, 28
2.0 mm	No	49, 50, 48
	Yes	42, 44, 44

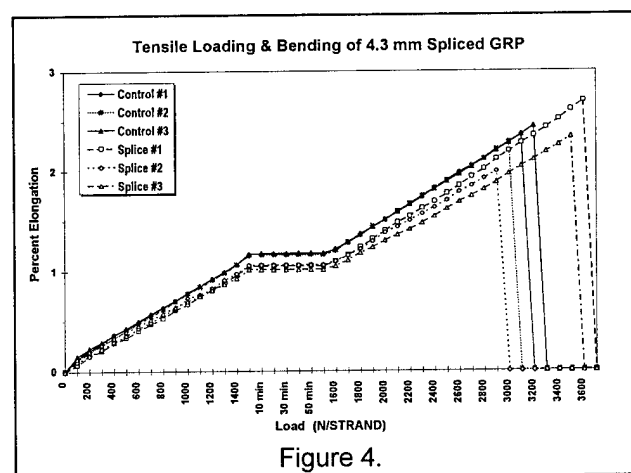
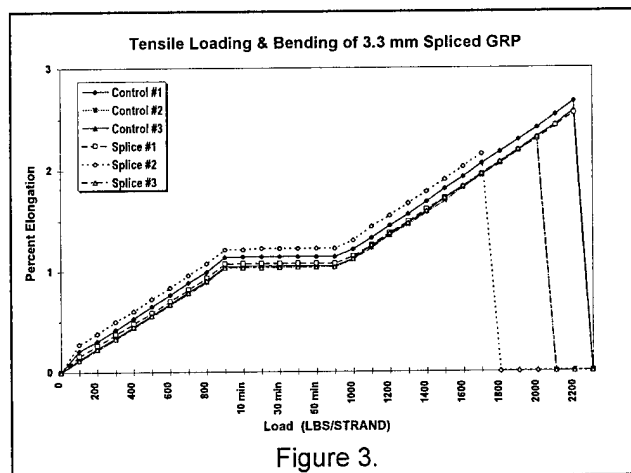
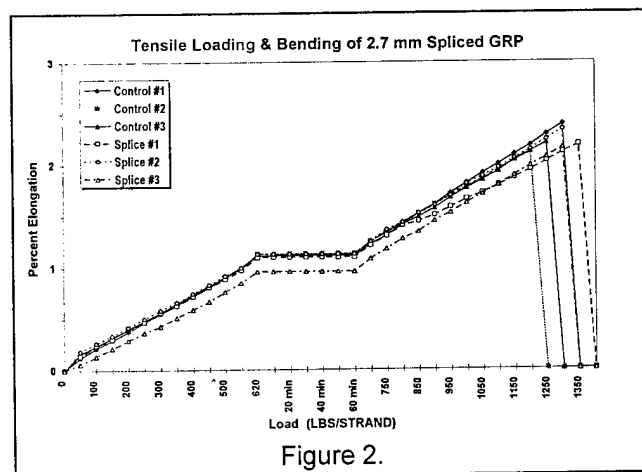
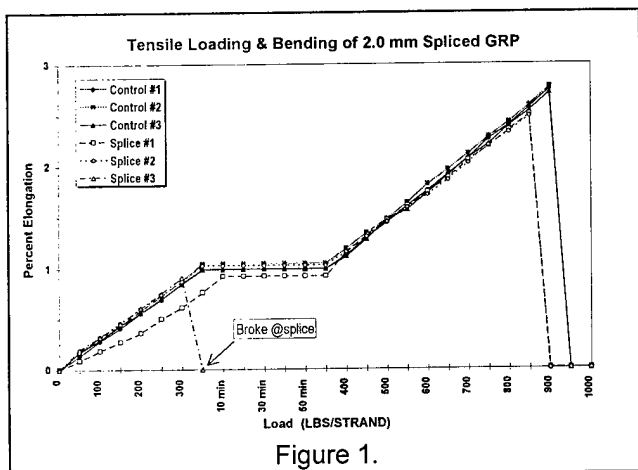
Tensile Loading & Bending Test

Unlike typical tensileometers, the cable tensile loading and bending apparatus controls the load (or stress) and measures the elongation (or strain). Since an extensometer was not used, the elongation measured is the relative movement of the crosshead, not the actual elongation of the element. For these reasons the tensile loading and bending graphs, shown in Figures 1 through 4, have percent elongation of the element plotted versus load. The curves were not corrected for initial slack present in the GRP elements when mounted on the apparatus, therefore, the curves do not overlap exactly and do not extrapolate through zero.

All specimens were tested by loading the specimen to approximately 1% elongation, holding that stress for one hour, then increasing the load until break. Note that for the spliced elements, the splice was placed on the mandrel (on the "bend") with the plane of the splice perpendicular to the direction of the bend. As can be seen from the figures, the

elongation increases linearly with load both before and after the one hour holding period. During the one hour holding period, no creep⁶ is exhibited in any of the elements. The loads and percent elongations at break appear to be random and do not appear to correlate with the presence or absence of splices for all specimens except one.

For all the sample sizes, shear-type breaks, occurring away from the splice, were observed with the exception of one of the 2.0 mm specimens which broke at the splice. The splice break in this 2.0 mm specimen appears to be an anomaly: a break of this low tension would normally have been screened out during the proof testing at 80% of rated strength. Since the samples were made to the lengths required for these tests, it may be that this one specimen missed proof testing. More likely, however, is that the sample may have been damaged during mounting on the LT&B apparatus.



Tables 10 and 11 summarize modulus and break properties, respectively, for the data shown in Figures 1 through 4. The modulus shown in Table 10 was calculated by taking the inverse of the slopes from the curves and dividing by the cross sectional area of the rods. As can be seen, the calculated modulus (converted to units of MPa) is essentially the same before and after the one hour hold at 1% strain. Even between sizes of GRP rods, there is very little difference compared with experimental error and resolution. Note that the resolution of load applied during the experiment is ± 222 N (or as shown in the graphs, ± 50 lbf) for the 2.0 and 2.7 mm samples and ± 444 N (± 100 lbf) for the 3.3 and 4.3 mm samples. This is especially pertinent to the data presented in Table 11.

Table 10. Average Modulus of GRP from LT&B

GRP Size	Sample Type	Modulus Before 1 hr Hold	Modulus After 1 hr Hold
2.0 mm	Unspliced	475 ± 11 MPa	424 ± 4 MPa
	Spliced	462 ± 9 MPa	457 ± 2 MPa
2.7 mm	Unspliced	449 ± 4 MPa	430 ± 20 MPa
	Spliced	472 ± 25 MPa	468 ± 56 MPa
3.3 mm	Unspliced	456 ± 15 MPa	434 ± 3 MPa
	Spliced	446 ± 25 MPa	440 ± 7 MPa
4.3 mm	Unspliced	437 ± 6 MPa	410 ± 1 MPa
	Spliced	478 ± 31 MPa	436 ± 39 MPa

Given the experimental resolution and the small number of specimens tested (only 3), the load and percent elongation at break data shown in Table 11 is relatively consistent and does not indicate problems that may be associated with unreliable splices. Because of the small number of specimens tested, it was not possible to apply Weibull statistics as in the tensile tests discussed below.

Table 11. Average % Elongation and Load @ Break

GRP Size	Sample Type	Approximate Load @ Break ^a	%Elongation @ Break ^b
2.0 mm	Unspliced	1213 ± 0 MPa	2.73 ± 0.04%
	Spliced ^c	1146 ± 0 MPa	2.49 ± 0.07%
2.7 mm	Unspliced	971 ± 39 MPa	2.18 ± 0.16%
	Spliced	1023 ± 22 MPa	2.18 ± 0.06%
3.3 mm	Unspliced	1110 ± 60 MPa	2.49 ± 0.15%
	Spliced	1023 ± 131 MPa	2.27 ± 0.26%
4.3 mm	Unspliced	972 ± 31 MPa	2.30 ± 0.06%
	Spliced	1045 ± 119 MPa	2.31 ± 0.36%

a) Resolution of load for experiment is ±222N (± 50 lbf). b) Corrected for initial slack. c) The datum from the premature break was censored.

Tensile Test

While the test was performed per GR-20,¹ the analysis of data was not. Although it is not clearly stated, it is assumed that GR-20 requires comparison of the median or average tensile strengths. However, in order to ensure that the spliced GRP meets the strength requirements of the cable, the minimum possible break load of the spliced GRP must be determined. One widely accepted method of analyzing failure probability is through Weibull distributions.⁷ By applying the data to a Weibull treatment, the slope and the intercept may be obtained. The intercept is of most interest here because it corresponds to the minimum break

load, i.e. all breaks should occur above this load. The results of treating the break load data using Weibull statistics is shown in Figures 5 and 6 where the probability of a break occurring at a specific load is plotted against the break strength.

Because of the difficulty in preparing the samples and testing, only five (5) specimens were tested. It is clear that improvements in accuracy of the results could have been realized with a larger population of specimens. This clearly would have been an advantage with the 2.0 mm samples where the linearity is not as good as with the 2.7 mm GRP elements. Notice also that there is a consistent reduction in strength between the unaged, unspliced GRP and the unaged, spliced GRP. The reduction may be due to pre-stressing around a ten inch (10") mandrel which is applied only to the spliced samples. As was observed from the LT&B testing, break locations are not typically within the splice section so it is unlikely that the splice itself is a contributor.

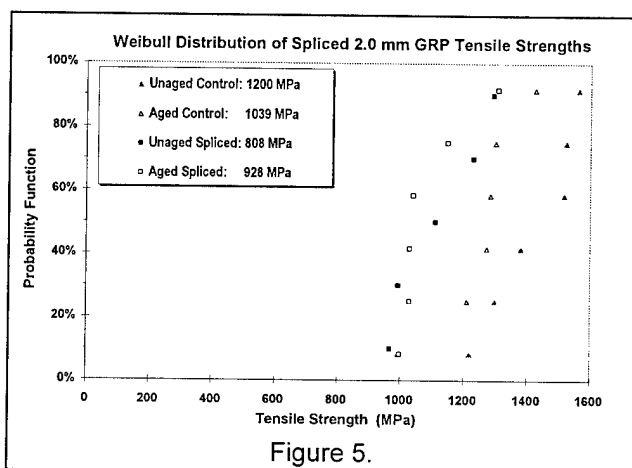


Figure 5.

Table 12. Weibull Results for 2.0 mm GRP

Sample	Slope	Median	Intercept	% Change
Unaged Unspliced	434 ± 55	1470	1200 ± 31 MPa	----
Aged Unspliced	417 ± 94	1248	1039 ± 54 MPa	-13%
Unaged Spliced	531 ± 47	1073	808 ± 31 MPa	-33%
Aged Spliced	327 ± 92	1091	928 ± 53 MPa	-22%

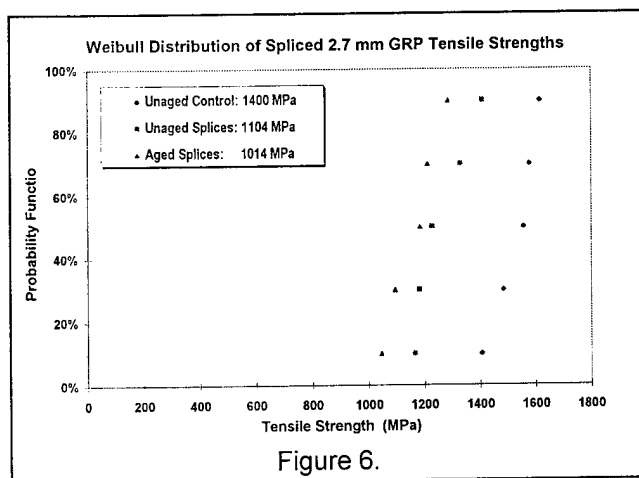
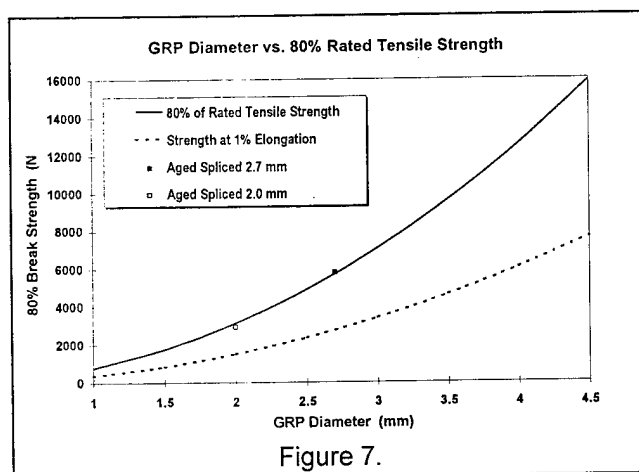


Table 13. Weibull Results for 2.7 mm GRP

Sample	Slope	Median	Intercept	% Change
Unaged Unspliced	257 ± 35	1528	1400 ± 20 MPa	0
Unaged Spliced	308 ± 48	1263	1104 ± 28 MPa	- 21%
Aged Spliced	301 ± 23	1165	1014 ± 13 MPa	- 28%



Shown in Figure 7 is a comparison between the strength at 1% elongation (dotted line) and 80% of the rated tensile strength of various GRP sizes. Included in the graph are the minimum tensile strengths of the 2.0 and 2.7 mm aged spliced rods as calculated by the Weibull intercepts. As can be seen, using the conservative minimum tensile strengths, both the 2.0 and the 2.7 mm aged spliced rods meet the requirement. However, cables are

typically designed to carry a rated load and maintain a cable strain level which will protect the enclosed fibers from excessive strain. For example, if the maximum load at 1% is conservatively set at 50,000 MPa, as the dotted line shows, the maximum cable load experienced would not even approach the 80% rated tensile strength line.

CONCLUSIONS

Various sizes of spliced and unspliced GRP rods were tested for mechanical and environmental reliability. Samples of spliced elements were subjected to standard mechanical tests to determine the robustness of the splices. It was clear from the outset that these tests were considered extreme in that it is very unlikely that any of the GRP rods would see these types of abuse under actual field conditions. GRP elements are typically embedded in the cable product and do not see the high degree of abrasion seen in tests like Cyclic Flex. The results from the twist and cyclic flex unaged samples show that there is little difference between spliced or unspliced samples. Only when the samples were tested beyond their design requirements and to failure were differences seen in some of the samples.

The results of the tensile loading and bending test demonstrate that the splices have no significant effect on the GRP tensile modulus, load at break, or elongation at break. For tensile testing, Weibull analysis was successfully applied to determine the minimum break strength of any GRP rod, whether aged or unaged, spliced or unspliced. Further, it was shown that the aged splices meet the Bellcore requirement for retention of 80% of rated tensile strength after aging. From a design standpoint, further restrictions can be imposed such that there is ample safety factor between design and ultimate strength values of the strength element.

ACKNOWLEDGMENTS

The authors would like to thank, from Sumitomo Electric Lightwave, Corp., Messrs. Ronald Smith and Edward Conroy for performing the experiments and Messrs. Ron Lindsay for providing helpful suggestions to the text. Thanks also go to Rick Beach and Doug Taylor of Neptco, Inc., for time and

effort conducting the Bellcore annual testing and producing all spliced samples.

¹ Bellcore GR-20-CORE, Issue 1, September 1994, *Generic Requirements for Optical and Fiber Optic Cable*, Section 6.1.3.

² TIA/EIA-455-104A, *Fiber Optic Cable Cyclic Flexing Test*, Telecommunications Industry Association, 2001 Eye Street, N.W., Washington, D.C. 20006, **1993**.

³ TIA/EIA-455-85A, *Fiber Optic Cable Twist Test*, Electron Industries Association, 2001 Eye Street, N.W., Washington, D.C. 20006, **1992**.

⁴ EIA-455-33A, *Fiber Optic Cable Tensile Loading and Bending Test*, Electron Industries Association, 2001 Eye Street, N.W., Washington, D.C. 20006, **1988**.

⁵ ASTM D 3916-84, *Test Method for Tensile Properties of Pultruded Glass Fiber-Reinforced Plastic Rod*, Vol. 8.02, American Society for Testing and Materials, 100 Barr Harbor Drive, West Conshohocken, PA 19428.

⁶ Creep is defined as a change in strain with a constant applied stress.

⁷ Nelson, W., *Accelerated Testing*, John Wiley & Sons, NY, 1990.

Paul E. Neveux Jr. obtained a B.S. in Chemistry and Biology from Antioch College, Yellow Springs, Ohio. After obtaining a Doctorate in Chemistry at The University of North Carolina at Chapel Hill, he held a post-doctoral fellowship investigating conducting liquid crystal polymers at Duke University, Durham, North Carolina. In 1986, he joined Sumitomo Electric and is currently Sr. Engineer, engaged in materials research and development, and supervisor of the Materials Laboratory. Dr. Neveux is an active member in the Telecommunications Industries Association and the American Chemical Society.

Stephen R. Stokes obtained a B.S. degree in Electrical Engineering from Virginia Polytechnic Institute and State University in 1988. He was employed by ITT Electro-Optical Products Division and, subsequently by Alcatel Cable Systems from 1980 to 1990 in the development of fiber optic measurement systems. From 1990 to 1991, he was employed by Galileo Electro-Optics Corporation as a design Engineer in the development of light guide and imagescope products. He has been employed by Sumitomo Electric Lightwave, Corp. since 1991 in the development of fiber optic cables and is currently manager of Product Design Engineering.

J. Scott Radley graduated from Providence College of Providence, Rhode Island with a BS in Business Management. He is currently Senior Sales Engineer for Composites with Neptco, Inc., and is responsible for domestic fiber optic manufacturers out of the Pawtucket, RI, facility.

Gregory V. Payne graduated from State University of New York at Buffalo with a BS degree in Industrial Technology. Greg is a member of ASQC with a Certificate of Quality Engineer and is currently P&QC Manager at Neptco's Granite Falls Facility.

BALLISTIC PROTECTION OF AERIAL CABLES A NEW ECONOMICAL SOLUTION WITH A SPECIAL IMPACT MODIFIED POLYAMIDE

Hochuli Martin
Manager Application Development for Cables
EMS-CHEMIE AG, CH-7013 Domat/Ems, Switzerland

ABSTRACT

Aerial cables are sometimes damaged by hunters shooting birds or using cables to adjust their gun sights. In the case of optical fibre cables, this can lead to a total loss of signal transmission requiring cable replacement.

A well known material for ballistic protection is woven aramid yarns. To reach an acceptable ballistic protection at least two or three such woven tapes have to be wound around the cable. As aramid yarns are very costly, the cable industry is still asking for a more economical solution.

EMS has studied the armouring properties and energy absorption behaviour of different polymer materials and their combination with aramid tapes. Special test methods, such as penetration tests with a steel bolt and shooting tests on plates were developed for that purpose. It was found that specially modified polyamides with high impact strength and good energy absorption properties in combination with a single aramid tape, gives the same protection as three similar aramid tapes used together. The cost of such a system is around half that of the aramid tape solution.

ARAMID YARN AS BALLISTIC PROTECTION

A well known material for ballistic protection is woven aramid yarns. Bullet proof clothes for the police or the army are made in this material. It is therefore logical to use a similar solution for cable protection. In order to reach an acceptable ballistic protection level at least two or three woven aramid tapes need to be wound around a cable (Fig.1). The additional costs

for a ballistic protected cable made with aramid fibres lie between 2.5 and 3.5 US\$ per meter dependent on the cable diameter. Not only the cable manufacturers but also the telecom companies are still asking for a more economical solution.

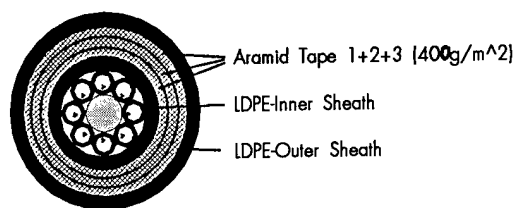


Fig. 1: Design for ballistic protected optical fibre cable as recommended today by aramid suppliers

An analysis of damaged cables has shown that the buffer tubes are often broken, even if the lead grain has not penetrated the aramid armouring. The reason for this is that the woven aramid yarns can hold back the grains but still transmit a high impact energy through the polyethylene layer to the buffer tubes.

The idea of this study was to find a material with good armouring as well as having energy absorption properties.

TEST METHODS FOR MATERIAL EVALUATION

Standard material test methods, like tensile test, shore hardness or impact strength only partially describes if a material has good armouring and energy absorption properties. On the other hand a direct evaluation of materials and armouring designs on cables would be very expensive in terms of time and costs. Because of this two special tests, a penetration energy test and a shot gun test on plates has been developed.

Penetration Energy Test

In this test a bolt penetrates a plate with high speed. The force can be measured and the energy calculated. Also the break behaviour, ductile or brittle, can be determined.

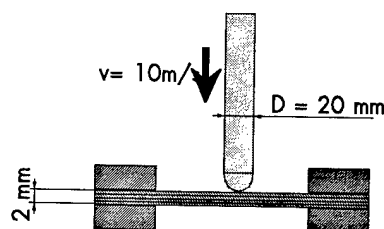


Fig. 2: Penetration Energy Test

Shot Test on Plates

A shot test as shown in fig. 3 was developed. The distance between the gun and the test plates was set at 15 m. In reality it is quite unrealistic that a hunter goes nearer closer 20 to 25 m, as otherwise the prey would contain too much lead rendering it unsuitable for eating! A 12/70 shot gun best quality N° 5 lead grain ammunition was used.

The armouring plates or tapes were fixed between two steel plates. The first plate was always a black HDPE plate 0.8 mm thick and the last plate was made in a brittle material and used as reference. The complete plate packet had a weight of approx. 1 kg and was mounted on a post without fixation.

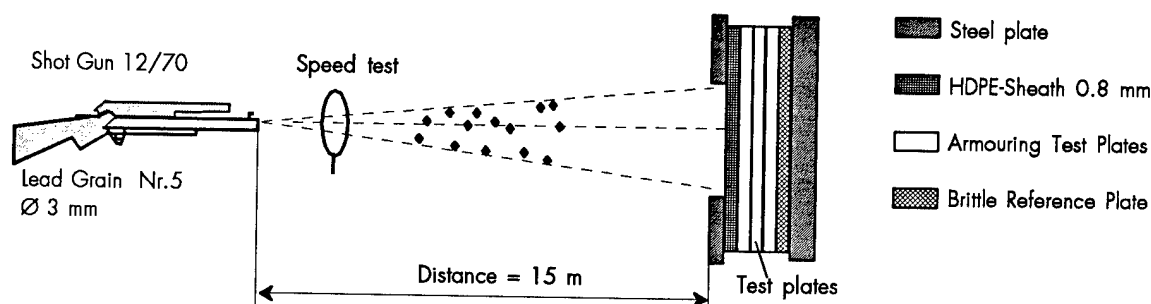


Fig. 3: Shot Test on Plates

TEST RESULTS

The penetration energy of a wide range of polymer

materials was measured for pre-evaluating. The following table (Table 1) shows only the results of the most interesting ones.

Material	Tensile-E-Modulus [MPa]	Shore-D-Hardness [-]	Penetration Energy [Nm]
HDPE black	650	58	62
Thermoplastic Polyester Elastomer(TPE)	200	55	67
Polyamide 6 natural *)	1100	67	40
Polyamide 6 modified *)	600	65	125
Polyamide 12 natural	1100	71	120
Polyamide 12 modified	950	68	-
Polyamide 12 elastomeric	300	63	110

*) all values in cond. state

Table 1: Penetration Energy, Tensile-E-Modulus and Hardness

packets of 3 plates with thickness 1.6mm were tested (Fig. 4). After selecting the best armouring materials, the modified PA6 and PA12 grades were also tested in combination with woven aramid tapes (Fig. 5).

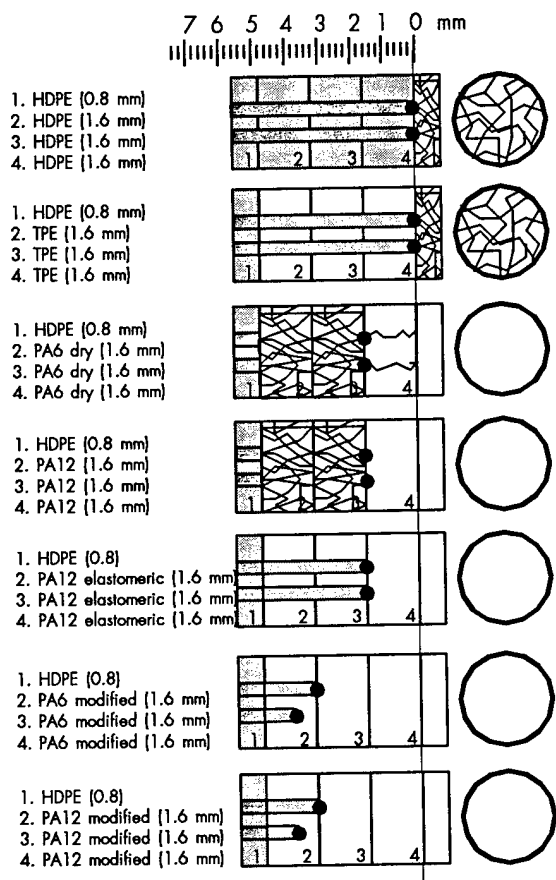


Fig. 4: Shot test results on plate packets

DISCUSSION OF THE RESULTS

The energy penetration test can give an initial impression of the armouring behaviour of a polymer material. But they also showed high penetration energy values for the PA12 natural and PA12 elastomeric grades, these excellent results were not however confirmed in the shot tests. Therefore the penetration energy test can not be used on its own for material evaluation.

The shots test on plates in combination with woven aramid tapes has shown that a combination of one

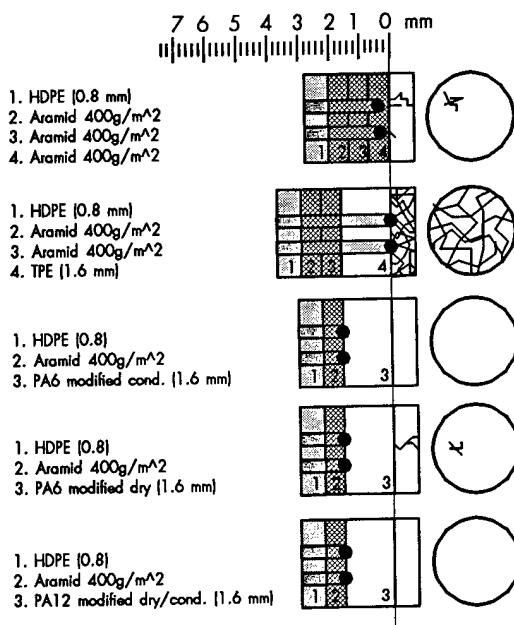


Fig. 5: Shot test results on plates in combination with woven aramid tapes

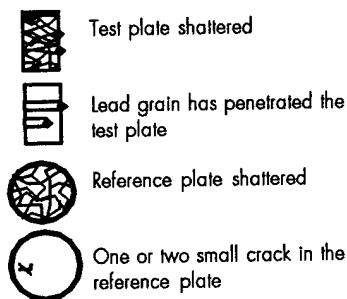


Fig. 6: Graphic legend to fig. 4 and fig. 5

plate made in a modified polyamide (1.6mm) and only one aramid tape (400g/m²) has the same armouring properties as three aramid tapes of the same thickness.

New Design for Ballistic Protected Cables

A cable design build according these new results according this study is shown in fig. 6. By replacing two of the costly aramid tapes with one armouring layer made in special modified polyamide saves 40 to 50 % on costs.

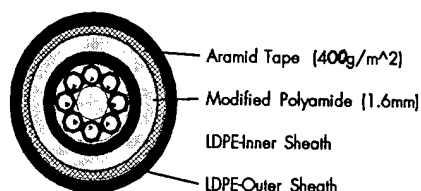


Fig. 6: Economical design for ballistic protected optical fibre cable with one polyamide and one aramid layer.

Polyamide 6 or Polyamide 12?

Polyamides tend to absorb humidity from the air. The humidity content in the polymer has a significant influence on the properties of most polyamides. A polyamide 6 for example undergoes changes in tensile-E-modulus from 3200 MPa in a dry state down to 1100 MPa in the cond. state. Polyamide 12 absorbs the lowest amount of moisture of all polyamides. The change in properties dependent on the humidity content can be ignored for polyamide 12. For the same reason, polyamide 12 has also better cold impact properties.

Therefore polyamide 12 would be the preferred material, especially for cables used in cold or humid climate conditions. Nevertheless the influence of humidity has to be tested in a further study.

CONCLUSION

The armouring properties and the energy absorption behaviour of different polymers was studied with two specially developed tests. It was found that specially modified polyamides with high impact strength and good energy absorption properties in combination with only one aramid tape, provides the same protection as three similar aramid tapes together. The cost of such a system is around half that of the aramid tape solution.

REFERENCES

Twaron Aramid Tapes as Ballistic Protection for Aerial Optical Fiber Cables; AKZO NOBEL; IN93/4364, Issue March 94

AUTHOR



Martin Hochuli
EMS-CHEMIE AG
Reichenastrasse
7013 Domat/Ems
Switzerland

Martin Hochuli (CH) was born in 1966. He received his engineering degree from HTL Brugg-Windisch (CH) in 1990. He joined EMS-CHEMIE AG in 1992 where he was first in charge of Technical Customer Service for Extrusion Applications.

Since 1994 Martin Hochuli is responsible for Application Developments in the Cable and Electrical Market Segment.

DEVELOPMENT & DESIGN APPROVAL OF TWO FIBRE, SINGLEMODE ENHANCED PERFORMANCE FIBRE UNIT (EPFU)

Paul Morris

Optical Fibres, Second Avenue, Deeside Industrial Park, Deeside,
Flintshire CH5 2NX, United Kingdom

ABSTRACT

This paper describes the successful design, development and design approval of a two fibre, singlemode enhanced performance fibre unit (EPFU) for British Telecommunications (BT). The paper details the history behind blown fibre technology, the initial design and development phase on three prototype products, the selection process to find the optimum product for the customer and the testing programme to gain provisional design approval from BT. The final stage of approval, took the form of a pilot trial under field conditions which was performed by the customer. Details were not available at the time of writing the paper but are hoped to be given at the conference.

INTRODUCTION

History

BT designed, developed and patented the blown fibre technology in 1983¹. The concept has been widely described in other papers, but in simple terms, it allows a bundle of fibres to be installed in a small duct (known as a microduct) using compressed air, allowing installation of the fibre with little or no tension on the fibres. The total installed cost of a blown fibre unit (including microducting) is equivalent to that of a conventional cable. However, the blown fibre approach helps to minimize stranded investment in installed fibre.² That is, fibre which is the wrong place and will never earn revenue. The first blown fibre units contained seven fibres, which were encapsulated in a two layer plastic structure, and were designed for use in microducts with an inside diameter of 6 mm. This unit was manufactured by Optical Fibres

(OF) under licence from BT until 1995, with a four fibre product being added to the portfolio in 1988. In the late 1980's, OF developed a single, blowable buffered fibre system³ which used U-V curable acrylate materials, rather than plastic. At about this time, BT requested the development of a second generation, four fibre unit, using acrylate materials. This was developed to give improved blowing times and distances, plus the ability to be installed into smaller bore microducts (inner diameter of 3.5 mm). This product was named "Enhanced Performance Fibre Unit" or EPFU for short. OF developed their own version of this product to meet BT's specification over the period 1992 to 1994 and commenced volume manufacture in 1995.

In 1995, it was indicated that a two fibre version of EPFU was required for local loop applications, which potentially could include connection to subscriber homes. A programme was initiated to develop a product which had the same diameter specification as the four fibre product, plus similar stripping and blowing qualities.

DESIGN PHASE

Initially, three designs incorporating different materials and structures were considered. Figure 1 shows the three designs, which are designated A, B and C respectively. Design A was a two fibre version of the four product; this comprised of three layers of different U-V curable acrylate materials. Design B comprised of two layers of acrylate material and Design C had three layers of acrylate, different to Design A. The outer layer of all three designs contained hollow glass microspheres, to aid blowing, and all designs used two singlemode fibres coated with CPC6 coating, and coloured with a tertiary

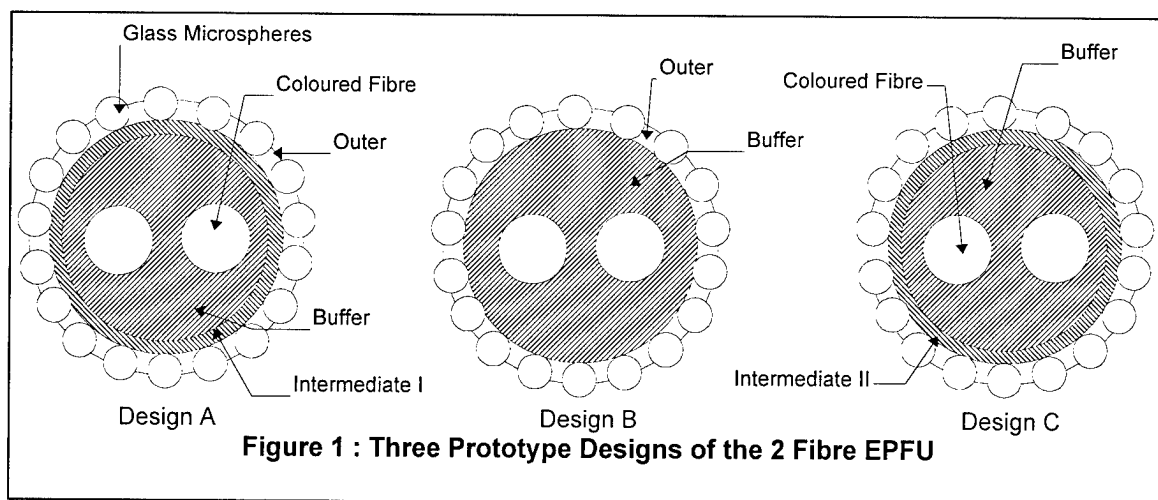


Figure 1 : Three Prototype Designs of the 2 Fibre EPFU

layer of DSM LTS U-V curable ink (blue and orange respectively). The nominal diameter and weight of the three designs were 0.93 mm and 0.75 g/m respectively.

At this stage, samples of the three prototypes were sent to the customer to evaluate the ease of stripping the fibres out of the EPFU structure. The result of this initial evaluation was that Design A was found the most difficult to strip of the three and was dropped from the development programme. This was probably due to the extra amount of inner material present in comparison to the four fibre product which stripped satisfactorily. Designs B and C were found to have stripping properties which met the customer's requirements, and OF was requested to put both designs through the second phase of testing to try and differentiate between them.

INITIAL TEST PHASE

Designs B and C were both subjected to a group of tests to see if any performance differences could be determined. This first round of testing was a subset of the full acceptance programme specified by BT, which is known as "Design Approval". Three units of the two designs were subjected to the following tests :

Strippability

A sample of each test unit was exposed to 0°C, 20°C and 40°C respectively for 24 hours and then stripped within five minutes of removal from the environment. The requirement was that two metres of the coloured fibres could be removed from the unit in a time not exceeding five

minutes, and that the fibres were free from unit coating materials. Both designs met the test requirements.

Blow Performance

A key parameter was the speed at which the unit may be installed into microducting, and two duct routes were specified; 700 metres and 300 metres. The latter route, although shorter, was more tortuous than the former 700 metre layout. The maximum allowable installation times were 40 minutes and 30 minutes for the 700 metre and 300 metre routes respectively. Both designs met the requirements, with average times of <30 minutes and <13 minutes for the 700 metre and 300 metre routes respectively. The average installation speed for both designs, in the two routes was 24 m/min.

Attenuation

Two kilometre lengths of each test unit were temperature cycled over the range -10°C to +60°C for three cycles. All the units measured met the customer's requirements. Graph 1 shows the 1310 nm and 1550 nm attenuation data for the two fibres from one of the Design B units. The performance of the other units was very similar to that illustrated in Graph 1.

Unit Mechanical Performance

There are three tests performed to characterise mechanical performance of the EPFU. These are crush, flexibility and unit "strength" or strain.

Crush. A 100 Newton load is applied via two steel plates, with dimensions of 100 mm², for 60 seconds.

Flexibility. This test takes the form of repeatedly wrapping and unwrapping four complete turns of the unit around a 40 mm diameter mandrel for ten cycles.

In both tests, the attenuation at 1550 nm is monitored whilst the tests are ongoing by using an LED light source and power meter, and the circularity of the unit is measured before and after the respective tests. The maximum allowable attenuation increase is 0.05 dB/km, whilst the ratio of the maximum and minimum diameters after the test shall not be greater than 0.05.

Strength. The unit was subjected to a load of $9.81 \times W$; where W is the unit mass (in kg/km) for ten minutes. This load was applied on apparatus normally used for fibre static fatigue analysis, which allowed a ten metre length of unit to be strained. The strain of the individual fibres was measured using a "time of flight" technique, thus allowing the fibre strain to be measured whilst the load was applied to the unit. The maximum allowable strain while under test was specified as 0.25%, with a maximum residual strain of 0.01% permitted after the load was removed.

Both designs met all the mechanical performance criteria described above, with no measurable differences between Design B and C noted.

INITIAL PHASE SUMMARY

As stated above, both Designs B and C met all the requirements of the first phase of testing, with the results being very similar; to the point where it was almost impossible to differentiate between the two designs. Whilst this work was ongoing, 2 kms samples had been sent to the customer for blowing and handleability trials. A design review was held between customer and ourselves, where both sides results were shared to enable a decision to be taken on which design of unit to select for the final phase of testing, and hopefully, customer approval.

Although, our test programme had shown little difference between the designs, it had been noted that Design B was somewhat "easier" to strip than C and "felt" a little less robust. The customer concurred with these rather subjective views, and thus Design C was selected for the final phase, since it offered good strippability and robustness, whilst meeting all other requirements.

SECOND TEST PHASE

The second phase of testing took the form of several environmental exposures, where one 2 km length of unit of Design C was tested in each environment. The testing programme was performed such that all the tests were conducted in parallel. The environments are described in Table 1.

Table 1 : Environmental Test Programme

Environment	Description	Requirements
Cold	-20°C for 96 hours in accordance with IEC 68-2-1	Attenuation at 1310 nm & 1550 nm ≤ 0.5 dB/km Unit colouring & identification shall remain distinguishable
Combined Temperature Change/High Humidity	-10°C/+65°C/93% RH, 10 cycles of 24 hour duration in accordance with IEC 68-2-38	Attenuation change at 1310 nm & 1550 nm ± 0.07 dB/km Unit colouring & identification shall remain distinguishable
Environmental Sequence		
Temperature Cycle - followed by :	-10°C/+60°C, dwell time of 1 hour, 3 cycles	Attenuation change at 1310 nm & 1550 nm ± 0.07 dB/km
20°C Water Immersion	20 \pm 2°C contaminated water for 1000 hours	Unit colouring & identification shall remain distinguishable
Hydrogen Generation	1 atm of H ₂ at 70°C for 1000 hours	H ₂ generated ≤ 1.54 mg/km

Cold Test

Graph 2 show the attenuation results at 1310 nm and 1550 nm for the unit tested in this environment. The data shows that there was virtually no change in the unit attenuation, and was well inside the specification.

Combined Temperature Change/High Humidity

Graph 3 shows the change in attenuation results for this test, which are within the requirement of ± 0.07 dB/km at both wavelengths.

Environmental Sequence

The temperature cycle is used as a conditioning period for the unit, and the results for this test have not been presented, as they are almost identical to those shown in Graph 1, and met the requirements of being within ± 0.07 dB/km. Graph 4 shows the change in attenuation at both 1310 nm and 1550 nm for the 1000 hour immersion in 20°C contaminated water, which again met the customer specification. The "contaminated" water is a solution of several chemicals which the customer specifies as being representative of the condition of water in their duct system. It is worth noting that the test unit has been kept immersed in the solution, and at the time of writing the paper, was still exhibiting similar results to those shown in Graph 4 - this after 570 days under test.

Hydrogen Generation

Two samples of unit were tested in one atmosphere of hydrogen at 70°C for 1000 hours, giving in both cases a measured level of hydrogen of 0.013 mg/km, well within the limit of 1.54 mg/km.

In summary, Design C performed well above the requirements set by the customer in this second phase of the programme. After examination of the results, BT issued provisional design approval for this design of two fibre, singlemode EPFU.

FINAL PHASE OF THE PROGRAMME

For the customer to issue full design approval, a pilot trial had to be performed using the product. At the time of writing this paper, the pilot trial was about to be run in two locations in the UK, to test the suitability of the product in the field, by field craftsmen.

CONCLUSIONS

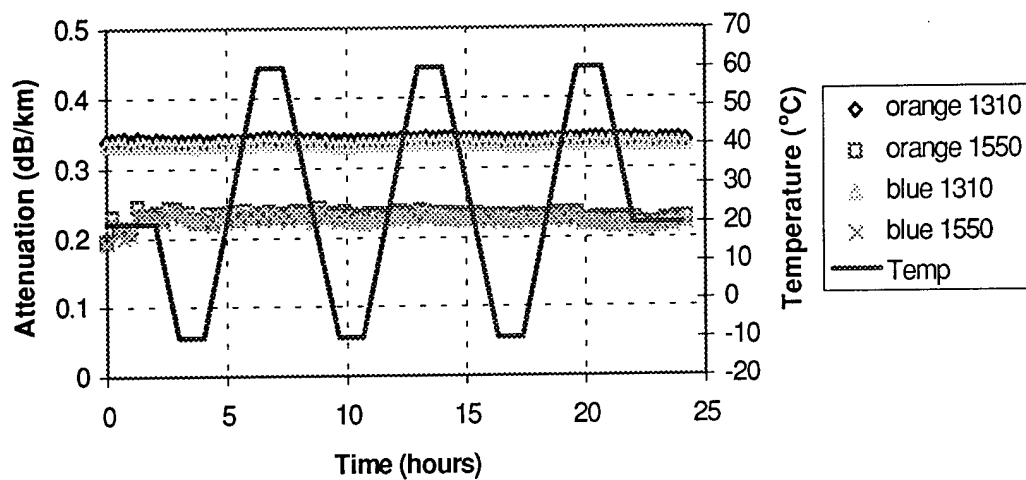
A two fibre, singlemode blown fibre unit (EPFU) has been successfully designed and developed, in cooperation with the customer. Pilot trials are under way to completely assess the product's performance under field conditions.

ACKNOWLEDGMENTS

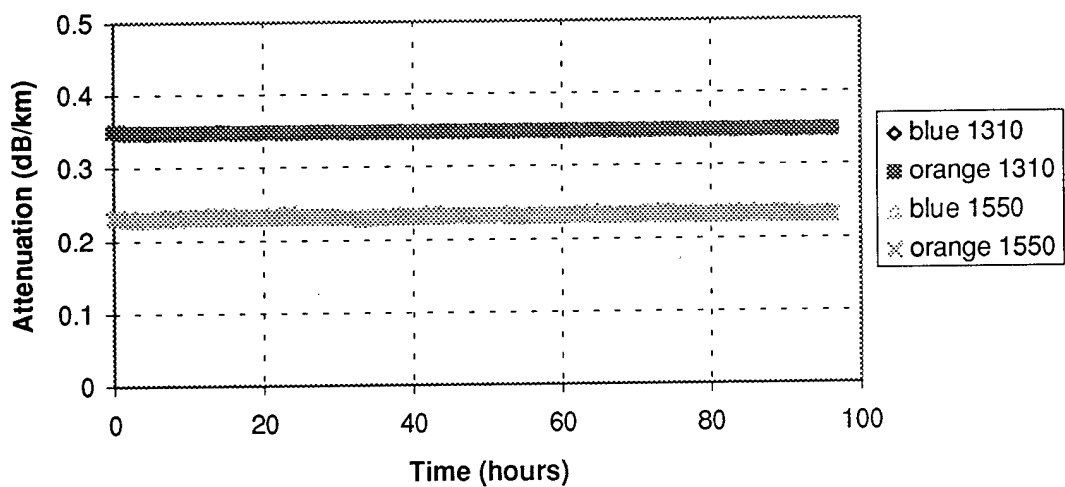
I would like to thank Jonathan Wells, Aidan Cadden, Sheila Williams and Austin Taunton, all of Optical Fibres, who performed the majority of the work and gave invaluable support in the preparation of this paper. I would also like to acknowledge the support and cooperation afforded by Ian Gauntlett of BT.

REFERENCES

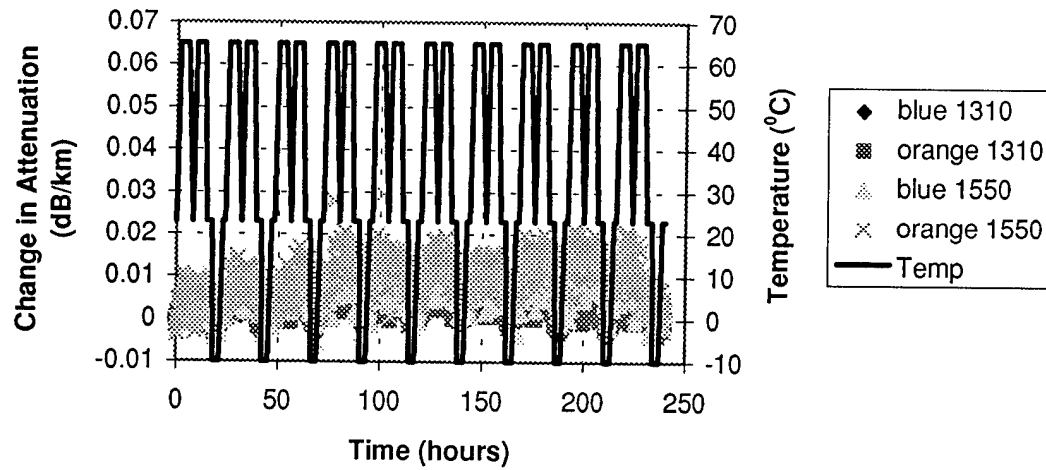
- ¹ Installation of optical fibre units using viscous drag of air by M H Reeve and S A Cassidy, BT Research Labs, Ipswich, UK; 9th European Conference on Optical Communications (1983), pp 239-42
- ² Communication Cables for Fibre in the Loop by V Abadia et al, BICC Cables; IWCS 1995, pp 659-73
- ³ BLOLITE blown fibre system performance by A Sadler, Optical Fibres Deeside, UK; EFOC/LAN'91, EFOC Proceedings (1991), pp 92-6



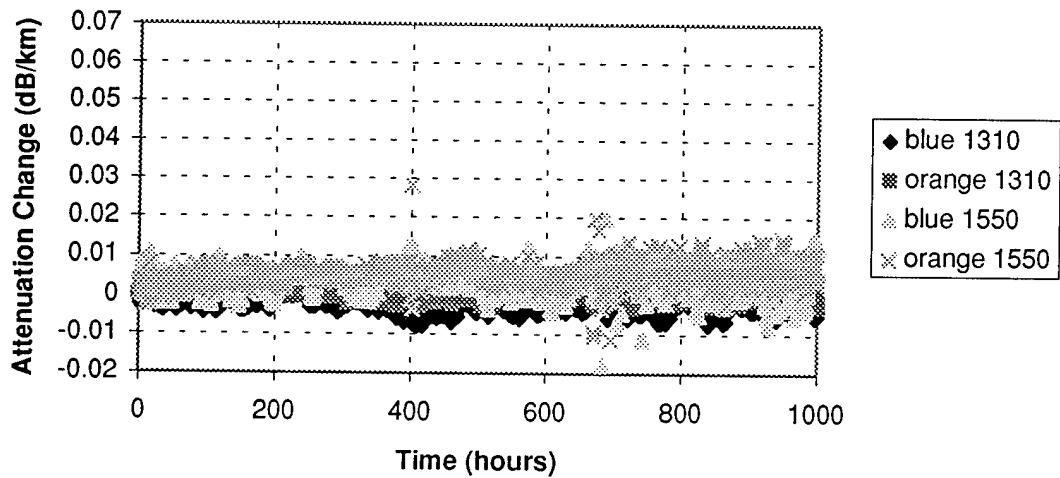
Graph 1 : Temperature Cycling Performance of Design B



Graph 2 : Attenuation Results from Cold Test



Graph 3 : Attenuation Results from Temperature/High Humidity Test



Graph 4 : Attenuation Results from Contaminated Water Immersion

AUTHOR



Paul Morris was born in 1961. After graduating in 1983 from Aston University, Birmingham with a honours degree in Physics, he joined BICC Cables as a Cable Design Engineer. In 1986, he joined Optical Fibres as Product Engineer. At present, he is Head of Product Engineering.

Optical Fibres, Second Avenue, Deeside Industrial Park, Deeside, Clywd, United Kingdom, CH5 2NX

A NOVEL METHOD FOR THE INSTALLATION OF LIGHTWEIGHT OPTICAL FIBRE UNITS INTO TUBING

J P Wells*, A Cadden*, G Brown^, P J Clayton^

* Optical Fibres, Deeside, Flintshire, Wales, UK

^ Mainetti (UK) Ltd, Jedburgh, Roxburghshire, Scotland, UK

ABSTRACT

The feasibility of installing lightweight units containing optical fibres into long lengths of small diameter tubing using pre-installed pulling threads has been examined. Various product designs have been evaluated. Designs of unit and tubing have been developed which have enabled units to be installed over lengths of up to 3km with acceptable pulling forces and optical performance after installation. The effect of bends has also been evaluated. Potential applications for the technology have been considered.

INTRODUCTION

Two main techniques have been used for the deployment of fibre in network installations, pulling and blowing.

The conventional method is to pull cables into ducts using a pulling member. Cables installed in this way are generally heavy in weight, being provided with a substantial measure of reinforcement. The philosophy behind this approach is that pulling exerts substantial forces on the optical fibre, and that the reinforcement is necessary to prevent excessive fibre strain.

The second approach uses the blown fibre technique discovered and developed by BT¹. A "cable" containing empty tubes is installed first, usually into a duct. Lightweight fibre units are then installed using a flow of fluid, usually air, into one or more of its tubes. Using a fluid has the effect that the propelling force exerted on the fibre unit is substantially the same throughout its length, and this force is less than the maximum force present in a cable that is being installed by pulling.

Accordingly, significant reinforcement of the fibre unit is not required.

The use of blown fibre technology in access networks and local area networks is now well proven. It has offered system designers a number of advantages over conventional cables, including;

- planning flexibility
- rapid fibre deployment
- deferment of fibre cost
- easy upgradeability
- ease of repair in the event of damage

Blown fibre has proved to be particularly suitable for use in the distribution and subscriber drop portions of access networks and for within building and campus type local area networks, where future fibre requirements and configuration are not easily predictable.

Investigation of the feasibility of pulling lightweight fibre units into tubes was initiated to determine whether benefits of blown fibre could be achieved using an approach offering potential advantages, such as simplicity of equipment, reduced environmental sensitivity and possibly smaller tube, higher speed or longer length capabilities.

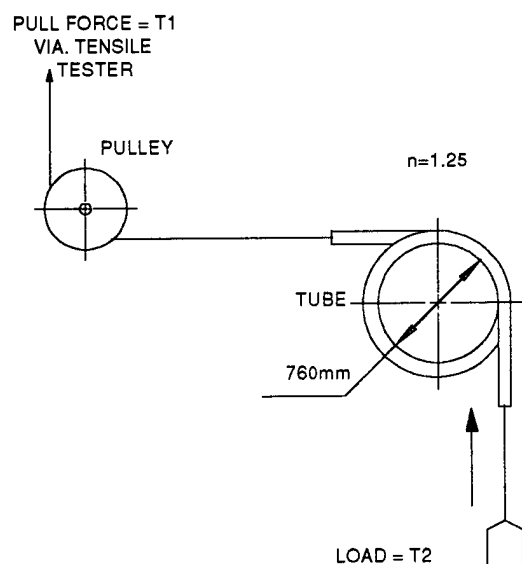
The concept of installing fibre units with little or no reinforcement was developed from the idea that by removing it from the design of a bundle of fibres the weight would be significantly reduced, resulting in reduced friction between the bundle and tube during installation. By removing the reinforcement provided to protect the fibres, the pulling forces on the fibre bundle may be sufficiently low that the fibres themselves may be able to withstand the forces comfortably.

CANDIDATE DESIGN SELECTION

A number of lightweight fibre unit designs were assembled, together with a number of alternative tube designs. The fibre units contained between one and four fibres, and were of between 0.5 and 1.7mm in diameter, while the tubes were of nominally 3.5mm inside diameter.

Dynamic friction coefficients for various combinations of units and tube designs were determined using a test rig as in fig 1.

Fig 1. Friction Test Rig



The force required to lift a 100g load at a fixed speed was determined, and from it the coefficient of friction calculated using equation 1;

$$\mu = (\log_n(T_1/T_2)) / 2\pi n \dots\dots\dots(1)$$

Coefficients of friction for various combinations are as Table 1.

On the basis of the test data fibre unit designs A and E, and tube design 1 were selected for initial pulling trials.

Table 1 Coefficient of friction μ for fibre units and tubes

Fibre Unit Type	Tube Design			
	1	2	3	4
A	0.105	0.124	0.162	0.241
B	0.122	0.142	0.146	0.212
C	0.183	0.205	0.215	0.259
D		0.160		
E	0.116	0.151		
F	0.189	0.302		

PULLING MEMBER SELECTION

The pulling member was selected based on friction performance, ease of connection to the fibre unit, cost, breaking tension, and ability to be installed within tubes during their extrusion. The rig indicated in fig 1 was used for friction determination. A variety of monofilaments and threads were evaluated, with and without lubricants. The candidate selected is a lightweight polyester braided thread, which, being of a tubular design can be directly connected to the fibre unit by sliding over the end of the unit then gripping the unit when tensioned. The thread/tube friction is lower than the fibre unit/tube friction, so the installation tension would rise during an installation, as unit enters the tube. The breaking tension of 8kg far exceeds planned installation tensions.

INITIAL PULLING TRIALS

A single tube, of design 1 containing a pulling member, was laid over a route of 1km in length, with a 180 degree bend of 1metre radius half way along the route.

The candidate units were connected to the pulling member, then pulled in using a manual winch. Despite the simplicity of the equipment used, the units were installed smoothly and rapidly, at a rate of over 100 metres/minute. Attenuation measurement made by OTDR indicated no change

between pre-installed and installed values. Tensions of less than 1kg were measured during the exercise. Inspection of the units after removal from the tube indicated no damage in the case of design A. Design E which comprised four fibres loosely contained in a thin extruded layer suffered some damage.

Fibre unit design A and tube design 1 were then evaluated in further installation tests over various routes. A powered winch, with continuous indication of pulling member tension, was used. Results are summarised in Tables 2 and 3.

Table 2 Influence of Installation Speed on Tension

Installed Length m	Included Bend Angle degrees	Installation Speed m/min	Typical Max Pulling Tension gf
1000	180	28	500
1000	180	40	600
3000	180	10	800
3000	180	28	1500

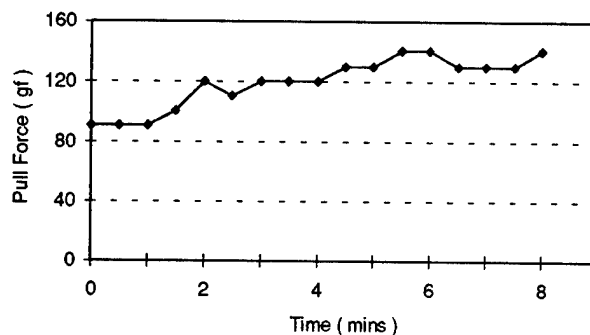
Table 3 Influence of Bend Angle on Installation Tension

Total Included Bend Angle degrees	Installation speed m/min	Installation Length m	Typical Max Pulling Tension gf
0	28	1100	500
180	28	1100	590
360	28	1100	810

All bends at pulling end.

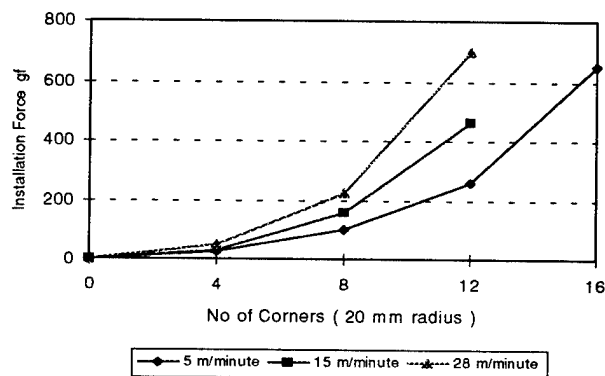
The influence of bends on installation tension was investigated over a more demanding 250 metre route in which nine 90 degree bends of 97mm diameter were spaced at 25 metre intervals. The installation tension profile is indicated in Fig 2.

Fig 2 Installation of Fibre Unit into Route with Bends (Installation speed 28m/minute)



Consideration was also given to tighter radius bends, of the type which could be experienced in office or residential applications, as shown in fig 3.

Fig 3 Pull into Route with Tight Bends



It was concluded from installations involving bends that;

- the products evaluated can be installed in routes containing significant bends.
- the apparent coefficient of friction between fibre unit and tube is higher for straight sections than for bends of less than 5 metres diameter.
- as the bend radius is reduced to 20mm the friction increases.

The influence of bend radius on friction coefficient could be usefully studied further.

WHAT IS A "SAFE" PULLING TENSION ?

In recommending a safe maximum pulling tension, several questions have been considered;

- how likely is fibre breakage, during installation and during the lifetime of the unit ?
- how strong is the unit to pulling member joint ?
- what tube or unit damage is experienced ?

Fibre Strength/Failure Considerations

The distribution of load between fibres contained within a fibre unit of design A was evaluated. A 10 metre length of a 2km unit was tensioned to 1046g and the strain on each fibre determined by the time of flight technique, using an EG&G SPL3 strain measurement system. A difference of only 0.017% strain was measured between the most and least strained fibres.

In the following analyses it has been assumed that these differences are insignificant and that the load has been equally shared between all fibres and that the fibres bear all of the load applied to the unit.

The probability of failure of any one of four fibres during an installation has been assessed using Weibull statistics². In a worst case where all of a 1km unit is under a tension of 1.5kg for two hours (strain on each fibre approximately 0.36%), the probability of failure during the installation would be much less than 1 in 100,000.

The probability of fibre failure during the operating lifetime is dependant on the residual strain in the unit. Residual strain has been experimentally determined using an artificially severe test route as indicated in fig 4. A unit was fully installed, to allow access to both ends. It was then pulled through further, while fibre strain was measured with the EG&G strain system, using the time of flight technique. As indicated in fig 5, the strain measured during installation was around 0.25%, but decayed to virtually zero once pulling was discontinued. The almost instant reduction in tension to zero has also been confirmed using mechanical measurements on units installed in longer routes, where tensions dropped from 2kg to less than 20g within minutes of completion of installation.

Fig 5. Plot of Fibre Strain Before, During and After Installation, Measured by Time of Flight Technique

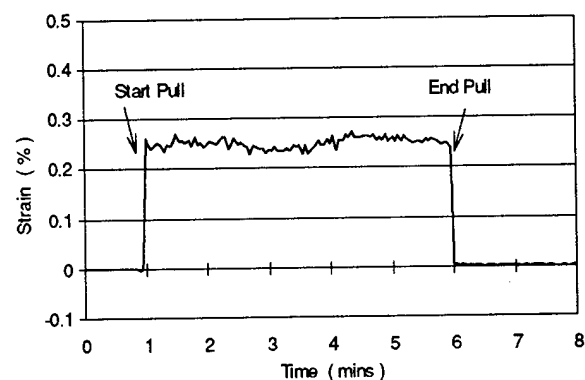
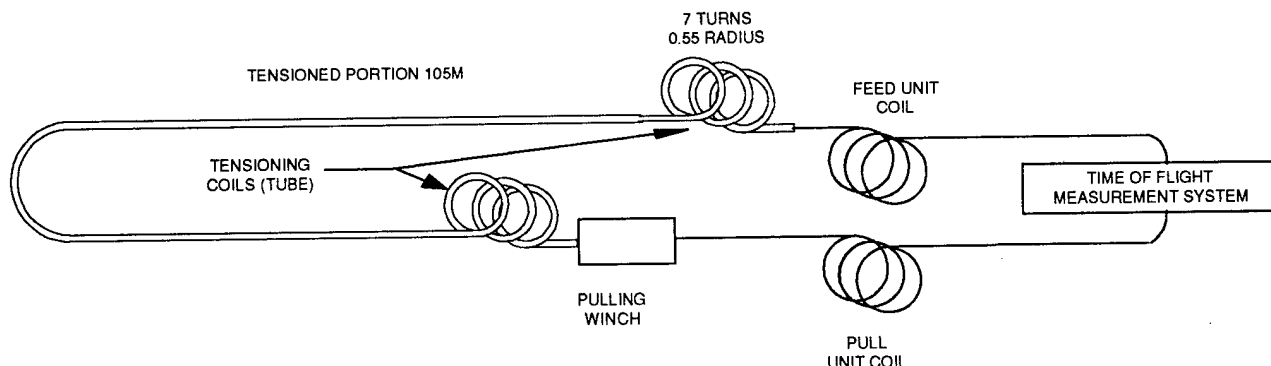


Fig 4 Residual Tension Test Layout



Using Weibull statistics it has been calculated that, for a fibre proof tested at 1% strain, if a 1km length was subjected to a residual strain of 0.28% for a lifetime of 25 years the probability of failure would be 1 in 100,000. As indicated above, residual strains have been found in practice to be insignificant.

Pulling Member/Fibre Unit Joint Strength

The breaking tension for the pulling member to fibre unit joint has been determined experimentally to be around 6kg.

Unit Wear Resistance

Units repeatedly installed over lengths totalling over 5km have been removed and inspected visually. The outer coatings have remained intact, even at elevated pull forces.

Pull Force Recommendation

Based on the above data it has been concluded that the recommended maximum pulling force of 1.5kg for a four fibre unit is safe with regard to fibre strength, pulling member to unit joint strength, and fibre unit coating integrity. In practice the maximum tension in a single pull is experienced only during the last few minutes of a pull. If the maximum recommended tension was being approached, the speed could be reduced to cause the tension to fall to more acceptable levels.

FIELD EXPERIENCE

The technology described has been used to provide fibre links to a number of business and residential premises.

Tubes have been assembled into bundles of up to 19 in a sheath, which is provided with an aluminium moisture barrier. Tube bundles have been pulled into ducts, and more heavily sheathed versions have been directly buried. Joints of tubes, and their pulling members, have been made to provide branched tubing routes, enabling the installation of unspliced links from a point to a number of destinations. Tubing joints have been contained in heat shrink or mechanical closures.

Pulling tensions required in the field have generally exceeded those experienced in early off-line testing, as indicated in the examples shown in Table 5.

Table 5 Examples of Pulled Fibre Installations

Route Length m	Formal Bends degrees	Route Type	Max Pull Tension gf
330	400	Direct Buried	330
390	210	Direct Buried	200
395	400	Direct Buried	1300
395	400	Ducted	300
690	1300	DB/Duct Mix	1500
1000	90	Ducted	1260

Optical results from all trials have been excellent, with no significant change in attenuation on installation.

Techniques of onward pulling have been developed, enabling the making of longer spliceless links installed in a series of pulls. Links of up to 3.4km have so far been provided using these techniques.

Conclusions drawn from the field trials include the following;

- the degree of bends experienced in practice generally far exceeds the predicted figures. Drawings are generally plan views and take little account of bends in the vertical plane. Obstacles such as lamp posts and driveways also have to be circumnavigated.
- higher pull forces are required for installation into ducted tube bundles than were required in the preliminary trials, which had used single, unsheathed tubes. The more rigid nature of the bundles and the set held by them effectively add bends to the routes.
- higher forces are required for installation into direct buried routes than for ducted routes, due to trench undulations and bending caused during refill.
- the maximum single pull installation distance for typical ducted routes is around 1000 metres, while for direct buried routes the maximum is around 500 metres. Longer distances can be achieved by onward pulling.

POTENTIAL APPLICATIONS FOR PULLED FIBRE TECHNOLOGY

Pulled fibre is particularly suited to applications where fibre demand is uncertain or likely to change. It is simple and relatively cheap to install tubing or tubing bundles, while fibre units with appropriate fibre counts can be quickly installed once requirements are clear. Concerns over prediction of capacity requirements for the future can be overcome by installation of multi-tube bundles and initial occupation of only one or two tubes, with other tubes available for future installation as necessary. The prime application for the technology is seen in provision of fibre to business or domestic premises.

- The simplest form could be provision of links from a node of a traditional cable into customer premises.
- The flexibility of joining and branching tubes makes it attractive in developing residential or business areas, where branched tube systems could be formed and subsequently pulled through without need for fibre splices at all branch points.
- A cable ring or branch could even be replaced with a larger tube count bundle, giving potential for installation of unspliced links all the way from an exchange to the customer.

Further potential for application exists in within building and campus type local networks. Low fire hazard tube bundle types have been developed to meet fire regulations. The installation equipment is compact, fume-free and quiet, such that it can be operated within occupied areas without disturbance.

The cost benefits of pulled fibre depend largely on the application architecture. In studies conducted to date costs have been less than for provision of conventionally cabled links, while providing additional benefits including future upgradeability.

FUTURE WORK

Further work is planned in a number of areas;

- development of tube and fibre unit designs to reduce friction and increase installation capability.

- modelling of route features to enable confident prediction of installation forces.
- evaluation of costs for alternative architectures.
- refinement of installation equipment.
- investigation of potential for reduction of tube dimensions.
- alternative tube and fibre counts.

CONCLUSIONS

The feasibility of installation of fibre units into long lengths of tubing by means of a lightweight pulling member has been demonstrated.

Studies have indicated that the reliability of the fibres is unlikely to have been worsened by the installation technique.

The products have already been used in active networks. Significant advantages over conventional cables, particularly in network planning flexibility have been identified for some portions of networks.

ACKNOWLEDGEMENTS

The authors would like to acknowledge the contributions made by many colleagues at Mainetti and Optical Fibres. The efforts of Colin Kirkpatrick of Mainetti have been particularly significant.

REFERENCES

1. Installation of optical fibre units using viscous drag of air, M H Reeve and S A Cassidy, BT Research Labs, Ipswich, UK; 9th European Conference on Optical Communications (1983), pp239-242
2. Optical Fibres Application Note AN3, Strength of Optical Fibres. Available on request.

BIOGRAPHIES



JONATHAN WELLS
Optical Fibres
Second Avenue
Deeside Industrial
Park, Deeside,
Flintshire, UK
CH5 2NX

Jonathan Wells has been with Optical Fibres for 11 years and is currently Head of Special Products. He received his B.Sc. honours degree in Chemical Engineering from the University of Leeds in 1982, and is a Chartered Engineer.



AIDAN CADDEN
Optical Fibres
Second Avenue
Deeside Industrial
Park, Deeside,
Flintshire, UK
CH5 2NX

Aidan Cadden has worked in a variety of technical roles within Optical Fibres for 11 years and is currently a Development Engineer within the Special Products department. He received his B.Sc. honours degree in Applied Chemistry (Polymer and Colour Science) from Queen's University Belfast in 1970.



GEORGE BROWN
Mainetti (UK) Ltd
Annfield Estate
Oxnam Road
Jedburgh, Roxburgh-
shire, UK, TD8 6NN

George Brown completed a degree in Economics at Hull University, in 1974. He joined Mainetti (UK) Ltd in 1979 as Factory Manager, with responsibility for injection moulding and extrusion activities. In 1986 he became General Manager of the Industrial Products Division and was then appointed as a Board Member. In 1996 he has been appointed as Chief Executive of Mainetti (UK) Ltd - Industrial Products.



PHIL CLAYTON
Mainetti (UK) Ltd
Burnfoot Industrial
Estate, Hawick,
Roxburghshire,
UK, TD9 8RW

Philip Clayton became a Chartered Mechanical Engineer in 1972 and worked at Fothergill and Harvey on the development of high performance plastic coatings and insulations for wires and cables. In 1982 he became Technical Manager with the high performance division of the GEC Cable Group. He joined Mainetti (UK) Ltd in 1994 and is currently developing miniature duct systems for the local loop fibre optic network.

EVALUATION OF THE ABF-MULTIPLEX INSTALLATION TECHNIQUE AND ITS APPLICATION IN CUSTOMER ACCESS OPTICAL FIBER NETWORK

Yoku Matsumoto Tadatoshi Kubo Mitsuhiro Ohta Kusuo Sanjo Kikaku Tokumaru

Kansai Electric Power Co., Inc. Osaka, JAPAN Sumitomo Electric Industries, Ltd. Osaka, JAPAN

ABSTRACT

In order to establish a communications network infrastructure for customers in the future information society, the Kansai Electric Power Co., Inc. (KEPCO) is promoting the construction of customer access optical fiber networks. But in providing access for each customer, the transmission routes will continually change as the number of customers changes.

The Air Blown Fiber (ABF) technique¹ has been used since 1988 as a optical fiber installation method which can cope with such transmission route changes. With the ABF technique, ABF units (i.e. slender optical fiber-bundle) is blown into previously laid slender pipe using compressed air, so the ABF unit can be installed or removed at any time.

In this paper, the Authors, we have verified the feasibility of applying the ABF technique to customer optical fiber networks. For instance the applications of this technique have been put into use in the systems for monitoring power distribution equipment at Expo '90 (the 1990 International Garden and Greenery Exposition) and at Kansai International Airport. Also, in order to enlarge the potential scope of application, we studied ABF units with multiple cores, and succeeded in installing 36-core ABF units.

With the conventional ABF technique, a second ABF unit cannot be laid in an ABF pipe already containing one ABF unit. However, if multiple ABF units could be passed through a single ABF pipe and then branch in any desired direction, transmission routes could adapt more flexibly to changes in the number of customers. Moreover, reducing the number of ABF pipes provides cost savings. Therefore feasibility study of the ABF-Multiplex installation technique that an additional ABF unit can be installed into an ABF pipe which is already

occupied by other ABF units was carried out. And we developed the tools necessary for installing additional ABF units and the equipment to enable the ABF units to branch in any direction.

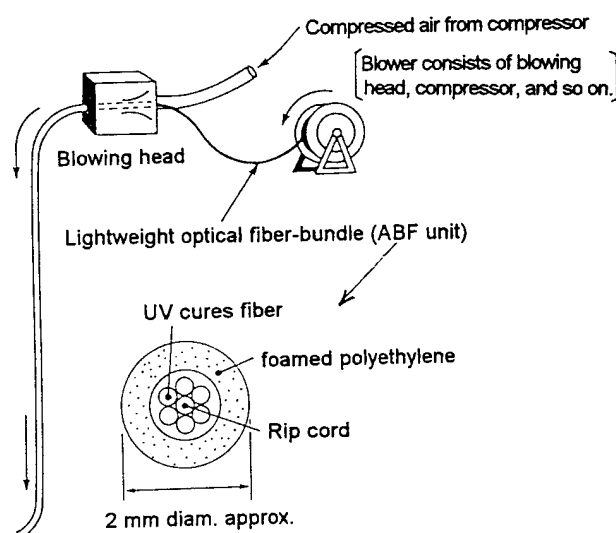


Fig. 1: ABF Technique

EVALUATION OF APPLYING THE ABF TECHNIQUE TO CUSTOMER ACCESS OPTICAL FIBER NETWORKS

With the ABF technique, ABF units (optical fiber-bundle covered with foamed polyethylene, light and slender) are installed in or removed from the ABF pipe (made of plastic) by compressed air blowing. ABF unit is usually contained 6-cores of optical fiber.

With this application, ABF pipe is frequently assembled with an underground power cable. Therefore the pipe must have sufficient outer diameter to avoid applying direct sidewall pressure to the ABF pipe when installing the ABF pipe assembled cable into the con-

duit. Consequently, in our experiment two types of pipe were used: one with inner diameter of 6mm and outer diameter of 8mm (simplified as "d_i 6mm /d_o 8mm" below), and another with d_i 8mm /d_o 10mm.

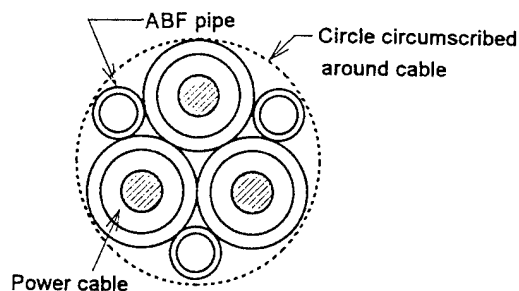


Fig. 2: Power Cable Assembled with ABF Pipe

Limit Blowing length of 6-core ABF Unit

The blow end pressure P_1 needed to blow an ABF unit the entire length through a pipe of length L_0 is given by the following formula.²

$$P_1 = \left\{ P_0^{\frac{7}{4}} + \frac{7}{4} L_0 \frac{0.3164 \rho}{2dg} \left(\frac{d}{v} \right)^{-\frac{1}{4}} (kA)^{-\frac{3}{4}} P_0^{\frac{3}{4}} Q^{\frac{7}{4}} \right\}^{\frac{4}{7}}$$

Where:

P_0 = Atmospheric pressure

L_0 = Pipe length

d = Pipe inner diameter

g = Gravitational acceleration

v = Kinematic viscosity of air

k = Cross-sectional coefficient determined by the combination of the pipe and ABF unit

A = Pipe cross-sectional area

Q = Air flow rate required at pipe outlet

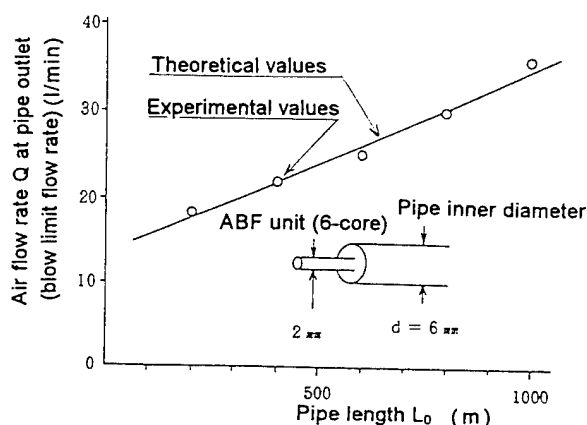


Fig. 3: Pipe Length L_0 and Flow Rate (Q) at Pipe Outlet (blow end pressure 7 kg/cm²)

Fig. 3 shows the relationship between the pipe length L_0 and the air flow rate at the pipe outlet (Q) when the blowing pressure at the end of the pipe is 7 kg/cm², and there is a good match between experimental and theoretical values. This makes it possible to calculate the required blowing pressure at the end pressure when the pipe length is fixed, as well as the limit blowing length when the blowing pressure is fixed.

Blowing Length and Blowing time

Fig. 4 shows the relationships between blowing length and blowing time, when a 6-core ABF unit is installed in an ABF pipe laid into 16 routes at different length (total length 7 km). We confirmed that blow time is not proportional to blowing length, but the longer the blowing length, the more time will be needed. In the case sets of blowers can be used in series setting to effectively install ABF unit was developed.

Based on the above results, KEPCO used the ABF technique to lay the optical fiber network necessary for constructing a power distribution equipment monitoring system at Expo '90, and for introducing an integrated distribution automation system for performing telemetering, remote load control and other tasks at Kansai International Airport.

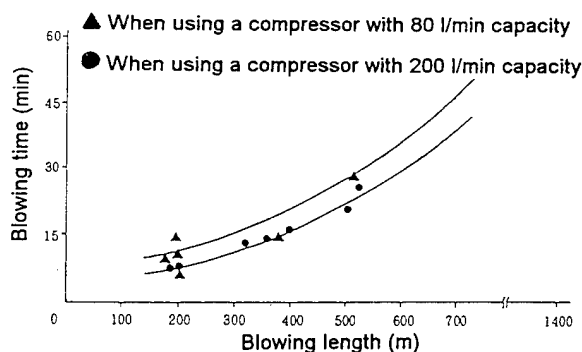


Fig. 4: Blowing Length and Blowing Time (6-core ABF unit)

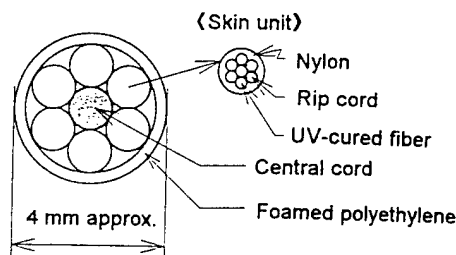


Fig. 5: 36-core ABF unit

VERIFICATION OF BLOWING CHARACTERISTIC OF A 36-CORE ABF UNIT

Structure of a 36-core ABF unit

The cross sectional structure of the 36-core ABF unit is shown in Fig. 5.

Verification of Basic Blowing Characteristics

In order to examine the basic blowing characteristics of a 36-core ABF unit, the blowing characteristics were verified using two types of ABF pipe which were wound respectively in one layer around the cylinder shown in Fig. 6. (Two types of ABF pipe: d_i 6mm / d_o 8mm and d_i 8mm / d_o 10mm)

It was impossible to blow the 36-core ABF unit into ABF pipe with d_i 6mm / d_o 8mm.

The blowing characteristics of the ABF pipe with d_i 8mm / d_o 10mm are given in Fig. 7. As shown in Fig. 7, it was possible to blow the 36-core ABF unit and make it reach to 250 m with constant speed, but the speed was sharply slow down when the unit exceeded position of 260 m. Therefore it is considered that the blowing length was limited within about 300 m.

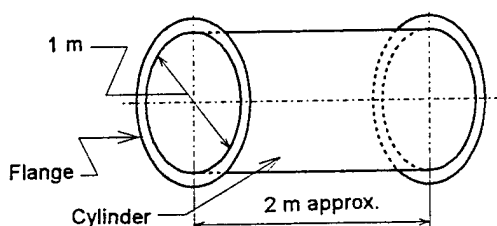


Fig. 6: Long Cylinder

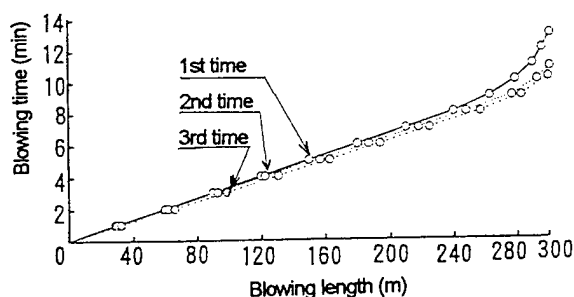


Fig. 7: Blowing Characteristics of 36-core ABF Unit (data with $n=3$)

BASIC VERIFICATION OF THE ABF-MULTIPLEX INSTALLATION TECHNIQUE

We defined the "ABF-Multiplex installation technique "

that an additional ABF unit can be installed into an ABF pipe which is already occupied by other ABF units.

Basic Characteristics of ABF-Multiplex Installation

The conventional ABF technique involves blowing only one ABF unit into a each ABF pipe. To examine the feasibility of the ABF-Multiplex Installation technique, initially we attached the branch connector shown in Fig. 8 to an ABF pipe (d_i 6mm / d_o 8mm) coiled with a diameter of 1 m at the ABF unit threading end as showing in Fig. 8. And then a 6-core ABF unit was installed into the ABF pipe, firstly through one inlet of the branch connector, finally another 6-core ABF unit was also successfully installed in the same ABF pipe via the other inlet.

Fig. 9 shows the relationship between blowing length and blowing time during ABF-Multiplex Installation. As Fig. 9 shows, we confirmed that additional ABF unit can be installed into 20-meter long ABF pipe.

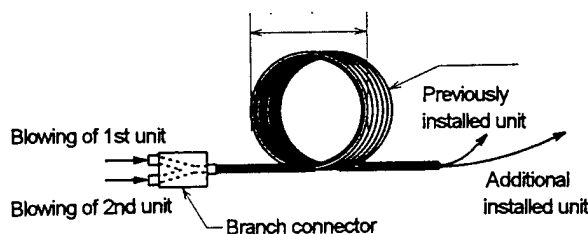


Fig. 8: Basic Concept of the ABF-Multiplex Installation

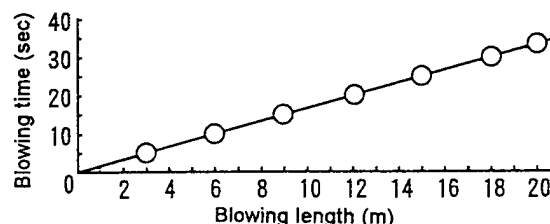


Fig. 9: Blowing Length and Blowing time for ABF-Multiplex Installation

Basic Characteristics with Long Pipe

Next, to examine the blowing characteristics for long pipes, we carried out ABF-Multiplex Installation for various length of ABF pipes (length 100-500 m) which were wound a single layer around the long cylinder

shown in Fig. 6. The basic characteristics for these cases were thus verified.

Table 1 shows the verification results. Table 1 shows that when there are units already installed, (even with the same conditions) there are some cases which were successfully blown into the entire length, and others which stopped somewhere in the way of pipe. The cause of the stopping is considered that the some points of previous installed ABF units present on obstacle to the additional ABF units. ABF pipe with d_i 8mm / d_o 10mm tends to be less susceptible to such stoppages than the ABF pipe with d_i 6mm / d_o 8mm. The d_i 8mm / d_o 10mm pipe also has more stable ABF-Multiplex Installation characteristics.

Where for the cases of that the additional ABF units can be successfully blown through the entire pipe with the length below 200 m, no matter the types of the pipe is d_i 6mm / d_o 8mm or d_i 8mm / d_o 10mm both, the blowing speed are at 33~44 mm. The presence of

previously installed units had almost no effect on blowing characteristics in such cases. However, for pipe length greater than 300 m, the installed units began to affect blowing performance. More over, it was found that the insulation of additional ABF units into a 500 m long pipe was impossible.

Through the above experiments, we confirmed the feasibility of the ABF-Multiplex installation technique which is possible to install ABF unit over distances of a few hundred meters, with one or two ABF units installed.

Blowing Characteristics with Various Branching Conditions

With the ABF-Multiplex installation technique, some branches of ABF pipe route can be connected to the trunk pipe somewhere, in which ABF units were installed. So we carried out experiments similar to such cases, and verified blowing characteristics under vari-

Table 1: Results of Verifying Basic Characteristics using Long Pipe

Experiment conditions	1	2	3	4	5	6	7	8	9	10	11	12	13	14	15				
Pipe type	d _i 6mm / d _o 8mm																		
Pipe length (m)	100			200			300			400			500						
Number of units previously installed	0	1	2	0	1	2	0	1	2	0	1	2	0	1	2				
Entire blowing ratio	3 / 3	2 / 3	2 / 3	3 / 3	3 / 3	2 / 3	3 / 3	3 / 3	0 / 3	1 / 3	1 / 1	◇	1 / 1	1 / 1	◇				
Experiment conditions	16	17	18	19	20	21	22	23	24	25	26	27	28	29	30	31	32	33	34
Pipe type	d _i 8mm / d _o 10mm																		
Pipe length (m)	100				200				300				400				500		
Number of units previously installed	0	1	2	3	0	1	2	3	0	1	2	3	0	1	2	3	0	1	2
Entire blowing ratio	3 / 3	3 / 3	3 / 3	—	3 / 3	3 / 3	3 / 3	2 / 3	3 / 3	3 / 3	3 / 3	0 / 3	1 / 1	1 / 1	0 / 1	◇	1 / 1	0 / 1	◇

(Note 1) In the figure A/B in the row labeled "Entire blowing ratio", A indicates the number of times the ABF unit was successfully blown laid into the entire length, and B indicates the number of times the experiment was carried out.

(Note 2) ◇ indicates that this case was not carried out.

Table 2: Pipe Length A-B-C Combinations (unit: m)

No	1	2	3	4	5	6	7	8	9
A	0			100			150		
B	0	50	100	0	50	100	0	50	100
C	150			100			50		

Trunk line: Pipe A to Pipe C

Branch line: Pipe B to Pipe C

Blowing sequence 1st unit = A→C (0 ABF units installed)

2nd unit = A→C (1 ABF unit installed)

3rd unit = B→C (2 ABF units installed)

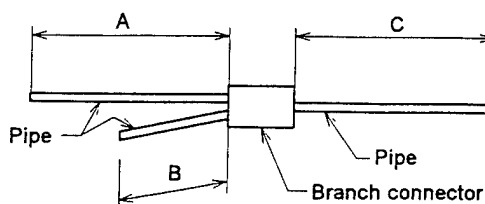


Fig. 10: Blowing Conditions of ABF pipes with Different Trunk Length and Branch Length

ous branching conditions. For the d_i 6mm / d_o 8mm ABF pipe, with the pipe length combinations indicated in Table 2 and Fig. 10. Three ABF units were blown in the following sequence: 1st unit A→C, 2nd unit A→C, 3rd unit B→C.

Table 3 shows the verification results. Under all sets of conditions, the blowing characteristics are almost the same with a blowing speed of 33-40 m/min, and there is almost no difference in blowing characteristics when the number of units installed previously less than two. These results confirmed that the presence of previously installed units has almost no affect on blowing conditions, (regardless of pipe branching) within the range checked in

Table 3: Results of Verifying Blowing Characteristics with Various Branch Conditions

Experiment conditions		1	2	3	4	5	6
Pipe length A-B-C combinations (m)	A	50			100		
	B	0	50	100	0		50
	C	150			100		
Entire length blowing ratio		3 / 3	3 / 3	3 / 3	3 / 3	3 / 3	3 / 3
Experiment conditions		7	8	9			
Pipe length A-B-C combinations (m)	A	150					
	B	0	50	100			
	C	50					
Entire length blowing ratio		3 / 3	3 / 3	3 / 3			

(Note) In the figure A/B in the row labeled "Entire length blowing ratio", A indicates the number of times the ABF was successfully laid into the entire length, and B indicates the number of times the experiment was carried out.

these experiments (i.e. pipe length 200-250 m). Consequently, we verified that ABF-Multiplex installation technique is highly feasible even if a branch is required to connected to the trunk pipe somewhere, as long as the pipe length is in the range 200-250 m.

DEVELOPMENT OF A PIPE BRANCHING TOOL FOR ABF-MULTIPLEX INSTALLATION TECHNIQUE

We defined that a "pipe branching tool for ABF-Multiplex installation technique" (hereafter referred to as the "branching tool") was a tool for ABF-Multiplex installation technique which allows a branch pipe to be connected at any location in an ABF pipe, in which there are installed ABF units. And it has been already developed.

The branching tool as shown in Fig. 11 is used to open the trunk pipe for making a new branch at any desired point of the pipe, in which there are installed 6-core ABF units, if a new 6-core ABF unit is required to install into the branch from that point.

The typical advantage of this branching tool we developed is that it can be attached to the ABF pipe easily without any cutting off the previously installed ABF units. In practical use, as shown in Fig. 12, the branching tool can be divided into two types: nozzle type (in which the branching tool is attached in the gap between the installed ABF unit and the ABF pipe) and a slit type (in which the branching tool is mounted on each ABF pipe, and the installed ABF unit is released to the outside of the tool via a slit in the tool). The slit

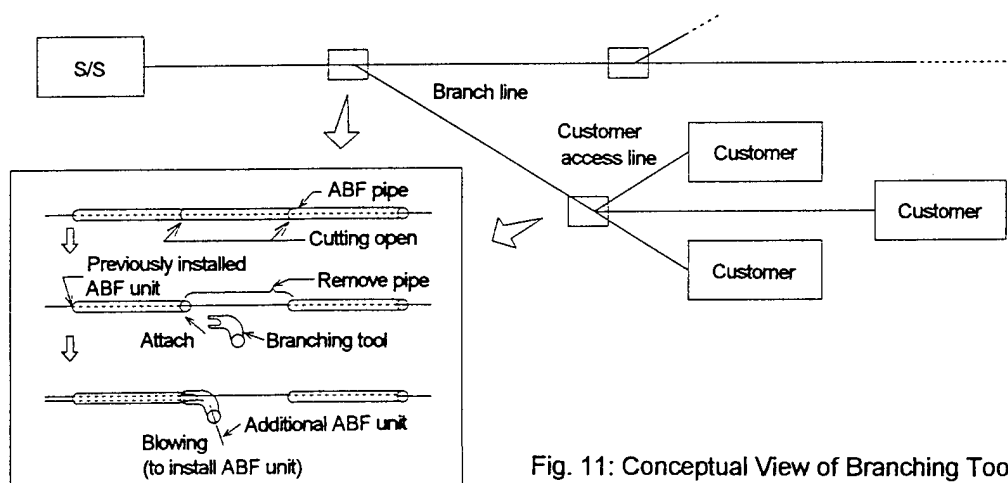


Fig. 11: Conceptual View of Branching Tool Utilization

type is furthermore classified according to the method of attaching on the ABF pipe as the cylindrical connector type and the 2 pieces-split type (in which the ABF pipe and the installed ABF units are held).

Table 4 shows the verification results, that ABF units were able to be blown by using each type of branching tool which were attached to an ABF pipe with d_i 6mm / d_o 8mm. These results show that the nozzle type offers the best performance.

DEVELOPMENT OF A BRANCHING UNIT WITH BRANCH SELECTION CAPABILITY

In order to install additional ABF units from a trunk pipe to a selected branch pipe, we developed a branching unit with branch selection capability

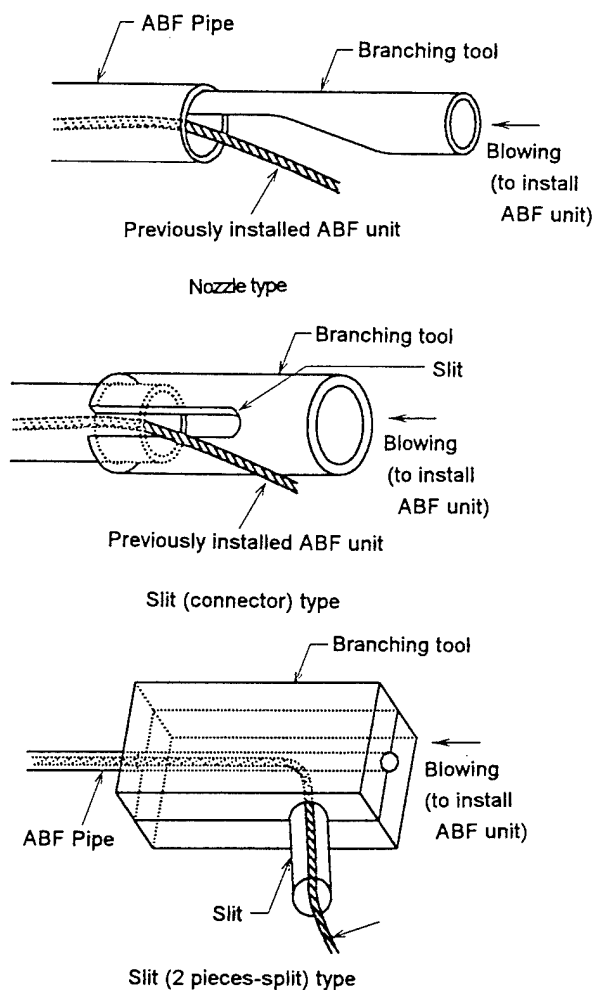


Fig. 12: Branching Tools

(hereafter referred to as a "branching unit") which an objective branch can be freely selectable.

As shown in Fig. 13, the branching unit is installed be-

Table 4: Verification Results of Blowing Characteristics Using Branching Tool

Experiment conditions	1	2	3	4	5	6	7	8	9
Branching tool type	Nozzle system								
Pipe length (m)	100			200			300		
Number of units previously installed	0	1	2	0	1	2	0	1	2
Entire length blowing ratio	◇	◇	◇	3/3	3/3	3/3	3/3	1/3	1/3
Experiment conditions	10	11	12	13	14	15	16	17	18
Branching tool type	Slit type								
Pipe length (m)	100			200			300		
Number of units previously installed	0	1	2	0	1	2	0	1	2
Entire length blowing ratio	3/3	0/3	◇	◇	◇	◇	◇	◇	◇
Experiment conditions	19	20	21	22	23	24	25	26	27
Branching tool type	Slit type								
Pipe length (m)	100			200			300		
Number of units previously installed	0	1	2	0	1	2	0	1	2
Entire length blowing ratio	3/3	1/3	0/3	3/3	0/3	◇	◇	◇	◇

(Note 1) In the figure A/B in the row labeled "Entire length blowing ratio", A indicates the number of times the ABF unit was successfully blown into the entire length, and B indicates the number of times the experiment was carried out.

(Note 2) ◇ indicates that this case was not carried out.

forehand (during pipe construction) at a branch point where the ABF pipe route branches from one trunk line into several branch lines. With this unit ABF units can be blown to go from the end of single pipe to the end of branch pipes.

The branching unit must therefore allow the selection of the objective pipe on the branch side in which the ABF unit is required to be installed.

There are two prototypes of branching unit we manufactured as show in Fig. 14, the single valve type and the double valve type. With the particular construction of these valve, the selective branch pipe can be opened for blowing ABF units into it, at the same time another pipe can be closed.

Each branching unit was connected to ABF pipes (d_i 6mm / d_o 8mm) with the different length shown in Table 5 and Fig. 16. The branch selection capability was verified by blowing in ABF units in the following se-

quence: 1st unit I→II, 2nd unit I→III, 3rd unit I→II.

Table 6 shows the verification results. In the cases, with both types of the valve, when ABF units were successfully blown into entire length, they also could be successfully blown into selective branch pipes. The results also show that the single valve type has slightly superior blowing performance.

On the other hand, the number of times that the ABF unit was successfully blown into entire length decreased as the length of pipe A increased, as shown in Fig. 15. But each case in which the stoppage was due to the ABF unit being caught by the branching unit. As shown in Fig. 16, since the valve of the twin valve type pushes the previously installed ABF unit, and this produces some resistance to obstruct to the additional ABF unit to go into the selective pipe. There is no problem in using the valve of a single valve type.

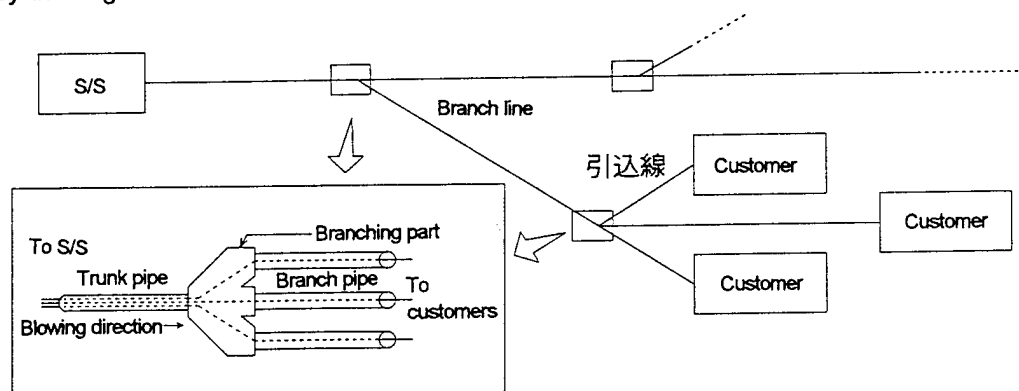


Fig. 13: Conceptual View of Branching Unit Utilization

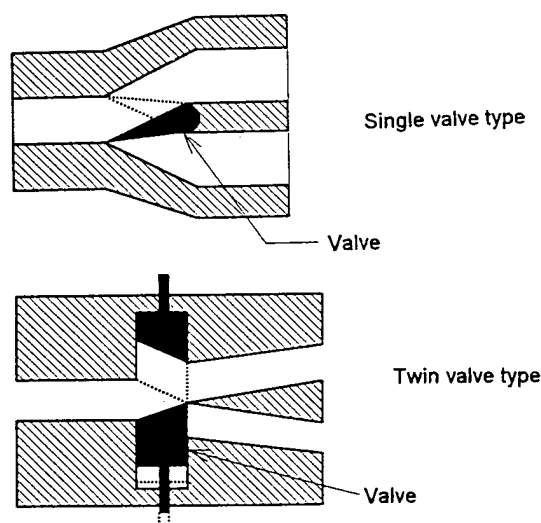


Fig. 14: Branching Unit Prototypes

Table 5: ABF Pipe Combinations
(unit: mm)

No	1	2	3
A	0	50	100
B	100	100	100

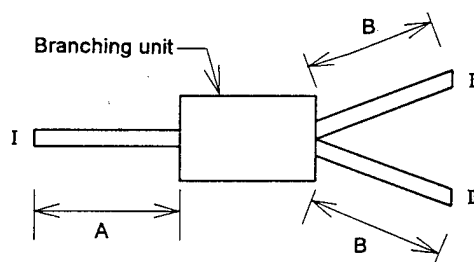


Fig. 15: ABF Pipe Blowing Conditions for Branching Unit Evaluation

Table 6: Verification Results of blowing Characteristics Branching Unit Using

Experiment conditions		1	2	3	4	5	6	7	8	9
Branching unit type		Single valve type								
Pipe length A-B combination	A	0			50			100		
	B	100			100			100		
Number of units previously installed		0	1	2	0	1	2	0	1	2
Entire length blowing ratio		3/3	3/3	3/3	3/3	2/3	3/3	3/3	1/3	0/3
Number of units into blowing the selective brunch pipe		3/3	3/3	3/3	3/3	2/3	2/3	3/3	1/3	0/3
Experiment conditions		10	11	12	13	14	15	16	17	18
Branching unit type		Twin valve type								
Pipe length A-B combination	A	0			50			100		
	B	100			100			100		
Number of units previously installed		0	1	2	0	1	2	0	1	2
Entire length blowing ratio		3/3	3/3	3/3	3/3	2/3	1/3	3/3	1/3	0/3
Number of units into blowing the selective brunch pipe		3/3	3/3	3/3	3/3	2/3	1/3	3/3	1/3	0/3

(Note) In the figure A/B in the row labeled "Entire length blowing ratio" and , "Number of units into blowing the selective brunch pipe". A indicates the number of times the ABF unit was successfully blown into the entire length, and the objective pipe and B indicates the number of times the experiment was carried out.

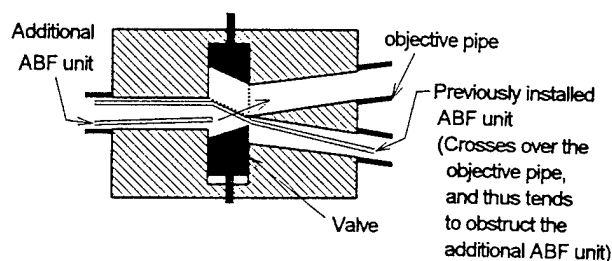


Fig. 16: Problems with the Twin-valve Type

CONCLUSION

In this report, we described experiments and showed the feasibility of applying the ABF technique to customer access optical fiber networks. And that the practical methods developed will allow the ABF technique to be used widely in customer access optical fiber networks. We investigated the blowing length limits for an ABF unit using a single blower, and thus realized that the blowing length could be extended by using an additional blower. In trying to increase the number of cores in each ABF unit, we realized that a 36-core ABF unit could be blown up to a distance of 300 m. Furthermore, in order to deal with the continually changing number of customers, we also developed a technique to allow additional ABF units to be installed. We successfully developed the tools necessary to support the ABF-Multiplex installation technique,

and equipment enabling the blowing of ABF units in any brunch.

This is an interim report on developed technology for installing ABF unit, in which an ABF pipe is assembled with an underground cable. However, the use of ABF pipes with larger inner and outer diameter would be viable when ABF pipe is laid independently, and the technology necessary to utilize this technique is now in development.

In the future, we will continue to make advances in constructing highly flexible customer access optical fiber networks incorporating the technology described in this paper.

REFERENCES

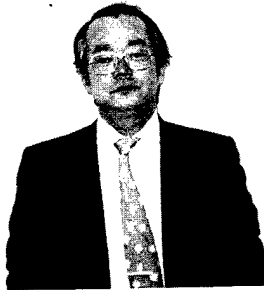
1. S.A. Cassidy, M.H. Reeve, Proceedings of IWCS '83 pp250-254 (1983)
2. Y. Matsumoto, et al., 1989 NATIONAL CONVENTION RECORD I.E.E. JAPAN No. 1177 (1989)

AUTHORS



Yoku Matumoto was born in Hyogo, JAPAN on April 28, 1943. He received the B.S. and M.S. degrees in Electrical Engineering from Kyoto University, Kyoto, in 1968. He joined Kansai Electric Power distribution network, development of power distribution equipment and distribution automation system. Currently, Mr. Matumoto is a general manager of Distribution Network Engineering Group, General Office of Customer Relations & Services.

His mailing address is 3-3-22 Nakanoshima Kita-ku, Osaka, 530-70 JAPAN



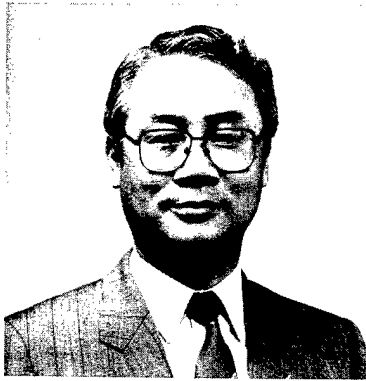
Tadatoshi Kubo was born in Mie, JAPAN on November 29, 1951. He received the B.S degree in Electrical Engineering from Osaka City University, Osaka, in 1975. He joined Kansai Electric Power Co., Inc. in 1975 and has been engaged in development of distribution automation system. Currently Mr. Kubo is a manager of Distribution Network Engineering Group, Office of Customer Relations & Services.

His mailing address is 3-3-22 Nakanoshima Kita-ku, Osaka, 530-70 JAPAN



Mitsuhiro Ohta was born in Osaka, JAPAN on November 28, 1961. He received the B.S. degree in Electrical Engineering from Osaka City University Osaka, in 1985. He joined Kansai Electric Power Co., Inc. in 1985 and has been engaged in development of transmission lines for distribution automation system. Currently, Mr. Ohta is a deputy manager of Distribution Network Engineering Group, General Office of Customer Relations & Services.

His mailing address is 3-3-22 Nakanoshima Kita-ku, Osaka, 530-70 JAPAN



Kusuo Sanjo was born in Hyogo, Japan on June 16, 1941. He received the B.S. degree in Electrical engineering from University of Tokyo, Tokyo, in 1964. He joined Sumitomo Electric Industries, Ltd. in 1964 and has been engaged in quality assurance, production engineering, design and development of high voltage XLPE cable & accessories. Currently, Mr. Sanjo is a director, Senior General Manager.

His mailing address is 1-1-3 Shimaya, Konohana-ku, Osaka, 554 JAPAN



Kikaku Tokumaru was born in oita on January 30, 1958. He received a B.S. degree in 1980 and M.S. degree in 1982 in electrical and electronics engineering from Toyohashi University of Technology. He joined in Sumitomo Electric Industries, Ltd. in 1982 and has been engaged in design of distribution cables. Currently, Mr. Tokumaru is a chief research associate of Energy Apparatus & Systems R & D Department.

His mailing address is 1-1-3 Shimaya, Konohana-ku, Osaka, 554 JAPAN

STUDY OF OPTICAL FIBER RIBBON STRUCTURAL DIMENSIONS

T. Kawano, M. Ito, T. Murase, H. Nakamura, T. Shiono, and M. Saegusa

Showa Electric Wire & Cable Co., Ltd.

1, Nabekura, Funaoka, Shibata-Machi, Shibata-Gun, Miyagi-Ken 989-16, Japan

1. ABSTRACT

A previous report on the lateral pressure properties of optical fiber ribbon found that finite element method (FEM) analysis and experiments indicate that the stress transmitted to optical fiber can be reduced by increasing the Young's modulus of the secondary coating and ribbon coating and by increasing their thickness.¹⁾

In this report, based on these results, a study was made of the ribbon thickness and material in a temperature region of -40 to 70°C using FEM and calculation of the shrinkage force. Fiber ribbon was made using the materials whose characteristics were determined in this study, and as a result of testing the lateral pressure properties and low-temperature properties of the fiber ribbon and the temperature properties of the cable, it was confirmed that the same performance can be ensured even if the ribbon thickness is reduced from 0.4 mm to 0.3 mm.

2. INTRODUCTION

As optical cable is made narrower, lighter, and at lower cost, studies have been carried out for reducing the thickness (0.3 mm) of mounted fiber ribbon.²⁾ One typical cable structure using fiber ribbon is a tape slot type cable, which has long provided adequate use results and good performance. In studies to

reduce the ribbon thickness, it has been possible to apply conventional cable structure design techniques, provided that the thinner fiber ribbon has undiminished performance. From this standpoint, this time we examined, for 4-fiber ribbon, thin ribbon (0.3 mm thick) having the same performance as previous ribbon (0.4 mm thick \times 1.1 mm wide), and we evaluated its performance in tight structure slotted core cable.

Because the lateral pressure properties are reduced when the fiber ribbon is made thinner, we conducted a stress analysis by FEM and made a selection of materials needed for ensuring the same performance at a constant temperature of 70°C even if the thickness of the fiber ribbon is reduced from 0.4 mm to 0.3 mm. Because the selected materials have a higher Young's modulus than previous materials, we studied the shrinkage force of the ribbon coating at low temperature. Based on the results of these studies, we fabricated various fiber ribbon and carried out a verification by testing the lateral pressure properties and low-temperature properties of the fiber ribbon and the temperature properties of the cable.

3. STRESS ANALYSIS BY THE FINITE ELEMENT METHOD

Using a model such as that shown in Figure 1,

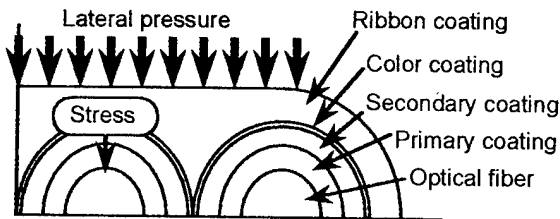


Fig. 1 Stress analysis model of 4-fiber ribbon

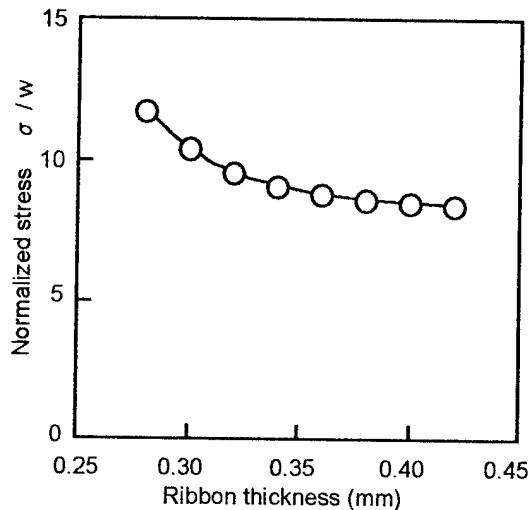


Fig. 2 Relationship between ribbon thickness and normalized stress

load(w) is applied to a 4-fiber ribbon from its thickness direction. Figure 2 shows the change in the normalized stress(σ/w) that is transmitted to the optical fiber surface when the ribbon thickness is varied. Here the parameters of fiber, primary coating, secondary coating, outside diameter of the color coating, and ribbon coating were held constant. As shown in Figure 2, as the ribbon is made thinner, the normalized stress increases, and the normalized stress with a ribbon thickness of 0.30 mm is about 1.2 times what it is with a ribbon thickness of 0.40 mm (23°C). When the ribbon is made thinner in this way without changing its material, its lateral pressure properties are reduced. Here we examined the material of the secondary coating and ribbon coating that yield the same lateral pressure properties as conventional products.

Table 1 Result of the stress analysis(0.30mm thick 4-fiber ribbon) by FEM (23°C)

		Young's modulus of the secondary coating (arb.unit)				
		0.7	1.0	1.3	1.7	2.0
Young's modulus of the ribbon coating (arb. unit.)	0.7	14.4	11.9	10.3	9.2	8.4
	1.0	12.4	10.3	9.0	8.0	7.3
	1.3	11.2	9.3	8.1	7.3	6.6
	1.7	10.3	8.6	7.5	6.7	6.1
	2.0	9.7	8.0	7.0	6.3	5.7

Table 2 Young's modulus of the coating materials (arb. unit)

		Temperature		
Material		-40°C	23°C	70°C
Secondary coating	Conventional material	3.2	1.0	0.2
	Material A	3.9	1.6	0.3
Ribbon coating	Conventional material	2.3	1.0	0.3
	Material B	2.7	1.3	0.3
	Material C	3.1	1.6	0.1

4. COATING MATERIALS OF THE SECONDARY COATING AND RIBBON COATING

UV resin (urethane acrylate type) was used for the coating materials. Table 1 lists the results of varying the Young's modulus of the secondary coating material and of the ribbon coating material when the ribbon thickness is 0.3 mm and determining the normalized stress by FEM. The region in which the normalized stress is at least as great as that for conventional products is indicated in Table 1 within a thick framework (box). Table 2 lists the properties of secondary coating materials and ribbon coating chosen to satisfy these conditions.

5. TEMPERATURE DEPENDENCE OF THE YOUNG'S MODULUS OF THE COATING MATERIAL

When the temperature at which fiber ribbon is used is set to -40 to 70°C, it is necessary to consider how the temperature affects the Young's modulus of the secondary coating material A and the ribbon coating materials B and C. Table 2 shows the Young's modulus

of each coating material at -40, 23, and 70°C. From Table 2, the Young's modulus is lower at a higher temperature, and the amount of the change differs depending on the coating material. Ribbon coating material B has a higher Young's modulus at high temperature than material C. This is because material B contains a higher proportion of alicyclic monomer, which has a high Young's modulus. In the following we consider the properties at high temperature and at low temperature.

5-1. AT HIGH TEMPERATURE

At high temperature, the Young's modulus is lower than at 23°C, so it is necessary to consider the reduction in the lateral pressure properties. Table 3 lists the results of determining the normalized stress when the Young's modulus of the coating material (secondary coating, ribbon coating) is varied in the same way as in Table 1. From the results of Table 3, within the thick framework (box) the normalized stress at 70°C is equal to or less than that of conventional products, and the optimum combination of coating materials here is material A for the secondary coating and material B for the ribbon coating.

Table 3 Result of the stress analysis (0.30mm thick 4-fiber ribbon) by FEM (70°C)

Ribbon coating \ Secondary coating	Conventional material	Material A
Conventional material	33.8	30.6
Material B	63.1	28.5
Material C	35.5	58.4

5-2. AT LOW TEMPERATURE

At low temperature, it is necessary to consider shrinkage due to the cold rather than the lateral pressure properties, because the Young's modulus is greater at low temperatures. This is because when the

shrinkage force is great, a loss increase arises due to micro-bends. In general, the shrinkage force F is expressed by formula (1).

$$F = (\sum E_i A_i K_i) \Delta T \quad \dots\dots (1)$$

E_i : Young's modulus of the primary coating, secondary coating, ribbon coating material
 A_i : cross-sectional area of the primary coating, secondary coating, ribbon coating
 K_i : coefficient of linear expansion of the primary coating, secondary coating, ribbon coating material

Figure 3 presents the shrinkage force/ ΔT by formula (1) for the ribbon coating material Young's modulus (here, the secondary layer is kept to material A in all cases). From Figure 3, the shrinkage force/ ΔT of the fiber ribbon of conventional products is 4.9×10^{-2} , and in order to make the shrinkage force less than that of conventional products when the ribbon thickness is 0.3 mm it is necessary to set the Young's modulus at low temperature to 2250 MPa or less. The selected materials satisfy this requirement.

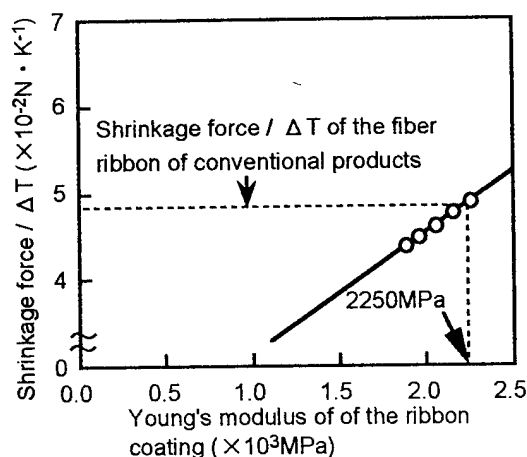


Fig. 3 Relationship between Young's modulus of the ribbon coating and shrinkage force/ ΔT .

6. PROTOTYPE EVALUATION RESULTS

6-1. LATERAL PRESSURE PROPERTIES

The 4-fiber ribbons listed in Table 4 were made using conventional materials and selected materials. These fiber ribbons were evaluated for their lateral pressure properties. The testing method is shown in Figure 4. The bobbin shown in the diagram has a radius of 165 mm and has stress application points having a radius of 1.25 mm at four locations around its circumference. One layer of fiber ribbon is wound over it (strand length: 120 m), and the difference in the transmission loss between before and after bobbin winding is measured by OTDR as the increase in the transmission loss. Both the measurement results and the stress analysis results are presented in Figure 5. From Figure 5, it was confirmed that the lateral pressure properties of 0.30 mm thick fiber ribbon using the selected materials provide performance at least equivalent to that of conventional products.

6-2. LOW-TEMPERATURE PROPERTIES

Low-temperature properties were evaluated using the conventional product and 0.30 mm-thick fiber ribbon using the selected materials. The results of evaluating the changes in the transmission loss over 72 hours at -40°C are given in Figure 6. It was confirmed that thin fiber ribbon and the conventional product have equivalent performance in transmission loss change.

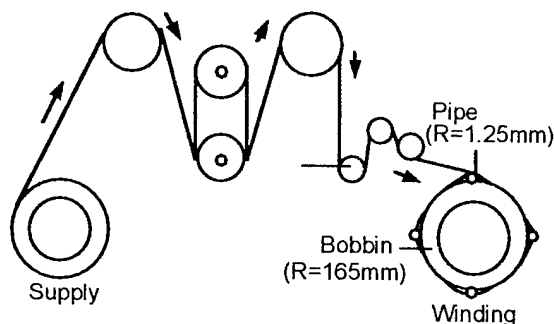


Fig. 4 Schematic diagram of loss increase measurement due to lateral pressure

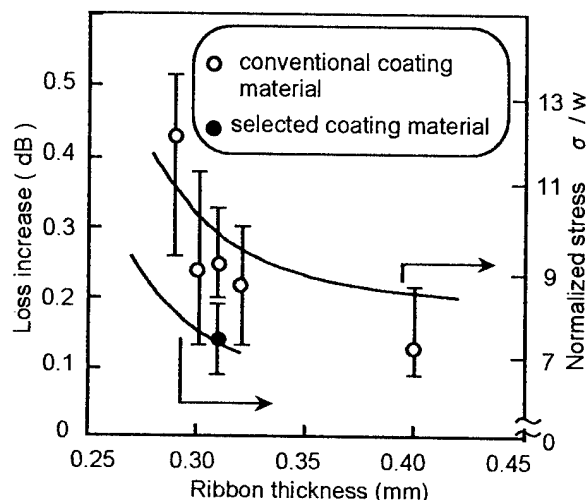


Fig. 5 Relationship between ribbon thickness and loss increase, normalized stress

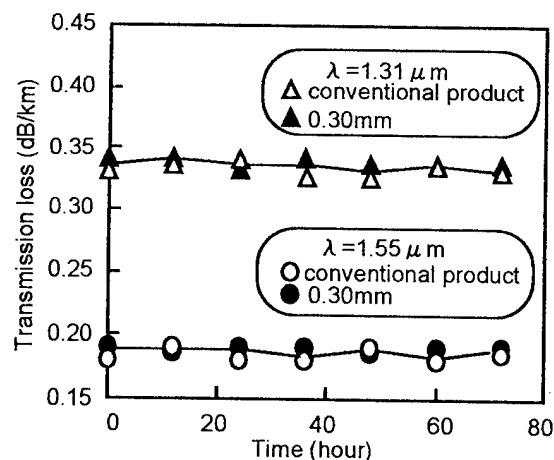


Fig. 6 Result of low temperature properties test

Table 4 Trial manufactured 4-fiber ribbons

Optical fiber		1.3 μ m single mode fiber					
Fiber	Secondary coating	Conventional material					Material A
	Outside diameter (mm)	0.25					
Fiber Ribbon	Ribbon coating	Conventional material					Material B
	Ribbon thickness (mm)	0.29	0.30	0.31	0.32	0.38	0.30
	Ribbon width (mm)	1.1					

6-3. CABLE EVALUATION (TEMPERATURE PROPERTIES)

We made slotted core fiber ribbon cable on which were mounted 0.30 mm-thick fiber ribbon using the selected materials. The cross-sectional structure of the cable is shown in Figure 7. Figure 8 shows the results of evaluating the thermal properties of this cable by heat cycle tests (-30 to 70°C, 3 cycles), along with the data for conventional product, obtained separately, shown for reference. Figure 8 shows the average values of test results obtained for each assigned temperature points for 3 temperature cycles. It was confirmed that thin fiber ribbon and the conventional product have equivalent performance in transmission loss change.

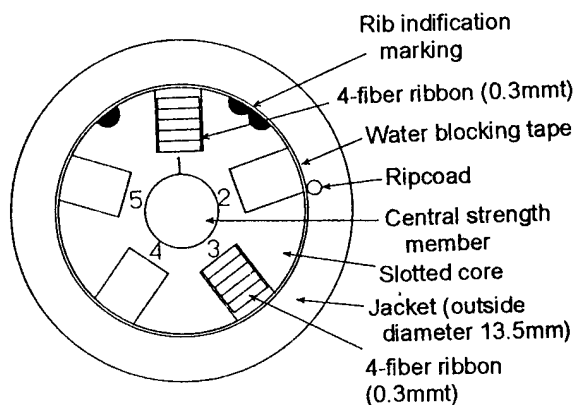


Fig. 7 Cross section of the slotted core cable

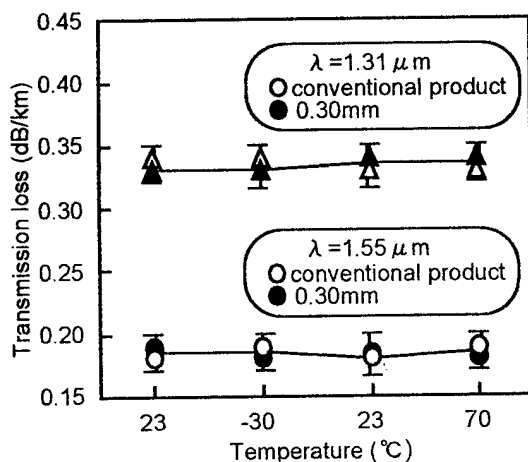


Fig. 8 Result of heat cycle test

7. CONCLUSION

Reducing the thickness of the fiber ribbon (to 0.30 mm) reduces its lateral pressure properties. Thus, from stress analysis by the finite element method and from calculation of the shrinkage force at low temperature, materials were selected that are needed to ensure the same performance as the conventional product (ribbon thickness 0.4 mm) at -40, 23°C, and 70°C. Thin (0.30 mm) 4-fiber ribbon and cable were made using these materials, and in an evaluation of their properties they were found to have performance equal to that of the conventional product. Thus it was learned that stress analysis by the finite element method, calculation of the shrinkage force at low temperature, and an evaluation method for verifying these are effective for designing the Young's modulus of the materials and the structure of the fiber ribbon.

8. REFERENCES

- 1) Murase, et al : "Mechanical properties of optical fiber ribbon" 44th IWCS, 485 (1995)
- 2) Iwata, et al : "Design and properties of ultra-dense optical cable with connectors on both ends" , Communication Society technical reports, CS95-49, OCS95-15 (1995)



Taketo Kawano

Showa Electric Wire
& Cable Co.,Ltd.,
1,Nabekura
Funaoka
Shibata-Machi
Shibata
Miyagi
Japan

T.Kawno received his M.S. degree from Scisence University of Tokyo in 1994. He is joined Showa Electric Wire & Cable Co.,Ltd., in 1994. He is an engineer working with the Optics & Communications engineering Dept.



Hiroshi Nakamura

Showa Electric Wire
& Cable Co.,Ltd.,
1,Nabekura
Funaoka
Shibata-Machi
Shibata
Miyagi
Japan

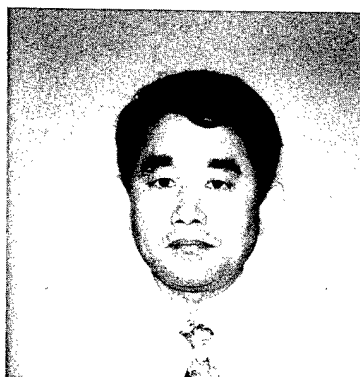
H.Nakamura received his B.E. degree from Shizuoka University in 1983. He is joined Showa Electric Wire & Cable Co.,Ltd., in 1983. He is an engineer working with the Optics & Communications engineering Dept.



Mitsuo Ito

Showa Electric Wire
& Cable Co.,Ltd.,
4-1-1
Minamihashimoto
Sagamihara
Kanagawa
Japan

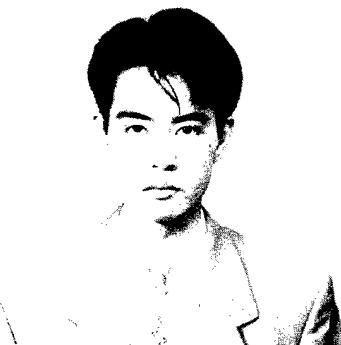
M.Ito passed from Yokohama Shoko Highschool in 1962. He joined Showa Electric Wire & Cable Co.,Ltd., in 1962. He is an engineer working with the Opto-Electronics R&D of Telecommunication R&D Dept.



Takeo Shiono

Showa Electric Wire
& Cable Co.,Ltd.,
1-1 Odasakae
Kawasaki-ku
Kawasaki
Kanagawa
Japan

T.Shiono received his Ph.D. degree in Chemical Engineering from the University of Tokyo in 1979. He joined Showa Electric Wire & Cable Co.,Ltd., in 1979. He is the manager of Electric Power R&D Dept.



Tomotaka Murase

Showa Electric Wire
& Cable Co.,Ltd.,
4-1-1
Minamihashimoto
Sagamihara
Kanagawa
Japan

T.Murase received his B.E. degree from Kanagawa University in 1993. He joined Showa Electric Wire & Cable Co.,Ltd., in 1993. He is an engineer working with the Opto-Electronics R&D of Telecommunication R&D Dept.



Masahiko Saegusa

Showa Electric Wire
& Cable Co.,Ltd.,
1,Nabekura
Funaoka
Shibata-Machi
Shibata
Miyagi
Japan

M.Saegusa received his B.E. degree from Yokohama National University in 1976. He is joined Showa Electric Wire & Cable Co.,Ltd., in 1976. He is the manager of the Optics & Communications engineering Dept.

DEVELOPMENT OF OPTICAL FIBER RIBBON MATERIALS WITH NOVEL SURFACE CHARACTER

Tsuyoshi Hirai, Junji Yoshizawa, Masanobu Sugimoto, Zen Komiya,
and, Takashi Ukachi

Tsukuba Research Laboratory, Japan Synthetic Rubber Co., Ltd.
25 Miyukigaoka Tsukuba, Ibaraki, 305 JAPAN

ABSTRACT

The smoothness of an optical fiber ribbon surface was correlated to surface cure measured by the Attenuated Total Reflection Infra-Red (ATR-IR) method. It was found that good surface cure of coatings was realized by employing appropriate photo initiator package and optimized UV dose. However, the highly slippery surface which seemed to be necessary for ribbon was not obtained only by optimizing these conditions. Addition of certain compounds such as poly-dimethylsiloxane compounds to the coatings was found to be effective to obtain slippery character of the surface and to eliminate surface tackiness completely.

Cured coatings with poly-dimethylsiloxane compounds were analyzed by using an Electron Probe Micro Analyzer (EPMA) and an X-ray Photoelectron Spectroscopy (XPS) to reveal the presence of poly-dimethylsiloxane on the surface. It was established that the selection of the poly-dimethylsiloxane had a key role to realize the

highly slippery surface of the cured coatings.

INTRODUCTION

Recent trend to high-count optical fiber cable has promoted shifting from a jelly filled structure to an optical fiber ribbon structure. Ribbon matrix materials for optical fiber should have properties such as, slippery surface, good break-out, high durability, low loss, and so on. Among these requirements, smooth and slippery surface of optical fiber ribbon is one of the most important factors for achieving not only cable performance, but also for high productivity. If the ribbon has tacky surface, it can be difficult to wind it neatly on a bobbin. Clumsy winding of ribbon may retard its production speed. The tacky surface may also cause loss increase when the cable is bent if the ribbons stick with each other in a groove. UV curable urethane acrylate coatings have been widely employed for ribbon matrix material because of high productivity and well balanced mechanical properties. However, it has been known that the cross link reaction of

acrylates induced by the UV irradiation is inactivated by contamination of oxygen in a UV curing chamber and consequently uncured tacky surface is obtained. The choice of appropriate photo initiator packages can provide the coatings which is less sensitive to the oxygen inhibition of the UV curing at the surface. Furthermore, addition of certain release agents to the ribbon matrix materials can also reduce the surface tackiness of the ribbon. However, few systematic study was provided on the structure-property relationship between the surface tackiness of the coatings and the photo initiator packages or the release agents.

In this paper, we report UV dose and/or photo initiators dependence of the surface character of ribbon matrix materials. The effect of addition of poly-dimethylsiloxane compounds on reducing surface tackiness of cured ribbon matrix materials was also investigated. We made spectroscopic analysis of the cured surface of coatings containing poly-dimethylsiloxane in order to elucidate the mechanism of reducing surface tackiness.

EXPERIMENTS

Material Preparation

The urethane acrylate coating, A-1 was formulated as the standard ribbon matrix material for optical fibers. The mechanical characteristics of the coating A-1 are listed in Table 1 along with its formulation. As shown in Table 1, the coating A-2 was also formulated only by replacing the photo initiator package of the coating A-1 in order to see the effect of photo initiators on the surface tackiness. Based on the

Table 1. Formulation and Physical Properties of Coatings, A-1 and A-2.

Formulation (wt%)	A-1	A-2
Oligomer A (Mw=2578)	39	38
Oligomer B (Mw=978)	28	28
Monomer A	14	14
Monomer B	9	9
Monomer C	8	8
Photo Initiator A	1.5	1.5
Photo Initiator B	0.2	1.0
Cured film properties ¹⁾		
Young's modulus (kg/mm ²)	75	76
Tensile strength (kg/mm ²)	5.0	4.8
Tensile elongation (%)	60	58

1) Cured at 1J/cm² under air. Film thickness is 200 μ m.

coating A-2, coatings S-1 to S-7 were formulated with using different kinds of poly-dimethylsiloxane compounds. Coatings, S-1 to S-3, were formulated with alcoxylated poly-dimethylsiloxanes having different kind of alchoxy side chains and different molecular weight. Coatings, S-4 to S-7, were also formulated with newly developed acrylated poly-dimethylsiloxanes having different molecular weight. The acrylated poly-dimethylsiloxane was synthesized from monohydroxyl terminated poly-dimethylsiloxane and diisocyanate end-capped with hydroxyl acrylate. The formulations of S-1 to S-7 are summarized in Table 2.

Evaluation of Surface Tackiness (Smear Testing)

The surface of the coating cured at 0.1 J/cm² under nitrogen or air atmosphere was rubbed by fingers to determine how the surface was tacky. The tackiness of cured surface was rated from "1" to "4". The rate "1" represents highest tackiness and "4" dose the lowest.

ATR-IR

The degree of surface cure of the coatings cured at desired UV dose was monitored

Table 2. Formulation of Coatings with Poly-dimethylsiloxane Compounds.

Mw	Silicone compound (wt%)						
	Alchoxy poly-dimethyl siloxane			Acrylated poly-dimethyl siloxane			
	G 3000	H 12000	I 20000	J 1000	K 2000	L 3000	M 4000
Coating							
S-1	1.5						
S-2		1.5					
S-3			1.5				
S-4				1.0			
S-5					1.0		
S-6						1.0	
S-7							1.0

by using the ATR-IR spectroscopy equipped with a zinc-selenide (Zn-Se) or germanium (Ge) prism.¹ The depth where infra-red ray penetrates into varies by the combination of the refractive indices between cured coatings and the prisms employed. One can detect information from the thickness of 3 μm by using the Zn-Se prism and from the thickness of 1 μm by using the Ge one. By using different kinds of prisms, consumption of acrylic double bond at the different depth of the coating surface was evaluated by monitoring the change of absorbance of IR band at 810 cm^{-1} assigned to the out-of-plane vibration of the C-H bond in acrylic group.

Measurement of Slipping Force

For the quantitative evaluation of slipping force of the cured ribbon matrix material, we developed a new measurement method as schematically drawn in Figure 1. The coating was drawn down on a glass plate with a thickness of 130 μm and cured at UV dose of 0.5 J/cm^2 under nitrogen. The resultant cured coating was cut into a 5 mm \times 10 mm specimen. The two pieces of the specimen were pasted on aluminum plates by a double-sided adhesive tape as the bottom surface of the

specimen faced aluminum plate. These specimens on the plates were held together as the each top surface faces each other with constant pressure, 0.5 kg/cm^2 , and the plates were pulled in opposite directions by using autograph to measure slipping force.

Analysis of the Surface and the Cross Section of Cured Coating

The EPMA revealed the distribution of the silicon atoms along the direction of coating thickness by analyzing the cross section of cured coating. The cured coating was cut by a microtome at liquid nitrogen temperature to give a cross section to give a planar mapping of the silicone atoms in the cross-sectional plane. The surface of the cured coating was analyzed by using the XPS method to evaluate the amount of silicon atoms on the cured surface. In order to obtain depth profile of the silicon atoms, the XPS analysis was made by using two different take-off angles.² By using a take-off angle, 15°, one can measure photoelectrons released from the thickness about 3 nm and by using one at 90° one can obtain photoelectrons from 10 nm thickness. A spot size of focused

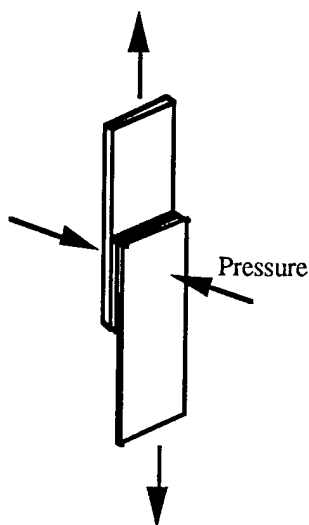


Figure 1. A schematic drawing of measurement method of slipping force of cured coatings.

X-ray was $1\text{ mm} \times 1\text{ mm}$.

RESULTS AND DISCUSSION

The results of the smear testing made on the coatings, A-1 and A-2 cured at different UV dose and at different atmosphere were summarized in Table 3 along with the degree of surface cure measured at the different thickness, $1\text{ }\mu\text{m}$ and $3\text{ }\mu\text{m}$, by using ATR-IR prisms, Zn-Se and Ge, respectively. Normalized reaction conversion was calculated and shown in Table 3. The normalized conversion is defined as the value that the reaction conversion obtained by ATR-IR measurement was divided by the reaction conversion of coating A-2 cured under nitrogen atmosphere with UV dose of 0.5 J/cm^2 . As shown in Table 3, the normalized reaction conversion at the very surface of the cured coatings correlates the tackiness evaluated by the

smear testing. Higher reaction conversion of cured surface tends to give less tacky surface. The poor degree of cure at the surface was caused by the oxygen inhibition of cross link reaction of acrylic double bonds. From the results listed in Table 3, at any UV dose rate, higher reaction conversion was obtained when curing was made under nitrogen atmosphere. The reaction conversion data obtained by using Ge prism for coating A-2 are lower than those obtained by using Zn-Se one. This indicates that the very surface of coating is easily affected by the oxygen contamination. Table 3 also indicates that the selection of photo initiator packages seems to be effective to increase the surface cure and to achieve less tacky surface. Although the coating A-2 showed the lower tackiness, the slipping force was measured to be 9.6 kg/cm^2 and was too high to be utilized as the matrix material.

One can reduce the oxygen inhibition by introducing inert gas to the UV curing chamber during drawing a ribbon. However it is very difficult to eliminate the oxygen contamination completely because the drawing rate of ribbon is too high to remove the adsorbed oxygen from the surface of the ribbon by blowing inert gas. We thus tried to reduce the surface tackiness of ribbon of which surface is not fully cured by adding some polydimethylsiloxane compounds.

Slipping forces measured on the coatings S-1 through S-7 are tabulated in Table 4. Although the degree of surface cure is relatively low, coatings S-1 through S-7 showed relatively low slipping force comparing to the

Table 3. Reaction Conversion of the Surface of the Cured Coatings and Results of the Smear Testing.

Condition	Under Nitrogen		Under Air		
Coating	A-1	A-2	A-1	A-2	
Smear test ranking ¹⁾	3	4	1	2	
ATR-IR prizm	Zn-Se	Zn-Se	Zn-Se	Ge	Zn-Se
Dose (J/cm ²)	Conversion (%)				
0.01	78	75	49	16	43
0.10	94	99	65	35	71
0.25	99	99	70	-	88
0.50	100	100	76	56	93

1) Coating cured at 0.1 J/cm² under nitrogen or air atmosphere. Film thickness is 200 μ m.

Table 4. Slipping Force of Cured Coatings with Different Kind of Poly-dimethylsiloxane Compounds.

Coating	A-2	S-1	S-2	S-3	S-4	S-5	S-6	S-7
Slipping force (kg/cm ²)	9.6	1.0	1.7	2.3	1.3	0.6	0.5	0.3

coating A-2. The coatings, S-1, S-2, and S-3 contain non-reactive alchoxy poly-dimethylsiloxane compounds. The solubility of the alchoxy poly-dimethylsiloxane employed in coating S-1 is measured to be less than 0.1 g of poly-dimethylsiloxane compound to the 10 g of coating resin. The solubility of the other poly-dimethylsiloxane compounds employed in coatings S-2 and S-3 were also to be 1 g and 10 g to the 10 g of coating resins, respectively. The poly-dimethylsiloxane compounds having less compatibility to the coating resins tend to make the cured surface more slippery. Because less compatible poly-dimethylsiloxane compounds can easily bleed out from the coating and tend to localize at the very surface of the cured coating. Resulting from these data, choosing a poly-dimethylsiloxane compound having appropriate compatibility to the coating is important to obtain slippery surface. However, the non-reactive poly-dimethylsiloxane compounds are supposed to be removed from the surface with time passing at elevated temperature

because the non-reactive poly-dimethylsiloxane compound does not participate the crosslinking network of the cured coating. We thus examined newly developed UV reactive poly-dimethylsiloxane compounds instead of the non-reactive ones.

Coatings S-4 through S-7 contain reactive, acrylated poly-dimethylsiloxane having different molecular weight of poly-dimethylsiloxane chain at constant concentrations (1.0 wt% to the resin). The slipping forces of these coatings S-4, S-5, S-6, and S-7 are much lower than those of coatings S-1, S-2, and S-3 which contain the non-reactive poly-dimethylsiloxane. Figure 2 plots the slipping force of cured coatings containing the reactive poly-dimethylsiloxanes as a function of molecular weight of poly-dimethylsiloxane chain. Higher molecular weight of poly-dimethylsiloxane chain gives the lower slipping force. This might be explained by the compatibility of poly-dimethylsiloxane to the coatings. The compatibility of the poly-

dimethylsiloxane compounds against the coating resins tends to decrease with an increase of molecular weight of siloxane chain, and resulting from this, the higher molecular weight of the reactive poly-dimethylsiloxane compound gives the lower slipping force.

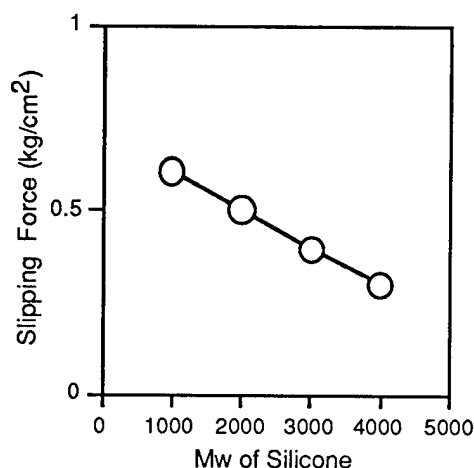


Figure 2. Slipping force of the coatings containing reactive poly-dimethylsiloxane compounds. Slipping force is plotted as a function of the molecular weight of poly-dimethylsiloxane chain.

Microscopic observation was made on the coating S-4 at uncured and cured states. As indicated in Figure 3 and 4, spherical particles with a diameter of 1 to 3 μm were found both in the uncured and cured coatings, respectively. In order to know the origin of these particles found in the coating, EPMA analysis was made on the cross section of the cured coating, S-4. Distribution of silicon atoms in the cross section of the cured coating was mapped as shown in Figure 5. The particles having a diameter of 1 to 3 μm were also seen in this figure. The spherical particles observed by the optical microscope correspond to the particles where

silicon atoms localized observed by EPMA. Due to the lower compatibility of the reactive poly-dimethylsiloxane compounds to the coating, the poly-dimethylsiloxane compound makes the phase-separated structure even in the cured state. However, the surface of the coating is damaged during preparation of samples, i.e., making cross-sectional specimens, it is hard to distinguish the existence of silicon atoms at the very surface of the coatings by EPMA method.

We thus analyzed the surface of the cured coating, S-4 by using XPS technique at the different penetration thickness. The cured coating S-4 was introduced in the XPS chamber to measure the density of silicon atoms at the 3 nm thickness by employing the take-off angle, 15°. An atomic ratio between silicon and carbon, Si/C, was determined by comparing the intensities of each peak and listed in Table 5. The atomic ratio, Si/C, of the reactive poly-dimethylsiloxane compound used in the coating S-4 was also calculated based on the molecular structure and listed in Table 5. The atomic ratio obtained at the 3nm thickness shows a good agreement with the calculated value. This indicates that the surface of the cured coating is covered by the thin layer of the poly-dimethylsiloxane compound. On contrary, the data obtained at the thickness of 10 nm by employing the take-off angle, 90°, showed that the atomic ratio of Si/C was almost one third to that obtained at 3 nm thickness. The body of cured coating contains phase-separated poly-dimethylsiloxane particles and the surface of the coating is covered by the thin layer of poly-dimethylsiloxane compound. This thin layer

Table 5. The Atomic Ratio Observed on the Surface of Cured Coating S-4 by using XPS Technique.

Sample	Ratio of atom Si/C
S-4 Cured film Measurement depth 3 nm	0.30
10 nm	0.11
S-4 Liquid (Calculated value)	0.001
Acrylated poly-dimethyl siloxane J (Calculated value)	0.26

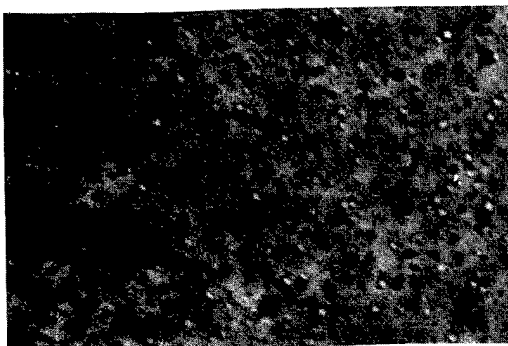


Figure 3. Microscopic observation of uncured resin, S-4 containing the reactive poly-dimethylsiloxane having a molecular weight of 1000. Magnification is 400.

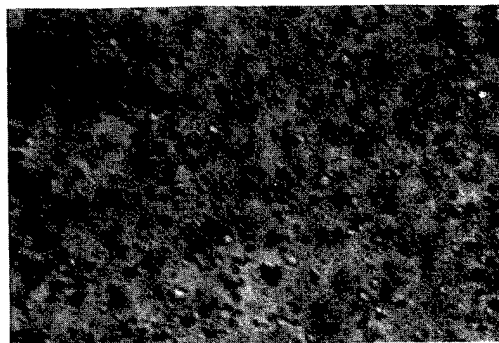


Figure 4. Microscopic observation of cured resin, S-4 containing the reactive poly-dimethylsiloxane having a molecular weight of 1000. Magnification is 400.

might be produced during coating by the following process. The phase-separated poly-dimethylsiloxane particles dispersed in the coating is broken by the high shear stress during coating and the poly-dimethylsiloxane molecules come up at the very surface of the coating due to the incompatibility between poly-dimethylsiloxane compound and coatings. Resulting from this, the poly-dimethylsiloxane compound bleeds out from the coating and is immediately immobilized by following UV dose. This immobilized thin layer of poly-dimethylsiloxane compound makes the coating surface highly slippery.

CONCLUSION

We discussed that the surface tackiness of the cured ribbon matrix materials was affected

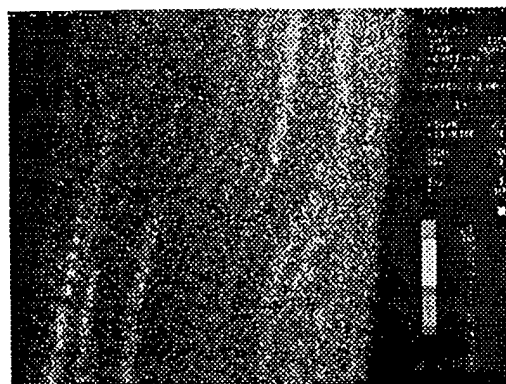


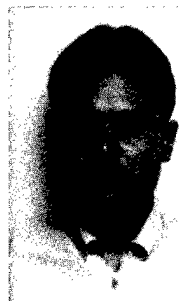
Figure 5. EPMA scanning for silicon atoms of the cross section of cured coating S-4. White dots represent localized silicon atoms.

by the photo initiator package employed in the coatings from the point of view of the reaction conversion of acrylic double bond at the surface. High reaction conversion was important to realize the less tacky surface of the coatings and was achieved by optimizing the photoinitiator employed. However, the selection of the

photoinitiator package was not sufficient to obtain highly slippery surface for ribbon matrix materials. We also demonstrated the effect of addition of poly-dimethylsiloxane compounds to the ribbon matrix materials to decrease the surface tackiness. We showed that the addition of the newly developed UV reactive poly-dimethylsiloxane compounds dramatically reduced the surface tackiness of cured coating. The spectroscopic, EPMA and XPS analysis of the coating containing the reactive poly-dimethylsiloxane compounds revealed that the surface of the cured coating was covered by thin layer of poly-dimethylsiloxane compound and this thin layer was effective to give a highly slippery character of the cured coatings.

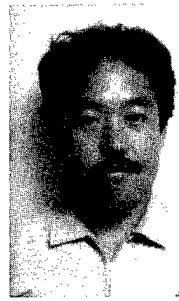
REFERENCE

- 1) S. Morita, Y. Naito, Z. Komiya, T. Naganuma, A. Fujimori, T. Ukachi, Proceedings 45th IWCS, 517 (1995).
- 2) Maria F. Ebel, Surf. Interface Anal., 3, 173 (1981).



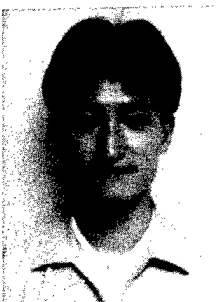
Tsuyoshi Hirai
Tsukuba Research
Laboratory,
Japan Synthetic Rubber
Co., Ltd
25 Miyukigaoka,
Tsukuba, 305
Japan

Tsuyoshi Hirai received his M. E. degree in Organic Chemistry from Toyohashi University of Technology and joined Japan Synthetic Rubber Co., Ltd. in 1993. He has been engaged in research and development of radiation curable materials for optical fiber coatings.



Zen Komiya
Tsukuba Research
Laboratory,
Japan Synthetic Rubber
Co., Ltd
25 Miyukigaoka,
Tsukuba, 305
Japan

Zen Komiya received his Ph. D. in Organic Chemistry from Hokkaido University in 1984 and joined Japan Synthetic Rubber Co., Ltd. He was engaged in research on development of new transparent plastics and currently has been engaged in research and development on radiation curable materials.



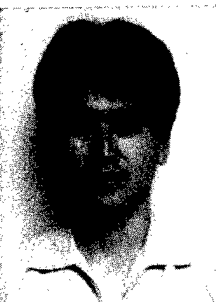
Junji Yoshizawa
Tsukuba Research
Laboratory,
Japan Synthetic Rubber
Co., Ltd
25 Miyukigaoka,
Tsukuba, 305
Japan

Junji Yoshizawa received his M. E. degree in Organic Chemistry from Tsukuba University and joined Japan Synthetic Rubber Co., Ltd. in 1995. He has been engaged in research and development of radiation curable materials for optical fiber coatings.



Takashi Ukachi
Tsukuba Research
Laboratory,
Japan Synthetic Rubber
Co., Ltd
25 Miyukigaoka,
Tsukuba, 305
Japan

Takashi Ukachi received his B. E. degree in Biophysics and Bioengineering from Osaka University and Ph. D. in Material Science from Kyushu University. He started his professional career at Japan Synthetic Rubber Co., Ltd. in 1976 and has been engaged in research and development of radiation curable materials.



Masanobu Sugimoto
Tsukuba Research
Laboratory,
Japan Synthetic Rubber
Co., Ltd
25 Miyukigaoka,
Tsukuba, 305
Japan

Masanobu Sugimoto received his M. E. degree in Material Science from Nagoya Institute of Technology and joined Japan Synthetic Rubber Co., Ltd. in 1991. He has been engaged in research and development of radiation curable materials for optical fiber coatings.

FIBER GRATINGS: TEMPERATURE AND MECHANICAL SENSITIVITY OF NARROW BAND TRANSMISSION FILTERS USING DIFFERENT PACKAGING SOLUTIONS

Stefano Pitassi, Francesco Pozzi, Andrea Marcone, Vittorio Spano

**SIRTI S.p.A. Cables and Optical Technologies
Cassina de Pecchi (Milano), Italy**

ABSTRACT

There is a considerable interest in the potential applications of gratings written directly in photosensitive optical fibers. These components are characterized by a mirror-like behaviour and mirrors play an important role in any optical system.

An attractive way to make a reflector integrated on a fiber is to generate a periodic refractive index variation along its length, whose control permits to determine the reflectivity amplitude, bandwidth and operating wavelength. Several devices can be realized with such kind of fiber integrated components, with low insertion loss: devices like tunable filters, wavelength selective filters with very narrow band, wavelength division multiplexers, DFB fiber lasers, gain amplifier equalizers, pump reflectors, dispersion compensators and sensors.

In-fiber Bragg grating technique represents one of the most encouraging method to produce optic reflectors with excellent spectral performances. Unfortunately it has, as a fundamental drawback, a substantial temperature and mechanical sensitivity which affects directly its reliability. This paper investigates environmental and mechanical effects on some fiber gratings in order to define the operating limits of the filter and therefore its specifications.

The main experimental results as well as different package solutions, that could be able to increase the stability of this kind of devices, will be discussed.

1. INTRODUCTION

Among the different techniques adopted to produce photoinduced gratings, one of the most encouraging method is derived from photolithography and uses a phase mask made of silica glass which does not absorb UV light. A laser beam at normal incidence is spatially modulated by a phase mask grating, thus resulting in an intensity pattern (with half the phase mask grating pitch) which generates an index modulation into the core of the Germanium doped photosensitive fiber. This technique is simple to use and can be easily transferred to an industrial plant.

1.1 Theoretical aspects

An in-fiber Bragg grating can be considered like an optic waveguide with a periodic distribution of the core refractive index. Two approaches are generally used to obtain solutions of propagation of electromagnetic radiation: Block-wave formalism and coupled-mode theory¹. The latter method consists, from a mathematical viewpoint, in expressing the electromagnetic wave as an expansion in the normal modes of an optical fiber with constant refractive index. Therefore the index modulation can be seen as a small perturbation δn that we can expand as a Fourier series and substitute in the wave equation.

Assuming further that only two modes are strongly coupled, the general propagation equations reduce to two, which involve the coupling coefficient C of unperturbed normal

modes and their propagation constant β . This leads in turn to a phase matching condition (or Bragg condition) that must be verified in order to assure a significant coupling between the modes. If broad-band radiation is launched into the fiber, only those wavelengths that are phase matched to the reflection are not transmitted, permitting to obtain a band pass filter.

In case of single-mode fibers, the Bragg condition and the coupling coefficient C are generally expressed as:

$$\lambda_B = 2 \cdot \Lambda \cdot n_{eff} \quad (1)$$

$$C = \frac{\pi \cdot n_{cl} \cdot \delta n \cdot \eta}{\lambda_B \cdot n_{eff}}$$

where Λ is the grating pitch, δn is the modulation depth of the index and η the overlap factor (i.e.: superposition integral of the two modes).

The coupling equations depend on the sign of the propagation constant, so that the coupling is generally divided into two categories: codirectional (the Bragg grating works in transmission) and contradirectional (the Bragg grating works in reflection). This results in two separate spectra (reflection and transmission) centered at the Bragg wavelength λ_B . Because of the configuration of narrow band filters, we are more interested in the grating reflectivity which shows a central peak R whose value depends on the coupling coefficient C and the whole length L of the grating^{1,2}:

$$R = \tanh^2(C \cdot L) \quad (2)$$

Aside from the main peak, the phase matching condition is not satisfied any more, and a decreasing series of sidelobes, due to multiple reflections, appear. The peak reflectivity of these sidelobes is still function of the parameters C and L and can be expressed as follows¹:

$$R = \frac{|C \cdot L|^2}{\left(p + \frac{1}{2}\right)^2 \cdot \pi^2 + |C \cdot L|^2} \quad (3)$$

$$p = 1, 2, 3, \dots$$

Finally the bandwidth $\Delta\lambda$ of the main peak is given approximately by³:

$$\frac{\Delta\lambda}{\lambda_B} = s \cdot \sqrt{\frac{\delta n^2}{n_0} + \frac{\lambda_B^2}{2n_0 L}} \quad (4)$$

where n_0 is the average refractive index in the core and s can assume values between 0.5 and 1 in case of weak and strong gratings respectively.

From these expressions it is evident that the longer the fiber and the higher the modulation depth, the greater is the peak reflection and the narrower its bandwidth.

1.2 Narrow band filter realization

The band pass filter is an all-fiber, compact device based on the Michelson interferometer scheme as shown in figure 1. It basically consists in a 3dB coupler with two ports devoted to the input and output signals (port 1 and 2 respectively) and the remaining two arms (port 3 and 4) used for inscribing the Bragg gratings. The device operation can be qualitatively explained as follows: light entering the input port (1) is halved by the coupler and separately reflected by the gratings at the opposite ports (3 and 4). If the optical path is accurately controlled, we get a constructive interference at the output port (2) and a destructive one at the input (1). In this way the resulting filter is potentially characterized by low insertion loss, high return loss and very narrow transmission bandwidth.

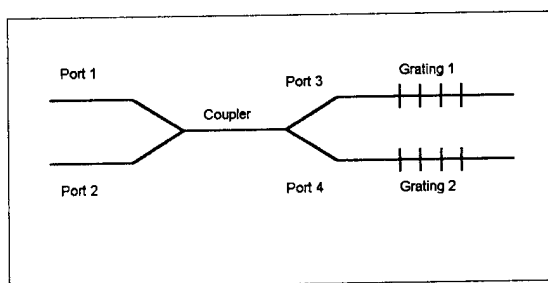


Fig.1 Scheme of the transmission filter

The packaging experiments have been carried out on fiber Bragg gratings supplied by different manufacturers and laboratories which are partners of the European ACTS Project A046 PHOTOS. Regarding the narrow band filters, they have been configured as a Michelson

interferometer realized inscribing two identical gratings on two arms of a 3dB fusion coupler, plus a zone where the optical path can be modified by UV trimming. More precisely fusion couplers have been inserted in steel cylinders with high H_2 pressure at room temperature in order to increase fiber photosensitivity, which represents the capacity of the fiber core to change its refractive index. After this step a UV exposure (242-248 nm range) allows the dissolved H_2 to react in the vitreous host, thus resulting in the observed permanent index variation. The inscription method, adopted for narrow band filter realization⁴, uses a glass phase mask that modulates the pulsed light from an excimer laser at 248 nm. The writing set-up includes also some optical elements for collimation, shaping and focalization of the UV beam.

2. BRAGG GRATING SENSITIVITY

Narrow band transmission filters are expected to be important components in wavelength-division-multiplexed systems, so that their stability over long time and under different installation condition is vital. This means that any package solution should assure an easy and safe handling of the filter, along with a thermal and mechanical reliability. On the basis of scheme in fig.1, a narrow band filter can be divided in two parts (one fusion coupler and two Bragg gratings), thus suggesting that the reliability problem can be solved separately for the coupler and the fiber grating. The former has already been studied while the latter seems to be rather complicated because of its environmental sensitivity. Therefore at this preliminary stage of filter development, our interest has been focused on temperature and stress dependence of optical gratings alone; in particular the transmission characteristics (bandwidth and Bragg wavelength) of several samples have been tested in order to define the specifications necessary for any further packaging study.

2.1 Temperature dependence

Temperature variations affect mainly the central wavelength λ_B which undergoes a nearly linear increase with temperature.

Table 1 Table of temperature grating sensitivity

Sensitivity	Grating A	Grating B	Grating C	Grating D
$\Delta\lambda/\Delta T$ [nm/°C] +10°C-+40°C	0.009	0.01	0.01	0.008
$\Delta\lambda/\Delta T$ [nm/°C] -40°C-+80°C	0.0078	0.0081	0.0075	0.0067

Measurements have been performed using a broadband source (ASE of an optical amplifier) and an optical spectrum analyzer while subjecting the fiber grating to temperature variation inside a climatic chamber. The slope is found to be equal or less than 0.01nm/°C (fig.2). The values reported in table 1 are simply calculated by dividing the whole wavelength shift by temperature range. We found that the grating sensitivity reduces if temperature extremes change from +10°C - +40°C (0.008÷0.01nm/°C) to -40°C - +80°C (0.0067÷0.0081nm/°C) as reported in table 1. These data are in good agreement with theoretical values that can be predicted taking into consideration either the thermal grating elongation or the thermal variation of the core refractive index.

Bragg wavelength [nm]

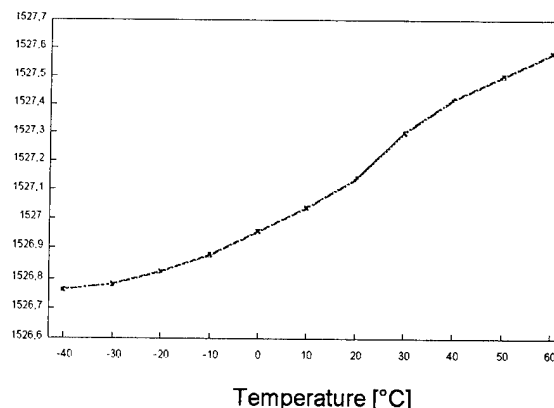


Fig.2 Fiber grating wavelength shift vs temperature

To obtain an expression for the wavelength shift we introduce the thermal expansion coefficient α and the thermo-optic coefficient ξ for Ge-doped silica into the equation (1). Such equation depends directly on effective index and grating pitch whose value is simply proportional to the length L . After some simple mathematics, the fractional

wavelength shift, due to temperature variation ΔT , is given by⁵:

$$\frac{\Delta \lambda_B}{\lambda_B} = (\alpha + \xi) \cdot \Delta T \quad (5)$$

$$\alpha = \frac{\partial L}{L \cdot \partial T}; \xi = \frac{\partial n}{n \cdot \partial T}$$

If we suppose that the parameters α and ξ have the values generally reported in literature⁴ ($0.55 \cdot 10^{-6} \text{C}^{-1}$ and $6.86 \cdot 10^{-6} \text{C}^{-1}$ respectively), the final temperature sensitivity is around $0.01 \text{nm}/^\circ\text{C}$ as experienced with our samples.

For what concerns filter bandwidth and peak reflectivity, our tests did not show any appreciable variation, thus confirming their weak temperature dependence (equations (2) and (3)).

2.2 Stress dependence

When an external force is applied to a transparent elastic medium like a fiber, the medium becomes birefringent like some crystals. This phenomenon is well known as the photoelastic effect, where anisotropy is produced in an optically isotropic medium and refractive index change is proportional to the mechanical stress. Such proportionality is generally expressed by photoelastic constants which take into account two different effects: a) the atoms move farther apart, under tensile stress, or closer together, under compressive force, b) the electron shell of the atoms are distorted causing a change in the medium polarizability. The effect is traditionally described by means of the change of the optical impermeability tensor. In case of tensile stress only (along fiber axes), we get the following index change induced by a strain ϵ :

$$\Delta n_{eff} = -\frac{1}{2} \cdot n_{eff}^3 \cdot [p_{12} - \nu(p_{11} + p_{12})] \cdot \epsilon \quad (6)$$

n_{eff} being the effective index in unperturbed conditions, p_{ij} the elastooptic coefficients and ν the Poisson's ratio. Using the expression (1) for the Bragg wavelength we have then the fractional wavelength shift due to strain optic effect.

A second contribution (opposite to the previous one) to the wavelength shift is due to

the geometrical variation of the grating pitch. The final result is therefore given by the following relationship⁵:

$$\frac{\Delta \lambda_B}{\lambda_B} = (1 - p_e) \cdot \epsilon \quad (7)$$

$$p_e = \frac{n_{eff}^2}{2} \cdot [p_{12} - \nu \cdot (p_{11} + p_{12})]$$

In literature p_e is reported to be nearly 0.2 for standard fiber, thus leading to a stress sensitivity of $1.2 \text{nm}/10^{-3}$ strain.

Tests made on many other samples provided by partners of the ACTS Project A046 PHOTOS have always shown a behaviour well approximated by a straight line with a slope of approximately 0.013nm/g . (table 2 and figure 3). In the experimental set-up the spontaneous emission of an optical amplifier is used as a source and an optical spectrum analyzer allows the measurement of transmission peak wavelength, while pulling the component with a controlled load by a high precision laboratory instrument. The characterization has been carried out with great finesse for load values lower than 100g. because this is the expected range of greater interest for the packaging.

Bragg wavelength [nm]

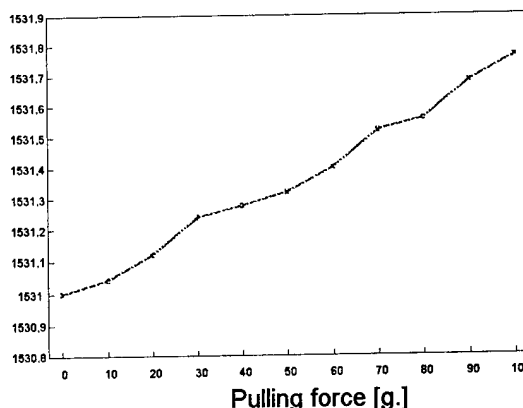


Fig.3 Fiber grating wavelength shift vs applied load

After the measurement has been completed and the stress relieved, the peak wavelength returns to its original value confirming that the grating operates in the linear region.

Finally no wavelength shift was noticed neither by bending (till 30mm curvature radius) nor by twisting the fiber grating.

Table 2 Table of stress grating sensitivity

Sensitivity	Grating A	Grating B	Grating C	Grating D
$\Delta\lambda/\Delta F$ [nm/g]	0.0132	0.013	0.0132	0.0131

3. PACKAGE DESIGN

On the basis of previous experimental results, concerning thermal and mechanical sensitivity of fiber Bragg gratings, it is now possible to study a package for narrow band filters. Our purpose is to obtain a cost effective, compact and totally passive component which is able to operate with a minimum temperature range of $+10^{\circ}\text{C}/+40^{\circ}\text{C}$. Under such conditions, the solution we have taken into consideration consists in a completely passive housing that exploits the thermal elongation of the fiber to compensate wavelength shift induced by a calibrated fiber tension.

An alternative choice regards the use of a Peltier cell (active housing) by which it is possible to keep the grating temperature stable even under strong environmental conditions. Obviously this solution is not cost effective any more, but could offer three distinct advantages: a) an high operating temperature range (may be $-30^{\circ}\text{C}/+60^{\circ}\text{C}$), b) the lack of any grating pretension which may affect the long-term reliability and c) the tunability of the component. Moreover, these same issues appear to be much more profitable in case of fiber grating compensators whose lengths vary from 5cm to 20cm, instead of few mm as with Bragg gratings for optic filters.

Before going into further details, it is interesting to notice that the filter reliability requires to solve separately the stability of the fusion coupler and that of the Bragg gratings, because of the difference in the their thermal and mechanical sensitivities. The solutions proposed herewith provide two separated pre-packages (one for the coupler and one for the two gratings) that are included into an external package whose main purpose is to make the filter mechanically resistant.

3.1 Fusion coupler pre-package

As illustrated in figure 1 a narrow band transmission filter is configured as a Michelson interferometer realized by inscribing two identical gratings on two arms

of a 3dB coupler. The technique adopted for coupler fabrication is the fusion process which consists in twisting two optical fibers and in fusing their controlled portion (fusion zone) while pulling. The result is a coupling region which operates in multimode condition and shows a strong bending sensitivity. Therefore any mechanical stress or thermal expansion/contraction which curves the coupling region should be rigorously avoided. The method we used to overcome the problem is to block, by means of resin, the twisted fibers on a half quartz tube whose thermal expansion coefficient is as close as possible to that of the silica. This guarantees a stable positioning of the fused zone (no bending effects) even if the coupler is subjected to strong temperature variations like $-40^{\circ}\text{C}/+80^{\circ}\text{C}$.

In other words, contrary to Bragg fiber gratings, it is preferable to permit fiber expansion with temperature, without any mechanical compensation.

In our narrow band filters the coupler pre-package is about 4cm long with an outer diameter of 1.5 mm.

3.2 Filter specifications

As follows from the data concerning thermal and mechanical sensitivity of Bragg gratings, we can now define the operating limits that a narrow band filter must guarantee. Bandwidth and central wavelength can be selected by properly controlling the grating pitch Λ , its modulation depth δn and length L (see equations 1-4). At this preliminary stage of the development we can assume a bandwidth not greater than 0.4nm, and this means that any package solution should be able to reduce wavelength shift as low as possible in order to avoid excessive insertion loss fluctuations with temperature. Supposing an operating temperature range of $-25^{\circ}\text{C}/+75^{\circ}\text{C}$, the grating wavelength should suffer about $\pm 0.5\text{nm}$ variation with respect to its value at room temperature in case of no compensation mechanism.

Our aim is to design a package able to undo as much as possible this effect.

3.3 Grating passive pre-package: table-top solution

A well known method to reduce the wavelength shifting with temperature consists in packaging the fiber grating under tension in such a way that the strain is relieved as the temperature rises. Therefore the upward thermal shift and the downward strain shift can combine in order to give an overall reduced temperature dependence. This can be accomplished by properly choosing two materials with different thermal expansion. In fig.4 we show the table-top mount concept⁶; It consists of an invar rod with two aluminium brackets screwed on it.

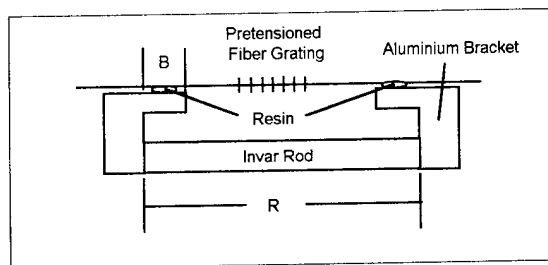


Fig.4 Table-top mount grating package

As the temperature increases the greater thermal expansion coefficient of the aluminium ($C_2=23.8 \cdot 10^{-6} \text{ } ^\circ\text{C}$), with respect to that of the invar ($C_1= 1.6 \cdot 10^{-6} \text{ } ^\circ\text{C}$), causes the distance between the blocking points to decrease, thus resulting in a strain reduction of fiber pretension. It is obviously necessary to design with great care the lengths of the rod and the brackets. Assuming 50°C temperature increase ΔT and 30mm fiber length L (which is the blocking point distance and includes the grating length), the blocking point approaching is expected to be about $12 \text{ } \mu\text{m}$ for a complete compensation (we assume $1.2\text{nm}/10^{-3}\text{strain}$ sensitivity and $0.01\text{nm}/^\circ\text{C}$ thermal sensitivity). Referring to fig.4, after some simple mathematics we obtain the length B of aluminium brackets and the length R of the invar rod by solving the following system:

$$\begin{aligned} L &= R - 2 \cdot B \\ X &= R + R \cdot C_1 \cdot \Delta T - 2 \cdot (B + B \cdot C_2 \cdot \Delta T) \end{aligned} \quad (8)$$

X being the blocking point distance after elongation due to temperature.

In the preliminary test we avoided using resin to block the fiber on the two aluminium brackets, and adopted a mechanical method based on a screw mechanism. Our main interest was to verify the feasibility of this solution without taking into consideration any influence of the resin which could reduce, if not optimized, the actual compensation. Figure 5 concerns the wavelength shift vs temperature for compensated and uncompensated Bragg grating (with constant pitch) that has been pretensioned with about 50g load.

Bragg wavelength [nm]

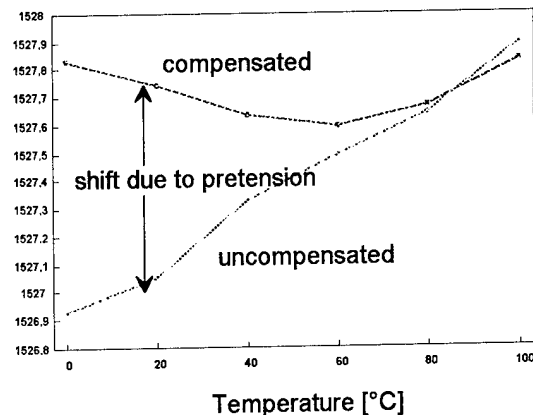


Fig.5 Wavelength shift vs temperature for compensated (table-top solution) and uncompensated Bragg grating

The final result demonstrates a significant reduction of the grating sensitivity ($0.2\text{nm}/100^\circ\text{C}$) and shows that, for $T < 60^\circ\text{C}$, the tension reduction exceeds the temperature influence (overcompensation) while, for $T > 60^\circ\text{C}$, the shift due to temperature becomes the dominant phenomenon (undercompensation).

The data reported in figures 6 and 7 refer to two samples packaged with different resins (A and B). A positive compensation action is still evident, even if the physical properties of the resin appear to be a fundamental factors in controlling the performance of the component (the problem is still under investigation). In fact we notice overcompensation in the case of resin A and undercompensation in the case of resin B.

This implies that, after the choice of the most reliable resin, it will be certainly necessary to optimize experimentally the distance between the blocking points of the grating.

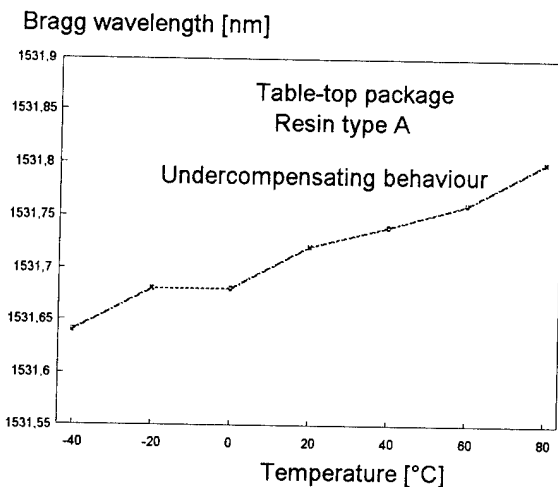


Fig.6 Temperature sensitivity of compensated grating (table-top solution with resin A)

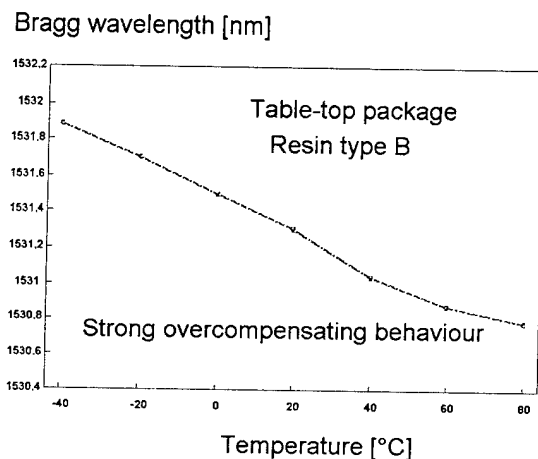


Fig.7 Temperature sensitivity of compensated grating (table-top solution with resin B)

Also it is worth remembering that, in all samples we packaged, fiber pretension experienced 10-20% reduction after resin curing, thus resulting in a lower maximum operating temperature of the component. Finally compensated gratings have been subjected to 4 subsequent temperature cycles (-40°C/+80°C) in order to investigate their long-term stability. Figure 8 shows a typical result which confirms the tendency of the component to gradually reduce its pretension. A possible explanation could be the slow movement of the resin, in particular at low temperature where the distance increase between blocking points, combined with the elastic strength of the fiber, subjects the resin to higher shearing stress.

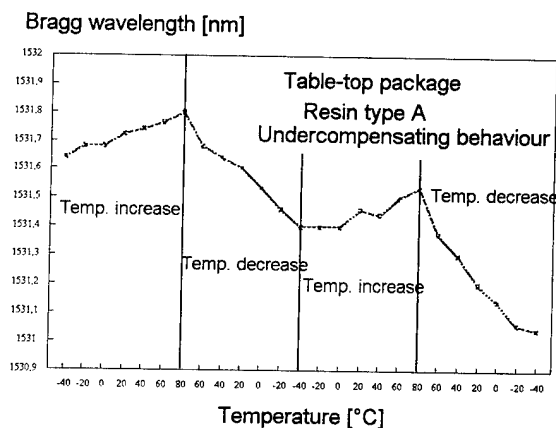


Fig.8 Long-term stability test of compensating grating (table-top solution with resin A)

3.4 Grating passive pre-package: bimetallic plate solution

This type of solution uses two metallic plates with different thermal expansion coefficient which are tightly bond each other, so that they appear as an only one piece, compact and low cost (fig.9).

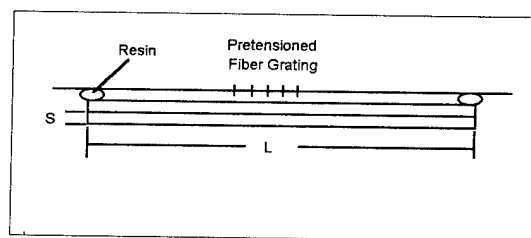


Fig. 9 Bimetallic plate grating package

As the temperature rises the two plates are expected to bend with the concavity in the same side of the plate with lower thermal expansion coefficient. In this way a temperature increase results in a fiber ends approaching and finally in a grating strain decrease.

Assuming 50°C temperature increase ΔT and 30mm fiber length L , the blocking point distance X after bending should be $12\mu\text{m}$ lower than L for a complete compensation, as calculated for the table-top solution. If L represents the length of the undeformed plates and C_1 and C_2 their thermal expansion coefficients (fig.9), the following relationships can be obtained by simple geometrical considerations:

$$L_1 = 2 \left(r + \frac{s}{2} \right) \cdot \arcsin \frac{X}{2r}$$

$$L_2 = 2 \left(r + \frac{3}{2} \cdot s \right) \cdot \arcsin \frac{X}{2r} \quad (9)$$

$$L_1 = L + L \cdot C_1 \cdot \Delta T$$

$$L_2 = L + L \cdot C_2 \cdot \Delta T$$

where s is the thickness of the metallic plates, L_1 , L_2 their lengths after bending and r the curvature radius. The design of the mount can be done by fixing a reasonable plate length (30 mm in our case) and choosing the materials and the thickness of the plate which best guarantee the requested blocking point approaching.

Figure 10 shows the temperature dependence of a prototype which consists of a constant pitch grating fixed to a 30mm long bimetallic plate. Its overcompensating behaviour demonstrates that the theoretical values for mechanical parameters (equation (9)) do not perfectly match the real ones, and an experimental optimization of the package is still necessary as in the case of table-top solution.

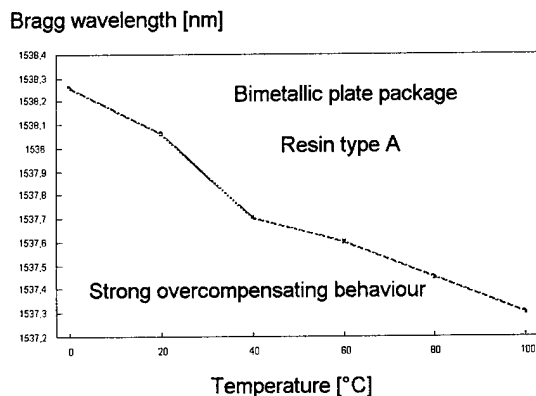


Fig.10 Temperature sensitivity of compensated grating (bimetallic plate solution with resin A)

3.5 Grating active pre-package: Peltier cell solution

In case it should be essential to avoid completely any wavelength shift due to temperature, the pre-package could consist in a Peltier cell with a simple driving circuits and a thermistor. This keeps the grating temperature stable over time by putting into

contact the fiber with the one side of the cell, and without any pretension mechanism. Climatic tests performed with commercially available Peltier cell have confirmed the ability of this package to assure a constant temperature of the grating (within $2\pm 3^\circ\text{C}$ tolerance) while the environmental temperature changes from -20°C to $+60^\circ\text{C}$.

4. CONCLUSIONS

This paper provides a description of different packaging techniques for in-fiber Bragg gratings that can be used in narrow band transmission filters. The results confirm the feasibility of the solutions proposed and demonstrate that the component should be able to work efficaciously in the temperature range $-25^\circ\text{C}/+75^\circ\text{C}$ with an overall wavelength shift of $0.2\div 0.3\text{nm}$. Better sensitivity can be achieved by optimizing the distance between blocking points or using a package with a particular geometry.

The major problem seems to be linked to the type of resin used for blocking the fiber and is actually under investigation. If the resin is subjected to high shearing stress (in particular at low temperature) the component gradually reduces grating pretension, thus resulting in a low long-term reliability.

5. ACKNOWLEDGMENTS

This study has been partially supported by the EEC, ACTS Project A046 PHOTOS. We also thank CSELT laboratories that provided us in-fiber Bragg gratings for packaging tests.

6. REFERENCES

- [1] A.Yariv, P.Yeh: "Optical wave in crystals" J.Wiley & Sons
- [2] R.Kashyap: "Photosensitive optical fibers: devices and applications", Optical Fiber Technology 1, pp.17-34, 1994
- [3] P.Russel et al.: "Optical Fiber Gratings", Physics World, October 1993
- [4] C.Bruschi et al.: "Progetto e realizzazione di reticoli ad alta riflettività in fibra ottica", Proceedings of Conference FOTONICA'95, Italy 1995

- [5] W.W.Morey et al., SPIE The International Society for Optical Engineering, 1989
[6] G.W.Yoffe et al.: "Temperature-compensated optical-fibers Bragg gratings", Proceedings of OFC Conference, 1995

Authors

Stefano Pitassi was born in Udine, Italy, in 1965. He received the doctor degree in Opto-Electronics Engineering from "Politecnico di Milano" in 1990. At the beginning of 1991 he joined R&D Dept. of SIRTl where he has been engaged in passive optical components as a Senior Engineer. He is involved in national and international standard committees (CENELEC) and had some papers published in national and international conferences.

Francesco Pozzi was born in Gallarate, Italy, in 1968. He received the doctor degree in Electronics Engineering from "Politecnico di Milano" in 1994. In 1995 he joined R&D Dept. of SIRTl where he has been engaged in passive optical components and optical amplifier as a Junior Engineer.

Andrea Marcone was born in Genova, Italy, in 1962. He received the doctor degree in Mechanical Engineering from "Politecnico di Milano". At the beginning of 1991 he joined R&D Dept. of SIRTl where he has been engaged in the project and development of accessories for telecommunication systems as a Senior Engineer.

Vittorio Spano was born in Lagonegro, Italy, in 1967. Since 1989 he has been working as technician in R&D Dept. of SIRTl where he has been engaged in the development of passive optical components

Mailing address: SIRTl S.p.A.
via E.Fermi 2,
20060 Cassina de Pecchi
Milano, Italy
Tel. +39.2.6677.5146
fax +39.2.6677.5199

STUDY OF THE HIGH-SPEED CONNECTION FOR PRE-CONNECTORIZED OPTICAL FIBER CABLES

Yoshikyo TAMEKUNI, Kei SUNAGA, Tomohiko UEDA,
Makoto HONJO, Toru YAMANISHI

Sumitomo Electric Industries, Ltd.
1, Taya-cho, Sakae-ku, Yokohama, 244 Japan

Abstract

In order to realize high-speed high-count cable connection, we produced the proto-type of 80-fiber connector and joint box.

Unit type 80-fiber connector is made of silicon and epoxy resin for the purpose of inhibiting the effect of moisture absorption. Low connector loss of less than 0.4dB has been achieved at the 80-fiber connector.

Utilizing the 80-fiber connectors and newly developed joint box, we estimated cable connection time. We realized less than 4 hours cable connection time for 4000 fibers.

1. Introduction

For construction of optical subscriber cable network, high-count high-density pre-connectorized cables are required¹. We had developed and reported 4000-fiber cable, 16-fiber ribbon and 16-fiber connector as the components for high-density cable technique^{2,3,4}. Furthermore, in order to shorten the cable connection time, to increase the fiber number of the optical multi-fiber connectors and to shorten the storage time of the excess fibers are required. So we developed 80-fiber connectors and new structure of cable joint box.

In this paper, the design concept and the properties of the proto-type models of unit type 80-fiber connectors, the design of joint box, and the estimation of the connection time utilizing the developed components are discussed.

2. 80-fiber connector

2.1 Structure of unit type 80-fiber connector

As the structure of 80-fiber connector, two types of 80-fiber connectors are considered. One is stacked-type connector, which is composed of five 16-fiber connectors, and the other is unit type connector (fig.1)⁵. As a primary step of the development for 80-fiber

connector, we had reported the stacked-type 80-fiber connector utilizing low-loss 16-fiber connectors⁴. Furthermore, in order to realize higher density of the optical fiber, we produced the proto-type models of unit type 80-fiber connector.

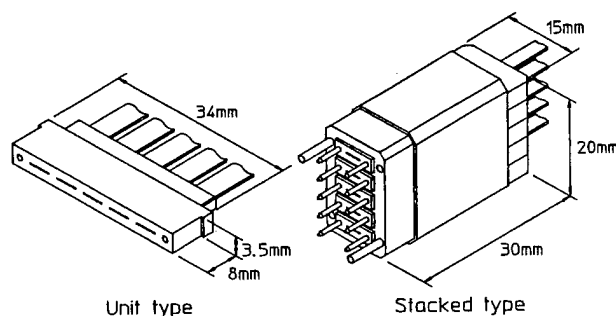


fig.1 Structure of 80-fiber connector

The design concept of conventional MT connector, less than 12-fiber connector, was applied to unit type 80-fiber connector. As shown in fig.2, a pair of 80-fiber connector consist of a pair of 80-fiber connector ferrules, two guide-pins and a clamp. Each ferrule has two guide-pin holes and eighty fiber positioning holes in a line between the two guide-pin holes. Five 16-fiber ribbons are fixed to the 80-fiber connector ferrule. The size of the connector is 34(W)*3.5(H)*8(L)mm, and the cross-section area is 1.49mm² / fiber, which is less than half of the stacked-type connector.

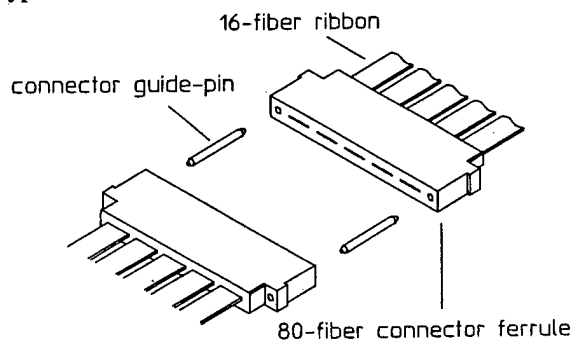


fig.2 Unit type 80-fiber connector

Averaged connection loss of 0.2dB is required for the optical fiber connector in the subscriber network¹. As the first step of the development of 80-fiber connector, we aimed at 0.4dB of average connector loss. The main cause of loss generation for this type optical fiber connector is the offset of the fiber positioning hole position (ferrule eccentricity error). The ferrule eccentricity error of 80-fiber connector ferrule is defined as the distance between the designed fiber positioning hole position and the actual position shown in fig.3. In order to realize the connector loss of 0.4dB, averaged ferrule eccentricity error must be within 1.1 μ m.

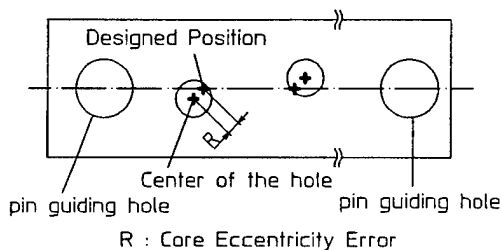


fig.3 Definition of ferrule eccentricity error

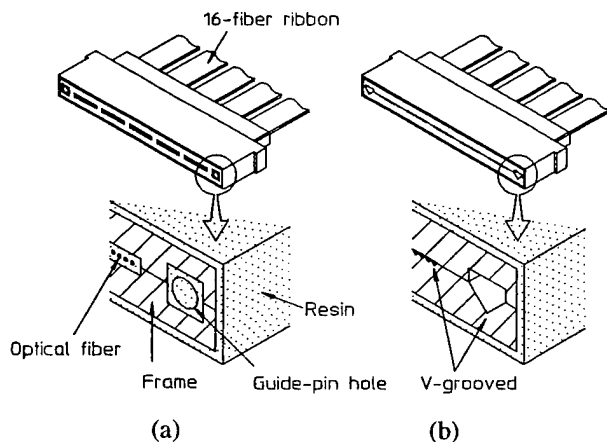


fig.4 Structure of 80-fiber connector ferrule

For the purpose of achieving this precision under every environment, we introduced new structure to the optical fiber connector ferrule. Our conventional MT connector ferrule is made of one material thermoset epoxy resin. However, plastics is generally easy to suffer the dimensional change by moisture absorption. Especially, in case of the 80-fiber connector, it was assumed that the tendency, not outstanding in conventional MT connector, may become prominent because of its size, which is about five times as long as that of MT connector. Considering the long time reliability as well, we adopted new structure as the 80-

fiber connector ferrule(fig.4). Inside the ferrule, it has the frame, which doesn't swell by moisture absorption. As the structure of the proto-type models, we produced two types of ferrules utilizing silicon as the material of the frame. One is silicon V-grooved (SV) connector (fig.4a), and the other is silicon frame (SF) connector (fig.4b).

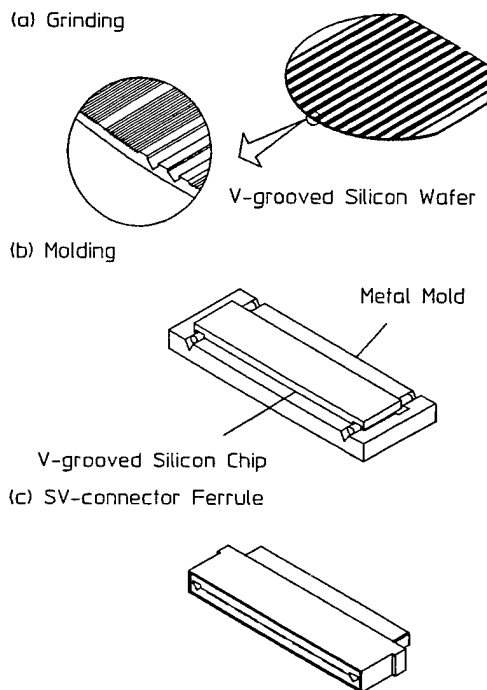


fig.5 Manufacturing process of SV connector ferrule

2.2 SV connector

SV connector is composed of V-grooved silicon chip covered with epoxy resin. It is manufactured by using precise grinding and transfer molding technique, as shown in fig.5. After grinded precisely, the V-grooved silicon chip is inserted into metal mold. Thermoset epoxy resin is supplied into the metal mold around the silicon chip and hardened by curing process. Silicon is the material which is comparatively easy to be grinded precisely. We had achieved 0.2dB connector utilizing the grinding technique. In case of 80-fiber connector ferrule, because the number of the V-grooves are high, more precisely we must control the grinding condition of the temperature, diamond wheel and grinding process. As well, the size of the connector ferrule is so thin and long that it is easy to warp in the molding process. In order to diminish the warp, we decided the molding condition by using an experiment planning method.

Using these technique, we tried to manufacture

SV connector ferrules. Fig.6 shows the distribution of ferrule eccentricity error of SV connector ferrules. Though ferrule eccentricity error become worse than the precision of silicon chip because of the warp, we achieved the precision of within averaged 1.2 μ m.

2.3 SF connector

SF connector is composed of silicon-frame covered with epoxy resin. This connector is manufactured by the similar process to SV connector. The main difference of the two structures is that, in SF connector, silicon is used only as the frame, which doesn't suffer the influence of the moisture, not as the alignment parts. Therefore the process of grinding precise V-groove is not necessary for SV connector. The surroundings of the guide-pin holes and fiber positioning holes are made of epoxy resin, and shaped by the molding insert pins in the metal mold. So as not to interfere to the molding insert pins in the metal mold, the silicon frame is designed to have enough space around each hole. We manufactured SF connector ferrules using the some molding condition as that of SV connector ferrule.

Fig.7 shows the distribution of ferrule eccentricity error of SF connector ferrules. The ferrule eccentricity error of averaged 1.0 μ m is attained.

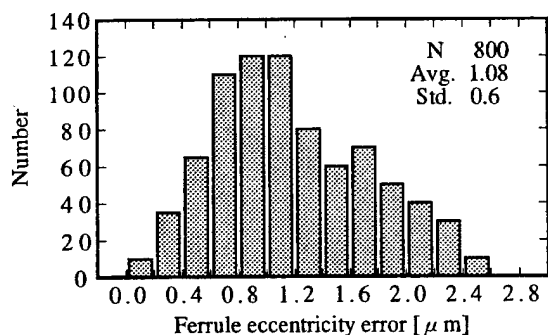


fig. 6 Distribution of ferrule eccentricity error (SV)

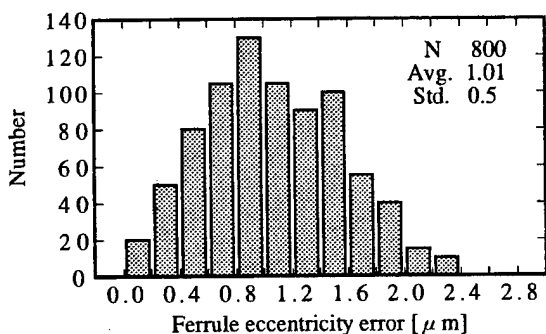


fig. 7 Distribution of ferrule eccentricity error (SF)

2.4 Connector loss of 80-fiber connector

We manufactured two types of 80-fiber connectors and estimated the connector loss using index matching gel. Fig.8 and fig.9 show the histograms of the connector loss against the master connector. We achieved low connector loss of averaged within 0.4dB for both type of the connectors. However, in order to realize the 0.2dB 80-fiber connector, further investigation to minimize the ferrule eccentricity error is necessary.

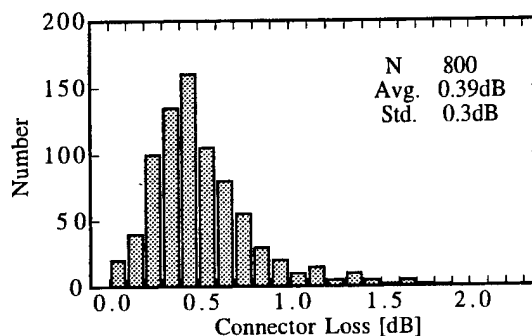


fig. 8 Distribution of connector loss (SV)

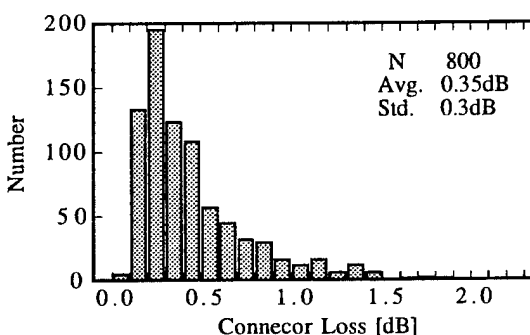


fig. 9 Distribution of connector loss (SF)

3. joint box

3.1 Joint box

In case of 4000-fiber cable connection, fifty pairs of 80-fiber connectors and excess fiber ribbon are stored in a joint box. For shortening the connection time, we developed new fiber storage method. Fig.10 shows the joint box. In the conventional enclosure, several pairs of connectors with excess fiber ribbons are stored in a sheet or a tray. But it takes much time to bind the excess fiber and to store them into the sheet. At the new storing method, in order to omit this process of individual storage, we designed the joint box so that all optical fiber ribbons can be handled together as a bundle in it. Five 16-fiber ribbons are bound to a bundle by spiral tubes because five 16-fiber ribbons are fixed to 80-fiber

connectors. 80-fiber connectors are positioned at the center of the joint box, and the fiber bundles are turned to the opposite direction in the joint box.

Cable jointing process of the optical fiber cable, in case of using this joint box, is as shown below. After the cable fixed to the joint box, fiber ribbons are turned to the opposite direction at around over the center. By adjusting the fix position of the optical fiber cable, it is possible to store the fiber ribbons of different length of the excess fiber (fig.11). The cable jointing process is finished by mating all the 80-fiber connectors at the center of the joint box.

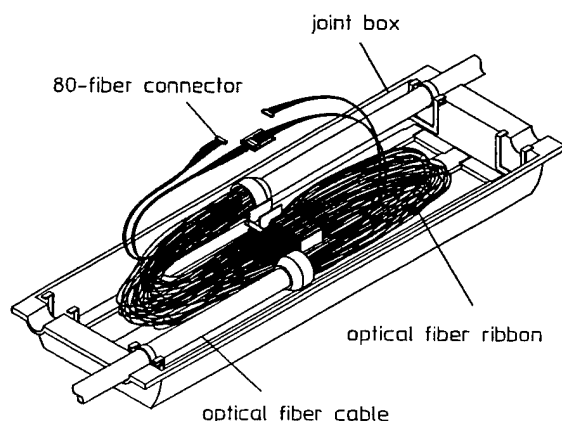


fig.10 New fiber storage method

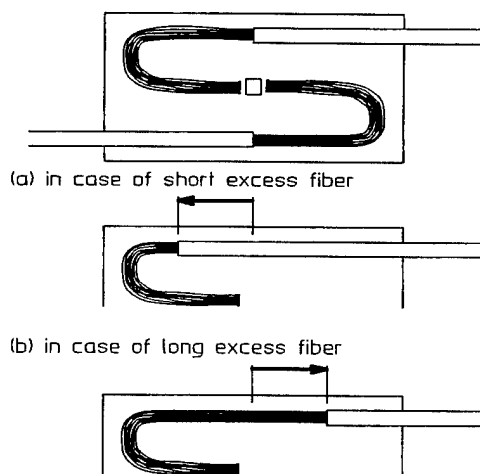


fig.11 adjusting method of the different length of excess fiber

3.2 Connector clamp

For shortening the connection time of the optical fiber connector, we designed a new part as the 80-fiber connector clamp. In case of conventional MT connector, as shown in fig. 12, metal clamp is utilized as the part to

press the connectors' endfaces one another and to keep the state of connection. In the mating process of MT connector, the set and removal of metal clamp is done with the tool. However, from the view of the workability, it is desirable that no special tool is required.

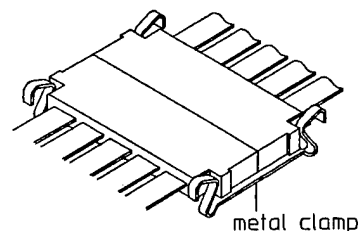


fig.12 Conventional metal clamp

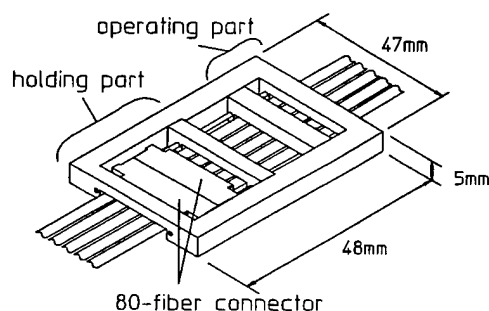


fig.13 Structure of new clamp

Fig.13 shows the new clamp for 80-fiber connectors. The new clamp consists of holding part and operating part. By picking and loosening the operating part, 80-fiber connector is loosened and pressed in the holding part. The cross section of the new clamp is 47(W)*5(H)mm. Connector loss with this connector clamp is the same as the loss with conventional metal clamp.

4. Estimate of connection time

We estimated the connection time of 4000-fiber using the proto-type of 80-fiber connectors, joint box and connector clamps. Two-hundred and fifty 16-fiber ribbons and fifty 80-fiber connectors were stored in the joint box. The measurement of the time was done from the removal of pulling head to the finish of installing the joint box.

Fig.14 shows the measured connection time of 4000-fiber. The connection time of within 4 hours is attained with these techniques. We can confirm that it took only a little time to store the excess fibers, especially by the effect of the new fiber storage structure.

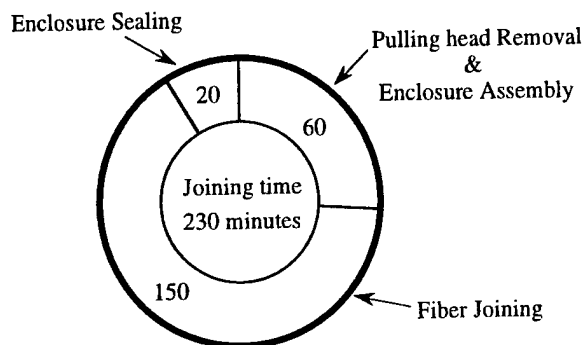


fig.14 Connection time of 4000 fiber

5. Conclusions

We designed the unit type 80-fiber connectors in two different ways considering of the long time reliability. We produced the proto-type of 80-fiber connector, and connector loss of within 0.4dB was attained. In order to shorten the cable connection time, instead of the conventional individual storage, we adopted and estimated the new method, at which fiber ribbons are handled as a bundle. From the view of the workability, we designed new structure of connector clamp.

Utilizing these components for high-density cable techniques, we estimated the connection time. The connection time of within 4 hours is attained with these techniques.

REFERENCES

- [1] S.Tomita, et al, 'Ultra High-density Optical Cable With Thin Coated Fiber and Multi-fiber Connector', IWCS 1993
- [2] K.Oishi, et al, 'Coating Design of Thin Coated Fiber for Ultra High-Count Optical Fiber Cable', IWCS 1993
- [3] W.Katsurashima, et al, 'Ultra-High-Count Optical Fiber Cable Using Single-Helical-Groove Unit', IWCS 1994
- [4] T.Ueda, et al, 'Development of 16-fiber Connectors for High-Speed Low-Loss Cable Connection', IWCS 1993
- [5] Nagasawa, et al, 'Single-Mode Multifiber Connectors for Future Large Scale Subscriber Network', 19th ECOC 1993



Yoshikyo Tamekuni

Sumitomo Electric Industries, Ltd.

1, Taya-cho, Sakae-ku
Yokohama, Japan

Yoshikyo Tamekuni recieved a B.E from Science University of Tokyo in 1991. He joined Sumitomo Electric Industries, Ltd in 1991, and has been engaged in research and development of optical connectors. He is an engineer of Communication R&D Department in Yokohama Research Laboratories.



Kei Sunaga

Sumitomo Electric Industries, Ltd.

1, Taya-cho, Sakae-ku
Yokohama, Japan

Kei Sunaga recieved a M.E. from Tohoku University in 1993. He joined Sumitomo Electric Industries, Ltd in 1993, and has been engaged in research and development of fiber joint box. He is an engineer of Communication R&D Department in Yokohama Research Laboratories.

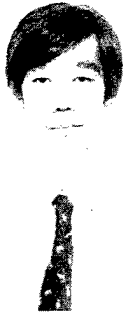


Tomohiko Ueda

Sumitomo Electric Industries, Ltd.

1, Taya-cho, Sakae-ku
Yokohama, Japan

Tomohiko Ueda recieved a B.E from Tokyo University in 1987. He joined Sumitomo Electric Industries, Ltd in 1987, and has been engaged in research and development of optical connectors. He is an engineer of Communication R&D Department in Yokohama Research Laboratories.



Makoto Honjo

Sumitomo Electric
Industries, Ltd.

1, Taya-cho, Sakae-ku
Yokohama, Japan

Makoto Honjo recieved a M.E from Osaka University in 1984. He joined Sumitomo Electric Industries, Ltd in 1984, and has been engaged in research and development of optical fiber, cable and jointing technologies. He is a senior engineer of Communication R&D Department in Yokohama Research Laboratories.

Toru Yamanishi

Sumitomo Electric
Industries, Ltd.

1, Taya-cho, Sakae-ku
Yokohama, Japan

Toru Yamanishi recieved a B.E from Hokkaido University in 1972. He joined Sumitomo Electric Industries, Ltd in 1972, and has been engaged in research and development of optical fiber, cable and jointing technologies. He is a manager of Optomechatronics Systems R&D Department in Yokohama Research Laboratories.

DEVELOPMENT OF A STACKED CONNECTION METHOD FOR HIGH DENSITY PRE-CONNECTORIZED 3000 FIBER CABLE.

Tetsuo Nozawa, Yasuhiro Tamaki and Hiroshi Yokosuka

Fujikura Ltd, Opto-Electronics Lab.

1440 Mutsuzaki, Sakura-shi, Chiba, 285, Japan

Abstract

We investigated rapid connection and storage technologies for a high density 3000 fiber pre-connectorized cable with pulling eye which can be used in existing ducts.

A flexible reinforced outer tube which has good storage efficiency and is mechanically strong was used for the connectorized pulling end. 375 pieces of 8 fiber MT connectors were stored within the end and it was possible to pull cable lengths of more than 500m within existing ducts having diameters of 75 mm.

The ability to change the connections was stressed in the jointing and an 8 fiber MT pair connection was used. By using a simple excess length storage (concentrated storage of connection points) method within the closure and the novel 5 connector stacked connection method, the overall cable jointing time was reduced to less than 6 hours which is half the time required presently.

1. Introduction

In line with the large scale implementation of ISDN, NTT's proposed Fiber To The Home (FTTH) optical access network plan has become an increasingly important task in Japan [1].

The key points in the efficient construction of user and access networks are increasing the fiber count of distribution cables, reducing the workload in cable installation and connection, and the efficient use of existing facilities [2]. High density, high count cables have been designed for use in existing underground ducts

having diameters of 75mm. We developed and implemented a 1000-fiber single slotted cable in 1995 [3], [4]. In the future, it is predicted that there will be a demand for even higher count cables.

MT connectors are very suitable for subscriber networks where connectors need to be switched easily. Recently, low losses of less than 0.15dB are possible for factory installed MTs. In the future, cables pre-connectorized with 8-fiber MT connectors on both ends will become important for fast cable connections.

This paper describes the design and performance of the pre-connectorized pulling end for a 3000 fiber cable, and the high count closure that uses the outer shell of a existing underground closure, and the stacked connection method which reduces the jointing time.

2. 3000-fiber Cable

Figure 1 shows the cross section of the developed 3000-fiber cable design. The maxi-

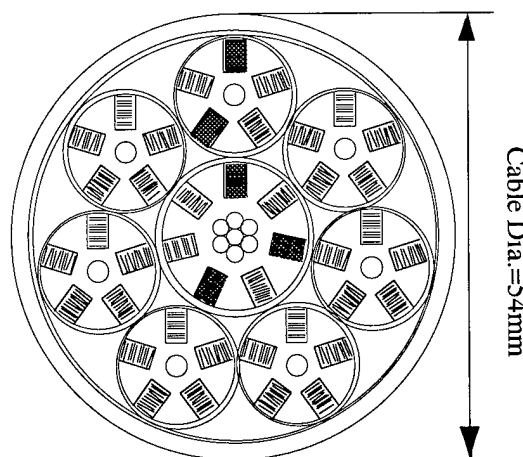


Fig.1 Cross section of the 3000-fiber cable

imum diameter of the cable is 54 mm. It comprises of a central slot and five sub-slots and uses ultra thin 8 fiber ribbons.

During the manufacture of the prototype, the fiber indicated in Fig.1 was monitored to determine the mechanical strength necessary for withstanding the rigors of cable installation.

3. Pre-connectorized Cable

The following conditions need to be met by the 3000 fiber connectorized pulling end. Firstly, it must accommodate and protect 375 pieces of MT connectors which terminate 3000 optical fibers. Next, a minimum storage radius of 20mm needs to be maintained. In addition it must have enough mechanical strength to withstand the stresses during cable installation. The investigations into each of these characteristics are described below.

3.1 Cable pulling end structure

We used a flexible reinforced outer tube (Fig.2) for the pre-connectorized pulling end. This structure has good space efficiency and can manage to store 375 MT connectors within a pulling end having a maximum outer diameter of 72 mm.

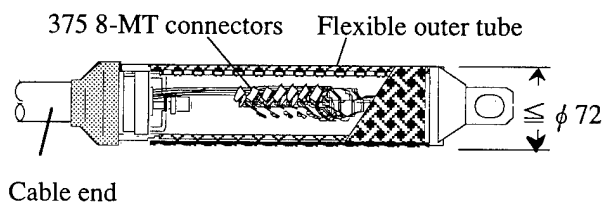


Fig.2. Cable pulling head structure

We proceeded to confirm that the pulling end could pass through a duct having a diameter of 75mm. Figure 3 shows the possible pulling end diameters that can pass through the 75 ϕ underground duct. The diameter of the prototype 3000 fiber connectorized pulling end is indicated on the figure. From the figure, it is confirmed that the pulling end could indeed

pass through the duct.

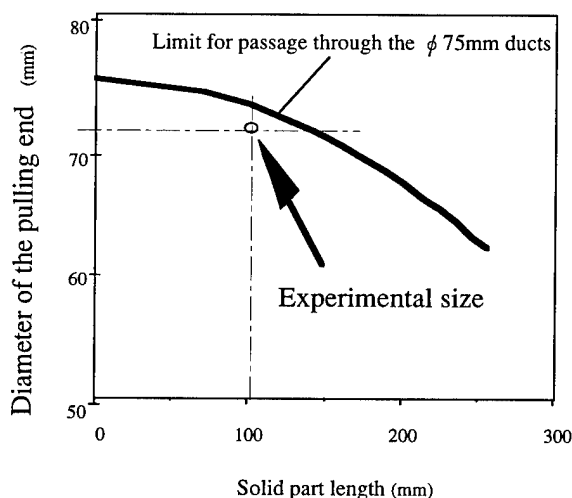


Fig. 3. Passage of the Cable pulling end through existing ducts

3.2 Mechanical strength

(1) Pulling stress

Since the clearance between a duct having a size of ϕ 75mm and a pulling end of ϕ 72mm is small, it was predicted that the resistance at bends would be fairly large. In addition, as the weight of the cable is large, the frictional resistance during installation is also expected to be very large.

A 3000 fiber cable has a free mass of approximately 1800kg/km. When 500m of this cable is installed horizontally and linearly within a duct of ϕ 75mm, the required pulling strength T_1 is

$$T_1 = 9.8 \mu \times \text{Cable weight/km} \times \text{Length} \\ = 9.8 \times 0.5 \times 1800 \times 500 / 1000 = 4410 (\text{N})$$

In general, several bends occur within a underground duct. The frictional resistance at these points tend to be higher than that along straight routes. We assumed a typical installation route as shown in figure 4 and investigations into the predicted pulling strength were carried out. In this simulation, we assumed the

frictional resistance around each curve guide to be the same as that of a straight route. The necessary pulling strength required for the same 500m was calculated for the case when bends of 10° , 20° and 30° occurred.

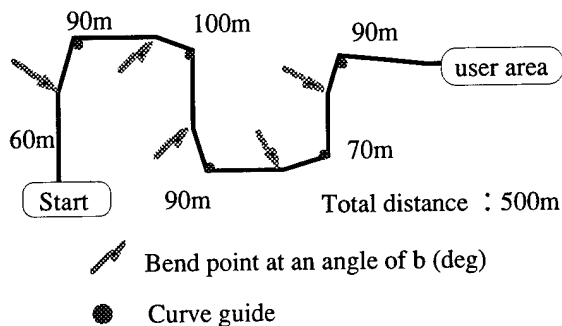


Fig. 4. Simulated route for cable installation

Figure 5 shows the calculated results of the pulling strength of an assumed cable installation route. The dotted line shows the load limit of existing cable installations using a curve guide.

In reality, the resistance of the termination as well as the maximum static friction cause a pulling force of close to 1 ton on the end. Therefore we designed the pulling end to withstand forces of up to 7800N.

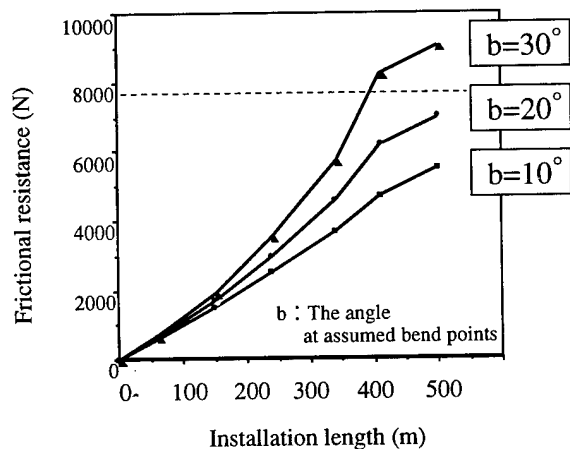


Fig. 5. The calculated pulling strength within an assumed cable installation route

(2) Mechanical strength tests

Reliability tests were carried out on the pulling end. Figure 6 shows the set up for the squeeze test. The insertion loss of the connector was measured when a force of 7800N was applied on the end and it was passed through a curved guide.

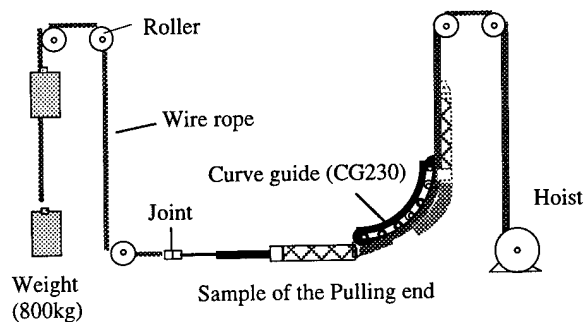
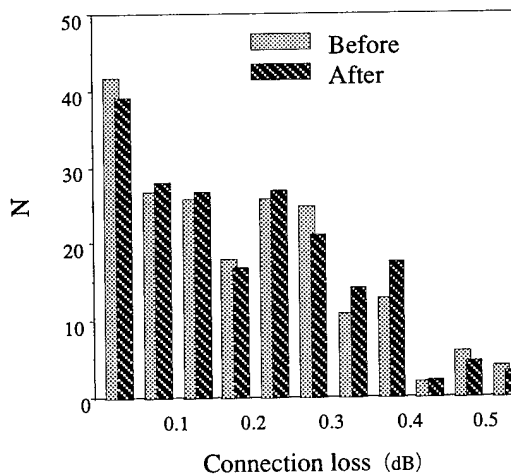


Fig. 6. Schematic of the Squeezing test

Figure 7 shows the insertion loss histogram of the connectors before and after the test. Taking into consideration the normal mating repeat-



	Test result	
	Before	After
N	200	200
Maximum	0.55 dB	0.52 dB
Minimum	0.00 dB	0.00 dB
Average	0.178 dB	0.181 dB

Fig. 7. Histogram of the test results of MT connection loss variation with tensile strength.

ability of connectors, there was hardly any change in the loss due to bending. We confirmed that the structure of the prototype connectorized pulling end afforded full protection to both the fibers and connectors.

4. High count closure

Presently, the largest capacity of underground closures used in Japan is 1000 fibers. Figure 8 shows a simplified structure of the closure.

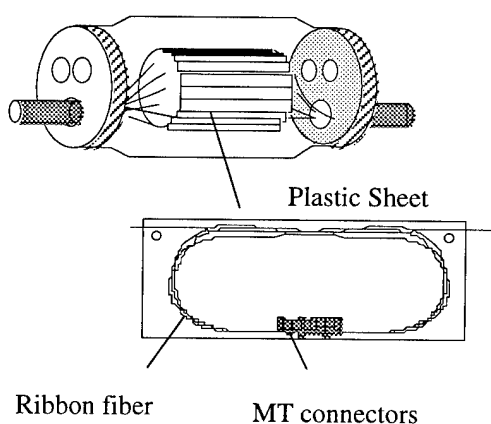


Fig. 8. Structure of existing underground closure

Most manholes are packed with cables. If the outer diameter of the closure was enlarged to accommodate 3000 fiber connections, this closure could not be used in existing manholes. So we devised a high density storage method for storing 3000 fibers within the present closure. Figure 9 shows a simplified structure of the closure. The connected MTs were stored in units of 5 within sub trays (connector trays). The sub trays were designed to accommodate fusion splices as well. The hanger tray was designed to accommodate 34 sub trays with a high density storage structure as shown in figure 9. In this experimental closure, three hanger trays can slide to the end of an upper or a lower tray, enabling easy access to all sub trays.

As for the storage of the fibers, instead of using the existing rounded storage method within the plastic case as shown in figure 8, a simplified half turn method within the sleeve was used.

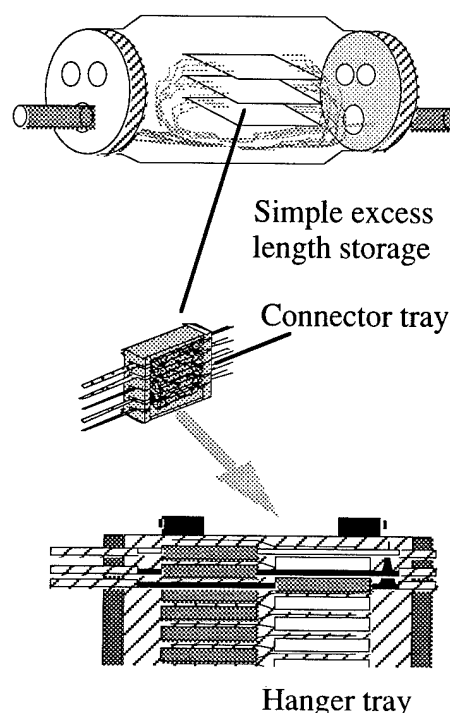


Fig. 9. Structure of the developed high count closure

5. Stacked connection method

Figure 10 shows the steps involved in the

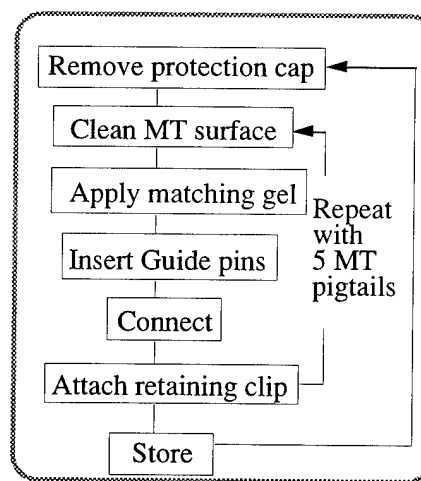


Fig. 10. Steps in jointing pre-connectorized Cables

connection of MT connectors. There were a large number of repeated operations involved in the basic 5 MT unit storage method which includes cleaning the MT end faces, application of matching gel, insertion of guide pins etc.

(1) Basic system

In order to carry out these operations simultaneously, a stacked connection method for 5 connectors was used during the connection process. Figure 11 shows the schematic of the stacked connection method. The stacked shells as shown in the figure have been already developed and used for 600- and 1000- fiber optical cable. The method has been proven to reduce by 30% the overall cable jointing time with the present closure.

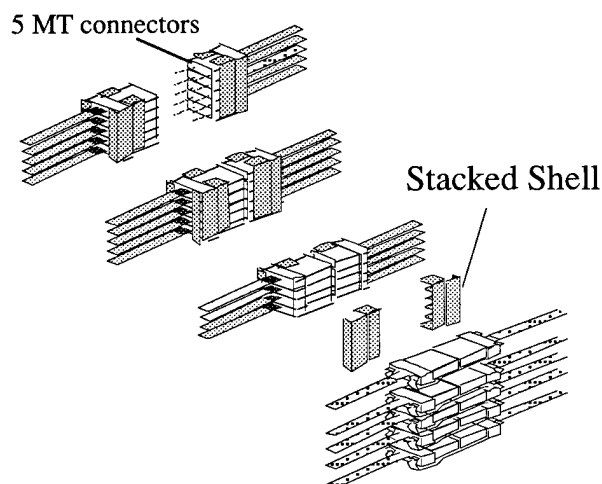


Fig.11. Schematic of a stacked connection method

(2) 5-pin applicator

The guide pins used for alignment were small having a diameter of $\phi 0.7\text{mm}$, and length $L=11\text{mm}$, they were difficult to handle in dark and narrow manholes. This small size of the guide pins has caused some difficulty in handling leading to reduced efficiency.

To solve the problem, at the first time, we developed a simple tool for inserting 5 guide pins simultaneously. Figure 12 shows the simultaneous insertion process of 5-guide pins with the 5-pins applicator.

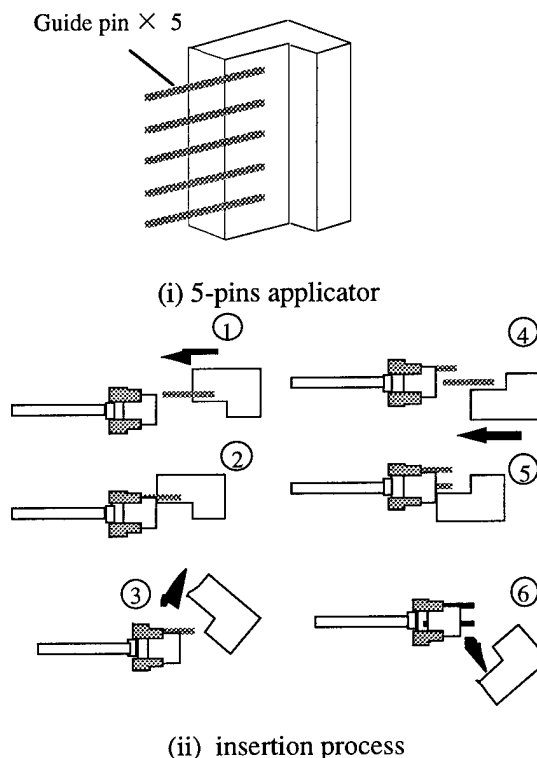


Fig.12. Simultaneous insertion process of 5-guide pins

(3) 10-pins applicator

Next, we developed a novel and simple tool for determining the position easily for inserting 10-guide pins. Figure 13 shows the simultaneous insertion process of 10-guide pins with the 10-pins applicator. In the case of the 5-pins applicator, the first operation is alignment with guide pin to the guide holes of MT connectors. This operation is a little difficult in dark manholes. But in the case of this 10-pins applicator, the alignment operation consists of placing the hollow portion of the applicator on the stacked connector surfaces. Even in manholes and other difficult environments, a fast and skillless operation has been realized with this tool.

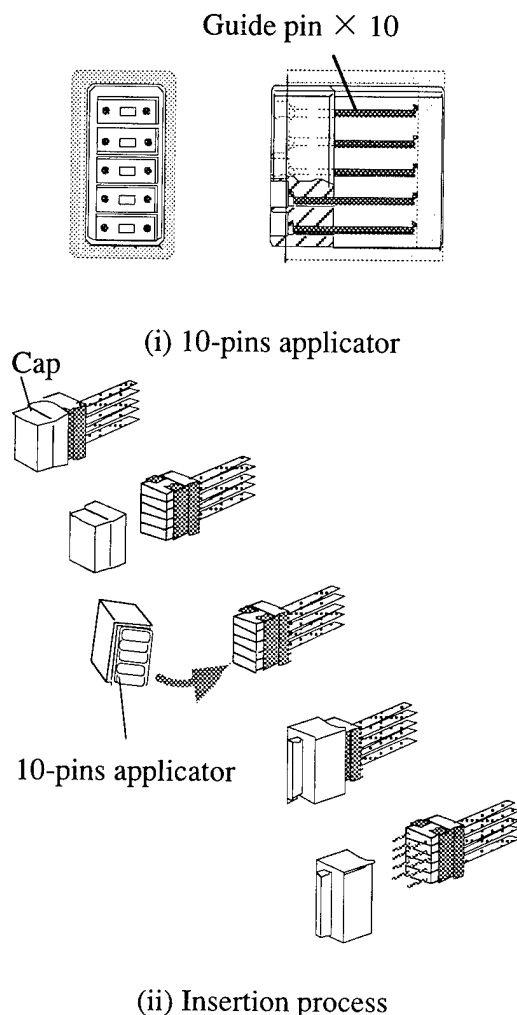


Fig.12. Simultaneous insertion process of 10-guide pins

(3) Experimental results

There are four operations in the storage procedure, removing the pulling end, assembling the closure, connecting and storing each cable, and sealing the closure. Up to now, in the actual field, in the case of 1000-fiber cable (connected with 4-MT connectors), the overall cable jointing time was over 10 hours. The installation is therefore regarded as a 2 day job. Assuming the conventional method was used for 3000 fiber cable (connected with 8-MT connectors), the overall jointing time would take over 14 hours.

Figure 13 compares the jointing time for 3000-fiber cables using the current method and each stacked connection methods. By using a simple excess length storage (concentrated

storage of connection points) method within the closure and 5 connector stacked connection method and simultaneous 10-guide pins insertion method, the time required for the entire cable jointing from the unraveling of the pulling end to the sealing of the closure took less than 6 hours, which is 60% the time required presently and can be carried out within a single working day.

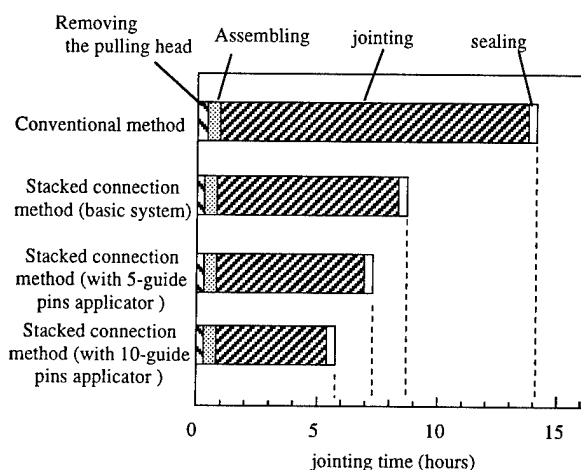


Fig. 13. Overall jointing time of the 3000 fiber cable

6. Conclusions

A novel rapid connection and storage technologies has been developed for a high density 3000 fiber pre-connectorized cable .

The ability to change the connections was stressed in the connection and an 8 fiber MT pair connection was used. By using a simple excess length storage (concentrated storage of connection points) method within the closure and the novel 5 connector stacked connection method using simultaneous 10-guide pin insertion tool, the overall cable jointing time was reduced to less than 6 hours which is half the time required presently.

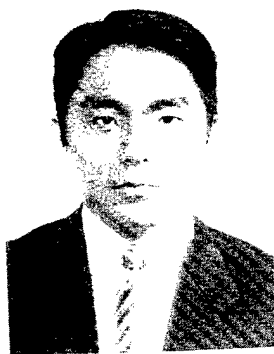
Reference

- [1] Y.Wakui, "The Fiber Optic Subscriber Network in Japan." , IEEE Communications Magazine, pp. 56-63, February 1994.

[2] H. Iwata, M. Matsumoto, Y. Ishino, S. Tomita, S. Nagasawa, T. Tanifuji, " Field Test Results for Pre-connectorized Cable with 16-fiber Ribbons", 43th IWCS, 1994

[3] H. Iwata, M. Tsutsumi, E. Nakamura, N. Matsumoto, M. Nozawa, S. Hayami, S. Nagasawa, T. Tanifuji, " Pre-connectorized 1000-fiber Single Slotted Core Cable", 44th IWCS, 1995

[4] N. Okada, K. Watanabe, K. Kobayashi, A. Sano, M. Miyamoto, " Development of single slotted-rod type 1000-fiber optical fiber cable for subscriber loop", 44th IWCS. 1995



Tetsuo NOZAWA

Opto-Electronics
Laboratory
Fujikura Ltd.

1440, Mutsuzaki,
Sakura-shi, Chiba,
285, Japan

Tetsuo Nozawa was born in 1962. He joined Fujikura Ltd. after his graduation from Keio University with a M.E. degree in 1988. He has been engaged in research and development of optical fiber and accessories.

He is now an engineer of the Fiber and Cable Accessory Department within Opto-Electronics Laboratory and a member of the IEICE of Japan.



Yasuhiro TAMAKI

Opto-Electronics
Laboratory
Fujikura Ltd.

1440, Mutsuzaki,
Sakura-shi, Chiba,
285, Japan

Yasuhiro Tamaki was born in 1955. He received the B.E. degree in mechanical engineering in 1977 from Saitama University.

He joined Fujikura Ltd. in 1982 and has been engaged in the research and development of telecommunication cables and accessories. He is now a manager in Fiber and Cable Accessory Department within Opto-electronics Laboratory and a member of the IEICE of Japan.



Hiroshi YOKOSUKA

Opto-Electronics
Laboratory
Fujikura Ltd.

1440, Mutsuzaki,
Sakura-shi, Chiba,
285, Japan

Hiroshi Yokosuka graduated in mechanical engineering from Tokyo Metropolitan Technical Junior College in 1967.

He has been engaged in development of telecommunication cables and accessories. He is now the general manager of the Fiber and Cable Accessory Department within Opto-Electronics Laboratory and a member of the IEICE of Japan.

CONNECTOR-TRANSFER TYPE COMPACT AND LOW INSERTION LOSS OPTICAL SWITCH FOR MULTI-FIBER RIBBONS

Tohru Sato, Makoto Okuda, Seiji Ohmizu, Takashi Shigematsu

The Furukawa Electric Co., Ltd., Yawata-kaigandori, Ichihara, Chiba 290, Japan

ABSTRACT

We have developed a compact manually-operated optical switch with a low insertion loss.

The optical switch has a pair of sixteen-fiber connectors using MT connector technology, then moving the connectors we can get switching action for a unit of eight-fiber ribbons at once. No index matching material to reduce reflection is used in the switch. Moreover, new switching mechanism is introduced into the switch. Therefore, we can get simple manual operation for switching and small outer dimensions of 50mm height, 35mm width, and 10mm thickness.

Using angled PC polishing technology, we have got mean insertion loss of 0.3dB and return loss of 45dB or high.

INTRODUCTION

We have been developed the real optical fiber subscriber network for the latest years in Japan, then the counts of optical fibers in the cables have got to a thousand. Now we have a serious issue of managing and maintaining tremendous counts of optical fiber economically. For easy and efficient management and maintenance, appropriate switching technology is necessary. From a point of view of application, the switch should be free from the conditions of

power supply as well.

The switching devices using micro-optical elements consisted of many parts and has complex optical system. This is disadvantage to reduce the cost and the size. Other switching devices with moving optical fiber connectors have much less complex mechanism, therefore, is getting better improvement in cost reduction than the former switch.¹ However, index matching material to reduce reflection prevents making smaller switches. At any way, we haven't had any manually-operated switch.

This paper reports the small in size, low in cost, and manually-operated optical switch which has low insertion loss and high return loss without index matching material.

2. STRUCTURE OF THE NEW SWITCH

2.1 Design concept

2.1.1 Using MT connector technology.

A low cost switch using the mechanism of moving multi-fiber connector was reported. We use a pair of sixteen-fiber connectors also, which is made of epoxy thermocuring material and has similar structure to MT connector.² The pair of connectors move on switching.

2.1.2 High return loss without matching index material.

The conventional switch with moving multi-fiber connectors needed index matching oil to reduce reflection, and had liquid proof construction. This made the switch larger. Angled PC connectors instead of index matching oil are introduced and the new mechanism protecting end faces of optical fibers on switching is developed for the new switch. The target optical characteristics are mean insertion loss of 0.5 dB or low and return loss of 40dB or high, which are same as those of MT connector.

2.1.3 No electric power required.

Keeping the application of the switch wider, the switch can be operated manually without any electric power. And for easy operation, the switching action is simple and all knobs for switching are concentrated on the same surface.

2.2 Basic switching action

The basic switching action of the conventional switch with moving connector was that one of two connectors moved in only perpendicular direction against the optical axis. A certain gap between connected fibers existed to protect the end faces of the fibers from scratching. And optical matching oil was required to reduce reflection and insertion loss.

The new switch has angled PC polished connectors. The end faces of fibers contact directly, so we need to develop new switching action. Shown in Figure 1, the action has three sub-actions, separating connectors, moving one of two connectors in the perpendicular direction against the optical axis, then connecting again.

Figure 2 shows the structure of the sixteen-fiber connector which is made of epoxy thermocuring material. The connector has four alignment-holes (*a*, *b*, *c*, and *d*) and two eight-

fiber ribbons are assembled on the connectors. The distance between alignment-holes *a* and *b*, *c* and *d*, and two ribbons are same. The end face of the connector is polished at an angle of eight degrees.

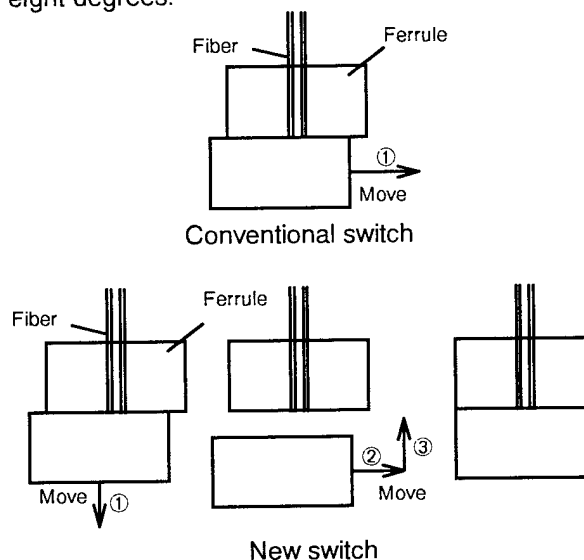


Figure 1 Comparison of switching actions

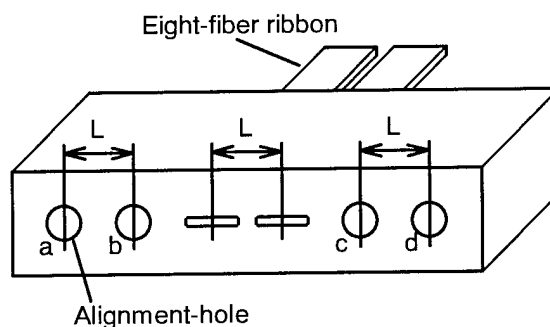


Figure 2 Structure of the sixteen-fiber connector

Figure 3 shows the basic switching action. Now two alignment-pins *X*, *Y* are fixed in the alignment-holes *a*, *c* of the connector 1. The optical fiber ribbon ① connects to the optical fiber ribbon ④ at normal state where the alignment-pins *X*, *Y* are inserted to the alignment-holes *b*, *d*, respectively. Then switching goes as following process. 1) the connector 1 goes backward until extracting the alignment-pins from the alignment-holes *b*, *d* completely. 2) the connector 2 slide in side direction. 3) the connector 1 goes forward until

inserting the alignment-pins into the alignment-holes *a*, *c* completely. Now the switch is at switched state where the optical fiber ribbon ① connects to the optical fiber ribbon ③ and the

optical fiber ribbon ② connects to the optical fiber ribbon ④.

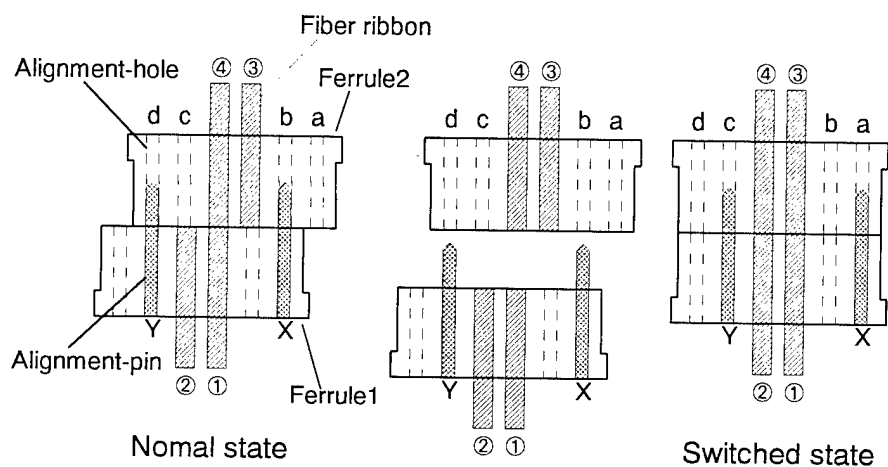


Figure 3 Basic switching action

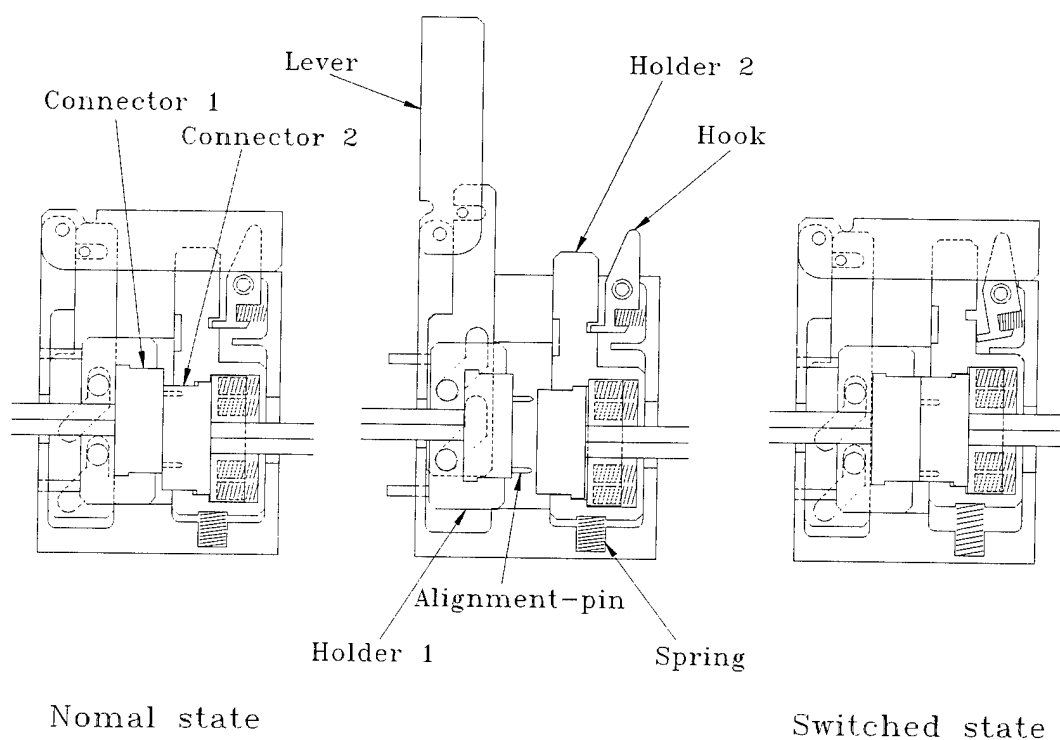


Figure 4 Structure of the switch

2.3 Details of the switch

Figure 4 shows the structure of the switch.

To realize easy manual operation, the switch has two independent mechanism, one for moving the connector 1 in front and behind and another for sliding the connector 2 in side direction. The action for connection and disconnection is operated with a lever. The motion of the lever is transmitted to the connector 1 converting into the motion in front and behind. At opening position of the lever, a hook and holder 2 appear. On changing state from normal to switched, the operation releasing the hook is done, on putting state back, the operation pressing the holder down is done. The lever and the hook are put on the same side of the switch. On closing the lever, no motion intending to move connector 2 can be operated, so the devices are protected from destruction.

The switch has two different levels of positioning precision. One is rough positioning depending on the precision of the holder 2 when the connectors are separated. At normal state, holder 2 are pressed against the hook by spring pressure, and at switched state, holder 2 are pressed against the wall of the switch cavity as well. Another is precise positioning depending on the precision of alignment-pins and alignment-holes of the connectors. Because the connector 2 are combined on the holder 2 with floating structure, the connectors can be connected as same precision as MT connector.

2.4 Exterior

The switch has compact dimension of 50mm height, 35mm width, and 10mm thickness because of eliminating matching index material and simple switching mechanism.

3. OPTICAL PERFORMANCES

3.1 Insertion loss

Insertion loss distributions at both normal state and switched state is shown in Figure 5. The number of fibers measured was 120 (five switches). We have got mean insertion loss of 0.30dB. This is same insertion loss level as MT connector.

3.2 Return loss

Return loss distribution is shown in Figure 6. We have got 46.0dB minimum return loss. Because of eight degree angled polish we have got high return loss without index matching material.

3.3 Thermal cycling test

The results of thermal cycling test are shown in Figure 7. The range of temperature is $-40 \sim +80^{\circ}\text{C}$. The upper plots are the results of insertion loss measured and the lower are the results of temperature. We have observed small loss change less than 0.1dB.

3.4 Cycle switching test

The results of the cycle switching test are shown in Figure 8. During 500 switching cycle, we have observed small loss change less than 0.1dB.

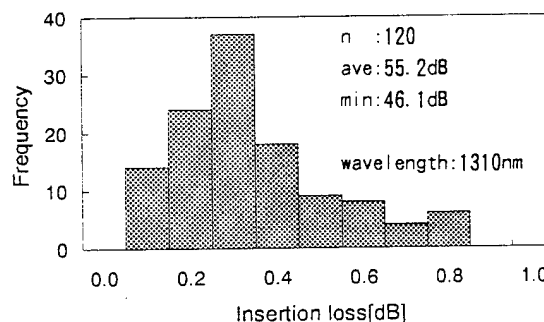


Figure 5 Insertion loss distribution

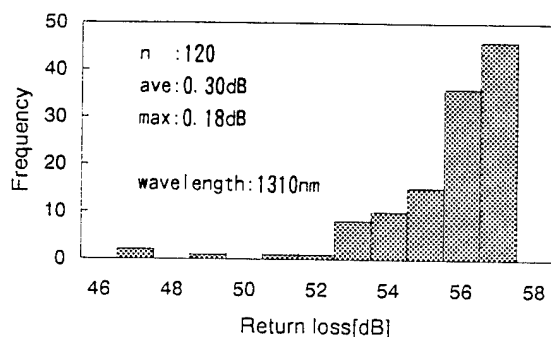


Figure 6 Return loss distribution

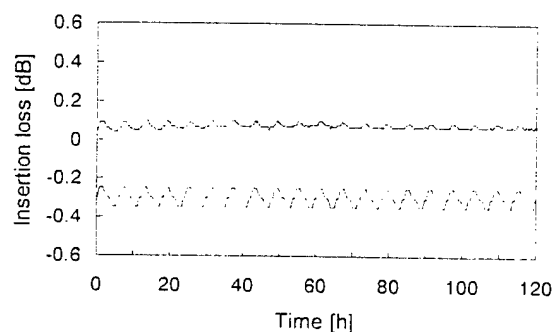


Figure 7 Result of thermal cycling test

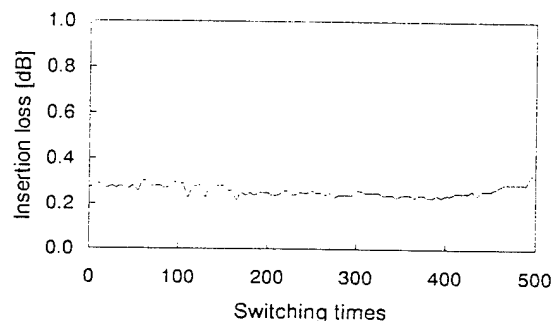


Figure 8 Result of cycle switching test

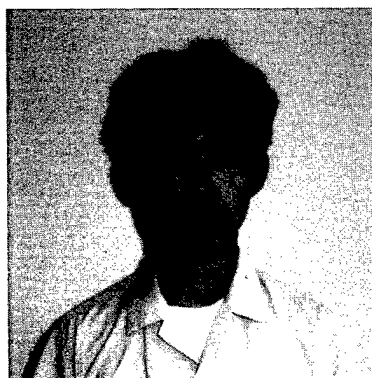
4. CONCLUSION

We have developed the new optical switch which doesn't have any index matching material and can be operated manually. The switch has compact dimension of 50mm(H) x 35mm(W) x 10mm(T). Moreover, we have got high optical performances of 0.3dB average insertion loss and 45dB minimum return loss, and good

stability during thermal cycling and cycle switching.

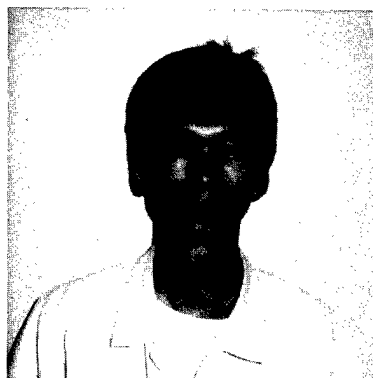
5. REFERENCES

- (1) M. Shimizu, K. Yoshida, and T. Ohta, "Mechanical Optical Switch for Single Mode Fiber," Trans. IEICE, vol. E76-B, NO.4, pp.370-374, 1993.
- (2) T. Haibara, S. Nagasawa, M. Matsumoto and M. Kawase, "Single-mode multifiber joining techniques for high-density high-count subscriber cables," Proceedings of 37th IWCS, 1989.



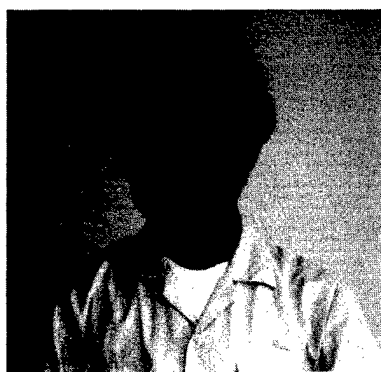
Tohru Sato
The Furukawa Electric Co., Ltd.
6, Yawata-kaigandori, Ichihara, Chiba, 290,
Japan

Tohru Sato was born in kanagawa, Japan, in 1967. He received the M.S. degree in applied physics from Tokyo Institute of Technology, Tokyo, Japan, 1993. He joined The Furukawa Electric Co., Ltd., in 1993. Since then he has engaged in development of optical fiber component.



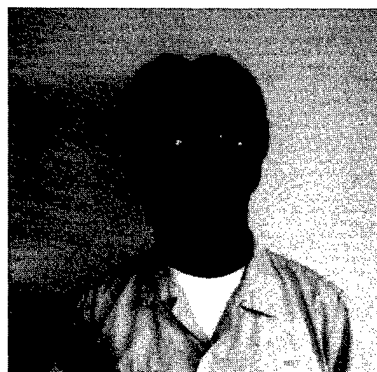
Seiji Ohmizu
The Furukawa Electric Co., Ltd.
6, Yawata-kaigandori, Ichihara, Chiba, 290,
Japan

Seiji Ohmizu was born in Nagasaki, Japan, in 1963. He joined The Furukawa Electric Co., Ltd., in 1982. Since then he has engaged in development of optical fiber switch.



Makoto Okuda
The Furukawa Electric Co., Ltd.
6, Yawata-kaigandori, Ichihara, Chiba, 290,
Japan

Makoto Okuda was born in Osaka, Japan, in 1965. He received the B.E. degree in electronics engineering from Mie University, Mie, Japan, 1989. He joined The Furukawa Electric Co., Ltd., in 1989. Since then he has engaged in development of optical fiber switch.



Takashi Shigematsu
The Furukawa Electric Co., Ltd.
6, Yawata-kaigandori, Ichihara, Chiba, 290,
Japan

Takashi Shigematsu was born in Shizuoka, Japan, in 1963. He received the B.E. degree in mechanical engineering from Yamagata University, Yamagata, Japan, 1986. He joined The Furukawa Electric Co., Ltd., in 1986. Since then he has engaged in development of optical fiber connector.

HIGH-RELIABILITY DISPERSION COMPENSATOR USING NEGATIVE SLOPE DCF

Ryuichi Sugizaki , Youichi Akasaka , Shin-ichi Arai , Kouichi Furukawa ,
Yoshihisa Suzuki , Tamotsu Kamiya and Hirotooshi Hondo

The Furukawa Electric Co.,Ltd Chiba Japan

ABSTRACT

In order to perform high speed and long distance optical transmission in 1550nm range using existing network line composed of 1.3 μ m zero dispersion single mode fiber (SMF), the dispersion compensator is required. Fiber type dispersion compensator is expected to use practically, because of their high reliability. In this study, dispersion compensating fiber (DCF) which can compensate first and second order dispersion of SMF was fabricated and the module with this fiber was evaluated transmission characteristics and reliability. The module is able to suppress the dispersion of 40km SMF from 700 ± 35 ps/nm to 0 ± 6 ps/nm in the wavelength range between 1530nm and 1560nm. The reliability is certified by heat-cycle test, anti-vibration test and anti-shock test. The results show that this dispersion compensator has high performance as a module of high speed and long distance transmission.

INTRODUCTION

Due to the development of EDFA, existing transmission systems using 1.3 μ m zero dispersion single mode fiber (SMF) are considered to be up-graded using in 1550nm range. As the attenuation loss in this range of SMF is lower than those of in 1300nm range, it is suitable for long distance transmission. However, SMF has a positive dispersion of about 17.5ps/nm/km at 1550nm. For using in 1550nm range high-bit-rate transmission system, some measures to compensate chromatic dispersion are necessary. DCF is suitable for dispersion compensation, because of its high reliability and a simple style. In order to perform WDM transmission, it is necessary to compensate not only chromatic dispersion but also dispersion slopes of SMF. Dispersion compensator using

negative dispersion slope DCF is the most suitable. Because it is possible to compensate both chromatic dispersion and dispersion slope of SMF at the same time.

The dispersion compensator is composed of optical fibers, it is treated as a optical module, and it is used for a component part of the up-grading system. Then, characteristics required for a dispersion compensator are high negative chromatic dispersion , negative slope, a small package and low insertion loss. DCF were wound on a small reel and packed it in a compact metallic case. Furthermore, Characteristics of anti-vibration and anti-shock are very important for module to practical use. We fabricated the dispersion compensator using the negative dispersion slope DCF and evaluated transmission characteristics and reliability.

FIBER FABRICATION

W-shaped profile fibers are suitable to compensate chromatic dispersion of SMF in 1550nm range because of their negative dispersion slopes. It is requested for WDM transmission to compensate not only chromatic dispersion, but also dispersion slope of SMF. We have found that the best parameter of W-shaped DCF is $\Delta^+ = 2.0\%$, $\Delta^- = -0.58\%$ as shown in fig 1. [1] We fabricated this structure by VAD method and optimized drawing conditions.

Table1 shows characteristics of the fabricated fiber. This DCF is -83ps/nm/km of chromatic dispersion, -0.24ps/nm²/km of dispersion slope, 0.73dB/km of attenuation loss and 113ps/nm/dB of figure-of-merit(FOM).

Bending loss characteristics are very important parameters to pack it into a smaller case.

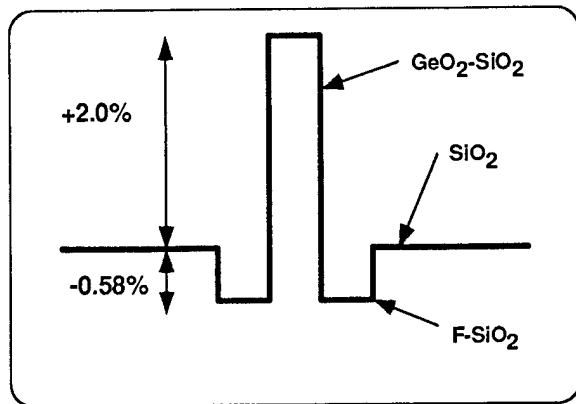


Fig.1 Refractive Index Profile of DCF

Bending losses of W-shaped profile fibers are sensitive. We measured bending loss characteristics of this fiber to determine the minimum coiling size. DCF's loss coiling to the small reel which has inner diameter of 60mm increased less than 9×10^{-4} dB/km. To coil small size and to avoid excess stress to DCF, inner diameter of coiling reel is fixed at 60mm. Since the chromatic dispersion of this DCF is -83 ps/nm/km, the DCF module for compensating 40km of SMF whose chromatic dispersion is 17.5ps/nm/km have about only 0.008dB of increased bending loss that is about 0.02% of total attenuation loss of DCF.

TABLE1 Characteristics of DCF

Item	Characteristics	Unit
Dispersion	-83	ps/nm/km
Dispersion Slope	-0.24	ps/nm ² /km
Attenuation Loss	0.73	dB/km
FOM	113	ps/nm/dB
Bending Loss @ ϕ 60mm	9×10^{-4}	dB/km
MFD	4.75	μ m

Notes:

All values except dispersion slope was measured at the wavelength of 1550nm. Dispersion slope was calculated in the range between 1530nm and 1560nm.

FIBER WINDING

We fabricated dispersion compensator of -700

ps/nm of total chromatic dispersion. This can compensate the chromatic dispersion of approximately 40 km SMF transmission line. We used 8.4km DCF of -83ps/nm/km dispersion to compose -700ps/nm. It was wound on a reel of outside diameter = 190 mm, inside diameter = 60 mm and thickness = 25 mm. During winding on a reel, it was controlled low tension. The loss change after winding on a reel was hardly observed. It was less than 0.1 dB.

PACKAGING

After winding on a reel, DCF was stored in a metallic case of 200mm(Depth) \times 230mm(Width) \times 30mm(Height). Both ends of DCF were spliced with SMF cords whose each length was 2m and diameter was 2mm. FC connectors with super physical contact (SPC) polishing were attached to SMF. Fig 2 shows an overview photograph of the fabricated module.

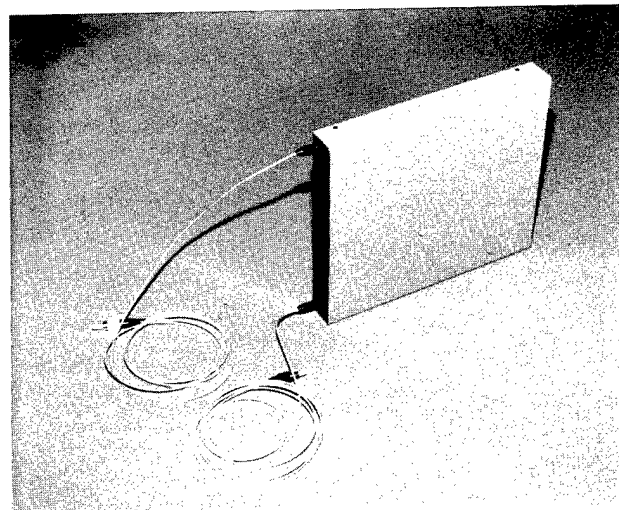


Fig.2 Overview of Dispersion Compensator

SPLICING

To achieve low concatenation loss using standard fusion splice technique of DCF and SMF is difficult because of difference of MFD. As DCF's MFD is an about 5μ m, which is approximately half of SMF's, splicing loss of mechanical concatenation of these fibers with connectors become more than 1 dB.

Fusion splicing of them was operated by using automatic splicer. We connected them by only fusion splicing and got 1dB splicing loss. After fusion splicing, we used Thermally-diffused Expanded Core (TEC) method. We did TEC with heating splicing point using micro-torch to diffuse

GeO₂ of a DCF's core. A concatenation loss of splice point decreased less than 0.2dB using TEC method of heating with micro-torch. We found TEC method was useful for connecting DCF and SMF.

TRANSMISSION CHARACTERISTICS

Attenuation loss characteristics of DCF module are important. It consists of fiber loss, increasing loss when fiber wound, splicing loss between DCF and SMF and insertion loss of both connectors. A total insertion loss of this module is 6.98 dB and this is enough low. Amount loss of 40km SMF and this compensator is less than 15dB and this value can be compensated by EDFA. Total FOM of this dispersion compensator is 100 ps/nm/dB.

The characteristics of this compensator is shown in table 2.

The total chromatic dispersion is -700ps/nm and does not change between before and after moduling. Dispersion slope between 1530nm and 1560nm is -1.99ps/nm².

The index for flat compensation has proposed as dispersion compensating rate. Dispersion Compensating Rate is as Eq.(1).[2]

Dispersion Compensating Rate (%) =

$$\frac{\text{Slope}_{\text{DCF}}}{\text{Slope}_{\text{SMF}}} \div \frac{\text{Dispersion}_{\text{DCF}}}{\text{Dispersion}_{\text{SMF}}} \times 100 \quad (1)$$

When the value of dispersion compensating rate is 100%, it means that dispersion compensator compensates a chromatic dispersion and dispersion slope of SMF completely at the same time. The compensation rate of this dispersion compensator becomes 86 % when SMF's chromatic dispersion and dispersion slope is 17.5ps/nm/km and 0.058ps/nm²/km, respectively. Fig.3 shows the total link dispersion versus wavelength. It shows total chromatic dispersion is suppressed ± 6 ps/nm between 1530nm and 1560nm, and it compensate existing transmission line of SMF to flatten dispersion fiber.

RELIABILITY TEST

This dispersion compensator was consist of only fibers, however, it was treated as an optical component for transmission systems in practical use. It is necessary to check up on temperature, anti-vibration, anti-shock characteristics for proving this reliability.

TABLE2
Characteristics of Dispersion Compensator

Item	Characteristics	Unit
Dispersion	-700	ps/nm
Dispersion Slope	-1.99	ps/nm ²
Compensating Rate	86	%
Insertion Loss	6.98	dB
Total FOM	100	ps/nm/dB
PMD	1.12	ps
PDL	< 0.1	dB
Connector Return Loss	-50	dB

Notes:

All values except dispersion slope was measured at the wavelength of 1550nm. Dispersion slope was calculated in the range between 1530nm and 1560nm.

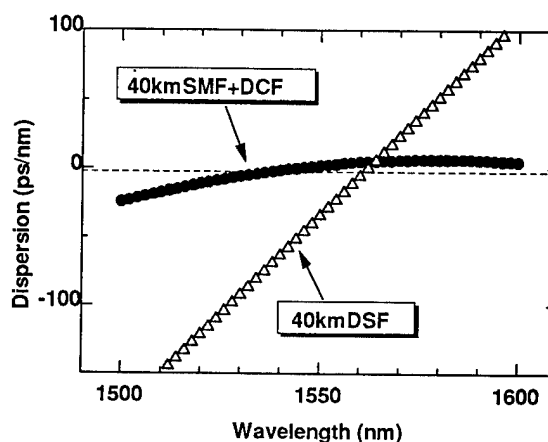


Fig.3 Total Link Dispersion

Temperature characteristics were measured in the range of -40 °C to +70 °C . Dispersion compensators are considered as rated for use in a controlled environment only. [3] It means the characteristics is requested in the range between 0°C and 40 °C. However, during transportation or in storage, dispersion compensator may be exposed to extremes in ambient temperature. There are not any changes on characteristics in the high and low temperature. The temperature-loss characteristic was shown in fig.4. This shows the attenuation characteristics between 0°C and +40°C are stable and there are not any changes

on characteristics after exposed to high and low temperature.

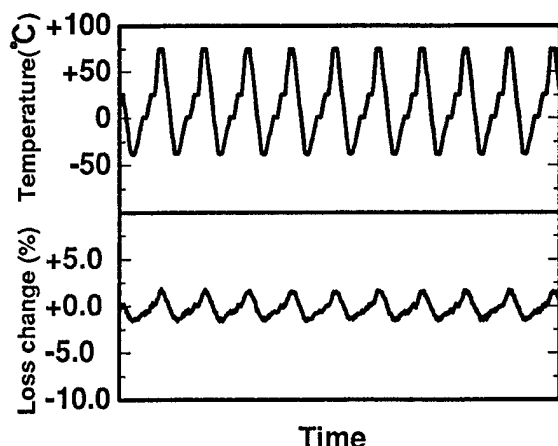


Fig.4 Temperature-Loss Characteristic

Anti-vibration and anti-shock characteristics were known as mechanical characteristics. Both of them are index for stability of characteristics. An anti-vibration character test of this is operated under between 10Hz and 45Hz frequency, 0.5mm amplitude, 3-axis and for 1hour at each axis. During the test, the loss change of more than 0.1dB was not observed. An anti-shock character test of this was operated under 100G acceleration, with 6ms, 3-axis, and tried 5times for each axis. DCF was wound very long length of 8.4km, it was capable of collapsing, however, collapsing was not observed after anti-vibration and anti-shock test.

It is accurate that the compensator have high reliability. The contents of experiment are shown in TABLE 3

TABLE3 Conditions of Mechanical Test

	Conditions
Anti-vibration	<ul style="list-style-type: none"> ● 10-45Hz ● 1 Hour ● 3-axis
Anti-shock	<ul style="list-style-type: none"> ● 100G ● 6ms ● 3-axis ● 5 times (each axis)

CONCLUSION

We fabricated dispersion compensator composed of DCF which can compensate dispersion of 40km SMF transmission line. And

total link dispersion was suppressed less than $\pm 6\text{ps/nm}$. We evaluated characteristics of temperature, anti-vibration and anti-shock test for reliability. And this dispersion compensator could be expect for the module which was used in long-distance and high-speed WDM transmission in 1550nm range.

REFERENCES

- [1] Y.Akasaka et al ECOC '95 We.B.2.4
- [2] T.Kamiya et al OECC '96 17C3-2
- [3] GR-2854-CORE Bellcore Sep. 1995



Ryuichi Sugizaki

The Furukawa Electric Co.,Ltd

6,Yawata-Kaigandori,Ichihara, Chiba, 290, Japan

Mr.Sugizaki graduated from Chiba Institute of Technology in 1990. He joined The Furukawa Electric Co., Ltd. and has been engaged in research and development of optical fiber. He is now a research engineer of functional material and device research department, opto-technology laboratory.



Shin-ichi Arai

The Furukawa Electric Co.,Ltd

6,Yawata-Kaigandori,Ichihara, Chiba, 290, Japan

Mr.Arai graduated from Tokyo Institute of Technology in 1991. He joined The Furukawa Electric Co., Ltd. and has been engaged in research and development of optical fiber. He is now a research engineer of functional material and device research department, opto-technology laboratory.



Youichi Akasaka

The Furukawa Electric Co.,Ltd

6,Yawata-Kaigandori,Ichihara, Chiba, 290, Japan

Dr.Akasaka has a B.S. degree in synthetic chemistry from Kyoto University and an M.S. and Ph.D. in industrial chemistry from University of Tokyo. He joined The Furukawa Electric Co., Ltd. in 1993 and has been engaged in research and development of optical fiber. He is now a research engineer of functional material and device research department, opto-technology laboratory.



Kouichi Furukawa

The Furukawa Electric Co.,Ltd

6,Yawata-Kaigandori,Ichihara, Chiba, 290, Japan

Mr.Furukawa graduated from Osaka University in solid state physics in 1985. He joined The Furukawa Electric Co., Ltd. and has been engaged in research and development of optical devices. He is now a senior research engineer of Research Department, opto-technology laboratory.



Yoshihisa Suzuki

The Furukawa Electric Co.,Ltd

6,Yawata-Kaigandori Ichihara, Chiba, 290, Japan

Mr.Suzuki graduated with the B.S. and M.S. degrees in chemical engineering from Tsukuba University in 1980 and 1982. He joined The Furukawa Electric Co., Ltd. and has been engaged in research and development of inorganic materials. He is now the chief of functional material and device research department, opto-technology laboratory.



Hirotooshi Hondo

The Furukawa Electric Co.,Ltd

5-1-9 Higashi-Yawata, Hiratsuka, Kanagawa, 254, Japan

Mr.Hondo graduated from Tohoku University in electrical engineering in 1969. He joined The Furukawa Electric Co.,Ltd. and has been engaged in development of telecommunication cables including optical fiber cable, almost during 25 years. During the time period, he was in design engineering department for 6 years and returned to R&D division . Now he is the General Manager of information and electronics laboratory.



Tamotsu Kamiya

The Furukawa Electric Co.,Ltd

6,Yawata-Kaigandori Ichihara, Chiba, 290, Japan

Dr.Kamiya received his Ph.D. degree from Waseda University in 1979. He joined The Furukawa Electric Co.,Ltd. and has been engaged in development of optical fiber including the preform and drawing processes, and he also engaged in manufacturing optical telecommunication cable. Now he is the Manager of Development Department, opto-technology laboratory.

2x400 SMF OPTICAL SWITCH USING AXIAL ALIGNMENT WITH COUNTERPART FIBERS IN A V GROOVE

Seiichi Naraoka, Sizuka Yamaguchi, Kazou Kamiko

The Furukawa Electric Co., Ltd.
6, Yawata-kaigandori, Ichihara, Chiba, 290, Japan

Abstract

Very lately developed, is a super-compact 2x400 optical switch, which volume referring to the mechanical part can be given as 270x105x55 mm. This new switch is found to feature connection loss of 0.4 dB or less, loss reproducibility of 0.1 dB or less, return loss of 40 dB or more, and durability of one million times or more.

1. Introduction

A large amount of fibers has been recently introduced to telephone communication cable, which must be monitored or inspected almost regularly by mean of optics. For switching, monitoring, and inspecting telephone communication cable, a measurement instrument should be selected be connected to each of hundreds of optical fibers. To date, 1x50 optical switch with approximate volume of 600 mm(W) x 300 mm(D) x 100 mm(H), has been used for switching over.⁽²⁾⁽⁶⁾ Along with increasing demand for space saving and further integration of communication cables, however, it becomes necessary to develop an outstandingly high-density optical switch. Authors has been developed this switch in order to achieve the target in table 1.

Table 1 The target characteristics

Item	Characteristics
Connection loss	< 0.4 dB
Repeatability	< 0.3 dB
Return loss	> 35 dB
Switching time(adjacent port)	< 3 sec
Switching time(maximum)	< 10 sec
Durability	>1 million times

2. Structure

2.1 Principle of switching

Usually a common single fiber connector is used for switching over optical switch. Each fiber connector requires area of 5 mm x 6 mm, inevitably resulting in a bulky device. On the conventional equipment, optical axial alignment is performed by means of holding force obtained from split sleeve on connector ferrule. In an attempt to address this problem, we have adopted direct movement of single-mode fiber with diameter of 0.125 mm for switch-over and connection.

A trial optical switch designed for this development is Fig. 1. The principle of switching is comprised of two mobile single mode fibers (125 μ m in cladding diameter, 9.5 μ m in mode field diameter), 400 fibers (50 eight-fiber ribbons) set in parallel and spaced 0.25 mm apart (as opposed to the mobile fibers), and a V groove plate with more than 400 grooves. Those 400 fibers are each glued in a V grooves. The two mobile fibers in V grooves are precisely brought in alignment with what to be connected (two of the 400), by holding them downward, using a holding mechanism.

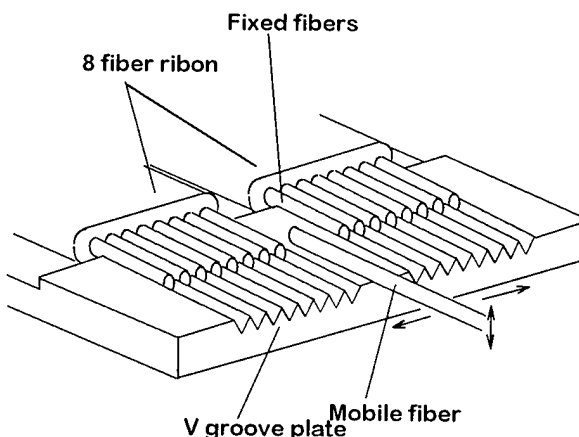


Figure 1 Principle of switching

The switching connection acts as follows :A mobile fiber held in a V groove is released and raised to clear top margins of V grooves. The fiber is slid at right angles with the fiber orientation, up to what to be connected to in a V groove. In the end, the holding mechanism lowers to hold the fiber.

The butting method as above described did give birth to an extraordinary compact unit, as contrasted with an optical switch involving a conventional SC connector. The trial optical switch is described about its tangible structure.

2.2 Switch structure

The switch structure of the trial optical switch in Fig. 2. This assembly consists of mobile fibers as in Fig. 1 a V groove plate, 400 fixed fibers a moving mechanism to move the mobile fibers and the holding mechanism to hold to set the mobile fibers in V groove. Those fibers and the mechanism are airtightly packed with matching oil in a casing. An array of 400 fibers in ribbons and two single mode fibers run out of one face of the casing. Two motor are provided each for the fiber moving and holding mechanisms. These moving motors were servo-motors, but at present they are pulse-motors, of which operation can be controlled with ease.

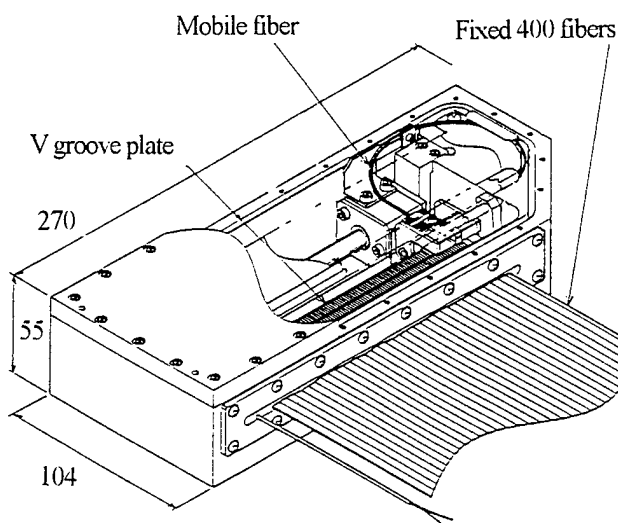


Figure 2 Switch structure

2.3 Switching mechanism

Fig. 3 presents the fiber moving mechanism. The moving assembly on which mobile fibers are fixed mount on a threaded guiding axis as a turning rod of a pulse motor. The turning motion slides the moving assembly with the fibers. The motor resolution is $25 \mu\text{m}$ a pulse. A proximity sensor is provided at the nearby motor, In this system it reacts when the moving assembly approaches, providing an original point for the sliding motion. Moving in a specific number of pulse from the original point, the fiber connection is carried out. Here what should be emphasized is to stop with accuracy. This switch has $\pm 35 \mu\text{m}$ of overall accuracy, which is judged satisfactory, considering the V groove opening $210 \mu\text{m}$ in width. Entering into the detail, the original point sensor shoes $\pm 10 \mu\text{m}$ of accuracy, while the pulse motor's motion shows ± 1 pulses ($\pm 25 \mu\text{m}$).

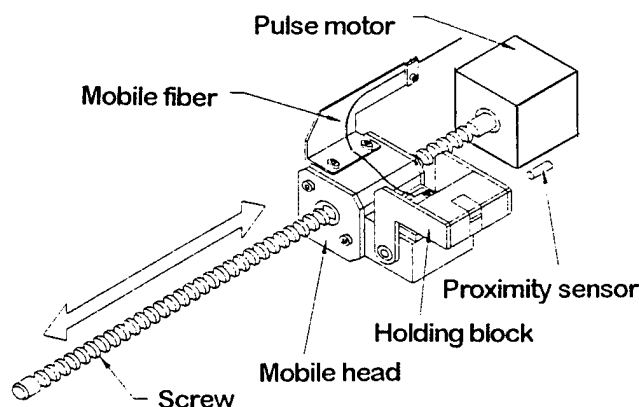


Figure 3 Fiber moving mechanism

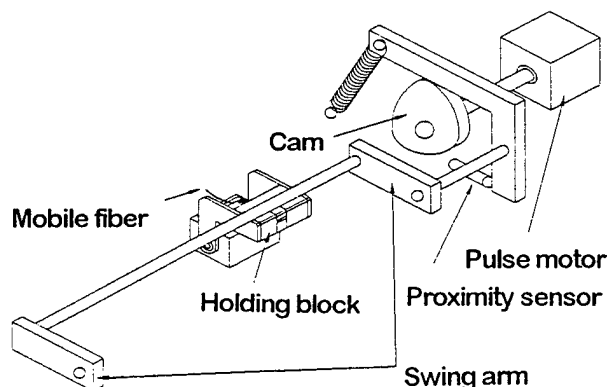


Figure 4 Fiber holding mechanism

Fig. 4 presents the fiber holding mechanism. A turntable fiber holder is provided on the moving assembly. A swing arm to be moving by a cam lobe holds the fiber holder downward. This action press the mobile fiber against the V groove. At the moment, the fiber holder only moves as linked up with the moving assembly, but the cam and arm never cooperate. The sensor has a L linkage to be moving by the cam lobe, which has a proximity sensor. The closest approach serves as the original point, from which a specific number of pulses are counted to determine the position where to hold the fiber.

2.4 Structure of connecting point

Fig. 5 presents structure of connecting point. Four hundred fibers are striped at the ends and laid in a V groove plate. They are glue at the coated segment and striped parts. The fixed fibers, which were glued and cut in a mass with a high-speed turning blade, vary in length at the fiber ends by less than $10\text{ }\mu\text{m}$. Fig. 5 cross-sectionally presents a fixed fiber as one out of the 400 and a mobile one held in V groove with a fiber holder.

Fiber end faces in alignment should never be allowed to rub against each other with flaw; a minute gap should be provided in-between. In this case, 20 to $30\text{ }\mu\text{m}$ of gap was set there. Matching oil was charged to interpose in the interface, for eliminating gap-caused loss.

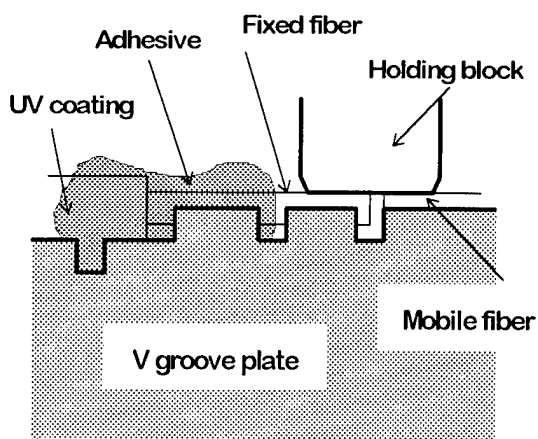


Figure 5 Structure of connecting point

Fig. 6 similarly shows a magnified connecting point. Four hundred fixed fibers were cut as angled at the ends to improve return loss. Since the gap was filled with matching oil, the connection loss was on trial reduced with a cutting angle of six degrees less than 90° . angled cutting and matching oil produced a high return loss.

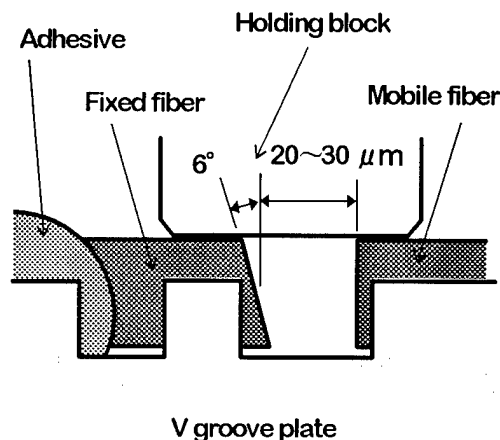
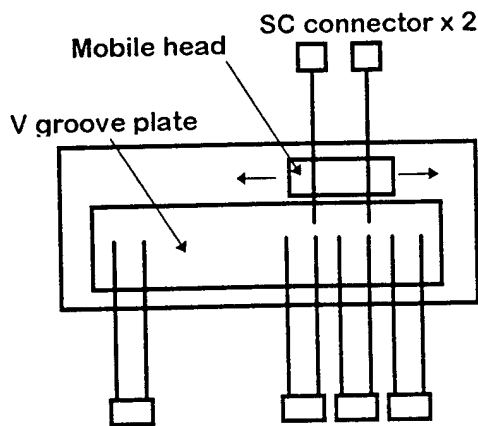


Figure 6 Structure of connecting point (2)

3. The characteristics of switch

3.1 Configuration and volume of switch

Fig. 7 shows optical configuration of this switch. Mobile fibers are equipped with single SC connectors at each end, while fixed 400 fibers are equipped with fifty MT connectors at each end. The outer dimensions of this switch is $270\text{ mm(W)} \times 104\text{ mm(D)} \times 55\text{ mm(H)}$ and one tenth of conventional type.



8MT connector x 50
Figure 7 Optical configuration

3.2 Connection loss

Fig. 8 shows the connection loss measurement setup. This switch has two connection points which are one SC connector and fiber switching point. A $1.3 \mu\text{m}$ wavelength LED light source was used. The histogram of connection loss is shown in fig. 9. The average connection loss was 0.178 dB. The maximum connection loss was 0.4 dB. The standard deviation was 0.088 dB.

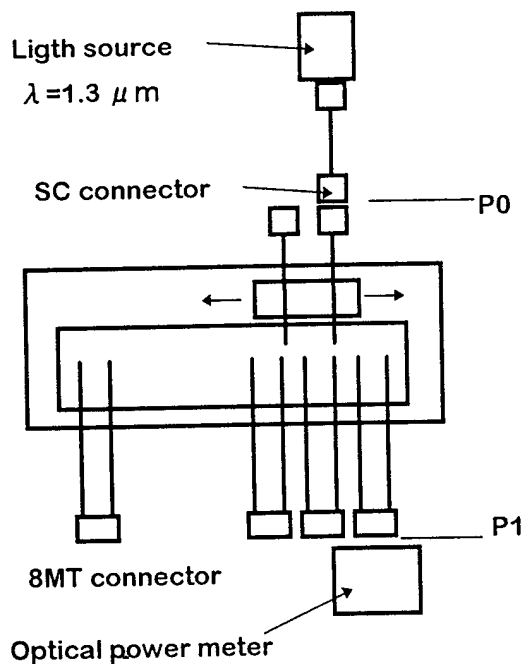


Figure 8 Loss measurement setup

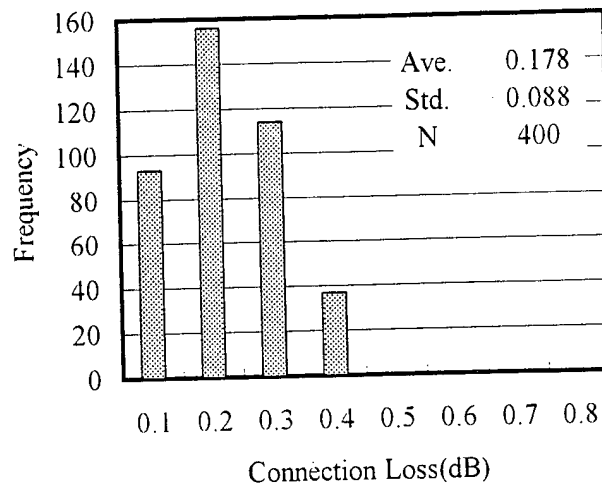


Figure 9 Connection loss histogram

3.3 Return loss

Fig. 10 shows the return loss measurement setup. A $1.3 \mu\text{m}$ wavelength LED light source was used. The average return loss was 44.0 dB. The minimum return loss was 40.4 dB.

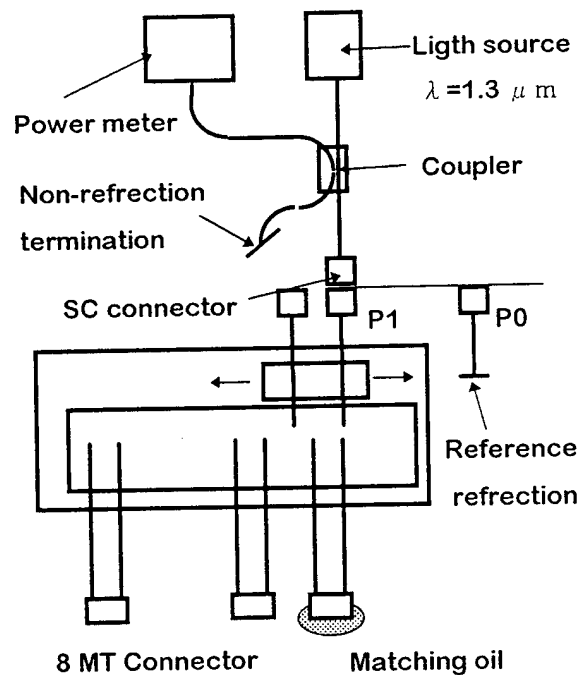


Figure 10 Return loss measurement setup

3.4 Switching time

The maximum switching time and the adjacent switching time were measured. The maximum switching time is mobile fibers stating from No. 1 fiber in fixed 400 fibers, switching to No. 400 fiber and the result is 7.5 sec. The adjacent switching

time is mobile fibers stating from one fiber, switching to adjacent fiber, the result is 2.1 sec.

3.5 Long-term endurance

This switch was examined for long-term endurance. The mobile fibers were connected to two of fixed 400 fibers (No. 137 and No. 153) by turns at random, where connection loss was measured at every 500th turn, following the measuring system in Fig. 8. The reproducibility of connection loss is shown in fig. 11. The result shows reproducibility of 0.1 dB or less in one million times.

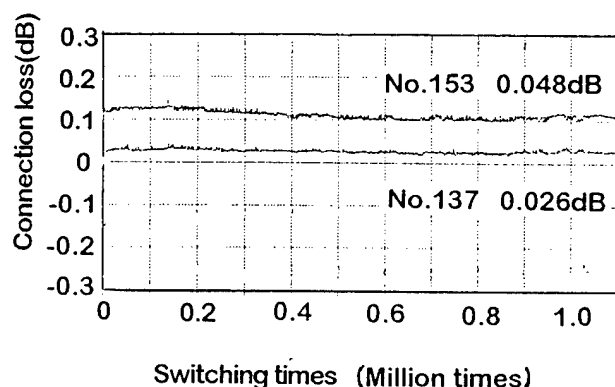


Figure 11 Reproducibility of connection loss

4. Conclusions

We have come up with 2 x 400 optical switch featuring outer dimensions of 270 mm(W) x 104 mm(D) x 55 mm(H). This new switch is found to feature connection loss of 0.4 dB or loss, loss reproducibility of 0.1 dB or less, return loss of 40 dB or more, and durability of one million times or more.

Reference

- (1)N. Tomita, et al., "Future prospects of automatic fiber testing system for fiber-optic subscriber loops", OECC '96 Tech. Dig., July 1996
- (2)N. Tomita, et al., "Optical fiber line support system,"NTT Rev., vol. 3 no. 1 pp 97-104,1991.
- (3)N. Tomita, et al., "Design and performance of a novel automatic fiber line testing system with OTDR for optical subscriber loops,"IEEE J. Light wave Technol., vol. 12, no. 5, pp. 717-726, May. 1994.
- (4)I. Nakanishi, et al. "Optical fiber selector with a fiber moving head and multi-fiber array", in Nat. Conv. Rec. IEICE, Sep 1995,B-651
- (5)N. Tomita, et al., "Automatic and optimum sensing of Fresnel reflections in optical fiber system with connectors using OTDR,"SPIE proc. vol. 2594, pp. 31-40, Oct. 1995
- (6)S. Naraoka, et al., "Development of automatic optical operation support system", in Nat. Conv. Rec. IEICE, Sep 1992,B-555



Seiichi Naraoka

The Furukawa
Electric Co., Ltd.

6, Yawata-
kaigandori
Ichihara, Chiba,
290, Japan

Seiichi Naraoka was born in Tokyo, Japan, in 1961. He received a B. E. degree in mechanical engineering from Tohoku University in 1985. He joined The Furukawa Electric Co., Ltd. In 1985 and has been engaged in research and development of joining technology and optical switches.



Sizuka Yamaguchi

The Furukawa
Electric Co., Ltd.

6, Yawata-
kaigandori,
Ichihara, Chiba,
290, Japan

Sizuka Yamaguchi was born in Fukui, Japan, in 1954. He joined The Furukawa Electric Co., Ltd. in 1975 and has been engaged in research and development of mechanical apparatus for automated assembly system.



Kazuo Kamiko

The Furukawa
Electric Co., Ltd.

6, Yawata-kaigandori,
Ichihara, Chiba, 290,
Japan

Kazuo Kamiko was born in Chiba, Japan, in 1960. He received A. B. E. degree in mechanical engineering from Chiba University in 1984. He joined The Furukawa Electric Co., Ltd. in 1984 and has been engaged in research and development of optical connectors and optical switches.

2 × 800 DIRECT FIBER TRANSFER OPTO-MECHANICAL SWITCH

Hiroshi Furukawa , Yoshikazu Nomura, Hiroshi Yokosuka
Fujikura Ltd, Opto-Electronics Lab.
Sakura-shi Chiba , Japan

ABSTRACT

We developed a low loss, highly reliable opto-mechanical switch which can be used for selecting a random fiber from an array of fibers.

The switch could be used for selecting from 800 fibers and we managed to realize a low connection loss of average 0.35 dB. By using a switching mechanism in which the fiber itself was directly moved, we succeeded in making the structure an extremely compact 160mm x 800mm x 45mm for an array of 800 fibers. The switching time was less than 0.8 s for adjacent fibers and less than 6 s for the maximum switching distance which is very fast for mechanical type switches.

This switch is being used in remote fiber test systems which are used for the efficient maintenance of optical fiber networks. Specifically, the switch is used for selecting fibers making up an optical access network which is being built as part of a FTTH network in Japan.

1. INTRODUCTION

With the aim of realizing a multimedia society, optical fiber networks are increasing yearly. Optical networks are progressing from trunk lines

to subscriber networks presently. An optical Remote Fiber Test System(RFTS) is an indispensable tool for the continued operation of such networks.

The fiber selector is an important element of the RFTS and is used to inject a test signal from the measurement equipment into any fiber in the subscriber network. In this way the condition of the fiber leading up to the subscriber premises can be determined. The switch needs to accommodate the increasingly higher count subscriber network cables. Therefore, it needs to have a large fiber array within a compact size, extremely low losses and superior operational functions.

We succeeded in developing a switch which satisfied the following requirements for the easy selection of a random fiber from an optical network.

1. Low connection loss
2. Compact size
3. Large fiber array
4. High speed switching
5. Low cost

In this paper we describe the steps involved in the development of the fiber switch which met

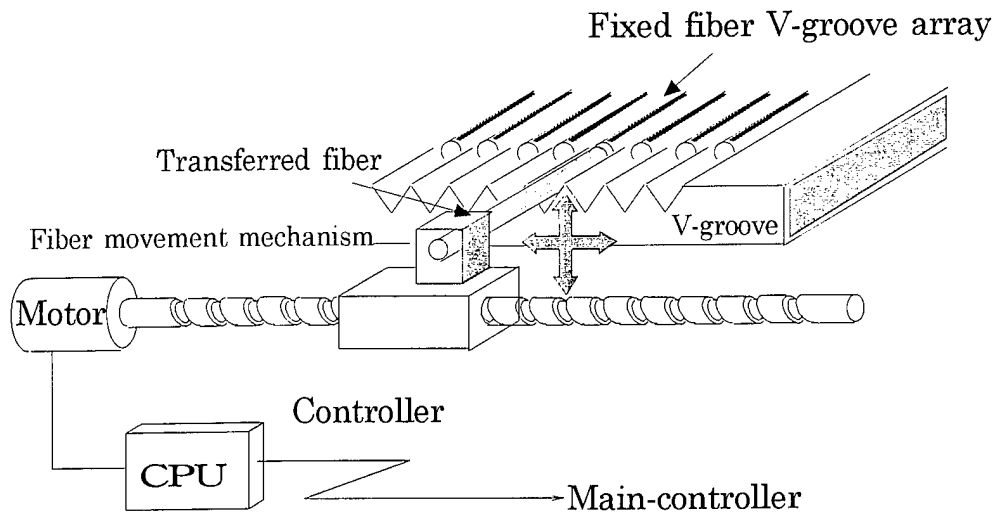


Fig.1

the above requirements starting from the mechanism to evaluation tests of the prototype.

2.DESIGN OF THE SWITCH

2.1 Principle of the switch

The direct fiber transfer mechanism in which the fiber itself is moved was developed for realizing a compact, high speed switch. The basic structure of the mechanism is shown in Fig. 1. The switch is made up of the following parts which are indicated in Fig. 1:

1. Fixed fiber V-groove array
2. Transferred fiber
3. Fiber movement mechanism
4. Controller

As the switch is made up of a small number of parts despite having a high fiber count, it has a low cost.

The principle of switching is as follows. 800 fibers are attached onto the fixed fiber V-groove array and the transferred fiber is moved along the

V-groove to mate with one of the 800 fibers. The pitch of the fibers on the V-groove array is 250 mm which is the same as that of ribbon fibers. This contributed to a structure which was not only small but was also versatile and had a low cost.

The pulse motor of the movement mechanism was matched to the pitch of the fixed fiber array and a ball screw was used for positioning. This allowed for a simple control process and high speed switching.

As for the controller, a CPU was used for positioning and the movement pitch was installed during the manufacture of the switch. The fiber number is selected by sending an external signal to the CPU. An RS-232C interface was used between the computer and the controller thus making possible remote control of the switch.

2.2 Positioning Mechanism

As shown in Fig. 2, by using the same V-groove for mating the fibers, a simple and easy

addition, by making the pitch of the V-grooves the same as that of ribbon fibers, the task of attaching the fibers to the array was simplified. This made the switch highly versatile and low cost.

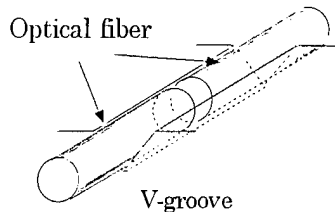


Fig.2

2.3 V-groove Termination

The termination of the V-grooves is the most important of the parts that make up the fiber switch. The structure of the termination is shown in Fig. 3.

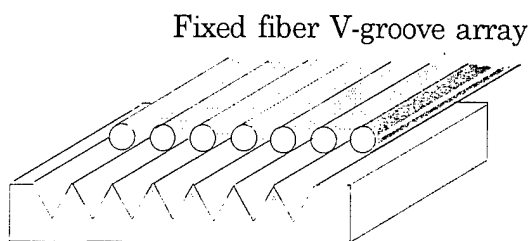


Fig.3

As shown in Fig.3, the technology used to obtain the high precision needed is of vital importance. The precision obtained in the machining of the depth and pitch of V-grooves was less than 1 mm. Next, the mirror finish dicing process used for the

fiber array V-grooves largely influences the connection and return loss characteristics of the switch.

The ribbon fibers were arranged and then attached to the V-groove and a cutting blade was then used to simultaneously polish and cut both the fibers and V-grooves. This resulted in an uniform mirror surface at the end faces as shown in Fig.4.

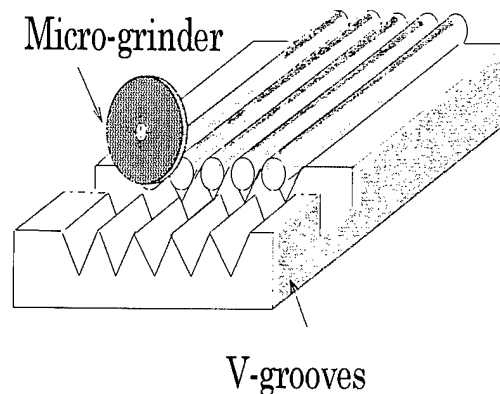


Fig.4

2.4 Structure of the Movement Mechanism

The complete switch is obtained by assembling the fixed fiber array, transferred fiber and movement mechanism. During this process, it is necessary to introduce index matching oil on the mating surface to reduce Fresnel losses and reflection.

Matching oil was placed within the assembly consisting of the movement mechanism and fibers. The assembly was then sealed to prevent any leakage. Stable optical characteristics were

obtained through this structure.

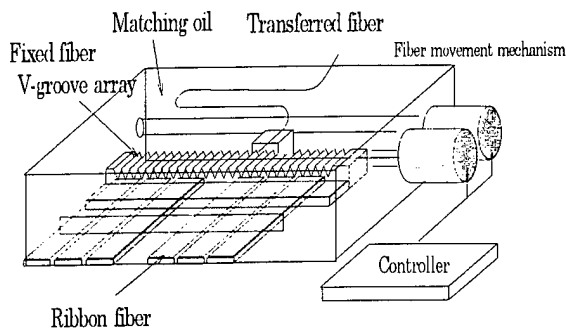


Fig. 5

2.5 Structure of prototype

The prototype switch which met the above design criteria was constructed. The structure of this switch is shown in Fig. 6. The results of optical evaluation tests and reliability are given below.

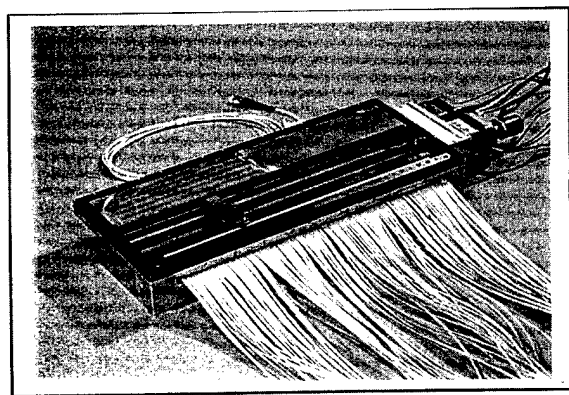


Fig. 6

3. PERFORMANCE

3.1 Insertion loss

The insertion loss histogram of the switch is shown in Fig. 7. Measurements were carried out for all 800 fibers on the fixed fiber array. A 1.31 mm LED light source was used for the test signal.

The insertion loss includes the internal loss of the switch and one SC connection.

The results showed that the average insertion loss was 0.35 dB with a maximum of 0.72 dB and a minimum 0.08 dB.

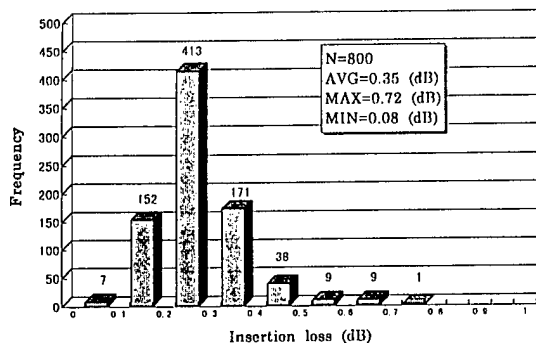


Fig. 7

3.2 Return loss

The return loss characteristics of the switch is shown in Fig. 8. A precision reflectometer was used to make the measurements for all 800 fibers. The return loss was greater than 50 dB for all the fibers.

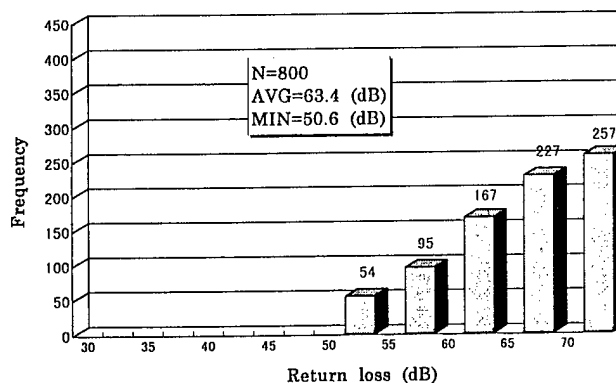


Fig. 8

3.3 Repeatability

The repeatability of the switch for 1000 switching operations was measured. Switching operations were carried out 1000 times for a given port and the insertion loss was measured. The switch had an extremely good repeatability of 0.01 dB.

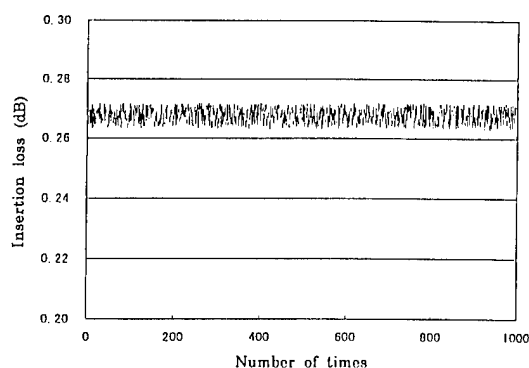


Fig.9

3.4 Switching time

The switching time required for adjacent ports of the switch is given in Fig. 10. During the switching process, the outgoing light signal cannot be detected. The switching time is defined to be the time when the light is not detected. The time required for switching to adjacent ports was less than 0.8 s and the time required for switching between the ports that are furthest apart was 0.01 dB.

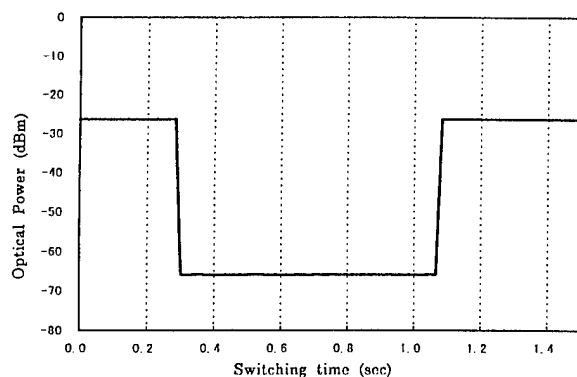


Fig.10

3.5 Temperature cycling

The optical characteristics of the switch when subjected to temperature cycling (0~50 deg C, 6hour cycle) is shown in Fig.11. The variation of the optical output during one cycle was less than 0.1 dB.

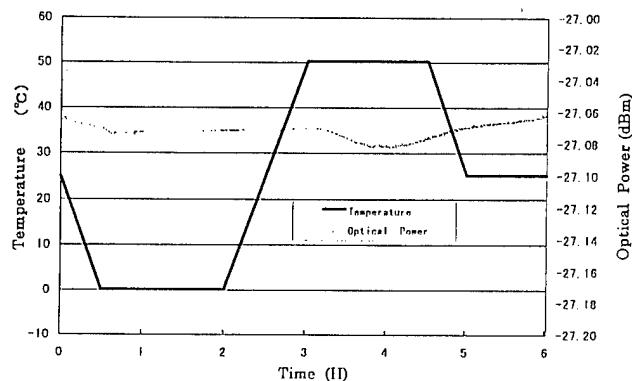


Fig.11

4. CONCLUSIONS

As a result of our development efforts, we succeeded in developing a high fiber count, high speed and compact switch with superior characteristics.

In addition, due to its simple structure, it is low cost and therefore has reached a adequate level for practical implementation.

In the future, we plan to implement this 2 x 800 switch in RFTS for subscriber networks to realize a highly reliable and easy to maintain optical network.

5. REFERENCES

- [1] I.Nakanishi, N.Tomita and, Y.Enomoto, "Optical Fiber Selector with a Fiber Moving Head and Multi-Fiber Array", Proceeding of the IEICE Communications Society Conference, B-651, pp.318, 1995.
- [2] Furukawa, N.Tomita, N.Yamazaki and H.Suda, "Very Compact Optical Fiber Selector Using Fiber Transfer and Fiber Axis Alignment

Techniques", Proceeding of the IEICE General Conference, B-986, 1994.

[3]

N. Tomita, H. Takasugi, T. Nakamura and K. Kurosawa, "Automatic Remote Optical Fiber Line Test and Administration System Design", Proceeding of the IEICE General Conference, B-888, 1990.

Hiroshi Furukawa



Opto-Electronics
Laboratory
Fujikura Ltd.

1440, Mutsuzaki,
Sakura-shi, Chiba,
285, Japan

Hiroshi Furukawa was born in 1959. He received the B.E. degree in mechanical engineering in 1984 from Chiba University.

He joined Fujikura Ltd. in 1984 and has been engaged in the research and development of telecommunication cable and accessories. He is now an engineer of the Fiber and Cable Accessory Department within Opto-Electronics Laboratory.

Yoshikazu Nomura



Opto-Electronics
Laboratory
Fujikura Ltd.
1440, Mutsuzaki,
Sakura-shi, Chiba,
285, Japan

Yoshikazu Nomura was born in 1951. He received the B.E. degree in mechanical engineering in 1975 from Shinsyu University.

He joined Fujikura Ltd. in 1975 and has been engaged in the research and development of telecommunication cable and accessories. He is now a manager in the Fiber and Cable Accessory Department within Opto-Electronics Laboratory.

Hiroshi Yokosuka



Opto-Electronics
Laboratory
Fujikura Ltd.
1440, Mutsuzaki,
Sakura-shi, Chiba,
285, Japan

Hiroshi Yokosuka graduated in mechanical engineering from Tokyo Metropolitan Technical Junior College in 1967.

He has been engaged in the development of telecommunication cable and accessories. He is now a General Manager of the Fiber and Cable Accessory Department within Opto-Electronics Laboratory and a member of IEICE of Japan.

HIGH SPEED AXIAL STRENGTH SETUP FOR THE MEASUREMENT OF THE «B» VALUE.

Authors: A. GOURONNEC, N. EVANNO.

France Telecom, Centre National d'Etudes des Télécommunications.

CNET/LAB/QFE/CDO

Technopole Anticipa

2 avenue Pierre Marzin

22307 LANNION, France.

Phone: 3396053443

Fax: 3396053427

ABSTRACT

Today most of the models used for optical fibres life-time calculations takes the factor «B» into account.

Characterizing the manufacturing conditions this factor is assumed to be constant. For measuring B, initial inert stress (σ_{ic}) has to be known. Recently, in literature some authors have presented different «B» values covering a very large range, from 10^{-8} to $1 \text{ GPa}^2 \cdot \text{s}$, principally resulting of the measurement methods used.

In France Telecom-CNET we have developped an experimental method to estimate «B». The method used is based on a high speed axial strength setup able to elongate the fibers from 60 Mpa/s to 1.0 TPa/s.

The very large stress rate range covered permits the direct measurement of the stress corrosion susceptibility parameter n (slope of the linear fit). Over 700 GPa/s the slope of the curve shows a knee and then a plateau corresponding to the the initial inert strength for the fibre tested. Using these value we can calculate «B». The paper gives values obtained for different optical fibres.

As conclusion we have measured with the same setup the stress corrosion susceptibility factor n and the environmental factor « B » for different commercial optical fibres.

Keywords:

Optical Fibre, Reliability, Mechanical testing.

1. INTRODUCTION.

Today, in the development of the optical access network, the deployment of the fibres is made under more severe conditions of installations. So, for optimising the reliability of the optical links, we have to predict the lifetime of the optical fibres used under these conditions.

Most of the models for lifetime calculations use the B parameter. So we have developed a new technique based on the principle of the very high axial pulling speed for the B measurement.

The first results are presented below.

2. PRINCIPLE OF THE MEASUREMENT.

As suggested by Charles [1] the evolution of the deepest flaw at the silica-

coating interface of an optical fibre is represented by the relation (1) below.

$$V = \frac{da}{dt} = AK_I^n \quad (1)$$

and $K_I = Y\sigma\sqrt{a}$ according to Griffith theory[2], where

* K_I is the stress intensity factor.

* Y is the geometrical factor ($\cong 1.24$ for silica fibres and elliptical shape of the flaws).

* σ is the stress level.

* n is the stress corrosion susceptibility parameter.

* a is the depth of the flaw.

* A is a constant.

Under a permanent (static fatigue) or a variable (dynamic fatigue) stress level the depth of the flaw grows until the fibre breaks at a critical stress intensity factor K_{IC} which is assumed to be constant in the Griffith concept [2]. Catastrophic failure occurs for

$$K_{IC} = Y \sigma_{ic} \sqrt{a}. \quad (2)$$

At a constant stress level it is possible to calculate the time to failure t_f [3]:

$$t_f = \frac{2}{\sigma^2 Y^2} \int_{K_I}^{K_{IC}} \frac{K_I}{V} dK_I \quad (3)$$

After calculation we have:

$$t_{fs} = \frac{2}{\sigma^2 Y^2 A(n-2) K_{IC}^{n-2}} \left[\left(\frac{\sigma_{ic}}{\sigma} \right)^{n-2} - 1 \right] \quad (4)$$

We have
$$B = \frac{2K_{IC}^{2-n}}{Y^2 A(n-2)} \quad (5)$$

The factor n is usually > 10 , so the approximate time to failure is now written as:

$$t_f = B \frac{\sigma_{ic}^{n-2}}{\sigma^n} \quad (6)$$

At a constant stress rate $\frac{d\sigma}{dt}$, by using the same calculations we have:

$$\sigma^{n+1} = \frac{2(n+1)}{AY^2(n-2)K_{IC}^{n-2}} (\sigma_{ic}^{n-2} - \sigma^{n-2}) \frac{d\sigma}{dt} \quad (7)$$

where σ_{ic} is the failure stress without slow crack grow giving

$$t_{fd} = B(n+1) \frac{\sigma_{ic}^{n-2}}{\sigma^n} \quad (8)$$

In each case we have σ_{ic} as the critical stress level corresponding to a catastrophic failure mechanism with no fatigue growing of the flaw. To reach such experimental conditions different way are possible: [4], [5], [6]:

* making the test in vacuum: this is not easy to do, and even in this case it is very difficult to completely pull out the molecules of water in the top of the weak flaws.

* By using a very high axial speed pulling test: thus it is possible to reach the catastrophic failure mechanism in a minimum of time, reducing drastically the chemical hydrolysis of the silica at the top of the weak flaw. So the σ_{ic} of the tested fibres can be evaluated as indicated below.

In France Telecom-CNET we have developed a new equipment able to reach pulling speeds of more than 6 meters per second, corresponding approximatively to stress rate of 1.0 Tpa/s. The setup is described in the next paragraph.

For measuring σ_{ic} we make the axial pulling test over a very large range of speeds (from 0.4 mm/s to 6.25 m/s). For each speed we measure 30 optical fibre samples of 0.5 meter length. Then we plot the result as LOG(strength) = LOG(stress rate). On this curve we observe two main parts, a linear part and then a plateau. The slope of the linear curve gives the n parameter, the plateau gives an evaluation of σ_{ic} . Using the results we calculate B with the relation given below:

$$\text{We have} \quad \sigma_f^{n-2} = \sigma_{ic}^{n-2} - \frac{1}{B} \int_{t_i}^{t_f} \sigma^n dt \quad (9)$$

$$\sigma_f^{n-2} = \sigma_{ic}^{n-2} - \frac{\sigma_f^{n+1}}{B(n+1) \frac{d\sigma}{dt}} \quad (10)$$

$$B = \frac{\sigma_f^{n+1}}{(n+1) \cdot \left(\frac{d\sigma}{dt} \right) \cdot [\sigma_{ic}^{n-2} - \sigma_f^{n-2}]} \quad (11)$$

3. THE EXPERIMENTAL SETUP.

The experimental setup is presented in figure 1. It is made of two main parts, one part for the lowest speeds (from 0.4 mm/mn to 80 mm/mn) and a second part for the highest speeds (from 80 mm/mn to 8 000 mm/mn). The equipment can pull samples of 0.5 meter to 1 meter length. In this experiment we have only tested 0.5 length fibres. The mobile mandrels are velocity controlled with an accuracy better than 1 % in the two tested range of speeds. The failure strength is measured with an accuracy of 0.1 % for the gauge sensor and the linearity of the response is better than 0.5 % for the electronic control output system. The strength system control used can measure forces from 0 to 200N. Figure 2 shows details of the clapping mandrels.

Figures 3 and 4 show as examples, two of the speed measurements done, giving at the upper part the speed trace and at the lower part the strength trace and the corresponding failure stress level obtained for the fibres under test. For the lowest speed the mobile mandrel reaches the indicated velocity after a short loading slope corresponding at 4 % of the sample length as shown on figure 4. For the highest speeds the mobile mandrel needs about 20 cm for reaching the indicated test velocity. So the test is performed under an impulsive pulling rate. For that the fibre is fixed on the mobile mandrel with the 0.5 meter length which is then down on the active mobile plate. So during the speed growing and speed stabilization time the fibre is free of axial stress. The fibre is instantaneously strengthened when the mobile mandrel has moved over the 0.5 meter corresponding to the length of the fibre under test.

On figure 2 we can see on the left part the high speed system with, at the top the mobile mandrel and at the bottom the static mandrel and the mobile plate used to pull out the mobile mandrel. All the tests are performed with 30 samples for each speed.

The results and our first conclusions are given below.

We are now working for going on a higher speed rate and also we are introducing in the setup, a direct real speed measurement system. Complementary results would be given during the paper presentation.

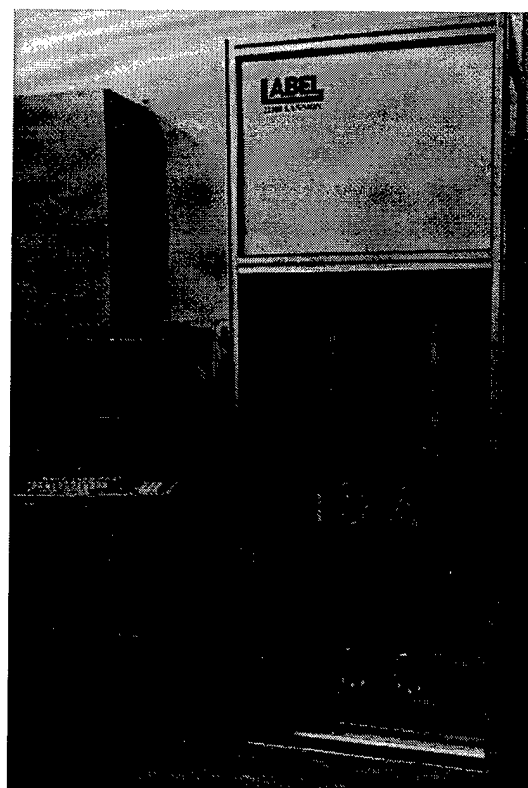


Fig 1: High Speed Pulling setup.

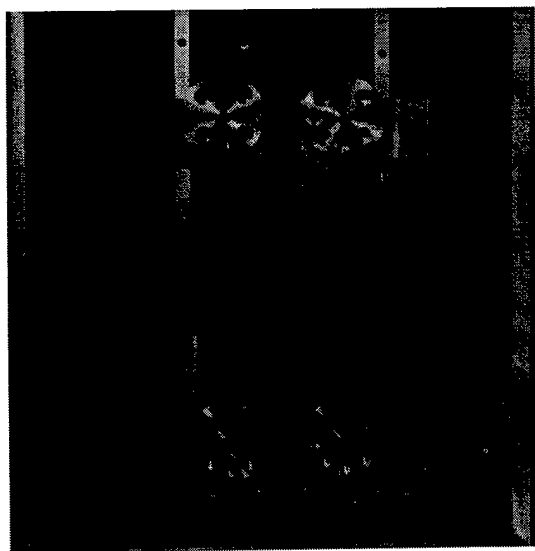


Fig 2: High Speed Pulling Setup: detail of clamping mandrels.

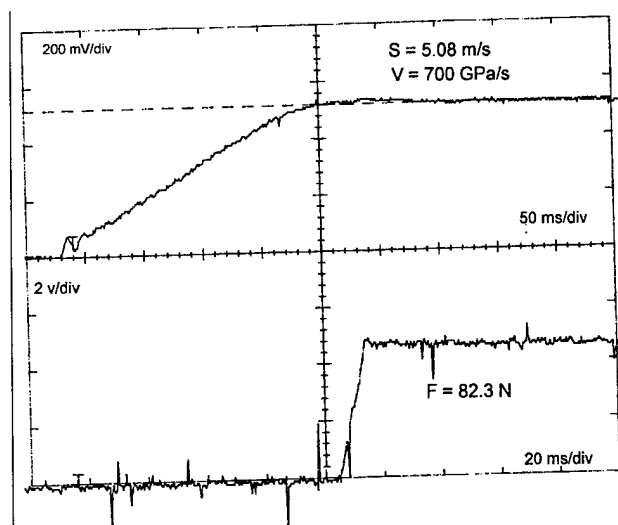


Fig 3: Example of velocity and strength diagram for the highest speed setup.

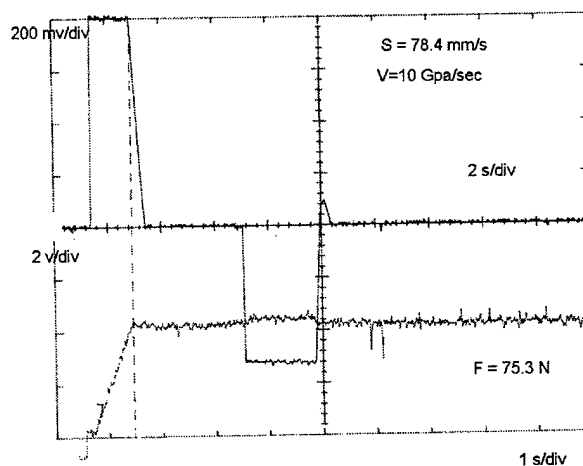


Fig 4: Example of velocity and strength diagram for the lowest speed setup.

4. RESULT ANALYSIS AND DISCUSSION.

In the figures 5 to 9 the general results obtained are given. We can observe two parts in the graphs: a linear fit from which we can calculate the n factor and an horizontal part from which we can deduce the initial inert stress σ_{ic} .

So from relation (11) we can calculate the B value for the highest stress rates.

All the results are given in the table 1.

For the 4 fibres tested, we can see that the n factors measured by the high speed test are in the same range as those measured by the IEC 793-1-3 method. Figures 6 and 9 show the cumulative failure probability issued from the high speed test. Figure 9 gives the 40 % probability failure stresses from 59 to 74 N respectively for 0.06, 0.1, 1 and 10 GPa/s. In figure 6, we can observe that after ageing the B value differs lightly as presented below in table 2. So we can notice that ageing effect has a low influence on the B value whereas the n factor increased strongly (from 17.5(unaged) to 32 (aged)).

	B (Fibre1 unaged)	B (Fibre 1 aged)
500 GPa/s	0.04 GPa ² .s	0.016 GPa ² .s
700 GPa/s	0.014 GPa ² .s	0.025 GPa ² .s

Table 2 : Fibre ageing effect on B value

For the highest stress rates (0.5 to 1TPa/s), the failure stresses measured often reach values of 7GPa. This seems to be lower than theoretical values presented by different authors [7].

For the fibres tested, we note that the B values calculated from the σ_{IC} measured are included between 0.01 and 0.2 GPa².s excepted for the fibre N°3. We can explain this fact by the difficulties encountered during clapping fibres on the pulling mandrels where the lower value has reached 0.002 GPa².s

So this high speed axial strength method permits to cover a very large range of stress rates. The B values obtained are in a relatively narrow scale. Using this method we have also measured the n factor.

5.CONCLUSION.

Different kinds of commercial optical fibres with the new generation of coatings have been tested under high speed axial strength test over a very large of stress rate. An evaluation of n factor and B value for different fibres has been made. Parameters B obtained cover a narrow scale of values (from 0.01 to 0.2 GPa².s).

The initial inert stress σ_{ic} , corresponding to "the plateau level", is quite constant for the different commercial fibres. This indicates that this parameter is a constant for the silica optical fibres.

6. ACKNOWLEDGEMENT.

The authors would like to thank all their colleagues who have performed the high speed strength measurements, J. MARTIN, Y. DUCHAFFAUT.

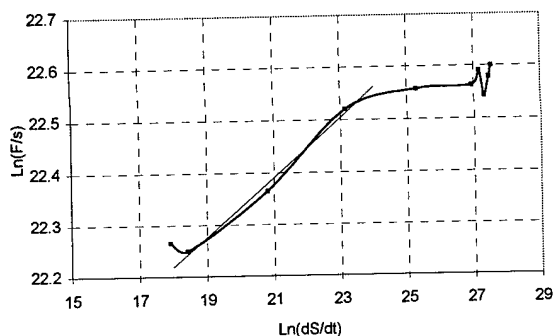
Particular thanks to P. RICHER from LABEL and to our colleagues G. LE MOIGNE, M. AUVRAY, J. MARTRET and R.BOURVA for the tests preparations and for the helpfull discussions and the setup optimisation.

We are grately to R. GOARIN for his encouragement and support for this work. We wish also to acknowledge A. MARIE for his help in results presentation.

7. REFERENCES.

- [1] R.J. CHARLES: "Static fatigue of glass I and II." J.A.P. 29 (1958), page 1549-1560.
- [2] GRIFFITH: "The phenomena of rupture and flow in solids." PHIL. ROY.Soc. (LONDRES) 221A (1920), page 163.198.
- [3] P.C.P BOUTEN: "Lifetime pristine optical fiber" - October 1987
- [4] G.S GLAESEMANN: "High speed strength testing of optical fibers". SPIE vol.2611 pp38-44
- [5] T.SVENSSON: "High strain-rate testing of optical fibres", Proc.37th IWCS (1988) 217.
- [6] N.EVANNO: CNET technical document
- [7] W.GRIFFIOEN, T.SVENSSON, B.FRIDERI CH: "Optical fiber inert strength and B-value", pp750-758 in proceedings of the 43rd International Wire&Cable Symposium, 1994

FIBRE N°1



$$n = 16.47$$

$$\sigma_{IC} = 6.535 \text{ GPa}$$

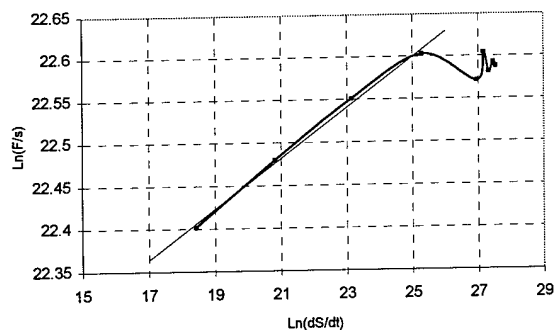
$$\text{For } 100 < d\sigma/dt \text{ (GPa/s)} < 850$$

$$0.014 < B(\text{GPa}^2 \cdot \text{s}) < 0.17$$

Note : by measurement (IEC 793-1-3), $n = 17.73$

Fig 5 : High speed measurement results for fibre N°1

FIBRE N°1 (aged 1000 hours in distilled water - 70°C)



$$n = 32.92$$

$$\sigma_{IC} = 6.487 \text{ GPa}$$

$$\text{For } 500 < d\sigma/dt \text{ (GPa/s)} < 900$$

$$0.015 < B(\text{GPa}^2 \cdot \text{s}) < 0.05$$

CUMULATIVE FAILURE PROBABILITY (for the 3 lowest speeds)

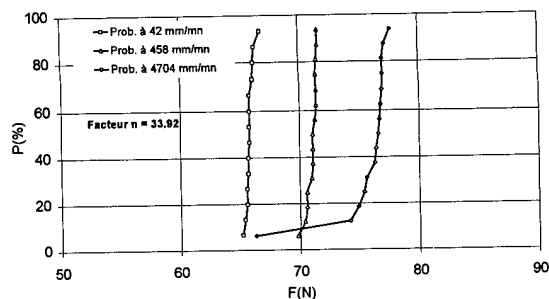
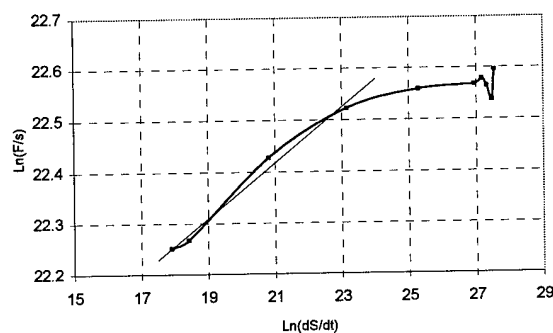


Fig 6 : High speed measurement results for fibre N°1 (aged 1000 hours in distilled water - 70°C)

FIBRE N°2



$$n = 17.54$$

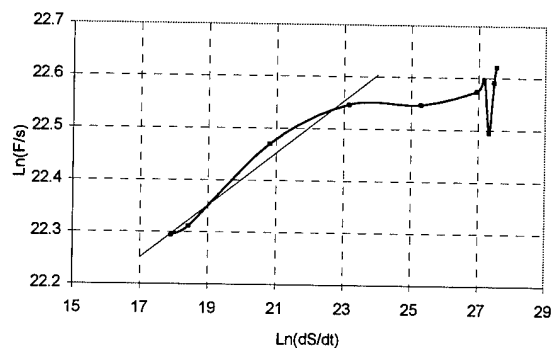
$$\sigma_{IC} = 6.508 \text{ GPa}$$

$$\text{For } 100 < d\sigma/dt \text{ (GPa/s)} < 850$$

$$0.01 < B(\text{GPa}^2 \cdot \text{s}) < 0.18$$

Fig 7 : High speed measurement results for fibre N°2

FIBRE N°3



$$n = 18.82$$

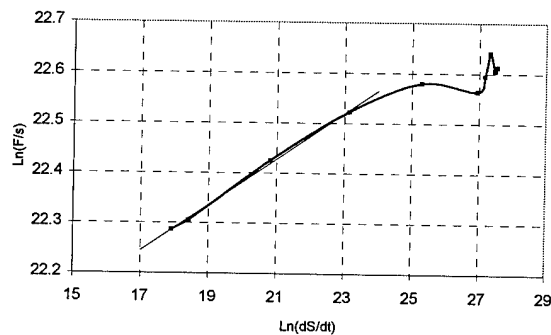
$$\sigma_{IC} = 6.672 \text{ GPa}$$

$$\text{For } 100 < d\sigma/dt \text{ (GPa/s)} < 850$$

$$0.002 < B(\text{GPa}^2 \cdot \text{s}) < 0.05$$

Fig 8 : High speed measurement results for fibre N°3

FIBRE N°4



$$n = 20.84$$

$$\sigma_{IC} = 6.618 \text{ GPa}$$

$$\text{For } 100 < d\sigma/dt \text{ (GPa/s)} < 850$$

$$0.015 < B(\text{GPa}^2 \cdot \text{s}) < 0.15$$

CUMULATIVE FAILURE PROBABILITY (for the 4 lowest speeds)

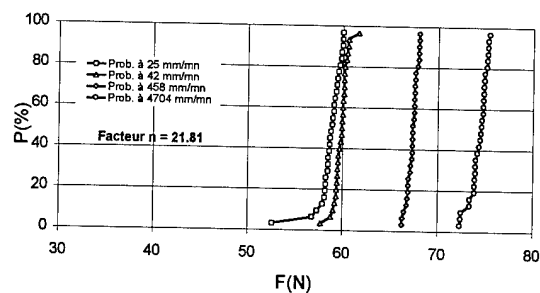
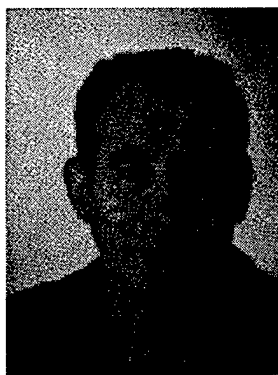


Fig 9 : High speed measurements results for fibre N°4

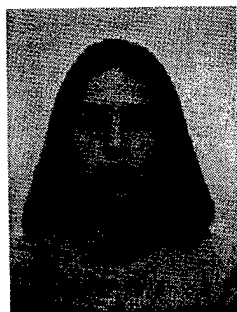
N°Fibre	Fibre Condition	n Factor	Inert initial Stress σ_{IC} (GPa)	Parameter B
1	unaged	16.47	6.535	For $100 < (\text{GPa/s}) < 850$ $0.014 < B(\text{GPa}^2 \cdot \text{s}) < 0.17$
1	aged (1000 hours in distilled water- 70°C)	32.92	6.487	For $500 < (\text{GPa/s}) < 900$ $0.015 < B(\text{GPa}^2 \cdot \text{s}) < 0.05$
2	unaged	17.54	6.508	For $100 < (\text{GPa/s}) < 850$ $0.01 < B(\text{GPa}^2 \cdot \text{s}) < 0.18$
3	unaged	18.82	6.672	For $100 < (\text{GPa/s}) < 850$ $0.002 < B(\text{GPa}^2 \cdot \text{s}) < 0.05$
4	unaged	20.84	6.618	For $100 < (\text{GPa/s}) < 850$ $0.015 < B(\text{GPa}^2 \cdot \text{s}) < 0.15$

Table 1 : General results measurements

8.Authors BIOGRAPHIES.



Alain GOURONNEC was born in 1946. He received his engineer degree from the CONSERVATOIRE NATIONAL DES ARTS ET METIERS in 1978. He joined the CNET in 1971 where he worked on the the pulling and multipulling of optical fibers studies. Then in 1986 he started to work on development and specification of telecommunication cables; since 1993 he is in charge of the evaluation and the qualification of optical fibers for FranceTelecom needs; he is also in charge of the optical fiber reliability studies in CNET.



Noella EVANNO was born in 1972. She's graduated from university RENNES I. She joined France Telecom-CNET where her research interest includes optical fibres reliability studies.

THE EFFECT OF DRAW CONDITIONS ON THE ZERO-STRESS AGING STRENGTH OF SILICA BASED OPTICAL FIBER

P.R. Stupak, M. Supczak, V.A. Cusanello, D. Mazzaresse, D. Roland, and M. Smith

SpecTran Communication Fiber Technologies, Inc., Sturbridge, MA.

ABSTRACT

The zero-stress aging strength of both doped and undoped (i.e., Suprasil) silica based fibers was investigated as a function of draw tension and aging time in pH10 solution at 85°C. For doped fibers produced by changing furnace temperature and holding draw speed constant the rate of zero-stress aging strength loss was not a function of compressive residual surface stress and potentially is a function of tensile residual stress. The zero-stress aged strength decreased with both increased aging time and draw speed for fibers produced by changing the draw speed at constant temperature. The fiber fabrication dependence of the zero-stress aging strength indicates that care must be exercised in interpreting aging strength results from fibers that do not have a well characterized process history.

INTRODUCTION

The combination of theoretical fracture mechanics with empirical stress corrosion crack growth laws has been successfully used to model time dependent strength reduction in glasses and ceramics containing well defined 'sharp' cracks¹. The mechanism involves diffusion of an aggressive molecule, usually water, to the highly strained crack tip. The presence of the reactive chemical effectively lowers the activation energy for rupture of the matrix material bond, thereby extending the sharp crack tip^{2,3}. The same mechanism was initially thought to govern the time dependent strength reduction of pristine silica based optical fibers⁴. However, the absence of 'sharp' cracks in high strength fibers and the observation of accelerated strength loss after long exposure times in harsh environments (i.e., fatigue

knee)⁵, indicated that a second mechanism was also operating.

Kurkjian et al.⁶ proposed that the second strength degradation mechanism was the growth of blunt 'pits' in the fiber surface formed by localized dissolution in regions of structural or compositional inhomogeneity. The pits serve as new stress concentration sites which result in decreased fiber strength with increasing pit growth. Recently, Innis and co-workers⁷ developed a theoretical model of the pit stress concentration as a function of the pit depth and radius. Pits are now thought to be responsible for the accelerated strength reduction occurring at the strength 'knee,' observed after aging fiber either under stress or under zero-stress conditions. Atomic force microscopy has been used to establish a correlation between pit roughness and degraded fiber strength, independent of the fiber coating type or presence of coating⁸.

While research has been conducted on the influence of humidity and temperature⁹, pH¹⁰, and coating and glass surface chemistry¹¹ on glass dissolution rate and fiber strength reduction, relatively little work has focused on the influence of fiber draw conditions on the aged strength properties of optical fiber.

Bouten et al.¹² investigated the draw tension dependence of the unaged and static fatigue aged strength of pure quartz Suprasil fiber and a highly doped fiber capable of developing draw induced residual surface tensile stress. The unaged and aged strength of the doped fiber decreased with increasing draw tension. The rate of aged strength loss increased with increased draw tension, suggesting that the residual and applied tensile stresses

combined to accelerate the stress-corrosion based static aging process.

Alternatively, Griffioen^{13,14} measured the zero-stress aging behavior of two fibers which were designed to have zero and compressive surface residual stress after draw, respectively. The aged strength of the fiber with compressive residual stress was greater than that of the zero stress fiber. However, the fiber surface chemistries were different and therefore did not allow a valid comparison.

The zero-stress aging strength of fibers, examined by Yuce et al.¹⁵, decreased as a function of aging time and decreased coating cure. The degree of cure was changed by varying the number of UV lamps and the draw speed to give both over and under-cured samples. It was concluded that the unreacted material in the under-cured coating was more easily extracted by the aging environment, allowing easier accessibility of the aggressive environment to the fiber surface.

The present work examined zero-stress aging strength of both doped and undoped (i.e., Suprasil) silica based fibers as a function of draw tension and aging time in pH10 solution at 85°C. Since equivalent draw tensions are obtained by varying either draw speed or furnace temperature, both conditions were studied to separate out the effects of each on aged strength. The rate of zero-stress aging strength loss was not a function of compressive residual surface stress and potentially is a function of tensile residual stress for doped fibers produced by changing furnace temperature and holding draw speed constant. The zero-stress aged strength decreased with both increased aging time and draw speed for fibers produced by changing the draw speed at constant temperature. The coating cure, measured by the amount of unbound material extracted, was found to be constant for fibers drawn over the same range of speeds, suggesting that the governing mechanism is not a function of bulk polymer cure. The fiber fabrication dependence of the zero-stress aging strength indicates that care must be exercised in interpreting aging strength results from fibers that do not have a well characterized process history.

SAMPLE FIBER PREPARATION

Three fiber types were considered in this study, including: 1) "Suprasil", synthetic quartz, 2) 62.5/125

µm (core/clad diameter) graded index, and 3) 89/125 µm step index fiber. A measure of the dopant level, the numerical aperture, for the graded and step index fibers was 0.275 and 0.290, respectively. The fiber samples for the three fiber types were each prepared from single preforms and all draw condition changes were completed during a single draw run. The draw tension ranged from 0.2N to 1.37N and was achieved by systematically changing either the furnace temperature or draw speed. All fibers were coated on-line using a commercially available UV curable acrylate. The same number of UV curing units were used for all conditions, meaning that fibers drawn as a function of speed were exposed to differing UV doses. For all draw conditions examined, precautions were taken to ensure that the final diameters of both the inner and outer coating layers did not deviate more than 2% from the nominal coated diameter. After draw, fibers were allowed to equilibrate under conditions of 23°C and 50% relative humidity for at least 72 hours prior to testing.

ZERO STRESS AGED STRENGTH TESTING

Sample preparation of fibers for zero stress aging consisted of forming loose coils of fiber, 305mm in diameter, for each fiber type and aging time. Coils were immersed into a large capacity (30 liter) polyethylene container filled with pH 10 buffer solution (Fisher Scientific SB115-20) maintained at 85±2°C for specified aging periods ranging from 12hr to twelve days. Fibers removed from the solution were allowed to dry and equilibrate in the 23°C and 50% relative humidity environment for 24hr prior to testing.

Strength testing was conducted with 0.5m gage length specimens fractured in axial tension using a rotary capstan fiber testing apparatus. Axial tension was used instead of two-point-bending to expose a greater fiber surface area to the applied tensile stress. The strain rate used in all cases was 4%/min. Thirty specimens were tested for each unique combination of fiber type, draw condition, and aging time. The Weibull moduli for unaged fibers exceeded 50 and were greater than 25 for all aged conditions with the exception of two cases.

Since the measured strength distributions were narrow, the slotted median strength symbol size served to approximately characterize the 25th and 75th percentile strengths. Draw speeds are reported as normalized values.

AGED STRENGTH: DRAW TENSION AS A FUNCTION OF FURNACE TEMPERATURE

The effect of draw tension (surface residual stress) on the rate of zero-stress aging strength loss was investigated initially. Draw tensions were established by changing the furnace temperature and holding draw speed constant to eliminate possible influences of fiber residence time in and below the furnace and the extent of coating cure due to changes in draw speed.

Figure 1 shows the median zero-stress aging strength of the Suprasil synthetic quartz fibers as a function of fiber aging time for draw tensions of 0.59, 0.98, and 1.37N. The fiber strength for all three draw tensions followed nearly the same aging curve, characterized by an immediate steep initial decline and converging to an apparent 'plateau' strength value at longer aging times. The superposition of the aging curves was anticipated due to the absence of dopant or draw induced residual stress in the pure quartz Suprasil fibers. The Suprasil fibers were therefore useful as low residual stress 'control' fibers.

In contrast, doped fibers are known to retain residual surface stresses originating from both thermal expansion mismatch of the core dopants and cladding glass, and superimposed draw stresses^{16,17}. The actual surface residual stresses for the doped fibers used in this study could not be accurately assessed using available experimental elasto-optic methods¹⁶. However, Figure 2 shows the approximate surface stresses as a function of draw tension calculated from a literature based model¹⁷. The graded index fiber surface residual stress was predicted to be compressive for the 0.2N and 0.59N draw tensions and tensile for the 0.98N and 1.37N conditions. The step index fiber surface remained compressive throughout the draw tension range employed. The step index fiber was used to evaluate the zero-stress aging mechanism over a broad range of stress without interactions from the 'stress corrosion' mechanism, which requires an applied tensile stress¹. The graded index fiber was used to examine both the zero-stress aging mechanism and the possibility of accelerated aging due to a combination of both zero-stress and stress corrosion mechanisms (i.e., tensile residual stress).

Figure 3 shows the median zero-stress aging strength as a function of aging time and draw tension for the step index and graded index fibers. The step index fiber aging curves exhibit the same shape as the

Suprasil fibers, but with a slightly lower unaged and plateau strength value. The aging curve for the graded index fiber exhibits a reduced rate of initial decline and a slightly higher convergent plateau strength at longer aging times, relative to the other two fiber types.

In contrast to the Suprasil fiber results, the strength curves for the step and graded index fibers are ranked approximately as a function of draw tension. Past work¹² suggests that the strength ranking, in the absence of aging effects, is due to the superposition of the applied tensile fracture stress and the residual fiber stress. The lower draw tension results in greater compressive residual stress at the surface (Figure 2) and therefore a greater applied tensile stress is required to cause failure from a surface flaw of a specified size. Any accelerating effects of aging would be observed as a greater separation of strength between draw tensions that would increase with time. Because the differences in strength are small for both fiber types, an alternative strength representation showing the stress difference between tension extremes as a function of aging time is illustrated in Figure 4.

The Suprasil fiber strength data in Figure 4 is a measure of the typical variation in the median stress for a fiber with no residual stress (i.e., 50 MPa). The draw induced residual stress of the step and graded index fibers, drawn at the tension extremes, add an additional 120 MPa and 33 MPa, respectively, to the 50 MPa 'baseline' variability (Figure 2). Therefore, excluding aging effects, the maximum strength difference for the step index fiber would be on the order of 170 MPa, and 83 MPa for the graded index fiber. Except for the value of 366 MPa observed for the one day aging time, the average strength difference for the step index fiber remained near the expected value of 170 MPa with no sustained divergence with aging time. A similar analysis comparing the other draw tensions gave the same negative result. In brief, zero-stress aging strength is not a function of compressive residual stress.

The strength difference for the graded index fiber drawn at the highest tension did diverge from the expected value of 83 MPa with increasing aging time. Since this fiber is thought to contain a surface tensile stress, it is suggested that a combination of zero-stress aging and "stress-corrosion" mechanisms may accelerate the zero-stress aging rate. Experiments using a preform capable of retaining

significant draw induced tensile surface residual stress are planned.

AGED STRENGTH: DRAW TENSION AS A FUNCTION OF DRAW SPEED

The second experiment examined the effect of the draw speed on the zero-stress aging strength. Draw tensions were established by changing the draw speed and maintaining a constant furnace temperature. Since the effect of compressive residual stress on zero-stress aging rate was not significant, only the Suprasil and graded index fibers were used in this experiment.

Both the Suprasil and graded index fiber zero-stress aged strength decreased as a function of increasing aging time and draw speed (Figure 5). The aged strength decreased more rapidly with aging time for higher draw speeds. Also, the strength difference between the curves at a given aging time decreased with increasing speed, suggesting that a limiting draw speed exists where no further increase in aging rate will occur. This was most apparent for the shorter aging times.

After longer aging times, the aged strength values tended toward convergence. Therefore the mechanism responsible for differentiating the aging rate as a function of draw speed is most important only for the shorter aging periods and has less influence for longer aging times. The duration of 'shorter' aging times may be very much longer for similar aging tests in less aggressive environments.

Three possible sources of the draw speed dependence of the zero-stress aged strength of the fibers used in this study include: 1) fiber residence time in the furnace, 2) fiber residence time in the ambient environment, and 3) differences in coating cure.

Zero-stress aging is thought to proceed through preferential chemical attack at sites of compositional or structural inhomogeneity causing the formation of pit-like defects in the fiber surface⁶. Differences in fiber residence time in the furnace could result in decreased perfection of the fiber surface after the preform neckdown region and therefore sites of increased structural inhomogeneity with increasing draw speed. However, differences in the surface perfection should also be reflected as differences in unaged strength. This was not observed since the unaged strengths of both fiber types were tightly distributed (Figure 5).

Modification of the bare fiber surface chemistry by the ambient draw environment prior to coating may also affect the zero-stress aging rate. For example, it is known that increases in the humidity of the ambient environment result in poorer coating adhesion¹⁸. Interactions between the atmosphere and fiber surface would be expected to be dependent on the time of exposure and therefore the draw speed.

The importance of the polymer coating as a physical barrier to external species and the influence of the coating on the chemical environment of the fiber surface has been recognized extensively^{5, 11, 19-21}. Mathewson and Kurkjian¹⁰ have shown that static fatigue behavior of coated and uncoated fibers differs significantly. The coated fibers exhibited a resistance to aging during short aging times due to coating barrier properties and then increased aging strength loss at longer testing times as the external environment reached the glass surface. These results suggest that the differences in the general shapes of the aging curves for each fiber type (i.e., Figures 1 and 3) are a result of differences in the coating. In contrast, the bare fibers used in Mathewson and Kurkjian's work¹⁰ exhibited a monotonic strength decrease during the same aging period.

Yuce et al.¹⁵ found that the zero-stress aging strength of fibers decreased as a function of decreasing extent of coating cure. The degree of cure was changed by varying the number of UV lamps and the draw speed to give over and under-cured samples. It was concluded that the unreacted material in under-cured coating was more easily extracted by the aging environment, allowing easier accessibility of the aggressive environment to the fiber surface. The fibers drawn in the present study were also exposed to varying UV dose rates since the number of UV cure units was held constant as the draw speed was changed. However, coating extraction tests²² conducted for fibers drawn and cured over the full range of draw speeds reported here yielded no significant difference in coating extractable content, indicating equal amounts of unbound material and equal levels of cure (Table 1). These results suggest that if the aging mechanism is coating related, the difference is not due to the bulk polymer cure.

Finally, zero-stress aging strength degradation rates, comparable to those reported for the fibers studied here, have been measured for a number of commercially available fibers from several manufacturers. The combination of this observation

with the processing dependence of the zero-stress aging strength reported in this study indicates that care must be exercised in interpreting aging strength results from fibers that do not have a well characterized process history.

CONCLUSIONS

The zero-stress aging strength of both doped and undoped (i.e., Suprasil) silica based fibers was investigated as a function of draw tension and aging time in pH10 solution at 85°C. The rate of zero-stress aging strength loss was not a function of compressive residual surface stress and potentially is a function of tensile residual stress for doped fibers produced by changing furnace temperature and holding draw speed constant. The zero-stress aged strength decreased with both increased aging time and draw speed for fibers produced by changing the draw speed at constant temperature. The coating cure, measured by the amount of unbound material extracted, was found to be constant for fibers drawn over the same range of speeds, suggesting that the governing mechanism is not a function of bulk polymer cure. The fabrication dependence of the zero-stress aging strength indicates that care must be exercised in interpreting aging strength results from fibers that do not have a well characterized process history.

ACKNOWLEDGMENTS

The authors gratefully acknowledge both the assistance of B. Bellerive and P. Chausse in conducting many of the fracture tests and SpecTran Communication Fiber Technologies for the permission to present and publish the results of this study.

REFERENCES

- 1) J.E. Ritter, "Assessment of Reliability of Ceramic Materials," in *Fracture Mechanics of Ceramics*, Vol 5, Eds. R.C. Bradt, A.G. Evans, D.P.H. Hasselman, and F.F. Lange, Plenum Press, NY (1984)227.
- 2) T.A. Michalske and S.W. Freiman, *J. Am. Ceram. Soc.*, 66(1983)284-288.
- 3) S.M. Wiederhorn, *J. Am. Ceram. Soc.* 55(1972)81-85.
- 4) W. Griffioen, *Opt. Eng.*, 33(1994)488-497.
- 5) C.R. Kurkjian and D. Inniss, *Opt. Eng.* 30(1991)681.
- 6) C.R. Kurkjian, J.T. Krause, and U.C. Paek, *J. Phys. C: Solid State Phys.* 43(1982)585.
- 7) D. Inniss, Q. Zhong, and C.R. Kurkjian, *J. Am. Ceram. Soc.*, 76(1993)3173-3177.
- 8) H.H. Yuce, J.P. Varachi, Jr., J.P. Kilmer, C.R. Kurkjian, and M.J. Matthewson, *OFC'92 Tech. Digest*, Postdeadline Paper- PD21, 1992.
- 9) W.J. Duncan, P.W. France, and S.P. Craig, "The Effect of Environment on the Strength of Optical Fiber," p. 309, in "Strength of Glass," Ed. C.R. Kurkjian, Plenum Press, New York, 1985.
- 10) M.J. Matthewson and C.R. Kurkjian, *J. Am. Ceram. Soc.*, 68(1985)177.
- 11) B.J. Stutnik, B.D. Munsey, and C.T. Bruckner, *Proc. Mat. Res. Soc. Symp.*, 88(1987).
- 12) P.C.P. Bouten, W. Herman, C.M.G. Jochem, and D.U. Wiechert, *J. Lightwave Tech.* 7(1989)555.
- 13) W. Griffioen, "Optical Fiber Reliability," PhD Thesis, Eindhoven University of Technology, 1995.
- 14) W. Griffioen, W. Ahn, A.T. de Boer, and G. Segers, *Proc. 40th IWCS* (1991)673.
- 15) H. Yuce, R.A. Fratz, O.S. Gebizlioglu, I.M. Plitz, and T.T. Volotinen, *IWCS 1993*, P. 857.
- 16) P.K. Backman, W. Hermann, H. Wehr, and D.U. Wiechert, *Applied Optics* 25(1986)1093.
- 17) P.K. Backman, W. Hermann, H. Wehr, and D.U. Wiechert, *Applied Optics* 26(1987)1175.
- 18) R.G. Huff and F.V. DiMarcello, *J. Lightwave Tech.* LT-3(1985)950.
- 19) H.C. Chandon, J.R. Petisce, J.W. Shea, C.R. Taylor, L.L. Blyler, D. Inniss, and L. Shepard, *IWCS 1992*, p. 239.
- 20) D.R. Roberts, E. Cuellar, L.M. Middleman, *SPIE*, Vol. 842, 1987, p. 32.
- 21) H.H. Yuce, *IWCS*, 1992, p.605.
- 22) FOTP-10, "Procedure for Measuring the Amount of Extractable Material in Coatings Applied to Optical Fibers," EIA/TIA-455-10, July 1991.

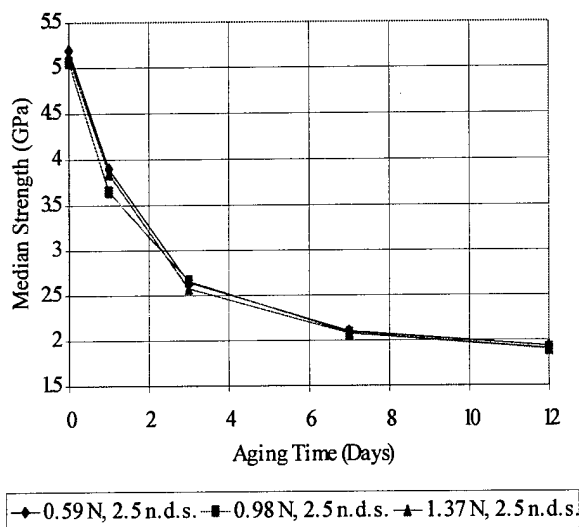


Figure 1: Suprasil median strength as a function of aging time - speed=constant, temperature=vary.
(The normalized draw speed is denoted "n.d.s.").

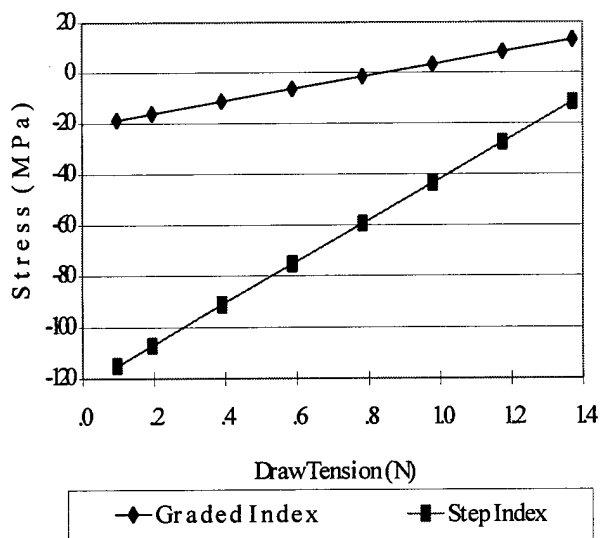


Figure 2: Calculated surface residual stress for the graded and step index fibers as a function of tension (after reference 17).

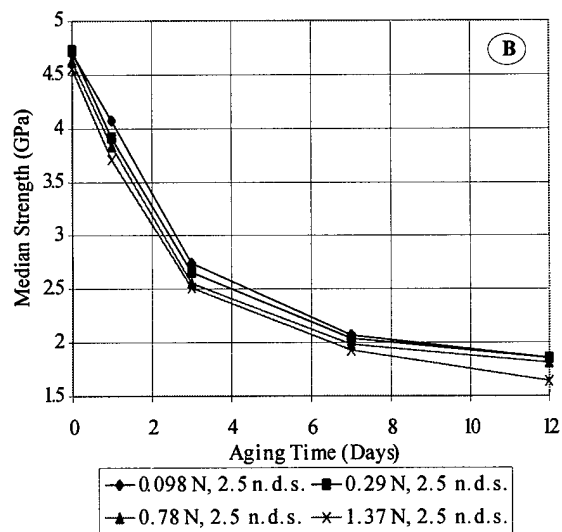
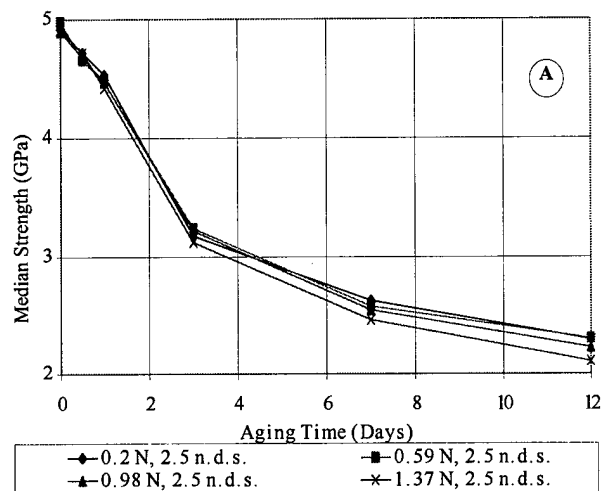


Figure 3: Zero Stress Aging Strength as a function of aging time and draw tension with speed=constant and temperature varying. Results are for A) Graded Index and B) Step Index.

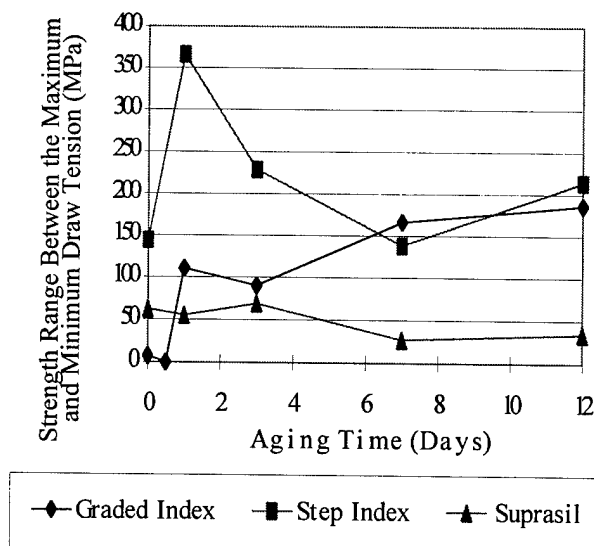


Figure 4: Stress range between the maximum and minimum draw tension as a function of aging time.

Normalized Draw Speed	Percent Polymerized
1	99.58
2.5	99.39
3.8	100.13
5.0	100.02

Table 1: Percentage of polymerization as a function of draw speed as measured by the coating extraction test (22). (Percent polymerization is defined as the percent of unextracted polymer divided by the unextracted polymer for a reference sample that was fully cured. Three replicates were conducted with a maximum range of error between extractable contents of $\pm 0.2\%$.)

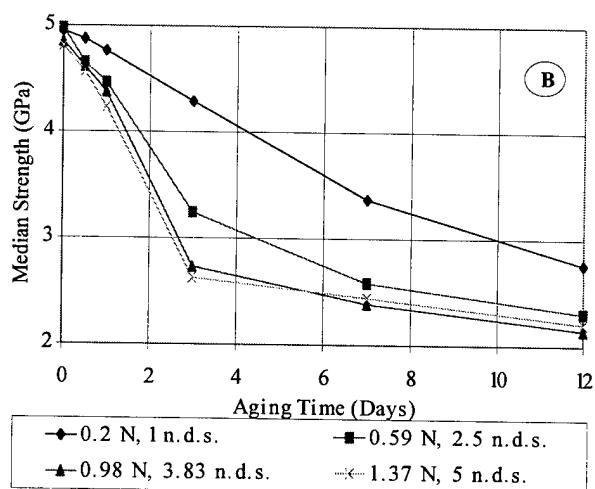
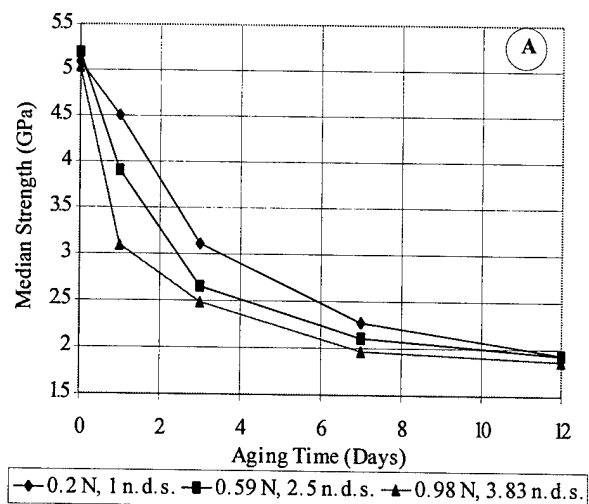
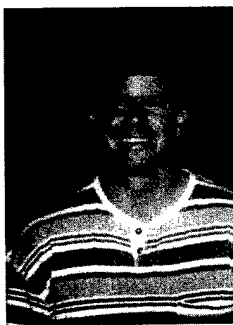
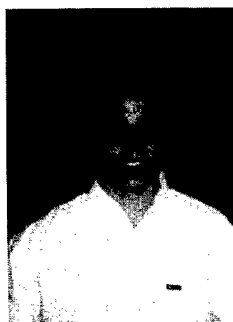


Figure 5: Zero stress aging strength as a function of aging time and draw speed with temperature = constant and speed varying. Results are shown for A) Suprasil and B) graded index.



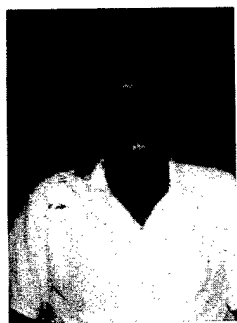
Peter R. Stupak is Engineering Manager at SpecTran Communication Fiber Technologies. He received a Ph.D. in Mechanical Engineering from the University of Massachusetts in 1992. After graduation he held a one-year postdoctoral position at the University of

Naples, Italy, studying the mechanical properties of glass reinforced polymers. After joining SpecTran in 1993, he spent three years working in R&D conducting research on the influence of the fiber draw process on fiber optical and mechanical properties.



Michael J. Supczak is a manufacturing engineer at SpecTran Communication Fiber Technologies. He received a Bachelor of Science degree in Mechanical and Aerospace Engineering from Cornell University and a Master of Science degree in Engineering Mechanics

from the University of Wisconsin-Madison. At SpecTran, Michael is focused on manufacturing process improvements. He has also worked extensively on the fatigue, fracture and reliability of optical fibers.



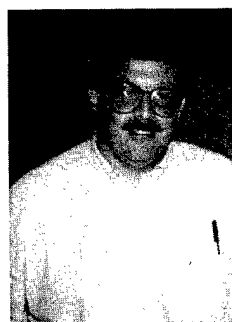
Victor Cusanello is a Draw Process/Project Engineer at SpecTran Communication Fiber Technologies. He has worked at SpecTran for 14 years, holding positions in preform and draw development and was responsible for the development of the

hermetic/polyimide draw process. Prior to joining SpecTran, Victor was employed by Valtec Corporation for three years where he held various positions in preform manufacturing and draw development.



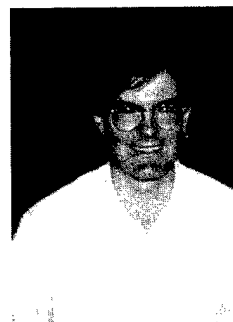
David Mazzaresse is a preform scientist at SpecTran Corporation. He received a B.S. in Chemical Engineering from Carnegie Mellon University and an M.S. in Electrical and Computer Engineering and a Ph.D. in Chemical Engineering from the University of

Massachusetts. Since joining the SpecTran R&D department in 1993, he has specialized in MCVD preform design and fabrication.



David K. Roland received his B.S. in Mathematics from Worcester State College. After working at Valtec Corporation as a member of the Optical R&D Staff, he joined SpecTran Corporation in 1983 as an Engineer. He is currently a Senior Development Engineer in

the Research and Development Department of SpecTran Corporation. In that position he supervises the measurement development and product qualification functions. His research interests include optical and mechanical measurement development and long term fiber reliability. He plays an active role in the establishment of US standards for optical fiber test procedures. He represents SpecTran in the Telecommunications Industry Association. He is chairman of the TIA Working Group on Step Index and Plastic Optical Fibers.



Malcolm Smith is a physicist who works in modeling of optical fiber properties. He received his Ph.D. in physics from Northeastern University in 1985, where he studied photoluminescence from multiple quantum well III-V semiconductor structures. He has worked

at Sandia National Laboratories and at Geo-Centers, Inc., where he was awarded a patent for a fiber optic three axis electric field sensor. Dr. Smith has been working primarily in the modeling of optical waveguides since joining SpecTran in 1992.

A SIMPLE OPTICAL FIBRE RELIABILITY MODEL FOR CABLE DESIGNERS

Frank Donaghy

Alcatel TCC, Liverpool, N.S.W., Australia

ABSTRACT

A generalised representation of time-to-failure under applied stress for optical fibres in cables and a standard flaw distribution function are used to derive a simple expression for failure probability. This model provides a dependable guide for the mechanical reliability of fibres installed in any cable design, and bypasses the complexities and uncertainty of interpretation which still prevail in classical failure models. The result is a simple graphical or mathematical reference for cable designers which provides safe proof test levels or maximum allowed strain for fibres under expected service conditions. The model is compatible with recent guidelines proposed by ITU SG15 for defining cable strength.

INTRODUCTION

Failure prediction for the electrical, optical and electro-optic components used in modern communications systems is a statistical process. Usually the mathematical form of the failure process for each type of device is assumed or inferred from accelerated ageing tests, and the failure statistics are determined by life-testing a sample population. In some cases devices intended for selection are screened by a part-ageing process i.e. a proof test. In general a rigorous and calibrated analytical model of the failure mechanism is not available, and it is therefore impossible to provide a guaranteed survival condition for a given component.

In this paper, corresponding principles are applied to the stress-induced failure of optical fibres due to fatigue to derive a straightforward reliability guide for proof tested fibres in communications cables. Most treatments of fibre reliability are based on a traditional crack growth model which invokes real physical quantities such as crack radius, stress intensity and inert strength.^{1,2,3,4} In reality however

the propagation of defects in optical fibre is only partially understood, and the physical constants which are needed to quantify it are only defined in the regime of established cracks which grow under the influence of an applied stress, intensified at the crack tip. It is well known among researchers in the field that this model does not completely describe the fatigue of high strength silica fibres. In addition there is considerable disagreement in the measured values of coefficients such as the popular constant 'B' which relates inert strength to measured strength.⁵

Despite this, fibre failure models used for cable design today still tend to rely on the crack growth concept alone. The theory is based on the original Charles/Evans model,^{1,2} and is used to derive either an absolute survival condition dependent on the minimum inert strength after the proof test, or a statistical model which delivers the fibre failure probability. In either case the theoretical treatment is a stumbling block for cable designers, who find it unnecessarily complex and difficult to integrate with the normal cable design process.

The alternative treatment presented below avoids this complexity by approaching the problem from a purely empirical and statistical viewpoint. This leads to a simple expression for the fibre failure probability which makes use only of empirical quantities, but is mathematically compatible with more traditional treatments i.e. gives the same result from the same initial assumptions.

SURFACE DEFECTS IN OPTICAL FIBRE

We begin by returning briefly to the issue of surface flaws in silica. As already mentioned, the regime of established cracks is not the only one to be considered when dealing with optical fibres. Figure 1 shows diagrammatically a fibre surface defect in three distinct phases which have been identified in different studies.

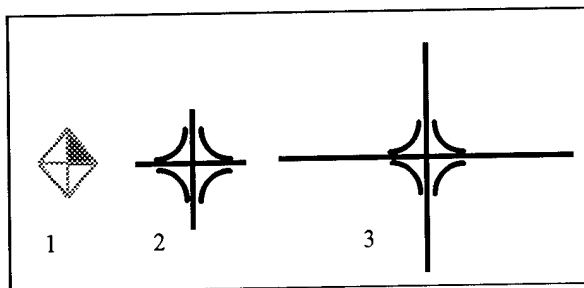


Figure 1. Phases of flaw growth in silica. The sub-threshold phase (1) results in crack initiation and early crack growth (2) leading to classical macroscopic cracks (3).

The sub-threshold phase applies to high strength samples in which there is a surface damage site comprising residual stress but no cracks.^{6,7} This type of defect is probably common in optical fibres as a result of particles impacting the fibre or preform surface in the drawing furnace. The coated fibre surface may even harbour micron-sized refractory particles in surface pits where cracks have not formed or have been annealed out. The sub-threshold phase culminates in an event, crack initiation, which is almost certainly accompanied by a downward step in the instantaneous strength of the sample.⁶

Cracks initiation occurs as a result of residual and applied stress, but will depend also on the fibre surface condition ie the degree of ageing that has occurred, and environmental factors such as humidity and pH.⁸ It is extremely difficult to model this theoretically. Post-threshold phases 2 and 3 may also apply in optical fibres,⁶ but the established crack phase is normally a relatively low-strength regime (up to 2-300MPa), compared to the 1GPa regime which is important in fibres.

Time to Failure Equation

It is probable therefore that the time to failure of high strength optical fibres under applied stress depends mainly on the propagation mechanism of sub-threshold defects and the environmental conditions which influence crack initiation, rather than on the growth of established cracks. Of these three processes, only the last is well understood. In summary, the physical mechanisms which cause delayed fracture of silica fibres are not readily modelled theoretically.

Fortunately a consistent and simple empirical relationship is found between the stress σ applied to samples of uniform initial strength and the

measured time to failure t . In fact both bulk silica and fibre samples are found to obey the relation

$$\sigma^n t = \text{constant.} \quad (1)$$

for uniform samples over a wide range of initial strength, but the index n varies from about 19 for short term tests in fibres to about 36 for established cracks in bulk silica.⁹ The value of around 19 for strong fibre has been shown to apply also to dry fibres of measured strength around 1GPa, due to deliberate damage.^{10,11} Fibres in longer term studies tend to display higher n values in the range 20-30, particularly in moist or acidic environments⁷ which promote surface ageing.

Equation (1) is the basis of the empirical design model. Many authors now believe that the variability of n is primarily due to the empirical power law formulation of equation (1). An exponential model provides a better fit and is probably a more correct representation theoretically,^{5,12,13} but for design purposes the power law is more convenient. The value of n must however be chosen conservatively.

Surface ageing due to moisture or chemical action on the fibre surface over long periods will be accompanied by a change in the value of the constant in equation (1), so that the increase in n may be associated with a shorter time to failure, as shown in Figure 2. The proof test conditions, viz dry, neutral and chemically inert, no longer apply to the long term prediction, and in these circumstances this and all other predictions based on the proof test are compromised.

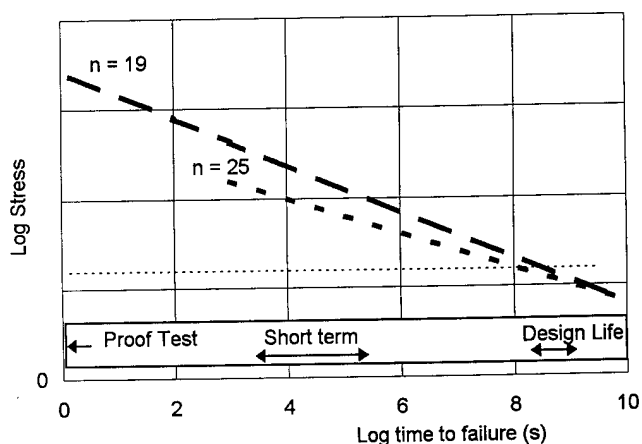


Fig. 2. Time to Failure extrapolations for varying n .

The assumption $n \leq 19$ is therefore recommended for use in all optical cable design. It is realistic for designs such as submarine cables where the fibre environment is benign and surface ageing is unlikely, and provides some insurance against unforeseen environmental action on the fibre surface. For cases where water penetration is expected a lower value, say 15, should be used.

Flaw Distribution Equation

To evaluate fibre failure probabilities, some assumptions must be made about the delivered fibre strength over long lengths. It is well known that manufactured optical fibres achieve very high average strengths due to a clean melt environment and the application of a protective coating immediately after drawing. Occasional weak points occur however due to surface damage, usually caused by residual refractory particles present either in the drawing furnace or in other regions of the drawing tower where the fibre is unprotected, including the coating material reservoir.

These so-called intrinsic and extrinsic flaws respectively form two quite distinct distributions. The intrinsic distribution can be observed easily by strength testing short fibre lengths; its distribution function is highly localised on the stress scale, and is generally described by a Weibull function whose slope index m is large (>50). The extrinsic distribution can only be observed in very long fibre lengths, as in modern draw towers such flaws are relatively infrequent, perhaps some km apart. Hence it is impractical to characterise the extrinsic flaw distribution by experiment as samples some tens of km in length would be needed. However the process of predicting the failure probability of hundreds or thousand of km of fibre in the field requires some knowledge of this distribution. Knowledge of the intrinsic distribution on the other hand is unnecessary: intrinsic flaws are not generally critical in cabled optical fibre except when very localised stressing such as accidental kinking takes place.

In this model the extrinsic distribution is described in terms of the failure probability of manufactured lengths L in a proof test of duration 1 second, where the maximum applied stress is σ_p . The distribution used is assumed to be exponential over the narrow strength range of interest (viz. close to the proof stress), on the grounds that the damaging particle sizes and their impact velocities will be essentially random. Calibration of the distribution is then readily achieved via the

statistics of failures in the proof test. Proof test yield in fact is the best available source of information on the strength of mass produced fibres today. The survival probability of fibres in a long cable will be seen to depend markedly on the frequency of extrinsic defects in the fibre draw process.

We therefore assign the following form to the distribution $P(\sigma_p)$, the probability of failure of a length L subjected to a nominal proof test cycle of maximum stress σ_p and duration 1 sec:

$$P(\sigma_p) = 1 - \exp(-KL\sigma_p) \quad (2)$$

The length dependence can be readily verified by considering the survival probability of several concatenated lengths. The scaling constant K depends on the average length drawn between failures in the proof test for a given value of σ_p , and will later be evaluated in those terms.

DERIVATION OF FAILURE PROBABILITY

By considering the change in inert strength resulting from individual stress-time events, the failure condition in equation (1) above may be generalised as follows.

For a fibre sample of (initial) inert strength σ_c the sum $S = \sum \sigma_i^n t_i$ for any combination of stress-time events which result in failure is independent of the individual stresses and times, including the failure stress. S depends only on σ_c .

This empirical deduction is mathematically provable and routinely used in the crack theory. The relationship holds for proof test failures as well as failures in the field ie (1) is valid down to $t < 1s$. This means that if, for example, a given fibre length has an a priori probability of breaking in a proof test at stress σ_p of duration t_p of say 50%, then its a priori probability of fracture during any events σ_i, t_i is also 50% if $\sum \sigma_i^n t_i = \sigma_p^n t_p$.

Then, if $P(\sigma_p)$ is the failure probability for a given manufactured fibre length in the proof test, $P(i)$ is the a priori probability of failure of this length after two or more events (σ_i, t_i) (the first of which is the proof test), and P_F is the figure which is to be calculated viz. the probability of failure during the remaining events (σ_i, t_i) , having survived the proof test, it is apparent that

$$P(i) = P(\sigma_p) + P_F [1 - P(\sigma_p)] \quad (3)$$

$P(i)$ may be evaluated as follows. Any sample fibre length has a fixed failure condition

$$S = \sum \sigma_i^n t_i = \sigma_{pc}^n t_p$$

for some proof stress σ_{pc} given by

$$\sigma_{pc} = (S/t_p)^{1/n}$$

The a priori failure probability $P(i)$ is therefore equal to $P(\sigma_{pc})$ which from equation (2) above is given by

$$P(i) = P(\sigma_{pc}) = 1 - \exp[-KL(S/t_p)^{1/n}] \quad (4)$$

Using equations (2) and (4) above, the conditional probability equation (3) may be solved for P_F , giving

$$P_F = 1 - \exp\{KL[\sigma_p - (S/t_p)^{1/n}]\} \quad (5)$$

It remains to present this design equation in its most useable form. A number of convenient simplifications are available. Firstly for a given proof test, the variable in the failure distribution becomes the yield length L , whose average or "expected" value L_0 for an exponential distribution occurs when the exponent is -1. Hence the constant K is given by

$$K = 1/L_0 \sigma_p$$

Secondly, since P_F will always be small, the approximation $1 - \exp(-x) = x$ applies. For the case where S comprises a fixed field stress σ_f for time t_f and the proof test, ie.

$$S = \sigma_p^n t_p + \sigma_f^n t_f$$

the result emerges in terms of the proof stress ratio:

$$\sigma_p/\sigma_f = \{1/t_f [(1 + L_0 P_F/L)^n - 1]\}^{-1/n} \quad (6)$$

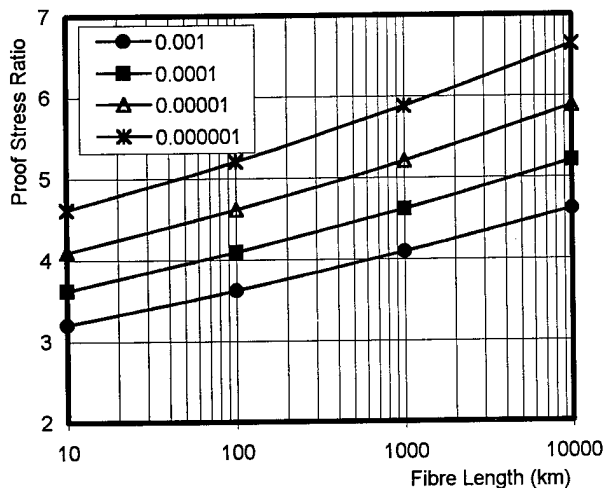


Fig. 3. Proof Stress ratio vs fibre length for four values of Failure Probability, 10 year life, $L_0 = 40$ km

noting that t_p has been eliminated by making it equal to 1 second, and t_f must therefore be measured in seconds or as a ratio to t_p . Alternatively the failure probability may be evaluated from prescribed proof test conditions from the expression

$$P_F = L/L_0 \{ (1 + \sigma_f^n t_f / \sigma_p^n)^{1/n} - 1 \} \quad (7)$$

These are the design equations; they are simple to apply and may be conveniently presented graphically or in spreadsheet form.

Fig. 3 gives an example of the variation of the proof stress ratio with fibre length for a number of target failure probabilities over 10 years of life. The value assumed for L_0 is 40 km, and the influence of this parameter under the same conditions is shown in Fig. 4.

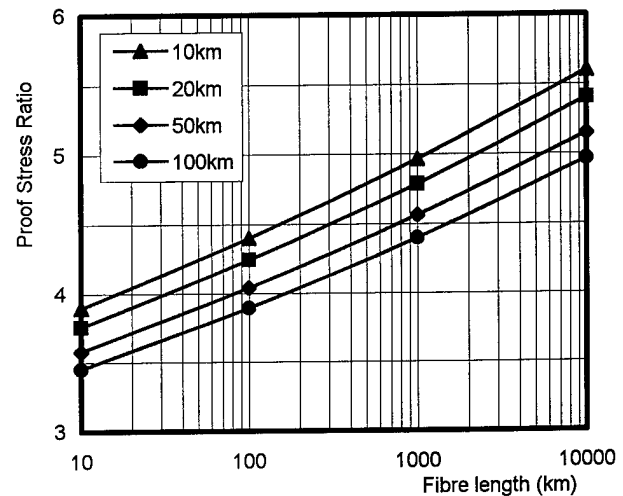


Figure 4. Proof Stress Ratio vs fibre length for 10^{-4} Failure Probability and four values of L_0 , 10 yr life.

Currently proof test yield is not normally revealed by fibre makers, but it can be seen that L_0 is a significant figure of merit for the fibre used to manufacture the cable. This can be a problem for cable makers without in-house or allied fibre manufacture. A contractual requirement could be imposed on the supplier to achieve yields between failures of say 15km minimum. An independent cable manufacturer can conservatively estimate a figure from delivered lengths and the location of splices, but this does not adequately allow for wastage and deliberate cutting to length. The

value of 15km for L_0 is recommended for use by designers in the absence of better information, as most fibre draw processes today are capable of this yield, particularly at low strain levels.

An interesting corollary of this probability model is that any fibres which survive an unforeseen stress event in the factory or field have in effect been re-proof tested, and their failure probability in subsequent service is not affected (in fact is lower). Absolute survival predictions based on the minimum possible inert strength after proof testing are spoiled by such events, which could lead to quite unnecessary scrapping of cable or fibre.

The model is particularly useful for establishing the reliability of splices, whose typical strength distribution can be measured and expressed as a Weibull function in place of equation 2. The corresponding derivation of the failure probability under field conditions is straightforward.

DESIGN PROCEDURE

The task confronting a cable designer, among other considerations, is to ensure that cabled fibres have a low probability of failure under the foreseeable mechanical stresses which the cable will experience. The simplest design approach is to specify the mechanical properties of the cable without reference to the fibres, such that it can handle all expected tensile stresses without significantly exceeding the elastic limit of the strength member and with a low level of residual strain. The cable strain under load is estimated during the design phase and later measured on prototypes. The fibre strain can be calculated from this after allowance for any slack and residual strain in the design, and it may also be measured by optical methods. The allowed fibre failure probability for the overall cable life should be pre-set at a low value, preferably 10^{-3} or less. The fibre model then allows calculation of the necessary proof stress ratio which assures this result.

Occasional events such as cable repairs, storms or installation mishaps resulting in periods of excessive cable strain should be allowed for separately from the lifetime conditions. In most cases these are the deciding factors which set the necessary proof test conditions, but they will generally apply only to relatively short lengths of cable. A submarine cable repair for example may

result in a section of cable being subjected to very high recovery strains and subsequently re-deployed, but the length of cable involved is unlikely to exceed 20km out of a total system length of perhaps several thousand km. Figs. 3 and 4 show that the cable length is a significant parameter in the calculation of failure probability. In addition a higher failure probability, eg 10^{-2} may be tolerable in such cases since a fibre break during a repair is not necessarily a major problem.

The new draft ITUT Recommendations G.oss³¹⁵ take due account of these factors in the derivation of the NPTS, NOTS and NTTS cable strength parameters, calling for fibre failure probabilities and actual cable lengths considered in each case.

Example

As an example the following parameters might be used in a typical repeated submarine cable repair where the cable will be in suspension for up to 48 hours, and the proof strain has been pre-set at 1.5% for 1 second.

N = No. of Fibres in Cable	4
L = Length of Cable (km)	10
t = Duration of app. Load (s)	1.73×10^5
n = stress corrosion index	19
P_F = Fibre Failure Probability	1×10^{-3}
L_0 = Proof Test Yield (km)	15

Using equation (6), (and substituting NL for L) the proof test ratio works out to be 2.45, which would set the maximum allowed fibre strain at around 0.63%. The corresponding cable strain will determine the NOTS (Nominal Operating Tensile Strength) for the design. Using a one hour period the result is 0.77% for the fibre, which will set the conditions for NTTS (Nominal Transient Tensile Strength). The converse calculation of failure probability given the applied strain using equation (7) is equally straightforward. The proof stress ratio and proof strain ratio are approximately the same, but fibre stress σ and % strain ϵ can be more accurately related by the expression¹⁴

$$\sigma = -11.9 \ln (1 - \epsilon / 17).$$

Finally, if required by the specification or the customer, all events may be included in the overall system reliability by simple addition of the individual failure probabilities chosen for each. Generally this will be a design specification to be included in equation (6) rather than an outcome of the design, and the above-mentioned standards could ultimately be extended to suggest an

appropriate failure probability or a range of failure probabilities for NPTS etc.

CONCLUSION

A designer's guide for fibre failure probability in optical fibre cables has been presented, making use only of empirically determined quantities.

The author is indebted to Yves Charles of Alcatel Submarine Networks, Calais, and Jon Steinar Andreasson of AKN Oslo, for valuable discussion.

REFERENCES

- ¹ R. J. Charles, "Static fatigue of glass," J. Appl. Phys., 29, 11, pp 1549-1560, 1958.
- ² A. G. Evans, "Slow crack growth in brittle materials under dynamic loading conditions," Int. J. Fract., 10, 2 pp 251-259, 1974.
- ³ R. Olshansky, R. D. Maurer, "Tensile strength and fatigue of optical fibres," J. Appl. Phys., 47, 10, p 4497, 1976.
- ⁴ J. E. Ritter, J. M. Sullivan, Jr., K. Jakus, "Application of fracture mechanics theory to fatigue failure of optical glass fibres," J. Appl. Phys., 49, 9, pp 4779-4782, 1978.
- ⁵ W. Griffioen, "Optical Fiber Mechanical Reliability", Append B, Ph.D thesis, Eindhoven University of Technology, 1994.
- ⁶ P. Dabbs, B. R. Lawn, "Strength and fatigue properties of optical glass fibres containing micro-indentation flaws," J. Amer. Ceram. Soc., 68, pp 563-569, 1985.
- ⁷ F. A. Donaghy, T. P. Dabbs, "Sub-threshold flaws and their failure prediction in long-distance optical fiber cables," J. Lightwave Tech. 6, 2, pp 226-232, 1988
- ⁸ T. P. Dabbs, B. R. Lawn, "Acid-enhanced crack initiation in glass," J. Amer. Ceram. Soc., 65, pp C37-C38, 1982.
- ⁹ S. M. Wiederhorn, in "Glass: Science and Technology", New York Academic, 5, p 58, 1980
- ¹⁰ F. A. Donaghy, D. R. Nicol, "Evaluation of the fatigue constant n in optical fibres with surface particle damage," J. Amer. Ceram. Soc., 66, pp 601-604, 1983.

¹¹ S. P. Craig, W. J. Duncan, P. W. France, J. E. Snodgrass, "The strength and fatigue of large flaws in silica optical fibre," 8th ECOC, Cannes, 1982

¹² T. A. Michalske, W. L. Smith, B. C. Bunker, "Fatigue mechanisms in high strength silica glass fibres," J. Amer. Ceram. Soc., 74, 8, pp 1993-96, 1991

¹³ M. Muraoka, H. Abé, "Subcritical crack growth in silica optical fibres in a wide range of crack velocities," J. Amer. Ceram. Soc., 79, 1, pp 51-57, 1996.

¹⁴ F. A. Donaghy, "The production and evaluation of high strength optical fibre", Ph.D. Thesis, University of New South Wales, 1982.

¹⁵ Draft ITU-T Recommendation G.oss3, Test Methods applicable to Optical Fibre Submarine Cable Systems - for completion at ITU-T SG15 in February 1997.



F. A. Donaghy
Alcatel TCC
1 Moorebank Avenue
Liverpool, NSW 2170
Australia

Frank Donaghy is a Physics graduate of the Queen's University, Belfast. He holds also a Master's degree in Opto-electronics, also from Queen's, and obtained his Ph.D. in optical fibre fabrication and fatigue from the University of New South Wales in 1982. He spent 10 years in fibre manufacturing technology development with AWA in Sydney before entering the submarine systems business with Australia's OTC, now Telstra, in 1987. In 1992 he joined Alcatel TCC, a new submarine cable system supplier based at Port Botany in Sydney, as Technical Manager.

EFFECT OF WATER QUALITY AND QUANTITY ON STRENGTH DEGRADATION OF FUSED SILICA FIBER IN WATER TESTS

Jette V. Overgaard, Peter Hasløv, Hanna Knuuttila, Andrea Mazzotti, Paola Regio, Torbjörn Svensson, Tarja Volotinen, Stephen Dodd

Tele Danmark Denmark, DRAKA-NKT Denmark, Nokia Cables Finland, FOS Italy, CSELT Italy, Telia Research Sweden, Ericsson Cables Sweden, Optical Fibers U K
COST 246 WG1.1 SG2

ABSTRACT

This paper presents round robin test results for a standard single mode fused silica fiber with an acrylate coating of commercial type. The aging conditions were: 100 %RH, deionized liquid water, tap water and jelly filled loose tube in water. The objective of the round robin test was to find which factors of the test conditions effect the fiber mechanical strength degradation in water; and to find standard conditions for water aging tests of fibers.

We have found that the water test conditions (such as fiber length, type of water, impurities, ions strengths, test vessel material, etc.) must be carefully defined in order to get repeatable and comparable test results. Strength degradation in water at +60 °C can vary from not at all to 70 % in a 90 day test. Our work is continued towards a complete recommendation of a standard. So far we can conclude that a test in deionized water in an inert, closed vessel with a defined amount of water per fiber length gives repeatable strength results.

INTRODUCTION

It is well known, that fibers in metal free cables buried in the humid ground will be exposed to water or 100% RH after some time. Occasionally, water also penetrate into splice boxes. These are arguments for studying the effect of water on strength and lifetime of fiber. Throughout the years numerous tests have been performed with fibers in water, and some telecom operators have included +60 °C water aging tests in their quality requirements. The proper test conditions are still a matter for discussions.. For natural aged fibers in installed cables and for laboratory aged cables, only modest reduction of strength has been reported. However, researchers have recently reported strength degradation results of optical

telecommunication standard fibers in water aging tests.

In COST 246^{*)} it was therefore decided to investigate which factors of the test conditions effect mechanical strength degradation of fiber after aging in wet environment. The conclusions of this work are based on a round robin test at eight laboratories of the COST 246 participants, and on a study of the chemical reaction mechanisms of silica in water¹.

BACKGROUND

In water tests, the amount of water per meter of fiber significantly exceeds the possible amount of water in filled cables. Results from such tests may therefore not be representative for the behavior in cables, and it is the aim of this work to find the most suitable amount of water for these kind of tests.

From the earlier published papers¹⁻¹⁴ it was imagined that a lot of factors may affect the strength degradation, but it was not known which factors would give the major or minor influences. Therefore we decided to test if the quantity and/or the quality of water does have an effect on the strength of the fibers.

From chemical reaction kinetics we would expect to find a direct proportional decrease in strength with the amount of water, if glass behaves as a normal heavy soluble compound.

The dissolution reaction of fiber glass will be arrested saturation¹⁴⁻¹⁵, and an equilibrium will establish at which the dissociation rate of silica is as large as the recombining rate.

^{*)} COST 246 is the European collaboration research action: "Materials and Reliability of Passive Optical Components and Fiber Amplifiers in Telecommunications Networks."

This situation would lead to a constant surface roughness implying a constant strength level dependent of the amount of water per amount of fiber.

If, on the other side, the dissolution of the glass stops because a protecting layer¹⁴⁻¹⁵ of silicic acid builds up on the surface, then the dissolution of the glass and the strength degradation will follow the same degradation mechanism independent of the amount of water.

The protecting layer will control the transportation speed of the ions and chemicals into and out of the glass surface. The surface roughening will develop at a much lower rate, which would look like leveling of strength at the same level independent of the amount of water.

EXPERIMENTS

The aging tests were performed with the same fiber at eight laboratories. The fiber is a single mode dual coated fiber with a diameter, $d_{\text{glass}} = 125 \pm 1 \mu\text{m}$, and is a commercial fiber of world wide application. It was cut in 100 m test samples arranged in free coils with a diameter, $D = 200 \text{ mm}$, and aged in water at 60°C . Each aging test included six coils which were aged in separate containers for respectively 1, 7, 14, 30 and 90 days, with no other materials in the container. Each laboratory used either different type of water (deionized, distilled or tap water) or different type of container material (stainless steel, glass, plastic) all with lids, or different amount of H_2O either as vapor 100 %RH or as liquid water: 0.2, 0.5, 5, 10, 50, or 200 l per 100 m fiber only supplying evaporated water. Fiber strength was measured by a standard tensile test method (IEC 793-1-B7A) at each laboratory using 31 samples of 0.5 m gauge length and 10 % per min. strain rate after preconditioning for 12 - 60 hours at standard room conditions ($23 \pm 2^\circ\text{C}$, $50 \pm 5 \text{ \%RH}$), under which conditions they were also measured.

The results from each coil are plotted in a Weibull distribution, using the procedure described in (IEC 793-1-B7A), from which the Weibull-parameters σ_0 and m were calculated, by Maximum likelihood method see example in Fig. 1.

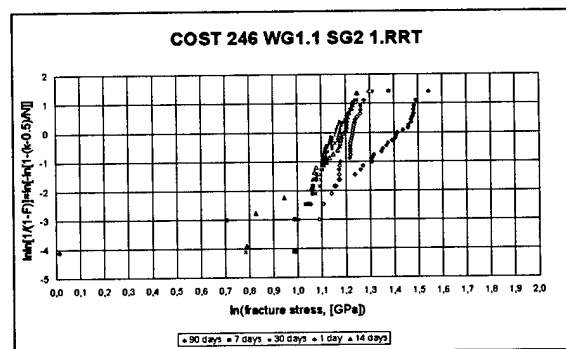


Fig. 1 Weibull curves for one test series

The reduction in strength during time is found by following the eventually decrease in σ_0 , Fig. 2.

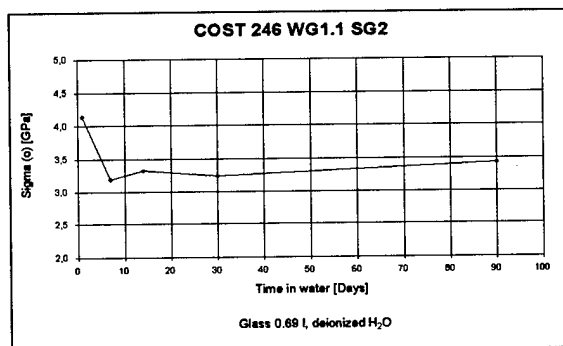


Fig. 2 The strength, σ_0 , as a function of time in water. Results from Fig. 1

RESULTS

The eight laboratories have performed 22 test series in this first round robin test.

The strength degradation

Fig. 3 shows a graph with the results from all the tests. See appendix 1 for a full scaled graph.

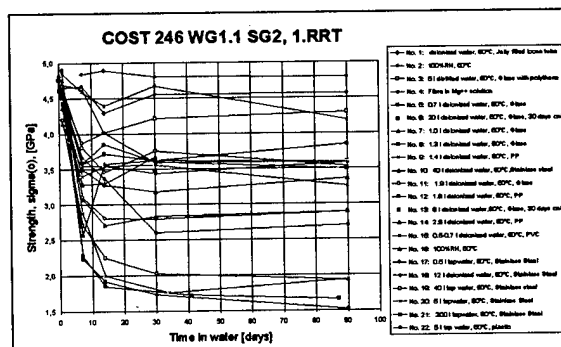


Fig. 3 Strength degradation from all the tests, curve 1 to 22

The first and most striking result obtained from this graph is, that the results are very different.

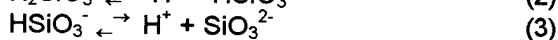
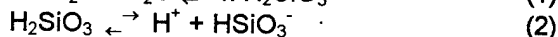
In some tests the fibers are not affected at all by the water whereas in other tests the strength degradation is very significant, showing down to 30 % of original strength. With such difference in results it is obvious that a standard procedure for tests in water or wet condition is required.

Looking at the results for the references (0 days) we can see that they vary only a little, from 4.60 to 4.81 GPa ($\sigma_{0, \text{mean}} = 4.71 \pm 0.07$ GPa), meaning that the inter laboratory correlation and measurement accuracy is good.

It can be distinguished that certain factors affects the result:

- Concentration of the water in humid (water molecules per volume of environment)
- Concentration of foreign molecules or ions in the liquid water from the water source, the container materials or from other sources, as (H^+ , Mg^{2+} , Cl^- , Metal ions ect.)

All chemicals that can influence the dissolution reaction of silica, equations 1-3, will effect the strength degradation.



Fiber in jelly, curve 1

The fibers in a tube with jelly, see Fig. 4 keep their strength throughout the hole test period of 90 days although they are wet.

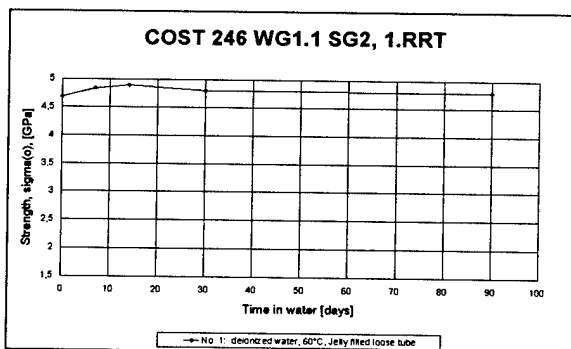


Fig. 4 Fibers in jelly, curve 1

This is believed to be an effect of at least three factors. One is the acidic jelly, as it is well known that acids preserve the silica from dissolution. Looking at equation 1-3 it is obvious that if we add acids, H^+ , or silicate ions SiO_3^{2-} to the water, the equations will be pushed to the left preserving the glass. So fibers are well protected in cables with jelly in wet conditions. Further more we know that jelly contains a tixotrophy agent consisting of silica

gels, which will contribute to the concentration of silicate ions. Meaning that an equilibrium in equation 1-3 will be reached faster stopping further dissolution of the glass. It is also believed that the jelly will act as a barrier and that it will fill the interstitial sites in the acrylate coating.

Fibers in humid environment, curve 2 and 16

The fibers in curve 2 show only a very little strength degradation throughout the test period, whereas the fibers in curve 12 degrade even more than those in liquid water. See Fig. 5

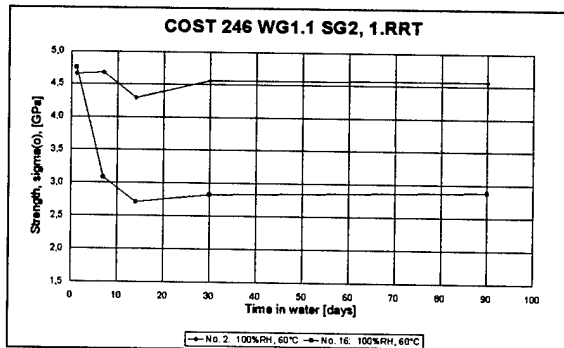


Fig. 5 Fibers in humid conditions, curve 2 and 16

Fibers exposed to humidity will be more affected by the water the higher the concentration of the water is, see equation 1. This means that the higher the humidity the higher the strength degradation.

In the tests shown in curve 2 and 16 we aimed at 100 %RH. In practice this figure is very difficult to obtain without risk for condensation on the fiber.

It was believed that both curves would lie above the curves for liquid water because fibers only wetted with vapor (~100 %RH or less) is less affected by the water than those aged in liquid water.

The difference in water concentration from e.g. 85 %RH to 95 %RH is very small compared to the concentration of water in liquid water which contains more than 7,000 times as many water molecules per unit of volume than vapor with 100 %RH at 60 °C.^{*)}

But the fibers in curve 16 show much higher strength degradation than all the fibers in liquid deionized water. This means that another factor must have influenced this results.

^{*)} 1 m³ air contains 130 g water at 100 %RH and 60 °C whereas 1 m³ liquid water contains 1000 kg water

During these tests it was noted that liquid water was dripping from the fiber indicating that the humidity had passed the dew point, which means that this test more likely was a liquid water test in running water than a humidity test. In this case the fiber could have been exposed to up to 800 l of water during the 90 days of test, as the humidity in the climate chamber is continuously expelled by the ventilation. In this case the fibers have been exposed to more water than in any of the other tests.

We made other tests in running tap water which are not included here as they were tested by two point bending. They seemed to show the opposite result. So test in running water is another issue to be investigated.

The quantity of water

We also tested if the amount of liquid water had any influence, as this will influence the concentration of the present ions coming from the container material or the water itself.

Except for curve 6, 13 and 15 all the fibers in curve 5 to 15, see Fig. 6 and Fig. 7, have been exposed to different amount of water in such a way that the container materials will influence the water in exactly the same way in all the tests.

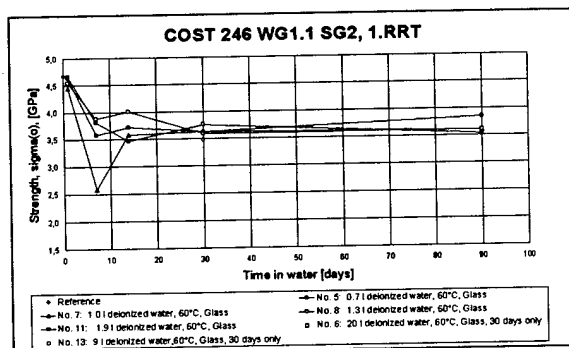


Fig. 6 Deionized water in glass containers, curves 5 to 8 and 11 and 13 of the combined plot

When we keep water in a container some of the inside surface is wet. Material from this wet surface will be dissolved into the water. In this test exactly 500 cm² wet surface per liter of water has been used. This implies that the container materials will contribute with exactly the same amount of chemicals to the water in all these tests and that every coil in a test series is aged in exactly the same normalized environment with respect to the exposed surface. Thus the difference from test series to test series is the volume of water not a difference in concentration of materials from the container. With this test

setup we can investigate the amount of water on the degradation of the fiber.

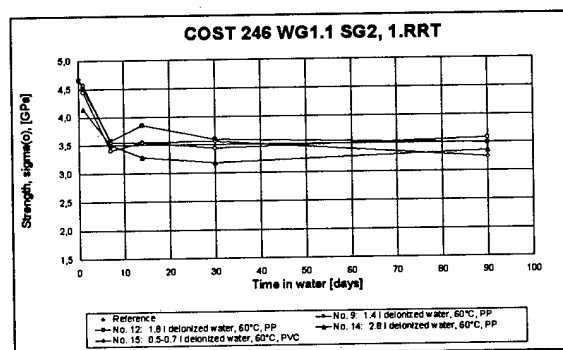


Fig. 7 Deionized water in polypropylene and PVC containers, curves 9,12,14 and 15

The fibers in Fig. 6 have been aged in glass containers, and the fibers in Fig. 7 in polypropylene containers. If there is no effect of the amount of water we would expect to find only one curve in Fig. 6 and Fig. 7 respectively and if there also is no effect of the container materials the curves in Fig. 6 and Fig. 7 would be identical.

We did not find a clear difference in the results. The amount of water did not influence the results in a significant way in the tests in this work.

In glass containers we also tested the influence from the wet container surface. The results after 30 days with 170 cm² and 220 cm² wet surface per l of water (in respectively 20 l and 9 l of water) can be seen in Fig. 6 curve 6 and 13. There is no difference in these results compared with the results from the containers with 500 cm² wet surface per l water. And the results are the same in the polypropylene containers indicating that we have an equilibrium concentration of silicate ions in all these tests and that the saturation originates from the water itself.

Even a strong ion exchanger can hardly extract silicate ions to a concentration as low as the equilibrium concentration for glass, which is around 10⁻⁶ moles per liter¹⁴. Silicates are the most abundant compound in the ground, so a lot of sand and rock material contribute to the concentration of silicate ions in water. This means that laboratory glass containers used in our tests do not contribute very much to the content of silicate ions in the water, meaning that for these glass containers it is not extremely important to keep the wet surface per volume of water constant. But as a good laboratory practice we should do so for the glass containers too in order not to make any mistakes later on. The degradation mechanism in the glass

fibers in deionized water is a very local chemical phenomenon at the surface of the fiber.

Tap water in stainless steel and plastic containers curve 17 and 19 to 22

Except for the fibers in curve 17 the fibers exposed to tap water in stainless steel containers show higher strength degradation than those in deionized water in glass or polypropylene containers Fig. 8

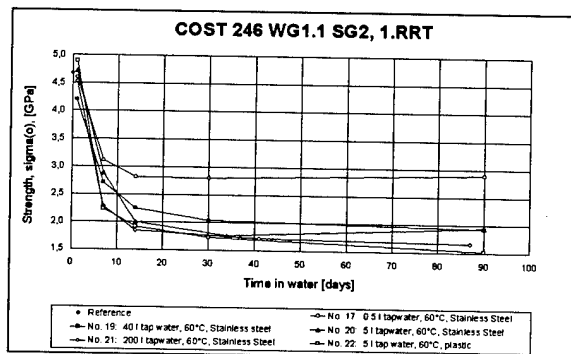


Fig. 8 Fibers in tap water in stainless steel containers

In most of these tests several factors are involved: Small amounts of chemicals from the tap water and/or small amount of metals from the stainless steel container and like all the other tests: the amount of water and the surface area of the fiber. The concentration of chemicals from the tap water is the same in all tests, meaning that these chemicals influence the strength degradation in the same way in all the tests. The metals from the stainless steel container have either reached equilibrium and are the same in all the tests, or the concentration is dependent of the wet surface of the container. This means that the concentration of metals is either the same in the two containers or is larger⁷⁾ in the container with 0.5 l see curve 17, compared to the container with e.g. 5 l in the same kind of stainless steel, see curve 20.

If the concentration had reach a saturation at the wet surface of the container we would expect to find the same strength degradation in all the tap water stainless steel tests. And we could not distinguish the effect of the two factors. But the results in the container with the largest wet surface are the strongest indicating that stainless steel metals reduce the degradation effect of the tap water which seems to be the case in curve 17 see Fig. 8. But it looks as if the effect of tap water

⁷⁾ Area of the wet surface pr. volume of water:

$$A_{\text{wet surface}} / V_{\text{water}} = (A_{\text{bottom}} + C_{\text{bottom}} H_{\text{water}}) / V_{\text{water}} =$$

$$((\pi/4) D_{\text{bottom}}^2 + \pi D_{\text{bottom}} H_{\text{water}}) / ((\pi/4) D_{\text{bottom}}^2 H_{\text{water}})$$

$$A_{0.5l} / V_{0.5l} = 600 \text{ cm}^2/\text{l}$$

$$A_{5l} / V_{5l} = 230 \text{ cm}^2/\text{l}$$

chemicals are the dominating factors resulting in an overall strength reduction. This is confirmed by the results of the fibres in tap water in plastic container curve 22 which has the highest strength reduction of all the tested fibres.

Deionized water in different container materials, curves 10,11,14,15 and 18

We also made some tests with deionized water in stainless steel containers. The results so far show that the strength degradation is smaller in deionized water than in tap water. But in lack of enough data it is too early to conclude what influence the stainless steel containers has in deionized water, as we in one container found the same strength degradation as in glass containers and in another container more strength degradation than in glass containers.

In this last test the quality of the deionized water was questioned. But the differences could also be caused by differences in the stainless steel alloy as stainless steel is a group of chemically different alloys of metals. In our tests we have used at least four different types of stainless steels. We are still studying the subject.

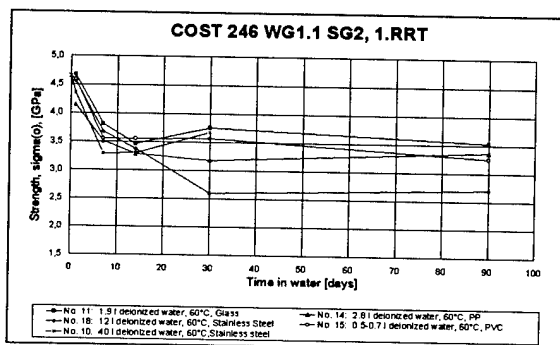


Fig. 9 Different container materials, curves: 10,11,14,15, and 18

Comparing the effect of the other container materials we have tested: glass, polypropylene and PVC we can only see some minor differences and they are not so different that we could see a significant influence from the container materials in these tests.

It looks like an unsolved paradox for fiber tests, that one of the most inert vessel materials available for laboratory tests is glass, as hardly any silica glass wear is as inert and pure as the silica of fibers, in which the over all impurity level is extremely low at the ppm-level.

This could be due to the idea that all chemical reactions with glass, including container walls, are surface governed reactions with local surface

saturation and equilibrium which implies very slow dissolution of the glass and other component from the glass wear. The same way we think it is for pure silica fiber. They do not contribute very much to the content of ions in the water.

Content of ions in tap water

Analysis of tap water from different sources around in Europe are shown in full scale in appendix 2.

It is obvious that the content of chemicals are not the same from place to place. From our results we can see that the chemicals in tap water influence the results and from some earlier work we have done¹⁻³ we know that the strength depends both of the ionic strength of the water but also of the concentration of the specific ions. This has also been reported by Wirth and Gieskes⁵. So for comparison tests tap water is not a good medium.

But for special purposes it could be a more realistic test medium than deionized water. In another COST 246 group, WG1.2, we are investigating what is the real environment for the fibers, in order to perform realistic tests. It seems that it depends on the outer sheet material of the cables, splice boxes and so on which ions can come in contact with the fibers. We do not know yet if tests in local tap water could be relevant for special uses. But for comparison tests deionized water is the best choice.

Magnesium in water

Mg^{2+} , found in tap water, is an interesting ion because it is known from inorganic chemistry reactions that it forms heavy soluble salts with SiO_3^{2-} , meaning that we could expect that the presence of large amounts of Mg^{2+} in tap water would precipitate the SiO_3^{2-} in the water and dissolve the glass resulting in strength degradation. But we found the opposite see Fig. 10, where it can be seen that the presence of magnesium almost preserve the glass. From Wirth and Gieskes⁵ we learned that this is due to the fact that the Mg^{+2} will bind not only to the free SiO_3^{2-} in the water, but also to partly bound ions on the glass surface, which are formed by the dissolution of the glass by water, see equation 1.

This $MgSiO_3$ may be chemically bonded to the surface of the glass and by that retard the dissolution rate. The strength degradation seems to be much smaller than in deionized water but up to now we have only this one result and it is still under investigation.

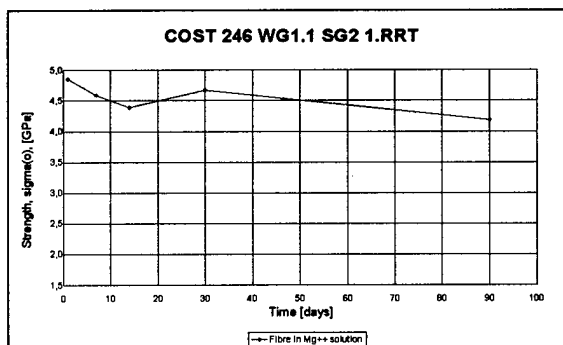


Fig. 10 The result with Mg^{2+} in the water

Factors that could have influenced the results

During this first round robin test we discussed that factors as preconditioning of the fibers before the tensile test or the accuracy and deviation of the load cell or the capstans and clamps could influence the test.

Load cell

We realized that it is important to specify not only the accuracy^{*)} but also the deviation^{**)} of the loadcell in the tensile tester, as we, in our test procedure, suggested a specific amount of repetitions of the strength measurements.

Very often when we discuss lifetime models we focus very much on the m value, meaning that it is very important that the deviation in the loadcell is not shadowing for the deviation in the fiber itself.

The accuracy of our load cells were very high - see the inter laboratory correlation- and applying a 31-fold strength measurements we were able to find acceptable estimations for σ_0 to be used for comparison.

Capstan and clamps

Beside the load cell one of the laboratories has demonstrated that different capstans and clamps of different sizes and of different materials can influence the results. This means that we have to define capstans and clamps to fasten fibres.

DISCUSSION

The strength degradation of optical fused silica fibres in water and humidity tests is dependent on the dissolution of the fiber silica glass to the water. The water will react and create a hydrolyzed silica layer with the outermost layers of the silica; and if

^{*)} Accuracy: X_{mean} close to X_{true} where X is a test result

^{**)} Deviation: Variations in X_i called s, where X_i is one test result

both the silica and the water was absolutely 100% pure the reaction would end up being extremely slow, defined by the diffusion of water in to the glass, as the degradation products would create a kind of protective layer of hydrolyzed silica. Only extremely small amounts of dissolution would take place. A local saturation is established at the surface. This is a very theoretical situation. In real environment and in our test we found, that small amount of chemicals can influence this protecting layer and either cause strength degradation or strength preservation.

In some of our tests we know the chemicals involved: H_2O , H^+ , SiO_3^{2-} , Mg^{2+} and we found that all the reactions were dependent of the concentrations of the involved chemicals not the amount. The quantity of the water plays a role in the definition of the concentration e.g. when the material from the container material is dissolved in the test water. In the tests with known chemicals easy chemical explanations can be found by looking at the dissolution reaction for silica even though we do not know all the chemicals in the primary coating. But when more chemicals are involved like both unknown chemicals in tap water, and unknown metals in stainless steel containers more complicated reactions must have occurred and no easy chemical explanations can be given. This means that the quality of the test water is very important for the results obtained.

So in order to get repeatable and comparable results, we need well defined water. The best applicant for that is deionized water. Tap water should only be used when the effect of a special local tap water is under investigation. Tap water could be relevant as a representative for local environments. We are not ready to choose a single container material for all kind of tests. So far we can conclude that we can make comparable and repeatable tests in high quality pure glass laboratory containers.

But it seems that we have to agree on a fixed wetted surface area per unit of volume of water, in order not to limit this kind of tests to containers of a special shape or size. This is especially important if we perform tests in stainless steel containers which may contribute to the chemically reactions. Stainless steel containers should be used if the affect of stainless steel is under investigation, which could be relevant as some splice boxes contain stainless steel.

CONCLUSIONS

Presence of contaminating ions in the water is an important factor of the test conditions for the mechanical strength decrease of standard fused silica fibers in water. They could originate from ions in tap water or dissolved from the different container materials.

We see a smaller strength decrease in deionized and distilled water than in tap water. We have found that tap water from different countries and sources contain ions in different concentrations, which gives different results. Therefore a reference test should be performed in deionized water, whereas tap water should be reserved for tests where it serves as a representative for local environments.

We see a larger decrease in strength in liquid water than in non condensed humidity at 60 °C. Meaning that it is the concentration of the water which is important for the results just as we would expect it from chemical reaction kinetics.

We do not see a significant decrease in fiber strength when we increase the amount of pure deionized liquid water, even though larger amount of water should give rise to larger amount of dissolved silica in order to keep an equilibrium concentration. But the glass contributes so little to the content of silica ions even in deionized water, that it is difficult to see if the amount of water or the wet glass container surface contributes to the reactions. This means that a saturation/equilibrium with silicate ions in respect to glass has occurred at the surface during the test period; and that dissolution in pure deionized water in glass containers is so little that differences in amount of water and amount of wet container surface is of minor importance for the strength degradation. A stable slow deterioration rate will be established, as long as no foreign ions are added to the water. During the tests all the strength degradations stopped at a constant level after 14 days aging.

However, when we compare the results with the 100 m fiber in respectively 0.5 l and 50 l tap water we see a larger decrease of strength in the larger amount of water. The reason is different concentration of metals from the stainless steel container material which, contribute more the larger the wet surface is compared to the water volume. The smallest container, 0.5 l, has the relatively largest wet surface. This means that stainless steel metals preserve the glass fiber from dissolution in these tests.

This also means that no saturation with metals is reached during the tests in stainless steel containers with tap water. If so the concentration of metals would have been the same giving the same strength degradation in the different stainless steel containers.

Normally the amount of water in these tests is extremely high when compared to the length of fiber in the cable. In real environment only small amounts of water are present in the cables at the fibers. In our tests we have found that the amount of water plays a minor role for the strength degradation.

But any way it is still a good laboratory practice to perform all tests with the same wetted surface per volume of water for a given length of fiber.

Aging of fibers in a jelly filled loose tube immersed into water did not cause any remarkable strength degradation. Jelly and tube protected the fiber by one or some of the reasons: colloidal silica powder in the jelly contribute to the concentration of dissolved silica, weakening the ion and residual spice transportation and lowering the pH-value at the silica surface. So we can conclude that fibers in cables with jelly are kept in a rather safe environment and tests with fibers directly in water are very severe compared to real environment. We do not know if these results can be generalized for all kinds of fibres.

FUTURE WORK

COST 246 is continuing the tests to find a good recommendation for the water test conditions

ACKNOWLEDGMENTS

We would like to thank following experts and co-authors for participation in the tests and contribution to the discussions:

- Dr. Charles Kurkjian, Bellcore
- The members of COST 246 WG1.1 SG2 "Aging tests" i.e. T. Breuls POF, F. Couchet Cabloptic, A. Gouronnec CNET, K. B. Jensen Draka NKT, P. Salina Swiss Telecom and Sennhauser EMPA
- Prof. M. Tomozawa, Rensselaer Polytechnic Institute, New York.
- Prof. M. J. Matthewson, Rutgers University

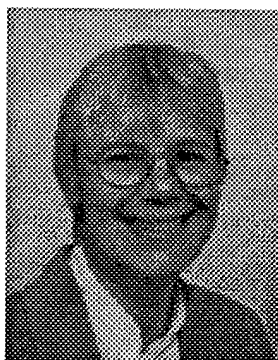
We also like to thank all the employees in the eight laboratories. Without their assistance this work could not have been accomplished.

REFERENCES

- 1 J. V. Overgaard, SPIE, Vol. 2611, (1995), p. 64 - 71.
- 2 T. T. Volotinen et al. SPIE Vol. 1973, (1993), p. 161 - 174.
- 3 L. Oksanen and H. Knuuttila, SPIE, Vol. 2290 (1994)
- 4 D. Innis et al., Proc. OFC, (1994), p. 244 - 245.
- 5 G. S. Wirth and J. M. Gieskes, J. Coll. Intr. Sci., Vol. 68, No 3, (1979), p. 492 -500.
- 6 V. Rondinella et al., Cer. Trans., Vol. 20 (1991), p. 171 -182.
- 7 Rondinella et al., SPIE Vol. 1366, (1990), p. 77 - 84.
- 8 M. J. Matthewson et al., Proc. OFC, (1991), paper ThG2, p. 152.
- 9 M. J. Matthewson et al., J. Am. Ceram. Soc., Vol. 74 (10), (1991), p.2592 - 98.
- 10 A. Bershtein et al., Sov. Phys. Solid State, Vol. 15, No. 11, (1974), p. 2173 - 2176.
- 11 W. J. G. Wijnen et al., J. Non-Cryst. Sol. Vol. 109, (1989), p. 85 - 94.
- 12 D. Dennis, D. L. Brownlow, C. R. Kurkjian; J. Am. Ceram. Soc. Vol. 75 n. 2, p. 364-68 (1991)
- 13 P. C. P. Bouten, D. J. Broer; SPIE vol. 2074; P. 59-70
- 14 I. Fanderlik, Glass Sci. Tech. 11, Prague (1991)
- 15 A. Fleming, J. Coll. Intr. Sci. Vol. 110, No 1, (1986), p. 40 - 64.
- 16 H. Yuce, OFC, paper PD2, p. 359-399 (1992).
- 17 R. Kurkjian et. al., SPIE Vol. 2611, (1995), p. 34 - 37.
- 18 J. Carr, Proc. IWCS, (1993), p. 394 - 398.
- 19 H. Scholze, Glass Nature Structure and Properties, NY 1991
- 20 Bailer, Moeller and Kleunberg, University Chemistry, Boston 1966

KEY WORDS

Optical fiber, strength degradation, quantity, quality, humidity, deionized water, tap water, ion concentration



Ms. J. V. Overgaard
Tele Danmark R&D
Telegade 2
DK-2630 Taastrup
Denmark

Jette Viig Overgaard is head of the Material Chemistry group at Tele Danmark R&D. She received her B.Sc. in Chemical Engineering from the Technical University of Copenhagen in 1973. In 1984 she joined Tele Danmark, and is especially involved in projects concerning reliability and lifetime of the materials in the fiber optical network. Member of COST 246 since 1987.



Mr. A. Mazzotti
FOS
Strada Provinciale 135
I-84091 Battipaglia Salerno
Italy

Andrea Mazzotti received the degree in Mechanical Engineering from University of Calabria in 1992. He joined FOS in 1994 as a researcher in the mechanical characterisation of optical fibres and since 1995 he is involved in the technology area. He is a member of COST 246 since 1995.



Ms. H. Knuuttila
Nokia Cables Fiber Optics
P.O. Box 419
00101 Helsinki
Finland

Hanna Knuuttila was born in 1968. She received the master's degree in Chemical Engineering in 1994 from the Helsinki University of Technology. She is working at Nokia Cables Fiber Optics group as a research engineer. Her work consists of the fiber reliability and fiber coating issues. Member of COST 246.



Dr. T. Volotinen
Ericsson Cables Telecom
Cables division
S-82482 Hudiksvall
Sweden

Tarja Volotinen is a senior specialist in optical fiber reliability at Ericsson Cables, Telecom Cables Division. She graduated from Helsinki University, Finland, 1978 with a M.Sc. and 1991 with a Ph.D. in physics. Since 1978 she has worked with optical fibers. In 1992-93 she worked as visitor scientist at Bellcore. She is chairman of European research action COST 246 titled "Materials and Reliability of Passive Optical Components and Fiber Amplifiers in Telecommunications Networks".



Ms. P. Regio
CSELT Optical Technologies
Via G. Reiss Romoli 274
I-10148 Torino
Italy

Paola Regio received her degree in Physics from the University of Torino in 1993 and prepared her thesis in CSELT on the mechanical properties of optical fibres. During the same year she joined CSELT and actually she is working in a group involved in the reliability research of the passive components of the optical network: in particular she works on the mechanical reliability of optical fibres. She is a member of COST 246 since 1994.

Mr. S. Dodd

Optical Fibres, Second Avenue, Deeside Industrial Park, Deeside, Flintshire CH5 2NX, United Kingdom

Stephen Dodd is Senior Product Engineer at Optical Fibres, UK. He received his B.Sc. from Manchester University in Physics and Electrical Engineering, 1985. Member of COST 246.

Dr. T. Svensson

Telia Research, S-136 80 Haninge, Sweden

Photo is presented elsewhere in this proceeding.

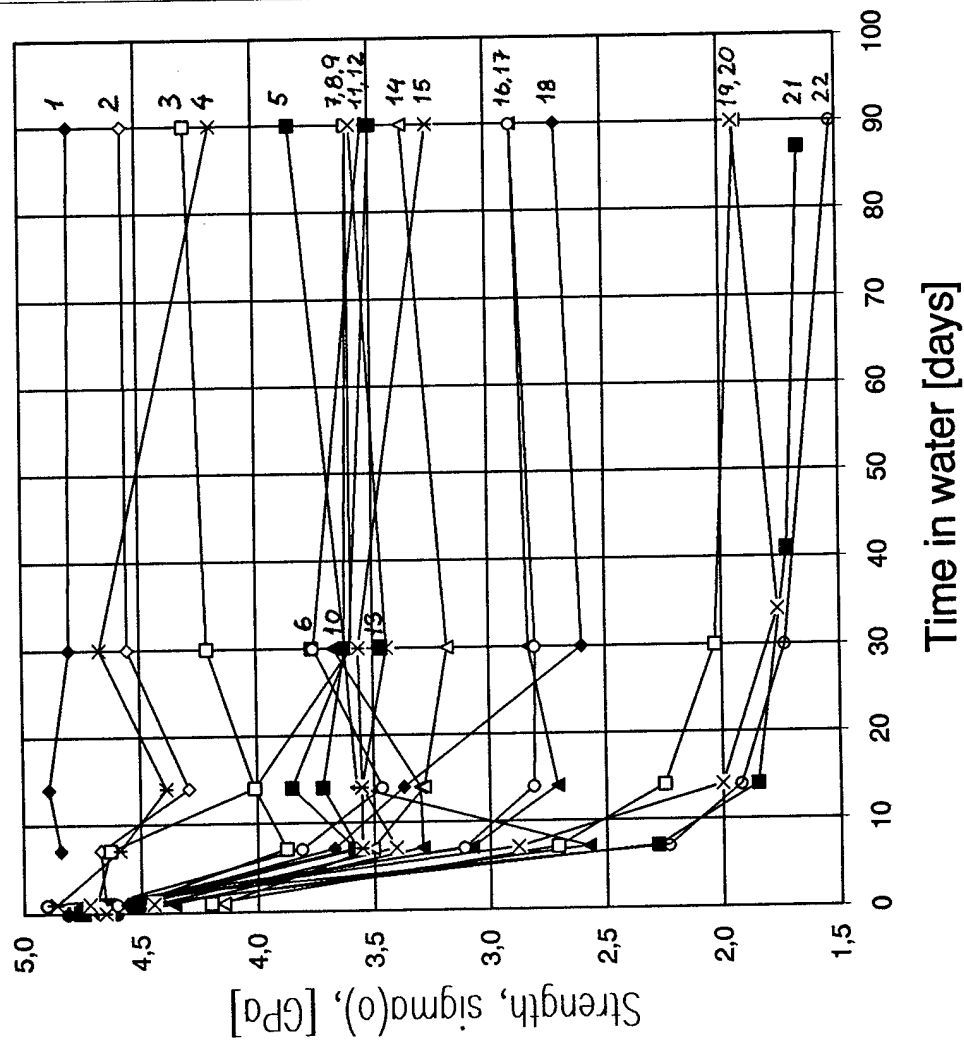
Torbjörn Svensson has a M.Sc. and Ph.D from Royal Institute of Technology, Stockholm. In 1985 he joined Telia where his major engagement was cable and fiber testing techniques, in which field he also holds a number of patents. He is now employed by Telia Research AB, working with the reliability of optical transmission systems and components. Member of COST 246.

Mr. P. Hasløv

DRAKA-NKT Optical Cable, Sognevej 13, DK-2605 Brøndby, Denmark

Peter Hasløv is M.Sc. in chemistry from Copenhagen Technical University 1974. Until recently he was employed at DRAKA-NKT Optical Cables. He was a member of COST 246 because of his capacity as specialist on polymers. He is now working at the Danish Technological Institute with technological assistance about plastic materials and components.

COST 246 WG1.1 SG2, 1.RRT



Analysis of tap water from different laboratories and sources:

Ions	Sweden ICP (mg/l)	Sweden (mg/l)	Denmark (mg/l)	Italy ICP (mg/l)	Italy ICP (mg/l)	Italy AAS (mg/l)	France ICP (mg/l)
Al ³⁺	<0.05			0.01	0.28	<0.005	
B ³⁺	<0.05						
Ba ²⁺	0.004						
Ca ²⁺	12	25		5.38	104	180	16.3
Cd ²⁺	<0.05			<0.024	0.01		
Cl ⁻							
Co ²⁺ /Co ³⁺	<0.05			0.001	0.01		3.5
Cr ²⁺ /Cr ³⁺ /Cr ⁶⁺	<0.05					<0.005	
Cu ¹⁺ /Cu ²⁺	0.05			0.07	0.01	0.005	
Fe ²⁺ /Fe ³⁺	0.01			0.08	0.04	0.01	
K ⁺	2.8	2.5	3.5	0.15	2.13		3.1
Li ¹⁺	<0.005			<0.031	0.01		
Mg ²⁺	4.9	4.8	17	1.57	31.14	140	6.2
Mn ²⁺ Mn ³⁺ Mn ⁴⁺ Mn ⁷⁺	<0.005			<0.007	<0.007	0.006	
Na ⁺	4.6	10	15	227.65	20.69		12.3
NH ₄ ⁺							0
Ni ²⁺ Mn ³⁺	0.07			0.03	0.04	0.036	
NO ₃ ⁻							24.6
Pb ²⁺ Pb ⁴⁺	<0.01			0.04	0.11		
Si ²⁺	0.04			0.16	4.08		
SO ₄ ⁻							13.8
Zn ²⁺	<0.01			1.20	2.13		
Si ²⁺ Si ⁴⁺ Si ⁻	10	0.34	0.15			28	

NOVEL INDEX PROFILE FOR IMPROVED LARGE EFFECTIVE AREA FIBER

P. Nouchi*, P. Sansonetti**, C. Le Sergent**

*Alcatel Fibres Optiques, Marcoussis, France

**Alcatel Alsthom Recherche, Marcoussis, France

ABSTRACT

Extensive design results are presented on several index profiles regarding their capability of yielding low-loss dispersion-shifted large-effective-area fiber with low bending and microbending loss. We find the new coaxial class of profiles, which includes a ring and a depressed center, offers the best combination of large effective area (up to $90\mu\text{m}^2$), small chromatic dispersion slope (as low as $0.065\text{ ps/nm}^2/\text{km}$) and low bending and microbending loss. This theoretical investigation has been validated on three index-profile types, that is trapezoid+ring profile and profiles from the coaxial family. The fiber samples we made were in very good agreement with the numerical prediction.

INTRODUCTION

Development of Erbium-doped fiber amplifier (EDFA) at $1.55\mu\text{m}$ has made possible high-performance transmission systems : high-bit-rate non-regenerated transmission over thousands of kilometers, as well as repeater-less transmission for hundreds of kilometers and Wavelength Division Multiplexing (WDM) transmission with high power. However, amplifier technology magnifies the effect of optical nonlinearities by increasing propagation distance and optical powers in the fibers, and eventually limits the system capacity.

Transmission-fiber non-linear effective area (A_{eff}) is a key parameter in describing optical nonlinearities. Commercial dispersion shifted fibers (DSF's) have an effective area around $50\text{--}55\mu\text{m}^2$, which is small compared to $80\text{--}85\mu\text{m}^2$ effective area of standard step fibers. It is clear that larger effective area for DSF's would lower nonlinear effects. For long-haul high-bit rate system, it would allow larger signal power, improved signal-to-noise ratio and longer repeater spacing;¹ for unrepeated systems, Stimulated Brillouin Scattering threshold would be increased² and four wave mixing effects in dense WDM systems would be diminished.³

Over the past two years, much research has been done on new designs for DSF's with increased effective area and acceptable level of bending and microbending loss, since bending and microbending loss are a major limitation for an operational installed fiber system. This led to new classes of fibers called LEA (Large Effective Area). For the first time, we demonstrated the feasibility of DSF with effective area increased up to $70\mu\text{m}^2$.⁴ This was made possible by carefully choosing the 6 opto-geometrical parameters of a trapezoid+ring index profile, which was called LEA1 (Large Effective Area). The system impact (longer repeater spacings) of LEA1 fibers was demonstrated in a 5 and 10 Gb/s soliton-loop experiment.^{5,6} Further work followed demonstrating higher effective area : from 80 to $90\mu\text{m}^2$ on a triangle+ring index profile⁷ and a double-ring profile,⁸ although microbending and bending loss are estimated to be high in these profiles. We recently demonstrated effective areas larger than $90\mu\text{m}^2$ with two novel designs.⁹ The first one, called LEA2 (or coaxial-type profile), is made of a germanium-doped ring with a fluorine-doped depressed center. The second one LEA3 (or coaxial+ring type) consists of a double ring with depressed center and inner ring. Some other works also include the ring profile, yielding effective areas $\sim 55\mu\text{m}^2$ and small chromatic dispersion slope (from 0.05 to $0.07\text{ ps/nm}^2/\text{km}$),¹⁰ and the dual-shape core (or pedestal) profile yielding effective areas $\sim 60\mu\text{m}^2$ but larger chromatic dispersion slope (from 0.10 to $0.12\text{ ps/nm}^2/\text{km}$).³

It is difficult however to compare performances of these various profiles because authors have different ways of evaluating bending and microbending loss. Bending losses are measured for a 30 mm radius in ref. 4 and 9 and 37.5 mm radius in ref. 7. They are measured with the pin-array test in ref. 8 and computed for a 15mm radius in ref. 3. The only direct microbending loss measurement is done in ref. 4 and 9 with the wire mesh test. Also, corresponding zero-dispersion wavelength data are not always given though larger effective areas are easier to get with the lowest zero dispersion wavelength.

In this paper, we present extensive design results regarding several well-known index profiles. This investigation allows us to compare, on a theoretical basis, the performances of each profile for given bending loss, and even chromatic dispersion slope. For each profile, we clearly put numbers on how the effective area is limited by bending, microbending loss and chromatic dispersion slope. From this work, we could define the index profiles of ref. 4 and 9 which are in very good agreement with numerical prediction. We find the new coaxial class of profiles, which includes a ring and a depressed center, offers the best combination of large effective area (up to $90\mu\text{m}^2$), small chromatic dispersion slope (as low as $0.065\text{ ps/nm}^2/\text{km}$) and low bending and microbending loss.

FIBER DESIGN

We present here an extensive investigation of most of the index profiles reported in the articles cited above, that is : (1) the ring profile of ref. 10; (2) the pedestal profile, close to the dual-shape core profile of ref. 3; (3) the trapezoid+ring index profile of ref. 4 and 7; (4) the coaxial profile of ref. 9 and (5) the coaxial+ring index profile of the same reference. All those profiles are depicted in Figure 1. We also recall the well-known results for the simple step index profile as reference data.

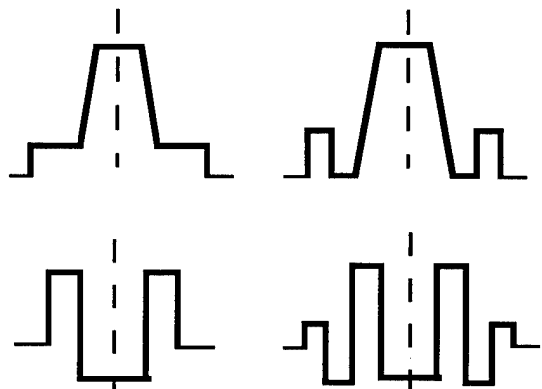


Figure 1: Schematic diagram of index profiles : pedestal, trapezoid+ring, coaxial, coaxial+ring.

We use a computer program that solves the scalar wave equation for arbitrary index profiles and wavelength. Once the propagation constant (or effective index) and fundamental mode field distribution is known, we can compute : mode field diameter Petermann 1 and 2 and effective area ; chromatic dispersion and chromatic dispersion slope, using Sellmeier formula for λ -dependence of silica, germanium and fluorine-doped silica refractive index¹¹. We can also compute bending

loss for any radius using the radiation model of ref. 12 and a microbending sensitivity parameter $S_{\mu c}$ that we defined according to ref. 13. This microbending sensitivity parameter allows us a good prediction of added microbending loss in cables. Following recommendations of the international standard committee UIT-T (G653), we essentially focus on bending loss in dB for 100 turns on a 30mm radius mandrel, the maximum acceptable level of loss being 0.5 dB. At last, we also look at the tolerance of chromatic dispersion to small fiber-parameter deviations. Small changes in chromatic dispersion with changes in core radius and core-cladding refractive index will insure a good control and a good reproducibility of chromatic dispersion during the manufacture process.

When studying a class of index profiles, we proceed the following way. For given bending loss α_{b0} and given chromatic dispersion C_0 at $1.55\mu\text{m}$, we scan through the adjustable profile parameters (from 2 to 6 depending on profile shape) to find the set of parameters yielding largest possible effective area. For the step index profile, there is only one index difference value Δn and one core radius value yielding α_{b0} and C_0 , but for more complicated profiles there are usually many sets of parameters yielding those two values, so that we can select the set of parameters defining the index profile with the largest effective area. Also, when scanning through profile parameters, core-cladding index difference Δn is limited to 15×10^{-3} to ensure good loss behavior. For complicated design with more than 3 adjustable parameters, chromatic dispersion slope changes over a wide range of values. In this case, as it will be detailed below, parameters yielding largest effective area are selected within a set value for chromatic dispersion slope.

This procedure is repeated for several bending loss values (100 turns on a 30 mm radius mandrel) ranging over four orders of magnitude up to 1 dB, so that we can follow exactly how the effective area is increasing when tolerance for bending loss is increasing. Again, by repeating the same procedure for all the profiles, we get the 6 solid curves shown in Figure 2 -each curve corresponding to one class of profile- so that we can compare the capability of each profile to yield high effective area within given bending loss. In Figure 2, chromatic dispersion value is set to about 0 ps/nm/km at $1.55\mu\text{m}$.

As it is well known, step-index profile would make a poor LEA fiber design. It yields the smallest effective areas from 40 to $50\mu\text{m}^2$ but with small chromatic dispersion slopes (about $0.06\text{ ps/nm}^2/\text{km}$) and Δn values around 10×10^{-3} .

The next profile on the curve is the ring profile with effective areas slightly larger, ranging from 45 to 55 μm^2 . As noticed in ref. 10, the ring mode-field radial distribution has a peculiar non-gaussian shape with an off-axis peak and a strong decay in the cladding, which makes it a good candidate for a LEA design. However, the intrinsic waveguide dispersion of the ring profile is very poor compared to that of a step-index profile so that this profile needs high Δn values to compensate for material dispersion. A high core-cladding index difference value tends to confine the mode and eventually cancels the positive effect of the field shape. Chromatic dispersion slopes values for the ring are similar to step index values, around 0.06 ps/nm²/km.

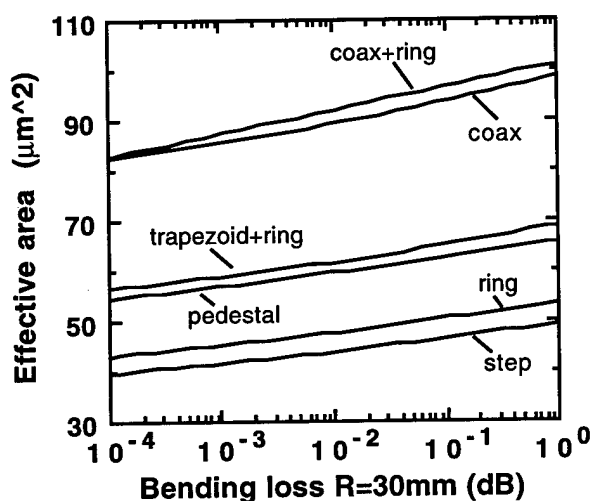


Figure 2 : Maximum effective area as a function of computed bending loss (100 turns on a 30 mm radius mandrel) for the 6 investigated index profiles. Pedestal, trapezoid+ring and coaxial+ring are also constant chromatic-dispersion-slope data at 0.08 ps/nm²/km, which corresponds to that of commercial DSF.

The next two curves correspond to more complicated design, pedestal and trapezoid+ring profiles, which have respectively 5 and 6 adjustable parameters (width, height, position of ring and width, height and shape of central trapezoid). The additional ring has a number of advantages regarding the field shape and the intrinsic waveguide dispersion : the field shape is also non-gaussian and waveguide dispersion can be tailored to values comparable to that of step index. Both profile allows a 10 μm^2 effective area gain compared to the ring profile, with effective area values up to 65 μm^2 . For those two profiles, chromatic dispersion slope covers a wide range of values for given bending loss and chromatic

dispersion. On the curves of Figure 2, it is set at about 0.08 ps/nm²/km, that is a value comparable to that of standard dispersion shifted fibers.

The last two curves of Figure 2 show a large improvement in the effective area. Effective area values range from 80 to almost 100 μm^2 over the bending loss values covered. These curves are associated with the class of coaxial index profile. The simple coaxial profile is made of a simple germanium-doped ring with a fluorine-doped depressed center. This type of profile was first theoretically studied in ref. 14. A design example was given for a dispersion shifted fiber with a larger index difference in the central dip (17×10^{-3}), than the index difference of the ring (7×10^{-3}), but such large index difference values for the depressed dip are difficult to achieve with current preform technology. By scanning through the 4 parameters, we find it is possible to define index profiles with Δn values lower than 10×10^{-3} for the fluorine-doped layer and lower than 15×10^{-3} for the ring. However, chromatic dispersion slope tends to be a little bit higher than typical DSF's, from 0.085 to 0.095 ps/nm²/km. Curve of figure 2 shows the 0.085 ps/nm²/km data point.

The second index profile (coaxial + ring) consists of a double ring with depressed center and inner ring and has eight adjustable parameters. It offers about the same combination of high effective area and low bending loss than the simple coaxial profile, while minimizing refractive index differences. This is also a profile which offers a wide range of chromatic dispersion slopes. The curve of figure 2 corresponds to constant-slope data at 0.08 ps/nm²/km. We believe the depressed central region offers a better trade-off between a large effective area and low bending loss. Again, this is due to the peculiar non-gaussian field shape, which is even more pronounced in the coaxial case : an enlarged extension inside the fiber core with the field maxima located near the ring and a sharp decay in the cladding. With this field shape, the effective area is always larger than the Petermann-II mode field area πW_{02}^2 . Also, the additional ring offers the possibility of tailoring the waveguide dispersion just as it did in the trapezoid case.

We next study the influence of chromatic dispersion slope on effective area values. Only the most complicated designs (pedestal, trapezoid+ring and coaxial+ring) offer enough parameters to yield very different propagation behavior and chromatic dispersion slopes. Constant-slope curves are shown on figure 3. Pedestal and trapezoid+ring profiles behave in the same way, that is the maximum allowable

effective area is not only limited by bending losses but also by chromatic dispersion slope. For pedestal profile, larger effective areas are obtained for chromatic dispersion slope values about 0.09 to 0.95 ps/nm²/km, but there is only a small gain of 5 μm^2 for the effective area compared to the 0.08 ps/nm²/km curve. Smallest effective area values are obtained with smaller slopes. The trapezoid+ring profile offers a wider range of chromatic dispersion slope and effective area values. Chromatic dispersion slopes can be as high as 0.12 ps/nm²/km and the gain in effective area as large as 10 μm^2 compared to the 0.08 ps/nm²/km curve. For both profiles, even higher slopes and effective areas could be obtained but with larger than $15 \times 10^{-3} \Delta n$ values. However, those high slopes profiles have a very poor tolerance of chromatic dispersion to small fiber parameter deviations.

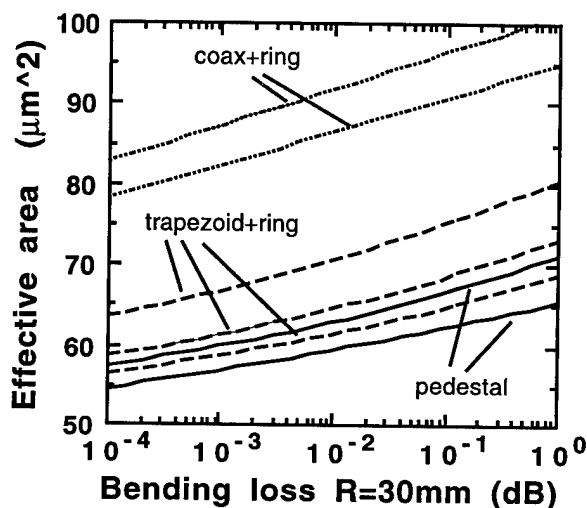


Figure 3: Maximum effective area as a function of computed bending loss (100 turns on a 30 mm radius mandrel) for constant chromatic dispersion slope value. From bottom to top, pedestal data correspond to 0.080 and 0.092 ps/nm²/km; trapezoid+ring data corresponds to 0.080, 0.092 and 0.112 ps/nm²/km; coaxial+ring data corresponds to 0.065 and 0.080 ps/nm²/km.

Coaxial+ring profile behaves in a very different way since it has its maximum effective area for slopes of around 0.08 ps/nm²/km. Figure 3 shows the 0.065 ps/nm²/km curve with a 5 μm^2 loss on the effective area value.

So far, we only focused on how bending loss limits the effective area. Bending loss mainly depends on how the field falls off in the cladding, but it does not fully take into account the mode field extension. As shown in ref. 13, microbending loss

depends strongly on the mode extension. It specifically depends on mode-field diameter Petermann 1, defined as the root mean square of near field intensity. Therefore, a good resistance to bending loss does not ensure a good resistance to microbending loss. Because low microbending loss is important for good cabling capability, we also studied the microbending behavior of these profiles. We use a microbending loss sensitivity parameter which includes both Petermann 1 diameter and how sharp the field decay is. On the scale we use, conventional DSF and standard step-index fibers have a microbending sensitivity of about 0.5 and 1 respectively.

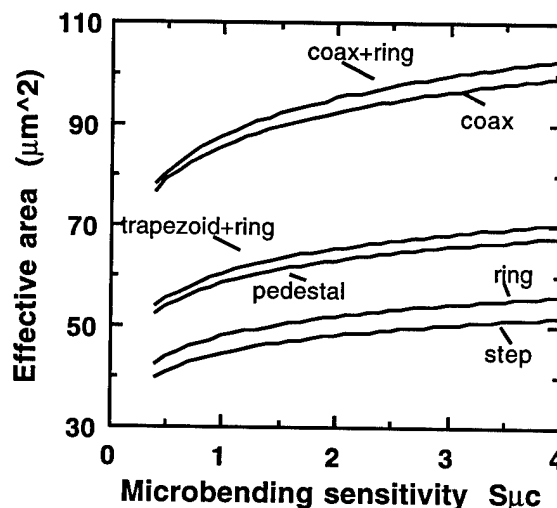


Figure 4: Maximum effective area as a function of computed microbending sensitivity for the 6 investigated index profiles. Pedestal, trapezoid+ring and coaxial+ring are also constant chromatic-dispersion-slope data at 0.08 ps/nm²/km, which corresponds to that of commercial DSF.

Figure 4 represents effective area of the profiles of figure 2 as a function of their computed microbending sensitivity. For microbending sensitivity comparable to that of standard fiber, we can expect effective areas between 85 and 90 μm^2 for the coaxial and coaxial+ring profile and about 60 μm^2 for the trapezoid+ring profile with a 0.08 ps/nm²/km chromatic dispersion slope. Figure 5 shows the constant-slope curves of figure 3 as a function of microbending sensitivity. For the trapezoid+ring index profile, an increased chromatic slope can lead to 70 μm^2 effective area with yet microbending sensitivity comparable to that of standard fiber.

This extensive theoretical investigation was used to define a few index profiles for large effective area fibers. Corresponding experimental results are presented in the next chapter.

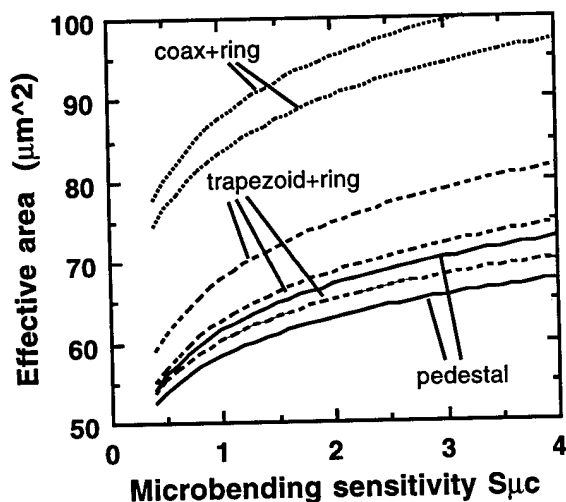


Figure 5 : Maximum effective area as a function of computed microbending sensitivity for constant chromatic dispersion slope value. From bottom to top, pedestal data correspond to 0.080 and 0.092 ps/nm²/km; trapezoid+ring data corresponds to 0.080, 0.092 and 0.112 ps/nm²/km; coaxial+ring data corresponds to 0.065 and 0.080 ps/nm²/km.

EXPERIMENTAL RESULTS

We first defined a trapezoid+ring profile with a 70 μm² effective area and a chromatic dispersion slope $\partial C/\partial \lambda = 0.1$ ps/nm²/km. This profile was called LEA1 and we made several sample fibers using the MCVD process. Figures 6 and 7 show histograms of measured chromatic dispersion and effective area at 1.558 μm, yielding respectively an average value 0.43 ps/nm/km and a distribution 72 ± 3 μm². The effective area was extracted from the Variable Aperture in the Field data, classically used to measure Petermann II mode field diameter. For this profile, πW_{02}^2 is a good approximation within 2% for this profile.

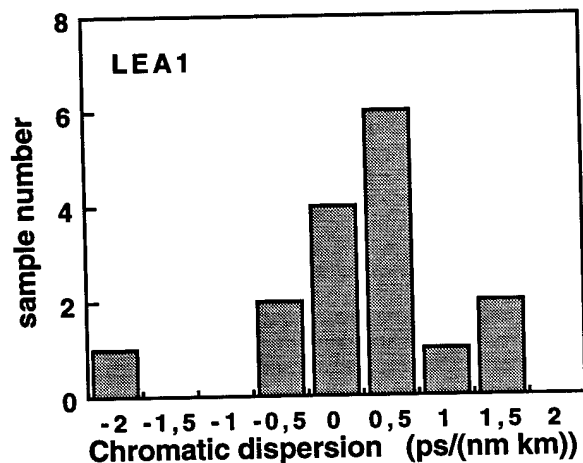


Figure 6 : Histogram of measured chromatic dispersion at 1.558 μm for sixteen LEA1 fiber samples.

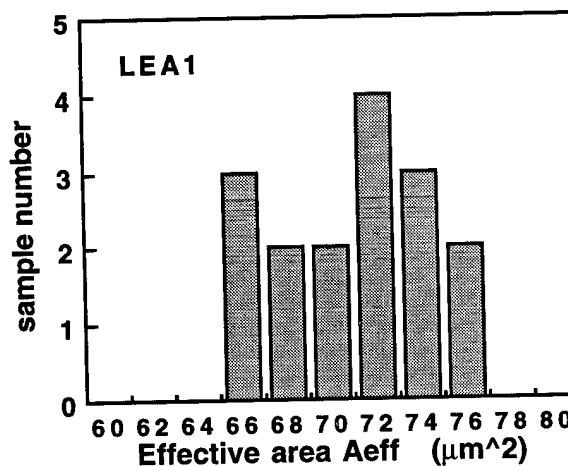


Figure 7: Histogram of measured effective area at 1.558 μm for sixteen LEA1 fiber samples.

We then defined a profile in the coax and coax+ring family, called respectively LEA2 and LEA3. Their profile parameters were chosen to yield (1) a microbending sensitivity equal to that of standard step fibers for both profiles and (2) a chromatic dispersion slope of about 0.085 ps/nm²/km for LEA2 profile and 0.065 ps/nm²/km for LEA3 profile. About 15 fiber samples of each profile were made. Measured chromatic dispersion at 1.55 μm is presented on Figures 8. Chromatic dispersion is well controlled between -2 and 2 ps/nm/km. We use a computer program which allows us to predict the measured chromatic dispersion within 1 ps/nm/km, from the index profile measured of preform. Figure 9 shows the measured chromatic dispersion slope at 1.55 μm yielding as expected, values around 0.086 ps/nm²/km for LEA2 profiles and 0.065 ps/nm²/km for LEA3 profiles. Two LEA3 samples have a larger slope due to slightly modified ring design.

We also compute the effective area from the classical Variable Aperture in the Far Field data used for measuring mode field diameter. Four out of the 32 samples have an effective area between 80 and 90 μm², while all the other samples have effective areas slightly larger than 90 μm². The fibers with the largest effective areas don't necessarily have the lowest zero dispersion wavelength, but they have the largest bending and microbending loss. We also measured PMD values, which can be as low as 0.05 ps/√km.

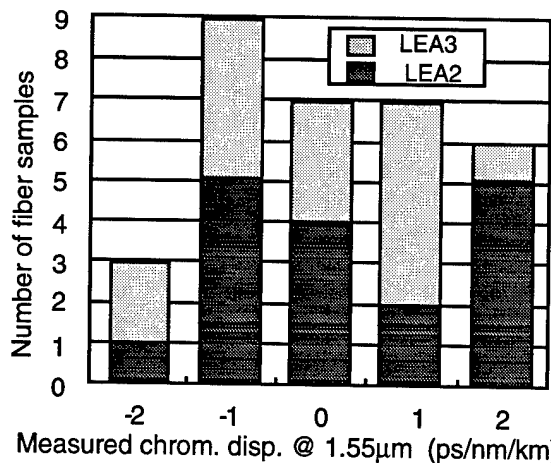


Figure 8: Histogram of measured chromatic dispersion at 1.55 μm for LEA2 and LEA3 fibers.

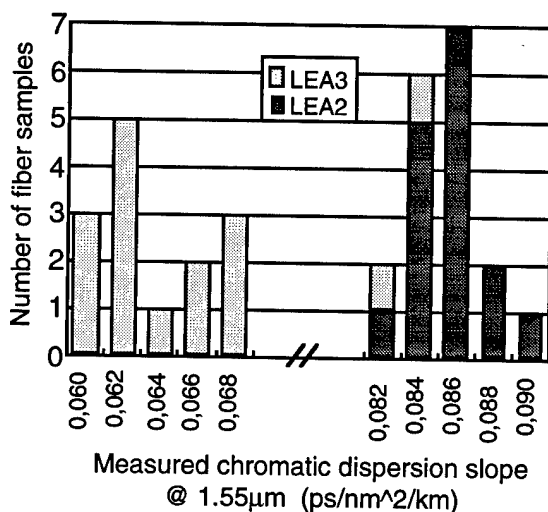


Figure 9: Measured chromatic dispersion slope at 1.55μm, for LEA2 and LEA3 fibers.

MCVD process has been improved for fluorine-doped deposition (down to -8×10^{-3}). We find that a fluorine-doped center combined with alternate fluorine-doped and germanium-doped layers yields excess loss if no special care is taken during the fiber process. Rayleigh scattering for fluorine-doped silica is reported to be comparable to that of Germanium-doped silica.¹⁵ Current fiber loss is as low as 0.23 dB/km, but we believe we can achieve theoretical limit of 0.21 dB/km.

At last, we find the resistance to bending loss is quite good for LEA2 and LEA3 fibers: the measured bending loss (100 turns for a 30 mm radius mandrel) is lower than 0.02 dB for all the fiber samples. Microbending loss was measured with the wire mesh test and was found to be comparable to that of standard step-index fibers.

Also, first cable trials with LEA2 fibers did not show any excess loss.

CONCLUSION

In this paper, we thoroughly investigated several index profiles to find how large the effective area can be for a dispersion shifted fiber, for given bending loss and microbending loss. The profiles we studied cover a wide range of effective area values (several $10 \mu\text{m}^2$). We find the best suited profiles corresponds to highly non-gaussian mode-field shape, and adjustable waveguide dispersion. For the first time, we present extensive data on two new designs which include a depressed central region. We believe the depressed central region offers a better trade-off between large effective area and low bending loss. We find those two profiles can offer effective areas up to $90 \mu\text{m}^2$, with very low bending loss and good microbending behavior, and also chromatic dispersion slopes comparable to that of commercial DSFs. Among all the profiles, the coaxial+ring family offers the best combination of large effective area, small chromatic dispersion slope, as low as that of standard step fibers, low splicing loss and low bending and microbending loss.

Following this extensive calculation, we made several fiber samples out of three index profiles: trapezoid+ring LEA1, coaxial LEA2 and coaxial+ring LEA3. Our results are in very good agreement with our numerical predictions.

[1] O. Audouin and J.P. Hamaide, 'Enhancement of amplifier spacing in long-haul optical links through the use of large effective area transmission fiber', IEEE Photonics Technol. Lett., Vol. 7, pp 1363-65, 1995.

[2] R. Yamauchi, 'Optical-fiber nonlinearity: measurements and counter measures,' OFC'95, Paper FD2, San Diego, Feb. 26 - Mar. 3, 1995.

[3] Y. Terasawa et al., 'Design optimization of Dispersion Shifted Fiber with enlarged Mode Field Diameter for WDM transmission,' IOOC'95, Paper FA2-2, Hong-Kong, June 25-26, 1995.

[4] P. Nouchi et al., 'Low loss single mode fiber with high nonlinear effective area,' OFC'95, Paper ThH2, San Diego, Feb. 26 - Mar. 3, 1995.

[5] B. Biotteau et al., 'Enhancement of soliton system performance by use of new large effective area fibres,' Electron. Letters., Vol.31, p. 2026-2027, 1995.

[6] J. P. Hamaide et al., '*Experimental 10 Gb/s sliding filter-guided soliton transmission up to 19 Mm with 63 km amplifier spacing using large effective area management*,' ECOC'95, Post-deadline Paper ThA.3.7, Bruxelles, Sept 18 - 21, 1995.

[7] Y. Liu et al., '*Single-mode dispersion-shifted fibers with effective area larger than $80\mu\text{m}^2$ and good bending performance*,' ECOC'95, Paper TuL.2.4, Bruxelles, Sept 18 - 21, 1995.

[8] Y. Liu et al., '*Large effective area dispersion-shifted fibers with dual-ring index profile*,' OFC'96, Paper WK15, San Jose, Feb. 26 - 29, 1996.

[9] P. Nouchi et al., '*Single-mode dispersion-shifted fibers with effective area larger than $80\mu\text{m}^2$ and good bending performance*,' ECOC'96, Paper MoB.3.2, Oslo, Sept 19 - 22, 1996.

[10] V. A. Bhagavatula et al., '*Dispersion-shifted single-mode fiber for high-bit-rate and multiwavelength systems*,' OFC'95, Paper ThH1, San Diego, Feb. 26 - Mar. 3, 1995.

[11] J. W. Fleming, '*Material dispersion in lightguide glasses*,' Electronics letters, vol. 14, p. 326-327, 1978.

[12] A. W. Snyder and J. D. Love, '*Optical Waveguide Theory*,' Chapman and Hall, New York, 1983.

[13] K. Petermann and R. Kuhne, '*Upper and lower limits of the microbending loss in arbitrary single mode fibers*,' Journal of Lightwave Technol., vol. LT4, p. 2-9, 1986.

[14] S. F. Mahmoud and A. M. Kharbat, '*Transmission characteristics of a coaxial optical fiber line*,' Journal of Lightwave Technology, vol. 11, pp. 1717-1720, 1993.

[15] M. Ohashi et al., '*Optical loss property of silica-based single-mode fibers*,' Journal of Lightwave Technology, vol. 10, pp. 539-543, 1992.



Pascale Nouchi
Alcatel Fibres Optiques
R&D department
Route de Nozay
91460 Marcoussis
France

Pascale Nouchi received an engineering degree in Physics and Chemistry from ESPCI in Paris, France in 1988. She received her Ph. D. degree in Optical Sciences from the University of Southern California in Los Angeles, in 1992. She then joined the Fiber Optic Department of Alcatel Alsthom Research center. She is now with Alcatel Fibres Optiques.

THERMAL AGING EFFECTS ON COAXIAL CABLE'S TRANSMISSION AND ITS LIFE EXPECTANCY

Lal M. Hore, Vincent J. Ferraro, Orlando G. Chavez, and Joseph D'Amico

Bellcore
Morristown, New Jersey 07962
USA

ABSTRACT

A number of technical papers have been published on the life expectancy of coaxial drop cables, but few on distribution coaxial cables. In this paper, the authors discuss the procedures and problems associated with the estimation of the life expectancy of the distribution coaxial cables. Disc and air dielectric, and foamed dielectric coaxial distribution cables were aged at 80, 90 and 100°C. Periodically, the attenuation of the cables was measured. In the absence of any industry's standard, we selected a ten percent increase in the initial attenuation as our failure criteria and have determined the failure points from each of the 80, 90 and 100°C attenuation data lines. An Arrhenius projection to the expected life of the coaxial distribution cable was made by plotting the time (on a logarithmic scale) required for a selected percent change in signal attenuation to occur in aged cables as a function of the aging temperature.

In addition, we compared the aging data on the dielectric properties of the molded dielectric test slabs which were aged in both open air and sealed air, simulating the cable cell of one particular coaxial cable design. Arrhenius projection was also made on the life expectancy of these dielectric materials used in the coaxial cable.

Finally, oxidative induction time (OIT) levels of the dielectric materials removed from the cables were also measured both before and after aging of the cable samples to find out if any correlation existed between the attenuation and the OIT.

INTRODUCTION

In the electronic super highway, coaxial cables are extensively used as an economical and readily available broadband link between the customers and the network. Cable television operators are extensive users of coaxial cables in their networks. Even in the telephony carrier network, coaxial cables of serrated seam design were used for many decades. With the advent of fiber optic cable, the use of serrated seam design of coaxial cables in the long haul circuits has been almost eliminated. In

the central offices, however, coaxial cables are still commonly used for interconnection between equipment.

Researchers in the past have published papers on the expected life of coaxial drop cables^{[1][2][3]}. Drop cables are designed differently than the hard-line coaxial distribution cables from the center and outer conductor materials selection point of view. Drop cables' short life can be attributed to the cable design, connector problems, installation practices, quality of cable materials used, environmental concerns, etc.

Hard-line coaxial distribution cables are designed either with foam dielectric, or air and disc dielectric. They may have different ratios of air to solid polyethylene materials and different stabilizers in the dielectric. Both the above designs require the use of adhesive material on the center conductor of the coaxial cable to help ensure bonding to the dielectric.

The life expectancy of coaxial distribution cables depends largely on the long term consistency of the dielectric properties, i.e. dielectric constant (ϵ), and dissipation factor ($\tan \delta$) of the dielectric materials, stabilizers and adhesive coating materials over a wide frequency and temperature range. Unless the center and outer conductor materials of coaxial cable are corroded, the aging of coaxial cables is not expected to produce any degradation in the transmission parameters, i.e. attenuation, structural return loss (SRL), characteristic impedance etc. attributable to changes in the metallic conductors alone. When coaxial cables are exposed to thermal aging, the stabilizers used in the dielectric are gradually depleted. As a result, the cable's dielectric properties are degraded and the coaxial transmission parameters can be affected adversely. Thermal aging of non-metallic components affects attenuation more than either SRL or impedance parameters. In the following design considerations, it will be evident that the dielectric materials play a significant role in the life expectancy of coaxial cable.

DESIGN CONSIDERATIONS

Attenuation (α) of a coaxial cable with solid center conductor can be expressed by the following expression:

Attenuation (α) = Attenuation due to conductors (α_C) + Attenuation due to dielectric (α_G)

In imperial units^[4], α is expressed as $\alpha = \alpha_C + \alpha_G =$

$$\left(\frac{2.39}{(\log D/d)} \cdot \sqrt{\epsilon} \cdot f \right) \cdot \left(\frac{\sqrt{\rho_1}}{d} + \frac{\sqrt{\rho_2}}{D} \right) + 2.77 \cdot \sqrt{\epsilon} \cdot f \cdot \tan \delta$$

dB/100ft.

Where,

D = inside diameter of outer conductors in inches

d = diameter of center conductor in inches

ϵ = effective dielectric constant of insulation

$\tan \delta$ = dissipation factor of insulation

f = frequency in MHz

ρ_1 = volume resistivity of center conductor in ohm-cm

ρ_2 = volume resistivity of outer conductor in ohm-cm

In the expression above, the first factor, α_C , depends primarily on the resistivities of both the conductor materials, conductor dimensions, signal frequency (f) and the effective dielectric constant, ϵ . The second factor, α_G , accounts for loss of the dielectric materials which include coaxial cable insulation, stabilizers blended with the insulation and the adhesive coating materials. In a Bellcore paper^[3], presented at the International Wire and Cable Symposium (IWCS) in 1995, it was shown that as coaxial drop cables are aged at higher temperatures, the stabilizers in their dielectrics are consumed, and attenuation increases. The oxidative induction time (OIT) of the drop cable's dielectric decreases substantially in the mean time and reaches a plateau. With the depletion of stabilizer, the cable's attenuation increases significantly.

CABLE MODELING WITH DIELECTRIC SLABS

Measurements of the dielectric properties with highly stabilized and partially stabilized slabs of polyethylene, aged in open air and sealed containers with a fixed ratio of air/solid dielectric corresponding to approximately 95% velocity of propagation (Vp), at different aging temperatures were conducted. The results showed that

the dielectric slabs initially were maintaining reasonably constant level of dielectric constant and dissipation factor. After a certain period of aging at elevated temperatures, both the dielectric constant and dissipation factor were found to increase at the same time. It was also noticed that the increase in the dielectric constant and dissipation factor started earlier with slabs that were aged at higher temperatures and also with partially stabilized slabs. From the equation for attenuation, it is reasonably clear that the increase in attenuation of coaxial cables after aging at elevated temperatures, is due to the increase in the two factors, $\sqrt{\epsilon}$ and $\tan \delta$. Thus, by determining the starting points of degradation of ϵ and $\tan \delta$ at different aging temperatures, it is feasible to make an Arrhenius projection of the life expectancy of the dielectric materials and also of the coaxial cable using them. In the following sections, test procedures, samples used and the results are presented.

Measurement of Dielectric Properties and Test Samples

The dielectric constant and dissipation factor at 1 MHz were measured for two different kinds of molded slabs of polyethylene, each 0.050" thick, one kind highly stabilized and the other partially stabilized, using Hewlett Packard "Q" meter.

One set of samples was aged in air circulation ovens at 100, 90 and 85°C. In the other set of tests, slabs were kept inside sealed glass beakers maintaining air/solid dielectric ratio of 14:1, simulating a coaxial cable cell of approximately 95% velocity of propagation, and oven aged at the above temperatures. Eight sealed beakers were prepared for each of the 100, 90 and 85°C oven tests. Open air aged slabs were measured periodically at room temperature until the dielectric constant and dissipation factor showed sign of degradation. At this point, measurements were discontinued. All sealed slabs were also measured for dielectric constant and dissipation factor before aging. During aging, individually contained sealed samples were opened and the measurements were made. The material slabs were discarded after measurements. This procedure was continued until the degradation of dielectric properties was observed.

The results presented in Table 1 show that at 100°C open air aging, both the dielectric constant and dissipation factor for the highly stabilized slabs began to increase significantly after about 14 weeks. The partially stabilized slabs showed degradation of both dielectric constant and dissipation factor after only about 2 weeks of aging. At 90°C open air aging, starting points of

degradation of dielectric properties were 26 weeks for highly stabilized slabs and for partially stabilized slabs it was three weeks. The corresponding periods for 85°C open air aging were about 31 weeks for highly stabilized, and five weeks for partially stabilized slabs.

The partially stabilized slabs were found to deteriorate earlier than the highly stabilized slabs at any temperature of oven aging. The higher the temperature of aging, the quicker was the deterioration. Full stabilization as opposed to partial stabilization was found to extend the life of the dielectric by a factor of about 6 to 9. This ratio is however expected to change depending on the extent of stabilization in both cases (See Table 1).

Table 1. Initiation of Dielectric Degradation
(Weeks)

Aging Temperature °C	Highly Stabilized Slab		Partially Stabilized Slab
	Sealed Air	Open Air	Open Air
100	36 - 38	14	2
90	67-72	26	3
85	>52	31	5

Material slabs, sealed and aged inside beakers having air/solid dielectric ratio of 14:1 were also measured periodically. At 100°C aging, deterioration of sealed samples was noticed after 36 - 38 weeks and at 90°C after 67-72 weeks. Aging at 85°C was discontinued after one year since no degradation was noticed within this period. The ratio of the starting point of dielectric degradation under sealed air aging to open air aging at both 100 and 90 °C is 2.6 average. In the absence of the 85°C failure data in sealed air aging, it has been assumed that the slopes of Arrhenius plots, shown in Figure 1, will be identical for both aging conditions with similar chemical reactions, and the slope of the projection line will change similarly at 90° C as observed by the earlier researchers^[5]. Under these assumptions, the life of the coaxial cables using the highly stabilized slabs can be predicted for the operating temperature range of 30 to 40 °C^[6].

The predicted life of the coaxial cable materials having air to solid dielectric ratio of 14:1 (95% Vp), is 11 years at 30° C, 9 years at 35° C and 8 years at 40° C constant operating temperatures (see Figure 1). There are a number of factors that would affect the actual life of coaxial cables using the above mentioned dielectric materials. These are: type and amount of stabilizers mixed with polyethylene dielectric pellets, air to solid polyethylene ratio, effect of adhesive/copolymer materials added to the dielectric, dispersion of stabilizers in the polyethylene pellets, environmental conditions during service life, signal frequency, etc.

TEST METHODS ON COAXIAL CABLES AND SAMPLES

In order to make a realistic prediction of the life of coaxial distribution cables under environmental aging conditions, a number of cable samples were selected for study. These cables, 250 to 500 feet long, were aged at 80, 90 and 100°C in forced air chambers. Before aging, attenuation of the cables was measured at room temperature. An HP 8753C Network Analyzer and an "S" Parameter 85046B Test Set were employed. The coaxial cables after aging for selected times were stabilized at room temperature for at least 24 hours before making any attenuation measurements between 5 MHz to 1 GHz at 51 individual frequency points.

The three samples A, B and C selected for the aging study were:

One of Disc and Air Dielectric Coaxial Distribution Cable, and two of Foam Dielectric Coaxial Distribution Cable.

ANALYSIS OF COAXIAL CABLE AGING DATA

Since attenuation is the primary transmission parameter that is affected the most by thermal aging, this parameter was measured periodically at room temperature on aged samples. At the time of writing this paper, measurements were completed up to 52 weeks of aging.

After 52 weeks of aging, the average increase in the attenuation in percent with respect to the initial values of the Coaxial Cable - Sample A in the frequency range of 5 to 1000 MHz was found to be 8% for 80°C, 9% for 90°C and 12% for 100°C aging. For the coaxial cable samples B and C, the corresponding increase in

attenuation varies approximately between 75 to 80% of those measured for Sample A.

ARRHENIUS PROJECTION OF CABLE LIFE

In the industry, there is no precise requirement as to how large an increase in attenuation is permitted for any system design. In the absence of any industry standard, we have arbitrarily selected a ten percent increase in attenuation as our failure criteria in projecting the cable life. We have drawn linear regression lines through the percentage increase in attenuation points versus aging periods for 100, 90 and 80°C data points. By extrapolating these attenuation data lines, we have determined the periods of aging that correspond to the 10% increase in attenuation points for 100, 90 and 80°C aging respectively for all three samples. If we consider a 7.5% increase in attenuation as the alternative failure criteria, the corresponding crossover points can also be determined for the above three temperatures.

An Arrhenius projection to the expected useful life of the coaxial distribution cable can be made by plotting the time (on a logarithmic scale) required for a selected percent change in signal attenuation to occur in aged cables as a function of the aging temperature. The effective operating temperature for the outdoor coaxial distribution cable is 30 to 40°C^[6]. The actual cable temperature however will vary depending on the geographical location and plant types (aerial, buried etc.) of the installation. The Arrhenius plots of the coaxial cable Sample A for both 10% and 7.5% failure points show that at 90°C the slope of the projection line changes. This observation as mentioned earlier in the paper (see Figure 1) was also made by other researchers^[5]. For coaxial cable samples B and C, similar procedures were followed to make an Arrhenius projection of coaxial cables at an operating temperature range of 30 to 40°C. Considering that the cable system is designed to limit the increase in attenuation to 10%, we have estimated the life expectancy of the three coaxial cable samples to range between 7 and 10 years within the operating temperatures of 30 to 40°C. If the system design is limited to 7.5% increase in attenuation, the estimated life of the coaxial cables will be 50% of those estimated for 10% increase in attenuation limit. As mentioned earlier, this estimate of the life expectancy is based on constant operating temperature of 30 to 40°C. In real situations, this is not the case throughout the day and night and throughout the year. Therefore, adjustment in the estimate must be made for accuracy.

OXIDATIVE INDUCTION TIME (OIT) MEASUREMENTS

To ensure adequate life of coaxial cables, the dielectric material should be stabilized with the proper quantity of stabilizers. The coaxial dielectric as mentioned earlier, is either foamed polyethylene, or polyethylene disc and air. In order to have bonding of the dielectric to the center conductor, a polymeric adhesive coating is applied over the center conductor. For the foamed polyethylene dielectric design, a pre-determined quantity of gas is injected during the extrusion of the dielectric. To ascertain the degree of stabilization of the cable dielectric, the concentration of stabilizers is determined by High Pressure Liquid Chromatography (HPLC) Test Method, and/or by measuring the oxidative induction time (OIT). The latter technique is commonly used by the industry to determine the degree of stabilization.

In this series of tests, OIT of the dielectric material from the distribution cable of three different samples A, B, and C were compared in accordance with ASTM D 4565^[8]. For each of the three samples, there were four coils (some 250 feet and some 500 feet long), one was unaged and three were aged for one year at 80, 90, and 100°C. From one end of each of these lengths, samples of the dielectric were cut from three places of the 3-foot cable samples: 1) the end of the length with a connector, 2) the end of the length without the connector and 3) the middle of the length. A circular disc was cut from the dielectric and then a wedge was cut lengthwise along the radius of the disc. These wedges, which were used as the samples, weighed between 4 and 9 milligrams. They were weighed using a balance scale manufactured by E.H. Sargent, but with a control panel made by the Mettler Instrument Corp. Using a Dupont Thermal Analyzer in conjunction with a TA Instruments 2100 Thermal Analyst system, these 36 samples were tested according to the procedure recommended by the ASTM method. Gas 1 was compressed nitrogen and Gas 2 was compressed oxygen. The equilibration temperature was 55.1°C +/- 0.1°C and the isothermal temperature was 181.7°C +/- 0.2°C.

The OIT was calculated using the heat flow vs. time curve generated by the Thermal Analyzer. The computer was used to draw a tangent to the portion of the curve parallel to the time axis and a tangent to the curve where it first changes its slope. The time at the intersection of these two tangents minus the time before oxygen was introduced into the chamber is the OIT.

The OIT measurements on PIC (Polyolefin Insulated Conductors) is traditionally used in the telephone

industry to ensure the life of telephone cables. The hard-line coaxial cable's OIT requirements are less stringent in comparison to the telephone cables because of the coaxial cable's dielectric media being sealed under an aluminum shield conductor.

The OIT of the dielectric materials collected from coaxial cable samples are shown in Table 6a, 6b, and 6c.

Table 6a: Oxidative Induction Time

(Minutes) - 80°C Aging

Sample	Section	Initial	After 52 Weeks	Percent of Original
A	End	135	94	
A	Mid	141	70	
A	Connector	47	58	
	Avg.	108	74	69
B	End	45	37	
B	Mid	35	33	
B	Connector	35	41	
	Avg.	38	37	96
C	End	112	43	
C	Mid	144	48	
C	Connector	100	38	
	Avg.	119	43	36

Table 6b: Oxidative Induction Time

(Minutes) - 90°C Aging

Sample	Section	Initial	After 52 Weeks	Percent of Original
A	End		52	
A	Mid		49	
A	Connector		39	
	Avg.	108	46	43
B	End		20	
B	Mid		28	
B	Connector		42	
	Avg.	38	35	91
C	End		27	
C	Mid		42	
C	Connector		96	
	Avg.	119	55	46

Table 6c: Oxidative Induction Time

(Minutes) - 100°C Aging

Sample	Section	Initial	After 52 Weeks	Percent of Original
A	End		155, 119	
A	Mid		21	
A	Connector		51	
	Avg.	108	86	80
B	End		19	
B	Mid		21	
B	Connector		33	
	Avg.	38	25	55
C	End		22	
C	Mid		6	
C	Connector		20	
	Avg.	119	16	13

Figure 2 shows stabilizer retention in percent of the original OIT values for samples A, B, and C after 52 weeks of aging at 80, 90, and 100°C. The OIT values as clearly evident in Tables 6a, 6b, and 6c and Figure 2 are widely scattered. The drop in the average value of OIT after 52 weeks of aging ranged from 13 to 80 percent for 100°C, 43 to 91 percent for 90°C, and 36 to 96 percent for 80°C aging. Even the same cable shows a wide spread of OIT values within a 3-foot section. Example: 100°C aged sample A show 155, 119, 21, and 51 minutes as OIT values. The wide variation of the stabilizer level between samples of the same cable section is a result of non-uniform stabilizer dispersion at the extruder line. After one year of aging, sample C appeared to have suffered the maximum loss of stabilizer at all three temperatures. The wide variation in the retention level of the OIT values on the aged samples, might have produced changes in the cell structure and morphology of the polymer. These conditions in the absence of sufficient degradation of the dielectric properties (i.e. ϵ , $\tan \delta$), can partly be attributed to the spread in the attenuation data. Since the production line extruder is not a high sheer mixer, there is also every reason to believe that the stabilizers were dispersed non-uniformly throughout the dielectric media during the cable extrusion process.

CONCLUSION

After the completion of coaxial cables and cable materials aging at elevated temperatures followed by the measurements of attenuation and stabilizer levels of the cable dielectric materials, the following conclusions were drawn:

1. The percent increase in the attenuation data shows scattered results. As a result, the projected life of the three coaxial samples are approximate. The estimated life of both foamed dielectric, and disc and air dielectric coaxial cables can range between 7 and 10 years within the constant operating temperature of 30 to 40°C. If 7.5% increase in attenuation is considered as a criteria of the cable degradation, the estimated life of the cables will be half of those estimated for 10% increase in attenuation.
2. The OIT data of the dielectric samples removed from the cables both before and after aging show wide variation. This can possibly be attributed to the non-uniform stabilizer dispersion at the extruder line.
3. Wide variation in the stabilizer level both before and after aging, and any possible change in the cell structure and morphology of the polymer could be attributed, at least partly, for the scattered attenuation data.

4. With the existing cable samples, accurate prediction of cable life is difficult for the reasons explained above.

5. The predicted life expectancy of the dielectric materials used in coaxial cable with approximately 95% velocity of propagation is close to the estimated life of the cable samples A, B and C based on 10% increase in attenuation.

6. Measurements of dielectric constant and dissipation factor of the coaxial cable dielectric materials aged inside sealed containers, and mixed with a fixed ratio of air to solid dielectric corresponding to a pre-determined V_p , at the frequencies of operation could possibly be used as an additional method of predicting the life expectancy of coaxial cables.

ACKNOWLEDGMENTS

The authors thank William McLaughlin, a Senior Mechanical Engineering Student of the University of Notre Dame in South Bend, Indiana, and currently a Summer Intern at Bellcore, for measuring the stabilizer levels of the dielectric materials from the cable samples. The authors also acknowledge with thanks the valuable suggestions of Dr. Trevor Bowmer of Bellcore and the help of Prasad V. Maddali, a contractor, in the preparation of the manuscript.

REFERENCES

1. K. L. Smith, "Drop Cable RF Leakage Throughout 20 Years of Service", Cable-81 NCTA Annual Convention, Technical Paper, 1981.
2. P.L. Key, et al., "Reliability of Coaxial Drops in the CATV Industry", National Fiber Optics Engineers Conference, Technical Paper, 1994.
3. J.N. D'Amico, et al., "The Deterioration of Transmission Characteristics and Coaxial Cable Longevity", published in International Wire and Cable Symposium (IWCS) Proceedings 1995, Pages 720-727.
4. Electrical Conductors Handbook, Published by Northern Electric Co; Ltd., 1968, page 167.
5. G. A. Schmidt, "Life Prediction of Filled Cables in Pedestal Terminals", Proceedings of the 36th International Wire and Cable Symposium (1977)
6. T.N. Bowmer, "Cracking of Foam-Skin Insulation in Pedestals", Proceedings of the 37th International Wire and Cable Symposium (1988) (Referenced)
7. GR-1399-CORE, Generic Requirements for Coaxial Distribution Cable, Issue 1, July 1994.

8. ASTM D-4565-94, Standard Method of Testing Physical and Environmental Performance Properties of Insulation and Jackets for Telecommunications Wire and Cable.



- **Lal M. Hore** is currently responsible for the preparation of Bellcore's Generic Requirements for Outside Plant Cables and the development of high speed transmission requirements for coaxial cable and other wire products. After receiving a M.Sc. Tech degree in Applied Physics from the University of Calcutta and a Dr. Tech. Degree from the Technical University of Budapest in Electrical Engineering, he joined Bell Northern Research in 1970 to design and develop communications cables. In 1972 Lal moved to General Cable Company where he worked as a manager in the Communications Cable Section and next as a Staff Project Manager in the Applications Engineering Section until 1987 when he joined Bellcore.

Dr. Hore has authored numerous technical papers on dielectric materials and telecommunications wire and cable and holds a number of patents on telecommunications cables.

- **Vincent J. Ferraro** is a member of the Distribution Network Components Group in Bellcore, Morristown, NJ. He joined AT&T Bell Laboratories in 1981 and worked at the Whippany, N.J. facility. In 1984 he joined Bellcore as a member of the Applied Research Area working on DSL, ADSL and Video on Demand prototypes. He is currently a team member who has responsibility for the analysis of Telecommunication Products, Coaxial Cable, Coaxial Components, and Hardware for deployment in the Outside Plant Environment.

- **Orlando Chavez** is a member of the Distribution Network Components Group in Bellcore, Chester, NJ. He joined Western Electric in 1968 and worked at the Phoenix Cable Plant until December 1983. In 1984 he started work for Bellcore's CSO Quality Assurance Group. In May 1994 he joined the DNC Group in Morristown. He is currently a team member who has responsibility for the test analysis of, Metallic Telecommunication Cable, Coaxial Components, Outside Plant Hardware, and Electrical Protection Devices.

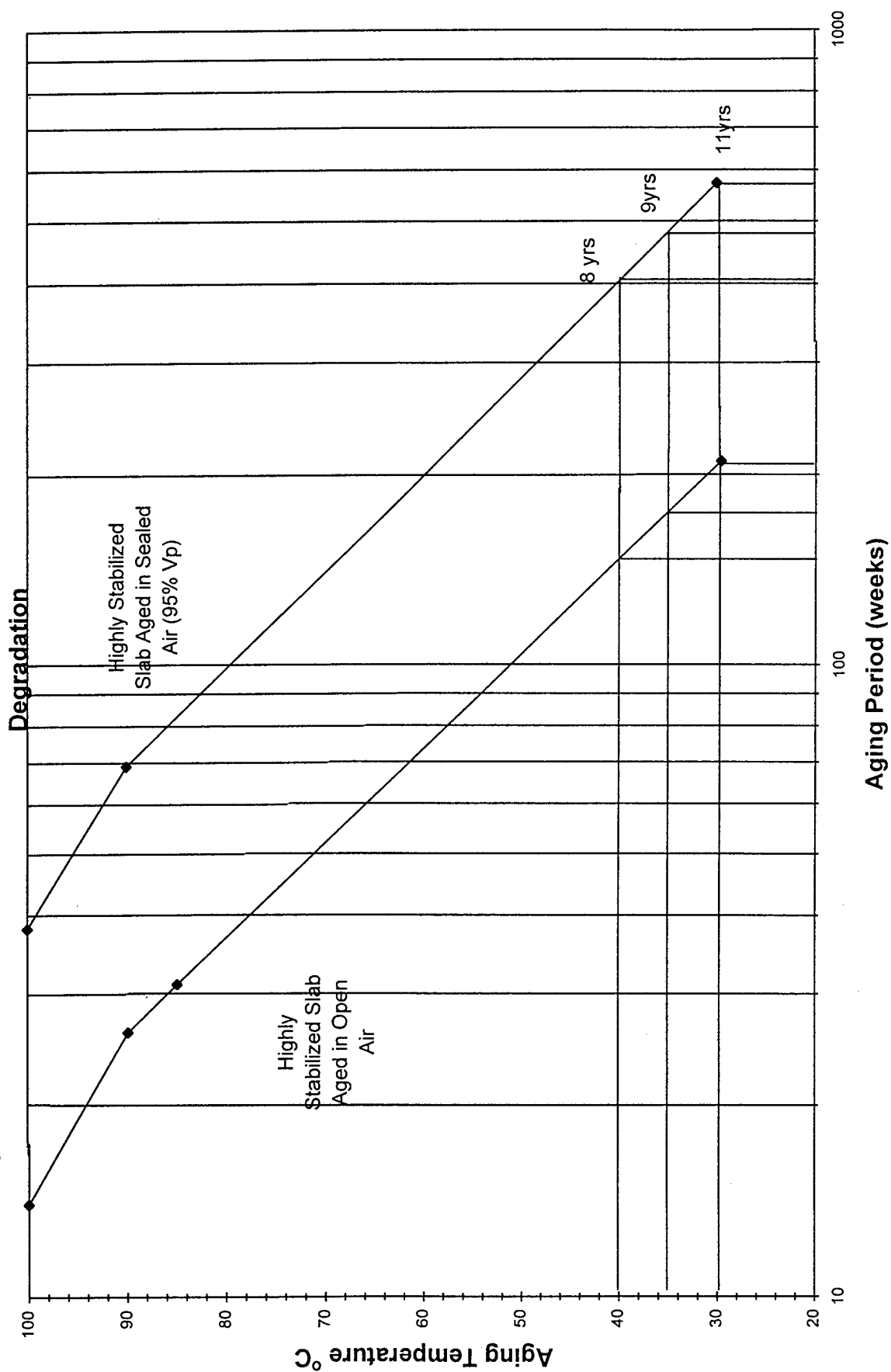


- **Joe D'Amico** is a member of the Distribution Network Components at Bellcore. He has worked on engineering and materials issues affecting all types of telecommunications and power cables in his career. Initially, he worked with communications cables at the Western Electric Company, later he joined the General Cable Company. There as a senior research physicist, he investigated the structure and composition of all types of telecommunications wire, cable and optical fiber as well as electrical power cables. Since 1985 Joe has worked for Bellcore, initially as a quality assurance engineer and since 1989 as a researcher and engineer in the Applied Research and in the Network and Product Integrity Organizations. Joe is a graduate of Seton Hall University. He received his MS degree from Fairleigh Dickinson University.

- All authors can be contacted at :

Bellcore
445 South Street
Morristown, NJ. 07960

Figure 1: Arrhenius Projection of Dielectric Materials (stabilized) Temperature Vs. Time of



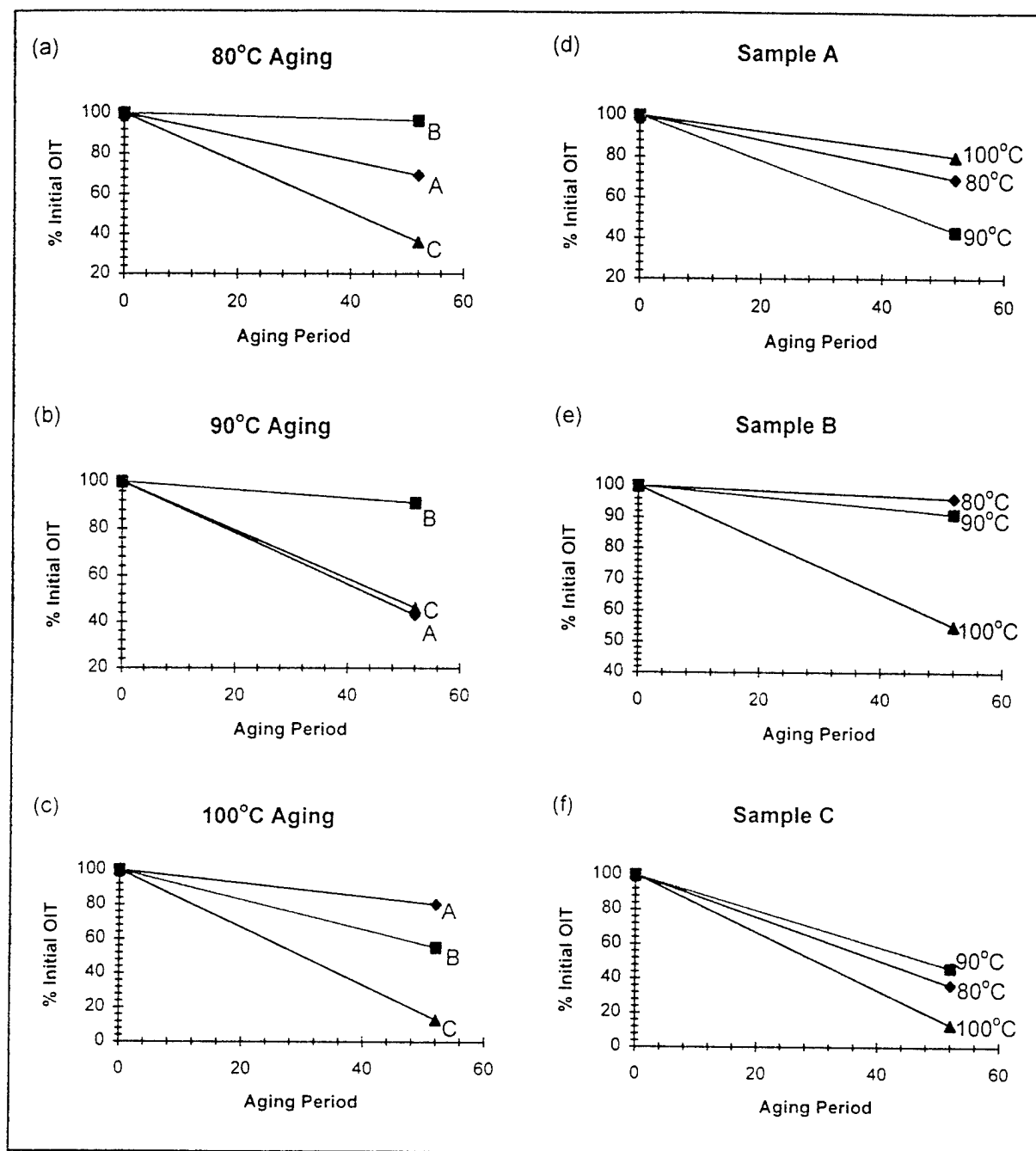


Figure 2: Stabilizer Retention in Percent of Original OIT

IMPROVING THE SHIELDING EFFECTIVENESS OF COAXIAL CABLES

Antonio R. Panicali

TELEBRAS R&D Center, Campinas, S. Paulo, BRAZIL

ABSTRACT

The phase velocity of electromagnetic waves propagating inside highly conductive materials is dramatically reduced compared to the corresponding free space value; as demonstrated in this paper, this property can be used to produce destructive interference between the residual waves leaking through the shield thus increasing the shielding effectiveness at least at some selected frequencies; the method is particularly valuable at low frequencies when high shielding effectiveness would require very thick shields. Experimental results described in this work demonstrate the validity of the method when applied to coaxial cables.

INTRODUCTION

As illustrated in Figure-1, the shielding effectiveness (SE) of good conductor is based on two different electromagnetic phenomena: (a) energy reflection at the interfaces between the free space and the shield and (b) signal attenuation along the propagation path inside the shielding material. Therefore increasing the SE with basis on properties (a) and (b) alone requires increasing the thickness of the shield which can lead to extremely bulky structures particularly at low frequencies.

The present work shows how the SE can be considerably increased, at least at some arbitrarily selected frequencies, by making use of another propagation property besides reflection and attenuation namely, the dramatic reduction on the associated phase velocity inside good conductors as compared to its corresponding free space value.

As it is well known [1], for frequencies below 10^{15} Hz the propagation constant inside good conductors (copper, aluminum etc.) can be approximated by:

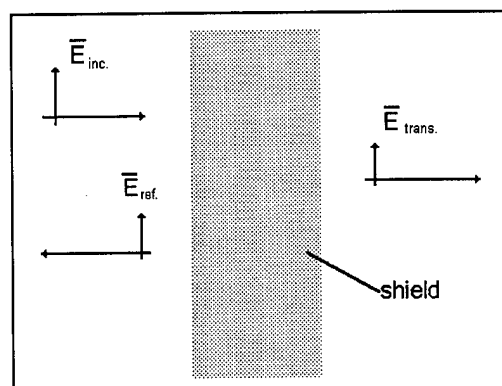


Figure 1- basic phenomena which take place on a conventional shield: reflection and absorption.

$$\gamma \cong \sqrt{-j\omega\sigma\mu} \quad (1)$$

where

$$\gamma = \alpha + j\beta$$

$$j = \sqrt{-1}$$

$$\omega = 2\pi f \quad (2)$$

f = frequency(Hz)

σ = conductivity(mho / m)

μ = permeability(henry / m)

For the case of copper

$$\sigma = 5.8 \times 10^7 \text{ (mho / m)}$$

and

$$\mu = 4\pi \times 10^{-7} \text{ (H / m)}$$

so that

$$\alpha = 15.1\sqrt{f} \text{ (nepers / m)} \quad (3)$$

$$\beta = 15.1\sqrt{f} \text{ (rad / m)}$$

and the corresponding phase velocity v_p will be given by

$$v_p = \frac{2\pi f}{\beta} = 0.4153\sqrt{f} \quad (m/s) \quad (4)$$

As an example, for a signal with $f = 10^5 \text{ Hz}$ propagating inside copper

$$\begin{aligned} v_p &= 131.3 \text{ m/s} \\ \lambda &= 1.131 \text{ mm} \end{aligned} \quad (5)$$

whereas in free space $\lambda_0 = 3000 \text{ m}$.

As described below, these drastic reductions on v_p and λ as compared to their corresponding free space values render it possible the creation of 180° phase shifts between portions of the signal passing through the shield so that they can be made to cancel, at least at some previously selected frequencies, thus increasing the resulting SE.

APPLICATION

Figure 2 shows two sections of a coaxial cable with lengths l_1 and l_2 ; let δ denote the corresponding difference between the thickness of the walls of the two sections. Let $\lambda_0 \gg (l_1 + l_2)$ denote the corresponding wavelength of the signal propagating inside the coaxial cable, between the center conductor and the coaxial shield; under these conditions the current flowing on the inner surface of the shield can be assumed to be in phase along the two sections. In fact, due to the finite conductivity of the shield, this current will not be restricted to the inner surface of the shield but will propagate through the material toward its outer surface. If multiple reflections inside the shield are neglected, the amplitude and phase of the current densities flowing on the outer surfaces of sections 1 and 2 will be related by $e^{-\delta\gamma}$. It is clear then that by choosing $\delta = \lambda/2$ and $l_1/l_2 = e^\pi$ at some frequency of interest, the total voltage between points **a** and **b**, see Figure 2, along

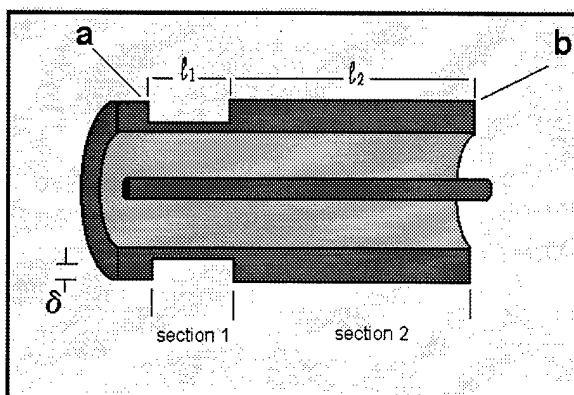


Figure 2- coaxial cable with improved SE: voltage across section 1 is canceled by voltage across section 2.

the external surface of the shield will be canceled except for some second order diffraction effects which may take place at the transition between the two sections.

EXPERIMENTAL RESULTS

Figure 3 shows the experimental setup used to validate the results of the previous sections where we have adopted:

$$\begin{aligned} l_1 &= 20 \text{ mm} \\ l_2 &= 462.8 \text{ mm} \\ \delta &= 0.324 \pm 0.04 \text{ mm} \end{aligned} \quad (6)$$

Figure 4 shows the voltage $V_{ab}(f)$ measured between points **a** and **b** along the external surface of the coaxial shield referred to the corresponding voltage at each frequency measured along a similar portion of a tube with total length $(l_1 + l_2)$ but not including a recessed section; $V_{ab}(f)$ is the sum of the voltages across the two sections of the coaxial shield, Figure 3. As indicated $V_{ab}(f)$ exhibit a well defined minimum at the frequency $f_m = 360 \text{ kHz}$ which results from the 180° phase difference between the voltages along the two sections thus corresponding to the 30 dB improvement of the SE.

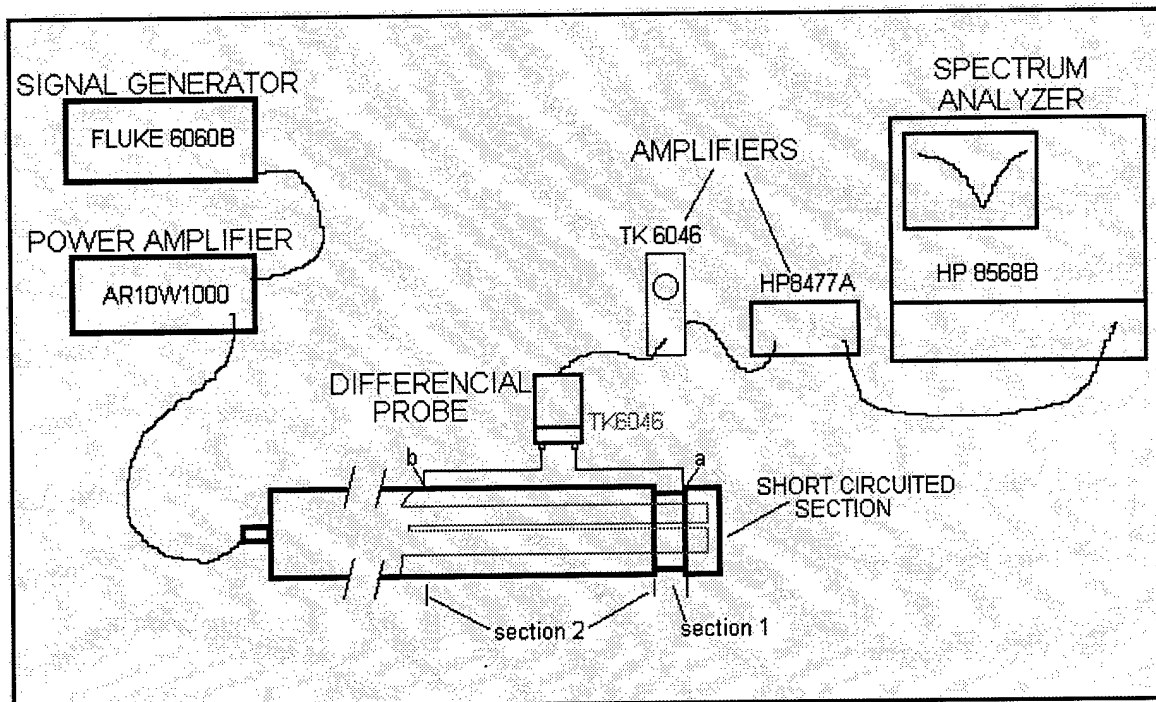


Figure 3- experimental setup for measuring SE.

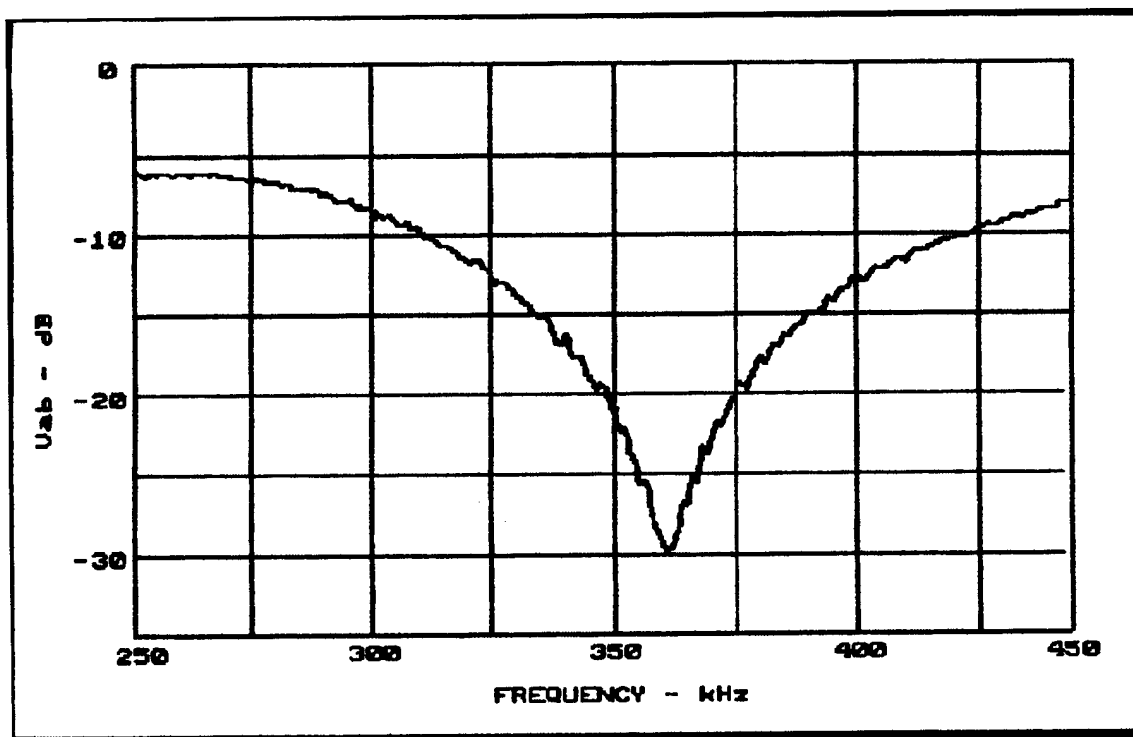


Figure 4- measured values of SE improvement.

With the value of δ given by (6) and imposing that $\delta = \lambda/2$ it is possible to compute from (3) the theoretical range of frequencies at which the minimum of $V_{ab}(f)$ should occur:

$$325.8\text{kHz} \leq f_m \leq 538.6\text{kHz}$$

which is in good agreement with the measured value.

CONCLUSIONS

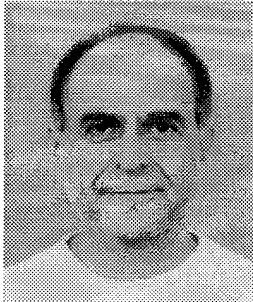
A method for improving the SE of highly conductive shields without increasing the thickness of the shield has been discussed: it makes use of the dramatic reduction on the phase velocity and the corresponding wavelength which takes place inside these materials in order to create cancellation effects between portions of the signal which

crosses the shield. As an application a coaxial cable with 30 dB improvement on its SE was designed and tested. In fact it is believed that a more significant SE improvement could have been achieved if tighter mechanical tolerances had been observed.

Clearly, the basic ideas discussed here are equally applicable to other types of structures such as planar shields. It is believed that the same principle can also be applied for obtaining very compact filters operating in the kilohertz band and below; in this sense the technique presented here may be considered as an alternative to the SAW (surface acoustic waves) principle.

REFERENCE

- 1- S.Ramo, J. R. Whinnery, T. van Duzer, "Fields and Waves in Communication Electronics", John Wiley & Sons Inc., Wiley International Ed., 1965, pp. 334,337.



Antonio R. Panicali
CPqD TELEBRAS
Caixa Postal 1579
Campinas, S Paulo
Brazil
cep 13.088-061
fax: +55 (19) 239-2179
e-mail:
jepanicali@cpqd.br

Msc-1968, PhD-1970 by the EE Department of the University of Illinois at Champaign - Urbana. Since 1972 he works as an independent consultant on EMC; he is also a permanent consultant for Telebras R&D Center. He is a Professor at the EE Department at the University of S. Paulo in SP - Brazil.

Optimization of Leaky Feeders for Broadband Wireless Communication Systems

Karl Schulze-Buxloh / Mark Davies

RFS kabelmetal, Division of kabelmetal electro GmbH,
Kabelkamp 20, 30179 Hannover, Germany

ABSTRACT

The implementation of wireless communications networks is growing world wide. They are operative in many different frequency bands - 70, 150, 450, 900, 1800/1900 MHz and beyond. In order to provide reliable coverage in tunnels and buildings, leaky feeders enjoy widespread use. Leaky feeders are normally coaxial cables with apertures punched into the outer conductor allowing electromagnetic fields penetration from the inside of the cable to the outside and vice versa.

In many cases, several radio services are desired to run concurrently in a tunnel or a building. This makes a broadband leaky feeder system a very favorable alternative to a configuration consisting of several antennas. This paper will describe leaky feeders in terms of transmission properties and it will show the procedure of choosing the optimum leaky feeder design for a given set of frequencies. Typical questions are:

- How far does the range of a leaky feeder, extend, and which are the limiting factors?
- How do the transmission properties change with frequency/leaky feeder length/leaky feeder size (diameter)?
- How do all the design parameters interact with one another, where are the degrees of freedom for optimization?
- What are the different effects if not one but several frequencies are to be considered as a bundle?

These questions will be investigated and various experimental results from measurements will be shown. The architecture of leaky feeder subsystems including amplifiers and also RF modulated fiber optic backbones will also be discussed.

Some examples will be shown from projects which have already been completed and future applications are to be foreseen.

It is shown that leaky feeders provide an optimal solution for broadband radio services in tunnels and buildings, particularly in view of recent developments to optimize certain parameters to practical system architecture. Present day requirements demand low losses and modularity of system integration, which are duly considered in leaky feeder development.

INTRODUCTION

Leaky feeders are employed to facilitate radio communication in areas where the free space propagation of electromagnetic waves using antennas is impaired or rendered impossible, e.g. in tunnels, mines, buildings etc. [1, 2]. Their main application fields are in the distribution of public services (police, fire brigade), for rebroadcasting and cellular radio.

Leaky feeders are inherently broadband in their transmission characteristics, comprising typically several octaves. In recent years, distributed communication services have multiplied and moved to ever higher carrier frequencies. This has led radiating cable developers to proceed in two different ways: firstly to optimize the cables performance at a particular frequency or frequency range, to cut equipment costs and secondly to further increase the bandwidth of the cable to carry as many services as possible, in order to achieve a high investment return on the installed cable. Several developments of frequency-optimized cable have been reported [3, 4, 5]. Here, we shall contrast this against a wide band optimization, noting that both have their defined fields of application.

FUNCTIONING PRINCIPLES OF LEAKY FEEDERS

Normal RF cables aim to transfer RF energy from one end to the other with a maximum of transverse screening to prevent loss of RF energy in transit and unwanted signals from entering the cable. Leaky feeders, on the other hand, are designed to allow RF signals to enter or leave the cable at any point by a deliberate reduction of the transverse screening.

A single or twin wire will act as a leaky feeder, as will a coaxial feeder or waveguide whose outer conductor allows some RF penetration. Single or twin wires show heavy longitudinal losses above FM frequencies whilst the size of waveguides below 3 GHz makes them prohibitively large and expensive. Most widespread is the use of leaky coaxial cables whose longitudinal losses, installation and expense are comparable to that of normal coaxial cables.

A number of leaky coaxial cable designs are in common use today. One of the earliest designs evolved from the conventional foam dielectric feeder with a corrugated outer conductor by milling a line of apertures into the finished outer conductor before jacketing (quasi-continuous slot cable). This type of cable has provided system designers with a reliable and adequate transmission medium for several decades. However, certain limitations of this cable design have become apparent recently as ever higher frequencies are introduced. As with all coaxial cables - radiating or not - the longitudinal losses increase with frequency, but, for the milled corrugated cable type, so also does the coupling loss (i.e. the free space loss between the signal in the cable and an external antenna). The overall losses thus increase drastically at high frequencies. This tendency, coupled with comparatively high manufacturing costs, is likely to reduce the application of this type of cable in coming years.

A different approach is also well established, that of simply using copper foil as the outer conductor and punching holes or slots in it. Apart from the obvious advantage in terms of manufacturing cost, the developer has considerably greater degrees of freedom in designing the slot structure. Although it is possible to emulate the performance of a

corrugated quasi continuous slot cable by punching a fine line of holes with corresponding spacing, the use of larger slots and larger spacing, of the order of the wavelength or greater, results in a performance more favorable to an extended frequency spectrum. Here, the coupling loss decreases at higher frequencies thus compensating to some extent the higher longitudinal losses. We can thus expect this design of cable to be the major player in future developments. Other designs are the continuous slot and coaxial braided cables, whose behavior is subject to similar limitations to the milled corrugated version in terms of degrees of freedom and losses at high frequencies.

INTERDEPENDENCE OF RADIATING CABLE PARAMETERS

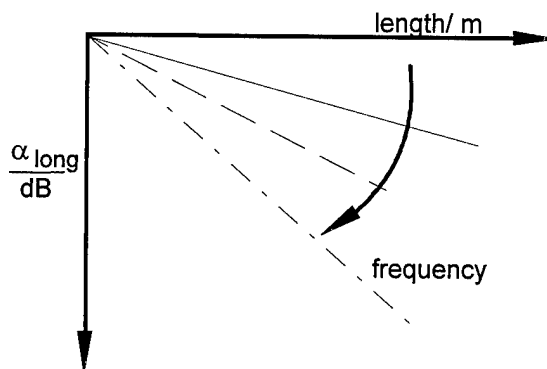
The electrical parameters of radiating cables are both interdependent and also a result of the cable's physical construction and dimensions. This is detailed below.

Frequency dependence

The longitudinal loss in dB is directly proportional to the length of the cable deriving from its exponential attenuation characteristic.

At higher frequencies, the longitudinal losses of coaxial cables also increase as shown in diagram A

Diagram A: Cable Losses increase with frequency

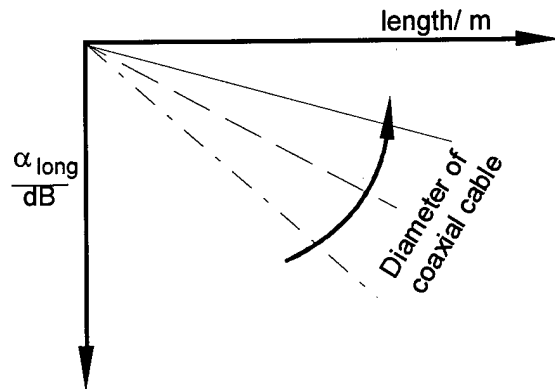


As the longitudinal losses of a radiating cable are higher than those of a non radiating coaxial cable, the latter provides a basis for radiating cable dimensioning as a minimum of longitudinal loss for a given cable diameter.

Cable Diameter

Longitudinal losses are reduced if the cable diameter is increased as shown in diagram B.

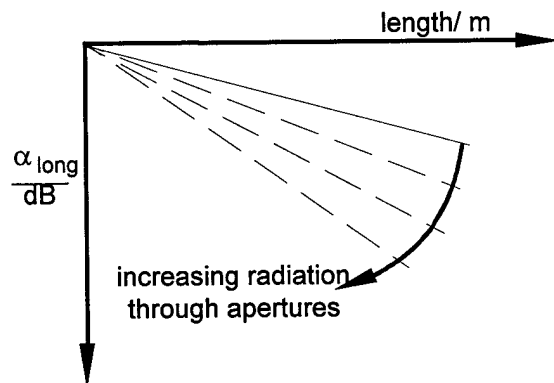
Diagram B: Cable Losses are reduced by increasing the diameter



Slot configuration

The radiated power from the slots results in increased longitudinal losses as shown in diagram C. However, there is no fixed dependency between radiated power and additional longitudinal loss. The choice of slot configuration must aim to radiate as much power as possible whilst keeping the additional longitudinal losses small. The degrees of freedom which can be exploited in the design procedure are, for example, slot size, slot form, slot pattern and slot spacing.

Diagram C: Cable Losses increase as more power is radiated



RELEVANCE OF PERFORMANCE PARAMETERS FOR SYSTEM DESIGN

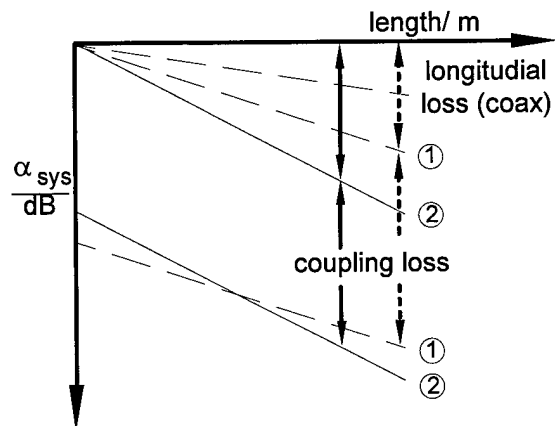
Overall loss

A figure of paramount importance for the designer is the overall loss of the radiating cable i.e. the sum of longitudinal loss and

coupling loss. It must not exceed the permissible system loss (transmitter power - receiver sensitivity) and for cellular services is normally of the order of 105 dB, because the permissible system loss of typically 130 dB is reduced by other losses (e.g. combiner, screening, body losses). For a given cable diameter, it is the objective of the developer to attain as much radiation from the cable as possible without having an adverse effect on the longitudinal attenuation.

The overall loss is indicated in diagram D. Two cables are depicted of the same nominal diameter but different degrees of radiation. The cable number ② shows higher radiation, which is reflected in higher longitudinal loss. The overall loss of a highly radiating cable such as ② is thus higher over long lengths in comparison to cable ① and results in a higher dynamic range.

Diagram D: Overall loss as the sum of longitudinal loss and coupling loss.



Dynamic range

Depending on the location of the mobile relative to a radiating cable, the path loss between base and mobile can vary considerably. This is not normally a problem when only base and mobile are involved, as one or both has a large dynamic range and Automatic Level Control (ALC) to compensate the near-far effect as well as sudden fluctuations caused by screening, multipath etc. However, where repeaters are involved (to compensate cable losses), and particularly if a fiber optic backbone is necessary (to overcome daisy chain limitations), the dynamic range of the uplink or reverse path becomes an issue. If the signal level becomes too low, it can disappear in the noise produced by a fiber link even if the output level is well above the threshold of the base

receiver. If it becomes too high it will produce in-the-band intermodulation products which degrade the signal.

These problems can be countered on the equipment side by using channel selective repeaters which repress intermodulation activity but are inflexible: channels are fixed and frequently cannot be altered without accessing the repeater. Another countermeasure is that of using wide band repeaters of increased linearity e.g. feed-forward technique. Both measures involve increased repeater expense.

It is therefore advantageous to employ radiating cables whose dynamic range is small [6]. Two factors contribute to the dynamic range

- (i) the longitudinal loss
- (ii) the fluctuation of the coupling loss

The dynamic range of each is characterized by its respective probability function, and the probability density function (PDF) of the overall loss is derived from the convolution integral of the two individual functions. The standard deviations of each are simply added to give the overall standard deviation.

In other words: small deviations of coupling loss are wasted on a cable whose longitudinal loss is great in comparison, and vice versa.

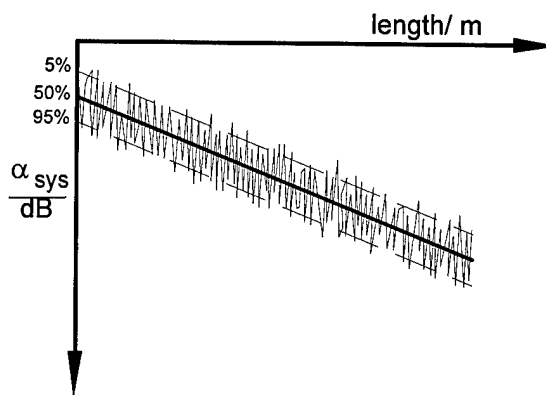
Reception probability

From the above, it can be seen that the overall loss of a transmission path over a radiating cable varies from point to point and results in a figure whose variation needs to be standardized in some form to allow reliable system planning.

An essential parameter is the reception probability or coverage, which states with what probability a particular overall loss figure is achieved or improved upon. Typical coverage factors chosen are 50 % and 95 %. A loss figure with 50 % probability indicates that at 50 % of the sampled locations a loss equal to or better than this figure is attained. Sometimes referred to as the median, this figure should not be confused with the average of all samples; the average does not give any indication of the probability of reception. In the same way, 95 % coverage denotes that 95 % of the sampled losses were at least as good as the figure indicated. Other coverage factors, notably

90 % and 98 %, are of interest in certain system designs. The derivation of coupling loss for a given reception probability is shown qualitatively in Diagram E.

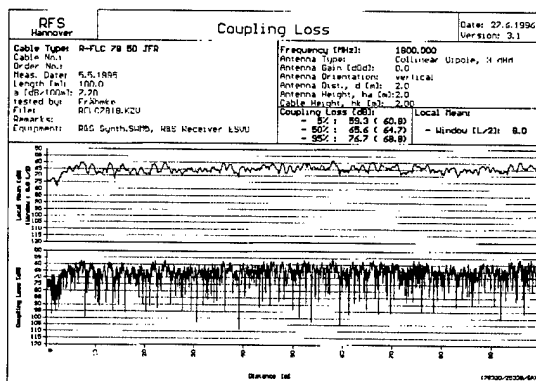
Diagram E: Derivation of reception probability from a fluctuating coupling loss.



It makes sense to define a figure to characterize the dynamic range. Dynamic range can be conveniently characterized as the difference in dB between the 95% and 5% coverage figure.

It should be noted in this connection that a true evaluation of the dynamic range is only possible if no integration or averaging of the sampled data takes place. In diagram F it is shown how the dynamic range (5 % - 95 %) of the coupling loss alone can be reduced from 17.4 dB down to an apparent 8 dB by substituting the actual measured data by a local mean (in this case over 4 wavelengths). Averaging or integrating only makes sense if it reflects the technology to be later employed by the operating service on the cable.

Diagram F: "Smoothing" effect of measuring coupling loss using a local mean in comparison to raw measured data



Environmental considerations

Dirt, moisture. Deposits of dirt, moisture containing salt or metallic dust are potential loss sources on the jacket of the radiating cable which can increase the longitudinal attenuation of certain cable designs [7]. This can be effectively countered by the RLF concept: keeping the slots far apart (preventing coupling loss degradation), or occasionally cleaning the cable for other slot configurations.

Cable stand-off from wall. If the cable cannot be installed with the specified stand-off (usually 8 cm), some adjustments need to be made to the losses. The effect on longitudinal losses is minimized by employing the RLF concept.

Periodic metallic fixtures Periodic metallic fixtures can induce standing waves in certain leaky feeder types. If such fixtures are unavoidable and correlate to the wavelength, again the RLF cable concept has proved unaffected.

DEFINING THE BAND

There is no clear-cut definition of where the operating frequency band of a radiating cable starts or finishes. It depends very much on the system employed and the length of cable required.

One of the most frequently asked questions among potential users of radiating cables is: what is the maximum distance between repeaters? The motivation is obvious: minimizing the use of repeaters in order to save on procurement, power consumption, monitoring and maintenance. To answer this question satisfactorily we shall assume a target overall loss of 105 dB with 95 % reception probability which reflects the system requirement for the majority of present day installations. From this premise we shall define maximum cable lengths for satisfactory operation.

OPTIMIZATION: NARROWING THE BAND

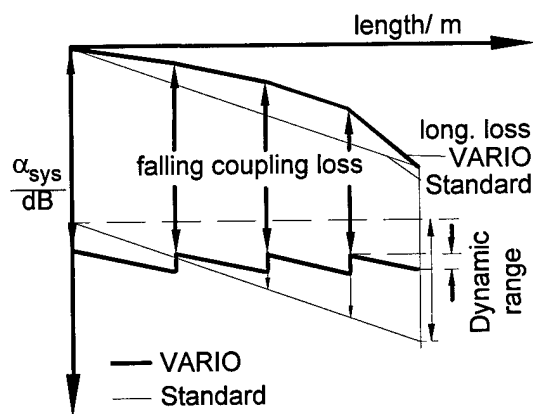
There are two radiating cable features which can be optimized towards a particular frequency or frequency band

- employment of the radiating mode
- using the vario principle

The radiating mode of a leaky feeder with periodic slot grouping begins at frequencies of $\frac{c}{2d}$ where c is the propagation velocity in the cable and d is the slot group period, and extends approximately 1 octave. In this range, there is a defined phase shift between waves from each slot group which is first order only, giving a regular radiation pattern comparable to that of a group antenna. The radiated signal level is higher and shows a very small mean fluctuation. This reduces the coupling loss, and the dynamic range of the coupling loss. Outside this frequency range the radiation is described as coupled mode, where either higher order superposition or random superposition disturb the regularity [8].

The vario principle is that of decreasing the coupling loss down the cable to compensate longitudinal losses, i.e. the further from the source, the more the cable radiates. This counters the dynamic range caused by longitudinal loss as indicated in diagram G, where a conventional cable is also shown for comparison [9, 10].

Diagram G: The VARIO principle: compensating longitudinal losses with a falling coupling loss.



Evidently it is advantageous to combine both features. We have developed vario type radiating mode cables showing a total dynamic range (5%-95%) of 8.4 dB at 960 MHz. In comparison, the same cable performs at 460 MHz with a dynamic range of 19.8 dB clearly showing the advantages of the radiating mode in combination with the vario principle. The transmission characteristics (which were obtained in an operational tunnel environment) are shown in diagrams H and I at the end of this paper. Overall losses at 960 MHz depend on the length chosen. For 250 m they are less

than 65 dB for 95 % coverage, well under the coupling loss figure alone of most conventional cables. The diagram shows results achieved in a tunnel, resulting in a highly uniform signal level. Combining the vario principle with the radiating mode is thus the perfect optimization for single band systems or bands up to an octave apart. Equipment costs are reduced by reducing the dynamic range and the avoidance of unnecessarily high radiation of power from the cable close to the source [11].

OPTIMIZATION: WIDENING THE BAND

By widening the band the aim is to be able to include as many services as possible on one cable. Since, irrespective of their radiating properties, all coaxial cables show increased longitudinal losses at higher frequencies, one evident requirement is that the coupling loss is reduced at these higher frequencies to counter this effect.

One example is a 1/2" cable developed for wide band coverage in buildings which has been shown to display considerable system related advantages over antennas [12]. As single lengths rarely exceed 100 m in such cases, longitudinal losses are less critical and 1/2" diameter is adequate [13]. The performance figures are as shown in Table 1.

Table 1: Electrical Parameters of 1/2" Radiating Cable

frequency (MHz)	Coupling Loss, 95 % (dB)	Longitudinal Loss (dB/100 m)
75	65	2.3
150	70	3.4
450	72	6.2
900	70	9.7
1800	66	23.3
1900	65	25.2

This results in the permissible lengths as indicated in Table 2.

Table 2: Maximum permissible lengths for 105 dB total loss with 95 % coverage using 1/2" Radiating Cable from Table 1

f (MHz)	length (m)
75	1732
150	1029
450	532
900	360
1800	167
1900	159

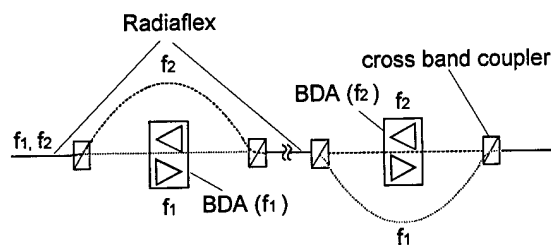
This enables a radiating cable network to be installed in most buildings which is transparent to frequency and need only be accessed from one single feeding point without further repeaters.

In contrast to building applications, the longitudinal loss of a cable in tunnels is also of importance, as it dictates the number of repeaters required, or the longest single length of cable which can be employed without boosting the signal. To meet present day requirements, the coupling loss of the cable should not exceed 105 dB for 95% coverage at any frequency between 75 MHz and 1.9 GHz.

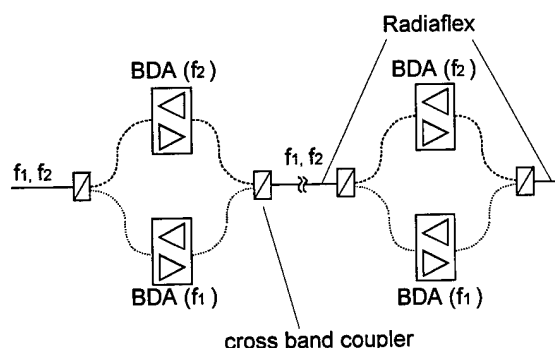
A multiband cable for use in tunnels will either include bi-directional amplifiers (BDA's) at regular intervals or employ a T-cell structure fed by a fiber optic backbone interfacing to the BDA's [14].

In each case, the aim is to attain a modular structure. This should consist of fixed lengths of cable between amplifiers. Evidently, the installed system will only be user friendly if amplifier units for each frequency band involved share the same location (equipment room, tunnel niches). Otherwise equipment sites will not have a standard equipment configuration, power supply requirements, replacement and maintenance cannot be standardized and bypass measures must be introduced to allow certain services to bypass certain amplifiers, see diagram J.

Diagram J: Comparison of separate sites with shared sites for BDA's



Separate Sites



Shared Sites

We have developed 1 5/8" cables to secure 500 m repeater spacing at all frequencies from 75 MHz to 1900 MHz assuming 105 dB overall loss and 95% coverage. We have exploited the significant drop in coupling loss which occurs when frequencies move into the radiating mode, to compensate the higher longitudinal losses at higher frequencies. In the example shown in Table 3, this effect makes the overall performance at 450 MHz and at 1900 MHz similar, see Table 4. This cable thus enables all present day mobile radio services to be integrated into a system architecture with an amplifier spacing of 500 m.

Table 3: Data of 1 5/8" Radiating Cable optimized for wide band transmission

frequency (MHz)	Coupling Loss, 95 % (dB)	Longitudinal Loss (dB/100 m)
75	88.4	0.59
150	97.7	0.87
450	96.7	1.66
900	81.5	2.60
1800	81.4	4.50
1900	80.9	4.80

Table 4: Maximum permissible lengths for 105 dB total loss with 95 % coverage using 1 5/8" Radiating Cable from Table 3

f (MHz)	length (m)
75	2814
150	839
450	500
900	904
1800	524
1900	502

CONCLUSION

The development of radiating cables in recent years has been twofold: a) optimizing towards a particular frequency and b) optimizing to the widest possible frequency spectrum.

In this paper we have noted further refinements of narrowing the band as well as criteria to be considered when widening the band.

We have introduced small diameter cables for use in buildings at all common mobile radio frequencies which provide a transparent net from a single feeding point.

In tunnels we have observed the need for a modular system architecture and single BDA sites for all services and developed cables to serve this need up to 1900 MHz. A basic prerequisite common to all cables striving to cover the spectrum is a coupling loss which falls at higher frequencies sufficiently to counter the rising longitudinal losses. This type of cable, once installed in a tunnel, provides a realistic basis for modular system upgrading in the future regardless of the frequencies to be accommodated and can be expected to find many diverse applications in the near future.

Diagram H: Overall losses of a VARIO type cable operating in the coupled mode (460 MHz)

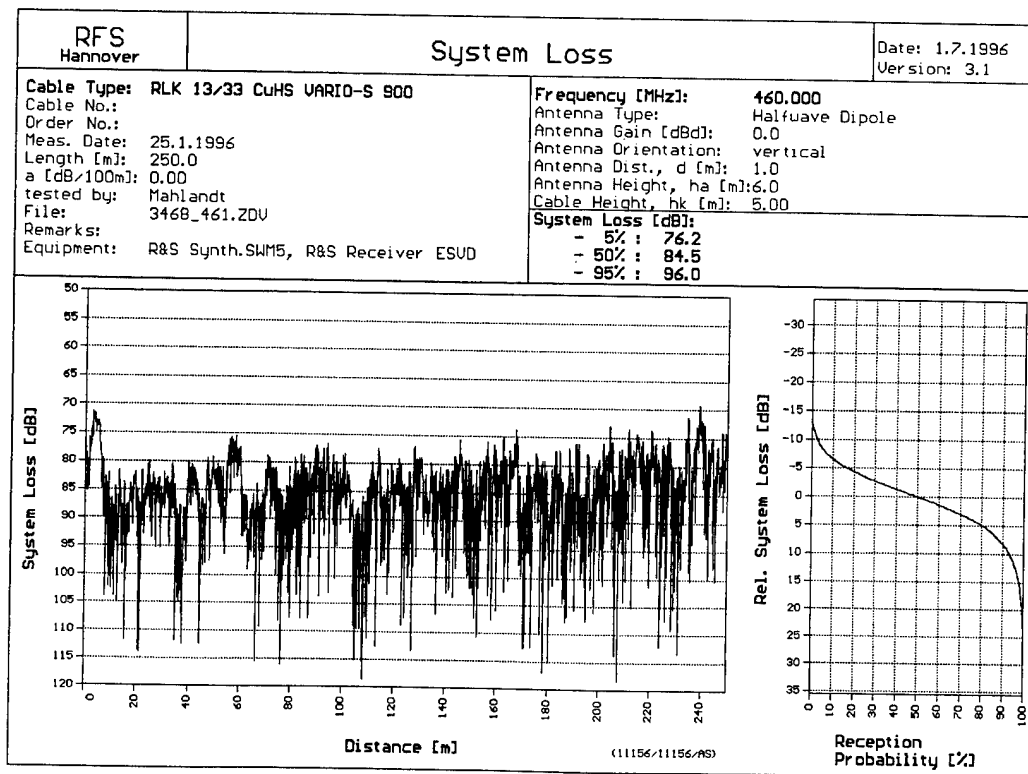
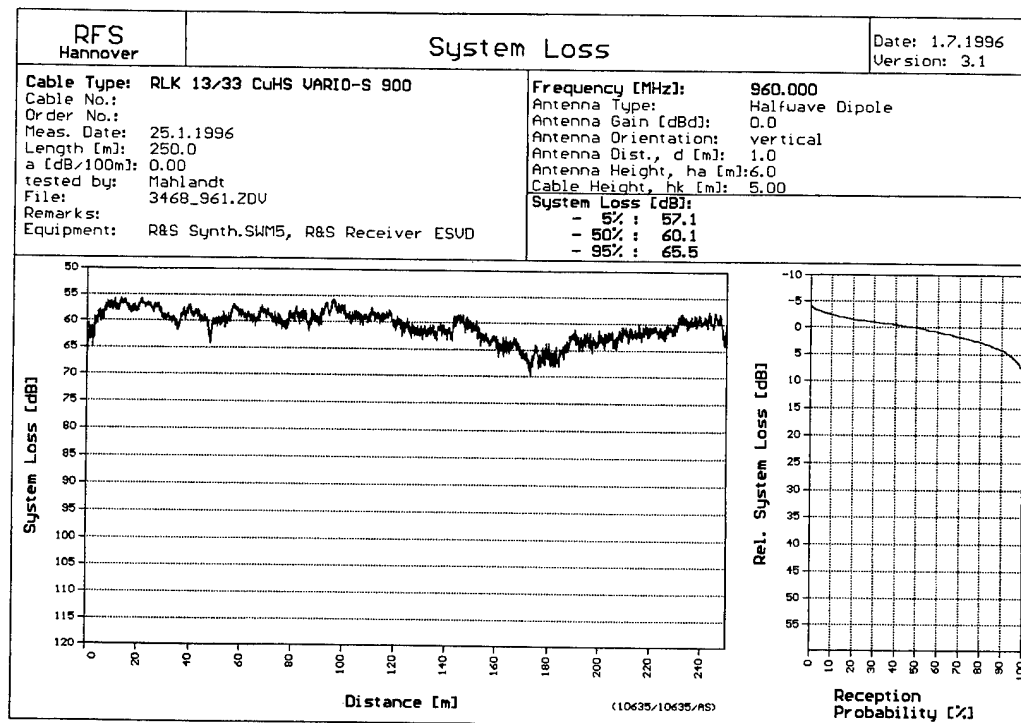


Diagram I: Overall losses of a VARIO type cable operating in the radiating mode (960 MHz) showing reduced dynamic range.



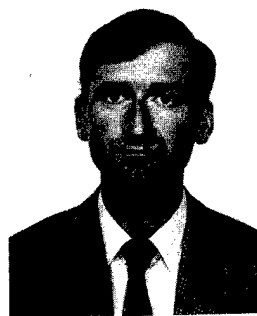
- [1] Jakubowski, R.: "Results of Distributed Antenna and Leaky Feeder Systems Tests at 800 MHz in the Washington D. C. Metro System Tunnels", 1994, IEEE 0-7803-1927
- [2] Schulze-Buxloh, K.: "Vergleichende Gegenüberstellung von Antennen und abstrahlenden Koaxialkabeln zur Tunnel- und Gebäudefunkversorgung", ITG-Diskussions-sitzung "Antennen für mobile Systeme", Starnberg 1996
- [3] Becker, H., Schulze-Buxloh, K.: "GSM-Parametermessungen im Düsseldorfer Rheinalleetunnel unter Verwendung eines "Repeater"-Verstärkers und eines optimierten strahlenden Kabels (VARIO 450/900)", ITG-Fachbericht 128, VDE-Verlag 1994
- [4] Hettstedt, H.: "Development and Applications of Leaky Feeders", Proc. Communications Systems for Tunnels, London, 1993, ITC Ltd. Verlag
- [5] Hettstedt, H., Coraiola, A., Heddebaut, M., Schulze-Buxloh, K., Boby, J., Baranowski, S., Lienard, M.: "Development and Applications of Radiating Cables for GSM Retransmission in Tunnels - The Optimization Problem", ATT and IVHS-Congress, Paris, 1994
- [6] Chappuis, J., Brun, S., Mazan, S.: "Breitbandige Tunnelfunkversorgung bei den Schweizerischen Bundesbahnen (SBB)", SIGNAL+DRAHT, 86 (1994), Heft 1/2, Tetzlaff Verlag
- [7] Rampalli S., Nudd, H. R.: "Recent Advances in the Designs of Radiating (Leaky) Coaxial Cables", Proc. IWCS '91
- [8] Levisse, A.: "Leaky or Radiating? Radiation Mechanisms of Radiating Cables and Leaky Feeders - Channel Tunnel Applications", Proc. IWCS '92
- [9] Coraiola, A., Schulze-Buxloh, K.: "Variable Leaky Feeders for Cellular Radio Systems", Proc. ICWC '92, IEEE Verlag 1992
- [10] Coraiola, A., Haag, H., Schulze-Buxloh, K., Thönessen, G.: "Leaky Coaxial Cable with Length Independent Antenna Receiving Level", Proc. IWCS '92
- [11] Coraiola, A., Brambilla, G.: "Multiservice Communications Plants for Long Tunnels", Proc. VNIS '91, Society of Automotive Engineers, Inc.
- [12] Torrance, J. M., Keller, T., Hanzo, L.: "Multi-Level Modulation in the Indoors Leaky Feeder Environment", 1996, IEEE 0-7803-3157-5/96
- [13] Hettstedt, H., Herbig, G., Spinner, C., Fischer, H., Schulze-Buxloh, K.: "Hausversorgung mit abstrahlendem Kabel - Meßergebnisse im Bereich 75 bis 1800 MHz", 2. ITG-Fachtagung "Mobile Kommunikation", Neu-Ulm, 1995, Tagungsband, VDE-Verlag
- [14] Brambilla, G., Haag, H., Schulze-Buxloh, K., Weiss, A.: "Optimized VARIO Leaky Feeders for 900 and 1800 MHz Frequency Bands with Optical Fibers Integrated in the Inner Conductor for Use in Mobile Radio Communication Systems in Tunnels and Buildings", Proc. IWCS '94



Karl Schulze-Buxloh

RFS kabelmetal
Sales Department
Hannover, Germany

Karl Schulze-Buxloh (40) graduated as a Dipl.-Ing. from Ruhr-University Bochum in 1986. He joined AEG KABEL for the development and sale of leaky coaxial cables. In May 1994 he joined RFS kabelmetal where he is a project sales engineer in the field of distributed communication systems and RF transmission lines.



Mark Davies

RFS kabelmetal
Project Sales
Hannover Germany

Mark Davies (39) obtained his Master's Degree at Cambridge University and an Engineering Diploma (Dipl.-Ing) from the University of Hagen. He has worked with kabelmetal in fiber optic R&D and RF technical sales before obtaining his present position as project sales manager for radiating cable systems.

STUDY ON HIGHLY EXPANDED INSULATION MATERIAL FOR COAXIAL CABLES BY NON-FLUOROCARBON FOAMING TECHNIQUE

Takashi Higashikubo Toshihiro Zushi Hirokazu Kuzushita
Kaneharu Suga Takumi Yamamoto Makoto Wada
Mitsubishi Cable Industries, Ltd.
Amagasaki, Japan

ABSTRACT

The authors studied expanded insulation materials and foaming technique in order to develop low-loss, large-size coaxial cable using a non-fluorocarbon blowing agent. An inert gas was selected among the non-fluorocarbon blowing agents. We found a new base polymer prepared by blending HDPE and LDPE to produce large size cables. As a nucleating agent, we selected boron nitride (BN) and found that the uniformity of cell depended on its particle size, surface area, and shape.

With the new expanded insulation material, we established a technique to produce — using a non-fluorocarbon blowing agent — large-size 39D (13/8inch) coaxial cable with highly expanded (80%) insulation. The developed cable was confirmed to be improved about 10% in transmission loss as compared with conventional cables.

1. INTRODUCTION

Coaxial cables with highly expanded (80%) material are used recently for antenna feeder for mobile communication and transmission line for cable TV system, which are increasing in demand. For these coaxial cables with highly expanded material, fluorocarbons have been generally used as the blowing agent. But from the viewpoint of environmental protection, it is desirable to develop a substitute. These cables are mostly applied in higher frequency bands where lower transmission loss is desired. But the use of conventional organic nucleating agents has limited the electrical properties of these cables. Because their decomposition residue in the insulating material have led to increase in transmission loss. In addition, it has been difficult to obtain a thickly expanded material for large-size

cables without fluorocarbon blowing agent.

In order to solve these problems, we have studied the constituent materials of the expanded insulation: the base polymer, blowing agent, and nucleating agent. We have also developed a new foaming technique.

2. EXPERIMENT

2.1. Materials

2.1.1. Base Polymer

As the base polymers we experimented high density polyethylene (HDPE), low density polyethylene (LDPE) and HDPE/LDPE blend with low ϵ , $\tan \delta$ and good foam extrusion processability. The properties of the studied polymer are shown in Tables 1 and 2 and HDPE/LDPE blend ratio are shown in Table 3.

2.1.2 Blowing Agent

Conventionally HCFC22 (a kind of fluorocarbon and low ozone depletion potential: 0.05) has been used as a blowing agent. Since HCFC22 is not free ozone depletion, it is not desirable for the environmental problem. We chose some non-fluorocarbon gases which were free from ozone depletion, chemically inert, nontoxic, non-flammable and easily available. These blowing agents were added to molten polymer (mixture of the base polymer and the nucleating agent) from a blowing agent inlet in the extruder. Properties of the blowing agents are shown in Table 4.

2.1.3. Nucleating Agent

We already have reported that BN gave a formulation having excellent electrical properties and good foam extrusion processability as nucleating agent.¹⁾ In this paper, we studied on foam extrusion processability of BN containing formulation with various particle size, surface area, and shape. Properties of nucleating agents

are shown in Table 5. These nucleating agents were added to base polymer in varied amounts.

2.2. Extrusion Equipment for Experiment

In this study we used laboratory scale 25mm ϕ to 30mm ϕ two stage extruder in order to estimate foam extrusion processability of each material. Its outline is shown in Fig.1.

2.2.2. Extrusion Screw

In general, non-fluorocarbon gas (ex. N_2) has low solubility for molten polymer. So that, we devised some screws for the first stage with good mixing properties between molten polymer and blowing agent. These structures are shown in Fig.2.

2.3. Experimental Method

2.3.1. Foam Extrusion Processability

The authors used the extruder shown in Fig.1 in order to evaluate foam extrusion processability. A mixture of a base polymer and a nucleating agent was fed into the first stage extruder, and blowing agent was added to it from a blowing agent inlet at high pressure. The temperature of the mixture was reduced to the suitable temperature for expansion during the second stage extruder. And the foamed insulation layer was extruded over a 0.813mm annealed copper wire with about 10mm in outer diameter. Void fraction (occupied fraction of foams) varied greatly with the injection amount of blowing agent. We evaluated maximum void fraction, foam structure and surface appearance of the foamed insulation layer.

2.3.2. Melt Property

Foam extrusion processability of base polymer depends upon melt properties of base polymer. We evaluated its melt tension (one of melt properties) of each base polymer by capillary rheometer. (capillary: $L = 8.0\text{mm}$, $D = 2.1\text{mm}$, piston speed: 10mm/min , draw rate: 5mm/min)

2.3.3. Hygroscopic Properties of Nucleating Agent

Since $\tan \delta$ of coaxial cable increases by a little moisture in insulation, it is important to evaluate hygroscopic property of nucleating agent. In the manufacturing process of coaxial cable, it is considered that the absorption of moisture occurs during between the extruded insulation process and the covering outer conductor process. We evaluated the hygroscopic properties of expanded

insulation materials with various nucleating agent. The experimental conditions are shown in Table 6.

2.4. Manufacturing a Coaxial Cable Using New Materials

A 39D (13/8inch) coaxial cable with 80% highly expanded insulation using new materials was manufactured by the coaxial cable manufacturing extrusion line. The electrical properties of the coaxial cable were evaluated. The outline of manufacturing extrusion line is shown in Fig.3.

3. RESULTS AND DISCUSSION

3.1. Materials Screening Tests

3.1.1. Base Polymer

Highly void fraction, uniform cell structure free of large void and smooth surface appearance are required for the foam insulation of thick, large-size coaxial cable. Therefore, we evaluated foam extrusion processability and melt property of base polymers. The evaluated results of processability and melt property of HDPE and LDPE are shown in Tables 7 and 8 and Figs.5 and 6.

On the whole, HDPE foam had smooth surface appearance, but had large void. No.1 in Table 7 had the most excellent foam extrusion processability. And the melt tension of No.1 was high and rised slowly at the extrudy temperature (about 140°C) on the part of die. (see Fig.5)

On the whole, LDPE foam had high void fraction, but not smooth surface appearance. Correlation between foam extrusion processability and melt tension of LDPE was not found. (see Fig.6)

On the HDPE/LDPE blend, we selected No.1 for HDPE and No.7 for LDPE. The relationship between maximum void fraction and blend ratio of HDPE/LDPE is shown in Fig.4. When HDPE/LDPE blend ratio was 15/85, the foam had the highest void fraction, smooth surface appearance and non-large void. On the case of thick, large-size foam insulation, it was found that HDPE/LDPE blend (ratio=15/85) was the most desirable as base polymer.

3.1.2. Blowing Agent

Results of measuring foam extrusion processability are shown in Table 9. It was found that GAS-C had good foam extrusion processability as good as HCFC22. We considered that GAS-C had high solubility for molten polymer as well as HCFC22, and the other gases had poor

solubility for molten polymer.

But GAS-C cannot raise pressure than 50kg/cm² at room temperature. Therefore it was difficult to use GAS-C as blowing agent at the manufacturing extrusion line(Fig.3). Because the molten polymer pressure was higher than 100kg/cm² at the part of gas injection zone. Therefore, it was necessary to improve the mixturability of molten polymer and GAS-B which had poor solubility

3.1.3. Nucleating Agent

The evaluated results of foam extrusion processability are shown in Table 10. BN-2 with medium particle size attained the smallest cell size and good uniformity, and BN-1 with small particle size and BN-3 with large particle size led to giant cell and un-uniformity. SEM photographs of BN-1, -2, -3 are shown in Fig.7. It is shown that BN-1 is condensed, BN-2 is independent and scale shape, and BN-3 is a large granule shape.

In the results, we considered that BN with a medium particle size (about 10 μ m) and scale shape had the highest nucleating effect, BN with a small particle size had the lowest nucleating effect because of condensation, and BN with large particle was few nucleating point because of a few numbers as unit volume.

The results of evaluating hygroscopic properties of inorganic powders are shown in Fig.8. Moisture contents of expanded insulation materials with inorganic powders are as low level as natural. On the other hand, the moisture content of that with ADCA or its decomposition residue increased with the progress of time. As the result it was clear that by using BN as nucleating agent no drying process was required.

3.1.4. Extrusion Screw

We estimated some kind of screws in order to improve the mixturability of molten polymer and GAS-B. (See 3.1.2) The evaluated results of foam extrusion processability of each screw by using GAS-B are shown in Table 11. We found that the highly expanded insulation more than 80% was obtained by using screw-Y or-Z. (see fig.2)

As the results, it was clear that in the case of using non-fluorocarbon gas with low solubility for molten polymer, highly void fraction was gotten, only when gas and molten polymer were mechanically mixed by screw with mixture element.

3.2. Manufacturing Coaxial Cable Using New Materials

Then the laboratory test results was applied to actual commercial cable manufacturing line, by using new materials.

We selected the HDPE/LDPE blend (ratio=15/85) as base polymer, non-fluorocarbon GAS-B as blowing agent, BN-2 as nucleating agent, and screw-Z as extrusion screw from the results of our study.

A 39D coaxial cables with 80% expanded insulation in void fraction, 17.3mm in inner conductor diameter and 46.5mm in outer conductor diameter were manufactured without drying process with the manufacturing extrusion line shown in Fig.3.

Evaluated electrical properties of coaxial cables with new materials and conventional materials are shown in Table 12. The cross section of the highly expanded insulation used new materials is shown in Fig.8.

It was confirmed that the developed cable had lower transmission loss than the conventional cable by about 10%.

4. CONCLUSIONS

We evaluated the expanded insulation materials and foaming technique in order to develop a low-loss, large-size coaxial cable using a non-fluorocarbon gas as blowing agent. HDPE/LDPE blend(ratio=15/85), a non-fluorocarbon gas and boron nitride were proved to be the best base polymer, blowing agent and nucleating agent, respectively. The new expanded insulation material and improved foaming technique, have enabled us to produce — with a non-fluorocarbon blowing agent (inert gas) — thick, large-size, 39D (13/8inch) coaxial cable with highly expanded materials. The electrical properties of the newly developed cable was improved about 10% in transmission loss as compared with the conventional cable.

5. ACKNOWLEDGMENT

The authors wish to thank Mr. T. Kaide, Y. Fujiwara, N. Matsuda and T. Takai for their direction, enlightening discussion and helpful suggestions. The authors also wish to thank Ms. M. Yamagishi and Mr. K. Hiroba for their invaluable assistance in the developmental work.

6. REFERENCES

- 1) Y.Morita et al., "New Extrusion Material for Highly Expanded Insulations for Coaxial Cable", 40th International Wire and Cable Symposium, p16-19 (1991)

Table 1 Properties of Base Polymer (HDPE)

	No.1	No.2	No.3	No.4	No.5	No.6
Density (g/cm ³)	0.943	0.943	0.952	0.946	0.965	0.960
Melt flow rate (g/10min)	0.9	1.8	0.4	0.8	8.0	5.0

Table 2 Properties of Base Polymer (LDPE)

	No.7	No.8	No.9	No.10	No.11
Density (g/cm ³)	0.920	0.920	0.921	0.919	0.917
Melt flow rate (g/10min)	2.0	3.0	5.0	3.5	2.0

Table 3 Blend Ratio of HDPE/LDPE (PHR)

	No.12	No.13	No.14	No.15
HDPE (No.1)	85	65	35	15
LDPE (No.7)	15	35	65	85

Table 4 Properties of Blowing Agents

	GAS-A	GAS-B	GAS-C	HCFC22
Boiling point (°C)	<-150	<-150	-78.5	-40.8
Critical temperature (°C)	<-100	<-100	31.0	96.0
Critical pressure (atm)	<50	<50	72.9	49.1

Table 5 Properties of Nucleating Agents

	BN-1	BN-2	BN-3
Average particle size (μ m)	1.8	10.5	40.0
Surface Area (m ² /g)	12.3	3.0	2.0
Shape	scale	scale	granule

Table 6 Experimental Conditions for Determining Hygroscopic

Properties of Inorganic Powders	
Nucleating agent	BN, ZrO ₂ , MgO
(Cont. ADCA and ADCA decomposition residue)	
Atmosphere	Room temperature, 90%RH
Sample	1mm HDPE sheet with 10wt% powder
Experimental apparatus	Karl-fischer moisture titrator

Table 7 Foam Extrusion Results of Base Polymer (HDPE)

	No.1	No.2	No.3	No.4	No.5	No.6
Maximum void fraction (%)	68	63	63	65	51	53
Foam structure ¹⁾	○	○	○	○	×	×
Surface appearance ²⁾	○	○	×	○	○	○

* Blowing agent : GAS-A, Nucleating agent : BN-1

1) Fine : ○, Giant : ×, 2) Smooth : ○, Rough: ×

Table 8 Foam Extrusion Results of Base Polymer (LDPE)

	No.7	No.8	No.9	No.10	No.11
Maximum void fraction (%)	65	65	66	62	60
Foam structure ¹⁾	○	○	○	○	×
Surface appearance ²⁾	×	×	×	×	×

* Blowing agent : GAS-A , Nucleating agent : BN-1

1) Fine : ○, Giant : ×, 2) Smooth : ○, Rough: ×

Table 9 Foam Extrusion Results of Blowing Agents

	GAS-A	GAS-B	GAS-C	HCFC22
Maximum void fraction (%)	70	73	85	82
Foam structure ¹⁾	○	○	○	○
Surface appearance ²⁾	○	○	○	○

* Base polymer : HDPE/LDPE=80/20, Nucleating agent : OBSH

1) Fine : ○, Giant : ×, 2) Smooth : ○, Rough: ×

Table 10 Foam Extrusion Results of Nucleating Agents

	BN-1	BN-2	BN-3
Maximum void fraction (%)	66	76	70
Average sell size (mm)	1.44	0.57	0.75
Foam structure ¹⁾	×	○	×
Surface appearance ²⁾	○	○	○

* Blowing agent : GAS-B、 Base polymer : HDPE (No.1)

1) Fine : ○, Giant : ×、 2) Smooth : ○, Rough: ×

Table 11 Foam Extrusion Results of Screw for Extrude

	Screw-X	Screw-Y	Screw-Z
Maximum void fraction (%)	76	80	85
Foam structure ¹⁾	○	○	○
Surface appearance ²⁾	○	○	○

* Blowing agent : GAS-B、 Base polymer : HDPE/LDPE=20/80、

Nucleating agent : OBSH

1) Fine : ○, Giant : ×、 2) Smooth : ○, Rough: ×

Table 12 Properties of Coaxial Cable Manufactured by Using New Materials

			New Cable ¹⁾	Conventional Cable ²⁾
Constituent of 80% expanded insulation	Base polymer		HDPE/LDPE	HDPE/LDPE
	Blowing agent		GAS-B	HCFC22
	Nucleating agent		BN-2	OBSH
Cable structure	Diameter of inner conductor (mm)		17.3	
	Diameter of core (mm)		43.0	
	Diameter of outer conductor (mm)		46.5	
	Diameter of PE jacket (mm)		51.0	
Electrical properties	Capacitance (PF/m)		71.0	71.3
	Characteristic impedance (Ω)		51	50
	Transm- ission loss (%) ³⁾	400MHz	92	100
		900MHz	91	100
		1500MHz	91	100
		2000MHz	91	100

1) No drying 2) Vacuum drying for 48hours at 70°C

3) Calculation as the transmission loss of conventional cable is 100%

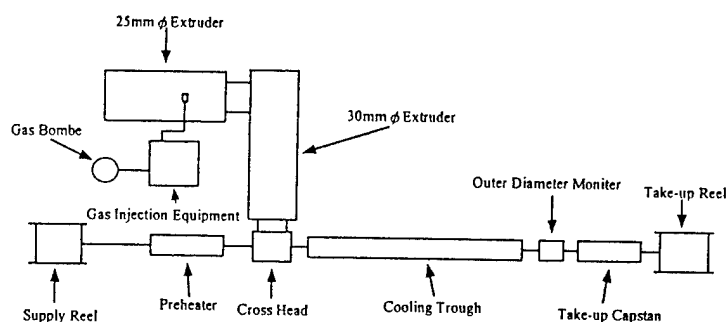


Fig. 1 25mm ϕ - 30mm ϕ Extrusion line for experiment

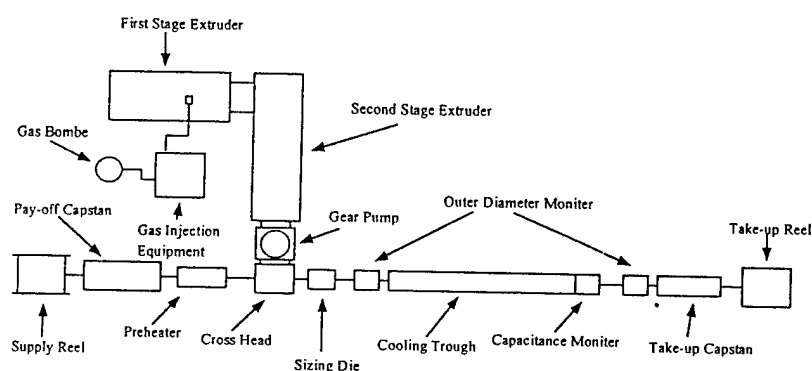


Fig. 3 Manufacturing extrusion line for coaxial cable core with highly expanded insulation

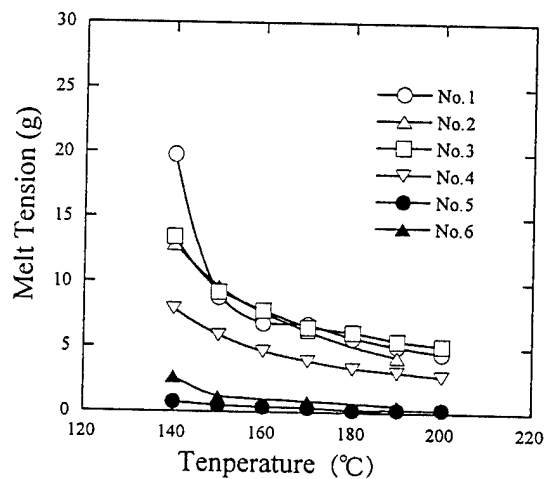
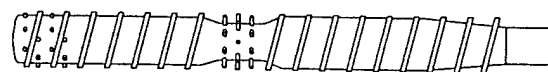


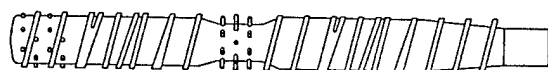
Fig. 5 Temperature dependence of melt tension of HDPE



Screw-X
(Conventional Vent Type Screw)



Screw-Y
(Vent Type Screw with Pin)



Screw-Z
(Vent Type Screw with Pin and Barrierable Mixing)

Fig. 2 Screw design for 25mm ϕ extruder

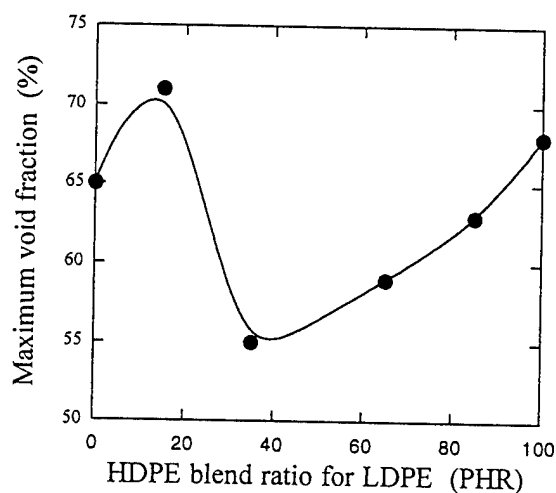


Fig. 4 Relationship between maximum void fraction and HDPE/LDPE blend ratio

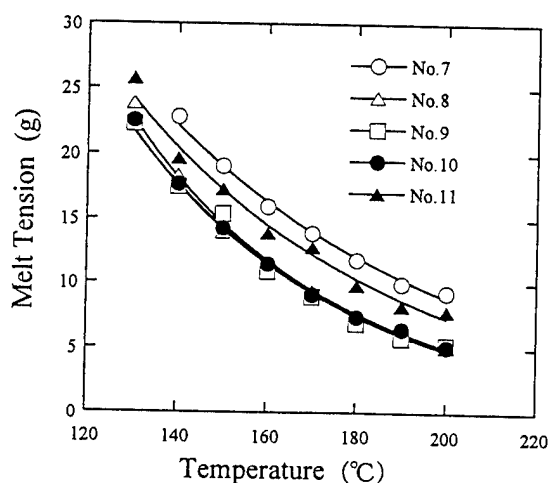


Fig. 6 Temperature dependence of melt tension of LDPE

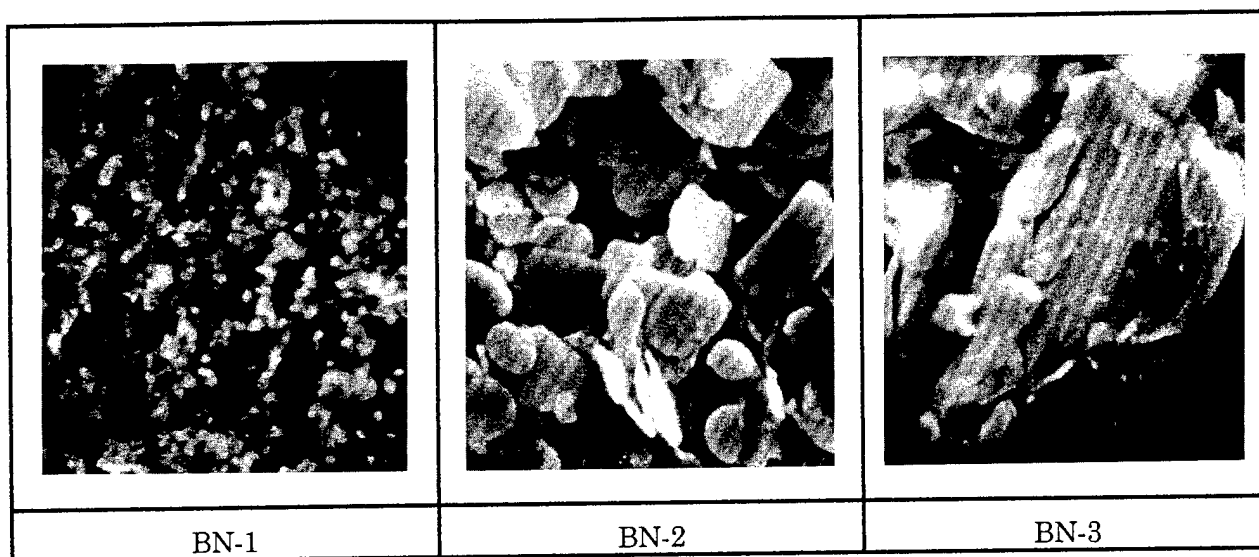


Fig. 7 SEM photographs of BN-1, BN-2, BN-3

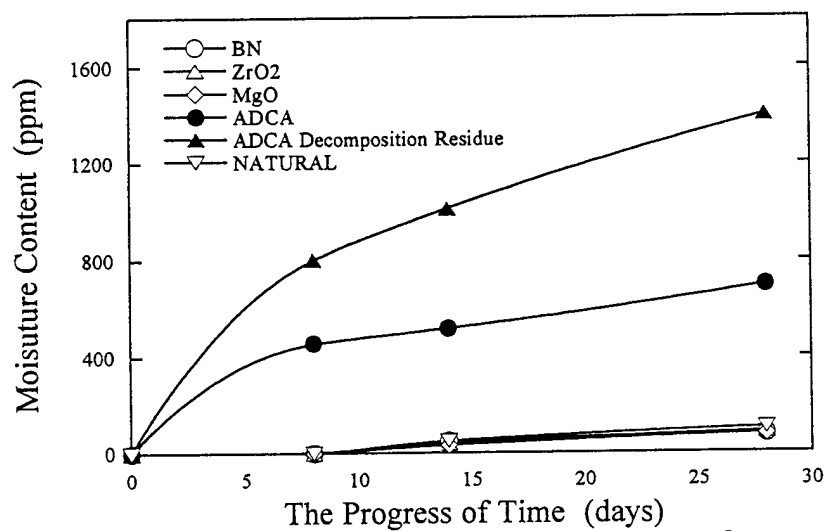


Fig. 8 Hygroscopic properties of inorganic powders

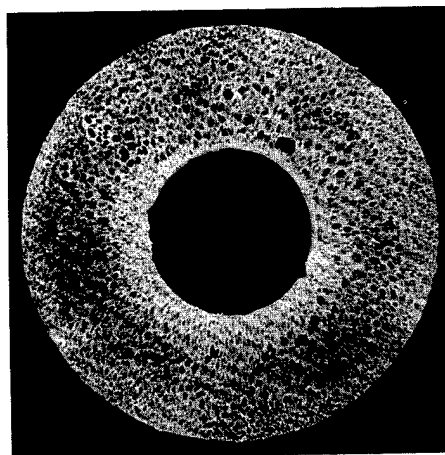
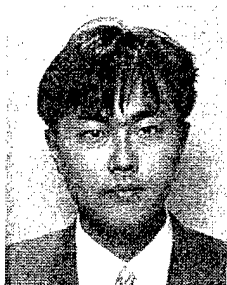


Fig. 9 Cross section of highly expanded insulation used new materials



Takashi Higashikubo

Mitsubishi Cable
Industries, Ltd.
8, Nishinocho
Higashimukaijima
Amagasaki-City
Hyogo-Pref, Japan

Mr. T. Higashikubo received a B.E. degree in Industrial Chemistry from Kyoto Institute of Technology in 1991. Then he immediately joined Mitsubishi Cable Industries, Ltd. And he has been engaging in the research and development of plastic materials for communication cables. He is now a engineer of Materials Research Dept.



Kaneharu Suga

Mitsubishi Cable
Industries, Ltd.
1-6-37,
Shirakatacho
Fukui-City
Fukui-Pref, Japan

Mr. K. Suga graduated from Amagasaki Industrial High School majoring in TV technology in 1967. Then he immediately joined Mitsubishi Cable Industries, Ltd. And he engaged in the quality control of high frequency communication cables. He is now a member of Fukui Works.



Toshihiro Zushi

Mitsubishi Cable
Industries, Ltd.
4-3, Ikejiri
Itami-City
Hyogo-Pref, Japan

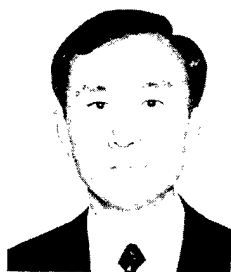
Mr. T. Zushi received a B.E. degree in Synthetic Chemistry from Okayama University in 1985. Then he immediately joined Mitsubishi Cable Industries, Ltd. And he has been engaging in the research and development of plastic materials for communication cables. He is now a member of Itami Works.



Takumi Yamamoto

Mitsubishi Cable
Industries, Ltd.
1-4-3, Marunouchi
Tiyoda-Ward
Tokyo-Pref, Japan

Mr. T. Yamamoto received a B.E. degree in Electrical Engineering from Kinki University in 1991. Then he immediately joined in Mitsubishi Cable Industries, Ltd. And he has been engineering in test plant and communication cable production. He is now a member of Tokyo Works.



Hirokazu Kuzushita

Mitsubishi Cable
Industries, Ltd.
8, Nishinocho
Higashimukaijima
Amagasaki-City
Hyogo-Pref, Japan

Mr. H. Kuzushita received B.E and M.E. degrees in Industrial Chemistry from Kyoto University in 1977 and 1979 respectively. Then he immediately joined Mitsubishi Cable Industries, Ltd. And he has been engaging in the research and development of plastic materials for communication cables. He is now a chief engineer of Materials Research Dept.



Makoto Wada

Mitsubishi Cable
Industries, Ltd.
8, Nishinocho
Higashimukaijima
Amagasaki-City
Hyogo-Pref, Japan

Mr. M. Wada received a B.E. degree in Mechanical Engineering from Kansai University in 1989. Then he immediately joined Mitsubishi Cable Industries, Ltd. And he engaged in production engineering of communication cables. He is now a engineer of Mechanical Equipment and Engineering Center.

MEASURING RF EMISSIONS FROM A MOVING COAXIAL DROP CABLE

By
Joseph N. D'Amico

Belcore
Morristown, New Jersey

Grant F. Apgar

Belcore
Red Bank, New Jersey

ABSTRACT

Historical CATV data suggests that the long term physical and electrical reliability of coaxial drop cables will be a major concern for service providers as new hybrid fiber coaxial networks are constructed. Determining the relative RF shielding reliability of coaxial drop cables has been difficult.

Belcore designed and constructed test equipment to measure the transmission of RF energy through the shields of coaxial drop cables while they are being bent or flexed. This report describes the test equipment and compares the shielding reliability of coaxial drop cables of different suppliers. It establishes that Belcore has developed a reliable means, available to the telecommunications industry, for comparing the long term shielding reliability of coaxial drop cables.

COAXIAL DROP CABLES AND RF EMISSIONS

Drop Cable Description

Coaxial drop cables are designed to carry high frequency radio waves (5 MHz to 1 GHz) from some distribution point to the user. The term "drop cable" applies both to those cables that are

suspended aurally as well as to those that are designed to be buried in the soil or placed within cable ducts. A coaxial cable consists of concentric inner and outer conductors. The radio frequency (RF) signal travels primarily on the outer surface of the inner conductor and on the inner surface of the outer conductor, i.e., the cable shield. The dielectric and the distance that separates the outer and inner conductors give the cable its characteristic impedance.

In practice, a typical CATV type coaxial drop cable consists of :

- A copper clad steel center conductor,¹
- Concentric within a foamed polyethylene plastic dielectric,
- Over which is placed an aluminum shield.

That shield usually consists of one of the three following constructions:

- a) The "Standard Shield": An aluminum foil/plastic laminated ribbon which is longitudinally wrapped and adhesively bonded to the central dielectric. Over this laminate is woven a braid consisting of 34 AWG bare aluminum wire which provides at least a 60% coverage of the foil.
- b) The "Triple Shield": A cable core with a "Standard Shield" over which is wrapped a

¹ The center conductor may also consist of solid copper (not common in the US) to enable the drop to carry electric current for powering applications

second aluminum foil/plastic tape laminate. It is not bonded to the other shields.

c) The "Quad Shield": A cable core with a "Triple Shield" over which is woven a second aluminum braid of less coverage than the first.

- Over the cable shield is extruded a black plastic jacket. Polyethylene is the preferred plastic for a buried cable jacket because of its high moisture impermeability while PVC ((poly) vinyl chloride) is usually used in the aerial plant. (It can easily be made fire resistant.) Some aerial cables are constructed with a coextruded steel messenger wire so as to be self supporting. Buried drop cables all contain a tacky waxy substance between the cable shield and jacket to inhibit water migration along the core.

This cable is designed to be flexible while preventing the emission of radio frequency (RF) energy to the outside environment. Repeated bending or flexing of the cable, however, causes its aluminum foil shield(s) to crack and its braid wires to break. Perforation of the cable shield permits both RF energy egress and ingress. Since the energy in the drop is relatively low, its emission usually doesn't interfere with broadcast transmission. To the same extent, however, RF waves in the environment can enter the drop cable, mix with the transmitted signal and eventually appear as noise.

Moreover, since the transmission of radio frequency information via coax is only permitted because it occurs in private "wave space", its intrusion into the public airways is forbidden. Cable operators must periodically demonstrate FCC compliance.

The Detection and Measurement of RF Emissions from Coaxial Cables

Radio frequency energy is easy to detect. The ubiquitous prevalence of radio and television receivers attest to this fact. However, we do encounter a two-fold problem. Firstly, we must detect the sought after signal, often in the presence of other interfering RF signals. Secondly, we must accurately quantify the desired signal. Any of several methods can be used to detect and measure the RF energy being emitted from a coaxial cable. Several are reviewed here. They may be characterized as:

A. Those methods that detect and measure the signal in an electromagnetically shielded environment, for example:

1. The Tri-axial Test Fixture - RF Energy Measurement By Transfer Impedance: A coaxial drop cable may be tested for RF emissions by placing it in the axial center of a metal (copper) pipe such that the shield of the cable under test becomes the coaxial inner conductor of the test fixture and its outer conductor becomes the inner surface of the metal tube. The test fixture's dimensions are such that the air between the test cable and the tube provides the desired characteristic impedance. The energy transferred to the cable's "new" outer shield, i.e., the pipe, is measured and compared to the input signal.ⁱ

2. The GTEM Cell: The shielding effectiveness of a cable is measured in this shielded chamber by the technique known as gigahertz transverse electromagnetic mode energy transfer. The geometry of the chamber prevents standing waves from being reflected and interfering with the test. Energy radiated through the cable shield is measured and compared with that transmitted or received by a calibrated antenna placed in the GTEM chamber in the test cable's location. A comparison between the test cable and the standard antenna provides the cable's shielding effectiveness.ⁱⁱ

3. The Anechoic Chamber: This chamber simulates an open air test site in a large electromagnetically shielded environment. Unlike the GTEM cell, standing waves are absorbed to prevent their interfering with the test. Here also a comparison is made between the cable and a standard antenna.

B. Those methods that detect and measure the RF energy in an open environment. This technique while conceptually simple, is made difficult by the electromagnetic noise that surrounds us all.

1. The Open Air Test Site or OATS - RF emissions from a coaxial drop cable can be detected and measured at an OATS facility by the use of a calibrated antenna at some fixed distance from the device under test. Some type

of compensation is necessary for that electromagnetic energy that will be present even at a well chosen test site. The anechoic chamber may be used to screen samples prior to testing in an OATS facility.

2. The Calibrated Magnetic Antenna or Close Field Probe - Radio signals can be measured in an unshielded radio environment using the calibrated magnetic antenna. This technique relies on the very close proximity of the device under test and functions by measuring the strength of the magnetic component of the electromagnetic wave while canceling out its electrical component. Consequently, the device under test must be physically properly oriented with respect to the close field probe. The magnetic field wave component from more distant objects becomes inconsequential since its energy decreases more rapidly than that of the electrical field component.

BELLCORE'S COAXIAL DROP CABLE RF EMISSIONS TEST SYSTEM

The Bellcore coaxial drop cable RF emissions tester consists of three basic components that are effectively linked together to form a system which generates RF signals, introduces them

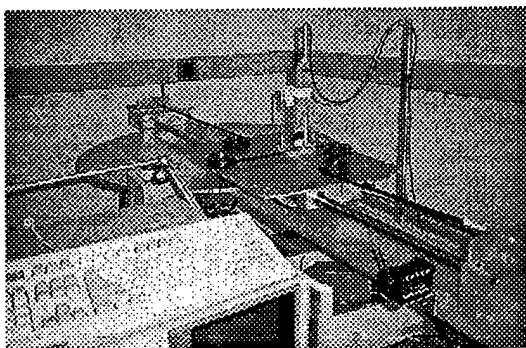


Figure 1

The Bellcore Coaxial Drop Cable RF Emissions Test System

into a moving coaxial cable and simultaneously detects and measures any energy which traverses the cable shield. The test is conducted to frequencies of over one gigahertz. The system is operated with measurements continuously taken until the cable becomes incapable of

transporting RF signals. While we may arbitrarily call that event "cable failure", its practical failure actually occurs much earlier with markedly increased RF emissions and changes in the cable's structural return loss (SRL). (Figure 1)

The Close Field Probe

The close field probe is a small calibrated magnetic antenna which is mounted on the moving test platform and positioned so as the cable, i.e., the device under test, passes the sensor, any radiated energy, i.e., emitted energy, is maximally coupled to the antenna. The probe² itself is a balanced magnetic field sensor that provides an output voltage proportional to the magnetic field strength at the tip of the probe. Both the radiated magnetic and electric fields couple to the probe. The magnetic field produces an electrical output while the electric field does not because of the design and construction of the probe. It uses a dual loop sensor and a balun to reject electrically coupled signals. Since the probe does not rectify the input signal, it passes both frequency and amplitude information to the measurement system. Because the circuitry is passive, only thermal noise, provides a small unwanted contribution to the system. Signal generation in the probe simply follows Faraday's Law of Induction.

Since the close field probe's circuitry is passive, there are losses to the strength of the input signal and those losses are not uniform. The antenna is not equally sensitive to all frequencies. To compensate for those losses, we utilize an antenna factor (AF), a value that varies with frequency and must be algebraically added to the measured data to obtain the actual strength of the measured signal.³ A constant, K, must also be added to account for any uniform gain or loss to the system.

² We used two probes to cover the frequency range of interest: The Hewlett-Packard Model HP 11941A for measurements to 30 MHz. and the Model HP 11940A for measurements from 30 MHz to 1 GHz

³ Refer to Hewlett-Packard Publications No. 11941-90001 and No. 11940-90004. The antenna factors (AF) are specific to the individual probes and are provided on the probes themselves.

$$H - \text{Field Strength (dB}(\mu\text{A/m)}) = V_{SA} + AF + K$$

Where:

V_{SA} = Voltage in dB μ V measured on the analyzer,
and

AF = Probe Antenna Factor in dB((μ A/m)/ μ V)

K = The uniform loss or gain in dB between the probe and the spectrum analyzer.

The contributors to the constant K are the preamplifier and the impedance matching pad. A preamplifier⁴ is inserted in the circuit between the close field probe and the spectrum analyzer, i.e., network vector analyzer. Its gain contribution is 28 dB with the low frequency probe and 25 dB with the high frequency probe. The gains are linear throughout their frequency ranges. The principal loss is contributed by the 50 Ω to 75 Ω impedance matching pad.⁵ It is inserted in the circuit between the preamplifier (50 Ω output) and the analyzer (75 Ω input). Its insertion loss of 5.7 dB is linear across the frequency range of interest. K is presented on the network analyzer's RF emissions graphs. Mathematical adjustments for the antenna factors and K have been made in all tabulated and graphic data but not on the network vector analyzer instrument generated RF emissions graphics.

The Test Bed And The Moving Test Platform

The test bed holds the drop cable sample while it is being tested. (Figure 2) It keeps the cable under constant uniform tension (approximately ten pounds force) and provides the support for the drive motor and speed reducers that propel the moving test platform. The moving test platform uniformly flexes the cable by forcing it to move around pulleys of specified diameter and to pass the close field (a.k.a. near field) probe. The probe is mounted on the test platform between two sets of two pulleys each. The geometry is such as to flex the cable evenly and oppositely. (Figure 3) Unless otherwise stated, the pulley radius is ten times that of the test cable, a cable bend radius specified as acceptable

⁴ Hewlett-Packard Preamplifier Model HP 8447F Option H64 dual preamplifier.

⁵ Hewlett-Packard Minimum Loss Pad Model 11852B, insertion loss: 5.7 dB linear

by most cable manufacturers. The near field probe is attached to the moving platform by a plastic support, the pulleys are of nylon, while the platform itself is made of aluminum, as is the main girder of the test bed beneath it. It was designed to prevent any spurious interaction of the metal test device with the sensor in the close field magnetic detector.

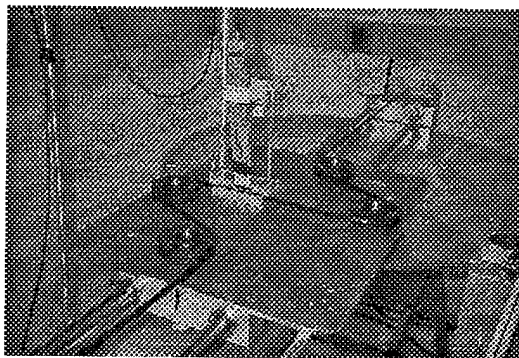


Figure 2

The Bellcore Coaxial Drop Cable RF Emissions Tester showing the close field probe mounted on the moving test platform.

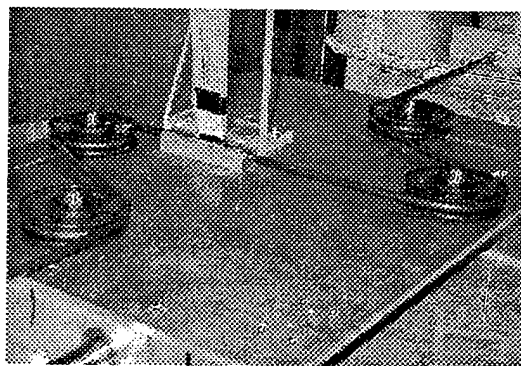


Figure 3

**The Bellcore Coaxial Drop Cable RF Emissions Tester
Detail of Cable Around Pulleys and In Contact With Probe**

As the moving test platform cycles back and forth over the six foot length of the test bed, the coaxial cable under test, which is affixed to the machine frame, is forced to bend or flex as shown in Figure 3. While almost the entire

length of the test cable bends over at least one pulley, only a 20 inch segment of the cable near its center and beginning 35 inches from the near end, i. e. the end closest to the signal source, is flexed over three pulleys. Static and dynamic measurements are recorded in this area. The sensing surface of the probe rides the surface of the cable between the two pulley sets. The cable itself is held under constant uniform tension by springs. The holding device measures any cable elongation and is equipped to stop the test should the elongation exceed a preset length. It also holds the 75 Ω terminating resistor. (Figure 4)



Figure 4

**The Bellcore Coaxial Drop Cable RF
Emissions Tester
Detail of Cable Tensioning Mechanism**

Electronic Instrumentation

The instrumentation consists of network vector analyzer which is both the radio frequency generator for the discrete source signals and the calibrated receiver for the measurement of the sensed RF emissions. It also measures the cable's structural return loss (SRL), i.e., the energy reflected by the structure of the cable itself. More specifically, the network analyzer sends into the cable under test RF energy at 1601 equally spaced discrete frequencies over the selected frequency range. The frequency span for these tests was usually from 10 MHz. to 1.210 GHz. While we are interested in data only to 1 GHz., we tested to the higher frequency so that when we examined the structural return loss, we could effectively remove the reflections

caused by the connectors and connecting cables. We utilized the time domain inverse Fast Fourier Transform (FFT) gating function of the network vector analyzer to perform that task. Meanwhile, the RF energy which traverses the cable shield at the location of the near field probe was received by that antenna. From the antenna it was transmitted to the preamplifier before being sent to the network analyzer. The network analyzer has two independent channels and is capable of acting as two (coupled) receivers. Its dynamic range is >100 dB enabling it to respond to very weak signals. The instrument's time domain function also allows us to localize defects in the test cable's structure.

In Summary

The Bellcore coaxial drop cable RF emissions tester provides data on the radio frequency emissions which escape through the shield of a coaxial drop cable:

- When they occur,
- Where they occur,
- When the cable is in motion, or
- While it is at rest.

It does so continuously until the cable becomes incapable of transporting radio frequency energy.

EXPERIMENTAL

Testing

While dozens of coaxial drop cables of various sizes, designs, manufacturer, etc. were tested for RF emissions with the Bellcore coaxial drop cable RF emissions tester, here to illustrate our test results, we report on two similar cables from two major manufacturers, herein noted as "A" and "B". The cables tested were Series 7 aerial cables with standard shields.

We simultaneously measured RF emissions through the cable shield, the cable's structural return loss (SRL) and characteristic impedance at frequencies of 10 MHz to 1 GHz. Bend pulley diameters of ten times that of the cable were used. Except for failure point static RF determinations, RF measurements were made on cables in areas that had been bent by three pulleys. When making SRL and characteristic

impedance measurements, the effects of test leads and connectors were removed by the time domain inverse Fast Fourier Transform (FFT) gating function of the network vector analyzer. We arbitrarily defined cable failure as that time in the cyclic bending of the drop cable when its structural return loss approached 0 dB. It usually occurred long after cable RF emissions had increased over 30 dB at high frequency.

RESULTS AND DISCUSSION

General

The test data developed by this program are voluminous. This fact can be appreciated if the reader understands that typically we recorded over twenty data scans of 1601 values each for both RF emissions and SRL for every sample tested. Such data, of necessity, must be averaged where possible and summarized for presentation. The data points provided in all tables and figures are averaged. Individual cables can consistently and reproducibly exhibit RF leakage at defect locations which can vary by

10 dB more or less than the average. This phenomenon is probably the result of localized cable shield rupture or fragmentation.

Please note that the RF emissions values are expressed as negative numbers. They are expressed in dB below signal generator power. The inserted power level has been adjusted for 0 dBm. The further below zero the RF emissions values are, the better is the cable shielding. Values shown in the tables as < or <= are below the measurement capabilities of the instrumentation. Also note that the close field probes are more sensitive to higher frequencies than they are to lower frequencies. If we compare test data from a cable in motion with data taken on the cable at rest, we see that the RF emissions from the cable in motion are greater than those from the cable at rest.

An examination of the data in Tables A and B also shows that the level of RF emissions detected through the shields of drop cables as they are bent or flexed is dependent on cable size, and that furthermore, it will vary from manufacturer to manufacturer.

**Coaxial Drop Cable
Series 6 - Aerial Standard Shield**

Cable Mfgr.	AT Freq. (MHz)	No. of Cycles Cable Flexed						At SRL	
		0	20	85	200	500	1000	Failure*	At Cycles
"A"	500	<= -68	<= -66	-55	-50	-40	-37	-40	2700
"B"	500	<= -68	<= -66	-64	-44				Halted**
"A"	1000	<= -74	-64	-45	-34	-24	-26	-27	2700
"B"	1000	<= -74	-69	-50	-36				Halted**

RF Emissions - dB Below Input Power
(Static Measurements)

*At Cycles Indicated, SRL approaches 0 dB.

**Limited Sample, Test Halted - Sample Used For GTEM Test

TABLE A

Coaxial Drop Cable Series 7 - Aerial Standard Shield

Cable Mfgr.	At Freq. (MHz)	No. of Cycles Cable Flexed					At SRL	
		0	20	85	200	500	Failure*	At Cycles
"A"	500	<= -66	-51	-39	-26	-33	-30	550
"B"	500	< -75	<= -76	<= -71	-58	-52	-53	900
"A"	1000	<= -71	-46	-30	-16	-18	-19	550
"B"	1000	<= -73	<= -76	-57	-42	-38	-35	900

RF Emissions - dB Below Input Power
(Static Measurements)

*At Cycles Indicated, SRL approaches 0 dB.

TABLE B

Electrical Deterioration of the Cable Core

The electrical deterioration of coaxial drop cables is described in detail using network analyzer produced graphics in Figures 5 through 7. It is summarized here.

Shield deterioration occurs early upon cable flexing so that often RF emissions have increased markedly by twenty flexing cycles. (Other test results have shown that cable shield emissions from some cables increased substantially after five bending cycles.) Yet changes in the cable's structural return loss at that point are minimal. If anything, the SRL curve appears to have become smoother, perhaps as a result of new scattered cable structure reflection locations. (Please note that the upward slope in the SRL graph that appears at both ends of the display is an artifact that results from the instrument's filtering utilized in the "Gating" process that was described earlier in this report.)

An examination of the cable's structural return loss and shield emissions prior to flexing the cable with the Bellcore Coaxial Drop Cable RF Emissions Test System is shown in Figure 5. The SRL is approximately 40 dBs down and the cable shield's RF emissions are so low as to be hidden by the instruments background noise. Figure 6 shows that the cable's shield leakage has increased by up to 50 dB at the higher

frequencies. The upper section of the graphic display shows that there has been little change in the SRL. Figure 7 describes cable failure. While cable shield emissions, which increased rapidly upon initial cable flexing, have continued to increase slightly (perhaps limited by the network analyzer's signal generator

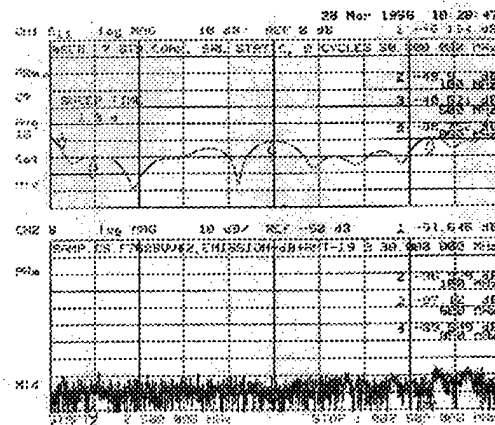


Figure 5

Network analyzer produced graphics showing coaxial drop cable structural return loss (SRL) [top] and cable shield emissions [lower] prior to cyclic flexing. The emissions shown here are beneath the analyzer's noise threshold.

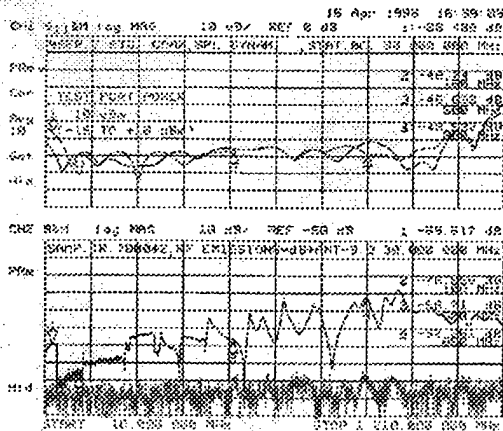


Figure 6

Network analyzer produced graphics showing coaxial drop cable structural return loss (SRL) [top] and cable shield emissions [lower] during cyclic flexing. The emissions [lower graph] shown here are up to 50 dB (higher curve) above the analyzer's noise threshold at higher frequencies (lower curve). The cable's structural return loss has not changed much.

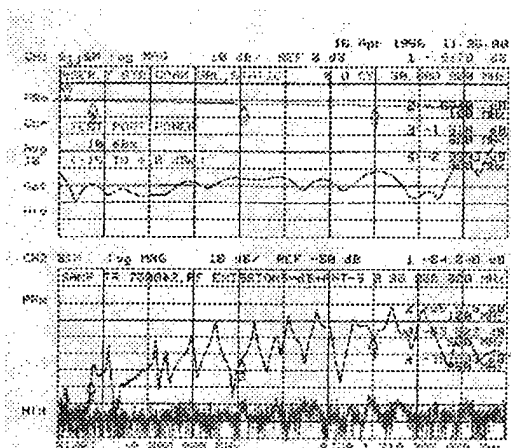


Figure 7

Network analyzer produced graphics showing coaxial drop cable structural return loss (SRL) [top] and cable shield emissions [lower] after cyclic flexing. The emissions [lower graph] shown here are over 50 dB (higher curve) above the analyzer's noise threshold (lower curve) at higher frequencies. The cable's structural return loss approaches

zero. The cable is incapable of transporting RF signals

capacity), the SRL remained relatively constant until, at defined cable failure, it quickly approached zero dB.

CONCLUSIONS

History has shown that coaxial drop cables are often the weak link in a CATV distribution plant. Within the past few years, telecommunications companies have recognized that the coaxial drop cable may be the most cost effective medium for delivering broadband services (telephony, video, data) the final step, from "curb" to home. This paper describes a test procedure to quantitatively compare the RF shielding reliability of coaxial drop cables. It describes the specialized test equipment that Bellcore designed and built to measure coaxial drop cable RF emissions.

We have concluded from our analysis of the physical reliability of coaxial drop cables that similar cables made by different manufacturers can vary widely in the integrity of their RF emissions shielding when bent or flexed.

Our analyses have established that the Bellcore coaxial drop cable RF emissions test system is a useful tool for measuring coaxial drop cable emissions. It is available to the telecommunications industry for comparing the shielding reliability of coaxial drop cables.

Part VII: Acknowledgments

The authors thank Ken Moyers, Lal Hore and Mark Carangi for their advice on the testing and the electrical measurements and William McLaughlin for performing much of the actual testing. They also thank Dr. P. Leland Key for his support and advice in developing this program and Robert Willis for shepherding it to completion.

References

ⁱ Society of Cable Telecommunications Engineers, Inc. (SCTE), Exton, PA, "Test Method for Transfer Impedance", preliminary, Document IPS-TP-011, 5/93

ⁱⁱ Society of Cable Telecommunications Engineers, Inc. (SCTE), Exton, PA, "Test Method for Shielding Effectiveness", preliminary, Document IPS-TP-403, 4/93

Joe D'Amico is a member of the Network and Product Integrity organization at Bellcore. He has worked on engineering and materials issues affecting all types of telecommunications and power cables in his career. Initially, he worked with communications cables at the Western Electric Company, later he joined the General Cable Company. There as a senior research physicist, he investigated the structure and composition of all types of telecommunications wire, cable and optical fiber as well as electrical power cables. Since 1985 Joe has worked for Bellcore, initially as a quality assurance engineer and since 1989 as a researcher and engineer in the Applied Research and in the Network and Product Integrity Organizations. Joe is a graduate of Seton Hall University. He received his MS degree from Fairleigh Dickinson University.



AUTHORS INDEX

Name	Page	Name	Page
Ahmed, K. A.	68	Chen, C.-H.	610
Akasaka, N.	471	Chen, C.-P.	511
Akasaka, Y.	888	Chen, K.	515
Akiyama, A.	695	Chen, K.-Y.	511, 515, 561
Aloisio, C. J.	302	Chen, S.-C.	614
Aoustin, H.	207, 599	Chen, W.-J.	604
Apgar, G. F.	977	Chiantore, A.	13
Arai, S.	888	Chien, C.-K.	554, 558
Araki, S.	322, 570, 695	Chou, S.-H.	561
Artingstall, L. P.	520	Clarke, M. A.	645
Arvidsson, B.	566	Clayton, P. J.	828
Asano, K.	312	Clyburn III, C. E.	359, 779
Backstrom, R.	184	Cocchini, F.	13
Baek, S.-D.	590	Cochard, S.	520
Ban, M.	471	Cogen, J. M.	167
Bark, P. R.	645	Cole, H. R.	554
Barraud, J. Y.	328	Collins, S. F.	68
Barton, R.	438	Cooke, H. G.	645
Baxter, G. W.	68	Cooper, S. A.	37
Bélanger, M.	751	Cressan, E.	100
Best, A. B.	1	Curado, P. J. P.	711
Biswas, D. R.	456	Cusanello, V. A.	914
Björkman, J.	547	Cyr, M. J.	50
Böhme, R.	43, 500	D'Amico, J.	946
Boitel, M.	207, 599	D'Amico, J. N.	977
Bonicel, J. P.	595	Daguillon, O.	100
Boscher, D.	340	Davies, M.	959
Bottanelli, M.	402	Dell, S.	520
Bouffant, O.	100	Di Censo, G.	92
Bourhis, J. F.	328	Di Francesco, A.	92
Bouvard, A.	353	Di Minico, C. T.	129
Bowmer, T. N.	479	Dodd, S.	928
Brault, D.	340	Dogi, S.	236
Bringuier, A. G.	779	Donaghy, F.	922
Brising, K.	18	dos Santos Rosa, D.	711
Brown, G.	485, 828	Dumont, D. P.	50
Brown, G. D.	167	Duprat, C. F. X.	1
Brown, R. J.	623	Dwivedi, A.	381
Burgess, D. M.	68, 704	Eng, Jr., W.	266
Cadden, A.	828	Eoll, C. K.	645
Cailleaux, J.-M.	207	Esposito, E.	92
Carones, G.	13	Evanno, N.	906
Carter, C. N.	60	Fedoroff, M.	27
Caudill, L. M.	184	Ferraro, V. J.	946
Chandan, H. C.	302	Filho, J. E.	711
Chang, S.-T.	610	Fontaine, G. N.	50
Chang, T.-C.	604	Foy, P. R.	479
Chapin, J. T.	184	Frantz, R. A.	479
Charles, Y.	8	Fujisaki, A.	253
Chastain, S. M.	369	Furukawa, H.	900
Chavez, O. G.	946	Furukawa, K.	888

Name	Page	Name	Page
Gaillard, P.	353	Jackson, K. W.	221, 623
Gallagher, D.	27	Jackson, W.	27
Gallagher, G.	718	Jansen, U.	43
Gandhi, P.	184	Jasik, J. S.	68
Gao, Z.	793	Jo, J. C.	85
Gebizlioglu, O. S.	456	Joly, B.	595
Gedde, U. W.	464	Kamei, Y.	532
Ginocchio, A.	13	Kamikatan, M.	689
Gitlits, G.	68	Kamiko, K.	894
Godo, S.	122	Kamiya, T.	888
Gouronnec, A.	906	Kang, H. J.	85
Grajewski, F.	201	Karlsson, S.	464
Griffioen, W.	485	Kasetani, T.	236, 253
Grooten, A. T. M.	485	Kashima, N.	638
Guenot, P. L.	679	Kato, Y.	312
Guerin, JY.	340	Kawano, T.	845
Guo, W.-Y.	614	Kemp, R. C.	68, 704
Ha, J. Y.	585, 391	Keogh, M. J.	167
Haigh, N. R.	60	Keon, B. J.	479
Halevi, C. H.	428	Kim, M.-G.	590
Han, K. H.	585, 391, 590	Kinard, M. D.	623
Hara, M.	506, 665	King, W. W.	228
Hasløv, P.	928	Kish, P.	287
Hata, Y.	407	Kiuchi, M.	527
Hattori, T.	471	Kmiec, C. J.	177
Hawkins, D. F.	485	Knight, I. G.	542
Hayashi, K.	236	Knuuttila, H.	928
Herman, L. E.	645	Kobayashi, K.	657
Higashikubo, T.	968	Koeman, H.	295
Hinoshita, S.	312, 726	Komiya, Z.	851
Hirai, T.	851	Konda, E.	506, 665
Hjorth, A.	490	Kroupa, K. M.	623
Hochuli, M.	817	Kubo, H.	695
Hoffart, M.	43, 500	Kubo, T.	835
Hög, G.	43, 500	Kubota, M.	214
Högström, P.-A.	464	Kuo, R.-S.	610
Holder, J.	353	Kurkjian, C. R.	456
Hondo, H.	888	Kuroiwa, M.	396
Honjo, M.	869	Kuyl, P. B.	736
Hore, L. M.	946	Kuzushita, H.	968
Hosoi, F.	506	Lai, K.-H.	511, 515
Hsiao, C.-M.	561	Lai, S.-W.	610
Hsiao, J.-M.	604	Latini, M. E.	711
Hsu, H.-P.	561, 604	Le Noane, G.	595
Hua, P. A.	1	Le Sergeant, C.	939
Huang, L.-J.	610	Le Traon, G.	100
Hughes, F. T.	575	Lee, B.-C.	391, 590
Hugo, P.	438	Lee, C.-C.	511, 515
Imamura, S.	495	Lee, Y. I.	85
Ishi, S.	726	Lee, Y. T.	585, 391, 590
Ishisaki, H.	495	Leech, J. R.	177
Ito, M.	537, 845	LeFevre, B. G.	228
Ito, T.	260	Legros, F.	340
Iwano, S.	374	LeNir, V.	751
Iwata, H.	638	Libert, J.-F.	8, 788
Jackman, W. S.	645	Lin, J.-C.	561

Name	Page	Name	Page
Lin, Y.-c.	561, 604	Nozawa, T.	875
Livingston, R. O.	645	Odom, R. I.	415
Lopez, A.	328	Ogawa, O.	689
Lord, B.	287	Oh, S.-K.	590
Louboutin, JP	340	Ohmizu, S.	882
Lu, M.-S.	610	Ohsono, K.	312
Lundergan, M. L.	37	Ohta, M.	835
Maglio, M.	246	Oka, R.	333
Mahe, T.	207	Okada, N.	657
Maillard, J.-J.	599	Oku, M.	665
Maki, H.	407	Okuda, M.	882
Mann, J. D.	479	Olsen, R.	449
Marcone, A.	860	Omori, T.	657
Markezich, R. L.	194	Omoto, K.	396
Matsuda, T.	407	Omura, H.	618, 669
Matsuda, Y.	471	Oohashi, K.	322, 570
Matsumoto, Y.	835	Opel, E.	631
Mazzarese, D.	914	Orcel, G. F.	328
Mazzotti, A.	928	Osaka, K.	580
McCormick, W. D.	415	Osmondson, B.	743
McNutt, C.	328, 353	Overgaard, J. V.	928
Mercereau, O.	679	Overton, B. J.	328
Mettler, S. C.	221	Panicali, A. R.	955
Mikawa, M.	214	Parente, M.	115
Miyamoto, M.	657, 689	Park, S. C.	85
Mlinarsky, F. I.	762	Payne, G. V.	809
Moalic, J.	100	Pecot, A.	207, 599
Momma, H.	495	Pereira Netto, A. C.	711
Moore, R. C.	302	Personne, J.	595
Morellec, D.	599	Petit, R.	100
Morimitsu, T.	214	Pfandl, W.	793
Moro, D.	246	Pitassi, S.	860
Morris, P.	821	Pitombo, C.	711
Murase, T.	845	Plitz, I. M.	479
Murata, A.	322, 570	Plumettaz, G.	485
Nagai, K.	665	Poumellec, B.	679
Nagatomi, K.	77	Pozzi, F.	246, 860
Nagatomi, O.	527	Preston, J.	520
Nakagawa, M.	260	Radley, J. S.	809
Nakamura, H.	253, 537, 845	Rampalli, S.	139
Nakao, N.	396	Regio, P.	928
Nakayama, A.	726	Richter, S.	500
Nakayama, H.	618, 669	Roland, D.	914
Naraoka, S.	894	Roman, R. C.	37
Nasu, H.	618, 669	Roussel, Y.	340
Neveux, Jr., P. E.	800, 809	Rowland, S. M.	60
Nielsen, M. W.	743	Rybinski, V. A.	277
Niiyama, S.	333	Saegusa, M.	845
Nijstad, H.	485	Saito, M.	665
Ninomiya, M.	260	Sandwith, C. J.	415
Nishida, T.	527	Sanjo, K.	835
Nishimura, A.	333	Sansonetti, P.	939
Nomura, Y.	900	Santana, M. R.	623
Nothofer, K.	43, 500	Sato, M.	374
Nouchi, P.	679, 939	Sato, T.	882
Nozawa, M.	638	Sawyer, D.	520

Name	Page
Schick, G.	115
Schulze-Buxloh, K.	959
Schürmann, H.	108
Sears, F. M.	645
Seidenberg, J.	108, 201
Sekiya, K.	236
Sepper, W.	438
Shibata, M.	695
Shigematsu, T.	882
Shimane, H.	312
Shimoohsako, K.	236
Shiono, T.	537, 845
Shiraishi, K.	537
Smith, J. L.	381
Smith, M.	914
Sodhi, S. S.	645
Sollenberger, N. W.	221, 302
Spano, V.	860
Stappers, V.	599
Stephenson, D. L.	228
Stieb, W.	201
Stöcklein, W.	793
Stokes, S. R.	809
Stringer, A.	68, 704
Stupak, P. R.	914
Suetsugu, Y.	77
Suga, K.	968
Sugimoto, M.	851
Sugizaki, R.	888
Sunaga, K.	869
Supczak, M.	914
Susaeta, L. M. M.	1
Susai, K.	253
Suzuki, A.	471
Suzuki, Y.	888
Svensson, T.	490, 547, 928
Tabaddor, P. L.	302
Tachikura, M.	374
Taguchi, T.	407
Taha, A. J.	60
Takagi, S.	333
Takenami, Y.	407
Tamaki, Y.	875
Tamekuni, Y.	869
Tanaka, S.	77
Tanifuji, T.	638
Tanskanen, J. K.	566
Taoka, S.	532
Tardif, D.	287
Tatat, O.	353
Taylor, C. R.	302
Tedder, C. L.	359
Tedeschi, A.	92
Tezuka, K.	618, 669
Thomas, P. M.	623
Thompson, G. O.	773

Name	Page
Thornton, J. A.	415
Thornton, J. W.	369
Tokumaru, K.	835
Toler, J. R.	554
Tomita, K.	396
Tomita, N.	374
Tomizu, D.	260
Traut, R. T.	50
Tsai, F.-Y.	515, 614
Turnipseed, J. M.	302
Ueda, T.	869
Ukachi, T.	851
van Wingerden, A.	485
Vanpouille, S.	328
Vergez, C.	595
Vincent, A.	595
Vogel, E. M.	479
Vokey, D.	718
Volotinen, T.	928
Wada, M.	968
Wade, S. A.	68
Wagman, R. S.	645
Wahl, W.	438
Walling, J.-H.	287, 751
Wang, C.-S.	511, 515
Wang, S.-W.	614
Watanabe, K.	580, 657, 726
Watanabe, T.	580
Wells, J. P.	828
Wieczorek, C. J.	479
Wildeman, G.	27
Wise, D. R.	415
Wright, W. F.	50
Yamada, K.	312
Yamaguchi, S.	894
Yamamoto, T.	968
Yamanishi, T.	869
Yokokawa, T.	77
Yokosuka, H.	875, 900
Yonezawa, K.	77
Yoshida, K.	214
Yoshii, Y.	396
Yoshimura, T.	236
Yoshioka, H.	527
Yoshizawa, J.	851
Young, K.	718
Yusa, H.	580
Zakoh, T.	407
Zamzow, P.	201
Zamzow, P. E.	108
Zushi, T.	968

45TH INTERNATIONAL WIRE AND CABLE SYMPOSIUM (IWCS) SYMPOSIUM COMMITTEE

IWCS STAFF

ELMER F. GODWIN
(President/Director)
GEF Associates
3A Buttonwood Drive
Shrewsbury, NJ 07702
Tel: (908) 389-0990 (Office)
Fax: (908) 389-0991 (Office)
E-mail: iwcs@monmouth.com

IRVING KOLODNY
(Director's Assistant)
80-56 230th street
Bellerose Manor, NY 11427
Tel & Fax: (718) 464-9197

PATRICIA HUDAK
(Administrative Assistant)
174 Main Street
Eatontown, NJ 07724
Tel: (908) 389-0990
Fax: (908) 389-0991
E-mail: iwcs@monmouth.com

1996 OFFICERS

RICHARD ROSSI
(Chairman)
General Cable Co.
300 Plainfield Road
Edison, NJ 08820
Tel: (908) 205-9460
Fax: (908) 205-9456

JAMES R. LEECH
(Vice-Chairman)
Union Carbide Corp.
Weston Canal Center
PO Box 450
Somerset, NJ 08875-0450
Tel: (908) 271-7935
Fax: (908) 271-7949
E-mail: ajrlp01@peabody.
sct.ucarb.com

XAVIER MANN
(Secretary)
AT&T Fitel
201 Adamson Industrial Blvd
Carrollton, GA 30117
Tel: (770) 830-6616
Fax: (770) 836-8820
E-mail: xmanna@attmail.com

INGE B. KOVACS
(Treasurer)
Consultant for Polychex Ltd
264 Harvard Drive
Hackettstown, NJ 07840
Tel: (908) 852-1610
Fax: (908) 852-1518

1996 COMMITTEE MEMBERS

NILS ARTLÖVE
Telia AB
Conductores Latincasa S.A. de C.V.
Av. Industrias Esp. 120
78090 San Luis Potosi, Mexico
Tel: +52-48-24-59-62
Fax: +52-48-24-59-81
E-mail: Nils.A.Artlove@telia.com

DR. STEPHEN HORNUNG
120/B67
British Telecom Laboratories
Martlesham Heath
Ipswich IP5 7RE
United Kingdom
Tel: +44-1473-644685
Fax: +44-1473-644142

DR. MAREK KAPUŚCINSKI
NORDX/CDT
150, Montreal-Toronto Blvd
Lachine, Quebec
Canada H8S 1B6
Tel: (514) 639-2328
Fax: (514) 639-2337

MICHEL ROUSSEAU
Alcatel Cable
30, rue des Chasses
BP 309
92111 Clichy Cedex
France
Tel: +33-1-4756-6900
Fax: +33-1-4756-6739

HIROTOSHI HONDO
The Furukawa Electric Co, Ltd.
Information & Electronics Laboratory
5-1-9 Higashiyawata
Hiratsuka, Kamagawa, 254, Japan
Tel: +81-463-24-8450
Fax: +81-463-24-8491
E-mail: hondo@ie.inf.furukawa.co.jp

LAURENCE JONES
Borealis Compounds, Inc.
176 Thomas Road
Port Murray, NJ 07865
Tel: (908) 850-6200
Fax: (908) 850-6268

PAUL M. KOPERA
Anixter Inc.
4711 Golf Road
Skokie, IL 60076
Tel: (708) 677-2600
Fax: (708) 674-3045
E-mail: paul.kopera@anixter.com

JOHN R. SICOTTE
Corning Inc
35 W. Market St., MP-RO-03
Corning, NY 14831
Tel: (607) 974-4447
Fax: (607) 974-7549
E-mail: SICOTTE_JR@corning.com

DR. FELIX P. KAPRON
Bellcore
445 South Street, MCC-1A104B
Morristown, NJ 07960-6438
Tel: (201) 829-5225
Fax: (201) 829-5965
E-mail: fkapron@notes.cc.
bellcore.com

FRED NARAYAN
Phelps Dodge International Corp.
2121 Ponce de Leon Blvd.
Coral Gables, FL 33134
Tel: (305) 447-4322
Fax: (305) 448-7250

DR. HOWARD WICHANSKY
Cdr, US Army CECOM
ATTN: AMSEL-RD-ST-WL-AW
Fort Monmouth, NJ 07703-5203
Tel: (908) 427-4713
Fax: (908) 427-2150
E-Mail: wichansk@doim6.monmouth.
army.mil

ADVISORY

DR. PETER R. BARK
Siecor Corporation
P.O. Box 489
489 Siecor Park
Hickory, NC 28603
Tel: (704) 323-6205
Fax: (704) 323-6264
E-mail: Peter_Bark@siecor.com

DAVE FALLOWFIELD
TELUS Advanced Communications
10039 102 Avenue
Edmonton, Alberta
Canada T5J 0E5
Tel: (403) 944-4272
Fax: (403) 426-3868
E-mail: davef@tac.net

LEO CHATTLER
DCM Industries, Inc.
2930 Faber Street
Union City, CA 94587
Tel: (510) 429-9500
Fax: (510) 429-1250

DIETER S. NORDMANN
(European Representative)
Kabelmetal Electro GmbH
P.O. Box 260; Kabelkamp 20
D30179 Hannover, Germany
Tel: +49-511-676-2020
Fax: +49-511-676-2664

MICHAEL A. DELUCIA
Consultant
Tel: (410) 721-2991
E-mail: mdelucia@clark.net

MANUEL R. SANTANA
Lucent Technologies
Bell Laboratories
2000 NE Expressway, Rm 1D32
Norcross, GA 30071
Tel: (770) 798-2754
Fax: (770) 798-4654
E-mail: msantana@lucent.com

CONSULTANTS

DR. REINER J. GERDES
TransTel Group Inc.
5555 Oakbrook Pkwy, Suite 110
Norcross, GA 30093
Tel: (770) 368-8343
Fax: (770) 368-8382
E-mail: rgerdes@transtelgroup.com

DR. RAYMOND E. JAEGER
SpecTran Corporation
50 Hall Road
Sturbridge, MA 01566
Tel: (508) 347-2261
Fax: (508) 347-2747

HANS A. MAYER
Olex Cables (A Division of Pacific Dunlop Ltd.)
207 Sunshine Road
Tottenham, VIC 3012
Melbourne, Australia
Tel: +61-3-9281-4240
Fax: +61-3-9314-1436

IWCS INTERNET HOME PAGE:
<http://www.iwcs.org/iwcs/>